EANM'19

Annual Congress of the European Association of Nuclear Medicine
October 12 – 16, 2019
Barcelona, Spain

Abstracts

European Journal of Nuclear Medicine and Molecular Imaging (2019) 46 (Suppl 1): S1–S952
10.1007/s00259-019-04486-2

This supplement was not sponsored by outside commercial interests. It was funded entirely by the association's own resources.

Dear colleagues, dear friends,

On behalf of the European Association of Nuclear Medicine, it is my great pleasure and honour to cordially invite you to the 32nd Annual EANM Congress in October 2019. This year, our Congress will take place in Barcelona, Spain. The city is world famous for its hospitality, its cultural attractions and its culinary highlights.

Molecular imaging is continuously expanding: it is increasingly being combined with advanced technologies such as artificial intelligence and has become a principal component of medical imaging. In the therapy field, targeted radiopharmaceuticals have been demonstrated to be effective and are increasingly used in a variety of clinical settings, often integrated with other therapeutic options. The ultimate goal is to design personalised, super-selective therapies and to identify more precise means of monitoring response to treatment in routine clinical practice.

In the last three years, the status of the EANM annual meeting as the world-reference congress in nuclear medicine has been confirmed. In order to maintain the high level of excellence, the 2019 EANM Congress will build on the traditions that are highly appreciated by all attendees, with the expansion of newer features. A specific educational track, implemented with the collaboration of the European School of Multimodality Imaging and Therapy, will include up-to-date teaching sessions, enriched pitfalls seminars and Continuous Medical Education interactive sessions. In all these active learning conferences, attendees will have the possibility to enhance their knowledge of multimodality imaging. A careful evaluation procedure relating to the speakers will be implemented in order to gain feedback and ensure that future interactive sessions continue to enjoy a positive response. With similar pedagogic intent, numerous multidisciplinary joint symposia, organised by several EANM Committees in collaboration with our sister societies, will offer an integrative approach to various topics relevant to the state of the art of our discipline.

All these learning sessions will not impact adversely on the predominant role of our Congress, which is to enable oral and electronic poster presentations on the latest achievements in clinical nuclear medicine, science and technology. On the contrary, the oral sessions will be enriched. Rapid Fire sessions will draw attention to the highly rated abstracts in specific fields, with a panel of top-level presentations followed by extensive discussions; this will provide attendees with an integrated and coherent view on a wide variety of topics. Furthermore, the concept of featured oral sessions in which an invited speaker places the presentations into a broader perspective will be generalised to the other oral presentations. The now well-established tracks M2M – Molecule to Man (basic and translational science) and Do.MoRe (radionuclide therapy and dosimetry) promise to promote high-quality research through interaction between basic and translational clinical scientists and to present the latest achievements and developments in the fields of clinical molecular imaging and nuclear medicine therapy. During plenary lectures, distinguished speakers will address the state of the art and new developments in clinical and allied sciences, covering a broad range of topics with the goal of fostering the provision of the best possible care for our patients.

I am particularly delighted that two young but very motivated and highly respected members of our European Nuclear Medicine community, Dr. Valentina Garibotto from Geneva, Switzerland, and Dr. Sarah Schwarzenböck from Rostock, Germany, will provide the traditional Highlights lecture.

For all these reasons, I cordially invite you to EANM'19 to actively participate in our 32nd Annual Congress, to meet and interact with friends and colleagues from all over the world, to discuss science, to learn about the exciting developments in nuclear medicine, to break away from the daily routine and to enjoy everything that the city of Barcelona has to offer.

Francesco Giammarile,
EANM Congress Chair 2017-2019

Saturday, October 12, 2019

						Room 111	Room 113	Room 114	Room 115	Room 116	
08:00 - 08:30											08:00 - 08:30
08:30 - 09:00											08:30 - 09:00
09:00 - 09:30						**Pre-Symposium 1** Inflammation & Infection Committee Systematic Reviews and Meta-Analyses of Diagnostic Test Accuracy (DTA)	**Pre-Symposium 2** Cardiovascular Committee / EACVI Quantification of Myocardial Blood Flow - Ready for Daily Practice?	**Pre-Symposium 3** Radiopharmacy + Oncology & Theranostics + Dosimetry Committee Alpha Therapy - Practical Aspects on Chemistry and Applications	**Pre-Symposium 4** Translational Molecular Imaging and Therapy + Drug Development + Radiopharmacy Committee We can't make it cool, but we can make it easier....	**Pre-Symposium 5** Dosimetry + Physics Committee Dosimetry from Image Reconstruction with Monte Carlo Modelling	09:00 - 09:30
09:30 - 10:00											09:30 - 10:00
10:00 - 10:30											10:00 - 10:30
10:30 - 11:00											10:30 - 11:00
11:00 - 11:30		**EANM Advisory Council Meeting**									11:00 - 11:30
11:30 - 12:00											11:30 - 12:00
12:00 - 12:30											12:00 - 12:30
12:30 - 13:00											12:30 - 13:00
13:00 - 13:30						**Pre-Symposium 6** Thyroid Committee / ESES An Update on Differentiated Thyroid Cancer (DTC) - Overview of Management	**Pre-Symposium 7** Neuroimaging Committee Reserve, Resilience and Protective Factors in AD - Contribution of Molecular Imaging	**Pre-Symposium 8** Oncology & Theranostics Committee / EAU PSMA Theranostics and Beyond	**Pre-Symposium 9** Physics + Dosimetry Committee Advances in Image Processing Techniques	**Pre-Symposium 10** Radiation Protection + Dosimetry Committee European Projects for Clinical Implementation of Dosimetry in Molecular Radiotherapy	13:00 - 13:30
13:30 - 14:00											13:30 - 14:00
14:00 - 14:30			**EANM Delegates' Assembly**								14:00 - 14:30
14:30 - 15:00											14:30 - 15:00
15:00 - 15:30											15:00 - 15:30
15:30 - 16:00											15:30 - 16:00
16:00 - 16:30											16:00 - 16:30
16:30 - 17:00			**EANM Members' Assembly**								16:30 - 17:00
17:00 - 17:30											17:00 - 17:30
17:30 - 18:00											17:30 - 18:00
18:00 - 18:30											18:00 - 18:30
19:30 - 20:30	**Opening Ceremony**										19:30 - 20:30

Sunday, October 13, 2019

	Auditorium	Room 311	Room 312	Room 117	Room 111	Room 112	Room 113	Room 114	Room 115	Room 116	Room 133/134	
08:00 - 08:30	101 CME 1 Dosimetry Committee An Educational Trip from Organ to Voxel-Based to Small Scale Dosimetry	102 Joint Symposium 1 Bone & Joint + Inflammation & Infection Committee / EULAR Bone Imaging in Chronic Inflammatory Joint Conditions	103 Joint Symposium 2 Cardiovascular + Translational and Molecular Imaging Therapy + Inflammation & Infection Committee / ESMI New Approaches for the More Specific Detection of Inflammatory Cells than FDG	104 Technologists' Opening (08:00-08:15) CTE 1 Technologist Committee / CAMRT / ANZSNM Technologist Approach to Global Dose Optimization	105 M2M - Parallel Session Improvement of PSMA Ligands	106 Do.MoRe - Rapid Fire Session Data Analysis	107 Pitfalls & Artefacts 1 - ICC* Paediatrics Committee Pitfalls and Artefacts in Paediatric Nephro-Urology	108 Clinical Oncology - Rapid Fire Session Prostate - BCR and More	109 Neuroimaging - Rapid Fire Session Kinetic Modeling and Computational Approach in Neuroimaging	110 Cardiovascular - Parallel Session Myocardial Blood Flow Quantification with SPECT	111 e-Poster Presentation Session 1 Oncology Oncology - Greatest Hits	08:00 - 08:30
08:30 - 09:00												08:30 - 09:00
09:00 - 09:30												09:00 - 09:30
09:30 - 10:00												09:30 - 10:00
10:00 - 10:30	201 Plenary 1 incl. Marie Curie Lecture Radiomics and Artificial Intelligence			204 Plenary 1 incl. Marie Curie Lecture (in Auditorium) Radiomics and Artificial Intelligence								10:00 - 10:30
10:30 - 11:00												10:30 - 11:00
11:00 - 11:30												11:00 - 11:30
11:30 - 12:00	301 CME 2 Oncology & Theranostics Committee NET - PRRT and More	302 Joint Symposium 3 Bone & Joint + Paediatrics Committee / EPOS Role of Bone SPECT/CT in Paediatric Population	303 Joint Symposium 4 Cardiovascular Committee / ASNC** New Development in Nuclear Cardiology - Ready for Prime Time?	304 CTE 2 Technologist + Radiation Protection Committee Risk and Incidents	305 M2M - Parallel Session Radionuclide Production	306 Do.MoRe - Parallel Session Diagnostic Dosimetry	307 Pitfalls & Artefacts 2 - ICC* Dosimetry Committee From Imaging to Dosimetry - Step-by-Step Patient Dosimetry	308 Clinical Oncology - Rapid Fire Session Prostate - BCR only	309 Thyroid - Rapid Fire Session Thyroid and Parathyroid		311 e-Poster Presentation Session 2 Inflammation & Infection + Translational and Molecular Imaging Therapy Infection and Inflammation - Clinical and Preclinical Studies	11:30 - 12:00
12:00 - 12:30												12:00 - 12:30
12:30 - 13:00												12:30 - 13:00
13:00 - 14:30	Lunch Symposium					Lunch Symposium	EANM Young Daily Forum		Lunch Symposium	Lunch Symposium		13:00 - 14:30
14:30 - 15:00	401 CME 3 Radiation Protection + Dosimetry Committee Metrological Aspects on the Implementation of Dosimetry in Radionuclide Therapy	402 Joint Symposium 5 Oncology & Theranostics Committee / EORTC The Future of Medical Imaging in Precision Medicine	403 Joint Symposium 6 Translational and Molecular Imaging Therapy + Cardiovascular + Inflammation & Infection Committee / AHA Imaging Inflammation as Major Determinant of Cardiovascular Diseases - New Tracers and Clinical Applications	404a Mini Course 1 (14:30-15:30) Technologist Committee Research Methodology 404b Mini Course 2 (15:45-16:45) Technologist Committee Stress Testing for Technologists	405 M2M - Parallel Session Antibody-Based Radionuclide Therapy	406 Do.MoRe - Parallel Session Image Reconstruction	407 Teaching Session 1 - ICC* Paediatrics + Thyroid + Translational and Molecular Imaging Therapy Committee Management of Thyroid Cancer in Children	408 Clinical Oncology - Rapid Fire Session New Tracers and Machine Learning	409 Thyroid - Parallel Session Thyroid Cancer	410 Clinical Oncology - Parallel Session Lung, Head & Neck and More	411 e-Poster Presentation Session 3 Neuroimaging Neurodegeneration, Amyloidosis and Neuroinflammation	14:30 - 15:00
15:00 - 15:30												15:00 - 15:30
15:30 - 16:00												15:30 - 16:00
16:00 - 16:30				404c Mini Course 3 (17:00 - 18:00) Technologist Committee Theranostics - Fundamental								16:00 - 16:30
16:30 - 17:00	501 CME 4 Radiopharmacy + Drug Development + Translational and Molecular Imaging Therapy + Oncology & Theranostics Committee Role of Extracellular Matrices in Cancer and Other Diseases	502 Joint Symposium 7 Physics + Dosimetry Committee / AAPM Interventional Nuclear Medicine	503 Joint Symposium 8 Cardiovascular Committee / EACVI Which Strategy for the Evaluation of Patients at the Time of Multi-Modality Cardiac Imaging?		505 M2M - Parallel Session Radiolabelled Peptides and Proteins	506 Do.MoRe - Parallel Session ^{177}Lu PRRT and other Preclinical & Clinical Dosimetry	507 Teaching Session 2 - ICC* Radiopharmacy + Inflammation & Infection + Oncology & Theranostics Committee Imaging Immune Cells	508 Clinical Oncology - Rapid Fire Session PRRT 4.0?	509 Neuroimaging - Parallel Session Movement Disorders and Neurotransmission	510 Cardiovascular - Parallel Session Cardiac Imaging - More than Perfusion	511 e-Poster Presentation Session 4 Paediatrics & Other Clinical Studies Joint Paediatrics & Other Clinical Studies	16:30 - 17:00
17:00 - 17:30												17:00 - 17:30
17:30 - 18:00												17:30 - 18:00

Monday, October 14, 2019

	Auditorium	Room 311	Room 312	Room 117	Room 111	Room 112	Room 113	Room 114	Room 115	Room 116	Room 133/134	
08:00 - 08:30	601 CME 5 Oncology & Theranostics + Bone & Joint Committee Radionuclide Molecular Imaging in Bone Tumours and Multiple Myeloma - Pearls, Patterns & Pitfalls	602 Joint Symposium 9 Neuroimaging Committee / ILAE Clinical Use of Brain Imaging for Patients with Epilepsy	603 Joint Symposium 10 Drug Development / SRS What is Molar Activity and When does it Impact PET Imaging?	604 Technologists Oral Presentations 1	605 M2M - Parallel Session Innovations in Bio-Nanotechnology	606 Do.MoRe - Parallel Session Preclinical Dosimetry - What is the Future?	607 Pitfalls & Artefacts 3 - ICC* Cardiovascular + Inflammation & Infection Committee Tips and Tricks in the Interpretation of Cardiac PET	608 Clinical Oncology - Parallel Session Breast and Gynaecological Cancers	609 Paediatrics - Parallel Session Paediatrics	610 Endocrine - Parallel Session Neuroendocrine Malignancies	611 e-Poster Presentation Session 5 Oncology Oncology - e-Poster All Stars	08:00 - 08:30
08:30 - 09:00												08:30 - 09:00
09:00 - 09:30												09:00 - 09:30
09:30 - 10:00												09:30 - 10:00
10:00 - 10:30	701 Plenary 2 Prostate Cancer-Reload			704 Plenary 2 (in Auditorium) Prostate Cancer-Reload								10:00 - 10:30
10:30 - 11:00												10:30 - 11:00
11:00 - 11:30												11:00 - 11:30
11:30 - 12:00	801 CME 6 Inflammation & Infection + Translational and Molecular Imaging Therapy + Radiopharmacy Committee Molecular Imaging Technologies for Infectious Diseases	802 Joint Symposium 11 Neuroimaging Committee / ISCBFM** New Applications for Hybrid Brain PET/MRI	803 Symposium 12 Physics Committee Digital Detection in Clinical NM (PET/SPECT)	804 Technologists Technologist e-Poster Presentation Sessions 1-4	805 M2M - Parallel Session PET Radiosynthesis	806 Do.MoRe - Parallel Session Clinical Dosimetry and Modeling	807 Pitfalls & Artefacts 4 - ICC* Oncology & Theranostics Committee PSMA Imaging	808 Clinical Oncology - Featured Session Implementing Radiomics into Technical Practice		810 Thyroid - Rapid Fire Session Prognostic Factors in DTC	Technologists e-Poster Presentation Session Slot	11:30 - 12:00
12:00 - 12:30												12:00 - 12:30
12:30 - 13:00												12:30 - 13:00
13:00 - 14:30	Lunch Symposium					Lunch Symposium	EANM Young Daily Forum		Lunch Symposium	Lunch Symposium		13:00 - 14:30
14:30 - 15:00	901 CME 7 Translational and Molecular Imaging Therapy Committee Imaging Immune Therapy	902 Joint Symposium 13 Neuroimaging Committee / EANO Low Grade Glioma	903 Joint Symposium 14 Dosimetry + Radiation Protection Committee / ICRP Radiological Protection in Therapy with Radiopharmaceuticals	904 CTE 3 Technologist Committee Preclinical Studies, from Bench to Bedside	905 M2M - Parallel Session Neurodegeneration and Neuroinflammation	906 Do.MoRe - Parallel Session Artificial Intelligence in Image Processing	907 Teaching Session 3 - ICC* Radiological Aspects of Thoracic Anatomy	908 Clinical Oncology - Featured Session Evaluating Immunotherapy - Where do we stand?	909 Special - Parallel Session Tomorrow's Experts Session - Best-Ranked Papers from the Under-30s	910 Inflammation & Infection - Parallel Session Inflammation & Infection - PET in Vascular Infection and Myocardial Inflammation	911 e-Poster Presentation Session 6 Cardiovascular Searching for Myocardial Ischemia	14:30 - 15:00
15:00 - 15:30												15:00 - 15:30
15:30 - 16:00												15:30 - 16:00
16:00 - 16:30												16:00 - 16:30
16:30 - 17:00	1001 CME 8 Thyroid Committee Secondary Effects of Radioiodine Treatment	1002 Joint Symposium 15 Oncology & Theranostics Committee / ESMO Immunological Landscape in Solid Tumours and its Implications in Response to Immunotherapy	1003 Joint Symposium 16 Dosimetry + Translational and Molecular Imaging Therapy Committee / ESTRO Dosimetry in Preclinical Setting to Determine Dose Limits and Extrapolation to Clinical Dosimetry	1004 CTE 4 Technologist Committee / SNMMI Technologist Guide Launch - Radiopharmacy: An Update	1005 M2M - Parallel Session Tumour Microenviroment & Cancer Biomakers	1006 Do.MoRe - Parallel Session Dosimetry for PSMA Radiopharmaceuticals	1007 Teaching Session 4 - ICC* Translational and Molecular Imaging Therapy + Drug Development Committee Chemical Entities that can Induce a Therapeutic Response in Vivo - Light vs Radioisotopes	1008 Clinical Oncology - Featured Session Hybrid PET/MRI - Quo Vadis?	1009 Neuroimaging - Parallel Session TAU Imaging	1010 Cardiovascular - Parallel Session Myocardial Blood Flow Quantification with PET	1011 e-Poster Presentation Session 7 Do.MoRe Image Reconstruction & Data Analysis	16:30 - 17:00
17:00 - 17:30												17:00 - 17:30
17:30 - 18:00												17:30 - 18:00

Tuesday, October 15, 2019

	Auditorium	Room 311	Room 312	Room 117	Room 111	Room 112	Room 113	Room 114	Room 115	Room 116	Room 133/134	
08:00 - 08:30	1101 CME 9 Cardiovascular Committee Non-Invasive Imaging Strategies in Heart Failure	1102 Joint Symposium 17 Oncology & Theranostics Committee / AIO Challenge Pancreatic Cancer	1103 Joint Symposium 18 Thyroid + Inflammation & Infection Committee / ETA Imaging on Thyroiditis	1104 Technologists Oral Presentations 2	1105 M2M - Parallel Session Immune Therapy	1106 Do.MoRe - Parallel Session I-131 Dosimetry and DNA Damage during Different Therapies	1107 Pitfalls & Artefacts 5 - ICC* Neuroimaging + Technologists Committee Brain PET and SPECT - Patients' Preparation and Acquisition	1108 Clinical Oncology - Parallel Session Radioguided Surgery	1109 Cardiovascular - Parallel Session Imaging the Vessel Wall	1110 Do.MoRe - Parallel Session Performance, Standardisation & Quality Control	1111 e-Poster Presentation Session 8 Bone & Joint Bone SPECT/CT - Clinical Imaging Pattern and Quantification Tools	08:00 - 08:30
08:30 - 09:00												08:30 - 09:00
09:00 - 09:30												09:00 - 09:30
09:30 - 10:00												09:30 - 10:00
10:00 - 10:30	1201 Plenary 3 Next Generation PET Technology in the Clinical Setting			1204 Plenary 3 (in Auditorium) Next Generation PET Technology in the Clinical Setting								10:00 - 10:30
10:30 - 11:00												10:30 - 11:00
11:00 - 11:30												11:00 - 11:30
11:30 - 12:00	1301 CME 10 Neuroimaging Committee / EAN EANM-EAN Recommendations for the Use of Brain 18 F-FDG-PET in Neurodegenerative Cognitive Impairment and Dementia	1302 Joint Symposium 19 Oncology & Theranostics Committee / EHA PET/CT Guided Treatment in Non-Hodgkin Lymphoma	1303 Joint Symposium 20 Thyroid Committee / ETA-CG / EFSUMB Thyroid Cancer Imaging and Biomarkers	1304 Technologists Oral Presentations 3	1305 M2M - Parallel Session Preclinical Developments in Infectious Diseases	1306 Do.MoRe - Parallel Session SPECT/CT Quantification & Data Analysis	1307 Pitfalls & Artefacts 6 - ICC* Cardiovascular Committee Pitfalls & Artefacts in Cardiac Imaging	1308 Clinical Oncology - Parallel Session Therapy Response Assessment - Conventional Criteria and More			1311 e-Poster Presentation Session 9 Do.MoRe Dosimetry	11:30 - 12:00
12:00 - 12:30												12:00 - 12:30
12:30 - 13:00												12:30 - 13:00
13:00 - 14:30					Lunch Symposium	Lunch Symposium	EANM Young Daily Forum		Lunch Symposium	Lunch Symposium		13:00 - 14:30
14:30 - 15:00	1401 CME 11 Physics + Cardiovascular Committee Advances in Quantitative Cardiac Imaging	1402 Joint Symposium 21 Oncology & Theranostics Committee / ESGO** Ovarian Cancer	1403 Joint Symposium 22 TBA	1404 CTE 5 Technologist Committee Patient Communication	1405 M2M - Parallel Session Targeting the Brain	1406 Do.MoRe - Parallel Session Radiobiology and Dosimetry for Radioembolisation Therapy	1407 Teaching Session 5 - ICC* Neuroimaging Committee Neuroimaging - Before Reading PET Scans	1408 Clinical Oncology - Parallel Session Therapy - PSMA and More	1409 Bone & Joint - Featured Session Bone SPECT/CT and PET/CT Quantification - A Clinical Tool for Diagnosis and Prognosis in Diffuse and Localised Skeletal Diseases	1410 General Nuclear Medicine - Parallel Session General Nuclear Medicine	1411 e-Poster Presentation Session 10 Oncology Oncology - Mixed Pickles	14:30 - 15:00
15:00 - 15:30												15:00 - 15:30
15:30 - 16:00												15:30 - 16:00
16:00 - 16:30												16:00 - 16:30
16:30 - 17:00	1501 CME 12 Paediatrics Committee Response Evaluation of Paediatric Sarcomas	1502 Joint Symposium 23 Oncology & Theranostics Committee / ENETS Theranostic in NEN - What is New?	1503 Joint Symposium 24 Translational and Molecular Imaging Therapy + Oncology & Theranostics Committee / EAU** / ERUS** Image Guided Therapies for Prostate Cancer	1504 CTE 6 Technologist Committee Parathyroid Imaging	1505 M2M - Parallel Session Preclinical Models in Translational Science	1506 Do.MoRe - Parallel Session New Concepts, Harmonisation and Standardisation in Radiomics	1507 Teaching Session 6 - ICC* Radiological Aspects of Abdominal Anatomy	1508 Clinical Oncology - Parallel Session Liver Selective Therapy - 90Y and Beyond	1509 Neuroimaging - Parallel Session Brain Tumours	1510 Clinical Oncology - Parallel Session It's in the Blood!	1511 e-Poster Presentation Session 11 Cardiovascular Imaging Cardiomyopathies	16:30 - 17:00
17:00 - 17:30												17:00 - 17:30
17:30 - 18:00												17:30 - 18:00

Wednesday, October 16, 2019

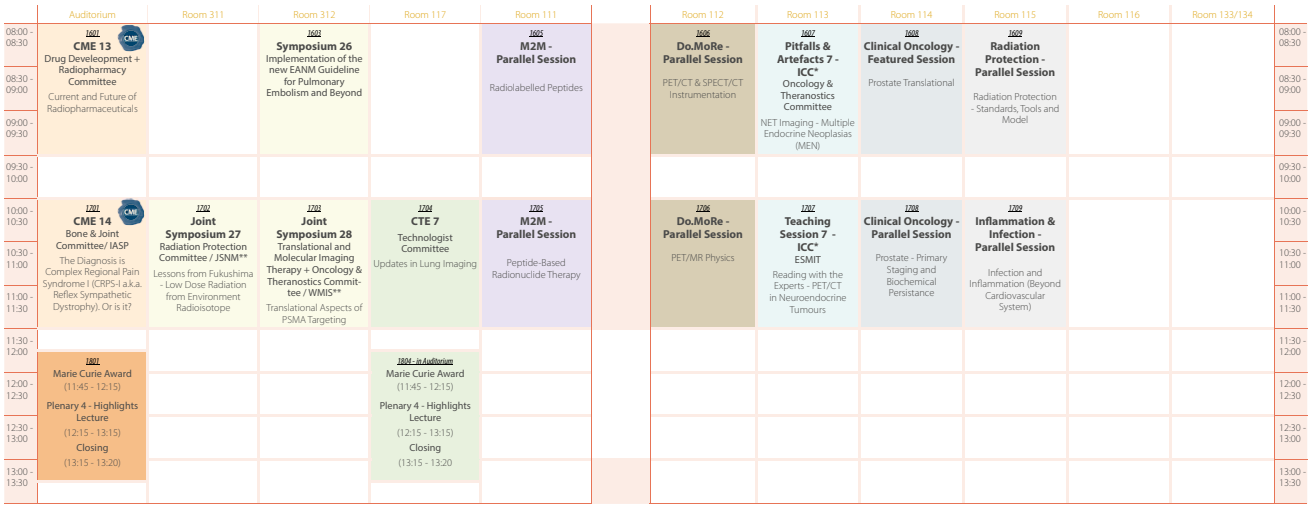

Oral Sessions

PS1

Pre-Congress Symposium 1 - Inflammation & Infection Committee: Systematic Reviews and Meta-Analyses of Diagnostic Test Accuracy (DTA)

Saturday, October 12, 2019, 9:00 - 12:00 Lecture Hall 111

PS-01
Introduction to Systematic Reviews and Meta-Analyses of Diagnostic Test Accuracy
G. Treglia; Imaging Institute of Southern Switzerland and Health Technology Assessment Unit, Ente Ospedaliero Cantonale, Bellinzona, SWITZERLAND.

PS-02
Formulating the Review Question and Planning Eligibility Criteria
G. Treglia; Imaging Institute of Southern Switzerland and Health Technology Assessment Unit, Ente Ospedaliero Cantonale, Bellinzona, SWITZERLAND.

PS-03
Systematic Search of Reports and Selection of Eligible Studies
B. Muoio; Oncology Institute of Southern Switzerland, Ente Ospedaliero Cantonale, Bellinzona, SWITZERLAND.

PS-04
Discussion

PS-06
Collecting Data and Performing the Quality Assessment
R. Sadeghi; Nuclear Medicine Research Center, Mashhad University of Medical Sciences, Mashhad, IRAN, ISLAMIC REPUBLIC OF.

PS-07
Pooling Indices Across Studies (Meta-Analysis)
Y. Takwoingi; Institute of Applied Health Research, University of Birmingham, Birmingham, UNITED KINGDOM.

PS-08
Analysis of Heterogeneity and Biases
Y. Takwoingi; Institute of Applied Health Research, University of Birmingham, Birmingham, UNITED KINGDOM.

PS-09
Discussion

PS2

Pre-Congress Symposium 2 - Cardiovascular Committee / EACVI: Quantification of Myocardial Flow Reserve ? Ready for Daily Practice?

Saturday, October 12, 2019, 9:00 - 12:00 Lecture Hall 113

PS-10
Pathophysiology of Coronary and Myocardial Flow Reserve
T. van de Hoef; Department of Cardiology, Academic Medical Centre, Amsterdam, NETHERLANDS.

PS-11
How to Quantify MBF?
M. Lubberink; PET Centre, Uppsala University Hospital, Uppsala, SWEDEN.

PS-12
MBF Quantification Based on SPECT
A. Manrique; Caen University Hospital, Department of Nuclear Medicine, Caen, FRANCE.

PS-14
MBF Quantification Based on PET
A. Saraste; University of Turku, Heart and PET Centre Hospital/Institute, Turku, FINLAND.

PS-15
MBF Quantification Based on CT
G. Pontone; Centro Cardiologico Monzino, IRCCS, University of Milan, Milan, ITALY.

PS-16
How to Implement MBF in Clinical Practice?
J. Knuuti; Heart and PET Centre, Turku, FINLAND.

PS-17
Discussion

PS3

Pre-Congress Symposium 3 - Radiopharmacy + Oncology & Theranostics + Dosimetry Committee: Alpha Therapy - Practical Aspects on Chemistry and Applications

Saturday, October 12, 2019, 9:00 - 12:00 Lecture Hall 114

PS-18
An Overview of Production and Radiochemistry of Alpha-Emitting Radionuclides
A. Morgenstern; European Commission, DG Joint Research Centre-JRC, Karlsruhe, GERMANY.

PS-19
Safe Handling of Alpha-Emitting Radionuclides During Preparation and Application of Radiopharmaceuticals
S. Holm; Klinik for Klinisk Fysiologi, Nuklearmedicin & PET, Copenhagen, DENMARK.

PS-20
Stability of Alpha-Emitting Radiopharmaceuticals - Impact on TATs
M. Benesova; German Cancer Research Center, Heidelberg, GERMANY.

PS-22
Recoil Effect and its Impact on TATs Dosimetry
N. Chouin; French Institute of Health and Medical Research, Nantes, FRANCE.

PS-23
Antibody Derivatives as a Vehicle for TAT - Advantages, Disadvantages, Future Prospects
S. Heskamp; Radboud Institute for Molecular Life Sciences, Nijmegen, NETHERLANDS.

PS-24
Future Directions for Targeted Alpha Therapy Beyond Prostate Cancer
M. Miederer; Department of Nuclear Medicine, University Medical Center Mainz, Mainz, GERMANY.

PS-25
Discussion

PS4

Pre-Congress Symposium 4 - Translational Molecular Imaging and Therapy + Drug Development + Radiopharmacy Committee: We can?t make it cool, but we can make it easier?.

Saturday, October 12, 2019, 9:00 - 12:00 Lecture Hall 115

PS-26
Too Many Regulations
O. Neels; German Cancer Research Center, Division of Radiopharmaceutical Chemistry, Heidelberg, GERMANY.

PS-27
Too Many "me too" Tracers
A. Gee; St Thomas' Hospital, Kings College London, Imaging Sciences Rayne Institute, London, UNITED KINGDOM.

PS-28
Too Expensive
B. Cornelissen; RRI, Dept.of Oncology, univ. of Oxford, Oxford, UNITED KINGDOM.

PS-30
Too Much Bias in Animal Experiments
M. Schottelius; TU Munich, Pharmaceutical Radiochemistry, Garching, GERMANY.

PS-31
Too Much Difficult Dosimetry
M. Konijnenberg; Erasmus MC, Radiology and Nuclear Medicine, Rotterdam, NETHERLANDS.

PS-32
Plenary Discussion with Focus on: How to Avoid Translational Hurdles

PS5

Pre-Congress Symposium 5 - Dosimetry + Physics Committee: Dosimetry from Image Reconstruction with Monte Carlo Modelling

Saturday, October 12, 2019, 9:00 - 12:00 Lecture Hall 116

PS-33
Statistical Reconstruction Methods - Principles
J. Gustafsson; Department of Medical Radiation Physics, Lund University, Lund, SWEDEN.

PS-34
An Introduction to Monte Carlo Calculations for Imaging and Dosimetry
M. Ljungberg; Department of Medical Radiation Physics, Lund University, Lund, SWEDEN.

PS-36
Problems Related to Dosimetry for Therapy Based on Quantitative SPECT Imaging
P. Minguez Gabina; Department of Medical Physics and Radiation Protection Gurutzeta/Cruces University Hospital 48903, Barakaldo, SPAIN.

PS-37
Examples of the Usefulness of Monte Carlo Modelling within a Reconstruction Process
H. de Jong; Department of Radiology, University Medical Center Utrecht, UMC, Utrecht, NETHERLANDS.

PS-38
Discussion and Concluding Remarks

PS6
Pre-Congress Symposium 6 - Thyroid Committee / ESES: An Update on Differentiated Thyroid Cancer (DTC) - Overview of Management

Saturday, October 12, 2019, 13:00 - 16:00 Lecture Hall 111

PS-39
Surgical Strategy at Initial Diagnosis
F. Sebag; Assistance Publique Hôpitaux de Marseille, Endocrine and Metabolic Surgery, Marseille, FRANCE.

PS-40
Strategies and Concepts Regarding Post-Surgery Radioiodine Treatment of DTC
E. Hindie; CHU hôpitaux de bordeaux Service Médecine Nucléaire, Bordeaux, FRANCE.

PS-41
Multiscale Prognostic Factors for the Management of DTC
L. Giovanella; Imaging Institute of Southern Switzerland, Clinic for Nuclear Medicine, Bellinzona, SWITZERLAND.

PS-43
Radioiodine Treatment for Metastatic DTC - How Much? How Many? How Often?
M. Luster; University of Marburg, Department of Nuclear Medicine, Marburg, GERMANY.

PS-44
Redifferentiation of Radioiodine Refractory DTC
S. Leboulleux; Nuclear Medicine and Endocrine Oncology, Gustave Roussy and Paris Saclay, Villejuif, FRANCE.

PS-45
Discussion

PS7
Pre-Congress Symposium 7 - Neuroimaging Committee: Reserve, Resilience and Protective Factors in AD ? Contribution of Molecular Imaging

Saturday, October 12, 2019, 13:00 - 16:00 Lecture Hall 113

PS-46
Reserve and Resilience in AD - Evolution of the Concept
P. Vemuri; Department of Radiology, Mayo Clinic, Rochester, MN, UNITED STATES OF AMERICA.

PS-47
Multimodal Interventions and Dementia Prevention
S. Sindi; Karolinska Institutet, Department of Neurobiology, Stockholm, SWEDEN.

PS-48
Functional Networks Underlying Cognitive Reserve
S. Morbelli; San Martino Hospital, Nuclear Medicine, Genoa, ITALY.

PS-49
Discussion

PS-51
Should we Considered Education as a Confounder on FDG-PET Diagnostic Accuracy in Alzheimer's Disease?
V. Garibotto; Nuclear Medicine and Molecular Imaging Division, Geneva University Hospitals, Geneva, SWITZERLAND.

PS-52
Contribution of Amyloid and Tau PET to the Understanding of Cognitive Reserve
M. Hönig; Department of Nuclear Medicine, University Hospital Cologne, Cologne, GERMANY.

PS-53
Meditation in the Ageing Population to Foster Reserve and Prevent Dementia
G. Chételat; Inserm UMR-S U1237, Normandie Univ, UNICAEN, GIP Cyceron, Caen, FRANCE.

PS-54
Discussion

PS8

Pre-Congress Symposium 8 - Oncology & Theranostics Committee / EAU: PSMA Theranostics and Beyond

Saturday, October 12, 2019, 13:00 - 16:00 Lecture Hall 114

PS-55
Defining the Landscape of Potential Candidates for PSMA-RLT
J. Walz; Institut Paoli-Calmettes Cancer Center, Department of Urology, Marseille, FRANCE.

PS-56
Overview of Clinical Data for 177Lu-PSMA
B. Krause; University of Rostock, Department of Nuclear Medicine, Rostock, GERMANY.

PS-57
PSMA RLT beyond 177Lu-PSMA
M. Eiber; Technische Universität München, Department of Nuclear Medicine, Munich, GERMANY.

PS-58
Discussion

PS-60
Overcoming Resistance to PSMA RLT
J. Czernin; University of California Los Angeles, Molecular and Medical Pharmacology, Los Angeles, CA, UNITED STATES OF AMERICA.

PS-61
Targets Beyond PSMA
J. Babich; Weill Cornell Medical College, Department of Radiology, New York, NY, UNITED STATES OF AMERICA.

PS-62
Discussion

PS9

Pre-Congress Symposium 9 - Physics + Dosimetry Committee: Advances in Image Processing Techniques

Saturday, October 12, 2019, 13:00 - 16:00 Lecture Hall 115

PS-63
Principles and Developments of Deep Learning Techniques in NM Image Processing
A. McMillan; University of Wisconsin, Department of Radiology, Madison, WI, UNITED STATES OF AMERICA.

PS-64
Whole Body Parametric PET/CT Imaging
N. Karakatsanis; Mount Sinai Hospital, Cornell University, New York, NY, UNITED STATES OF AMERICA.

PS-66
Functional Volume Segmentation - State of the Art
M. Hatt; INSERM, LaTIM, University of Western Britanny, Brest, FRANCE.

PS-67
Quantitative SPECT/CT Imaging
I. Armstrong; Nuclear Medicine Department, Manchester University Hospital NHS Trust, Manchester, UNITED KINGDOM.

PS-68
MC vs Non-MC Dose Estimation for Radionuclide Therapy
M. Ljungberg; Department of Medical Radiation Physics, Lund University, Lund, SWEDEN.

PS10

Pre-Congress Symposium 10 - Radiation Protection + Dosimetry Committee: European Projects for Clinical Implementation of Dosimetry in Molecular Radiotherapy

Saturday, October 12, 2019, 13:00 - 16:00 Lecture Hall 116

PS-69
Calibration protocols for quantitative imaging developed within the MRTDosimetry project
A. Robinson; National Physical Laboratory, Teddington, UNITED KINGDOM.

PS-70
Multicentre Quantitative Imaging Exercises and Dosimetry Tool Intercomparison in the MRTDosimetry Project
J. Tran-Gia; University of Würzburg, Department of Nuclear Medicine, Würzburg, GERMANY.

PS-71
Multicentre Quantitative Imaging Exercises and Dosimetry Tool Intercomparison in the MRTDosimetry Project
N. Calvert; The Christie NHS Foundation Trust, Manchester, UNITED KINGDOM.

PS-72
Discussion

PS-74
Intercomparison for Lu-177 Imaging in the Netherlands
S. Peters; Radboudumc, Radiologie & Nucleaire Geneeskunde, Nijmegen, NETHERLANDS.

PS-75
The Role of CT in Image-Based Dosimetry
K. Sjögreen-Gleisner; Lund University, Medical Radiation Physics, Lund, SWEDEN.

PS-76
Medirad I-131 Multicentre Trial Set-Up
F. Leek; Royal Marsden Hospital, Joint Department of Physics, Sutton, UNITED KINGDOM.

PS-77
Discussion

101
CME 1 - Dosimetry Committee: An Educational Trip from Organ to Voxel-Based to Small Scale Dosimetry

Sunday, October 13, 2019, 8:00 - 9:30 Auditorium

OP-001
Organ Level Dosimetry
J. Gear; Royal Marsden NHS Foundation Trust, Joint Department of Physics, Sutton, UNITED KINGDOM.

OP-002
Voxel Level Dosimetry
N. Chouin; French Institute of Health and Medical Research, Nantes, FRANCE.

OP-003
Small Scale Dosimetry - Not so Appealing, but...It's just Dosimetry
P. Bernhardt; University of Gothenburg, Department of Radiation Physics, Gothenburg, SWEDEN.

102
Joint Symposium 1 - Bone & Joint + Inflammation & Infection Committee / EULAR: Bone Imaging in Chronic Inflammatory Joint Conditions

Sunday, October 13, 2019, 8:00 - 9:30 Lecture Hall 311

OP-006
Bone SPECT/CT Versus MRI in Rheumatologic Patients
H. Palmedo; Institute for Radiology and Nuclear Medicine, Bonn, GERMANY.

OP-007
Impact of FDG-PET/CT in Patients with PMR
O. Gheysens; Nuclear Medicine and Molecular Imaging, Department of Imaging and Pathology, University Hospitals Leuven, Leuven, BELGIUM.

OP-008
Imaging of Osteoblast-/OsteoclastActivity in New Bone Formation in Rheumatologic Patients
X. Baraliakos; Rheumazentrum Ruhrgebiet, Herne, GERMANY.

103
Joint Symposium 2 - Cardiovascular + Translational and Molecular Imaging Therapy + Inflammation & Infection Committee / ESMI: New Approaches for the More Specific Detection of Inflammatory Cells than FDG

Sunday, October 13, 2019, 8:00 - 9:30 Lecture Hall 312

OP-009
Device Infection
F. Caobelli; Department of Nuclear Medicine, Universitätsspital Basel, Basel, SWITZERLAND.

OP-010
Cardiac Remodeling
J. Thackeray; Department of Nuclear Medicine, Hannover Medical School, Hannover, GERMANY.

OP-011
Atherosclerosis
J. Bucerius; Klinik für Nuklearmedizin, Universitätsmedizin Göttingen, Georg-August-Universität, Göttingen, GERMANY.

OP-012
Myocarditis
C. Rischpler; University Hospital Essen, Essen, GERMANY.

OP-013
Discussion

104

CTE 1 - Technologist Committee / ANZSNM / CAMRT: Technologist Approach to Global Dose Optimization

Sunday, October 13, 2019, 8:00 - 9:30 Lecture Hall 117

OP-014a
Opening Technologist's Track
A. Santos; Hospital Cuf Descobertas, Nuclear Medicine Department, Lisbon, PORTUGAL.

OP-014b
Dose Optimization Principles
P. Fragoso-Costa; University Hospital Essen, Clinic for Nuclear Medicine, Essen, GERMANY.

OP-015
Dose Reference Levels in Nuclear Medicine
E. Bailey; Royal North Shore Hospital, Department of Nuclear Medicine, Sidney, AUSTRALIA.

OP-016
PET/CT Dose Optimization and Occupational Exposure
T. Alden; BC Cancer Agency, Vancouver, CANADA.

OP-017
Cardiac Imaging Methods for Dose Reduction
L. Camoni; Università & Spedali Civili di Brescia, Brescia, ITALY.

105

M2M - Parallel Session: Improvement of PSMA Ligands

Sunday, October 13, 2019, 8:00 - 9:30 Lecture Hall 111

1OP-018
Novel ^{177}Lu-labeled albumin-binder-conjugated PSMA-targeting agents with extremely high tumor uptake and superior tumor-to-kidney therapeutic index
H. Kuo[1], Z. Zhang[1], C. Uribe[1], H. Merkens[1], C. Zhang[1], F. Bénard[1,2], K. Lin[1,2];
[1]Department of Molecular Oncology, BC Cancer, Vancouver, BC, CANADA, [2]Department of Radiology, University of British Columbia, Vancouver, BC, CANADA.

Aim/Introduction: The use of an albumin binder has been shown to improve tumor uptake of prostate specific membrane antigen (PSMA)-targeting radiopharmaceuticals. We recently reported ^{177}Lu-HTK01169[1], a ^{177}Lu-PSMA-617 derivative that delivered 8.3-fold higher absorbed dose to LNCaP tumor xenografts than ^{177}Lu-PSMA-617, at the expense of a lower tumor-to-kidney therapeutic index. We systematically investigated different linkers and albumin binders to maximize the therapeutic index of PSMA-binding radiopharmaceuticals. We aimed to develop novel radiopharmaceuticals that combine the effects of an improved linker with optimized albumin binders to maximize the tumor-to-kidney therapeutic index. **Materials and Methods:** Two novel PSMA-binding radiopharmaceuticals derived from the glutamate-ureido-lysine backbone, HTK03121 and HTK03123, were synthesized using a solid-phase approach. HTK03121 and HTK03123 were synthesized with a linker containing the lipophilic 3-(9-anthryl)-L-alanine and tranexamic acid, with the addition of albumin-binding motifs 4-(p-chlorophenyl)butanoyl]-Gly (HTK03121) and 4-(p-methoxyphenyl)butanoyl]-Gly (HTK03123). ^{177}Lu labeling was conducted in acetate buffer (pH 4.5). SPECT/CT and biodistribution studies were performed in LNCaP tumor-bearing mice. Radiation dosimetry in mice was calculated using the OLINDA v.1.2. **Results:** SPECT/CT imaging showed that both ^{177}Lu-HTK03121 and ^{177}Lu-HTK03123 had very high and sustained tumor uptake and were excreted mainly via the renal pathway. The blood retention values (%ID/g) at 1, 4, 24, 72 and 120h were 22.6±5.35, 15.3±2.07, 4.33±0.88, 0.75±0.19 and 0.23±0.05, respectively for ^{177}Lu-HTK03121 and 14.1±1.01, 7.30±1.39, 0.71±0.29, 0.16±0.01 and 0.09±0.06, respectively for ^{177}Lu-HTK03123. Tumor uptake values of ^{177}Lu-HTK03121 and ^{177}Lu-HTK03123 all peaked at 24h (104±20.3 and 70.8±23.7 %ID/g, respectively), and remained stable up to 120h post-injection. For a 350-mg lesion size, the dose delivered to tumors were 13,316 and 13,498 mGy/MBq for ^{177}Lu-HTK03121 and ^{177}Lu-HTK03123 compared to 846 mGy/MBq for ^{177}Lu-PSMA-617. Kidney doses were 15.8, 15.2 and 2.82 mGy/MBq for ^{177}Lu-HTK03121, ^{177}Lu-

HTK03123 and ^{177}Lu-PSMA-617, for tumor-to-kidney absorbed dose ratios of 843, 888 and 300 respectively. Thus, compared to ^{177}Lu-PSMA-617, ^{177}Lu-HTK03121 delivered 15.7-fold higher absorbed dose to tumor and a 2.8-fold improvement in the tumor-to-kidney dose ratio. ^{177}Lu-HTK03123 delivered 16.0-fold higher absorbed dose to tumor, a 2.96-fold improvement in the tumor-to-kidney dose ratio. **Conclusion:** We report novel PSMA-targeting radiopharmaceuticals that showed, in a mouse model of prostate cancer, very high tumor uptake, 15.7- and 16.0-fold higher absorbed dose to tumors and superior tumor-to-kidney therapeutic ratios compared to ^{177}Lu-PSMA-617. These compounds have the potential to improve treatment safety and efficacy using significantly lower quantities of ^{177}Lu, and are promising candidates for clinical translation. **References:** Kuo H-T, et al. Molecular Pharmaceutics 2018;15:5183-5191.

OP-019

Development of a new class of albumin-binding PSMA radioligands

C. Mueller[1], *L. Deberle*[2], *C. A. Umbricht*[1], *M. Benesova*[2], *F. Borgna*[1], *V. J. Tschan*[1], *K. Zhernosekov*[3], *R. Schibli*[2];
[1]*Paul Scherrer Institute, Villigen-PSI, SWITZERLAND,* [2]*ETH Zurich, Zurich, SWITZERLAND,* [3]*ITG GmbH, Garching, GERMANY.*

Aim/Introduction: A number of albumin-binding radioligands, targeting the prostate-specific membrane antigen (PSMA), have been developed for radionuclide therapy of metastasized prostate cancer [1]. ^{177}Lu-PSMA-ALB-56 consists of a DOTA-functionalized PSMA ligand with a p-tolyl-based albumin-binding entity which resulted in high tumor accumulation and, hence, improved therapeutic efficacy compared to ^{177}Lu-PSMA-617 [2]. High blood activity levels would be limiting for therapy due to the risk of bone marrow toxicity. The aim of this study was, therefore, the development of a new class of PSMA ligands with a weak albumin binder and variable linker entities to enable fine-tuning of kinetic properties. **Materials and Methods:** Four glutamate-urea-lysine-based PSMA ligands were synthesized using solid-phase chemistry in analogy to the previously described synthesis of PSMA-ALB-56 [1]. The p-tolyl-entity was replaced with an isobutyl-phenyl-propanoic acid-(Ibu)-based entity and connected either directly or via a negatively (Dα), neutral (N) or positively (DAB) charged linker to the **ε**-amino group of the lysine residue. ^{177}Lu-labeling was performed under standard conditions and the new PSMA radioligands were tested using PSMA-positive PC-3 PIP and PSMA-negative PC-3 flu tumor cells. Binding properties to plasma proteins were determined using an ultrafiltration assay. Biodistribution and SPECT/CT imaging studies were performed in PC-3 PIP/flu tumor-bearing Balb/c nude mice. **Results:** The PSMA ligands were obtained in moderate yields of 3-15% at high purity (>99%). ^{177}Lu-labeling was achieved at up to 100 MBq/nmol with >96% radiochemical purity. PSMA-binding affinity (K_D: 18-38 nM) and internalization into PSMA-positive PC-3 PIP tumor cells were in the same range for all radioligands, however, binding to proteins of human plasma was most pronounced for the ^{177}Lu-Ibu-PSMA and ^{177}Lu-Ibu-Dα-PSMA (95%) followed by ^{177}Lu-Ibu-N-PSMA (93%) and ^{177}Lu-Ibu-DAB-PSMA (89%). Similar observations were made in biodistribution studies where ^{177}Lu-Dα-PSMA showed the most pronounced blood retention and highest tumor uptake. ^{177}Lu-Ibu-DAB-PSMA revealed the best tissue distribution profile with high tumor uptake (65% IA/g at 4 h p.i. and 52% IA/g at 24 h p.i.) and most favorable tumor-to-blood dose ratios as compared to the other three candidates and ^{177}Lu-PSMA-ALB-56. **Conclusion:** ^{177}Lu-Ibu-DAB-PSMA was identified as the most promising candidate of this new class of albumin-binding radioligands. The favorable tissue distribution profile warrants in-depth investigations of the therapeutic potential of this new PSMA-targeting radioligand in tumor-bearing mice, which will be decisive for a potential future clinical translation. **References:** [1] Lau et al. Bioconjug Chem 2019, 30:487 [2] Umbricht et al. Mol Pharm 2018; 15:2297

OP-020

A Sarcophagine Containing PSMA Ligand for Targeting Prostate Cancer with $^{64/67}$Cu

J. M. Kelly[1], *S. Ponnala*[1], *A. Nikolopoulou*[1], *N. Zia*[2], *C. Williams Jr.*[1], *P. S. Donnelly*[2], *J. W. Babich*[1];
[1]*Weill Cornell Medicine, New York, NY, UNITED STATES OF AMERICA,* [2]*University of Melbourne, Melbourne, AUSTRALIA.*

Aim/Introduction: The use of PSMA-targeted small molecules to image or treat late-stage prostate cancer is a clinically validated concept. Although the tissue distribution of small molecule ligands is typically rapid, the longer half-life of ^{64}Cu ($t_{1/2}$=12.7 h) may offer logistical advantages over ^{68}Ga or ^{18}F without compromising image resolution[1]. An additional benefit of ^{64}Cu is that it forms a chemically identical theranostic pairing with ^{67}Cu ($t_{1/2}$=2.58 d, β^-=100%), improving dosimetry and patient selection. Recently, we described novel trifunctional PSMA-targeting ligands with high tumor uptake and therapeutic index[2], but the complexation of copper by DOTA is suboptimal. Sarcophagine chelators such as MeCOSar complex copper ions efficiently and with high stability[3,4]. We therefore aimed to develop a trifunctional sarcophagine ligand for PSMA-targeted theranostics with $^{64/67}$Cu. **Materials and Methods:** RPS-085 was synthesized by conjugation of a PSMA-targeting moiety, an N^{ε}-(2-(4-iodophenyl)acetyl)lysine albumin binding group, and a bifunctionalized MeCOSar chelator. The IC_{50} of metal-free RPS-085 was determined by competition binding in LNCaP cells. Radiolabeling was performed at 25°C in 0.5 M NH_4OAc, pH 5-6. ^{64}Cu-RPS-085 was administered intravenously to male BALB/c mice bearing LNCaP xenograft tumors. The mice (n=4/time point) were sacrificed at 4, 24, and 96 h post injection (p.i.) for biodistribution. **Results:** ^{64}Cu-RPS-085 was radiolabeled in nearly quantitative yield in 20 min. The metal-free complex was a potent inhibitor of PSMA (IC_{50} = 29±2 nM). Accumulation of the tracer was primarily evident in tumor and kidneys. Activity in all other tissues, including blood, was less than 1 %ID/g. Tumor activity was 12.9±1.4 %ID/g at 4 h p.i., and remained at 9.8±1.3 %ID/g at 48 h p.i. By contrast, activity in the kidney peaked at

4 h (13.7±2.3 %ID/g) and cleared to 1.6±0.05 %ID/g at 48 h p.i. At 24 h p.i., the tumor-to-kidney ratio was 3.4±0.7, the tumor-to-blood ratio was 490±152, and the tumor-to-muscle ratio exceeded 10000. **Conclusion:** ^{64}Cu-RPS-085 combines rapid tissue distribution with prolonged retention in LNCaP xenograft tumors. Good contrast to background is evident by 4 h p.i., leading to an imaging window from 4-48 h p.i. Preliminary biodistribution studies indicate that tumor-to-background ratios increase with time, suggesting that the pharmacokinetic profile of ^{64}Cu-RPS-085 would be suitable for PSMA-targeted radioligand therapy with ^{67}Cu. **References:** [1] Conti M, Eriksson L. EJNMMI Phys. 2016;3:8. [2] Kelly J, et al. Eur J Nucl Med Mol Imaging. 2018;45:1841-1851. [3] Paterson BM, et al. Dalton Trans. 2014;43:1386-1396. [4] Gourni E, et al. Mol Pharm. 2015;12:2781-2790.

OP-021

In vitro and in vivo evaluation of the new ^{99m}Tc labelled PSMA tracers for prostate cancer diagnosis

M. Maurin[1], *A. E. Sikora*[2], *M. Orzełowska*[2], *U. Karczmarczyk*[2], *P. Garnuszek*[2];
[1]*National Centre for Nuclear Research Radioisotope Centre POLATOM, Otwock, POLAND,* [2]*(1)National Centre for Nuclear Research Radioisotope Centre POLATOM, Otwock, POLAND.*

Aim/Introduction: Prostate cancer is the second commonly occurring malignance in men. The selection of an effective therapy form depends on the proper assessment of the disease progression. The prostate-specific membrane antigen (PSMA) is becoming increasingly recognized as a viable target for imaging and therapy of prostate and other types of cancer. In the present work we synthesized and investigated the series of HYNIC-PSMA conjugates with differentiated construction of the linker between the PSMA pharmacophore and HYNIC chelator. The aim of this study was to compare the biological properties in vitro and in vivo of the developed PSMA tracers. **Materials and Methods:** The HYNIC-PSMA conjugates (PSMA-T1,T2,T3 and T4) were synthesised using standard fmoc based solid support synthesis followed by HPLC purification. IC_{50} values of these compounds were determined by competitive binding assay on LNCaP cell membranes using radio-iodinated (^{131}I)MIP1095 radioligand with known high affinity to PSMA (IC_{50}=0.3). As the reference substances, the PSMA11 and PSMA617 were used. The HYNIC-PSMA inhibitors were labelled with ^{99m}Tc in the presence of tricine and EDDA co-ligands and $SnCl_2$ as reducing agent. The binding affinity of ^{99m}Tc-HYNIC-PSMA tracers was evaluated carrying out the studies on LNCaP cell membranes (PSMA positive). The non-specific binding was determined using PC3 membranes known not to express PSMA. The preliminary biodistribution of ^{99m}Tc-HYNIC-PSMA tracers (T1,T2,T3 and T4) was conducted in normal Balb/c mice 4h piv. The selected ^{99m}Tc-PSMA-T4 tracer was further tested for pharmacokinetics in normal Wistar rats and Balb/c Nude mice with subcutaneously induced tumors using LNCaP cells. **Results:** The IC_{50} values of the three HYNIC-PSMA conjugates (T1,T3 and T4) were assessed at the level below 100nM, what means ca. 8 times lower value than obtained for PSMA11. The biodistribution study of ^{99m}Tc-HYNIC-PSMA conjugates showed that ^{99m}Tc-PSMA-T4 was characterized by the fastest elimination with urine and the significantly lowest accumulation in kidneys (37%ID/g 4h piv) - the critical organ for the labelled HYNIC-PSMA. The pharmacokinetic study in tumour-bearing mice showed very high accumulation of ^{99m}Tc-PSMA-T4 in tumors (20-30%ID/g), constant over 24h and impressive T/M ratios (230 and 550, 2 and 6h piv, respectively). **Conclusion:** In the conducted studies the ^{99m}Tc-PSMA-T4 was pointed out as the most promising candidate for SPECT imaging of the prostate cancer. The in vitro and in vivo studies showed a very high affinity of this tracer to PSMA, comparable to radiolabeled PSMA-617 inhibitor and much better than PSMA-11 used for PET diagnostics of prostate cancer. **References:** None.

OP-022

Sensitivity and specificity of 18F DCFPyL (PSMA agent) compared to MR in biochemically recurrent prostate cancer patients

L. Lindenberg[1,2], *E. Mena Gonzalez*[1], *B. Turkbey*[1], *I. Lim*[1], *Y. McKinney*[1], *J. Weaver*[1], *P. Eclarinal*[1], *A. Forest*[1], *A. Hankin*[3], *A. Couvillon*[3], *E. Schott*[4], *W. Dahut*[3], *D. Citrin*[4], *S. Harmon*[5], *E. Bergvall*[6], *A. Lindenberg*[6], *A. Ton*[1], *S. Adler*[5], *J. Eary*[7], *P. Choyke*[1];
[1]*Molecular Imaging Program, National Cancer Institute, NIH, Bethesda, MD, UNITED STATES OF AMERICA,* [2]*F. Edward Hebert School of Medicine, Uniformed Services University of the Health Sciences, Bethesda, MD, UNITED STATES OF AMERICA,* [3]*Center for Cancer Research, National Cancer Institute, NIH, Bethesda, MD, UNITED STATES OF AMERICA,* [4]*Radiation Oncology Branch, National Cancer Institute, NIH, Bethesda, MD, UNITED STATES OF AMERICA,* [5]*Clinical Research Directorate, Frederick National Laboratory for Cancer Research sponsored by the National Cancer Institute, Bethesda, MD, UNITED STATES OF AMERICA,* [6]*Ft Belvoir Community Hospital, Ft Belvoir, VA, UNITED STATES OF AMERICA,* [7]*Cancer Imaging Program, National Cancer Institute, NIH, Bethesda, MD, UNITED STATES OF AMERICA.*

Aim/Introduction: We prospectively studied prostate cancer patients with biochemical recurrence and no evidence for disease on conventional imaging with 18F DCFPyL PET/CT and multiparametric MRI of the pelvis. **Materials and Methods:** In this IRB approved trial, analysis was done on 30 prostate cancer patients with biochemical recurrence (average PSA 3.56 ng/mL, range 0.44-9.97 ng/mL) who underwent whole-body ^{18}F-DCFPyL-PET/CT at 2 h p.i (299.9±15.5 MBq), and multiparametric pelvic MRI, 2 weeks apart. PET/CT and MR were independently read by nuclear medicine physicians and a radiologist, without knowledge of findings from either scan. Histologic biopsies were obtained from all. **Results:** Definitive prior therapy for the population included 14 who underwent radiation therapy, 8 prostatectomies and 8 with a combination of both. 18F DCFPyL detected a total of 91 lesions while MR detected 43. Only 6 lesions seen on 18F DCFPyL were outside the MRI field of view. In the prostate bed, 18F DCFPyL detected 21

lesions and MR detected 30, of which 12 were concordant. 18F DCFPyL detected 40 pelvic lymph nodes while MR reported 9 of which 4 were concordant. 18F DCFPyL detected 30 metastatic lesions consisting of soft tissue, bone and lymph nodes above the aortic bifurcation. MR detected 4 metastatic lesions in bone and a lymph node above the aortic bifurcation. A pubic bone lesion was concordant on both scans. Histologic validation was available from 69 biopsy specimens. MR and 18F DCFPyL were concordant with biopsy results in 42 sites. Histology was concordant only with MR in 8 lesions and with 18F DCFPyL alone in 17 lesions. One concordant MR and 18F DCFPyL lesion was false positive. There were no concordant false negatives. MR was false positive in 6 specimens while 18F DCFPyL was false positive in 2 sites. MR was false negative in 9 lesions and 18F DCFPyL was false negative in 8. 18F DCFPyL sensitivity 74%, specificity 92%, with MR sensitivity 70%, specificity 81%. Concordant MR/18F DCFPyL findings showed sensitivity 100% and specificity 97%. **Conclusion:** 18F DCFPyL and MR each had high sensitivity and specificity in biochemically recurrent prostate cancer patients with a slight advantage for 18F DCFPyL. Concordant findings with both modalities significantly increased sensitivity and specificity suggesting combined use would enhance clinical practice. **References:** None.

OP-023

^{18}F-siPSMAs: A Novel Class of Radiofluorinated PSMA Inhibitors

D. Di Carlo[1], *V. Prasad*[2], *A. Beer*[2], *H. Wester*[1];
[1]*Technical University of Munich, Garching bei München, GERMANY,* [2]*Ulm University Medical Center, Ulm, GERMANY.*

Aim/Introduction: Inspired by the series of Radiohybrid PSMA inhibitors (rhPSMAs) recently developed in our group, we designed and evaluated another novel class of ^{18}F-labeled PSMA ligands (siPSMAs) comprised of a Silicon Fluoride Acceptor (SiFA) moiety and non-chelator based pharmacokinetic modifiers. While the SiFA-moiety provides very fast and efficient radiofluorination, the modifier composition is decisive for the pharmacokinetic performance in vivo. Here we present the preclinical results of some selected siPSMAs differing in the modifier sequence with special regard to the most promising inhibitor siPSMA-14. **Materials and Methods:** siPSMA ligands containing a urea-based binding motif linked by a spacer with a pharmacokinetic modifier in close proximity to a SiFA-moiety were synthesized via solid phase peptide synthesis. Direct radiofluorination of the SiFA-based PSMA inhibitors was achieved by isotopic exchange within 5 min at room temperature followed by fast tracer purification via solid phase extraction. For in vitro characterization, $logP_{(o/w)}$ values as well as binding affinities (IC_{50}) on PSMA-expressing LNCaP cells were determined. Small animal µPET imaging and biodistribution studies were carried out on LNCaP tumor-bearing CB17-SCID mice. **Results:** Novel siPSMA ligands exhibit suitable lipophilicities ($logP_{(o/w)}$: -3.0 to -4.0) as well as high binding affinities. Biodistribution studies of ^{18}F-siPSMA-11 and ^{18}F-siPSMA-14 in mice showed high tumor uptake of up to 15 %ID/g at 1 h p.i. and low activity accumulation in non-target tissues and bones. Based on the high binding affinity, convenient lipophilicity and excellent biodistribution, siPSMA-14 was found to be the most promising candidate for first clinical studies in patients. **Conclusion:** siPSMA inhibitors stand out for their simple and fast radiofluorination as well as for their good in vitro properties. Furthermore, tracer lipophilicity and thus excretion route and kinetics can easily be adjusted by the composition of the pharmacokinetic modifier leading to ligands with favorable in vivo distribution. The promising preclinical assessment of ^{18}F-siPSMA-14 was confirmed in an encouraging proof-of-concept study in prostate cancer patients. **References:** None

OP-024

[^{111}In]In-IRDye700DX-PSMA ligands for targeted photodynamic therapy of PSMA-expressing tumors

Y. H. W. Derks[1], *H. I. V. Amatdjais-Groenen*[2], *A. Kip*[1], *G. M. Franssen*[1], *J. K. van der Kamp*[1], *D. W. P. M. Löwik*[2], *O. C. Boerman*[1], *M. Rijpkema*[1], *S. Lütje*[3], *S. Heskamp*[1];
[1]*Radboud university medical center, Nijmegen, NETHERLANDS,* [2]*Radboud university, Nijmegen, NETHERLANDS,* [3]*University Hospital Bonn, Bonn, GERMANY.*

Aim/Introduction: Incomplete resection of prostate cancer (PCa) and its metastases may lead to disease recurrence and consequently poor patient outcome. To obtain complete resection of tumor tissue, prostate specific membrane antigen (PSMA) targeting multimodal ligands containing both a radiolabel and a photosensitizer may be used for intra-operative tumor detection, delineation, and tumor-targeted photodynamic therapy (tPDT). Previously we produced a selection of 12 multimodal PSMA ligands which demonstrated both radionuclide and fluorescence imaging potential for PCa. Here, we selected the multimodal ligand with the most favorable tumor targeting properties and evaluated its potential for PSMA tPDT. **Materials and Methods:** The multimodal PSMA ligand PSMA-N064 consists of a PSMA-binding motif, a linker, the photosensitizer IRDye700DX and the chelator DOTAGA. In vitro, therapeutic efficacy of this ligand was evaluated using PSMA-transfected LS174T and PSMA-negative wild-type LS174T cells, which were incubated with PSMA-N064 followed by 100 J/cm² NIR light irradiation (3-10 min). Additionally, PSMA-N064 (3 nmol/mouse) mediated tPDT, using 150 J/cm² NIR light irradiation, was tested in BALB/c nude mice bearing PSMA⁺ LS174T-PSMA xenografts >30 mm³. Tumor growth and survival after tPDT (2h p.i.) was compared to control mice that received NIR-light irradiation or tracer injection only (n=5 mice per group). **Results:** In vitro a dose-dependent PSMA-specific loss of cell viability was observed after 100 J/cm² NIR irradiation, ranging from 29% ± 7.0% (3 nM) to 84% ± 2.6% (30 nM, P<0.001). Moreover, in a first in vivo feasibility study it was shown that PSMA-N064-mediated tPDT may lead to tumor growth delay and a prolonged median survival. In mice treated with tPDT the time interval until tumors reach a size of 500

mm³ (12.8 ± 1.1 days) was longer compared to only NIR-light irradiated (10 ± 4.9 days) or only tracer injected control mice (6.4 ± 1.7 days, P<0.05). In addition, tPDT prolonged survival (defined as tumor growth >1000 mm³, humane endpoint) in treated mice (16 days) compared to the two control groups (12 and 10 days, respectively). **Conclusion:** Here, we demonstrated the feasibility of PSMA-targeted PDT using the newly developed PSMA-N064 multimodal ligand. In the future, this ligand will be used for intra-operative tumor detection and PSMA-tPDT. Use of tPDT during surgery can facilitate removal of unresectable tumor rest and positive surgical margins, potentially leading to improved surgical outcomes of PCa patients. **References:** This work was supported by EKFS (2016-A64) and the Dutch Cancer Society (NKB-KWF 10443/2016-1).

OP-025

Assessment of in vivo biodistribution and treatment efficacy of ^{177}Lu PSMA-R2 and ^{177}Lu-PSMA-617 on mice bearing prostate cancer tumors

V. Muzio[1], *L. Ravasi*[1], *L. Sacchetti*[1], *L. Fugazza*[1], *S. Bacot*[2], *M. Debiossat*[2], *M. Ahmadi*[2], *C. Montemagno*[2], *C. Ghezzi*[2], *A. Broisat*[2];
[1]*Advanced Accelerator Applications, a Novartis company, Geneva, SWITZERLAND,* [2]*Univ. Grenoble Alpes, Inserm, CHU Grenoble Alpes, Grenoble, FRANCE.*

Aim/Introduction: Comparison of the in vivo biodistribution and the treatment efficacy of ^{177}Lu PSMA-R2 and ^{177}Lu-PSMA-617 in mice with prostate cancer grafts. **Materials and Methods:** PSMA positive-PC3-PIP were subcutaneously implanted in athymic nude mice in the left flank. A single injection of 111MBq of 177Lu-PSMA-R2 or 177Lu-PSMA-617 or of saline was performed approximately two weeks later, concomitantly to randomization into groups of similar average tumor volumes expressed in mm³ . SPECT/CT imaging was performed in a subset of 12 mice (6 from ^{177}Lu-PSMA-R2 group and 6 from ^{177}Lu-PSMA-617 group). Acquisitions were performed 24h post injection of ^{177}Lu-PSMA-R2 and ^{177}Lu-PSMA-617. Tumor volumes were monitored daily and expressed either as absolute values in mm3 or as a volume relative to that measured the day of the 177Lu-PSMA- R2, 177Lu-PSMA-617 or saline administration. Tumor growth curves were compared using two-ways ANOVA from the day of first injection to day 14. **Results:** Absolute tumor volumes were significantly reduced in the 177Lu-PSMA-R2 and 177Lu-PSMA-617 groups vs control group (p<0.001). Similarly, tumor volumes from 177Lu-PSMA-R2 and 177Lu-PSMA-617 groups were significantly reduced in comparison to control group (p<0.001). No differences were observed between the tumor volumes of the treated groups. At later time points (14-36 days), the tumors of the control group started to reach the 1500mm³-limit volume as opposed to those of the treated groups. Control mice were therefore euthanized. Although 177Lu-PSMA-R2 and 177Lu-PSMA-617 were no longer administered, a tumor regression was observed in both groups. By day 36th, tumors were no longer detectable in 5 out of 10 tumors from 177Lu-PSMA-R2 group and 4 out of 10 tumors from 177Lu-PSMA- 617 group. Mean tumor volume was of 13.9±23.6 and 11.1±10.4 in 177Lu- PSMA-R2 and 177Lu-PSMA-617 groups, respectively. No statistical differences were found in tumor growth under 177Lu-PSMA-R2 or 177Lu-PSMA-617 treatment. SPECT/CT data acquired on 6 mice from each 177Lu-group showed strong 177Lu- PSMA-R2 and 177Lu-PSMA-617 uptakes at tumor level 24h p.i. with very low uptake elsewhere. VOI quantification confirmed visual observation. Interestingly, after 14 days of a single dose of 111 MBq of 177Lu-PSMA-R2 or 177Lu-PSMA-617, similar tumor growth was observed between 177Lu-PSMA-R2 and 177Lu-PSMA-617 treated mice despite this different tumor uptake at 24h. **Conclusion:** 177Lu-PSMA-R2 and ^{177}Lu-PSMA-617 have a similar biodistribution in mice inoculated with PSMA positive-PC3-PIP tumor grafts. Similar significant reduction of tumor size was observed, despite the difference in clearance from tumor tissue. **References:** None.

106

Do.MoRe - Rapid Fire Session: Data Analysis

Sunday, October 13, 2019, 8:00 - 9:30 Lecture Hall 112

OP-026

Standardized Radiomics of Clinical Myocardial Perfusion Stress SPECT Images to Determine Coronary Artery Calcification Score

S. Ashrafinia[1], *P. Dalaie*[1], *M. Salehi Sadaghiani*[1], *T. H. Schindler*[2], *M. G. Pomper*[1], *A. Rahmim*[3];
[1]*Johns Hopkins University, Baltimore, MD, UNITED STATES OF AMERICA,* [2]*Washington University at St. Louis, St. Louis, MO, UNITED STATES OF AMERICA,* [3]*University of British Columbia, Vancouver, BC, CANADA.*

Aim/Introduction: Myocardial perfusion stress SPECT(MPSS) is an established diagnostic test for patients suspected with coronary-artery-disease(CAD). Meanwhile, coronary-artery calcification(CAC) scoring obtained from diagnostic CT is a highly-specific test, offering incremental diagnosis information in identifying patients with significant CAD yet normal MPSS scan[1]. Nonetheless, CAC scoring is not commonly performed/reimbursed in a wide community setting. Our aim is to quantify heterogeneity of uptake via radiomics of 'normal' MPSS scans to enable prediction of CAC scores, identifying subclinical CAD. **Materials and Methods:** 428 patients were collected with normal (non-ischemic) MPSS (8-30mCi ^{99m}Tc-Sestamibi) with consensus reading. NM physician verified images (iteratively-reconstructed/attenuation-corrected) to be free from fixed perfusion-defect/artifactual attenuation. 3D images were automatically-segmented into 4 regions-of-interest(ROI), including myocardium+3vascular segments (LAD-LCX-RCA). We developed standardized environment for radiomics analysis(SERA)[2] and calculated 215 3D radiomic features in compliance with image-biomarker standardization

initiative (IBSI)[3], ensuring reproducibility of this study. Isotropic-cubic-voxel-ROIs (no resampling/interpolation needed) were discretized using fixed-bin-number discretization into 8 grey-levels (GLs) (2^2,...,2^9). We first performed two-phase blind-to-outcome feature-selection: A)Removing: A-1)three smallest GLs (very-low dynamic-range), A-2)two highest-GLs (causing highly-correlated features ρ>0.9), and A-3)GL=128 (indifferent statistical properties), ultimately selecting GL=64, similar to findings from our previous study[4]. B)Post-feature calculation: removing features with B-1)identical values, B-2) very-low dynamic-range, B-3)varieties of higher-order feature-classes, B-4)redundant features(ρ=1), and B-5)highly-correlated features (Spearman ρ>0.95). Next, we ran multivariate analysis to predict CAC scores from i) radiomics, ii) clinical-features, iii) radiomics+clinical-features. We performed randomly-selected 60%/25%/15% training/validation/testing. Training started from a constant fit, following iteratively adding/removing features (stepwise-regression) based on sorted univariate-Spearman-correlation with CAC-scores, invoking Akaike-information-criterion (AIC) to discourage overfitting. Validation was run similarly, with the training output-model as initial fit. We shuffled training-validation sets 20 times, then found the best model using log-likelihood to evaluate the test-set. The sensitivity to test-set was further reduced by running the entire operation 50 times, then employing Fisher's method to verify significance of independent tests. **Results:** Feature-selection significantly reduced 8×215 features to 56. Median Absolute Pearson's-correlation coefficient|p-value for 3 feature-pools(radiomics,clinical,combined) were: (0.15±0.11,0.38±0.08,0.41±0.05)|(0.1,0.001,0.0006), (0.24±0.06,0.35±0.08,0.41±0.05)|(0.05,0.004,0.0007), (0.07±0.05,0.24±0.1,0.28±0.09)|(0.4,0.06,0.02) (0.06±0.05,0.16±0.06,0.24±0.06)|(0.4,0.2,0.05) for Myocardium-LAD-LCX-RCA, respectively. Results demonstrate combined features enhance the significance of CAC score prediction across all segments. **Conclusion:** Our multivariate model enabled the significant prediction of CAC scores at all cardiac segments when combining standardized-radiomics with clinical features, suggesting radiomics adds diagnostic/prognostic value to standard MPSS for wide clinical usage. **References:** [1] Shaw, et-al, Radiology, vol.228, no.3, pp.826-833, 2003. [2] Ashrafinia, PhD Thesis, 2019. [3] Zwanenburg, et-al., arXiv:1612.0700s3. [4] Ashrafinia, et al., Medical Physics. Vol.44. No.6, 2017.

OP-027

A novel myocardial perfusion phantom: performing 'ground truth' flow measurements to evaluate accuracy of flow quantification with SPECT

M. E. Kamphuis[1], *G. de Vries*[1], *M. Saaltink*[2], *J. Verschoor*[2], *A. Agool*[2], *M. J. W. Greuter*[3,1], *C. H. Slump*[1], *R. H. J. A. Slart*[3,1];
[1]*University of Twente, Enschede, NETHERLANDS,* [2]*Ziekenhuisgroep Twente, Hengelo, NETHERLANDS,* [3]*University Medical Center Groningen, Groningen, NETHERLANDS.*

Aim/Introduction: Quantitative PET myocardial perfusion imaging (MPI) can standardize detection of coronary artery disease and improve diagnostic accuracy in patients with balanced ischemia. Emerging SPECT technology may enable quantitative evaluation as well, but proof hereof is still in its infancy. We aim to contribute to 'ground truth' validation of quantitative SPECT-MPI by evaluating the accuracy of flow quantification using a novel myocardial perfusion phantom. **Materials and Methods:** The in-house built perfusion phantom mimics the anatomy and (patho-) physiology of left ventricular first-pass perfusion. Pumped continuous flow is conducted through a 3D printed left ventricle and aorta, which branches into coronary arteries that are connected to three myocardial modules. These represent the microcirculation of the main coronary territories. The modules are interchangeable and can consist of different tissue fillings. Flow sensors are incorporated into the setup as 'ground truth' flow measure. Flow distribution is controlled by adjustable end-resistances, which also enables simulation of local perfusion deficits. As with patients, a radioactive tracer is administered and a dynamic myocardial perfusion scan is started simultaneously to monitor tracer distribution. The resulting time activity curves (TACs) serve as input for myocardial blood flow quantification. The absolute difference between measured and computed flow (in mL/min/g) is used as measure of accuracy. In the phantom experiments, we used standard clinical protocols for SPECT-MPI (D-SPECT, Spectrum Dynamics) and subsequent flow quantification (4DM Corridor software). We injected 500 MBq ^{99m}Tc-tetrafosmin at an aorta flow of 2-5L/min. The flow into the individual myocardial modules varied between 20-100mL/min and module fillings varied (e.g. different types of sponge materials). **Results:** The obtained TACs inside the simulated left ventricle match physiological values. The area under the curve remains the same for the different aortic flow rates, but the maximum of the curve goes down and smears out over a longer period when lowering the flow. The TACs corresponding to myocardial tissue segments have a relatively fast washout of less than 20s. An aortic and myocardial flow of 2 and 100mL/min, respectively, resulted in the longest washout time. **Conclusion:** This study highlights the design and realization of a novel myocardial perfusion phantom to contribute to ground truth validation of quantitative SPECT-MPI. First testing showed promising results, as both geometry and tracer distribution resemble left ventricular microcirculation. Subsequent evaluation of quantitative SPECT-MPI accuracy is in progress. **References:** None.

OP-028

Initial evaluation of an automated high temporal resolution data-driven motion correction for rubidium cardiac relative perfusion PET

I. Armstrong[1], *C. Hayden*[2], *P. Arumugam*[1];
[1]*Manchester University NHS Foundation Trust, Manchester, UNITED KINGDOM,* [2]*Siemens Medical Solutions USA, Inc., Knoxville, TN, UNITED STATES OF AMERICA.*

Aim/Introduction: Vasodilator stress, due to predominantly respiratory side effects, can introduce varying degrees of patient

motion during rubidium cardiac PET. The most commonly observed is periodic patient motion due to tidal breathing and non-periodic motion due to cardiac creep. Motion can degrade perfusion images and is time dependant; in extreme cases rendering images non-diagnostic. In contrast to SPECT, motion correction during PET imaging is challenging. It can be performed by aligning reconstructed dynamic images but is labour-intensive and requires frames to be sufficiently long to avoid noisy data but intra-frame motion can be a potential problem. This work evaluates a prototype automated data-driven high-temporal resolution motion correction strategy. **Materials and Methods:** 10 rubidium stress and rest images (20 images total) from a Siemens Biograph Vision with evidence of motion blurring were included. Frame-by-frame motion correction (FBFMC) was performed by manually aligning and summing twelve 15-second dynamic frames from 120 to 300 seconds post infusion of rubidium-82. Data-driven motion correction (DDMC) was performed by automatically locating and tracking the myocardium within a sub-volume of raw projection data with a temporal resolution of one second. The offset in the axial direction within each one second frame was determined with a precision of 1mm and shifted to a reference position. Non-corrected (NC), FBFMC and DDMC data were reviewed by an experienced physician. Image quality was rated non-diagnostic, adequate or good while perceived motion was rated as none, mild, moderate or severe. Intra-frame motion still present in the FBFMC 15-second frames was determined from the DDMC position tracking. **Results:** For image quality, 7/20 NC images were good, 5/20 adequate and 8/20 NC non-diagnostic; 8/20 FBFMC images were good, 7/20 adequate and 5/20 non-diagnostic; 19/20 DDMC images were good and 1/20 was adequate. Of the 8 non-diagnostic NC images, 5 were still considered non-diagnostic with FBFMC and the other 3 were rated adequate whereas all 8 were rated good with DDMC. Intra-frame motion of up to 42 mm was present in the FBFMC frames highlighting the limitation of this technique. **Conclusion:** Effective motion correction requires high temporal resolution and is not possible by post-reconstruction image-based methods. This new automated data-driven method is promising from our preliminary data. While neither of these methods are used in current clinical practice, further work on a larger cohort of patients and assessment of clinical impact is required to make it routine. **References:** None.

OP-029

Value of Digital PET in Myocardial Perfusion Imaging Using Rubidium-82 PET

S. S. Koenders[1,2], *J. A. van Dalen*[3], *P. L. Jager*[1], *S. Knollema*[1], *J. R. Timmer*[4], *C. H. Slump*[2], *J. D. van Dijk*[1];
[1]*Isala hospital, Department of Nuclear Medicine, Zwolle, NETHERLANDS,* [2]*Technical Medicine Centre, University of Twente, Enschede, NETHERLANDS,* [3]*Isala hospital, Department of Medical Physics, Zwolle, NETHERLANDS,* [4]*Isala hospital, Department of Cardiology, Zwolle, NETHERLANDS.*

Aim/Introduction: The use of PET for myocardial perfusion imaging (MPI) is increasing rapidly due to the increased availability of strontium-82/rubidium-82 (Rb-82) generators, high accuracy and the possibility of quantifying myocardial blood flow (MBF). Recently, PET systems with digital photon counting technology have become available. These PET systems have an increased temporal and spatial resolution but the effect on image quality or visibility of perfusion defects in PET MPI is still unknown. Our aim was to determine the value of a digital PET system in comparison to a conventional PET system in MPI using Rb-82. **Materials and Methods:** We prospectively included 30 patients who underwent rest and regadenoson-induced stress Rb-82 MPI using a conventional PET system (D690, GE Healthcare). In addition, patients underwent rest and stress Rb-82 PET within three weeks on a digital PET system (Vereos, Philips Healthcare). A nuclear medicine physician and cardiologist scored the image quality on a 4-point grading scale and assessed the existence of possible defects in both the rest and stress scans. The images were presented in random order and readers were blinded for the type of scanner used. The image quality, defect interpretation and the quantitative MBF and myocardial flow reserve (MFR) values were compared between both PET systems. **Results:** Image quality was graded fair in 20% (6/30) of the conventional scans versus 10% (3/30) of the digital PET scans. Moreover, 60% (18/30) of the conventional scans was graded good and 20% (6/30) excellent versus 50% (15/30) good and 40% (12/30) excellent for the digital PET scans ($p<0.03$). In addition, the defect interpretation differed in 2 out of the 30 scans ($p=0.5$). Whereas these two scans were scored as normal on the conventional PET, they were interpreted as ischemic on the digital PET. There were no significant differences between both systems in rest MBF ($p\geq0.3$), stress MBF ($p\geq0.11$) and MFR ($p\geq0.5$). **Conclusion:** Digital PET provides better image quality than conventional PET and flow measurements seem comparable between the two systems. Nevertheless, defect interpretation may still differ. Additional studies are required to confirm this. **References:** None.

OP-030

Cross validation of quantitative assessment of global cardiac function through hybrid PET/MR images

A. Villagran Asiares[1], *T. Vitadello*[2], *J. Cabello*[3,4], *T. Ibrahim*[5], *S. Nekolla*[1];
[1]*Nuclear Medicine Department, Klinikum rechts der Isar, School of Medicine, Technical University of Munich, München, GERMANY,* [2]*Medizinische Klinik, Klinikum rechts der Isar, School of Medicine, Technical University of Munich, München, GERMANY,* [3]*Ex-Nuclear Medicine Department, Klinikum rechts der Isar, School of Medicine, Technical University of Munich, München, GERMANY,* [4]*Siemens, Nokxvill, TN, UNITED STATES OF AMERICA,* [5]*Kardiologie, Medizinische Klinik und Poliklinik, Klinikum rechts der Isar der TUM, München, GERMANY.*

Aim/Introduction: The assessment of left ventricular (LV) function via the ejection fraction (EF) is widely used with

almost all imaging modalities. So far, these techniques, acquired separately, were correlated but inter-study variability was significant. Therefore, more cross validation studies of EF obtained from a hybrid PET/MR images are needed to evaluate the effects arising from separately scans. However, in MR modalities the ECG signal used for EF calculation is distorted by the magnetic fields; potentially causing the missing of some R-peaks detections. This can produce a wrong delineation of the cardiac phases in the PET images, resulting in a motional blur. The aim of this work was to compare different PET histogramming methods proposed to solve it. **Materials and Methods:** List-mode FDG PET and cine MR images from cardiac PET/MR viability examination of 19 patients were used. Three methods of PET histogramming were tested: 1) the standard approach (STD) defines relative bin widths dividing each RR interval in equal gates and include all of R-peaks detected, 2) relative bin width with beat-rejection (BR) adds a beat rejection that allows the elimination of RR intervals outside a user-defined window, 3) fixed bin width (FW) uses a single width gate for each subject, obtained from an optimal RR interval. For each method, the LV end-diastolic (EDV), end-systolic volumes (ESV) and EF were obtained. **Results:** The EF value, and the volumes obtained from both modalities showed positive linear correlations. However, EF (STD:43+/-11%, BR:48+/-12%, FW:46+/-11%) and EDV (STD:144+/-37 ml, BR:148+/-36 ml, FW:148+/-38 ml) were underestimated and ESV (STD:80+/-29 ml, BR:78+/-30 ml, FW:81+/-32 ml) overestimated compared with MR (EF:52+/-13 %, EDV:156+/-43 ml, ESV:75+/-32 ml). Additionally, significant differences in EF were found with STD and FW compared with MR ($p < 0.01$). Bland-Altman analysis for EF, EDV and ESV, between PET methods and MR reported biases below 9%, 12,5 ml and 6 ml, respectively; while the limits of agreements were lower than 36%, 159 ml and 78 ml, but still clinically not negligible. The BR method showed the best performance. Considering the linear regression between the modalities, BR method provided the best overall correlation in EF (slope:0.68 and Pearson coefficient (r):0.74) and EDV (slope:0.52 and r:0.62), while in the case of ESV, FW performs best (slope:0.74 and r:0.79). **Conclusion:** Ejection Fraction assessed with PET and MR in simultaneously acquisitions have a positive association, but there are still relevant differences depending on the PET histograming method. **References:** None.

OP-031

Effect of collimator characteristics on ^{123}I-MIBG phantom imaging using Monte Carlo simulation

K. Okuda[1], *K. Nakajima*[2], *C. Kitamura*[3], *Y. Kirihara*[3], *J. Taki*[2], *M. Hashimoto*[1], *S. Kinuya*[2];
[1]*Kanazawa Medical University, Kahoku, JAPAN,* [2]*Kanazawa University, Kanazawa, JAPAN,* [3]*FUJIFILM Toyama Chemical Co., Ltd., Tokyo, JAPAN.*

Aim/Introduction: We have proposed a standardization method using a dedicated ^{123}I-metaiodobenzylguanidine (MIBG) phantom for the determination of a heart-to-mediastinum count ratio for the calibration of the collimator characteristics (1-2). The purpose of this study was to clarify the relationship between collimator characteristics and a calibration factor in a Monte Carlo simulation study using a dedicated phantom for cardiac ^{123}I- MIBG imaging. **Materials and Methods:** A digital phantom was created from the ^{123}I-MIBG phantom image acquired with X-ray computed tomography. The SIMIND Monte Carlo program was used to obtain ^{123}I-MIBG planar images, which were generated from various collimator specifications: collimator hole diameters were 1, 2, 3, 4, and 5 mm; septa thicknesses were 0.10, 0.45, 0.80, 1.15, and 1.50 mm; and collimator lengths were 20, 30, 40, 50, and 60 mm. Planar MIBG imaging was simulated with 256 × 256 matrix and energy window of ^{123}I was set to 159 keV ± 7.5 %. The calibration factor was calculated from the planar image using a dedicated software program, and defined as a conversion coefficient. The conversion coefficient value shows an approximate range of 0.5 to 0.9, corresponding to low-energy (LE) to medium-energy (ME) collimators. The conversion coefficient was compared with that from a phantom image database, which consisted of 705 image sets. **Results:** A total of 125 planar phantom images were generated with the digital phantom. When ^{123}I-MIBG phantom imaging with the LE, extended LE (ELE), and ME collimators was simulated, the conversion coefficients for LE, ELE, and ME were 0.52, 0.75, and 0.85, respectively. The conversion coefficients derived from simulated MIBG planar images were equivalent to those from the phantom image database (mean LE, ELE, and ME values were 0.54 ± 0.04, 0.75 ± 0.03, and 0.88 ± 0.04, respectively). When the collimator hole diameter and length were set as 1.0 mm and 30 mm, respectively, conversion coefficients for the septa thicknesses of 0.10, 0.45, 0.80, 1.15, and 1.50 mm were 0.52, 0.67, 0.72, 0.74, and 0.77, respectively. **Conclusion:** The Monte Carlo program successfully simulated ^{123}I-MIBG phantom imaging and conversion coefficients in the various collimator specifications. The collimator septal thickness was a prominent component in ^{123}I-MIBG phantom simulation. When the collimator specifications are determined, the conversion coefficients can be estimated without ^{123}I-MIBG phantom scan. **References:** (1) Verschure DO, et al. J Nucl Cardiol 2017:1-7. (2) Nakajima K, et al. J Nucl Cardiol 2014;21:970-8.

OP-032

Impact of deep learning artificial intelligence approaches on amyloid PET diagnosis

M. Schürer[1], *K. T. Chen*[2], *T. Jochimsen*[1], *M. Rullmann*[1], *M. Patt*[1], *S. Tiepolt*[1], *M. Schroeter*[3], *C. Weise*[4], *D. Saur*[4], *G. Zaharchuk*[2], *O. Sabri*[1], *H. Barthel*[1];
[1]*Department of Nuclear Medicine, University of Leipzig Medical Center, Leipzig, GERMANY,* [2]*Radiology, Stanford University, Stanford, CA, UNITED STATES OF AMERICA,* [3]*Max Planck Institute for Human Cognitive and Brain Sciences, Leipzig, GERMANY,* [4]*Department of Neurology, University of Leipzig Medical Center, Leipzig, GERMANY.*

Aim/Introduction: Deep learning artificial intelligence approaches have a great potential to simplify and improve medical imaging. This might, in case of PET imaging, also refer to

shorten scan times/reducing tracer doses. In this present study we evaluated whether this is the case for [18F]Florbetaben amyloid PET/MRI. **Materials and Methods:** We prospectively acquired list-mode [18F]Florbetaben brain PET/MRI scans (300MBq, scan start 90min p.i.) of 40 patients ("new data", 21 female, age=64±11yrs). The PET data were reconstructed for a (clinical standard) 20min scan duration as well as for 1min scan duration. For the 1min scan duration data, different deep learning approaches (a U-net was pre-trained with previous low-dose PET/MRI data and was either (AI1) directly applied to new data or (AI2) trained further with the new data, or trained from scratch based on (AI3) new data only or (AI4) all existing data) were applied. All PET data were analyzed visually (3 blinded experts, binary score for amyloid load and 5-point score for image quality with 5 being the highest score for excellent image quality) and semi-quantitatively (composite SUVRs, reference: cerebellar cortex, Hermes BRASS software). The 20min scan duration majority visual read served as standard to truth (SoT). **Results:** According to the SoT, 19 and 21 patients were amyloid-positive and -negative, respectively. Mean sensitivity and specificity for the three blinded readers were 100% and 95%, 100% and 78%, 100% and 100%, 100% and 100%, and 100% and 100% for the 1min, 1min+AI1, 1min+AI2, 1min+AI3, and 1min+AI4 data, respectively. Image quality in visual analysis was 2.5±0.3, 3.0±0.3, 4.0±0.3, 3.9±0.1and 3.8±0.1. Cohen's d effect sizes for the composite SUVRs according to amyloid state in SoT were significantly higher in the 1min+AI1/4 as compared to the 1min data (2.38/2.64/2.33/2.59 vs. 1.79). **Conclusion:** Using a trained neural network, scan duration in [18F]Florbetaben amyloid PET/MRI can be reduced down to 1min without losing diagnostic quality. This would alternatively translate to a reduction of tracer dose/radiation exposure by 95%. In conclusion, the deep learning artificial intelligence approach developed has great potential to improve patient convenience/throughput and/or reduce tracer costs. **References:** None.

OP-033

DASciS software: a scintigraphic tool able to evaluate the scintigraphic load of bone disease as a survival predictor in mCRPC Radium-223 patients

V. Frantellizzi, M. D. Ippoliti, M. Conte, G. De Vincentis;
Sapienza University of Rome, Rome, ITALY.

Aim/Introduction: Alpha-emitter ^{223}Radium-dichloride is associated to a clear survival benefit and significant bone pain palliation in CRPC patients with symptomatic bone metastases. Increase in Overall Survival (OS) is strictly associated to 6-cicles therapy's administration. Bone Scan Index (BSI) is defined as the percentage of total amount of bone metastasis on whole-body scintigraphic images. To calculate BSI values we used DASciS software, developed by an engineering team of "Sapienza" University of Rome. Aim of our observational, prospective, non randomized study was to assess the load of bone disease at starting and in the time course of Ra-223 treatment, in mCRPC patients, as an overall survival (OS) predictor. **Materials and Methods:** Bone scintigraphies of 127 mCRPC patients treated with 223Ra were collected before, during and after the therapy. Follow-up images were taken after 3 months, 6 months and one year. DASciS software was used to process bone scans and BSI was calculated. BSI values were analyzed alone and together with 3-PS (prognostic score based on basal values of Hb, PSA and ECOG-PS) in order to evaluate the OS predictive power of these parameters. **Results:** Employing DASciS software 546 scintigraphies were analyzed, (127 basal, 211 intermediate, 87 final, 60 after 3 months, 38 after 6 months and 23 after one year). Both the univariate (HR: 1,8, 1,61-2,02, p=0,001) and the multivariate (HR: 1,82, 1,56-2,10, p=0,001) analysis -adjusted for BMI, age, Gleason Score, number of previous systemic treatments, basal PSA, tALP, Hb, PLT, ECOG-PS- confirm the OS prediction power of basal BSI (Percentage of bone disease are: 0-3% = 28 months of median survival (MoMS), 3%-5% = 11 MoMS, more than 5% = 5 MoMS). The association of BSI with 3-PS have however the best OS prediction power (AUC=91%). **Conclusion:** Load of bone disease first of 223Ra treatment is an excellent predictor of OS and DASciS software is an accurate tool to calculate BSI. BSI and 3-PS together represent a unique multidimensional evaluation of mCRPC patients at basal conditions and are very useful for the stratification of patients who are candidates to 223Ra treatment. Despite EMA recommendation, the calculation of the bone disease extension percentage instead of number of lesions appears to be a more reliable tool for patients recruitment. **References:** A 3-variable prognostic score (3-PS) for overall survival prediction in metastatic castration-resistant prostate cancer treated with 223Radium-dichloride. Ann Nucl Med. 2017 Dec 28; V 32 (2), 142-148, 1. DOI 10.1007/s12149-017-1228-6

OP-034

Impact of PET/CT image reconstruction parameters on patient dose distributions for quantitative ^{90}Y liver radioembolization

X. Hou[1], H. Ma[2], P. Esquinas[3], S. Tolhurst[1], F. Benard[4], D. Liu[1], A. Celler[1];
[1]Radiology Department, University of British Columbia, Vancouver, BC, CANADA, [2]Department of Physics and Astronomy, University of British Columbia, Vancouver, BC, CANADA, [3]IBM Watson Health Imaging, Mississauga, ON, CANADA, [4]Department of Molecular Oncology, BC Cancer, Vancouver, BC, CANADA.

Aim/Introduction: ^{90}Y-radioembolization is a well-established treatment option for nonsurgical patients with liver tumours. Measuring the dose distribution with ^{90}Y PET/CT scans could be useful for dose verification and to investigate tumour response to treatment. However, ^{90}Y PET images are typically of very poor quality due to the low intensity of positrons from ^{90}Y. Regularized reconstruction algorithms have recently been introduced in clinical scanners to iterative reconstruction algorithm to reach convergence while minimizing image noise. The aim of this work was: 1) to evaluate regularized image reconstruction parameters to optimize image quality and quantification accuracy using

phantom studies, and 2) to investigate their impact on the dose distributions in lesions and healthy livers in patient studies. **Materials and Methods:** The IEC-NEMA phantom (9.7L) and six spheres (0.5-26mL), filled with ^{90}Y activities (0.325MBq/mL and 2.45MBq/mL, respectively) were scanned using GE-D690 PET/CT camera. Images were reconstructed with OSEM (standard) and the Q.Clear regularized reconstruction method (β-parameter ranging 0-8000), both with the time-of-flight option enabled. The reconstruction parameters were optimized for image quality by evaluating the background noise and contrast-to-noise ratios; while, the hot and cold contrast recovery coefficients were used for evaluating image quantification accuracy. Then, the optimized reconstruction parameters were applied to PET/CT scans obtained from five subjects following ^{90}Y-radioembolization studies. Dose maps of healthy liver parenchyma and tumours were estimated using the MIM software. The variabilities (coefficients of variation (COV)) of dose volume histograms, D_{max}, D_{mean}, D_{70}, and V_{100Gy} for the entire range of investigated reconstructions were assessed. **Results:** Generally, superior image quality was obtained from Q.Clear compared to OSEM reconstructions. The β-parameter optimized for best image quality was found to be in the range of 2000 - 2500 and equal to 300 for best quantification accuracy. In order to estimate how different reconstructions influence dose distributions, β-parameter ranged from 300-8000 were applied to patient studies. For D_{mean}, D_{70}, and V_{100Gy}, the COVs were <7% for all five patients; whereas, the COVs for D_{max} were >15%. **Conclusion:** There was a clear advantage of using regularized (Q.Clear) over conventional OSEM reconstruction to maximize image quality and quantitative accuracy for PET imaging studies performed after ^{90}Y-radioembolization studies. However, the β-parameter used in Q.Clear reconstructions needs to be carefully selected based on the study objectives, since its value will largely influence the visual quality of reconstructed images, as well as quantification accuracy and dose distribution in tumours and healthy liver. **References:** None.

OP-035

Impact of high energy co-emitted gamma quanta on quantification of Sc-44

F. Rosar[1,2], *H. G. Buchholz*[2], *M. Piel*[3], *F. Rösch*[3], *M. Schreckenberger*[2];
[1]*Department of Nuclear Medicine, Saarland University Medical Center, Homburg, GERMANY,* [2]*Department of Nuclear Medicine, Johannes Gutenberg-University, Mainz, GERMANY,* [3]*Institute of Nuclear Chemistry, Johannes Gutenberg-University, Mainz, GERMANY.*

Aim/Introduction: Scandium-44 is a promising PET nuclide with a half-life of 3.97 h and a β^+ fraction of 94.27 %. Several preclinical and clinical trials have been performed using Sc-44 labeled tracers e.g. Sc-44-PSMA-617 or Sc-44-DOTATOC. In contrast to the F-18, Sc-44 emits additional γ quanta (E= 1157 keV), which may influence the PET data acquisition. In this study we investigated the differences in coincidence energy spectra of Sc-44 compared to F-18 and analyzed its influence on quantification. **Materials and Methods:** A series of phantom measurements with Sc-44 and F-18 at different activity concentrations were performed using Mediso nanoScan PET/MR. Raw data were analyzed with respect to different energy windows. After iterative 3D reconstruction, a quantitative image VOI analysis was performed by using PMOD. **Results:** In comparison to F-18, Sc-44 showed a different energy spectrum of coincidences with a higher Compton peak, lower 511 keV peak and higher background due to its additional γ quanta. For Sc-44, 16.9-20.1 % of acquired coincidences were detected in an energy window of 400-600 keV in contrast to 19.3-23.7 % for F-18. On average, the reconstructed activity of Sc-44 was 19.5% lower than that of F-18. **Conclusion:** The co-emission of γ quanta of Sc-44 leads to a different energy spectrum in the raw data in comparison to F-18. As a consequence, lower activity was detected for Sc-44 in the reconstructed images. Therefore, an additional correction factor should be applied in further studies, in particular for quantification and dose calculations. **References:** None.

107

Pitfalls & Artefacts 1 - Interactive Clinical Cases - Paediatrics Committee: Pitfalls and Artefacts in Paediatric Nephro-Urology

Sunday, October 13, 2019, 8:00 - 9:30 Lecture Hall 113

OP-036

Dynamic Renal Scintigraphy

A. Santos;
Hospital Garcia de Orta,E.P.E., Nuclear Medicine Department, Almada, PORTUGAL.

OP-037

Static Cortical Scintigraphy

Z. Bar-Sever;
Schneider Children´s Medical Center, Department of Nuclear Medicine, Petach Tikva, ISRAEL.

OP-038

Radionuclide Cystography

L. Biassoni;
Great Ormond Street Hospital for Children NHS Foundation Trust, Department of Radiology, London, UNITED KINGDOM.

108

Clinical Oncology - Rapid Fire Session: Prostate - BCR and More

Sunday, October 13, 2019, 8:00 - 9:30 Lecture Hall 114

OP-039

Impact of application of furosemide combined with hydration on the halo artefact and intensity of tracer accumulation in the urinary bladder in ^{68}Ga PSMA-11 PET/CT

C. Uprimny[1], *A. Kroiss*[2], *B. Nilica*[2], *H. Svirydenka*[2], *E. Elmisgheri*[2], *C. Decristoforo*[2], *E. Guggenberg*[2], *G. di Santo*[2], *I. Virgolini*[2];
[1]*Medical University of Innsbruck, Gaimberg, AUSTRIA,*
[2]*Medical University of Innsbruck, Innsbruck, AUSTRIA.*

Aim/Introduction: Comparative study to assess systematically the influence of hydration and application of furosemide on the occurence of the halo artefact, a photopenic artefact surrounding the urinary bladder, that might be present on ^{68}Ga-PSMA-11 PET/CT images. **Materials and Methods:** 200 consecutive prostate cancer patients referred for ^{68}Ga-PSMA-11 PET/CT were included. Four groups receiving different preparation prior to imaging, comprising 50 patients each, were compared. Group one: no intervention. Group two: intravenous hydration with 500 ml sodium chloride after tracer application. Group three: intravenous hydration with 500 ml sodium chloride and 20 mg furosemide injected after tracer application. Group four: intravenous hydration with 500 ml sodium chloride and 40 mg furosemide injected after tracer application. Images were analysed visually to judge whether halo artefact was present. In addition intensity of tracer uptake in the urinary bladder was measured semiquantitatively with calculation of maximum standardised uptake value (SUV_{max}). **Results:** In group one (no preparation) ten patients (20 %) demonstrated a halo artefact surrounding the urinary bladder with a median SUV_{max} of 66.9 (range: 9.3 - 349.9) of the urinary bladder. In group two (intravenous hydration only) in seven patients (14 %) the halo artefact was present with a median SUV_{max} of 21.8 (range: 9.0 - 170.6) in the urinary bladder. In group three (20 mg furosemide) and group four (40 mg furosemide) no halo artefact could be found. Median SUV_{max} of the urinary bladder in group three and four was 8.9 (range: 2.3 - 32.1) and 9.7 (range: 2.3 - 26.8), respectively. The difference in number of halo artefact and median SUV_{max} of urinary bladder between group one and group three and four was statistically significant ($p < 0.001$). Although median SUV_{max} was significantly reduced between group one and two, number of halo artefact in these two groups did not differ significantly. No significant difference of results could be observed in patients receiving 20 mg furosemide and those injected with 40 mg furosemide. **Conclusion:** Intravenous injection of 20 mg furosemide combined with 500 ml sodium chloride significantly reduces the halo artefact and median SUV_{max} of the urinary bladder in ^{68}Ga-PSMA-11 PET/CT in comparison to patients receiving no preparation and patients receiving only hydration with 500 ml sodium chloride. **References:** None.

OP-040

Next-generation PET is a sensitive and reproducible biomarker of early CRPC

M. M. Weber[1], *C. E. Kurek*[2], *F. Barbato*[1], *C. Rischpler*[1], *M. Eiber*[3], *T. Maurer*[4], *B. Hadaschik*[5], *K. G. Herrmann*[1], *A. Wetter*[6], *F. P. Wolfgang*[1];
[1]*University Clinic Essen, Department of Nuclear medicine, Essen, GERMANY,* [2]*University Clinic Essen, Deparment of Nuclear medicine, Essen, GERMANY,* [3]*Department of Nuclear Medicine, Klinikum Rechts der Isar, Technische Universität München, Munich, GERMANY,* [4]*Martini-Clinic and Department of Urology, University Clinic Hamburg-Eppendorf (UKE), Hamburg, GERMANY,* [5]*Department of Urology; University Hospital Essen, Essen, GERMANY,* [6]*Institute of Diagnostic and Interventional Radiology and Neuroradiology; University Hospital Essen, Essen, GERMANY.*

Aim/Introduction: At early diagnosis of castration-resistant prostate cancer (CRPC), PSA measurement is limited by fluctuations and conventional imaging by low detection probability. We thus aim to assess the value of PSMA-PET/CT as biomarker at early CRPC. **Materials and Methods:** We screened our local database (n=1369) for patients with histopathologically proven prostate cancer, rising PSA despite effective androgen-deprivation therapy and PSA ≤ 3. CT and PSMA-PET/CT scans of eligible patients (n=46) were anonymized and interpreted independently by three blinded readers. Patients were stratified by PSA (<1.0; 1-0-2.0; 2.0-3.0); primary endpoint was the per-patient detection rate. Secondary endpoints were the per-region detection rate, interobserver agreement and risk factors for PET positivity or M1-disease. **Results:** PSMA-PET/CT was positive in 74% of patients. 28% patients had local disease only, 46% patients had M1-disease (26% bone, 4% visceral). Interobserver agreement was substantial/almost perfect (Fleiss' kappa 0.80, 95% confidence interval 0.63-0.97) for PET. Factors typically associated with adverse outcome (e.g. Gleason Score ≥8, PSA doubling time≤6 months) were not associated with PET positivity or M1-disease. **Conclusion:** PSMA-PET/CT localizes prostate cancer in more than two thirds of patients with pre/early CRPC, even before PSA exceeds the 2 ng/mL threshold. PSMA-PET/CT is a sensitive and reproducible biomarker of disease that may allow earlier diagnosis and guided treatment of CRPC. **References:** None.

OP-041

Benefit of CT urography in ^{68}Ga-PSMA-11 PET with low dose CT

F. Rosar[1], *M. Hügle*[1], *M. Ries*[1], *S. Maus*[1], *M. Bartholomä*[1], *T. Stemler*[1], *H. Bohnenberger*[1], *P. Fries*[2], *F. Khreish*[1], *S. Ezziddin*[1];
[1]*Department of Nuclear Medicine, Saarland University Medical Center, Homburg, GERMANY,* [2]*Department of Radiology,*

Saarland University Medical Center, Homburg, GERMANY.

Aim/Introduction: Accuracy of ^{68}Ga-PSMA-11 PET/CT may be hampered by ureter accumulation. Depending on localization and configuration it may mimic lymph node metastases. We evaluated the benefit of intravenous CT contrast agent for urography in ^{68}Ga-PSMA-11 PET with low dose CT to help to differentiate between lymph node metastasis and urinary tract activity. **Materials and Methods:** Retrospective analysis of n=247 PET/CT scans (Biograph 40 mCT, 124±17 MBq ^{68}Ga-PSMA-11, 60 min p.i. image-acquisition, iterative 3D OSEM algorithm (3 iterations, 24 subsets), low dose CT (120 keV, max. 30 mAs)) for primary staging, biochemical recurrence or local therapy planning. For urography, a reduced amount of 30 ml contrast agent (370-400 mg iodine/ml) was applied 10 minutes prior to image acquisition. All foci of potential pathologic radiotracer accumulation were reviewed and analysed. The success of achieving a contrasted ureter was verified by measuring Hounsfield units in the ureter. All foci were rated and scored by at least three experienced physicians to assess the provided benefit of urography. In addition, the imaging outcome for further decision making was evaluated. **Results:** By CT urography, it was possible to identify each ureter on low dose CT, with its major part contrasted. In 120/247 PET/CT scans (48.6 %) with 189 sites of (peri)ureteral accumulation urography increased the diagnostic confidence. In 60 (24.3 %) scans, urography was rated important for decision making. In 36 of 189 sites, the tracer accumulation would not have been attributable to lymph node metastases or ureter excretion without urography. In 42 (17.0 %) scans, urography-enhanced PET-CT reading was clinically relevant (up-/downstaging) with potential impact on subsequent patient care. In 30 of these 42 cases (12.1 % of all), change in treatment would have resulted from misdiagnosed focus without urography. **Conclusion:** Additional administered contrast agent for CT-urography benefits the interpretation of ^{68}Ga-PSMA-11 PET with low dose CT by increasing diagnostic confidence in the differentiation of lymph node metastases and urinary tract activity. A subsequent change in patient management will result in a small but significant subset (12% in our cohort). Reduced contrast amount of 30 ml (370-400 mg iodine/ml) applied 10 minutes prior to image acquisition is adequate to identify the ureter on low dose CT. **References:** None.

OP-042

Prospective intra-patient comparison of ^{18}F-Fluciclovine and ^{68}Ga-PSMA-11 PET/CT in biochemical recurrence of prostate cancer after definitive therapy

***B. Pernthaler**, H. Kvaternik, R. Kulnik, C. Gstettner, R. M. Aigner;*
Medical University Graz, Department of Radiology, Division of Nuclear Medicine, Graz, AUSTRIA.

Aim/Introduction: To compare ^{18}F-Fluciclovine to ^{68}Ga-PSMA-11 PET/CT in patients with biochemical recurrence of prostate cancer. To evaluate the advantages, disadvantages and comparability of these PET tracers. **Materials and Methods:** Prospective study of 58 patients with biochemical recurrence of prostate cancer after definitive primary therapy (radical prostatectomy, radiation therapy). ^{18}F-Fluciclovine and ^{68}Ga-PSMA-11 PET/CT were performed within a time window of median 9,4 days with standardized image acquisition protocols and interpretation criteria. The performance of both tracers were evaluated on a patient- and region-based analysis. **Results:** The patient-level detection rate for prostate cancer recurrence was 79.3% in ^{18}F-Fluciclovine and 82.8% in ^{68}Ga-PSMA-11 (p=0.64). Local recurrence was detected in 22/58 (37.9%) patients on ^{18}F-Fluciclovine PET/CT and only in 16/58 patients (27.6%) on ^{68}Ga-PSMA-11 PET/CT (p=0.03). In 6/58 patients (10.4%) local recurrence could only be detected in ^{18}F-Fluciclovine scans. Local pelvic lymph node recurrence was detected in 27/58 patients (46.6%) on ^{18}F-Fluciclovine PET/CT and in 29/58 patients (50.0%) on ^{68}Ga-PSMA-11 PET/CT (p=0.71). Local pelvic lymph node recurrence was only detected on ^{68}Ga-PSMA-11 scan in 3/58 patients (5.2%), and on ^{18}F-Fluciclovine scan in 1/58 patients (1.7%). Extrapelvic lymph node metastases were detected in 24/58 patients (41.4%) on ^{18}F-Fluciclovine PET/CT and in 30/58 patients (51.7%) on ^{68}Ga-PSMA-11 PET/CT (p=0.26). In 6/58 patients (10.4%), distant lymph node metastases were only detected on ^{68}Ga-PSMA-11. Bone metastases were detected in 15/58 patients (25.9%) on ^{18}F-Fluciclovine PET/CT and in 21/58 patients (36.2%) on ^{68}Ga-PSMA-11 PET/CT (p=0.23). In 8/58 patients (13.8%), bone metastases were only detected on ^{68}Ga-PSMA-11 scan, and on ^{18}F-Fluciclovine scan in 2/58 patients (3.5%). **Conclusion:** The strength of ^{18}F-Fluciclovine in comparison to ^{68}Ga-PSMA-11 lies in detecting local recurrence of prostate cancer especially when located in close anatomic relation to the urinary bladder. In the detection of distant metastases ^{18}F-Fluciclovine is almost comparable to ^{68}Ga-PSMA-11 PET/CT, with heterogeneity of tracer-avid disease across both scans. **References:** None.

OP-043

Impact of late pelvic acquisition on ^{68}Ga-PSMA-11 PET/CT positivity rate and inter-rater reliability analysis

***D. Nicolotti**, F. Ceci, E. Pilati, B. Dionisi, I. Cerio, M. Finessi, V. Liberini, R. Passera, G. Bisi, D. Deandreis;*
Nuclear Medicine Unit, Department of Medical Sciences, University of Turin, AOU Città della Salute e della Scienza di Torino, Turin, ITALY.

Aim/Introduction: The primary aim of this study was to evaluate the impact of late-pelvic scan on ^{68}Ga-PSMA-11-PET/CT accuracy in localizing recurrent prostate cancer (PCa). Secondary objective was the comparison of inter-rater reliability between standard images and late acquisition, both in a per-patient and per-region analysis. **Materials and Methods:** ^{68}Ga-PSMA-11-PET/CT is performed in our institution through a prospective, single-centre, study (protocol P-5315) in hormone-naïve recurrent PCa. Data of the first 65 consecutive patients

who performed late-pelvic acquisition were retrospectively analysed. Administered activity was 2.5 (±0.5) MBq/Kg. Vertex to mid-thigh images were acquired at 60 (±10) minutes post-injection, 2.5 minutes per bed-position. Late-pelvic images were acquired at 120 (±15) minutes post-injection, 6 minutes per bed-position, 2 beds centered on pelvis. All images were acquired by the same scanner (Philips Gemini Dual-Slice EXP PET/CT) and interpreted by three independent experienced readers (R1=EP, R2=DN, R3=FC) using the same workstation (GE Advantage). Both acquisitions were interpreted in a per-patient and per-region (prostate bed; pelvic lymph-nodes; pre-sacral lymph-nodes; pelvic bones) analysis, using a 3-point scale (not suspected for PCa[0], undetermined[1] and suspected for PCa[2]). The impact of late-pelvic acquisition was evaluated as reader's confidence (decreasing of undetermined findings rate) and number of lesions detected. The degrees of agreement were assessed using intraclass correlation coefficients (ICC) and their CI95%, using a 2-way mixed, single measure, consistency model. ICC was interpreted as follow: 0.0, poor; 0.0-0.20, slight; 0.21-0.40, fair; 0.41-0.60, moderate; 0.61-0.80, substantial; 0.81-1.00, almost-perfect reproducibility. **Results:** Overall ^{68}Ga-PSMA-11-PET/CT positivity rate increased from standard to late-pelvic acquisition: R1=43.07% to 60%, R2=49.23% to 64.62%, R3=40% to 55.38%, respectively. The reduction ratio of undetermined scans was: R1=18.46% (21.54% to 3.08%), R2=15.39% (21.54% to 6.15%), R3=15.38% (18.46% to 3.08%). All readers detected additional findings in late-scan compared to standard: R1=66 to 68; R2=64 to 72; R3=61 to 68. In the per-patient analysis the inter-observer agreement resulted substantial in standard scan (ICC=0.802, CI95%=0.733-0.834) and improved to almost-perfect in late-pelvic acquisition (ICC=0.851, CI95%=0.785-0.900). In the per-region analysis the inter-observer agreement improved especially in the prostate bed (ICC-standard=0.531, CI95%=0.390-0.661; ICC-late=0.606, CI95%=0.476-0.721), which remains however the more difficult district to evaluate, with moderate agreement. Despite high incidence of undetermined findings, pelvic lymph-nodes reached almost-perfect agreement both in standard (ICC=0.839, CI95%=0.770-0.892) and late-pelvic acquisition (ICC=0.878, CI95%=0.824-0.920). **Conclusion:** Our results show that the late-pelvic scan increases the overall ^{68}Ga-PSMA-11-PET/CT positivity rate and the number of detected lesions, improves reader's confidence and allows better inter-observer reproducibility. **References:** None.

OP-044

Interobserver and intraobserver agreement of PSMA PET/CT according to miTNM and PSMA-RADS criteria

E. Demirci[1], *R. Akyel*[2], *B. Caner*[1], *N. Alan-Selçuk*[1], *S. Güven Mese*[3], *L. Kabasakal*[4];

[1]*Yeditepe University, Department of Nuclear Medicine, Istanbul, TURKEY,* [2]*Sisli Etfal Training and Research Hospital, Istanbul, TURKEY,* [3]*Yeditepe University, Department of Medical Oncology, Istanbul, TURKEY,* [4]*Istanbul University-Cerrahpasa, Department of Nuclear Medicine, Istanbul, TURKEY.*

Aim/Introduction: Limited data is available about the interobserver variability of PSMA PET/CT and intraobserver variability has not been published. We aimed to investigate intra- and interobserver agreement for 68Ga-PSMA PET/CT interpretations according to miTNM and PSMA-RADS reporting templates and identify PET/CT findings with high variability and investigate diagnostic confidence levels of readers at specific PSMA PET/CT findings. We also investigated clinical outcome of interobserver variability. **Materials and Methods:** Patients (n=136) were selected with simple randomization. Anonymized images were evaluated by four experienced readers independently according to miTNM and PSMA-RADS templates. Diagnostic confidence levels of all findings also reported. Results evaluated with Feiss kappa test or intraclass correlation coefficients test(ICC) using 2-way mixed model for absolute agreement. **Results:** Readers agreed substantially for N and almost-perfectly for M categories (k=0.71 95%CI:0.67-0.79 and 0.78 95%CI:0.74-0.82). Moderate agreement was observed for initial T staging (k=0.63 95%CI:0.59-0.66). According to six-quadrant prostate reporting template, moderate or substantial agreement were observed for intraprostatic lesion localization (k=0.48 - 0.62). However, almost perfect interobserver agreement was observed for number of intraprostatic sites (ICC: 0.90 - %95CI:0.86-0.93). In Gleason Group 1 (GS 3+3) moderate reproducibility was observed (κ=0.531 %95CI:0.34 - 0.722). In Gleason Group ≥2 substantial reproducibility was observed (κ= 0.655 %95CI 0.55-0.761). Substantial agreement was observed for vesicula seminalis invasion (k=0.622 - 95%CI:0.533-0.71). All readers reported lower diagnostic confidence levels for «T3a» compared to other T stages (p<0.01). Three readers reported lower diagnostic levels for «T0» compared to other T stages (p<0.001). Two readers reported lower diagnostic confidence levels in patients with N1 compared to N0&2. In 12% (n=16) of the patients, only one reviewer reported clinically significant discordance (amendable errors with peer-review). In 9% (n=12) of the patient, the disagreement influences clinical management 3.8%(n=5). Almost-perfect intraobserver agreement was observed for 5-scale PSMA-RADS criteria (ICC=0.90 95%CI: 0.865-0.934). If lesions are grouped as benign (Score 1-2), suspicious (3) and malignant (4-5) moderate agreement was observed (k=0.5-95%CI:0.434-0.564). **Conclusion:** PSMA PET has a substantial interobserver agreement and an almost perfect intra-observer agreement levels. Interobserver variance has a limited effect on clinical decisions. PSMA PET/CT has the highest interobserver agreement levels among the modalities used for imaging of prostate cancer. Lower (still moderate) interobserver agreement calculated for intraprostatic lesion localization due to limitation of 6-quadrant template. Peer-review significantly increases reproducibility and reliability of PSMA PET/CT. miTNM template is better for standardization of PSMA-PET reporting, compared to PSMA-RADS template. **References:** None.

OP-045

Evaluation of [^{68}Ga]Ga-PSMA-PET/CT in therapy response assessment of PSMA-targeted radionuclide therapy in patients with castration resistant prostate cancer

J. Kurth[1], *J. Kretzschmar*[1], *M. Heuschkel*[1], *G. Kundt*[2], *O. W. Hakenberg*[3], *B. J. Krause*[1], *S. M. Schwarzenboeck*[1];
[1]*Department of Nuclear Medicine, Rostock University Medical Center, Rostock, GERMANY,* [2]*Institute for Biostatistics and Informatics in Medicine and Ageing Research, Rostock University Medical Center, Rostock, GERMANY,* [3]*Department of Urology, Rostock University Medical Center, Rostock, GERMANY.*

Aim/Introduction: Aim of this study was to retrospectively evaluate the value of [^{68}Ga]Ga-PSMA-PET/CT in monitoring early and late response to PSMA-targeted radionuclide therapy (Lu-177/Y-90) in castration resistant prostate cancer patients. **Materials and Methods:** 38 patients were referred for [^{68}Ga]Ga-PSMA-PET/CT before the first cycle (PET 1), after one/two cycles (PET 2) and after a mean of 3 cycles (range 3 to 5 cycles) (PET 3) of PSMA radioligand therapy (Lu-177/Y-90) for patient-based therapy response assessment. PET-based therapy response was assessed according to EORTC and PERCIST criteria, for PET 2 vs. 1 (early response assessment, ERA) as well as for PET 3 vs. 1 (late response assessment, LRA). PET-classified response was compared to the results of ERA and LRA based on clinical criteria (best clinical response) and percentual change in PSA. Additionally, relationship between change of SUV_{max}/SUV_{mean} and PSA (early and late, respectively) was evaluated. Prognostic value of initial SUV_{max} and SUV_{mean} was assessed. **Results:** About 76% of the patients were classified as SD or PR (SD: 65.2%; PR: 10.9%) by clinical criteria and 77% by change in PSA as response criterion (SD: 46.7%; PR: 31.1%). However, by PET-based response assessment approx. 95% were classified as SD or PR (PERCIST: SD 23.9%; PR: 71.7%; EORTC: SD 23.9%; PR: 69.6%). Cohens kappa analysis showed no statistically significant concordance between EORTC/PERCIST based and clinical criteria/PSA-based ERA and LRA; kappa < 0.2. No statistically significant correlation was found between change in SUV and PSA in ERA and LRA; r < 0.1, for both ERA and LRA. No statistically significant prognostic value of initial SUV_{max} and SUV_{mean} could be shown. **Conclusion:** Pretherapeutic [^{68}Ga]Ga-PSMA-PET/CT is an essential prerequisite to detect sufficient expression of the molecular target. However, a significant correlation between [$_{68}$Ga]Ga-PSMA-PET/CT based and clinical criteria/PSA-based therapy response assessment during the early and late course of PSMA targeted therapy could not be shown. The role of [^{68}Ga]Ga-PSMA-PET/CT in this setting has to be evaluated in further studies. **References:** None.

OP-046

Preliminary results on response assessment using PSMA molecular imaging in patients with metastatic prostate cancer undergoing abiraterone

C. Liu, *S. Hu, X. Xu, S. Song, Y. Zhang;*
Fudan university cancer center, Shanghai, CHINA.

Aim/Introduction: A well-recognized barrier to therapy response assessment in castration-resistant prostate cancer (CRPC) is the lack of reliable surrogate markers of response to treatment coupled with a potentially exaggerated reliance on changes in serum prostate-specific antigen (PSA) as an indicator of treatment efficacy. Functional imaging modalities have been advocated as important markers of disease response and progression to different tumor entities.The aim of this study was to investigate the role of ^{99m}Tc-HYNIC-PSMA SPECT/CT in the early treatment evaluation and outcome prediction in patients with CRPC treated with long-term abiraterone. **Materials and Methods:** ^{99m}Tc-HYNIC-PSMA SPECT/CT was performed in 68 CRPC patients before and after 3-6 months treatment with abiraterone. Treatment response was assessed according to RECIST 1.1 and PERCIST 1.0 criteria, respectively. A decrease in serum PSA level of ≥50% was defined as biochemical response (BR). Univariate and multivariate Cox regression models addressed potential predictors of progression-free survival (PFS) and overall survival (OS). **Results:** Declines in PSA level of ≥50% were seen in 21 of 68 (31%) patients. The concordance rate between SPECT and BR was 81% (Cohen κ = 0.60; 95% CI, 0.33-0.90;P ≤ 0.01), higher than for that between SPECT and CT with 55% (κ = 0.40; 95% CI, 0.23-0.68; P ≤ 0.01), as well as that between CT and BR with 40% (κ = 0.43; 95% CI,0.26-0.67, P ≤ 0.05). In univariate analysis, PSA decline and PSMA SPECT/CT response predicted PFS and OS. In multivariate analysis, only PSMA SPECT/CT (progression vs nonprogression) remained significant for PFS and OS (p = 0.013 and p = 0.022, respectively). **Conclusion:** Early PSMA SPECT/CT can predict clinical outcome in CRPC beyond PSA response and conventional CT approach. Our data support further studies on PSMA SPECT/CT for abiraterone monitoring and outcome prediction in patients with CRPC. **References:** None.

OP-047

Monocentric Intraindividual Comparison of ^{68}Ga-RM2 and ^{68}Ga-PSMA PET/CT in mCRPC

M. Heuschkel, *J. Kurth, O. W. Hakenberg, S. Nitsch, S. M. Schwarzenböck, B. J. Krause;*
Rostock University Medical Center, Rostock, GERMANY.

Aim/Introduction: ^{68}Ga-PSMA PET/CT is the standard imaging procedure in recurrent Prostate Cancer. Beyond PSMA, different agents addressing other targets in Prostate Cancer have been developed, such as the GRPr-antagonist RM2. As well as PSMA it can equally be labeled with ^{68}Ga and ^{177}Lu in a theranostic approach. First evaluations in early stage recurrent Prostate Cancer showed a high detection rate of ^{68}Ga-RM2 PET/CT and overlap with PSMA in this population (Minamimoto et al. JNM 2016). The aim of this retrospective study was an intraindividual comparison of ^{68}Ga-RM2 and ^{68}Ga-PSMA PET/CT for lesion detection in patients with advanced metastatic castration resistant Prostate Cancer (mCRPC). **Materials and Methods:** At the University Medical Center of Rostock we scanned 38 mCRPC patients with ^{68}Ga-PSMA as well as ^{68}Ga-RM2 to identify PSMA

or RM2 positivity as prerequisite for radionuclide treatment with either ^{177}Lu-PSMA or ^{177}Lu-RM2. Visual uptake and semiquantitative parameters (SUVmax and SUVpeak) were compared in 277 metastatic reference lesions (5 local, 96 lymph nodes, 146 bone, 18 liver, 5 lung, 7 others). **Results:** In the visual assessment 3/38 patients showed neither PSMA- nor RM2-positive lesions. The remaining 35 patients showed a PSMA uptake of any grade, of whom only 3 showed a higher, 17 a much lower and 13 no RM2 uptake. 2/38 patients showed complementary RM2-positive / PSMA-negative and RM2-negative / PSMA-positive lesions. SUVmax and SUVpeak were significantly higher for PSMA than for RM2 subsuming all reference lesions ($p < 0.001$) as well as in separate analysis of local recurrence ($p = 0.043$), lymph node ($p < 0.001$), bone ($p < 0.001$) and liver metastases ($p = 0.022$). **Conclusion:** Most of the included advanced mCRPC patients showed a higher number of PSMA- than RM2-positive lesions and a higher uptake in ^{68}Ga-PSMA compared to ^{68}Ga-RM2 PET/CT. Nearly no tumor lesion showed a high PSMA and RM2 uptake at the same time, so there seems to be a different biological behavior of tumor cells. The small amount of patients with missing or only faint PSMA but high RM2 uptake maybe could benefit from the use of ^{68}Ga-RM2 in restaging or in a theranostic approach including ^{177}Lu-RM2-therapy. **References:** Minamimoto R et al., Pilot Comparison of ^{68}Ga-RM2 PET and ^{68}Ga-PSMA-11 PET in Patients with Biochemically Recurrent Prostate Cancer. J Nucl Med. 2016 Apr;57(4):557-62.

OP-048

Localizing biochemical recurrence of prostate cancer using ^{68}Ga-PSMA-11 PET/CT and ^{11}C-acetate PET/CT

N. Regula, *V. Kostaras, S. Johansson, C. Pulido, E. Lindström, M. Lubberink, I. Velikyan, J. Sörensen;*
Uppsala University Hospital, Uppsala, SWEDEN.

Aim/Introduction: ^{68}Ga-PSMA-11 PET/CT is increasingly used for staging of prostate cancer (PCa), but no comparative studies with ^{11}C-acetate are available. This study aims to compare the performance of ^{68}Ga-PSMA-11 PET/CT and ^{11}C-acetate to locate the PCa recurrence in patients with biochemical relapse. **Materials and Methods:** Twenty-nine PCa patients, with PSA relapse after primary curative therapy, recruited from 2017-2018 were prospectively evaluated. PET/CT examination using ^{11}C-acetate and ^{68}Ga-PSMA-11 was performed on a Discovery MI scanner (GE Healthcare, Waukesha, WI). All available clinical data was recorded and evaluated. All highly suspicious lesions of local recurrence, regional or distal lymph node metastases and bone metastases were counted and evaluated regarding uptake intensity (SUV_{mean}, SUV_{max}) and tumor volume (TV) for both tracers. Total TV and total lesion activity (TLA_{mean}: summed SUV_{mean}*TV; TLA_{max}: summed SUV_{max}*TV) were calculated. PSA at time of scan, the instrumental clinical finding at time of relapse, was correlated with findings of both scans. **Results:** Patients with median PSA of 5 ng/mL at time of PET scan (range 0.36-240 ng/mL) were included in this study. Median Gleason sum at time of diagnosis was 7. All pathological lesions showed higher uptake on ^{68}Ga-PSMA-11 PET/CT (SUV_{max} 23.4±24.1) compared to ^{11}C-acetate PET/CT (6.7±3.9; p=0.001). ^{68}Ga-PSMA-11 PET/CT identified more lesions in 11 patients, less lesions in eight patients, identical in seven patients, same number of lesions but at different regions in one patient. Significantly more lymph node (n=107 vs n=80, McNemar test p=0.002) and bone lesions (n=54 vs n=35, McNemar test p=0.0001) were detected on ^{68}Ga-PSMA-11 PET/CT. Nine patients (31%) with median PSA of 6.9 at time of scan showed upgraded disease status on ^{68}Ga-PSMA-11 PET/CT, whereas 17 patients (59%) showed no change and 3 patients (10%) had downgraded disease status, compared to ^{11}C-acetate PET/CT. Both scans were negative in two patients. PSA at time of scan correlated better with ^{68}Ga-PSMA-11 PET/CT (spearman ρ >0.69, p<0.001) than ^{11}C-acetate PET/CT (ρ>0.40, p<0.03). TLA_{max} had the highest correlation (ρ =0.80, p<0.0001) among the two modalities. **Conclusion:** ^{68}Ga-PSMA-11 PET/CT identified significantly more suspicious lymph node and bone metastases compared to ^{11}C-acetate PET/CT. PSA at time of scan was well correlated with the findings on ^{68}Ga-PSMA-11 PET/CT. **References:** None.

OP-049

Impact of ^{18}F-PSMA-1007 Ligand PET/CT in Multimodal Imaging of Recurrent Prostate Cancer

L. Dronka[1,2], *M. Radziņa*[1,2], *M. Tirāne*[1,2], *L. Zemniece*[1], *M. Kalniņa*[3,2], *L. Roznere*[3,2], *V. Lietuvietis*[4], *A. Freimanis*[4], *E. Vjaters*[5];
[1]*Institute of Radiology, Pauls Stradins Clinical University Hospital, Riga, LATVIA,* [2]*Riga Stradins University Radiology Research Laboratory, Riga, LATVIA,* [3]*Riga Stradins University Nuclear Medicine Clinic, Riga, LATVIA,* [4]*Center of Urology, Riga East University Hospital, Riga, LATVIA,* [5]*Center of Urology, Pauls Stradins Clinical University Hospital, Riga, LATVIA.*

Aim/Introduction: Prostate cancer is generally a significant medical problem worldwide. Accurate localization of recurrent prostate cancer at low PSA values is a major challenge. Radiopharmaceutical ^{18}F-PSMA-1007 has some advantageous characteristics in recurrent prostate cancer diagnostics. The aim of this study was to evaluate the diagnostic performance of the ^{18}F-PSMA-1007 in patients with recurrent PCa, correlating with PSA levels, Gleason score(GS) and MRI Imaging results. **Materials and Methods:** This comparative prospective study included 20 PCa patients with biochemical relapse (mean age 64.15 ± 6.2 years) referred for 18F-PSMA PET/CT. Whole-body PET/CT imaging was performed in all patients 120 min. after injection of 376 ± 71,92 MBq ^{18}F-PSMA-1007. Prostatectomy and radiation therapy has been performed in 90% (N=18) and 40% (N=8) of the patients, respectively. PET/CT scans results were compared with GS, PSA level, doubling time and MRI Imaging results. **Results:** PET/CT confirmed pathological findings in 16/20 patients, 80%, respectively. MRI data was available for 13/20 patients and 76,9 % (N=10) showed local recurrence findings also in MRI while regional lymph nodes were detected by PET/CT vs. MRI, 11 vs. 5 cases, respectively (p=0.001). The higher SUVmax values were measured in pathological lymph

nodes (range 2.7-21.3), main reduced detection on MRI was seen when SUVmax did not exceed value 10. The overall mean PSA level in study group was 1.62 ng/ml (range 0.38-21.6 ng/ml). The mean PSA doubling time - 2,63 months with high correlation to Gleason score (rs=0.747; p=0.001). The mean PSA level in PET positive finding group was 4,39 ng/ml, in PET negative finding group - 0,74 ng/ml. The median GS was 7 (range 5-9), and 75% (N=12) had a score above 7 (with prevalence of 3+4), the rate of pathological scans in these patients was 94% (N=11). In all cases, when GS exceed value 7, local and nodal PET/CT finding was positive. Overall method sensitivity was for PET/CT and MRI for local recurrence 83% vs 100% and for regional lymph nodes Se 100% vs. 62% with 37 % of false negative MRI nodes and 13% of false negative local recurrence results PET/CT (p=0.001). **Conclusion:** ^{18}F-PSMA-1007 PET/CT is superior to MRI in detection of recurrent PCa in regional metastatic lymph nodes, with substantial false negative results for local recurrence where MRI should be applied as confirmative method. Results are highly dependent on PSA level increase and Gleason score, confirming result stability in the groups with GS>7 and PSA doubling time>2.6 months. **References:** None.

OP-050

Detection of biochemical recurrance of prostate cancer following radical prostatectomy through 18F-rhPSMA-7 positron emission tomography

L. Ulbrich[1], *M. Groenke*[2], *A. Wurzer*[3], *L. Jooss*[2], *T. Maurer*[4], *S. Kropf*[5], *T. Horn*[6], *H. Wester*[3], *W. Weber*[2], *M. Eiber*[2];
[1]*MRI/TUM, Munich, GERMANY,* [2]*Department of nuclear medicine, Klinikum rechts der Isar, TUM, Munich, GERMANY,* [3]*Chair of Pharmaceutical Radiopharmacy, TUM, Munich, GERMANY,* [4]*Martini-Klinik, UKE, Hamburg, GERMANY,* [5]*Scintomics GmbH, Fuerstenfeldbruck, GERMANY,* [6]*Department of Urology, Klinikum rechts der Isar, TUM, Munich, GERMANY.*

Aim/Introduction: The new theranostic PSMA-targeting agent 18F-rhPSMA-7 allows fast radiolabeling with 18F and radiometals and shows only minimal renal excretion. Aim of this retrospective study was to evaluate the effficancy of 18F-rhPSMA-7PET in patients with biochemical recurrance (BCR) of prostate cancer after radical prostatectomy. **Materials and Methods:** The 18F-rhPSMA-7PET/CT or PET/MRI datasets of patients with non-castrate BCR after radical prastatectomy imaged between June 2017 and June 2018 were retrospectively reviewed. One experienced nuclear medicine physician recorded all lesions suspicious for recurrent prostate cancer. Correlations between the detection rates and the patients' PSA level, their primary Gleason score and previous therapy (androgen deprivation therapy [ADT] and external beam radiation therapy [EBRT]) were evaluated. **Results:** 532 patients were included. Their median PSA level was 0.97 ng/mL (range, 0.01-372 ng/mL). The median uptake time between injection and start of the PET-scan was 76 min (range, 50-220 min). The median injected activity of 18F-rhPSMA-7 was 332 MBq (range: 142-486 MBq).423 (79.5%) patients with pathological findings were identified by 18F-rhPSMA-7 PET. 38.5% (15/39) patients with a PSA < 0.2 ng/mL presented with suspicious lesions. The detection rates were 63.8% (81/127), 86.5% (90/104), 85.3% (87/102) and 93.8% (150/160) at PSA levels of 0.2-< 0.5, 0.5-< 1, 1-< 2 and ≥ 2 ng/mL, respectively. Local recurrence was present in 42.1% (224) patients. Loco-regional, retroperitoneal and supraphragmatic lymph node metastases were observed in 41.4% (220), in 16.6% (88) and in 6.8% (36) of the patients, respectively. Findings indicating bone and visceral metastases were presented in 21.1% (112) and 4.0% (21) of patients. Higher detection rates were present in patients with an initial Gleason score ≥ 8 compared with scores ≤ 7 (85.0 vs. 77.2%, p<0.0001). Previous EBRT or ADT within 6 months prior imaging did not influence the detection rate (82.2% vs. 77.5%, p=0.185; 84.6% vs. 78.0%, p=0.114), respectively. **Conclusion:** 18F-rhPSMA-7 PET offer high detection rates in patients with BCR after radical prostatectomy appear. These data indicate superiority to previous published data for 68Ga-PSMA-11. **References:** None.

109

Neuroimaging - Rapid Fire Session: Kinetic Modeling and Computational Approach in Neuroimaging

Sunday, October 13, 2019, 8:00 - 9:30 Lecture Hall 115

OP-051

Classification of [^{18}F]Florbetapir brain PET studies in cognitively normal subjects using a Convolutional Neural Network

R. Boellaard, *B. de Vries, T. Timmers, J. Ebenau, S. Verfaillie, F. Heeman, M. Cysouw, W. van der Flier, B. van Berckel, M. Yaqub, S. Golla;*
Amsterdam University Medical Centers, VUMC, Amsterdam, NETHERLANDS.

Aim/Introduction: [^{18}F]Florbetapir (AV45) positron emission tomography (PET) studies allow for in vivo assessment of amyloid deposition. Presence of amyloid deposition is usually assessed visually, which is highly dependent on observer training and experience. These visual reads can be difficult in case of low amyloid depositions, e.g. in cognitively normal individuals. The aim of this work was to develop, train and validate a Convolutional Neural Networks (CNN) able to discriminate between amyloid negative and positive PET scans. **Materials and Methods:** 133 AV45-PET images (101 negative and 32 positive) were acquired at 50-70 min post-injection on a Philips Gemini TF-64 PET/CT scanner and visually assessed by an experienced nuclear medicine physician in the context of the SCIENCe project. AV45-PET SUV_R images using cerebellum as reference region were first spatially aligned (MNI). A 2D-CNN was

developed consisting of 4 convolution layers, two max-pooling layers, batch-normalisation and one sigmoid output layer. Next, 106 (80%) scans were used to train a 2D-CNN. During training data balancing was achieved by oversampling the amyloid positive scans and data augmentation was achieved by rotating, flipping, zooming and translating the images. Overfitting was avoided by applying dropouts. To study the impact of spatial resolution on the CNN model performance, PET images were additionally smoothed with 5 and 10 mm FWHM Gaussian kernels. The 2D CNN model performance was tested using the 27 (20%) unused scans, yielding accuracy, sensitivity and specificity. **Results:** The model classified amyloid negative and positive scans with 100% accuracy. Applying 5 and 10 mm Gaussian smoothing to the 20% test scans resulted in an accuracy of 96.3% and 81.5%, respectively, and a specificity of 94.4% and 72.2%, respectively. Retraining the 2D CNN model using the lower but matched resolution images recovered the accuracy to 100% and 92.6% and the specificity to 100% and 77.8% for the 5 and 10 mm smoothed data, respectively. **Conclusion:** A 2D CNN was developed, trained and tested and showed very promising classification performance for amyloid PET scans in a SCD patient cohort. However, decreased image quality/image resolution impacts the performance of the 2D-CNN, which can partly be resolved by retraining the model using the lower and matched resolution images. **References:** None.

OP-052

Machine-learning based interpretation of I-123 FP-CIT scans allows high-accuracy detection of Parkinson's Disease

M. Dotinga[1,2], *J. D. van Dijk*[1], *B. N. Vendel*[1], *C. H. Slump*[2], *J. A. van Dalen*[1];
[1]*Isala, Zwolle, NETHERLANDS,* [2]*University of Twente, Enschede, NETHERLANDS.*

Aim/Introduction: Dopamine transporter SPECT imaging with I-123-FP-CIT allows for visualisation of dysfunction of the dopaminergic system, which is characteristic of Parkinson's Disease (PD). Interpretation of scans based on visual assessment and semi-quantitative analysis imposes limitations as the latter requires a site-specific reference database that is often not available. Our aim was to develop a machine learning (ML)-based approach for interpretation of I-123-FP-CIT scans and determine its added value in clinical practice. **Materials and Methods:** We retrospectively included a consecutive cohort of 130 patients that underwent I-123-FP-CIT SPECT imaging (Discovery D670, GE Healthcare) and had a clinically confirmed diagnosis. Patients were labelled as either having PD or a diagnosis other than PD (non-PD) and divided into a training set (58 PD, 32 non-PD) and validation set (25 PD, 15 non-PD) using stratified random sampling. The training set was used to build a linear support vector machine (SVM) classifier to discriminate PD from non-PD using I-123-FP-CIT striatal uptake ratios, age and gender as input features. Ratios were obtained by means of semi-quantitative analysis (Xeleris 4.0, GE Healthcare) and comprised specific binding in striatum, caudate nucleus and putamen as well as a putamen/caudate index for both left and right hemisphere. A stratified, 10-times repeated 10-fold cross-validation was conducted to perform model optimization using mean accuracy and F_1-score as evaluation measures. Subsequently, the derived SVM model was tested on the validation set. I-123-FP-CIT scans and corresponding ratios of the validation set were scored as either PD or non-PD by two expert nuclear medicine physicians following European guidelines. Overread from a third expert was performed in case of disagreement. Next, their prediction performance was compared to that of the SVM model. **Results:** The highest mean prediction accuracy and F_1-score as found by cross-validation were 94.3% and 0.956, respectively. Testing the derived SVM model on the validation set, an accuracy of 95.0%, sensitivity of 96.0% and specificity of 93.3% were obtained. Prediction performance did not differ from visual assessment of PD, obtaining an equivalent accuracy, sensitivity and specificity of 95.0%, 96.0% and 93.3% ($p > 0.99$), respectively. **Conclusion:** ML-based interpretation of I-123-FP-CIT scans results in accurate discrimination of PD from non-PD identical to standard visual assessment, thereby encouraging implementation of this SVM model as diagnostic aid in clinical practice. **References:** None.

OP-053

Prognostic power of psoas muscles structure and metabolism in amyotrophic lateral sclerosis

A. Miceli[1], *M. Donegani*[1], *R. Lai*[2], *S. Morbelli*[1], *V. Ceriani*[1], *A. Borra*[1], *S. Raffa*[1], *M. Bauckneht*[3], *S. Capitanio*[3], *C. Campi*[4], *G. Sambuceti*[1], *M. Piana*[1], *C. Marini*[5];
[1]*DISSAL University of Genoa, Genoa, ITALY,* [2]*SPIN Institute, CNR, Genoa, ITALY,* [3]*IRCCS Policlinico San Martino, Genoa, ITALY,* [4]*DIMED, Padova University Hospital, Padua, ITALY,* [5]*CNR Institute of Molecular Bioimaging and Physiology (IBFM), Milan, ITALY.*

Aim/Introduction: Amyotrophic lateral sclerosis (ALS) is a lethal degeneration of upper and lower motor neurons. Median survival, from onset to death, is extremely variable and, to date, no reliable prognostic factors have been validated. Recent literature suggests a primary role of skeletal muscle and its derived signals in ALS progression. To verify this hypothesis, in the present study we evaluated whether ALS is associated with alteration in FDG uptake and total volume of both psoas as a sample of skeletal muscles already used for prognostic stratification in different disorders. **Materials and Methods:** We analyzed 54 ALS patients with spinal onset consecutively submitted to PET/CT imaging. These data were compared with the corresponding findings in an age-and sex-matched control population. A computational 3D method was used to extract psoas muscle's volumes from CT images and to evaluate total muscle volume and attenuation coefficient. In co-registered PET images, FDG accumulation was defined by average standardized uptake value (a-SUV) and the heterogeneity of its distribution expressed by SUV standard deviation (SUV-SD). Psoas volume was normalized for the ideal body weight. **Results:** Average psoas attenuation coefficient was similar in patients and controls (39±9 vs 38±11 Housfield

units, respectively, ns). By contrast, ALS was associated with a significant reduction in Psoas volume (221±74 mL vs 262±85 mL; p<0.01). This difference persisted when normalization for ideal body weight was considered (3.54±1.02 vs 4.12±1.33 mL/Kg; p<0.05). Similarly, at PET imaging, a-SUV was significantly lower in patients than in controls (0.77±0.21 vs 0.90±0.18; p<0.01). Finally, heterogeneity of psoas a-SUV, expressed by SUV-SD, predicted overall survival rate at Kaplan-Meyer analysis (p<0.05) with a predictive power that was confirmed by univariate as well as by multivariate Cox analysis (p<0.02). **Conclusion:** ALS is associated with a reduction in volume and FDG uptake of psoas muscles. The heterogeneity of glucose metabolism within this muscular district is related to disease aggressiveness. **References:** None.

OP-054

Abnormal I-123 MIBG scan can be identified by artificial neural network: possible application to Lewy body diseases

K. Nakajima[1], *S. Watanabe*[1], *K. Maruyama*[2], *A. Inaki*[1], *H. Wakabayashi*[1], *K. Okuda*[3], *S. Kinuya*[1];
[1]*Kanazawa University, Kanazawa, JAPAN,* [2]*Wolfram Research Inc., Tokyo, JAPAN,* [3]*Kanazawa Medical University, Kahoku, JAPAN.*

Aim/Introduction: ^{123}I-meta-iodobenzylguanidine (mIBG) has been used in neurology, and most of the studies have used a heart-to-mediastinal average count ratio (HMR) for diagnosis of Lewy-body diseases. This study aimed to determine abnormal mIBG scan with low cardiac uptake, which is typically observed in Lewy-body diseases, without specifying regions of interest (ROI), using machine learning algorithm. **Materials and Methods:** Anterior ^{123}I-mIBG images with normal uptake (n=72, 148 scans) and low uptake (n=55, 110 scans) were used as the training database of machine learning including neural network (Mathematica, Wolfram Research). Anterior planar mIBG images (20 minutes and 3 hours) were directly input without any preparations, and the probability of abnormality was judged from 0 (abnormal uptake or absent uptake) to 1 (normal uptake). In addition to visual interpretation of normal/abnormal, conventional quantitation method of HMR was calculated using heart and mediastinum ROI. Accuracy of determining normal or abnormal uptake was examined using receiver operating characteristic (ROC) analysis. The accuracy of the model was also tested with additional consecutive patients with Lewy-body diseases, amyloidosis, and other diseases (n=25, 50 scans; 15 scans with HMR&lt2.0). **Results:** The best classifier among those we studied was constructed by an artificial neural network consisting of 10 layers (256x256-matrix grayscale images for encoder, two classes of normal and abnormal as output). Probability of abnormality was 0.997±0.013 in patients with abnormal or low uptake, and 0.003±0.001 in patients with normal uptake (t ratio=663, p&lt0.0001). A dataset of 196 scans were randomly selected for the training, and 60 scans (abnormal/normal = 30/30) were used as the validation set. This processing was repeated 10 times. Average ROC area under the curve was 0.97 (range 0.93-1.00), accuracy 0.91 (0.87-0.97), true positive rate 0.88 (0.80-0.97), and true negative rate 0.93 (0.90-0.97). Calculated HMR was 2.71±0.70 in normal cases, and 1.78±0.71 in abnormal cases (t ratio=9, p&lt0.001), and some overlap of ranges was observed for HMR. In additional patients for the validation, when thresholds of HMR=2.0 and probability of 0.5 were used for contingency analysis, 86% of the data showed complete agreement (Pearson X^2=23, p&lt0.0001). **Conclusion:** Machine learning with appropriately trained neural network successfully classified mIBG images into normal and abnormal scans. Since anterior image was the only input without predefined ROI on the heart and mediastinum, machine learning could be a novel approach to classify patients with Lewy-body diseases. **References:** None.

OP-055

The impact of multi-center PET data harmonization on the classification performance of deep learning networks in neurological imaging

R. Fahmi, *L. Sibille;*
Siemens Medical Solutions USA, Inc., Knoxville, TN, UNITED STATES OF AMERICA.

Aim/Introduction: Comparison, longitudinal assessment, and quantification of multi-center PET data are challenging mainly due to differences in scanner resolutions. Harmonization methods reduce inter-center variability and facilitate comparisons of such PET data, typically by smoothing the data to match a lower target resolution across used scanners. In this work, we investigated the impact of harmonizing ADNI-PET data on the classification of FDG and amyloid images into Alzheimer's (AD) and normal-controls (NC) using a convolutional-neural-network (CNN). **Materials and Methods:** Longitudinal FDG and AV45 datasets corresponding to 479 subjects (222-AD, 257-NC) were obtained from the ADNI database for a total of 801 FDG (343-AD, 458-NC) and 654 AV45 (168-AD, 486-NC) datasets. For each dataset, both non-harmonized (summed image of co-registered dynamic frames in native space) and harmonized (processed image that included smoothing with scanner-specific filter to achieve 8mm FWHM), registered to MNI space, were separately used to train two identical CNNs designed to classify AD versus NC subjects. A 10-fold cross-validation scheme was used to evaluate classification performances. For each dataset, seven coronal slices (7x91x91) sparsely covering the brain were selected as CNN inputs, and went through four layers, each composed of a 2D convolution and a max-pooling operation. Outputs of these layers were aggregated and used for class prediction (AD or NC). Each CNN was trained to minimize the cross-entropy error using Adam optimizer with leaky ReLu activation for each layer, using a learning rate of 0.05 and dividing by 10 every 50 epochs until convergence. The classification performance using harmonized and non-harmonized data from the same subjects were compared and McNemar test was used to assess the effect of harmonization on classification performance. **Results:** Classification sensitivity, specificity, accuracy, and area-under-

the-curve (AUC) were as follows: i) FDG (88.3%, 91.7%, 90.2%, and 0.956) for non-harmonized versus (87.1%, 90.8%, 89.3%, and 0.955) for harmonized data; and ii) AV45 (76.7%, 93.5%, 89.2%, and 0.921) for non-harmonized versus (78.2%, 89.9%, 87.0%, and 0.919) for harmonized data, respectively. No significant difference in class assignment consistency was found for FDG (McNemar p=0.90) but this difference was significant for AV45 (p=0.027). **Conclusion:** We demonstrated that deep learning potentially overcomes the variability in multi-center PET FDG and amyloid data for image-based classification of AD versus NC subjects using CNN. For both tracers accuracy was higher for non-harmonized data. We carefully suggest that harmonization of multi-center brain PET data is not required for accurate disease classification with deep learning. **References:** None.

OP-056

^{18}F-Choline PET Kinetic Modeling with Arterial Sampling in Patients with High Grade Glioma

S. Rubí[1], *P. Bibiloni*[2], *M. Valiente*[1], *C. González*[2], *M. Villar*[1], *J. Molina*[1], *M. Brell*[1], *J. Chinchilla*[1], *M. López*[1], *A. Mir*[2], *M. González*[2], *C. Peña*[1];
[1]*Hospital Universitari Son Espases / IdiSBa, Palma de Mallorca, SPAIN,* [2]*Scopia Research Group, University of Balearic Islands, Palma de Mallorca, SPAIN.*

Aim/Introduction: 18F-fluoromethylcholine (FCho) has gained interest as a PET radiotracer in the assessment of gliomas, but full kinetic analysis has not yet been reported in this setting. Following its transport across the blood-brain-barrier (BBB), FCho is intracellularly phosphorylated by choline-kinase. Our aim is to characterize the uptake kinetics of FCho in high-grade-gliomas (HGG), as a required step for its rational use as a clinical diagnostic tool. **Materials and Methods:** Eighteen patients with suspected initial diagnosis of HGG underwent a 45min dynamic brain PET scan immediately after a FCho bolus injection, from which a VOI-based tumoral time-activity-curve was extracted. Plasma input functions were obtained using manual arterial blood sampling from a radial catheter, and parent fractions for metabolite correction were determined by thin-layer-chromatography. These data were fitted to several 1- and 2-tissue-compartment models, the best of which was selected through the Akaike-Information-Criteria (AIC). Parametric images of the main kinetic rate constants were also generated for each patient. We finally assessed the correlation between the kinetic parameters and the tumor SUV on static images, both for VOI-based and voxel-based approaches. **Results:** The 2-tissue-compartment model accounting for blood volume fraction (vB) yielded the lowest AIC score in all patients and was selected as the best model. The reversible step parameter k_4 was either small compared to the other exchange rate constants (in 12/18 patients) or even fitted to zero (in 6/18 patients): K_1 [median(range): 0.14 (0.06-0.30)ml·cm^{-3}·min^{-1}], k_2 [0.11 (0.01-0.28)min^{-1}], k_3 [0.16 (0.00-0.46) min^{-1}], k_4 [0.02 (0-0.03)min^{-1}], vB [0.08 (0.04-0.15)]. The perfusion/BBB transport rate constant K_1 and the influx macroparameter $K_i = K_1 * k_3 / (k_2 + k_3)$ were clearly the most identifiable parameters and both showed a positive linear correlation (r^2=0.66 and 0.69 respectively) with the SUVmax of the tumor on the VOI-based analysis. Parametric images of Ki were obtained through a voxel-based Patlak analysis, and a good correlation was shown between these K_i parametric images and SUV images in each patient (r^2=0.95[median]; 0.62-0.99[range]). Following surgery, a glioblastoma was confirmed in 16 patients, while the other two had a diagnosis of metastasis. **Conclusion:** FCho uptake kinetics in HGG is best explained by an irreversible or near irreversible 2-tissue-compartment model with blood volume fraction vB. The good linear relationship between the SUV and the K_1 rate constant suggests a strong influence of the perfusión/BBB transport step on FCho tumor uptake. Clinical routine SUV images may serve as an adequate surrogate for the K_i influx rate parametric images. **References:** None.

OP-057

Quantification of aromatase binding in the human brain using [^{11}C]cetrozole PET

M. Jonasson[1], *P. Nordeman*[2], *H. Wilking*[1], *G. Antoni*[1,2], *I. Sundström Poromaa*[2], *M. Lubberink*[1,2], *E. Comasco*[2];
[1]*Uppsala University Hospital, Uppsala, SWEDEN,* [2]*Uppsala University, Uppsala, SWEDEN.*

Aim/Introduction: Aromatase is an enzyme that converts androgens to estradiol and estrone in the brain and it is considered to play a role in different personality traits such as aggression and sexual behaviour. The aim of this study was to evaluate tracer kinetic models, as well as effect of scan duration on outcome parameters, for quantitative analysis of the novel aromatase PET ligand [^{11}C]cetrozole. **Materials and Methods:** Data from ten subjects, with three 90 min dynamic [^{11}C]Cetrozole PET scans each at baseline and after two different challenges, were included in this study. Arterial blood was sampled for measurement of blood radioactivity and metabolite analysis, to obtain a plasma-input function, in eight of the scans. VOI-based analysis was performed using single-tissue (1TCM) and two-tissue (2TCM) reversible plasma-input compartment models and Logan graphical analysis, in the eight scans with plasma data. In addition, simplified reference tissue models (SRTM) and reference Logan analysis were performed for all thirty scans with cerebellum as reference region. The optimal reference model was used for evaluation of decreased scan duration of 60 min. Five VOIs were included in the evaluation; thalamus, hypothalamus, putamen and raphae, obtained from a probabilistic VOI template on co-registered T1-MRI images, and amygdala, obtained by manually drawing a 70% isocontour VOI on the uptake images. Correlation and agreement between the plasma-input and reference methods, as well as for the full and decreased scan duration, were assessed by linear regression. **Results:** 2TCM performed better than 1TCM according to Akaike criteria in all cases except one, but was not able to robustly determine individual parameters. Plasma Logan distribution value ratio (DVR) agreed well with the 2TCM DVR and was used for validation of the reference models. Correlation and agreement between plasma Logan DVR-1 and reference Logan

DVR-1 was very high (R^2=1.00, slope=1.00) and slightly lower for SRTM binding potential (BP_{ND}) values (R^2=0.96, slope=0.86). Reference Logan was used for analysing the shortened data sets showing a high correlation and agreement for DVR-1 values between the full scan length and the 60 min data sets (R^2=0.98, slope=0.94). **Conclusion:** Reference Logan DVR-1 and SRTM BP_{ND} values were highly correlated with plasma Logan DVR-1. Reference Logan showed a higher agreement to the plasma-input model and was chosen as the optimal reference model for VOI-based analysis. Reference Logan generated robust and quantitatively accurate results for a shortened scan, indicating that 60 min scan duration is sufficient for [^{11}C]cetrozole PET. **References:** None.

OP-058

Kinetics and 28 day test-retest repeatability and reproducibility of [^{11}C]UCB-J brain PET imaging

H. Tuncel[1], *R. Boellaard*[1], *E. F. J. De Vries*[2], *P. Kopschina Feltes*[2], *S. C. J. Verfaillie*[1], *E. M. Coomans*[1], *E. E. Wolters*[1], *S. P. Sweeney*[3], *J. M. Ryan*[3], *M. Ivarsson*[3], *B. A. Lynch*[3], *P. Schober*[1], *P. Scheltens*[4], *R. C. Schuit*[1], *A. D. Windhorst*[1], *P. P. De Deyn*[2], *B. N. M. van Berckel*[1], *S. S. V. Golla*[1];
[1]*Amsterdam UMC, Amsterdam, NETHERLANDS,* [2]*UMCG, Groningen, NETHERLANDS,* [3]*Rodin Therapeutics, Cambridge, MA, UNITED STATES OF AMERICA,* [4]*Alzheimer Center Amsterdam, Amsterdam, NETHERLANDS.*

Aim/Introduction: [^{11}C]UCB-J is a novel radioligand that binds to synaptic vesicle glycoprotein 2A (SV2A) which is present in neuronal presynaptic terminals. [^{11}C]UCB-J Positron emission tomography (PET) imaging enables quantification of brain synaptic density in individual regions and may be used to study response to therapies in clinical trials. The main objective of this study is to determine the 28-day test-retest repeatability (TRT) of quantitative [^{11}C]UCB-J brain PET imaging in Alzheimer's disease (AD) patients and healthy controls. **Materials and Methods:** In this ongoing multicentre study 9 healthy and 5 AD subjects have been included (age 64.2±5.9, 7 male - 7 female). Subjects underwent two 60 minutes dynamic [^{11}C]UCB-J PET scans (radiotracer dose of 370±58 MBq) with an interval of 28 days. Arterial blood sampling and metabolite analysis were performed to generate a metabolite corrected plasma input function. Various compartmental models +/- blood volume correction (V_B) have been evaluated and the optimal model(s) has been assessed using Akaike criterion. Volumes of distribution (V_T) and tracer delivery (K_1) have been estimated using both 1T2k_V_B and 2T4k_V_B models. Data were also analyzed using a simplified reference tissue model (SRTM) with centrum semiovale (SO, white matter) (Koole et al., EJNMMI 2019) as reference region, providing estimates of BP_{ND}. We also examined the effect of plasma input model choice on model preferences, parameter estimation and TRT. **Results:** After intravenous injection, [^{11}C]UCB-J showed rapid kinetics. Based on AIC, both 1T2k_V_B and 2T4k_V_B described the [^{11}C]UCB-J kinetics equally well. V_T obtained from both models were similar, suggesting that a 1T2k_V_B model can be used to assess the in vivo kinetics. No significant difference in semiovale V_T between AD and healthy subjects were observed (p>0.05). Preliminary analysis showed that the mean TRT for V_T and SRTM BP_{ND} were -5.7 %±9.7 and -3.2%±14.5, respectively, for all subjects across all the different brain regions. Whole brain grey matter TRT for V_T and SRTM BP_{ND} were -3.4%±4.3 and -2.6%±6.0 respectively. **Conclusion:** [^{11}C]UCB-J kinetics can be well described by a plasma input single tissue compartment model and reliable fits can be obtained with a 60 min scan duration for both plasma input and reference tissue models, consistent with earlier reports (Finnema et al., JCBFM 2018). Our preliminary analysis shows TRT performance for V_T and BP_{ND} of <10% and <15% (1 SD), respectively, across brain regions and indicates adequate repeatability of [^{11}C]UCB-J PET for application in longitudinal clinical research. **References:** None.

OP-059

ViQuant: an open-source PET/MRI pipeline for non-invasive determination of cerebral metabolic rate of glucose

L. Shiyam Sundar[1], *O. Muzik*[2], *L. Rischka*[1], *A. Hahn*[1], *R. Lanzenberger*[1], *M. Hienert*[1], *E. Klebermass*[1], *M. Bauer*[1], *I. Rausch*[1], *E. Pataraia*[1], *T. Traub-Weidinger*[1], *T. Beyer*[1];
[1]*Medical University of Vienna, Vienna, AUSTRIA,* [2]*Wayne State University School of Medicine, Detroit, MI, UNITED STATES OF AMERICA.*

Aim/Introduction: To introduce ViQuant, a fully-automated MATLAB-based processing pipeline for PET/MRI to non-invasively determine the cerebral metabolic rate of glucose (CMRGlc) images. **Materials and Methods:** The ViQuant pipeline requires the following inputs: (1) PET list-mode data, (2) attenuation correction (AC) map, (3) MR angiography (MRA) images, (4) T1-w MRI and (5) MR navigators. No other user interaction is required. The processing pipeline includes three main components: (i) a component (IC) generating an image-derived input function (IDIF) , (ii) a component that creates MRGlc images(QC) and (iii) a report-generating component (RC). The IC component calculates an IDIF by first defining a volume-of-interest through automated segmentation of the MRA. This is followed by MR navigator-based motion correction (MC) and an MR-based partial volume correction (PVC). In addition, AC maps are aligned with the PET emission data prior to reconstruction. Once an accurate IDIF is calculated, it is used to generate MRGlc images based on a voxel-wise Patlak analysis. Finally, a report is generated with a list of regional MRGlc values. To validate the pipeline, 10 healthy volunteers underwent [18F] FDG test-retest PET/MRI examinations in an integrated PET/MR (Siemens Biograph mMR). The imaging protocol consisted of a 60 min list-mode PET acquisition, with parallel MR acquisitions consisting of MRA, MR navigators and T1-w MR. Arterial blood samples (AIF) were collected as reference standard. Pseudo-CT images derived from T1-w MR were used for AC. Quantification accuracy of non-invasive determination of MRGlc was assessed against the reference standard of MRGlc values derived using arterially sampled blood (AIF) based on the absolute percentage

difference (APD) in regional MRGlc values determined in the following 6 brain regions: corpus callosum (CC), brainstem (BS), cerebellum (CB), thalamus (TH), anterior cingulate cortex (ACC) and the superior frontal cortex (SFC). **Results:** The APD between CMRGlc values obtained from AIF and IDIF were: (5.9 ±3.2%) for CC, (5.9 ±3.3%) for BS, (5.8 ±3.4%) for CB, (5.5 ±3.1%) for ACC, (5.8 ±3.14%) for TH and (5.9 ±3.3%) for the SFC. The total processing time was ~6h on a dedicated high-end PC. **Conclusion:** We have developed a fully-automated open-source processing pipeline which allows non-invasive determination of absolute MRGlc values in a clinical setting. The obtained CMRGlc values were validated to be within 6% of those determined using arterial sampling. At present, our processing pipeline is limited to data obtained from a Siemens PET/MR scanner due to its dependency on the e7 reconstruction tools. **References:** None.

OP-060

How to convert F18-Flutemetamol centiloid SUVr to Centiloid scale values ? A simple-method using PNEURO 3.9 software

R. Lhommel[1], *B. Hanseeuw*[1], *V. Malotaux*[2], *j. Cerman*[3], *A. Ivanoiu*[1]; [1]*Cliniques Universitaires Saint-Luc, UCLouvain, Brussels, BELGIUM,* [2]*Institute of Neuro-Science (IONS), UCLouvain, Brussels, BELGIUM,* [3]*Memory Disorder Clinic, Charles University and Motol University Hopsital, Praha, CZECH REPUBLIC.*

Aim/Introduction: F18-Flutemetamol/Vizamyl PET is a validated surrogate biomarker to reveal the amyloid brain status of patients presenting neurodegenerative disorders, either by visual or semi-quantitative analysis (SUVr). However, alternative tracers and quantification methods complicates the possibility to compare clinical results between centers. In 2015, Klunk proposed a methodological approach based on C11-PIB PET to harmonize and reports semi-quantitative results on the same reference level scale (the so-called centiloid scale). This approach was then endorsed by the Global Alzheimer's Association Interactive Network (GAAIN) to help centers to calibrate and report their data whatever the type of Amyloid PET tracer and quantification method used. We report here the sequential calibration steps based on this approach to convert Flutemetamol SUVr to the centiloid scale using the PNEURO3.9 software. **Materials and Methods:** The PNEURO 3.9 (PMOD,Zurich) maximum_probability_workflow based on 3DT1 MRI segmentation was used to retreat C11-PIB/FLUT PET scans and compute $SUVr_{centil.}$ values (cortical centil.vois/whole cerebellum-reference). Two historical patients population were downloaded from the GAAIN website to qualify the PNEURO3.9 workflow. Step1:PMOD3.9 workflow validation for C11-PIB PET: n=79 (34 YHC-45 AD;C11-PIB/MRI; GAAIN, Klunk). Step2:FLUT versus C11-PIB $SUVr_{centil.}$ comparison and convertion of $SUVr_{centil.}$ to centiloid scale values; n=74 (24 YHC&50 AD; F18-Flutemetamol/C11-PIB/MRI; GAAIN, GE Healthcare). Statistical analysis and data plot fitting were computed using PRISM 8.0. **Results:** Step1 population analysis performed by PNEURO3.9 demonstrated an excellent correlation between the PMOD3.9 Centiloid scale values derived from the C11-PIB SUVrcentil. compared to the Klunk reported data (R^2: 0.9988;Y=1.004X-0.06600), validating the PMOD3.9 workflow based on the author criteria (R^2 >0.98; slope/intercept between 0.98;1.02/-2;2). For the step2 population, an excellent correlation was found between the PMOD 3.9 and published SUVrcentil. for the n=74 pairs of F18-FLUT/C11-PIB (R^2: 0.9945/0.9959). The correlation between the F18-FLUT and C11-PIB SUVrcentil. was also very similar to those reported (R^2:0.95 vs 0.96). The PMOD3.9 derived-equation to convert FLUT SUVrcentil. to centiloid scale values was Centil.val=115.4x$FLUT_{SUVr}$-113.2 (R^2:0.9501) compared to Centil.val=116.5x$FLUT_{SUVr}$-114.7 (R^2:0.9617). **Conclusion:** PNEURO 3.9 workflow seems a robust method to reproduced GAAIN data and derived centiloid scale values from Flutemetamol $SUVr_{centil.}$ values. **References:** Klunk et al. Alzheimers Dement, 2015. http://www.gaain.org/centiloid-project

110

Cardiovascular - Parallel Session: Myocardial Blood Flow Quantification with SPECT

Sunday, October 13, 2019, 8:00 - 9:30 Lecture Hall 116

OP-061

The Clinical Value of Quantitative Myocardial Blood Flow Derived by Dynamic ^{99m}Tc-sestamibi MPI Using A Cardiac-dedicated CZT Camera in Patients with Suspected Coronary Artery Disease

F. Liu[1], *S. Wang*[1,2], *Y. Shiau*[1], *Y. Wu*[1,2,3]; [1]*Department of Nuclear Medicine, Far Eastern Memorial Hospital, New Taipei City, TAIWAN,* [2]*Department of Nuclear Medicine, National Taiwan University Hospital and National Taiwan University College of Medicine, Taipei City, TAIWAN,* [3]*Division of Cardiology, Cardiovascular Medical Center, Far Eastern Memorial Hospital, New Taipei City, TAIWAN.*

Aim/Introduction: SPECT myocardial perfusion imaging (MPI) is a clinical mainstay with static imaging protocol and semi-quantitatively assessed for perfusion abnormalities. Dynamic cardiac SPECT is a new quantitative index of stenosis severity and ischemic burden by the assessment of myocardial flow reserve (MFR) and myocardial blood flow (MBF). Our aim is to evaluate the incremental value of dynamic SPECT in the detectability of multi-vessel coronary artery disease (CAD). **Materials and Methods:** Consecutive patients with suspected CAD, who underwent dynamic ECG-gated dipyridamole MPI using a cardiac-dedicated CZT camera (D-SPECT) and invasive/or computed tomography coronary angiography within 6 months were retrospectively reviewed. Subjects with history of coronary interventions in the past 90 days were excluded. Dynamic imaging data were analyzed using commercial Corridor 4DM software package, and static perfusion and volumetric data

were analyzed utilizing QPS/QGS software, which provided automatically plots according to the 17-segment model, and subsequently divided into three main vascular territories (LAD, LCX, RCA). Significant stenosis was defined as ≥ 50% luminal stenosis. The performance of static perfusion data, including summed stress, rest and difference scores (SSS, SRS and SDS), and dynamic perfusion data, namely post-stress and resting MBF (MBFs, MBFr) and MFR were compared at the vessel-level. The statistical significance was p<0.05. **Results:** A total of 50 patients with 139 stenotic vessels were included, 29 with multi-vessel disease (58%), and 11 patients (22%) with myocardial infarction (MI). Both global and regional MBFs showed a significant correlation with global and regional SSS (r=-0.67 and -0.38~-0.68, p≤0.001, respectively). Globally increased SSS, SDS and impaired MBFs, MFR were significantly associated with significant CAD. In vessel-based analysis, SSS and SDS failed to detect LAD, LCX diseases, except SSS in RCA disease. Post-stress MBF successfully detected LAD, LCX and RCA diseases, while MFR could only detect LAD disease. Using receiver operating characteristic (ROC) curve analyses, the best cutoff value of global MBFs to predict CAD was 2.4ml/g/min (area under the curve: 0.569, p=0.005), but the best cut-off value of MFR was not found. **Conclusion:** We validated a clinically available method for MFR quantification by dynamic ^{99m}Tc-perfusion SPECT utilizing a CZT camera, which improves the detectability of multi-vessel CAD, and post-stress MBF is a better parameter than MFR and static data. **References:** None.

OP-062

Impact of spline fitting of dynamic CZT SPECT data on the assessment of myocardial blow flow and flow reserve

N. Coudrais[1], *D. Agostini*[1,2], *C. Nganoa*[1], *M. Bouthiba*[3], *P. Tager*[1], *V. Roule*[1], *N. Roth*[4], *F. Beygui*[1,2], *A. Manrique*[1,2,5];
[1]*CHU Côte de Nacre, Caen, FRANCE,* [2]*Normandy University, Ea 4650, FRANCE,* [3]*EA 4650, Caen, FRANCE,* [4]*Spectrum Dynamics Medical Ltd, Caesarea, ISRAEL,* [5]*Cyceron PET Center, Caen, FRANCE.*

Aim/Introduction: Spline fitting allows to interpolate a sequence of temporal data, generating temporal and spatial smoothing of dynamic perfusion studies. We aimed to assess the impact of spline fitting on the assessment of myocardial blood flow and flow reserve using dynamic CZT perfusion SPECT. **Materials and Methods:** We retrospectively analyzed CZT dynamic myocardial perfusion SPECT previously acquired in 28 consecutive patients in the framework of the Waterday [1] study (clinicaltrials.gov: NTC 02278497) using a DSPECT camera (Spectrum Dynamics, Caesarea, Israel). The CZT SPECT data were processed without (DY) and with (SF) applying a spline fitting function using a commercially available software (4DM, Invia, Ann Arbor, MI). All reconstructed frames were automatically segmented to extract the vascular input function and the myocardial uptake curve, and a one-compartment model was used to estimate global uptake values. SPECT myocardial blood flow (MBF) derived using Leppo correction and flow reserve (MFR) were compared to 15O-water PET data quantified using the Carimas 2.4 software (Turku PET Centre, Turku, Finland). **Results:** Rest and stress SPECT MBF values were similar with or without spline fitting (rest: 1.178 ± 0.385 vs 1.120 ± 0.457; and stress: 3.209 ± 0.880 vs 3.151 ± 0.758 for DY and SF respectively). At stress, both DY and SF MBF were increased compared to PET MBF (2.882 ± 0.967, p<0.05 vs SF, p<0.01 vs. DY). At rest, DY but not SF MBF was significantly increased vs. PET MBF (1.027 ± 0.237, p<0.05 vs DY). Correlations to PET MBF were similar using DY (r= 0.90, p<0.0001) or SF (r= 0.88, p<0.0001) but the difference between SPECT and PET was optimized using SF (0.18±0.58, p<0.05) compared to DY (0.24±0.51, p<0.001). The differences observed in terms of MBF yielded no difference on the assessment of MFR (DY: 2.93 ±1.13, SF: 3.15±1.15, PET: 2.83±0.81, all p-values= ns). **Conclusion:** Spline fitting had only a limited impact on the quantitative assessment of myocardial blow flow and flow reserve using dynamic CZT SPECT.

References: [1] Agostini D et al. Eur J Nucl Med Mol Imaging. 2018;45(7):1079-1090.

OP-063

Evaluation of global and regional coronary flow reserve by routine perfusion SPECT, without first pass study

L. Philippe*, C. Prunier-Aesch, Y. El Yaagoubi;*
Medecine Nucleaire Tourangelle, Chambray-les-Tours, FRANCE.

Aim/Introduction: Multi-vessel disease is frequently a cause of false negative myocardial perfusion SPECT. The global reduction of perfusion is difficult to see on the images. Scintigraphic measurement of Coronary Flow Reserve (CFR), usually performed by dynamic SPECT or dynamic PET can decrease false negative study. We developed an original method to evaluate the CFR, using routine SPECT 99mTc-tetrofosmin (1 day Stress-Rest protocol), without 1st pass acquisition. **Materials and Methods:** Myocardial uptake being related to myocardial perfusion, the counts ratio stress/rest represents CFR. Successively, 5 corrective factors are applied (completely automatic) at stress and rest , on myocardial short axis slices (Software Aladdin language - Xeleris GE) 1. Subtraction of the stress residual activity in the rest images 2. Normalization of the injected tracer activity 3. Normalization of the time duration acquisition 4. Consideration of the flow depending tetrofosmin myocardial extraction. 5. Normalization of the central ventricular pixel counts The 5 cumulative applications produce global Coronary Reserve Index (CRI), and regional CRI (rCRI) corresponding to the 3 coronary territories (LAD, LCx and RCA). These processings have been applied to 32 patients addressed to our institution for routine myocardial stress (exercise, dipyridamole, or regadenoson) and rest SPECT; they underwent also Invasive Coronary Angiography (ICA). **Results:** The CRI evaluations were compared to ICA considered as gold standard. ICA indicates 7 normal patients and 25 Coronary Artery Disease (CAD) patients. CRI mean is 3.65 ± 2.10 for normal patients, and 1.57 ± 0.56 for CAD patients. We found 14 CAD patients with normal perfusion SPECT and low CRI. The optimal cut-off CRI to separate normal and CAD patients is 2.20.

Considering this CRI value, we obtain: Sensitivity 92%, Specificity 86%, Positive Predictive Value 96%, and Negative Predictive Value 75%. Among the 25 CAD patients, 8 present multi-vessel epicardial disease with abnormal global CRI. Analysis of the 3 regional CRI, shows that the difference between the maximal and the minimal rCRI, normalized with the global CRI, is smaller for the multi-vessel disease (0.36 ± 0.45) than for the 17 others CAD patients (0.11 ± 0.08). A diffuse decrease of rCRI may indicate multi-vessel epicardial disease and/or microvascular disease. **Conclusion:** Evaluation of global CRI and rCRI by routine 99mTc-tetrofosmin SPECT is feasible. Using this evaluation after the routine SPECT reconstruction,with no additional time (fully automatic process) improves efficiency of perfusion SPECT analysis. Sensitivity and Positive Predictive Value are excellent. **References:** None.

OP-064

Absolute myocardial blood flow and coronary flow reserve derived by dynamic single photon emission computed tomography: correlation with invasive coronary angiography results in patients with multivessel coronary artery disease

K. Zavadovskiy, A. Mochula, A. Baev, A. Maltseva, S. Andreev; Cardiology Research Institute, Tomsk National Research Medical Centre, Russian Academy of Sciences, Tomsk, RUSSIAN FEDERATION.

Aim/Introduction: To assess relative myocardial perfusion, absolute myocardial blood flow (MBF) and coronary flow (CFR) reserve by dynamic single photon emission computed tomography on cadmium-zinc-telluride gamma camera in patients with multivessel coronary artery disease (MVCAD). **Materials and Methods:** 38 patients with coronary artery disease (mean age 60±9,5 years; 52 men;) were enrolled. According to quantitative invasive coronary angiography results all the patients were divided into two groups: 1) multivessel CAD: 12 patients with the two-vessel disease and 24 patients with three-vessel disease; 2) non-multivessel CAD: consisted of 22 patients with nonobstructive disease and 12 patients with one vessel disease. Within one week all patients underwent the assessment of myocardial perfusion (SSS, SRS, SDS), stress and rest MBF (ml/min/g), CFR and flow difference (FD) by dynamic 99mTc-Sestamibi CZT SPECT. **Results:** The mean SYNTAX score was 16.5±11.The values of summed stress score were significantly (p< 0.01) different in patients with and without multivessel CAD: 7.5 (IQR 5;10) and 4 (IQR 4;8), respectively. Summed rest score and difference score did not differ significantly in these two groups. The values of global stress MBF, CFR and FD were significantly (p<0.01) lower in patients with multivessel disease than in non multivessel CAD group: 0.43 ml/g/min (IQR 0.29; 0.52) versus 0.67 ml/g/min (IQR 0.53; 0.81); 1.38 (IQR 1.13; 1.64) versus 2.09 (IQR 1.59; 2.7); 0.1 ml/g/min (IQR 0.04; 0.19) versus 0.32 ml/g/min (IQR 0.19; 0.53), respectively. The correlations between SYNTAX and stress MBF (r=-0.6; p=0.00006), CFR (r=-0.58; p=0.0001), FD (r=-0.6; p=0.00009), were stronger than between SYNTAX and SSS (r=0.37; p=0.02), SDS(r=0.39; p=0.02). Based on univariate logistic regression the following indexes allow to predict MVCAD significantly: stress MBF per 0.1 unit increase (OR 0.75; CI 0.62-0.91; p=0.005); CFR (OR 0.12; CI 0.04-0.38; p=0.0003); FD per 0.1 unit increase (OR 0.72; CI 0.57-0.91; p=0.0016 and SSS (OR 1.21; CI 1.06-1.39; p=0.004); SDS (OR 1.19; CI 1.01-1.14; p=0.03). Based on the ROC analysis it was revealed that the areas under the ROC curves were higher for stress MBF (0.81;CI 0,71-0,9) CFR (0.8; CI 0,68-0,88) and FD (0.78; CI 0,67-0,87) than for SSS (0.68; CI 0,55-0,79) and SDS (0.64; CI 0,51-0,75). **Conclusion:** Our results found out that dynamic SPECT indexes reflect the severity of coronary artery lesion better than standard MPI. Absolute myocardial blood flow indexes derived by CZT could be useful in clinical practice in the management of patients with multivessel CAD. **References:** None.

OP-065

Low-dose Dynamic Myocardial Perfusion Imaging by CZT-SPECT in the Identification of Obstructive Coronary Artery Disease

T. Mannarino[1], W. Acampa[1], A. Genova[1], P. Buongiorno[1], G. De Simini[1], A. D'Antonio[1], L. Piscopo[1], M. De Risi[1], F. Volpe[1], E. Zampella[1], C. Nappi[1], R. Assante[1], V. Gaudieri[1], M. Petretta[2], A. Cuocolo[1];
[1]Department of Advanced Biomedical Sciences, University Federico II, Naples, ITALY, [2]Department of Translational Medical Sciences, University Federico II, Naples, ITALY.

Aim/Introduction: Dynamic CZT-SPECT may be used to measure myocardial blood flow (MBF) and myocardial perfusion reserve (MPR). The aim of our study was to evaluate MBF and MPR using a low-dose CZT-SPECT protocol in patients with suspected or known coronary artery disease (CAD) and to investigate the accuracy of dynamic data in predicting obstructive CAD. **Materials and Methods:** We analyzed 150 patients (102 men, mean age 65±8 years) with suspected or known CAD. All patients underwent dynamic CZT-SPECT after the injection of 185 MBq and 555 MBq of ^{99m}Tc-sestamibi for rest and stress imaging, respectively. Standard rest and stress acquisition were performed at the end of each dynamic scan. Summed stress score (SSS) >3 was considered as abnormal. Obstructive CAD was defined as ≥75% stenosis at coronary angiography. **Results:** In the overall population, global MPR was significantly lower (P<0.05) in patients with abnormal (2.4±0.7) as compared to those with normal (2.7±0.8) myocardial perfusion imaging. Significant correlations between MPR and SSS (r=-0.213, P<0.01) and between MPR and total perfusion defect (TPD) (r=-0.217, P<0.01) were found. In a subgroup of 60 patients with available coronary angiographic data, MPR (2.11±0.56 vs. 2.72±0.65, P=0.001) and stress MBF (2.71±0.85 vs. 3.43±0.95 ml/min/g, P=0.009) were significantly lower in patients with (n=17) compared to those without (n=43) obstructive CAD. At univariable logistic regression analysis, male gender, SSS, TPD, stress MBF, and MPR resulted significant predictors of obstructive CAD. At multivariable regression

analysis only male gender (P<0.01) and MPR (P<0.005) were significant predictors of obstructive CAD. Accordingly, in the 180 individual vessels analyzed, regional stress MBF (2.79±0.94 vs. 3.35±1.07 ml/min/g, P=0.015) and regional MPR (2.18±0.81 vs. 2.74±0.81, P=0.002) were significantly lower in vessels with (n=25) compared to those without (n=155) obstructive CAD. **Conclusion:** MPR assessed by low-dose dynamic CZT-SPECT showed good correlation with myocardial perfusion imaging findings in patients with suspected or known CAD and it could be useful in predicting obstructive CAD. **References:** None.

OP-066

Comparison of SPECT Myocardial Blood Flow Quantification and MPI for Detection of Myocardial Ischemia in Patients with Intermediate Coronary Stenosis Disease

L. Wang[1], *R. Ma*[1], *M. Wang*[1], *B. Hsu*[2], *W. Fang*[1];
[1]*Chinese Academy of Medical Sciences & Fuwai Hospital, Beijing, CHINA,* [2]*University of Missouri-Columbia, Columbia, MO, UNITED STATES OF AMERICA.*

Aim/Introduction: Evaluation of myocardial ischemia is crucial for patients with intermediate coronary stenosis disease. Quantification myocardial blood flow (MBFQ) using technetium labeled myocardial perfusion tracers and dedicated SPECT cameras has become clinically feasible. Comparison of SPECT MBFQ, myocardial flow reserve (MFR) and myocardial perfusion imaging (MPI) has not been studied. **Materials and Methods:** Patients with suspected or known coronary artery disease who were scheduled for SPECT MPI were consented to receive an adjunct dynamic SPECT (DySPECT) scan for MBFQ under the same rest and stress test. Subjects with intermediate disease defined as a coronary lesion with a visually estimated percentage diameter stenosis ranging from between 50 and 80% were included. Image processing of MBFQ employed full physical corrections for reconstruction of DySPECT images, one-tissue compartment for kinetic modeling, and corrections for ^{99m}Tc-Sestamibi extraction and rest rate-pressure-product to quantify stress MBF, rest MBF and MFR using a dedicated SPECT MBFQ software. Flow values in myocardium were further converted to corresponded flow statuses defined by the Gould's flow diagram[1] with slight modification. The patient-based positive diagnosis of MBFQ met one of two independent criteria as 1) ≥3.01% extent of myocardium within ischemia-steal combined flow status or 2) ≥20.3% extent of myocardium within moderate abnormal and ischemia-steal combined status. MFR alone as criteria defined ischemia when MFR <1.74. Interpretation of MPI images were conducted by three experienced readers in a consented reading session. MPI was considered abnormal when SSS ≥4 or SDS ≥2 or index of transient ischemia dilation ≥1.19. The patient-based diagnostic performance SPECT MBFQ, MFR and MPI for detecting myocardial ischemia were compared. **Results:** A total of 126 patients were included. Among this population, 71 patients presented with multi-vessel disease and 55 patients showed one-vessel disease. 68 patients (50.0%) showed abnormal results on MBFQ, which was significantly higher than the abnormal rate of MFR (58/126, 46.0%, p=0.000) and MPI (30/126, 23.8%, p-0.012). In patients with multi-vessel intermediate disease, MBFQ also showed more abnormal results (40/71, 56.3%) than MFR (28/71, 39.4%, p=0.000) and MPI (33.3%, 14/71, p=0.013), suggesting more myocardial ischemia was found by MBFQ. In patients with one-vessel disease, there was no significant difference in diagnosing myocardial ischemia of three methods. **Conclusion:** SPECT MBFQ detected more myocardial ischemia than MFR alone and traditional MPI for patients with intermediate disease, especially for patients with multi-vessel intermediate disease. **References:** [1] JACC Cardiovasc Imaging. 2012 Apr;5(4):430-40.

OP-067

Diagnostic performance of myocardial perfusion imaging with conventional and CZT single photon emission computed tomography in detecting coronary artery disease: a meta-analysis

R. Green, *V. Cantoni*, *T. Mannarino*, *A. Genova*, *R. Assante*, *V. Gaudieri*, *C. Nappi*, *E. Zampella*, *P. Buongiorno*, *M. Petretta*, *W. Acampa*, *A. Cuocolo*;
University Federico II, Naples, ITALY.

Aim/Introduction: Stress myocardial perfusion imaging (MPI) with SPECT accounts for the majority of tests currently performed for ischemia detection in patients with known or suspected coronary artery disease (CAD). The novel gamma cameras with semiconductor cadmium-zinc-telluride (CZT) detectors allowed an improvement in image accuracy and acquisition time. We performed a meta-analysis to compare the diagnostic performance of conventional SPECT (C-SPECT) and CZT-SPECT systems in detecting angiographically proven CAD. **Materials and Methods:** Studies published between January 2000 and February 2018 were identified by PubMed and Web of Science databases search. We included studies assessing C-SPECT or CZT-SPECT as a diagnostic test to evaluate patients for the presence of CAD, defined as at least 50% diameter stenosis on invasive coronary angiography. A study was eligible regardless of whether patients were referred for suspected or known CAD. For each eligible study, data were extracted to estimate sensitivity, specificity, and diagnostic odds ratio (OR) with 95% confidence interval (CI). The bivariate random-effects model was used to calculate the pooled summary estimates for sensitivities and specificities for both cameras. **Results:** We identified 40 eligible articles (25 C-SPECT and 15 CZT-SPECT studies) including 7334 patients (4997 in C-SPECT and 2337 in CZT-SPECT studies). The pooled sensitivity and specificity were 85% (95% CI 79-89) and 66% (95% CI 56-74) for C-SPECT and 89% (95% CI 86-91) and 69% (95% CI 61-75) for CZT-SPECT imaging studies. The area under the curve was slightly higher for CZT-SPECT (0.89, 95% CI 0.86-0.92), compared to C-SPECT (0.83, 95% CI 0.80-0.86) (P=0.03); accordingly, the summary diagnostic OR was 17 (95% CI 13-22) for CZT-SPECT and 11 (95% CI 7-15) for C-SPECT (P=0.04). The accuracy of the two tests slightly

differs between C-SPECT and CZT-SPECT (chi-square 11.28, P=0.04). However, we were unable to demonstrate if the subtle difference in global accuracy was due to sensitivity (chi-square 2.13, P=0.14) or specificity (chi-square 0.21, P=0.65), also when separate variances for each test were allowed in the models. At meta-regression analysis, no significant association between both sensitivity and specificity and demographical and clinical variables considered was found for C-SPECT and CZT-SPECT studies. **Conclusion:** C-SPECT and CZT-SPECT have good diagnostic performance in detecting angiographically proven CAD, with a slightly higher accuracy for CZT-SPECT. This result supports the use of the novel gamma cameras in clinical routine practices also considering the improvements in acquisition time and radiation exposure reduction. **References:** None.

201/204

Plenary 1: Radiomics and Artificial Intelligence (incl. Marie Curie Lecture)

Sunday, October 13, 2019, 10:00 - 11:15 Auditorium

OP-068
Radiomics - Predictive and Prognostic Modelling using Multimodality Imaging
D. Visvikis;
INSERM UMR1101, LaTIM, CHRU Morvan, Bat 1, et 1, Brest, FRANCE.

OP-069
Artificial Intelligence in Nuclear Oncology
R. Hustinx;
Centre Hospitalier Universitaire, Service de Médecine Nucléaire, Liège, BELGIUM.

OP-070
Marie Curie Lecture: Artificial Intelligence in Brain Imaging
M. Forsting;
UK Essen, Institut für Diagnostische und Interventionelle Radiologie und Neuroradiologie, Essen, GERMANY.

301

CME 2 - Oncology & Theranostics Committee: NET - PRRT and More

Sunday, October 13, 2019, 11:30 - 13:00 Auditorium

OP-071
PET/CT Imaging of PPGL in the Era of Genomic Disease Characterization (EANM/SNMMI 2019 Guidelines)
D. Taïeb;
Department of Nuclear Medicine, La Timone University Hospital, CERIMED, Aix-Marseille University, Marseille, FRANCE.

OP-072
Long-Term Outcome of PRRT and Predictors of Outcome
M. Gabriel;
Allgemeines Krankenhaus Linz, Institut für Nuklearmedizin und Endokrinologie, Linz, AUSTRIA.

OP-073a
PRRT - Individualized Dosimetry vs. Fixed Dose Scheme
A. Haug;
University Clinic of Nuclear Medicine, Medical University of Vienna, Vienna, AUSTRIA.

OP-073b
PRRT Treatment Sequencing and Combinations
R. Hicks;
Department of Nuclear Medicine and PET, Peter MacCallum Cancer Institute, Melbourne, AUSTRALIA.

302

Joint Symposium 3 - Bone & Joint + Paediatrics Committee / EPOS: Role of Bone SPECT/CT in the Paediatric Population

Sunday, October 13, 2019, 11:30 - 13:00 Lecture Hall 311

OP-074
Bone Scan with SPECT/CT in the Assessment of Bone Viability
I. Roca;
Vall d'Hebron University Hospital, Pediatric Nuclear Medicine Unit, Nuclear Medicine Department, Barcelona, SPAIN.

OP-075
SPECT/CT of the Jaw in Condylar Hyperplasia
K. Strobel;
Luzerner Kantonsspital (LUKS), Department of Radiology and Nuclear Medicine, Lucerne, SWITZERLAND.

OP-076
Complex Adolescent Foot Pain - Clinical Scenarios and Management
D. Eastwood;
Great Ormond Street Hospital for Children NHS Foundation Trust, Department of Orthopaedics, London, UNITED KINGDOM.

OP-077
SPECT/CT in Complex Adolescent Foot Pain - Initial Experience
L. Biassoni;
Great Ormond Street Hospital for Children NHS Foundation Trust, Department of Radiology, London, UNITED KINGDOM.

303

Joint Symposium 4: Cardiovascular Committee / ASNC: New Development in Nuclear Cardiology - Ready for Prime Time?

Sunday, October 13, 2019, 11:30 - 13:00 Lecture Hall 312

OP-078
Whole-Body CZT Camera for Cardiac Imaging
D. Agostini;
Department of Nuclear Medicine, Caen University Hospital, Caen, FRANCE.

OP-079
Quantification of Myocardial Blood Flow with SPECT
R. Nkoulou;
Department of Nuclear Medicine, University Hospital Geneva, Geneva, SWITZERLAND.

OP-080
Measurement of Left Ventricular Dyssynchrony
P. Soman;
University of Pittsburgh Medical Center, Division of Cardiology and The Heart and Vascular Institute, Pittsburgh, UNITED STATES OF AMERICA.

OP-081
Artificial Intelligence and Deep Learning
P. Slomka;
University of California Los Angeles, Department of Imaging Cedars-Sinai Medical Center, Los Angeles, CA, UNITED STATES OF AMERICA.

304

CTE 2 - Interactive - Technologist + Radiation Protection Committee: Risk and Incidents

Sunday, October 13, 2019, 11:30 - 13:00 Lecture Hall 117

OP-082a
Risks and Incidents in Nuclear Medicine: A Medical Physics Perspective
K. Bacher;
Ghent University, Department of Medical Physics, Ghent, BELGIUM.

OP-082b
Discussion

OP-083a
Potential Risk and Incidents in HotLab
A. Socan;
University Medical Centre, Department of Nuclear Medicine, Ljubljana, SLOVENIA.

OP-083b
Discussion

OP-084a
Management of Risks and Incidents in Nuclear Medicine
G. Testanera;
St Bartholomew's Hospital, Department of Nuclear Medicine, London, UNITED KINGDOM.

OP-084b
Discussion

305

M2M - Parallel Session: Radionuclide Production

Sunday, October 13, 2019, 11:30 - 12:45 Lecture Hall 111

OP-085
Cyclotron Production of ^{68}Ga Using Enriched ^{68}Zn Foils
J. Siikanen[1], E. Jussing[2,3], S. Milton[2], C. Steiger[2], J. Ulin[3], T. Tran[2,3], E. Samén[2,3];
[1]Karolinska University Hospital, Department of Medical

Radiation Physics and Nuclear Medicine, Stockholm, SWEDEN, [2]Karolinska University Hospital, Department of Radiopharmacy, Stockholm, SWEDEN, [3]Karolinska Institute, Department of Clinical Neuroscience, Stockholm, SWEDEN.

Aim/Introduction: Increased use of biomarkers for diagnostics of neuroendocrine tumors and prostate cancer has amplified the clinical demand for ^{68}Ga. For sites with access to a cyclotron, the high price and limited availability/activity output of ^{68}Ge/^{68}Ga generators are strong motivators for production of ^{68}Ga ($T_{1/2}$=68 min) via the ^{68}Zn(p,n)^{68}Ga-reaction. To expand production capacity over generators and also over liquid cyclotron solution targets the aim of this work is to optimize and automate solid target ^{68}Ga production using enriched ^{68}Zn-foils. **Materials and Methods:** Enriched (98.80 % ^{68}Zn, 0.46 % ^{64}Zn, 0.43 % ^{66}Zn, 0.29 % ^{67}Zn, 0.02 % ^{70}Zn) zinc foils (CMR, 15.5 mm diameter, 0.10 mm thick) were pneumatically transferred to a solid target system (Comecer EDS/PTS) and irradiated with 25 µA protons (PETtrace, GE Healthcare). Proton energy was degraded to a nominal 12.6 MeV to minimize co-production of long lived ^{67}Ga. Separation of ^{68}Ga from zinc was programmed and automated with a separation module (I.e Comecer, Taddeo PRF). In these initial trials foils were dissolved with 12 M HCl. The solution was diluted to 6 M HCl and passed over a UTEVA resin (Triskem, 100 mg) to trap gallium and to remove zinc and other metals. Gallium was then eluted with 1.2 ml water. Radionuclidic purity (RNP) was determined with an energy and efficiency calibrated HPGe-detector. **Results:** Irradiation of 136 min (i.e two half-lives) yielded up to 48 GBq of ^{68}Ga (saturation yield = 2.6 GBq/µA) in the foil at end of bombardment (EOB). Transfer (5 min) and gallium isolation (16 min) requires 21 min after EOB. Decay corrected trapping/elution on the UTEVA resin itself exceeds 93 %. Up to 29 GBq of ^{68}Ga was eluted with 1.2 ml of water at end of separation. RNP in the eluate was 99.98 % at EOB. Other gamma lines corresponded to ^{66}Ga (0.010 %) and ^{67}Ga (0.015 %). This equates to an RNP above 98% out to 7.7 hrs post-EOB. **Conclusion:** This setup produces approximately 20 times more activity than eluates from new generators (1.5 GBq). Solid target production using foils do not require any plating techniques. By using a 0.25 mm thick ^{68}Zn foil, we estimate that production of approximately 140 GBq may be possible. Ongoing ICP-MS and titration studies are underway to assess alignment with current generator formulations. **References:** None.

OP-086

Multi-Curie Production of Gallium-68 on a Biomedical Cyclotron

J. Kumlin[1], *J. H. Dam*[2,3], *C. J. Chua*[1], *S. Borjian*[1], *A. Kassaian*[1], *B. Hook*[1], *S. Zeisler*[1], *P. Schaffer*[1], *H. Thisgaard*[2,3];
[1]*ARTMS, Vancouver, BC, CANADA,* [2]*Department of Nuclear Medicine, Odense University Hospital, Odense, DENMARK,* [3]*Department of Clinical Research, University of Southern Denmark, Odense, DENMARK.*

Aim/Introduction: With increasing clinical demand for gallium-68, the commercial ^{68}Ge/^{68}Ga generators fail to supply sufficient amounts of this short-lived isotope. In this study we develop and evaluate an automated method for multi-Curie production of gallium-68 using solid targetry. **Materials and Methods:** Gallium-68 was produced by irradiation of an enriched zinc-68 solid target (on silver backing) in an ARTMS QIS on a GE PETtrace cyclotron. Beam currents up to 80 µA were applied for up to 120 min with a proton energy of 13 MeV. After end-of-bombardment (EOB), the targets were automatically transferred to a dissolution cell (ARTMS) in connection to a GE FASTlab 2 synthesizer unit. The targets were dissolved in hot, concentrated HCl followed by radiochemical separation of gallium-68 from the target material on the FASTlab 2. **Results:** Irradiation was performed using up to 80 µA for 120 min, producing up to 194 GBq (5.24 Ci) of gallium-68 at the end of separation from an expected >370 GBq (>10 Ci) gallium-68 at EOB. The fully automated dissolution/separation was performed in 35 min. Multiple productions were analyzed according to Ph. Eur. Monograph draft[1] and found to comply with all tests completed to date. Analysis of metal impurities using ICP-OES is in progress. Importantly, the radionuclidic purity (RNP) was high and allowed for a shelf-life of up to 7 h based on RNP alone. In every instance the radiochemical purity was above 99.9%. Radiolabeling of DOTATATE and PSMA-HBED-11 were performed in high yields (>95%) and in clinically acceptable molar specific radioactivity (≥ 24 MBq/nmol, non-optimized). This indicates a low amount of metallic impurities in the produced gallium-68, i.e., similar to what is observed for the generator-produced isotope. **Conclusion:** We have developed and evaluated an automated method for production of up to isolated 194 GBq gallium-68 chloride in high radionuclidic and radiochemical purity - expected to be suitable for compounding and subsequent clinical use. **References:** [1] Gallium (^{68}Ga) Chloride (Accelerator-Produced) Solution for Radiolabelling, Ph. Eur. Monograph draft 3109

OP-087

Characterization of TrisKem Actinide resin for separation of ^{51,52g}Mn from target material

K. Barrett[1], *E. Aluicio- Sarduy*[1], *S. Happel*[2], *C. Kutyreff*[1], *A. Olson*[1], *K. Seely*[1], *P. Ellison*[1], *T. Barnhart*[1], *R. Nickles*[1], *J. Engle*[1];
[1]*University of Wisconsin- Madison, Madison, WI, UNITED STATES OF AMERICA,* [2]*TrisKem International, Bruz, FRANCE.*

Aim/Introduction: Radio-manganese shows promise for a variety of nuclear medical applications including radiolabeling antibodies, monitoring pancreatic beta cell viability [1], and as dual PET/MR imaging agents [2]. Cyclotron-produced ^{51}Mn or ^{52g}Mn must be chemically separated from target materials to render the radiotracers suitable for in vivo use. This process has previously been accomplished only using multiple sequential columns, unwieldy liquid/liquid extractions, or complicated precipitation methods. We studied the TrisKem Actinide (AC) resin to investigate its potential to isolate ^{51,52g}Mn from bulk iron,

chromium, and common trace metal contaminants. **Materials and Methods:** Both batch and dynamic column experiments were performed to characterize the AC resin's affinity for representative masses of various metallic constituents. For batch resin experiments, solutions containing Fe, Mn, Co, Zn, Cu and Cr were loaded onto columns containing 100 mg resin equilibrated with varying concentrations of HNO_3 and HCl. These columns were agitated for 30 min. Afterwards, the solution was pushed through the resin, and concentrations of each metal were assayed by Microwave Plasma - Atomic Emission Spectroscopy and HPGe (FWHM @ 1333 keV = 1.6 keV) to quantify the metal mass adhered to the resin and eluted in solution. Affinity constants were calculated from these data for Fe, Cr, and Mn. Batch experiment results were used to design dynamic column experiments. A column containing 500 mg of resin was equilibrated with 5 mL of 0.05 M HNO_3. A dissolved and reconstituted target solution was then loaded onto the column and washed with 46 mL of .05 M HNO_3. In this wash, Cr, Fe, and other trace metals eluted from the column while Mn was retained. The Mn was eluted in 2 mL of 5 M HNO_3. **Results:** The results collected from both batch resin experiments and preliminary dynamic column experiments show promising results for a quick and efficient separation chemistry of ^{51,52g}Mn from bulk target material. **Conclusion:** We hope to determine a quantified separation factor from multiple dynamic column experiments, as well as binding efficiency with cheltors such as DOTA, EDTA, and PCTA. These final characterizations of the separation method using TrisKem AC resin will provide insight to the potential application of radio-manganese in nuclear medicine. **References:** [1] Fonslet, J. et al. (2017). Optimized procedures for manganese-52: Production, separation and radiolabeling. Applied Radiation and Isotopes. [2] GJ Topping et al.,"Manganese-52 Positron Emission Tomagraphy Tracer Characterization and Initial Results in Phantoms and In Vivo."Med Phys (2013).

OP-088

^{161}Tb Purification by High Performance Ion Chromatography (HPIC) from Irradiated ^{160}Gd

M. Ooms[1], *A. R. Burgoyne*[1], *B. Ponsard*[1], *D. Elema*[1], *T. Cardinaels*[1,2]; [1]*SCK-CEN, Institute for Nuclear Materials Science, Mol, BELGIUM,* [2]*KU Leuven, Department of Chemistry, Leuven, BELGIUM.*

Aim/Introduction: ^{161}Tb has many attractive properties (half-life of 6.9 d, β- decay energy of 593 keV, conversion and Auger electron emission) for targeted radionuclide therapy with peptides and antibodies [1]. ^{161}Tb can be produced via neutron irradiation of ^{160}Gd in a nuclear reactor, such as BR2 (flux of circa 10^{14} neutrons cm^{-2} s^{-1}) at SCK•CEN. The aim of this project was to develop a fast and easy method to purify small amounts (circa 250 MBq) of n.c.a. ^{161}Tb with high specific activity, for radiolabeling studies and in-house chelator design. **Materials and Methods:** 0.5 mg Enriched ^{160}Gd (98.2%) was loaded in a quartz ampoule under vacuum and irradiated at SCK•CEN. Initial irradiations (ϕ_0 = 3.67x10^{11} neutrons cm^{-2} s^{-1}) were performed at the BR1 reactor to test the separation procedure using tracer amounts. Following a 2 day cooling time, the ampoules were transported to the lab for processing. High performance ion chromatography (HPIC) was used to separate ^{161}Tb from the target matrix on a strong cation exchange resin by elution with α-hydroxyisobutyric acid (α-HIBA). Gamma spectrometry and inductively coupled plasma mass spectrometry (ICP-MS) were used for ^{161}Tb characterization and quantification. To show that the $^{161}TbCl_3$ can be used for radiolabeling, we performed some radiolabeling experiments with DOTA derivatives as a proof of concept. **Results:** With the use of a step-wise gradient elution of α-HIBA ^{161}Tb was separated from the Gd target material. 50 kBq ^{161}Tb (specific activity of 49.2 GBq/mg ^{161}Tb) was collected in one fraction of circa 1 ml. Gamma spectrometry analysis pre- and post-purification showed successful separation of the 161Tb from the ^{159}Gd (363.3 keV γ-emission). ^{161}Tb was characterized and quantified by the analysis of the 25.5 (22%), 48.9 (16%), 57.2 (2%) and 74.6 (10%) keV γ-emissions [2]. ICP-MS analysis of the produced ^{161}Tb is still ongoing. Initial radiolabeling experiments with DOTA derivatives however showed high radiolabeling yields could be achieved with our $^{161}TbCl_3$ solution. **Conclusion:** Preliminary results show that a fast and efficient method to purify MBq amounts of n.c.a. ^{161}Tb has been developed. Further irradiations in the BR2 reactor are in progress to validate the procedure, analyse the radiochemical purity and yield by using higher activities and thus leading to regular production of ^{161}Tb for in-house research at SCK•CEN. **References:** [1] Kostelnik, T.I. and C. Orvig, Chemical Reviews, 2018. 119, 902-956.[2] Tuli, J.K., Nuclear Data Sheets, 1974. 13, 493-547.2. Tuli, J.K., Nuclear Data Sheets, 1974. 13, 493-547.

OP-089

The development of ^{161}Tb production and its characterization towards clinical application

N. van der Meulen[1], *N. Gracheva*[1], *Z. Talip*[1], *S. Heinitz*[1], *J. Zeevaart*[2], *U. Koester*[3], *P. V. Grundler*[1], *C. Favaretto*[1], *C. Bailat*[4], *Y. Nedjadi*[4], *T. Duran*[4], *F. Juget*[4], *R. Schibli*[1], *C. Mueller*[1]; [1]*Paul Scherrer Institut, Villigen, SWITZERLAND,* [2]*Necsa, Brits, SOUTH AFRICA,* [3]*Institut Laue-Langevin, Grenoble, FRANCE,* [4]*Institute of Radiation Physics (IRA), Lausanne, SWITZERLAND.*

Aim/Introduction: ^{161}Tb ($T_{1/2}$ = 6.89 d) is a therapeutic radiolanthanide which shows similar decay characteristics and chemical behaviour to that of ^{177}Lu. While ^{177}Lu is currently regarded as the "gold standard" of radionuclide therapy, the therapeutic effect of the former may be superior as a result of its co-emission of conversion and Auger electrons [1]. The production of ^{161}Tb was reported previously [2], however, further development and improvement of the ^{161}Tb purification process took place and will be presented. The product was characterized and the ^{161}Tb purity compared with that of ^{177}Lu. **Materials and Methods:** Enriched ^{160}Gd oxide targets were irradiated at the SAFARI-1 (South Africa) reactor and the high flux reactor of ILL (France), as well as the spallation-induced neutron source (SINQ) at PSI, Switzerland, using the $^{160}Gd(n,\gamma)^{161}Gd \rightarrow ^{161}$Tb

nuclear reaction to produce a no-carrier-added (n.c.a.) product. ^{161}Tb separation from the target material was performed using cation exchange chromatography, while the desired ^{161}Tb was concentrated using extraction chromatography before elution of the final product in a small volume. The pH, radionuclidic and radiochemical purity of $^{161}TbCl_3$ was determined, with the radiolabeling capacity of ^{161}Tb monitored over a two-week period post processing. The product was assessed metrologically towards future instrument calibration. The ^{161}Tb was characterized and half-life measurements performed, using various forms of detection, to ensure accuracy of activity measurements. **Results:** Irradiations of enriched $^{160}Gd_2O_3$ targets, followed by chemical separation, resulted in yields of 8-20 GBq ^{161}Tb. The final product was obtained with a >80% separation yield and activity concentration of 11-21 MBq/μL. The radionuclidic purity of $^{161}TbCl_3$ was ≥99.9% at End of Separation (EOS) with the ^{160}Tb impurity, produced by the ^{159}Tb(n,γ) reaction, determined to be ≤0.007% of the total ^{161}Tb activity at EOS. DOTANOC was labelled with ^{161}Tb at 180 MBq/nmol specific activity at a labelling efficiency of ≥99%. The radiolabelling yield of DOTA with ^{161}Tb was comparable to n.c.a. ^{177}Lu over a two-week period. The half-life measurements of ^{161}Tb are ongoing. **Conclusion:** High yields of $^{161}TbCl_3$ in a quantity and quality suitable for high-specific radiolabelling, useful for preclinical and potential clinical application, was produced using a variety of irradiation sources and an innovative chemical separation method. **References:** [1] Müller et al. Eur. J. Nucl. Med. Mol. Imaging 2014; 41: 476-85. [2] Lehenberger et al. Nucl. Med. Biol. 2011; 38: 917-24.

OP-090

Target development and chemical separation for radioantimony production

A. Olson[1], *P. A. Ellison*[1], *E. Aluicio-Sarduy*[1], *T. Kostelnik*[2,3], *J. Mynerich*[3], *T. E. Barnhart*[1], *R. J. Nickles*[1], *V. Radchenko*[2,3], *J. W. Engle*[1]; [1]*Department of Medical Physics, University of Wisconsin Madison, Madison, WI, UNITED STATES OF AMERICA,* [2]*Medicinal Inorganic Chemistry Group, Department of Chemistry, University of British Columbia, Vancouver, BC, CANADA,* [3]*Life Sciences Division, TRIUMF, Vancouver, BC, CANADA.*

Aim/Introduction: The Auger and conversion electron emitting radionuclide ^{119}Sb ($t_{1/2}$ = 38.5 h) is a candidate for targeted radionuclide therapy (TRT) due to highly localized energy deposition of its emitted low energy electrons [1]. Antimony-119 can be produced using ^{119}Sn(p,n)^{119}Sb reactions initiated by proton irradiation on small cyclotrons, providing a scalable production route [1]. Our efforts build upon previous work in Sn target development and chemical separation [2] with a focus on producing radioantimony suitable for chelation-based labeling of biological targeting vectors. **Materials and Methods:** At the University of Wisconsin Madison, thick, electrodeposited ^{nat}Sn targets [3] were irradiated with 16 MeV protons using a GE PETtrace, producing various radioisotopes of antimony. Chemical separation techniques explored and optimized included liquid-liquid separation, cation exchange (AG 50W-8X), and extraction chromatography. Chelation reactions with trithiol chelator, designed and synthesized by the Jurrisson Radiochemistry group at the University of Missouri [4], and Sb-chelate stability in mouse serum were monitored using analytical HPLC. **Results:** Various Sb radioisotopes were produced from ^{nat}Sn, with ^{120m}Sb ($t_{1/2}$= 5.76 d), ^{122}Sb ($t_{1/2}$= 2.74 d), and co-produced ^{117m}Sn ($t_{1/2}$= 14.0 d) used as tracers for development and optimization of chemical separation techniques. The cation exchange separation method developed produces a separation factor between Sn and Sb of >10^4 and resulted in chemical purity and Sb speciation suitable for chelation. Reactions resulting in trithiol chelation of radioantimony isolated via cation exchange chromatography were fast (<30 min) and efficient (>95%). Recycling techniques that enable recovery of enriched ^{119}Sn are being developed and will be discussed. **Conclusion:** Radioisotopes of antimony were produced via proton irradiation of ^{nat}Sn, chemically separated, and stably chelated, with ongoing studies into the recycling of target material for future application of enriched ^{119}Sn targets for ^{119}Sb production. **References:** [1] H. Thisgaard and M. Jensen, "Production of the Auger emitter 119Sb for targeted radionuclide therapy using a small PET-cyclotron," Appl. Radiat. Isot., 2009. [2] H. Thisgaard, M. Jensen, and D. R. Elema, "Medium to large scale radioisotope production for targeted radiotherapy using a small PET cyclotron," Appl. Radiat. Isot., 2011.[3] P. Møller and L. P. Nielsen, Advanced Surface Technology, 2nd ed. 2013.[4] A. J. DeGraffenried, Y. Feng, C. L. Barnes, A. R. Ketring, C. S. Cutler, and S. S. Jurrison, "Trithiols and their Arsenic Comounds for Potential Use in Diagnostic and Therapeutic Radiopharmaceuticals," Nucl Med Biol, vol. 43, no. 5, pp. 288-295, 2016.

306

Do.MoRe - Parallel Session: Diagnostic Dosimetry

Sunday, October 13, 2019, 11:30 - 12:45 Lecture Hall 112

OP-091

Radiation Dosimetry of ^{18}F - AzaFol as the the first Folate Receptor-alpha (FRα) directed PET-Tracer

S. Gnesin[1], *J. Mueller*[2], *I. Burger*[3], *A. Meisel*[4], *M. Choschzick*[5], *C. Mueller*[6], *R. Schibli*[7], *S. M. Amethamey*[7], *J. O. Prior*[8], *N. Schaefer*[8]; [1]*Institute of Radiation Physics, Lausanne University Hospital and University of Lausanne, Lausanne, SWITZERLAND,* [2]*Department of Radiology and Nuclear Medicine, Cantonal Hospital St Gallen, St. Gallen, SWITZERLAND,* [3]*Department of Nuclear Medicine, Kantonsspital Baden, Baden, SWITZERLAND,* [4]*Department of Internal Medicine - Hematology & Oncology, Stadtspital Waid, Zurich, SWITZERLAND,* [5]*Institute for Pathology and Molecular Pathology, University Hospital of Zurich, Zurich, SWITZERLAND,* [6]*Center for Radiopharmaceutical Sciences ETH-PSI, Paul Scherrer Institute, Villigen-PSI, Villigen, SWITZERLAND,* [7]*Department of Chemistry and Applied Biosciences, ETH*

Zurich, Zurich, SWITZERLAND, [8]Department of Nuclear Medicine and Molecular Imaging, Lausanne University Hospital and University of Lausanne, Lausanne, SWITZERLAND.

Aim/Introduction: The FRα has evolved to a valuable diagnostic and therapeutic target in different cancer entities. Here we present the first in-human radiation dosimetry results of a prospective, multicentric trial (NCT03242993) evaluating the ^{18}F-AzaFol as the first clinically-assessed PET-tracer targeting the FRα. **Materials and Methods:** The prospective, multi-centric study was conducted in three Swiss academic hospitals. Eligible patients (n=6) presented a histologically confirmed ovarian cancer or adenocarcinoma of the lung with measurable lesions in the standard of care imaging modality with an indication for systemic treatment. All patients had TOF-PET acquisitions at 5, 10, 15, 30, 40, 50 and 60 minutes after the intravenous injection of 327 MBq (SD=37, range: 299-399 MBq) of 18F-AzaFol. Source organ segmentation for brain, thyroid, lungs, heart, liver, spleen, stomach, kidneys, prostate (in men), red marrow, intestines, whole body, for the choroid plexuses and for tumors (primary carcinoma and metastases) was performed using the PMOD software based on sequential PET/CT data. Time integrated activity coefficients (TIAC) were calculated by bi-exponential analytical integration of the time activity curves for $0 \leq t \leq 60$min then assuming mono-exponential physical decay to infinite. Organ absorbed doses (AD) and patient effective doses (ED) where assessed using the OLINDA/EXM v.2.0 software using a urinary voiding period of 1h. The OLINDA/EXM sphere model was used to obtain AD in tumors. Dose estimates in patients were compared with those extrapolated from a previous study in mice [1]. **Results:** No patient had any serious adverse event related to the experimental substance. The organs receiving the highest AD were the urinary bladder wall, the liver, the kidneys and the small intestine (51.3, 50.6, 44.9 and 26.2 µGy/MBq respectively). Considering a 1h urinary voiding time, the ED across our patient cohort and for the gender-averaged reference person were of 18.3±2.7 and 20±1.4 µSv/MBq respectively. ED in human exceeded the value of 13.2 µSv/MBq obtained from pre-clinical data. A specific biologic uptake and a significant AD (30 µGy/MBq) were reported for the choroid plexuses. Average AD in tumors was 26.4 µGy/MBq (range: 9.6-47.1 µGy/MBq). **Conclusion:** ^{18}F-Azafol is a PET agent with favourable dosimetric properties and reasonable radiation dose burden in patients (comparable to ^{18}F-FDG), which merits further evaluation to assess its performance in patients with ovarian and lung adenocarcinoma. **References:** [1] T. Betzel et al, Chem. 2013 Feb 20;24(2):205-14.

OP-092

Biodistribution and radiation dosimetry study of ^{68}Ga-FAPi-46 PET imaging in patients with various cancers

C. Meyer[1,2], M. Dahlbom[1,2], J. Czernin[2], S. Vauclin[3], T. Lindner[4], U. Haberkorn[4], J. Calais[2];
[1]Physics & Biology in Medicine Interdepartmental Graduate Program, UCLA, Los Angeles, CA, UNITED STATES OF AMERICA, [2]Department of Molecular & Medical Pharmacology, UCLA, Los Angeles, CA, UNITED STATES OF AMERICA, [3]DOSIsoft SA, Cachan, FRANCE, [4]Department of Nuclear Medicine, University Hospital Heidelberg, Heidelberg, GERMANY.

Aim/Introduction: Targeting cancer-associated fibroblasts (CAFs) has become an attractive goal in research and industry given that CAFs can constitute as much as 90% of tumor stroma. The serine protease, fibroblast activation protein (FAP), is highly overexpressed in CAFs, suggesting FAP as a promising stromal target(1). The recently developed quinolone-based FAP-inhibitor PET tracer, ^{68}Ga-FAPI-46, has demonstrated encouraging results with high tumor-to-background ratios (TBR) in patients with various cancers(2). Here we present a biodistribution and radiation dosimetry study of ^{68}Ga-FAPi-46 PET imaging in cancer patients. **Materials and Methods:** Radiotracer synthesis and image acquisition were conducted at the University of Heidelberg; image analysis and dosimetry were performed at UCLA. Six patients with different cancers underwent serial PET/CT ^{68}Ga-FAPi-46 scans at three time points following radiotracer injection: 10 minutes, 1.2 hours, and 3.3 hours (injected activity range 214-246 MBq). Source organ contouring and activity accumulation was calculated using PLANET®Dose (DOSIsoft SA, Cachan, France). The source organs consisted of the kidneys, bladder, liver, heart, spleen, bone marrow, and uterus. OLINDA/EXM was used to fit the organ activity kinetic data with a monoexponential decay function and integrated according to MIRD formalism to yield total body and organ absorbed doses. Standardized uptake values (SUV) and TBR were generated from the contoured tumor and source organ volumes. Spherical volumes in muscle and blood pool were also obtained for TBR. **Results:** At all timepoints, the highest organ SUV was observed in the kidneys. Tumor and organs SUVs decreased with time whereas TBRs increased with time. The highest TBRs at 3.3 hours were observed with the marrow (32.2), muscle (23.1), spleen (19.6), and liver (17.3). The organs with the highest absorbed doses are the kidneys (1.66E-02 mGy/MBq), followed by the heart wall (1.11E-02 mGy/MBq) and liver (1.01E-02 mGy/MBq). The average total body effective dose is 7.84E-03 mSv/MBq - similar to reported values for related FAP-inhibitors(3). Thus for administration of 200 MBq ^{68}Ga-FAPi-46 the total body effective dose is 1.57 mSv ± 0.26 mSv, in addition to approximately 3.7 mSv from one low-dose CT attenuation scan. **Conclusion:** ^{68}Ga-FAPi-46 PET/CT imaging is safe: for administration of 200 MBq(5.4 mCi) of ^{68}Ga-FAPi-46 the whole body effective dose including CT is 5.3 mSv. The biodistribution study showed high TBRs increasing over time, suggesting high diagnostic performance and favorable tracer kinetics for potential therapeutic applications. **References:** [1]Hamson et al.(2014) Proteomics Clin. Appl., 8(5-6):454-463. [2]Kratochwil et al.(2019) JNM, Epub ahead of print.[3]Giesel et al.(2018) JNM, 60(3):386-392.

OP-093

Patient-Specific Estimates of Organ Dose in Paediatric ^{18}FDG PET/CT Imaging Studies

F. Fahey[1,2], *C. Kofler*[3], *B. Sexton-Stallone*[1], *R. Reddy*[1], *R. MacDougall*[1], *W. Bolch*[3];
[1]*Boston Children's Hospital, Boston, MA, UNITED STATES OF AMERICA,* [2]*Harvard Medical School, Boston, MA, UNITED STATES OF AMERICA,* [3]*Crayton Pruitt Family Dept. of Biomedical Engineering, University of Florida, Gainesville, FL, UNITED STATES OF AMERICA.*

Aim/Introduction: Hybrid imaging using PET/CT provides crucial clinical information for a variety of paediatric conditions. Fahey et al. [1] noted that currently there are no standard guidelines for the CT portion of a PET/CT in children. At Boston Children's Hospital (BCH), a diagnostic-quality (Dx) CT is acquired over essential portions of the field-of-view, with low-dose attenuation correction (AC) CT applied to the remainder of the PET field-of-view. The objective of this study was to estimate CT and FDG organ and effective doses in a cohort of BCH patients undergoing FDG PET/CT. **Materials and Methods:** The UF/NCI phantom library was used to estimate organ dosimetry on 163 PET/CT scans performed on 100 children imaged at BCH (47 females, 53 males; 1 - 19 years, mean 11.4 years). For the PET component, organ dose coefficients from the UF/NCI reference phantom library were interpolated across patient weight to determine patient-specific organ dose coefficients. These coefficients were scaled by FDG administered activity recommendations from the North American Guidelines for children and adolescents [2]. For the CT component, patients were matched by height/weight to individual phantoms within the UF/NCI phantom library. CT parameters as well as scan length and body region imaged were taken into consideration. An attenuation-based algorithm was applied to account for tube current modulation (TCM). Patients in the cohort were scanned with specific BCH AC and Dx protocols. **Results:** Effective dose of the FDG PET component ranged from 4.1 to 9.2 mSv (average 5.8 mSv). The effective doses of the CT component for AC and Dx scans ranged from 0.01 to 3.04 mSv (average 0.9 mSv) and 0.19 to 11.2 mSv (average 4.1 mSv), respectively. For the combined PET/CT, effective doses for the AC and Dx scans ranged from 4.8 to 9.6 mSv (average 6.9 mSv) and 5.3 to 17.7 mSv (average 10.1 mSv), respectively. The FDG, CT and total PET/CT effective doses all varied with body weight. **Conclusion:** This work demonstrates the dependence of paediatric PET/CT effective dose (FDG, CT and total) on body weight. The CT effective dose also depends on scan type (AC or Dx) and CT acquisition parameters (kVp, effective mAs, scan length and body region imaged) as well as the use of TCM. This work also highlights the range of effective dose typical in paediatric PET/CT imaging. **References:** 1. Fahey FH, et al. J Nucl Med. 2017;58:1360-1366. 2. Treves ST, et al. J Nucl Med. 2016;57:15N-18N.

OP-094

Dosimetric Impact of Modeling the Epiphyseal Plates in Pediatric ^{99m}Tc-MDP Studies

J. L. B. Brown[1], *Y. Li*[2], *B. Sexton-Stallone*[3], *X. Cao*[3], *D. Plyku*[2], *E. C. Frey*[2], *S. T. Treves*[3], *F. H. Fahey*[3], *G. Sgouros*[2], *W. E. Bolch*[1];
[1]*University of Florida, Gainesville, FL, UNITED STATES OF AMERICA,* [2]*Johns Hopkins University, Baltimore, MD, UNITED STATES OF AMERICA,* [3]*Harvard Medical School, Boston, MA, UNITED STATES OF AMERICA.*

Aim/Introduction: ^{99m}Tc labeled methylene diphosphonate (MDP) is a commonly used radiopharmaceutical for imaging skeletal regions of high bone turnover. These regions include fractures, infections, and tumors. In pediatric patients, ^{99m}Tc-MDP will also localize within the epiphyseal plates. Present biokinetic models given by the ICRP do not account for increased uptake. The present study aims to quantify the dosimetric impact of epiphyseal plate uptake through explicit modeling of the epiphyseal plates within the femur of the reference 10-year-old. The simulation study employs polygon mesh models of cortical bone, medullary marrow, distal and proximal trabecular spongiosa, and epiphyseal plates. Polygon mesh Monte Carlo (MC) radiation transport is a recent advancement that supersedes the implementation of memory intensive voxel models. **Materials and Methods:** The UF/NCI reference 10-year-old phantom used in the study was modified to include epiphyseal plates in the long bones. To create the epiphyseal plates, a Boolean splitting operation is performed at the location of the epiphyseal plate and two planes that are separated 0.08 mm. This operation results in a 0.08-mm structure representing the epiphyseal plate. Phantom triangle mesh structures are converted to a tetrahedral mesh using Tetgen. MC radiation transport was performed using PHITS to assess doses to all structures in the model. **Results:** Results were generated using an isolated femur where the epiphyseal plates of the proximal femoral head, greater trochanter and the distal femoral head were modeled. Cortical bone, spongiosa, and epiphyseal plates were then independently simulated as source regions using the ^{99m}Tc decay scheme. This approach allows the assessment of varying levels of activity for each source organ. Results for femur active marrow dose are shown to be highly dependent on the percent of total femur activity localized in the epiphyseal plate. For all structures, increasing the ^{99m}Tc-MDP activity concentration within the epiphyseal plates lowers the absorbed dose to active bone marrow in the 10-year femur. Future efforts will extend this modeling approach to all skeletal sites, and for all reference patient ages. **Conclusion:** This work demonstrates the need for incorporating epiphyseal plates in long bones for pediatric dosimetry. The assumption of a uniform uptake across all bone surfaces leads to an overestimation of active marrow dose in comparison to that assuming some uptake to the growth plates. Future work will incorporate epiphyseal structures in all other regions of the pediatric skeleton. **References:** Acknowledgements: Grant R01 EB013558 from the National Institute for Biomedical Engineering and Bioengineering.

OP-095

Radiation dosimetry of nasally administered PET agents using computer simulations

J. O' Doherty[1,2], *E. Hippelainen*[3,4], *C. Mangini*[5], *D. Hamby*[6], *N. Singh*[7];
[1]*Sidra Medicine, Doha, QATAR,* [2]*Weill Cornell Medicine Qatar, Doha, QATAR,* [3]*Helsinki University Hospital, Helsinki, FINLAND,* [4]*University of Helsinki, Helsinki, FINLAND,* [5]*Rennaisance Code Development, Corvallis, OR, UNITED STATES OF AMERICA,* [6]*Renaissance Code Development, Corvallis, OR, UNITED STATES OF AMERICA,* [7]*Oxford University, Oxford, UNITED KINGDOM.*

Aim/Introduction: The intranasal (IN) administration of radiopharmaceuticals is of interest in being a viable route for the delivery of radiopharmaceuticals that do not ordinarily cross the blood brain barrier (BBB) [1]. For this imaging technique to be viable in a patient population, certain conditions need to be met for clinical use, for example good image quality and safety and efficacy of the administration. This work provides initial dosimetry calculations related to the safety of performing such experiments in patients. **Materials and Methods:** We utilized an analytical equation and VARSKIN software to estimate the radiation dose to the skin tissue inside the nasal cavity assuming a homogenous distribution of F-18 and C-11 radiotracers. Furthermore, we performed a direct Monte Carlo simulation of radiation transport in tissue, and estimated radiation dosimetry to organs of interest such as the eyes, thyroid and brain by way of calculation of dose factor (DF) values used in dosimetry calculations. **Results:** Analytical and VARSKIN calculation methods estimated absorbed radiation doses to the skin of the nasal cavity of approximately 11 mGy/MBq and 7 mGy/MBq per hour for 18F and 11C radiotracers administered via IN. Direct Monte Carlo simulations of radiation transport resulted in DF values from nasal cavity to the thyroid, eyes and brain of $1.72x10^{-6}$, $1.93x10^{-6}$ and $3.51x10^{-6}$ mGy/MBq·s respectively for F-18 radiotracers and $1.8x10^{-6}$, $1.95x10^{-5}$ and $3.54x10^{-6}$ mGy/MBq·s for C-11 radiotracers respectively. **Conclusion:** Dosimetric concerns about IN administrations of PET radiotracers should be considered before human use. Depending on the administered amount of activity via the IN route, values presented in this work can be used for assessment of dosimetric concerns. Based on these calculations, absorbed dose and thus safety of IN administration of future study protocols can be balanced with requirements for good image quality. **References:** [1] N Singh, M Veronese, J O'Doherty, T Sementa, S Bongarzone, D Cash, C Simmons, M Arcolin, P K Marsden, A Gee, F ETurkheimer. Assessing the feasibility of intranasal radiotracer administration for in brain PET imaging. Nuc Med Biol, 66, 32-39, 2018

307

Pitfalls & Artefacts 2 - Interactive Clinical Cases - Dosimetry Committee: From Imaging to Dosimetry ? Step-by-Step Patient Dosimetry

Sunday, October 13, 2019, 11:30 - 13:00 Lecture Hall 113

OP-096

Dosimetry for Radioembolisation with 90Y Microspheres

C. Chiesa;
Nuclear Medicine, Foundation IRCCS Istituto Nazionale Tumori, Milan, ITALY.

OP-097

Dosimetry for 177Lu-PSMA Therapy

G. Böning;
Ludwig-Maximilians-University of Munich - University Hospital, Department of Nuclear Medicine, Munich, GERMANY.

OP-098

Dosimetry for 177Lu-PSMA Therapy

H. Illhan;
Ludwig-Maximilians-University of Munich - University Hospital, Department of Nuclear Medicine, Munich, GERMANY.

OP-099

Dosimetry for Alpha-Particle Emitters

C. Hindorf;
Skåne University Hospital, Department of Radiation Physics, Lund, SWEDEN.

OP-100

Step by Step Estimation of Uncertainty on Absorbed Dose

J. Gear;
Royal Marsden NHS Foundation Trust, Joint Department of Physics, Sutton, UNITED KINGDOM.

308

Clinical Oncology - Rapid Fire Session: Prostate - BCR only

Sunday, October 13, 2019, 11:30 - 13:00 Lecture Hall 114

OP-101

68Ga-PSMA PET/CT in biochemical recurrent prostate cancer: an international multi-institutional prospective study promoted by the IAEA

E. Estrada Lobato[1], *S. Fanti*[2], *J. Cerci*[3];
[1]*International Atomic Energy Agency, Vienna, AUSTRIA,* [2]*Universita di Bologna, Bologna, ITALY,* [3]*Quanta Diagnóstico e Terapia, Curitiba, BRAZIL.*

Aim/Introduction: Biochemical recurrence is a major problem in patients with Prostate Cancer(PCa), rising PSA occurs in 20-30% of patients treated with radical prostatectomy and up to 60% in patients treated with external radiotherapy. Standard practice for suspected recurrence in PCa includes computed tomography(CT), bone scintigraphy(BS); MR and PET have been suggested. The most accurate tracer used so far is Prostate Specific Antigen(PSMA), but there is lack of reliable data, as most of the published studies have been limited by retrospective design, single institution approach, small sample size and lack of follow-up data/reference standard. Therefore, this prospective, multicentric, international study was planned to evaluate the accuracy of 68GaPSMA-PET/CT in evaluating patients with biochemical recurrent PCa; the study was promoted and supported by IAEA. We report the first interim analysis. **Materials and Methods:** Patients with PCa who have undergone primary definitive treatment and with rising PSA were recruited in the study from 17 centres in 15 countries (Azerbaijan, Brazil, Colombia, India, Israel, Italy, Jordan, Lebanon, Malaysia, Mexico, Pakistan, Poland, South Africa, Turkey, and Uruguay); all centres obtained ethical clearance for prospective patient recruitment. Images and data were centrally reviewed; data were collected for positivity rate, detection rate, site of findings, impact on patient management and clinical follow-up. **Results:** 842 patients have been enrolled since 2017, while full data are available for 704 cases. Overall 68GaPSMA-PET/CT was positive in 423 (60.1%); lesions were identified locally (prostate/prostatic bed) in 169 cases; pelvic lymph nodes in 214 cases; bone in 137 cases and in other locations in 93 cases. There was a clear relationship between PSMA positivity and Gleason score: detection rate was 54.3% in patients with Gleason 7, 61.3% in Gleason 8, 76.0% in Gleason 9 and 76.9% in Gleason 10. Also, there was a clear relationship between lesions identification and PSA values: detection rate was 44.1% for PSA <1, 61,9% for PSA ≥1 and <2, 81.4% for PSA ≥2 and <4, and 87.1% in PSA >4. **Conclusion:** This is the largest multicenter trial on PSMA-PET reported so far; the data are in line with existing literature regarding diagnostic performances of PSMA PET in biochemical recurrent PCa. No relevant difference of the accuracy was noted among the participating countries, while the major clinical role that PET may play in this setting was confirmed. Those preliminary data from the first international multicentric trial are supporting the benefits of the use of 68Ga-PSMA PET/CT. **References:** None.

OP-102

^{68}Ga-PSMA PET/CT in patients with recurrent prostate cancer after radical treatment: prospective results in 1000 patients

P. Caroli[1], *U. De Giorgi*[1], *M. Celli*[1], *L. Fantini*[1], *A. Moretti*[2], *R. Galassi*[2], *V. Di Iorio*[1], *F. Ferroni*[1], *A. Romeo*[1], *M. Caracciolo*[3], *G. Paganelli*[3], *F. Matteucci*[1];
[1]*IRCCS IRST, Meldola, ITALY,* [2]*Ospedale Morgagni-Pierantoni, Forlì, ITALY,* [3]*Ospedale S. Anna, Ferrara, ITALY.*

Aim/Introduction: We studied the usefulness of 68Ga-prostate-specific membrane antigen (PSMA) PET/CT for detecting relapse in a prospective series of patients with biochemical recurrence (BCR) of prostate cancer (PCa) after radical treatment. **Materials and Methods:** Patients with BCR of PCa after radical surgery and/or radiotherapy with or without androgen-deprivation therapy were included in the study. 68Ga-HBED-CC-PSMA was prepared according to national regulations, good radiopharmaceutical practice (GRP) as outlined in EANM guidelines, using an Eazy® synthesis module (Eckert and Zieckert, Germany).68Ga-PSMA PET/CT scans performed from the top of the head to the mid-thigh 60 min after intravenous injection of 150 ± 50 MBq of 68Ga-PSMA were interpreted by two nuclear medicine physicians. 68Ga-PSMA PET/CT scans were performed on a Biograph mCT Flow® (Siemens Healthineers, Erlangen Germany). Acquisition was made on Flow mode (0,7 mm/sec) in 3D mode. The results were correlated with prostate-specific antigen (PSA) levels at the time of the scan (PSApet), Gleason score and patient age. When available, 68Ga-PSMA PET/CT scans were compared with 18F-choline PET/CT scans routinely performed within 1 month previously. **Results:** From November 2015 to October 2018, 1000 PCa patients with BCR were evaluated. Their median age was 72.4 years (+/- 10.3 years) and their median PSApet was 2 ng/ml (0,2 - 19 ng/ml). 68Ga-PSMA PET/CT localized one or more suspected PCa lesions detected in 653 patients (62.3%). Lesions limited to the pelvis, i.e. the prostate/prostate bed and/or pelvic lymph nodes (LNs), were detected in 415 patients (63%). At least one distant lesion (LNs, bone, other organs) was detected in 238 patients (37%). For PSA categories 0.2-0,5, 0,51-1, 1,01-2 and >2 ng/ml, 47,9%, 60,9%, 68,6%, and 87,3% of the scans were positive respectively. **Conclusion:** Our experience confirms 68Ga-PSMA PET/CT as a highly sensitive and accurate restaging tool in biochemically-relapsing prostate cancer with negative or equivocal conventional imaging also for PSA < 1.0 ng/ml.These results support the use of 68Ga-PSMA PET/CT in the clinical setting for an early localization of biochemical recurrence. **References:** None.

OP-103

The impact of clinical factors and inter-site variation on detection of recurrent prostate cancer with ^{18}F-fluciclovine PET/CT and subsequent management decisions: data from the FALCON trial

G. Cook, FALCON study group;
King's College London, London, UNITED KINGDOM.

Aim/Introduction: The FALCON study aimed to confirm the clinical benefit of PET radiotracer, ^{18}F-fluciclovine, through its impact on management decisions for men with recurrent prostate cancer. Here, we explore the impact of clinical factors and variations between recruitment sites on the ^{18}F-fluciclovine detection rate (DR) and subsequent management decisions. **Materials and Methods:** Data were collected at 6 UK sites from men with a first episode of prostate cancer recurrence after curative-intent treatment who were now being considered for radical salvage treatment. Patients who received androgen-deprivation therapy during the preceding 3 months were excluded. PSA and Gleason scores were recorded pre-scan.^{18}F-Fluciclovine PET/CT was conducted and interpreted according to standard protocols. The patients' management plans were recorded before and after scanning to document any post-scan amendments to plans. **Results:** In total, 104 patients (median age, 67 years; median PSA, 0.79 ng/mL; 15.4% with Gleason score ≥8) underwent ^{18}F-fluciclovine PET/CT. Inter-site variation was noted for the number of patients recruited per site (range: 3-37), the median PSA value (inter-site range: 0.25-5.00 ng/mL), the proportion of patients with Gleason score ≥8 (inter-site range: 0-33%), the scanning equipment used (5 PET/CT systems were used across the 6 sites), and the median activity of ^{18}F-fluciclovine administered per site (inter-site range: 343.3-373.0 MBq). The overall patient-level DR was 56%. Detection was broadly proportional to PSA and ranged from 33% (6/18) at PSA ≤0.2 to 100% (8/8) at PSA >10.0 ng/mL. Inter-site variation was also noted in DRs; across sites, the overall patient-level DR ranged from 23% to 95%, while the patient-level DR at PSA ≤1.0 ng/mL ranged from 13% to 50%. The site with the highest median PSA (5 ng/mL) reported the highest overall DR (95%). Low patient numbers limited meaningful analysis, however, Gleason scores ≤7 were associated with a lower DR (53%) compared with scores ≥8 (69%). Scores ≥9 showed the highest extraprostatic detection (31% vs 19% for scores ≤6). In total 66/104 (63%) of patients had a management change post-scan. Across sites, the proportion of patients with a post-scan management change ranged from 15% to 100%. In general, the sites with the highest DRs showed the highest proportion of post-scan management changes. **Conclusion:** This UK-wide study showed inter-site variation in patient characteristics, ^{18}F-fluciclovine DR and proportion of post-scan management changes. ^{18}F-Fluciclovine showed acceptable performance at low PSA. Lesions, particularly in extraprostatic regions were more common among patients with higher Gleason scores. **References:** None.

OP-104

^{68}Ga-PSMA-11 PET localizes residual prostate cancer after salvage lymph node dissection in a multicenter retrospective study

A. Farolfi[1], *M. Weber*[2], *F. Barbato*[2], *H. Ilhan*[3], *A. Gafita*[4], *M. Eiber*[4], *J. Calais*[5], *A. Afshar-Oromieh*[6], *A. Wetter*[7], *B. Hadaschik*[8], *D. Pianori*[9], *S. Fanti*[1], *U. Haberkorn*[10], *K. Herrmann*[2], *W. P. Fendler*[2];
[1]*Nuclear Medicine Department, S.Orsola Hospital, University of Bologna, Bologna, ITALY,* [2]*Department of Nuclear Medicine, University Hospital Essen, Essen, GERMANY,* [3]*Department of Nuclear Medicine, University Hospital Munich, Ludwig-Maximilians-Universität (LMU), Munich, GERMANY,* [4]*Department of Nuclear Medicine, Klinikum rechts der Isar, Technical University Munich, Munich, GERMANY,* [5]*Ahmanson Translational Theranostics Division, Department of Molecular and Medical Pharmacology, University of California Los Angeles (UCLA), Los Angeles, CA, UNITED STATES OF AMERICA,* [6]*Department of Nuclear Medicine, Bern University Hospital, Bern, SWITZERLAND,* [7]*Department of Radiology, University Hospital Essen, Essen, GERMANY,* [8]*Department of Urology, University Hospital Essen, Essen, GERMANY,* [9]*Department of Biomedical and Neuromotor Sciences, University of Bologna, Bologna, ITALY,* [10]*Department of Nuclear Medicine, Heidelberg University Hospital, Heidelberg, GERMANY.*

Aim/Introduction: In patients with prostate cancer (PCa) recurrence confined to the pelvic lymph nodes the main aim of metastases-directed therapy is to delay androgen deprivation therapy and improve cancer-specific survival. The aim of this study was to identify regions at risk for residual disease in patients with PSA persistence after salvage lymph node dissection (SLND) using ^{68}Ga-PSMA-11 PET (PSMA-PET). **Materials and Methods:** 21 patients were included in this multicenter retrospective study with the following inclusion criteria: a) SLND for PCa; b) persistently elevated post-operative PSA levels (≥0.1 ng/mL) ≥6 weeks after SLND; c) PSMA-PET performed within 12 months after SLND. Moreover, a subgroup analysis was performed in 15 patients with both PSMA-PET pre-SLND and PSMA-PET post-SLND. Images analysis was performed by three independent nuclear medicine physicians applying the molecular imaging TNM system PROMISE. Lesions were confirmed by histopathology/biopsy, presence of lesion on correlative CT/MRI/bone scan or change in size/disappearance/appearance on follow-up CT/MRI/bone scan. Furthermore, management after PSMA-PET was documented when available. **Results:** PSMA-PET identified PCa-lesions in 81% (17/21) of patients with PSA persistence after SLND at a median PSA level of 1.1 ng/mL (IQR, 0.2-12.0 ng/mL). The probability of detection of Tr, N1, M1 or multiple lesions was positively associated with PSA PET (p=0.039). In the patient-based analysis disease confined to the pelvis was detected in 43% of patients (9/21), with predominant pelvic nodes disease (8/21, 38%). Most frequently affected pelvic nodal regions were internal iliac (8/21, 38%). In the subgroup analysis (PSMA-PET before and after SLND), 60% (9/15) of patients had at least one lesion already detected at baseline (PET persistence) and 27%

(4/15) had previously undetected lesions (PET recurrence). Most frequently affected nodal regions with PET persistence were internal iliac (5/9), obturator (3/9) and external iliac (3/9). PSMA-PET was performed before SLND with a median time of 2 months (IQR, 1-2 months). Validation was available in 6/21 patients (29%) and 9/9 validated regions were true positive. Management after PSMA-PET was recorded in 8/21 patients (38%). **Conclusion:** In this multicenter retrospective study, ^{68}Ga-PSMA-11 PET detected disease in more than 80% of patients with PSA persistence after salvage lymph node dissection. Most common sites of persistent disease were within the internal iliac region. Our data suggests a role for PSMA-ligand PET for both staging before salvage surgery and early restaging after salvage surgery in case of PSA persistence. **References:** None.

OP-105

Prostate-Specific Membrane Antigen Positron-Emission Tomography (PSMA-PET) in High-Risk Nonmetastatic Castration-Resistant Prostate Cancer (nmCRPC) SPARTAN-like Patients Negative by Conventional Imaging

W. Fendler[1,2], *M. Weber*[1], *A. Iravani*[3], *M. S. Hofman*[3], *J. Calais*[2], *J. Czernin*[2], *H. Ilhan*[4], *F. Saad*[5], *E. J. Small*[6], *M. R. Smith*[7], *P. M. Perez*[6], *T. A. Hope*[6], *I. Rauscher*[8], *A. Londhe*[9], *A. Lopez-Gitlitz*[10], *S. Cheng*[11], *T. Maurer*[8], *K. Herrmann*[1], *B. Hadaschik*[12], *M. Eiber*[8];
[1]*Department of Nuclear Medicine, University of Duisburg-Essen and German Cancer Consortium (DKTK), partner site University Hospital Essen, Essen, GERMANY,* [2]*Department of Molecular and Medical Pharmacology, University of California Los Angeles, Los Angeles, CA, UNITED STATES OF AMERICA,* [3]*Department of Cancer Imaging, Peter MacCallum Cancer Centre, Melbourne, AUSTRALIA,* [4]*Department of Nuclear Medicine, Ludwig Maximilian University, Munich, GERMANY,* [5]*Centre Hospitalier de l'Université de Montréal, Université de Montréal, Montréal, QC, CANADA,* [6]*Helen Diller Family Comprehensive Cancer Center, University of California San Francisco, San Francisco, CA, UNITED STATES OF AMERICA,* [7]*Massachusetts General Hospital Cancer Center and Harvard Medical School, Boston, MA, UNITED STATES OF AMERICA,* [8]*Department of Nuclear Medicine, Klinikum rechts der Isar, Technical University of Munich, Munich, GERMANY,* [9]*Janssen Research & Development, Titusville, NJ, UNITED STATES OF AMERICA,* [10]*Janssen Research & Development, Los Angeles, CA, UNITED STATES OF AMERICA,* [11]*Janssen Research & Development, Raritan, NJ, UNITED STATES OF AMERICA,* [12]*Department of Urology, University of Duisburg-Essen and German Cancer Consortium (DKTK), partner site University Hospital Essen, Essen, GERMANY.*

Aim/Introduction: In SPARTAN, patients with nmCRPC assessed by conventional imaging benefited from the addition of apalutamide to ongoing androgen deprivation therapy (ADT).[1] PSMA-PET detects localized and metastatic PC with superior sensitivity to conventional imaging. We retrospectively characterized disease extent using PSMA-PET in SPARTAN-like patients and evaluated risk factors for distant metastases (M1 disease) detected by PSMA-PET. **Materials and Methods:** A total of 200 patients with nmCRPC at high risk of developing metastases (prostate-specific antigen doubling time [PSADT] ≤ 10 months, or Gleason score [GS] ≥ 8) who had no identifiable extrapelvic metastases on prior conventional imaging were assessed with PSMA-PET. Detection rate on PSMA-PET, including local/pelvic and distant M1 disease, was determined. Association of baseline age ≥ 65 years, GS ≥ 8, PSA ≥ 5.5 ng/mL, PSADT ≤ 6 months, pelvic nodes (N1 disease), and prior local therapy with M1 disease in the PSMA-PET cohort was assessed using univariate and multivariate analyses. SPARTAN patients were stratified by risk factors for PSMA-PET-detected M1 disease and analyzed using Cox proportional-hazards models. **Results:** Baseline characteristics of PSMA-PET and SPARTAN patients were generally similar. PSMA-PET detected PC in 196/200 (98%) patients; 55% had local recurrence, 54% had N1 disease, 55% had any extrapelvic distant metastatic disease despite being negative on conventional imaging; 24% were diagnosed with local recurrence only, 29% with oligometastatic (1-3 lesions), and 46% with polymetastatic disease. PSA ≥ 5.5 ng/mL (OR, 2.0; 95% CI, 1.1-3.6; p = 0.03), pN1 disease (OR, 2.7; 95% CI, 1.2-6.0; p = 0.01), prior prostatectomy/salvage external radiation therapy (OR, 4.6; 95% CI, 2.0-11.0; p < 0.01), and prior external radiation therapy only (OR, 3.1; 95% CI, 1.5-6.2; p = 0.02) were significantly associated with M1 disease detected by PSMA-PET. All clinically relevant subgroups of SPARTAN patients, including patients with independent predictors of PSMA-PET-M1 disease, significantly benefited from apalutamide. **Conclusion:** PSMA-PET-positive CRPC patients were similar to those at high-risk of developing metastases from SPARTAN. Apalutamide added to ongoing ADT showed significant benefit in all clinically relevant subgroups of SPARTAN patients, including patients with risk factors for distant metastases detected by PSMA-PET but negative by conventional imaging. Therefore, apalutamide plus ADT should be considered for patients negative by conventional imaging but positive by PSMA-PET (stage migration). The added value of PSMA-PET over PSADT in patients with high-risk nmCRPC should be explored in prospective studies. **References:** 1. Smith et al. N Engl J Med. 2018;378:1408-1418.

OP-106

Prognostic value of PSMA PET-derived skeleton tumor burden parameters for overall survival in patients undergoing radium-223 treatment

A. Gafita[1], *H. Wang*[1], *M. Krönke*[1], *W. Weber*[1], *R. Tauber*[2], *M. Eiber*[1];
[1]*Technical University Munich, School of Medicine, Department of Nuclear Medicine, Munich, GERMANY,*
[2]*Technical University Munich, School of Medicine, Department of Urology, Munich, GERMANY.*

Aim/Introduction: Prostate-specific membrane antigen (PSMA)-targeted PET imaging showed enhanced accuracy in lesion detection compared to conventional imaging in patients with prostate cancer. Radium-223 is a bone-targeted treatment for symptomatic metastatic castration-resistant prostate cancer (mCRPC) patients. Bone-scan-index (BSI) showed high predictive value for survival rate in patients

undergoing radium-223. The aim of this retrospective analysis was to evaluate the prognostic value of baseline PSMA-PET derived skeleton tumor burden parameters for OS in patients undergoing radium-223. **Materials and Methods:** Patients who underwent radium-223, received a PSMA PET/CT and had available lab values prior to the treatment were considered. qPSMA was used for bone lesion segmentation using a fixed SUV-threshold of 3. Bone PSMA-avid tumor volume (bPSMA-TV) and bone PSMA-total lesion (bPSMA-TL) were used as output parameters. Baseline alkaline phosphatase (ALP) values were extracted from the database. Baseline tumor burden parameters were divided into two groups by medians and into tertile by 25th and 75thpercentiles. Kaplan-Meier curves and log-rank test were used to evaluate the association of bPSMA-TV, bPSMA-TL and ALP with OS. **Results:** Fifty-four patients were included in the analysis. Median PSMA-TV, PSMA-TL and ALP were 502mL, 3255 and 191 U/L. Median OS was 17.5 (95%CI: 3.2-43.6) months and 6 patients were alive at the end of follow-up period. When divided by medians, a trend towards a higher median survival for low vs. high tumor burden was noticed for bPSMA-TV and bPSMA-TL and ALP (19.2 vs. 16.6 months, 19.5 vs. 16.6 months and 19.2 vs. 14.2 months; p=0.33, p=0.33 and p=0.26, respectively). When divided by percentiles, a longer survival rate was noticed among patients with low (<144mL) vs. moderate vs. high (>1374mL) bPSMA-TV with a median OS of 24.4 vs. 14.2 vs. 6.8 months, respectively (p=0.003). No significant difference was noticed among patients with low (<1434) vs. moderate vs. high (>10174) bPSMA-TL with a median OS of 19.5 vs. 17.2 vs. 11.5 months, respectively (p=0.22). For ALP a significantly longer median survival was observed among patients with low (<121 U/L) vs. moderate vs. high (>393 U/L) levels: 21.4 vs. 19.5 vs. 6.8 months, respectively (p=0.01). **Conclusion:** Baseline PSMA PET-derived skeleton tumor burden parameters showed promising results for OS prediction. Compared to ALP, PSMA-TV showed a tendency to better differentiate survival rates in patients with high vs. moderate tumor burden. Advanced analyses including larger patients cohort are warranted to establish the role of PSMA-targeted PET imaging in the framework of radium-223. **References:** None.

OP-107

Prediction Nomogram for ^{68}Ga-PSMA-11 PET/CT in different clinical settings of PSA failure after radical treatment for prostate cancer

F. Ceci[1,2], *L. Bianchi*[3], *M. Borghesi*[3], *G. Polverari*[2], *A. Briganti*[4], *A. Farolfi*[2], *R. Schiavina*[3], *E. Brunocilla*[3], *P. Castellucci*[2], *S. Fanti*[2];
[1]*University of Turin, Turin, ITALY,* [2]*Metropolitan Nuclear Medicine, S.Orsola-Malpighi Hospital, University of Bologna, Bologna, ITALY,* [3]*Department of Urology, S.Orsola-Malpighi Hospital, University of Bologna, Bologna, ITALY,* [4]*Unit of Urology/Division of Oncology, Urological Research Institute, IRCCS San Raffaele Hospital, Milan, ITALY.*

Aim/Introduction: The prompt identification of the site of prostate cancer (PCa) recurrence with ^{68}Ga-PSMA-11-PET/CT may change the disease management, potentially improving the survival outcomes. Objective: to develop a clinical nomogram to predict ^{68}Ga-PSMA-11-PET/CT positivity in different clinical settings of PSA failure. **Materials and Methods:** Design: seven-hundred-three (n=703) PCa patients with confirmed PSA failure after radical therapy were enrolled. Each patient underwent ^{68}Ga-PSMA-11-PET/CT to identify the site of recurrence. Patients were stratified according to different clinical settings of recurrence (first-time biochemical recurrence [BCR]: group-1; BCR after salvage therapy: group-2; biochemical persistence after radical prostatectomy [BCP]: group-3; advanced stage PCa before second-line systemic therapies: group-4). All patients never received AR-targeted therapies and chemotherapy. Outcome measurements and statistical analysis: First, we assessed ^{68}Ga-PSMA-11-PET/CT positivity rate. Second, multivariable logistic regressions analyses were used to determine which co-variates independently predicted positive scan. Third, regression-based coefficients were used to develop a nomogram predicting positive ^{68}Ga-PSMA-11-PET/CT result and 200 bootstrap resamples were used for internal validation. Fourth, Receiver operating characteristic (ROC) analysis was used to identify the most informative nomogram's derived cut-off to predict the positive scan. Decision curve analysis (DCA) were implemented to quantify nomogram's clinical benefit in clinical practice. **Results:** ^{68}Ga-PSMA-11-PET/CT positivity rate was 51.2 % (CI95% 46.8%-71.3%), while was 40.3% in group-1, 54% in group-2, 60.5% in group-3, 86.9% in group-4 (p<0.001). Median PSA=0.7 ng/mL (IQR 0.4-1.3). At multivariable analyses Gleason-grade, PSA, PSAdt and clinical setting were independent predictors of a positive scan (all p≤0.04). A nomogram based on covariates included in the multivariate model demonstrated a bootstrap-corrected accuracy of 82%. At ROC analysis, 40% resulted the best nomogram's cut-off. Applying this cut-off, 282/703 patients (40.1%) would be spared ^{68}Ga-PSMA-11-PET/CT and positive ^{68}Ga-PSMA-11-PET/CT would be missed in 55 patients (15.3%). The sensitivity, specificity and NPV associated with 40% as cut-off were 84.7%, 66.2%, and 80.5%, respectively. Finally, in DCA, the nomogram revealed clinical net benefit when the threshold probabilities of positive ^{68}Ga-PSMA-11-PET/CT is >10%. **Conclusion:** We developed and internally validated the first nomogram aimed at predicting the likelihood of ^{68}Ga-PSMA-11-PET/CT positivity in different stages of PSA failure. This novel nomogram proved its good accuracy to predict a positive ^{68}Ga-PSMA-11-PET/CT results. The 40% cut off was the most informative threshold probability to predict positive ^{68}Ga-PSMA-11-PET/CT. This tool might be markedly important as a guide to clinicians in the best use of PSMA-based PET imaging, in order to select the best treatment option. **References:** None.

OP-108

^{68}Ga-PSMA-11 PET/CT in hormone-naïve recurrent prostate cancer: a prospective, single-center study in patients eligible for salvage therapy

F. Ceci[1], *D. G. Nicolotti*[1], *E. Pilati*[1], *A. Guarneri*[2], *B. Lillaz*[3], *R. Passera*[1], *V. Liberini*[1], *M. Finessi*[1], *M. Bellò*[1], *P. Gontero*[3], *U. Ricardi*[2], *D. Deandreis*[1];
[1]*Nuclear Medicine, Department of Medical Sciences, University*

of Turin, Turin, ITALY, [2]Radiation Oncology, Department of Oncology, University of Turin, Turin, ITALY, [3]Urology, Department of Surgery, University of Turin, Turin, ITALY.

Aim/Introduction: Primary objective: to assess the efficacy of ^{68}Ga-PSMA-11-PET/CT to detect recurrent location(s) in hormone-naïve prostate cancer (PCa) patients. Secondary objectives: 1) to evaluate changes in clinical management occurred after ^{68}Ga-PSMA-11-PET/CT; 2) to determine which covariates independently predict positive scan; 3) to assess ^{68}Ga-PSMA-11-PET/CT performance in different clinical setting of PSA relapse. **Materials and Methods:** This is a prospective, open-label, observational, single-centre study in hormone-naïve PCa patients (protocol P-5315). All patients, were recruited at the uro-oncological tumour board of University Hospital of Turin. Patients were investigated with ^{68}Ga-PSMA-11-PET/CT at single referral centre between November 2016 and January 2019. Inclusion criteria: 1) proven PCa; 2) radical therapy (radical prostatectomy [RP] or radiotherapy); 3) proven biochemical recurrence (BCR) or biochemical persistence (BCP); 4) hormone-naïve patients; 5) PSA<1.5 ng/mL or any PSA in case of negative choline-PET/CT. Exclusion criteria: 1) not eligible for salvage therapy; 2) inability to tolerate PET scan; 3) concurrent malignancy. Changes in clinical management and definition of clinical settings of PSA relapse were defined by a single-centre tumour board. Clinical settings: BCP after RP (group-1); first-time BCR (group-2); BCR after salvage therapy (group-3). Multivariable logistic regressions analyses were used to determine independent predictors of positive ^{68}Ga-PSMA-11-PET/CT. **Results:** Two-hundred twenty-three (n=223) consecutive patients have been prospectively enrolled: median PSA=0.65 ng/mL (0.2-8.9); median PSAdt=9.3 months (0.4-144.6). 96.9% received RP as primary therapy, while 3.1% received radiotherapy. Overall positivity rate for ^{68}Ga-PSMA-11-PET/CT was 38.6% (CI95% 32.2%-45.3%). Disease confined to pelvis (prostate bed and/or lymph-nodes) was detected in 19.3% of cases, while distant locations (extra-pelvic nodes, bone or visceral) were observed in 19.3%. Overall, 153 PSMA positive lesions were detected. Secondary objectives: 1) taking into consideration clinical, laboratory and imaging data derived by ^{68}Ga-PSMA-11-PET/CT, the multidisciplinary tumour board changed in 35.4% of cases the treatment planned prior to PET scan. 2) PSA, PSAdt and T stage≥3a were independent predictors of a positive scan (all p<0.03). The same features resulted independent predictors of distant PCa locations. 3) ^{68}Ga-PSMA-11-PET/CT positivity rate was 56% in group-1, 23.3% in group-2, 47.2% in group-3. Positivity rate was significantly different among different clinical stages of PSA relapse (p=0.001). **Conclusion:** This study attested the overall good performance of ^{68}Ga-PSMA-11-PET/CT to detect recurrent locations in hormone-naïve PCa, influencing the subsequent therapy management. PSA, PSAdt, T stage and different clinical settings should be taken into consideration by referent physicians, since these parameters showed significant association with ^{68}Ga-PSMA-11-PET/CT positivity rate. **References:** None.

OP-109

68Ga-PSMA-11 PET-CT study in prostate cancer patients with biochemical recurrence and non-contributive 18F-Choline PET-CT: impact on therapeutic decision-making and biomarker changes

C. Rousseau[1,2], A. Michaud[1], M. Barbaud[1], C. Morvant[1], B. Maucherat[1], M. Le Thiec[1], D. Rusu[1], A. Morel[1], V. Fleury[1], M. Colombié[1], A. Rauscher[3], M. Frindel[3], P. Baumgartner[3], N. Fleury[4], L. Campion[5], F. Kraeber-Bodéré[1,2];
[1]ICO Cancer Center, Nuclear Medicine Unit, St Herblain, FRANCE, [2]CRCINA, University of Nantes, INSERM UMR1232, CNRS-ERL6001, Nantes, FRANCE, [3]ICO Cancer Center, Pharmacy Unit, St Herblain, FRANCE, [4]ICO Cancer Center, DRCI, St Herblain, FRANCE, [5]ICO Cancer Center, Biometrics Unit, St Herblain, FRANCE.

Aim/Introduction: The aim of this retrospective study was to investigate the impact of 68Ga-PSMA-11 PET/CT on current management of recurrence prostate cancer patients with negative PET/CT F-Choline. **Materials and Methods:** Eighty-nine patients with previously negative 18F-Choline (FCH) were enrolled (PSA from 0.28 to 24.6 ng/mL). PET images were recorded 1 hour after injection of 150 MBq of 68Ga-PSMA. Referring patient physician was asked about the care before and after PSMA PET imaging to determine the influence of PSMA results on therapeutic strategy. Six months after the end of treatment, a PSA assay was requested to evaluate therapeutic efficacy. **Results:** Sixty-nine among the 89 patients (77,5%) had a positive PSMA PET/CT. Detection rates were 85.6% and 89.4% for serum PSA levels lower than 2 ng/ml, and > 2 ng/ml, respectively. Three hundred and one lesions were detected: 235/301 in lymph nodes (78.1%), 38/301 as metastatic sites (bone, mostly on axial skeleton, or lung) (12.6%) and 28/301 in the prostate bed (9.3%). The majority of lesions were detected in lymph nodes: in particular with 71.5% pelvic nodes, on the other hand with 17.9% of para-aortic nodes and 10.6% with sus diaphragmatic location. For the para-aortic and sub-diaphragmatic node locations, initial surgical management associated with pelvic salvage radiotherapy were the most common initial management which could explain the frequently supra-pelvic node recurrence. The median number of lesions per patient was 2 [ranging from 0 to 67]. No particularity of the PSA serum level, doubling time or PSA velocity at the time of PSMA PET-CT could explain why 68Ga-PSMA PET-CT was unable to detect any suspicious tumor lesions in 20 patients. Thanks to PSMA PET/CT, therapeutic management changed in 59/69 patients (84.9%). With a follow-up of 5.7 ± 1.8 months, 62/89 (69.6%) PSA assays after treatment guided by PSMA PET-CT were collected. For 43.5% (27/62) of patients, the serum PSA level was lower than 0.2 ng/mL and a total PSA decrease of over 50% in 35 (56.5%) patients was obtained. **Conclusion:** Performing a PSMA PET-CT when FCH PET-CT was negative allows the recurrence localization in more 80% of patients and this had a major clinical impact, as it resulted in treatment change in more than 80% of patients as well as a significant decrease in PSA levels in more than 55% of them. **References:** None.

OP-110

Multi-phasic 68Ga-PSMA PET/CT in detection of early recurrence in prostate cancer patients with PSA < 1 ng/ml: a prospective study of 105 cases

M. Beheshti[1,2], *R. Manafi-Farid*[3], *F. M. Mottaghy*[4], *W. Loidl*[5], *H. Geinitz*[6], *W. Langsteger*[7];
[1]*Nuclear Medicine, University Hospital, RWTH University, Aachen, GERMANY,* [2]*Nuclear Medicine, Paracelsus Medical University, Salzburg, AUSTRIA,* [3]*Research Center for Nuclear Medicine, Tehran University of Medical Sciences, Tehran, IRAN, ISLAMIC REPUBLIC OF,* [4]*University Hospital, RWTH University, Aachen, GERMANY,* [5]*Urology, Ordensklinikum, Linz, AUSTRIA,* [6]*Radiation Oncology, Ordensklinikum, Linz, AUSTRIA,* [7]*PET-CT Center, St. Vincent's Hospital, Ordensklinikum, Linz, AUSTRIA.*

Aim/Introduction: The main objective of this prospective study was to determine the impact of multi-phasic acquisition of 68Ga-PSMA PET/CT in the detection of local recurrence in prostate cancer (PCa) patients in early stage of biochemical recurrence with PSA level < 1 ng/ml. In addition, 68Ga-PSMA PET/CT positivity were correlated with clinical parameters. **Materials and Methods:** 105 patients (mean age 66.9±8.3) with biochemical recurrence and PSA level < 1 ng/ml were enrolled in this study. All patients have been subjected to initial prostatectomy with additional radiation therapy in 19.3% (26/135) and anti-hormonal therapy in 7.4% (10/135) through the disease course. A multi-phasic imaging including dynamic acquisition (1-8 min. p.i.) from prostate bed, standard whole-body images (60 min. p.i.) and delayed studies (120-150 min. p.i.) from pelvis, were performed. 68Ga-PSMA PET/CT positivity was also correlated with primary clinical findings (i.e. initial PSA, Gleason score, T-stage, positive surgical margin). **Results:** Overall, 91 lesions were detected in 47.6% (50/105) of patients, of whom 18 were classified as local recurrence, 48 as malignant lymph node in pelvis, and 25 distant metastases. The detection rates were 27.8% (5/18), 45.0% (27/60), and 66.7% (18/27) for PSA < 0.2 ng/ml, 0.2 ≤ PSA < 0.5 and 0.5 ≤ PSA < 1, respectively. Standard whole-body images showed significantly higher detection rate in the pelvic region in comparison with dynamic phase (p-value=0.039). However, there was no significant difference in 68Ga-PSMA PET positivity between standard and delayed imaging (p-value=0.38). Nevertheless, reviewing the findings in all acquisition phases resulted in better determination of the equivocal lesions leading to higher diagnostic accuracy in 21.9% (23/105) of patients. Trigger PSA and history of antiandrogen treatment were the significant predictor of 68Ga-PSMA PET/CT positivity. **Conclusion:** 68Ga-PSMA PET/CT revealed promising results for early detection of recurrent disease even in PCa patients with PSA ≥0.5 - <1.0 ng/ml. However, it showed limited value in cases with PSA level < 0.5 ng/ml.Stand-alone dynamic imaging seems to have no appreciable additive value in the detection of local recurrences or pelvic lymph node metastases. However, performing multi-phasic 68Ga-PSMA PET/CT imaging may provide additional information leading to better determination of findings in about 20% of PCa patients with low PSA of <1 ng/ml. **References:** None.

309

Thyroid - Rapid Fire Session: Thyroid and Parathyroid

Sunday, October 13, 2019, 11:30 - 12:45 Lecture Hall 115

OP-111

The role of thyroid scintigraphy with Tc-99m in the era of FNAC and molecular markers

S. Sophocleous;
Diagnostic center Agios Therissos, Strovolos, Nicosia, CYPRUS.

Aim/Introduction: In Cyprus with known iodine deficiency, thyroid nodules are found in ~15% of the adults. Recent investigations show that approximately 10% of them are malignant, mainly diagnosed with FNAC. The use of thyroid scintigraphy in the work-up of thyroid nodules has been dramatically decreased during last years. It is only used in cases with low TSH level. Consequently autonomous functioning thyroid nodules (AFNT) with normal TSH are rarely diagnosed and the number of unnecessary performed FNAC on these lesions is unknown. **Materials and Methods:** We investigate the prevalence of AFTN with normal TSH level. Between 01.01.2011 and 31.12.2018, 1505 nuclear scans were performed, in two groups.In the first group we performed 1220 thyroid scan with Tc-99m to investigate the behavior of 2000 nodules found on ultrasound. In the second group, of 285 patients with hyperparathyroidism a dual tracer scan with Sestamibi and Tc-99m was performed. We used the Pertechnetate scan to investigate the behavior of 90 incidentally found nodules on ultrasound. **Results:** On the first group we demonstrated AFNT in 30% of the cases. On the second group AFNT was found in 20/90 (22%). **Conclusion:** Thyroid scan using Tc-99m is able to pick up the AFNT especially in multinodular goiters. The Tc-99m used in the dual tracer technique is a successful method to evaluate the presence of AFNT. In patients with thyroid nodules and normal TSH level to avoid unnecessary FNAC, a thyroid scan must be performed, especially in regions with iodine deficiency. **References:** LITERATURESurvey on thyroid diseases in Cyprus 2005CANCER ARCHIVE(Urojod test 1997, thyrochem 2015). (ATA,ETA). guidelines

OP-112

Is there a role for semiquantitative parameters to characterize incidental focal thyroid uptake on (18)F-FDG PET/CT study?

R. Durmo[1], *D. Albano*[1], *M. Bonacina*[1], *M. Gazzilli*[1], *E. Cerudelli*[1], *F. Dondi*[2], *A. Mazzoletti*[2], *P. Bellini*[2], *F. Bertagna*[2], *R. Giubbini*[2];
[1]*Nuclear Medicine, Spedali Civili di Brescia, Brescia, ITALY,* [2]*Nuclear Medicine, University of Brescia and Spedali Civili di Brescia, Brescia, ITALY.*

Aim/Introduction: Thyroid incidental uptake (TIU) on fluorine-18 fluorodeoxyglucose PET/CT (FDG PET/CT) is defined as an uptake newly detected in patients who underwent imaging for non thyroid diseases. The clinical significance of TIU in FDG PET/CT studies remains controversial. The aim of this large retrospective study was to (a) establish the prevalence and pathological nature of focal TIU, (b) to establish possible metabolic PET parameters cut-off over which a malignant lesion should be suspected and (c) to assess a gender correlation of PET/CT parameters and malignancy. **Materials and Methods:** We retrospectively reviewed a total of 41169 patients who underwent a FDG PET/CT for non thyroid diseases between January 2012 and December 2018. A TIU was diagnosed in 695 (1.6%) patients (159 male; 536 female; average age 64). Of 695 TIU, 184 (26.4%) underwent further investigation to determine the nature of the uptake. We measured the maximum standardized uptake value body weight (SUVmax), SUVmean, lean body mass (SUVlbm), body surface area (SUVbsa), metabolic tumor volume (MTV), total lesion glycolysis (TLG) of TIU. Receiver operating curves (ROC) were calculated to determine optimal cut-off values between malignant and benign lesions. Moreover semiquantitative metabolic parameters between benign and malignant TIU were compare using T-test. **Results:** Fifty-seven (22 male, 35 female) of the 184 patients who underwent ultrasound guided fine-needle aspiration biopsy or thyroidectomy had malignant disease (31%), 98/184 (29 male; 63 female) were benign (53.3%) and 29/184 (8 male, 21 female) were indeterminate (15.7%) at cytological examination in absence of surgery. The ROC derived cut-off was SUVmax=7.27 (sensitivity=78.6, specificity=56.1, AUC=0.713), SUVmean=3.84 (sensitivity=74.5, specificity=54.4, AUC=0.663), SUVlbm=4.8 (sensitivity=77.3, specificity=63.2, AUC=0.719), SUVbsa=2.14 (sensitivity=82.3, specificity 56.1, AUC=0.79), MTV=1.5 (sensitivity=80.6, specificity 41.8, AUC=0.592) and TLG=8.6 (sensitivity=71.4, specificity 45.5, AUC=0.509). A statistical significant difference at T-test was observed between benign and malignant SUVmax, SUVmean, SUVlbm, SUVbsa ($p<0.05$). Metabolic tumor volume (MTV and TLG) were not significant different between malignant and benign lesion. There were not significant statistical difference in the semiquantitative parameters between female and male patients ($p>0.05$). **Conclusion:** There is a relatively high possibility of a malignant lesion in TIU. Semiquantitative parameters could be a useful tool in the assessment of TIU, however there are no safe and definitive cut-off values to discriminate between malignancy and benign lesion. **References:** None.

OP-113

Technetium-99m MIBI Scintigraphy Contribution In The Assessment Of Cold Thyroid Nodule

A. Chehboun[1], *D. Foudil*[1], *Q. Naili*[1], *M. Serir*[2], *L. Bougrina*[3], *L. Griene*[4], *S. E. Bendib*[2], *S. Mimouni-Zerguini*[1];
[1]*Endocrinology Unit-Pierre and Marie Curie Center, Algiers, ALGERIA,* [2]*Radiology Unit-Pierre and Marie Curie Center, Algiers, ALGERIA,* [3]*Cytology Unit-Pierre and Marie Curie Center, Algiers, ALGERIA,* [4]*Hormonology Unit-Pierre and Marie Curie Center, Algiers, ALGERIA.*

Aim/Introduction: Thyroïde nodules are common in endocrine pathology. Relatively, thyroid cancer is less frequent, but affects the thyroid nodule management. The fine needle aspiration biopsy (FNAB) is the gold standard test. Nevertheless, Technetium-99m-MIBI scintigraphy represents a supplementary alternative in difficult cases. Objectives of the study: Evauate the diagnostic value of technetium-99m methoxyisobutylisonitrile (^{99}mTC-MIBI) scintigraphy in the assessment of cold thyroid nodules. **Materials and Methods:** Prospective study of 203 operated patients with nodular goiter (NG). The total number of cold nodules on ^{99}mTc-pertechnetate scans was 380, confirmed by ultrasonography and measured more than 10mm or equal. The thyroid scan was performed 15 min and 120 min after i.v. injection of 555 MBq of ^{99}mTc-MIBI. ^{99}mTC-MIBI uptake in the nodule compared with that in surrounding normal thyroid tissue was scored for both early and delayed images as follows: 0, cold; 1, decreased; 2, equal; 3, increased. Semi-quantitative analysis was performed using a lesion to non-lesion ratio on early (ER) and delayed images (DR). Additionally, a retention index (RI) was calculated using the formula RI= (DR-ER) x 100/ER. The malignancy criteria were a positive retention and increased uptake in the nodule in the early and delayed images. And these data was compared to histopathological results. **Results:** Histopathologically, the nodules were found to be well-differentiated cancer in 29 cases, medullary cancer in 3, poorly differentiated cancer in 5 and benign in 343 cases. None of the malignant nodules were cold on MIBI at the early and delayed images. An increased uptake in both early and delayed images was found in 24 malignant nodules (64.9%) from whom 18 (75%) with a positive retention index. A receiver operating characteristic analysis was performed to determine threshold value for the RI as 1.95 with an area under the curve (AUC) of 0.65. When nodules with increased uptake in both the early and delayed images and a positive retention index were considered as malignant, sensitivity, specificity, positive predictive value, negative predictive value and accuracy were 0.49, 0.96, 0.56, 0.95 and 0.91. The highest sensitivity (0.95) was obtained at multivariate analysis by logistic regression, when both score 2+3 at only delayed images with a positive retention index were considered as malignant **Conclusion:** ^{99}mTC-MIBI scintigraphy could be helpful in the preoperative assessment of thyroid nodules, particularly, those with non diagnostic or indeterminate cytology. **References:** None.

OP-114

Diagnostic performance of technetium-99m (^{99m}Tc) methoxy-isobutyl-isonitrile (MIBI) for differentiation of malignant from benign thyroid nodules with indeterminate or non-diagnostic fine needle aspiration cytology (FNAC)

I. Iakovou, *E. Giannoula, A. Kalaitzoglou, V. Mpalaris, K. Michailo, G. Arsos;*

Academic Dpt Of Nuclear Medicine,
Papageorgiou Hsp, Thessaloniki, GREECE.

Aim/Introduction: Thyroid nodules are common, their prevalence being largely dependent on the identification method ranging from 4-7% when identified by palpation to 20-75% when detecting by ultrasound techniques. FNAC is a part of the diagnostic algorithm to detect or exclude thyroid malignancy. However, there is a large range in the percentage of non-diagnostic and indeterminate FNACs raising the need for new molecular imaging techniques to further characterize thyroid nodules. Although, ^{99m}Tc-MIBI has been initially introduced for myocardial perfusion and parathyroid scintigraphy, it has also a role as a non specific radiopharmaceutical for tumor imaging and in particular for diferentiating malignant from benign lesions in patients with non-diagnostic and indeterminate FNACs of thyroid nodules. The objective of the current work is to evaluate the utility of ^{99m}Tc-MIBI thyroid scintigraphy in differentiating malignant from benign thyroid nodules with indeterminate or non-diagnostic cytology. **Materials and Methods:** We retrospectively evaluated 23 patients affected by thyroid nodules with either indeterminate (16, 69.5%), class III or IV according to the Bethesda system or non-diagnostic (7, 30.5%) cytology. Planar images of the thyroid were acquired 10 and 60 minutes after ^{99m}Tc-MIBI administration, early and late SPECT images were applied when needed and wash-out index (WOI) was used as a quantitative method to evaluate thyroid nodules. All patients underwent total/near total thyroidectomy and scintigraphic results were compared to histological findings. **Results:** Twelve out of 23 patients were diagnosed with differentiated thyroid cancer (DTC) (7 papillary TC and 5 follicular TC) and the remaining with benign adenomas. Malignant nodules were detected by WOI with a threshold of -19%. Therefore, overall sensitivity, specifcity, PPV and NPV were 100%, 63.4%, 66.6% and 100%, respectively. **Conclusion:** In conclusion, semiquantitative ^{99m}Tc-MIBI scintigraphy imaging analysis is a useful tool in differential diagnosis of thyroid nodules with non-diagnostic and indeterminate FNAC. **References:** Thyroid nodules with indeterminate cytology: molecular imaging with ^{99}mTc-methoxyisobutylisonitrile (MIBI) is more cost-effective than the Afirma gene expression classifier. Heinzel A, Müller D, Behrendt FF, Giovanella L, Mottaghy FM, Verburg FA.Eur J Nucl Med Mol Imaging. 2014 Aug;41(8): Select item 23529672Diagnostic performance of (99m)Tc-MIBI scan in predicting the malignancy of thyroid nodules: a meta-analysis. Treglia G, Caldarella C, Saggiorato E, Ceriani L, Orlandi F, Salvatori M, Giovanella L.Endocrine. 2013 Aug;44(1):70-8.

OP-115

Comparison of ^{18}F-fluorocholine PET-CT to ^{11}C-methionine PET-CT for the localisation of hyperfunctioning parathyroid tissue in primary hyperparathyroidism

***C. Mathey**, C. Keyzer, G. Van Simaeys, N. Trotta, S. Lacroix, B. Corvilain, S. Goldman, R. Moreno-Reyes;*
Erasme hospital, Bruxelles, BELGIUM.

Aim/Introduction: To investigate the diagnostic performance of ^{18}F-fluorocholine (FCH) PET/CT compared to ^{11}C-methionine (MET) PET/CT in the localisation of hyperfunctioning parathyroid tissue in patients with primary hyperparathyroidism (pHTP) in case of negative or inconclusive ^{99m}Tc-sestaMIBI SPECT (MIBI) findings. **Materials and Methods:** Fifty-eight patients with biochemical evidence of pHTP and negative or inconclusive MIBI were referred for evaluation by MET and FCH-PET/CT for pre-surgical localisation of hyperfunctioning parathyroid tissue. The PET/CT results were classified into 3 categories (positive, inconclusive or negative) based on the nodular aspect of tracer uptake and the visualisation of corresponding nodules on the CT. The PET/CT results were confronted to the surgical and histopathological findings used as gold standard. **Results:** Fifty-three patients with a median serum calcium level of 2.67+/-0.17 mmol/L and PTH level of 72+/-78 ng/L were included for analysis. FCH PET/CT was positive in 39 patients (74%), inconclusive in 3 (6%) and negative in 11 (21%) compared to 30 (57%), 4 (7%) and 19 (36%) respectively for MET PET/CT. FCH localised 13 additional foci (10 positive and 3 inconclusive) compared to MET. Twenty-six patients (sex F/M ratio16/10) underwent surgery and 31 lesions were resected (22 adenomas, 6 hyperplasia, 2 cancers, and 1 normal gland). FCH PET/CT correctly localised 26 lesions in 24/26 (92%) patients compared to 21 lesions in 20/26 (77%) patients localised by MET PET/CT. Per patient-based sensitivity and PPV were 96% and 96% for FCH vs. 87% and 95% for MET. Per lesion-based sensitivity and PPV were respectively 84% and 93% for FCH vs. 70% and 91% for MET (p=0,0010). At the follow-up, twenty-one (81%) patients were considered cured after the surgery while 3 (12%) patients have a biological recurrence of hypercalcaemia. **Conclusion:** FCH was found significantly more sensitive than MET for lesion detection and localisation of hyperfunctioning parathyroid tissue in case of negative or inconclusive MIBI scan. **References:** None.

OP-116

Added Value Of Fluorocholine (FCH) PET/CT To sestaMIBI Scintigraphy/SPECT (Sc) And Ultrasonography (US) For Preoperatory Detection Of Hyperfuntionning Parathyroid (PT) Glands In Patients With Hyperparathyroidism (HPT) And Chronic Kidney Disease (CKD)

***J. Talbot**[1], J. Zhang-Yin[2], T. Delbot[3], M. Tassart[4], I. Anton[2], S. Balogova[2], F. Montravers[2], P. Haymann[5], S. Périé[6], M. Gauthé[2], S. Gaujoux[7];*
[1]Hopital Tenon, Paris, FRANCE, [2]Hopital Tenon, Nuclear Medicine, Paris, FRANCE, [3]Hopital Cochin, Nuclear Medicine, Paris, FRANCE, [4]Hopital Tenon Radiology, Paris, FRANCE, [5]Hopital Tenon, Explorations fonctionnelles, Paris, FRANCE, [6]Hopital Tenon, ORL, Paris, FRANCE, [7]Hopital Cochin, Endocrine Surgery, Paris, FRANCE.

Aim/Introduction: Since the publication in 2014 of our pilot study about ^{18}F-fluorocholine (FCH)-PET/CT in hyperparathyroidism (HPT), evidence have been widely provided on its ability to detect parathyroid (PT) adenomas in case of primary HPT and non-conclusive sestaMIBI scintigraphy/

SPECT (Sc) and ultrasonography (US). In contrast, there are few data on FCH PET/CT performance when HPT is associated with chronic kidney disease (CKD). Detection of PT hyperplasia predominant in this setting is limited with Sc. We determined the added value of FCH PET/CT in this context. **Materials and Methods:** HPT was diagnosed and parathyroidectomy planned in 74 CKD patients. Based on the results of on-site reading (OR) of Sc and US performed by specialists of PT imaging, the surgeon considered that the location of abnormal PTs was unclear and referred those patients to FCH PET/CT from 2012 until 2018. Masked reading (MR) of Sc and FCH PET/CT was also performed. The equivocal results of readings were considered negative. The standard-of-truth was histology after parathyroidectomy and follow-up to rule out recurrent HPT and consider non-resected PT as normal. **Results:** According to the selection criteria, ORs of Sc and US were both negative in 24 patients, discrepant in 17, only US-positive in 28, only Sc-positive in 5. The overall patient-based positivity-rate (PBPR) was 74% for FCH, 19% for Sc and 55% for US.60 patients (80%) underwent parathyroidectomy; histology of 109 resected glands was hyperplasia in 61, adenoma in 30 and normal in 18. According to OR, gland-based sensitivity was 71% for FCH, 20% for Sc, 44% for US and specificity 99%, 98% and 90%, respectively. Results of MR were sensitivity 77% for FCH, 16% for Sc; specificity 99% and 98%. When Sc and US were both negative, FCH had a PBPR of 63% a gland-based sensitivity of 62% (OR) 76% (MR) and a 100% specificity. When US was positive and Sc negative, gland-based sensitivity was 58% for US vs. 66% (OR) 79% (MR) for FCH. OR gland-based sensitivity according to the KDIGO categories G2, G3, G4-5 respectively, was 67%, 79%, 90% for FCH; 15%, 29%, 40% for Sc and 43%, 50%, 50% for US. **Conclusion:** FCH appeared effective for detecting abnormal PT in patients with HPT and CKD G2 to G5. When Sc and US were non-contributive or discrepant to detect abnormal PTs, FCH PET/CT showed added value, improving the positivity rate and the gland-based sensitivity compared with both Sc and US. **References:** None.

OP-117

Preoperatory ^{18}F-fluorocholine PET/CT performed in patients undergoing hemodialysis locates hyperfunctioning parathyroid glands and may show brown tumours

J. T. Zhang-Yin[1], *S. Perie*[2], *M. Gauthe*[1], *I. Anton*[1], *H. Fessi*[3], *J. Haymann*[4], *P. Ronco*[3], *F. Montravers*[1], *S. Balogova*[1], *J. Talbot*[1];
[1]*Service de Médecine Nucléaire, Hôpital Tenon, Paris, FRANCE,* [2]*Service d'ORL, Hôpital Tenon, Paris, FRANCE,* [3]*Service de Néphrologie hémodialyse, Hôpital Tenon, Paris, FRANCE,* [4]*Service de l'Exploration rénale fonctionnelle, Hôpital Tenon, Paris, FRANCE.*

Aim/Introduction: In patients undergoing hemodialysis (HD), nuclear functional imaging has the advantage to display and localize orthotopic and ectopic hyperfunctioning parathyroid glands (PT) prior to initial parathyroidectomy (PTX) and in case of post-surgical recurrence. In primary hyperparathyroidism (HPT), ^{18}F-fluorocholine (FCH) PET/CT has shown superior performance compared to sestaMIBI scintigraphy or SPECT/CT. No data on its diagnostic performance are currently available in HPT of HD. Brown tumours (BT) are rare skeletal anomalies that occur in case of prolonged HPT. They result from increased osteoclastic activity, often related to chronic kidney failure. We also aimed to determine the ability of FCH PET/CT to detect BT in HPT of HD. **Materials and Methods:** We included in this retrospective study all HPT patients on HD referred to our center between 2013 and 2018. FCH PET/CT was acquired on the neck and the thorax; if bone lesions were visible on PET or on CT, a complementary whole-body acquisition was performed. **Results:** In 41 patients on HD (13 with kidney transplant), 50 FCH PET/CTs were performed (16 for recurrent HPT post-PTX). 36 patients were then (re)operated. Initial PTX in 25 patients found 72 abnormal PT of which 62 were FCH-positive (detection-rate DR=86%); reoperation in 11 patients found 11 abnormal PT all FCH-positive (DR=100%). In 6 patients, were also found multiple osteolytic lesions with substantially increased FCH uptake, among them, 3 had more than 5 osteolytic lesions. BT was diagnosed based on histology in 2 patients, in 1 patient on the post-PTX change of the bone lesions on CT from osteoclastic to osteoblastic scars, and on the typical aspect of BT on CT in the last 3 patients. **Conclusion:** In patients on hemodialysis with hyperparathyroidism, FCH PET/CT showed a high detection-rate for abnormal parathyroid glands, particularly in case of post-PTX recurrence. This complete success in case of recurrent hyperparathyroidism may be explained by the increased metabolism of the gland which was left alone after initial PTX. Furthermore, brown tumours showed a substantially increased uptake of FCH. In this context, brown tumours must be considered among the causes of osteolytic lesions with increased FCH uptake. Thus, FCH PET/CT represents a powerful "One-stop-shop" examination, since it appears to be very sensitive for preoperatory detection of the abnormal parathyroid glands, and since it can guide parathyroidectomy, the most effective option for correcting the metabolic trouble of the bone revealed by high FCH uptake and responsible for brown tumours. **References:** None.

OP-118

Contribution of dual time point F-18 fluorocholine PET/CT for challenging pre-operative parathyroid imaging in primary hyperparathyroidism

L. M. Vija[1], *E. Gabiache*[2], *P. Pascal*[1], *S. Kanoun*[2], *L. Dierickx*[2], *C. Renaud*[3], *B. Jean*[3], *B. Herbault-Barres*[4], *S. Brillouet*[5], *S. Grunenwald*[6], *M. Vialon*[6], *P. Caron*[6], *F. Courbon*[2];
[1]*Nuclear Medicine,Institut Universitaire de Cancerologie IUCTO, ICR, Toulouse, FRANCE,* [2]*Nuclear Medicine, Institut Universitaire de Cancerologie IUCTO, ICR, Toulouse, FRANCE,* [3]*Thoracic Surgery, University Hospital-CHU, Toulouse, FRANCE,* [4]*Pathology, Institut Universitaire de Cancerologie IUCTO, ICR, Toulouse, FRANCE,* [5]*Institut Universitaire de Cancerologie IUCTO, ICR, Toulouse, FRANCE,* [6]*Endocrinology, University Hospital-CHU, Toulouse, FRANCE.*

Aim/Introduction: When cervical ultrasound and Tc-99m MIBI scans are not informative, second-line imaging should

be considered for preoperative localization of pathologic parathyroid glands. Dual time point F-18 fluorocholine PET/CT (FCH PET/CT) combines molecular (PET) and morphological (CT) information with uptake modifications within time, increasing sensitivity for parathyroid gland detection. However, the optimal time point for image acquisition for FCH PET/CT remains under debate. We evaluate image acquisition time point for the localization of pathologic parathyroid glands on FCH PET/CT as well as detection rates and sensitivities in patients with primary hyperparathyroidism **Materials and Methods:** Patients with primary hyperparathyroidism explored with a dual time point FCH PET/CT (at 10 and 60 minutes post injection) and with post-operative histological parathyroid analysis have been prospectively included in the study. Early versus late acquisitions have been analyzed both on visual and semi-quantitative analysis. **Results:** Thirty-seven patients (13 men, 24 women, mean age 51 years (20-80) with primary hyperparathyroidism [serum calcium 2.79 mmol/l (2.4-2.91), PTH levels 108.6 ng/L (57-190)] had dual time FCH PET/CT, 34 of them after a negative or discordant US/Tc-99m-sestaMIBI scans. On visual analysis, uptake of pathologic parathyroid glands was similar on early versus late FCH PET/CT in 27 patients, in 1 patient early image acquisition was more intense, whereas in 8 patients (22 %) uptake was better visible on late acquisition. There was a tendency on FCH uptake increase in pathologic parathyroid glands on late images ($p = 0.24$), with a significant increase of parathyroid to thyroid ratio on semi quantitative analysis (SUVmax lesion/ thyroid; $p = 0.01$). On a per-lesion analysis, FCH-PET/CT sensitivity, specificity, positive and negative predictive values were 86 %, 33 %, 96 % and 11 % respectively. On a per-patient analysis, Se, Sp, PPV, NPV were 82 %, 14 %, 86 % and 11 %. FCH-PET/CT imaging made to remove successfully pathologic glands in 34 patients (adenomas $n = 31$, hyperplasia $n = 3$), with a global cure rate of 92 % and cure rate related to FCH contribution of 65 %. **Conclusion:** With FCH-PET/CT in second line imaging of primary hyperparathyroid patients, most pathologic parathyroid glands are adequately visualized on early imaging; for several patients, parathyroid adenomas are better visualized on late time points. Therefore in pre-operative parathyroid characterization, FCH-PET/CT with dual time acquisition remains a useful option when first-line imaging and early time FCH PET/CT are not informative. **References:** None.

YDF1

EANM Young Daily Forum

Sunday, October 13, 2019, 13:00 - 14:30 Lecture Hall 113

YDF-1

How to Meet More Great People at the EANM Congress

R. Sheppard;
EANM Moderator, London, UNITED KINGDOM.

401

CME 3 - Radiation Protection + Dosimetry Committee: Metrological Aspects on the Implementation of Dosimetry in Radionuclide Therapy

Sunday, October 13, 2019, 14:30 - 16:00 Auditorium

OP-119

Introduction

K. Sjögreen-Gleisner;
Lund University, Medical Radiation Physics, Lund, SWEDEN.

OP-120

Requirements for the Dosimetry-Guided, Multi-Center Clinical Trial SELIMETRY

J. Wadsley;
Weston Park Cancer Centre, Sheffield, UNITED KINGDOM.

OP-121

Priorities of Dosimetry in Clinical Radionuclide Therapy - The Italian Agreement Between National Nuclear Medicine and Medical Physics Associations

C. Chiesa;
Nuclear Medicine, Foundation IRCCS Istituto

Nazionale Tumori, Milan, ITALY.

OP-122

European Initiatives to Ensure Traceable Dosimetry Across Countries and Centers

M. Lassmann;
Universitaetsklinikum Wuerzburg, Klinik fuer Nuklearmedizin, Würzburg, GERMANY.

402

Joint Symposium 5 - Oncology & Theranostics Committee / EORTC: The Future of Medical Imaging in Precision Medicine

Sunday, October 13, 2019, 14:30 - 16:00 Lecture Hall 311

OP-123

The Future of Theranostic Radionuclide Approaches

U. Haberkorn;
Heidelberg University Hopsital, Department of Nuclear Medicine, Heidelberg, GERMANY.

OP-124

Companion Diagnostics in Drug Development

G. van Dongen;
Amsterdam University Medical Center, Department of Radiology & Nuclear Medicine, Amsterdam, NETHERLANDS.

OP-125
Total Body PET-CT for Pharmacokinetic Analysis
S. Vandenberghe;
University of Ghent, Department of Electronics and information systems, Gent, BELGIUM.

OP-126
The Use of Artificial Intelligence in Precision Medicine
I. Buvat;
Unité Imagerie Moléculaire In Vivo, CEA/DRF/Service, Hospitalier Frédéric Joliot, Orsay, FRANCE.

OP-127
Panel Discussion

403

Joint Symposium 6 - Translational and Molecular Imaging Therapy + Cardiovascular + Inflammation & Infection Committee / AHA: Imaging Inflammation as Major Determinant of Cardiovascular Diseases ? New Tracers and Clinical Applications

Sunday, October 13, 2019, 14:30 - 16:00 Lecture Hall 312

OP-128
New Concepts, New Targets
J. Thackeray;
Department of Nuclear Medicine, Hannover Medical School, Hannover, GERMANY.

OP-129
SPECT and PET in Cardiac Infection and Inflammation
C. Lauri;
Department of Nuclear Medicine and Molecular Imaging, "Sapienza" University of Rome. -Sant'Andrea Hospital, Rome, ITALY.

OP-130
PET Imaging of Inflammatory Alterations in Ischaemic and Non-Ischaemic Disease
F. Caobelli;
Department of Nuclear Medicine, Universitätsspital Basel, Basel, SWITZERLAND.

OP-131
A Clinical Perspective
V. Taqueti;
Cardiac Stress Laboratory, Brigham and Women's Hospital, Harvard Medical School, Boston, MA, UNITED STATES OF AMERICA.

OP-132
Discussion

404a

Mini Course 1 - Technologist Committee: Research Methodology

Sunday, October 13, 2019, 14:30 - 15:30 Lecture Hall 117

OP-133
Research Methodology for Technologists
C. Malamateniou;
Division of Midwifery and Radiography, City University of London, London, UNITED KINGDOM.

405

M2M - Parallel Session: Antibody-Based Radionuclide Therapy

Sunday, October 13, 2019, 14:30 - 16:00 Lecture Hall 111

OP-134
Targeted alpha therapy with ^{212}Pb-NNV003 is efficient in treatment of ibrutinib-resistant chronic lymphocytic leukaemia in preclinical models
A. Saidi[1], H. Heyerdahl[2], A. Maaland[2], J. Torgue[3], J. Dahle[2];
[1]Orano Med SAS, Paris La Défense, FRANCE, [2]Nordic Nanovector ASA, Oslo, NORWAY, [3]Orano Med LLC, Plano, TX, UNITED STATES OF AMERICA.

Aim/Introduction: Approximately 90,000 cases of chronic lymphocytic leukaemia (CLL) and non-Hodkgin's lymphoma (NHL) are expected annually in the US. Standard of care includes chemotherapy combined with anti-CD20 antibodies and Bruton's tyrosine kinase inhibitor ibrutinib. While these therapies are initially effective, most patients inevitably relapse. CD37 is under clinical evaluation as a therapeutic target for B-cell malignancies. Alpha-emitting radionuclides have demonstrated potential for targeted therapies due to the short alpha track, causing localized cytotoxicity. Orano Med and Nordic Nanovector developed a targeted alpha therapy combining the CD37-specific antibody NNV003 with the alpha-particle-emitting radioisotope ^{212}Pb. We previously reported that ^{212}Pb-

NNV003 is effective in disseminated animal models using CD37-expressing NHL and CLL cell lines (1). Here we compare the efficacy of ^{212}Pb-NNV003 with ibrutinib in a disseminated mouse model using the ibrutinib-resistant cell line MEC-2. **Materials and Methods:** The efficacy and tolerability of a single dose ^{212}Pb-NNV003 treatment were evaluated in disseminated models using human CLL (MEC-2) and Burkitt's lymphoma (Daudi) cells. Comparison to therapeutic doses of ibrutinib was investigated in the MEC-2 model. R2G2 or CB17-SCID mice were injected intravenously with 2.5×10^6 MEC-2 or 10×10^6 Daudi cells on day 0, followed by intravenous injection of ^{212}Pb-NNV003 (2.5, 5 or 7.5 µCi in Daudi model and 5, 10, 15 or 20 µCi in MEC-2 model) or daily oral administration of ibrutinib (12.5 or 25 mg/kg) starting on day 2 (n=10-12 per group). ^{212}Pb-cetuximab (unspecific isotype control), unlabelled NNV003 and NaCl were used as controls. **Results:** ^{212}Pb-NNV003 treatments resulted in survival of 67-91% of the mice 26 weeks after Daudi cell injection, and 30-90% of the mice 27 weeks after MEC-2 cell injection. Control mice presented a median survival of 7-8 weeks in the Daudi model and 4.9-9.3 weeks in the MEC-2 model. ^{212}Pb-NNV003 showed a significantly prolonged survival compared to ibrutinib and controls ($p < 0.0001$). 15 and 20 µCi ^{212}Pb-NNV003 resulted in survival of 100% and 70% of mice 15 weeks after MEC-2 cell injection. Ibrutinib treated animals presented a median survival of 4.3-4.4 weeks, comparable to the NNV003 and saline groups (4.1 and 4.4 weeks). Mice receiving ^{212}Pb-cetuximab presented a median survival of 7 weeks. **Conclusion:** The study shows that a single injection ^{212}Pb-NNV003 is safe and effective for the treatment of CD37 positive CLL and NHL in preclinical models, with promising efficacy in an ibrutinib-resistant CLL model. Further clinical testing is warranted. **References:** 1. Saidi et al., Blood, 2018, 132 Suppl1:4422

OP-135

Preclinical study with ^{212}Pb-rituximab as an alpha-radioimmunotherapy for Non-Hodgkin's Lymphoma

I. Quelven[1,2], *J. Monteil*[1,2], *A. Saidi*[3], *J. Torgue*[4], *M. Cogne*[2], *S. Durand-Panteix*[2];
[1]*Limoges University Hospital, Limoges, FRANCE,* [2]*CRIBL, CNRS UMR 7276, INSERM 1262, Limoges, FRANCE,* [3]*Orano Med SAS, Paris, FRANCE,* [4]*Orano Med LLC, Plano, TX, UNITED STATES OF AMERICA.*

Aim/Introduction: Non-Hodgkin's Lymphoma (NHL) is the 8thmost commonly diagnosed cancer in men and 11thin women. Despite significantly improved response rate and survival, many relapses are observed. Radioimmunotherapy (RIT) is an emerging second line option for NHL. RIT with beta-emitters (Bexxar®, Zevalin®) has been developed but presented hematological toxicity. The development of RIT with alpha-emitters is attractive because of the high linear energy transfer (LET) and short path length of alpha-radiation in tissues, resulting in higher tumor cell killing and lower toxicity to surrounding tissues. In this study, we investigated the potential of alpha-RIT with ^{212}Pb-rituximab. ^{212}Pb is used as an in vivo generator of the high-energy alpha-particle emitting radionuclide ^{212}Bi (1). **Materials and Methods:** Biodistribution of $^{203/212}$Pb-rituximab was evaluated in vivo by SPECT-CT imaging and post-mortem. Acute toxicity studies (survey, hematological and renal parameters) were performed in order to determine the safety profile and safe administration doses. To evaluate tumor biodistribution and in vivo efficacy of ^{212}Pb-rituximab, a mice lymphoma model was used: 8-week-old C57BL/6JRj mice were injected intravenously with 25 x 10^3 EL4-hCD20-Luc cells (mouse lymphoma cell line). Mice were treated either 11 days or 20 to 30 days post-cell injection with 277.5 kBq ^{212}Pb-rituximab or controls (including 277.5 kBq ^{212}Pb-irrelevant mAb, cold rituximab and saline). Therapeutic efficacy was monitored by bioluminescence imaging (BLI) and overall survival. **Results:** ^{212}Pb-rituximab biodistribution studies shows about 20% ID/g tumor uptake and that liver and spleen are the organs at risk. Acute toxicity was observed at 555 kBq with a reduced mice survival. Transient and reversible hematological toxicity was observed from 277.5 kBq treatment dose. Mice treated with ^{212}Pb-rituximab 20 to 30 days post cell injection (BLI-detectable tumors) exhibited marked tumor growth inhibition compared to controls, with a median survival of 28 days for ^{212}Pb-rituximab-treated group instead of 9 to 13 days for control groups. Strongly improved median survival (above 105 days) was observed for mice treated with ^{212}Pb-rituximab 11 days after cell injection, whereas median survival was reached 36.5 days post-treatment for ^{212}Pb-irrelevant mAb, 64 days for cold rituximab and 27 days for saline control. **Conclusion:** These results show ^{212}Pb-rituximab efficacy on a murine syngeneic lymphoma model with significant tumoral regression and increased survival. This study highlights alpha-RIT potency in B-NHL treatment. **References:** (1) K. Yong and M.W. Brechbiel, Dalton Trans. 2011

OP-136

Preclinical evaluation of CEA-PRIT, a novel pretargeted alpha therapy regimen for treatment of CEA-positive tumours with ^{212}Pb

S. Frost[1], *A. Pichard*[1], *A. Haas*[2], *H. P. Grimm*[3], *A. Mouchotte*[1], *A. Colmont*[1], *O. Freytag*[1], *J. Torgue*[4], *S. Colombetti*[1], *C. Klein*[1], *P. Umaña*[1];
[1]*Roche Pharma Research and Early Development, Zürich, SWITZERLAND,* [2]*Roche Pharma Research and Early Development, Penzberg, GERMANY,* [3]*Roche Pharma Research and Early Development, Basel, SWITZERLAND,* [4]*Orano Med LLC, Plano, TX, UNITED STATES OF AMERICA.*

Aim/Introduction: Pretargeted radioimmunotherapy (PRIT) optimizes delivery of radioactivity to malignant cells, by allowing tumour-targeting bispecific antibodies (BsAb) to distribute within target tissue before administering a small radiolabelled molecule that efficiently binds to pretargeted sites or is rapidly excreted. This dissociation of targeting and irradiation can minimize the exposure of healthy tissues while increasing the tumour absorbed dose, especially using short-lived radionuclides such as ^{212}Pb ($t_{1/2}$ = 10.6 h), an in vivo generator of the highly cytotoxic alpha emitter ^{212}Bi ($t_{1/2}$ = 60.6 min). Here we

describe CEA-PRIT, a novel pretargeted alpha therapy regimen using a CEA-DOTAM bispecific antibody and ^{212}Pb for PRIT of carcinoembryonic antigen (CEA)-positive tumours. **Materials and Methods:** Mice with subcutaneous CEA-expressing BxPC3 xenografts were injected with a pretargeting BsAb with specificity for CEA and 1,4,7,10-Tetrakis(carbamoylmethyl)-1,4,7,10-tetraazacyclododecane (DOTAM). Circulating BsAb was neutralized after 4-7 days using a dextran-based clearing agent; 2-24 h later, the radiolabelled effector molecule ^{212}Pb-DOTAM was injected. The three-step PRIT cycle was repeated twice with 2 weeks between radioactive injections for efficacy assessment. Tumour volumes were estimated through calipering, and the biodistribution assessed 5 min-48 h after the radioactive injection. **Results:** A pretargeting BsAb was generated that binds bivalently with pM affinity to CEA and fM affinity to Pb-DOTAM. A single CEA-PRIT cycle of 0.37 or 1.11 MBq significantly delayed tumour growth compared with control groups in an activity-dependent manner in the BxPC3 model. Three cycles of 0.37 or 1.11 MBq prolonged tumour control further, with the strongest inhibition demonstrated after three cycles of 1.11 MBq. However, 1.11 MBq caused significant weight loss, whereas 0.37 MBq was well tolerated. Subsequent studies using 0.74 MBq demonstrated good multiple-cycle tolerability, and dosimetry of the optimized regimen confirmed the ^{212}Pb-targeting specificity to tumour compared with normal tissues; the tumour uptake reached 43% of the injected activity per gram of tissue (IA/g) at 6 h p.i., whereas kidneys had a maximum of 12% IA/g 5 min p.i., decreasing to 4% IA/g 2 h p.i. In vivo proof-of-concept was also demonstrated using other targets, such as HER2. **Conclusion:** The preclinical studies demonstrated therapeutic efficacy of the novel CEA-PRIT approach, combining the high cytotoxicity and short half-life of ^{212}Pb/^{212}Bi with highly efficient and specific tumour targeting for safe treatment of CEA-expressing tumours. Translation of the described CEA-PRIT scheme to a phase I trial is foreseen in the near future based on these encouraging results. **References:** None.

OP-137

^{212}Pb-labelled monoclonal antibodies: A PBPK model for treatment planning in Targeted Alpha-particle Therapy (TAT)

N. Zaid, *N. Begum, P. Kletting, A. Beer, G. Glatting;*
Department of Nuclear Medicine, Ulm Universiy, Ulm, GERMANY.

Aim/Introduction: There is growing interest in ^{212}Pb-labelled monoclonal antibodies (mAbs) as promising targeted in vivo generators of alpha particles. A first physiologically-based pharmacokinetic (PBPK) model for describing the pharmacokinetics and dosimetry is presented as a step towards treatment planning in Targeted Alpha-particle Therapy (TAT). **Materials and Methods:** A compartmental model for tumour and dose limiting organs, e.g. kidneys (0.33 l) and plasma (2.75 l) was developed and implemented in the modelling software SAAMII. The model was constructed based on physiological, chemical and physical properties with parameter values from the literature. The dose of bound and unbound radiopharmaceuticals and free radionuclides in the tumour (0.02 l), kidneys and plasma were calculated for various injected amounts and activities. The contribution to dose and equivalent dose in the investigated organs were calculated for each radionuclide by using a weighting factor of 5 for alpha particles. The required activities and amounts were estimated for a prescribed tumour absorbed dose of 30 Gy for different molar activities. The excretion of free ^{212}Bi after being released from the chelator due to a preceding disintegration was studied by including a physiological kidney model[1]. Kidney parameter values were estimated in a separately developed excretion model for stable Bi (208.9 u). **Results:** The prescribed dose in tumour of 30 Gy was achieved by an injection of 82 MBq ^{212}Pb with a molar activity of 10.9 TBq/µmol; the corresponding dose to kidneys and plasma were 8 and 0.7 Gy. The relative contributions of ^{212}Pb_β, ^{212}Bi_β, ^{212}Bi_α, ^{208}Tl_β and ^{212}Po_α to absorbed dose in the tumour were 8%, 14%, 21%, 3% and 54%, to the kidneys 8%, 13%, 21%, 6% and 52%, and to the plasma 8%, 13%, 20%, 7% and 52%, respectively. Alpha particle emissions contribute more than 88% to the equivalent doses in organs of investigation. For molar activities of 1.1 and 0.1 TBq/µmol, the absorbed dose in both plasma and kidneys increased by 1% and 8% for the fixed prescribed tumour dose. **Conclusion:** The developed basic ^{212}Pb-labelled mAbs model allows the simulation of the biokinetics of radiolabelled and unlabelled mAbs and released free radionuclides in the body. Thus, it holds promise to predict optimal dosing regimens (activity and amounts) for prescribed doses to tumours using different radiopharmaceuticals. Ongoing improvements, e.g., inclusion of other organs, degradation, microdosimetry, will allow generating hypotheses for optimal treatment planning using ^{212}Pb-labelled species. **References:** Kletting et al., J Nucl Med 2016;57:503-508.

OP-138

In vitro and in vivo evaluation of bismuth-213 labeled anti-HER2 nanobodies

Y. Dekempeneer;
Vrije Universiteit Brussel, Brussel, BELGIUM.

Aim/Introduction: This study investigates a novel targeted therapy which combines the α-emitter bismuth-213 (^{213}Bi) and HER2-targeting nanobodies (Nbs) to selectively kill HER2^{pos} metastases in breast- and ovarian cancer. The use of nanobodies as vehicles in TAT is promising due to their excellent in vivo properties, high target affinity and specificity, fast diffusion and clearance kinetics. Moreover, Nbs show good tumor penetration due to their small size. The aim of this study is to develop and evaluate the stability up to 105 min after labeling, in vitro binding characteristics and cytotoxicity on HER+ SKOV-3 cells, and the in vivo biodistribution of [^{213}Bi]DTPA HER2 targeting Nb. **Materials and Methods:** First, a ^{213}Bi-labeled-Nb was developed, using p-SCN-Bn-CHX-A**″**-DTPA as bifunctional chelator. Due to the 46 min half-life of ^{213}Bi, the ^{213}Bi labeling reaction and quality control of the resulting radioconjugate

was performed in a very short time frame to limit significant radioactivity losses. In vitro saturation binding assay, clonogenic assay, IncuCyte® live cell imaging and double strand break ex vivo immunofluorescence staining were performed on HER2^{pos} cells to determine the affinity and cytotoxicity of [^{213}Bi]DTPA-Nb. Its biodistribution and maximum tolerated dose was analyzed in relevant mouse models. **Results:** Under optimized labeling conditions, the [^{213}Bi]DTPA-Nb remained stable up to 100 min with a radiochemical purity ≥ 95%. In vitro, [^{213}Bi]DTPA-Nb bound HER2^{pos} SKOV-3 cells in a HER2-specific way. [^{213}Bi]DTPA-anti-HER2Nb resulted in a high cytotoxic effect significantly different from the [^{213}Bi]DTPA-controlNb. High tumor uptake was reached 15 min after injection. Extremely low uptake values were observed in normal tissues at all time points. [^{213}Bi]DTPA-Nb was excreted via the kidney into the urine, leading to a kidney retention of the radioconjugate of 59.9±5.1 %ID/g at 60 min post injection. Coinfusion of 150 mg/kg gelofusine resulted in a 2-fold reduction of the kidney retention at all time points. The injection of [^{213}Bi]DTPA- control Nb resulted in 0.3±0.03 %ID/g tumor uptake 60 min post injection, which was confirmed by a significant decrease in double strand DNA damage compared to the [^{213}Bi]DTPA-anti-HER2Nb injected group. **Conclusion:** Here we describe for the first time the successful labeling of an anti-HER2 Nb with the α-particle emitter ^{213}Bi, using a DTPA derivative, resulting in high yields with excellent preservation of affinity for its HER2 target, high in vivo stability and high tumor-to-background ratios. This study shows that [^{213}Bi]DTPA-Nb is a promising new radioconjugate for targeted α-particle therapy and supports its further development. **References:** None.

OP-139

^{177}Lu-NNV003 Shows Potential Synergy with Venetoclax or Olaparib In Diffuse Large B-cell Lymphoma (DLBCL) and Mantle Cell Lymphoma (MCL) Cell Lines

A. H. Repetto-Llamazares[1], *A. F. Maaland*[1,2], *M. M. Malenge*[1,2], *H. Heyerdahl*[1], *S. Patzke*[1,3], *T. Stokke*[3], *A. Hansen Ree*[2], *A. Kolstad*[4], *J. Dahle*[1];
[1]*Nordic Nanovector ASA, Oslo, NORWAY,* [2]*Institute of Clinical Medicine, University of Oslo, Oslo, NORWAY,* [3]*Institute for Cancer Research, Oslo University Hospital, Oslo, NORWAY,* [4]*Department of Oncology, Oslo University Hospital, Radiumhospitalet, Oslo, NORWAY.*

Aim/Introduction: The next generation anti-CD37 radioimmunoconjugate ^{177}Lu-NNV003 (Humalutin®) has previously shown therapeutic activity in preclinical models of non-Hodgkin lymphoma by inducing DNA damage, antibody dependent cellular cytotoxicity and apoptosis in the targeted cells. In this study we have combined ^{177}Lu-NNV003 with an inhibitor of DNA damage repair, the poly(ADP-ribose) polymerase (PARP) inhibitor olaparib, or the anti-apoptotic protein BCL-2 inhibitor venetoclax to test for potentially synergistic interactions in treatment of DLBCL and MCL cell lines. **Materials and Methods:** The effect of the combination of ^{177}Lu-NNV003 with venetoclax or olaparib in DLBCL cell lines DOHH2, SUDHL-4, U2932 and WSU-DLCL2, and MCL cell lines Granta519 and Rec-1 was evaluated by the Ray Design Methodology. Five rays per cell line were defined (two rays corresponding to the drugs alone and 3 rays with their combination). Cells were treated for 24 hours and their metabolic activity was measured at days 3, 4 and 5 after seeding. The interaction index for each ray (I_r) was calculated using the Loewe additivity model with 10% threshold, where $I_r < 0.9$ is synergistic, $0.9 < I_r < 1.1$ is additive and $I_r > 1.1$ is antagonistic interaction. In addition, RNA was extracted from all cell lines 24 hours after treatment with single treatments or drug combinations and mRNA sequenced using an Illumina TruSeq stranded mRNA kit. **Results:** Values of I_r varied between 0.3 and 1.8 depending on cell line, ray and day of measurement. Synergism was evident in all cell lines for at least one ray and one day of measurement, except for the combination of ^{177}Lu-NNV003 and venetoclax in U2932 and DOHH2 cells, where additivity/antagonism was observed in all measurements. The cell lines showing highest synergy were WSU-DLCL2 for both combinations and U2932 for the combination of ^{177}Lu-NNV003 with olaparib. Here, $I_r < 0.9$ was found for most rays and days of measurement. Differences in sensitivity observed between cell lines were not correlated to sensitivity to BH3 (DLBCL) or ATM status (MCL) as described in the literature. Hence mRNA sequencing data will be explored for potential differential gene expression (DGE) signatures. **Conclusion:** We have shown that ^{177}Lu-NNV003 can act synergistically with venetoclax or olaparib in DLBCL and MCL cell lines. DGE analysis may identify gene expression signatures predictive of synergy. If these findings can be translated to the clinic, it will allow identification of patients that could benefit from the combination of these drugs. **References:** None.

OP-140

^{90}Y-NM600 improves survival in a clinically relevant immunologically cold melanoma model when combined with immunotherapies

J. Grudzinski, *R. Patel, R. Hernandez, R. Brown, L. Zangl, P. Carlson, P. Sondel, J. Weichert, Z. Morris;*
University of Wisconsin, Madison, WI, UNITED STATES OF AMERICA.

Aim/Introduction: We have previously shown that 1.85 MBq of ^{90}Y-NM600, calculated to deliver 2.5 Gy to the tumor, enhances tumor response to external beam radiotherapy (XRT) and both immune checkpoint inhibition and in situ vaccine at both irradiated and distant unirradiated B78 melanoma tumors. The aim of this study is to investigate whether ^{90}Y-NM600 can enhance efficacy in a more clinically relevant melanoma cancer model consisting of a primary, an occult secondary, and micrometastases. **Materials and Methods:** Mice with both large primary (200 mm^3) and occult secondary (non-palpable on day of treatment) B78 heterotopic melanoma tumors were injected IV with B16 melanoma cells on the day of treatment to create micrometastases. The primary tumor was subsequently irradiated with 12 Gy of XRT, which is required to establish an in-situ vaccine (IS), and the mice were injected IV with enough

^{90}Y-NM600 (TRT) to deliver 2.5 Gy of absorbed tumor dose. On Days 4, 7, and 10, mice were injected IP with anti-CTLA4 and PD1 (ICI). Day 6 through Day 10, the primary tumors were injected intratumorally with IL2 + anti-GD2 mAb (IS). Mice were monitored out to Day 60 for survival and tumor volume. Mice who were complete responders (CRs) were re-challenged with B78 cells on the flank at Day 90. Treatment groups consisted of TRT, ICI, or IS alone, or in combination with each other. Reason for death was assessed at Day 90. **Results:** All the mice within the control, TRT, IS, and TRT + ICI groups were dead by Day 90. Eighty-percent of the control group succumb to metastases and 20% succumb to the primary; while, 100% of the mice within the TRT only and TRT + ICI groups died from the primary. ICI was the only monotherapy that had survivors with 20% of the mice still alive at Day 90. In the ICI alone group, 60% died from the primary and 20% died from the metastases. However, 60% of the mice who received TRT + IS and 50% of the mice who received ICI + IS were still alive. Surprisingly, the mice who received TRT + ICI + IS all survived. Of these mice that survived, 83% were tumor free and rejected a re-challenge of B78 cells. **Conclusion:** Low dose ^{90}Y-NM600 can improve response to both local (IS) and systemic (ICI) immunotherapy treatments in "cold" tumors that normally do not respond to immune checkpoint blockade alone. **References:** None.

OP-141

Biodistribution and Therapeutic Efficacy of ^{211}At-labelled Farletuzumab in a Disseminated Ovarian Cancer Mouse Model

S. Palm[1], *E. Aneheim*[1], *T. Bäck*[1], *A. Hallqvist*[1], *R. Hultborn*[1], *L. Jacobsson*[1], *H. Jensen*[2], *S. Lindegren*[1], *P. Albertsson*[1];
[1]*University of Gothenburg, Gothenburg, SWEDEN,*
[2]*Rigshospitalet, Copenhagen, DENMARK.*

Aim/Introduction: Alpha-emitter astatine-211 ($t_{½}$ = 7.2h), labelled to high-affinity monoclonal antibody MX35, has previously shown promise as an adjuvant treatment of ovarian cancer, where any remaining microscopic tumors are typically contained within the peritoneal lining. Here we explore the use of farletuzumab, a mAb with a more complex antigen targeting and release pattern. The rationale was to see if a mAb with a seemingly multi-compartmental binding characteristics could be beneficial for our presumed clinical setting, where both cancer single cells and micrometastases up to ~1 mm need to be eradicated. The aim was to evaluate the biodistribution and therapeutic effect of ^{211}At-farletuzumab in in-vitro and pre-clinical experiments and, using our models for radiation dosimetry, to translate the findings to expected results in the clinical setting. **Materials and Methods:** Anti-human FOLR1 farletuzumab was labelled with ^{211}At and used for biodistribution and therapeutic efficacy studies. Control groups included ^{211}At-labelled MX35 and rituximab. For biodistribution, mice (n=28) were inoculated subcutaneously with 1×10^{7} NIH:OVCAR-3 cells in 0.1 mL, in the scapula region. Four weeks thereafter, the longest axes of the tumors were 5-7 mm, and mice were i.v. injected (0.1 mL in the tail vein) radiolabeled antibodies for biodistribution. Mice were administered either 450 kBq ^{211}At-farletuzumab (n=16); or with a combination of 150 kBq ^{125}I-trastuzumab and 450 kBq ^{211}At-MX35 (n=12). At 1, 3, 10 and 22 h, mice were sacrificed and tumors and organs weighted and measured for radioactivity in a gamma-well counter. Therapeutic efficacy was investigated on 63 mice sorted into four groups. All mice were inoculated i.p. with 2×10^{6} NIH:OVCAR-3 cells in a single-cell suspension. Specific or control (sham) treatments, all in 0.7 mL, were delivered i.p. twelve days after cell inoculation. A specific group (A; n=22) received 0.7 MBq ^{211}At-Farletuzumab together with trace amounts (10 kBq) of ^{125}I-Rituximab. One control group (B; n=22) received 0.7 MBq irrelevant ^{211}At-Rituximab. Another control (C; n=11) received unlabelled farletuzumab; and one group (D; n=8) received PBS only. **Results:** The biodistribution of ^{211}At-farletuzumab was similar to that with ^{125}I as radiolabel, and also to that of ^{211}At-labeled MX35 antibody. The tumor-free fraction (TFF) of the three control groups of mice (PBS, unlabeled farletuzumab, and irrelevant ^{211}At-rituximab) was 12%, 9% and 14%, respectively. TFF after treatment with ^{211}At-farletuzumab was 91%. **Conclusion:** The current pre-clinical work-up of intraperitoneal therapy with ^{211}At-farletuzumab, delivered at clinically relevant ^{211}At-mAb radioactivity concentrations and specific activities, warrant further clinical testing. **References:** None.

406

Do.MoRe - Parallel Session: Image Reconstruction

Sunday, October 13, 2019, 14:30 - 16:00 Lecture Hall 112

OP-142

Quantitative and Clinical Evaluation of a Block-Sequential Regularized Expectation Maximization Reconstruction Algorithm for 18F-FDG PET-CT in Oncology

E. Tragardh[1], *D. Minarik*[1], *H. Almquist*[2], *U. Bitzén*[2], *S. Garpered*[1], *E. Hvittfelt*[1], *B. Olsson*[2], *J. Oddstig*[2];
[1]*Skåne University Hospital, Malmö, SWEDEN,*
[2]*Skåne University Hospital, Lund, SWEDEN.*

Aim/Introduction: Block-sequential regularization expectation maximization (BSREM), commercially Q.Clear (GE Healthcare, Milwaukee, WI, USA) is a reconstruction algorithm that allows for a fully convergent iterative reconstruction leading to higher image contrast compared to conventional reconstruction algorithms, while also limiting noise. The noise penalization factor β controls the trade-off between noise level and resolution. The aim was to evaluate the influence of different β values for different activity time products (ATs = administered activity x acquisition time) in whole-body ^{18}F-fluorodeoxyglucose (FDG) positron emission tomography with computed tomography

(PET-CT) regarding quantitative data, interpretation, and quality assessment of the images. **Materials and Methods:** Twenty-five patients with known or suspected malignancies, referred for clinical ^{18}F-FDG PET-CT examinations acquired on a silicon photomultiplier (SiPM) PET-CT scanner, were included. The data were reconstructed using BSREM with β values of 100 - 700 (increments of 100) and ATs of 4 - 16 MBq/kg*min/bed (acquisition times of 1, 1.5, 2, 3, and 4 min/bed). One nuclear medicine physician identified two lesions per patient with slight to moderate hypermetabolism. Noise level in the liver, lesion SUV_{max}, and lesion SUV_{peak} were calculated for ATs of 4-16. Image quality and lesion detectability were assessed by four nuclear medicine physicians for ATs of 4 and 6. **Results:** The noise level decreased with increasing β values and ATs. Lesion SUV_{max} varied considerably between different β values and ATs. The highest median lesion SUV_{max} was found with an AT of 4 and a β of 100 (6.7, interquartile range 2.7) and the lowest with an AT of 16 and a β of 700 (2.6, interquartile range 1.3). SUV_{peak} were stable over the range of ATs and decreased less than SUV_{max} with increasing β values. For an AT of 6 (in our case 1.5 min/bed), the best image quality was obtained with a β of 600 and the best lesion detectability with a β of 500. AT of 4 generated poor-quality images and false positive uptakes due to noise. **Conclusion:** For oncologic whole-body ^{18}F-FDG examinations on a SiPM-based PET-CT, we propose using an AT of 6 (i.e. 4 MBq/kg and 1.5 min/bed) reconstructed with BSREM using a β value of 500 - 600 in order to ensure image quality and lesion detection rate as well as a high patient throughput. We do not recommend using AT < 6 since the risk of false positive uptakes due to noise increases. **References:** None.

OP-143

Momentum acceleration of the block sequential regularized expectation maximization algorithm as applied to General Electric's Q.Clear PET image reconstruction algorithm

C. Schmidtlein[1], *J. Guo*[2,3], *Y. Lin*[3], *A. Krol*[4], *S. Li*[5], *S. Ahn*[6], *C. Stearns*[7], *Y. Xu*[2];

[1]*Memorial Sloan Kettering Cancer Center, New York, NY, UNITED STATES OF AMERICA,* [2]*Old Dominion University, Norfolk, VA, UNITED STATES OF AMERICA,* [3]*Sun Yat-sen University, Guangzhou, CHINA,* [4]*State University of New York Upstate Medical University, Syracuse, NY, UNITED STATES OF AMERICA,* [5]*Guangdong University of Technology, Guangzhou, CHINA,* [6]*GE Global Research, Niskayuna, NY, UNITED STATES OF AMERICA,* [7]*GE Healthcare, Milwaukee, WI, UNITED STATES OF AMERICA.*

Aim/Introduction: Regularized PET image reconstruction can produce high quality PET images but is computationally expensive, requiring substantial computing resources. This study presents a momentum modification to the block sequential regularized expectation maximization (BSREM) algorithm as implemented by General Electric known as Q.Clear with the purpose of accelerating the convergence of this algorithm (1-5). **Materials and Methods:** Momentum is implemented as an additional update step using a weighted difference of the image from the most recent update step with that from the last one (3,6). We utilize a novel step weighting and compare its performance by experiments using both simulated and clinical data. In our simulated experiments we use realistic patient derived images over a wide range of counts. **Results:** In both simulated and clinical experiments we show that our momentum modification, with some parameter tuning, improves convergence as much as a factor of 2, while all other algorithm and regularization parameters are fixed. Other momentum approaches, such as Nesterov's momentum, perform well with small subset sizes but fail to improve convergence for larger subsets and lower count data. We show similar improved convergence with un-regularized reconstruction as well. **Conclusion:** This modification, with minimal additional computational overhead, can improve the convergence rate of the BSREM PET algorithm as implemented by GE in Q.Clear, as well as the un-regularized version of this algorithm. However, the optimal momentum step-size and subset relaxation parameters are data dependent complicating use and need further research. **References:** 1. Ahn S, Fessler JA. Globally convergent image reconstruction for emission tomography using relaxed ordered subsets algorithms. Medical Imaging, IEEE Transactions on. 2003;22:613-626.2. 2. Nuyts J, Beque D, Dupont P, Mortelmans L. A concave prior penalizing relative differences for maximum-a-posteriori reconstruction in emission tomography. IEEE Transactions on nuclear science. 2002;49:56-60.3. 3. Lin Y, Schmidtlein CR, Li Q, Li S, Xu Y. A Krasnoselskii-Mann algorithm with an improved EM preconditioner for PET image reconstruction. IEEE transactions on medical imaging. 2019.4. 4. Ross S. Q. Clear. GE Healthcare, White Paper. 2014:1-9.5. 5. Ahn S, Ross SG, Asma E, Miao J, Jin X, Cheng L, Wollenweber SD, Manjeshwar RM. Quantitative comparison of OSEM and penalized likelihood image reconstruction using relative difference penalties for clinical PET. Physics in Medicine & Biology. 2015;60:5733. 6. Nesterov Y: A method of solving a convex programming problem with convergence rate O (1/k2). in Soviet Mathematics Doklady 1983. pp. 372-376.

OP-144

Systematic inaccuracies in the timing offset calibration may lead to large reconstructed transaxial asymmetries in the GE SIGNA PET/MR MP24

G. Schramm, A. Rezaei, J. van Aalst, D. Van Weehaeghe, M. Koole, J. Nuyts, K. Van Laere;

KU/UZ Leuven, Department of Imaging and Pathology, Division of Nucelar Medicine, Leuven, BELGIUM.

Aim/Introduction: Recently we showed that systematic inaccuracies in crystal timing offset calibration procedures can lead to substantial transaxial asymmetries in PET images reconstructed with TOF OSEM. Moreover, we proposed a data-driven method to compensate for those inaccuracies [1]. In this retrospective analysis, we investigate to what extent PET image quantification in our GE SIGNA PET/MR (software version MP24)

was affected by inaccuracies in the timing offset calibration. **Materials and Methods:** First, we retrospectively analyzed TOF OSEM PET reconstructions of 20cm homogeneous cylindrical phantom acquisitions from 15 different calibration periods between Sep 2015 and Dec 2018. Transaxial asymmetries in the reconstructed images were calculated in different directions (horizontal, vertical and oblique) by evaluating the relative difference between 6 sectors of 2D annulus ROIs with inner and outer radius of 68mm and 82mm, respectively. Second, we retrospectively analyzed TOF OSEM reconstructions of 7 static [^{18}F]FDG brain data sets of healthy controls (2F/5M, age 56±12 years), where uptake is supposed to be essentially left-right symmetric, all acquired in one timing offset calibration period in Jan 2017. Left-right asymmetries of ROI mean values in pairs of homologous ROIs of the AAL2 atlas were calculated in MNI space. Moreover, the analysis was repeated with TOF OSEM reconstructions of the same data sets with corrected timing offsets using the method of [1]. **Results:** In the phantom measurements, we observed transaxial asymmetries of more than 5% in 9 out of 15 calibration periods. The asymmetries were predominantly in the horizontal (left-right) direction and varied strongly between calibrations. The biggest asymmetries were up to 10%. In the brain data sets, the regionally averaged left-right asymmetries of ROI means were (mean ± std. dev.): (7.0±5.4)% frontal, (6.9±5.6)% parietal, (8.8±4.6)% temporal, (7.1±4.5)% occipital, (3±5.3)% cerebellum. After the data-driven correction of the timing offset inaccuracies, those values decreased to: (1.5±4.0)% frontal, (-0.7±4.5)% parietal, (-0.2±5.3)% temporal, (-1.4±2.3)% occipital,(-2.2±5.3)% cerebellum. After an update to software version MP26 in Jan 2019, the inaccuracies in the crystal timing offset calibration procedures were strongly reduced which was verified by an additional phantom measurement. **Conclusion:** Inaccuracies in the timing offset calibration of the GE SIGNA PET/MR (MP 24) lead to substantial time varying transaxial left-right asymmetries of up to 10% in TOF OSEM reconstructions which can be corrected for by applying the method of [1]. **References:** [1] Rezaei et al., "Data driven time alignment for TOF-PET", 2017 IEEE Nuclear Science Symposium and Medical Imaging Conference (NSS/MIC)

OP-145

Quantitative Optimization of High Definition Neurologic Imaging for Digital PET/CT

K. Binzel, *A. Adelaja, J. Zhang, M. V. Knopp;*
The Ohio State University Wexner Medical Center, Columbus, OH, UNITED STATES OF AMERICA.

Aim/Introduction: To assess the accuracy of high definition image reconstruction methodologies provided by digital photon counting PET (dPET) for neurologic imaging applications. **Materials and Methods:** A Hoffman brain phantom was filled with 31 MBq ^{18}F in the background volume and four spheres with volumes ranging from 2ml to .125 ml were filled with 235.0 kBq, 98.4 kBq, 47.0 kBq and 18.5 kBq of ^{18}F as well as two spheres filled with distilled water. The spheres were placed throughout the volume of the phantom. The phantom was imaged on a digital photon counting PET/CT (Philips Vereos). Ten runs of five minute acquisitions were repeated with the brain 256 mm field of view (FOV) and the whole body 576 mm FOV. Each acquisition was reconstructed using listmode data with high definition (HD) 2x2x2 mm voxel volumes / 288x288 matrix with 3 iterations and subsets ranging from: 23, 21, 19, 17, 15, 13, 11, 9, 7 and 5. Point spread function (PSF) only, Gaussian only, a combination of both or no filters were enabled. Sixteen regions of interests (ROIs) were placed in background regions as well as over the spheres. **Results:** The most accurate quantitative results regarding hot spheres were determined when no filters were set for all subsets. The combination of both PSF and Gaussian filters was slightly less accurate, but better than Gaussian alone which gave an underestimation of activity concentrations. There was little difference between the 256mm brain FOV and the 576 mm whole body FOV when no filter was applied. For the brain FOV, the average recovery coefficients (RCs) of the hot spheres were similar within reconstructions with different subsets, ranging from 1.08, 1.04 and 1.00 for the 11, 7 and 5 subset reconstructions, respectively. For the whole body FOV with no filter the RCs were similar, averaging 1.09, 1.08 and 1.01 for the 11, 7 and 5 subsets, respectively. With the background ROIs, all reconstruction settings showed similar accuracy. **Conclusion:** Next-generation digital photon counting PET/CT allows for high definition imaging of the brain with accurate and robust quantification. Phantom analysis showed that excellent image quality can be achieved using both brain and whole body field of view by adjusting reconstruction settings, such as the number of subsets per iteration. Quantitative accuracy is maintained over the range of reconstruction settings, due in part to the quality of counts in the PET data resulting from digital photon counting. **References:** None.

OP-146

Clinical impact of Spatially Variant Positron Range Correction for ^{68}Ga-DOTATATE and ^{68}Ga-PSMA PET/CT

A. Berger[1], *J. Cal-Gonzalez*[1], *S. Rasul*[2], *M. Hacker*[2], *M. Grahovac*[2], *R. A Latiff*[3], *G. Schembri*[4], *I. Rausch*[1], *T. Beyer*[1], *P. Kench*[3];
[1]*QIMP Team, Center for Medical Physics and Biomedical Engineering, Medical University of Vienna, Vienna, AUSTRIA,* [2]*Division of Nuclear Medicine, Department of Biomedical Imaging and Image-guided Therapy, Medical University of Vienna, Vienna, AUSTRIA,* [3]*Discipline of Medical Radiation Science and Brain and Mind Centre, Faculty of Health Sciences, The University of Sydney, NSW, AUSTRALIA,* [4]*Department of Nuclear Medicine, Royal North Shore Hospital, St Leonards, NSW, AUSTRALIA.*

Aim/Introduction: To evaluate the clinical impact of spatially variant positron range correction (PRC) for ^{68}Ga-DOTATATE and ^{68}Ga-PSMA PET/CT. **Materials and Methods:** Five patients with neuroendocrine tumor and 10 with prostate cancer underwent ^{68}Ga-DOTATATE and ^{68}GA-PSMA PET/CT examinations on a Siemens Biograph mCT system, respectively. The PET data was reconstructed using standard clinical settings. In addition, a

post-reconstruction, tissue dependent PRC was performed of all data-sets. A direct comparison of the PRC and non-PRC images was performed by two nuclear medicine specialists independently. The image quality was classified on a 4-point scale considering noise, contrast, and spatial resolution. Absolute changes in scores of 1 and 2 points was classified as mild to moderate and high change, respectively. SUV_{max} of up to 3 noticeable lesions and SUV_{mean} of the liver was measured for PRC and non-PRC images. **Results:** PRC improvements in contrast were rated by reviewer1 / reviewer 2 as mild to moderate in 73% / 87% of the patients. Improvements in spatial resolution were denoted as mild to moderate in 60% / 80% and as high in 27% / 13% of the patients. PRC-induced degradation of noise properties were denoted as mild to moderate in 53% / 60% and as high in 13% / 27% of the patients. The PRC-induced change of SUV (max) of all detected lesions was denoted by reviewer1 / reviewer 2 as 35.8%±18.5% / 32.6%±19.7% and of SUV (mean) of liver as 1.0%±0.1% / 11.25%±7.8%. Note each reviewer may have selected different lesions for analysis. After PRC mild to moderate degradation in overall image quality was denoted in 20% / 86%, no change was denoted in 27% / 7% and mild to moderate improvement of overall image quality was denoted in 53% / 7% of the patients. **Conclusion:** Images corrected with PRC revealed in all reviewed cases a detectable change in the image quality. PRC can improve contrast and spatial resolution in ^{68}Ga-DOTATATE and ^{68}Ga-PSMA PET/CT. However, how these changes are perceived are highly reader dependent. As expected, the deconvolution used in the PRC induces noise, leading to a mild to moderate degradation of the subjective scoring of overall image quality for one of the readers. Image quality may be improved by different filtering/reconstruction of the PRC data. Acknowledgements: The financial support of Siemens Healthineers is gratefully acknowledged. **References:** None.

OP-147

Feasibility of Quantitative SPECT of Radionuclides used in Targeted Alpha Therapy

M. Ghaly[1,2], *B. He*[2], *Y. Du*[1], *G. Sgouros*[1,2], *E. C. Frey*[1,2];
[1]*Johns Hopkins University, Baltimore, MD, UNITED STATES OF AMERICA,* [2]*Radiopharmaceutical Imaging and Dosimetry (Rapid), LLC, Baltimore, MD, UNITED STATES OF AMERICA.*

Aim/Introduction: There is a great deal of current interest in and high potential for radiopharmaceutical therapy using alpha emitters. The most commonly used parent radionuclides are Ra-223, Th-227, Ac-225, and Pb-212. Accurate dosimetry is important for these therapies in the regulatory process, for rational dose escalation and optimal therapy. Accurate dosimetry requires a knowledge of the activity distribution. However, quantitative imaging of these radionuclides is challenging. They all have multiple daughters and complex decay schemes with overlapping x-ray and gamma emissions. For Pb-212, there is a high abundance 2.6 MeV photon emitted by Tl-208 that easily penetrates even high-energy collimators. Th-227 has Ra-223 as a daughter and knowing the distribution of the daughter can be important for accurate dosimetry. **Materials and Methods:** We have developed a framework for comparing the potential energy windows and collimators in terms of a signal-to-noise ratio criterion that considers unscattered photons passing through the collimator holes as the signal. The quantum noise resulting from photons scattered in the body and those penetrating through the septa, scattering in the septa, or backscattering in the compartment behind the crystal is considered noise. Using this, we have selected the acquisition energy windows and collimators for these radionuclides. We have also developed a general framework for modeling the image formation process of multiple radionuclides into multiple energy windows and incorporated this into an iterative reconstruction code for estimating the activity distribution of one or more radionuclides. We have performed phantom studies demonstrating the feasibility of quantitative SPECT reconstruction of the activity distributions of radionuclides used in alpha therapy. This includes Pb-212, Ra-223, Th-227, and Ac-225. We have performed physical phantom experiments using simple geometries and Monte Carlo simulations of anthropomorphic phantoms to evaluate the accuracy of this method. **Results:** For Pb-212, the presences of a high energy photon from Tl-208 results in substantial septal penetration and scatter and backscatter. While an HEGP collimator provided a higher signal-to-noise ratio, an MEGP collimator provided acceptable images. For Pb-212, Th-227, and Ra-223, we obtained accuracies of better than 10% in physical phantoms for spheres ~5 cm in diameter. For Th-227 we obtained accuracies of better than 10% for simultaneously estimating the activities of Ra-223 and Th-227. For Ra-223, simulation studies indicate accuracies on the order of 10% for organs. **Conclusion:** The results of this work demonstrates the . **References:** None.

OP-148

Artefacts reduction in cardiac SPECT images by using a novel reconstruction algorithm Maximum a Posteriori with local regularization

N. Denisova[1], *A. Ansheles*[2], *V. Sergienko*[2], *H. Kertész*[3], *T. Beyer*[3], *I. Kolinko*[1,4];
[1]*Institute of Theoretical and Applied Mechanics, Novosibirsk, RUSSIAN FEDERATION,* [2]*National Medical Research Center of Cardiology, Moscow, RUSSIAN FEDERATION,* [3]*Medical University of Vienna, Vienna, AUSTRIA,* [4]*Novosibirsk State University, Novosibirsk, RUSSIAN FEDERATION.*

Aim/Introduction: Clinical methods are limited in studying the causes of artefacts associated with mathematical aspects of reconstruction algorithms and methods. In this work, a novel Maximum a Posteriori (MAP) reconstruction algorithm with local regularization is developed to increase the resolution and to improve the quality of reconstructed images. The aim of this work is to evaluate the proposed algorithm in artefacts reduction in cardiac SPECT imaging. **Materials and Methods:** Joint clinical and simulation studies are performed. A special

mathematical model of torso (MMT) was designed which plays the role of virtual patient and models spatial distribution of 99mTc-MIBI in thoracic organs. The MMT is easy transformed to study patients with various constitutions and different myocardial left ventricle (LV) forms. MMT was sampled on grids 128*128*128 and 64*64*64. Computer simulations of the SPECT/CT myocardial perfusion imaging (MPI) procedure were performed. Projection (raw) data were calculated for 32 and 64 angular views over an arc extending from the right anterior oblique to the left posterior oblique in accordance with acquisition protocol of MPI SPECT. Standard OSEM and a novel MAP reconstruction algorithm with local regularization were applied for images reconstruction. Two types of artefacts were studied: false apical defects and artefacts of extra-cardiac activity. The simulation results were verified by comparing to the clinical data. Clinical MPI studies were performed in the National Medical Research Center of Cardiology (Moscow) by using the Philips Bright View XCT SPECT/CT hybrid system with low-energy high-resolution (LEHR) collimator. **Results:** The results of simulations have shown that the cause of false apical defects is not associated with attenuation correction, as it was discussed in some clinical studies, but it is related to the LV form and to the limitations of the standard OSEM reconstruction algorithm. Severity of false apical defects was decreased by 10-15% using the proposed MAP algorithm. It is shown that extra-cardiac activity artifacts are reduced by using the MAP algorithm with local regularization. **Conclusion:** Joint clinical and simulation studies in nuclear cardiology may be considered as a first-line approach in analyzing sources of possible artifacts and pitfalls. The proposed MAP algorithm with local regularization has shown as a promising approach to improve resolution of reconstructed images and to reduce artefacts in cardiac SPECT images. **References:** None.

OP-149

Dependence Of Error Propagation Due To An Incorrect Attenuation Map On PET Time-of-Flight Resolution

E. C. Emond[1], *A. Bousse*[2], *A. M. Groves*[1], *B. F. Hutton*[1], *K. Thielemans*[1];
[1]*University College London, London, UNITED KINGDOM,*
[2]*Université de Bretagne Occidentale, Brest, FRANCE.*

Aim/Introduction: In recent years, PET time-of-flight (TOF) scanners have become available with improved timing resolution, with many groups aiming towards a TOF FWHM of 100ps or below. For TOF, in addition to the increase in SNR, it has been observed that the impact of inaccurate attenuation maps is reduced [1]. However, it is unclear whether a local error in attenuation values causes errors in distant parts of the reconstructed image. The aim of this work is to investigate the impact of incorrect attenuation (μ) maps in PET systems with improved time resolution. **Materials and Methods:** Simulations were performed for a uniform cylinder and XCAT phantom based on the geometry of the GE 690 discovery, but with TOF resolution varying from 70ps to 1000ps. For the cylinder, a 12-mm diameter central area of incorrect attenuation (μ reduced by 15%) was introduced in order to understand the error propagation in terms of distance to the incorrect μ values. For the thorax phantom, both lungs were assigned μ values 15% lower than the true values. TOF MLEM reconstructions were performed over the range of TOF resolution values using STIR, iterating until close to convergence. The influence of TOF resolution on the propagated errors was then studied for regions drawn inside or outside the region of incorrect μ values (lung versus heart). **Results:** For the cylinder, with low TOF resolution the errors are dominated by local effects; however, as TOF resolution improves, the local error decreases linearly but the error in more distant parts of the image increase significantly (e.g. by a factor of 10 at 100ps compared to 400ps at 2.1cm off-centre). The same trend is verified in the XCAT simulation. The errors within the lung decrease with improved TOF resolution (from 13.11% to 4.63%), whereas bias in the left ventricle increased by a factor of 3.2 at 70ps compared to 600ps (from 0.67% to 2.15%). **Conclusion:** Superior TOF resolution aids quantification in regions where the attenuation is not accurately known (e.g. effect of density changes in the lungs induced by motion). However, this is accompanied by significant increase in bias in areas remote from the incorrect attenuation. Future improvement of TOF resolution could result in unforeseen bias in PET quantification. **References:** [1] A. Mehranian and H. Zaidi, 10.2967/jnumed.114.148817

407

Teaching Session 1 - Interactive Clinical Cases - Paediatrics + Thyroid + Translational and Molecular Imaging Therapy Committee: Management of Thyroid Cancer in Children

Sunday, October 13, 2019, 14:30 - 16:00 Lecture Hall 113

OP-150

Paediatric DTC Management

A. Piccardo;
E.O. Ospedali Galliera, Dapartment of Nuclear Medicine, Genoa, ITALY.

OP-151

Molecular Imaging in Paediatric DTC

F. Van Leeuwen;
Leiden University Medical Center, Interventional Molecular Imaging Laboratory, Leiderdorp, NETHERLANDS.

OP-152

Radioiodine Dosimetry and Therapy in Paediatric DTC Patients

M. Luster;
University of Marburg, Department of Nuclear Medicine, Marburg, GERMANY.

408
Clinical Oncology - Rapid Fire Session: New Tracers and Machine Learning

Sunday, October 13, 2019, 14:30 - 16:00
Lecture Hall 114

OP-153

Radiomics from [18F]PSMA PET-CT with machine learning as a novel biomarker in primary prostate cancer

M. Cysouw[1], *B. H. Jansen*[1], *K. C. van der Zande*[1], *B. M. de Vries*[1], *R. J. van Moorselaar*[2], *A. N. Vis*[2], *O. S. Hoekstra*[1], *T. van de Brug*[3], *D. E. Oprea-Lager*[1], *R. Boellaard*[1];
[1]*Amsterdam UMC, Vrije Universiteit Amsterdam, dept. of Radiology and Nuclear Medicine, Amsterdam, NETHERLANDS,* [2]*Amsterdam UMC, Vrije Universiteit Amsterdam, dept. of Urology, Amsterdam, NETHERLANDS,* [3]*Amsterdam UMC, Vrije Universiteit Amsterdam, dept. of Epidemiology and Biostatistics, Amsterdam, NETHERLANDS.*

Aim/Introduction: In primary prostate cancer (Pca) patients, accurate staging and risk stratification is crucial to guide treatment and optimize patient outcomes. Visual assessment of [18F]PSMA PET-CT has been demonstrated not to be suitable for these purposes. However, high-throughput extraction of quantitative features from these [18F]PSMA PET-CT images could improve sensitivity for metastatic deposits or yield additional data on unfavorable tumor characteristics. The aim of this study was to investigate the potential of [18F]PSMA PET-CT radiomics and machine learning models as novel biomarkers in primary Pca. **Materials and Methods:** 61 patients with biopsy-proven Pca underwent whole body [18F]DCFPyL (PSMA) PET-CT at 120min post-injection before planned radical prostatectomy with extended pelvic lymph node dissection. Primary tumors were delineated using both a 50%peak and 41%max background-adapted thresholds. Per primary tumor we extracted 480 radiomics features on morphology, intensity, and grey-level co-occurrence. Random Forest, Support Vector Machine, Neural Network, and Logistic Regression with optimized hyperparameters were combined with several data normalization, feature selection, and (training) data balancing methods. We assessed whether the models could discriminate between i) ≤7 vs >7 post-surgery Gleason score, ii) pathological T2 vs. T3 tumors, and iii) absence or presence of pathology-proven lymph node and/or distant metastases. The models were trained and tested in a 10 times repeated 4-fold cross-validation, each fold yielding test scores from unseen data. Model performance was assessed using the mean receiver-operator-curve integral (AUC) and mean weighted accuracy. Model stability was assessed using the coefficient-of-variation (COV%). **Results:** The highest performance was observed for prediction of presence of pathology-proven metastatic disease, with a mean AUC of 0.98±0.03 (COV 3.4%) and a weighted accuracy of 0.93±0.06. For discrimination between high vs. low Gleason score, the best model had a mean AUC of 0.83±0.12 (COV 14.6%) and a weighted accuracy of 0.84±0.09. For T2 vs. T3 tumors, the best model had a mean AUC of 0.69±0.14 (COV 20.5%) and a weighted accuracy of 0.65±0.10. Scores from 41%max delineation were higher than those of 50%peak, but absolute differences in model performance were small. **Conclusion:** Machine learning models using [18F]PSMA PET-CT primary prostate tumor radiomics are robust and highly accurate in predicting presence of metastatic disease. A lower classification accuracy was observed for post-surgery Gleason score and tumor stage, indicating that the biological basis of radiomics features could be partly independent from these histopathological tumor characteristics. The additive value of these radiomics features to clinical nomograms merits further investigation. **References:** None.

OP-154

Comparison Of Ga-68 PSMA PET/MRI With Textural Analysis Data In Transitional Zone Prostate Tumors: Preliminary Results Of An On-Going Study

L. L. Uslu[1], *S. Tuncer*[2], *B. Bakır*[2], *S. Ozel Yildiz*[3], *C. Demirdag*[4], *E. Güner*[5], *S. Sager*[1], *H. B. Sayman*[1], *K. Sonmezoglu*[1];
[1]*Istanbul University-Cerrahpasa, Cerrahpasa Medical Faculty, Department of Nuclear Medicine, Istanbul, TURKEY,* [2]*Istanbul University, Istanbul Medical Faculty, Department of Radiology, Istanbul, TURKEY,* [3]*Istanbul University, Istanbul Medical Faculty, Department of Biostatistics, Istanbul, TURKEY,* [4]*Istanbul University-Cerrahpasa, Cerrahpasa Medical Faculty, Department of Urology, Istanbul, TURKEY,* [5]*Health Sciences University, Bakırköy Sadi Konuk Training and Research Hospital, Department of Urology, Istanbul, TURKEY.*

Aim/Introduction: Multiparametric prostate MRI (mp-MRI) is an effective imaging modality for detection of primary prostate lesions. MRI textural analysis was introduced to improve the detection of primary prostate lesions, especially in the transitional zone of the gland. Ga-68 PSMA PET on the other hand was shown to be superior to mp-MRI in detection of primary prostate lesions. The aim of our study is to compare textural analysis method and Ga-68 PSMA PET/MRI in transitional zone tumors. **Materials and Methods:** Data obtained from 21 patients who underwent hybrid Ga-68 PSMA PET/MRI for prostate cancer between August 2017 and January 2019 for the on-going prospective clinical study were retrospectively analyzed. All patients had radical prostatectomy operation following imaging. Sixty-two textural analysis were deduced from each manually contoured whole transitional zone on axial T2-weighted (T2W), diffusion-weighted images (DWI) (b value=1400s/m²) and apparent diffusion coeffient (ADC) map which was obtained from b value=0-50-800 s/mm². Textural features of transitional zone were compared to PSMA expression on the corresponding PET images. T-test and Mann-Whitney U test were used for comparison of textural features of transitional zone on three different sequences. **Results:** Twenty-one patients had mean 13.74 ng/ml (range=4.1-41) PSA value. Among 21 men, 9 patients had positive tumoral PSMA uptake on transitional zone whereas 12 patients had no PSMA uptake on the transitional

zone. One patient had no DWI on b value=1400 s/m² among 12 patients. Nine patients who had PSMA uptake on transitional zone had statistically significantly higher mean signal intensity on DWI textural analysis compared to PSMA negative group (p=0.024). There is no difference between skewness, kurtosis and standart deviation values on three different sequences on transitional zone among PSMA positive and negative groups. **Conclusion:** Although T2W imaging is the dominant MRI sequence to evaluate transitional zone tumors, we could not find a significant difference in textural analysis parameters using T2W sequence. DWI (b=1400 s/m²) signal intensity on the other hand was shown to detect transitional zone tumors similar to Ga-68 PSMA PET/MRI. Therefore, combined usage of textural analysis with dominant T2W MRI sequence and Ga-68 PSMA PET/MRI may add up to each other to increase the diagnostic accuracy in transitional zone tumors. **References:** 1. Bates A, et al. Eur Radiol. 2017;27:5290-8. 2. Patel N, et al. Clin Radiol. 2018, https://doi.org/10.1016/j.crad.2018.11.007; 3. Wang Y et al. Magn Reson Imaging. 2019;60:76-84.

OP-155

Preliminary evaluation of PSMA PET/MR radiomics for primary staging in patients with prostate cancer

E. Solari[1], *A. Gafita*[2], *B. Laurent*[3], *T. Amiel*[4], *R. Tauber*[4], *D. Visvikis*[3], *W. Weber*[2], *M. Eiber*[2], *M. Hatt*[3], *S. G. Nekolla*[1];
[1]*Department of Nuclear Medicine, Klinikum rechts der Isar, München, GERMANY,* [2]*Department of Nuclear Medicine, School of Medicine, Technical University Munich, München, GERMANY,* [3]*LaTIM, INSERM, UMR 1101, Univ. Brest, Brest, FRANCE,* [4]*Department of Urology, School of Medicine, Technical University Munich, München, GERMANY.*

Aim/Introduction: Magnetic resonance imaging (MRI) radiomics have shown promising results in prostate cancer (PC) staging. Prostate specific-membrane antigen (PSMA)-targeted PET/MR imaging showed enhanced accuracy in PC lesion detection compared to conventional imaging. Therefore, in the present analysis we aimed to evaluate the potential of applying handcrafted PSMA PET-MR radiomics for PC staging. **Materials and Methods:** Patients with PC who underwent PSMA PET/MR in a primary staging setting were included in the analysis. Histopathologic results (Gleason score (GS)) obtained during radical prostatectomy were collected. The entire prostate organ was segmented in PET and T2 MR images. For PET, a semi-automatic FLAB segmentation (LaTIM, Brest) was used, whereas a manual segmentation was carried out on the MR images. Image biomarker standardization initiative (IBSI)-compliant handcrafted features were extracted from both PET and MR images. The cohort was split into training and validation using stratified K-fold cross-validation with 10 folds. The benefit of performing imbalance correction (random oversampling, SMOTE) was evaluated. Principal component analysis (PCA) was performed for dimensionality reduction (2 to 20 components). A radial-basis support vector machine (SVM) model with hyperparameter tuning was trained for the classification of GS by groups (≤7, 8, ≥9). The average accuracy, specificities and sensitivities of the best classifiers on the validation data is reported. **Results:** 130 patients were included in the analysis. 64% (83) of the patients exhibited a GS of 7, 21% (27) a GS of 8 and 15% (20) a GS of 9. Slightly better results were obtained with SMOTE oversampling compared to random and no oversampling. The 10-fold averaged classification accuracy of PET-MR radiomics (77%) as well as sensitivities (GS≤7: 78%, GS=8: 83%, GS≥9: 80%) and specificities (GS≤7: 82%, GS=8: 83%, GS≥9: 96%) were superior to PET-only radiomics (acc.: 73%; sens.: 83%, 50%, 60%; spec.: 73%, 87%, 92%) and T2-only radiomics (acc.: 67%; sens.: 89%, 33%, 40%; spec.: 69%, 86%, 79%). **Conclusion:** The strongly imbalanced dataset justifies the necessity of balancing strategies in training the model. The combined information gathered from PET and MR radiomic features improved performance compared to PET-only and MR-only. Further analyses including a larger and more balanced patient cohort and advanced radiomics are warranted. (This project is funded by the European Union's Horizon 2020 research and innovation programme under the Marie Sklodowska-Curie grant agreement No 764458) **References:** None.

OP-156

Machine Learning to Detect Prostate Cancer Recurrence using ^{18}F-Fluciclovine PET

G. A. Davidzon[1], *J. Lee*[2], *H. Yang*[3], *H. Song*[1], *C. Harrison*[1], *A. Iagaru*[1];
[1]*Stanford University, Stanford, CA, UNITED STATES OF AMERICA,* [2]*Asan Medical Center University of Ulsan College of Medicine, Seoul, KOREA, REPUBLIC OF,* [3]*Dimensional Mechanics, Seattle, WA, UNITED STATES OF AMERICA.*

Aim/Introduction: Development of machine learning (ML) classifiers for cancer detection in medical images has shown promise. Recent work using convolutional neural networks (CNN) has focused on the classification of positron emission tomography (PET) using ^{18}F-fluorodeoxyglucose (FDG). ^{18}F-Fluciclovine is a relatively newly FDA-approved radiopharmaceutical indicated when prostate cancer (PC) biochemical recurrence (BCR) is suspected based on elevated prostate specific antigen (PSA) levels following prior treatment. We evaluated the performance of a 3D-CNN to detect BCR PC using ^{18}F-Fluciclovine PET scans. **Materials and Methods:** 179 consecutive ^{18}F-Fluciclovine PET/CT scans were performed at Stanford University between Dec 2017 and Feb 2019 in 163 PC patients who had prior treatments and suspected recurrence. Patients' age and serum PSA level at the time of PET were 71.8 +/- 9.1 years and 35.2 +/- 225.3 (range 0.05-2975.0 ng/mL). To augment the model's accuracy and reduce computational expense, the pelvis, which is the region most commonly affected by early recurrence and metastases was included. Studies were classified as normal (N), abnormal (A), and indeterminate (I) based on the clinical reports. N-scans were those with the expected biodistribution of ^{18}F-Fluciclovine and A-scans included those with focal radiopharmaceutical uptake in the prostate gland or bed, in lymph nodes and/or the skeleton. A training set of 150

cases (A=106, N=38, and I=6) and a test set of 29 cases (A=24, N=4, and I=1) were randomly allocated. ResNet 3D model with 14 layers was built to classify the data into 3 classes. The model's performance was calculated on a test set to assess for sensitivity, specificity, and AUC by ROC curve analysis. **Results:** Sensitivity and specificity to determine the abnormality for the test set were 91.7% and 75.0% in the ROC analysis (criterion of 0.701) and area under the curve (AUC) was 0.896 (p<0.001). **Conclusion:** 3D-CNN architecture showed good performance for detection of BCR PC using ^{18}F-Fluciclovine PET. Further work is warranted to confirm results in larger and prospective cohorts of patients. **References:** None.

OP-157

^{68}Ga-NODAGA-exendin-4 PET/CT for the diagnosis and localization of focal congenital hyperinsulinism

M. Boss[1], *P. Shah*[2], *W. Brenner*[3], *O. Blankenstein*[3], *C. Rottenburger*[4], *M. Brom*[1], *A. Eek*[1], *M. Buitinga*[1], *M. Gotthardt*[1];
[1]*Radboudumc, Nijmegen, NETHERLANDS,* [2]*Great Ormond Street Hospital, London, UNITED KINGDOM,* [3]*Charite University Hospital, Berlin, GERMANY,* [4]*University of Basel Hospital, Basel, SWITZERLAND.*

Aim/Introduction: Congenital hyperinsulinism (CHI) is the most common cause of persistent and recurrent hypoglycemia in neonates. The focal subform of CHI, is caused by focal islet cell hyperplasia. In contrast to the diffuse subform of CHI, it can be cured with partial pancreatectomy or limited lesionectomy. For this, it is crucial to diagnose focal CHI and precisely localize the lesion. With [^{18}F]F-DOPA PET, the current standard technique for non-invasive detection of focal CHI, about 15% of focal lesions are missed. The stable glucagon-like peptide-1 analogue exendin-4 specifically binds the glucagon-like peptide 1 receptor on pancreatic beta cells. ^{68}Ga-labeled exendin has already been shown to detect insulinomas with high sensitivity. In this multicenter trial we included prospective as well as retrospective data of patients with CHI who underwent both [^{18}F]F-DOPA PET and [^{68}Ga]Ga-NODAGA-exendin-4 PET to compare the effectiveness of these two imaging techniques for the diagnosis and localization of focal CHI. **Materials and Methods:** We analyzed data of 14 CHI patients with a median age of 5 (2.2-9.4) months. All patients underwent [^{18}F]F-DOPA PET (according to standard procedure of each institute) and [^{68}Ga]Ga-NODAGA-exendin-4 PET with a median time of 4 (3 - 8) days between the procedures. For [^{68}Ga]Ga-NODAGA-exendin-4 PET, 1 hour dynamic acquisitions started at the time of injection, or 10 minute static acquisitions started 45 minutes post injection were obtained after injection of 1.6 MBq/kg [^{68}Ga]Ga-NODAGA-exendin-4 with a lower limit of 20 MBq (maximally 0.12 µg/kg). Quantitative analysis of all positive [^{18}F]F-DOPA PET and GLP-1R PET/CT scans was performed by a non-blinded observer. **Results:** Suspicious lesions were detected in 7 patients. These patients underwent surgery and presence of a focal lesion was confirmed by histopathology in all these patients. Patients were cured after surgery. Analysis using histopathology as a reference standard showed a higher sensitivity of [^{68}Ga]Ga-NODAGA-exendin-4 PET (100% (CI 60-100%)) than [^{18}F]F-DOPA PET (57% (CI 18-90%)). SUV_{max} ratios between visually identified focal lesions and the area in the pancreas with the next highest tracer uptake are higher in GLP-1R PET than [^{18}F]F-DOPA PET (1.83 ± 0.75 and 1.47 ± 0.43 respectively). **Conclusion:** In this study we provide the first evidence of the possibility of diagnosis and localization of focal CHI using [^{68}Ga]Ga-NODAGA-exendin-4 PET. These first results show a better sensitivity and image quality of [^{68}Ga]Ga-NODAGA-exendin-4 PET compared to [^{18}F]F-DOPA PET, demonstrating the potential of [^{68}Ga]Ga-NODAGA-exendin-4 PET as a novel diagnostic tool for focal CHI. **References:** None.

OP-158

[^{68}Ga]Ga-NODAGA-exendin-4 PET/CT for the localization of insulinomas

M. Boss[1], *K. Mikkola*[2], *M. Brom*[1], *A. Eek*[1], *M. Buitinga*[1], *O. Eriksson*[3], *D. Wild*[4], *V. Prasad*[5], *A. Brouwers*[6], *F. Pattou*[7], *H. Hofland*[8], *P. Nuutila*[2], *M. Gottthardt*[1];
[1]*Radboudumc, Nijmegen, NETHERLANDS,* [2]*University of Turku, Turku, FINLAND,* [3]*Uppsala University, Uppsala, SWEDEN,* [4]*University Basel Hospital, Basel, SWITZERLAND,* [5]*Charite University Hospital of Berlin, Berlin, GERMANY,* [6]*University Medical Center Groningen, Groningen, NETHERLANDS,* [7]*University Hospital Lille, Lille, FRANCE,* [8]*Erasmus Medical Center, Rotterdam, NETHERLANDS.*

Aim/Introduction: Insulinomas are usually small, single, benign pancreatic neuroendocrine tumors. Precise preoperative localization of these tumors is essential for successful surgical treatment. The current standard imaging techniques CT, MRI and somatostatin receptor (SSTR) PET have limited sensitivity. The stable glucagon like peptide-1 (GLP-1) analog exendin specifically binds to the GLP-1 receptor (GLP-1R), which is markedly overexpressed in most insulinomas. [^{68}Ga]Ga-DOTA-exendin-4 PET/CT has been shown to be feasible for detection of insulinomas with a higher sensitivity than MRI. Replacing the chelator DOTA by NODAGA in the labeling process ensures higher specific activities, allowing imaging with sub-pharmacological peptide doses. We have performed a prospective multicenter imaging study in which we compared the effectiveness of [^{68}Ga]Ga-NODAGA-exendin-4 with all current standard non-invasive imaging procedures for the localization of insulinomas. **Materials and Methods:** 42 adults aged 24-62 with biochemically proven hyperinsulinemic hypoglycemia were included. PET/CT images were obtained one and two hours after injection of 95-105 MBq ^{68}Ga-NODAGA-exendin-4 (5-7 µg). Current standard imaging, consisting of CT or MRI and SSTR PET, was performed within 8 weeks of ^{68}Ga-NODAGA-exendin-PET in all patients. A patient-based analysis was performed with histopathology as a reference standard. **Results:** Suspicious lesions were identified in 33 patients. 31 of these patients underwent surgery after which presence of an insulinoma was confirmed histopathologically. Plasma glucose values normalized after the procedure in all these patients without further hypoglycemic episodes. Analysis showed that

[68Ga]Ga-NODAGA-exendin-4 PET localized insulinomas with a higher accuracy and sensitivity (90.6% and 93.5% respectively) than conventional imaging (78.1% and 80.6% respectively) and SSTR PET (59.4% and 61.3% respectively). In 12.5% of patients, a correct diagnosis and decision to perform surgery was only reached after [68Ga]Ga-NODAGA-exendin-4 PET. This novel technique therefore significantly influenced the clinical management of the patients in this population. The median size of the lesions identified by GLP-1R PET was 12 (10 - 18) mm, including 5 lesions smaller than 10 mm, showing the excellent sensitivity of the technique. The lower peptide dose used in this study compared to previous studies with [68Ga]Ga-DOTA-exendin-4 (4-7 µg vs. 12-24 µg) resulted in fewer occurrences of nausea (5% vs. 27% of patients). **Conclusion:** This study demonstrates the superior performance of [68Ga]Ga-NODAGA-exendin-4 PET/CT compared to current standard imaging modalities for pre-operative localization of benign insulinomas. Because of its high sensitivity and excellent imaging quality, [68Ga]Ga-NODAGA-exendin-4 PET/CT could have the potential to become the primary diagnostic imaging modality in patients with hyperinsulinemic hypoglycemia. **References:** None.

OP-159

Lesion detection by [89Zr]Zr-DFO-girentuximab and [18F]FDG-PET in patients with newly diagnosed metastatic renal cell carcinoma

S. Verhoeff[1], *S. C. van Es*[2], *E. Boon*[1], *E. van Helden*[3], *L. Angus*[4], *S. G. Elias*[5], *S. F. Oosting*[6], *E. H. Aarntzen*[1], *A. H. Brouwers*[2], *T. C. Kwee*[2], *S. Heskamp*[1], *O. S. Hoekstra*[3], *H. Verheul*[3], *G. J. C. Zwezerijnen*[3], *C. Menke-van der Houven van Oordt*[3], *A. A. M. van der Veldt*[4], *E. G. E. de Vries*[2], *O. C. Boerman*[1], *W. T. A. van der Graaf*[7,1], *W. J. G. Oyen*[8,9,1], *C. M. L. van Herpen*[1];

[1]*Radboud University Medical Center, Nijmegen, NETHERLANDS,* [2]*University Medical Center Groningen, Groningen, NETHERLANDS,* [3]*Amsterdam University Medical Center, Amsterdam, NETHERLANDS,* [4]*Erasmus University Medical Center, Rotterdam, NETHERLANDS,* [5]*Julius Center for Health Sciences and Primary Care, Utrecht, NETHERLANDS,* [6]*Univeristy Medical Center Groningen, Groningen, NETHERLANDS,* [7]*Antoni van leeuwenhoek, Amsterdam, NETHERLANDS,* [8]*Rijnstate Arnhem, Arnhem, NETHERLANDS,* [9]*Humanitas University, Milan, ITALY.*

Aim/Introduction: The objective of this study is to evaluate the potential of contrast-enhanced CT, [89Zr]Zr-DFO-girentuximab-PET and [18F]FDG-PET for detection of clear cell renal cell carcinoma (ccRCC) lesions in patients with a good or intermediate prognosis metastatic ccRCC according to the International Metastatic Database Consortium risk model, allowing to safely observe the course of disease in a period of so-called watchful waiting. **Materials and Methods:** Between February 2015 and March 2018, 42 patients with recently (<6 months) diagnosed mccRCC with a good or intermediate prognosis, were enrolled in the IMaging PAtients for Cancer drug selecTion (IMPACT)-renal cell cancer (RCC) study, conducted at 4 Dutch academic medical centers. Patients underwent a diagnostic CT of the chest, abdomen and pelvis, a whole-body [89Zr]Zr-DFO-girentuximab PET (37 MBq, 4 days p.i.), and a whole-body [18F]FDG-PET according to EARL guidelines. The [89Zr]Zr-imaging procedures were harmonized. Scans were independently reviewed and lesions of ≥10 mm and lymph nodes of ≥15 mm on CT were analyzed. For lesions with [89Zr]Zr-DFO-girentuximab or [18F]FDG-uptake visually exceeding background, maximum standardized uptake values (SUV_{max}) were measured. **Results:** In total 449 lesions were detected by ≥1 modality (median 7 per patient; inter quartile range 4.25-12.75) of which 42% in lung, 22% in lymph nodes and 10% in bone. Combined [89Zr]Zr-DFO-girentuximab-PET and CT detected most lesions (91%, 95%CI:87-94) compared to CT alone (56%, 95%CI:50-62, p=0·001) and combined CT and [18F]FDG-PET (84%, 95%CI:79-88, p<0·005). Overall, the median number of two involved organs per patient as determined by CT alone increased to three per patient with the addition of either [89Zr]Zr-DFO-girentuximab and [18F]FDG-PET (range: 1-7; p<0.005), without adjusting for 9 lesions outside of the CT field-of-view. The increase in the number of lesions was mainly due to a better detection of bone and soft tissue lesions by PET compared to CT alone. The [89Zr]Zr-DFO-girentuximab SUV_{max} in metastatic lesions varied greatly (range, 3.8 to 230.8), and was highest in adrenal gland and metastatic kidney lesions and lowest in lung lesions (median SUV_{max} 69.9 and 61.1 vs. 9.4, respectively). **Conclusion:** In newly diagnosed good and intermediate prognosis metastatic ccRCC patients eligible for watchful waiting, the addition of [89Zr]Zr-DFO-girentuximab-PET and [18F]FDG-PET to standard of care diagnostic CT leads to an increased lesion detection compared to standard diagnostic CT only. The clinical and potential prognostic relevance of PET using [89Zr]Zr-DFO-girentuximab and [18F]FDG in ccRCC patients warrants further investigation. **References:** None.

OP-160

Theranostic [64/67Cu]SARTATE Clinical Trial - Uptake and retention of [64/67Cu]SARTATE within meningioma

G. P. Schembri[1], *C. Yin*[1], *K. Willowson*[1], *A. Hedt*[2], *E. Lengyelova*[2], *M. Parker*[2], *C. Biggin*[2], *M. Harris*[2];

[1]*Royal North Shore Hospital, St Leonards, AUSTRALIA,* [2]*Clarity Pharmaceuticals, Sydney, AUSTRALIA.*

Aim/Introduction: Somatostatin receptors (SSTR) are expressed in 60-100% of meningioma and peptide receptor radionuclide therapy (PRRT) utilising radiolabelled somatostatin analogues has been demonstrated used in the management of these tumours. SARTATE is a somatostatin peptide analogue that can be labelled with 64Cu or 67Cu. We report preliminary findings in a first in human trial utilising [67Cu]SARTATE. **Materials and Methods:** [67Cu]SARTATE is being evaluated in a Phase I-IIa multidose trial with recurrent or progressive grade I-III meningioma (ACTRN12618000309280). Between July 2018 and April 2019, 5 patients with histologically confirmed GRADE I to III meningioma underwent a baseline [64Cu]SARTATE PET/CT scan on a Siemens Biograph mCT. Three patients went on

to have therapy with [^{67}Cu]SARTATE. Quantitative SPECT/CT was performed on a Siemens Intevo camera and processed using in house quantification software. Lesion analysis was performed using MIM software. On the baseline ^{64}Cu PET/CT studies, SUV_{max}, SUV_{peak} and SUV_{mean} were calculated at 1h, 4h and 24h time points. For the ^{67}Cu SPECT/CT data, quantitative data was assessed at 1h, 4h, 24h and 96h time points. **Results:** Five patients PET/CT studies were analysed. Three subjects proceeded to therapy with 11 treatments being completed. Average SUV_{max} at 1h was 15.8 (26.6 to 4.2), stable at 4h at 15.8 and reduced to 7.7 by 24h. Retention compared to 1h values were similar across SUV measures. Based on SUV_{peak}, [^{64}Cu]SARTATE retention in each patient's intracranial lesion remained high for the first 4h with average 97% retention at that time point. Between 4 and 24h, there is clearance, with 50% remaining at 24h. One patient had increasing uptake with >100% retention at 24h. Serial ^{67}Cu SPECT/CT demonstrated a similar pattern with slightly faster clearance rates. 88% retention was evident at 4h, 45% at 24h and 9% at 96h. Individual lesions demonstrated greater variation. At 4h, the retention range was 75% to 100%, at 24h, 23% to 66%, and at 96h 2% to 23%. **Conclusion:** There is excellent initial uptake of [Cu]Sartate radiopharmaceuticals into meningioma with high retention in the first 4h. Tumour clearance rates were similar between ^{64}Cu and ^{67}Cu products on this initial data. At 24h, there was approximate 50% average retention for the ^{64}Cu and ^{67}Cu. The theranostic pair of ^{64}Cu and ^{67}Cu Sartate may have a role in the management of these tumours. **References:** Hick RJ Et al: First-in-human trial of 64Cu-SARTATE PET imaging of patients with neuroendocrine tumours ....J Nucl Med. 2018 Nov 15

OP-161

Results of a Phase I/IIa study using ^{68}Ga-NeoBOMB1 in oligometastatic GIST

L. Gruber[1], *C. Decristoforo*[2], *C. Uprimny*[2], *P. Kaeopookum*[2], *L. Jimenez*[3], *G. Glatting*[4], *P. Hohenberger*[5], *S. Schönberg*[6], *F. Orlandi*[7], *M. Mariani*[7], *W. Jaschke*[1], *I. Virgolini*[2];
[1]*Department of Radiology, Medical University Innsbruck, Innsbruck, AUSTRIA,* [2]*Department of Nuclear Medicine, Medical University Innsbruck, Innsbruck, AUSTRIA,* [3]*Medical Radiation Physics/Radiation Protection, Universitätsmedizin Mannheim, Medical Faculty Mannheim, Heidelberg University, Mannheim, GERMANY,* [4]*Medical Radiation Physics/Radiation Protection, Universitätsmedizin Mannheim, Medical Faculty Mannheim, Heidelberg University; Medical Radiation Physics, Department of Nuclear Medicine, Ulm University, Mannheim, Ulm, GERMANY,* [5]*Division of Surgical Oncology and Thoracic Surgery, Medical Faculty Mannheim, Heidelberg University, Mannheim, GERMANY,* [6]*Institute of Clinical Radiology and Nuclear Medicine, University Medical Center Mannheim, Medical Faculty Mannheim, Heidelberg University, Mannheim, GERMANY,* [7]*Advanced Accelerator Applications, Colleretto Giacosa TO, ITALY.*

Aim/Introduction: Gastrin releasing peptide receptors (GRPRs) are potential molecular imaging targets in a variety of tumours. Recently, a ^{68}Ga-labelled antagonist to GRPRs, NeoBOMB1, was developed for PET. We here report on the outcome of a Phase I/IIa clinical trial (EudraCT 2016-002053-38) within the EU-FP7 project MITIGATE (grant 602306) in patients with oligometastatic gastrointestinal stromal tumours (GIST). **Materials and Methods:** The main objectives were evaluation of safety, biodistribution, dosimetry and preliminary diagnostic performance of ^{68}Ga-NeoBOMB1 in patients with advanced TKI-treated GIST using PET/CT. Nine patients with histologically confirmed GIST and unresectable primary or metastases were included. Eight patients had a documented first-line TKI-resistance to imatinib. ^{68}Ga- NeoBOMB1 was prepared using a kit procedure with a licensed ^{68}Ge/^{68}Ga generator. 3MBq/kg body weight were injected intravenously and safety parameters were assessed. PET/CT included dynamic and 1, 2 and 3-4h static PET imaging for dosimetric calculations and pharmacokinetics (including blood sampling and urine collection). Tumour targeting was assessed on a per-lesion and per-patient basis. **Results:** ^{68}Ga- NeoBOMB1 was prepared with high radiochemical purity (>97%). Patients received 176MBq (mean) corresponding to 50µg of NeoBOMB1. Treatment was well tolerated with only transient mild adverse events (maximum CTCAE grade 1) apparent within 4 weeks after application. Dosimetric calculations (n=6 patients) revealed a mean adsorbed effective dose of 0.0287±0.06mSv/MBq with highest organ doses to the pancreas (0.274 ± 0.099 mSv/MBq). Mean plasma half-life was 27.3min with primarily renal clearance (mean 25.7±5.43% of injected dose after 4h). Plasma metabolite analysis revealed good stability, but only metabolites in urine. 5 patients showed a significant tumour uptake with increasing SUV values (SUVmax 2h p.i. between 4.3 and 25.9) and contrast over time. 4 patients had no tumour specific accumulation. A correlation between CT contrast-enhancement and ^{68}Ga-NeoBOMB1 was found. **Conclusion:** This Phase I/IIa provides human safety data for ^{68}Ga-NeoBOMB1, a promising radiopharmaceutical for targeting GRPR-expressing tumours. Pharmacokinetics are suitable for PET imaging and radiation dose is comparable to other ^{68}Ga-radiopharmaceuticals in clinical routine. In this preliminary evaluation of TKI-resistant GIST patients uptake of ^{68}Ga-NeoBOMB1 was variable, potentially depending on the degree of GRPR expression. PET imaging of other tumour entities expressing GRPR, such as breast, prostate or lung cancers is currently under investigation in a continuing Phase II study possibly also leading to a theragnostic pathway with the corresponding Lu-177 counterpart. **References:** None.

OP-162

The role of FAPI-PET/CT for patients with lower gastrointestinal malignancies - first clinical experience

S. A. Koerber[1,2,3], *F. Staudinger*[4], *C. Kratochwil*[4], *T. Lindner*[4], *P. Flechsig*[4], *H. Rathke*[4], *M. Roehrich*[4], *K. Herfarth*[1,2,3], *J. Debus*[1,2,5], *U. Haberkorn*[4,6], *F. L. Giesel*[4,6,7];
[1]*Department of Radiation Oncology, Heidelberg University Hospital, Heidelberg, GERMANY,* [2]*Heidelberg Institute of Radiation Oncology (HIRO), Heidelberg, GERMANY,* [3]*National Center for Tumor diseases (NCT), Heidelberg, GERMANY,* [4]*Department of*

Nuclear Medicine, Heidelberg University Hospital, Heidelberg, GERMANY, [5]Clinical Cooperation Unit Radiation Oncology, German Cancer Research Center (DKFZ), Heidelberg, GERMANY, [6]Clinical Cooperation Unit Nuclear Medicine, German Cancer Research Center (DKFZ), Heidelberg, GERMANY, [7]German Cancer Consortium (DKTK), Heidelberg, GERMANY.

Aim/Introduction: For radiotherapy planning and oncological management, reliable staging tools are essential. Recent development of positron-emission tomography (PET) - imaging using tracers that act as fibroblast-activation-protein inhibitors (FAPI) demonstrated promising preclinical and clinical results (Ref. 1,2). The current study aimed to evaluate the role of FAPI-PET/computed tomography (CT) for primary malignancies located within the lower gastrointestinal tract. **Materials and Methods:** FAPI-PET/CT was performed in seven patients with metastasized colon cancer and three patients with metastasized rectal cancer; in addition two patients underwent FAPI-PET/CT for primary staging. All patients were referred for improved delineate target volume for planned external-beam radiotherapy. A Biograph mCT Flow scanner (Siemens, Erlangen/Germany) was used for PET/CT, imaging was performed 10min and 1h after injection of 122-312 MBq 68Ga-FAPI-04. We quantified tumor uptake by standardized uptake value (SUV) max and SUVmean (60% isocontour). **Results:** PET/CT detected multiple FAPI-positive nodes, liver lesions as well as bone and pulmonary lesions for colon and rectal cancer patients. SUVmax values ranged from 5.5 to 16.5 for patients with colon cancer and 3.7 to 14.1 for patients with rectal cancer, respectively. The highest SUVmax was observed for patients with anal cancer. The cohort demonstrated a FAPI-uptake of 17.9/ 19.1 within the primary tumor, while no suspicious lesion was detected in nodes or organs outside the pelvis. Compared to conventional imaging, we observed an excellent detection rate for FAPI-PET/CT due to eminent tumor-to-background ratio. **Conclusion:** For patients with lower gastrointestinal malignancies, FAPI-PET/CT was able to demonstrate promising results with regard to intense tumor uptake and image contrast. Considering some benefits when using FAPI imaging (no diet/ fasting, short interval between injection of the tracer and start of the exam), FAPI-PET/CT may open up new applications like staging or non-invasive tumor characterization for patients with malignant tumors of the lower gastrointestinal tract. **References:** (1) Kratochwil C, Flechsig P, Lindner T, Abderrahim L, Altmann A, et al.: FAPI-PET/CT: Mean intensity of tracer-uptake (SUV) in 28 different kinds of cancer. J Nucl Med. 2019 Apr 6. pii: jnumed.119.227967. doi: 10.2967/jnumed.119.227967. [Epub ahead of print] (2) Giesel FL, Kratochwil C, Lindner T, Marschalek MM, Loktev A, et al.: 68Ga-FAPI PET/CT: Biodistribution and Preliminary Dosimetry Estimate of 2 DOTA-Containing FAP-Targeting Agents in Patients with Various Cancers. J Nucl Med. 2019 Mar;60(3):386-392. doi: 10.2967/jnumed.118.215913. Epub 2018 Aug

OP-163

Non-invasive imaging of tumor-associated fibroblasts by^{68}Ga-FAPI-PET/CT - first experience in head and neck cancer

S. Serfling[1], *Y. Zhi*[2], *A. Schirbel*[1], *T. Lindner*[3], *A. Scherzad*[2], *S. Hackenberg*[2], *E. Gerhard-Hartmann*[4], *U. Haberkron*[3], *C. Lapa*[1], *A. Buck*[1];

[1]*Department of Nuclear Medicine, University Hospital Würzburg, Würzburg, GERMANY,* [2]*Department of ENT, University Hospital Würzburg, Würzburg, GERMANY,* [3]*Department of Nuclear Medicine, University Hospital Heidelberg, Würzburg, GERMANY,* [4]*Department of Pathology, University Würzburg, Germany, Würzburg, GERMANY.*

Aim/Introduction: Positron emission tomography/computed tomography (PET/CT) with radioactively labeled 2-deoxy-2-(^{18}F) fluoro-D-glucose(^{18}F-FDG) is the standard for nuclear medicine imaging of head and neck cancer (HNC). However, specificity of this approach is hampered by reactive or inflammatory changes that require a number of various samples for histopathological examination during diagnostic endoscopy.The fibroblast activation protein (FAP) is a transmembrane glycoprotein overexpressed by so-called "cancer-activated fibroblasts" that are present in over 90 % of epithelial carcinomas. Recently, a radiolabeled diagnostic inhibitor for non-invasive visualization of FAP was developed (^{68}Ga-FAPI). The aim of this study was to investigate the value of ^{68}Ga-FAPI in patients with newly diagnosed HNC. **Materials and Methods:** In this ongoing study, four patients with treatment-naïve primary tumors of the tonsils were enrolled. ^{68}Ga-FAPI-PET/CT was performed 1h after i.v. injection of 136-156 MBq ^{68}Ga-FAPI-04. Imaging results (including mean (SUV_{mean}) and maximum (SUV_{max}) standardized uptake values) were compared to ^{18}F-FDG-PET/CT and histolopathologic work-up. For calculation of tumor-to-normal (T/N) ratios, tumor uptake was related to uptake in the contralateral healthy tonsil. **Results:** All tonsil carcinomas were ^{18}F-FDG and ^{68}Ga-FAPI positive. SUV_{mean} and $SUV_{max}$for ^{18}F-FDG and ^{68}Ga-FAPI were 17.5±3.3 and 27.4±6.3 (^{18}F-FDG) as well as 12.5±5.5 and 18.0±5.9 (^{68}Ga-FAPI), respectively. In contrast to ^{18}F-FDG, ^{68}Ga-FAPI demonstrated higher T_{max}/N ratios of 7.8±3.2 vs. 6.1±3.3. ^{68}Ga-FAPI uptake in the tumors was confirmed by immuno-histochemical staining of the resected tissue. **Conclusion:** In comparison to ^{18}F-FDG, ^{68}Ga-FAPI could enable a better differentiation between tumor tissue and inflammatory changes. In the future, ^{68}Ga-FAPI-PET/CT might serve as a useful tool in the work-up of HNC. **References:** None.

OP-164

A Pilot Study of Anti-HER2 Affibody Molecule ^{68}Ga-MZHER2 in HER2-positive Gastric Cancer Patients

X. Guo*, N. Zhou, H. Zhu, Z. Yang;*

Peking University Cancer Hospital & Institute, Beijing, CHINA.

Aim/Introduction: The purpose of this study was to develop a HER2-targeted affibody ^{68}Ga-NOTA-MAL-MZHER2 and confirmed the possibility of clinical transformation. We measured the safety, bio-distribution of ^{68}Ga-NOTA-MAL-

MZHER2, and determine its feasibility of detecting bone metastases in HER2-positive noninvasively. **Materials and Methods:** ^{68}Ga-NOTA-MAL-MZHER2 successfully translated to clinical PET imaging [ethical approval no. 2018KT61]. Four HER2-positive and two HER2-negative gastric cancer patients with bone metastases by contrast enhanced MRI, CT or pathology were included. Whole-body PET/CT were performed at 1, 2, and 3 h after injection of approximately 185±18.5 MBq of the probe ^{68}Ga-NOTA-MAL-MZHER2. Volumes of interest were drawn on all clearly identifiable source organs to evaluate the bio-distribution of the probe. Each patient also underwent standard ^{18}F-FDG PET/CT for comparison analysis. **Results:** NOTA-MAL-MZHER2 was efficiently radiolabeled with ^{68}Ga over a 99% radio-chemical purity and 1 GBq/μmol specific activities. No adverse effects were noticed in all patients from 0 to 6 hour after tracer's injection. Regarding the bio-distribution of HER2-targeted agents ^{68}Ga-NOTA-MAL-MZHER2, predominant uptake was in kidneys and liver at 1, 2 and 3 h. And uptake was also noted in the lacrimal glands, salivary glands, spleen, and small bowel. This was different from the ^{18}F-FDG distribution. The results of the study showed that the best time for assessment of bone metastases was 2 h after the injection. Co-injection of 500 μg HER2-affibody was optimal to reduce the uptake in normal hepatic tissue. In four HER2-positive cases, 13 metastatic bone lesions could be clearly visualized by ^{68}Ga-NOTA-MAL-MZHER2 PET/CT with the SUVmax of 26.01 ± 12.36 (range, 12.3~52.6), which was significantly different from that of ^{18}F-FDG ($p < 0.001$), with the SUVmax of 6.51± 2.51 (range, 2.6~12). In two HER2-negative cases, ^{18}F-FDG showed obvious uptake (SUVmax 16.08 ± 8.67, range 7.3~28.1) of 13 metastatic bone lesions and low uptake on ^{68}Ga-NOTA-MAL-MZHER2 (SUVmax 4.0 ± 1.50, range 2~6.3). There were obviously differences among metastatic bone lesions uptake in HER2 positive and HER2 negative level in ^{68}Ga-NOTA-MAL-MZHER2 at 2 h imaging ($p< 0.0001$). **Conclusion:** We produced clinical grade ^{68}Ga-NOTA-MAL-MZHER2 agent for HER2 targeting PET imaging. And a pilot PET/CT imaging demonstrated a favorable bio-distribution, safety profile. Compared with ^{18}F-FDG, it showed better detection capability of bone metastases from HER2-positive gastric cancer. And ^{68}Ga-NOTA-MAL-MZHER2 holds a great potential for noninvasive detection of metastatic bone lesions in patients with HER2-positive gastric cancer. **References:** None.

409

Thyroid - Parallel Session: Thyroid Cancer

Sunday, October 13, 2019, 14:30 - 16:00 Lecture Hall 115

OP-165

Thyroid Imaging Reporting And Data System (TIRADS) and Tc99m-MIBI-scintigraphy for the assessment of differentiated thyroid carcinomas and follicular neoplasms

S. Schenke[1,2], R. Klett[3], P. Wagner[4], M. Zimny[5], M. C. Kreissl[1];
[1]Department of Radiology and Nuclearmedicine, University Hospital Magdeburg A.ö.R., Magdeburg, GERMANY,
[2]ÜBAG Nuclearmedicine Hanau, Giessen, GERMANY,
[3]ÜBAG Nuclear Medicine Hanau, Giessen, GERMANY,
[4]Department of Radiology and Nuclear Medicine, University Hospital Magdeburg A.ö.R., Magdeburg, GERMANY,
[5]ÜBAG Nuclearmedicine Hanau, Hanau, GERMANY.

Aim/Introduction: Thyroid Imaging Reporting And Data System (TIRADS) is helpful for sonographic risk stratification of thyroid nodules (TN). However, there is a lack of data for the TIRADS classification of the follicular variant of papillary thyroid carcinoma (FVPTC), follicular carcinoma (FTC), and follicular adenoma (FA) compared to the classical papillary thyroid carcinoma (PTC). MIBI-Imaging has a high negative predictive value for the exclusion of thyroid malignancy in hypofunctioning TN. Aim of this analysis was to compare PTC, FTC, FVPTC, and FA using three different variants of TIRADS and MIBI-Imaging. **Materials and Methods:** We retrospectively analyzed MIBI-Imaging studies performed between 2010 and 2016. Inclusion criteria were a hypofunctioning TN, available B-mode ultrasound and histopathological diagnosis. All nodules were retrospectively classified according to Kwak-TIRADS, EU-TIRADS, and K-TIRADS. MIBI-imaging (planar/SPECT images 60 minutes p.i.) was visual categorized as MIBI positive (hypointense and isointense pattern of the TN compared to the paranodular MIBI uptake) and MIBI negative (hypointense pattern of the TN). **Results:** We included 226 patients (177 female) with TN (198 benign, 28 malignant TN). Among 28 malignant TN, we found 17 (61%) PTC, 5 (18%) FVPTC, and 6 (21%) FTC. 42 (21%) of the benign nodules were FA. When using Kwak-TIRADS > 4B as as a marker for high risk nodules, we found 90.5% of the FA, 100% of the FTC, 80% of the FVPTC, and 47.1% of the PTC to be below this cutoff. We found similar results for K-TIRADS. Using EU-TIRADS 54.8% of the FA, 66,6% of the FTC, 60% of the FVPTC, and 29.3% of the PTC were classified as EU-TIRADS 3 and 4. All PTC and FVPTC were MIBI positive, and 83.3% of the FTC and 73.8 % of the FA were MIBI positive. **Conclusion:** Using TIRADS for the risk stratification of thyroid nodules, FVPTC and FTC may be missed. MIBI-imaging seems to detect FVPTC and FTC better. However, neither TIRADS nor MIBI-scintigraphy is able to differentiate between FA and FTC or FVPTC. **References:** None.

OP-166

Variations in radioiodine ablation - decision making after total thyroidectomy

O. C. Maas[1], *M. Maas*[1], *P. M. Putora*[2], *C. M. Panje*[3], *J. Blautzik*[4], *M. Brühlmeier*[5], *I. Engel-Bizik*[6], *L. Giovanella*[7], *A. Haldemann*[8], *M. E. Kamel*[9], *S. Kneifel*[10], *C. Rottenburger*[11], *N. Schäfer*[12], *M. A. Walter*[13], *S. Weidner*[14], *F. Forrer*[1];
[1]*Cantonal Hospital St. Gallen, Dept. of Radiology and Nuclear Medicine, St. Gallen, SWITZERLAND,* [2]*Dept. of Radiation Oncology, University of Bern, Bern, SWITZERLAND,* [3]*Cantonal Hospital St. Gallen, Dept. of Radiation Oncology, St. Gallen, SWITZERLAND,* [4]*Hirslanden Klinik St. Anna Luzern, Dept. of Radiology and Nuclear Medicine, Lucerne, SWITZERLAND,* [5]*Cantonal Hospital Aarau, Dept. of Radiology and Nuclear Medicine, Aarau, SWITZERLAND,* [6]*University Hospital Zurich, Dept. of Radiology and Nuclear Medicine, Zurich, SWITZERLAND,* [7]*Ospedale Regionale di Lugano Civico, Medicina nucleare e Centro PET-CT, Lugano, SWITZERLAND,* [8]*Triemli Spital Zurich, Dept. of Nuclear Medicine, Zurich, SWITZERLAND,* [9]*Hôpital du Valais, Servie Médince Nucléaire, Sion, SWITZERLAND,* [10]*Cantonal Hospital Graubünden, Dept. of Radiology and Nuclear Medicine, Chur, SWITZERLAND,* [11]*University Hospital Basel, Dept. of Radiology and Nuclear Medicine, Basel, SWITZERLAND,* [12]*CHUV Lausanne, Service Médcine Nucléaire, Lausanne, SWITZERLAND,* [13]*HUG, Service Médcine Nucléaire, Geneva, SWITZERLAND,* [14]*Inselpital Bern, Dept. of Radiology and Nuclear Medicine, Bern, SWITZERLAND.*

Aim/Introduction: The role of radioiodine treatment following total thyroidectomy for differentiated thyroid cancer is changing. At the latest, the major revision of the American Thyroid Assiciation (ATA) Management Guidelines for Patients with Thyroid Nodules and Differentiated Thyroid Cancer in 2015 [1] changed treatment recommendations dramatically in comparison to the European Association of Nuclear Medicine (EANM) 2008 guidelines [2]. We hypothesize that there is marked variability between the different treatment regimes used today. **Materials and Methods:** We performed a decision-tree based analysis of management strategies from all Swiss hospitals offering radioiodine treatment to map current practice within the community. Within this analysis [3], we collected data on treatment activities administered and treatment preparation as well as decision criteria. **Results:** Our survey clearly points out that for low risk DTC patients follow-up only after thyroidectomy is recommended in some places while being offered RIA with significant doses in other hospitals. E.g. for pT1b tumors without evidence of metastases the level of agreement ranges from 50% to 75% voting for RIT depending on histologic features; if treated administered activities of I-131 range from 1.1 GBq to 3.0 GBq. For intermediate and high risk patients radioiodine treatment is recommended in general. However, dosing and treatment preparation (rTSH vs. THW) vary distinctly. **Conclusion:** Currently existing variety between treatment recommendation after total thyroidectomy for DTC at Swiss Nuclear Medicine facilities reflects differences in clinical guidelines as different stimulation methods and activity ranges are suggested.The recently proposed different approach on RIA therapy, based on integrated post-surgery assessment and clear defined aims of RIA therapy [4] and results of ongoing prospective randomized studies are likely to reduce uncertainty in approaching RAI treatment in DTC patients. **References:** 1. Haugen, B.R., 2015 American Thyroid Association Management Guidelines for Adult Patients with Thyroid Nodules and Differentiated Thyroid Cancer: What is new and what has changed? Cancer, 2017.123(3):p.372-381. 2. Luster, M., et al., Guidelines for radioiodine therapy of differentiated thyroid cancer. European Journal of Nuclear Medicine and Molecular Imaging, 2008. 35(10): p.1941. 3. Panje, C.M., et al., Applied Swarm-based medicine: collecting decision trees for patterns of algorithms analysis. BMC Med Res Methodol, 2017.17(1):p.123. 4. Tuttle, R.M., et al., Controversies, Consensus, and Collaboration in the Use of I-131 Therapy in Differentiated Thyroid Cancer: A Joint Statement from the ATA, the EANM, the SNMMI, and the ETA. Thyroid, 2019.29(4):p.461-470.

OP-167

Braf V600E mutation analysis in low and intermediate risk papillary thyroid carcinoma

I. López Villar*, T. Navarro Martínez, P. Jane Soler, J. Bonilla Plaza, A. Martínez Lorca, J. Pérez Iruela, M. Orduña Díez;*
Ramón y Cajal University Hospital, Madrid, SPAIN.

Aim/Introduction: B-Raf protein plays a role in regulating the MAP Kinase/ERKs signaling pathway but its prognostic value in papillary thyroid carcinoma (PTC) is still a matter of debate. This study aimed to evaluate BRAF V600E impact on the radioiodine therapy decision in low and intermediate risk (PTC). **Materials and Methods:** A retrospective observational study was conducted from January 2014 to December 2016, at Universitary Hospital, of 140 patients with PTC (T1-T3N0NxM0, T1-T3N1M0). The patients were divided into two groups: The first group with BRAF V600E mutation 53% (74/140): of them 41% age < 55 years and 59% age > 55 years. The second group without BRAF V600E mutation 47% (66/140): of them 39 % age < 55 years and 61% age > 55 years. The association between clinicopathological characteristics and BRAF mutation were evaluated and also compared based on the ongoing risk stratification (age, gender, histology and tumor staging). All patients underwent a total thyroidectomy with or without lymphatic dissection. The response to treatment was evaluated one year after treatment with 131I (2,9-5,5 GBq), considering a complete response when TG was less than 1 ng / ml (after stimulation with recombinant TSHrh), antiTG antibody <20 IU and negative total body scan. Thyroid uptake of 131I was visually evaluated and graded with semiquantitative score. **Results:** We studied 140 PTC patients without distant metastases, with positive BRAF mutation in 53% (74/140). 41 men (29%) and 99 women (71%), age range from 8 to 77 years (mean 59). There was an excellent response in the first group with BRAF mutation (94% vs 90%) and also an excellent response in the second group without BRAF mutation (88% vs 92%) p> 0.05 not significant, for the two groups. Significant association was observed between BRAF mutation and gender, proportion of male with positive mutation 60% (20/41), but not associate with a worse prognosis. In the 140 PTC the somatic

BRAF mutation does not associate with less radiodine uptake according our semiquantitative score p> 0.05. **Conclusion:** No significant difference in clinical outcome, was observed between these two groups (BRAF V600E mutation status), in patients with PDT free of metastasis. Significant association was observed between BRAF mutation and gender male. No correlation with loss of radioiodine uptake at the sodium/iodine symporter (NIS) promoter in this retrospective study. Although it requires long-term evolutionary studies. **References:** None.

OP-168

Additional Value of ^{131}I SPECT/CT in the Management of Patients with Differentiated Thyroid Carcinoma

I. Marini[1,2], *M. Maussier*[1,2], *G. Perotti*[1], *M. Salvatori*[1,2];
[1]*Unità Operativa Complessa di Medicina Nucleare, Fondazione Policlinico Universitario A. Gemelli IRCCS, Roma, ITALY,* [2]*Istituto di Medicina Nucleare, Università Cattolica del Sacro Cuore, Roma, ITALY.*

Aim/Introduction: Differentiated thyroid carcinoma (DTC) is the most common endocrine cancer in adult patients (1% of all malignant tumors). Patients undergoing ^{131}I treatment or diagnostic examination are generally evaluated with planar whole-body scans only. SPECT/CT has demonstrated to be a promising tool in improving anatomical localization and detection rate. The aim of our study was to determine the additional value of SPECT/CT imaging in the assessement and in the management of patients affected by DTC. **Materials and Methods:** we retrospectively enrolled 106 patients affected by DTC (68 female, median age 45.7, range 10-86 years), who underwent ^{131}I post-therapeutic or diagnostic whole-body scan and a subsequent SPECT/CT, after total thyroidectomy, in our centre from June 2016 to December 2018. A total number of 121 whole body scans (105 post-therapeutic and 16 diagnostic) and corresponding SPECT/CT has been considered. The images were acquired within 2-3 days after oral radioiodine administration (range 1-7.4 GBq, median 3.31 GBq, for post-therapeutic scans and a median dose of 0.196 GBq for diagnostic scans). The TNM stage was determined according to the TNM classification 8th edition. Two experienced nuclear medicine physicians blindly reviewed both the planar and SPECT/CT images and separately evaluated the N and M stage, the number of metastatic lesions, the anatomical localization of uptake and the management they would have proposed for every case. **Results:** in comparison with planar imaging only, SPECT/CT helped distinguish a total number of 138 more lesions (p 0.0012). It improved anatomical localization of 112 foci of uptake. The addictional use of SPECT/CT changed the N stage in 11 cases (9.1 %) and the M stage in 32 cases (26.4%), both reducing or upgrading the stage. SPECT/CT also helped excluding a total number of 29 false positive findings. The proposed management (additional ^{131}I therapy, surgery, RT) changed in 31 cases (25.6%). In 19 cases (15.7%) the clarification of equivocal foci of uptake would have avoided further unnecessary investigations or treatments. **Conclusion:** in patients with DTC the additional use of SPECT/CT ameliorates the correct definition of the TNM stage, improving detection rate and correct localization of both nodal and metastatic lesions and reduces the number of equivocal findings on planar imaging. The changes in TNM scores may significantly influence the subsequent management of these patients. **References:** None.

OP-169

Thirteen-year Outcome of a Prospective Randomized Phase III study: 1.1 GBq and 3.7 GBq of Radioiodine Are Equally Effective in Ablation Therapy for Papillary and Follicular Thyroid Cancer

V. Ahtiainen, *L. Vaalavirta, M. Tenhunen, H. Joensuu, H. Mäenpää; Helsinki University Hospital, Comprehensive Cancer Center, Helsinki, FINLAND.*

Aim/Introduction: The optimal activity of radioiodine (I-131) administered for ablation therapy in papillary and follicular thyroid cancer after thyroidectomy remains unknown in a long-term (>10 years) follow-up. Some, shorter follow-up studies suggest that activities 1.1 GBq and 3.7 GBq are equally effective. We evaluated the long-term outcomes after radioiodine treatment to extend current knowledge about the optimal ablative dose of I-131. **Materials and Methods:** One hundred and sixty consecutive adult patients (129 females, 31 males; mean age 46 ± 14y, range 18-89 y) diagnosed with histologically confirmed papillary or follicular thyroid cancer, were randomized in a prospective, phase III, open-label, single-centre study during 2000-2004, to receive either 1.1 GBq or 3.7 GBq of I-131 after thyroidectomy. At randomization, patients were stratified according to the histologically verified cervical lymph node status and were prepared for ablation using thyroid hormone withdrawal. No uptake in the whole-body scan with I-131 and serum thyroglobulin concentration less than one ng/mL at 4-8 months after treatment was considered successful ablation. **Results:** Median follow-up time was 13.0 years (mean 11.0 ± 4.8 y; range 0.3-17.1 y). Altogether 81 patients received 1.1 GBq with successful ablation in 45 (56 %) patients. Thirty-six patients (44%) needed one or more extra administrations to replete the ablation. Of these, 4 (8.9%) and 5 (14%) patients relapsed, respectively. Of the 79 patients treated with 3.7 GBq, 45 (57%) had successful ablation after one administration of radioiodine and 34 (43%) needed several treatments. Of these, 2 (4.4%) and 9 (26.5%) patients relapsed, respectively. The groups did not differ in the proportion of patients relapsing (p=0.591). Three (1.9%) of the patients died from thyroid cancer during the follow-up, all in the higher activity group. **Conclusion:** During follow-up of median 13 years, 1.1 GBq is as effective as 3.7 GBq in the radioiodine treatment after thyroidectomy in papillary and follicular thyroid cancer. **References:** Mäenpää HO, et al., Low vs. High Radioiodine Activity to Ablate the Thyroid after Thyroidectomy for Cancer: A Randomized Study, PLoS One. 2008 Apr 2;3(4):e1885. Schlumberger M, et al., Strategies of Radioiodine Ablation in Patients with Low-Risk Thyroid Cancer, N Engl J Med. 2012 May 3;366(18):1663-73.

OP-170

Predictive factors of recurrence in patients with indeterminate or incomplete biochemical response after radio-iodine therapy in patients followed for differentiated thyroid carcinoma

M. Chafai El Alaoui[1], *A. Kelly*[1], *F. Kwiatkowski*[1], *B. Barrès*[1,2], *C. Valla*[1], *B. Lardet*[1], *M. Batisse-Lignier*[3], *I. Tauveron*[3,4], *F. Cachin*[1,2], *S. Maqdasy*[3,4];
[1]*Centre Jean Perrin, Clermont-Ferrand, FRANCE,* [2]*UMR INSERM 1240 IMOST UCA, Clermont-Ferrand, FRANCE,* [3]*CHU Gabriel Montpied, Clermont-Ferrand, FRANCE,* [4]*GReD UMR UCA - CNRS 6293 - INSERM U1103, Aubière, FRANCE.*

Aim/Introduction: The aim of this study was to identify predictive factors of recurrence in patients presenting with high stimulated serum-thyroglobulin (sTg) value on the first evaluation of response 6 to 9 months after radioiodine therapy (RAI), in differentiated thyroid carcinoma. **Materials and Methods:** This is a retrospective study from our database concerning 1688 patients followed in our center for differentiated thyroid carcinoma from 1990 to 2010. Complete response after surgery and RAI was considered for 923 patients according to the European Recommendations. Metastatic patients, patients presenting with structural disease on iodine scintigraphy performed 6 to 9 months after RAI or neck ultrasonography, or with serum thyroglobulin antibodies were excluded. Finally, 145 patients (8.5%) with isolated high value of sTg were analyzed ; mean follow-up was 8.7 years [0.6-19.7] in this population. Recurrence rate (defined as structural local or metastatic recurrence) was calculated and statistical analysis of recurrence-free survival was based on Kaplan Meier curves. Predictive factors of recurrence were identified using Log Rank tests on univariate analysis and Cox Model on multivariate analysis. **Results:** Recurrence rate was statistically different between the three groups individualized based on sTg value [sTg<1: 16/923 (1.7%); sTg 1-5µg/l: 12/111(10.8%); sTg>5: 10/34 (29.4%), $p<10^{-21}$]. The Kaplan Meyer curves show a statistically significant difference of recurrence-free survival between the three groups (Log-Rank : $Chi^2 = 57.594$ / d.d.l. = 2 ; $p < 10^{-7}$). Univariate analysis identified tumor size (T), metastatic lymph nodes (N), male sex, initial serum thyroglobulin (before RAI) and sTg as factors influencing recurrence-free survival. On multivariate analysis, only the tumor size appeared as a predictive factor of recurrence when value of sTg exceeded 5µg/l . There was no significant difference in terms of recurrence-free survival in the T1 subgroup whether sTg<1 or sTg 1-5µg/l ($p<10^{-7}$). A reduced recurrence-free survival is observed in other cases when sTg>1 ($p<10^{-5}$). **Conclusion:** A cutoff of sTg below 5 µg/l on the first evaluation of response to RAI for differentiated thyroid cancer can be considered as a good factor of long recurrence-free survival when tumor size is less than 2 cm. A reduced recurrence-free survival was observed in other cases when sTg>1. **References:** None.

OP-171

Prognosis estimation with the ratio of largest tumor diameter to total tumor diameter in multifocal T1 differentiated thyroid cancer

M. Araz, P. Akkus, C. Soydal, E. Ozkan, M. K. Kir;
Ankara University, Ankara, TURKEY.

Aim/Introduction: To evaluate the prognostic importance of the ratio of the largest tumor diameter to total tumor diameter in multifocal T1 papillary thyroid carcinoma following radioiodine ablation (RAI). **Materials and Methods:** We retrospectively reviewed 487 T1 differentiated thyroid cancer patients who received RAI were reviewed. 176 patients with multifocal tumors were included in the analysis. Diameter ratio (DR) was defined as the largest tumor diameter divided by total tumor diameter in multifocal disease. Patients were divided into two groups according to a cutoff which was determined as the mean values of total tumor diameter and DR. Relationship between DR and the the largest tumor diameter with gender, histopathological subtypes, capsular or vascular invasion, extrathyroidal extension were analyzed with Chi-Square test. Additionally to analyze the prognostic importance of DR and the largest tumor diameter, Kaplan Meier Test was used to predict the clinical outcome and the disease progression. **Results:** Multicentricity was recorded in 176/478 patients (36.1%), among which the contralateral lobe was involved in 112/478 patients (23%). Thus, a total of 176 patients aged >18y were involved (34M, 142F, mean age: 43.13 ±11.65 years min:20, max:83). Mean diameter of the largest tumor was 1.07±0.54cm (min:0.08cm,max:2cm) and mean RAI ablation dose applied was 100.38±24.93mCi (min:75, max:200mCi). Capsular and vascular invasion was found in 76/176 (43.2.%) and 10/176 (5.7%) patients respectively. Mean follow up was 103.55±42.49 months (min:20, max:228). 154/176 (87.5%) of the patients were under remission with an excellent therapy response, but disease remained persistent in 18 (10.2%) patients and recurrence was observed in 4/176 (2.3%) patients. Disease progression was found in 6/176 (3.4.%) patients. DR was significantly correlated with contralateral lobe involvement, capsular invasion and male gender ($p<0.001$, $p<0.05$ and $p<0.05$ respectively). No recurrence, persistant disease or progression was found in patients with a total tumor diameter <1cm ($p<0.05$). On survival analysis, none of these factors were found to be associated with clinical outcome and progression. **Conclusion:** The ratio of the largest tumor diameter to total tumor diameter calculated in patients with multifocal tumors was correlated with male gender, contralateral lobe involvement and capsular invasion and can be a predictive parameter for aggressiveness. However, it does not seem to be a negative prognostic factor in patients who receive radioiodine ablation treatment for multifocal papillary T1 tumors. Multifocality is not an important factor affecting clinical course of the disease in tumors with largest tumor diameter <1cm. **References:** None.

OP-172

Serum miRNAs measurements and diagnostic radioiodine whole body scintigraphy can be useful diagnostic tool in early identifying of persistent disease in differentiated thyroid cancer (DTC) patients with uninformative Tg values

A. Campenni[1], *M. Aguennouz*[2], *A. Vento*[1], *F. Polito*[2], *A. D. Comis*[1], *R. M. Di Giorgio*[2], *F. Panasiti*[1], *R. M. Ruggeri*[3], *S. Baldari*[1]; [1]*Department of Biomedical and Dental Sciences and Morpho-Functional Imaging, Nuclear Medicine Unit, University of Messina, Messina, ITALY,* [2]*Department of Clinical and Experimental Medicine, Unit of Neurology, University of Messina, Messina, ITALY,* [3]*Department of Clinical and Experimental Medicine, Unit of Endocrinology, University of Messina, Messina, ITALY.*

Aim/Introduction: Serum thyroid-tumor associated micro-RNAs (miRNAs) have been recently evaluated as novel potential biomarkers in the management of differentiated thyroid cancer(DTC), mainly in patients whose Tg is "uninformative" (e.g positive Tg-antibodies/indeterminate biochemical response). Aim of our study was to evaluate the role of miRNAs-(221,222,375,155,146b) in early detection of persistent disease in radioiodine treated DTC patients. **Materials and Methods:** We prospectively collected serum samples from 89 patients (65 F, 24 M) undergone (near)-total-thyroidectomy [(near)-TT] for papillary thyroid cancer (PTC) (n= 49) or benign thyroid disease (BTD) (n=49). miRNAs levels in bloodstream were evaluated at 131-radioiodine therapy (RaIT), 2 months after (near)-TT [basal evaluation], six [i.e. eight months after (near)-TT] (first follow-up) and twelve months later (second follow-up) in PTC patients and two and eight months after (near)-TT (basal evaluation and first follow-up, respectively) in BTD patients. miRNAs levels were also evaluated in twenty gender-age matched healthy-controls. The ratio between miRNAs levels of PTC/BTD patients and healthy-controls was reported as fold-change and considered significant if it was ≥2 and p-value ≤0.05. In PTC patients, the response to RaIT was verified at second follow-up by means of basal and rhTSH-stimulated Tg measurements, neck-ultrasonography, diagnostic 123/131-radioiodione whole body scintigraphy (Dx-WBS). Patients were classified in two categories: (I)Excellent response; (II)indeterminate/incomplete bio-chemical and/or structural response. **Results:** At basal evaluation, miRNAs levels did not differ in DTC vs BTD patients (p>0.05), but they were significantly higher in both groups of patients than in healthy controls (p<0.05). At first follow-up, all BTD patients and 41/49 DTC patients showed a reduction of miRNAs levels ≥50%. In eight DTC patients, the reduction of miRNAs (namely miR-221, miR-222 and miR-146b) levels was <50%. At second follow-up, these 8 patients had persistent loco-regional disease, as demonstrated at Dx-WBS; their miRNAs (miR-221, miR-222 and miR-146b) levels did not change compared to first follow-up. In 3/8 patients, basal-Tg was less than 1 ng/ml while in 2 cases basal-Tg was ≥1 ng/ml. In 3 patients, TgAb levels did not decrease. The remaining 41 DTC patients showed an excellent-response to RaIT at second follow-up. **Conclusion:** In our PTC patients, response to RaIT was early predicted by serum miRNAs levels reduction six months after RaIT. A reduction rate <50% of miRNAs 221,222 and 146b should be considered predictive of persistent disease, thus suggesting a more aggressive follow-up. Dx-WBS allowed to identify all patients with persistent disease, confirming to be a useful tool in DTC follow-up. **References:** None.

410

Clinical Oncology - Parallel Session: Lung, Head & Neck and More

Sunday, October 13, 2019, 14:30 - 16:00 Lecture Hall 116

OP-173

FLT-PET And FDG-PET/CT For The Detection Of Relapse Following Definitive Radiotherapy In Non-small Cell Lung Cancer. Preliminary Results

T. Christensen[1,2], *S. W. Langer*[3], *K. R. Larsen*[4], *G. F. Persson*[5], *A. G. Amtoft*[1], *H. H. Johannesen*[1], *S. H. Keller*[1], *A. Kjær*[1,2], *B. M. B. Fischer*[1]; [1]*Dept. of Clinical Physiology, Nuclear Medicine & PET, Rigshospitalet, University of Copenhagen, Copenhagen, DENMARK,* [2]*Cluster for Molecular Imaging, University of Copenhagen, Copenhagen, DENMARK,* [3]*Dept. of Oncology, Rigshospitalet, University of Copenhagen, Copenhagen, DENMARK,* [4]*Dept. of Pulmonary Medicine, Bispebjerg Hospital, University of Copenhagen, Copenhagen, DENMARK,* [5]*Dept. of Oncology, Herlev Hospital, University of Copenhagen, Copenhagen, DENMARK.*

Aim/Introduction: Diagnosing relapsed lung cancer after radiotherapy is challenging. CT and ^{18}F-fluorodeoxyglucose (FDG)-PET/CT have a low specificity in this setting. Further, changes may evolve differently after normofractionated radiotherapy (nRT) and stereotactic body irradiation (SBRT). ^{18}F-fluorothymidine (FLT)-PET is considered a more cancer specific tracer compared to FDG-PET. Therefore, we investigated if FLT-PET could improve diagnosis of relapse in patients treated with nRT and SBRT. **Materials and Methods:** Lung cancer patients suspected for relapse after radiotherapy were consecutively included in this prospective clinical study. Patients were stratified dependent on initial treatment: nRT or SBRT. FDG-PET/CT and FLT-PET/CT were conducted no more than three weeks apart. PET scans were evaluated visually, blinded for previous PET-scans. Lung lesions were evaluated as malignant, benign or inconclusive. FDG- and FLT-PET from the same patient were evaluated at least three months apart. Maximum standardized uptake value (SUV_{max}) was measured in the worst graded lesion in each patient. Differences in malignant vs benign lesions were tested with an independent t-test. Sensitivity and specificity were analysed for FDG-PET/CT and FLT-PET. The reference standard was based on histology if available, otherwise on independent review of subsequent imaging, conference decisions, and clinical course within 6 months after FLT-PET. **Results:** We present the results from the

first 40 patients. All patients had radiotherapy for non-small cell lung cancer; nRT to 66 Gy (n=20) or SBRT to 45-66 Gy (n=20). Twenty-two patients received concurrent chemotherapy (19 nRT-patients; 3 SBRT-patients). FLT-PET was performed 35-581 days after radiotherapy (median 225 days). FDG- and FLT-PET were conducted 1-17 days apart (median 6 days). During follow up, 12/20 nRT-patients and 10/20 SBRT-patients had relapse. SUV_{max} was significantly higher in relapsed vs benign lesion within the entire cohort (mean FDG-SUV_{max}: 10.9 (95 % CI: 8.5-13.3) vs. 5.1 (3.4-6.9); p<0.001; mean FLT-SUV_{max}: 4.3 (3.1-6.5) vs. 2.5 (1.8-3.3); p=0.007). The sensitivity of FDG-PET/CT was 100 % (95 % CI: 85-100 %) within the entire cohort. The specificity of FDG-PET/CT was 61 % (36-83 %); lowest in nRT-patients (50 % vs. 70 %). The sensitivity of FLT-PET was 64 % (41-83 %), lowest in nRT-patients (58 vs. 70 %). The specificity of FLT-PET was 100 % (81-100 %). **Conclusion:** FDG-SUV_{max} and FLT-SUV_{max} were higher in lesions with relapse than benign lesions. The specificity of FLT-PET was 100 %, making FLT-PET promising for non-invasive diagnosis of relapse after RT with the potential to obviate invasive procedures in some patients. **References:** None.

OP-174

A comparison of quantitative and qualitative assessment for the diagnosis of malignancy in solitary pulmonary nodules using ^{18}Fluorine Fluorodeoxyglucose Positron Emission Tomography/Computed Tomography (PET-CT) in the multicentre SPUtNIk trial

S. Dizdarevic[1], *J. R. Weir-McCall*[2], *S. Harris*[3], *L. A. Little*[4], *J. Jones*[5], *K. A. Miles*[6], *R. C. Rintoul*[7], *N. R. Qureshi*[8], *J. Madden*[4], *K. Eichhorst*[4], *L. Durcan*[4], *K. Cozens*[4], *L. Pike*[9], *D. Sinclair*[9], *R. Eaton*[10], *A. Shah*[10], *L. Brindle*[11], *A. Cook*[4], *S. George*[3], *on behalf of the SPUTNIK investigators, F. Gilbert*[2];
[1]*Imaging and Nuclear Medicine Department, Brighton and Sussex University Hospitals NHS Trust, Brighton, UNITED KINGDOM,* [2]*Department of Radiology, University of Cambridge School of Clinical Medicine, Cambridge, UNITED KINGDOM,* [3]*Public Health Sciences and Medical Statistics, University of Southampton, Southampton, UNITED KINGDOM,* [4]*Southampton Clinical Trials Unit, University of Southampton, Southampton, UNITED KINGDOM,* [5]*Centre for Innovation and Leadership in Health Sciences, University of Southampton, Southampton, UNITED KINGDOM,* [6]*Institute of Nuclear Medicine, University College London, London, UNITED KINGDOM,* [7]*Department of Thoracic Oncology, Papworth Hospital, Cambridge, UNITED KINGDOM,* [8]*Department of Radiology, Royal Papworth Hospital NHS Foundation Trust, Cambridge, UNITED KINGDOM,* [9]*Division of Imaging Sciences and Biomedical Engineering, King's College London, London, UNITED KINGDOM,* [10]*Radiation Protection Department, East and North Hertfordshire NHS Trust, Stevenage, UNITED KINGDOM,* [11]*Faculty of Health Sciences, University of Southampton, Southampton, UNITED KINGDOM.*

Aim/Introduction: 18Fluorine-Fluorodeoxyglucose-Positron Emission Tomography-Computed Tomography (PET-CT) plays a key role in the characterisation of indeterminate solitary pulmonary nodules (SNPs). Both qualitative scoring of the nodule uptake in reference to the mediastinal blood pool and quantitative scoring using SUVmax have been proposed. To date these have been examined in single centre, single vendor or retrospective multicentre descriptive studies. The objective of our study was to compare qualitative and quantitative criteria for the diagnosis of SNPs in a prospective multicentre multivendor environment. **Materials and Methods:** 380 (M 53%, F 47%) patients were recruited to the SPUtNIk trial at 16 sites accredited by the UK PET Core Lab. The inclusion criteria were the presence of a dominant SPN on CT ≥8 and ≤30 mm on axial plane with no ancillary evidence of malignancy. PET-CT scans were analysed and reported locally by PET physicians. Qualitative assessment used a five-point scale compared to the mediastinal blood pool. Quantitative measures included SUVmax. The study's end points were: the diagnosis of lung cancer via biopsy/histology or a diagnosis of benign or non-lung cancer via either biopsy or radiological 2-year follow-up. Receiver Operating Characteristic (ROC) curve analysis was performed for the ordinal grading and SUVmax, with sensitivity and specificity calculated at a prespecified SUVmax cutoff of 2.5, and a visual score of uptake equal to or greater than the mediastinum. Exploratory analysis of SUVmax as a continuous variable was also performed. **Results:** 311 (81.8%) participants with a baseline PET/CT completed follow-up with an outcome status at two years. The overall incidence of lung cancer was 61% (189/311). Mean size diameter of SPN was 15.4±5.4mm at baseline CT. The area under the ROC were 0.81 (95% CI 0.77; 0.86) for qualitative grading and 0.85 (95% CI 0.81;0.90) for SUVmax. The sensitivity and specificity were 77.8% (95% CI 71.3;83.1%) and 74.6% (66.2;81.5%) for qualitative uptake ≥ the mediastinal blood pool and 75.1% (95% CI 68.5;80.8%) and 80.8% (95% CI 72.9;86.9%) for pre-specified SUVmax cutoff of ≥2.5 The optimal SUVmax threshold with the best balance between sensitivity and specificity was ≥1.95, which yielded a sensitivity, specificity and diagnostic accuracy of 87.3 (95% CI 81.8;91.3%), 70% (95% CI 61.3;77.5%), 80.1 (95 CI 75.3;84.1%), respectively. **Conclusion:** In this multicentre multivendor prospective study, quantitative analysis was more accurate than qualitative grading of the nodule uptake for the diagnosis of malignancy in solitary pulmonary nodules with the optimal SUVmax threshold of ≥1.95. **References:** None.

OP-175

Assessment of Pulmonary Lobar Perfusion Fraction and Prediction of Postoperative Function in Lung Cancer Patients

C. von Nida[1], *L. Titze*[2], *P. T. Meyer*[1], *B. Passlick*[2], *C. Goetz*[1];
[1]*Department of Nuclear Medicine, Medical Center of the University of Freiburg, Faculty of Medicine, University of Freiburg, Freiburg, GERMANY,* [2]*Department of Thoracic Surgery, Medical Center of the University of Freiburg, Faculty of Medicine, University of Freiburg, Freiburg, GERMANY.*

Aim/Introduction: When planning surgical treatment of

lung cancer, preoperative assessment of the lung function is an established tool to predict the expected residual function after surgery in particular in patients with borderline function. Lung perfusion scans are recommended in clinical routine - however multiple quantification methods are described and used to predict the postoperative function. The aim was to compare the prediction accuracy of planar and truly 3D-analysis methods based on CT-anatomy in a pre-operative pool of patients. **Materials and Methods:** 100 patients (mean age 68+/-8 years, 63% male) bearing operable lung cancer with borderline lung function were referred to pre-operative lung quantification and included. Perfusion planar- and SPECT-data with subsequent low-dose CT were acquired after injection of 174+/-9 MBq Tc99m-MAA (Siemens Symbia Intevo 6, Siemens Healthcare GmbH, Erlangen, Germany) and reconstructed. Planar analysis was performed using the model-based (upper, median and lower vertical zone) Mende approach (T. Mende et al., Nucl Med, 1990) for the calculation of the lobar fractions. 3D-analysis used a CT-based segmentation and VOI transfer to the co-registered perfusion-SPECT (3D-Lung Quantification, HERMES Medical Solutions, Stockholm). All patients underwent pulmonary function tests (PFT) including FEV1 and DLCO prior to surgery. This PFT-assessment was used in combination with the scintigraphic planar and 3D lobar fractions to calculate the predicted FEV1 and DLCO according to the extent of the pulmonary resection. Comparison between the predicted values for each method (n=100) as well as a direct comparison to post-operative PFT-values (n=16, subgroup of operated patients) were performed using T-tests, Correlation tests and Bland-Altman analyses. **Results:** In our population significant differences ($p<0.05$) were found between the results from planar imaging and 3D-methods for the right upper lobe (23% of the tumors) and the left lower lobe (11% of the tumors). Correlation between predicted and measured PFT was also higher for the 3D-analysis compared to the Mende approach (Spearman's correlation coefficient 0.62 vs 0.45). **Conclusion:** The lobar perfusion values obtained by an anatomically driven 3D-quantification differed significantly from the ones obtained from the traditional planar approach in 34% of the patients in our group and showed the most accurate prediction of post-operative PFTs - affecting potentially the operability of the tumors in individual patients. Considering these preliminary results, we recommend using 3D-anatomically driven methods whenever available. **References:** None.

OP-176

First comparison of [18F]-FMISO and [18F]-FAZA for PET imaging of hypoxia in lung cancer before surgery

S. Thureau[1,2], *N. Piton*[3], *P. Gouel*[2], *R. Modzelewski*[2], *A. Dujon*[4], *J. Baste*[5], *J. Melki*[5], *P. Rinieri*[5], *C. Peillon*[5], *S. Hapdey*[2], *J. Sabourin*[3], *J. Picquenot*[6], *P. Bohn*[2], *P. Vera*[2];

[1]*Department of Radiation Oncology, Henri Becquerel Cancer Center and Rouen University Hospital, & QuantIF – LITIS [EA (Equipe d'Accueil) 4108], Rouen, FRANCE,* [2]*Department of Nuclear Medicine, Henri Becquerel Cancer Center and Rouen University Hospital, & QuantIF – LITIS [EA (Equipe d'Accueil) 4108 – FR CNRS 3638], Faculty of Medicine, University of Rouen, Rouen, FRANCE,* [3]*Rouen University Hospital, Department of Pathology and Normandie University, UNIROUEN, Inserm U1245, Rouen University Hospital, Rouen, FRANCE,* [4]*Clinic of Cedre, Rouen, FRANCE,* [5]*Unit of General and Thoracic Surgery, Rouen University Hospital, Rouen, FRANCE,* [6]*Department of Pathology, Henri Becquerel Cancer Center, Rouen, FRANCE.*

Aim/Introduction: Hypoxic areas are typically treatment resistant areas especially radiotherapy. For NSCLC, several studies have proposed to increase the dose of radiotherapy on these volumes defined by FMISO. In Head and Neck cancers, the same approach was performed with FAZA or FMISO, but these two tracers have never been compared in NSCLC. **Materials and Methods:** 20 patients were included before surgery for localized NSCLC cancer and benefited from three pre-surgical PET scans: FDG-PET, FMISO-PET and FAZA-PET. For each patient, the PET data of the three tracers were compared with each other, and compared to immunohistochemical analysis (CD34, GLUT-1, CAIX, LDH-5, MCT-4, HIF1-Alpha) after tumor removal. **Results:** 19 patients were definitively included in this trial: 4 women and 15 men, with a mean age of 67 ± 7.4 years. For FDG PET, the SUVmax was 12.3 (± 5.4) and the volume with a thresholding at 40% of SUVmax was 23.2 cc (± 19.2). 18 lesions had a significant uptake (SUV max greater than 1.4) for the F-Miso and 17 for FAZA. The mean SUV max was respectively 3 (± 1.36) with a mean volume of 25.8 cc (± 25.8) for FMISO and 2.16 (± 0.7) with a mean volume of 13.06 cc (± 13.76) for FAZA. The SUV max F-Miso was greater than SUV max FAZA ($p= 0.0003$).There was a good correlation between the SUV max F-Miso and SUV max FAZA at 0.88 (0.72 to 0.95) and a good correlation at 0.732 (0.42 to 0.89) for the volume with a thresholding at 1.4 but there were no correlation between SUV max FDG and SUV max F-Miso nor FAZA. The immunohistochemical analysis was not correlated to hypoxia PET whatever the staining. **Conclusion:** This study confirms the very good correlation of the two tracers of hypoxia and the superiority of FMISO over FAZA. Unfortunately, there is no correlation with immunohistochemical analysis. **References:** None.

OP-177

Breath-Hold with High-Resolution, High-Sensitivity SiPM PET/CT: Higher FDG Uptake Detected in Neoplastic Lung Nodules

M. Jreige, *M. Meyer, G. Allenbach, M. Pappon, M. Nicod Lalonde, N. Schaefer, J. O. Prior;*

Lausanne University Hospital, Lausanne, SWITZERLAND.

Aim/Introduction: Accurate pulmonary nodules characterization is highly important considering its impact on management and prognosis. The introduction of the latest PET/CT scanners combing ultra-dynamic range, high-sensitivity detector technology (SiPM), faster time-of-flight and breath-hold (BH) application may allow optimal visualization and

uptake quantification in smaller lesions. Herein, we investigated the outcome of a single 20-second-BH PET/CT acquisition as compared to the standard free-breathing (FB) one and its effects on metabolic lung nodule characterization. **Materials and Methods:** We retrospectively analyzed all PET/CT examinations from June 2018 to March 2019 acquired on a Siemens Biograph Vision 600 with a lung dedicated BH-acquisition in addition to standard FB-acquisition. Only nodules confirmed malignant on histopathological analysis or considered highly suspicious for primary or secondary malignancy based on their radiologic progression on CT scan were included and metabolic characteristics (SUVmax, SUVmean, MTV, TLG and Signal-to-Background Ratio=SBR) were compared between both acquisitions. **Results:** Forty nodules reported as highly suspicious in 30 patients were included. The mean nodule size, SUVmax, SUVmean, MTV, TLG and SBR were 12.4±5.3mm, 9.3±7.4g/mL, 5.3±4.4g/mL, 1.4±2cm³and 10.2±23.9g and 23.9±22.2(1) in FB and 13.2±5.3mm, 14.4±10.7g/mL, 7±4.8g/mL, 1.3±1.6cm³, 13.3±28.8g and 45.9±37.9(1) in BH, respectively. Both SUVmax and SBR were significantly higher in BH compared to FB, p=0.016 and p=0.002, respectively. Concordance analysis showed a statistically significant increase of 45%, 20% and 70% of the SUVmax, TLG and SBR values in BH compared to FB. Using BH, MTV was comparable and lung background was slightly, but significantly lower (-4%, p=0.03). **Conclusion:** BH with high-resolution, high-sensitivity latest generation SiPM PET/CT allowed to detect higher metabolic activity in lung nodules categorized as highly suspicious with a better visualization due to a higher SBR in comparison to FB. This increased detectability may help to increase the sensitivity and specificity of malignant nodule PET/CT characterization. **References:** [1] Sonni I, Baratto L, Park S, et al. Initial experience with a SiPM-based PET/CT scanner: influence of acquisition time on image quality. EJNMMI Phys. 2018 Apr 18;5(1):9. [2] Johnson GB, Peller PJ, Kemp BJ, et al. Future of thoracic PET scanning. Chest. 2015 Jan;147(1):25-30.

OP-178

18 Fdg Pet Ct Therapeutic And Pronostic Impact In The Initial Assessment Of Head And Neck Squamous Cell Carcinomas A Retrospective Study Of 477 Patients

J. Leclere[1], *O. Delcroix*[2], *P. Robin*[2], *S. Querellou*[2], *P. Le Roux*[2], *C. Guezennec*[2], *L. Ollivier*[3], *U. Schick*[3], *J. Rousset*[4], *G. Valette*[1], *R. Abgral*[2];
[1]*Department of Head and Neck Surgery, Brest University Hospital, Brest, FRANCE,* [2]*Department of Nuclear Medicine, Brest University Hospital, Brest, FRANCE,* [3]*Department of Radiotherapy, Brest University Hospital, Brest, FRANCE,* [4]*Department of Radiology, Brest Military Hospital, Brest, FRANCE.*

Aim/Introduction: Accurate initial staging of head and neck squamous cell carcinoma (HNSCC) is essential for appropriate treatment planning and outcome prediction. 18-FDG PET-TDM performance to detect regional lymph node metastasis, distant metastasis or synchronous primary cancer has already been demonstrated. The objective of this study was to evaluate 18-FDG PET/CT therapeutic and prognostic impact in the initial assessment of patients with HNSCC cancer. **Materials and Methods:** From 2004 to 2014, 477 consecutive patients with HNSCC were included (414M/63W; mean age 62). Conventional work-up (CWU) with clinical examination, endoscopy, cervical contrast-enhanced CT and/or contrast-enhanced MRI and chest CT, was compared with 18-FDG PET/CT. A group of cancer specialists met to determine if 18-FDG PET/CT had caused an impact on the therapeutic decision, classifying changes as minor - type 1 (modification of NM staging and/or discovery of synchronous cancer), moderate - type 2 (modification of the surgical procedure or target volume in radiotherapy) or major - type 3 (change of treatment type). Three-year follow-up data were collected. **Results:** A total of 221 patients (46.3%) were affected by any therapeutic impact, and 94 of them (19.5%) had different treatment due to 18-FDG PET/CT (type 2 or 3). Type 2 and 3 therapeutic impact was statistically equivalent between the stage I/II subgroup and the stage III/IV subgroup (p=0.02). 3-year overall survival of patients with 18-FDG PET/CT upstaging was significantly lower than patients with identical staging (44.2% vs 59.8% respectively, p=0.002). In the CWU stage I/II subgroup, 29 of them (22%) upstaged to stage III/IV following the 18-FDG PET/CT; their 3-year overall survival was significantly lower than that of concordant stage I/II patients (54.8% vs 82.6%, p=0.001). CWU stage III/IV patients with 18-FDG PET/CT downstaging had better overall survival than others (64.8% vs 44.4% p=0.01). **Conclusion:** Systematic 18-FDG PET/CT in the initial assessment of HNSCC should be discussed at any stage since it allows restaging with a significant impact on therapeutic management. **References:** None.

OP-179

^{18}F-FDG-PET/CT for the assessment and prognostication Cardiac Tumors

J. Meng[1], *X. Li*[2], *H. Zhao*[3], *M. Yun*[3], *W. Dong*[3], *M. Kreissl*[4], *X. Zhang*[3];
[1]*Beijing Anzhen Hospital, Capital Medical University, BeiJing, CHINA,* [2]*Medical University of Vienna, Vienna, AUSTRIA,* [3]*Beijing Anzhen Hospital, Capital Medical University, BeiJing, CHINA,* [4]*University Hospital Magdeburg, Magdeburg, GERMANY.*

Aim/Introduction: We sought to evaluate ^{18}fluorine-fluorodexoyglucose (^{18}F-FDG) PET/CT in distinguishing benign from malignant tumors, and for predicting all-cause mortality in patients with cardiac neoplasias. **Materials and Methods:** We retrospectively analyzed consecutive diagnosed patients with cardiac tumors (n = 58) undergoing ^{18}F-FDG PET/CT for staging. Thirty-three ("performance population": 20 female, age 51 ± 13 years) had histopathological data, the gold standard in assessing performance of the ^{18}F-FDG variables, maximum standardized uptake value (SUV_{max}) and maximum tumor to background ratio (TBR_{max}). Optimal SUV_{max} and TBR_{max} cut-offs identifying malignancy were derived by receiver-operating characteristics analysis, then used to stratify 54 patients with follow-up data ("survival population": 28 female, age 51 ± 14 years) into "benign" or "malignant subgroups;" subgroups' overall

survival, assessed by Kaplan-Meier methodology, was compared by log-rank testing. Prognostic power was evaluated by Cox regression analysis. **Results:** In the performance population, 13 patients had benign, 21 malignant cardiac lesions, by histopathology. Calculated optimal cut-offs indicating malignancy were: SUV_{max}=4.22, with 100% sensitivity/91.7% specificity vs TBR_{max}=1.6, with 100% sensitivity/ 91.7% specificity. Mean SUV_{max} and TBR_{max} were significantly lower in patients with benign primary tumors (n=13) versus their counterparts with malignant primary tumors (n =9) or secondary tumors (n = 11) (SUV_{max}: 2.43 ± 1.56 versus 9.96 ± 4.02 versus 15.94 ± 7.69; TBR_{max}: 1.09 ± 0.63 versus 4.12 ± 1.44 versus 6.83 ± 3.22; all p < 0.001). Lifespan was significantly shorter in malignant subgroups versus corresponding benign subgroups (p=0.001). SUV_{max} ≥4.22 and TBR_{max} ≥1.59 independently predicted mortality (respective hazard ratios [95% CIs] 9.54, [2.18-41.84], p = 0.003, 47.434, [1.399-1608], p = 0.032). **Conclusion:** In patients with cardiac tumors, ^{18}F-FDG uptake can be used to differentiate benign versus malignant lesions with high accuracy, and to foretell mortality. **References:** None.

OP-180

Metabolic Behavior And Prognostic Role Of Pretreatment ^{18}F-FDG PET/CT In GIST

D. Albano[1,2], *M. Bonacina*[1], *R. Durmo*[1], *E. Cerudelli*[1], *M. Gazzilli*[1], *F. Dondi*[1], *A. Mazzoletti*[1], *P. Bellini*[1], *F. Bertagna*[3], *R. Giubbini*[3];
[1]*Spedali Civili Brescia, Brescia, ITALY,* [2]*Univeristy of Brescia, Brescia, ITALY,* [3]*Spedali Civili Brescia and University of Brescia, Brescia, ITALY.*

Aim/Introduction: Our aim was to investigate the metabolic features of GIST and whether the tumor stage, tumor risk group, epidemiological (age, gender), histological (Ki-67 index, mitotic index) and morphological (tumor size) variables might be related to 18F-FDG-PET/CT results. Moreover, we investigated the prognostic impact of baseline PET/CT parameters on outcome survival. **Materials and Methods:** Thirty-five patients with histologically proven GIST were retrospectively enrolled; all patients underwent baseline 18F-FDG-PET/CT before any treatment. The PET images were analyzed visually and semi-quantitatively by measuring the maximum SUVbody weight (SUVbw), SUVlean body mass (SUVlbm), SUVbody surface area (SUVbsa), metabolic tumor volume (MTV) and total lesion glycolysis (TLG). For the entire population, receiver operating characteristic curve analysis was used to identify the optimal cutoff point of semiquantitative parameters in the light of PFS and OS. Survival curves were plotted according to the Kaplan-Meier method. **Results:** Twenty-nine (82%) patients had positive 18F-FDG-PET/CT, while the remaining 6 had no increased FDG-uptake. 18F-FDG-avidity was significantly associated with mitotic index, tumor stage and tumor risk group and not correlated with other features. Semiquantitative PET/CT parameters correlated only with tumor risk group. At a median follow-up of 36 months, progression of disease occurred in 16 patients with an average time of 21 months; death occurred in 7 with an average of 36 months. The estimated 2-year PFS and OS rates were 60% and 78%, while 3-year PFS and OS rates were 41% and 75% respectively. In multivariate analysis, only baseline MTV, TLG and positive PET/CT confirmed to be independent prognostic factors for PFS (p=0.032, p=0.046 and p=0.045). No metabolic parameters were correlated with OS. **Conclusion:** In conclusion, we have demonstrated that 18F-FDG pathological uptake in GIST occurred in 82% of the population evaluated, being independently associated with mitotic index, stage and tumor risk groups. Semiquantitative metabolic PET/CT parameters (SUVbw, SUVlbm, SUVbsa, MTV and TLG) were not correlated with any histological, epidemiological and morphological features analyzed except of tumor risk group. Moreover FDG-avidity and the metabolic tumour features (MTV and TLG) were the only parameters significantly correlated with survival rates. **References:** None.

404b

Mini Course 2 - Interactive - Technologist Committee: Stress Testing for Technologists

Sunday, October 13, 2019, 15:45 - 16:45 Lecture Hall 117

OP-181

Stress Testing for Technologists

M. Attard;
Isala, Radiology and Nuclear Medicine Department, Zwolle, NETHERLANDS.

501

CME 4 - Radiopharmacy + Drug Development + Translational and Molecular Imaging Therapy + Oncology & Theranostics Committee: Role of Extracellular Matrices in Cancer and Other Diseases

Sunday, October 13, 2019, 16:30 - 18:00 Auditorium

OP-182

Extra Cellular Matrix - A Target in the Future?!

M. Behe;
Paul Scherrer Institut, Centre of Radiopharmaceutical Sciences, Villigen, SWITZERLAND.

OP-183

Molecular Imaging of Collagen and Oxidized Collagen in Fibrosis

P. Caravan;
Massachusetts General Hospital (MGH) & Harvard Medical

School (HMS), Athinoula A. Martinos Center for Biomedical Imaging, Charlestown, MA, UNITED STATES OF AMERICA.

OP-184
Imaging of Activated Fibroblasts in ECM
U. Haberkorn;
Heidelberg University Hopsital, Department of Nuclear Medicine, Heidelberg, GERMANY.

502
Joint Symposium 7 - Physics + Dosimetry Committee / AAPM: Interventional Nuclear Medicine

Sunday, October 13, 2019, 16:30 - 18:00 Lecture Hall 311

OP-185
Nuclear Medicine Approaches in Guiding Surgical Procedures - Review and Current Status
F. Van Leeuwen;
Leiden University Medical Center, Interventional Molecular Imaging Laboratory, Leiderdorp, NETHERLANDS.

OP-186
Methodological Aspects of PET/CT Guided Interventions
A. Kirov;
Memorial Sloan-Kettering Cancer Center, Department of Medical Physics, New York, NY, UNITED STATES OF AMERICA.

OP-187
Future Perspectives of Radioembolization Interventional Methods
M. Lam;
University Medical Center Utrecht, Department of Radiology and Nuclear Medicine, Utrecht, NETHERLANDS.

OP-188
NM Guided Focused Ultrasound - A Potential Future Application
A. Melzer;
University of Leipzig, Innovation Centre for Computer Assisted Surgery, Leipzig, GERMANY.

OP-189
All Speakers: Panel Discussion, Questions

503
Joint Symposium 8 - Cardiovascular Committee / EACVI: Which Strategy for the Evaluation of Patients at the Time of Multi-Modality Cardiac Imaging?

Sunday, October 13, 2019, 16:30 - 18:00 Lecture Hall 312

OP-190
Which Role for Cardiac CT(A) in CAD?
D. Andreini;
Centro Cardiologico Monzino, Milan, ITALY.

OP-191
Which Role for MPI in CAD?
J. Knuuti;
Heart and PET Centre, Turku, FINLAND.

OP-192
Which Role for Cardiac MRI in Infiltrative Cardiomyopathies?
M. Fontana;
Royal Free Hospital, UCL, London, UNITED KINGDOM.

OP-193
Which Role for SPECT and PET in Infiltrative Cardiomyopathies?
O. Lairez;
University Hospital Toulouse, Toulouse, FRANCE.

505
M2M - Parallel Session: Radiolabelled Peptides and Proteins

Sunday, October 13, 2019, 16:30 - 18:00 Lecture Hall 111

OP-194
Preclinical theranostic study of anti TEM-1 scFv-Fc fusion proteins
J. Delage[1], *A. Faivre-Chauvet*[2], *J. Fierle*[3], *N. Schaefer*[1], *G. Coukos*[1], *S. Dunn*[3], *J. Prior*[1], *D. Viertl*[1];
[1]*Lausanne University Hospital and University of Lausanne, Lausanne, SWITZERLAND,* [2]*Nantes University Hospital and University of Nantes, Nantes, FRANCE,* [3]*Ludwig Center for Cancer Research and University of Lausanne, Lausanne, SWITZERLAND.*

Aim/Introduction: TEM-1 (tumor endothelial marker-1) is a single pass transmembrane cell surface glycoprotein and has been described as a suitable and safe candidate for cancer therapy. Therefore, a panel of anti TEM-1 scFv-Fc fusion antibody constructs isolated from naïve human antibody by phage display has been developed in Lausanne. We decided to radiolabel and study them in vitro in a novel theragnostic approach paradigm. **Materials and Methods:** Four scFv-Fc fusion antibody constructs tested for purity (electrophoresis) and affinity to TEM-1 (flow cytometry) were used (2B11, 78Fc, 1C1, 1C1m). Each fragment was conjugated to p-SCN-Bn-DOTA using different excess molar ratio in buffer pH 9. After a 1-hour coupling reaction time, the non-coupled ligand was eliminated by ultrafiltration on 50kD filters. The number of chelates grafted by antibody was evaluated both with a radiolabeling test and mass spectrometry analysis (MALDI). The immune fraction of the modified antibody was measured by flow cytometry, using TEM-1 positive (SK-N-AS, neuroblastoma) and negative (HT-1080, fibrosarcoma) cells lines The purity and the stability of the native and of the conjugated antibodies were evaluated up to one year by HPLC. Each fragment of antibody (500pmol) was labeled with ^{177}Lu (non-carrier added, 20MBq) in ammonium acetate buffer (0,4M; pH 5,6). To determine radiolabeled antibody immunoreactivity, Lindmo assays were performed on SK-N-AS cell lines **Results:** Purity of scFv-fc fragments were confirmed by electrophoresis. MALDI analysis showed that the concentration of 20 equivalents of DOTA (4 to 6 DOTA fixed per antibody) was the best for the radiolabeling. In flow cytometry, the binding of conjugated fragments was similar to the native antibodies showing that the conjugation did not affect TEM-1binding. HPLC profile of the native fragments and of the conjugated antibodies was stable at one year. The labeling with ^{177}Lu was successful with a radiochemical purity up to 95%. Immunoreactivity of 2B11 and 78Fc was less than 20% whereas immunoreactivity of 1C1m and 1C1 was respectively 80% and 90%. **Conclusion:** We could select 2 fusion antibodies candidates (1C1 and 1C1m) with successful radiolabeling and radioimmunoreactivity properties. The next step will be to test them in vivo in murine xenografts models with biodistribution and therapeutic studies towards a future translation in patients. **References:** None.

OP-195

Comparison Of Affibody- And Antibody Fragments-based Caix Imaging Probes In Mice Bearing Renal Cell Carcinoma Xenografts

J. Garousi[1], *F. Huizing*[2], *A. Vorobyeva*[1], *B. Mitran*[3], *K. Andersson*[4], *C. Dahlsson Leitao*[4], *F. Frejd*[1], *J. Löfblom*[4], *J. Bussink*[2], *A. Orlova*[3], *S. Heskamp*[5], *V. Tolmachev*[1];
[1]*Department of Immunology, Genetics and Pathology, Uppsala University, Uppsala, SWEDEN,* [2]*Department of Radiation Oncology, Radboud University Medical Center, Nijmegen, NETHERLANDS,* [3]*Department of Medicinal Chemistry, Uppsala University, Uppsala, SWEDEN,* [4]*Department of Protein Science, KTH Royal Institute of technology, Stockholm, SWEDEN,* [5]*Department of Radiology and nuclear medicine, Radboud University Medical Center, Nijmegen, NETHERLANDS.*

Aim/Introduction: Carbonic anhydrase IX (CAIX) is a molecular target for several types of anti-cancer therapeutics. Hypoxia-independent overexpression of CAIX is frequent in renal cell carcinomas (RCC) and might be used for targeted treatment of disseminated tumors. However, CAIX can be expressed heterogeneously, particularly in granular cell and mixed cell RCC. Radionuclide molecular imaging of CAIX-expression could be a potential non-invasive tool to select patients who can benefit from CAIX-targeting therapy. Antibody-based and small non-immunoglobulin scaffold protein-based radionuclide imaging are two possible approaches approaches. The aim of this study was to compare the imaging properties of the new tracer [^{111}In]In -DOTA-HE$_3$-ZCAIX:2 with the currently available tracers [^{99m}Tc]Tc(CO)$_3$-HE$_3$-ZCAIX:2 and [^{111}In]In-DTPA-G250(Fab')$_2$. **Materials and Methods:** Recombinantly produced ZCAIX:2 containing a unique C-terminal was site specifically conjugated with maleimido derivative of DOTA chelator. DOTA-ZCAIX:2 was labeled with ^{111}In. In vitro binding specificity, cellular processing and affinity was measured using SK-RC-52 (7× 10^5 binding sites/cell) renal cell carcinoma cell-line. The biodistribution of [^{111}In]In-DOTA-ZCAIX:2 was directly compared with [^{99m}Tc]Tc(CO)$_3$-HE$_3$-ZCAIX:2 and [^{111}In]In-DTPA-G250(Fab')$_2$ in female BALB/C nu/nu mice bearing SK-RC-52 xenografts. Specificity of [^{111}In]In-DOTA-ZCAIX:2 binding was tested by saturation of CAIX in xenografts using 100-fold excess of non-labelled ZCAIX:2. **Results:** LC-MS data confirmed the identity and purity of DOTA-HE$_3$-ZCAIX:2. The radiochemical purity of all labelled conjugates was over 99%. In vitro, [^{111}In]In-DOTA-ZCAIX:2 bound specifically to CAIX-expressing cells and internalization was slow. The apparent dissociation constants were 1.2, 6 and 0.12 nM for [^{111}In]In-DOTA-HE$_3$-ZCAIX:2, [^{99m}Tc]Tc(CO)$_3$-HE$_3$-ZCAIX:2 and [^{111}In]In-DTPA-G250(Fab')$_2$, respectively. In vivo, the tumor uptake of [^{111}In]In-DOTA-ZCAIX:2 was highly specific. The tumor uptake at 4 h after injection was 15±3, 7±1, and 6±1%ID/g for [^{111}In]In-DOTA-HE$_3$-ZCAIX:2, [^{99m}Tc]Tc(CO)$_3$-HE$_3$-ZCAIX:2 and [^{111}In]In-DTPA-G250(Fab')$_2$, respectively. Tumor-to-blood ratios were 63±11, 23±2, and 2.1±0.2 for these tracers. At 24 h after injection, [^{111}In]In-DTPA-G250(Fab')$_2$ demonstrated tumor uptake of 5±1 %ID/g and tumor-to-blood ratio of 67±12. ^{111}In-DOTA-HE$_3$-ZCAIX:2 provided significantly higher tumor-to-liver, tumor-to-lung and tumor-to-bone ratios compared to both [^{99m}Tc]Tc(CO)$_3$-HE$_3$-ZCAIX:2 (parental variant) and [^{111}In]In-DTPA-G250(Fab')$_2$. These ratios are essential for imaging of CAIX expression in major metastatic sites of RCC. MicroSPECT/CT imaging confirmed the biodistribution data. **Conclusion:** [^{111}In]In-DOTA-HE$_3$-ZCAIX:2 provided the highest tumor-to-organ ratios and imaging contrast. Therefore, this probe can be considered as the most promising tracer to image CAIX-expressing in RCC metastases. **References:** None.

OP-196

Pharmacodynamic changes of FAP-targeted IL2 variant immunotherapy assessed with [68Ga]Ga-DOTA-Siglec-9 in B16-FAP melanoma mice

R. Siitonen[1], *H. Virtanen*[1], *H. Liljenbäck*[1,2], *O. Moisio*[1], *X. Li*[1], *C. Klein*[3], *T. Nayak*[3], *S. Jalkanen*[4], *A. Roivainen*[1,2];
[1]*Turku PET Centre, University of Turku, Turku, FINLAND,* [2]*Turku Center for Disease Modeling, University of Turku, Turku, FINLAND,* [3]*Roche Pharma Research and Early Development, Roche Innovation Center Basel, Basel, SWITZERLAND,* [4]*MediCity Research Laboratory, University of Turku, Turku, FINLAND.*

Aim/Introduction: Vascular adhesion protein 1 (VAP-1) is up-regulated at the sites of inflammation and supports contacts between leukocytes and inflamed endothelium. Sialic acid binding Ig-like lectin 9 (Siglec-9) is a leukocyte ligand for VAP-1 and [68Ga]Ga-DOTA-Siglec-9 can be used for PET imaging of inflammation and cancer (1). Interleukin-2 (IL-2) based immunotherapy is an efficient therapy against cancers but toxic. We evaluated B16-fibroblast activated protein (FAP)-transfected melanoma tumors in mice with longitudinal [68Ga]Ga-DOTA-Siglec-9 PET/CT imaging during novel tumor stroma targeted engineered immunocytokine FAP-IL2v immunotherapy. **Materials and Methods:** B16-FAP murine melanoma cells were subcutaneously inoculated in immunocompetent C57BL/6J mice and divided into anti-FAP-IL2v treatment and PBS groups. The progression of tumor growth was monitored with external caliper. At 9 days after the inoculation of the cells, a 30-min dynamic [68Ga]Ga-DOTA-Siglec-9 PET/CT was performed as a baseline measurement. Thereafter, the mice were treated with intravenously injected anti-FAP-IL2v (n=12) or PBS (n=12) and the injections were repeated 3 days later. Subsequent PET/CT imaging were performed 3, 5 and 7 days after the baseline imaging. Mice were sacrificed 5 or 7 days after the baseline imaging and tumors were cut into cryosections for ex vivo autoradiography. **Results:** At the end of the study, the size of the tumors were similar in anti-FAP-IL2v and PBS groups (P=0.73 at day 7). However, the tumor uptake of [68Ga]Ga-DOTA-Siglec-9 was significantly higher in anti-FAP-IL2v treated mice compared to PBS group (day 7: tumor-to-muscle ratio 2.6 ± 0.091 vs. 2.1 ± 0.17, P=0.026). This was confirmed by tumor autoradiography analyses (37 ± 2.6 vs. 29 ± 2.2 PSL/mm², P=0.035). There were no differences between groups 3 or 5 days after the baseline imaging. [68Ga]Ga-DOTA-siglec-9 PET uptake results correlated well with tumor volume (r=0.48, P<0.0001). **Conclusion:** Although anti-FAP-IL2v treatment had no effect on tumor growth, the results suggest that it induced VAP-1 expression detected by [68Ga]Ga-DOTA-Siglec-9 in tumors and the [68Ga]Ga-DOTA-Siglec-9 PET/CT imaging has potential as a useful method for assessing pharmacodynamic changes during the anti-FAP-IL2v immunotherapy. **References:** (1) Aalto K. et al. Blood 2011;118(13):3725-33

OP-197

[89Zr]-N-sucDf-Amc-2Nal -KuE (89Zr-DANKE) offers a prolonged time frame for prostate cancer imaging with potentially improved tumor detection

S. Muñoz Vázquez[1], *H. Endepols*[1], *T. Fischer*[1], *B. Zimmermanns*[1], *S. Tawadros*[2], *V. Marmann*[1], *A. Drzezga*[1], *K. Schomäcker*[1];
[1]*Clinic of Nuclear Medicine, Cologne, GERMANY,*
[2]*Decentralized Animal Husbandry Network of the Faculty of Medicine University of Cologne, Cologne, GERMANY.*

Aim/Introduction: The detection of prostate carcinoma lesions by means of PSMA-PET is usually realized in within few hours after injections with the available radiotracers such as e.g. [68Ga]PSMA11 or [18F]JK-PSMA7. It cannot be expected that the optimum contrast is achieved within such short time of biodistribution. Therefore, in order to overcome this limitation, we have proposed a new PSMA-binding compound that exploits the longer physical half-life (78h) of 89Zr: [89Zr]DANKE. **Materials and Methods:** EuK-2Nal-Amc-N-sucDf-Fe was provided by ABX GmbH (Radeberg) and is formed by the pharmacophore EuK coupled to a naphthylic linker, and the chelator agent N-sucDf-Fe. The N-sucDF-Fe moiety functionalizes the molecule for labeling with 89Zr. The [89Zr]DANKE was characterized in vitro by the calculation of the corresponding K_d value, the cellular uptake and the internalization in LNCaP cells. Its biodistribution in vivo was studied with LNCaP prostate tumor xenograft in mice and PET-imaging experiments were conducted on a Focus 220 micro PET scanner. Analogue experiments and compound characterization were carried out with [68Ga]PSMA11 and [18F]JK-PSMA7. **Results:** [89Zr]DANKE was labeled in a radiochemical purity ≥99.9%. [89Zr]DANKE, [68Ga]PSMA 11 and [18F]JK-PSMA7 showed high affinity for LNCaP cells of around 5 nM. The internalization to cell-associated activity ratios of [89Zr]N-sucDf-Amc-2Nal-KuE at 1 h, 2 h and 3 h was comparable to those of [68Ga]PSMA11 and [18F]JK-PSMA7. [89Zr]-DANKE showed very high stability in PBS and human serum until 7 d at 37 °C. At 2 h, all radiotracers showed a comparable tumor uptake of approximately 20% ID/g. The biodistribution profiles of [89Zr]DANKE in normal tissues at 2 h and 4 h post injection were found to be similar to those of [68Ga]PSMA11 (p<0.0001) and [18F]JK-PSMA7 (p<0.0001). [89Zr]DANKE allowed the acquisition of small animal PET-images with demarcated tumor after 24 h and 52 h p.i., showing that over time the compound remains in the tumor with very low activity in background except for the kidneys. The analysis of the PET-images also revealed that the tumor-to-background ratio is increasing over time. **Conclusion:** This study demonstrates that the tumor uptake and the biodistribution in normal tissues of [89Zr]DANKE is comparable to [68Ga]PSMA11 and [18F]JK-PSMA7. The small animal PET data suggest that [89Zr]DANKE remains in the tumor up to 52 h p.i. with increasing tumor/background ratio. Together with the long half-life of the [89Zr]-label, this novel tracer may therefore allow late PET-acquisition with improved lesion detection. **References:** None.

OP-198

Renal Radioactivity Accumulation In Mice Injected With Radiometal Labeled Affibody Molecules, Is Reduced By Maleate And Fructose

M. Altai[1], *A. Vorobyeva*[1], *A. Orlova*[2], *V. Tolmachev*[1], *J. Garousi*[1];
[1]*Immunology, Genetics and Pathology, Uppsala, SWEDEN,*
[2]*Department of Medicinal Chemistry, Uppsala, SWEDEN.*

Aim/Introduction: Advances in biotechnology have led to the development of alternatives to monoclonal antibodies for targeted radionuclide-based imaging and therapy. Affibody molecules were successfully implemented for radionuclide molecular imaging applications both in preclinical and clinical settings. However, the high renal retention of radiometal-labeled affibody molecules hampered their use in targeted radionuclide therapy. Affibody molecules (7 kDa) are readily filtered by glomeruli and subsequently reabsorbed. Like many peptide-based agents, the reabsorption of radiolabeled affibody molecules is mainly due to endocytosis in the proximal tubule cells. We have shown earlier that this process is independent on the nature of binding-site and is not mediated by the megalin-cubulin endocytic receptors complex. This study evaluates the effect of several drugs on the renal uptake, processing and retention of the 99mTc radiolabeled anti-HER2 affibody molecule $Z_{HER2:2395}$. For this we have tested the effect of probenecid (organic anion transport inhibitor), furosemide (loop diuretic), mannitol (osmotic diuretic), colchicine (microtubule inhibitor) as well as maleate and fructose (ATP depleting agents) on renal activity post ^{99m}Tc-$Z_{HER2:2395}$ injection. **Materials and Methods:** Twenty eight NMRI normal mice were divided into 7 groups (n=4). All groups were injected with 1 µg ^{99m}Tc-$Z_{HER2:2395}$ affibody molecule. In six of the groups mice were pre injected with, probenecid (20 mg/kg, 1 h, i.p.), furosemide (2.5 mg/kg, 5 min, i.v.), mannitol (400 mg/kg, 5 min, i.v.), colchicine (1 mg/kg, 5 h, i.p.), maleate (400 mg/kg, 5 min., i.v.) and fructose (50 mmol/kg. 5 min, i.p.) prior to the injection of ^{99m}Tc-$Z_{HER2:2395}$ affibody molecule. The last group was preinjected with PBS (control). Mice were sacrificed 4 h post affibody injection and organs were collected and measured for activity. Autoradiographic images of the kidneys from treated mice were acquired and compared with controls. **Results:** Preinjection of probenecid, furosemide, mannitol and colchicine did not influence renal-associated activity post ^{99m}Tc-$Z_{HER2:2395}$ injection. Preinjection of the ATP depleting agents, fructose (50 mmol/kg. 5 min, i.p) and maleate (400 mg/kg, 5 min., i.v.) led to the reduction of renal associated radioactivity by 33 % and 51%, respectively, compared to the control group. Autoradiographic images showed that the accumulation of radioactivity post ^{99m}Tc-$Z_{HER2:2395}$ injection was in the renal cortex. Both fructose and maleate significantly reduced this cortical accumulation of radioactivity, however at different levels. **Conclusion:** A presumed mechanism of action for both fructose and maleate may be attributed to disruption of ATP-mediated cellular uptake and endocytosis processes of ^{99m}Tc-$Z_{HER2:2395}$ in tubular cells. **References:** None.

OP-199

EPI-PEG-DOTA: Novel androgen receptor ligand as an alternative to PSMA ligands

F. Braun[1], *S. Muñoz*[1], *V. Marmann*[1], *T. Fischer*[1], *H. Endepols*[1], *M. von Brandenstein*[2], *M. Pietsch*[3], *A. Drzezga*[1], *K. Schomäcker*[1];
[1]*University of Cologne, Clinic of Nuclear Medicine, Cologne, GERMANY,* [2]*University of Cologne, Clinic of Urology, Cologne, GERMANY,* [3]*University of Cologne, Institute of Pharmacology, Cologne, GERMANY.*

Aim/Introduction: Prostate carcinomas (PC) not only overexpress PSMA but also different subtypes of the androgen receptors (AR). Therefore, they can be used as an alternative target for radioactive vectors. In contrast to numerous ligands with high AR affinity, the chlorohydrin-modified bisphenol-A based "EPI" shows even irreversible AR binding, thus EPI-derivatives provide promising ligands for use in radionuclide based targeting of PC. Here, we present a new radioactive vector, the EPI-PEG-DOTA, labeled with ^{68}Ga and ^{177}Lu and its accumulation rate in PC cells in ovo. **Materials and Methods:** For the labeling with ^{68}Ga and ^{177}Lu, EPI-064 ligand was modified with the linker PEG_3 and the chelator DOTA to generate the compound EPI-PEG-DOTA (EPD). EPD was synthesized and tested for radiochemical purity, cell binding, and in vitro stability. The pharmacodynamic properties of this compound were tested with the chicken egg chorioallantoic membrane (CAM)-culture. LNCaP tumor cells were CAM-xenotransplantated and cultured. Then the ^{68}Ga-labeled EPD, and for reason of comparison, [^{18}F]FDG and [^{18}F]PSMA7 were injected into the bloodstream of chicken embryo. The uptake was monitored by a small animal positron emissions tomography (PET)-scanner. Subsequently, the activity uptake was monitored in the tumor tissue and blood and compared with the accumulation of the control tracers [^{18}F]PSMA7 and [^{18}F]FDG. **Results:** The successful synthesis of the EPD-precursor was proven by ^{13}C, ^{1}H-NMR and mass spectrometry. The labeling of EPD yielded a purity of >98% for ^{177}Lu and >96% for ^{68}Ga with a specific activity of 40 MBq/nmol with sufficient cell binding. In case of [^{177}Lu]EPD, after 48h a value of 92% for the stability in human serum was found. Examination of the pharmacokinetic properties observed in ovo showed significant accumulation of [^{68}Ga]EPD in the tumor tissue. The tumor-to-blood ratio of PET-derived uptake after 30 min was 1.82 in the case of [^{68}Ga]EPD and 2.99 in the case of [^{18}F]PSMA7. With [^{18}F]FDG, only tumor/blood ratios <1 were observed. **Conclusion:** The novel compound EPD appears to be a promising candidate for the future use as PC targeting agent particularly in cases with low or lacking PSMA-expression. **References:** None.

OP-200

Evaluation of Bivalent GRPR Radioligands for Targeting Prostate Cancer

N. Romantini[1], *S. Dobitz*[2], *M. Alam*[1], *M. Spillmann*[1], *R. Schibli*[1], *X. Deupi*[1], *H. Wennemers*[2], *P. Berger*[1], *M. Behe*[1];
[1]*Paul Scherrer Institute, Villigen, SWITZERLAND,* [2]*Federal Institute of Technology (ETH), Zurich, SWITZERLAND.*

Aim/Introduction: Targeted radiotherapy (TRT) aims at the destruction of tumor tissue by radioactivity specifically delivered to neoplastic lesions. Since the gastrin-releasing peptide receptor (GRPR) is overexpressed on prostate cancer cells, it is an ideal target for TRT. In this project, ^{177}Lu-labeled bivalent peptides are evaluated as high affinity ligands for GRPR. Two agonistic recognition motifs are fused on a rigid oligoproline backbone in different distances from each other (10, 20 or 30 Å), forming the three compounds BBN-10, BBN-20 and BBN-30. A monovalent oligoproline-backbone-based compound (BBN-00) as well as the well-characterized agonist AMBA served as references. **Materials and Methods:** We determined the receptor-mediated cellular uptake of all compounds as well as the biodistribution of BBN-20, BBN-00 and AMBA in tumor-bearing mice 4 h post-injection. Moreover, we established assays to explore the influence of bivalent ligands on G-protein and arrestin dependent receptor signaling using luciferase complementation and BRET assays. **Results:** All bivalent compounds showed significantly higher cellular uptake (BBN-10: 29.2 ± 2.3%, BBN-20: 28.2 ± 2.5% and BBN-30: 20.2 ± 3.5%) than the monovalent reference BBN-00 (7.0 ± 1.4%) but could not outperform the literature reference AMBA (43.5 ± 3.5%) probably due to steric hindrance of the oligoproline backbone. Moreover, the cellular uptake was clearly distance-dependent since BBN-30 showed significantly lower uptake than BBN-10 and BBN-20. Signaling assays confirmed that all oligoproline-based ligands maintained their agonistic characteristics and induced G-protein as well as arrestin recruitment. The biodistribution study of BBN-20 resulted in a 1.5- to 2-fold increase in tumor uptake in comparison to the monovalent BBN-00 and AMBA. Furthermore, both oligoproline-based compounds showed a decreased uptake in healthy receptor-expressing organs such as the pancreas, leading to improved tumor-to-pancreas ratios (AMBA: 0.07 ± 0.02, BBN-00: 0.26 ± 0.05, BBN-20: 0.26 ± 0.09). **Conclusion:** We show that bivalency is a promising strategy to increase the uptake into receptor-positive cells in vitro. This favorable effect depends on the distance between the recognition motifs. Furthermore, a biodistribution study of the bivalent compound BBN-20 resulted in higher tumor accumulation compared to the literature reference. **References:** None.

OP-201

Imaging of Prostate Cancer in Therapy-Naive Patients Using the GRPr Antagonist ^{68}Ga-SB3

I. L. Bakker[1], *A. C. Fröberg*[1], *M. B. Busstra*[1], *J. F. Verzijlbergen*[1], *M. Konijnenberg*[1], *I. Schoots*[1], *G. J. L. H. van Leenders*[1], *E. de Blois*[1], *J. Veenland*[1], *W. M. van Weerden*[1], *T. Maina*[2], *B. A. Nock*[2], *M. de Jong*[1]; [1]*Erasmus MC, Rotterdam, NETHERLANDS,* [2]*INRASTES, NCSR "Demokritos", Athens, GREECE.*

Aim/Introduction: The prostate cancer (PCa) target gastrin releasing peptide receptor (GRPr) shows overexpression in early disease. The gallium-68-labelled GRPr-antagonist Sarabesin 3 (^{68}Ga-SB3) was selected after excellent results in (pre)clinical pilot studies. The aim of this phase I study was to assess the safety and to validate ^{68}Ga-SB3 PET-CT imaging of primary PCa tumors in patients scheduled for prostatectomy. Secondary aims included GRPr-expression levels, dosimetry and optimal thresholding. After previously published primary data we are now ready to present our complete dataset. **Materials and Methods:** We included ten therapy-naive PCa patients scheduled for prostatectomy. ^{68}Ga-SB3 (185±39MBq, 40±5µg) was administered, followed by an intensive PET-CT imaging protocol. Surgically obtained prostate tissue was cut following a template. Pathologists determined tumor localizations, Gleason Scores (GS), and in vitro autoradiography was performed. Time-activity curves (TAC) were used to estimate residence times. Recalculation to standard volumes, effective dose to the body, as well as absorbed doses to organs were calculated using IDAC dose 2.1 model. MRIs were matched to PET-CT by hand registration and trans-axial whole-prostate histopathological overlays were created. ROC curves of PET thresholding and tumor positivity on histopathology were calculated. **Results:** Administration of ^{68}Ga-SB3 proceeded without side effects. PET-CT imaging visualized lesions in 8 out of 10 patients. A total of 15 lesions were found in pathological evaluation of 10 patients, 5x GS6, 9x GS7 and 1x GS8. PET-CT imaging had a sensitivity of 82% in low Gleason disease (GS3+3 and GS3+4). PET showed 2 false positives and missed 2 tumor foci. Autoradiography of PCa tissue showed heterogeneous GRPr-expression and was negative in 4 patients. The PET-negative patients had at least one GRPr negative tumor. Of autoradiography-positive patients, SUV_{max} showed significant correlation to GRPr expression levels. Effective dose was 0.0144 mSv/MBq (1h voiding interval ICRP103), similar to other ^{68}Ga labeled compounds. Quick renal excretion kinetics were observed. GRPr-rich pancreas showed high physiological uptake, highest absorbed dose was therefore found in this organ (0.198 mGy/MBq), followed by bladder wall and kidneys. In the PET positive patients PET/CT-MRI-histopathology matching was performed. Optimal imaging time did not show significant differences between 60 or 150 min post injection. Optimal threshold was 35% SUV_{max} (range 35%-75%). **Conclusion:** Based on this data we showed the potential of ^{68}Ga-SB3 PET-CT as a diagnostic tool in the imaging of early PCa. **References:** None.

506

Do.MoRe - Parallel Session: ^{177}Lu PRRT and other Preclinical & Clinical Dosimetry

Sunday, October 13, 2019, 16:30 - 18:00 Lecture Hall 112

OP-202

In vitro dose-response comparison of [177Lu]Lu-labelled somatostatin receptor agonist and antagonist

G. Tamborino[1,2], *M. De Saint-Hubert*[1], *L. Struelens*[1], *S. Dalm*[2], *E. Ruigrok*[2], *M. De Jong*[2], *J. Nonnekens*[2,3], *M. W. Konijnenberg*[2]; [1]*Research in Dosimetric Applications, Belgian Nuclear*

Research Centre (SCK•CEN), Mol, BELGIUM, [2]Department of Radiology & Nuclear Medicine, Erasmus MC, University Medical Center Rotterdam, Rotterdam, NETHERLANDS, [3]Department of Molecular Genetics, Erasmus MC, University Medical Center Rotterdam, Rotterdam, NETHERLANDS.

Aim/Introduction: Peptide receptor radionuclide therapy (PRRT) using radiolabeled somatostatin receptor (SST) is very effective for treatment of neuroendocrine metastatic tumors. Recent studies indicate that radiolabeled SST antagonists show better tumor targeting during clinical imaging and preclinical therapy, despite little to no internalization in the cancer cells. However, preclinical studies are often limited to activity uptake, with no correlation between the delivered absorbed dose and the biological end-point. This study aims to calculate the absorbed dose to the nucleus for [^{177}Lu]Lu-DOTA-Tyr3,octreotate (^{177}Lu-DOTA-TATE, SST agonist) and [^{177}Lu]Lu-DOTA-JR11 (^{177}Lu-DOTA-JR11, SST antagonist), for comparison with DNA damage induction. **Materials and Methods:** Time-activity curves were determined for 177Lu-DOTA-TATE and 177Lu-DOTA-JR11 uptake in medium, membrane-bound and internalized-fractions of U2OS+SST2 cells during 4h incubation and 6 days follow-up. An upgraded version of our previously developed dosimetry model[1], implementing polygonal mesh (PM) structures to realistically represent the cells within Geant4, was used to determine the absorbed dose-rate as function of time and absorbed dose to the nucleus at the end of the 4h-incubation, as well as cumulated over the 6 days follow-up. Visualization of p53 binding protein 1 (53BP1) foci was used to determine the number of DNA double-strand breaks (DSBs), after 4h incubation with 2.5 MBq/ml of [177Lu]Lu-diethylene-triamine-pentaacetic acid (177Lu-DTPA), 177Lu-DOTA-TATE and 177Lu-DOTA-JR11. **Results:** After 4h-incubation, most of ^{177}Lu-DOTA-JR11 uptake (80% ± 29%) was membrane bound, whereas most of ^{177}Lu-DOTA-TATE uptake (78% ± 31%) was internalized. The total ^{177}Lu-DOTA-JR11 uptake was 2.4 times higher than ^{177}Lu-DOTA-TATE, however, the SST antagonist uptake caused only 1.6 more DSBs compared to the SST agonist, demonstrating that total uptake does not correlate well to the number of 53BP1 foci. A good linear correlation (R^2=0.95) between the absorbed dose to the nucleus after 4h Lu-DTPA (0.34Gy±0.00), ^{177}Lu-DOTA-TATE (0.49Gy±0.03) and ^{177}Lu-DOTA-JR11 (0.70Gy±0.07) and the corresponding number of repair foci (3.63±0.58, 9.91±0.58, 15.28±0.77, 24.88±1.18, respectively) was found. Hence, the absorbed dose delivered by the antagonist after the first 4h was 43±22% more than the agonist. Dose-response models for cell survival after 6 days need to be established but, from preliminary calculations, 177Lu-DOTA-JR11 is expected to lead to much lower survival than 177Lu-DOTA-TATE. **Conclusion:** Our cellular dosimetry model is currently successful in predicting the number of DNA foci and we are eager to show it can predict cell survival. This will lead to better understanding of dose-response models and repair mechanisms at low dose-rate. **References:** [1] G. Tamborino, et al. EANM Congress 2018

OP-203

Absorbed doses to kidneys based on one or two SPECT measurements versus three SPECT measurements in 777 patients with neuroendocrine tumours receiving ^{177}Lu-DOTATATE therapy

M. Sandstrom[1,2], *D. Granberg*[1], *A. Sundin*[1], *M. Lubberink*[1,2]; [1]*Nuclear medicine & PET, Uppsala University, Uppsala, SWEDEN,* [2]*Medical physics, Uppsala University Hospital, Uppsala, SWEDEN.*

Aim/Introduction: As in all therapies using ionizing radiation, a patient-specific optimization of the delivered radiation should be performed in therapy with ^{177}Lu-DOTATATE. At our centre, the number of treatments is based on the absorbed dose (AD) to the kidneys. For logistical reasons, estimation of absorbed doses should be performed with as few measurements as possible. The aim of the present work was to study how well kidney AD and effective half-life (t_{eff}) estimations using methods with one or two measurement points agree with the method we use today that is based on three imaging points. **Materials and Methods:** 777 patients (333 female and 444 male) with neuroendocrine tumors with high somatostatin receptor expression were included. SPECT/CT over the abdomen were acquired at 24, 96 and 168 h after start of infusion of ^{177}Lu-DOTATATE. AD and t_{eff} were calculated using single exponential fits to data from 3 measurements (24-96-168) or two measurements (24-96 and 24-168). In addition, absorbed doses were calculated using a single measurement, assuming t_{eff} 50 h (96/50h). Bias of AD and t_{eff} values relative to those based on the three-point measurement were calculated. To test statistical significance a Wilcoxon matched-pairs signed rank test with a P-value of 0.05 for significance was used. Median, Min and Max of the deviations were also calculated. **Results:** Bias versus AD(24-96-168) was -3%(-20-72) (Median (Min-Max)) for AD(24-96), 3%(-22-30) for AD(24-168) and -7%(-51-27) for AD(96/50h). The bias for t_{eff} in the AD calculations versus AD(24-96-168) was -9% (-53-63) for AD(24-96) and 0% (-9-4) for AD(24-168). In all tests there was a small but significant difference for the whole group. In about 15% of the patients the bias in t_{eff} was more than 20% when ignoring the 168-h scan. In about 5-10% of the patients AD differed more than 20% for all methods that excluded the 168-h measurement. Using a fixed limit of the absorbed dose to the kidneys, this would mean that these patients would be given either too many or too few treatments. **Conclusion:** Although absorbed dose calculations based on only one or two measurement points may serve as a good approximation for the majority of patients, it leads to substantial errors affecting the number of given treatments in about 10% of patients. Since this is a radiation treatment a high precision for all patients is warranted, and three measurements, or at least inclusion of a late 168-h measurement, are recommended. **References:** None.

OP-204

Quantitative SPECT/CT voxel-based dosimetry in ^{177}Lu-octreotate PRRT: the selection of the reference timepoint for deformable CT registration impacts on the calculated absorbed dose to target tissues

A. Desy[1,2], *G. F. Bouvet*[1,2], *D. Mirando*[3], *A. S. Nelson*[3], *J. M. Beauregard*[1,2];
[1]*Department of Medical Imaging and Oncology Division of Research Center, CHU de Québec - Université Laval, Quebec City, QC, CANADA,* [2]*Department of Radiology and Nuclear Medicine and Cancer Research Center, Université Laval, Quebec City, QC, CANADA,* [3]*MIM Software Inc., Cleveland, OH, UNITED STATES OF AMERICA.*

Aim/Introduction: Dosimetry based on serial quantitative SPECT (QSPECT)/CT imaging allows personalizing ^{177}Lu peptide receptor radionuclide therapy. When performing voxel-based dosimetry using deformable CT registration, the first timepoint scan is typically set as the reference, to which other scan(s) are registered[1]. Our aim was to investigate if selecting another timepoint as the reference would impact on the calculated absorbed doses to target tissues. **Materials and Methods:** Data from 22 consecutive patients with neuroendocrine tumours enrolled in the P-PRRT trial (NCT02754297) were analysed using a voxel-based dosimetry software package (MIM SurePlan™ MRT). Following the first injection of ^{177}Lu-octreotate (8.9±2.0 GBq), two QSPECT/CTs were acquired at 23.3±1.3 (Day-1) and 70.9±1.4 hours (Day-3) post-injection. A deformable registration of one CT to the other was performed and applied to the corresponding QSPECT, and the 3D dose map was calculated. This was repeated twice, with Day-1 and Day-3 CTs as the reference, respectively. Resulting absorbed doses to target tissues (kidney, spleen and tumour) were compared using (i) the maximum dose ($Dose_{max}$), and (ii) the isodose volume (Vol_{iso}). For the kidney and the spleen, the latter was defined as the volume of the lowest integer isodose allowing isolation of the tissue, while for the tumour, the 20 Gy field-of-view isodose was used. **Results:** 53 of 60 (88%) evaluable target tissue samples had a higher $Dose_{max}$ when Day-3 was the reference timepoint. Selecting Day-1 as the reference resulted in a median (IQR) $Dose_{max}$ that was lower by -8.4% (-13.4% to -5.6%), -8.9% (-11.0% to -3.4%), and -11.4% (-18.5% to -2.8%) for the kidney, spleen and tumour, respectively. Similarly, 40 of 60 (67%) tissue samples had a larger Vol_{iso} with Day-3 as the reference. Fixing Day-1 lowered Vol_{iso} by -4.3% (-14.3% to 1.5%), -7.2% (-21.1% to 3.2%), and -2.3% (-15.4% to 4.9%), respectively. Our provisional hypothesis is that inconsistencies in the QSPECT vs. CT alignment, along with slight redistribution of counts in the co-registered QSPECT matrix, may translate into activity underestimations in the high-uptake regions. The impact of this on voxel dose calculations could be amplified when Day-3, the most contributory scan, is registered to Day-1. **Conclusion:** QSPECT/CT voxel-based ^{177}Lu dosimetry is affected by the choice of the reference scan for deformable registration. Using a later timepoint as the reference may be preferable for estimating absorbed doses to high-uptake tissues.
References: 1. Jackson PA et al. Med Phys 2013;40(11):112503.

OP-205

Personalized OAR dosimetry in patients with NET: preliminary results of a Phase II study

E. Tonini[1], *M. Longo*[1,2], *S. Di Biaso*[3], *A. Barboni*[1], *A. Turra*[1], *L. Longo*[3], *G. Di Domenico*[3], *L. Uccelli*[4], *S. Panareo*[4], *C. Cittanti*[4], *I. Santi*[4], *I. Rambaldi*[4], *M. Bartolomei*[4];
[1]*Arcispedale Sant'Anna Hospital, Medical Physics Unit, Ferrara, ITALY,* [2]*Sapienza University of Rome, Ph. D. Program in Morphogenesis & Tissue Engineering, Rome, ITALY,* [3]*Dipartimento di Fisica e Scienze della Terra, Ferrara University, Ferrara, ITALY,* [4]*Arcispedale Sant'Anna Hospital, Nuclear Medicine Unit, Ferrara, ITALY.*

Aim/Introduction: Peptide-receptor radionuclide-therapy (PRRT) represents the treatment of choice for patients affected by neuroendocrine-tumours (NET) and has been mostly administered in subsequent induction-cycles. Kidneys and bone-marrow (BM) toxicities are the dose limiting factor in PRRT, which has to be administered to not exceed cumulative absorbed-dose (AD) of 23 and 2 Gy to kidneys and BM respectively. The present study aims to accurately perform kidneys and BM dosimetry of patients treated with PRRT both at first- and last-administration cycle in order to use the dosimetric results to guide the administration of safe activities after the first-cycle and to verify dosimetry at the last-cycle. **Materials and Methods:** Forty-eight patients with NET have been treated at Arcispedale Sant'Anna (Ferrara, Italy) between 2018 and 2019 according to the FENET-2016 protocol, which includes 5-cycles of ^{177}Lu-DOTATOC administrations used alone or in combination with ^{90}Y-DOTATOC on second and fourth cycle. SPECT/CT images were acquired on first- and fifth-cycle at 1, 24 and 48 h after the administration of the ^{177}Lu- DOTATOC. For each patient, kidneys and BM doses were calculated at first- and fifth-cycle. The activity concentration in kidneys was calculated according to MIRD scheme; the image-based method was applied for calculating AD to BM (using L2-L4 activity concentration). The MIM software was used for contouring, image coregistration and statistics while OLINDA for the AD calculation. For patients treated in combination with the two radionuclides, dose calculation was also performed for ^{90}Y, scaling the activities in kidneys and BM to correct for the difference in half-life. Dosimetric results between first- and fifth-cycle were compared as well as those obtained with two radionuclides. **Results:** The administered activities per cycle have been from 1.9 to 5.5 GBq. The kidneys AD per unit activity lie between 0.2÷1.2 Gy/GBq and 1.5÷4.0 Gy/GBq, while BM AD per unit activity are between 0.01÷0.04 Gy/GBq and 0.07÷0.20 Gy/GBq for treatment with ^{177}Lu and ^{90}Y respectively. ^{90}Y absorbed-doses are approximately a factor of five higher than those with ^{177}Lu. The cumulative doses resulted from 5 to 27 Gy for kidneys and from 0.3 to 1.1 Gy for BM, with differences between first- and fifth-cycle from 0 to 40%. **Conclusion:** Routine dosimetry for personalized treatment of patients underwent ^{177}Lu- and ^{90}Y-DOTATOC treatments also administered in combination has been successfully established in our institution. Comparing ^{177}Lu and ^{90}Y dosimetric results has provided a useful method to guide the clinicians in using

combined treatment modality. **References:** None.

OP-206

Absorbed dose calculation considering organ mass variation for patients treated with Luthatera

E. Mora Ramirez[1,2], *A. Vergara-Gil*[1], *J. Ocampo-Ramos*[1], *J. Pouget*[3], *P. Kotzki*[3,4], *L. Santoro*[4], *E. Deshayes*[3,4], *M. Bardies*[1];
[1]*CRCT, UMR 1037, INSERM, Université Toulouse III Paul Sabatier, Toulouse, FRANCE,* [2]*Universidad de Costa Rica, Escuela de Fisica, CICANUM, San Jose, COSTA RICA,* [3]*Institut de Recherche en Cancérologie de Montpellier, Montpellier, FRANCE,* [4]*Nuclear Medicine Department, Institut Régional du Cancer de Montpellier, Montpellier, FRANCE.*

Aim/Introduction: Molecular Radiotherapy (MRT) dosimetry requires sequential quantitative SPECT/CT at different time points to assess pharmacokinetics in order to compute the absorbed dose delivered to the patient. Due to organ movements or wrong positioning of the patient, organ mass can vary at each time point. Yet, most often clinical MRT dosimetry assumes constant organ mass. The aim of this work is to integrate organ mass variation in the case of peptide receptor radionuclide therapy dosimetry. **Materials and Methods:** Two patients (1F, 1M) treated with Lutathera® were previously reported[1]. The same patients were reprocessed using the Dosisoft workstation. Manual segmentation of liver, spleen and left/right kidneys was performed using the CT at each time point. The definition of the absorbed dose rate at each time point requires adjusting the reference S-value by the organ mass ratio between reference model and patient: $S_{pat}(t) = S_{ref} \times [M_{ref}/M_{pat}(t)]$. The activity-mass concentration at each time point was integrated, considering no activity at t=0 and a mono-exponential fit from the first time point to infinity, and multiplied by the time-invariant product ($S_{ref} \times M_{ref}$). These results were then compared to previous calculations using OLINDA V2[2] where S-values were adjusted from the model to the patient but assumed no time-related organ mass variation (one reference time was selected to perform segmentation). **Results:** For liver, spleen and L/R kidneys, the average organ mass and standard deviation were 1673.4±31.6g, 102.2±6.8g, 127.7±6.2g, 114.5±6.8; 1448±59.7g, 263.1±65.6g, 175.2±30.4g, 182.8±18.7g for the female and male patient respectively. Absorbed dose estimations for liver, spleen and L/R kidneys were 15.9Gy, 4.0Gy, 3.3Gy, 3.8Gy and 1.1Gy, 4.2Gy, 2.6Gy, 2.5Gy for the female and male patient respectively. In the case of OLINDA V2 the absorbed dose results were for liver, spleen and kidneys 17.8Gy, 3.8Gy, 3.6Gy (for both kidneys) and 1.1Gy, 4.5Gy, 2.7Gy (for both kidneys) for female and male patient, respectively. The relative variation between results from the 2 approaches was between -10.6 and 4.8% among all organs and for both patients. **Conclusion:** The proposed method is indicated whenever important mass variations in time are observed. Further investigations will consider organ mass variation and integration of absorbed dose rates obtained using the local energy deposition assumption, convolution or Monte Carlo modelling of radiation transport and energy deposition.

References: [1]Mora-Ramirez et al. Eur J Nucl Med Mol Imaging **45**(Suppl 1), S180 (2018).[2]M. Stabin and A. Farmer, J. Nucl. Med. **53**(Suppl 1), 585 (2012).

OP-207

Cellular dose-response models for [177Lu]Lu-DOTA-Tyr3,octreotate radionuclide therapy compared to external beam radiotherapy

G. Tamborino[1,2], *M. De Saint-Hubert*[1], *L. Struelens*[1], *M. W. Konijnenberg*[2], *M. de Jong*[2], *J. Nonnekens*[2,3];
[1]*Research in Dosimetric Applications, Belgian Nuclear Research Centre (SCK•CEN), Mol, BELGIUM,* [2]*Department of Radiology & Nuclear Medicine, Erasmus MC, University Medical Center Rotterdam, The Netherlands, Rotterdam, NETHERLANDS,* [3]*Department of Molecular Genetics, Erasmus MC, Rotterdam, The Netherlands, Rotterdam, NETHERLANDS.*

Aim/Introduction: To investigate the applicability of different dose-response models for in vitro radiobiological experiments with Peptide Receptor Radionuclide Therapy (PRRT) in comparison to the well-established linear-quadratic (LQ) model. **Materials and Methods:** We upgraded our previously developed dosimetry model [1], implementing 9 polygonal mesh structures (PM) to realistically represent the cell on Geant4 and assuming instant translocation of the radionuclide to the Golgi (G). After wash-out, we tested two hypotheses: (1) re-localization in the cytoplasm (Cy) and (2) permanent incorporation in the G. This model was used to determine the absorbed dose to the nucleus for cells undergoing [177Lu]Lu-DOTA-Tyr3,octreotate PRRT treatment. Clonogenic survival assays were performed for [177Lu]Lu-DOTA-Tyr3,octreotate (0.1-2.5 MBq/ml) and for an x-ray irradiation characterized by 86 keV of average energy (0.5-4 Gy). The LQ, repairable-conditionally repairable (RCR) and linear model (L) were used to fit the data. **Results:** Contrary to the results found with the truncated cone representation of the cell [1], the absorbed dose per decay (S-value) for the PM structures is not increased if the radionuclide is localized in Cy rather than cell membrane. However, if the internalised fraction of activity is assumed to be translocated into the G, the S-value increases on average +64% and up to +149%, depending on the cell morphology. The absorbed dose to the nucleus was 2.8-3 fold less, when modeling the cells realistically using PMs compared to MIRD-spheres. Testing hypothesis 2, the absorbed dose to the N (0.2-2.9 Gy) increases on average with a factor of 1.38 compared to hypothesis 1 (0.1-2.1 Gy), corresponding to survival fractions 60%-40% for the range of tested activities. The L-model, preferred by the Akaike Information Criterion, relies on the assumption of a high α/β or a short sub-lethal damage repair half-life, which would lead to ignore the quadratic term of the LQ-model. The RCR model instead, favored by the F-test, assumes that the repair system can be triggered only by potentially repairable damage, not detected at very low doses; this would explain the over-response in the low-dose region and could be fostered by the affinity with the so-called inverse dose-rate effect. **Conclusion:**

Our cellular dosimetry model showed different dose-response correlations for PRRT compared to EBRT. The flattening of the LQ-curve is representative of protracted exposures, whilst the RCR model predicts the hypersensitivity in the low-dose region, possibly explained by dose-rate dependent repair mechanisms. **References:** [1] G. Tamborino, et al. EANM Congress 2018.

OP-208

Preliminary dosimetric study with177-Lutetium Peptide Receptor Radionuclide Therapy for Pediatric Patients with neuroendocrine tumors

B. Cassano[1], *E. Genovese*[1], *C. Polito*[1,2], *M. Longo*[3,4], *S. Donatiello*[1], *A. Napolitano*[1], *T. Insero*[1], *S. Valeri*[5], *M. Pizzoferro*[6], *A. Serra*[7], *M. C. Garganese*[6], *V. Cannatà*[1];
[1]*IRCCS Bambino Gesù Children's Hospital, Medical Physics Unit, Rome, ITALY,* [2]*Sapienza University of Rome, Molecular Medicine Department, Rome, ITALY,* [3]*Arcispedale Sant'Anna Hospital, Medical Physics Unit, Ferrara, ITALY,* [4]*Sapienza University of Rome, Ph. D. Program in Morphogenesis & Tissue Engineering, Rome, ITALY,* [5]*Tor Vergata Postgraduate School of Medical Physics, Rome, ITALY,* [6]*IRCCS Bambino Gesù Children's Hospital, Nuclear Medicine Unit/Imaging Department, Rome, ITALY,* [7]*IRCCS Bambino Gesù Children's Hospital, Oncoemathology Unit, Rome, ITALY.*

Aim/Introduction: Peptide receptor radionuclide therapy (PRRT) with 177Lu-labelled peptides is an effective strategy for the treatment of metastatic/non-resectable neuroendocrine tumours (NETs) in adults, but its use is uncommon in pediatric patients. The aim of this study is to report our initial experience in 3 pediatric patients with evidence of cellular expression of somatostatin (SSTR) treated with 177Lu-DOTATATE. **Materials and Methods:** 2 patients (PAT-1 and PAT-2) affected by relapsed/refractory metastatic high-risk neuroblastoma (rrmHRNBL) and 1 patient (PAT-3) with phaeochromocytoma were enrolled in this study. PAT-1 and PAT-2 were previously treated according to SIOPEN HRNB 01 protocol including 131I-MIBG as second-line treatment. PAT-1 and PAT-2 received 4 cycles of palliative PRRT (4.4 GBq in the 1st cycle in PAT-1, 7.4 GBq per administration in the other cycles) and PAT-3 is actually in treatment (he was administered twice). To reduce kidneys uptake, the patient received an intravenous infusion with bioarginine 20 g (body surface scaled) in 1200 ml of NaCl solution over 4 h starting 30 min before the administration. In a time-window ranging from 0.5 to 144 h, 6 whole-body and static planar images, 11 blood samples and 9 acquisitions with a NaI external probe at 2 meters distance were collected. Red Marrow (RM) and renal dosimetry were performed according to the MIRD method and kidney toxicity was monitored assessing creatinine levels **Results:** PAT-1, PAT-2, PAT-3, cumulative absorbed dose was 1.1, 0.6, 0.4 Gy for RM and 26, 22, 11 Gy for kidney respectively. Kidney absorbed dose per activity administered was 0.98, 0.96, 0.91 Gy/GBq with a maximum intra-variability, measured as the maximum percentage difference, of 6.3%. The creatinine values show the absence of acute toxicity to kidneys. No disease regression was observed but early symptoms improvement (mild flushing) was registered in only one patient. **Conclusion:** Our preliminary experience suggests that PPRT might be a safe and new valuable tool for palliative intent in pediatric patients affected by NETs. The main observed advantages are the improvement of life quality with symptoms relief, the absence of kidney toxicity and the short duration of hospitalization. Although the small number of evaluated patients we observed that the absorbed dose per administered activity was in line to the values reported in the literature for the adult patients and it is slightly constant for the duration of the treatment. Due to the lack of pediatric standard dose limits for kidney further investigation are needed. **References:** None.

OP-209

Biodistribution and dosimetry of a single dose of [^{177}Lu]Lu-DOTA^{ZOL} in patients with mCRPC

V. Kramer[1,2], *R. Fernandez*[1], *W. Lehnert*[3], *J. Flores*[1], *C. Soza-Ried*[1], *J. Ribbeck*[2], *M. Ceballos*[1], *E. Eppard*[2], *L. Jiménez-Franco*[3], *A. Kluge*[3], *M. Meckel*[4], *F. Roesch*[5], *H. Amaral*[1,2];
[1]*Center for Nuclear Medicine & PET/CT Positronmed, Santiago de Chile, CHILE,* [2]*Positronpharma SA, Santiago, CHILE,* [3]*ABX-CRO, Dresden, GERMANY,* [4]*Isotope Technologies Garching, München, GERMANY,* [5]*Institute of Nuclear Chemistry, Johannes Gutenberg-University, Mainz, GERMANY.*

Aim/Introduction: Palliative treatment of bone metastasis using radiolabelled bisphosphonates is a well-known concept and proven to be safe and effective. A new, theranostic radiotracer for bone palliation, is [^{177}Lu]LuDOTA-Zoledronic acid ([^{177}Lu]Lu-DOTA^{ZOL}), which has improved pharmacokinetics when compared to established radiopharmaceuticals. In this study, safety and dosimetry of therapeutic doses of [^{177}Lu]Lu-DOTA^{ZOL} were evaluated based on a series of SPECT/CT images and blood samples. **Materials and Methods:** Eight patients with bone metastasis from mCRPC (71±8.6 y) and progression under conventional therapies were evaluated by laboratory tests and PSMA-PET/CT to confirm absence of soft tissue lesions. After receiving a single dose of 5778±328.2 MBq [^{177}Lu]Lu-DOTA^{ZOL}, patients underwent venous blood sampling (5, 15, 30 min and 1.5, 6, 24 and 48 h p.i.) and 3D SPECT/CT imaging from top of the head to upper thigh using a pre-calibrated SPECT/CT camera at 1.5, 6, 24, 48 h and 7 d p.i. Tumor lesions and volumes were defined by objective criteria on pre-therapeutic PSMA-PET/CT scans and volumes of interest for organs and tumors were defined on SPECT/CT scans. Red bone marrow activity uptake was conservatively estimated from venous blood samples (RMBLR = 1.00). QDOSE, OLINDA/EXM_v1.1 and IDAC-Dose_v2.1 were used for dosimetric evaluations and calculation of absorbed organ doses for red marrow, kidneys, skeleton without tumor and tumor lesions. **Results:** [^{177}Lu]Lu-DOTA^{ZOL} showed fast uptake and high retention in bone lesions and very fast clearance from blood stream in all patients. Average retention in tumor lesions was 0.02 %ID/g at 6 h p.i. and approximately 0.01 %ID/g at 170 h p.i. with a high variability between patients, due to variations localization and size of lesions (mass range

from 0.63 g to 99.24 g). In this cohort, average doses in bone tumor lesions, kidneys, red bone marrow and bone surface were 4.21, 0.17, 0.36 and 1.19 mGy/MBq, respectively. Using the most conservative estimation, red bone marrow was found to be the dose limiting organ for all patients. A median injected activity of 3.5 GBq will not exceed the defined threshold of 2 Gy for the red bone marrow. **Conclusion:** The dosimetry calculations indicate that [^{177}Lu]Lu-DOTA^{ZOL} has a very favourable therapeutic index for the treatment of osteoblastic bone metastases caused by prostate cancer. The predicted therapeutic index is superior, compared to other radiopharmaceuticals used in the treatment of bone metastasis. Personalised dosimetry will, however, be required to avoid hematotoxicity for individual patients. **References:** Meckel et al;EJNMMI Radiopharmacy and Chemistry;2016,1-14.

507

Teaching Session 2 - Interactive Clinical Cases - Radiopharmacy + Inflammation & Infection + Oncology & Theranostics Committee: Imaging of Immune Cells

Sunday, October 13, 2019, 16:30 - 18:00 Lecture Hall 113

OP-210

Introduction

P. Laverman;
Radboud University Nijmegen Medical Centre, Department of Radiology & Nuclear Medicine (757), Nijmegen, NETHERLANDS.

OP-211

Basics of Immune Cells - Expression, Role and Targeting Possibilities

E. Aarntzen;
Radboud Universtiy Medical Center, Department of Radiology and Nuclear Medicine, Nijmegen, NETHERLANDS.

OP-212

Methods for Immune Cell Radiolabeling

R. Torres Martin de Rosales;
St Thomas' Hospital / King's College London, School of Biomedical Engineering & Imaging Sciences, London, UNITED KINGDOM.

OP-213

Imaging of Immune Cell - From Preclinical to Clinical

M. Kneilling;
Eberhard Karls Universtiy, Werner Siemens Imaging Center, Department of Preclinical Imaging and Radiopharmacy, Department of dermatology, Tübingen, GERMANY.

OP-214

Discussion/General Questions

508

Clinical Oncology - Rapid Fire Session: PRRT 4.0?

Sunday, October 13, 2019, 16:30 - 18:00 Lecture Hall 114

OP-215

LUTATHERA® in first line therapy of G2 and G3 GEP-NETs (the NETTER-2 study)

D. Ferone[1], *M. Pavel*[2], *P. Kunz*[3], *W. de Herder*[4], *P. Santoro*[5], *A. Wegener*[5], *P. Broberg*[5], *L. Ravasi*[5], *S. Singh*[6];
[1]*IRCCS AOU San Martino - IST, Genova, ITALY,* [2]*FAU Erlangen-Nurnberg, Erlangen, GERMANY,* [3]*Stanford University School of Medicine, Stanford, ON, CANADA,* [4]*Erasmus MC Rotterdam, Rotterdam, NETHERLANDS,* [5]*Advanced Accelerator Applications, a Novartis company, Geneva, SWITZERLAND,* [6]*University of Toronto, Toronto, ON, CANADA.*

Aim/Introduction: The pivotal Phase III NETTER-1 study showed that LUTATHERA® provided a significant increase in PFS to patients with progressive midgut neuroendocrine tumors compared to those treated with 60 mg octreotide LAR. The NETTER-1 patient population included 34.5% of patients with G2 and 65.5% with G1 NET while G3 were excluded. Only patients progressive on somatostatin analogs (SSAs) were eligible (2nd line), SSA-naïve patients were excluded. The aim of the NETTER-2 study is to determine if LUTATHERA® in combination with octreotide LAR prolongs PFS in patients (including adolescents ≥15 years of age and > 40 kg) with somatostatin receptor positive, high proliferative rate (G2 with Ki67 index ≥10% and G3 with Ki67 ≤ 55%) advanced GEP-NETs, when given as a first line treatment in comparison to treatment with high dose (60 mg) octreotide LAR. Both SSA-naïve as well as patients previously treated with SSAs in the absence of progression are eligible. Patients with high pace of disease progression, which would warrant first-line chemotherapy in the opinion of the investigator, are excluded. **Materials and Methods:** In this multicenter, stratified, open-label, randomized, comparator-controlled Phase III study, 222 patients will be randomized (2:1 randomization ratio) to receive treatment with LUTATHERA® (7.4GBq/200 mCi x 4 administrations every 8± 1 weeks; cumulative dose: 29.6 GBq/800mCi) plus octreotide LAR (30 mg every 8 weeks during LUTATHERA® treatment and every 4 weeks after last LUTATHERA® treatment) or high dose octreotide LAR (60 mg every 4 weeks). Randomization will be stratified by Grade (G2 vs G3) and tumor origin (pNET vs other origin). The primary end point is PFS between the two treatment arms (centrally assessed according to RECIST 1.1). Secondary endpoints include objective response rate, quality of life, disease control rate, safety, side-effect profile, and overall survival. In the control arm, any RECIST progressive

patient (based on central assessment) has the option to enroll for post-progression cross-over, to receive maximum 4 cycles of LUTATHERA® (7.4 GBq/200 mCi x 4 cycles; cumulative dose: 29.6 GBq / 800mCi) plus 30 mg octreotide LAR every 8 weeks. **Results:** Not available yet **Conclusion:** An advanced GEP-NET (G2 and G3) patient population including adolescents ≥15 years will be assessed in NETTER-2 to evaluate a potential new first line radioligand therapy (RLT) option for these patients with high risk profile and high unmet medical need. **References:** None.

OP-216

Prognostic value of ^{18}F-FDG PETCT in a large cohort of 495 patients with advanced neuroendocrine neoplasms (NENs) treated with peptide receptor radionuclide therapy (PRRT)

J. Zhang[1], *Q. Liu*[2,1], *H. R. Kulkarni*[1], *A. Singh*[1], *C. Schuchardt*[1], *K. Niepsch*[1], *R. P. Baum*[1];
[1]*THERANOSTICS Center for Molecular Radiotherapy & Precision Oncology, ENETS Center of Excellence, Zentralklinik Bad Berka, Bad Berka, GERMANY,* [2]*Department of Nuclear Medicine, Peking Union Medical College (PUMC) Hospital, Chinese Academy of Medical Science & PUMC, Beijing, CHINA.*

Aim/Introduction: To evaluate the role of ^{18}F-FDG PET/CT in a large cohort of 495 patients with advanced neuroendocrine neoplasms (NENs) who were treated with peptide receptor radionuclide therapy (PRRT) and had long-term follow-up. **Materials and Methods:** 495 patients (M 299; mean age 59.0±10.7 y; G1:G2:G3:NA=117:245:29:104; pancreatic NEN: n=199, midgut: n=139, CUP: n=49, rectum: n=20, lung: n=38, stomach: n=8, thymus/mediastinum: n=4, other: n=38) received PRRT with ^{177}Lu and/or ^{90}Y labeled somatostatin analogs (DOTATATE or DOTATOC), and were studied with both, ^{68}Ga-SSTR and ^{18}F-FDG PET/CT at baseline before PRRT. Kaplan-Meier analysis, log-rank test (Mantel-Cox), and Cox regression analysis were performed for survival analysis. **Results:** 382 (77.2%) patients were classified as ^{18}F-FDG-positive and 113 (22.8%) as ^{18}F-FDG-negative before PRRT. 3 (0.6%) patients were with tumors uptake on ^{68}Ga-SSTR PET of grade 1 (SUVmax=liver), whereas 161 (32.5%) patients of grade 2 (liver<SUVmax≤15), 106 (21.4%) of grade 3 (SUVmax≤20) and 225 (45.5%) of grade 4 (SUVmax>20). The median follow-up was 94 months. For all patients, the median PFS was 19.6 months and the median OS was 59.4 months. The median OS of patients with pancreatic, midgut and bronchopulmonary NEN were 54.4 months, 77.8 months and 46.2 months, respectively. For patients with ^{18}F-FDG PET- positive, the median PFS was 18.5 months and the median OS was 53.2 months. Patients with ^{18}F-FDG PET-negative, had a median PFS of 24.1 months and a median OS of 83.1 months. A significant difference was found for both, PFS and OS, as $p = 0.0015$ and $p < 0.0001$, respectively. In the pancreatic NENs subgroup, the median OS was 114.3 months in ^{18}F-FDG-negative group and 52.8 months in ^{18}F-FDG PET-positive group ($p = 0.0006$). In the midgut NENs subgroup, the median OS was 95.3 months in ^{18}F-FDG-negative group and 62.1 months in ^{18}F-FDG PET-positive group. For patients with positive ^{18}F-FDG uptake, and a ratio of the SUVmax on ^{68}Ga-SSTR PET to the SUVmax on ^{18}F-FDG PET > 2, the median OS was 53.0 months, compared toh 43.4 months in those patients with a ratio <2 ($p = 0.0296$). For those patients with no ^{18}F-FDG uptake, the median OS were 108.3 vs 76.9 months for a SUVmax >15.0 and a SUVmax ≤15.0 on ^{68}Ga-SSTR PET, respectively. **Conclusion:** ^{18}F-FDG PET/CT is an independent prognostic factor in patients with NEN treated with PRRT. High uptake on ^{68}Ga-SSTR PET/CT combined with negative ^{18}F-FDG PET/CT is associated with a better long-term prognosis. **References:** None.

OP-217

Influence of Pretreatment with Everolimus and/or Sunitinib on the Acute Hematotoxicity of ^{177}Lu-DOTATATE PRRT

E. Medaer*, C. Verslype, E. Van Cutsem, J. Dekervel, P. Clement, K. Nackaerts, O. Gheysens, K. Goffin, S. Jentjens, K. Van Laere, C. M. Deroose;*
UZ Leuven, Leuven, BELGIUM.

Aim/Introduction: Peptide receptor radionuclide therapy is a validated treatment for somatostatin receptor overexpressing neuroendocrine tumors. The NETTER-1 trial has demonstrated a pronounced positive effect on progression-free-survival compared to high dose somatostatin agonists, with a strong tendency towards overall survival benefit. Our PRRT cohort consists of patients with heavy pretreatment with targeted agents, due to requirements for reimbursement within the Belgian healthcare system. Everolimus is approved for primary pancreatic, lung and non-functional intestinal NETs, sunitinib for primary pancreatic NETs. Our aim was to determine the influence of pretreatment with everolimus and/or sunitinib on acute hematotoxicity of PRRT. **Materials and Methods:** We analyzed the records of 90 consecutive patients treated with ^{177}Lu-DOTATATE PRRT (1 to 4 cycles of 7.4 GBq) at the University Hospital Leuven, between November 2013 and July 2018. Eight patients were excluded (incomplete data). All 82 included patients were assigned to 2 groups according to their pretreatment: no targeted agents (naïve; N=41), or pretreated (with everolimus, sunitinib or both; N=41). The end point was the acute hematotoxicity, defined as the nadir value between start of PRRT and the 3-months follow-up period after the last PRRT administration, using the Common Terminology Criteria for Adverse Events (CTCAE) 4.03 classification. Any grade and grade 3/4 toxicity was examined. Fisher exact test was used for statistical analysis. **Results:** The primary tumor site was small intestine in 37 patients, pancreas in 25, unknown in 7, lung in 5, colon in 4, paraganglioma in 2 patients and menigeoma and pheochromocytoma each in 1 patient. No statistically significant differences in acute hematotoxicity were seen in the pretreated cohort vs. the naïve cohort for hemoglobin (any grade: 100% vs. 100%; grade 3/4: 12% vs. 22%), neither for leucocytes (any grade: 59% vs. 63%; grade 3/4: 10% vs. 7%), nor for neutrophils (any grade: 56% vs. 59%; grade 3/4: 5% vs. 7%), lymphocytes (any grade: 98% vs. 90%; grade 3/4: 49% vs. 37%) or platelets (any

grade: 61% vs. 61%; grade 3/4: 15% vs. 15%). Limitations of this study are its retrospective nature, potential bias in the lack of use of targeted agents in patients more susceptible to toxic effects, and the limited number of patients and events. **Conclusion:** In a cohort of patients pretreated with everolimus and/or sunitinib, we could not demonstrate a significant influence of everolimus or sunitinib on the acute hematotoxicity of ^{177}Lu-DOTATATE PRRT. **References:** None.

OP-218

Peptide Receptor Radionuclide Therapy using SSTR antagonists: biokinetics and dosimetry of Lu-177 DOTA-LM3

C. Schuchardt, S. Wiessalla, A. Singh, J. Zhang, H. R. Kulkarni, D. Mueller, R. P. Baum;
Theranostics Center for Molecular Radiotherapy and Molecular Imaging, Bad Berka, GERMANY.

Aim/Introduction: Peptide Receptor Radionuclide Therapy (PRRT) is used to treat patients with somatostatin receptor (SSTR) positive tumors. Recent studies show a higher tumor detection rate in PET/CT studies using SSTR antagonists compared to SSTR agonists. The aim of the present investigations was to determine the biokinetics and dosimetry of the Lu-177 labelled antagonist DOTA-LM3. **Materials and Methods:** 11 patients with neuroendocrine neoplasms (aged 64+/-12 years) were included in the analysis. High SSTR expression was verified before treatment by Ga-68 NODAGA-LM3 PET/CT. The administered activity ranged from 2.8 to 7.3 GBq Lu-177 DOTA-LM3. Biokinetics were determined based on planar whole body scintigraphiy & SPECT/CT and dosimetry calculations were performed (OLINDA 2.0). To analyze the kinetics, we used the following parameters: effective half-life (HL in hours) and uptake (%IA, fraction of injected activity), which were calculated using the fit of the time-dependent activity curve to a mono- or bi-exponential function. **Results:** Very intense uptake in the tumor lesions as well as significant uptake in the kidneys, spleen and liver was observed in all patients. There was rapid clearance of tracer from whole body with a HL of 56-93 hours. The maximum renal uptake at 20h p.i. was 15% IA (mean 7%IA) and showed a wash-out with HL of 47-159 hours. The highest uptake in the spleen was observed at 3h p.i. with 5%IA and an exponential decline with a HL of 74-156h. The liver also demonstrated moderate uptake at 20h p.i. up to 7% IA and a HL of 67-75 hours. Concerning malignant lesions we distinguished between bone (8) and liver (9) metastases. The maximum uptake at 20h p.i. was 11.9% IA for liver and 1.3% IA for bone metastases. All tumor lesions followed an exponential decline with a long mean HL of 111 hours. The following organ- and tumor doses were calculated: Whole body 0.12+/-0.03 Gy/GBq (0.07-0.18 Gy/GBq); kidneys 2.3+/-0.9 Gy/GBq (0.5-3.6 Gy/GBq); liver 0.39+/-0.05 Gy/GBq (0.35-0.44Gy/GBq); spleen 3.4+/-1.6 Gy/GBq (1.2-5.4Gy/GBq); bone lesions 1-57 Gy/GBq; liver lesions 15-81 Gy/GBq. **Conclusion:** As already demonstrated in PET/CT studies with antagonists, these first results show a high accumulation of the antagonist DOTA-LM3 in metastases. Despite the also high mean absorbed organ doses, PRRT using antagonist appears to be promising, as significantly high tumor doses are achieved. These preliminary results have to be verified in further studies with a higher amount of patients and better statistics. **References:** None.

OP-219

Analysis of patient diaries in the NETTER-1 Study

R. Srirajaskanthan[1], *J. Strosberg*[2], *E. Wolin*[3], *B. Chasen*[4], *M. Kulke*[5], *D. Bushnell*[6], *M. Caplin*[7], *R. P. Baum*[8], *T. Hobday*[9], *A. Hendifar*[10], *P. Santoro*[11], *P. Broberg*[11], *A. Demange*[11], *K. Öberg*[12], *P. Ruszniewski*[13], *L. Ravasi*[11], *E. Krenning*[14];
[1]*Kings College Hospital, London, UNITED KINGDOM,* [2]*Moffitt Cancer Center, Tampa, FL, UNITED STATES OF AMERICA,* [3]*Montefiore Einstein Center for Cancer Care, Bronx, NY, UNITED STATES OF AMERICA,* [4]*University of Texas MD Anderson Cancer Center, Houston, TX, UNITED STATES OF AMERICA,* [5]*Boston Medical Center, Boston, MA, UNITED STATES OF AMERICA,* [6]*University of Iowa, Iowa City, IA, UNITED STATES OF AMERICA,* [7]*Royal Free Hospital, London, UNITED KINGDOM,* [8]*Zentralklinik, Bad Berska, GERMANY,* [9]*Mayo Clinic College of Medicine, Rochester, MN, UNITED STATES OF AMERICA,* [10]*Cedars Sinai Medical Center, Los Angeles, CA, UNITED STATES OF AMERICA,* [11]*Advanced Accelerator Applications, a Novartis company, Geneva, SWITZERLAND,* [12]*University Hospital, Uppsala University, Uppsala, SWEDEN,* [13]*Hopital Beaujon and Paris Diderot University, Clichy, FRANCE,* [14]*Erasmus Medical Center, Rotterdam, SWEDEN.*

Aim/Introduction: The NETTER-1 trial primary statistical analysis showed a clinically and statistically significant PFS benefit with ^{177}Lu-DOTATATE vs. high-dose octreotide. ^{177}Lu-DOTATATE treatment was also correlated with a significant delay in time to deterioration in HRQoL. Patients were asked to record presence or absence of a range of symptoms in a daily diary. **Materials and Methods:** A Mixed Model Repeated Measures (MMRM) was used to analyze the change, compared to baseline. The symptoms considered to judge the overall disease status were abdominal pain, diarrhea and cutaneous flushing. The number of days with symptoms during the previous period was calculated for each visit (week=0, 4, 8, etc.). At baseline, the number of days with symptoms was counted over the previous 6 weeks, whereas the time frame between visits lasted 4 weeks. **Results:** The estimated number of days with symptoms declined significantly more in the ^{177}Lu-DOTATATE arm compared to the octreotide arm. Table 1 is showing the difference in change and the confidence intervals. **Conclusion:** Analysis of symptom diaries confirms that ^{177}Lu-DOTATATE can palliate clinically relevant symptoms when compared to high-dose octreotide. **References:** None.

OP-220

First Results of Targeted Alpha Peptide Receptor Radionuclide Therapy Using Ac-225 DOTATOC for Progressive Metastatic Neuroendocrine Neoplasms

H. R. Kulkarni, J. Zhang, A. Singh, C. Schuchardt, R. P. Baum;
Theranostics Center for Molecular Radiotherapy and Precision Oncology, Zentralklinik Bad Berka, Bad Berka, GERMANY.

Aim/Introduction: Peptide receptor radionuclide therapy (PRRT) using beta emitters like Lu-177, is an established treatment option for somatostatin receptor positive neuroendocrine neoplasms (NENs). Alpha-particles, due to their much higher linear energy transfer, result in more double-stranded DNA breaks. Therefore, alpha-particle emitters could have a higher therapeutic efficacy, when used for PRRT. We present our first experience of targeted alpha PRRT (TA-PRRT) in progressive metastatic NENs. **Materials and Methods:** Thirteen NEN patients with widespread metastases, having progressed after previous PRRT (2 - 9 cycles) using beta-emitters (Lu-177 / Y-90), received totally 23 cycles of Ac-225 DOTATOC. The primary tumors were pancreas (n=4), midgut (n=3), paraganglioma-pheochromocytoma (n=2), unknown (n=2), lung and kidney (each n=1) TA-PRRT was performed using a mean administered activity of 9.7 MBq (5 - 19 MBq), including 5 intra-arterial applications in 4 patients. All laboratory parameters (including complete blood picture 2-weekly, renal, hepatic function etc.) were regularly monitored. The objective response was evaluated by Ga-68 DOTATOC PET/CT. **Results:** The treatment (both intra-arterial and intravenous) was very well tolerated by all patients. There was no hematological toxicity; no worsening of counts even in patients with pre-existing anemia or pancytopenia. No evidence of hepatic or renal toxicity was noted. Ga-68 DOTATOC PET/CT at 3 months after therapy revealed an objective response in 85 % of the patients, including partial remission in 4 patients (31 %) and stable disease in 7 patients (54 %). Whereas, the disease continued to progress in 2 patients (15 %). **Conclusion:** Targeted alpha PRRT administering Ac-225 DOTATOC appears to be feasible, safe and effective in progressive metastatic NENs, refractory to beta emitters Lu-177 and Y-90. **References:** None.

OP-221

Predictive factors for short-term haematotoxicity during peptide receptor radionuclide therapy

D. M. V. Huizing, M. W. J. Versleijen, I. Walraven, M. M. Geluk - Jonker, M. E. T. Tesselaar, J. J. M. A. Hendrikx, B. J. de Wit - van der Veen, M. P. M. Stokkel;
Netherlands Cancer Institute, Amsterdam, NETHERLANDS.

Aim/Introduction: The goal of this study was to identify pre-treatment parameters associated with haematotoxicity during peptide receptor radionuclide therapy (PRRT), as moderate haematotoxicity already affects therapy management. **Materials and Methods:** A retrospective study was performed in patients with a neuroendocrine tumour, treated with PRRT in the Netherlands Cancer Institute between March 2016 and February 2019, and from whom a pre-therapy ^{68}Ga-DOTATATE PET/CT was available. Patients previously treated with PRRT were excluded. PRRT regimen comprised four administrations of ~7.4 GBq ^{177}Lu-DOTATATE every 10 weeks. Haematological parameters were measured every 3, 6 and 8.5 weeks after each administration or more frequent on clinical indication. Haematotoxicity was classified if either Hb <5.5 mmol/L, leukocytes <3.0×10^9/L, neutrophil granulocytes <1.0×10^9/L, or thrombocytes <75×10^9/L between start of PRRT until 10 weeks after cycle four, comparable to Common Terminology Criteria for Adverse Events (CTCAE) grade ≥2. General patient and tumour characteristics, previous therapies, baseline laboratory values and the volume and number of bone metastases were evaluated. Bone metastases were segmented using 40% SUV_{peak} threshold on pre-therapy ^{68}Ga-DOTATATE PET/CT. Univariate logistic regression and correlation analysis was performed to identify baseline variables associated with haematotoxicity. **Results:** In total 82 patients were included, of whom 60 (73.2%) completed four administrations and eleven (13.4%) are still continuing treatment. Eleven (13.4%) patients had to discontinue therapy, of which three patients due to persistent haematotoxicity. Haematotoxicity in one of the four blood parameters was observed in 29/82 (35.4%) patients. A postponed next administration and reduced activity was used in 9/29 patients, while only postponement or reduced activity was used in 2/29 and 5/29 patients, respectively. No intervention was applied in 13/29 patients. Toxicity was most frequently observed in leukocytes (20/82, 24.4%), followed by thrombocytes (13/82, 15.9%), Hb (8/82, 9.8%) and the least in neutrophil granulocytes (2/82, 2.4%). In univariate analyses, baseline thrombocyte levels between 87-208×10^9/L [OR 3.8 (95% CI 1.22-11.92)] were predictive for haematotoxicity (p-value = 0.015). In detail, baseline thrombocytes between 87-208×10^9/L were associated with leukopenia [OR 6.93 (95% CI 1.69-28.44)] and thrombocytopenia [OR 5.92 (95% CI 1.14-30.65)]. In addition, a significant (p-value <0.001) but low correlation (Spearman's rho = 0.54) was observed between baseline and lowest thrombocyte value. **Conclusion:** In roughly 20% of patients PRRT regime was modified due to haematotoxicity. Baseline thrombocyte values ≤208×10^9/L were associated with increased risk for haematotoxicity (CTCAE grade ≥2). No correlation with other parameters and between baseline thrombocyte values and thrombocytopenia was observed. **References:** None.

OP-222

Amino Acid Solutions in Premedication Peptide Receptor Radionuclide Therapy (PRRT) with Lutathera®: a Tolerance Study

P. Courault[1], V. Habouzit[1], A. Deville[1], L. Mele[1], N. Bouzehouane[1], F. Bour[1], E. Levigoureux[1,2], C. Bolot[1], C. Bournaud[1];
[1]Hospices Civils de Lyon, Groupement Hospitalier Est, Bron, FRANCE, [2]Université Lyon 1 Claude Bernard, Lyon, FRANCE.

Aim/Introduction: Co-infusion of amino-acid solutions during PRRT reduces tubular reabsorption of Lutathera® (^{177}Lu-oxodotreotide), thus minimizing nephrotoxicity of the radiopeptide. In our nuclear medicine center, patients have been treated with two different types of amino acid perfusions: a commercial solution (CS) containing 10% of amino-acid and a 2.5% Lysine-Arginine hospital preparation produced by a referral laboratory. The aim of this study was to analyze the tolerance of the two amino acid perfusions. **Materials and Methods:** Medical files of the patients have been analyzed with double checking. Data were gathered from paper or informatics folders and nurse traceability sheets. Parameters recorded were: sex, age, primitive site of the tumor, type of amino acid perfusion, adverse events (AE) and their OMS grades, antiemetic premedication, clearance of the creatinine and kalemia. **Results:** From February 2016 to February 2019, 76 patients (male 55%, mean age = 63 years-old) were treated for a total of 235 cycles. Primitive tumor site was small intestine (73%), then pancreas (15%), bronchial (5%), rectum (5%) and other (2%). AE occurred in 69% (n=82/119) of cycles with CS as compared to 18% (n=21/116) in the Lysine-Arginine group (p<0.0001). One patient declined to continue PRRT after the first cycle, because of grade 4 vomiting with the CS. Most frequent AE consisted in nausea and vomiting (n=83/103), flush (n=10/103), headache (n=6/103) or diarrhea (n=6/103). In the CS group, AE were mostly graded 4 in the OMS scale (n=24/82), whereas they were graded 1 in the Lysine-Arginine group (n=13/21). Thanks to the reduction of AE, patients received on average 3.2 and 1.4 lines of antiemetics before CS administration or Lysine-Arginine. Interestingly, 10 patients (36 cycles) received both solutions. Sixty-four percent (n=11/17) of these cycles with the CS were complicated by AE versus 15% (n=3/19) of cycles with Lysine-Arginine (p=0.005). Mean creatinine clearance was identical before and after PRRT cycles, whatever the amino acid infusion. Three patients underwent a temporary degradation of renal failure from stage 2 to 3: one in CS group and two in Lysine-Arginine group. Four patients (6 cycles) were closely follow-up 1 or 2 days after PRRT for the kaliemia and no significant variation was observed. **Conclusion:** The Lysine-Arginine preparation offers a better tolerance than the commercial solution. Short term follow-up did not disclosed difference regarding nephroprotective effect of both preparations. The change for Lysine-Arginine allowed a reduction of the antiemetic premedication from 4 to 1 molecule. **References:** None.

OP-223

Favourable outcome in patients with metastatic pheochromocytomas and paragangliomas treated with ^{177}Lu-DOTATATE

A. Vyakaranam[1,2], *J. Crona*[1], *E. Thiis-Evensen*[3], *P. Hellman*[1], *O. Norlén*[1], *D. Granberg*[2], *U. Garske-Román*[4], *K. Fröss-Baron*[1], *M. Sandström*[1], *A. Sundin*[1];
[1]*Uppsala University, Uppsala, SWEDEN,* [2]*Akademiska Sjukhuset, Uppsala, SWEDEN,* [3]*Oslo Metropolitan University, Oslo, NORWAY,* [4]*Department of Nuclear Medicine, Sahlgrenska University Hospital, Gothenburg, SWEDEN.*

Aim/Introduction: Peptide receptor radiotherapy (PRRT) with ^{177}Lu-DOTATATE, has emerged as a promising therapy for neuroendocrine tumors. PRRT has been used both as first-line and salvage treatment in small cohorts of patients, world-wide, diagnosed with pheochromocytoma (PCC) and paraganglioma (PGL). **Materials and Methods:** This was a retrospective cohort study including 22 patients with histopathologically confirmed PCC and PGL, two were localized and 20 metastatic. 13/22 patients were tested for gene abnormalities,7 patients had SDHx-related mutations, 2 patients with mutations in NF-1 gene and 4 patients were sporadic. Radiological response utilized RECIST 1.1 and toxicity was graded according to CTCAE4 criteria. Visually rated decrease (>50%) of tumor accumulation as compared to scintigraphy during the first cycle was considered as scintigraphic response. Reduction in plasma chromogranin A ≥50% was considered as biochemical response. **Results:** 7.4 GBq per cycle of ^{177}Lu-DOTATATE (median 4, range 3-11 cycles) was administered as first-line therapy in 13 patients or because of progressive disease in 9 patients. Partial response (PR) was achieved in two and stable disease (SD) in 20 patients. The median overall survival (OS) in months was 49.6 (range 8.2-139) and median progression free survival (PFS) was 21.6 (range 6.7-138). The median best response on CT according to RECIST 1.1, across the cohort was -10 % (range 0 to -65%). The time to best response was median 14.4 months (range 4.7 to 128 months). Scintigraphic response was seen in 9/19 (47%) patients. In 7 out of 15 evaluable patients (47%) biochemical response was achieved and 2 (13%) showed an increase in plasma chromogranin A. Subgroup analysis showed that low Ki-67 (<15%) was associated with longer OS (p=0.013) and PFS (p=0.005). PRRT as first-line therapy was found associated with increased OS (p=0.041).No hematological or kidney toxicity grade 3-4 was registered. **Conclusion:** ^{177}Lu-DOTATATE therapy was associated with favorable outcome and low toxicity. High Ki-67 (≥15%) and PRRT received because of progression on previous therapy, could constitute negative predictive factors for OS. **References:** None.

OP-224

A standardized and simplified dosimetric approach for PRRT in patients with neuroendocrine tumor

E. Tonini[1], *S. Di Biaso*[2], ***M. Longo***[1,3], *A. Barboni*[1], *A. Turra*[1], *L. Uccelli*[4], *S. Panareo*[4], *C. Cittanti*[4], *M. Bartolomei*[4];
[1]*Arcispedale Sant'Anna Hospital, Medical Physics Unit, Ferrara, ITALY,* [2]*Dipartimento di Fisica e Scienze della Terra, Ferrara University, Ferrara, ITALY,* [3]*Sapienza University of Rome, Ph. D. Program in Morphogenesis & Tissue Engineering, Rome, ITALY,* [4]*Arcispedale Sant'Anna Hospital, Nuclear Medicine Unit, Ferrara, ITALY.*

Aim/Introduction: Since July 2018, Neuroendocrine Tumour (NET) patients are being treated with peptide-receptor radionuclide-therapy (PRRT) at Arcispedale Sant'Anna of Ferrara, according to the FENET 2016 protocol, that includes the use of both ^{177}Lu-DOTATOC and combined ^{177}Lu/^{90}Y-DOTATOC. The

aim of the study is to propose a shorter but patient-tailored dosimetric procedure to provide significant data for an accurate evaluation of each patient. **Materials and Methods:** Forty-eight patients are treated with systemic administration of a cumulative activity between 11 and 28 GBq. The treatment is fractionated in 5-cycles, each ranging from 1.9 to 5.5 GBq (for ^{177}Lu-DOTATOC and ^{177}Lu/^{90}Y-DOTATOC). Dosimetric evaluation is performed after the 1° cycle to modulate the activity of the further 2°, 3° and 4° cycles and it is repeated after the 5° to assess the variation in term of uptake volume, absorbed dose and BED on lesions and critical organs. A validated and simplified method based on 3 SPECT/CT at 1, 24, 48-hours after administration was developed. The MIM® software was used by an automated workflow that allows contouring the volume of interest (VOI) regarding lesions and kidneys on sequential fused images and co-registered. Image counts were then corrected for scatter, attenuation and partial volume effects. The absorbed dose have been computed through OLINDA2.0 and the BED in the selected VOI has been also obtained. **Results:** A high variability in tumor absorbed doses per unit activity was observed due to variability in target volume [16÷490 ml]; reported values are from 0.6 to 10.8 Gy/GBq and from 0.6 to 3.0 Gy/GBq at 1° and 5° cycle respectively. ^{90}Y kidney and lesions absorbed doses are a factor of 4 and 5 higher than those with ^{177}Lu; BED resulted in a mean value of 42 Gy. For ^{177}Lu-DOTATOC the mean absorbed dose in kidneys has been found of 3.1 Gy [1.0÷6.5 Gy], while the BED is 3.4±0.9 Gy, with an effective half-time of 42.0±5.4 h. For ^{90}Y-DOTATOC the mean absorbed dose in kidneys is 7.8 Gy [4.7÷12.1 Gy] with a BED of 9.3±3.2 Gy and an effective half-time of 26.0±7.1 h. **Conclusion:** The final aim of this work is to ensure a dosimetric evaluation to all patients undergoing PRRT. MIM® software has allowed us to standardize the method by working accurately and with a great saving of time. Our results suggest that a dosimetric evaluation at both 1° and 5° cycle is advisable in order to provide a precision-treatment. **References:** None.

OP-225

177Lu-DOTATATE in advanced neuroendocrine tumours: real word data from SEPTRALU registry

M. Mitjavila Casanovas[1], *C. Field*[2], *P. Bello*[3], *Z. Nogareda Seoane*[4], *L. García-Cañamaque*[5], *J. Arbizu*[6], *A. Rotger*[7], *P. Gajate*[8], *M. Castellón*[9], *M. Muros*[10], *A. Teulé*[11], *A. Repetto*[12], *M. Miguel Martinez*[13], *M. Estorch*[14], *P. Jimenez Fonseca*[15], *A. Carmona-Bayona*[16];

[1]*Nuclear Medicine HU Puerta de Hierro Majadahonda, Madrid, SPAIN,* [2]*Nuclear Medicine Hospitales Madrid, Madrid, SPAIN,* [3]*Nuclear Medicine, HU La Fe, Valencia, SPAIN,* [4]*Nuclear Medicine, HU Lucus Augusti, Lugo, SPAIN,* [5]*Nuclear Medicine, Hospitales Madrid, Madrid, SPAIN,* [6]*Nuclear Medicine, Clínica Universidad de Navarra, Pamplona, SPAIN,* [7]*Nuclear Medicine, Hospital Universitario Gregorio Marañón, Madrid, SPAIN,* [8]*Medical Oncology, HU Ramón y Cajal, Madrid, SPAIN,* [9]*Nuclear Medicine, HU Virgen de la Arrixaca, Murcia, SPAIN,* [10]*Nuclear Medicine,HU Virgen de Las Nieves, Granada, SPAIN,* [11]*Medical Oncology, ICO-Bellvitge, Barcelona, SPAIN,* [12]*Nuclear Medicine, HU Son Espases, Palma de Mallorca, SPAIN,* [13]*Nuclear Medicine HU Burgos, Burgos, SPAIN,* [14]*Nuclear Medicine HU Sant Pau, Barcelona, SPAIN,* [15]*Medical Oncology, Hospital Universitario Central de Asturias, Oviedo, SPAIN,* [16]*Medical Oncology, Hospital Universitario Morales Meseguer de Murcia, Universidad de Murcia, UMU, IMIB, Murcia, SPAIN.*

Aim/Introduction: Radionuclide therapy is effective in advanced neuroendocrine tumors (NET), but we lack multicentre data from real word patients. The aim of this paper has been to describe the caracteristics of patients with advanced NET´s and to show the results in efficacy, tolerance and toxicity of treatment with 177Lu-DOTATATE (PRRT) in our national experience. **Materials and Methods:** The data is taken from the national multicenter study SEPTRALU. Researchers from 18 centers (oncologists, endocrinologists, nuclear medicine physicians) recruited 177 patients. Toxicity was registered according to CTCAE v3.0 criteria. The best response and maximum toxicity were reported. Survival was assessed according to Kaplan-Meier method and Cox model. **Results:** 177 patients were recruited (49.7% women) with median age of 58 years (18-89) and a good performance status (ECOG 1-2) 89.3%. 61% were functioning NETs with Ki-67 <20% in 91%. The most common primary tumor location was gastrointestinal 41%, followed by pancreatic 39%. The most common metastasis location was the liver 83.6%, followed by lymph nodes 42.4% and bone 27.1%. Prior to PRRT they had received a median of 4 lines of treatment (1-7). 64.2% of the patients received 4 PRRT cycles, and in 96% of them 7.4 GBq. Of 101 patients assessed by RECIST 1.1 criteria, they reached partial response 25.7% (n = 26), complete response 3.9% (n = 4), stable disease 55.4% (n = 56) and progression 14.8% (n = 15). The median progression free survival and overall survival were 24.3 months (IC95% 21.3-NA) and 28.1 months (24.6-NA) respectively. Toxicity G3-G4 was registered in 9% (n = 16), the most common: haematologic (4.1%, n = 7), asthenia (2.9%, n = 5), and nephrotoxicity (1.1%, n = 2). In the multivariate analysis, the factors associated with overall survival were ECOG-PS (HR 1.16, p = 0.001), Ki-67%, HR 1.02 (p = 0.026), extra-liver/extra-lymph nodes metastases (HR 2.63, p = 0.018). **Conclusion:** In our serie of patients from the real world, meaning more heterogeneous than in clinical trials, we have confirmed that therapy with 177Lu-DOTATATE is safe and effective. It is necessary to understand the pattern of use of PRRT in daily practice to be able to understand the cost-effectiveness of this therapy. **References:** None.

509

Neuroimaging - Parallel Session: Movement Disorders and Neurotransmission

Sunday, October 13, 2019, 16:30 - 18:00 Lecture Hall 115

OP-226

Multi-Centre Evaluation of the New-Generation Tau PET Tracer [^{18}F]PI-2620 in Progressive Supranuclear Palsy

H. Barthel[1], M. Brendel[2], T. van Eimeren[3], K. Marek[4], L. Beyer[2], M. Song[2], C. Palleis[2], G. Respondek[5], J. Sauerbeck[2], J. Hammes[3], M. Barbe[3], Ö. Onur[3], F. Jessen[3], J. Rumpf[1], M. L. Schröter[1], M. Rullmann[1], A. Schildan[1], J. Classen[1], G. Höglinger[5], P. Bartenstein[2], V. Villemagne[6], A. Drzezga[3], J. Seibyl[4], O. Sabri[1], PI-2620 in PSP Study Group;

[1]Leipzig University, Leipzig, GERMANY, [2]Ludwig-Maximilian University Munich, Munich, GERMANY, [3]University of Cologne, Cologne, GERMANY, [4]Invicro, New Haven, CT, UNITED STATES OF AMERICA, [5]Technical University Munich, Munich, GERMANY, [6]University of Melbourne, Melbourne, AUSTRALIA.

Aim/Introduction: Progressive supranuclear palsy (PSP) is a 4-repeat (4R) tauopathy for which post mortem histopathology of brain region-specific tau deposits is considered the diagnostic gold standard, and for which establishing a clinical diagnosis may be challenging. Respective in vivo PET imaging would potentially allow not only for improved early and differential diagnosis, but also for more rationalized anti-tau drug trial stratification/therapy monitoring. The available first-generation tau PET tracers have major limitations, especially in imaging PSP patients. [^{18}F]PI-2620 is a second-generation tau tracer which, due to its low non-specific binding and relative high affinity for 4R tau, might be a suitable alternative. Thus, a multi-centre evaluation was conducted to investigate this question. **Materials and Methods:** Twenty patients (71±6y, n=10 female) with probable or possible PSP-Richardson syndrome (RS) according to the MDS-PSP criteria (PSP rating scale: 38±17; range 13-71) underwent [^{18}F]PI-2620 PET at five different centres, together with ten matched healthy controls (HCs) and ten disease controls (multi-system atrophy, Parkinson's disease, Alzheimer's disease). Multilinear reference tissue modelling with cerebellar reference served for calculation of 0-60min p.i. distribution volume ratios (DVRs). DVRs in PSP target regions (globus pallidus, substantia nigra, nucleus subthalamicus, nucleus dentatus) were compared between PSPs, HCs, and disease controls, and controlled for potential imaging centre, age and gender effects. In parallel, globus pallidum PSP and HC slices were subjected to [^{18}F]PI-2620 in vitro autoradiography (with/without blocking with 10µM ^{19}F-PI2620). **Results:** When compared to the HCs, elevated [^{18}F]PI-2620 DVRs were observed in the PSP patients in the globus pallidus (1.17±0.09 vs. 1.00±0.06; p<0.001), the nucleus subthalamicus (1.20±0.08 vs. 1.05±0.09; p=0.002), and the nucleus dentatus (1.13±0.05 vs. 1.07±0.04; p=0.032). The disease controls showed no significant differences in the above target regions when compared to the HCs (p>0.9). Even in PSP patients with low disease severity (PSP rating scale ≤30; n=6), the globus pallidum DVRs were significantly higher compared to the HCs (1.19±0.07 vs. 1.00±0.06; p=0.004). In vitro autoradiography showed displaceable tracer binding in the globus pallidus of PSP patients, but not in HCs. **Conclusion:** This preliminary multi-centre data indicate a diagnostic value of dynamic [^{18}F]PI-2620 PET imaging in PSP, potentially both for early and differential diagnosis. More studies, in both PSP-RS and non-PSP-RS patients and also with regard to the question of whether static PET imaging might suffice in establishing a binary diagnosis are thus warranted. **References:** None.

OP-227

A Multiple-modality Pattern of Multiple System Atrophy Based on FDG PET/CT and MRI

L. Li[1], S. Peng[2], P. Wu[1], J. Ge[1], J. Lu[1], J. Wang[1], Y. Ma[2];

[1]Huashan Hospital, Shanghai, CHINA, [2]Feinstein Institute for Medical Research, New York, NY, UNITED STATES OF AMERICA.

Aim/Introduction: This study established multiple system atrophy related brain network (MSARP) based on multiple-modality images and proved their comparable values in diagnostic specificity **Materials and Methods:** We selected 20 MSA (14M/6F, age: 57.6±7.7y, HY: 3.3±0.8, UPDRS: 30.5 ±18.6, duration: 1.7±0.9y), 20 PD (12M/8F, age: 62.5±8.3y, HY: 2.0±0.7, UPDRS: 19.9±7.7, duration: 3.2±2.3y), 20 PSP (13M/7F, age: 65.0±7.9y, HY: 3.1±1.1, UPDRS: 24.3±12.2, duration: 2.9±1.9y), and 20 healthy control subjects (5M/15F, age: 61.7±6.1y) who underwent FDG PET and arterial spin labeling (ASL) and structural imaging (T1). We used multimodal images of patient and control groups separately to establish brain network. Structural MRI data was segmented into maps of gray matter and white matter using voxel-based morphometry to detect local changes in brain tissue volume. Maps of CBF were extracted from ASL images. All PET/MRI images were coregistered to the subject's structural MRI scan and spatially normalized into the standard MNI brain space, then were smoothed using a Gaussian filter with the width of 6-10 mm (FWHM) depending on signal-to-noise ratio characteristics of a particular imaging modality. Network analysis were performed separately in each category of patients for FDG PET, ASL and T1 MRI data using matlab 2013 by applying a voxel-based spatial covariance mapping algorithm known as Scaled Subprofile Modeling based on principal component analysis (SSM/PCA), whose expression could best discriminate the patients from the controls in a logistical regression model along with bootstrap resampling. Network scores were z-transformed using the mean and standard deviations of healthy control subjects in the original derivation cohort for each imaging modality. **Results:** Three versions of MSARP were generated, which came from 3~4 PCs accounting for 20~40% of subject × voxel variance. There were similar effects of group in MSARP scores among all subjects with FDG/CBF/GM data (ANOVA: F[3,76] ≥30.4,

p<0.0001) with differential elevation in MSA relative to NC/PSP/PD. These scores correlated positively with duration in MSA (regression analysis: r=0.552, p=0.012; FDG only). MSARP scores exhibited excellent accuracy in discriminating MSA from NC and PD (ROC analysis: AUC≥0.988±0.014 [SE], CI: 0.96-1.00) or the three other groups (AUC≥0.943±0.025, CI: 0.90-1.00) with FDG/CBF/GM data. The discrimination of MSA vs PSP was greater with FDG (AUC≥0.920±0.045, CI: 0.83-1.00) than with CBF/GM data (AUC≥0.848±0.061, CI: 0.73-0.99) **Conclusion:** This study produced highly robust MSARP across different modalities which may provide a reliable and objective marker of MSA in clinical diagnosis **References:** None.

OP-228

Variability of Dopaminergic Degeneration Patterns in Multiple System Atrophy: Data-driven Approaches of Dopamine Transporter PET

R. Lee, J. Shin, H. Choi, H. Kim;
Seoul National University Hospital, Seoul, KOREA, REPUBLIC OF.

Aim/Introduction: Multiple system atrophy (MSA) is a progressive neurodegenerative disorder with highly variable clinical presentations. Even though striatonigral dopaminergic degeneration is a typical neuropathological feature, its spatial pattern which can be evaluated by PET imaging in accordance with the clinical presentation of MSA has not yet been clarified. Here, we identified variable dopamine degeneration patterns of F-18 FP-CIT PET in MSA using a data-driven method. **Materials and Methods:** Sixty-eight MSA patients who underwent F-18 FP-CIT PET/CT between 2009 and 2018 were retrospectively enrolled. For quantitative analysis, the PET images were spatially normalized and transformed to binding-ratio (BR) maps using occipital lobe as a reference region. As conventional quantification methods, the BR for putamen and caudate (BR_{put} and BR_{cau}) were calculated. To identify voxel-wise patterns with a data-driven approach, principal component analysis (PCA) was employed and correlated with the clinical presentation. The pattern of imaging data was also visualized by 2-dimensional projection using t-distributed stochastic neighborhood embedding (t-SNE). **Results:** Of the 68 subjects, 42 presented with Parkinsonian subtype of MSA (MSA-P), 16 presented with cerebellar subtype of MSA (MSA-C), and 10 presented with both features of MSA subtypes (MSA-PC) (mean age, 61.8 ± 9.5 years; disease duration, 7.3 ± 3.4 years). The BR_{put} was significantly lower in MSA-P patients than in MSA-C patients (2.6 ± 0.4 vs. 3.0 ± 0.5, p = 0.003). Each principal component (PC) represents a specific pattern of degeneration: PC1 and PC2 was associated with the entire putamen and posterior putamen, respectively. PC3 was associated with caudate and FP-CIT binding of dorsal raphe nuclei. PC1 and PC2 showed a significant difference between MSA-P and MSA-C patients (-0.7 ± 3.0 vs. 1.2 ± 4.0, p = 0.023 and -0.4 ± 1.2 vs. 0.9 ± 1.1, p = 0.001). PC2 and PC3 were associated with patients' age (r= 0.42, p < 0.001; r = -0.42, p <0.001, respectively). Moreover, MSA patients with decreased PC2 were related to relatively good response to the L-DOPA (t= 2.5, p = 0.02). **Conclusion:** MSA shows variable dopamine degeneration patterns according to the FP-CIT PET. The dopamine degeneration pattern identified by PET through a data-driven approach may contribute to the refining subtypes of MSA as well as to explain various clinical presentations. **References:** None.

OP-229

Differential Diagnosis of Parkinsonism using a 3D Deep Residual Convolutional Neural Network based on 18F-FDG PET Imaging

P. Wu[1], Y. Zhao[2], J. Wang[3], N. Navab[2], I. Yakushev[4], W. Weber[4], M. Schwaiger[4], S. Huang[5], P. Cumming[6], A. Rominger[6], C. Zuo[1], K. Shi[6];
[1]PET Center, Huashan Hospital, Fudan University, Shanghai, CHINA, [2]Department of Computer Science, Technische Universität München, Munich, GERMANY, [3]Department of Neurology, Huashan Hospital, Fudan University, Shanghai, CHINA, [4]Department of Nuclear Medicine, Technical University of Munich, Munich, GERMANY, [5]Department of Molecular and Medical Pharmacology, UCLA, Los Angeles, CA, UNITED STATES OF AMERICA, [6]Department of Nuclear Medicine, University of Bern, Bern, SWITZERLAND.

Aim/Introduction: Idiopathic Parkinson's disease (IPD) and atypical parkinsonian syndromes (APS) have similar symptoms at early disease stage, making the differential diagnosis difficult. 18F-FDG PET and machine learning can discriminate metabolic patterns for the differential diagnosis of parkinsonism [1]. We recently introduced deep learning to differentiate these syndromes based on projected 2D images of the 18F-FDG PET volumes [2], which may miss some characteristic features due to dimension reduction. Therefore, we aimed to develop an automated diagnosis framework operating directly on 3D image volumes based on a sufficient database. Furthermore, we depicted in salience maps the decision mechanism of the deep learning method. **Materials and Methods:** 920 patients with evident parkinsonian features underwent 18F-FDG PET imaging and were subsequently diagnosed by movement disorders specialists as IPD (n=502), multiple system atrophy (MSA, n=239) and progressive supranuclear palsy (PSP, n=179), respectively. We developed a 3D deep residual convolutional neural network comprising a total of 18 layers. The residual connections included in this network were helpful for simplifying its optimization. We generated saliency maps using the guided back-propagation method [3]. Five-fold cross validation was applied to evaluate the proposed network, which was implemented in the TensorFlow platform and accelerated by a NVIDIA Titan-XP GPU. **Results:** We cross-validated the diagnostic efficiency of the neural network in the 542 patients with clinically definite diagnosis after pretraining in the 378 patients with clinically probable diagnosis. The proposed framework achieved 98.9% sensitivity, 90.0% specificity, 98.4% PPV and 95.0% NPV for the classification of IPD, versus 98.8, 82.5, 96.1, and 96.0% for the classification of MSA, and 87.1, 97.8, 96.1, and 94.1% for the classification of PSP respectively. The figure demonstrates fused saliency maps of subjects (N=15)

with IPD, MSA, or PSA, showing main saliency in (A) the right prefrontal cortex, (B) the bilateral thalamus and putamen, and (C) the midbrain and left lingual gyrus. **Conclusion:** We successfully developed a 3D deep residual convolutional neural network for automated differential diagnosis of IPD and atypical parkinsonism with excellent diagnostic accuracy. The greatest salience was in expected regions of the basal ganglia, but initial findings also implicate high order visual cortex and prefrontal cortex. The method is currently under detailed assessment in a separate group of several hundred parkinsonian patients, and with emphasis on the interpretation of the saliency maps in diagnosis. **References:** [1] Tang et al. Lancet Neurol 2010 [2] Wu et al. SNMMI 2018 [3] Springenberg, J.T., arXiv:1412.6806

OP-230

^{123}I-FP-CIT reference values from subjects with non-degenerative Parkinsonism, comparable to values from healthy volunteers

C. Scheiber[1], *G. Platsch*[2], *S. Gouttard*[1], *S. Thobois*[1,3], *S. Zuehlsdorff*[4], *R. Fahmi*[4];
[1]*HCL- Groupement Hospitalier Est, Lyon, FRANCE,* [2]*Siemens AG Healthcare, Erlangen, GERMANY,* [3]*Hopital Neurologique, Lyon, FRANCE,* [4]*Siemens Medical Solutions USA, Inc., Knoxville, TN, UNITED STATES OF AMERICA.*

Aim/Introduction: The distinction between degenerative Parkinsonism and other entities without dopaminergic lesion (e.g., atypical tremors and drug-induced-parkinsonism (DIP)) are frequent indications of ^{123}I-FP-CIT. In addition to visual interpretation of ^{123}I-FP-CIT scans, semi-quantification and comparison to reference values are often needed, in particular for equivocal cases. To overcome the challenges of multi-center variability and the difficulty to recruit healthy volunteers, we generated ^{123}I-FP-CIT references from individuals with various neurological diseases without dopaminergic-degeneration, scanned at a single center following the same protocol, and compared them to references from healthy-volunteers. **Materials and Methods:** From a pool of 1,884 patients scanned on a SymbiaT2 (Siemens Healthineers) with low-energy-high-resolution collimators between Jan-2008 and Dec-2015, 256 subjects with normal ^{123}I-FP-CIT imaging and a clinical diagnosis follow-up of 4.8±1.3 years to ensure that they did not develop degenerative-Parkinsonian-syndrome, were initially selected based on visual (2 readers) and (in-house) semi-quantitative assessments (SC). Corresponding SPECT-projections and CT-images were further assessed by a trained physician (GP) who kept 237 subjects (120 male, 117 female, age: 62.2±15.7 [16-88]), the majority of which (49.8%) had either ET or DIP. A younger group (8.85%) had attention-deficit/hyperactivity disorder. Scans were acquired 3hrs post-injection of ~185MBq of ^{123}I-FP-CIT with (rotational radius≤15cm, matrix: 128x128, 120 projections over 360°, and zoom=1.23 x 1.23). Images were reconstructed with Flash3D (10-iterations, 8-subsets, CTAC, TEW scatter-correction, and 8mm-Gauss post-filtering). Using syngo.via® (Siemens Healthineers), we computed regional striatal-binding-ratios (SBRs), caudate-to-putamen-ratios (C2PRs), and asymmetries on predefined striatal volumes-of-interest. We used linear-regression to correct for age-dependency of SBRs and to allow comparisons to age-matched references. Left and right SBRs were averaged to generate one reference SBR per region. C2PRs and asymmetries were independent of age. Women had higher SBRs than men but without statistical significance. We compared our results to ENCDAT-database[1]. **Results:** Overall average percent-decline of uptake per-decade was 4.56%. Slope, intercept, and R^2-value of linear-regression were, respectively: striatum (-0.016, 4.03, 0.27), caudate (-0.0145, 4.0, 0.22), and putamen (-0.018, 4.06, 0.32). In comparison with uncalibrated ACSC-ENCDAT results, we found comparable regression parameters according to gender (see tables). **Conclusion:** Our ^{123}I-FP-CIT reference values, generated from individuals with various neurological conditions without dopaminergic degeneration scanned at a single center, have similar distribution as a function of age as values from healthy-volunteers. Co-morbidities (e.g., diabetes, hypertension) didn't seem to increase the variance when compared to healthy subjects, making it possible for clinicians to build their own normal ^{123}I-FP-CIT databases from day-to-day practice. **References:** [1]Varrone et al.--EJNMMI'2013;40(2):213-27.

OP-231

Neuroprogressive character of sigma-1 receptor pathophysiology in unmedicated patients with acute major depressive disorder as investigated by (-)-[^{18}F] Fluspidine PET

P. Meyer[1], *M. Strauss*[2], *G. Becker*[1], *S. Hesse*[1], *K. Bednasch*[2], *B. Ettrich*[2], *S. Wilke*[1], *F. Zientek*[1], *M. Rullmann*[1], *J. Luthardt*[1], *S. Fischer*[3], *M. Patt*[1], *B. Wünsch*[4], *P. Brust*[3], *O. Sabri*[1];
[1]*Department of Nuclear Medicine, University of Leipzig, Leipzig, GERMANY,* [2]*Department of Psychiatry and Psychotherapy, University of Leipzig, Leipzig, GERMANY,* [3]*Department of Neuroradiopharmaceuticals, Institute of Radiopharmaceutical Cancer Research, Helmholtz-Zentrum Dresden-Rossendorf, Research Site Leipzig, Leipzig, GERMANY,* [4]*Institute for Pharmaceutical and Medicinal Chemistry, University of Münster, Münster, GERMANY.*

Aim/Introduction: We have previously shown that the sigma-1 receptor (Sig-1R) availability is increased in unmedicated acute MDD (MDD) using (-)-[^{18}F]Fluspidine PET. In order to assess whether this pathophysiology is progressive, we investigated the relationship between Sig-1R availability and duration of disease (DD), number of depressive episodes (DE) and severity of acute depressive symptoms (Hamilton Depression Rating Scale, HAMD) in this now completed first-in-human (-)-[^{18}F]Fluspidine PET trial. **Materials and Methods:** Patients with moderate to severe MDD (n=18; 32±12 years; 9 females; DD 6±8 years; DE 3±1 years; HAMD: 20±4) were studied using (-)-[^{18}F]Fluspidine PET (300 MBq, ECAT Exact HR+) and compared with sex-/age-matched healthy controls (HC; n=16; 32±13ys [n.s.]; 9 females [n.s.]). VOI analyses were performed and regional distribution

volumes (V_T) were estimated by kinetic modeling (0-210 min p.i.; 2TCM; metabolite correction). **Results:** In MDD, compared with HC, V_T was higher especially within the fronto-temporal, anterior cingulate and insular cortices, amygdala, striatum, thalamus and ncl. raphe (P<0.005). Positive correlations were found between HAMD and V_T within the anterior and posterior cingulate and insular cortices, ncl. caudatus and thalamus (r=0.43 to 0.57, P<0.05, adjusted for DD, BMI).Negative correlations were found between DD and V_T within the orbitofrontal cortex and hypothalamus (r=-0.40 to -0.47, P<0.05, adjusted for severity of MDD) and between DE and V_T within the hypothalamus, orbitofrontal, temporo-parietal and cingulate cortices, striatum, thalamus and cerebellum (r=-0.42 to -0.60, P<0.05, adjusted for severity of MDD). **Conclusion:** Using (-)-[^{18}F]Fluspidine PET, we showed for the first time increased cortico-(para-)limbic Sig-1R availability during the DE of MDD, as compared with HC, that was associated with the severity of acute depressive symptoms (HAMD). Remarkably, in MDD, there is a negative correlation between DE or DD and Sig1-R availability, especially within orbitofrontal cortices and hypothalamus as well as within various (sub)cortical-(para)limbic and cerebellar brain regions. Although verification by longitudinal (-)-[^{18}F]Fluspidine PET studies is needed, our findings suggest a neuroprogressive character of Sig-1R pathophysiology in MDD. **References:** None.

OP-232

[18F]Fluspidine and [18F]Fallypride PET study to evaluate sigma-1 receptor (S1R) and dopamine 2 / dopamine 3 receptor (D2/3R) occupancy by pridopidine in healthy volunteers (HV) and patients with Huntington disease (HD)

P. Meyer[1], *I. D. Grachev*[2,3], *G. Becker*[1], *M. Bronzel*[4], *D. Marsteller*[5], *G. Pastino*[5], *O. Voges*[4], *L. Rabinovich*[5], *H. Knebel*[5], *F. Zientek*[1], *M. Rullmann*[1], *B. Sattler*[1], *M. Patt*[1], *E. Strauss*[6], *A. Kluge*[4], *J. Savola*[5], *M. F. Gordon*[5], *M. Geva*[7], *S. Hesse*[1,8], *H. Barthel*[1], *M. R. Hayden*[7], *O. Sabri*[1]; [1]*Department of Nuclear Medicine, University of Leipzig, Leipzig, GERMANY,* [2]*Teva Branded Pharmaceutical Products R&D, Inc, Malvern, PA, UNITED STATES OF AMERICA,* [3]*Guide Pharmaceutical Consulting, LLC, Millstone Twp, NJ, UNITED STATES OF AMERICA,* [4]*ABX-CRO Advanced Pharmaceutical Services Forschungsgesellschaft mbH, Dresden, GERMANY,* [5]*Teva Branded Pharmaceutical Products R&D, Inc, Frazer, PA, UNITED STATES OF AMERICA,* [6]*AFL – Arzneimittelforschung Leipzig GmbH, Leipzig, GERMANY,* [7]*Prilenia Therapeutics Development Ltd., Herzliya, ISRAEL,* [8]*Integrated Research and Treatment Centre (IFB) Adiposity Diseases, University of Leipzig, Leipzig, GERMANY.*

Aim/Introduction: Pridopidine is an investigational drug which was initially designed as dopamine stabilizer to treat motor symptoms in HD. Interestingly, as shown previously in-vitro and in rats, pridopidine has much higher affinity to S1Rs as compared to D2/3Rs. S1R, located intracellularly at the endoplasmic reticulum and mitochondria interface, may mediate neuroprotection and enhancement of mental dysfunction. Thus, in order to improve the understanding about the mechanism of action of pridopidine and the observed clinical outcomes in prior clinical trials, we quantitatively assessed, using S1R-specific (S)-(-)-[^{18}F]Fluspidine and D2/3R-specific [^{18}F]Fallypride PET, the S1R occupancy (S1RO) and D2/3R occupancy (D2/3RO) by pridopidine at previously used clinical doses in the brain of HVs and HD patients. **Materials and Methods:** Eleven male HVs (27 ± 2yrs; pridopidine 90mg to 0.5mg in 6 dose groups) and 3 male HD patients (43 ± 13yrs, pridopidine 90mg) were studied twice before and 2hrs following single oral doses of pridopidine using (S)-(-)-[^{18}F]Fluspidine PET (300 MBq, 0-90min p.i., Siemens PET/MRI). Distribution volume (V_T) was quantified using kinetic modeling (1TCM; metabolite correction). In addition, four male HVs (29 ± 5yrs) were studied twice using [^{18}F]Fallypride PET (200 MBq, 0-210min p.i.) before and 2hrs following a single oral dose of pridopidine (90mg). Binding potential (BP_{ND}) was assessed using a simplified reference tissue model (cerebellum as reference region). VOI-analyses were performed. For each subject/tracer, the receptor occupancy (RO) was calculated by Lassen plot analysis. **Results:** A typical non-linear sigmoid-shaped dose response relation for S1RO was established in HVs for pridopidine doses ranging from 0.5mg to 90mg. In HVs, there was a high degree of S1RO (87 ± 3% to 91 ± 4%) across all brain regions at pridopidine doses ranging from 22.5mg to 90mg. S1RO only dropped below 50% after reducing the pridopidine dose to 1mg (43%). The lowest possible dose of 0.5mg pridopidine still achieved a blocking rate of 18%. In HD, very similar to HVs, there was a high degree of S1RO (87 ± 7%, n.s.) for a pridopidine dose of 90mg. In contrast, in HVs there was only negligible D2/3RO (3 ± 2%) for pridopidine 90mg. **Conclusion:** Our PET findings indicate that after single dose of 90mg (exposure correlates with 45mg bi-daily at steady state), pridopidine shows full (approx. 90%) S1RO but only minimal (approx. 3%) D2/3RO. These data provide significant clarification about the mechanism of action/clinical effects of pridopidine. **References:** None.

OP-233

Simultaneous Sigma-1 Receptor PET/Multimodality MRI of the Effect of Pridopidine in Huntington Disease Patients and Healthy Volunteers

H. Barthel[1], *P. M. Meyer*[1], *M. Rullmann*[1], *G. Becker*[1], *M. Bronzel*[2], *D. Marsteller*[3], *G. Pastino*[3], *O. Voges*[2], *L. Rabinovich*[3], *H. Knebel*[3], *F. Zientek*[1], *B. Sattler*[1], *M. Patt*[1], *E. Strauss*[4], *A. Kluge*[2], *J. Savola*[3], *M. F. Gordon*[3], *M. Geva*[5], *S. Hesse*[1], *M. Hayden*[5], *I. D. Grachev*[3,6], *O. Sabri*[1]; [1]*University Hospital Leipzig, Leipzig, GERMANY,* [2]*ABX-CRO, Dresden, GERMANY,* [3]*Teva Branded Pharmaceutical Products R&D, Frazer, PA, UNITED STATES OF AMERICA,* [4]*Arzneimittelforschung Leipzig, Leipzig, GERMANY,* [5]*Prilena Therapeutics Development, Herzliya, ISRAEL,* [6]*Guide Pharmaceutical Consulting, Millstone Twp, NJ, UNITED STATES OF AMERICA.*

Aim/Introduction: Pridopidine is currently under development as a drug to maintain functional capacity or to provide functional benefit in Huntington disease (HD). Its pharmacological effect is mainly mediated via sigma-1 receptor (S1R) interaction. Little is

known so far about how this interaction exerts different brain processes in vivo. It was, thus, the aim of this simultaneous PET/MRI study to investigate the pridopidine effect on neurotransmission, brain perfusion, metabolism, and functional connectivity. **Materials and Methods:** This is a sub-study of a brain PET study which evaluated the S1R and dopamine-2 receptor occupancy by pridopidine in healthy volunteers (HVs) and HD patients (abstract no. 2019-S-1338-EANM). Here, the data of 3 HD patients (age 43±13yrs) and those of 7 HVs (age 29±3yrs) are presented. All subjects underwent simultaneous brain PET/multimodality MRI (up to 390min p.i., 3T Siemens Biograph mMR) under baseline conditions and after a single oral dose of 90mg pridopidine. MRI included arterial spin labelling (ASL, pulsed sequence, VOI and SPM analysis, global normalisation, relative cerebral blood flow [rCBF]), resting-state fMRI (BOLD sequence, seed-based: basal ganglia, sensory-motor and default mode networks [DMN]), and proton MR spectroscopy (MRS, axial slice through striatum, 10 ROIs, each creatine [Cr]), choline [Cho], inositol [Ins], and glutamine/glutamate peaks, reference: N-acetylaspartate [NAA] peak). S1R occupancy was determined by (S)-(-)-[18F]Fluspidine PET and VOI analysis, 1-tissue compartment modelling (metabolite-corrected arterial input), and Lassen plot analysis. **Results:** In HVs, 90mg pridopidine (i) occupied 91±4% of the S1Rs (n=4), (ii) decreased rCBF in temporal cortical (p=0.009) and cerebellar (p=0.007) areas, (iii) decreased Ins/NAA in white matter (p=0.037), and (iv) increased connectivity within the basal ganglia network (4/7 subjects) and DMN (6/7 subjects). In HD, the drug effect was not different with regard to S1R occupancy. While no drug effects on rCBF were observed in HD, pridopidine increased Cr/NAA (p=0.050) and Cho/NAA (p=0.018) in the putamina as well as functional connectivity within the default mode (3/3 patients) network. **Conclusion:** Pridopidine in a clinically tested dose of 90mg intensively acts on S1Rs with multiple associated (and at least in parts differential between HD patients and HVs) effects on brain perfusion, metabolism, and functional connectivity. Especially the positive effect on the DMN network connectivity provides further support for pridopidine improving functional impairment in HD. However, these data indicate that pharmacological PET/MRI is a useful tool to improve understanding of drug effects in the brain on a multi-modality level in a one-stop shop approach. **References:** None.

510

Cardiovascular - Parallel Session: Cardiac Imaging - More than Perfusion

Sunday, October 13, 2019, 16:30 - 18:00 Lecture Hall 116

OP-234

Detection of Thrombi inside LVADs using ^{18}F-GP1 PET/CT - Preliminary Results

V. Hugenberg[1], *W. Burchert*[1], *R. Preuß*[1], *N. Koglin*[2], *M. Berndt*[2], *A. Stephens*[2], *C. Feldmann*[3], *A. Kassner*[4], *H. Milting*[4];
[1]*Institute for Radiology, Nuclear Medicine and Molecular Imaging, Heart and Diabetes Center North Rhine Westphalia, University Hospital, Ruhr University Bochum, Bad Oeynhausen, GERMANY,* [2]*Life Molecular Imaging GmbH, Berlin, GERMANY,* [3]*Department of Cardiothoracic, Transplantation and Vascular Surgery (HTTG), Hannover Medical School, Hannover, GERMANY,* [4]*Clinic for Thoracic and Cardiovascular Surgery, Erich & Hanna Klessmann Institute, Heart and Diabetes Center North Rhine Westphalia, University Hospital, Ruhr University Bochum, Bad Oeynhausen, GERMANY.*

Aim/Introduction: Left ventricular assist devices (LVADs) offer benefits for patients with severe congestive heart failure. Thromboembolic events like intra-pump thrombi, thrombi in inflow cannula or outflow graft are difficult to detect. Therefore, sensitive and specific diagnosis of pump thrombus remains a clinical dilemma. Currently, increased erythrocyte hemolysis, changes in LVAD power consumption and suggestive echocardiography are indirect evidences to suspect a pump thrombus. The LVAD titanium housing complicates the application of noninvasive imaging techniques like MRI, CT or ultrasound. Therefore, a targeted nuclear medicine approach using PET/CT would be of clinical impact for the direct detection of a pump thrombus. ^{18}F-GP1, a novel small-molecule PET tracer, targets the glycoprotein IIb/IIIa receptor on activated platelets and was investigated for the imaging of thrombi in acute arterial and venous thrombosis. The objective of this work is to explore the feasibility of the direct imaging of a pump thrombus inside LVADs using ^{18}F-GP1 PET/CT. **Materials and Methods:** The radiosynthesis of ^{18}F-GP1 was optimized for GMP-production. ^{18}F-GP1 PET/CT was performed with adult patients who had symptoms of a pump thrombus. Explanted thrombi were characterized by western blot using an HRP-labeled antibody against CD41. **Results:** GMP-compliant radiosynthesis of ^{18}F-GP1 was realized via an automated two-step procedure starting with the direct nucleophilic substitution of the Boc-protected tosylate precursor, followed by deprotection and HPLC purification. ^{18}F-GP1 was obtained in radiochemical yields of 39±3% (decay corrected; rcp>98%) in 76-79 min (n=4) from EOB. Preliminary preclinical studies revealed that ^{18}F-attenuation by LVAD titanium (1 mm) was 26-33%. Patients (n=5) suspected of having an intra-pump thrombus or a thrombus in the outflow graft were examined by ^{18}F-GP1 PET/CT. Focal ^{18}F-GP1 uptake was observed in two patients inside the LVAD or in the outflow graft, three patients were ^{18}F-GP1-negative. After PET imaging two patients (one ^{18}F-GP1-positive, one ^{18}F-GP1-negative) underwent LVAD replacement. The clotted material derived from the explanted LVADs confirmed the presence of GPIIb/IIIa receptors on the ^{18}F-GP1-positive thrombus, while no receptors could be detected on fibrin material of the ^{18}F-GP1-negative case, confirming the imaging findings from the respective PET/CT scans. Symptoms of the other ^{18}F-GP1-negative patients were likely not caused by a pump thrombus. **Conclusion:** ^{18}F-GP1 PET/CT is feasible for the specific detection of thrombi

inside of LVADs. Furthermore, a differentiation between thrombi and fibrin plaques might be of impact for therapy decision and individualized patient management. **References:** Chae, EJNMMI Research (2019) 9:3. Kim, J Nucl Med (2019) 60:224.

OP-235

Sex Hormones Preserve Cardiac Sympathetic Integrity Following Myocardial Injury

A. Haider[1,2], *S. Bengs*[1,2], *M. Maredziak*[1,2], *A. Portmann*[1,2], *G. Warnock*[1], *F. Montecucco*[3], *A. Akhmedov*[2], *A. Müller Herde*[4], *C. Keller*[4], *S. D. Krämer*[4], *R. Schibli*[4,1], *L. Mu*[4,1], *P. A. Kaufmann*[1], *S. M. Ametamey*[4], *C. Gebhard*[1,2];
[1]*University Hospital Zurich, Zurich, SWITZERLAND,* [2]*University of Zurich, Zurich, SWITZERLAND,* [3]*University of Genoa, Genoa, ITALY,* [4]*ETH Zurich, Zurich, SWITZERLAND.*

Aim/Introduction: Activation of the sympathetic nervous system is an initial physiological stress response facilitating inotropic and chronotropic adaptation of the heart. However, sympathetic overdrive following acute myocardial infarction (MI) - as observed predominantly in women - has been linked to poor survival. Underlying mechanisms for the female predisposition to persistent stress-induced adrenergic activation remain elusive. The aim of this study was to assess the extent to which sex hormones regulate sympathetic activity in the absence of myocardial injury as well as following acute myocardial infarction using small animal Positron-Emission-Tomography (PET). **Materials and Methods:** Gonodectomized and sham-operated FVB/N mice of both sexes were scanned following tail-vein injection of [^{11}C]meta-hydroxynorephedrine ([^{11}C]mHED), a widely used PET probe in preclinical and clinical assessment of the cardiac sympathetic system. Subgroups of each animal cohort were subjected to ischemia-reperfusion (I/R) injury prior to in vivo cardiac imaging. [^{11}C]mHED uptake was analysed in the myocardium and standardized uptake values (SUVs) were used to compare sympathetic activity among different cohorts (n ≥ 5 for each cohort). **Results:** Female sham-operated mice generally exhibited higher myocardial [^{11}C] mHED uptake compared to their male counterparts, however, these sex-differences vanished in gonodectomized animals. In the absence of I/R injury, gonadal hormone deprivation resulted in significantly higher myocardial [^{11}C]mHED uptake in both sexes. All mice exposed to sex hormones displayed preserved [^{11}C]mHED uptake following I/R injury. In contrast, withdrawal of sex hormones resulted in cardiac sympathetic overdrive following I/R injury. **Conclusion:** Sex hormones modulate baseline cardiac sympathetic tone and preserve cardiac sympathetic integrity following I/R injury in mice. Given (1) the detrimental role of sympathetic overactivation following myocardial injury in women, and (2) the potential role of sex hormones in preventing sympathetic overdrive, assessment of cardiac sympathetic integrity may provide important prognostic information in postmenopausal women and elderly men. **References:** Law, M.P., et al., Molecular imaging of cardiac sympathetic innervation by 11C mHED and PET: from man to mouse? Journal of Nuclear Medicine, 2010. **51**(8): p. 1269-1276. Brodde, O.-E. and K. Leineweber, Autonomic receptor systems in the failing and aging human heart: similarities and differences. European journal of pharmacology, 2004. **500**(1-3): p. 167-176.

OP-236

Early inflammatory chances of myocardial ischemia-reperfusion injury can be detected with vascular adhesion protein-1-targeting PET imaging

A. Autio[1,2], *S. Uotila*[1], *V. Kytö*[3], *M. Kiugel*[1], *H. Liljenbäck*[1,4], *T. Saanijoki*[1], *J. Knuuti*[1], *S. Jalkanen*[2], *A. Saraste*[1,3], *A. Roivainen*[1,4];
[1]*Turku PET Centre, Turku, FINLAND,* [2]*University of Turku, Medicity Research Laboratory, Turku, FINLAND,* [3]*Heart Center, Turku University Hospital and University of Turku, Turku, FINLAND,* [4]*Turku Center for Disease Modeling, University of Turku, Turku, FINLAND.*

Aim/Introduction: Vascular adhesion protein-1 (VAP-1) mediates leukocyte trafficking into inflamed tissue (1). Sialic acid-binding Ig-like lectin 9 (Siglec-9) is a leukocyte ligand for VAP-1 and [^{68}Ga]Ga-DOTA-Siglec-9 peptide can be used as a positron emission tomography (PET) tracer for in vivo imaging of inflammation (2). We hypothesized that [^{68}Ga]Ga-DOTA-Siglec-9 would detect the inflammatory processes associated with myocardial ischemia-reperfusion (I-R) injury. **Materials and Methods:** The myocardial uptake of [^{68}Ga]Ga-DOTA-Siglec-9 was evaluated in rats subjected to temporary myocardial ischemia by transient surgical ligation of the left coronary artery (LCA). The LCA was ligated for 8-12 minutes (group 1, n=6) or 20 minutes (group 2, n=12) followed by a reperfusion of 24 hours. In addition, group 3 consisted of rats with 8 minutes ligation and 4-6 hours reperfusion (n=3). Sham-operated rats (n=2-4) were studied as controls. Animals were injected with [^{68}Ga]Ga-DOTA-Siglec-9 (27±13 MBq) and after 30 min, hearts were excised, cut in short-axis slices and stained with triphenyltetrazolium chloride (TTC) for detection of myocardial injury. Dynamic PETand contrast-enhanced CT imaging were performed for a subset of animals. [^{68}Ga]Ga-DOTA-Siglec-9 uptake in the whole heart was measured by ex vivo gamma counting. More detailed radioactivity distribution in cryosections of the left ventricle was measured by autoradiography. Luminal VAP-1 induction was evaluated by immunohistochemical staining of intravenously injected anti-VAP-1 antibody. **Results:** All animals in group 2 showed large TTC negative area of myocardial injury. PET imaging of this group showed significantly increased tracer uptake in the injured myocardial area compared to remote myocardium (1.5-fold, p=0.014). Ex vivo gamma counting of excised hearts showed increased tracer accumulation in group 2 (p=0.010) and group 3 (p=0.033) compared to sham-operated controls. Autoradiography analysis showed significantly higher [^{68}Ga]Ga-DOTA-Siglec-9 uptake in the injured area compared to non-ischemic myocardial area in group 2 (p=0.002) but differences in group 1 and group 3 were insignificant. The immunohistochemical staining showed VAP-1 positive vessels in the ischemic left ventricle areas in groups 2 and 3. **Conclusion:** The [68Ga]Ga-DOTA-Siglec-9 accumulates in the areas of

myocardial ischemia-reperfusion injury in rats and it reflects VAP-1 expression. **References:** 1. Salmi M, Jalkanen S. Trends Immunol. 2001.2. Aalto K, Autio A, Kiss EA et al. Blood. 2011.

OP-237

Comparison of a new ^{68}Ga-radiolabelled PET imaging agent sCD146 and RGD peptide forin vivoevaluation of angiogenesis in mouse model of myocardial infarction

M. Anais, *P. Garrigue, S. Fernandez, F. Hubert, L. Balasse, P. Brige, A. Bouhlel, G. Hache, M. Blot Chabaud, F. Rochais, F. Dignat-George, B. Guillet;*
Aix marseille university, Marseille, FRANCE.

Aim/Introduction: We recently reported that hindlimb ischemia induces an post-ischemic tissue increase of angiomotin (AMOT) expression, which provides a promising target for therapy and imaging. In this previous work, we validated an AMOT-targeting ^{68}Ga-radiolabled radiotracer (^{68}Ga-sCD146) in peripheral ischemia. This present work aimed to perform the first in vivo evaluation of ^{68}Ga-sCD146 imaging compared to ^{68}Ga-RGD$_2$ and ^{18}F-FDG imaging on a myocardial infarction mice model. **Materials and Methods:** Myocardial infarction was induced by permanent ligation of the left anterior descending coronary artery and myocardial perfusion evaluated by Doppler ultrasound imaging at Day 30 post-surgery and by ^{18}F-FDG PET imaging at Days 16 and 30 post-surgery. NODAGA-conjugates of sCD146 were synthetized and radiolabeled with ^{68}Ga. ^{68}Ga-sCD146 and ^{68}Ga-PRGD$_2$ (5-10MBq) PET imaging was performed on SHAM and myocardial infarction mice respectively at 15-22 and 14-23 days post-surgery using µPET/CT (nanoPET/CT®, Mediso). **Results:** On Day 16, ^{18}F-FDG PET imaging confirmed myocardial infarction, radiotracer uptake infarct area (5.19±4.10%ID/g) was significantly decreased compared to the viable heart (30.71±7.25%ID/g) (P<0.0001, n= 7). ^{68}Ga-sCD146radiochemical purity was 93.1%±2.0 (n=10) and stability in serum evaluated up to 2 hours at 90±1.5%. In mice, ^{68}Ga-sCD146 showed a rapid plasmatic clearance (6.0±2.0min) and a pharmacokinetic profile compatible with PET imaging. In myocardial infarction model, heart to muscle (H/M) ratio of ^{68}Ga-sCD146 uptake 90min after injection showed a radiotracer uptake in infarct area at Day 15 (H/M=3.23±0.82; n=7) significantly higher than in sham (H/M=2.03±0.25; n=7), (P=0.02). ^{68}Ga-PRGD$_2$ didn't show a significantly higher uptake ratio in myocardial infarction model at Day 14 (H/M=2.67±1.36; n=6) compared to sham (H/M=1.64±0.81 n=6), (p=0.11). We didn't find any significant differences for both tracers between ischemic heart and sham heart at 22 and 23 days post-surgery (^{68}Ga-sCD146: $H/M_{ischemic}$=2.52±0.94, H/M_{sham}=2.02±0.56);(^{68}Ga-PRGD$_2$, $H/M_{ischemic}$=0.95±0.19, H/M_{sham}=0.65±0.12). Interestingly, we also observed a significant correlation between H/M ratio assessed by ^{68}Ga-sCD146 imaging on Day 15 and the latest perfusion of heart assessed by ^{18}F-FDG on Day 30 (R^2=0.58;n=7, P=0.04). **Conclusion:** Based on the increased AMOT expression we recently reported in peripheral ischemia, this work demonstrated for the first time a transient increase of AMOT expression 15 days after myocardial infarction in mouse model assessed by ^{68}Ga-sCD146 TEP imaging. We observed a higher TEP signal compared to ^{68}Ga-PRGD$_2$. Then, correlation study showed that early post-ischemic ^{68}Ga-sCD146 uptakes (Day 16) correlated with delayed later hearth perfusion allows us to postulate that ^{68}Ga-sCD146 could represent a promising and innovative radiotracer to predict post-ischemic heart recovery. **References:** None.

OP-238

Feasibility and potential time reduction of simultaneous 99mTc-tetrofosmin and 123I-BMIPP dual-tracer imaging with cadmium-zinc-telluride detectors in patients with acute myocardial infarction

S. Nakano[1], *Y. Yamada*[1], *T. Muramatsu*[1], *S. Nishimura*[1], *N. Okano*[2], *I. Matsunari*[2], *K. Fukushima*[3];
[1]*Department of Cardiology, International Medical Centre, Saitama Medical University, Hidaka, Saitama, JAPAN,* [2]*Division of Nuclear Medicine, Department of Radiology, Saitama Medical University, Moro, Saitama, JAPAN,* [3]*Department of Nuclear Medicine, International Medical Centre, Saitama Medical University, Hidaka, Saitama, JAPAN.*

Aim/Introduction: Simultaneous perfusion-metabolism dual imaging is clinically useful. However, use of Tc rather than Tl as a perfusion tracer has been challenging due to its proximate photo-peak with BMIPP, resulting in poor resolution. This drawback could be overcome by improved properties of cadmium-zinc-telluride (CZT)-based scanners. We aim to investigate feasibility and potential time reduction of 99mTc-tetrofosmin and 123I-BMIPP dual-tracer imaging using a Discovery NM/CT 670 CZT. **Materials and Methods:** Thirty patients having undergone primary percutaneous coronary intervention for acute myocardial infarction underwent single-(Tc-tetrofosmin (TF) or I-BMIPP first) followed by simultaneous Tc-TF/I-BMIPP dual-tracer imaging. To examine feasibility, QGS and QPS values of dual-imaging were compared with those of single-imaging. To verify clinical utility, inter-rater concordance between two radiologists was also assessed. Next, referenced images of dual-imaging with acquisition time of approximately 16 minutes were reframed to produce images with shortened acquisition time, and the values were compared among various acquisition times. **Results:** The QGS/QPS values were comparable between the single- and dual-imaging (intra-class correlation (ICC) coefficients for summed motion score: 0.95, summed thickened score: 0.98, summed rest score (SRS) for Tc-TF: 0.97, SRS for I-BMIPP: 0.95). The inter-rater concordance for detection of infarction and perfusion-metabolism mismatch was significant (P < 0.001). The QPS values with acquisition time of 8, 4 and 2 minutes showed good consistency with 16 minutes (the lower 95% CI of ICC >= 0.8). The QPS values for Tc-TF with shortened acquisition times (8, 4 , and 2 minutes) also showed good consistency with those with 16 minutes. However, the QPS values for I-BMIPP with 2 minutes were not consistent with 16 minutes (the lower 95% CI of ICC < 0.8). **Conclusion:** The

(semi-)quantitative values of myocardial function, perfusion, and fatty acid metabolism were closely comparable between the dual-tracer and single-tracer modes, suggesting clinical feasibility of the novel CZT-based scanner for the simultaneous Tc-TF/I-BMIPP dual-tracer acquisitions. The QGS and QPS values obtained from images with shorter acquisition times (8, 4, and 2 minutes) correlated with the values obtained from images with a reference acquisition time of 16 minutes. However, tracer-specific predisposition should be considered, as the QPS values for I-BMIPP with acquisition time of 2 minutes were inconsistent with those with 16 minute. In summary, simultaneous Tc-TF/I-BMIPP dual-tracer imaging with the novel CZT scanner may be clinically feasible, and time reduction can be possible in view of potential tracer-specific predisposition. **References:** None.

OP-239

Low septal to lateral wall ^{18}F-FDG ratio is a marker of mechanical dyssynchrony in non-ischemic CRT candidates

G. Degtiarova[1,2], P. Claus[3], J. Duchenne[4,5], M. Cvijic[4], H. J. Verberne[6], G. Schramm[1], J. Nuyts[1], J. Voigt[4,5], O. Gheysens[1,2];
[1]Nuclear Medicine and Molecular Imaging, Department of Imaging and Pathology, KU Leuven, Leuven, BELGIUM, [2]Nuclear Medicine and Molecular Imaging, University Hospitals Leuven, Leuven, BELGIUM, [3]Cardiovascular Sciences, Cardiovascular Imaging and Dynamics, KU Leuven, Leuven, BELGIUM, [4]Cardiovascular Diseases, University Hospitals Leuven, Leuven, BELGIUM, [5]Cardiovascular Sciences, Cardiology, KU Leuven, Leuven, BELGIUM, [6]Radiology and Nuclear Medicine, Amsterdam UMC, location AMC, University of Amsterdam, Amsterdam, NETHERLANDS.

Aim/Introduction: Presence of mechanical dyssynchrony is associated with favorable response to cardiac resynchronization therapy (CRT)[1]. Better understanding of the pathophysiological changes, induced by mechanical dyssynchrony, may improve patient selection for CRT. In this study, we investigated the effect of mechanical dyssynchrony on regional myocardial metabolism and absolute perfusion assessed with ^{18}F-FDG and ^{13}N-NH3 PET/CT in non-ischemic patients selected for CRT. **Materials and Methods:** 30 consecutive patients underwent static ^{18}F-FDG (using a hyperinsulinemic euglycemic clamping) and resting dynamic ^{13}N-NH3 PET/CT scans 1 week before CRT implantation. Regional ^{18}F-FDG uptake and absolute myocardial blood flow (MBF, kinetic modelling) were analyzed in the septal and lateral wall and for both, septal-to-lateral wall ratios (SLR) were calculated. Based on the presence of mechanical dyssynchrony (either septal flash or apical rocking or both) on echocardiography, patients were divided into 2 groups - with (n=23) and without (n=7) mechanical dyssynchrony. **Results:** A significantly higher mean ^{18}F-FDG SUV in the lateral wall was observed compared to the septum in the group with mechanical dyssynchrony (SUVmean lateral wall: 11.19±4.10 vs SUVmean septum: 5.58±2.65, p<0.0001), while in the group without dyssynchrony ^{18}F-FDG distribution was not different between the walls (SUV mean lateral wall: 8.31±2.50 vs SUV mean septum:7.33±2.88, respectively, p=0.3). Similarly, absolute MBF was significantly different between the regions in the dyssynchrony group (lateral wall: 0.92±0.23 ml/g/min vs septum: 0.57±0.11 ml/g/min, p<0.0001), whereas in the non-dyssynchrony group absolute MBF was more homogeneous (lateral wall: 0.77±0.21 ml/g/min vs septum: 0.61±0.23 ml/g/min, p=0.16). Patients with mechanical dyssynchrony had a significantly lower ^{18}F-FDG SLR (0.50±0.13) compared to patients without dyssynchrony (0.86±0.23, p=0.02). However, no significant difference in MBF SLR was observed between both groups (dyssynchrony: 0.67±0.17 vs non-dyssynchrony: 0.80±0.21, p=0.2). Moreover, ROC analyses showed that ^{18}F-FDG SLR was highly predictive of the presence of mechanical dyssynchrony (area under the curve 0.91, p<0.0001) with an optimal cut-off value of 18F-FDG SLR ≤0.74 (sensitivity 100%, specificity 83%). MBF SLR didn't show any significance for predicting mechanical dyssynchrony. **Conclusion:** Non-ischemic heart failure patients with mechanical dyssynchrony demonstrate heterogeneous regional metabolism and MBF compared to non-dyssynchrony group. However only ^{18}F-FDG-SLR is the significant predictor of the presence of mechanical dyssynchrony and might be associated with CRT response. **References:** 1.Stankovic I, Prinz C, Ciarka A, Daraban AM, Kotrc M et al. Relationship of visually assessed apical rocking and septal flash to response and long-term survival following cardiac resynchronization therapy (PREDICT-CRT). Eur Heart J Cardiovasc Imaging. 2016 Mar;17(3):262-9.

OP-240

Cardiac ^{123}I-mIBG scintigraphy as a tool to optimize CRT patient selection

D. O. Verschure[1], E. Poel[1], V. Frantellizzi[2], G. De Vincentis[2], O. Gheysens[3], J. R. de Groot[1], H. J. Verberne[1];
[1]Amsterdam University Medical Center, Amsterdam, NETHERLANDS, [2]Sapienza - University of Rome, Rome, ITALY, [3]University Hospitals Leuven, Leueven, BELGIUM.

Aim/Introduction: Cardiac resynchronization therapy (CRT) is a disease modifying therapy in patients with chronic heart failure (CHF). Eligibility for CRT is based on QRS duration and NYHA functional capacity only. However, one-third of CHF patients does not benefit from CRT. Moreover, CRT is associated with malfunction and high costs. In addition there is no consensus on how to assess CRT response best. This study evaluated whether ^{123}I-mIBG assessed cardiac sympathetic activity could optimize CRT patient selection. **Materials and Methods:** 78 stable CHF subjects from Italy and the Netherlands (age 66.8 ± 9.6 years, 73% male, LVEF 25.2 ± 6.7%) referred for CRT-Defibrillator implantation were enrolled. All subjects underwent planar ^{123}I-mIBG scintigraphy prior to CRT implantation. Early and late heart-to-mediastinum (H/M) ratio and ^{123}I-mIBG washout (WO) were calculated. Improvement of LVEF (>35%), QRS duration (<150 msec) and NYHA functional class between baseline and 1 year follow-up were used as parameters of CRT response. **Results:** Response to CRT using QRS duration occurred in 36

patients, NYHA functional class and LVEF identified 33 patients each. Of all three response parameters only improvement of LVEF could be independently predicted by late H/M ratio (p=0.009). None of the other myocardial 123I-mIBG parameters was associated with CRT response. **Conclusion:** In stable CHF myocardial late H/M ratio was associated with improvement of LVEF as a measure of CRT response. Therefore cardiac ^{123}I-mIBG could be seen as a tool to optimize the selection of CHF subjects who might benefit from CRT. **References:** None.

OP-241

Prediction of cardiac death using 123I-MIBG: comparison between statistical and machine learning models for serious arrhythmic events and heart failure death

K. Nakajima[1], *T. Nakata*[2], *T. Doi*[3], *K. Maruyama*[4];
[1]*Kanazawa University, Kanazawa, JAPAN,* [2]*Hakodate Goryoukaku Hospital, Hakodate, JAPAN,* [3]*Teine Keijinkai Hospital, Sapporo, JAPAN,* [4]*Wolfram Research Inc, Tokyo, JAPAN.*

Aim/Introduction: Although we have been working on the prediction of sudden cardiac death (SCD) and heart failure death (HFD) using ^{123}I-meta-iodobenzylguanidine (mIBG) in patients with chronic heart failure (CHF), an appropriate classifier model to predict serious arrhythmic events (ArE) has yet to be determined. The aim of this study is to establish the model for predicting ArE using Japanese multicenter cohort database with machine learning (ML) method. **Materials and Methods:** A total of 525 patients (66±14 years, male 72%) with CHF was used for creating the statistical and machine learning (ML) models that are implemented on the Wolfram Language. ArE comprised SCD, serious arrhythmic events and appropriate therapy by implantable cardioverter defibrillator within a two-year follow-up period. A multivariable statistical model used four variables of age, left ventricular ejection fraction, NYHA functional class, and heart-to-mediastinum ratio (HMR) that was calculated with an anterior planar mIBG image. To develop ML models, in addition to 4 variables as above, a total of 14 variables were used; sex, MIBG washout rate, estimated glomerular filtration rate, ischemic etiology, b-type natriuretic peptide, hemodialysis, diabetes, hypertension, dyslipidemia, and anemia. The training of ML was performed with randomly selected 392 patients (75%), and the remaining patients (25%) were used for validation. The accuracy of the models was compared using receiver-operating characteristic (ROC) analysis with area under the curve (AUC) analysis and contingency table analysis. **Results:** During the follow-up of 2 years, 7% and 20% of the patients experienced ArE and HFD, respectively. To predict cardiac events including both HFD death and ArE, the four-variable logistic model and ML-based classifier model showed ROC-AUC of 0.88 and 0.88, respectively (p=0.82). To predict ArE specifically, the ML model showed better AUC of 0.83 compared with the statistical model AUC of 0.67 (p=0.049). The contingency table analysis for ArE events also showed a higher likelihood ratio by the ML model than that by the statistical model (p=0.0002 and 0.04, respectively). The best cutoff probability to predict ArE was 10%, with sensitivity 90% and specificity 69% by the ML model. **Conclusion:** The accuracy of the ML model with 14 variables and that of the four-variable statistical model were comparable in predicting cardiac events. However, the ML model showed a better predictive accuracy for ArE and seems promising to predict serious arrhythmic events in patients with CHF. **References:** Statistical model from European Heart Journal - Cardiovascular Imaging 2018;19: 749-756.

404c

Mini Course 3 - Technologist Committee: Theranostics - Fundamental

Sunday, October 13, 2019, 17:00 - 18:00 Lecture Hall 117

OP-242

General Aspects of Theranostics in Nuclear Medicine

S. Mirzaei;
Department of Nuclear Medicine with PET-Center, Wilhelminenspital, Vienna, AUSTRIA.

OP-243

Theranostics for Technologists in the Context of NET

N. Gulliver;
Department of Nuclear Medicine & PET-CT | King's College Hospital NHS Foundation Trust | Denmark Hill, London, UNITED KINGDOM.

601

CME 5 - Oncology & Theranostics + Bone & Joint Committee: Radionuclide Molecular Imaging in Bone Tumours and Multiple Myeloma - Pearls, Patterns & Pitfalls

Monday, October 14, 2019, 8:00 - 9:30 Auditorium

OP-244

Radionuclide Molecular Imaging in Primary Bone Tumours

T. Van den Wyngaert;
Antwerp University Hospital, Nuclear Medicine, Edegem, BELGIUM.

OP-245

Radionuclide Molecular Imaging of Bone Metastases

G. Gnanasegaran;
Royal Free Hospital, Nuclear Medicine, London, UNITED KINGDOM.

OP-246

Radionuclide Molecular Imaging in Multiple Myeloma

C. Nanni;
S.Orsola-Malpighi Hospital, Policlinico S.Orsola Malpighi Bologna, Nuclear Medicine, Bologna, ITALY.

602

Joint Symposium 9 - Neuroimaging Committee / ILAE: Clinical Use of Brain Imaging for Patients with Epilepsy

Monday, October 14, 2019, 8:00 - 9:30 Lecture Hall 311

OP-247

The Use of MRI for Patients with Epilepsy and the Need of Multimodal Imaging for the Clinician

P. Federico;
Hotchkiss Brain Institute, Cumming School of Medicine, University of Calgary, Calgary, CANADA.

OP-248

FDG-PET for Partial Epilepsy Revisited

F. Chassoux;
Sainte-Anne Hospital, Neurosurgery Department, Paris, FRANCE.

OP-249

The Role of Ictal SPECT in the Presurgical Evaluation of Patients with Drug-Resistant Epilepsy

W. Van Paesschen;
UZ Leuven, Neurology Department, Leuven, BELGIUM.

603

Joint Symposium 10 - Drug Development Committee / SRS: What is Molar Activity and When does it Impact PET Imaging?

Monday, October 14, 2019, 8:00 - 9:30 Lecture Hall 312

OP-250

What do I Need to Know? Basic Concepts of Mass in Radionuclide Imaging

S. Bongarzone;
King's College London, Division of Imaging Sciences and Biomedical Engineering, London, UNITED KINGDOM.

OP-251

Optimal Molar Activity is a Precondition for a Sensitive and Specific Molecular Imaging in Oncology

V. Tolmachev;
Biomedical Radiation, Institute of Oncology, Radiology and Clinical Immunology, Uppsala, SWEDEN.

OP-252

Mass Effect of PET Radioligands for Neuroscience

C. Halldin;
Karolinska Institute, Department of Clinical Neuroscience, Stockholm, SWEDEN.

604

Technologists: Oral Presentations 1

Monday, October 14, 2019, 8:00 - 9:30 Lecture Hall 117

OP-253

Ability of artificial intelligence to diagnose coronary artery stenosis using hybrid images of coronary computed tomography angiography and myocardial perfusion SPECT

H. Yoneyama[1], *K. Nakajima*[1], *J. Taki*[1], *H. Wakabayashi*[1], *T. Konishi*[1], *K. Okuda*[2], *T. Shiburani*[3], *M. Onoguchi*[3], *S. Kinuya*[1];
[1]*Kanazawa University Hospital, Kanazawa, JAPAN,*
[2]*Kanazawa Medical University, Kanazawa, JAPAN,*
[3]*Kanazawa University, Kanazawa, JAPAN.*

Aim/Introduction: Detecting culprit coronary arteries in patients with ischemia using only myocardial perfusion single-photon emission computed tomography (SPECT) can be challenging. This study aimed to improve the detection of culprit regions using an artificial neural network (ANN) to analyze hybrid images of coronary computed tomography angiography (CCTA) and myocardial perfusion SPECT. **Materials and Methods:** This study enrolled 59 patients with stable coronary artery disease (CAD) who had been assessed by coronary angiography within 60 days of myocardial perfusion SPECT. Two nuclear medicine physicians interpreted the myocardial perfusion SPECT and hybrid images with four grades of confidence, then drew regions on polar maps to identify culprit coronary arteries. The gold standard was determined by the consensus of two other nuclear cardiology specialist based on coronary angiography findings and clinical information. The ability to detect culprit coronary arteries was compared among experienced nuclear cardiologists and the ANN. Receiver operating characteristics (ROC) curves were analyzed and areas under the ROC curves (AUC) were determined. **Results:** Using hybrid images, observer

A detected CAD in the right (RCA), left anterior descending (LAD), and left circumflex (LCX) coronary arteries with 83.6%, 89.3%, and 94.4% accuracy, respectively and observer B did so with 72.9%, 84.2%, and 89.3%, respectively. The ANN was 79.1%, 89.8%, and 89.3% accurate for each coronary artery. Diagnostic accuracy was comparable between the ANN and experienced nuclear medicine physicians. The AUC was significantly improved using hybrid images in the RCA region (observer A: from 0.715 to 0.835, p = 0.0031; observer B: from 0.771 to 0.843, p = 0.042). To detect culprit coronary arteries in perfusion defects of the inferior wall without using hybrid images was problematic because the perfused areas of the LCX and RCA varied among individuals. **Conclusion:** Hybrid images of CCTA and myocardial perfusion SPECT are useful for detecting culprit coronary arteries. Diagnoses using artificial intelligence is comparable to that by nuclear medicine physicians. **References:** 1) Nakajima K, Okuda K, Watanabe S, Matsuo S, Kinuya S, Toth K, et al. Artificial neural network retrained to detect myocardial ischemia using a Japanese multicenter database. Ann Nucl Med. 2018;32:303-10. 2) Nakajima K, Kudo T, Nakata T, Kiso K, Kasai T, Taniguchi Y, et al. Diagnostic accuracy of an artificial neural network compared with statistical quantitation of myocardial perfusion images: a Japanese multicenter study. Eur J Nucl Med. 2017;44:2280-3.

OP-254

The ratio between RPP in stress and rest in patients with and without myocardial ischemia as assessed by $^{13}NH_3$ PET/CT

C. Bulder, S. V. Lazarenko, F. M. van der Zant, W. A. M. Broos, R. J. J. Knol;
Noordwest Ziekenhuisgroep, Alkmaar, NETHERLANDS.

Aim/Introduction: The rate pressure product (RPP) is a widely used hemodynamic parameter and a good predictor of myocardial oxygen consumption. In the present study, RPP-ratios (ratio between RPP_{stress} and RPP_{rest}) were compared for groups of patients with proven myocardial ischemia as assessed with $^{13}NH_3$ myocardial perfusion PET/CT versus patients without ischemia. Also, the relation between the RPP-ratios and cardiac flow reserves (CFR) of both groups was investigated. **Materials and Methods:** Data of 181 patients (90 M, 91 F) who underwent an adenosine-induced pharmacologic stress $^{13}NH_3$ PET/CT were analyzed. Of these, 66 patients showed evidence of myocardial ischemia at myocardial perfusion PET/CT (ischemic group) whereas the other 115 patients had no signs of ischemia and normal myocardial blood flow (non-ischemic group). The RPP was calculated using the following formula: heart rate (HR) * systolic blood pressure. Subsequently, the RPP ratio was calculated by using the following formula: RPP stress / RPP rest. An independent t-test was used to evaluate the difference in RPP-ratio between both groups. Next, the correlation between the RPP-ratio and the CFR (myocardial blood flow stress/myocardial blood flow rest) was assessed using a Pearson's correlation test for both groups. **Results:** The RPP ratio differs significantly between the ischemic and non-ischemic group (p=0,03). The mean ± SD in the ischemic group was 1,31±0,27 and in the non-ischemic group this was 1,44±0,30. The (positive) correlation between the RPP-ratio and the CFR is statistically significant (p=0.00) for both groups. However, the correlation was shown to be negligible for the non-ischemic group (r^2=0.09) and weak for the ischemic group (r^2=0,25). **Conclusion:** RPP-ratios are significantly different for patients with and without myocardial ischemia. However, a correlation between the RPP-ratio and the CFR in the non-ischemic group is negligible and only weak in the ischemic group. **References:** None.

OP-255

Studies On Sterile Filters In The Preparation N-13 Ammonia Injection

C. Oh, S. Kim, J. Shin, M. Cha, Y. Ji, S. Choi;
Samsung Medical Center, Seoul, KOREA, REPUBLIC OF.

Aim/Introduction: In the preparation process for N-13 ammonia injections, there were radioactive medicines adsorbed on sterile filters remarkably. Hereby, we have compared the adsorption rate and quality test on Millex GS filter and Satorious Minisart filter, both representativly hydrophilic sterilizing filters, also evaluated which filter is more accommodative for N-13 ammonia injection production. **Materials and Methods:** The filters used for sterilization of N-13 ammonia injections were Millex GS filter (pore size : 0.22 μm, Merk Millipore, Ireland) and Satorious Minisart filter (pore size : 0.2 μm, Satorious, Germany), which are generally used to strain aqueous solutions. After the N-13 ammonia passes through each sterilization filter, the adsorption rate of the filter (n = 10) is determined by measuring not only the radioactivity through the filter but also the amount of radioactivity remaining in it using a Dose calibrator. The N-13 ammonia injections after the each filter is tested by the quality control test to conform to the European Pharmacopoeia standard. **Results:** The ratio of radioactivity passed through Millex GS indicated 29.0 ± 17.6 %, Satorious Minisart filters output was 80.9 ± 3.2%, respectively. Each ratio of radioactivity adsorbed on the sterile filter was 71.0 ± 17.6% for Millex GS and 19.1 ± 3.2 % for the Satorious Minisart filters, respectively. Furthermore, on the ratio of filtered radioactivity, Using Satorious Minisart filter showed about 2.8 times higher than using Millex GS filter. The quality testing of N-13 ammonia injections through each filter met the European Pharmacopoeia standard. **Conclusion:** The Millex GS filter is composed of cellulose acetate and cellulose nitrate, whereas the Satorious Minisart filter is composed only of cellulose acetate. Therefore, the presence of cellulose nitrate on the membrane seems to have made differences. The quality control test results of the radioactive medicines filtered using both filters also met the European Pharmacopoeia standards without any net differences even after impurities concerns. In this hospital, the loss of radioactive medicines caused by the adsorption of filters was minimized by the use of Satorious Minisart filter in the preparation process of N-13 ammonia injection, thereby increasing the synthetic yield. **References:** None.

OP-256

The Importance of Timing of MRAC Acquisition on Co-Registration in PET/MR Cardiac Stress Examinations

M. Thueringer, M. Hofbauer, S. Epp, E. von Felten, D. Patriki, T. Fuchs, R. R. Buechel;
University Hospital Zurich, Zurich, SWITZERLAND.

Aim/Introduction: Cardiac examinations with N^{13}-ammonia are scanned in two PET parts, each lasting 18 minutes. Before starting the PET stress scan, adenosine is injected over two minutes. After starting the PET scan, the MR-attenuation correction (MRAC) is scanned first as default. Adenosine injection is stopped after six minutes at the latest. Due to the stress the adenosine creates, the diaphragm and therefore the heart are moving more at the beginning of the PET in comparison to the end. The aim of the study is to improve the accuracy of the co-registration of the MRAC to the PET images. **Materials and Methods:** The standard workflow is as follows: 1.) Start of the adenosine injection 2.) Start of the PET scan directly followed by the acquisition of the MRAC 3.) N^{13}-Ammonia injection 4.) End of the adenosine injection. 30 patients were scanned using the GE Signa PET/MR. In order to improve the co-registration of the MRAC to the PET images, we moved the MRAC to the very end of the PET task, when the effects of the adenosine have subsided. The MRAC must be acquired within the 18-minute PET task, so it can be used for the reconstructions. Four patients (ongoing) were scanned that way. **Results:** Performing the standard workflow, MRACs had to be shifted manually (R/L, A/P, S/I) after every examination to gain a correct co-registration in the dynamic PET reconstruction of the first seven minutes. No manual shift of the MRACs was needed when it had been acquired at the end of the PET task. **Conclusion:** The alternative workflow reduces effort both on doctors' side who provide the shift values and on technologists' side who set up the additional PET reconstructions manually. Another advantage is the time factor, because the gap between end of exam and start of reading shortens significantly. Since the reconstructions with shifted MRACs can only be set up, after all PET/MR examinations are finished and the reconstruction time itself is around 25 minutes. The alternative workflow is therefore more efficient and saves time. The only action it requires is moving the MRAC down to the end of the PET task, which can be set as default in the scan protocol. **References:** None.

OP-257

Investigation into Method for Radiolabelling Erythrocytes with Tc-99m for Use in Red Cell Volume

W. A. Sanders, J. Croasdale, A. Notghi;
SWBH NHS Trust, Birmingham, UNITED KINGDOM.

Aim/Introduction: Use of Cr-51 Sodium Chromate for in-vitro labelling of RBC's (Red Blood Cells) has been the gold standard for many years, and its withdrawal means a new radiolabelling method for Red Cell Mass studies is required. Red Cells have been radiolabelled with Tc-99m for various imaging studies; however, its use for Red Cell Mass studies has not been fully explored; in particular whether it gives an accurate Red Cell Mass value and whether the label is stable. Using current methods for radiolabelling RBC with Tc-99m for imaging studies, this study aims to establish whether labelling efficiency is satisfactory, to assess the need for EDTA as a stabilising agent, and to assess stability of radiolabelled RBC over the desired shelf life (up to 2 hours). **Materials and Methods:** Previous methods of radiolabeling RBC have been evaluated and a proposed method established. The procedure is to be performed using venous blood samples from healthy volunteers. Dilute Stannous Chloride will be added to 10ml of blood, after incubation 4% Edetate solution is to be added before centrifuging the blood to obtain the packed RBC's. To the RBC 10MBq of Tc-99m is added and incubated for 5 minutes. After which the sample is washed with saline and the supernatant measured to calculate the labelling efficiency (LE). A total of 4 samples have been processed using the Edetate solution and 4 samples without. At t = 0, 1 and 2hrs the samples are centrifuged and the supernatant measure to calculate the stability. **Results:** Total mean LE for labelling method without using EDTA was 92%, with EDTA mean LE was also 92%. Mean percentage loss after two hours without EDTA was 3.9%, using EDTA was 3.1%. **Conclusion:** The use of Tc-99m to radiolabel RBC has been shown to give high labelling efficiency with acceptable in vitro stability, The use of EDTA to stabilise the product and bind any free stannous ions did not impact the final labelling efficiency or the in vitro stability of the final labelled cells. Future work will look to confirm in vivo stability of the label by assessing thyroid uptake, and by measuring freeTc-99m in urine and blood plasma. **References:** None.

OP-258

Review of protocol change for SLN injections in patients with breast cancer

P. J. Campbell, H. Sharman, C. Caro;
The Royal Marsden NHS FT, London, UNITED KINGDOM.

Aim/Introduction: The purpose of the service review was to investigate the efficacy of the new standard of practice to reduce the presence of air artefacts on ultrasound for patients undergoing sentinel lymph node injections and enhance patient flow through departments. Previously there would be an air bubble behind the Tc99m Nanocolloid to "push" the tracer out of the syringe due to the small volume (0.1mls). This technique was replaced by retrieving more tracer and purging the air from the syringe. **Materials and Methods:** 142 patients (49 2 day protocol and 93 same day protocol) using the new technique were retrospectively investigated along with 92 of the previous method. (63 same day and 29 2 day protocols). Counts measured at the injection site, number of "hot" sentinel lymph nodes detected and use of blue dye was documented. Cases were excluded if the counts were omitted from the operation notes **Results:** The study showed some interesting

results. Previous studies using sulphur colloid have indicated that a one day protocol has marginally better axillary drainage whilst the two day protocol is still within limits. This single centre study showed that 14% of patients having SLNI using the old technique required the addition of blue dye to identify the sentinel lymph nodes compared to 20% of those requiring a two day protocol. Comparing this to the new airless technique we can see the one day protocol has a 24% requirement for the blue dye whereas the 2 day protocol has a 10% necessity for the blue dye. This could be as a result of an increased activity injected median 12.56MBq for the air push technique and 14.51MBq for the airless technique. However this is contraindicated when studying the median values for the 2 day protocol: 31.6MBq for the air push and 37.5MBq for airless. This could show that a larger activity for a 2 day protocol than initially proposed could result in better sentinel node detection and a value as close to 10MBq as practicable for the same day injections. **Conclusion:** To conclude the 2 day protocol performs better than the same day injections for sentinel node detection with the new airless technique. This allows for a smother patient flow through the department and minimal surgical delays arising from difficulties obtaining ultrasound images due to the presence of air artefacts. However careful consideration should be given to patient preference and convenience. **References:** None.

OP-259

Twin Peaks: Should we use Dual Energy Windows for [^{75}Se] SeHCAT Studies?

A. List, *B. Stiles, A. Paramithas;*
St George's University Hospitals NHS Foundation Trust, London, UNITED KINGDOM.

Aim/Introduction: Gamma emissions from ^{75}Se occur at two principle energies, 136keV and 264keV. This presents a choice for the Nuclear Medicine department undertaking SeHCAT (GE healthcare) studies; collect data from both - maximising total number of counts; or use only the higher energy emission - reducing the chance of interference from other sources. The former is our current clinical protocol. The aims of this study were to; determine if using only the higher energy window (HEW) gives equivalent results to using dual energy windows (DEW); and to assess whether interference from other sources are likely to have a clinically significant effect on the calculated result. **Materials and Methods:** 141 SeHCAT patients were reviewed retrospectively. Their 7-day retention was calculated using both DEW and HEW and classified as: normal (≥15%), mild Bile Acid Malabsorption (BAM) (<15%), moderate BAM (<10%) or sever BAM (<5%). A phantom study was performed using a 370kBq ^{75}Se-SeHCAT capsule taped to the back of a water-filled phantom and imaged using the clinical protocol. Imaging was repeated with 400MBq of ^{99m}Tc placed outside and then inside the room. **Results:** DEW classified 95 patients as normal, 14 mild, 16 moderate, 16 severe BAM. HEW gave 94 Normal, 15 mild, 15 moderate, 17 severe BAM. Of 141 patients 2 changed category; in one case the retention changed by 0.2%, but changed classification due to rounding; the second changed from 7% to 2% (moderate to severe). Overall mean difference between the two methods was 0.8% retention. The addition of ^{99m}Tc in the room caused an 18% increase in raw counts for DEW and 1.0% for HEW, when background corrected this changed to DEW 0.7% and HEW 1.1%. ^{99m}Tc outside the room increased raw counts in DEW by 0.6% and HEW by 0.7%. **Conclusion:** Results calculated with both methods were 99% comparable, with only 1 patient significantly changing - most likely due to a transient source adding counts to the lower energy window, demonstrating the potential risk of including the lower energy peak. External sources are only problematic if they change during the procedure. The decision to include/exclude the lower energy peak will depend on local factors such as department layout and session arrangements. Our working conclusion is to continue with DEW but use the low and high windows separately as a QA step. Further measurements and analysis are ongoing and will be presented at the conference. **References:** None.

OP-260

Establishing Local Dose Reference Levels for Low-dose CT Scans Associated with SPECT and PET Imaging Examinations - Experience at Sultan Qaboos University, Oman

Y. Bouchareb[1], *N. Tag*[2], *A. Al-Jabri*[2], *N. Makhmari*[2], *A. Al-Haji*[2], *H. Al-Dhuhli*[2];
[1]*Sultan Qaboos University, Muscat, OMAN,* [2]*Sultan Qaboos University Hospital, Muscat, OMAN.*

Aim/Introduction: The purpose of this study was to develop effective local dose reference levels (LDRL) for use within SPECT-CT and PET-CT services in order to monitor and audit locally devised low-dose CT protocols associated with the most frequent SPECT/CT and PET/CT imaging examinations performed at our institution. **Materials and Methods:** A retrospective study included a total of 589 adult patients who have undergone SPECT/CT and PET/CT scanning over a period of 24 months was performed. Patients were scanned on the Siemens Symbia SPECT/CT T16 and mCT 128 slices PET/CT Siemens scanners. The 589 patients' scans consisted of: 181 whole body PET/CT scans, 140 SPECT/CT bone, 113 myocardial perfusion imaging SPECT/CT, 87 thyroid post-ablation scans, 41 parathyroid and 27 octreotide SPECT/CT scans. Low-dose CT scans, performed as part the PET/CT and SPECT/CT imaging examinations, were only used for attenuation correction and localisation at our institution. The CT dosimetry data (CTDIvol, DLP and exposure settings) which was documented on RIS and PACS, was collected for all patients scans. The mean, standard deviation (SD) and third quartile were then calculated for CTDIvol (mGy) and DLP (mGy.cm) for each SPECT/CT examination group and whole body PET/CT examinations. The effective dose range was calculated for each examination group using the k-factors devised by Shrimpton et al (2006) for effective dose per DLP (mSv/mGycm). **Results:** The calculated LDRLs are given

as follows (third quartile DLP (mGy.cm), third quartile CTDIvol (mGy)): PET whole body: 251, 2.3; SPECT bone: 246, 5.0; SPECT myocardial perfusion imaging: 191, 6.9; SPECT Parathyroid, 319, 6.7; SPECT Octreotide: 183, 2.8 and SPECT thyroid post-ablation: 280, 5.5. The estimated effective dose range (min - max) was: (0.7 - 6.1), (0.4 - 1.1), (1.3 - 6.6), (1.3 - 8.7), (0.6 - 9.1), (1.05 - 10.3) for PET whole body, SPECT myocardial perfusion imaging, SPECT Octreotide, SPECT parathyroid, SPECT bone and SPECT thyroid post-ablation, respectively. The differences between these results and the published literature are believed to be mainly due to differences in local practices. **Conclusion:** The development of LDRLs has facilitated careful monitoring and could act as a trigger to investigate any reported CT dose that exceeds the LDRL set. The on-going aim is to validate these LDRLs with regular audit to provide a robust service provision that is in-keeping with the ALARA principle. This will ensure that LDRLs are not routinely exceeded, or prompt investigation if otherwise. **References:** Shrimpton PC et al, BJR 2006.

OP-261

Estimation of radiation dose to the eye lens of patients undergoing PET/CT scan with lowdose-CT compared to diagnostic-CT head

E. C. Streefkerk, *T. Young - Mylvaganan, J. olde Heuvel, D. Huizing, B. de Wit - van der Veen;*
Cancer institute, Amsterdam, NETHERLANDS.

Aim/Introduction: The eye lens is the most radiosensitive organ; too much radiation exposure can lead to cataract formation. The International Commission on Radiological Protection (ICRP) Publication 118 recommended a threshold for lens opacities of 0.5Gy[1]. Modern positron emission tomography (PET) imaging includes a computed tomography (CT) scan for attenuation correction and anatomical reference. In this study we want to estimate the radiation dose to the eye lens of patients undergoing a low dose-CT compared to a standard diagnostic-CT, and between different PET/CT protocols. With these results we aim to optimize our acquisition protocols considering the ALARA principle. **Materials and Methods:** We retrospectively reviewed PET/CTs in three acquisition categories, Head/Neck (2mm), Whole-body (5mm) and PSMA (2mm) starting January first 2018. These were compared to Diagnostic CT Brain (1mm) and Face (1mm). The PET/CT patients were scanned on the GEMINI TF Big Bore (Philips, Netherlands). The diagnostic CTs were scanned on the Aquilion CX (Toshiba, Japan). The DICOM information from all scans was analyzed using OSIRIX software. The slice including the eye lens was used to extract the $CTDI_{vol}$ (mGy). A conversion factor for adults CF_{age} was derived[2]. Using the following equation an estimation of the lens dose was made. $D_{lens} = CF_{age} \times CTDI_{vol}$ **Results:** A total of 60 scans were analyzed. For the low dose-CT component the mean radiation dose to the lens was 3.4mGy (range 0.9-9.0mGy). The Head/Neck protocol has a dose that is three times lower than the Whole-body or PSMA protocol. In comparison, the diagnostic-CT gave a mean dose of 43.0mGy (range 7.1-79.2mGy) to the lens. **Conclusion:** The low dose-CT is less than a tenth of the diagnostic-CT. The whole-body acquisition has the highest radiation dose to the lens. The difference between the Head/Neck and the other protocols can be explained by the positioning of the arms. The arms are commonly positioned above the head to improve PET imaging quality of the body. Considering the ALARA principle a change in positioning of the patient or scan range can be opted. **References:** 1 ICRP, 2012. ICRP Statement on Tissue Reactions / Early and Late Effects of Radiation in Normal Tissues and Organs - Threshold Doses for Tissue Reactions in a Radiation Protection Context. ICRP Publication 118. Ann. ICRP 41(1/2). 2 Januzis, Natalie Ann (2016). Radiation Dose to the Lens of the Eye from Computed Tomography Scans of the Head. Dissertation, Duke University.

605

M2M - Parallel Session: Innovations in Bio-Nanotechnology

Monday, October 14, 2019, 8:00 - 9:30 Lecture Hall 111

OP-262

Ultrasound-Induced Mircobubble Cavitation For Optimisation Of Tumour Uptake Of Liposome-Based Chemo-Radionuclide Therapy

K. A. Vallis, *E. Thomas, J. Menon, J. Owen, S. Wallington, M. Gray, I. Skaripa-Koukelli, R. Carlisle;*
University of Oxford, Oxford, UNITED KINGDOM.

Aim/Introduction: Nanoparticles (NP) allow active targeting of cancer for diagnostic and therapeutic applications through incorporation of multiple functional components. However, the low penetration of NP into tumours sometimes hinders their efficacy. In this study, ultrasound plus microbubbles were used to promote the intra-tumoural delivery of a novel liposome (LP) for chemo-radionuclide therapy. The epidermal growth factor receptor (EGFR) is over-expressed by many types of cancer, making it an attractive molecular target. **Materials and Methods:** Liposomes were loaded with doxorubicin (Dox) and surface modified by addition of epidermal growth factor (EGF) peptide conjugated to DTPA for radiolabelling with indium-111 (^{111}In). Human breast cancer cell lines with high and low EGFR expression (MDA-MB-468 and MCF7 respectively) were used to study selectivity of liposomal uptake, subcellular localisation of drug payload, cytotoxicity (by clonogenic assay) and DNA damage (by immunostaining for gamma-H2AX). Liposome extravasation following ultrasound-induced cavitation of microbubbles (SonoVue) was studied using a tissue-mimicking phantom. In vivo stability, pharmacokinetic profile and biodistribution were evaluated following intravenous administration of ^{111}In-EGF-LP to mice bearing subcutaneous MDA-MB-468 xenografts. The influence of ultrasound-mediated cavitation on the delivery of ^{111}In-EGF-LP into tumours was

studied. **Results:** Liposomes were loaded efficiently with Dox, surface decorated with ^{111}In-EGF and showed selective uptake in MDA-MB-468 compared to MCF7 cells. Following EGF binding to EGFR, Dox was released in the intracellular space and ^{111}In-EGF shuttled to the cell nucleus. Radioactivity accumulated to a greater extent in the nuclei of MDA-MB-468 compared to MCF7 cells (16.8 +/- 0.9% vs. 2.2 +/- 0.7% of the internalized activity). DNA damage and cell kill were greater in MDA-MB-468 than MCF7 cells. In addition, Dox and ^{111}In were shown to have an additive cytotoxic effect in MDA-MB-468 cells. Ultrasound-mediated cavitation increased the extravasation of liposomes in an in vitro gel phantom model. In vivo, the application of ultrasound plus microbubbles increased tumour uptake by 66% $p<0.05$) despite poor vascularisation of MDA-MB-468 xenografts (as shown by DCE-MRI). **Conclusion:** ^{111}In-EGF-DOX-LPs are promising for targeted cellular uptake and drug delivery. In vivo, ultrasound plus microbubbles enhance delivery to tumour. The extent of tumour vascularisation is likely a critical determinant of success of this delivery strategy and will be further studied. **References:** None.

OP-263

Activated Gold Nanoparticles Conjugated with 68Ga-DOTA-PEG(4)-BBN(7-14) for Targeting Tumours Expressing GRP Receptors

D. Niculae[1], *L. E. Chilug*[1,2], *R. M. Serban*[1,3], *A. J. Abrunhosa*[4], *R. A. Leonte*[1], *R. Turcu*[5], *A. Nan*[5], *V. Lavric*[2];
[1]*Horia Hulubei National Institute for Physics and Nuclear Engineering IFIN-HH, Bucharest (Magurele), ROMANIA,* [2]*University Politehnica of Bucharest, Faculty of Applied Chemistry and Materials Science, Bucharest, ROMANIA,* [3]*University of Bucharest, Faculty of Biology, Bucharest, ROMANIA,* [4]*CIBIT/ICNAS Institute for Nuclear Sciences Applied to Health, University of Coimbra, Coimbra, PORTUGAL,* [5]*National Institute for Isotopic and Molecular Technologies, Cluj-Napoca, ROMANIA.*

Aim/Introduction: Nanoparticles have recently emerged as innovative tools for cancer diagnosis and therapy. Their functionalization with biorecognition molecules (ligands), forming targeted drug delivery systems, can make them suitable for early detection of tumors, patient management and therapy follow-up, using molecular imaging techniques. The aim of this study was to investigate the potential as an imaging agent of activated N-Hydroxysuccinimide gold nanoparticles functionalized with ^{68}Ga-DOTA-PEG(4)-BBN(7-14) to target GRP (gastrine releasing peptide) receptors, overexpressed on colorectal cancer cells HT-29/HCT116 and prostate cancer cells DU-145.**Materials and Methods:** The morphology and size distribution of gold nanoparticles obtained were examined by TEM/SEM coupled with energy dispersion spectroscopy (EDS) technique and, after functionalization, by UV-Vis spectroscopy and DLS. The Gold NPs were functionalized with PEG(4)-BBN (7-14), previously radiolabelled with Ga-68 using DOTA as a chelating agent. The obtained radiolabeled nanoconjugate was incubated with neuroendocrine colorectal cancer cell line HT-29/ HCT116 and prostate cancer cells DU-145, expressing GRPRs. We investigated the specific binding of bombesin-like peptide sequence PEG(4)-BBN(7-14) to GRP receptors by comparing the receptor interaction with radiolabeled ^{68}Ga-DOTA-PEG(4)-BBN(7-14) in the presence of an cold competitor antagonist ligand. **Results:** In vitro binding kinetics assessment showed over 60% radioisotope retention inside tumor cells in the presence of AuNPs, higher than ^{68}Ga-DOTA-PEG(4)-BBN(7-14) alone. This result is attributed to the possibility that AuNPs bind to several peptides on the cell surface and promote a higher internalization rate by receptor mediated endocytosis. Biodistribution studies were performed on tumor bearing nude mice, and the results show high tumor uptake of the radiolabeled nanoconjugates. **Conclusion:** The combination of size-controlled distribution of nanoparticles, functionalization with bio-recognition peptides and PET radioisotope labelling has resulted in highly promising imaging probes. ^{68}Ga-DOTA-PEG(4)-BBN(7-14) shows very promising results regarding in vitro and in vivo behavior. Further investigations are to be performed to determine the detailed dosimetry and pharmacokinetics and to extend the potential use to targeted radionuclide therapy, by use of highly cytotoxic potency of alpha radionuclides transported close to the cell nuclei. **References:** Livia E. Chilug et al., In vitro binding kinetics study of gold nanoparticles functionalized with 68Ga-DOTA conjugated peptides, J Radioanal Nucl Chem (2017) M. E. Panait et al., Biological Effects Induced by 68Ga-Conjugated Peptides in Human and Rodent Tumor Cell Lines, Int J Peptide Res Therapeutics (2018)

OP-264

Direct radiolabeling of ^{89}Zr-silica gadolinium nanoparticles (^{89}Zr-AGuIX®) for tumor targeting via long term EPR effect and in vivo clearance characterization in 9L brain tumor model

V. Tran[1], *B. Jego*[1], *A. Winkeler*[1], *A. Bouleau*[1], *F. Lux*[2], *O. Tillement*[2], *B. Kuhnast*[1], *C. Truillet*[1];
[1]*Laboratoire Imagerie Moléculaire In Vivo (IMIV), Service Hospitalier Frédéric Joliot, CEA, Inserm, Univsité Paris Sud, CNRS, Université Paris-Saclay, Orsay, FRANCE,* [2]*Institut Lumière Matière, UMR 5306, Université Claude Bernard Lyon 1, CNRS, Université de Lyon, Villeurbanne, FRANCE.*

Aim/Introduction: High-Z nanoparticles (NP) are attracting great attention as sensitizers for radiotherapy.[1] A major challenge is to characterize and quantify intratumoral NP distribution spatially and temporally in order to optimize delivered dose in the tumor area with minimal effect on normal tissues. Our aim is to assess the use of PET to quantitatively image ultrasmall silica gadolinium NP (AGuIX®), a promising nanosensitizer currently under phase 2 clinical trial.[2] We are interested in using ^{89}Zr, a long-lived positron emitter, which allows longitudinal monitoring of tumor-specific accumulation of NP. Labeling ^{89}Zr on a nanostructure often requires introducing a chelator such as DFO.[3] This would probably affect its properties in vivo and necessitates new approval application. In this study, we

have shown that AGuIX® can be directly labeled with ^{89}Zr. Then labeled particles can be used to follow tumor uptake in a preclinical glioma model. **Materials and Methods:** AGuIX® was labeled while taking advantage of free DOTA groups on the particle with ^{89}Zr-oxalic acid in different conditions. Stability of the radiotracer has been tested in vitro with fetal bovine serum and mouse plasma. Transmetalation assays have been performed with different endogenous ions i.e. Fe^{3+}, Zn^{2+}, Ca^{2+}, Cu^{2+}. Syngeneic tumor model was established by stereotactically implanting 9L gliosarcoma cells into the striatum of Fisher rats' brain. PET-CT images were acquired at different time points after injection of labeled NP. Organs were collected for ex vivo analysis. **Results:** Complete labeling was achieved even at mild condition. ^{89}Zr- AGuIX® were stable in different in vitro conditions. 9L tumor growth was assessed by ^{18}F-FDG PET and histology. Expectedly, PET images post ^{89}Zr-AGuIX injection showed NP accumulation in the tumor. Long half-life of ^{89}Zr allowed longitudinal follow-up of this accumulation, which lasted more than 24 h in accordance with previous studies. NP accumulation was confirmed by autoradiograms of brain sections. In addition, ex vivo biodistribution indicated that labeled NP were not retained in major organs and eliminated mainly via the kidneys. **Conclusion:** We have demonstrated that AGuIX® can be directly labeled with ^{89}Zr in simple conditions, which can be readily applied for GMP manufacturing. Labeled NP was stable and showed promising results for translational brain tumor imaging. **References:** 1. Rancoule, C. et al. Cancer Lett. 375, 256-262 (2016).2. Lux, F. et al. Br. J. Radiol. 20180365 (2018).3. Truillet, C. et al. Mol. Pharm. 13, 2596-2601 (2016).

OP-265

Radiolabelling endothelial microvesicles and evaluating their in vivo biodistribution in healthy and ischemic mice

P. Garrigue[1], *R. Giraud*[1], *A. Moyon*[1], *V. Nail*[2], *S. Simoncini*[3], *L. Balasse*[4], *S. Fernandez*[5], *A. Bouhlel*[4], *F. Dignat-George*[6], *B. Guillet*[1], *F. Sabatier*[6];

[1]*C2VN INSERM 1263 INRA 1260 CERIMED Aix-Marseille Université APHM, Marseille, FRANCE,* [2]*CERIMED Aix-Marseille Université APHM, Marseille, FRANCE,* [3]*C2VN INSERM 1263 INRA 1260 Aix-Marseille Université, Marseille, FRANCE,* [4]*C2VN INSERM 1263 INRA 1260 CERIMED Aix-Marseille Université, Marseille, FRANCE,* [5]*CERIMED Aix-Marseille Université, Marseille, FRANCE,* [6]*C2VN INSERM 1263 INRA 1260 Aix-Marseille Université APHM, Marseille, FRANCE.*

Aim/Introduction: Microvesicles (MVs) are of great interest as biological markers in cardiovascular and oncologic diseases, but they are also currently evaluated as biotherapeutic agents. However, although their characterization and their purification/isolation method are now well established, to date there is no published data about their systemic biodistribution after intravenous administration. The aims of this work were to develop the radiolabeling of endothelial MVs to characterize their in vivo biodistribution in healthy mice by isotopic imaging, and to evaluate their biodistribution in a mouse model of ischemia and their impact on revascularization. **Materials and Methods:** Large amounts of MVs were generated from primary cultures of HUVECs after TNFα stimulation. [^{99m}Tc]Tc-AnnexinV radiolabeling (AnV-128, AAA) technically enabled to obtain radiolabeled MVs with a suitable yield for isotopic imaging. A purification-concentration method of these MVs was then validated on specific size-exclusion columns, to inject a purified and concentrated suspension of MVs to the animal. Stability in serum at 37°C was assessed up to 2h after labeling. MVs biodistribution was quantified on microSPECT/CT imaging data of healthy mice up to 3h after injection (n=6). MVs biodistribution was also quantified after i.v. injection in a mouse model of hindlimb ischemia (2-5.10^6 MVs/100µL, n=7 mice) while a control group (n=4 mice) was i.v. injected with 100µL PBS. Angiogenic activation and blood flow in the hindlimbs were respectively evaluated by [^{68}Ga]Ga-RGD_2 microPET/CT (on days 3,4,7,10 post-ischemia) and by LASER-Doppler on days 1,3,7,14,21,28 days post-ischemia. **Results:** Labeling yield didn't exceed 5% but remained compatible with preclinical isotopic imaging. Radiolabeling stability as well as physical integrity of the MVs were confirmed up to 2h after labeling. Quantifications showed an accumulation of radiolabeled MVs in the liver, intestines and kidneys of healthy mice. A significant higher MVs SPECT signal was found in the ischemic hindlimb compared to the contralateral 2h post-injection (*p=0.0467). On day 3, [^{68}Ga]Ga-RGD_2 microPET/CT quantifications showed a significant higher ipsi- to contralateral signal ratio in the MVs group (**p=0.0082). We observed a better, earlier reperfusion in the MVs group (***p<0.0001). We highlighted the intensity of the reperfusion was significantly, positively correlated with the intensity of the number of MVs retained in the ischemic hindlimb (r=0.9883, *p=0.0117). **Conclusion:** These preliminary data enabled to quantify endothelial MVs in vivo biodistribution, and for the first time the appreciation of a correlation between the intensity of the radiolabelled MVs SPECT signal and the therapeutic effect on revascularization. **References:** None.

OP-266

Novel radiolabeled silicon dyes for bimodal scintigraphic and optical imaging

T. Kanagasundaram[1,2], *M. Schäfer*[1], *C. Kramer*[1], *E. Boros*[3], *K. Kopka*[1];

[1]*German Cancer Research Center (DKFZ), Division of Radiopharmaceutical Chemistry, Im Neuenheimer Feld 280, Heidelberg, GERMANY,* [2]*Institute of Inorganic Chemistry, Heidelberg University, Im Neuenheimer Feld 270, Heidelberg, GERMANY,* [3]*Stony Brook University, Department of Chemistry, New York, NY, UNITED STATES OF AMERICA.*

Aim/Introduction: Radiolabeled fluorescent dyes are crucial for bimodal imaging and currently in demand for scintigraphic and optical imaging. These dyes show unique optical properties such as high quantum yields and extinction coefficients (1). Organic fluorophores are well-known for fluorescent light-guided intraoperative surgery. The goal of this work was developing near-infrared (NIR) light-emitting Si-rhodamines

for scintigraphic and optical imaging. We have synthesized these first-in-class dyes for their subsequent conjugation to the SPECT-compatible radiometal technetium-99m with the aim to elucidate their potential as sentinel lymph node detecting agents. Moreover, PET-compatible Si-rhodamine conjugation to exemplary prominent tumor targeting binding vectors such as the PSMA-binding motif has also been performed. The introduced dyes are intended to be used for noninvasive SPECT or PET imaging (prestaging) followed by light-guided R0-tumor-resection. **Materials and Methods:** The combination of scintigraphic and optical imaging leads to new approaches in tumor imaging and resection. This powerful strategy enables the differentiation of healthy and affected tumor tissues. We have developed dyes with absorption and emission properties in the near-infrared region of ca. 660 nm. The synthesized dyes are belonging to the silicon (Si)-rhodamine family. We utilized the dyes for copper(I)-catalyzed alkyne-azide [3+2]-cycloaddition with alkyne-functionalized biomolecules to receive respective 1,2,3-triazoles for complexing the prominent SPECT-radiometal technetium-99m. Furthermore we have designed another DOTA-functionalized 1,2,3-triazole for complexing the PET-radiometal gallium-68. Finally, the dyes were characterized using NMR-, UV/VIS/NIR-spectroscopy and mass spectrometry. **Results:** The conventional synthesis of novel Si-rhodamines through xanthone building blocks provided novel amino- and azide-functionalized Si-rhodamines with overall yields of 60%. The azide-functionalized Si-rhodamines were converted with PSMA-inhibitor functionalized alkynes adapted from the PSMA-617 binding motif and L-propargylglycine to the corresponding 1,2,3-triazoles (2). Already determined extinction coefficients up to 120.000 $M^{-1}cm^{-1}$ and quantum yields of 0.45 show promising results, making them potentially useful for optical imaging. Furthermore the dyes were prepared as precursors for technetium-99m and gallium-68-labeling. For that purpose different chelators (e.g. DOTA) were used. Corresponding rhenium-Si-rhodamines [used as "cold" technetium-surrogate] were characterized as well. **Conclusion:** A variety of novel NIR fluorescent dyes based on the Si-rhodamine lead structure were synthesized and chemically characterized. We successfully developed non-radioactive analogues of putative NIR dyes for bimodal scintigraphic and optical imaging and their radiolabeling precursors. Furthermore, our first-in-class radiolabeled silicon dyes are subject of current and future biological evaluation. **References:** (1) T. Nagano et al., J. Am. Chem. Soc. 2012, 134, 5029-5031. (2) K. Kopka et al., J. Nucl. Med. 2015, 56, 914-920.

OP-267

A Reinjection Study of Sn-117m Colloid to Treat Canine Osteoarthritis Shows Safety and Efficacy

C. A. Doerr[1], *J. M. Donecker*[1], *N. R. Stevenson*[1], *G. R. Gonzales*[1], *J. C. Lattimer*[2];
[1]*Serene, LLC, The Woodlands, TX, UNITED STATES OF AMERICA,* [2]*University of Missouri, Columbia, MO, UNITED STATES OF AMERICA.*

Aim/Introduction: Homogeneous Sn-117m colloid (HTC) is commercialized in the US as a treatment for osteoarthritis (OA) in dogs using radiosynoviorthesis (RSO). Human clinical trials using ascorbic homogeneous Sn-117m colloid (AHTC) will commence in Canada in 2019. The outcome of safety and efficacy of repeat therapeutic RSO injections in canines may be applicable to human subjects. **Materials and Methods:** 10 dogs previously enrolled in a prospective trial to treat elbow OA with one of three doses of HTC intra-articular injection were enrolled in a re-injection trial if their symptoms remained unchanged or worsened by canine brief pain inventory (cBPI) or force-plate analysis after 6-12 months. These dogs received an additional RSO procedure with the commercial dose (1.7 mCi per elbow normalized for a 50 lb/22.7kg dog) in both elbows (n=20) and were followed for 12 months for safety and efficacy. Therapeutic success by cBPI was defined as either (1) improvement of >1 for pain severity score (PSS) AND >2 for pain interference score (PIS), or (2) improvement of >1 for PSS OR >2 for PIS. Therapeutic success by clinician's lameness examination was defined as significantly improved p values between the two assessment time points. Therapeutic success by force plate was demonstrated by improvement of >5% at any time point in the peak vertical force (PF) or the mean vertical impulse (IMP). Safety was assessed by analysis of CBC and blood chemistry, joint fluid, UA, and by owner and clinician assessment. **Results:** The per protocol group of 9 dogs (18 elbows) showed therapeutic improvement in three assessments. cBPI success using PSS AND PIS demonstrated improvement over baseline of up to 37.5% during 12 months. cBPI success using PSS OR PIS demonstrated improvement over baseline of up to 75.0% during 12 months. Force plate evaluation demonstrated improvement in PF or IMP in up to 66.7% of subjects over 180 days. Clinician's lameness examination showed no statistical improvement. There were no safety issues noted associated with HTC. **Conclusion:** The therapeutic success and demonstrated safety of reinjection using HTC for OA in dogs provides support for similar use in humans. **References:** None.

OP-268

^{68}Ga-labeled carbon nanoparticles for ventilation PET/CTimaging: physical properties study and comparison with Technegas®

F. Blanc-Béguin[1], *P. Eliès*[2], *N. Kervarec*[3], *P. Robin*[1], *R. Tripier*[2], *C. Lemarié*[1], *S. Hennebicq*[1], *C. Tromeur*[1], *P. Salaün*[1], *P. Le Roux*[1];
[1]*Brest university hospital, Brest, FRANCE,* [2]*Brest occidental university, Brest, FRANCE,* [3]*Brest occidental university, Brest, FRANCE.*

Aim/Introduction: For lung imaging, ventilation PET/CT is now possible with ^{68}Ga-labeled carbon nanoparticles. Radiolabeling can be performed using the same synthesis device as Technegas® (Cyclopharm Ltd, Australia), by substituting ^{99m}Tc with ^{68}Ga. Several studies showed promising results of ventilation PET images for regional lung function assessment. However, no study has assessed the physical properties of ^{68}Ga-labeled carbon nanoparticles. The aim of this study was to assess the

size, shape, mass and particles composition of ^{68}Ga-labeled carbon nanoparticles, as compared with ^{99m}Tc-labeled carbon nanoparticles. **Materials and Methods:** ^{68}Ga and ^{99m}Tclabeled carbon nanoparticles were produced using an unmodified Technegas generator, following the usual technique proposed for Technegas production. Approximately 50 MBq of $^{68}GaCl_3$ and 700 MBq of $^{99m}TcO_4^-$ Na^+ were introduced in the carbon crucible, respectively. Nanoparticles were collected using an aerosol collector PA 2000 (Algade®) on a cellulose filter and on a Transmission Electron Microscopy (TEM) grids coated with a carbon film. The size and shape of particles were studied by TEM (JEOL JEM 1400). The mass of carbon particles was studied by Time-Of-Flight Mass Spectroscopy (TOF-MS) (spectrometer Bruker Autoflex III SmartBeam) from a solution obtained by infusing the cellulose filters in methanol. The particles composition was assessed using scanning electron microscopy (SEM) (HITACHI S-3200N) coupled with EDX analysis. **Results:** On TEM, the mean diameter of ^{68}Ga and ^{99m}Tc-labeled carbon nanoparticles was 22.6±17.3 nm and 66.8±50.2 nm ($p<0.05$), respectively. The diameter of both particles was consistent with previously published data for ^{99m}Tc-labeled carbon nanoparticles, ranging from 5 to 400 nm (Lloyd et al. PMID: 7641756; Lemb et al. PMID: 8053994). Both ^{99m}Tc and ^{68}Ga labeled carbon nanoparticles had similar shape with primary hexagonally structured particles. Mass spectra of ^{68}Ga and ^{99m}Tc- labeled carbon nanoparticles showed the same 326 and 327 daltons peaks, suggesting the presence of similar particles in both aerosols. EDX spectra demonstrated higher percentage of Sodium and Chlorine atoms in ^{99m}Tc labeled carbon nanoparticles, consistent with the composition of ^{99m}Tc eluate. However, the composition in Carbon and Oxygen of both particles was similar. **Conclusion:** Using a Technegas generator in the usual clinical way, ^{68}Ga and ^{99m}Tc-labeled carbon nanoparticles demonstrated similar shape, mass and particles composition. ^{68}Ga-labeled carbon nanoparticles were significantly smaller than ^{99m}Tc labeled particles, but remained in the range of previously published data for ^{99m}Tc-labeled carbon nanoparticles. This data support the use of ^{68}Ga-labeled carbon nanoparticles for the assessment of ventilation regional lung function with PET imaging. **References:** None.

OP-269

Recoil retention and therapeutic efficacy of ^{225}Ac-containing polymersomes

R. Raavé[1], *R. M. de Kruijff*[2], *A. Kip*[1], *J. Molkenboer-Kuenen*[1], *A. Morgenstern*[3], *F. Bruchertseifer*[3], *S. Heskamp*[1], *A. G. Denkova*[2]; *[1]Radboudumc, Nijmegen, NETHERLANDS, [2]Delft University of Technology, Delft, NETHERLANDS, [3]European Commission, Joint Research Centre, Directorate for Nuclear Safety and Security, Karlsruhe, GERMANY.*

Aim/Introduction: Alpha emitters can play an important role in cancer treatment. With their high linear energy transfer and short range, alpha particles are ideal for localized cell killing. However, upon emission of an alpha particle, the radioactive daughter nuclides experience a recoil energy of about 100-200 keV which is much larger than the energy of any chemical bond, resulting in the daughter nuclide breaking free from any targeting agent. These daughter can accumulate in healthy tissue as kidneys, resulting in toxicity. Here, we evaluate the retention of the ^{225}Ac recoiling daughter ^{213}Bi entrapped in poly-butadiene-poly-ethylene oxide (PBD-PEO) polymersomes in vivo, both upon intravenous as well as intratumoral administration. Furthermore, the suitability of ^{225}Ac-containing polymersomes as therapeutic agents is assessed upon intratumoral injection. **Materials and Methods:** Polymersomes (100 nm) were labeled with ^{225}Ac through DTPA chelation or through co-precipitation within $InPO_4$ nanoparticles were injected intravenously in healthy mice, and intratumorally in MDA-MB-231 tumor-bearing BALB/c nude mice, and the retention of the ^{213}Bi daughter nuclide was determined. Concentration of ^{213}Bi in the blood, spleen, kidneys and tumor was compared to that of ^{225}Ac. The tumor retention and therapeutic effect of ^{225}Ac-containing polymersomes upon intratumoral injection was compared to ^{225}Ac-DOTA, PBS or no treatment in MDA-MB-231 tumor-bearing BALB/c nude mice. **Results:** ^{225}Ac recoil daughter retention in $InPO_4$ nanoparticles in polymersomes showed a significant ($p<0.05$) two-fold increased retained fraction of ^{213}Bi in the blood compared to ^{225}Ac in DTPA-polymersomes (0.14 ± 0.07 vs. 0.06 ± 0.03) in healthy mice. When injected intratumorally, polymersomes showed good retention in tumor tissue (244 ± 74 %ID/g and 289 ± 130 %ID/g at 1 and 7 days p.i, respectively), whereas ^{225}Ac-DOTA was rapidly cleared from the tumor (10 %ID/g and 5 %ID/g at 1 and 7 days p.i, respectively). The two treatment groups showed a remarkable therapeutic efficacy (complete inhibition of tumor growth in 7/8 and 6/8 for ^{225}Ac polymersome- and ^{225}Ac-DOTA treated tumors, respectively) with no tumor-related deaths over the treatment period, while the survival of the PBS control group was significantly ($p<0.05$) decreased over the course of the experiment. Out of the PBS injected tumors and non-treated tumors only 1/8 and 2/8 of the tumors showed inhibition of growth, respectively. **Conclusion:** The observed polymersome retention in tumor tissue and tumor growth inhibition of xenografts treated with ^{225}Ac-labeled polymersomes indicate that targeted alpha therapy with polymersomes has potential for long-term irradiation of tumors upon intratumoral injection. **References:** None.

606

Do.MoRe - Parallel Session: Preclinical Dosimetry - What is the Future?

Monday, October 14, 2019, 8:00 - 9:30 Lecture Hall 112

OP-270

NM600, a theranostic alkylphosphocholine chelate, shows promise as a universal tumor-targeting agent

J. Grudzinski, *R. Hernandez, I. R. Marsh, R. B. Patel, E. Aluicio-Sarduy, J. Engle, Z. Morris, B. Bednarz, J. Weichert; University of Wisconsin, Madison, WI, UNITED STATES OF AMERICA.*

Aim/Introduction: We characterized the in vivo biodistribution and tumor selectivity of ^{86}Y-NM600, a theranostic alkylphosphocholine radiometal chelate with broad tumor selectivity, in a variety of syngeneic and xenograft preclinical cancer models (n=15) and estimated the tumor and normal organ dosimetry of ^{90}Y-NM600 in these models. We have shown previously that precise tumor dosimetry of ^{90}Y-NM600 is important when combined with immunotherapies. **Materials and Methods:** Mice bearing heterotopic or orthotopic tumors (breast, lymphoid, sarcoma, melanoma, oral, prostate, pancreatic, lung and colon) were injected intravenously (IV) with 9.25-9.75 MBq of ^{86}Y-NM600 and imaged longitudinally out to 72 hours using microPET/CT. Percent injected activity per gram (%IA/g) for each volume-of-interest (VOI) was measured at each time point for the organs of interest. Mice were euthanized after the final time point and the tumor and organs of interest were counted with an automatic gamma counter. Absorbed doses delivered by ^{90}Y-NM600 per injected activity (Gy/MBq) were estimated using an inhouse Monte Carlo platform. Mice bearing B78 flank tumors were injected with a prescription of ^{90}Y-NM600 that delivered 2.5 Gy of absorbed tumor dose and was compared to an equivalent absorbed dose delivered via external beam radiotherapy (XRT) using tumor volume as a measure of response. Histology and complete blood counts (CBC) were analyzed in naïve C57BL/6 mice who were injected with 9.25 MBq of ^{90}Y-NM600 at 5, 10, and 28 days post injection (p.i.). **Results:** PET imaging showed consistent tumor accumulation and retention across all tumor models investigated with little off-target retention of NM600 except for in the liver, which is characteristic of hepatobiliary metabolism. The tumor uptake was highest in the TC11 breast, MOC2 oral, and 4T07 breast cancer models, reaching peak concentrations of **11.68 ± 0.52%IA/g (n=2)**, **9.76 ± 1.02 %IA/g (n=3)**, and **9.28 ± 0.55 %IA/g (n=3)** respectively, at approximately 24-48 hr post injection. These corresponded to tumor dose estimates of **3.97 ± 0.04 Gy/MBq**, **3.13 ± 0.37 Gy/MBq, and 2.98 ± 0.18 Gy/MBq**, respectively. In the toxicity study, there were no visible signs of acute toxicity by histology, and perturbation of hematological parameters was transient when observed, returning to pre-therapy levels after 28 days. **Conclusion:** NM600 is a theranostic agent with a unique ability to selectively target and safely deliver precise radiation to a variety of cancer types, presenting a unique opportunity for PET image guided TRT and combination with immunotherapies. **References:** None.

OP-271

Pharmacokinetic variability of vector labeled Actinium-225 and the in vivo generated decay daughters Francium-221 and Bismuth-213 in murine models

A. Josefsson, J. R. Nedrow, S. R. Banerjee, M. G. Pomper, G. Sgouros, R. F. Hobbs;
Johns Hopkins University School of Medicine, Baltimore, MD, UNITED STATES OF AMERICA.

Aim/Introduction: Actinium-225 has lately become a popular α-particle emitter and has been used both pre-clinically and clinically against several types of cancers. Actinium-225 ($T_{1/2}$=10 days) have in its decay chain a total net emission of four α-particles and two β-particles. Actinium-225 is labeled to the targeting vector using a chelator. The chemical bond between the chelator and the ^{225}Ac-atom is weak (~10eV), and after the first α-particle is emitted the bond is broken due to the high recoil energy (~100keV) of the atom. Consequently the ^{225}Ac decay daughters (^{221}Fr, ^{217}At, ^{213}Bi, ^{213}Po, ^{209}Tl and ^{209}Pb) are no longer bound to the vector and are free to relocate within the in vivo system. The α-particle emitting decay daughters with the longest half-life are ^{221}Fr ($T_{1/2}$=4.9 minutes) and ^{213}Bi ($T_{1/2}$=45.6 minutes). These are decay daughters in the ^{225}Ac decay chain that emit a gamma ray that can be either measured or imaged. In this study we investigated the pharmacokinetics in murine models of different ^{225}Ac-labeled vectors (7.16.4 antibody against breast cancer; PSMA small molecule against prostate cancer) and the in vivo generated unbound decay daughters ^{221}Fr and ^{213}Bi. **Materials and Methods:** The mice were injected i.v. with ^{225}Ac-labeled vectors and sacrificed at specific time-points p.i. The organs/tissues were directly after sacrifice harvested and measured in a gamma counter in 1 minute intervals for a duration up to 5 hours. Bi-exponential functions were fitted to the measured activity to determine the amount of vector labeled ^{225}Ac and unbound ^{221}Fr and ^{213}Bi within the organs/tissues. **Results:** All murine models showed accumulation of unbound ^{213}Bi in the kidneys, accounting for ~60% of the absorbed dose. The main supplier of ^{213}Bi to the kidneys was the liver for the small molecule and the blood for the antibody. In addition, within the kidneys the vector labeled ^{225}Ac was uniformly distributed for the antibody, and non-uniform for the small molecule and unbound ^{213}Bi, suggesting need for small scale dosimetry for more accurate calculations. **Conclusion:** This study demonstrate that different targeting vectors for delivery of ^{225}Ac alters the pharmacokinetics and suppliers of the unbound decay daughters. These properties are important for translation to clinical studies as in vivo imaging cannot distinguish between the vector labeled ^{225}Ac and the unbound decay daughters ^{221}Fr and ^{213}Bi. This results in an overestimation of the absorbed dose to the kidneys and an underestimation of the absorbed dose to the supplying organ/tissues. **References:** None.

OP-272

Organic melanin nanoparticles targeting prostate-specific membrane antigen (PSMA) and multimodality imaging for human prostatic cancer xenograft model

L. Xia[1], Z. Cheng[2], H. Zhu[1], Z. Yang[1];
[1]Peking university cancer hospital, Beijing, CHINA, [2]Stanford University, San Francisco, CA, UNITED STATES OF AMERICA.

Aim/Introduction: Prostate-specific membrane antigen is widely used for the diagnosis and therapy of prostatic cancer. The introduction of the nuclide-labelled PSMA targeted positron-

emitting-tomography/computed-tomography (PET/CT) tracer has proven highly sensitive for the detection of prostate cancer. But radionuclide imaging still has the disadvantages of low resolution and difficult to detect microlymph node metastases. Multimodal imaging has been an important research direction and uses a versatile, integrated contrast agent to provide complementary imaging information for disease diagnosis and treatment evaluation. Nanoparticles are the most widely used contrast agents or carriers for multimodal imaging due to their excellent properties. Herein, we used safer organic melanin nanoparticles as a carrier and surface-loaded PSMA-11 to construct a prostatic cancer targeted nanoprobe (PSMA-PEG-MNP). **Materials and Methods:** Organic melanin nanoparticles are prepared from naturally produced biopolymers. The biocompatible PEG was modified on the surface and the PSMA-11 was bound by condensation reaction. MNPs have excellent photoacoustic imaging (PAI) functions and can directly label metal nuclide ^{64}Cu and magnetic resonance contrast agent Fe^{3+} without a coupling agent. Therefore, MNPs can be used not only for photoacoustic imaging, but also for PET and MRI. The LNCaP prostatic tumor xenograft model with high PSMA expression was constructed to evaluate the multimodal imaging ability of (^{64}Cu, Fe^{3+}) PSMA-PEG-MNP. **Results:** (^{64}Cu, Fe^{3+}) PSMA-PEG-MNP showed good imaging abilities in PAI, MRI and PET imaging. The PA images showed that the photoacoustic signal in the LNCaP tumor site gradually increased with time, and the LNCaP xenograft showed a clear increase in the T1-weighted signal intensity after injection with Fe-PSMA-PEG-MNP at 24 h compared to that in the prescan. Micro-PET imaging and biodistribution showed that the uptake of LNCaP tumor (7.03 ± 0.45% ID/g) was significantly higher than that in the control PC-3 models (2.25 ± 0.41% ID/g) after injection with (^{64}Cu, Fe^{3+}) PSMA-PEG-MNP at 24 h. **Conclusion:** The (^{64}Cu, Fe^{3+}) PSMA-PEG-MNP was successfully applied to multimodal imaging in prostatic cancer model with high PSMA expression. This nanoparticle may be considered for clinical trials since it combines the numerous advantages of organic nanoparticles. **References:** None.

OP-273

Direct Comparison of Theranostic [$^{124/131}$I]-NM404 and [$^{124/131}$I]-MIBG Dosimetry in a Murine Xenograft Model of Neuroblastoma

I. R. Marsh, J. J. Grudzinski, R. Hernandez, J. P. Weichert, M. Otto, B. P. Bednarz;
University of Wisconsin-Madison, Madison, WI, UNITED STATES OF AMERICA.

Aim/Introduction: Neuroblastoma is the most common extracranial solid tumor in children. For patients with metastatic disease, ^{131}I-meta-iodobenzylguanidine (^{131}I-MIBG) molecularly targeted radiotherapy (MTRT) is a standard treatment. However, 10% of neuroblastoma tumors are not MIBG-avid and patients are left with limited treatment options. 18-(p-iodophenyl) octadecyl phosphocholine (NM404) is a radioiodinated alkylphospholipid ether analog with confirmed uptake in more than 80 preclinical cancer models and has potentially broad applicability in pediatric oncology. The goal of this study was to compare subject-specific dosimetry for theranostic ^{131}I-NM404 and ^{131}I-MIBG MTRT using PET/CT imaging of ^{124}I-NM404 and ^{124}I-MIBG in a murine xenograft model of MIBG-avid neuroblastoma. **Materials and Methods:** NSG mice bearing a NB1691-hNET neuroblastoma flank tumor were administered with 9.2 MBq of ^{124}I-NM404 or 9.7 MBq of ^{124}I-MIBG via lateral tail vein injection (n=4 each). Sequential microPET/CT scans were acquired at 1, 24, 48, 72, 96, and 120 h post-injection for ^{124}I-NM404 and at 1, 4, 24, 48, and 72 h post-injection for ^{124}I-MIBG, to account for the relatively faster biological clearance. CT-based contours of the flank tumor and contralateral muscle were overlaid on the PET volumes and in vivo pharmacokinetics were reported in %ID/g. Using the PET image volumes and a Geant4 Monte Carlo based dosimetry platform, the integral prescription dose (Gy/MBq) delivered by ^{131}I-NM404 and ^{131}I-MIBG was estimated. The tumor-to-muscle ratio (TMR) of integral prescription dose was used to compare the tumor-selectivity of the agents. **Results:** In vivo pharmacokinetic analysis showed tumor-selective uptake of both ^{124}I-NM404 (2.9 %ID/g at 44 h) and ^{124}I-MIBG (2.3 %ID/g at 4h). Subject-specific tumor dosimetry predicted an integral prescription dose of 0.07 Gy/MBq for ^{131}I-MIBG which was significantly lower than the 0.64 Gy/MBq predicted for ^{131}I-NM404. This discrepancy arose from the fundamental differences in uptake and biological clearance such that MIBG was entirely excreted by 48 h whereas NM404 exhibited prolonged uptake and retention beyond 120 h. The TMR of each MTRT agent's prescription integral dose provides a more apt comparison with 1.8 ± 0.6 for ^{131}I-MIBG and 2.3 ± 1.0 for ^{131}I-NM404. **Conclusion:** Our results show that ^{124}I-NM404 and ^{124}I-MIBG exhibit similar levels of tumor-specificity towards neuroblastoma in an MIBG-avid murine model. This suggests that ^{131}I-NM404 MTRT could potentially achieve therapeutic efficacy comparable to what has been established for ^{131}I-MIBG. **References:** None.

OP-274

Demonstration of significantly heterogeneous intratumoural [177Lu]Lu-PSMA-617 dose deposition in a preclinical model of prostate cancer using ex vivo digital autoradiography

J. R. Crawford[1], H. Kuo[1], C. F. Uribe[1], C. Zhang[1], J. Rousseau[1], Z. Zhang[1], K. Lin[1], F. Benard[1,2];
[1]BC Cancer, Vancouver, BC, CANADA, [2]University of British Columbia, Vancouver, BC, CANADA.

Aim/Introduction: For emerging targeted ^{177}Lu therapies, understanding the relationship between absorbed dose and therapeutic outcome provides a basis to optimize delivery parameters for maximum efficacy. Tumours are inherently heterogeneous with a complex microenvironment, which can lead to heterogeneity in deposited radiation dose. The relationship between calculated dose and efficacy may be inaccurately described if non-uniform radiotracer

distributions are not considered in the model. We developed a method for determining volumetric intratumoural activity and corresponding dose rate distributions using an ex vivo digital autoradiography system (BetaIMAGER DFine, Biospace Lab) dedicated to beta-particle detection. Preclinical ^{177}Lu distributions were imaged in vivo with μSPECT (U-SPECT^{+}/CT, MILabs) and ex vivo by autoradiography. Dose rate distributions were interpreted using corresponding histological sections. **Materials and Methods:** NRG mice bearing subcutaneous LNCap tumours were administered 37 MBq of [^{177}Lu]Lu-PSMA-617 via tail-vein injection one day before μSPECT imaging. Tumours were then harvested and frozen with dry ice. Tumour sections 16 μm in thickness were collected at intervals of 160 μm throughout each tumour and imaged using the BetaIMAGER DFine. Three-dimensional activity distributions were constructed in Matlab from high resolution planar images of the complete set of serial sections. Each image was aligned using intensity-based image registration followed by interpolation between adjacent sections to estimate activity distributions at 0.08x0.08x0.08 mm3 voxel size. Corresponding dose rate distributions were calculated by convolving each activity distribution with a dose kernel calculated with GATE 8.1 simulating a 177Lu point-source in water. **Results:** Serial beta-dedicated autoradiography with 3D analysis demonstrated significant intratumoural heterogeneity for [^{177}Lu]Lu-PSMA-617 dose rate distributions. The observed intratumoural distribution was significantly more complex than a simple relationship between a central void with radiotracer accumulation at the periphery. Histological sections (HE stain) confirmed a tight spatial correlation between connective or necrotic tissue and voids in the activity distributions. Even after convolving with a dose kernel, very significant intratumoral dose heterogeneity persisted, with higher dose delivered to clusters of tumour cells compared to necrotic areas or connective tissue. **Conclusion:** These results confirm that intratumoural heterogeneity in delivered radiation dose can be very significant in human prostate cancer models following [^{177}Lu]Lu-PSMA-617 administration, even taking into account the path length of beta-particle emissions. This may significantly affect the accuracy of image-based dosimetry estimates performed using low resolution imaging methods. Further research is needed on how to best model this effect and establish an accurate dose-response relationship to take into account intratumoural heterogeneity. **References:** None.

OP-275

Similarities and differences of dosimetry between meta-[^{211}At]astatobenzylguanidine (^{211}At-MABG) and meta-[^{123}I] iodobenzylguanidine (^{123}I-MIBG) as companion diagnostic drug

N. Ukon[1], *S. Zhao*[1], *K. Yoshinaga*[2], *K. Washino*[2], *M. Aoki*[1], *K. Nishijima*[1], *S. Shimoyama*[1], *C. Tan*[1], *K. Washiyama*[1], *N. Oriuchi*[1], *K. Takahashi*[1], *T. Higashi*[3], *H. Ito*[1,4];
[1]*Advanced Clinical Research Center, Fukushima Medical University, Fukushima, JAPAN,* [2]*National Institute of Radiological Science, Chiba, JAPAN,* [3]*Department of Molecular Imaging and Theranostics, National Institute for Quantum and Radiological Sciences and Technology (QST), Chiba, JAPAN,* [4]*Department of Radiology and Nuclear Medicine, Fukushima Medical University, Fukushima, JAPAN.*

Aim/Introduction: The meta-[^{211}At]astatobenzylguanidine (^{211}At-MABG) has possibility for treatment of malignant pheochromocytoma. In case of clinical application, ^{211}At-MABG requires dosimetry. ^{211}At-MABG needs a companion diagnostic imaging agent for dosimetry such as meta-[^{123}I] iodobenzylguanidine (^{123}I-MIBG). In this regard, the purpose of the study was to evaluate the similarities and differences of dosimetry between ^{123}I-MIBG and ^{211}At-MABG in normal mice. **Materials and Methods:** In this biodistribution study, male normal mice (BALB/cCrSlc, 9 weeks old) received intravenously either 997kBq of ^{123}I-MIBG or 483kBq of ^{211}At-MABG. The radioactivity levels (%ID/g) in the tissues were determined at 1 min, 30 min, 1 h, 3 h, 6 h, 12 h and 24 h after injection (n = 5 in each group) using a gamma counter. The absorbed radiation dose for each compound was calculated by OLINDA EXM ver. 2.0. **Results:** ^{211}At-MABG and ^{123}I-MIBG showed very similar biodistribution profiles in normal mice at every time point. Both drugs showed higher uptake in heart and adrenal glands. Specifically, at 6h, ^{123}I-MIBG and ^{211}At-MABG accumulation were similar in heart and adrenal gland, respectively. ^{123}I-MIBG showed lower uptake in lung and liver compared to ^{211}At-MABG. In contrast, ^{123}I-MIBG showed higher uptake in thyroid than did ^{211}At-MABG, suggesting that dehalogenation may occur more easily in ^{123}I-MIBG than in ^{211}At-MABG. The absorbed dose of ^{211}At-MABG showed a value close to ^{211}At-MIBG (^{211}At-MIBG means estimated the extrapolated radiation dosimetry for ^{211}At-MABG using ^{123}I-MIBG-biodistribution.) because of similar biodistribution in normal mice. However, the absorbed dose of ^{211}At-MABG was higher in the stomach wall (1.60 vs 0.98 Gy/MBq), lung (1.23 vs 0.78 Gy/MBq) and bladder (1.63 vs 1.04 Gy/MBq) than dose of ^{211}At-MIBG. Moreover, the absorbed doses of ^{211}At-MIBG to thyroid gland was markedly higher (4.60 vs 1.79 Gy/MBq) than dose of ^{211}At-MABG. **Conclusion:** At each time point, the trends for biodistribution of ^{211}At-MABG and ^{123}I-MIBG were almost similar in normal mice. A certain level of difference was observed in heart and adrenal gland, in which have higher density of noradrenalin transporter compared to other organs. Therefore, ^{123}I-MIBG may be used for dosimetry and imaging for treatment decisions for ^{211}At-MABG radiotherapy as a companion drug. However, it should be noted that thyroid grand of the absorbed dose of ^{211}At-MABG has lower than the absorbed dose of ^{211}At-MIBG. ^{123}I-MIBG biodistribution data needs certain adjustments to compensate for possible under- or over-estimation of ^{211}At-MABG absorbed dose. **References:** None.

OP-276

Radiation doses from terbium-161 compared to lutetium-177 in single tumor cells and micrometastases

E. Hindie[1], *M. E. Alcocer-Avila*[2], *C. Morgat*[1], *C. Champion*[2];
[1]*Bordeaux University Hospital, Bordeaux, FRANCE,* [2]*Centre Lasers Intenses et Applications, Bordeaux University, Talence, FRANCE.*

Aim/Introduction: Targeted radionuclide therapy is a very promising modality for treating minimal residual disease, occult micrometastases and single tumor cells. However, the radionuclide needs to be appropriately selected. Indeed, radiation doses delivered with traditional beta emitters decrease as the size of tumors decreases (Hindié et al, 2016). Terbium-161 is a medium-energy beta radionuclide like lutetium-177 and with similar chemistry (Müller et al, 2018). However, terbium-161 abundantly emits conversion and Auger electrons which can increase the dose to micrometastases. **Materials and Methods:** We used the Monte Carlo code CELLDOSE to compare the effectiveness of lutetium-177 and terbium-161 at irradiating single cells (14µm cell diameter with 10µm nucleus diameter) or small tumor clusters consisting in a central cell surrounded by 18 neighbouring cells. We here studied the dose to the nucleus of the single cell according to various distributions of the radionuclides: either at cell membrane, cytoplasmic, homogeneous in the cell, or only intranuclear. For the tumor cluster we studied the dose to the nucleus of the central cell considering the various distributions of the radionuclides. For both radionuclides, the simulations were run assuming that 1 MeV was released per µm³ (1436 MeV/cell). **Results:** For the single cell, the dose to the nucleus was substantially higher with terbium-161 compared to lutetium-177, whatever the radionuclide distribution: 5.0 Gy vs 1.9 Gy in case of cell membrane distribution; 8.3 Gy vs 3.0 Gy for intracytoplasmic distribution; 19.5 Gy vs 5.8 Gy in case of homogeneous distribution; and 38.6 Gy vs 10.7 Gy in case of intranuclear location. The dose to the central cell increased with the addition of the 18 neighbors, but remained higher for terbium-161 compared to lutetium-177. For example, in the case of cell membrane distribution, the dose to the nucleus of the central cell was 15.1 Gy with terbium-161 and 7.2 Gy with lutetium-177. **Conclusion:** Terbium-161 should be a better candidate than lutetium-177 for irradiating single tumor cells and micrometastases, whatever the radionuclide distribution is. **References:** Hindié E, Zanotti-Fregonara P, Quinto MA, Morgat C, Champion C. Dose Deposits from 90Y, 177Lu, 111In, and 161Tb in Micrometastases of Various Sizes: Implications for Radiopharmaceutical Therapy. J Nucl Med. 2016; 57: 759-64. Müller C, Domnanich KA, Umbricht CA, van der Meulen NP. Scandium and terbium radionuclides for radiotheranostics: current state of development towards clinical application. Br J Radiol. 2018; 91: 20180074.

607

Pitfalls & Artefacts 3 - Interactive Clinical Cases - Cardiovascular + Inflammation & Infection Committee: Tips and Tricks in the Interpretation of Cardiac PET

Monday, October 14, 2019, 8:00 - 9:30 Lecture Hall 113

OP-277

Quantification of MBF

M. Lubberink;
PET Centre, Uppsala University Hospital, Uppsala, SWEDEN.

OP-278

Viability

A. Saraste;
University of Turku, Heart and PET Centre Hospital/Institute, Turku, FINLAND.

OP-279

Endocarditis

F. Rouzet;
Bichat Hospital, Paris, FRANCE.

OP-280

Sarcoidosis

L. Leccisotti;
Fondazione Policlinico Universitario A. Gemelli IRCCS, Rome, ITALY.

608

Clinical Oncology - Parallel Session: Breast and Gynaecological Cancers

Monday, October 14, 2019, 8:00 - 9:30 Lecture Hall 114

OP-281

^{18}F-FDG PET/CT in Locally Advanced Cervical Cancer: prognostic value of pre- and post-treatment examination and the role of metabolic PET features in this setting

G. M. Lima[1], *G. Dondi*[2], *L. Muraglia*[3], *A. Matti*[3], *N. Naselli*[4], *A. G. Morganti*[5], *A. M. Perrone*[2], *P. De Iaco*[2], *M. Tredici*[1], *P. Castellucci*[3], *C. Nanni*[3], *M. Farsad*[1], *S. Fanti*[3];
[1]*Nuclear Medicine Department, Bolzano Hospital, Bolzano, ITALY,* [2]*Department of Gynecology, S.Orsola-Malpighi Hospital, University of Bologna, Bologna, ITALY,* [3]*Nuclear Medicine Department, S.Orsola-Malpighi Hospital, University of Bologna, Bologna, ITALY,* [4]*Radiology Department, S.Orsola-Malpighi Hospital, University of Bologna, Bologna, ITALY,* [5]*Radiation Oncology Department, S.Orsola-Malpighi Hospital, University of Bologna, Bologna, ITALY.*

Aim/Introduction: Primary aim was to evaluate the prognostic value of 18F-FDG PET/CT in locally advanced cervical cancer, by investigating the association between both baseline and post-treatment PET features and the Overall Survival (OS). Secondary aim was to investigate whether metabolic baseline PET and clinical parameters may play a role as predictors of treatment response. **Materials and Methods:** one hundred and seventeen patients were retrospectively enrolled. Each patient underwent a 18F-FDG PET/CT both at baseline and after chemoradiation. Post-treatment PET/CT were classified according to EORTC criteria and then grouped as complete metabolic responders (CMR) and non-complete metabolic responders (N-CMR). Baseline PET/CT parameters and post-treatment PET/CT results were tested to investigate their possible correlation with prognosis, using Kaplan-Meier analysis and Cox's proportional hazard model. Baseline PET/CT parameters were also tested to investigated their possible role as predictors of response to therapy. **Results:** As regards the pre-treatment scan, the Cox regression survival analysis showed a significant association between baseline MTV and OS (p=0.005). As regards the post-treatment scan, the Kaplan-Meier analysis showed a highly significant difference in OS between the CMR and N-CMR groups (p<0.0001). As regard the prediction to metabolic response to therapy, baseline MTV, TLG and Nodal PET-positivity demonstrated to be independent predictors of response (respectively, p=0.001, p=0.004, p =0.005). **Conclusion:** In our cohort of patients, baseline MTV values and post-treatment PET results are reliable prognostic tools. MTV, TLG and Nodal PET-positivity are independent predictors of metabolic response to chemoradiation therapy in locally advances cervical cancer. **References:** None.

OP-282

Predictive value of Visceral Fat Activity Assessed by Preoperative F-18 FDG PET/CT for omental Metastasis in Patients with Epithelial Ovarian Cancer

S. Choi[1], *J. Eo*[1], *E. Lee*[1], *S. Kim*[2];
[1]*Korea University Guro Hospital, Seoul, KOREA, REPUBLIC OF,*
[2]*Korea University Anam Hospital, Seoul, KOREA, REPUBLIC OF.*

Aim/Introduction: Epithelial ovarian cancer(EOC) cells could directly spread from the primary tumor in to peritoneal cavity and disseminate to organs in the abdomen. EOC preferentially metastasizes to the omentum. Dysregulated visceral adipose tissue(VAT) secretes various pro-inflammatory adipokines related to systemic inflammation which play key roles in metastasis. ^{18}F-FDG PET/CT is a well-established imaging method for evaluation of functional VAT activity. The aim of this study was to investigate the predictive role of functional VAT activity evaluated by preoperative F-18 FDG PET/CT for omental metastasis in patients with EOC. **Materials and Methods:** Ninety-patients(age 53.8 ±14.5) with EOC who underwent ^{18}F-FDG PET/CT before the surgery were included in this study. PET parameters (maximum SUV of the primary tumor, VAT SUVmax, and subcutaneous adipose tissue SUVmax) were measured. And age, histology, FIGO stage, tumor grade were recorded. We performed analysis of PET parameters for predicting the omental metastasis. **Results:** The patients with omental metastasis showed higher VAT SUVmax(0.79 ± 0.14 vs. 0.69 ± 0.16, p=0.006) and tumor SUVmax(7.53 ± 2.53 vs. 5.99 ±3.87, p=0.042) than the patients without omental metastasis. In addition, VAT SUVmax was significantly associated with distant metastasis. An optimal cut-off VAT SUVmax of 0.725 was proposed for predicting omental metastasis with a sensitivity of 70.6% and specificity of 53.6% (area under the curve: 0.66; p=0.012) **Conclusion:** VAT SUVmax is significantly associated with omental metastasis in EOC patients. Furthermore, VAT SUVmax can be useful as a complementary factor in predicting omental metastasis. **References:** None.

OP-283

Imaging in breast cancer staging: MRI of the breast versus dedicated breast PET and whole body PET/CT

D. Grigolato[1], *A. Invento*[2], *F. Pellini*[2], *M. Zuffante*[1], *M. Cucca*[1], *E. Biggi*[1], *F. Padovano*[1], *M. Naseri*[1], *E. Fiorio*[3], *Q. Piubello*[4], *G. P. Pollini*[2], *M. Ferdeghini*[1];
[1]*Nuclear Medicine Dept, Azienda Ospedaliera di Verona, Verona, ITALY,* [2]*Oncologic Surgery Department, Complex Operative Unit of Breast Surgery - Breast Unit, Azienda Ospedaliera di Verona, Verona, ITALY,* [3]*Department of Oncology, Azienda Ospedaliera di Verona, Verona, ITALY,* [4]*Department of Diagnostic and Pathology, Azienda Ospedaliera di Verona, Verona, ITALY.*

Aim/Introduction: To assess the accuracy of two diagnostic modalities, whole body PET/CT with dedicated breast positron emission tomography and MRI of the breast and their retrospective fusion in patients with breast cancer. **Materials and Methods:** One hundred patients were retrospectively analyzed, age ranged from 30 to 49 years with a clinical stadium I-III at diagnosis. They where divided into five groups according to the following characteristics: single cancer, multicentric/multifocal lesions, pectoral invasion, prosthesis holders and patients receiving preoperative chemotherapy. All patients underwent 3T MRI of the breast and FDG PET/CT before surgery or chemotherapy. A standard whole body PET/CT scan was immediately followed by a dedicated breast positron emission tomography with acquisition of two beds in high resolution in prone position of the upper thorax including the axilla (dbPET). Biologic prognostic parameters obtained at diagnosis and, after surgery, pathological results were correlated with metabolic features (SUVmax). **Results:** Primary multifocal/multicentric lesions were better identified by MRI in all groups, a good correlation in the detection of single lesions was noticed among the two methods. There was one false positive (FP) result at MRI and 5 false negative (FN) cases at dbPET, all patients with infiltrating lobular cancer (ILC), low grade and low Ki-67, but fusion dbPET-MRI correctly changed the results in all these patients. PET/CT identified 15 metastatic patients at diagnosis, then confirmed at CT and/or MR. Bone metastases were discovered in 13 patients, liver and lung lesions in 3 patients,

and single cases with periocular soft tissue lesion, adrenal gland and brain metastasis, the latter identified by MRI. MRI was more sensitive in defining pectoral invasion in 8 women, while dbPET showed high accuracy in detecting cutaneous infiltration, internal mammary chain involvement in 6 cases and macrometastatic axillary lymph nodes in 44 women, whereas partial, micrometastatic involvement of axillary lymph nodes was only ruled out with sentinel lymph node biopsy (SLNB). MRI was more precise in defining prosthesis state and their relationship with the pectoral muscle. Whole body PET/TC was useful in the evaluation of chemotherapy response or disease progression and dbPET had great correlation with pathological response to neoadjuvant chemotherapy ($p < 0.001$). **Conclusion:** MRI alone or fusion dbPET-MR are among the best breast cancer diagnostic modalities allowing the more appropriate surgical approach or identifying patients for preoperative chemotherapy. Whole body PET/CT may become a part of the routine workup staging of high risk patients except for ILC. **References:** None.

OP-284

First results of molecular imaging (FDG and FES) in prospective study for selecting second line hormonotherapy in estrogen receptors positive metastatic breast cancer patients

B. Maucherat[1], *A. Leduc-Pennec*[2], *N. Fleury*[3], *L. Ferrer*[4,5], *E. Bourbouloux*[6], *H. Simon*[7], *M. Le Thiec*[1], *D. Rusu*[1], *V. Fleury*[1], *M. Colombie*[1], *A. Morel*[1], *F. Kraeber-Bodere*[1,5], *L. Campion*[8,5], *C. Rousseau*[1,5];
[1]*ICO Cancer Center, Nuclear Medicine Unit, Saint Herblain, FRANCE,* [2]*University Hospital, Nuclear Medicine Unit, Brest, FRANCE,* [3]*ICO Cancer Center, DRCI, Saint Herblain, FRANCE,* [4]*ICO Cancer Center, Physics Unit, Saint Herblain, FRANCE,* [5]*CRCINA, University of Nantes, INSERM UMR1232, CNRS-ERL6001, Nantes, FRANCE,* [6]*ICO Cancer Center, Oncology Unit, Saint Herblain, FRANCE,* [7]*University Hospital, Oncology Unit, Brest, FRANCE,* [8]*ICO Cancer Center, Biometrics, Saint Herblain, FRANCE.*

Aim/Introduction: About 70% of primitive breast cancers had positive estrogen receptors (ER) and may benefit from hormonotherapy. However, ER expression in breast cancer metastases is heterogeneous and about 15% of metastases lost this expression over time. Biopsies were not possible systematically. 16α-18Fluoro-17β-Oestradiol (^{18}FES) is a radiopharmaceutical which predict the response to the first line hormonotherapy. The aim of this prospective study (NCT03442504) was to determine the predictive value of PET at the patient level, before a second line hormonotherapy (2nd-HT) on the FDG response obtained at 6 weeks of treatment. **Materials and Methods:** We prospectively included 12 ER+ metastatic breast cancer patients, HER2 negative, in progression despite first line hormonotherapy. For the complete study, 60 patients will be included. Due to 2nd-HT proposed by oncologist, we performed ^{18}FES PET-CT (^{18}FES-BL) and ^{18}FDG PET-CT (^{18}FDG-BL) at baseline in the month before the new treatment introduction. Follow-up with ^{18}FDG PET-CT and CT were performed to detect treatment response, particularly with a first FDG PET-CT at 6 weeks (^{18}FDG-6W). Semi-quantitative data were extracted from ^{18}FES-BL, ^{18}FDG-BL and ^{18}FDG-6W, and compared to the progression free survival (PFS) during the 2nd-HT treatment, among which SUVmax and adapted thresholded Total Tumour Volume (TTV). **Results:** At breast cancer diagnosis, 6 patients (50%) had lymph node metastases and 5 (41,6%) had visceral metastases. After first line hormonotherapy, only one patient had no positive FES (FES+) lesion while more than 40 FDG positive (FDG+) lesions were detected. Eleven patients (91,6%) had between 3 and more than 40 FES+ lesions. Three patients (25%) had more FES+ lesions than FDG+ lesions, 4 patients (33,3%) had more FDG+ lesions than FES+ and 5 patients (41,7%) had as many FES+ lesions as FDG+. Despite the 2nd-HT started, no significant result was found for the semi-quantitative data outside a likely poor prognosis of ^{18}FDG-BL TTV ($p=0.079$). We noted a trend for a better PFS when the ^{18}FES-BL TTV was greater or equal to the ^{18}FDG-BL TTV. Comparing ^{18}FDG-BL and ^{18}FDG-6W, a ^{18}FDG-BL TTV greater or equal to the ^{18}FES-BL TTV seemed predict the stability or progression of the ^{18}FDG-6W TTV. **Conclusion:** ^{18}FES PET-CT seemed to be interesting for the 2nd-HT response prediction. These results must be confirmed with the the following study patients. **References:** None.

OP-285

Frequency Of Incidental Focal Breast Lesions Identified By 18f-FDG PET/CT

L. Petersen, *J. D. Andersen*, *H. D. Zacho*;
Department of Nuclear Medicine, Aalborg University Hospital, DENMARK.

Aim/Introduction: Incidental focal uptake of 18F-FDG in the breast on PET/CT is rare. However, there is very few and often quite small studies from Europe. Here we report data from Denmark, a country with wide access to PET/CT as part of a free, public health care system. **Materials and Methods:** All PET/CT scans from a seven-year period (2010-2017) were electronically searched for specific words and phrases indicative of breast lesions. Potentially eligible PET/CT scans were manually reviewed for incidental findings. All patients with known, suspected or previous cancer of the breast were excluded. Patients with diffuse FDG breast uptake were excluded. The extent of clinical, pathology, and imaging follow up were reviewed among patients with focal FDG uptake. **Results:** A total of 19.551 PET/CT scans performed in the 7-year period of which 64 patients (0.3%) presented with an incidental, focal FDG-avid lesion of the breast. There were 63 women and 1 man with a mean age of 67 ± 15 year. The main reasons for referral were staging of known cancer (45%) or suspected cancer (28%). Five percent of the patients were referred with a non-cancer indication. Fifty-two patients (81%) had a follow up, mostly with biopsy (n=39), clinical evaluation (n=7), or imaging (n=6). Twelve patients had no follow up, mostly due to disseminated malignant disease. Thirty-three patients had biopsy-verified cancer (33 primary breast lesions, 2 metastases), i.e. 52% among the 64 patients

with a focal FDG breast uptake. However, the malignancy rate was 85% among patients with a biopsy (33 of 39 patients). The most frequently malignant lesion was ductal carcinoma (n=23). **Conclusion:** We found a very low rate of incidental, focal FDG uptake in the breast in patients evaluated on PET/CT in Denmark. However, the malignancy rate was high among these patients, in particular in patients who had a follow up biopsy. We recommend biopsy in patients with focal uptake of FDG in the breast. **References:** None.

OP-286

To evaluate the role of F-18 FDG-PET/CT in different molecular subtypes of breast cancer for prognostication

R. Kumar, *S. Arora, A. Passah, A. Prashanth, N. Mohan, A. R. Vuthaluru, C. Bal;*
AIIMS, New Delhi, INDIA.

Aim/Introduction: To find out whether, 18F-FDG PET/CT can be used as prognostic marker for survival outcome in MBC, taking into consideration different molecular subtypes. **Materials and Methods:** A total of 136 breast cancer patients who underwent 18F-FDG PET/CT and having documented receptor status were included in this analysis. The patients were divided into 3 subgroups, group 1 (ER+, PR+/-, Her 2neu-), group 2 (ER+/-, PR+/-, Her 2neu+) and group 3 (ER-, PR-, Her 2neu-)-triple negative breast cancer (TNBC). Patients were followed till at least 1year after their last PET-CT study. **Results:** Among three pathological groups, lymph nodal metastases was seen in 26/49 (53%) in group 1, 32/62 (51%) in group 2 and 19/25 (76%) in group 3. There was significant difference between three groups regarding presence of lymph nodal metastases (p=0.09). Skeletal metastases was noted in 24/49 (49%), 21/62 (33%) and 12/25 (48%) in three groups respectively, with no significant difference in distribution (p=0.2). Liver metastases was noted in 8/49 (16%), 6/62 (9%) and 2/25 (8%) in three groups respectively, with no significant difference in distribution (p=0.4). Lung metastases was noted in 10/49 (20%), 21/62 (33%) and 8/25 (32%) in three groups respectively, with no significant difference in distribution (p=0.2). Among Semiquantitative PET parameters, SUVmax (mean, SD): 5.2(6.7) in Group 1, 4.8(3.6) in group 2 and 8.8 (5.08) in group 3), significant difference in SUVmax value of primary breast lesions was noted among three groups (p=0.04). Group three (TNBC) lesions had highest SUVmax values, compared to group 1 (p=0.03) and group 2 (p=0.01). Although within group 3, no significant difference between SUVmax values of primary lesions were noted among patients who expired or were alive at last follow up. No significant difference in SUVmax value of extra primary lesions, were noted among the three groups. On follow up, significant difference regarding survival outcome was noted among three groups (18/49 (36%) in group 1, 19/62(30%) in group 2 and 18/25 (72%) in group 3 (p=0.001). Also, on subgroup analysis, using age (younger patient group (<45year) showed increased mortality compared to age group (>45 years) (p=0.04). **Conclusion:** TNBC patients showed more metabolic activity of primary lesion and worse survival outcome compared to other groups. 18F-FDG PET-CT can provide role as prognostic marker in different molecular subtypes of breast cancer. **References:** None.

OP-287

Retrospective Analysis Of Baseline FDG PET/CT In Prognostication Of Locally Advanced Breast Cancer

Z. Nayeem, *S. Shah, N. Purandare, A. Agrawal, A. Puranik, V. Rangarajan;*
Tata Memorial Centre, Mumbai, INDIA.

Aim/Introduction: To correlate metabolic parameters on baseline 18 F FDG PET/CT with outcomes i.e., disease free survival (DFS) and progression free survival (PFS) in cases of locally advanced (LABC) and metastatic breast cancer (MBC) respectively. **Materials and Methods:** This was a retrospective observational study. Female patients with biopsy proven locally advanced breast cancer referred to our department for baseline 18 F FDG PET/CT scan during the period of Jan 2011 to June 2015 with minimum follow up of 3 years were included in the study. Patients were segregated into LABC and MBC. Recurrence in cases of LABC and progression in cases of MBC were confirmed by clinical/ radiological follow up. Suitable cut-off points for SUV max, SUV mean, MTV and TLG for primary tumor and whole body MTV were obtained using receiver operating characteristic curve. Survival curves for DFS and PFS were constructed by using the Kaplan-Meier method. **Results:** 130 female patients who met inclusion criteria were included in the study. 86 patients were LABC and 44 patients were MBC. On follow up, 25 out of 86 patients of LABC developed recurrence (mean DFS -65 months). On analysis MTV of primary tumor showed significant correlation with DFS with cut-off value of 20.51 (53 months v/s 72 months) (p value- 0.036). While TLG of primary tumor showed trend towards statistically significant value. 36 out of 44 patients of MBC developed progression (mean PFS - 23 months). On analysis whole body MTV showed statistically significant correlation with progression free survival with cut-off value of 83.24 (8 v/s 18 months) (p value-0.05). Rest of the metabolic parameters did not show any statistically significant correlation. **Conclusion:** MTV of primary tumor is a prognostic factor in determination of recurrence in case of LABC and whole body MTV is a prognostic factor in determination of MBC. Prospective multicenter studies in a larger homogenous patient cohort and longer follow up are required for the validation of these observations **References:** None.

OP-288

Using 18F-FDG-PET/CT for Response Monitoring of Metastatic Breast Cancer: Interrater Agreement and Reliability of PERCIST and Visual Assessment

J. Sørensen[1,2], *M. H. Vilstrup*[2], *J. Holm*[2], *M. Vogsen*[1,2,3], *J. Bülow*[2], *L. Ljungstrøm*[2], *M. G. Hildebrandt*[1,2,4], *O. Gerke*[1,2];
[1]*Department of Clinical Research, University of Southern Denmark, Odense, DENMARK,* [2]*Department of Nuclear*

Medicine, Odense University Hospital, Odense, DENMARK, [3]Department of Oncology, Odense University Hospital, Odense, DENMARK, [4]Center for Innovative Medical Technology, Odense University Hospital, Odense, DENMARK.

Aim/Introduction: Palliative medical treatment is indicated for metastatic breast cancer (MBC) along with response evaluation at regular intervals[1]. Accurate response monitoring is becoming increasingly important, and FDG-PET/CT may have the potential to monitor treatment response accurately. The PERCIST criteria[2] may perform with better agreement between observers than qualitative assessment. The aim of this study was to compare the interrater agreement and reliability of the semi-quantitative PERCIST criteria to qualitative visual assessment in response evaluation of MBC. Furthermore, to investigate the intrarater agreement when comparing each rater's visual assessment to their own respective PERCIST assessment. **Materials and Methods:** We performed a retrospective study on FDG-PET/CT in women with MBC who received treatment at Odense University Hospital. Patients were recruited from September 2017 to December 2017, and data from medical files and scans were analysed retrospectively for consenting women. Three specialists in nuclear medicine categorized response evaluation by qualitative assessment and standardized one-lesion PERCIST assessment based on SULpeak measurements[2]. The scans were categorized into complete metabolic response, partial metabolic response, stable metabolic disease, and progressive metabolic disease. **Results:** A total of 37 patients with 179 scans were included. Visual assessment categorization yielded moderate agreement with an overall proportion of agreement between raters of 0.52 (95% CI 0.44-0.66) and a Fleiss kappa estimate of 0.54 (95% CI 0.46-0.62). PERCIST response categorization yielded substantial agreement with an overall proportion of agreement of 0.65 (95% CI 0.57-0.73) and a Fleiss kappa estimate of 0.68 (95% CI 0.60-0.75). The difference in proportions of agreement between overall estimates for PERCIST and visual assessment was 0.13 (95% CI 0.06-0.21; p=0.001), that of kappa was 0.14 (95% CI 0.06-0.21; p<0.001). The overall intrarater proportion of agreement was 0.80 (95% CI 0.75-0.84) with substantial agreement by a Fleiss kappa of 0.74 (95% CI 0.69-0.79). **Conclusion:** Semi-quantitative PERCIST assessment achieved significantly higher level of overall agreement and reliability compared to qualitative assessment among three raters. The achieved high levels of intrarater agreement indicated no obvious conflicting elements between the two methods. PERCIST assessment may therefore give more consistent interpretations between raters as well as between institutions when using FDG-PET/CT for response evaluation in MBC. **References:** [1]Cardoso F et al. Ann Oncol. 2018;29:1634-57. doi:10.1093/annonc/mdy192. [2]Wahl RL et al. J Nucl Med. 2009;50 Suppl 1:122S-50S. doi:10.2967/jnumed.108.057307.

609

Paediatrics - Parallel Session: Paediatrics

Monday, October 14, 2019, 8:00 - 9:30 Lecture Hall 115

OP-289

[18]F-FET PET/MRI for CNS-Tumors in Children and Adolescents

L. Marner[1,2], *K. Nysom*[3], *A. Sehested*[3], *L. Borgwardt*[2], *R. Mathiasen*[3], *R. Mathiasen*[3], *P. S. Wehner*[4], *O. M. Henriksen*[2], *M. Lundemann*[2], *C. Thomsen*[5], *L. Bøgeskov*[6], *J. Skjøth-Rasmussen*[6], *H. Broholm*[7], *D. Scheie*[7], *M. Juhler*[6], *L. Højgaard*[2], *I. Law*[2];
[1]*Department of Clinical Physiology and Nuclear Medicine, University Hospital Bispebjerg, Copenhagen, DENMARK,* [2]*Department of Clinical Physiology, Nuclear Medicine and PET, University Hospital Rigshospitalet, Copenhagen, DENMARK,* [3]*Department of Pediatrics and Adolescent Medicine, University Hospital Rigshospitalet, Copenhagen, DENMARK,* [4]*Hans Christian Andersen Children's Hospital, University Hospital Odense, Odense, DENMARK,* [5]*Department of Diagnostic Radiology, Zealand University Hospital, Roskilde, DENMARK,* [6]*Department of Neurosurgery, University Hospital Rigshospitalet, Copenhagen, DENMARK,* [7]*Department of Pathology, University Hospital Rigshospitalet, Copenhagen, DENMARK.*

Aim/Introduction: [18]F-fluoro-ethyltyrosine ([18]F-FET) positron emission tomography (PET) improves diagnostic accuracy in adult patients with gliomas. We aimed to 1) determine accuracy for detecting tumor using [18]F-FET PET and MRI versus MRI alone in children and adolescents with CNS tumors and 2) test the clinical impact of the scans. **Materials and Methods:** Ninety-seven patients (57 males, 40 females, median age 10.1 years, range 0-33 years) with primary pediatric CNS tumors were included consecutively and prospectively, and a total of 169 hybrid [18]F-FET PET/MRI (n=140) or PET/CT scans were performed at time of diagnosis, recurrence, or before or after treatment. For the estimation of a lesion-based accuracy for detection of tumor, the reference standard was operation, biopsy, or follow-up. The accuracies between MRI, PET, and PET/MRI were compared using McNemar's test, correcting for possible correlation between lesions belonging to the same patient. Clinical impact was assessed by sequential clinical decision making, first with only MRI and then with additional [18]F-FET PET available. As scans were performed consecutively for research purposes, the majority were not clinically indicated. The clinically indicated scans were identified before the [18]F-FET PET scan was available, and were cases of anticipated impact of the PET scan due to important clinical decisions combined with an equivocal MRI. **Results:** For treated lesions, the sensitivity/specificity/accuracy for PET/MRI was 0.88(0.82-0.94)/1.00(0.82-1.00)/0.91(0.87-0.96), as compared to MRI alone 0.93(0.89-0.97)/0.48(0.30-0.70)/0.81(0.75-0.89), p=0.31/p=0.0001/p=0.044. Of the 151 scans rated for clinical impact, the addition of [18]F-FET PET to MRI added extra relevant

information in 28% and influenced the clinical management in 8%. Of the 30 ^{18}F-FET PET scans that were beforehand identified as clinically indicated (e.g. due to equivocal MRI), 40% added new information and 33% influenced clinical management. **Conclusion:** We collected a large dataset of ^{18}F-FET PET scans in a broad spectrum of pediatric tumor types. Interpretation of MRI can be challenged by unspecific contrast enhancement especially after treatment procedures. PET showed higher specificity (p=0.0001) and using the combined information from PET and MRI showed a significantly higher accuracy for detecting pediatric tumors of 0.91 vs. 0.81 for treated lesions (p=0.04). Further, the addition of ^{18}F-FET PET influenced clinical management in 8% of all scans and in 33% of the clinically indicated scans. In conclusion, ^{18}F-FET PET is useful in cases of pediatric brain tumors with difficult clinical decision making, as 33% of scans influence clinical management in this group of patients. **References:** None.

OP-290

Diagnostic and Prognostic Role of 18F-DOPA PET/CT in children affected by Neuroblastoma: Comparison with 123I-mIBG scan

G. Bottoni[1], *G. Ferrarazzo*[2], *A. Cistaro*[3], *M. Puntoni*[4], *G. Morana*[5], *S. Sorrentino*[6], *P. Zucchetta*[7], *M. Ugolini*[8], *M. Conte*[6], *M. Pescetto*[9], *M. Lattuada*[9], *A. Garaventa*[6], *L. Giovanella*[10], *E. Lopci*[11], *A. Piccardo*[12]; [1]*Nuclear medicine unit Ospedali Galliera, Genova, ITALY,* [2]*Nuclear medicine unit, Pavia, ITALY,* [3]*Department of Nuclear Medicine, Galliera Hospital, Genoa, ITALY,* [4]*Clinical Trial Research Unit, Galliera Hospital, Genoa, ITALY,* [5]*Neuroradiology Unit, IRCCS Istituto Giannina Gaslini, Genova, ITALY,* [6]*Unit of Pediatric Oncology, IRCCS G. Gaslini Genoa, ITALY,* [7]*Department of Nuclear Medicine, University Hospital of Padova, Padova, ITALY,* [8]*Medical Physics Department, Galliera Hospital, Genoa, ITALY,* [9]*Anaesthesiology Department, Galliera Hospital, Genoa, ITALY,* [10]*Clinic of Nuclear Medicine and Molecular Imaging, Imaging Institute of Southern Switzerland, SWITZERLAND,* [11]*Department of Nuclear Medicine, Humanitas Research Hospital, Rozzano, ITALY,* [12]*Nuclear medicine unit, Galliera Hospital, Genoa, ITALY.*

Aim/Introduction: We aim to validate the diagnostic role of ^{18}F-DOPA PET/CT, at the time of first staging, in children affected by Neuroblastoma (NB) and to investigate the ability of this technique in the assessment of treatment response. Lastly, we investigated the prognostic value of ^{18}F-DOPA at onset and after chemotherapy. **Materials and Methods:** We included children affected by NB at onset. All patients underwent, before and after chemotherapy, ^{18}F-DOPA PET/CT and ^{123}I-mIBG whole-body scan (WBS) with additional SPECT/CT.The ^{18}F-DOPA PET/CT results were compared with those of ^{123}I-mIBG WBS. For each modality, a patient-based (PBA) and lesion-based-analysis (LBA) was performed and sensitivity calculated. Specific scoring systems applied to ^{123}I-mIBG WBS and to ^{18}F-DOPA PET/CT were also calculated and the association between these parameters, the principal NB risk-factors and outcome was evaluated. **Results:** We enrolled 16 high and 2 intermediate-risk NB patients. On the PBA, the sensitivity of ^{123}I-mIBG WBS and ^{18}F-DOPA PET/CT in detecting primary tumours, soft tissue metastases and bone/bone marrow metastases was 83%, 50%, 92% and 94%, 92% and 100% respectively. On the LBA, the sensitivity of ^{18}F-DOPA PET/CT in detecting soft tissue and bone/bone marrow metastases was 86% and 99%; significantly higher than that ^{123}I-mIBG WBS (41% and 93%). After chemotherapy, on the PBA, the sensitivity of ^{123}I-mIBG WBS and ^{18}F-DOPA PET/CT in detecting primary tumours, soft tissue metastases and bone/bone marrow metastases was 72%, 33%, 38% and 83%, 75% and 54% respectively. On the LBA, the sensitivity of ^{18}F-DOPA PET/CT in detecting soft tissue and bone/bone marrow metastases was 77% and 86%; significantly higher than that ^{123}I-mIBG WBS (28% and 69%). Over a median follow-up of 29.3 months, 8 cases of disease progression and 5 deaths occurred. At multivariate level, the ^{18}F-DOPA WBMB, evaluated after therapy, wasthe only factor independently associated to disease progression free survival. **Conclusion:** ^{18}F-DOPA PET/CT is more sensitive than ^{123}I-mIBG WBS to stage NB patients and to evaluate disease persistence after chemotherapy. In time-to-event analyses,^{18}F-DOPA WBMB, evaluated after chemotherapy, remained the only risk factor independently associated to disease progression. **References:** None.

OP-291

Metastatic differentiated thyroid cancer in paediatric patients - radioiodine treatment after thyroid hormone withdrawal or rhTSH stimulation

D. Handkiewicz-Junak, A. Kropinska, A. Ledwon, J. Roskosz, D. Kula, A. Kluczewska, T. Olczyk, E. Paliczka, Z. Puch, B. Jarzab; M.Sklodowska Curie Memorial Institute – Cancer Center Gliwice Branch, Gliwice, POLAND.

Aim/Introduction: Distant metastases are diagnosed in about 20% of children with DTC. Radioiodine is the treatment of choice, however, there are limited data on optional preparation for it. The aim of our retrospective study was to evaluate the effectiveness of radioiodine treatment after thyroid hormone withdrawal (THW) and rhTSH stimulation in metastatic paediatric DTC. **Materials and Methods:** From 501 children diagnosed with DTC during the years 1988- 2018, 72 (14.4%) had distant metastases (lungs - 66, bones - 2, both- 4). All 72 children were treated with radioiodine after THW (group A:46 patients) or combination of rhTSH and THW cycles (group B: 26 patients). Median cumulated radioiodine activity was 16.8 GBq. **Results:** Median time of observation in the whole group of patients was 11.5 years and was longer in group A (13 vs. 5 years, $p < 0.05$) During the last radioiodine treatment complete scintigraphic response was achieved in 63% and biochemical CR (Tg <2 ng/ml) in 24% ($p < 0.05$). Complete scintigraphic and biochemical response increased respectively to 86% and 40% during the last follow-up on TSH stimulation. During the last follow-up suppressed Tg decreased below 1 ng/ml in 70% of children. When we compared last radioiodine treatment in group A and B there was no statistically significant difference in scintigraphic

(58% vs. 72%) or biochemical (25% vs. 18.5%) complete response. However, during last follow up on TSH suppression complete biochemical response was higher in group A (84% vs. 46%, p < 0.05). In 6 patients treated under rhTSH stimulation only (no THW) complete biochemical and scintigraphic response was achieved respectively in 1/6 (17%) and 5/6 (83%) patients. No lung fibrosis nor secondary malignancies were diagnosed during follow-up **Conclusion:** Our study confirms that radioiodine treatment of disseminated DTC in children/adolescents is safe and effective. To confirm complete remission long follow-up is necessary since the response is extended in time. rhTSH seem not to decrease response rate to radioiodine treatment and the observed difference between groups are probably related to shorter follow-up time after rh-TSH. **References:** None.

OP-292

Significance Of Interim PET/CT And Lugano Criteria For Early Response Evaluation With 18F-FDG-PET/CT In Pediatric Lymphoma--A Part Of Report On IAEA Multicentric Prospective Study

K. Bashir Mir[1], *I. Iaea*[2], *S. A. Bukhari*[1], *S. Batool*[1], *S. Fatima*[1];
[1]*Nuclear Medicine And Oncology Institute, Islamabad, PAKISTAN,*
[2]*International Atomic Energy Agency, Vienna, AUSTRIA.*

Aim/Introduction: Pediatric lymphoma is third most common childhood malignancy with relapse rate of 5-20%. 18F-FDG PET/CT is an excellent tool for staging and monitoring disease in adult lymphoma but there is no validated standardized criteria for evaluation of treatment response by PET/CT in pediatric Lymphoma. Aims: To establish the significance of interim PET/CT (iPET/CT) in the treatment response evaluation of pediatrics Lymphoma and to evaluate the prognostic impact of Lugano criteria (LC) in the evaluation of pediatric 18F-FDG PET/CT in pediatric lymphoma. **Materials and Methods:** Between 2013-2017 PET/CT studies performed for staging and interim response evaluation in 35 patients (n=35), <18 years of age of pediatric Lymphoma after taking informed consent. Whole body PET/CT (head to toe) was done. Staging PET/CT (sPET/CT) and early response evaluation after 2 cycles of chemotherapy, iPET/CT was done. We prospectively reviewed results of sPET/CT and iPET/CT and in some patients with end of treatment (EOT) PET/CT, and their 18 months follow up after start of therapy to asses complete response (CR) and incomplete response (NCR) of the treatment given. PET/CT findings were evaluated using visual and quantitative variables eg, Deauville criteria, Luganos criteria, measurement of bulk of lesion in baseline and interim and differences in values of SUV Max and Mean in both s and i PET/CT . LC scores of 1-3 was considered negative, LC- ,4-5 was taken as LC +. **Results:** n= 35, Age (Years) 7.8 +_ 3.7, Sex Ratio (M: F) (28 :07), Type (HL: NHL) 30:05). Comparison of baseline and interim PET/CT scans were done on the basis of Deauville criteria, measurement of bulk of lesion in baseline and interim, difference in the values of SUV max and SUV mean and LC in both sPET/CT and iPET/CT. Long term follow up of patients showed that patients in which iPET/CT showed good response, (n=27) showed complete response, with event free survival of more than 18 months, mostly in Hodgkin's Lymphoma. Moreover LC+ studies were independently and significantly associated with overall increased mortality and with more events in these patients. **Conclusion:** Good response in interim PET/CT is strong & independent predictor of prognosis with event free survival of more than 18 months without relapse in pediatric Lymphoma and LC+ 18F FDG PET/CT in interim evaluation is significantly and independently associated with increased overall mortality and more events. **References:** 1. Weiler-Sagie M,et all, 18F-FDG Avidity in Lymphamoa Readdressed, J Nucl Med 2010;51: 25-30.

OP-293

Prognostic value of interim-PET in paediatric Hodgkin lymphoma: the role of qPET

S. Pacella[1], *C. Landoni*[1], *M. Arosio*[2], *E. De Ponti*[3], *S. Morzenti*[3], *C. Crivellaro*[1], *F. Elisei*[2], *M. Spinelli*[4], *A. Sala*[4], *L. Guerra*[2];
[1]*University of Milano Bicocca, Milano, ITALY,* [2]*Nuclear Medicine Department, ASST Monza San Gerardo Hospital, Monza, ITALY,* [3]*Medical Physics Department, ASST Monza San Gerardo Hospital, Monza, ITALY,* [4]*Fondazione MBBM ASST Monza San Gerardo Hospital, Monza, ITALY.*

Aim/Introduction: 18-Fluorodeoxyglucose (FDG) positron emission tomography/computed tomography (PET/CT) is an useful tool for staging and for the evaluation of response to therapy in Hodgkin lymphoma (HL); interim-PET has also a prognostic role. Our study aimed to evaluate the prognostic role of r-PET in paediatric HL by calculating qPET , that is the ratio of SUVpeak of a reference lesion to the liver SUVmean. **Materials and Methods:** 63 children (32 males, mean age 13, range 5-17) with newly diagnosed HL, stage I-IV disease (14 stage I- IIA, 49 stage IIB-IVB) were retrospectively evaluated. All patients underwent a pre-treatment 18F-FDG PET/CT (baseline PET) and after 2, 3 o 4 cycles of chemotherapy (restaging-PET; r-PET) according to the therapeutic group. r-PET scans were evaluated according to Deauville Score (DS) criteria. DS 1-3 classified r-PET as negative, and DS 4-5 as positive. A qPET threshold ≥ 1.3 classified r-PET as positive for disease (Hasenclever et al. 2014). Disease related major events (death and disease relapse) were correlated to r-PET results according both to DS and qPET using the Fisher exact text, with a p value < 0.05 considered as significant. **Results:** The median follow-up was 44 months for DFS and 55 months for OS; at last follow-up, 53 children were in complete remission , 2 had progression and died and 8 relapsed. According to DS r-PET resulted negative in 53 patients (84%) and positive in 10 (16%). There was no statistical difference between r-PET results and the presence of relapse (p-value 0.19); conversely there was a statistical difference between r-PET results and the number of exitus with a higher value in r-PET positive group (p-value 0.023). The positive predictive value (PPV) and negative predictive value (NPV) of r-PET to predict exitus were 100% and 87%. The mean values of qPET in relapsed and not relapsed patients were 1.32 (median 0.86, range 0.46-3.93) and 0.91 (median 0.84, range 0.34-5.27) respectively,

without statistical difference between the two groups (p-value 0.07). Conversely qPET values in dead and alive patients were 0.91 (average value; median value 0.83; range 0.34-5.27) and 3.11 (average value; median value 3.11; range 2.29-3.93) respectively with statistically significant difference (p-value 0.01); the PPV and NPV of qPET to predict exitus were 100 % and 92%. **Conclusion:** Our study suggests that DS and qPET are both strong predictors of exitus with a slightly better performance of qPET in terms of NPV. **References:** Hasenclever et al. 2014

OP-294

^{18}F-FDG-PET-CT in Paediatric Langerhans Cell Histiocytosis: Extension, Diagnosis, Recurrence and Treatment Response Evaluation

J. Alors-Ruiz[1], *C. Sábado-Álvarez*[2], *A. A. Cardozo-Saavedra*[3], *I. Roca-Bielsa*[3], *A. García-Burillo*[3], *J. Castell-Conesa*[3];
[1]*Nuclear Medicine Department. Hospital Clínico Universitario Virgen de la Victoria, Málaga, SPAIN,* [2]*Paediatric Oncology and Haematology Department. Hospital Universitari Vall d'Hebrón, Barcelona, SPAIN,* [3]*Nuclear Medicine Department. Hospital Universitari Vall d'Hebrón, Barcelona, SPAIN.*

Aim/Introduction: At first clinical approach, Langerhans Cell Histiocytosis (LCH) may be a systemic and severe disease or just monosymptomatic. And the evolution of the disease may be a spontaneous resolution or a rapid systemic progression, including death. PET-CT with ^{18}F-FDG is used both for initial diagnosis and for the treatment response assessment. Paediatric series published until now have a limited number of cases and follow-up evaluations. **Materials and Methods:** From January 2010 till March 2019, 41 paediatric patients have been submitted to ^{18}F-FDG-PET-CT under the clinical suspicion of LCH (later confirmed), for treatment response assessment of LCH during and after chemotherapy and in case of recurrence suspicion: mean age 5.3 ± 4.1 years; age range 6 months to 17.6 years. A total number of 63 ^{18}F-FDG-PET-CT have been performed corresponding to the 41 patients: 37 initial evaluation, 10 response assessment, 7 recurrence suspicion and 9 after treatment. **Results:** Results in ^{18}F-FDG-PET-CT have classified the patients in single-system involvement in 26 patients (63.4%): 17 single site and 9 multiple sites. 15 patients (36.6%) were assigned to multisystem group, 10 with risk organs involvement (spleen, liver, bone marrow and central nervous system). At diagnosis, bone system is the most frequently involved, with bone lytic lesions (32 patients, 78%). Other initial presentations includes: skin involvement (10 patients), diabetes insipidus (4 patients), haemophagocytic syndrome (3 patients), lung involvement (1 patient) and soft tissue (1 patient).26 patients received chemotherapy (based on prednisone/vinblastine protocols). Based on ^{18}F-FDG-PET-CT results and clinical evaluation, complete resolution, stable lesions and progression were present in 27%, 46% and 27%, respectively. **Conclusion:** ^{18}F-FDG-PET-CT is an all-in-one technique in LCH, with clinical usefulness for the initial extension diagnostic, in case of clinical suspicion of recurrence, for treatment response assessment (interim) and at end of treatment. **References:** 1: Mueller WP, Melzer HI, Schmid I, Coppenrath E, Bartenstein P, Pfluger T. The diagnostic value of ^{18}F-FDG PET and MRI in paediatric histiocytosis. Eur J Nucl Med Mol Imaging. 2013 Feb;40(3):356-63.2: Lee HJ, Ahn BC, Lee SW, Lee J. The usefulness of F-18 fluorodeoxyglucose positron emission tomography/computed tomography in patients with Langerhans cell histiocytosis. Ann Nucl Med. 2012 Nov;26(9):730-7.3: Phillips M, Allen C, Gerson P, McClain K. Comparison of FDG-PET scans to conventional radiography and bone scans in management of Langerhans cell histiocytosis. Pediatr Blood Cancer. 2009 Jan;52(1):97-101.4: Kaste SC, Rodriguez-Galindo C, McCarville ME, Shulkin BL. PET-CT in pediatric Langerhans cell histiocytosis. Pediatr Radiol. 2007 Jul;37(7):615-22.

OP-295

Might STAGING 18FDG-PET stratify prognosis in Osteosarcoma and Ewing sarcoma?

C. Olianti[1], *R. Di Dato*[1], *M. Allocca*[1], *A. Tamburini*[2], *C. Caporalini*[2], *R. Sciagra*[1];
[1]*University Hospital of Careggi, Florence, ITALY,*
[2]*University Hospital Meyer, Florence, ITALY.*

Aim/Introduction: To identify at staging18FDG-PET-CT the biological aspects of Osteosarcoma (OS) and Ewing'Sarcoma (ES) able to stratify the risk of poor response to therapy or relapse, and correlate them with progression free survivor (PSF). **Materials and Methods:** SUVmax (Standardized Uptake Value) of lesion, MTV41% (Tumor Volume), TLG41% (Tumor Lesion Glycolysis), FDG%necrosis, cylindrical or ellipsoid morphology are evaluated in 48 patients with OS (26) and ES (22), age 4-29 years (mean 15.06+/-5.8) in staging18FDG-PET-CT. Data-comparisons (t-student, test-U of Mann-Whitney) are performed with histological outcome (Huvos for OS, Picci for ES) and histological%necrosis, dividing the cohort in Poor/Good responders, Kaplan-Meier curves for 5years-PFR are builded, and ROC-analysis for cut-off evaluation performed. **Results:** Statistical-analysis shows a significant difference ($p<0.05$) between OS and ES cohort for SUVmax (mean+/-SD: 7.06+/-3.82 OS vs 4.43+/-2.93 ES), MTV (mm3: 93.46+/-170.78 OS vs 39.87+/-23.18 ES) and TLG (355.75+/-128.81 OS 128.81+/-127.56 ES) and significant difference ($p<0.05$) of SUVmax and TLG41% between GoodES and PoorES (mean+/-SD: respectively 2.75+/-1.18 vs 6.78+/-3.75, $p<0.02$ and 59.5+/-33 vs 220.59+/-159.75, $p<0.005$). SUVmax cut-off of 3.4 and TLG41% cut-off of 136.13 correlate with GoodES and PoorES stratification (AUC 0,83; $p<0.05$), not for OS; they also indicate a 86% risk of relapse (5y-PSF) if higher and 50% (5y-PSF) if lower (Kaplan-Meier). FDG%necrosis respect tumor volume (mm^3 : 253,86+/-273,57 OS vs 257.68 +/-276,21 ES) is 17% in OS and 13% in ES. Age at staging is 15.6+/-6 years for OS and 14.4+/-5.7 years for ES ($p>0.05$), otherwise a cut-off of 12.5y is found for GoodES and PoorES stratification (AUC 0,82, $p<0.05$), not for OS, and it indicates a 92% risk of relapse (5y-PSF) if higher and a 20% of risk of relapse (5y-PSF) if lesser (Kaplan-Meier). Cylindric morph. is found in 15.4% of OS, 25% of

GoodOS and 75% of PoorOS, and in 50% of ES, 62.5% of GoodES and 37.5% of PoorES, ($p < 0.05$). Ellipsoid morph. is found 84.6% of OS, 52% of GoodOS and 48% of PoorOS, and in 50% of ES, 55% for GoodES and 45% for PoorES. Ellipsoid and cylindrical morphologies correlate respectively with a 14% and 50% risk of relapse (5y-PSF Kaplan-Meier Curves) independently from the tumor-site if arms, axial skeleton or pelvis. **Conclusion:** Preliminary data seem to assess prognostic value of SUVmax, TLG, age at staging and morphology in ES only. A trend is suggested in OS to investigate with a larger cohort of patients. **References:** None.

OP-296

Assessment of future remnant liver function in pediatric patients with liver malignancies

Y. Likar, *K. Chaurasiya, E. Kireeva, I. Vdovina, M. Chetchasova, D. Akhaladze;*
Dmitry Rogachev National Research Center of Pediatric Hematology, Oncology and Immunology, Moscow, RUSSIAN FEDERATION.

Aim/Introduction: Liver malignancies are 3rdmost common malignant tumors of the abdominal/retroperitoneal cavity in children. Surgery remains the most important treatment for liver tumors. Post-resection liver failure remains a major problem, which requires accurate preoperative assessment of future remnant liver function (FRL-F). Recently a novel method was presented using ^{99m}Tc-mebrofenin hepatobiliary scintigraphy (HBS) for estimation of the FRL-F in adults. It has been shown that the threshold value of FRL-F >2.7 %/min/m^{2}minimizes the postoperative liver failure. The aim of our study is to evaluate the role of preoperative HBS for estimation of the FRL-F in pediatric patients with liver malignancies. **Materials and Methods:** Twenty-nine pediatric patients with liver malignancies (aged from 27 days to 16.7 years) were included in this study. All patients underwent HBS for estimation of the FRL-F before surgery. The study was performed immediately after intravenous injection of ^{99m}Tc-mebrofenin using standard protocol with the two dynamic phases and SPECT/CT of the liver. Venous phase of CECT was used for more accurate segmentation of liver. The boundary of future remnant liver was drawn manually. **Results:** In 12 patients right side extended hemihepatectomy was performed, the FRL-F was evaluated in S2, S3 segments and ranges from 1.2 to 11.7 %/min/m^2. In 8 patients right hemihepatectomy was performed, the FRL-F was evaluated in S2, S3, S4 segments and ranges from 2.8 to 19.3 %/min/m^2. In 3 patients left hemihepatectomy was performed, the FRL-F was evaluated in S5, S6, S7, S8 segments and ranges from 27.1 to 29.5 %/min/m^2. In 6 patient atypical resection was performed, the FRL-F value was evaluated in S2, S3, S6 and S7 segments and ranges from 5.8 to 14.1 %/min/m^2. At the initial diagnosis the FRL-F value was less than 2.7 %/min/m^{2}in 3 patients (1.2, 1.5, 2.4 %/min/m^2), after chemotherapy the FRL-F values was increased up to 9.0, 4.5 and 5.7 %/min/m^2, respectively. No one has developed post-resection hepatic failure following one month after liver resection. **Conclusion:** Our results demonstrated that recent method of ^{99m}Tc-mebrofenin hepatobiliary scintigraphy for estimation of the FRL-F in adults can be successfully used in children. In the most of the patients value of FRL-F was more than 2.7 %/min/m^2 before surgery, which can be explained by lack of severe parenchymal diseases in children. FRL-F value in pediatric patients increases after chemotherapy. To obtain reliable data it is necessary to continue the study with further recruitment and analysis. **References:** None.

610

Endocrine - Parallel Session: Neuroendocrine Malignancies

Monday, October 14, 2019, 8:00 - 9:30 Lecture Hall 116

OP-297

[^{18}F] DOPA PET/CT for the evaluation of primary or recurrent medullary thyroid carcinoma

E. Rainer, *S. Rasul, C. Scheuba, M. Mayerhöfer, P. Mazal, A. Haug, M. Hacker, S. Li;*
Medical university of Vienna, Vienna, AUSTRIA.

Aim/Introduction: Basal calcitonin (bCT) and carcinoembryonic antigen (CEA) can be used as tumor markers for diagnosis and follow-up of MTC. [^{18}F]DOPA-PET/CT has been reported to be useful for the detection of primary or recurrent MTC. However, so far, no data have been published concerning the possible relation between the sCT levels and the results of [^{18}F]DOPA-PET/CT as well as possible gender differences in [^{18}F]DOPA-PET results. The aim of this study is to evaluate a possible correlation between bCT- or sCT levels and tracer uptake of [^{18}F]DOPA. Furthermore, we want to assess possible gender differences in the results of [^{18}F]DOPA-PET. **Materials and Methods:** 148 [^{18}F]DOPA-PET/CT examinations in 50 patients (26 female, 24 male patients, mean age 59± 14 years, range 24 to 84) with histologically verified primary or recurrent MTC were included. 5 patients presented with hereditary MTC. Serum bCT and CEA were measured in all patients. Calcium stimulation test was performed in 42 of the 50 patients. SUVmax was calculated for each lesion. Correlation and cutoff values were determined with SPSS Statistics using Pearson's correlation, Chi square test and ROC curves. **Results:** Positive [^{18}F]DOPA-PET/CT results were shown in 127 examinations with a case-related sensitivity of 86%. 43 patients had positive [^{18}F]DOPA-PET/CT scans with a sensitivity of 86%. 22 male patients (92%) had positive findings in [^{18}F]DOPA-PET/CT, whereas only 21 female patients (80%) were positive in the [^{18}F]DOPA-PET/CT. However, we found no significant difference in sensitivity between female and male patients. All 5 patients (100%) with hereditary MTC had positive PET/CT scans. Significant correlations were found between bCT and SUVmax ($p<0,01$) as well as between sCT and SUVmax ($p<0,01$). 119 examinations with positive [^{18}F]DOPA-PET/CT had

bCT levels >82 pg/mL with a sensitivity of 90% and a specificity of 67%. [^{18}F]DOPA-PET/CT was positive in 53 examinations with sCT levels >1714 pg/mL with a sensitivity of 73% and a specificity of 63%. Cutoff value for CEA values >4 ng/L had a sensitivity of 80% and a specificity of 64%. **Conclusion:** Tracer-uptake of [^{18}F]DOPA (SUVmax) correlates significantly with bCT and sCT. We observed higher sensitivity of [^{18}F]DOPA-PET/CT in male patients than in female patients, however no significant difference was shown. Higher sensitivity of [^{18}F]DOPA-PET/CT tends to be found in patients with hereditary MTC as compared to patients with sporadic MTC. [^{18}F] DOPA-PET/CT may be especially useful in patients with bCT levels >82 pg/mL or sCT levels >1714 pg/mL or CEA >4ng/L. **References:** None.

OP-298

Diagnostic Value of ^{18}F-Fluorocholine PET/CT for the Detection of Recurrent Medullary Thyroid Carcinoma

J. Jamsek[1], *M. Hocevar*[2], *D. Bergant*[2], *K. Zaletel*[1], *S. Rep*[1], *B. Peric*[2], *L. Lezaic*[1];
[1]*University Medical Centre Ljubljana, Ljubljana, SLOVENIA,*
[2]*Institute of Oncology Ljubljana, Ljubljana, SLOVENIA.*

Aim/Introduction: Medullary thyroid carcinoma (MTC) recurrence after primary surgery is found in 15-50% of patients. Our group recently reported the usefulness of ^{18}F-Fluorocholine (^{18}F-FCH) in primary MTC staging. Following those findings, we wanted to assess the role of ^{18}F-FCH PET/CT in biochemical recurrence of MTC. Preliminary results are presented. **Materials and Methods:** Twenty MTC patients (8 male, 12 female; aged 33-74 years) with biochemical recurrence (calcitonin > 10 ng/L) after primary surgery performed an ^{18}F-FCH PET/CT between May 2014 and March 2017 with a minimal follow-up of 2 years. ^{18}F-FCH PET/CT examination included a three-phase scan of the head, neck and upper mediastinum (5 min, 45 min and 90 min post application) and a whole-body scan (60 min post application). Calcitonin and CEA levels before the PET/CT scan were measured. Suspicious lesions were either histologically analysed after surgery or evaluated based on FNAB or follow-up imaging. Results with $p < 0.05$ were considered statistically significant. **Results:** ^{18}F-FCH PET/CT was positive in 16/20 patients (80%) with calcitonin > 10 ng/l, and in 13/14 patients (93%) with calcitonin > 150 ng/l. Based on PET/CT, 8 patients were reported as having only neck metastases (5 diagnosed on follow-up imaging; 1 MTC and 2 benign on histology), while 12 were reported as having distant metastases (7 diagnosed on follow-up imaging; 2 MTCs and 2 benign on histology; 1 lesion unconfirmed). Lesions defined as distant metastases on PET/CT were visualized in the mediastinum (6/12), bones (5/12), liver (3/12), distant lymph nodes and soft tissues (2/12) and lungs (1/12). One patient had diffuse sclerotic bone lesions visible on CT that were not ^{18}F-FCH avid (histologically unconfirmed finding). For neck metastases ^{18}F-FCH PET/CT had 100% sensitivity (95% CI 48-100%) and 65% specificity (95% CI 43-84%). The sensitivity of ^{18}F-FCH PET/CT for the detection of distant metastases was 83% (95% CI 36-100%). Patients positive on ^{18}F-FCH PET/CT had higher calcitonin (median 562.8 [IQR 243.9-2589.3] vs 35.8 [IQR 30.1-79.1] ng/l, Wilcoxon signed-rank $p = 0.01115$) and CEA levels (median 9.7 [IQR 7.3-35.5] vs 4 [IQR 2.7-6.2] µg/l, Wilcoxon signed-rank $p = 0.1482$) in comparison to ^{18}F-FCH PET/CT negative patients. **Conclusion:** ^{18}F-FCH appears to be a promising radiotracer for visualization of MTC recurrence with detection rates similar to ^{18}F-FDOPA. Further evaluation of our data and comparison with other imaging modalities are needed to define the role of ^{18}F-FCH PET/CT in the management of MTC recurrence. **References:** None.

OP-299

Normal and Abnormal Adrenal glands' Standard Uptake Values in ^{123}I mIBG scintigraphy for diagnosis of Pheochromocytoma and Paraganglioma

R. Gregory[1], *E. Nowosinska*[1], *Y. Bouchareb*[2], *M. Burniston*[1];
[1]*Barts Health NHS Trust, London, UNITED KINGDOM,*
[2]*College of Medicine & Health Sciences Sultan Qaboos University Hospital, Muscat, OMAN.*

Aim/Introduction: Iodine-123 mIBG scintigraphy is the standard imaging method for diagnosis of pheochromocytoma and paraganglioma. Pheochromocytoma develops in the adrenal glands and it is challenging to distinguish abnormal uptake from the physiological uptake in the adrenal medulla. The aim of this work is to show whether quantitative imaging can be used to aid distinction between normal and abnormal (tumour) adrenal gland uptake. **Materials and Methods:** Sixteen patients' ^{123}I mIBG SPECT/CT scans for suspected pheochromocytoma or paraganglioma were analysed. These scans were performed using medium-energy general purpose collimators on SPECT/CT systems that had been calibrated for ^{123}I imaging. The injected activity and patient's weight were used to calculate standard uptake values (SUVs). The maximum SUV in the adrenal glands were recorded. The mean SUV in a 3cm spherical VOI defined in the right liver lobe was used to calculate the adrenal glands-to-liver ratios (ALRs) [1]. The normal and abnormal SUVs and ALRs were compared, using an unpaired two-tailed t-test assuming unequal variance. **Results:** Seven of the patients were diagnosed with pheochromocytoma, 5 with paraganglioma and 4 were found to have no neuroendocrine disease. The average ±standard deviation(range) mean SUV in the liver was 2.14±0.93 (0.76-3.59). The average maximum SUV in the normal adrenal glands in patients found to have no disease was 5.83±2.25 (2.44-8.91) and the corresponding ALRs were 2.45±0.98 (1.23-4.39). The average maximum SUV in 7 abnormal adrenal glands of the pheochromocytoma patients was 27.58±33.32 (7.00-102.22) with ALRs of 10.82±8.33 (4.40-28.47). For the extra-adrenal masses of the paraganglioma patients the average maximum SUV was 31.84±33.32(15.05-45.41) with ALRs of 20.22±12.16(7.13-33.52). These differences between the normal and abnormal ALRs were statistically significant with a p-value of 0.038; however the maximum SUVs were not statistically different (p-value 0.135). There were no statistical differences between the extra adrenal paraganglioma

lesion and pheochromocytoma abnormal adrenal SUVs or ALRs (p-values 0.769 and 0.181 respectively). **Conclusion:** The statistically significant difference between the ALRs for the normal and abnormal adrenal glands without overlap in the range of values shows this semi-quantitative approach to be useful in the pheochromocytoma diagnosis. However the maximum SUVs were not statistically different for this group of patients and the range of SUVs did overlap. Therefore the ALR effectively adjusts to the physiological uptake using the liver uptake, which was shown to vary widely for these patients. This investigation is to continue. **References:** 1. van Berkel A et al. J Nucl Med. 2015 Jun;56(6):839-46.

OP-300

May It Be A New Parameter Of 18F-FDG PET/CT In Differentiating Between Benign And Malignant Adrenal Lesions: Adrenal Densitometabolic Index

E. Ciftci[1], *T. Y. Erdil*[2], *Ü. Erkorkmaz*[3], *H. T. İlçe*[1];
[1]*Sakarya University, School of Medicine, Research And Training Hospital, Department of Nuclear Medicine, Sakarya, TURKEY,* [2]*Marmara University, School of Medicine, Research And Training Hospital, Department of Nuclear Medicine, Istanbul, TURKEY,* [3]*Sakarya University, School of Medicine, Research And Training Hospital, Department of Biostatistics, Sakarya, TURKEY.*

Aim/Introduction: Several reports have documented the ability of PET/CT to differentiate benign from malignant adrenal diseases focusing on the ability of functional and metabolic advantages of PET. This study evaluates the diagnostic importance of a new parameter that consisting of the densitometric and metabolic proporties of the lesion measured by 18F-FDG PET/CT in differentiating between benign and malignant adrenal lesions in cancer patients. **Materials and Methods:** In this retrospective study, we evaluated 18F-FDG PET/CT parameters of adrenal lesions of follow-up cancer patients referred to our clinic between January 2017 and April 2019. Diagnosis of adrenal malignant lesions was based on interval growth, reduction after chemotherapy or MRI findings. For PET images, the ROI was placed within the adrenal mass while avoiding peripheral area. Also, ROIs were placed at the same level of an adrenal mass on the unenhanced CT images. Based on these values, a new parameter "Adrenal Dansitometabolic index (ADMI)" was calculated as the square root of the multiplication of SUVmax and HU values. Besides this, also analysis of mostly used metabolic parameters such as SUVmax (maximum standard uptake value) and Tumor SUVmax/ Liver SUVmean ratio (T/LR), morphologic and metabolovolumetric parameters as Hounsfield Units (HU), metabolic tumor volume (MTV) and total lesion glycolysis (TLG) of adrenal lesions were calculated. PET/CT parameters were assessed using the Mann-Whitney U test and receiving operating characteristic analysis. **Results:** 204 adrenal lesions in 181 cancer patients (121M/60F; mean±SD age 65±10.6 years) underwent FDG PET/CT for tumor evaluation. Of those 115 malign, 89 benign adrenal lesions were exist. ADMI values (median (%25-75)) were 4.6 (1.7-6.5) and 16.9 (13.4-19.5); SUVmax were 3 (2.3-3.4) and 8.6 (6.3-12.2); HU were 7.8 (-1.2-14.8) and 31.8 (26.9 and 36.9); TLG were 8 (4.4-14.3) and 27.9 (17-56.6) and T/LR 1 (0.8-1.3) and 3.4 (2.5-4.9) in benign and malignant adrenal lesions, respectively. Based on AUC, adrenal lesion ADMI, SUVmax and T/LR had the similar highest diagnostic performance for predicting malignant lesions (AUC:0.991, 0.992 and 0.988 p=0.000), respectively. Multivariate logistic regression analysis revealed that adrenal lesion SUVmax and ADMI was an independent predictive factor for malignancy rather than TLG. **Conclusion:** Using a new parameter that consist of metabolic and morphologic feature of the adrenal lesions (ADMI) was statistically highly significant for differentiating benign from malignant lesions, with high NPV. This analytic technique may facilitate diagnosing of the adrenal lesions but needs further large series studies. **References:** None.

OP-301

Metabolic tumour volume on FDG PET predicts survival for patients with neuroendocrine tumours (NENs)

D. Chan[1,2], *G. Schembri*[2], *P. J. Roach*[2], *M. Johnson*[2], *N. Pavlakis*[2], *S. Clarke*[2], *D. L. Bailey*[2], *E. Bernard*[2];
[1]*University of Sydney, St Leonards, AUSTRALIA,* [2]*Royal North Shore Hospital, St Leonards, AUSTRALIA.*

Aim/Introduction: 18-Fluorodeoxyglucose (FDG) PET avidity in NENs has been associated with higher grade disease. FDG avidity and high SUV_{max} have been demonstrated to predict poor outcome. Quantitative metrics of FDG PET, specifically metabolic tumour volume (MTV) and total lesion glycolysis (TLG), have been shown to be prognosticators in other malignancies, but these have not been investigated to date in NETs. **Materials and Methods:** Patients with NEN undergoing ^{18}F-FDG at Royal North Shore Hospital were retrospectively included (2012-18). Images were analysed using MIM software version 6.8.3, with automated segmentation (SUV cutoff of 4) followed by contour verification by a nuclear medicine physician and manual segmentation where required. Variables collected included patient age, histological grade, MTV, TLG, and SUV_{max}/SUV_{mean}. The primary outcome was overall survival (OS), and the secondary outcome was progression-free survival (PFS). Univariate (UV) and multivariate (MV) analyses were performed for OS and PFS for MTV and TLG separately. For univariate analysis, the median MTV and TLG were used to dichotomize the cohort. MTV/TLG for NENs of different histological grade were compared using ANOVA. **Results:** 190 patients were included (median age 63.5, 49% female). Primary site: 42% small bowel, 32% pancreas, 15% other GI, 6% lung, 6% other. Grade for GEPNENs: G1 37%, G2 40%, G3 15%, unknown 8%. Median MTV was 4.83mL and TLG was 29.22. Patients with high MTV had worse median OS compared to those with low MTV (29.7mo vs not reached, HR 4.1, 95% CI 2.25-7.49, p<0.00001). Considered as a continuous variable, MTV predicted for poorer OS on UV (p<0.00001) and MV (p=0.003) analysis. Whilst histological grade was significant on both UV and MV, SUVmax was significant on UV (p<0.00001) but not MV (p=0.76). Tumours of higher grade

had higher MTV (mean MTV - G1: 39.6mL, G2: 107mL, G3: 337mL; p=0.0001 by ANOVA). **Conclusion:** Quantitative analysis of FDG PET in NEN is feasible. High MTV/TLG are predictors of poor prognosis in NEN. Further analyses are underway to investigate a larger cohort of NEN patients. **References:** 1. Binderup et al, Functional imaging of neuroendocrine tumors: a head-to-head comparison of somatostatin receptor scintigraphy, 123I-MIBG scintigraphy, and 18F-FDG PET, J Nucl Med. 2010 May;51(5):704-12. 2. Bahri et al, High prognostic value of 18F-FDG PET for metastatic gastroenteropancreatic neuroendocrine tumors: a long-term evaluation. J Nucl Med. 2014 Nov;55(11):1786-90. doi: 10.2967/jnumed.114.144386. Epub 2014 Oct 6.

OP-302

Texture analysis of dual tracer 68Ga-DOTATOC and 18F-FDG PET/CT for preoperative risk assessment in pancreatic neuroendocrine neoplasms

P. Mapelli[1,2], *M. Salgarello*[3], *S. Pasetto*[3], *S. Partelli*[1,4], *P. Rancoita*[5], *J. Doraku*[3], *F. Muffatti*[4], *V. Andreasi*[1,4], *L. Gianolli*[2], *M. Falconi*[1,4], *M. Picchio*[1,2];
[1]*Vita-Salute San Raffaele University, Milan, ITALY,* [2]*Nuclear Medicine Department, IRCCS San Raffaele Scientific Institute, Milan, ITALY,* [3]*Department of Nuclear Medicine, Sacro Cuore Don Calabria Hospital, Negrar, ITALY,* [4]*Pancreatic Surgery Unit, Pancreas Translational & Clinical Research Centre, IRCCS San Raffaele Scientific Institute, Milan, ITALY,* [5]*University Centre of Statistics in the Biomedical Sciences, Vita-Salute San Raffaele University, Milan, ITALY.*

Aim/Introduction: Aim of the present study is to carry on an explorative assessment of texture features, obtained from 68Ga-DOTATOC and 18F-FDG PET/CT images that might define a preoperative risk profile in patients affected by pancreatic neuroendocrine neoplasms (PanNENs). **Materials and Methods:** A retrospective analysis was performed including61 patients (38 males, 23 females; mean age: 58.4 years, range 15-84) who underwent both a 68Ga-DOTATOC and a 18F-FDG PET/CT before surgery for PanNEN between 2011 and 2017. For all patients histological and follow-up data were available. PET/CT scans were qualitatively interpreted. Texture analysis (TA) was applied to PET images of both scans; volumetric region of interests (VOIs) were drawn on positive findings and Chang-Gung Image Texture Analysis (CGITA) software package for statistical radiomics metrics was used. Selected texture features from both scans (intensity variability-IV; size zone variability-SZV; Zone percentage-ZP; Entropy; Homogeneity, Dissimilarity; Coefficient of Variation-CoV) were analysed with appropriate regression models to evaluate their possible role in predicting tumour characteristics (size, grade G2 vs G1, lymphnodal involvement, angioinvasion). Bonferroni's correction was applied to account for multiple testing. P-values less than 0.05 were considered significant. **Results:** According to the 2017 WHO classification, 18 patients had G1, 39 G2 and 4 had G3 PanNEN. The mean Ki-67 index was 7.1% (range: 0.9-65). 68Ga-DOTATOC TA: SZV, Entropy and IV were significantly positively predictive for tumour dimension (p=0.0002, p<0.0001 and p=0.0007, respectively), remaining significant also when adjusting for multiple testing (p=0.0023, p<0.0001 and p=0.0105, respectively). Entropy was significantly positively predictive for G (p=0.0236, but was not confirmed after p-value adjustment: p=0.3302). ZP was predictive for the number of involved lymph nodes (p=0.0372, but not confirmed after p-value adjustment: p=0.5215). Co-V was predictive for disease-free survival at 24 months (p=0.0055), not confirmed after p-value adjustment, probably due the low number of events (n=6). 18F-FDG TA: IV, SZV and homogeneity were significantly positively predictive for tumour dimension (p<0.0001, p<0.0001 and p=0.0017, respectively) also when adjusting for multiple testing (p= p<0.0001, p=0.0004 and p=0.0231, respectively); IV and SZV were positively predictive for angioinvasion (p=0.0134 and p=0.0034, respectively) with only SZV confirmed after p-value adjustment (p= 0.0481). **Conclusion:** Specific texture features derived from preoperative 68Ga-DOTATOC and 18F-FDG PET/CT could non-invasively predict specific tumour characteristics. The retrospective nature of the study and its limitations (i.e. small sample, unbalance of G categories) advocate the need of a further validation on larger prospective cohorts. **References:** None.

OP-303

Texture analysis of ^{68}Ga-DOTATATE positron emission tomography and computed tomography images as a prognostic biomarker in adults with neuro-endocrine cancers treated with ^{177}Lu-DOTATATE

C. Atkinson[1], *B. Ganeshan*[2], *M. Gaze*[2], *R. Endozo*[2], *S. Wan*[2], *M. Aldridge*[2], *A. Groves*[2], *K. Miles*[2], *J. Bomanji*[2];
[1]*Queens Hospital, Romford, UNITED KINGDOM,* [2]*University College London Hospitals, London, UNITED KINGDOM.*

Aim/Introduction: Neuroendocrine tumors (NETs) are a rare, heterogeneous group of cancers whose behavior can be hard to predict. A better understanding of prognosis would aid individualized management decisions. We aim to demonstrate the prognostic potential of tumor heterogeneity and avidity in NETs using PET and CT textural analysis (PTA & CTTA) and standardized uptake values (SUV). **Materials and Methods:** The baseline 68Gallium-DOTATATE PET/CT scans of 49 prospectively recruited patients with NETs (carcinoid, pancreatic, thyroid, head and neck, catecholamine-secreting and unknown primary tumours) treated with 177Lutetium-DOTATAE at a tertiary center were retrospectively analyzed. Non-contrast CT and PET heterogeneity was assessed using a commercially available TexRAD texture analysis software (TexRAD Ltd www.texrad.com, part of Feedback Plc, Cambridge, UK) which employed a filtration-histogram technique. Regions of interest were drawn around the most prominent metastases of each patient (up to 5 tumour foci) as seen on the 68Ga-DOTATATE PET scan. Gallium uptake on PET was quantified as SUVmax and SUVmean. Association between imaging and clinical markers with progression-free (PFS) and overall survival (OS) were assessed using univariate Kaplan-Meier and multivariate Cox regression

analysis. **Results:** Amongst all available clinical factors, presence of lung metastases significantly predicted worse PFS (p=0.026) and having thyroid primary NET negatively impacted on OS (p=0.012). Measures of texture heterogeneity (quantified as kurtosis, entropy and skewness) on filtered (coarse texture scale) CT and unfiltered PET images predicted PFS (CT coarse kurtosis: p=0.05, PET entropy: p=0.01, PET skewness: p=0.03) and OS (CT coarse kurtosis: p=0.05, PET entropy: p=0.01, PET skewness p=0.02). Conventional PET parameters such as SUV_{max} and SUV_{mean} showed trends towards predicting outcome but did not reach statistical significance. Multivariate Cox analysis identified that CTTA (coarse kurtosis: HR=2.57, 95%CI=1.22-5.38, p=0.013) was an independent predictor of PFS and PTA (unfiltered skewness: HR=9.05, 95%CI=1.19-68.91, p=0.033) independently predicted OS. **Conclusion:** ^{68}Ga-DOTATATE PET/CT texture heterogeneity and SUV measurements could act as prognostic biomarkers in NETs and potentially playing a key role in risk stratifying these patients. **References:** None.

OP-304

Decreased administered activity for ^{68}Ga-DOTATATE with preserved assessed image quality

A. Stenvall[1], *L. Jönsson*[1,2], *B. Olsson*[3], *A. Svensson*[3], *G. Brolin*[1], *H. Almquist*[3], *C. Hindorf*[1];
[1]*Radiation Physics, Skåne University Hospital, Lund, SWEDEN,* [2]*Department of Medical Radiation Physics, Lund University, Lund, SWEDEN,* [3]*Department of Clinical Physiology and Nuclear Medicine, Skåne University Hospital, Lund, SWEDEN.*

Aim/Introduction: For PET/CT tumour imaging with ^{68}Ga-DOTA-conjugated peptides, an injected activity of 100-200 MBq ^{68}Ga-DOTATATE is recommended by guidelines. Due to limited total activity of ^{68}Ga-DOTATATE per batch produced, the aim of this study was to evaluate if a lower activity could be administered with preserved image quality by optimization of image reconstruction parameters. **Materials and Methods:** Ten patients were included and the NEMA-IQ-phantom with spheres with diameter 37-10 mm and the Jaszczak-phantom with spheres with diameters of 15.4-4 mm were filled with activity concentrations of ^{68}Ga corresponding to tumours in high activity background (e.g. liver) (41 kBq/ml, 10 kBq/ml, SBR4) and tumours in low activity areas (represented by fat) (12 kBq/ml, 0.3 kBq/ml, SBR40). In our clinical protocol patients are administered 2.5 MBq/kg body weight and imaged 3 minutes/bed position (Discovery MI), then reconstructed with a block-sequential regularization expectation maximization reconstruction with a beta-value of 500 (Q.Clear). The 3-minute patient and phantom images were re-reconstructed to 1 and 2 minutes/bed position with beta-values from 100 to 1200 in steps of 100. Circular ROIs were drawn in liver and fat in the patient images, and in spheres and background in the CT central slice of the phantoms. Max, mean and standard deviation (std) were noted. Signal to noise ratios (SNR=mean/std) was calculated in the phantom background and in liver and fat. Recovery curves (ratio of measured and true activity concentration) were determined for the spheres. Patient images were assessed for image quality by one expert reader. Scores were given by a five-grade scale (1=unacceptable to 5=very high image quality). **Results:** Similar SNR were obtained in the truncated phantom and patient images for a 2-minute acquisition time with beta-value 700 and 1-minute acquisition time with beta-value 1100, compared to the clinical protocol (3min;beta500). The recovery of the 2-minutes images and the 1-minute images was within +-10% for sphere sizes 10-37 mm and up to -30% for smaller spheres relative to the 3-minute images. The SNR was retained in liver and fat and the scored image quality was considered equivalent for the three reconstructions: 2.1 (3min;beta500), 2.2 (2min;beta700) and 2.0 (1min;beta1100). **Conclusion:** Our study shows that it is possible to administer 0.8 MBq/kg with an acquisition time of 3 minutes, with preserved assessed image quality, constant SNR and a limited decrease in the recovery when the beta-value is increased, i.e. a higher number of patients per batch can be examined. **References:** None.

612

UEMS/EBNM Clinical Audit Session & New Fellows of EBNM

Monday, October 14, 2019, 8:00 - 9:30 Meeting Room 118/119

OP-305

Introduction & Welcome

J. O. Prior;
Médecine nucléaire, Centre Hospitalier Universitaire Vaudois, Médecine nucléaire, Lausanne, SWITZERLAND.

OP-306

Quality in Nuclear Medicine

M. Hall;
Royal Free Hospital, Nuclear Medicine, London, UNITED KINGDOM.

OP-307

Implementation of Quality Systems in Nuclear Medicine - Why It Matters. An Outcome Analysis of the IAEA's QUANUM

D. Paez;
IAEA, Vienna, AUSTRIA.

OP-308

Quality Improvement with Self-Assessments

J. T. Liukkonen;
STUK - Radiation and Nuclear Safety Authority in Finland, Helsinki, FINLAND.

OP-309a
Clinical Audits in Switzerland - Results of the Pilot Phase and Outlook
R. Hesselmann;
Bundesamt für Gesundheit, Strahlenschutz, Bern, SWITZERLAND.

OP-309b
Presentation of the Accredited Centers since last EANM 2018
J. O. Prior;
Médecine nucléaire, Centre Hospitalier Universitaire Vaudois, Médecine nucléaire, Lausanne, SWITZERLAND.

OP-309c
Presentation of the Accredited Centers since last EANM 2018
S. Mirzaei;
Wilhelminenspital der Stadt Wien, Institute of Nuclear Medicine with PET-Center, Vienna, AUSTRIA.

OP-309d
FEBNM Examination - Certificate Handover to the New Fellows
A. Boubaker;
Service de Medecine Nucleaire, Clinique de La Source, Institut de Radiologie, Lausanne, SWITZERLAND.

OP-309e
Group Pictures for New Accredited Centers and New FEBNM Members

701/704

Plenary 2: Prostate Cancer ? Reload

Monday, October 14, 2019, 10:00 - 11:15 Auditorium

OP-310
Introduction
S. Fanti;
Policlinico S.Orsola, University of Bologna, Radiological Sciences - Nuclear Medicine, Bologna, ITALY.

OP-311
^{18}F-1007PSMA
F. Giesel;
University of Heidelberg, Department of Nuclear Medicine, Heidelberg, GERMANY.

OP-312
^{68}Ga-11PSMA
M. Eiber;
Technische Universität München, Department of Nuclear Medicine, Munich, GERMANY.

OP-313
^{18}F-DCFPyL
M. Pomper;
John Hopkins Hospital , Radiology, Nuclear Medicine and Molecular Imaging, Baltimore, UNITED STATES OF AMERICA.

OP-314
Others
K. Herrmann;
Universitätsklinikum Essen, Nuclear Medicine, Essen, GERMANY.

OP-315
Is there Life Beyond PSMA Tracer?
C. Decristoforo;
Medical University Innsbruck, Department of Nuclear Medicine, Innsbruck, AUSTRIA.

OP-316
PSMA Therapy - Where are we now?
R. Hicks;
Department of Nuclear Medicine and PET, Peter MacCallum Cancer Institute, Melbourne, AUSTRALIA.

801

CME 6 - Inflammation & Infection + Translational and Molecular Imaging Therapy + Radiopharmacy Committee: Molecular Imaging Technologies for Infectious Diseases

Monday, October 14, 2019, 11:30 - 13:00 Auditorium

OP-317
Imaging of Bacterial and Pathogen Infections, Infectious Disease Specialist's Point of View
M. Roestenberg;
Leiden University Medical Center, Department of Infectious diseases and parasitology, Leiden, NETHERLANDS.

OP-318
Imaging of Bacterial and Pathogen Infections, Nuclear Medicine's Point of View
M. Sathekge;
Steve Biko Academic Hospital, University of Pretoria, Department of Nuclear Medicine, Pretoria, SOUTH AFRICA.

OP-319
Novel Approaches to Image the Pathogen, Radiopharmacy's Point of View
C. Decristoforo;
Medical University Innsbruck, Department of Nuclear Medicine, Innsbruck, AUSTRIA.

802

Joint Symposium 11 - Neuroimaging Committee / ISCBFM: New Applications for Hybrid Brain PET/MRI

Monday, October 14, 2019, 11:30 - 13:00 Lecture Hall 311

OP-323
Brain PET/MRI - Where Are We Now?
H. Barthel;
University Hospital Leipzig, Nuclear Medicine, Leipzig, GERMANY.

OP-324
Brain PET/MRI for Neuromodulation
C. Sander;
Harvard Medical School, A. A. Martinos Center for Biomedical Imaging, Boston, MA, UNITED STATES OF AMERICA.

OP-325
Brain PET/MRI in Epilepsy
M. Koepp;
University College London, Institute of Neurology, London, UNITED KINGDOM.

OP-326
Quantification and Standardization in Brain PET/MRI
R. Boellaard;
Dept. of Radiology and Nuclear Medicine, Amsterdam University Medical Centres, location VUMC, Amsterdam, NETHERLANDS.

OP-327
Summary and General Discussion

803

EANM Symposium 12 - Physics Committee: Digital Detection in Clinical NM (PET & SPECT)

Monday, October 14, 2019, 11:30 - 13:00 Lecture Hall 312

OP-328
The Physics of SiPM PET Detection
M. Lubberink;
PET centre, Department of Radiology, Oncology and Radiation Science, Uppsala, SWEDEN.

OP-329
The Clinical Aspects of SiPM PET
T. Mognetti;
Centre Léon Bérard, Département de Médecine Nucléaire et de Radioprotection, Lyon, FRANCE.

OP-330
The Physics of Large FOV CZT Detection
L. Imbert;
Centre Hospitalier Universitaire de Nancy, service de médecine nucléaire, Nancy, FRANCE.

OP-331
The Clinical Aspects of Large FOV CZT
A. Verger;
Centre Hospitalier Universitaire de Nancy, service de médecine nucléaire, Nancy, FRANCE.

OP-332
The Clinical Aspects of Large FOV CZT
P. Declerck;
Clinique Saint-Jean, service de médecine nucléaire, Brussels, BELGIUM.

805

M2M - Parallel Session: PET Radiosynthesis

Monday, October 14, 2019, 11:30 - 12:45 Lecture Hall 111

OP-333

Pd catalyzed cross coupling of [^{11}C]MeLi and its application in the synthesis and evaluation of a potential tracer for vesicular acethylcholine transporter (VAChT)

H. Helbert[1,2], B. Wenzel[3], W. Deuther-Conrad[3], G. Luurtsema[1], W. Szymanski[1,2], P. Brust[3], B. Feringa[2], R. Dierckx[1], P. Elsinga[1]; [1]UMCG, Groningen, NETHERLANDS, [2]RUG, Groningen, NETHERLANDS, [3]Helmholtz-Zentrum Dresden-Rossendorf, Leipzig, GERMANY.

Aim/Introduction: The short half-life of ^{11}C ($t_{1/2}$ = 20.33 min) requires ultra-fast reactivity in order to perform efficient labelling of PET tracers. A recently discovered cross-coupling methodology[1] enables the coupling between aryl bromides and organolithium reagents within seconds and therefore can be an attractive strategy to access ^{11}C-labelled compounds. In this work several clinically relevant structures were labelled via this method. The scope of the reaction was further explored and expanded, allowing radiolabelling of highly reactive compounds, such as aldehydes. Then we focused our attention on the development of a new potential tracer for vesicular acetylcholine transporter (VAChT) which was enabled by this novel cross-coupling of [^{11}C]MeLi. **Materials and Methods:** [^{11}C]MeLi was prepared via lithium-halogen exchange by trapping [^{11}C]MeI in a solution of n-BuLi. The prepared [^{11}C]MeLi was further reacted in a Pd catalyzed cross-coupling reaction with aryl bromides at r.t. for 4 minutes. After quench and evaporation of the solvent - or cartridge purification when the reaction was done on a synthesis module - the mixture was directly purified by HPLC. A series of synthesized vesamicol derivatives were subjected to affinity studies. **Results:** Several clinically relevant structures with application in breast cancer imaging and early diagnosis of Alzheimer's disease had been successfully labelled and the procedure was later on automatized using a cassette based synthesis module. Employing this same methylation strategy, novel potential tracers for VAChT were synthesized and evaluated in vitro, identifying a compound with good selectivity for VAChT versus σ1 and σ2 receptors. **Conclusion:** A new labelling methodology was successfully applied to the synthesis of clinically interesting radiotracers, providing the purified target molecules in R.C.Y. ranging from 34% to 56% within 30 to 40 minutes (EOB). This procedure offers new opportunities in the development of novel tracers, illustrated by the synthesis of a novel VAChT tracer. **References:** [1]Heijnen D, Tosi F, Vila C, Stuart M, Elsinga P, Szymanski W, Feringa B. Angew. Chem. Int. Ed. **2017**, 56 (12), 3354-3359.

OP-334

Optimization of manufacturing process of [^{11}C]-DMDPA for phase II clinical study

S. Krajewski[1], L. Steczek[1], J. Ambroziak[1], J. Radłowska[1], P. Kaźmierczak[2], O. Shamni[3], S. Cohen[3], E. Mishani[3], J. Włostowska[1]; [1]Research & Development Centre, Synektik S.A., Warszawa, POLAND, [2]Faculty of Pharmacy, Medical University of Warsaw, Warszawa, POLAND, [3]Cyclotron/Radiochemistry/ MicroPET Unit, Hadassah Hebrew University Hospital, Hadassah Medical Organization, Jerusalem, ISRAEL.

Aim/Introduction: The potential of [^{11}C]dimethyldiphenyl-ammonium ([^{11}C]-DMDPA) as a PET-myocardial perfusion imaging (MPI) agent has already been demonstrated [1]. Phase I clinical study confirmed that single doses of [^{11}C]-DMDPA were safe and well tolerated by healthy male subjects when administered as a single IV bolus injection. Furthermore, [^{11}C]-DMDPA showed a low radiation exposure in human subjects, therefore it is a very good candidate for MPI. The aim of our study was to optimize the API synthesis process together with quality control methods for phase II clinical study. **Materials and Methods:** [^{11}C]-DMDPA was synthetized as previously described [1] using Eckert&Ziegler Modular-Lab Standard: [^{11}C] CO_2 was reduced to [^{11}C]CH_3I, activated to [^{11}C]CH_3OTf, reacted with methyldiphenylamine (MDPA) to give [^{11}C]-DMDPA and purified. The optimized synthesis parameters were: $LiAlH_4$ and MDPA concentration, reaction times, solvent and purification cartridge used. The obtained API solution was transferred to the Clio dispenser through initial sterilizing filter, where the product was formulated by addition of saline solution. The product was sterilized by a final filtration. The radiochemical and chemical purity were measured by HPLC using Waters XTerra Column. The following method parameters were optimized: gradient, flow and UV wave length to give reliable results in the shortest analysis time. The quality of manufactured [^{11}C]-DMDPA was confirmed by PET acquisitions carried out on male Wistar rats. **Results:** The most favorable synthesis conditions were: 0.1 M $LiAlH_4$ in THF with distillation time of 170 s, [^{11}C]CH_3OTf and MDPA reaction conducted without solvent for 180 s, using for purification one Waters CM short cartridge. The total radiosynthesis time was reduced to ≤ 25 min, [^{11}C]-DMDPA was obtained in activities up to 30 GBq, with radiochemical yield up to 63% (decay corrected). The product with highest radiochemical purity was achieved when dichloromethane was used as a solvent, while reaction in pure MDPA gave the highest yield with the purity not less than 95%. The most favorable HPLC analysis conditions were: 14.9 min gradient time with flow of 1.3 ml/min, using 210 nm for determination of DMDPA and MDPA concentrations. The validation parameters were: accuracy, intermediate precision, repeatability and linearity, which met acceptance criteria. The biodistribution results were in good agreement with those obtained by O. Jacobson et al. [1]. **Conclusion:** The synthesis parameters of [^{11}C]-DMDPA and HPLC method were optimized to ensure reproducible and convenient manufacturing process for phase II clinical study.

References: [1] O. Jacobson et al. Nuc. Med. Biol. **2013**, 40, 967-973.

OP-335

Selection Of The Optimal Macrocyclic Chelators For Labelling With ^{111}In And ^{68}Ga Improves Contrast Of Her2 Imaging Using Engineered Scaffold Protein Adapt6

J. Garousi[1], E. Witting[2], S. Lindbo[2], A. Vorobyeva[1], M. Altai[1], M. Oroujeni[1], B. Mitran[3], A. Orlova[3], S. Hober[4], V. Tolmachev[1];
[1]Department of Immunology, Genetics and Pathology, Uppsala University, Uppsala, SWEDEN, [2]Department of Protein Science, KTH Royal Institute of technology, Stockholm, SWEDEN, [3]Department of Medicinal Chemistry, Uppsala University, Uppsala, SWEDEN, [4]Department of Protein Science, KTH Royal Institute of technology, Uppsala, SWEDEN.

Aim/Introduction: Albumin-binding domain-derived affinity proteins (ADAPTs) are one of the smallest (5 kDa) non-immunoglobulin engineered scaffold proteins. These probes have been designed for imaging of therapeutic targets expressed in disseminated cancers for personalizing medicine. Previous optimization studies demonstrated that positioning of DOTA chelator at C-terminal of anti-HER2 $(HE)_3$DANS-ADAPT6-GSSC improves biodistribution properties for both ^{68}Ga and ^{111}In labels. The available data for other scaffold proteins suggested that selection of an optimal combination of radionuclide and chelator improves imaging sensitivity. The aim of this study was to evaluate the influence of the commonly used macrocyclic chelators on tumour-to-organ ratios and select the best variant of ADAPT6 labeled with ^{68}Ga and ^{111}In for PET and SPECT, respectively **Materials and Methods:** Recombinantly produced $(HE)_3$DANS-ADAPT6-GSSC was site specifically conjugated with maleimido derivatives of macrocyclic chelators DOTA, DOTAGA, NOTA and NODAGA. All labelled conjugates were purified using size-exclusion Nap-5 columns. In vitro specificity and cellular processing were studied using HER2-expressing SKOV-3 and BT474 cell lines. Female BALB/C nu/nu mice bearing SKOV-3 (1.6×10^6 receptors/cell) xenografts were used to evaluate biodistribution of the radioconjugates with ^{68}Ga at 3h and with ^{111}In at 3h and 24 h. Mice bearing HER2-negative Ramos xenografts were used for in vivo specificity evaluation. **Results:** LC-MS data confirmed the identity and purity of the constracts. The radiochemical purity of all conjugates were over 98%. No release of radioactivity was observed 3h after incubation with 500-molar excess of EDTA. In vitro, all probes bound specifically to HER2-expressing cells and internalization was slow. In vivo, all conjugates rapidly cleared from blood through the kidneys, but renal reabsorption was high. Significantly higher uptake of all conjugates ($p < 0.0005$) in HER2-expressing compared to HER2-negative xenografts demonstrated HER2-specificity. The analysis revealed that there was no significant difference between tumor uptakes of all variants. In the case of ^{68}Ga, NOTA and NODAGA conjugates cleared significantly ($p<0.05$) faster from blood and normal tissues than DOTA and DOTAGA conjugates. On the opposite, DOTA and DOTAGA conjugates cleared faster in the case of ^{111}In. Accordingly, tumor-to-organ ratios for conjugates with rapider clearance was higher. **Conclusion:** An optimal combination of ADAPT6 targeting agent, radionuclide and macrocyclic chelator increased the sensitivity of imaging. ^{68}Ga-ADAPT6-NODAGA provided the highest tumour-to-organ ratios for blood, muscles and major metastatic sites (lung, liver and bone). ^{111}In-ADAPT6-DOTA provided the highest tumour-to-organ ratios. This study provides evidences for correlation between labelling chemistry and imaging sensitivity. **References:** None.

OP-336

Fluorescein-based ^{18}F labeled probe for pre-targeted PET imaging of cancer cells

***H. Helbert[1,2]**, D. Samplonius[1], S. Blok[1], V. Böhmer[1,2], G. Luurtsema[1], R. Dierckx[1], B. Feringa[2], P. Elsinga[1], W. Helfrich[1], W. Szymanski[1,2];*
[1]UMCG, Groningen, NETHERLANDS, [2]RUG, Groningen, NETHERLANDS.

Aim/Introduction: Bispecific antibodies (BsAb) that at the same time contain binding sites for targets on cancer cells and for specific small molecules[1] offer the possibility for smart pre-targeting approach. In this approach, the antibody is first administered to the patient, and after some time (usually >24 h) the small molecules, modified with for example a short-lived radionuclide for PET imaging, is injected with the aim to visualize the tumor. The availability of BsAb with affinity for different tumors, yet the same small molecule, lends versatility to this approach. Specifically, fluorescein has emerged as the small molecule of choice[2] to bind to BsAb and therefore we aim for developing a tracer based on its core for imaging of various tumors. **Materials and Methods:** The synthesis of the precursor involves a modification of the fluorescein with the introducing an alkyne moiety. The [^{18}F]fluoro-azide compound was synthesized from its corresponding tosylate by [^{18}F]F$^-$. After HPLC-purification, the [^{18}F]fluoro-azide was used in a copper(I)-catalyzed alkyne-azide cycloaddition "click" reaction[3],[4],[5] with the modified fluorescein to afford the final radiotracer [^{18}F]TPF. The binding of [^{18}F]TPF to bispecific antibodies was then evaluated in vitro. **Results:** [^{18}F]TPF was synthesized in 2 steps from [^{18}F]F$^-$, the whole labeling procedure takes 2h affording [^{18}F]TPF in 37% RCY (d.c.). The compound was then formulated and was found to be stable in its formulated form as well as in human serum for several hours (>95% after 2h30). In vitro evaluation of the tracer shows significant specific binding with bispecific antibodies PD-L1/FITC (2.9%) and MCSP/FITC (3.3%) immobilized on agar beads. **Conclusion:** A novel tracer based on a fluorescein core was developed for pre-targeted PET imaging. The radiotracer was stable and could be easily synthesized via copper(I)-catalyzed click reaction. From in vitro assays, we obtained a proof of principle of its ability to bind to bispecific antibodies allowing specific imaging of various cancer cells with a single tracer. **References:** [1] R. E. Kontermann, U. Brinkmann Drug Discovery Today **2015**, 20 (7), 838-847 [2] B. Micheel, P. Jantscheff, V. Böttger, G. Scharte, G. Kaiser, P. Stolley and L. Karawaje Journal of Immunological Methods **1988**, 111, 89-94 [3] Huisgen, R., Angew. Chem. Int. Ed. **1963,** 75 (13), 565-598. [4] B. T. Worrell, J. A. Malik, V. V. Fokin Science, **2013**, 340, 6131, 457-460. [5] L. Mirfeizi, L. Campbell-Verduyn, R. A. Dierckx,

B. L. Feringa and P. H. Elsinga, Curr. Org. Chem. **2013**, 17, 2108-2118.

OP-337

Radiopharmacological Evaluation of Cyclohexanediamine-Triazole-Peptide Conjugates Labeled via the Al^{18}F-Approach

W. Sihver[1], *J. Böhme*[1,2], *M. Walther*[1], *R. Wodtke*[1], *F. Reissig*[1,3], *C. Mamat*[1], *C. Neuber*[1], *M. Ullrich*[1], *J. Pietzsch*[1,3], *H. Pietzsch*[1];
[1]*Helmholtz-Zentrum Dresden-Rossendorf, Dresden, GERMANY,* [2]*Ernst-Abbe-Hochschule Jena, University of Applied Sciences, Jena, GERMANY,* [3]*Technische Universität Dresden, Faculty of Chemistry and Food Chemistry, Dresden, GERMANY.*

Aim/Introduction: The Al^{18}F-labeling method is as modern technique an alternative to conventional ^{18}F-labeling procedures that allows radiofluorination of biomolecules such as peptides and proteins in a one-step procedure in aqueous solution [1]. In search for versatile applicable chelators, which allow stable binding of both ^{18}F and radiometals such as ^{68}Ga or ^{111}In, a cyclohexanediamine-triazole-chelator was designed. This chelator was conjugated via copper-catalyzed azide-alkyne cycloaddition (CuAAC) to the well-known binding motif (glutamate-urea-lysine) of the prostate-specific membrane antigen (PSMA) [2-5] complemented by 2-azidoacetyl moiety as linker unit (ligand L1). Furthermore, ligand L2 was synthesized bearing a 6-azidohexanoyl moiety as linker to investigate the influence of the linker on the stability of final ^{18}F or radiometal complex. The aim of this study was to investigate the radiopharmacological potential of L1 and L2 after radiolabeling regarding binding properties, cell internalization, and in vivo behavior in a murine prostate cancer model. **Materials and Methods:** For the in vitro assays PSMA-positive LNCaP cells were used. The incubation with the respective radiolabeled ligand (RCY>95%) was terminated via a cell harvester. Internalization experiments were carried out by the "acid wash" method. In vivo studies (biodistribution and small animal PET) were performed with mice bearing a prostate tumor. **Results:** In competition assays versus [^{177}Lu]Lu-PSMA-617 ("gold standard"), the affinity of non-labeled L1 and L2 was slightly lower than that of PSMA-617. Saturation analysis of [^{68}Ga]Ga-L1, [^{111}In]In-L1, and [^{18}F]F-L1 binding on LNCaP homogenate was comparable to [^{18}F]F-L2 binding. The obtained K_d values were in a range of 20 to 30 nM. Internalization experiments with LNCaP cells revealed a lower uptake of the differently labeled L1 and L2 conjugates compared to [^{64}Cu]Cu-PSMA-617. Furthermore, in vivo behavior of both [^{18}F]F-L1 and [^{18}F]F-L2 was investigated in prostate carcinoma bearing mice by biodistribution experiments and small animal PET imaging. Thereby, PSMA dependent tumor uptake could be observed. **Conclusion:** After successful radiolabeling, the conjugates L1 and L2 showed promising binding properties towards PSMA. The chelator presented here offers a flexible platform for radiolabeling of peptides or proteins for various PET and SPECT applications. **References:** [1] F. Cleeren, Bioconjugate Chem. 2016, 27, 790. [2] K. Kopka, J. Nucl. Med. 2017, 58,17S. [3] H.R. Kulkarni, Br. J. Radiol. 2018, 91, 20180308. [4] Y. Tolkach, Breast Cancer Res.Treat. 2018, 169, 447. [5] M.C. Haffner, Hum. Pathol. 2009, 40, 1754.

OP-338

In vivo evaluation of [^{18}F]-5-fluoroaminosuberic acid ([^{18}F]FASu) isomers as PET imaging agents for different cancer types

M. Colovic[1,2], *H. Yang*[1], *H. Merkens*[2], *N. Colpo*[2], *F. Benard*[2,3], *P. Schaffer*[1,3,4];
[1]*TRIUMF, Vancouver, BC, CANADA,* [2]*BC Cancer Research Centre, Vancouver, BC, CANADA,* [3]*Department of Radiology, University of British Columbia, Vancouver, BC, CANADA,* [4]*Department of Chemistry, Simon Fraser University, Burnaby, BC, CANADA.*

Aim/Introduction: 5-[^{18}F]fluoroaminosuberic acid ([^{18}F]FASu) is a novel positron emission tomography (PET) tracer, which exhibits uptake specific to system x_c^-, and has shown favourable tumor uptake in lymphoma, ovarian and breast cancer xenografts in mice. With two optically active centres (positions 2- and 5-), [^{18}F]FASu synthesis by the commonly used Kryptofix 2.2.2/K_2CO_3-facilitated fluorination method results in four diastereomers. We recently reported the synthesis of the optically pure 2S-[^{18}F]FASu from chiral precursors and found that this isomer is preferentially taken up by tumour cells, when compared to 2R-[^{18}F]FASu. The aim of this study was to compare the 5-position diastereomers to the racemic (2S,5R/S-) mixture as PET agents in three different tumour models. **Materials and Methods:** Cell uptake, biodistribution and PET imaging in mice bearing glioblastoma (U-87), breast (MDA-MB-231) and prostate (PC-3) cancer xenografts were carried out using the 5-position diastereomers and the 2S,5R/S- racemic mixture. In vivo imaging studies were performed on a Siemens Inveon μPET/CT scanner at 2h post-injection (p.i.) on animals inoculated with MDA-MB-231 tumours, and at 1h p.i. on U-87 and PC-3 tumour-bearing mice. **Results:** We successfully visualised the xenografts with all three tracer conformations. Quantitatively, the 5-position racemic mixture (2S,5R/S-) displayed similar image contrast compared to the 5-position diastereomers. The 2S,5S-[^{18}F]FASu conformation had clearer delineation of U-87 and PC-3 xenografts. Tumour uptake of the isomers was blocked with coinjection of the cold standard, aminosuberic acid (ASu), confirming target specificity. Biodistribution data indicated that PC-3 tumours had the highest tracer uptake and tumour-to-background ratios. Accumulation (%ID/g) of 2S,5R/S-, 2S,5S- and 2S,5R-isomers in the tumours were 9.19±1.14, 8.00±1.41, and 7.16±2.13 at 1h p.i. Two-way ANOVA/Tukey's multiple comparisons test yielded adjusted p values of 0.8141 and 0.5459 for 2S,5R/S- v. 2S,5S- and 2S,5R/S- v. 2S,5R- isomer comparisons respectively, and 0.8992 for the tumour uptake comparison between 2S,5S- and 2S,5R-enantiomers. The corresponding tumour-to-muscle ratios were 33.68±9.52, 31.42±4.54, and 25.33±4.97, respectively. One-way ANOVA test showed no statistically significant differences between the groups (p value = 0.1701). MDA-MB-231 tumours had the lowest uptake, at

1.13±0.12 %ID/g in the case of 2S,5S-[^{18}F]FASu and 1.25±0.67 %ID/g in the case of 2S,5R-[^{18}F]FASu, at 2h p.i. **Conclusion:** We found that in the case of [^{18}F]FASu, chirality at the 5- position does not greatly affect tracer biodistribution or tumour uptake in all three tumour models studied. Furthermore, this work shows potential utility of [^{18}F]FASu for detection of glioblastoma and prostate cancer. **References:** None.

806

Do.MoRe - Parallel Session: Clinical Dosimetry and Modeling

Monday, October 14, 2019, 11:30 - 12:45 Lecture Hall 112

OP-339

Influence of affinity and total ligand amounts on pharmacokinetics and absorbed doses of PSMA-specific ligands: A simulation study

N. Begum[1], *G. Glatting*[1], *M. Eiber*[2], *A. Beer*[1], *P. Kletting*[1];
[1]*Ulm University, Ulm, GERMANY,* [2]*Technical University of Munich, Munich, GERMANY.*

Aim/Introduction: For theranostic approaches ligands that can be used for both diagnostics and therapy are developed. However, it is unclear whether ligands optimized for imaging are also ideal candidates for radionuclide therapy, because of different target values (activity concentrations vs absorbed doses) and different administered ligand amounts. Therefore, the aim was to investigate the effect of affinity and injected amount of prostate-specific membrane antigen (PSMA)-specific ligands on the activity concentrations for imaging and the absorbed doses for therapy. **Materials and Methods:** In this study, a recently published whole-body physiologically based pharmacokinetic (PBPK) model for PSMA-specific ligands was implemented in Simbiology/MATLAB and was used for simulations based on 13 virtual patients. The affinity is described by the dissociation constant KD=koff/kon. Therefore, simulations with metastatic castration-resistant prostate cancer (mCRPC) were conducted for KD of 0.01-10 nM and molar amounts of 1-1000 nmol. The normalized activity concentration after injection (68Ga-PSMA at 1 h and 18F-PSMA at 2 h) for imaging and the absorbed doses (177Lu-PSMA activity: (7.3±0.3) GBq) for therapy were calculated for tumour, background and organs at risk (OARs). **Results:** Imaging shows similar concentrations in tumours for KD of 0.1-1 nM and for amounts of 1-32 nmol. A KD=0.01 nM only leads to the highest uptake if the amount of substance is optimized. The activity concentration 2 h after injection of the 18F-PSMA simulations results in significantly higher values compared to 68Ga-PSMA (e.g. by a factor of 1.3±0.1, using an amount of 10 nmol, a typically administered amount for imaging). In therapy, the reduction of KD led to a significant increase in the absorbed dose in tumours. Using an amount of 100 nmol, a typically administered amount for therapy, relative to KD=10 nM, the absorbed doses increased by factors of 4±1, 7±5 and 10±8 for KD of 1, 0.1, and 0.01 nM, respectively. Favourable tumour-to-kidney ratios could be obtained for all KD when choosing the optimal amount. **Conclusion:** For imaging with the commonly used amount of 1-10 nmol, a significant improvement in tumour uptake is achieved with an increase in affinity only with a KD 1-0.1 nM compared to KD=10 nM. A measurement at 2 h p.i (18F-PSMA) is advantageous. For therapy, the increase in affinity has a large influence on absorbed doses in tissues with high perfusion. Therefore, especially for ligands with high affinity, both, the given amount and activity must be optimized to achieve the maximum tumour-to-kidney ratio **References:** None.

OP-340

Image quality of a ^{90}Y pretreatment procedure for radioembolisation

B. Kunnen, *M. M. A. Dietze, A. J. A. T. Braat, M. G. E. H. Lam, M. A. Viergever, H. W. A. M. de Jong;*
UMC Utrecht, Utrecht, NETHERLANDS.

Aim/Introduction: Prior to ^{90}Y radioembolisation, 150 MBq of ^{99m}Tc-magroaggregated albumin (MAA) is administered to simulate the distribution of ^{90}Y-loaded microspheres. This pretreatment procedure is performed to estimate the lung shunt fraction (LSF), to detect potential extrahepatic depositions, and to quantify the liver parenchymal dose. The accuracy of the pretreatment scan is currently limited, since the MAA particles and microspheres behave differently. Ideally, ^{90}Y microspheres would also be used for the pretreatment procedure, but making such use inherently safe would limit activity to about 100 MBq[1], which makes imaging challenging. Safe estimation of ^{90}Y-based LSF has been suggested to be feasible.[1] This study investigates if it is also possible to accurately detect extrahepatic depositions and quantify liver parenchymal dose for low activity ^{90}Y pretreatment scans. **Materials and Methods:** An anthropomorphic thorax phantom with three extrahepatic depositions (2.0, 4.2 and 8.2 mL) was filled with ^{90}Y chloride to acquire an LSF of 5.3% and a tumour to non-tumour ratio (T/N) of 7.9. PET/CT (Siemens Biograph mCT) and SPECT/CT (Siemens Symbia T16) images were acquired at 2.0 GBq (typical treatment dosage) and 100 MBq (theoretically safe pretreatment dosage). The LSF, T/N, and liver parenchymal dose were measured. In addition, a radioembolisation patient (3.1 GBq injected activity at time of imaging) received posttreatment PET/CT and SPECT/CT and was additionally scanned with short acquisition times to simulate 100 MBq ^{90}Y pretreatment scans. All SPECT scans were reconstructed with in-house Monte Carlo-based reconstruction software and PET scans were reconstructed using clinical software. **Results:** At a pretreatment activity of 100 MBq ^{90}Y, PET/CT overestimated LSF (+10 pp), underestimated liver parenchymal dose (-3 Gy/GBq), and could not detect extrahepatic depositions. SPECT/CT could detect all three extrahepatic depositions and was as

accurate for the low as the high activity scan in estimating LSF (-0.7 pp at 100 MBq, -0.2 pp at 2.0 GBq), and liver parenchymal dose (-0.3 Gy/GBq at 100 MBq, +0.2 Gy/GBq at 2.0 GBq). The simulated pretreatment PET/CT patient scan was very noisy and was not representative for the high activity posttreatment scan. The simulated pretreatment SPECT/CT patient scan showed comparable activity distribution as compared to the high activity posttreatment scan. **Conclusion:** The reconstructions of a 100 MBq ^{90}Y pretreatment procedure are representative of a high activity posttreatment ^{90}Y scan when acquired with quantitative SPECT/CT. **References:** 1.Kunnen et al. Radioembolization lung shunt estimation based on a ^{90}Y pretreatment procedure: a phantom study Med Phys. 2018; 45(10):4744-4753.

OP-341

TOF-PET/CT enables valuable EUD estimations in heterogeneous ^{90}Y distributions

M. Hesse, S. Walrand, F. Jamar, R. Lhommel;
Cliniques Universitaires Saint-Luc, Brussels, BELGIUM.

Aim/Introduction: Several studies have shown the superior quality of TOF-PET/CT for ^{90}Y imaging, providing better evaluation of the absorbed dose distribution in the tissues and improving dose-response analyses. We recently unified the patient dose-response relationship for resin and glass ^{90}Y microspheres by using the Jones-Hoban equivalent uniform dose (EUD) derived from the PET/CT imaging and assuming a radio-sensitivity α of 0.036 Gy^{-1}. The aim of this study is to evaluate the accuracy of this PET based EUD estimation in known heterogeneous activity distributions. **Materials and Methods:** A hot rod insert (diameters: 4.8, 6.4, 7.9, 9.5, 11.1, 12.7 mm) placed at the bottom of a cylindrical Jaszczak phantom set in the vertical position was imaged on a 590ps TOF-PET. A typical patient attenuation was reached by adding a 13cm-thick attenuating support under the phantom. A two bed 20min/position acquisition was performed after pouring a 3GBq ^{90}Y - 300ml DTPA water solution into the phantom, resulting in a 115 Gy mean absorbed dose in the 6 sectors. The acquisition was repeated after adding 300ml DTPA water solution reducing the mean absorbed dose to 57 Gy. These doses are typical values used as response threshold for glass and resin spheres, respectively. The PET spatial resolution was modeled and the EUDs were computed using a ^{90}Y dose kernel. True EUDs were computed from the phantom drawing using a radio-sensitivity extracted from EBRT in vivo studies (1). **Results:** All rods larger than 7 and 6 mm were visible for the 57 and 115 Gy setups, respectively. Using the same 0.036 Gy^{-1} α value, a good agreement (deviation < 8%) was found for both setups between the PET based EUDs data and the true values for rod diameters larger than 9 mm. Such heterogeneity scales are typically observed in biopsies post ^{90}Y liver radio-embolization. EUD overestimation of about 30% was observed for the smaller rod sectors. **Conclusion:** This study confirms the PET ability to image heterogeneous ^{90}Y distribution allowing an accurate EUD estimation. This explains the good patient dose-response obtained previously for both microspheres types. Moreover TOF-PET/CT based EUD formalism is the preferred dosimetric technique as it takes into account distribution heterogeneities due to variable microspheres activities tuned by decay and to differences in tumor vascularization. **References:** (1) Tai A, Erickson B, Khater KA, Allen X. Estimate of radiobiologic parameters fromclinical data for biologicallybased treatment planning for liver irradiation. IntJRadiatOncol Biol Phys (2008) 70:900-7. doi:10.1016/j.ijrobp.2007.10.037.

OP-342

Personalized dosimetry for liver cancer radioembolization using computational fluid dynamics

***E. Roncali**, A. Taebi, M. Rusnak, B. Spencer, D. Caudle, C. Foster, C. T. Vu;*
University of California, Davis, CA, UNITED STATES OF AMERICA.

Aim/Introduction: Yttrium-90 (Y-90) transarterial radioembolization (TARE) uses radioactive microspheres injected into the hepatic artery to deliver internal radiation therapy to liver tumors. One of the major challenges in making TARE more effective is the lack of reliable dosimetry methods for dose prediction and dose verification. We present a patient-specific dosimetry approach for personalized treatment planning based on computational fluid dynamics (CFD) simulations of the microsphere transport combined with Y-90 physics. **Materials and Methods:** We developed a three-step CFD dosimetry tool based on the individual patient Cone-beam CT (CBCT) angiograms performed in standard-of-care radioembolization planning: (1) segment the hepatic arterial tree from the patient CBCT, (2) predict the microsphere distribution using CFD with boundary conditions, (3) calculate the absorbed dose based on the microsphere distribution with Y-90 physics modeling. The hepatic arterial tree was segmented for 2 patients from CBCT images acquired during treatment planning with an Artis Zeego (Siemens Healthineers). The microsphere transport was predicted using multiscale CFD modeling [1]. The predicted microsphere distribution was convolved with a Y-90 dose kernel computed with GATE [2] to calculate the dose distribution. These patients were enrolled in pilot study for which they received an additional positron emission tomography (PET) scan after radioembolization to image the Y-90 distribution. **Results:** The CBCT angiograms of two subjects were used to segment the hepatic arterial tree. The segmented structures included one inlet at the CHA, and 23 and 46 outlets for subject 1 and 2. The smallest detected outlet diameter was ~0.5 mm, indicating the ability of our method to segment small vessels. The vessels feeding the tumors, the liver Couinaud segments, and the injection points were identified using the CBCT images and the 2D digital subtraction angiograms (DSA) acquired during the planning. Here the microsphere transport was assumed to follow that of the blood, which allowed us to calculate a distribution of the spheres at the outlets and calculate the subsequent dose distributions. We qualitatively compared the predicted dose with the Y-90 PET images acquired 2h after the microsphere delivery. **Conclusion:**

We demonstrate the feasibility of developing a complete framework for personalized Y-90 microsphere simulation and dosimetry, using patient-specific input parameters. **References:** 1. Westerhof, N., J.W. Lankhaar, and B.E. Westerhof, The arterial Windkessel. Med Biol Eng Comput, 2009. **47**(2): p. 131-41. 2. Jan, S., Ongoing developments in GATE and what to expect in upcoming versions, in IEEE NSS/MIC, Gate User Meeting. 2015: San Diego, USA.

OP-343

Improving resolution recovery factors using 3D printed phantoms and Monte Carlo for quantitative imaging and dosimetry

J. Gear, F. Leek, G. Flux;
Royal Marsden NHSFT, Sutton, UNITED KINGDOM.

Aim/Introduction: Accurate absorbed dose calculations require recovery factors applied post-reconstruction to correct for partial volume effects. The IEC PET phantom is widely available with insert diameters ranging from 10 to 37mm, which whilst appropriate for PET are too small to fully characterise the recovery curve of SPECT isotopes such as Lu-177 or I-131. The aim of the study was to improve characterisation of the recovery curve and reduce standard uncertainty in recovery factors by complimenting the IEC phantom images with those using 3D printed inserts and Monte Carlo derived images. **Materials and Methods:** Nine 3D-printed spheres with internal diameters of 8 to 65mm where designed and manufactured using a Connex photopolymer 3D printer. An adapted lid for the IEC phantom was manufactured to mount the spheres. Inserts were filled with Lu-177, I-131 and Tc-99m. Images were acquired on a Siemens Symbia SPECT/CT system equipped with the appropriate collimator. A SIMIND Monte Carlo simulation was also performed of the SPECT/CT system with a cylindrical phantom containing spherical inserts of diameter 10 - 80mm. All real and simulated SPECT images were quantitatively reconstructed using an OSEM algorithm using attenuation and scatter correction but without collimator detector response. VOIs matching the known insert volume were drawn over the reconstructed images and the recovery coefficient taken as the ratio of the mean activity concentration measured in the VOI to the known concentration. **Results:** With the additional images the recovery curve could be properly characterised up to volumes of 300ml, compared to only 26ml for the standard inserts. Recovery curves, fitting parameters and associated uncertainties for the different datasets were generated according to EANM guidelines. The standard uncertainty in fit parameters was reduced by 15% and 20% when 3D printed and Monte Carlo derived datasets were included. For a Lu-177 lesion of volume of 150ml the calculated recovery factor varied from 0.81 to 0.74 when the additional datasets were included. **Conclusion:** The ability to extend the recovery curve data beyond the insert volumes within the IEC phantom is essential for accurate image quantification and dosimetry. 3D printed inserts are a useful and cost effective tool for achieving this. Monte Carlo simulations enable characterisation of volumes beyond that practically measurable and enables scope to extend this work for different shaped inserts with varying lesion to background concentration ratios. These phantoms have been used for quantification in the SOLLID and MEDIRAD clinical trials. **References:** None.

OP-344

Quantification of the Trabecular Bone Volume Fraction with Dual Energy Quantitative CT to Calculate Patient-Specific Radionuclide S Values for Bone Marrow Dosimetry

M. Salas Ramírez, J. Tran-Gia, U. Gbureck, A. Kosmala, M. Lassmann;
University of Würzburg, Würzburg, GERMANY.

Aim/Introduction: The correlation between bone marrow toxicity and absorbed dose in radionuclide therapies is still not well defined. Improvements of the techniques for patient-specific skeletal dosimetry have led to the development of increasingly realistic 3-dimensional geometry models for Monte-Carlo simulation of radiation transport. These models require as inputs marrow cellularity (obtained by MR imaging) and trabecular bone volume fraction (TBVF) in the patient bone marrow to calculate patient-specific radionuclide S values for bone marrow dosimetry. Therefore, the aim of this study was to validate a phantomless post-reconstruction quantification method which enables the calculation of TBVF for bone marrow dosimetry in molecular radiotherapy based on dual energy quantitative computed tomography (DEQCT). **Materials and Methods:** First, a phantomless post-reconstruction DEQCT method based on x-ray beam profile and detector sensitivity function was implemented for a dual source computed tomography (DSCT) system and a SPECT/CT. The method was validated in a homemade phantom composed of five 50-ml vials; three of them contained hydroxyapatite (HA) in different concentration in a water equivalent medium, the last two contained a mix of agar, paraffin (fat) and hydroxyapatite (HA). Additionally, the European Spine Phantom (ESP) was used to simulate the vertebral geometry. Bone mineral content (BMC) of each phantom vertebra and bone mineral density (BMD) in the spongiosa region of each phantom vertebra were measured with the DEQCT method and dual-energy x-ray absorptiometry (DEXA). Furthermore, the BMC was measured in lumbar vertebrae 1 (LV_1) and 2 (LV_2) of a patient using DEQCT and DEXA. Lastly, the TBVF was quantified in the spongiosa region of each vertebra. **Results:** Measured values of HA volume fraction and nominal values in the homemade phantom showed good correlation (maximum error: 14.2%). Quantification of BMC (whole vertebra) and BMD (spongiosa) in the ESP showed a good agreement between measured values and nominal values (relative error [0.69%, 7.45%] for $BMC_{SPECT/CT}$, [1.10%, 7.71%] for BMC_{DSCT}, [5.44%, 31.96%] for $BMD_{SPECT/CT}$, and [10.0%, 59.38%] for BMD_{DSCT}). Quantification of BMC in the patient vertebrae showed relative errors of 7.61% (LV_1) and -8.39% (LV_2) between DEXA and DSCT. The TBVF values were 0.071 (LV_1) and 0.072 (LV_2). **Conclusion:** Our study shows that DEQCT using a commercial hybrid SPECT/

CT system enables the quantification of TBVF in a clinical setting. However, this method is sensitive to the image reconstruction kernel and the chemical description of the reference material and requires a good characterization of the x-ray beam and detector. **References:** None.

OP-345

Towards a Patient-Specific Kidney Dosimetry in Radionuclide Therapy

J. Tran-Gia, H. Neumayer, M. Lassmann;
University of Würzburg, Würzburg, GERMANY.

Aim/Introduction: SPECT/CT-based quantification of sub-organ activities is one of the major challenges in radionuclide therapies. The aim of this study was to fabricate a patient-specific two-compartment kidney phantom (medulla and cortex) and validate it with a post-therapy SPECT/CT of the same patient (Lu-177-DOTATATE). **Materials and Methods:** To enable a good differentiation of cortex and medulla, but also a validation of the resulting activity distribution, a patient for whom a venous-phase contrast-enhanced full-dose CT as well as a post-therapy SPECT/CT acquisition were available, was selected. Segmentation of the kidney was performed in 3D Slicer [1]: First, a 3D volume around the right kidney was cropped out of both CTs, and the full-dose CT was co-registered to the low-dose CT (affine registration). Next, medulla and cortex were separately segmentated based on the co-registered venous-phase CT and exported as STL-files. Further modelling of the kidney phantom was performed in Autodesk Netfabb 2019: After generating shells from both segmentations (shell thickness: 1mm), filling tubes and attachment rods were inserted. The cortex was split into two separate shells for separate printing. A stereolithography 3D printer (Form 2, Formlabs) was used for manufacturing the phantom. After 3D printing (resin: Clear V4), the three parts were processed as suggested by the manufacturer. After agglutination using a two-compoment adhesive, plastic threads were glued into the filling tubes (M4) and the attachment rod (M6). Finally, the entire phantom was clear coated. A Lu-177 SPECT/CT acquisition was performed (phantom mounted in Jaszczak cylinder, activity concentration ratio of 5:1 [cortex:medulla]). The total kidney activity of 62.6 MBq was based on the patient data. Acquisition parameters were the same for patient and phantom. **Results:** The venous-phase contrast-enhanced CT image considerably facilitated the differentiation of cortex and medulla. Although, in general, a good visual match between the SPECT reconstructions of patient and re-printed kidney was achieved, minor differences were found in the cortex-medulla border region. This could potentially be improved by varying the cortex-medulla activity concentration ratio. As many Lu-177-labelled radiopharmaceuticals are accumulating in large parts in the renal tubules in this border region, a three-compartment model (cortex, medulla, intermediate tubules region) would further improve the image quantification. **Conclusion:** Additional imaging information such as contrast-enhanced CT or dedicated MRI techniques should be exploited for prototyping nuclear medicine phantoms. This represents a major step towards a quantification of sub-organ activity distributions which could, eventually, facilitate reliable absorbed dose calculations for radionuclide therapies. **References:** [1] Thomas;PhysMedBiol;2016;61(22).

807

Pitfalls & Artefacts 4 - Interactive Clinical Cases - Oncology & Theranostics Committee: PSMA Imaging

Monday, October 14, 2019, 11:30 - 13:00 Lecture Hall 113

OP-346

Common Pitfalls of ^{68}Ga-PSMA 11

C. Artigas;
Ist Bordet, Nuclear Medicine, Brussels, BELGIUM.

OP-347

Un-usual Findings and Pitfalls of Different PSMA Compounds

F. Ceci;
University of Turin, Nuclear Medicine, Torino, ITALY.

OP-348

Pitfalls and Variants of ^{68}Ga-PSMA 11 in CRPC - Implications for RLT

W. Fendler;
University of Essen, Nuclear Medicine, Essen, GERMANY.

808

Clinical Oncology - Featured Session: Implementing Radiomics into Technical Practice

Monday, October 14, 2019, 11:30 - 13:00 Lecture Hall 114

OP-349

Scenarios and Challenges in Clinical Implementation of Radiomics

D. Visvikis;
INSERM UMR1101, LaTIM, CHRU Morvan, Bat 1, et 1, Brest, FRANCE.

OP-350

Extraction of histogram and texture features from parametric ^{18}F-FET PET images for molecular-genetic and histologic differentiation of gliomas

L. Kaiser[1], M. Grosch[2], S. A. Ahmadi[2], M. Unterrainer[1], A. Holzgreve[1], E. Mille[1], A. Gosewisch[1], J. Brosch[1], B. Suchorska[3], N. Navab[4], J. C.

Tonn[3], S. Ziegler[1], P. Bartenstein[1], N. L. Albert[1], G. Böning[1];
[1]Department of Nuclear Medicine, University Hospital, LMU Munich, Munich, GERMANY, [2]German Center for Vertigo and Balance Disorders, University Hospital, LMU Munich, Munich, GERMANY, [3]Department of Neurosurgery, University Hospital, LMU Munich, Munich, GERMANY, [4]TUM Department of Informatics, Technical University of Munich, Munich, GERMANY.

Aim/Introduction: Besides an improvement of PET instrumentation or radiopharmaceutical properties, current research is focussed on various methods aiming to enhance image read-out. For glioma classification, static and kinetic parameters extracted from dynamic ^{18}F-FET PET data have proven to be clinically relevant. In this study, histogram and texture radiomic features were derived from the respective parametric images calculated on a voxel basis. **Materials and Methods:** 322 patients with a newly diagnosed glioma were included: 128 IDH-Mutant, 194 IDH-wildtype (IDHmut/wt); 91 low-, 231 high-grade gliomas (LGG/ HGG). Glioma volumes-of-interest (VOI) were segmented with the clinically established 1.6 x background threshold, whereby a crescent shaped VOI on the contralateral side served as background VOI. Subsequent histogram and texture analysis was performed using the following parametric images: tumour-to-background ratios ($TBR_{5\text{-}15}$, $TBR_{5\text{-}20}$, $TBR_{10\text{-}30}$, $TBR_{20\text{-}40}$), late slope ($Slope_{15\text{-}40}$), time-to-peak (TTP), distribution volume ratio (DVR) from Logan-reference tissue model, and net influx rate K_i/V'_T from Patlak-reference tissue model. For each parametric image a total of 94 radiomic features was extracted. Univariate and multivariate ROC-analyses using logistic regression were performed with 5-fold cross-validation with stratified folds, aiming to identify IDHwt or HGG gliomas. **Results:** The highest area-under the ROC curve (AUC) averaged over 5 folds was obtained for features derived from early static $TBR_{5\text{-}15}$ images and the related parametric images TTP, $Slope_{15\text{-}40}$, and K_i/V'_T (a). Parameters derived from the highly correlated $TBR_{20\text{-}40}$ and DVR images tended to yield lower AUC values (b). For the first parameter category (a) the highest univariate AUC values (>0.79) were obtained with simple first order statistics such as mean, median, percentage volume histograms (PVH), and percentiles. In contrast to this, the features with the highest AUCs within the second parameter group (b) comprised more elaborate texture features, which still yielded only moderate AUCs (<0.77). Multivariate analysis based on simple mean values from each parametric image yielded an AUC of 0.86 for the identification of IDHwt gliomas and 0.80 for the identification of HGG. Inclusion of the remaining features provided only a moderate improvement (IDHwt 0.87; HGG 0.83). **Conclusion:** Although texture features allow for an improved classification of gliomas in case of $TBR_{20\text{-}40}$ and DVR as opposed to mean values, an incorporation of first order parameters describing ^{18}F-FET kinetics is highly recommended. Besides multi-parametric information, a further incorporation of information from other imaging modalities might be of interest for future studies aiming to provide an elaborate description of the tumour microenvironment. **References:** None.

OP-351

18F-FDG PET/CT radiomic predictors of molecular markers expression in oral cavity squamous cell carcinoma

***Y. G. Abdelhafez[1,2]**, Y. Dou[1], L. Nardo[1], T. Yen[3], C. Liao[3], A. J. Chaudhari[1];*
[1]University of California Davis, Sacramento, CA, UNITED STATES OF AMERICA, [2]South Egypt cancer Institute, Assiut University, Assiut, EGYPT, [3]Chang Gung Memorial Hospital and Unviersity, Linkou, TAIWAN.

Aim/Introduction: To evaluate the association between radiomic features extracted from pre-operative 18F-FDG PET/CT in patients with advanced stage oral cavity squamous cell carcinoma (OCSCC) and pathological molecular markers expression. **Materials and Methods:** The study retrospectively included 99 patients with advanced stage OCSCC (pathologic TNM stage III=26, IV=73; 93 males, 6 females; median age 49 years, range: 29-89). All patients had biopsy-proven SCC of oral cavity, locally- or loco-regionally advanced disease with no distant metastasis (M0), and a staging 18F-FDG PET/CT scan. Patients were treated with surgical resection of the primary tumor followed by adjuvant chemo(radio)therapy. The maximum pathologic axial tumor size was 33±17 mm. Primary tumor from PET images was segmented using absolute isocontour threshold of 40% of the maximum standard uptake value (SUV). Using TextIriX, a texture analysis plugin developed for OsiriX by our group, a total of 78 radiomic features (including shape by graphics algorithms, first order, and texture features) were extracted. SUVs within the segmented volume were normalized between the minimum and maximum values, then discretized into 64-bins to construct the grey-level matrices. No spatial resampling was used. Receiver operating characteristics (ROC) curves and area under the curve (AUC) of the extracted features were plotted against molecular markers status of the primary tumor including TP53, EGFR, BRAF, PIK3CA, FGFR3 and HRAS. **Results:** Small-area low gray-level emphasis was associated with TP53 expression (n=63/99) with AUC of 0.63 (95% confidence interval [95%CI] 0.52-0.74); p=0.03. The following radiomic features were significantly associated with EGFR expression (n=6/99): maximum 2D (AUC:0.78, 95%CI:0.66-0.90; p=0.02) & 3D diameters, major & minor axis length, mesh & voxel volumes, surface area, and run-length non-uniformity, size-zone non-uniformity, and dependence non-uniformity. Axis length (AUC:0.72, 95%CI:0.57-0.87; p=0.03), gray-level non-uniformity dependence non-uniformity, size-zone non-uniformity, run-length non-uniformity, mesh & voxel volumes, and surface area were significantly associated with BRAF expression (n=9/99). Both large-dependence (AUC:0.73, 95%CI:0.61-0.85; p=0.002) and large-area low-gray-level emphasis were significantly associated with PIK3CA expression (n=80/99). Kurtosis was marginally associated with FGFR3 expression. No features were predictive of HRAS status. **Conclusion:** Radiomic features, extracted from pre-operative 18F-FDG PET/CT images of the primary tumor of advanced stage OCSCC patients, are associated with the expression of some important molecular markers including TP53, EGFR, BRAF and PIK3CA. **References:** None.

OP-352

Baseline FDG-PET/CT Radiomics to Predict Outcome in Lung Cancer Patients Treated with Surgery

M. Kirienko[1], *L. Cozzi*[1], *L. Antunovic*[2], *E. Voulaz*[3], *A. Chiti*[3], *M. Sollini*[1];
[1]*Humanitas University, Milan, ITALY,* [2]*Humanitas Clinical and Research Center - IRCCS, Rozzano (Milan), ITALY,* [3]*Humanitas University, Humanitas Clinical and Research Center - IRCCS, Milan, ITALY.*

Aim/Introduction: The study aimed to identify a radiomic signature (from FDG-PET and/or CT) capable of predicting disease-free and overall survival (DFS and OS) in non-small cell lung cancer (NSCLC) patients undergoing surgery. **Materials and Methods:** This was an update of a retrospective single-center study. Inclusion criteria: patients with a pathological diagnosis of NSCLC, surgically treated between 01/01/2011 and 30/11/2016 in our institution, and availability of baseline FDG-PET/CT. Exclusion criteria: age <18 years. A cohort of 259 patients (M:F=177:82, mean age 70±8.4 years) was selected. Then, we randomly assigned the patients to a training and a validation group. Lung lesions were semi-automatically segmented on PET images applying a 40% of SUVmax threshold using a commercial software (PET VCAR, General Electric). Textural features from both CT and PET were calculated using LifeX (www.lifexsoft.org, [1]) and used as predictors. R platform was used for statistical analysis. Kaplan-Meier analysis was used to test the ability of the models to stratify patients with different outcomes. Covariables significant at univariate analysis were fed into a multivariate Cox proportional hazard regression model that was used to predict DFS and OS. Cox-Snell residuals were used to verify the goodness of the Cox model. **Results:** One hundred thirty patients experienced relapse, 69 died; 40 patients were lost at follow-up and excluded from the DFS prediction analysis. For the whole cohort, median DFS and OS were 17 (range 1-89) and 28 (range 1-89) months, respectively. In the training dataset, the radiomic CT, PET and PET+CT-based models were able to identify low-risk and high-risk patients with respect to DFS (p=0.021, and p=0.007). In the validation dataset the CT, PET and PET+CT-based models confirmed to be able to predict low vs high-risk disease (p=0.025, p=0.0009, and p=0.025). Within the OS analysis, in the training dataset radiomic CT, PET and PET+CT-based models provided the following performance in differentiating low-risk from high-risk patients: p=0.60, p=0.08, and p=0.035, while in the validation dataset the CT, PET and PET+CT-based models showed stratification ability with the following significance: p=0.05, p=0.08, and p=0.05. **Conclusion:** A radiomic signature, for either CT, PET or PET/CT images, has been identified and validated for the prediction of disease-free survival in NSCLC patients treated with surgery. The combination of PET and CT features was able to stratify lung cancer patients with respect to overall survival. These findings confirmed our previous results, supporting the prognostic role of radiomics. **References:** 1.Cancer Research 2018;78(16):4786-4789.

OP-353

Baseline Radiomic CT Features Differentiate Mediastinal Masses As Thymic Neoplasms Or Lymphomas

G. Ninatti[1], *M. Kirienko*[1], *L. Cozzi*[1,2], *E. Voulaz*[2], *F. Ricci*[2], *C. Carlo-Stella*[1,2], *P. Zucali*[2], *A. Chiti*[1,2], *M. Sollini*[1];
[1]*Humanitas University, Pieve Emanuele (MI), ITALY,* [2]*Humanitas Clinical and Research Center, Rozzano (MI), ITALY.*

Aim/Introduction: To evaluate the ability of computed tomography (CT) radiomic features to classify prevascular mediastinal masses as thymic neoplasms or lymphomas. **Materials and Methods:** This is a retrospective single-center study. Inclusion criteria: pathologically assessed either thymic neoplasia or lymphoma with at least one mediastinal localization, and availability of baseline non-contrast enhanced CT. Exclusion criteria: age <16 years; mediastinal lymphoma lesion <4 cm. We selected 108 patients (M:F=47:61, median age 48, range 17-79) and divided them into a training and a validation group. Mediastinal masses were manually delineated using LIFEx and Eclipse software. Two different resampling settings (1x1x4 and 2x2x2) were used. Radiomic features (n=41) were extracted using the LIFEx software and used as predictors in linear discriminant analysis (LDA) with backward stepwise variable insertion to classify the lesions. Different radiomic models considering segmentation software and resampling setting were built. Additionally, a clinical model was built considering age, sex, B symptoms, lymphadenopathies, autoimmune disorders, and white blood cell count. Scoring metrics included sensitivity, specificity, accuracy and analysis of the receiver operating characteristic curves in terms of area under the curve (AUC). Wilcoxon paired test was used to compare the AUCs of the validation models. A p value <0.05 was considered significant. R platform and SPSS were used for statistical analysis. **Results:** Fifty-five patients (27 males, 28 females) were affected by thymic neoplasia (52 thymoma, 3 thymic carcinoma) and 53 (20 males, 33 females) by lymphoma (39 Hodgkin, 12 Non-Hodgkin, and 2 Grey-zone Lymphoma); median age of 62 (range 26-79) and 36 (range 17-79) years, respectively. The radiomic model that resulted to have the highest performance selected 13 CT radiomic features. In the training group, sensitivity, specificity, accuracy and AUC resulted 88.2±5.5, 94.3±3.9, 91.3±4.4 and 0.93±0.05, respectively; in the validation group, the same metrics resulted 76.2±7.0, 77.8±5.5, 76.9±6.0 and 0.84±0.06, respectively. The clinical model included 4 clinical variables selected by LDA. In this model, the training group values for sensitivity, specificity, accuracy and AUC resulted 88.2±5.5, 82.9±6.4, 85.5±;6.3 and 0.95±0.05, respectively; while the same metrics in the validation group resulted 95.2±7.0, 88.9±8.9, 92.3±8.5 and 0.98±0.07, respectively. No statistically significant difference was found between the AUC of the best radiomic and the clinical model. **Conclusion:** CT radiomic model had similar performances to the clinical one, proving the potential to play a crucial role in asymptomatic patients differentiating thymic masses from lymphomas and, in a selected clinical setting, avoiding invasive diagnostic procedures. **References:** None.

OP-354

Contribution of tumour blood-flow for prediction of response to neoadjuvant chemotherapy in breast cancer using 18F-FDG PET/CT

N. Payan[1], *B. Presles*[1], *J. M. Vrigneaud*[1,2], *A. Cochet*[1,2];
[1]*ImViA laboratory, EA 7535, University of Burgundy, Dijon, FRANCE,* [2]*Department of Nuclear Medicine, Georges-François Leclerc Cancer Centre, Dijon, FRANCE.*

Aim/Introduction: The aim of this prospective study is to assess the contribution of tumour blood flow (BF) and tumour metabolism heterogeneity in the prediction of pathological complete response (pCR) to neoadjuvant chemotherapy (NAC) in patients with newly diagnosed breast cancer (BC). **Materials and Methods:** One hundred and ninety-seven newly diagnosed BC patients underwent a 18F-FDG PET/CT exam before any treatment. Tumour BF and tumour metabolism were extracted from dynamic first-pass and delayed PET images respectively. Standard PET parameters and texture features (TF) were computed from BF and metabolic parametric PET images. The pCR was defined as the absence of residual invasive cancer after NAC in primary tumour and lymph nodes. Multivariate logistic regressions were performed to predict pCR using (a) only clinical characteristics such as tumour histological type, hormonal receptors, (b) using clinical and metabolic tumour features and (c) using clinical, metabolic and perfusion tumour parameters. Five stratified k-fold cross-validation experiments, with 80% of the population selected for the training set and 20% for the testing set, were performed. After univariate feature selections performed on the training sets, hyperparameter optimization, done via inner cross validations, were then carried out to maximise the f1 score as recommended for unbalanced classes (pCR: ~25%). Generalisation errors were evaluated on the independent test sets through three metrics, the f1 score, the area under the receiver operating characteristics curve (AUC) and the accuracy. **Results:** Models including clinical, metabolic and perfusion tumour features yielded to the best test prediction results, with f1 values ranging from 0.44 to 0.67, AUC values from 0.64 to 0.85 and accuracy values from 0.70 to 0.87. In comparison, the f1 score, the AUC and the accuracy of the models using clinical and metabolic features ranged from 0.40 to 0.63, from 0.61 to 0.75 and from 0.73 to 0.82, respectively. For the predictions based on clinical features only, results varied from 0.30 to 0.71 for the f1 score, from 0.53 to 0.78 for the AUC and from 0.63 to 0.87 for the accuracy. For all models including clinical, metabolic and perfusion tumour features, various TFs, such as correlation or entropy, were selected during the univariate selection process which highlights the prognostic value of these parameters. **Conclusion:** This study showed that the association of tumour BF with tumour metabolism and clinical parameters enables to improve the pCR prediction and highlighted TFs as significant prognostic variables. **References:** None.

OP-355

Radiomic features of glucose metabolism enable prediction of bone marrow involvement in mantle cell lymphoma

M. Mayerhoefer, *C. Riedl, H. Schöder;*
Memorial Sloan Kettering Cancer Center, New York, NY, UNITED STATES OF AMERICA.

Aim/Introduction: Mantle cell lymphoma (MCL) is a rare subtype of B-cell Non-Hodgkin lymphoma, and can be associated with an aggressive or, less frequently, an indolent course. Bone marrow infiltration, which is routinely assessed by bone marrow biopsy (BMB) is present in about 60% of the cases at the time of diagnosis. It was therefore the aim of this study to determine whether [18F]FDG-PET/CT-derived radiomic features are predictive of bone marrow infiltration in MCL, alone or in combination with laboratory findings. **Materials and Methods:** Ninety-seven treatment-naïve MCL patients who had undergone [18F]FDG-PET/CT as well as iliac crest bone marrow biopsy (BMB) were retrospectively included. Standardized uptake values (SUVmax, SUVmean, and SUVpeak) and 16 co-occurrence matrix radiomic features were extracted from metabolic tumor volumes of the bony pelvis on pre-therapeutic [18F]FDG-PET/CT. Kendall's correlation coefficients in combination with Lasso regression analyses was used to determine the three best radiomic features for prediction of bone marrow involvement. This step was repeated for different absolute and relative thresholds of bone marrow involvement according to histology: Abs10% (absolute involvement >10% of the total analyzed bone marrow); Abs20%; Rel10% (involvement >10% of the cellular/red bone marrow); and Rel20%. A multi-layer perceptron neural network was then used for prediction of bone marrow involvement, with training-to-validation dataset ratios of 70% to 30% percent, using only radiomic features, and then, separately, also including LDA (lactate dehydrogenase) and white blood count (WBC). Median areas under the receiver operating characteristic curve (AUC) based on five repetitions of the classification step, respectively, were used as main outcome measures. **Results:** In total, 67/97 patients (69.1%) of the patients showed bone marrow involvement at BMB, whereas involvement rates were 35/97 (36.1%) for Abs10%, 31/97 (32.0%) for Abs20%, 41/97 (42.3%) for Rel10%, and 34/97 (35.1%) for Rel20%. Based solely on [18F]FDG-PET/CT-derived radiomic features, median AUC values were 0.77 for Abs10%, 0.73 for Abs20%, 0.70 for Rel10%, and 0.72 for Rel20%. Based on the combination of radiomic features and laboratory features, median AUC values were 0.81 for Abs10%, 0.79 for Abs20%, 0.73 for Rel10%, and 0.76 for Rel20%. **Conclusion:** In MCL, radiomic features of glucose metabolism may be useful for prediction of bone marrow involvement. Results may be further improved by a combination of [18F]FDG-PET/CT-derived radiomic features with laboratory parameters. **References:** None.

810

Thyroid - Rapid Fire Session: Prognostic Factors in DTC

Monday, October 14, 2019, 11:30 - 12:45 Lecture Hall 116

OP-356

Radioiodine In Differentiated Thyroid Carcinoma: Can Diagnostic Pre-Ablation Scintigraphy Optimize Treatment?

E. J. de Koster[1], *T. Sulaiman*[2], *J. F. Hamming*[2], *A. Schepers*[2], *M. Snel*[2], *F. H. P. van Velden*[2], *L. de Geus-Oei*[2], *D. Vriens*[2];
[1]*Radboud University Medical Centre, Nijmegen, NETHERLANDS,*
[2]*Leiden University Medical Centre, Leiden, NETHERLANDS.*

Aim/Introduction: Changing insights and ongoing global debate regarding postoperative radioiodine (I-131) administration in differentiated thyroid carcinoma (DTC) also stir up the discussion on whether pre-ablation diagnostic scintigraphy (DxWBS) could optimize treatment. **Materials and Methods:** Post-therapy I-131 whole-body scintigraphy (TxWBS) data were retrospectively qualitatively and semi-quantitatively assessed in a blinded manner for clinically relevant findings that would have influenced the course of treatment, had they been detected on pre-ablation scintigraphy. This included a thyroid remnant, lymph node metastasis and distant metastasis. Uptake counts in the thyroid bed were measured using an isocontour-based volume-of-interest on SPECT/CT images. Thyroid remnant size was semi-quantitatively assessed through a background- and volume-corrected value for the relative additional iodine uptake in the thyroid bed above background (remnant-to-background ratio), to correct for inter-patient and time-specific variability. Next, clinical, histopathological and surgical parameters were evaluated for their association with thyroid remnant size and treatment success. Successful treatment was defined as no clinical, biochemical (i.e. serum thyroglobulin (Tg) <0.5 ng/mL in absence of Tg-antibodies) or structural (i.e. on imaging) evidence of disease at nine months. **Results:** 97 consecutive DTC patients were included. TxWBS findings included a thyroid remnant in 89 (92%) patients, suspicion of lymph node metastasis in 26 (27%) and unexpected distant metastasis in 6 (6%). Pre-ablative knowledge of these findings could have influenced management in 48 (50%) patients. On multivariable linear regression analysis, surgery with oncological intent and surgery performed by two dedicated thyroid surgeons were independently associated with a smaller thyroid remnant. Multivariable logistic regression analysis demonstrated that one or more surgeries at a referring hospital, aggressive tumour histopathology, histopathological lymph node metastasis and new lymph node metastasis on TxWBS were independently associated with an unsuccessful treatment. Thyroid remnant size was not associated with treatment success. All 13 (100%) TNM-stage pN1 patients in whom additional lymph node metastases were detected on TxWBS had an unsuccessful treatment, opposite 19 of 31 (61%) pN1 patients without additional lymph node metastases on TxWBS (p=0.009). **Conclusion:** Pre-ablation DxWBS could optimize DTC risk stratification and patient-tailored I-131 administration. Selective application of DxWBS is recommended in patients with pN1 stage or patients at risk for in situ lymph node metastases, in whom DxWBS results could change the course of treatment and potentially improve treatment outcome. Although it enables fitted I-131 dosimetry and accurate Tg-based follow-up, DxWBS is not recommended to determine thyroid remnant size: it is unrelated to treatment success. **References:** None.

OP-357

Clinical implications of radioactive iodine - avid metastatic lymph nodes on post-ablation whole body scans in 1-4cm differentiated thyroid cancer

R. Gao, *X. Jia*, *Y. Wang*, *L. Yang*, *G. Zhang*, *A. Yang*;
The First Affiliated Hospital of Xian Jiaotong Universit, Xi'an, CHINA.

Aim/Introduction: Controversy exists in surveillance of low-risk differentiated thyroid cancer (DTC), especially in cases with 1-4 cm tumors. The risk of recurrence/metastasis was suggested to be estimated based on their response to initial therapy. However, the specific value of radioactive iodine (RAI) -avid lymph node metastasis (mLN) revealed in whole body scans (RxWBS) as a predictor of recurrent or progressive structural disease was not clear till now. **Materials and Methods:** We performed a retrospective review of patients with 1-4 cm DTC who were treated from January 2015 to January 2018. Enrolled patients received total thyroidectomy and RAI, followed by a radioiodine whole body scan. Patients revealed distant metastasis or lost of follow-up were excluded for further analysis. The clinical, pathologic, and incidence of RAI-avid mLN on RxWBS were reviewed, and the risk factors related to recurrence and/or metastasis were analyzed. **Results:** In total, 401 patients with 1-4 cm tumors were enrolled. The median age was 45 years (range, 14-88 years) with 289 women. More than half tumors manifested capsule invasion (82.54%) and 19.20% demonstrated gross extra thyroidal extension. 89.53% (359/401) cases received lymph node dissection and metastatic disease was found in 76.88% (276/359). The median RAI dose administered was 4.44 GBq (range, 2.96-47.63 GBq) and RAI-avid mLN was found in 28.43% (114/401) on RxWBS. After a median follow-up of 28 months (range, 11-91 months), recurrent/metastatic disease was detected in 17.52% (65/371) of the patients. Significantly higher incidence of recurrence was found in patients who demonstrated RAI-avid mLN after initial therapy as compared with those who did not ($p < 0.001$).The univariate analysis identified gross extrathyroidal extension, more than 5 lymph node metastasis, and RAI-avid mLN as significant and independent risk factors for recurrence or metastasis ($p < 0.005$). In a multivariate analysis, RAI-avid mLN appeared to be the only significant risk factor for recurrent /metastatic disease after initial therapy (HR, 17.457; 95% CI, 8.760 - 34.788; $p < 0.001$). **Conclusion:** RAI-avid mLN is a significant risk factor for disease

recurrence/metastasis in 1-4 cm DTC. More careful surveillance is suggested in patients demonstrated RAI-avid mLN after initial treatment. **References:** None.

OP-358

Prognosis of high-risk papillary thyroid cancer patients with pre-ablation stimulated Tg <1 ng/mL

T. Tian, Y. Kou, R. Huang, B. Liu;
West China Hospital, Sichuan University, Chengdu, CHINA.

Aim/Introduction: The prevalence of undetectable pre-ablation stimulated thyroglobulin (s-Tg) and its clinical implications in high-risk papillary thyroid cancer (PTC) patients have been less described. We attempted to investigate the rate of tumor recurrence in PTC patients initially classified as high risk but with pre-ablation s-Tg< 1 ng/mL and negative anti-Tg antibody (TgAb). **Materials and Methods:** In order to have follow-up period of at least 5 years for each patient, PTC patients consecutively seen at our department from May 2008 to June 2013 with the following characteristics were selected: (i) classified as ATA high risk on the basis of the tumor histopathological features; (ii) submitted to adjuvant ^{131}I therapy after total thyroidectomy; (iii) a postoperative pre-ablation s-Tg<1 ng/mL and negative TgAb. **Results:** Among 767 high risk PTC patients submitted to adjuvant ^{131}I therapy, 69 patients met inclusion criteria. Sixty seven patients (97.1%) were diagnosed as classical PTC, the remaining 2 patients (2.9%) as follicular variant PTC. When evaluated 9-12 months after ^{131}I therapy, 67 patients (97.1%) were classified as excellent response. Two (2.9%) patients had a s-Tg >1 ng/mL (<3 ng/mL) in the absence of apparent disease detected by imaging methods (indeterminate response). During a median follow-up duration of 5.6 years, recurrence was observed in only 2 (2.9%) patients. The 67 (97.1%) patients without tumor recurrence were not submitted to any additional therapy, and all had a suppressed Tg <1 ng/mL in the last assessment. **Conclusion:** High-risk PTC patients with pre-ablation s-Tg < 1 ng/mL and negative TgAb had a favorable prognosis. **References:** None.

OP-359

Comparisons between Thyroid Hormone Withdrawal and Recombinant Human Thyroid-stimulating Hormone Administration for Radioiodine Ablation in Patients with Intermediate-risk to High-risk Differentiated Thyroid Cancer

***Y. Iizuka**, T. Katagiri, K. Ogura, M. Inoue, K. Nakamura, T. Mizowaki;*
Kyoto University, Kyoto, JAPAN.

Aim/Introduction: Radioactive iodine (RAI) ablation is performed to destroy residual normal thyroid tissue after the surgical resection of differentiated thyroid cancer (DTC). Two methods are used to prepare the subjects for RAI ablation: thyroid hormone withdrawal (THW) and administration of recombinant human thyroid-stimulating hormone (rhTSH). The methods were equally effective in low-risk to intermediate-risk DTC, according to the American Thyroid Association. However, a few studies reported differences in the intermediate- to high-risk DTC. This study aimed to compare the clinical outcome between the methods. **Materials and Methods:** Between May 2012 and October 2018, 136 patients who underwent ablation with high dose (3,700 MBq) RAI for DTC, without any macroscopic residual lesions or metastatic lesions after surgical resection, were retrospectively evaluated. Patients were excluded if distant metastasis was confirmed during RAI ablation or if the outcome could not be confirmed; thus, 112 patients were evaluated. Patients either underwent a 3-week I restriction with thyroxine withdrawal or a 2-week I restriction with rhTSH administration. We measured the thyroglobulin (Tg) concentration and performed ^{131}I scintigraphy (370 MBq) 3 to 12 months after RAI ablation. The initial success of RAI ablation was defined as the disappearance of the uptake of ^{131}I at the thyroid bed and Tg concentration <2.0 ng/mL. Patients who did not undergo ^{131}I scintigraphy were evaluated based on the Tg value, and those who had anti-Tg antibodies were evaluated based on ^{131}I scintigraphy. The results of ablation were compared between the groups using the Fisher's exact test, and the TSH levels and estimated glomerular filtration rate (eGFR) using the Welch's t-test. **Results:** The THW and rhTSH groups included 47 and 65 patients, respectively, and the intermediate-risk and high-risk groups included 63 and 49 patients, respectively. There was no patient classified into the low-risk group. In the THW and rhTSH groups, the initial RAI ablation goal was achieved in 30/47 (63.8%) and 46/65 patients (70.8%), respectively (p=0.54); mean±standard deviation of the TSH levels was 120.9±49.7 μIU/mL and 272.1±102.4 7 μIU/mL, respectively (p<0.01); and eGFR (treatment/pre-treatment) was 0.81 and 0.98, respectively (p<0.01). In the intermediate-risk and high-risk groups, the initial RAI ablation goal was achieved in 43/63 patients (68.3%) and 33/49 (67.3%), respectively (p=1.0). **Conclusion:** There were no significant differences in initial success of RAI ablation between the preparation methods. However, patients in the rhTSH group showed higher TSH levels and retained eGFR. **References:** None.

OP-360

Interleukin-6 is over-expressed in Differentiated thyroid cancer and could act as the prognostic factor for disease persistence or recurrence

Z. Guo-Qiang;
Department of Nuclear Medicine, Shanghai Jiao Tong University Affiliated Sixth People's Hospital, Shanghai, CHINA.

Aim/Introduction: It has been repeatedly reported that Differentiated thyroid cancer (DTC) was associated with inflammatory microenvironment, evidenced by a mixture of immune cells and cytokines within or surrounding primary thyroid cancer. Interleukin-6 (IL-6) acts as the pro-inflammatory cytokine to maintain the chronic inflammatory environment in the microenvironment and has been reported to be an independent prognostic factor in melanoma patients. This study

was to evaluate the relationship between the IL-6 expression in DTC and clinicopathologic factors and Disease-free survival (DFS). **Materials and Methods:** Immunohistochemistry staining was conducted to evaluate the expression level of IL-6 in a total of 108 DTC tumor and corresponding para-carcinoma tissues. **Results:** IL-6 expression was positive in 72.2% (78/108) of DTC tumor tissues, which was significantly higher than in corresponding non-tumor tissue (p=0.002). The expression level of IL-6 was associated with tumor pathological type (p=0.021), lymph node metastasis (p=0.021), distant metastasis (p=0.036) and disease persistence or recurrence (p=0.032). Univariate analysis of factors influencing DFS shows that DFS was associated with the IL-6 expression level (p=0.028), tumor size (p=0.005) and TNM stage (p=0.010). In multivariate Cox regression analysis, positive IL-6 expression in tumor tissue was significantly associated with worse DFS (Hazard Ratio 5.813 [confidence interval 1.471-22.727], p=0.013). **Conclusion:** IL-6 is overexpressed in differentiated thyroid cancer and associated with the aggressiveness of the disease and could act as a factor to predict the prognosis of DTC patients. **References:** None.

OP-361

Radioiodine-refractory thyroid cancer, looking for predictive factors

M. Guiote Moreno[1,2], *A. M. Santos Bueno*[1,2], *J. Márquez Fernandez*[1], *J. C. Prieto Prieto*[1], *M. Albalá González*[1], *E. Rodriguez Cáceres*[1], *R. Carlos Zamora*[1], *J. A. Vallejo Casas*[1,2];
[1]*Hospital Universitario Reina Sofía, Cordoba, SPAIN,* [2]*Instituto Maimonides de Investigación Biomédica, Cordoba, SPAIN.*

Aim/Introduction: To analyze the data of radioiodine-refractory thyroid cancer patients diagnosed with PET/CT ^{18}F-FDG; and its correlation with dedifferentiated tumor with possible predictive factors. **Materials and Methods:** We recruited 61 patients with differentiated thyroid cancer who underwent surgical and ablative treatment with ^{131}I that presented an incomplete response. A PET-CT with ^{18}F-FDG was performed between the years 2015-2019 to patients, after stimulation with rTSH and a negative ^{131}I wholebody scan. Refractory and dedifferentiated tumors were considered in patients that had positive results in PET/CT scans. Age, sex, histology, tumoral staging, treatment ^{131}I dosage, biochemical levels of thyroglobulin and antibody anti-thyroglobulin were taken into account in these patients. A hypothesis contrast was obtained for each one of these variables and the dedifferentiated variable to calculate if they correlate using the chi square for the qualitive variables and the U Mann-Whitney-Wilcoxon for the cuantitative variables. **Results:** 28 patients were suggestive of dedifferentiated tumor on PET/CT; 18 were women and 10 were men with a mean age of 57 (SD ± 16,7 years). Total thyroidectomy and ^{131}I ablation was performed predominantly on stage III (47%) papillary thyroid cancer (89%) with a mean dose of 5,1 Gbq (SD ± 2,8 Gbq). Statistical significance was seen only with age and tumor diagnosis after analyzing the variables with the dedifferentiated tumor (W = 123.5, p-value = 0.00005323), tumoral staging (X-squared = 11.884, df = 3, p-value = 0.007791), Tg basal values (W = 67.5, p-value = 0.0005168) and stimulated Tg (W = 100, p-value = 0.0006464), with a strong association. Therefore these values should be taken into account in patients with suspected dedifferetiated thyroid tumors. 5 of these patients were submitted to surgery, 6 are in treatment with Sorafenib/Levantinib and the rest are in close surveillance. **Conclusion:** PET/CT ^{18}F-FDG is a very sensitive diagnostic technique for radioiodine-refractory thyroid cancer patients. Basal and stimulated Tg, age at the moment of diagnosis and tumor staging are predictive factors that need to be taken into account for an early diagnosis and better management; they demonstrate a significant correlation with the risk of tumoral dedifferentiation. **References:** None.

OP-362

Contrast-Enhanced ^{18}F-FDG PET/CT in Detection of Recurrent/Metastatic Radioiodine Negative Differentiated Thyroid Carcinomas

P. Koranda[1], *H. Polzerová*[1], *L. Quinn*[1], *E. Buriánková*[1], *R. Formánek*[1], *M. Halenka*[2], *M. Mocňáková*[3], *M. Kamínek*[1];
[1]*Dept. of Nuclear Medicine, Univ. Hosp. and Palacký University, Olomouc, CZECH REPUBLIC,* [2]*Dept. of Internal Medicine III, Univ Hosp., Olomouc, CZECH REPUBLIC,* [3]*Dept. of Surgery II, Univ Hosp., Olomouc, CZECH REPUBLIC.*

Aim/Introduction: Localization of radioiodine-negative remnants or recurrences of differentiated thyroid carcinomas (DTCs) is mandatory because only it allows to effectively cure the patients using a locoregional treatment. The aim of this study was to assess the diagnostic value of ^{18}F-FDG PET/CT in this indication. **Materials and Methods:** A total of 160 patients (pts) with suspicion of recurrent DTC and negative ^{131}I scans in the period 2009-2018 underwent contrast-enhanced ^{18}F-FDG PET/CT. Examination was performed in 150 pts due to a positivity of TSH-stimulated thyroglobulin (TSH-Tg) (in case of TSH-Tg < 2 µg/l suspicious sonography or high-risk disease was also a condition of PET/CT indication) and in 10 cases due to persistent elevation of anti-Tg. Only the first ^{18}F-FDG PET/CT examinations were evaluated, all subsequent examinations of the same patient were excluded. **Results:** Contrast-enhanced ^{18}F-FDG PET/CT was true positive in 76/160 (48%) cases - false positive in 4/160 (3%). Subgroup of 26 patients with TSH-Tg 0 < 2 µg/l and suspicious sonography or high-risk patients: true positive 7 (27%), false positive 1 (4%). Subgroup of 46 patients with TSH-Tg 2 < 10 µg/l: true positive 20 (43%), false positive 2 (4%). Subgroup of 78 patients TSH-Tg >10 µg/l: true positive 43 (55 %), false positive 1 (1%). Subgroup of 10 patients with anti-TG pathology: true positive 6 (60%). Incidentally 2 other malignancies and 1 interstitial lung disease were detected. The surgery or external beam radiotherapy or targeted imunotherapy was subsequently performed in 56, 19 and 2 cases, respectively. Treatment management plan was changed in 61/160 patients (38%). **Conclusion:** Contrast-enhanced ^{18}F-FDG PET/CT is able to identify recurrent/metastatic radioiodine-negative DTCs in an important part of patients with elevation of TSH-Tg or

with another suspicion of metastases. The detection rate of recurrences increases with increase of TSH-Tg. Nevertheless the number of positive findings in patients with low positive level of TSH-Tg represent a significant part of examinations. Therefore, it is not possible to set a TSH-Tg limit for ^{18}F-FDG PET/CT indication. TSH-stimulated ^{18}F-FDG PET/CT is an efficient diagnostic tool with a significant impact on therapy. **References:** None.

OP-363

Course of disease and outcome in patients with poorly differentiated thyroid cancer: a single center study

F. Ahmaddy, V. Wenter, P. Bartenstein, S. Lehner, H. Ilhan, A. Todica;
Department of Nuclear Medicine, University Hospital, LMU Munich, Munich, GERMANY.

Aim/Introduction: Poorly differentiated thyroid cancer (PDTC) is a rare but very aggressive variant of thyroid carcinoma. Due to the relative rarity of the disease, studies on diagnostic and treatment findings are limited. Therefore, we investigated the clinical course of these patients. **Materials and Methods:** A retrospective analysis was conducted in 47 patients with histologically proven PDTC, who were treated between 2005 and 2019 at the Department of Nuclear Medicine of the University Hospital of Munich. All patients underwent total thyroidectomy, followed by adjuvant radioiodine ablation (RAI). Clinico-pathological features, Tg levels, 131-I Uptake in whole body scan and FDG-Uptake in PET/CT were analyzed. A stimulated Tg level below 0.5 ng/ml was defined as undetectable. **Results:** The mean age at diagnosis was 57±18 years (55% females) and mean follow-up was 7 years. According to the 7th TNM classification, 22% of patients had pT1b/pT2-stage disease, 70% pT3, 8% pT4a/b. At initial presentation, 28% of patients had regional lymph node metastases and 19% extrathyroidal extension and 4% showed R1 resection. A mean I-131 activity dose of 5.8±2.0 GBq was applied at initial RAI. 68% patients underwent further RAI therapy treatment cycles. At initial presentation 72% of patients (N=34) showed no distant metastases. 28% of the patients (N=13) already showed distant metastases at initial presentation. During follow-up, 32% (N=15) showed no evidence of disease (NED), 34% (N=16) showed persistent disease, out of which in 12 patients structural disease was diagnosed during follow-up. Recurrence occurred in 6% (1 patient biochemical, 2 patients structural). During follow-up FDG-PET was available in 96% of patients with distant metastases (22/23) of whom all patients showed a pathological uptake. Out of these patients with distant metastases only 5 patients were radioiodine positive. At the time of last follow-up 36% (N=17) showed NED, 9% (N=4) persistent biochemical disease and 47 % (N=22) structural disease. 3 patients (6%) were lost to follow-up. Disease related death was reported in 5 patients until last follow-up. **Conclusion:** Poorly differentiated thyroid cancer is acting more aggressively than well differentiated forms of thyroid cancer, with a high number of patients with distant metastases at initial presentation and an increasing number of patients with structural disease during follow-up. These patients show uptake almost exclusively in FDG-PET/CT with only a small fraction demonstrating positive iodine uptake. Thus, rendering FDG-PET/CT the imaging method of choice for these patients during follow-up. **References:** None.

OP-364

A Prospective Study of the Effect of Radioiodine Therapy on Ovarian Reserve Function in Patients with Differentiated Thyroid Carcinoma

W. Miao, R. Lin;
The First Affiliated Hospital of Fujian Medical University, Fuzhou, CHINA.

Aim/Introduction: The aim of this study was to prospectively assess the effect of radioiodine therapy (RAIT) on ovarian reserve function for the patients with DTC. **Materials and Methods:** Seventy-six pre-menopausal women (34.1±6.8years) pathologically diagnosed with DTC planning to receive RAIT after surgery were recruited for this study, of which 8 subjects underwent the twice RAIT. Serum FSH, LH, estradiol(E2), progesterone(P), TSH and anti-Müllerian hormone (AMH) levels during the early follicular phase were measured before and 1, 2, 3, 6, 9 and 12 months after RAIT (M0, M1, M2, M3, M6, M9, M12). **Results:** ① The mean AMH levels were 2.15(0.92-3.74), 1.21(0.52-2.82), 1.19(0.28-2.22), 1.20(0.38-3.28), 2.10(0.65-3.59), 1.95(0.44-3.45) and 1.59(0.44-4.55) ng/mL respectively at M0, M1, M2, M3, M6, M9, M12. The AMH level at M2 was significantly lower than that at M0 (P=0.021), while no significant difference was found among other time points (P > 0.05).② The descent rates of AMH level based on M0 were(49.0%±23.4%), (46.1%±25.5%), (42.0%±23.7%), (33.1%±20.5%), (36.0%±22.9%) and(25.4%±17.6%) at M1, M2, M3, M6, M9, M12, respectively. The number at M1 was significantly higher than that at M6, M9 and M12 (P=0.003, P=0.038 and P=0.002) and the number at M12 was significantly lower than that at M1, M2 and M3 (P=0.002, P=0.008 and P=0.034).③ The AMH levels after the second RAIT were lower than that after the first RAIT, the descent rates showed the opposite trend, but no statistically significant relation was found between the two therapy (P> 0.05).④ At M1, AMH descent rate was positively correlated with age (r=0.381, P=0.000) and negatively correlated with basic AMH level (r=-0.358, P=0.002). The descent rate of AMH had no correlation with the age at menarche, BMI, ^{131}I dose, Hashimoto's thyroiditis and the interval time between surgery and RAIT(P>0.05). ⑤ The difference in FSH, LH, E2 and P levels among all time points were found to be insignificant (P> 0.05). ⑥50.7% (38/75) patients had menstrual disorders after RAIT. But there was no significant difference in AMH decent rates and age between patients with menstrual disorder and those with normal menstruation (P>0.05). **Conclusion:** This study prospectively showed that ovarian reserve declined rapidly after RAIT, with a partial recovery in the subsequent follow-up. **References:** None.

OP-365

Clinical study on the effect of TSH suppression on left ventricular systolic synchrony in patients with DTC

R. Wang[1], *I. Yang*[1], *S. Jin*[2], *B. Wu*[1], *X. Han*[1], *Y. Liu*[1], *B. Liu*[1];
[1]*Nuclear Medicine Department, the First Affiliated Hospital of Zhengzhou University, Zhengzhou, CHINA,* [2]*Nuclear Medicine Department, Zhe Jiang Cancer Hospital, Hangzhou, CHINA.*

Aim/Introduction: To investigate the effect of TSH suppression therapy on left ventricular systolic synchrony in patients with DTC. **Materials and Methods:** Patients with differentiated thyroid cancer who underwent TSH suppression were treated with gating myocardial perfusion imaging before suppression, 6 months, 12 months, and 24 months after suppression. The left ventricular systolic synchrony parameter was obtained including phase angle, phase standard deviation, and entropy. Patients with differentiated thyroid cancer who do not require TSH suppression therapy in the same age group are normal controls. Data were tested for covariance by SPSS 19.0 with age as a covariate to analyze the effect of TSH suppression on left ventricular systolic synchrony. **Results:** After TSH suppression treatment, the phase angle, phase standard deviation, and entropy of the experimental group gradually increased with time. However, at 6 months and 12 months of suppression, there was no statistical difference compared with the control group. There were statistical differences in phase angle, phase difference, and entropy at 24 months, with p values of 0.006, 0.007, and 0.001, respectively. **Conclusion:** This study used GMPI to evaluate the left ventricular systolic synchrony in patients with PTC after TSH suppression. Long-term TSH suppression led to left ventricular systolic synchrony, suggesting early intervention. **References:** None.

YDF2

EANM Young Daily Forum

Monday, October 14, 2019, 13:00 - 14:30 Lecture Hall 113

YDF-2

Presentation Skills for Medical Professionals

R. Sheppard;
EANM Moderator, London, UNITED KINGDOM.

901

CME 7 - Translational and Molecular Imaging Therapy Committee: Imaging Immune Therapy

Monday, October 14, 2019, 14:30 - 16:00 Auditorium

OP-366

Imaging of Immunological Targets

W. Weber;
Nuclear Medicine Department, Klinikum rechts der Isar, Technische Universität München (TUM), Munich, GERMANY.

OP-367

Current State of Imaging in Assessment of Immunotherapy

C. Bodet-Milin;
Nuclear Medicine Department, University Hospital, CRCINA, INSERM, CNRS, Université d'Angers, Université de Nantes, Nantes, FRANCE.

OP-368

Emerging Imaging Concepts in Immuno-Oncology

M. Schottelius;
TU Munich, Pharmaceutical Radiochemistry, Garching, GERMANY.

902

Joint Symposium 13 - Neuroimaging Committee / EANO: Low Grade Glioma

Monday, October 14, 2019, 14:30 - 16:00 Lecture Hall 311

OP-369

Imaging Low Grade Glioma

N. Albert;
Ludwig-Maximilians-Universität, Dept of Nuclear Medicine, Munich, GERMANY.

OP-370

State of the Art Neurosurgical Management in Low Grade Glioma

J. Tonn;
Ludwig-Maximilians-Universität, Dept. Neurosurgery, Munich, GERMANY.

OP-371

Non-Surgical Management of Low Grade Glioma

M. van den Bent;
Erasmus MC Cancer Center, Brain Tumor Center, Rotterdam, NETHERLANDS.

903

Joint Symposium 14 - Dosimetry + Radiation Protection Committee / ICRP: Radiological Protection in Therapy with Radiopharmaceuticals

Monday, October 14, 2019, 14:30 - 16:00 Lecture Hall 312

OP-372

ICRP framework for Individual Absorbed Dose Estimation

W. Bolch;
University of Florida, Biomedical Engineering, Gainesville, FL, UNITED STATES OF AMERICA.

OP-373

Justification and Optimisation of Protection in Radiopharmaceutical Therapy Patients

G. Flux;
Royal Marsden NHS Trust & Institute of Cancer Research, Joint Department of Physics, Sutton, UNITED KINGDOM.

OP-374

EANM Framework for Individualized Treatment Planning and Dose Verification

C. Stokke;
Oslo University Hospital, Rikshospitalet, Intervention Centre, Oslo, NORWAY.

904

CTE 3 - Technologist Committee: Preclinical Studies, from Bench to Bedside

Monday, October 14, 2019, 14:30 - 16:00 Lecture Hall 117

OP-375

How to Develop the Ideal Radiopharmaceutical

G. Bormans;
Ku Leuven, Radiopharmacy Department, Leuven, BELGIUM.

OP-376

Preclinical PET Imaging and Quantification

M. Koole;
UZ Gasthuisberg, Nuclear Medicine and Molecular Imaging, Leuven, BELGIUM.

OP-377

Nanobody Applications for Radionuclide Imaging and Therapy - Process from Camel to Patient

M. Keyaerts;
UZ Brussels, Nuclear Medicine, Brussels, BELGIUM.

905

M2M - Parallel Session: Neurodegeneration and Neuroinflammation

Monday, October 14, 2019, 14:30 - 16:00 Lecture Hall 111

OP-378

First-in-human investigating and translational study of ^{18}FS3-1 a novel alpha-synuclein PET tracer

B. Hooshyar Yousefi[1], K. Shi[2], T. Grimmer[3], R. Arakawa[4], H. Wester[3], C. Halldin[4], M. Schwaiger[3], W. Weber[3], I. Yakushev[3], T. Arzberger[5];
[1]Phillips University of Marburg, Marburg, GERMANY, [2]University of Bern, Bern, SWITZERLAND, [3]Technical university of Munich, Munich, GERMANY, [4]Karolinska Institutet, Stockholm, SWEDEN, [5]Ludwig-Maximilians University of Munich, Munich, GERMANY.

Aim/Introduction: α-Synuclein aggregates (α-syn) imaging in the living brain would enable to diagnose and track the degree and location of α-synucleinopathies over time. We have been developing several small molecule diagnostic probes based on 4,4′-diaryl-2,2′-bithiazole suitable for quantification of α-syn by nuclear medicine imaging. Recently, we studied ^{18}FS3-1 as a promising lead compound for noninvasive, specific imaging of a-syn as opposed to other proteopathies (e.g. Aβ and tau). Here, we report the results of studies aimed at the clinical translation of FS3-1 lead by PET using α-syn E46K mutant rat model as well as in nonhuman primates (NHP) and first-in-human investigation. **Materials and Methods:** The ^{18}FS3-1 shows 3nM affinity for α-syn and high selectivity (120 fold) for Aβ and tau was labeled with the Neptis module. The brain-specific binding kinetics were investigated in 12 month-old rats with E46K α-syn mutation and controls using dynamic PET coregistered to a 7T-MRI. Furthermore, in collaboration with Karolinska Institute, we studied its brain uptake kinetics and plasma stability in NHP. Preliminary toxicology studies carried out in mice. Patients with α-synucleinopathy underwent dynamic PET imaging for 120 min in Siemens mMR. The image data were spatially normalized based on MRI using PMOD. Images were analyzed by comparing binding potentials (BP) obtained using

a reference tissue model, and distribution volume (DV). **Results:** The comparisons of distribution volume showed statistically significant differences between a-syn E46K rats and controls for the substantia nigra, cerebellum, thalamus, and brainstem. In NHP FS3-1 showed initial brain uptake of up to 1.4% ID (1.3 SUV) and a rapid washout with marginally increases in later time points (up to 0.4SUV at 120min). FS3-1 showed no toxic effect at 154nmol/Kg dose in mice and higher than 55% 120 min p.i. in vivo stability in monkey plasma. The specific binding of FS3-1 was detected in the cases with underlying α-synucleinopathies. **Conclusion:** The suitable uptake kinetics in rats and NHP and target affinity suggests that FS3-1 is promising selective α-syn tracer that may allow for the first non-invasive imaging of αsynuclein aggregates in patients with dementia with Lewy bodies or Parkinson's disease. Further human investigation and new candidates optimization and their translation study are in progress. **References:** Wester HJ, Yousefi BH Compounds binding to neuropathological aggregates US20170157274A12.

OP-379

Discovery and preclinical characterization of [^{18}F]PI-2620, a next generation tau PET tracer for the assessment of tau pathology in Alzheimer's disease and other tauopathies

A. Mueller[1], *H. Kroth*[2], *F. Oden*[1], *F. Capotosti*[2], *M. Berndt*[1], *J. Molette*[2], *H. Schieferstein*[1], *V. Darmency*[2], *J. Castillo-Melean*[1], *E. Vokali*[2], *H. Schmitt-Willich*[1], *D. Hickman*[2], *A. Pfeifer*[2], *S. Poli*[2], *L. Dinkelborg*[1], *A. Stephens*[1];
[1]*Life Molecular Imaging, Berlin, GERMANY,* [2]*AC Immune SA, Lausanne, SWITZERLAND.*

Aim/Introduction: Tau deposition in the brain is a key pathologic feature of Alzheimer's disease (AD) and other neurodegenerative disorders. PET is currently explored for detection of aggregated tau in these diseases. Several PET tracers targeting tau-aggregates have been described and tested in humans. Limitations have been reported for first-generation Tau tracers regarding their selectivity. In our screening campaign we utilized the Morphomer™ library to identify pyrrolo[2,3-b:4,5-c'] dipyridine core structures with high affinity for aggregated Tau. Further characterization showed compounds containing this moiety had significantly reduced MAO-A binding compared to pyrido[4,3-b]indole-derivatives like AV1451. Here we present preclinical data of ten fluoropyridine regioisomers attached to the pyrrolo[2,3-b:4,5-c']dipyridine scaffold, leading to compounds with superior properties. **Materials and Methods:** Tau binding of fluoropyridine regioisomers and AV1451 was evaluated in competition binding-assays using AD brain-homogenate. Off-target binding of the ten compounds and AV1451 was evaluated using radiolabeled MAO-A/B and beta-amyloid binders. Compounds were radiolabeled with ^{18}F and brain-PK properties were evaluated in NMRI-mice by Micro-PET imaging. The most promising compounds were further characterized by (micro)ARG and PET imaging in NHPs. **Results:** Using human AD brain-homogenates, pIC_{50} values ranging from 7.35 to 8.42 were measured for the fluoropyridine regioisomers. The majority of compounds showed no binding to MAO-A or B and 8/10 regioisomers showed no measurable binding to beta-amyloid. 8/10 compounds were successfully radiolabeled with ^{18}F and brain-uptake was evaluated by PET imaging in NMRI-mice. The brain-uptake ranged from 2.1-8.2 % ID/g for those compounds. Five compounds showed defluorination in mice. Three compounds showed excellent wash-out properties in mice with peak brain-uptake-to-60 min ratios > 20. Two compounds showed a comparable preclinical profile based on their affinity and PK-properties and were further characterized in NHPs and for binding to Tau-aggregates in PSP. **Conclusion:** Preclinical characterization of the ten fluoropyridine regioisomers showed that small changes of the same general scaffold can surprisingly result in significantly changed properties with respect to tau-binding, off-target binding and PK properties of the different compounds. Based on these results, PI-2620 was selected as candidate for clinical validation. This compound displayed high affinity for tau-aggregates in AD and PSP brain-homogenate competition-assays. Specific binding to aggregated tau was demonstrated by ARG and micro-ARG on AD and PSP brain sections, whereas no specific binding was observed on brain sections from non-demented donors. PI-2620 showed excellent selectivity with no off-target binding to beta-amyloid or MAO-A/B. Good brain-uptake and fast wash-out were observed in mice and NHPs. **References:** None.

OP-380

Characterization of the Serotonin 2A receptor selective PET tracer (R)-[^{18}F]MH.MZ in the human brain

V. Kramer[1,2], *A. Dyssegaard*[3], *J. Flores*[2], *C. Soza-Ried*[2], *F. Roesch*[4], *G. Moos Knudsen*[3], *H. Amaral*[1,2], *M. Herth*[5,6];
[1]*Positronpharma SA, Santiago de Chile, CHILE,* [2]*Center for Nuclear Medicine & PET/CT Positronmed, Santiago, CHILE,* [3]*Center for Integrated Molecular Brain Imaging, Rigshospitalet, Copenhagen, DENMARK,* [4]*Institute of Nuclear Chemistry, Johannes Gutenberg-University, Mainz, GERMANY,* [5]*Department of Drug Design and Pharmacology, University of Copenhagen, Copenhagen, DENMARK,* [6]*Department of Clinical Physiology, Nuclear Medicine & PET, Rigshospitalet, Copenhagen, DENMARK.*

Aim/Introduction: The serotonin receptor subtype 2A is of significant clinical interest due to its relevance in diseases such as depression, Alzheimer's disease, or schizophrenia and as target for hallucinogenic drugs and atypical antipsychotics. The radiolabelled antagonist (R)-[^{18}F]MH.MZ has been identified as a promising PET imaging agent for quantification of 5-HT_{2A}Rs, combining an excellent selectivity profile (as for [^{11}C]MDL 100907) with the favorable isotopic properties of fluorine-18. In this study, we aimed to evaluate the potential of (R)-[^{18}F]MH.MZ in the human brain by PET. **Materials and Methods:** Nine healthy volunteers (HCs) underwent (R)-[^{18}F]MH.MZ PET imaging at baseline for 180 min. 5/9 HCs participated in additional arterial blood sampling and metabolite analysis during PET imaging. 4/9 participated in a second PET scan after ketanserin pretreatment to determine specificity of (R)-[^{18}F]MH.MZ. Regional time-activity

curves of 17 brain regions were analyzed comparing different kinetic modeling approaches (1TCM, 2TCM, Logan, SRTM, …) and stability of outcome measures was evaluated. **Results:** Highest uptake was determined in 5-HT_{2A}R rich cortical regions with distribution volumes (VTs) of approximately 4.5-5.0 and BP_{ND}s of 1.5. No radiometabolism was observed. 1- and 2-TCM resulted in similar outcome measure, whereas reference tissue models resulted in a stable and predictable overestimation. (R)-[^{18}F]MH.MZ displayed specific binding and could be blocked by pretreatment with ketanserin. Moreover, outcomes measures were stable after 100-110 minutes allowing a 5% deviation to the control. **Conclusion:** (R)-[^{18}F]MH.MZ is a suitable PET tracer to image and quantify the 5-HT_{2A}R system in humans. In comparison to [^{11}C]MDL 100907, faster and more precise outcome measure could be obtained using (R)-[^{18}F]MH.MZ. We believe that (R)-[^{18}F]MH.MZ has the potential to become the antagonist radiotracer of choice to investigate the human 5-HT_{2A}R system. **References:** Herth MM, Kramer V, Piel M, Palner M, Riss PJ, Knudsen GM, et al. Synthesis and in vitro affinities of various MDL 100907 derivatives as potential ^{18}F-radioligands for 5-HT_{2A} receptor imaging with PET. Bioorg Med Chem. 2009;17(8):2989-3002.

OP-381

A minimally-invasive approach to quantify P2X7 receptor occupancy using ^{18}F-JNJ-64413739 dynamic PETMR and MRA-driven image-derived input function

N. Mertens[1], *M. Schmidt*[2], *A. Hijzen*[2], *P. Ravenstijn*[2], *K. Van Laere*[1], *M. Koole*[1];
[1]*University Hospital and KU Leuven, Leuven, BELGIUM,*
[2]*Janssen Research & Development, Beerse, BELGIUM.*

Aim/Introduction: ^{18}F-JNJ-64413739, a selective P2X7-inhibitor, has been extensively evaluated as a candidate PET-ligand. A 2-tissue compartment model (2TCM) with arterial blood sampling was identified as the most suitable kinetic model for ^{18}F-JNJ-64413739 brain PET quantification in humans, since no reference region could be identified. In the context of a P2X7-PET dose occupancy study, we evaluated a minimally-invasive approach by limiting arterial blood sampling to baseline conditions and combine baseline blood-to-plasma ratios and metabolite fractions with an image-derived input function (IDIF) using MR-angiography (MRA) on a simultaneous PETMR-system, to calculate post-dose distribution volumes (V_T). This non-invasive approach to estimate post-dose regional V_T was validated by comparing post-dose MRA-IDIF based V_T and corresponding occupancy with full arterial blood sampling. **Materials and Methods:** 4 healthy volunteers (M;30.8±13.7yrs) underwent a 90-min dynamic ^{18}F-JNJ-64413739 PET scan (84-155 MBq, GE Signa PETMR) with arterial blood sampling under baseline and P2X7-antagonist dosing conditions at antagonist T_{max}. Two subjects received a second post-dose scan (later timepoint), resulting in 6 pairs of baseline and post-dose scans. V_T was calculated using 2TCM with sampled arterial blood and metabolite-corrected plasma input function (IF), while occupancy was estimated using a Lassen plot (PMOD,v4.0). These values were considered as gold standard. First, baseline blood-to-plasma ratios and metabolite fractions were combined with sampled, post-dose arterial blood IF for calculating post-dose V_T and occupancy. Second, baseline blood-to-plasma ratios and metabolite fractions were combined with post-dose IDIF as arterial blood IF. IDIF was extracted by defining carotids and background volume-of-interest (VOI) guided by time-of-flight MRA (TOF-MRA), acquired simultaneously at the beginning of the dynamic PET. Correction for partial volume effects between arterial blood and background was optimized by comparing baseline IDIF with sampled baseline blood IF. Results of both approaches were compared with the gold standard by a Bland-Altman analysis. **Results:** Similar post-dose V_T were found for all regions by using baseline blood-to-plasma ratio and metabolisation information (4.1% bias,95%CI[-3.4%;11.5%] for cortex). For the IDIF-approach, similar results were found with a slightly higher bias (7.4%,95%CI[-8.2%;23.0%]). Occupancy was observed with -1.8% bias (95%CI[-9.0%;5.3]) for the first approach, while for the IDIF-approach the bias increased to -5.8% (95%CI[-19.2%;7.5%]). **Conclusion:** A post-dose IDIF, guided by TOF-MRA, can be used as arterial blood IF and can be combined with baseline blood-to-plasma ratios and metabolite fractions for accurate post-dose P2X7-quantification, thus avoiding the need for repeated invasive arterial blood sampling in pharmaceutical dosing studies, thereby increasing flexibility in study design. **References:** None.

OP-382

The influence of high-fat diet on neuroinflammation and D_2 receptor availability in a rat model of Parkinson`s disease

L. Reali Nazario[1,2], *A. Dellink*[3], *R. Moraga-Amaro*[1], *B. Lima Giacobbo*[1], *A. Schildt*[1], *R. A. J. O. Dierckx*[1], *C. Maria Moriguchi Jeckel*[2], *R. Souza da Silva*[2], *J. Doorduin*[1], *E. F. J. de Vries*[1];
[1]*University Medical Center Groningen, Groningen, NETHERLANDS,* [2]*Pontifícia Universidade Católica do Rio Grande do Sul, Porto Alegre, BRAZIL,* [3]*University of Groningen, Groningen, NETHERLANDS.*

Aim/Introduction: Lifestyle can influence on the incidence and progression of Parkinson's disease (PD) (Paul et al., 2019). However, the underlying molecular mechanisms in the brain are still unknown. The objective of this study is to evaluate the effect of a high-fat diet (HFD) on neuroinflammation (^{11}C-PBR28) and the D_2-receptor (^{11}C-Raclopride) availability in the brain of a rat model of PD. **Materials and Methods:** Nine weeks old male Wistar rats were fed with either a HFD (60% fat) or a standard diet (STD; 10% fat) for three months. The bodyweight and food intake were measured twice a week and a glucose tolerance test (GTT) was performed every month. After two months of diet the animals were submitted to stereotactic surgery injecting a low dose of 6-OHDA (2x 3µg) in the right striatum. Static ^{11}C-PBR28 and ^{11}C-Raclopride PET scans were performed two days before and one month after the surgery. Tracer uptake in the striatum

was measured and expressed as SUV. GraphPad Prism 7.02 and IBM SPSS 23 were used for statistical analysis. **Results:** After three months, animals on HFD had 8.9% higher bodyweight than those on STD ($p<0.038$). The surgery caused a temporary small decrease in bodyweight in both groups. No difference in the glucose tolerance test between the STD and HFD groups were found in the first two months, but in the third month the HFD group did show a slower recovery of glucose levels, suggesting a pre-diabetic state. In the HFD group, ^{11}C-PBR28 uptake in the 6-OHDA-injected caudate putamen significantly increased (33%; $p=0.0193$) between both PET scans. This effect was not observed in the contralateral striatum, nor in the STD group. ^{11}C-Raclopride PET showed significantly lower uptake in all regions of the striatum in the HFD group than in the STD group ($p<0.05$). After the surgery this effect disappeared, except for the right accumbens core ($p<0.05$). ^{11}C-Raclopride PET did not reveal any effect of 6-OHDA injection. **Conclusion:** HFD significantly reduced D_2 receptor availability in rat striatum, but this effect was no longer present one month after 6-OHDA injection. Moreover, the HFD aggravated 6-OHDA-induced neuroinflammation in the Parkinson model. Both observations suggest a detrimental role of the HFD-induced pre-diabetic state on the onset or progression of Parkinson's disease. **References:** Paul KC, et al. The association between lifestyle factors and Parkinson's disease progression and mortality. Disord. 2019 Jan;34(1):58-66.

OP-383

TSPO-targeting ^{18}F-CB251 PET/MR in an intracranial LPS induced neuro-inflammation model: comparative analysis with bioluminescence imaging of peripheral immune cells

K. Kim[1,2], *H. Kim*[1], *S. Bae*[1,2], *Y. Kim*[1,2], *J. Na*[1], *C. Lee*[1], *M. Lee*[3], *G. Ko*[2], *K. Kim*[2], *J. Paeng*[2], *G. Cheon*[2], *K. Kang*[2], *S. Kim*[4], *J. Chung*[3], *E. Kim*[3], *J. Lee*[2], *B. Lee*[4], *H. Youn*[3];
[1]*Samsung cancer institute, Seoul, KOREA, REPUBLIC OF,* [2]*Seoul National University, Seoul, KOREA, REPUBLIC OF,* [3]*Seoul National University Hospital, Seoul, KOREA, REPUBLIC OF,* [4]*Seoul National University Bundang Hospital, Seoul, KOREA, REPUBLIC OF.*

Aim/Introduction: Imaging the inflamed region and the interaction of immune cells in the brain is important because neuro-inflammation is a primary defence mechanism and closely related to neurodegenerative disease. Here, we established multi-modalities imaging using PET/MR imaging with a recently developed TSPO-targeting radionuclide PET probe, ^{18}F-CB251, for detecting neuro-inflammation in a mouse harbouring intracranial lipopolysaccharide (LPS)-induced regional inflammation. In addition, since the infiltration of peripheral immune cells exacerbated neuro-inflammation to greater neuro-toxic levels, we monitored peripheral immune cells infiltration in neuro-inflammation with bioluminescence imaging by adoptive transfer of luciferase expressing splenocytes into the inflamed mouse. **Materials and Methods:** Lipopolysaccharide (LPS) was used to induce regional inflammation in the right striatum of a mouse brain (anteroposterior, +1.8; mediolateral, +2.0; dorsoventral,-3.0) using a Hamilton syringe (Stoelting, IL, USA). Splenocytes (2 x 10^7) were isolated from luciferase expressing transgenic mice (B6.LucTg), and adoptively transferred to recipient B6 (C57BL/6) mouse by intravenously injection for visualizing immune cell localization with bioluminescence imaging. Simultaneous PET/MR scans were acquired using ^{18}F-CB251 activity at a dose ranging from 9.25 to 11.1 MBq per mouse. To monitor the effect of anti-inflammatory drug with our multimodal imaging, mice were also treated with an inflammatory cytokine inhibitor, CDDO-methyl ester (200 nM, 3 times). **Results:** ^{18}F-CB251 was specific to the cells with the different TSPO expression, and activated immune cells. Simultaneous ^{18}F-CB251 PET/MR showed that ^{18}F-CB251 radioactivity was co-registered with the MR signals in the same region of LPS-injected mouse. Luciferase-expressing splenocytes were clearly localized at the LPS-injected site of the right striatum, indicating that peripheral immune cells were infiltrated in the LPS-induced inflammatory region of brain. Though BLI signals from peripheral immune cells in the inflamed region of mouse brain were very sensitive to measure the degree of inflammation, they were only detectable in the mouse brain under the skin. On the other hand, ^{18}F-CB251-PET radioactivity targeting TSPO successfully reflected the anti-inflammatory effect of CDDO-Me by quantitatively assessing the degree of neuro-inflammation without invasive methods. **Conclusion:** Our multi-modal imaging modalities with ^{18}F-CB251-PET/MR and BLI have great potential to detect neuro-inflammation and to evaluate the efficacy of anti-inflammatory drugs for pre-clinical studies, and ^{18}F-CB251-PET targeting TSPO can be suggested as an effective method to investigate severity of neuro-inflammatory diseases for clinical applications. **References:** None.

OP-384

Synthesis Of A Potential Cannabinoid Receptor Subtype 2 (CB2) Receptor Binding Ligand, Nucleophilic [^{18}F] Fluorination and First Preclinical Results

D. Modemann, *C. Bouter, A. Kreyenschmidt, C. Breunig, D. Stalke, J. Wiltfang, C. Sahlmann, Y. Bouter, B. Meller;*
Georg-August University Göttingen, Göttingen, GERMANY.

Aim/Introduction: There is evidence that cerebral inflammatory processes play a central role in the development of neurodegenerative diseases. These processes are characterized by the activation of microglia which is associated with the expression of CB2 in this cell type. Therefore the visualization of CB2 is of major interst. 3-acylindoles shows high affinities to CB1 and CB2.[1] Depending on substitution, the selectivity towards one receptor subtype could be achieved. The substitution with tetramethylcyclopropyl group lead to receptor ligands with high selectivity for CB2. Based on this, (1-(3-[^{18}F]fluoropropyl)-1H-indol-3-yl)(2,2,3,3-tetramethylcyclopropyl)methanone was chosen as a potential tracer for the nuclear imaging of CB2 receptors. **Materials and Methods:** A [^{19}F]fluorine-substituted reference compound and a tosylated precursor

were synthesized and characterized (^{1}H, ^{13}C, ^{19}F NMR). In both cases indole was first acylated followed by N-alkylation. [^{18}F] Fluoride was dried by azeotrope distillation using MeCN and $TBAHCO_3$. The precursor (40 µmol) was substituted in MeCN (5 min, 85 °C) and isolated by SPE- and HPLC-purification. Log P was determined by measurement of activity distribution between n-octanol and aqueous phosphate buffer (pH 7.4). Protein plasma binding was measured after incubation of the tracer in fresh human blood plasma, followed by protein precipitation and activity measurement. Additionally the tracer was incubated with CB2-expressing cell lines (HEK 293), the blocking of the receptor was performed by coincubation with HU308, a high affine CB2 Agonist. **Results:** The non-radioactive reference compound was obtained in 66% total yield and the corresponding tosylate-precursor was synthesized with 73% total yield, both in a four-step synthesis. The radioactive tracer was synthesized on a commercially available module (Neptis Perform, Ora) in up to 38% RCY and molar activities of up to 67 GBq/µmol (6-16 nmol carrier per Batch). The log P of the tracer was 3,83±0,04 (shake-flask method). Furthermore, protein-plasma binding was 81%. In blocking experiments using HU308 in CB2-expressing HEK cultures the cell-bound tracer fraction could be significantly reduced time-dependently (40–50%, $p<0.05$). **Conclusion:** A new potential tracer for nuclear imaging of CB2 in CNS was synthesized. The automated radio synthesis can be performed on a commercially available module and delivered the tracer in good yield and high molar activity. First preclinical evaluations were performed and present results are quite promising. **References:** [1] J. M. Frost et al. J. Med. Chem. **2010**, 53, 295-315.

906

Do.MoRe - Parallel Session: Artificial Intelligence in Image Processing

Monday, October 14, 2019, 14:30 - 16:00 Lecture Hall 112

OP-385

Low-count PET reconstruction using deep learning: application to FDG imaging of Hodgkin lymphoma during deep inspiration breath hold

M. Gæde, *C. N. Ladefoged, A. K. Berthelsen, A. Loft, F. L. Andersen; Rigshospitalet, Copenhagen University, Copemhagen, DENMARK.*

Aim/Introduction: Deep inspiration breath-hold (DIBH) can reduce radiation doses to the lungs, heart, and cardiac structures without compromising target dose in Hodgkin Lymphoma (HL) during radiation therapy. ^{18}F-FDG PET/CT is the choice for diagnostic and planning of HL and thus needs to be acquired in DIBH. Today, this is performed in a series of self-monitored breath-hold scans producing an averaged fulltime PET scan. Recently, methods utilizing deep learning (DL) for denoising have been proposed, but the impact on clinical accuracy has yet to be established. In this study we aim to use a DL network for noise reduction of short time DIBH PET scans and validate the accuracy using standard clinical metrics. **Materials and Methods:** 62 patients injected with 4 MBq/kg ^{18}F-FDG was imaged on a Siemens mCT. Six PET repetitions of 20 sec over the lung were acquired in DIBH followed by CT. Images was reconstructed using PSF modeling 3i21s, fully anonymized and cropped to 256x256 voxels. The first DIBH scan were used as input to the DL network along with the CT and the average of the 6 scans (in total 120 seconds scanning time) representing ground truth. We used 3D U-net with four blocks in the encoding part, each consisting of strided convolution, dropout and ReLU activation function. 8 adjacent image residuals (full time - short time) were used as input along with the CT. We used MAE as loss function, learning rate of 10^{-4} and trained for 2000 epochs. We used a 2-fold setup each using 48 patients for training. During validation, we predicted the residual noise, which was added to the single short-time DIBH images to obtain a denoised PET image. Metabolic tumor volumes were delineated on the 28 validation images by a nuclear medicine specialist. SUV mean and standard deviation are reported. **Results:** Visual inspection showed high resemblance of the denoised images compared to full time PET images. Tumor outline showed no visible change. SUV mean was reproduced in all tumors with a mean error of -4.0% [-17% - 13%]. Relative change in noise level (SD) in the tumors was -7% [-29% - 11%]. Outliers were located in the noisy images at the ends of the scanning field. **Conclusion:** We have demonstrated that by using residual training a DL network can be used to reduce the scanning protocol from 6 repetitions to just a single breath-hold PET without loss of clinical quality. **References:** None.

OP-386

Deep Learning segmentation of planar thyroid scintigraphy: application of U-net for cold nodules detection

F. Hanin[1], *M. Destiné*[1], *J. Marques-Trindade*[2], *I. Mathieu*[1], *B. Willemart*[1];
[1]*CHU UCLouvain Namur, Namur, BELGIUM,*
[2]*Neuralys Diagnostics, Brussels, BELGIUM.*

Aim/Introduction: Deep Learning covers the use of neural networks build with several layers of artificial neurons (or perceptrons). A specific network design called U-net allows to segment images. This network was trained and tested on 99mTc - thyroid planar scintigraphies for segmentation and test if such network can detect cold nodules. **Materials and Methods:** The same operator retrospectively manually segmented 1135 thyroid scintigraphies. Consecutive masks were generated from ROIs and used as ground truth. Data augmentation was performed on the data by horizontal flip to reach a total of 2270 images and corresponding masks. Dice loss function was used for training on an 1800 images batch, and testing was applied on 470 remaining images. The training was performed using keras 2.2.0 and Tensorflow-GPU 1.8 as backend installed on ubuntu 17.10 running CUDA 9.2 for two NVIDIA GTX 1070 GPUs.

Training of the network was performed with various batch sizes (from 1 to 20) and epochs (40 to 200). Dice value was computed for each test image, except for thyroids with no uptake (mask entirely negative, dice coefficient is not computable). **Results:** Best network performance was obtained by training with batches size of 2 and 150 epochs. Dice values on 427 test segmentations were: mean 0,98 ± 0,01; maximal value 0,992; minimal value 0,78; median value 0,983. Visual assessment of each of the 470 test images showed 29 wrong segmentations (6,1 %). Cold nodules were correctly included inside of the thyroid even when the uptake was visually similar to the background. **Conclusion:** Deep Learning shows interesting promises for diagnostic assistance. The training process is long, requires massive computing power and is subject to flaws as overfitting; however, these results show that specific tasks can be learned by artificial neural networks and even recognize cold nodules as part of the thyroid. Further research and data pooling are required to develop clinically valuable tools. **References:** U-Net keras code implementation used, https://github.com/petrosgk/Kaggle-Carvana-Image-Masking-Challenge.

OP-387

Automated Cervical Primary Tumor Functional Volume Segmentation in PET Images

A. Iantsen[1], *F. Lucia*[2], *M. Ferreira*[3], *P. Bonaffini*[4], *I. Masson*[5], *A. Mervoyer*[5], *C. Reinhold*[4], *P. Lovinfosse*[3], *R. Hustinx*[3], *M. De Cuypere*[3], *F. Kridelka*[3], *U. Schick*[2], *D. Visvikis*[1], *M. Hatt*[1];
[1]*LaTIM, INSERM, UMR 1101, University Brest, Brest, FRANCE,* [2]*Radiation Oncology Department, University Hospital, Brest, FRANCE,* [3]*Centre Hospitalier Universitaire de Liège, Liège, BELGIUM,* [4]*Department of Radiology, McGill University Health Centre (MUHC), Montreal, QC, CANADA,* [5]*Department of Radiation Oncology, Institut de Cancérologie de l'Ouest, Nantes, FRANCE.*

Aim/Introduction: Radiomics studies, radiotherapy treatment planning and response assessment mostly rely on manual or semi-automatic tumor segmentation in medical images such as MRI, CT and PET. The use of convolutional neural networks (CNNs) is relevant for fully automatic tumor delineation. However, this approach is challenging, especially in a multicentric context with images having different properties. Currently, most of the published studies have been devoted to the use of CNNs for automatic tumor segmentation in MRI and CT, whereas considerably less attention have been paid to PET images. Moreover, the majority of studies on applying CNNs for PET have used only datasets with small cohorts of patients from one or two centers. Our goal was to investigate the use of CNNs for fully automatic tumor delineation on PET images in a multicentric context and the challenging case of cervical cancer, where the primary tumor functional volume is often close to the bladder. **Materials and Methods:** We collected FDG PET images of 252 cervical cancer patients from five different institutions located in Europe and Canada. All ground-truth labels were determined by clinical experts that followed the same annotation procedure. We developed a versatile pipeline (data preprocessing, CNN architecture, the training procedure and the data augmentation strategy) that can be successfully applied for tumor segmentation on PET images and that is nearly indifferent to image properties specific for a particular center. We used a 3D-version of the popular U-Net model as a benchmark and presented its modified version that demonstrated significantly better results on our dataset. To estimate the performance of the model, we used cross-validation where each fold was comprised of only samples from a particular institute. A number of metrics including Dice similarity coefficient (DSC), sensitivity and positive predictive value were used for evaluation. **Results:** The designed CNN obtained good average accuracy for all considered institutes (DSC of 0.82 ±0.03) without requiring any change in the whole pipeline. Most importantly, it was able to learn in most cases not to include the nearby bladder in the resulting segmentation mask, hence allowing for a fully automated primary tumor functional volume delineation. **Conclusion:** We showed that CNNs can be successfully implemented for fully automatic tumor delineation on PET images without the need for user input, even in a multicentric context. The described general pipeline can be implemented with minimal modifications to solve a variety of segmentation tasks for PET images. **References:** None.

OP-388

Fully automated computations of putamen and caudate-based clinical measures in ^{18}F-FE-PE2I-PET/CT dopamine transport imaging using deep learning segmentation

L. Anderberg[1], *C. N. Ladefoged*[1], *K. Korsholm*[2], *L. Friberg*[2], *M. Lonsdale*[2], *I. Law*[1], *F. L. Andersen*[1];
[1]*Department of Clinical Physiology, Nuclear Medicine and PET, Rigshospitalet, Copenhagen, DENMARK,* [2]*Department of Clinical Physiology and Nuclear Medicine, University Hospital of Bispebjerg and Frederiksberg, Copenhagen, DENMARK.*

Aim/Introduction: The aim of this project was to develop a fully automated and practically useful method of delineating putamen and caudate for the newly introduced PET-tracer, ^{18}F-FE-PE2I, in the context of diagnosing Parkinsonism, and thus removing a time-consuming step required in computing clinically relevant measures. **Materials and Methods:** 170 patients ^{18}F-FE-PE2I PET/CT scanned for clinically uncertain Parkinsonism over a continuous eight month period were selected and divided for training/validation sets (80/20). The validation set had 24 abnormal and 10 normal PET scans. A 10-minute static PET-acquisition was performed 30-minutes after an i.v. injection of 200 MBq ^{18}F-FE-PE2I. Preprocessing of the data consisted in intensity normalization, skull stripping and spatial normalization to MNI space. A 3D U-net CNN was trained on ground-truth segmentations of putamen and caudate derived semi-manually on both CT and ^{18}F-FE-PE2I PET data. Patch shape was 80x48x48, stride one, sigmoid activation function on final layer, batch size 10, learning rate 5x10-5, generalized Dice loss, max pooling with pool size 2^3 and image augmentation was used. In validation, VOI-specific Dice-scores

were computed, as well as specific binding ratios (SBR's) relative to cerebellar gray matter and putamen-caudate activity ratios as the clinically relevant semi-quantitative metrics. **Results:** For normal and abnormal scans the Dice-scores for putamen mean (SD; range) were 97.6 (0.3; 97.2 - 97.9) and 89.3 (4.9; 79.1 - 96.9), respectively, and for caudate 96.3 (0.8; 95 - 97.5) and 83.7 (8.8; 72 - 98.1), respectively. The mean difference in putamen-SBR given the two segmentations (neural network minus ground-truth) for normal and abnormal scans were mean (SD; range) 0.03 (0.02; 0.01 - 0.05) and 0.62 (0.12; -0.10 - 0.38), respectively. For both methods, separation between normal and abnormal patients was perfect in the validation set, leading to an AUC of 1.0 in both cases. Similar results were observed for the putamen-caudate activity ratios. Inference time was approximately 5 seconds/scan. **Conclusion:** Using a 3D U-net CNN is a viable and computationally efficient method for delineating putamen and caudate and thus computing clinically relevant measures used in diagnosing Parkinsonism using 18F-FE-PE2I PET/CT. Main obstacles are associated with abnormal scans for which activity in both structures is reduced. Yet in terms of clinical measures, separability between abnormal and normal patients remained intact. **References:** None.

OP-389

Performance assessment of Artificial Intelligence-supported lesion classification in a heterogenous 18F-FDG PET/CT population

C. Von Gall, D. Thomas, V. Shah, L. Sibille, B. Spottiswoode; Siemens Medical Solutions USA, Inc., Knoxville, TN, UNITED STATES OF AMERICA.

Aim/Introduction: Artificial intelligence (AI) in PET/CT reading could support routine tasks, such as the identification of physiological uptake. As a prerequisite, the technology should perform robustly in a heterogeneous patient cohort. The aim of this work is to assess the performance of a deep learning algorithm that classifies 18F-FDG uptake in a such a population. **Materials and Methods:** 181 PET/CT scans were evaluated using a convolutional neural network [CNN], that was trained previously with 18F-FDG scans of lung cancer and lymphoma cases from two scanner types [1].The evaluation data consisted of lung cancer, lymphoma, melanoma, colorectal and other cancer types [27.1%,26%,9.4%,4%, and 24.3%, respectively]. In 9.4% the underlying disease was not available. Data was acquired on TruePoint, mCT, Horizon and Vision Biograph PET/CT scanner generations (4%,19%,57% and 20%,respectively) (Siemens Medical Solutions USA, Inc.).Acquisition and reconstruction methods consisted of OSEM and OSEM3D PSF-ToF (214ps to 540ps), with Gaussian post filter FWHM's varying from 0 to 5 mm. None of the data used for this evaluation was part of the initial development, training or testing of the AI algorithm. Automated segmentation was performed by identifying significant uptake using PERCIST recommendations (SUVpeak,Liver VOI) and segmenting using 42% of max[2]. The liver VOI was manually re positioned to cover normal hepatic tissue if necessary.The segmentation results were processed by the AI algorithm and classified into physiological or non-physiological. Two experienced nuclear medicine physicians (CvG,DT) reviewed the results independently and corrected the proposed classification if necessary. Both physicians were blinded to the disease type and patients'history and only findings with agreement between the two physicians were considered **Results:** The performance of the algorithm for 5744 findings with reader agreement was [sensitivity/specificity/accuracy/precision]: Overall [0.97/0.99/0.99/0.97]; Disease type: Lung cancer [0.99/1.00/1.00/0.99]; Lymphoma [0.98/0.99/0.99/0.98]; Melanoma [0.84/01.00/0.99/0.97]; Colorectal cancer [0.93/1.00/0.99/1.00]; Other cancer types [0.93/0.99/0.98/0.92]; Scanner type: TruePoint [0.98/1.00/0.93/1.00]; Horizon [0.97/0.99/0.98/0.95]; mCT [0.95/1.00/0.99/0.98]; Vision [0.99/0.99/0.99/0.96]. **Conclusion:** These results demonstrate robustness of the AI algorithm to disease type, scanner model and reconstruction parameters. This suggests that this approach may be suitable for routine clinical work. **References:** [1] Sibille et al. PET Uptake Classification in Lymphoma and Lung Cancer using Deep Learning, Proc. SNMMI, Philadelphia, (2018) [2] Wahl, R. et al, From RECIST to PERCIST: Evolving Considerations for PET Response Criteria in Solid Tumors. J Nucl Med 50, 122S-150S (2009).

OP-390

Consensus of machine learning pipelines for outcome prediction relying on clinical and radiomics features from ^{18}F-FDG PET/CT images in non-small cell lung cancer

M. Hatt[1], S. Sepehri[1], T. Upadhaya[2], D. Visvikis[1], C. Cheze Le Rest[2]; [1]INSERM, Brest, FRANCE, [2]CHU Milétrie, Poitiers, FRANCE.

Aim/Introduction: Radiomics consists in extracting a large number of quantitative features from medical images and combining these features with clinical variables in order to predict patients outcome, tumor sub-type or gene expression. Given the potentially very large number of features compared to the usually limited number of patients, machine (deep) learning (ML) is today a crucial part of the methodological toolbox used for radiomics analyses. In this work we evaluated the interest of combining several classifiers to improve the prediction performance. **Materials and Methods:** We implemented and optimized three popular ML methods: random forest (RF), support vector machines (SVM), -both with embedded features selection- and logistic regression (LR) -with stepwise feature selection- for predicting overall survival (OS) relying on clinical variables and ^{18}F-FDG PET/CT radiomics features in a cohort of 145 non-small cell lung cancer patients with stage 2 and 3, which was split into a training set (67%, n=97) and a testing set (33%, n=48) using stratified sampling, ensuring similar outcome, number of events and clinical characteristics in both sets. The set endpoint for this study was to identify patients with OS below the median (15 months). The outputs of the three ML pipelines were then aggregated through majority voting in order to derive a consensus classification. The classification accuracy was

used to evaluate the performance in the testing set. **Results:** In the training set, the 3 different ML pipelines selected slightly different sets of features (25, 27 and 37 variables for RF, SVM and LR) and reached similar although slightly different accuracy (90%, 95% and 74% for RF, SVM and LR respectively). In the testing set the accuracy was 68%, 67% and 65% for RF, SVM and LR respectively. The majority voting of their outputs reached a higher performance (accuracy of 100% in the training set and 75% in the testing set). **Conclusion:** Different ML pipelines reached similar accuracy in predicting the notoriously difficult endpoint of survival in NSCLC. Implementing simple majority voting of these outputs allowed to increase the accuracy. Even though the level of accuracy reached can seem relatively low (~75%), the resulting prognostic stratification is higher than when relying on clinical stage (58%), and of interest for clinical practice as it could help identifying patients with higher risk amongst stage II and III patients, that could benefit from intensified treatment and/or more frequent follow-up after treatment. **References:** None.

OP-391

Radiogenomics analysis of PET/CT images in lung cancer patients: Conventional radiomics versus deep learning

I. Shiri[1], *G. Hajianfar*[1], *S. Ashrafinia*[2,3], *E. Jenabi*[4], *M. Oveisi*[1,5], *A. Rahmim*[6,7];
[1]*Department of Biomedical and Health Informatics, Rajaie Cardiovascular Medical and Research Center, Iran University of Medical Science, Tehran, IRAN, ISLAMIC REPUBLIC OF,* [2]*Department of Radiology and Radiological Science, Johns Hopkins University, Baltimore, MD, UNITED STATES OF AMERICA,* [3]*Department of Electrical and Computer Engineering, Johns Hopkins University, Baltimore, MD, UNITED STATES OF AMERICA,* [4]*Research Center for Nuclear Medicine, Shariati Hospital, Tehran University of Medical Sciences, Tehran, IRAN, ISLAMIC REPUBLIC OF,* [5]*Department of Computer Science, University of British Columbia, Vancouver, BC, CANADA,* [6]*Departments of Radiology and Physics & Astronomy, University of British Columbia, Vancouver, BC, CANADA,* [7]*Department of Integrative Oncology, BC Cancer Research Centrer, Vancouver, BC, CANADA.*

Aim/Introduction: Analysis of the mutation status of epidermal growth factor receptor (EGFR) and Kirsten rat sarcoma viral oncogene (KRAS) mutations arefrequently used as treatment management tools in non-small cell lung cancer (NSCLC). The objective of this study was to investigate and compare EGFR andKRAS mutation status in PET images using conventional radiomics (explicit-feature-extraction) versus deep learning (implicit-feature-extraction). **Materials and Methods:** 147 NSCLC patients were included in the study, where 32 had effective EGFR mutations, 37 had KRAS mutations, and 110 and 115 had no EGFR or KRASmutations, respectively. Tumors were segmented by semiautomatic method from the PET images (expert radiologist). For conventional radiomics analysis,images were first discretized into 64 bin levels. 105 features were subsequently extracted from the lesions, including statistical (SUV), shape, GLCM, GLSZM, GLRLM, NGTDM and GLDM. Following feature extraction, we apply a union on embedded feature selection with different methods to get a set of useful features. After getting the union, we investigated correlations between features to eliminate high correlate features. The selected features were fed into different classifiers including decision tree(DT), bagging, gradient boosting (GB), random forest (RF), ada-boost (AB), logistic regression (LR), support vector machine (SVM), naïve Bayesian (NB), LASSO, multi-layer perceptron (MLP), and an ensemble of the above methods. By comparison, our deep learning framework included a 3D deep convolution neural network (CNN) composed of 3×3×3 convolutions, batch norm, LeakyReLU, and 2×2×2 max pooling blocks followed by fully connected layers. The final layer is a softmax for binary classification. We evaluated the performance of classifiers using receiver operating characteristic (ROC) area under the curve (AUC) analysis with 10-fold cross validation. **Results:** NB and RF with AUCs of 75.04 and 72.02 had the highest performance in predicting EGFR and KRAS mutations, respectively. Ensemble methods hadAUCs of 86.98 and 77.05 for predicting EGFR and KRAS, respectively. Finally, CNN had AUCs of 89.95 and 79.02 in predicting EGFR and KRAS mutations,respectively. **Conclusion:** Radiogenomics analysis of PET images in NSCLC patients was undertaken to link PET uptake and heterogeneity quantitation with genomics. Ensemble learning in the context of radiomics analysis can result in significantly higher performance compared to individual learning models, while deep learning (CNN; implicit feature extraction) showed the highest performance in prediction of EGFR and KRAS status. The results of the current study indicate the potential of advanced machine learning methods within radiogenomics analysis towards non-invasive prediction of mutation status in patients with NSCLC. **References:** None.

OP-392

Towards fully automated image processing in the clinic

J. Taylor, *P. Metherall;*
Sheffield Teaching Hospitals, Sheffield, UNITED KINGDOM.

Aim/Introduction: Machine learning has huge potential in Nuclear Medicine for increasing efficiency and improving accuracy. In particular, numerous authors have demonstrated high performance in segmentation, classification and regression tasks. However, many studies are based on assumptions which may not be reflective of the clinic, for instance using research rather than clinical data. Implementation for routine patient care has so far been limited. This study aims to demonstrate the performance of established machine learning methods for two routine nuclear medicine processing tasks, currently performed manually in clinic: 1) segmentation of the myocardium in MPS stress-rest scans (the segmentation mask being used to guide a rigid registration, to quantify differences in patient position) and 2) segmentation of the left ventricle blood pool for ejection fraction estimation on MUGA scans. Automating either of these tasks would achieve significant reductions in workload.

Materials and Methods: A large set of historical clinical data was used for both applications: 9604 MPS studies (stress and rest), acquired from a GE Discovery 530nm camera and 4092 MUGA scans acquired from a range of different gamma cameras, all with manually drawn segmentation masks, were extracted from the archives at Sheffield Teaching Hospitals. In each case a convolutional neural network was trained on 80% of the data using niftynet software (www.niftynet.io). For segmentation of the myocardium on MPS data the highres3dnet architecture was used. For the MUGA ejection fraction task, an architecture based on U-net was adopted. 10% of the data was set aside for validation and 10% for testing. Automatically generated segmentation masks were compared to those generated manually in terms of Dice scores. Output quantities from both processing tasks were also compared between automated and manual methods. **Results:** For task 1) a mean Dice of 0.85 was achieved on test data. Patient offset measurements gave a mean difference of -0.006mm when using the automatically generated segmentation, rather than the manual one (far smaller than the reconstructed pixel size). For task 2) automatic segmentations have so far been compared to manual across the whole cardiac cycle (i.e. treating the MUGA scan as a 3D dataset, with each slice representing a single cardiac phase). Preliminary results have demonstrated a mean Dice of 0.75. **Conclusion:** Existing machine learning technology can achieve high performance for routine nuclear medicine processing tasks. Fully automated patient positioning checks have now been implemented in the local department based on these results **References:** None.

907

Teaching Session 3 - Interactive Clinical Cases: Radiological Aspects of Thoracic Anatomy

Monday, October 14, 2019, 14:30 - 16:00 Lecture Hall 113

OP-393

Radiological Aspects of Thoracic Anatomy

T. Lynch;
Belfast, UNITED KINGDOM.

OP-394

Radiological Aspects of Thoracic Anatomy

N. Magee;
Belfast City Hospital, Belfast, UNITED KINGDOM.

OP-395

Radiological Aspects of Thoracic Anatomy

K. McManus;
Belfast, UNITED KINGDOM.

908

Clinical Oncology - Featured Session: Evaluating Immunotherapy - Where do we stand?

Monday, October 14, 2019, 14:30 - 16:00 Lecture Hall 114

OP-396

Scientific Programme

TBA;
TBA.

OP-397

Total Metabolic Tumor Volume (TMTV) correlates with treatment failure after CD19 CAR T-cell therapy in patients with relapsed/refractory diffuse large B-cell lymphoma (DLBCL)

L. S. Vercellino[1], *J. Paillassa*[1], *A. Martineau*[1], *S. Chevret*[1], *R. Di Blasi*[1], *S. Bernard*[1], *E. De Kerviler*[1], *V. Meignin*[1], *M. Meignan*[2], *P. Merlet*[1], *C. Thieblemont*[1];
[1]*Hôpital Saint Louis, Paris, FRANCE,* [2]*LYSA Imaging Henri Mondor University Hospitals, Créteil, FRANCE.*

Aim/Introduction: Despite significant clinical benefit in relapsed/refractory diffuse large B-cell lymphoma (R/R DLBCL), patients treated with autologous anti-CD19 chimeric antigen receptor (CD19 CAR) T-cells may experience early relapse/progression within the first 90 days after infusion. High total metabolic tumor volume (TMTV) measured with 18F-FDG PET/CT before R-CHOP is significantly associated with the outcome of patients with DLBCL. The aim of our study was to evaluate if high TMTV measured immediately before infusion was associated with early relapse in patients with R/R DLBCL treated with CAR T-cells. **Materials and Methods:** We performed a retrospective cohort analysis including consecutive patients treated with CAR T-cells for R/R DLBCL between June 2018 and February 2019. Median follow-up was 86 days (range: 15-198). TMTV was measured on pre-infusion PET/CT with either the 41% SUV_{max} threshold method ($TMTV_{41\%}$), or a fixed threshold of SUV>4 (TMTV4), using the free semiautomatic software Fiji. Total Lesion Glycolysis (TLG) was calculated for each method. Relapse and progression were determined based on the Lugano criteria. Predictive factors associated with relapse were assessed using univariate (10% level) then multivariate Cox models. To measure the predictive accuracy of TMVT for relapse, cumulative / dynamic ROC curves were used. **Results:** 31 patients received CD19 CAR T-cells. The median age was 48 years (range: 23-77), with 20, 5 and 6 patients having R/R DLBCL, primary mediastinal B-cell lymphoma and transformed follicular lymphoma, respectively. Tumor bulk >5 and>10 cm was reported in 12 (39%) and 7 (23%), respectively. Median $TMTV_{41\%}$ was 37.9 cm^3 (range: 1.44-630.9) and median TMTV4 was 48 cm^3 (range: 0-940). Median TLG41% was 294.3 g (range: 2.43-6685.2) and median TLGSUV4 was 379.5 g (range: 0-781.839). Treatment failure occurred in 11 patients, with a median time of

18 days (range: 4-119). IPI (p=0.045) and aaPI (p=0.09), number of previous lines (p=0.01), C-reactive protein (p=0.002), Albumin (p=0.005), Ferritin (p=0.001), lactate dehydrogenase (p=0.0006), most intense SUVmax (p=0.09), $TMTV_{41\%}$(p=0.003) and $TMTV_{SUV4}$ (p=0.006), $TLG_{41\%}$ (p=0.003), TLG_{SUV4} (p=0.010) were significantly associated with relapse by univariate analyses. After multivariate analysis and model selection, only the number of previous lines (HR 1.66, CI95% [1.10;2.52], p 0.016), and $TLG_{41\%}$ (HR 4.46, CI95% [1.58-12.6], p 0.005) were predictive of relapse. Similar results were reached with $TMTV_{SUV4}$ (HR 4.91, CI95% [1.47-16.5], p 0.010). **Conclusion:** In our cohort, TMVT and TLG at baseline were correlated to relapse in patients with R/R DLBCL treated with CAR T-cells. **References:** None.

OP-398

Value of FDG-PET/CT radiomic features in predicting response to anti-programmed death 1 (PD-1) antibodies treatment in refractory Hodgkin Lymphoma patients

M. Sollini[1], *M. Kirienko*[1], *L. Cozzi*[2], *C. Torrisi*[2], *L. Antunovic*[2], *E. Tabacchi*[3], *L. Calderoni*[3], *C. Nanni*[3], *A. Alessi*[4], *E. Seregni*[4], *S. Fanti*[3], *A. Guidetti*[4], *F. Ricci*[2], *P. Corradini*[4,5], *P. Zinzani*[3], *C. Carlo Stella*[1,2], *A. Chiti*[1,2];
[1]*Humanitas University, Pieve Emanuele, ITALY,* [2]*Humanitas Clinical and Research Center, IRCCS, Rozzano, ITALY,* [3]*Policlinico S.Orsola – University of Bologna, Bologna, ITALY,* [4]*Fondazione IRCCS Istituto Nazionale dei Tumori, Milan, ITALY,* [5]*University of Milan, Milan, ITALY.*

Aim/Introduction: To assess the predictive role of positron emission tomography (PET)-derived radiomic features in patients affected by refractory Hodgkin Lymphoma (HL) undergoing checkpoint inhibitor treatment. **Materials and Methods:** This retrospective multicenter study evaluated HL patients who performed a PET/CT before the initiation of anti-programmed death 1 (anti-PD-1) monoclonal antibodies. The volume of interest (VOI) of the target lymph node (the largest in transverse diameter and/or with the highest maximum standardized uptake value (SUVmax)) - was semi-automatically defined on PET images with a threshold of 40% of the SUVmax using a commercial software (PET VCAR, GE Healthcare, Waukesha, WI, USA). The features were extracted using LifeX software (http://www.lifexsoft.org, [1]). The dataset was geographically split into training (center 1) and validation (centers 2 and 3) sets. Combinations of imaging features were used as predictors in k-nearest neighbors after principal component analysis reduction. Moreover, clinical parameters (age, sex, bone disease) were tested as predictors. Treatment response was assessed according to Lyric criteria. Patients were classified as responders (stable disease, partial or complete response) and non-responders (progressive disease).The discriminative ability of the models to identify responders and non-responderswas calculated as true positive, true negative, false positive, and false negative. Statistical analysis was performed using STATA. **Results:** Fifty-seven HL patients, 36 in the training set (M:F=21:15) and 21in the validation cohort (M:F=15:6)were analyzed. Mean age was 32±10 and 37±14 years in the training and validation sets, respectively. Fourteen patients had bone disease (14/36) in the training set, and 9/21 in the validation set. Eleven and 10 patients were classified as responders in the training and validation sets, respectively. Six radiomics features (SUVmean, TLG, NGLDM_Coarseness, GLRLM_LRLGE, GLZLM_GLNU, GLZLM_ZP) were fed into the model. The radiomics model correctly predicted all patients as responders and non-responders in both the training and validation cohorts. The clinical model correctly identified 11/11 patients as responders and 22/25 patients as non-responders in the training set. The clinical model correctly predicted all patients as responders and non-responders in the validation cohort. **Conclusion:** Radiomics features performed slightly better than clinical parameters in predicting checkpoint inhibitor treatment outcome. Patients who benefit from checkpoint inhibitor treatment can be successfully selected by pre-treatment PET/CT textural features. **References:** 1. Cancer Research 2018;78(16):4786-4789.

OP-399

^{18}FDG PET/CT in the early assessment of NSCLC response to immunotherapy: results from a prospective study

O. Humbert, *N. Cadour, M. Paquet, D. Chardin, J. Otto, J. Darcourt; Centre Antoine-Lacassagne, Nice, FRANCE.*

Aim/Introduction: Few data are available regarding the role of ^{18}FDG-PET to monitor non-small cell lung cancer (NSCLC) response to immunotherapy. This prospective study aimed to describe the PET response patterns to immunotherapy and their association with clinical outcome. **Materials and Methods:** Fifty patients with metastatic NSCLC were prospectively included before pembrolizumab or nivolumab initiation. FDG-PET scan was performed at baseline and after 7 weeks of treatment ($PET_{Interim}1$). On $PET_{Interim}1$, different criteria/parameters of tumor response were assessed (PERCIST; ΔSUV; new lymph nodes or visceral lesion(s)). If a first PERCIST progressive disease (PD) without clinical worsening was observed, the treatment was continued and a subsequent FDG-PET scan ($PET_{interim}2$) was performed at 3 months of treatment. If a second PERCIST PD was assessed, a homogeneous progression of lesions (termed immune progressive disease: $iPD_{homogeneous}$) was distinguished from a heterogeneous one (termed immune dissociated response: iDR). Pseudo-progression (PsPD) was defined as a delayed PERCIST response or stability after a first PD. $PET_{interim}2$ was confronted to patients' clinical status for therapeutic management. A durable clinical benefit (DCB) of immunotherapy was defined as treatment continuation over a 6-month period. The association between $PET_{interim}1$ parameters, $PET_{interim}2$ evolutive profiles and DCB were assessed. **Results:** Using PERCIST on $PET_{interim}1$, 42% (21/50) of patients showed a response or stable disease, most of them (18/21) reached a DCB. In contrast, 58% (29/50) showed a PD, but more than one third (11/29) were misclassified as they finally reached a durable clinical benefit of immunotherapy. None of the standard $PET_{interim}1$ parameters could accurately identify non-responding

patients with early treatment failure. Treatment was continued in 19/29 of patients despite a first PD. The subsequent $PET_{interim}2$ demonstrated $iPD_{homogeneous'}$ iDR and PsPD in 47%(9/19), 26%(5/19) and 25%(5/19), respectively. Whereas no patients with $iPD_{homogeneous}$ experienced a DCB, all patients with iDR and PsPD reached a clinical benefit to immunotherapy. **Conclusion:** In patients with a PERCIST progressive disease on a first interim FDG-PET, a subsequent exam will identify more than half of them with iDR and PsPD, both patterns being strongly associated with a favorable clinical outcome. **References:** None.

OP-400

Combined Pre-Treatment Metabolic Tumor Burden on 18F-FDG PET/CT and Derived Neutrophils to Lymphocytes Ratio as Prognostic and Predictive Biomarkers in Advanced Non-Small Cell Lung Cancer Patients Treated with Immune Checkpoint Inhibitors

R. Seban[1,2], *L. Mezquita*[2], *L. Champion*[1], *A. Berenbaum*[2], *A. Botticella*[2], *C. Le Péchoux*[2], *C. Caramella*[2], *L. Cabel*[1], *M. Massiani*[1], *L. Dercle*[2], *S. Grimaldi*[2], *S. Leboulleux*[2], *D. Planchard*[2], *N. Girard*[3], *B. Besse*[2];

[1]*Institut Curie - René Huguenin, Saint-Cloud, FRANCE,* [2]*Gustave Roussy, Villejuif, FRANCE,* [3]*Institut du Thorax Curie-Montsouris, Paris, FRANCE.*

Aim/Introduction: We aimed to evaluate if a score combining Metabolic Tumor Burden (MTB) on pretreatment 18F-FDG PET/CT and derived Neutrophils to Lymphocytes Ratio (dNLR) could predict clinical outcomes in patients with advanced non-small cell lung cancer (NSCLC) treated with immune checkpoint inhibitors (ICIs). **Materials and Methods:** In this retrospective bicentric study, we enrolled 105 patients (80 for training and 25 for validation) with advanced NSCLC who underwent baseline 18F-FDG PET/CT before ICI initiation between July 2013 and October 2018. Clinical, biological (including dNLR=neutrophils/[leukocytes minus neutrophils]), pathological and PET parameters (including MTB) were evaluated. MTB was defined as the sum of the Metabolic Tumor Volume of all hypermetabolic lesions, measured with setting a margin threshold as 42% of SUVmax. A score based on MTB (high if > to the median value and dNLR (high if >3), was developed, characterizing 3 groups (good, 0 factors; intermediate, 1 factor; poor, 2 factors). A multivariate prediction model was developed using Cox models for progression-free survival (PFS) and overall survival (OS) and a logistic regression for disease control rate (DCR). **Results:** In the training cohort, median follow-up was 11.6 months (95%CI 7.7-15.5). Sixty-four and 52 patients experienced progression and death, respectively. DCB was 40%. Median PFS and OS were 2.5 (95%CI 1.6-3.3) and 9.2 (95%CI 6.2-12.2) months, respectively. In multivariate analyses, MTB>median (75cm³) and dNLR>3 were associated with shorter OS (HR 2.5, 95%CI 1.3-4.7, p=0.004 and HR 3.3, 95%CI 1.6-6.4, p=0.001, respectively). Median OS for good, intermediate, and poor score was 35.0 (95%CI 14.6-55.4), 12.5 (95%CI 6.6-18.5) and 2.4 (95%CI 1.9-2.9) months and median PFS was 9.8 (95%CI 5.2-14.4), 2.7 (95%CI 1.7-5.8) and 1.4 (95%CI 0.8-2.0) months (both p<0.001). The score also correlated with response. The good prognosis group was associated with DCR, with an OR of 8.5 (95%CI, 2.3-31.5, p=0.001), which was even higher than those determined with MTB or dNLR alone (OR 3.5, p=0.01 and 3.6, p=0.008, respectively). Results were reproducible in the validation cohort for OS, PFS, and DCR. **Conclusion:** Pretreatment score, combining MTB and dNLR, was correlated with worse outcomes for ICI. This innovative scoring approach could improve the selection of appropriate candidates and might be useful for identifying NSCLC patients unlikely to benefit from treatment with an ICI. **References:** None.

OP-401

FDG-PET/CT Imaging Of Immune-related Adverse Effects In Patients With Cutaneous Melanoma Treated With Pembrolizumab

A. Sabaté-Llobera[1], *P. C. Notta*[2], *M. Martínez de Bourio*[2], *L. Jiménez-Colomo*[3], *J. Martín-Liberal*[3], *M. Cortés-Romera*[2], *J. Marcoval*[4], *J. L. Vercher-Conejero*[2], *C. Gámez-Cenzano*[2];

[1]*PET Unit, Department of Nuclear Medicine-IDI. Skin Cancer Multidisciplinary Team. Hospital Universitari de Bellvitge-IDIBELL, L'Hospitalet de Llobregat (Barcelona), SPAIN,* [2]*PET Unit, Department of Nuclear Medicine-IDI. Hospital Universitari de Bellvitge-IDIBELL, L'Hospitalet de Llobregat (Barcelona), SPAIN,* [3]*Department of Medical Oncology-ICO. Skin Cancer Multidisciplinary Team. Hospital Universitari de Bellvitge-IDIBELL, L'Hospitalet de Llobregat (Barcelona), SPAIN,* [4]*Department of Dermatology. Skin Cancer Multidisciplinary Team. Hospital Universitari de Bellvitge-IDIBELL, L'Hospitalet de Llobregat (Barcelona), SPAIN.*

Aim/Introduction: Pembrolizumab is a PD-1 inhibitor that has demonstrated to improve progression-free survival and overall survival in patients with advanced melanoma*. However, it is not exempt of secondary effects, mostly due to blocking the inhibitory pathways of T-cell activation, which can cause autoimmune-like pathology. We describe different immune-related adverse effects (IRAE) detected on FDG-PET/CT in patients treated with this immune checkpoint inhibitor. **Materials and Methods:** Retrospective review of prospectively collected data of 13 patients (8 women) with cutaneous melanoma treated with pembrolizumab due to systemic disease relapse. All of them had FDG-PET/CT scans performed before initiating systemic therapy and at different time-points during treatment. FDG-PET/CT detection of possible IRAE was reported and evaluated, both clinically and/or in subsequent FDG-PET/CT studies. **Results:** Seven patients (53.8%) presented findings suggestive of IRAE at follow-up FDG-PET/CT; six of them (87.5%) were women. The most common adverse effect was thyroiditis (3 patients), followed by sarcoid-like reactions (2 patients), aortitis (1 patient), and arthritis/synovitis (1 patient). In 6 cases, these effects appeared after 2-8 cycles of pembrolizumab, while one of the sarcoid-like reactions appeared 2 months after finishing the treatment (36 cycles). All thyroiditis presented with hypothiroidism parameters at blood tests and were treated

with levothyroxine. Both cases with sarcoid-like reactions were histologically confirmed, one through an endobronchial ultrasound bronchoscopy and the other one with a cutaneous biopsy. The patient with arthritis/synovitis complained of articular pain, while the one with aortitis was asymptomatic; no blood tests with inflammatory parameters were performed in this patient, and vascular wall activity persisted in subsequent FDG-PET/CT. Among patients with IRAE, four reached a metabolic complete response (57.1%), one a partial response, and two progressed (28.6%). Of those who had not IRAE, five were progressing (83.3%), and one had stable disease after having progressed at 2 cycles of pembrolizumab. **Conclusion:** IRAE are frequently evidenced in FDG-PET/CT of patients treated with pembrolizumab for cutaneous melanoma, being thyroiditis the most common in our series. Despite the little number of patients analysed, those with IRAE seem to have a better response to treatment. **References:** Robert C, Schachter J, Long GV, et al. Pembrolizumab versus Ipilimumab in Advanced Melanoma. N Engl J Med 2015; 372:2521-32.

909

Special - Parallel Session: Tomorrow?s Experts Session - Best-Ranked Papers from the Under-30s

Monday, October 14, 2019, 14:30 - 16:00 Lecture Hall 115

OP-402

First extensive preclinical evaluation of PSMA-specific tracers for prostate cancer radioligand therapy

E. Ruigrok, *S. U. Dalm, E. de Blois, N. van Vliet, D. C. van Gent, J. Haeck, C. de Ridder, D. Stuurman, M. W. Konijnenberg, W. M. van Weerden, M. de Jong, J. Nonnekens;*
Erasmus MC, Rotterdam, NETHERLANDS.

Aim/Introduction: Prostate specific membrane antigen (PSMA) is overexpressed in >90% of prostate cancer (PCa) cases. Therefore, various radiolabeled PSMA-targeting tracers are clinically applied for PCa imaging and radioligand therapy (RLT). The PSMA binding affinities and biodistribution of these tracers however, have not yet been compared. Furthermore these PSMA-targeting radiotracers show toxicity in other PSMA-expressing organs, such as the salivary glands. A proper evaluation therefore is essential to determine the best performing tracer, however, such evaluation is currently missing. This study is the first extensive preclinical evaluation of the clinically relevant PSMA targeting tracers DOTA-PSMA-617, DOTA-PSMA-I&T together with nanobody DOTA-JVZ-007 using PSMA expressing cell lines and PCa patient-derived xenografts (PDXs). **Materials and Methods:** In vitro displacement assays were performed on PSMA-expressing cells (LNCaP, DU145-PSMA, U2OS-PSMA) and cryosections of PSMA-positive PDXs (PC295), which were incubated with the 3 [^{177}Lu]Lu-labeled tracers together with increasing concentrations of unlabeled tracers to determine the relative binding affinities. To assess tumor-specific binding, autoradiography assays were performed on cryosections of human salivary- and renal tissue incubated with the [^{177}Lu]Lu-labeled PSMA-tracers with or without an excess of the same unlabeled tracer. The in vivo biodistribution patterns of [^{177}Lu]Lu-DOTA-PSMA-617 and [^{177}Lu]Lu-DOTA-PSMA-I&T were determined in athymic nude mice bearing PC295 PDXs. Mice were intravenously injected with the [^{177}Lu]Lu-labeled tracers (30MBq/0.3nmol) and sacrificed 4h, 8h, or 24h post injection (p.i.) (n=4 per group). Organs and blood were collected and tracer uptake was measured. **Results:** In vitro displacement studies revealed high and PSMA-specific binding affinity for all three tracers with IC50 values in the nanomolar range. [^{177}Lu]Lu-DOTA-JVZ-007 could not be displaced by DOTA-PSMA-617 and DOTA-PSMA-I&T, suggesting this tracer to target an alternative PSMA binding site. Autoradiography assays showed a ±90% lower tumor binding of [^{177}Lu]Lu-DOTA-JVZ-007 and interestingly, a 4-times lower tumor-to-kidney and tumor-to-salivary gland ratio as compared to [^{177}Lu]Lu-DOTA-PSMA-617 and [^{177}Lu]Lu-DOTA-PSMA-I&T. In vivo biodistribution assays revealed a comparable average tumor uptake of [^{177}Lu]Lu-DOTA-PSMA-617 and [^{177}Lu]Lu-DOTA-PSMA-I&T of ±5% at all time points. However, [^{177}Lu]Lu-DOTA-PSMA-I&T showed a ±40x higher uptake in the kidneys at 4h and 8h p.i. resulting in an unfavorable tumor-to-kidney ratio. **Conclusion:** While in vitro binding characteristics for [^{177}Lu]Lu-DOTA-PSMA-617 and [^{177}Lu]Lu-DOTA-PSMA-I&T are highly comparable, [^{177}Lu]Lu-DOTA-PSMA-617 has a more favorable biodistribution in mice with a higher tumor-to-kidney ratio compared to [^{177}Lu]Lu-DOTA-PSMA-I&T. Concerning [^{177}Lu]Lu-JVZ-007, the significantly lower in vitro binding of this tracer to the salivary and renal tissue is very favorable and underlying reasons are being explored further. **References:** None.

OP-403

Synthesis and Preclinical Evaluation of GRPR/PSMA Bispecific Heterodimers for the Theranostics Application in Prostate Cancer

A. Abouzayed, *C. Yim, B. Mitran, S. Rinne, V. Tolmachev, M. Larhed, U. Rosenström, A. Orlova;*
Uppsala University, Uppsala, SWEDEN.

Aim/Introduction: Prostate cancer is one of the most prevalent and deadliest cancers in men worldwide. Several prostate cancer cell markers have been identified, including gastrin-releasing peptide receptors (GRPR) and prostate-specific membrane antigens (PSMA). GRPR and PSMA are overexpressed in the majority of prostate cancer samples with GRPR expression being higher in earlier stages and PSMA expression increasing with the disease progression. The aim of this study was to develop and evaluate GRPR/PSMA bispecific heterodimers for the management of prostate cancer. The heterodimers consist of urea derivative PSMA-617 and bombesin-based antagonistic analogue RM26 (D-Phe-Gln-Trp-Ala-Val-Gly-His-Sta-Leu-NH_2) linked via X-triazolyl-Tyr-PEG2 (X= PEG2 (BO530), $(CH_2)_8$ (BO535),

or none (BO536)). The heterodimers can be radioiodinated with I-123 for SPECT imaging, I-124 for PET imaging, or I-131 for therapeutic purposes. **Materials and Methods:** The heterodimers were synthesized by solid phase peptide synthesis, radiolabeled with I-125, and evaluated in vitro for their binding specificity, cellular retention, and affinity towards GRPR and PSMA. In vivo specificity was studied on mice bearing PC-3 (GRPR+) or LNCaP (PSMA+) xenografts for all heterodimers. [^{125}I]I-BO530 was further evaluated in PC-3pip (GRPR+/PSMA+) xenografted mice 1, 3, 24 and 72 h pi. MicroSPECT/CT scans were acquired 3, 24 and 72 h pi. **Results:** The heterodimers were radiolabeled with I-125 with high radiochemical yields. After HPLC purification radioiodinated heterodimers bound specifically to GRPR and PSMA in vitro. The half-maximal inhibitory concentrations were 8-25 nM for GRPR and 95-127 nM for PSMA. The heterodimers demonstrated high degree of activity retention in PC-3pip cells (after 24 h incubation 65% of initially bound activity were cell associated). In vivo, only [^{125}I] I-BO530 demonstrated in vivo specificity to both GRPR and PSMA receptors. The biodistribution study of [^{125}I]I-BO530 in mice bearing GRPR+/PSMA+ xenografts showed relatively slow for small peptides blood clearance that resulted in high tumor activity uptake (21±3%ID/g at 1 h pi). While activity uptake in normal organs rapidly decreased, activity uptake in tumors was stable between 3 and 24 h pi (30-35%ID/g). Already 24 h pi activity uptake in tumors exceeded all other organs, including excretory organs. At 72 h pi activity uptake decreased only 2-fold. The SPECT/CT images confirmed ex vivo results. **Conclusion:** The radioiodinated PSMA-617/RM26 heterodimer [^{125}I]I-BO530 is a promising agent for the theranostics application in prostate cancer. **References:** None.

OP-404

Parameterized Mathematical Modelling of Positron Range Effects in PET/MRI

A. Berger[1], *J. Cal-Gonzalez*[1], *I. Rausch*[1], *H. Kertesz*[1], *J. Herraiz*[2], *A. López-Montes*[2], *M. Conti*[3], *T. Beyer*[1];
[1]*QIMP Team, Center for Medical Physics and Biomedical Engineering, Medical University of Vienna, Vienna, AUSTRIA,* [2]*Grupo de Física Nuclear and UPARCOS, Universidad Complutense de Madrid, Madrid, SPAIN,* [3]*Siemens Medical Solutions, Knoxville, TN, UNITED STATES OF AMERICA.*

Aim/Introduction: Positron range (PR) limits the spatial resolution of PET imaging and it is affected by magnetic fields in PET/MR systems, causing an axial elongation of the PR that degrades image quality and introduces artefacts [1]. Here, we present a mathematical modelling approach of PR in the presence of external magnetic fields that can be used for PR correction. **Materials and Methods:** GATE (GEANT4 Application for Tomographic Emission) simulations [2] of point sources of various radionuclides with significant positron emission energies (^{18}F, ^{68}Ga, ^{82}Rb and ^{124}I) were performed in three different tissues (water, lung and bone). Simulations were performed for static magnetic fields (B_0) of 0T, 1.5T, 3T, 5T, 7T and 9.4T set along the main PET system axis (z-axis). The distribution of positron annihilation points was modelled as a direct product of (i) the radial distribution of annihilation events and (ii) a 1D height-distribution that intrinsically models the impact of B_0 according to the performed simulations [3]. Mean positron range (Rmean) was calculated from the simulation output. **Results:** Elongated annihilation point distributions were observed for high B0 for all simulated isotopes. The line profiles of positron annihilation points of ^{124}I/^{68}Ga show a relative reduction of 2D positron range of up to 53%/62%, measured perpendicular to the B_0 axis for a field of 9.4T respectively. Absolute reduction of mean positron range (Rmean) for ^{18}F/^{68}Ga in water (0.32/1.94 mm), bone (0.09/0.34 mm) and lung (1.58/6.89 mm) was seen for increasing B_0 from 0.0T to 9.4T. General agreement of simulated PR with measured values was 3.0% / 9.1% for ^{18}F / ^{68}Ga respectively [4]. **Conclusion:** A parameterized mathematical model to calculate PR in magnetic field was established based on Monte Carlo simulations that correctly estimates PR for various B_0 field strengths. The inclusion of this model into PR correction algorithms is work in progress and it will be presented at the conference. **References:** [1] Kolb A. et. al. Shine-Through in PET/MR Imaging: Effects of the Magnetic Field on Positron Range and Subsequent Image Artifacts. JNM 2015 [2] Stute et al., Monte Carlo simulations of clinical PET and SPECT scans: impact of the input data on the simulated images. Phys Med Biol 2011 [3] Blanco A. Positron range effects on the spatial resolution of RPC-PET. IEEE Nucl Sci Symp Conf Rec 2006 [4] J Cal-González et. al. Positron range estimations with PeneloPET. Phys Med Biol 2013.

OP-405

CTCA based assessment of endothelial shear stress and functional significance of coronary lesions: relationship and comparative performance in predicting impaired vasodilating capability by PET myocardial perfusion imaging

G. E. Kalykakis[1,2], *A. Antonopoulos*[3], *T. Pitsargiotis*[1,4], *P. Kafouris*[5,1], *P. Siogkas*[6], *A. Giannopoulos*[7], *R. Liga*[8], *P. Kaufmann*[7], *A. Scolte*[9], *G. Pelosi*[8], *O. Parodi*[8], *J. Knuuti*[10], *D. Neglia*[8], *D. Fotiadis*[11], *C. Anagnostopoulos*[1];
[1]*Biomedical Research Foundation Academy Of Athens, Athens, GREECE,* [2]*Ionian University-Department of Informatics, Kerkyra, GREECE,* [3]*General Hospital of Athens Hippocrates, Athens, GREECE,* [4]*University of Patras-Department of mechanical engineering and aeronautics, Patra, GREECE,* [5]*National & Kapodistrian University of Athens-Department of informatics and communication, Athens, GREECE,* [6]*Biomedical Research Institute - FORTH, Ioannina, GREECE,* [7]*University Hospital Zurich, Zurich, SWITZERLAND,* [8]*Institute of Clinical Physiology, Pisa, ITALY,* [9]*Leiden University Medical Center, Leiden, NETHERLANDS,* [10]*Turku PET Centre, Turku, FINLAND,* [11]*University of Ioannina, Ioannina, GREECE.*

Aim/Introduction: Interrogation of functional significance of coronary lesions and shear stress forces acting on atherosclerotic plaques detected by CCTA has become feasible through

application of computational fluid dynamics in CTCA datasets. Our aim was to investigate a) the relationship of local endothelial shear stress (ESS) with anatomic, morphologic and functional characteristics of coronary stenoses and b) the comparative performance of ESS and virtual functional assessment index (vFAI), a validated surrogate of FFRCT, in predicting impaired coronary vasodilating capability assessed by PET perfusion imaging in patients with stenoses of intermediate severity in CTCA. **Materials and Methods:** Thirty-two patients (21 male, mean age 65.6 ± 7.2 years) with intermediate pre-test likelihood of coronary artery disease (CAD), who were enrolled in the EVINCI and SMARTool projects and had undergone CTCA and PET myocardial perfusion imaging using ^{15}O-water or ^{13}N-ammonia, were included in the study. PET was considered positive for abnormal vasodilating capability when >1 contiguous segments showed both stress MBF ≤2.3 mL/g/min and MFR ≤ 2.5 for^{15}O-water or <1.79 mL/g/min and ≤ 2.0, for ^{13}N-ammonia respectively. A previously validated vFAI threshold of 0.85 was used as predictor of impaired vasodilating capability. ESS computation was based on a mean aortic pressure of 100 mmHg for the inlet and a mean mass resting blood flow rate 0.00105 kg/s for the outlet. ESS was calculated in the full length of the stenosis and the mean value was obtained. High-risk atherosclerotic plaque characteristics, (calcified-non calcified volume, thickness, eccentricity, plaque burden), were extracted in the lesions using image analysis techniques in the CTCA datasets. **Results:** Sixty-two coronary segments were evaluated. Forty-one lesions with stenosis 31-50% and 21 lesions with stenosis 51-70% were identified. ESS was higher in the latter (3.0, IQ: 1.85 to 5.24 vs. 1.8, IQ: 1.39 to 3.6, p=0.04). There was a moderate positive correlation between ESS and plaque burden (r=0.675, p<0.0001) and a weak negative correlation (r=-0.3, p=0.017) between the former and vFAI. ESS was not different in stenoses with impaired vasodilating capacity compared to those without (2.5, IQ: 1.70-6.92 vs. 1.85, IQ: 1.32-3.84, p=0.25), but vFAI was (0.75, IQ:0.65-0.79 vs 0.87, IQ:0.82-0.93,p=0.002).The latter was also a good predictor of impaired coronary vasodilating capability (AUC=0.840, CI:0.69-0.93, p<0.0001). **Conclusion:** ESS is related with stenosis severity and atherosclerosis plaque burden. It is weakly associated with vFAI, but in contrast to the latter does not appear to be a predictor of impaired coronary vasodilating capability. **References:** None.

OP-406

VoxelWise Analysis of Dynamic^{18}FFET PET Enables NonInvasive Prediction of IDH Genotype in Newly Diagnosed Glioma

A. Holzgreve[1], *M. Unterrainer*[1], *L. Kaiser*[1], *F. Vettermann*[1], *B. Suchorska*[2], *J. Tonn*[2], *P. Bartenstein*[1], *N. Albert*[1];
[1]*LMU Munich University Hospital, Dept. of Nuclear Medicine, Munich, GERMANY,* [2]*LMU Munich University Hospital, Dept. of Neurosurgery, Munich, GERMANY.*

Aim/Introduction: Prognosis of glioma patients notably relies on mutation of the isocitrate dehydrogenase (IDH) gene and non-invasive methods for the prediction of the IDH genotype are much sought-after. Voxel-wise analysis of dynamic ^{18}FFET PET has recently been introduced as a reader-independent tool for in vivo characterisation of glioma. However, the value of voxel-wise analysis of dynamic ^{18}FFET PET for non-invasive prediction of IDH genotype is hitherto unknown. **Materials and Methods:** 322 patients with a newly diagnosed FETpositive glioma were included (194 IDH wildtype, 128 IDH mutant). All patients underwent dynamic ^{18}FFET PET imaging and contrast-enhanced MRI prior to surgery. The biological tumor volume in PET was defined by the established threshold of 1.6 × background activity (2040 min p. i.). Voxel-wise analysis of static and dynamic PET parameters was performed, e. g. tumortobackground ratios (TBR) or the percentage of tumor voxels with a time-to-peak lower than 12.5 min ($\%TTP_{\leq 12.5}$). Optimal cutoffs to predict an IDH wildtype status were chosen according to Youden's index following ROC analysis and the positive and negative predictive values were calculated. **Results:** IDH wildtype gliomas showed generally a higher uptake intensity than IDH mutant gliomas (e.g. TBR_{max} 3.32 vs. 2.79; p=0.01) and a higher percentage of voxels with a short TTP ($\%TTP_{\leq 12.5}$ 34% vs. 7%; p<0.01). TBR analyses did not reveal reliable cutoff values for the discrimination between IDH wildtype and IDH mutant gliomas. Conversely, voxel-wise TTP analysis was able to discriminate between IDH wildtype and IDH mutant gliomas: In the overall group, $\%TTP_{\leq 12.5}$ (cutoff >22%) predicted an IDH wildtype status with a PPV of 89% (NPV 69%). 113 gliomas did not show contrast-enhancement in MRI (40 IDH wildtype, 73 IDH mutant). In this subgroup, $\%TTP_{\leq 12.5}$ with a cutoff of >24% predicted an IDH wildtype status with a PPV of 75% (NPV 83%). By adding a subsequent TBR_{max} analysis (cutoff >2.06) PPV could be increased to 100% (n=32 IDH wildtype gliomas). **Conclusion:** Voxelwise analysis of dynamic ^{18}FFET PET enables the non-invasive prediction of the prognostically pivotal IDH mutation status in gliomas at initial diagnosis. Especially in the critical subgroup of non-contrast enhancing gliomas, the combination of static and dynamic voxel-wise ^{18}FFET PET analyses further increases the diagnostic accuracy. **References:** None.

OP-407

Histologically-confirmed diagnostic efficacy of ^{18}F-rhPSMA-7 positron emission tomography for lymph node staging of patients with high risk primary prostate cancer

L. Jooss[1], *M. Kroenke*[1], *A. Wurzer*[2], *K. Schwamborn*[3], *L. Ulbrich*[1], *T. Maurer*[4], *S. Kropf*[5], *T. Horn*[6], *B. Haller*[7], *H. Wester*[2], *W. Weber*[1], *M. Eiber*[1];
[1]*Department of Nuclear Medicine, Klinikum rechts der Isar, TUM, Munich, GERMANY,* [2]*Chair of Pharmaceutical Radiopharmacy, TUM, Munich, GERMANY,* [3]*Institute of Pathology, TUM, Munich, GERMANY,* [4]*Martini-Klinik, UKE, Hamburg Eppendorf, GERMANY,* [5]*Scintomics GmbH, Fuerstenfeldbruck, GERMANY,*
[6]*Department of Urology, Klinikum rechts der Isar, TUM, Munich, GERMANY,* [7]*Institute of Medical Statistics and Epidemiology, Klinikum rechts der Isar, TUM, Munich, GERMANY.*

Aim/Introduction: ^{18}F-rhPSMA7 is a new PSMA (prostate specific membrane antigen)-targeting agent with the advantage of both efficient labeling with ^{18}F and radiometals and a minimal renal excretion. This retrospective analysis investigates the diagnostic efficacy of ^{18}F-rhPSMA7 PET for lymph node staging compared to morphological imaging (CT and MRI) for patients with primary high-risk prostate cancer, validated by histopathology. **Materials and Methods:** Data from 58 patients with high risk prostate cancer (defined by D'Amico) who were staged with ^{18}F-rhPSMA7 PET/CT or PET/MRI between July 2017 and June 2018 was analysed. Median pre-scan PSA was 12.4 ng/mL (range, 1.2-81.6 ng/mL). Median injected activity of ^{18}F-rhPSMA-7 was 327 MBq (range, 132-410 MBq), with a median uptake time of 79.5 min (range, 60-153 min). All patients underwent subsequent radical prostatectomy and extended pelvic lymph node dissection. PET and morphological datasets were rated independently by an experienced reader for the presence of lymph node metastases. Results were compared to histopathological findings on a patient and templated based manner. **Results:** Lymph node metastases were present in 18 patients (31.0%) located in 52 of 375 templates (13.9%). On patient-based analyses ^{18}F-rhPSMA-7 PET showed a sensitivity of 72.2%, a specificity of 92.5% and an accuracy of 86.2%. Morphological imaging resulted in 50.0%, 72.5% and 65.5%, respectively. On template-based analyses the sensitivity, specificity and accuracy of ^{18}F-rhPSMA-7 PET were 53.8%, 96.9% and 90.9%, and those of morphological imaging were 9.6%, 95.0% and 83.2%, respectively. ROC analyses showed ^{18}F-rhPSMA-7 PET to perform significantly better than morphological imaging on both patient (AUCs of 0.858 vs. 0.649, p=0.012) and template-based analyses (AUCs of 0.765 vs. 0.589, p<0.001). Median histopathological size of lymph node metastases missed in ^{18}F-rhPSMA-7 was 3.5 mm (range: 0.3-15 mm). **Conclusion:** ^{18}F-rhPSMA-7 PET is superior to morphological imaging for lymph node staging of high risk primary prostate cancer. Its diagnostic efficacy is similar to published data for other PSMA-ligands. **References:** D'Amico AV, Whittington R, Malkowicz SB, et al. Biochemical outcome after radical prostatectomy, external beam radiation therapy, or interstitial radiation therapy for clinically localized prostate cancer. JAMA 1998;280:969-974.

OP-408

SUV-based interpretation is better for prognosting response than Deauville Score in Hodgkin Lymhpoma patients

E. Texte[1], *J. Lequesne*[2], *P. Vera*[1], *A. Stamatoullas-Bastard*[3], *S. Becker*[1];
[1]*Centre Henri Becquerel, Nuclear Medicine Dpt, Rouen, FRANCE,*
[2]*Centre Henri Becquerel, Statistical analysis Dpt, Rouen, FRANCE,*
[3]*Centre Henri Becquerel, Haematology Dpt, Rouen, FRANCE.*

Aim/Introduction: To evaluate the prognostic role of Tumor/Liver ratio (TLr) and SUVmax reduction (ΔSUVmax) in patients with Hodgkin Lymphoma (HL) at interim and end-of-treatment FDG PET-CT and to compare these methods with visual interpretation (Deauville-Score). **Materials and Methods:** 374 patients who received primary treatment with ABVD or BEACOPP therapy were retrospectively analyzed. All patients underwent FDG-PET/CT at baseline and end-of-treatment (PETeot) and 348 during treatment after 2 (PET2) or 4 (PET4) courses of chemotherapy. The receiver operating characteristic (ROC) curves were used to determined optimal cut-offs of TLr (SUVmax target residual lesion/SUVmax liver) at PET2, PET4 and PETeot. ΔSUVmax optimal cut-offs were also determined with ROC curves at PET2 and PET4. Positive and negative predictive values were calculated and compared to Deauville score for predicting progression free survival (PFS)**.** Cox proportional-hazards model was performed to test the relationship between the study variables and survival rates. Survival curves were estimated using Kaplan-Meier analysis. **Results:** Median follow-up was 56.6 months. TLr optimal cut-offs were 1.66 at PET2, 1.35 at PET4 and 1.29 at PETeot. ΔSUVmax optimal cut-off were -73% at PET2 and -69% at PET4. TLr, ΔSUVmax and Deauville Score were strong predictors of clinical outcome with a better positive predictive values (PPV) for TLr and ΔSUVmax and similar negative predictive values (PPV were 33%, 40% and 58% at PET2 and 53%, 67% and 70% at PET4 for DS, deltaSUVmax and TLr respectively). In univariate analysis, the three interpretation methods were statistically significant (p<0.001 for PFS and OS). In multivariate analysis, only TLr was an independent prognostic factor for PFS at PET2, PET4 and PETeot and ΔSUvmax was an independent prognostic factor at PET4. BEACOPP treatment was also statistically significant for survival rates. Chemotherapy regimen combined with PET results according to TLr identified 4 groups with very different outcome: i) patients treated with BEACOPP and a negative PET, ii) patients treated with ABVD and a negative PET, iii) patients treated with BEACOPP and a positive PET, iiii) patients treated with ABVD with a positive PET. These 4 groups had a 89.1%, 84.8%, 64.8% and 25.4% 2y-PFS (p<0.0001) respectively at PET4. **Conclusion:** TLr is a strong predictor of therapeutic response during interimPET whether it is used after two or four courses of chemotherapy and at the end of treatment and can outperform Deauville Score. DeltaSUVmax is an independent prognostic factor at PET4. Larger prospective studies should be done to validate these cut-offs. **References:** None.

OP-409

Integrating radioguidance during robot-assisted laparoscopic surgery - In-human evaluation of a DROP-IN gamma probe

M. N. van Oosterom[1,2], *P. Dell'Oglio*[1,3], *P. Meershoek*[1,2], *T. Maurer*[4], *P. J. van Leeuwen*[2], *E. M. K. Wit*[2], *H. G. van der Poel*[2], *F. W. B. van Leeuwen*[1,2,3];
[1]*Interventional Molecular Imaging Laboratory, Department of Radiology, Leiden University Medical Center, Leiden, NETHERLANDS,*
[2]*Department of Urology, Netherlands Cancer Institute-Antoni van Leeuwenhoek Hospital, Amsterdam, NETHERLANDS,*
[3]*ORSI Academy, Melle, BELGIUM,* [4]*Martini-Clinic, University Medical Center Hamburg-Eppendrof, Hamburg, GERMANY.*

Aim/Introduction: In the surgical management of prostate cancer, robot-assisted laparoscopic surgery has rapidly evolved into a routine procedure. While the robot offers many advantages, it can also create challenges e.g. when attempting to apply radioguided surgery using a rigid laparoscopic gamma probe. The limited maneuverability of such a probe restricts lesion identification when low-activity lesions are situated in close proximity to a high-activity background. Furthermore, in the robot-assisted setup, the surgeon relies on the bedside assistant for probe positioning. To regain autonomy and to increase maneuverability during radioguidance, by allowing the (wristed) robotic tools to position the probe, we created a tethered DROP-IN gamma probe in 2014 and translated it into humans in 2018 [1-4]. We have successfully demonstrated in vivo use of this technology during the SN procedure and PSMA-targeted lymphatic salvage procedure in prostate cancer using proof-of concept studies. In the current study, we evaluate the technique in a larger SN patient cohort and make an in-depth comparison with respect to the traditional laparoscopic gamma probe and fluorescence guidance. **Materials and Methods:** 25 prostate cancer patients were included, all scheduled for a SN procedure, extended pelvic lymph node dissection and prostatectomy. After intraprostatic injections of (indocyanine green-)^{99m}Technetium-nanocolloid, preoperative SN identification was performed using lymphoscintigraphy and SPECT/CT. Surgical excision of the SNs was assisted by a combination of DROP-IN radioguidance, traditional laparoscopic radioguidance and Firefly fluorescence guidance. **Results:** 44 SNs were resected under DROP-IN gamma probe guidance (average of 1090 counts in vivo and 1681 ex vivo). 91% of these could also be detected using fluorescence imaging in vivo (95% ex vivo). 17 SNs (39%) were also surgically pursued with a laparoscopic gamma probe (average of 742 counts in vivo and 969 counts ex vivo). As a result of the restricted maneuverability in specific anatomical locations (i.e. right cloquet, right paravesical, right communis and left iliaca externa regions), one quarter of these nodes could not be (clearly) identified without the help of either the DROP-IN or Firefly modalities **Conclusion:** This clinical study further underlines that the DROP-IN gamma probe technology has the potential to bring radioguided surgery within reach of robot-assisted procedures. Due to improved maneuverability, the DROP-IN probe even indicated an increased detection rate with respect to the traditional laparoscopic gamma probe. **References:** [1] M.N.vanOosterom et al., Am_J_Nucl_Med_Mol_Imaging, 2016 [2] B.Fuerst et al., IEEE_Trans_Med_Imaging, 2016 [3] P.Meershoek et al., Eur_J_Nucl_Med_Mol_Imaging, 2019 [4] F.W.B.vanLeeuwen et al., Clin_Nucl_Med, in_press.

910

Inflammation & Infection - Parallel Session: PET in Vascular Infection and Myocardial Inflammation

Monday, October 14, 2019, 14:30 - 16:00 Lecture Hall 116

OP-410

18F-FDG-PET accuracy for diagnosis of Infective Endocarditis compared to Duke echocardiographic criteria

M. Gazzilli[1], R. Durmo[1], D. Albano[1], E. Cerudelli[1], M. Bonacina[1], F. Dondi[1,2], A. Mazzoletti[1,2], P. Bellini[1,2], F. Bertagna[1,2], R. Giubbini[1,2]; [1]Azienda Socio Sanitaria Territoriale degli Spedali Civili di Brescia, Brescia, ITALY, [2]Università di Brescia, Brescia, ITALY.

Aim/Introduction: In the latest update of the European Society of Cardiology (ESC) guidelines echocardiography, contrast-enhanced CT, radiolabelled leucocyte SPECT/CT and [18F]FDG-PET/CT are been included in the diagnostic flow chart for the management of infective endocarditis (IE). The aim of this study is to analyse the diagnostic accuracy of [18F]FDG-PET/CT in the detection of IE. **Materials and Methods:** We retrospectively analyzed 105 patients (M:F=54:51, mean age 62 years, range 18-88) who underwent 18F-FDG-PET/CT scan for suspicious of IE, diabetic patients were excluded. PET/CT images were analyzed qualitatively and semi-quantitatively by measuring maximum and mean Standardized Uptake Value (SUVmax and SUVmean) of the suspected lesion. These results were compared with the echocardiographic findings, according to major Duke criteria, and the clinical final diagnosis. **Results:** Comparing PET/CT report and clinical final diagnosis revealed a Sensitivity of 96,3% (87.25-99.55 95%CI), Specificity of 92.59% (82.11-97.94% 95%CI), Negative Predictive Value of 96,15% (86.49-98.99% 95%CI), Positive Predictive Value of 92.86% (83.49-97.10% 95%CI) and of Accuracy 97.22% (92.10-99.42 95% CI), in presence of adequate preparation to reduce the physiological myocardial uptake of 18F-FDG: a low carbohydrate, high protein, high fat diet starting 72 hours before the examination. The transthoracic and/or transesophageal echocardiograph findings showed a Sensitivity of 48.84% (33.31%-64.54% 95%CI), Specificity of 52.23% (40.12%-66.02% 95%CI), Negative Predictive Value of 60% (50.79%-68.55% 95%CI), Positive Predictive Value of 42% (32.57%-52.06% 95%CI)and of Accuracy 51.43% (41.47%-61.30% 95%CI). The echocardiograph accuracy in the detection of IE is considerable reduced in presence of prosthetic valves (PVE) due to the artefacts. PET/CT has shown greater accuracy than the echocardiograph in the evaluation of the response of antimicrobial therapy (97% vs 62%) and in the study of cardiovascular implantable electronic device (CIED) infections or local device infection the accuracy is not comparable. Furthermore, PET/CT confirmed its ability to identify extra-cardiac sites of [18F]FDG uptake in patients with other diseases (pneumonias, vasculitis, vascular prosthesis infections,

spondylodiscitis, mediastinitis, etc). In two cases PET/CT allowed to diagnose unknown tumors. **Conclusion:** Our preliminary results suggested the high accuracy of PET/CT in the diagnosis and follow-up of IE on native valve (NVE), prosthetic valve (PVE) and CIED; PET/CT ability to provide other diagnoses and/or incidental diagnosis. An adequate preparation strategy for cardiac PET/CT imaging is critical to the accuracy of IE detection because complete suppression of physiologic 18F-FDG uptake by normal myocardium facilitates the detection of inflammation in the heart. **References:** None.

OP-411

Quantitative analysis of 18F-Fluorodeoxyglucose uptake by PET/CT for detection infective endocarditis

M. Gazzilli[1], *R. Durmo*[1], *D. Albano*[1], *E. Cerudelli*[1], *M. Bonacina*[1], *F. Dondi*[1,2], *A. Mazzoletti*[1,2], *P. Bellini*[1,2], *F. Bertagna*[1,2], *R. Giubbini*[1,2];
[1]*Azienda Socio Sanitaria Territoriale degli Spedali Civili di Brescia, Brescia, ITALY,* [2]*Università di Brescia, Brescia, ITALY.*

Aim/Introduction: Infective endocarditis (IE) outcome largely depends on early diagnosis and treatment, despite developments in the imaging and microbiological techniques the final diagnosis of IE often remain a challenging. 18F-FDG PET/CT was recently introduced as a new tool for the diagnosis of IE, especially in patients with prosthetic valve and ICD. The aim of this study is to demonstrate that higher accuracy can be obtained using quantitative methodology to analyze PET/CT. **Materials and Methods:** A series of 108 consecutive patients (M:F=57:51, mean age 62 years, range 18-88) with suspected IE were analyzed; diabetic patients were excluded. After clinical assessment and echocardiographic exams, the patients underwent to FDG PET/CT imaging after adequate preparation to reduce the physiological myocardial uptake of 18F-FDG (a low carbohydrate, high protein, high fat (LCHPHF) diet starting 72 hours prior the scan). PET/CT images were analyzed qualitatively: 2 nuclear physicians indipendently reviewed fusion and maximum intensity projection images and they classified suspect lesions uptake of FDG into 3 patterns (none, focal or diffuse). For quantitative analysis, we obtained SUVmax, heart-to-blood pool (H/BP) SUV ratio, and heart-to-liver (H/L) SUV ratio. The SUVmax in the suspect lesions, H/BP SUV ratio, H/L SUV ratio were analyzed using receiver operating charateristic (ROC) curves, displaying sensitivity and specificity at various cut-off values. **Results:** Of the 108 patients enrolled in the study, 53 had a clinical final diagnosis of IE. The SUVmax of the suspect lesion was significantly higher in patients with IE compared with non-IE patients (8,6 ± 6,02 vs 4,42 ± 2,03). The area under the ROC curve was 0.976 for SUVmax. Using a cut-off value of 3,32, the sensitivity was 90,6 (79,3-96,8 95% CI) and specificity was 94,5 (84,9-98,8 95%CI) for diagnosing IE, wich could be more accurate than visual analysis. **Conclusion:** When evaluated by quantification of myocardial suspect lesions FDG PET/CT imaging, in patient with adeguate diet preparation, provides high sensitivity and specificity for diagnosing IE. **References:** None.

OP-412

Diagnostic and therapeutic impact of wholebody FDG PET/CT in patients suspected of infective endocarditis on native or prosthetic valve: the prospective multicenter TEPvENDO study

F. Rouzet[1], *B. Mahida*[1], *S. Tubiana*[1], *M. Esposito-Farese*[1], *E. Ilic-Habensus*[1], *A. Bourdon*[2], *E. Chevalier*[3], *N. Piriou*[4], *O. Morel*[5], *O. Humbert*[6], *A. Devillers*[7], *B. Grégoire*[8], *C. Laouenan*[1], *B. Iung*[1], *X. Duval*[1];
[1]*Bichat hospital, Paris, FRANCE,* [2]*Lapeyronie Hospital, Montpellier, FRANCE,* [3]*Nancy hospital, Nancy, FRANCE,* [4]*Nantes hospital, Nantes, FRANCE,* [5]*Besançon hospital, Besancon, FRANCE,* [6]*Dijon hospital, Dijon, FRANCE,* [7]*Centre Eugène Marquis, Rennes, FRANCE,* [8]*Hospices Civils de Lyon, Lyon, FRANCE.*

Aim/Introduction: FDG-PET/CT has been integrated in the 2015 European society of cardiology (ESC) guidelines as a major Duke criterion in patients suspected of infective endocarditis (IE) on prosthetic valve (PV). The benefit with native valves (NV) is not well established. The aim of the study was to prespectively assess the diagnostic and therapeutic impacts of systematic whole-body FDG PET/CT in patients suspected of IE on PV or NV. **Materials and Methods:** Consecutive patients referred for high suspicion of IE in 8 french tertiary care hospitals underwent FDG PET/CT. ESC-2015-modified Duke criteria were applied and therapeutic plans were established jointly by two experts immediately before and after FDG PET/CT completion. The final diagnosis was established as the Duke classification at 6 months **Results:** 140 patients have been enrolled in the study (70 PV and 70 NV; 34 and 46 classified as definite IE before FDG PET/CT, respectively). FDG abnormal cardiac uptake was present in 64 (45.7%) patients (47 [67.2%] PV and 17 [24.3%] NV) but was considered related to IE in 42.9% and 15.7%, respectively ($p<0.001$). FDG extracardiac uptake was present in 44.3% and 51.4% of PV and NV, respectively. IE classification was modified in 24.3% and 5.7%, respectively ($p=0.005$); net reclassification index as compared to final diagnosis was 20% and 4.3%, respectively. Therapeutic plans were modified in 21.4% and 31.4% ($p=0.02$) in PV and NV patients, respectively. Taken together, patients for whom FDG PET/CT modified care had more frequently an inconclusive echocardiography ($p<0.001$) or were classified as possible IE at inclusion ($p=0.04$). The nature of the cardiac valve was not a determinant of the overall benefit. **Conclusion:** Systematic FDG PET/CT significantly impacted diagnostic classification and therapeutic plans in patients suspected of IE with both PV and NV. **References:** Clinical Trials: NCT02287792.

OP-413

Advanced texture features analysis of [^{18}F]FDG-PET/CT imaging in patients with infective endocarditis

R. Zanca[1], *A. Marciano*[1], *F. Bartoli*[1], *S. Vitali*[1], *R. Doria*[2], *U. Conti*[3], *E. Lazzeri*[1], *R. Slart*[4], *A. Glaudemans*[4], *P. Erba*[1];
[1]*Regional Center of Nuclear Medicine, Department of Translational Research and New Technology in Medicine, University of Pisa*

and AOUP, Pisa, ITALY, [2]Unit of Infectious Diseases, Univerisity of Pisa and AOUP, Pisa, ITALY, [3]Division of Cardiology, Univerisity of Pisa and AOUP, Pisa, ITALY, [4]Medical Imaging Center, Department of Nuclear Medicine and Molecular Imaging, University of Groningen, University Medical Center Groningen, Pisa, ITALY.

Aim/Introduction: [18F]FDG-PET/CT has been recently introduced in the diagnostic algorithm for the diagnosis of infective endocarditis (IE). [18F]FDG PET/CT positivity at the valve site, which is a major criteria of the 2015 ESC criteria, is generally characterized by visual analysis, but sometimes it can be difficult to differentiate between infection and reactive inflammation. The advantage of semiquantitative assessment is still matter of discussion. In this study we evaluated the value of advanced texture features analysis for diagnosing IE. **Materials and Methods:** In this work we prospectively evaluated a series of [18F]FDG PET/CT scans in 226 patients (M:F =139:87, mean age 66 ± 18 years, median age 72, range 13-86) with suspected IE (native valve endocarditis (NVE) =52, prosthetic valve endocarditis (PVE) biological =116 and PVE mechanical =58) studied at the AOUP Pisa and the University Medical Center Groningen between January 2015 to April 2019. Images were analysed (1) visually to define different patterns of uptake (focal versus diffuse), (2) by semiquantitative parameters (SUVmax, SUVmean ,SUVstd, TLA) and (3) with advanced texture features (a total of 44 features). To this aim we used LIFEx software (www.lifexsoft.org) from semiautomatically segmented PET images with Advantage Workstation GE. Results were compared based on the confirmed diagnosis of EI, type of valve, microbiology and biochemical markers. Presence and duration of antimicrobial treatment at the time of PET/CT was also considered. Statistical analysis was performed with JMP Statistical Discovery™. **Results:** Texture features analysis allowed to identify a different signature in patients with confirmed IE and without IE (sensitivity 84%, specificity 84%), in patients with IE on native valve and prosthetic valve (sensitivity 97%, specificity 97%), in presence of focal versus diffused pattern of uptake, as shown in Table 1. Ongoing antimicrobical treatment and its duration has significant impact on texture features, in particular when long lasting. In addition, patients with MSSA infection also presented with a specific signature (sensitivity 89%, specificity 89%). **Conclusion:** Our results demonstrated the feasibility of the textural feature analysis in patients with suspected. We found added value in the differential diagnosis between patients with confirmed IE, both in NVE and PVE and in patients with MSSA infection. Ongoing antimicrobical treatment and its duration impact on texture features, in particular when long lasting. **References:** None.

OP-414

Effect of image artifacts on texture analysis in mechanical prosthetic valve endocarditis

R. Zanca[1], *A. Marciano*[1], *F. Bartoli*[1], *S. Vitali*[1], *E. Lazzeri*[1], *R. Slart*[2], *A. Glaudemans*[2], *P. Erba*[1];
[1]*Regional Center of Nuclear Medicine, Department of Translational Research and New Technology in Medicine, University of Pisa and AOUP, Pisa, ITALY,* [2]*Medical Imaging Center, Department of Nuclear Medicine and Molecular Imaging, University of Groningen, University Medical Center Groningen, Groningen, NETHERLANDS.*

Aim/Introduction: Several studies have shown that the semiquantitative parameters are influenced by the distortion of the signal generated by valve prosthesis, especially mechanical (PVEm), in the diagnosis of Endocarditis with [18F]FDG PET/CT. Accordingly, the use nonattenuation-corrected (NAC) images for a correct diagnosis is recommended. Our group is currently working on radiomics analysis of [18F]FDG PET/CT images in IE. Thus, we are interested in understanding the possible impact of metal artifacts on images analysis. In this preliminary study we aim to investigate the influence of image artifacts on radiomic analysis in prosthetic valves endocarditis. **Materials and Methods:** This is a preliminary analysis of the first 20 consecutive patients (M:F =15:5, mean age 57 ± 16.20 years, median age 56, range 26-80) with PVEm studied prospectively with [18F]FDG PET/CT at AOUP Pisa in January 2017. We performed semiautomatically segmentation of [18F]FDG PET/CT attenuation-corrected images and NAC images on the same patients with LIFEx software (www.lifexsoft.org). Texture features was also performed using LIFEx package. Statistical analysis was performed with JMP Statistical Discovery$_{tm.}$ **Results:** No significant difference in the texture features analysis (total of 44 features) in attenuation-corrected images and NAC images were found. On the contrary, semiquantitative parametetrs (SUVmax, SUVmean, SUVstd, TLA) were significantly different in the two groups (SUVmean p- value <0.001; SUVstd p- value <0.001; SUVmax p- value <0.001; TLA p- value <0,001). **Conclusion:** Despite preliminary and in a small number of patients, our data suggest that texture features analysis is much less influenced by image artifacts as compare to semiquantitative parameters. Therefore, the use of texture features is feasible also in presence of metal artifacts, representing a more accurate analysis. The next steps of this work will be the analysis of motion effects artifacts on texture analysis results. **References:** None.

OP-415

18F-FDG PET/CTand Radiolabeled Leukocyte Scintigraphy for the Diagnosis of Infected Aortic Aneurysms

P. Mention[1], *L. Omarjee*[2], *J. Brosseau*[1], *O. Couturier*[1], *M. Ammi*[1], *J. Picquet*[1], *P. Abgueguen*[1], *V. Rabier*[1], *H. Rakotonirina*[1], *F. Lacoeuille*[1];
[1]*CHU Angers, Angers, FRANCE,* [2]*CHU Rennes, Rennes, FRANCE.*

Aim/Introduction: Computed tomography angiography (CTA) plays a key role in the management of patients with aortic aneurysms. But it can be inconclusive in patients whom infected aortic aneurysm is suspected. The incremental diagnostic value of 18F-FDG PET/CT and radiolabeled leukocyte scintigraphy (RLS) has already been reported in endocarditis. The aim of this study was to compare the respective performance of 18F-FDG PET/CT and RLS for the diagnosis of IAA. **Materials and Methods:**

^{18}F-FDG PET/CT and RLS were performed on 18 patients admitted for clinically suspected IAA and inconclusive CTA results. The results of ^{18}F-FDG PET/CT and RLS were analyzed separately by experienced physicians blinded to both the results of the other imaging technique and patient outcome. Final diagnosis of IAA was established based either on the bacteriological analyses of excised tissues or by experienced infectious disease specialists and vascular surgeons. **Results:** Of the 18 patients, 9 were classified as infected. Sensitivity, specificity, positive predictive value, negative predictive value and accuracy were 89%, 89%, 89%, 89% and 89% for ^{18}F-FDG PET/CT and 75%, 100%, 100%, 79% and 89% for RLS respectively. Discrepancies between the results of ^{18}F-FDG PET/CT and RLS occurred in 4 patients (22%). In patients with IAA, 2 had true positive ^{18}F-FDG PET/CT results (Coxiella Burnetti and Yersinia Enterolitica) and 1 had true positive RLS results (Coxiella Burnetti). The last patient with a discrepancy (non-IAA) had false positive ^{18}F-FDG PET/CT. **Conclusion:** ^{18}F-FDG PET/CT offers higher sensitivity while RLS offers higher specificity for the detection of active infection in patients with suspected infectious aortic aneurysms. A sequential strategy consisting of ^{18}F-FDG PET/CT imaging followed by RLS when patients had positive ^{18}F-FDG PET/CT results without obvious bacteriological data may be of relevance. **References:** None.

OP-416

Reference values for abnormal uptake of 68Ga-DOTATOC in patients with myocardium inflammation

S. Boughdad, M. Meyer, E. Pruvot, P. Pascale, K. Casagrande, J. Costes, J. Delage, M. Jreige, N. Schaefer, J. Prior;
CHUV, Lausanne, SWITZERLAND.

Aim/Introduction: Suspicion of myocardial inflammation (MINF) is a common referral for FDG PET/CT scan, which has demonstrated good diagnostic performance to detect abnormal uptake. However, it requires a strict low-carbohydrate diet ideally over several days, which prevents its realization in the emergency setting. Conversely, ^{68}Ga-DOTATOC, a somatostatin analogue targeting SSTR 2 (Somatostatin Receptor 2) without such restrictions, appears as an attractive alternative. SSTR 2 is expressed by active inflammatory cells, especially lymphocytes present in MInf. Thus, we compared myocardial metabolic uptake in clinically symptomatic patients with MINF (MINF+) to a control group of patients with neuro-endocrine tumors without cardiac symptoms (NET). **Materials and Methods:** Patients were recruited from March-April 2019 at our institution and received 2 MBq/kg of ^{68}Ga-DOTATOC intravenously with a PET/CT acquisition 90 minutes after. Visual and quantitative analyses of myocardial uptake were assessed. Visual analysis was considered positive if myocardial uptake was easily distinguishable from the intracavitary activity of the left ventricle (LV). For quantitative analysis, the following myocardial SUV measurements Max, Peak and Mean were extracted from different regions: sidewall of the LV, apex and interventricular septum. We calculated ratios for each region between SUVmax(M) or SUVpeak(M) of the myocardium and SUVmean(LV) inside the LV. We used t-tests for independent samples to compare SUVs and ratios values between MINF+ and NET groups and ROC analysis to assess diagnostic performance. **Results:** Sixteen patients were included, 6 in MINF+ group (4 females/2 males ; 50±22y) and 10 in NET group (4 females/6 males ; 57±17y). All patients in MINF+ group had abnormal ^{68}Ga-DOTATOC myocardial uptake, hence positive scans, whereas none was seen in NET group. Acquisition time was similar in MINF+ and NET group respectively (105±16 vs. 95.3±4.7min, p=0.17). Absolute SUV values did not show consistent significant differences between groups, for instance at the LV free wall: SUVmax and SUVpeak in MINF+ vs NET patients: 1.4±0.4 and 1.2±0.4 vs 2.2±1.0 and 1.1±0.3 respectively, (p>0.05 for both). Conversely, SUVmax(M)/SUVmean(LV) and SUVpeak(M)/SUVmean(LV) ratios were significantly greater in all myocardial regions (p<0.0001 for both) in MINF+ vs NET patients, with the latter showing the best accuracy on ROC analysis (Table 1). **Conclusion:** ^{68}Ga-DOTATOC PET/CT appears as a reliable option to visualize myocardial inflammation in clinically symptomatic patients. A quantitative assessment of myocardial uptake using the SUVpeak(M)/SUVmean(LV) ratio can separate patients with from those without myocardial inflammation with optimal accuracy. These results need to be validated prospectively in a larger population. **References:** None.

OP-417

Comparison of 68Ga-DOTANOC PET/CT with cardiac MRI for imaging inflammation in cardiac sarcoidosis

P. Kaushik, C. Patel, G. Gulati, S. Seth, N. Parakh, R. Kumar, R. Guleria, C. Bal;
All India Institute of Medical Sciences, New Delhi, INDIA.

Aim/Introduction: The diagnosis of cardiac sarcoidosis is often challenging due to lack of a gold standard investigation. Endomyocardial biopsy has poor sensitivity due to sampling errors and other tests like ECG, echocardiography, serum ACE etc are not very sensitive or specific. FDG PET/CT has been used for imaging inflammation in cardiac sarcoidosis for diagnosis, follow up and prognostication. However, the major limitation of FDG PET/CT is the inability to achieve adequate suppression of physiological FDG uptake in the myocardium in all patients despite prolonged fasting, dietary modification or other interventions. 68Ga-DOTANOC can be a useful alternative to FDG as it binds to somatostatin receptors expressed on inflammatory cells and does not show any significant physiological uptake. The aim of our study was to compare 68Ga-DOTANOC PET/CT and myocardiac perfusion SPECT with cardiac MRI for detecting inflammation in patients with clinical suspicion of cardiac sarcoidosis. **Materials and Methods:** 21 consecutive patients with clinical suspicion of cardiac sarcoidosis were included in the study. Of these, 9 patients had biopsy proven extracardiac sarcoidosis. All patients underwent cardiac 68Ga-DOTANOC PET/CT and cardiac MRI. Any focal increased uptake on 68Ga-DOTANOC PET/CT was considered as positive. On cardiac MRI, presence of T2 hyperintensity with late gadolinium

enhancement (LGE) was taken as positive. Considering CMR as gold standard we calculated sensitivity, specificity, PPV and NPV of 68Ga-DOTANOC PET/CT for detecting inflammation. **Results:** A total of 14 patients were positive on 68Ga-DOTANOC PET/CT. CMR revealed both T2 hyperintensity and LGE in 10 patients (suggestive of ongoing inflammation) and only LGE without T2 hyperintensity in 11 patients (suggestive of fibrosis). Therefore, 10 patients were considered as positive on CMR. Both 68Ga-DOTANOC PET/CT and CMR were positive in 9 patients and both were negative in 6 patients. One patient was positive on CMR but did not show any abnormal 68Ga-DOTANOC uptake. There were 5 patients who were categorised as negative on CMR but showed abnormal focal 68Ga-DOTANOC uptake. All of these 5 patients had LGE without T2 hyperintensity of CMR. Considering CMR as gold standard, the sensitivity, specificity, PPV and NPV of 68Ga-DOTANOC PET/CT for detecting ongoing inflammation were 90%, 54.5%, 64.3% and 85.7% respectively. The percent concordance between the two modalities was 71.4%. **Conclusion:** 68Ga-DOTANOC is an alternative tracer which may be used for PET imaging of inflammation in cardiac sarcoidosis. **References:** None.

1001

CME 8 - Thyroid Committee: Secondary Effects of Radioiodine Treatment

Monday, October 14, 2019, 16:30 - 18:00 Auditorium

OP-418

General Aspects of Radiobiology in Radioiodine Therapy

C. D'Alessandria;
Nuklearmedizinische Klinik und Poliklinik, Klinikum Rechts der Isar, Technische Universität München, Munich, GERMANY.

OP-419

Deterministic Effects of Radioiodine Treatment
P. Spanjol;
University Hospital, University of Geneva, Department of Nuclear Medicine, Geneva, SWITZERLAND.

OP-420

Stochastic Effects of Radioiodine Treatment
P. Radojewski;
Charité – Universitätsmedizin Berlin, Klinik für Nuklearmedizin, Berlin, GERMANY & University Hospital, University of Geneva, Department of Nuclear Medicine, Geneva, SWITZERLAND.

1002

Joint Symposium 15 - Oncology & Theranostics Committee / ESMO: Immunological Landscape in Solid Tumours and its Implications in Response to Immunotherapy

Monday, October 14, 2019, 16:30 - 18:00 Lecture Hall 311

OP-421

Prognostic and Predictive Role of Tumour Immune Landscape
J. Haanen;
Medical Oncology and Molecular Oncology & Immunology Divisions, The Netherlands Cancer Institute, Amsterdam, NETHERLANDS.

OP-422

Immunoscore and its Introduction in Clinical Practice
J. Galon;
INSERM, Laboratory of Integrative Cancer Immunology (Team 15), Cordeliers Research Center, Paris, FRANCE.

OP-423

Advanced Techniques for the Assessment of Tumour Immunological Profile
E. Lugli;
Laboratory of Translational Immunology, Humanitas Clinical and Research Center, Rozzano, ITALY.

OP-424

Immune-PET, Tumour Metabolism and Patterns of Response to Immunotherapy
E. Lopci;
Istituto di Ricerca e Cura a Carattere Scientifico (IRCCS), HUMANITAS (Rozzano), Nuclear Medicine, Milan, ITALY.

OP-425

Discussion

1003

Joint Symposium 16 - Dosimetry + Translational and Molecular Imaging Therapy Committee / ESTRO: Dosimetry in Preclinical Setting to Determine Dose Limits and Extrapolation to Clinical Dosimetry

Monday, October 14, 2019, 16:30 - 18:00 Lecture Hall 312

OP-426

Variable Proton RBE - Is it Time to Reconsider the Dose Limits for Normal Tissues?

I. Toma-Dasu;
Stockholm University and Karolinska Institutet, Medical Radiation Physics, Stockholm, SWEDEN.

OP-427

The Physics of Radiobiology for Alpha-Particle Radionuclide Therapy Effects

R. Hobbs;
Johns Hopkins University, Radiation Oncology, School of Medicine, Baltimore, MD, UNITED STATES OF AMERICA.

OP-428

The Biology of Radiobiology Markers for Dose-Effects in Radionuclide Therapy

J. Nonnekens;
Erasmus MC, Radiology & Nuclear Medicine and Genetics, Rotterdam, NETHERLANDS.

1004

CTE 4 - Technologist Committee / SNMMI: Technologist's Guide Launch - Radiopharmacy: An Update

Monday, October 14, 2019, 16:30 - 18:00 Lecture Hall 117

OP-429

Technologist's Guide Launch

M. Attard;
Isala, Radiology and Nuclear Medicine Department, Zwolle, NETHERLANDS.

OP-430

Generators used in Nuclear Medicine

M. Crosthwaite;
Virginia Commonwealth University, Richmond, VA, UNITED STATES OF AMERICA.

OP-431

Theoretical Basics of Radiopharmacy

Z. Wimana;
Institut Jules Bordet, Nuclear Medicine/ Radiopharmacy, Brussels, BELGIUM.

1005

M2M - Parallel Session: Tumour Microenvironment & Cancer Biomarkers

Monday, October 14, 2019, 16:30 - 18:00 Lecture Hall 111

OP-432

The Case for SUV75 as an Imaging Biomarker of Response to Therapy in FDG-PET Imaging of Triple Negative Breast Cancer (TNBC) Patient-Derived Tumor Xenografts (PDX)

K. Shoghi, S. Li, T. Whitehead, S. Roy, L. Strong, N. Fettig, R. Wahl, M. Savaikar;
Washington University School of Medicine, St. Louis, MO, UNITED STATES OF AMERICA.

Aim/Introduction: Inter- and intra heterogeneity of patient-derived tumor xenografts (PDX) present several challenges in developing optimal quantitative pipelines to assess response to therapy. The objective of this work was to perform radiomics analysis in preclinical FDG-PET of triple negative breast cancer (TNBC) PDX towards an optimal metric of response to therapy **Materials and Methods:** Three TNBC PDX sub-types served as a preclinical platform to develop and optimize preclinical FDG-PET/CT quantitative image metrics of response to therapy. Considerations in this effort include variability in tumor growth rate and tumor size, solid tumor vs. tumor heterogeneity and necrotic tumor, impact of tumor necrosis and whole tumor vs. optimal selection of tumor slices or volumes-of-interest. Three experiments were performed. In the first experiment, a test-retest protocol was implemented on consecutive days to assess the reproducibility of FDG-PET metrics. In the second experiment, we assessed the impact of repeated imaging on the survival of PDX under a therapeutic regiment. In the third experiment, we evaluated optimal image metrics of response to therapy. FDG-PET imaging was performed at baseline and +4 days and +7 days following therapy. Therapy was administered at baseline and weekly for a period of four weeks. Tumor volumes were measured weekly by the caliper. Volumes of interest (VOI) were drawn on co-registered CT images to define tumors. The

reproducibility, accuracy, and variability of radiomics metrics of FDG-PET were evaluated by Pearson correlation coefficient (PCC), bias correction factor (BCF), and Lin's concordance correlation coefficient (LCC). Image metrics at baseline and change in FDG-PET uptake from baseline were used to predict/assess response to therapy. The sensitivity, specificity, precision, accuracy, and negative predictive value (NPV) of baseline and change image metrics were used to identify predictors of response to therapy. **Results:** Repeated imaging had an impact on the survival of PDX mice undergoing therapy. Not surprisingly, measures of SUV_{max} exhibited poor precision in test-retest studies while SUV_{mean} exhibited highest precision in solid tumors. Image metrics which capture the top 75% of tumor voxels (SUV_{75}) yield consistent test-retest performance in both solid and tumors with necrotic phenotype. In agreement with these findings, image metrics of SUV_{75} also scored highest in sensitivity, specificity, precision, and accuracy in assessing response to therapy. **Conclusion:** SUV75 is an optimal imaging biomarker of response to therapy in FDG-PET imaging of TNBC PDX **References:** None.

OP-433

First-in-humans Evaluation of [^{99m}Tc]-ADAPT6, a Novel Scaffold Protein for Visualizationof HER2 Expression

V. Tolmachev[1], *O. Bragina*[2], *E. von Witting*[3], *J. Garousi*[1], *R. Zelchan*[2], *I. Sinilkin*[2], *A. Medvedeva*[2], *A. Doroshenko*[2], *A. Vorobyeva*[1], *S. Lindbo*[3], *J. Borin*[3], *N. Tarabanovskaya*[2], *S. Hober*[3], *V. Chernov*[2];
[1]*Uppsala University, Uppsala, SWEDEN,* [2]*Tomsk National Research Medical Center of the Russian Academy of Science, Cancer Research Institute, Tomsk, RUSSIAN FEDERATION,* [3]*KTH-Royal Institute of Technology, Stockholm, SWEDEN.*

Aim/Introduction: Transmembrane receptor tyrosine kinase human epidermal growth factor 2 (HER2) is a molecular target for the monoclonal antibodies trastuzumab and pertuzumab, the antibody-drug conjugate trastuzumab-DM1 and the tyrosine kinase inhibitor lapatinib. High expression of HER2 is a predictive biomarker for response of breast cancer to HER2-targeting therapies. Evaluation of the HER2 levels in breast tumours can be done by radionuclide molecular imaging which is a non-invasive and effective approach. ADAPTs are novel class of engineered affinity proteins created using the scaffold of the albumin-binding domain of protein G (42 amino acids). Using a combinatorial library, the molecule ADAPT6 was selected and shown to bind HER2 with an affinity of 1.3 ± 0.4 nM. For imaging purpose, the affinity to albumin was obliterated by the introduction of three point mutations. Preclinical studies demonstrated that the use of [^{99m}Tc]-Tc$(CO)_3$ provides stable labelling with a radiochemical purity of over 95 %. [^{99m}Tc]-ADAPT6 provided high-contrast specific imaging of HER2-expressing xenografts in mice. The aim of this first-in-human study was to evaluate safety and dosimetry of [^{99m}Tc]-ADAPT6. **Materials and Methods:** Ten patients with primary breast tumours were included in the study. The injected activity was 397±117 MBq (range, 318-450 MBq). The injected protein doses were 200 µg (one patient), 500 µg (6 patients) and 1000 µg (3 patients). The tomographic imaging was performed at 2, 6, 8 and 24 h after injection. Blood samples were taken at 20 min, 2, 4 and 6 h to evaluate elimination half-life of the tracer. The health status was monitored during imaging. **Results:** No adverse effects were observed after injection of [^{99m}Tc]-ADAPT6. Elimination half-life in blood was 180 min.The highest uptake in normal tissues was in kidney followed by uptake in liver. Some uptake was also visualized in salivary glands. Primary tumours were visualized in all 10 patients, although a small tumour (less than 8 mm) was visualized with lower contrast. Auxiliary lymph node metastases were visualized in three patients. **Conclusion:** This first-in-human study shows that [^{99m}Tc]-ADAPT6 is safe, has favourable dosimetry characteristics and can provide images of HER2-expressing primary breast tumours and auxiliary lymph node metastases. Thus, [^{99m}Tc]-ADAPT6 is a promising tool for evaluation of HER2 expression in breast cancer using SPECT. The novel scaffold-based format of targeting probes, ADAPT, is very promising for development of targeting agents for radionuclide molecular imaging. **References:** None.

OP-434

Enhanced apoptosis in response to glucose metabolism and oncogene driver co-targeting in non-small cell lung cancer

V. De Rosa[1], *C. Terlizzi*[2], *F. Iommelli*[1], *E. Leggiero*[3], *L. Pastore*[4], *S. Del Vecchio*[2];
[1]*Institute of Biostructures and Bioimaging, National Research Council, Naples, ITALY,* [2]*Department of Advanced Biomedical Sciences, University of Naples "Federico II", Naples, ITALY,* [3]*CEINGE Advanced Biotechnologies, Naples, ITALY,* [4]*Departement of Molecular Medicine and Medical Biotechnology, University of Naples "Federico II", Naples, ITALY.*

Aim/Introduction: Inhibition of MET and EGFR signaling in oncogene-driven non-small cell lung cancer (NSCLC) causes modulation of proliferation, apoptosis and glucose metabolism. The aim of the present study was to test whether co-targeting of glucose metabolism and oncogene drivers enhances tumor response to tyrosine kinase inhibitors (TKIs) in NSCLC. To this end, pyruvate dehydrogenase kinase 1 (PDK1), a key glycolytic enzyme favoring the conversion of pyruvate to lactate, was stably downregulated in oncogene-driven NSCLC cell lines exposed or not to selective TKIs. **Materials and Methods:** H1993 and H1975 cells were stably transfected with scrambled (shCTRL) or PDK1-targeted (shPDK1) shRNA and then treated with MET inhibitor crizotinib (1 µM), double mutant $EGFR^{L858R/T790M}$ inhibitor WZ4002 (1 µM) or vehicle for 48 h. Effects of PDK1 knockdown on glycolytic cascade was evaluated by western blotting and biochemical assays. Furthermore, levels of cyclin D1, PARP, cleaved caspase 3, lamin a/c along with several members of Bcl-2 family were determined by western blot analysis in shCTRL and shPDK1 transfected cells in response to treatment or vehicle. Finally, to understand the mechanisms underlying tumor response to PDK1 knockdown and oncogene

driver inhibition, we also analyzed protein-protein interactions at the mitochondrial/endoplasmic reticulum interface by immunoprecipitation. **Results:** Both shPDK1 H1993 and H1975 cells showed a dramatic reduction of PDK1 protein levels as compared to shCTRL cells. Knockdown of PDK1 in both cell lines did not cause significant changes in glycolytic cascade, ATP production and glucose consumption. The same decrease of cyclin D1 was observed in shCTRL and shPDK1 cells exposed to crizotinib or WZ4002 indicating that downregulation of PDK1 did not significantly affect proliferation. Conversely, increased levels of apoptotic markers were found in shPDK1 cells as compared to shCTRL cells, both treated with TKIs. These findings indicate that PDK1 downregulation is able to potentiate the effects of TKIs thus enhancing apoptotic tumor response. Analysis of mitochondrial fractions showed a PDK1-dependent pattern of protein-protein interaction suggesting the assembly of large macromolecular complexes at the mitochondrial/endoplasmic reticulum interface. **Conclusion:** Our findings indicate that co-targeting of PDK1 and oncogene driver is able to potentiate the effects of TKIs thus enhancing apoptotic tumor response. **References:** None.

OP-435

^{90}Y-NM600 targeted radionuclide therapy immunomodulates the tumor microenvironment of prostate tumors

R. Hernandez, C. Zahm, E. Aluicio-Sarduy, H. Potluri, J. Grudzinski, C. Massey, A. Bitton, J. Engle, D. McNeel, J. Weichert;
University of Wisconsin, Madison, WI, UNITED STATES OF AMERICA.

Aim/Introduction: Immunotherapies are potentially curative treatments for metastatic cancers but are ineffective against metastatic prostate cancer (PC) due to an immunosuppressive tumor microenvironment (TME). External-beam radiation therapy can elicit a proinflammatory response in irradiated tumors but is prohibitively toxic in a scenario of disseminated disease. Our goal is to employ [^{90}Y]Y-NM600 targeted radionuclide therapy (TRT) to systemically condition the tumor microenvironment of PC for an enhanced response to immunotherapy. **Materials and Methods:** Immunocompetent male FVB mice were implanted with syngeneic prostate cancer (MyC-CaP) tumors (n=3). Tumor-bearing mice were administered 9.25 MBq of the positron-emitting [^{86}Y]Y-NM600 and static PET/CT scans were acquired at 3, 24, 48, and 72 h post-injection. [^{86}Y]Y-NM600 uptake in MyC-CaP tumors and normal tissues was quantified via a region-of-interest analysis of the images, from which [^{90}Y]Y-NM600 TRT dosimetry was estimated. The radiation dose and time dependency of the immunomodulatory effects of [^{90}Y]Y-NM600 in the TME of MyC-CaP tumors was determined by flow cytometry and immunohistochemistry, while systemic hematopoietic toxicity was monitored via CBC analysis. In treatment studies, mice bearing MyC-CaP grafts (200 mm^3; n=5) were administered 1.85, 5.55, or 11.1 MBq [^{90}Y]Y-NM600 monotherapy or in combination with an anti-PD-1 mAb (100 µg) weekly for 3 weeks and tumor growth was monitored for 45 days. **Results:** Longitudinal PET/CT imaging showed selective uptake and retention of [^{86}Y]Y-NM600 in MyC-CaP tumors that allowed the delivery of an estimated [^{90}Y]Y-NM600 dose to the tumor of 1.97 Gy/MBq. Mice treated with [^{90}Y]Y-NM600 at 4, 10, or 20 Gy showed a marked reduction in CD45+ tumor-infiltrating lymphocytes (TIL). Both CD8+ and CD4+ TIL populations declined, but only CD8+ numbers recovered at day 14 post-injection. Notable changes in the phenotype of surviving CD8+ T-cells were observed with a marked reduction in the expression of 4-1BB activation marker and the checkpoint molecules LAG-3, CTLA-4, and PD-1. Recovery to pre-treatment CD8+ phenotype was seen at day 14. PD-L1 expression in tumor cells also increased indicating the induction of IFN-γ related response to radiation. TME immunomodulation was achieved without systemic hematopoietic toxicity. Combination of [^{90}Y]Y-NM600 and anti-PD-1 immunotherapy resulted in enhanced anti-tumor response compare to each monotherapy. **Conclusion:** Our preliminary data suggest that TRT induces profound immunological effects in TME by modifying the phenotype and abundance of TIL populations and upregulating checkpoint ligands in tumors cells, effects that can be leveraged to enhance the response of PC tumors to checkpoint blockade immunotherapy. **References:** None.

OP-436

Podocalyxin, a new target for radioimmunotherapy of pancreatic cancers

J. Rousseau[1], P. H. W. Chan[2], H. Merkens[1], K. Gitschtaler[1], L. Li[3,4], P. Bergqvist[2], N. Colpo[1], C. Uribe[1], C. Orvig[3], C. Roskelley[5], K. M. McNagny[6], K. Lin[1], I. Samudio[2], F. Benard[1];
[1]Molecular Oncology, BC Cancer, Vancouver, BC, CANADA, [2]Biologics Division, CDRD, Vancouver, BC, CANADA, [3]Medicinal Inorganic Chemistry Group, Department of Chemistry, UBC, Vancouver, BC, CANADA, [4]Life Sciences Division, TRIUMF, Vancouver, BC, CANADA, [5]Department of Cellular and Physiological Sciences, UBC, Vancouver, BC, CANADA, [6]Department of Medical Genetics, UBC, Vancouver, BC, CANADA.

Aim/Introduction: Podocalyxin (PODXL) is a sialoglycoprotein involved in mobility and invasiveness of pancreatic tumor cells and thus a promising target to treat advanced pancreatic cancer and/or metastases by radioimmunotherapy (RIT). PODXL-447 is a high affinity monoclonal antibody that recognizes a PODXL tumor-selective glyco-epitope. The aim of this study was to develop a RIT strategy to treat pancreatic cancer using PODXL-447. **Materials and Methods:** H4pypa conjugated PODXL-447 (H4pypa:PODXL-447 ratio 3:1) was radiolabeled with ^{177}Lu. Radiochemical purity and specific activities were determined by iTLC-SG chromatography and size exclusion chromatography using HPLC. Immunoreactivity was determined using MIA PaCa-2 cells. Biodistribution studies were performed at 4, 24, 72, 168 and 240h post-injection (p.i) in MIA PaCa-2 tumor-bearing mice (13.9±0.3 µg, 3.2±0.1 MBq, n=8/group). Dosimetry was also performed. To determine the maximum tolerated dose (MTD), increasing activities of ^{177}Lu-pypa-PODXL-447 were injected in

healthy mice and blood cell counts were monitored p.i (4.1, 8.4, 17.8 MBq, 25.7±0.6 µg, n=8/group). A RIT assay was performed in MIA PaCa-2 tumor-bearing mice at 2/3 of the MTD as compared to controls injected with unlabeled H4pypa-PODXL-447 (14.6±0.3 µg, n=6-7/group). **Results:** H4pypa-PODXL-447 was effectively radiolabeled with ^{177}Lu (radiochemical purity >99%, 0.6-2.5 MBq/µg, immunoreactivity >85%). Significant tumor uptakes, with high tumor to background ratios, were observed 4h and until 72h p.i (15.6±4.7 and 13.5±4.4 %ID/g, respectively), and dropped at Day 7 (5.0 ± 0.9 %ID/g, p=0.0001). The absorbed dose to the tumor was 1.2 Gy/MBq. ^{177}Lu-H4Pypa-PODXL-447 showed a dose-dependent hematological toxicity with a MTD of 8.4 MBq (transient toxicity: 11 and 12% of platelets and leukocytes remaining at nadir, recovery observed at 56 and 40 days p.i, respectively). As compared to H4pypa-PODXL-447 (controls), the MIA Paca-2 tumor volumes treated with 5.8 MBq of ^{177}Lu-pypa-PODXL-447 remained unchanged up to 14 days p.i (415±180 versus 62±45 mm³, respectively, p=0.0004). After 14 days, ^{177}Lu-pypa-PODXL-447 treated tumors began to increase in size and remained significantly smaller than the controls 26 days p.i (196±100 versus 870±245 mm³, respectively, p=0.0001). At 40 days p.i the survival rate was 71.4% for the ^{177}Lu-pypa-PODXL-447 group versus 16.7% for the controls (tumor size: 519±139 and 1108±204 mm³ for the remaining mice, respectively, p=0.0026). **Conclusion:** ^{177}Lu-pypa-PODXL-447 enabled control of tumor growth in a preclinical RIT study using a PODXL-positive pancreatic cancer model. The use of a fractionated protocol, a pretargeting strategy and/or α-emitters might decrease toxicity and increase the radiation dose that could be delivered to tumors. **References:** None.

OP-437

Fluorine-18 Labeled FAPI-Tracers For PET Imaging

T. Lindner[1], *A. Altmann*[1,2], *F. L. Giesel*[1], *C. Kratochwil*[1], *C. Kleist*[1], *S. Kraemer*[1], *J. Debus*[3,4], *W. Mier*[1], *U. Haberkorn*[1,2,5];
[1]*Nuclear Medicine, University Hospital Heidelberg, Heidelberg, GERMANY,* [2]*Clinical Cooperation Unit Nuclear Medicine, German Cancer research Center (DKFZ), Heidelberg, GERMANY,* [3]*Dept. of Radiation Oncology, University Hospital Heidelberg, Heidelberg, GERMANY,* [4]*Clinical Cooperation Unit Radiation Oncology, German Cancer research Center (DKFZ), Heidelberg, GERMANY,* [5]*Translational Lung Research Center Heldelberg, German Center for Lung Research, Heidelberg, GERMANY.*

Aim/Introduction: Recently the DOTA-based radiotracers FAPI-04 and -46 which target the fibroblast activating protein (FAP) of cancer associated fibroblasts were successfully tested for PET imaging and targeted radionuclide therapy. This imaging method is especially valuable in case of malignancies with low glucose uptake, which are not easily detectable by FDG-PET/CT such as pancreatic cancer. Since the use of Ga-68 limits batch-sizes to 2-4 GBq and the half-life of 68 min is relatively short, Ga-68 FAPI tracers have to be produced on site and in time. To overcome these disadvantages radiotracers for labeling with the longer-lived F-18 were developed, which is produced in common cyclotrons. This would offer centralized radiopharmaceutical production and distribution as well as longer time slots for application. **Materials and Methods:** Ten FAPI-derivatives were synthesized as precursors for incorporation of F-18 as aluminum fluoride complexes or as 6-fluoronicotinamides. The radiolabeled compounds were tested in vitro for their ability to bind FAP transfected HT-1080 cells and their respective EC_{50}-value. Additionally the specificity was affirmed by a negative control with DPP4 transfected HEK cells. The most promising tracer was identified by PET imaging in HT-1080-FAP xenografts. Further characterization included an organ distribution study and a test for stability in serum. Finally a first clinical application was performed. **Results:** All compounds showed excellent performance in vitro. The initial 6-flouronicotinamide derivatives showed a disadvantageous biliary excretion. Although this could be averted by insertion of hydrophilic amino acids into the linker region, the accumulation in the xenografted tumor was also suppressed. The AlF-labeled compounds FAPI-42 and -52 also revealed an unfavorable biliary excretion in PET experiments, while these tracers showed fast renal clearance if labeled with Ga-68. The lower lipophilicity of FAPI-74, -75 and -76 reduced the fraction of the biliary elimination and enabled high tumor-to-background ratios for FAPI-74 and -75. This result could also be confirmed in a clinical application of FAPI-74 for PET/CT imaging of a lung cancer patient. **Conclusion:** The different elimination pathways of Ga-68 and AlF-18 labeled NOTA-compounds show the sensitivity of FAPI-tracers towards changes of physicochemical properties. The interfering biliary excretion could be suppressed in case of AlF-18 complexes while maintaining high tumor accumulation. This was achieved by reducing the lipophilicity via insertion of additional charges or incorporation of the 2-cyanopyrrolinine residue of FAPI-02. Possessing excellent performance in PET imaging as well as a feasible synthesis, FAPI-74 is a promising precursor for clinical F-18 based FAPI-imaging. **References:** None.

OP-438

Theranostics targeting fibroblast activation protein in the tumor stroma: [^{64}Cu] and [^{225}Ac] labelled FAPI-04 in pancreatic cancer xenograft mice

T. Watabe[1], *Y. Shirakami*[2], *K. Kaneda-Nakashima*[3], *Y. Liu*[1], *T. Lindner*[4], *K. Ooe*[1], *A. Toyoshima*[2], *S. Naka*[5], *E. Shimosegawa*[1], *U. Haberkorn*[4], *F. Giesel*[4], *J. Hatazawa*[6];
[1]*Osaka University Graduate School of Medicine, Suita, Osaka, JAPAN,* [2]*Institute for Radiation Sciences, Osaka University, Suita, Osaka, JAPAN,* [3]*Osaka University Graduate School of Science, Suita, Osaka, JAPAN,* [4]*University Hospital Heidelberg, Heidelberg, GERMANY,* [5]*Osaka University Hospital, Suita, Osaka, JAPAN,* [6]*Research Center for Nuclear Physics, Osaka University, Suita, Osaka, JAPAN.*

Aim/Introduction: Fibroblast activation protein (FAP), which is known to promote tumor growth and progression, is overexpressed in cancer associated fibroblasts of many

human epithelial cancers. Since its expression is minimal in normal organs, FAP is an excellent target for the theranostics in oncology. In this study, we used longer half-life radionuclides, [^{64}Cu] (half-life = 12.7 hrs) and [^{225}Ac] (half-life = 10 days), for the labelling of FAP inhibitor (FAPI), to evaluate the biodistribution and treatment effect in mice with human pancreatic cancer xenografts. **Materials and Methods:** Male nude mice were prepared by subcutaneous injection with human pancreatic cancer cells (PANC-1 or MIAPaCa2, n=4 for each, respectively). Dynamic and delayed PET scans 2.5 hrs after injection of [^{64}Cu] FAPI-04 (7.9 ±0.6 MBq), and static scans one hour after injection of [^{68}Ga]FAPI-04 (3.6 ±1.4 MBq) were acquired using the same cohort mice. Immunohistochemical staining was also performed to confirm the FAP expression in the tumor xenograft using FAP-alpha antibody. For the radioligand therapy, [^{225}Ac]FAPI-04 (34 kBq) was injected into PANC-1 xenograft mice (n=3). Tumor size was monitored and compared to control mice (n=3). **Results:** Dynamic imaging of [^{64}Cu]FAPI-04 showed a rapid clearance through kidneys and a slow washout of the tumors. Delayed PET imaging of [^{64}Cu]FAPI-04 showed mild uptake in the tumors and relatively high uptake in the liver and intestine. SUVmean of [^{64}Cu]FAPI-04 and [^{68}Ga]FAPI-04 were 0.13 ± 0.03 and 0.08 ± 0.01 in the PANC-1 xenograft, 0.14 ± 0.03 and 0.08 ± 0.02 in the MIAPaCa2 xenograft, 0.04 ± 0.01 and 0.02 ± 0.01 in the muscle, 0.12 ± 0.03 and 0.10 ± 0.01 in the heart, 1.46 ± 0.33 and 0.21 ± 0.08 in the liver, 0.40 ± 0.19 and 0.06 ± 0.02 in the intestine, 0.34 ± 0.07 and 0.19 ± 0.03 in the kidneys, and 4.36 ± 2.93 and 21.92 ± 21.47 in the bladder, respectively. Accumulation in the tumor or normal organs were significantly higher in [^{64}Cu]FAPI-04 compared to [^{68}Ga]FAPI-04 except for the heart, and excretion in the urine showed higher trend in [^{68}Ga]FAPI-04 compared to [^{64}Cu]FAPI-04. Immunohistochemical staining using FAP-alpha antibody revealed the abundant FAP expression in the stroma of both PANC-1 and MIAPaCa2 xenografts. [^{225}Ac]FAPI-04 injection showed significant tumor growth suppression in the PANC-1 xenograft mice compared to the control mice. **Conclusion:** This study showed the feasibility of theranostics using [^{64}Cu] FAPI-04 and [^{225}Ac]FAPI-04 for the treatment of FAP-expressing pancreatic cancer. **References:** None.

OP-439

A Small Molecule Trifunctional Ligand for Fibroblast Activation Protein-α (FAP)-Targeted Theranostics

J. M. Kelly, S. Ponnala, T. M. Jeitner, A. Nikolopoulou, C. Williams Jr., B. Hu, J. W. Babich;
Weill Cornell Medicine, New York, NY, UNITED STATES OF AMERICA.

Aim/Introduction: Fibroblast activation protein-alpha (FAP) is a marker of cancer-associated fibroblasts, a major regulator of the tumor microenvironment[1]. FAP is upregulated in many cancers and is minimally expressed in normal tissue[2]. The radiometallated small molecule FAP inhibitors FAPI-02 and FAPI-04 show promising tumor delineation and minimal background accumulation in human cancer patients[3,4], but significant tumor washout is evident even by 3 h post injection (p.i.)[5]. We have previously developed trifunctional ligands that bind prostate-specific membrane antigen (PSMA) and serum albumin to improve dose to tumor and therapeutic index[6,7]. Our aim was to develop a trifunctional small molecule ligand with improved tumor uptake and retention for FAP-targeted radiotherapy. **Materials and Methods:** RPS-309 comprises a 7-quinolynoyl)-glycyl-2-cyanopyrrolidine group derivatized with DOTA and 2-(4-iodophenyl)acetic acid using a polyethylene glycol (PEG) linker group. The IC_{50} was determined by a competition binding assay in SW872 cells. The ligand was radiolabeled with ^{68}Ga and evaluated by microPET/CT imaging and biodistribution in female BALB/c nu/nu mice bearing SW872 xenograft tumors. Specificity for FAP was determined by co-administration of non-radioactive ligand (35 nmol). **Results:** RPS-309 potently inhibited FAP. ^{68}Ga-RPS-309 clearly demarcated SW872 xenograft tumors (5.4±0.3 %ID/g at 30 min p.i.), and was retained for up to 3 h p.i. (5.0±0.3 %ID/g). Renal clearance was the predominant route of excretion, and activity in the blood remained high at 3 h p.i. The tumor-to-kidney ratio increased from 1.05±0.16 at 30 min p.i. to 1.73±0.11 at 3 h p.i. Uptake in bone and pancreas was consistent with native murine FAP expression[8], and was eliminated by co-administration of a blocking dose of non-radiolabeled ligand. By this method, tumor uptake was also dramatically reduced. **Conclusion:** ^{68}Ga-RPS-309 shows high affinity and specificity for FAP. Uptake in SW872 xenograft tumors is high in spite of the modest expression of FAP in this cell line, with tumor-to-tissue ratios exceeding 1 as early as 30 min p.i. Sustained tumor retention over 3 h suggests that RPS-309 may be suitable for FAP-targeted radiotherapy with longer-lived radionuclides. **References:** [1] Siveke JT. J Nucl Med. 2018;59:1412-1414. [2] Puré E, Blomberg R. Oncogene 2018;37:4343-4357. [3] Loktev A, et al. J Nucl Med. 2018;59:1423-1429. [4] Lindner T, et al. J Nucl Med. 2018;59:1415-1422. [5] Giesel FL, et al. J Nucl Med. 2019;60:386-392. [6] Kelly J, et al. Eur J Nucl Med Mol Imaging. 2018;45:1841-1851. [7] Kelly JM, et al. J Nucl Med. 2018. doi:10.2967/jnumed.118.221150. [8] Roberts EW, et al. J Exp Med. 2013;210;1137-1151.

1006

Do.MoRe - Parallel Session: Dosimetry for PSMA Radiopharmaceuticals

Monday, October 14, 2019, 16:30 - 18:00 Lecture Hall 112

OP-440

Patient-specific 3D Monte-Carlo-based bone marrow dosimetry for Lu-177-PSMA therapy and the potential value of Tc-99m-anti-granulocyte antibody SPECT/CT for image-based 3D active bone marrow localisation

A. Gosewisch[1], H. Ilhan[1], S. Tattenberg[1], A. Mairani[2], K. Parodi[3], J. Brosch[1], L. Kaiser[1], F. Gildehaus[1], A. Todica[1], S. Ziegler[1], P. Bartenstein[1], G. Böning[1];
[1]Department of Nuclear Medicine, University Hospital Munich, Munich, GERMANY, [2]Heidelberg Ion Beam Therapy Center, University Hospital Heidelberg, Heidelberg,

GERMANY, [3]Department of Medical Physics, Ludwig-Maximilians-Universität München, Munich, GERMANY.

Aim/Introduction: The bone marrow (BM) is a main risk organ during Lu-177-PSMA therapy of mCRPC patients. Classical BM dosimetry relies on phantom-based S-values, however, mCRPC patients often present with a high bone lesion load, which leads to a heterogeneous and patient-specific activity accumulation close to potentially BM-bearing sites and which may significantly interfere with the distribution of active BM. The aim was to investigate Monte Carlo (MC) simulations of the BM absorbed dose and the potential value of image-based BM localisation. **Materials and Methods:** This study is based on the first therapy cycle of 11 patients (3.7-6 GBq Lu-177-PSMA-DKFZ-617). Each patient obtained a pre-therapeutic Ga-68-HBED-CC-PSMA PET/CT, therapeutic quantitative Lu-177 SPECT acquisitions of the abdomen 24 (CT), 48, and 72 h p. i., a Lu-177 whole-body planar scintigraphy 24 h p. i., and five blood samples 30 and 80 minutes p. i. and 24, 48, and 72 h. Lesions, kidneys and the remainder of the body (ROB) were segmented from the Ga-68 PET/CT volume and filled with the respective Lu-177 activities. BM absorbed doses were simulated using FLUKA, assuming first, an unaltered BM distribution (MC1), or second, a displacement of active BM from the direct location of bone lesions (MC2). Results were compared to absorbed dose estimates from S-values (SMIRD), with ROB (including tumors), kidneys and blood considered as source regions, and correlated with the post-therapeutic decrease of lymphocytes, total white blood cells, haemoglobin level and platelets. For two patients, an additional pre-therapeutic Tc-99m-anti-granulocyte antibody SPECT/CT was performed for BM localisation. **Results:** Median BM absorbed doses were 130, 37, and 11 mGy/GBq for MC1, MC2, and SMIRD. Significant correlation with the decrease of platelet counts was found, with highest correlation for MC2 (MC1: r=-0.60, p=0.05, MC2: r=-0.75, p<0.01, SMIRD: r=-0.62, p=0.04). For both investigated patients, BM localisation via Tc-99m-anti-granulocyte antibody SPECT/CT indicated a displacement of active BM from the direct location of lesions similar to model MC2, and led to a reduction in the BM absorbed dose of 40 and 41 % compared to MC1. **Conclusion:** Higher absorbed doses were observed for MC-based models than for SMIRD, however, for MC2 all BM absorbed dose values were still below the threshold of 2 Gy. MC1 partialy resulted in critical values, but this method may lead to too exaggerated absorbed doses by neglecting BM displacement by the metastasis. Image-based BM localisation might be beneficial for identified risk patients. **References:** None.

OP-441

Machine learning to predict post-therapy dosimetry for ^{177}Lu-PSMA I&T treatment

K. Shi[1], *S. Xue*[1], *A. Gafita*[2], *C. Dong*[2], *Y. Zhao*[2], *G. Tetteh*[2], *B. H. Menze*[2], *A. Afshar-Oromieh*[1], *M. Eiber*[2], *A. Rominger*[1];
[1]*University of Bern, Bern, SWITZERLAND,* [2]*Technical University of Munich, Munich, GERMANY.*

Aim/Introduction: The emerging PSMA-targeted radionuclide therapy (RLT) is an effective treatment for metastatic castration-resistant prostate cancer (mCRPC). The European council mandates that treatments should be planned according to the radiation doses delivered to individual patients [1,2]. However, there is no clinically simple but practical method to predict the dosimetry before RLT, which hampers the realization of treatment planning. Therefore, we aimed to prove the concept to employ machine learning methods to predict the post-therapy dosimetry. **Materials and Methods:** Retrospectively 17 patients with metastatic castration-resistant prostate cancer (mCRPC) treated with ^{177}Lu-PSMA I&T RLT were included in this study. Only those cycles with ^{68}Ga-PSMA-HEBD-CC PET/CT directly before the treatment and at least 3 planar and 1 SPECT/CT dosimetry imaging were selected. Totally 30 cycles of treatments were considered for this proof-of-concept study. Organ-based mean and max SUV uptake were obtained from pretherapy PET/CT scans. Dosimetry was calculated for kidney, liver, spleen and salivary glands using Hermes Hybrid Dosimetry 4.0. Two machine learning methods, a 3-layer fully connected neural network artificial neural network (ANN) and a random forest regression (RFR) model, were established. 10-folder cross validation was applied to verify the trained network. Our results were compared with population-based dosimetry from literature. **Results:** ANN has better performance than RFR in the dose prediction for liver and salivary glands, while worse performance for kidney and spleen. Combining the advantages, machine learning achieved the dosimetry prediction error of 18.7±16.0% for kidney, 31.4±27.0% for liver, 24.3±16.2% for salivary glands and 32.1±31.4% for spleen. In contrast, the prediction based on literature population mean has significantly larger error (p<0.01), 46.2±50.4% for kidney, 99.5±238.7% for liver, 705.7±377.7% for salivary glands, 62.3±58.9%. **Conclusion:** The proof of concept study shows that machine learning can significantly reduce the prediction error compared to generally population-based estimation. Artificial intelligence may provide a practical solution to improve the dosimetry-guided treatment planning for RLT. **References:** 1. Stokke et al. EJNMMI Phys 2017 2. Flux et al. Eur J Nucl Med Mol Imaging 2018.

OP-442

Lu-177 PSMA Radioligand therapy: Does the pretherapeutic SUV in Ga-68 PSMA PET/CT predict the therapeutic tumor uptake and absorbed tumor dose?

C. Schuchardt*, S. Wiessalla, A. Singh, J. Zhang, H. R. Kulkarni, D. Mueller, R. P. Baum;*
Theranostics Center for Molecular Radiotherapy and Molecular Imaging, Bad Berka, GERMANY.

Aim/Introduction: Theranostics of metastatic prostate cancer is becoming more and more important. Ga-68 PSMA PET/CT enables accurate detection of metastases with high diagnostic sensitivity and specificity and provides quantitative and reproducible data that can be used to select patients for molecular radiotherapy using PSMA-targeted radioligand

therapy (PRLT) with Lu-177 PSMA ligands. The aim of our study was to determine whether the pretherapeutic SUV can be used to predict the therapeutic Lu-177 PSMA tumor uptake and mean absorbed dose. **Materials and Methods:** 57 patients suffering from metastatic prostate cancer (aged 70+/-8 years) were included in the analysis. High PSMA expression was verified before treatment by Ga-68 PSMA PET/CT and SUVmean and SUVmax of target lesions were determined. PRLT was performed with a mean activity of 6.9 +/- 1.4 GBq Lu-177 PSMA. Biokinetics were determined based on planar whole body scintigraphy & SPECT/CT and dosimetry calculations were performed (OLINDA 2.0). SUVs were compared with the tumor uptake at 20h p.i. and absorbed doses per injected activity (D/A). The correlation between SUV values and uptake/absorbed doses was tested using Spearman rank correlation analysis. **Results:** Analyzed were 114 metastases of 57 patients; 80 bone, 30 lymph node and 4 liver lesions. The SUVmean ranged from 1.7 to 45.1, SUVmax ranged from 2.1 to 253.7. The mean Lu-177 PSMA uptake at 20h p.i. was 0.5 %IA (% of injected activity) and the mean absorbed dose 7Gy/GBq. The correlation of SUV and D/A was r=0.40 (SUVmean) and r=0.43 (SUVmax), both significant with p< 0.001. SUV and uptake also showed positive significant correlations: r=0.33 (SUVmean) and r=0.37 (SUVmax). Because the SUV represents only the uptake at the time of acquisition, while the absorbed dose is based on uptake and associated half-life (HL), we distinguished between lesions with short HL<50h and lesions showing long HL>50h. For short HL, the correlation of SUV and uptake was r=0.32 (SUVmean) and 0.35 (SUVmax), p<0.05. The strongest correlation was found for SUV and D/A for lesions showing long HL: r=0.45 (SUVmean) and r=0.53 (SUVmax), both p<0.001. **Conclusion:** Significant correlations between SUV and uptake/ absorbed dose prove that the pretherapeutic Ga-68 PSMA PET/CT may predict tumor uptake and absorbed doses. Indicating lesions with low SUV or high SUV could help to select suitable or inappropriate candidates for PRLT. However, larger series are needed to confirm and validate these results. **References:** None.

OP-443

Biodistribution and dosimetry of a single dose of albumin-binding ligand [^{177}Lu]Lu-PSMA-ALB-56 in patients with mCRPC

V. Kramer[1,2], *R. Fernandez*[1], *W. Lehnert*[3], *J. Flores*[1], *E. Eppard*[2], *C. Soza-Ried*[1], *L. Jiménez-Franco*[3], *M. Benesova*[4,5], *C. Umbricht*[4], *R. Schibli*[4,5], *M. Meckel*[6], *A. Kluge*[3], *C. Müller*[4,5], *H. Amaral*[1,2];
[1]*Center for Nuclear Medicine & PET/CT Positronmed, Santiago, CHILE,* [2]*Positronpharma SA, Santiago, CHILE,* [3]*ABX-CRO, Dresden, GERMANY,* [4]*Center for Radiopharmaceutical Sciences ETH-PSI-USZ, Villingen, SWITZERLAND,* [5]*Department of Chemistry and Applied Biosciences, ETH Zurich, Zürich, SWITZERLAND,* [6]*Isotope Technologies Garching, München, GERMANY.*

Aim/Introduction: PSMA-targeted radioligand therapy with lutetium-177 is an effective treatment option for metastatic, castration-resistant prostate cancer (mCRPC). Small molecule inhibitors (e.g. PSMA-617, PSMA-I&T) show good tumor-to-blood and kidney ratios but high salivary gland uptake. In contrast, antibodies (e.g. huJ591) show high tumor retention with almost no uptake in salivary glands but relevant hematotoxicity. Ligand-optimization by enhancing blood circulation time with albumin-binding moieties has shown to be feasible [1]. The aim of this study was to evaluate safety and dosimetry of a single therapeutic dose of the albumin-binding [^{177}Lu]Lu-PSMA-ALB-56. **Materials and Methods:** Ten patients (71±8.3 y) with mCRPC and progression under conventional therapies participated in laboratory tests and PSMA-PET/CT to evaluate target expression. After injection of a single dose of 3344±390.5 MBq [^{177}Lu]Lu-PSMA-ALB-56 [2], patients underwent venous blood sampling (5, 15, 30 min and 1.5, 6, 24 and 48 h p.i.) and 3D SPECT/CT imaging (head to upper thigh at 1.5, 6, 24, 48 h and 7 d p.i.). Tumor lesions and volumes were defined on pre-therapeutic PSMA-PET/CT scans. Red bone marrow uptake was conservatively estimated from venous blood samples (RMBLR = 1.0). QDOSE, OLINDA/EXM v1.1 and IDAC-Dose 2.1 were used for dosimetric evaluation and calculation of mean absorbed organ doses for salivary glands, kidneys, red bone marrow, and tumor lesions. **Results:** [^{177}Lu]Lu-PSMA-ALB-56 showed slow clearance from blood with highest uptake at 24 h p.i. in the kidneys and salivary glands and 24-48 h p.i. in tumor lesions. Compared with other therapeutic PSMA radiopharmaceuticals, [^{177}Lu]Lu-PSMA-ALB-56 showed higher absorbed doses in tumor (6.64±6.92 mGy/MBq), but also in kidneys and red bone marrow (2.55±0.93 and 0.27±0.07 mGy/MBq, respectively). The absorbed dose to the salivary glands was lower (0.87±0.43 mGy/MBq) as compared to the dose delivered by [^{177}Lu]Lu-PSMA-617. The red bone marrow was found to be the dose-limiting organ with injectable mean activities of 7300 MBq without exceeding 2 Gy as maximum tolerated dose. **Conclusion:** Treatment with a single dose of [^{177}Lu]Lu-PSMA-ALB-56 delivers higher doses to tumor lesions, but dose calculations imply that the injected activities and number of treatment cycles have to be considered carefully with respect to the higher absorbed doses to kidneys and red marrow. Tumor/salivary glands absorbed dose ratios was significantly increased, but tumor/kidneys absorbed dose ratios for [^{177}Lu]Lu-PSMA-ALB-56 was significantly lower, in comparison to ^{177}Lu-based PSMA radiopharmaceuticals without albumin-binding properties. **References:** [1] Lau et al. Bioconjug Chem 2019, 30:487 [2] Umbricht et al. Mol Pharm 2018; 15:2297.

OP-444

Optimized sampling schedules for renal dosimetry of ^{177}Lu-PSMA I&T regarding the hybrid planar-SPECT/CT method

A. Rinscheid[1,2], *P. Kletting*[1,2], *J. Allmann*[3], *A. Allmann*[3], *M. Eiber*[3], *A. J. Beer*[2], *G. Glatting*[1,2];
[1]*Medical Radiation Physics, Department of Nuclear Medicine, Ulm University, Ulm, GERMANY,* [2]*Department of Nuclear Medicine, Ulm University, Ulm, GERMANY,* [3]*Department of Nuclear Medicine, Klinikum Rechts der Isar, Technische Universität München, Munich, GERMANY.*

Aim/Introduction: Kidneys are an organ at risk in ^{177}Lu-PSMA therapy. For renal dosimetry, time-integrated activity coefficients (TIACs) of the kidneys are determined. However, in practice the sampling schedules are not optimized for this purpose. A modified version of a recently developed method was used to determine optimal sampling schedules for ^{177}Lu-PSMA I&T therapy. **Materials and Methods:** Biokinetic data of 13 patients with metastatic castration-resistant prostate cancer (mCRPC) during ^{177}Lu-PSMA I&T therapy and a whole-body physiologically based pharmacokinetic (PBPK) model were used to create virtual patients. The virtual patients were used to generate renal time-activity curves considered as ground-truth. The 2640 investigated sampling schedules consisted of three planar whole-body images to determine the patient-specific biokinetics and a quantitative SPECT/CT to correctly scale the determined biokinetics, i.e. compensating for the systematic error of the planar image data. All investigated sampling schedules were clinically feasible regarding working hours, comprised of time points < 200 h, had a planar image up to 4 h after administration of the radiopharmaceutical and a SPECT/CT simultaneously to one planar image. For each sampling schedule for the planar images, noise was added to the virtual patients' time-activity data (log-normally distributed, total standard deviation: 20 %, ratio of systematic to stochastic error $r_{syst/stoch}$: 1:3, 1:1, 3:1). A mono-exponential fit function was fitted to the simulated data. The analytically calculated "planar" TIACs were subsequently scaled with the activity value (log-normal, standard deviation: 5 %) of the simulated SPECT/CT. For each virtual patient and each sampling schedule, 10,000 replications were performed. The optimal sampling schedule was defined based on the lowest variability of all simulated TIACs averaged over all virtual patients. **Results:** Planar images at (4, 68-72, 116-124) h with an additional quantitative SPECT/CT at 68-72 h were the optimal sampling schedules for all investigated ratios $r_{syst/stoch}$. Using this measurement scheme and assuming $r_{syst/stoch}$ = 1:1, a median of 13 % (range: 6 %, 19 %) of the determined TIACs of the investigated population deviated more than 10 % from the ground-truth values. Variations of the second planar measurement including the SPECT/CT from the optimal time point to e.g. about 24 h results in higher percentage values of 27 % (13 %, 60 %). Variations of the third time point in the range of 96 h and 124 h had negligible effects. **Conclusion:** This simulation study showed that an accurate dosimetry with the hybrid planar-SPECT/CT method is feasible using three planar images around (4, 68-72, 116-124) h and one SPECT/CT at 68-72 h. **References:** None.

OP-445

Evaluation of a Highly-Automated Dosimetry Tool-Chain for Lu-177-Therapies

P. Ritt[1], *M. Cachovan*[2], *A. H. Vija*[3], *T. Kuwert*[1];
[1]*Clinic for Nuclear Medicine, Erlangen, GERMANY,* [2]*Siemens Healthcare GmbH, Molecular Imaging, Forchheim, GERMANY,* [3]*Siemens Medical Solutions USA, Inc., Molecular Imaging, Hoffman Estates, MI, UNITED STATES OF AMERICA.*

Aim/Introduction: Personalized dosimetry in nuclear medicine relies on many individual steps: Points of time-activity-curve (TAC) are derived from emission imaging, models are fit to TAC, area-under-the-curve (AUC) is extracted and converted to organ-wise absorbed dose by application of S-values, derived from MIRD phantoms. Current clinical dosimetry is predominantly manual, time-consuming, and non-standardized. Its complexity hinders its extension to fully 3-D based one. Siemens developed a dedicated 3-D, voxel-based dosimetry tool-chain, consisting of xSPECT Quant technique and Dosimetry Research Tool (DRT), which automates and integrates all steps of 3-D dosimetry. Aims of our study were to evaluate factors causing deviations of manual and automatic dosimetry. We introduce the experimental setup enabling this investigation and first results, which characterize differences between TAC data obtained by standardized NIST-traceable xSPECT Quant (xQ) technique and facility-specific phantom-calibrated Flash3D (fQ). **Materials and Methods:** In 21 patients undergoing either Lu-177-PSMA (n=12) or -DOTATOC (n=9) therapy, dosimetry of kidneys, liver, and spleen was performed. Image data were acquired from SPECT at 4h, 24h (as SPECT/CT), 48h, 72h p.i. on a Symbia T2. Organ-VOIs were defined manually on CT data. 3-D SPECT data in absolute units (Bq/ml) were obtained based on xQ and fQ. Siemens' DRT was used to automatically co-register data with the VOI-defining CT, for extracting organ-wise TAC, fitting (mono-exponential), and calculating AUC. Additionally, fitting and AUC determination were carried out with commercial software (Graphpad PRISM 5). Deviations between following items were analyzed: -TAC-fit parameters and AUC as calculated by DRT and PRISM 5 -TAC points and resulting AUCs obtained from xQ and fQ. **Results:** Seven of 80 organ-fits resulted in implausible half-lives (>physical) and were excluded from further analysis. Deviations between TAC-fit parameters derived by DRT and PRISM were in remaining cases <0.03% for effective half-life / intercept and <0.2% for AUC. Average deviations between xQ and fQ data were 4.8±5.2%, 5.7±4.6%, 3.3±4.5%, and 8.9±13.8% for left kidney, right kidney, liver, and spleen, respectively. Resulting AUC deviation was 6.2±6.3% (0.3-24.3%), 7.6±5.6 (1.2-22.5%), 3.3±3.4% (0.1-12.1%), and 11.1±11.6% (1.3-20.9%) for left kidney, right kidney, liver, and spleen, respectively. Visual assessment of higher-deviation datasets hinted towards residual inaccuracies in registration between reconstructed SPECT data and CT. **Conclusion:** Deviations in TAC fitting were negligible, consequently these sub-routines of DRT could be considered validated. Relatively low deviations between xQ and fQ were found. These deviations directly propagate to absorbed dose values, if these are obtained by multiplication with S-values. **References:** None.

OP-446

^{225}Ac-PSMA prediction dosimetry: the role of mannitol and glutamate tablet for organ at risk preservation

A. Sarnelli[1], *M. L. Belli*[1], *F. Cesarini*[1,2], *E. Mezzenga*[1], *V. Di Iorio*[1], *M. Monti*[1], *P. Caroli*[1], *F. Matteucci*[1], *E. Tardelli*[1], *S. Nicolini*[1], *S. Severi*[1], *G. Paganelli*[1];
[1]*Istituto Scientifico Romagnolo per lo Studio e la Cura*

dei Tumori (IRST) IRCCS, Meldola, ITALY, [2]Alma Mater Studiorum - Università di Bologna, Bologna, ITALY.

Aim/Introduction: For novel alpha particle Peptide Receptor Radio Therapy treatments, dosimetry evaluation is of paramount importance for toxicity evaluation prevision. Dose limiting organs in PSMA (Prostate-Specific Membrane-Antigen) based PRRT therapy are salivary glands and kidneys. A strong and unexpected xerostomia toxicity was observed for ^{225}Ac-PSMA therapy [1]. A phase-II trial is ongoing at our Institute, with the administration of ^{177}Lu-PSMA treatments in combination with mannitol intra-venous infusion and iron mineral glutamate oral administration (candy) combined with ice-pack external application in order to reduce kidneys and salivary glands uptake, respectively. Based on ^{177}Lu-PSMA data, we evaluated the impact of administered organ preservation drugs on ^{225}Ac-PSMA uptake, assuming a similar uptake guided by PSMA substrate. **Materials and Methods:** ^{225}Ac-PSMA prediction dosimetry was performed on 10 patients treated with 5.5 GBq(5pts) and 4.4 GBq(5pts) of ^{177}Lu-PSMAPRRT. Sequential whole-body planar images and blood samples were acquired at 1h,16-24h,36-48h and 120h post-injection. Data were corrected for scatter, attenuation, background and anterior/posterior view geometric mean. ^{177}Lu time-activity curves were corrected for ^{225}Ac physical decay, and assumed in equilibrium for all daughters. OLINDA adult male phantom was used for whole body(WB), kidneys, liver and red marrow(RM) dose estimation with remainder of the body inclusion, while spherical model was used for parotid and submandibular glands (PGs,SGs). Absorbed dose for each daughter was calculated and summed for the total dose estimation. Correction for single mass organ (based on pre-PRRT PET-CT) and patient weight was introduced. **Results:** 10 patients were enrolled, Dosimetry was performed on first cycle for all patients except 3 (second cycle); median age was 68y(range:53-85). Single or bi-exponential time-activity curve fitting were considered. Median(range) effective half-life were 30.9h (27.2-67.4) for PGs, 34.0h (16.1-70.1) SGs, 48.3h (12.9-70.7) kidneys, 67.0h (15.0-240) liver, 6.90h (2.60-15.2) RM and 79.5h (17.5-110) for remainder WB. For dose calculation, RBE=5 was used for alpha particle weight, 1 for beta/photon component. Median(range) doses were 0.50 $Sv_{RBE=5}$/MBq (0.28-2.73) for PGs, 0.62 $Sv_{RBE=5}$/MBq (0.26-1.19) SGs, 0.72 $Sv_{RBE=5}$/MBq (0.25-1.82) kidneys, 0.11 $Sv_{RBE=5}$/MBq (0.05-017) liver, 0.05 $Sv_{RBE=5}$/MBq (0.03-0.14) RM and 0.04 $Sv_{RBE=5}$/MBq (0.02-0.11) for WB. A reduction more than 50% for salivary gland mean dose is observed compared to previously published data (2.33 $Sv_{RBE=5}$/MBq[1]). **Conclusion:** The possibility to reduce salivary glands uptake in ^{225}Ac-PSMA PRRT treatment with the administration of combined therapy was estimated. Our results are promising, but should be confirmed with effective ^{225}Ac-PSMA therapy and post-injection evaluation in terms of toxicities and treatment outcome. **References:** [1]Kratochwil 2017;JNM:58(10),1624-1631.

1007
Teaching Session 4 - Interactive Clinical Cases - Translational and Molecular Imaging Therapy + Drug Development Committee: Chemical Entities that can Induce a Therapeutic Response in Vivo ? Light vs Radioisotopes

Monday, October 14, 2019, 16:30 - 18:00 Lecture Hall 113

OP-447
PDT General Overview

T. Hasan;
Wellman Center for Photomedicine, Harvard Medical School, Massachusetts General Hospital, Boston, MA, UNITED STATES OF AMERICA.

OP-448
PDT Strategies for Recurrent Head and Neck Cancer

B. Karakullukçu;
The Netherlands Cancer Institute, Antoni van Leeuwenhoek Hospita, Department of Head and Neck Surgery and Oncology, Amsterdam, NETHERLANDS.

OP-449
PDT and the Dosimetry of Light

M. Konijnenberg;
Erasmus MC, Radiology and Nuclear Medicine, Rotterdam, NETHERLANDS.

1008
Clinical Oncology - Featured: Hybrid PET/MRI - Quo Vadis?

Monday, October 14, 2019, 16:30 - 18:00 Lecture Hall 114

OP-450
10 Years PET/MRT – Was it Worth the Effort?

P. Veit-Haibach;
University of Toronto, Department Medical Imaging, Toronto, ON, CANADA.

OP-451

Texture analysis of 2-point Dixon Images acquired during PET/MRI: Technique and Initial Experience in Colorectal Cancer

B. Ganeshan, D. Walls, L. Hoy, S. Wan, K. Miles, A. Groves; University College London Hospital, London, UNITED KINGDOM.

Aim/Introduction: To describe the technique and initial results obtained from MR texture analysis (MRTA) of 2-point Dixon images acquired during PET/MRI in patients with colorectal cancer. **Materials and Methods:** Simultaneous Fluorodeoxyglucose PET/MRI was performed prospectively in 30 consecutive patients with primary colorectal cancer (20 male, 10 female; mean age: 63.9 years; range 42-83 years). MRI acquisitions included 2-point Dixon sequences and diffusion weighted imaging with mapping of apparent diffusion coefficient (ADC). Parametric images of fractional water content (FWC) generated from Dixon sequences underwent MRTA using commercially available software (TexRAD, Feedback Medical Ltd, Cambridge, UK). A filtration step highlighting image features of specified sizes as determined by the spatial scaling factor (SSF) preceeded quantification of texture using statistical parameters derived from histograms of filtered images of FWC within the primary colorectal cancer. FWC and MRTA were assessed for inter-operator agreement and correlated against tumor stage, ADC histogram analysis and overall survival. **Results:** Tumor FWC (mean: 0.889; range: 0.180 - 0.978) correlated significantly with the kurtosis of the ADC histogram (rs=-0.429, p=0.018) but not with ADCmean (rs=0.164, p=0.388). The standard deviation of tumor FWC correlated with tumor stage (rs=0.419, p=0.021). Inter-operator agreement for MTRA was excellent (intra-class correlation coefficients > 0.8) for all parameters except skewness at SSF=2 and was superior to histogram analysis of unfiltered FWC images. MRTA expressed as entropy correlated with the kurtosis of ADC histograms at multiple SSF values (rs = 0.399, p=0.029 for SSF=6) and was associated with overall survival (p=0.0089 for SSF=2). **Conclusion:** MRTA of tumor water fraction images shows good inter-operator agreement, correlates with ADC histogram analysis and relates to overall survival in primary colorectal cancer. MRTA can potentially assess tumor heterogeneity from MR images acquired routinely during simultaneous PET/MRI evaluation of primary colorectal cancer. **References:** None.

OP-452

^{18}F-FDG PET/MR in discriminating between malignant and benign pancreatic cystic neoplasms (PCNs)

H. Xing[1], *B. Hou*[2], *W. Zhu*[1], *H. Ding*[3], *X. Li*[4], *Y. Hu*[5], *H. Xue*[2], *F. Feng*[2], *K. Lv*[6], *X. Wu*[7], *F. Li*[1], *Z. Jin*[2], *D. Li*[5], *L. Huo*[1], *Y. Zhao*[5];
[1]*Department of Nuclear Medicine, Peking Union Medical College Hospital, Chinese Academy of Medical Science & Peking Union Medical College, Beijing Key Laboratory of Molecular Targeted Diagnosis and Therapy in Nuclear Medicine, Beijing, CHINA,* [2]*Department of Radiology, Peking Union Medical College Hospital, Chinese Academy of Medical Science & Peking Union Medical College, Beijing, CHINA,* [3]*Center for Biomedical Imaging Research, Department of Biomedical Engineering, School of Medicine, Tsinghua University, Beijing, CHINA,* [4]*Division of Nuclear Medicine, Department of Biomedical Imaging and Image-guided Therapy, Medical University of Vienna, Vienna, AUSTRIA,* [5]*Department of General Surgery, Peking Union Medical College Hospital, Chinese Academy of Medical Science & Peking Union Medical College, Beijing, CHINA,* [6]*Department of Doppler Ultrasonic, Peking Union Medical College Hospital, Chinese Academy of Medical Science & Peking Union Medical College, Beijing, CHINA,* [7]*Department of Gastroenterology, Peking Union Medical College Hospital, Chinese Academy of Medical Science & Peking Union Medical College, Beijing, CHINA.*

Aim/Introduction: Cystic lesions of the pancreas are common and increasingly detected in the primary care setting. Noninvasive determination of malignancy is of major interest for patient therapeutic management. We aim to evaluate the diagnostic performance of ^{18}F-FDG PET/MRI in preoperative assessment of patients with pancreatic cystic neoplasms (PCNs). **Materials and Methods:** Twenty-seven Patients (9 male, 54.1 ±12.8 yrs) with suspected PCNs underwent ^{18}F-FDG PET/MR using a GE Signa PET/MRI scanner prior to resection or endoscopic ultrasound-guided fine-needle aspiration. MR protocol included T_1-weighted, T_2-weighted and diffusion-weighted sequences. ^{18}F-FDG was injected with 3.7-7.4mbq/kg 144 ± 56 min before scan. According to the revisions of international consensus Fukuoka guidelines 2017 and European evidence-based guidelines on pancreatic cystic neoplasms 2018, cystic lesions were characterized and classified to subtypes of intraductal pancreatic mucinous neoplasm (IPMN), serous cystic neoplasm (SCN), mucinous cystic neoplasm (MCN) and solid pseudopapillary neoplasm (SPN) based on MRI anatomical features including lesion size and main duct involvement. Tumor with high-grade dysplasia and invasive pattern were defined as malignance based on the histological examinations. Patients were grouped into malignant (n = 8, IPMN=7, pancreatic ductal adenocarcinoma=1) and benign (n=16, IPMN=6, SCN=7, MCN=3) groups. Pancreatic pseudocyst (n=3) were excluded from analysis. Regions of interest (ROIs) were defined on the lesions on MRI. The maximum standardized uptake value (SUVmax) of placed RIOs was assessed on PET. The uptake ratio (SUVR) was calculated by SUVmax of the lesion targeted to the liver (mean of SUV of 1 cm ROI). Corresponding calculation of sensitivity, specificity, and accuracy of SUVR to differentiate malignance and benign tumors, and the Receiver Operating Characteristic curve analysis (ROC) were performed. **Results:** SUVR values (4.97 ± 3.72) in malignant group were significantly elevated than those in benign group (0.87 ± 0.32) (P = 0.017) To differentiate malignance from benign, the threshold value of SUVR=1.75 was associated total sensitivity, specificity, and accuracy were 75%, 100% and 91.7% respectively. Area under the ROC curve was 0.852 with significance level of P = 0.0047. **Conclusion:** FDG/MRI PET might provide incremental diagnostic value in differentiation between benign and malignant pancreatic cystic neoplasms. **References:** None.

OP-453

Fully hybrid PET/MRI with 18F-FDG in preoperative staging of endometrial cancer: initial experience

P. Mapelli[1,2], *G. Ironi*[3], *A. Bergamini*[1,4], *F. Fallanca*[2], *L. Bocciolone*[4], *P. Scifo*[2], *V. Bettinardi*[2], *R. Cioffi*[1,4], *G. Taccagni*[5], *M. Petrone*[4], *E. Rabaiotti*[4], *L. Gianolli*[2], *G. Mangili*[4], *F. De Cobelli*[1,3], *M. Picchio*[1,2]; [1]*Vita-Salute San Raffaele University, Milan, ITALY,* [2]*Nuclear Medicine Department, IRCCS San Raffaele Scientific Institute, Milan, ITALY,* [3]*Radiology Department, IRCCS San Raffaele Scientific Institute, Milan, ITALY,* [4]*Unit of Obstetrics and Gynaecology, IRCCS San Raffaele Scientific Institute, Milan, ITALY,* [5]*Pathology Unit, IRCCS San Raffaele Scientific Institute, Milan, ITALY.*

Aim/Introduction: 18F-FDG PET/CT and Magnetic resonance imaging (MRI) have complementary roles in the management of patients with endometrial cancer. Aim of the present study is to present the emerging clinical value of fully hybrid 18F-FDG PET/MRI in preoperative assessment of endometrial cancer. **Materials and Methods:** Twelve patients with endometrial cancer candidate to surgery underwent 18F-FDG PET/MRI (SIGNA PET, General Electric Medical Systems, Wakesha, Wisconsin, USA) for staging purpose from December 2018 to April 2019. A dedicated PET/MRI protocol has been optimized: a simultaneous PET/MR whole-body (WB) scan started approximately 60 minutes after 18F-FDG injection; a second PET/MRI study, corresponding to a single PET-FOV, has been acquired centered over the pelvis at the end of the WB scan. This latter acquisition provided: high statistic PET scan and large FOV axial T2w and high-resolution small FOV T2-w FSE (fast spin echo) PROPELLER of the pelvis; a small field of view (FOV) diffusion-weighted acquisition (DWI) on primary tumor; dynamic contrast enhances (DCE) MRI of the primary tumor; large FOV axial fat-saturated T1-weighted sequence of the pelvis before and after contrast agent administration; a small FOV high-resolution 3D fat-saturated T1-weighted sequence of the uterus after contrast agent administration. Six out of 12 patients already have histological data available. **Results:** Patients' median age was 65 yrs (range: 52-86). All patients well tolerated the 18F-FDG PET/MRI scan although the duration time of the study (approximately 60 minutes). 18F-FDG PET/MRI identified the primary tumour in all 12 patients. Using a threshold of 40%, mean value (range) of SUVmax, SUVmean, MTV and TLG of the primary tumours were 25.5 (5.1-72.4), 15.5 (2.6-44), 18.7 (0.8-71.2), 277.7 (3.9-1026.1). Additionally, in 4/12 patient lymphnodal involvement has been detected. Mean value (range) of SUVmax, SUVmean, MTV and TLG of the positive lymphnodes were 8.5 (3.9-16.5), 4.8 (2-9.4), 3.3 (0.8-8.4), 10.1 (4.6-17.2). Regarding the 6 patients with available histology, 4/6 had endometrial type tumour, 1/6 had mixed-serous carcinoma and 1/6 presented a malignant mixed-mullerian tumour. Among the 4/12 patients with lymphnodal involvement detected by PET/MRI, for 3/4 histology confirmed lymphnodal metastases while in 1/4 histology showed chronic reactive lymphadenitis. **Conclusion:** Simultaneous 18F-FDG PET/MRI scan is feasible and well tolerated in patients with endometrial cancer candidate to surgery. This preliminary experience highlight an emerging clinical role of this hybrid technique with clinical relevance. **References:** None.

OP-454

The role of PET/MR imaging, PSA and patient age in risk prediction for lesions from prostate cancer

L. Papp[1], *C. P. Spielvogel*[2], *M. Grahovac*[3], *T. Beyer*[1], *M. Hacker*[3]; [1]*QIMP team, Center for Medical Physics and Biomedical Engineering, Medical University of Vienna, Vienna, AUSTRIA,* [2]*Christian Doppler Laboratory for Applied Metabolomics, Medical University of Vienna, Vienna, AUSTRIA,* [3]*Division of Nuclear Medicine, Medical University of Vienna, Vienna, AUSTRIA.*

Aim/Introduction: PET/MRI together with clinical values, such as PSA and patient age play an important role in prostate cancer management. Nonetheless, the importance of PET and MRI modalities in low-high risk prediction is still unknown. This study compared PSA and patient age with modality-specific in-vivo features to estimate their relative importance in risk prediction. **Materials and Methods:** 74 prostate patients were included having a multi-parametric PET/MRI with 8 modalities: ^{18}F-FMC and ^{18}F-FMC+^{68}Ga-PSMA$^{HBED-CC}$ (dual-tracer) PET, furthermore, T2, ADC, iAUC, KEP, Ktrans and Ve MRI. Based on annotated, full-mount histopathological slices, 120 lesions representing different Gleason patterns were delineated from the PET/MRI dataset (Hermes Nuclear Diagnostics, Sweden). Clinical PSA value and patient age features were merged with 56 highly repeatable (multi-centric variation <5%) in vivo features (7 feature x 8 modality) [1]. A low risk (<=Gleason 3) vs. high risk (>=Gleason 4) predictive model was established over the 58 features [2]. Predictive performance was estimated by 1000-fold Monte Carlo (MC) cross-validation with 80% training and 20% validation sets in each fold. The PSA, patient and modality-specific feature weights of the established predictive models over the MC folds were averaged and normalized to the sum of 1.0. This way, relative importance of PSA, patient and the 8 imaging modalities in predicting low-high risk could be compared. **Results:** The low-high risk predictive model performance was: SENS 72%, SPEC 77%, ACC 75%, PPV 76% and NPV 73%. The feature weight ratios were the following: PSMA (50%), PSA (10%), patient age (10%), T2 (8%), ADC, and VE (5% each), iAUC, KEP, Ktrans and FMC (3% each). **Conclusion:** PSMA PET-derived features together with PSA and patient age features appear to be highly important to predict low-high risk of prostate cancer lesions. FMC and MRI modalities had a significantly lower importance (overall 30%) in predicting low-high risk of prostate lesions. As the FMC PET had 3% importance, we consider that the dual-tracer PET acquisition did not introduce significant bias to PSMA-derived features. **References:** Papp L., et al: Optimized feature extraction for radiomics analysis of 18F-FDG-PET imaging. JNM 2018, 10.2967/jnumed.118.217612 Papp L., et al: Glioma Survival Prediction with Combined Analysis of In Vivo ^{11}C-MET PET Features, Ex Vivo Features, and Patient Features by Supervised Machine Learning. JNM, 2018(59):892-899.

OP-455

Ga68 PSMA PET/MRI in newly diagnosed prostate cancer patients: Correlation of Ga68 PSMA uptake in intraprostatic lesion with disease stage

U. Aydos[1], *U. Akdemir*[1], *S. Gulbahar*[1], *I. Gonul*[2], *N. Karabacak*[1], *T. Alkibay*[3], *L. Atay*[1];
[1]*Gazi University Medical Faculty Department of Nuclear Medicine, Ankara, TURKEY,* [2]*Gazi University Medical Faculty Department of Pathology, Ankara, TURKEY,* [3]*Gazi University Medical Faculty Department of Urology, Ankara, TURKEY.*

Aim/Introduction: Our purpose in this study was to evalute the clinical value of the degree of Ga68 PSMA uptake in intraprostatic lesions for the prediction of nodal and distant metastases in newly diagnosed prostate cancer patients. **Materials and Methods:** The data of 62 newly diagnosed prostate cancer patients who underwent pretreatment whole body Ga68 PSMA PET/MRI were analyzed retrospectively. For the quantitative analysis, the highest SUVmax of intraprostatic lesions were used. We also studied a visual assessment of Ga68 PSMA uptake to evaluate the presence of local lymph node and distant metastases in PET/MRI images. Distant metastases were divided into two groups according to the number of metastatic lesions (oligometastatic if ≤3 lesions and multimetastatic if >3 lesions). Pretreatment PSA values, Gleason scores, medium and high risk groups according to Gleason scores (7 and 8-10, respectively) were also noted. **Results:** The median age of our patient group was 65,0 ± 7,6 years. SUVmax of intraprostatic lesions were moderately correlated with the Gleason scores (R= 0.461; p=0.001). PSA levels also showed a moderate correlation with both Gleason scores (R= 0.367; p=0.014) and SUVmax (R= 0.372; p=0.018). When SUVmax measurements were analyzed according to Gleason risk groups, significantly higher values were observed in the high risk group compared to the medium risk group (14.8 ± 8.6 vs 7.2 ± 4.6; t: 3.947 and p<0.001). SUVmax of intraprostatic lesions were higher in the multimetastatic group (22.4 ± 10.6) than the oligometastatic group (11.3 ± 6.2) and the nonmetastatic group (11.1 ± 7.4), but the differences reached statistical significance only for the comparison between the multimetastatic and the nonmetastatic groups (One-way ANOVA, post-hoc test: Bonferroni p=0.019). In the medium risk group (n=25), there were no metastatic patients and all of the metastatic patients were seen in the high risk group (n=31). When the relationship between risk groups and the presence of local lymph node metastases was analyzed, the patients with multiple pathological lymph nodes were in the high risk group. In medium risk group there was only one patient with lymph node metastasis. **Conclusion:** The degree of Ga68 PSMA uptake in intraprostatic lesions in newly diagnosed prostate cancer patients correlated with the presence of lymph node and distant metastases. Ga68 PSMA SUVmax levels of intraprostatic lesions were found to be approximately two fold higher in the high risk group compared to medium risk group and in multimetastatic group compared to nonmetastatic group. **References:** None.

OP-456

Can the number of tumour feeding vessels predict hypoxia in breast cancer? A study using combined ^{18}F-FMISO PET-MRI

J. Carmona-Bozo[1], *R. Manavaki*[1], *G. Baxter*[1], *R. Woitek*[1], *A. Patterson*[1], *E. Provenzano*[1,2], *T. Frayer*[1], *M. Graves*[1], *F. Gilbert*[1];
[1]*University of Cambridge, Cambridge, UNITED KINGDOM,* [2]*Cambridge University Hospitals NHS Foundation Trust, Cambridge, UNITED KINGDOM.*

Aim/Introduction: To investigate the relationships between hypoxia (^{18}F-FMISO-PET), tumour perfusion (DCE-MRI) and the number of feeding vessels in breast cancer. **Materials and Methods:** Imaging was performed using a GE Signa PET-MRI scanner on 28 patients with biopsy-confirmed breast cancer. A 60-min simultaneous PET-MRI scan was performed following injection of 300 MBq ^{18}F-FMISO and a 2-hour uptake period. Hypoxic status was assessed using the influx rate constant K_i determined through Patlak-plot analysis, using a population-based arterial input function derived from existing data. Perfusion parameters were derived from DCE-MRI data using the extended Tofts model (K_{trans}). Tumour feeding vessels (FV) were counted on maximum intensity projection (MIP) images generated from the maximally enhancing phase of the DCE-MRI (approximately corresponding to phase 22). Tumours positive for oestrogen or progesterone receptors were classified as hormone receptor positive (HR+). Associations between imaging parameters and FV were assessed via Spearman correlation. **Results:** 28 patients/ 31 primary breast cancers were assessed (HR+: n=30; HR-: n=1; ductal: n=20; lobular: n=6; mixed: n=3; mucinous; n=2; Grade: I: n=3; II: n=15; III: n=13). Tumour longest diameter ranged between 11 and 53-mm. The median number of tumour feeding vessels was 9 (range: 1-39). An inverse correlation was observed between K_i and the number of feeding vessels (rho=-0.10; p=0.58). A positive relationship was observed between K_{trans} and FV (rho=0.10; p=0.56). There was a significant positive correlation between tumour size and the number of tumour feeding vessels (rho=0.45; p=0.01). **Conclusion:** K_i mean, which is a marker of hypoxia, had a negative relationship with breast cancer feeding vessels and a positive relationship with tumour vascularity (K_{trans}). A statistically significant relationship was found between the number of feeding vessels and tumour size. **References:** None.

1009

Neuroimaging - Parallel Session: TAU Imaging

Monday, October 14, 2019, 16:30 - 18:00 Lecture Hall 115

OP-457

Tau-PET Correlates with Neuropathology Findings

V. Lowe[1], *E. S. Lundt*[1], *S. M. Albertson*[1], *H. Min*[1], *P. Fang*[1], *S. A. Przybelski*[1], *M. L. Senjem*[1], *C. G. Schwarz*[1], *K. Kantarci*[1], *B. Boeve*[1], *D. T. Jones*[1], *J. F. Tranovich*[2], *F. S. Hanna Al-Shaikh*[2], *D. Knopman*[1], *C. R.*

Jack Jr.[1], *D. W. Dickson*[2], *R. C. Petersen*[1], *M. E. Murray*[2];
[1]*Mayo Clinic, Rochester, MN, UNITED STATES OF AMERICA,*
[2]*Mayo Clinic, Jacksonville, FL, UNITED STATES OF AMERICA.*

Aim/Introduction: Correlation of tau positron emission tomography findings to autopsy data is important to understand the sensitivity and specificity of tau positron emission tomography for neurofibrillary pathology and the relationship of this neuroimaging method to commonly used neuropathologic schemes (1). We evaluated a group of participants who had brain autopsy to assess tau deposition and its relationship with tau-positron emission tomography signal seen antemortem. **Materials and Methods:** Autopsies were performed on 26 participants from the Mayo Clinic who had antemortem tau-positron emission tomography with flortaucipir within 30 months. Flortaucipir positron emission tomography standardized uptake value ratios were determined by a composite brain meta-region (amygdala, entorhinal cortex, fusiform, parahippocampal, and inferior temporal and middle temporal gyri) normalized to the bilateral cerebellar crus gray matter. An optimal flortaucipir uptake ratio cut-point to identify those with Alzheimer's disease primary or secondary neuropathologic diagnoses was determined. Autopsy diagnosis and Braak tangle stage of the participants were compared to flortaucipir imaging findings. Comparison of quantitative tau burden at autopsy to regional flortaucipir signal was also performed. **Results:** Autopsy diagnoses included Alzheimer's disease (n=11), pathological aging (n=1), globular glial tauopathy (n=1), primary age-related tauopathy (n=3), Lewy body disease (n=9), and hippocampal sclerosis (n=1). A flortaucipir cut-point of 1.29 was determined to be optimal. Flortaucipir was elevated in all participants with Alzheimer's disease. Those with Braak tangle stages of IV or greater all had elevated flortaucipir signal. Three Lewy body disease participants and a globular glial tauopathy participant also had elevated flortaucipir signal. Quantitative measurement in temporal lobe regions of tau burden at autopsy and flortaucipir signal were highly correlated (rho's from 0.61 to 0.70, p <0,002). **Conclusion:** Elevated flortaucipir signal seen with an Alzheimer's disease specific cortical meta-region reflects Braak stage IV or greater neuropathology. Some participants with Lewy body disease had elevated flortaucipir signal in the meta-region but the signal intensity was low (not greater than 1.5 in this group) and was likely due to minimal or early tau pathology in this group. Participants with primary age-related tauopathy, and hippocampal sclerosis did not show elevated flortaucipir signal above the cut-point. A secondary neuropathologic diagnosis in the Alzheimer's disease spectrum can be represented by a minimally positive flortaucipir signal. Flortaucipir signal is a valid biomarker of the neurofibrillary tangle pathology of Alzheimer's disease. **References:** 1. Braak H, Braak E. Neuropathological stageing of Alzheimer-related changes. Acta Neuropathol 1991; 82(4): 239-59.

OP-458

Changes in synaptic density in relation to tau deposition in prodromal Alzheimer's disease: a dual protocol PET-MR study

H. R. J. Vanhaute[1], *J. Ceccarini*[2], *L. Michiels*[3], *S. Sunaert*[4], *R. Lemmens*[3], *L. Emsell*[4], *M. Vandenbulcke*[5], *K. Van Laere*[2];
[1]*Nuclear Medicine and molecular imaging, Department of Geriatric Psychiatry, University Hospitals Leuven; department of imaging and pathology, Catholic University Leuven, Leuven, BELGIUM,* [2]*Nuclear Medicine and molecular imaging, University Hospitals Leuven; department of imaging and pathology, Catholic University Leuven, Leuven, BELGIUM,* [3]*Department of Neurology, University Hospitals Leuven; Laboratory for neurobiology, Catholic University Leuven; Center for Brain and disease research, VIB-KU Leuven, Leuven, BELGIUM,* [4]*Department of Imaging and pathology, Translational MRI; Catholic University Leuven, Leuven, BELGIUM,* [5]*Department of Geriatric Psychiatry, University Hospitals Leuven, Leuven, BELGIUM.*

Aim/Introduction: Synaptic loss and deposition of neurofibrillary tangles (NFT) are known, early pathophysiological changes in the AD course, already detectable in prodromal stages[1,2]. Both events correlate with early cognitive impairment[2,3]. Hyperphosphorylated tau could cause loss of synaptic connections[4], leading downstream to cognitive dysfunction, but the exact neuropathological sequence remains largely unknown. In a multitracer PET-MR study we simultaneously assessed synaptic density, by ^{11}C-UCB-J, and deposition of NFT, by ^{18}F-MK-6240, in patients with amnestic mild cognitive impairment (aMCI) and healthy controls (HC) to gain insight in the temporal distribution of these two hallmarks of cognitive decline. **Materials and Methods:** Nine aMCI patients (70.1±5.5years, 3F/6M, MMSE 22-28) and 9 HC (68.0±6.3years, 5F/4M, MMSE 28-30) underwent static ^{11}C-UCB-J (60-90min post-injection (p.i.), 221.2±83.7MBq), ^{18}F-MK-6240 (90-120min p.i., 139.1±22.7MBq) and ^{11}C-PIB PET scans (40-60min p.i., 197.3±52.5MBq) on a GE Signa 3T PET-MR and neuropsychological tests. We studied SUVR images for ^{11}C-UCB-J and ^{18}F-MK-6240 using respectively the centrum semiovale[5] and the cerebellar grey matter[6] as reference region. Grey matter (GM) atrophy was assessed with voxel-based morphometry using T1-weighted MR images (P_{uncorr}<0.001,K_{ext}>200 voxels). Voxelwise group analysis (SPM12) and volume-of-interest (VOI) based correlation analyses (Hammers N30R83 atlas PMODv3.9) were conducted. We expressed the relationship between regional changes in synaptic density and tau deposition by VOI-based Z-scores of SV2A and tau. **Results:** We observed GM reductions in the aMCI group in the superior and inferior temporal gyrus, hippocampus, precuneus, middle occipital gyrus and parietal cortices. Compared to HC, aMCI patients had a decrease in SV2A binding in the medial temporal lobe (MTL), adjacent lateral temporal gyri and insula (T>5.3; decrease: 13-20%). We revealed increased ^{18}F-MK-6240 binding in the MTL, spreading to the parietal and occipital cortex (T>3.5; increase: 51-102%). The decrease in synaptic density and increase in tau deposition remained present in the mesotemporal

regions after correcting for PVE. In the MTL, higher tau accumulation was inversely related to lower synaptic density (Z-scores;p=0.02,r=-0.79). Decreased performance on cognitive screening and episodic memory tests was highly significantly associated with decreased SV2A binding and increased tau deposition in the hippocampus(MMSE:p<0.0001,r=0.80; RAVLT delayed recall:p<0.0004,r>0.75). **Conclusion:** aMCI subjects have high tau deposition and synaptic density loss mainly in key regions known to be involved in early cognitive impairment, indicating that these early pathological changes are interrelated in the MTL. Longitudinal data will provide further insight in the temporal aspects of this relationship. **References:** 1Scheff,S.W.et al;Biochem.Pharmacol;88,517(2014) 2Nelson,P.T.et al;J.Neuropathol.Exp.Neurol;71,362-81(2012) 3Terry,R.D.et al;Ann.Neurol;30,572-580(1991) 4Pooler,A.M.et al;Neuropharmacology;76PtA,1-8(2014) 5Koole,M.et al;Eur.J.Nucl.Med.Mol.Imaging;46,396-406(2019) 6Pascoal,T.A.et al;Alzheimers.Res.Ther;10,74(2018).

OP-459

[^{18}F]flortaucipir PET strongly correlates to cognition across the clinical Alzheimer's disease continuum, independently of CSF tau

E. Wolters[1], *R. Ossenkoppele*[1,2], *S. C. J. Verfaillie*[1], *E. M. Coomans*[1], *T. Timmers*[1], *D. Visser*[1], *H. Tuncel*[1], *A. D. Windhorst*[1], *R. Boellaard*[1], *W. M. van der Flier*[1], *C. E. Teunissen*[1], *P. Scheltens*[1], *B. N. M. van Berckel*[1];
[1]*Amsterdam UMC VUmc, Amsterdam, NETHERLANDS,*
[2]*Lund University, Lund, SWEDEN.*

Aim/Introduction: Tau pathology can be measured in cerebrospinal fluid (CSF) and by [^{18}F]flortaucipir PET in vivo. The aim of this study was twofold. First we examined associations between CSF total tau (t-tau) and phosphorylated tau(p-tau) with [^{18}F]flortaucipir PET across the clinical Alzheimer's disease (AD) continuum, and second we investigated associations of CSF-tau and [^{18}F]flortaucipir PET with cognitive performance. **Materials and Methods:** We included 51 MCI/ AD patients (all amyloid-positive, age: 65±6 years, MMSE: 24±4) and 24 subjective cognitive decline(SCD) subjects (28% amyloid-positive, age: 65±6 years, MMSE: 28±1). Dynamic 130 minute [^{18}F]flortaucipir PET scans were performed to generate global binding potential (BP_{ND}) images using receptor parametric mapping. Cognitive assessment consisted of MMSE and composite scores of four cognitive domains. Pearson's partial correlations and voxel-wise linear regressions were used to investigate associations between CSF-tau and tau-PET; both adjusted for age, sex and time lag between lumbar puncture(LP) and tau-PET. Linear regression models were used to assess the relationships between CSF-tau and tau-PET with cognition(model 1; separate models for CSF and PET) and assessed the independent effects of CSF t-tau and tau-PET on cognition(model 2, with both CSF t-tau and [^{18}F] flortaucipir BP_{ND} as predictor). Models were adjusted for age, sex, education and time lag between assessments. **Results:** Overall, global [^{18}F]flortaucipir BP_{ND} was positively correlated with CSF p-tau (r=0.55) and t-tau (r=0.59). Within groups, correlations were stronger for SCD subjects than MCI/AD patients (r=0.76 for p-tau; r=0.81 for t-tau vs. r=0.38 for p-tau; r=0.42 for t-tau). Voxel-wise analyses across all subjects showed significant associations between widespread cortical [^{18}F]flortaucipir binding (right>left) and CSF-tau, whereas in SCD a temporoparietal pattern was seen. When entered simultaneously (model 2), global [^{18}F]flortaucipir BP_{ND}, but not CSF tau biomarkers, was associated with MMSE and all four cognitive domains across all subjects. In MCI/AD, worse MMSE, attention and executive functions were only associated with global [^{18}F]flortaucipir BP_{ND}. **Conclusion:** There is a strong relationship between tau CSF and [^{18}F]flortaucipir PET, particularly in cognitively normal subjects. Independently of CSF-tau, [^{18}F]flortaucipir PET strongly correlates to cognition in AD, but not in SCD. This suggests that tau PET may more accurately reflects the disease stage than CSF tau. **References:** None.

OP-460

Cortical Binding Characteristics of ^{18}F-PI-2620 Differentiate the Clinically Predicted Tau Isoform in Suspected 3/4-Repeat and 4-Repeat Tauopathies

M. Song[1], *H. Barthel*[2], *T. van Eimeren*[3], *K. Marek*[4], *L. Beyer*[1], *C. Palleis*[1], *J. Sauerbeck*[1], *J. Hammes*[3], *F. Jessen*[3], *D. Saur*[2], *M. Schroeter*[2], *A. Schildan*[2], *O. Barret*[4], *D. Russell*[4], *A. Stephens*[5], *J. Levin*[1], *J. Classen*[2], *G. Hoeglinger*[6], *P. Bartenstein*[1], *V. Villemagne*[7], *A. Drzezga*[3], *J. Seibyl*[4], *O. Sabri*[2], *M. Brendel*[1];
[1]*LMU, Munich, GERMANY,* [2]*University of Leipzig, Leipzig, GERMANY,* [3]*University of Cologne, Cologne, GERMANY,* [4]*Molecular NeuroImaging, New Haven, CT, UNITED STATES OF AMERICA,* [5]*Life Molecular Imaging, Berlin, GERMANY,* [6]*DZNE, Munich, GERMANY,* [7]*University of Melbourne, Melbourne, AUSTRALIA.*

Aim/Introduction: Pathological accumulation of hyperphosphorylated microtubule-associated tau protein underlies a wide range of neurodegenerative disorders. Tau proteins consist of different isoforms, characterized by the number of repeats (R) of microtubule binding sites. Preliminary evidence suggests the novel second-generation tau PET tracer ^{18}F-PI-2620 is able to visualize the predominantly 3/4R-tauopathy Alzheimer's disease (AD) and the mainly 4R-tauopathies corticobasal syndrome (CBS) and progressive supranuclear palsy (PSP), but - apart from the obvious topographical differences - likely with a different magnitude of affinity among them. The aim of this study was to determine whether, in PET-positive cortical regions, the presence of 3/4R- vs. 4R-tauopathies can be differentiated by the binding characteristics of ^{18}F-PI-2620. **Materials and Methods:** ^{18}F-PI-2620 PET data of twenty-three patients (72±9y) with suspected 3/4R-tauopathy (clinical AD; n=12) and suspected 4R-tauopathy (clinical CBS/PSP; n=11), all visually PET-positive in cortical regions, were included in this project. ^{18}F-PI-2620 PET scans were acquired 0-60min p.i. and distribution volume ratios (DVR, cerebellar reference) were calculated after coregistration to an ^{18}F-PI-2620 template in the MNI space. Visually presumed tau-positive cortical volumes of interest (VOIs) in frontal, parietal, temporal or occipital regions

were delineated as target regions by semi-automatized thresholding. Target-to-cerebellum ratios in six 5-min frames (30-60min p.i.) were plotted as a linear function of time to calculate the individual slope in the late binding phase. Mean DVR values, mean 30-60min SUVRs, and slopes were compared between suspected 3/4R- and 4R-tauopathies. Receiver operating characteristics were used to calculate the area under the curve (AUC) for discriminating suspected 3/4R- vs. 4R-tauopathy by all three read-outs. **Results:** Tau-positive cortical regions in suspected 3/4R-tau cases had significantly higher mean ^{18}F-PI-2620 DVR (1.61±0.17 vs. 1.25±0.08, p<0.001) and mean 30-60 min SUVR (2.13±0.31 vs. 1.44±0.18, p<0.001) values when compared to suspected 4R-tau cases. Slope of the late binding phase was steeper in suspected 3/4R-tau cases when compared to suspected 4R-tau cases (0.75 ±0.69 vs. -0.19±0.55, p=0.002). AUC for prediction of a suspected 3/4R-tauopathy was highest for SUVR 30-60 min (AUC: 0.970), followed by DVR (AUC: 0.962), and the slope (AUC: 0.845). **Conclusion:** ^{18}F-PI-2620 binding characteristics in tau-positive cortical brain regions differentiate clinically suspected 3/4R-tauopathies from 4R-tauopathies. Unequal slopes of SUVR in the late binding phase when comparing 3/4R- and 4R-tauopathies might reflect different ^{18}F-PI-2620 binding properties to different tau isoforms. The impact of variable tau extent and disease severity on these results will need to be addressed in this ongoing evaluation. **References:** None.

OP-461

Amyloid and tau PET relate to memory loss in cognitively normal individuals: the SCIENCe project

*E. Wolters[1], T. Timmers[1], R. Ossenkoppele[1], **S. C. J. Verfaillie**[1], D. Visser[1], P. Scheltens[1], M. E. Schmidt[2], K. van den Bosch[1], R. Boellaard[1], S. S. V. Golla[1], W. M. van der Flier[1], B. N. M. van Berckel[1];*
[1]VUmc, Amsterdam, NETHERLANDS, [2]Janssen Research and Development, Beerse, BELGIUM.

Aim/Introduction: Subjective cognitive decline (SCD) may reflect the earliest changes associated with Alzheimer's disease (AD). The aim of this study was to investigate the regional associations between tau pathology, amyloid-β and cognition in cognitively unimpaired individuals with subjective cognitive decline (SCD). **Materials and Methods:** We included 53 participants with SCD who underwent both dynamic [^{18}F]Flortaucipir (tau) and [^{18}F]Florbetapir (amyloid-β) PET scans and neuropsychological testing. We used receptor parametric mapping to create [^{18}F]Flortaucipir and [^{18}F] Florbetapir binding potential (BP_{ND}) images with cerebellar gray matter as reference region. Data were analyzed using a global cortical region-of-interest (ROI) for [^{18}F]Florbetapir and ROIs reflecting early (entorhinal), intermediate (lateral temporal (LTL)) and late tau deposition (global cortical) for [^{18}F] Flortaucipir. Neuropsychological test scores were z-transformed and combined into composite scores for memory, attention, executive functions and language. We used linear regression analyses to assess associations between I) [^{18}F]Florbetapir BP_{ND} and [^{18}F]Flortaucipir BP_{ND} (age and sex adjusted), II) [^{18}F] Florbetapir BP_{ND} and cognition and III) [^{18}F]Flortaucipir BP_{ND} and cognition (models II & III age, sex and education adjusted). **Results:** Participants were 66±7 years old, 47% female, Mini Mental State Examination (MMSE) was 29±1, and 38% were amyloid-β positive on visual read of [^{18}F]Florbetapir PET. Global [^{18}F]Florbetapir BP_{ND} was correlated with [^{18}F]Flortaucipir BP_{ND} in all ROIs (range βs: 0.61-0.74, all p<0.001). Higher [^{18}F]Florbetapir BP_{ND} was associated with lower memory scores (β=-0.31, p<0.05). In addition, higher entorhinal (β=-0.28, p<0.05), but not LTL or neocortical [^{18}F]Flortaucipir BP_{ND} were associated with worse memory performance (β=-0.17, p=0.22 and β=-0.12, p=0.32). When we modeled [^{18}F]Florbetapir BP_{ND} and entorhinal [^{18}F]Flortaucipir BP_{ND} simultaneously, the associations with memory were no longer significant ([^{18}F]Flortaucipir: β=-0.18, p=0.26; [^{18}F]Florbetapir BP_{ND}: β=-0.19, p=0.25). Non-memory domains were not related to [^{18}F]Florbetapir or [^{18}F]Flortaucipir BP_{ND}. **Conclusion:** In cognitively unimpaired individuals with SCD, amyloid-β and tau are tightly linked across brain regions. Increased global amyloid-β and tau in early AD-related regions were both associated with worse memory performance. These associations were strongly dependent on each other, providing support for the notion that in this early stage, amyloid-β and tau are associated with symptoms equally. **References:** None.

OP-462

Longitudinal Dynamic [18F]Flortaucipir PET Reveals Increased Early Stage Tau Pathology in Individuals with Subjective Cognitive Decline

*D. Visser[1], R. Ossenkoppele[2,3], S. C. J. Verfaillie[1], T. Timmers[1,2], E. E. Wolters[1,2], H. Tuncel[1], **E. M. Coomans**[1], M. E. Schmidt[4], R. Boellaard[1], B. Windhorst[1], P. Scheltens[2], W. M. van der Flier[2,5], B. N. M. van Berckel[1];*
[1]Department of Radiology & Nuclear Medicine, Amsterdam Neuroscience, Vrije universiteit Amsterdam, Amsterdam UMC, Amsterdam, NETHERLANDS, [2]Alzheimer Center Amsterdam, Department of Neurology, Amsterdam Neuroscience, Vrije Universiteit Amsterdam, Amsterdam UMC, Amsterdam, NETHERLANDS, [3]Clinical Memory Research Unit, Lund University, Lund, SWEDEN, [4]Janssen Research & Development, Beerse, BELGIUM, [5]Department of Epidemiology and Biostatistics, Vrije Universiteit Amsterdam, Amsterdam UMC, Amsterdam, NETHERLANDS.

Aim/Introduction: Tau pathology is related to clinical progression in Alzheimer's disease (AD). Longitudinal tau PET imaging in preclinical stages of AD may help to identify individuals at risk of progression. Individuals with subjective cognitive decline (SCD) may suffer from preclinical AD. As dynamic scanning protocols allow for accurate quantitative measures of tracer retention over time, the aim of this study was to investigate whether there is a change in tau pathology, as measured with dynamic [^{18}F]Flortaucipir (FTP) PET, in subjects with SCD over a time period of two years. **Materials and Methods:** In an ongoing sub-study of the SCIENCe project,

we included 20 SCD subjects (age 66±8, 45% female, MMSE 29±1, 25% [^{18}F]Florbetapir PET positive based on visual read). All subjects underwent a 90 minute dynamic [^{18}F]Florbetapir PET scan at baseline and a 130 minutes dynamic [^{18}F]FTP PET scan at baseline and 2±0.06 (1.9-2.1) year follow-up. Parametric images were generated using receptor parametric mapping (RPM; reference region cerebellar grey matter) to extract non-displaceable binding potential (BP_{ND}). For [^{18}F]FTP three non-overlapping regions-of-interest reflecting early (medial temporal), intermediate (limbic) and late stage (neocortical) tau pathology were selected. Analyses were performed using ANOVA for repeated measures, adjusting for age and sex. To examine the interaction effect of amyloid pathology, global [^{18}F]Florbetapir BP_{ND} was added in additional analyses. **Results:** We found a significant increase in [^{18}F]FTP BP_{ND} in the medial temporal region, F(1,17)=5.205, p=0.036, reflecting an average increase in tau pathology from 0.01 to 0.02 BP_{ND} over the two year period. No significant [^{18}F]FTP BP_{ND} changes were found for the limbic and neocortical regions, F(1,17)=1.654 and 1.660, p>0.05. Addition of global [^{18}F]Florbetapir BP_{ND} to the model revealed an interaction effect in the limbic and neocortical regions (both p<0.05), attributable to a larger increase in [^{18}F] FTP BP_{ND} in amyloid positive individuals. Data collection is still ongoing. **Conclusion:** Over a two year period, quantitative imaging revealed an increase in tau pathology only in early stage tau pathology regions in SCD subjects. Individuals with higher amyloid load showed relatively higher levels and larger increases in intermediate and late stage tau pathology, supporting the hypothesis that amyloid facilitates the spread of tau pathology. **References:** None.

OP-463

Incremental Value Of Tau Burden Quantified By ^{18}F-AV-1451 PET/CT Over Conventional ^{11}C-PIB And ^{18}F-FDG PET/CT For Alzheimer'S Disease

S. Chen[1], *Y. Leung*[1], *L. Au*[2], *Y. Lau*[2], *V. Mok*[2], *C. Ho*[1];
[1]*Hong Kong Sanatorium & Hospital, Hong Kong, HONG KONG,*
[2]*The Chinese University of Hong Kong, Hong Kong, HONG KONG.*

Aim/Introduction: Recommended by the Alzheimer's Association, diagnosis of Alzheimer's disease (AD) is now based on in vivo biomarkers of abnormal β-amyloid (Aβ) and tau burden. In Aβ+ patients, tau burden is a continuous variable, not only for AD diagnosis but also useful for tracking disease progression. In this study, we investigated the capability of ^{18}F-AV-1451 (^{18}F-T807) tau PET/CT to quantify the severity of neurological impairment by correlation with ^{18}F-FDG PET/CT. **Materials and Methods:** From Feb 2018 to Feb 2019, 54 patients (M:22, F:32; age range:43-79years, mean=65.9±8.2years) with decreased short-term memory, with/without cognitive impairment, and no history of stroke or other neurodegenerative disease, were recruited. They all underwent 3-tracers PET/CT within 1 week: ^{18}F-FDG at 30 minutes, ^{11}C-PIB at 35 minutes, ^{18}F-T807 at 85 minutes, each with a 10-min static acquisition. Global cortical-to-cerebellum SUV ratio (SUVR) was calculated for both ^{11}C-PIB and ^{18}F-T807 PET. ^{11}C-PIB $SUVR_{amyloid}$>=1.30 and ^{18}F-T807 $SUVR_{tau}$>=1.14 were taken as the cut-off for diagnosis of AD by our prior reported studies. ^{18}F-FDG PET was assessed visually and by z-score (MIMNeuro) for regional hypometabolism. AD severity was assessed by 4-degrees of ^{18}F-FDG hypometabilism to assess neuronal injury:normal, mild, moderate, marked. Correlation analysis was performed between 4-degrees of AD severity and $SUVR_{tau}$ & $SUVR_{amyloid}$ respectively. **Results:** 30/54 patients had negative ^{11}C-PIB PET ($SUVR_{amyloid}$=1.12±0.06), as well as negative ^{18}F-T807 ($SUVR_{tau}$=1.04±0.05) and ^{18}F-FDG, thus effectively excluded from AD. 24/54 patients were found to have abnormal Aβ ($SUVR_{amyloid}$=1.52±0.16), of whom 18/24 also had abnormal tau ($SUVR_{tau}$=1.39±0.22), thus classified as biological AD (PIB+/T807+), while 6/24 without abnormal tau ($SUVR_{tau}$=1.06±0.04) as AD-pathologic-change (PIB+/T807-). ^{18}F-FDG PET was negative in all (6/6) patients with AD-pathologic-change. Based on the predefined 4-degrees of ^{18}F-FDG hypometabolism, 5/18 AD patients had no neuronal injury, 6/18 mild, 6/18 moderate, 1/18 marked. The tau burden strongly correlated with AD severity measured by the 4-degrees of neurological impairment (r=0.828, P<0.05); but Aβ burden correlated poorly (r=0.160, P>0.05). One-way ANOVA showed significant difference in tau among patients with AD-pathological-change and 4-degrees of AD severity ($SUVR_{tau}$=1.06±0.04, 1.21±0.03, 1.30±0.12, 1.57±0.16, 1.84±0.00, P<0.05); but no significant difference in Aβ ($SUVR_{amyloid}$=1.42±0.08, 1.56±0.19, 1.46±0.07, 1.68±0.19, 1.43±0.00, P>0.05). **Conclusion:** ^{11}C-PIB PET/CT is valuable for excluding AD and predicting AD pathology at an earlier phase. Concomitant ^{18}F-T807 PET/CT may provide quantitative assessment of tau burden to allow serial measurement and longitudinal tracking of AD pathology, thus useful not just for pre-symptomatic diagnosis, but also for monitoring severity and progression of AD. **References:** None.

OP-464

Early-Phase ^{18}F-PI-2620 Tau-PET Imaging as a Surrogate Marker of Neurodegeneration

L. Beyer[1], *A. Nitschmann*[1], *H. Barthel*[2], *T. van Eimeren*[3], *K. Marek*[4], *C. Palleis*[1], *J. Sauerbeck*[1], *M. Song*[1], *J. Hammes*[3], *F. Jessen*[3], *D. Saur*[2], *M. Schroeter*[2], *A. Schildan*[2], *O. Barret*[4], *D. Russell*[4], *A. Stephens*[5], *J. Levin*[1], *J. Classen*[2], *G. Hoeglinger*[6], *P. Bartenstein*[1], *V. Villemagne*[7], *A. Drzezga*[3], *J. Seibyl*[4], *O. Sabri*[2], *M. Brendel*[1];
[1]*LMU, Munich, GERMANY,* [2]*University of Leipzig, Leipzig, GERMANY,* [3]*University of Cologne, Cologne, GERMANY,* [4]*Molecular NeuroImaging, New Haven, CT, UNITED STATES OF AMERICA,* [5]*Life Molecular Imaging, Berlin, GERMANY,* [6]*DZNE, Munich, GERMANY,* [7]*University of Melbourne, Melbourne, AUSTRALIA.*

Aim/Introduction: Tauopathies are a collective of neurodegenerative diseases with the uniting feature of misfolded and accumulated tau protein in different parts of the brain. For the first-generation tau and several amyloid PET tracers, it has been shown that early after tracer administration PET images reflect perfusion and can as such, due to the neurovascular coupling evident in the brain, act as a surrogate of glucose

metabolism as determined by ^{18}F-fluorodeoxyglucose (FDG)-PET. Thus, we aimed to analyse the early-phase PET images of the second-generation tau tracer ^{18}F-PI-2620 to explore its potential as a neurodegeneration biomarker surrogate. **Materials and Methods:** Patients (n=20) were referred from dementia experts for imaging with different suspected tauopathies (n=7: Alzheimer's disease; n=6: progressive supranuclear palsy; n=7: corticobasal syndrome). All patients underwent ^{18}F-FDG-PET in a clinical setting and data had been reconstructed in a static 30-50 min frame. ^{18}F-PI-2620 PET was performed in a full dynamic 0-60 min setting. Single frames (6x30s, 4x60s, 4x120s, 9x300s) and regional cerebral blood flow estimate R_1 maps were likewise computed from the dynamic ^{18}F-PI-2620 images. Volumes of interest (VOIs) were placed in the bilateral frontal, parietal, temporal, and occipital cortices, as well as in the central region and the striatum. Associations between the resulting semi-quantitative early-phase ^{18}F-PI-2620 and ^{18}F-FDG-PET standard uptake value ratios (cerebellar reference region) were investigated by calculating Pearson's correlation coefficients (Rs). **Results:** Highest agreement of single ^{18}F-PI-2620 frames and ^{18}F-FDG-PET was found for frames between 60 and 180 seconds (all R of all regions >0.6). The agreement strongly deteriorated after 420 seconds p.i. (mean R<0.4). Summed 1-3 min frames indicated a significant agreement between early phase ^{18}F-PI-2620 frames and ^{18}F-FDG-PET in all target regions (mean R: 0.66±0.13) with highest agreement in the parietal cortex (bilateral R=0.81, both p<0.001) and lowest agreement in the right frontal cortex (R=0.47, p=0.038). ^{18}F-PI-2620 R_1 maps also indicated a good agreement with ^{18}F-FDG-PET in most target regions (mean R: 0.58±0.13) with highest agreement in the left temporal cortex (R=0.76, p<0.001) and lowest agreement in the right frontal cortex (R=0.36, p=0.117). Comparisons of visual clinical reads are pending. **Conclusion:** Early-phase images of the second-generation tau tracer ^{18}F-PI-2620 show high accordance with FDG PET images and can, thus, be used as a surrogate of neurodegeneration. If also valid for clinical assessment, this could provide the opportunity to classify two (tau and neuronal injury) biomarkers with one procedure in a dual-phase "one-stop shop" PET imaging protocol. **References:** None.

1010

Cardiovascular - Parallel Session: Myocardial Blood Flow Quantification with PET

Monday, October 14, 2019, 16:30 - 18:00 Lecture Hall 116

OP-465

Association between pericoronary fat thickness and coronary vascular function in patients with suspected coronary artery disease and normal myocardial perfusion imaging

C. Nappi[1], *V. Gaudieri*[1], *R. Assante*[1], *E. Zampella*[1], *G. De Simini*[1], *A. Giordano*[1], *T. Mannarino*[1], *A. D'Antonio*[1], *R. Green*[1], *V. Cantoni*[1], *M. Petretta*[2], *W. Acampa*[1], *A. Cuocolo*[1];
[1]*Department of Advanced Biomedical Sciences, Federico II University, Naples, ITALY,* [2]*Department of Translational Medical Sciences, University Federico II, Naples, ITALY.*

Aim/Introduction: Myocardial perfusion reserve (MPR) is a sensitive indicator of vascular damage in patients with cardiovascular risk. It has been suggested that pericoronary fat thickness (PCFT) may have a local pro-atherosclerotic effect. However, the association between PCFT and coronary vascular function has not been fully investigated. We evaluated the relationships of PCFT and hyperemic myocardial blood flow (MBF) and MPR in patients with suspected CAD and normal myocardial perfusion imaging. **Materials and Methods:** From a pool of 1550 subjects referred to stress-rest Rb-82 PET/CT, 582 patients with suspected CAD and normal myocardial perfusion imaging (summed stress score<3) were considered. Regional PCFT, defined as the maximum fat thickness (mm) between the surface of the heart and the visceral epicardium surrounding the 3 main coronary arteries, and CAC score were measured on CT images. The mean value of the 3 regional PCFT was used to calculate the mean PCFT. Myocardial perfusion was assessed using standardized segmentation of 17 myocardial regions. Absolute MBF was computed from dynamic rest and stress imaging series. MPR was defined as the ratio of hyperemic to baseline MBF and considered reduced when<2 **Results:** Among 582 patients included, 106 (18%) had reduced and 476 (82%) normal MPR. Compared to patients with normal MPR, those with impaired MPR were older (64±13 years vs. 59±13 years, P<0.001) and showed higher prevalence of hypertension (89% vs. 74%, P<0.002) and diabetes mellitus (40% vs. 22%, P<0.002). Baseline MBF did not differ between patients with normal and impaired MPR. On the contrary, patients with impaired MPR had a blunted response to pharmacological stressor (1.99±0.61 vs. 2.89±0.70, P<0.001) and higher mean PCFT values (11.6±1.9 mm vs. 10.93±1.9 mm, P<0.005) compared to those with normal MPR. At univariate linear regression analysis, age, hypertension, diabetes, CAC score, and mean PCFT were significant predictors of reduced hyperemic MBF and impaired MPR, while male gender predicted only a reduced hyperemic MBF (all P<0.005). Although baseline MBF was not associated with PCFT, a significant correlation of global and regional PCFT and corresponding hyperemic MBF was found for left anterior descending, left circumflex, and right coronary arteries (all P<0.001). Such a relationship was also seen between left circumflex coronary artery PCFT and corresponding MPR (P<0.001). **Conclusion:** In patients with suspected CAD and normal MPI, there is a significant association of global and regional hyperemic MBF with PCFT suggesting a local effect of pericoronary fat on underlying coronary vascular function. **References:** None.

OP-466

Quantitative myocardial perfusion ^{82}Rb-PET assessed by hybrid PET/coronary-CT: normal values and diagnostic performance

M. T. Freitag, J. Bremerich, D. Wild, P. Haaf, M. J. Zellweger, F. Caobelli;
University Hospital Basel, Basel, SWITZERLAND.

Aim/Introduction: No conclusive data exist on normal values of quantified myocardial blood flow on ^{82}Rb-PET/CT under stress (sMBF) and rest (rMBF). We aimed to assess normal reference values for MBF on a hybrid PET/coronary-CT scanner and to test their diagnostic performance in patients with suspected coronary artery disease (CAD). **Materials and Methods:** Patients underwent sequential cardiac ^{82}Rb-PET/CT (Siemens Biograph mCT 128) with stress/rest (Adenosine) and integrated CT-based coronary angiography (CTCA). Patients were classified as normal (<50% stenosis on CTCA and summed stress score [SSS]=0) and with CAD (>50% stenosis, any SSS). sMBF, rMBF and myocardial flow reserve (MFR) were calculated both globally and in each vascular territory by Syngo MBF (Siemens). On static PET images, ischemia was visually assessed and defined as summed difference score ≥2. Mann-Whitney-U test was used for comparison of non-parametric data across groups, ROC-analysis was performed to determine diagnostic accuracy in identifying ischemia. Flow values are given in ml/g/min as mean±SD. **Results:** Of overall 357 patients included (male/female 53%/47%, aged 61.1±10.3 years, body-mass-index 28.9±6.3 kg/m², 21% diabetics, 57% with arterial hypertension), 225 patients were classified as normal and 132 as with CAD. sMBF and MFR were significantly higher in normal patients than in patients with CAD (3.64±0.68 vs. 3.05±0.77, p<0.0001; 3.09±0.86 vs. 2.73±0.77, p=0.0002). rMBF was not different (1.28±0.40 vs 1.19±0.34, p=0.06). In the right coronary artery (RCA), sMBF[RCA] in normal vessels was higher than in stenotic ones (3.84±0.89 vs 3.31±1.14, p=0.008). Both rMBF[RCA] and MFR[RCA] were not different (1.27±0.44 vs. 1.19±0.48, p=0.14; 3.29±1.03 vs. 3.06±1.23, p=0.13). In the circumflex artery (RCX), sMBF[RCX] and MFR[RCX] in normal vessels were significantly higher than in stenotic ones, (3.26±0.76 vs. 2.50±0.86, p<0.0001; 2.84±0.83 vs. 2.17±0.69, p<0.0001). rMBF[RCX] was similar between normal and stenotic vessels (1.24±0.38 vs. 1.19±0.24, p=0.99). In the left anterior descending artery (LAD) sMBF[LAD] and MFR[LAD] in normal vessels was higher than in stenotic ones (3.53±0.72 vs. 2.89±0.79, p<0.0001; 3.00±0.83 vs. 2.46±0.75, p<0.0001). rMBF[LAD] was similar (1.26±0.38 vs. 1.25±0.35, p=0.99). Global sMBF yielded superior accuracy in identifying myocardial ischemia over MFR (AUC 0.75 vs. 0.63, p<0.003). Optimal threshold for sMBF was 3.5 ml/g/min (sensitivity 87.5%, specificity 48.7%, negative predictive value (NPV) (96%). **Conclusion:** The assessed normal reference values for global sMBF provided higher diagnostic accuracy than MFR with respect to stenosis detection. Using sMBF-threshold of 3.5 ml/mg/min on ^{82}Rb-PET/CT yielded similar NPV (96%) as CTCA to rule out ischemia (1). **References:** (1) Meijboom et al. JACC 2008;52:2135-44.

OP-467

Prognostic value of coronary vascular dysfunction assessed by hybrid rubidium-82 PET/CT imaging in patients with resistant hypertension

V. Gaudieri[1], W. Acampa[1], R. Assante[1], E. Zampella[1], C. Nappi[1], T. Mannarino[1], M. Panico[2], A. D'Antonio[1], M. Raddi[1], M. Petretta[3], M. Memmott[4], P. Arumugam[4], A. Cuocolo[1];
[1]Department of Advanced Biomedical Sciences, University Federico II, Naples, ITALY, [2]Institute of Biostructure and Bioimaging, National Council of Research, Naples, ITALY, [3]Department of Translational Medical Sciences, University Federico II, Naples, ITALY, [4]Nuclear Medicine Centre, Manchester University NHS Foundation Trust, Manchester, UNITED KINGDOM.

Aim/Introduction: Aim of this study was to evaluate if impaired vasodilator function, assessed by ^{82}Rubidium (^{82}Rb) PET/CT imaging, carries to an increased cardiovascular risk in patients with resistant hypertension (RH). **Materials and Methods:** A total of 518 hypertensive patients without overt coronary artery disease and normal myocardial perfusion (summed stress score <3) at stress-rest ^{82}Rb PET/CT imaging were studied. Hypertension was defined as resistant when the concurrent use of three different antihypertensive agents failed to lower blood pressure to target values. Coronary artery calcium (CAC) score were categorized into 4 groups (0, 0.1-99.9, 100-399.9 and ≥400). Left ventricular (LV) ejection fraction reserve was calculated as the difference of stress and rest ejection fraction. Baseline and hyperemic myocardial blood flow (MBF) were automatically measured. Myocardial perfusion reserve (MPR) was defined as the ratio of hyperemic to baseline MBF and considered reduced when <2. The endpoints were cardiac death, nonfatal myocardial infarction, coronary revascularization, and admission for heart failure. **Results:** Over a median of 38 months (interquartile range 26 to 50 months), 22 cardiac events (4.2% cumulative event rate) occurred: 3 cardiac deaths, 4 myocardial infarctions, 5 revascularization procedures and 10 admissions for heart failure. Patients with events compared to those without were older (70±14 vs. 61±12 years, P<0.001) and had a higher prevalence of RH (59% vs. 24%, P<0.001), a higher prevalence of CAC ≥400 (36% vs. 18%, P<0.05), a lower hyperemic MBF (2.15±0.74 vs. 2.58±0.82 ml/g/min, P <0.05) and a lower MPR (2.14±0.86 vs. 2.58±0.70, P<0.01). At univariable Cox regression analysis, age (P<0.001), RH (P=0.001), MPR (P<0.005), and LV ejection fraction reserve (P<0.05) were significant predictors of events. At multivariable analysis, age (P<0.01), RH (P<0.05), and MPR (P<0.05) were independent predictors of events. Patients with RH and impaired MPR showed the worst outcome. Event-free survival was lower in patients with RH and impaired MPR compared to those with controlled hypertension and impaired MPR (P<0.001). Differently, the best outcome was observed in patients with controlled hypertension and preserved MPR. **Conclusion:** Coronary vascular dysfunction by ^{82}Rb PET/CT in patients with RH can help in identify a higher risk of cardiovascular events. Thus, MPR could be useful in the risk assessment and for patient's management, guiding alternative potential therapeutic strategies aimed to directly improve MPR. **References:** None.

OP-468

Quantitative PET with [13N] -Ammonia in the Detection of Functional Significance of Intermediate Stenoses of Coronary Arteries

D. Ryzhkova, D. Zverev;
National Almazov Medical Research Centre, St.Petersburg, RUSSIAN FEDERATION.

Aim/Introduction: The assessment of diagnostic and prognostic values of quantitative PET with [13N] -ammonia to identify the functional significance of intermediate stenoses of coronary arteries. **Materials and Methods:** 80 patients (M:F 61:19, 63±10,1 years) with intermediate stenoses of one and more coronary arteries (50%-70%) were included in the study. Dynamic PET/CT scanning with [13N] -ammonia was performed twice at rest and during pharmacological test with adenosine. Low-dose CT scan was used for attenuation correction of PET data. Regional absolute myocardial blood flow and coronary flow reserve (CFR) were quantified automatically using commercially available Corridor4DM CFR software (Invia, Ann Arbor, Michigan). Fractional flow reserve (FFR) measurement was applied to assess the functional significance of intermediate coronary stenoses. According to the guidelines we considered the normal value of CFR >2.3 [1] and FFR ≥ 0.8 [2]. **Results:** 91 coronary arteries with intermediate stenosis (50%-70%) were included in analysis. We observed the agreement between CFR and FFR data in identification of functional significance of intermediate stenoses of coronary arteries in 78% of all cases. The sensitivity of PET with [13N] -ammonia was 82%, specificity - 77%, accuracy - 78%. FFR and CFR disagreed in 22% of all cases, mainly when FFR remained normal, but CRF was below the reference values. The positive prognostic value of [13N] -ammonia PET was 53%. We found the significant correlation between CFR and myocardial mass index (r=0,68, p<0,05). Moreover, patients with 2 type of diabetes mellitus had CFR below the normal values while FFR was ≥ 0.8 . The negative prognostic value of [13N] -ammonia PET was high - 93%. **Conclusion:** Quantitative [13N] -ammonia PET is an effective method to rule out the functional significance of intermediate coronary stenoses. Ventricular myocardial hypertrophy and 2 type of diabetes mellitus contribute on impairment of coronary microcirculation and leads to decrease CFR in territory supplied by coronary artery with intermediate stenosis and normal FFR. **References:** 1. Dilsizian, V., Bacharach, S.L., Beanlands, R.S. et al. ASNC imaging guidelines/SNMMI procedure standard for positron emission tomography (PET) nuclear cardiology procedures J. Nucl. Cardiol. (2016). doi:10.1007/s12350-016-0522-3 2. 2014 ESC/EACTS Guidelines on myocardial revascularization / European Journal of Cardio-Thoracic Surgery. - 2014. - V. 46. - P. 517-592.

OP-469

Combined evaluation of regional coronary artery calcium and myocardial perfusion by ^{82}Rb PET/CT in predicting lesion-related outcome

E. Zampella[1], W. Acampa[1], R. Assante[1], T. Mannarino[1], A. Genova[1], C. Nappi[1], A. D'Antonio[1], V. Gaudieri[1], M. Panico[2], M. Petretta[3], P. Arumugam[4], A. Cuocolo[1];
[1]Department of Advanced Biomedical Sciences, University Federico II, Naples, ITALY, [2]Istitute of Biostructrure and Bioimaging, National Council of Research, Naples, ITALY, [3]Department of Translational Medical Sciences, University Federico II, Naples, ITALY, [4]Department of Nuclear Medicine Central Manchester Foundation Trust, Manchester, UNITED KINGDOM.

Aim/Introduction: Cardiac imaging with PET/CT allows measurement of coronary artery calcium (CAC), myocardial perfusion and myocardial perfusion reserve (MPR). We evaluated the prognostic role of the combined assessment of regional CAC score, ischemic total perfusion defect (ITPD) and MPR in predicting lesion-related outcome in patients with suspected coronary artery disease (CAD). **Materials and Methods:** We studied 206 patients referred to ^{82}Rb PET/CT and with available coronary angiographic data. At coronary angiography a stenosis ≥50% was considered significant. Regional CAC score was categorized as <300 and ≥300 and regional ITPD in <5% and ≥5%. Regional MPR was considered reduced when <2. The outcome end points were cardiac death, target vessel-related myocardial infarction, or unstable angina requiring coronary revascularization (ischemia-driven target vessel revascularization). When identification of culprit vessel was not possible the endpoint was assigned to all the stenotic vessels of those patients. **Results:** During a median follow-up of 34 months, 41 events occurred in vessels with significant stenosis (n=199), while only 6 events were observed in vessels without stenosis (n=419) (P<0.001). Compared to vessels without event, those with event showed higher CAC score and ITPD, and lower hyperemic myocardial blood flow and MPR (all P<0.001). At Cox regression multivariable analysis, CAD ≥50% (P<0.001), CAC score ≥300 (P<0.01) and MPR <2 (P<0.01) resulted as independent predictors of events. At incremental analysis, the addition of CAC score ≥300 to coronary angiography findings, significantly increased global χ2 of the model (P<0.001). The addition of MPR <2 to coronary angiography findings and CAC score, further increased the χ2 (P<0.01). In vessels with significant stenosis, the recursive partitioning and regression trees analysis for the identification of events produced five terminal groups. The initial split was on CAC score values. For vessels with CAC <300 and MPR ≥2, no further split was performed, while vessels with MPR <2 were further stratified by ITPD. For vessels with CAC ≥300 a further stratification was performed only by MPR. The worst prognosis was observed in vessels with CAC ≥300 and MPR <2 and in vessels with CAC <300, MPR <2 and ITPD ≥5% (both P <0.001) **Conclusion:** A combined use of CAC score and MPR can help to predict more accurately the lesion-related outcome in the presence of significant CAD. Thus, these measurements may be useful in the identification of stenotic vessels at higher

risk of events, in which a more aggressive treatment should be taken into account. **References:** None.

OP-470

Evaluation Of Quantitative Cmr Perfusion Imaging By Comparison With Simultaneous ^{15}O-water-pet

T. Kero[1], *E. Johansson*[2], *M. Engström*[3], *K. Eggers*[1], *L. Johansson*[2], *H. Ahlström*[1], *M. Lubberink*[1];
[1]*Uppsala University, Uppsala, SWEDEN,* [2]*Antaros Medical, Mölndal, SWEDEN,* [3]*GE Healthcare, Uppsala, SWEDEN.*

Aim/Introduction: We assessed the quantitative accuracy of cardiac perfusion measurements using dynamic contrast-enhanced MRI with simultaneous ^{15}O-water PET as reference with a fully integrated PET-MR scanner. **Materials and Methods:** 15 patients underwent simultaneous DCE MRI and 15O-water PET scans at rest and adenosine-stress on an integrated PET-MR scanner. Correlation and agreement between MRI- and PET-based global and regional MBF values were assessed using correlation and Bland Altman analysis. **Results:** Three subjects were excluded due to technical problems. Global mean (± SD) MBF values at rest and stress were 0.97 ± 0.27 and 3.19 ± 0.70 mL/g/min for MRI and 1.02 ± 0.28 and 3.13 ± 1.16 mL/g/min for PET (p=0.66 and p=0.81). The correlations between global and regional MRI- and PET-based MBF values were strong (r=0.86 and r=0.75). The biases were negligible for both global and regional MBF comparisons (0.01 and 0.00 mL/min/g for both), but the limits of agreement were wide for both global and regional MBF, with larger variability for high MBF-values. **Conclusion:** The correlation between simultaneous MBF measurements with DCE MRI and 15O-water PET measured in an integrated PET-MRI was strong but the agreement was only moderate indicating that MRI-based quantitative MBF measurements is not ready for clinical introduction. **References:** None.

OP-471

Appropriate Coronary Revascularization Can Be Accomplished If Myocardial Perfusion Is Assessed With Cardiac PET Prior To Treatment Decision

S. Akil[1,2], *F. Hedeer*[1], *J. Oddstig*[1], *T. Olsson*[1], *J. Jogi*[1], *D. Erlinge*[1], *M. Carlsson*[1], *H. Arheden*[1], *C. Hindorf*[1], *H. Engblom*[1];
[1]*Lund university, Lund, SWEDEN,* [2]*Princess Norah Bint AbdulRahman University, Riyadh, SAUDI ARABIA.*

Aim/Introduction: Current guidelines for coronary revascularization in stable coronary artery disease (CAD) recommends the use of non-invasive stress-testing prior to treatment (1). Still, many patients undergo percutaneous coronary intervention (PCI) based on clinical symptoms and angiographic findings. The aim of this study was to investigate if appropriate revascularizations are accomplished in clinical routine and to determine the potential added value of guiding revascularization by quantitative assessment of myocardial perfusion with cardiac PET prior to intervention. **Materials and Methods:** Thirty-three patients (10 females) with suspected or established CAD who had been referred for a clinical coronary angiography (CA) with possibility for PCI were included. Adenosine stress and rest ^{13}N-NH_3 positron emission tomography (PET), cardiac magnetic resonance (CMR) and cardiopulmonary exercise test were performed 4±3 weeks before and 5±1 months after CA. The angiographer was blinded to the PET, CMR and exercise test results. The decision to perform PCI in conjunction with CA was based on available clinical data and CA findings, according to clinical routine. Regional and global coronary flow reserve (CFR) by PET, left ventricular function by CMR, presence of myocardial infarction by CMR and peak oxygen uptake (VO_2 peak) were quantified before and after the CA. CFR<2.0 was considered abnormal. **Results:** A PCI was performed in 19/33 patients. In 41% (11/27) of the revascularized vessel territories, a normal regional CFR was found prior to the PCI and no improvement in CFR was found at follow-up (p=0.9). However, vessel territories with regional CFR<2.0 at baseline improved significantly after PCI (p=0.003). No significant change was found between baseline and follow-up regarding global CFR, left ventricular ejection fraction or VO_2 peak. Of the 14 patients not undergoing PCI, 5 had CFR<2 in one or more coronary territories. **Conclusion:** Assessment of quantitative myocardial perfusion, by cardiac PET, prior to revascularization could lead to more appropriate use of coronary angiography when managing patients with stable coronary artery disease. Thereby, unnecessary angiographies and subsequent revascularizations can be avoided. **References:** 1. Task Force M, Montalescot G, Sechtem U, Achenbach S, Andreotti F, Arden C, et al. 2013 ESC guidelines on the management of stable coronary artery disease: the Task Force on the management of stable coronary artery disease of the European Society of Cardiology. Eur Heart J. 2013;34(38):2949-3003.

OP-472

Preserved stress myocardial flow can predict of improvement of contractile function in the patients with non ischemic dilated cardiomyopathy

E. Kong, *I. Cho*, *C. Lee*, *D. Shin*;
Yeungnam university hospital, Daegu, KOREA, REPUBLIC OF.

Aim/Introduction: NH_3 myocardial perfusion PET(N-PET) not only has a high diagnostic power for coronary artery disease, but also enables quantitative analysis of myocardial blood flow, thus enabling diagnosis of microvascular disease. We decided to investigate whether adenosine stress (Ad-St) N-PET can provide clinically useful information to predict prognosis in patients with dilated cardiomyopathy (DCM). **Materials and Methods:** From Oct 2015 to Aug 2018, 92 patients underwent both Ad-St N-PET and cardiac MRI for the evaluation of DCM. After except for patients with incomplete initial testing, loss of follow-up, or severe systemic disease, 63 patients (46 males) was finally enrolled. Patients were measured stress myocardial flow with Ad-St N-PET and myocardial fibrosis by LGE MRI.

LVEF and LV end diastolic diameter (LVEDD) were measured by echocardiography. We evaluated the factors that can predict the improvement of cardiac function (LVEF 10%) based on follow - up echocardiography. **Results:** Fifty (57 y-o) patients with nonischemic (Nis) DCM and 13 (65 y-o) with ischemic(Is) DCM, baseline LVEF was 27.5% and 29.2%, and LVEDD was 62.5 mm and 61.8 mm, respectively. LGE was observed in 67% of Nis-DCM patients and 100% in Is-DCM. Stress flow was 1.52 and 1.15, respectively, and 42% and 65% of patients showed functional improvement. In Nis-DCM patients, function improving patients group (n=21) had more female ratio (48% vs. 24%), younger patients (51.5 y-o vs 61.4 y-o) 86%), less LGE (38% vs 86%) and higher stress flow (1.74 vs 1.36) than non-improving group. However, there was no significant difference in baseline LVEF and LVEDD. For prediction of functional recovery, LGE was sn 62%, sp 86%, PPV 76.5% and NPV 75.7%, and the stress flow was 62%, 86%, 76.5% and 75.7%, respectively. Of the 7 patients with no LGE but low stress flow, 4 had no functional recovery and one expired within one year. Of the 4 patients with LGE but maintained stress flow, 2 had no improvement, but one of them had a 19% decrease in LVEDD, so clinically improved 3 patients. If LGE and stress flow were mismatched, stress flow predicted better at 7/11. **Conclusion:** We can predict of improvement of LVEF by the stress myocardial blood flow rate was over 1.9 mL / min / g or absence of LGE in patients with non-ischemic dilated cardiomyopathy. Stress ammonia PET was able to provide additional information on prognosis prediction compared with LGE in cardiac MRI. **References:** None.

1101

CME 9 - Cardiovascular Committee: Non-Invasive Imaging Strategies in Heart Failure

Tuesday, October 15, 2019, 8:00 - 9:30 Auditorium

OP-473

When and How Should I Look for Myocardial Ischemia or Viability?

F. Hyafil;
Department of Nuclear Medicine, Bichat University Hospital, Paris, FRANCE.

OP-474

When and How Should I Look for Cardiac Amyloidosis?

R. Slart;
University Medical Center Groningen, University of Groningen, Groningen, NETHERLANDS.

OP-475a

When and How Should I Look for Cardiac Dyssynchrony?

M. Hacker;
Department of Biomedical Imaging and Image-guided Therapy, Vienna, AUSTRIA.

OP-475b

When and How Should I Look for Cardiac Innervation?

H. Verberne;
Academic Medical Center, Department of Nuclear Medicine, Amsterdam, NETHERLANDS.

1102

Joint Symposium 17 - Oncology & Theranostics Committee / AIO: Challenge Pancreatic Cancer

Tuesday, October 15, 2019, 8:00 - 9:30 Lecture Hall 311

OP-476

Diagnostic Challenges of PDAC

A. Scarpa;
University of Verona, Department of Pathology and Diagnostics, Verona, ITALY.

OP-477

Treatment Algorithm of PDAC

J. Siveke;
Universitätsklinikum Essen, Department of Medical Oncology, Essen, GERMANY.

OP-478

Challenge Diagnostic Imaging of PDAC

P. Veit-Haibach;
University of Toronto, Department Medical Imaging, Toronto, ON, CANADA.

OP-479

Is PDAC an Indication for Radioligand Therapy?

F. Giesel;
University of Heidelberg, Department of Nuclear Medicine, Heidelberg, GERMANY.

1103

Joint Symposium 18 - Thyroid + Inflammation & Infection Committee / ETA: Imaging on Thyroiditis

Tuesday, October 15, 2019, 8:00 - 9:30 Lecture Hall 312

OP-480

Thyroiditis - Clinical Appraisal and Ultrasound Features

C. Buffet;
Hopital Pitie Salpetriere, Thyroid Unit, Paris, FRANCE.

OP-481

Thyroid Scintigraphy and Uptake in Patients with Thyroiditis - Is there a Current Role?

L. Giovanella;
Imaging Institute of Southern Switzerland, Clinic for Nuclear Medicine, Bellinzona, SWITZERLAND.

OP-482

Thyroiditis at PET Imaging with Different Tracers - Interpretation Criteria and Reporting

G. Treglia;
Imaging Institute of Southern Switzerland and Health Technology Assessment Unit, Ente Ospedaliero Cantonale, Bellinzona, SWITZERLAND.

1104

Technologists: Oral Presentations 2

Tuesday, October 15, 2019, 8:00 - 9:30 Lecture Hall 117

OP-483

Prevention of activated brown adipose tissue in F^{18}-FDG-PET-imaging in children and adolescents - Which measures are effective?

C. Pötzsch[1], *S. Naumann*[1], *L. Kurch*[1], *T. W. Georgi*[1], *M. Weckesser*[2], *S. Klutmann*[3], *D. Schmidt*[4], *K. Herrmann*[5], *J. Sciuk*[6], *D. Hasenclever*[7], *C. Mauz- Körholz*[8], *D. Körholz*[8], *O. Sabri*[1], *R. Kluge*[1];
[1]*Department of Nuclear Medicine, University of Leipzig, Leipzig, GERMANY,* [2]*Department of Nuclear Medicine, University of Münster, Münster, GERMANY,* [3]*Department of Nuclear Medicine, University Hospital Eppendorf, Hamburg, GERMANY,* [4]*Department of Nuclear Medicine, University of Erlangen, Erlangen, GERMANY,* [5]*Department of Nuclear Medicine, University of Essen, Essen, GERMANY,* [6]*Department of Nuclear Medicine, University of Augsburg, Augsburg, GERMANY,* [7]*Institute for Medical Informatic, Statistics and Epidemiology, University of Leipzig, Leipzig, GERMANY,* [8]*Department of Pediatric, Hamatology and Oncology, University of Gießen, Gießen, GERMANY.*

Aim/Introduction: FDG accumulation in activated brown adipose tissue (ABAT) complicates PET assessments in children and adolescents. Preventive measures (PM) as warming or the administration of non-selective beta-blockers (BB) have been described. The aim of our German-wide study was the evaluation of the effectiveness of these PM to prevent ABAT. **Materials and Methods:** The study included 267 children or adolescents with Hodgkin lymphoma treated in 48 German hospitals within the EuroNet-PHL-C2 trial. The severity of ABAT was assessed in 589 PET-CT or PET-MRI examinations by two experienced technologists using a five point scale (none, low, intermediate, strong (s) and very strong (vs)). In addition, the thickness of the pelvic soft tissue and the weather at the time point of the PET scan were determined. The individual PM (warming, BB (with dose), both, others) were delivered by the 48 local PET centers. **Results:** In 528/589 cases, the PMs were determinable. 165 patients (31%) did not receive any PM, 243 patients (46%) were warmed only, 36 patients (7%) received BB only, and 84 patients (16%) got both warming and BB. ABAT was detected in 28 % of the PET without PM, in 14% with warming, in 14% with BB and in 8% with both warming and BB. S or vs ABAT was detected in 14% without PM, in 5% with warming, in 3% with BB and in 0% with combined BB and warming. Presence of ABAT was strongly correlated with the outdoor temperature (p= 0.000235) but not with the thickness of the pelvic soft tissue layer (p= 0.787). **Conclusion:** In Germany, very different PMs are used to avoid ABAT. Without PM, more than every fourth PET study was affected by ABAT. Both, warming and the administration of BB proved to be effective measures; the combination of both was the most effective way to reduce ABAT. **References:** None.

OP-484

Combined 18F-Fluorocholine and 11C-Methionine PET-CT for parathyroid adenoma localization: a pilot acquisition protocol

A. Pereira Gomes, L. Silva;
Erasme Hospital, Anderlecht, BELGIUM.

Aim/Introduction: Aim: Localization of parathyroid adenomas is now possible with 18F-Fluorocholine (18F-FCH) PET-CT imaging, although very limited data are available in literature about this subject. This prospective study aims to describe an acquisition protocol for parathyroid adenoma localization using 18F-FCH. **Materials and Methods:** Methods: Twenty patients with hyperfunctioning parathyroid were enrolled in this study and underwent two different exams, both performed using a Philips Gemini Dual PET-CT. The first one (as our standard of truth) was performed with 555 MBq of 11C-Methionine (11C-MET) administered intravenously (IV). An emission scan, 20 min post IV, was obtained for 7 min at each of 3 bedpositions centred to the neck, upper and medium mediastinum and co-

registered with a low-dose CT. The second one, and with the patient positioned inside of the PET tunnel, 4 MBq/Kg 18F-FCH was injected on IV at the same time of the first scan: a dynamic emission scan centered on the neck (1 bed-position) during 15 min. Immediately after, a second emission scan centered to the neck, upper and medium mediastinum for also 7 min at each of 3 bed-positions. Subsequently, 60 min post IV, a third emission scan was acquired equally to the second one. The total of three emissions scans were co-registered with a second low-dose CT. The dynamic images were reframed by summing up images every 5 min to facilitate interpretation and all images were reconstructed by iterative method (2 iterations and 21 subsets). Three experienced observers started to analyse all images in which the highest value of lesion contrast should be expected at the optimal scan time. **Results:** Results: We succeeded to set up a one-day protocol for both 18F-FCH and 11C-MET PET acquisitions for patients with a suspicion of parathyroid adenoma. The protocol included a dynamic acquisition for the 18FFCH, which allows data acquisition on the washout kinetics. Dynamic data might indeed improve the diagnostic value of the procedure. **Conclusion:** Conclusion: To the best of our knowledge there are no studies describing an acquisition protocol for parathyroid adenoma localisation using two tracers in a single session. This study suggested that the acquisition protocol mentioned is possible and might reinforce the diagnostic. Notwithstanding a larger database is needed for further investigation. **References:** None.

OP-485

Dual time-point ^{18}F-Flutemetamol PET protocol for the imaging of neurodegenerative and amyloid biomarkers in mild cognitive impairment

A. Ruzza, *L. Filippi, G. Cicco, P. Basile, R. Pirisino, O. Bagni;*
Santa Maria Goretti Hospital, Latina, ITALY.

Aim/Introduction: According to recently published international recommendations, diagnosis of Alzheimer's Disease (AD) should be based on a specific pathological biomarker network termed AT(N), including detectable bioumoral or imaging hallmarks of amyloid burden (A), tau protein aggregates (T) and neurodegeneration (N). Our aim was to evaluate a dual time-point protocol for Positron Emission Tomography (PET) with ^{18}F-flutemetamol (FMM) for the contextual evaluation of both blood flow impairment (as hallmark of neurodegeneration) and amyloid burden in patients with mild cognitive impairment (MCI). **Materials and Methods:** We enrolled 16 patients (9 women, 7 men, mean age 66,6 + SD) with clinical diagnosis of MCI. All the subjects were injected intravenously with ^{18}F-FMM (dose 185 MBq) and hydrated with 500 ml of saline (0.9 % sodium chloride). In all cases PET-CT was acquired through a Discovery ST device (GE Healthcare). Dual time-point brain PET/CT was acquired according to the following protocol: an early phase (EPH) consisting of a short acquisition with the duration of 6 minutes, starting immediately post injection, followed by a late phase (LPH) at 90 minutes post injection with the standard duration of 20 minutes. Images both for EPH and LPH were reconstructed using an ordered subset expectation maximization iterative algorithm (OSEM-SV, VUEPoint HD; GE Healthcare, 2 iterations, 30 subsets), matrix 256x256; full width at half maximum: 5 mm. EPH images were visually evaluated. LPH images were evaluated by visual and quantitative (CortexID Suite, GE Healthcare) examination. **Results:** Among the 16 patients, five presented perfusion defects typical for AD at EPH, the remaining subjects did not show any relevant perfusion defects. All the subjects, who showed hypoperfusion at the EPH, were positive for amyloid burden at the LPH. Of note, three of them had previously performed perfusional SPECT (n= 1) or FDG PET (n= 2) that revealed hypoperfusion or hypometabolism patterns substantially in agreement with the results obtained with amyloid PET at EPH. At LPH, nine patients were positive for amyloid burden both at visual and quantitative analysis. None of the patients who were negative at the EPH presented significant amyloid deposition at the LPH. **Conclusion:** These preliminary results suggest that our dual-time point protocol for FMM PET might represent a reliable tool for the dual imaging of neurodegenerative and amyloid biomarker in MCI. **References:** None.

OP-486

Further Reduction Of [^{18}F]-fdg Activity Applied In Clinical Routine For State-of-the-art 3d Tof Pet/ct Systems: Is It Feasible?

J. Pilz, *L. Hehenwarter, J. Holzmannhofer, G. Schweighofer-Zwink, C. Pirich;*
Department of Nuclear Medicine and Endocrinology, University Hospital Salzburg, Paracelsus Medical University, Salzburg, AUSTRIA.

Aim/Introduction: A reduction of the [^{18}F]-FDG activity applied may become feasible in the clinical setting due to the ongoing technical innovation implemented into PET/CT systems. Currently, the [^{18}F]-FDG activity applied is 4 MBq per kg bodyweight and the acquisition time is set to 75 seconds per bed position at our nuclear medicine department. The aim of this study is to investigate the performance of a 3D state-of-the-art PET/CT scanner including TOF technology with respect to the minimum acquisition time where adequate image quality is still maintained. The minimum acquisition time could be translated to a reduced [^{18}F]-FDG activity. **Materials and Methods:** A NEMA NU2 body phantom containing a lung insert in the center, six spheres varying in size and a background compartment, was filled with [^{18}F]-FDG according to the European Association of Nuclear Medicine Research Ltd. (EARL) specifications. A Philips Ingenuity TF PET/CT system was used to scan the phantom with two bed positions of five minutes. Various datasets with different acquisition times were analyzed afterwards. The PET datasets were reconstructed by a blob-based ordered-subsets expectation maximization (OSEM) TOF algorithm using a matrix of 144×144 pixels. Image data were evaluated by the calculation of mean and maximum activity

concentration recovery coefficients (RCs) for each sphere of the NEMA phantom and the determination of the coefficient of variation (COV) of the background compartment. Adequate image quality was predefined by RCs meeting EARL criteria and a COVmax < 0.15. **Results:** The following RCs were achieved for the image data with an acquisition time of 57 seconds per bed position: 37mm sphere (meanRC 0.85; maxRC 1.09), 28mm sphere (meanRC 0.78; maxRC 1.04), 22mm sphere (meanRC 0.77; maxRC 1.09), 17mm sphere (meanRC 0.63; maxRC 0.89), 13mm sphere (meanRC 0.53; maxRC 0.75) and 10mm sphere (meanRC 0.36; maxRC 0.49). The COVmax of the image dataset was equal to 0.136. All EARL criteria were met by the 3D TOF Philips Ingenuity TF PET/CT system using a reduced scan time of 57 seconds. **Conclusion:** Minimizing the scan time/activity applied for [^{18}F]-FDG studies is feasible in clinical routine. Experimental imaging data reveal that the Philips Ingenuity TF system still shows adequate image quality in terms of EARL criteria using a reduced acquisition time of 57 seconds per bed position. This implies a [^{18}F]-FDG activity reduction from 4 MBq to 3 MBq per kg BW in clinical routine. Patient studies validating these assumptions are currently under way. **References:** None.

OP-487

Automated preparation and dispensation of ^{68}Ga-DOTATOC on the same synthesizer - impact on the dosimetric exposure of technologists compared to manual practice

M. Frindel[1], *N. Varmenot*[1], *A. Rauscher*[1], *P. Baumgartner*[1], *F. Delaunay*[1], *C. Rousseau*[1], *F. Kraeber-Bodere*[1,2];
[1]*Institut de Cancérologie de l'Ouest, Saint-Herblain, FRANCE,* [2]*CHU de Nantes, Nantes, FRANCE.*

Aim/Introduction: The use of gallium-68 in nuclear medicine imaging is continuously increasing. In a previous study, we have evaluated the dosimetric impact of radiolabeling with 68Ga, and have shown for the DOTATOC that it could lead to significant equivalent doses for technologists. As the SOMAKIT-TOC® kit requires manual preparation as well as dispensation of the patient dose, in this work, we have evaluated the dosimetric benefit of automating these processes. **Materials and Methods:** SOMAKIT-TOC® was purchased from Advanced Accelerator Applications and Galliapharm® (1850 MBq) generator from Eckert&Ziegler. Manual preparation of 68Ga-DOTATOC was performed according to the instructions in the SOMAKIT-TOC® SPC. Automated preparation was developed on the ModularLab PharmTracer® synthesizer (Eckert&Ziegler) with slightly customized C1-EL-01 cassette. This includes the elution, the injection of the buffer, the heating and finally a transfer from the reaction kit vial to a sterile/shielded vial. The dispensation step only requires to connect a shielded syringe to a tubing of the cassette and to enter the volume corresponding to the prescribed activity (150 MBq/patient) in the program starting parameters. Exposures of extremities of the technologist were measured for automated preparation and dispensation for three runs and compared to those with manual process. OSL pellets (LANDAUER) were used to measure the cumulative dose. Dosimeters are placed on fingers pulp and base. **Results:** Regarding the preparation step, the volume of buffer has been set to 0.6 ml that allows a variation of the elution volume of 4 to 5.8 ml while remaining within the pH range [3.2-3.8]. The heating setpoint (110°C during 510 s) has been adjusted in order to obtain the same endpoint temperature into the vial as compared to the manual preparation. Concerning the dosimetric impact to extremities, the median [min, max] radiation exposure per syringe was 132 µSv [70, 273] vs. 315 µSv [28, 875] respectively for the automated vs. the manual practice. The extrapolated annual equivalent dose lead to 86 mSv [46; 177] and 205 mSv [18; 569], respectively for automated vs. manual 68Ga-DOTATOC labeling. **Conclusion:** Automation of 68Ga-DOTATOC preparation and dispensation is effective to reduce technologist's extremities exposition by a factor 2 to 3. This automation is applicable to other kits and permit the wide spread of the 68Ga use with low dosimetric impact for the technologists. **References:** None.

OP-488

PET/CT SiPM: Feasibility of a breath-hold acquisition in a clinical routine

M. Pappon, *M. Jreige, C. Beigelman, P. Genoud, J. Prior;*
CHUV, Lausanne, SWITZERLAND.

Aim/Introduction: Recently introduced high-resolution SiPM PET/CT allows high-sensitivity pulmonary breath-hold acquisition, which is of particular interest in lung nodule characterization. This technique helps to overcome long acquisition time and image quality degradation secondary to breath movements. Herein, we report our first practical experience with an additional breath-hold PET/CT acquisition integrated in clinical routine. **Materials and Methods:** We retrospectively reviewed all PET/CT examinations between January 2019 and March 2019 that were acquired on our SiPM PET/CT (Siemens Biograph Vision 600) with an additional breath-hold (BH) acquisition applied in clinical routine for lung nodules/metastasis investigation. We reported the lung apnea duration achieved by patients (=combined time of consecutive CT and PET acquisitions). The total time added to the examination, as well as the dose differences between total body PET/CT and lung breath-hold PET/CT were also reported. **Results:** A total of 28 patients were included (16M/12F), with an average BMI of 24.4±4.3kg/m² and an injected dose of 145±35MBq of ^{18}F-FDG (2MBq/kg). All patients managed to maintain a success apnea for a duration of 30.8±7.7s, independently of their BMI (Spearman's rho=-0.30, p=0.12) or gender (p=0.116). We observed a significant positive correlation between BH-apnea duration and age (rho=0.40, p=0.036). All BH CT scans were acquired using an ultra-low dose setup with mA modulation resulting in a significantly lower DLP of 15.3±9.2mGy·cm compared to 416±109mGy·cm for the whole-body acquisition (p<0.005) with averaged added dose of 3.7%. The average time difference between the BH and whole-body acquisitions were

15.2±1.4min. **Conclusion:** All patients managed to maintain the relatively short apnea time necessary to obtain BH PET/CT acquisition. Use the ultra-low dose CT protocol resulted in a very low additional dose to patients; high speed acquisition with notably short time between BH and whole-body exams allowed to maintain comparable results between both sequences, which is especially important for quantification purposes. **References:** None.

OP-489

Clinical Benefit Of Routine True-whole-body ^{18}F-fdg Pet/ct For Patients With Malignant Melanoma

A. M. van den Berk, J. P. Esser;
Meander Medical Centre, Amersfoort, NETHERLANDS.

Aim/Introduction: Malignant melanoma (MM) is one of the most lethal carcinomas worldwide and its incidence is increasing. It is an aggressive tumour with often lymphatic and haematogenous spread to any part of the body. Therefore, for screening it is recommended to make an ^{18}F-FDG PET/CT scan from vertex to toes (true-whole-body) instead of the typical scan in oncology from vertex to thigh (partial-whole-body). Consequences of extending the scan are increased patient's radiation exposure and doubled scan-time. By doubling scan-time, fewer patients can be scanned per day and the chance of motion artefacts increases. We retrospectively looked if there is indeed a clinical benefit for true-whole-body scanning. **Materials and Methods:** ^{18}F-FDG PET/CT scans and their reports, performed between March 2006 and March 2018 at the Meander Medical Centre in Amersfoort, the Netherlands, were retrospectively reviewed. Criteria for inclusion into the study were: ^{18}F-FDG PET/CT performed for staging, restaging or surveillance of proven MM. ^{18}F-FDG PET/CT performed as true-whole-body scan (from vertex to toes). Availability of complete patient care reports. We reviewed all ^{18}F-FDG PET/CT scans as well as the reports. Location of primary tumour, metastases located in the region vertex to thigh and/or in the lower extremities were registered. **Results:** We reviewed 284 ^{18}F-FDG PET/CT examinations. A total of 212 scans, performed in 165 patients, met the inclusion criteria. We excluded 15 scans, as they did not image patient's lower extremities. Clinical information was incomplete in another 57 scans, these patients came from other hospitals. No metastases were found in 78 scans (36.8%). Metastases in the region vertex to thigh were found in 102 scans (48.1%). Another 24 scans (11.3%) showed metastases in at least one lower extremity as well as in the partial-whole-body-region. Lower extremity metastases only, were found in 8 scans (3.8%). In all of these 8 cases, the primary tumour was also located in the lower extremities. No scan showed metastases in the lower extremities when the primary tumour was not located in the lower extremities. **Conclusion:** True-whole-body ^{18}F-FDG PET/CT (vertex-toes) has no useful additional information in patients with MM compared to partial-whole-body ^{18}F-FDG PET/CT (vertex to thigh) unless the primary tumour is/was located in the lower extremities. **References:** None.

OP-490

The role of ultra-low dose (0.04mCi/kg) ^{18}F-Sodium Fluoride (NaF) PET/CT in the evaluation of metastatic bone disease

M. Al-Daas, T. Al-Ahmad, A. Esmail, S. Usmani, F. Marafi;
Jaber Al-Ahmad Center for Molecular Imaging, Shuwaikh, KUWAIT.

Aim/Introduction: Fluorine-18-sodium fluoride (^{18}F-NaF) PET/CT have been widely used in the detection of metastatic bone cancer. We have previously demonstrated that ^{18}F-NaF PET/CT has high diagnostic accuracy in with low dose of 0.06 mCi/kg [[i]]. In the present work, we investigate whether these superior imaging characteristics are preserved in ultra-low dose of 0.04mCi/kg. **Materials and Methods:** We prospectively enrolled 16 patients with (mean BMI 30.11 ± 6.48 kg/m²; mean age 48 years [range 18 - 72]) and referred for ^{18}F-NaF PET/CT for the osseous metastatic staging. All the patients underwent ^{18}F-NaF PET/CT scan using an advanced digital PET/CT system in JACMMI (GE Discovery MI) after injection of 0.04 mCi/kg of ^{18}F-NaF. Images were acquired for 2 minutes per bed then reconstructed using different time intervals (2 min, 1:30 min and 1 min/bed). Images were also reconstructed using Bayesian penalized likelihood reconstruction (Q.Clear) with beta (β) value of 700. Signal-to-noise-ratio was measured in the third lumber vertebra (L3) and analyzed semi-quantitatively. Diagnostic test characteristics were calculated using traditional methods. Means with standard deviations and proportions with 95% confidence intervals are reported. **Results:** The results of the 16 patients show that when comparing 2 min/bed images with 1 min/bed a highly significant difference in the Signal-to-noise ratio (SNR) with a p-value of 0.018 using Wilcoxon Signed-Rank Test. On the other hand, the 2 mins/bed compared with the 1:30 mins/bed shows a non-significant change with the SNR with a p-value of 0.509. **Conclusion:** ^{18}F-NaF PET/CT retains its high diagnostic accuracy and confidence with ultra-low dose of 0.04 mCi/kg. Dose can be reduced to this level by using ultra-sensitive digital PET/CT cameras. **References:** [1]. Usmani S, Marafi F, Ahmed A, et al. Diagnostic challenge of staging metastatic bone disease in the morbidly obese patients: A primary study evaluating the usefulness of 18F-Sodium Fluoride (NaF) PET-CT. Clin Nucl Med. 2017;42:829-836.

OP-491

Experiences from the Technologist Point of View: Automatic Nuclear Medicine DICOM Image Observer Tool for Quality Management

M. Szoliková, F. Nagy, Á. K. Krizsán, K. Kukuts, S.Barna, Z. Hascsi, I. Garai, A. Forgác;
ScanoMed Kft., Debrecen, HUNGARY.

Aim/Introduction: The header of a stored DICOM (Digital Imaging and Communications in Medicine) file comprise a number of data elements, including information related to the patient, the imaging system as well as the acquired data

set. Quality Management Bot (Q-Bot), a software tool was developed at our institute, which is capable to give feedback to the technologists about improper injected activity, radiopharmaceutical uptake time and patient ID mismatches. **Our aim** was to introduce the Q-Bot in the clinical routine, to inspect the DICOM records regularly for quality assurance (QA) purposes. **Materials and Methods:** DICOM files acquired on three PET/CT systems (GE, Philips, Mediso) and on three SPECT systems (Mediso) were included in this study. Metadata regarding to patient data (patient ID, patient weight and height, age), radiopharmaceutical (radionuclide, injected amount of radioactivity, measurement time), acquisition parameters (scan start, acquired counts) were monitored continuously for five months. The Q-Bot tool provides evaluated information on unexpected outliers compared to the standardized protocol parameters of the above mentioned categories, while allowing the correction of them by the assigned staff members. 4358 bone ^{99m}Tc scintigraphy and 3416 ^{18}F-FDG PET/CT DICOM images were evaluated with the Q-Bot. **Results:** When considering all the inspected patient scans approximately 4% of all cases showed outliers compared the standardized protocols. Several simple typo errors (patient ID, weight, height, injected activity) were found and repaired continuously. The revealed deviations from the acquisition protocol (e.g. uptake time delay) were identified and discussed. Applied dose to the patient in case of manual injection of radiopharmaceutical was identified as a high risk point for the occurrence of systematic error by the Q-Bot tool. **Conclusion:** Q-Bot as an automatic inspector has significant potential in QA, especially when large amount of patient data is generated on a daily basis. Continuous feedback from such a QA tool enables the detection of both systematic and random errors, and therefore, ensures high quality work of the staff members of a nuclear medicine center. **References:** None.

1105

M2M - Featured Session: Immune Therapy

Tuesday, October 15, 2019, 8:00 - 9:30 Lecture Hall 111

OP-492

TBA

M.Kneilling;
Eberhard Karls Universtiy, Werner Siemens Imaging Center, Department of Preclinical Imaging and Radiopharmacy, Department of dermatology, Tübingen, GERMANY.

OP-493

In vivo Cell Tracking with A Cell Membrane Thiol Targeting Dual PET and Fluorescent Bioconjugation Reagent

***T. T. Pham**, C. Davis, J. Maher, R. Yan;*
King's College London, London, UNITED KINGDOM.

Aim/Introduction: Cell-based therapies offer a novel and rapidly developing technology that has great potential to ameliorate human disease. One fundamental challenge in the successful development and clinical application of cellular therapeutics is the need to better understand the in vivo behaviour of adoptively infused cell products. We envisage that a dual PET and fluorescent cell labelling reagent will harness the synergistic property of both imaging modalities to visualise the labelled cells across the cellular to whole body scales. By placing the dual imaging reagent extracellularly, the cytotoxicity and radiation damages to the cells would be minimised**. Materials and Methods:** We radiosynthesised a novel dual-modality trifunctional labelling reagent, ^{124}I-Green-dithiophenolmaleimide. It equips with: (i) a long half-life positron emitter, iodine-124 ($t_{1/2}$=4.2 days) for longitudinal cell tracking with PET; (ii) a clinically approved green fluorescent reporter, fluorescein for micro-scale fluorescence cell imaging; (iii) a dithiophenolmaleimide moiety for cell membrane thiol bioconjugation. The cellular distribution of the dual labelling reagent, its cell radiolabelling efficiency, and radiolabel retention were evaluated on Jurkat, murine multiple myeloma 5T33, and human T cells, respectively, in vitro. The in vivo migration of the dual labelled Jurkat cells was investigated using sequential PET/CT imaging in male NSG mice (n=3) over 7 days. **Results:** The ^{124}I-Green-dithiophenolmaleimide was prepared with radiochemical yields of 71±1% (n=3) determined by HPLC. The confocal images revealed the cell surface localisation of the ^{124}I-Green-dithiophenolmaleimide on both Jurkat and 5T33 cells. The radiolabelling efficiency of Jurkat, 5T33, and human T cells (5 x 10^6) were 20.4±2.9%, 61.7±1.1%, and 27.0±2.0% (n=3), respectively. Notably, 67.6±1.7% (n=3) of total radioactivity still retained in Jurkat cells 7 days post labelling without apparent impact on its viability and reproducibility. When ^{124}I-Green-dithiophenolmaleimide dual labelled Jurkat cells were intravenously injected to NSG mice, the cell migration from lung to liver was detected with PET over 7 days. **Conclusion:** A dual PET and fluorescent cell labelling reagent, ^{124}I-Green-dithiophenolmaleimide was prepared in excellent RCYs. It labelled various cell lines through their membrane thiols with good labelling efficiency and prolonged radiolabel retention. The cell membrane localisation of the ^{124}I-Green-dithiophenolmaleimide was confirmed by confocal fluorescence imaging. The longitudinal monitoring of the in vivo distribution and migration of the dual labelled Jurkat cells was achieved with PET/CT imaging. These promising results warrant future labelling of the therapeutic cells with the ^{124}I-Green-dithiophenolmaleimide for in vivo tracking study using PET/CT. **References:** None.

OP-494

Evaluation of [^{18}F]FDG uptake after anti PD-1 therapy in mice

***M. Ogawa**, M. Tomita, H. Yasui, K. Higashikawa, K. Nakajima, T. Shiga, Y. Kuge;*
Hokkaido University, Sapporo, JAPAN.

Aim/Introduction: Immune checkpoint inhibitors such as PD-1 inhibitors have attracted attention in cancer therapy. However, PD-1 inhibitors are not effective to all patients. In anti PD-1 therapy, it is important to evaluate metabolism in the cancer microenvironment, as this helps to clarify the pathological conditions. Herein, we evaluate the early effects of PD-1 therapy on [^{18}F]FDG uptake in vivo in mice, focusing on cell distribution and glycolysis in cancer cells. **Materials and Methods:** Mice melanoma cells (B16F10) was inoculated subcutaneously to C57BL/6 mice. Anti PD-1 antibody treatment was started when tumor presence was confirmed. Anti-mouse PD-1 antibody (250 μg) was administered twice (i.p, 5 days apart) to the mice. FDG-PET/CT imaging was performed just prior to initiating therapy and at 7 days after the initiation of anti PD-1 treatment initiation. After PET imaging on day 7, the mice were sacrificed, and their organs were dissected. For ex vivo validation, tissues were weighed, and radioactivity was measured. Also, flow-cytometry was performed to assess immune cell (CD8$^+$ T cells, CD4$^+$ T cell, Treg, macrophage and dendritic cell) populations, and expression of GLUT1 and hexokinase II in tumors. **Results:** Anti PD-1 antibody treatment did not significantly inhibit tumor growth during our observation period (7 days). [^{18}F]FDG uptake to tumor was significantly higher in anti-PD-1 antibody treated mice (8.06 ± 0.48 %ID/g) than non-treated mice (4.02 ± 1.03 %ID/g) after anti PD-1 treatment. Difference in [^{18}F]FDG uptake to tumor was negligible between anti-PD-1 antibody treated mice and control mice before the treatment. Ex vivo validation shows that [^{18}F]FDG uptake in the spleen and blood did not differ between treatment group and non-treatment group. Flow-cytometry analysis showed that CD8$^+$ T cells and CD4$^+$ T cells were slightly increased by anti-PD-1 antibody treatment, however, infiltration of immune cells (CD8$^+$ T cells, CD4$^+$ T cells, Tregs, macrophages and dendritic cells) was around 1%, and thus, immune cells should not be responsible for the increase in [^{18}F]FDG uptake. Anti PD-1 treatment significantly increased glucose transporter 1 (GLUT1) and hexokinase II expression in CD45$^-$ cancer cells, indicating that anti PD-1 treatment increased glucose metabolism in cancer cells. **Conclusion:** This study is the first to assess early changes in [^{18}F]FDG uptake by anti PD-1 treatment in a mouse B16F10 melanoma model. We found that anti PD-1 therapy increases glucose metabolism in cancer cells, at the point when anti PD-1 therapy does not cause significant inhibition of tumor growth. **References:** None.

OP-495

[18F]AlF-RESCA-IL2 for imaging activated T-cells

I. Antunes[1], *E. L. van der Veen*[2], *F. V. Suurs*[2], *F. Cleeren*[3], *G. Bormans*[3], *P. H. Elsinga*[1], *R. A. J. O. Dierckx*[1], *M. N. Lub-de Hooge*[4], *E. G. E. de Vries*[2], *E. F. J. de Vries*[1];
[1]*University of Groningen, University of Medical Center of Groningen, Dept. of Nuclear Medicine and Molecular Imaging, Groningen, NETHERLANDS,* [2]*University of Groningen, University of Medical Center of Groningen, Dept. of Medical Oncology, Groningen, NETHERLANDS,* [3]*University of Leuven, Dept. of Pharmacy and Pharmacology, Laboratory for Radiopharmaceutical Research, Groningen, NETHERLANDS,* [4]*University of Groningen, University of Medical Center of Groningen, Dept. of Hospital and Clinical Pharmacy, Groningen, NETHERLANDS.*

Aim/Introduction: Interleukin-2 is glycoprotein that binds with high affinity to IL2 receptors (IL2R) that are overexpressed on activated T-cells. These activated T-cells are involved in autoimmune diseases but also play a major role in the tumor immune response. Previously we have developed N-(4-[^{18}F]-Fluorobenzoyl)interleukin-2 ([^{18}F]FB-IL2) which has been successfully used for detecting activated T-cells in rodents [1]. The complexity and time-consuming GMP-compliant production of [^{18}F]FB-IL2 led us to develop the simplified PET tracer, [^{18}F]AlF-RESCA-IL2 [2]. Here we present its affinity for activated T-cells in comparison to [^{18}F]FB-IL2. **Materials and Methods:** The stability of [^{18}F]AlF-RESCA-IL2 was tested in human serum (TCA precipitation) over time (n=3). Its affinity for activated T-cells was tested: i.) in vitro, in an binding assay containing activated peripheral blood mononuclear cells (PBMCs) (48h, n=3); non-activated PBMCs (48h, n=3) and freshly non-activated PBMCs (0h, n=3) ii.) in vivo, where a 60 min dynamic PET scan of [^{18}F]AlF-RESCA-IL2 (2.10±2.41 MBq) followed by ex-vivo biodistribution was performed in SCID mice inoculated with activated PBMCs in Matrigel in the absence/presence of an excess of IL2 (PBMCs, n=6 and PBMCs+IL2, n=6) and in SCID mice inoculated only with Matrigel (Controls, n=6). Similar assays were performed with [^{18}F]FB-IL2 for comparison. **Results:** Al[^{18}F]F-RESCA-IL2 was obtained with a radiochemical yield of 2.4±1.6% (c.f.d. from the start of synthesis) and radiochemical purity (>95%) within 90 min.[^{18}F]AlF-RESCA-IL2 showed high stability in human plasma with >90% of the tracer remaining intact after 60 min. PET images clearly showed the presence of activated PBMCs in the SCID mice injected with [^{18}F]AlF-RESCA-IL2 or [^{18}F]FB-IL2. Biodistribution of [^{18}F]AlF-RESCA-IL2 in mice (60 min, p.i) showed higher uptake in activated PBMCs (2.00±1.37 %ID/g) than in the Matrigel without PBMCs (0.52±0.37 %ID/g, p=0.017). [^{18}F]FB-IL2 showed similar higher uptake in activated PBMCs (2.03±0.52 %ID/g) than in the Matrigel without PBMCs (0.86±0.25%ID/g, p=0.016). [^{18}F]AlF-RESCA-IL2 (0.65±0.26 %ID/g, p=0.06) an [^{18}F]FB-IL2 (1.15±0.49 %ID/g, p=0.048) showed reduced uptake in activated PBMCs when blocked with an excess of IL2. **Conclusion: :** [^{18}F]AlF-RESCA-IL2 can be obtained in similar yields as [^{18}F]FB-IL2, but in a shorter time (90 vs. 150 min). The new [^{18}F]AlF-RESCA-IL2 showed increased binding towards activated T-cells, indicating that this tracer might be used to image activated T-cells. **References:** [1] Di Gialleonardo et al., J. Nuc. Med., 2012, 53(5):679-86 [2] Antunes et al., Eur. J. Nucl. Med. Mol. Imaging, 2018, 45 (Suppl 1):S78.

OP-496

Imaging CD8+ T cell tumor infiltration following radiotherapy

P. Wierstra, *R. Raavé, G. Sandker, M. Boswinkel, J. Molkenboer-Kuenen, G. Adema, J. Bussink, M. Gotthardt, E. Aarntzen, S. Heskamp;*
Radboudumc, Nijmegen, NETHERLANDS.

Aim/Introduction: Immunotherapy is considered a new cornerstone in cancer treatment by its profound and durable clinical responses in patients with various types of cancer. However, only a subgroup of patients respond to immunotherapy and methods for accurate early response monitoring are lacking. Noninvasive quantitative imaging of CD8+ cytotoxic T cells can provide dynamic and spatial information of anti-tumor response. Therefore, we developed an ^{111}In-labeled antibody to image influx of CD8+ T cells in irradiated tumors in a syngeneic mouse tumor model. **Materials and Methods:** An anti-mouse CD8 antibody (clone: YTS 169.4) was conjugated with NCS-DTPA and labeled with indium-111. Immunoreactivity, IC_{50}, internalization, and K_d were determined using CD8+ TK1 mice lymphoma cells. Subsequently, CT26 tumor bearing BALB/c mice were intravenously injected with 8.5 µg (8.5 MBq) [^{111}In]In-DTPA-CD8 antibody. SPECT/CT imaging was performed at 4h, 24h, 48h and 72h after injection. In a separate experiment, C57Bl/6 mice bearing bilateral B16-F1 tumors received right-side external beam irradiation (1x10Gy). After 24h, mice received either: 8.1 MBq [^{111}In]In-DTPA-CD8 antibody (8.5 µg, n=10) or 8.7 MBq [^{111}In]In-DTPA-Isotype control (8.5 µg, n=10) followed by SPECT/CT at 48h post irradiation. **Results:** In vitro assays showed the immunoreactive fraction was 44%, IC_{50} was 1.77 nM and K_d was 3.83 nM. CD8+ T cell containing organs (lymph nodes, spleen and duodenum) were clearly visible on SPECT scans at all time points. SPECT quantification showed significantly increased uptake of [^{111}In]In-DTPA-CD8 antibody in irradiated B16-F1 tumors compared to non-irradiated tumors in the radiation naïve mice (13.65 ± 0.83 vs. 9.95 ± 1.65 %ID/g ± SD, p = 0.005). Uptake of control IgG showed no differences between irradiated or non-irradiated tumors (4.70 ± 1.04 vs. 5.06 ± 0,96, p = 0.92). Further analysis of the SPECT scans indicated the presence of tertiary lymphoid structures in the tumor periphery also showing increased CD8 uptake in irradiated tumors, which was confirmed by immunohistochemistry. Further immunohistochemical analysis tumor and normal tissues is ongoing. **Conclusion:** The anti-CD8 antibody showed specific uptake in CD8+ T cell containing tissues in vivo, but tumor uptake was limited due to low number of CD8+ T cells present. We demonstrated that irradiation induces a significant increase in tracer uptake in B16-F1 tumors. These differences were shown to be specific for an increase in CD8+ T cells. In the future, this tracer has potential for in vivo evaluation of CD8+ T cell infiltration and could assist in immunotherapy response monitoring. **References:** None.

OP-497

PET Imaging For Tracking Immunologically Competent Cells With Zirconium-89 Labeling Method In Murine Syngeneic Transplantation Model

T. Sasaki[1], *M. Akehi*[1], *T. Sadahira*[1], *K. Hagihara*[2], *R. Watanabe*[2], *Y. Ishimoto*[2], *N. Komatsu*[2], *K. Wakita*[2], *M. Watanabe*[1];
[1]*Okayama university, Okayama, JAPAN,*
[2]*Daiichi Sankyo Co., Ltd., Tokyo, JAPAN.*

Aim/Introduction: The development of cell-based therapy and cancer immunotherapy would benefit from noninvasive and systemic cell tracking methods. In this study, we report a cell labeling method with ^{89}Zr to track immunologically competent cells in vivo and evaluate their whole body distribution by positron emission tomography (PET) imaging. **Materials and Methods:** [^{89}Zr]oxinate$_4$ was synthesized and its uptake was measured in splenocytes and CD8+ T cells isolated from spleens of C57BL/6 mice. [^{89}Zr]oxinate$_4$ was synthesized by modifying a previously reported method (1). Zirconium-89 in 0.1 M oxalic acid was neutralized to pH 7- 8 with 1.0 M Na_2CO_3 and added to a glass reaction vial containing 1 mg/ml 8-hydroxyquinoline solution. After being rotated at room temperature overnight, the organic phase was separated by centrifugation and concentrated under the reduced pressure to give the [^{89}Zr]oxinate$_4$, which was dissolved in 10-20 µl dimethyl sulfoxide and diluted with saline. [^{89}Zr]oxinate$_4$ (1.4-7.1 MBq) in 500 µl saline was added to 500 µl of the cell suspension (1.0 - 4.0 × 10^7 cells) and incubated for 30 min at room temperature. After incubation, the tubes were centrifuged (5 min, 500 ×g) twice, supernatant was removed and the activities of the supernatant and the cell pellet were measured for calculating labeling efficiency and specific activities. Radiolabeled cells were injected intravenously into C57BL/6 mice and PET/CT images were acquired 0 to 10 days after administration. **Results:** Labeling efficiencies were determined ranging from 8.0 to 38.2 % and the specific activity ranged from 18.9 to 34.5 mBq/cell. Splenocytes and CD8+ T cells were visualized with PET imaging and kinetics of immunologically competent cells were assessed in mice. Splenocytes and CD8+ T cells were mainly distributed in the spleen 1 to 10 days after injection. **Conclusion:** We have developed long half-life PET tracers for immunologically competent cells. Zirconium-89 was taken up by splenocytes and CD8+ T cells and whole body distribution of these radiolabeled cells was detectable in mice for a long duration. **References:** (1) Eur J Nucl Med Mol Imaging (2015) 42:278-287 DOI 10.1007/s00259-014-2945-x.

OP-498

Is [^{89}Zr]PD-L1 a useful tool to capture an immune response to oncolytic virotherapy?

J. Hoebart, *C. Da Pieve, F. Raes, D. M. Ciobota, G. Smith, A. Melcher, K. J. Harrington, G. Kramer-Marek;*
The Institute of Cancer Research, London, UNITED KINGDOM.

Aim/Introduction: Oncolytic virotherapy (OV) has recently attracted a lot of attention in the field of cancer immunotherapy as several studies have indicated its potential to enhance the therapeutic response of immune checkpoint blockade when both were used in a combination regimen[1]. However, little is still known about the immunological impact of oncolytic viruses on the tumour and the body as a whole. Therefore, we aimed to investigate the effect of OV by imaging programmed death receptor ligand 1 (PD-L1), which is considered as a major marker of an interferon-driven, antiviral immune response. PD-

L1 PET performed during and after OV might elucidate the dynamics of the anti-viral immune response and ultimately help to optimise the clinical application of this therapeutic strategy. **Materials and Methods:** The murine head and neck cancer cell line MOC2, and its variants MOC2-Luc and MOC2-Luc-PD-L1, were used in vitro and grown as subcutaneous tumours in immunocompetent mice. An anti-mouse PD-L1 mAb was conjugated with desferrioxamine (DFO) and labelled with zirconium-89 (^{89}Zr). The radiotracer specificity was characterised in vitro (0.3-0.5 MBq) and in vivo (biodistribution via automated γ-counting and autoradiography) at multiple time points post-injection (2.0-10.0 MBq). Reovirus, a non-genetically modified dsRNA virus, administered intratumourally or intravenously was used for OV (repeated dosing) which was followed up by PET imaging with [^{89}Zr]PD-L1. **Results:** [^{89}Zr]PD-L1 showed high receptor specificity in vitro. In vivo studies demonstrated high accumulation of the tracer in MOC2 tumours at 48 hr (%ID/g = 29.4±2.9) and at 96 hr (%ID/g = 25.1±1.9) post-injection, with tumour-to-blood ratios of 5.4±0.5 and 18.0±4.9, respectively. Autoradiograms of tumour sections confirmed heterogeneous tracer distribution within the tumour and IHC staining of consecutive sections the presence of PD-L1. The pilot-study investigating OV showed markedly increased [^{89}Zr]PD-L1 uptake in the spleen, a major organ of systemic immune response, as well as in the tumour of reovirus-treated animals at 96 hr post-treatment. The radioactivity level in the blood, i.e. circulating activated immune cells, remained relatively low among both groups. In addition, IHC staining of PD-L1 on tumour and spleen sections confirmed the PET findings. **Conclusion:** Our results suggest that [^{89}Zr]PD-L1 PET has great potential to capture changes of systemic and intratumoural PD-L1 status and further support PD-L1 as an imaging biomarker of immune response to OV. **References:** [1] Samson, A., et al., Intravenous delivery of oncolytic reovirus to brain tumor patients immunologically primes for subsequent checkpoint blockade. Sci Transl Med, 2018. 10(422).

1106

Do.MoRe - Parallel Session: I-131 Dosimetry and DNA Damage during Different Therapies

Tuesday, October 15, 2019, 8:00 - 9:30 Lecture Hall 112

OP-499

Lesion dosimetry in metastatic thyroid cancer treated with ^{131}I:standardization of SPECT-TC calculation method with an in-house software tool and preliminary texture analysis results

E. Richetta[1], *M. Poli*[1], *A. Rienzo*[1], *D. Valentini*[2], *B. Peiretti Paradisi*[1], *V. Garbaccio*[3], *R. Pellerito*[1], *A. Muni*[2], *D. Deandreis*[3], *M. Stasi*[1];
[1]*AO Ordine Mauriziano, Torino, ITALY,* [2]*Ospedale Civile Santi Antonio e Biagio e Cesare Arrigo, Alessandria, ITALY,* [3]*AOU Citta della Salute e della Scienza, Torino, ITALY.*

Aim/Introduction: The ^{131}I treatment is an effective option for metastatic thyroid cancer. Lesion dosimetry is suggested by EU Directive 59/2013 and national regulations to optimize the patient's management but commercial software are not always accessible. Aim of this project granted by our Regional Oncological Network is to develop an in-house software to standardize dosimetric method among centers. **Materials and Methods:** Lesion dosimetry is performed after the ^{131}I therapy (4 SPECT-CT @ 4,24,48, 96 h p.a. ,Siemens SymbiaIntevoT2, 64 views, 256x256, ITSCAC, partial volume effect and dead-time corrected, absolute calibration). In the standard approach both lesions definition and doses (MIRD sphere model) are manually performed. An in-house MATLAB tool was developed to automatized the process: images co-registration, automatic lesion segmentation, cumulated-activity curve fitting, mean dose calculation. The software was tested on a spheres phantom filled with liquid ^{131}I (13 MBq/ml, volumes: cylinder 130 ml, spheres 11.5, 5.6, 2.6, 0.5 ml) and on 6 patients (37 lesions, mean activity 6061 MBq, 3716÷9286 MBq). Volumes, activity and doses calculated with MATLAB code were compared to the standard calculation method. For 4 patients (29 lesions) texture features (LIFEx) and mean doses were correlated to the treatment response in the ROC curve analysis. **Results:** Phantom analysis confirmed a good agreement between standard method and MATLAB tool. Percentage variations were in mean (±1SD) -1±2 % for the volumes of cylinder and spheres, -9.5±11.6 % for the cumulated-activity and becomes 10.3±7 % when doses were compared (limit volume > 2.7 ml to avoid not acceptable variations ~ 105%). Also patient dosimetry comparison suggests that the automatized tool is effective for dose calculation: mean variation (±1 SD) were -0.1 ± 1.6 % (max 3 %), 0.1 ± 48 % (max 7%) and 1.2 ± 4.8 % (max -13 %) for volume, activity and dose respectively. Mean doses correlate with treatment outcome (AUC 0.61, threshold 81 Gy) but some texture features seem to better predict the tumor response (HGZE: AUC 0.72, HGRE: AUC 0.68, skewness and kurtosis 0.67) in these preliminary results. **Conclusion:** Lesion dosimetry and texture-analysis in metastatic thyroid cancer 131I treatment are effective tools for patient management. The standardization of the dose calculation was achieved and verified with the software. This allowed to share the dosimetric protocol to other nuclear medicine unit to the aim of dose comparisons. Preliminary dose-response correlation investigated both for dose and texture features needs further investigations with a larger dataset. **References:** None.

OP-500

Retrospective evaluation of a single time point dosimetry method for radioiodine treatment of hyperthyroidism

E. Amato[1,2], *A. Campenni*[1,3], *R. M. Ruggeri*[4], *L. Auditore*[1,2], *S. Baldari*[1,3];
[1]*Department of Biomedical and Dental Sciences and Morphofunctional Imaging, University of Messina, Messina, ITALY,* [2]*Istituto Nazionale di Fisica Nucleare, Catania, ITALY,* [3]*Nuclear Medicine Unit, University Hospital "G. Martino", Messina, ITALY,* [4]*Department of Clinical and Experimental Medicine, Unit of Endocrinology, University of Messina, Messina, ITALY.*

Aim/Introduction: The treatment of hyperthyroidism with ^{131}I radioiodine is a safe and effective therapy, in which a diagnostic uptake curve is used to pre-determine the patient-specific activity to be administered. Aim of this study was to retrospectively evaluate the accuracy of a dosimetric approach based on a model presented in Ref. 1 of mono-exponential clearance following instantaneous uptake, relying on a single time uptake measurement. We extended the model to account for a non-instantaneous uptake phase. **Materials and Methods:** Our population consisted in 69 mixed hyperthyroid patients, of which 43 were affected by Plummer Disease, 13 by Toxic Multi-Nodular Goiter and 13 by Graves Disease. They were treated according to the results of a dosimetric protocol based on six times of measurement (3-6-24-48-72/96-168 hours). Time-integrated activity and radiation absorbed doses were estimated using a unique uptake measurement at 168 hours, both exploiting the original model considering an instantaneous uptake followed by mono-exponential clearance, and our extended model for non-instantaneous uptake. Results were compared with the dosimetric protocol based on six points and with a simplified time schedule based on a three time points schedule at 6-24-168 hours. Results were also compared to patients' final functional status (i.e. euthyroidism, hypothyroidism or hyperthyroidism). **Results:** Time-integrated activity calculated by the single time approach provide relative per cent differences up to ±20% with respect to the reference dosimetric protocol, whereas errors expected from the model presented in Ref. 1 should be within ±10%. This difference can be partly ascribed to the variability of the average population half-lives with type of hyperthyroidism, and partly on the intrinsic limitations of the model. On the other hand, a fit procedure based on a simplified time schedule at 6-24-168 hours showed errors within ±5%. **Conclusion:** The dosimetry based on three time measurements confirms to be the most accurate choice.From the operational point of view, the three times schedule requires only one more appearance of the patient at the nuclear medicine center (at 24 hours); differently, the single late time measurement approach, needs twice the presence of the patient, namely for administration and late measurement. Consequently, when, for practical reasons, three time measurements are not achievable, the single time point may be an acceptable alternative. **References:** Madsen, et al. Technical Note: Single time point dose estimate for exponential clearance. Med Phys. 2018;45:2318-2324.

OP-501

Salivary gland dosimetry of differentiated thyroid cancer patients treated with ^{131}I-NaI after near-total thyroidectomy

J. Taprogge[1,2], *F. Leek*[1,2], *J. Gear*[1,2], *I. Murray*[1,2], *G. Flux*[1,2];
[1]*Royal Marsden Hospital NHSFT, London, UNITED KINGDOM,*
[2]*The Institute of Cancer Research, London, UNITED KINGDOM.*

Aim/Introduction: Salivary glands have sodium iodine symporters and can take up ^{131}I-NaI which is used in differentiated thyroid cancer patients (DTC) after thyroidectomy. Several studies have reported salivary gland hypofunction and xerostomia after treatment with ^{131}I-NaI but controversy remains over whether absorbed doses correlate with clinically observed toxicity. The aim of this study was to assess inter- and intra-patient variability of effective half-lives and absorbed doses to parotid and submandibular salivary glands. **Materials and Methods:** 19 patients with DTC were treated with 3000 MBq of ^{131}I-NaI following near-total thyroidectomy. SPECT scans of the head and neck were performed at 24, 48, 72 and 96 hours and the maximum absorbed dose to the left and right parotid and submandibular salivary glands estimated. The voxel with maximum uptake was used for the calculations to avoid issues due to volume delineation. Instantaneous uptake was assumed and time activity curves were fitted with a single exponential decay function to obtain cumulated activities and half-lives. Unpaired and paired t-tests were used to identify any statistical significant inter- and intra-patient variability of half-lives and cumulated activity of parotid and submandibular salivary glands. **Results:** Median effective half-lives of ^{131}I-NaI in the parotid and submandibular salivary glands were found to be 16.3 hours (Range: 4.8 - 39.7 hours) and 14.8 hours (Range: 7.2 - 43.9 hours), respectively. The difference in half-life between parotid and submandibular salivary glands was found to be not statistically significant (p=0.63). Median cumulated activity in the maximum pixel was measured to be 2.6 MBq.h (Range: 1.1 - 8.8 MBq.h) and 2.0 MBq.h (Range: 0.9 - 7.5 MBq.h) in parotid and submandibular salivary glands, respectively. No significant difference in cumulated activity between the two types of salivary glands was observed (p=0.06). Paired t-tests showed no significant difference between half-lives and cumulated activities of left and right parotid salivary glands (p=0.17 and p=0.13) or submandibular salivary glands (p=0.83 and p = 0.07)) of individual patients. **Conclusion:** Effective half-lives and cumulated activities in salivary glands are comparable between patients. No significant inter-patient variability between left and right parotid and submandibular salivary glands could be identified. **References:** None. Acknowledgments: The MEDIRAD project has received funding from the Euratom research and training programme 2014-2018 under grant agreement No 755523.

OP-502

The MEDIRAD multi-national I-131 dosimetry study for thyroid ablation and adjuvant therapy: current status

F. Leek[1], *J. Taprogge*[1], *R. Gregory*[2], *K. Newbold*[1], *F. Verburg*[3], *M. Luster*[3], *T. Schurrat*[3], *J. Trans-Gia*[4], *U. Eberlein*[4], *C. Lapa*[4], *A. K. Buck*[4], *M. Lassmann*[4], *E. Mora-Ramirez*[5,6,7], *A. Vergara-Gil*[5,6], *M. Bardies*[5,6], *D. Vallot*[8], *F. Courbon*[9], *L. Vija*[9], *G. Flux*[1];
[1]*The Royal Marsden NHS Foundation Trust & Institute of Cancer Research, London, UNITED KINGDOM,* [2]*Barts Health NHS Trust, London, UNITED KINGDOM,* [3]*University Hospital Marburg, Marburg, GERMANY,* [4]*University Hospital Würzburg, Würzburg, GERMANY,* [5]*INSERM, UMR 1037, Université Toulouse III Paul Sabatier, Toulouse, FRANCE,* [6]*Centre de Recherches en Cancérologie de Toulouse, Toulouse, FRANCE,* [7]*University of*

Costa Rica, Physics School, CICANUM, San Jose, COSTA RICA, [8]Institut Universitaire du Cancer, Toulouse, FRANCE, [9]IUCT-Oncopole, Toulouse Oncology Institute, Toulouse, FRANCE.

Aim/Introduction: Current practice for post-thyroidectomy radioiodine therapy (RAIT) in the treatment of differentiated thyroid cancer (DTC) is based on activity administered resulting in a wide range of absorbed doses being delivered to the remnant and normal organs. As internal dosimetry is seldom routinely performed there is currently very little evidence for the correlation between the absorbed dose delivered and response. This Horizon 2020 MEDIRAD[1] multi-centre multi-national prospective observational study aims to accurately determine the absorbed doses to healthy organs and thyroid remnants from radioiodine ablation. The relation between patient biokinetics, patient-specific radiosensitivity and the success of thyroid ablation and acute to mid-term toxicity will be assessed. **Materials and Methods:** One hundred patients with histologically proven DTC and a clinical indication for RAIT will be recruited. Three centres will recruit low-risk patients, the fourth intermediate-risk; 1.1 or 3.7GBq I-131-NaI will be administered, according to local protocol. Gamma cameras have been calibrated for high activity quantitative I-131 imaging, characterising count losses due to dead-time and partial volume effects (PVE). A flexible patient data acquisition protocol for dosimetry has been developed to allow for inter-centre variabilities with respect to access to hybrid imaging, existing camera workloads and local radiation protection regulations. The imaging protocol mandates a minimum of four WB planar scans (24-96 hours post-administration) plus a SPECT(/CT) at 48 hours between the base of skull and upper thighs. A comprehensive compartmental model is being developed for high activity radioiodine biokinetics following thyroidectomy. Biomarker studies will be performed for 20 patients with gamma-H2AX as a marker of both radiation damage to the DNA and of radiosensitivity. **Results:** All four centres participating in this study have been set-up. Three Siemens Intevo SPECT/CTs, one Siemens Symbia S SPECT and one GE Discovery 670 SPECT/CT were characterised. The GE SPECT/CT system had a system volume sensitivity of 57.8cps/MBq compared to Siemens SPECT/CTs with sensitivities ranging from 79.1-91.9cps/MBq. Recovery curves for count losses due to the PVE were determined. The mean system dead-time factor at 1.1 GBq was 1.07±0.0266. **Conclusion:** The first European network able to perform standardised quantitative radioiodine imaging for dosimetry has been established with the potential for expansion to other centres. The dosimetric methods and tools developed will provide the basis for a subsequent large-scale observational epidemiological study of acute, mid- and long-term risk from absorbed doses delivered to normal organs. **References:** [1] EC Horizon 2020 NFRP-9.

OP-503

Dosimetric analysis and clinical outcome for patient with High-Risk Neuroblastoma administered with high-activity therapy of 131I-mIBG

B. Cassano[1], *C. Polito*[1,2], *E. Genovese*[1], *M. Longo*[3,4], *S. Donatiello*[1], *A. Napolitano*[1], *T. Insero*[1], *S. Valeri*[5], *M. F. Villani*[6], *A. Castellano*[7], *M. C. Garganese*[6], *V. Cannatà*[1];
[1]*IRCCS Bambino Gesù Children's Hospital, Medical Physics Unit, Rome, ITALY,* [2]*Sapienza University of Rome, Molecular Medicine Department, Rome, ITALY,* [3]*Arcispedale Sant'Anna Hospital, Medical Physics Unit, Ferrara, ITALY,* [4]*Sapienza University of Rome, Ph. D. Program in Morphogenesis & Tissue Engineering, Rome, ITALY,* [5]*Tor Vergata Postgraduate School of Medical Physics, Rome, ITALY,* [6]*IRCCS Bambino Gesù Children's Hospital, Nuclear Medicine Unit/Imaging Department, Rome, ITALY,* [7]*IRCCS Bambino Gesù Children's Hospital, Oncoemathology Unit, Rome, ITALY.*

Aim/Introduction: Patients with relapsed/refractory metastatic high-risk neuroblastoma (rrmHRNBL) are very difficult to treat and they have a very poor prognosis. High-activity therapy is a useful and safe treatment for children with rrmHRNBL and tandem modality administration consists of two administrations of 131I-metaiodobenzylguanidine (131I-mIBG). The aim of this study was to report the absorbed dose to whole-body (WB), red marrow (RM) and tumours in order to correlate them with clinical outcome of the patients. **Materials and Methods:** 15 patients (9 boys and 6 girls, age range [3;20] years) with rrmHRNBL treated between 2016-2019 with tandem high-activity therapy giving in total 29 administrations of 131I-mIBG (one patient was administered once) were enrolled. WB and RM dosimetry has been performed according to MIRD and EANM guidelines, collecting WB data, with an external probe at 2 meters distance, and blood samples at 0.5-h, 6-h, 24-h, 30-h, 48-h, 72-h and 144-h after the administration. The first administration was weight-based (444 MBq/kg) [6.6;17.5] GBq, while the second one was dosimetry-based, achieving 4 Gy to WB. For ten patients five static images were acquired in the time window [2;144] h and the absorbed dose to lesions have been assessed following the conjugated view method. The response was visually assessed by comparing the CT and 123I-mIBG-SPECT/CT scans obtained before therapy with those obtained between 8-10 weeks after 123I-mIBG, and it was graded according to the semiquantitative SIOPEN mIBG score system. **Results:** The injected activity at the second administration varies from 12.6 to 17.9 GBq while the dose per activity remains constant between first and second administration. The cumulative absorbed dose ranging from [2.5;4.8], [0.7;2.4], [13;464] Gy for the WB, the RM and lesions respectively. After 131I-mIBG therapy, combined with chemotherapy, 4 patient achieved partial remission, 7 showed stable disease and 3 had progressive disease. All patients showed grade 3 of haematological toxicity (neutropenia, anaemia and thrombocytopenia). At the end of the study, 5 patients died after 7-24 months from treatment. **Conclusion:** The dosimetric approach is necessary to perform a patient-specific treatment. The dose per administered activity, performed at the first administration, is a good predictor for

the second treatment in order to inject the maximum tolerable activity to the patients. High-activity therapy, in combination with chemotherapy treatment, is well tolerated and effective in patients with rrmHRNBL. We observed benefits in the treatment of relapse/progression, improving survival rates without severe toxicities. **References:** None.

OP-504

Imaging DNA Damage in vivo following [^{177}Lu] Lu-DOTATATE therapy in a model of pancreatic neuroendocrine cancer

E. O'Neill[1], *V. Kersemans*[1], *P. Allen*[1], *S. Terry*[2], *J. Baguña Torres*[1], *S. Smart*[1], *B. Quan Lee*[1], *N. Falzone*[1], *K. Vallis*[1], *M. Konijnenberg*[3], *M. de Jong*[3], *J. Nonnekens*[3], *B. Cornelissen*[1];
[1]*University of Oxford, Oxford, UNITED KINGDOM,*
[2]*King's College London, London, UNITED KINGDOM,*
[3]*Erasmus MC, Rotterdam, NETHERLANDS.*

Aim/Introduction: Molecular Radiotherapy (MRT) using [^{177}Lu] Lu-DOTATATE is an effective treatment against somatostatin receptor expressing neuroendocrine tumours (NETs). This beta-particle emitting radiopharmaceutical binds to receptors on tumour cells, irradiating the tumour locally, causing DNA damage, tumour cell death, and tumour regression. Despite its frequent and successful use in the clinic, little or no radiobiological considerations are taken into account at the time of treatment planning or delivery, and treatment is usually administered as a standard dose and number of cycles without consideration for peptide uptake, dosimetry, or radiobiological and DNA damage effects in the tumour. Here, we visualise and quantify the extent of DNA damage following [^{177}Lu]Lu-DOTATATE therapy using SPECT imaging with [^{111}In]In-anti-γH2AX-TAT, which visualises the well-studied DNA double strand break signalling protein, γH2AX. This work is a proof-of-principle study of this in vivo non-invasive biodosimeter, for use with therapeutic radiopharmaceuticals. **Materials and Methods:** Six cell lines were exposed to external beam radiotherapy (EBRT) or [^{177}Lu]Lu-DOTATATE, after which the number of γH2AX foci and clonogenic survival were measured. Mice bearing CA20948 somatostatin receptor positive tumour xenografts were treated with [^{177}Lu]Lu-DOTATATE or sham-treated, and co-injected with [^{111}In]In-anti-γH2AX-TAT, [^{111}In]In-IgG-TAT control, or PBS. **Results:** Clonogenic survival following EBRT was cell line specific, indicating varying levels of intrinsic radiosensitivity. In vitro, cell lines treated with [^{177}Lu]Lu-DOTATATE, clonogenic survival decreased and γH2AX foci increased in cells expressing high levels of somatostatin receptor subtype 2 (SST2). Mice treated with [^{177}Lu]Lu-DOTATATE resulted in a significant increase in [^{111}In]In-anti-γH2AX-TAT uptake compared to non-treated mice (P=0.0033) at 72 h, or the non-specific control compound [^{111}In]In-IgG-TAT, with or without ^{177}Lu treatment (P<0.0001). Ex vivo measurements revealed a partial correlation between [^{177}Lu]Lu-DOTATATE uptake and γH2AX foci induction between different regions of CA20948 xenograft tumours, suggesting different parts of the tumour may react differentially to [^{177}Lu]Lu-DOTATATE irradiation. **Conclusion:** [^{111}In]In-anti-γH2AX-TAT allows monitoring of DNA damage following [^{177}Lu] Lu-DOTATATE therapy, and reveals heterogeneous damage responses. **References:** None.

OP-505

Alpha Particles Induce DNA Damage in Leukocytes during Treatment with Ra-223

S. Schumann[1], *M. Lassmann*[1], *C. Lapa*[1], *R. Muhtadi*[2], *H. Scherthan*[2], *U. Eberlein*[1];
[1]*Department of Nuclear Medicine, University of Würzburg, Würzburg, GERMANY,* [2]*Bundeswehr Institute of Radiobiology affiliated to the University of Ulm, Munich, GERMANY.*

Aim/Introduction: Irradiation with the α-emitter Ra-223 creates densely packed DNA damage tracks along particle trajectories (α-tracks) in exposed cells. These α-tracks can be visualized by immunofluorescent staining with γ-H2AX+53BP1 antibodies and used as a biomarker for α-particle exposure. The aim of this study was to investigate the time- and dose-dependency of the number of α-tracks in blood leukocytes of patients undergoing their first therapy with Ra-223. **Materials and Methods:** Blood samples from prostate cancer patients (n=9) were taken before the administration of Ra-223 dichloride (55 kBq per kilogram bodyweight) and nominally 1.5 h, 3 h and 4 h after the administration. One or two blood samples were taken on subsequent days (n=4; 24 h up to 96 h after administration) and one sample four weeks after treatment (n=3). In each blood sample, the activity was quantified using a calibrated, high purity germanium detector and integrated time-activity curves were used to calculate the absorbed doses to the blood, assuming that the complete energy by α- and β-particles emitted by Ra-223 and its progeny is deposited locally in the blood. For the quantification of γ-H2AX+53BP1 positive α-tracks, leukocytes were separated, fixed in ethanol and immunofluorescently stained. The number of α-tracks was evaluated manually in 100 nucleated cells per sample in a fluorescence microscope. **Results:** The absorbed doses to the blood up to 4 h after administration were below 6 mGy in all samples. For the three patients with five time-points, it was possible to calculate the total absorbed dose to the blood, which ranged between 4 mGy and 16 mGy. The number of α-tracks in 100 cells ranged from 0 to 7. In the samples taken before the administration, only one α-track was observed in one patient's sample, while the other eight patients did not show any α-tracks. The average number of α-tracks 4 h after administration was 2.9 per 100 cells. In all late samples (24 h up to 4 weeks after administration), the number of α-tracks was still elevated (minimum 1 and maximum 6 per 100 cells). **Conclusion:** Even at absorbed doses to the blood < 16mGy, there was an increased frequency of α-particle-induced DNA damage carrying leukocytes, which in some cases, persisted even four weeks after the treatment. Our results highlight the sensitivity of the γ-H2AX+53BP1 DNA damage test even after internal exposure to extremely low absorbed doses. **References:** None.

OP-506

Determination of S-values and characterization of direct damage to DNA induced by Auger electrons from Copper-64

J. Carrasco[1], *J. Ramos-Mendez*[2], *M. Avila-Rodroguez*[3];
[1]*Instituto Politécnico Nacional, CDMX, MEXICO,* [2]*University of California, San Francisco, CA, UNITED STATES OF AMERICA,* [3]*Universidad Nacional Autónoma de México, CDMX, MEXICO.*

Aim/Introduction: The radioisotope Cu-64 possesses unique propierties that can serve the dual rol of diagnostic and theraphy [1]. The therapeutic potential of Cu-64 lies on its emissions of Auger electrons, provided its internalization to the cell nucleus, but to date, have not been evaluated in detail. The Monte Carlo Track Structure (MCTS) simulations are recognized as the most accurate theoretical tools to evaluate the biological effects of ionizing radiation at the DNA-scale. The aim of this research work was to determine the S values and evaluate the number of double-trand-breaks caused by Auger electrons from CU-64. **Materials and Methods:** TOPAS-nBio was used to simulate the complete trajectories of Delta rays, Auger and Coster Kroing electrons generated from the decay of Cu-64 on water. The S-values were calculated for different target-source configurations simulating the cell (C) and the cell nucleus (N) as concentric spheres of 5µm and 4µm , respectively, the cytoplasm (Cy) as intermediate region, and the cells surface (Cs). For estimation of the direct damage to the DNA, the DBSCAN algorithm was used to calculate the number of double strand breaks that are produced in the nucleus cell. Additionally, ionization clusters were calculated in a model of 10-base-pair segment of DNA to obtain the average ionization cluster produced by a source of Cu-64 as a function of distance to the DNA segment. **Results:** The determined S values are in good agree with the values reported by the MIRD Committee To the best of our knowledge this is the first time that S values are obtained for Cu-64 by using MCTS calculations. The number of double breakings obtained for Cu-64 for the configuration N←N, N←C, and N←Cs were 0.0187±0.001, 0.0317±0.0005, and 0.0125±0.0002, respectively. The cluster size shows a direct dependence on the position of the source in relation to the DNA, showing a fast decrease as the source gets apart from the DNA segment. **Conclusion:** Micro and nanodosimetric parameters of Cu-64 were characterized with track-structure simulations, these quantities can be used to calculate absorbed dose when Cu-64 is internalized in the cell, in addition to the total number of double breaks within the nucleus cellular through data of biodistribution of Cu-64 in the cell. **References:** [1] M.A. Avila Rodriguez, C. Rios, J. Carrasco Hernandez, et al., Biodistribution and Radiation Dosimetry of [64Cu]Copper Dichloride: First in Human Study in Healthy Volunteers, Eur J Nucl Med Mol Imaging Research. 7, 98 (2017).

1107

Pitfalls & Artefacts 5 - Interactive Clinical Cases - Neuroimaging + Technologists Committee: Brain PET and SPECT ? Patients? Preparation and Acquisition

Tuesday, October 15, 2019, 8:00 - 9:30 Lecture Hall 113

OP-507

Challenges Related to Acquisition of Brain PET and SPECT in Patients with Neurological Diseases - A Technical Overview

M. Mada;
MRC Cognition and Brain Sciences Unit, Cambridge, UNITED KINGDOM.

OP-508

Pitfalls and Artefacts Related to Preparation and Acquisition of Brain FDG PET

M. Bauckneht;
Nuclear Medicine Unit, San Martino Hospital, University of Genoa, Genoa, ITALY.

OP-509

Pitfalls and Artefacts Related to Preparation and Acquisition of Dopaminergic Imaging

E. van de Giessen;
Department of Nuclear Medicine, Academic Medical Center, University of Amsterdam, Amsterdam, NETHERLANDS.

OP-510

Pitfalls and Artefacts Related to Preparation and Acquisition of PET AA-Imaging in Brain Tumours

I. Law;
Department of Clinical Physiology, Nuclear Medicine and PET, University of Copenhagen, Copenhagen, DENMARK.

1108

Clinical Oncology - Parallel Session: Radioguided Surgery

Tuesday, October 15, 2019, 8:00 - 9:30 Lecture Hall 114

OP-511

Diagnostic values of real time F-18 FDG PET/CT guided metabolic biopsy for diagnosis of Lymphoma

B. Mittal, R. Kumar, H. Singh, A. Bhattacharya, G. Prakash, P. Malhotra;
Postgraduate Institute of Medical Education & Research, Chandigarh, INDIA.

Aim/Introduction: Conventional image guided biopsy is subjected to sampling error with varying diagnostic accuracy. In this prospective study, we aimed to evaluate the diagnostic values of real time PET/CT guided metabolic biopsies from the FDG avid nodal or extra-nodal sites in clinically suspected cases of lymphoma or suspected cases of relapse. **Materials and Methods:** In this prospective study, patients were recruited for PET/CT guided metabolic biopsy in proven or suspected cases of lymphoma. The site of biopsy was planned from the most accessible FDG avid lesion in each case. The biopsies were done using a dedicated automated-robotic-arm assisted device, and a real-time samples were retrieved after confirming the position of the needle-tip within target lesion with regional PET/CT. To check the accuracy of the procedure, histopathology reports were reviewed. For confirmation of negative results, clinical or imaging follow-up was done and the diagnostic values of the procedure was calculated. The procedure related complication were also evaluated. **Results:** Ninety-six patients (56 males, 40 female) with age 39.6±17.1 (range 17-85) years were enrolled for biopsies from nodal or extra-nodal sites. Of these 51 patients were suspected cases of lymphoma, while 45 patients had suspected recurrence on prior PET/CT images. Biopsy target were nodal in 59 patients while extra-nodal in 37 patients (bone or marrow lesions - 28, lung-1, liver- 1, and pancreas 3, spleen-1, cutaneous soft tissue mass-3). Adequate tissue was obtained in all the patients to yield a pathological diagnosis except three (93/96) and repeat biopsy confirmed the lymphomatous involvement. Pathology revealed lymphoma in 86/93 patients while tuberculosis in four, plasmacytoma, IgG4 related disease and sarcoidosis one each. The findings revealed 84 true-positive, zero false-positive, seven true-negative and three false-negative lesions. The procedure revealed a sensitivity, specificity, PPV, NPV and accuracy of 96.6%, 100%, 100%, 70.0% and 96.9% respectively for establishing a diagnosing of lymphoma. No procedure related complications were encountered during or after the procedure. **Conclusion:** PET/CT guided metabolic biopsy from nodal and extra-nodal site is safe and accurate method for a pathological diagnosis and shown a very high diagnosis performance for evaluation of lymphomatous involvement. PET/CT-guided biopsy is a practical approach for isolated lesions with no discernible morphological change on CT images. **References:** None.

OP-512

Sentinel Lymph Node Biopsy in breast cancer with ^{99m}Tc-Tilmanocept (LYMPHOSEEK®): A descriptive analysis of our experience in 9 centers in Spain

S. Vidal Sicart[1], M. Rioja-Martin[2], A. Prieto[3], E. Goñi[4], I. Gómez[5], M. Albalá[6], L. Lumbreras[7], L. León[8], J. Gómez[9];
[1]Hospital Clinic Barcelona, Barcelona, SPAIN, [2]Hospital Universitario Ramon y Cajal, Madrid, SPAIN, [3]Hospital Puerta de Hierro, Madrid, SPAIN, [4]Complejo Hospitalario de Navarra, Pamplona, SPAIN, [5]Hospital General Universitario Gregorio Marañón, Madrid, SPAIN, [6]Hospital Universitario Reina Sofia, Córdoba, SPAIN, [7]Hospital Regional Universitario de Málaga, Málaga, SPAIN, [8]Hospital Rey Juan Carlos, Madrid, SPAIN, [9]Hospital Torrecárdenas, Almería, SPAIN.

Aim/Introduction: Sentinel lymph node (SLN) biopsy is the standard of care in axillary staging of clinically node-negative breast cancer patients. ^{99m}Tc-Tilmanocept is a novel receptor-targeted radiopharmaceutical in Europe indicated for imaging and intraoperative detection of SLNs in breast cancer, melanoma or oral cavity squamous cell carcinoma. **Aim:** To describe results in clinical practice with ^{99m}Tc-Tilmanocept in breast cancer patients scheduled for SLN biopsy. **Materials and Methods:** Retrospective multicenter analysis of 352 patients (98.9% women, mean age 59 years, mean body mass index (BMI) 27), with T1-T3 N0-N1 breast cancer, who underwent SLN biopsy from September 2017 to October 2018 in 9 Spanish centers. An average dose of 87.4 (± 28.4) MBq was administered in patients with two-day protocol and 57.7 (± 19.5) MBq with one-day protocol. SLN biopsy was identified using preoperative lymphoscintigraphy and intraoperative gamma probe. Local protocols used for SLN localization were not changed throughout the study. Statistical analysis was done with SPSS v25.0. Differences were considered significant when the value was < 0.05. **Results:** Two-day protocol was used in 89.2% of cases. Forty-five (12.8%) of patients received neoadjuvant systemic therapy previously to SLN biopsy. Final report was unavailable in 17 patients (4.8%). SLN detection rate with ^{99m}Tc-Tilmanocept was 96.1% (96.5% in those clinically N0 and 94.9% in N1 patients). More than 78% of patients showed 1 or 2 SLN (mean 1.73) in lymphoscintigraphy (range 0-8). Intradermal injection results in better SLN detection rate than peri-intratumoral injections. In 3.9% of the patients, a SLN could not be detected in lymphoscintigraphy and it was significantly related to the radiotracer's injection area. Her2 tumor patients had 3.33 times higher probability to non-visualization of SLN. No significant differences in successful identification of a SLN were found due to patient age, BMI, sex or tumor localization. During surgery 6/13 patients without SLN visualization achieved a SLN retrieval with gamma probe. Pathology report showed negative SLN in 239 patients (71.3%). The percentage of positive SLN was

higher in patients below 50 years old (31.9%) versus those with more than 50 years (23.7%). Overall sensitivity was 97.7% and false negative rate was 2.3%. No adverse side-effects were reported. **Conclusion:** ^{99m}Tc-Tilmanocept is a new radiotracer for lymphatic mapping and SLN biopsy that shows good results in breast cancer SLN biopsy whatever protocol is used in a heterogeneous breast cancer population with a sensitivity better than expected and false negative rate lower than expected. **References:** None.

OP-513

Sentinel lymph node biopsy with ^{99m}Tc- Tilmanocept in oral cavity cancer: Our experience

M. Albala Gonzalez, A. Santos Bueno, A. Dean Ferrer, M. Estero Serrano De La Cruz, M. Sanchez Frias, A. Acosta Collado, J. Marquez Fernandez, J. Prieto Prieto, V. Guiote Moreno, J. Vallejo Casas;
Hospital Universitario Reina Sofia, Cordoba, SPAIN.

Aim/Introduction: In oral cavity cancer, the presence of cervical lymph node metastases reduces survival by up to 50%. Selective sentinel lymph node biopsy (SLNB) can detect metastases in patients without clinical or radiologic lymph node disease. ^{99m}Tc-Tilmanocept is a novel receptor-targeted radiotracer, whose smaller molecular size and its specific binding to CD206 receptors on the surfaces of macrophages within lymph nodes allow faster injection site clearance than ^{99m}Tc-nanocolloids. Our aim is to evaluate the use of ^{99m}Tc-Tilmanocept administration in oral cavity cancer SLNB. **Materials and Methods:** A prospective study of patients with oral cavity tumors measuring less than 4cm, T1(73%) & T2 with clinical/radiological N0 stage, attending our unit and scheduled for SLNB. Four peritumoral ^{99m}Tc-Tilmanocept injection were administered. Planar images were obtained immediately and 2 hours post-injection and in a late phase SPECT/CT. Surgery was performed the next day. **Results:** 13 patients (mean age 72; 8 men), were recruited. Surgery was performed in only 11 patients, one was ruled out for clinical reasons, and the other was rescheduled and switched to ^{99m}Tc-nanocolloids. Tumor location was 54% tongue, 23% mouth floor, 15% buccal mucosa and 8% lip. At least one SLN was detected in all patients. A mean of 2,4 nodes were removed per patient (range 1-5). Only one patient presented positive bilateral SLN's as isolated tumoral cells and for clinical reasons was treated with cervical radiotherapy. Disease progression was only detected in the patient with positive lymph nodes after a mean follow-up of 8.7 months (6-12 months). Disease relapse has not been detected in the others patients. Currently the false-negative rate is 0%. In static imaging and in SPECT/CT there was less activity in the injection site, providing a clear differentiation between the SLN, especially levels 1A and 1B and the injection site. This clear differentiation has been observed in all tumor locations, including mouth floor. In one patient, the procedure was performed with both radiotracer. The same lymphatic drainage patterns was observed, with a better visualization of 1B bilateral lymph nodes with ^{99m}Tc-Tilmanocept, because in level 1B bilateral lymph nodes ^{99m}Tc-nanocolloids presented shine-through phenomenon, and the left one could not be identified clearly. **Conclusion:** According to our experience, the radiotracer ^{99m}Tc-Tilmanocept is a good option for oral cavity cancer selective SLNB, improving the shine-through phenomenon, with better delimitation between the injection site and nearby SLN, mainly levels 1A and 1B, proving high value in floor-of-mouth tumors. **References:** None.

OP-514

Image-guided Occult Lesion Localization for Non-Palpable Breast Cancer Tumors

J. R. Orozco Cortés, A. Badenes Romero, G. Garrigos Ortega, B. Cueto Cañadas, I. Latorre Agraz, P. Abreu, T. Mut, D. Balaguer, R. Vila, S. Pelaez, E. Caballero Calabuig, M. Plancha, M. Reyes, R. Martinez;
Hospital Universitario Dr Peset, Valencia, SPAIN.

Aim/Introduction: The use of gamma probes and Tc-99m colloids for radioguided occult-lesion localization (ROLL) is replacing guidewire localization in breast cancer in Europe. However, ROLL could be further improved by adding intraoperative SPECT imaging to assess tumor margins **Materials and Methods:** 19 patients with non-palpable breast cancer tumors (<1.5 cm diameter) were injected intratumorally with 37 - 148 MBqof 99m-Tc-nanocolloids 24 hours before surgeryunder ultrasound targeting the lesion center. Early planar scintigraphy and freehand SPECT (fhSPECT) were obtained to control no leakage. Intraoperatively, fhSPECT was used to obtain 5 images: pre-incision, during resection, tumor bed and twice on specimen. The first, to define the incision site. During resection, to decide surgery extension of all 6 borders guided by the distance from the center of maximum activity to the border with the gamma probe provided by system. After resection, fhSPECT was used to image specimen and to estimate security margins. If distance from the center of maximum activity to the margins was <10 mm, resection was extended. Specimens were further imaged using mammography (RxM). Histology was considered gold standard for margins involvement. We compared the time spent intraoperatively with fhSPECT vs RxM and assessed the concordance of fhSPECT with RxM, and both with histology. Predictive values (PPV and NPV) were calculated **Results:** Preoperative imaging showed no leakage in any patient. Every fhSPECT scan lasted 2 minutes, resulting in acceptable image quality (total imaging time 10 minutes). RxM time was 20min. Surgery total time was 85 min (40-129min).Compared to histology, fhSPECT/RxM resulted in 5/6 false negatives (margin considered sufficient, but histologically affected (R1)); 1/0 true positive (margin considered too small and R1); 7/7 false positive (margin considered too close, but unaffected (R0)); and 9/9 true negative (margin considered sufficient and R0). NPV was 64.3% vs. 60%. PPV, 14.3% vs. 0%. Concordance between fhSPECT and RxM was 13/19 (68.4%). Concordance of fhSPECT versus histology was 10/19 (52.6%), and of RxM versus histology was 9/19 (47.3%). **Conclusion:** Border delimitation using SPECT-Portable is a useful and efficient procedure, requiring an optimized and multidisciplinary protocol. fhSPECT

does not prolong surgery because the time used for patient is 10 minutes. Provided non-inferiority of fhSPECT compared to RxM in this short group, it could potentially replace RxM for specimen control. Modifying this protocol by adding tumor to margins distance could reduce false negative rate for fhSPECT. Such modification is being evaluated in a larger patient group **References:** None.

OP-515

Sentinel Lymph Node Biopsy After Neoadjuvant Chemotherapy In Breast Cancer Patients; Correspondence With Molecular Subtypes

P. de la Riva Pérez, C. Calvo Moron, T. Cambil Molina, F. García Gómez, A. Agudo MartÍnez, G. Sabatel Hernández, M. Molina Mora; Hospital Macarena, Sevilla, SPAIN.

Aim/Introduction: To present both the results obtained by the Sentinel Lymph Node Biopsy (SLNB) technique after neoadjuvant chemotherapy in patients with breast cancer and initial N (+)/(-), and the existing connection with the different molecular subtypes. **Materials and Methods:** We included 167 breast cancer patients(mean age 52.4 years). Intending to perform conservative surgery, we treated the patients with neoadjuvant chemotherapy to try to reduce the tumor size. The nodal state at the beginning was N(-) in 119 patients and N(+) in 48. It was necessary to demonstrate axillary negativity in the last group after ultrasound. Molecular subtypes: 5(2,7%) luminal A, 59(35,3%) luminal B, 48(28,64%) luminal-HER2+, 18(11,11%) HER2+ and 37(22,15%) triple(-). We carried out lymphoscintigraphy after the injection of 3 mCi of ^{99m}Tc-nanocolloids the day before the intervention. We located the sentinel node intraoperatively with mixed technique(radiotracer and blue dye) using gammaprobe and intraoperative portable gamma camera. Once we analyzed the SN (OSNA), we decided intraoperatively whether to perform or not lymphadenectomy depending on indications from last consensus. We classified all data analyzed (identification rate (IR), presence of SN (+)/(mic+) and performing lymphadenectomy) by the initial state of the axilla and the molecular subtypes. **Results:** Result according to N (initial) and molecular subtypes: IR was 72.9% in the N (+) inital group and 96.6% in the N (-) group (2.06 SN removed/patients). We obtained the lowest identification rates in the luminal groups with initial N (+) (see table). We avoided unnecessary lymphadenectomy were in 58,3% of the N (+) initial patients. With respect to the 30 dissections made, 40% (12/30) were (+). 53.84% of the ALND after failure of the technique in the N (+) initial group were positive (7/13). **Conclusion:** SLNB after neoadjuvant chemotherapy is still subject of debate. This is mainly because, according to the literature, the identification rates of the sentinel node and the rate of false negatives involved in the validation of the test fluctuate heavily, especially in N + initial.We obtained the lowest IR in the luminal groups, although the luminal A group would be biased due to its small sample size.We avoided unnecessary lymphadenectomy in 58,3% of N(+) initial patients. Long-term monitoring of patients will be necessary because of lack of TFN. **References:** None.

OP-516

Sentinel lymph node status versus tumor characteristics, neutrophil to lymphocyte ratio, C-reactive protein levels and C-reactive protein to albumin ratio-prognostic factors for primary cutaneus melanoma

S. Stojanoski, N. Manevska, T. Makazlieva, D. Miladinova; Medical Faculty, Skopje, NORTH MACEDONIA.

Aim/Introduction: The aim of this study was to identify tumor characteristics of primary malignant melanoma, neutrophil to lymphocyte ratio (NLR), C - reactive protein (CRP) levels and C - reactive protein to albumin ratio (CRP/Alb) predictive of sentinel lymph node (SLN) positive status and their impact on disease recurrence, melanoma specific survival (MSS), disease free survival (DFS) and overall survival (OS) period. **Materials and Methods:** 100 patients with primary malignant melanoma, clinically staged T1b/T2+ (1-4mm thick) N0, M0 underwent SLN detection procedure. Tumor characteristics, NLR, CRP levels and CRP/Alb ratio were analyzed in correlation with SLN status. The optimal cutoff values of NLR and CRP/Alb were determined by the receive operative characteristics (ROC) analysis. Univariate and multivariate Cox regression analyses, t - test for continuous or X^2 test for categorical variables and Kaplan-Meier curve analyses were performed to assess factors predicting SLN positive status, regional recurrence rate, DFS, MSS and OS period. **Results:** We identified Breslow`s thickness (OR=1,51; 95% CI 1,02-2,01; p=0,034), presence of ulceration (p=0,041), lymphocytic infiltration (OR=0,42; 95% CI 0,18-0,99; p=0,02), high mitotic rate (p=0,031), high Ki67 index (p<0,01), high NLR (HR=2,45; 95% CI 1,52-3,34; p<0,01), increased CRP levels (HR=1,53; 95% CI 1,33-1,75; p<0,001) and high CRP/Alb ratio (HR=2,01; 95% CI 1,15-3,52; p=0,016) as independent predictors of SLN positive status. SLN status was the strongest predictor (HR=0,241; 95% CI 0,45-1,01; p=0,04) of DFS, MSS and OS period. **Conclusion:** We confirmed Breslow's thickness, presence of ulceration, lymphocytic infiltration extent, high mitotic rate, high Ki67 index, high NLR, increased CRP levels and high CRP/Alb ratio as factors predictive of SLN metastatic involvement. We also confirmed SLN status to be the most significant independent predictor of DFS, MSS, OS and risk of regional recurrence. **Key words:** neutrophil to lymphocyte ratio, c - reactive protein to albumin ratio, prognostic factors, melanoma, sentinel lymph node **References:** None.

OP-517

The value of ^{99m}Tc-nanocolloid reinjection in vulva cancer patients with non-visualisation of a contralateral sentinel node

C. Brouwer[1], *H. J. M. A. Zijlmans*[2], *M. P. M. Stokkel*[2], *B. van der Hiel*[2]; [1]*The Netherlands Cancer Institute-Antoni van Leeuwenhoek, Amsterdam, NETHERLANDS,* [2]*the Netherlands Cancer Institute-Antoni van Leeuwenhoek, Amsterdam, NETHERLANDS.*

Aim/Introduction: The aim of this study was to evaluate whether in vulva tumors located within 1 cm of the midline but not involving the midline 99mTc-nanocolloid reinjection after initial non-visualization of a sentinel lymph node (SLN) in the contralateral groin has clinical value. **Materials and Methods:** From November 2013 until November 2018 patients with vulvar carcinoma underwent preoperative SLN lymphoscintigraphy including planar imaging and SPECT/CT after four intradermal injections of 99mTc-nanocolloid surrounding the tumor. Demographic data, visualization of sentinel nodes ipsi- and contralateral, reinjection, surgical procedures, pathology results and follow up was registered retrospectively. Data was categorized by primary tumor location as midline, within 1 cm of the midline but not involving the midline and more than 1 cm of the midline. **Results:** Eighty patients with stage T1b vulvacarcinoma and mean age of 67 years underwent SLN lymphoscintigraphy, of which thirty-nine patients had a tumor within 1 cm of the midline but not involving the midline. In this category, eight cases had initially non-visualization of a contralateral SLN. After reinjection in six patients, four contralateral sentinel node biopsies (SNB) were performed and two contralateral lymph node dissections (LND). In none of these six patients metastases were found. In two remaining patients with non-visualization and without reinjection, follow up of 18 months did not show any disease recurrence. Of the thirty-one patients with visualization of a contralateral SN after first injection, no SNB contained metastases, neither were contralateral lymph node metastases found in follow up.In contrast, in four out of thirty-one patients with a midline tumor, metastases were found in a contralateral sentinel node which were all visualized after first injection. In three patients with non-visualization of the contralateral SN, no metastases were found after reinjection followed by SNB, LND or SNB without reinjection. **Conclusion:** In this retrospective analysis, no metastases in contralateral lymph nodes were found in any of the patients with vulvar carcinoma localized within 1 cm of the midline but not involving the midline, either by SNB, LND or during follow-up. In this respect, reinjection after non-visualization of a contralateral SLN may not have clinical value. **References:** None.

OP-518

Head-to-head comparison of two radiocolloids with different particle size for sentinel lymph node imaging using lymphoscintigraphy and SPECT/CT

D. Rietbergen[1], *P. Meershoek*[1], *M. Donswijk*[2], *M. Klop*[2], *R. Valdes Olmos*[1,2], *F. van Leeuwen*[1], *J. vd Hage*[1,2]; [1]*Leids Universitair Medisch Centrum (LUMC), Leiden, NETHERLANDS,* [2]*NKI-AVL, Amsterdam, NETHERLANDS.*

Aim/Introduction: The purpose of this study was to compare the drainage patterns of two radiotracers with different particle size (PS) in melanoma patients scheduled for sentinel lymph node (SLN) biopsy. Based on a head-to-head comparison of ICG-99mTc-nanocolloid (PS 5-80nm) with 99mTc-Senti-Scint (PS 100-600nm), we evaluated their drainage pattern and sentinel lymph node localization using lymphoscintigraphy and SPECT/CT. Further, we studied whether the increased particle size could reduce the amount of non-SLNs, while preserving the SLN identification. **Materials and Methods:** Twenty-five patients (mean age: 56.9y, range: 25-79y) with a melanoma scheduled for SLN biopsy prior to (re)excision of the primary lesion (scar) were prospectively included. The localisation of the primary lesion was as follows: head and neck region (n=6), the trunk (n=11) and extremities (n=8). All patients followed a two-day procedure. On the first day, 99mTc-Senti-Scint was injected in 4 intradermal depots around the primary lesion or scar. Injection points were marked on skin with indelible ink to facilitate reproducibility in the administration of the second tracer. The second day, after planar images to control resting lymph node radioactivity, ICG-99mTc-nanocolloid was injected following the same protocol. The paired planar and SPECT/CT images of both tracers were evaluated with respect to drainage to lymph node basins, SLN visualisation and non-SLN uptake. **Results:** Twenty-four out of 25 patients were evaluable. One patient was excluded since the SPECT data were not completed. SLN visualisation rate was 100% for ICG-99mTc-nanocolloid and 96% for 99mTc-Senti-Scint, whereas uptake in non-SLNs was found in respectively 71% (17/24) and 61% (14/23). Concordance rate in drainage to 45 lymph node basins was 91% (41/45) with discordant findings for two melanomas in head/neck and one in clavicular area. Unique lymph node basins were seen in 44/45 (98%) for ICG-99mTc-nanocolloid and 42/45 (93%) for 99mTc-Senti-Scint. **Conclusion:** Although ICG-99mTc-nanocolloid led to SLN visualisation in all patients this was accompanied by a tendency to visualize more non-SLNs. The high reproducibility of both tracers appears to minimize the difference in particle size as a factor influencing SLN imaging in melanoma. However, some caution mainly for lesions located in head and neck, which needs to be evaluated in a separate head-to-head comparison including a larger series of patients, is necessary. **References:** None.

1109

Cardiovascular - Parallel Session: Imaging the Vessel Wall

Tuesday, October 15, 2019, 8:00 - 9:30 Lecture Hall 115

OP-519

Fully-automated production of [^{18}F] ligands of Lipoprotein-associated phospholipase A2 for PET imaging of atherosclerosis

E. Jestin[1], *F. Guibbal*[2], *S. Bénard*[1], *V. Meneyrol*[1], *I. Ait-Arsa*[1], *F. Gimié*[1], *O. Meilhac*[2];
[1]*GIP CYROI, Sainte Clotilde, FRANCE,* [2]*Université de la Réunion/ UMR DéTROI, Sainte Clotilde, FRANCE.*

Aim/Introduction: Atherosclerosis and its associated clinical complications are major health issues in industrialized countries. Accurate diagnostic methods for early detection of atherosclerotic plaque remains a major challenge to providing appropriate medical care. Lipoprotein-associated phospholipase A_2 (Lp-PLA_2) was demonstrated to play an important role in atherogenesis and is overexpressed in plaques prone to rupture. Various Lp-PLA_2 inhibitors have been developed but failed to prevent plaque complication. We diverted the use of these high-affinity ligands for PET imaging. We report here the automated radiosynthesis of Lp-PLA_2 [^{18}F]-ligands. These radiotracers were tested in vivo and ex vivo. **Materials and Methods:** Starting from two aryl-BPin precursors, alcohol-enhanced Cu-mediated ^{18}F-fluorination was performed in a Tracerlab FXFN. [^{18}F]KF was eluted from QMA cartridge with KOTf/K_2CO_3 and dried with MeCN. Precursors, $Cu(OTf)_2$ and Pyridine were added to the reaction vessel in NMP/n-BuOH and heated at 110°C for 20 min. The radiotracers were isolated by prep-HPLC and formulated in Saline/EtOH (5%). Quality controls were realized prior mice injections. Stability studies were performed in buffer and plasma. ApoE KO mice were chosen as atherosclerosis models and C57Bl/6 as control mice. 15±5MBq were injected intravenously in 3 ApoE KO and 3 C57Bl/6. PET imaging acquisitions were performed during 15 min after injection. Heart and aorta were dissected, blood-flushed and imaged. Human atherosclerotic carotids samples were tested by incubating 30±5MBq of radiotracers at 37°C. After washing the samples with saline, PET acquisitions were carried out. All the in vivo and ex vivo experiments were compared with [^{18}F] FDG. **Results:** Starting from 45GBq, two Lp-PLA_2 [^{18}F]-ligands were obtained with an automation system yielding 99±0.5% radiochemical purities and up to 270GBq/µmol. Stability studies have shown no degradation, confirming their suitability for mice injection. PET imaging with radiolabeled ligands has shown a strong accumulation in ApoE KO aortas that was not observed with [^{18}F]FDG. No accumulation was observed in C57Bl/6 aortas either with Lp-PLA_2 [^{18}F]-ligands or with [^{18}F]FDG. In carotid endarterectomy samples, [^{18}F]FDG displayed a weak signal only in the stenosed complicated plaque sample. Both radiotracers were able to significantly accumulate in complicated and non-complicated parts of atherosclerotic carotid samples. **Conclusion:** Two Lp-PLA_2 [^{18}F]-ligands were successfully obtained on automated module through a Cu-mediated [^{18}F]-fluorodeboronation of aryl-BPin with excellent RCP and specific activities. The preclinical and ex vivo studies have shown the suitability of these two candidates for the detection of Lp-PLA_2 within the atherosclerotic plaque. **References:** Guibbal F et al. Bioorg Med Chem Lett. 2018;28(4):787-792.

OP-520

Functional and Metabolic Reprogramming of Bone Marrow Myeloid Cells in Patients with Atherosclerosis

M. P. Noz[1], *S. Bekkering*[1], *L. Groh*[2], *T. Nielen*[2], *E. Lamfers*[2], *S. El Messaoudi*[1], *N. Van Royen*[1], *E. Rutten*[1], *H. Dolstra*[1], *E. M. M. Smeets*[1], ***E. H. J. G. Aarntzen***[1], *M. Bremmers*[1], *W. Van der Velden*[1], *E. Huys*[1], *F. Preijers*[1], *L. A. B. Joosten*[1], *M. E. Gomes*[2], *M. G. Netea*[1], *N. P. Riksen*[1];
[1]*Radboud University Nijmegen Medical Center, Nijmegen, NETHERLANDS,* [2]*Canisius Wilhelmina Hospital, Nijmegen, NETHERLANDS.*

Aim/Introduction: Atherosclerosis is the major cause of cardiovascular diseases. Monocyte-derived macrophages play a central role in the development and progression of atherosclerotic plaques. Monocytes can adopt a long-term pro-inflammatory phenotype after brief exposure to atherogenic stimuli, which has been termed trained immunity. In animal models, this occurs due to functional and metabolic reprogramming at the level of myeloid progenitors in the bone marrow. We recently reported that circulating monocytes of patients with atherosclerosis have a long-term pro-inflammatory phenotype associated with an increased glycolytic metabolism. In this study, we explored whether innate immune reprogramming in patients with atherosclerosis occurs in bone marrow progenitors. **Materials and Methods:** Patients with and without severe coronary atherosclerosis (calcium score 400+ on CT-scan and total plaque score 4+ on CCTA) underwent vene puncture, bone marrow aspiration and ^{18}F-FDG PET-CT scanning. Cytokine production capacity was assessed after ex vivo stimulation of PBMCs from peripheral blood, and mononuclear cells (MNC's) from the bone marrow aspirate. In addition, cellular metabolism was assessed with Seahorse technology. With flow cytometry, cells of the peripheral blood and bone marrow compartment were characterised. Vascular wall inflammation and bone marrow tissue activation were determined in specified regions of interests, and expressed as target to background ratios (TBR). **Results:** 13 Patients and 13 controls were included (60±10; 52±10 years, all men). Cytokine production capacity of PBMCs and MNCs was higher in patients with atherosclerosis (e.g. LPS TNFα, p-value less than 0.05). Similarly, oxygen consumption and extracellular acidification rates of MNCs was increased (max ECAR p-value less than 0.05), but no difference in circulating monocytes was observed. No significant changes in monocyte subsets or expression markers were observed. Vascular

wall, splenic and bone marrow ^{18}F-FDG uptake revealed no differences. **Conclusion:** Patients with severe coronary atherosclerosis, in addition to the circulating monocytes, the mononuclear cell fraction from the bone marrow also shows pro-inflammatory functional reprogramming. With regard to underlying mechanisms, both oxygen consumption as well as glycolysis are increased in these cells. This study confirms pro-atherogenic reprogramming of myeloid precursors in the bone marrow, which reveals a potential novel target for preventive pharmacotherapy in these patients. **References:** None.

OP-521

The Presence Of Brown Adipose Tissue Protects Against Arterial Inflammation In Young Healthy Adults

O. Hedesan[1,2], A. Gruber[1,3], C. T. Herz[2], M. E. Mayerhöfer[4], F. Langer[5], G. Prager[5], M. Hacker[1], F. W. Kiefer[2], A. R. Haug[1,3];
[1]Department of Biomedical Imaging and Image-guided Therapy, Division of Nuclear Medicine, Medical University of Vienna, Vienna, AUSTRIA, [2]Clinical Division of Endocrinology and Metabolism, Department of Medicine III, Medical University of Vienna, Vienna, AUSTRIA, [3]Christian Doppler Laboratory for Applied Metabolomics (CDL AM), Medical University of Vienna, Vienna, AUSTRIA, [4]Department of Biomedical Imaging and Image-guided Therapy, Division of General and Pediatric Radiology, Medical University of Vienna, Vienna, AUSTRIA, [5]Division of General Surgery, Department of Surgery, Medical University of Vienna, Vienna, AUSTRIA.

Aim/Introduction: Energy dissipation through the promotion of brown adipose tissue (BAT) has recently evolved as a promising concept in the fight against obesity and metabolic disease. Upon activation, BAT combusts fatty acids and thus lowers plasma lipid levels protecting thereby against the development of atherosclerosis. Recent data have shown a negative correlation between the presence of BAT and arterial inflammation. Here, we aim to investigate the degree of arterial inflammation in young, healthy adults undergoing a ^{18}F-FDG PET/CT study for the detection of BAT. **Materials and Methods:** : 94 healthy participants (age 30.1±0.8; 50 females, 44 males; 38 lean and 56 obese) enrolled in a prospective imaging study underwent two consecutive ^{18}F-FDG PET/CT examinations at thermoneutrality and after BAT activation using personalized cooling protocols. BAT was segmented according to BARCIST criteria. Based on these criteria the participants were classified as BAT-positive (n = 42; 25 lean and 17 obese) and BAT-negative (n = 52; 13 lean and 39 obese). The arterial inflammation was assessed in accordance with the EANM guidelines. **Results:** Lean subjects showed lower aortic inflammation compared to obese, both in the aortic arch (2.5±0.07 vs. 2.7±0.06, p = 0.04) but not and in the ascending aorta (2.8±0.1 vs.2.9±0,08, p = 0.23). The presence of BAT was associated with significantly lower arterial inflammation in the aortic arch (ArchAo) and in the ascending aorta (AscAo) (BAT+ vs. BAT-: 2.40±0.07 vs. 2.81±0.06, p < 0.001 and 2.68±0.08 vs. 3.02±0.09, p = 0.003). In obese subjects, the differences in arterial inflammation between BAT+ and BAT- were even more pronounced (ArchAo: 2.31±0.1 vs 2.88±0.07, p < 0.001; AscAo 2.56±0.11 vs 3.07±0.09, p = 0.001) whereas no significant differences were observed in the lean cohort (ArchAo: 2.45±0.09 vs 2.56 ± 0.14, p = 0.55 and AscAo: 2.71±0.11 vs. 2.81±0.21, p = 0.70). Furthermore, in obese subjects, we noticed strong negative correlations between BAT activation parameters (volume, SUV_{mean}) and arterial inflammation in ArchAo (volume R = -0.54, p = 0.02; SUV_{mean} R = -0.53, p = 0.02) and AscAo (volume R = -0.6, p = 0.01; SUV_{mean} R = - 0.32, p = n.s). **Conclusion:** There is a strong negative correlation between brown fat activity and arterial inflammation suggesting a protective role of brown adipose tissue against atherosclerosis in young, healthy subjects. This effect was particularly pronounced in obese subjects. **References:** None.

OP-522

The birth of calcific plaques: the significance of focal 18F-NaF hot spot within the arterial walls, analyzed on sequential PET/CT

F. Fiz[1], C. Campi[2], S. Morbelli[3], A. Piccardo[4], C. la Fougère[1], M. Piana[5], G. Sambuceti[3];
[1]Nuclear Medicine Unit, Department of Radiology, University of Tübingen, Tübingen, GERMANY, [2]Nuclear Medicine Unit, Department of Medicine, University of Padua, Padua, ITALY, [3]Nuclear Medicine Unit, Department of Healt Sciences, University of Genoa, Genoa, ITALY, [4]Nuclear Medicine Unit, Ente Ospedaliero Ospedali Galliera, Genoa, ITALY, [5]Department of Mathematics, University of Genoa, Genoa, ITALY.

Aim/Introduction: Vascular uptake of 18F-Natrium Fluoride (NaF) on PET/CT has been linked to active calcium deposition within arterial calcifications (AC). However, it is unclear whether focal NaF uptake in segments without evidence of calcification can predict the future appearance of AC in the same area.In this study, we analyzed the density of the arterial wall in areas with or without focal NaF uptake. Furthermore, we tested whether an increase in mean density or the appearance of a visible calcification can be observed on a follow-up PET/CT **Materials and Methods:** 55 patients (25 females, mean age 71±7 years) were retrospectively enrolled. Each patient had undergone 2 consecutive NaF-PET for clinical reasons (spaced 18±11 months apart). On each baseline PET, a VOI was created on all focal uptakes with no evidence of calcfications within the abdominal aorta wall, (hot-spot, HS1). A ROI with the same area was created on a control segment of the aorta wall, with neither focal NaF uptake nor calcification (CS1). Both HS1 and CS1 were then copied on the corresponding position of the follow-up PET/CT: these VOIs were labeled HS2 and CS2, respectively. Mean and maxiumum Hounsfield density (HUmean and HUmax) as well as bloodpool-corrected SUV (target-to-background ratio, TBR) were calculated in all VOIs; in case of appearance of focal calcification in HS2, an Agastone-like calcium score was calculated with a dedicated software tool. **Results:** A total of 125 HS1 were identified; a focal calcification appeared on 54 of HS2 (43,2%). In patients were new calcifications appeared, interval between the first and the second PET/CT was 25±12

months. Baseline HS1 TBR correlated with the calcium score of the AC within HS2 (R=0.7, p<0.01). HUmean and HUmax were higher in HS1 than in CS1 (48±8 Vs. 40±7, p<0.001; 122±53 and 88±17, p<0.01, respectively). HUmean increased from HS1 to HS2 (up to 61±14, p<0.01); conversely, no density variation could be described between CS1 and CS2. **Conclusion:** Focal NaF accurately describes the microscopic calcium deposition within the vessel wall: high-uptake areas have higher density than the ones without visible uptake; moreover, mean density tends to increase in focal uptake segments. Focal uptake can predict the appearance of visible calcifications; however, a longer observation period might be required to demonstrate this phenomenon. **References:** None.

OP-523

Arterial Wall Inflammation, Increased Hematopoiesis and Macrophage Activation in Patients with Primary Aldosteronism

*C. D. C. C. Van der Heijden[1], E. M. M. Smeets[1], **E. H. J. G. Aarntzen**[1], M. P. Noz[1], H. Monajemi[2], S. Kersten[1], C. Kaffa[1], A. Hoischen[1], J. Deinum[1], L. A. B. Joosten[1], M. G. Netea[1], N. Riksen[1];*
[1]Radboud University Nijmegen Medical Center, Nijmegen, NETHERLANDS, [2]Rijnstate Hospital, Arnhem, NETHERLANDS.

Aim/Introduction: Primary hyperaldosteronism (PA) is the most common form of secondary hypertension. Patients with PA have a strongly increased risk of cardiovascular diseases (CVD), which is independent of blood pressure. Animal models showed that aldosterone induces pro-inflammatory changes in innate immune cells and accelerates atherosclerosis, but human data are scarce. Here, we aimed to assess arterial wall inflammation, bone marrow activation, and innate immune cell activation in patients with PA. **Materials and Methods:** We performed ^{18}F-FDG PET/CT imaging in 15 patients with PA and 15 matched controls with essential hypertension (EHT) after a 24h low carbohydrate diet and overnight fasting prior to infusion of ^{18}F-FDG (2 MBq/kg) and 120 minutes incubation time. ^{18}F-FDG uptake was assessed in 8 regions of interest (ROIs): carotid arteries, wall of the ascending, descending and abdominal aorta, iliac arteries, bone marrow (L2-L3), spleen and liver. The maximal standardized uptake value (SUV_{max}), and target-to-background-ratio (TBR) were assessed. The TBR was calculated from arterial SUV_{max} and background activity in the low-thoracic aortic blood pool. For the hematopoietic ROIs, TBR was calculated as the ratio of the splenic or bone marrow SUV_{max} and the mean background activity in the liver. We assessed several circulating markers of inflammation in plasma and ex vivo cytokine production of peripheral blood mononuclear cells (PBMC) with ELISA. Furthermore, flow cytometry was used to classify monocyte subsets. CD14^{pos}MACS-isolated monocytes stored at baseline were processed for RNA sequencing. **Results:** ^{18}F-FDG uptake was significantly higher in the carotid arteries, descending and abdominal aorta, and iliac arteries of patients compared to controls; and ^{18}F-FDG uptake correlated with aldosterone level in both cohorts. Moreover, ^{18}F-FDG uptake in the bone marrow was higher in patients, which coincided with a higher monocyte-to-lymphocyte ratio. While circulating inflammatory markers, ex vivo cytokine production, and the transcriptome of circulating monocytes were similar between patients and controls, macrophages from PA patients showed significantly higher TNFA expression. Moreover, macrophages from healthy donors cultured in serum of PA patients showed increased pro-inflammatory cytokine production compared to macrophages cultured in EHT serum. **Conclusion:** We show that patients with PA have a higher ^{18}F-FDG uptake in the arterial wall than EHT controls. This associates with enhanced hematopoietic activity in the bone marrow, changes of the peripheral blood cell composition and increased inflammatory activity of monocyte-derived macrophages. These mechanisms explain, at least in part, the increased CVD risk in patients with PA and reveal novel pharmacological targets. **References:** None.

OP-524

Alterations of peripherial micorcirculation in Diabetes mellitus and Obesity

***M. Miko*[1,2], *J. Varga*[3], *F. Nagy*[2], *M. Emri*[3], *M. Kaplar*[4], *A. Forgacs*[2], *I. Garai*[2,2];**
[1]Deparment of Medical Imaging, University of Debrecen, Debrecen, HUNGARY, [2]Scanomed Ltd., Debrecen, HUNGARY, [3]Division of Nuclear Medicine and Translational Imaging, Medical Imaging Department, Faculty of Medicine, University of Debrecen, Debrecen, HUNGARY, [4]Department of Internal Medicine, Faculty of Medicine, University of Debrecen, Debrecen, HUNGARY.

Aim/Introduction: The number of people with obesity and diabetes is continously growing. These are important metabolic drivers of cerebrovascular and cardiovascular diseases as well as peripheral neuropathy. Damage to the microcirculation is the basis for these conditions.In our study we investigated peripheral perfusion in these two metabolic diseases and its correlation with laboratory parameters and neuropathy. **Materials and Methods:** In this prospective study, 57 patients with controlled type 2 diabetes mellitus (T2DM) (mean age:52±9.6) and 46 patients with obesity (50.6±7.9) were recruited. BMI was 34.1±5.9 in T2DM and 38.1±6.1 in the obese group. Quantitative Tc99m HMPAO (Mediradiopharma, Hungary) SPECT/CT (AnyscanFlexSC, Mediso, Hungary) studies were performed to assess peripheral microcirculation in the legs. Patients with known symptomatic peripheral circulation abnormalities were excluded from the study. For the SUVmean calculation, fixed sized spheric VOIs (volume of interest) were drawn in the calf musculature bilaterally. Neurometer testing (NM-01/CPT) was used for evaluating sub-clinical peripheral nerve dysfunction. For statistical analysis, Shapiro normality test, Wilcoxon test and paired Spearman correlation was done. **Results:** There were no significant differences of calculated SUVmean values in right and left legs in both groups, neither were there any in neurometer testing. However, leg perfusion was significantly lower in the diabetic group predominantly on the left side (p=0.015 right leg, p=0,00065 left leg). Neurometer data showed correlation

with HBA1C in the diabetic group, but none with leg perfusion. There was no correlation between neurometer test results and leg perfusion in the obese group. We also investigated the correlation of BMI, age and leg perfusion. BMI showed positive correlation with mean leg perfusion (rho=0,36, p=0,001) and no correlation with age was found. **Conclusion:** Quantitative leg perfusion SPECT/CT with Tc99m HMPAO is a sensitive method for evaluating subclinical perfusion abnormalities, providing complementary information for early assessment of peripheral neuropathy in diabetes. Further investigation is needed to understand the background of correlation of leg perfusion and BMI. **References:** None.

OP-525

FDG PET/CT Provides Additional Information on Characterization Vascular Lesions in Addition to Clinical Assessment in Takayasu Arteritis Patients

E. Incerti[1], *F. Fallanca*[1], *U. Pajoro*[1], *E. Tombetti*[2], *M. Papa*[3], *G. Ironi*[1,3], *E. Baldissera*[4], *P. Mapelli*[1,5], *F. De Cobelli*[3,5], *L. Gianolli*[1], *A. A. Manfredi*[4,5], *M. Picchio*[1,5];
[1]*Unit of Nuclear Medicine, IRCCS San Raffaele Scientific Institute, Milan, ITALY,* [2]*Department of Biomedical and Clinical Sciences, "L. Sacco" Hospital, Milan, ITALY,* [3]*Unit of Radiology and Experimental Imaging Center, IRCCS San Raffaele Scientific Institute, Milan, ITALY,* [4]*Unit of Internal Medicine and Clinical Immunology, IRCCS San Raffaele Scientific Institute, Milan, ITALY,* [5]*Vita-Salute San Raffaele University, Milan, ITALY.*

Aim/Introduction: Takayasu arteritis (TA) is a rare granulomatous disease of unknown etiology, affecting the aorta and its major branches. The first goal of therapy is prevent progression of inflammation in vascular lesions. Disease activity evaluation defined according to National Institutes of Health criteria is very important for therapeutic decision. The aim is to verify if activity PET and functional lesion characterization provide more additional information to clinical assessment in TA patients. **Materials and Methods:** Sixty-two patients according to American College of Rheumatology Criteria was recruited in this retrospective monocentric study at the IRCCS San Raffaele Hospital from April 2013 to April 2017 (56 women and 6 men; mean age: 48 years, range: 18-81 years). All patients underwent FDG PET/CT and MRI examinations, with a median interval of 1 month (range: 0-6 months). All vascular lesions was evaluated in PET/CT with both qualitative (positive/negative, visual scale 0-3, uptake aspect), and semi-quantitative (maximum standardized uptake value - SUVmax) methods. Correlation of PET evaluation versus serum biomarkers values as C-reactive protein (CRP), erythrocyte sedimentation rate (ESR) and pentraxin 3 (PTX3) was also performed. **Results:** PET was positive in 28/62 and negative in 34/62 patients, but all patients showed at least one vascular lesions at MRI. PET has detected 108 positive vascular lesions with a median SUVmax value of 2.8 (range: 1.1-7.0). Visual scale analysis showed score 3.0 (> liver uptake) in 22/62, 2.0 (= liver uptake) in 7/62, 1.0 (< liver uptake) in 14/62, and 0 (no uptake) in 19/62 patients. Aspect of FDG uptake was focal in 8/62, widespread inhomogeneous in 25/62 and widespread homogeneous in 9/62 patients. In positive PET patients, mean CRP value was 7.9 mg/L (range: 0.0-39.6), mean ESR value was 21 mm/1h (range: 1-73), and mean PTX3 value (13/28 patients) was 5.69 ng/ml (range: 2.16-15.70). In negative PET patients, median CRP was 9.0 mg/L (range: 0.3-65.5; p-value: 0.421), mean ESR value was 28 mm/1h (range: 2-78; p-value: 0.195), and mean PTX3 (18/34 patients) value was 7.74 ng/ml (range: 2.93-22.70; p-value: 0.132). **Conclusion:** PET/CT provide additional information on functional characterization of the vascular lesions in TA patients over disease activity measures, mainly based on systemic inflammation. Further prospective study is necessary to correlate FDG PET uptake with MRI enhancement in vascular lesions, and to clarify the clinical relevance and the predictive value of this imaging approach for the disease progression and the best treatment strategy. **References:** None.

OP-526

Aorta Inflammation spatial heterogeneity in Erdheim-Chester Disease: ^{18}F-Fluorodeoxyglucose Positron Emission Tomography-Computed Tomography

M. Nikpanah*, F. Farhadi, M. Ahlman, B. R. Gochuico, W. A. Gahl, J. I. Estrada Veras, E. C. Jones, K. J. O'Brien, B. Saboury;*
National Institutes of Health, Bethesda, MD, UNITED STATES OF AMERICA.

Aim/Introduction: To quantitatively investigate whether vascular inflammation is uniform across the length of the aorta in patients with Erdheim-Chester Disease (ECD). **Materials and Methods:** This retrospective study was performed on 11 ECD patients. FDG-18 PET/CT images acquired at presentation to our institute were used for data analysis. For each patient, the aorta was segmented from aortic valve to aortic bifurcation using 2mm slice thickness CT images. Binary masks were extracted and resized to 256x256 to fit dimensions of attenuation corrected PET images for image multiplication. Pixel values were exported and standardized using blood pool in vena cava as a measure for Target to Background Ratio (TBR), a previously published method[1]. Mean of pixel values in each slice standardized with background was used to quantify aortic inflammation in each slice. Aorta was divided into 4 anatomic locations (1. Ascending 2. Thoracic 3. Supra-renal abdominal (diaphragm-renal artery); and 4. Infra-renal abdominal (renal artery-bifurcation)). Repeated measures analysis of variance was used to investigate differences in aortic inflammation among these 4 anatomic locations. **Results:** Median TBR (inter-quartile range) was 1.34 (1.11, 1.66), including 1.41 (1.04, 1.7), 1.32 (1.08, 1.62), 1.36 (1.16, 1.69), and 1.34 (1.11, 1.7) for ascending, thoracic, supra-renal, and infra-renal aorta, respectively. Repeated-measure analysis of variance showed differences ($P < 0.001$) in TBR values between 4 sections of aorta. **Conclusion:** The extent of aortic inflammation in ECD patients may vary across the length of the aorta, from the aortic valve to the aortic bifurcation. **References:** Rudd, J. H., Myers, K. S., Bansilal, S., Machac, J., Woodward, M., Fuster, V., ... & Fayad, Z. A. (2009). Relationships among regional arterial inflammation,

calcification, risk factors, and biomarkers: a prospective fluorodeoxyglucose positron-emission tomography/computed tomography imaging study. Circulation: Cardiovascular Imaging, 2(2), 107-115.

1110

Do.MoRe - Parallel Session: Performance, Standardisation & Quality Control

Tuesday, October 15, 2019, 8:00 - 9:30 Lecture Hall 116

OP-527

Variability in NEMA NU 2-2012 performance measurements of all sixteen Discovery MI digital time-of-flight PET-CT systems in the Nordic countries

M. Lubberink[1,2], E. Ilan[1,2], A. Moreno[2], J. Oddstig[3], S. Leide Svegborn[4], P. Braad[5], M. Nowak Lonsdale[6], T. Hjørnevik[7], L. Gyland Mikalsen[7], V. Gjervan[8], T. Tolvanen[9], O. Sipilä[10], C. Hindorf[3], E. Trägårdh[4];
[1]Uppsala University, Uppsala, SWEDEN, [2]Uppsala University Hospital, Uppsala, SWEDEN, [3]Skåne University Hospital, Lund, SWEDEN, [4]Skåne University Hospital, Malmö, SWEDEN, [5]Odense University Hospital, Odense, DENMARK, [6]Bispebjerg Hospital, Copenhagen, DENMARK, [7]Oslo University Hospital, Oslo, NORWAY, [8]Østfold Hospital Kalnes, Grålum, NORWAY, [9]Turku University Hospital, Turku, FINLAND, [10]Helsinki University Hospital, Helsinki, FINLAND.

Aim/Introduction: Sixteen 4-ring Discovery MI PET-CT scanners (GE Healthcare; 1) were installed in the Nordic countries (Sweden, Denmark, Norway and Finland) during the last two years. During all installations the manufacturer's clinical specialist, in collaboration with a local medical physicist, performed the acceptance testing. This presented a unique possibility to address inter-scanner variability of test results with minimal influence of experimenter variation and variation in local customs and workflows. The aim of the present work was to assess the variability between NEMA performance results across scanners. **Materials and Methods:** NEMA NU 2-2012 tests for spatial resolution, sensitivity, count rate performance and scatter fraction, and image quality of 16 4-ring Discovery MI PET-CT scanners, installed between September 2016 and September 2018, were included. This scanner contains 36 rings of 3.95 x 5.3 x 25 mm LYSO detectors coupled to silicone photomultipliers in a block detector configuration (4x9 LYSO crystals to 3x6 SiPMs). Detector ring diameter is 74.4 cm and transaxial and axial field of view (FOV) are 70 and 20 cm, respectively. **Results:** Spatial resolution (mean of all directions) using OSEM (without time of flight and resolution recovery) was 3.9 mm (range, 3.8-4.1) at 1 cm, 4.3 mm (range, 4.2-4.5) at 10 cm, and 5.4 mm (range, 5.2-5.6) at 20 cm from the centre of the FOV. The mean sensitivity of all scanners was 13.6 cps/kBq (range, 12.7 to 14.8). Mean peak NEC rate was 182.5 kcps (range, 168.5-199.5) and mean activity concentration at which peak NEC was reached was 22.8 kBq/mL (range, 21.2-25.3). Mean scatter fraction was 41.1% (range, 39.9-42.1), and mean maximum count loss below peak NEC was 3.4% (range, 1.8-5.4). Hot sphere contrast ranged from 52.5% (range, 44.7-61.8) for the 10 mm sphere to 78.3% (range, 73.0-84.1) in the 22 mm sphere, and cold sphere contrast as measured in the 37 mm sphere was 89.5% (range, 87.7-91.4). **Conclusion:** Variability in NEMA NU 2-2012 measurements was highest for the count loss measurement (coefficient of variation 28%) and lowest in the spatial resolution measurement at 10 cm in radial direction (1.2%). Variability in sensitivity values was 4.3%. Further measurements will be conducted to assess to what extend these variations can be attributed to experimental uncertainty rather than true variations between scanners. **References:** 1. Hsu et al, J Nucl Med 2017.

OP-528

Harmonisation of PET/CT Performance for Brain Studies

E. E. Verwer[1], S. V. S. Golla[1], A. Kaalep[2], M. Lubberink[3], F. H. P. van Velden[4], V. Bettinardi[5], M. M. Yaqub[1], T. Sera[6], S. Rijnsdorp[7], A. A. Lammertsma[1], R. Boellaard[1];
[1]Amsterdam University Medical Centers, location VUmc, Amsterdam, NETHERLANDS, [2]North Estonia Medical Center Foundation, Tallinn, ESTONIA, [3]Uppsala University hospital, Uppsala, SWEDEN, [4]Leiden University Medical Center, Leiden, NETHERLANDS, [5]IRCCS Scientific Institute San Raffaele, Milan, ITALY, [6]EANM Research Limited (EARL), Vienna, AUSTRIA, [7]BovenIJ hospital, Amsterdam, NETHERLANDS.

Aim/Introduction: For clinical brain PET studies, performed within multi-center or longitudinal settings, harmonisation of image quality and quantification is imperative. Given the different characteristics of brain PET versus oncology PET, current EARL criteria may be inadequate. In this study, prototype standards specific for brain PET harmonisation were developed. **Materials and Methods:** A Hoffman 3D Brain Phantom, modelling a human brain with grey matter (GM) recovery coefficient (RC) of 1 and white matter (WM) RC of 0.25, filled with ~35 kBq·mL^{-1} [^{18}F]FDG, was scanned on 12 clinical PET/CT systems (4 GE, 4 Philips, 4 Siemens, including a digital system of each vendor). Data were reconstructed into 30 min frames using various reconstruction protocols: with/without resolution modelling (PSFon/PSFoff), time-of-flight and vendor specific settings. The resulting 81 images were co-registered to a PET image template (voxel size 1.17x1.17x2.00 mm^3) containing volumes of interest (VOI) for deriving various metrics, e.g. total phantom activity, RC_{GM}, RC_{WM}, $RC_{mid\text{-}phantom\text{-}cold\text{-}spot}$, GM/WM ratio (GMWMr) and left/right hemisphere activity ratio (LRr). To address inaccuracies in calibration and activity measurements, RC were calculated based on both injected activity and image derived total phantom activity. Harmonisation criteria were defined such that for each PET/CT system at least one reconstructed image complied. **Results:** Bias and its variability among systems were smaller for image based RC than injected

activity based RC (0.97±0.03 vs 0.92±0.04). Notable differences were observed between PSF_{ON} and PSF_{OFF}: RC_{GM}=0.98±0.02, 0.95±0.03; GMWMr=4.05±0.22, 3.63±0.26; $RC_{mid\text{-}phantom\text{-}cold\text{-}spot}$=0.030±0.011, 0.043±0.013; Vendor specific differences were found for all metrics. Based on these results, RC_{GM} for both PSF_{ON} and PSF_{OFF} were defined as harmonisation standards. Minimum RC_{GM} bandwidths, ensuring at least one compliant scan per system, were PSF_{ON}-RC_{GM}=[0.95-1.00] leading to PSF_{ON}-GMWMr=[3.73-4.67], PSF_{ON}-LRr_{GM}=[0.94-1.03], PSF_{ON}-$RC_{mid\text{-}phantom\text{-}cold\text{-}spot}$=[0.020-0.065]; and PSF_{OFF}-RC_{GM}=[0.87-0.98], leading to PSF_{OFF}-GMWMr=[3.25-4.67], PSF_{OFF}-LRr_{GM}=[0.94-1.03], PSF_{OFF}-$RC_{mid\text{-}phantom\text{-}cold\text{-}spot}$=[0.020-0.071]. In addition, each image was compared with an average reference image, derived from one scan per system with RC_{GM} nearest to the mid-bandwidth value. An upper limit to the root mean squared difference over all brain region voxels (RMSD) <0.08 compared with the average reference image was found to further harmonise image quality. **Conclusion:** A combination of an RC_{GM} bandwidth of [0.95-1.00] for PSF_{ON} and [0.87-0.98] for PSF_{OFF} with RMSD<0.08 was found to identify scans of comparable image quality. $RC_{mid\text{-}phantom\text{-}cold\text{-}spot}$ showed SD>35%, which may preclude the use of a low uptake reference region. These prototype standards can now be tested prospectively to validate and/or refine the underlying harmonisation criteria. **References:** None.

OP-529

Imaging performance of Siemens Vision 600 and GE Discovery MI-5 evaluated on phantoms with focus on detection and quantification of sub-centimeter lesions

O. L. Munk, L. P. Tolbod;
Aarhus University Hospital, Aarhus, DENMARK.

Aim/Introduction: Our aims were: 1) to evaluate imaging performance of the new Siemens Vision 600 (Vision) and GE Discovery MI-5 (MI-5) 'digital' PET/CT systems; 2) to optimize image reconstruction parameters for clinical scans with focus on detection of small lesions and quantification of their tracer uptake; and 3) to evaluate recovery coefficients (RCs) using different reconstruction settings to harmonize image quality from the two scanners. **Materials and Methods:** Four phantoms were filled with ^{18}FDG in the 4:1 activity concentration ratio recommended in the NEMA NU2-2018 standard. (1) NEMA Image Quality Phantom with 6 hot spheres with inner diameter range (IDR) 10-37 mm; (2) Jaszczak SPECT Phantom with 6 hot spheres IDR 4-12 mm and a hot rod insert IDR 4.8-12.7 mm; (3) custom-made wall-less gel phantom with 12 hot spheres IDR 3-12 mm in a cold background; and (4) Mini Deluxe SPECT phantom with cold rods IDR 1.2-4.8 mm. The four phantoms were first scanned on MI-5 and then on Vision. We scanned with full bed-overlap to have uniform counting statistics and reconstructed images corresponding to 1.5 minute per bedposition. The time per bedposition was prolonged on the Vision to adjust for radioactive decay. Images reconstructed using clinically relevant sets of reconstruction parameters were evaluated using PMOD 4.0. For all spheres, RCmean and RCmax were measured inside sphere-shaped volumes of interests with the same diameter as the hot spheres. Images of hot and cold rods were inspected visually to assess spatial resolution. Coefficient of Variations (CoV) were measured in the uniform background of the Jaszczak Phantom. **Results:** For the Vision (4 iterations, 5 subsets, 2 mm Gauss filter, voxel size 1.65x1.65x1.65mm^3) and MI-5 (3 iterations, 16 subsets, 2 mm Gauss filter, voxel size 1.82x1.82x2.80mm^3) the RC ranges were respectively: (NEMA) RCmean 0.61-0.88, RCmax 1.04-1.46 vs RCmean 0.59-0.88 and RCmax 1.11-1.47; (Jaszczak) RCmean 0.30-0.67, RCmax 0.32-1.42 vs RCmean 0.35-0.63 and RCmax 0.42-1.16; (Wall-less gel phantom): RCmean 0.07-0.65 and RCmax 0.09-1.09 vs RCmean 0.06-0.63 and RCmax 0.08-1.21. In both images, 6.6 mm hot rods and 4.8 mm cold rods could be separated. CoV were 7.8% vs 9.3%. **Conclusion:** The scanners can produce similar SUV recoveries as function of sphere size with CoV well below the commonly accepted 15% level. Preliminary results indicate that Vision produced slightly higher RCmean with lower CoV. More sets reconstruction parameters will be explored including using continuous bed motion scans (Vision) and Q.Clear image reconstruction (MI-5). **References:** None.

OP-530

Quality Control of PET/MRI systems: Consensus Recommendations from a European Network of Hybrid Imaging Sites (HYBRID)

A. Valladares[1], S. Ahangari[2], T. Beyer[1], R. Boellaard[3], Z. Chalampalakis[4], C. Comtat[4], L. DalToso[5], A. E. Hansen[2], M. Koole[6], J. Mackewn[5], P. Marsden[5], J. Nuyts[6], S. Poth[7], E. Solari[8], I. Rausch[1];
[1]Medical University of Vienna, Vienna, AUSTRIA, [2]Department of Clinical Physiology, Nuclear Medicine and PET, Rigshospitalet, University of Copenhagen, Copenhagen, DENMARK, [3]Department of Radiology and Nuclear Medicine, VU University Medical Centre, Amsterdam, NETHERLANDS, [4]Service Hospitalier Frédéric Joliot, IMIV, CEA, INSERM, CNRS, Univ. Paris-Sud, Orsay, FRANCE, [5]King's College London & Guy's and St Thomas' PET Centre, School of Biomedical Engineering and Imaging Sciences, King's College London, London, UNITED KINGDOM, [6]Nuclear Medicine and Molecular Imaging, University Hospitals Leuven and KU Leuven, Leuven, BELGIUM, [7]Department of Nuclear Medicine, University Hospital Tuebingen, Tuebinguen, GERMANY, [8]Department of Nuclear Medicine, Technical University of Munich, Munich, GERMANY.

Aim/Introduction: Dual-modality PET/MR imaging provides information valuable for patient management and, moreover, for novel applications of radiomics and machine learning. The highest quality of PET/MR image data is required to fuel subsequent single site and multi-centre data pooling and analysis. This contribution aims at developing a consensus on the minimum level of QC required for routine PET/MRI as seen by a consortium of experienced hybrid imaging sites. **Materials and Methods:** The HYBRID consortium is an innovative training network funded by the European Commission (MSCA #764458) involving 23 partner organizations including eight imaging sites

highly experienced in clinical PET/MRI as well as three vendors of PET/MRI systems. All PET/MRI centres within HYBRID were surveyed to collect information about local QC tests and testing frequencies for the PET/MRI systems. The survey was based on QC tests for the PET and MR imaging systems by international guidelines and recommendations. These tests include, for example, image uniformity, normalization, image quality for the PET component, and central frequency, coil check, geometry accuracy for the MRI modality. Survey responses and information provided by the vendors about implemented QC measures as well as existing recommendations on QC for PET and MRI, served as the basis for discussions to reach a consensus on QC procedures for PET/MRI. **Results:** The survey revealed that all sites perform the PET daily QC test implemented by the vendor; however, significant variations were noted for other routine PET QC tests and testing frequencies. Furthermore, higher variability of QC measures between the centres was reported for the MRI component. Based on the survey results as well as existing recommendations by professional imaging associations, a consensus on QC measures for PET/MRI was reached; it includes the daily QC as implemented by the vendor, a quarterly cross-calibration measurement also including the assessment of uniformity and a yearly IQ test for the PET component of the systems. For the MRI component, the consensus includes regular coil checks and a quarterly MR IQ test including the assessment of signal-to-noise ratios and artefacts. **Conclusion:** Significant variations in currently implemented QC measures for PET/MRI are seen between PET/MRI centres. Therefore, we propose a set of QC measures to ensure the proper function of the PET/MRI system as a consensus recommendation for PET/MRI QC in the HYBRID consortium. (This work has received funding from the European Union's Horizon 2020 research and innovation programme under the MSCA No. 764458.) **References:** None.

OP-531

Clinical trial qualification of PET-CT scanners in onco-haematological clinical trials performed with ^{68}Ge pre-filled phantom permits to achieve a lower inter-scanner variability respect to standard ^{18}F phantoms

F. Bergesio[1], *A. De Maggi*[1], *F. Dalmasso*[1], *M. Coronado*[2], *L. Ceriani*[3], *L. Guerra*[4], *S. Chauvie*[1];
[1]*Medical Physics Unit, S. Croce e Carle Hospital, Cuneo, ITALY,* [2]*Nuclear Medicine Department,La Paz University Hospital, Madrid, SPAIN,* [3]*Nuclear Medicine Department, Oncology Institute of Southern Switzerland, Bellinzona, SWITZERLAND,* [4]*Nuclear Medicine Department, S. Gerardo Hospital, Monza, ITALY.*

Aim/Introduction: The aim of this study was to compare the Clinical Trial Qualification (CTQ) adopted by the Italian Foundation on Lymphoma (FIL), the Grupo Espanol de Linfomas/Transplante Autologo de Medula Osea (GELTAMO), the International Extranodal Lymphoma Study Group (IELSG) and the SwissGroup for Clinical Cancer Research (SAKK). **Materials and Methods:** The CTQ process consisted in the scanning with the default acquisition and reconstruction parameters used for whole-body oncological PET/CT studies of the same model of NEMA/IEC image quality phantom. In the standard approach the phantom background and spheres were filled with a ^{18}F solution by local imaging experts. In the other approach the phantom's background and the six spheres were all pre-filled with a ^{68}Ge epoxy. All the images were analysed by Cuneo CoreLab. Background activity concentration (BAC) was defined as the difference between the average activity concentration in a large homogenous region and the expected activity concentration. Sphere to background ratio (SBR) was defined as the ratio between the maximum of the activity concentration in the largest 37 mm diameter sphere and the BAC. Inter-scanner variability (ISV) was estimated as the 95% confidence level of BAC and SBR. The ^{18}F phantom was used in IELSG, GELTAMO and FIL-1 (first phase) clinical trials while the ^{68}Ge phantom was used in SAKK and FIL-2 (second phase). **Results:** 122/151(81%) PET/CT scanners fulfilled the CTQ with the first procedure. CTQ was reached at the first round in 38% of the cases, while in 32%, 12% and 18%, two, three or more than three iterations, were required, respectively. The ISV were 21.4%, 51.6% and 56.9% for BACUQP, BACIQ and SBR respectively. 34/34(100%) PET/CT scanners fulfilled the CTQ with the second procedure. The CTQ was reached at the first round in 82% of the cases, while in 15%, 0% and 3%, two, three or more than three iterations, were required, respectively The ISV were 22.7%, 21.4% for BACIQ and SBR. Iteration to reach CTQ was defined as an interaction between the Cuneo CoreLab and the local personnel regarding the data, phantom preparation, infrastructural problems. **Conclusion:** ^{68}Ge approach permits to achieve a lower inter-scanner variability respect to ^{18}F one. Indeed, ISV of both BAC and SBR are reduced of 2-3 times. This is mostly due to the difficulty in phantom preparation (in particular in sphere filling) for ^{18}F phantom. Moreover, the number of iterations required to achieve the clinical trial qualification is much lower. **References:** None.

OP-532

Low dose CT for attenuation correction in PET. Validation of quantification for different patient sizes

A. Törnblom[1,2], *J. Siikanen*[1], *D. Thor*[1], *M. Bolin*[1];
[1]*Karolinska University Hospital, Department of Medical Radiation and Nuclear Medicin, Stockholm, SWEDEN,* [2]*Stockholm University Fysikum, Department of Medical Radition Physics, Stockholm, SWEDEN.*

Aim/Introduction: Despite the relatively low dose generated by Attenuation Correction CT (ACCT) (0.5 mSv - 1 mSv) in PET examinations, the ALARA principle is still applicable. The currently used ACCT standard protocol in our clinic uses 7.6 effective mAs (eff-mAs) and 120 kVp, but reducing eff-mAs and/or kVp would decrease patient dose and facilitate an increased number of research subjects. A CT reconstruction algorithm called Quantification Achieved Consistently (Q.AC.) (Lonn, 2012) has recently been developed to enable reduced doses from ACCT, while preserving quantitative PET data. The purposes of

this study were to investigate possible limitations of the Q.AC. with respect to patient size, and to optimise protocols, aiming at minimising ACCT dose in terms of $CTDI_{vol}$. **Materials and Methods:** Measurements were performed with a GE PET/CT Discovery system, which offers Q.AC. reconstruction. The NEMA NU-2 protocol was followed to quantify PET quality, including evaluations of background variability (N), hot- and cold-sphere contrast (Q) and relative count error in the artificial lung in the phantom centre (DClung).Two phantoms were used; the NEMA body phantom (30 cm laterally/23 cm anterior posterior), here representing paediatric patients and small-sized adults, and the same phantom with an additional (20 cm laterally/4 cm anterior posterior) ellipsoid plastic (PMMA) extension ring, representing mid- and large-sized patients. ACCTs were acquired with 15 eff-mAs values, range [2.3 - 260], in combination with four kVp values [80, 100, 120, 140] and reconstructed with two algorithms (Q.AC. and a regular soft CT algorithm). PET reconstructions were performed based on each eff-mAs, kVp and CT-reconstruction combination. **Results:** Quantitatively similar results to the standard protocol were achieved with the Q.AC. using (2.3 eff-mAs and 80 kVp) for the NEMA body phantom, respectively (2.3 eff-mAs and 120 kVp) for the phantom with additional extension ring. Accordingly, the $CTDI_{vol}$ may be reduced to 1/10 of that for the standard protocol for paediatric patients and small-sized adults, respectively to 1/3 for mid- and large-sized patients. **Conclusion:** This study indicates that the Q.AC. CT reconstruction algorithm enables accurate PET results at lower ACCT eff-mAs and kVp settings than the currently used clinical standard protocol. For paediatric patients and small-sized adults, a reduction of $CTDI_{vol}$ by approximately 90% may be achieved, while for mid- and large-sized patients, the $CTDI_{vol}$ can be reduced by approximately 70% without loss of quantitative PET data. **References:** None.

OP-533

Dose optimization for pediatric FDG whole body PET/CT

M. van Gent, *V. C. Hamming, J. E. Schaar, A. W. J. M. Glaudemans, A. T. M. Willemsen;*
University of Groningen, University Medical Center Groningen, Groningen, NETHERLANDS.

Aim/Introduction: It was shown by De Groot et al.[1] that a quadratic relationship between body mass (BM) and administered FDG dose (A) is required to ensure a constant image quality of FDG-PET/CT in adult patients (≥18 years). However, the EANM guidelines for pediatric FDG-PET/CT prescribe a nearly linear relationship between BM and dose[2]. The aim of this pilot study was to investigate whether a linear BM and dose relationship results in constant image quality in pediatric FDG-PET/CT scans. **Materials and Methods:** Twenty whole body FDG-PET/CT scans of patients (median age 9.5 years, range 0 to 18 years) were included. Scans were acquired on either a Siemens Biograph mCT40 (n=7) or mCT64 (n=13) between November 2017 and February 2019 using the standard local protocol i.e. 3 MBq/kg FDG, 2 min/bed position and reconstructed with iterative OSEM3D reconstruction with point-spread-function and time-of-flight (OSEM3D+PSF+ToF). Some patients underwent a longer scantime/bed to compensate for radioactive decay during schedule delays. The mean and standard deviation (SD) for a volume of interest in a homogeneous part of the liver were determined and the signal-to-noise ratio (SNR = Mean/SD) was used as a measure for image quality. Corrections were performed for scantime: $SNR_L = SNR/\sqrt{(time)}$ as well as scan time and activity: $SNR_{norm} = SNR/\sqrt{(A*time)}$. A linear regression between SNR (and SNR_L) and BM was performed to test whether image quality varied with BM. $p<0.05$ was considered significant. SNR_{norm} was fitted with a power function: $SNR_{fit} = a*BM^{-b}$. Note that image quality would become independent of BM, if A*time scales as BM^{2b}. **Results:** Where BM of children and adults overlapped, SNR, SNR_L and SNR_{norm} values were consistent with literature. SNR slightly, but significantly, decreases with body mass: SNR=8.8-0.034*BM (p=0.022). However, SNR_L does not: SNR_L=5.5-0.010*BM (p=0.22). The optimal fit was found to be $SNR_{fit} = 3.2*BM^{-0.52}$. **Conclusion:** Contrary to adult FDG-PET/CT[1], the results of this pilot study indicate that in pediatrics image quality is constant for a linear relationship between BM and administered FDG dose. Accordingly, the EANM guidelines for pediatric FDG-PET/CT seem accurate. It should be noted that this is a preliminary study that includes only twenty patients and it should be further investigated with a larger group to confirm these initial findings. **References:** [1]. de Groot et al. Optimized dose regimen for whole-body FDG-PET imaging. EJNMMI Res. 2013;3:63. [2]. Amthauer et al. Guidelines for 18F-FDG PET and PET-CT imaging in paediatric oncology. Eur J Nucl Med Mol Imaging. 2008;35:1581-8.

OP-534

Optimization of Yttrium-90 PET/CT Acquisition Time on a SiPM-PET/CT during Selective Internal Radiation Therapy

J. Labour[1,2], *A. Martin*[1], *P. Boissard*[1], *T. Baudier*[1], *P. Veyrat Durebex*[1], *D. Delliage*[1], *D. Sarrut*[1,2], *J. N. Badel*[1];
[1]*Centre Léon Bérard, Lyon, FRANCE,* [2]*CREATIS, Lyon, FRANCE.*

Aim/Introduction: We investigated the impact of acquisition time on the quantification of Yttrium-90 PET images acquired with a SiPM-based PET/CT for post-selective internal radiation therapy (SIRT). The aim is to reduce acquisition time without compromising the image quality and quantification accuracy[1]. The work presents preliminary results towards achieving a standard protocol for post-SIRT PET imaging[2]. **Materials and Methods:** List-mode data for 6 patients who underwent PET/CT imaging after SIRT was gathered. Data for each patient were analyzed regarding ^{90}Y uptake in several regions of interest (ROI) defined as: the total liver drawn on the CT image, three perfused regions obtained from PET thresholding at 10, 20 and 40 % of the maximum value, non-perfused regions defined as the total liver minus each respective threshold-based perfused ROI. Thanks to the list-mode data, reconstructions were performed at different time intervals ranging from 1 to 15 minutes for 1 bed position. Images were reconstructed with pixels of 2mm using OSEM

iterative algorithm with 15 updates (3 subsets, 5 iterations), time of flight and point spread function modeling. A post-reconstruction Gaussian filter of 2mm full width at half maximum (FWHM) was used in all reconstructions. The aim of ^{90}Y-PET is to quantitatively estimate the absorbed dose delivered to the perfused region. Therefore, voxel-level quantitative information for each ROI was assessed, including the total number of counts and the mean of the activity concentration (Bq/mL) for each ROI. The noise present in the images were evaluated as the standard deviation on the mean activity concentration for each patient. The relative percentage differences of each reconstructed image according to the reference 15 minutes acquisition were computed. **Results:** For each patient, 9 min acquisition was found to be necessary to obtain less than 10% difference in the mean activity concentration with 15 min acquisition.This percentage falls below 5% when 11 minutes acquisition was used. Below 9 min, large differences appears (up to 20% for 7 min acquisition). Down to 11 min, the relative percentage difference on standard deviation stays below 5%. **Conclusion:** Image acquisition duration can be reduced by up to 40% if a 10% difference with the reference image is tolerated, improving patient comfort during scan. **References:** [1]Zhang et al. "Feasibility of accelerating Yttrium-90 PET by Optimizing PET Volume Overlap", J Nucl Med, 57:1425-2016 [2] Wright et al. "Theranostic Imaging of Yttrium-90", BioMed Res Int, 2015:481279-2015.

1201/1204

Plenary 3: Next Generation PET Technology in the Clinical Setting

Tuesday, October 15, 2019, 10:00 - 11:15 Auditorium

OP-535

Cardiovascular Molecular Imaging Beyond Perfusion - Ready for Prime Time?

F. Hyafil;
Department of Nuclear Medicine, Bichat University Hospital, Paris, FRANCE.

OP-536

Cardiac PET/MRI

C. Rischpler
University Hospital Essen, Essen, GERMANY.

OP-537

DAT Markers - Should PET replace SPECT?

A. Varrone;
Karolinska Institutet, Department of Clinical Neuroscience, Stockholm, SWEDEN.

1301

CME 10 - Neuroimaging Committee / EAN: EANM-EAN Recommendations for the Use of Brain 18 F-FDG-PET in Neurodegenerative Cognitive Impairment and Dementia

Tuesday, October 15, 2019, 11:30 - 13:00 Auditorium

OP-538

Assessing FDG-PET Diagnostic Accuracy Studies to Develop Recommendations for Clinical Use in Dementia

F. Nobili;
University of Genoa and Polyclinic San Martino Hospital, Department of Neuroscience (DINOGMI), Genoa, ITALY.

OP-539

Clinical Utility of FDG-PET for the Differential Diagnosis Among the Main Forms of Dementia

J. Arbizu;
University of Navarra, Clinica Universidad de Navarra, Department of Nuclear Medicine, Pamplona, SPAIN.

OP-540

Clinical Utility of FDG-PET in Parkinson's Disease and Atypical Parkinsonism Associated with Dementia

S. Morbelli;
San Martino Hospital, Nuclear Medicine, Genoa, ITALY.

1302

Joint Symposium 19 - Oncology & Theranostics Committee / EHA: PET/CT Guided Treatment in Non-Hodgkin Lymphoma

Tuesday, October 15, 2019, 11:30 - 13:00 Lecture Hall 311

OP-541

Response Assessment - The Haematologist's Perspective

J. Zijlstra;
Amsterdam UMC, Afdeling Hematologie, Amsterdam, NETHERLANDS.

OP-542

Staging - The Radiotherapist's Perspective

G. Mikhaeel;
Guy's Cancer Centre, Department of Clinical Oncology, London, UNITED KINGDOM.

OP-543

Impact of Metabolic Tumour Volume

A. Segolène Cottereau;
Cochin Hospital, Department of Nuclear Medicine, Paris, FRANCE.

1303

Joint Symposium 20 - Thyroid Committee / ETA-CG / EFSUMB: Thyroid Cancer Imaging and Biomarkers

Tuesday, October 15, 2019, 11:30 - 13:00 Lecture Hall 312

OP-544

Molecular Biomarkers

C. Colombo;
Università di Milano, Milan, ITALY.

OP-545

Ultrasound and Cross-Sectional Radiology

M. Radzina;
Pauls Stradins Clinical University Hospital, Institute of Diagnostic Radiology, Department, Riga, LATVIA.

OP-546

Molecular Imaging and Circulating Biomarkers

L. Giovanella;
Imaging Institute of Southern Switzerland, Clinic for Nuclear Medicine, Bellinzona, SWITZERLAND.

1304

Technologists: Oral Presentations 3

Tuesday, October 15, 2019, 11:30 - 13:00 Lecture Hall 117

OP-547

Long-term trends in occupational radiation exposure and associated health risks among technologists performing nuclear medicine procedures: new findings and future research directions

C. Kitahara[1], *M. Bernier*[2], *M. Van Dyke*[3], *C. Yoder*[4], *M. Doody*[1], *S. Simon*[1], *M. Linet*[1], *B. Alexander*[5], *D. Villoing*[1];
[1]*National Cancer Institute, Rockville, MD, UNITED STATES OF AMERICA,* [2]*Institute for Radiological Protection and Nuclear Safety, Laboratory of Epidemiology, Fontenay-aux-Roses Cedex, FRANCE,* [3]*Emory University, Atlanta, GA, UNITED STATES OF AMERICA,* [4]*Independent consultant, Weddington, NC, UNITED STATES OF AMERICA,* [5]*University of Minnesota, Minneapolis, MN, UNITED STATES OF AMERICA.*

Aim/Introduction: The field of nuclear medicine has changed and expanded rapidly since its inception in the mid-20th century. A surge of new radiopharmaceuticals and increased demand for nuclear medicine procedures, particularly in the United States, has led to a growing interest in occupational radiation exposure doses and associated health risks to nuclear medicine technologists. However, data on this topic have been extremely limited. **Materials and Methods:** We evaluated trends in work history practices and badge doses and assessed radiation-related risks in a large cohort of more than 110,000 radiologic technologists, the U.S. Radiologic Technologists (USRT) study. **Results:** In the USRT cohort, technologists who reported ever working with nuclear medicine procedures (n=22,039 in 1994-1998) had modest but significant elevated risks of all-cause and all-cancer mortality, myocardial infarction incidence, incidence of squamous cell carcinoma of the skin, mortality from cancers of the breast and lung, and cataracts during the follow-up period. Among 4,406 technologists who completed a detailed nuclear medicine work history survey in 2013-14, the reported weekly frequency of performing diagnostic nuclear medicine procedures, particularly cardiac and positron emission tomography (PET), increased over calendar time, while the frequency of performing therapeutic procedures remained stable. Trends in annual badge doses through 2015 mirrored these practice patterns, with consistently higher doses to technologists performing cardiac and PET scans versus those performing general nuclear medicine and, to a much greater extent, general radiologic procedures, particularly within the last two decades. Estimation of organ-specific occupational radiation doses for individual technologists (in progress) will allow for comprehensive retrospective and prospective investigations of radiogenic cancer and other disease risks. We also recently conducted a pilot study evaluating work history practices and dosimeter readings for an independent sample of U.S. technologists first certified in nuclear medicine in 1980 or later. Doses were slightly higher than the USRT sample but still well below established occupational limits (median: 1.4 to 3.3 mSv/year since 1992); like the USRT, doses were increasingly variable over time and higher doses were associated with PET versus general nuclear medicine. **Conclusion:** Our results suggest that nuclear medicine technologists may be among the most highly-exposed medical radiation worker populations in the United States currently, and that these higher doses may be related to increased radiation-related risks. These findings may inform radiation protection and dose monitoring efforts in nuclear medicine departments. **References:** None.

OP-548

177Lu peptide receptor radionuclide therapy, availability, radioprotection, cost: comparison of two administration methods

F. Herbaut[1], *S. Boukhlef*[1], *N. Lheureux*[2], *J. Legrand*[1], *B. Dekyndt*[1];
[1]*CHRU Lille, Lille, FRANCE,* [2]*CHU Amiens, Amiens, FRANCE.*

Aim/Introduction: Lutathera® (^{177}Lu peptide receptor radionuclide therapy) indication is the treatment of somatostatin receptor-positive gastroenteropancreatic neuroendocrine tumors (GEP-NETs) inoperable or metastatic. The summary of the product characteristics references an administration method consisting in gravity method from its original vial, which requires no preparation step. Since 2017, for almost 100 infusions, this one hasn't been adopted in the Lille University Hospital for the respect of infusion's good practices. So, a syringe infusion pump (SIP) has been set-up, which leads to a preparation constraint (transfer to a 50 mL syringe). A "reference-like method" is used in the Amiens Hospital Center, which requires a thorough rinsing corresponding to 10 times the vial volume. The aim of this study is to compare the two administration methods with: the percentage of administrated activity, the staff hand dosimetry and devices costs. **Materials and Methods:** Respectively 20 and 11 Lutathéra®'s preparations have been studied for Lille and Amiens. The initial vial, syringe and residual devices activities have been measured with a dose calibrator and expressed in percentage of total vial activity. Staff hand dosimetry is estimated on 3 preparation procedures for both administration methods. In the Lille Center, the dosimetry has been calculated thanks to dose rate measured. In Amiens center, the dosimetry has been measured on three fingers with single point radiation monitoring nanoDot dosimeters. The devices cost were calculated for preparation/administration steps. **Results:** The 50 ml syringe of SIP contains 94.6% (+/-3%) of total vial activity, with residual activity estimated at 3.2%. The "reference-like method" leads to an infusion of 98.9% (+/-0.2%) of total activity. With SIP, a theoretical staff hand dose of 29.41µSv has been calculated. For "reference-like method", dosimetry measured from 18.83 to 43.57µSv, according to concerned finger. The devices cost was 2.77€ for "reference method". For SIP, devices costs of preparation and administration steps have been separated, and represent respectively 2.93€ and 1.53€. **Conclusion:** The SIP does not increase staff exposure. However, a loss of medication results of the syringe conditioning, but all doses are included in the 5% acceptable range. The rinsing volume is essential to obtain the percentage of total activity infused for "reference-like method". The total devices cost is nearly equivalent for both infusion methods and low in contrast on the drug cost. The syringe preparation could be optimized to reduce staff hand exposure : the use of anti-reflux valve will reduce the three-way stop cock manipulation. **References:** None.

OP-549

The Impact of Metastable Lutetium-177 on a Nuclear Medicine Department

A. Brown;
Oregon Health and Science University, Portland, OR, UNITED STATES OF AMERICA.

Aim/Introduction: In the United States, Lutetium-177 is being used to treat patient's with gastro-entero-pancreatic neuroendocrine tumors with the FDA approved radiopharmaceutical Lutathera, which is manufactured by Advanced Accelerator Applications. In addition, Radiomedix, is manufacturing Lutetium-177-PSMA to treat patients with metastatic prostate cancer as part of a phase III clinical trial which is run by Endocyte. Each company uses a different process to manufacture the Lutetium, one of which adds a small amount of metastable Lutetium-177 which has a 160.4 day half-life. Without the metastable component, Lutetium-177 has a 6.65 day half-life. The difference in manufacturing methods may lead to differences in handling and disposing of the radioactive material. The purpose here is to share a single institution's experience, OHSU, with Lutetium-177 from different manufacturers. **Materials and Methods:** After administration of the radionuclide therapy, any radioactive waste is stored in a secure area to decay in storage. With a half-life of 6.65 days, our process is to check for any residual activity at approximately 65 days or 10 half-lives. After this decay period, we compared residual activity in multiple vials between manufacturer's which had the same calibration date or were within one or two days of each other. For this comparison, we measured the vial in a dose calibrator and also withdrew 1cc from each vial and measured the counts per minute using a Perkin Elmer Wizard well counter. **Results:** When comparing waste from each manufacturer which had the same calibration date or were within one or two days of each other, we noticed that measured counts per minute from the well counter were 200% higher for vials from AAA. This phenomenon is consistent across all vials that were compared. We believe this is directly correlated to the metastable component that can be found in Lutetium-177 from AAA. The prolonged presence of radioactivity in the vials from AAA have required us to use a third-party company for disposal of this radioactive waste, which has led to increase in space needed for decay in storage and an additional operating cost to properly handle this material. **Conclusion:** In summary, Lutetium-177 has become a vital tool for radionuclide therapy, however, there are important considerations for decay and disposal of the radioactive waste which vary based on the method of production. Having this information available when starting new programs and service lines is critical to long term success and compliance with regulatory agencies. **References:** None.

OP-550

Analysing and improving working procedures in radiopharmacy laboratories in three European countries

G. De Mol[1], *H. François*[1], *T. Säilä*[2], *T. Starc*[3], *T. Taatila*[2], *S. Rep*[3], *H. Mol*[1];
[1]*Odisee vzw, Brussel, BELGIUM,* [2]*Department of Radiography and Radiotherapy, Tampere University of Applied Sciences, Tampere, FINLAND,* [3]*Faculty of Health Sciences, University of Ljubljana, Ljubljana, SLOVENIA.*

Aim/Introduction: The finger doses of technologists preparing radiopharmaceuticals can be quite high, exceeding the annual dose limits. Recommendations to reduce radiation exposure

for standard nuclear medicine procedures were developed. Despite these efforts, differences in preparing and administering radiopharmaceuticals exist. The aim of the project was to improve a daily routine in three European countries focusing on radiation protection and aseptics in radiopharmacy. **Materials and Methods:** All together 15 healthcare professionals from 10 hospitals in three countries participated in the project. In a first-round participants were asked to film their daily radiopharmaceutical preparation. These films were analysed using a checklist based on the human health campus of the IAEA, with a focus on sterility and radiation protection. A score was given on 56 items during the different stages. Participants wore finger dosimeters over a period of three to four weeks to see if a correlation could be found between the procedures used and the dose to the fingers. In February 2019 participants started an eight weeks on-line refresher-course which addressed different aspects of radiopharmacy work. The course contained tasks, readings, videos and discussions. In a second round the filming process and finger dosimetry were repeated. **Results:** The baseline results varied between countries. Based on analysed films 57% scores were positive. This means that in the three countries 43% of the manipulations in the hot lab did not comply with the IAEA guidelines. For some items only a few complied with IAEA guidelines. When only the manipulations related to radiation safety are considered 56% of all participants comply with the guidelines. Regarding the manipulations related to sterility 46% of all technologists complied to the guidelines. These results ask for attention since there is a strong urge for sterility when preparing material for injecting patients. The results from finger dosimeters are not yet available. Course feedback will be available in summer and second round finger dosimeter results in late summer. **Conclusion:** The results of the first-round show that there is a need to improve daily routines in the radiopharmacy laboratories in the participating countries. The results also show that the IAEA guidelines might need an update. An online refresher course on daily routine in the radiopharmacy laboratory was presented to the participants. We expect to have data on the impact of this course on daily routine and finger doses of the participants in late summer or early autumn 2019. **References:** None.

OP-551

An MRT Shares Her Experience: When Health Care Provider Becomes the Patient

L. Rimanic;
British Columbia Institute of Technology, Burnaby, BC, CANADA.

Aim/Introduction: As an experienced NM technologist and educator I was confident in my ability to provide excellent patient care. In 2014, I was diagnosed with breast cancer and I transitioned from health care provider to patient. Being on the opposite side of the health care equation has taught me valuable lessons that I will share with the audience. This presentation will demonstrate how best practice can be utilized to optimize the patient's experience. **Materials and Methods:** Audience members will be reminded of the importance of practicing excellence in their work and will realize that meticulous work habits can have a profound impact on patient outcomes. The presentation will examine the effect of waiting time and waiting room design on patient satisfaction and cooperation and give options for improving the waiting room experience. The phenomenon of "awfulizing" will be introduced and I will identify how time management and technologist efficiency can calm this behavior. **Results:** Research shows that changes to waiting room design can have a significant impact on patient satisfaction and cooperation. Technologist attention to work habits and more effective time management can reduce awfulizing. **Conclusion:** Becoming a patient provides a unique perspective on how to optimize patient care. It is hoped that sharing the knowledge gained through this experience will be of value to all medical professionals. **References:** None.

OP-552

Amyloid Positron Emission Tomography (PET) scanning: Process and pathway pitfalls and review

L. Alves*, B. Williams, D. Vilic, Z. Win;*
Imperial College Healthcare NHS Trust, London, UNITED KINGDOM.

Aim/Introduction: Alzheimer's disease(AD) is the most common cause of dementia in elderly and its global burden is expected to grow with the increase of life expectancy. Definitive diagnosis of AD is a complex process requiring a plethora of neuropsychological and imaging tests. One of the common features of definitive AD diagnosis is the presence of extracellular plaques composed of insoluble beta-amyloid (amyloid deposits). The identification of amyloid plaques, with PET and 18F-labeled radiopharmaceuticals (18F-florbetapir, 18F-florbetaben, and 18F-flutemetamol) is now considered a powerful tool for assisting in AD diagnosis[1]. **Materials and Methods:** At Imperial College Healthcare NHS Trust we have successfully scanned over 350 Amyloid PET patients since 2016. The aim of this project is to analyse the process in place, from the tracer production to the report and assess its benefits and pitfalls, from a technologist point of view: the booking process and information dissemination to the patient/carer; the waiting time for appointments; the patient experience during preparation and injection; and facilities compared to dementia friendly environments.Data regarding the number of scans performed versus cancelled and cancellation reasons was also retrieved and analysed **Results:** Being in hospital can be a disorientating and frightening experience for a person with dementia, even in early stages. Although the scan is not invasive (except for venepuncture) the full process can be quite difficult, starting with appointment booking. Straightforward information is given to the patient/carer previously to the appointment but we still experience a high rate of same-day cancellations. This happens mainly due to memory problems. Another observed distressing moment is short notice cancellations related to tracer availability and/or delivery. This issue also increases

waiting lists and the worry that comes with that prolonged wait. We have also perceived that patients, due to behavioral problems inherent to dementia (fear, panic, disorientation), also contribute to same day cancellations and artifacts and poor quality images due to movement during the acquisition. **Conclusion:** In conclusion we assess that although the department has been very successful in amyloid PET scanning, a more dementia-friendly environment (colour coding rooms and doors, large clocks on the walls, a more relaxing waiting area) and developed training in dementia awareness for staff would definitely improve patient experience and consequently lead to a more efficient department. **References:** 1. Filippi, L. et al. '18F-labeled radiopharmaceuticals for the molecular neuroimaging of amyloid plaques in Alzheimer's disease', Am J Nucl Med Mol Imaging, 2018, vol.8, no.4, pp. 268-281.

OP-553

Opening minds to Lean management in Nuclear Medicine

J. Lemos, D. Vieira, N. Arantes, P. Costa;
Nuclear Medicine Department, School of Health, Polytechnic Institute of Porto (ESS|P.Porto), Porto, PORTUGAL.

Aim/Introduction: Nuclear Medicine (NM) is in constant technological evolution, challenging often professionals to be up to most recent standards and practices. In this sense, teaching NM should not be limited on the transmission of technical and scientific knowledge but also on opening minds to, for example, different management philosophies. Therefore, Nuclear Medicine students should be capable to change behaviours/practices and be concerned to search continuous improvement. To reach this standard, NM Department at our institution decided to implement the application of Lean Philosophy (management culture/philosophy focused on reducing various types of waste) in NM, in a process involving students, teachers and alumni. **Materials and Methods:** We used several Lean tools: Gemba walk to detect problems; Brainstorming to "label" 12 wastes (1.Over production, 2.Stock, 3.Transport, 4.Waiting, 5.Motion, 6.Over processing, 7.Defects, 8.Human capital, 9.Design of products and services, 10.Inappropriate systems, 11. Energy, 12.Materials); A3 thinking, 5S (Sort, Set in order, Shine, Standardize, Sustain) and Visual management to solve/minimize the problems/wastes detected. Surveys were used to assess satisfaction degree amongst students, teachers and alumni related to changes implemented in NM laboratory and office, and with Lean Philosophy Workshops. **Results:** Students and teachers walked in NM laboratory (place of practical classes) and identified many problems or "wastes" (such as wasting time looking for materials or excess of material boxes). After applying 5S and visual management, students and teachers considered that Laboratory use was optimized resulting in more productive practical classes. Teacher's office was also a Lean intervention target. This approach developed a Communication Board that contributed to improve communication between teachers (reflected in shorter and more productive meetings). We organized two Lean Philosophy Workshops open to alumni and professionals. Workshop participants evaluated provided training actions positively and showed motivation to engage participation in future sessions. **Conclusion:** Students have expressed great interest about Lean Philosophy, reflected in 3 major points: the large number of students who participated (voluntarily) at Lean workshops; good results obtained in the satisfaction surveys; students considering doing their final course work in LEAN Philosophy by submitting projects in this subject to viability analysis. We sow the seeds of Lean management on their minds and we are already reaping the first fruits. **References:** None.

OP-554

Barriers And Limitations For Nuclear Medicine Technologists' Research In Spain

R. García Gorga[1,2], C. Romero Magdalena[3], N. Vega de Andrea[1], L. Rincon Gayán[1], I. Herrera Peco[3];
[1]Sociedad Española de Graduados y Técnicos en Radiología, Madrid, SPAIN, [2]Servei de Medicina Nuclear, Hospital Universitari Parc Taulí, Sabadell, SPAIN, [3]Health Sciences College, Alfonso X El Sabio University, Madrid, SPAIN.

Aim/Introduction: We conducted a qualitative cohort study aimed at detecting possible determinants of the low scientific production of Spanish radiographers. A survey was designed to characterize the profile of the professionals and the work environment. We also sought to establish a relationship between perceived barriers and different variables such as work experience, contractual situation and type of work center. **Materials and Methods:** After receiving the acceptance of the research ethics committee of the Alfonso X El Sabio University, an online survey (Google Forms) was distributed from January to February 2019. The global sample was composed of 595 Medical Imaging and NM Technologists recruited from Spanish Hospitals. For the statistical analysis we use the SPSS 20.0. **Results:** Results showed that 37% (n=220) of participants detect the existence of research barriers meanwhile 63% (n=375) couldn't identify any kind of research barrier in hospitals where they carry out their activity. Participants identify 17 different research barriers related to environment situation (extrinsic barriers) and personal situation (intrinsic barriers). It was found that 35% (208) of the participants were men, compared to 63.2% (376) who were women, 1.8% (11) preferred not to indicate their gender. Grouped by age intervals, 61.4% of the participants were older than 36 years ($p < .001$). Regarding the ability to find barriers, we observed significant differences when analyzing years of experience ($p < .000$), type of contract ($p < .000$) and work in a University Hospital ($p < .001$). No differences were found, both by sex and type of management of the work center or job position performed by the professionals ($p > .05$ in all cases). Based on years of experience, we observed that starting in the 21st year, a greater number of barriers are detected. The most significant are; Access to research resources ($p < .016$); Lack of funding ($p < .043$); Lack of dedicated time to clinical level ($p < .003$). On the other hand, a significative relation was found between work in a University Hospital

and negative perception by others of NMT ability (p <.001). Finally, when comparing the type of contract it was observed a significative relation to Negative perception by other, lack of support for leaders, workload and lack of recognition (p<.001 applicable in all cases). **Conclusion:** Our results have shown that work experience, years as NM technologist, and work in a University Hospital, were related to the capability to find and describe barriers and limitations to research projects. **References:** None.

OP-555

Nuclear Medicine Technologists: Professional Identity - Can leadership profiles makes a difference?

A. Martins[1,2,3], *I. Faro de Albuquerque*[4], *G. Cunha*[3];
[1]*Higher School of Health of the Portuguese Red Cross, Lisbon, PORTUGAL,* [2]*Joaquim Chaves Saúde, Lisbon, PORTUGAL,* [3]*Lisbon School of Health Technology, Lisbon, PORTUGAL,* [4]*NOVA-SBE, Lisbon, PORTUGAL.*

Aim/Introduction: The aim of the study is to identify, provide and explore some management outputs data on Nuclear Medicine Technologists (NMT) in Portugal like professional identity, work engagement, leadership profiles and analyze their impact on perceived organizational performance. There is no data about management outputs on NMT in Portugal. Leadership profiles characterization and assessment of their influence on motivation and effective outputs of professional performance have been demonstrated an important role in human resources management. **Materials and Methods:** 67 NMT answered an online survey that assesses their perceptions about their leadership styles, their professional identity, work engagement and perceived organizational performance. Data were statistical treated and one theoretical model that correlates the variables studied has been proposed and tested. The wished leadership profile also was assessed. **Results:** These professionals have revealed a professional identity that reflects a moderate to great integration between their personal identity and their identity in the profession. Higher values of work engagement were obtained than those found in other health professions such as nursing. The perceived performance was also high in most cases. The leadership profile with the highest scores was the "Mentor Leader" in the case of Nuclear Medicine. With the application of the proposed theoretical model, we can prove that work engagement moderate the relation between professional identity and perceived organizational engagement, and we have also been able to prove statistically assesses focused on flexibility (focused on people and teamwork and focused on innovation, change and professional performance) positively measure the relationship between work engagement and perceived organizational performance. On the other hand, convergent, control-focused leadership models (focused on the hierarchy or the achievement of results) negatively mediate the relationship between work engagement and perceived performance. **Conclusion:** This study allowed obtaining characteristics of the NMT professionals of the for which data were not yet available in Portugal. The proof that leadership mediates the relationship between how we are integrated into our workplaces and the way we perceive these same places in terms of their performance, brings new importance in betting on training and discuss leadership as the theme for obtaining of new human resources policies and professional solutions in the area of Nuclear Medicine. This information can be used to help develop strategies to meet those needs through work redesign and leadership behavior development. **References:** None.

1305

M2M - Parallel Session: Preclinical Developments in Infectious Diseases

Tuesday, October 15, 2019, 11:30 - 12:45 Lecture Hall 111

OP-556

^{111}In-PCTA-VRC07 a Radiolabeled Broadly Neutralizing Antibody For HIV Imaging in Mice

D. Viertl[1], *T. Denoël*[1], *F. Cicone*[1], *C. Müller*[2], *C. Fenwick*[1], *G. Pantaleo*[1], *J. O. Prior*[1];
[1]*Lausanne University Hospital and University of Lausanne, Lausanne, SWITZERLAND,* [2]*University Hospital of Zürich, Zürich, SWITZERLAND.*

Aim/Introduction: Broadly neutralizing antibodies (bNAbs) targeting several HIV-1 envelope (Env) epitopes are currently being investigated as a new curative approach against HIV-1 infection. Radiolabeled bNAbs are prospective novel tracers for translational investigation of HIV-1 infection in vivo imaging. In this study, the bNAb VRC07 was conjugated with the versatile macrocyclic ligand p-SCN-Bn-PCTA. The construct was radiolabeled with indium-111 and evaluated in vitro and in vivo in a tumour bearing mice HIV-1 model. **Materials and Methods:** VRC07 was conjugated with ten equivalents of p-SCN-Bn-PCTA at pH 9.5. The immunoaffinity of PCTA-VRC07 was tested by flow cytometry using HeLa243 cells that stably express the HIV-1 NL4.3 Env and Tat proteins. Chelation of PCTA-VRC07 was obtained with 113 MBq indium-111 for one hour at 37 °C and pH 4.5 in NH_4OAc. Immunoreactive fraction assay with ^{111}In-PCTA-VRC07 was done using serial dilution of HIV-1 Env glycoprotein gp120 heptamer coated on microplate. Biodistribution of ^{111}In-PCTA-VRC07 was studied in female BALB/c nude mice bearing xenografts of HeLa243 and control HeLa tumours. Three animals per time point were sacrificed at 24, 48 and 120 hours after injection of 0.5 Mbq ^{111}In-PCTA-VRC07. SPECT/CT scans were acquired at the same time points after injection of 15 Mbq ^{111}In-PCTA-VRC07 in three additional mice. Expression of gp120 was confirmed by immunoblotting ex vivo in the same tumours. **Results:** Flow cytometry histograms of immunolabeled HeLa243 with PCTA-VRC07 and VRC07 were overlapping showing retained affinity for HIV-1 Env proteins after PCTA conjugation. As shown in SEC-HPLC and iTLC, the

radioimmunoconjugate ^{111}In-PCTA-VRC07 was obtained in 99% radiolabeling yield and thus used without purification. An immunoreactive fraction of ^{111}In-PCTA-VRC07 for gp120 greater than 70% was calculated. At 48 hours, ^{111}In-PCTA-VRC07 uptake was significantly higher in the HeLa243 tumours than in HeLa tumours (control), respectively 16.8 ± 1.0 versus 11.7 ± 2.0 % IA/g (t test, P = 0.017, n = 3). At 120 hours, 9.8 ± 2.0 % IA/g of ^{111}In-PCTA-VRC07 was found in the HeLa243 tumour, 10.0 ± 0.9 % IA/g in the liver, 5.1 ± 2.0 % IA/g in the control tumour, 4.3 ± 0.3 % IA/g in the spleen and 3.5 ± 0.4 % IA/g in the blood. SPECT images confirmed the preferential uptake of ^{111}In-PCTA-VRC07 in HeLa243 tumours compared to HeLa control tumours. **Conclusion:** Using the innovative radioimmunoconjugate ^{111}In-PCTA-VRC07 directed against gp120, in vivo SPECT imaging of HIV-1 Env proteins was possible in a HeLa243 tumour bearing mice model. **References:** None.

OP-557

Imaging infections: evaluation of antimicrobial peptide 99mTc-DPAH-UBI29-41 as a specific agent

*M. Zorkaltsev[1], A. Pershina[1], **V. Udodov**[1], V. Ivanov[1], M. Larkina[1], E. Stasyuk[2], A. Rogov[2], A. Lushchyk[3], N. Shevtsova[1], V. Zavadovskaia[1];*
[1]Siberian State Medical University, Tomsk, RUSSIAN FEDERATION, [2]National Research Tomsk Polytechnic University, Tomsk, RUSSIAN FEDERATION, [3]Institute of Bioorganic Chemistry, Minsk, BELARUS.

Aim/Introduction: Development of radiopharmaceutical for detection septic inflammation using the original approach to radiolabelling of antimicrobial peptide UBI29-41. **Materials and Methods:** UBI29-41 was produced by solid phase peptide synthesis using Fmoc-protected amino acids. Succinimid-1-yl 6-(bis(pyridin-2-ylmethyl)amino)hexanoate (DPAH-NHS ester) was used as the chelating agent for 99mTc. DPAH-NHS ester in ethanol was added to UBI29-41 in PBS and incubated for 2 hours at room temperature and then for 24 hours at 4°C. DPAH-UBI29-41 was purified using a PD Minitrap™ G-10 column (GE Healthcare, UK). The radiolabeling was accomplished in two steps using CRS KIT to form the [99mTc(CO)3(H2O)3]+ intermediate, which was neutralized before UBI29-41 addition. The vial was heated at 70°C for 60 min, and then, the radiolabeled peptide UBI29-41 was purified using columns C18 Sep-Pak. The radiochemical yield and radiochemical purity were determined by iTLC in PBS. The in vitro stability test was performed by incubating the radiolabeled peptide with 5000-fold molar excess of histidine in PBS for 3 h. Control samples were incubated in PBS. The osteomyelitis (n=6) and sterile bone inflammation models (n=6) were developed in rats. 99mTc-DPAH-UBI29-41 was intravenously injected into the tail vein at a dose of 18.5 mBq. Then sequential recording of 5 minute images was performed for 1 hour using SPECT Philips BrightView. Scans were interpreted on the basis of bacterial culture, laboratory tests and three-phase bone scanning. **Results:** The radiochemical yield of 99mTc-DPAH-UBI29-41 was 80% and radiochemical purity was 96%. Each milliliter 99mTc-DPAH-UBI29-41 of in physiologic saline at the end of synthesis contained approximately 50 MBq of 99mTc activity and 3.8 nmol DPAH-UBI29-41.The stability assay, including analysis in the presence of histidine excess, showed no adverse effects on radiochemical purity. Scan after 99mTc-DPAH-UBI29-41 administration showed accumulation of radionuclide in femur of rats with microbial bone inflammation, whereas no signals change are observed in rats with sterile LPS-induced inflammation. Quantitative analysis revealed a maximum mean target-to-nontarget ratio of 2.72 [1.96-2.87] at 35 min, which decreased to 2.35 [1.71-2.42] at 60 min. No adverse reactions were observed during image acquisition and within 3 day after the study. **Conclusion:** Antimicrobial peptides derived from ubiquicidine (UBI29-41) were successfully labeled by 99mTc using chelator DPAH-NHS ester. 99mTc-DPAH-UBI29-41 with high radiochemical purity (96%) and stability was produced. The scintigraphy with 99mTc radiolabeled UBI29-41 peptides provided highly accurate detection and differentiation of infection and sterile inflammation in rat model of osteomyelitis. **References:** None.

OP-558

In vivo imaging of infection with 99mTc-Labelled Human Beta-Defensin-3 in a Rat Model

G. A. Follacchio[1,2], A. Pala[1], S. Scaccianoce[3], F. Monteleone[1], M. Liberatore[1];
[1]Sapienza University of Rome, AOU Policlinico Umberto I, Nuclear Medicine Unit, Rome, ITALY, [2]Department of Molecular Medicine, Sapienza University, Rome, ITALY, [3]Sapienza University of Rome, Department of Human Physiology and Pharmacology, Rome, ITALY.

Aim/Introduction: In clinical practice, differentiation of infection from aseptic inflammation represents a major issue. Nevertheless, none of the commercially available compounds (labelled granulocytes, anti-granulocyte antibodies, 67Ga-citrate, labelled immunoglobulin-G, 18F-FDG) is capable of this differentiation, producing a not negligible false-positive rate. The current gold standard imaging procedure, scintigraphy with labelled leukocytes, is furthermore characterized by a time-consuming sequence of cell separation and radiolabelling requiring highly-trained personnel due to the hazard of blood-borne infections. Recently, our group evaluated the antimicrobial peptide Human β-Defensin-3 (HBD-3) as a potential radiotracer for specific infection imaging, reporting a reliable labelling procedure with 99m-technetium and testing its toxicity in a rat model [1,2]. Aim of the present study was to evaluate 99mTc-HBD-3 in vivo imaging potential in differentiating infection from sterile inflammation in a rat model. **Materials and Methods:** Recombinant HBD-3 was radiolabeled with 99mTc. Radiolabelling yield and specific activity of the compound were calculated. An experimental model involving S.aureus-induced infection and carrageenan-induced aseptic inflammation was realised in five Wistar rats. Serial planar scintigraphic acquisitions were performed from 15' to 180' after 99mTc-HBD-3 intravenous administration. Radiotracer uptake in infected versus non-infected sites was evaluated qualitatively and semiquantitatively.

ROIs were drawn on the infection site, inflammation site and background. Radiotracer uptake in each ROI was expressed in terms of average counts and Target-to-NonTarget (T/NT) ratios were calculated. **Results:** Radiolabelling yield of 99mTc-HBD-3 was 70% with a specific activity of 6-8 MBq/µg. Despite an intense activity in the abdominal region, a significant and progressive 99mTc-HBD-3 uptake was observed in S.aureus-induced infection site compared to sterile inflammation and background. Maximum average T/NT ratio (5.7-fold higher in infection site vs inflammation site) was observed at 140'. **Conclusion:** In vivo imaging with 99mTc-HBD-3 in a rat model of S.aureus-induced infection showed a favourable uptake in the infection site compared to sterile inflammation and background. These promising findings, together with previous in vitro and ex vivo results on 99mTc-HBD-3 targeting capacity and toxicity, further confirm 99mTc-HBD-3 as a novel potential candidate for specific infection imaging. **References:** 1. Liberatore M, Pala A, Scaccianoce S, et al. Microbial Targeting of 99mTc-Labeled Recombinant Human Beta-Defensin-3 in an Animal Model of Infection: a Feasibility Pilot Study. J Nucl Med 2009; 50:823-826 2. Liberatore M, Anagnostou C, Scaccianoce S, et al. Toxicity assessment of 99m-Technetium-labeled human beta-defensin-3 in CD1 mice. Hell J Nucl Med 2015; 18:233-237.

OP-559

Multiplexing during host-guest mediated pre-targeting of bacteria

M. Welling[1], *N. Duszenko*[1,2], *D. M. van Willigen*[1], *W. K. Smits*[3], *M. Roestenberg*[2], *T. Buckle*[1], *F. W. B. van Leeuwen*[1,4];
[1]*Interventional Molecular Imaging Laboratory, Department of Radiology, Leiden University Medical Center, Leiden, NETHERLANDS,* [2]*Department of Parasitology and Department of Infectious Diseases, Leiden University Medical Center, Leiden, NETHERLANDS,* [3]*Department of Medical Microbiology, Section Experimental Bacteriology, Leiden University Medical Center, Leiden, NETHERLANDS,* [4]*Laboratory of BioNanoTechnology, Department of Agrotechnology and Food Sciences, Wageningen University & Research, Wageningen, NETHERLANDS.*

Aim/Introduction: Cyclodextrin (CD)-based host-guest interactions with adamant have demonstrated value during the functionalization of stem-cells and to generate a pre-targeting-based alternative for hepatic radioembolization [1-3]. An obvious next step in the technological validation of this approach is the pre-targeting of transplanted cells in vivo. We validated this concept using a bacterial colonization study with Staphylococcus aureus. **Materials and Methods:** Bacteria (Staphylococcus aureus) were labeled with a radiolabeled, adamantane-containing antimicrobial peptide (^{99m}Tc-(Ad-Gly)$_2$-Lys-UBI$_{29-41}$; guest). An ^{111}In-labeled Cy5$_{0.5}$CD$_9$PIBMA$_{39}$ polymer served as host vector, yielding the bimodal agent ^{111}In-Cy5$_{0.5}$CD$_9$PIBMA$_{39}$. Mice were either (1) intra-hepatically or (2) intra-muscularly infected with 1x10^8 viable ^{99m}Tc-(Ad-Gly)$_2$-Lys-UBI$_{29-41}$-labeled S. aureus (n=6 mice per model). Twenty four hours after host administration, ^{111}In-Cy5$_{0.5}$CD$_9$PIBMA$_{39}$ was administered intravenously. Dual-isotope SPECT imaging, %ID/g and fluorescence studies were performed at 4 h (model 1) or 24 h (model 2) allowing multi modal imaging of the individual vectors and assessment of the host-guest complexation in vivo. Imaging of guest vector ^{111}In-Cy5$_{0.5}$CD$_9$PIBMA$_{39}$ in mice without an infection served as control. **Results:** Dual-isotope SPECT imaging of host-guest interactions revealed pre-targeting was efficient in both colonization models as binding of the guest vector to the host was seen in both the liver and the muscle. Quantitative assessment revealed that after intra-hepatic administration the hepatic accumulation of the host vector was nearly 4 times higher at 4 h post-injection (27.1 ± 11.1 %ID/g, $p < 0.001$) compared to hepatic uptake of the host vector in mice that did not received an injection with the bacterial host (7.6 ± 2.3 %ID/g). In the intra-muscular model, the accumulation of the host vector in the infected muscle at 24 h post-injection was two-fold higher (4.4 ± 0.7 %ID/g, $p < 0.001$) than in control muscle (2.1 ± 0.3 %ID/g). Fluorescence imaging confirmed co-localization in the liver or infected muscle. **Conclusion:** Supramolecular host-guest complexation can efficiently be used as pretargeting strategy during bacterial infection models. The obtained results demonstrate the feasibility of using such an approach during bacterial colonization studies, thereby highlighting the technologies potential to advance the field of nanomedicine. **References:** M. Rood et al., Sci Rep 2017; 7:39908. S. Spa et al., Theranostics 2018; 8(9):2377-2386. M. Welling et al., J Contr Rel 2019;293:126-134.

OP-560

An animal model of foreign body infection for the development of quantitative infection imaging

B. Mahida[1], *R. Aid*[2], *J. Aerts*[1], *F. Andreata*[3], *L. Louedec*[2], *F. Chau*[4], *F. Rouzet*[5];
[1]*Department of Nuclear Medicine, Bichat University Hospital, Assistance Publique– Hôpitaux de Paris, Paris, FRANCE,* [2]*INSERM Unité 1148 Bichat University Hospital, Paris, FRANCE,* [3]*INSERM, Bichat University Hospital, Paris, FRANCE,* [4]*University Paris Diderot-Paris 7, Paris, FRANCE,* [5]*Department of Nuclear Medicine, Bichat University Hospital, Assistance Publique– Hôpitaux de Paris, University Paris Diderot-Paris 7, Inserm Unité Mixte de Recherche 1148, Paris, FRANCE.*

Aim/Introduction: The diagnosis of foreign body infection such as prosthetic material or implanted cardiac device is challenging. Many animal models of infection were reported but usually lack standardization and reproducibility (size and concentration of the septic inoculum) preventing a quantitative approach to infection imaging. ^{99m}Tc-labelled polymorphonuclear cells (PMNs) SPECT is acknowledged as the current benchmark of infection imaging. Our study aimed to design a standardized experimental rat model of chronic infection and to validate this approach using ^{99m}Tc-labelled PMNs SPECT/MRI. **Materials and Methods:** Experiments were performed in Lewis (syngenic) rats. Foreign body consisted in a disc-shaped (6 mm diameter x 3 mm width) polysaccharide bioscaffold (AlgiMatrix™ 3D Culture System). Septic inoculum consisted of Staphylococcus aureus (strain HM1054), a major opportunistic pathogen. Bioscaffolds

were incubated with 20 µL of either HM1054 solution (10E4 CFU/ml corresponding to 200 CFU/ scaffold) or 0.9% NaCl solution for controls. Two septic bioscaffolds (M1,M2) were implanted on the right flank of 4 rats (n=8), control bioscaffolds (C) were implanted on the opposite flank for aseptic inflammation (n=4). Separated (PMNs) were obtained from bone morrow of syngenic animals and labelled with ^{99m}Tc-HMPAO. Labelling efficiency was measured over 24 hours, after labeling. ^{99m}Tc-labelled PMNs were injected 9 days after bioscaffolds implantation, SPECT/MRI was acquired 24 hours later. Quantitative analysis compared the uptake of infected vs. control bioscaffolds. Reproducibility was assessed by comparing ratios of uptake intensity between each infected bioscaffold in the same rat (M1/C vs. M2/C). Then quantitative autoradiography and histologic staining (Massons's trichrome) of bioscaffolds were performed. **Results:** Labelling efficiency was stable over time (89% at 24 hours). ^{99m}Tc-labelled PMNs uptake was visually detectable on SPECT around all infected bioscaffolds and none on control bioscaffolds. There was a significant difference between infected and control bioscaffolds Σ(M1,M2)= 2.3±0.9 vs. ΣC=0.27±0.9 (p=0.004). There was no significant difference between ratios of infected bioscaffolds M1/C =9.6[7.9-12.5] vs. M2/C =9.9[6.7-11.9] (p=0.9 Mann Whitney test).Autoradiography confirmed diffuse uptake in all infected bioscaffolds. Comparative analysis of autoradiography and histopathologic staining showed the co-localization of tracer uptake and granulocytes infiltration. Bacteriological analysis of explanted bioscaffolds showed living bacteria on infected bioscaffolds and none on controls. **Conclusion:** This study validates the experimental infection model with standardized and reproducible parameters, detectable with ^{99m}Tc-labelled PMNs. These results pave the way to further comparison between the conventional ^{99m}Tc-labelled PMNs SPECT and quantitative approach based on novel PET agents. **References:** None.

OP-561

FDG uptake pattern can predict the success of bacterial cancer therapy

A. Chong[1], *J. Min*[2], *H. Nguyen*[2], *J. Ha*[1], *K. Kim*[2];
[1]*Chosun University Hospital, Gwangju, KOREA, REPUBLIC OF,* [2]*Chonnam National University Hospital, Gwangju, KOREA, REPUBLIC OF.*

Aim/Introduction: The number of studies about cancer therapy with engineered bacteria (BCT) such as Salmonella or Escherichia is increasing including phase I clinical studies [1, 2]. Not only by deliver therapeutic agents, but also those bacteria themselves have some cancer-suppression effect[2]. One of the mechanisms of BCT is via immune stimulation [2, 3]. In our lab, we have studied BCT for several years and we found that in some objects, their response to BCT was less than others. F-18 FDG is widely used for cancer and inflammation evaluation. The aim of this study is to find out whether F-18 FDG uptake pattern can predict the result of BCT and to find out FDG uptake pattern after BCT. **Materials and Methods:** BCT was done by intravenous injection of engineered attenuated Salmonella typhimurium (SLΔppGpp/lux) to total 15 male BALB/c mice with tumor (CT26 cells) in their right thigh. Scanning with animal PET/CT with F-18 FDG was done at various time points after injection. Tumor volume was observed till 16-17 DPI. FDG uptake (SUVmax, SUVmean), tumor volume, and growth rate were analyzed. **Results:** FDG tumor uptake was decreased on 1-2 DPI (day post injection). It increased again from 4 DPI. Amount of SUVmean decrease on 1-2 DPI is strongly correlated with tumor volume suppression (rank correlation rho 0.867, p=0.0025). With cutoff value >0.43 (change of SUVmean at 1-2 DPI) we can expect tumor volume increase would be no larger than 500 mm^3 at 16-17 DPI (sensitivity 100% & specificity 83.3%). **Conclusion:** After BCT, FDG tumor uptake decreased on 1-2 DPI and increased again from 4 DPI. We can predict the result of BCT with F-18 FDG PET by change of SUVmean. **References:** 1.Kim, K., et al., A novel balanced-lethal host-vector system based on glmS. PLoS One, 2013. 8(3): p. e60511.2.Zheng, J.H. and J.J. Min, Targeted Cancer Therapy Using Engineered Salmonella typhimurium. Chonnam Med J, 2016. 52(3): p. 173-84.3.Nguyen, V.H. and J.J. Min, Salmonella-Mediated Cancer Therapy: Roles and Potential. Nucl Med Mol Imaging, 2017. 51(2): p. 118-126.

1306

Do.MoRe - Parallel Session: SPECT/CT Quantification & Data Analysis

Tuesday, October 15, 2019, 11:30 - 12:45 Lecture Hall 112

OP-562

Convolutional neural network-based denoising allows 67% reduction of scan time or tracer dose in dopamine transporter SPECT

M. Nazari[1,2], *S. Kimiaei*[1], *M. Ehrenburg*[3], *A. Kluge*[1], *R. Bucher*[4];
[1]*ABX - CRO advanced pharmaceutical services, Dresden, GERMANY,* [2]*TU-Dresden, Dresden, GERMANY,* [3]*Pinax Pharma, Bad Liebenwerda, GERMANY,* [4]*University Medical Center Hamburg-Eppendorf, Hamburg, GERMANY.*

Aim/Introduction: Dopamine transporter (DAT) SPECT is the most frequent nuclear medicine brain imaging procedure. Typical scan duration of 30-50 minutes presents a burden for many patients. It is also associated with considerable risk of head motion during the scan resulting in artefacts that might compromise the interpretation of the reconstructed SPECT images. Deep learning-based methods have been found promising for enhancement / denoising of medical images. Aim of the present study was to test a convolutional neural network (CNN) for denoising of DAT SPECT images. **Materials and Methods:** Reconstructed DAT SPECT images in the anatomical space of the Montreal Neurological Institute of 656 different subjects were obtained from the database of the Parkinson's

Progression Markers Initiative, 446 patients with Parkinson's disease (PD) and 210 healthy controls. Two-dimensional slab view images of 12mm thickness were obtained by averaging transversal slices through the striatum. A 67% reduction of scan time was simulated by adding white Gaussian noise to each slab view. The corresponding noise level was estimated from dynamic DAT SPECT scans in which the total scan duration had been split into 3 frames. Ten 60/20/20 random splits of the subject sample were used to train, validate, and test a CNN (inspired by Alex-Net and denoising auto-encoder methodology) with a combination of loss functions based on the pixel value differences and the structural difference between the estimated image (from the noisy one) and the true image. The area under the receiver operating characteristic curve (AUC) of the specific putaminal binding ratio (SBR, mean of both hemispheres) for identification of PD patients in the test set was used as clinically relevant performance measure (putamen ROI of the AAL atlas). **Results:** The mean absolute pixelwise difference between the CNN-denoised images and the true images was 1.8% (compared to 6.7% for the noisy images). The CNN-denoised images provided a small AUC improvement not only compared to the noisy images but also compared to the ground truth: 0.994±0.005, 0.986±0.009, and 0.990±0.007, respectively. **Conclusion:** These results suggest that CNN-based denoising allows considerable reduction of scan time and/or tracer dose in DAT SPECT. Further improvement might be achieved by training the CNN using larger datasets and/or use raw projection data prior to image reconstruction for denoising. **References:** None.

OP-563

Deep Image Denoising in SPECT

M. Reymann[1,2], *T. Würfl*[1], *P. Ritt*[3], *B. Stimpl*[1], *M. Cachovan*[4], *H. A. Vija*[5], *A. Maier*[1];
[1]*Friedrich-Alexander University Erlangen-Nürnberg, Pattern Recognition Lab, Erlangen, GERMANY,* [2]*Erlangen Graduate School in Advanced Optical Technologies (SAOT), Erlangen, GERMANY,* [3]*Clinic for Nuclear Medicine, University Hospital Erlangen, Erlangen, GERMANY,* [4]*Siemens Healthineers, Erlangen, GERMANY,* [5]*Siemens Medical Solutions USA, Inc., Malvern, PA, UNITED STATES OF AMERICA.*

Aim/Introduction: Single Photon Emitted Computed Tomography (SPECT) images are characterized by a high degree of image noise, which is due to the low photon count at the detector. Recently, several deep learning-based approaches for image denoising have been proposed for low-dose Computed Tomography (CT). We investigate their suitability for SPECT denoising. **Materials and Methods:** In order to have a groundtruth for training the networks, a Monte Carlo Simulation was set up with the SIMIND software, where in total 24 SPECT acquisitions of brains, lungs, livers and skeleton were simulated with the XCAT phantom. Pairs of noisy and clean SPECT images were then used for training the neural networks. The networks tested were the U-Net as proposed by Heinrich et al. [1], the convolutional denoising autoencoder (CNN DAE) proposed by Gondara et al. [2] and a custom U-Net that had a depth of 4 layers with 2 convolutions, Batch Normalization and ReLU in each layer. Training of the networks was done with the hyperparameters as described in the original publications. **Results:** The best denoising performance of the neural networks was achieved by either the CNN DAE when measured with the Structural Similarity (SSIM) index of 0.933 or by the custom U-Net with a Peak Signal to Noise Ratio (PSNR) of 30.03 dB. This corresponded to a signal quality improvement of 0.09 compared to the noisy input when measured with the SSIM, or 5.9 dB when measured with the PSNR. The denoised SPECT images showed improved visual appearance, however, gain in image quality was not as distinct as on low-dose CT data. We assume this was due to the image characteristics of SPECT images, which are characterized by few distinct image values and a more heterogeneous pixel intensity distribution compared to CT data. **Conclusion:** Image characteristics in SPECT pose a special challenge to deep learning-based image denoising methods, as the signal is sparse and contains a high degree of noise. We believe this, in conjunction with the limited number of samples explains the weaker benefit in performance in SPECT when compared to low-dose CT data. We assume that with a more diverse training set and specialized loss function suitable for SPECT data , we can further increase performance. **References:** [1] Gondara, L. (2016). Medical image denoising using convolutional denoising autoencoders. IEEE ICDMW-2016. [2] Heinrich, M. , Stille, M., Buzug, T. (2018). Residual U-Net Convolutional Neural Network Architecture for Low-Dose CT Denoising. CDBME-2018.

OP-564

Optimization of myocardial perfusion imaging protocol for digital SPECT/CT imaging system

R. Hirvilammi[1], *M. Seppänen*[1,2], *J. Knuuti*[2], *T. Noponen*[1,3];
[1]*Department of Clinical Physiology and Nuclear Medicine, Turku University Hospital, Turku, FINLAND,* [2]*Turku PET Centre, Turku University Hospital, Turku, FINLAND,* [3]*Department of Medical Physics, Turku University Hospital, Turku, FINLAND.*

Aim/Introduction: Digital SPECT/CT scanner offers better spatial resolution and sensitivity compared to traditional analogical SPECT/CT. Myocardial perfusion imaging (MPI) is somewhat challenging imaging procedure which has several parameters affecting the images. New features of digital SPECT/CT allows optimization of clinical image acquisition protocols. The aim of this study was to develop optimal MPI imaging protocol for digital NM/CT 670 CZT SPECT/CT (GE Healthcare, Tirat Hacarmel, Israel). **Materials and Methods:** Data of 30 MPI patients imaged using list-mode acquisition in Turku University Hospital were used retrospectively. Sinograms were reformatted with Xeleris 4.0 Lister software using 15 parameter combinations and total of 900 new sinograms were reconstructed with QPS/QGS software (Cedars Sinai Medical Center, Los Angeles, USA). Statistical analysis was carried out using SPSS (IBM, Armonk, USA). Visual analysis was performed by comparing bull's eye pictures. **Results:** Using 16 gates instead of 8 gated-SPECT

results in significantly higher ejection fraction (EF) (rest: 50.00 ± 11.89% vs. 53.63 ± 13.20% (p < 0.001) and stress: 51.23 ± 11.00% vs. 54.47 ± 12.41% (p < 0.001)). Using narrower ±3% energy window instead of ±7.5% results in significantly larger ischemic regions (rest: 0.5% (0 - 4%) vs. 3.5% (1 - 6.75%) (p < 0.020) and stress: 2% (0.25 - 5.75%) vs. 6% (1 - 9.75%) p < 0,001)). Decreasing time per view from 20 to 15 s in stress study does not significantly chance the size of ischemic region (p = 0.792). Optimal setting combination using 16 gates, ±3% energy window and 30 s / 15 s (rest / stress) time per projection results in significantly larger EF (rest: 50.00% ± 11.89 % vs. 52.90% ± 14.57% (p < 0.001) and stress: 51.23% ± 11.00% vs. 54.07 ± 11.3 % (p < 0.001)) and significantly larger ischemic region (rest: 0.5% (0% - 4%) vs. 4.5% (2% - 7.75%) (p < 0.001) and stress 2% (0.25% - 5.75%) vs. 5.5% (2% - 11%) (p < 0.001)). Visual analysis verified the clinically meaningful increase of ischemic region mostly in stress study. **Conclusion:** Using more gates in gated-SPECT allows better tracking of cardiac volumes which results in more accurate assessment of EF. The increase of ischemic regions in stress studies seems to be caused by the decreased amount of scattered photons due to narrower energy window. It seems to be possible also to reduce imaging time or injected activity by 25% in our cardiac protocol. **References:** None.

OP-565

Optimisation Of A General Purpose CZT SPECT/CT For Tomography

***N. Bird**, D. Gillett;*
Addenbrooke's Hospital, Cambridge, UNITED KINGDOM.

Aim/Introduction: The aim was to investigate whether image quality improvements with a general purpose solid state gamma camera, compared to a conventional camera, would allow reduction in acquisition times. The focus was myocardial perfusion tomography which will be the majority of the workload for this camera. **Materials and Methods:** The camera under investigation was a GE Discovery NM/CT 670CZT comparisons were made with a NM/CT 670 fitted with LEHR collimators. Energy resolution, planar spatial resolution and sensitivity were measured conforming to NEMA (1) protocols as far as possible. Reconstructed resolution in scatter was measured using a NEMA SPECT Triple line source phantom using a radius 21 cm, reconstructing with and without resolution recovery correction (2). Clinical myocardial perfusion images were simulated using a torso phantom with a cardiac insert, CT was used for attenuation correction. Images were reconstructed with and without scatter correction and resolution recovery correction **Results:** Comparing the CZT system results with the conventional system: Energy resolution for Tc-99m was 6.0% compared with 9.3%. Planar spatial resolution @ 10 cm was 7.3 mm compared with 7.4 mm. Sensitivity was 82 cps/MBq compared to 70 cps/MBq. Reconstructed resolution was 14.1/14.3/11.0 mm for central/radial/tangential measurements compared with 12.3/11.9/8.6 mm. With resolution recovery the resolution was 9.9/9.0/7.5 mm compared with 8.3/7.2/5.9 mm. Analysis of the cardiac phantom images showed very similar overall image quality for the same number of acquired counts. **Conclusion:** The energy resolution of the CZT system is significantly better than for conventional systems, potentially improving image quality due to reduction in scatter. The collimator fitted to the CZT system gives an 18% increase in sensitivity compared to using LEHR collimators on the conventional camera with similar resolution at 10 cm. However it would appear the resolution drops off rapidly with distance so that reconstructed resolution may be significantly poorer in clinical tomographic images. Simulating clinical Myocardial Perfusion images demonstrated that the overall effect of system differences mean that an 18% reduction in acquisition time would be justifiable. **References:** (1)Performance Measurements of Gamma Camera NU 1-2007, NEMA. (2)Evolution for cardiac White Paper, GE Medical Systems.

OP-566

Lutetium-177 SPECT Quantification: A Multi-Center, Multi-Vendor Comparison

***S. Meyer Viol**[1], S. M. B. Peters[2], N. R. van der Werf[3,1], F. H. P. van Velden[4], N. de Jong[4], M. Konijnenberg[3], A. Meeuwis[2], M. Gotthardt[2], C. Beijst[1], H. W. A. M. de Jong[1], M. Segbers[3];*
[1]UMC Utrecht, Utrecht, NETHERLANDS, [2]Radboudumc, Nijmegen, NETHERLANDS, [3]Erasmus MC, Rotterdam, NETHERLANDS, [4]Leiden University Medical Center, Leiden, NETHERLANDS.

Aim/Introduction: Quantitative SPECT imaging in targeted radionuclide therapy with lutetium-177 holds great potential for individualized treatment based on dose assessment. Application of universal dose targets requires a standardized method for SPECT quantification. The purpose of this multi-center study is to evaluate quantitative accuracy and inter-system variations of different SPECT/CT systems with corresponding commercially available quantitative reconstruction algorithms, as part of an important step towards a vendor independent standard for quantitative lutetium-177 SPECT. **Materials and Methods:** Four state-of-the-art SPECT/CT systems were included: Discovery™ NM/CT 670Pro (GE Healthcare), Symbia Intevo™ and two Symbia™ T16 (Siemens Healthineers). Quantitative accuracy and inter-system variations were evaluated by repeatedly scanning a cylindrical phantom with 6 spherical inserts (0.5-113mL). A sphere-to-background activity concentration ratio of 10:1 was used. Acquisition settings were standardized: medium energy collimator, body contour trajectory, photon energy window of 208 keV (±10%), adjacent 20% lower scatter window, 2x64 projections, 128x128 matrix size, and 40s projection time. Reconstructions were performed with vendor/center specific reconstruction and quantification algorithms GE Q.Metrix™, Siemens xSPECT Quant™, Siemens Broad Quantification™ and Siemens Flash3D™ using vendor recommended settings. In addition, raw data was reconstructed using Hermes SUV SPECT™ with standardized reconstruction settings to obtain vendor neutral quantitative reconstructions for all systems. Volumes of interest (VOI) for the spheres were obtained by applying a 50% threshold of the sphere maximum voxel value corrected for background activity. For each sphere the mean recovery

coefficient (RC_{mean}) of three repeated measurements was calculated, defined as the mean imaged activity concentration divided by the actual activity concentration. Accuracy was defined as the inter-system average of RC_{mean}. Inter-system variations (%) were defined as the range of RC_{mean} divided by the accuracy. **Results:** Accuracy of RC_{mean} decreased from 0.79 to 0.13 with decreasing sphere volume for vendor/center specific reconstructions, while accuracy of RC_{mean} decreased from 0.84 to 0.14 for vendor neutral reconstructions. Inter-system variations of RC_{mean} with vendor/center specific reconstructions were between 4-58% depending on sphere size, and improved to 6-11% with vendor neutral reconstructions. These results are preliminary, as the Discovery™ NM/CT data must still be analyzed and included. **Conclusion:** Despite using a standardized approach for acquisition and image analysis of multi-vendor lutetium-177 SPECT/CT, inter-system variations in quantification of up to 58% remain. By standardizing reconstruction methods, inter-system variations in quantification can be reduced drastically, paving the way for application of individualized treatment and universal dose limits. **References:** None.

OP-567

Reproducibility and Accuracy for a Phantom with Lutetium-177 Filled Spherical Inserts Using two Different SPECT/CT Quantitation Methods; Implications for Tumour Dosimetry After ^{177}Lu-lilotomab satetraxetan Treatment

J. Blakkisrud[1,2], *L. T. G. Mikalsen*[1], *A. Løndalen*[1,3], *C. Stokke*[1,4];
[1]*Division of Radiology and Nuclear Medicine, Oslo University Hospital, Oslo, NORWAY,* [2]*Dept. of Physics, University of Oslo, Oslo, NORWAY,* [3]*Faculty of Medicine, University of Oslo, Oslo, NORWAY,* [4]*Dept of Life Sciences and Health, Oslo Metropolitan University, Oslo, NORWAY.*

Aim/Introduction: Accurate quantitation of radioactivity is fundamental for tumour dosimetry. At our centre, we treat lymphoma patients with ^{177}Lu-lilotomab satetraxetan, targeting the CD37 antigen. Multiple post-therapy SPECT/CT-scans are obtained with the aim of performing tumour dosimetry. The amount of activity administrated is relatively low (approximately 1 GBq), and the lesions are often small (down to a few milliliters). Consequently, the images can be prone to intrascan motion due to prolonged acquisition periods. In this work, we used a phantom to evaluate accuracy and interscan reproducibility for two candidate quantitation methods. **Materials and Methods:** A NEMA IEC Body Phantom Set without the lung-insert was used. Spheres with diameters of 10, 13, 17, 22, 28, and 37 mm were filled with 0.25 MBq/ml of lutetium-177. Sphere to background ratios of 1:0 (no background), 32:1 and 16:1 were used. The chosen activity level and ratios reflect our patient acquisitions for the described treatment. The scans were repeated three times for each ratio. Two quantitation methods were explored. Recovery-coefficient (RC) method: A volume of interest (VOI) was placed around the physical boundary of each sphere. Margin-based method: Spherical VOIs with radial margins of 0-15.6 mm were placed around the spheres. For both methods the activity within the VOI were derived. For the latter method, the optimal margins were defined when the expected activity was reproduced, and the overall best margin chosen for all quantitations. The relative difference between the maximum and the minimum activity found for the three repeated scans was used as a measure of interscan reproducibility. The difference between the two methods was tested with a Wilcoxon signed-rank test. **Results:** For the margin-based method, the additional margins reproducing the sphere activity best were 8.16, 9.91, and 11.5 mm (approximately 4, 5, and 6 voxels) for background contrast ratios of 1:0, 32:1 and 16:1, respectively. The mean relative interscan differences across all background ratios were 0.31, 0.12, 0.08, 0.07, 0.04, and 0.02 for spheres of increasing diameters for the RC-method, and 0.28, 0.08, 0.06, 0.06, 0.04, and 0.01 for the margin-based method using an overall considered optimal margin of 9.98 mm. There was an overall significant difference between the two methods (p=0.006). **Conclusion:** Both methods provide interscan reproducibility in the order of 1-10 %, except for the smallest sphere which may prove challenging to quantify accurately. Further work will include investigations of motion effects, to more closely simulate the patient scanning. **References:** None.

OP-568

Automated, robust and agile organ segmentation for voxel-based dose planning

M. Nazari[1,2], *A. Kluge*[1], *S. Kimiaei*[1];
[1]*ABX - CRO advanced pharmaceutical services, Dresden, GERMANY,* [2]*TU-Dresden, Dresden, GERMANY.*

Aim/Introduction: Voxel-based dose planning systems require delineation of organs at risk. Today, segmentations are either done manually or in a semi-automated manner which is time-consuming, error prone, operator-dependent and require significant expertise. The main goals of this work are: a) to extend, combine and/or optimize the architecture of an existing Convolutional Neural Network (CNN) to obtain a fast, robust and accurate CT-based organ segmentation method. b) to train the CNN with an inhomogeneous set of CT scans and validate the CNNs usability for daily practice. **Materials and Methods:** Our CNN was a modified attention based neural network and Recurrent-CNN executed in two stages inspired by MASK r-cnn operated in 2.5 mode. In the first step, the network calculates a Region of Interest (ROI) covering the sought organ. In the second step, the ROI is fine-tuned. Two steps network eliminated the prerequisite of preprocessing of the images. The designed CNN was trained and evaluated using a database of 200 3D CT scans with the livers and kidneys segmented obtained from various sources. The data sets were hence acquired with different scanners and acquisition protocols. Overall, the matrix size was 512 x 512 with the slice spacing ranging from 0.4 to 6.5 mm and the in-plane resolution from 0.55-1.0 mm. 150 of the CT scans were selected randomly for training, 10 sets for validation and 40 sets for final testing. **Results:** The global Dice-Coefficient accuracy obtained for the segmented livers was 93.0% and 94.1% for kidneys. The average CPU time required to segment

each of the 2.5 D slices on a 1.7 GHz Intel Core i7 was 2.5 seconds. The time to segment an entire liver and kidneys using a standard gaming GPU (approx. price €600) was less than 1 sec. **Conclusion:** Based on our preliminary evaluation, we conclude that the proposed approach provides a fast and adequately accurate way to accelerate voxel-based dosimetry. Our fully automated, yet robust method can also facilitate the broader acceptance of 2.5D and 3D dosimetry in the routine practice. Finally, the general ability of our segmentation algorithm, using transfer learning, will allow us to extend its usage to delineation of other organs such as spleen, heart and bladder with moderate efforts. **References:** This project has received funding from the European Union's Horizon 2020 research and innovation programme under the Marie Skłodowska-Curie grant agreement No 764458.

1307

Pitfalls & Artefacts 6 - Interactive Clinical Cases - Cardiovascular Committee: Pitfalls & Artefacts in Cardiac Imaging

Tuesday, October 15, 2019, 11:30 - 13:00 Lecture Hall 113

OP-569
SPECT/CT
C. Nappi;
Institute of Biostructures and Bioimaging, Naples, ITALY.

OP-570
PET/CT
R. Sciagra;
Department of Experimental and Clinical Biomedical Sciences, University of Florence, Florence, ITALY.

OP-571
Cardiac-Centered Gamma Cameras
O. Lairez;
University Hospital Toulouse, Toulouse, FRANCE.

OP-572
Hybrid Imaging
C. Rischpler;
University Hospital Essen, Essen, GERMANY.

1308

Clinical Oncology - Parallel Session: Therapy Response Assessment - Conventional Criteria and More

Tuesday, October 15, 2019, 11:30 - 13:00 Lecture Hall 114

OP-573
Value Of FDG PET/CT To Evaluate The Efficacy Of Regorafenib In Locally Advanced Non_Resectable/ Metastatic Biliary Tract Tumors: The REACHIN Study
R. Lhommel[1], *L. Guillaume*[1], *I. Borbath*[1], *S. Goldman*[2], *J. Van Laethem*[2], *A. Demols*[2];
[1]*Cliniques Universitaires Saint-Luc, UCLouvain, Brussels, BELGIUM,* [2]*Hôpital Universitaire Erasme - ULB, Brussels, BELGIUM.*

Aim/Introduction: The REACHIN study is a double blinded randomized placebo controlled phase II trial aiming to evaluate the safety and efficacy of regorafenib for patients with locally advanced (non-resectable)/metastatic biliary tract tumors progressing after gemcitabine and platinum based chemotherapy. Primary endpoint was PFS and secondary endpoints were response rate (using RECIST 1.1), OS and safety. The tumor early response-to-treatment was evaluated separately by DWI-MRI and FDG PET/CT. The result of the FDG PET/CT sub-study is presented here. **Materials and Methods:** Between May 2014 and February 2018, 66 patients were recruited and randomized (1:1) to received either Best Supportive Care (BSC)+Placebo (Control arm) or BSC+Regorafenib (160mg per day 21 days on, 7 days off, treated arm) until progression/ unacceptable toxicity. From them, 29 patients (control n=15/ Rego n=14) were willing and eligible to participate to the PET/ CT window sub-study, comparing the FDG tumor metabolism at baseline and after two weeks of arm-regimen-based treatment. The main inclusion criteria was at least one FDG positive lesion (primary/metastases) at baseline, with a Tumor/Liver-uptake-ratio ≥1.4. Two independent PET/CT readers were blinded of the patient's randomization and clinical results during the scans review and tumor sites delineation (MIMvista software). Metabolic parameters considered for the statistical analysis (PRISM 8) were SUVbw_max, SUVbw_peak, Metabolic-Tumor-Volume (MTV) and Total-Lesion-Glycolysis (TLG=MTVx SUVbw_ mean). A 3cm diameter sphere was also placed within the non-tumor healthy liver as reference. **Results:** Primary endpoint was met with significantly increase of the PFS from 1.5 to 3 months, p=0.004 (ASCO GI 2019). For the PET window study, both ΔSUVmax, ΔMTV and ΔTLG (%change from baseline) show a significant decline between baseline and FU scan for the treated group (P=0.0151*;0.037**; 0.0056**) compared to the placebo arm. The main tumor SUVmax was significantly decreased in the treated group but not in the control arm (P=0.0353* vs 0.5614). Both TLG and MTV significantly progressed in the control arm (p= 0.0004***; 0.0002***;) while a stabilization/NS progression

was observed in the treatment arm (P=0.3910 ; 0.2412). There was no relevant treatment's related impact on the reference-liver-uptake (P=0.381(ctrl); 0.6149(rego)). **Conclusion:** Despite a limited number of patients, FDG PET/CT seems performant to discriminate early positive metabolic tumor changes in patients treated with regorafenib as compared to the control/placebo group. Additional analysis are ongoing to estimate if these early changes also correlate with the final clinical output parameters (PFS, OS). **References:** Regorafenib after failure of gemcitabine (...). Demols A. et al. ASCO GI 2019, abstract 345.

OP-574

[^{18}F]fluciclatide Pet As A Biomarker Of Response To Combination Therapy Of Pazopanib And Paclitaxel In Platinum-resistant/refractory Ovarian Cancer

R. Sharma[1], *P. O. Valls*[1], *M. Inglese*[1], *S. Dubash*[1], *M. Chen*[1], *H. Gabra*[1], *A. Montes*[2], *A. Challapalli*[1], *M. Arshad*[1], *G. Thakaran*[1], *E. Chambers*[1], *T. Cole*[1], *J. Lozano-Kuehne*[1], *T. D. Barwick*[1], *E. O. Aboagye*[1];
[1]*Imperial college london, London, UNITED KINGDOM,* [2]*Guys and St Thomas' NHS Trust, London, UNITED KINGDOM.*

Aim/Introduction: Angiogenesis is a hallmark of cancer and a therapeutic target in a number of tumour types including ovarian, colorectal and renal cell carcinoma. Despite their therapeutic activity, anti-angiogenic agents are associated with significant side-effects, a key consideration in the palliative setting. The main limitation of anti-angiogenics is the paucity of imaging response biomarkers allowing early identification of non-responders and cessation of ineffective, potentially toxic treatment. Integrins $\alpha_v\beta_3$ and $\alpha_v\beta_5$ are both up-regulated in tumor-associated vasculature. [^{18}F]Fluciclatide is a novel PET tracer that has high affinity for integrins $\alpha_v\beta_{3/5}$. We performed a phase Ib study of combinatorial therapy with pazopanib and weekly paclitaxel, followed by maintenance pazopanib in patients with platinum-resistant/refractory ovarian cancer. The primary outcome of which was to ascertain whether [^{18}F]fluciclatide-PET could be used as a pharmacodynamic (PD) marker of pazopanib effect following 1 week of single agent therapy. The secondary endpoints were to assess the relationship between [^{18}F] fluciclatide uptake with pharmacokinetics (PKs) of pazopanib and with circulating markers of angiogenesis. **Materials and Methods:** We conducted an open-label, phase Ib study in patients with platinum resistant/refractory ovarian cancer. Patients received 1 week of single agent pazopanib (800mg daily) followed by combination therapy with weekly paclitaxel 80mg/m². Following completion of 18 weeks of combination therapy, patients continued with single agent pazopanib until disease progression. Dynamic [^{18}F]Fluciclatide-PET imaging was conducted at baseline and after 1 week of pazopanib. Response (RECIST 1.1), toxicities and survival outcomes were recorded. Circulating markers of angiogenesis were assessed with therapy. **Results:** Fourteen patients were included in the intention-to-treat analysis. Complete and partial response was seen in seven patients (54%). Median progression free survival (PFS) was 10.63 months, and overall survival (OS) was 18.5 months. Baseline [^{18}F]fluciclatide uptake was predictive of long PFS. Elevated baseline circulating angiopoietin and fibroblast growth factor (FGF) were predictive of greater reduction in $SUV_{60,mean}$ following pazopanib. Kinetic modelling of PET data indicated a reduction in K_1 and K_i following pazopanib indicating reduced radioligand delivery and retention. **Conclusion:** In a phase 1b study of combination therapy of the anti-angiogenic pazopanib and paclitaxel followed by maintenance pazopanib, [^{18}F]fluciclatide-PET uptake parameters were observed to be predictive clinical outcome indicating an anti-angiogenic response. **References:** None.

OP-575

Combination of ^{18}F-FDG PET/CT-based Metabolically Active Tumor Volume and Early Metabolic Response Significantly Improves Outcome Prediction in Metastatic Colorectal Cancer: results from two prospective development and one external validation cohort

E. Woff[1], *A. Hendlisz*[1], *L. Salvatore*[2], *F. Marmorino*[3], *A. Falcone*[3], *D. Genovesi*[4], *A. Giorgetti*[4], *G. Critchi*[1], *T. Guiot*[1], *H. Levillain*[1], *N. Plouznikoff*[1], *P. Flamen*[1];
[1]*Institut Jules Bordet, Brussels, BELGIUM,* [2]*Fondazione Policlinico Universitario Agostino Gemelli IRCCS, Rome, ITALY,* [3]*Azienda Ospedaliera Universitaria Pisana, Pisa, ITALY,* [4]*Fondazione Toscana "Gabriele Monasterio", Pisa, ITALY.*

Aim/Introduction: This study aimed to develop and validate a model integrating baseline metabolically active tumor volume (MATV) and early metabolic response (mR) among clinical prognostic factors in metastatic colorectal cancer (mCRC) patients. **Materials and Methods:** The development cohort included chemorefractory mCRC patients enrolled in two prospective Belgian multicenter non-randomized trials evaluating multikinase inhibitors as last line therapy. The validation cohort prospectively included mCRC patients from Italian centers treated with chemotherapy and bevacizumab as first line. Baseline MATV was defined as the sum of metabolically active volumes of all target lesions identified on the baseline ^{18}F-FDG PET/CT. Early metabolic non-responder patients were identified when at least one target lesion showed no significant decrease of SUV_{max} (<15%). Univariate analyses for overall and progression-free survival (OS/PFS) were performed to assess the prognostic values of MATV and early mR and multivariate analyses to assess their prognostic independency along with clinical factors (age, gender, BMI, ECOG PS, and KRAS status). **Results:** MATV, early mR, and clinical factors were evaluable respectively in 216 and 122 patients of the development and validation cohorts. In univariate analyses, baseline MATV and early mR were strongly related to outcome (OS/PFS) in both cohorts. Multivariate analyses identified in the development cohort two independent negative predictors for OS (high MATV and BMI<30) and PFS (high MATV and early mNR), and in the validation cohort three for OS (high MATV, early mNR, poor PS) and PFS (high MATV, early mNR, KRAS mutated). A model

combining baseline MATV and early mR allowed to identify three risk groups for OS and PFS respectively with different median OS/PFS in the development (12.1 vs 6.7 vs 3.8 months for the low, intermediate and high-risk groups; p<0.001 for OS and 4.9 vs 2.9 vs 1.3 months; p<0.001 for PFS) and validation cohorts (40 vs 25.3 vs 15.7 months; p<0.001 for OS and 15.3 vs 10.6 vs 7.7 months; p<0.001 for PFS). **Conclusion:** This study demonstrates the robustness of combined baseline MATV and early mR as prognostic biomarkers for OS/PFS in mCRC, independently of patients' treatment. As independent predictors of outcome, combining these biomarkers allowed to improve risk stratification for OS and PFS in both the development and validation cohorts. **References:** None.

OP-576

Multimodal Radiomic Imaging: Evaluation of ^{18}F-FDG-PET and CE-CT as an early Imaging Biomarker for Prognostication and Response Prediction after Radiochemotherapy using Cetuximab in Head and Neck Squamous Cell Carcinoma

B. Sah[1,2,3], *M. Bogowicz*[4], *S. Tanadini-Lang*[4], *O. Riesterer*[4,5], *C. Leissing*[6], *J. Heverhagen*[2], *G. Studer*[4,7], *M. W. Huellner*[1], *P. Veit-Haibach*[1,3,8];
[1]*Department Nuclear Medicine, University Hospital Zurich and University of Zurich, Zurich, SWITZERLAND,* [2]*Department of Diagnostic, Interventional, and Pediatric Radiology, Inselspital, University of Bern, Bern, SWITZERLAND,* [3]*Department of Diagnostic and Interventional Radiology, University Hospital Zurich, Zurich, SWITZERLAND,* [4]*Department of Radiation Oncology, University Hospital Zurich, Zurich, SWITZERLAND,* [5]*Department of Radiation Oncology, Kantonsspital Aarau, Aarau, SWITZERLAND,* [6]*University of Zurich, Zurich, SWITZERLAND,* [7]*Department of Radiation Oncology, Kantonsspital Luzern, Luzern, SWITZERLAND,* [8]*Joint Department of Medical Imaging, University of Toronto, Toronto, ON, CANADA.*

Aim/Introduction: This study investigated the value of F-18-Fluorodeoxyglucose-positron-emission-tomography (PET) radiomics in comparison to contrast-enhanced-computed-tomography (CE-CT) radiomics in a) evaluation of progression free survival after radio-chemo-therapy, and b) identifying patients who will be free of recurrence of head and neck squamous cell carcinoma (HNSCC) as early as one week after end of radiochemotherapy. **Materials and Methods:** Following Institutional Ethics Committee approval and informed consent, a total of 59 patients with histologically proven and locoregionally advanced HNSCC were prospectively enrolled in this single-center randomized study, and scheduled for curative radiochemotherapy including cetuximab and cisplatin. PET and CE-CT were acquired on the same machine. Patients underwent PET/CE-CT imaging at 3 time points: pre-treatment (PET/CE-CT1), 1 week post primary radiochemotherapy (PET/CE-CT2) and 3 months post primary radiochemotherapy (PET/CE-CT3). 154 radiomic features of first, second, and higher order, glucose uptake (SUVmax), and Hounsfield units (HU) were extracted from the primary tumor at each time point separately. Delta radiomics/values ([posttreatment feature value – pretreatment feature value]/pretreatment feature value) following treatment were calculated for each parameter (PET2, CE-CT2, PET3, CE-CT3). Association of features to non-/recurrence, progression free survival (PFS), and between the different modalities was evaluated (Spearman's Rho "ρ"). A p-value of <0.05 was considered statistically significant. **Results:** 38 patients were free of recurrence during follow-up period (52+/-22 month; range 8-89). PFS was 38+/-26 month (range 2-83). There was no significant correlation between patients with/without recurrence, and SUVmax (p=0.17, 0.65, 0.94) or HUmean (p=0.17, 0.40, 0.05) at the 3 imaging time points. None of the PET/CE-CT1, but delta radiomics of 4 PET2 (0.02<p<0.04), 1 CE-CT2 (p=0.03), 9 PET3 (0.001<p<0.02), and 6 CE-CT3 (0.01<p<0.04) features could significantly predict the development of a recurrence. SUVmax and HUmean at 3 imaging time points were not significantly correlated to PFS (ρ=-0.25,-0.06,-0.11 for SUVmax and ρ=0.10,-0.07,-0.27 for HUmean). Pre-treatment values and proportional differences of selected significant radiomic features showed weak (PET1: -0.29<ρ<0.32; CT1: -0.31<ρ<0.30), weak to moderate (PET2: -0.44<ρ<0.39; CT2: -0.38<ρ<0.26), and moderate (PET3: -0.47<ρ<0.60; CT3: -0.36<ρ<0.38) correlation to PFS. Comparison of respective radiomic features between PET and CE-CT showed weak to moderate correlation at 3 imaging time points (0.24<ρ<0.76, -0.05<ρ<0.55, -0.02<ρ<0.39). **Conclusion:** Radiomics in a multimodality approach might be a complementary tool for response prediction and prognostication of patients with HNSCC as early as 1 week after primary radiochemotherapy. **References:** None.

OP-577

Prediction Of Therapeutic Response And Long-term Outcomes By EORTC Criteria And Percist In Breast Cancer Following Two Courses Of Neoadjuvant Chemotherapy

W. Lian, *C. Liu*, *Z. Yang*, *S. Song*, *Y. Zhang*;
Fudan University Shanghai Cancer Center, Shanghai, CHINA.

Aim/Introduction: To investigate the predictive value of ^{18}F-FDG PET/CT for pathological response and disease recurrence in breast cancer patients during neoadjuvant chemotherapy (NAC). **Materials and Methods:** Consecutive PET/CT scans in 128 operable breast cancer female patients at baseline and after two courses of NAC were retrospectively analyzed using the European Organization for Research and Treatment of Cancer (EORTC) criteria and Positron Emission Tomography Response Criteria in Solid Tumors (PERCIST). The concordance between these criteria was determined using Cohen's κ coefficient. Metabolic changes between scans for predicting pathological complete response (pCR) were evaluated with diagnostic test and receiver operating characteristic (ROC) analysis. Molecular subtypes were taken into consideration in the analysis. Kaplan-Meier plots and Cox regression analysis for the correlation with progression-free survival (PFS) were performed. **Results:**

Ninety-two patients were finally enrolled. CMR was determined in 36 patients with EORTC criteria and 35 with PERCIST, and the κcoefficient was 0.988. Thirty-three patients showed postoperative pCR. The sensitivity, specificity, positive predictive value (PPV), negative predictive value (NPV), and accuracy for pCR prediction were 69.7% (23/33), 77.9% (46/59), 63.9% (23/36), 82.1% (46/56), and 75.0% (69/92) with EORTC criteria, respectively, and 69.7%(23/33), 79.7%(47/59), 65.7%(23/35), 82.5%(47/57), and 76.1%(70/92) with PERCIST, respectively. The decline percentage of maximum standardized uptake value (SUVmax), total lesion glycolysis (TLG), and metabolic tumor volume (MTV) were found to be moderately distinguished pCR from non-pCR with the area under the curves (AUCs) of 0.715, 0.743, and 0.754, respectively ($p = 0.001$, $p < 0.001$, and $p < 0.001$). Nineteen (20.7%) of the 92 patients relapsed at a median follow-up period of 48.7 months (20.6-84.1 months). The univariate Cox analysis indicated that complete metabolic response (CMR) by EORTC ($p = 0.017$) and PERCIST ($p = 0.021$), and HER2 overexpression ($p = 0.037$) were significantly related to a longer PFS. The multivariate analysis suggested that CMR by EORTC was considered to be an independent predictor to disease recurrence ($p = 0.017$). **Conclusion:** The sensitivity and specificity of both EORTC criteria and PERCIST were relatively suboptimal to predict pCR. However, EORTC criteria were more valuableapproaches than PERCIST for predicting progression-free survival in operable breast cancer patients following two cycles of NAC. **References:** None.

OP-578

EORTC versus PERCIST 1.0 Criteria In The Evaluation Of Response To Neoadjuvant Chemotherapy In Inoperable High-grade Serous Ovarian Carcinoma. Which One Best Predicts An Optimal Interval Surgery?

A. Sabaté-Llobera[1], *J. Robles-Barba*[2], *A. Palomar-Muñoz*[2], *J. Mestres-Martí*[2], *B. Pardo*[3], *M. T. Climent*[4], *E. Llinares-Tello*[2], *J. Ponce*[4], *C. Gámez-Cenzano*[2];
[1]*PET Unit, Nuclear Medicine Department-IDI. Gynecologic Oncology Multidisciplinary Team. Hospital Universitari de Bellvitge-IDIBELL, L'Hospitalet de Llobregat (Barcelona), SPAIN,* [2]*PET Unit, Nuclear Medicine Department-IDI. Hospital Universitari de Bellvitge-IDIBELL, L'Hospitalet de Llobregat (Barcelona), SPAIN,* [3]*Department of Medical Oncology-ICO. Gynecologic Oncology Multidisciplinary Team. Hospital Duran i Reynals-IDIBELL, L'Hospitalet de Llobregat (Barcelona), SPAIN,* [4]*Department of Gynecology. Gynecologic Oncology Multidisciplinary Team. Hospital Universitari de Bellvitge-IDIBELL, L'Hospitalet de Llobregat (Barcelona), SPAIN.*

Aim/Introduction: Debulking surgery is the primary staging and treatment procedure for patients with ovarian cancer. However, maximal debulking is not always possible in high stage disease, so neoadjuvant chemotherapy (NACT) followed by interval cytoreduction is a therapeutic alternative. This study aims to evaluate the response to NACT by FDG-PET/CT, applying both EORTC and PERCIST 1.0 criteria, trying to determine which method best predicts the possibility to achieve an optimal surgery. **Materials and Methods:** Thirty-eight women diagnosed with primarily inoperable high-grade serous ovarian cancer (FIGO IIIB-IV) were retrospectively studied. All of them underwent two PET/CT scans: one at diagnosis (PET1) and another one after 3 or 4 cycles of standard NACT with taxol/carbo (PET2). Metabolic parameters for response evaluation (SUVmax for EORTC and SULpeak for PERCIST 1.0) were obtained both at PET1 and at PET2. Response to treatment was classified as complete metabolic response (CMR), partial metabolic response (PMR), stable metabolic disease (SMD), and progressive metabolic disease (PMD). Concordance between both evaluation criteria was assessed using Cohen's kappa. Relation between the type of response and optimal surgery for each method was calculated using the Chi-square test. **Results:** Final response analysis was performed considering only infradiaphragmatic disease, as supradiaphragmatic lesions (detected in 60.5% of patients) did not modify the surgical decision. According to EORTC criteria, 11 patients (28.9%) reached a CMR, 25 (65.8%) a PMR, 1 (2.6%) showed SMD, and 1 PMD. Considering PERCIST 1.0 criteria, 11 patients (28.9%) had a CMR, 23 (60.5%) a PMR, 3 (7.9%) had SMD, and 1 had PMD. Concordance between both methods was excellent (k=0.90), with inconsistent results in 2 patients (5.3%), both changing from PMR with EORTC to SMD with PERCIST 1.0. Optimal surgery was achieved in 30 patients (78.9%). Chi-square test showed no differences between reaching a CMR or a PMR and the possibility to achieve an optimal surgery, neither considering EORTC criteria (p=0.418), nor when applying PERCIST 1.0 (p=0.523). **Conclusion:** EORTC and PERCIST 1.0 criteria have an excellent correlation to evaluate response to NACT in inoperable high-grade serous ovarian carcinoma. None of the two methods shows significant differences between reaching a CMR or a PMR and the possibility to achieve an optimal surgery. **References:** None.

OP-579

Response Assessment to Immunotherapy with PD1 Inhibitors Using Metabolic Tumor Volume on ^{18}F-FDG PET/CT

G. Ferreira*, S. F. Castro, I. L. Sampaio, L. S. Violante, J. P. Teixeira, H. Duarte;*
Instituto Português de Oncologia do Porto Francisco Gentil, Porto, PORTUGAL.

Aim/Introduction: Immunotherapy with checkpoint inhibitors (CPIs) directed towards the programmed cell death protein 1 (PD1) produces durable responses in a variable yet small proportion of metastatic melanoma patients. While response assessment based on ^{18}F-FDG PET/CT may be able to early identify non-responders, inflammatory response induced by CPIs could limit the accuracy of currently used PET-based criteria. We evaluated the association between response based on total metabolic tumor burden and prognosis in patients with metastatic melanoma treated with PD-1 inhibitors. **Materials**

and Methods: We analyzed patients with metastatic melanoma treated with pembrolizumab and nivolumab between 2017 and 2018. From this cohort, 30 consecutive subjects performing ^{18}F-FDG PET/CT scans before and after treatment initiation were included and followed until last observation or death (median 8.1 months, IQR 8.03). Median time between start of treatment and response assessment was 11.0 weeks (IQR 3.07). Response was defined according to interval change in total-body metabolic tumor volume (MTV), adopting the same thresholds to define response as PET Response Criteria in Solid Tumors (PERCIST). Unlike PERCIST, appearance of new lesions was not necessarily considered disease progression. Chi-square and Log Rank tests were used to compare overall survival (OS) between groups and multivariable cox regression to determine prognostic factors. Agreement between MTV-based and PERCIST criteria was assessed. **Results:** According to MTV-based criteria, 18 (60.0%) patients had progressive disease (PD), 7 (23.3%) partial response (PR) and 5 (16.7%) complete response (CR). In patients with PD, OS at 6 months was 55.6%, vs 100% (p=0.009) in responders (PR and CR). Moreover, none of the responders died during the entire follow-up time, while patients with PD had a median OS of 6.9 months (95% CI 3.8-10.0, p<0.001). Multivariable analysis identified MTV quantitative decrease between scans to significantly associate with survival (HR 1.06, 95% CI 1.02-1.09, p=0.001), independently of age, gender and baseline total-body tumor load. There was substantial agreement between MTV-based and PERCIST criteria (κ=0.689, p<0.001). Importantly, 2 patients with PR according to MTV-based criteria were classified as PD in PERCIST due to the appearance of new lesions. These regressed spontaneously during follow-up, accounting for a phenomenon of pseudoprogression. **Conclusion:** In patients with metastatic melanoma treated with anti-PD1 agents, response assessment according to MTV interval change on ^{18}F-FDG PET/CT imaging was significantly associated with OS. This method may overcome the problems associated with pseudoprogression, allowing for better stratification of patients with progressive disease based on standard PERCIST criteria. **References:** None.

OP-580

Immune-Metabolic-Prognostic Index (IMPI): Combination of 18F-FDG PET/CT and Peripheral Blood Biomarkers in Patients with NSCLC Treated with Checkpoint Inhibitors

A. Castello[1], *L. Toschi*[2], *S. Rossi*[2], *E. Mazziotti*[1], *E. Lopci*[1];
[1]*Nuclear Medicine, Humanitas Clinical and Research Hospital - IRCCS, Rozzano (MI), ITALY,* [2]*Oncology and Hematology, Humanitas Clinical and Research Hospital - IRCCS, Rozzano (MI), ITALY.*

Aim/Introduction: To investigate whether metabolic parameters evaluated by ^{18}F-FDG PET/CT and peripheral blood biomarkers can be associated with clinical outcomes in patients affected by metastatic NSCLC and treated with immune checkpoint inhibitors (ICI). **Materials and Methods:** The trial was registered at http://www.clinicaltrials.gov (NCT03563482). We prospectively enrolled 33 patients (21 male, 12 female, mean age 75) with NSCLC and treated with ICI from April 2017 to December 2018. Complete blood cell counts before and after 8 weeks of treatment were measured. Likewise, all patients underwent ^{18}F-FDG PET/CT at baseline, while 25 patients after 8 weeks of treatment. Response assessment was according to EORTC criteria. Progression-free survival (PFS) and overall survival (OS) were determined and compared using the Kaplan-Meier method and the log-rank test. Multivariate analysis for PFS and OS were performed using the variables that were significant on univariate analysis by Cox proportional hazard regression analysis. Median follow-up was 11.3 months (range 1-17 months). **Results:** We found a progressively increase of neutrophil-to-lymphocyte ratio between baseline and after 8 weeks (ΔNLR) among response groups (median ΔNLR -19.8% for partial metabolic response, +29.6% for stable metabolic disease, and +180.8% for progressive metabolic disease, p=0.03). In multivariate analysis, low post-treatment NLR (< 4.9) and total lesion glycolysis (post-TLG< 541.5 ml) were independently associated with both PFS (HR 0.273; 95%CI, 0.92-0.806 and HR, 0.295; 95%CI, 0.092-0.806, respectively) and OS (HR 0.044; 95%CI, 0.007-0.275 and HR, 0.204; 95%CI, 0.042-0.988, respectively). Afterwards, we developed an immune-metabolic prognostic index (IMPI), based on post-NLR < 4.9 and post-TLG < 541.5 ml, classifying 3 groups: high risk, 2 factors; intermediate risk, 1 factor; low risk, 0 factors. Median PFS for low, intermediate and high risk was 7.8 months, 5.6 months, and 1.8 months, respectively (p<0.001). Likewise, median OS was 15.2 months, 13.2 months, and 2.8 months, respectively (p<0.001). **Conclusion:** Combination of both immune (post-NLR < 4.9) and metabolic (post-TLG < 541.5) biomarkers, was associated with longer PFS and OS. This result could better characterize the tumor biology and aid oncologists for identifying NSCLC patients who likely need to change therapy. However, further larger studies are warranted to establish IMPI as predictor of outcome. The Italian Association for Research on Cancer (AIRC - Associazione Italiana per la Ricerca sul Cancro) is acknowledged for the support on research. **References:** None.

YDF3

EANM Young Daily Forum

Tuesday, October 15, 2019, 13:00 - 14:30 Lecture Hall 113

YDF-3

Be Stronger - Managing Work Stress and Building Your Resilience

R. Sheppard;
EANM Moderator, London, UNITED KINGDOM.

1401

CME 11 - Physics + Cardiovascular Committee: Advances in Quantitative Cardiac Imaging

Tuesday, October 15, 2019, 14:30 - 16:00 Auditorium

OP-581
Quantification in SPECT - Current State and Perspectives
M. Hakulinen;
Kuopio University Hospital, Imaging Centre, Department of Clinical Physiology and Nuclear Medicine, Kuopio, FINLAND.

OP-582
Quantification in PET - Current State and Perspectives
I. Armstrong;
Nuclear Medicine Department, Manchester University Hospital NHS Trust, Manchester, UNITED KINGDOM.

OP-583
Quantification in CT - Current State and Perspectives
M. Dewey;
Charité, Radiology, Berlin, GERMANY.

1402

Joint Symposium 21 - Oncology & Theranostics Committee / ESGO: Ovarian Cancer

Tuesday, October 15, 2019, 14:30 - 16:00 Lecture Hall 311

OP-587
Staging, Prognosis and Relapse Detection - The Clinician's Point of View
A. Ferrero;
Academic Division Gynaecology and Obstetrics - University of Torino, Mauriziano Hospital, Torino, ITALY.

OP-588
Staging, Prognosis and Relapse Detection with PET/CT and PET/MR - The Nuclear Medicine Physician's Point of View
R. Delgado Bolton;
San Pedro Hospital - Centre for Biomedical Research of La Rioja (CIBIR), Servicio Riojano de Salud (SERIS), Department of Diagnostic Imaging (Radiology) and Nuclear Medicine, Logroño - La Rioja, SPAIN.

OP-589
Response Assessment with Imaging - The Clinician's Point of View
M. Rosendahl;
Rigshospitalet - Copenhagen University Hospital, Copenhagen, DENMARK.

OP-590
Response Assessment with PET/CT and PET/MR - The Nuclear Medicine Physician's Point of View
N. Aide;
University Hospital, Department of Nuclear Medicine and Medical Physics, Caen, FRANCE.

1403

Joint Symposium 22

Tuesday, October 15, 2019, 14:30 - 16:00 Lecture Hall 312

Session details not finished as per date of publishing

1404

CTE 5 - Interactive - Technologist Committee: Patient Communication

Tuesday, October 15, 2019, 14:30 - 16:00 Lecture Hall 117

OP-596
Health Communication - Design Thinking
D. Miranda;
National School of Public Health, Lisbon, PORTUGAL.

OP-597
Patient Welfare and Advocacy - A View from the Inside
M. Lee;
EANM, Patient and Public Involvement and Engagement, London, UNITED KINGDOM.

OP-598
Risk Communication - Why and How to Communicate about Ionizing Radiation?
T. Perko;
Belgian Nuclear Research Centre, Mol, BELGIUM.

1405

M2M - Parallel Session: Targeting the Brain

Tuesday, October 15, 2019, 14:30 - 16:00 Lecture Hall 111

OP-599

Development of novel ^{11}C- labeled ASEM analogs for detection of neuronal nicotinic acetylcholine receptors (α7-nAChR)

S. Nag[1], Z. Jia[1], P. Datta[1], P. M. Azpiazu[1], R. Arakawa[1], K. Varnäs[1], L. Lemoine[1], G. Kuang[2], H. Ågren[2], B. Långström[3], C. Halldin[1];
[1]Karolinska Institutet, Stockholm, SWEDEN, [2]Royal Institute of Technology, Stockholm, SWEDEN, [3]Uppsala University, Stockholm, SWEDEN.

Aim/Introduction: The homo-pentameric alpha 7 receptor is one of the major types of neuronal nicotinic acetylcholine receptor (α7-nAChR) related to cognition, memory formation, and attention processing. The mapping of α7-nAChR by PET draws a lot of attention to understand mechanism and the progress of CNS diseases such as AD, PD, schizophrenia. Several PET ligands have been explored for imaging of the α7-nAChR, but [^{18}F]ASEM is so far the most interesting for in vivo quantification of α7-nAChR in human. The aims of this study were i) to explore the binding profile of ASEM derivatives by in silico methods ii) label the suitable derivatives with ^{11}C/^{3}H and to evaluate some binding characteristics in vitro and in vivo. **Materials and Methods:** All molecular dynamics simulations were carried out using the GROMACS 4.6.7 code. The Glide utility of the Schrodinger software package was used for molecular docking and the Bennett Acceptance Ratio (BAR) method was used to carry out free energy calculations. Five analogs of ASEM (KIn 74, KIn 75, KIn 84, KIn 85 and KIn 83) were labeled with ^{11}C and KIn 83 was additionally labeled with ^{3}H. Binding properties were evaluated using autoradiography (ARG) and PET measurements in a few non-human primates (NHPs). Radiometabolites were measured in NHPs plasma using gradient radio HPLC. **Results:** Five ASEM analogs were chosen for radiolabeling depending on the docking score, free energy calculation and feasibility of the radiolabeling. All compounds were successfully radiolabeled with purity >99%. Evaluation with ARG showed that only [^{11}C]KIn83 (0.01 MBq/ml) binds to α7-nAChR in rat brain. Competition studies showed that 80% of the total binding was displaced by adding 10 μM of unlabeled KIn83 and ASEM. Further ARG were performed with [^{3}H]KIn83, replicating the results obtained with [^{11}C]KIn83. In vivo [^{11}C]KIn83 brain uptake was relatively low (1.6 SUV at peak) compared to [^{18}F]ASEM (4.4 SUV). Regional distribution of [^{11}C]KIn83 was similar to [^{18}F]ASEM, with relatively high uptake in thalamus, cortex and basal ganglia. Low uptake was observed in cerebellum and white matter. Radiometabolism of [^{11}C]KIn83 was relatively fast. **Conclusion:** Preliminary evaluation of KIn 83 by ARG with both ^{11}C and ^{3}H as well as in vivo evaluation in NHP showed favorable properties for imaging α7-nAChR despite the relatively lower brain uptake. Acknowledgements: Support from the Swedish Foundation for Strategic Research (SSF, RB13-0192) **References:** None.

OP-600

Synthesis and bioevaluation of a novel TSPO-selective PET probe, [^{18}F]BS224 with low binding sensitivity to TSPO polymorphism

I. Song[1], S. Lee[2], B. Lee[1,3], S. Kim[1,2,3];
[1]Department of Nuclear Medicine, Seoul National University Bundang Hospital, Seongnam, KOREA, REPUBLIC OF, [2]Graduate School of Convergence Science and Technology, Seoul National University, Suwon, KOREA, REPUBLIC OF, [3]Center for Nanomolecular Imaging and Innovative Drug Development, Advanced Institutes of Convergence Technology, Suwon, KOREA, REPUBLIC OF.

Aim/Introduction: Selective TSPO-ligand could provide a powerful imaging tool to detect and monitor several inflammatory brain disorders[1]. However, single nucleotide polymorphism in the TSPO gene influences the binding affinity of TSPO ligands, eventually leading to a binding profile classification according to each genotype[2]. Thus, novel ligand, which has no dependency of the polymorphism on the binding affinity for TSPO, is urgently needed. This study aimed to develop and evaluate a novel TSPO-selective PET imaging agent, [^{18}F]BS224, which is unaffected from TSPO polymorphism. **Materials and Methods:** [^{18}F]BS224 were synthesized by two different precursors, respectively: i)diaryliodonium salts (condition A); ii)pinacol boronate ester (condition B). Both conditions for aromatic [^{18}F]fluorination was optimized in various phase transfer catalysts, solvents, temperatures, and catalysts. [^{18}F]BS224 (R_t=34 min) was collected from semi-preparative HPLC(Xterra Semi-preparative C18 column, 10x250 mm, 10 μm; 50% acetonitrile-water, UV 250 nm, flow rate: 5.0 mL/min). We prepared 294FT cell transfected with wild TSPO gene(TSPO wild) or A147T point mutant gene(TSPO mutant). Cellular uptake assay of [^{3}H]PK11195, [^{18}F]PBR28, and [^{18}F]BS224 was performed and the radioactivity of the samples was normalized by the protein concentration of each sample. **Results:** A new aromatic fluorine-substituted imidazo[1,2-a]pyridine analogue, BS224, showed a subnanomolar affinity(K_i=0.51 nM). Using condition A, [^{18}F]BS224 was synthesized with 18-25% radiochemical yield(RCY). In condition B, much higher RCY of [^{18}F]BS224(63.6%) was shown in the presence of copper(II)triflate and pyridine in dimethylformamide. Finally, the radio-synthesis of [^{18}F]BS224 was optimized by using condition B including HPLC purification. The RCY of the final product was 39±6.8 % (n=3, decay-corrected) with high molar activity(127 GBq/μmol) and radiochemical purity(>99 %). Log D and in vitro human serum stability were 2.78±0.04 and >99% after 2 h incubation, respectively. Cellular uptake ratios (Wild/Mutant) of [^{3}H]PK11195, [^{18}F]PBR28, and [^{18}F]BS224 were 1.29, 4,79 and 1.24, respectively. Cellular uptake of [^{18}F]BS224 in TSPO mutant was significantly reduced compared to that in TSPO wild. However, in the case of [^{3}H]PK11195 and

[18F]BS224, the cellular uptakes were similar between TSPO wild and mutant. **Conclusion:** Aromatic [18F]fluorination of BS224 was successfully performed by nucleophilic substitution of the corresponding pinacol boronate ester precursor using [18F] fluoride. [18F]BS224 was showed with a little dependency of the polymorphism on the cellular uptake. Based on these results, [18F]BS224 is a promising TSPO PET imaging agent overcoming the TSPO polymorphism. **References:** [1] G. Kreutzberg, et al. (1997) Journal of neurocytology, 26, 77-82.[2] Owen DR, et al. (2012) J Cereb Blood Flow Metab. 32, 1-5.

OP-601

In Vivo Visualization Of Cerebral Cell Proliferation And Neurogenesis After Bilateral Labyrinthectomy In The Rat By Serial [18F]FLT Imaging

C. Branner[1,2], A. Krämer[1,2], M. Lindner[1,2], A. Gosewisch[1,2], M. Grosch[1], S. Lindner[2], R. Oos[2], P. Bartenstein[2], S. Ziegler[2], A. Zwergal[1,3]; [1]German Center for Vertigo and Balance Disorders (DSGZ), University Hospital, LMU Munich, Munich, GERMANY, [2]Department of Nuclear Medicine, University Hospital, LMU Munich, Munich, GERMANY, [3]Department of Neurology, University Hospital, LMU Munich, Munich, GERMANY.

Aim/Introduction: Neurogenesis contributes to plasticity in the adult brain and is considered to be involved in structural remodelling following inner ear lesions. The current study aimed at examining changes in cerebral cell proliferation in the rat following bilateral labyrinthectomy (BL) by serial [18F]FLT-µPET and histochemistry. **Materials and Methods:** 12 SD rats underwent BL through transtympanic injection of bupivacaine and arsanilic acid. Rats were followed up until 9 weeks post BL. Spatial orientation and locomotion were tested in a rewarded T-maze task to monitor behavioural changes. A [18F]FLT-µPET scan with probenecid pre-treatment (following a modified protocol by Tamura et al., 2016) was acquired once weekly to depict cerebral cell proliferation in vivo. Histochemistry after BrdU-injection was performed on corresponding days in a subgroup of animals to verify neurogenesis in vitro. The results were compared to a dataset of healthy controls. **Results:** T-maze testing revealed differences between BL rats and healthy controls: Locomotor velocity was significantly higher and the spatial orientation performance significantly worse in BL rats compared to controls until 9 weeks post-surgery. Histochemistry showed a decreased number of BrdU-labeled proliferating cells in the hippocampal dentate gyrus(DG) and subventricular zone(SVZ) at 2 to 6 weeks post BL ($p<0.05$). In the BL group cell proliferation remained 40% lower in DG compared to controls, while it recovered to the levels of controls in the SVZ until 9 weeks post BL. In the vestibular nuclei(VN) BrdU-positive cells were twice as frequent in BL animals as in controls on day3 post-surgery. In relatively good accordance with histochemical results, BL rats displayed a reduced [18F]FLT-uptake in the SVZ until 9 weeks and in the DG until 6 weeks post-surgery ($p<0.005$). The VN showed an increase in [18F]FLT-uptake especially directly after and 9 weeks after BL ($p<0.005$). **Conclusion:** Changes of cerebral cell proliferation appear after a bilateral vestibular lesion in the VN, hippocampal DG and SVZ. [18F]FLT imaging is a feasible method to depict differential regulations in these neurogenic niches over time in vivo. As the number of proliferating cells is rather small in the adult brain, [18F]FLT-based experiments need to be done in larger groups and with probenecid pre-treatment to depict changes in neurogenesis. **References:** Tamura, Y., et al. Noninvasive Evaluation of Cellular Proliferative Activity in Brain Neurogenic Regions in Rats under Depression and Treatment by Enhanced [18F] FLT-PET Imaging. Journal of Neuroscience 36, 8123-8131 (2016).

OP-602

Preclinical comparison of the first generation Tau PET tracer AV1451 and two next-generation Tau PET tracers, MK-6240 and PI-2620

***A. Mueller**[1], H. Kroth[2], F. Oden[1], F. Capotosti[2], M. Berndt[1], J. Molette[2], H. Schieferstein[1], E. Vokali[2], J. Castillo-Melean[1], H. Schmitt-Willich[1], D. Hickman[2], A. Pfeifer[2], S. Poli[2], L. Dinkelborg[1], A. Stephens[1]; [1]Life Molecular Imaging, Berlin, GERMANY, [2]AC Immune SA, Lausanne, SWITZERLAND.*

Aim/Introduction: Intracellular Tau deposition is a key pathologic feature of Alzheimer's disease (AD) and other neurodegenerative disorders. Positron emission tomography could be an important tool for the detection of Tau aggregates in the brain in AD and other tauopathies. Several tracers have been described and are being administered clinically. First-generation Tau PET tracers have reported limitations, particularly off-target binding. Here we present a preclinical comparison of the first-generation tracer AV1451 and two next-generation tracers, PI-2620 and MK-6240. **Materials and Methods:** Compounds were evaluated for affinity and selectivity to aggregated Tau using human brain homogenates and 4R-Tau fibrils. The non-specific component was measured using homogenate binding assays with brain tissue from non-demented controls. Specific off-target binding was measured in competition assays using radiolabeled MAO-A/B and beta-amyloid binders. Compounds were further characterized by autoradiography (ARG) on AD brain sections. The binding was compared to the corresponding signals on brain tissues of non-demented control subjects. The pharmacokinetic profiles of the 18F-labeled test compounds were evaluated in mice. **Results:** All three compounds showed high affinity for Tau-aggregates in AD brain homogenate competition assays (IC_{50}: AV1451 <1 nM; MK-6240 1nM, PI-2620 1.8 nM). None of the compounds displayed binding to beta-amyloid. However, AV1451 showed also significant, high-affinity binding in brain homogenates of non-demented controls. The ratio of specific to non-specific binding was 2, 15, and 28 for AV1451, MK-6240 and PI-2620, respectively. In contrast to AV1451 and MK-6240, PI-2620 also showed high affinity binding to recombinant 4R-Tau fibrils IC_{50} (4 nM). PI-2620 binding to 4R-Tau was confirmed by homogenate binding-assays and autoradiography on PSP brain slices. Binding to MAO-A (IC_{50} 22 nM) as well as to MAO-B (78 nM) was found for AV1451, but not for the other two compounds. PI-

2620 and MK-6240 showed excellent PK characteristics in mice PET studies (peak uptake-to-60 min of 24 and 29 respectively). The brain washout of AV1451 was slower (ratio peak-to-60 min: 7). Minor defluorination was found in this experiment for MK-6240 and AV1451, but not for PI-2620. **Conclusion:** All three tracers demonstrate high affinity binding to human tau-aggregated in AD. The first-generation tracer AV1451 showed significant binding in control tissue lacking tau-aggregates which can be attributed partly to MAO-A/B. This off-target binding is probably also responsible for reduced brain wash-out in mice. In contrast to the other two compounds, PI-2620 demonstrated the ability to bind to 4R-Tau using recombinant fibrils, PSP brain homogenate and ARG. **References:** None.

OP-603

Hyperactivation of neutrophils in Alzheimer's disease transgenic mice by ^{68}Ga-PEG-cFLFLFK PET imaging

Y. Kong, Y. Guan;
PET Center, Huashan Hospital, Fudan University, Shanghai, CHINA.

Aim/Introduction: Neutrophils play a critical role in the innate immune system. Neutrophil hyperactivation has been identified as a biomarker of Alzheimer's disease (AD)[1]. However, there is still no in vivo imaging tool to study the activation of neutrophils in AD dynamically. ^{68}Ga-PEG-cFLFLFK, an antagonist of the neutrophil formyl peptide receptor (FPR) with a high binding affinity, has been developed as a specific tracer to probe the activation of neutrophils. In this study, we aim to detect the variation of neutrophil in the AD transgenic mice by ^{68}Ga-PEG-cFLFLFK. **Materials and Methods:** In this study, we used the B6;129-Psen1tm1Mpm Tg(APPSwe,tauP301L)1Lfa/Mmjax mouse model, which was confirmed by RT-PCR. Open field test, morris water maze, high plus maze and Y-maze test were performed to evaluate the status of the mice. ^{68}Ga-PEG-cFLFLFK was synthesized by the previously reported[2]. Serial microPET was used to investigate the uptake of tracer in the AD transgenic mice and control at different ages. **Results:** Behavior test results confirmed the impairment of learning and memory in AD transgenic mice. PET imaging 60 min after tracer injection indicated that %ID/g mean of brain for AD transgenic group that was higher, respectively, compared with control group. Furthermore, the radioactivity uptake of heart in AD transgenic group was significantly higher than control. **Conclusion:** These results indicated that increased activation of neutrophil in the heart and brain of AD mice. ^{68}Ga-PEG-cFLFLFK PET imaging is a sensitive approach for studying the status and mechanism of neutrophil on AD. **References:** 1. Dong Y, Lagarde J, Xicota L. Ann Neurol. 2018 Feb;83(2):387-405 2. Landon W. Locke, Mahendra D. Chordia, Yi Zhang. J Nucl Med. 2009 May ; 50(5): 790-797.

OP-604

Preclinical validation of [^{18}F]2FNQ1P, a specific PET radiotracer of 5-HT$_6$ receptors in rat, pig, non-human primate and human brain tissues

S. Emery[1,2], S. Fieux[3], B. Vidal[3], F. Liger[4], T. Billard[5], P. Courault[2,1], S. Bouvard[2], L. Zimmer[2,1,4], S. Lancelot[2,1,4];
[1]Hospices Civils de Lyon, Neurological Hospital, Lyon, FRANCE, [2]Lyon Neuroscience Research Center (UMR 5292, U 1028), University of Lyon, University Lyon 1, Lyon, FRANCE, [3]Lyon Neuroscience Research Center (UMR 5292, U1028), Lyon, FRANCE, [4]Cermep-In Vivo Imaging, Groupement Hospitalier Est, Lyon, FRANCE, [5]Institute of Chemistry and Biochemistry (ICBMS-UMR CNRS 5246), University of Lyon, Lyon, FRANCE.

Aim/Introduction: Subtype 6 of serotonin receptor (5-HT$_6$) is one of the more recently serotonin receptor identified, first in rat and then in human brain. The distribution of 5-HT$_6$ receptors in human is mainly in the striatum, but also in the pre-frontal cortex and the hippocampus. The 5-HT$_6$ receptor is a G protein-coupled receptor that as recently emerged as a new target for neuropharmacology since it plays a vital role in memory and cognitive processes, reinforcing its status as an emerging target in antidementia therapeutic agents. The aim of this study is to perform in vitro and in vivo pharmacological characterization of [^{18}F]2FNQ1P, a new radiotracer of 5-HT$_6$ receptors, in rat, pig, non-human primate, and human tissues. **Materials and Methods:** In vitro autoradiography and saturation binding assays were performed in post-mortem brain tissues from, rat, pig, non-human primate and healthy controls. Serum stability of [^{18}F]2FNQ1P after incubation in serum at 37°C for 2h was assess in all species. We studied brain unmetabolized radiotracer fraction and biodistribution in rats. **Results:** In all species, autoradiography revealed high binding levels in regions whith high density of 5-HT$_6$ receptors as striatum or pre-frontal cortex. A blocking effect was observed using an excess of antagonist specific ligand (SB258585), suggesting that the binding was specific. In binding assays, K_D and B_{max} values were respectively 1.34 nM and 0.03 fmol.mg^{-1} in rat, 0.60 nM and 0.04 fmol.mg^{-1} in pig, 1.38 nM and 0.07 fmol.mg^{-1} in non-human primate, and 0.93 nM and 0.17 fmol.mg-1 in healthy controls. Excellent serum stability of [^{18}F]2FNQ1P was observed for 2h. In rat, the amount of radioactivity from unmetabolized [^{18}F]2FNQ1P in brain was superior 99% at 5 minutes and decreased to 87% at 40 minutes with pre-injection of ciclosporin. In biodistribution studies, the highest concentration of radioactivity was found in the lungs (up to 3.5+/- 1.2 %ID/g) and kidneys (up to 2.0 +/- 0.7 %ID/g) at 15 minutes p.i but theses concentrations decreased after 60 minutes to 0.7 +/- 0.1 %ID/g and 0.9 +/- 0.1 %ID/g, respectively. **Conclusion:** The new data confirm the interest of [^{18}F]2FNQ1P as the first fluorinated and specific radiotracer for molecular imaging of serotonin 5-HT$_6$ receptors. A first in man PET study will ultimately determine the utility of [^{18}F]2FNQ1P as a PET radioligand. **References:** None.

OP-605

Exploring the impact of different aggression access levels in striatal dopaminergic system: a ^{11}C-raclopride PET study

R. Moraga-Amaro[1], *P. K. Feltes*[1], *B. L. Giacobbo*[1], *I. L. Alves*[2], *S. F. de Boer*[3], *C. M. Moriguchi-Jeckel*[4,5], *R. A. J. O. Dierckx*[1], *J. Doorduin*[1], *E. F. J. de Vries*[1];

[1]*Department of Nuclear Medicine and Molecular Imaging, University Medical Center Groningen, University of Groningen, Groningen, NETHERLANDS,* [2]*Department of Radiology and Nuclear Medicine, VU Medical Center, Amsterdam, NETHERLANDS,* [3]*Behavioural Neuroscience Unit, Neurobiology Department, Groningen Institute for Evolutionary Life Sciences, University of Groningen, Groningen, NETHERLANDS,* [4]*Biomedical Gerontology, Pontifical Catholic University of Rio Grande do Sul (PUCRS), Porto Alegre, BRAZIL,* [5]*Brain Institute of Rio Grande do Sul (BraIns), Pontifical Catholic University of Rio Grande do Sul (PUCRS), Porto Alegre, BRAZIL.*

Aim/Introduction: Excessive aggression is a major source of death and social stress, constituting a significant problem for public health. Understanding the mechanisms underlying the development of aggressive behaviour could help to control it. Interestingly, winning aggressive confrontations results in self-reinforcing pleasurable effects, suggesting a role for the reward system. The aim of this study was to compare the impact of two protocols of aggression with different levels of intensity on dopaminergic D2 receptor availability in the brain. **Materials and Methods:** Repeated social defeat model was used to train animals for aggression. 16 weeks old male outbred Long Evans rats (residents) were housed together with a tubal-ligated female Long Evans rat at least one week before the experimental phase. During aggression trials, females were removed from the cage and Wistar rats (intruders; 8 weeks old) were introduced. Attack latency (AL) was measured and used as a proxy for aggression. After submission, the intruder was either placed inside a wire mesh cage to allow closer resident-intruder interaction (close interaction group), or by a plexiglass partition, allowing visual and olfactory interaction, but not physical (mild interaction group). Residents with an AL higher than 60s were defined as non-aggressive control group. All animals underwent ^{11}C-raclopride PET scans (D2-receptor), either at least 2 weeks after the last resident-intruder interaction (control and close interaction group), or one day after an intruder exposure (mild interaction group). Binding potential (BP_{ND}) values in the striatal areas were obtained through the simplified reference region (SRTM) model , using the cerebellum as reference. **Results:** A significantly increased tracer uptake was found in the Nucleus Accumbens (NA) of close interaction animals when compared to controls ($p<0.05$), but not in mild interaction animals. Additionally, an increased tracer uptake was found in the Caudate Putamen (CPu) of close ($p<0.05$) and mild interaction animals ($p<0.001$), as compared to the control group. Correlations between BP_{ND} in NA and AL were found only in the control and close interaction groups ($p<0.05$). **Conclusion:** Increased levels of D2 receptor tracer binding in the NA and CPu were demonstrated when animals have access to higher levels of aggression (i.e. close intruder-resident interaction, instead of mild interaction). Only D2 receptor binding in NA was related with the attack latency of the animals, a brain region extensively associated with addiction and rewarding experiences. Therefore, we hypothesize that access to repetitive winning confrontations might lead to habit-forming escalated forms of aggression. **References:** None.

OP-606

Clinical applicability of a mathematical model for FET PET uptake kinetics in brain tumor patients

C. Lerche[1], *T. Radomski*[1], *P. Lohmann*[1], *C. Regio-Brambilla*[1], *L. Tellmann*[1], *J. Scheins*[1], *E. Rota Kops*[1], *H. Herzog*[1], *K. Langen*[1], *J. N. Shah*[1,2,3];

[1]*Institute of Neuroscience and Medicine 4, INM-4, Forschungszentrum Jülich GmbH, Jülich, GERMANY,* [2]*Institute of Neuroscience and Medicine 11, INM-11, JARA, Forschungszentrum Jülich GmbH, Jülich, GERMANY,* [3]*JARA - BRAIN - Translational Medicine, Aachen, GERMANY.*

Aim/Introduction: Several studies have demonstrated that changes of the tracer accumulation of O-(2-[18F]fluoroethyl)-L-tyrosine (18F-FET) in cerebral gliomas during the first hour after injection are variable depending on their grade of malignancy. Extraction of the parameter that describes the dynamic uptake behaviour is currently not possible in a clinical setting. The aim of this work was the evaluation of a recently developed method for extracting dynamic behaviour using a non-linear model for the ^{18}F-PET time activity curve (TAC). Emphasis was placed on enabling the use of the method in a clinical setting with limited acquisition times of about 20 to 40 min. **Materials and Methods:** The class of functions given by $\log(u)=\log(A)+0.5\log(t)-\kappa\sqrt{t}$ successfully reproduces all typically observed uptake kinetics of ^{18}F-FET, where $u=u(t)$ is the ^{18}F-FET uptake as a function of time, A is the amplitude parameter and κ is the curve shape parameter. The model was fitted to the average TACs obtained from all voxels inside the segmented tumour volume. The PET acquisition was started with the injection of the tracer, but only TAC data points obtained from reconstructed time frames lying between 20 and 40 min p.i. were included in the fit. We evaluated the model in PET images from 11 low-grade (LGG) and 16 high-grade (HGG) gliomas and with different dynamic framing schemes: 5 x 240 s, 6 x 200 s, 7 x 170 s, and 8 x 150 s. Results were also compared to a linear model and to results obtained using the complete 4-50 min p.i dynamic PET data. Diagnostic performance for identification of HGG was assessed by ROC curve analyses (with LOOCV) using the results from neuropathology as reference. **Results:** Diagnostic performance for HGG identification was best (accuracy=0.89, sensitivity=0.94, specificity=0.82, false rate (LOOCV)=0.15) when using the empirical model together with the complete PET data. Diagnostic performance for HGG identification for 20-40 min p.i. was best when using the linear model with 7x170sec framing (accuracy=0.78, sensitivity=0.63, specificity=1, false rate=0.22). Results for using the non-linear model with the same framing were slightly worse (accuracy=0.74, sensitivity=0.63,

specificity=0.91, false rate=0.26). **Conclusion:** The linear model fit and the non-linear model fit can be used in a typical clinical setting to assess the ^{18}F-FET uptake kinetics with an accuracy of 78% and 74%, respectively. However, using the entire dynamic PET data allows a more reliable identification of HGG. **References:** None.

1406

Do.MoRe - Parallel Session: Radiobiology and Dosimetry for Radioembolisation Therapy

Tuesday, October 15, 2019, 14:30 - 16:00 Lecture Hall 112

OP-607

The need for standardised activity measurements of ^{166}Ho-poly (L-lactic acid) microspheres for radioembolization therapy

K. M. Ferreira[1], *A. J. Fenwick*[1,2], *N. C. Ramirez*[1], *S. Chen*[3]; [1]*National Physical Laboratory, Teddington, UNITED KINGDOM,* [2]*Cardiff University, Cardiff, UNITED KINGDOM,* [3]*Quirem Medical B.V., Deventer, NETHERLANDS.*

Aim/Introduction: Radioembolization with Holmium-166 poly (L-lactic acid) microspheres (^{166}Ho-MS) is used to treat patients with inoperable liver tumours[1-3]. The total activity administered to the patient is typically determined using a radionuclide calibrator at the hospital. For each radionuclide, the radionuclide calibrator has a dial setting which is determined for a specific well-defined geometry in a standard position. A previous study highlighted the differences in the radionuclide calibrator response for liquid and microspheres forms when measuring radionuclides such as ^{90}Y[4]. In this work, the differences between measuring ^{166}Ho-chloride solution and ^{166}Ho-MS were investigated to consequently improve activity measurement of ^{166}Ho-MS. Calibration factors and volume correction factors were determined for the glass V-vial that will be used for delivery of ^{166}Ho-chloride solution,^{166}Ho-MS pre-therapy scout and ^{166}Ho-MS therapy vials. **Materials and Methods:** To understand the differences between chloride solution and microspheres, a series of glass vials with known activities were prepared at different densities (1.005g/cm^3-1.437g/cm^3) to mimic the density of ^{166}Ho-chloride and ^{166}Ho-MS. The vials were measured on an Atomlab-500, Capintec CRC-12 and the NPL secondary standard ionisation chamber (NPL IC). To confirm the results obtained from the density tests, additional vials were prepared by adding ^{166}Ho-chloride to inactive microspheres to mimic the scout and therapy geometries. For the volume correction factors a glass vial was prepared with 0.1g of ^{166}Ho-chloride solution and measured on each system. Incremental volumes of inactive carrier were then added to the vial with measurements being taken on each system between fills. Additional tests were performed using both scout (60mg ^{166}Ho-MS) and therapy (600mg ^{166}Ho-MS) vials to determine the effect of settling of the active microspheres within the glass vial. **Results:** The density tests demonstrated that differences of up to 30% can be observed for different commercial radionuclide calibrators. Settling tests showed discrepancies of up to 10% depending on the time of the measurement after shaking the vial. Volume tests indicate corrections of up to 5%. New dial settings and respective uncertainties were determined for both geometry types. **Conclusion:** Similarly, to the findings for ^{90}Y-microspheres, this study showed significant differences in calibration factors for ^{166}Ho-MS and ^{166}Ho-chloride solution for various commercially available radionuclide calibrators, highlighting the need to calibrate them individually for different measurement geometries. **References:** [1]Smits, et al. Lancet Oncology. 2012 Nov;13(11):e464. [2]Prince,J.F. et al. J Nucl Med. 59(4): 582-588(2018) [3]Radosa,C.J. et al. Cardiovascular and Interventional Radiology 42(3):405-412(2019) [4]Ferreira,K.M. et al. Appl. Radiat. Isot. 109, 226-230(2016).

OP-608

^{166}Ho-Only Versus ^{166}Ho-DI: A Qualitative And Quantitative Assessment

M. Stella, *A. Braat, M. Lam, H. de Jong, R. van Rooij; University Medical Center, Utrecht, NETHERLANDS.*

Aim/Introduction: With the increase in radioembolization procedures, the need for accurate dosimetry is compelling. To this purpose, an automatic protocol for healthy liver dosimetry based on dual-isotope (DI) SPECT imaging combining Holmium-166 (^{166}Ho) and Technetium-99m phytate (^{99m}Tc), was developed: ^{166}Ho-microspheres being used as scout and therapeutic particle and ^{99m}Tc to identify the healthy liver[1]. However, image quality is potentially compromised due to crosstalk: ^{99m}Tc influences ^{166}Ho image due to downscatter and vice versa. This study investigates the effect ^{99m}Tc downscatter has on ^{166}Ho dosimetry, by comparing ^{166}Ho-SPECT reconstructions of patient scans acquired before and after additional administration of ^{99m}Tc (referred to as ^{166}Ho-only and ^{166}Ho-DI respectively). **Materials and Methods:** The ^{166}Ho-only and ^{166}Ho-DI SPECT scans were performed in short succession, minimizing patient motion between acquisitions. Images were reconstructed using clinically available iterative reconstruction software, including attenuation and scatter correction. To compensate for ^{99m}Tc downscatter, its influence in the ^{166}Ho photopeak window was accounted for in the DI image reconstruction using energy window based scatter correction methods. The qualitative comparison was performed by independent blinded comparison by two experienced nuclear medicine physicians (>5 years) which assessed 65 pairs of SPECT/CTs, expressing their preference for either ^{166}Ho-DI or ^{166}Ho-only SPECT. Inter-observer agreement was tested by Cohen's kappa coefficient. For the quantitative analysis, two small volumes of interest, VOI_{TUMOR} and $VOI_{HEALTHY}$, were manually delineated on the ^{166}Ho-only reconstruction and then transferred to the co-registered ^{166}Ho-DI reconstruction. Absorbed dose within the resulting VOI_{TUMOR} and $VOI_{HEALTHY}$ was calculated based

on the planned therapeutic activity. **Results:** The qualitative assessment showed no distinct preference for either the ^{166}Ho-only or ^{166}Ho-DI SPECT with a kappa value = 0.093. Quantitative analysis indicated that the difference in mean absorbed dose between ^{166}Ho-DI and ^{166}Ho-only in the tumor region was -7.88 ± 9.75 Gy and -4.68 ± 3.77 Gy in healthy region. These differences were regarded as acceptable by treating physicians, considering the different aims within tumor and healthy liver: maximize treatment effectiveness while minimizing dose to healthy tissue. The Pearson correlation coefficient between ^{166}Ho-only and ^{166}Ho-DI for absorbed dose was 0.99 for VOI_{TUMOR} and 0.95 for $VOI_{HEALTHY}$. **Conclusion:** The dual isotope protocol enables satisfying ^{166}Ho-DI reconstructions within the clinical reconstruction framework, which will allow an automatic estimation of absorbed dose in both tumor and healthy liver and improve the current therapeutic activity calculation method, thus introducing true personalized dosimetry. **References:** [1]Braat, A. et al. J. Nucl. Med. 57, 1423 (2016).

OP-609

MAA-based Dosimetry predicts Tumor Response and Outcome in Patients with Hepatocellular Carcinoma after Selective Internal Radiation Therapy (SIRT)

J. Mutschler[1], *V. Gumpp*[2], *P. T. Meyer*[1], *C. Goetz*[1];
[1]*Department of Nuclear Medicine, Medical Center of the University of Freiburg, Faculty of Medicine, University of Freiburg, Freiburg, GERMANY,* [2]*Comprehensive Cancer Center Freiburg CCCF, Medical Center of the University of Freiburg, Faculty of Medicine, University of Freiburg, Freiburg, GERMANY.*

Aim/Introduction: Radioembolization of liver malignancies with Y90-loaded microspheres is an effective strategy in unresectable hepatocellular carcinoma (HCC). In the planning of selective internal radiation therapy (SIRT) both Lung- and Liver-Dosimetry are considered using models assuming a uniform distribution of microspheres but inapt to predict tumor response. In contrast published optimized predictive models using MAA-based dosimetry prior to therapy can provide good estimates of absorbed doses in tumor and healthy liver. Our aim was here to correlate the MAA-based dosimetry with tumor response and to assess its impact on median overall survival (OS) in patients treated with SIRT. **Materials and Methods:** 79 evaluable HCC lesions were retrospectively included from 27 unresectable HCC patients (median age 66 years) who underwent SIRT in our department (SIR-Spheres, Sirtex Medical Limited, Sydney, Australia). Three-dimensional predictive voxelized dose maps were computed from the Tc99m-MAA SPECT/CT data (PMOD Technologies LLC, Zürich, Schweiz) and the administered Y90-activities. Mean absorbed dose (Dmean) was evaluated for both tumor and healthy liver. The tumor response (assessed by volumetric changes 12 weeks after SIRT) and the overall survival were evaluated and their relationship with dosimetry was analyzed. Tumors were dichotomized in "responder" and "non-responder" according to the mRECIST criteria. A cutoff value was determined for Dmean using ROC analysis and the Youden-index. Kaplan-Meier estimate was used to describe OS curves. **Results:** A tumor Dmean cutoff of 112 Gy (sensitivity 0.65, specificity 0.85 and accuracy 0.79) was determined to predict tumor response. Dmean was substantially lower in healthy liver and showed an important variability (42+/-22 Gy) without occurrence of radioembolization-induced liver disease. In patients bearing multiple liver lesions Dmean values were pooled and a patient-based cutoff was determined. Patients with Dmean pooled > 95 Gy had an OS = 26 months, significantly longer (p=0.057) than the others (OS = 6 month). **Conclusion:** In unresectable HCC patients undergoing SIRT, tumor absorbed dose assessed using MAA-based dosimetry clearly correlates with tumor response and is also associated with prolonged OS. Pretreatment dosimetry may be used routinely to achieve a fully patient-adapted approach allowing treatment optimization or intensification - including higher tumor irradiation and minimizing risks of liver toxicity. Further studies are needed to confirm these findings and to evaluate the maximal tolerated liver dose. **References:** None.

OP-610

Modeling the biological effectiveness of non-uniform dose distributions delivered from selective internal radiation therapy

B. Bednarz;
University of Wisconsin, Madison, WI, UNITED STATES OF AMERICA.

Aim/Introduction: Recently, the SARAH trial, a large randomized phase 3 study in patients with advanced hepatocellular carcinoma (HCC), showed no benefit in terms of overall survival after receiving ^{90}Y-loaded resin microsphere selective internal radiation therapy (SIRT)[1]. These negative results could partially be explained by the absence of biologically-based dosimetric endpoints to prescribe the injected activity. This work describes a general method for assessing the biological effects of non-uniform dose distributions on tumors treated with SIRT. **Materials and Methods:** The approach is based on the concept of biologically effective dose (BED). Three different BED models are considered: (1) standard linear-quadratic dependent cell kill with dose-rate effects, (2) same as (1) but also accounting for proliferation, and (3) same as (2) but also accounting for immune system response. Tumor absorbed dose distributions were modeled as normal distributions with means μ [50 Gy,200 Gy] and standard deviations σ [0.25 Gy,100 Gy] based on PET/MR data measured at our institution and found in the literature. Using these models the equivalent uniform dose (EUD) was calculated for varying levels of non-uniformity. Although adjustable, it was assumed that the tumors had a repair half-time of 0.5 hrs, a repopulation time of 7 days, an $\alpha/\beta = 10$ and a α=0.35 Gy^{-1}. For the immune system model the immune cell interaction constant was set to 0.14 day^{-1} and the probability of immune cell destruction per immune cell interaction was set to unity. **Results:** The relative effectiveness values range from 1 to 1.23 for the parameters considered. The BED varied only slightly between the different models with a maximum difference of -1.2% between model (2) and (1) and 0.27% between model (3) and (1). The EUD changed significantly as a function of the BED

uniformity index σ/ μ in the tumor. **Conclusion:** The general method used in this work can be integrated into an image-based dosimetry workflow that could lead to improved prescription strategies for SIRT. The large uncertainties associated with the parameters used in this study could potentially be reduced by evaluating clinically-relevant biomarkers in patient samples or in vitro, which is an active area of ongoing research. **References:** [1]Vilgrain V et al. Lancet Oncol. 2017; 18: 1624-1636.

OP-611

Voxel-based Dosimetry in the Liver: Yttrium-90 Microspheres Radioembolization After SBRT

P. Ferreira[1], *F. P. M. Oliveira*[1], *R. Parafita*[1,2], *P. S. Girão*[3], *P. L. Correia*[3], *O. Pares*[1], *D. C. Costa*[1];
[1]*Champalimaud Centre for the Unknown, Champalimaud Foundation, Lisbon, PORTUGAL,* [2]*Mercurius Health, Lisbon, PORTUGAL,* [3]*Instituto de Telecomunicações, Instituto Superior Técnico - Universidade de Lisboa, Lisbon, PORTUGAL.*

Aim/Introduction: Voxel-based dosimetry of planning tumor volume (PTV) and normal liver volume (NLV) has been performed for several years in stereotactic body radiotherapy (SBRT). In this work we propose a methodology to implement voxel-based dosimetry for liver radioembolization using Yttrium-90 (^{90}Y) glass microspheres. Voxel-wise biological effective dose (BED) distributions of a patient previously treated with SBRT were combined with newly generated ^{90}Y-microspheres liver radioembolization BED distributions for further analysis. **Materials and Methods:** A patient with pancreatic carcinoma and a single liver metastasis was studied. The metastasis was previously irradiated with 48 Gy (10 MV SBRT) in three sessions and ten months later the patient underwent radioembolization due to disease progression. Radioembolization followed the glass microspheres manufacturer's protocol. This involved the assessment of the Technetium-99m (^{99m}Tc) labelled macroaggregated albumin (MAA) distribution captured pre-treatment with planar images and single-photon emission computed tomography (SPECT). Based on the microspheres manufacturer's protocol, a ^{90}Y-microspheres activity of 3.239 GBq was administered in one session via the right hepatic artery. Post-treatment ^{90}Y-microspheres positron emission tomography (PET) images were used to verify the ^{90}Y-microspheres distribution and to calculate the voxel-wise absorbed liver dose distribution. Voxel-wise BED distributions of both treatments was computed and summed to obtain the total BED [1]. Median BED was then computed in the PTV and NLV defined in the radioembolization volumetric imaging studies. **Results:** SBRT median absorbed doses were 48 Gy and 5 Gy in the PTV (190 cm³) and NLV (1880 cm³), respectively. Regarding the radioembolization, median absorbed doses were 78 Gy and 10 Gy respectively in the PTV (510 cm³) and NLV (1416 cm³). After computing the voxel-wise BED on both treatment distributions, the total voxel-wise BED distribution was obtained. The total BED median PTV (510 cm³) and NLV (1416 cm³) were respectively 168 Gy and 22 Gy. **Conclusion:** In this patient, based on the absorbed dose and BED, at least twice as much activity could have been administered during radioembolization keeping the NLV dose at safe values. Thus, we believe there is room for improvement in the microspheres manufacturer's protocol by attempting better treatment personalization, for instance, estimating the dose distribution based on the SPECT-MAA pre-treatment images to optimize the ^{90}Y-microspheres activity to be administered. Voxel-based dosimetry may be an important tool in the evaluation of personalized treatment efficacy and toxicity. **References:** [1] M. Cremonesi et al., "Radioembolization of Hepatic Lesions from a Radiobiology and Dosimetric Perspective", Front Oncol, 4(210):1-20, 2014.

OP-612

Key role of personalized dosimetry in dose adjustement for selective internal radiotherapy : retrospective study of patients treated with yttrium-90 resin microspheres

C. Subreville[1], *J. Pinaquy*[2], *J. Miguel*[1], *S. Buj*[2], *L. Bordenave*[2], *F. Debordeaux*[1];
[1]*Radiopharmacy - Bordeaux University Hospital, Bordeaux, FRANCE,* [2]*Department of Nuclear Medicine - Bordeaux University Hospital, Bordeaux, FRANCE.*

Aim/Introduction: Liver tumors present a high mortality rate. Curative treatments aren't feasible for all patients. Selective internal radiotherapy (SIRT) with yttrium-90-labeled microspheres is widely used for the treatment of patients with liver cancer. Single-photon and emission computed tomography/ computed tomography (SPECT/CT) with ^{99m}Tc-macroaggregated albumin (MAA) is used for the treatment planning. Several methods were proposed to calculate the activity of the treatment, but currently there is no real consensus in terms of absorbed dose to tumor and healthy liver. A dosimetric analysis using the dosimetry software, Simplicit^{90}Y®, was realized to define doses to the tumor and healthy liver, and to determine a threshold tumor dose that could predict progression-free survival. **Materials and Methods:** Patients suffering from hepatocellular carcinoma (HCC) and treated with ^{90}Y-labeled resin microspheres between 2013 and 2018 were included in a retrospective study. Simplicit^{90}Y® was used retrospectively to define the volumes of interest (VOIs) and to calculate the dose in each VOIs based on ^{99m}Tc-MAA SPECT/CT. Tumor, liver and healthy liver volumes were delineated with CT. The perfused volume was determined using adaptive thresholding method based on ^{99m}Tc-MAA SPECT/CT. A threshold tumor dose was calculated using receiver operating characteristic analysis with ^{99m}Tc-MAA SPECT/CT to predict a progression-free period over 6 months with a sensitivity of 100%. Time to progression of the target lesions (TTPL) and overall survival (OS) were evaluated using Kaplan-Meier tests and this comparison was based on a log-rank test. **Results:** Twenty-two patients were evaluated in retrospective study, including 18 patients with portal vein thrombosis (PVT). The mean injected activity was 0,96 ± 0,43 GBq. The mean dose delivered to the tumor was 140,0 ± 71,1 Gy and to the healthy liver was 13,3 ± 7,8 Gy. A threshold tumor dose of 105 Gy was determined with a sensitivity of 100% and a specificity of 70%. For patients with tumor dose of less than

105 Gy, median OS was 9 months (95% CI: 5-22 months) and TTPL was 3 months (95% CI: 2-6 months) versus 38 months (95% CI: 22-NC months) and 33 months (95% CI: 19-NC months), respectively, for those with a tumor dose of 105 Gy or more (P= 0,004 and P=0,0002). **Conclusion:** Personalized dosimetry based on ^{99m}Tc-MAA SPECT/CT is predictive of TTPL and OS in patients with HCC. The customized dosimetry software is essential to optimize treatment planning. **References:** None.

OP-613

Tumor control probability in the limit of high heterogeneity applied to Y-90 radioembolization therapy

P. Roberson, T. Devasia, Y. K. Dewaraja;
University of Michigan, Ann Arbor, MI, UNITED STATES OF AMERICA.

Aim/Introduction: Radiobiologic modeling in radioembolization (RE) has had some success in relating dosimetry estimates to treatment outcome. A challenge is to incorporate the expected heterogeneity of clonogen number and radiosensitivity into the model. Here, we use the formula in the limit of high heterogeneity[1], applied at the voxel level, to perform a preliminary description of tumor control probability (TCP). **Materials and Methods:** We express the voxel TCP for the ith voxel with biological equivalent dose BED_i using parameters BED_{50}= the equivalent dose required to control 50% of the tumor population and γ_{50}= the normalized slope of the TCP curve at 50% TCP. $TCP(BED_i)=1/2*erfc[SQRT(\pi*(1+\xi^2)/(\{BED_i/BED_{50}\}^2+\xi^2)*\gamma_{50}*(1-BED_i/BED_{50})]$where ξ is the ratio of relative standard deviations for log clonogen number and radiosensitivity. The tumor $TCP=\Pi_i^M [TCP(BED_i)]^{n_i}$ where $\Sigma_i^M n_i=1$ and the $\{n_i, BED_i\}$ represent the M-voxel tumor BED-DVH. The study population included primary and secondary intrahepatic malignancies treated with Y-90 RE using glass microspheres. Patients underwent Y-90 PET/CT imaging and retrospective dosimetry. The data set included 51 tumors in 20 treatments, split (22 tumors in 10 treatments) hepatocellular carcinoma (HCC) and (29 tumor in 10 treatments) metastatic (MET). Tumor control was determined using mRECIST criteria and a mean follow-up time of 16 weeks (range 7 to 33 weeks). Curve fitting maximized $\Pi_j[(TCP_j)^{z_j}*(1-TCP_j)^{(1-z_j)}]$ for binary outcome, z_j, over all tumors, j. **Results:** The optimum fit was found for large ξ, implying a probit-like fit curve where log-clonogen heterogeneity was dominant. There was no dependence of TCP on tumor volume. Optimum fit values were BED_{50}= 187 Gy and γ_{50}= 0.31 for the full data set (51 tumors in 20 treatments, AUC=0.74, sensitivity 82%, specificity 65%, calculated using a threshold corresponding to 50% TCP). Optimum fit values for the MET only dataset was BED_{50}=155 Gy and γ_{50}=0.44 (29 tumors in 10 treatments, AUC=0.83, sensitivity 96%, specificity 71%). mRECIST criteria implies a positive response if all but one of 6 partitions are controlled, for an apparent radiosensitivity (= $\ln(6)/BED_{50}$) of ~0.01 Gy^{-1}. **Conclusion:** The high heterogeneity formula was successfully used to describe tumor response as determined by mRECIST criteria for a voxelized TCP model. Optimum fits required the heterogeneity parameter set for log clonogen heterogeneity dominant. **References:** [1]Corlone MC, Warkentin B, Stavrev P, Fallone G. Fundamental form of a population TCP model in the limit if large heterogeneity. Med Phys 33:1634(2006).

OP-614

Inter-observer variability of ^{90}Y PET/CT dosimetry in hepatocellular carcinoma after glass microspheres transarterial radioembolization

N. Meyers, A. Jadoul, C. Bernard, R. Hustinx;
University hospital of Liege (division of nuclear medicine and oncologic imaging), Liege, BELGIUM.

Aim/Introduction: Strong correlation has been demonstrated between tumor dose and tumor response, and between healthy liver dose and side effects. Individualized dosimetry is increasingly recommended in the current clinical routine. However, hepatic and tumor segmentation could be complex in some cases. The aim of this study is to assess the reproducibility of the tumoral and non-tumoral liver dosimetry in selective internal radiation therapy (SIRT). **Materials and Methods:** Twenty-three patients with hepatocellular carcinoma (HCC) who underwent SIRT with glass microspheres (TheraSpheres®) were retrospectively included in the study, for a total of 25 treatments (1,98 +- 1,23 GBq). The mean absorbed doses in tumoral liver (TD) and non-tumoral liver (NTD) were determined using Simplicit90YTM software by three independent observers. The tumor and and non-tumor volumes were measured on the ^{90}Y PET/CT performed 24 hours after the treatment. One dosimetry dataset was obtained as part of the routine clinical practice by a medical physicist helped by a nuclear medicine (NM) physician with 10 years of experience in SIRT (A). The second was performed by a NM physician with 4-year experience (B). The third was performed by a resident with limited experience and who first performed 10 dosimetry assessments as a training (C). Inter-observer agreement was evaluated using the inter-class correlation coefficients (ICC), coefficients of variation (CV), and Bland-Altman plots. **Results:** A strong agreement was observed between all three readers for estimating the healthy liver volume (ICC: 0.98) and the non-tumoral liver dose (ICC: 0.97). Agreement was lower for tumor volume delineation (ICC : 0.94) and particularly for tumor dose (ICC : 0.73), especially for high values as shown by the Bland-Altman plots. Regarding TD, the CV(%) was 26.5, 26.9 and 20.2 between observers A-B, A-C and B-C, respectively. Regarding NTD, it was 8.5, 12.7 and 9.4. With a target dose >200Gy for the tumor and <50 Gy for the non-tumor liver, 7/25 patients (tumor) and 2/25 patients (non tumor) fell in different categories, i.e. target reached/not reached, depending on the observer. **Conclusion:** Using a standardized methodology, the estimation of the NTD is highly reproducible. Although the reproducibility of the assessment of tumor irradiation is overall quite high, large variations may be observed in a limited number of patients. **References:** None.

1407

Teaching Session 5 - Interactive Clinical Cases - Neuroimaging Committee: Neuroimaging ? Before Reading PET Scans

Tuesday, October 15, 2019, 14:30 - 16:00 Lecture Hall 113

OP-615

Introduction to PET/CT Acquisition of the Brain

J. Dickson;
University College Hospital, Institute of Nuclear Medicine, London, UNITED KINGDOM.

OP-616

Quantification for Dummies

R. Boellaard;
Dept. of Radiology and Nuclear Medicine, Amsterdam University Medical Centres, location VUMC, Amsterdam, NETHERLANDS.

OP-617

MRI and CT - Abnormal Findings Relevant for PET Reading

E. van de Giessen;
Department of Nuclear Medicine, Academic Medical Center, University of Amsterdam, Amsterdam, NETHERLANDS.

1408

Clinical Oncology - Parallel Session: Therapy - PSMA and More

Tuesday, October 15, 2019, 14:30 - 16:00 Lecture Hall 114

OP-618

177Lu PSMA-617 in advanced castration resistant prostate cancer patients:dosimetry and preliminary evaluation of IRST 185.03 phase II prospective study

M. Sansovini[1], *A. Sarnelli*[1], *S. Severi*[1], *F. Foca*[1], *M. Celli*[1], *M. Monti*[1], *S. Nicolini*[1], *E. Tardelli*[1], *M. Belli*[1], *F. Matteucci*[1], *M. Giganti*[2], *V. Di Iorio*[1], *U. De Giorgi*[1], *G. Paganellli*[1];
[1]*IRST, Meldola (FC), ITALY,* [2]*University of Ferrara, Ferrara (FE), ITALY.*

Aim/Introduction: Introduction/aim: Radio-ligand therapy (RLT) with ^{177}Lu-PSMA-617 is a promising option for patients (pts) with metastatic castration-resistant prostate-cancer (mCRPC). A prospective single arm, open label phase-II study (EUDRACT/RSO,2016-002732-32) on mCRPC started at IRST (Meldola, Italy) in April 2017. The study was designed to define efficacy, toxicity and the minimal effective dosage of ^{177}Lu-PSMA-617in mCRPC pts. Protective agents for salivary glands and kindey were co-administered and dosimetry was carried-out. **Materials and Methods:** Pts with histologically confirmed advanced mCRPC (PCWG3 criteria) previously treated with docetaxel, abiraterone or enzalutamide were enrolled in the study if the diagnostic PET/CT ^{68}Ga-PSMA images showed clear uptake (tumor to background ratio >2.5) at tumor sites previously assessed by CT or MRI. Folic polyglutamate tablets were orally administered as parotid glands (PGs) protectors and 500 mL of a 10% mannitol solution was intravenously infused to reduce kidney uptake before the injection of 3.7-5.5 GBq of ^{177}Lu-PSMA-617 repeated 4 times at interval of 8-12 weeks. The adsorbed dose calculation was performed with MIRD formalism (OLINDA/EXM software). Bryant and Day design taking into account the injected activity and the toxicity was used to estimate the sample size **Results:** At February 2019, 43 eligible pts were preliminary evaluated on response, toxicity and dosimetry. A concomitant decreased of PSA > 30% and objective response at post therapy whole body scan(pt WBS) was observed in 26 (60 %) pts after the first or 2nd cycle. Fifteen of 26 pts had more than 50% PSA reduction. Early PD within 4 months was reported in 18 (41%) of cases. Two pts (4.8%) had G3 and 8 pts (19.5%) had G2 haematological toxicity. Only three pts (6.9%) had mild G1 salivary gland toxicity and 8 (19.5%) had G1 renal toxicity. The median adsorbed doses(10 pts scanned) were 0.48 mGy/MBq (range: 0.33-2.63) for PGs, 0.70 mGy/MBq (0.26-1.07) for kidneys, 0.044 mGy/MBq (0.023-0.067) for red marrow and 0.04 mGy/MBq (0.02-0.11) for the whole body **Conclusion:** In this prospective phase II study, preliminary evaluation on response, toxicity and dosimetry confirms that ^{177}Lu-PSMA-617 RLT is safe and active in mCRPC pts. In advanced and end-stage patients, 3.7-5.5 GBq of ^{177}Lu-PSMA-617 per cycle can be safely injected and produced imaging responses at PSMA ptWBS along with significant PSA decrease. Toxicity outcomes and dosimetry data would indicate that the co-administration of polyglutamate tablets and mannitol solution can reduce side effect for salivary glands and kidneys **References:** None.

OP-619

Tandem PSMA Radioligand Therapy Using Ac-225 and Lu-177 in Advanced Prostate Cancer: Safety and Efficacy

H. R. Kulkarni, J. Zhang, A. Singh, A. Mishra, C. Schuchardt, R. P. Baum;
Theranostics Center for Molecular Radiotherapy and Precision Oncology, Zentralklinik Bad Berka, Bad Berka, GERMANY.

Aim/Introduction: PSMA radioligand therapy (PRLT) using Ac-225 labelled PSMA ligands is very effective, but xerostomia is dose-limiting. Lu-177 PSMA, on the other hand, is relatively safe, but there is a failure rate of up to 30 %. Hence an effective treatment with limited adverse effects is warranted for Lu-177 PSMA-refractory metastatic castration resistant prostate cancer (mCRPC) and for patients with disseminated bone and bone marrow metastases. The aim of our study was to analyze the safety and efficacy of tandem PRLT, administering Lu-177 and Ac-225 labelled PSMA ligands concomitantly. **Materials and Methods:** Tandem PRLT was performed in 43 patients with mCRPC (median

Gleason score 8) applying a combination of Lu-177 and Ac-225 (mean administered activity 4.0 GBq and 4.5 MBq, respectively) labelled PSMA ligand concomitantly. All laboratory parameters (including complete blood picture 2-weekly, renal function etc.) were regularly monitored. The patients were clinically followed up for Karnofsky performance score, visual analog scale for pain, and any other clinical symptoms, as documented on dedicated patient questionnaires. The objective response was evaluated by Ga-68 PSMA PET/CT. Serum PSA response was documented at least monthly. **Results:** Eight patients (18.6 %) complained of increasing pain (requiring intensification of analgesia for 1-2 days), most probably due to post-therapeutic flare. The most common symptom noted in 20 patients (46.5 %) was obstipation, requiring laxatives for short time. There was no worsening of pre-existing mild xerostomia in 2 patients (status post previous Lu-177 PSMA radioligand therapy and after EBRT of cervical spine metastases. Mild (G1-G2) xerostomia occurred as a new symptom in 8 patients (18.6 %) after treatment. G3 thrombocytopenia, G2 anemia and leucocytopenia were noted in 1 patient with progressive disease. Otherwise, there was no hematological toxicity; no worsening of counts even in patients with pre-existing anemia or pancytopenia. The median OS is not yet reached and median PFS was 6.9 months after follow-up of 14 months. On Ga-68 PSMA PET/CT, 27 (62.7 %) patients had partial remission, 5 (11.8 %) had a mixed pattern of disease and 11 (25.5 %) patients progressed. **Conclusion:** Tandem PLRT concomitantly administering Ac-225 and Lu-177 PSMA seems to be feasible, safe and effective in end-stage metastatic prostate cancer refractory to Lu-177 PSMA. It eventually permits dose estimations. The administered radioactivity of Ac-225 PSMA can be lowered and the risk of dose-limiting toxicity be minimized. There might be a potential synergistic effect using two radionuclides with different emission characteristics. **References:** None.

OP-620

Prognostic Tumor Markers In Men With Prostate Cancer Undergoing [^{177}Lu]Lu-PSMA-617

A. Yordanova[1], *P. Linden*[1], *S. Hauser*[1], *G. Feldmann*[1], *R. Fimmers*[1], *M. Essler*[1], *S. Holdenrieder*[2], *H. Ahmadzadehfar*[1];
[1]*University Hospital Bonn, Bonn, GERMANY,* [2]*Technical University of Munich, Munich, GERMANY.*

Aim/Introduction: Currently, prostate-specific membrane antigen-radioligand therapy (PSMA-RLT) is considered a last-line treatment option in advanced castration-resistant prostate cancer (CRPC). Despite these patients' poor prognosis, accurate estimation of their overall survival (OS) is essential to determining whether benefits exist from the treatment and whether loss of valuable time and unnecessary side effects can be avoided. The aim of the present study is to evaluate whether various biochemical markers can predict OS in men undergoing PSMA-RLT and whether the changes assessed after the first cycle of PSMA-RLT correlate with the OS. **Materials and Methods:** The tested tumor markers in this retrospective analysis were alkaline phosphatase (ALP), bone-specific alkaline phosphatase (BAP), prostate-specific antigen (PSA), lactate dehydrogenase (LDH), chromogranin A (CgA), and pro-gastrin-releasing peptide (pro-GRP). For the evaluation, we performed blood tests before each PSMA-RLT cycle and during follow-up visits (which were 2-3 months apart). All patients were followed up until their deaths. To test the correlations between the tumor markers and survival, we conducted log rank tests for the univariate analysis and the Cox proportional-hazards regression model with stepwise variable addition for the multivariate analysis. The significance level was set at $p < 0.05$. **Results:** The study included 137 patients who received a total of 487 PSMA-RLT cycles between January 2015 and November 2017. Of the tested biochemical tumor markers, baseline ALP (120 U/l cut-off) and LDH (248 U/l cut-off) correlated significantly with survival post-PSMA-RLT ($p < 0.001$ for both markers). Stable and/or decreased values in most of the initially abnormal parameters were associated with significantly better OS; these parameters were ALP ($p = 0.009$), LDH ($p = 0.005$), PSA ($p < 0.001$), and pro-GRP ($p = 0.013$). The BAP and ALP responses also correlated significantly with survival in patients with bone metastases ($p = 0.002$ and $p < 0.001$, respectively). Baseline PSA (400 ng/mL cut-off), pro-GRP (63 pg/mL cut-off) and CgA levels (100 ng/mL cut-off), as well as CgA changes after the first cycle, were not significant predictors of OS. **Conclusion:** Along with established tumor marker PSA, ALP, LDH, BAP, and pro-GRP were correlated with the OS of the prostate cancer patients who underwent PSMA-RLT. **References:** None.

OP-621

Response evaluation of ^{177}Lu-PSMA-617 RLT using PSA, Chromogranin A, and LDH in 100 patients

H. Rathke[1], *T. Holland-Letz*[2], *W. Mier*[1], *P. Flechsig*[1], *E. Mavriopoulou*[1], *M. Roehrich*[1], *K. Kopka*[3], *M. Hohenfellner*[4], *F. Giesel*[1], *U. Haberkorn*[1], *C. Kratochwil*[1];
[1]*Heidelberg University Hospital, Heidelberg, GERMANY,* [2]*German Cancer Research Center, Heidelberg, GERMANY,* [3]*Division of Radiopharmaceutical Chemistry, German Cancer Research Center (DKFZ), Heidelberg, Germany, Heidelberg, GERMANY,* [4]*Heidelberg University Hospital, Department of Urology, Heidelberg, GERMANY.*

Aim/Introduction: Partial neuroendocrine differentiation is common in prostate cancer (PCa), especially in high risk PCa and over time in up to 40 % of PCa patients, caused by selection pressure [1]. Neuroendocrine differentiation is associated with poor prognosis [2] and could affect PSMA-expression and radio-sensitivity. Aim of this work was to evaluate possible predictive lab markers for ^{177}Lu- Prostate specific Membrane Antigen (PSMA)-617- radioligand therapy (RLT). **Materials and Methods:** 100 patients with metastasized castration resistant prostate cancer (mCRPC) and PSMA-RLT were selected. Prostate specific antigen (PSA) as a secretory marker of prostate cancer cells, Chromogranin A as marker for neuroendocrine cells and lactate dehydrogenase (LDH) as a marker for cell turnover were selected for evaluation. PSA, Chromogranin A and LDH were

checked before each cycle of PSMA-RLT and for restaging. To assess tumor uptake, post-therapeutic scintigraphy was evaluated visually regarding quantitative tumor uptake and its homogeneity. **Results:** In total, 211 cycles of ^{177}Lu-PSMA therapy were evaluated. 35 patients had partial remission (PR), 16 patients stable disease (SD), 15 patients mixed response (MR) and 36 patients progression of disease (PD). All patients with partial remission had a normal baseline LDH and in majority a PSA <200 ng/ml. Chromogranin A doubling had an increased risk for progression with an Odds Ratio (OR) of 3.089 (KI 1.302 - 7.332). Normal LDH implied a reduced risk for progression with an OR of 0.094 (KI 0.017 - 0.518). Mainly intense tumor uptake in metastasis (uptake > salivary glands in the 24h p.i. emission scan) was a prerequisite to achieve PR with an OR of 60.265 (KI 5.038-720.922). **Conclusion:** Elevated LDH had an increased risk for progression of disease in PSMA-RLT. Doubling of Chromogranin A conducted into higher risk for non-response and PD. Furthermore, an increased risk for liver metastases was detectable with elevated Chromogranin A. Most beneficial constellation of lab parameters was a high tumor uptake in combination with a low LDH in patients before PSMA-RLT. High tumor uptake was a prerequisite to achieve PR. However, there were also several patients with PD despite high tumor uptake, indicating additional resistance mechanisms beyond tumor-dose. **References:** 1. Aparicio A, Logothetis CJ, Maity SN. Understanding the lethal variant of prostate cancer: power of examining extremes. Cancer Discov. 2011;1:466-468. 2. Hong P, Guo RQ, Song G, et al. Prognostic role of chromogranin A in castration-resistant prostate cancer: A meta-analysis. Asian J Androl. 2018;20:561-566.

OP-622

Preliminary Evaluation of Tumor Uptake and Laboratory Parameters After a Single Dose of ^{177}Lu-RM2 Radioligand Therapy in Metastatic Castrate-Resistant Prostate Cancer

R. Fernández[1], *V. Kramer*[2], *A. Hurtado de Mendoza*[1], *J. Flores*[1], *H. Amaral*[1,2];
[1]*Center for Nuclear Medicine & PET/CT Positronmed, Santiago, CHILE,* [2]*Positronpharma SA, Santiago, CHILE.*

Aim/Introduction: RM2 is a synthetic bombesin receptor antagonist that targets gastrin-releasing peptide receptors (GRPr). GRPr are highly overexpressed in several human tumors, including prostate cancer, providing a promising target for imaging and radionuclide therapy. Initial experiences with ^{68}Ga-RM2 PET/CT showed renal clearance, high physiologic uptake in the pancreas and suggested that this tracer could detect relapse of prostate cancer and metastases with high contrast in some patients. Aim: To evaluate early effects on blood tests after a single dose of ^{177}Lu-RM2 in patients with metastatic castration-resistant prostate cancer (mCRPC). **Materials and Methods:** The local ethical committee approved the study, and informed consent was obtained in all patients. Four patients (mean age ± SD, 72 ± 4,3 y) with late-stage mCRPC underwent both, ^{68}Ga-PSMA-11 and ^{68}Ga-RM2 PET/CT for target evaluation and laboratory workup according to the protocol. All patients received a single dose of 5,6 GBq ^{177}Lu-RM2. Laboratory parameters were evaluated at week 1, 4 and 8 post-injection, including blood count, creatinine serum levels, amylase and PSA values; these were compared to baseline values. A p value of < 0,05 was considered statistically significant. **Results:** Both PET/CT scans showed comparable tracer uptake and SUV values in tumor lesions, outside the expected physiological biodistribution. As expected, ^{177}Lu-RM2 accumulated well in tumor lesions and showed stable binding for at least seven days, as demonstrated by 3D SPECT/CT and planar images. Interestingly, ^{177}Lu-RM2 uptake in pancreatic tissue showed washout and reduced binding after 24-48h. No significant differences were found when comparing basal levels of red blood cells, leukocytes, platelets, creatinine or amylase levels after 1, 4 and 8 weeks from therapy. Although two patients showed a partial response during the first weeks, PSA values at 8 weeks remained stable or slightly elevated when compared to baseline. **Conclusion:** In this small cohort of patients with mCRPC, treatment with a single dose of ^{177}Lu-RM2 was well tolerated and no adverse effects were observed, proving the feasibility of ^{177}Lu-RM2 PRRT. Despite stable binding to tumor lesions, no therapeutic PSA-response was observed and additional work is needed to evaluate the real benefit of this novel theranostic agent. **References:** None.

OP-623

Efficacy of radium 223 in radioactive iodine refractory bone metastases from thryoid cancer: Preliminary results of a single arm Phase II trial

S. Zerdoud[1], *D. Deandreis*[2,3], *A. Maillard*[4,5], *I. Borget*[4,5], *C. Bournaud*[6], *L. Leenhardt*[7], *M. Terroir*[2], *A. Al Ghuzlan*[8], *M. Schlumberger*[2], *S. Leboulleux*[2];
[1]*Institut Universitaire du cancer Toulouse Oncopole, Toulouse, FRANCE,* [2]*Nuclear Medicine and Endocrine Oncology, Gustave Roussy and Paris Saclay, Villejuif, FRANCE,* [3]*Department of Medical Science, University of Turin, Turin, ITALY,* [4]*Biostatistics and Epidemiology Department, Gustave Roussy, Villejuif, FRANCE,* [5]*Fac. de médecine - UVSQ, INSERM, Université Paris-Saclay, 94805, Villejuif, FRANCE,* [6]*Nuclear Medicine, Groupement Hospitalier Est, Lyon, FRANCE,* [7]*Endocrine Oncology, Hôpital Pitié-Salpêtrière, Paris, FRANCE,* [8]*Pathology, Gustave Roussy and Paris Saclay, Villejuif, FRANCE.*

Aim/Introduction: Radium 223 is a therapy for symptomatic bone metastases from castration resistant prostate cancer. The aim of this trial was to evaluate the efficacy of Radium-223 in patients with bone metastases from radioactive iodine refractory (RAIR) thyroid cancer (TC). **Materials and Methods:** Multicenter prospective single arm two-stage Simon Phase II trial (NCT02390934). Primary objective establish efficacy of 3 monthly Radium-223 administrations by PERCIST FDG PET/CT criteria in RAIR TC patients with bone metastases without visceral metastases or progressive visceral metastases. Secondary objectives was to establish efficacy

of 6 monthly administrations of Radium-223 by FDG PET/CT according to PERCIST criteria, response on 99mTc-HMDP bone scan and 18 NaF PET/CT after 3 and 6 monthly administrations of Radium-223, and during treatment: monthly clinical benefits, changes serum bone markers and thyroglobulin levels and assess safety of Radium-223 according to NCI CTCAE version 4. **Results:** For first step analysis: 10 patients were prospectively enrolled between July 2015 and December 2017 (4 M; 6F Median Age 74 y, range 62-76). Papillary (n=5), Follicular (n=3) and Poorly differentiated TC (n=2). Delay between discovered first bone metastases and inclusion: 6 years (3-10). Bone lesions in the axial skeleton: all patients (median number: 4, 1-9) and bone lesions in peripheral skeleton 3/10. Median RAI treatments before Radium-223: 4 (3-6). Delay between last RAI treatment and inclusion was 3 yrs (1-5). Patients received previously external radiation therapy (n=9), interventional radiology treatment (n=3) and surgery (n=8). 9/10 patients received 6 cycles of radium 223. At FDG PET/CT PERCIST criteria, after: 3 monthly Radium 223 administrations patients presented 6/10 Stable Disease (SD) and 4/10: Progressive Disease (PD). One patient stopped Radium 223 for bone skeletal event needing urgent surgery. After 6 monthly Radium-223 administrations, 5/9 SD and 4/9 PD. At bone scan and at 18 NaF PET/CT, after 6 cycles of Radium 223, patients presented 9/9 SD and 8/9 SD and 1/9 Partial Response (PR) respectively. After 6 cycles of Radium not significant and durable reduction thyroglobulin and ALP levels. During the treatment only 1 grade 3 neutropenia, but during follow up 1 patient developed acute myeloid and 1 promyelocitic leukemia. **Conclusion:** According to metabolic response at FDG PET, preliminary data suggest no evidence of Radium-223 efficacy in RAI refractory TC patients with bone metastases. Long term follow up is ongoing to confirm these preliminary data. Furthermore awareness of long term toxicity is needed. **References:** None.

OP-624

Novel CT guided 188-rhenium Brachytherapy Device For Local Primary And Secondary Lung Malignancies

H. Belhadj-Tahar[1], *J. Chen*[2], *J. Zhao*[2], *J. Song*[3], *M. Quan*[2], *C. Li*[1], *X. Gu*[2], *G. Yang*[1], *Y. Gao*[2];
[1]*AFPREMED (French Association of Medical Research Advancement), Toulouse, FRANCE,* [2]*Shanghai East Hospital, School of Medicine, Shanghai East Hospital (China), Shanghai, CHINA,* [3]*Shanghai East Hospital, School of Medicine, Shanghai East Hospital (China), Shanghai, CHINA.*

Aim/Introduction: Stereotactic brachytherapy for extensive local tumors offers a very effective treatment option locally without significant complications in medically impaired patients who are not amenable to surgery. In this context, we have recently developed a new potential anticancer agent from Poly-L-Lysins dendrimer as a delivery nano system loaded with diffusible Imidazolic probes complexed with ^{188}Rhenium (physical half-life: 17hrs; with β: 2.12MeV, 71.1% and 1.965MeV, 25.6% and γ : 155keV, 15.1%) for targeting in particular hypoxic tumors resistant to conventional cancer treatments. The aim of the study reported herein was to evaluate the feasibility of this minimally invasive, percutaneous brachytherapy technique for tumor treatment in the lung. In addition, we assessed the safety and efficacy profiles of a novel nano-device derived from [^{188}Re] rhenium-ligand as radioactive ligand loaded 5th generation poly-L-lysins dendrimer in patients with unresectable Lung Malignancies. **Materials and Methods:** The experiment agent " ^{188}Rhenium-ImDendrim" is consisting of 5th generation poly-L-lysins dendrimer (172,3 kDa, 20 nM) mixed with nitro-imidazole-methyl-1,2,3-triazol-methyl-di-(2-pycolyl) amine at GMP grade (Gift from Nano-Gun-Technology NGT) and labelled with ^{188}Rhenium. The study was approved by Shanghai East Hospital ethics commette. 5 Patients received "^{188}Rhenium-ImDendrim" directly into lung tumors under CT-guidance, at an activity level of 162 MBq/cc of tumor (range 2 to 7 cm; mean diameter, 4 cm) . For voluminous tumors (>65 cc) the dose is given in divided injection spaced 2 weeks apart (Tumor of 115cc: 2 administrations, Tumor of 180cc: 3 administrations). Toxicity was assessed by the nature, incidence, and severity of adverse events (Common Toxicity Criteria scores) and by hematology and clinical chemistry parameters. At $T_{0.5hr}$, T_{4hr}, T_{24hr}, T_{36hr} , T_{72hr} post- administration patients get a control scintigraphy with SPECT gamma camera . The response to treatment is evaluated thanks to PET/CT Standardized Uptake Values (SUVs). **Results:** Stereotactic administrations of "^{188}Rhenium-ImDendrim" were successfully carried out in all patients under local anesthesia. The radioactive product diffuses in all tumoral volume and remains 72 hours post-administration with no significant diffusion out site of injection. One of the 5 patients reported discrete transitive hemoptysis as adverse events, but no serious events were attributable to the study device. All targeted tumors were responding at 12 weeks, with two complete responses. **Conclusion:** Percutaneous single and iterative administrations of this novel ^{188}Rhenium-Imdendrim brachytherapy device into lung cancers are safe and well tolerated. The initial data on therapeutic response are promising. **References:** Belhadj-Tahar and coll. Journal Clinical Oncology 2018 36:15.

OP-625

First Clinical Experience using 177Lu-Zoledronate for the Treatment of Skeletal Metastases in Breast Cancer: 68Ga-NODAGA-ZOL PET-CT imaging for patients eligibility and follow-up

F. Novruzov[1], *J. Aliyev*[2], *S. Rahimzade*[3], *R. Shukurov*[1], *J. Šimeček*[4], *L. Mehmetbeyli*[1], *Z. Allahverdiyeva*[5], *E. Mehdi*[1];
[1]*Department of Nuclear Medicine, National Centre Of Oncology, Baku, AZERBAIJAN,* [2]*Department of General Surgery, National Centre Of Oncology, Baku, AZERBAIJAN,* [3]*Department of Woman Health, National Centre Of Oncology, Baku, AZERBAIJAN,* [4]*Isotope Technologies Garching GmbH, Garghing, GERMANY,* [5]*Department of Medical Oncology, Central Clinical Hospital, Baku, AZERBAIJAN.*

Aim/Introduction: Metastatic bone cancer is a common and severe complication in advanced diseases. Around 70% of all

metastatic patients eventually develop bone metastases. In total, 60% to 75% of metastasis in breast cancer is diagnosed as bone metastasis at first. Radionuclide therapy is shown to be useful and cost effective in relieving bone pain in metastatic diseases and may be more effective when combined with chemotherapy. Herein we evaluate the response to 177Lu-DOTA-Zoledronate treatment and report the 68Ga-NODAGA-Zoledronate PET/CT findings of a breast cancer patient with multiple bone-only metastases in the axial and appendicular parts of the skeleton. **Materials and Methods:** A 65-year-old breast cancer patient with multiple bone-only metastases was referred for staging. 18F-NAF PET-CT performed before and 2 months after the pain treatment with 3700 MBq of 177-DOTA-Zoledronic acid. The eligibility for radionuclide treatment was determined with 68Ga-NODAGA-Zoledronate acid (192 MBq for 66 kg of weight) PET-CT imaging. The patient's blood test results (Hb: 15.1 g/dL, total white cell count: 8.21 × 103/µL, plt:277 109/L) made her eligible for the therapy with the bone-seeking agent. Patient also received 2 cycles of chemotherapy (adriamycin and cytoxan). Complete blood count, liver function tests, oncomarkers and blood creatinine were noted before and during the treatment. **Results:** The baseline 18-F NAF and 68Ga-Zoledronate PET/CT showed multiple intense and identical lytic lesions throughout the axial skeleton. In comparison with the pre-treatment 18F-NaF PET/CT images the SUVmax values of lesions were decreased up to 7 times. The patient gradually reduced the usage of the pain relief medication (fentanyl 50 mcg/hr, transdermal patch) which she took every 3 days and stopped using at all over one month. The main adverse effect was pancytopenia detected after 5 days, lasted nearly 7 weeks, which was difficult to differentiate whether this was due to the radionuclide treatment or concurrent/ongoing chemotherapy. **Conclusion:** Due to better physical properties of 177Lu compared to other bone pain palliation agents like (153Sm and 188Re), 177Lu-Zoledronate could be used as a potential new candidate in clinical trials for bone pain palliation therapy. This case illustrates the benefit of 68Ga-NODAGA-ZOL PET/CT in skeletal metastases of breast cancer to assess potential for radionuclide therapy with 177-Lu DOTA-Zoledronate and monitor treatment. **References:** None.

1409

Bone & Joint - Featured Session: Bone SPECT/CT and PET/CT Quantification - A Clinical Tool for Diagnosis and Prognosis in Diffuse and Localised Skeletal Diseases

Tuesday, October 15, 2019, 14:30 - 16:00 Lecture Hall 115

OP-626

Bone SPECT/CT and PET/CT Quantification - A Clinical Tool for Diagnosis and Prognosis in Diffuse and Localised Skeletal Diseases

T. Van der Wyngaert;
Antwerp University Hospital, Nuclear Medicine, Edegem, BELGIUM.

OP-627

Quantifying skeletal burden in fibrous dysplasia using Sodium Fluoride PET/CT

W. van der Bruggen[1,2], M. Hagelstein-Rotman[3], L. de Geus-Oei[2], F. Smit[4], S. P. D. S. Dijkstra[5], N. M. Appelman-Dijkstra[3], D. Vriens[2];
[1]Dept. of Nuclear Medicine, Slingeland Hospital, Doetinchem, NETHERLANDS, [2]Section of Nuclear Medicine, dept. of Radiology, Leiden University Medical Center (LUMC), Leiden, NETHERLANDS, [3]Center for Bone Quality, dept. of Internal Medicine, division of Endocrinology, Leiden University Medical Center (LUMC), Leiden, NETHERLANDS, [4]Dept. of Nuclear Medicine, Alrijne Hospital, Leiderdorp, NETHERLANDS, [5]Dept. of Orthopaedic surgery, Leiden University Medical Center (LUMC), Leiden, NETHERLANDS.

Aim/Introduction: To quantify Na^{18}F-PET/CT uptake in relation to clinical and biochemical parameters of fibrous dysplasia (FD) severity and healthy bone (HB) metabolism. Secondary aims: to compare different normalizations for volume of distribution, to determine the reproducibility of Na^{18}F-PET/CT uptake parameters in HB and FD and to relate Na^{18}F-uptake to skeletal burden score (SBS) and antiresorptive therapy and pain measured by Brief Pain Inventory (BPI). **Materials and Methods:** In a prospective pilot study (n=20), Na^{18}F-PET/CT parameters of HB and FD were determined by two independent readers to define the cut-off defining increased bone uptake, optimized normalization and interobserver agreement. Na^{18}F-PET/CT FD-parameters were related to SBS, serum biomarkers, medication, and clinical parameters. **Results:** Physiological bone standardized uptake value (SUV) was best normalized, but displayed large interpatient variation (total range 4.1-13.7 g/mL), with very high interobserver agreement (ICC=0.964). FD-burden defined by patient-specific SUV-cutoffs reached near-perfect agreement for SUVpeak (ICC=0.994) and total lesion fluorination (TLF) (ICC=0.999). TLF correlated weakly with SBS (R^2=0.384, p=0.047). TLF correlated positively with serum alkaline phosphatase (R^2=0.571, p=0.004) and procollagen type 1 N-terminal propeptide (R^2=0.621, p=0.002), SBS did not (p>0.06). SBS and TLF both correlated with increased fibroblast growth factor-23 (FGF-23) (R^2=0.596, p=0.007 and

R^2=0.541, p=0.015, respectively). TLF was higher in use of bisphosphonates (p=0.038), SBS was not. Average BPI-scores correlated to increased FGF-23, work-related BPI-scores to higher SBS (R^2=0.518, p=0.024), higher TLF (R^2=0.478, p=0.036) and to higher levels of FGF-23 (R^2=0.567, p=0.034). **Conclusion:** Individualized Na^{18}F-PET/CT SUV cut-offs reproducibly discriminated HB from FD and were well-normalized. The strong relations of bone formation serum markers with Na^{18}F-PET/CT FD-burden measurements suggest clinical relevance over SBS as an adjunct instrument in FD patients before treatment initiation. The correlation of both imaging modalities with increased work-related BPI-scores also indicates clinical applicability. Moreover, SBS is known to remain stationary irrespective of use of medication, whereas TLF on Na^{18}F-PET/CT was higher in baseline patients using antiresorptive therapy. This makes Na^{18}F-PET/CT a promising tool to quantitatively measure treatment efficacy in the follow-up of FD patients. To our experience, the advantages of Na^{18}F-PET/CT clearly outweigh the disadvantages over technetium bone scintigraphy. Depending on local availability and cost-effectiveness depending on costs and reimbursement, we foresee a more prominent role for Na^{18}F-PET/CT in primary diagnosis and follow-up of FD patients. **References:** None.

OP-628

^{18}F-NaF uptake by fibrous dysplasia bone lesions is positively associated with bone turnover markers (BTMs)

G. Z. Papadakis[1,2], *G. C. Manikis*[2], *A. H. Karantanas*[1,2], *K. Marias*[2], *U. Bagci*[3], *P. Florenzano*[4], *M. T. Collins*[4], *A. M. Boyce*[4];
[1]*Department of Radiology, Medical School, University of Crete, Heraklion, GREECE,* [2]*Computational Biomedicine Laboratory (CBML), Institute of Computer Science (ICS), Foundation for Research and Technology Hellas (FORTH), Heraklion, GREECE,* [3]*Center for Research in Computer Vision, University of Central Florida, Orlando, FL, UNITED STATES OF AMERICA,* [4]*National Institute of Dental and Craniofacial Research (NIDCR), Bethesda, MD, UNITED STATES OF AMERICA.*

Aim/Introduction: Fibrous dysplasia (FD) of bone is a benign skeletal disorder characterized by the replacement of normal bone and normal bone marrow with abnormal fibro-osseous tissue leading to significant morbidity. ^{18}F-NaF is a bone seeking PET-agent, which targets bone processes characterized by increased bone surface exposed to blood flow, such as the processes encountered in FD. Aim of the current study was to explore potential associations between FD-related ^{18}F-NaF activity in the entire skeleton, with established markers of bone activity, like serum levels of alkaline phosphatase (Alk Phos) and osteocalcin (OC), and urine levels of N-terminal telopeptide (NTX). **Materials and Methods:** Fifteen FD patients underwent whole-body ^{18}F-NaF PET/CT studies at the NIH Clinical Center. PET scans from the vertex of the skull to the plantar surface of the feet were obtained 62.36 ± 6.11 (mean ± SD) minutes (range: 58 - 76) after intravenous administration of an average ± standard deviation of 2.81 ± 0.83 mCi of ^{18}F-NaF (range: 0.92 - 4.98). Low dose, non-contrast, non-diagnostic CT scans were acquired for localization and attenuation correction purposes. FD-related ^{18}F-NaF activity was assessed by using MIM vista (version 6.5.9). Firstly, a VOI encompassing the entire skeleton was drawn, and afterwards a SUVmax threshold-based approach -customized per patient- was employed in order to include all FD-related bone uptake. Separate VOIs encircling all areas above the SUVmax threshold set by the user, were automatically generated and areas with physiologic or non-FD related ^{18}F-NaF activity (e.g. activity in the urinary tract, inflammatory uptake) were manually removed. Subsequently, FD-related ^{18}F-NaF activity in the entire skeleton determined as the product of SUVmean multiplied by the total volume (TV) of all skeletal ^{18}F-NaF positive FD lesions (TA = SUVmean × TV) was obtained automatically. **Results:** Pearson's correlation test revealed that skeletal FD-related ^{18}F-NaF activity was positively associated with serum levels of alkaline phosphatase ($r = 0.758$, $P < 0.01$), and osteocalcin ($r = 0.707$, $P = 0.01$), as well as urine levels of NTX ($r = 0.739$, $P = 0.02$). (P-values adjusted for false discovery rate) **Conclusion:** Skeletal FD-associated ^{18}F-NaF activity strongly correlates with bone turnover markers, suggesting that ^{18}F-NaF PET/CT accurately reflects underlying bone metabolic processes encountered in FD. These findings strongly imply the employment of this imaging modality for the in vivo assessment of FD activity, holding promise to serve as a surrogate endpoint for accurate determination of disease activity. **References:** None.

OP-629

Prognostic utility of ^{18}F-NaF PET/CT imaging for fractures in patients with fibrous dysplasia of bone

G. Z. Papadakis[1,2], *G. C. Manikis*[2], *A. H. Karantanas*[1], *K. Marias*[2], *U. Bagci*[3], *P. Florenzano*[4], *M. T. Collins*[4], *A. Boyce*[4];
[1]*Department of Radiology, Medical School, University of Crete, Heraklion, GREECE,* [2]*Computational Biomedicine Laboratory (CBML), Institute of Computer Science (ICS), Foundation for Research and Technology Hellas (FORTH), Heraklion, GREECE,* [3]*Center for Research in Computer Vision, University of Central Florida, Orlando, FL, UNITED STATES OF AMERICA,* [4]*National Institute of Dental and Craniofacial Research (NIDCR), Bethesda, MD, UNITED STATES OF AMERICA.*

Aim/Introduction: Fibrous dysplasia (FD) of bone is a benign skeletal disorder characterized by the replacement of normal bone and normal bone marrow with abnormal fibro-osseous tissue leading to significant morbidity. ^{18}F-NaF is a bone seeking PET-agent, which targets bone processes characterized by increased bone surface exposed to blood flow, such as the processes encountered in FD. Aim of the current study was to explore potential prognostic utility of ^{18}F-NaF-PET/CT for fractures in FD patients. **Materials and Methods:** Fifteen FD patients underwent whole-body ^{18}F-NaF-PET/CT studies at the NIH Clinical Center. PET scans from the vertex of the skull to the plantar surface of the feet were obtained 62.36±6.11 (mean±SD) minutes (range: 58

- 76) after intravenous administration of an average±standard deviation of 2.81±0.83 mCi of ^{18}F-NaF. Low dose, non-contrast, nondiagnostic CT scans were acquired for localization and attenuation correction purposes. FD-related ^{18}FNaF activity was assessed by using MIM vista (version 6.5.9). Firstly, a VOI encompassing the entire skeleton was drawn, and afterwards a SUVmax threshold-based approach -customized per patient- was employed in order to include all FD-related bone uptake. Separate VOIs encircling all areas above the SUVmax threshold set by the user, were automatically generated and areas with physiologic or non-FD related ^{18}F-NaF activity (e.g. activity in the urinary tract, inflammatory uptake) were manually removed. Subsequently, the following FD-related ^{18}F-NaF parameters were automatically obtained from the extracranial skeleton (i.e., total skeleton without the skull): Total Volume (TV) of all ^{18}F-NaF positive FD lesions, and total lesions activity determined as the product of SUVmean multiplied by the total volume (TV) of the ^{18}F-NaF positive FD lesions (TA = SUVmean × TV) detected in the extracranial skeleton. **Results:** TV of extracranial FD showed very strong correlation with lifetime fractures (Spearman's rank correlation coefficient rho = 0.897, P < 0.001) and mean fractures per year (rho = 0.873, p < 0.001). Similarly, TA of extracranial FD was strongly associated with lifetime fractures (rho = 0.87, p < 0.001) and mean fractures per year (rho = 0.844, p < 0.001). **Conclusion:** Total volume (TV) and total activity (TA) of ^{18}F-NaF avid bone lesions in the extracranial skeleton is of prognostic utility for fractures in patients diagnosed with FD of the bone. This data suggests prognostic application of ^{18}F-NaF PET/CT imaging for selection of FD patients with increased risk for bone fractures. **References:** None.

OP-630

Quantitative ^{99m}Tc-DPD-SPECT/CT for the detection of prosthetic loosening in patients with hip- and knee joint replacement - an interim Analysis of a prospective imaging study

M. Braun[1], *M. Cachovan*[2], *A. H. Vija*[3], *G. Pagenstert*[4], *D. Wild*[1], *M. Kretzschmar*[1];
[1]*University Hospital of Basel, Clinic of Radiology and Nuclear Medicine, Basel, SWITZERLAND,* [2]*Siemens Healthcare GmbH, Molecular Imaging, Forchheim, GERMANY,* [3]*Siemens Medical Solutions USA, Inc., Molecular Imaging, Hoffman Estates, IL, UNITED STATES OF AMERICA,* [4]*University Hospital of Basel, Department of Orthopedic Surgery, Basel, SWITZERLAND.*

Aim/Introduction: To evaluate the diagnostic performance of standardized quantitative ^{99m}Tc-DPD-SPECT/CT with and without use of anatomical bone segmentation as well as with and without mitigation for CT metal artefact reduction in patients with painful knee and hip joint prostheses suspicious for loosening. **Materials and Methods:** Thirteen consecutive patients with a total of 22 prostheses (13 hip and 9 knee prostheses) underwent ^{99m}Tc-Dicarboxypropandiphosphate(DPD)-SPECT/CT 3h after injection of ^{99m}Tc-DPD (mean dose 697MBq). Quantitative reconstruction was performed with Siemens xSPECT-Quant and xSPECT-Bone, with and without iMAR-reconstruction of CT data which show high Z-material streak artefacts. SUVmax means were correlated to intraoperative findings or clinical outcome after 1 year (standard of comparison). Cut-off values and accuracy of the different reconstructions were calculated using receiver operator characteristics (ROC) and compared to the accuracy of visual SPECT/CT readings by a senior physician and a trainee blinded for the quantitative data and clinical outcome. **Results:** SUVmax were significantly higher in loose prostheses compared to stable prostheses, with all methods of quantification used (p=0.018-0.001). For xSPECT Bone quantification, diagnostic accuracy was 91% without iMAR (cut-off SUVmax 13.4, sensitivity 88%, specificity 93%). With iMAR, accuracy of xSPECT Bone was 95% (Cut-off SUVmax 13.8, sensitivity 100%, specificity 93%). For xSPECT Quant without iMAR, accuracy was 85% (Cut-off SUVmax 10.3, sensitivity 100%, specificity 83%). For xSPECT Quant with iMAR, accuracy was 83% (Cut-off SUVmax 11.1, sensitivity 88%, specificity 86%). Diagnostic accuracies of blind-readers were 79% for an experienced reader, and 71% for a trainee. **Conclusion:** This interims analysis provides first evidence that quantitative uptake values of periprosthetic bone metabolism using ^{99m}DPD-SPECT/CT with xSPECT Quant and Bone reconstructions has a higher accuracy compared to conventional scan reading underlining the high potential of quantification as a biomarker for the diagnosis of prosthetic loosening. The use of iMAR reconstructed CT in the xSPECT Quant and xSPECT Bone reconstruction only mildly impacts attenuation correction but improves image quality of CT and xSPECT Bone. **References:** None.

OP-631

Prognostic value of NaF-PET/CT in non-instrumented posterolateral lumbar fusion

C. Constantinescu[1], *R. Piri*[1,2], *O. Gerke*[3], *M. Andersen*[4], *P. Høilund-Carlsen*[1,2];
[1]*Department of Nuclear Medicine, Odense University Hospital, Odense, DENMARK,* [2]*Research Unit of Clinical Physiology and Nuclear Medicine, Department of Clinical Research, University of Southern Denmark, Odense, DENMARK,* [3]*Odense University Hospital, Odense, DENMARK,* [4]*Center for Spine Surgery and Research, Sygehus Lillebælt, Odense, DENMARK.*

Aim/Introduction: Non-instrumented posterolateral lumbar fusion is the treatment of choice in Scandinavia for spinal stenosis patients with degenerative spondylolisthesis. Positron emission tomography (PET) with 18F-sodium fluoride (NaF) is an imaging modality capable of showing ongoing calcium deposition in vivo. We aimed to investigate the prognostic value of NaF-PET/CT performed in this category of patients one month after treatment with non-instrumented posterolateral lumbar fusion. **Materials and Methods:** 18 patients (median 66.5 years, range 60-78, 13 females) underwent 90-minute NaF-PET/CT one month after surgery for degenerative spondylosis. Fusion status was determined using high resolution CT within a year of surgery. Clinical characteristics including walking distance, VAS score of back pain (VAS-B), Oswestry Disability Index questionnaire (ODI),

and European Quality of Life - 5 Dimensions questionnaire (EQ-5D) were assessed before surgery and 1 year after. The changes in clinical parameters between the time points were compared with the graft NaF uptake in each patient. **Results:** Only 4 of 18 patients experienced fusion, which was bilateral and multilevel in all four. The median graft uptake (range) in fused patients was 1178(961-1279) SUV compared to 1333(474-27817) SUV in non-fused patients (p = 0.93). The corresponding partial volume corrected values were 1282(962-9535) SUV and 1341(481-27842) SUV (p = 0.35). Fused patients showed a median increase in walking distance of 737 (0-985) meters compared to 855(360-985) in non-fused patients (p = 0.29), a median decrease in VAS-B of 4.3(0-8.3) vs 3.8(0.1-8.5) (p=0.92), a median decrease in ODI of 25(12-54) vs 29.5(4-38) (p=0.56), and a median change in EQ-5D of 0.279(0.53-0.674) vs 0.277(0-0.611) (p = 0.56). Graft NaF uptake was not significantly correlated with walking distance (p = 0.3), VAS-B (p = 0.62), ODI (p = 0.22) or EQ-5D (p = 0.78). **Conclusion:** Total NaF uptake in the graft region measured one month after surgery was not able to predict change in any of the measured clinical parameters from baseline to one year after surgical treatment. However, there was no difference either in the change of clinical parameters suggesting that the examined sample of patients and the fraction of patients with fusion were too small to allow detection of potential differences. **References:** None.

OP-632

The role of ^{18}F-NaF PET/CT imaging in the assessment of patients undergoing spinal fusion surgery

A. Sammartano, M. Scarlattei, G. Baldari, S. Migliari, F. Tartara, L. Ruffini;
Azienda Ospedaliero-Universitaria di Parma, Parma, ITALY.

Aim/Introduction: Lumbar intercorporal fusions are performed to treat symptomatic segmental degeneration or instability in the spine. After spinal fusion surgery patients may have recurrent symptoms requiring standard evaluation by clinical examination and conventional imaging. However, CT and/or MRI will often show extensive and nonspecific postoperative changes. ^{18}F-fluoride is a PET tracer depicting blood flow and osteoblastic activity. Aim of this study was to assess osteoblastic activity in the spine as sign of local reparative process after implantation of intersomatic cages using ^{18}F-NaF PET/CT imaging **Materials and Methods:** Fifteen patients with intercorporal fusions were submitted to a PET/CT scan with ^{18}F-NaF. Time interval between fusion surgery and the PET/CT examination was variable according to symptoms recurrence ((1 day-3 years). The level of surgery was mainly L4-L5 and L5-S1. PET dynamic images of the specific spine tract were acquired immediately after i.v. injection of ^{18}F-NaF on a hybrid scanner Discovery IQ (GE Healthcare). Whole-body PET/CT was acquired from base of skull to pelvis 60 minutes after tracer injection and late image after 90 minutes on the site of cages. In all patients, a non-diagnostic CT was acquired for attenuation correction. **Results:** PET imaging with 18F-NaF PET/CT was performed in 15 patients (6 female and 9 male, mean age 59 years, age range 41-77 years). Administerd activity was 1,5-3,7 MBq/Kg. Images were evaluated by two independent expert nuclear medicine physicians. Uptake was defined as linear if present along the vertebral contour or focal. Linear (9) or focal (2) uptake was revealed in all patients without changes at different acquisition time. In 3 patients tracer uptake was multilevel. SUVmax ranged from 5.8 to 7.3 (mean 6.4, median 6.2). Four patients were submitted to surgery **Conclusion:** In this pilot investigation, ^{18}F-NaF PET/CT imaging showed potential utility for evaluation of recurrent symptoms after spinal fusion surgery by identifying those patients requiring surgical management. 18F-fluoride uptake was variable at different time between surgery and PET scan suggesting a role in understanding osteoblastic reparative bone reaction and its correlation with persistence or recurrence of symptoms. **References:** None.

1410

General Nuclear Medicine - Parallel Session: General Nuclear Medicine

Tuesday, October 15, 2019, 14:30 - 16:00 Lecture Hall 116

OP-633

Renal Clearance Function Index - a New Quantitative Parameter of a Dynamic Renal Scintigraphy

K. Filipczak[1], P. Cichocki[2], M. Surma[2], A. Plachcinska[1], J. Kusmierek[2];
[1]Department of Quality Control and Radiological Protection, Medical University of Lodz, Lodz, POLAND, [2]Department of Nuclear Medicine, Medical University of Lodz, Lodz, POLAND.

Aim/Introduction: Assessment of a kidney function by the dynamic renal scintigraphy (DRS) is based both on the visual analysis of sequential scintigraphic images and a course of renographic curves with respect to T_{max} and $T_{1/2}$, as well as a split function (SF). The relative nature of SF makes it impossible to reliably assess the real efficiency of renal parenchyma in some situations. Therefore, a parameter was determined which reflects a kidney function in an absolute way and could expand diagnostic capabilities of DRS in many clinical situations. **Materials and Methods:** The study involved 138 kidneys, from adult patients with measured serum creatinine level. Standard dynamic renal scintigraphy was performed, with detector field of view covering kidneys as well as heart. A ^{99m}Tc-EC radiopharmaceutical, in activity of 111MBq, was used. A sequence of 120 images (10s acquisition each) was acquired, then processed with the in-house developed method. This method included among others generation of a cardiac curve (from the cardiac ROI), standardization of cardiac and renographic curves (dividing them by the area under the cardiac curve) and calculation of a clearance function index (CFi) for each kidney. For the purpose of assessment of inter-observer

variability of the method, definition of ROIs, curves generation and calculation of CFi was done twice, by two operators. In addition to the renoscintigraphic study, a glomerular filtration rate value was estimated (eGFR) for each patient using the MDRD formula (taking into account patient creatinine level, age and sex). Based on the SF, eGFR coefficients were estimated separately for each kidney (KeGFR). The obtained values of CFi and SF were compared with the KeGFRn values. **Results:** The correlation coefficient between CFi and KeGFR was high - 0.83 and statistically significant (p<0.0001) - significantly higher than the correlation coefficient between SF and KeGFR, which was 0.65 (p<0.0001). Correlation between CFi values obtained by two operators was very high (0.99) and statistically significant (p<0.0001). **Conclusion:** The generated renal clearance function index (CFi) is a new absolute, non-relative and reproducible parameter, describing a clearance function of each kidney separately, which can be compared between patients. It can be useful in assessment of the damage of a kidney parenchyma, especially in clinical situations when the usefulness of the relative percentage uptake is limited. **References:** None.

OP-634

Effect of adenosine infusion on renal blood flow (RBF) during stress Rb-82 PET/CT

G. Allenbach, N. Testart, M. Meyer, M. Nicod Lalonde, J. Prior; Lausanne University Hospital, Lausanne, SWITZERLAND.

Aim/Introduction: Rb-82 dynamic perfusion PET is used to quantify myocardial blood flow. With the extended field of view in newest PET scanners it becomes possible to measure renal Rb-82 uptake opening the door to renal blood flow quantification. Our aim is to measure the effect of adenosine infusion on renal blood flow (RBF) using Rb-82 in patient with coronary heart disease. **Materials and Methods:** We selected 16 consecutive patients referred for suspicion of myocardial ischemia, 6 with normal myocardial perfusion imaging (no ischemia) and normal myocardial flow reserve (>2) and 9 with stress ischemia and a reduced flow reserve (<2). Myocardial 6-min adenosine stress and rest PET acquisitions were obtained after injection of 300-700 MBq of Rb-82. On the 6-minutes dynamic PET series 3 spherical VOI were placed on the upper pole of each kidney. A VOI on the aorta was used for vascular input function. Using the PMOD software, a 1-compartment model was used to compute K1 without further corrections applied. **Results:** Mean RBF at rest was 1.33±0.39 ml/min/g in the non ischemic group and 1.03±0.3 0ml/min/g in the ischmic group. Mean RBF at stress was 1.39±0.28 ml/min/g for the non ischemic group and 0.85±0.36 ml/min/g (0.91-1.81) for the group with myocardial ischemia with a significant difference (p=.012). We observed a decrease of 19% RBF under adenosine perfusion in the group known for myocardial ischemia and an increase of 2% in the group without ischemia. **Conclusion:** Assessment of RBF during cardiac perfusion scan is possible. Adenosine stress seems to induce a reduction of RBF in patient with myocardial ischemia, and had no effect on RBF in a group without myocardial ischemia. **References:** None.

OP-635

Tailoring the sampling time of single-sample GFR according to renal function: is the proposal in the British Nuclear Medicine Society GFR guidelines practical and supported by evidence?

S. Townrow[1], H. McMeekin[1], M. Burniston[1], F. Wickham[2], B. Fongenie[2], D. McGowan[3], C. Porter[3], A. Bradley[4], M. Memmott[4], N. Vennart[5], M. Barnfield[6];
[1]Barts Health NHS Trust, London, UNITED KINGDOM, [2]Royal Free London NHS FT, London, UNITED KINGDOM, [3]Oxford University Hospitals NHS FT, Oxford, UNITED KINGDOM, [4]Manchester University NHS FT, Manchester, UNITED KINGDOM, [5]Gateshead Health NHS FT, Gateshead, UNITED KINGDOM, [6]Leeds Teaching Hospitals NHS Trust, Leeds, UNITED KINGDOM.

Aim/Introduction: In the UK, GFR studies have been routinely determined using a slope intercept calculation with the blood plasma samples taken typically in the range from 2 - 6 hours post injection. The revised 2018 BNMS GFR guidelines recommend a single-sample technique with the sampling time dictated by the expected renal function, but this is not known with any accuracy before the test. We aimed to assess whether the sampling regime suggested in the guidelines is optimal, and determine the expected error in GFR result if the anticipated eGFR differs significantly from the GFR measured in the study or venous sampling occurs at the wrong time. We can then infer the degree of flexibility in the sampling regime. **Materials and Methods:** Data from over 8000 patients referred for GFR assessment at 6 different UK hospitals for a variety of indications were reviewed. The difference between the single-sample (Fleming) GFR result at each sample time and the slope-intercept GFR result in routine clinical use at each hospital was calculated. Data points were excluded if the sample was taken outside a series of time windows around the intended time. A further analysis was performed on 660 patients who had completed a more thorough 9 point area-under-the-curve study for renal clearance up to 8 hours post-injection, to determine if there was any systematic variation between slope intercept and single-sample GFR results. **Results:** The optimal sampling time is determined based on the accuracy (bias) and reproducibility (precision) of the result. At low GFR (< 60 ml/min/1.73m²) single-sample measurements are more precise at longer sampling times, but also show a systematic positive bias of up to 6 ml/min/1.73m² compared with the slope intercept values. At intermediate GFR (60 - 100 ml/min/1.73m²) single-sample results are both accurate and precise when the blood sample is taken between two and four hours post-injection. For higher GFR values the study becomes imprecise if the blood sample is collected later than 2 hours post-injection, and there is a systematic negative bias of up to 10 ml/min/1.73m² compared with the slope intercept values. **Conclusion:** The data supports the approach of the guidelines and demonstrates a reassuringly wide range of sample times for an acceptably accurate single-sample GFR result. This needs to be further validated with a reference technique out to 24 hours post injection rather than a limited sample slope-intercept GFR calculation. **References:** None.

OP-636

Utility Of The Isotopic Renogram And SPECT/CT In The Urinary Leaks Diagnosis And Management In Patients With Renal Transplantation

J. Gómez Hidalgo, M. Ruiz Gómez, P. Turbay Eljach, N. Álvarez Mena, A. Sainz Esteban, M. Alonso Rodríguez, C. Gamazo Laherrán, B. Pérez López, M. González Soto, R. Ruano Pérez;
Hospital Clínico Universitario de Valladolid.
Medicina Nuclear, Valladolid, SPAIN.

Aim/Introduction: to evaluate the contribution of the isotopic renogram, early and delayed planar image and delayed SPECT/CT to the diagnosis of urinary leakage in patients with kidney transplantation. **Materials and Methods:** we studied 394 patients who underwent cadaver kidney transplantation from January 2011 to December 2016. Twenty-four hours after transplantation we performed a 30 minutes renogram study focusing on the abdomen in anterior projection after the administration of 370 MBq of ^{99m}Tc-DTPA, followed by planar images at 30 and 180 minutes post-injection. In 81 of these patients we performed isotopic renogram controls. In addition, 46 patients underwent delayed abdominal SPECT/CT (22 cases at 24 hours post-transplant and 24 patients in renogram controls). **Results:** of the 394 patients (age: 59.0+/-13, 275 men), in 46 urine leak was suspected. Isotopic renogram with early and delayed planar images and delayed SPECT/CT were performed in all of them, confirming urinary leak in 17 (4.3% of the total and 36.9% of the diagnostic suspicions) and ruling out the urinary leakage in the rest. Of the 17 patients with urinary leak, in 15 cases the delayed planar image and SPECT/CT were necessary for the diagnosis (location and extension) and in the other 2 patients the SPECT/CT confirmed the diagnosis suspicion and improved the localization and extension. Of the 17 patients with urine leakage, 6 were diagnosed in the scintigraphic image performed 24 hours post-transplant and 11 cases in the renogram controls performed at 6 days (2 patients), 8, 9, 10 (2 patients), 11, 12, 22, 28 and 40 days post-transplant (mean: 9.88 days and median: 8 days). All cases of urinary leakage resolved satisfactorily after scintigraphic diagnosis. **Conclusion:** the renogram in transplant patients allows detecting urinary leaks as a surgical complication, facilitating the implementation of corrective measures at an early stage. Delayed planar imaging and SPECT/CT are especially useful in the diagnosis of urinary leakage, improving the assessment of its extension and location. **References:** None.

OP-637

Quantification of pulmonary function using hybrid SPECT/CT in normal subjects

C. C. M. Fernandez, E. Silvera, S. Rodriguez, A. Damian, R. Ferrando;
Clinics Hospital, University of the Republic, Montevideo, URUGUAY.

Aim/Introduction: Planar perfusion scintigraphy with 99mTc-MAA allows a non-invasive preoperative quantification of regional lung function in patients with pulmonary malignancies and compromised function. However, subdividing lung parenchyma into rectangular regions of interest, as done on planar images, poorly reflects true lobar anatomy. SPECT/CT allows analyzing pulmonary function based on individual 3D perfusion obtained through low dose CT segmentation. The aim of our study was to determine 3D normal values of perfusion for the whole lungs and each pulmonary lobe using SPECT/CT. **Materials and Methods:** We performed a unicenter retrospective analysis including 20 normal subjects (9 males; mean age 60 years, range 36-84) without history of lung pathology, derived to our center for pulmonary perfusion scintigraphy with 99mTc-MAA. After intravenous injection of 200 MBq planar images in standard projections and SPECT/low-dose CT images were acquired in a Mediso AnyScan 16 gamma camera. Data was analyzed using Mediso Lung Lobe Segmentation software to determine relative perfusion and relative volumes. **Results:** A total of one hundred lobes were quantified. In females the results of segmented quantification (mean [CI 95%], perfusion/volume) were: right upper lobe: 36.3(31.9-40.7) / 36.0 (32.2-36.0), middle lobe 5.1 (3.9-6.3) / 6.9 (5.4-8.2), right lower lobe 14.0 (11.3-16.7) / 12.6 (10.4-14.9), total right lung 55.3 (53.0-57.8) / 55.8 (54.3-57.3), left upper lobe 27.3 (25.3-29.3) / 30.4 (28.4-32.4) left lower lobe 17.3 (14.1-20.4) / 15.1 (11.8-18.4) and total left lung 46.4 (42.8-49.9) / 45.1 (42.5-47.6). In males: 29.9 (25.2-34.6) / 26.8 (23.1-30.4), 9.7 (7.1-12.2) / 12.0 (10.0-14.0), 15.3 (11.2-19.5) / 15.7 (12.4-18.9), 55.1 (52.0-58.2) / 55.2 (53.2-57.3), 28.6 (25.2-32.1) / 28.2 (25.3-31.1), 16.4 (13.9-18.9) / 17.7 (14.5-20.9) and 44.9 (41.2-48.0) / 44.8 (42.7-46.8), respectively. Middle lobe perfusion was lower in women than in men ($p = 0.003$). No differences in other lobes or total lungs were detected. **Conclusion:** We report normal values of relative total lung and lobar perfusion for hybrid SPECT/CT imaging. Tridimensional quantification can provide valuable information to guide surgical decisions and estimate postoperative outcomes, particularly when a lobectomy is planned. **References:** None.

OP-638

The Role of Tc-99m MAA SPECT-CT in Evaluation of Lung Lobar Perfusion in Patients with Chronic Obstructive Pulmonary Disease (COPD) Prior to Lung Volume Reduction Surgery (LVRS)

E. Trahair, E. Nowosinska, N. Sizer, K. Lau, G. Sotiropoulos, A. Balan, T. O'Shaughnessy, R. Williams, D. Waller, M. Burniston;
Barts Health NHS Trust, London, UNITED KINGDOM.

Aim/Introduction: COPD patients are routinely referred for lung perfusion imaging to quantify lobar perfusion prior to lung volume reduction surgery (LVRS). Traditionally planar imaging is performed and lung perfusion quantification is calculated on anterior and posterior images by dividing the lungs into three equal size ROIs. Whilst this method gives some indication of regional lung function, it does not accurately represent the lung lobes. It is accepted that a more useful result for surgical planning would be accurate lobar perfusion contributions,

and it is proposed that SPECT-CT would allow for calculation of lobar perfusion. **Materials and Methods:** Patients referred for pre-surgery lung perfusion imaging with Tc99m-MAA underwent both planar and SPECT imaging. Diagnostic CT images were registered with reconstructed SPECT data and used for segmentation of lung lobes using Hermes Hybrid 3D Lung Lobe Quantification software in order to calculate lobar perfusion contributions. Planar perfusion quantification was performed by dividing each lung into three equal size ROIs. Additionally, as a complementary result for surgical planning, CT scans were analysed using StratX Lung Analysis Platform to quantify emphysema destruction in the lungs. Where available, lung function test results were also collected. **Results:** Within a 6 month period 74 patients were evaluated (43 male, 31 female), mean age 65 (range 37-82). Perfusion contributions of left and right lung correlated well between planar and SPECT imaging methods with no significant difference found. Lobar perfusion results from planar and SPECT methods differed by an average of 11% (range 0-35%), which was statistically significantly different ($p<0.01$), and in some cases indicated a different target lobe for LVRS. Comparison with the results of quantitative analysis of emphysema destruction on CT scans will also be included in the presentation. **Conclusion:** SPECT-CT for lung perfusion provides more anatomically correct delineation of lung lobes, leading to more accurate lobar quantification results. This technique could have a significant impact on LVRS planning and critically could prevent mis-targeting a lobe that makes a significant contribution to lung function. **References:** None.

OP-639

Evaluating the Need for Anti-Coagulation Therapy in Patients with a Small Pulmonary Thromboembolic Burden on VQ Scan

P. Maliha[1], *G. Chaussé*[1], *V. Tagalakis*[2], *A. Ciarallo*[1];
[1]*McGill University Health Center, Montreal, QC, CANADA,*
[2]*Jewish General Hospital, Montreal, QC, CANADA.*

Aim/Introduction: Introduction of single photon emission computed tomography ventilation/perfusion (SPECT V/Q) imaging has resulted in the increased detection of small perfusion defects previously not seen with conventional ventilation/perfusion imaging. This leads to an increased number of patients diagnosed with pulmonary embolism (PE) and, consequently treated with anticoagulation. Studies comparing computed tomography angiography (CTA) to planar VQ imaging have shown that CTA increases the number of PE diagnoses without impacting PE mortality, raising the question of the relevance of anticoagulation in small PE. We postulate that anticoagulation therapy may have little impact in patients diagnosed with small PEs on VQ scintigraphy, since a low embolic burden in absence of other comorbidities is unlikely to increase the risk of mortality. Our aim is to assess the clinical outcome of subjects with subsegmental mismatched defects on VQ scintigraphy. **Materials and Methods:** We performed a retrospective chart review of all VQ studies performed in January to December 2015 at the Jewish General Hospital, Canada to identify patients with small perfusion abnormalities. Subjects were included if the V/Q scan revealed small subsegmental VQ mismatches (defined as <50% of a pulmonary segment). Subjects were excluded if there was documented prior PE or DVT or if there were any large VQ mismatches (defined as >50% of a pulmonary segment). In addition to a chart review, we measured the number of PE recurrences in addition to PE and bleeding related morbidity. **Results:** Of the 543 VQ scans reviewed, 44 V/Q scans in 44 subjects revealed only subsegmental VQ mismatches and were included in the study. Of the 44 subjects included, 11 were excluded due to history of PE. Ultimately, 26 subjects not anticoagulated and 7 anticoagulated subjects had follow-up for approximately 900 +/- 400 days from the day of the VQ scan. Each VQ scan revealed 1 to 4 subsegmental mismatches. No subjects suffered PE recurrence requiring medical intervention and 1 anticoagulated subject had a minor bleed (which did not require change in therapy or a transfusion). **Conclusion:** Our study suggests that subjects with small subsegmental mismatches on VQ scintigraphy do not carry a significant risk of PE related morbidity or mortality, regardless of anticoagulation status. Therefore, clinicians can potentially forego anti-coagulation therapy in this subset of patients and therefore avoid potential hemorrhagic complications, which in and of themselves carry a significant risk of morbidity and mortality. However, this observation requires validation with a randomized prospective study. **References:** None.

OP-640

Initial Evaluation of the Protocol to Assess the Function of Future Remnant Liver After Major Hepatectomy by Means of Hepatobiliary Scintigraphy and SPECT/CT Imaging with 99mTc-Mebrofenin

M. Nevares Herrero*, P. Mínguez Gabiña, A. Esteban Figueruelo, R. Valverde Jorge, I. Fernández Tercero, E. Rodeño Ortiz de Zárate, M. Prieto Calvo, A. Valdivieso López;*
Hospital Universitario de Cruces, Barakaldo, SPAIN.

Aim/Introduction: Hepatobiliary scintigraphy (HBS) with ^{99m}Tc-mebrofenin has been used as a quantitative method to evaluate liver function. The use of SPECT/CT has allowed a more accurate measurement of segmental liver functionality. **Materials and Methods:** Since August 2017, in patients with major liver resection, except for left hepatectomy with non-compromised liver, CT volumetry and HBS+SPECT/CT with ^{99m}Tc-mebrofenin have been performed. From the latter test, the function of the future remnant liver (FRL-F) (%/min/m²) and the HIBA index (%) were obtained. For these indexes, cutoff values for liver failure of 2.7%/min/m² and 15%, respectively, have been reported. Morbidity was classified by Dindo-Clavien, and liver failure was measured by the IGSLS and 50/50 scores. **Results:** A total of 20 patients were included, two of them being excluded preoperatively (progression). Cholangiocarcinoma was the most common diagnosis (50%), followed by colorectal liver metastases (44.4%). Of all patients, 55.6% were female with a

median (min-max) age of 68y (35-83). Fifteen patients (83.3%) were considered preoperatively as compromised liver but only one patient (5.6%) was cirrhotic. Seven patients (38.9%) had a preoperatively biliary drainage and three patients (16.6%) had right portal vein embolization. In two patients (11.1%) an ALPPS procedure was performed. Eight patients (44.4%) had postoperative morbidity but in only two patients (11.1%) was ≥ IIIb. Two patients (11.1%) developed post-resection liver failure, associated to portal thrombosis. From the CT volumetry, the median liver remnant weight and percentage of liver remnant were 620g (336-1270) and 40% (24-75), respectively. From the SPECT/CT, the median percentage of liver functionality of the FLR was 51% (28-89). The median FRL-F and HIBA index were 2.4%/min/m² (0.5-8.9) and 19% (7-50), respectively. Both, the FRL-F and the HIBA index followed a normal distribution, and a good correlation was found between them (r=0.75). Of all patients, 56% had a FLR-F and 33% a HIBA-index below the cutoff values for liver failure. The two patients that showed liver failure had FRL-F below the cutoff value (both patients 2.2%/min/m²) but HIBA-indexes (17% and 26%) above it. **Conclusion:** In patients that undergo major liver resection, HBS+SPECT/CT with ^{99m}Tc-mebrofenin is a simple technique to calculate the function of the future remnant liver (FLR-F and HIBA index). A higher number of patients will be needed in order to look for a correlation between those indexes and the risk of post-resection liver failure. **References:** None.

1501

CME 12 - Paediatrics Committee: Response Evaluation of Paediatric Sarcomas

Tuesday, October 15, 2019, 16:30 - 18:00 Auditorium

OP-641

Response of Paediatric Sarcomas - Does it Matter?

S. Bielack;
Klinikum der Landeshauptstadt Stuttgart gKAöR – Olgaspital, Department of Paediatric Oncology, Stuttgart, GERMANY.

OP-642

Radiological Response Evaluation of Paediatric Sarcomas

T. von Kalle;
Klinikum der Landeshauptstadt Stuttgart gKAöR – Olgaspital, Department of Paediatric Radiology, Stuttgart, GERMANY.

OP-643

Response Assessment in Paediatric Sarcomas - Value of Nuclear Medicine Techniques

M. Parisi;
Seattle Children's Hospital, Department of Paediatric Radiology and Nuclear Medicine, Seattle, WA, UNITED STATS OF AMERICA.

1502

Joint Symposium 23 - Oncology & Theranostics Committee / ENETS: Theranostic in NEN - What is New?

Tuesday, October 15, 2019, 16:30 - 18:00 Lecture Hall 311

OP-644

Overview on NEN Treatment - Current Options and Clinical Needs

M. Pavel;
Department of Medicine 1 Division of Endocrinology, Friedrich Alexander University Erlangen – Nürnberg, Erlangen, GERMANY.

OP-645

Overview on NEN Diagnosis

V. Ambrosini;
University of Bologna, S.Orsola-Malpighi Hospital, Department of Experimental Diagnostic and Specialized Medicine, Nuclear Medicine, Bologna, ITALY.

OP-646

Update on PRRT - When and How

L. Bodei;
Memorial Sloan Kettering Cancer Center, Department of Radiology, Targeted Radionuclide Therapy Molecular Imaging and Therapy Service, New York, NY, UNITED STATES OF AMERICA.

OP-647

New Treatment Options

D. Wild;
University Hospital Basel, Division of Nuclear Medicine, Basel, SWITZERLAND.

OP-648

Discussion

1503

Joint Symposium 24 - Translational and Molecular Imaging Therapy + Oncology & Theranostics Committee / EAU / ERUS: Image Guided Therapies for Prostate Cancer

Tuesday, October 15, 2019, 16:30 - 18:00 Lecture Hall 312

OP-649
Hardware Development for Targeted Prostate Cancer Therapies
F. Collamati;
Istituto Nazionale di Fisica Nucleare, Department of Physic, Rome, ITALY.

OP-650
Molecular Targeting Strategies for Salvage Prostate Cancer Surgery
T. Maurer;
University of Hamburg-Eppendorf (UKE), Martini-Klinik Prostate Cancer Center, Hamburg-Eppendorf, GERMANY.

OP-651
Focal Therapy for Prostate Cancer
J. Walz;
Institut Paoli-Calmettes Cancer Center, Department of Urology, Marseille, FRANCE.

1504

CTE 6 - Technologist Committee: Parathyroid Imaging

Tuesday, October 15, 2019, 16:30 - 18:00 Lecture Hall 117

OP-652
Comparison of 99mTc-MIBI and 18F-Cholin Scintigraphy in Localization of Hyperfunctioning Parathyroid Tissue
L. Lezaic;
University Medical Centre, Department of Nuclear Medicine, Ljubljana, SLOVENIA.

OP-653
11C-Methionine PET-CT Imaging in Hyperparathyroidism
G. Pepe;
Humanitas Research Hospital, Department of Nuclear Medicine, Milan, ITALY.

OP-654a
The Role of a Technologist in the Preparation of Acquisition Protocols and the Processing of Image Data
S. Rep;
University Medical Centre Ljubljana, Department of Nuclear Medicine, Ljubiana, SLOVENIA.

OP-654b
The Role of a Technologist in the Preparation of Acquisition Protocols and the Processing of Image Data
G. Testanera;
St Bartholomew's Hospital, Department of Nuclear Medicine, London, UNITED KINGDOM.

1505

M2M - Parallel Session: Preclinical Models in Translational Science

Tuesday, October 15, 2019, 16:30 - 18:00 Lecture Hall 111

OP-655
Characterization Of The Apolipoprotein E-deficient Rat As Novel Model For Atherosclerosis Imaging
J. Sijbesma, A. van Waarde, S. Kristensen, I. Kion, U. J. F. Tietge, J. L. Hillebrands, H. Buikema, D. Nakladal, F. Liu, H. H. Boersma, R. A. J. O. Dierckx, R. H. J. A. Slart;
UMCG, Groningen, NETHERLANDS.

Aim/Introduction: The apolipoprotein E-deficient (apoE-/-) mouse is a well-established preclinical model of atherosclerosis. Lipoprotein clearance is impaired in this model, resulting in elevated plasma levels of remnant cholesterol which stimulates the development of atherosclerotic plaques. Positron emission tomography (PET) plays an important role in visualizing and understanding plaque development but the small size of the mouse is a limitation. Vessels are hard to detect, formed plaques are often smaller than the camera resolution and rapid arterial blood sampling is technically challenging. ApoE-/- rats have recently become available. Thus, we aimed to answer the following questions: 1.Is the apoE-/- rat suitable for imaging of atherosclerosis? 2.At which age become plaques detectable in this model? **Materials and Methods:** For a baseline scan (at age 8 weeks), apoE-/- (n=10) and wild type (WT) rats (Long-Evans) (n=10) were injected with 60 MBq ^{18}F-FDG. Plasma cholesterol was measured. After 3h a CT scan was performed followed by a 20-min static PET scan. Animals received a high fat/cholesterol diet after the baseline scan. The scan procedure was repeated at week 4, 12, 26 and 51. After the final scan, aortic tissue was collected for future analysis. The CT data was used to calculate the % of body fat. Uptake of ^{18}F-FDG in the aortic root and abdominal aorta was calculated. **Results:** Plasma

cholesterol levels in apolipoprotein B-containing lipoproteins were substantially increased after 4 weeks of high/cholesterol diet in the apoE-/- rats and kept increasing until the end of the study versus the WT rats where levels stay stable. Body weight and the % of body fat increased faster in the apoE-/- rats, but were similar for both strains at the end of the study. The SUVmean of FDG in the aortic arch increased in both strains, but was significantly higher ($p<0.001$) in apoE-/- versus WT rats at week 26 and 51. Tracer uptake in the abdominal aorta showed a similar pattern, but with a significantly higher ($p<0.05$) uptake in the apoE-/- rats already at week 12. Immunohistochemical staining of the collected tissues is ongoing. **Conclusion:** The apoE-/- rat is a promising model for atherosclerosis imaging. The model shows elevated plasma circulating levels of cholesterol in proatherogenic apoB-containing lipoproteins of total and LDL cholesterol. PET imaging shows differences in FDG uptake in aortic arch and abdominal aorta after 12 weeks when feeding a high fat/cholesterol diet. Immunohistochemical staining has to confirm if this is plaque formation. **References:** None.

OP-656

Systemic effects of SGLT2-Inhibition in healthy mice

B. K. Geist, T. Balber, S. Bugayong, E. Klebermass, L. Nics, A. Pillinger, S. Rasul, H. Regele, A. Zacher, M. Hacker;
Medical University Vienna, Vienna, AUSTRIA.

Aim/Introduction: SGLT2 inhibitors such as Dapagliflozin are anti-diabetic drugs which primarily inhibit the re-absorption of glucose by the sodium-glucose transporter SGLT2 in the kidneys, leading to an increased glucose excretion and thus a decreased blood glucose level. Additionally, also positive effects on other organs have been reported recently. In particular, the cardio-protective effect of SGLT2 inhibition in the heart is not fully understood yet. Therefore, a mice study was performed with dynamic combined positron emission and computer tomography (PET/CT). **Materials and Methods:** The study ran from autumn 2018 to May 2019, involving one group with 16 diabetes type 2 and one with 16 healthy mice, whereby half of the animals were treated with Dapagliflozin. Dynamic PET/CT scans were performed using one glucose analogue with low (FDG: 2-[18F]Fluor-2-desoxy-D-glucose) and one with high SGLT2 affinity (Me4: α-methyl-4-deoxy-4-[18F]FDG). From the fused images, the uptake after 40 minutes of brain, liver, kidneys, bladder and heart was calculated. Furthermore, a kinetic modeling and a immunohistological analysis will be performed. **Results:** So far, the healthy group was evaluated. In the brain, Me4 uptake was 70 % lower ($p < 0.0001$) compared to FDG, Dapagliflozin had no impact on both tracers. In the liver, Me4 uptake was higher by 55 % ($p = 0.002$), Dapagliflozin lead to a decrease by 47 % ($p = 0.002$). In the heart, Me4 uptake was small and 76 % lower than FDG uptake ($p < 0.001$). Dapagliflozin decreased Me4 uptake by 46 % ($p < 0.001$), but it increased FDG uptake by 35 % ($p = 0.04$). Further results on the diabetes group, immunohistological analysis and kinetic modeling will be presented. **Conclusion:** The study confirms that Me4 is less suitable for the brain (although SGLT2 is expressed), since it does not cross the blood brain barrier [1]. SGLT2 can be found in the liver [2], which therefore responds to Dapagliflozin. In the heart, SGLT1 is expressed, playing an important role in cardiac protective mechanisms [3]. Although only the immunohistological analysis can complete the picture, an increased FDG and decreased Me4 uptake after Dapagliflozin treatment might be indirect reactions: as observed in the kidneys [4], SGLT1 expression could be increased due to SGLT2 inhibition. **References:** 1. Yu AS et al, doi: 10.1152/ajpcell.00296.2010. 2. Sabolic I et al, doi: 10.1152/ajpcell.00450.2011 3. Kashiwagi Y et al, doi: 10.1371/journal.pone.0130605 4. Song P et al, doi: 10.1517/14728222.2016.1168808.

OP-657

Molecular imaging characterization of Distraction Osteogenesis model

L. Balasse[1], F. Roseren[2,3], A. Moyon[1], S. Fernandez[4], P. Garrigue[1], G. Hache[1], M. Pithioux[2,3], B. Guillet[1];
[1]Aix Marseille Univ, C2VN, CERIMED, Marseille, FRANCE, [2]Aix Marseille Univ, CNRS, ISM, Marseille, FRANCE, [3]Aix Marseille Univ, APHM, CNRS, ISM, Sainte-Marguerite Hospital, Institute for Locomotion, Department of Orthopaedics and Traumatology, Marseille, FRANCE, [4]Aix Marseille Univ, CERIMED, Marseille, FRANCE.

Aim/Introduction: Distraction osteogenesis (DO) is a surgical procedure widely used for limb lengthening to treat limb length discrepancy. DO procedure is divided into three distinct phases. The latency period starts after callotasis surgery (A), followed by the distraction period (B). When the desired elongation is reached, the external fixator is then locked, and consolidation period is initiated (C). To date, if limb lengthening is efficient, the duration of phase C needed to remove external fixator, remains hard to set, causing a high risk of fracture. This work aimed to characterize, using molecular imaging, callus regeneration, angiogenesis and osteoblastic activity in rat model of DO during Phases A, B and C. **Materials and Methods:** A DO rat model (1) were applied to 6 male rats. Animals were weekly monitored during the phases A (6 days), B (10 days), C (6 weeks) by µCT, µTEP and µSPECT to quantify the bone density, angiogenesis and bone metabolism. Angiogenesis were longitudinally evaluated using 10±0.5 MBq of [^{68}Ga]-RGD. PET images were acquired 1h after injection on Mediso-NanoPET-CT. Bone metabolism were longitudinally monitored using 30±1.5 MBq of [^{99m}Tc]-HMDP. Planar SPECT images were acquired 4h after injection on Mediso-NanoSPECT-CT. Quantitative region-of-interest (ROI) analysis of PET and SPECT images were performed with Vivoquant software (Invicro®) and tissue uptake values presented as ratio of fractured bone on contralateral bone (i/c). **Results:** Molecular imaging showed that activation of angiogenesis and osteogenesis both started on Day 6 after the surgery during Phase A, increased progressively during Phase B up to the end of the phase to an C : i/c ratios of 5.6±1.2 and 2.59±0.4 respectively for [^{68}Ga]-RGD and [^{99m}Tc]-HMDP imaging. Then [^{68}Ga]-RGD TEP signal start to decrease and normalized 2

weeks after the end of phase C and [^{99m}Tc]-HMDP SPECT signal normalized 4 weeks after the end of phase C. **Conclusion:** This is the first report of molecular imaging characterization of DO model. DO induced strength and sustained activations of both angiogenesis and osteogenesis that persists several weeks after distraction. Osteogenesis activation is more sustained than angiogenesis. This work shows that molecular imaging can be an efficient imaging tool to evaluate new optimization of DO procedure and that PET and SPECT imaging could be a valuable tool to determine whether the bone reconstruction phase should be extended and decrease the risk of fracture for which occurrence after removal remain frequent. **References:** (1) M. Pithioux and al., 2017.

OP-658

124I-trastuzumab for noninvasive HER2 detection: From patient-derived xenograft models to gastric cancer PET imaging

X. Guo, *N. Zhou, Z. Chen, H. Zhu, Z. Yang;*
Peking University Cancer Hospital & Institute, Beijing, CHINA.

Aim/Introduction: Here we sought to develop the trastuzumab probe labeled with the positron emission tomography (PET) radionuclide 124I (T1/2 =100.32 h), which has a long physical decay time, to evaluate the safety, distribution, internal dosimetry, and initial PET images of human epidermal growth factor receptor 2 (HER2)-positive lesions in gastric cancer patients. **Materials and Methods:** In the animal study, we injected 14.8 MBq 124I-trastuzumab/124I-hIgG1 into HER2-positive (n = 20) and HER2-negative (n=20) gastric cancer patient-derived xenograft (PDX) models for micro-PET imaging and in vivo biodistribution. Then, 124I-trastuzumab was successfully translated to clinical PET imaging [ethical approval no. 2018KT48]. Six patients with metastatic gastric cancer underwent 124I-trastuzumab PET imaging. Each patient received an intravenous injection of 74±17 MBq 124I-trastuzumab along with 10 mg trastuzumab, and the PET scans were acquired at 1, 24, 48 h. The radioactivity data were obtained by drawing regions of interest on the PET images, and the multiorgan biodistribution and internal dosimetry data of the probe were evaluated. Each patient underwent 18F-FDG PET/CT as a comparison. **Results:** In the micro-PET imaging study, 124I-tratuzumab exhibited a significantly higher tumor uptake than 124I-IgG1 ($p = 0.0002$) in HER2-positive PDX models at 24 h postinjection. The low uptake levels of 124I-tratuzumab ($p = 0.0004$) in HER2-negative PDX models at 24 h further confirmed the specific binding of the radioprobe. In the clinical study, 29 lesions (18 HER2-positive lesions and 11 HER2-negative lesions) were selected for image analysis. The PET images showed that the best time for assessing 124I-tratuzumab uptake in the tumors was 24 h postinjection, and 10 mg cold trastuzumab was adequate to reduce nonspecific liver uptake. There were clear differences in tumor uptake between HER2-positive and HER2-negative lesions at 24 h ($p< 0.0001$). In HER2-negative lesions, there were significant differences in tumor uptake between 124I-trastuzumab and 18F-FDG ($p< 0.0001$), which further confirms the specific binding of 124I-trastuzumab. No toxicities or adverse reactions were observed in any of the patients. **Conclusion:** We successfully synthesized, evaluated the quality control and applied the 124I-trastuzumab PET radiotracer. The findings of the micro-PET imaging study confirmed that 124I-trastuzumab was useful and specifically bound to HER2-positive tumors. The findings of the clinical study indicated that the use of 124I-trastuzumab PET was feasible for identifying HER2-positive lesions in patients with primary and metastatic gastric cancer and for the quantitative differentiation of HER2-positive and HER2-negative lesions. **References:** None.

OP-659

Prospective Theranostic Treatment Planning for Patient-Specific Low-Dose Molecularly Targeted Radiotherapy to Enhance Immunotherapeutic Response

I. R. Marsh, *R. Hernandez, M. Turek, E. Aluicio-Sarduy, J. J. Grudzinski, R. Patel, P. Carlson, M. Otto, P. M. Sondel, J. W. Engle, Z. Morris, J. P. Weichert, D. Vail, B. P. Bednarz;*
University of Wisconsin-Madison, Madison, WI, UNITED STATES OF AMERICA.

Aim/Introduction: External beam radiotherapy (EBRT) delivering immunomodulatory dose to localized disease has been shown to enhance tumor response to checkpoint inhibition immunotherapies. In metastatic disease, where the utility of EBRT is limited, we are investigating the use of molecularly targeted radiotherapy (MTRT) with a radiolabeled alkylphosphocholine analog (^{86}Y/^{90}Y-NM600) to deliver immunomodulatory dose to all tumor sites. In preclinical murine models, we have demonstrated a cooperative therapeutic effect with immunotherapies and ^{90}Y-NM600 MTRT delivering as little as 2 Gy to tumors. Here, we present a preliminary report on patient-specific ^{86}Y-NM600 derived dosimetry for ^{90}Y-NM600 MTRT treatment planning and delivery in an ongoing first-in-canine theranostic study. **Materials and Methods:** A 45 kg canine companion presenting with metastatic osteosarcoma was administered 178 MBq of ^{86}Y-NM600, and serial PET/CT scans were acquired at 2.5, 24, and 48 h post-injection. Regions of interest (ROIs) were expertly-contoured at each timepoint based on the fused PET/CT images. Decay-corrected ^{90}Y-NM600 PET/CT biodistributions were modeled in Geant4 Monte Carlo simulations to produce absorbed dose rate (ADR) distributions at each timepoint. Voxel-level ADR distributions were integrated over time to estimate the prescription dose (Gy/GBq) within temporally coregistered ROIs. Following confirmation of tumor-specific uptake, ^{90}Y-NM600 was prescribed to achieve a mean dose of 2 Gy to the lowest-uptake lesion while limiting exposure to red marrow. **Results:** PET/CT imaging confirmed specificity and persistent accumulation of ^{86}Y-NM600 in tumors (3.4-4.2 SUV mean at 48 h) and the dosimetry workflow for theranostic ^{90}Y-NM600 MTRT was completed within 5 days. The estimated prescription dose of 3.2 Gy per injected GBq in the lowest-uptake lesion suggested the administration of 0.62 GBq of ^{90}Y-NM600

MTRT to deliver 2.0-2.6 Gy to all tumors. Dose delivered by ^{86}Y-NM600 imaging studies was negligible. Dose to red marrow was estimated at 1.1 Gy based on lumbar vertebrae marrow. The liver and kidneys received a tolerable 2.6 and 3.2 Gy, respectively. Following treatment with MTRT, the subject exhibited a favorable adverse event profile. **Conclusion:** We demonstrate here the first use of patient-specific prospective dosimetry for theranostic ^{90}Y-NM600 MTRT treatment planning in this first-in-canine osteosarcoma patient. These preliminary results indicate the feasibility of patient-specific theranostic MTRT to deliver optimal immunomodulatory radiation that potentially enhances immunotherapeutic response. **References:** None.

OP-660

PET imaging of the glucagon receptor in non-human primate

I. Velikyan[1], *O. Eriksson*[1], *T. Haack*[2], *M. Bossart*[2], *A. Evers*[2], *I. Laitinen*[2], *P. J. Larsen*[3], *O. Plettenburg*[2], *G. Antoni*[1], *L. Johansson*[4], *S. Pierrou*[4], *M. Wagner*[2];
[1]*Department of Medicinal Chemistry, Uppsala University, Uppsala, SWEDEN,* [2]*Sanofi-Aventis, Frankfurt, GERMANY,* [3]*Grunenthal GmbH, Aachen, GERMANY,* [4]*Antaros Medical AB, Molndal, SWEDEN.*

Aim/Introduction: The Glucagon receptor (GCGR) is an emerging target in anti-diabetic therapy. Reliable biomarkers for in vivo activity on the GCGR, in the setting of dual glucagon like peptide 1/ glucagon (GLP-1/GCG) receptor agonism, are currently unavailable. Positron Emission Tomography (PET) tracer [^{68}Ga]Ga-DO3A-S01-GCG was previously shown to bind to the GCGR with high affinity and specificity in vitro and in vivo in rats [1]. Here, we investigated [^{68}Ga]Ga-DO3A-S01-GCG as a biomarker for GCGR occupancy in liver in non-human primates by PET. **Materials and Methods:** The GCGR targeting properties of [^{68}Ga]Ga-DO3A-S01-GCG was evaluated by dynamic PET in non-human primates by a dose escalation study design where up to 67µg/kg DO3A-S01-GCG peptide mass was co-injected. The test-retest reproducibility in non-human primate, as well as the effect on [^{68}Ga]Ga-DO3A-S01-GCG by pre-treatment with an acylated glucagon agonist was also investigated by PET/CT imaging. **Results:** [^{68}Ga]Ga-DO3A-S01-GCG bound to GCGR rich liver in vivo in a dose-dependent manner. Negligible peptide mass effect was observed for DO3A-S01-GCG doses of <0.2 µg/kg. In vivo K_d for [^{68}Ga]Ga-DO3A-S01-GCG in liver corresponded to 0.7 µg/kg indicating high potency. The test-retest reproducibility was 5.7±7.9% and pre-treatment with an acylated glucagon agonist incurred an occupancy of 61.5±9.1% in liver. Predicted human absorbed doses would allow for repeated annual [^{68}Ga]Ga-DO3A-S01-GCG PET examinations. **Conclusion:** PET radioligand [^{68}Ga]Ga-DO3A-S01-GCG is a novel quantitative biomarker of in vivo GCGR occupancy determination in non-human primates. **References:** Velikyan I, et al. First-in-class Positron Emission Tomography tracer for the Glucagon receptor. EJNMMI Res (2019) 9(1):17.

OP-661

The potential of PET/CT imaging as a clinical evidence method for the early detection of Duchenne muscular dystrophy (DMD) in female carriers- a study in genetically modified pigs

M. J. Lindner[1], *L. M. Fonteyne*[2], *B. Keßler*[2], *A. Bollenbacher*[1], *E. Kemter*[2], *A. Todica*[1], *S. Nekolla*[3], *P. Bartenstein*[1], *E. Wolf*[2], *S. Ziegler*[1];
[1]*Department of Nuclear Medicine, University Hospital Munich, Munich, GERMANY,* [2]*Gene Center and Department of Biochemistry, Molecular Animal Breeding and Biotechnology, LMU Munich, Munich, GERMANY,* [3]*Department of Nuclear Medicine at Technische Universität München, Munich, GERMANY.*

Aim/Introduction: DMD is the most common neuromuscular disease in juvenile age. The x-chromosomally recessive heredity leads to a degeneration of the muscle fiber and substitution of muscles by fat and connective tissue. Importantly, heart muscle is affected preclinically and clinically as cardiomyopathy. The therapy consists of symptomatic treatment. Female carrier subjects may, although not suffering from DMD, also develop cardiac symptoms. In this study, quantitative PET/CT imaging of genetically modified DMD carrier pigs was used to test for presymptomatic detection of muscular dystrophy. **Materials and Methods:** The study was performed on 3 months old genetically modified DMD (n=5) and wildtype pigs (n=3) on a clinical PET/CT scanner (Siemens Biograph). A non-contrast enhanced CT scan was acquired first, followed by a 60 min dynamic ECG-triggered PET measurement of the heart, starting at the time of injection of F18-FDG (300MBq) into the lateral ear vein. Afterwards, whole-body FDG distribution was measured in 8 bed positions from 60-90 min p.i.. Pigs were monitored by ECG, respiratory rate, and blood-glucose-level. The volumes-of-Interest (VOI´s) were defined firstly by the left ventricle of the heart. Ejection fraction (EF in %), endsystolic volume (EsVol in ml), and enddiastolic volume (EdVol in ml) were determined. Secondly, FDG uptake in skeletal muscle was determined by placing a VOI on the longissimus thoracis muscle. **Results:** Compared to wild type animals, cardiac ejection fraction was 7% lower in DMD pigs. Mean enddiastolic (endsystolic) volume was 7 % (15%) less in DMD pigs. Group average of mean standard uptake value (SUV) in the whole longissimus thoracis muscle was 0.50 in DMD and 0.32 in wildtype pigs. Mean standard deviation in the whole-muscle VOI was 0.26 in DMD and 0.16 in wildtype. Further, an asymmetry of SUV between the right and left part of the muscle was found (mean group deviation right: 10%; left: 29%). No statistical significance was found in this preliminary study with low number of animals. **Conclusion:** A reduction of the cardiac function and an increase of the regional radioactivity concentration in the musculus longissimus thoracis could be measured in the genetically modified DMD pigs compared to wildtype animals. These results may reflect early impairment of cardiac function and potential changes in muscle metabolism in DMD-carriers. Thus, FDG imaging may guide in identifying signs of DMD in carrier subjects. The animal number will be increased for improved statistics. Further studies will correlate imaging results with tissue samples. **References:** None.

OP-662

Pharmacokinetic modelling of P-glycoprotein function at the blood-brain barrier with [18F]MC225 PET in non-human primates

L. Garcia Varela[1], *W. M. Arif*[1], *D. Vállez García*[1], *T. Kakiuchi*[2], *H. Ohba*[2], *S. Nishiyama*[2], *T. Tago*[3], *P. H. Elsinga*[1], *H. Tsukada*[2], *N. A. Colabufo*[4], *R. A. J. O. Dierckx*[1], *A. van Waarde*[1], *J. Toyohara*[3], *R. Boellaard*[1], *G. Luurtsema*[1];
[1]*University of Groningen, Groningen, NETHERLANDS,* [2]*Central Research Laboratory, Hamamatsu Photonics KK, Hamamatsu, JAPAN,* [3]*Research Team for Neuroimaging, Tokyo Metropolitan Institute of Gerontology, Tokyo, JAPAN,* [4]*University of Bari Aldo Moro, Bari, ITALY.*

Aim/Introduction: Impaired P-glycoprotein (P-gp) function can lead to the onset of neurodegenerative disease or to drug resistance. [18F]MC225 has been developed as a weak substrate aimed to measure increases and decreases of the P-gp function. The tracer was initially evaluated in mice and rats. In this study, we extended these evaluations by investigating [18F]MC225 kinetics in non-human primates with a particular emphasis on assessing robust parameters to estimate the P-gp function. Moreover, since short PET scans are desirable, the pharmacokinetics were explored at different acquisition times (10-, 20-, 30- and 60-min). **Materials and Methods:** Three non-human primates underwent two 91-min-dynamic PET scans with arterial blood sampling, one at baseline and another after P-gp inhibition (8mg/Kg tariquidar). Metabolite-corrected plasma and whole-blood time-activity curves were used as input function for pharmacokinetic modeling. For each acquisition time, the preferred model was chosen according to the Akaike Information Criterion (AIC), and the volume of distribution (V_T), the overall net influx rate constant (K_i), the influx constant (K_1), and the Standardized Uptake Values (SUV) were estimated. Differences were assessed by Generalized Estimated Equations (GEE). Linear regression analysis and Bland-Altman plots were used to measure agreement between the parameters. **Results:** According to AIC, a reversible 2-tissue compartment model (2-TCM) is the model of choice for a 91-min scan. For 30- and 60-min PET scans, the preferred model was an irreversible 2-TCM. For 10- and 20-min scans, a 1-TCM resulted in lowest AIC. After the treatment, the V_T increases 31% ($p<0.001$) and the K_1 36% ($p<0.001$) using 91-min scan. The analysis did not find significant differences among the K_1 values at different acquisition times, and their correlations were very good (e.g. K_1 at 20-min =0.17 vs. 91-min =0.18, $p<0.01$, $R^2=0.984$). However, the results showed a poor agreement between K_1 and V_T (e.g. 91-min $R^2=0.116$ at baseline and $R^2<0.01$ after-treatment) and between K_1 and K_i (e.g. 60-min $R^2=0.613$ at baseline and $R^2=0.114$ after-treatment), and K_1 and SUV (e.g. 91-min $R^2=0.04$ at baseline and $R^2=0.56$ after-treatment). **Conclusion:** Our results support the use of K_1 as the parameter of choice to measure P-gp function with [18F]MC225. Although, alterations in the blood flow should be considered carefully during the study design to minimize confounders during K_1 estimation. Moreover, a 0-20 min scan seems to be sufficiently reliable to estimate P-gp function using a 1-TCM fit. **References:** None.

1506

Do.MoRe - Parallel Session: New Concepts, Harmonisation and Standardisation in Radiomics

Tuesday, October 15, 2019, 16:30 - 18:00 Lecture Hall 112

OP-663

A Study of Radiomic Features Robustness for 68Ga-DOTATOC PET/CT in Neuroendocrine Tumors

V. Liberini[1], *E. Gallio*[2], *O. Rampado*[2], *B. De Santi*[3], *B. Dionisi*[1], *F. Ceci*[1], *E. Pilati*[1], *M. Finessi*[1], *M. Bellò*[1], *G. Bisi*[1], *F. Molinari*[3], *D. Deandreis*[1];
[1]*Nuclear Medicine Unit, Department of Medical Sciences, University of Turin, Turin, ITALY,* [2]*Medical Physics Unit, AOU Città della Salute e della Scienza, Turin, ITALY,* [3]*Biolab, Department of Electronics and Telecomunications, Politecnico di Torino, Turin, ITALY.*

Aim/Introduction: The use of 68Ga-DOTATOC PET/CT as a prognostic and predictive tool of heterogeneity in neuroendocrine tumors (NET) is gaining importance.The aim of this study was to evaluate the impact of different reconstruction and segmentation methods on the identification of repeatable and reliable radiomic features (RFs). **Materials and Methods:** To evaluate the robustness of RFs, we retrospectively analyzed data from two different cohorts of patients that performed a 68Ga-DOTATOC PET/CT scan (Philips Dual GEMINI) for NET disease: "algorithm cohort" including 22 patients to evaluate the robustness in function of reconstruction algorithms; "naive cohort" including 49 treatment-naive patients, for which the primary NET location was foregut (7/49), midgut (11/49), pancreatic (22/49) and bronchial (9/49). For the "algorithm cohort", all datasets were reconstructed using three different algorithms: 3D-RAMLA (standard), iterative and filtered backprojection. In both the cohorts, contouring was performed on a total of 116 lesions with two different contouring methods: manual contours using the software LIFEx (v. 4.81, www.lifexsoft.org) by two operators and semi-automatic edge-based method using a MATLAB (MathWorks) homemade code. For each region of interest (ROIs), SUVmax fixed thresholds (20, 30 and 40%) were applied and three different intensity rescale factors were employed (0-60, 0-80, min-max of the SUV of the ROI). 45 RFs (25 texture, 6 histogram, 4 shape indices and 10 conventional PET features) were extracted using LIFEx. The impact of the different parameters on RFs was assessed by Intra-class Correlation Coefficients (ICC) using statistical R software (www.r-project.org). A RF was considered robust if ICC was > 0.8. **Results:** According to the different reconstruction algorithms, all 45 RFs were considered robust (ICC > 0.9). According to the different segmentation methods, a moderate inter-observer variability was observed for manual methods and 80% of 45 RFs appeared to be robust. The comparison of manual and semi-automatic contouring methods highlighted robustness for only 38% of RFs. Furthermore, ROI-thresholds and intensity rescale factors affected the repeatability of RFs. Only GLZLM-GLNU

RF was stable according to all different parameters analyzed, while the GLRLM RFs group and entropy histogram resulted to be robust according to all different analyzed parameters, except for intensity rescale factors. **Conclusion:** This study allowed to evaluate the impact of methodological aspects on the assessment of RFs robustness at ^{68}Ga-DOTATOC PET/CT. To investigate different biological behaviours of NET with a radiomic approach, contouring methods and intensity rescale factors should be carefully evaluated in order to use repeatable RFs. **References:** None.

OP-664

Multi-level multi-modality fusion radiomics: application to PET and CT imaging for improved prognostication of head and neck cancer

W. Lv[1,2], *S. Ashrafinia*[3,4], *J. Ma*[1], *L. Lu*[1], *A. Rahmim*[2,4,5];
[1]*School of Biomedical Engineering, Southern Medical University, Guangzhou, CHINA,* [2]*Department of Integrative Oncology, BC Cancer Research Centre, Vancouver, BC, CANADA,* [3]*Department of Electrical & Computer Engineering, Johns Hopkins University, Baltimore, MD, UNITED STATES OF AMERICA,* [4]*Department of Radiology, Johns Hopkins University, Baltimore, MD, UNITED STATES OF AMERICA,* [5]*Departments of Radiology and Physics, University of British Columbia, Vancouver, MD, CANADA.*

Aim/Introduction: Intra-tumor heterogeneity plays a key role in tumor development and responses to therapy. Radiomics analysis, incorporating measurement of heterogeneity, has been extensively investigated on individual imaging modalities. By contrast, multi-modality radiomics analysis has been much less commonly performed, and if applied, is usually performed by concatenation of features from different modalities. However, such an approach may not be able to effectively integrate the supplementary information provided by different modalities. Thus, the purpose of this study was to investigate a multi-level fusion strategy to combine the information provided by PET and CT at the image-, matrix- and feature-levels towards improved prognosis of multi-center head & neck cancer. **Materials and Methods:** 296 patients scanned with FDG-PET/CT imaging from 4 centers were collected from The Cancer Imaging Archive (TCIA). Three outcomes recurrence-free survival (RFS), metastasis-free survival (MFS) and overall survival (OS) were considered. 127 radiomics features were extracted from (1) PET images alone; (2-7) PET and CT images fused via wavelet-based fusion (WF) with CT-weights of 0.2, 0.4, 0.6 and 0.8, gradient transfer fusion (GTF), and guided filtering-based fusion (GFF); (8) fused matrices (sumMat), constructed by considering the voxel relationships in PET and CT simultaneously; (9-10) fused features constructed via feature averaging (avgFea), and feature concatenation (conFea); and finally, (11) use of CT images alone. Top 10 features with higher concordance index (C-index) in univariate Cox analysis were selected, and multivariate model was constructed by Akaike information criteria (AIC). **Results:** For RFS prediction, PET (C-index: 0.62±0.08) and WF0.6 (C-index: 0.61±0.05) showed higher performance than other 9 strategies (C-index: 0.55-0.59). For MFS prediction, PET (C-index: 0.69±0.09), WF0.8 (C-index: 0.69±0.09) and sumMat (C-index: 0.67±0.10) showed higher performance than other 8 strategies (C-index: 0.62-0.65). For OS prediction, WF0.8 showed highest C-index of 0.64±0.02 compared with other 10 strategies (C-index: 0.58-0.63). **Conclusion:** Models constructed by image-level fusion outperformed matrix- and feature-level fusion, as well as use of single modality, indicating that integrating information at earlier stages (i.e. merging metabolic information from PET and anatomic information from CT voxel by voxel) can capture more useful characteristics. **References:** 1.Wong, A.J., et al., Radiomics in head and neck cancer: from exploration to application. Transl Cancer Res, 2016. 5(4): p. 371-382. 2.Lv, W., et al., Radiomics Analysis of PET and CT Components of PET/CT Imaging Integrated with Clinical Parameters: Application to Prognosis for Nasopharyngeal Carcinoma. Mol Imaging Biol, 2019, doi: 10.1007/s11307-018-01304-3.

OP-665

Comparison of machine learning-driven lesion classifiers in PET/MR images of prostate cancer patients

L. Papp[1], *C. P. Spielvogel*[2], *M. Grahovac*[3], *T. Beyer*[1], *M. Hacker*[3];
[1]*QIMP team, Center for Medical Physics and Biomedical Engineering, Medical University of Vienna, Vienna, AUSTRIA,* [2]*Christian Doppler Laboratory for Applied Metabolomics, Medical University of Vienna, Vienna, AUSTRIA,* [3]*Division of Nuclear Medicine, Medical University of Vienna, Vienna, AUSTRIA.*

Aim/Introduction: Positron Emission Tomography (PET) plays an important role in tumour characterization. Lately, the use of radiomics analysis of PET images has shown potential to positively impact diagnostic work-up of oncology patients. However, various radiomics features were reported to be sensitive to multi-centric imaging protocol variations. Here, we compared different Gleason pattern classifiers in prostate PET/MRI studies built on four multi-centric coefficient of variation (CoV) radiomic feature groups [1]. **Materials and Methods:** 74 prostate patients were included in this study having a multi-parametric prostate PET/MRI including 8 series: ^{18}F-FMC and ^{18}F-FMC+^{68}Ga-PSMA$^{\text{HBED-CC}}$ (dual-tracer) PET, furthermore, T2, ADC, iAUC, KEP, Ktrans and Ve MRI. Based on Gleason-annotated, full-mount histopathological slices, 120 lesions were delineated from each study (Hermes Nuclear Diagnostics, Sweden). Overall 589 radiomics features were extracted from the 8 series of each of the 120 lesions based on optimized radiomics [1]. Features were categorized as CoV<5%, CoV<10%, CoV<20% and all-CoV according to [1]. For each of the four CoV categories, a low risk (<=Gleason 3) vs. high risk (>=Gleason 4) machine learning predictor was established [2]. 1000-fold Monte Carlo cross-validation with 20% held-out sets was performed to estimate the sensitivity (SENS), specificity (SPEC), accuracy (ACC), positive-predictive-value (PPV) and negative-predictive-value (NPV) of the four predictive models. **Results:** The accuracy of the low-high risk predictive models over four CoV feature categories were 75% (CoV<5%), 76% (CoV<10%), 78% (CoV<20%) and 77%

(all-CoV). The performance values of the CoV<5% low-high risk model were SENS 72%, SPEC 77%, PPV 76% and NPV 73%. The same values for the all-CoV model were SENS 74%, SPEC 80%, PPV 78% and NPV 75%, respectively. **Conclusion:** The accuracy of a low-high risk prediction model for prostate cancer PET/MRI varied minimally between 75% and 78%, thus, pointing to the ability to effectively reduce the number of features to the most repeatable ones (CoV<5%). This helps simplifying the complexity of relevant prediction models. **References:** Papp L., et al: Optimized feature extraction for radiomics analysis of 18F-FDG-PET imaging. JNM 2018, 10.2967/jnumed.118.217612 Papp L., et al: Glioma Survival Prediction with Combined Analysis of In Vivo ^{11}C-MET PET Features, Ex Vivo Features, and Patient Features by Supervised Machine Learning. JNM, 2018(59):892-899.

OP-666

Harmonization strategies based on ComBat for mutlicentric radiomics studies

R. Da-ano[1], F. Lucia[2], M. Vallières[1], P. Bonaffini[3], I. Masson[4], A. Mervoyer[4], C. Reinhold[3], U. Schick[1,2], D. Visvikis[1], M. Hatt[1]; [1]LaTIM, INSERM, UMR 1101, Univ Brest, Brest, FRANCE, [2]Radiation Oncology department, University Hospital, Brest, FRANCE, [3]Department of Radiology, McGill University Health Centre (MUHC), Montreal, QC, CANADA, [4]Department of Radiation Oncology, Institut de Cancérologie de l'Ouest, Nantes, FRANCE.

Aim/Introduction: Multicentric studies are needed to demonstrate the clinical potential value of radiomics as a prognostic tool. However, variability in scanner models, acquisition protocols and reconstruction settings are unavoidable and radiomic features are notoriously sensitive to these factors. A statistical harmonization method called ComBat was developed to deal with the "batch effect" in gene expression microarray data and was used in radiomics studies to deal with the "center-effect". A modified version called M-ComBat was later introduced. Our goal was to develop and evaluate hybrid techniques based on ComBat, intended to improve the predictive ability of the models developed on data from a "reference" center and validated on others. **Materials and Methods:** The hybrid ComBat methods were developed by adding bootstrap from the obtained initial batch-wise estimates and used Monte Carlo method to obtain the final batch-wise estimates, denoting them B-ComBat and BM-ComBat. 92 IBSI-compliant radiomic features extracted from FDG-PET and MRI sequences (T1, T1c, T2 and ADC maps) of 197 cervical cancer patients treated with radiochemotherapy in 3 centers (Brest, n = 119, Nantes, n = 50 and Montreal, n = 28) were exploited. After splitting untransformed or harmonized features (harmonized using 4 ComBat versions) 70/30 in training and testing sets, models to predict recurrence were built using 3 approaches: i) multivariate regression (MR) with 10-fold cross validation after feature selection based on LASSO, ii) Random Forest (RF) and iii) Support Vector Machine (SVM). They were compared using Area Under the Curve (AUC) and balanced accuracy (BAC). **Results:** Noticeably, our proposed bootstrap modification (B-ComBat and BM-ComBat) slightly but consistently improved the predictive ability of the developed models. In MR with LASSO, B-ComBat outperformed ComBat (AUC 0.92 vs. AUC 0.91 and BAC 84% vs. 82%) and BM-ComBat also outperformed M-ComBat (AUC 0.92 vs. AUC 0.91 and BAC 84% vs. 82%). With RF, B-ComBat outperformed ComBat (AUC 0.93 vs. AUC 0.90 and BAC 85% vs. 83%) and BM-ComBat also outperformed M-ComBat (AUC 0.93 vs. AUC 0.90 and BAC 91% vs. 83%). Also in SVM, B-ComBat outperformed ComBat (AUC 0.93 vs. AUC 0.92 and BAC 84% vs. 83%) and BM-ComBat also outperformed M-ComBat (AUC 0.93 vs. AUC 0.92 and BAC 85% vs. 84%). **Conclusion:** The hybrid bootstrapped ComBat(B-ComBat and BM-ComBat) versions are modifications to an acknowledged method that seem to provide slight improvement with the performance of predictive radiomics models in a multicentric context, whatever machine learning technique is used. **References:** None.

OP-667

A Concept to Simulate Heterogeneities in a Combined PET/CT Phantom for Standardised Radiomic Features Analysis

A. Valladares, T. Beyer, L. Papp, E. Salomon, I. Rausch; Medical University of Vienna, Vienna, AUSTRIA.

Aim/Introduction: Recently, textural features in medical images have been proposed as potential biomarkers for in-vivo disease characterization. However, standardized imaging procedures and pre-processing protocols are mandated to ensure repeatability. Here, we propose a simple concept for simulating heterogeneity in a PET and CT phantom for assessing the variability of textural features. **Materials and Methods:** Three conical tubes (d=31mm, h=110mm) were partly filled with different sizes of acrylic spheres (tube 1: 1.6mm; tube 2: 50%(1,6mm)/50%(6,3mm) and tube3: 6.3 mm diameter) resulting in a homogeneous (spheres free)- and a heterogeneous area separated from each other with a plastic grid. The tubes were filled with an aqueous solution containing [18F]-FDG (20 kBq/mL). Two identical arrangements (test/retest) of these three tubes were centered in the field-of-view of a Siemens Biograph TPTV PET/CT system and scanned using a standard oncological protocol. From the resulting CT and PET images, SUVs and HUs as well as six selected textural features, reported as robust features in a PET/CT multi-centre study [1], were calculated from volumes-of-interests (2.2 mL) placed in the homogeneous and heterogeneous regions of each tube by using the software LIFEx [2]. Changes in extracted parameters between the homogeneous and the heterogeneous areas were calculated as percentage-differences. **Results:** Average SUV and HU for the homogeneous regions were 4.5±0.1 and 11.1±3.8 respectively. SUV and HU changed by tube 1 (test/retest): -62%/-63% and 652%/688%; tube 2: -65%/-66% and 668%/672% and tube 3: -61%/-61% and 609%/624%, respectively. The changes in evaluated features from the heterogeneous regions with respect to the ones extracted from the homogeneous areas were highly variable for both, the PET and CT images. For example, PET

images presented changes of 24% to 55% for correlation, 24% to 55% for entropy and 16 to 171% for coarseness. **Conclusion:** With using different acrylic spheres as filling material in a radioactive aqueous solution, it was possible to alter radiomics feature values extracted from PET and CT images. Therefore, this concept seems promising for building a reproducible an easy to handle heterogeneity phantom. (This work has received funding from the European Union's Horizon 2020 research and innovation programme under the Marie Skłodowska-Curie grant agreement No. 764458). **References:** [1] L Papp et al. J Nucl Med 2018. DOI:10.2967/jnumed.118.217612. [2] C Nioche, et al. Cancer Research 2018; 78(16):4786-4789. www.lifexsoft.org.

OP-668

Experimental Multicenter And Multivendor Evaluation Of Pet Radiomic Features Performance Using 3d Printed Phantom Inserts

E. Pfaehler[1], *J. van Sluis*[1], *B. B. J. Merema*[1], *P. Van Ooijen*[1], *R. C. M. Berendsen*[2], *F. H. P. Van Velden*[3], *R. Boellaard*[4];
[1]*University Medical Center Groningen, Groningen, NETHERLANDS,* [2]*Zuyderland Medical Center, Heerlen, NETHERLANDS,* [3]*Leiden University Center, Leiden, NETHERLANDS,* [4]*VU Medical Center, Amsterdam, NETHERLANDS.*

Aim/Introduction: The sensitivity of radiomic features to several confounding factors, such as image reconstruction settings, makes clinical use challenging. To use radiomic features in a clinical setting, they have to be comparable across institutions and scanner types. In order to investigate the impact of harmonized image reconstruction settings on feature consistency, a multicenter phantom study was performed using 3D printed phantom inserts reflecting realistic tumor shapes and heterogeneity uptake. **Materials and Methods:** Tumours extracted from real PET/CT scans of patients with non-small cell lung cancer served as model for three 3D printed phantom inserts. Different heterogeneity patterns were realized by printing separate compartments that can be filled with different activity solutions. The inserts were placed in the NEMA image quality phantom and scanned repeatedly. Firstly, a list-mode scan was acquired and five statistical equal replicates were reconstructed. Secondly, the phantom was scanned four times on the same scanner. Thirdly, the phantom was scanned on six different PET/CT systems. All images were reconstructed using EARL-compliant and the locally clinically-preferred reconstructions. The EARL-compliant reconstructions were performed without (EARL1) or with (EARL2) point-spread function (PSF). Images were analyzed with and without resampling to 2 mm cubic voxels. Images were discretized with a fixed bin width (FBW) of 0.25 and a fixed bin number (FBN) of 64 bins. The intraclass correlation coefficient (ICC) of each scan setup was calculated and compared across reconstruction settings. An ICC above 0.75 was regarded as good correlation. **Results:** The percentage of features yielding a good ICC was the largest for the statistical equal replicates (70%- 91% for FBN, 90%-96% for FBW discretization). For the scans acquired on the same system, the percentage decreased, but the majority of features still resulted in a high ICC (FBN: 52%-63%, FBW: 75%-85%). The percentage of features yielding a high ICC decreased more in the multicenter setting. In this case, the percentage of features yielding a high ICC was larger for images reconstructed with (harmonizing) EARL-compliant reconstructions: e.g. 40% for EARL1, 60% for EARL2 vs. 21% for the clinically-preferred setting for FBW discretization. When discretized with FBW and resampled to isotropic voxels, this benefit was more pronounced. **Conclusion:** EARL-compliant reconstructions harmonize a wide range of radiomic features. FBW discretization and a sampling to isotropic voxels, pronounces the benefits of EARL-compliant reconstructions. **References:** None.

OP-669

Adding the Temporal Domain to PET Radiomic Features

W. A. Noortman[1,2], *D. Vriens*[1], *C. H. Slump*[2], *J. Bussink*[3], *T. W. H. Meijer*[3], *L. F. de Geus-Oei*[1,2], *F. H. P. van Velden*[1];
[1]*Leiden University Medical Center, Leiden, NETHERLANDS,* [2]*University of Twente, Enschede, NETHERLANDS,* [3]*Radboud University Medical Center, Nijmegen, NETHERLANDS.*

Aim/Introduction: Currently, in PET imaging, textural radiomic features are derived from static images and express heterogeneity in the spatial distribution of radiotracer uptake. However, changes in uptake over time might contain additional information concerning tumour biology. This study introduces novel texture features that are derived from the temporal domain using dynamic images, aiming to assess the amount of information of these dynamic texture features and features derived from parametric images compared to conventional features derived from static images. **Materials and Methods:** Thirty-five patients with non-small cell lung carcinoma underwent dynamic ^{18}F-FDG-PET/CT scans. The time frame of 50-60 min p.i. was used as static scan. Parametric glucose metabolic rate images were created using Patlak analysis (15-60 min). The dynamic images consisted of 16 frames of 150 s acquired 10-50 min p.i.. Volume of interest (VOI) delineation of lesions was performed on static and parametric images; static VOIs were used for dynamic series. 90 intensity, shape and texture features were extracted from static and parametric images, using PyRadiomics 2.0. Following the approach of Hu et al. (IEEE ISBI 2006) in proteomics, 22 dynamic grey level cooccurrence matrix (GLCM) and 16 dynamic grey level run length matrix (GLRLM) features were extracted from the dynamic frames. Static and parametric texture features were calculated bidirectionally for 13 angles; dynamic features only included the unidirectional temporal domain. Following the approach of Yip et al. (Phys Med Biol. 2016), population-based fixed bin widths were dependent on the range of voxel values and number of voxels within the VOI. Comparison of parametric and dynamic features with static features was performed with Spearman rank correlation, $\rho>0.7$ is considered to be high. **Results:** Five dynamic GLCM features showed a negligible to moderate correlation with any

static feature, indicating potential additional information to existing features. All other dynamic features, including GLRLM, showed a high correlation with at least one static feature. Three out of 90 parametric features did not show a high correlation with corresponding static features, but showed a moderate correlation (ρ>0.61). **Conclusion:** This study suggests that, for NSCLC, certain dynamic GLCM radiomic features show additional information compared to static features. In extension to Tixier et al. (J Nucl Med 2016), equivalent features indicated no additional information in radiomics derived from parametric images; other features only gave a minimal suggestion of additional information. Future studies should assess whether there is a clinical benefit of dynamic radiomics over static radiomics. **References:** None.

OP-670

Dose distribution radiomics: a new paradigm for assessment of radioligand therapy

X. Hou[1], *W. Lv*[2], *J. Buregaurd*[3,4], *A. Celler*[1], *A. Rahmim*[5,1];
[1]*Radiology Department, University of British Columbia, Vancouver, BC, CANADA,* [2]*Department of Biomedical Engineering, Southern Medical University, Guang Zhou, CHINA,* [3]*Department of Medical Imaging and Oncology Division of Research Center, CHU de Québec – Université Laval, Quebec, QC, CANADA,* [4]*Department of Radiology and Nuclear Medicine and Cancer Research Center, Quebec, QC, CANADA,* [5]*Department of Integrative Oncology, BC Cancer Research Centre, Vancouver, BC, CANADA.*

Aim/Introduction: Personalized dosimetry in radioligand-therapy (RLT) is increasingly recognized as an important procedure for ensuring patient safety and improving treatment efficacy. Furthermore, radiomics has gained increasing acceptance as a powerful tool for assessment of radiological images. Here we propose a paradigm of dose-distribution radiomics towards improved assessment of RLT. It is known that radiomics features can be affected by image generation and processing methods. In this work, we applied radiomics to voxelized dose maps from RLT and investigate features' robustness when varying segmentation, discretization and dose calculation methods. **Materials and Methods:** Ten patient kidney datasets (the main organ-at-risk) from ^{177}Lu-DOTA-TATE therapy were analyzed. Three SPECT/CT scans, acquired at around 4h(D0), 23h(D1) and 70h(D3) after injection, were used for dose estimations. Four fixed-thresholds (20%-50%) were employed in kidney segmentations. Voxelized dose-maps were obtained using seven methods: (M1) from unfiltered images, and images processed with 3x3x3(M2) and 5x5x5(M3) box-filters with time-activity-curves (TACs) determined for each voxel; and (M4-M7) based on activity distributions from images on D0, D1, D3 and the mean of all images to scale the TACs obtained from the entire organs to individual voxels. In total, 280 dose-maps were used in radiomics analysis. Five discretization (bin=16/32/64/128/256) with 43 radiomics features (from histogram and GLCM, GLRLM, GLSZM, NGTDM matrices) were applied to each dose-map. Reproducibility of the radiomics features with respect to dose-map generation parameters was assessed using the intra-class correlation coefficient (ICC). **Results:** Varying dose calculation methods, among all the segmentation and discretization methods, the mean values of ICCs were >0.8 for 31/43 features; while, large variations were found in 1/13 GLRLM and 6/13 GLSZM features. When varying segmentations, features highly depended on the dose calculation methods. For M1-M3, only 5/43 features showed ICCs>0.8, but 24/43 features showed ICCs>0.8 for M4-M7. Poor ICCs were observed in all histogram, 5/9 GLCM, 4/13 GLRLM and 5/13 GLSZM features. Varying bin sizes of discretization, besides 2/3 histogram, 2/9 GLCM and 1/5 NGTDM non-robust features, ICCs for other features were >0.8 for any given segmentation and dose calculation methods. **Conclusion:** Radiomics features in dose-maps from RLT were investigated. Their robustness to segmentation highly depended on dose-map calculation methods. Features obtained from dose-maps based on organ-based TACs showed high and consistent reproducibility for most radiomics features. This analysis can serve for selection of reproducible dose-map radiomics features towards improved assessment of RLT and prediction of outcome in future efforts. **References:** None.

1507

Teaching Session 6 - Interactive Clinical Cases - Radiological Aspects of Abdominal Anatomy

Tuesday, October 15, 2019, 16:30 - 18:00 Lecture Hall 113

OP-671

Radiological Aspects of Abdominal Anatomy

T. Lynch;
Belfast, UNITED KINGDOM.

OP-672

Radiological Aspects of Abdominal Anatomy

N. Magee;
Belfast City Hospital, Belfast, UNITED KINGDOM.

OP-673

Radiological Aspects of Abdominal Anatomy

K. McManus;
Belfast, UNITED KINGDOM.

1508

Clinical Oncology - Parallel Session: Liver Selective Therapy - 90Y and Beyond

Tuesday, October 15, 2019, 16:30 - 18:00 Lecture Hall 114

OP-674

Survival outcomes for transarterial Y-90 radioembolization with glass microspheres in hepatocellular carcinoma patients: a single-institution experience

S. C. Kappadath, A. Mahvash, J. Long, M. Abdelsalam, R. Avritscher, B. Chasen, A. Kaseb, J. Kuban, R. Murthy, B. Odisio, A. Teyateeti, H. Macapinlac, A. Teyateeti;
UT MD Anderson Cancer Center, Houston, TX, UNITED STATES OF AMERICA.

Aim/Introduction: Y90 transarterial-radioembolization (90Y-TARE) with glass-microspheres has shown efficacy in patients with unresectable hepatocellular carcinoma (HCC). The aim of this study is to investigate prognostic factors and stratify the overall survival (OS) for unresectable HCC patients in our institution who underwent 90Y-TARE. **Materials and Methods:** A retrospective study on HCC patients that underwent 90Y-TARE at our institution from November 2010 to November 2018 (n=181). According to institutional algorithm, 90Y-TARE (TAREalone) is an option for patients with tumor involvement ≤50% of liver (tumor≤50%). 90Y-TARE with sorafenib (TARE+sorafenib) was reserved for tumor involvement >50% of liver (tumor>50%) and/or more advanced/aggressive disease features (ADF, defined as infiltrative/ill-defined HCC, presence of macrovascular invasion, portal vein tumor thrombus (PVT), or extrahepatic disease (EHD)). Patients having contraindication to sorafenib would receive 90Y-TARE alone (TAREpalliative) or other treatments (TARE+other). OS was defined as time from date of first 90Y-TARE to death from any cause or last follow-up. Survival function was estimated by Kaplan-Meier analysis. Multivariate Cox proportional-hazards was used to identify prognostic factors. **Results:** Median (range) of patient age was 65 (15-85) with 136 (75%) males. Majority of patients were BCLC stage B (25%) or stage C (71%), multifocal HCC (84.5%), bi-lobar involvement (64%), and tumor≤50% (65%). EHD and PVT were present in 20% and 24% of patients. The median follow-up time was 49.4 months (range 2.4-96.4). Median OS for the patient cohort was 13.4 months (95%CI 9.7-17.2) with no significant difference when stratified by treatment strategy: TAREalone vs TARE+sorafenib vs TARE+other vs TAREpalliative. OS stratified by disease burden and treatment strategy were: 1) tumor≤50% without ADF treated with TAREalone (n=58) 21.6 months (95%CI 5.9-37.3); 2) tumor≤50% with ADF treated with TAREalone (n=17) 8.8 months (95%CI 5.9-11.7) or with TARE+sorafenib (n=36) 18.4 months (95%CI 3.6-33.2), p=0.04; 3) tumor>50% irrespective of ADF treated with TAREalone (n=12) 6.2 months (95%CI 2.6-9.8) or with TARE+sorafenib (n=42) 10.3 months (95%CI 5.8-14.8), p=0.22. On multivariate analysis, the significant independent prognostic factors for OS for patients receiving TAREalone was alpha fetoprotein (AFP) levels (<400 vs ≥400; HR = 0.345 (95%CI 0.12-0.97), p=0.04) and for patient receiving TARE+sorafenib was tumor involvement (tumor≤50% vs tumor>50%; HR = 0.52 (95%CI 0.29-0.93), p=0.03). **Conclusion:** OS of individual HCC patients undergoing TARE strongly related to AFP, disease burden, and ADF. Intolerance of patients to sorafenib substantially decreased median OS by 9.6 months for patients with tumor≤50% and ADF and by 4.1 months for patients with tumor>50%. **References:** None.

OP-675

Effect of transarterial Re188 lipiodol therapy on survival outcome in hepatocellular carcinoma with portal vein thrombosis

S. Datta Gupta, S. Shamim, S. Gamanagatti, Shalimar, P. Gupta, M. A. Khan, M. B. Mallia, V. Chirayil, A. K. Dash, C. S. Bal;
All India Institute of Medical Sciences, New Delhi, INDIA.

Aim/Introduction: Hepatocellular carcinoma (HCC) is the sixth most common malignancy globally with a rising trend owing to increase in non-alcoholic liver cirrhosis. At presentation nearly 40% of patients are inoperable with existing portal vein tumor thrombosis. Recommended treatment in this group of patients is tyrosine kinase inhibitors (TKIs), which improve overall survival from 3-4 months to 6-9 months. However, tolerability and compliance to TKIs is poor. Our objective was to assess the efficacy and survival outcome of Re188 lipiodol trans arterial radionuclide therapy in HCC with PVT. **Materials and Methods:** Patients of HCC with PVT with baseline radiological diagnosis on MRI with Eastern Co-operative Oncology Group (ECOG) performance status ≤2 and Child Pugh score A or B were recruited from Liver Cancer Clinic. Baseline serum alpha-fetoprotein (AFP) was obtained for biochemical follow-up. Lipiodol was labeled with Re-188 using either HDD or N-DEDC kits and empirical dose of Re188-lipiodol was estimated. Patients underwent an initial scout scan (~185MBq Re188 lipiodol) to look for dose distribution in lungs and normal liver parenchyma, prior to injection of therapeutic dose. Thereafter, therapeutic dose was injected trans-arterially as close to tumor feeding vessel as possible. Planar and SPECT imaging was done at 12, 24 and 48hrs. Radiological response on MRI (mRECIST) and biochemical response with serum AFP was assessed every three months and survival was assessed at the end of 6 months from last therapy. **Results:** Fifteen therapies were given in fourteen patients (12 male, 2 female) with median age of 62 years (range: 41-70 years). In eight out of fifteen therapies Re188-HDD lipiodol was injected and in seven therapies Re188-N-DEDC lipiodol was injected, with overall mean injected dose of 2.6GBq±0.4. Radiological response was assessed in 13 patients and biochemical in 10. Radiological complete response was noted in 3 patients, objective response rate was 31% and disease control rate was 85%. Biochemical response (fall of s. AFP≥50%) was noted in 6 patients. Median follow-up period was of 7 months. Survival assessed at 3 and 6 months was 93% and 80% respectively.

Conclusion: In patients of HCC with PVT, Re188 lipiodol therapy appears to be effective in disease control as well as prolonging survival, comparable to TKIs. Further studies at a larger scale may be appropriate to determine its efficacy in comparison to TKIs and establish its role as an alternative treatment option in these patients. **References:** None.

OP-676

Impact of personalized treatment in HCC patients treated with resin 90Y-microspheres: preliminary results of a randomized clinical trial

L. Strigari[1,2], S. Ungania[1], S. Rea[1], A. Annovazzi[1], G. Pizzi[1], G. Vallati[1], G. Iaccarino[1], S. De Niccolo[1], R. Sciuto[1];
[1]Regina Elena Institute IFO, Rome, ITALY, [2]St. Orsola Malpighi University Hopital, Bologna, ITALY.

Aim/Introduction: The aim of the study is to demonstrate a survival benefit in HCC patients treated with resin 90Y-microspheres (μs) when a dosimetry-based patient-specific activity is administered compared to a standard treatment with BSA method in a randomised clinical study. **Materials and Methods:** A prospective double- blinded RCT on 140 HCC patients is now ongoing comparing patients receiving the resin Y90-microspheres activity based on BSA methods (Arm 1: 70 pts) or personalized dosimetry (Arm 2: 70 pts). Patients are also stratified by BLCB stage. CT and PET imaging are acquired before and after therapy. For each enrolled HCC patient both previsional dosimetry, performed using 99mTc-MAA, will be calculated using SPECT-CT imaging and MIM tool, as well as the post-SIRT dosimetry will be determined. Patient blood samples will be also collected before, 30 days and 3 months after SIRT treatment. AFP and PIVKA-II will be determined at baseline and post-SIRT at different time points. Based on dose response models developed by IRE-IFO group, the association between patient outcome (overall survival, time to progression, local tumor control and toxicity) and accurate dosimetry and biomarkers will be investigated. **Results:** Until now 14 unresectable HCC patients (age range 51-84 yrs) with a minimum follow-up of three months were enrolled in the study: six patients in Arm 1 and eight patients in Arm 2. Nine pts were in BCLC stage B and five pts in BCLC stage C. Administered Y90 activity ranged from 1.2 GBq to 2.7 GBq (mean value 1.52 GBq). Mean activity calculated by BSA resulted 1.71 +/- 0.26 SD; mean activity calculated by 3D dosimetry resulted 1.3 +/- 0.37 SD. The administered activity was statistically different between the two methods ($p<0.05$) with a trend of lower activity by using the 3D dosimetric approach. Post- treatment dosimetry evidenced that administered activity in Arm 2 provided at least therapeutic dose to lesion (>120Gy) while sparing normal liver (<40Gy in all patients). At clinical follow-up only 1/8 pts of Arm 2 presented transient liver toxicity while 2/6 pts of Arm 1 presented a significant and persistent liver flure. Objective response was observed in 3/6 pts of Arm 1 and in 9/9 pts of Arm 2. **Conclusion:** The selection of administered activity based on an accurate previsional patient specific dosimetry may result in an optimized resin Y90-μs treatment with a better tumor control and lower toxicity. **References:** None.

OP-677

Survival Analysis of Advanced HCC Treated with Yttrium-90 Radioembolization: A 10-year single-center experience

***S. Bilgiç**, M. S. Sağer, B. Akovali, O. E. Şahin, E. Kaymak, R. L. Uslu Beşli, S. Asa, L. Kabasakal, H. B. Sayman, K. Sönmezoğlu;*
Istanbul University-Cerrahpasa, Istanbul, TURKEY.

Aim/Introduction: Yttrium-90 treatment is widely used in patients with hepatocellular cancer. Patients who had no chance of surgery and were not eligible for transarterial chemoembolization were included in our study. This study was planned to determine the effectiveness of the treatment and to evaluate the overall survival. **Materials and Methods:** A total of 127 patients with HCC who presented to our department between January 2009 and December 2018 were reviewed. 50 of these patients with appropriate hepatic arterial perfusion findings were treated. This study presents data of a retrospective cohort. Overall survival was estimated using Kaplan-Meier method **Results:** The average age was 66.67 years (46 - 83 years). The median time of overall survival was 11.18 months (1-77). Two- and five- year survivals are 20% and 6%, respectively. In stage of BCLC B, median survival period calculated as 16.08 ±4.63 months. The median survival period BCLC C stage, on the other hand, calculated as 9.31 ±3.06 months ($p=0.32$). When the distribution was analyzed, survival was observed as 18.04 (± 5.55) months in the unilobar group and 8.84 (± 2.98) months in the group with bilobar distribution ($p = 0.02$). Survival rate was found to be 15.21 (± 4.05) months in the extrahepatic metastasis group and it was 23.92 (± 4.99) months in the non metastatic group. **Conclusion:** In the literature, treatment-free survival in BCLC B and C group HCC patients was reported as 9.5 and 3.4 months, respectively (1). The mean survival of 16.08 and 9.31 months in the patients whom we provide treatment shows the benefit of the treatment.Median overall survival in studies on Y-90 SIRT treatment varies significantly from other sources (7-27 months) (2, 3). This problem is based on clinical experiences, patient selection and the variety in practice. **References:** 1.Khalaf, N., et al., Natural History of Untreated Hepatocellular Carcinoma in a US Cohort and the Role of Cancer Surveillance. Clin Gastroenterol Hepatol, 2017. 15(2): p. 273-281.e1.2.Salem, R., et al., Institutional decision to adopt Y90 as primary treatment for hepatocellular carcinoma informed by a 1,000-patient 15-year experience. Hepatology, 2018. 68(4): p. 1429-1440.3.Vilgrain, V., et al., Efficacy and safety of selective internal radiotherapy with yttrium-90 resin microspheres compared with sorafenib in locally advanced and inoperable hepatocellular carcinoma (SARAH): an open-label randomised controlled phase 3 trial. Lancet Oncol, 2017. 18(12): p. 1624-1636.

OP-678

Clinical Follow-up after Imaging and Dosimetry for Yttrium-90 (^{90}Y) Liver Radioembolization Using a SiPM-based PET/CT Scanner

H. Duan, M. H. Khalaf, L. Baratto, S. Srinivas, D. Sze, A. Iagaru; Stanford University, Stanford, CA, UNITED STATES OF AMERICA.

Aim/Introduction: To evaluate the response rate and survival of patients treated with Yttrium-90 (^{90}Y) radioembolization following personalized dosimetry and high-quality imaging using SiPM-based PET/CT. **Materials and Methods:** Thirty patients (19 males, 11 females; 47 - 88 years old) with advanced hepatic malignancies were prospectively enrolled. According to their tumor, they were treated with resin or glass microspheres. Pre-therapy ^{99m}Tc MAA SPECT/CT and post-therapy ^{90}Y PET/CT images were analyzed. Tumor and normal liver dose was calculated using SurePlan (MIM) software. ^{90}Y PET/CT scans were obtained in a single bed position for 20 minutes using a SiPM-based PET/CT scanner and reconstructed as 10- and 15-min datasets. Image quality was evaluated using the 5-point Likert scale. **Results:** The mean administered activity was 2.3 GBq ^{90}Y microspheres. Mean tumor dose estimated from ^{99m}Tc MAA SPECT/CT was 99.13 Gy vs. 111.53 Gy from ^{90}Y PET/CT. For normal liver, a mean dose of 28.41 Gy was estimated from ^{99m}Tc MAA SPECT/CT and 21.04 Gy from ^{90}Y PET/CT. ^{99m}Tc MAA SPECT/CT yielded great accuracy as there was no significant divergent tumor or normal liver dose between ^{99m}Tc MAA SPECT/CT and ^{90}Y PET/CT (p=0.667 vs. 0.134). Image quality for ^{90}Y PET/CT was similar at 10 min and 15 min scan time (Likert-scale 4.4 ± 0.6 vs. 4.6 ± 0.5). Our preliminary data show 12 (66.7%) patients had partial response, 1 (5.5 %) stable disease and 5 (27.8%) had progressive disease at 3 months follow up. Five patients passed away after a mean of 5 months. Median survival was 11.5 months. In a sub-analysis, patients treated with resin microspheres vs. glass microspheres had a mean survival of 12.6 vs. 10.3 months, respectively. **Conclusion:** Our preliminary data show a high response rate and median survival of 11.5 months in this cohort. The administered activity may be adjusted to yield the desired 120 Gy in the tumor based on the estimated tumor dose from ^{99m}Tc MAA SPECT/CT. The SiPM-based PET/CT scanner showed excellent image quality even at a reduced scan time of 10 min, acquired with only one bed position. That may allow for inclusion of ^{90}Y PET/CT in routine clinical workflow. However, more patients have to be evaluated to confirm these findings. **References:** None.

OP-679

Evaluation of Utility of Low Dose Yttrium-90 for Radioembolization Treatment Planning Using SPECT/CT and PET/CT - A phantom study

N. Kokabi[1], I. Sethi[1], D. Mir[1], D. M. Schuster[1], J. S. Lee[2], S. Kappadath[3], B. Risk[4], J. R. Galt[1];
[1]Emory University School of Medicine, Atlanta, GA, UNITED STATES OF AMERICA, [2]Radiology Associates of Florida, Sarasota, FL, UNITED STATES OF AMERICA, [3]University of Texas MD Anderson Cancer Center, Houston, TX, UNITED STATES OF AMERICA, [4]Emory Rollins School of Public Health, Atlanta, GA, UNITED STATES OF AMERICA.

Aim/Introduction: To determine the utility of low-dose yttrium-90 (Y-90) for liver radioembolization (RE) treatment planning using SPECT/CT and PET/CT. Specifically, 1) to calculate lung shunt fraction (LSF) and 2) to determine tumor to normal liver activity ratio (TNR). **Materials and Methods:** A torso anthropomorphic phantom with lung and liver chambers was filled initially with 148 MBq and 510 MBq liquid Y-90 solution in the lungs and liver respectively for LSF of 22.4%. Liver activity included 2 fillable spheres simulating hypervascular tumors with initial TNR of 13.9. After imaging with SPECT/CT and PET/CT, more activity was added to the non-tumor liver, lowering the LSF to 14% and TNR to 7. Imaging was repeated and more activity was again added to the liver, lowering the LSF to 10% and TNR to 4.6. Liver activity ranged from 222-877 MBq throughout the study (~10-30% of usual Y-90 therapeutic dose depending on glass vs. resin microspheres used). SPECT/CT imaging was obtained with medium energy collimation and dual energy windows (primary: 108 keV, 32%; secondary: 360 keV, 28%) for 40 minutes total imaging time. A fraction of the counts from the secondary window was subtracted from the primary window to compensate for septal penetration of high energy bremsstrahlung as scatter correction. PET/CT with time-of-flight was obtained with 15 minutes/bed position over 2 bed positions. Volumes of interest were placed over the lungs, liver, the spheres (simulating tumors) on the corresponding CT images and activities were then calculated using MIM V5.6 (MIM Software Inc., Cleveland, Ohio, USA). **Results:** For the true LSF's of 22.5%, 14%, and 10.2%, the SPECT/CT estimated the LSF's to be 18.1%, 10.6% and 7.2%, respectively, and PET/CT estimated them to be 25.2%, 16.1% and 15.5%, respectively. Quantitative evaluation of TNR was compromised because Y-90 came out of suspension and adhered to walls and the sphere mounting rods which was apparent on PET due to superior spatial resolution. For the true TNR's of 13.9, 7 and 4.6, SPECT/CT estimated TNR's to be 6.2, 4.2 and 3.2, respectively and PET/CT estimated them to be 9.6, 5.7 and 3.9, respectively. **Conclusion:** Low-dose Y-90 can be used as a direct surrogate marker for Y-90 RE treatment planning. The under and over estimation of LSF by SPECT and PET, respectively and the underestimation of TNR by both imaging modalities are in part likely related the artificial milieu of the phantom study. Further in-vivo studies are warranted. **References:** None.

OP-680

HCC Radioembolization with Yttrium-90 Polymer Beads (SIR-Spheres):^{99m}Tc-MAA SPECT/CT based dosimetry correlation with survival and tumor response

M. Rodari[1], G. Tosi[1], V. Pedicini[1], D. Poretti[1], E. Lanza[1], R. Muglia[2], K. Marzo[1], M. Sollini[2], A. Chiti[2,1];
[1]Humanitas Clinical and Research Hospital, Milan, ITALY, [2]Humanitas University, Milan, ITALY.

Aim/Introduction: Aim of this study was to evaluate correlation of ^{99m}Tc-MAA SPECT/CT based dosimetry with survival and tumor response in HCC patients treated with ^{90}Y-labelled polymer (SIR-Spheres). **Materials and Methods:** A retrospective analysis was performed on 49 consecutive patients (8 females, 41 males, mean age 69) affected by advanced HCC, treated with radioembolization (TARE). Before treatment, all patients were subjected to a preliminary study with ^{99m}Tc-MAA SPECT/CT to evaluate tumor and organ at risk (OAR) absorbed doses and to predict the number of microspheres that could pass to the systemic blood circulation. Tumor absorbed dose was calculated using a partition model method. Forty-nine procedures were performed, including dual-lobe treatments in eight patients. Overall survival (OS) was evaluated using Kaplan-Meier curve and objective response was assessed using modified RECIST criteria assessed on CT performed two and six months after treatment. **Results:** Median OS of the entire cohort was 15.1 months. The median tumor absorbed dose was 193 Gy. Twenty-nine patients who received tumor absorbed dose > 150 Gy had significantly longer survival when compared to those receiving a dose <150 Gy (median 17.5 months versus 11.5 months). Moreover, Overall survival (OS) correlated to the presence and degree of portal venous invasion. Patients without portal venous invasion had longer OS when compared to those with portal venous invasion (median 18.2 months versus 11.8 months). Patients with main portal venous invasion had 8.9 months OS, while those with segmental venous invasion had 13 months OS. Objective response rate (OR) was 36 % and associated with higher tumor absorbed dose. **Conclusion:** In our series, we found a better overall survival (OS) in patients that received tumor absorbed dose >150 Gy. Main portal venous invasion was correlated with poor overall survival (OS). **References:** None.

1509

Neuroimaging - Parallel Session: Brain Tumours

Tuesday, October 15, 2019, 16:30 - 18:00 Lecture Hall 115

OP-681

Prognostic value of dynamic ^{18}F-FET PET in oligodendrogliomas

F. J. Vettermann, M. Unterrainer, B. Suchorska, J. Herms, P. Bartenstein, J. Tonn, N. L. Albert;
Ludwig-Maximillians-University, Munich, GERMANY.

Aim/Introduction: In the updated 2016 WHO classification gliomas are stratified into separate entities according to their molecular genotype with different prognoses. IDH-mutant, 1p/19q-codeleted gliomas (oligodendrogliomas) have a favourable outcome compared to astrocytic tumors or glioblastomas. With regard to the longer survival, treatment decisions have to be made carefully and have to weigh up the risk of treatment-associated morbidity. Therefore we evaluated the role of dynamic ^{18}F-FET PET as prognostic biomarker in oligodendroglioma. **Materials and Methods:** Seventy-five patients with newly diagnosed, untreated oligodendrogliomas with IDH-mutation and 1p/19q-codeletion (WHO grade II n=58 and III n=17) and dynamic ^{18}F-FET PET were included. ^{18}F-FET PET parameters (maximum/mean tumor-to-background ratios [TBR_{max}, TBR_{mean}], minimal time-to-peak [TTP_{min}]) were correlated with the clinical outcome in terms of progression-free survival (PFS) as defined by RANO criteria using Kaplan-Meier estimates and uni-/multivariate analyses. **Results:** During a median follow-up time of 67.5 months, 43/78 patients showed tumor progression. The median PFS was 57.0 months. In the univariate analysis, WHO grade (II vs. III: median PFS 64.0 vs. 39.0 months, p=0.035) and TTP_{min} (≤25 vs. >25 min: median PFS 50.0 vs. 104.0 months, p=0.021) were associated with the clinical outcome, whereas age, contrast enhancement, Karnofsky-Performance-Score, surgical procedures, $TBR_{max/mean}$ and BTV were not (p>0.05). In the multivariate analysis both WHO grade (hazard ratio 2.4 (CI: 1.2-4.9), p=0.019) and TTP_{min} (hazard ratio 2.4 (CI: 1.1-5.2), p=0.021) remained significant prognostic factors for PFS. **Conclusion:** In IDH-mutant, 1p/19q-codeleted oligodendrogliomas, the WHO grade and TTP_{min} are independent prognostic parameters for the PFS. A TTP_{min} of >25 min identified patients with a favourable outcome (PFS twice as long). Therefore, the evaluation of dynamic ^{18}F-FET PET in addition to histopathology and the molecular genetic profile seems useful for the characterization of gliomas and might help to individualize the treatment. **References:** None.

OP-682

Prognostic value of FDG-PET/CT in recurrent/refractory CNS lymphoma receiving Ibrutinib-based therapies

***S. Krebs**, J. Wolfe, I. Mellinghoff, C. Grommes, H. Schoder;*
Memorial Sloan Kettering Cancer Center, New York, NY, UNITED STATES OF AMERICA.

Aim/Introduction: Quantitative PET imaging biomarkers for primary central nervous system lymphoma (PCNSL) have not yet been established. This study evaluated the prognostic value of pretreatment FDG PET/CT-based measurements for treatment response, progression-free survival (PFS) and overall survival (OS) to ibrutinib-based treatment regimen in recurrent/refractory (r/r) PCNSL and secondary CNS lymphoma (SCNSL). **Materials and Methods:** Eligible patients had r/r PCNSL/SCNSL, age≥18, ECOG≥2, normal end-organ function, and unrestricted number and type of prior therapies. In patients with SCNSL disease, systemic disease needed to be absent. Participants received either single agent ibrutinib (560 mg, 840 mg) or ibrutinib in combination with methotrexate (HD-MTX; at 3.5g/m2 every 2 weeks) with or without rituximab. Pretreatment FDG-PET/CT scans were prospectively analyzed. Lesion volumes were measured by three-dimensional threshold-based volume of interest (VOI) analyses for FDG-PET uptake and referring to PET/CT images in all patients. The VOIs were overlaid on

the tumors covering the entire lesion. We determined the maximum standardized uptake values (SUVmax), MTV (volume encompassed by a 42% isocontour around the voxel with the highest PET uptake), and TLG (calculated by multiplying MTV by SUVmean). **Results:** 46 patients underwent single agent therapy, 15 combination therapy. FDG PET/CT scans of 57/61 patients with (r/r) PCNSL and SCNSL were analyzed. 16 patients had no measurable disease on PET. A total of 85 lesions were identified, and maximum standardized uptake values (SUVmax), metabolic tumor volume (MTV), total lesion glycolysis (TLG), were measured, lesion sum determined and correlated with progression free survival (PFS). Median SUVmax was 19.7 (3.7-47.9), MTV 1.8 (0.3-32.4) and TLG 18.8 (0.5-709.5). High SUVmax was correlated with lower PFS. In patients with a SUVmax >20, PFS has 3.4 months, whereas patients with a SUVmax <20 had a PFS of 10.8 months. **Conclusion:** In patients with CNS lymphoma receiving an ibrutinib-based regimen, SUVmax of >20 appears to be a prognostic factor. Validation in a larger clinical trial will be performed. **References:** None.

OP-683

Biological-tumour-volumes in standard and early summation ^{18}F-FET PET images distinctly exceed contrast-enhancementin patients with IDH-wildtype glioma

M. Unterrainer, *K. von Rohr, L. Kaiser, C. Diekmann, V. Ruf, J. Herms, P. Bartenstein, M. Niyazi, J. Tonn, N. L. Albert;*
University of Munich, Munich, GERMANY.

Aim/Introduction: In patients with IDH-wildtype glioma, the contrast-enhancement (CE) on MRI usually represents the target of local treatments such as resection and radiotherapy. PET using ^{18}F-FET enables detection of metabolically active tumour parts beyond CE on MRI. Especially, even larger metabolically active tumour parts were seen in early ^{18}F-FET PET summation images. However, the spatial correlation of CE and PET-derived tumour volumes in IDH-wildtype gliomas remains unknown and was analysed in this study. **Materials and Methods:** Patients with de-novo IDH-wildtype glioma WHO grade III/IV undergoing ^{18}F-FET PET and MRI prior to any further therapy were included. On ^{18}F-FET PET, the biological-tumor-volume (BTV) was assessed (1.6 x background-activity) within standard (20-40 minutes) and early (5-15 minutes) summation images (eBTV). On MRI, the volume of CE was delineated. The spatial correlation between CE, BTV and eBTV was assessed using the Dice-similarity-coefficient (DSC). **Results:** 164 patients with IDH-wildtype glioma were included (99/164 (60%) glioblastoma WHO grade IV, 65/164 (40%) anaplastic astrocytoma WHO grade III). Of these, 157/164 (96%) were ^{18}F-FET-positive and 130/164 (79%) showed CE on MRI. 27/34 (79%) patients without CE were ^{18}F-FET-positive; vice versa, 0/7 (0%) ^{18}F-FET-negative patients showed CE on MRI. Overall, CE was significantly smaller than BTV (13.6±18.5 vs. 26.6±24.8 ml, p<0.001) and eBTV (32.1±26.7 ml, p<0.001), whereas eBTV was significantly larger than BTV (32.1±26.7 vs. 26.6±24.8 ml, p=0.001). Hence, there was a poor spatial correlation of CE / BTV (DSC 0.31±0.22) and CE / eBTV (DSC 0.33±0.21) and a moderate spatial correlation of BTV and eBTV (DSC 0.75±0.19). The DSC was significantly lower in WHO grade III compared to WHO grade IV gliomas correlating CE / BTV (DSC 0.22±0.21 vs. 0.34±0.21, p=0.005) and CE / eBTV (DSC 0.26±0.21 vs. 0.36±0.21, p=0.024). **Conclusion:** In IDH-wildtype gliomas, the PET-derived BTVs distinctly exceed the CE on MRI in both standard and early summation images with a poor spatial correlation only; especially in WHO grade III gliomas. Moreover, eBTV also exceeds BTV with a moderate spatial correlation. These vast spatial discrepancies suggest that metabolically active tumour on ^{18}F-FET PET should be implemented into resection and radiotherapy planning. **References:** None.

OP-684

The Role of ^{11}C-methionine PET in Patients with Negative/Undetermined Diffusion-Weighted Magnetic Resonance Imaging (DWI-MRI): Correlation with Histology and Molecular Biomarkers in Operated Glioma

A. Castello[1], *A. Bizzi*[2], *M. Riva*[3], *M. Rossi*[3], *F. Pessina*[3], *B. Fernandes*[4], *M. Grimaldi*[5], *E. Mazziotti*[6], *P. Navarria*[7], *L. Bello*[3], *E. Lopci*[1];
[1]*Nuclear Medicine, Humanitas Clinical and Research Hospital - IRCCS, Rozzano (MI), ITALY,* [2]*Neuroradiology, Fondazione IRCCS Istituto Neurologico Carlo Besta, Milan, ITALY,* [3]*Oncological Neurosurgery, Humanitas Clinical and Research Hospital - IRCCS, Rozzano (MI), ITALY,* [4]*Pathology, Humanitas Clinical and Research Hospital, Rozzano (MI), ITALY,* [5]*Neuroradiology, Humanitas Clinical and Research Hospital, Rozzano (MI), ITALY,* [6]*Nuclear Medicine, Humanitas Clinical and Research Hospital, Rozzano (MI), ITALY,* [7]*Radiotherapy and Radiosurgery, Humanitas Clinical and Research Hospital, Rozzano (MI), ITALY.*

Aim/Introduction: Our aim was to assess ^{11}C-methionine PET and Diffusion-Weighted Magnetic Resonance Imaging (DWI-MRI) diagnostic accuracy and the prognostic value in patients with gliomas candidate to neurosurgery. **Materials and Methods:** Patients (n=124) who underwent 11C-methionine PET and DWI-MRI in the diagnostic and preoperative stage were retrospectively enrolled. The reference standard was established by histology after neurosurgery. Images were interpreted by visual evaluation for DWI-MRI and by both visual and semi-quantitative analysis, expressed by SUVmax, SUVratio (ratio of SUVmean in the tumor to SUVmean in contralateral normal cortex) and metabolic tumor burden (MTB), for 11C-methionine PET. Kaplan-Meier survival analysis was performed. The median follow-up was 14.3 months (range 2-73 months). Correlations between metabolic parameters and Ki-67 were evaluated. **Results:** 47 high-grade gliomas (HGG), 77 low-grade gliomas (LGG) were diagnosed. On visual assessment, sensitivity and specificity for differentiating HGG from LGG were 80.8% (38/47) and 59.7% (46/77) for DWI-MRI, and 95.7% (35/47) and 41.5% (32/77) for ^{11}C-methionine PET. On semi-quantitative analysis the sensitivity, specificity and the area under the curve by ROC analysis, respectively, were 78.7%, 71.4%, and 80.4% for SUVmax, 78.7%, 70.1%, and 81.1% for SUVratio, and 74.5%, 61%, and 76.7% for MTB. In patients with negative DWI-RMI, median PFS

was longer in those with SUVmax<3.6 (median not reached vs 34.2 months, p=0.004), SUVratio<2.4 (median not reached vs 21.5 months, p<0.001), and MTB<7 (median not reached vs 45.7 months, p=0.018). When we analyzed patients with LGG and negative DWI-RMI, only SUVratio<2.4 and MTB<7 were associated with longer PFS (p=0.016 and p=0.024, respectively). Regarding molecular profile, in patients with negative DWI-RMI and IDH wild type, SUVmax and SUVratio were higher compared to those with IDH mutated (p=0.025 and p=0.01, respectively). In the same cohort, patients with 1p/19q codeletion showed a tendency to have higher SUVmax (p=0.067) compared to those without codeletion. No significant difference was found regarding MGMT promoter methylation status. Finally, we demonstrated a positive correlation among metabolic parameters by ^{11}C-methionine PET and Ki-67, in all gliomas as well as in those with negative DWI-MRI (SUVmax rho=0.515, SUVratio rho=0.488, and MTB rho=0.477). **Conclusion:** ^{11}C-methionine PET was highly sensitive for the differentiation between LGG and HGG both by visual and semi-quantitative evaluation. In patients with negative DWI-MRI, ^{11}C-methionine PET was predictive of PFS, hence allowing to identify gliomas with worse prognosis and helping clinicians to tailor therapy approach. ^{11}C-methionine PET metrics correlated significantly with proliferative index and the IDH status. **References:** None.

OP-685

Molecular-genetic and histologic differentiation of gliomas based on characteristic ^{18}F-FET PET pharmacokinetics

L. Kaiser[1], M. Unterrainer[1], A. Holzgreve[1], M. Grosch[2], S. A. Ahmadi[2], E. Mille[1], A. Gosewisch[1], J. Brosch[1], B. Suchorska[3], J. C. Tonn[3], S. Ziegler[1], P. Bartenstein[1], N. L. Albert[1], G. Böning[1];
[1]Department of Nuclear Medicine, University Hospital, LMU Munich, Munich, GERMANY, [2]German Center for Vertigo and Balance Disorders, University Hospital, LMU Munich, Munich, GERMANY, [3]Department of Neurosurgery, University Hospital, LMU Munich, Munich, GERMANY.

Aim/Introduction: Various static and kinetic parameters derived from dynamic ^{18}F-FET PET data have shown clinical relevance for glioma classification. The aim of this study was to correlate heuristic with pharmacokinetic modelling parameters, and to assess the relevance for molecular-genetic and histologic glioma classification. **Materials and Methods:** A total of 322 newly diagnosed gliomas were included: 128 IDH-mutant, 194 IDH-wildtype (IDHmut/wt); 91 low-, 231 high-grade (LGG/HGG). We investigated 1- and 2-tissue compartment models (1/2TC) with/ without blood volume fraction (V_B) using an image-derived input function (IDIF), linear models (Logan and Patlak) with IDIF or reference tissue input, and the following heuristic parameters: early/ late tumour-to-background ratios ($TBR_{5\text{-}15'}$ $TBR_{20\text{-}40}$), late slope ($Slope_{15\text{-}40}$), and time-to-peak (TTP). The ability to identify an IDHwt or HGG glioma was assessed with univariate and multivariate ROC-analysis using 5-fold cross-validation with stratified folds. **Results:** In 63% a reversible $2TC_{VB}$ model was preferred (Akaike). While $TBR_{20\text{-}40}$ was strongly correlated with DVR (ρ=0.92), an increasing kinetic was associated with an elevated net-influx-rate K_1 from Patlak plots (ρ>0.8), and an early peak or negative slope was associated with an elevated K_1 (ρ>0.53) and k_2 (ρ>0.72) from $1TC_{VB}$, and K_1 (ρ>0.34) and k_4 (ρ>0.56) from $2TC_{VB}$. Despite significantly elevated distribution-volumes (V_T) in tumour tissue compared to background, V_T was not able to differentiate between glioma grades in univariate analysis (AUC for identification of IDHwt <0.59; AUC for identification of HGG <0.52). Relative values (DVR or $TBR_{20\text{-}40}$) yielded slightly better results. The highest AUC values were obtained for $TBR_{5\text{-}15}$ (0.78; 0.80), TTP (0.78; 0.72), $Slope_{15\text{-}40}$ (0.83; 0.78), and the parameters from Patlak plots (0.82; 0.79) and $1TC_{VB}$ (K_1: 0.75; 0.75 and k_2: 0.72; 0.73). Multivariate analysis yielded an AUC of 0.86 for the identification of IDHwt and 0.82 for the identification of HGG gliomas. **Conclusion:** The characteristic kinetics of aggressive gliomas could be described with pharmacokinetic model parameters. The best results for molecular-genetic and histologic glioma classification were obtained with multivariate analysis incorporating static and kinetic ^{18}F-FET PET parameters. A validation study based on stereotactic biopsies is ongoing. **References:** None.

OP-686

Dynamic ^{68}Ga-DOTATATE PET/MRI and Patlak analysis for enhanced diagnosis of intracranial meningioma

***N. Karakatsanis**, M. Skafida, E. Lin, M. Roytman, B. Liechty, T. Schwartz, S. Pannullo, J. Osborne, J. Ivanidze;*
Weill Cornell Medical College, New York, NY, UNITED STATES OF AMERICA.

Aim/Introduction: Meningiomas are the most common intracranial tumors. They are often slow-growing tumors without noticeable early symptoms, but potentially life threatening with increasing size and high likelihood of recurrence. Contrast enhanced MRI is the gold standard for meningioma diagnosis and treatment planning but with limitations in accurately differentiating recurrence from post-treatment effects. ^{68}Ga-DOTATATE is a PET radiotracer with high target affinity in somatostatin receptors 2 (SSTR2) previously utilized for the characterization of gastrointestinal neuroendocrine tumors. Meningiomas exhibit high expression rates of SSTR2. The aim of this study was to evaluate the usefulness of dynamic ^{68}Ga-DOTATATE PET/MRI and Patlak uptake rate (Ki) analysis in a prospective clinical cohort of patients with meningioma. **Materials and Methods:** A cohort of 20 patients with clinically suspected or pathology proven meningioma were imaged over a period of 6 months. Dynamic PET/MRI was performed at 10-50 +/-5 minutes post ^{68}Ga-DOTATATE injection. For 12 randomly selected patients, the PET list data were binned to 5-min frames, followed by reconstruction of the respective dynamic PET images and subsequent Patlak Ki analysis. SUV_{mean} values over post-injection time and Ki scores were extracted from target regions, corresponding to identified meningiomas or suspected post treatment effects, using the superior sagittal

sinus as reference uptake. Post-injection time-SUV_{mean} curves and regional Ki scores were evaluated to determine the rate of ^{68}Ga-DOTATATE uptake in the target against the reference regions. Moreover, the last 10min of PET data were binned into a single frame and the respective static PET images were reconstructed. **Results:** From the static ^{68}Ga-DOTATATE/MR images, 50 meningiomas were identified (median: 2 per patient, range 0-14). In the sub-cohort of 12 patients, the high Ki scores (Ki>0.015ml/min/g) from Patlak analysis of the dynamic PET data confirmed the previously identified meningiomas, while in 4 cases a very low uptake rate (Ki<0.009ml/min/g) suggested post-treatment effects even in presence of suspicious MRI findings. Distinctively higher Ki rates of ^{68}Ga-DOTATATE uptake were evaluated for meningioma relative to post-treatment effects ($p<0.01$) positively correlated with parenchymal and osseous invasion. Finally, the contrast of SUV_{mean} in meningioma over post-treatment effect regions continuously increased with the maximum ratio attained later than 45min post injection. **Conclusion:** Dynamic ^{68}Ga-DOTATATE PET/MRI and Patlak Ki analysis can enhance the differentiation between meningioma and post-treatment effects at no additional scan time relative to static PET/MR. The unique multi-parametric features of dynamic ^{68}Ga-DOTATATE PET/MRI may facilitate a more accurate diagnosis of intracranial meningioma. **References:** None.

OP-687

^{68}Ga PSMA PET/MRI in THE DIFFERENTIATION of LOW and HIGH GRADE GLIOMAS

E. Akgun, *M. Y. Akgun, C. Isler, M. Uzan, H. B. Sayman;*
IUC Cerrahpasa Medical Faculty, Istanbul, TURKEY.

Aim/Introduction: The increased expression of prostate specific membrane antigen on the neovasculature of tumors enables uptake of 68Ga PSMA on brain tumors (1). Based on this fact, we investigated if there was a relationship between SUV measurements and tumor grades using the images obtained with 68Ga PSMA PET/MR in patients pre-diagnosed as low grade glioma (LGG) or high grade glioma (HGG). **Materials and Methods:** From thirty-five out of 38 patients whose pathological examination revealed glial tumor, a total of 42 lesions located on separate anatomic localizations were evaluated. SUV (max/mean/peak) values and grade relationship were evaluated based on each lesion while mitosis, Ki-67 were evaluated for each patient. Endothelial proliferation, necrosis was only evaluated in HGGs, Alpha thalassemia/mental retardation syndrome X-linked (ATRX) mutation was evaluated in astrocytomas. **Results:** Grade, Ki-67, mitosis and necrosis and SUV (max/mean/peak) values were found statistically significant in correlation. The parameter with the highest correlation coefficient was mitosis. (For SUVmax r = 0.64, p = 0). The correlation of endothelial proliferation in HGGs was not statistically significant. There was no significant difference between the SUV values of ATRX mutant and nonmutant cases. When Grade II and III were considered as the first group and IV as the second group, the cutoff values were found to be for SUVmax 2.30, for SUVmean 0.21 and for SUVpeak 0.63. When lesions were grouped as LGG and HGG, the cutoff values were 1.15 for SUVmax, 0.06 for SUVmean and 0.21 for SUVpeak. In the diagnosis of HGG, PET's sensitivity is higher than MRI but there is no statistically difference in specificity (PET sensitivity 85.7% specificity 85,7%; MR sensitivity 71.4% specificity 85.4%). **Conclusion:** 68Ga PSMA PET imaging is found to be particularly useful in differentiating Grade IV glial tumors from lower grades. This finding is thought to be important in the differentiation of relapse from postoperative tissue changes and utility of 177Lu PSMA treatment (2). Thanks to the PET/MRI technique, that patients can undergo simultaneous PET and MRI in one stop. **References:** 1. Nomura N, Pastorino S, Jiang P, Lambert G, Crawford JR, Gymnopoulos M et al. Prostate specific membrane antigen (PSMA) expression in primary gliomas and breast cancer brain metastases. Cancer Cell Int 2014; 14 :26.2. Sasikumar A, Kashyap R, Joy A, Charan Patro K, Bhattacharya P, ReddyPilaka VK, et al. Utility of 68Ga-PSMA-11 PET/CT in Imaging of Glioma-A Pilot Study. Clin Nucl Med. 2018 Sep; 43(9): e304-e309.

1510

Clinical Oncology - Parallel Session: It's in the Blood!

Tuesday, October 15, 2019, 16:30 - 18:00 Lecture Hall 116

OP-688

Comparison between tumour metabolism derived from 18F-FDG-PET/CT and accurate cytogenetic stratification in newly diagnosed multiple myeloma patients

Y. E Silva[1], *J. Riedinger*[1], *D. Caillot*[2], *M. Chrétien*[2], *J. Corre*[3], *A. Cochet*[1], *C. Tabouret-Viaud*[1];
[1]*Unicancer Georges-François Leclerc Cancer Center, Dijon, FRANCE,* [2]*University Hospital François Mitterrand, Dijon, FRANCE,* [3]*Institut Universitaire du Cancer-Oncopole, Toulouse, FRANCE.*

Aim/Introduction: p.p1 {margin: 0.0px 0.0px 0.0px 0.0px; font: 12.0px 'Helvetica Neue'; color: #454545} 18-Fluorodeoxyglucose Positron Emission Tomography (18F-FDG-PET/CT) is a useful tool for baseline staging in newly diagnosed Multiple Myeloma (MM). This monocentric retrospective study aimed at examining the relation between baseline tumour metabolism and LINEAR PREDICTOR (LP)-score, a new cytogenetic stratification score. **Materials and Methods:** p.p1 {margin: 0.0px 0.0px 0.0px 0.0px; font: 12.0px 'Helvetica Neue'; color: #454545} From June 2011 to March 2019, 104 patients addressed to our institution for staging of newly diagnosed MM were included. Thirty-nine patients were included in a preliminary study in order to determine which threshold of significance for calculation of total metabolic tumor volume (TMTV) / total lesion glycolysis (TLG) is the most associated with progression rate in MM, between four per-patient adapted thresholds, absolute threshold at SUV_{max}2.5, relative threshold at 41% of SUV_{max}. For the remaining 65

patients, LP score was determined on systematic iliac crest bone marrow samples. Obtained on CD138-sorted bone marrow plasma cells, this new composite cytogenetic stratification is a 6-marker based weighted score using FISH+/- single nucleotide polymorphism arrays (deletion 17p, translocation (4;14), trisomy 5, trisomy 21, 1q gain, deletion 1p32). We then correlated TMTV / TLG calculation and LP-score using a Kruskall-Wallis test, and diffuse bone marrow involvement (DBI) on PET (based on hepatic background as threshold of positivity) and cytogenetic data using a Chi-squared test. **Results:** p.p1 {margin: 0.0px 0.0px 0.0px 0.0px; font: 12.0px 'Helvetica Neue'; color: #454545} In the preliminary study, $TMTV_{bm}/TLG_{bm}$ calculation (with bone marrow threshold) was correlated more significantly to 2-year progression rate than other methods (p=0.023 and 0.033 respectively, corresponding AUC = 0.739+/-0.085 and 0.723+/-0.085 respectively) and was the only method associated with 3-year progression rate (p=0.029 and 0.039 respectively). The distribution of $TMTV_{bm}/TLG_{bm}$ values among the 3 LP-score categories was almost stochastic, without any significant association (p=0.70). There was also no significant association between $TMTV_{bm}/TLG_{bm}$ and any of the 6 cytogenetic abnormalities included in LP-score calculation except for trisomy 21 (trend for significance: p=0.09 and 0.11 respectively). We didn't find significant association between DBI and cytogenetics, either (p=0.29). **Conclusion:** p.p1 {margin: 0.0px 0.0px 0.0px 0.0px; font: 12.0px 'Helvetica Neue'; color: #454545} There is no significant association between tumour metabolism assessed with 18F-FDG-PET/CT and LP-score cytogenetic stratification in patients with newly diagnosed MM, suggesting a potential complementarity of these biomarkers for prognostic stratification. **References:** None.

OP-689

^{11}C-acetate Is The Preferred Tracer Over ^{18}F-FDG In PET/CT Evaluation Of Active Multiple Myeloma: A Follow-up Study With A Larger Cohort Of Patients

G. C. L. Ho, *S. Chen, S. Cheung, Y. Leung, K. Cheng, K. Wong, Y. Wong, K. Wu, R. Liang;*
Hong Kong Sanatorium & Hospital, Hong Kong, HONG KONG.

Aim/Introduction: Our pilot study in 2014 suggested that ^{11}C-acetate is a more appropriate PET tracer than ^{18}F-FDG for early detection of active multiple myeloma (MM) and measurement of MM tumor burden. In this follow-up study, we extended our investigation to a larger cohort of clinically-suspected MM patients in order to verify that ^{11}C-acetate is indeed the preferred PET tracer to evaluate the metabolic pathology of MM. **Materials and Methods:** From Aug 2014 to July 2018, 195 patients clinically suspected of MM (M:F=102:93; age range:32-90years, mean=64.0±13.4years) were referred by hematologists for dual-tracer (^{11}C-acetate, ^{18}F-FDG) PET/CT. The PET criteria for active MM were defined as: (1) focal bone lesions (FBLs) with visually increased ^{11}C-acetate or ^{18}F-FDG uptake; and/or (2) diffusely increased marrow metabolism with L3 vertebra ^{11}C-acetate SUV_{max}_L3>=3.8 or ^{18}F-FDG SUV_{max}_L3>=3.0, (L3 as an index site to measure tumor burden in diffuse MM validated by prior study). The gold standard was bone marrow examination and trephine biopsy with immunohistochemistry. Patients with other hematological disorders found by trephine biopsy were excluded. **Results:** 160 patients (M:F=81:79; age range:33-90years, mean=64.2±12.8years) were finally included. Patho-histochemical examinations confirmed 95 patients with active MM (who required treatment), 16 with indolent smoldering MM (SMM), 25 with monoclonal gammopathy of unknown significance (MGUS), 24 with active marrow with/without reactive plasmacytosis. Of the 95 active MM patients, ^{11}C-acetate PET/CT identified 78/95 (82.1%) versus ^{18}F-FDG 53/95 (55.8%), P<0.05. All 17/95 patients negative on ^{11}C-acetate PET/CT were also negative on ^{18}F-FDG PET/CT; however, ^{11}C-acetate could identify 25/42 (59.5%) active MM missed by ^{18}F-FDG. Of the 53/95 patients detected by both tracers, 51/53 had MM lesions more avid for ^{11}C-acetate than ^{18}F-FDG (respectively SUV_{max}_L3=5.6±1.7 vs. 3.6±1.3, P<0.05) and/or with greater number of ^{11}C-acetate-avid FBLs than ^{18}F-FDG. ^{11}C-acetate PET/CT was negative in indolent SMM (16/16=100%), MGUS (21/25=84%), active marrow with/without reactive plasmacytosis (23/24=95.8%) with an overall specificity 92.3% (60/65). ^{18}F-FDG PET/CT could not correct any of the 5 false positive cases by ^{11}C-acetate and had a lower specificity (54/65=83.1%). **Conclusion:** With a larger cohort, we found that ^{18}F-FDG offered no incremental value over ^{11}C-acetate and verified that ^{11}C-acetate is the preferred tracer for PET/CT diagnosis of active MM, potentially useful in 3 management scenarios: to confirm or rule out active MM, to suggest observation versus initiation of treatment in SMM, or to observe in simple plasma cell dyscrasia not yet requiring active treatment. **References:** None.

OP-690

Prognostic role of baseline 18F-FDG PET/CT metabolic parameters in elderly Hodgking lymphoma

A. Mazzoletti[1], *D. Albano*[2], *F. Dondi*[1], *M. Bonacina*[2], *R. Durmo*[2], *E. Cerudelli*[2], *M. Gazzilli*[2], *P. Bellini*[1], *F. Bertagna*[1], *R. Giubbini*[1];
[1]*Università degli Studi di Brescia, Brescia, ITALY,*
[2]*Spedali Civili di Brescia, Brescia, ITALY.*

Aim/Introduction: Hodgkin Lymphoma (HL) is an aggressive lymphoma subtype with high 18F-FDG avidity at 18F-FDG-PET/CT but no validated criteria in treatment evaluation and prediction of outcome are currently available. The prognosis of HL in elderly patients (aged over 65 years) is considerably poor especially in comparison with young patient and the reason of this poor outcome is yet unclear. The aim of this study was to investigate whether the metabolic baseline 18F-FDG PET/CT parameters can predict prognosis in elderly HL. **Materials and Methods:** Between January 2006 and January 2019, 73 (average age 73,5; 38 men and 35 women) patients with histologically proven Hodgkin Lymphoma who underwent baseline 18F-FDG-PET/CT were retrospectively enrolled. Seventy-two patients diagnosed with HL were cured with standard chemotherapy

regimens, 13 of them received also radiation therapy and just 1 patient received only radiation therapy. PET images were analyzed visually and semi-quantitatively by measuring the maximum standardized uptake value body weight (SUVbw), the maximum standardized uptake value lean body mass (SUVlbm), the maximum standardized uptake value body surface area (SUVbsa), total metabolic tumor volume (MTV) and total lesion glycolysis (TLG). For the entire population, receiver operating characteristic curve analysis was used to identify the optimal cutoff point of semiquantitative parameters in the light of progression free survival (PFS) and overall survival (OS). Survival curves were plotted according to the Kaplan-Meier method. **Results:** All baseline PET/CT were positive showing increased 18F-FDG uptake in nodal and/or extranodal lesions. At a median follow up of 31,4 months (range 1-101), the median PFS and OS were respectively 20,7 and 31,4 months with a 2-year and 3-year PFS of 54% and 42% and a 2-year and 3-year OS of 68% and 41% respectively. Relapse or progression of disease occurred in 29 patients with an average time of 14,8 months from the baseline PET/CT and death occurred in 21 patients with an average time of 17,2 months. SUVbw, SUVlbm and SUVbsa were significantly related to PFS (respectively p=0,03; p=0.003; p=0,009) and only SUVbw was related to OS (p=0,03). Metabolic tumor volumes (MTV and TLG) were not related with outcome survival. **Conclusion:** In conclusion, in our study we demonstrated that several metabolic tumour features (SUVbw, SUVlbm and SUVbsa) were significantly correlated with PFS, while only SUVbw with OS. MTV and TLG were not related with outcome survival. **References:** None.

OP-691

Determining the optimal segmentation method for assessing metabolic tumor volume in ^{18}FDG-PET-CT scans in relapsed/refractory classical Hodgkin lymphoma

J. Driessen[1], *G. J. C. Zwezerijnen*[2], *J. J. Eertink*[3], *M. J. Kersten*[1], *O. S. Hoekstra*[2], *J. M. Zijlstra*[3], *R. Boellaard*[2];
[1]*Department of Hematology, Amsterdam UMC, University of Amsterdam, Cancer Center Amsterdam and LYMMCARE (Lymphoma and Myeloma Center), Amsterdam, NETHERLANDS,* [2]*Department of Radiology and Nucleair Medicine, Amsterdam UMC, Vrije Universiteit Amsterdam, Cancer Center Amsterdam, Amsterdam, NETHERLANDS,* [3]*Department of Hematology, Amsterdam UMC, Vrije Universiteit Amsterdam, Cancer Center Amsterdam, Amsterdam, NETHERLANDS.*

Aim/Introduction: Baseline metabolic tumor volume (bMTV) is increasingly studied as a prognostic factor for relapsed/refractory classical Hodgkin lymphoma (R/R cHL). However, there is no consensus on a standard segmentation method for assessing bMTV. The aim of this pilot study was to derive bMTV with 6 semi-automatic segmentation methods and a manual approach and to investigate the correlation of bMTV among all segmentation methods. **Materials and Methods:** We selected 20 EARL compliant baseline ^{18}FDG-PET-CT scans of R/R cHL patients. Six semi-automatic segmentation methods were applied using an in-house developed software "Accurate": two fixed thresholds (SUV4.0 and SUV2.5), two relative thresholds (A50P: a contrast corrected 50% of SUVpeak, and 41max: 41% of SUVmax), and 2 majority vote methods, MV2 and MV3 selecting delineations of ≥2 and ≥3 of previously mentioned methods, respectively. After removing regions with physiological uptake, quality scores (QS) were given to each segmentation by two reviewers (JD, GZ): QS-1, complete selections containing all visible tumor localizations after minimal observer-interaction; and QS-2 for incomplete selections. Besides, quality of the segmentation was rated: A, for good visual delineation of lesions; B, for too narrow delineation; and C, for too large delineation. Semi-manual segmentation was done by adjusting the most complete semi-automatic method. We used Spearman's correlations to compare all semi-automatic methods. Bland-Altman analysis was performed to compare semi-automatic with semi-manual segmentation. **Results:** SUV2.5, A50P, MV3, 41max, SUV4.0 and MV2 had QS-1 in respectively 65%, 55%, 55%, 50%, 45% and 40% of cases, with QS-1A in 45%, 25%, 30%, 35%, 40% and 15% of all scans. Segmentation quality was not significantly different in patients with advanced stage or primary refractory disease. However, in scans containing lesions close to regions with physiological uptake (n=8), only 37.5% (SUV4.0 and 41max), 25% (SUV2.5), 13% (MV3) and 0% (MV2 and A50P) had QS-1A. The median bMTV was 39.3, 35.8, 35.3, 31.0, 21.7 and 21.5 mL for A50P, MV2, MV3, 41max, SUV2.5 and SUV4.0, and 39.2 mL with semi-manual segmentation. Spearman coefficients were lowest for SUV2.5 (0.39-0.61). High correlations were shown between all other methods (0.70-0.92, p-values <0.001). Bland-Altman analysis showed the highest agreement between 41max and semi-manual segmentation. **Conclusion:** Semi-automatic bMTV segmentation often does not result in good quality segmentations. This indicates that semi-automatic segmentation should be supervised and manually adapted. Since bMTV using different segmentation methods correlated well, the optimal method may be best identified based on ease of use and clinical performance. **References:** None.

OP-692

Prognostic Value of Baseline Total Metabolic Tumor Volume Measured on FDG PET in Patients with Richter Syndrome

X. Palard[1], *A. Girard*[1], *H. Mesbah*[1], *A. Tempescul*[2], *A. Devillers*[1], *P. Salaün*[2], *L. Haumont*[1], *T. Lamy*[3], *F. Le Jeune*[1], *C. Pontoizeau*[1];
[1]*Centre Eugène Marquis, Rennes, FRANCE,* [2]*CHRU, Brest, FRANCE,* [3]*CHU, Rennes, FRANCE.*

Aim/Introduction: Richter syndrome (RS) derives from the rare transformation of chronic lymphocytic leukemia (CLL) into an aggressive lymphoma, most commonly of the diffuse large B cell lymphoma (DLBCL) type. It is a rare complication with an unfavorable prognosis, so the identification of prognostic factors at diagnosis is needed. Extracted from the FDG PET, the baseline Total Metabolic Tumor Volume (TMTV) is a known independent predictor of outcome in aggressive de novo lymphoma. The aim

of the study was to investigate the prognostic value of TMTV for patients with transformation of CLL into DLBCL. **Materials and Methods:** We performed a retrospective review of 28 consecutive patients with transformation of CLL into DLBCL who had undergone baseline FDG PET from January 2012 to April 2018. Overall survival rates were estimated using the Kaplan-Meier method. Univariate analysis was perfomed using log-rank tests with an optimal cut-off point for binary outcomes and compared with others prognostic factors for multivariate analysis using Cox proportional hazards models. The parameters (at the time of diagnosis) tested were: gender, age, performans status, IPI score, serum LDH level, serum platelet count, the presence or not of prior therapies for CLL, Ann Arbor stage, Bulky or not, SUVmax, SUVmean and TMTV. **Results:** The median age of patients was 71 years old. During the follow-up period (median 19 months), 14 patients died. Median baseline TMTV was 80 cm^3 (5 - 2500 cm^3). Only low serum platelet count, high serum LDH level, and high TMTV at the time of the transformation were predictive of overall survival. The 4-year estimates of overall survival were 75 % in the low metabolic burden group (TMTV ≤1200 cm^3) and 35 % in the high metabolic burden group (TMTV >1200 cm^3). The estimated median overall survival time was 11 months for the high metabolic burden group compared to 191 months for the low metabolic burden group (p=0.02). The multivariate analysis did not found any significant association of these parameters with the overall survival. **Conclusion:** The TMTV extracted from FDG PET at the moment of the transformation of CLL into DLBCL is a predictor of overall survival. **References:** None.

OP-693

Baseline FDG-PET/CT detects bone marrow involvement in follicular lymphoma and provides relevant prognostic information

R. Nakajima[1], *A. J. Moskowitz*[2], *L. Michaud*[3], *A. Mauguen*[4], *H. Schöder*[1];
[1]*Memorial Sloan Kettering Cancer Center, Department of Radiology, Molecular Imaging and Therapy Service, New York, NY, UNITED STATES OF AMERICA,* [2]*Memorial Sloan Kettering Cancer Center, Department of Medicine, Division of Hematologic Oncology, Lymphoma Service, New York, NY, UNITED STATES OF AMERICA,* [3]*Memorial Sloan Kettering Cancer Center, Molecular Imaging and Therapy Service, New York, NY, UNITED STATES OF AMERICA,* [4]*Memorial Sloan Kettering Cancer Center, Department of Epidemiology and Biostatistics, New York, NY, UNITED STATES OF AMERICA.*

Aim/Introduction: To evaluate the diagnostic performance of ^{18}F -FDG PET/CT images for the detection of bone marrow involvement (BMI) and determination of prognosis in patients with follicular lymphoma (FL) before treatment. **Materials and Methods:** Patients were identified from our institutional database, records of patients with FL diagnosed from 2002-2016 in a single hospital and who had undergone both FDG-PET/CT and bone marrow biopsy (BMB) prior to treatment were retrospectively reviewed. BMI was identified by a positive-BMB result and/or focal skeleton FDG uptake in PET/CT (BM-positive by PET) irrespective of the BMB result. We assessed the correlation of PET findings with BMB results, progression free survival (PFS), and overall survival (OS). **Results:** In total, 247 patients with FL were included, of whom 111 (44.9%) were judged to have BMI; 80 were identified by BMB and 76 were identified by FDG-PET/CT. PET identified BMI cases that were not identified by BMB and upstaged 24 patients to stage IV, of those, 10 patients from I or II to IV. In contrast, BMB identified BMI not identified by FDG-PET/CT, which changed-stage 32 patients to stage IV, of whom, 6 patients from I or II to IV. The sensitivity, negative predictive value (NPV), and accuracy of FDG-PET/CT to detect BMI by BMB were 56%, 80%, and 73%, respectively. However, if BM-positive by PET and positive BMB were both considered separately sufficient to detect true BMI, the sensitivity, negative predictive value (NPV), and accuracy were 68% 80% and 86% for FDG-PET/CT, and 72% 81%, and 87% for BMB, respectively. As a secondary aim, we compared the prognosis of BMI, as detected by FDG-PET/CT or BMB. Sixty-one patients had progressive disease or died, and 25 patients died during the follow-up period. Univariate analysis of PFS demonstrated that high FLIPI (>2), BM-positive by PET, and positive BMB were associated with lower PFS ($p = 0.05, 0.001$, and 0.01). Also, high FLIPI and BM-positive by PET were associated with lower OS ($p = 0.009$ and < 0.001). In multivariate analysis, BM-positive by PET was the only independent predictor of PFS and OS ($p = 0.002$). **Conclusion:** Combined FDG-PET/CT and BMB have greater accuracy for identifying BMI in FL than BMB alone does. Thus, baseline FDG-PET/CT contributes to accurate staging of FL, with potential impact on treatment choice. BMI by PET also provides relevant prognostic information. **References:** None.

OP-694

Quantitative Assessment of [^{18}F]FDG PET Images in Patients with Hodgkin Lymphoma: Is It Affected by Contrast-Enhanced CT Attenuation Correction?

C. Voltin[1], *J. Mettler*[1], *R. Boellaard*[2], *G. Kuhnert*[1], *M. Dietlein*[1], *P. Borchmann*[1], *A. Drzezga*[1], *C. Kobe*[1];
[1]*University Hospital of Cologne, Cologne, GERMANY,* [2]*VU University Medical Centre, Amsterdam, NETHERLANDS.*

Aim/Introduction: The reliability of visual and quantitative response assessment may be impaired due to inconsistent scanning protocols and image reconstruction methods of 2- deoxy-2-[^{18}F]fluoro-D-glucose ([^{18}F]FDG) positron emission tomography (PET). Hence, this study investigates the impact of contrast-enhanced computed tomography (CT) attenuation correction in patients with Hodgkin lymphoma. **Materials and Methods:** In 10 consecutive patients undergoing either staging or response assessment, [^{18}F]FDG PET images were attenuation corrected once on the basis of unenhanced CT and additionally using contrast-enhanced CT. Reconstruction was performed in both cases with ordered subset expectation maximization (OSEM) and ultra high definition (UHD) algorithm. While SUV_{max}

and SUV_{peak} were obtained from tumour tissue, SUV_{max} and SUV_{mean} were determined within the background regions liver and mediastinal blood pool. **Results:** After switching to contrast-enhanced CT attenuation correction, SUV_{max} and SUV_{peak} in lymphoma tissue increased on average by 2.55±3.24 (p=0.018) and 3.64±3.22% (p=0.008) with OSEM and by 4.59±5.49 (p=0.005) and 3.84±5.65% (p=0.005) with UHD reconstruction. In the liver, SUV_{max} and SUV_{mean} showed a mean rise of 7.15±4.27 (p=0.005) and 6.97±2.18% (p=0.005) after OSEM, compared to 7.24±6.59 (p=0.017) and 6.29±2.83% (p=0.005) after UHD reconstruction. Mediastinal SUV_{max} and SUV_{mean} increased on average by 10.82±4.89 (p=0.005) and 12.40±3.73% (p=0.005) in the OSEM data sets and by 13.11±14.93 (p=0.005) and 11.50±12.19% (p=0.005) in the UHD images. **Conclusion:** Since the use of CT contrast fluids results in a stronger SUV increase within the liver and mediastinal blood pool than within lymphoma tissue, this may have clinical consequences regarding visual and quantitative response assessment. Ideally, CT scans for PET attenuation correction should therefore be performed in the absence of a contrast agent. **References:** None.

OP-695

Characterization Of Post-transplant Lymphoproliferative Disorder With Semi-quantitative FDG-PET/CT

F. Montes de Jesus, W. Noordzij, X. Kahle, M. Nijland, E. Verschuuren, R. Dierckx, T. van der Meerten, W. van der Bij, G. Huls, T. Kwee, A. Glaudemans;
University Medical Center Groningen, Groningen, NETHERLANDS.

Aim/Introduction: One of the most dire complications of hematopoietic stem cell (HSCT) and solid organ transplantation (SOT) is the development of post-transplant lymphoproliferative disorder (PTLD). PTLD compromises a broad spectrum of disorders classified by the 2017 World Health Organization (WHO) in non-destructive, polymorphic, monomorphic and classic Hodgkin lymphoma. Distinct morphologies are associated with a more favorable clinical course and better response to initial treatment. Reduction of immunosuppression, commonly used as first-line treatment, has been associated with higher response rates in non-destructive and polymorphic PTLD, while a more aggressive therapy is advised for monomorphic PTLD. Biopsy is the reference standard for PTLD diagnosis and classification, but may not always be safely possible. Therefore, there is a need for non-invasive imaging-based tools. **Materials and Methods:** All patients with histopathologically proven PTLD at the UMC Groningen were included in this study between January 2010 to March 2019. FDG-PET/CT scans were performed on a Siemens Biograph mCT camera, according to EANM procedure guidelines for tumor imaging and reconstruction parameters compliant with EARL recommendations. Semi-quantitative measurements (SUV_{max}, SUV_{peak} and SUV_{mean}) were performed using dedicated Hermes Hybrid 3D software with the "Tumor Finder" application. Semi-quantitative measurements were obtained from the biopsy site or in cases in which a biopsy was performed before the scan from the nearest lymph node in the same lymph node region **Results:** In total 41 patients were included. From those, 27 were monomorphic PTLD and 14 were "other PTLD morphologies", including non-destructive (n=4), polymorphic (n=9) and Hodgkin-like PTLD (n=1). Median SUV_{max}, SUV_{peak}, SUV_{mean} values were statistically significantly higher in monomorphic PTLD than in "other PTLD morphologies (p<0.05): SUV_{max}, 17 (range 3.3-64) for monomorphic PTLD vs 6.1 (2.9-24) for other PTLD morphologies; SUV_{peak} 15 (range 2.7-53) vs 4.8 (range 2.2-19) and SUV_{mean} 7.3 (range 2.4-16) vs 4.3 (range 1.9-9.3). **Conclusion:** Semi-quantitative FDG-PET/CT measurements may be helpful to discriminate monomorphic from "other PTLD subtypes". However we observed a wide range of values for all semi-quantitative measurements explored, with value overlap between monomorphic PTLD and "other PTLD morphologies". Semi-quantitative quantification may provide an indication of PTLD classification but biopsy is still warranted for definite classification. **References:** Swerdlow, S. H. et al. International Agency for Research on Cancer, 2017. Krishnamurthy et al, Int. J. Surg. Pathol. 2010. Trappe, R. et al. Lancet Oncol. 2012. Chiou, F. K. et al. Transplantation 2018. Dierickx, D. et al. Blood 2015

1601

CME 13 - Drug Develeopment + Radiopharmacy Committee: Current and Future of Radiopharmaceuticals

Wednesday, October 16, 2019, 8:00 - 9:30 Auditorium

OP-696

PET Radiopharmaceuticals of Recent Years from a Radiopharmaceutical Chemist's Perspective

A. Windhorst;
VuMc, Amsterdam, NETHERLANDS.

OP-697

Current Value of PSMA-Targeting Ligands in Diagnostic and Therapeutic Nuclear Medicine

C. Kratochwil;
Heidelberg University Hospital, Heidelberg, GERMANY.

OP-698

Established, Emerging and Future Radionuclides - Which will we use in 2030?

U. Köster;
ILL, Grenoble, FRANCE.

1603

EANM Symposium 26: Implementation of the new EANM Guideline for Pulmonary Embolism and Beyond

Wednesday, October 16, 2019, 8:00 - 9:30 Lecture Hall 312

OP-700

Pulmonary Embolism, Clinical Probabilities, Difficulties and Challenges

M. Monreal Bosch;
Hospital Universitario Germans Trias, Badalona, Barcelona, SPAIN.

OP-701

V/P SPECT-Performance and Gamuts. Importance of follow up Patients with PE

G. Schembri;
University of Sydney, Nuclear Medicine and PET, Sydney, AUSTRALIA.

OP-702

When should we use Hybrid Imaging?

H. Verberne;
Academic Medical Center, Department of Nuclear Medicine, Amsterdam, NETHERLANDS.

OP-703

Importance of Ventilation SPECT for Diagnosing other Cardiopulmonary Diseases and Calculating the Total Lung Function

M. Bajc;
University Hospital Lund, Department of Clinical sciences, Lund, SWEDEN.

1605

M2M - Parallel Session: Radiolabelled Peptides

Wednesday, October 16, 2019, 8:00 - 9:30 Lecture Hall 111

OP-704

Gallium-68 labelled minigastrin analogue for high sensitivity PET imaging of cholecystokinin-2 receptor expressing tumours

E. von Guggenberg[1], *M. Klingler*[1], *P. Garnuszek*[2], *R. Mikołajczak*[2], *B. Janota*[2], *A. Hubalewska-Dydejczyk*[3], *M. Kieć-Klimczak*[3], *E. Przybylik-Mazurek*[3], *I. Virgolini*[1];
[1]*Department of Nuclear Medicine, Medical University of Innsbruck, Innsbruck, AUSTRIA,* [2]*Radioisotope Centre POLATOM, National Centre for Nuclear Research, Otwock, POLAND,* [3]*Department of Endocrinology, Jagiellonian University, Medical College, Krakow, POLAND.*

Aim/Introduction: Cholecystokinin-2 receptors (CCK2R) are expressed at high incidence in different tumours including medullary thyroid carcinoma (MTC), small cell lung cancer, gastroenteropancreatic neuroendocrine tumours and others. CCK2R based PET imaging keeps high promise to improve the staging and follow-up of patients with persistent disease or recurrence. Evaluation of the CCK2R status additionally forms the basis for the selection of patients for peptide receptor radionuclide therapy with therapeutic radionuclides. CCK2R targeting represents a highly personalised theranostic approach for different tumours with limited treatment options. A kit for ^{68}Ga-labelling was developed for a new minigastrin analogue in order to facilitate the clinical translation. **Materials and Methods:** The kit formulation was based on a new DOTA-conjugated minigastrin analogue with site-specific amino acid substitutions in the C-terminal receptor specific sequence. The receptor affinity and targeting profile was evaluated using A431 human epidermoid carcinoma cells stably transfected with human CCK2R (A431-CCK2R) as well as mock transfected cells (A431-mock). In displacement assays the CCK2R affinity of the unlabelled peptide and of the chelates with different trivalent metals was analysed. The tumour uptake and pharmacokinetics of the peptide radiolabelled with Ga-68, as well as In-111 and Lu-177, was studied in female BALB/c nude mice with subcutaneous tumour xenografts. The performance of the kit for ^{68}Ga-labelling was tested for up to one year. First clinical translation of PET imaging was pursued in patients with advanced MTC. **Results:** The peptide analogue with C-terminal amino acid substitutions displayed retained high CCK2R affinity. The modifications in the linear peptide analogue also enhanced the stability against enzymatic degradation improving the targeting properties. Rapid clearance from non-target tissue together with highly improved tumour uptake was observed in the mouse tumour model. A tumour uptake of >20% IA/g was observed in A431-CCK2R xenografts, whereas the uptake in A431-mock xenografts was <1% IA/g. Labelling with Ga-68 within a long-term kit storage of up to one year was carried out with a radionuclide incorporation of 98.4±0.3% and a radiochemical purity of 95.7±0.8% at preparation. Within 3 h after preparation, a radiochemical purity of 91.4±0.7% was met. The injection of ^{68}Ga-DOTA-MGS5 was well tolerated by the first patient examined. Besides physiological uptake in stomach a focal uptake was observed in the liver. **Conclusion:** A new highly specific peptide analogue targeting CCK2R was developed for PET imaging. The successful application for PET imaging lays the basis for the future therapeutic use. **References:** None.

OP-705

Novel Radiolabelled CCK$_2$R Antagonists: Design, Synthesis and In Vitro Evaluation

D. Novak[1,2], *M. Anderluh*[2], *R. Mansi*[3], *T. Tomašič*[2], *M. Krošelj*[1], *P. Kolenc Peitl*[1];

[1]*University Medical Centre Ljubljana, Ljubljana, SLOVENIA,* [2]*University of Ljubljana, Faculty of Pharmacy, Ljubljana, SLOVENIA,* [3]*Division of Radiopharmaceutical Chemistry, University Hospital Basel, Basel, SWITZERLAND.*

Aim/Introduction: The cholecystokinin-2/gastrin receptor (CCK_2R) is (over)expressed in several tumour types and therefore represents a suitable target for the development of the radiolabelled ligands. To bypass the possible adverse pentagastrin test-like effects of currently evaluated CCK_2R agonists, we considered the transition to antagonists (CCK_2R-ANTs), supported by the fact that the agonist-induced internalization is not required for successful imaging. The low molecular weight antagonist Z-360 offers a solid base for the development of radiolabelled CCK_2R-ANTs due to its subnanomolar affinity and high selectivity for CCK_2R[1]. The aim of the present study was to design, synthesize and evaluate novel DOTAconjugated CCK_2R-ANTs, followed by comparison to the selected agonist CP04 (DOTA-(D-Glu)$_6$-Ala-Tyr-Gly-Trp-Met-Asp-Phe-NH_2) in in vitro pre-clinical studies. **Materials and Methods:** Structurebased in silico drug design using the calculated homology model of CCK_2R (PDB code: 2RH1) was applied to define the optimal distance between the targeting (Z-360) and the chelate (DOTA) moieties. A series of 10 compounds with different hydrophilic spacers were synthesized manually on solid phase, while DOTA coupling was performed in solution. After purification by RP-HPLC, the compounds were characterized by ESIMS and analytical RP-HPLC. The inositol monophosphate-based functional assay (IPOne®) on A431CCK_2R+ cell line was used for screening and SAR optimization of the (DOTA)conjugates and their corresponding cold-labelled compounds. LogD experiments on radiolabelled CCK_2R-ANTs were performed by shake-flask method. Selected radioligands, based on the lowest IC_{50} values and optimal hydrophilicity, were chosen for protein binding and serum stability studies. In vitro evaluation on A431-CCK_2R+ cells was performed for the most promising conjugates. **Results:** Due to the lipophilic character of Z-360, conjugates with hydrophilic spacers were designed. Based on the values of the scoring function and visual inspection of docked structures, the minimal spacer length of three amino acids was determined. All conjugates showed purities >95% and exhibited antagonistic properties assessed by the functional assay (IC_{50}: from 0.08±0.01 nM to 64.9±15.7 nM). The logD values varied between -1.51±0.01 and -2.57±0.03. Selected radiolabelled CCK_2R-ANTs exhibited high metabolic stability (>90% intact compounds at 24h) and <10% of radioactivity detected in protein bound fraction. In preliminary studies, the best candidate ^{111}InCCK_2RANT**1** showed lower cell associated radioactivity but higher B_{max} as compared to ^{111}In-CP04. **Conclusion:** A series of novel radiolabelled CCK_2R ligands with confirmed antagonistic properties was successfully designed, synthesized and brought to cell based in vitro evaluation. Further in vitro comparison studies are on-going. **References:** 1. Grabowska, AM. Regul. Pept. 2008; 146: 46-57.

OP-706

One step closer to clinical translation: Notably enhanced localization of [^{111}In]SG4 in CCK_2R-positive xenografts in mice treated with Entresto®

P. Kanellopoulos[1,2], *A. Kaloudi*[1], *M. de Jong*[3], *E. P. Krenning*[4], *B. A. Nock*[1], *T. Maina*[1];

[1]*Molecular Radiopharmacy, INRASTES, NCSR "Demokritos", Athens, GREECE,* [2]*Molecular Pharmacology, School of Medicine, University of Crete, Heraklion, GREECE,* [3]*Department of Radiology & Nuclear Medicine, Erasmus MC, Rotterdam, NETHERLANDS,* [4]*Cyclotron Rotterdam BV, Erasmus MC, Rotterdam, NETHERLANDS.*

Aim/Introduction: We have recently proposed the administration of the neprilysin (NEP) inhibitor phosphoramidon (PA) to increase the in vivo stability and tumor targeting of biodegradable peptide radiotracers. This methodology turned out to be very effective in stabilizing radiolabeled des-Glu$^{6\text{-}10}$ gastrin analogs in peripheral mouse blood, leading to remarkable enhancement of radiotracer uptake in CCK_2R-expressing xenografts while renal accumulation remained favorably low. Translation of this promising concept in the clinic requires the use of a NEP-inhibitor that is safe and effective. In the present study, we investigated the biological profile of [^{111}In]SG4 ([^{111}In-DOTA,Nle^{15}]MG11) in mice bearing CCK_2R-positive tumors treated with the FDA approved drug Entresto® compared to non-treated controls. **Materials and Methods:** [^{111}In]SG4 was injected in healthy Swiss albino mice without or with co-injection of the NEP-inhibitor sacubitrilat (0.3 mg sacubitrilat/kg body weight); a third mice group received orally a slurry of the FDA-approved drug Entresto® (containing 50 mg of the sacubitrilat-prodrug sacubitril/kg body weight) by gavage 30 min in advance. Blood samples collected 5 min postinjection (pi) were analyzed by RP-HPLC. Biodistribution was conducted in SCID mice bearing a double A431-CCK_2R(+/-) tumor model. [^{111}In]SG4 was injected alone in mice 30 min after gavage of Entresto®, or in untreated mice, or together with sacubitrilat; animals were sacrificed at 4 h pi and biodistribution was conducted. For SPECT/CT mice were treated or not with Entresto® 30 min prior to radioligand injection and were likewise sacrificed at 4 h pi. **Results:** While 11.5±3.2% (n=4) of [^{111}In]SG4 were detected intact in peripheral mouse blood at 5 min pi, by Entresto® or sacubitrilat-treatment the percentage of intact radiotracer reached 78.4±2.5% (n=3) and 72.7±2.4% (n=3), respectively. A likewise impact of orally administered Entresto® or iv-injected sacubitrilat was observed on the uptake of [^{111}In]SG4 in the A431-CCK_2R(+) xenografts, which notably increased at 4 h pi from 2.2±0.6%ID/g (n=3) to 9.6±1.7%ID/g (n=5) and 8.1±1.4%ID/g (n=3), respectively. In contrast, renal values as well as uptake in the A431-CCK_2R(-) tumors remained low and unaffected by such treatment. These results could be visualized by SPECT/CT. **Conclusion:** This study has shown that per os administration of the FDA-approved drug Entresto® or iv-coinjection of the respective NEP-inhibitor sacubitrilat in mice impressively improved the stability of circulating [^{111}In]SG4. Consequently, the radioligand localization in CCK_2R-expressing tumors was effectively enhanced whereas renal values remained

low. These results are very significant for the translation of the in-situ NEP-inhibition concept in the clinic. **References:** None.

OP-707

Novel radiolabelled neurotensin analogues containing silylated amino acid for improved neurotensin receptor-1 (NTS_1) targeting

*A. Chastel[1,2,3], R. Fanelli[4], S. Previti[4], D. Vimont[2,3], P. Zanotti-Fregonara[5], B. Guillet[6,7], P. Garrigue[6,7], L. Balasse[6], P. Fernandez[1,2,3], E. Rémond[4], E. Hindié[1,2,3], F. Cavelier[4], **C. Morgat**[1,2,3];*
[1]Nuclear Medecine Department, University Hospital of Bordeaux, Bordeaux, FRANCE, [2]University of Bordeaux, INCIA, UMR5287, Bordeaux, FRANCE, [3]CNRS, INCIA, UMR5287, Bordeaux, FRANCE, [4]Institut des Biomolécules Max Mousseron, IBMM, UMR-5247, CNRS, Université de Montpellier, ENSCM, Montpellier, FRANCE, [5]Houston Methodist Research Institute, Houston, TX, UNITED STATES OF AMERICA, [6]Aix-Marseille University, INSERM, Institut National de la Recherche Agronomique, Centre de Recherche en Cardiovasculaire et Nutrition, Marseille, FRANCE, [7]Centre Européen de Recherche en Imagerie Médicale, Marseille, FRANCE.

Aim/Introduction: The neurotensin receptor-1 (NTS_1) is overexpressed in numerous cancers such as pancreatic cancer, lung cancer or breast cancer. To date, radiolabelled neurotensin analogues suffer from low plasmatic stability and thus insufficient availability for high uptake in tumors. We report the development of new ^{68}Ga-radiolabelled neurotensin analogues with improved properties through introduction of silylated amino acid (DOTA-APAC-Lys-Lys-Pro-Tyr-TMSAla-Leu-OH = JMV6658 and DOTA-APAC-Lys-Lys-Pro-Tyr-Ile-TMSAla-OH = JMV6659) or introduction of natural amino acids (DOTA-APAC-Lys-Lys-Pro-Tyr-Ile-Leu-OH = JMV6660) in the minimal bioactive sequence NT[8-13]. JMV6661, based on the unmodified sequence (DOTA-APAC-NT[8-13]), serves as reference compound. **Materials and Methods:** Affinity of precursors JMV6658, JMV6659, JMV6660 and JMV6661 was studied by competition experiment in recombinant CHO cells over-expressing NTS_1. All analogues were then radiolabelled with ^{68}Ga. Plasmatic stability was determined in human plasma. Cellular uptake, efflux and saturation binding assays (regarding NTS_1 and NTS_2) were performed on HT-29 cells. Finally, the most potent analogue was studied in nude mice bearing HT-29 xenograft using µPET/CT imaging up to 2h. Biodistribution was assessed on sacrificed animals after imaging. Estimation of human absorbed doses was calculated using OLINDA/EXM software. **Results:** Affinity of precursors JMV6658, JMV6659, JMV6660 and JMV6661 were 4877 ± 1173 nM, 34.5 ± 1.4 nM, 1919 ± 1253 nM and 540 ± 129 nM, respectively. Plasmatic half-lives for ^{68}Ga-JMV6658, ^{68}Ga-JMV6659, ^{68}Ga-JMV6660 and ^{68}Ga-JMV6661 were 10.95, 11.09, 1.77 and 3.75 minutes, respectively. In saturation binding assays, ^{68}Ga-JMV6659 showed the highest NTS_1-affinity and selectivity (Kd_{NTS1} = 6.29±1.37 nM, Kd_{NTS2} = 225.5±34.0 nM), whereas ^{68}Ga-JMV6660 and ^{68}Ga-JMV6661 showed only moderate affinity and selectivity for NTS_1 and ^{68}Ga-JMV6658 showed no affinity. NTS_1-mediated internalization in HT-29 cells was 61.5 ± 1.6% for ^{68}Ga-JMV6659, 70.1 ± 9.7% for ^{68}Ga-JMV6660 and 66.8 ± 25.1% for ^{68}Ga-JMV6661, whereas ^{68}Ga-JMV6658 did not internalize. The efflux of ^{68}Ga-JMV6659 was 45.6 ± 1.2% at 1h, while the other ^{68}Ga-radiolabelled peptides showed higher efflux (60.4 ± 7.3% - 76.2 ± 9.3% at 1h). In mice, ^{68}Ga-JMV6659 showed urinary excretion, as well as early and unprecedented high uptake in HT-29 tumor beginning at 3min and reaching 7.58 ± 0.54%ID/g at 2h. Co-injection of neurotensin (180µg) significantly decreased tumor uptake to 1.4 ± 0.7%ID/g ($p<0.05$). Kidneys, blood and spleen showed also NTS_1-mediated uptake of ^{68}Ga-JMV6659. Mean effective dose was 0.023 ± 0.006 mSv/MBq. **Conclusion:** Following introduction of silylated amino acid TMSAla, we identified ^{68}Ga-JMV6659 as a lead compound for PET imaging of tumors expressing NTS_1 due to its very favorable properties. **References:** None.

OP-708

cCPE Peptides for SPECT Imaging of Claudin-4 Overexpression in Pancreatic Cancer

J. Baguna Torres[1], *M. Mosley[1], S. Koustoulidou[1], S. Hopkins[1], S. Knapp[2], A. Chaikuad[2], M. Kondoh[3], K. Tachibana[3], V. Kersemans[1], B. Cornelissen[1];*
[1]Radiobiology Research Institute, University of Oxford, Oxford, UNITED KINGDOM, [2]Structural Genomics, University of Oxford, Oxford, UNITED KINGDOM, [3]Graduate School of Pharmaceutical Sciences, Osaka University, Osaka, JAPAN.

Aim/Introduction: Overexpression of tight junction protein claudin-4 has been detected in primary and metastatic pancreatic cancer tissue, and is associated with better prognosis in patients[1,2]. Non-invasive measurement of claudin-4 expression by imaging methods could provide a means for accelerating detection and stratifying patients into risk groups. Clostridium perfringens enterotoxin (CPE) is a natural ligand for claudin-4 and holds potential as a targeting vector for molecular imaging of claudin-4 overexpression. A GST-tagged version of the C-terminus of CPE (cCPE) was previously used to delineate claudin-4 overexpression by SPECT, but showed modest binding affinity and slow blood clearance in vivo[3]. **Materials and Methods:** Based on the crystal structure of cCPE, a series of smaller-sized $cCPE_{194-319}$ mutants (S313A, H194, S307A+N309A+S313A, D284A and L254F+K257D) with putatively improved binding affinity for claudin-4 were generated by site-directed mutagenesis[4]. All peptides were conjugated site-specifically on a C-terminal cysteine using maleimide-DTPA to enable radiolabelling with ^{111}In. The binding affinity of all radioconjugates was evaluated in claudin-4-overexpressing Panc-1 cells and HT1080 negative controls. The specificity of all cCPE mutants to claudin-4 was assessed in hCLDN3/hCLDN4-HT1080 stably transfected cell lines. SPECT imaging of BALB/c nude mice bearing Panc-1 or HT1080 xenografts was performed to determine the claudin-4-targeting ability of these peptides in vivo. **Results:** Uptake of all cCPE-based radioconjugates was significantly higher in Panc-1 cells compared to HT1080 negative controls. All peptides showed a marked improvement in affinity

for claudin-4 in vitro when compared to ^{111}In-cCPE.GST (K_d values of 2.2±0.8, 3±0.1, 5.5±1.1, 8.3±2.8 and 9.4±0.5 vs. 14.8±1.3 nM). Blood clearance of all cCPE probes, as measured by SPECT, was considerably faster when compared to that of ^{111}In-cCPE.GST ($t_{1/2}$<2 min). All radiopeptides showed significantly higher accumulation in Panc-1 xenografts than HT1080 tumours at 90 min post-injection (2.7±0.7, 2.3±0.9, 2±0.4, 2±0.2 and 6.3±0.6 vs. 0.4±0.1, 0.5±0.1, 0.3±0.1, 0.7±0.1 and 0.7±0.1 %ID/g; P<0.01, P<0.01, P<0.05, P<0.05 and P<0.001 respectively). **Conclusion:** These optimised cCPE-based SPECT imaging agents show great promise as claudin-4-targeting vectors for in vivo imaging of claudin-4 overexpression in pancreatic cancer. **References:** 1. Nichols et al, 2004, Am J Clin Pathol 121:226-30; 2. Tsutsumi et al, 2012, Ann Surg Oncol 19:491-99; 3. Mosley et al, 2015, J Nucl Med 56:745-51; 4. Van Itallie et al, 2008, J Biol Chem 283(1):268-74.

OP-709

The Effect of a Cationic Linker on the Pharmacokinetics of ProBOMB2, a Novel Bombesin Derivative

I. Bratanovic, C. Zhang, Z. Zhang, H. Kuo, N. Colpo, J. Pan, K. Lin, F. Bénard;
British Columbia Cancer Research Center, Vancouver, BC, CANADA.

Aim/Introduction: Gastrin-releasing peptide receptor (GRPR), a G-protein coupled receptor, is aberrantly expressed in prostate, breast and lung cancers, among others, and has been targeted for molecular imaging with bombesin (BBN) derivatives. We recently developed [^{68}Ga]Ga-ProBOMB1 [1], based on the [Leu^{13}ψAA^{14}]BBN family, which showed faster radioactivity clearance from background organs compared to [^{68}Ga]Ga-NeoBOMB1. Moderate normal organ uptake, particularly in the pancreas, was still observed with [^{68}Ga]Ga-ProBOMB1. Herein, we designed ProBOMB2, a novel ProBOMB1 derivative with a cationic linker, radiolabeled with ^{68}Ga, and evaluated its pharmacokinetic properties in tumor-bearing mice with positron emission tomography (PET) imaging and biodistribution studies. **Materials and Methods:** ProBOMB2 (DOTA-Pip-D-Phe-Gln-Trp-Ala-Val-Gly-His-Leu-ψ(CH_2N)-Pro-NH_2) was synthesized by solid-phase peptide synthesis. A cationic 4-amino-(1-carboxymethyl) piperidine (Pip) linker and a 1,4,7,10-tetraazacyclododecane-1,4,7,10-tetraacetic acid (DOTA) chelator were conjugated to the N-terminus of the peptide sequence. Fmoc-Leu-ψ(CH_2N)-Pro-OH was synthesized in solution phase prior to solid-phase peptide synthesis via the STAB-H mediated reductive amination of Fmoc-leucine aldehyde with L-proline. ProBOMB2 was radiolabeled with ^{68}Ga in acetate buffer followed by HPLC purification. PET imaging for [^{68}Ga]Ga-ProBOMB2 and biodistribution studies were performed in immunocompromised mice bearing PC-3 prostate cancer xenografts. To verify the specificity of the tumor uptake, blocking experiments with co-injection of [D-Phe^6,Leu-NHEt^{13},des-Met^{14}]Bombesin(6-14) were also performed. **Results:** [^{68}Ga]Ga-ProBOMB2 was obtained with 56% decay-corrected radiochemical yield and > 95% radiochemical purity. Using [^{68}Ga]Ga-ProBOMB2, PC-3 tumor xenografts were clearly visualized in PET images with excellent contrast at 1 h post injection (p.i.). [^{68}Ga]Ga-ProBOMB2 was excreted primarily through the renal pathway with minimal background radioactivity accumulation Based on biodistribution studies, the tumor uptake of [^{68}Ga]Ga-ProBOMB2 was 10.43 ± 1.25 percent injected dose per gram (%ID/g) at 1 h p.i., without significant normal organ uptake. Importantly, pancreas and kidney uptake remained low at 1.06 ± 0.22 and 1.82 ± 0.26 %ID/g. The tumor-to-blood and tumor-to-muscle uptake ratios of [^{68}Ga]Ga-ProBOMB2 were 20.31 ± 2.35 and 88.73 ± 46.51 at 1 h p.i.. Co-injection with the blocking agent reduced average uptake of [^{68}Ga]Ga-ProBOMB2 in tumors by 66% at 1 h p.i. **Conclusion:** Our data suggest that with a cationic linker, [^{68}Ga]Ga-ProBOMB2 showed improved tumor uptake and minimal normal organ uptake, particularly in the pancreas. This compound is a promising radiotracer for PET imaging of GRPR expression in cancers. **References:** [1] Lau J, et al. ACS Omega 2019; 4: 1470.

OP-710

Evaluation of [^{68}Ga]Ga-BL02 for Imaging the C-X-C Chemokine Receptor 4: Leveraging a Glutamate-based Linker

D. Kwon[1], *Z. Zhang*[1], *J. Zeisler*[1], *C. Uribe*[2], *C. Zhang*[1], *J. Lau*[3], *K. Lin*[1,4], *F. Benard*[1,4];
[1]*Department of Molecular Oncology, BC Cancer, Vancouver, BC, CANADA,* [2]*Functional Imaging, BC Cancer, Vancouver, BC, CANADA,* [3]*National Institute of Biomedical Imaging and Bioengineering, National Institutes of Health, Bethesda, MD, UNITED STATES OF AMERICA,* [4]*Department of Radiology, University of British Columbia, Vancouver, BC, CANADA.*

Aim/Introduction: Based on LY2510924, a peptide targeting the C-X-C chemokine receptor type 4 (CXCR4), we developed [^{68}Ga]Ga/[^{177}Lu]Lu-BL01, a theranostic pair for PET imaging and radiotherapy. We hypothesized that the addition of a tri-glutamate linker between the targeting pharmacophore and DOTA chelator (BL02) would reduce liver uptake and promote renal clearance. **Materials and Methods:** BL02 was synthesized via solid phase peptide synthesis. A Lys(ivDde) residue was added at the C-terminus of LY2510924 (cyclo[(Phe-Tyr-Lys(iPr)-D-Arg-2-Nal-Gly-D-Glu]-Lys(iPr)-NH_2). The ivDde protecting group was removed with hydrazine and 3 Glu residues and a DOTA chelator were added sequentially to the ε-amine. BL02 was radiolabeled with [^{68}Ga]$GaCl_3$ and biodistribution studies were performed on immunocompromised mice inoculated with Daudi Burkitt lymphoma cells. PET imaging studies were performed with [^{68}Ga]Ga-BL02, with blocking studies performed with pre-injection of LY2510924. An unpaired t-test with unequal variances was performed using Microsoft Excel. **Results:** [^{68}Ga]Ga-BL02 was synthesized with a 71±5% (n=4) radiochemical yield, >99% radiochemical purity and 216±106 GBq/μmol (n=4) molar activity. Imaging/biodistribution studies demonstrated primarily renal clearance, with negligible liver uptake. Daudi xenografts were clearly visualized on PET images at 1 and 2 h post-injection (p.i.), with biodistribution data showing uptake

values of 9.14±2.95 %ID/g and 8.66±2.15 %ID/g respectively. No other organs demonstrated higher uptake. The tumour-to-blood, tumour-to-liver, tumour-to-spleen, and tumour-to-muscle ratios at 2 h p.i. were 123.97±39.91, 15.16±2.88, 39.28±16.86 and 219.05±58.12 respectively, showing agreement with PET images. Finally, pre-injection of LY2510924 reduced tumour uptake by 91.6% (0.767 %ID/g at 1 h p.i.), demonstrating the target specificity of [^{68}Ga]Ga-BL02. Despite lower absolute tumour uptake at 2 h p.i. compared to [^{68}Ga]Ga-BL01 (10.2±2.56 %ID/g and 15.3±1.86 %ID/g at 1 and 2 h p.i. ($p<0.0001$)), [^{68}Ga]Ga-BL02 had higher tumour-to-organ ratios at 2 h p.i. than [^{68}Ga]Ga-BL01 (13.33±2.14, 1.66±0.22, 1.83±0.29 and 52.87±2.26 for blood ($p<0.0005$), liver ($p<0.0001$), spleen ($p<0.005$) and muscle ($p<0.0005$), respectively). **Conclusion:** [^{68}Ga]Ga-BL02 with a tri-glutamate linker demonstrates markedly enhanced imaging properties over previously reported [^{68}Ga]Ga-BL01 due to improved pharmacokinetics and tumour-to-non target ratios. [^{68}Ga]Ga-BL02 shows significant promise as a CXCR4-targeting PET imaging agent. **References:** None.

OP-711

Lower binding potential of GLP-1 receptor in the pancreas as a consequence of diet-induced obesity

C. Malbert[1], *A. Chauvin*[2], *F. Le Gouevec*[2], *J. Georges*[2], *M. Genissel*[2];
[1]*Aniscan, INRA, Saint-Gilles, FRANCE,* [2]*UEPR, INRA, Saint-Gilles, FRANCE.*

Aim/Introduction: GLP-1 receptor agonists are capable of effective weight reduction in obese subjects. However, the weight loss in response to treatment is heterogeneous depending on BMI. This might be the consequence of a lower GLP-1 receptor density since the reduced expression of the receptor has been already demonstrated at the vascular level in obese. This study aimed to evaluate the hypothesis of lower GLP-1 receptor density in obese vs. lean using a preclinical model of diet-induced obesity. **Materials and Methods:** GLP-1 receptor density was quantified in the pancreas of 16 adult miniature pigs, eight being obese (80 ± 5 kg) while the remaining lean (42 ± 3 kg). PET-CT (Discovery ST, GE) dynamic imaging was performed for one hour in anesthetized animals after the IV administration of [^{68}Ga]Ga-DO3A-VS_Cys^{40}-Exendin-4 (1), (7 ± 4.2 MBq; 0.1 µg/kg). The radiolabelled compound was produced using an automated GRP synthesizer (Scintomics - GRP series 2013), and quality control was performed with UV-radioHPLC. Input arterial function was continuously recorded using an extemporaneous external arterial -venous loop between the femoral artery and the saphenous vein. Abdominal organs VOIs were drawn from CT and PET images using ITK-snap software. Pancreas PET data were fitted to a single and two tissues compartment models using Pmod software, and binding potential was calculated as the ratio between K_1*k_3 and k_2*k_4. **Results:** [^{68}Ga]Ga-DO3A-VS_Cys^{40}-Exendin-4 showed a clear pancreatic uptake in lean animals but the difference in uptake between the pancreas and the other abdominal organs was less in obese. The fitting of the time-activity curve is more accurate with a two tissues compartment model compared to a single one as indicated by a lower Akaike information criterion (21 ± 4 vs. 54 ± 14). Binding potential in obese was one-tenth (0.024395 ± 0.000523) of that observed in lean subjects (0.2056 ± 0.00328) primarily as a consequence of reduction in K1 (0.0406 ± 0.00072 vs 0.0092 ± 0.000149 ml/ccm/min in lean vs obese). **Conclusion:** The use of ^{68}Ga labeled GLP-1 receptor agonist allow to demonstrate a massive down-regulation of GLP-1 receptor within the pancreas of obese versus lean adult pigs. While this lower binding potential might explain the clinically reduced efficacy of GLP-1 receptor agonist, it also opens a new pharmacological avenue aimed towards weight reduction. **References:** (1) - Ericksson O et al, Species differences in pancreatic binding of DO3A-VS-Cys^{40}-Exendin4. Acta diabetes, 2017, 54: 1039-1045.

1606

Do.MoRe - Parallel Session: PET/CT & SPECT/CT Instrumentation

Wednesday, October 16, 2019, 8:00 - 9:30 Lecture Hall 112

OP-712

Head-to-head comparison of a Si-photomultiplier-based and a conventional photomultiplier-based PET-CT system

J. Oddstig[1], *G. Brolin*[1], *E. Trägårdh*[2], *D. Minarik*[3];
[1]*Radiation Physics, Lund, SWEDEN,* [2]*Clinical Physiology and Nuclear Medicine, Malmö, SWEDEN,* [3]*Radiation Physics, Malmö, SWEDEN.*

Aim/Introduction: Recently, a novel generation of PET-scanners, based on silicon (Si)-photomultiplier (PM) technology, was introduced. Concurrently, there has been a development of new reconstruction methods, with the aim of increasing the detection of small lesions without increasing the noise level. The combination of new detector technology and new reconstruction algorithms have been found to increase image quality. However, it is currently unknown to what extent the improved image quality is due to hardware improvements or improved reconstruction algorithms. The aim of this study was to compare the ability to detect small hotspots in phantoms using a SiPM-based (GE Discovery MI) and a conventional PM-based PET-CT scanner (GE Discovery 690), with identical reconstruction protocols in order to isolate the properties of the hardware. **Materials and Methods:** Two different phantoms (NEMA-body and Jasczcak) with small fillable spheres (31µl-26.5ml) and different sphere-to-background ratios (SBR) were scanned in one bed position of 10minutes on both scanners. The acquired data were rebinned into sinograms corresponding to different acquisition durations (15s - 600s) and reconstructed using identical reconstruction parameters on both scanners. ROI were drawn in all images in spheres and in background. The recovery coefficient (RC) and $sphere_{peak}/background_{peak}$-

value were calculated and compared between the scanners. The detectability of each sphere at each acquisition time was graded on a three-level scale: clearly visible (2), visible but not distinguishable from background noise (1), and not visible (0). The sensitivity was calculated as the sum of the scores divided with the highest possible score. **Results:** RC-curves for the NEMA body phantom was near-identical for both scanners at SBR 10:1 and acquisition times 90-600s. For smaller spheres (31-500µl) in the Jaszczak phantom, the sphere/background-ratio was 1.22 higher for the MI scanner at SBR 15:1. The ratio decreased for lower SBR, with a ratio of 1.03 at SBR 3.85:1. Regarding the detectability of spheres, the sensitivity was 99% and 97% for the MI and 690, respectively, for SBR 15:1. For SBR 7.5, the sensitivity was 91% and 96% for the MI and 690, respectively. For SBR 3.85:1, the sensitivity was 68% and 62% for the MI and 690, respectively. **Conclusion:** Marginally better detectability in small spheres at low noise levels was seen for the SiPM-based scanner but the difference was smaller at higher noise levels. It was difficult to detect differences between the scanners, suggesting that the SiPM-based detectors are not the primary reason for improved image quality. **References:** None.

OP-713

Comparison of Siemens Biograph Vision 600 and Biograph mCT PET-CT scanners

***S. Eberl**, J. Verschuer, A. Waugh, A. Hughes, M. J. Fulham;*
Royal Prince Alfred Hospital, Sydney, AUSTRALIA.

Aim/Introduction: Our aim was to compare the latest generation Siemens Biograph PET-CT, the SiPMT-based Vision 600, to the previous generation, traditional PMT-based Biograph mCT. **Materials and Methods:** We used the Biograph Vision 600 Edge (128-slice CT) with an axial PET FOV of 26 cm and the Biograph mCT (128-slice CT) with a PET axial FOV of 21 cm. We compared: i) NEMA NU-2 acceptance tests, ii) Hoffman brain phantom acquisitions, iii) SNMMI chest phantom acquisitions and, iv) clinical image quality for patients who had scans on both scanners, using 18F-FDG / 68Ga-PSMA / 68Ga-Dotatate, within a 3-month period. All FDG PET-CT scans were done using a FDG-dose based on BMI and scanner sensitivity. All acquisitions were undertaken using continuous bed motion (CBM). Bed speed, CT parameters and PET reconstructions were identical /matched for both scanners; 'matched' since the Biograph Vision is limited to 5 subsets. Hence we used 16 iterations 5 subsets on the Vision 600 and 4 iterations 21 subsets on the mCT. **Results:** The Vision 600 Edge had a sensitivity of 15.2 cps/kBq when compared to 9.44 cps/kBq for the mCT which was 1.6 times higher hence the injected dose of FDG was reduced by a factor of 1.6. FWHM transverse resolution @10cm was 5.0 mm for the mCT and 4.2 mm for the Vision 600. In the clinical activity range, the NECR at the same activity was 1.6 times higher for the Vision 600 and the activity required to achieve same NECR was a factor of about 2 lower on the Vision 600. The TOF resolution was 217 ps for the Vision 600 and 530 ps for the mCT. There was improved image quality in the cortical gyri, posterior fossa nuclei and central mediastinal lesion on the phantom studies and on the clinical scans where there was more confident detection of small sites of disease. For 68Ga-PSMA studies when there were high SUVs in the kidneys and bladder there was a more marked artefact on the Vision 600 that was not corrected by the prompt gamma and scatter correction. **Conclusion:** The Biograph Vision has superior image quality at a lower injected activity when compared to the mCT for FDG whole body PET-CT scans. Image quality, however, for 68Ga-PSMA scans was inferior to the mCT when tracer excretion was high which suggests further optimisation of the reconstruction parameters are required. **References:** None.

OP-714

Continuous Bed Motion Acquisition for Clinical PET Systems With a Sparse Block Rings Configuration

***N. A. Karakatsanis**, S. A. Zein, S. A. Nehmeh;*
Weill Cornell Medical College, New York, NY, UNITED STATES OF AMERICA.

Aim/Introduction: To implement continuous bed motion (CBM) acquisition for clinical PET systems with sparse block rings configuration, and assess its value on image quality (IQ). **Materials and Methods:** The Siemens Biograph™ mMR is a clinical PET/MR scanner consisting of 8 compact block rings with 3.2cm axial block dimension and 25.8cm axial field-of-view (AFOV). List-Mode PET data of the NEMA IQ phantom with 4:1 spheres-to-background ratio were acquired for 30min. A sparse block rings configuration (sparse-mMR) was adopted by setting to zero all counts measured at detector pair positions associated with at least one even block ring. Sparse CBM acquisitions with constant speeds were implemented along an axial distance of two blocks (16 detector rings, 6.4cm) to compensate for the axial gaps. Sparse CBM acquisitions were simulated by axially shifting the stationary mMR projection data by a different number of detector rings each time, from 0 (reference axial position) to 15, then removing the counts associated with even block rings at each shifted position and shifting back the sparse data to the reference position. This process was repeated for all 16 positions and the corresponding output data were added to produce the sparse CBM sinogram. The input data for each step was sampled from independent PET lists corresponding to 16 different periods of equal duration. Sparse-mMR CBM data of 304, 608, 912 and 1216 seconds and the respective PET image quality metrics were compared against that achieved with stationary 304sec acquisitions using the mMR and a compact-½mMR configuration. The latter included only the 4 central block rings. All PET data were reconstructed with 3D-OSEM (1 iteration, 21 subsets, 4mm FWHM Gaussian post-filtering, no Time-of-Flight) using the component-based normalization factors of each configuration. **Results:** In all images, no artifacts were observed, and all spheres were detected. Contrast recovery differences between the three scanner configurations were within 7% for 304sec scans. The image background variability for 304sec scans increased on average from 4.03% for mMR to 6.80% and 7.60% for the compact-½mMR and sparse-mMR with CBM, respectively.

A 4.12% background variability was achieved with the sparse configuration for 1216sec scans. Image noise uniformity across the AFOV subscribed by the compact-½mMR was superior in mMR and sparse-mMR CBM images relative to compact-½mMR. **Conclusion:** CBM compensates for the gap effects in the axial sensitivity of PET systems with sparse block rings configurations thereby improving uniformity in image noise and detectability across the AFOV. **References:** None.

OP-715

PET2020 HRS: Maximization of sensitivity and resolution using axial extension and patient adaptive rings in a high resolution long axial FOV scanner

S. Vandenberghe[1], *M. Geagan*[2], *N. Efthimiou*[3], *M. Stockhoff*[1], *C. Thyssen*[1], *M. Akl*[1], *V. Keereman*[1], *C. Vanhove*[1], *M. Koole*[4], *R. Van Holen*[1], *J. Karp*[2];
[1]*Universiteit Gent, Ghent, BELGIUM,* [2]*University of Pennsylvania, Philadelphia, PA, UNITED STATES OF AMERICA,* [3]*University of Hull, Hull, UNITED KINGDOM,* [4]*KU Leuven, Leuven, BELGIUM.*

Aim/Introduction: We propose a whole-body imager with transformable geometry that allows optimal detector positioning and has superior spatial resolution and sensitivity for a reasonable number of detectors. The proposed European PET system (PET2020) is based on high resolution monolithic detector technology and has in standard mode a 70-cm transverse diameter and axial FOV of 70 cm, optimized for cost, single organ and high throughput body scan imaging. Here we present an additional upgrade or research mode (High Resolution Sensitivity, HRS) for this system with axial and transverse adaptation by linear motors and advanced mechanics. **Materials and Methods:** To accommodate the increasing interest in total body imaging research, we depart from the fixed diameter ring design of most PET systems. The first step is an axial extension of the 70 cm long scanner into a 140 cm long scanner (without any additional detectors). By splitting each initially fully populated ring into two half-populated rings (even or odd detectors), gaps are evenly spread over thr detector surface. The additional advantage of this design is that the gaps enable to reduce the bore diameter to a radius of 35 cm per detector ring. The proposed mechanics for this adaptive ring system is one motor per ring driving one mechanical aperture (similar to the shutter mechanism in optical cameras), on which the detectors are mounted. **Results:** Even for 50 % gaps in the 140 cm configuration with 70 cm diameter, results show that there is sufficient redundancy to obtain high quality data with iterative reconstruction methods. By adapting to the closest circle enclosing the patient, resolution is improved (less acolinearity) and the sensitivity is further enhanced. In the limit of a completely closed 35 cm diameter system with 140 cm axial length, the sensitivity will be even higher than a 2m long PET system as it has a larger solid angle. In this mode, an isotropic (DOI information) spatial resolution of 1.5 mm is expected over the complete field-of-view as acolinearity will have a smaller contribution. **Conclusion:** The adaptive design has interesting applications for molecular imaging research: by translating the patient head to the middle of the system, brain scans can be performed with very high resolution, sensitivity and with simultaneous body imaging. The system has very high resolution, high sensitivity and is adaptive so it can outperform and replace organ specific PET systems, making it a general-purpose PET system. **References:** None.

OP-716

Digital SPECT: Collimator Design and CZT Crystal Thickness Affect General Purpose Solid State Camera Characteristics Facilitating Dual Isotope ^{99m}Tc/^{123}I Quantitation

J. Kennedy[1,2], *R. Lugassi*[1], *Z. Keidar*[1,2];
[1]*Rambam - Health Care Campus, Haifa, ISRAEL,* [2]*B. and R. Rappaport School of Medicine, Technion – Israel Institute of Technology, Haifa, ISRAEL.*

Aim/Introduction: To compare the characteristics of a digital general purpose solid state cadmium zinc telluride (CZT) SPECT/CT camera (CZTC), for three hardware configurations, to a standard SPECT sodium iodide camera (NaIC), and to compare dual isotope ^{99m}Tc/^{123}I quantitation. **Materials and Methods:** Spatial resolution, sensitivity, and energy resolution were compared for CZTC (Discovery 670 CZT) and NaIC (Discovery 670). CZTC comprised 5 mm thick CZT crystals with 50 mm long collimator holes (CZTC50). Reconfigurations gave 45 mm long collimator holes (CZTC45) and then the same with 7.25 mm thick CZT crystals (CZTC7p25). Additional spatial resolution measurements beyond National Electrical Manufacturers Association (NEMA) methods included using an adaptive filter for CZTC and acquiring at distances 0 to 24 cm from each detector. Dual isotope ^{99m}Tc/^{123}I SPECT images of a Jaszczak phantom with an Esser lid were acquired on CZTC7p25 and NaIC for a 40 kBq/mL background radiotracer concentration and target-to-background ratios of 8:1 for the hot vials. The phantom acquisitions were repeated for separate ^{99m}Tc and ^{123}I single tracer acquisitions and standardized uptake values (SUV) were compared. **Results:** The CZTC7p25 planar sensitivity (84.8 cps/MBq per head) was superior to NaIC (75.9 cps/MBq), CZTC45 (70.5 cps/MBq), and CZTC50 (56.6 cps/MBq). The NEMA spatial resolution for CZTC7p25 (7.1±0.1 mm) was comparable to NaIC (7.3±0.1 mm). The spatial resolution of CZTC7p25 was superior to NaIC for distances within 11 cm of the detector head, giving 2.5±0.2 mm and 4.0±0.1 mm respectively at closest approach. Measured with an adaptive filter, the spatial resolution of CZTC45 (5.3±0.1 mm), CZTC50 (5.6±0.4 mm), and CZTC7p25 (5.9±0.1 mm) were comparable. The energy resolution of CZTC50 (5.6 %), CZTC45 (5.5 %), and CZTC7p25 (5.4 %) were all superior to NaIC (9.2 %). The SUV of the largest hot vials of the dual isotope ^{99m}Tc image was 8.7 g/mL for both CZTC7p25 and NaIC, with a background of 1.6 g/mL instead of 1.0 for both. The 60 % extra background counts were attributable to down-scatter from the ^{123}I energy window. In the dual isotope ^{123}I image, 4 % extra counts were attributable to the ^{99m}Tc energy window for NaIC

and <0.2 % for CZTC7p25. **Conclusion:** Decreasing collimator hole length and increasing CZT crystal thickness substantially improved the sensitivity of a clinical digital SPECT camera without significantly degrading its spatial resolution or energy resolution, and provided no crosstalk into the ^{123}I image for dual isotope ^{99m}Tc/^{123}I quantitation. **References:** None.

OP-717

Performance Evaluation of a Novel Multi-Pinhole Collimator for Dopamine Transporter SPECT

K. Tecklenburg, I. Apostolova, S. Klutmann, R. Buchert; University Medical Center Hamburg-Eppendorf, Hamburg, GERMANY.

Aim/Introduction: There is a general tradeoff between count sensitivity (-> statistical noise) and spatial resolution (-> contrast recovery) in conventional SPECT associated with photon collimation using parallel-hole or fan-beam collimators. Multi-pinhole (MPH) collimator technology, very successful in small animal SPECT, has potential for concurrent improvement of count sensitivity and contrast recovery also in clinical SPECT of 'small' organs. This study evaluated a novel MPH collimator specifically designed for clinical dopamine transporter (DAT) SPECT. **Materials and Methods:** The 3-dimensional count sensitivity profile of a triple head SPECT system (Mediso AnyScan® TRIO) equipped with the MPH collimator was measured with a Tc-99m point source placed on the lattice points of a 1 cm grid covering the whole field-of-view (FOV). Measurements of an anthropomorphic striatum phantom were performed with varying striatum-to-background activity concentration ratios. MPH projection data were reconstructed using the iterative reconstruction algorithm (TeraTomo™) of the SPECT system software with default parameter settings for patient scans. Recovery of the striatum-to-background (S/B) contrast was assessed by the contrast recovery coefficient (CRC = (measured S/B - 1) / (true S/B - 1)). Count sensitivity and phantom measurements were also performed with a 2-head SPECT system with LEHRHS collimators (filtered backprojection) and fan-beam collimators (OSEM reconstruction with ENC-DAT settings). Finally, a patient referred to DAT SPECT because of suspicion of Parkinson's disease was scanned with both the 2-head LEHRHS and the 3-head MPH system. **Results:** The FOV of the 3-head MPH system is shifted about 8 cm towards the patient to simplify positioning. Nevertheless, the MPH sensitivity profile is almost symmetrical around its peak. Total sensitivity in the peak is 620 cps/MBq compared to 225 cps/MBq and 190 cps/MBq for the 2-head fan-beam and LEHRHS system, respectively. Sensitivity of the MPH system decreases towards the edges of the FOV. The full width of the sensitivity profile at 200 cps/MBq is 21 cm (transaxial) and 11 cm (axial), which requires precise patient positioning in the FOV. Average contrast recovery in putamen (left/right) is 0.74 with MPH SPECT, 0.56 with fan-beam SPECT and 0.48 with LEHRHS SPECT. The patient scan demonstrates very good image quality of MPH SPECT with almost PET-like delineation of putamen and caudate nucleus, clearly superior to LEHRHS SPECT. **Conclusion:** MPH DAT SPECT provides improved count sensitivity and striatum-to-background contrast recovery compared to DAT SPECT with parallel-hole and fan-beam collimators. Improved sensitivity opens the possibility to reduce scan time and/or tracer dose. **References:** None.

OP-718

Evaluation of general-purpose CZT SPECT/CT scanner for dual-isotope parathyroid imaging

T. E. Noponen[1,2], R. Hirvilammi[2], M. Seppänen[2], V. Tunninen[3]; [1]Department of Medical Physics, Turku University Hospital, Turku, FINLAND, [2]Department of Clinical Physiology and Nuclear Medicine, Turku University Hospital, Turku, FINLAND, [3]Department of Clinical Physiology and Nuclear Medicine, Satakunta Central Hospital, Pori, FINLAND.

Aim/Introduction: Dual-isotope SPECT/CT with ^{99m}Tc-sestamibi and ^{123}I is highly sensitive and specific for parathyroid scintigraphy for the localization of hyperfunctioning parathyroid adenomas. Cadmium zinc telluride (CZT) gamma-camera provides a superior energy resolution compared to conventional NaI(Tl) scintillator camera, which can be especially beneficial in the dual-isotope imaging of ^{99m}Tc and ^{123}I. We studied the capabilities of CZT SPECT camera on parathyroid imaging using a synthetic thyroid-parathyroid phantom. **Materials and Methods:** A standard Jaszczak phantom including a thyroid-parathyroid insert was used. The synthetic thyroid was eccentrically attached in the middle of phantom. On the thyroid surface, four synthetic spherical parathyroid adenomas with the inside diameter of 7.9, 6.2, 5.0 and 4.0 mm were taped. All adenomas had the ^{99m}Tc activity concentration of 2.1 Mbq/ml and the thyroid ^{99m}Tc concentration of 451.0 kBq/ml and ^{123}I concentration of 395.6 kBq/ml. The background activity concentration was 36.2 kBq/ml. The phantom was scanned using standard clinical protocols with Discovery NM/CT 670 CZT camera (GE Healthcare, Tirat Hacarmel, Israel) and with Symbia T6 SPECT/CT camera (Siemens Healthineers, Erlangen, Germany). Energy windows in Symbia were 140 keV ± 5.0% for ^{99m}Tc and 159.0 ± 5.0% for ^{123}I and in CZT 139.7 keV ± 7.3% for ^{99m}Tc and 160.4 keV ± 6.5% for ^{123}I. The Lister program of Xeleris 4.0 server (GE Healthcare) was used to regenerate the CZT data sets with the ±3% energy windows. A SPECT subtraction software (Hermes Medical Solutions, Stockholm, Sweden) was employed to remove the thyroid background activity from the reconstructed parathyroid ^{99m}Tc-image utilizing the reconstructed thyroid ^{123}I-image. Finally target-to-background ratios (TBRs) were calculated from the subtracted parathyroid adenoma images. **Results:** CZT camera provided higher TBRs for all sizes of parathyroid adenomas when compared with Symbia images. When images scanned with a standard protocols and reconstructed with a FWHM = 7 mm post-filter were compared, the adenomas of CZT images had 38,1 - 46,1% higher TBRs than those of Symbia images. In the regenerated CZT images with the ±3% energy windows, the TBRs were 67,6 - 94,9% higher

compared to Symbia images. When the FWHM = 3-mm post-filtered images were compared, adenomas scanned with CZT have 68,9 - 125,1% higher TBRs than the adenomas scanned with Symbia. **Conclusion:** The general-purpose CZT scanner with high energy-resolution can produce the subtraction SPECT images with much higher TBRs than conventional NaI(Tl) scanner. CZT scanner performance even improves when its energy windows are made narrower. **References:** None.

OP-719

Slant-hole collimation system for high-resolution molecular imaging gamma tomosynthesis

M. Longo[1,2], *R. Pani*[3], *R. Pellegrini*[4], *M. Cinti*[4], *V. Frantellizzi*[4], *G. De Vincentis*[3];
[1]*Sapienza University of Rome, Ph. D. Program in Morphogenesis & Tissue Engineering, Rome, ITALY,* [2]*Arcispedale Sant'Anna Hospital, Medical Physics Unit, Ferrara, ITALY,* [3]*Department of Radiological Sciences, Oncology and Anatomical Pathology, Sapienza University of Rome, Rome, ITALY,* [4]*Department of Molecular Medicine, Sapienza University of Rome, Rome, ITALY.*

Aim/Introduction: It is well known that without the ability to detect small lesions, indicative of early stage disease, molecular imaging technique has limited clinical utility. This study investigates a novel gamma tomosynthesis (GT) method based on a slant-hole collimation system (SHCS) which, mounting to a conventional gamma, is able to perform high-resolution three-dimensional imaging. This study aims to evaluate the sensitivity, spatial resolution and imaging potentials of the SHCS with clinical gamma camera and breast phantom and to compare the system with conventional SPECT imaging. **Materials and Methods:** The SHCS has the remarkable feature to be modular, consisting of independent collimation elements able to tilt according to variable angles [–45° to +45°]. The SHCS allows to acquire planar images at different angles which are then reconstructed using the Shift And Add (SAA) method. The proposed collimator and reconstruction methodology were validated through experimental measurements using the SHCS on a clinical gamma camera. Spatial resolutions were measured in reconstructed GT images of a point source at different source-to-collimator distances, while sensitivity was evaluated over the range of slant angles using a disk source. Image contrast (IC) and contrast to noise ratio (CNR) of sub-centimeters tumors were evaluated using a breast phantom containing a background activity and two spheres filled with ^{99m}Tc to simulate lesions at two depths. GT images of the breast phantom were also compared with those obtained with a circular-orbit scan SPECT acquisition. **Results:** The proposed system allows to reach planar spatial resolutions ranging from 9 to 14 mm over a depth range of 6-10 cm; spatial resolution in the depth dimension becomes two times greater than the other two dimensions. The gamma tomosynthesis has an average spatial resolution better than that resulted from circular-orbit SPECT scan where spatial resolutions are always restricted between 20 and 30 mm. The measured sensitivity decreased from approximately 9 cps/μCi to 6 cps/μCi varying the slant angle from 0° to 45°. The measured IC and CNR of GT reconstructed images demonstrated that it was possible to obtain significant imaging improvement compared to SPECT. **Conclusion:** The proposed GT based SHCS demonstrated the potential for superior spatial resolution and contrast compared to conventional SPECT acquisition. Differently from the currently used SPECT, a conventional gamma camera equipped with the SHCS could be located in a fixed position at the minimum distance from the patient, thus improving detection, localisation and characterisation of sub-centimetre lesions. **References:** None.

1607

Pitfalls & Artefacts 7 - Interactive Clinical Cases - Oncology & Theranostics Committee: NET Imaging ? Multiple Endocrine Neoplasias (MEN)

Wednesday, October 16, 2019, 8:00 - 9:30 Lecture Hall 113

OP-720

Genomics of MEN - Diagnostic Strategy and Pitfalls

M. North;
Hôpital Cochin AP-HP, Service de Génétique et Biologie Moléculaires, Paris, FRANCE.

OP-721

Imaging MEN 1

J. Talbot;
Hôpital Tenon AP-HP & Sorbonne Université, Médecine Nucléaire, Paris, FRANCE.

OP-722

Imaging MEN 2

S. Balogova;
St.Elisabeth Oncology Institute, Comenius University of Bratislava, Nuclear medicine, Bratislava, SLOVAKIA.

1608

Clinical Oncology - Featured Session: Prostate Translational

Wednesday, October 16, 2019, 8:00 - 9:30 Lecture Hall 114

OP-723

Scientific Programme

F. van Leeuwen;
Leiden University Medical Center, Interventional Molecular Imaging Laboratory, Leiden, NETHERLANDS.

OP-724

Bispecific anti-GRPR/PSMA heterodimer for PET and SPECT diagnostic imaging of prostate cancer

B. Mitran[1], *Z. Varasteh*[2], *E. Puuvuori*[1], *A. Abouzayed*[1], *S. S. Rinne*[1], *V. Tolmachev*[1], *M. Larhed*[1], *U. Rosenström*[1], *A. Orlova*[1];
[1]*Uppsala University, Uppsala, SWEDEN,* [2]*Technische Universität München, München, GERMANY.*

Aim/Introduction: Prostate Specific Membrane Antigens (PSMA) and Gastrin-Releasing Peptide Receptors (GRPR) are well-validated biomarkers that are overexpressed in most prostate cancers (PCa). Given the complexity and heterogeneity of PCa, targeting both receptors using bispecific radiotracers could improve the diagnostic accuracy and therapeutic outcome. The aim of this study was to develop a GRPR-PSMA bispecific heterodimer for SPECT and PET imaging of PSMA and GRPR expression in PCa. **Materials and Methods:** Bispecific anti-GRPR/PSMA dimer NOTA-DUPA-RM26 was produced using a combination of solid-phase and manual peptide synthesis and was labeled with ^{111}In and ^{68}Ga. The heterodimer was evaluated towards stability, targeting specificity, binding affinity, and cellular processing on PC3pip cell line expressing both PSMA and GRPR. In vivo specificity was studied 1 h pi in mice bearing PC3pip xenografts. Biodistribution was studied 1, 3 and 24 h pi for ^{111}In-NOTA-DUPA-RM26, or 1 and 3 h pi for ^{68}Ga-NOTA-DUPA-RM26. Tumor uptake was confirmed by preclinical SPECT/CT and PET/CT imaging. **Results:** The heterodimer was successfully labeled with ^{111}In and ^{68}Ga with radiochemical yields exceeding 99% for ^{111}In and 98% for ^{68}Ga. The radiolabeled heterodimers demonstrated high stability and retained binding specificity to PSMA and GRPR. Cellular processing assay revealed a low degree of internalization for ^{111}In-NOTA-DUPA-RM26. IC50 values for ^{nat}In-NOTA-DUPA-RM26 were 4±1 nM towards GRPR and 0.4±0.2 μM towards PSMA. In vivo binding specificity tests performed at 1h pi revealed partially blockable tumor uptake when co-injected with excess of either PSMA- or GRPR-targeting agents. A pronounced blocking effect was observed for ^{111}In and ^{68}Ga-labeled heterodimer when co-injected simultaneously with PSMA- and GRPR-targeting agents. Biodistribution over time revealed a fast clearance of radioprobes from blood and normal organs via renal excretion. Tumor uptake exceeded the uptake in all normal organs including excretory organs for both ^{111}In and ^{68}Ga-labeled analogs at 1h pi. Interestingly, ^{68}Ga-NOTA-DUPA-RM26 had a significantly lower tumor uptake (8±2%ID/g) compared to ^{111}In-NOTA-DUPA-RM26 (12±2%ID/g), but a two-fold higher uptake in liver at 1h pi. The faster clearance of radioactivity from normal tissues compared to tumor lead to an overall increase in tumor-to-organ ratios for both ^{111}In and ^{68}Ga-labeled analogs at 3h pi. At 24h pi, however, tumor-to-organ ratios decreased for ^{111}In-NOTA-DUPA-RM26. MicroPET/CT and microSPECT/CT scans confirmed the ex vivo data. **Conclusion:** Anti-GRPR/PSMA dimer NOTA-DUPA-RM26 labeled with galium-68 (for PET) and indium-111 (for SPECT) is a suitable candidate for imaging of GRPR and PSMA expression in PCa already at 1h pi. **References:** None.

OP-725

Introduction of an amylase cleavable linker to PSMA-617 - a novel strategy for the reduction of salivary gland uptake in endoradiotherapy of prostate cancer

A. Baranski[1,2], *T. Lindner*[3], *R. Tönnesmann*[1,2], *P. T. Meyer*[1,2], *W. Mier*[3], *M. Eder*[1,2];
[1]*Department of Nuclear Medicine, University Medical Center Freiburg, Faculty of Medicine, University of Freiburg, Freiburg im Breisgau, GERMANY,* [2]*Division of Radiopharmaceutical Development, German Cancer Consortium (DKTK), partner site Freiburg, and German Cancer Research Center (DKFZ), Heidelberg, Freiburg im Breisgau, GERMANY,* [3]*Department of Nuclear Medicine, Heidelberg University Hospital, Heidelberg, GERMANY.*

Aim/Introduction: The treatment with alpha- or beta-emitter labeled PSMA-617 represents a promising approach in the clinical management of metastasized, hormone-refractory prostate cancer. However, the concomitant irradiation of salivary glands remains the main dose-limiting side effect thereby significantly reducing patient's quality of life. Thus, strategies minimizing the salivary gland uptake of PSMA-617 are urgently needed. **Materials and Methods:** After introduction of the amylase cleavable linker to PSMA-617, the PSMA-binding properties of the novel compound were analyzed by competitive binding and internalization experiments in human PSMA expressing LNCaP cells. To further investigate the cleavability of the linker in vitro the ^{177}Lu-labeled compound was incubated in the presence of α-amylases. Biodistribution and μPET studies were performed in LNCaP tumor-bearing mice (BALB/c nu/nu) to determine first data on tumor uptake and pharmacokinetic properties. **Results:** The cleavable derivative of PSMA-617 retained high binding affinity, specific cell uptake and was effectively internalized into the PSMA expressing cell line LNCaP. The cleavability of the linker was proven by in vitro enzymatic cleavage using α-amylases isolated from human salivary gland. In first in vivo studies the tumor uptake and pharmacokinetic profile of the novel modified compound showed only minor changes compared to PSMA-617 at 1 h and 4 h p.i.. **Conclusion:** The introduction of an amylase cleavable linker to PSMA-617 was accompanied by only minor impact on the binding properties, tumor uptake and the pharmacokinetic characteristics. As the amylase cleavability of the novel compound was shown in the presented in vitro proof-of-concept, further studies need to investigate the related in vivo properties. The first preclinical data on a cleavable derivative of PSMA-617 emphasize the potential of this strategy to minimize dose-limiting side effects for an improved therapy of prostate cancer. **References:** None.

OP-726

^{68}Ga-RM2 PET/CT in Patients with Newly Diagnosed Intermediate- or High-Risk Prostate Cancer

A. Iagaru, *L. Baratto*, *H. Duan*, *N. Hatami*, *C. Mari*, *G. Davidzon*;
Stanford University School of Medicine, Stanford, CA, UNITED STATES OF AMERICA.

Aim/Introduction: ^{68}Ga-RM2 is a synthetic bombesin receptor antagonist that targets gastrin-releasing peptide receptors (GRPR). GRPR are highly overexpressed in several human tumors, including prostate cancer (PC). In this study we evaluated ^{68}Ga-RM2 PET/CT in patients with newly diagnosed intermediate- or high-risk PC **Materials and Methods:** We enrolled 22 men, 50-78 year-old (mean±SD: 62.5±6.7). Images were acquired 42-72 minutes (mean±SD: 54.4±7.6) after injection of 3.3-6.7 mCi (mean±SD: 3.9±0.7) of ^{68}Ga-RM2. ^{68}Ga-RM2 PET/CT findings were compared to concurrent preoperative pelvic MRI (n=20) and ^{68}Ga-PSMA11 PET (n=10). Findings were also correlated with prostate saturation biopsy (n=22) and post-prostatectomy whole-mount pathology (n=16). Six participants decided to undergo radiation therapy. **Results:** The cohort included 9 participants with intermediate-risk and 13 participants with high-risk PC, with PSA 3.3-28.0 ng/ml (mean±SD: 9.8±6.2) at diagnosis. Preoperative ^{68}Ga-RM2 PET identified intraprostatic cancer foci in all 22 patients (45 lesions), whereas mpMRI alone identified PIRADS 4 or 5 lesions in 17/20 patients (21 lesions vs. 35 lesions on ^{68}Ga-RM2 PET) and PIRADS 3 in 1/20 patients (2 lesions vs. 1 lesion on ^{68}Ga-RM2 PET). mpMRI was negative in 2/20 patients (3 lesions on ^{68}Ga-RM2 PET). ^{68}Ga-RM2 PET demonstrated focal uptake in non-enlarged pelvic lymph nodes in 4 patients. Final pathology confirmed nodal metastases in 3 patients and follow-up imaging confirmed nodal metastasis in 1 patient. One patient with normal pelvic nodes on PET/CT had nodal metastases on post-surgery histopathology. ^{68}Ga-RM2 PET and ^{68}Ga-PSMA11 PET done 1-12 days (mean±SD: 4.4±4.3) apart identified 19 and 18 intraprostatic lesions, respectively, as well as 2 and 3 pelvic lymph nodes, respectively. Non-congruent findings between ^{68}Ga-RM2 PET and ^{68}Ga-PSMA11 PET were recorded in 4/10 patients (intraprostatic lesions in 3 patients and nodal lesion in 1 patient). **Conclusion:** Our preliminary results suggest that ^{68}Ga-RM2 PET can accurately detect intermediate- and high-risk prostate cancer. In addition, it appears to have better performance when compared to mpMRI and similar performance to ^{68}Ga-PSMA11 PET. These findings need to be confirmed in larger studies. **References:** None.

OP-727

PSMA PET/CT and Sentinel Node Biopsy for Primary Lymph Node Staging in Prostate Cancer

F. Hinsenveld[1], *E. M. K. Wit*[1], *P. J. Van Leeuwen*[1], *O. R. Brouwer*[1], *M. L. Donswijk*[1], *C. N. Tillier*[1], *E. Vegt*[1], *H. A. M. Van Muilekom*[1], *M. Van Oosterom*[2], *F. W. B. Van Leeuwen*[2], *H. G. Van der Poel*[1];
[1]*Netherlands Cancer Institute Antoni van Leeuwenhoek, Amsterdam, NETHERLANDS,* [2]*Leiden University Medical Center, Leiden, NETHERLANDS.*

Aim/Introduction: To determine the diagnostic capabilities of combined prostate-specific membrane antigen positron emission tomography/computed tomography (PSMA PET/CT) and sentinel node (SN) biopsy in PSMA PET/CT negative patients for the primary lymph node (LN) staging in prostate cancer (PCa) patients. **Materials and Methods:** Between January 2017 and March 2019, all patients with primary diagnosed PCa who underwent a preoperative PSMA PET/CT (^{68}Ga or ^{18}F-DCFPyL) followed by robot-assisted radical prostatectomy and extended pelvic lymph node dissection (ePLND) were included. All patients with intermediate- or high-risk PCa, but without suspected LN metastases on PSMA PET/CT were considered candidates for SN biopsy with indocyanine green-^{99m}Tc-nanocolloid (ICG-^{99m}Tc-nanocolloid) or ^{99m}Tc-nanocolloid with free ICG as used tracers. **Results:** Of 53 patients, 22 had a positive PSMA PET/CT and 31 received subsequent SN biopsy after negative PSMA PET/CT. In total, 23 patients (43%) were pN1, of which 17 patients (74%) with positive PSMA PET/CT and 6 (26%) with a negative PSMA PET/CT and subsequent SN biopsy. The combined use of SN biopsy and PSMA PET/CT identified all patients with LN metastases found at ePLND (100% sensitivity) and performed correct nodal staging in 48 of 53 patients (91%). The five incorrectly staged patients had a false-positive PSMA PET/CT, two of whom had a biochemical recurrence with LN metastases in the ePLND field seen on repeated PSMA PET/CT, implying that an incomplete ePLND was performed. SN biopsy identified significantly smaller LN metastases (median diameter of 2.0 mm interquartile range [IQR] 1.0-3.8) than PSMA PET/CT (5.5 mm IQR 2.6-9.3; p=0.007). SNs outside the standard ePLND template were identified and resected in eight cases, of which one was positive for metastases. **Conclusion:** Combining both modalities led to a 91% accuracy for nodal staging in primary diagnosed PCa. Adding SN biopsy in patients with a negative PSMA PET/CT increases the combined sensitivity to 100% for detecting nodal metastases at ePLND. **References:** None.

OP-728

High Repeatability Of Dynamic ^{82}Rubidium-PET/CT For Tumor Blood Flow Imaging In Prostate Cancer -a Test-Retest Study

M. Jochumsen[1,2], *K. Bouchelouche*[1,2], *K. B. Nielsen*[3], *M. Borre*[4,2], *J. Frøkiær*[1,2], *J. Sörensen*[1,2], *L. P. Tolbod*[1];
[1]*Aarhus University Hospital, Dept. of Nuclear Medicine and PET-Centre, Aarhus, DENMARK,* [2]*Aarhus University, Dept. of Clinical Medicine, Aarhus, DENMARK,* [3]*Aarhus University, Dept. of Public Health, Section for Biostatistics, Aarhus, DENMARK,* [4]*Aarhus University Hospital, Dept. of Urology, Aarhus, DENMARK.*

Aim/Introduction: Non-invasive tumor blood flow (TBF) measurement may be used for monitoring disease progression in patients diagnosed with prostate cancer. Recently, we validated dynamic ^{82}Rubidium (^{82}Rb) positron emission tomography (PET) for quantification of TBF in prostate cancer patients (1), but we did not assess the repeatability of this method. Given the paucity of test-retest data, the potential clinical impact of dynamic ^{82}Rb PET cannot be evaluated. We here aim to determine the repeatability of TBF measurement with dynamic ^{82}Rb PET. **Materials and Methods:** Ten prostate cancer patients were prospectively included. Each patient underwent two ^{82}Rb PET scan sessions within one week, each

consisting of both a dynamic pelvic and a cardiac ^{82}Rb PET to obtain a blood image-derived input function. **Results:** ^{82}Rb PET K1 can be measured in prostate tumors with a repeatability of 31.9%, a within-subject coefficient of variance of 11.5%, and an excellent intraclass correlation of 0.98. **Conclusion:** Dynamic ^{82}Rb PET measures TBF in prostate cancer with a high repeatability that allows detection of actual changes in blood flow between repeated measurements if the change (relative to the mean) is above 32%. Dynamic ^{82}Rb PET K1 could be precise and consistent enough to draw conclusions on an individual patient basis. **References:** 1.Jochumsen MR, Tolbod LP, Pedersen BG, et al. Quantitative tumor perfusion imaging with (82)Rubidium-PET/CT in prostate cancer - analytical and clinical validation. J Nucl Med. 2019 (epub ahead of print).

OP-729

Prospective comparison of ^{68}Ga-RM2 PET/CT and ^{68}Ga-PSMA-617 PET/CT for initial staging of prostate cancer

*R. Schollhammer[1,2,3], H. De Clermont Gallerande[4], G. Robert[5], M. Yacoub[6], F. Lamare[4,7,8], N. Balamoutoff[4], D. Vimont[7,8], E. Hindie[4,7,8], P. Fernandez[4,7,8], **C. Morgat**[4,7,8];*

[1]Service de Médecine Nucléaire,CHU Bordeaux, Bordeaux, FRANCE, [2]Université de Bordeaux, INCIA, UMR 5287, Talence, FRANCE, [3]CNRS, INCIA, UMR 5287, Talence, FRANCE, [4]Service de Médecine Nucléaire,CHU Bordeaux, F-33076, Bordeaux, FRANCE, [5]Service d'Urologie, CHU Bordeaux, F-33076, Bordeaux, FRANCE, [6]Service d'Anatomopathologie, CHU Bordeaux, F-33076, Bordeaux, FRANCE, [7]Université de Bordeaux, INCIA, UMR 5287, F-33400, Talence, FRANCE, [8]CNRS, INCIA, UMR 5287, F-33400, Talence, FRANCE.

Aim/Introduction: PSMA (Prostate Specific Membrane Antigen) and GRP-R (Gastrin Releasing Peptide Receptor) are overexpressed on prostatic cancer cells and can be targeted with a PSMA inhibitor such as ^{68}Ga-PSMA-617 (Liu 2018) or a GRP-R antagonist such as ^{68}Ga-RM2 (Touijer 2019). GRP-R-targeting and PSMA-targeting have been compared in patients with biochemically recurrent prostate cancer (Minamimoto 2016) but not at primary staging. We aimed to compare ^{68}Ga-PSMA-617 PET/CT and ^{68}Ga-RM2 PET/CT at initial staging of prostate cancer. **Materials and Methods:** We prospectively enrolled 10 treatment-naïve patients with biopsy-confirmed prostate cancer (two with Gleason score (GS) 6; three with GS 7(3+4), one with GS 7(4+3) and four with GS ≥ 8). ^{68}Ga-PSMA-617 PET/CT and ^{68}Ga-RM2 PET/CT were randomly performed before prostatectomy with imaging at 1 hour and 2 hours after injection (2MBq/kg). Manual (MS) and automatic (AS) segmentation were performed on each PET imaging using PMOD software and segmentations were then compared to histology (standard-of-truth). Prostatectomy samples were analyzed by an experimented pathologist who identified and staged each lesion according to GS. Each prostatectomy slice available was scanned for comparison between PET and histologic segmentation. Uptake intensity (SUV_{max}) and signal-to-noise ratio (SNR) relative to non-lesional prostate gland parenchyma were analyzed. Per-lesion analysis was performed on final GS (prostatectomy). Lesions < 0.1 cm³ were excluded. **Results:** Using AS, ^{68}Ga-RM2 PET/CT showed better sensitivity (Se) than ^{68}Ga-PSMA-617 PET/CT: (0.85 vs 0.75) and better specificity (Sp) (0.89 vs 0.60). MS found similar Se (0.94 vs 0.93) but better Sp (0.89 vs 0.80) with ^{68}Ga-RM2 PET/CT. SNR of ^{68}Ga-RM2 PET/CT was high whatever the GS was; while ^{68}Ga-PSMA-617 PET/CT exhibited higher SNR in high GS ($p = 0.044$). Finally, in low GS, SNR of ^{68}Ga-RM2 PET/CT was significantly higher than ^{68}Ga-PSMA-617 PET/CT ($p = 0.004$). **Conclusion:** To our knowledge, this is the first study comparing PSMA- and GRPR-based imaging for initial local staging of prostate cancer. The results showed great diagnostic performance of ^{68}Ga-RM2 PET/CT compared to ^{68}Ga-PSMA-617 PET/CT to characterize low Gleason score tumors. ^{68}Ga-PSMA-617 PET/CT is promising for initial staging of high Gleason score tumors. We are enrolling more patients to confirm the results of these innovative imaging modalities. **References:** Touijer KA, Michaud L, Vargas Alvares Ha et al (2019) Eur Urol Oncol. 2(2):166-173 Liu C, Liu T, Zhang n, Liu Y et al (2018) Eur J Nucl Med Mol Imaging. 45(11):1852-1861 Minamimoto R, Hancock S, Schneider B et al (2016) J Nucl Med. 57(4):557-562.

1609

Radiation Protection - Parallel Session: Radiation Protection - Standards, Tools and Models

Wednesday, October 16, 2019, 8:00 - 9:30 Lecture Hall 115

OP-730

Reporting Incidents In Therapeutic Nuclear Medicine. A New IAEA Tool

M. Marengo[1], *D. Gilley[2], J. Vassileva[2], F. Fahey[3], L. Dimmick[4], B. R. Thomadsen[5], T. Ell[6];*

[1]University of Bologna, Bologna, ITALY, [2]IAEA, Vienna, AUSTRIA, [3]Children's Hospital and Harvard Medical School, Boston, MA, UNITED STATES OF AMERICA, [4]Medical Radiation Safety, Nuclear Regulatory Commission, Rockville Pike, MD, UNITED STATES OF AMERICA, [5]University of Wisconsin, Madison, WI, UNITED STATES OF AMERICA, [6]Foothills Hospital, Calgary, AB, CANADA.

Aim/Introduction: The role of nuclear medicine therapeutic treatments is established and expanding, thanks to new radiopharmaceuticals that allow targeting malignancy with a high level of selectivity, releasing only limited radiation dose to healthy tissues, and considering the potential of the theragnostic approach. In the vast majority of cases, these treatments are well tolerated by patients and have limited deleterious effects. Nevertheless, in a complex, highly structured discipline like nuclear medicine, there remains the probability of procedural errors, unexpected events or unforeseeable aspects that may lead to inappropriate delivery of the therapy, undesired patient exposure or other consequences potentially harmful to patients. Limited, but significant reports are effectively presented in the

current scientific literature. **Materials and Methods:** Incident reporting systems are a tool in health institutions to monitor unexpected events, incidents and close calls, activate corrective actions and provide useful information to the clinicians to prevent repetitions. The IAEA introduced SAFRON in 2012, a web-based system for incident reporting in radiotherapy. A meeting on prevention of incidents in nuclear medicine held in May 2018, with participation of an international, multidisciplinary panel of experts, produced a series of recommendations including extending SAFRON to incidents in nuclear medicine therapeutic applications. These include therapies with radiopharmaceuticals and radioactive medical devices such as SIRT. A specific task group convened in November 2018, reviewed existing reports and experiences, and develop the parameters of the application, define the scheme of incident models, the modality of registration and the possible safety barriers. **Results:** The new addition to the SAFRON platform is under development at the IAEA with expectations that it will be tested and available in the second half of 2019. The introduction of data is easy and anonymous, guaranteeing the privacy of patients and reporting institutions, but nevertheless making possible for professionals in the field to obtain relevant information on incidents, their modality, consequences and possibilities for mitigation, and contributing then to diffuse knowledge and learn from previous lessons. Participating facilities will be able to use SAFRON NM as their local incident learning system as well as contributing to an international incident learning system looking for opportunities to improve the safety systems and reduce potential errors. **Conclusion:** SAFRON NM is a state of the art, safe and effective incident learning tool that the IAEA will make available to the nuclear medicine community to foster prevention of incidents and improve the safe administration of radionuclide therapy. **References:** None.

OP-731

Development of a radiation protection precaution calculator for personalised patient-specific precautions post-SIRT therapy

S. Cournane, J. McCavana, M. Manley, J. McCann, J. Lucey;
St Vincent's University Hospital, Dublin 4, IRELAND.

Aim/Introduction: Yttrium-90 (90Y) microspheres are used for selective internal radiation therapies (SIRTs) to treat patients with hepatocellular carcinoma (HCC) or metastatic colon cancer to the liver, with doses of up to 150Gy delivered per treatment. 90Y, a pure beta emitter, with a half-life of 64.2 hours, decay energy of 0.94 MeV and mean tissue penetration length of 2.5mm, is ideal for delivering high radiation doses to precise volumes of diseased tissue. The resultant beta exposure from the patient post-therapy is, thus, negligible; however, there can be a considerable associated Bremsstrahlung radiation exposure component. There is very little literature on the associated dose rates from SIRT patients post therapy, and none discussing the challenges of radiation protection (RP) precautions encountered within the European Union jurisdiction where dose constraints of 0.3mSv are employed. Further, there is a dearth of work on patient-specific radiation protection precautions. Accordingly, the aim of this work is, firstly, to establish the dose rates from patients post-therapy, followed by modelling the doses received to patient family members. Finally, this work will present a personalised radiation protection precautions calculator, optimising precautions for family members taking into account patient-specific administered activities and living circumstances. **Materials and Methods:** Dose rates from patients treated since 2016, measured using a Thermo Electron RadEye G-10 immediately after 90Y microspheres infusion at various distances will be presented. Normality and Log-normality will be investigated using the Shapiro-Wilks test. Dose rates will be used to calculate radiation doses received by family members (partner and child, respectively) and carers based on interaction patterns described in the literature, and using in-house estimates. **Results:** Examining our SIRT patient cohort as if following interaction patterns with children will demonstrate the 0.3mSv dose constraint being exceeded in the majority of cases. Hence, this work will show the need for RP restrictions considering local dose constraints. Furthermore, by assigning dose contributor weighting factors to each of the distance components for each proximity model, and accounting for duration, a radiation protection precautions calculator will be presented. This will provide a means of optimising patient-specific precautions taking into account personal circumstances and administered activities. **Conclusion:** We demonstrate the need for radiation protection precautions for those individuals in regular contact with SIRT patients. Further, we will present a radiation protection precaution calculator designed for optimising radiation protection precautions taking the patient-specific circumstances and administered activities into account. **References:** None.

OP-732

Construction of Safety Standards for Short-half-life Alpha Emitters by Grant of Nuclear Regulatory Agency of Japan

M. Hosono[1], T. Yamada[2], N. Oriuchi[3], N. Ukon[3], K. Nagatsu[4], T. Ito[2], H. Yamanishi[2], T. Matsuda[2], A. Hachisuka[5], Y. Nakamura[6];
[1]Kindai University Faculty of Medicine, Osaka-Sayama, JAPAN, [2]Kindai University Atomic Energy Research Institute, Higashi-Osaka, JAPAN, [3]Fukushima Medical University, Fukushima, JAPAN, [4]National Institute of Radiological Sciences, Chiba, JAPAN, [5]National Institute of Health Sciences, Tokyo, JAPAN, [6]Japan Radioisotope Association, Tokyo, JAPAN.

Aim/Introduction: Theranostics approaches using radiopharmaceuticals currently continue to develop in nuclear medicine worldwide, and it is expected that alpha emitters will enhance substantially the efficacy of radionuclide therapy over the next decades as we have seen emerging application of radium-223 dichloride to castration-resistant prostate cancer with bone metastases, Nuclear Regulatory Agency of Japan organized and supported projects for application of alpha emitters in basic and clinical researches since 2017. The

purpose of this study, granted by the Agency, was to propose novel principles of radiation safety in laws and guidelines so that research and development of radionuclide therapy technologies using nuclides including short-half-life alpha emitters are carried out under rational safety control based on scientifically accumulated data. **Materials and Methods:** We identified and examined major issues on optimization of protection from the viewpoint of the personnel engaged in production and use of radiopharmaceuticals and from that of the general public in consideration of novel application of therapeutic radiopharmaceuticals by conducting surveys at facilities in Japan and overseas. **Results:** We surveyed situations on safety control of alpha emitters at facilities including National Institute of Radiological Sciences (Chiba, Japan) and Fukushima Medical University (Fukushima, Japan) which own accelerators for producing alpha emitters in Japan. We also visited University of Göteburg (Göteburg, Sweden), ARRONAX (Nantes-Saint Herblain, France), and IRSN (Institut de Radioprotecion et Sûreté Nucléaire, Saclay, France), and investigated use, disposal, technical standards, GMP production, and regulations regarding of short-half-life alpha emitters including astatine-211 and actinium-225. We summarized the findings by overviewing different situations at the facilities. **Conclusion:** We listed the present and future needs of research and development for alpha radiopharmaceuticals in relation to clinical demands, safety management, and regulatory issues. As a result, we recognized that scientific evidence should be accumulated in order to establish safety management in facilities and to revise current regulations in accordance with the international basic safety standards for conventional and novel radiopharmaceuticals. **References:** Radiation protection in therapy with radiopharmaceuticals. International Journal of Radiation Biology 2019 in press. Published online: 28 Sep 2018. Introduction of the targeted alpha therapy (with Radium-223) into clinical practice in Japan: learnings and implementation. Annals of Nuclear Medicine 2019;33:211-221. Perspectives for concepts of individualized radionuclide therapy, molecular radiotherapy, and theranostic approaches. Nuclear Medicine and Molecular Imaging 2019 in press.

OP-733

Nationwide Survey in Finland: Optimisation Principle Should Not Be Forgotten

J. T. Liukkonen, J. Suutari;
Radiation and Nuclear Safety Authority, Helsinki, FINLAND.

Aim/Introduction: Optimisation is a basic principle in radiation protection. In this study optimisation is considered as a general imaging protocol modification, not as a patient-wise. In this study we investigated the role of optimisation in SPECT-CT and PET-CT facilities in Finland. The study focused on nuclear imaging. **Materials and Methods:** A Webropol survey was conducted to all nuclear medicine licensees in Finland. In addition optimisation will be assessed by onsite inspections. **Results:** Answers to the survey were received from all licensees (N=24). According to the answers optimisation is a multidisciplinary process. Nuclear medicine physician and radiologists resources limits frequency of optimisation in some hospitals. Absence of written protocols for optimisation was reported widely. New national or international guidelines and recommendations are the most common initiative for optimisation. In many cases optimisation process was originated from self assessment, collegial interaction and EANM recommendations. Surprisingly, commissioning a new scanner did not always lead to optimisation. Median optimisation frequencies for ten year period for kidney function SPECT, total body bone isotope imaging, upper body PET and whole body PET were 2, 1, 1.5 and 2 respectively. Image quality was the main aim in optimisation and it was not compromised during optimisation in any reported cases. On the other hand approximately in half of the cases activity and image quality were not changed. **Conclusion:** Optimisation as a basic principle is insufficiently applied. This calls for systematic and documented optimisation as a regular practise. We conclude that this would increase optimisation frequencies remarkably. Furthermore, as optimisation is a basic principle, it should be a integral part of commissioning. Self assessment, collegial interaction and EANM recommendations provide foundation for optimisation and sufficient resources for optimisations should be assured. The result that in half of the cases the activity was not changed aligns with national and European statistics. Based on this study, STUK will emphasize optimisation in the inspection program for year 2020. We propose that 1) this study should be carried out in other countries as well 2) EANM facilitates development of optimisation 3) special attention should be paid on administrated activities. **References:** None.

OP-734

Dynamic absorbed dose calculations to the urinary bladder wall for the ICRP compartmental models of iodide and technetium

M. Andersson[1], *S. Mattsson*[1], *L. Johansson*[2];
[1]*Medical Radiation Physics, Malmö, SWEDEN,* [2]*Radiation Physics,Umeå University, Umeå, SWEDEN.*

Aim/Introduction: The urinary bladder wall is a radiosensitive organ that can receive a high absorbed dose from radiopharmaceuticals used even in diagnostic nuclear medicine. The commonly used method to calculate the absorbed dose to the urinary bladder wall is to apply absorbed fractions or S-values derived for a static volume of the content e.g. 200 mL for adult males. However, there are some dynamic models to estimate the photon and electron absorbed dose contributions to the inner surface or the mean absorbed dose to the bladder wall. These models have only been applied on adults and use descriptive biokinetic models for the transfer of radionuclides. The aim of this work is to estimate the absorbed dose, based on Monte Carlo-simulated dynamic urinary bladders and the ICRP compartmental biokinetic models of iodide and pertechnetate. The calculations include sex specific absorbed

dose and estimations for preadults of 15- 10- 5- 1-year and newborn. **Materials and Methods:** S-values were calculated for different volumes of the content with a fix mass of the wall. As an approximation a spherical shape was assumed. Calculations were based on anatomical and physiological data of the reference sets of values given in ICRP Publication 89. The reference values were given for both male and female subjects of six different ages: newborn, 1-, 5-, 10-, 15-years, and adult. The elemental compositions of the urinary bladder wall and content were taken from the ICRP Publication 110. **Results:** For adult male assuming a urinary flow rate of 1600 ml/day, an initial urine volume of 100 ml, a voiding volume at 300 ml and a residual volume of 30 ml, the cumulated activity will for intravenously administered activity of Tc-99m pertechnetate be 30 % lower than assuming a 3.5 hour voiding interwall. The absorbed dose to the urinary bladder wall will be 64% lower also applying the dynamic S-values on the dynamic case. Using the same biological parameters for intravenous intake of I-131 iodide, the cumulated activity will be 60 % higher for the dynamic case and the mean absorbed dose to the urinary bladder wall 30 % lower. **Conclusion:** This project aims to perform more realistic calculation of absorbed dose to the urinary bladder calculations. This is done by tracking the activity in the urinary content at each time on compartment models and applying the time dependent activity to urinary flow and Monte Carlo simulated S-values. **References:** None.

OP-735

Eye lens dose estimation in Peptide Receptor Radionuclide Therapy: Monte Carlo simulations versus experimental measurements

F. Fioroni[1], *P. Ferrari*[2], *E. Grassi*[1], *A. Chendi*[1,3], *M. Bertolini*[1], *V. Piccagli*[1], *A. Filice*[1], *A. Versari*[1], *F. Mariotti*[2], *M. Iori*[1];
[1]*AUSL-IRCCS, Reggio Emilia, ITALY,* [2]*ENEA, Radiation Protection Institute, Bologna, ITALY,* [3]*Postgraduate School in Medical Physics, University of Bologna, Bologna, ITALY.*

Aim/Introduction: The increasing role played by Peptide Receptor Radionuclide Therapy (PRRT) has provided a larger use of unsealed beta-emitter in medicine. The objective of this work is to assess eye lens doses using methods of computational dosimetry and to compare them with experimental measurements performed during PRRT administration. **Materials and Methods:** The administration of ^{90}Y/^{177}Lu-radiolabelled derivatives is usually performed manually, using an infusion system. In the present work only ^{90}Y administration is considered.The vial, the shielding and the polyethylene catheter have been reproduced with their specific composition and densities. The source was simulated as an electron spectrum of 0.93 MeV and 2.23 MeV (mean and maximum), generated inside the vial and the catheter. Dose equivalents were scored at 50, 100 and 150 cm distance from the vial and at three different heights (0, 50,100 cm) from its mid-plane.The eye lens dose of the physician was assessed by 3 dosimeters positioned next to the eyes during the administration phase. **Results:** The greatest contribution of dose due to electrons is when the radiopharmaceutical flows through the catheter. At 50 cm distance from the vial axis, the simulated Hp(3) for electron varies from 203 uSv h^{-1}GBq^{-1}, at the same height of the vial and catheter, to 110 uSv h^{-1}GBq^{-1}at 50 cm height and to 34 uSv h^{-1}GBq^{-1}at 100 cm height. At the same heights, but at 150 cm distance from the vial axis, these values decrease respectively to 22 uSv h^{-1}GBq^{-1}, 17 uSv h^{-1}GBq^{-1} and 11 uSv h^{-1}GBq^{-1}. Considering an uncertainty of 5% for the simulations and 10% for the dosemeters, such values are quite in agreement with the measurements that varies from a minimum of 10 uSv h^{-1}GBq^{-1} and a maximum of 280 uSv h^{-1}GBq^{-1}(mean 89 uSv h^{-1}GBq^{-1}, median 48 uSv h^{-1}GBq^{-1}). The variation are consistent with the intrinsic variability of the practice (different operators, different distance, difficulties during the infusion, etc...). **Conclusion:** The satisfactory agreement between dosemeters and simulations allows employing the evaluated data to study the exposure of the medical personnel performing PRRT. From the general results, a value of the order of 50 uSv h^{-1}GBq^{-1}can be assumed. That means that for a single administration of 20 GBq of ^{90}Y, with the operator remaining 15 minutes near the patient, Hp(3) can reach 0.25 mSv. With such figures, the maximum dose to the eye lens can be reached after 80 treatments. Further evaluations will be carried out for ^{177}Lu. **References:** None.

OP-736

Novel Nanotech Antioxidant Cocktail for Protection from Ionizing Radiation during Bone Scans

M. Gorenberg[1], *N. Eiza*[1], *M. Ziv*[1], *Y. Hadid*[1], *I. Volovic*[2], *A. Shalata*[1];
[1]*Bnai Zion Medical Center-Technion, Haifa, ISRAEL,*
[2]*Bnai Zion Medical Center, Haifa, ISRAEL.*

Aim/Introduction: Exposure to ionizing radiation produces oxygen-derived free radicals in the tissue, these free radicals then interact with nearby DNA, causing double strand breaks (DSB). These DNA lesions are usually efficiently repaired, however, DSB misrepair can lead to chromosomal translocations and therefore initiate carcinogenesis (1). A novel nanotech protective drinkable cocktail (PCK) of non-toxic radical-scavenging of 10 potent antioxidants was developed . We investigated the protective effect of this novel nanotech antioxidant cocktail in suppressing formation of gamma -ray induced DSBs DNA lesions in patients undergoing Bone Scans. **Materials and Methods:** Sixteen patients (5 women, 11 men; mean age, 46.9.2 years; range, 27-90 years) undergoing technetium-99m methylene diphosophonate (99mTc MDP) bone scans were prospectively recruited. Six patients receive the PCK before radiotracer injection (CKT group) and 10 patients receive no CKT (control group). None of these patients had had any ionizing imaging procedures in the past seven days or chemotherapy/radiotherapy within the prior six months before bone scan. The average radiotracer activity injected was 922 MBq (range: 888-925 MBq). Peripheral blood lymphocytes (PBLs) were isolated from blood samples drawn directly before the bone scan radiotracer injection and 120 minutes later. DNA DSBs

were detected by γH2AX immunofluorescence staining and quantified (in terms of γH2AX % of doted cells) with automated digital microscopy in each of the two blood samples to assess any significant differences. Statistical analysis was performed with pair t test. The study was approved by the local ethics committee, and written informed consent was obtained from each patient. **Results:** PBLs from blood taken before radiotracer injection showed a median of 22% γH2AX doted cells (range 7.4-58.2) in the control group as compared with a median of 19.5% γH2AX (range 11-24.4) for the CKT group (NS). PBLs from blood taken 120 minutes after injection increase to a median of 39% γH2AX doted cells (range 27.7-70) in the control group (P< 0.005) as compared with an increase to a median of 21.5 % γH2AX (range 15.5-28.6) for the CKT group (NS), consistent with evidence of CKT radiation protection from a single ionizing radiation study. **Conclusion:** In patients undergoing 99mTc MDP bone scans, treatment with a novel oral nanotech cocktail of antioxidants before scanning significantly prevented DNA damage in PBLs. **References:** 1.Ward JF. DNA Damage Produced by Ionizing Radiation in Mammalian Cells: Identities, Mechanisms of Formation, and Reparability. Prog Nucleic Acid Res Mol Biol. 1988;35(C):95-125. doi:10.1016/S0079-6603(08)60611-X.

1701

CME 14 - Bone & Joint Committee / IASP: The Diagnosis is Complex Regional Pain Syndrome I (CRPS-I a.k.a. Reflex Sympathetic Dystrophy). Or is it?

Wednesday, October 16, 2019, 10:00 - 11:30 Auditorium

OP-737
Contemporary Consensus and Controversies in Diagnosis and Management of CRPS-I
R. Atkins;
University of Bristol, Orthopaedic Surgery, Bristol, UNITED KINGDOM.

OP-738
Role for Imaging in Diagnosis and Management of CRPS-I
F. Paycha;
Nuclear Medicine Department, University Hospital Lariboisière, Paris, FRANCE.

OP-739
Role for Imaging in Alternate Diagnoses Usually Confused with CRPS-I
E. Rust;
Nuclear Medicine Department, Clinique du Diaconat-Roosevelt, Mulhouse, FRANCE.

1702

Joint Symposium 27 - Radiation Protection Committee / JSNM: Lessons from Fukushima - Low Dose Radiation from Environment Radioisotope

Wednesday, October 16, 2019, 10:00 - 11:30 Lecture Hall 311

OP-741
Doses and Likely Health Effects in Fukushima
N. Takamura;
Dept of Global Health, Medicine and Welfare, Atomic Bomb Disease Institute, Nagasaki University, Nagasaki, JAPAN.

OP-742
Controversies and Challenges of the Linear No Threshold Model
R. Wakeford;
Manchester University, Newcastle, UNITED KINGDOM.

OP-743
Supporting Fukushima - The Nuclear accident's Consequences on the Region
K. Kanai;
Faculty of Applied Sociology, Kindai University, Osaka, JAPAN.

OP-744
Special Aspects of Radiation Induced Paediatric Thyroid Cancer
C. Reiners;
University Hospital Würzburg, Würzburg, GERMANY.

OP-745
Discussion

1703

Joint Symposium 28 - Translational and Molecular Imaging Therapy + Oncology & Theranostics Committee / WMIS: Translational Aspects of PSMA Targeting

Wednesday, October 16, 2019, 10:00 - 11:30 Lecture Hall 312

OP-746
Biology of PSMA
J. Grimm;
Memorial Sloan Kettering Cancer Centre, New York, NY, UNITED STATES OF AMERICA.

OP-747

Update on PSMA Tracers

M. G. Pomper;
John Hopkins Hospital, Radiology, Nuclear Medicine and Molecular Imaging, Baltimore, MD, UNITED STATES OF AMERICA.

OP-748

Clinical Relevance PSMA Targeting

F. Giesel;
University of Heidelberg, Department of Nuclear Medicine, Heidelberg, GERMANY.

1704

CTE 7 - Technologist Committee: Updates in Lung Imaging

Wednesday, October 16, 2019, 10:00 - 11:30 Lecture Hall 117

OP-751

New PET Radiotracers for Lung Imaging

D. Albano;
Spedali Civili of Brescia, Nuclear Medicine Department, Brescia, ITALY.

OP-752

Metabolic Volumes Delineation for External Beam Radiotherapy and its Prognostic Role in Lung Cancer

W. Cholewinski;
The Greater Poland Cancer Centre, Nuclear Medicine Department, Poznan, POLAND.

OP-753a

Radiomic Features in Non-Small-Cell Lung Cancer FDG-PET/CT Studies

M. Kirienko;
Humanitas University, Department of Biomedical Sciences, Milan, ITALY.

OP-753b

Discussion

1705

M2M - Parallel Session: Peptide-Based Radionuclide Therapy

Wednesday, October 16, 2019, 10:00 - 11:30 Lecture Hall 111

OP-754

Intra-tumoral somatostatin receptor 2 heterogeneity confers differential radionuclide therapy response in preclinical neuroendocrine tumor models

D. Feijtel[1], *G. N. Doeswijk*[1], *N. S. Verkaik*[1], *J. C. Haeck*[1], *M. Konijnenberg*[1], *C. Angotti*[2], *D. Chicco*[2], *D. C. van Gent*[1], *M. de Jong*[1], *J. Nonnekens*[1];
[1]*Erasmuc MC, Rotterdam, NETHERLANDS,* [2]*Advanced Accelerator Applications, A Novartis Company, Colleretto Giacosa, ITALY.*

Aim/Introduction: Patients with neuroendocrine tumors (NETs) often suffer from metastases at the time of diagnosis, which limits the possibility for resection as an effective treatment. For the localization of NETs, targeting of somatostatin receptor subtype-2 (SST2), that is highly expressed on tumor cells, with radiolabeled somatostatin analogues is a diagnostic standard. By labeling with radionuclides that cause DNA damage, this diagnostic tool has been transformed into a treatment: peptide receptor radionuclide therapy (PRRT). PRRT with [^{177}Lu]Lu-DOTA-Tyr3-octreotate has been proven effective in improving both progression-free- and overall survival and quality of life, however complete cure is rare. We conducted this study to improve the current understanding of the effects of PRRT on tumor to ultimately increase the therapeutic efficacy. **Materials and Methods:** BALB/c-nude mice were engrafted with NCI-H69, a SST2-overexpressing cancer cell line. These mice were treated with 30MBq/0,5µg/mouse [^{177}Lu]Lu-DOTA-Tyr3-octreotate (non-curative dose, as per previous experience in animal models), scanned using SPECT/MRI and sacrificed at different time-points up to 14 days post-treatment. Organs were excised for biodistribution measurement. Biological parameters such as DNA damage response, proliferation and SST2 expression were analyzed using immunohistochemical- and immunofluorescent stainings. These parameters were also investigated in NCI-H69 in vitro and in Ca20948, a pancreatic NET cell line, in vitro and in vivo. Finally, pancreatic NETs from patients were analyzed to confirm our findings. **Results:** In vivo results show intra-tumoral heterogeneity in DNA damage and subsequent cell death induction in NCI-H69 tumors, despite a homogeneous vascular distribution. We observe that DNA damage response processes induced by a non-curative dose are transient in nature, after which tumor relapse occurs. Heterogeneity of the response in tumor tissue can be attributed to non-homogeneous SST2 expression. We observe that high SST2-expressing regions/cells show a higher level of DNA damage in vitro and in vivo, indicating a potential concordance with the therapeutic response. As we also confirmed SST2 heterogeneity in resected

pancreatic NETs from patients, the effects of such parameters in a clinical setting warrant further investigation. **Conclusion:** In this research we investigated direct effects of PRRT in preclinical NET models and mapped important radiobiological parameters. Tumoral intrinsic biological properties, such as regional SST2-expression levels, appear to be relevant in determining the therapeutic response and efficacy. **References:** None.

OP-755

First in human dosimetry of [^{177}Lu]RM2: A gastrin-releasing peptide receptor antagonist for targeted radiotherapy of metastasized castration resistant prostate cancer

J. Kurth, B. J. Krause, C. Bergner, S. M. Schwarzenboeck, M. Heuschkel;
Rostock University Medical Center, Rostock, GERMANY.

Aim/Introduction: Besides PSMA prostate cancer cells also express gastrin-releasing peptide receptor (GRPr) which is therefore an attractive target for theranostic approaches. High affinity GRPr antagonist (RM2) for use as diagnostic imaging agent was developed by Mansi et al. [1], offering the opportunity to label it with beta-emitting radiometals for therapeutic purposes. Aim of this study was to calculate absorbed doses for critical organs for [^{177}Lu]Lu-RM2 administration in a group of mCRPC patients, that lost or showed lower PSMA accumulation after initial [^{177}Lu]Lu-PSMA-617 therapy. **Materials and Methods:** 35 patients suffering from mCRPC, without adequate treatment options for approved therapies received [^{68}Ga]Ga-RM2-PET/CT. 4 patients (mean age of 68y (range:60-80ys)) were recruited for therapy; 2 of them also received a 2nd therapy cycle. Therapies were conducted in accordance with the German Medicines Law (AMG,§13[2b]). Mean activity was 4.5±0.9GBq. For dosimetry, patients underwent planar WB-scintigraphy and SPECT/CT imaging (Siemens Symbia T6) of the upper and lower abdomen at approximately 1h, 24h, 48h and 72h p.i. along with blood sampling. SPECT/CT was quantitatively reconstructed with corrections for scatter, attenuation and detector blurring. Absorbed doses for kidneys, pancreas, liver, spleen, gallbladder and tumor lesions were calculated from SPECT/CT data according to RADAR dosimetry scheme using OLINDA/EXM2.1. Individual organ masses were extracted from CT. Absorbed dose to bone marrow was calculated according to EANM-guideline [2]. **Results:** Therapy was well-tolerated by all patients and no side effects were observed. A highly increased uptake in tumor lesions and pancreas was seen within the first 1 h. Mean organ doses were 1.10±0.44Gy/GBq in the pancreas, 0.35±0.14Gy/GBq in the kidneys, 0.05±0.02Gy/GBq in the liver, 0.07±0.02Gy/GBq in the gallbladder wall, 0.10±0.06Gy/GBq in the spleen and 15.9±5.5mGy/GBq for the red bone marrow. The mean dose estimated for tumor lesions was 6.2±3.0Gy/GBq. **Conclusion:** Application of GRPr antagonist [^{177}Lu]Lu-RM2 is suitable for targeted radiotherapy of mCRPC, as it shows high tumor uptake and rapid clearance from normal organs. Absorbed doses in tumor lesions are therapeutically relevant. Critical organ receiving the highest absorbed dose was the pancreas. However, the critical dose limit for the pancreas is 50 to 60 Gy, which is far from limiting the administration of higher activities and the application of further treatment cycles. Our results suggest that the activity administered for each cycle could be increased to maximize absorbed dose of tumors and metastases. **References:** [1] Mansi R et al. EJNMMI. 2011 Jan;38(1):97-107[2] Hindorf C et al. EJNMMI. 2010 Jun; 37(6):1238-50.

OP-756

Chemical Conjugation Of Evans Blue Derivative Prolongs Blood Half-life And Improves The Integrin $\alpha_v\beta_3$-targeted ^{177}lu-radionuclide Therapy In A Patient-derived Xenograft Model Of Lung Adenocarcinoma

L. Zhao[1], *H. Chen*[1], *K. Fu*[1], *D. Fan*[2], *Z. Guo*[3], *H. Wu*[1], *O. Jacobson*[4], *Q. Lin*[1], *X. Chen*[5];
[1]*The First Affiliated Hospital of Xiamen University, Xiamen, CHINA,* [2]*Beijing Tiantan Hospital, Beijing, CHINA,* [3]*Center for Molecular Imaging and Translational Med, Xiamen, CHINA,* [4]*9000 Rockville Pike, Bethesda, MD, UNITED STATES OF AMERICA,* [5]*NIBIB/NIH, Bethesda, MD, UNITED STATES OF AMERICA.*

Aim/Introduction: The arginine-glycine-aspartic acid (RGD) peptide has high activity and specificity in various malignancies as an imaging agent. However, the short blood half-life is the main hurdle of RGD peptide as a radiotherapeutic agent for the treatment of integrin $\alpha_v\beta_3$-expressing tumors. In this study, we developed an "add-on" molecule Evans blue (EB) to moderate albumin binding that prolongs half-life in the blood, allows radiolabeling for imaging and targeted radiotherapy. **Materials and Methods:** The EB-RGD were radiolabeled with ^{177}Lu for SPECT imaging and integrin $\alpha_v\beta_3$-targeted radiotherapy, respectively, and compared to the peptides without the "add-on" (EB) in a patient-derived xenograft (PDX) models of lung adenocarcinoma (LUAD). **Results:** Samples of LUAD were obtained from patients undergoing operation, and the PDX ($\alpha_v\beta_3$ high expression) models of LUAD were subsequently established by implanting cancer fragments into nude mice. In ^{177}Lu-DOTA-EB-RGD SPECT imaging, the tumor to background ratio (T/B) reached 14.63 ± 3.82 at 24 h, and remained 12.02± 1.76 at 72 h post injection. The ex vivo biodistribution result showed that tumor uptake of EB-RGD reached the peak (14.96 ± 6.71 %ID/g) at 48 h post-injection (p.i.) and remained stable (14.00 ± 3.18) at 96 h p.i.. Regarding targeted radiotherapy, starting from day 12 after the treatment, significant differences in the tumor volume were observed between ^{177}Lu-DOTA-EB-RGD treated groups (Group B: 21.6 MBq, tumor volume = 35.6 ± 15.8 mm3; Group D: 13.5 MBq, tumor volume = 125.1 ± 55.4 mm3) and saline /^{177}Lu-DOTA-RGD monomer treated groups (Groups A: saline, tumor volume = 472.8 ± 203.0 mm3 ; Group C: 21.6 MBq, tumor volume = 305.9 ± 65.6 mm3). These differences increased over time (P <0.01), and the tumors in both ^{177}Lu-DOTA-EB-RGD treated group became unmeasurable by 28 days post initial treatment. No systemic toxicity due to radiotherapy was observed in all groups by monitoring animal body weight.^{18}F-FDG PET imaging 7 days post-injection of ^{177}Lu-DOTA-EB-RGD showed decreased uptake, indicating reduced

glucose utilization. **Conclusion:** Conjugation of our novel "add-on" molecules to RGD peptides showed a prolonged circulation half-life and enhanced tumor accumulation in integrin $\alpha_v\beta_3$-expressing tumors, and can transform drugs into theranostic entities. Furthermore, our PDX model is the available, validated PDX model for LUAD, and preclinical data suggests that ^{177}Lu-DOTA-EB-RGD may be an effective treatment option for LUAD patients with high integrin $\alpha_v\beta_3$ expression. **References:** None.

OP-757

Chelation of Radium-223 for Targeted Radionuclide Alpha Particle Therapy

D. Abou[1], *N. A. Thiele*[2], *M. Longtine*[1], *A. L. Villmer*[1], *J. J. Wilson*[2], *D. L. J. Thorek*[1];
[1]*Washington University School of Medicine, Saint Louis, MO, UNITED STATES OF AMERICA,* [2]*Cornell University, Ithaca, NY, UNITED STATES OF AMERICA.*

Aim/Introduction: There is currently tremendous interest in targeted alpha particle therapy as these emissions have short path lengths with high linear energy transfer. Radium-223 dichloride is the first approved agent in this space; it is administered as a free ion with bone seeking properties. Alpha emitters delivered directly to cancer cells themselves may have improved therapeutic properties, and agents are currently under evaluation using peptides and antibodies as targeting vectors. To date, Radium-223 has not been used as a targeted agent because of the challenges in achieving robust chelation for radiolabeling and in vivo use. We have investigated the coordination of an 18-membered macrocyclic ligand to achieve rapid and stable chelation of Radium-223 with significant biomedical potential. **Materials and Methods:** Radium-223 was produced using an in house microgenerator from radiochromatographic purification from source Actinium-227/Thorium-227. MACROPA chelator (10mM) was used to label approximately 37kBq of Radium-223 and assessed at room temperature; pH 6. Instant thin layer chromatography in running buffers of either 10mM EDTA or 10mM NaOH were used for quality control and complexation efficiencies along with autoradiography by phosphor storage screen exposure. Radio/UV FPLC was conducted to test biological stability of chelated Radium-223 in biological conditions. Animals (n=5, male, FVB) purchased from Charles River Laboratories were administered 3.7kBq activity and biodistribution performed at early (15min) and late (24h) times after tail vein injection; and were compared to Radium-223 dichloride in 30mM citrate. **Results:** Radium-223 was rapidly complexed by MACROPA in buffer. RadioTLC were developed and validated to confirm stable complexation of the isotope in vitro. Challenge with serum proteins did not lead to decomplexation. In vivo biodistribution of the complex demonstrated rapid renal clearance and nearly quantitative excretion to the urine verifying in vivo stability. In contrast, and as expected, Radium-223 dichloride in citrate was found in the skeletal compartment and gastrointestinal tract. **Conclusion:** We have demonstrated stable and rapid chelation of Radium-223 using an 18-membered macrocycle. This four alpha particle emitting radionuclide is widely available, and has the potential to significantly reinforce the emerging targeted alpha particle armamentarium. **References:** None.

OP-758

Alpha Particle Emiting Radium-223 in Combination Therapy: Potential and Pitfalls

D. L. Thorek[1], *D. S. Abou*[1], *M. Longtine*[1], *P. Kushwaha*[2], *R. C. Riddle*[2], *B. Baumann*[1];
[1]*Washington University School of Medicine, St. Louis, MO, UNITED STATES OF AMERICA,* [2]*Johns Hopkins University School of Medicine, Baltimore, MD, UNITED STATES OF AMERICA.*

Aim/Introduction: Radium-223 dichloride is a first in class alpha particle emitting radiopharmaceutical for treatment of bone metastatic castrate resistant prostate cancer (bmCRPC). Localizing to the active bone surface through physicochemical affinity at sites of bone metastases, it produces four potent cytotoxic alpha particles through its decay scheme. This mechanism of action has been viewed as orthogonal to conventional pharmacological treatments of bmCRPC and multiple ongoing clinical trials are being evaluated to test the value of multi-agent treatment of bmCRPC. One trial investigating abiraterone (a CYP17 inhibitor that blocks androgen synthesis) with Radium-223, ERA-223 (NCT02043678), was halted early after a higher incidence of skeletal events and poorer survival versus each agent alone. We have developed advanced small animal models of bmCRPC to evaluate combination treatments of Radium-223. Our work demonstrates the potential for synergies, as well as significant toxicities, in the emerging alpha particle combination space. **Materials and Methods:** Radium-223 was produced using an in house microgenerator from radiochromatographic purification from source Actinium-227/Thorium-227. Hormonal (dutastaride, enzalutamide, abiraterone acetate, androgens) and chemo-therapies (docetaxel, mitoxantrone) were tested alone or in combination with Radium-223 dichloride in animal models of bone metastases (FVB bearing Hi-Myc metastases). Castrate animals were kept on hormonal therapy prior to and after radiopharmaceutical administration. Excised bone tissues were evaluated by high resolution microCT for standard morphometry, dual labeled calcein/alizuran for bone turnover, and gene expression analysis (AR, OCN, RUNX) as well as counted ex vivo for administered activity. **Results:** We show that Radium-223 accumulates at sites of bone metastasis in skeletal models of metastasis, with therapeutic benefit. Upon combination, Radium-223 distribution does not significantly change; and in the case of abiraterone + Radium-223 slightly but significantly decreases. No significant changes in the morphological properties of the bone (including BV/TV, cortical area or trabecular thickness) are noted. Several combinations lead to changes in gene expression of bone tissue samples, in particular abiraterone + Radium-223 with significant upregulation of resoptive processes indicating severe adverse effects of co-administration of these agents. **Conclusion:** Our

data suggest that rational combinations of Radium-223 can have synergy but that negative outcomes from overlapping toxicities can be severe. Our findings with abiraterone and Radium-223 may in part elucidate findings in ERA-223. This work may have import for the expanding number of alpha particle therapies in trial, for their real-world use in combination with other therapies. **References:** None.

OP-759

Targeted alpha therapy of recurrent glia tumors : clinical experience with ^{225}Ac-Substance-P

L. Krolicki[1], *F. Bruchertseifer*[2], *J. Kunikowska*[1], *H. Koziara*[3], *B. Krolicki*[3], *M. Jakuciński*[1], *D. Pawlak*[4], *C. Apostolidis*[2], *R. Rola*[5], *A. Merlo*[6], *A. Morgenstern*[2];
[1]*Medical University of Warsaw, Warszawa, POLAND,* [2]*European Commission, Joint Research Centre, Directorate for Nuclear Safety and Security, Karlsruhe, GERMANY,* [3]*Department of Neurosurgery, Institute of Oncology, Warszawa, POLAND,* [4]*Radioisotope Centre POLATOM, National Centre for Nuclear Research, Warszawa, POLAND,* [5]*Department of Neurology, Military Institute of Aviation Medicine, Warszawa, POLAND,* [6]*University of Basel, Basel, SWITZERLAND.*

Aim/Introduction: Treatment of patients with recurrent glioma is very limited. Introduction of new options of treatment is critically important for this group of patients. Gliomas are characterized by a high expression of receptors for Substance -P (SP), regardless of the histological grading. Therefore, SP labeled with alpha emitters was used for local application into the tumour. Local application reduces systemic adverse effects of the drug as well as the protective effect of the Blood-Brain-Barrier. Moreover, alpha rays have many advantages: tissue range is less than 100 µm; hypoxia and cell cycle are not critical to the effect of radiation. Initially, ^{213} Bi was used for labeling of SP; bismuthium is convenient for labeling of peptides, and short T1/2 of ^{213}Bi ($T_{1/2}$ = 46 min) is beneficial for radiation protection. Currently, 225Ac was introduced. It seems that a diverse range of energy, as well as longer T1/2 (10 days) should favor a better distribution of the radiopharmaceutical into the tumor. **Materials and Methods:** 13 patients with histologically confirmed recurrence of the glia tumor grade II-IV were treated: group A - patients with grade II - III WHO (5 patients), group B - patients with grade IV (8 patients). All patients received a standard treatment (surgery + radio-chemo-therapy). When a recurrence/progression was diagnosed, an intracavitary/intratumoral injection of 20-40 MBq ^{225}Ac-SP was applied every 2 months (1-7 injections). Monitoring of toxicity and overall survival was indicated as the first goal of the study. The study was approved by the Ethical Committee of the Medical University of Warsaw. **Results:** In group A: PFS was 4.8 (median) months, OS from primary diagnosis was 114.7 months, OS from diagnosis of recurrence - 38.0 months, and OS from start of radioisotopic treatment - 26.5 months. In group B: : PFS was 3.0 (median) months, OS from primary diagnosis was 21.3 months, OS from diagnosis of recurrence - 10.9 months, and OS from start of radioisotopic treatment - 5.0months. **Conclusion:** Intracavitary/intratumoral injection of ^{225}Ac-substance P is tolerated well. Only mild temporary adverse effects (edema, epileptic seizures, aphasia) were observed. It seems that the presented method using 225Ac is promising and requires further clinical trials. **References:** None.

OP-760

Targeted alpha therapy using astatine (^{211}At) labelled phenylalanine: preclinical study in glioma xenograft mice

T. Watabe[1], *K. Kaneda-Nakashima*[2], *Y. Liu*[1], *Y. Shirakami*[3], *K. Ooe*[1], *A. Toyoshima*[3], *E. Shimosegawa*[1], *T. Nakano*[4], *A. Shinohara*[5], *J. Hatazawa*[4];
[1]*Osaka University Graduate School of Medicine, Suita, Osaka, JAPAN,* [2]*Osaka University Graduate School of Science, Suita, Osaka, JAPAN,* [3]*Institute for Radiation Sciences, Osaka University, Suita, Osaka, JAPAN,* [4]*Research Center for Nuclear Physics, Osaka University, Suita, Osaka, JAPAN,* [5]*Graduate School of Science, Osaka University, Toyonaka, Osaka, JAPAN.*

Aim/Introduction: Upregulation of amino acid transport as well as glucose transport was generally observed in malignant tumors. Phenylalanine derivatives are focusing attention for its specific tumor targeting, especially through L-type amino acid transporter-1 (LAT1). In the present study, we aimed to evaluate the treatment effect of alpha emitter astatine labelled phenylalanine (^{211}At-Phe) using xenograft model of malignant brain tumor. **Materials and Methods:** Cellular uptake analysis was performed using the cell line of C6 glioma, U-87MG, and GL261. Uptake inhibition was evaluated by adding either phenylalanine (Phe) or 2-aminobicyclo-(2,2,1)-heptane-2-carboxylic acid (BCH), an inhibitor of system L amino acid transporters. Tumor xenograft models were prepared by subcutaneous injection of C6 glioma in immunodeficient nude mice (n=12) and GL-261 in C57BL/6mice (n=12) with preserved immune function, respectively. ^{211}At-Phe was injected into 3 groups (each n=3) of C6 glioma mice (0,1, 0.5, and 1MBq, respectively) and GL261 mice (n=7, 1MBq). Planar imaging was performed at 30min and 3hr after the administration of ^{211}At-Phe to evaluate the uptake in the tumor using percent injected dose (%ID) and absorbed dose (Gy). Tumor size (mm^3) was monitored by the caliper measurement and compared among the injected groups and control mice. **Results:** Cellular uptake analysis showed significant uptake inhibition in C6 glioma (13.6 ± 6.1 %), U-87MG (27.9 ± 3.0 %), and GL261 (4.6 ± 1.0 %) after adding BCH, suggesting the large contribution of ^{211}At-Phe uptake via system L of amino acid transporter. Planar imaging showed early distribution and wash-out of ^{211}At-Phe in the C6 glioma tumor (3.7 ± 0.8 %ID at 30min and 1.5 ± 0.2 %ID at 3hrs). Absorbed dose was estimated as 1.7± 0.6 (Gy/MBq) in the C6 glioma tumor. In the evaluation of treatment effect, tumor growth suppression was observed in C6 glioma xenograft in a dose-dependent manner. Relative ratios of tumor size compared to the control were 0.56 in 0.1MBq, 0.42 in 0.5MBq, and 0.30 in 1MBq one month after the injection of ^{211}At-Phe, respectively. In GL261

xenograft mice, growth suppression effect was also observed (relative tumor size: 0.24). **Conclusion:** This study showed the treatment effect of ^{211}At-Phe in the xenograft models of malignant brain tumor, suggesting its potential applicability to the alpha therapy targeting amino acid transporter (system L) for cancers. **References:** None.

OP-761

Preliminary results on ^{225}Ac-DOTATATE Targeted Alpha Therapy in Metastatic Gastroenteropancreatic Neuroendocrine Tumors: First Clinical Experience on Safety and Efficacy

S. Ballal, M. P. Yadav, C. Bal;
All India Institute of Medical Sciences, New Delhi, INDIA.

Aim/Introduction: The objective of this study was to investigate and present the early results on the safety and efficacy of ^{225}Ac-DOTATATE targeted alpha therapy (TAT) in patients with advanced, progressive, ^{177}Lu-DOTATATE refractory, somatostatin receptor (SSTR) positive, metastatic gastroenteropancreatic neuroendocrine tumors (GEP NETs). **Materials and Methods:** This study was approved by the Institute Ethics Committee (IEC No:517/2018). We recruited 35 patients (mean age, 55.3±6.3years range: 46-72 years) who either reached the maximum limit of ^{177}Lu-DOTATATE therapy cycles or were refractory to ^{177}Lu-DOTATATE therapy. Systemic TAT was performed in all the patients with ^{225}Ac-DOTATATE (100 KBq/Kg body weight) at an interval of 8 weeks . The patients were treated between April 2018 to April 2019 with a median follow-up duration of 9 months (range: 2 - 13 months). Treatment-related side effects were assessed every 2 weeks on the basis of physical examination, vital signs, laboratory results (hematologic, kidney and liver function levels) and adverse events graded according to the CTCAE v5.0. Efficacy assessment included morphological and molecular tumor responses measured by diagnostic contrast-enhanced ^{68}Ga-DOTANOC PET/CT scans according to RECIST 1.1 and PERCIST 1 criteria, respectively. **Results:** The most common adverse effects (AEs) were nausea, vomiting, gastritis, and appetite loss, but were limited to grade 1 or 2. Majority of the patients experienced these AEs at the time of amino acid infusion which was administered during ^{225}Ac-DOTATATE therapy and was resolved after few hours of amino acid infusion. All the other AEs such as fatigue or asthenia, diarrhoea, appetite loss, abdominal pain, abdominal distension, weight loss, peripheral edema, headache, dizziness, and flushing were also identified which were limited to grade 1 or 2, except for 1 patient with grade 3 abdominal distension and fatigue. None of the patients experienced grade 3 or 4 hematotoxicity, renal insufficiencies or hepatotoxicity. In a median follow-up duration of 9 months, morphological response assessment was assessed in 26 patients which revealed complete remission in 1, partial remission in 16, and Stable disease in 9 patients. Similarly, molecular tumor response evaluation in 26 patients revealed complete remission in 1 patient, partial remission in 18, and stable disease in 7 patients. There were no treatment related deaths. **Conclusion:** Our initial results indicate ^{225}Ac-DOTATATE TAT safe with low and transient side-effects. It add to a new dimension in the treatment of end-stage GEP-NET who have exhausted all the standard treatment options. **References:** None.

1706

Do.MoRe - Parallel Session: PET/MR Physics

Wednesday, October 16, 2019, 10:00 - 11:30 Lecture Hall 112

OP-762

Zero Echo Time MR Attenuation Correction Method on the GE SIGNA PET/MR: Comparison with CT Based Attenuation Correction in Dynamic PET Brain imaging

A. Firouzian[1], G. Delso[2], R. McCutcheon[3,4,5], M. Nour[3,4,5], O. Howes[3,4,5], W. Hallett[1];
[1]Invicro, London, UNITED KINGDOM, [2]GE Healthcare, London, UNITED KINGDOM, [3]King's College London, London, UNITED KINGDOM, [4]Medical Research Council, London, UNITED KINGDOM, [5]Imperial College London, London, UNITED KINGDOM.

Aim/Introduction: In PET imaging on combined PET/MR scanners MR-based attenuation correction (MRAC) methods are used to correct for the effects of scattering and absorption of gamma radiation as it travels from within the subject's body to reach the PET detectors. This is challenging for brain imaging, where the head bones make a significant contribution to attenuation and scatter but do not produce a strong signal, at least in conventional MR imaging. We present a comparison between CT based attenuation correction, as used in a conventional PET/CT scanner, and an MR method based on a zero echo time sequence sensitive to bone, as implemented on the GE SIGNA PET/MR, in dynamic PET brain imaging. **Materials and Methods:** 10 healthy subjects in a study evaluating ^{11}C-PHNO brain uptake gave informed consent to take part in this methodology study. Subjects underwent a 90 min PET/MR scan on a GE SIGNA PET/MR scanner, as well as a low dose head CT scan for attenuation correction purposes, on a Siemens Biograph 6 TruePoint PET/CT scanner on the same day as one of their PET/MR scans. Dynamic PET images were generated using the PET/MR reconstruction pipeline with attenuation correction based on both the CT scan (CTAC), and on a zero echo time MR sequence acquired on the PET/MR (MRAC-ZTE). Two regional outcome measures were calculated from the dynamic PET series above: the non-displaceable binding potentials (BP_{ND}) estimated from kinetic modelling of ^{11}C-PHNO over the 90min scan immediately post-injection, and the standard uptake values (SUVR) averaged over 60-90min post-injection, both with respect to cerebellum grey matter. **Results:** The average percentage BP_{ND} difference between CTAC and MRAC-ZTE based dynamic PET data is 0.3% ± 0.9% ranging from -4.6% to 8.8% for brain regions with significant uptake (BP_{ND}>0.5). The average percentage SUVR difference between

CTAC and MRAC-ZTE based data for the same regions is 0.3% ± 0.4%, ranging from -3.8% to 3.6%. **Conclusion:** Quantitative measurements on PET images reconstructed using ZTE based attenuation correction implemented on the GE SIGNA PET/MR were very similar to those obtained using CT based attenuation correction, supporting the use of ZTE based attenuation correction for fully quantitative PET brain imaging. This agrees with our previous findings using a different PET tracer (^{11}C-Ro15-4513) [1]. **References:** [1] Firouzian A, Delso G, Hallett W, Comparison of MR based Attenuation Correction Methods with CT Based Attenuation Correction in Dynamic Brain PET Imaging, EJNMMI (2018) 45 (Suppl 1):S695.

OP-763

Deep Direct Attenuation Correction of Brain PET images using Emission Data and Deep Convolutional Encoder-Decoder for application to PET/MR and dedicated brain PET scanners

I. Shiri[1], *P. Ghafarian*[2,3], *P. Geramifar*[4], *K. Ho-Yin Leung*[5,6], *M. Oveisi*[7,8], *A. Rahmim*[9,10], *M. Ay*[1,11];
[1]*Research Center for Molecular and Cellular Imaging, Tehran University of Medical Sciences, Tehran, IRAN, ISLAMIC REPUBLIC OF,* [2]*Chronic Respiratory Diseases Research Center, National Research Institute of Tuberculosis and Lung Diseases (NRITLD), Shahid Beheshti University of Medical Sciences, Tehran, IRAN, ISLAMIC REPUBLIC OF,* [3]*PET/CT and Cyclotron Center, Masih Daneshvari Hospital, Shahid Beheshti University of Medical Sciences, Tehran, IRAN, ISLAMIC REPUBLIC OF,* [4]*Research Center for Nuclear Medicine, Shariati Hospital, Tehran University of Medical Sciences, Tehran, IRAN, ISLAMIC REPUBLIC OF,* [5]*Department of Biomedical Engineering, Johns Hopkins University, Baltimore MD, UNITED STATES OF AMERICA,* [6]*Department of Radiology and Radiological Science, Johns Hopkins University, Baltimore MD, UNITED STATES OF AMERICA,* [7]*Department of Biomedical and Health Informatics, Rajaie Cardiovascular Medical and Research Center, Iran University of Medical Science, Tehran, IRAN, ISLAMIC REPUBLIC OF,* [8]*Department of Computer Science, University of British Columbia, Vancouver, BC, CANADA,* [9]*Departments of Radiology and Physics & Astronomy, University of British Columbia, Vancouver, BC, CANADA,* [10]*Department of Integrative Oncology, BC Cancer Research Centre, Vancouver, BC, CANADA,* [11]*Department of Medical Physics and Biomedical Engineering, Tehran University of Medical Sciences, Tehran, IRAN, ISLAMIC REPUBLIC OF.*

Aim/Introduction: Attenuation correction (AC) is one of the main nontrivial obstacles in PET/MRI and dedicated Brain PET systems. Different methods have been proposed to address the AC of PET images. Recent developments in the field of Machine learning have enable new approaches to cross modality mapping. The main aim of this study is to explore the possibility of inferring the attenuation corrected PET image directly from the non-attenuation corrected image using deep convolutional auto encode decoder. **Materials and Methods:** In total 100 patients brain PET data were used in current study. DeepDAC consists of a paired encoder and decoder. Non attenuation corrected (NAC) PET images are treated as the network input in encoder part and decoder part try to reconstruct pixel-wise continuously-valued of measured attenuated corrected (MAC) PET image. The DeepDAC was trained using 80 randomly-selected data and evaluated in the remaining 10 subjects and 10 patient as external validation set. Quality of the synthesized images, was quantitatively assessed by different image quality parameters. Variability of image quantification was assessed by radiomic features (SUVmax, SUVmean,TLG and and second and high order texture) in 83 brain region delineated based on Hammers N30R83 maximum probability atlas. Reliability of measurement determined by pixel-wise Relative Errors (%) with respect to radiomics features values (RFV) in CTAC PET images and t-test statistical analysis. **Results:** RMSE values were (1.19±0.5) e-2 and (1.19±0.49) e-2 for testing and external validation set. PSNR and SSIM value for test and external validation were 38.70±3.54, 39.22±3.65 and 0.988± 0.006, 0.989±0.006 respectively. RE of SUVmean was -0.1 ± 2.14 for all region and only three region has significant difference with MAC image, however the mean of difference of this region were 0.02 with range of -0.83 - 1.18. SUVmax has mean RE of -3.87 ± 2.84 for all brain regions and 17 regions in brain had significant difference from MAC image with mean RE of -3.99 with range of -8.46 - 0.76. Homogeneity from GLCM had highest number (Twenty) of sub region with significant difference from MAC with mean RE of 7.22 but in all brain sub region mean RE of homogeneity were 2.5 ± 3.65. **Conclusion:** The present study demonstrated that direct AC of PET image using deep auto encoder decoder is a promising technique for brain PET images. Deep learning technique pave the road toward emission-based AC in PET images applicable in PET/MRI and dedicated Brain PET scanners. **References:** None.

OP-764

PET/MRI attenuation correction in the pelvic region with a statistical decomposition method

E. Wallstén, *J. Axelsson, J. H. Jonsson, C. Thellenberg Karlsson, T. Nyholm, A. Larsson;*
Department of radiation sciences, Umeå University, Umeå, SWEDEN.

Aim/Introduction: Quantification in PET/MRI is of importance, and its accuracy is currently limited by the MR based attenuation correction estimate. A common method for attenuation correction of the pelvic region is based on a 2-echo Dixon MRI sequence for segmentation of fat and water and does not account for bone. In this work, we evaluate a new method for attenuation correction using an algorithm based on statistical decomposition of a T2 weighted MRI scan. **Materials and Methods:** Substitute CT images (sCTs) were calculated from T2 weighted MRI scans with a statistical decomposition algorithm, originally developed for MRI-based radiotherapy dose-planning [1]. These sCTs benefits from having bone density information included, in addition to fat and water information. Prostate cancer patients from the PARAPLY study [2] were retrospectively

selected, scanned with PET/MRI ^{11}C-Acatate and CT the same day. The stand-alone CT images were transformed to the same geometry as the PET and MR images, using a non-rigid registration. CT images, generated sCT images, and the Dixon-based attenuation maps (MRAC), all in the same geometry, were together with the PET raw data used to reconstruct attenuation-corrected PET images using the PETrecon toolbox [GE Healthcare]. The two MR-based attenuation corrections were compared to the CT-based attenuation correction with root mean squared error (RMSE). Lesion analysis will also be reported. PET/MRI images were acquired on a Signa PET/MRI (GE Healthcare), and the CT images on a Brilliance Big Bore (Phillips Healthcare). The study will include 12 patients and a subset of 6 patients has been analyzed so far and is presented here. **Results:** Soft tissue in-between pelvic bone structures were overestimated with 13% in MRAC-PET, and the error was reduced to 5% with sCT attenuation corrected PET (sCT-PET). For the whole patient volume, an average underestimation of 6% was found in the MRAC-PET, compared to 1% for sCT-PET. RMSE within the body was reduced with a factor 2.5 with sCT-PET (RMSE=3.6%), compared to MRAC-PET (RMSE=8.8%). **Conclusion:** Applying sCT from statistical decomposition as a base for calculation of attenuation maps reduces quantification errors in PET-images of the pelvic region compared to the common Dixon based method. **References:** [1] Siversson, C., Nordström, F., Nilsson, T., Nyholm, T., Jonsson, J., Olsson, L. E. (2015). Technical Note : MRI only prostate radiotherapy planning using the statistical decomposition algorithm. Medical Physics, 10(42), 6090-6097. https://doi.org/10.1118/1.4931417 [2] ClinicalTrials.gov ID NCT01962324

OP-765

Evaluating the Effect of Bone Attenuation and Scatter Correction Methods on PET Quantification in ^{68}Ga-uPAR-PET/MRI

S. Ahangari[1], *M. Ø. Fosbøl*[1], *S. Kurbegovic*[2], *H. H. Johannesen*[1], *B. W. Jakoby*[3], *F. Büther*[4], *A. Loft*[1], *A. Kjær*[1,5], *F. L. Andersen*[1], *A. E. Hansen*[1];
[1]*Department of Clinical Physiology, Nuclear Medicine and PET, Rigshospitalet, University of Copenhagen, Copenhagen, DENMARK,* [2]*Department of Urology, Copenhagen Prostate Cancer Center, Rigshospitalet, University of Copenhagen, Copenhagen, DENMARK,* [3]*Siemens Healthcare GmbH, Erlangen, GERMANY,* [4]*Department of Nuclear Medicine, University Hospital Münster, Albert-Schweitzer-Campus 1, Münster, GERMANY,* [5]*Cluster for Molecular Imaging, University of Copenhagen, Copenhagen, DENMARK.*

Aim/Introduction: PET/MRI is a promising diagnostic method for prostate cancer patients. In clinical practice, halo artifacts can occur around bladder due to e.g. suboptimal PET scatter correction (SC) [1,2]. Scatter and attenuation correction are related because the attenuation map is utilized for single scatter simulation [1]. The aim was therefore to investigate the effects of bone inclusion in MRAC as well as varying SC methods on PET quantification in pelvis PET/MRI with ^{68}Ga-uPAR (^{68}Ga-NOTA-AE105). **Materials and Methods:** Thirty-two patients from an ongoing prostate cancer study underwent PET/MRI (Siemens Biograph mMR) [single bed, 20 minutes p.i. 200 MBq ^{68}Ga-UPAR]. Patients had crossed arms over the chest, and arms did not enter the FOV at the level of prostate. PET was reconstructed using vendor-provided Dixon-based MRAC with and without an atlas-based bone segmentation, and with relative and absolute SC methods (3D OP-OSEM, 3 iterations, 21 subsets, 4 mm Gaussian filter). The halo artifact was defined as the patient volume with less than 50% of activity in reference muscle [gluteus maximus away from bladder] and excluding adipose tissue. A prostate ROI was defined on anatomical MRI excluding a 1 cm margin to the bladder. **Results:** The appearance of the halo varied greatly between patients, with only a few cases showing a severe artifact. Overall, inclusion of bone in MRAC and absolute as opposed to relative SC resulted in the best image quality. The median size of the halo artifact was 320 cm³ (absolute SC, no bone), 1176 cm³ (relative SC, no bone) 130 cm³ (absolute SC, bone) and 441 cm³ (relative SC, bone). No significant correlation of relative halo size with SUV_{max}/SUV_{mean} of bladder, injected dose per weight or patient cross-sectional area was observed. SUV_{mean} of prostate was 2.3 (absolute SC, no bone), 1.5 (relative SC, no bone), 2.3 (absolute SC, bone,) and 1.8 (relative SC, bone). **Conclusion:** Halo artifacts were observed for ^{68}Ga-uPAR PET/MRI. Absolute SC with bone inclusion resulted in the smallest halo. Relative halo size did not depend on SUV of bladder, as observed also by Noto et al. [1] but not by Heußer et al [2], which however, had much higher bladder uptake. Prostate activity depended on SC method, and on bone inclusion for relative SC. Including bone in MRAC can be a contributing factor to PET quantification bias in ^{68}Ga-uPAR PET/MRI. **References:** [1] Noto, Benjamin, et al. EJNMMI research (2017) [2] Heußer, Thorsten, et al. PloS one (2017)

OP-766

One-stop-shop fully integrated dynamic PET-MRI for the characterization of lung lesions : a feasibility study

F. L. Besson[1,2], *B. Fernandez*[3], *S. Faure*[4], *A. Seferian*[5], *O. Mercier*[6], *X. Mignard*[5], *E. Blanchet*[7], *S. Mussot*[6], *S. Bulifon*[5], *D. Mitilian*[6], *A. Chetouani*[7], *F. Bouderraoui*[7], *L. Mabille*[6], *H. Cherkaoui*[8], *A. Botticella*[9], *C. Caramella*[9], *P. Pradere*[6], *C. Le Pechoux*[9], *E. Fadel*[6], *D. Planchard*[9], *B. Besse*[9], *C. Comtat*[7], *P. Gervais*[7], ***V. Lebon***[7], *E. Durand*[1,2];
[1]*Department of Nuclear Medicine Hopitaux Universitaires Paris Sud, APHP, Le Kremlin-Bicêtre, FRANCE,* [2]*IR4M unit UMR8081 Paris Sud-CNRS, Orsay, FRANCE,* [3]*GE Healthcare, Orsay, FRANCE,* [4]*Laboratoire de mathématiques Université Paris Sud-CNRS, Orsay, FRANCE,* [5]*Department of respiratory medicine, Hopitaux Universitaires Paris Sud, APHP, Le Kremlin-Bicêtre, FRANCE,* [6]*Thoracic Oncology Institute, Université Paris-Sud, Hopital Marie Lannelongue, Le Plessis-Robinson, FRANCE,* [7]*Service Hospitalier Frederic Joliot, Université Paris Sud, CEA, Orsay, FRANCE,* [8]*CEA-Neurospin, Université Paris-Saclay, Gif sur Yvette, FRANCE,* [9]*Thoracic Oncology Institute, Université Paris-Sud, Gustave Roussy, Villejuif, FRANCE.*

Aim/Introduction: To assess the feasibility of a fully integrated dynamic PET-MRI approach applied to the characterization of lung lesions specifically. **Materials and Methods:** A total of 9 patients underwent a one-hour dynamic PET-MRI imaging protocol for suspected lung cancer. FDG PET and DCE MRI full kinetic analyses (Sokoloff and extended Toft models respectively), together with DWI-ADC and T1/T2-mapping were performed. All the PET-MRI data were warped into the same isotropic reference space before analyses. For each lung lesion, voxel-wise 3D maps of 14 biological features / 4 main categories were computed using an in-house fully integrative multimodal post-processing pipeline developed for this purpose specifically : perfusion/vascularization (Ktrans, Kep, Ve and Vp); metabolism (SUV, k1, k2, k3, Ki, Vb, and MRGlu); diffusion (ADC); and tissular characterization (T1 and T2 mapping). For each lesion, voxel-wise monotonic relationships between all the PET-MRI features were explored (Spearman correlations). Finally, all the lesions were partitioned by using multidimensional unsupervised gaussian mixture approach, and features profiles / relationships were explored at the supervoxel regional level. **Results:** Relationships between the perfusion/vascularization, metabolism, diffusion and tissular feature categories differed among the lesions. At the feature level, strong correlations (absolute r value superior to 0.5) were observed for the perfusion/vascularization features pairs and the metabolic feature pairs. At the category level, absolute r values were inferior to 0.5 for the vast majority of the feature pairs. Combining the 14 features together, unsupervised clustering provided 2 to 4 supervoxels depending on the lesion. At the supervoxel regional levels, feature profiles differed, as well as their monotonic relationships. **Conclusion:** Our one-stop-shop fully integrative dynamic PET-MRI protocol provided 14 biological features (4 main categories) in the same examination. For all lesions, the heterogeneity of features profiles / relationships at the regional supervoxel level highlights the unique capability of PET-MRI to get better insight of the biological characterization of lung masses. **References:** Dennis Vriens, Eric P Visser et al. Methodological considerations in quantification of oncological FDG PET studies. Eur J Nucl Med Mol Imaging 2010;37(7):1408-1425. Khalifa F, Soliman A et al. Models and methods ofr analyzing DCE-MRI: a review. Med Phys 2014;41(12):124301. Divine MR, Katiyar P et al. A population based Gaussian mixture model incorporating 18F-FDG-PET and DW-MRI quantifies tumor tissue classes. J Nucl Med. 2016;57:473-79.

OP-767

PET/MRI for Radiotherapy Planning: Dosimetric Evaluation of Deep Learning Synthetic CT from MR for Head and Neck Cancer Patients

A. Olin[1], *C. N. Ladefoged*[1], *A. E. Hansen*[1], *K. Håkansson*[2], *A. Kjær*[1,3], *J. H. Rasmussen*[4], *A. K. Berthelsen*[1,2], *B. M. Fischer*[1], *F. L. Andersen*[1]; [1]*Department of Clinical Physiology, Nuclear Medicine & PET, Rigshospitalet, Copenhagen Ø, DENMARK,* [2]*Department of Oncology, Section of Radiotherapy, Rigshospitalet, Copenhagen Ø, DENMARK,* [3]*Cluster for Molecular Imaging, Rigshospitalet, Copenhagen Ø, DENMARK,* [4]*Department of Otorhinolaryngology, Head & Neck Surgery and Audiology, Rigshospitalet, Copenhagen Ø, DENMARK.*

Aim/Introduction: Combined PET/MRI as a one-stop-shop imaging modality for radiotherapy (RT) planning holds great potential. However, information about electron density, normally provided by CT, is a prerequisite for attenuation correction of PET and for RT dose calculations. Here, we create a deep learning approach for synthetic CT (sCT) generation based on MR imaging of head and neck cancer (HNC) patients, acquired in RT treatment position and evaluate the effect on dose calculations. **Materials and Methods:** Eight patients referred for RT of HNC underwent PET/MRI (Siemens Biograph mMR) after routine FDG-PET/CT planning scan. In both scans, the patients were fixated in treatment position. Rigid registration between planning CT and MR Dixon images was performed. A deep learning convolutional neural network for sCT generation, similar as previously described [1], was implemented. The network was trained using full-slice 3D volumes of Dixon (in-phase and opposed-phase) images as input, and the voxel-to-voxel matched CT as output. The network was initialized by a pretrained model with 811 brain scanned patients and then fine-tuned using the HNC patients. Network training and evaluation was performed in a leave-one-out process. RT treatment plans (VMAT) were derived in Eclipse (Varian Medical Systems Inc) and optimized on the planning CT. The plans were copied onto the sCT and dose distributions were recalculated. Cumulative dose volume histograms (DVH) and the relative differences in mean (ΔD_{mean}), maximum (ΔD_{max}), near-maximum ($\Delta D_{2\%}$), and near-minimum ($\Delta D_{98\%}$) absorbed doses for different organs at risk and planning target volume of primary tumor and involved nodes (PTV1) between the two dose calculations were calculated. **Results:** A sCT was derived for each patient in under 10 seconds. Currently, dose calculations were performed on five of the eight patients. The average relative difference (±standard deviation) in DVH points between dose calculations from CT and sCT for the different volumes were: PTV1 ($\Delta D_{2\%}$= 0.60±0.66%, $\Delta D_{98\%}$= -0.08±1.02%, ΔD_{mean}= 0.40±0.40%), left parotid (ΔD_{mean}= -0.56±0.67 %), right parotid (ΔD_{mean}= -0.07±0.51%), spinal cord (ΔD_{max}= 0.37±0.71%). **Conclusion:** These preliminary results suggest that our proposed method for sCT generation produces dose calculations that are similar to CT. The low differences in the DVH points and the prospect of using the sCT for attenuation correction of PET is a promising step towards using PET/MRI for one-stop-shop RT planning. **References:** [1] Ladefoged, Claes Nøhr, et al. "Deep learning based attenuation correction of PET/MRI in pediatric brain tumor patients: Evaluation in a clinical setting." Frontiers in neuroscience 12 (2018): 1005.

OP-768

Comparison of simultaneous arterial spin labeling MRI and ^{15}O-H_2O PET measurements of regional cerebral blood flow in rest and altered perfusion states

O. Puig, *O. M. Henriksen, M. B. Vestergaard, A. E. Hansen, F. L. Andersen, C. N. Ladefoged, E. Rostrup, H. B. W. Larsson, U. Lindberg,*

I. Law;
Department of Clinical Physiology, Nuclear Medicine and PET, Rigshospitalet, Copenhagen, DENMARK.

Aim/Introduction: Arterial spin labelling (ASL) is a non-invasive magnetic resonance imaging (MRI) technique that may potentially provide fully quantitative regional cerebral blood flow (rCBF) images. However, before using it in clinical routine it needs to be validated against the clinical gold-standard, fully quantitative ^{15}O-H_2O-positron emission tomography (^{15}O-H_2O-PET). We aimed to compare both techniques by performing repeated and simultaneous quantitative ASL-MRI and ^{15}O-H_2O-PET scans in different perfusion states acquired in a hybrid PET/MRI scanner. **Materials and Methods:** 14 healthy young males were studied twice in resting state, during hyperventilation and after acetazolamide (post-ACZ), yielding a total of 63 (26 in resting state, 18 during hyperventilation and 19 post-ACZ) combined simultaneously acquired PET/MRI datasets in total. Each ^{15}O-H_2O-PET was acquired dynamically for 4 min. with arterial sampling after the injection of 500MBq ^{15}O-H_2O i.v. and modelled using a 2-compartment 1-tissue model[1]. The ASL sequence was a 7 min. multi post-labeling delay 2D pseudo-continuous ASL (PCASL) with full brain coverage quantified with BASIL in FSL using Buxton's method[2]. Fully quantitative measurements of global and regional CBF and CBF reactivity from both techniques were compared. **Results:** Average global CBF by ASL-MRI and ^{15}O-H_2O-PET were not significantly different in any state (40.0±6.5mL/100g/min and 40.6±4.1mL/100g/min respectively in rest, 24.5±5.1mL/100g/min and 23.4±4.8mL/100g/min, respectively during hyperventilation, and 59.1±10.4mL/100g/min and 64.7±10.0mL/100g/min respectively post-ACZ). Average reactivity by ^{15}O-H_2O-PET and ASL-MRI were not significantly different. An overall, strong correlation between the two methods was found across all states and volunteers (slope=1.01, R^2=0.82), while the correlations within individual states, although significant, had a lower slope and poorer correlation (rest: slope=0.26, R2=0.05; hyperventilation: slope=0.73, R^2=0.47; and post-ACZ slope=0.55, R^2=0.37). Correlations between the methods for absolute and relative reactivity were also weak, but significant. ^{15}O-H_2O PET and ASL rCBF showed a similar regional distribution, although ASL yielded significantly higher perfusion and absolute reactivity in highly vascularized areas (cingulate and insula) and lower perfusion in areas close to air-bone interface due to susceptibility induced artifacts in MRI (orbitofrontal cortex, inferior temporal cortex and cerebellum). **Conclusion:** ASL-MRI and ^{15}O-H_2O-PET measurements of global CBF and rCBF are highly correlated across different perfusion states, but with moderate correlation in measurements of hemodynamic reactivity and systematic differences in regional distribution. Hence, caution is advised when using PCASL for reactivity studies, and further evaluation in clinical studies is needed. **References:** 1.Ohta S, et. al.JCBFM.1996;16:765-780. 2.Buxton RB, et. al.MRM.1998;40:383-396.

OP-769

Design and performance of a compact preclinical scanner for simultaneous PET/MR acquisitions at 7 T

A. Courteau[1], J. McGrath[2], P. M. Walker[3,1], R. Pegg[2], G. Martin[2], R. Garipov[2], P. Doughty[2], A. Cochet[1,4,3], F. Brunotte[1,4,3], J. M. Vrigneaud[4,1];
[1]ImViA laboratory, EA 7535, University of Burgundy, Dijon, FRANCE, [2]MR-Solutions Ltd, Guildford, UNITED KINGDOM, [3]CHU François Mitterrand, Dijon, FRANCE, [4]Georges-François Leclerc Cancer Centre, Unicancer, Dijon, FRANCE.

Aim/Introduction: Preclinical PET/MR imaging requires a high field but compact system, easy to install in a preclinical nuclear imaging environment, with a low sensitivity to temperature variations, and a low electric noise. A simultaneous PET/MR system has been developed to fit these requirements. It combines a cryogen-free superconducting 7 T magnet and SiPM-based PET detectors offering compensation of depth of interaction effects. **Materials and Methods:** The 7 T magnet has a length of 0.8 m, a diameter of 1 m, and a weight of 600 kg. The 5-gauss line is just 1.1 m from the magnet and no Faraday cage is required around the imaging room. The liquid helium-free superconductive magnet avoids the need of regular helium and nitrogen supply. The MR gradients strength is 240 mT/m. The fully integrated PET insert consists of sixteen planar modules gathered in two octagons with a 117 mm inner diameter. Each module contains a dual layer of LYSO:Ce scintillation crystals coupled to 144 Sens-L J-series SiPMs with high photon detection efficiencies. Temperature correction is integrated to the detectors. Axial fields of view are 103 mm in PET and 80 mm in MR imaging. A specially designed bore shield reduces drastically the electric noise both in MR imaging and in rodents monitoring devices. A performance assessment study complying with the NEMA-NU4-2008 standard and a compatibility study based on the ACR MRI QA Guide were performed. **Results:** Thanks to its dual ring-like geometry, the microPET offered a peak absolute sensitivity of 7.5% with an energy window of 250-750 keV. No distinguishable difference was found between noise equivalent count rates measured with and without MR pulsing. PET characteristics remained stable over all tested MR operating conditions. Good count rate linearity was observed on the reconstructed images up to 50 MBq. Regarding MR imaging, the homogeneity of both static magnetic field and radiofrequency were not significantly affected by the integration of the PET scanner. **Conclusion:** As a conclusion, despite a compact magnet design, MR field homogeneity meets the existing state-of-the-art performances. Regarding PET, high sensitivity and high counting rates are the strong points of this integrated system. These results also suggest that mutual interferences between both modalities does not impact imaging data qualitatively nor quantitatively. Moreover, simultaneous PET/MR acquisitions on mice and rats have been successfully performed on the system using various radiotracers. **References:** None.

1707

Teaching Session 7 - Interactive Clinical Cases - ESMIT: Reading with the Experts - PET/CT in Neuroendocrine Tumours

Wednesday, October 16, 2019, 10:00 - 11:30 Lecture Hall 113

OP-770

PET/CT with ^{68}Ga-Radiolabelled SSTR Analogues - Interactive Clinical Cases Presentation

V. Ambrosini;
University of Bologna, S.Orsola-Malpighi Hospital, Department of Experimental Diagnostic and Specialized Medicine, Nuclear Medicine, Bologna, ITALY.

OP-771

PET/CT with [^{18}F]DOPA - Interactive Clinical Cases Presentation

S. Balogova;
St.Elisabeth Oncology Institute, Comenius University of Bratislava, Nuclear medicine, Bratislava, SLOVAKIA.

OP-772

Wrap-up and Conclusions

P. Erba;
Nuclear Medicine, Department of Translational Research and New Technology in Medicine, University of Pisa and Azienda Ospedialiero Universitaria Pisana, Pisa, ITALY.

1708

Clinical Oncology - Parallel Session: Prostate - Primary Staging and Biochemical Persistance

Wednesday, October 16, 2019, 10:00 - 11:30 Lecture Hall 114

OP-773

Comparison of ^{18}F-PSMA-1007 PET/CT, whole-body MRI and ^{99m}Tc-HMDP SPECT/CT to planar bone scintigraphy and CT in primary staging of intermediate or high-risk prostate cancer

S. Malaspina[1], *M. Anttinen*[2], *O. Ettala*[2], *I. Jambor*[3], *J. Kemppainen*[1], *M. Sandell*[4], *I. Rinta-Kiikka*[5], *S. Kajander*[1], *J. Schildt*[6], *E. Saukko*[7], *K. Timonen*[8], *P. Rautio*[9], *T. Noponen*[10], *J. Saunavaara*[4], *H. Aronen*[4], *M. Seppänen*[11], *P. Boström*[2];
[1]*Turku PET Centre, Turku University Hospital, Turku, FINLAND,* [2]*Department of Urology, Turku University Hospital, Turku, FINLAND,* [3]*Department of Radiology, Icahn School of Medicine at Mount Sinai, New York, NY, UNITED STATES OF AMERICA,* [4]*Medical Imaging Centre of Southwest Finland, Turku University Hospital, Turku, FINLAND,* [5]*Department of Radiology, Tampere University Hospital, Tampere, FINLAND,* [6]*Department of Clinical Physiology and Nuclear Medicine, Helsinki University Central Hospital, Helsinki, FINLAND,* [7]*Department of Diagnostic Radiology, University of Turku, Turku, FINLAND,* [8]*Department of Clinical Physiology, Central Hospital of Central Finland, Jyväskylä, FINLAND,* [9]*Department of Clinical Physiology, North Karelia Central Hospital, Joensuu, FINLAND,* [10]*Department of Clinical Physiology and Nuclear Medicine, Turku University Hospital, Turku, FINLAND,* [11]*Department of Clinical Physiology, Nuclear Medicine and Turku PET Centre, Turku University Hospital, Turku, FINLAND.*

Aim/Introduction: Current EAU guidelines strongly recommend abdominopelvic computer tomography and bone scintigraphy in primary staging of high-risk prostate cancer (PCa). Nevertheless, both modalities have limited accuracy for staging PCa metastases. Several other potentially more accurate imaging modalities are available including SPECT/CT, PSMA PET/CT and whole-body MRI. This trial aims to compare these imaging modalities to the traditional ones. **Materials and Methods:** This ongoing ethics-approved, prospective, registered, single-center trial enrolls patients with primary unfavorable intermediate or high-risk PCa according to EAU risk group classification. After consent, patients undergo ^{99m}Tc-HMDP planar bone scintigraphy (BS) and contrast-enhanced abdominopelvic and chest CT as a clinical standard. Research scans include ^{99m}Tc-HMDP SPECT/CT, ^{18}F-PSMA-1007 PET/CT and 1.5 T whole-body MRI with diffusion weighted imaging. Two separate modality-based specialists review each modality blinded for other modalities. Reported regions include bony skeleton, regional lymph nodes (LN), extra regional LNs and visceral lesions. In addition to overall metastasis-status, regions and lesions are reported either benign, equivocal or malignant. Pessimistic analysis (equivocal considered malignant) is performed in case of equivocal modality consensus. Based on clinical data, including all imaging modalities and follow-up information (imaging, histology and PSA), ground truth is defined on patient-level. **Results:** To date, 50 patients have undergone all imaging modalities. Mean age was 69 years. Eighteen (36%) presented with intermediate and 32 (64%) with high-risk PCa. Median PSA was 12 ng/ml (range: 3-2000). Twenty-eight (56%) had metastatic disease and the rest presented with localized or locally advanced disease. Of the patients with metastasis, 17(34%) had bone-only metastasis, 3(6%) nodal-only, 4(8%) bone and nodal, 1(2%) bone and visceral, and 3(6%) bone, nodal, and visceral metastases. In patient-level pessimistic analysis, sensitivity of BS, CT, SPECT/CT, whole-body MRI, and PSMA PET/CT were 0.23, 0.36, 0.46, 0.42 and 0.86, respectively. The corresponding specificity and AUC values were 0.75, 0.59, 0.73, 0.81, 0.91 and 0.49, 0.47, 0.59, 0.62, 0.88, respectively. Furthermore, PSMA PET/CT revealed metastatic disease in 16% (8/50) of patients where all the other modalities were negative. **Conclusion:** Compared to traditional imaging modalities, ^{18}F-PSMA-1007 PET/CT appears to be a more accurate diagnostic tool for primary staging in intermediate or high-risk prostate cancer. Therefore this method could serve as a new reference standard. **References:** None.

OP-774

Prospective evaluation of ^{68}Ga-PSMA PET/CT in primary prostate cancer diagnosis - final results of a dedicated trial

E. Lopci, G. Lughezzani, A. Castello, A. Saita, P. Colombo, N. M. Buffi, N. Lo Iacono, R. Hurle, K. Marzo, L. Leonardi, R. Peschechera, A. Benetti, S. Zandegiacomo, L. Pasini, P. Casale, P. Diana, G. Bevilacqua, E. Mazziotti, L. Balzarini, A. Chiti, G. Guazzoni, M. Lazzeri;
Humanitas Clinical and Research Hospital - IRCCS, Milano, ITALY.

Aim/Introduction: The current study is designed to test the diagnostic performance of ^{68}Ga-PSMA PET/TC for primary diagnosis in a selected subset of patients with suspicious prostate cancer (PCa). **Materials and Methods:** For this prospective trial, from January 2017 till December 2018, we enrolled and addressed to ^{68}Ga-PSMA PET/CT consecutive patients having a persistently elevated PSA and/or PHI (prostate health index) suspicious for PCa, negative digital rectal examination, and at least one negative biopsy were enrolled. The cohort comprised patients with either a negative/equivocal mpMRI (PIRADS v2. ≤2) or absolute/relative contraindications to mpMRI. All patients underwent whole body ^{68}Ga-PSMA PET/CT 60 minutes after radiopharmaceutical injection (185-250MBq). Focal PSMA uptake superior to background activity was considered for the analysis and outlined for target biopsy. Semi-quantitative measures for all lesions comprised SUVmax and SUVratio-to-background. Sensitivities, specificities, and accuracy were calculated based on pathology results. **Results:** Overall, 97 patients were enrolled in the study: 70 patients (72%) had already performed a mpMRI with either a negative result for PCa (n=22) or positive mpMRI, but previous negative biopsy. ^{68}Ga-PSMA PET/TRUS fusion biopsy was performed in 64 patients (66%), total 114 regions of interest (ROIs), whereas in the remaining cases (34%) the indication for biopsy was not confirmed. According to pathology, 23 patients (34%) with 41 ROIs had evidence of PCa: 8 patients (16 ROIs) resulted Gleason score (GS) 6, 13 patients (21 ROIs) resulted GS 7 (3+4 or 4+3), 1 patient (2 ROIs) GS 8 and 1 patient (2 ROIs) GS 10. In 14 patients with previous positive mpMRI and negative biopsy, PCa presence was demonstrated after ^{68}Ga-PSMA PET/CT: 3 GS 6 and 11 GS 7. Mean SUVmax and SUVratio-to-background for all PCa lesions resulted statistically significantly higher than in benign lesions (p<0,001): in particular, mean SUVmax and mean SUVratio were 10.6 versus 4.1, and 4 versus 1.5, respectively. ROC analysis performed for optimal cut-off points demonstrated that a SUVmax >5.4 and a SUVratio >2.2 could identify clinically significant PCa (GS ≥7) with an accuracy of 81% e 90%, respectively. **Conclusion:** In patients with a high suspicion of cancer, despite previously negative biopsy and/or mpMRI, ^{68}Ga-PSMA PET/CT is capable to detect malignant lesions and identify with a high accuracy clinically relevant PCa. **References:** Lopci E, Saita A, Lazzeri M, et al. J Urol. 2018 Jul;200:95-103.Lopci E, Guazzoni G, Lazzeri M. Radiology. 2018 May;287:725-726.Lazzeri M, Lopci E, Lughezzani G, et al. Eur J Hybrid Imaging. 2017;1:9.

OP-775

arallel comparison of 68Ga-Prostate Specific Membrane Antigen PET-CT and PRIMUS in primary prostate cancer diagnosis

E. Lopci, G. Lughezzani, A. Castello, A. Saita, P. Colombo, N. M. Buffi, N. Lo Iacono, R. Hurle, K. Marzo, L. Leonardi, R. Peschechera, A. Benetti, S. Zandegiacomo, L. Pasini, P. Casale, P. Diana, G. Bevilacqua, E. Mazziotti, L. Balzarini, A. Chiti, G. Guazzoni, M. Lazzeri;
Humanitas Clinical and Research Hospital - IRCCS, Milano, ITALY.

Aim/Introduction: To compare the diagnostic performance of ^{68}Ga-PSMA PET/TC with PRIMUS (prostate risk identification using micro-ultrasound) in the primary diagnosis of prostate cancer (PCa) in patients with previously negative biopsy. **Materials and Methods:** From September till December 2018, we enrolled 28 patients candidate to ^{68}Ga-PSMA PET/TRUS (transrectal ultrasound) fusion biopsy and compared them with PRIMUS. The present analysis is embedded into a larger diagnostic trial investigating the role of ^{68}Ga-PSMA PET/CT in PCa diagnosis of patients having a persistently elevated PSA and/or PHI (prostate health index) suspicious for PCa, negative digital rectal examination, with either negative or contraindication to mpMRI, and at least one negative biopsy. All patients underwent parallel ^{68}Ga-PSMA PET/CT and micro-ultrasound for biopsy indication. Focal PSMA uptake superior to background activity was considered for the analysis and outlined for target biopsy. Semi-quantitative measures for all lesions comprised SUVmax and SUVratio-to-background. PRIMUS classification was performed according to standard criteria: score 1&2 benign; score 3 suspicious, score 4&5 significant disease. The two imaging modalities were statistically compared and diagnostic performance calculated based on pathology results. **Results:** Overall, 20 patients were addressed to ^{68}Ga-PSMA PET/TRUS fusion biopsy following the examinations. In the remaining cases, the indication was not confirmed. Two patients resulted having a GS 6 PCa, 7 patients had a GS 7 (3+4 or 4+3), 1 patient had a GS 8 PCa and 13 patients presented with benign findings (prostatitis/BPH). Mean SUVmax and SUVratio for all PCa lesions resulted statistically significantly higher than in benign lesions (p=0,041 and 0.011, respectively): in particular, mean SUVmax was 5.5 versus 4.1, and mean SUVratio was 2.3 versus 1.5, respectively for PCa and benign findings. By using optimal cut-off points as reference, ^{68}Ga-PSMA PET/CT demonstrated an overall accuracy of 83% for SUVmax ≥5.4 and 94% for SUVratio ≥2.2 in the detection of clinically significant PCa (GS≥7). On counterpart, PRIMUS results were as follows: score 3 in 9 patients (45%), score 4 in 10 patients (50%) and 1 patient with score 5. When considering only score 4&5, PRIMUS demonstrated an overall accuracy of 61% in detecting clinically significant PCa. **Conclusion:** In comparison to PRIMUS, ^{68}Ga-PSMA PET/CT shows a higher diagnostic performance and is capable of detecting clinically relevant PCa in patients with a high suspicion of cancer. **References:** Lughezzani G, et al. European Urology Oncology, 2018, In PressLopci E, et al. J Urol. 2018;200:95-103. Pavlovich CP, et al. Urol Oncol. 2014;32:34.e27-32.

OP-776

Validation of gallium-68 PSMA-PET/CT for primary lymph node staging in prostate cancer patients

L. van Kalmthout[1], *H. van Melick*[2], *J. Lavalaye*[2], *R. Meijer*[1], *A. Kooistra*[3], *J. de Klerk*[3], *A. Braat*[4], *P. Kaldeway*[5], *B. de Keizer*[1], *M. Lam*[1]; [1]*Academic hospital, Utrecht, NETHERLANDS,* [2]*St. Antonius Ziekenhuis, Nieuwegein, NETHERLANDS,* [3]*Meander Medisch Centrum, Amersfoort, NETHERLANDS,* [4]*UMC Utrecht, Utrecht, NETHERLANDS,* [5]*St. Anotnius Hospital, Nieuwegein, NETHERLANDS.*

Aim/Introduction: In many centers, gallium-68 (^{68}Ga) prostate specific membrane antigen (PSMA)-PET/CT imaging is currently implemented in the standard diagnostic work-up of prostate cancer (PCa). However, prospective validation of diagnostic accuracy in initial staging of PCa is lacking. This study evaluates diagnostic accuracy of ^{68}Ga-PSMA-PET/CT in detection of lymph node metastases (LNMs). **Materials and Methods:** From October 2017 up to October 2018, newly diagnosed PCa patients with negative bone scan and >10% risk of LNMs (MSKCC-nomogram) were prospectively included if tumor board considered them candidates for extended pelvic lymph node dissection (ePLND). After informed consent was signed, patients underwent ^{68}Ga-PSMA PET/CT prior to ePLND. Two blinded experienced nuclear medicine physicians examined all scans; disagreements were solved by the introduction of a third reader. Scan results were evaluated in a second tumor board meeting for possible change of management (CoM), being either ePLND-template extension, ePLND cancellation (e.g. in case of positive distant lesions following biopsy) or other management strategies. Histopathological examination was performed by dedicated uropathologists. Sensitivity, specificity, positive (PPV) and negative predictive value (NPV) for the detection of LNMs were calculated using histopathology as reference. Statistical analyses were performed using SPSS Statistics v24. **Results:** A total number of 103 patients were eligible for analysis. Ninety-seven ePLNDs were performed. Forty-one patients (42.3%) had a total of 89 LNMs. Seventeen of these patients were PET-positive, resulting in a patient-based sensitivity, specificity, PPV and NPV for the detection of LNMs of respectively 41.5%, 89.4%, 73.9% and 67.6%. Side-based sensitivity, specificity, PPV and NPV was 37.7%, 92.2%, 64.5% and 79.8%; template-based sensitivity, specificity, PPV and NPV was 37.3%, 94.3%, 55.0% and 89.0%. CoM due to PSMA findings was observed in 13 patients (12.6%): In six patients, ePLND-template was extended. ePLND was cancelled in another six patients, either because of PCa-positive extrapelvic lesions following biopsy (n=2); clinical parameters with suspected ≥M1a-disease on PET (n=3) and M1a-disease confirmed by CT thorax (n=1). Radiation therapy following ePLND (0/18 positive lymph nodes) was given in one patient with a PET-positive rib lesion. **Conclusion:** This prospective analysis in newly diagnosed PCa patients shows that ^{68}Ga-PSMA PET/CT detects LNMs with high specificity and moderate sensitivity. Furthermore, PET-imaging leads to significant CoM. **References:** None.

OP-778

Interobserver Agreement of ^{68}Ga-PSMA-11 PET/CT images interpretation

C. Derwael[1], *O. Lavergne*[2], *P. Lovinfosse*[1], *V. Nechifor*[1], *D. Waltregny*[1], *R. Hustinx*[1], *N. Withofs*[1]; [1]*CHU, Liège, BELGIUM,* [2]*CHR, Liège, BELGIUM.*

Aim/Introduction: Prostate-specific membrane antigen (PSMA)-ligand PET/CT has already provided promising results in prostate cancer imaging yet simple and reproductible reporting criteria are still lacking. This study aimed at retrospectively evaluating the reproducibility of ^{68}Ga-PSMA-11 PET/CT images interpretation according to prostate cancer molecular imaging standardized evaluation (PROMISE) criteria and reproducibility of PSMA-reporting and data systems (RADS) version 1.0 was also studied[1,2]. **Materials and Methods:** Forty-two patients with newly diagnosed histologically proven intermediate or high-risk prostate cancer, eligible for radical prostatectomy with pelvic lymph node dissection and who underwent ^{68}Ga-PSMA-11 PET/CT before surgery were retrospectively included. Three nuclear medicine physicians (2 experienced; 1 trainee) independently reviewed PET/CT images blinded to clinicopathologic data. Interpretation of ^{68}Ga-PSMA-11 PET/CT images was based on PROMISE criteria including miTNM classification and lesions miPSMA expression score visual estimation[1]. For a given scan, findings were further categorised according to PSMA-RADS version 1.0 (not applicable to the primary tumour) [2]. Consensus among reviewers was measured (Cohen's kappa and Krippendorff's coefficients) and guideline for interpreting degree of agreement followed Nanni et al. method[3]. All lymph nodes short and long axes were measured and correlation between lymph nodes size and miPSMA expression score was tested (Spearman Correlation, p &lt 0.05 considered significant). **Results:** Agreement between observers was substantial (coefficients 0,61-0.80) for almost all criteria: miTNM staging, localisation of metastases and lymph nodes, miRADS classification, localisation and evaluation of PSMA's level of expression of the primary tumour and miPSMA expression score of bone and visceral metastases. The only criterion for which interobserver agreement was only moderate (Krippendorff's coefficient = 0,53) was lymph nodes miPSMA expression score. A statistically significant correlation was found between miPSMA expression score and lymph nodes size (p &lt 0.05). This study pointed out that PSMA expression of reference organs for the estimation of miPSMA expression score might be variable between individuals, especially for the distinction between liver activity (miPSMA expression score 2) and parotid activity (miPSMA expression score 3). **Conclusion:** This study showed interobserver substantial agreement of PROMISE criteria for the interpretation of ^{68}Ga-PSMA-11 PET/CT images except for the estimation of miPSMA expression score of positive lymph nodes that can be hampered by the interindividual variability of reference organs PSMA expression. **References:** 1. Eiber et al. J Nucl Med, 2018 March. 59(3) : 469-478; 2. Rowe SP and al. Eur Urol. 2018; 73:485-487; 3. Nanni, C. et al. Eur J Nucl Med Mol Imaging (2018) 45: 712-719.

OP-779

Performance of ^{68}Ga-PSMA-11 PET in patients with PSA persistence after radical prostatectomy for the detection of residual prostate cancer: a multicenter retrospective study

A. Farolfi[1], *A. Gafita*[2], *J. Calais*[3], *M. Eiber*[2], *A. Afshar-Oromieh*[4], *F. Spohn*[5], *F. Barbato*[6], *M. Weber*[6], *H. Ilhan*[7], *V. Cervati*[1], *A. Wetter*[8], *B. Hadaschik*[9], *A. Briganti*[10], *J. Walz*[11], *D. Pianori*[12], *S. Fanti*[1], *U. Haberkorn*[5], *K. Herrmann*[6], *W. P. Fendler*[6];
[1]*Nuclear Medicine Department, S.Orsola Hospital, University of Bologna, Bologna, ITALY,* [2]*Department of Nuclear Medicine, Klinikum rechts der Isar, Technical University Munich, Munich, GERMANY,* [3]*Ahmanson Translational Theranostics Division, Department of Molecular and Medical Pharmacology, University of California Los Angeles (UCLA), Los Angeles, CA, UNITED STATES OF AMERICA,* [4]*Department of Nuclear Medicine, Bern University Hospital, Bern, SWITZERLAND,* [5]*Department of Nuclear Medicine, Heidelberg University Hospital, Heidelberg, GERMANY,* [6]*Department of Nuclear Medicine, University Hospital Essen, Essen, GERMANY,* [7]*Department of Nuclear Medicine, University Hospital Munich, Ludwig-Maximilians-Universität (LMU), Munich, GERMANY,* [8]*Department of Radiology, University Hospital Essen, Essen, GERMANY,* [9]*Department of Urology, University Hospital Essen, Essen, GERMANY,* [10]*Department of Urology, Division of Oncology, Urological Research Institute, IRCCS Ospedale San Raffaele, Milan, ITALY,* [11]*Department of Urology, Institut Paoli-Calmettes Cancer Centre, Marseille, FRANCE,* [12]*Department of Biomedical and Neuromotor Sciences, University of Bologna, Bologna, ITALY.*

Aim/Introduction: PSA persistence after radical prostatectomy (RP) is associated with adverse outcome in patients with prostate cancer (PCa). Our aims were to define positivity rate, regions of high risk for residual disease and impact on management of PSMA-ligand PET in patients with PSA persistence. **Materials and Methods:** 210 patients were retrospectively selected from the 6 participating centers and included in the study according to the following inclusion criteria: a) RP for PCa; b) persistently elevated post-operative PSA levels (≥0.1 ng/mL) ≥6 weeks after surgery; c) PSMA-ligand PET performed within 12 months after RP. Positivity rate, impact on management and positive-predictive value were determined. In patients with additional PSMA-ligand PET before RP (n=33) a subgroup analysis was performed to determine PET-based disease persistence and recurrence. Anonymized imaging datasets were evaluated independently by three experienced nuclear medicine physicians employing the molecular imaging TNM system PROMISE. **Results:** PSMA-ligand PET identified PCa-lesions in 68% (143/210) of patients with PSA persistence at a median PSA level of 1.1 ng/mL. Detection rate significantly increased in accordance with PSA levels at time of scan (p<0.001). Overall, 36% (76/210) patients had disease limited to the pelvis while 30% (64/210) of patients had distant lesions. The most commonly involved regions were obturator (47%) and presacral/mesorectal (42%). In the subgroup analysis (PSMA-ligand PET before and after surgery), 45% (15/33) of patients had at least one lesion already detected at baseline (PET persistence), 24% (8/33) had previously undetected lesions (PET recurrence), and 30% (10/33) were PET negative after RP. Most PET positive pelvic nodes presented with intense tracer uptake (median SUV_{max}=10.1), however 71% were not enlarged by CT/MRI criteria (median short diameter=0.80 cm). PSMA-ligand PET positive predictive value was 87%. Initiation of systemic therapy was significantly associated with presence of distant lesions on PSMA-ligand PET (p=0.001). According to multivariable regression analysis, PSA and ISUP grade were associated with the presence of Tr/N1 and/or M1 disease; whereas T stage ≥3a was associated only with the presence of M1 disease (OR 7.64, CI95% 1.66-35.08; p=0.01). **Conclusion:** In this multicenter retrospective study, PSMA-ligand PET detected disease in more than two thirds of patients with PSA persistence after radical prostatectomy. Most common sites of persistent disease were within the obturator and presacral/mesorectal regions. Extra-pelvic regions however frequently harbored persistent prostate cancer. Our data suggests a role for PSMA-ligand PET to identify residual disease in high-risk patients. **References:** None.

OP-780

Salvage radiotherapy guided by 68Ga-PSMA-11 PET/CT in patients with biochemical persistence (BCP) after radical prostatectomy for prostate cancer

F. Ceci[1], *D. Nicolotti*[1], *E. Pilati*[1], *A. Guarneri*[2], *S. Bartoncini*[2], *M. Finessi*[1], *V. Liberini*[1], *G. Bisi*[1], *U. Ricardi*[2], *D. Deandreis*[1];
[1]*Nuclear Medicine, Department of Medical Sciences, University of Turin, Turin, ITALY,* [2]*Radiation Oncology, Department of Oncology, University of Turin, Turin, ITALY.*

Aim/Introduction: Introduction: prostate cancer (PCa) patients with persistent high PSA levels (BCP) after radical prostatectomy (RP) showed less favourable survival rates. Thus, localizing the residual disease after surgery is crucial to precisely define the planned target volume (PTV) of salvage radiotherapy (SRT). Objective: to evaluate the impact of ^{68}Ga-PSMA-11-PET/CT on SRT planning in BCP patients. **Materials and Methods:** Design: ^{68}Ga-PSMA-11-PET/CT is performed in our institution through a prospective, single-center, open-label study (prot. P-5315) in hormone-naïve PCa. We performed a retrospective sub-analysis in BCP patients matching these inclusion criteria: 1) RP as primary therapy; 2) PSA-nadir >0.1 ng/mL at 8 weeks after RP; 3) No adjuvant/salvage therapy or hormonal-therapy performed after RP; 4) all patients considered eligible for SRT in prostate bed; 5) PET scan performed within 12 months from RP. Changes in clinical management and SRT planning were defined by a singlecentre multidisciplinary tumour board. Population characteristics: twenty-eight (n=28) patients matched all inclusion criteria and were analysed. ISUP grade <=3 (n=11/28), >=4 (n=17/28); stage >=pT3a (n=17/28); pN1 (n=7/28); R1 (n=16/28). Median/mean PSA-nadir=0.34/0.48 ng/mL (0.1-3.3); median/mean PSAdt=2.8/7.1 months (0.6-44.6); median/mean PSAvel=0.8/3.1 ng/mL/year (range 0.1-24.7). **Results:** Overall results: ^{68}Ga-PSMA-11-PET/CT detection rate was 57.1% (CI95% 37.4%-75.0%). Median/mean PSA at time of imaging=0.53/1.06 ng/mL (range 0.22-8.9). Prostate bed relapse only was detected

in 3.6% of cases. Intra-pelvic relapse (pelvic lymph-nodes with/without prostate bed) was detected in 21.4%,.The presence of at least one extra-pelvic lesion (extra-pelvic nodes and/or bone) was detected in 32.1%. of cases. Oligometastatic disease (1-3 PSMA positive lesions) was detected in 53.6% of cases. SRT planning: in 46.4% of patients (13/28), SRT in prostate bed was confirmed as intended before PET scan. In 53.6% of patients SRT planning was changed: 7/28 patients performed SRT in prostate bed and additional stereotactic radiotherapy (SBRT) on PET positive findings. In 2/28 cases PTV was modified including only PET positive pelvic nodes without standard radiotherapy in prostate bed. SRT was aborted in 5/28 patients and ADT was administrated instead. In 1/28 case SRT was aborted and pelvic lymph-node dissection was performed. **Conclusion:** In this patient-series, ^{68}Ga-PSMA-11-PET/CT proved its role in BCP setting detecting disease outside prostate bed in 53.5% of cases and SRT planning was modified due to the integration of ^{68}Ga-PSMA-11-PET/CT results into the decision-making process. These data may suggest the presence of extended disease not detected by conventional imaging prior to surgery and highlight the importance of PET imaging in BCP setting. **References:** None.

1709

Inflammation & Infection - Parallel Session: Infection and Inflammation (Beyond Cardiovascular System)

Wednesday, October 16, 2019, 10:00 - 11:30 Lecture Hall 115

OP-781

A comparison of the diagnostic value of MRI and Whole body 18F-FDG PET/CT in diagnosis of spondylodiscitis. A comparison of the diagnostic value of MRI and Whole body 18F-FDG-PET/CT in diagnosis of spondylodiscitis

C. Altini, A. Branca, R. Ruta, G. Santo, C. Ferrari, A. Niccoli Asabella, N. Merenda, G. Rubini;
Nuclear Medicine Unit, Interdisciplinary Department of Medicine – University of Bari "Aldo Moro", Bari, ITALY.

Aim/Introduction: Magnetic resonance Imaging (MRI) is considered the most accurate technique for the diagnosis of spondylodiscitis while currently 18F-FDG PET/CT has been proposed in doubtful cases. The aim of this study was to compare the role of 18F-FDG PET/CT and MRI in the diagnosis of spondylodiscitis. **Materials and Methods:** 66 patients with suspected spondylodiscitis (48 male, 18 female; mean age 63 years; range: 11-90 years) who performed 18F-FDG PET/CT were retrospectively analyzed. MRI were performed on average 19 days before 18F-FDG PET/CT (range: 3-36 days). Cohen's K was applied to evaluate the agreement between the two techniques in all patients and in subgroups who performed whole-spine, two-districts, one-district MRI respectively. **Results:** Considering all patients, 18F-FDG PET/CT and MRI were both positive for spondylodiscitis in 53/66 (80%) patients, the two techniques were both negative in 6/66 (9%),18F-FDG PET/CT was negative while MRI was positive in 7/66 (11%). The agreement was moderate (K=0.579). Twenty-eight/66 (42%) patients performed whole-spine MRI: 18F-FDG PET/CT and MRI were both positive in 21/28 (75%), the two techniques were both negative in 3/28 (11%), 18F-FDG PET/CT was negative while MRI was positive in 4/28 (14%). The agreement was moderate (K=0.529). Considering the 21/28 with positivity of the two techniques, in 15/21 patients the same lesions were identified, in 5/21 MRI identified lesions in two districts while 18F-FDG PET/CT only in one, in 1/21 patients 18F-FDG PET/CT identified one lesion more than MRI. Nineteen/66 (29%) patients performed two-districts MRI: 18F-FDG PET/CT and MRI were both positive in 13/19 (68%), the two techniques were both negative in 3/16 (16%), 18F-FDG PET/CT was negative while MRI was positive in 3/16 (16%). The agreement was moderate (K=0.574). Considering the 13/19 with positivity of the two techniques, in 11/13 patients the same lesions were identified, in 1/13 MRI identified lesions in two districts while 18F-FDG PET/CT only in one, in 1/13 patients 18F-FDG PET/CT identified one lesion more than MRI. In the subgroup of 19/66 (29%) patients who performed one-district MRI, 18F-FDG PET/CT and MRI were both positive and completely concordant for lesions identified that were respectively: cervical in 1/19 (5%), dorsal in 5/19 (26%), lumbar in 13/19 (69%). **Conclusion:** Our results confirm the 18F-FDG PET/CT diagnostic value in the diagnosis of spondylodiscitis, comparable to MRI for the entire spine evaluation. It can be considered a valid alternative to MRI, in particular in patients who cannot perform it. **References:** None.

OP-782

Predictive Potential of Nonstandard Quantitative Imaging Features in Diabetic Foot

A. Marciano[1], J. Beukinga[2], Z. Keidar[3], M. Kurash[3], R. Zanca[1], A. W. J. M. Glaudemans[2], P. A. Erba[1], R. H. J. A. Slart[2];
[1]Regional Center of Nuclear Medicine, Department of Translational Research and New Technology in Medicine, Univerisity of Pisa and AOUP, Pisa, ITALY, [2]Medical Imaging Center, Department of Nuclear Medicine and Molecular Imaging, University of Groningen, University Medical Center Groningen, Groningen, NETHERLANDS, [3]Department of Nuclear Medicine, Rambam Health Care Campus, Haifa, ISRAEL.

Aim/Introduction: [^{18}F]FDG PET/CT is an accurate imaging modality for the diagnosis of diabetic foot complications. Currently, images are generally visually assessed and quantitative analysis is limited to simple metrics like maximum standardized uptake value, target/background ratio analysis. The goal of this work was to assess the predictive potential of nonstandard quantitative imaging features in the differentiation between soft tissue and bone infections in diabetic foot. **Materials and Methods:** Within a retrospective trial, we evaluated a series of 47 patients (mean age 58±9 years, median age 58 years, range

40-81) with possible diabetic foot infection. PET/CT images were acquired about 45-60 mins after [^{18}F]FDG administration (mean dose 376±107 MBq/kg of body weight, median dose 376 MBq/kg, range 185-580). In order to perform the texture analysis, we segmented lesions using three different methods, two semiautomatic and one manual. The semiautomatics segmentations were delineated with a threshold fixed at 20% and 40% of the relative SUVmax on PET; with the manual method, we delineated the segmentations on CT (LDCT). Radiomics texture features (46 features) were extracted using the LIFEx package. The information resulting from the texture features analysis for all the segmentations method were correlated with the presence of Osteomyelitis, Soft Tissue Infections and Inflammation, using microbiological findings as reference. Data were analyzed by multivariate analysis, linear discriminant analysis. The Spearman correlation coefficient two-sided Wilcoxon rank sum test or Kruskal-Wallis test were used and corrected for multiple testing using the Bonferroni-Holm method (significance level $\alpha = 0.05$). Statistical analysis was performed with JMP Statistical Discovery™. **Results:** Texture features analysis allowed to discriminate the presence of osteomyelitis, soft tissue infections and inflammation (Table 1). The best overall performance was obtained using the semiautomatic segmentations with a fixed threshold at 40%, with the AUCs of 0.93 for Osteomyelitis, 0.90 for Soft Tissue Infections, 0.96 for inflammations, respectively. **Conclusion:** Our preliminary results suggest a predictive potential of nonstandard quantitative imaging features in the differentiation between inflammation and infection as well between soft tissue and bone involvement in diabetic foot infection. **References:** None.

OP-783

Handling of doubtful WBC scintigraphies in patients with prosthetic joint infections

G. Lauretti, C. Lauri, D. Riolo, S. Tetti, A. Signore;
Nuclear Medicine Unit, Dept of Medical-Surgical Sciences and of Translational Medicine, "Sapienza" University of Rome, Rome, ITALY.

Aim/Introduction: The aim of this study is to find the appropriate protocol in order to evaluate 99mTc-HMPAO-labelled WBC scintigraphy when the qualitative analysis is uncertain by using alternative tools like semi-quantitative analysis and/or bone marrow scintigraphy with 99mTc-nanocolloids. **Materials and Methods:** Retrospective study on 566 patients referred for suspected hip and knee prosthetics infection (PJI). 99mTc-HMPAO-WBC images were acquired at 30', 3h and 20h and image interpreted according to EANM guidelines. Amongst these, 37 patients had a doubtful scan and 20 performed also a bone-marrow scintigraphy in order to evaluate match or mismatch. Inclusion criteria for "doubtful cases" were: A) small non significant increase of activity in the suspected region at late images; B) increase of medullary activity with time that does not allow easy visualization of peri-prosthetic bone activity; C) small increase of extent pf uptake in the suspected region at late images without increase of activity; D) soft tissue infection that does not allow to clearly evaluate the bone; E) small increase of activity with time in the suspected region with similar increase activity in bone marrow; F) residual activity in the suspected region in the follow-up study after therapy; G) unmodified activity with time in the suspected region but with clear decrease of medullary and background activity. We performed semi-quantitative analysis considering as positive findings the increase of T/B value between early and delayed images with four different cut-off values (5%-10%-20%-30%). **Results:** Semi-quantitative analysis using as parameter the increase of T/B ratio with cut-off of 20% between early and delayed images is the most reliable tool when qualitative analysis is not clear, as it shows the highest accuracy (85%) with high negative predictive value (81%). The region chosen for background calculation should be the contralateral joint by drawing mirror ROI. Only in cases B or D, when bone marrow activity increases or is stable over time, the background can be chosen on the iliac crest or any other bone-marrow site. Combining bone marrow scintigraphy with WBC scan showed high positive predictive value (100%). **Conclusion:** In case of "doubtful" qualitative analysis a semi-quantitative analysis can be performed on delayed and late images. If T/B increases of >20% over time, a PJI should be considered. If T/B does not increase >20%, a bone-marrow scintigraphy should be performed in order to rule out or confirm the PJI. **References:** None.

OP-784

Is the^{18}F-FDG-PET/CT able to characterize fibrosing diseases?

Y. K. Henao Celada, A. Mari Hualde, J. Orcajo Rincon, D. Zamudio Rodriguez, A. Rotger Regí, J. J. Ardila Mantilla, J. Atance Garcia de la Santa, J. C. Alonso Farto;
Hospital General Universitario Gregorio Marañon, Madrid, SPAIN.

Aim/Introduction: To evaluate the utility of ^{18}F-FDG-PET / CT in the diagnosis of fibrosing disease. **Materials and Methods:** A retrospective descriptive study including all patients who underwent at least one ^{18}F-FDG-PET/CT, diagnosed of fibrosing disease by conventional image and / or histology, from December/2016 to March/2019 in the HGUGM. 20 patients were recruited (15M and 5F, 3: 2), whose average age was 61.2 years. They were categorized into 2 groups based on the presence of IgG4 infiltrate in the fibrous tissue: Group1: IgG4-related disease (IgG4-RD) and Group2: non-IgG4 fibrosing disease (No-IgG4-FD). Clinical, analytical (IgG4 serum levels) and histology were collected, as well as qualitative (morphologic and metabolic) and semi-quantitative (SUVmax) findings of the ^{18}F-FDG-PET/CT study. **Results:** 9 out of 20 patients were included in group1 due to the presence of IgG4 infiltration and 11 were included in group2 due to the absence of it. 100% of them showed morphological alterations in ^{18}F-FDG-PET / CT concordant with previous conventional images or with clinical suspicion. 70% (14/20) presented pathological ^{18}F-FDG uptake, mostly afecting more than one organ. The highest prevalence metabolically active locations were: retroconal fat (n: 4),

salivary glands (n: 2), pleura / mediastinum (n: 3), periaortic / retroperitoneal tissue (n: 3) and visceral (n: 2) . In group1 (IgG4-RD) the following morphological findings were found: 4 orbital and facial affectation, 2 visceral (autoimmune pancreatitis and biliary fibrosis), 2 thoracic (pleural and mediastinal) and 1 retroperitoneal. 100% (9/9) of the lesions, showed an increase in glycidic consumption, mean SUVmax: 5.1 (range 2.1-9.1). In group 2 (EF-No IgG4) the CT showed: 4 patients with orbital pseudotumor, 5 retroperitoneal fibrosis, 1 soft tissue fibrosis and 1Erdheim Chester disease. 5/11 patients (46%) presented an increase in metabolic activity associated with fibrosing lesions, SUVmax average: 5.3 (2.9-6.4). All patients were receiving immunosuppressant treatment at the time of the study, with the exception of 2 patients in the group2. Only 1/20 patient showed elevation of serum IgG4. **Conclusion:** ^{18}F-FDG-PET / CT is a useful tool for locating fibrosing disease, both with presence or absence of IgG4 infiltration, also adding information about its inflammatory activity with respect to other conventional imaging techniques. All patients with IgG4-RD have metabolic activity in any of their fibrosing lesions, more frequently than no-IgG4-FD do, although there is no clear difference in the locations or in its intensity. **References:** None.

OP-785

The Significance Of Inverted-"V" Shaped Prostatic FDG Uptake As A Diagnostic Clue for IgG4-Related Prostatitis

K. Nakatani, K. Yoshino, T. Koyama;
Kurashiki Central Hospital, Kurashiki, Okayama, JAPAN.

Aim/Introduction: FDG-PET/CT has been considered to provide functional information about the disease activity in patients with IgG4-related disease (IgG4-RD), and several typical manifestations are well-known in the pancreas as well as submandibular glands and periaortic soft tissue. As for the prostate, much less is known about the specific features of IgG4-related prostatitis and about how to differentiate from benign prostatic hyperplasia (BPH). Recently, inverted-"V" shaped prostatic FDG uptake has been reported as helpful to diagnose autoimmune pancreatitis. Our aim was to investigate the significance of this sign in the differential diagnosis of IgG4-related prostatitis from BPH. **Materials and Methods:** All the study population underwent FDG-PET/CT scan between 05/2012-01/2019. The cases included were 25 male patients (age: 56-83) who met the comprehensive diagnostic criteria for IgG4-RD 2011 (Umehara et al.), histopathologically or clinically; the controls were 22 healthy male individuals (age: 52-80) who studied for cancer screening and turned out to have BPH. The visual shape of FDG uptake distribution in the prostate were compared, as well as their SUVmax, between the cases and the controls. Furthermore, the intensity of FDG uptake in the prostatic glands was compared using one-way ANOVA among the IgG4-RD cases with inverted-"V" uptake, those without inverted-"V" uptake, and the controls. **Results:** The IgG4-RD cases had a slight tendency to show higher prostate SUVmax (3.7±1.5; range 2.0-7.5) than the controls with BPH (3.0±0.9; range 2.1-6.2) (P=0.044, unpaired t-test), even with a substantial overlap. 10/25 of the IgG4-RD cases showed inverted-"V" shaped prostatic uptake, whereas none of the controls showed this pattern (P=0.0008, Fisher's exact test); the controls with intense FDG uptake showed either punctate or wedge-shaped patterns. The one-way ANOVA showed significant difference among the three groups (P=0.0002), and post-hoc Tukey's test revealed that the prostate SUVmax of the IgG4-RD cases with inverted-"V" uptake (4.8±1.2; range 3.1-7.5) was significantly higher than the prostate SUVmax of the IgG4-RD cases without inverted-"V" uptake (3.0±1.3; range 2.0-3.8), and was also significantly higher than the prostate SUVmax of the controls with BPH. **Conclusion:** Inverted-"V" shaped prostatic FDG uptake, specifically observed in IgG4-RD patients, should be a diagnostic clue for IgG4-related prostatitis, which would be expected to provide an important information to achieve less-invasive biopsy. **References:** 1) Umehara H et al. Comprehensive diagnostic criteria for IgG4-related disease (IgG4-RD), 2011. Mod Rheumatol. 2012;22:21-30
2) Zhang J et al. ^{18}F-FDG PET/CT helps differentiate autoimmune pancreatitis from pancreatic cancer. BMC Cancer. 2017;17:695.

OP-786

Diagnostic validity of (S)-4-(3-[^{18}F]Fluoropropyl)-L-glutamic acid ([^{18}F]FSPG) positron emission tomography/computed tomography (PET/CT) for the assessment of disease activity in patients with inflammatory bowel disease: a phase 2 pilot study

D. Lee[1], *M. Seo*[2], *B. Ye*[3], *S. Park*[3], *S. Chae*[1], *S. Hwang*[3], *S. Lee*[1], *S. Oh*[1], *J. Kim*[4], *S. Na*[5], *N. Koglin*[6], *M. Berndt*[6], *A. Stephens*[6], *D. Moon*[1];
[1]*Department of Nuclear Medicine, Asan Medical Center, University of Ulsan College of Medicine, Seoul, KOREA, REPUBLIC OF,* [2]*Department of Nuclear Medicine, Ulsan University Hospital, University of Ulsan College of Medicine, Ulsan, KOREA, REPUBLIC OF,* [3]*Department of Gastroenterology and Inflammatory Bowel Disease Center, Asan Medical Center, University of Ulsan College of Medicine, Seoul, KOREA, REPUBLIC OF,* [4]*Department of Nuclear Medicine, Hanyang University Medical Center, Hanyang University College of Medicine, Seoul, KOREA, REPUBLIC OF,* [5]*Department of Radiology, Uijeongbu St. Mary's Hospital, College of Medicine, The Catholic University of Korea, Seoul, KOREA, REPUBLIC OF,* [6]*Life Molecular Imaging GmbH, Berlin, GERMANY.*

Aim/Introduction: Assessment of disease activity in inflammatory bowel disease (IBD), comprising ulcerative colitis (UC) and Crohn's disease (CD), is important for guiding subsequent therapy. [^{18}F]FSPG can image x_c^- transporter activity with PET. We aimed to explore the validity of [^{18}F]FSPG PET/CT for evaluating ileocolonic inflammation in patients with IBD. **Materials and Methods:** We conducted a prospective study enrolling patients with definite UC or CD, aged 19 to 79 years, with symptoms suggestive of active IBD. All patients underwent endoscopy within 7 days prior to or after [^{18}F]FSPG PET/CT. Abdominopelvic PET/CT imaging was performed after injection of 200 MBq of [^{18}F]FSPG. Increased [^{18}F]FSPG uptake in the bowel compared to the liver was interpreted as positive

for active inflammation. Endoscopic assessment of disease activity was performed using Ulcerative Colitis Endoscopic Index of Severity (UCEIS) for UC (≥ 2 as active disease), and Crohn's Disease Endoscopic Index of Severity (CDEIS) for CD (≥ 3 as active disease). **Results:** Between August 2018 to January 2019, ten patients with UC (median age 42, 6 males), and 10 with CD (median age 28, 9 males) were enrolled. Endoscopic diagnosis of active inflammation was made in six with UC, and eight with CD. [^{18}F]FSPG PET/CT was positive in four of six patients with UC (67%), and all eight with CD (100%). [^{18}F] FSPG PET/CT could correctly diagnose endoscopic remission in two of four with UC (50%), and all two CD (100%). Summed maximum standardized uptake value (SUVmax) of bowel segments in UC did not show a significant correlation with clinical and laboratory markers of disease activity (P>0.05), but it showed a strong correlation with UCEIS (ρ=0.79, P=0.006), and histological score (Robarts Histopathology Index: ρ=0.83, P=0.003). In CD, summed SUVmax had a strong correlation with C-reactive protein (ρ=0.94, P<0.001), fecal calprotectin (ρ=0.98, P<0.001), Crohn's Disease Activity Index (ρ=0.70, P=0.025), and CDEIS (ρ=0.90, P<0.001), but not with histological score (Colonic and Ileal Global Histologic Disease Activity Score: n=6, P>0.05). Twelve of 47 bowel segments in patients with UC and 24 of 41 segments in patients with CD showed active lesions in endoscopy, and sensitivity and specificity of [^{18}F]FSPG PET/CT in identifying active bowel lesions were 75% (9/12), and 86% (30/35), respectively for UC, and 71% (17/24), and 94% (16/17), respectively for CD. SUVmax showed a strong correlation with segmental UCEIS (ρ=0.66, P<0.001), and segmental CDEIS (ρ=0.61, P<0.001). **Conclusion:** [^{18}F]FSPG PET/CT imaging may noninvasively assess disease activity status of IBD. **References:** None.

OP-787

Noninvasive Diagnosis and Monitoring of Pneumonia using Pathogen-Specific ^{18}F-Fluorodeoxysorbitol (FDS) PET

*U. Granados[1], **A. A. Ordoñez**[2,3], L. M. Wintaco[4,1], C. A. Bedoya[2,3], S. Frey[5], J. D. Sanchez[2,3], F. R. D'Alessio[6], H. T. Ravert[5], D. P. Holt[5], R. F. Dannals[5], M. G. Pomper[5], S. K. Jain[2,3,5];*

[1]Unidad de Medicina Nuclear, Hospital Internacional de Colombia, Fundación Cardiovascular de Colombia, Bucaramanga, COLOMBIA, [2]Center for Infection and Inflammation Imaging Research, Johns Hopkins University School of Medicine, Baltimore, MD, UNITED STATES OF AMERICA, [3]Department of Pediatrics, Johns Hopkins University School of Medicine, Baltimore, MD, UNITED STATES OF AMERICA, [4]Universidad del Rosario, Unidad de Medicina Nuclear, Hospital Internaciona, Bogotá, COLOMBIA, [5]Russell H. Morgan Department of Radiology and Radiological Sciences, Johns Hopkins University School of Medicine, Baltimore, MD, UNITED STATES OF AMERICA, [6]Division of Pulmonary and Critical Care Medicine, Department of Medicine, Johns Hopkins University School of Medicine, Baltimore, MD, UNITED STATES OF AMERICA.

Aim/Introduction: Imaging tools such as chest X-ray, computed tomography (CT) are frequently used in the management of pulmonary infections. However, they can be notoriously difficult to interpret as they rely on the presence of nonspecific structural abnormalities that often occur late in the disease process and can mimic other pathologies. Therefore, invasive procedures are frequently needed to diagnose infections. Enterobacteriaceae (E. coli, Klebsiella spp., Enterobacter sp., Salmonella sp., etc.), a family of rod-shaped Gram-negative bacteria that normally inhabit the gastrointestinal tract, are the most common cause of Gram-negative bacterial infections in humans and a predominant cause of hospital-acquired pneumonia. We have previously demonstrated that 2-^{18}F-fluorodeoxysorbitol (^{18}F-FDS), synthesized from ^{18}F-FDG, can be used to specifically localize infections due to Enterobacteriaceae and monitor the efficacy of antibiotic treatment in animal models. Therefore, we hypothesized that ^{18}F-FDS PET could be used to noninvasively detect and monitor Enterobacteriaceae pneumonia in patients. **Materials and Methods:** We prospectively enrolled patients with microbiologically confirmed pneumonia due to Enterobacteriaceae as well as controls with an inflammatory or oncologic pulmonary disease without infection. Patients were injected with 370 MBq of ^{18}F-FDS and PET/CT performed 1- and 2-hours post-injection. A follow-up ^{18}F-FDS PET/CT was also performed in a subset of infected patients after the initiation of antibiotic to monitor the efficacy of the treatments. **Results:** Seven patients, three with Enterobacteriaceae infection and four controls, with a mean age of 64.5 ± 5.2 years were imaged. The mean administered activity was 322.9 ± 29.6 MBq (range, 284.9 - 357.42 MBq). There were no adverse or clinically detectable pharmacologic effects in any of the subjects. ^{18}F-FDS PET was able to specifically detect and localize pulmonary infections in all the three patients. PET activity was significantly higher in infected lesions compared with sterile, inflammatory (P=0.004) or neoplastic pulmonary lesions (P<0.001) demonstrating specificity for infectious lesions. Finally, ^{18}F-FDS PET was also able to monitor the efficacy of antibiotic treatment, demonstrating a decrease in signal intensity and correlating with clinical improvement. **Conclusion:** We present the first-in-human results of a novel bacteria-class specific PET imaging tracer for rapid and specific detection of pulmonary infections due to Enterobacteriaceae. ^{18}F-FDS clears rapidly from the lungs, is safe and well tolerated in patients. These preliminary data support the potential role of ^{18}F-FDS as a clinically translatable tracer for the specific detection of Enterobacteriaceae infections in humans. **References:** None. none

OP-788

Real-Time Imaging of Human Skin Invasion by Fluorescently Labelled (Radiation-Attenuated) Schistosoma mansoni Parasites

C. de Korne[1], B. M. F. Winkel[1], M. R. Dalenberg[1], D. M. van Willigen[1], A. W. Hensbergen[1], E. C. de Jong[2], M. Roestenberg[1], F. W. B. van Leeuwen[1];

[1]LUMC, Leiden, NETHERLANDS, [2]AMC, Amsterdam, NETHERLANDS.

Aim/Introduction: With around 54 million people infected with the parasite Schistosoma mansoni (Sm), schistosomiasis is considered as one of the most devastating parasitic diseases. After penetrating the skin, Sm larvae, termed cercariae, transform into schistosomula and stay intradermally for several days. During the skin stage interaction with the dermal immune system can take place, which makes this stage a promising target for schistosomiasis vaccine development. It is, however, unclear how the skin invasion takes place exactly. To allow for imaging of the initial skin invasion, we have developed a tracer-based method that supports real-time tracking of the multicellular Sm cercaria. Using this method, we compared the skin penetration of non-attenuated (NA) and radiation-attenuated (RA) Sm cercariae. Moreover, we have studied the dermal immune response they induced after invasion. **Materials and Methods:** Sm cercariae were shed from water snails and half of them were attenuated by irradiating them to a total dose of 20 krad. To enable tracking of the cercariae, they were labelled with a translocator protein targeting fluorescent dye. Fluorescence confocal microscopy movies were obtained of NA cercariae (n=45) and RA cercariae (n=35) penetrating human skin explants, available from plastic surgery, and their invasion behaviour was analysed. Following infection, the dermal immune response after exposure to RA cercariae was assessed and compared to the exposure to NA cercariae. **Results:** The labelling strategy yielded brightly fluorescent cercariae. Monitoring the invasion of the cercariae in human skin explants confirmed the infectious potential of both the NA and RA cercariae, for both groups 51% of the tracked cercariae entered the human skin within 30 min. Three different types of skin invasion were seen: 1) full body penetration, lodged in epidermis (NA cercariae: 17%, RA cercariae: 28%), 2) full body penetration, reached the basal membrane (NA cercariae: 61%, RA cercariae: 22%) and 3) tail shedding, reached the basal membrane (NA cercariae: 22%, RA cercariae: 50%). Analysis of the dermal immune response revealed that exposure to NA cercariae induced a regulatory immune response (enhanced production of IL-10, IL-6 and MIP-1α), which was less well mastered by the RA cercariae. **Conclusion:** In addition to the more well-known single cell tracking studies we have now demonstrated that similar technologies may apply for multicellular parasites. As such, imaging studies can be used to help understand the dermal immune response. With that, molecular imaging provides a valuable tool on the path towards effective vaccine development. **References:** None.

Plenary 4: Highlights Lecture

Wednesday, October 16, 2019, 12:15 - 13:15 Auditorium

OP-789

Highlights Lecture

V. Garibotto;
Nuclear Medicine and Molecular Imaging Division, Geneva University Hospitals, Geneva, SWITZERLAND.

OP-790

Highlights Lecture

S. Schwarzenböck;
Rostock University Medical Center, Department of Nuclear Medicine, Rostock, GERMANY.

Scientific e-Poster Presentation Sessions

111

e-Poster Presentation Session 1 - Oncology: Oncology - Greatest Hits!

Sunday, October 13, 2019, 8:00 - 9:30 Room 133/134

EPS-001

Visualization of sentinel lymph nodes in gynecological cancer patients

I. Sinilkin[1], V. Chernov[1], A. Medvedeva[1], R. Zelchan[1], O. Bragina[1], A. Chernyshova[1], L. Kolomiets[1], M. Ochirov[1], E. Stasyuk[2], V. Skuridin[2];
[1]Tomsk National Research Medical Center of the Russian Academy of Sciences, Tomsk, RUSSIAN FEDERATION, [2]Tomsk Polytechnic University, Tomsk, RUSSIAN FEDERATION.

Aim/Introduction: To evaluate the diagnostic efficacy of a new radiopharmaceutical ^{99m}Tc- aluminum gammoxide for the detection of sentinel lymph nodes (SLN) in gynecological cancer patients. **Materials and Methods:** The study included 60 patients with endometrial cancer T1a-bNxM0 (n = 30) and cervical cancer T1a-bNxM0 (n = 30). The day before the operation, 2-4 submucosal injections of ^{99m}Tc-Alotech at a dose of 20 MBq per injection site were made to the cervix. Patients underwent single photon emission computed tomography (SPECT) of the pelvic region 18 hours after administration of the radiocolloid. Evaluation of the results of the study was carried out both visually and the intensity of the radiopharmaceutical uptake in the SLN was compared with the injection site. To improve the topographic localization of the sentinel lymph nodes, a multimodal technique was used, consisting in combining the results of the SPECT and MRI. Radioguide intraoperative detection of sentinel lymph nodes using a gamma probe was carried out. After removal of the sentinel lymph nodes, pelvic lymph node dissection was performed to examine the condition

of the remaining lymph nodes. **Results:** Sentinel lymph nodes were detected in all patients by SPECT and radioguide mapping. In three (5%) cases one SLN were found, in 57 (95%) patients - 2 bilateral SLN were visualized. In 78.3% of cases SLN were located in the region of the external and internal iliac vessels, and in all cases the location of the SLN was determined by SPECT/MRI study. The excised SLNs were evaluated by urgent cytology with subsequent routine histological examination. By urgent cytology in 9 SLN metastatic lesions were and two patients had micrometastases. **Conclusion:** The use of radiopharmaceutical ^{99m}Tc- aluminum gammoxide in patients with gynecological cancer allows you to identify SLN with sensitivity and specificity of 100%. The use of the multimodal SPECT/MRI fusion allows accurately indicate the anatomical localization of the SLN. **References:** None.

EPS-002

Evaluation of PSMA Expression Changes on PET/CT Before and After Initiation of Novel Antiandrogen Drugs (Enzalutamide or Abiraterone) in Metastatic Castration-Resistant Prostate Cancer Patients

*N. Plouznikoff[1,2], **C. Artigas**[1], S. Sideris[3], T. Gil[3], N. Martinez-Chanza[3], T. Roumeguere[4], A. Peltier[5], P. Flamen[1];*
[1]Department of Nuclear Medicine, Institut Jules Bordet, Université Libre de Bruxelles (ULB), Brussels, BELGIUM, [2]Department of Nuclear Medicine, Centre Hospitalier de l'Université de Montréal (CHUM), Montreal, QC, CANADA, [3]Department of Oncology, Institut Jules Bordet, Université Libre de Bruxelles (ULB), Brussels, BELGIUM, [4]Department of Urology, Hôpital Erasme, Université Libre de Bruxelles (ULB), Brussels, BELGIUM, [5]Department of Urology, Institut Jules Bordet, Université Libre de Bruxelles (ULB), Brussels, BELGIUM.

Aim/Introduction: Novel androgen deprivation therapies are currently indicated for castration-resistant prostate cancer patients. The aim of this study was to retrospectively investigate the association between ^{68}Ga-labeled Prostate-Specific Membrane Antigen (PSMA) expression changes on PET/CT and the response to treatment, mainly based on Prostate-Specific Antigen (PSA) levels, following the start of enzalutamide or abiraterone in metastatic castration-resistant prostate cancer (mCRPC) patients. **Materials and Methods:** We retrospectively reviewed all ^{68}Ga-PSMA-11 PET/CT scans performed at our institution from November 2014 to March 2019. We included mCRPC patients with a first ^{68}Ga-PSMA PET/CT performed <2 months before the start of enzalutamide or abiraterone, and a second ^{68}Ga-PSMA PET/CT performed <1 year after (with no modification in therapy between scans). 11 and 15 patients were included in the enzalutamide and abiraterone arms, respectively. All associated clinical records were reviewed. The biological data was used to distinguish PSA-non-responders (increasing PSA following the start of therapy or the nadir thereafter) and PSA-responders (decreasing PSA following the start of therapy or the peak thereafter). The PSMA PET/CT response was assessed visually by two independent nuclear medicine physicians. Patients were classified as PSMA-non-responders (≥1 new PSMA-expressing metastases, majority of PSMA-expressing metastases increasing in intensity, or stable PSMA-expression of the disease) or PSMA-responders (complete disappearance of pathologic PSMA uptake, or majority of PSMA-expressing metastases decreasing in intensity). Descriptive statistics and measures of associations (two-sided Fisher's exact test and Phi coefficient) were calculated. **Results:** For enzalutamide and abiraterone, the median delay between the first ^{68}Ga-PSMA PET/CT and the start of therapy was 8 (IQR:7-16) and 24 (IQR:8-30) days, respectively. The median delay between the start of therapy and the second ^{68}Ga-PSMA PET/CT was 110 (IQR:76-124) and 87 (IQR:71-242) days, respectively. PSA-response and PSMA-response were perfectly associated for both enzalutamide (8 PSA/8 PSMA-non-responders, 3 PSA/3 PSMA-responders; p=0.006, Phi=1.000) and abiraterone (11 PSA/11 PSMA-non-responders, 4 PSA/4 PSMA-responders; p=0.001, Phi=1.000). No isolated PSMA flare was detected, as PSA-response was always associated with a decrease in PSMA-expression on the second PET/CT. **Conclusion:** This retrospective study suggests that, after a median follow up of 3 months under enzalutamide or abiraterone, PSMA expression changes on PET/CT are strongly associated with PSA response. No PSMA-expression flare was found, but an early and limited flare phenomenon cannot be excluded. Prospective studies are needed to better understand PSMA expression dynamics following the start of enzalutamide and abiraterone, along with its potential role in response assessment. **References:** None.

EPS-003

Neoadjuvant Pazopanib Treatment In High-risk Soft Tissue Sarcoma: A Quantitative Dynamic ^{18}F-FDG PET/CT Study Of The German Interdisciplinary Sarcoma Group

***C. Sachpekidis**[1,2], I. Karampinis[3], J. Jakob[4], B. Kasper[5], K. Nowak[6,7], L. Pilz[8], U. Attenberger[9], T. Gaiser[10], H. G. Derigs[11], M. Schwarzbach[12], P. Hohenberger[3], A. Dimitrakopoulou-Strauss[1], U. Ronellenfitsch[3,13];*
[1]Clinical Cooperation Unit Nuclear Medicine, German Cancer Research Center, Heidelberg, GERMANY, [2]Nuclear Medicine Dept, Bern University Hospital, Bern, SWITZERLAND, [3]Division of Surgical Oncology and Thoracic Surgery, University Medical Center Mannheim, Mannheim, GERMANY, [4]Department of General, Visceral and Child Surgery, University Medical Center Göttingen, Göttingen, GERMANY, [5]Interdisciplinary Tumor Center Mannheim, Sarcoma Unit, Mannheim University Medical Center, Mannheim, GERMANY, [6]Division of Surgical Oncology and Thoracic Surgery, University Medical Center Mannheim, Heidelberg, GERMANY, [7]Department of Abdominal, Vascular and Thoracic Surgery, Romed Klinikum, Rosenheim, AUSTRIA, [8]Medical Faculty Mannheim, University of Heidelberg, Mannheim, GERMANY, [9]Institute of Clinical Radiology and Nuclear Medicine, University Medical Center Mannheim, Mannheim, GERMANY, [10]Institute of Pathology, University Medical Center Mannheim, Mannheim, GERMANY, [11]Department of Hematology and Oncology, Klinikum Frankfurt-Hoechst, Frankfurt am Main, GERMANY, [12]Department of Surgery, Klinikum Frankfurt-Hoechst, Frankfurt am Main, GERMANY, [13]Department of Abdominal, Vascular, and Endocrine Surgery, University Hospital Halle, Halle (Saale), GERMANY.

Aim/Introduction: The outcome of high-risk soft tissue sarcoma (STS) is poor with radical surgery being the only potentially curative modality. Pazopanib is a multikinase inhibitor approved for treatment of metastatic STS. Most recently, the German Interdisciplinary Sarcoma Group (GISG-04/NOPASS) trial has shown that preoperative pazopanib therapy is not effective for unselected high-risk STS, using metabolic response in ^{18}F-FDG PET/CT as primary endpoint; nevertheless, relevant treatment effects were observed in selected patients. Herein, we evaluate the potential role of kinetic analysis of ^{18}F-FDG data derived from application of dynamic PET/CT in response assessment to pazopanib of STS patients scheduled for surgical resection. **Materials and Methods:** Sixteen STS patients treated with pazopanib as neoadjuvant therapy before surgery were enrolled in the analysis. All patients underwent dynamic PET/CT prior to and after pazopanib treatment. Data analysis consisted of visual (qualitative) analysis of the PET/CT scans, semi-quantitative evaluation based on SUV calculations, and quantitative analysis of the dynamic ^{18}F-FDG PET data based on two-tissue compartment modeling as well as on a non-compartmental model based on the calculation of the fractal dimension of the time-activity curves. Resection specimens were histopathologically assessed and the percentage of regression grade was recorded. Time to tumor relapse/progression was also calculated. **Results:** In the follow up 12/16 patients (75%) were alive without relapse, while four patients (25%) relapsed, among them one patient who died. Mean histopathological regression was 26%. The studied population was dichotomized according to mean value of the percentage of histopathological regression after pazopanib as a cutoff. Using the 30% regression grade as threshold, 6/14 patients (43%) showed partial remission (PR), while stable disease (SD) was seen in the rest of 8 evaluable patients (57%). Although semi-quantitative evaluation showed no statistically significant change of $SUV_{average}$ and SUV_{max}, ^{18}F-FDG kinetic analysis revealed a significant decrease of the perfusion-related parameter K_1. The dichotomization of the studied population according to histopathologic regression grade showed no statistically significant differences between the PR and SD groups. **Conclusion:** Although the widely used PET parameter SUV did not show significant response, the perfusion-related kinetic parameter K_1 -reflecting the carrier-mediated transport of ^{18}F-FDG from plasma to tumor- significantly decreased as a marker of response to pazopanib in STS. This finding could be due to the anti-angiogenic effect of pazopanib. ^{18}F-FDG PET parameters did not show any association to histopathological regression as response to the treatment. **References:** None.

EPS-004

Role of Metabolic Response by ^{18}F-FDG PET/CT Added to iRECIST in NSCLC Patients Treated with Immune Checkpoint Inhibitors

A. Castello[1], *L. Toschi*[2], *S. Rossi*[2], *E. Mazziotti*[1], *E. Lopci*[1];
[1]*Nuclear Medicine, Humanitas Clinical and Research Hospital - IRCCS, Rozzano (MI), ITALY,* [2]*Oncology and Hematology, Humanitas Clinical and Research Hospital - IRCCS, Rozzano (MI), ITALY.*

Aim/Introduction: To investigate the role of metabolic response with ^{18}F-FDG PET/CT in patients with non-small cell lung carcinoma (NSCLC) treated with Immune Checkpoint Inhibitors (ICI). **Materials and Methods:** The trial was registered at http://www.clinicaltrials.gov (NCT03563482). We analyzed data from 25 patients (16 male, 9 female, mean age 75) with NSCLC treated with ICI prospectively enrolled from April 2017 to December 2018. ^{18}F-FDG PET/CT and contract enhanced CT were performed at baseline and after 8 week of treatment in all patients. Response assessment was evaluated according metabolic and morphological criteria based on EORTC and iRECIST, respectively. As metabolic parameters, we utilized also metabolic tumor volume (MTV), total lesion glycolysis (TLG), as well as their percentage changes (ΔSUVmax, ΔMTV, and ΔTLG). With a median follow-up of 11.3 months, response criteria we mutually compared and correlated to progression-free survival (PFS). **Results:** Based on metabolic response, after 8 weeks of ICI we identified 8 (32%) partial metabolic response (PMR), 11 (44%) stable metabolic disease (SMD), and 6 (24%) progressive metabolic disease (PMD). Median values for the other metabolic parameters resulted ΔSUVmax=+8.21%, ΔMTV=+67.7% and ΔTLG=+37.6%. On the other hand, 5 (20%) partial response (PR), 11 (44%) stable disease (SD), and 9 (36%) progressive disease (PD) were identified according to morphological criteria. On log rank test, EORTC response classified as PMR vs SMD/PMD resulted significantly correlated to PFS (p=0.014). Univariate analysis with Cox proportional hazards determined a statistically significant association to PFS also for ΔSUVmax (p=0.009), ΔMTV (p=0.03), and ΔTLG (p=0.013). Moreover, in patients with PR and SD according to iRECIST, there was a significant difference in PFS based on metabolic response (median not reached for PMR vs 6 months for SMD/PMD, p=0.023; HR 0.229). **Conclusion:** Metabolic response by ^{18}F-FDG PET/CT allows for the prediction of patients with longer PFS during therapy with ICI. The added value of EORTC criteria is confirmed for patients presenting with a PR or SD according to iRECIST. The Italian Association for Research on Cancer (AIRC - Associazione Italiana per la Ricerca sul Cancro) is acknowledged for the support on research. **References:** None.

EPS-005

The evaluation of tumor response to neoadjuvant chemotherapy for esophageal cancer using PERCIST 1.0-multicenter study

H. Kaida[1], *K. Kitajima*[2], *M. Nakajo*[3], *M. Ishibashi*[4], *R. Minamimoto*[5], *K. Hirata*[6], *K. Nakatani*[7], *T. Yasuda*[1], *K. Ishii*[1];
[1]*Kindai University Faculty of Medicine, Osaka-Sayama, JAPAN,* [2]*Hyogo College of Medicine, Nishinomiya, JAPAN,* [3]*Graduate School of Medical and Dental Sciences, Kagoshima University, Kagoshima, JAPAN,* [4]*School of Medicine, Tottori University, Yonago, JAPAN,* [5]*National Center for Global Health and Medicine, Tokyo, JAPAN,* [6]*Hokkaido University Graduate School of Medicine, Sapporo, JAPAN,* [7]*Kurashiki Central Hospital, Kurashki, JAPAN.*

Aim/Introduction: To evaluate tumor response to neoadjuvant chemotherapy (NAC) and predict esophageal squamous cell carcinoma recurrence using Positron Emission Tomography Response Criteria in Solid Tumors (PERCIST) 1.0. **Materials and Methods:** Our study population was collected from seven institutions in Japan, and comprised of 180 patients (153 men and 27 women) who underwent fluorodeoxyglucose-positron emission tomography/computed tomography (FDG-PET/CT) before and after NAC prior to planned surgical resection. The median age of our population was 66 (range, 38-78) years. Patients were divided into responder and non-responder based on pathological response, and the pathological response of both primary tumor and lymph node metastasis was evaluated. The PET parameters including peak standardized uptake value corrected for lean body mass (SULpeak) and total lesion glycolysis (TLG) were measured to evaluate PERCIST to both primary lesion and lymph node metastasis. To examine the diagnostic performance of each parameter in discriminating pathological responder, receiver operating curve (ROC) analysis was conducted, and the best cut-off point in each parameter was determined. The difference between responder and non-responder about PET parameters and clinicopathological variables was investigated using the Mann-Whitney U, Chi-squared or Fisher's exact test. The Cox proportional hazard model was used to evaluate the effects of PET parameters and clinicopathological variables for progression free survival (PFS). Survival curves were drawn using the Kaplan-Meier method and the significant difference between survival curves was tested with the log-rank test. **Results:** Complete metabolic response (CMR), partial metabolic response (PMR), stable metabolic disease (SMD), and progressive metabolic disease (PMD) were seen in 31 101, 40, and 8 patients, respectively. Seventy-nine (43.9%) of 180 patients showed pathologic responder. An optimal percent decrease in SULpeak of 52.2% was found to have a sensitivity of 87.3%, and accuracy of 68.9%, and that of TLG of 87.3% did a sensitivity of 84.8%, specificity of 59.4%, and accuracy of 70.6%. There was a significant correlation between pathologic response and PERCIST ($P<0.001$). Eighty-three (46.1%) of the 180 patients developed recurrent disease. Multivaraite Cox regression analysis showed that PERCIST, %SULpeak reduction rate, number of pathological lymph nodes, and resection level were significantly associated with longer PFS (PERCIST; HR=2.134; P=0.03, %SULpeak reduction rate; HR=1.025; $P<0.001$, number of pathological lymph nodes: HR=2.370; P=0.001, resection level: HR=0.235; $P<0.001$). **Conclusion:** PERCIST 1.0 may be useful for predicting pathological response and prognosis after NAC in esophageal squamous cell carcinoma patients. **References:** None.

EPS-006

18F-FDG PET/CT metabolic/volumetric parameters evaluation to predict response to neoadjuvant chemotherapy (NAC) and prognostic value in patients withTriple-Negative breast cancer (TNBC)

G. Paone[1], *S. Di Lascio*[2], *F. Quattrocchi*[3], *T. Ruberto*[1], *G. Treglia*[1], *L. Ceriani*[1], *L. Giovanella*[1];

[1]*Department of Nuclear Medicine and PET/CT Centre, Imaging Institute of Southern Switzerland, Lugano-Bellinzona, SWITZERLAND,* [2]*Department of Medical Oncology, Oncology Institute of Southern Switzerland, Bellinzona, SWITZERLAND,* [3]*Department of Nuclear Medicine, University of Messina, Messina, ITALY.*

Aim/Introduction: The aim of this study was to assess response to NAC and prognostic value considering dynamic evolution of metabolic/volumetric parameters measured on 18F-FDG PET/CT in TNBC. **Materials and Methods:** We retrospectively analyzed 42 patients with TNBC, who performed a staging PET/CT before and after neo-adjuvant chemotherapy. Treatment-related changes in SUVmax, MTV and TLG were evaluated (ΔSUVmax, ΔMTV and ΔTLG) in the primary tumor. To identify the optimal cut-off value of these parameters a receiver-operating curve analysis was performed. Kaplan-Meier method was used to evaluate prognostic value. The associations between early metabolic/volumetric changes, pathological complete response (pCR), and event-free survival (EFS) were examined **Results:** Of the 42 patients, 10 (24%) achieved pCR, 14 (33%) relapsed and 10 of them died (median FU, 33 mo). No relapse was observed in patients with pCR (0.001). An optimal percent of decrease in SUVmax (cutoff value ΔSUVmax 86%, p 0.0001), MTV (cutoff value ΔMTV 99%, p 0.0001) and TLG (cutoff value ΔTLG 99%, p 0.0001) had the best predictive value in terms of pCR. No significant correlation was found with SUVmax, MTV and TLG absolute value. ΔSUVmax 84% (p 0.0026), ΔMTV 59% (p 0.0014) and ΔTLG 70% (p 0.0026) were significantly associated with EFS yielding the best prediction of recurrence **Conclusion:** Our data suggest that only the dynamic variation of 18F-FDG PET/CT metabolic/volumetric parameters is a predictive marker for pCR and EFS following NAC in TNBC. In the future, this could be a further tool to evaluate the response to NAC addressing to different therapeutic strategies **References:** None.

EPS-007

^{18}F-5-FPN: A Strikingly Fascinating and Potential Probe for Monitoring Photothermal Therapy Response in Malignant Melanoma

X. Lan*, Y. Wang, Y. Zhang, R. An;*
Union Hospital, Tongji Medical College, Huazhong University of Science and Technology, Wuhan, CHINA.

Aim/Introduction: The increasing global burden and the markedly breakthroughs in therapy of malignant melanoma (MM) make urgent demands on efficient response evaluation. In our previous researches, ^{18}F-5-fluoro-N-(2-(diethylamino)ethyl) picolinamide (^{18}F-5-FPN) exhibited high sensitivity, specificity and affinity to melanin. Photothermal therapy (PTT) exploits melanin to absorb and convert light energy into heat, which could kill tumor cells. The aim of this study was to further explore the feasibility of ^{18}F-5-FPN PET to evaluate PTT therapy for MM, and comparing with that of ^{18}F-FDG. **Materials and Methods:**

Nude mice bearing B16F10 (melanoma cell) or MDA-MB-231 (breast cancer cell) were irradiated with an 808 nm laser for PTT. Survival analysis with Kaplan-Meier plots and Log-rank test was exploited to observe the therapy efficacy of PTT. ^{18}F-5-FPN and ^{18}F-FDG PET imaging were performed before and after PTT for therapy response evaluation in mice bearing B16F10 until 17 days after treatment. Furthermore, three different models, B16F10, MDA-MB-231 bearing nude mice and inflammatory models were prepared, and performed ^{18}F-FDG and ^{18}F-5-FPN PET imaging to further assess the specificity of ^{18}F-FDG and ^{18}F-5-FPN. **Results:** Melanin in B16F10 tumors successfully transformed optical energy into heat, and apparently framework destruction of tumor tissue and extensive necrosis were discovered by HE staining after 24 h of PTT. PTT prolonged the median survival of B16F10 models compared with untreated B16F10 mice (34 d vs. 9.5 d, P<0.001). The mean tumor uptakes of ^{18}F-5-FPN on Day 2 (7.52 ± 3.65 %ID/g) and Day 6 (0.22 ± 6.00 %ID/g) after PTT were much lower than that those of before treatment 18.33 ± 4.98 %ID/g (P < 0.01). However, no significance existed between the ^{18}F-FDG uptakes on Day 1 after PTT and before treatment (6.18 ± 1.18 %ID/g vs. 6.54 ± 0.84 %ID/g, P > 0.05), and the tumor uptakes on Day 5 elevated to 8.69 ± 2.75 %ID/g. For the three different models, ^{18}F-5-FPN only accumulated in B16F10 tumor with 20.36 ± 4.38 %ID/g, but not in the MDA-MB-231 tumor (2.72 ± 0.49 %ID/g) and inflammation (1.14 ± 0.30 %ID/g). However, high uptakes of ^{18}F-FDG were seen in all three models. **Conclusion:** Compared with ^{18}F-FDG, ^{18}F-5-FPN PET imaging was capable of estimating PTT response in MM, successfully monitored the occult recurrence after therapy, and perfectly distinguished MM from inflammation and other carcinomas. This potential probe may provide a new approach for precise and effective response evaluation, timely management of therapeutic regimen and sensitive follow-up. **References:** None.

EPS-008

Clinical Efficacy of Radiosynoviorthesis (RSV) in Elbow Joint Systemic Arthritis

I. Iakovou, T. Kotrotsios, E. Giannoula, A. Kalaitzoglou, C. Sachpekidis, G. Arsos;
Academic Dpt Of Nuclear Medicine, Papageorgiou Hsp, Thessaloniki, GREECE.

Aim/Introduction: To retrospectively evaluate the long term efficacy of radiosynoviorthesis (RSV) in patients with systemic (rheumatoid or psoriatic) arthritis of the elbow joint. **Materials and Methods:** 29 painful despite pharmacotherapy elbow joints of 28 patients (22 females, 67+-3 years old enrolled the study. They were intra-articularly injected with 2mci of 169Er citrate under x-ray guidance. In the pretherapeutic bone scan, all joints presented an positive blood pool image, indicative for active local synovitis. Joint functional status and pain were assessed by a visual analog scale (VAS) of ten steps: 1 - lack of any impairment to 10 - total disability just before (less than a week), a month and a year after treatment. **Results:** Twenty five in 28 patients (26 in 29 joints -90%) responded to therapy reporting a pronounced improvement in their manual activities as documented by the decrease of the mean VAS score prior to treatment from 8,3+-1,6 to 2,8+-1,9 (p<0,05) 12 months after RSV. **Conclusion:** RSV is a highly effective procedure in elbow's systemic arthritis active synovitis. **References:** [Radiosynovectomy for the treatment of rheumatoid arthritis of the elbow joint]. Rozeboom S, Dörr U, Bihl H. Nuklearmedizin. 2001 Jun;40(3):91-7.

EPS-009

FDG PET/CT for early prediction of response to neoadjuvant therapy in HER2+ breast cancer: validation in a multicentric population

S. Tisserand[1], *S. Kanoun*[1], *J. Blanc*[1], *B. Coudert*[1], *A. Berriolo-Riedinger*[1], *F. Cachin*[2], *L. Champion*[3], *O. Humbert*[4], *P. Salaun*[5], *T. Mognetti*[6], *K. Kerrou*[7];
[1]*Centre Georges François Leclerc, Dijon, FRANCE,* [2]*Centre Jean-Perrin, Clermont-Ferrand, FRANCE,* [3]*Institut Curie, Paris, FRANCE,* [4]*Centre Antoine Lacassagne, Nice, FRANCE,* [5]*CHU Morvan, Brest, FRANCE,* [6]*Centre Léon Bérard, Lyon, FRANCE,* [7]*Hopital Tenon, Paris, FRANCE.*

Aim/Introduction: Neoadjuvant therapy (NAC) including trastuzumab is a standard treatment in locally advanced breast cancer (BC) overexpressing HER2. Achieving pathologic complete response (pCR) at surgery is linked with better clinical outcome. Previous monocentric studies have shown the utility of FDG-PET/CT for early prediction of response in this setting, thanks to a high negative predictive value to identify nonresponders. However, multicentric validation is lacking and there are contradictory results regarding the best predictor of pCR, (early metabolic changes, or low residual metabolism after 1 or 2 cycles of therapy). The aim of this study was to determine in a multicentric population, the best metabolic parameters derived from FDG-PET/CT for early prediction of pCR after one cycle of NAC in HER2+ BC **Materials and Methods:** Patients were initially recruited in the AVATAXHER trial (EUDRACT 2009-013410-26), a prospective phase II multicentric study (26 participating centres) designed to investigate whether the addition of bevacizumab could improve the proportion of patients achieving pCR in patients unlikely to respond to treatment, based on FDG-PET/CT. For this ancillary study, only patients receiving conventional NAC (6 cycles of docetaxel+trastuzumab) were included. Each patient had FDG PET/CT before the first and second cycle of therapy in order to evaluate baseline and residual tumour metabolism (SUV_{max}, SUV_{peak}, SUV_{mean}, MTV, TLG). The tumour metabolic response (ΔSUV_{max}, ΔSUV_{peak}, ΔSUV_{mean}, ΔMTV, ΔTLG) was also calculated **Results:** Sixty-one patients were included. Of them, 34 (56%) reached pCR. There was no significant association between baseline tumour metabolism and pCR. In univariate analysis, low residual metabolism was significantly associated with pCR when considering SUV_{max} (p = 0.01, AUC=0.66), SUV_{mean} (p = 0.006, AUC=0.66) and SUV_{peak} (p = 0.003, AUC=0.69). Tumour metabolic response was also correlated with pCR when considering ΔSUV_{max} (p = 0.001, AUC=0.71), ΔSUV_{peak} (p = 0.0009, AUC 0.72),

and ΔSUV_{mean} (p=0.002, AUC=0.71). Volume-based parameters, either baseline, residual or early changes, did not correlate with pCR. In multivariate analysis, ΔSUV_{max} remained an independent predictive factor of pCR (OR=8.87, p = 0.002) with high SBR grade **Conclusion:** Our results confirm the utility of FDG-PET/CT for early prediction of pCR after NAC in HER2+ BC. Among the various metabolic parameters tested, ΔSUV_{max} appears to be the most robust and appropriate in this multicentric population **References:** None.

EPS-010

Pathologic neck node metastasis in Patients With Gynecologic Malignancy with neck node uptake on the F-18 FDG PET/CT

S. Yoon;
Department of Nuclear Medicine, Health Promotion Center, H plus New Yang-Ji Hospital, Department of Nuclear Medicine, Cheil General Hospital, Seoul, KOREA, REPUBLIC OF.

Aim/Introduction: Metastatic neck nodes limited to the lower neck including supraclavicular node are usually associated with primary malignancies below the clavicle. Prognosis of neck node metastasis of gynecologic malignancy is considered significant due to possibilities of combined further distant metastasis. We evaluated the pathologic type of primary malignant lesion and frequency of pathologic proven node metastasis in the patients with neck lymph nodal uptake on the F-18 fluorodeoxyglucose (FDG) PET-CT in the gynecologic cancer patients. **Materials and Methods:** Between April 2009 and December 2018, retrospectively 1600 patients with pathological-proven gynecologic malignancies including cervix cancer, endometrial cancer and ovarian cancer were evaluated. Thirty patients were suspected of neck lymph node metastasis in PET/CT and underwent a sono-guided neck lymph node biopsies. We evaluated the primary pathologic malignant lesion and histologic type of node metastasis in the patients with node metastasis in the neck. We evaluated the primary pathologic malignant lesion and the tumor marker in the patients with only single node metastasis in the neck. **Results:** Metastastic neck node on the PET-/CT in the patient with gynecologic malignancy was suspected in 30/1600 patients. 11 patients among 30 proven by sono guided aspiration biopsy of the neck nodes had node metastasis, other 19 patients showed benign reactive nodes. Among 11 patients with pathologically proven neck node metastasis, 7 among 17 cervical malignant lesion (41%) and 3 among 7 endometrial malignant lesion (43%) showed pathologic proven metastatic nodes. Histologic cell types showed 3 metastatic adenocarcinoma, 6 metastatic squamous cell carcinoma, 1 metastatic adenosquamous cell carcinoma and 1 lymphoma. Six patients (55%) among 11 patients with pathological proven neck node metastasis had pathologically only single neck node metastasis without any evidence of other metastatic nodes/lesions. Four cervix carcinoma with single neck node metastasis had normal tumor marker. One ovarian carcinoma also had normal tumor marker level. Only another one endometrial carcinoma showed elevated CA-125 **Conclusion:** Cervical carcinoma was the most common type of gynecologic malignancy with neck node metastasis. Six among 11 patients with neck node metastasis showed only single node metastasis without any metastasis outside the neck. And five patients with only single neck node metastasis had normal tumor marker level. Cervical carcinoma was the most common type of gynecologic malignancy with single node metastasis and normal tumor marker. We should attend suspicious neck node uptake on PET-CT albeit only single node uptake and normal tumor marker. **References:** None.

EPS-011

Bone marrow FDG uptake and correlation with bone marrow plasma cell infiltration rate and plasma cell morphology in Multiple Myeloma patients

A. Paschali[1], *E. Panagiotidis*[1], *P. Mitsakis*[1], *N. Papadopoulos*[1], *T. Triantafyllou*[2], *E. Giannoula*[1], *M. Kotzasarlidou*[1], *E. Verrou*[2], *P. Konstantinidou*[2], *V. Chatzipavlidou*[1], *E. Katodritou*[2];
[1]*Department of Nuclear Medicine, Theageneio Cancer Hospital, Thessaloniki, GREECE,* [2]*Department of Hematology, Theageneio Cancer Hospital, Thessaloniki, GREECE.*

Aim/Introduction: Multiple Myeloma (MM) is characterized by markedly heterogeneous phenotypic, genetic and clinical presentation. Aim of our study was to investigate possible correlations between bone marrow (BM) diffuse FDG uptake, plasma cell infiltration rate and plasma cell morphology. **Materials and Methods:** Thirty-three patients with MM either at diagnosis (n=11) or at relapse (n=22) were eveluated (M/F: 19/14, median age 62.5, range: 38-80, IgG: 19, IgA: 6, light-chain: 7, IgD: 1, ISS1: 12, ISS2: 14, ISS3: 7). High risk cytogenetics detected by FISH, including t(4;14), del17p and 1q+ were observed in 5 patients and t(11;14) was detected in 2 patients. Whole body 18F-FDG PET/CT studies were evaluated visually and semi quantitatively with the following parameters included in the analysis: BM metabolic state, number (Fn) and SUVmax of focal PET lesions, osteolysis number (Ln), presence and site of extramedullary disease (EM), paramedullary lesions (PM) and fractures(Fr), according to the IMPeTUs criteria (Nanni et al, EJNM 2018). For each patient we calculated the SUVmax ratio pelvis/liver using a circular region of interest (ROI) in the central portion of the liver far away from its edge, and a ROI within the pelvis (to include iliac crests and sacrum/L5) taking care not to include focal areas or other abnormality. Bone marrow aspirates of the iliac crest were performed within 4 weeks around the PET/CT examination. According to the plasma cell morphology we separated patients in groups of good, moderate and poor differentiation. **Results:** The rate of clonal plasma cells (PCs) in the BM at the time of PET evaluation was ≥20% in 27/33 patients (PCs of good differentiation: 18/33, PCs of moderate/poor differentiation:15/33). In these 27 patients the patterns of skeletal FDG uptake were: diffuse (n=8), diffuse+focal (n=10), focal (n=6) and negative (n=3). Moderate or poor differentiation morphology and BM plasma cell infiltration rate≥20% both

positively correlated with increased SUVmax pelvis/liver (p=0.05 and 0.02, respectively). Limb's marrow involvement (femurs and humerals) was observed in all patients with diffuse axial marrow involvement, being more evident in those of moderate/poor differentiation. PM or EM disease significantly correlated with PCs' morphology (p<0.05). Plasma cell morphology or rate of BM infiltration did not correlate with PET skeletal pattern, focal sites on PET or lytic lesions on CT. **Conclusion:** These preliminary data suggest that the sensitivity of PET in the detection of diffuse BM infiltration is dependant on plasma cell morphology and increases with the degree of undifferentiation. **References:** None.

EPS-012

^{68}Ga-PSMA PET/CT whole-body tumor burden in patients with biochemical recurrence of prostate cancer

***A. Biggi Mattiolli**, M. C. L. Lima, M. Camacho, C. D. Ramos, A. O. Santos, E. Etchebehere;*
Medicina Nuclear de Campinas, Campinas, BRAZIL.

Aim/Introduction: In solid tumors, metabolic tumor volume (MTV) and total lesion glycolysis (TLG) in ^{18}F-FDG PET/CT studies showed to correlate with prognosis. In prostate cancer patients submitted to Ra-223 therapy, fluoride tumor volume and total fluoride uptake on lesions in ^{18}F-Fluoride PET/CT have shown to correlate with prognosis[1]. However, the determination of PSMA-^{68}Ga tumor burden of PSMA in lesions (whole-body PSMA tumor volume-PSMA-TV and the whole-body total uptake-PSMA-TL) in ^{68}Ga-PSMA PET/CT has not been extensively studied[2]. The objective of this project is to evaluate whether the serum PSA values and clinical parameters are associated with PSMA-TV and PSMA-TL. **Materials and Methods:** We retrospectively evaluated 211 patients with prostate cancer submitted to ^{68}Ga-PSMA PET/CT due to biochemical recurrence. In ^{68}Ga-PSMA PET/CT positive studies, the tumor burden parameters PSMA-TV and PSMA-TLG were calculated with a semi-automatic software (MFS tool; Syngo.Via VB20; Siemens Medical Solutions, Chicago, IL). The images were then reviewed to exclude any areas of physiologic uptake and to include pathologic areas with relatively low uptake. PSMA tumor burden metrics were correlated to clinical the following parameters age, free PSA levels (PSAf), total PSA levels (PSAt), Gleason score and the highest SUVmax lesion. **Results:** Among the 140 patients that underwent ^{68}Ga-PSMA PET/CT studies, 114 were positive and thus used to calculate the PMSA-TV and PSMA-TL tumor burden parameters. The mean PMSA-TV was 28.54 cm^3 and PMSA-TL was 207.99. There was a direct correlation between age and the PMSA-TV (p = 0.0056) and PSMA-TL (p = 0.0004) values. Higher PSAf and PSAt levels were associated with higher tumor burden values of PMSA-TV (p = 0.0002 and p <0.0001, respectively) and of PSMA-TLV (p <0.0001 and p <0.001, respectively). The SUVmax values only showed a direct and positive correlation with PSMA-TL (p <0.0001). **Conclusion:** In biochemical recurrence of prostate cancer, the whole-body tumor burden on ^{68}Ga-PSMA PET/CT has a direct and positive correlation with serum PSA values and age. Further work is needed to establish if PSMA-TL and PSMA-TV is a strong and independent prognostic imaging biomarker able to determine therapy response. **References:** 1. Etchebehere EC et. al. Prognostic factors in patients treated with 223Ra: the role of skeletal tumor burden on baseline 18F-fluoride PET/CT in predicting overall survival. J Nucl Med 2015. 2. Schmidkonz C et. al. 68Ga-PSMA-11 PET/CT-derived metabolic parameters for determination of whole-body tumor burden and treatment response in prostate cancer. Eur J Nucl Med Mol Imaging 2018.

EPS-013

Retrospective cohort study to assess the prognostic value of baseline necrosis on PET-CT imaging in Hodgkin lymphoma

***I. Chen**, N. Borges, L. Winn, W. Osborne, G. Petrides;*
Freeman Hospital, Newcastle Upon Tyne, UNITED KINGDOM.

Aim/Introduction: Identifying prognostic markers at diagnosis is essential to determine optimal tailored therapy for patients. The presence of necrosis has been shown to be associated with inferior outcomes in patients with diffuse large B cell lymphoma (1). This retrospective cohort study assesses whether necrosis at baseline correlates with clinical outcomes in patients with Hodgkin lymphoma. **Materials and Methods:** All available baseline PET-CT scans of patients diagnosed with Hodgkin lymphoma between January 2015 and December 2016 at a large UK teaching hospital were reviewed for evidence of tumour necrosis by a consultant radionuclide radiologist with a specialist interest in lymphoma. Potential necrosis identified on PET-CT was then confirmed visually and quantitatively on alternative imaging. The presence or absence of necrosis was correlated with prognostic markers (Total Metabolic Volume (TMV), Total Lesion Glycolysis (TLG) International Prognostic Index (IPI) (Hasenclever Index)) and response assessment (metabolic response, current remission status, relapse outcome and mortality). **Results:** Fifty three patients' PET-CT scans were reviewed in total. Ten patients were confirmed to have necrosis on both PET-CT and alternative imaging. The presence of necrosis was associated with increased total mortality (40%) vs no necrosis (16%); Kaplan Meier survival analysis demonstrated a significant difference between the necrosis cohort compared with the no necrosis cohort using the log rank test (p = 0.042). The presence of necrosis did not correlate with other prognostic markers (TMV, TLG or IPI). **Conclusion:** The presence of necrosis on baseline PET-CT scan in patients receiving frontline treatment for Hodgkin lymphoma significantly correlates with increased patient mortality. Tumour necrosis did not significantly correlate with other prognostic markers. Identifying high risk patients at diagnosis is important. The current UK practice of delivering more intensive frontline therapy to patients with a high IPI is suboptimal and intensifying treatment after a positive interim PET scan is also associated with poor outcomes. Robust prognostic markers at diagnosis are a priority for the management of patients with Hodgkin Lymphoma. This study has identified a new independent prognostic marker in Hodgkin Lymphoma and prospective

clinical trials are required. **References:** 1. Adams HJA, de Klerk JMH, Fijnheer R, Dubois SV, Nievelstein RAJ, Kwee TC. Prognostic value of tumor necrosis at CT in diffuse large B-cell lymphoma. Eur J Radiol. 2015 Mar;84(3):372-377.

EPS-014

Metabolic Tumor Volume Predicts Short-Term Progression After Immunotherapy in Non Small Cell Lung Cancer

***D. Chardin**, M. Paquet, J. Darcourt, J. Otto, O. Humbert;*
Centre Antoine Lacassagne, Nice, FRANCE.

Aim/Introduction: Baseline markers are needed to predict outcome after immunotherapy. This study aimed to investigate the predictive value of total metabolic tumor volume (MTV) measured from baseline [^{18}F]-fluorodeoxyglucose positron emission tomography/computed tomography (FDG-PET/CT) in patients with non-small cell lung cancer (NSCLC) treated with immunotherapy. **Materials and Methods:** From February 2017 to September 2018, 54 patients scheduled to initiate immunotherapy (pembrolizumab or nivolumab) as their first or later systemic treatment for metastatic NSCLC were prospectively evaluated in this non-randomized, current-care study in our institution. FDG PET was performed at baseline. Standardized uptake values of lesion with the highest uptake (SUV_{max}) was measured. Total MTV was obtained using à threshold based on 41% of the SUV_{max} in each lesion. Short-term progression was defined as progression and treatment stop within 3 months after the beginning of immunotherapy. Deaths within a 6 month follow up period were recorded. Univariate analyses and ROC analyses were performed to identify predictors of short-term progression. **Results:** Mean patient's age was 63±10 years. The pathological subtype was squamous cell carcinoma and adenocarcinoma in 80% and 20% of patients, respectively. On PET, median SUV_{max} was calculated at 14.2 [range: 6.3-64.0] and median MTV was measured at 31mL [range:2mL-308mL]. Sixteen patients presented with short-term progression after immunotherapy. By univariate analyses, a higher MTV was significantly associated with short-term progression (cut-off=31mL, HR=7.14; 95% CI: 1.6-45.9; p=0.006). A short-term progression was observed in 46% of patients with MTV >31 mL vs 11% of patients with MTV < 31mL. SUV_{max} did not show any correlation with short-term progression (p>0.05). ROC curve analysis of MTV to predict short-term progression revealed an AUC of 0.81 (95% CI: 0.69-0.92). Concerning overall survival, 7/27 patients with an MTV > 31 mL died during the 6 months follow-up, whereas 3/27 deaths were observed in patients with MTV < 31mL. **Conclusion:** MTV has a potential value in predicting short-term progression after immunotherapy in patients with NSCLC. Indeed, a high MTV is associated with a higher risk of short-term progression and could predict death within 6 months. **References:** None.

EPS-015

[^{68}Ga]Ga-PSMA-11 PET/CT For Monitoring Response to Treatment in Metastatic Prostate Cancer - is there an Added Value over Standard Follow-up?

***J. Kuten**, D. Sarid, O. Yossepowitch, N. J. Mabjeesh, E. Even-Sapir;*
Tel Aviv Sourasky Medical Center, Tel Aviv, ISRAEL.

Aim/Introduction: The aim of the current study was to assess whether, and to what extent, follow-up PSMA-based PET/CT studies add value to the routine clinical follow-up during treatment of patients with metastatic prostate cancer (PCa). **Materials and Methods:** The study cohort was composed of 52 patients with metastatic PCa who underwent [^{68}Ga]Ga-PSMA-11 PET/CT imaging and PSA level measurements before and during treatment. Response was categorized as improvement, stable disease and disease progression by serum PSA dynamics and compared to change in imaging findings on pre- and post-treatment PET/CT. McNemar's test was used to assess agreement between PET/CT- and PSA-based response to treatment. **Results:** Most patients (65.4%) had compatible biochemical- and imaging- based response to treatment. However, in 18/52 patients (34.6%) imaging and biochemical response, were discrepant. In 5/52 patients (9.6%) PET/CT "upstaged" and in 13/52 (25%) it "downstaged" disease compared to biochemical assessment. Discrepancy between imaging and biochemical response was most prominent in biochemically-stable patients (90.9%), followed by patients with biochemical-progression (33.3%) and only in 8.7% of patients with biochemical improvement. In 22 of 30 patients (73.3%) with longer follow-up, imaging response was relevant for treatment choice. Relevance of imaging response was reflected by its ability to assess individual lesions in case of heterogeneous lesion response, appearance of new lesions, and identification of lesions requiring specific attention such as targeting radiotherapy. **Conclusion:** Results of this retrospective analysis show that biochemical response to treatment and [^{68}Ga]Ga-PSMA-11 PET/CT-based response assessment differ in a third of metastatic PCa patients, often in view of the ability of imaging to allow for lesion-based and not only patient-based analysis. Monitoring response during treatment by [^{68}Ga]Ga-PSMA-11 PET/CT is relevant for decision-making and choosing treatment in the majority of patients. **References:** None.

EPS-016

Artificial intelligence can discriminate between focal and normal bone/bone marrow uptake in lymphoma patients staged with FDG-PET/CT- a descriptive study

***M. Sadik**[1], A. Krupic[1], A. Dudás[1], J. Lopez Urdaneta[1], J. Ulén[2], O. Enqvist[3,2], P. Andersson[4], L. Edenbrandt[1];*
[1]Nuclear Medicine, Gothenburg, SWEDEN, [2]Eigenvision AB, Malmö, SWEDEN, [3]Chalmers University of Technology, Gothenburg, SWEDEN, [4]Hematology, Gothenburg, SWEDEN.

Aim/Introduction: Localized bone marrow involvement

on FDG-PET/CT in newly diagnosed lymphoma patients has prognostic implications. A growing body of evidence suggest that FDG-PET/CT can replace bone marrow biopsy in some patients, avoiding unnecessary procedures and pain. As a first step we aim to study whether artificial intelligence (AI) can discriminate between localized and normal bone/bone marrow uptake. **Materials and Methods:** All newly diagnosed Hodgkin lymphoma (HL) and diffuse large B-cell lymphoma (DLBCL) patients who had undergone a staging PET/CT between 2011-2016 at Sahlgrenska University hospital were retrospectively included. Information regarding bone and bone marrow involvement were extracted from the final clinical assessment done by hematologists. In a previous work AI was trained to find the skeletal anatomy (1). Bone less than 7 mm from the bone surface were removed to isolate the bone marrow. A threshold was defined as the average SUV + 2 SD for the vertebral bone marrow. Any bone marrow voxels with SUV above this threshold were classified as lesion and the total lesion uptake (TLU) was calculated as (average lesion SUV - threshold) x (total lesion volume in mL). A TLU > 0,8 was considered pathological. **Results:** The total cohort consisted of 151 patients, of whom 72 (48%) patients were female. Median age was 34 years (10-85 years). Most patients had HL (87%) and the rest DLBCL. Eighteen patients were classified as having focal uptake by AI. Of those, 14 patients (78%) were classified as true positive and 4 (22%) as false positive. 133 patients were classified as normal by AI resulting in 127 (95%) patients classified as true negative and six (5%) as false negative. **Conclusion:** Our results show that AI can differentiate between normal and pathological bone/bone marrow uptake. This method can highlight pathological regions to focus the physician's attention and in the future standardize the PET/CT image reading. **References:** (1) Lindgren Belal S, Sadik M, Kaboteh R, Enqvist O, Ulén J, Poulsen MH, Simonsen J, Høilund-Carlsen PF, Edenbrandt L, Trägårdh E. Deep learning for segmentation of 49 selected bones in CT scans: First step in automated PET/CT-based 3D quantification of skeletal metastases. Eur J Radiol. 2019 Apr;113:89-95.

311

e-Poster Presentation Session 2 - Inflammation & Infection + Translational and Molecular Imaging Therapy: Infection and Inflammation - Clinical and Preclinical Studies

Sunday, October 13, 2019, 11:30 - 13:00 Room 133/134

EPS-017

Possible pharmacological treatment interactions in autologous leucocytes labelling technique with 99mTc-HMPAO in patients with knee/hip prosthesis

E. Dobra, B. Martínez de Miguel, E. Orihuela Pantoja, V. Mendi Barcina, H. García Ruiz, E. Martínez Montalbán;
Hospital Universitario La Paz, Madrid, SPAIN.

Aim/Introduction: Determine if the patient´s pharmacological treatment influences the labelling procedure of autologous leucocytes with 99mTc-HMPAO. **Materials and Methods:** We did a prospective study between May 2018 and April 2019 with a total of 72 patients with knee/hip prosthesis. All patients underwent study with 99mTc-HMPAO autologous leucocytes. Pharmacological treatment was collected from the patient's medical records. The drugs have been classified into 6 groups: 1=NSAID(Non-Steroidal Anti-Inflammatories), 2=Statins, 3=Corticosteroids, 4=PPI(Proton-Pump Inhibitor), 5=BDZ(Benzodiazepines), 6=ACEI(angiotensin-converting enzyme inhibitors).Labelling efficiency was calculated by dividing the final activity of labelled leucocytes by the activity before removing the wash supernatant. In our Radiopharmacy Unit a 60% limit is tolerable for patients over 12 years of age. The labelling mean activity of 99mTc-HMPAO was 24.5% ±1.80. In all cases % RQP(radiochemical purity) ≥80% with mean %RQP= 95.93±2.37. The statistical analysis was performed with SPSS program (descriptive statistical test with frequencies, means and standard deviation) and quantitative comparisons with the Mann-Whitney and Wilcoxon W tests. **Results:** The groups of drugs that showed a statistically significant association with the labelling efficiency were: 3=Corticoids and 5=BDZ. In the group of patients who received corticosteroids, mean labelling efficiency was 59.65% ±6,40 with a confidence interval of 95% (56.65; 62.65) and p = 0.0001. On the other hand the patients who did not take corticosteroids labelling efficiency had a mean of 67.10% ±6.68 with a 95% confidence interval (65.22; 68.98). The group of benzodiazepines the mean was 62.37% ±3.54 with 95% confidence interval (60.66; 64.08). The patients who did not take benzodiazepines the mean was 65.96% ±8.17 with a confidence interval of 95% (63.69; 68.24) with p = 0.017. In groups 1,2,4 and 6 no statistical significance was detect: 1=NSAIDs: 67.26% ±6.96 decreases to 63.92% ± 7.39; p=0,074 2=Statins: 65.50% ±7.47 to 64.19% ±7.29; p=0,399 4=PPI: 64.84% ±7.89 to 65.38% ± 6,15; p=0,82 6= ACEI: 64.92% ±7.95 to 65.19% ±5.94; p=0,700 **Conclusion:** According to the results obtained, we can affirm that, the treatments with NSAIDs, Statins, PPI, ACEI do not seem to have an influence on the leucocyte labelling and the corticoids and benzodiazepines, produce a decrease in the labelling efficiency, so that special attention should be paid to these treatments as they can negatively affect the leucocyte labelling with 99mTc-HMPAO. **References:** None.

EPS-018

Differential diagnosis of Adult-onset Still's disease and other connective tissue diseases with FDG PET/CT

Q. Wang, X. Zhou;
Peking University People's Hospital, Beijjing, CHINA.

Aim/Introduction: Adult-onset Still's disease (AOSD) is often difficult to diagnose because it is lack of characteristic clinical manifestations. In order to explore the value of FDG PET/CT in the differential diagnosis, we retrospectively analyzed the FDG PET/CT images in AOSD patients and other connective tissue

diseases(CTD) patients. **Materials and Methods:** Within the patients with fever of unknown origin who underwent FDG PET/CT examination, data of 46 with AOSD and 53 with other CTD were retrospectively studied, and 40 subjects with negative PET/CT in the same period were taken as the control group. Imaging characteristics of AOSD was firstly observed by visual judgment and SUV_{max} was respectively measured as a quantitative parameter in the spleen, bone marrow and blood pool in each cases. When abnormal lymph node was found, the SUV_{max} was measured on the lymph node with maximal diameter. ROC curve was used to analyze the differential diagnosis threshold. Significance of FDG PET/CT for the diagnosis of AOSD was evaluated, according to the image diagnostic criteria set on current study. **Results:** On FDG PET/CT examinations, abnormal uptake was found in 45/46 of the AOSD patients, including spleen (44), bone marrow (45) and lymph nodes (35), while above uptakes can also be seen in 44/53 of other CTD patients. However, SUV_{max} of spleen, bone marrow and lymph nodes in AOSD group was all significantly higher than that in the other CTD group, although the SUV_{max} of spleen and bone marrow in other CTD group were all significantly higher than that of control group. In addition, compared with the control group, FDG distribution was lower in on blood pool and liver in AOSD patients, but no statistic difference was found between the AOSD patients and other CTD patients. If taken the following two or more as the diagnostic criteria for AOSD, a diagnostic sensitivity, specificity and accuracy of 95.7%, 94.3% and 94.9% will be obtained, respectively: (1) spleen $SUV_{max} \geq 2.6$ and/or bone marrow $SUV_{max} \geq 3.1$; (2) multiple reactive hyperplastic lymph nodes with a symmetrical distribution mainly in neck and axillary lymph region and $SUV_{max} \geq 3.1$, (3) no abnormal uptake in other organs except the above nonspecific uptake. **Conclusion:** AOSD have characteristic imaging manifestations on FDG PET/CT, and it can help for differentiating AOSD from other connective tissue diseases. **References:** None.

EPS-019

Role of FDG PET/CT and MRI co-registration for diagnosis and follow-up of malignant external otitis: Preliminary results

L. Rodriguez-Bel[1,2], *M. Cortés-Romera*[1,2], *F. Cruellas-Taischik*[3,2], *M. Santín-Cerezales*[4,2], *A. Sabaté-Llobera*[1,2], *E. Llinares-Tello*[1,2], *A. Palomar-Muñoz*[1,2], *M. Martínez de Bourio-Allona*[1,2], *C. Gámez-Cenzano*[1,2];
[1]*PET-Unit. Department of Nuclear Medicine, L'Hospitalet De Llobregat, Barcelona, SPAIN,* [2]*Hospital Universitari de Bellvitge-IDIBELL, Barcelona, SPAIN,* [3]*Department of Otorhinolaryngology, L'Hospitalet De Llobregat, Barcelona, SPAIN,* [4]*Deparment of Infectious diseases, L'Hospitalet De Llobregat, Barcelona, SPAIN.*

Aim/Introduction: Malignant otitis externa (MOE) is an infrequent but severe infectious disorder that is generally caused by Pseudomonas aeruginosa, mostly affecting elderly diabetic patients. Progression of the disease from the external auditory canal may lead to osteomyelitis of the skull base resulting in potentially fatal intracranial complications. This life-threatening condition can be difficult to diagnose and treat. This study aimed to investigate the usefulness of ^{18}F-FDG PET/CT co-registered with MRI in determining disease extent and treatment response in patients clinically diagnosed of MOE. **Materials and Methods:** Nine subjects were enrolled in the study (7 diabetic); mean age: 62 years (range: 22-84 y). Sixteen FDG PET/CT studies were evaluated: 6 in the initial diagnosis and 10 to determinate treatment response. A dedicated head and neck (HN) acquisition was performed as well as images from mid-thigh to the base of the skull. FDG PET scans were co-registered with MRI when available (69% studies). We evaluated the extent of disease on the basis of visual interpretation on PET/CT or co-registered FDG-PET/MRI images. In addition, SUVmax was measured in the lesions. **Results:** All the scans showed pathological FDG uptake (mean: 7,5; range 3,6-13,4). Imaging located skull base osteomyelitis or intracranial extension (69%), soft tissue involvement and erosive changes of temporal bone (19%) and soft tissue and cartilaginous involvement (12% of scans). Ten studies (62,5%) were used to evaluate response to treatment. We observed an increase of FDG uptake (50%), a significant decrease/metabolic normalization (40%) or no significant changes (10% of them) .In patients with significant uptake antibiotic treatment was continued and when the scan demonstrated no or substantially reduced FDG uptake treatment was stopped. MRI alone failed to correctly classify response to treatment in two of these studies. **Conclusion:** The diagnostic challenge in MOE lies in the fact that no single modality is able to address the scope of the disease. FDG PET/CT is a reliable imaging modality for determining disease extent and specially treatment response, because it allows an objective quantitative measurement for tracer accumulation. MRI images alone are less useful than FDG PET/CT for treatment monitoring. PET co-registered to MRI combines functional and high-resolution anatomical imaging. Further studies are needed to assess the role of FDG PET/RM as first-line diagnostic imaging in MOE. **References:** A.M.J.L. van Kroonenburgh, W.L. van der Meer. R. J. P. Bothof. Advanced Imaging Techinques in Skull Base Osteomyelitis Due to Malignant Otitis Externa. Curr Radiol Rep (2018) 6:3. https://doi.org/10.1007/s40134-018-0263-y

EPS-020

Diagnostic impact of Ga-SPECT/CT using quantitative analysis for patients with lower-limb osteomyelitis

Y. Nishikawa, *Y. Fukushima, S. Kirinoki, G. Takagi, M. Miyamoto, S. Kumita;*
Nippon Medical School Hospital, Tokyo, JAPAN.

Aim/Introduction: Lower-limb osteomyelitis is caused by various conditions, such as diabetes mellitus, collagen diseases, and trauma. Since patients with this disease occasionally require amputations, early diagnosis and risk stratification are important to improve their outcomes. While Ga-scintigraphy is commonly used for diagnosing inflammatory diseases, the diagnostic performance of conventional planar imaging for localized

lesions is limited. This study aimed to estimate the diagnostic performance of Ga-SPECT/CT using quantitative analyses for patients with lower-limb osteomyelitis. **Materials and Methods:** A total of 103 consecutive patients between April 2012 and October 2016, who were suspected of lower-limb osteomyelitis, were included in this study. All patients underwent Ga-scintigraphy via both planar and SPECT/CT imaging. The image findings of osteomyelitis were assessed both visually and quantitatively. In the visual analysis, localized accumulations higher than background were determined as positive lesions (planar and SPECT/CT imaging scores). In the quantitative analysis via SPECT/CT images, the inflammation-to-background ratio (IBR) was calculated by dividing the maximum count in the osteomyelitis lesion by mean count in both distal femur bone marrow as background. The maximum standardized uptake value (SUVmax) in the osteomyelitis lesion was also calculated using GI-BONE. The diagnoses were confirmed based on the patients' outcomes and pathological examinations, and the diagnostic performances of the planar and SPECT/CT imaging for lower-limb osteomyelitis were compared. For the evaluation of the prognostic performances of quantitative indicators, all patients were observed over 3 years from initial Ga-SPECT/CT for the occurrence of major adverse events (MAE), which was defined as recurrence of osteomyelitis, major leg amputation, or fatal event. **Results:** The number of patients with and without osteomyelitis was 54 and 49, respectively. Compared with planar imaging (sensitivity: 91% and specificity: 18%), SPECT/CT imaging showed a higher accuracy (sensitivity: 91% and specificity: 96%) for the diagnosis of lower-limb osteomyelitis. Whereas the visual planar imaging score showed no difference between patients with and without osteomyelitis, both IBR and SUVmax were significantly higher in the osteomyelitis patients compared with the patients without osteomyelitis (14.33 vs. 2.11 and 7.04 vs. 1.71, both $p < 0.001$). MAE occurred in 36 out of 54 osteomyelitis patients. In the multivariate Cox proportional hazards regression analysis, both IBR and SUVmax were found to be the independent prognostic factors (both $p < 0.001$). **Conclusion:** Ga-SPECT/CT using quantitative parameters, such as IBR and SUVmax, may have a high diagnostic performance for patients with lower-limb osteomyelitis compared with the planar imaging. **References:** None.

EPS-021

One year survival in patients with lead-associated endocarditis after transvenous lead extraction: the importance of pocket involvement

R. Bonfiglioli, *L. Calderoni, R. Mei, S. Lorenzetti, G. Massaro, J. Frisoni, C. Martignani, S. Fanti, I. Diemberger;*
Azienda ospedaliero-universitaria S.Orsola-Malpighi, Bologna, ITALY.

Aim/Introduction: Cardiac implantable electronic device infections (CIEDI) represent a life-treating condition with a poor prognosis even after transvenous lead extraction (TLE). The aim of this study was to find the predictors of poor prognosis after TLE according to the presence of lead-associated endocarditis (LAE). **Materials and Methods:** We performed a single center prospective observational study in a population of consecutive patients referred for TLE to a tertiary hospital for the treatment of CIEDI. **Results:** We enrolled 105 consecutive patients with confirmed CIEDI, 81% male, aged 72.7 years. LAE was observed in 49 patients and CIED pocket involvement in 81. 24/49 of the patients with LAE were free from pocket involvement (both at inspection and at FDG-PET). Comparing baseline characteristics, patients with LAE free from pocket involvement more frequently occurred after first implant (54% vs. 24%; p=0.030) and >6 months after last CIED procedure (88% vs. 48%; p=0.003) without any other significant differences in terms of implanted hardware or comorbidities. TLE was performed in all the patients, requiring powered sheaths in 64/105, two subjects experiencing a major complication secondary to a vascular tear promptly repaired by the cardiac surgeon who also completed lead extraction. One year mortality was significantly higher in patients with LAE without pocket involvement, while survival was almost superimposable between patients with pocket CIEDI and patients with LAE and pocket involvement. **Conclusion:** Patients with LAE without CIED pocket involvement usually develop CIEDI after >6 months after their first device implant. These subgroup of patients require better characterization in view of the bad prognosis despite complete TLE. **References:** None.

EPS-022

^{99m}Tc-PYP scintigraphy detects transthyretin-related cardiac amyloidosis; a substitute for biopsy?

P. Valsamaki, *E. Kastritis, I. Dialoupi, A. Dimopoulos, V. Papantoniou;*
University General Hospital "Alexandra", Athens, GREECE.

Aim/Introduction: Cardiac amyloidosis (CA) is caused by extracellular deposition of a misfolded and insoluble protein, namely amyloid. The underlying pathophysiologic mechanism is hitherto ultimately identified by endomyocardial biopsy combined with immunohistochemical parameters/mass spectroscopy. Imaging with cardiac US/MRI provides non-specific findings. We herein suggest the use of technetium-99m pyrophosphate (^{99m}Tc-PYP) scintigraphy for defining cardiac amyloidopathy subtype, specifically transthyretin-related CA (ATTR), whether familial or wild-type (senile). **Materials and Methods:** Sixty-one patients [50 males, aged (mean±SD) 69.4±11.2y; 11 females, aged 73.3±7.6y] with suspected ATTR, underwent myocardial scintigraphy (planar and tomographic) 1-3h after iv administration of 555-925 MBq ^{99m}Tc-PYP. Myocardial radiotracer uptake was assessed optically (grade 0-3) and semiquantitatively, using two regions of interest (ROI); over the heart (H) and over the contralateral hemithorax (CL), to estimate the H/CL count ratio. We applied a cut-off H/CL value of 1.5 to differentiate patients bearing ATTR versus light-chain CA (AL). Diagnosis was confirmed by biopsy and/or laboratory investigation. **Results:** Diffuse intense

myocardial uptake verified semi-quantitatively in 19 men and 4 women by ^{99m}Tc-PYP scintigraphy, was consistent with ATTR, 12 men and 3 women bearing the wild-type. Faint or no myocardial tracer uptake with H/CL ratios <1.5, was found in 38 patients (16 diagnosed with AL). Detection of ATTR in our study population by ^{99m}Tc-PYP scintigraphy was accomplished with 100% sensitivity and specificity. **Conclusion:** Our data indicate that ^{99m}Tc-PYP scintigraphy, a non-invasive, low-cost, and widely available modality, identifies patients with the ATTR subtype and may prove a valuable tool for earlier diagnosis and screening, substituting for biopsy as well as optimizing therapeutic and prognostic implications. **References:** 1. Banypersad SM, Moon JC, Whelan C et al. Updates in cardiac amyloidosis: a review. J Amer Hear Assoc 2012; 1: e000364. 2. Chee CE, Lacy MQ, Dogan A et al. Pitfalls in the diagnosis of primary amyloidosis. Clin Lymphoma Myeloma Leuk 2010; 177-80. 3. Gonzalez-Lopez E, Gallego-Delgado M, Guzzo-Merello G, et al. Wild-type transthyretin amyloidosis as a cause of heart failure with preserved ejection fraction. European Heart Journal 2015;36:2585-94. 4. Bokhari S, Castaño A, Pozniakoff T, et al. 99mTc-pyrophosphate scintigraphy for differentiating light chain cardiac amyloidosis from the transthyretin-related familial and senile cardiac amyloidoses. Circ Cardiovasc Imag2013; 2: 195-201. 5. Castano A, Haq M, Narotsky D, et al. Multicenter experience of planar technetium pyrophosphate cardiac imaging: Does preferential cardiac uptake predict survival in patients with ATTR cardiac amyloidosis? ISA INTERNATIONAL SOCIETY OF AMYLOIDOSIS 2016; 39.

EPS-023

The Utility of ^{18}F-FDG PET/CT In The Diagnosis Of Infectious Endocarditis

D. Tamayo-Carabaño, *I. Acevedo-Bañez, R. Fernández-López, R. Álvarez-Pérez, J. Jiménez-Hoyuela-García;*
Hospital Universitario Virgen del Rocío, Sevilla, SPAIN.

Aim/Introduction: Evaluated the utility of ^{18}F-FDG PET/CT performed in patients with suspected infectious endocarditis(IE). **Materials and Methods:** Personal history of each patient was assessed: previous valvular or endovascular surgery or prosthesis, time elapsed since surgery, results of transthoracic echocardiography and antibiotic treatment prior to the procedure. All patients were administered a ^{18}F-FDG dose standardized by weight, and by size in pediatric cases, one hour before image acquisition. Images were analyzed measuring the SUVmax of the areas of pathological uptake, describing the character of the uptake, the Deauville scale, a captation scale of the uncorrected images, the persistence of the pathological focus and the modification of the SUVmax in the delayed images. **Results:** We included 32 studies between June2016 and October2018, conducted in 29 adult and 3 pediatric patients, 25 were men and 7 women with a median age of 68 years. The reason for requesting the study was fever-of-unknown-origin in 19 cases and bacteremia demonstrated with positive blood cultures in 13. The 93.75% of the patients had a prosthetic heart valve and/or an endovascular prosthesis, with a median of 27 months from surgery to the scan. Prior to the study, only 8 transthoracic echocardiograms were suspects. A special preparation for cardiac assessment was performed in 87.5% of the cases. The 87.5% of the cases received antibiotic therapy before the scan. Were considered metabolically positive for IE 19 cases, 9 were negative and 4 were not evaluable due to physiological uptake by the myocardium. In the positive cases, the average SUVmax was 5.08; the Deauville scale was 4 in 12 patients and 5 in 7 cases; the scale of uncorrected images was 2 in 14 patients and 3 in 5. A delayed image of the thoracic region was performed in 78,9% of the cases, with persistence of the focus and an average SUVmax of 6.3, increasing the uptake in 73.3% of the cases. A final diagnosis of suggestive was obtained in 5, definitive in 14 and rejected in 9. A sensitivity of 82.6%, specificity of 100%, positive predictive value of 100% and negative predictive value of 55.5% was demonstrated. **Conclusion:** Although ^{18}F-FDG PET/CT is included in the diagnostic algorithm of IE, there is no consensus in the protocol, preparation and interpretation of the images. The model that we have followed compiled from several research, seems a suitable option to diagnose this disease that warrants a thorough and early treatment. **References:** None.

EPS-024

Diagnostic accuracy of ^{67}Ga-citrate scintigraphy in left ventricular assist device (LVAD) infection

K. Matsunaga, *F. Soeda, D. Katayama, M. Watanabe, T. Watabe, H. Kato, M. Tatsumi, E. Shimosegawa, J. Hatazawa;*
Osaka University, Suita city, JAPAN.

Aim/Introduction: LVAD is used in supporting end-stage heart failure patients. One of the major complications is infection of the LVAD or driveline. In Japan ^{67}Ga-citrate scan is reimbursed by health insurance system in the diagnosis of infection, however the usefulness of ^{67}Ga-citrate scan in LVAD associated infection has not been examined. The aim of this study was to evaluate the usefulness of ^{67}Ga-citrate scan in the diagnosis of LVAD related infection. **Materials and Methods:** Twenty-nine ^{67}Ga-citrate scans (27 scans with additional SPECT/CT, 1 scan with additional SPECT and 1 scan with only planar image) performed between January and December 2015 with 19 patients supported with LVAD were retrospectively analyzed. The patients were referred to our department with a suspicion of LVAD related infection or fever of unknown origin. An infection was defined according to the adverse event definition of the Interagency Registry of Mechanically Assisted Circulatory Support. ^{67}Ga-citrate scintigraphy was performed 3 days following intravenous administration of 111 MBq ^{67}Ga-citrate. Images were obtained using a dual-head gamma camera (Symbia T6 or Symbia Intevo, Siemens Healthcare) and high-resolution, medium-energy collimators. Whole-body anterior and posterior images were acquired with a scan speed of 10 cm/min using 20% window energy peaks of 93, 184 and 300 keV. SPECT/CT was additionally performed following whole-body scan, focused on the chest

and the abdomen. The data acquisition included 180° rotation, 5° angle step, and 30-s-per-frame acquisition time using a 128 x 128 matrix. CT based attenuation correction was used. Iterative reconstruction was performed. All scans were reviewed by a reader experienced in ^{67}Ga scan analysis, who was blinded to the final clinical diagnosis. The scans were visually evaluated for the presence of an infection along the driveline, conduits and pump housing. The abnormal uptake was graded as positive for an infection. **Results:** Sensitivity, specificity, positive and negative predictive value were 85, 94, 92, 88 % for planner image and 92, 94, 92, 94 % for SPECT/CT. In false negative cases of planner image, the uptake of infection site located near sites of physiological uptake such as liver. **Conclusion:** ^{67}Ga-citrate scan was useful in the diagnosis of LVAD infection. **References:** None.

EPS-025

Role of 18F-FDG PET/CT in Diagnostics of Infective Endocarditis in Patients with Prosthetic Valves and Implantable Cardiac Devices

D. Pursanova, *L. A. Bockeria, I. P. Aslanidi, O. V. Mukhortova, I. V. Shurupova, T. A. Katunina, T. A. Trifonova;*
A.N.Bakoulev National Medical Research Center of Cardiovascular Surgery of the Ministry of Health of Russian Federation, Moscow, RUSSIAN FEDERATION.

Aim/Introduction: 18F-FDG PET/CT has potential to improve the early diagnosis of infectious endocarditis (IE) and its complications in patients with fever of unknown origin after valve replacement and/or cardiac device implantation. Purpose: To investigate the usefulness of 18F-FDG PET/CT in the detection of IE in patients after cardiac surgery. **Materials and Methods:** This prospective analysis included results of 18-FDG PET/CT examinations performed in 35 patients with fever of unknown origin and suspected IE after: heart valve replacement (n=19), pacemaker implantation (n=9) and both procedures (n=7). Examinations were performed on PET/CT scanner (Biograph-64, Siemens) 90 min after 18F-FDG injection (175-200Mbq). All patients were on low-carbohydrate diet for 48 hours before PET-scan and fasted for at least 15 hours before it. Final diagnosis was made based on clinical and laboratory (n=35), as well as intraoperative data (n=28). **Results:** Overall, the diagnosis of IE was confirmed in 27 and ruled out in 8 patients. PET/CT results allowed to confirm IE in 93% (25/28) of patients: in prosthetic valve (n=18), in generator pocket and along the leads (n=7). In addition, whole body PET/CT results revealed other foci of infection in these patients: along the ascending aorta prosthesis (n=4), in native valve (n=2), soft tissue infiltrates of the anterior chest wall (n=2), sternum (n=2), lung (n=1) and spleen (n=1). Importantly, 88% (22/25) patients with true positive PET/CT results had negative or doubtful laboratory and instrumental data: sterile blood cultures (n=14) and/or negative (n=7) or doubtful (n=10) results of echocardiography. Moreover, in two of these patients, the diagnosis of IE was made based on clinical and PET/CT data, while the results of both blood cultures and echocardiography were negative.PET/CT results allowed to rule out the infectious process in 88% (7/8) of patients: in prosthetic valve (n=5), in generator pocket and along the leads (n=2). Of these, in one case the cause of fever was identified - lung inflammation. Other 6 negative results were confirmed by follow-up clinical and laboratory data during 6+3 months. Sensitivity, specificity and accuracy of 18F-FDG PET/CT in the diagnosis of IE were 93%, 88% and 92%, respectively. Positive and negative predictive value - 96% and 78%. **Conclusion:** 18F-FDG PET/CT proved to be a useful diagnostic tool in patients with suspected IE after valve replacement and/or cardiac device implantation, and should be included in the algorithm for early diagnosis. PET/CT results also allow to detect extracardiac complications in these patients. **References:** None.

EPS-026

Diagnostic accuracy of 18F-FDG digital PET/CT in the detection of infective endocarditis on native and prosthetic valves and intracardiac devices: Preliminary results in a reference medical center

M. Mallón Araujo, *E. Abou Jokh, V. Pubul Núñez, M. d. Pombo Pasín, M. Garrido Pumar, L. Garcia Bernardo, A. Martínez-Monzonis, A. Martínez de Alegría Alonso, Á. Ruibal Morell;*
CHUS, Santiago De Compostela, SPAIN.

Aim/Introduction: Infective endocarditis (IE) is a pathology that remains a medical challenge despite the great technological advances, thus requiring a multidisciplinary approach to improve its fatal prognosis. Digital PET/CT has been recently developed to offer an improvement in quality image, volumetric resolution, quantitative accuracy and higher sensitivity. The aim was to evaluate the diagnostic accuracy of 18F-FDG digital PET/CT in the early diagnosis of IE. **Materials and Methods:** We retrospectively evaluated 38 patients (10 women and 28 men) with possible IE regarding Duke´s criteria, 8 of them with native valves (NV), 20 prosthetic valves (PV) and 10 intracardiac devices (ID). All patients underwent analytical and microbiological tests, a transesophageal echocardiogram (TEE) and a 18F-FDG digital PET/CT scan (Phillips Vereos PET-TC model); the results of each test were compared between them. The final diagnosis of EI was reached according to the modified Duke´s criteria. All patients underwent a low carbohydrate diet and the administration of 50UI of sodium heparin 15 minutes before the injection of 18F-FDG. **Results:** Out of thirty-eight patients suspected of IE, the diagnosis was confirmed in 20 cases (52,6%). 18F-FDG digital PET/CT was positive in 15 patients, 10 showing FDG uptake on cardiac valves (3 native and 7 prosthetic), 2 on intracardiac devices and 3 on both (valves and devices). 18F-FDG PET/CT had a 33,3% sensitivity (S) for IE on NV and 85.7% on PV and ID and a 100% specificity (E) on NV and 93.7% in PV and ID. The TEE had a S and an E for NV of 50% and 100% respectively, and a S and a E for VP and DI of 14.2% and 100% respectively. **Conclusion:** ^{18}F-FDG digital PET/CT has proven to be a sensitive technique with a high diagnostic value in patients suspected of IE with prosthetic valves and intracardiac devices. Its utility

decreases in patients with IE on NV, in which TEE presented a higher sensitivity thus a better diagnostic value. **References:** None.

EPS-027

Evaluation of [18F]FDG-PET/CT for initial diagnosis and healing assessment after therapy in extra-pulmonary tuberculosis

L. Sarda-Mantel[1], *J. Kaoutar*[2], *T. Alfaiate*[3], *A. Lopes*[4], *K. Benali*[5], *L. Vercellino*[6], *N. Mikail*[5], *M. Soussan*[7], *C. Lemarignier*[6], *F. Mechai*[7], *S. Le Nagat*[8], *F. Montravers*[9], *O. Deradji*[10], *E. Durand*[11], *T. Goulenok*[12], *D. Ponscarme*[13], *P. Yéni*[2], *C. Laouénan*[3,14], *C. Rioux*[2];
[1]*APHP Hôpital Lariboisière Service de Médecine Nucléaire, Paris, FRANCE,* [2]*APHP Hôpital Bichat Service de Maladies Infectieuses, Paris, FRANCE,* [3]*APHP Hôpital Bichat Département d'Epidémiologie Biostatistique et Recherche Clinique, Paris, FRANCE,* [4]*APHP Hôpital Lariboisière Service de Médecine Interne, Paris, FRANCE,* [5]*APHP Hôpital Bichat Service de Médecine Nucléaire, Paris, FRANCE,* [6]*APHP Hôpital Saint-Louis Service de Médecine Nucléaire, Paris, FRANCE,* [7]*APHP Hôpital Avicennes Service de Médecine Nucléaire, Paris, FRANCE,* [8]*APHP Hôpital Tenon Service de Maladies Infectieuses, Paris, FRANCE,* [9]*APHP Hôpital Tenon Service de Médecine Nucléaire, Paris, FRANCE,* [10]*APHP Hôpital Kremlin-Bicêtre Service de Maladies Infectieuses, Paris, FRANCE,* [11]*APHP Hôpital Kremlin-Bicêtre Service de Médecine Nucléaire, Paris, FRANCE,* [12]*APHP Hôpital Beaujon Service de Médecine Interne, Paris, FRANCE,* [13]*APHP Hôpital Saint-Louis Service de Maladies Infectieuses, Paris, FRANCE,* [14]*IAME UMR 1137, Paris, FRANCE.*

Aim/Introduction: In extra-pulmonary tuberculosis forms, the bacteriological evidence of cure most often cannot be obtained, the evolution of conventional imaging is poorly understood, raising the need for other tools for therapeutic evaluation. The aim of this study was to evaluate [18F]FDG-PET before and after antibiotherapy, assuming that it could provide useful information for therapeutic management. **Materials and Methods:** We performed a multicenter prospective study including 55 patients with definite or probable lymph node or bone tuberculosis. Patients were followed until 12 months after end-of-treatment [EOT]. Additionally to usual biological, histological and morphological explorations, [18F]FDG-PET was performed at diagnosis (PET1) and at EOT (PET2). Patients were considered cured at EOT if adherence to treatment was at least 80% and if they did not relapse one year after EOT. The [18F]FDG-PET variables studied were the sum (ΣSUVmax) and average (MSUVmax) of the SUVmax measured in each site considered as lesioned. **Results:** Eleven of 55 patients were secondarily excluded, 20 were lost to follow-up. PET1 and PET2 were completed respectively in 42 and 35 patients. PET1 was positive in 41 of 42 (97.6%) patients (ΣSUVmax: 35.5 [19.6-59.9], MSUVmax: 6.6 [5.7-8.8]). It retrieved unknown lesions in 32.4% of cases, which induced a modification of therapy duration in 5.4% of cases. PET2 was positive in 29/35 (82.8%) patients (ΣSUVmax: 5.5 [2.4-10.5], MSUVmax: 2.8 [1.6-3.6]), and retrieved unknown lesions in 7.7% of cases, which did not induce modification of patient management. Three of 26 patients (11.5%) had recurrence during follow-up related to bacterial resistance. Eighteen patients were considered cured and 6 uncured at EOT. Fourteen cured patients (77.8%) and all uncured patients had abnormal PET2. PET1 ∑SUVmax and MSUVmax were higher in uncured than in cured patients (p<0.01). Δ∑SUVmax and ΔMSUVmax between PET1 and PET2 were not different between cured and uncured patients: -88.3%[-93.7;-55.5] vs -68.3%[-77.1;-68.8] (p=0.24), and -64.6%[-74.9;-25.8] vs -54.3%[-57.7;-25.9] (p=0.31). PET2 MSUVmax showed the highest AUC on ROC curves for the diagnosis of healing or residual disease at EOT: (0.79[0.57;1.00]). MSUVmax above 3.7 had a sensitivity of 82.3%, and a specificity of 80.0% to diagnose residual disease at EOT. **Conclusion:** [18F]FDG-PET/CT at diagnosis was positive in 97.6% and discovered unknown lesions in 32.4% of cases. ∑SUVmax and MSUVmax clearly decreased on PET2 at EOT in cured patients, but abnormal hot spots persisted in 77.8% of them. MSUVmax above 3.7 on PET2 was the best criteria to diagnose residual disease at EOT. **References:** None.

EPS-028

Cardiac Amyloidosis : The Utility Of Tc-99m PYP Scintigraphy In Etiologic Evaluation Of Dilated Cardiomyopathy

S. Fukuzawa, *S. Okino, H. Ishiwaki, Y. Iwata, T. Uchiyama, N. Kuroiwa, N. Oka, S. Furihata, N. Shibayama, M. Inagaki; Funabashi Municipal Medical Center, Funabashi, JAPAN.*

Aim/Introduction: Cardiac amyloidosis (CA) presents initially with mild LV diastolic dysfunction, progressing to classical restrictive cardiomyopathy and finally even dilated cardiomyopathy(DCM) like stage with end-stage heart failure. Tc-99m PYP scintigraphy in the absence of evidence of a monoclonal gammopathy was diagnostic for transthyretin cardiac amyloidosis (ATTR-CA), providing a cost-effective and non-invasive technique with a specificity and positive predictive value of nearly 100%. The aim of study is to identify ATTR-CA as a specific cause in which Tc-99m PYP scintigram may be useful in the etiologic evaluation of DCM patients. **Materials and Methods:** 68 patients with the diagnosis as DCM between 2012 Apr. and 2017 Mar. in our heart center were included. All the subjects were underwent Tc-99m PYP cardiac imaging, also echocardiographic, MIBG scintigraphic and clinical variables were gathered. Retention of Tc-99m PYP in the heart was assessed using both a semiquantitative visual score (range, 0 [no uptake] to 3 [uptake greater than bone]). **Results:** 4 of 68 patients (5.9%) were detected underlying ATTR-CA using Tc-99m PYP imaging (Score of 2~3). Patients with amyloid deposition were older, and had a lower left ventricular ejection fraction and H/M ratio of MIBG scan. During a five-year follow-up period, survival was significantly worse if patients had amyloid deposition compared with no deposition subjects, according to a Kaplan-Meier analysis. **Conclusion:** Our results demonstrate that Tc-99m PYP imaging, when used as a part of a comprehensive clinical evaluation, can help identify transthyretin amyloidosis in 5% of

patients presenting with unexplained dilated cardiomyopathy. **References:** 1) Bokhari S, Shahzad R, Castano A, et al : Nuclear imaging modalities for amyloidosis. J Nucl Cardiol 21 : 175-184, 2014.

EPS-029

Gallium-68 labelled pyoverdines for Pseudomonas aeruginosa infection imaging

M. Petrik[1], *E. Umlaufova*[1], *V. Raclavsky*[2], *A. Palyzova*[3], *V. Havlicek*[3], *Z. Novy*[1], *C. Decristoforo*[4], *M. Hajduch*[1];
[1]*Institute of Molecular and Translational Medicine, Faculty of Medicine and Dentistry, Palacky University, Olomouc, CZECH REPUBLIC,* [2]*Department of Microbiology, Faculty of Medicine and Dentistry, Palacky University, Olomouc, CZECH REPUBLIC,* [3]*Institute of Microbiology of the Czech Academy of Sciences, Prague, CZECH REPUBLIC,* [4]*Clinical Department of Nuclear Medicine, Medical University Innsbruck, Innsbruck, AUSTRIA.*

Aim/Introduction: Pyoverdines (PVDs) are highly specific siderophores excreted by several Pseudomonas species. Siderophores have potent affinity for iron and are employed for iron delivery by almost all microorganisms. Iron is an essential nutrient and is also a key factor in the virulence of many pathogens. Replacing iron in siderophores by radiometal, such as gallium-68, opens approaches for targeted imaging of infections by means of PET. Pseudomonas aeruginosa (P.a.) is one of the most common pathogens causing life-threatening pneumonia, which is associated with high mortality and morbidity, especially in immunocompromised patients. Here we report on the preclinical evaluation of selected Ga-68 labelled PVDs produced by P.a. for imaging of P.a. infections. **Materials and Methods:** PVDs isolated from different P.a. strains were labelled with Ga-68 in sodium acetate. Partition coefficient, protein binding and stability in various media were determined up to 120min incubation time. In vitro uptake of ^{68}Ga-PVDs was studied in different microbial cultures. In vivo biodistribution was determined in normal Balb/c mice 30 and 90 min p.i.. PET/CT imaging of ^{68}Ga-PVDs was performed in P.a. animal infection models and compared with clinically used radiopharmaceuticals. **Results:** Studied PVDs were labelled with ^{68}Ga with high (>95%) radiochemical purity. The resulting complexes showed hydrophilic properties (log P = -3), low protein binding (<5%) and high stability in human serum (>95%). In vitro uptake of ^{68}Ga-PVDs displayed different levels of uptake in studied P.a. strains as well as in other tested microorganisms. In normal mice, all studied ^{68}Ga-PVDs showed similar results manifested by rapid renal excretion and low blood values up to 90min p.i.. PET/CT imaging of ^{68}Ga-PVDs in P.a. infected animals showed different levels of accumulation in infected tissue corresponding to in vitro results and better distribution than other, clinically used radiopharmaceuticals. **Conclusion:** We have shown that different PVDs can be labelled with Ga-68 with high affinity and radiochemical purity. ^{68}Ga-PVDs revealed suitable in vitro characteristics and excellent pharmacokinetics. In vitro uptake of ^{68}Ga-PVDs in tested microbial cultures was diverse even within the microbial species. ^{68}Ga-PVDs can be used for imaging of P.a. infections and show better pharmacokinetics than clinical radiopharmaceuticals. **References:** We gratefully acknowledge the financial support of Technology Agency of the Czech Republic (Project No. TE01020028) and the Czech Science Foundation (Project No. 19-10907S).

EPS-030

Radiolabelling and in vivo biodistribution studies of a lipid-protein based enterotoxigenic E. Coli vaccine after intranasal and transdermal administration using polymeric microneedle patches

G. Quincoces[1], *Á. Erhard*[1], *M. Collantes*[1], *Y. Pastor*[2], *J. Uranga*[3], *J. Simon*[1], *M. Ecay*[1], *C. Gamazo*[2], *I. Peñuelas*[1];
[1]*University Clinic of Navarra, Pamplona, SPAIN,* [2]*University of Navarra, Pamplona, SPAIN,* [3]*USCAL, Pamplona, SPAIN.*

Aim/Introduction: Infections by enterotoxigenic Escherichia coli (ETEC) are a top cause of children diarrhea and travelers' diarrhea. The success of an ETEC vaccine will depend on the appropriate combination of the right antigens delivered through appropriate routes to produce optimal protective immune responses. The objective of this work is to radiolabel the selected vaccine antigens (heat-labile toxin, HT) and analyze its biodistribution in vivo in mice by two different routes of administration: intranasal and transdermal using polymeric microneedle patches. **Materials and Methods:** Radiolabeling of HT antigen (1 mg) was performed by ^{99m}TcO4 reduction with $SnCl_2$·2H2O. Radiochemical purity was checked by thin layer chromatography. Microneedle patches were prepared after Wire Electrical Discharge Machining (wire EDM) a stainless-steel cast of 122 quadrangular pyramid microneedles (11x11 matrix, 250X300 µm). Silicon molds were prepared from the SS cast. HT antigen was radiolabeled and added to a 40% Gantrez solution that was poured onto the silicon molds to generate the microneedle patches. After centrifugation solid polymer-based patches were created after RT 4h drying. For intranasal administration, 10 µl of the radiolabeled complex were placed inside each nostril of Balb-c mice: ^{99m}Tc-HT (20 µg/3.14 MBq, n=4) and negative control (free ^{99m}TcO4$^-$, 4.99 MBq, n=4). For transdermal administration the microneedle patches were placed on the ear of BALB/c mice and fixed with sticking plaster (20 µg/2.40 MBq, n=4; free ^{99m}TcO4$^-$, 2.70 MBq, n=4). In vivo biodistribution studies were performed by SPECT/CT 1, 4, and 24 hours post-administration and quantified by drawing VOIs over CT images. Animals were euthanized and extracted organs measured ex vivo in a gamma-counter for the calculation of the percentage of injected dose (% ID/organ). **Results:** HT antigen radiolabeling proceeded with >95-97% yield, thus avoiding the need for further purification. SPECT / CT images and the organ count showed that after nasal administration HT-antigens remain in the nasal area and move onto the intestine, with a very different distribution to control animals; 75% of the dose was eliminated at 6 h. Transdermal administration shows a much slower elimination, compatible with very slow

absorption. **Conclusion:** The radiolabeling of HT-samples was achieved in an efficient manner. SPECT/CT images and ex vivo counting confirmed that the intranasal administration achieves a retention of HT samples in the nasal and intestinal mucosa sufficient for an effective immunization. While additional studies are needed to achieve good absorption, microneedle patches seem to be a promising route of administration. **References:** None.

EPS-031

Differential ^{18}F-FDG uptake in bacteria and yeast cells-associated prosthetic joint infection strains

***M. Rua**, J. Simón, M. Collantes, M. Ecay, F. Carmona-Torre, Á. Erhard, J. Payo-Ollero, G. Quincoces, J. Leiva, A. Valentí-Azcárate, J. Del Pozo, I. Peñuelas;*
Clínica Universidad de Navarra, Pamplona, SPAIN.

Aim/Introduction: Chronic prosthetic joint infection (PJI) is associated with significant morbidity and socioeconomic burden. Since Fluorine-18-fluorodeoxyglucose (^{18}F-FDG) is able to pinpoint bacteria and yeast metabolism, our objective was to quantitatively compare the uptake of PJI-relevant clinical isolated and reference strains of bacteria and yeast cells using in vitro experiments **Materials and Methods:** Six different bacteria and yeast clinical isolates were selected from patients diagnosed with chronic PJI (S. epidermidis, S. aureus, P. acnes, E. ludwigii, P. aeruginosa and C. albicans) and only in one case from a chronic prosthetic heart valve infection (E. coli). Identification of clinical strains was performed using MALDI-TOF (Matrix-Assisted Laser Desorption/Ionization-Time Of Flight). Additionally five reference strains (ATCC) were also studied as control. In vitro uptake of ^{18}F-FDG in reference strains and clinical isolates was compared using three independent experiments and nine replicates. The radiotracer (37±11 MBq/ml) was incubated with cultures of all the species at 37ºC for 2 hours, pelleted by centrifugation and washed with PBS. Microorganisms were counted by culturing in agar media before and after the experiment to control the growth. ^{18}F-FDG uptake was measured using a gamma counter. **Results:** ^{18}F-FDG in vitro accumulation of Gram-positive bacteria was higher (mean = 5092 Bq/10^6 CFU) when compared to Gram-negative (mean = 120 Bq/10^6 CFU). Among bacteria, S. epidermidis clinical strain showed the highest uptake (7928 ± 3305 Bq/10^6 CFU). Clinical and reference yeast cells (C. albicans) showed a thousand times higher ^{18}F-FDG uptake in vitro than any bacteria strain (mean clinical and reference strain = 1.2 ± 0.7 MBq/10^6 CFU). Interestingly, P. aeruginosa incorporated virtually no ^{18}F-FDG (mean clinical and reference strain = 4 ± 6 Bq/10^6 CFU) and showed a decrease in the number of bacteria during the experiment that was not observed in the other species. **Conclusion:** Yeast cells (eukaryotic) presented unexpected higher uptake compared to bacteria. The lack of ^{18}F-FDG uptake both in the clinical isolate and the ATCC strain of P. aeruginosa and the observed decrease in growth might be due to a higher radiosensibility of this specie. Since virtually all bacterial strains associated with PJI showed ^{18}F-FDG uptake in variable amounts and chronic PJI has a reduced inflammatory component due to low virulence factors, ^{18}F-FDG could provide an in vivo diagnostic tool for this clinical problem. **References:** None.

EPS-032

Design and performance evaluation of a fully automated system for the synthesis of the gram-negative specific radiotracer ^{18}F-fluoro-deoxy-sorbitol

***J. Simon**, Á. Erhard, G. Quincoces, M. Rúa, M. Collantes, M. Ecay, I. Peñuelas;*
Clínica Universidad de Navarra, Pamplona, SPAIN.

Aim/Introduction: [^{18}F]fluorodeoxysorbitol ([^{18}F]FDS) is a gram-negative specific radiotracer that can be obtained by a simple reaction from the widely available [^{18}F]fluorodeoxyglucose. This tracer could potentially be used in the diagnosis of otherwise undetectable infections like prothesis-associated infection. The aim of this work is to design, construct and evaluate the performance of a completely automated system for the synthesis of [^{18}F]FDS that yields a high purity product in a short time, while also allowing the synthesis of other radiotracers. **Materials and Methods:** Five different Eckert&Ziegler modular units were used: motorized syringe, Peltier reactor, electrovalve, three-way valve ramp and a six-way valve module. The user interface and synthesis sequence for the system were programmed using the Modular-Lab software. 250-370 MBq of [^{18}F]FDG were added into the reactor, and subsequently reduced with 0,5 mL of a 4 mg/mL freshly prepared $NaBH_4$ aqueous solution. After 15 minutes in the reactor at 35 ºC the reaction was stopped with 1,4 mL of a HCl/Sodium acetate solution (0,4 and 0,9 M for each respectively). After neutralization to pH 6,5-7,5 with 0,2 mL of NaOH 1M, the product was purified through an Alumina N Light Sep-Pack and sterile-filtered. Thin Layer Cromatografy using silica-gel based plates and 95:5 acetonitrile-water mixture was used to evaluate the purity of the products (Rf ([^{18}F]FDS): 0,2). **Results:** A fully functional automatic synthesis system (hardware, user interface and program) for the synthesis of the [^{18}F]FDS has been developed. The time-corrected radiochemical yield was 81 ± 6 % after 26 ± 2 min synthesis time, while our old manual system took 41 ± 7 min and gave a 66 ± 14 % yield. TLC showed no traces of unreacted [^{18}F]FDG. The pH for the automatic systems product was always 6,5, while the manual method needed 0,05-0,15 mL of additional NaOH. The produced tracer has successfully been used for PET imaging in animal models of prosthetic infection. **Conclusion:** A system for the fully-automated production of [^{18}F]FDS has been created. This new system provides a 15% improvement in the radiochemical yield and a 38% reduction of the time required for the synthesis. The synthesis with the automatic module also showed an increased reproducibility, with lower variability in the yield, time and final pH. Moreover, the system has also been used for the synthesis of [^{18}F]-2-fluoro-paraaminobenzoic acid ([^{18}F]FPABA, other bacterial specific radiotracer) with minimal alteration of the configuration of the system. **References:** None.

EPS-033

^{68}Ga-citrate PET/CT findings in experimental acute appendicitis induced rabbits: preliminary results

A. Gültekin, O. Uzunlu, A. Uğur, D. Yüksel;
Pamukkale University Medical Faculty, Denizli, TURKEY.

Aim/Introduction: Acute appendicitis (AA) is the most common abdominal surgical emergency all around the world. Lifetime risk of AA is about 7% to 8%. It is most commonly seen in second and third decades of life. Preferred treatment for AA is surgery. Diagnosis of acute appendicitis is sometimes difficult. In addition to imaging methods such as ultrasonography and computed tomography, infection imaging methods have been used for diagnosis in some limited cases. ^{67}Ga-citrate is a radiopharmaceutical that has traditionally been used in infection and inflammation imaging. However, due to its disadvantages, it is not used much now. ^{68}Ga-citrate and ^{67}Ga-citrate are an analog molecule. Half-life of ^{68}Ga is much shorter than ^{67}Ga. It is suitable for imaging in PET/CT devices and provides a good image resolution. The aim of this study was to investigate the use of ^{68}Ga-citrate in experimentally induced with AA rabbits. **Materials and Methods:** Twelve rabbits from New Zeland lineage (oryctogalus cuniculus) weigthing approximately 2750 grams each were included. The animals were divided into two groups. Appendicus of AA group rabbits was ligated from 10 cm distal. The abdomens of 6 rabbits in the sham group was opened. Their appendices were touched and their abdomens are closed again. Both groups were imaged with ^{68}Ga-citrate PET/CT for 12-24-36 hours after the formation of AA model. For ^{68}Ga-citrate PET/CT imaging, the ^{68}Ga citrate was synthesized as home made. Whole body scans were made after each 60 minutes of injection of about 37 mBq of ^{68}Ga-citrate through the ear vein. At the 36th hour, all rabbits were appendectomized. Appendices were sent to the pathology laboratory for histopathological examination. **Results:** Macroscopically, 3 of 6 rabbits undergoing appendectomy had perforated appendicitis, 2 had suppurative appendicitis, and 1 had gangrenous appendicitis. Appendices of the sham group rabbits were completely normal in macroscopically. In all AA modeled rabbits, ^{68}Ga citrate was successfully visualized AA localisation after the 12th hour. The ^{68}Ga citrate showed the increased uptake in the AA region within hours. **Conclusion:** ^{68}Ga citrate has quite good uptake in the appendicitis region in the AA model created in rabbits. However, high uptake of ^{68}Ga-citrate in kidneys, liver, spleen and very high blood pool activity are the most important limiting factors. This study is ongoing. In AA, the relationship between histopathological signs of inflammation and ^{68}Ga-citrate involvement will be shown. **References:** None.

411

e-Poster Presentation Session 3 - Neuroimaging: Neurodegeneration, Amyloidosis and Neuroinflammation

Sunday, October 13, 2019, 14:30 - 16:00 Room 133/134

EPS-034

Clinical outcome of Amyloid PET: interim analysis of the Spanish Registry of amyloid PET

J. Arbizu[1], G. Marti[1], C. Lorenzo-Bosquet[2], C. Gamez[3], M. Gomez-Rio[4], C. Marsal[5], M. Balsa[6], B. Rodriguez-Alfonso[7], A. Garcia-Vicente[8], R. Larumbe[9], E. Caballero[10], A. Gomez-Grande[11], P. Sopena[12], L. Dominguez-Gadea[13], A. Rotger[14], V. Camacho[15], J. Boan[16], P. Tamayo[17], A. Perissinotti[18], I. Peñuelas[1], C. Carnero[4], P. Martinez-Lage[19], I. Carrio[15], on behalf of the Spanish Registry of Amyloid PET and PET ADDS Consortium;
[1]Clinica Universidad de Navarra, Pamplona, SPAIN, [2]Hospital Universitario Vall d´Hebron, Barcelona, SPAIN, [3]Hospital Universitario de Bellvitge, Barcelona, SPAIN, [4]Hospital Universitario Virgen de las Nieves, Granada, SPAIN, [5]Complejo Hospitalario de Toledo, Toledo, SPAIN, [6]Hospital Universitario de Getafe, Madrid, SPAIN, [7]HospitalUniversitario Puerta de Hierro, Madrid, SPAIN, [8]Complejo Hospitalario de Ciudad Real, Ciudad Real, SPAIN, [9]Complejo Hospitalario de Navarra, Pamplona, SPAIN, [10]Hospital Universitario Dr. Peset, Valencia, SPAIN, [11]Hospital Universitario 12 de Octubre, Madrid, SPAIN, [12]Hospital 9 de Octubre, Valencia, SPAIN, [13]Hospital Universitario La Paz, Madrid, SPAIN, [14]Hospital Universitario Gregorio Marañon, Madrid, SPAIN, [15]Hospital Universitario de la Santa Creu i Sant Pau, Barcelona, SPAIN, [16]Hospital Ruber Internacional, Madrid, SPAIN, [17]Complejo Asistencial Universitario de Salamanca, Salamanca, SPAIN, [18]Hospital Clinic, Barcelona, SPAIN, [19]CITA Alzheimer Foundation, San Sebastian, SPAIN.

Aim/Introduction: To evaluate the influence of amyloid PET on planned prescription of Alzheimer´s disease (AD) drugs in subjects with progressive cognitive impairment of uncertain aetiology. **Materials and Methods:** A multicentric prospective observational clinical study of patients with objective cognitive impairment evaluated for suspected AD and referred for an Amyloid-PET scan was conducted. The study consisted on a monitored collection of clinical and image case record forms filled by neurologists and nuclear physicians of 18 centres on a digital platform. Specifically, neurologists were asked about therapeutic planning according to the suspected aetiological diagnosis as well as diagnostic confidence pre- and post-PET scan. A mixed effects logistic regression modelof factors associated with change in AD drug therapy was fitted considering age, gender, education level, dementia, AD diagnosis, PET result, diagnostic confidence and controlled by centre random effects. **Results:** 210 out of 369 patients with complete pre- and post-PET data set were evaluated. Median

age was 68 years [IQR 63-73] and 55.6% were females. Subjects were clinically evaluated by dementia specialists: 60.4% were MCI and 39.6% were demented. Median age in MCI patients was 69 years [IQR 64-74], and 69 years [IQR 63-74] in dementia patients (p=0.735). 50% of MCI cases and 64.5% of dementia patients were females (p=0.048). Median MMSE in MCI was 26 [IQR 24-28], and 20 [IQR 18-24] in dementia (p<0.001). Pre-PET aetiological diagnoses were AD 86.3% (typical AD 50%, atypical AD 36.3%), and non-AD 13.7%. The percentages of Amyloid-PET positivity in typical AD were 71.6% in MCI and 82.8% in dementia patients; in atypical AD were 46.9% in MCI and 52.9% in dementia; and in the non-AD were 38.5% in MCI and 60% in dementia. Changes of planned AD drugs (start, stop and modification) between pre- and post-PET was 42.2%. Multivariable analysis of factors associated with AD treatment changes (Table 1) showed significant interaction between PET scan results and pre-PET primary aetiological diagnosis (p=0.001). **Conclusion:** Amyloid PET result has a significant influence on the clinicians´ planned management of patients with cognitive impairment of uncertain aetiology, including dementia syndrome. In our experience, the probability of changes in the prescription of AD drugs increases when atypical AD or non-AD diagnoses are suspected **References:** None.

EPS-035

Simultaneous 3T Quantitative Susceptibility Mapping MRI and Amyloid PET in Dementia

M. Rullmann[1,2], *S. Tiepolt*[1], *A. Schäfer*[2,3], *T. H. Jochimsen*[1], *M. L. Schroeter*[2], *M. Patt*[1], *O. Sabri*[1], *H. Barthel*[1];
[1]*Department of Nuclear Medicine, University of Leipzig, Leipzig, GERMANY,* [2]*Max-Planck-Institute for Human Cognitive and Brain Sciences, Leipzig, GERMANY,* [3]*Siemens Healthcare GmbH, Diagnostic Imaging, Magnetic Resonance, Research & Development, Erlangen, GERMANY.*

Aim/Introduction: It is known that, in Alzheimer's disease (AD), cerebral Aß plaques contain/are surrounded by excessive iron. As iron is paramagnetic, it can be detected by certain MRI methods, like Quantitative Susceptibility Mapping (QSM). So far, most QSM MRI studies in patients with the clinical diagnosis of AD found an increase of iron-sensitive MR signals in the putamen and other deeper brain structures. The aim of this exploratory study was to examine whether these results translate to simultaneous 3T amyloid PET/MRI. **Materials and Methods:** We retrospectively analyzed the QSM MRI/C-11-PiB PET data of 11 healthy controls (HCs, 7 female; 65±3yrs) as well as 16 Aβ PET-positive (12 female; 69±9yrs) and 10 Aβ PET-negative (6 female; 73±8yrs) dementia patients. The data were analyzed regionally using the AAL template (PMOD). A ROC analysis combined with the calculation of Youden's index was performed to determine QSM cut-off values. Outcome measures for the MRI data were regional QSM values, and for the PET data regional SUV ratios taking the cerebellar cortex as reference region. **Results:** Compared to the HCs, the Aβ PET-positive patients showed higher QSM values in putamen (0.049±0.033vs.0.002±0.031; p=0.006), while the Aβ-negative patients showed lower QSM values in the caudate nucleus (0.003±0.027vs. 0.051±0.039; p=0.006). ROC analysis revealed the following threshold QSM values: to differentiate between Aβ PET-positive patients and HCs: putamen: -0.0014ppm (sensitivity: 0.88, specificity: 0.55, Youden's index: 0.43); to differentiate between Aβ PET-negative patients and HCs: caudate nucleus: -0.0184ppm (sensitivity: 0.82, specificity: 0.60, Youden's index: 0.42). Putaminal QSM values showed a trend towards a significant correlation with the MMSE scores (ρ=-0.340, p=0.053). Furthermore, in the Aβ PET-positive patients, the putaminal QSM values were significantly correlated with the composite neocortical SUVRs (ρ=-0.574, p=0.020). **Conclusion:** Compared to the HCs, patients with amyloid biomarker-supported AD showed significantly higher QSM values in the putamen, and non-AD patients significantly lower QSM values in the caudate nucleus. These data indicate that QSM on hybrid 3T PET/MRI has potential in determining the difference in iron content in deeper brain regions and in relation to the pathophysiological process. The results encourage further investigations in well-defined patient cohorts to clarify the value of QSM/magnetic susceptibility in the course of neurodegenerative diseases. **References:** None.

EPS-036

Validation of a pseudoreference region approach using [18F]DPA714 in ALS patients

D. Van Weehaeghe[1], *N. Zürcher*[2], *C. Tseng*[2], *M. Koole*[1], *M. Alshikho*[3], *J. Hooker*[2], *J. De Vocht*[4], *P. Van Damme*[4], *K. Van Laere*[1], *N. Atassi*[3];
[1]*Department of nuclear medicine and biomedical imaging, University Hospital Leuven, Leuven, BELGIUM,* [2]*Athinoula A. Martinos Center for Biomedical Imaging, Massachusetts General Hospital, Harvard Medical School, Boston, MA, UNITED STATES OF AMERICA,* [3]*Neurological Clinical Research Institute, Massachusetts General Hospital, Harvard Medical School, Boston, MA, UNITED STATES OF AMERICA,* [4]*Department of Neurology, University Hospital Leuven, Leuven, BELGIUM.*

Aim/Introduction: Amyotrophic lateral sclerosis (ALS) is a devastating motor neuron disease. Neuroinflammation, reflected by glial activation, has been observed using [^{11}C] PBR28,[^{11}C]PK1195 and [^{18}F]DPA714, mainly in the (pre)motor cortex and correlates with clinical parameters (1-7). Although full dynamic modelling is the gold standard, genotype differences increase inter-subject variability and long dynamic scans are only feasible in early stage ALS due to fast progression and bulbar symptoms. Studies using [^{11}C]PBR28 in ALS have already successfully used pseudoreference regions (3-7). [^{18}F]DPA714 has a similar effect size as [^{11}C]PBR28 however, the [^{18}F]-labelling facilitates distribution and enables multiple scans using one single production. In this work, we aim to validate the use of a pseudoreference region approach using [^{18}F]DPA714 in ALS. **Materials and Methods:** 7 healthy volunteers (HV,51.9±17.3y, all mixed affinity binders (MAB), 4F) and 6 ALS patients (61.7±6.7y, 3 high AB-3 MAB, 2F) underwent a 60-minute [^{18}F]DPA714 (145±21 MBq injected activity) PET-MR scan with full kinetic modelling. V_T

maps (Logan approach) were calculated in Pmod v3.9. $SUVR_{40-60}$ using cerebellum (CBL), occipital cortex (OC) and whole brain without ventricles (WB-ventricles) were created. After region-based partial volume correction (Freesurfer v6.0), the ratios of mean (pre)motor over mean OC, CBL and WB-ventricles were calculated for V_T and $SUVR_{40-60}$ to correct for genotype. Student t-test was performed to compare ALS to HV and Pearson was used to correlate V_T maps and $SUVR_{40-60}$ (SPSS v25). Additionally, surface based comparisons between ALS and HV on $SUVR_{40-60}$ images were performed after Gaussian smoothing (1 and 6 mm) (projection factor 0.5, $p_{uncorr}<0.05$, $p_{cluster\ FWE-corr}<0.05$) (Freesurfer v6.0). **Results:** Increased [18F]DPA714 signal (10%) in the (pre) motor cortex was observed as measured by V_T (gold standard) using OC(p=0.029) and by $SUVR_{40-60}$ using OC (p=0.049) and WB-ventricles (p=0.025). A trend was observed for V_T using WB-ventricles (p=0.082). Surface-based comparisons showed similar results. Highly significant correlations were observed between V_T and $SUVR_{40-60}$ for OCC (r=0.83, p<0.001), CBL (r=0.97, p<0.001) and WB-ventricles (r=0.94, p<0.001)). **Conclusion:** Reference region $SUVR_{40-60}$ values provide similar and even more robust results as V_T obtained by full quantification Additionally, $SUVR_{40-60}$ correct for genotype, so no arterial sampling is needed and short static scans can be sufficient with highest sensitivity using WB-ventricles as pseudoreference region. In conclusion, these results indicate that instead of 60-minute full kinetic modelling with arterial sampling, a static 20-minute scan is sufficient for [18F]DPA714 ALS analysis. **References:** 1.Turner. et.al.Neurobiol Dis.2004 2.Corcia.et.al.PLoS ONE.2012 3.Zürcher. et.al.Neuroim Clin.2015 4.Albrecht.et.al.JNM.2018 5.Ratai.et.al. Neuroim Clin.2018 6.Alshikho.et.al.Neurology.2016 7.Alshikho. et.al.Ann Neurol.2018

EPS-037

Influence of APOE genotype on α4β2 nicotinic acetylcholine receptor binding in mild Alzheimer's dementia as assessed by (-)-[18F]Flubatine PET

P. Meyer[1], *S. Wilke*[1], *S. Hesse*[1,2], *G. Becker*[1], *M. Rullmann*[1], *M. Patt*[1], *J. Luthardt*[1], *G. Wagenknecht*[3], *A. Hoepping*[4], *R. Smits*[4], *B. Sattler*[1], *S. Tiepolt*[1], *W. Deuther-Conrad*[5], *H. Barthel*[1], *P. Schönknecht*[6], *P. Brust*[5], *O. Sabri*[1];

[1]*Department of Nuclear Medicine, University of Leipzig, Leipzig, GERMANY,* [2]*Integrated Research and Treatment Centre (IFB) Adiposity Diseases, University of Leipzig, Leipzig, GERMANY,* [3]*Electronic Systems (ZEA-2), Central Institute for Engineering, Electronics and Analytics, Research Centre Juelich, Juelich, GERMANY,* [4]*ABX advanced biochemical compounds GmbH, Radeberg, GERMANY,* [5]*Department of Neuroradiopharmaceuticals, Institute of Radiopharmaceutical Cancer Research, Helmholtz-Zentrum Dresden-Rossendorf, Research Site Leipzig, Leipzig, GERMANY,* [6]*Department of Psychiatry and Psychotherapy, University of Leipzig, Leipzig, GERMANY.*

Aim/Introduction: The question of whether the presence of the APOE ε4 allele impacts α4β2 nicotinic acetylcholine receptor (α4β2-nAChR) availability in Alzheimer's dementia (AD) was so far mainly studied post-mortem, and is subject of a controversial debate. We aimed to answering this question in vivo using the recently developed α4β2-nAChR-specific radioligand (-)-[18F] Flubatine and PET. **Materials and Methods:** Non-smoking, drug-naïve AD-APOE ε4+ (n=7; 76±6ys; 6 females; MMSE 24±3) and AD-APOE ε4- (n=9; 75±7ys; 7 females; MMSE 24±2, n. sign. vs. AD-APOE ε4+) were investigated using (-)-[18F]Flubatine (370 MBq, ECAT Exact HR+, 0-90min p.i.) and compared with non-smoking healthy controls (HC; n=13; 72±4ys; 7 females). For quantification of the α4β2-nAChR availability, kinetic modeling (1TCM, Logan) was performed and the distribution volume (V_T) was calculated. VOI analyses of a-priori selected brain regions and exploratory SPM analyses were carried out (ANCOVA, significance at P<0.05 and T>3.0; P<0.003). **Results:** Compared with HC, in AD-APOE ε4+, there was significantly lower V_T within the basal forebrain, hippocampus, amygdala, and fronto-temporal cortices. Compared with HC, in AD-APOE ε4-, voxel-based analysis revealed significantly lower V_T in minor clusters within the fronto-temporo-parietal and posterior cingulate cortices. In AD-APOE ε4+, directly compared with AD-APOE ε4-, there was significantly lower V_T within the basal forebrain, hippocampus, amygdala, fronto-temporal, and cingulate cortices. **Conclusion:** Using the recently developed (-)-[18F]Flubatine and PET, we demonstrated for the first time in-vivo the influence of APOE ε4 on α4β2-nAChR availability in mild AD. In contrast to earlier studies, we show that the APOE ε4 genotype modulates the α4β2-nAChR pathophysiology in AD. If replicated in larger cohorts, our findings encourage adjusting cholinergic drug therapy to the APOE genotype in patients with AD. **References:** None.

EPS-038

Assessment of Centiloid [18F]flutemetamol values relative to CERAD-style pathology categories from a well characterised autopsy cohort

C. J. Buckley[1], *M. Battle*[1], *G. Farrar*[1], *C. Foley*[1], *A. Smith*[1], *D. Thal*[2];

[1]*GE Healthcare Pharmaceutical Diagnostics, Amersham, UNITED KINGDOM,* [2]*2.Department of Neurosciences, KU Leuven, Leuven, BELGIUM.*

Aim/Introduction: [18F]flutemetamol Centiloid (CL) values from a PET-only SUVR analysis pipeline were compared to autopsy-determined neuritic plaque densities assessed by a numeric CERAD-style method[1] (mCERAD) with a view to determining the band of CL values associated with the numerical equivalents of neuritic plaque mCERAD categories of none, sparse, moderate or frequent with a view to identifying the Centiloid band of values for those accumulating amyloid pathology in early stages **Materials and Methods:** [18F]flutemetamol PET images were made in 106 subjects in life and pathology CERAD scores of neuritic plaque densities were measured post-mortem. The PET images were analysed using an adaptive template-based PET-only pipeline (AmyPype) to provide SUVR Centiloid values from these subjects. Post-mortem histopathology assessments were from 8 regions. Neuritic plaque densities using Bielschowsky

silver-staining were made to obtain quantitative regional pathology scores aligned with CERAD style scoring. Each subject's pathology was considered abnormal if any region had a numeric mCERAD score greater than the boundary between sparse and moderate. Particular emphasis is given to the Centiloid values in subjects whose levels of pathology are positive, but below accepted autopsy thresholds. **Results:** CL values for the mCERAD bands are shown in Table 1. **Conclusion:** The Centiloid values in the cases which had pathology but were below mCERAD positive thresholds had a median value of ~17 with most of the values lying below 28 Centiloids. The subjects in this band which had Centiloid values of greater than 28 had Thal phases 3 to 5 indicating the likely role of diffuse plaques in elevating the Centiloid scores. For those cases which had border-line positive pathology, the majority had Centiloid values above 50. However, there were 4 cases below 30 Centiloid. These cases typically had pathology scores that were regionally variable which, though positive by mCERAD rules, the averaging out the PET signal in the large Centiloid cortical VOI produced a net lower value. In summary, subjects with Centiloid values between 15 and 30 are highly likely to be accumulating amyloid pathology which may not have reached the density required to show as visually abnormal by PET. **References:** 1. Ikonomovic et. al. Acta Neuropathologica CommunicationsNeuroscience of Disease2016 4:130

EPS-039

18F-ML-104 Tau Positron Emission Tomography/Computed Tomography: a potential biomarker for mild cognitive impairment due to Alzheimer's disease

J. Jaleel, *M. Tripathi, V. Baghel, S. T. Arunraj, P. Kumar, A. Dey, C. Bal; All India Institute of Medical Sciences, New Delhi, INDIA.*

Aim/Introduction: Tau positron emission tomography/computed tomography (PET/CT) enables invivo imaging of the spatial distribution pattern of neurofibrillary tau tangles in the brain. We have previously demonstrated increased tau deposition in temporo-parietal regions in Alzheimer's dementia (AD) and early AD in comparison to normal controls (paper in communication). This study was undertaken to evaluate the tau distribution pattern in patients with amnestic mild cognitive impairment (MCI). **Materials and Methods:** Twenty eight patients, who were diagnosed clinically as amnestic MCI (MMSE ≥ 24) in the geriatric memory clinic, were included in the study. Ten normal controls, were also recruited. Each MCI patient underwent ^{18}F- Fluorodeoxyglucose (^{18}F-FDG) PET/CT on the basis of which they were divided into two groups- those showing a metabolic pattern consistant with early AD (shown to beat a greater risk of developing overt AD) and those who did not reveal any metabolic abnormality. All patients and controls were taken up for the ^{18}F-ML-104 Tau PET/CT (Neptis-ORA). The tau PET/CT images were independently evaluated using region of interest drawn over bilateral frontal, parietal, medial temporal, lateral temporal lobes, posterior cingulate, precuneus and cerebellum.The standardised uptake value ratios were calculated ($SUV_{region}/SUV_{cerebellum}$) and compared in the two groups (based on FDG PET/CT patterns) and with normal controls. Significance was evaluated statistically using Mann Whitney U test. **Results:** Maximum ^{18}F-ML-104 retention was noted in the medial temporal lobes in both the FDG hypometabolism group (mean SUVR-1.63) and the no-hypometabolism group (mean SUVR-1.48), with a significant difference between groups (p=0.04). There was a significant difference in retention of the tracer in the lateral temporal (p=0.02), precuneus (p=0.03) and posterior cingulate (p=0.03) cortex between the two groups. Compared to controls, tracer retention was significantly increased in all the regions evaluated in both groups (p <0.01). **Conclusion:** We could demonstrate a significant increase in tau deposition in amnestic MCI patients with a metabolic pattern consistant with early AD on FDG PET. This suggest the utility of tau PET as a biomarker for MCI patients who are likely to progress to AD dementia. **References:** None.

EPS-040

Sex Modulates the ApoE ε4 Effect on Tau Brain Deposition measured by^{18}F-AV-1451 PET in Individuals with Normal Aging and Mild Cognitive Impairment

R. Wang[1,2], *M. Liu*[1], *X. Chen*[1], *Y. Zhou*[3];
[1]*Peking University First Hospital, Beijing, CHINA,* [2]*Peking University International Hospital, Beijing, CHINA,* [3]*Johns Hopkins University School of Medicine, Baltimore, MD, UNITED STATES OF AMERICA.*

Aim/Introduction: To evaluate sex differences in the association between apolipoprotein E type 4 allele (ApoE ε4) carrier status and brain tau deposition measured using ^{18}F-AV-1451 positron emission tomographic (PET) imaging among mild cognitive impairment (MCI) participants. **Materials and Methods:** Preprocessed ^{18}F-AV-1451 tau and ^{18}F-AV-45 amyloid PET images, T1-weighted structural magnetic resonance imaging (MRI) scans, demographic information, and cerebrospinal fluid (CSF) total tau (t-tau) and phosphorylated tau (p-tau) measurements from 108 MCI subjects (mean age 78.3 (7.4) years) in the Alzheimer's Disease Neuroimaging Initiative (ADNI) database were included.After downloading pre-processed images from ADNI, an iterative reblurred Van Cittertiteration partial volume correction (PVC) method was applied to all PET images. MRIs were used for PET spatial normalization. Regions of interest (ROIs) were defined in standard space, and standardized uptake value ratio (SUVR) images relative to cerebellum were computed. ApoE ε4 by sex interaction analyses on ^{18}F-AV-1451 and CSF tau (t-tau, p-tau)were assessed using generalized linear models. Correlation between ^{18}F-AV-1451 SUVR and CSF tau (t-tau, p-tau) were calculated. **Results:** After applying PVC and controlling for age, education level and global cortical ^{18}F-AV-45 SUVR, we found that the entorhinal cortex, amygdala, fusiform, parahippocampal gyrus, posterior cingulate, and occipital ROIs exhibited a significant ApoE ε4 by sex interaction effect(FDR P<0.05) among MCI individuals. There were significant ApoE ε4 by sex interaction effect in CSF t-tau and p-tau.^{18}F-AV-1451 SUVR in all 6 ROIs with ApoE ε4 by sex interaction was significantly

correlated with CSF p-tau and t-tau. **Conclusion:** Our findings suggest that women are more susceptible to ApoE ε4-associated accumulation of neurofibrillary tangles during preclinical stages of AD compared to males, and may also be more cognitively resilient to higher loads of tauopathy. Both CSF tau (p-tau, t-tau) and brain tau PET are robust quantitative biomarkers for studying ApoE ε4 by sex effects on tau brain deposition in MCI. The strongest genetic risk factor for AD is the ApoE ε4. We report that sex modulates the relationship between ApoE ε4 carrier status and brain tau deposition (a quantitative endophenotype in AD) in individuals with MCI. These new findings improve our understanding of the role of sex and ApoE ε4 as risk factors in preclinical AD and help develop precision-medicine based therapeutics. **References:** None.

EPS-041

At first sight - Can gray matter/white matter boundary delineation or partial volume effect correction improve the visual read of [18F]Florbetaben PET images?

M. Rullmann[1,2], *S. Tiepolt*[1], *K. Messerschmidt*[1], *T. Gerhards*[1], *M. Schürer*[1], *S. Hesse*[1,2], *D. Saur*[3], *C. Weise*[3,4], *M. L. Schroeter*[4], *J. Classen*[3], *O. Sabri*[1], *H. Barthel*[1];
[1]*Department of Nuclear Medicine, University of Leipzig, Leipzig, GERMANY,* [2]*IFB AdiposityDiseases, Leipzig University Medical Center, Leipzig, GERMANY,* [3]*Department of Neurology, University of Leipzig, Leipzig, GERMANY,* [4]*Day Clinic of Cognitive Neurology, University of Leipzig, Leipzig, GERMANY.*

Aim/Introduction: Beta-amyloid (Aß) PET tracers like [18F] Florbetaben are approved for clinical use via binary visual evaluation for the existing (Aß-negative) or missing (Aß-positive) contrast between specific gray matter (GM) and non-specific white matter (WM) uptake. Consequently, a priori reader training focusses on evaluating the GM/WM contrast within the PET images. Of note, the influence of partial volume effects (PVEs) is so far not considered in this clinical routine visual read. Thus, we tested the hypothesis that amyloid PET read can be improved by WM/GM boundary superimposition and/or PVE correction. **Materials and Methods:** Six nuclear medicine physicians (three experts, three novices after reader training) blindly and independently evaluated 480 [18F]Florbetaben PET datasets (90-110min p.i.) including 20% duplicates and four modalities: (A) Standard PET images, (B) PET images with superimposed WM/GM boundaries (individual T1 MPRAGE MRI, segmentation in SPM12), (C) PVE-corrected (Van-Cittert deconvolution approach) PET images, (D) combined B and C. Evaluation included binary diagnosis and diagnostic confidence (five-point Likert scale). Results of the clinical consensus board served as standard of truth. Sensitivity, specificity, accuracy, multi-rater Fleiss' kappa and percentage of agreement for duplicates were assessed for all four modalities. Differences in sensitivity, specificity, accuracy and confidence were tested by paired t-tests. **Results:** Assessment (A) showed high sensitivity, specificity, accuracy and confidence (97%, 82%, 90%, 81%, respectively). Here, experts and novices did not significantly differ. Assessment (B) decreased sensitivity (-7%, p=0.04) while specificity increased (+10%, p=0.004). Assessment (C) only decreased sensitivity (-6%, p=0.05). Assessment (D) decreased sensitivity (-14%, p=0.002) and increased specificity (+15%, p=0.003). As compared to assessment (A), inter-reader agreement was higher for assessment (B) (0.80, $p=5\times10^{-211}$ vs. 0.76, $p=2\times10^{-192}$). Intra-reader agreement did not relevantly differ between the assessment types (85-90%). **Conclusion:** Standard visual evaluation of [18F]Florbetaben PET images already has high sensitivity, which cannot be further improved by the approaches tested. Reliability and at the expense of sensitivity, specificity can, however, be increased by superimposing WM/GM contrast and/or PVE correction of the PET data. A prospective evaluation of this promising approach is warranted. **References:** None.

EPS-042

Baseline Assessments of Striatal Amyloid Plaque Load, Hippocampal and Ventricular Volumes via [18F] flutemetamol PET and MRI Imaging Predicts Clinical Progression to pAD in a 3-year Observational aMCI Cohort Study

L. Chedumbarum Pillay[1], *P. Wilkens*[2], *C. J. Buckley*[3];
[1]*University of Oxford, Oxford, UNITED KINGDOM,* [2]*GE Healthcare, Marlborough, MA, UNITED STATES OF AMERICA,* [3]*GE Healthcare, Amersham, UNITED KINGDOM.*

Aim/Introduction: By clinicopathological diagnostic requirements for Alzheimer Disease (AD), a minimum load of both Aß and neurofibrillary tau tangles (NFTs) should be present. Amyloid imaging is therefore critically limited in this regard. Post-mortem studies have indicated a stronger association, however, between striatal Aß deposition and advanced NFT Braak stages. Further to amyloid measures, structural MRI neurodegenerative biomarkers are a key consideration to be able to identify individuals with mild cognitive impairment (MCI) due to AD. In addition to assessments of striatal amyloid plaque burden, we investigate cortical thickness atrophy of the medial temporal structures, hippocampal atrophy and ventricular dilation in an aggregate measure of neuronal injury (N), with respect to their statistical predictive performance in amnestic MCI (aMCI) to probable AD (pAD) progression and survival rates over a three-year observation period. **Materials and Methods:** Facilitating our analysis were the baseline [18F] flutemetamol PET and 3D T1 MRI scans of 231 aMCI subjects obtained in a three-year GE Healthcare led Phase-III clinical trial comprising of cross-sectional PET/MR imaging and longitudinal clinical evaluation. Subjects' baseline PET and MRI images were pre-processed and co-registered in FSL v5.0. A striatal volume of interest (VOI) based on an average pAD [18F]flutemetamol PET image was used to quantify striatal uptake by means of a SUVr_pons ratio. Cortical thicknesses and hippocampal volume were derived in FreeSurfer v6.0. Frontal-lateral ventricular dilation was estimated in FSL. **Results:** Of the 95 Blinded Image Evaluated (BIE) Amyloid-Positive (A+) aMCI subjects,

those who progressed to pAD (N=51) had a mean(SD) bilateral striatal SUVr_pons of 0.87(0.11), and those who remained aMCI (N=26, excl. 18 middle censored), 0.75(0.11). Striatal uptake was therefore significantly higher amongst BIE A+ subjects who had progressed to pAD (p=2.5e-05, Mann-Whitney U-test). Following ROC analysis, also associated with striatal uptake was an AUC of 0.80. Cortical thickness measures of the entorhinal (ENT) and parahippocampal (PHC) cortices over the full cohort had respective mean(SD)s of [Non-Converters: 3.2(0.42), Converters: 2.9(0 .49)] and [Non-Converters: 2.6(0.3), Converters: 2.46(0.28)], and respective AUCs of 0.30 and 0.30. We thus omit cortical thickness measures in our aggregate measure of neuronal injury, and accounting for hippocampal atrophy and ventricular dilation achieve sensitivity and specificity rates of 0.82 and 0.77, and improved hazard rates of up to 67% compared to (cortical) amyloid positivity status alone. **Conclusion:** Baseline striatal amyloid load, hippocampal volume and ventricular dilation provide markedly improved statistical predictive performance rates in aMCI progression to clinical pAD. **References:** None.

EPS-043

Direct quantification of native-space amyloid PET via end-to-end training of a deep learning

J. Kim, H. Choi, J. Paeng, G. Cheon, K. Kang, D. Lee; Department of Nuclear Medicine, Seoul National University, Seoul, KOREA, REPUBLIC OF.

Aim/Introduction: Accurate quantification of amyloid PET is crucial for the estimation of amyloid load in the gray matter as a biomarker for Alzheimer's disease. So far, the quantification has required complicated preprocessing steps including structural MR-based segmentation and normalization. It has been difficult to perform the quantification as a clinical routine because of no unified method of multiple centers and time and effort for the processing. Here, we developed a deep learning model to quantify amyloid PET via the end-to-end training using native-space multiple center PET images. **Materials and Methods:** Amyloid PET data from the Alzheimer Disease Neuroimaging Initiative were used. 850 baseline florbetapir PET images were used as a training/validation set and 366 florbetapir PET images as 2-year follow-up were used as an independent test set. We also validate the model using 89 florbetaben PET data. We designed a 3-d convolutional neural network model for the direct quantification. The end-to-end training of deep learning model was performed using native-space PET images as inputs and standardized uptake value ratios (SUVR) previously calculated by MR-based preprocessing as outputs. SUVR of 4 cortical subregions (frontal, cingulate, parietal, and temporal) were estimated using the deep learning model. The composite SUVR was obtained by the mean value of the 4 subregional SUVR. The model performance was estimated by mean absolute errors of the composite SUVR and correlation coefficients using a Pearson correlation. Bland-Altman plots were drawn to evaluate bias and errors of the deep learning-based estimation. **Results:** The mean absolute error of the composite SUVR of training and test sets were 0.031 and 0.064. The mean absolute error of florbetaben PET as an independent test set was 0.057. The correlation coefficients were 0.99, 0.93, and 0.93 for the training set, test set of florbetapir PET, and florbetaben PET, respectively. Samples were divided into two groups, amyloid-positive and negative, using a predefined cutoff value of the composite SUVR. The agreement measured by Cohen's kappa of two quantification methods, approaches of full-processing with MR and deep learning, was 0.84 and 0.78 for test sets of florbetapir PET, and florbetaben PET, respectively. The Bland-Altman plots showed the agreement without bias for the quantification. **Conclusion:** We suggest a feasible quantification method for amyloid PET with the end-to-end training of deep learning. For our approach, structural MR and multiple preprocessing steps are not required. Furthermore, it shows reliable quantification results of PET images obtained from multiple centers. **References:** None.

EPS-044

Comparison of Centiloid Scaling Values with Visual Read Assessment in a Pathology Verified Autopsy Cohort

M. Battle[1], C. Buckley[1], A. Smith[1], G. Farrar[1], D. R. Thal[2], J. Molineuvo[3], O. Hansson[4,5];
[1]GE Healthcare, Amersham, UNITED KINGDOM, [2]Department of Neurosciences, KU Leuven, Leuven, BELGIUM, [3]Barcelona Brain Research Centre, Barcelona, SPAIN, [4]Clinical Memory Research Unit, Department of Clinical Sciences Malmö, Lund University, Lund, SWEDEN, [5]Memory Clinic, Skåne University Hospital, Malmö, SWEDEN.

Aim/Introduction: Centiloid scaling has been established as a method of standardising quantitative image analysis for measuring the uptake of βamyloid imaging PET tracers in Alzheimer's disease (AD), with process pipeline equations reported by various groups [1,2,3]. The "Standard" Centiloid methods, described by Klunk et.al.[4], utilise both PET and MR scans with defined regions of interest. Here the utility of Centiloid scaling in a cohort of subjects with no MRI scans was investigated. AmyPype-derived Centiloid (^{AmyP}Centiloid) values for [^{18}F]flutemetamol were calculated and compared against visual read outcomes for the PET images. This is compared to the pathology status. **Materials and Methods:** Using an in-house developed software platform (AmyPype) the Centiloid Volume of Interest (VOI) regions were applied to 104 [^{18}F] flutemetamol images obtained from subjects who were part of a larger autopsy study. Images had been assessed as either normal (n=34) or abnormal (n=70) by majority visual read. SUVR and ^{AmyP}Centiloid values for the VOI regions were calculated. A comparison of the SUVR and ^{AmyP}Centiloid classifications with the visual assessment reads were made. **Results:** SUVR and ^{AmyP}Centiloid values were ranked in ascending order and plotted for each subject. For the SUVR and Centiloid values, the threshold between normal and abnormal subjects as defined by visual reads were determined. A comparison of the ^{AmyP}Centiloid prediction, based on a threshold cut-off of 40 for an autopsy

based normal/abnormal classification , gave an 89% (93/104) agreement with the visual read assessment. Interestingly, in the cases where there was disagreement between the visual assessment and the ^{AmyP}Centiloid prediction, ^{AmyP}Centiloid predictions agreed with at least one reader in 45% (5/11) cases. **Conclusion:** Centiloid values provide quantifiable information that can complement the visual read assessment. For the cases where there was disagreement between readers, the availability of Centiloid values may have provided additional guidance in almost half (45%) of the cases. Centiloid scaling has some limitations in sensitivity, based on the application global VOIs, and these are discussed by Buckley et al. **References:** 1. Battle MR, et al. EJNMMI Res 2018. 2. Rowe C, et al. EJNMMI 2017. 3. Navitsky M, et al. Alzheimer's & Dementia. 2016. 4. Klunk WE, et al. Alzheimer's & Dementia 11, 2015. 5. Thurfjell L, et al. J Nucl Med, 2014.

EPS-045

Validation of a Visual Assessment Strategy for 18F-Flortaucipir PET

A. Dodich[1], *A. Rochat*[1], *I. Mainta*[2], *C. Noirot*[2], *P. Andryszak*[3], *B. Rakotomiaramanana*[3], *G. B. Frisoni*[3], *V. Garibotto*[1,2];
[1]*NIMTlab, Neuroimaging and Innovative Molecular Tracers Laboratory, University of Geneva, Geneva, SWITZERLAND,* [2]*Nuclear Medicine and Molecular Imaging Division, Diagnostic Department, Geneva University Hospitals, Geneva, SWITZERLAND,* [3]*Memory Center and LANVIE - Laboratory of Neuroimaging of Aging, Department of Rehabilitation and Geriatrics, Geneva University Hospitals, Geneva, SWITZERLAND.*

Aim/Introduction: The presence of pathological changes characterizing Alzheimer's Disease can be assessed by amyloid (A) and tau (T) imaging biomarkers, with important possible implications in clinical practice. A key step is the reliable assessment of the biomarker measure and threshold for positivity. We developed a visual assessment (VA) strategy for 18F-flortaucipir PET and we tested its interrater agreement as well as its consistency with quantitative (QA) assessment. **Materials and Methods:** 120 subjects with available 18F-flortaucipir PET and T1-weighted MRI images were selected from the ADNI dataset. They were characterized by heterogeneous clinical (55 cognitive normal, 65 cognitive impaired) and A status (53 A+ and 67 A-). Raters were instructed through a standard visual analysis procedure, including images synchronization and display on a continuous color map with the cerebellar crux set approximately at the 30% of the scale. Each reader provided as output an estimated Braak stage and its level of confidence (5-level scale). Blinded visual reads were conducted by three raters. QA and definition of T positivity was based on two automated algorithms (Schwarz et al., 2018) and literature-based global and regional cut-points for standardized uptake value ratio (SUVR). Agreement between T positivity defined through VA (based on the classification performed by the majority of readers) and QA was evaluated through Cohen's kappa. Finally, we compared the global SUVR through independent sample t-test in T+ vs T- sub-groups based on VA consensus. **Results:** Raters showed a substantial agreement in visual classification, with a kappa ranging between 0.68 and 0.78 (percentage of agreement 87%-91%), and an average confidence in the interval 3.4-4.5. Global SUVR was significantly different in T+ vs T- subjects classified according to VA consensus ($t(118)=5.64$, $p<0.001$). In the assessment of the T status based on QA, the agreement between different methods ranged from 0.33 to 0.66. The comparison of QA and VA showed the highest agreement between VA and a regional-based SUVR cut-point (medial temporal regions: k=0.48, CI95% 0.32-0.64, percentage of agreement 78%). **Conclusion:** This is the first study proposing and testing a standardized VA for flortaucipir images. Readers performing VA obtained a substantial interrater agreement, higher than the agreement observed between different QA approaches. **References:** 1. A. J. Schwarz et al., Topographic staging of tau positron emission tomography images. Alzheimers Dement **10**, 221-231 (2018). 2. S. Mishra et al., AV-1451 PET imaging of tau pathology in preclinical Alzheimer disease: Defining a summary measure. Neuroimage **161**, 171-178 (2017).

EPS-046

AmyPype: an automated system to quantify AMYPAD's [^{18}F]flutemetamol and [^{18}F]florbetaben images including regional SUVR and Centiloid analysis

C. J. Buckley[1], *C. Foley*[1], *M. Battle*[1], *E. Grecchi*[1], *G. Farrar*[1], *J. Gispert*[2], *I. Lopes-Alves*[3], *F. Barkhof*[3], *A. A. Lammertsma*[3], *S. Bullich*[4], *D. Altomare*[5], *G. B. Frisoni*[5], *C. Moro*[5], *V. Garibotto*[6], *J. Cardoso*[7], *M. Modat*[8];
[1]*GE Healthcare Pharmaceutical Diagnostics, Amersham, UNITED KINGDOM,* [2]*BarcelonaBeta Brain Research Centre, Barcelona, SPAIN,* [3]*Amsterdam UMC, Vrije Universiteit, Amsterdam, NETHERLANDS,* [4]*Life Molecular Imaging, Berlin, GERMANY,* [5]*Laboratory of Neuroimaging of Aging (LANVIE), University of Geneva, Geneva, SWITZERLAND,* [6]*Division of Nuclear Medicine and Molecular Imaging, University Hospitals of Geneva, Geneva, SWEDEN,* [7]*Centre for Medical Image Computing, UCL, London, UNITED KINGDOM,* [8]*Dementia Research Centre, London, UNITED KINGDOM.*

Aim/Introduction: AMYPAD is a multi-centre pan European public-private partnership funded by Innovative-Medicines-Initiative aimed at understanding the added value of amyloid PET imaging in the clinical workup of subjects with cognitive complaints and for understanding the process of amyloid deposition in the AD pathology continuum. In particular for the clinical workup scenario, AmyPype was designed to allow the harmonized (including Centiloid[1]) quantitative assessment of [^{18}F]flutemetamol and [^{18}F]florbetaben amyloid PET without the need for individual's structural MRI images. **Materials and Methods:** Amyloid PET images (static or dynamic) are co-registered with a pre-defined adaptive negative/positive PET template. Next, individual images are transformed into MNI152 space based on previously known transformation matrix these

templates. Next, a grey-matter parcellated cortical-volume of interest (VOI) mask is applied to the images, together with a Centiloid Cortical mask and whole cerebellum reference region. The application runs on a GE Advantage Workstation. Centiloid GAAIN data were used to validate the process pipeline, as described in the methods by Klunk et al. (2015). In-house data were used to validate the [18F]flutemetamol process and determine the Centiloid conversion equation (available on the GAAIN website). For [18F]florbetaben, data was also obtained from the GAAIN website and used to validate the process **Results:** Amypype is able to receive PET-only amyloid scans in batch and output ascii tables of regional and composite SUVR values together with Centiloid values for both [18F] flutemetamol and [18F]florbetaben PET images. Additionally, where a normal database was available (currently only for [18F] flutemetamol), voxel wise Z-scores relative to the regional and voxel level normal database images are reported. Validation was achieved by comparing the output of AmyPype with the Centiloids obtained through the GAAIN two step validation approach. The difference between the Centiloid values obtained with AmyPype compared to the standard MR-driven pipeline[1] were substantially less than 1% on average for all cohorts and both tracers. **Conclusion:** AmyPype provides a robust Centiloid amyloid quantification process platform that allows quick and easy batch processing of PET-only images for both [18F]flutemetamol and [18F]florbetaben. Centiloid scaling and the derived process reports, can complement visual reads and provide additional quantitative information to better-aid patient selection and management. **References:** 1. Klunk et. al. Alzheimers Dement. 2015 Jan; 11(1):1-15

EPS-047

Evaluation of a visual interpretation method for Flortaucipir PET imaging

I. Sonni[1,2], *O. H. Lesman-Segev*[3], *S. L. Baker*[2], *D. Korman*[4], *G. D. Rabinovici*[3,2], *W. J. Jagust*[4,2], *S. M. Landau*[4];
[1]*University of California, Los Angeles, CA, UNITED STATES OF AMERICA,* [2]*Lawrence Berkeley National Lab, Berkeley, CA, UNITED STATES OF AMERICA,* [3]*University of California, San Francisco, CA, UNITED STATES OF AMERICA,* [4]*University of California, Berkeley, CA, UNITED STATES OF AMERICA.*

Aim/Introduction: We aimed to evaluate a visual interpretation method for the qualitative assessment of 18F-AV-1451 (Flortaucipir - FTP) Tau PET scans in clinical settings. **Materials and Methods:** 274 subjects (137 ADNI, 137 UCSF/BACS, tables 1 and 2) scanned with FTP-PET were selected. FTP-PET images (smoothed to 4mm, non-normalized, not co-registered to MRI to resemble a clinical scenario) were qualitatively interpreted independently by two readers. Readers were blinded to clinical information and to SUVR values. The rating scheme was purely visual and started with adjusting the color scale based on binding to inferior cerebellum. The rating provided 1) a global visual score (0-to-14 scale), obtained by assessing the binding severity (0-to-2 ROI score) in 7 cortical regions (medial, inferior and lateral temporal, medial and lateral parietal, frontal and occipital), and summing all individual ROI's scores together; 2) a FTP distribution pattern among one of four pre-determined distribution patterns**:** 1.negative scan 2.temporal binding only 3.AD-like 4.non-AD like binding patterns. The results of the visual interpretation were compared to global FTP SUVR, amyloid status and clinical diagnosis. Negative and positive predictive values of the distribution pattern based on clinical diagnosis were calculated. Inter-rater reliability was calculated. **Results:** Average of the two readers' global visual scores were significantly associated with global FTP SUVR (r=0.69 for ADNI, r=0.84 for UCSF/BACS). Mean visual scores within each diagnostic category were lower for amyloid negative subjects than for amyloid positive subjects. Visual scores were correlated with diagnosis (tables 3 and 4): controls had the lowest scores, MCIs intermediate, and AD the highest values. Patients with non-AD dementia had an average visual rating similar to healthy controls. The low rate of false negative scans (clinically diagnosed AD described as having a visual FTP pattern different from AD) determined a high NPV (80% and 89% for ADNI and 97% and 98% for UCSF/BACS). PPV was 60% and 76% for ADNI and 84% and 94% for UCSF/BACS). Inter-rater agreement on global visual scores was strong (linear weighted Kappa for ADNI=.61, for UCSF/BACS=.83). Inter-rater agreement on the definition of distribution pattern was also good with an overall full agreement in 66% of cases (60% in ADNI and 71% in UCSF/BACS). **Conclusion:** Our data show that this purely visual rating scheme strongly correlates with FTP global quantification and clinical diagnosis. Inter-rater reliability is strong. This visual method is a reliable, reproducible and promising alternative approach to Tau measurement in clinical settings. **References:** None.

EPS-048

A kinetics-based approach to amyloid PET semi-quantification

S. Capitanio[1], *E. Peira*[2], *M. Corosu*[2], *S. Morbelli*[3], *M. Bauckneht*[3], *M. Pardini*[4], *D. Arnaldi*[4], *C. Vellani*[5], *D. D'ambrosio*[6], *V. Garibotto*[7], *F. Assal*[8], *B. Paghera*[9], *G. Trifiro*[5], *U. Guerra*[10], *F. Nobili*[4], *G. Frisoni*[11], *A. Chincarini*[2];
[1]*IRCCS Ospedale Policlinico San Martino, Genova, ITALY,* [2]*Istituto Nazionale di Fisica Nucleare (INFN), Genova, ITALY,* [3]*IRCCS Ospedale Policlinico San Martino; Nuclear Medicine Unit (DISSAL), University of Genoa, Genova, ITALY,* [4]*IRCCS Ospedale Policlinico San Martino; Dept of Neuroscience (DINOGMI), University of Genoa, Genova, ITALY,* [5]*Nuclear Medicine Unit, ICS Maugeri IRCCS, Pavia, ITALY,* [6]*Medical Physics Unit, ICS Maugeri IRCCS, Pavia, ITALY,* [7]*Nuclear Medicine and Molecular Imaging Division, University Hospitals and University of Geneva, Geneva, SWITZERLAND,* [8]*Division of Neurology, Department of Clinical Neurosciences, Geneva University Hospitals, Geneva, SWITZERLAND,* [9]*Nuclear Medicine Unit, ASST Spedali Civili, Brescia, ITALY,* [10]*Nuclear Medicine, Fondazione Poliambulanza, Istituto Ospedaliero, Brescia, ITALY,* [11]*Laboratory of Neuroimaging of Aging (LANVIE), University of Geneva; Memory Clinic, University Hospital of Geneva, Geneva, SWITZERLAND.*

Aim/Introduction: To date, amyloid-PET assessment consists in a visual binary evaluation of the scan (negative/positive) optionally supported by semi-quantification techniques. Regional cerebral blood flow (rCBF) changes between patients and intra-patient could hamper longitudinal evaluation. The aim of our work was to develop and validate a semi-quantification method (TDr) for amyloid-PET scans based on tracer kinetics information through a dual-time point acquisition and customized on the individual patient anatomic and pathophysiological characteristics, which does not need any template or MRI-coregistration. **Materials and Methods:** We retrospectively enrolled 143 subjects (aged 54-87) with clinical suspicion of AD who underwent to 18F-florbetapir PET/CT in 4 clinical italian centers. An early (E) 5 minutes PET/CT static acquisition was performed soon after tracer injection as a proxy of brain perfusion, followed by a late (L) 20 minutes static acquisition after 45 minutes. High rCBF regions were concentrated in the cortical gray matter and were used to delineate the uptake regions of interest (ROIs). Time-delayed ratio (TDr) was then calculated as the ratio between the average intensities in the ROIs from E onto the reference ROI on L. TDr values were compared to the binary visual assessment and to two validated semi-quantification methods (cortical-cerebellar SUVr and ELBA method, a SUVr-independent approach). TDr area under the receiver operating characteristic curve (AUC) was measured for negative versus positive scans. **Results:** TDr showed excellent performance with respect to the binary visual assessment (AUC=0.99) with very good accuracy both on the whole dataset and on single center cohorts. It significantly correlated with both SUVr and ELBA although it related better with ELBA as evidenced by the correlation coefficients on the negative and positive classes separately. **Conclusion:** TDr is a highly accurate semi-quantification method that requires minimal image processing, it is independent on predefined ROI, does not require MR coregistration and implies a negligible added patient discomfort. In clinical setting, the use of TDr could lead to a very robust index of amyloid load particularly suitable for measuring longitudinal changes in monitoring disease progression or treatment response. **References:** Schmidt et al. The influence of biological and technical factors on quantitative analysis of amyloid PET: Points to consider and recommendations for controlling variability in longitudinal data. Alzheimers Dement 2015;11:1050-68. Chincarini et al. Standardized Uptake Value Ratio-Independent Evaluation of Brain Amyloidosis. J Alzheimers Dis 2016;54:1437-57.Cecchin et al. A new integrated dual time-point amyloid PET/MRI data analysis method. Eur J Nucl Med Mol Imaging 2017;44:2060-72.

EPS-049

Translocator Protein in 4R Tauopathies - Experience from the ActiGliA Study

J. Sauerbeck[1], *L. Beyer*[1], *S. Schönecker*[2], *C. Palleis*[2], *G. Höglinger*[3], *E. Schuh*[4], *R. Boris*[5], *G. Rohrer*[2], *S. Sonnenfeld*[2], *K. Bötzel*[2], *A. Danek*[2], *A. Rominger*[6], *J. Levin*[2], *B. Matthias*[7];
[1]*Dept. of Nuclear Medicine, University of Munich, Muenchen, GERMANY,* [2]*Klinikum der Universität München, Klinik und Poliklinik für Neurologie, Muenchen, GERMANY,* [3]*Klinikum Rechts der Isar, Technische Universität München, Neuro-Kopf-Zentrum, Muenchen, GERMANY,* [4]*Klinikum der Universität München, Institut für Klinische Neuroimmunologie, Muenchen, GERMANY,* [5]*Klinikum der Universität München, Klinik für Psychiatrie und Psychotherapie, Muenchen, GERMANY,* [6]*Inselspital Bern, Universitätsklinik für Nuklearmedizin, Bern, SWITZERLAND,* [7]*Dept. of Nuclear Medicine, University of Munich, LMU Munich, Muenchen, GERMANY.*

Aim/Introduction: Corticobasal Syndrome (CBS) is a rare clinical condition with heterogeneous underlying diseases. The most frequent neuropathological diagnoses of CBS patients are either the 3R/4R tauopathy Alzheimer's disease (AD) or the 4R tauopathies Corticobasal Degeneration (CBD) and Progressive Supranuclear Palsy (PSP). Microglia, the cerebral innate immune cells, have been shown to be dysfunctional in AD, CBD and PSP. In our interdisciplinary study "Activity of Cerebral Networks, Amyloid and Microglia in Aging and Alzheimer's Disease (ActiGliA)", we generate multimodal prospective imaging and fluid biomarker data in CBS patients. Here we want to focus on 18kDa translocator protein (TSPO)-PET, which is a biomarker for microglial activity. **Materials and Methods:** Until now 30 patients with suspected 4R tauopathy, 21 patients (66 ± 10; 15 f/ 6 m) with probable CBS and 9 patients with probable PSP (67 ± 7; 6 f/ 3 m), according to current diagnosis criteria underwent ^{18}F-GE-180 TSPO-PET. All images (60-80 min time window) were scaled by the temporal lobe and standardized uptake value ratios (SUVR) were generated in cortical (central region) and subcortical (putamen, globus pallidus, thalamus, nucleus subthalamicus, substantia nigra, nucleus dentatus) brain regions known to be affected in 4R tauopathies. SUVR values were compared between CBS and PSP and against ten healthy controls (HC). ^{18}F-flutemetamol amyloid-PET served to confirm a negative amyloid status in all patients. **Results:** We find significantly increased TSPO-PET SUVR values in the comparison of CBS versus HC in the central region, putamen, thalamus, nucleus subthalamicus, substantia nigra and nucleus dentatus (all $p < 0.05$). Significantly increased TSPO-PET SUVR values in PSP versus HC were observed in the central region, globus pallidus and thalamus (all $p < 0.05$). In the direct comparison of clinical CBS and PSP patients, there were higher TSPO-PET SUVR values in the central region (+6% $p < 0.05$) but there were no significant differences in subcortical areas. **Conclusion:** CBS and PSP patients show an elevated ^{18}F-GE-180 signal in disease associated brain regions, indicating a potential of TSPO-PET to serve as biomarker for microglial activation in 4R tauopathies. Pronounced cortical TSPO activation in the central region of CBS patients fits to the known predilection site of this phenotype. Ongoing longitudinal measures of TSPO activation and clinical severity in this prospective cohort will elucidate if microglial activation has a predictive potential on the clinical course in 4R tauopathies. **References:** None.

EPS-050

[11C]PK11195 PET Quantification Analysis in Multiple Sclerosis and Healthy Subjects: Preliminary Results

P. N. Schuck[1], *A. S. Araújo*[1], *C. M. Dartora*[1], *L. D. Narciso*[2], *M. A. Andrade*[1], *C. S. Matushita*[1,3], *M. Koole*[4], *A. M. Marques da Silva*[1,3], *J. Becker*[1,3];
[1]*PUCRS, Porto Alegre, BRAZIL,* [2]*Western University, London, ON, CANADA,* [3]*Bralns, Porto Alegre, BRAZIL,* [4]*KU Leuven, Leuven, BELGIUM.*

Aim/Introduction: To investigate [11C]PK11195 PET quantification in brain white matter (WM) and gray matter (GM) regions in relapsing-remitting multiple sclerosis (RRMS) subjects and healthy controls (HC). **Materials and Methods:** Eight HC (30±9 years, 75±10 kg) and eighteen RRMS subjects (29±9 years, 67±15 kg) underwent [11C]PK11195 PET/CT and MRI. Dynamic 60min post-injection list-mode PET/CT were acquired in a GE Discovery600, with (341±64) MBq. I Attenuation and motion correction images were reconstructed using VUE PointHD algorithm, 32 subsets, 2 iterations, and smoothing filter 4.0 mm FWHM. T1-weighted MR from each subject was co-registered to the first 10 min static PET. Thalamus, caudate, putamen, pallidum, cerebellar cortex, cerebellar WM, hippocampus, brainstem, apparently normal WM, whole GM and juxtacortical and periventricular regions (JPV) binding were calculated using image-derived input function (IDIF) extracted from MR segmented carotid in each subject. Two tissue compartment model (2TCM) and Logan graphical method (LGM) were used to calculate the total distribution volume (VT) with IDIF from t*=20min and t*=40min. Group normality was tested using Shapiro-Wilk, and VT comparison between RRMS and healthy groups was evaluated with one-way ANOVA ($p<0.05$). **Results:** Using 2TCM, only JPV VT (RRMS=0.72±0.20; HC=0.92±0.28; $p=0.047$) was significantly different between groups. LGM (t*=20min) did not shown VT differences between groups. LGM (t*=40min) showed VT statistical differences between groups in caudate, GM, cerebellar GM, thalamus, putamen, brainstem, and JPV (RRMS=0.70±0.19; HC=0.84±0.09; $p=0.049$). JPV VT was different between RRMS and HC, both with 2TCM and LGM t*=40min. Although there was substantial heterogeneity in [11C]PK11195 binding in RRMS subjects, caudate VT seems correlated with the disease, considering lesions usually appear around this region [1]. Decreased GM and cerebellar GM suggests demyelination in RRMS, in agreement with other studies [2,3]. **Conclusion:** [11C]PK11195 in RRMS cortical and JPV regions seem related to the gradual vanishing of myelin fibres towards the chronic degenerative phase, providing potential indicators of disease progression. Further studies are required to determine the association between [11C]PK11195 binding and MS phase. **References:** [1] Thompson et al. The Lancet Neurology, 2018.[2] Pitt et al. Arch Neurol 2010.[3] Debruyne et al. EJN, 2003.

511

e-Poster Presentation Session 4 - Paediatrics & Other Clinical Studies: Joint Paediatrics & Other Clinical Studies

Sunday, October 13, 2019, 16:30 - 18:00 Room 133/134

EPS-051

Use of Iterative Reconstruction for Dose Optimisation of Paediatric ^{99m}Tc MDP Bone SPECT

F. Fahey[1,2], *J. Ouyang*[3,2], *X. Cao*[1], *Z. Levin*[3], *B. Sexton-Stallone*[1], *A. Falone*[1], *K. Zukotynski*[4], *N. Kwatra*[1,2], *R. Lim*[3,2], *Z. Bar-Sever*[5], *S. Treves*[6], *G. El Fakhri*[3,2];
[1]*Boston Children's Hospital, Boston, MA, UNITED STATES OF AMERICA,* [2]*Harvard Medical School, Boston, MA, UNITED STATES OF AMERICA,* [3]*Gordon Center of Medical Imaging, Massachusetts General Hospital, Boston, MA, UNITED STATES OF AMERICA,* [4]*McMaster University, Hamilton, ON, CANADA,* [5]*Schneiders Children's Medical Center of Israel, Petah Tikva, ISRAEL,* [6]*Brigham and Women's Hospital, Boston, MA, UNITED STATES OF AMERICA.*

Aim/Introduction: An observer study showed paediatric bone SPECTs using half the ^{99m}Tc MDP activity reconstructed using ordered subset expectation maximization with 3D resolution recovery (OSEM3D) yielded similar/better image quality to filtered back-projection (FBP) with full activity [1]. That study relied on subjective image-quality evaluation. This investigation compares diagnostic performance for paediatric bone SPECTs using localization receiver operating characteristic (LROC) analysis. **Materials and Methods:** Sixty-six normal bone SPECTs (13 boys, 53 girls, 10-17 years, mean 14.9 years) using administered activities consistent with the North American guidelines [2] were downloaded from the Boston Children's Hospital (BCH) database. These were acquired over 360°; thus, reconstructing data from one or both detectors simulated 2 count/activity levels (half vs full). "Features" simulating focal stress reactions/fractures were electronically inserted into posterior elements of the lumbar spine (L3 - L5) and reconstructed twice (OSEM3D and FBP). A teaching (N=32) and study set (N=400) were generated. Five experienced nuclear medicine physician observers were informed that a feature was present in L3, L4 or L5 on the left or right in half of the cases with no feature in the other half. For each case, observers identified the most likely feature location and ranked the likelihood of its presence on a 6-point scale (definitely, probably, possibly negative/possibly, probably, definitely positive). Observers first reviewed the training set where they were informed if each case were negative or positive and its location for positive cases. The observers then evaluated the 400 study cases. Using LROC analyses, the area under the curve (AUC) and standard deviation were determined for the pooled observer results. Differences were compared using one-tailed Student's t-test for dependent means. **Results:** OSEM3D yielded slightly higher performance than FBP (AUC = 0.783 ±

0.020 vs 0.749 ± 0.021). OSEM3D led to higher sensitivity but yielded contrast enhancement of small features leading to lower specificity. For OSEM3D and FBP, the full-count performance was significantly higher than with half counts (OSEM3D: 0.783 ± 0.020 vs 0.678 ± 0.024; FBP: 0.749 ± 0.021 vs 0.671 ± 0.025, p = 0.0021). OSEM3D did not perform considerably better than FBP with half counts (0.678 ± 0.024 vs 0.671 ± 0.025, p = 0.22). **Conclusion:** Iterative reconstruction yielded slightly higher performance than FBP (higher sensitivity/lower specificity). Reducing dose by half yielded significantly lower performance. **References:** 1. Stansfield EC, et al. Radiology. 2010;257:793-801. 2. Treves ST, et al. J Nucl Med. 2016;57:15N-18N.

EPS-052

Reducing paediatic patient radiation exposure during [18F]-PET/CT: The effect of reduced tracer dose and reconstruction methods on image quality

H. Kertesz[1], *T. Beyer*[1], *T. Traub-Weidinger*[2], *J. Cal-Gonzalez*[1], *M. Hacker*[2], *T. Kitsos*[3], *K. London*[3], *P. L Kench*[4];
[1]*QIMP Team, Center for Medical Physics and Biomedical Engineering, Vienna, AUSTRIA,* [2]*Division of Nuclear Medicine, Department of Biomedical Imaging and Image-guided Therapy, Medical University of Vienna, Vienna, AUSTRIA,* [3]*Nuclear Medicine Department, The Children's Hospital at Westmead, Sydney, AUSTRALIA,* [4]*Discipline of Medical Radiation Sciences and Brain and Mind Centre, Faculty of Health Sciences, The University of Sydney, Sydney, AUSTRALIA.*

Aim/Introduction: To assess image quality, by quantification of noise, at reduced count levels for whole-body [18F]FDG-PET/CT studies of paediatric oncology patients in relation to different image reconstruction algorithms. **Materials and Methods:** This study is ongoing. To date, nine paediatric oncology patients were included (4F/5M, (13±4)-y/o, 16.2≤BMI≤24.0). Subjects were injected with a mean activity concentration of (3.8±08) MBq/kg, and underwent routine [18F]FDG-PET/CT whole-body examinations on a Siemens Biograph mCT system with TOF capability (500ps). Emission data was collected in list mode (LM) format and preprocessed to simulate a reduction of the injected [18F]FDG activity by randomly removing counts from the original LM (100%) to achieve activity levels of 75%, 50%, 35%, 20% and 10%. Following attenuation and scatter correction, all emission data was reconstructed using the vendor e7-tools with OSEM and OSEM plus resolution recovery (PSF), and PSF plus time-of-flight (TOF) information. A 5mm FWHM Gaussian post-filter was applied during all reconstructions. Four spherical volumes-of-interests (VOIs) were defined in the right-lung, liver, left-thigh muscle and in the mediastinum. We report, noise and the signal-to-noise ratio (SNR) for each VOI and image reconstruction. **Results:** When using OSEM, the mean noise levels were on the order of (17-44)% in the lung, (10-28)% liver, (14-31)% mediastinum and (17-51)% thigh muscle for 100% counts. For PSF, the noise levels were reduced by 18% (lung), 16% (liver), 14% (mediastinum) and 13% (muscle), while the SNR was increased by 24% (lung), 21% (liver), 17% (mediastinum.) and 17% (muscle). Assuming that image noise levels below 20% are acceptable for clinical work-up, VOI analysis of the liver and mediastinum, indicated this level to be achieved at 50% counts, or more when using OSEM. At this level of counts, noise levels in the lung and thigh muscle was slightly higher 22% and 24% respectively. For PSF these noise levels could be reduced to 18% (lung) and 21% (muscle). **Conclusion:** Ongoing evaluations of WB-[18F]FDG-PET/CT images of paediatric patients indicate a 50% dose reduction potential when using a 20% acceptable threshold on noise levels and iterative reconstruction with PSF. Adding TOF information is likely to promote further dose reduction. This quantitative analysis of reference regions in pilot data will be complemented by qualitative grading of image quality by clinical experts. Ethics approval 2019/ETH00138. The financial support of the Austrian FWF Project I3451-N32 is gratefully acknowledged. **References:** None.

EPS-053

Impact of 18F-FDG PET/CT in Therapy Management of Pediatric Patients with Bone and Soft Tissue Sarcomas

E. Riera[1], *S. Ortiz*[1], *P. Bassa*[1], *M. Soler*[1], *P. Pérez*[2], *M. Garraus*[2], *E. Inarejos*[2], *I. Barber*[2], *J. García*[1];
[1]*CETIR-ASCIRES, Barcelona, SPAIN,* [2]*Hospital Sant Joan de Déu, Esplugues de LLobregat, Barcelona, SPAIN.*

Aim/Introduction: We have evaluated the impact of 18F-FDG PET/CT on the early therapy follow-up of a group of pediatric patients with primary bone tumors and soft-tissue sarcomas. **Materials and Methods:** From 2007 through 2018, 12 children with Bone Sarcomas and 11 children with Soft Tissue Sarcomas were evaluated by 18F-FDG PET/CT for early post-therapy study and follow-up treatment response. Primary Bone Tumors: 1 Osteosarcoma (7 y-o) and 11 Ewing Sarcoma ($\bar{x}$: 8.5 y-o; range: 2-12 y-o). Soft Tissue Sarcomas: 4 embrionary Rhabdomyosarcoma ($\bar{x}$: 6.7 y-o; range: 2-13 y-o) and 5 Alveolar Rhabdomyosarcoma ($\bar{x}$: 10 y-o; range: 2-14 y-o) and 2 Synovial Sarcoma ($\bar{x}$: 9.5 y-o). A total of 82 PET/CT studies, with normal blood glucose levels, were acquired with a PET/CT Philips Gemini-GXL 1 hour +/- 10 min. after intravenous injection of 4.6 mBq/Kg of 18F-FDG. mA and KV CT acquisition parameters were set to pediatric procedure. All PET relevant findings and SUVmax were assessed and correlated with CT and MRI findings and histology results whenever available. **Results:** Primary Bone Tumors: - Two out of 12 patients with negative PET in the early post-therapy study remained negative in the follow-up PET studies. None of them died over the time of analysis. - Two out of 12 patients with negative PET in the early post-therapy study became positive in the follow-up PET studies. One patient died over the time of analysis. - Eight out of 12 patients with positive PET in the early post-therapy became positive in the follow-up PET studies. Four patients died over the time of analysis. Soft tissue Sarcomas: - Nine out of 11 patients with negative PET in the early post-therapy study remained negative in the follow-up PET studies. None of them died over the time of analysis. - Two out of 11 patients with

positive PET in the early post-therapy reduced SUVmax uptake on primitive lesions and no new lesions appeared in the follow-up PET studies. None of them died over the time of analysis. **Conclusion:** 18F-FDG PET/CT is a useful imaging procedure for post-therapy follow-up of primary bone tumors and soft tissue sarcomas in pediatric patients. Moreover, the early post-therapy study showed prognostic value. **References:** None.

EPS-054

Normal [11C]-metionine PET uptake in the brain in children before and after treatment

D. Susin, T. Skvortsova;
N.P. Bechtereva Institute of human brain, Saint-Petersburg, RUSSIAN FEDERATION.

Aim/Introduction: Tumors of the central nervous system are the most common form of solid tumors in children age 0-14 years. Subtentorial location and the midline of the brain are the most frequent localization of embryonic and glial tumors in children. Normally increased [^{11}C]-methionine uptake in some brain structures makes it difficult to distinguish healthy brain tissue from the tumor process and to find an appropriate reference region to determine the metabolic activity of the lesion. The purpose of our study was determine distribution of [^{11}C]-methionine (Met) in the structures of posterior cranial fossa on PET/CT imaging of pediatric brain in control and after treatment. **Materials and Methods:** The children between 2 and 15 years old were divided in two group. In the first group (n=30) we included children examined with suspicion on brain tumor that has not been confirmed. Second group consisted of 17 children after combined treatment of tumors in the posterior cranial fossa without any residual tumor tissue. A PET studies were performed on a GE Discovery 710 PET/CT scanner according to the standard protocol. Different ROIs were drawn on PET-Met images including pons, cerebellum, thalamus and frontal cortex. A circle ROI of 10 mm in diameter was placed in the site of maximum Met uptake in the structure of interest. Different uptake indexes (UI) were calculated: pons to cerebellum ratio (PCR), pons to thalamus ratio (PThR), pons to brain cortex ratio (PBR). The differences between control UI measurements and post-treatment UI values were tested using M-W test. **Results:** In the control group PCR, PThR and PBR were 1.11 ± 0.16, 1.21 ± 0.17, 1.38 ± 0.17 (mean ± SD), respectively. After the combined treatment of tumors in the posterior cranial fossa PCR, PThR and PBR were 1.19 ± 0.13, 1.27 ± 0.17, 1.58 ± 0.21 (mean ± SD), respectively. Significant differences was found in PBR between two groups. There were no differences was fond in PThR and PCR. **Conclusion:** The results should be taken into account in the diagnosis of childhood tumors in the posterior cranial fossa and in monitoring of their treatment. **References:** None.

EPS-055

Risk stratification using 18 FDG PET/CT in high risk neuroblastomas :Is it comparable with ^{131}I-metaiodobenzylguanidine (MIBG)-??

C. V. Bongulwar[1], S. Shah[2], N. Purandare[2], A. Agrawal[2], V. Rangarajan[2];
[1]National Cancer Institute, Nagpur, INDIA, [2]Tata Memorial Hospital, Mumbai, INDIA.

Aim/Introduction: Radio iodinated metaiodobenzylguanidine (mIBG) is an established imaging modality in neuroblastoma. Semiquantiative scoring -SIOPEN [International Society of Pediatric Oncology Europe Neuroblastoma Group] and Modified Curie using radiolabelled MIBG are used for prognostication in high risk neuroblastomas. The present study aims to use 18F -fluorodeoxyglucose (FDG) for semiquantitative scoring and compares it with mIBG scores thereby validating it for risk stratification. **Materials and Methods:** Data of 90 patients were retrospectively analyzed diagnosed to have stage IV high risk neuroblastoma. MIBG scans were assessed according to the SIOPEN and the modified Curie scoring method. Similarly 18 F FDG PET/CT scans were also scored using these semi quantitative systems. The paired scans were compared at initial staging and end of induction therapy. A Curie score of </=2 and > 2 and a SIOPEN score </=4 and >4 (best cutoff) described in previous studies was used to classify these scans into low and high risk and subsequently correlated with the clinical course of the disease. **Results:** At initial staging there was a statistically significant difference between the Curie-FDG scores of (10.94 ± 10.0)as compared to mIBG score of (7.99 ± 9.00)with an increase of 2.94 with p=0.001.Also for SIOPEN -FDG scores of (20.00 ± 26.00) against mIBG (11.72 ± 20.00) with a difference of 8.27 and p=0.12.At end of induction therapy there was no statistically significant difference (p >0.01)between the Curie FDG and MIBG scores. Using the standard cut off values for Curie and SIOPEN scores 18 patients show discordance out of which 6 patients (33%) showed disease progression or death. **Conclusion:** Modified CURIE score and SIOPEN score using 18F FDG shows an incremental value over MIBG score and can be correlated with the clinical outcome of the disease. The Modified Curie and SIOPEN score can be validated using 18 F FDG PET/CT establishing their role in risk stratification . **References:** Borris decoralis et al Boris Decarolis, Christina Schneider, Barbara Hero, Thorsten Simon, Ruth Volland, Frederick Roels,Markus Dietlein, Frank Berthold, and Matthias Schmidt Iodine-123 Metaiodobenzylguanidine Scintigraphy Scoring allows Prediction of Outcome in Patients With Stage 4 Neuroblastoma:Results of the Cologne Interscore Comparison Study2013 -JCO Matthay KK, Edeline V, Lombroso J, et al: Correlation of early metastatic response by123Imetaiodobenzylguanidinescintigraphy with overall response and event-free survivalin stage IV neuroblastoma. J Clin Oncol 21:2486-2491, 2003.

EPS-056

Role of Large bowel transit scintigraphy in children with chronic constipation

K. Tigapuram, K. Seetharaman, A. Bhattacharya, S. Lal, B. R. Mittal, R. Bolia;
PGIMER, Chandigarh, INDIA.

Aim/Introduction: To evaluate usefulness of large bowel transit scintigraphy in management of children with chronic constipation **Materials and Methods:** We retrospectively analysed data of 53 patients (36 M, 17 F) aged 2-15 (median 7) years who presented with complaints of constipation, over a period of 3 years (January 2016-January 2019). The mean duration of symptoms was 2 years and 9 months (range 1 month - 9 years). Twenty-four of the 53 patients also had pallor on clinical examination and 24 had history of retentive measures being taken. Whole bowel transit scintigraphy was performed after oral administration of 5 mCi of Tc-99m sulphur colloid (SC) labelled solid meal. Sequential static images were acquired hourly from 1 to 4 hours and delayed images at 6hr, 8hr, 24hr, 28hr and 36hrs (if required), in simultaneous anterior and posterior projections using a dual-head gamma camera. Gastric emptying time (GET) was also assessed in 26 patients. The scan findings were interpreted visually, based on intestinal transit of activity. Tracer transit to the sigmoid colon / rectum by 24 hours was regarded as normal, while persistent retention of activity upto the ascending / transverse colon till 28-36 hours was interpreted as delayed colonic transit. All patients were started on standard medical treatment after the scan. Clinical response to treatment was assessed in 37 patients till April 2019. **Results:** Of the 53 patients, 24 patients had a delayed large bowel transit time and one had rapid transit time. Of the 26 patients who had also undergone GET evaluation, 1 patient had delayed gastric emptying with normal whole bowel transit time and one had rapid GET. On follow-up, the patients were divided into two groups, one in which symptoms persisted and the other in which constipation was relieved or controlled with medication. In patients with persisting symptoms (n=18), delayed large bowel transit was seen in 14 and normal transit in 4. In the group in which symptoms were either relieved or controlled with medication (n=19), delayed large bowel transit was seen in 1 and normal transit in 18. On applying Fisher exact test, the differences in large bowel transit time results were significantly different between the two groups (p=0.0001). **Conclusion:** Large bowel transit scintigraphy is a useful non-invasive investigation to evaluate children with constipation. Patients with normal large bowel transit times are more likely to respond to standard medical treatment than patients with delayed transit times. **References:** None.

EPS-057

Hepatobiliary scintigraphy for pediatric biliary atresia: a single-institution experience

W. Wong, K. Chu, B. Kung, T. Au Yong;
Nuclear Medicine and Clinical PET Centre, Queen Elizabeth Hospital, Hong Kong, HONG KONG.

Aim/Introduction: The purpose of this study was to evaluate the diagnostic accuracy of hepatobiliary scintigraphy for biliary atresia. **Materials and Methods:** A retrospective analysis of 186 infants (122 males and 64 females, median age of 52 days) at Queen Elizabeth Hospital between January 2008 and February 2019 was performed. Demographic details, laboratory data, results of ultrasonography are also evaluated. **Results:** Among the 186 infants, 18 patients (9.7%) were diagnosed to have biliary atresia. Sensitivity, specificity, positive predictive value and negative predictive value of hepatobiliary scan were found to be 100% , 95%, 69%, and 100% respectively. For full-term infant subgroup, positive predictive value is even higher (83%). There is greater proportion of false-positive cases in preterm infants than full-term infants, and repeated hepatobiliary scintigraphy was found to be able to pick up 38% of false positive cases. **Conclusion:** This study shows that hepatobiliary scintigraphy is highly sensitive and specific, particularly among full-term infants. Low positive predictive value among preterm infants can be improved by repeating follow-up scintigraphy. **References:** 1. Kwatra N et al. (2013) Phenobarbital-enhanced hepatobiliary scintigraphy in the diagnosis of biliary atresia: two decades of experience at a tertiary center. Pediatr Radiol. 43:1365-1375. 2. Zeissman HA (2014) Hepatobiliary scintigraphy in 2014. JNM. 55:1-9.

EPS-058

Age & puberty are major determinants of response to radioiodine in children and adolescents with differentiated thyroid cancer

S. S. Singh, A. Sood, A. Bhattacharya, B. R. Mittal, G. Kumar, A. S. Shekhawat;
Post graduate institute of medical education and research (PGIMER), Chandigarh, INDIA.

Aim/Introduction: Age and pubertal status have been speculated to affect the disease course and response to radioiodine therapy in children with differentiated thyroid cancer (DTC). Factors influencing post-operative risk stratification and applicability of response to initial treatment (RTT) classification have barely been explored in children. We aimed to assess the effect of age and number of surgically-excised metastatic lymph nodes on recurrence risk stratification and RTT (at 1.5 years follow-up) in children and adolescents. **Materials and Methods:** Clinical, surgical & radioiodine treatment and follow-up (minimum 1.5 years) data of 47 DTC patients (between years 2010-2018), ≤ 20 years of age was retrospectively analyzed. Mean age at symptom presentation was 15±3.8

years (range 5.5-20) and median follow-up duration was 3.6 years (range 1.5 -8.5 years). Patients were stratified into three age-groups, namely, pre-pubertal (≤10 years; n=7), pubertal (11-15years,n=12) and post-pubertal (16-20years, n=28). All patients underwent total/near-total thyroidectomy; 46 patients received radioiodine therapy. More than 5 surgically-resected metastatic lymph nodes was used as cut-off to determine minimal and extensive nodal disease (in central and/or lateral nodal stations) while applying postoperative pediatric ATA recurrence risk stratification. RTT reclassification, (ATA guidelines for adult DTC 2015) was used to assess response to therapy at 1.5 years under which patients with excellent & indeterminate responses deemed as responders and biochemical & structurally incomplete responses as having persistent disease. **Results:** Overall, resolution of radioiodine avid disease was significantly more in post-pubertal age group (p<0.00001) than pubertal (p=0.004) and pre-pubertal age groups. There was a significantly larger percentage of responders among post-pubertal patients than in pubertal age-group (60% vs 42%, p= 0.04). None of the pre-pubertal patients were rendered radioiodine negative at the 1.5-year follow-up. At the end of median follow-up of 3.5 years, 23/47 patients (49%) were deemed as responders. Using >5 metastatic lymph nodes chosen as cut-off for recurrence risk estimation, 45% (n=19), 43% (n=18) and 14% (n=5) patients were categorized under high, intermediate and low risk groups of recurrence, respectively. At the end of median follow-up of 3.5 years, all patients (100%) in low risk group were rendered as responders whereas responders in intermediate and high-risk groups were 67% and 26%, respectively. **Conclusion:** Age and pubertal status are major determinants of response to initial therapy in children & adolescents with DTC. Incorporation of number of metastatic lymph nodes into recurrence risk classification systems help in predicting response to radioiodine in this age-group. **References:** None.

EPS-059

Predictors Of Radioiodine Therapy Effectiveness In Children And Adolescents With Graves' Disease

P. O. Rumyantsev, D. Dzeytova, A. Trukhin, M. Sheremeta, V. Yasuchenya, K. Slaschuck, M. Degtyarev, S. Serzhenko, Y. Sirota, V. Nikitaev;
Endocrinology Research Center, Moscow, RUSSIAN FEDERATION.

Aim/Introduction: Graves' disease (GD) - common cause of hyperthyroidism in different age groups, including children and adolescents. Treatment with ^{131}I requires individual dosimetry-based justification of therapeutic activities to improve effective outcome and acceptable safety. **Materials and Methods:** The article describes 56 children and adolescents (f - 50, m - 6) aged from 8 to 17 years (14.2 ± 0.7 years) with GD. Follow-up ranged 6 - 36 months (18.8 ± 2.8). Thyroid volume varied from 7.1 to 94.5ml (34.7 ± 5.3ml), ^{99m}Tc-pertechnetate uptake met 1.8 to 41.2% range (15.1 ± 3.0%), ^{131}I maximum uptake was observed between 10 and 60% (42.5 ± 2.7%). The severity of Graves' orbitopathy (GO) was assessed. ATD medication ranged 3 - 144 months (37.8 ± 8.3), in some cases thyrotoxicosis recurred during ATD reduction. Calculation of ^{131}I activity was based on ^{131}I kinetic investigation. Prescribed ^{131}I activities, specific ^{131}I activity and absorbed doses rates at maximum ^{131}I uptake varied from 534 to 1396MBq (889 ± 58MBq), 4.1 to 27.0MBq/ml (14.4 ± 1.4MBq/ml), and 0.44 to 2.9Gy/h (1.6 ± 0.2Gy/h). TSH, fT3, fT4 levels were checked every month after the treatment. After 6 months were assessed; TSH, fT4, fT3, TSH receptor Ab ,thyroid ultrasound. **Results:** The first week after radioiodine therapy (RIT) 11 (20%) children complained of moderate pain when swallowing, which lasted 7-10 days. Hypothyroidism, euhyroidism, thyrotoxicosis developed within 6 months after the treatment in 46 (82.1%), 1 (1.8%) and 9 (16.1%) patients, respectively. Four children received the second RIT: hypothyroidism developed in 3 cases, in one case it was euthyroidism. Fourteen (78%) children with GO signs had no worsening, 3 (16.7%) children showed a progression of exophthalmos with a subsequent improvement, only 1 (5.6%) child showed significant deterioration. The thyroid volume decrease ranged from 12.2 to 94.3% (average 70.0 ± 4.7%). Thus, the predictors of hypothyroidism development are the thyroid volume (P <0.001); TRAb (P = 0.009); specific ^{131}I activity (MBq/g), (P = 0.009); thyrotoxicosis recurrence during ATD reduction (P = 0.017). Age, gender, GO, prescribed activity of ^{131}I did not significantly affect the treatment outcome. **Conclusion:** RIT is an effective and safe method of GD management in children and adolescents. The main predictors of RIT effectiveness in children and adolescents with GD are the thyroid volume, and specific^{131}I activity. Further clinical investigation and advancement of individual dosimetry-based methodology are required to improve treatment outcome and safety of RIT. **References:** None.

EPS-060

Will pulmonary embolism diagnosis still be made with ventilation/perfusion imaging?

P. Bonnefoy[1], N. Prevot[1], G. Mehdipoor[2], A. Sanchez[1], B. Bikdeli[3], J. Lima[4], L. Font[5], A. Gil-Díaz[6], P. Llamas[7], J. Aibar[8], L. Bertoletti[9], M. Monreal[10], RIETE investigators;
[1]CHU Saint-Etienne, Saint-Etienne, FRANCE, [2]Cardiovascular Research Fondation, New York, NY, UNITED STATES OF AMERICA, [3]Division of Cardiology, Department of Medicine, New York-Presbyterian Hospital, Columbia University Medical Center/ New York-Presbyterian Hospital, New York, NY, UNITED STATES OF AMERICA, [4]Department of Pneumonology, Hospital Universitario de Valme, Sevilla, SPAIN, [5]Department of Haematology, Hospital de Tortosa Verge de la Cinta, Tarragona, SPAIN, [6]Department of Internal Medicine, Hospital Universitario de Gran Canaria Dr. Negrín, Las Palmas, SPAIN, [7]Department of Haematology, Hospital Universitario Fundación Jiménez Díaz, Madrid, SPAIN, [8]Department of Internal Medicine, Hospital Clínic, Barcelona, SPAIN, [9]Service de Médecine Vasculaire et Thérapeutique, CHU Saint-Etienne, Saint-Etienne, FRANCE, [10]Universitari Germans Trias i Pujol, Badalona, Barcelona, SPAIN.

Aim/Introduction: Ventilation/perfusion (V/Q) lung scan was the first noninvasive imaging test validated to replace invasive pulmonary angiography in the diagnosis of acute pulmonary embolism (PE). Although there is no precise numerical data about quantitative evolution, it appears as a second line test after computed tomography pulmonary angiography (CTPA). We aim to report contemporary data about the relative utilization and the patient characteristics associated with use of V/Q scanning. **Materials and Methods:** From the data of RIETE (Registro Informatizado Enfermedad ThromboEmbolica) registry, including patients diagnosed with acute symptomatic PE, we evaluate the number of patients per year diagnosed with V/Q or CTPA from 2007 to 2017. Characteristics of these patients were also studied. **Results:** Over the entire 11-year period, 26,540 patients with acute PE were included. CTPA was performed in 87.7% of patients compared to 7.8% for V/Q scan. The number of PEs diagnosed by V/Q scan decrease from 288 in 2007 to 107 in 2017 (compared to 1,635 and 1,760 respectively for CTPA), a V/Q scan reduction about 62,8% ($p<0.001$). In multivariate analysis, patients diagnosed with V/Q scan were older (72.7 vs. 66.7 years, $p <0.001$) and more likely to present severe renal insufficiency (odds ratio [OR]: 10.6; 95% confidence interval [CI]: 7.49-15.0), chronic lung disease (OR: 1.50; 95%CI: 1.07-2.11), diabetes (OR: 2.04; 95%CI: 1.50-2.77) or chronic heart failure (OR: 1.87; 95%CI: 1.25-2.80) than patients diagnosed with CTPA. **Conclusion:** The rate of V/Q scan in diagnosed PE is relatively low but stabilized in recent years. Patients diagnosed with V/Q scanning are older, and more frequently have renal insufficiency, diabetes, chronic lung disease or chronic heart failure than those diagnosed by CTPA. Pulmonary embolism diagnosis still be made with ventilation/perfusion imaging, which appears as an essential tool in some frail patients. **References:** None.

EPS-061

Findings in Lung Perfusion and Ventilation-Perfusion Scintigraphy in patients with suspicion of Chronic Thromboembolic Pulmonary Hypertension

G. Guzmán, *M. Calderón, L. Nieto, M. Falgás, P. Navarro, M. Sangrós, S. Álvarez, L. De la Cueva, D. Abós;*
Hospital Universitario Miguel Servet, Zaragoza, SPAIN.

Aim/Introduction: To study the findings in 99mTc-macroaggregated albumin lung perfusion scintigraphy (LPS) and 99mTc- pertechnetate lung ventilation - perfusion scintigraphy (V/Q), in patients with clinical and echocardiographic suspicion for pulmonary hypertension (PH), and in those who are not confirmed left heart or lung disease as single causes of PH, by the treating doctor. **Materials and Methods:** We collected all consecutives lung scintigraphies of patients with suspect of pulmonary embolism (PE) chronic/residual, as a cause of PH, attended between January of 2017 and April of 2019.We performed a review of the scintigraphic findings, observing whether they have been compatible with a diagnosis of suspected chronic thromboembolic pulmonary hypertension (CTEPH). We used modified PIOPED diagnostic criteria for V/P scintigraphy and PISAPED criteria for LPS.We also reviewed the history of left heart disease, pulmonary disease, previous thromboembolisms, scleroderma and right - left SHUNT as possible cause of PH. The frequency of PE is calculated, and it is related to the basic pathology of the patients and to the background of previous PE. **Results:** 36 lung perfusion scintigraphy and 15 V/Q scintigraphy of 50 patients, aged between 37 and 87 years, 25 female and 25 male, were selected. 30/50 of the patients (60%) had lung disease (chronic obstructive pulmonary disease, obstructive sleep apnea and interstitial lung disease), 20/50 (40%) had left heart disease (cardiomyopathy and valvulopathies) and 12/50 (24%) had history of PE. Seven patients (12%), had diagnosis of PE in the scintigraphy. Of these, 3/7 (43%) had history of lung disease and 1/7 (14%) of left heart disease. We highlight that 6/7 patients (85%) had history of PE, of which 50% (3/6) had associated lung and/or heart disease simultaneously. On the other hand, among the 12 patients with previous history of PE, 6 (50%) had scintigraphic signs of residual pulmonary embolism, while among the 38 patients without previous PE, only 1 patient had signs of embolism on the scan (2.6%). Thus, the risk of probable CTEPH is 19 times higher among patients with documented prior PE. One patient with right-left SHUNT and 4 patients with scleroderma, showed a normal scintigraphy **Conclusion:** 1. Lung scintigraphy is capable to identify CTEPH, in patients with history of documented previous PE, even in a population with high prevalence of lung and cardiac disease, therefore, allowing an adequate treatment for those patients with CTEPH. 2. In those patients without previous PE, lung scintigraphy shows less benefit. **References:** None.

EPS-062

Differences in Pulmonary Ventilation / Perfusion Scintigrahpic in Patients with Chronic Thromboembolic Disease with or without Pulmonary Hypertension

J. C. Cañadas Salazar, *F. Gomez-Caminero Lopez, S. Cadenas Menéndez, P. Álvarez Vega, P. Garcia-Talavera San Miguel, A. C. Peñaherrera Cepeda, M. Martin Lopez, J. Villanueva Curto, C. Riola Parada, M. Tamayo Alonso;*
Sacyl, Salamanca, SPAIN.

Aim/Introduction: To compare the scintigraphic findings and the possible differences observed after ventilation / perfusion scintigraphy (V/Q) in patients diagnosed with chronic pulmonary thromboembolism (CTEP) with confirmed pulmonary hypertension (PH) and patients with CTEP without HP. **Materials and Methods:** We reviewed 387 lung ventilation and perfusion scans of patients with suspected chronic PE from July 2015 to April 2019, of which 33 cases of CTEP were confirmed. 470MBq ^{99m}Tc-DTPA was administered as an aerosol for the ventilation study and 185MBq of ^{99m}Tc-MAA was administered intravenously for the perfusion study. Planar images were acquired in anterior, posterior and oblique posterior and right projections. Visual analysis of each of the studies was carried out. The number of defects visualized, distribution according to lobes and the existence of cardiomegaly were defined. **Results:** Of

the 33 patients who presented scintigraphic criteria suggestive of CTEP, 15 were males (45,5%) and 18 females (54,5%) with a total mean age of 76 years (range 34-86). Of these, 15 were clinically and radiologically diagnosed of PH. In this group of patients, the distribution of most defects was subsegmental and predominantly superior and right, observing defects in almost all patients (67%) and indirect signs of cardiomegaly (73%). without HP the distribution of the defects was similar. Regarding the number of segments and subsegments affected according to the criterion of both Nnuclear Physicians, greater number of defects were observed in patients with TEPC + HP (51) than in those with only TEPC (36) and greater subsegmental involvement (45). Although there were obvious differences visually, the statistical significance was not reached due, probably, to the small number of the sample. There were no differences in the existence or not of cardiomegaly. **Conclusion:** Pulmonary V/Q scintigraphy demonstrated a greater number of perfusion defects in patients who were diagnosed with CTEP + PH, despite the small sample size of patients included in the study. The greater number of perfusion defects and their distribution help confirm the diagnosis of suspected CTEP with HP. **References:** 1. Fedullo, P.F. Clinical manifestations and diagnosis of chronic thromboembolic pulmonary hypertension. [Online]. Available from: {{configCtrl2.info.canonicahttps://uptodate.publicaciones.saludcastillayleon.es/contents/clinical-manifestations-and-diagnosis-of-chronic-thromboembolic-pulmonary-hypertension?search=Pulmonary%20embolism&topicRef=8253&source=related_link#referencesIUrl}} [Accessed 25 April 2019].

EPS-063

Scintigraphic quantification of pulmonary perfusion - comparison between planar and tomographic acquisition

M. Victor, S. Carmona, S. Chin, A. I. Santos;
Hospital Garcia de Orta, E.P.E., Almada, PORTUGAL.

Aim/Introduction: Pulmonary perfusion quantification, being of major importance for pulmonary surgery or transplantation, has been performed in planar images. However, this mode of acquisition is being replaced by tomography, and there is no established equivalence between these two types of acquisition for the quantification of pulmonary perfusion. Our aim was to evaluate this equivalence, to facilitate follow-up evaluation of each patient. **Materials and Methods:** We retrospectively analysed all 47 patients (14 males and 33 females, median age=62[P25:47;P75:75]years) that performed both planar and tomographic pulmonary scintigraphies in our department. To evaluate the quality of the perfusion images, we calculated the ratio of counts/sec between the perfusion and ventilation images, in both anterior (median=4.23[P25:3.08;P75:6.45]) and posterior (median=4.25[P25:3.22;P75:6.24]) planar projections. To calculate the percentage of counts obtained for each lung or thirds of each lung, three image data were used: Group 1 (G1) - Planar acquisition; Group 2 (G2) - the sum of two anterior and two posterior projections of the tomographic study; Group 3 (G3) a 2D image obtained by sum of all coronal slices of the tomographic reconstruction. Relative perfusion was calculated in G1 and G2 using the geometric mean of counts and in G3 using the counts obtained in the 2D image. The Wilcoxon signed rank test, a non-parametric test for related samples, was used to evaluate the statistical significance of the differences. **Results:** We found no statistically significant difference between G1 and G2, regarding relative perfusion of the: entire right lung (p=0.057), right superior third (p=0.607), entire left lung (p=0.057), left superior third (p=0.404), left middle third (p=0.262) and left inferior third (p=0.759); however, there was a statistically significant difference between the values regarding the middle right third (p=0.05) and the inferior right third (p=0.011). Comparing G1 and G3, we found no statistically significant difference regarding the: right superior third (p=0.081), right inferior third (p=0.146) and left middle third (p=0.337); statistically significant difference was found for the: entire right lung (p=0.000), right middle third (p=0.000), entire left lung (p=0.000), superior left third (p=0.000) and inferior left third (p=0.000). **Conclusion:** According to our results, for the purpose of pulmonary scintigraphy quantification, tomographic acquisition data might be compared with the planar one, when using the sum of two anterior and two posterior frames of the tomographic study, and only for the ratio between the two lungs. This should still be confirmed with larger series and reproducibility evaluation. **References:** None.

EPS-064

Lung Aerosol Scintigraphy in Diabetic Patients Without Pulmonary Symptoms

K. Kota, N. Pandit;
JIPMER, Pondicherry, INDIA.

Aim/Introduction: Diabetes mellitus is one of the most common chronic diseases in nearly all countries, and continues to increase in numbers. Retinopathy, neuropathy, nephropathy, and cardiovascular dysfunction are common diabetic complications and are basically caused by vascular damage. Pulmonary complications of diabetes are frequently disregarded. This is mainly because the alveolar-capillary system is characterized by a great micro vascular reserve, and pulmonary abnormalities are commonly subclinical in Diabetic patients. Aerosol clearance from the lung is an indirect evaluation of capillary permeability. In this study we aim to compare the Aerosol clearance in Diabetic patients who have Diabetic complications and who do not have complications and both are without pulmonary symptoms. **Materials and Methods:** The inclusion criteria include Diagnosed cases of Diabetes on follow up and without any pulmonary Symptoms at the time of study with Age more than 18 years and up to 60 years. The exclusion criteria include History of smoking; with any other known pulmonary or cardiac disorders; Respiratory tract infections within 6 weeks; Pregnancy and breastfeeding. In this study we divided Diabetic patients into two groups. One with known Diabetic complications (Group 1) and the other without complications (Group 2).

Lung aerosol Scintigraphy was performed using Tc-99m DTPA Aerosols. After aerosol inhalation for 3 minutes, we acquired a 30 minutes dynamic scan using Siemens Symbia T6 gamma camera using 64x64 matrix. We calculated the $T_{1/2}$ for DTPA clearance by drawing a standard ROI on lung fields excluding the central area. **Results:** Total 58 patients are evaluated, in which 26 (M: F = 4:22) are in Group 1 and 32 (M: F=13:19) are in group 2. Mean (Standard deviation) $T_{1/2}$ in Group 1 is 51.031 (15.1498) and in Group 2 is 62.115 (14.4895). Mean difference is compared using simple unpaired T test with 95% confidence interval, which is statistically significant ($p<0.05$). **Conclusion:** The significant difference in clearance pattern in both the groups suggests there is impaired permeability in Group 2 patients. With this study we can assume that Lung Aerosol scintigraphy can detect the changes in vascular permeability even before the patients are symptomatic. So Lung Aerosol Scintigraphy can be used as a baseline evaluation in diabetic patients, especially in those who are planned for inhalational insulin therapy as vascular permeability is important for insulin to reach into circulation. **References:** None.

EPS-065

Utility Of ^{99m}Tc-MAA Scintigraphy And SPECT/CT For The Diagnosis Of Peritoneal Leakage In Dialyzed Patients with End Stage Kidney Disease

B. Pérez López, *P. J. Turbay Eljach, J. Gómez Hidalgo, N. Álvarez Mena, S. Sanz Ballesteros, M. A. Ruíz Gómez, C. Gamazo Laherrán, M. Alonso Rodríguez, M. J. González Soto, A. Sainz Esteban, R. Ruano Pérez;*
Hospital Clínico Universitario de Valladolid, Valladolid, SPAIN.

Aim/Introduction: Dialysis fluid leakage (DFL) represents a major noninfectious complication of peritoneal dialysis (PD). It is a consequence of the loss of peritoneal membrane integrity. When DFL occurs into subcutaneous tissues, it is sometimes occult and difficult to diagnose. An early diagnosis in these patients is important to prevent significant morbidity and mortality. Our aim was to evaluate the utility of peritoneal scintigraphy and SPECT/CT using macroaggregated albumin tagged with ^{99m}Tc (^{99m}Tc-MAA) to assess the diagnosis of DFL. **Materials and Methods:** We reviewed patients from April 2014 to April 2019 referred to our Nuclear Medicine deparment with clinical suspicion of DFL.All patients underwent a peritoneal scintigraphy with ^{99m}Tc-MAA. Planar images were obtained 15 minutes after the infusion of ^{99m}Tc-MAA in the peritoneal cavity and 2 hours after the drainage. A SPECT/CT of the target region was also performed after the late images. We also recommended to patients to do exercises to increase intraabdominal pressure. As variables, we evaluated demographic data, PD duration, scintigraphy detection capability, utility of SPECT/CT, grade of uptake (low, moderate and high) and leakage location. **Results:** A total of 8 patients were reviewed (5 women and 3 men), average age 62.2 years old (range 49-76 years) and mean duration of the PD of 17 months.They presented edema as a clinical sign, being abdominal the most frequent location followed by scrotal edema. A reduction of ultrafiltration was also observed in all patients.Regarding peritoneal scintigraphy result, DFL was detected in 100% of cases. Foci detected in after drainage images, presented moderate uptake in 2 cases and high in 6. Periumbilical region was the most frequent leak location (50%), followed by inguinal region (37.5%) and pelvis (12.5%) in the planar images. When evaluating leakage location by SPECT/CT was observed that the foci detected in periumbilical region were located in the subcutaneous cellular tissue. Inguinal foci were located in the left inguinal canal and both scrotal sacs. Pelvic focus was placed in right paravesical area. **Conclusion:** Peritoneal leakage is a possible complication of peritoneal dialysis that can be easily confirmed by ^{99m}Tc-MAA scintigraphy. The inclusion of SPECT/CT images increase confidency in the results obtained. **References:** None.

EPS-066

Replacing the 3 hours imaging in ^{75}Se-SehCAT bile acid malabsorption investigations with a calculated value

L. Duchstein, *C. Hædersdahl, J. Nielsen, A. Flensborg;*
Bispebjerg and Frederiksberg Hospital, Dept. of Clinical Physiology and Nuclear Medicine, Copenhagen NV, DENMARK.

Aim/Introduction: We report a study carried out alongside our clinical routine aiming to replace the 3-hour imaging investigation after administration of tauroselcholic (selenium-75) acid (^{75}Se-SeHCAT) to patients referred for quantification of bile acid absorption. The current method used for carrying out a SeHCAT investigation in Denmark follows Williams et al. [1]: 1. administration of a ^{75}Se- SeHCAT capsule 2. gamma camera imaging 3 hours after administration 3. repeated imaging 7 days after administration. The photon flux from the patient after 3 hours is essentially determined by attenuation of photons in the patient's body, since no redistribution has taken place yet. It can therefore be estimated based on the patient's weight and height. Smout et al. [2] proposed a logarithmic approach, but we could not fit that to our existing data. Instead, we propose: $Cps=activity[kBq]\cdot(a\cdot height[m]/(b\cdot weight[kg])^2+c)$ Where: Cps are the calculated counts per second, activity is the administered ^{75}Se activity in kBq, height is the patients' height in m, weight is the patients' weight in kg and a, b and c are fitting parameters that are dependent on the setup and the gamma camera **Materials and Methods:** In total 170 patients were included (104 women, age 18-90 years, body-mass-index (BMI) between 17.1kg/m^2 and 47.2kg/m^2). Administered dose of ^{75}Se-SeHCAT was between 222kBq and 450kBq. In addition to our clinical routine we recorded the weight and height of our test patients. The data of the first 13 patients were used to establish the best fit of the parameters a, b and c specific to our setup. These parameters were then used to predict count rates of the 3 hours investigation for the remaining patients and these were compared to the count rates actually measured. **Results:** According to our 3-hour imaging 80 patients showed a significantly reduced reabsorption of bile acid (below 15%), 90 patients were healthy. The calculated values showed as

well 80 with malabsorption and 90 healthy patients. Using the measured counts after 3 hours as a gold standard, the calculation produced 4 false positive and 4 false negatives. A Bland-Altman plot shows a higher deviation with increased retention. **Conclusion:** Using the patient's weight and height, we can reliably estimate the number of counts measured by a gamma camera 3 hours after administration of ^{75}Se- SeHCAT, thereby sparing the patient for one investigation and 3 hours waiting time. **References:** [1] Williams et al. Gut 1991; 32:1004-6 [2] Smout et al, EANM 2016 EP723.

611

e-Poster Presentation Session 5 - Oncology: Oncology - e-Poster All Stars

Monday, October 14, 2019, 8:00 - 9:30 Room 133/134

EPS-067

Prognostic value of volumetric parameters of on F-18 FDG PET/CT in patients with uterine carcinosarcoma in predicting progression free survival and overall survival

S. Kim, W. Kang;
Severance Hospital, Yonsei University College of Medicine, Seoul, KOREA, REPUBLIC OF.

Aim/Introduction: This study was aimed to analysis the prognostic value of volumetric parameters on preoperative F-18 fluorodeoxyglucose positron emission tomography/computed tomography (FDG PET/CT) in patients diagnosed with uterine carcinosarcoma for predicting progression free survival (PFS) and overall survival (OS). **Materials and Methods:** Fifty eight women (median age : 60 (range 30-81 years old)) were included who pathologically confirmed uterine carcinosarcoma and underwent F-18 PET/CT before surgery from June 2006 to November 2016. Maximum standardized uptake value (SUVmax) of primary tumor was obtained. Also, we estimated metabolic tumor volume (MTV) and total lesion glycolysis (TLG) of primary tumor using fixed SUV of 2.5 as the threshold for determining the contouring margins around the tumor. Optimal cut-off values of continuous variables were determined by receiver operating characteristic (ROC) curve. PFS and OS were evaluated using Log-rank test and Cox regression test. **Results:** The median duration of PFS was 24.7 months (range 1.4-123.1 months). Twenty six patients (44.8 %) experienced recurrences. The median duration of OS was 62.4 months (range 3.1-127.5 months), and 21 (36.2 %) patients died. In the univariate analysis, age, size, CA 125 level, SUVmax, MTV, and TLG were significant prognostic factors for predicting PFS. In the multivariate analysis, TLG was the only significant prognostic factor for PFS. (p= 0.006, hazard ratio (HR) 4.131, 95 % confidence interval (CI) 1.508-11.313) For predicting OS, age, size, myometrial involvement, lymphovascular space (LVS) invasion, CA 125 level , SUVmax, and TLG were significant prognostic factors in the univariate analysis. LVS invasion (p= 0.022, HR 3.403, 95 % CI 1.195-9.696) and CA 125 level (p= 0.006, HR 5.592, 95 % CI 1.657-18.866) were the significant prognostic factors in the multivariate analysis. **Conclusion:** Preoperative TLG was the most significant factor for predicting recurrence in patients with uterine carcinosarcoma. For predicting OS in uterine carcinosarcoma, LVS invasion and CA 125 level were the more significant prognostic factors than F-18 FDG PET parameters. **References:** None.

EPS-068

The use of the updated EARL harmonization of 18F-FDG PET-CT in patients with lymphoma yields significant differences in Deauville score compared with previous EARL recommendations

*J. Ly[1,2], D. Minarik[3], L. Edenbrandt[4], P. Wollmer[2], **E. Trägårdh**[2,5,6];*
[1]Department of Radiology, Kristianstad Hospital, Kristianstad, SWEDEN, [2]Department of Translational Medicine, Lund University, Malmö, SWEDEN, [3]Radiation Physics, Skåne University Hospital and Lund University, Malmö, SWEDEN, [4]Department of Clinical Physiology and Nuclear Medicine, Sahlgrenska University Hospital, Region Västra Götaland, Gothenburg, SWEDEN, [5]Department of Clinical Physiology and Nuclear Medicine, Skåne University Hospital, Malmö, SWEDEN, [6]Wallenberg Centre for Molecular Medicine, Lund University, Lund, SWEDEN.

Aim/Introduction: The Deauville score (DS) is a classification system which distinguishes treatment response in patients with lymphoma. The standardized uptake value (SUV) of a lesion in positron emission tomography with computed tomography (PET-CT) is compared to the SUV in reference organs which results in five numerical categories, 1-5. The rapid development in PET-CT software algorithms and hardware affects SUV and consequently DS, which may lead to different medical decisions and treatment. Local preferences in scanner settings vary widely, therefore the EANM Research Ltd. (EARL) harmonization program from the European Association of Nuclear Medicine (EANM) makes it possible to unify scanning results and produce multicentre studies. This program was recently updated to accommodate modern PET-CT technology. We have investigated the discordance in DS calculated from patients with lymphoma referred for 18F-fluorodeoxyglucose (FDG) PET-CT reconstructed with three different algorithms: the newly introduced block-sequential regularization expectation maximization algorithm commercially sold as Q.Clear (QC, GE Healthcare, Milwaukee, WI, USA), compliant with the updated EARL recommendations, and two settings compliant with the previous EARL recommendations ($EARL_{lower}$ and $EARL_{upper}$, representing the lower and upper limit of the EARL recommendations). **Materials and Methods:** 52 patients with non-Hodgkin and Hodgkin lymphoma were included (18 females and 34 males). The patients were scanned on a Si-photomultiplier based PET-CT system (Discovery MI, GE Healthcare, Milwaukee, WI, USA) after being injected with 4 MBq/kg 18F-FDG and an accumulation time of 60 min. Segmentation of mediastinal

blood pool and liver were semi-automatically performed, whereas segmentation of lesions was done manually. From these segmentations, SUV_{max} and SUV_{peak} were obtained and DS calculated for the three different reconstructions described above. **Results:** There was a significant difference in DS between the QC algorithm and $EARL_{lower}$ / $EARL_{upper}$ ($p<0.0001$ for both) but not between $EARL_{lower}$ and $EARL_{upper}$ ($p=0.102$) when SUV_{max} was used. For SUV_{peak}, there was a significant difference between QC and $EARL_{lower}$ ($p=0.001$), but not for QC vs $EARL_{upper}$ ($p=0.071$) or $EARL_{lower}$ vs $EARL_{upper}$ ($p=0.102$). Five non-responders (DS 4-5) for QC were classified as responders (DS 1-3) when $EARL_{lower}$ / $EARL_{upper}$ was used, both when SUV_{max} and SUV_{peak} were investigated. **Conclusion:** DS classification is significantly changed when comparing the updated with the previous EARL recommendation. In select cases, the discordance in DS would affect choice of medical treatment. Specifically, the previous EARL recommendations were more often prone to classify patients as responders. **References:** None.

EPS-069

Comparison of criteria for the indication of axillary lymph node dissection in patients with breast cancer and positive sentinel lymph node biopsy

D. Vega Perez, *M. Tabuenca Mateo, M. Martin Ferrer, E. Martinez Albero, V. Godigna Guilloteau, A. Galiana Moron, S. Ruiz Solis, J. Estenoz Alfaro;*
Hospital 12 de Octubre, Madrid, SPAIN.

Aim/Introduction: Our objective is to compare the criteria for the indication of axillary lymph node dissection (ALND) in patients with breast cancer and positive sentinel lymph node biopsy (SLNB), according to the Sociedad Española de Senología y Patología Mamaria (SESPM) guidelines and to those of the ACOSOG Z0011 study, to determine which method is superior in the indication of ALND in our clinical practice. **Materials and Methods:** A retrospective study of 124 women with breast cancer (32 excluded due to lack of information) selected consecutively between 2013-2019, with positive SLNB (analyzed using the OSNA method), and to whom a posterior ALND was performed. The patients had an average age of 56.5 years (between 34 and 87 years) with tumor T stage, 5% T1b, 37% T1c, 44% T2 and 11% T3. Of these, 69% had a histology of infiltrating ductal carcinoma, 18% infiltrating lobular carcinoma and 13% others. Regarding the histochemical type, 49% luminal A, 44% Luminal B, 5% HER2 + and 2% triple negative. A total of 222 sentinel lymph nodes were analyzed, with a mean of 2.4 (between 1 and 6) per patient.We reviewed the ALND indication in all patients according to ACOSOGZ0011 criteria (tumor of> 3 cm, with histological grade II-III, negative hormone receptors, HER2 +, triple negative, with lymphovascular invasion or more than 2 positive sentinel nodes) and that of SESPM (tumor burden greater than 25,000 copies of sentinel node mRNA with OSNA analysis, modified according to our clinical experience). **Results:** Of the total of 92 patients, 35% had ALND positive and 65% negative. With the application of the ACOSOGZ0011 criteria, ALND was indicated in 15% of the patients, and application of that of the SESPM indicated in 75%. The sensitivity to perform ALND obtained in our sample with the ACOSOGZ0011 criteria was 25%, while the sensitivity with that of the SESPM was 80%. **Conclusion:** The application of the SESPM criteria, using a tumor burden greater than 25,000 copies, gives us a higher sensitivity to perform ALND in our patients, obtaining better results than with the ACOSOGZ0011 criteria, however, these discordant results are probably related to the low number of patients in our study. On the other hand, the ACOSOGZ0011 criteria provided a higher specificity. Therefore, it could be useful to include some of their criteria in that of the SESPM in order to create a single guide and achieve a greater sensitivity and specificity. **References:** None.

EPS-070

Impact of 18F-FDG PET/CT comparing to MRI in primary staging and treatment approach of anal cancer

M. Beheshti[1,2], *R. Manafi-Farid*[3], *A. Beheshti*[4], *H. Wundsam*[5], *F. M. Mottaghy*[1], *H. Geinitz*[6], *W. Langsteger*[7];
[1]*Nuclear Medicine, University Hospital, RWTH University, Aachen, GERMANY,* [2]*Nuclear Medicine, Paracelsus Medical University, Salzburg, AUSTRIA,* [3]*Research Center for Nuclear Medicine, Tehran University of Medical Sciences, Tehran, IRAN, ISLAMIC REPUBLIC OF,* [4]*Ludwig Maximilian University, Munich, GERMANY,* [5]*Visceral Surgery, Ordensklinikum, Linz, AUSTRIA,* [6]*Radiation Oncology, Ordensklinikum, Linz, AUSTRIA,* [7]*PET-CT Center, St. Vincent's Hospital, Ordensklinikum, Linz, AUSTRIA.*

Aim/Introduction: Accurate staging is imperative to preserve anal sphincter and enhance the quality of life. In this study, we evaluated the additive value of 18F-FDG-PET/CT in the initial staging and management of Anal Carcinoma. Also, we assessed the prognostic significance of pre-treatment intensity of 18F-FDG uptake. **Materials and Methods:** Fifty-four patients with anal carcinoma who underwent both semi-whole body 18F-FDG-PET/CT and MRI of pelvis for primary staging and treatment planning were included in this study. The interval between 2 imaging modalities had to be no longer than 4 weeks. Data regarding primary tumor, lymph-nodes (anorectal, iliac, and inguinal regions), and metastatic lesions were compared. The additional relevant information provided by 18F-FDG-PET/CT impacting the management was assessed. Also, patients were followed (mean of 41.5±29.3 months) to determine true/false findings, as well as find a correlation between SUVmax of the lesions and disease-free-survival. **Results:** Discordant findings were found in 46.30% (25/54) of patients (5 in T; 1 in T and N; 18 in N; and 1 in M stage). T-stage appeared higher in 3.70% of patients and lower in 7.40% on 18FDG-PET/CT. Discordant findings regarding the region of involved lymph-nodes were observed in 35.18% of patients in a total number of 30 regions. There were20 more involved regions on 18FDG-PET/CT and 7 more on MRI;threeregionswere positive on MRI and negative on 18FDG-PET/CT. N-stage was incongruent in 22.22% (higher in 14.82% on 18F-FDG-PET/CT and in 7.40% higher on MRI).

18FDG-PET/CT resulted in true up-staging in 9.26% and down-staging in 3.70% of patients. 18F-FDG-PET/CT was negative in 12.96% of patients with perirectal lymph-node involvement leading to erroneous down-staging in only 3.7%. Moreover, 18F-FDG-PET/CT resulted in management change in 24.08% of patients (18.52% received more radiation, 3.70% received less, and one patient (1.86%) underwent palliative therapy). Finally, an adverse relation was observed between metabolic lymph-node involvement and complete response to treatment (p=0.006). No significant correlation was demonstrated between disease-free-survival and metabolic activity of the primary tumor (p=0.127) or lymph-nodes (p=0.478) by means of SUVmax. **Conclusion:** 18F-FDG-PET/CT provided more accurate staging in about 13% of patients and led to change in treatment management in 24% of cases. However, MRI was superior in the detection of anorectal lymph-nodes. No significant prognostic advantage was demonstrated using semi-quantitative parameters of 18F-FDG-PET/CT. Nevertheless, 18F-FDG-PET/CT seems to play a pivotal role in treatment planning of Anal Carcinoma. **References:** None.

EPS-071

The value of PSMA-based ^{18}F-DCFPyL PET/CT imaging in patients with biochemical recurrence prostate cancer after primary local therapy

E. Mena[1], *B. Turkbey*[1], *L. Lindenberg*[1], *S. A. Harmon*[2], *I. Lim*[1], *S. Adler*[2], *A. Ton*[1], *A. N. Forest*[2], *P. Eclarinal*[1], *Y. L. Mckinney*[1], *J. Weaver*[2], *D. Citrin*[3], *W. Dahut*[3], *J. F. Eary*[3], *P. L. Choyke*[1];
[1]*Molecular Imaging Program. NCI. NIH, Bethesda, MD, UNITED STATES OF AMERICA,* [2]*Clinical Research Directorate, Frederick National Laboratory of Cancer Research sponsored by the NCI, Bethesda, MD, UNITED STATES OF AMERICA,* [3]*NCI. NIH, Bethesda, MD, UNITED STATES OF AMERICA.*

Aim/Introduction: To investigate lesion detection rate of ^{18}F-DCFPyL PET/CT, a PSMA targeted PET agent, in patients with biochemical relapse prostate cancer after primary local therapy. **Materials and Methods:** This is a prospective IRB-approved study including 90 patients with documented biochemical recurrence (average PSA of 4.2 ng/mL, range 0.21-35.5 ng/mL) after primary local therapy, either with radical prostatectomy (n= 38), radiation (n=27) or combination therapy (n=25), with negative conventional anatomical imaging. Patients underwent whole-body ^{18}F-DCFPyL-PET/CT at 2 h p.i (299.9±15.5 MBq). PSMA-PET lesion detection rate was correlated with pre-scan PSA levels. **Results:** Seventy patients (77.8%) showed a positive PSMA-PET scan, identifying a total of 287 suspicious lesions: 37 in the prostate bed, 210 lymph nodes, and 40 bone/organ distant sites; 11 patients had a negative scan and 9 patients showed indeterminate lesions, which were also considered as having a negative scan. The detection rates were 47.6% (n=10/21), 50% (n=5/10), 88.9% (n=8/9), and 94.0% (n=47/50) for PSA levels of >0.2 to <0.5, >0.5 to 1.0, >1 to 2.0, and ≥ 2.0 ng/mL, respectively. Out of 70 patients with positive PSMA-PET scan, tumor recurrence was confirmed in 67.1% of the cases at least for one site, by either biopsy (n=31), or matched multiparametric MRI (n=16); 2 patients had negative biopsy and 21 patients had lesions not amenable for biopsy or refused biopsy. **Conclusion:** ^{18}F-DCFPyL-PET imaging is helpful in identifying suspicious lesions in 77.8% of patients with biochemical recurrence prostate cancer; and importantly, it reveals a high number of positive imaging findings in the range of low PSA values (<0.5 ng/mL), which might substantially impact further clinical management. **References:** 1) Giesel FL, Will L, Kesch C, Freitag M, Kremer C, Merkle J, Neels OC, Cardinale J, Hadaschik B, Hohenfellner M, Kopka K, Haberkorn U, Kratochwil C. Biochemical Recurrence of Prostate Cancer: Initial Results with [^{18}F]PSMA-1007 PET/CT. J Nucl Med. 2018 Apr;59(4):632-635. 2) Caroli P, Sandler I, Matteucci F, De Giorgi U, Uccelli L, Celli M, Foca F, Barone D, Romeo A, Sarnelli A, Paganelli G. ^{68}Ga-PSMA PET/CT in patients with recurrent prostate cancer after radical treatment: prospective results in 314 patients. Eur J Nucl Med Mol Imaging. 2018 Nov;45(12):2035-2044.

EPS-072

Usefulness of combined analysis by both FDG-PET and diffusion MRI in predicting overall survival in biliary cancer

S. Nagamachi[1], *M. Nonokuma*[1], *Y. Mizutani*[2], *T. Terada*[2], *K. Yoshimitsu*[1];
[1]*Fukuoka University, Fukuoka Prefecture, JAPAN,* [2]*Miyazaki University, Miyazaki Prefecture, JAPAN.*

Aim/Introduction: Both Total lesion glycolysis (TLG) calculated by FDG-PET and apparent diffusion coefficient (ADC) calculated by diffusion MRI are useful for predicting overall survival (OS) in biliary cancer. However, few researches predicting OS of biliary cancer by the combined analysis with FDG-PET and diffusion MRI have been reported. We investigated the usefulness of combined analysis by both FDG-PET and diffusion MRI in predicting OS of biliary cancer. **Materials and Methods:** Forty-two biliary cancer patients (27 females and 15 males, mean age 67.7) were analyzed retrospectively. Although tumor location (Extra-hepatic19, Intra-hepatic 9, Papilla of Vater14) and stages were various (I 4, II 9 III19, IV10), all cases were undertaken surgical resection and given post-operative chemotherapy (gemcitabine /cisplatin). Both pre-operative FDG-PET and MRI diffusion images were analyzed retrospectively. The values of TLG (g) were calculated by multiplication of total volumes more than 40% of SUVmax and SUV mean value on FDG-PET/CT. ADC mean values were measured within the tumor ROI on the ADC map imaged by 3T MRI with b value 1000.We divided all patients in the four subgroups according to the value of TLG and ADC mean obtained in pre-therapy examinations. The cut-off values of each examination were 30g and 1300 s/mm² respectively. We compared OS (days) among the four groups, namely the group with high TLG and low ADC mean (n=12), the group with high TLG and high ADC mean (n=11), the group with low TLG and low ADC mean (n=11) , the group with low TLG and high ADC mean group (n=8). We also compared various parameters, including tumor locations and stages, among four subgroups.

Results: The mean value of each OS was 481, 557, 941 and 959 days respectively. The OS of high TLG and low ADC mean was significantly shorter compared with those of each low TLG groups (481 vs. 941 days, 481 vs. 959 days). Although there was no statistical significance, each low ADC mean group showed shorter OS compared with those of each high ADC mean groups (481 vs. 557 days, 941, vs. 959 days). Regarding other clinical parameters including pathological stages, there was no statistical significance among four subgroups. **Conclusion:** The patients group with both high TLG and low ADCmean had poor prognoses compared to other groups.In planning treatment of biliary cancer, combined analyses of TLG by FDG-PET and ADC mean by MRI is useful in order to stratify and predict OS. **References:** None.

EPS-073

"Complete" whole-body 18F-FDG PET-CT scan in malignant supradiafragmatic cutaneous melanoma. Does it have any added value?

N. Bustos, G. Bruno, C. Gonzalez, S. Traverso, M. Arceluz, P. Corona, M. Namias;
Fundación Centro Diagnostico Nuclear, Buenos Aires, ARGENTINA.

Aim/Introduction: The aim of this study was to determinate if "complete" whole body (head-to-toe) PET/CT acquisition protocol has a added value in the assessment of patients with supradiaphragmatic primary malignant cutaneous melanoma: Our experience in 212 patients. **Materials and Methods:** We retrospectively evaluated 389 patients with cutaneous melanoma who underwent staging or restaging PET/CT between 2008 and 2014, and selected those whose primary lesion was supradiaphragmatic located (212/389). All abnormal hypermetabolic areas and morphologic lesions related to the primary disease were recorded, focusing mainly on findings in lower extremities. **Results:** A total of 3.3% (7/212) of patients had lesions in lower limbs using whole body scan PET/CT. Most of the patients had primary melanoma lesions on trunk (128/212), while upper extremities (49/212) and head and neck (39/212) were the following locations per frequency. The percentage of patients with potentially suspicious metastases on lower limbs where 1.8% for trunk primary lesions and 1.4% for those situated at head and neck. Only two patients (0.9%) with primary lesions at external ear and trunk had lower limb metastases as unique finding, changing the staging thus the treatment; whereas the rest of the patients (5/212) had already more extensive disease with secondary involvement in lungs and distant lymph nodes. No CNS (central nervous system) metastases where found. It is emphasized that no patients with primary melanoma on upper limb had secondary involvement at lower extremities in our study. **Conclusion:** Primary cutaneous melanoma with supradiaphragmatic location had low incidence of lower limbs metastases. Whole body (head-to-toe) acquisition protocol in these cases has no added value in the assessment of the disease, so it might not be necessary to routinely include lower extremities beyond the mid thighs. Standard PET / CT scanning protocol from the skull to mid thighs would be suitable in most cases, in addition it has the benefit of a shorter acquisition time and less radiation exposure. **References:** None.

EPS-074

Assessment Of Abdominal Resectability With FDG-PET/CT In Locally Advanced Ovarian Cancer

A. Caresia Aróztegui[1], J. Del Riego Ferrari[2], Y. García García[3], L. Ribot Luna[4], B. Morillas Oliveras[4], I. Costa Tranchsel[5], J. Martín Miramon[1], A. Rodríguez Revuelto[1], M. Moragas Solanes[1], Z. Bravo Ferrer[1], J. Antoni Vives[4], L. Bernà Roqueta[1];
[1]Nuclear Medicine Department, Parc Taulí Hospital Universitari, Sabadell, SPAIN, [2]Radiology Department, Parc Taulí Hospital Universitari, Sabadell, SPAIN, [3]Oncology Department, Parc Taulí Hospital Universitari, Sabadell, SPAIN, [4]Gynecology Department, Parc Taulí Hospital Universitari, Sabadell, SPAIN, [5]Pathology Department, Parc Taulí Hospital Universitari, Sabadell, SPAIN.

Aim/Introduction: In locally advanced ovarian cancer the primary treatment is debulking surgery followed by chemotherapy. Surgery is recommended in patients who can be debulked upfront to no residual tumour. Therefore, there are some specific criteria against primary surgical approach (Diffuse deep infiltration of the root of small bowel mesentery; large and diffuse carcinomatosis of the small bowel, extensive involvement of superior abdomen or multiple visceral metastases). In case of inoperable disease, neoadjuvant chemotherapy with interval surgery should be planned. The aim of this study is to evaluate the capability of FDG-PET/CT to assess abdominal resectability in advanced ovarian cancer, before surgery (primary or interval surgery). **Materials and Methods:** Unicenter, restrospective, observational study included 35 patients (age 63.11, range 40-82 years) with clinical and radiological suspicion of primary advanced ovarian cancer. All patients underwent contrast enhanced PET/CT before surgery. Based on criteria against surgical approach, patients were classified as resectable or non resectable. Sensitivity, specificity, NPV, PPV and accuracy for PET/CT to predict complete surgical resectability were calculated (R0). **Results:** Thirty-one patients were concordant (18 patients were considered resectables by PET/CT and surgery, 13 patients were considered non resectables by PET/CT and surgery). Only 4 patients were discordant: 1 patient presented inoperable milliary carcinomatosis, not visible by PET/CT. The other 3 patients were finally resectables but it seems not by PET/CT (large and diffuse carcinomatosis of the small bowel or extense involvement of superior abdomen). For detection of abdominal resectability, PET/CT presented a sensitivity of 85.7% (95% CI:64-97), specificity 92.8%(95% CI:66-100), NPV 81.2%(95% CI:54-96), PPV 94.7%(95% CI:74-100) and accuracy of 88.57%(95% CI:73-96). PET/CT also revealed extrabdominal distant metastases in 9/35 patients (29%), mainly represented by supradiaphragmatic lymph nodes (8/9 patients), associated with additional metastases in pleura and/or liver. **Conclusion:** In locally advanced ovarian cancer, PET/CT had good results in assessment of surgical abdominal resectability, especially in

terms of specificity, PPV and accuracy. PET/CT could be helpful in patients with questionable initial terapeutic decision, due to its ability to detect additional unsuspected extraabdominal disease. **References:** None.

EPS-075

TNF alfa therapy and radiosynoviorthesis in patients with rheumatoid arthritis

M. Szentesi[1], *Z. Mangel*[1], *Z. Nagy*[2], *G. Csőre*[3], *P. Géher*[1]; [1]*Department of Rheumatology, Polyclinic of the Hospitaller Brothers of St. John of God, Budapest, HUNGARY,* [2]*Polyclinic of the Hospitaller Brothers of St. John of God, Budapest, HUNGARY,* [3]*St. Andrew Hospital for Rheumatic Diseases, Hévíz, HUNGARY.*

Aim/Introduction: The treatment of patients with rheumatoid arthritis (RA) has been spectaculary changed since the 1950's. Introduction of the steroid compounds and their local application, the chemical and radionuclide synovectomy, surgical synovectomy, use of non steroid drugs, the basic treatment and the spread of biological therapy are the most important steps. Introduction of the biological therapy has changed the quality of life for these patients. During biological therapy sometimes 1 or 2 joints could be affected by inflammation. In this cases always the question is how to solve the problem. Change of the biological or basic therapy, use surgical synovectomy or radiosynovectomy (RSO)? **Materials and Methods:** In our reumatological department 2100 patients with RA were treated with biological therapy between 2002 and 2018. In 100 patients we applied RSO because of the inflammation of the knee joint during biological therapy. We made a long term follow-up in 82 patient. All participants provided written informed consent. 82 participants inflammatory knee joint disease was diagnosed on the basis of the American College of Rheumatology. 70 of 82 patients with rheumatoid arthritis were seropositive, 12 seronegative. Steinbrocker functional stadium II was observed in 72, stadium III in 10. Mean age of 18 male and 76 female patients was 51.4 years (range 24-79) years. In 42 patients the right knee, in 40 the left knee was treated by radiosynovectomy. Mean duration of disease was 8.3 years (range 0.5-25), of synovitis (6.3month (range 3-8) Mean number of punctions of the treated joint prior to radiosynovectomy was 4,2 per patient and of steroid administrations prior to radiosynovectomy 3,0. In 15 patients a systemic steroid therapy has been performed. **Results:** During the study period, inflammation decreased. In the first 3 years excellent and good results were recorded in 81,2%. 3 years after radiosynoviorthesis 82.2% of patients did not need another punction. Before the knee inflammation patients were in complete remission which status has been achieved after RSO as well. DAS: 2,4+-0,4. **Conclusion:** 1. RSO is an effective method to treat the inflammation of the knees. 2. RSO performed during biological tehrapy is as effective as in the case of patients without biological therapy. 3. In case of a successful RSO there is no need for biological or basic therapy neither for surgical synovectomy. 4. However an intraarticular injection has a low risk for infection it is recommended to avoid the biological therapy during the RSO. **References:** None.

EPS-076

^{18}F-FDG PET/CT based BRAFV600 prediction in melanoma

H. Saadani[1], *B. van der Hiel*[1], *E. A. Aalbersberg*[1], *I. Zavrakidis*[1], *J. B. A. G. Haanen*[1], *O. S. Hoekstra*[2], *R. Boellaard*[2], *M. P. M. Stokkel*[1]; [1]*Netherlands Cancer Institute, Amsterdam, NETHERLANDS,* [2]*Amsterdam UMC, Vrije Universiteit Amsterdam, Cancer Center Amsterdam, Amsterdam, NETHERLANDS.*

Aim/Introduction: Approximately 50% of melanomas contain a BRAF mutation, which causes tumor growth, cell proliferation and metastasis. BRAF mutation determination is the decisive factor for commencing first line BRAF inhibition in metastatic melanoma. The potential of PET/CT based prediction in melanoma has been mainly explored in conventional PET features and visual assessments whereas current developments in precision medicine increase the need for in-depth tumor characterization, which can be enabled by radiomics analysis. The aim of this study was to predict BRAFV600 mutation status with both conventional- and radiomics ^{18}F-FDG PET/CT features, while exploring several methods of feature selection in melanoma radiomics. **Materials and Methods:** Seventy unresectable stage III/IV melanoma patients who underwent a baseline ^{18}F-FDG PET/CT scan were identified. Patients were assigned to the BRAFV600 group or BRAF wild-type group according to mutational status. ^{18}F-FDG uptake quantification was performed on the three lesions with the highest FDG uptake per organ region, diameter ≥2 cm or MATV ≥4.2 cm^3 by SUVmax50% based semi-automatic lesion delineation. Four hundred eighty radiomics features and four conventional PET features (SUVmax, SUVmean, SUVpeak and total lesion glycolysis) were extracted per lesion. Six different feature selection methods (a correlation matrix of all radiomics features, a correlation matrix of all radiomics features with the conventional PET features SUVpeak, MATV, and TLG; a principle component analysis, selecting features from prior studies, a penalized binary logistic regression analysis of all radiomics features, and a random forest model of all radiomics features) were implemented and ten-fold cross validated predictive models were built for each. Model performances were evaluated with Area Under the Curves (AUC) of the Receiver Operating Characteristic (ROC) curves. **Results:** Thirty-five BRAFV600 mutated patients (100 lesions) and thirty-five BRAF wild-type patients (79 lesions) were analyzed. AUCs predicting the BRAFV600 mutation varied from 0.54-0.62 and were susceptible to feature selection method. The best AUCs were achieved by feature selection based on literature, a penalized binary logistic regression model and random forest model. No significant difference was found between the BRAFV600 and BRAF wild-type group in conventional PET features, nor predictive value. **Conclusion:** BRAFV600 mutation status is not associated with- nor can be predicted with conventional PET features, while radiomics features were of low predictive value (AUC=0.62). We showed feature selection methods influence predictive model performance, describing and evaluating six unique methods. Detecting BRAFV600 status in melanoma based on ^{18}F-FDG PET/CT alone does not yet provide clinically relevant knowledge. **References:** None.

EPS-077

Phase I clinical trial using a novel CCK_2 receptor-localizing radiolabelled peptide probe for personalized diagnosis and therapy of patients with progressive or metastatic medullary thyroid carcinoma - final results

A. Hubalewska-Dydejczyk[1], *R. Mikolajczak*[2], *C. Decristoforo*[3], *P. Kolenc-Peitl*[4], *P. A. Erba*[5], *K. Zaletel*[4], *H. Maecke*[6], *T. Maina*[7], *M. Konijnenberg*[8], *P. Garnuszek*[2], *M. Trofimiuk-Müldner*[1], *E. Przybylik-Mazurek*[1], *I. Virgolini*[3], *M. de Jong*[8], *A. C. Froberg*[8], *C. Rangger*[3], *G. Goebel*[3], *L. Scarpa*[3], *B. Glowa*[9], *K. Skórkiewicz*[9], *L. Lezaic*[4], *B. Solnica*[1], *D. Fedak*[1], *P. Gawęda*[1], *A. Sowa-Staszczak*[1], *B. A. Nock*[7], *D. Bergant*[4], *S. Rep*[4], *V. Lenda-Tracz*[9];
[1]*Jagiellonian University, Krakow, POLAND,* [2]*NCBJ POLATOM, Otwock-Swierk, POLAND,* [3]*Medical University, Innsbruck, AUSTRIA,* [4]*University Medical Center, Ljubljana, SLOVENIA,* [5]*University of Pisa, Pisa, ITALY,* [6]*University Medical Center, Freiburg, GERMANY,* [7]*National Center for Scientific Research Demokritos, Athens, GREECE,* [8]*Erasmus MC, Rotterdam, NETHERLANDS,* [9]*University Hospital, Krakow, POLAND.*

Aim/Introduction: We aim to present the final results of the translational study: GRAN-T-MTC in the innovative field of targeted radionuclide therapy in advanced medullary thyroid cancer (MTC). In this phase I study held within the multinational cooperation (ERA-NET,TRANSCAN), the ^{111}In-labelled CCK_2 receptor (CCK_2R)-seeking ligand (DOTA-$(DGlu)_6$-Ala-Tyr-Gly-Trp-Met-Asp-Phe-NH_2 (CP04) was tested. The justification for the project was the limited efficacy of available imaging and treatment options (including tyrosine kinaseinhibitors) and a high expression of CCK_2Rs on MTC lesions. **Materials and Methods:** The study consisted of a preclinical (WP1) and clinical (WP2) part. WP1 aimed to establish a clinically useful formulation for radiolabelled peptide CP04. The primary objectives of WP2 were to determine: i) the safety of CP04 intravenous administration, ii) the biodistribution and dosimetry of [^{111}In] CP04 in cancer and normal tissues, iii) the critical organs, and iv) the ability of the biomarker to visualize MTC lesions. In phase 1A (4 patients) two peptide amounts, both radiolabelled with [^{111}In] (200 ± 10% MBq), were administered: 10 µg as a safety step in the first applications of CP04 and 50 µg as the amount representative of potential therapy with [^{177}Lu]CP04. After safety assurance, only 50 µg of ^{111}InCP04 was applied (phase 1B). Patients were randomized into two arms: with and without the co-administration of gelofusine (a renoprotective agent). Overall, sixteen patients were enrolled in the study. During [^{111}In]CP04 administration, blood samples were taken forthe purpose of dosimetry, pharmacokinetics and measurement of the calcitonin and procalcitonin concentration in the blood. www.clinicaltrials.gov: ID:NCT03246659; EudraCTnumber: 2015000 80538 **Results:** The positive results of [^{111}In]CP04 stability, radiolabelling, and toxicity studies (WP1) enabled the development of a clinically useful formulation for radiolabelled CP04. The Investigator's Brochure and IMPD were prepared.All the study goals of the clinical trial were achieved. The safety of [^{111}In]CP04 intravenous injection was confirmed. The biomarker was able to detect even unknown MTC lesions. Biodistribution and dosimetry data demonstrated CP04 as a promising targeting vector also for radionuclide with therapeutic properties (^{177}Lu). Gelofusine co-injection unambiguously showed a reduction of tracer retention in the kidneys, which can be crucial for planning future treatment. **Conclusion:** The project has provided a novel, promising diagnostic tool for MTC patients. ^{111}In-CP04 has been proven as a safe, sensitive and highly specific imaging biomarker. The favorable dosimetry results justify action to initiate clinical trials of therapeutic efficacy assessment with the CP04 labelled with a beta emitting therapeutic radionuclide (^{177}Lu). **References:** None.

EPS-078

Comparison of ^{68}Ga-PSMA and ^{18}F-FDG PET/CT in Multiple Mieloma: Preliminary Results

C. D. Ramos[1], *F. C. Frasson*[1], *S. P. M. Souza*[1], *G. B. Oliveira*[1], *V. P. Castro*[1], *F. V. Pericole*[1], *E. C. S. C. Etchebehere*[1], *M. C. L. Lima*[1], *E. M. R. Brunetto*[1], *J. Mengatti*[2], *E. B. Araujo*[2], *C. A. Souza*[1], *I. Lorand-Metze*[1], *A. O. Santos*[1];
[1]*University of Campinas, Campinas, BRAZIL,* [2]*Nuclear and Energy Research Institute (IPEN), Sao Paulo, BRAZIL.*

Aim/Introduction: ^{18}F-FDG PET/CT has been used to detect active lesions of multiple myeloma (MM), but image interpretation may be challenging in patients with mild lesion uptake because of physiological FDG accumulation in the bone marrow. Recent case reports (1,2) have suggested the use of ^{68}Ga-labeled prostate-specific membrane antigen (PSMA) as a possible tracer for MM evaluation. This study aimed to compare these two imaging modalities in the MM. **Materials and Methods:** Ten consecutive patients with biopsy proven MM (6 female, mean age 67.7 ±8.1 years) were submitted to whole body ^{18}F-FDG and ^{68}Ga-PSMA PET/CT with a time interval of 1-7 days between procedures. Two patients were under initial staging, 3 with disease relapse and 5 under follow-up after treatment. ISS score was 1, 2 and 3 for respectively 4, 2 and 4 patients. Two experienced nuclear physicians analyzed images by consensus. All lesions were counted and had their maximum SUVs measured in both procedures. **Results:** A total of 90 lesions were detected in 9/10 patients. FDG detected 50/90 lesions in 8 patients and PSMA 83/90 lesions in 9 patients. Both procedures did not identify any active lesion in 1 patient. Forty lesions were detected only by PSMA and 7 only by FDG. Both tracers identified 43 lesions, but with intra-lesion mismatch pattern in 6 lesions, found in 4 different patients. Different lesions with uptake of only FDG or PSMA in the same patient were found in 3 patients. The 50 FDG and the 83 PSMA avid lesions had a median SUV of 3.8 (1.3-37.8) and 6.8 (1.3-51.3), respectively ($p<0.0001$). The median SUVs of the 43 lesions with uptake of both tracers were respectively 4.0 (1.3-37.8) and 9.1 (1.3-51.3) for FDG and PSMA ($p<0.0001$). FDG and PSMA respectively identified 8 and 11 soft tissue lesions. Benign lesions with FDG uptake had minimal or no uptake of PSMA. The absence of physiological uptake in the brain or in normal bone marrow made it easier to identify MM lesions in PSMA than in FDG

images. **Conclusion:** Our preliminary results suggest that ^{68}Ga-PSMA PET/CT may be a good alternative for detecting active lesions in patients with MM. Neoangiogenesis is the supposed mechanism of PSMA uptake in MM. ^{18}F-FDG and ^{68}Ga-PSMA might have a complementary role in these patients, due to the marked genomic heterogeneity of the disease. **References:** (1)Baerentzen S, et al. Clin Nucl Med 2017;42(10):790-792. (2) Rauscher I, et al. Clin Nucl Med 2017;42(7):547-548.

EPS-079

Diagnosis of Pelvic Insufficiency Fractures in Oncology Patients: Radiological Findings and Role of Tc99m MDP SPECT/CT imaging

V. Sabaliauskas, S. Tiškevičius;
National Cancer Institution, Vilnius, LITHUANIA.

Aim/Introduction: Diagnosing pelvic insufficiency fractures (PIFs) in oncology patients is a challenge to radiologists and recognition of imaging features is essential in order to avoid misdiagnosis of bone metastases and prevent patients from inaccurate treatment. The aim of this study is to assess risk factors, clinical and imaging findings of PIFs and evaluate a diagnostic role of single-photon emission computed tomography/computed tomography (SPECT/CT) in diagnosing PIFs in oncology patients. **Materials and Methods:** This study is based on a retrospective analysis of 42 oncology patients (from August 2006 till March 2019) with PIFs who underwent computed tomography (CT), magnetic resonance imaging (MRI) of pelvis and radionuclide whole body scan (WBS) followed by pelvic SPECT/CT. The analysis included radiological findings, clinical information, time-to-onset, follow-up time, risk factors and complications associated with radiation therapy. **Results:** Median age at onset of PIF was 68.5 years (range: 52-87 years). 34 of patients (81%) were postmenopausal women. The median follow-up time was 12 months (range: 8-48 months). 32 patients (76.2%) presented with clinical symptoms. 35 patients (83.3%) received pelvic radiotherapy (RT). The median time for the development of PIFs after the completion of RT was 13 months (range: 2-36 months). PIFs were most frequently observed in the sacrum (80.1%). Fracture lines or sclerotic lines were seen on CT and/or MRI scans in 25 of 40 patients, and osteosclerosis with no visible fracture lines was observed in 17 of 42 patients. On CT and/or MRI scans 16 radiological changes were interpreted as benign, 9 as malignant, and 17 abnormalities were undetermined. All of the lesions were observed on SPECT/CT; only 5 (11.9%) of 42 lesions were undetermined and needed further follow-up. Postmenopausal state and prior RT were concluded as the main risk factors for the development of PIFs. **Conclusion:** SPECT/CT should be included in the differential diagnostics when radiological features of pelvic bone pathology on CT or MRI are undetermined or PIFs are suspected. PIFs must always be considered in oncology patients with pelvic pain, especially in postmenopausal state and after RT. For patients with risk factors of PIFs, bone density screening and precise review of the most common fracture sites are recommended. **References:** None.

EPS-080

Meet 99mTc-tilmanocept as next generation radiotracer with the requirements for improved sentinel node imaging?

D. Rietbergen, L. Pereira Arias-Bouda, J. vd Hage, R. Valdes Olmos;
Leids Universitair Medisch Centrum (LUMC), Leiden, NETHERLANDS.

Aim/Introduction: Radiotracers with small particle size have been associated with a successful sentinel node (SN) visualisation; however, in many cases concomitant non-SN lymph node uptake may difficult image interpretation and radioguided procedures at the operating room. Recently, 99mTc-tilmanocept, with an average molecular size of 7 nm, has become available in Europe; due to the improved receptor affinity of its mannose component in surface macrophages this tracer is aimed to combine increased uptake in SN with a rapid clearance from injection site. We evaluated 99mTc-tilmanocept for SN imaging in patients with breast cancer and melanoma scheduled for SN biopsy after interstitial tracer administration. **Materials and Methods:** In 25 patients scheduled for SN biopsy (mean age: 63y, range: 45-81y) planar images were acquired 10 and 120 min after administration of 74Mbq 99mTc-tilmanocept in order to evaluate lymphatic drainage as well as uptake ratios between injection site (IS), SN and non-SN. SPECT/CT was performed immediately after delayed planar images to enable anatomical lymph node localisation. **Results:** SNs were visualized in all patients (100%), in 13 of them (52%) without visible non-SN uptake on both planar images and SPECT/CT. Number of SNs was concordant between early and delayed images in all patients excepting two (92%). In 21 patients tracer migrated to one lymph node basin (LNB), in three to 2 and in one to 4. When IS was included (N=21) on image IS/SN ratio per LNB at 2h decreased with an average of 69.3% (range:15-98%) in comparison with 15-min ratio. SN/non-SN 2h ratio in 12 LNB with visible non-SNs averaged 6.8 (range:2.3-15.6). In 7 patients with two SNs SN1/SN2 ratio averaged 1.6 on early images and 1.7 on delayed. **Conclusion:** Despite its small particle size 99mTc-tilmanocept appears to amply meet the requirements for improved SN imaging in breast cancer and melanoma on the basis of early and persistent SN visualisation frequently without non-SN lymph nodes. This is accompanied by rapid migration from the injection site together with increasing SN uptake as expressed by decreasing IS/SN ratios, and, in the case of visible non-SNs, an adequate delayed SN/non-SN ratio. Further head-to-head comparison of 99mTc-tilmanocept with standard SN radiotracers in larger series of patients is necessary to establish its role as first choice option in SN procedures. **References:** None.

EPS-081

Integrating Clinical Experience Into Radiomics For Reducing The False Positive Rate Of ^{18}F-FDG PET/CT Diagnosis In Patients With Suspected Lung Cancer

F. Kang[1], *W. Mu*[2], *J. Gong*[3], *W. Qin*[3], *J. Tian*[2], *J. Wang*[1];
[1]*Department of Nuclear Medicine, Xijing Hospital, Xi'an, CHINA,* [2]*Key Laboratory of Molecular Imaging of Chinese Academy of Sciences, Institute of Automation, Chinese Academy of Sciences, Beijing, CHINA,* [3]*Life Sciences Research Center, School of Life Sciences and Technology, Xidian University, Xi'an, CHINA.*

Aim/Introduction: The high false positive rate (FPR) of ^{18}F-FDG PET/CT in lung cancer screening represents a severe challenge for clinical decision-making. This study aimed to develop a clinical-translatable radiomics nomogram for reducing the FPR of PET/CT in lung cancer diagnosis, and to determine the impact of integrating manual diagnosis to the performance of the nomogram. **Materials and Methods:** Among 3947 lung cancer patients diagnosed with ^{18}F-FDG PET/CT, 157 malignant and 111 benign patients were enrolled and divided into training and test cohorts. The data of manual diagnosis were retrospectively recorded. A total of 4338 features were extracted from CT, thin-section CT, PET and PET/CT, and the four radiomics signatures (RS) were then generated by LASSO method. A hybrid nomogram integrating PET/CT RS and manual diagnosis was developed using multivariable logistic regression. The performances of RS and hybrid nomogram were validated through key discrimination index and clinical benefit. **Results:** The FPR of manual diagnosis was found to be 30.63%. Among the four RS, PET/CT RS exhibited the best performance. By integrating manual diagnosis, the hybrid nomogram demonstrated lowest FPR and highest C-index and Youden index (YI) in both training and test cohorts (FPR: 5.36% and 9.09%, C-index: 0.982 and 0.924, YI: 85.78% and 75.53%, respectively). The hybrid nomogram respectively corrected 78.57% and 37.50% among FPR cases produced by PET/CT RS, without significantly sacrificing its sensitivity. The net benefit of hybrid nomogram appeared highest at < 85% threshold probability. **Conclusion:** The established hybrid nomogram integrating PET/CT RS and manual diagnosis can significantly reduce FPR, improve diagnostic accuracy and enhance clinical benefit compared to manual diagnosis. The performance of this hybrid nomogram is superior to PET/CT RS without manual diagnosis integration, indicating the importance of clinicians' judgement as an essential information source for improving radiomics diagnostic approaches. **References:** None.

EPS-082

Impact of Metabolic Switch in HCC Patients Treated with Sorafenib - A Proof-of-concept Trial

E. Lopci*, A. Castello, N. Personeni, T. Pressiani, V. Smiroldo, E. Mazziotti, L. Rimassa;*
Humanitas Clinical and Research Hospital - IRCCS, Milano, ITALY.

Aim/Introduction: Sorafenib is an inhibitor of multiple small molecules involved in hepatocyte proliferation and neoangiogenesis used in the last decade to treat advanced hepatocellular carcinoma (HCC). Recently, a preclinical trial has shown that response to sorafenib is associated to a metabolic shift towards aerobic glycolysis, with increased glucose consumption and lactate production, as early as 12 hours following sorafenib administration. To text this observation in humans, we decided to conduct a proof-of-concept trial investigating the role of metabolic shift detected on FDG PET in predicting survival and tumor response in patients with advanced HCC during treatment with sorafenib. **Materials and Methods:** For this study, we prospectively enrolled advanced HCC patients candidate to therapy with sorafenib and undergoing FDG PET/CT before treatment, after 24 hours, and at day 7. Response evaluation was performed after 8 weeks according to the modified Response Evaluation Criteria in Solid Tumors (mRECIST). All clinical variables, including alpha-fetoprotein, and metabolic parameters (i.e. SUVmax; metabolic tumor volume, MTV; total lesion glycolysis, TLG; and their variations) were compared to treatment response and correlated to PFS and OS, based on a median follow-up of 5.3 months. The trial was registered: www.clinicaltrials.gov (NCT02977754). **Results:** Overall, thirteen patients (10 male, 3 female, median age 69) were enrolled for this proof-of-concept trial between August 2016 and August 2018. According to mRECIST, among the 10 patients who were evaluated after 8 weeks, six (60%) patients obtained SD, four (40%) PD, and no objective responses were reported. As expected, median SUVmax, MTV, and TLG resulted lower in patients with stable disease than progressive disease according mRECIST (p=0.019). Considering the overall cohort, we demonstrated a significant negative correlation between ΔSUVmax at 24 hours and at 1 week (rho= -0.733, p=0.016). Metabolic parameters and ECOG Performance Status (PS) resulted significantly correlated to PFS and OS at univariate analysis, while on multivariate analysis, only median MTV at 1 week was found as independent prognostic factor for PFS (p=0.033). **Conclusion:** Our study indicates that FDG PET/is able to evaluate metabolic shift at 24 hours and early treatment response as early as after 1 week of treatment in patients with advanced HCC undergoing sorafenib therapy. Moreover, metabolic parameters and ECOG PS result predictive and prognostic factors to PFS and OS, with MTV at 1 week appearing as an independent prognostic factor for PFS. **References:** Llovet JM, et al. NEJM 2008; 359:378-390. Tesori V, et al. Sci Rep (2015) 5:9149.

EPS-083

Incidental finding of 68Ga-prostate-specific membrane antigen (PSMA) uptake in the thyroid gland in patients with prostate cancer: A single-center cross sectional study

L. Petersen*, F. Gossili, H. D. Zacho;*
Department of Nuclear Medicine, Aalborg University Hospital, Aalborg, DENMARK.

Aim/Introduction: 68Ga-prostate-specific membrane antigen (PSMA) PET/CT has become a well established imaging method for evaluation of patients with prostate cancer. However, numerous cases have revealed PSMA uptake in a large variety of other conditions than prostate cancer. Such findings often represent other malignancies, but also a wide range of benign conditions may show PSMA uptake. PSMA uptake in thyroid cancer has been reported. The aim of present study was to describe the frequency of focal, pathologic PSMA uptake in the thyroid gland leading to further investigations, and to assess the frequency of malignant findings in a large patient cohort with prostate cancer. **Materials and Methods:** We retrospectively identified all patients referred for a 68Ga-PSMA PET/CT at the department of Nuclear Medicine, Aalborg University Hospital, Denmark between 11th of May, 2015 and 12th of February, 2019. Patients with focal, pathologic PSMA uptake in the thyroid gland were retrieved and follow up was conducted based on medical charts, blood samples, additional imaging and histology when available. **Results:** A total of 321 68Ga-PSMA PET/CT were performed in patients with prostate cancer (mean age 68, range 47-83 years). 68Ga-PSMA avid lesions in the thyroid gland were observed in 9 patients (2.8 %) (mean age 70 years, range 52-78 years). Further investigations were conducted in all of the patients, and seven patients underwent biopsy of the thyroid gland. The biopsy was without malignancy in four patients, one biopsy was intermediate and two biopsies were suspicious of malignancy. Based on the results of the biopsy and other clinical indication, five men underwent hemi-thyroidectomy, which revealed a synchronous primary papillary thyroid cancer in one patient, metastases from a renal cell carcinoma in the second patient and finally, in three patients no malignancy was present in the thyroid. Thus, malignancy was verified in two of nine (22 %) PSMA avid lesion in the thyroid gland. **Conclusion:** Pathologic, focal PSMA uptake in the thyroid tissue in prostate cancer patients is a rare condition. However, such findings should be further investigated as these findings may represent metastatic or primary malignancy of the thyroid gland. **References:** None.

911

e-Poster Presentation Session 6 - Cardiovascular: Searching for Myocardial Ischemia

Monday, October 14, 2019, 14:30 - 16:00 Room 133/134

EPS-084

SPECT Myocardial Blood Flow measurement with a dedicated cardiac CZT camera for Coronary Artery Disease screening: correlation with cardiovascular risk

M. Bailly[1], *F. Thibault*[1], *M. Courtehoux*[2], *G. Metrard*[1], *M. Ribeiro*[2];
[1]*CHR Orléans, Orleans, FRANCE,* [2]*CHRU Tours, Tours, FRANCE.*

Aim/Introduction: Dedicated CZT cardiac cameras have been shown to provide accurate measurements of absolute myocardial blood flow (MBF) and flow reserve (MFR). PET MBF studies using either Rb-82 or N-13-ammonia have shown that MFR was predictive of major adverse cardiovascular (CV) events. In this study we evaluate the correlation between SPECT global MFR measurement and clinical cardiovascular risk (CVR). **Materials and Methods:** Patients referred for Myocardial Perfusion Imaging (MPI) for Coronary Artery Disease (CAD) screening between June 2018 and March 2019 were included. Clinical symptoms and CVR factors were collected to classify patients in 3 groups: moderate, high and very high risk. HeartScore (SCORE) according to the European Society of Cardiology was calculated. SPECT data were acquired on a CZT-based pinhole cardiac camera in listmode using a stress (249 ± 17 MBq) / rest (508 ± 29 MBq) one-day Tc-99m-tetrofosmin protocol. Kinetic analysis was done with FlowQuant™software using a 1-tissue-compartment model and converted to MBF using a previously determined extraction fraction correction. Statistical analysis was performed using Prism 8™. **Results:** 87 patients (39 male, 48 female) were included and classified in 3 clinical CVR groups: 31 moderate, 13 high and 43 very high risk. Mean SCORE was 3.9%. Mean global MFR was 2.50 ±0.91. 25 patients (29%) had impaired CFR (using a threshold of 2), whereas only 7 patients had pathological MPI. MFR wasn't significantly different between the three groups of CVR (p=0.08), nor according to patient symptomatology (p=0.31). There was a significant correlation with the SCORE (p=0.03) and the number of CVR factors (p=0.02). Excepting dyslipidemia (p=0.011) and family history of coronary artery disease (p<0.05), we did not notice any significant correlation between impaired MFR and other CVR factors (p=0.07 for smoking, p=0.17 for hypertension and p=0.29 for diabetes). Impaired MFR was significantly associated to microalbuminuria (p<0.05), using a urinary albumin to creatinine ratio threshold of 20mg/g. **Conclusion:** MFR measured during MPI for CAD screening on CZT camera is significantly correlated with the SCORE and the number of CVR factors. Impaired MFR was also significantly associated with microalbuminuria, reflecting microvascular dysfunction. Adding MFR to MPI could dramatically increase CAD diagnostic confidence and provide prognostic information. **References:** None.

EPS-085

Correlation Of Coronary Calcium Burden And Myocardial Perfusion Assessed By Myocardial Perfusion SPECT/CT

S. Cho[1], *J. Kim*[1], *S. Yoo*[2], *S. Kang*[2], *S. Kwon*[2], *J. Min*[2], *H. Song*[1], *H. Bom*[2];
[1]*Chonnam National University Hospital, Gwang-ju, KOREA, REPUBLIC OF,* [2]*Chonnam National University Hwasun Hospital, Jeollanam-do, KOREA, REPUBLIC OF.*

Aim/Introduction: We assessed the correlation between coronary calcium scoring performed by low-dose attenuation correction CT (AC-CT) and myocardial perfusion on myocardial

perfusion SPECT/CT. **Materials and Methods:** We retrospectively included 225 patients with low-to-intermediate (≤ 90%) pretest probability, who underwent myocardial perfusion SPECT/CT equipped with low-dose attenuation correction CT (AC-CT) for evaluation of coronary artery disease. Patients with previous coronary artery disease, clinically suspected heart failure or left ventricular ejection fraction < 45% or wall motion abnormality on echocardiography, heart rate > 75/min, other valvular or myocardial diseases were excluded. Agatston calcium score (ACS) was calculated for each patient's resting AC-CT images. Total perfusion deficit (TPD) was calculated for stress and resting SPECT images, and ischemic TPD was also calculated (stress TPD - resting TPD). Abnormal SPECT was defined as stress TPD ≥ 5% or ischemic TPD ≥ 3%. Clinical implications of ACS by AC-CT were analyzed in terms of its correlation with TPD and its relationship with myocardial perfusion status against other coronary risk factors. **Results:** Total ACS by AC-CT showed positive correlations with both stress TPD ($r = 0.360$, $p < 0.001$) and resting TPD ($r = 0.369$, $p < 0.001$), but not with ischemic TPD ($r = 0.065$, $p = 0.335$). SPECT was abnormal in 52 (23%) patients and total ACS by AC-CT was significantly higher in patients with abnormal SPECT, as compared to those with normal SPECT (319.3 ± 681.5 vs 121.2 ± 319.3, $p = 0.049$). Multivariate analysis revealed that total ACS ≥ 100 was the only clinical factor related to abnormal SPECT result. **Conclusion:** Higher coronary calcium burden on SPECT/CT was predictive of abnormal myocardial perfusion. **References:** Ghadri JR et al. Coronary Calcium Score as an Adjunct to NuclearMyocardial Perfusion Imaging for Risk StratificationBefore Noncardiac Surgery. J Nucl Med 2012; 53:1-6.

EPS-086

SPECT Myocardial Perfusion Imaging Reveals Increased Myocardial Perfusion Entropy in a Rodent Model of Type 2 Diabetes Prone to Coronary Microvascular Dysfunction

A. Carabelli[1,2], *M. Canu*[2], *A. Fraguas-Rubio*[2], *J. Leenhardt*[3], *A. Broisat*[2], *J. Miranda*[2,4], *G. Vanzetto*[1,2], *D. Fagret*[3,2], *M. Desvignes*[4], *L. Djaileb*[3,2], *C. Ghezzi*[2], *G. Barone-Rochette*[1,2], *L. Riou*[2];
[1]*Grenoble - Alpes University Hospital - Cardiology Dpt, Grenoble, FRANCE,* [2]*INSERM U1039 Radiopharmaceutiques Biocliniques, Grenoble, FRANCE,* [3]*Grenoble - Alpes University Hospital - Nuclear Medicine Dpt, Grenoble, FRANCE,* [4]*GIPSA-lab, UMR CNRS 5216, Grenoble, FRANCE.*

Aim/Introduction: Type 2 diabetes (T2D) is a major risk factor for coronary microvascular dysfunction (CMD). The role of CMD in the occurrence of cardiovascular events (CVE) is increasingly being recognized. However, no noninvasive method is currently available for the routine evaluation of CMD. The anti-diabetic, glucagon-like peptide-1 analog Liraglutide decreases CVE. We hypothesized that enhanced, pixel-by-pixel signal analysis from thallium-201 SPECT myocardial perfusion images (MPI) allowing the quantification of myocardial perfusion entropy (MPE) would allow the assessment of MPE variations related to CMD in a preclinical model of T2D. **Materials and Methods:** Thirty-nine male Sprague-Dawley rats were equally divided into control (CTL), diabetic (T2D) and liraglutide-treated (T2D-LIR) groups. T2D and T2D-LIR animals were fed a high-fat diet and received an intraperitoneal injection of streptozotocin (35 mg/kg) to induce diabetes. T2D-LIR rats were treated with Liraglutide (4 weeks, 300 µg/kg/day subcutaneously). Heart structure and function were assessed with transthoracic doppler echocardiography. CMD was assessed through MPE quantification from thallium-201 stress (dobutamine) SPECT MPI using an original and patented algorithm. **Results:** T2D rats were hyperglycemic as compared with CTL animals (5.5 ± 0.5 g/L vs 1.1 ± 0.3 g/L, $P<0.001$) and had a significantly lower left ventricular (LV) ejection fraction (LVEF) (65 ± 4% vs 74 ± 9%, $P<0.01$), decreased LV shortening fraction (LVSF, 37 ± 3.% vs 46 ± 10%, $P<0.05$), higher indexed LV mass (5.5 ± 1 g/m^2 vs 3.8 ± 0.7 g/m^2, $P<0.001$) and increased LV end diastolic diameter (8.7 ± 0.4 mm vs 7.5 ± 0.6 mm, $P<0.001$). Liraglutide partially restored glycemia (3.9 ± 0.6 g/L, $P<0.05$ vs CTL and T2D) and totally restored LVEF and LVSF (72 ± 7% and 43 ± 4%, P=NS vs CTL). MPE was significantly increased in T2D rats (7.6 ± 0.5 vs 7.1 ± 0.5, $P<0.05$), but was not significantly improved in T2D-LIR rats despite being not significantly different from that of CTL animals (7.4 ± 0.4, P=NS vs CTL & T2D). **Conclusion:** T2D induced by a high-fat diet and a moderate dose of streptozotocin resulted in increased MPE, likely reflecting CMD. Liraglutide did not affect MPE, suggesting that CMD may not be a major target of liraglutide in the present experimental model. The relevance of MPE for the assessment of CMD warrants further clinical investigation. **References:** None.

EPS-087

Prognostic value of myocardial perfusion entropy quantified from SPECT myocardial perfusion images

L. Djaileb[1,2], *A. Seiller*[1,3], *A. Fraguas-Rubio*[1], *J. Leenhardt*[1,2], *A. Martin*[4], *J. Poujol*[1], *A. Broisat*[1], *J. Miranda*[1,3], *G. Vanzetto*[1,4], *D. Fagret*[1,2], *M. Desvignes*[3], *C. Ghezzi*[1], *L. Riou*[1], *G. Barone-Rochette*[1,4];
[1]*INSERM U1039 Radiopharmaceutiques Biocliniques, Grenoble, FRANCE,* [2]*Grenoble - Alpes University Hospital - Nuclear Medicine Dpt, Grenoble, FRANCE,* [3]*GIPSA-lab, UMR CNRS 5216, Grenoble, FRANCE,* [4]*Grenoble - Alpes University Hospital - Cardiology Dpt, Grenoble, FRANCE.*

Aim/Introduction: Single-photon emission computed tomography (SPECT) myocardial perfusion imaging (MPI) for the assessment of myocardial ischemia provides valuable prognostic value. However, the risk stratification of patients with type 2 diabetes mellitus (T2D) remains suboptimal. Recent studies have highlighted the role of coronary microvascular disease in the occurrence of coronary symptoms in this population. We hypothesized that enhanced signal analysis from SPECT myocardial perfusion images may allow insights into the coronary microvascular status. More specifically, we hypothesized that myocardial perfusion entropy (MPE) as a surrogate marker of microvascular disease quantified from SPECT myocardial perfusion images may provide an incremental prognostic value in T2D patients independently

from the routinely performed assessment of myocardial ischemia. **Materials and Methods:** T2D patients with very high cardiovascular risk were studied (n=166, 65±12 years). Ischemia was assessed by SPECT myocardial perfusion imaging (MPI). In addition, SPECT MPI was used for the quantification of rest and stress MPE using an original algorithm providing a global value of MPE from reconstructed rest and stress SPECT images. The primary end point was major adverse cardiac events (MACEs) defined as cardiac death, Q-wave myocardial infarction (MI) and myocardial revascularization >3 months after SPECT. **Results:** 46 patients underwent MACEs over a median follow-up of 4.6 years. Significant differences in stress MPE were observed between patients with and without MACEs (4.19±0.46 vs. 3.93±0.39; p≤.01). By Kaplan-Meier analysis, the risk of MACEs was significantly higher in patients with higher stress MPE (log-rank p≤.01). Stress MPE was significantly associated with the risk of MACEs (hazard ratio: 2.80, p≤.01) after adjustment for clinical and imaging risk factors as identified from preliminary, univariate analysis and including age, hypertension and ischemia. The risk of overfitting was controlled by internal validation procedures such as LASSO, stepwise and random forests selections on time-to-MACEs Cox models. A competing risk event ("other deaths") slightly overestimated Cox estimates. However, the impact of informative censorship as assessed by Fine-Gray subdistribution hazard estimates proved to be marginal. The incremental prognostic value of MPE over clinical risk factors was quantified using nested models showing improved AIC, improved reclassification (global continuous Net Reclassification Improvement [NRI]: 70.1, global Integrated Discrimination Improvement [IDI]: 6.6%), improved discrimination (change in c-statistic : 0.69 vs 0.74), and improved time-dependent AUC (0.71 vs 0.77 at 4 years of follow-up). **Conclusion:** Stress MPE provided independent and incremental prognostic information for the prediction of MACEs in diabetic patients. **References:** None.

EPS-088

Significance of microalbuminuria in predicting silent myocardial ischemia (SMI) in patients with type 2 diabetes using myocardial perfusion imaging

M. Assadi[1], *T. Emami*[1], *Z. Naeimei*[1], *A. Salehifard*[1], *D. Iranpour*[1], *M. Kalantarhormozi*[1], *Z. Azizmohammadi*[2], *E. Jafari*[1];
[1]*Bushehr University of Medical Sciences (BUMS), Bushehr, IRAN, ISLAMIC REPUBLIC OF,* [2]*Shahid Beheshti University of Medical Sciences (BUMS), Tehran, IRAN, ISLAMIC REPUBLIC OF.*

Aim/Introduction: In light of increased risk of cardiovascular events and the poor prognosis of coronary artery disease (CAD) in diabetic versus non-diabetic patients and with respect to the importance of early diagnosis of CAD in this status, the study was aimed to assess the importance of microalbuminuria in predicting silent myocardial ischemia (SMI) in patients with type 2 diabetes using myocardial perfusion imaging . **Materials and Methods:** This study included 120 patients with diabetes type 2, but without previously known CAD or any cardiac symptoms that were stratified into two groups based on presence/absence of microalbuminuria. All participants underwent CAD evaluation using MPS gated SPECT imaging. Other clinical and laboratory indices were also recorded. **Results:** Studied population consisted of 120 patients (84 male 70%; 36 female 30%) with mean age of 9.90± 58.61). In total, asymptomatic ischemia was detected in 78 (65% of the included diabetic patients. Stress induced ischemia was found in 56 patients (87.5%) of Alb^+ group and in 22 patients(39.3%) of Alb^- group. The frequency of stress induced ischemia was 10.81 times higher in the patients with micro albuminuria compared to Alb^- ones(p<0.001 , OR:10.81, 95% CI:4.33-26.99). Likewise , no correlation was found between the presence of stress induced ischemia and therapy type, diabetes duration , history of evident retinopathy , history of hypertension and serum levels of HbA1C (p > 0.05). **Conclusion:** The current study showed that abnormal MPI findings are significantly more common in diabetic patients with microalbuminuria. With respect to low cost and availability of urine albumin detection tests, it might be as a biomarker for prediction of silent myocardial ischemia in diabetic population. **References:** None.

EPS-089

Prognostic value of coronary artery calcium and myocardial perfusion reserve in patients with and without diabetes mellitus

R. Assante[1], *W. Acampa*[1], *E. Zampella*[1], *C. Nappi*[1], *T. Mannarino*[1], *V. Gaudieri*[1], *M. Panico*[2], *V. Cantoni*[1], *R. Green*[1], *M. Petretta*[3], *M. Memmott*[4], *P. Arumugam*[4], *A. Cuocolo*[1];
[1]*Department of Advanced Biomedical Sciences, University Federico II, Naples, ITALY,* [2]*Institute of Biostructure and Bioimaging, National Council of Research, Naples, ITALY,* [3]*Department of Translational Medical Sciences, University Federico II, Naples, ITALY,* [4]*Nuclear Medicine Centre, Manchester University NHS Foundation Trust, Manchester, UNITED KINGDOM.*

Aim/Introduction: We assessed the prognostic value of combined measures of structural abnormalities and coronary vasodilator function by ^{82}Rb PET/CT in diabetic and nondiabetic patients with suspected coronary artery disease (CAD). **Materials and Methods:** A total of 985 patients (251 with and 734 without diabetes mellitus) without overt CAD, referred to ^{82}Rb PET/CT as part of their diagnostic program were studied. CAC score was categorized into two groups (<400 and ≥400). Myocardial perfusion reserve (MPR) was considered reduced when <2. The outcome was a composite end-point of cardiac death, nonfatal myocardial infarction and unstable angina requiring coronary revascularization. **Results:** Follow-up was 93% complete during a mean period of 41±16 months. During follow-up, 59 events occurred (6% cumulative event rate). Event rate was significantly higher in diabetic patients as compared to nondiabetic subjects (P<0.001). In both diabetic and nondiabetic patients event rate significantly increased with increasing of CAC score categories (P<0.05). Similarly, event rate was significantly higher in the presence of impaired MPR in both groups of patients with

and without diabetes (both P<0.05). At multivariable Cox analysis, CAC score ≥400 and impaired MPR were independent predictors of events in both diabetic and nondiabetic patients (both P<0.05). Event free survival was not significantly different between diabetic and nondiabetic patients with impaired MPR and CAC <400 (P=0.26). Differently, event free survival was lower in diabetic patients with impaired MPR and CAC score ≥400 compared to nondiabetic patients (P<0.05). **Conclusion:** In patients with suspected CAD atherosclerosis burden and coronary vascular function were independent predictors of cardiac events in both diabetic and nondiabetic patients. However, in patients with impaired MPR and CAC score ≥400, the presence of diabetes was associated with lower event free survival. **References:** None.

EPS-090

Prospective diagnostic performance of semi-conductor SPECT myocardial perfusion imaging: wall thickening analysis overcomes the lack of prone acquisition

L. Djaileb[1,2], B. Dubois[3], N. de Leiris[1], A. Seiller[1], J. Leenhardt[1], M. Canu[1], A. Broisat[1], G. Vanzetto[1,4], D. Fagret[1,2], M. Desvignes[5], C. Ghezzi[1], L. Riou[1], G. Barone-Rochette[1,4];
[1]INSERM U1039 Radiopharmaceutiques Biocliniques, Grenoble, FRANCE, [2]Grenoble - Alpes University Hospital - Nuclear Medicine Dpt, Grenoble, FRANCE, [3]CH Métropole Savoie, Chambéry, FRANCE, [4]Grenoble - Alpes University Hospital - Cardiology Dpt, Grenoble, FRANCE, [5]GIPSA-lab, UMR CNRS 5216, Grenoble, FRANCE.

Aim/Introduction: The routine acquisition of combined prone and supine SPECT myocardial perfusion images remains limited despite the associated improvement in diagnostic and prognostic accuracies. Our aim was to determine whether the assessment of regional wall thickening (WT) in addition to myocardial perfusion from stress supine acquisitions could overcome the lack of prone acquisition and the corresponding decrease in the diagnostic performances of SPECT myocardial perfusion imaging (MPI) in patients with known or suspected coronary artery disease (CAD). **Materials and Methods:** 41 patients (123 vessels) with known or suspected CAD were prospectively recruited for systematic prone and supine thallium-201 stress SPECT myocardial perfusion imaging using a semi-conductor, cardiac dedicated SPECT camera. The diagnostic performances of SPECT MPI were determined for various image sets including non-gated, supine images (supine NG), non-gated, combined prone and supine acquisitions (prone & supine NG), and gated supine acquisition allowing the evaluation of WT in addition to that of perfusion from NG images (supine NG+WT). Invasive coronary angiography (ICA) and fractional flow reserve (FFR) as the gold standard. Myocardial perfusion was scored using a 5-point scale (0 = normal, 1 = equivocal, 2 = moderate, 3 = severely reduced radiotracer uptake, 4 = no detectable uptake) and a 17-segment model of the left ventricle leading to summed stress score values (SSS). Patients were classified as positive for the presence of ischemia if SSS≥2. Additional WT analysis was used to classify myocardial perfusion as pathological when a myocardial segment with a SSS≥2 also presented with a WT abnormality. Significant CAD was defined by the presence of ≥90% stenosis/occlusion or fractional flow reserve ≤ 0.80 in the presence of a ≥50% coronary stenosis. **Results:** Upon per patient analysis, the occurrence of false positives was significantly higher in supine NG images (36.6%) than in both prone & supine NG and supine NG+WT image sets (9.8% and 7.8%, respectively, p<0.05 vs supine NG) (see Figure). Consequently, specificity decreased from prone & supine NG to supine NG images (86.2% vs. 48.3%, p=0.003) and was restored when using supine NG+WT images (88.5%, p=NS vs prone & supine NG), with no compromise in sensitivity (91.7%, 91.7%, 83.3%, respectively, p=NS for all comparisons). Similar results were observed upon per vessel analysis. **Conclusion:** The diagnostic performances of supine stress SPECT MPI are restored compared with combined prone & supine acquisitions when WT assessment in the ischemic segments is used as an additional diagnostic criterion. **References:** None.

EPS-091

Comparison of the prognostic value of PET and SPECT in patients with coronary artery disease: A meta-analysis

H. Chen, R. Wang, J. Wei, C. Fan;
West China Hospital of Sichuan University, Chengdu, CHINA.

Aim/Introduction: The prognostic value of single-photon emission computed tomography (SPECT) myocardial perfusion imaging (MPI) has been fully evaluated in the past few decades. For now, the positron emission tomography (PET) is widely used clinically. However, whether the prognostic value of PET MPI superior to SPECT MPI is still unknow. We performed a meta-analysis to compare the negative predictive value (NPV) of normal PET MPI and SPECT MPI in patients with known or suspected coronary artery disease (CAD). **Materials and Methods:** Studies published between January 2000 to June 2018 were identified by database search. We included studies using PET or SPECT to evaluate patients with known or suspected CAD and providing data on clinical outcomes with a follow-up time ≥1 year. **Results:** A total of 20 eligible articles (9 PET MPI and 11 SPECT MPI) were finally included, recruiting 16,387 patients in PET and 21,936 patients in SPECT. The negative predictive value (NPV) for hard events (cardiac death and nonfatal myocardial) was 97.53% (95% confidence interval, CI 95.67-98.88) in PET and 97.22% (95% CI 96.14-98.13) in SPECT, resulting in estimated event rate after negative test (ERNT) equal to 2.47% (95% CI 1.12-4.33) and 2.78% (95% CI 1.87-3.86) respectively. The corresponding annualized event rate (AER) after a negative test was 0.73% and 0.63%. **Conclusion:** The negative prognostic value of PET MPI and SPECT MPI for hard events in patients with known or suspected CAD are similar and comparable. Further studies of prognostic value of PET MPI are still needed. **References:** None.

EPS-092

Predictability of Coronary Flow Reserve and Geriatric Nutrition Risk Index for poor prognosis in the Patients with Dialysis dependent End-stage Renal Disease

S. Ohshima[1], *N. Umemoto*[2], *R. Ito*[1], *T. Sakakibara*[1], *H. Hori*[1], *T. Murohara*[3];
[1]*Nagoya Kyoritsu Hospital, Nagoya, JAPAN,* [2]*Ichinomiya Municipal Hospital, Ichinomiya, JAPAN,* [3]*Nagoya University Graduate School of Medicine, Nagoya, JAPAN.*

Aim/Introduction: Ischemic heart disease (IHD) is an important issue to be resolved in the patients with dialysis dependent end-stage renal disease (dd-ESRD). Coronary flow reserve (CFR) measured using ^{13}N-ammonia positron emission tomography (^{13}N-NH_3-PET) myocardial perfusion imaging (MPI) is an established and reliable parameter for detecting coronary artery disease and prediction for cardiovascular event and mortality. On the other hand, it is shown that dd-ESRD patients with malnutrition status have poor prognosis. In previous studies, we reported the relationship between low geriatric nutrition risk index (GNRI) and poor prognosis in the patients with dd-ESRD. In this study, we investigated the predictability of CFR and GNRI in dd-ESRD population. **Materials and Methods:** Consecutive 306 dd-ESRD patients, who were performed ^{13}N-NH_3-PET MPI for suspected IHD, were studied. Patients undergone any revascularization within 60 days after $^{13}NH_3$-PET MPI were excluded in this analysis. Patients were classified into 4 groups according the median value of CFR (1.99) and GNRI (97.73); Low CFR-Low GNRI group (n=77), High CFR-Low GNRI group (n=76), Low CFR-High GNRI group (n=78) and High CFR-High GNRI group (n=75). We followed up to 1,544 days (median 833 days) about all-cause mortality, cardiovascular (CV) mortality and major adverse cardiovascular and cerebrovascular event (MACCE). **Results:** There was no mortality event in High CFR-High GNRI group. Kaplan-Meyer analysis showed that there were statistically differences in each group (all-cause mortality; log rank $p<0.01$, CV mortality; log rank $p=0.02$, MACCE; log rank $p<0.01$). **Conclusion:** Dd-ESRD patients with low CFR and malnutrition status would have poorer prognosis than the patients without them. **References:** None.

EPS-093

Prognostic value of coronary flow reserve in patients with suspected or known coronary artery disease referred to myocardial perfusion imaging by positron emission tomography: a meta-analysis

V. Cantoni, *R. Green, T. Mannarino, R. Assante, V. Gaudieri, E. Zampella, C. Nappi, G. Agliata, M. Petretta, W. Acampa, A. Cuocolo; University Federico II, Naples, ITALY.*

Aim/Introduction: Coronary vascular dysfunction is related to poor cardiovascular prognosis in patients with suspected or known coronary artery disease (CAD). We conducted a meta-analysis to evaluate the prognostic value of coronary flow reserve (CFR) assessed by positron emission tomography (PET) in predicting adverse cardiovascular events in patients with suspected or known CAD. **Materials and Methods:** A search in electronic databases was conducted including PubMed and Embase for studies published in English language until April 2019. The studies were included in the analysis if they evaluated CFR by PET in patients with suspected or known CAD, providing data on adjusted hazard ratio for the occurrence of adverse events. Because of the large heterogeneity experienced and to minimize the effect of confounding, we considered separately the hazard ratio derived from multivariate regression analyses for the occurrence of both hard events, defined as cardiac death and nonfatal myocardial infarction, and all adverse events. Summary risk estimates for impaired CFR by PET were derived in random effect regression analysis and causes of heterogeneity were determined in meta-regression analysis. **Results:** We identified 13 eligible articles including 9,090 patients with suspected or known CAD with a mean follow-up of 3.17±0.55 years. All studies reported the hazard ratio for the occurrence of all adverse events. The pooled hazard ratio was 1.57 (95% confidence interval 1.16-2.11). Among the included publications, five studies reported the hazard ratio for the occurrence of hard events. The pooled hazard ratio was 2.51 (95% confidence interval 1.73-3.64). At meta-regression analysis we found an association between the hazard ratio for all adverse events and clinical variables (family history of CAD and prior myocardial infarction) and between the hazard ratio for hard events and demographic (male gender) and clinical variables (diabetes mellitus, arterial hypertension, and prior coronary revascularization). **Conclusion:** The results of this meta-analysis suggest that in patients with suspected or known CAD an impaired CFR is associated with adverse cardiovascular events. However, the large heterogeneity in study population underlines the need for further investigations to maximize the prognostic role of CFR. **References:** None.

EPS-094

Diagnostic Performance of Attenuation Corrected Myocardial Perfusion Imaging for Coronary Artery Disease: A Meta-analysis of Vessel-based Data

J. Huang[1,2], *C. Huang*[3,2], *R. Yen*[1], *K. Ko*[1], *C. Lu*[1,2], *K. Chien*[3,2], *Y. Wu*[4];
[1]*Department of Nuclear Medicine, National Taiwan University Hospital and National Taiwan University College of Medicine, Taipei, TAIWAN,* [2]*Institute of Epidemiology and Preventive Medicine, College of Public Health, National Taiwan University, Taipei, TAIWAN,* [3]*Department of Internal Medicine, National Taiwan University Hospital and National Taiwan University College of Medicine, Taipei, TAIWAN,* [4]*Department of Nuclear Medicine, and Cardiology Division of Cardiovascular Medical Center, Far Eastern Memorial Hospital, New Taipei City, TAIWAN.*

Aim/Introduction: Myocardial perfusion imaging (MPI) with single photon emission computer tomography (SPECT) is a well-established tool for the diagnosis of coronary artery disease (CAD). Soft tissue attenuation is a common artifact which limits

the diagnostic accuracy of MPI. Attenuation artifacts showed different patterns in the three territories supplied by coronary arteries. The aim of this study was to determine whether and how attenuation correction (AC) improved diagnostic performance of MPI in different coronary artery supplied territories, using coronary angiography as reference standard. **Materials and Methods:** Pubmed and EMBASE were searched until April 2019 for studies evaluating AC MPI for the diagnosis of CAD with vessel-base data. Methodological quality was assessed using the Quality Assessment of Diagnostic Accuracy Studies tool. For each study, the sensitivity, specificity, diagnostic odds ratio and area under summary receiver operating characteristic curve, along with 95% confidence intervals (CIs), were calculated to determine the diagnostic accuracy of AC vs. non-attenuation corrected (NAC) MPI. A bivariate mixed-effect model was applied for pooling the data. **Results:** Out of 332 articles, 21 studies (2,417 patients) were identified including 18 studies with data of CAD at patient-level, 20 studies with data of LAD and RCA ischemia and 19 studies with data of LCX ischemia. Significant improvement of specificity (0.77 versus 0.56 in overall CAD, 0.87 versus 0.59 in RCA) and diagnostic odds ratios (16 versus 8 in overall CAD, 18 versus in RCA) after AC were shown in overall CAD and RCA stenosis. Improvement of area under summary receiver operating characteristic curve were also noted. MPI showed similar diagnostic performance in detecting LAD and LCX stenosis with or without AC. There was a trend of decreased sensitivity after AC, but none were significant. Details of pooled estimates for detecting RCA stenosis were shown in the table. **Conclusion:** The results from this study suggested that attenuation correction should be applied to myocardial perfusion imaging to improve the diagnosis of CAD, especially in detecting RCA stenosis for better specificity. **References:** None.

EPS-095

Comparison between computer-based analysis and expert reading in the interpretation of MPI studies

***G. Angelidis**, V. Valotassiou, S. Alexiou, I. Tsougos, D. Psimadas, C. Tzavara, A. Ziaka, E. Baniora, E. Theodorou, C. Ziangas, A. Tzitzani, M. Kournouti, M. Asproudi, P. Georgoulias;*
University Hospital of Larissa, Larissa, GREECE.

Aim/Introduction: Quantitative parameters are widely used in the interpretation of myocardial perfusion imaging (MPI) studies. We aim to compare the automated measurements of SSS (summed stress score), SRS (summed rest score), and SDS (summed difference score) using Emory Cardiac Toolbox, Myovation, and Quantitative Gated SPECT software, with the expert scoring in patients who underwent coronary angiography. **Materials and Methods:** The sample consisted of 143 patients with mean age 63.9 years, who underwent 99mTc-tetrofosmin gated SPECT studies. Each study was blindly evaluated by two independent observers, and the mean SSS, SRS, and SDS values were recorded. One experienced observer blindly interpreted the coronary angiography studies; a stenosis of the vessel lumen >50% (and/or fractional flow reserve ≤0.80) was considered haemodynamically significant, while the presence of a stenosis in the left mainstem was considered equivalent to a two-vessel disease (angiographic score: 0-3). The concordance of the software packages with the expert reading (mean values) and the angiographic score, was evaluated with the computation of intraclass correlation coefficients (ICCs) and Bland-Altman 95% confidence intervals for limits of agreement. Wilcoxon signed rank test were used to evaluate median differences, and agreement was further analyzed by comparing the categorized by percentiles measures of SSS, SRS and SDS with weighted Kappa coefficients. **Results:** The agreement between the two observers evaluating MPI studies was very good (ICC for interrater agreement >0.8). ICCs between the three software packages and the expert scoring were mainly moderate to good (ICCs range: 0.41-0.8), but poor for SDS (ICCs<0.4). Paired comparisons for SSS, SRS and SDS showed significantly different values for the expert scoring, as compared to the three packages ($p<0.001$). Weighted Kappa coefficients were used to compare the agreement of expert scoring with the packages, after categorizing SSS, SRS and SDS in specific intervals defined by percentiles. For all comparisons Kappa coefficients were low (<0.4), indicating a not acceptable agreement. Furthermore, Bland-Altman 95% confidence intervals for limits of agreement were widely indicating that the average discrepancy between the expert scoring and software was large enough. Correlation coefficients of expert SSS, SRS and SDS with angiographic score were significant and high ($r=0.65$ for SSS, $r=0.68$ for SDS and $r=0.42$ for SRS, $p<0.001$), while the correspondence correlation between the three packages estimates for SSS, SRS and SDS with angiographic score were low ($r<0.3$) **Conclusion:** Expert reading correlated significantly better with angiographic results, in comparison to software packages. **References:** None.

EPS-096

Causative factors of prolonged myocardial ischemic damage shown on hybrid cardiac fatty-acid metabolism SPECT/CT in patients with coronary artery disease after coronary artery bypass grafting

***Y. Fukushima**, Y. Ishii, T. Kiriyama, T. Nitta, S. Kumita;*
Nippon Medical School, Tokyo, JAPAN.

Aim/Introduction: Patients with coronary artery disease (CAD) undergoing coronary artery bypass grafting (CABG) occasionally have prolonged myocardial ischemic damage, shown on cardiac fatty-acid metabolism SPECT using ^{123}I-BMIPP. However, causes of persistent myocardial ischemic damage in this population are unknown. Despite their severe CAD and complicated hemodynamics, hybrid cardiac SPECT/CT can provide comprehensive diagnoses, including myocardial ischemic damage distribution, coronary artery lesion distribution, and their relationship. This study aimed to examine the causative factors of persistent ischemic myocardial damage using hybrid cardiac fatty-acid metabolism SPECT in patients with CAD after CABG. **Materials and Methods:** A total of 192

consecutive patients between April 2016 and March 2019, who underwent cardiac rest-stress perfusion SPECT and fatty-acid metabolism SPECT using Discovery NM 530c after CABG, were included in this study. Among them, 125 patients who received cardiac CT (CCT) using Revolution CT and hybrid cardiac SPECT/CT imaging using CardIQ Fusion were analyzed. On cardiac SPECT, the myocardial accumulation defect diagnoses were determined, and SSS, SRS, SDS, summed BMIPP defect score (SBS), and summed perfusion-metabolism mismatch score (SMS) were quantified using a 17-segment model with a 5-point-grading system. Coronary artery segments, including coronary artery bypass grafts, were assessed on CCT. With hybrid cardiac SPECT/CT images, coronary artery territories were confirmed. Furthermore, the regional difference score (RDS) and regional mismatch score (RMS) in each coronary territory were calculated. Causative factors for myocardial residual perfusion-metabolism mismatch (RPMM) were examined comparing with patients' clinical and imaging findings. Moreover, the relationships between regional coronary artery stenosis, RDS, and RMS were assessed. **Results:** The interval between CABG and cardiac SPECT was 17 ± 44 months. The myocardial segment number with ischemic myocardial damage was 4 ± 3, and SMS was significantly higher than SDS (6 ± 5 vs. 3 ± 3, $p < 0.001$). There was no correlation between SMS and the duration from CABG to cardiac SPECT ($p = 1.000$). The significant causes of RPMM were SDS ($p = 0.007$), previous myocardial infarction ($p = 0.003$), LVEF ($p = 0.023$), and concomitant ischemic cardiomyopathy ($p = 0.049$). RMS was correlated with RDS ($p < 0.001$) but showed no correlation with regional coronary artery stenosis ($p = 1.000$). **Conclusion:** Ischemic myocardial damage, shown by hybrid cardiac fatty-acid metabolism SPECT/CT, is likely to persist for a long period due to several causes, such as residual myocardial ischemia, low LVEF, and comorbid ischemic cardiomyopathy in patients with CAD undergoing CABG. **References:** None.

1011

e-Poster Presentation Session 7 - Do.MoRe: Image Reconstruction & Data Analysis

Monday, October 14, 2019, 16:30 - 18:00 Room 133/134

EPS-097

Value of ultra-high resolution reconstructions in small-lesion detection with FDG-PET

T. J. Gerritse[1,2], *D. Koopman*[1,2], *A. H. J. Oostdijk*[1], *H. Arkies*[1], *P. L. Jager*[1], *C. H. Slump*[2], *J. A. van Dalen*[3];
[1]*Isala, Department of Nuclear Medicine, Zwolle, NETHERLANDS,* [2]*Technical Medicine Centre, Enschede, NETHERLANDS,* [3]*Isala, Department of Medical Physics, Zwolle, NETHERLANDS.*

Aim/Introduction: We know that decreasing the image voxel-size to 2x2x2mm³ in FDG-PET reconstructions improves the image resolution and thereby small lesion detection [1]. The use of 1x1x1 mm³ voxel reconstructions may even further improve small lesion detection. Our aim was to evaluate the value of these ultra-high-resolution (uHR) reconstructions, compared to high-resolution (HR) 2x2x2 mm³ reconstructions, to improve small lesion detection in patients with cancer. **Materials and Methods:** We included 31 consecutive cancer patients who underwent FDG-PET/CT (Vereos, Philips Healthcare) that revealed at least one FDG-avid lesion <6mL. For each FDG-positive lesion SUV_{max}, SUV_{mean} and lesion volume were determined, up to a maximum of 5 lesions per patient, in both HR and uHR images. Furthermore, we determined the noise level in each PET image, defined by the ratio of the standard deviation and mean pixel value in healthy liver tissue. In a qualitative analysis two expert readers performed a blinded side-by-side comparison between HR and uHR images. Based on image contrast, noise, and diagnostic confidence, they stated their preference. In case of disagreement, a third expert reader was consulted to reach consensus per image. **Results:** In total 112 FDG-positive lesions (volumes: 0.1-5.2mL) were included. Using uHR reconstructions, mean lesion volume decreased from 0.70 to 0.47 mL (33%±26%, $p<0.001$) while both the average SUV_{max} and SUV_{mean} increased with 12%±8% ($p<0.001$). The mean noise level increased with 11%±7% ($p<0.001$). Visually, there was no significant preference for either uHR or HR: readers had no preference (4 patients) or only a minor preference for either uHR (15 patients) of HR (12 patients). **Conclusion:** With uHR reconstructions, small lesion detection is less hampered by the partial-volume effect, resulting in higher SUVs and decreased lesion volumes as compared to HR reconstructions. However, noise levels increased as well, cancelling out the effect of enhanced uptake values, as confirmed by a visual analysis by experts. Hence, we expect that the value of uHR image reconstruction in small lesion detection with FDG-PET is limited. **References:** 1. D. Koopman, J. A. Van Dalen, M. C. M. Lagerweij, H. Arkies, J. De Boer, A. H. J. Oostdijk, C. H. Slump, and P. L. Jager, "Improving the Detection of Small Lesions Using a State-of-the-Art Time-of-Flight PET/CT System and Small-Voxel Reconstructions," J. Nucl. Med. Technol., vol. 43, no. 1, pp. 21-27, 2015.

EPS-098

Optimizing Image Reconstruction on Digital PET

E. G. Simons-Winters[1,2], *D. Koopman*[1,2], *P. L. Jager*[1], *C. H. Slump*[2], *J. A. van Dalen*[1];
[1]*Isala, Department of Nuclear Medicine, Zwolle, NETHERLANDS,* [2]*Technical Medicine Centre, University of Twente, Enschede, NETHERLANDS.*

Aim/Introduction: PET imaging with digital photon counting technology is associated with better spatial resolution, however, at the expense of increased noise-levels. We aimed to determine an image reconstruction that provides the best small lesion detectability without unnecessary noise for FDG-PET using a digital PET system. **Materials and Methods:** We performed a phantom study with the NEMA image quality

phantom and micro-phantom (sphere diameters: 4-37 mm) using a digital PET system (Vereos PET/CT, Philips Healthcare). We used 2x2x2 mm³ voxels and compared six different OSEM reconstruction settings (51, 45, 39, 34, 26 and 21 updates (=iterations x subsets)). For every setting, the effect of applying no filter and post-smoothing Gaussian filters of 2 and 4 mm was determined as well. Noise-levels were calculated by dividing the standard deviation to mean pixel value in a background area of the NEMA-phantom. Furthermore, we determined contrast recovery coefficients based on the mean activity (RC_{mean}) and maximum activity (RC_{max}) in all spheres in both phantoms. In the patient study, the reconstruction settings providing the lowest noise-levels without impairing RCs, were tested on FDG-PET scans of patients with breast cancer (n=5) and lung cancer (n=19). We measured SUV_{max} and SUV_{mean} of 81 FDG-avid lesions and noise-levels in the liver. **Results:** In the phantom study, the highest noise was found for 51 updates without filtering. Noise decreased with 14% for 45 updates and 22% for 39 updates ($p<0.01$). RC_{mean} and RC_{max} were similar for those reconstructions ($p>0.12$). By further reducing the number of updates, both noise and RCs decreased, especially for the smaller spheres. For all updates, applying a 2 mm filter resulted in decreasing noise levels (9-19%, $p\leq0.03$) and decreasing RCs (3-4%, $p<0.01$). A 4 mm filter led to a noise reduction of 14-39% ($p\leq0.03$) and a RC decrease of 10-12% ($p<0.01$). Consequently, on patient data we applied 51, 45 and 39 updates without filtering. Noise-level decreased with 6% for 45 updates and with 13% for 39 updates when compared to 51 updates ($p<0.01$). For all lesions (size: 0.1-8.1 mL), SUV_{mean} and SUV_{max} were similar between updates. **Conclusion:** Adequate image quality for a digital PET system using the OSEM reconstruction algorithm requires a limited number of updates. The lowest noise-level without impairing small lesion detectability can be obtained using 2x2x2 mm³ voxels with 3 iterations x 13 subsets (39 updates) without post-smoothing filter. Post-smoothing filtering only results in a reversed effect. **References:** None.

EPS-099

The impact of Q.Clear reconstruction algorithm of ^{18}F-FDG PET on the staging of lymphoma

M. Wyrzykowski[1], *R. Czepczyński*[1,2], *M. Ruchała*[3];
[1]*Dept. of Nuclear Medicine Affidea, Poznan, POLAND,*
[2]*Poznan University of Medical Sciences, Poznań, POLAND,*
[3]*Poznan University of Medical Sciences, Poznan, POLAND.*

Aim/Introduction: Q.Clear is a Bayesian penalized-likelihood reconstruction algorithm for PET that was implemented by GE Healthcare on their new scanners. Q.Clear allows to achieve more effective convergence in images that results in more accurate standardized uptake value (SUV) measurement. Previously Q.Clear has been shown to be superior to ordered subset expectation maximization algorithm (OSEM) in phantom studies, as well as in liver metastates, lung nodules and mediastinal lymph nodes in lung cancer. The aim of the study was to determine whether Q.Clear influences lymphoma staging in comparison to OSEM. **Materials and Methods:** We retrospectively analyzed 70 ^{18}F-FDG PET/CT studies of 33 females and 37 males with the diagnosis of lymphoma, performed between the years 2015-2018. Our group included 34 patients with Hodgkin lymphoma and 36 patients with non-Hodgkin lymphoma. The median age was 46.5 and (range: 6 to 84 years). The routine ^{18}F-FDG PET/CT images were obtained using Discovery IQ scanner (GE Healthcare). The PET scans were reconstructed using two different algorithms with the same normalisation correction factors and with CT-based attenuation correction. Penalisation factor (beta) of 350 was used for Q.Clear reconstruction algorithm. For both algorithms lymphoma staging was performed using modified Ann Arbor 4-stage system. Additionally SUVmax values of mediastinal blood pool (MBPS), liver and lesion with the highest metabolic activity - target lesion were measured and compared. **Results:** Of total 70 PET/CT initial studies, 69 were concordant with regard to the stage. Only in 1 study, the Q.Clear algorithm increased the stage from 1 to 2. The staging difference was not statistically significant ($p=0.31$). In all 70 studies, SUVmax values measured in the target lymphoma lesions were higher when measure with Q.Clear. SUVmax values of MBPS measured with Q.Clear where higher than measured with OSEM in 20/70 and lower - in 26/70 cases. In the remaining 24/70 cases SUVmax values were equal with both algorithms. The SUVmax values of the liver were higher with Q.Clear in 21/70 cases, lower - in 32/70 and equal - in 17/70 cases. **Conclusion:** In spite of the influence of Q.Clear on the SUVmax values of target lesions and reference regions, the use of this reconstruction algorithm has no impact on lymphoma staging. **References:** None.

EPS-100

Feasibility of Ra-224 SPECT/CT imaging in a therapeutic setting —a phantom study

C. Stokke[1,2], *L. Mikalsen*[1], *T. Bønsdorff*[3], *Ø. Bruland*[1,4,3];
[1]*Oslo University Hospital, Oslo, NORWAY,* [2]*Oslo Metropolitan University, Oslo, NORWAY,* [3]*Oncoinvent AS, Oslo, NORWAY,* [4]*University of Oslo, Oslo, NORWAY.*

Aim/Introduction: In preparation for an upcoming clinical trial using Ra-224 in dosages from 1 to 7 MBq, we have evaluated the possibility for direct SPECT/CT imaging of the agent's distribution. The principle emitter of imageable gamma is Pb-212, but other nuclides, including Ra-224 itself, also contribute. There are also high and very high energy photons up to 2615 keV from Tl-208, which scatter in the collimator and patient bed and decrease contrast, making an optimized protocol important. **Materials and Methods:** Using the NEMA IEC PET Body Phantom without the lung insert, the phantom spheres were filled with Ra-224-RaCl dissolved in an EDTA solution. 28 kBq/ml at the time of scan (total activity 1.36 MBq) and no background activity was used. Imaging was performed on a Siemens Symbia Intevo Bold SPECT/CT system using high energy (HE) and medium energy (ME) collimators and a 20 % energy window at 240 keV, with dual 5 % scatter windows, 60 views and a 30 min acquisition

time. Reconstructions were performed using the Flash3d and the Tomo Reconstruction workflow, with 16mm Gaussian post filters and CT-based attenuation correction. Datasets were reconstructed with and without scatter, using 20 mm Gaussian filter on the scatter windows. Reconstructions were performed at 25 different levels; from 5 to 900 iterations x subsets. The visibility of a lesion was defined as having a local maximum. **Results:** The image quality obtained indicate that we can detect accumulations of the agent as low as 14 kBq (activity of smallest sphere). Imaging is possible using both collimators; however, ME was preferable due to a higher degree of visibility of the two smallest spheres. Still, the HE collimator did have greater contrast for the two largest spheres. Scatter correction was found to increase the contrast of the four largest spheres relative to their immediate surroundings, but reduce the visibility of the two smallest spheres. In general, the reconstructions benefited from relatively high numbers of updates, approximately 30 to 100. With the employed level of post filtering, artefacts in the sphere shapes were not observed. **Conclusion:** Imaging of relatively low activities of Ra-224 is feasible. Overall, we recommend the use of the ME collimator on this system. For small uptakes nearby high activity regions, attenuation correction only may be preferable, but in general the combination of attenuation and scatter correction seems to provide higher contrast. (Mikalsen LTG, Bønsdorff T, Bruland ØS, Stokke C.) **References:** None.

EPS-101

Development of a Novel Simulation and Image Reconstruction Toolkit for PET and PG Imaging

M. Safari[1], *A. Zoglauer*[2], *G. Lovatti*[1], *V. Anagnostatou*[1], *M. Nitta*[1], *H. Tashima*[3], *P. Thirolf*[1], *T. Yamaya*[3], *K. Parodi*[1];
[1]*Ludwig-Maximilians-Universität München, Munich, GERMANY,* [2]*Space Sciences Laboratory, University of California, Berkeley, CA, UNITED STATES OF AMERICA,* [3]*National Institute of Radiological Science, National Institutes for Quantum and Radiological Science and Technology (QST), Chiba, JAPAN.*

Aim/Introduction: Positron emission tomography (PET) imaging of the beta+-activity induced during ion beam therapy is one of the most clinically investigated methods for 3D in-vivo ion range verification. Along with the rapid improvements in the capabilities of detectors and in-beam PET systems, the necessity of using more reliable simulation software with dedicated analysis tools for spatial reconstruction of the PET-like positron-annihilation radiation and prompt gamma-ray (PG) emission is becoming more important. In this study the Medium-Energy Gamma-ray Astronomy library (MEGAlib) has been further developed in order to use this toolkit as a standard simulation and image reconstruction framework for PET imaging in addition to its established features for PG imaging. **Materials and Methods:** The MEGAlib software was equipped with the Toolkit for Multivariate Analysis (TMVA), which provides a ROOT-integrated machine-learning environment for a better and more accurate classification of various event types (Compton scattering, PET, and others).The uncertainty of the reconstructed PET image was improved by applying an analytic correction in the reconstruction of each line of response (LOR) based on the time-of-flight (TOF) information, along with attenuation and scattering probabilities.The PET scanner geometry used in this study resembled the PET component of the Whole Gamma Imaging (WGI) detector from NIRS-QST (16x16x4-DOI array of 2.8x2.8x7.5mm^{3}GSO, in four rings with 66cm diameter). A spherical PMMA phantom with 5cm radius was used in this work. The performance of the MEGAlib in the reconstruction of PET events was investigated by considering the accuracy of the TMVA machine-learning algorithm and performance of TOF and attenuation-scattering corrections. **Results:** The accuracy of the TMVA machine learning has been found to be 90%. Implementation of the TOF information into the PET image reconstruction could improve the signal-to-noise ratio (SNR) of the PET images up to 88% for a coincidence time resolution of 500ps. Comparing the detected PET photons of a point positron source positioned inside a PMMA phantom and air at the center of the PET scanner revealed that using the attenuation-scattering corrections could significantly improve the signal lost inside the PMMA phantom by up to 64%. **Conclusion:** This study showed that the upgraded MEGAlib software could be used as a promising simulation and image reconstruction framework for PET imaging, which in combination with its proven capabilities in the context of Compton imaging makes it a valuable toolkit to facilitate research projects for PET, PG imaging, and novel hybrid detection schemes in ion therapy monitoring. **References:** None.

EPS-102

Impact of reconstruction settings and respiratory motion correction strategies on image quality and quantitation with ^{68}Ga in phantom studies

T. Q. Christensen[1], *P. Braad*[2];
[1]*Department of Clinical Engineering, Region of Southern Denmark, Esbjerg, DENMARK,* [2]*Department of Nuclear Medicine, Odense University Hospital, Odense, DENMARK.*

Aim/Introduction: Respiratory motion causes blurring in PET/CT and inaccurate quantitative values. Neuroendocrine tumors (NETs) are often detected in the lung and liver, areas with a high degree of respiratory motion. Diagnosis of NETs are frequently done with ^{68}Ga-radiopharmaceuticals. We designed a phantom study to study the impact of reconstruction settings and respiratory motion correction strategies on image quality and quantification in lung and liver lesions in ^{68}Ga-PET. **Materials and Methods:** A NEMA/IEC torso phantom with six fillable spherical inserts with diameters ranging between 10 and 37 mm was filled with a homogeneous aqueous solution of ^{68}Ga and scanned on a GE Discovery MI (GE Healthcare) PET/CT scanner at lesion-to-background ratios (LBRs) of 2.5:1, 5:1 and 10:1. Acquisition times and background concentrations corresponded to typical liver concentrations in clinical ^{68}Ga-DOTATOC PET-scans. Reconstructions were done using block

sequential regularized expectation maximization (BSREM) at penalization values (β) of 300-1000. Contrast recovery (CR), background variability (BV) and contrast-to-noise ratios (CNR) were compared. The impact of respiratory motion correction was studied in the CIRS Dynamic Thorax Phantom with movable spheres of 0.5, 2.5 and 8 ml. PET scans were performed without background activity in lung equivalent tissue and at LBRs of 2.5:1, 5:1, and 10:1 of aqueous ^{68}Ga solutions while spheres were moved with patient-like respiratory motion patterns at amplitudes of 0, 5, and 10 mm respectively. The impact of GE's motion correction methods Q.Static and Q.Freeze on lesion detectability, lesion size, and lesion activity quantification was analyzed. **Results:** With increasing β values a small decrease in CR was seen with an average relative difference from β=300 to β=1000 of -8.1% (-19.2 to -1.9) and a bigger decrease in BV of -32.8% (-46.9 to -18.9) which lead to an improved CNR of 37.5% (19.1 to 69.9). The results were confirmed qualitatively although differences in the images were not apparent at values of 700 and above. The image quality and quantitative accuracy were greatly improved with Q.Freeze at all motion displacements and LBRs. Q.Static showed improvements at the highest motion displacement amplitudes but not significantly at 5 mm and below. **Conclusion:** Optimization of the reconstruction and the use of respiratory motion strategies can improve the image quality and quantitative accuracy of ^{68}Ga PET/CT scans. A high BSREM β value increases image quality at a small expense of quantitative accuracy. Q.Freeze seems favorable in all situations and Q.Static in most. **References:** None.

EPS-103

Optimizing image reconstruction for lesion assessment with I-124 PET

D. Koopman[1,2], *I. M. Spenkelink*[1,2], *P. L. Jager*[1], *H. Arkies*[1], *C. H. Slump*[2], *J. A. van Dalen*[3];
[1]*Isala, Department of Nuclear Medicine, Zwolle, NETHERLANDS,* [2]*Technical Medicine Centre, Enschede, NETHERLANDS,* [3]*Isala, Department of Medical Physics, Zwolle, NETHERLANDS.*

Aim/Introduction: Iodine-124 (I-124) PET/CT scans are performed in follow-up of patients treated for differentiated thyroid carcinoma. For FDG-PET, it has been shown that decreasing the image reconstruction voxel-size from 4x4x4 mm³ to 2x2x2 mm³ improves the image resolution and thereby small lesion detection [1]. It is unknown if small voxel reconstructions are beneficial for I-124 PET as well. Different reconstruction settings may be preferred due to the low-count statistics of I-124 PET. Our aim was to optimize the image reconstruction for lesion assessment with I-124 PET. **Materials and Methods:** We included 10 patients who were treated for thyroid cancer and underwent PET/CT imaging (Ingenuity TF, Philips Healthcare) 24h and 96h after administration of 74 MBq I-124. All patients had thyroid remnants and/or metastases visible on PET. Images were reconstructed 4 times using two voxel-sizes (standard 4x4x4 mm³ and small 2x2x2 mm³) and two relaxation settings (0.5 and 1.0), indicating a smoothing and a non-smoothing filter. Two expert readers visually evaluated the image quality of the 80 reconstructions by ranking the 4 reconstructions per scan. For quantitative assessment, we measured SUV_{max} of the thyroid remnants and signal-to-noise ratio ($SNR=SUV_{max}/\sigma$), where σ was defined by the standard deviation in a background area above the lungs. **Results:** The smooth standard-voxel reconstruction was preferred above the other reconstructions for both the 24h and 96h scans. The quantitative analysis (24h scans) showed that the average SUV_{max} increased from 5.4 (smooth standard-voxel) to 5.8 (non-smooth standard-voxel) to 10.8 (smooth small-voxel) to 11.6 (non-smooth small-voxel) ($p<0.01$). However due to increased noise levels, the average SNR decreased from 76 on smooth small-voxel images to 47, 52 and 46 for the other three reconstructions respectively ($p<0.01$). For the 96h scans we found similar quantitative trends. **Conclusion:** Smooth standard-voxel reconstructions provide the best visual and quantitative assessment of lesions with I-124 PET. For each radiopharmaceutical, evaluation of different reconstruction settings is required for optimized PET imaging. **References:** Koopman D. et al. Improving the detection of small lesions using a state-of-the-art time-of-flight PET/CT system and small-voxel reconstructions. J Nucl Med Technol 2015.

EPS-104

Value of Non-TOF Reconstruction from TOF Compressed Data for High Resolution TOF Scanner

V. Panin;
Siemens Medical Solutions USA, Knoxville, TN, UNITED STATES OF AMERICA.

Aim/Introduction: The new Siemens Biograph Vision PET/CT scanner provides both improved spatial resolution and improved TOF resolution by about 210 ps. Although raw Vision data are significantly increased in size, good TOF resolution allows their substantial compression in the azimuthal and polar angle dimensions without a loss of spatial resolution. While the so-called histo-projection format was developed solely for TOF reconstruction, pseudo non-TOF reconstruction from these data is still possible. TOF reconstructions are very sensitive to the time calibration errors. We developed a non-TOF reconstruction, which is unaffected by the time calibrations, as a tool used in the object-based timing calibration approach to obtain accurate time alignment in high performance, high time resolution PET scanners. **Materials and Methods:** TOF compressed data are additionally compressed over the TOF dimension to generate pseudo non-TOF data. Since correction factors are TOF dependent, non-TOF reconstruction will require modification of the update equation in the commonly-used OSEM algorithm, which stays TOF intrinsically. In the analytical 3D DIFT algorithm, convergence into the non-TOF format is performed in the Fourier domain by using only part of the available data. The NEMA IQ phantom and its various degree, post-smoothed reconstructions were used in construction of the smallest sphere (10 mm diameter)-to-background value ratio versus background variability trade-off curve. Additionally,

uniform cylinder data were produced with detector timing residual offsets of about 40ps when an approximate time calibration procedure was used and with the most exact time alignment procedure. **Results:** At the same noise level, small sphere recovery was reduced by more than 10% in non-TOF analytical reconstruction. A relatively small misalignment produces detectable bias in the TOF uniform cylinder reconstructed image, in the form of image non-uniformity of more than five percent. Both iterative and analytical algorithm non-TOF reconstructions from the same cylinder data do not reproduce this TOF image non-uniformity. This property can be used to correct time offsets during the scanner time calibration, and allows for accurate time calibration. **Conclusion:** Pseudo non-TOF reconstruction from TOF compressed data is inferior to TOF reconstruction in bias noise trade-off, but it is insensitive to the time alignment imperfections. **References:** None.

EPS-105

Detectability of small objects in positron emission tomography/ computed tomography images with Bayesian penalized likelihood reconstruction

M. Macnab[1], *T. J. Biggans*[2], *F. I. Mckiddie*[1], *M. I. Pether*[1], *J. B. Straiton*[1], *R. T. Staff*[1];
[1]*NHS Grampian, Aberdeen, UNITED KINGDOM,*
[2]*NHS Tayside, Dundee, UNITED KINGDOM.*

Aim/Introduction: This study investigated the small lesion (3mm-7mm) visual detection gains brought about by Bayesian penalized likelihood reconstruction (BPLR) (Q.Clear, GE Healthcare) in positron emission tomography/ computed tomography (PET/CT) phantom images when compared to a more conventional high definition attenuation corrected ordered subset maximisation (HDAC OSEM) reconstruction (Vue Point HD, GE Healthcare). **Materials and Methods:** Lesions within a phantom were constructed using insoluble putty, removing the requirement for Perspex walls usually used to separate different compartments. This design eliminated the partial volume effects brought about by these compartmental walls in conventional phantoms. 70 inactive and 93 (^{18}F) active lesions, with diameters of 3mm, 5mm or 7mm were suspended in active backgrounds at varying contrast ratios (2:1 to 32:1) within a NEMA 2012 phantom. PET/CT images were acquired with a GE Discovery 710 and reconstructed using both BPLR with a penalization coefficient of 400 and HDAC OSEM (2 iterations, 24 subsets). Images were presented to three blinded experienced observers, who were asked to identify lesions and assign confidence ratings. These responses were used to create free receiver operator characteristic (FROC) and alternative FROC curves. Image contrast to noise ratio (CNR) for lesions with each reconstruction was found for comparison. **Results:** Moderate visual detection gains were seen for active, 'hot', lesions with BPLR over OSEM. When split by subset, these improvements were significant for 5mm and a lesion to background ratio of 8:1. No significant differences were seen for the identification of inactive, 'cold', lesions of any size. Significantly higher CNR values were found for BPLR compared to HDAC OSEM for active lesions. The significant improvements in CNR with BPLR over OSEM did not consistently accompany improvements in detection. **Conclusion:** BPLR was found to provide superior small 'hot' lesion detection when compared to a more conventional HDAC OSEM approach. No advantages were found for the detection of 'cold' lesions. Collectively these results indicate a superior performance of BPLR over HDAC OSEM. These gains, however, do not appear to be universal for all simple detection tasks. Furthermore, in this case more conventional measures of estimating quality gains, such as CNR, were shown to not directly map onto the performance of these visual tasks. **References:** None.

EPS-106

NEMA NU 2-2007 Measurements and GATE Monte Carlo Simulations of GE Signa integrated PET/MR for Pure and Non-Pure Positron Emitters

P. R. R. V. Caribe[1], *M. Koole*[2], *A. Diogo*[3], *Y. D'Asseler*[1], *T. Deller*[4], *S. Vandenberghe*[1];
[1]*Medical Imaging and Signal Processing – MEDISIP Ghent University, Ghent, BELGIUM,* [2]*Division of Nuclear Medicine and Molecular Imaging – UZ/KU Leuven, Leuven, BELGIUM,* [3]*Faculty of Sciences of the University of Lisbon, Lisbon, PORTUGAL,* [4]*GE Healthcare, Waukesha, WI, UNITED STATES OF AMERICA.*

Aim/Introduction: NEMA characterization of PET systems is generally done with ^{18}F. However, other PET isotopes such as ^{68}Ga and ^{90}Y are gaining clinical importance as they are of specific interest for oncological applications and for follow up of radionuclide therapy. However, the physical properties of these PET isotopes are quite different and there may be a larger interference with the magnetic field of the MR compared to ^{18}F. Therefore, it is relevant to determine the performance of PET/MR for those clinically relevant and commercially isotopes. **Materials and Methods:** The aim was divided into two parts: (1) NEMA NU 2-2007 tests were performed for characterizing the spatial resolution (SR), sensitivity, image quality (IQ) and NECR for ^{18}F, ^{68}Ga, and ^{90}Y. NECR was performed using ^{18}F and ^{68}Ga. (2) Modelling of a realistic GATE Monte-Carlo model of the GE Signa PET/MR to investigate the Sensitivity, NECR and the effect of the 3T MR field on positron range using ^{18}F, ^{11}C,^{15}O, ^{13}N, ^{68}Ga and 82Rb. These simulated results were compared with the NEMA measurements. **Results:** NEMA tests for ^{18}F, ^{68}Ga and ^{90}Y resulted in substantially different system characteristics. The SR is about 1mm larger in the axial direction (compared to^{18}F). The impact of this lower resolution is also visible in the recovery coefficients of the smallest spheres of ^{68}Ga in IQ tests, where clearly lower values are obtained compared to ^{18}F. The differences in sensitivity are due to the scale factor from the positron emission fraction of the isotopes. The peak NECR was lower than for 18F and appears at higher activities. The peak NECR were: 216.8, 217.6, 212.0, 216.4, 207.1 and 173.5 kcps for ^{18}F, ^{11}C, ^{15}O, ^{13}N, ^{68}Ga and ^{82}Rb respectively. The positron range is a tissue-dependent and reduces in the x/y-direction by a factor

3-4 when compared to z-direction for the higher positron energy emitters. Comparing to the measurements, the detectability of this transversal reduction was affected by the spatial resolution of the system. **Conclusion:** The system performance of GE Signa integrated PET/MR was substantially different, in terms of NEMA SR, IQ and NECR for ^{68}Ga compared to ^{18}F. For ^{90}Y the resolution is comparable to ^{68}Ga and the low number of counts leads to a large variability in the IQ measurements. The transversal direction is significantly affected by the 3T MR field and the spatial resolution of the system is limited to detect this reduction. **References:** None.

EPS-107

Relying on deep convolutional neural networks on PET/CT images for stage II and III non-small cell lung cancer outcome prediction

M. Ibrahim[1], *D. Visvikis*[1], *C. Cheze Le Rest*[2], *M. Hatt*[1];
[1]*Laboratory of Medical Information Processing, Brest, FRANCE,* [2]*CHU Mllitaire, Poitiers, FRANCE.*

Aim/Introduction: To design a deep convolutional neural network based workflow for non-small cell lung cancer (NSCLC) outcome fully automated prediction, i.e. without the need for tumor segmentation, as is usually required for radiomic analyses. **Materials and Methods:** Several modified versions of 3D deep convolutional neural networks (CNN, e.g., C3D and Inception) were evaluated using computed tomography (CT) images as input. The proposed workflow is divided into two modules. The first consists of a primary tumor detector relying on a 3D CNN trained on two publicly available datasets of CT scans (1397 and 888 patients) with or without lung nodules/tumors (not necessarily NSCLC). This CNN was also trained to classify the detected lesion as normal or cancerous. This trained tumor detector was then evaluated in 3 different cohorts of patients with NSCLC (110, 422 and 61 patients). The goal is to feed only the image region containing the primary tumor to a second CNN trained specifically for outcome prediction. We assumed that training would be more efficient if the CNN can focus on the primary tumor only instead of the whole image. Two different methods were compared to design this second module: first, a modified version of the 3D CNN used in the first module (detector) with transfer learning using the tumor region as input. Second, we created 8×8 tiles where each tile has the size of 64×64 pixels as 2D input representing the entire 3D region containing the tumor as a training data and ability to classify patients below or above the median overall survival in the three NSCLC cohorts was evaluated. **Results:** The accuracy of the trained CNN for differentiating normal from cancerous nodule in the two lung CT scans datasets was 86%. It was able to correctly detect the primary tumor in 70% of patients, detected only partial areas of the tumor in 30% of patients and failed for the remaining 10% patients. The best accuracy for outcome prediction for patients with tumor correctly detected by the first module was 70% using 2D networks. **Conclusion:** The availability of large datasets is usually a crucial requirement for efficient training of CNN. Our work shows that by relying on a two-step approach these requirements can be in part alleviated. Further experiments are ongoing to improve the accuracy of the prediction as well the tumor detection with the addition of the PET component in case of PET/CT scans. **References:** None.

EPS-108

Fuzzy Radiomics: A novel approach to minimizing the effects of target delineation on radiomic models for PET

L. Papp[1], *I. Rausch*[1], *M. Hacker*[2], *T. Beyer*[1];
[1]*QIMP team, Center for Medical Physics and Biomedical Engineering, Medical University of Vienna, Vienna, AUSTRIA,* [2]*Division of Nuclear Medicine, Medical University of Vienna, Vienna, AUSTRIA.*

Aim/Introduction: In-vivo characterization of tumours with radiomic features from Positron Emission Tomography (PET) imaging is currently of great interest to clinical researchers. However, the different lesion delineation approaches significantly affect radiomic models. Here, we seek to integrate fuzzy logics into the process of radiomics feature extraction in order to address uncertainties arising from variations in lesion delineation. **Materials and Methods:** PET images from NEMA IQ studies performed on 13 PET/CT systems [1] were included. In each PET the largest sphere (d=37mm) was delineated with two automated approaches to generate 3-dimensional binary volumes-of-interest (VOI) masks: the first method built on dichotomized fuzzy clustering (DFC), while the second method employed gradient maximization (GM) to identify optimal boundaries of lesions. In addition, a third approach, a fuzzy delineation (FD) was executed, which provided a non-binary probability VOI mask over the largest sphere. Thirteen radiomic features with <20% multi-centric variations [2] were extracted from the DFC, GM and FD VOI masks in each of the 13 PET images. The binary VOI masks were used for classic radiomics calculations that considered binary membership of voxels, while the fuzzy VOI mask was used for modified radiomics calculations, handling non-binary probability membership voxel values. Coefficients-of-variation (CoV) were calculated for each feature and delineation method across the 13 PET. Finally, the mean of the feature CoVs across features was calculated to describe the average multi-centric variation of each delineation method. **Results:** The mean CoV across all features of the fuzzy mask (FD) was 21%, compared to 37% (DFC) and 63% (GM). **Conclusion:** Fuzzy radiomics appears to be a promising approach to minimize variations of radiomic features in a multi-centric environment compared to the selected binary delineation methods, thus, supporting efforts towards reproducible quantitative radiomics in large data cohorts. **References:** 1. Rausch I., et al; Variation of system performance, quality control standards and adherence to international FDG-PET/CT imaging guidelines. A national survey of PET/CT operations in Austria. Nuklearmedizin 2014;53(6):242-248 2. Papp L., et al: Optimized feature extraction for radiomics analysis of 18F-FDG-PET imaging. JNM 2018, 10.2967/jnumed.118.217612.

EPS-109

Towards automated whole-body MTV/TLG calculation using artificial intelligence uptake classification

C. Von Gall, D. Thomas, L. Sibille, V. Shah, B. Spottiswoode; Siemens Medical Solutions USA Inc, Knoxville, TN, UNITED STATES OF AMERICA.

Aim/Introduction: Whole-body Total Lesion Glycolysis [TLG] and metabolic tumor volume [MTV]-based therapy assessments using Fluorodeoxyglucose [18F-FDG] are gaining clinical interest. However, such measurements are tedious to perform in cases with a large number of findings. The aim of this work was to investigate workflow improvements offered by an Artificial Intelligence (AI) algorithm which classifies uptake in 18F-FDG PET/CT scans. **Materials and Methods:** An existing convolutional neural network [CNN] trained to classify uptake in PET/CT as physiological or non-physiological [1] was augmented with ~120,000 physiological findings generated by applying multiple SUV thresholds. The training data was limited to lung cancer and lymphoma patients scanned with 18F-FDG on two scanner types. This study evaluates the refined CNN on 181 independent PET/CT datasets (not used for training or testing the AI algorithm) consisting of lung cancer, lymphoma, melanoma, colorectal and other cancer types [27.1%, 26%, 9.4%, 4%, 24.3%]. In 9.4% the underlying disease was not available. Data was acquired on Biograph TruePoint, mCT, Horizon and Vision PET/CT scanner generations (4%, 19%, 57%, 20%)(Siemens Medical Solutions USA, Inc.) Findings were identified using PERCIST recommendations (SUVpeak>1.5*liverSUVmean+2SDs) and segmented using 42% of SUVmax. All findings were reviewed by two experienced nuclear medicine physicians [CvG, DT], who were blinded to the disease type and patient history. If required, additional seed-point-based segmentations were added manually. All findings were classified by the CNN, and manually corrected if necessary. Analysis was performed for findings where both readers agreed, and workflow improvements were assessed by the number of manually added findings and classification corrections. **Results:** A total of 5744 findings were identified resulting in an average of 31.7±27.5 (mean±stdev) total findings per patient of which 5.7±11.8 were non-physiological. Manually added findings and characterization changes per patient were 0.4±1.2 and 0.4±1.0, respectively. **Conclusion:** AI assisted PET/CT analysis can optimize complex workflows to facilitate whole-body MTV/TLG measurements. This approach enables whole body MTV/TLG to be calculated with an average of 0.8 clicks per patient compared to creating 5.7 manual segmentations, an 86% reduction in manual clicks.However, interobserver disagreement may bias the workflow impact and additional sub-analysis is warranted to confirm the overall improvements. **References:** 1.Sibille et al. PET Uptake Classification in Lymphoma and Lung Cancer using Deep Learning, Proc. SNMMI, Philadelphia, (2018)2. Wahl, R. et al. From RECIST to PERCIST: Evolving Considerations for PET Response Criteria in Solid Tumors. J Nucl Med 50, 122S-150S (2009).

EPS-110

A Deep Learning Model to Predict a Classification of Tc-99m ECD SPECT of the Brain by Using Different Pre-trained Models

*Z. Lin[1], F. P. Tseng[1], **Y. C. Ni**[1], P. Y. Chiu[2], G. U. Hung[3], M. C. Pai[4]; [1]Institute of Nuclear Energy Research, Taoyuan, TAIWAN, [2]Show Chwan Memorial Hospital, Changhua, TAIWAN, [3]Chang Bing Show Chwan Memorial Hospital, Changhua, TAIWAN, [4]National Cheng Kung University, Tainan, TAIWAN.*

Aim/Introduction: To develop an aggregation algorithm that predicts the classification of Alzheimer disease (AD) and normal cognition at Tc-99m ECD SPECT of the brain by using small dataset and different pre-trained models. **Materials and Methods:** In Taiwan, dementia population was about 270,000 people at the end of 2017, with a prevalence of about 8 percent. There is an ongoing program to collect Tc-99m ECD SPECT images from AD, DLB, VaD and age-various control subjects. First in order to neglect the deviation between different centers, the images in this study were chosen from one hospital. The images of 53 AD patients and 32 healthy people (from 2014 to 2019) were collected. Final clinical diagnosis was recorded. The pre-trained models including InceptionV3, Xception, DenseNet121, ResNet50 and VGG16 and were fine-trained on 93 % of the dataset and tested on the remaining 7%. After each model has been fine-trained, final predictions were based on the aggregated testing results of the fine-trained models and analyzed with F1 score for performance evaluation. **Results:** The F1 scores were 0.67, 0.57, 0.86, 0.86 and 0.8 for InceptionV3, Xception, DenseNet121, ResNet50 and VGG16 respectively. And the F1 score of the aggregation algorithm is 0.86. The F1 score of the aggregation algorithm was highest as the one of ResNet50 and VGG16. **Conclusion:** By using limited data from Tc-99m ECD SPECT of the brain, different models of architecture with fine-training achieved various performance results. However, the aggregation algorithm achieved better results and avoided worse performance from choosing a model improperly. **References:** None.

EPS-111

Integrating respiratory gating into PET/CT and PET/MR: evaluating an improved clinical workflow

***E. Solari**, C. Kruschke, S. Schachoff, B. Bogdanovic, A. Winter, M. Mustafa, W. Weber, S. G. Nekolla; Klinik der Nuklearmedizin, Klinikum rechts der Isar, TUM, München, GERMANY.*

Aim/Introduction: Respiratory motion correction (RMC) is available on PET/CT and PET/MR systems to improve diagnostic accuracy by reducing motion blurring. However, increased scan times and logistical overhead hinder its widespread clinical use. Therefore, we investigated whether an integration with continuous bed motion (CBM) scanning addresses these limitations for PET/CT, and if similar results could be

achieved with PET/MR that does not allow CBM. **Materials and Methods:** Patients undergoing [18F]-FDG (n=20) and [18F]-PSMA (n=8) PET/CT examinations were scanned with CBM and a respiration monitor belt (RMB). As reference, [18F]-PSMA PET/MR examinations (n=9) were acquired with a long (15 min) single-bed-position pelvis acquisition protocol with RMB. CBM PET scan speed was reduced from 1.1 mm/sec to 0.5 mm/sec during half of the scan area, with 40% duty cycle. For PET/MR, 40% and 50% duty cycle corrections were compared. Complete and expiration phase images were compared using a three-point score (poor, sufficient, good) for signal to noise ratio (SNR) and definition of kidney and lesions. Quantitative comparisons included liver and bladder ROI (5cm radius sphere) SNR, as well as lesion statistics: mean, standard deviation (SD), lesion volume (40% iso-contour VOI). **Results:** We observed reduced scores in overall background SNR (2.4 vs 2.9) but increased visual definition of lesions (2.6 vs 2.1) and kidneys (3.0 vs 2.3). The quantitative analysis confirmed a reduced SNR in liver on RMC images (4.8±2.6 vs 7.8±1.3 for FDG, 5.0±1.2 vs 8.8±1.5 for PSMA). An overall reduction in tumor volume was achieved (ΔVmean[%]= -9.85 ±18.39), most significantly in liver (-26.8±19.7) and lung (-15.8±18.7) lesions, and smaller in abdominal (-6.2±9.8) and prostate (-2.0±4.1) lesions. For PSMA PET/MR studies, most lesions were located in the prostate. The SNR in bladder was smaller on RMC images (40% RMC: 4.5±0.7; 50% RMC: 5.1±0.8; NO RMC: 6.9±1.0), whereas lesion size [%] in prostate was slightly reduced (-0.7±8.7 for 40% RMC, -4.4±11.8 for 50% RMC), similar to the results for PET/CT. **Conclusion:** The combination of respiratory gating and CBM (PET/CT) showed improved lesion definition and significantly altered uptake statistics, especially for thorax lesions. For prostate lesions, both PET/CT and PET/MR protocols showed a small reduction in tumor sizes, with significant SNR loss. Enhanced preparation and examination times need to be put into consideration depending on the scan area, especially for high throughput settings.(This project is funded by European Union's Horizon 2020 research and innovation programme under the Marie Sklodowska-Curie grant agreement No 764458) **References:** None.

EPS-112

Quantitative Characterization Of Tumors In PET: A Comparison Of Three Texture Analysis Software Packages

M. Larobina, R. Solla, R. Megna;
Institute of Biostructure and Bioimaging, National Research Council, Naples, ITALY.

Aim/Introduction: To compare differences in texture feature values computed by three different software packages on ^{18}F-FDG-PET images. **Materials and Methods:** PET images from 15 patients with head and neck cancer were processed with three different freeware software: CGITA version 1.4, LIFEx version 4.6, and Metavol/Ptexture version 20181009. First, for each of the three software, patient's lesions were segmented using the 40% of the SUV_{max}. Second, for each lesion a total of 38 textural features representing the common group of features among all packages, were extracted: 4 conventional: Metabolic Tumor Volume, SUV_{max}, SUV_{mean}, SUV_{std}; 3 histogram-based features: Skewness, Kurtosis, Entropy; 6 grey level co-occurrence matrix (CM) features: Homogeneity^{CM}, Energy^{CM}, Correlation^{CM}, Contrast^{CM}, Entropy^{CM}, Dissimilarity^{CM}; 11 grey level run-length matrix (RLM) features: SRE^{RLM}, LRE^{RLM}, LGRE^{RLM}, HGRE^{RLM}, SRLGE^{RLM}, SRHGE^{RLM}, LRLGE^{RLM}, LRHGE^{RLM}, GLNU^{RLM}, RLNU^{RLM}, RP^{RLM}; 11 grey level size-zone matrix (SZM) features: SZE^{SZM}, LZE^{SZM}, LGZE^{SZM}, HGZE^{SZM}, SZLGE^{SZM}, SZHGE^{SZM}, LZLGE^{SZM}, LZHGE^{SZM}, GLNU^{SZM}, SZNU^{SZM}, ZP^{SZM}, and 3 neighbourhood grey level difference matrix (NDM) features: Coarseness^{NDM}, Contrast^{NDM}, Busyness^{NDM}. Finally, the texture features collected by the three software packages were analysed and compared. To evaluate the agreement among texture features across packages a non-parametric Kruskal-Wallis test was used. Differences in radiomic features between each couple of software packages were assessed using a subsequent Dunn test. Correlation between texture features was assessed via Spearman coefficient (r). The Bonferroni correction for multiple comparisons and a significance level of .05 were used for all the tests. **Results:** Metabolic Tumor Volume, SUV_{max}, SUV_{mean}, and SUV_{std} showed a good agreement across the three software. For the histogram-based features, the agreement was good for Skewness and Kurtosis. For high-order features, a good agreement was found for: Homogeneity^{CM}, Contrast^{CM}, and Dissimilarity^{CM}; HGRE^{RLM}, SRHGE^{RLM}, LRLGE^{RLM}, GLNU^{RLM}, and RLNU^{RLM}; SZE^{SZM}, LZE^{SZM}, HGZE^{SZM}, SZHGE^{SZM}, LZHGE^{SZM}, GLNU^{SZM}, and SZNU^{SZM}; Coarseness^{NDM} and Busyness^{NDM} features. The agreement was better between LIFEx vs. Metavol (95%, 36 features of 38) and worse between CGITA vs. Metavol (63%, 24 features of 38) and CGITA vs. LIFEx (60%, 23 features of 38). All features resulted highly correlated ($r>=0.7$, $p<.001$) in comparing LIFEx vs. Metavol, while 5 of 38 features (13%) were found not in agreement and slightly or not correlated ($r<0.7$, $p<.001$) in comparing CGITA vs. LIFEx, and CGITA vs. Metavol. **Conclusion:** Some texture discrepancies across software packages exist. It could be interesting to further investigate the origin of these differences and how these can affect radiomic analyses conducted using different software packages. **References:** None.

EPS-113

Accuracy of 18F-FDG brain activity quantification on the GE SIGNA PET/MR system with MR derived attenuation correction

P. Braad[1,2], T. L. Andersen[1,2], P. Grupe[1];
[1]Department of Nuclear Medicine, Odense C, DENMARK, [2]Department of Clinical Research, University of Southern Denmark, Odense, DENMARK.

Aim/Introduction: Combined ^{18}F-FDG PET/MR has potentially a large clinical value for the diagnostic work-up of dementia and other neurodegenerative diseases. However, the lack of MR signal from bony structures challenges stable activity quantification and thus, until recently, attenuation correction in clinical studies could only be performed without bone

segmentation. GE Healthcare has recently introduced the Zero Echo Time MR-sequence (ZTE) to extract signals from bones in head scans. Before routine implementation of PET/MR for 18F-FDG brain scans we wanted to compare the quantitative performance of the ZTE attenuation method to conventional PET/CT (CTAC) attenuation correction and the standard PET/MR method without bone segmentation (MRAC). **Materials and Methods:** 10 dementia patients referred for 18F-FDG PET/CT were scanned on PET/CT and subsequently on the GE SIGNA PET/MR system (GE Healthcare) using the same activity injection. PET/MR attenuation correction was performed using MRAC, ZTE and with CT attenuation maps extracted from the PET/CT. PET/MR images were reconstructed with and without time-of-flight (TOF). T1 weighted MR images were registered to a NURBS-based HUman Brain (NHUB) Phantom containing 98 segmented brain regions using the ITK based Elastix toolbox. Calculated transformations were applied on reconstructed PET images. Average ^{18}F-FDG radionuclide activities were calculated in all segmented brain regions for all patients and reconstruction methods. Median patient activities in brain regions were compared to activities in PET/MR images reconstructed with the CTAC method. **Results:** Average ^{18}F-FDG brain activities were 2% lower on images reconstructed with MR-derived attenuation maps compared to the reference images reconstructed with CTAC. With MRAC and ZTE, activity quantification inaccuracy was <5% in the majority of brain regions but as large as 10% in some outer parts of the brain. With ZTE based attenuation correction images appeared more homogenous and the uniformity of activity quantification accuracy in bone-near brain regions and lower parts of the brain was improved. TOF reduced the maximum median brain region activity quantification inaccuracy by 5% and further enhanced image quality, particularly in regions with a high scatter content. **Conclusion:** With ZTE attenuation correction and TOF reconstruction methods, clinical 18F-FDG PET/MR brain studies can be performed with activity quantification inaccuracies of <5%. **References:** None.

1111

e-Poster Presentation Session 8 - Bone & Joint: Bone SPECT/CT - Clinical Imaging Pattern and Quantification Tools

Tuesday, October 15, 2019, 8:00 - 9:30 Room 133/134

EPS-114

The role of SPECT/CT for diagnosis of planatar fascitis and Achilles tendinopathy

I. Hyun, *B. Kim, Y. Kim, M. Lee;*
Inha University Hospital, Incheon, KOREA, REPUBLIC OF.

Aim/Introduction: We evaluated the role of SPECT/CT of foot and ankle in evaluation of heel pain (HP) for diagnosis of plantar fasciitis (PF) and Achilles tendinopathy (AT). **Materials and Methods:** A total of 47 patients with HP were enrolled. Orthopedic clinician made preliminary clinical diagnosis (CD) of HP according to physical examinations and patient's symptom. Provisionally, typical plantar HP was regarded as PF and posterior HP was diagnosed as AT. Patients with atypical pain were categorized into inconclusive group. Radiographs and SPECT/CT of foot and ankle were acquired. On SPECT/CT, plantar uptake of calcaneus in relation to the attachment point of plantar fascia was diagnosed as PF and posterior uptake of the calcaneus in relation to the Achilles tendon was regarded as AT. The results of preliminary CD were compared with visualization of bony activity on SPECT/CT. The radiographic findings of ankle spurs including plantar spur, Haglund's deformity, and Achilles spurs were also compared with presence of bony activity. Additional findings on SPECT/CT were also evaluated. **Results:** Among 47 patients, 26 patients were clinically diagnosed PF in 18 and AT in 8 patients by well-localized typical HP. In these 26 patients with typical HP, preliminary CD matched SPECT/CT in 88% (23/26) of patients. The prevalence of ankle spurs with bony activity was 48% (16/33) of lesions. SPECT/CT showed additional information related to coexistent pathologies in 12% (3/26) of patients (metatarsal bone fracture: 1, osteoarthritis: 1 and idiopathic neuropathy: 1). In 21 patients with atypical HP, SPECT/CT made the diagnosis of PF and AT in 67% (14/21) of patients by visualization of bony uptake in plantar or posterior calcaneus. The prevalence of ankle spurs with bony activity was 35% (6/17) of lesions. SPECT/CT provides additional information related to coexistent pathologies in 33% (7/21) of patients (arthritis: 3, chondrosarcoma: 1, delayed union of fibular fracture: 1, symptomatic accessory navicular bone: 1 and simple bone cyst: 1). **Conclusion:** In typical and atypical heel pain. bony activity of SPECT/CT showed good outcome for diagnosis of PF and AT. Also, it gives information for hidden pathologies of foot and ankle not suspected by clinicians. Therefore, SPECT/CT imaging can improve diagnostic accuracy of PF and AT in patients with HP, and it will enable confident therapeutic planning by showing hidden pathologies with HP, especially in atypical HP. **References:** None.

EPS-115

Bilateral Osteochondritis Dissecans Of The Ankle Joints In A Young Female

I. El Bez, *R. Tulbah, I. Munir, F. Alghamlas, M. Alharbi;*
KFMC, nuclear medicine department, Riyadh, SAUDI ARABIA.

Aim/Introduction: Osteochondritis dissecans (OCD) of bilateral ankles is very rare, with few reported cases of bilateral OCD of both medial part of the talus. We report a case of 25 year old lady, medical student, with bilateral osteochondritis dissecans in ankles; who was diagnosed with plain radiographs, magnetic resonance imaging and triphase bone scan with SPECT-CT. **Materials and Methods:** The patient was a 25 year-old women. She came to the orthopedic clinic of orthopedics Department

in king Fahad Medical City Riyadh, with a complaint of pain and swelling in both ankles for around three months.The pain began insidiously in both ankles, without any history of trauma. It's not improved with non-steroidal anti-inflammatory drugs and worsened after exercise practice. The patient underwent radiographs of the bilateral foot and of the bilateral ankle on anterior, posterior and lateral view radiographs, as well as MRI of the wright foot. Triphase bone scan was performed. The patient received approximately 814 MBq of Technetium-99m MDP intravenously. Limited Flow and blood pool images of the bilateral ankle and foot were immediately performed, as well as delayed spots views and SPECT-CT of the same area. **Results:** The patient underwent radiographs of the bilateral foot and of the bilateral ankle on anterior, posterior and lateral view radiographs, and bilateral osteochondral lesions are noted in the medial talar domes with no radiographic evidence of displaced fragment. MRI of the right foot was requested, which revealed moderate to severe chondropathy involving the medial talar dome articular cartilage suggesting OCD.Limited Flow and blood pool images of the bilateral ankle and foot were immediately performed, as well as delayed spots views and SPECT-CT of the same area. The flow and the blood pool images involving the bilateral ankle and foot demonstrate bilateral symmetrical increased uptake within the ankles. The delayed planar and SPECT-CT images demonstrate significant symmetrical increase activity involving the bilateral medial talar domes. **Conclusion:** In conclusion, we propose that the diagnosis of OCD of bilateral ankles should be kept in mind in young adults with a history of trauma or repetitive microtrauma. For imaging, MRI is usually sufficient. The tri-phase bone scintigraphy is sensitive and specific in determining the mechanical stability of OCD lesions. The addition of SPECT-CT increases the clinical accuracy due to increased contrast resolution and anatomical localization. **References:** None.

EPS-116

Diabetic patients with suspected foot osteomyelitis: new method for evaluating hybrid images SPECT-WBC/MRI based on a score system

*V. Udodov[1], M. Zorkaltsev[1], V. Zavadovskaia[1], **M. Zamyshevskaia**[1], A. Kurazhov[1], E. Grigoriev[2], N. Vegerin[1];*
[1]Siberian State Medical University, Tomsk, RUSSIAN FEDERATION, [2]Cancer Research Institute, Tomsk, RUSSIAN FEDERATION.

Aim/Introduction: The abstract presents the possibilities of the software combined SPECT-WBC/MRI in the detection of osteomyelitis in patients with diabetic foot syndrome. **Materials and Methods:** 80 patients with diabetes type I and II, suspected osteomyelitis were studied (35 (43.7%) males and 45 (56.3%) females, mean age 58.4 ± 12.3 years). The study included patients with neuropathic (n = 27), ischemic (n = 3) and neuroischemic (n = 50) DFS forms. All patients underwent scintigraphy with 99mTc-HMPAO labeled leukocytes (370 MBq; SPECT Philips Brightview) and magnetic resonance imaging (Siemens Magnetom Essenza 1.5T; T1WI, T2WI, PD-FSat). Fusion of SPECT and MRI was performed in the program RView 9.06 (Colin Studholme). **Results:** All patients were divided into two groups: the first group (n = 42) for developing the scoring system, the second group (n = 38) for testing the scoring system. In the first group diagnostic indicators of typical symptoms of osteomyelitis were calculated. The scoring system was based on the positive predictive value. Each symptom has received a certain amount of scores: radiopharmaceutical differential accumulation iqual 1,56 - 4, fistula - 4, bone marrow edema - 3, radiopharmaceutical hyperfixation in one or two foot bones - 3, bone destruction - 2, soft tissue disorganization - 2, soft tissue swelling - 1, tenosynovitis - 1. According to the results of the ROC analysis, the threshold value of the presence of osteomyelitis was obtained with a score of more than 12. This quantitative criterion was extremely highly specific and sensitive (Se = 95.5% Sp = 100.0%). **Conclusion:** The study shows a high diagnostic efficiency of the SPECT / MRI-based scoring system in detection of osteomyelitis in patients with diabetic foot syndrome (sensitivity 95.5% and specificity 100.0%). **References:** None.

EPS-117

Irradiated sciatic pain as an unusual presentation of osteoid osteoma in distal limb bone

***J. Uña**, C. Alvarez Gonzalez, C. Cardenas Negro, A. Allende Riera, F. de Leon Garcia;*
Servicio Canario Salud, Santa Cruz de Tenerife, SPAIN.

Aim/Introduction: We present an atypical case of an adult with classic irradiated right sciatic pain with affectation of L3-S1 roots. It was initially treated as lumbar pain with imaging and neurophysiological evidence that guided it. **Materials and Methods:** After multiple ineffective conservative treatments and two year of evolution, even with worsening of the involvement of the right S1 root, it was decided to track the pelvis with an MRI and later the body with a 99mTc-HMDP bone scintigraphy. An osteoid osteoma was detected on the right tibia on the scan, later confirmed with SPECT-CT and a simple Rx. It was treated by radiofrequency ablation of the nidus and irradiated pain disappeared without further analgesia. **Results:** After reviewing the available scientific literature in Pubmed with the search terms "osteoid osteoma and radicular pain" and "osteoid osteoma and irradiated" we have found articles that refer to the presence of osteomas with irradiated radicular pain in the proximal bones of both extremities. None of the articles that we found referred pain like our patient's with osteoma in distal limb. Osteoid osteomas with pathologic electromiography are described in femur or humerus. Thus to the best of our knowledge this is the first patient described in the literature with osteoid osteoma in distal limb and sciatic type irradiated pain with positive tests describing neural lesions. **Conclusion:** Bone scintigraphy with phosphonates remains a useful test to determine the presence of unsuspected lesions in patients with clinical conditions that do not respond to usual therapy. In addition, the possibility offered by modern gamma cameras to perform hybrid studies facilitates the diagnosis and

location of injuries, making patient management faster and more efficient. **References:** Stoffelen D, Martens M, Renson L, Fabry G. Osteoid osteoma as a cause of knee pain. A review of 10 cases.Acta Orthop Belg. 1992;58(4):395-9. L Kiers, L K Shield, W G Col. Neurological manifestations of osteoid osteoma. Archives of Disease in Childhood 1990; 65: 851-855. Bea Muñoz M, Jiménez Álvarez M., Pérez Vallina J.R., Medina Sánchez M. Osteoid osteoma of the proximal femur preenting as knee pain: A well-known problem difficult to diagnose. Doi: 10.1016/j.anpedi.2009.04.16. Saqtas E, Gokkus K, Aydin AT. Intra-Articular Osteoid Osteoma as a Cause of Anteromedial Knee Pain. Case Rep Orthop. 2017;2017:5846368. doi: 10.1155/2017/5846368. Epub 2017 May 2. Ebrahimzadeh M.H., Ahmadzadeh-Chabock H.,Ebrahimzadeh A.R. Osteoid Osteoma: A Diagnosis for Radicular Pain of Extremities. Orthopedics. November 2009 -Volume 32 · Issue 11.DOI: 10.3928/01477447-20090922-23.

EPS-118

Mazabraud's syndrome a new case report

Z. Jemni[1,2], A. Ezzine[1,2], H. Chekir[3], H. Boudrigua[1], M. Ben Fredj[1,2], S. Mensi[1], T. Dardouri[1], H. Charfi[1], R. Sfar[1], M. Nouira[1,2], K. Chatti[1];
[1]Nuclear medicine department, Sahloul university hospital, Sousse, TUNISIA, [2]LR12ES02, University of Sousse, Faculty of medicine of Sousse, Sousse, TUNISIA, [3]Imaging Department, Sahloul university hospital, Sousse, TUNISIA.

Aim/Introduction: Polyostotic fibrous dysplasia (FD) in association with intramuscular myxomas is a rare condition. Only few case reports are mentioned in the literature and this is known as Mazabraud's syndrome. We present this case report to enlighten the value of radionuclide bone scintigraphy and SPECT/CT in the diagnosis of FD and subsequently in referring to other clinical syndromes. **Materials and Methods:** A 50-year-old female patient was referred to our department in order to underwent a whole-body bone scan for suspicion of skeletal metastases on the basis of osteolytic bone lesions incidentally discovered on a CT-scan. The patient then proceeded directly for SPECT/CT for anatomic location and further evaluation. **Results:** Tc-99m MDP whole body scan showed multiple sites of increased tracer uptake, including the skull and the right facial bones, multiple ribs, pelvis and bones of both lower limbs. The SPECT/CT findings showed expanding, cystic lesions with ground glass density, corresponding to bone scan abnormalities .Overall, it was interpreted as consistent with polymelic subtype of a fibrous dysplasia of the bone. On further examination, the patient was found to have a large sessile tumor of right arm with a separate soft tissue swelling within the biceps muscle, notably asymptomatic, painless on palpation.Blood samples were requested revealing that alkaline phosphatase were greater than four times the upper limit of normal and hormonal tests were correct. The soft tissue tumor on excision and histopathological examination was found to be intramuscular myxoma. The combination of the above two, called Mazabraud's syndrome is being reported. **Conclusion:** Polyostotic (FD) may closely mimic the appearance of bony metastatic disease. Its association with intramuscular myxomas in the Mazaraud's syndrome, should be known and recognized as a benign differential diagnosis of bone metastases to not misguide the clinicians and the patient for further therapeutics and explorations. **References:** None.

EPS-119

Hypertrophic Osteoarthropathy as a warning in bone scintigraphy

L. S. Torres, V. Alves, A. Oliveira, J. Pereira;
Centro Hospitalar Universitário S. João, Porto, PORTUGAL.

Aim/Introduction: Hypertrophic osteoarthropathy (HO) is a syndrome characterized by abnormal proliferation of the skin and periosteum mainly at the extremities. Clinical and imaging features include digital clubbing, periostosis of tubular bones, and synovial effusions. Secondary HO is associated with lung cancer, other pulmonary disorders, and several other conditions. In this study, we aim to review the findings and value of bone scintigraphy for this syndrome, while also assessing its possible causes. **Materials and Methods:** After retrospective review of our patient database from April 2009 to April 2019, bone scintigraphies reported as demonstrating or possibly demonstrating HO were selected. A diagnosis of HO was considered in patients with a scintigraphic pattern of diffusely increased uptake along the cortical margins of long bones. Every bone scintigraphy was performed with an acquisition of anterior and posterior static images, taken 3-4h after i.v. injection of approximately 925 MBq of ^{99m}Tc-HDP. **Results:** 51 patients met the inclusion criteria for HO on bone scan. All 51 patients showed higher activity of ^{99m}Tc-HDP in the lower limbs (3 only in the femur and 1 only in the tibia), 21 (41%) also in the upper limbs (9 only in the humerus, 2 only in the radio/ulna) and 1 (2%) in the clavicles. In 7 (14%) of the patients, ^{99m}Tc-HDP uptake in the affected bones was asymmetrical. 40 patients (78%) had diagnosed lung carcinoma, and 7 (14%) others had known conditions associated with HO, namely lung metastasis (n=3), other pulmonary disorders (n=3; COPD, tuberculosis, interstitial pulmonary disease) and colorectal cancer (n=1). Of the 4 patients with no apparent cause for HO at the time of the bone scan, 1 patient was afterwards diagnosed with lung metastasis due to breast cancer, 1 patient is still in staging for breast cancer, and only 2 remain with no likely cause for HO (breast and prostate carcinomas with no known metastasis). **Conclusion:** As described in previous literature, HO affects mainly the lower limbs, is usually, though not always, symmetrical in its presentation, and remains highly linked to malignancy. Due to its easily recognizable pattern, bone scintigraphy remains a simple and powerful tool to help in the detection of HO, and can serve as a warning sign for an underlying causal condition, be it malignant or benign, pulmonary or otherwise. **References:** None.

EPS-120

Comparison of conventional MDP bone scan and Somatostatin Receptor PET CT in detection of active Rheumatoid Arthritis

S. Shamim, A. Behra, R. Gupta, G. Arora, S. Datta Gupta, C. Bal; All India Institute of Medical Sciences, Delhi, INDIA.

Aim/Introduction: Rheumatoid arthritis (RA) despite various available treatment options is considered an incurable disease. The treatment is predominantly composed of drugs for symptomatic relief and a class of drugs known as disease modifying anti-rheumatic drugs (DMARDs). Despite these available treatment options, some patients are not able to achieve satisfactory clinical results and some patients are outright refractory to all available treatment options. Such patients may require modification of treatment protocols and new treatment options. Recently, few studies have reported radiotracer uptake of somatostatin receptor (SSR) analogues in chronic inflammatory sites including active RA [1,2]. SSR targeted imaging may provide a novel method for RA evaluation. This study thus aims to investigate the potential utility of SSR PET imaging in RA as compared to ^{99m}Tc-MDP bone scan, which is already an established modality for detection of active joint inflammation. **Materials and Methods:** Nineteen patients (>18years) with clinical diagnosis of RA were included in the study. The patients underwent skeletal scintigraphy and ^{68}Ga-DOTANOC PET/CT. 3-phase bone scan was done post-intravenous (i.v.) injection of 20mCi ^{99m}Tc-MDP. ^{68}Ga-DOTANOC PET/CT was acquired from head to toe, 30 min post-i.v. injection of 2mCi ^{68}Ga-DOTANOC. Both bone and PET/CT scan images were visually assessed independently by two experienced nuclear medicine physicians. **Results:** Nineteen patients (16 female; 3 male) of clinically proven RA, with mean age of 41.9 ± 12 years were included in the study. In 19 patients, 196 joints were clinically positive. Of these 196 joints, 157 joints (80%) were positive on Tc-99m MDP scan and 151 joints (77%) were positive on ^{68}Ga-DOTANOC scan. The difference in the detection efficiency between ^{99m}Tc-MDP and ^{68}Ga-DOTANOC scan was found to be insignificant ($p < 0.7$). **Conclusion:** From this study of comparative evaluation of conventional ^{99m}Tc-MDP bone scan and SSR PET/CT in articular manifestation of RA**,** we conclude that ^{68}Ga-DOTANOC and MDP bone scan are equally efficient in the detection of RA with an added advantage of therapeutic potential with ^{68}Ga-DOTANOC. However, further evaluation with larger sample size is warranted. **References:** 1. Vanhagen PM, Markusse HM, Lamberts SW, Kwekkeboom DJ, Reubi JC, Krenning EP. Somatostatin receptor imaging. The presence of somatostatin receptors in rheumatoid arthritis. Arthritis Rheum. 1994; 37(10):1521-1527 2. Anzola-Fuentes LK, Chianelli M, Galli F, Glaudemans AWJM, Martin Martin L, Todino V, et al. Somatostatin receptor scintigraphy in patients with rheumatoid arthritis and secondary Sjögren's syndrome treated with Infliximab: a pilot study. EJNMMI Res. 2016; 6(1):49.

EPS-121

Assessment of instablity in thoracolumbar burst fractures using bone scintigraphy

M. Seo[1], J. Choi[2], J. Kim[3], S. Park[3]; [1]Ulsan University Hospital, Ulsan, KOREA, REPUBLIC OF, [2]Dongkang Medical Center, Ulsan, KOREA, REPUBLIC OF, [3]Ulsan University Hospital, University of Ulsan College of Medicine, Ulsan, KOREA, REPUBLIC OF.

Aim/Introduction: Unstable thoracolumbar burst fractures (TLBF) require surgical management because they may result in varying degrees of neurologic deficit, especially when the Thoracolumbar Injury Classification and Severity (TLICS) score is over 4. The aim of this study was to evaluate whether a bone scintigraphy using a proposed scoring system can accurately assess instability in TLBF. **Materials and Methods:** Among TLBF patients who underwent bone scintigraphy between January 2015 and August 2017, 52 patients who underwent imaging work-up {bone scintigraphy and magnetic resonance imaging (MRI)} before operation were chosen for analysis. Instability of TLBF was determined by clinical and imaging assessments. The TLICS score was also determined. Bone scintigraphy was visually evaluated with a proposed scoring system {S_T (total score) = S_B (body score, 5 points) + S_P (spinous process score, 2 points)}. Diagnostic performance of the scoring system in assessing instability of TLBF was assessed. **Results:** Among 52 TLBF, 34 (65.4%) were unstable fractures and 31 (59.6%) had TLICS score > 4. $S_T \geq 4$ was an optimal cut-off for assessing instability after receiver operating characteristic curve analysis. The diagnostic performance of the proposed scoring system ($S_T \geq 4$) for assessing unstable TLBF were as follows; sensitivity 61.8%, specificity 94.4%, positive predictive value (PPV) 95.5%, and negative predictive value (NPV) 56.7%. Diagnostic performance of $S_T \geq 4$ for assessing lesions with TLICS score > 4 were as follows; sensitivity 58.1%, specificity 81.0%, PPV 81.8%, and NPV 56.7%. **Conclusion:** Bone scintigraphy using the proposed scoring system shows high specificity and PPV for detecting TLBF that are unstable or have TLICS score > 4. This scoring system may be of use in deciding surgical management of TLBF. **References:** None.

EPS-122

Tc-99m-DPD xSPECT Bone Scan Quantification of Subchondral Bone Uptake: An Updated Analysis in Osteoarthritic Knee Assessment

M. Jreige, N. Schaefer, P. Omoumi, J. O. Prior, M. Nicod-Lalonde; Lausanne University Hospital, Lausanne, SWITZERLAND.

Aim/Introduction: Bone scintigraphy with Tc-99m labeled DPD can identify osteoblastic reactions within the spectrum of osteoarthritic (OA) bone changes with a high sensitivity, especially at the knee level. The aim of this study was to investigate the emerging role of Tc-99m DPD absolute uptake quantification with xSPECT/CT in normal and osteoarthritic

tibial and patellar subchondral bone and to correlate obtained SUV to CT density using Hounsfield units (HU). **Materials and Methods:** We retrospectively assessed 14 patients (mean age 50±15 years) with no/minimal knee OA and 18 patients (aged 62±11y) with advanced knee OA and contralateral total knee replacement. Quantitative xSPECT/CT (Symbia Intevo, Siemens Healthineers, Erlangen, Germany) was acquired and SUV quantified on post-processed images using SUVmax, SUVmean (g/mL) in tibial and patellar subchondral bone. HU of the same regions of interest were measured on CT. **Results:** A total number of 18 osteoarthritic knees were analyzed showing a mean tibial and patellar SUVmax, SUVmean (g/mL) and CT density (HU) of 6.6 ±2.9, 4.1±1.6 and 263±80 and 8.1±4, 5.4±2.8 and 374±86, respectively. In 14 knees with no/minimal OA mean corresponding tibial and patellar SUVmax, SUVmean (g/mL) and CT density (HU) were 3.5±1.2, 2.2±0.8 and 261±36 and 3.8±1.8, 3.8±1.8, and 306±69 respectively. Comparison of both SUVmax and SUVmean between the OA and no/minimal OA groups showed a statistically significant difference for tibial and patellar SUVmax and SUV mean (all p<0.0008). CT density was statistically different between the OA and no/minimal OA groups only in patellar region (p=0.02). We found a positive correlation between SUVmax and SUVmean with CT density (HU) in tibial subchondral bone in the group with no/minimal OA (rho=0.839, p<0.0005 and rho=0.672, p=0.0001), but not in the OA group (both p<0.81). **Conclusion:** This study showed significant differences in Tc-99m-DPD uptake on bone scan between OA and no/minimal OA in the subchondral tibial and patellar bone based on quantitative data analysis. There were significantly higher SUVmax and SUVmean in OA group but no difference in CT density (HU) of the subchondral tibial bone. Thus, integrating quantitative analysis of bone scan might be valuable in increasing sensitivity for initial detection, stratification and evolution assessment of knee OA. **References:** [1]McCrae , Shouls J, Dieppe P,et al. Scintigraphic assessment of osteoarthritis of the knee joint. Ann Rheum Dis. 1992 Aug; 51(8): 938-942.[2]Kraus VB, Worrell TW, Renner JB,et al. High prevalence of contralateral ankle abnormalities in association with knee osteoarthritis and malalignment. Osteoarthritis Cartilage. 2013 Nov;21(11):1693-9.

EPS-123

Quantitative three-phase 99mTc-MDP scintigraphy in the assessmenmt of loosening of total knee endoprostheses in patients with equivocal imaging findings

M. Beheshti[1,2], *Z. Paymani*[3], *R. Ortmaier*[4], *C. Schiller*[5], *F. Fitz*[5], *F. Masoumi*[6], *J. Hochreiter*[7], *W. Langsteger*[5];
[1]*Nuclear Medicine, University Hospital, RWTH University, Aachen, GERMANY,* [2]*Nuclear Medicine, Paracelsus Medical University, Salzburg, AUSTRIA,* [3]*Research Center for Nuclear Medicine, Tehran University of Medical Sciences, Tehran, IRAN, ISLAMIC REPUBLIC OF,* [4]*Orthopedics surgery, Ordensklinikum, Linz, AUSTRIA,* [5]*Nuclear Medicine, St. Vincent's Hospital, Ordensklinikum, Linz, AUSTRIA,* [6]*Orthopaedics Surgery, Tabriz University of Medical Sciences, Tabriz, IRAN, ISLAMIC REPUBLIC OF,* [7]*Orthopaedics surgery, Ordensklinikum, Linz, AUSTRIA.*

Aim/Introduction: The purpose of this study was to determine whether quantitative three-phase 99mTc-MDP bone scintigraphy can provide accurate thresholds for predicting loosening in symptomatic patients with knee total endoprostheses. **Materials and Methods:** A total of 125 patients of knee total endoprostheses (TEP) (126 K - TEP) suffering pain symptoms were retrospectively included in this study. For the quantification of the 3-phase skeletal scintigraphy, the ratio of pathological peri-prosthetic tracer uptake to normal bone was evaluated. In case of visually equivocal findings, the change in ratios was analyzed between 2 examinations at the 6-month interval whether cut-off point could be found to predict loosening. The imaging interpretations were validated by the 6 months clinical course or the revision operation. **Results:** The quantitative analysis enhances the predictive value of loosening in the region of the "tibial plateau" in equivocal cases at a cut-off of 1.55 (AUC = 0.52) with a sensitivity of 50% and specificity of 57% in early images. Six months follow up images of equivocal cases reveal a cut off of 1.53 (AUC79%) with 71% sensitivity and 79% specificity. The percentage of the ratio changes in the follow-up control for the detection of a loosening process rises at a cut-off of 3.88% in the "tibial plateau" (sensitivity 87%, specificity 89%, AUC = 0.94, p = 0.056). **Conclusion:** Exclusive uptake ratios are not sufficient to predict loosening in equivocal cases. While increased uptake ratios with time in quantitative three-phase bone scintigraphy improves the predictive value for the recognition of a loosening process in cases with K-TEP equivocal imaging findings. **References:** None.

EPS-124

Bone SPECT/CT in patients with persistent low back pain after lumbar spine stabilization

R. García Jiménez*, Y. Herrera-Martinez, E. López Rodríguez, P. Fernandez-Rodríguez, J. Jiménez-Hoyuela García;*
Hospital Universitario Virgen del Rocio, Sevilla, SPAIN.

Aim/Introduction: The incidence of low back pain after lumbar stabilization surgery (LSS) is observed in 10-20% of cases. There are limitations in the sensitivity and specificity of conventional imaging techniques (radiography, CT and MRI), conditioning the presence of errors in the diagnosis in 20% of cases. The aim of this study was to determine the sensibility of bone SPECT/CT as a diagnostic method in patients with low back pain after LSS **Materials and Methods:** Descriptive, cross-sectional, retrospective study was performed. A total of 96 consecutive patients with lumbar pain after LSS, who underwent ^{99m}Tc-HDP bone SPECT/CT from January 2010 to December 2018 were included in this study. The sensitivity, specificity and accuracy of ^{99m}Tc-HDP bone SPEC/CT were determined. Results were confirmed with surgery results or with clinical variables. **Results:** 96 patients were included (41,7% men, 58,3% women) with an average age of 52,9 ± 12,3 years. In 92,7% the LSS was initially indicated by degenerative causes, while the 7, 3% by traumatic causes. In 47,8% of patients the arthrodesis of more than two

joints were performed. Image study was performed on average 52,2 months after the first surgery (range 4-360 months). The most frequent diagnosis by bone SPECT/CT was "Insufficient stabilizing function", followed by "mobilization of the material" and "Insufficient stabilizing function with mobilization of the material". The SPECT/CT was negative in 12,5% of the cases. The sensitivity of the test was 94% with a specificity of 53,8% (PPV: 92%; NPV 58%). Diagnostic accuracy was 88,5%. Subsequently, 25,5% of the cases required surgery, 43.7% were managed in the unit of pain, and 31,6% were treated by medical treatment. **Conclusion:** Bone SPECT/CT has high sensitivity for diagnosis of the etiology of low back pain in patients with previous LSS. Its systematic use may improve the precocity and efficiency of treatment in these cases, especially in those cases with inconclusive conventional imaging. **References:** None.

EPS-125

Utility of SPECT-CT in the follow-up of patients undergoing cervical intersomatic arthrodesis

M. Moreno-Caballero[1], *A. Moreno-Flores*[2], *A. Martínez-Esteve*[1], *P. Jiménez-Granero*[1], *A. Cobo-Rodríguez*[1], *J. Infante-de la Torre*[1], *J. Serrano-Vicente*[1], *J. Rayo-Madrid*[1];
[1]*Departamento de Medicina Nuclear. Hospital Universitario de Badajoz, Badajoz, SPAIN,* [2]*Departamento de Neurocirugía. Hospital Universitario de Badajoz, Badajoz, SPAIN.*

Aim/Introduction: To evaluate the usefulness of SPECT-CT ^{99m}Tc-HDP in patients undergoing cervical spinal fixation with intersomatic cage system (Cervios®) and its possible contribution to the diagnosis of pseudoarthrosis. **Materials and Methods:** A retrospective pilot study including 13 subjects, 8 women and 5 men, average age: 52.1 years [32-72]. Of these, 4 were asymptomatic, 9 with persistent cervical pain or signs of myelopathy. All of them underwent SPECT-CT study (Symbia T2®, GE Healthcare). Median of 39 months [9-132] between surgery and scintigraphy. The images were visually interpreted independently by 2 nuclear physicians, with clinical blinding. A scale of 3 degrees was used according to the intensity of uptake (mild, moderate or intense). Subsequently, a quantitative analysis was carried out using rectangular 35 mm ROIs in summative slices of the tomographic image. The ratio of counts per pixel in the arthrodesed area to the one measured on adjacent healthy vertebra was calculated, obtaining an index of asymmetry. The results were finally compared with the Gold standard established: clinical evolution for 7 individuals and surgical reintervention in 6. **Results:** Five patients presented arthrodesis in 2 levels, being the most frequently intervened C5-C6 (53.8%). Of the 9 symptomatic patients, only 3 confirmed the presence of pseudoarthrosis due to surgical reoperation (3/9). In the remaining 6 (6/9), 3 did not show graft mobility during reoperation and in 3 others surgery was ruled out, 2 due to radiological imaging and 1 for mild symptomatology. The 4 asymptomatic patients remained stable during the period considered. All showed increased uptake of the radiotracer in the arthrodesed area, with a degree of visual agreement between both observers of 80%. The asymmetry index obtained for symptomatic patients was 1.8 while for asymptomatic patients it was 1.6. There was no difference between the group of symptomatic patients with surgically confirmed pseudoarthrosis and in those who discarded this disease. In 2 symptomatic patients without pseudoarthrosis (2/6), facet and intervertebral osteodegenerative activity was associated at different levels. **Conclusion:** Our preliminary results suggest a probable causal relationship between the increase in osteoblastic activity in the arthrodesis and the biomechanical characteristics of the fixation material. We propose a simple and reproducible quantification method that contributes to the diagnosis of pseudoarthrosis. However, more patients and standardization of the follow-up criteria are needed to clarify its usefulness. **References:** None.

EPS-126

Usefulness of bone SPECT/CT for the prediction of bone graft viability after maxillofacial reconstruction with vascularized bone grafts

H. Kim[1], *S. Ha*[1], *E. Shin*[1], *J. Lee*[2,3], *K. Ahn*[2,3], *J. Ryu*[1,3];
[1]*Department of Nuclear Medicine, Asan Medical Center, Seoul, KOREA, REPUBLIC OF,* [2]*Department of oral and maxillofacial surgery, Asan Medical Center, Seoul, KOREA, REPUBLIC OF,* [3]*University of Ulsan College of Medicine, Seoul, KOREA, REPUBLIC OF.*

Aim/Introduction: The accurate assessment of bone graft viability is important in patients who had maxillofacial reconstructive surgery with vascularized bone graft after resection of mandible or maxilla. Bone scintigraphy has proved to be of value for non-invasive, simple and effective in postoperative assessment of bone graft. Hybrid imaging of single photon emission computed tomography (SPECT) and computed tomography (CT) has more advantages by providing complex anatomical information of maxillofacial region and attenuation correction of SPECT images. We performed this study to evaluate the performance of bone SPECT/CT in the prediction of bone graft viability after maxillofacial reconstruction with vascularized bone grafts. **Materials and Methods:** We retrospectively reviewed the medical record and images of 34 consecutive patients (M:F=23:11, age 26 - 89 years) who underwent bone SPECT/CT with ^{99m}Tc-DPD or ^{99m}Tc-HDP at about one week (5 - 8 days) after reconstructive surgery of mandible (n=28) or maxilla (n= 6) with vascularized bone graft between February 2014 and March 2019. Fibular free flap (n=21) or iliac crest free flap (n= 13) were used, and 11 patients had reconstructive surgery with 2 segments of bone graft. Patients were clinically followed for at least one month (range 5 - 61, median 13 months), and the final diagnosis of non-viable graft was surgically confirmed. For visual analysis of bone SPECT/CT images, two readers who blind to clinical information scored the uptake degrees of each bone graft segment in comparison with those of calvarium as follows; 0 = absence of tracer uptake, 1 = decreased uptake, 2 = same degree of uptake, and 3 = increased uptake. **Results:** In the visual analysis of bone graft

uptake on SPECT, the anatomical CT information from hybrid images was helpful for discriminating bone graft uptake on SPECT from adjacent stump end of maxilla or mandible, or soft tissue uptake of surgical bed. Forty-one of all 45 bone graft segments were scored more than 1, and all of them were viable graft and uneventful during follow-up. Four bone grafts had score 0 (absence of tracer uptake), and all of them were surgically removed and confirmed as nonviable bone graft with osteonecrosis. **Conclusion:** Absent tracer uptake in the vascularized bone graft on bone SPECT/CT at one week after reconstructive surgery could be used to predict the graft failure. Bone SPECT/CT would be useful for the assessment of vascularized bone graft at risk after maxillofacial reconstruction. **References:** None.

EPS-127

Bone SPECT/CT in the early diagnosis of calciphylaxis

Y. Herrera-Martinez, J. Martín-Marcuartu, P. Fernández-Rodríguez, J. Jiménez-Hoyuela García, R. García Jiménez;
Hospital Universitario Virgen del Rocío, Seville, SPAIN.

Aim/Introduction: Calciphylaxis is an uncommon understood vascular calcification disorder with the subsequent necrosis of skin and soft tissues, affecting patients with end-stage renal disease (ESRD). Two-year mortality rates from sepsis ranges from 50% to 80%. In this context, early diagnosis and subsequent treatment are necessary. The aim of this study is to determine the sensibility of the bone SPECT/CT as a diagnostic method in patients with skin lesions suggestive of calciphylaxis. **Materials and Methods:** Descriptive, cross-sectional, retrospective study was performed. A total of 46 consecutive patients with skin lesions suggestive of calciphylaxis, who underwent ^{99m}Tc-HDP bone SPECT/CT from July 2011 to January 2019 were included in this study. The sensitivity, specificity and accuracy of ^{99m}Tc-HDP bone SPEC/CT were determined. Results were confirmed with the histological analysis and the response to treatment with sodium thiosulfate. **Results:** Forty-six patients (71,7% women, 28,3% men) were included in this study with an average of 65,5 ± 11,4 years. The 91,3% of the patients had ESRD and were in hemodialysis, 8,7% of them had not renal disease. Lesions were localized in the lowers limbs in the 73,9% of the cases (34 of 46). Hybrid image was performed on average 147 days after the appearance of the lesions (range 14-700 days). Histological analysis was performed in 54,4% of the cases (25 of 46). The sensibility of the test was 100% with a specificity of 31,25% (PPV: 73%; NPV 100%). Diagnostic accuracy was 76%. Histopathology was positive in 48% of the cases (12 of 25). **Conclusion:** Bone SPECT/CT is a non-invasive tool with a high sensibility for the diagnosis of calciphylaxis. Its indication in early stages of the disease could improve the early diagnosis and specific treatment. It also avoids performing skin biopsy, which can have serious complications such as septicemia. **References:** None.

EPS-128

A Novel Sn-117m Colloid for Human Radiosynoviorthesis Clinical Trials

N. R. Stevenson[1], *C. A. Doerr*[1], *G. R. Gonzales*[1], *J. Simon*[2], *A. Bendele*[3];
[1]*Serene, LLC, Buford, GA, UNITED STATES OF AMERICA,* [2]*IsoTherapeutics Group, LLC, Angleton, TX, UNITED STATES OF AMERICA,* [3]*Bolder BioPATH, Inc., Boulder, CO, UNITED STATES OF AMERICA.*

Aim/Introduction: In patients with advanced arthritis, direct injections of a radio-colloid into affected joints (radiosynoviorthesis a.k.a. radiosynovectomy) is used therapeutically to relieve pain and increase mobility. Isotopes such as Y-90, Re-186 and Er-169 are in routine clinical use. Recently, a Sn-117m (γ 159 keV, 86% ; e^- ~140 keV, 112% ; $t_{½}$ 14d) homogeneous colloid (HTC) has become available for treating canine osteoarthritis (OA) [1]. This product was modified with ascorbic acid (causing a color change) to differentiate it for human use. Studies were undertaken to demonstrate comparable physical and safety characteristics so that the product can be used in human trials. **Materials and Methods:** The addition of a small quantity of ascorbic acid to commercially available HTC results in a color change from yellow/orange to white. We anticipated that all other characteristics would remain unchanged as determined by measurements of particle size distributions, pH, endotoxicity, sterility, stability and free tin in solution performed in accordance with the established cGMP manufacturing procedures. Additionally, a study was undertaken to demonstrate that there were no in-vivo differences between the two products. Fourteen Sprague-Dawley rats (~ 120 g) were placed in 2 groups based on sex, totaling 7 male and 7 female rats in this study. All rats received HTC injected in the left knee, and the ascorbic acid homogeneous Sn-117m hydroxide colloid (AHTC) injection in the right knee. The planned dose administration was nominally 20 µCi (740 kBq) per injection for every rat, which scales in humans to about 12 mCi (444 MBq) or double the highest anticipated human knee dose. All rats were sacrificed at 42 days and both knees of each rat were harvested and fixed in formalin. The knees were sent for histopathological examination and a comparison of the left and right tissues. **Results:** There were no significant differences observed in the physical characteristics between the two colloidal preparations other than the desired color change. No significant histopathological differences were observed between the HTC and AHTC treated joints. **Conclusion:** An ascorbic Sn-117m homogeneous colloid has been developed specifically for human use. Other than the appearance (color) the physical and in-vivo characteristics are identical to the well-studied canine HTC product. The AHTC will now be used in upcoming human clinical trials in Canada. **References:** 1. "Intraarticular Injection of a Tin-117m Radiosynoviorthesis Agent In Normal Canine Elbows Causes No Adverse Effects", Journal of Veterinary Radiology & Ultrasound, DOI: 10.1111/vru.12757 (2019).

1311

e-Poster Presentation Session 9 - Do.MoRe: Dosimetry

Tuesday, October 15, 2019, 11:30 - 114:30 Room 133/134

EPS-129

Predictive value of ^{99m}Tc-MAA SPECT-CTbased dosimetry before radioembolization of liver tumors

P. D'abadie, R. Lhommel, S. Walrand, M. Hesse, N. Amini, P. Goffette, I. Borbath, F. Jamar;
Cliniques Universitaires Saint Luc, Brussels, BELGIUM.

Aim/Introduction: ^{99m}Tc- macroaggregated albumin SPECT/CT(^{99}Tc-MAA) is performed before ^{90}Y liver radioembolization (RE) for evaluating lung shunt, ruling out extrahepatic deposition and sometimes for calculating the delivered activity for treatment using the partition model[1,2]. ^{99m}Tc-MAA is then considered as a surrogate to ^{90}Y-microspheres to predict tumor and liver absorbed doses. The aim of this study is to assess the value of the dosimetry based on ^{99m}Tc-MAA SPECT-CT compared to the real distribution of ^{0}Y-microspheresobserved with ^{90}Y PET-CT. **Materials and Methods:** Patients treated by RE in our institution between 2011 and 2018 for hepatocellular carcinoma and cholangiocarcinoma were studied. 53 treatments and 136 lesions were analyzed. Tumor volumes of interest (VOIs) were delineated using the baseline imaging (arterial contrast enhanced MRI ou CT scan). VOIs were fused with ^{99m}Tc-MAA SPECT and ^{90}Y PET using PMOD 3.7 for calculation of a tumor to total liver ratio (T/L). Mean doses (D_{Y90} and D_{MAA}) and Dose Volume histogram (DVH) were calculated using the MIRD formula with input of the delivered activity of ^{90}Y microspheres and of the ratio $T/L_{(MAA\ or\ 90Y)}$. Using DVH, the minimal dose deposited in 66% of the tumor volume (D66) was calculated. Patients were categorized as a function of the catheter's position during the ^{99}Tc-MAA and ^{90}Ymicrospheres injections. Correlations were analyzed using the Spearman's coefficient (R) and the accuracy of the prediction was studied using the standard error of the estimate (SEE). **Results:** Regarding only treatments realized in the same angiographic conditions (25 treatments, 58 treatments), the correlation was strong (R=0,78) but the linear regression demonstrates a significant risk of error (SEE=76 Gy). A better correlation was found after exclusion of angiographies with injections in the proximity of an arterial bifurcation (R=0,88, SEE=56 Gy). Using DVH and D_{66}, results were quite similar in both conditions (R=0,71, SEE=57 Gy and R=0,82, SEE= 51 Gy). **Conclusion:** Despite good catheter positioning, our study failed to confirm an accuracy in ^{99}Tc-MAA dosimetry. In clinical practice, this dose estimation would not guarantee to avoid liver toxicity in case of dose escalation based on the partition model. Moreover, DVH applied to ^{99}Tc-MAA SPECT/CT is not predictive in many cases. **References:** 1- Padia SA et al. J Vasc Interv Radiol 28:1-15, 2017.2- Garin E et al. Eur J Nucl Med Mol Imaging 43:559-75, 2016.

EPS-130

Radiation Dosimetry for ^{99m}Tc-labeled PSMA-I&S

S. Urbán, I. Farkas, Z. Besenyi, L. Pávics;
University of Szeged, Szeged, HUNGARY.

Aim/Introduction: Prostate-specific membrane antigen (PSMA) is a metallopeptidase expressed predominantly in prostate cancer (PCa) cells. Recently, PSMA has shown promising results in patients with PCa. The aim of this study was to estimate the radiation dosimetry of ^{99m}Tc-PSMA-I&S in healthy volunteers. **Materials and Methods:** 4 healthy man volunteers (mean age 65.2 ± 5.6 y) were injected with 561-828 MBq of ^{99m}Tc-PSMA-I&S. Whole-body anterior and posterior PSMA scintigraphies (WB) was performed at 1, 2, 3, 6 and 24 h after radiopharmaceutical administration using a triple head gamma camera (AnyScan Trio SPECT/CT, Mediso Medical Imaging Systems Ltd.), equipped with low energy, high-resolution collimators (LEHR). Additionally, SPECT/CT images were acquired at 6 h after p. i. with the same device. Regions of interest were drawn on WB and SPECT/CT images for source organs (salivary glands, kidneys, liver, spleen, small intestine, urinary bladder) and the whole body. Dose factors from the OLINDA/EXM software was used to determine organ absorbed dose and equivalent doses using the RADAR method. **Results:** Physiological uptake in salivary glands, kidneys, liver, spleen, small intestine and urinary bladder was seen. Salivary glands with highest mean organ absorbed dose (0.0207 mSv/MBq) were the critical organs followed by liver (0.0117 mSv/MBq), spleen (0.0086 mSv/MBq), small intestine (0.0084 mSv/Mbq), kidneys (0.0049 mSv/Mbq) and urinary bladder wall (0.0039 mSv/MBq). The mean effective dose was found to be 0.0044 mSv/Mbq, which means 3.29 ± 0.51 mSv effective dose using 740 MBq PSMA I&S. Measured absorbed doses and effective doses are similar to previously reported ^{99m}Tc-EDDA/HYNIC-iPSMA (3.42 ± 0.78 mSv/740 MBq) [1] and much lower than the ^{99m}Tc-MIP-1404 (6.5 mSv/740 MBq) and the ^{99m}Tc-MIP-1405 (5.82 mSv/740 MBq) [2]. **Conclusion:** To the best of our knowledge, this is the first report on radiation dosimetry of ^{99m}Tc-labeled PSMA-I&S in healthy volunteers. PSMA-I&S is found to be a safe diagnostic agent with similar effective dose to ^{99m}Tc-EDDA/HYNIC-iPSMA. **References:** [1] C. Santos-Cuevaset al. ^{99m}Tc-labeled psma inhibitor: Biokinetics and radiation dosimetry in healthy subjects and imaging of prostate cancer tumors in patients. Nuclear Medicine and Biology, 52:1 - 6, 2017. [2] S. Vallabhajosula et al. ^{99m}Tc-labeled small-molecule inhibitors of prostate-specific membrane antigen: Pharmacokinetics and biodistribution studies in healthy subjects and patients with metastatic prostate cancer. Journal of Nuclear Medicine, 55(11):1791-1798, 2014.

EPS-131

Correlation between lesion absorbed dose and relative variation of the ^{99m}Tc-HDP lesion uptake before the first cycle and after the sixth cycle in patients treated for metastatic castration resistant prostate cancer with ^{223}Ra

P. Minguez Gabiña, A. Gomez de Iturriaga Piña, A. Esteban

Figueruelo, M. Nevares Herrero, R. Valverde Jorge, I. Fernandez Tercero, E. Rodeño Ortiz de Zarate;
Osakidetza, Barakaldo, SPAIN.

Aim/Introduction: We looked for a possible correlation between relative variation of the ^{99m}Tc-HDP uptake in bone lesions and lesion absorbed dose in patients with metastatic castration resistant prostate cancer (mCRPC) treated with ^{223}Ra. **Materials and Methods:** Ten patients were included in the study. Absorbed doses of the lesions with the higher ^{99m}Tc-HDP uptake were determined for the first cycle of the ^{223}Ra therapy. The ^{223}Ra activity in the lesions was obtained from planar imaging at 3d and 7d after ^{223}Ra administration, and the time-integrated activity from a mono-exponential curve determined by those two time-points. The lesion volume was obtained from ^{99m}Tc-HDP SPECT/CT imaging and the S-value calculated for unit-density spheres of that volume. A correction for the bone mass density was applied to the calculated lesion absorbed dose. For the lesions for which dosimetry had been performed, in the ^{99m}Tc-HDP WBSs performed before the first cycle and after the sixth cycle were administered, the mean value of the counts in the ROIs encompassing them, C_{ROI}, was determined. As the time between the ^{99m}Tc-HDP injection and the WBS was not the same for all patients, C_{ROI} was made relative to the femur uptake. The relative variation of C_{ROI} between the two WBSs, ΔC_{ROI}, was obtained. In order to analyse the effect on ΔC_{ROI} of other variables, a multivariate analysis was performed including the lesion absorbed doses, the received concomitant therapies (abiraterone, enzalutamide, external beam radiotherapy) and the total number of lesions. **Results:** The absorbed dose of 29 lesions was determined. Values of ΔC_{ROI} and of the absorbed doses followed a normal distribution, with mean±1SD values of 46±32% of 1.4±0.Gy, respectively. A logarithmic correlation was obtained between ΔC_{ROI} and the lesion absorbed dose (Pearson's correlation coefficient of 0.86). The multivariate analysis concluded that the effect of other variables on ΔC_{ROI} was no significant in relation to that of the lesion absorbed dose. **Conclusion:** We found a strong correlation between the relative variation of the mean value of the counts in the ROIs encompassing lesions in the ^{99m}Tc-HDP WBSs performed before the first cycle and after the sixth cycle and the lesion absorbed dose determined for the first cycle of the ^{223}Ra therapy. These results show that determining lesion absorbed doses may be useful in order to evaluate the evolution of those lesions in the treatment of mCRPC with ^{223}Ra. **References:** None.

EPS-132

NCINM: an internal dosimetry software using ICRP and NCI pediatric and adult computational phantoms

***D. Villoing**, C. Lee;*
National Cancer Institute at the National Institutes of Health, Rockville, MD, UNITED STATES OF AMERICA.

Aim/Introduction: Nuclear medicine (NM) procedures make up about 25% of the per capita medical effective dose in the United States[1]. Thorough investigation of health risks associated with NM procedures relies on the accuracy of the radiation dose assessment and hence on the human anatomy models in use. Existing organ dose estimation tools are limited to simplified anatomy models or fixed body morphometry. To fill the research gaps, we developed a new dose calculation tool using advanced human anatomy models. **Materials and Methods:** We adopted the twelve National Cancer Institute (NCI) pediatric and adult phantoms[2] developed from patient computed tomography images as well as the two adult reference computational phantoms[3] from the International Commission on Radiological Protection (ICRP). Specific Absorbed Fractions (SAFs) were calculated for photon and electron on the NCI phantoms for 68 source and 55 target regions using the MCNPX Monte Carlo radiation transport code[4]. SAFs for the two adult ICRP reference phantoms were adopted from the ICRP Publication 133[5]. S values were then derived from the SAFs for 299 radionuclides commonly used in nuclear medicine[6]. A graphical user interface-based computer program, named National Cancer Institute dosimetry system for Nuclear Medicine (NCINM), was finally developed to facilitate data input and output. **Results:** The ratios of the iodine-131 S values from the NCI phantoms to those from the ICRP ones were on average 0.96±0.10σ and 0.92±0.59σ for eight major organs in the adult male and female phantoms in case of self-absorption and cross-irradiation, respectively. The ratios of the iodine-131 S values from the NCI phantoms to those from OLINDA/EXM 1.0[7](based on the ORNL stylized phantoms) were on average 0.91±0.15σ and 1.34±0.62σ for eight major organs in the adult and pediatric phantoms in case of self-absorption and cross-irradiation, respectively. **Conclusion:** A good agreement was overall observed between iodine-131 S values from the NCI phantoms series vs. the ICRP 110 reference phantoms, both of which have realistic anatomy compared to the ORNL stylized phantoms. Greater differences were, however, revealed in S values between the NCI phantoms and the stylized phantoms (OLINDA), especially for cross-irradiation, which emphasizes the importance of realistic human anatomy models in S value calculations. The NCINM program will be useful for epidemiologic studies of risk and patient dose monitoring in NM procedures. **References:** [1]NCRP Report 160 (2009) [2]Lee et al (2010)[3]ICRP Publication 110 (2009) [4]Briesmeister JF (2000) [5]ICRP Publication 133 (2016) [6]ICRP Publication 107 (2008) [7]Stabin et al (2005).

EPS-133

Validation of a voxel based MRT dosimetry software module for 3D slicer

***D. P. Rushforth**, J. Jear, I. Murray, G. Flux;*
The Royal Marsden NHS Foundation Trust, Sutton, UNITED KINGDOM.

Aim/Introduction: Dosimetry for Molecular Radiotherapy can be complex and time consuming. An in-house dosimetry module, was designed to speed up and simplify this process.

Voxelised calculations were used to enable 3D visualisation and analysis. The aim of this project was to validate this approach against conventional region based dosimetry, particularly to evaluate those factors relevant to voxel dosimetry including higher noise to signal ratios. **Materials and Methods:** Written in python for the open-source platform, 3D Slicer, the module calculates absorbed doses at both voxel and region levels. Time activity curves are fitted using least squares minimisation, with constraints to compensate for voxel noise. Final absorbed doses can be determined using either local deposition (LD) or fast convolution (FC). Validation was performed using a SPECT scan of a 3D-printed anthropomorphic phantom with known activities of Y90 in liver, spleen, kidney and lesion compartments. The acquired image was used to replicate a set of time-activity images with voxel half-lives of 24 hours. Absorbed doses calculated using LD and FC were compared to results obtained using region based calculations and Olinda Dose Factors. To determine the effect of image noise on voxel based calculations, simulated datasets were created comprising three uniform images containing 128^3 voxels with effective half-lives ranging from 1/3 to 1 times the physical half-life. A random Gaussian number generator was used to add noise and produce a range of datasets with coefficients of variation (CoV) ranging from 0 to 100%. **Results:** LD and FC gave absorbed organ doses for the phantom dataset that were on average within 3.4% (SD=0.01%) and 1.6% (SD=0.02%) of the conventional methodology respectively. Data were unaffected by the presence of image noise when doses were calculated using average VOI activities. When fitting at the voxel level a 0.017% difference was observed for noise levels up to a CoV of 10%. For the dataset used, noise in the dose map was 40% less than that present in the original images. **Conclusion:** The module provides a simple and efficient solution for performing dosimetry reducing the time required from 5 hours to 20 minutes. The results derived are in good agreement with our previous methodology and the constraints used for the voxel calculations have a negligible effect on the resulting doses. Further work will investigate the quantitative impact of different registration methods (rigid and deformable) and explore alternate methods for reporting voxel dose information. **References:** None.

EPS-134

Geant4/GATE ion source implementation for internal dosimetry applications

A. Vergara Gil[1], *M. Chauvin*[1], *G. Kayal*[1,2], *J. Ocampo*[1], *M. Bardies*[1];
[1]*CRCT, UMR 1037, INSERM, Université Toulouse III, Paul Sabatier, Toulouse, FRANCE,* [2]*SCK.CEN, Belgian Nuclear Research Centre, Boeretang, BELGIUM.*

Aim/Introduction: In Geant4, the ion source implementation allows the full integration of isotope decay within simulations [1]. This feature has not been tested for internal dosimetry of complex decay chains in GATE. The aim of this work is to study the dosimetric implications of the use of ion source for several radionuclides currently used in Nuclear Medicine. **Materials and Methods:** We tested two ways of modelling a radioactive source within GATE (version 8.2): manual spectrum input (from [2]) and explicit radioactive decay process modelling (ion source). To implement the comparison, simulations in cubes of various materials (15) were set up. Cubes were made large enough to account for the deposition of most emitted energy (>99%).We considered 12 radioactive isotopes relevant in a context of nuclear medicine: ^{32}P, ^{51}Cr, ^{89}Sr, ^{90}Y, ^{131}I, ^{153}Sm, ^{177}Lu, ^{186}Re, ^{188}Re, ^{192}Ir, ^{212}Pb, ^{223}Ra. Absorbed doses per decay (S factors) were calculated for 10^7 primaries (manual spectrum input) or 10^7 Bq.s (ion source). **Results:** The comparison between manual spectrum input and ion source yield little differences (<1%) for simple decay. In complex decay chains, more important differences (>10%, 160% for ^{223}Ra) were observed. This was explained by the presence within the chain of semi-stable daughters (mainly alpha) with very long half-lives. These are fully accounted for in ion source decay process, even though the secular equilibrium is never achieved in practice. Geant4 handles this with a pre-equilibrium decay models that are not currently implemented in GATE. Using ion source requires less user input since it explicitly models nucleus decay (all emitted particles); the input should be given in Bq.s, whereas for manual spectrum input, the total number of simulated particles and type should be entered. Furthermore, the ion source implementation uses a variance reduction technique to model all decay chains [1]. As a consequence, the simulation time to get the same statistics is lower for complex emission spectra (average 3 times for ^{51}Cr, 5 times for ^{131}I, 2.55 for ^{177}Lu and 17.8 times for ^{223}Ra). **Conclusion:** The validation results show that ion source is an accurate yet efficient way to model isotope decay for nuclear medicine dosimetry. Yet we recommend caution when using it in GATE simulations involving radioactive nuclides who contain decay chains. **References:** 1 Steffen Hauf et al. IEEE Trans Nuclear Science 60.4 (2013); 2 K.F. Eckerman and A. Endo. J. Nucl Med 50.12 (2008).

EPS-135

Customisation of Internal Dosimetry Phantoms by Using the OpenDose SAFs Generated for the ICRP Voxel Phantom

A. Malaroda[1], *E. McKay*[2];
[1]*St Vincent's Hospital Sydney, Sydney, AUSTRALIA,*
[2]*St George Hospital, Sydney, AUSTRALIA.*

Aim/Introduction: The OpenDose project [1] is generating a database of Specific Absorbed Fractions (SAFs) for the 140 regions of the ICRP Publication 110 voxel phantoms. One major application of this data is the computation of internal dosimetry for arbitrary radio-pharmaceuticals. Existing software such as OLINDA/EXM or IDAC provide a hard-coded set of source and target regions which do not necessarily match, for example, the sources for which residence time data might be available. There is a need for software which enables the construction of customised dosimetric phantoms where source and target regions are comprised of arbitrary sets of composable parts from the OpenDose database or other SAF

collections. **Materials and Methods:** A packaging module was implemented for the OpenDose calculator [2]; this allows subsets of the SAFs generated by the OpenDose project to be combined, as mass-fraction weighted sums, to form SAFs for composite source and target regions. The module was validated by estimating dose depositions for the radio-iodide model described by the ICRP Publication 128. The model comprised 12 sources (blood, thyroid, salivary glands, liver, kidneys, bladder, stomach wall, stomach contents, small, upper-large and lower-large intestine contents) and 22 targets (as in OLINDA/EXM, except for bone surfaces which can not be simulated in voxel models) constructed from 26 and 53 components of the ICRP voxel phantom respectively. The phantom's composite SAFs were compared against SAFs generated by direct Monte Carlo simulation using a previously validated GATE macro [3]. **Results:** Excellent agreement was observed between the composite SAFs and the SAFs estimated by the GATE Monte Carlo simulation, with differences of less than 5% in more than 90% of the source-target combinations. In general, percentage differences were less than 10% except for the combinations: thyroid <-- bladder (~18%), skin <-- salivary glands (~18%), testes <-- salivary glands (~14%) and skin <-- thyroid (~14%). **Conclusion:** Composition of SAFs from separate sources and targets provides a viable and flexible alternative to hard-coding SAFs into internal dosimetry software. **References:** 1. Chauvin M, et al; Physica Medica, 42(1): 32-33 (2017) 2. Mckay E, Malaroda, A; Australas Phys Eng Sci Med (2019) 42: 285 3. Mckay E, Chatrie F, Malaroda, A; Australas Phys Eng Sci Med (2018) 41: 245.

EPS-136

Feasibility study of using monocrystalline silicon as a dosimeter for neutron capture therapy

M. Anikin, *I. Lebedev, N. Smolnikov, A. Naymushin; National Research Tomsk Polytechnic University, Tomsk, RUSSIAN FEDERATION.*

Aim/Introduction: During preclinical studies of interaction of ionizing radiation with biological objects exact experimental determination of dosimetric fields is necessary. In this paper, aspects of using nuclear purity monocrystalline silicon plates as accumulative dosimeters during NCT are considered. **Materials and Methods:** The essence of the method for determining thermal neutrons fluence using monocrystalline silicon is transmutation of Si-31 nuclei into P-32 after interaction with thermal neutron. Since electrical conductivity of silicon depends, inter alia, on presence of impurities, it is possible to unambiguously determine the relationship between specific electrical resistance of silicon and amount of P-32 formed. The method of dose measuring involves installation of a thin (less than 1 mm) silicon plate with a diameter of more than 15 mm in front of the irradiated sample. The location of the plate is chosen so that the surface of plate is perpendicular to radiation beam and located as close as possible to surface of the biological object. Silicon monocrystalline plate has small cross-section of interaction with neutrons of all energies, so there is practically no effect on the process of NCT. Measurements of changes in electrical resistivity are carried out by the four point probe method, manually or automatically. **Results:** In the framework of this work, the conditions for using monocrystalline silicon plates to determine dose during the NCT were determined. The relationships between the determined conductivity of plates with distribution of thermal neutrons over the volume of a biological object for ionizing radiation beams with different spectral characteristics have been developed. **Conclusion:** The advantages of the proposed method are that P-32 formed is a stable isotope and its inclusion in the silicon crystal ensures that information on the accumulated dose is preserved for an extremely long period of time. In this way, it is possible to restore information about modes of irradiation after any arbitrary period of time. In this case, the sample is not subject to aging, ultraviolet radiation, oxidation, or exposure to high temperatures. At the same time, measurement accuracy in therapeutic range (10^11-10^13) of thermal neutron fluence is measured with high accuracy, since in this fluence range that a sharp drop in electrical resistivity is observed.The disadvantage of this method is the need to pre-calibrate silicon samples on each neutron beam, since in the general case the nature of the change in the conductivity of silicon will depend on the spectrum of neutron radiation. **References:** None.

EPS-137

Effects of timing and number of SPECT acquisition on biodistribution and dose evaluation in hepatocellular carcinoma patients treated with ^{188}Re SSS Lipiodol radioembolization

K. Delaunay[1,2], *E. Garin*[3,4,5], *Y. Rolland*[6], *N. Lepareur*[3,5], *S. Laffont*[3], *V. Ardisson*[3], *J. Edeline*[7,4,5];
[1]*Paris Diderot University, Paris, FRANCE,* [2]*Bichat Claude Bernard University Hospital, Department of Nuclear Medicine, Paris, FRANCE,* [3]*Comprehensive Cancer Institute Eugene Marquis, Department of Nuclear Medicine, Rennes, FRANCE,* [4]*University of Rennes 1, Rennes, FRANCE,* [5]*INSERM INRA UMR 1241 NuMeCan, Rennes, FRANCE,* [6]*Comprehensive Cancer Institute Eugene Marquis, Department of Radiology, Rennes, FRANCE,* [7]*Comprehensive Cancer Institute Eugene Marquis, Department of Medical Oncology, Rennes, FRANCE.*

Aim/Introduction: Phase one trial Lip Re 1 (NCT 01126463) results are promising concerning ^{188}Re-SSS Lipiodol radioembolization in hepatocellular carcinoma [1]. In order to develop a simple dosimetry protocol that could reduce the number of imaging time points, we evaluated the impact of the number of SPECT acquisition on the biodistribution and dose evaluation. **Materials and Methods:** Quantification of tumor and target organs uptake (in % of detected activity, DA) of ^{188}Re-SSS Lipiodol evaluated on SPECT/CT studies performed at 1, 6, 24, 48- and 72-hours post-administration with biological elimination corrected. Evaluation of tumor and target organs absorbed doses using MIRD formalism. Relative quantification and the dose estimation in each organ derived from each of

these 5 subsets and derived from one, two- or three-time subsets were compared to those obtained using all five data points. Variability of the relative quantification and the dose evaluation were calculated as percent difference. **Results:** Between May 19, 2010 and September 1, 2017, six patients were administered 1645±361MBq of ^{188}Re-SSS Lipiodol. Based on 5 data points of SPECT studies (reference quantification): 90.96±1.15% of activity was detected in the liver, with 65.96±1.12% of DA in the tumor. 25.0±1.29% of DA was in the healthy liver and 9.03±0.55% in the lungs, with 5.48±0.55% in the right and 3.65±0.61% in the left lungs. Using one, two and three time SPECT subset, biodistribution quantification ranged from (compared to the reference value): -3,13 to 1.71% in whole liver, -3.84 to 1.27% in the tumor, -14.73 to 5.56% in healthy liver, -21.61 to 32.87% in right lung and -10.63 to 29.41% in left lung. Based on 5 times SPECT studies (reference dose), mean absorbed doses were as follows: 7.9±3.7Gy to whole liver, 42.7±34.0Gy to tumour, 10.2±3.7Gy to healthy liver, and 1.5±1.2Gy to lungs. Using one, two- and three-time SPECT subset, dose calculation ranged from (compared to the reference value): -8.74 to 1.56% in whole liver, -17.56 to 1.24% in the tumor, -18.75 to 6.57% in healthy liver, -16.49 to 29.97% in lungs. **Conclusion:** Biodistribution quantification and dose evaluation based on one, two- or three-time subsets are reliable for whole liver, tumor and healthy liver. **References:** [1] Delaunay K, Edeline J, Rolland Y, Lepareur N, Laffont S, Palard X, et al. Preliminary results of the Phase 1 Lip-Re I clinical trial: biodistribution and dosimetry assessments in hepatocellular carcinoma patients treated with 188Re-SSS Lipiodol radioembolization. Eur J Nucl Med Mol Imaging. 2019.

1411

e-Poster Presentation Session 10 - Oncology: Oncology - Mixed Pickles

Tuesday, October 15, 2019, 14:30 - 16:00 Room 133/134

EPS-138

Is it reliable to perform radioguided surgery with Magnetic Resonance Imaging after neoadjuvant chemotherapy in patients with breast cancer?

S. Fuertes Cabero*, V. Martinez de Vega, S. Linares, U. Vera Schmülling, G. Hernandez Cortes, R. Sainz De La Cuesta, R. Murillo, L. Gonzalez Cortijo, A. Maldonado Suarez;*
H. Universitario Quironsalud Madrid, Pozuelo de Alarcón (Madrid), SPAIN.

Aim/Introduction: To evaluate if it is reliable to perform radioguided surgery with breast Magnetic Resonance Imaging (MRI) after neoadjuvant chemotherapy in patients with breast cancer. The study evaluated the correlation with the pathological histological response and follow-up of the disease. **Materials and Methods:** This is a retrospective study performed from October-2011 to April-2015. 71 breast cancer patients treated with neoadjuvant chemotherapy were enrolled in this study. The diagnosis was performed: breast and axillary ultrasound, breast MRI and mammography. During the treatment, MRI was performed in the middle and at the end of treatment. The response at the end of the treatment by MRI was classified as: Complete Response (RC): Disappearance of the enhancement, Subtotal Response (SR): Punctate uptake <4mm and Partial Response (PR): Tumor Remains > 4 mm. To evaluate the pathological histological response we used The Miller and Payne system. The day before surgery an intralesional dose of 99mTc-nanocolloid (activity of 4 mCi and 0.2 ml volume) was injected guided with MRI using a titanium needle. The site of injection and lymphatic drainage were confirmed by scintigraphy image. Intraoperative lesion and sentinel lymph node were localized and excised during surgery using a gamma probe. In some cases were necessary to administer blue day. **Results:** The 100% of the patients got a complete surgical excision of primary breast tumour with free margins. Lymphoscintigraphy showed drainage in 89% patients. When we analyzed the correlation between MRI-response and the pathological histological response: 82.2% patients with CR corresponded G5 and 15.5% G4. 50% patients with SR corresponded G5 and 41.7% G4. 50% patients with RP corresponded G3, 17% G2 and 33.3% G4 and G5. 5-years Follow-up Media, 94.4 % patients were free disease. **Conclusion:** Our results demonstrate MRI radioguided surgery after neoadjuvant chemotherapy is a reliable technique for complete excision nonpalpable breast lesions and to avoid recurrences. We found a good correlation between MRI-response and the pathological histological response. **References:** None.

EPS-139

PSMA Expression according to different Prostate Cancer Bone Metastases subtypes

P. I. d. P. Soeiro[1]*, R. Silva*[1,2]*, G. Costa*[1,3]*, J. Pedroso de Lima*[1,2,3]*;*
[1]*Centro Hospitalar e Universitário de Coimbra, Coimbra, PORTUGAL,* [2]*Instituto de Ciências Nucleares Aplicadas à Saúde, Coimbra, PORTUGAL,* [3]*Faculdade de Medicina da Universidade de Coimbra, Coimbra, PORTUGAL.*

Aim/Introduction: Prostate cancer (PCa) has historically been associated with blastic bone metastases, but hybrid imaging and, more recently, [^{68}Ga]Ga-PSMA PET/CT have shown that other types, although less frequent, are also present. Furthermore, the scientific literature implies that lytic lesions are associated with aggressive PCa phenotypes.The aim of this study was to evaluate PSMA expression of different PCa bone metastasis subtypes, as assessed by [^{68}Ga]Ga-PSMA PET/CT uptake. **Materials and Methods:** All PCa patients referred to our center, between October 2015 and March 2019, for [^{68}Ga]Ga-PSMA PET/CT with bone metastasis were included. Only staging and restaging scans performed in a first biochemical relapse setting were accepted. Castration resistant PCa and patients submitted to palliative systemic therapies (as chemotherapy or ADT) were also rejected. All bone metastasis of significant size (above 15mm) were classified according to morphology as blastic,

lytic, mixed or undetectable. Size, SUVmax and Hounsfield units were also recorded. **Results:** A total of 725 [^{68}Ga]Ga-PSMA PET/CT scans were performed during the designated time window. One hundred and eighty seven patients presented with bone metastasis, of which only 43 (70±9.2 46-87 years) fulfilled the inclusion criteria. We analysed 216 lesions: 100 blastic, 42 mixed, 38 lytic and 36 undetectable by CT. The pelvis was the most frequent location (77), followed by the spine (65), costal grid (34) and lower limbs (13). The average SUVmax for all subtypes was 9.0 g/ml (±9.0, 1.1-68.0). SUVmax was not statistically different between the different bone metastasis subtypes (Kruskal-Wallis, p: 0,065). **Conclusion:** PSMA expression, as assessed by [^{68}Ga]Ga-PSMA PET/CT uptake, was not statistically different between the diverse bone metastasis subtypes. **References:** None.

EPS-140

Ga68 PSMA or F18-Fluciclovine: When & Why - A Comparative Review of early clinical experience in a UK centre

M. Didier, *S. Vinjamuri;*
The Royal Liverpool and Broadgreen University Hospitals NHS, Liverpool, UNITED KINGDOM.

Aim/Introduction: Due to various regulatory and commissioning restrictions, Centres across the world are allowed to use different tracers to characterize the prostate, pelvis and bones in patients with possible recurrent prostate cancers. Temporary suspension of our Ga68 PSMA (PSMA) scanning service enabled us to attain approval and use a relatively newer tracer F18-Fluciclovine (FLUC). Given this opportunity we sought to make some comparison of the clinical usefulness of these two tracers. In the absence of direct comparison of usage of the two tracers in the same patient, we decided to have a "real-world experience" comparison between the two tracers in cohorts matched for age and risk status. **Materials and Methods:** 31 patients scanned (age range 57 to 80) with FLUC since March 2019 were therefore matched with 31 matched patients from our cohort of 370 patients scanned with PSMA between 2016 -19 . We then analysed the patterns of avidity (ie prostate, pelvic nodes or bones/distant metastases or combinations of these). **Results:** The largest proportion of the patients were found within the age ranges 65 to 70 (n=13) and 70 to 75 (n=9) and there were more high risk group patients (n=20). The net overall positivity rate for FLUC was 74% (23) compared to 84% (26) for PSMA. The FLUC scan identified more local prostatic avidity (13/23 vs 8/26 for PSMA), while the PSMA scan identified more extra-prostatic sites of avidity (21/26 vs 14/23 for FLUC). In the more common ages of presentation to us, PSMA identified more disease in both groups of 65 to 70 (FLUC 50% vs PSMA 70%) and 70 to 75 (FLUC 50% vs PSMA 89%). When these results were interpreted in the clinical context, the comparative detection rates were for High Risk (FLUC 60%; PSMA 76%); Intermediate risk (FLUC 0%; PSMA 75%;] and Low Risk (FLUC 0%; PSMA 100%) (2 cases had unknown risk status). **Conclusion:** In this small study limited due to its retrospective nature, we found subtle differences between the use of FLUC and PSMA. Both scans were more useful in the high risk group, and FLUC scans were more likely to be abnormal in the 65 to 70 age group while PSMA scans were more likely to be abnormal in the 70 to 75 age group. Further analysis across a bigger comparative cohort involving multiple centres may be helpful to identify specific roles for each tracer. **References:** None.

EPS-141

Risk-stratification of significant prostate cancer by 18F-choline PET/MRI is more accurate and cost-effective than multi-parameter MRI alone

M. R. Piert[1], *M. S. Davenport*[1], *C. Barnett*[1,2], *J. S. Montgomery*[1], *E. Lee*[1,3], *X. Shao*[1], *L. P. Kunju*[1], *B. Denton*[1];
[1]*University of Michigan, Ann Arbor, MI, UNITED STATES OF AMERICA,* [2]*RTI Health Solutions, Research Triangle Park, NJ, UNITED STATES OF AMERICA,* [3]*Department of Information and Statistics, Chungnam National University, Daejeon, KOREA, REPUBLIC OF.*

Aim/Introduction: A prospective single-arm clinical trial (NCT01751737) was conducted to determine the diagnostic efficacy and cost-effectiveness of 18F-choline PET/MRI to detect Gleason ≥3+4 prostate cancer. **Materials and Methods:** Before targeted and systematic prostate biopsy, multi-parametric MRI and 18F-choline PET/CT were performed in 56 subjects with 90 Likert score 3-5 MRI target lesions, using a 18F-choline target-to-background ratio (TBR) >1.58 to indicate a positive 18F-choline result. MRI-targeted- and standard prostate biopsies were performed after registration of real-time transrectal ultrasound with T2-weighted MRI. A mixed-effects logistic regression was applied to measure the performance of MRI vs. 18F-choline PET/MRI (based on prospective Likert and retrospective PI-RADS version 2 scores). Health and economic consequences of 18F-choline PET/MRI for detection of Gleason ≥3+4 cancer were assessed using a Markov model of prostate cancer onset and progression. The cost-effectiveness of PET/MRI strategies was compared to universal standard biopsy, MRI alone with biopsy only for PI-RADS=3-5 lesions, and MRI alone with biopsy only for Likert=4-5 lesions. For each MRI strategy, either no biopsy or standard biopsy could be performed after a negative MRI. Deaths averted, quality-adjusted life years (QALYs), cost, and incremental cost-effectiveness ratios (ICERs) were estimated. **Results:** The per-patient accuracy of systematic and targeted biopsy based on MRI alone was 69.6% for Likert=4-5 scores. The best-performing PET/MRI strategy that selected all high-risk (Likert=5) plus any Likert=4 lesion with elevated 18F-choline TBR>1.58 improved the accuracy to 92.9% (p=0.002). Also, selecting all PI-RADS=5 lesions plus any PI-RADS=3-4 lesion with 18F-choline TBR>1.58 was significantly more accurate (91.1%) than MRI alone (accuracy=75%;p=0.016). When 18F-choline PET/MRI was negative, standard biopsy was more expensive and had lower QALYs than performing no biopsy. The screening strategy that performed 18F-choline PET/MRI with Likert scoring ($22,706/QALY gained relative to MRI alone) recommended standard and targeted biopsy for men with positive imaging

and no biopsy for men with negative imaging, and reduced the number of biopsies by 35% compared to MRI alone. When comparing the same policies using PI-RADS, hybrid 18F-choline PET/MRI cost $46,867/QALY gained relative to MRI alone. In threshold analysis, the best strategy among those considered remained cost-effective when sensitivity and specificity of PET/MRI and combined biopsy were simultaneously reduced by 20 percentage points, indicating robustness of the conclusions to model parameter estimates. **Conclusion:** 18F-choline PET/MRI for detection of Gleason ≥3+4 primary prostate cancer is more accurate and cost-effective than MRI alone, mainly by reducing the number of unneeded biopsies and therapies. **References:** None.

EPS-142

Comparison of ^{68}Ga-PSMA-11 and ^{18}F-DCFPyL in prostate cancer patients with biochemical recurrence after prostatectomy

L. van Kalmthout[1], *M. Wondergem*[2], *B. Jansen*[3], *H. van Melick*[4], *D. Oprea-Lager*[3], *A. Vis*[3], *J. de Klerk*[5], *F. van der Zant*[2], *M. Lam*[1]; [1]*Academic hospital, Utrecht, NETHERLANDS,* [2]*Noordwest Ziekenhuisgroep, Alkmaar, NETHERLANDS,* [3]*Academic hospital, Amsterdam, NETHERLANDS,* [4]*St. Antonius Ziekenhuis, Nieuwegein, NETHERLANDS,* [5]*Meander Medisch Centrum, Amersfoort, NETHERLANDS.*

Aim/Introduction: ^{68}Gallium (^{68}Ga)-labeled PET tracers, e.g. ^{68}Ga-PSMA-11, targeting the prostate-specific membrane antigen (PSMA) receptor are increasingly used to localize the site of recurrence in patients with a biochemical recurrence (BCR) of prostate cancer (PCa). Labeling of PSMA tracers with fluor-18 (^{18}F), e.g. ^{18}F-DCFPyL, leads to improved image quality and may enhance the detection of metastases. The present study aims to assess the detection performance of ^{18}F-DCFPyL PET/CT compared to ^{68}Ga-PSMA PET/CT in patients with a BCR after prostatectomy. **Materials and Methods:** From 2015 up to 2018, 160 consecutive patients, scanned with either ^{68}Ga- PSMA or ^{18}F-DCFPyL for BCR (PSA-level: 0.5-3.5 ng/ml) after prostatectomy in four hospitals in the Netherlands, were retrospectively analyzed. Imaging was performed according to standard acquisition protocols using ^{68}Ga-PSMA-11 (n = 80; 1.5-2.0 MBq/kg, PET 60 min post-injection) or ^{18}F-DCFPyL (n = 80, 3.0 MBq/kg, PET 120 min post-injection). Both tracers were compared on basis of site of tumor recurrence, number of detected lesions and PSA-stratified detection rates. Statistical analyses were performed using SPSS Statistics version 24. **Results:** The overall detection rate of ^{68}Ga-PSMA PET/CT and ^{18}F-DCFPyL PET/CT was 71.3% and 74.4% (p = 0.795), respectively. For PSA-levels of 0.5-1.0, 1.0-1.5, 1.5-2.0, 2.0-2.5, 2.5-3.0 and 3.0-3.5 ng/ml, PSA-stratified detection rate of ^{68}Ga-PSMA was 63.6%, 75.0%, 83.3%, 84.6%, 66.7% and 100%. Detection rate of ^{68}F-DCFPyL in these PSA-categories was 62.1%, 73.7%, 90%, 100.0%, 80.0%, 100.0%. Differences in detection rate were not found to be statistically significant. **Conclusion:** Our data suggest that the diagnostic performance of both ^{68}Ga-PSMA-11 and ^{18}F-DCFPyL in the setting of biochemical recurrence of PCa post-prostatectomy is comparable. **References:** None.

EPS-143

Prognostic role of the Total Metabolic Tumor Volume (TMTV) and the Total Lesion Glycolysis (TLG) in the definition of clinical outcome and response to therapy in Hodgkin's Lymphoma

M. Spallino[1,2], *M. Cuzzocrea*[1], *E. De Ponti*[3], *S. Bolis*[4], *I. Casaroli*[4], *C. Landoni*[1,5], *L. Guerra*[5];
[1]*Nuclear Medicine Department, University Milan Bicocca, Milan, ITALY,* [2]*ASST Grande Ospedale Metropolitano Niguarda, Milan, ITALY,* [3]*Medical Physics Department, San Gerardo Hospital ASST, Milan, ITALY,* [4]*Hematology Department, San Gerardo Hospital ASST, Monza, ITALY,* [5]*Nuclear Medicine Department, San Gerardo Hospital ASST, Monza, ITALY.*

Aim/Introduction: Recent papers showed that the TMTV and TLG assessed in baseline-PET are correlated to prognosis and consequently could be used to optimize the treatment strategy, but published results are sometimes discordant. In this work we evaluate whether quantitative parameters in baseline-PET are correlated to overall-survival (OS), disease-free-survival (DFS) and treatment response in patients with Hodgkin's Lymphoma (HL) treated at our Hematology Division. **Materials and Methods:** 163 patients (94men; mean age: 38y(18-81) with newly diagnosed HL, stage I-IV (11stage I, 49stage IIA, 34stage IIB, 33stage III, 36stage IV) referred to our Hospital were retrospectively evaluated. We calculated the semiquantitative parameters at baseline-PET using PET viewer add-on of FIJI software with a fixed threshold of 41% of the maximum. Sum rank test was performed to evaluate statistical differences between the semiquantitative parameters in patients with different outcome. Receiver operating characteristics (ROC) analysis was performed to evaluate the best threshold to discriminate patients' prognosis. **Results:** Overall, baseline-PET of 158/163 HL patients were evaluated for quantitative parameters. Median follow up duration was 40 months, 5 patients died and 11 relapsed.In dead and alive patients, median MTV values were 269.5 (87.3-546.5) vs 84.6 (3.5-590.9) (p=0.036) respectively and median TLG values were 2772.1 (341.7-3724.1) vs 492.4 (15.5-4596.8) respectively (p=0.029). According to ROC analysis, a TMTV cut-off value of 269.5 mL showed a sensitivity, specificity and accuracy respectively of 60%, 88.2% and 87.3% to identify patients with good vs worse prognosis; the same figure for TLG were 60%, 96.7% and 95.6% with a cut-off value of 2772.1. Kaplan Meier curves showed an OS significantly different in patients with low and high TMTV (p=0.05) and TLG (p<0.05). We classified patients with Deauville Score (DS) 1-2-3 at interim-PET as responders and patients with DS 4-5 as non-responders. TMTV and TLG were good to discriminate responder vs non-responder patients with the sum rank test (p=0.07 and 0.05 respectively).No statistically significant difference was found comparing metabolic parameters relative to relapsed and non-relapsed patients. **Conclusion:** We demonstrated

the correlation between baseline-PET metabolic parameters and clinical outcome in terms of prognosis and response to therapy defined by interim-PET. These results are promising but confirmation in a larger series is requested, particularly to increase patients with worse prognosis. If these results will be validated in a larger population, TMTV and TLG, in addition to other imaging parameters (interim-PET), can be useful benchmark to stratify patient prognosis and modulate the treatment strategy. **References:** None.

EPS-144

Bone Marrow Evaluation In Initial Staging Of Follicular Lymphoma. 18F-FDG PET/CT Versus Bone Marrow Biopsy

M. Cortes Romera[1], *S. Mercadal-Vilchez*[2], *A. Palomar-Muñoz*[1], *A. Sabaté-Llobera*[1], *F. Climent-Esteller*[3], *E. Llinares-Tello*[1], *E. Gonzalez-Barca*[2], *C. Gámez-Cenzano*[1];
[1]*Unit PET/CT (IDI)- Department of Nuclear Medicine. Hospital U. de Bellvitge-IDIBELL., L'Hospitalet De Llobregat (Barcelona), SPAIN,* [2]*Department of Hematology. ICO. Hospital Duran i Reynals-IDIBELL., L'Hospitalet De Llobregat (Barcelona), SPAIN,* [3]*Department of Pathology. Hospital U. de Bellvitge-IDIBELL, L'Hospitalet De Llobregat (Barcelona), SPAIN.*

Aim/Introduction: Bone or bone marrow focal FDG uptake in PET/CT is highly sensitive to detect bone marrow involvement(BMI) in HL and in aggressive NHL, obviating the need of a bone marrow biopsy(BMB). However, there are limited data to support this procedure in other histologies, such as follicular lymphoma(FL). The aim of this study is to assess the utility of PET/CT and its concordance with BMB in the detection of BMI in FL. **Materials and Methods:** Ninety-two patients(45 women, mean age 60.8 years) diagnosed with FL(de novo or relapsed) underwent an FDG-PET/CT. Patients with transformed or grade 3B FL, as well as those without a BMB or with non-valuable BMB findings were excluded. BMB was used as reference standard. PET images were evaluated visually and semiquantitatively. PET was considered positive for BMI at the visual assessment when there was diffuse bone marrow uptake(BMU) over liver(BMU>L), when it was equal to liver and there was also BMU in the limbs(BMU=L+E), or when there was a focal/multifocal/heterogeneous BMU pattern. Semiquantitative assessment was performed using the ratio between SUV(max and mean) of the left iliac crest and the liver. Concordance and agreement between PET(using visual analysis) and BMB were analyzed. Accuracy(A), sensitivity(S), specificity(Sp), and positive and negative predictive values(PPV and NPV, respectively) between visual and semiquantitative analysis were calculated. **Results:** Histological grading based on WHO classification showed: grade 1-2 in 59, 3A in 28, and "non-gradable" in 5 patients. PET/CT detected BMI in 42 cases(45%), and BMB in 38(41%). A substantial agreement was obtained between both techniques(Cohen's kappa 0.647). Concordant results between PET/CT and BMB were obtained in 76 patients(83%): 32 with positive PET/CT(13 uni-/multifocal, 3 heterogeneous, 13 diffuse(BMU>L) and 3(BMU=L+E) and BMB results(42%) and 44 with negative PET/CT and BMB results(58%). Discordant results were obtained in 16 cases(17%), 10 of them with positive PET/CT and negative BMB(2 diffuse BMU>L, 1 diffuse BMU=L+E, and 7 uni/multifocal pattern), and 6 with negative PET/CT and positive BMB. A, S, Sp, PPV and NPV were 83%,84%,81%,76% and 88%, respectively, for visual analysis; 75%,56%,88%,77% and 74%, respectively for semiquantitative analysis using the ratio SUVmaxBMU/liver; and 73%,43%,94%,84% and 70%, respectively, using the ratio SUVmeanBMU/liver. **Conclusion:** PET/CT detects more BMI in FL compared to BMB. Concordance between both techniques is high. Around 30% of patients with a focal uptake at the PET/CT had a negative BMB, while more than 80% with a diffuse pattern had a positive BMB. **References:** None.

EPS-145

Impact of interim FDG PET/CT on Hodgkin Lymphoma adult patients at King Hussein Cancer Center (KHCC), Jordan

A. N. K. Al-Ibraheem, F. Anwer, A. Khalaf;
King Hussein Cancer Center, Amman, JORDAN.

Aim/Introduction: The aim of this study was to assess the value of interim FDG PET/CT in predicting response to treatment of HL patients at KHCC. **Materials and Methods:** We retrospectively reviewed the records of HL patients who underwent FDG PET/CT between January 2014 and December 2017. 254 patients were included in this study whose records comprised initial PET, interim PET after cycle 2 or cycle 4 of ABVD and end of therapy PET. All had their PET scans in KHCC.The Deauville 5-point scoring (5-ps) was considered for the classification of patients as complete metabolic responders (CMR) if patients achieved 5-ps 1-3 in interim PET or as non-complete metabolic responders (nCMR) if patients achieved 5-ps 4 and 5. The decision of the multidisciplinary team based on the results of the end of treatment PET were adopted to classify patients as having complete response (CR) or residual active disease (RAD). **Results:** Our patient cohort are illustrated in the table below. Interim FDG-PET scan (either after cycle 2 or cycle 4 of ABVD therapy) was classified as CMR in 188/254 (74%) with their final FDG-PET showed CR in 185/188 (98.4%) of cases and 3 (1.6%) patients with RAD within the first 6 months follow up. In the remaining 66 (26%) patients, interim FDG-PET was nCMR with Score 4 in 60 patients (23.6%) and Score 5 in 6 patients (2.4%). In the aforementioned 60 patients with 5-ps 4 who continued the ABVD protocol, end of treatment FDG- PET imaging showed RAD in 25 patients (41.6%) of patients, CR in 30 patients (50%) and indeterminate response in 5 patients (8.4%).Statistical analysis revealed that interim FDG- PET after 2 or 4 cycle of ABVD had a negative predictive value of 98.4% and positive predictive value of 45.4%. Significant percent of patients with nCMR, particularly Deauville score 5, didn't achieve further response on this ABVD regimen at the end of treatment. **Conclusion:** This study showed that interim FDG-PET/CT scan after cycle 2 or 4 has a valuable role in predicting response to ABVD treatment

in HL. Patients with nCMR Deauville score 5 in interim PET commonly would have RAD at the end of treatment. Escalating of treatment in this group should be advocated. **References:** None.

EPS-146

Usefulness of gradient tree boosting for predicting histological subtype and EGFRmutation status of non-small cell lung cancer on ^{18}F FDG-PET/CT

S. Koyasu, M. Nishio, H. Isoda, Y. Nakamoto, K. Togashi;
Graduate School of Medicine, Kyoto University, Kyoto, JAPAN.

Aim/Introduction: To develop and evaluate a radiomics approach for classifying histological subtypes and epidermal growth factor receptor (EGFR) mutation status in lung cancer. **Materials and Methods:** PET/CT images of NSCLC Radiogenomics were obtained from public databases and used to establish two datasets, respectively to classify histological subtypes (156 adenocarcinomas and 32 squamous cell carcinomas) and EGFR mutation status (38 mutant and 100 wild-type samples). Seven types of imaging features were obtained from PET/CT images of lung cancer. Two types of machine learning algorithms were used to predict histological subtypes and EGFR mutation status: random forest (RF) and gradient tree boosting (XGB). The classifiers used either a single type or multiple types of imaging features. In the latter case, the optimal combination of the seven types of imaging features was selected by Bayesian optimization. Receiver operating characteristic analysis, area under the curve (AUC), and 10-fold cross-validation were used to assess the performance of the approach. **Results:** In the classification of histological subtypes, the AUC values of the various classifiers were as follows: RF, single type: 0.759; XGB, single type: 0.760; RF, multiple types: 0.720; XGB, multiple types: 0.843. In the classification of EGFR mutation status, the AUC values were: RF, single type: 0.625; XGB, single type: 0.617; RF, multiple types: 0.577; XGB, multiple types: 0.659. **Conclusion:** The radiomics approach to PET/CT images, together with XGB and Bayesian optimization, is useful for classifying histological subtypes and EGFR mutation status in lung cancer. **References:** None.

EPS-147

AI-based Detection of Lung Lesions in FDG-PET/CT from Lung Cancer Patients

L. Edenbrandt[1], *R. Kaboteh*[1], *S. Salehian*[1], *J. Ulen*[2], *O. Enqvist*[2,3], *P. Borrelli*[1];
[1]*Sahlgenska University Hospital, Gothenburg, SWEDEN,* [2]*Eigenvision, Malmö, SWEDEN,* [3]*Department of Electrical Engineering, Chalmers University of Technology, Gothenburg, SWEDEN.*

Aim/Introduction: Staging lung cancer is one of the most common indications for FDG-PET/CT in nuclear medicine departments. PET/CT is used both to differentiate between malignant and benign pulmonary nodules and to assess mediastinal lymph nodes and distant metastases. Our aim is to develop a completely automated method based on artificial intelligence (AI) for the analysis of FDG-PET/CT in patients with known or suspected lung cancer. In this project we take the first step and focus on the detection of abnormal lung lesions. **Materials and Methods:** A total of 81 patients, who underwent FDG-PET/CT due to suspected lung cancer or for the management of known lung cancer were studied. The patient group was divided into a training (80%) and a validation (20%) group. A nuclear medicine specialist manually marked abnormal lung lesions in all FDG-PET/CT studies.A convolutional neural network (CNN) was trained to classify each image voxel as either background or lung lesion. The input to the network was the PET and CT images along with an organ mask, marking the lungs, vertebrae and the heart. The organ mask was automatically generated from the CT image using a different CNN [1]. To focus on detection rather than exact delineation, the boundaries of each annotated lesion were marked as don't-care in the training.The output of the CNN was processed by removing spurious voxels far away from the lungs as well as components smaller than 0.1 ml. The remaining connected components are then treated as detected lesions. **Results:** A total of 26 abnormal lesions were detected in 16 of the 17 patients of the validation group. The lesion sensitivity was 91% and the positive predictive value was 85%. One of the 17 patients did not have any abnormal lesions and the AI-method correctly marked no lesions in this case. **Conclusion:** A completely automated AI-based method can be used to detect lung lesions with high accuracy. In future studies we will apply AI-methods for the assessment of lymph nodes and distant metastases. These type of clinical decision support tools appears to have significant clinical potential. **References:** [1]. Lindgren Belal S, Sadik M, Kaboteh R, Enqvist O, Ulén J, Poulsen MH, Simonsen J, Høilund-Carlsen PF, Edenbrandt L, Trägårdh E. Deep learning for segmentation of 49 selected bones in CT scans: First step in automated PET/CT-based 3D quantification of skeletal metastases. Eur J Radiol. 2019 Apr;113:89-95.

EPS-148

Efficacy and toxicity profile of low dose 177 Lutetium-Ethylenediamine tetra methylene phosphonate (177Lu-EDTMP) for bone pain palliation in patients with skeletal metastases

A. S A, D. Halanaik, N. Pandit, M. Ponnusamy;
JIPMER, Pondicherry, INDIA.

Aim/Introduction: Radionuclide therapy has the advantage in comparison to other modalities for pain palliation in targeting all the involved skeletal metastasis sites simultaneously. It is associated with fewer side effects. The only side effect is dose limiting transient myelosuppression. There is paucity of data on therapeutic efficacy and safety profile of low dose 177Lu-EDTMP in terms of the degree of pain relief, performance status

and toxicity profile for bone pain palliation. We conducted a prospective observational study to assess the efficacy and toxicity profile of low dose 177Lu-EDTMP for bone pain palliation in patients with skeletal metastases. **Materials and Methods:** Patients with multiple painful bone metastasis documented on 99mTc-MDP bone scan within last 8 weeks were being included for 177Lu-EDTMP therapy. Pain and performance were assessed using visual analog scale, Karnofsky performance scale and mobility score. Pre-therapy haemogram was in the range as in inclusion criteria. Patients were given 0.37 MBq/kg body weight of 177Lu-EDTMP intravenously on out-patient basis. Whole body scan was done after 2 hours to document radiopharmaceutical distribution. All patients were followed up at 4, 8 and 12 weeks post-therapy. Blood hemogram is advised following therapy every fortnightly up to 12 weeks. The VAS pain score, mobility score and Karnofsky performance scores (KF score) were recorded at 4, 8 and 12 weeks. **Results:** 20 patients who completed the follow up of 3 months were included in the analysis. The VAS Pain, KF score, mobility score and blood parameters were expressed as mean and standard deviation. The changes in continuous variables at different time point were assessed by using one-way repeated measure of ANOVA. It was observed that the pain response assessed by VAS score has significantly decreased ($p<0.05$). KF score showed statistically significant change ($p<0.05$). Mobility score improved but was not statistically significant ($p>0.05$). The blood parameters were in the normal range during the entries period of follow up. But there was statistically significant decrease in WBC count ($p<0.05$). **Conclusion:** Low dose 177Lu-EDTMP was effective in reducing pain in patients with skeletal metastasis. The performance of the patient was improved. The only observed toxicity was myelosuppression mostly affecting the WBC count. But the WBC count came to normal by the end of the 3 month follow up. So 177 Lu-EDTMP in low dose is definitely a promising radionuclide in bone pain palliation. **References:** None.

EPS-149

Design of a Bimodal Ligand of Neurotensin Receptor 1 for ^{68}Ga-PET Imaging and Fluorescence-Guided Surgery of Pancreatic Cancer

E. Renard[1], *P. A. Dancer*[2], *C. Portal*[3], *F. Denat*[1], *A. Prignon*[4], *V. Goncalves*[1];
[1]*Institut de Chimie Moleculaire de l'Université de Bourgogne, Université Bourgogne Franche-Comté, Dijon, FRANCE,* [2]*Kaer Labs, Nantes, FRANCE,* [3]*Edinburgh Molecular Imaging, Edinburgh, UNITED KINGDOM,* [4]*Laboratoire d'Imagerie Moleculaire Positonique, Sorbonne Université, Paris, FRANCE.*

Aim/Introduction: Pancreatic cancer is the 4th leading cause of death by cancer in Europe. This cancer has a poor prognosis, which is due to late clinical presentation, rapid progression and limited effect of chemotherapy. Moreover, 30 to 50% of patients who have had surgery, relapse because of the difficulty to accurately delineate tumor margins. Therefore, there is real need to develop new methods that improve both the diagnosis and the accuracy of tumor resection. An interesting target involved in the proliferation and progression of pancreatic cancer is the neurotensin receptor 1 (NTSR1). In this study, we describe the development and in vivo evaluation of PET/fluorescent imaging agents targeting NTSR1. **Materials and Methods:** Five bimodal imaging agents were synthesized, based on the structure of the NTSR1 peptide agonist NT20.3. The radiometal chelator, (R)-NODAGA, and three cyanine 5 derivatives were conjugated to the N-terminal lysine residue. Several spacers were introduced. The affinity of ligands for NTSR1 was determined in vitro after ^{nat}Ga labeling. The compounds were radiolabeled with ^{68}Ga and their biodistribution was evaluated on nude mice bearing a subcutaneous xenograft of AsPC1 (human pancreatic adenocarcinoma) cells. PET images were acquired 1 h post injection. Mice were sacrificed and the uptake of tracers into different organs was measured by gamma-counting. Fluorescence images were recorded at different times and tumors were removed through fluorescence-guided surgery. **Results:** Bimodal imaging agents were obtained with an overall yield of 10 to 33%. In vitro studies confirmed the high affinity of all compounds for NTSR1 with Ki values in the nanomolar range. Spacers did not have a significant impact on affinity for the receptor. In contrast, the addition of sulfonate groups resulted in a decrease in affinity. The radiolabeling with ^{68}Ga was achieved with good radiochemical yields (95%) and purity (>99%). PET imaging studies allowed us to identify the compound [^{68}Ga]-NODAGA-Lys(Cy5**)-PEG_2-[Me-Arg^8, Tle^{12}]-NT(7-13), as the one showing the most promising pharmacokinetic profile. Biodistribution data showed a high tumor uptake (2.6%ID/g 90 min p.i.) with a high tumor-to-normal tissues ratio. Similar results were obtained by fluorescence imaging and confirmed during the fluorescence-guided resection of tumor masses. **Conclusion:** A novel peptide-based bimodal imaging agent for NTSR1-positive tumors was developed. This compound showed high tumor uptake and fast clearance from non-targeted organs, leading to high contrast in PET and fluorescence imaging. These results highlight the potential of this agent for the diagnosis and the fluorescence-guided surgery of pancreatic cancer. **References:** None.

EPS-150

PSMA-targeting hybrid tracers based on heterobifunctional cyanine spacer moieties - tuning the pharmacokinetic properties and exploring dye interaction with PSMA

A. Hensbergen[1], *T. Buckle*[1], *D. M. van Willigen*[1], *M. Schottelius*[2], *M. M. Welling*[1], *F. A. van der Wijk*[1], *H. G. van der Poel*[3], *T. Maurer*[4], *H. Wester*[2], *F. W. B. van Leeuwen*[1];
[1]*Leiden University Medical Center, Leiden, NETHERLANDS,* [2]*Technische Universität München, Garching, GERMANY,* [3]*The Netherlands Cancer Institute, Amsterdam, NETHERLANDS,* [4]*Martini Klinik, Hamburg, GERMANY.*

Aim/Introduction: Precision surgery provides means to improve patient outcome after prostate cancer surgery. Herein

radical resection can be promoted via visualisation of tumour margins and (local) metastases. The prostate-specific membrane antigen (PSMA) has been shown to support staging of the disease via preoperative nuclear imaging and has helped realize radioguided tumour resections. Ideally, the latter approach is complemented with the ability to optically detect lesions. As the chemical composition of the linker moiety has been critical in PSMA radiotracer development, the same should be true for the development of hybrid (radioactive and fluorescent) tracer analogues. Here, the relationship between the linker moiety and overall hybrid tracer performance was structurally studied by exploring the use of heterobifunctional Cy5 molecules that act as a linker between an EuK moiety and a MAS_3 chelate. **Materials and Methods:** A panel of five EuK-(X)Cy5(X)-MAS_3 (X = SO_3^- or Ar) PSMA-specific hybrid tracers was synthesized. The effect of the C- or N- terminal dye functionalisation was evaluated through assessment of the lipophilicity, (photo) physical properties, serum interactions, chemical stability, ability to target PSMA in vitro (confocal microscopy) and PSMA receptor affinity (IC_{50} with ([^{125}I]I-BA)KuE)). Following radiolabelling with ^{99m}Tc (40 MBq), in vivo SPECT imaging, quantitative biodistribution analysis (%ID/g; 1 nmol) and ex vivo fluorescence imaging was conducted in BALB/c nude mice (n = 6/tracer) with orthotopically transplanted PSMA-positive PC346C tumours. **Results:** Synthesis yielded EuK-Cy5-MAS_3, EuK-(SO_3^-)Cy5-MAS_3, EuK-Cy5(SO_3^-)-MAS_3, EuK-(Ar)Cy5-MAS_3, EuK-Cy5-(Ar)-MAS_3. Presence of a SO_3^- moiety resulted in preferable photophysical properties (higher brightness) and serum interactions (binding and chemical stability). All tracers allowed tumour visualization with SPECT and fluorescence imaging. C- or N-terminal dye functionalisation was shown to directly influence in vitro and in vivo tracer performance; clear differences were seen in tracer affinity (IC_{50} range: 19.2 ± 5.8-175.3 ± 61.1 nM) and in vivo characteristics (e.g., tumour-to-prostate and tumour-to-muscle ratio: respectively 5.4-31.7 and 9.3-465.8). [^{99m}Tc]EuK-(SO_3)Cy5-MAS_3 showed the highest affinity and most favourable in vivo characteristics, i.e., highest tumour-to-background and low renal (18.4 ± 8.5 %ID/g), splenic (1.0 ± 1.2 %ID/g), and salivary gland (0.02 ± 0.01 %ID/g) uptake. **Conclusion:** Incorporation of bifunctional Cy5 bridging dyes between an EuK moiety and a MAS_3 chelate in PSMA-targeting tracers was shown to be feasible. Next to influencing the receptor affinity, systematic variation in C- and N-terminal substitution of the cyanine backbone of the EuK-(X)Cy5(X)-MAS_3 hybrid tracers was shown to exert influence on the optical properties and in vivo performance. **References:** None.

EPS-151

PSMA Targeted Nuclear Robotic Surgery: Preliminary Results

B. Yilmaz Gunes[1], *S. Sahin*[2], *N. Ergul*[1], *H. F. Baytekin*[3], *Y. Colakoglu*[2], *D. Sokmen*[4], *V. Tugcu*[4], *A. I. Tasci*[2], *T. F. Cermik*[1];
[1]*Istanbul Research and Training Hospital, Nuclear Medicine Department, Istanbul, TURKEY,* [2]*Istanbul Bakirkoy Dr. Sadi Konuk Research and Training Hospital, Urology Department, Istanbul, TURKEY,* [3]*Istanbul Bakirkoy Dr. Sadi Konuk Research and Training Hospital, Pathology Department, Istanbul, TURKEY,* [4]*Istanbul Bahcelievler Memorial Hospital, Urology Department, Istanbul, TURKEY.*

Aim/Introduction: Prostate-specific membrane antigen (PSMA)-targeted positron emission tomography / computed tomography (PET/CT) is successful imaging modality in prostate cancer (PC). But many centers do not have Germanium/Gallium (Ga)-68 generator and/or PET/CT. Also, reliable identification of small and/or atypically localized lymph nodes (Ln) during robotic surgery is challenging. In this prospective multicenteric study, feasibility of tracer production using ^{99m}Technetium (Tc)-based PSMA-11 sterile cold kit, imaging procedure and accuracy with single photon emission tomography/computed tomography (SPECT/CT), technique and feasibility of ^{99m}Tc-based PSMA-radioguided robot-assisted laparoscopic radical prostatectomy (^{99m}Tc-PSMA-RG-RALRP) for Ln dissection of primary PC patients were evaluated. **Materials and Methods:** 9 primary PC patients (Mean age 65,7 years) with intermediate (n:2) or high (n:7) risk score who had PSMA receptor affinity according to Ga-68 PSMA-11 PET/CT were enrolled. ^{99m}Tc-labelled PSMA-ligand (^{99m}Tc-PSMA-I&S) was injected iv. (Mean 630 MBq; range 555-770 MBq). 61.6±7.8 min. after the injection, whole body planar scintigraphy and abdominopelvic SPECT/CT were performed. Mean time to start ^{99m}Tc-PSMA-RG-RALRP with DaVinci XI robotic platform and laparoscopic gamma probe was 18±1.7 h after injection. Radioactive rating (positive vs negative; according to background activity) of resected tissue was compared with the findings of postoperative histopathology. Physiological and pathological uptakes of organs and tissues for both imaging modalities were compared visually and quantitatively with maximum and mean standard uptake values vs. region of interest and volume of interest counts. **Results:** ^{99m}Tc-PSMA-I&S was prepared in 2 hours with > %96 purity. Physiological radiotracer distribution were similar for both imaging modalities visually but PC lesions were much more visible on PET/CT. Late imaging with SPECT/CT could able to visualize lesions better. Mean operation time and mean console time were 6 h and 4.6 h, respectively. No patient suffered from complication related to surgery. Post-operative Gleason score were 7 (n:6), 8 (n:1) and 9 (n:2). Dissected locoregional Ln number were 23,3 ± 7,8 (Range: 12 - 39) .Total dissected lymph nodes were 210 with only 2 of them were metastatic. These results were exactly the same with per-operative probe counts. **Conclusion:** According to preliminary findings of this ongoing study, ^{99m}Tc-PSMA-RG-RALRP seems to be of high value in patients with localized PC and loco-regional Ln metastases which may shorten the operation time and make surgeon feel more comfortable. If Tc-99m PSMA-I&S SPECT/CT is used for only imaging purpose, late imaging up to 20 hours is recommended. For operation patient selection based on 68Ga-PSMA PET imaging is crucial. **References:** None.

EPS-152

Impact of Ga-68 PSMA PET/CT on diagnosis and staging of hepatocellular carcinoma

C. Gundogan[1], *N. Ergul*[1], *M. S. Cakir*[2], *T. Aksoy*[1], *N. O. Kilickesmez*[2], *T. F. Cermik*[1];
[1]*University of Health Sciences, Istanbul Training and Research Hospital, Clinic of Nuclear Medicine, Istanbul, TURKEY,* [2]*University of Health Sciences, Istanbul Training and Research Hospital, Clinic of Radiology, Istanbul, TURKEY.*

Aim/Introduction: In this study, we investigated the diagnostic impact of staging Ga-68 Prostate Specific Membrane Antigen (PSMA) PET/CT on patients with Hepatocellular Carcinoma (HCC). **Materials and Methods:** Twelve Child Pugh (CP)-A and 2 CP-B HCC patients (13 M, 1 F; mean age 68.3±5.9 [range 58-76] years) were enrolled in this prospective study. All patients underwent PSMA-PET/CT scan and F-18 fluorodeoxyglucose (FDG) PET/CT scan which performed within 30 days of each other. Magnetic resonance imaging (MRI) was performed to all patients before included in the study. The maximum standardized uptake value (SUVmax) was measured for primary tumors, lymph nodes and distant metastases in PSMA-PET/CT and FDG-PET/CT. In addition to SUVmax, tumor-to-liver (T/L) and tumor-to-background (T/B [gluteus medius muscle]) taken into consideration Liver tumors defined on PET/CT scans compared with MRI. Histopathology confirmed only in 6 patients. **Results:** In PET/CT imaging, increased PSMA uptake was observed in11 patients, mild uptake was observed in two patinets and no uptake was observed in one patient. (mean±SD SUVmax 20.9±11.7). Five patients tumors were non-FDG avid, three patients showed mild FDG uptake and six patients showed increased FDG uptake (mean±SD SUVmax 9±5.3). PSMA uptake mean ratio for T/B was significantly higher in primary tumors compared with FDG (p = 0.001). However, PSMA uptake mean ratio for T/L in primary tumors was higher than FDG, no significant difference was found (p=0.16). In our study group, 61 (98%) lesions were detected with PSMA-PET/CT, while FDG-PET/CT detected only 30 (48%) lesions. Seven (50%) patients had high-AFP-secreting tumors (>200 ng/mL) and 5 (35%) had low-AFP-secreting (<20 ng/mL) tumors. We did not find a relationship between AFP levels and PSMA or FDG uptake. Three patients had abdominal metastatic lymph nodes in PSMA-PET/CT and one of them was non-FDG avid. Abdominal metastatic lymph nodes uptake in PSMA-PET/CT was higher than FDG-PET/CT in 2 of 3 patients. On the other hand, three patients had mediastinal lymph nodes and these lesions had higher SUVmax values in FDG-PET/CT than PSMA-PET/CT. Biopsy results from subcarinal and right lower paratracheal lymph nodes of one of these patients were reported as anthracosis. **Conclusion:** In patients with HCC, PSMA-PET/CT is superior to FDG-PET/CT as a molecular imaging modality, and we think PSMA-PET/CT may be a potential new method in the diagnosis of primary tumors and metastatic lesions. **References:** None.

EPS-153

Texture analysis of 18F-choline uptake in prostate gland of patients with untreated cancer: relationship with the Risk Assessment Score, additional prostate biopsy findings and patient's outcome

M. Cuzzocrea[1], *L. Florimonte*[1], *V. Longari*[1], *G. Santaguida*[1,2], *E. Orunesu*[1], *M. Castellani*[1];
[1]*Nuclear Medicine Department, Fondazione IRCCS Cà Granda Ospedale Maggiore Policlinico, Milan, ITALY,* [2]*Università degli Studi di Milano, Milan, ITALY.*

Aim/Introduction: PET/CT imaging with 18F-choline for staging prostate cancer patients is currently used in selected cases when there is a high risk of local or distant metastases on the basis of PSA levels, Gleason Score and T grade (Risk Assessment Score: RAS). Radiomics features of PET/CT prostate images could provide additional information to predict the outcome of these high-risk patients. Aim of the study was to assess the relationship between texture analysis of 18F-choline prostate gland uptake and patient's outcome. **Materials and Methods:** PET/CT images of 42 males (mean age: 67.6; range: 49-84 yrs) with increased PSA levels (median value 9.3; range: 2.4-329) and histological diagnosis of prostate cancer, were retrospectively evaluated. The radiomics features and metabolic parameters of prostate gland were calculated for each patient along with RAS. Univariate analysis was performed to assess the relationship of the single parameters with the patient's outcome expressed in terms of stable disease or biochemical progression at follow-up (median: 19.8 months; range 3-47). The performance of continuous variables was assessed by comparing area under curves (AUC) at ROC analysis. Independent predictors of outcome were also assessed with Cox model multivariate analysis. **Results:** Among 38 texture features derivable from PET images analysis, 19 were statistically different (p≤0.03) in patients with stable disease and biochemical progression. Significant differences (p<0.01) were also observed in RAS and SUV values. At ROC analysis of radiomic and metabolic features, the best performance for predicting patients outcome was observed when grey level co-occurrence matrix contrast (GLCM_contrast; AUC 0.828; p< 0.001) and grey-level zone length matrix High Gray-level Zone Emphasis (GLZLM_HGZE; AUC=0.858; p<0.001) were used. In particular, a sensitivity (Se), specificity (Sp), positive predictive value (PPV) and negative predictive value (NPV) of 77.8, 87.9, 63.6 and 93.5 respectively, was calculated for GLZLM_HGZE (cut-off = 151.4) in the prediction of the different outcome. Similar results was reported for GLCM_contrast (Se 77.8; Sp 84.8; PPV 58.3; NPV 93.3; cut-off= 9.9). At Cox regression, both radiomic parameters were found to be independent variables in the prediction of a different outcome. **Conclusion:** These preliminary data suggest that texture analysis of prostate 18F-choline uptake is feasible and some radiomic features are related to the prognosis. However, the creation of prognostic/predictive models able to consider the multiplicity of texture features and an increase of the sample size of patents are mandatory. **References:** None.

EPS-154

Feasibility of Intra Arterial LU-177 DOTA TATE Therapy in Metastatic Neuroendocrine Tumors with Liver Dominant Disease - "A Novel Theragostic Approach to Augment Therapeutic Potential"

A. A. Rajan, S. Sumati;
Gleneagles Global Hospitals, Chennai, INDIA.

Aim/Introduction: Few recent preclinical and clinical studies have demonstrated a higher first pass effect with a higher tumoral uptake in the early phases of intra-arterial administration of Ga-68 DOTANOC and In-111 DOTANOC imaging of liver metastasis in neuroendocrine tumors [1,2]. It has been hypothesized that this novel approach could be translated into theragnostics. The aim of this study was to assess the safety, tolerability and efficacy of intra arterial Lu-177 DOTA TATE therapy in patients with liver dominant metastasis in well differentiated NETs. **Materials and Methods:** Four patients with well differentiated NET liver dominant metastasis were given 4 cycles of 200 mCi of Lu-177 DOTATATE therapy intra arterially at interval of 8 weeks through selective hepatic arterial cathrterization. All patients received bilobar hepatic arterial infusions. All patients were administered aminoacid infusions for 4-6 hours starting pretherapy and continued post therapy infusions. Their complete blood counts, liver function, renal function and coagulation profiles were assessed within 2 weeks prior to each treatment cycle, in the immediate post therapy period and within 6 weeks post treatment. Radiological assessment and tumor markers were also assessed pre and post treatment. **Results:** Significant reduction in serum chromogranin A levels with partial reduction in size and tracer uptake in all patients were noted. None of the patients experienced any acute side effects or unexpected complication during therapy or in the immediate post therapy period. No RILD or renal toxicity seen during the course of therapy and even after the last cycle. Liver functions remained stable with improved quality of life. **Conclusion:** Our initial experience of intra-arterial administration of Lu-177 DOTA TATE therapy in patients with liver dominant metastasis is promising, feasible, safe and tolerable treatment. Survival benefits evaluation is ongoing and will be evaluated on subsequent follow up. **References:** 1. Kratochwil C, et al. Hepatic arterial infusion enhances DOTATOC radiopeptide therapy in patients with neuroendocrine liver metastases. Endocr Relat Cancer. 2011;18(5):595-602. doi: 10.1530/ERC-11-0144. 2. Pool SE, Kam B, Breeman WAP. Increasing intrahepatic tumour uptake of 111 In-DTPA-octreotide by loco regional administration. Eur J Nucl Med Mol Imaging. 2009;36:S427. NETs - Neuroendocrine Tumors. RILD - Radiation induced liver disease.

1511

e-Poster Presentation Session 11 - Cardiovascular: Imaging Cardiomyopathies

Tuesday, October 15, 2019, 16:30 - 18:00 Room 133/134

EPS-155

Spect Imaging Of Tspo Expression In Rat Myocardial-Infarction- Reperfusion Models With $^{99}Tc^{M}$ -labeled Tspo Ligand Cb86

X. Su, F. Su, W. Dong, J. Li, Z. Guo;
Zhongshan Hospital Xiamen University, Xiamen, CHINA.

Aim/Introduction: Objective The purpose of this study is to develop a specific TSPO-targeting $^{99}Tc^{m}$ -labeled agent ($^{99}Tc^{m}$-DTPA-CB86) for single-photon-emission- computed-tomography (SPECT) imaging of TSPO expression in myocardial-infarction-reperfusion rat models. **Materials and Methods:** After SPECT/CT imaging with $^{99}Tc^{m}$-DTPA-CB86 at 1, 2, 4, 12, and 36 h after myocardial- infarction-reperfusion, the models were validated by ex vivo autoradiography, TTC staining, and immunohistochemistry and in vivo echocardiography and classical ^{18}F-FDG PET metabolic imaging. **Results:** The $^{99}Tc^{m}$-DTPA-CB86 SPECT/CT showed that the infarcted myocardium (Fig.1**)** could be visualized with high quality as early as 1 h and still clearly identified at 36 h after myocardial-infarction-reperfusion and that TSPO up-regulation was still visible at 36 h after myocardial-infarction-reperfusion. In the biodistribution study, high uptakes in the infarcted myocardium (0.39 ± 0.03, 0.46 ± 0.06, 0.52 ± 0.07, and 1.97 ± 0.12% ID/g at 1, 2, 4, 12, and 36 h after myocardial-infarction-reperfusion, respectively) were observed that were much higher than that of normal myocardium. The highest uptake was reached at 36 h after myocardial-infarction-reperfusion, which agreed well with the SPECT/CT imaging results. In addition, the radioactivity uptakes of the infarcted myocardium in both the biodistribution and SPECT imaging could be blocked effectively by excess amounts of unlabeled DTPA-CB86, indicating the high specificity of $^{99}Tc^{m}$-DTPA-CB86 to TSPO (Fig.2,3**)**. **Conclusion:** $^{99}Tc^{m}$-DTPA-CB86 may serve as a powerful TSPO-expression diagnostic probe for evaluating lesions and monitoring therapy responses in patients with cardiovascular diseases. **References:** None.

EPS-156

Comparison between 99mTc-sestamibi/123I-BMIPP mismatch and reverse redistribution of 99mTc-sestamibi using cadmium-zinc-telluride SPECT system in patients with acute myocardial infarction

S. Hida, Y. Fujita, Y. Igarashi, T. Hatano, T. Morishima, C. Shiba, T. Chikamori;
Tokyo Medical University Hospital, Tokyo, JAPAN.

Aim/Introduction: Although both 99mTc-sestamibi/123I-BMIPP mismatch and reverse redistribution of 99mTc-sestamibi in patients with acute myocardial infarction (AMI) are significant markers for predicting functional recovery in the infarcted territory in chronic phase, few studies compare them by simultaneous dual-isotope imaging with 99mTc-sestamibi/123I-BMIPP using cadmium-zinc-telluride (CZT)SPECT system. **Materials and Methods:** We evaluated 63 consecutive patients with AMI who had undergone simultaneous dual-isotope 99mTc-sestamibi:370MBq/123I-BMIPP:111MBq SPECT using Discovery NM530c within 8±4 days after PCI. Simultaneous dual-isotope imaging time ware 8 min for both 1 hour (early) and 4 hours (delayed) after administration of isotopes. The estimated radiation exposure was 5.1 mSv. Each SPECT image was assessed with a 17-segment model using a 5-point scoring system, and regional scores related to each coronary territory was calculated. When 123I-BMIPP defect scores were higher than those of the 99mTc-sestamibi defect scores in infarcted territory, it was considered as 99mTc-sestamibi/123I-BMIPP mismatch. And when 99mTc-sestamibi defect scores in the delayed image were greater than those in the early image in infarcted territory, it was considered as a reverse redistribution of 99mTc-sestamibi. We assessed the frequency of respective findings and compared defect scores in the infarcted territory. **Results:** The number of each infarcted related coronary arteries was 29 in LAD, 26 in RCA and 8 in LCX. Of 63 patients, 99mTc-sestamibi/123I-BMIPP mismatch were more frequent than reverse redistribution of 99mTc-sestamibi (71% vs 43%; p=0.036). And the scores of 99mTc-sestamibi/123I-BMIPP mismatch were greater than those of reverse redistribution of 99mTc-sestamibi in the infarcted territory (4.0±3.3 vs 0.8±1.7; p=0.0001). And similar results were observed with respect to each infarcted related coronary arteries. **Conclusion:** In the simultaneous 99mTc-sestamibi/123I-BMIPP dual-isotope imaging at rest with low radiation exposure using CZT SPECT system, the presence of 99mTc-sestamibi/123I-BMIPP mismatch was more frequently observed than that of reverse redistribution of 99mTc-sestamibi in the infarcted territory. The further examination is needed for their prediction of functional recovery in chronic phase. **References:** None.

EPS-157

Integrated FDG PET/MR imaging for the evaluation of myocardial viability in patient with acute myocardial infarction

E. Kong[1], *I. Cho*[1], *C. Lee*[1], *D. Shin*[1], *B. Ahn*[2];
[1]*Yeungnam university hospital, Daegu, KOREA, REPUBLIC OF,* [2]*School of Medicine, Kyungpook National University, Daegu, KOREA, REPUBLIC OF.*

Aim/Introduction: The gold standard to identify viable myocardium is FDG PET imaging. An alternative method is Late Gd enhancement technique (LGE) by cardiac MRI. Although both approaches are valuable to predict functional recovery, the studies for acute myocardial infarction (AMI) are limited. We compared the predictability of functional recovery between FDG PET and MRI, based on the regional wall motion abnormality (RWMA) improvement. **Materials and Methods:** Eleven patients (mean age 60.5 y-o, 9 males) with AMI (4 NSTEMI and 7 STEMI) underwent simultaneous PET/MRI. Myocardium was defined 'PET viable(PET-V)' of ≥50% FDG uptake or as 'MRI viable(MR-V)' when LGE transmurality of ≤50% was present. Eight patients also underwent myocardial perfusion SPECT. We compared the viability between FDG and LGE including the perfusion. Clinical follow-up with echocardiography were reviewed. **Results:** Nine patients received successful PCI, 1 patient was failed to PCI and 1 patient was performed PCI after PET/MR scan. No patient met cardiac event during follow period (8-42 months). Five patients showed PET-V and 4 of them showed also MR-V. Another 5 patients showed PET-non-viable (PET-NV) and all of them also showed MR-NV. One patient showed reverse FDG uptake: infarcted myocardium showed increased FDG uptake, he showed MR-NV. 8/9 with concordant PET/MRI results showed similar lesion size, only one patient showed diffuse FDG defect with focal LGE at LAD territory. Via echocardiography, 3 patients had no RWMA, 2 patients had improvement RWMA, 5 patients showed no improvement and one patient showed worsening of RWMA. No RWMA or improvement RWMA group (viable group) was consisted of 2 PET-V/MR-V, 2 PET-NV/MR-NV and 1 PET-V/MR-NV. The worsening RWMA or no change RWMA group (non-viable group) was consisted of 2 PET-V/MR-V, 2 PET-NV/MR-NV and 1 reverse PET/MR-NV. Two patients without RWMA showed normal perfusion SPECT. Two patients with improvement of RWMA showed larger perfusion defects than metabolic defects. Four patients of non-viable group showed matched perfusion-metabolism defect. **Conclusion:** The simultaneous assessment of FDG uptake and LGE is feasible. However, the predictability of viability is not satisfactory. Perfusion could improve to predict viability. In case of discordant between PET and MRI findings, FDG uptake was a better predictor for functional recovery. **References:** None.

EPS-158

A Comparison Between Ora Glucose Load And Acipimox/Asa/Insulin Administration Efficiency In Stimulating Myocardial Uptake Of Fdg

I. Schiorlin*, S. Casagrande, C. Gobbo, S. Scotti, D. De Palma;*
ASST Sette Laghi, Varese, ITALY.

Aim/Introduction: 18-FDG PET/CT is a well established tool for evaluating the presence of viable myocardium into necrotic post-infarction cardiac walls. The main technical problem is to address myocardial metabolism toward glucose consumption. In non-diabetic patients, this is normally obtained by oral glucose load (OGL). Diabetic patients represent a challenging group. The (2005) EANM/ESC procedural guidelines for myocardial perfusion imaging in nuclear cardiology suggests, in diabetic patients, the use of an hypolipemic drug, Acipimox, coupled with ASA and insulin (AAI). Nevertheless, literature search found less than 10 papers published on this topic in the

last 10 years, including some in animals. We began to use this protocol in diabetic patients five years ago. Now we reviewed our experience, assessing semiquantitatively the AAI protocol efficiency in comparison to the established OGL protocol **Materials and Methods:** we select 44 (37 males and 7 females) patients in which 18-FDG PET/CT was requested in search of viable myocardium. 29 underwent to OGL, 15 to AAI protocol. In the first group, FDG was administered when glycemia fell about 20-30 mg% after the peak, whilst the AAI protocol followed strictly the EANM GL published schedule, with no more than 2 hours between patient arrival and FDG administration. FDG PET was always performed 75 min after FDG administration (2.5 MBq/kg) with a single-bed 10-min acquisition with a four ring PET/CT scanner (Siemens Biograph MCi). The scans were evaluated semiquantively. Semi-quantitative evaluation was made tracing two identical VOIs into the cardiac blood pool and into the myocardial portion with the highest uptake. We than took into account the myocardial and blood pool SUVmax and the ratio between for comparing the capability of both protocols to stimulate myocardial glucose consumption. **Results:** The OGL group had a mean myocardial SUVmax of 6.61 +2.71, a mean cardiac blood pool SUVmax of 2.15 +0.52 and a mean myocardial/blood ratio of 3.2. The AAI group has 8.76 +5.01, 2.58 +0.91, 3.43 respectively. These values show no statistical difference at the Wilcoxon test. **Conclusion:** Although in a small group of patients, our data support the hypothesis that the AAI protocol in diabetics is at least as effective as OGL (in non-diabetics) in stimulating myocardial FDG uptake. This protocol seems then more effective in respect to literature reported results for OGL in diabetics, and with the practical advantage of a fixed maximum duration time. **References:** None.

EPS-159

Effect of intramyocardial injection of erytropetin stimulated autologus bone marrow cells on myocardial perfusion in patients with chronic myocardial ischemia - SPECT ^{99m}Tc-MIBI study

S. Minin, A. Fomichev, N. Nikitin, A. Chernyavskiy;
Meshalkin National Medical Research Center, Novosibirsk, RUSSIAN FEDERATION.

Aim/Introduction: To evaluate the changes of myocardial perfusion using ^{99m}Tc-MIBI single-photon emission computed tomography (SPECT) after the intramyocardial implantation of erythropoietin preconditioned autologous bone marrow cells (ABMC) in laser channels during coronary artery disease surgery. **Materials and Methods:** Randomized study of 40 patients (mean age 58 ± 6.9 лет, 9 females) with diffuse and (or) distal right coronary artery disease (RCA). Patients of the study group (n = 23) underwent coronary artery bypass grafting (CABG) of the left coronary artery (LCA) system and intramyocardial implantation of erythropoietin preconditioned ABMC in the left ventricular inferior wall. Patients of the control group (n = 17) underwent CABG of the LCA system only. ^{99m}Tc-MIBI SPECT performed 1-2 days before and 12 months after surgery. **Results:** In study group after 12-month follow-up the summed stress score in a typical RCA supply area (SSS_{RCA}) improved from 7.0 [5.5; 10.5] to 4.0 [1.0; 5.5] (p <0.01), summed rest score (SRS_{RCA}) improved from 3.0 [0.0; 7.0] to 1.0 [0.0; 3.5] (p <0.01), and summed different score (SDS_{RCA}) improved from 3.0 [1.0; 4.0] to 1.0 [0.0; 2.0] (p = 0.03). Control group patients after 12-month follow-up showed the significant improvement of SSS_{RCA} only - from 8.0 [6.0; 12.0] to 5.0 [4.0; 7.0] (p <0.01). **Conclusion:** After 12-month follow-up in patients with diffuse and (or) distal RCA disease, the procedure of intramyocardial implantation of the erythropoietin preconditioned ABMC in laser channels is safety and induces the improvement of myocardial perfusion. **References:** None.

EPS-160

Relationship between myocardial cardiac fibrosis and myocardial denervation in non-ischemic idiopathic dilated cardiomyopathy

***F. Heurtebize**, N. Deleval, E. Gayat, A. Benada, A. Cescau, J. Laissy, L. Sarda, A. Cohen-Solal;*
Lariboisière, Paris, FRANCE.

Aim/Introduction: Myocardial ^{123}I-MIBG scintigraphy (MIBG) and cardiac magnetic resonance (CMR) are used to evaluate cardiac sympathetic denervation and myocardial fibrosis respectively, in patients with reduced left ventricular ejection fraction (LVEF) heart failure. We evaluated potential concordance between denervation and fibrosis for pathophysiological purpose in non-ischemic idiopathic dilated cardiomyopathy (DCM). **Materials and Methods:** Thirty-eight symptomatic DCM patients, referred for MIBG and CMR within 3 months, were included retrospectively between 2011 and 2018 at Lariboisière University Hospital. Myocardial innervation was quantified using heart-to-mediastinum ratio (H/M) determined on 4hours (late)-post injection thoracic planar anterior images. Myocardial fibrosis was quoted as present (late gadolinium enhancement LGE+) or absent (LGE-) on CMR. **Results:** Mean age was 52 ± 15 years (28 men). Mean LVEF and BNP level were respectively reduced to 30 ± 9% and increased to 211 (77-642) ng/L. Mean late H/M ratio was decreased to 1.51 ± 0.21 (normal ≥ 1.8). Sixteen patients (42%) had CMR LGE. The concordance score between severe denervation (H/M<1.6) and presence of fibrosis (LGE +) was 0.52. Eleven patients (46%) with severe denervation were LGE +, versus 36% (n=5) of patients with no or mild denervation (H/M ≥ 1.6) (NS). BNP appeared higher in the severe denervation group with fibrosis, than in the no or mild denervation group without fibrosis. The anteriority of the disease didn't seem to be different between these groups. **Conclusion:** In non-ischemic idiopathic dilated cardiomyopathy, concordance between myocardial denervation assessed by cardiac ^{123}I- MIBG scintigraphy and the presence of myocardial fibrosis assessed by LGE on CMR was low. This suggests that denervation does not reflect presence of myocardial fibrosis in DCM, and may be only related to sympathetic increased tone. The rate of fibrosis was comparable in patients with severe myocardial denervation and

in patients with no or mild denervation. **References:** Jacobson AF, Senior R, Cerqueira MD, Wong ND, Thomas GS, Lopez VA, et al.Myocardial iodine-123 meta-iodobenzylguanidine imaging and cardiac events in heart failure.Results of the prospective ADMIRE-HF study. J Am Coll Cardiol. 18 mai 2010;55(20):2212-21. Assomull RG, Prasad SK, Lyne J, Smith G, Burman ED, Khan M, et al.Cardiovascular magnetic resonance, fibrosis, and prognosis in dilated cardiomyopathy. J AmColl Cardiol. 21 nov 2006;48(10):1977-85.

EPS-161

Correlation Between Left Ventricular Mechanical Dyssynchrony And ^{123}I-metaiodobenzylguanidine Uptake In Pediatric Heart Disease Patients

M. Ota[1], *S. Kasama*[2], *K. Omoya*[3], *T. Yamamoto*[1];
[1]*Gifu Prefectural General Medical Center, Gifu, JAPAN,* [2]*Nara Medical University Hospital, Kashihara, JAPAN,* [3]*Awano Children's Clinic, Gifu, JAPAN.*

Aim/Introduction: In general, neuronal uptake of norepinephrine is impaired in the failing myocardium. ^{123}I-Metaiodobenzylguanidine (MIBG) has become known as a reliable indicator of cardiac sympathetic activity. MIBG has been used to assess myocardial sympathetic nervous activity and severity of heart failure (HF). On the other hand, Gated Myocardial Perfusion SPECT (GMPS) tended to be used for estimation of only ischemia in pediatric cardiology. Recently, a newly developed program, EXINI heart (ExH) software, enabled the evaluation of Left Ventricular (LV) mechanical dyssynchrony using GMPS in adult heart disease. We could observe that small heart effect on end systolic volume and ejection fraction were significantly improved by using ExH with magnified GMPS. Moreover Plasma Brain Natriuretic Peptide (BNP) concentrations has been studied in emergency department to establish the severity of acute HF. Many studies had shown that decreased uptake of MIBG is associated with LV dyssynchrony. However, to our knowledge, it is no data on childhood HF about relationship between LV mechanical dyssynchrony and uptake of MIBG. The aim of this study was assessed in pediatric heart disease patients to relationship between the cardiac neuronal function using MIBG and severity of HF using BNP concentrations, and to relationship phase analysis using GMPS and severity of HF using BNP concentrations . **Materials and Methods:** The population is consecutive 34 pediatric heart disease patients (aged 2.5±2.2 year-old <15year old) including complex Congenital Heart Disease (CHD) of suspect HF . The subjects were received ^{99m}Tc-Sestamibi (MIBI) GMPS at rest and MIBG scintigraphy. MIBI GMPS was performed before and 1 month after performed MIBG scintigraphy and measured BNP concentrations. Cardiac sympathetic activity was assessed by MIBG scintigraphy as the delayed Heart-to-Mediastinum ratio (H/M ratio) and the Washout Ratio (WR). LV mechanical dyssynchrony as the PhaseSD and the Bandwidth was determined by ExH software using MIBI GMPS. It was assessed to relationship delayed H/M ratio, WR, PhaseSD, Bandwidth with BNP concentrations. **Results:** LogBNP was significantly correlated with Delayed H/M (r= 0.688 p<0.0001) and with WR (r= 0.585 p<0.0001). LogBNP was significantly correlated with LV mechanical dyssynchrony (with PhaseSD r=0.618 p<0.0001, with Bandwidth r=0.618 p<0.001). **Conclusion:** It was significantly relationship between LV mechanical dyssynchrony and BNP concentrations, between uptake of MIBG and BNP concentrations. These results suggest that LV mechanical dyssynchrony in pediatric heart disease patients can serve as a novel diagnostic tool to evaluate the severity of HF. **References:** None.

EPS-162

Cardiac sympathetic activity and dyssynchrony in prediction of cardiac resynchronization therapy response in heart failure patients

A. Mishkina, *K. Zavadovsky, V. Saushkin, M. Gulya, D. Lebedev, Y. Lishmanov;*
Cardiology Research Institute, Tomsk National Research Medical Centre, Russian Academy of Sciences, Tomsk, RUSSIAN FEDERATION.

Aim/Introduction: Cardiac resynchronization therapy (CRT) is considered an effective treatment method in improving outcomes on HF patients. But 25-30% of CRT patients do not show significant response despite following current guidelines. The aim of this study is to evaluate the prognostic significance of cardiac sympathetic activity and dyssynchrony in cardiac resynchronization therapy efficacy. **Materials and Methods:** This study included 28 chronic heart failure patients (mean age of 56.5±10.2 years; 17 male). Before CRT all patients underwent ^{123}I-metaiodobenzylguanidine (^{123}I-MIBG) scintigraphy for cardiac sympathetic activity evaluation. Early and delayed heart to mediastinum ratios (eH/M and dH/M) as well as ^{123}I-MIBG washout rate (WR) were calculated. Before CRT and six months after all patients underwent gated blood-pool SPECT (GBPS) for left and right ventricular end-systolic (ESV) and end-diastolic (EDV) volumes, ejection fraction (EF) and dyssynchrony (intra- and interventricular) evaluation. All scintigraphic images were acquired on Discovery NM/CT 570c, equipped with CZT gamma-camera. **Results:** Six months after CRT all patients were divided into two groups: (1) responders (n=15) - LV ESV decreased by ≥15% or LV EF increased by ≥5%; (2) non-responders (n=13) - LV ESV decreased by <15% and LV EF increased by <5%. Prior to CRT, significant differences in the following preoperative scintigraphic parameters between responders and non-responders were found: eH/M (2.42 and 1.87; p<0.05), dH/M (1.89 and 1.78; p<0.05), LV EDV (271 and 299; p<0.05); LV ESV (206 and 227; p<0.05) and interventricular dyssynchrony (109 ms and 62 ms; p<0.05). According to univariate logistic regression analysis dH/M per 0.1 unit increase (odds ratio=1.87; 95% confidence interval 1.03-3.38, p=0.0002) and interventricular dyssynchrony (odds ratio=1.027; 95% confidence interval 1.008-1.046, p=0.005) were the only independent predictors of response to CRT. The ROC-analysis showed that dH/M (cut of point - 1.49; sensitivity - 89%, specificity - 100%), WR (cut of point

- 36%; sensitivity - 67%, specificity - 100%) and interventricular dyssynchrony (cut of point - 61.9 ms; sensitivity - 92%, specificity - 64%) had the greatest prognostic significance. **Conclusion:** In chronic heart failure patients preoperative values of delayed H/M and interventricular dyssynchrony are independent predictors of response to CRT. ^{123}I-MIBG scintigraphy and GBPS can be used as additional criteria for predicting the effectiveness of CRT. Acknowledgment: Grant of the President of the Russia Federation (No. MK-3947.2018.7) **References:** None.

EPS-163

The value of gated blood-pool SPECT-derived cardiac dyssynchrony in the cardiac resynchronization therapy response prediction

V. Saushkin, *A. Mishkina, V. Shipulin, A. Mochula, D. Lebedev, K. Zavadovsky;*
Cardiology Research Institute, Tomsk National Research Medical Center of the Russian Academy of Sciences, Tomsk, RUSSIAN FEDERATION.

Aim/Introduction: To evaluate the cardiac mechanical dyssynchrony (based on the GBPS results**)** for the selection of patients with non-ischemic CHF for cardiac resynchronization therapy. **Materials and Methods:** We examined 22 patients with non-ischemic CHF, 12 of them were observed six months after CRT. All patients underwent gated blood-pool SPECT (GBPS). Phase images using the first harmonic Fourier transform were computed. The phase standard deviation (PSD), histogram bandwidth (HBW) and phase entropy (E) were used as an indicator of mechanical dyssynchrony for the both ventricles. **Results:** Mechanical dyssynchrony of both ventricles before CRT was increased. Median value PSD LV was 48°(35-55°), PSD RV 33°(23-43°), HBW LV 192°(126-216°), HBW RV 78°(54-210°), E LV 69%(66-75%), E RV 58%(56-71%). Six months after CRT 7(58%) respondents were identified. We divided the patients into two groups and compared phase parameters. It was found that the PSD (LV=38,6°, RV=26,1°) and HBW (LV=147,6°, RV=87,0°) in the responders group were significantly lower than in the non-responders group (PSD (LV=56,8°, RV=61,2°); HBW (LV=234,0°, RV=175,2°). The value of phase entropy between both groups is statistically not different (Responders: E LV=68%; E RV=57,5%. Non-responders: E LV=75%; E RV=64%). Receiver operating characteristic curve analysis demonstrated that the cutoff value of PSD LV ≤ 47,8° (sensitivity 74%, specificity 80%), PSD RV ≤ 33° (sensitivity 75%, specificity 80%), HBW LV ≤ 192° (sensitivity 87,5%, specificity 90%) and HBW RV ≤ 78° (sensitivity 75%, specificity 80%) for predicting a good response to CRT. **Conclusion:** Radionuclide evaluation of mechanical dyssynchrony of the left and right ventricles allow assessing the prognosis of CRT in patients with non-ischemic CHF. **Acknowledgment:** Grant of the President of the Russia Federation (No. MK-3947.2018.7) **References:** None.

EPS-164

Detection of left ventricular dyssynchrony in hypertensive patients using phase dyssynchrony analysis in gated myocardial perfusion SPECT

S. Fatima[1], *S. T. Butt*[1], *M. A. Saeed*[1], *A. Ammar*[1], *K. B. Mir*[1], *N. Ahmed*[1], *Z. Chiragh*[2];
[1]*Nuclear Medicine, Oncology & Radiotherapy Institute (NORI), Islamabad, PAKISTAN,* [2]*Gurayat General Hospital, Al-Qurayyat, SAUDI ARABIA.*

Aim/Introduction: LV systolic and diastolic dysfunction and dys-synchrony are not uncommon in patients with treatment naive hypertension. Diastolic dys-synchrony has been associated with increasing incidence of heart failure, cardiovascular morbidity, and mortality. The objective of our study was to assess left ventricular (LV) dys-synchrony in hypertensive patients with normal systolic function using GATED myocardial perfusion imaging (GMPS) in comparison with Two dimensional echocardiographic (2DE) evaluations. **Materials and Methods:** 73 enrolled individuals were divided into two groups. Group A included 42 hypertensive patients with good LV systolic function (ejection fraction more than 50%) and narrow QRS on the ECG less than120 ms).Group B included 31 age-matched and sex-matched healthy volunteers and represented the control group. All participants underwent GMPS and 2DE . GMPS with 99mTc tetrofosmin was performed to assess LV dyssynchrony using phase analysis. Acquired images were then submitted to the Emory Cardiac Toolbox for phase analysis. Summed Two quantitative indices were calculated from the phase arrays of all patients: (i) histogram bandwidth, which includes 95% of the elements of the phase distribution, and (ii) phase SD, which is the SD of the phase distribution. 2DE was performed and standard 2D and color Doppler data, triggered to the QRS complex, were saved in cine-loop format. LV end-systolic volume (LVESV) and LV end-diastolic volume were derived from the conventional apical 2- and 4-chamber views, and LVEF was calculated. **Results:** The hypertensive group had no significant perfusion abnormalities (SDS <2) as compared to control group ($p<0.05$). In addition, treatment naïve hypertensive (57.6%) and normal controls(42.4%) had comparable baseline characteristics, except for histogram bandwidth (166°±6.7° vs. 109°± 6.32° ($P<0.05$) and phase SD (54.9°±18.7° vs. 33.1±13.9° ($P<0.05$), which were significantly larger in hypertensives compared with controls ($P <0.05$). There was no correlation between dys-synchrony and perfusion abnormalities in both groups. The severity of dys-synchrony is significantly related to the LV mass, septal wall thickness, posterior wall thickness, and left ventricular end-diastolic dimension. **Conclusion:** Patients with systemic hypertension and normal systolic function demonstrate LV dys-synchrony by GMPS. Systolic dys-synchrony may identify hypertensive patients at risk for the development of further complications, and who may benefit from more intensive hypertension control at an earlier stage in their disease process. **References:** Folks RD, Rt N, Cooke CD, Garcia E V. Optimizing gated myocardial perfusion imaging processing for phase analysis. J Nucl Cardiol. 2016;23:1348-54. Peix, A., Karthikeyan, G.,

Massardo, T. et al. J. Nucl. Cardiol. (2019). https://doi.org/10.1007/s12350-018-01589-5.

EPS-165

The value of stress gated blood pool SPECT in prognosis of early postoperative period course in patients with ischemic cardiomyopathy

V. Shipulin, *K. Zavadovsky, S. Andreev, A. Pryakhin, V. Shipulin; Cardiology Research Institute, Tomsk National Research Medical Centre, Russian Academy of Sciences, Tomsk, RUSSIAN FEDERATION.*

Aim/Introduction: To assess the course of early postoperative status in patients with ischemic cardiomyopathy (ICM) based on preoperative stress gated blood pool SPECT (GBPS) results. **Materials and Methods:** The total of 44 patients with ICM were enrolled. Prior to surgery all patients underwent GBPS at rest and at stress (increasing doses of dopamine according to the protocol 5/10/15 μg/kg /min). The duration of each step was 5 minutes. Patients were divided into 2 groups: 1)n=12, with a complicated course of the early postoperative period (death, the usage of intra-aortic balloon pump, inotropic support for more than 5 days with the need to stay in the UAR); 2)n=32, with uncomplicated postoperative course. The following parameters were calculated: left and right ventricular end-systolic (ESV) and end-diastolic (EDV) volumes, ejection fraction (EF), ejection and filling rates (PER,RFR,TTPF,MFR/3) as well as dyssynchrony indices. **Results:** According to univariate U-test mots GBPS indexes had statistically significant differences between two groups. Univariate logistic regression analysis showed that the following GBPS parameters allow predicting the severity of early postoperative period, measured at rest: LV EF OR 0,888 (CI 0,815 - 0,965, p=0,001); LV ESVI OR 1,033 (CI 1,012 - 1,054, p<0,001); LV SD OR 1,0052 (CI 1,013 - 1,092, p=0,003); LV Bandwidth OR 1,012 (CI 1,002 - 1,023, p=0,008); RV EF OR 0,945 (CI 0,909 - 0,985, p=0,022); RV PFR OR 0,291 (CI 0,111 - 0,764, p=0,006). Parameters measured at stress: LV EF OR 0,933 (CI 0,877 - 0,993, p=0,01); LV EDVI OR 1,018 (CI 1,003 - 1,045, p=0,034); LV ESVI 1,035 (CI 1,014 - 1,056, p<0,001); RV EDV OR 1,014 (CI 1,005 - 1,022, p<0,001); LV SVI OR 0,248 (CI 0,071 - 0,854, p=0,02). In multivariate logistic regression LV EF at rest (OR 0,866 (CI 0,795 - 0,956, p=0,004) and RV EDV at stress (OR 1,016 (CI 1,007 - 1,025, p<0,001) were significantly associated with complicated course of early postoperative period. According to the ROC analysis, the area under the curve (AUC 0,810; CI 0,712 - 0,886, p<0,0001) for multivariate logistic regression model [LV EF at rest and RV EDV at stress] was significantly (p<0.05) higher than that for each factor separately (0,717 and 0,694 respectively). **Conclusion:** Left and right ventricular volumes and contractility parameters obtained from stress GBPS are associated with the course of an early postoperative period in patients with ICM. Stress GBPS could be useful in the preoperative evaluation of such patients. **References:** None.

EPS-166

Assessment of chemotherapy-induced systolic and diastolic myocardial impairments using gated perfusion SPECT

A. A. Ansheles, *Y. A. Prus, E. I. Vasilenko, I. V. Sergienko, V. B. Sergienko;*
National Medical Research Center of Cardiology, Moscow, RUSSIAN FEDERATION.

Aim/Introduction: Currently, advances in treatment led to improved survival of patients with cancer, but have also increased morbidity and mortality due to treatment side effects. Cardiotoxicity is the most common complication of chemotherapy, which must be evaluated at certain points. The aim of current research was to evaluate the effect of anthracyclines on the contractile (systolic and diastolic) function of myocardial left ventricle (LV) by using myocardial perfusion SPECT with ^{99m}Tc-MIBI. **Materials and Methods:** 52 patients (19 men, 33 women) referred to chemotherapy (substantially with anthracyclines), underwent gated myocardial perfusion SPECT/CT at rest before the onset of therapy and after 4 courses. Regarding functional assessment of LV, we evaluated the following parameters: ejection fraction (EF) and peak ejection rate (PER) as systolic indicators, peak filling rate (PFR), mean filling rate at first third of diastole (MFR/3), and time to peak filling (TTPF) as markers of diastolic function, as well as end systolic and diastolic volumes (ESV, EDV, ml) as markers of probable LV dilation. **Results:** LV systolic and diastolic function parameters in patients after 4 courses of chemotherapy worsened in a parallel manner. Rest LVEF before and after 4 courses was 64±14 and 59±12%, respectively, p=0.053, mostly due to systolic ejection function impairment (PER decreased from 3.26±0.96 to 2.81±0.74 EDV/s, p<0.01) and mild LV dilation (EDV increased from 78.2±25.4 to 87.6±26.6 ml, p=0.07, and ESV increased from 32.2±19.8 to 38.6±20.6 ml, p=0.11). Overall peak filling rate was decreased from 2.94±0.93 to 2.57±0.83 EDV/s, p=0.03, while MFR/3 and TTPF changes were not statistically reliable: MFR/3 decreased from 1.58±0.44 to 1.46±0.37 EDV/s, p=0.14, that led to TTPF prolongation from 154±34 to 163±36 ms, p=0.19. **Conclusion:** Our findings suggest that patients pass through systolic and diastolic myocardial function impairments during anthracyclines chemotherapy. While diastolic dysfunction is known to be the first phase of doxorubicin cardiomyopathy and chronic heart failure development, we observed parallel decrease of LV systolic function. We assume those impairments to be reversible, but not immediately after therapy completion. Gated myocardial perfusion SPECT enables additional evaluation of LV systolic and diastolic function and is reliable for dynamic assessment of chemotherapy cardiotoxic effects. **References:** None.

EPS-167

Potential of imaging modalities as gatekeeper prior to endomyocardial biopsy in patients suspected of cardiac sarcoidosis: Ga-67 SPECT vs F-18 FDG PET

K. Takanami, *K. Takase*;
Tohoku University Hospital, Sendai, JAPAN.

Aim/Introduction: Endomyocardial biopsy may be required to confirm the diagnosis of cardiac sarcoidosis (CS) in cases of negative extracardiac biopsy. However, endomyocardial biopsy has low sensitivity due to the focal nature of the disease. We examined whether low-invasive imaging modalities including Ga-67 SPECT and F-18 FDG PET could enhance appropriate endomyocardial biopsy indication in patients suspected of CS. **Materials and Methods:** This study included 39 patients with clinically suspected CS, who underwent F-18 FDG PET, Ga-67 SPECT and myocardial biopsy. A nuclear medicine specialist classified the myocardium F-18 FDG uptake as positive when nonuniform or diffuse high F-18 FDG uptake were observed, and classified the myocardial Ga-67 uptake as positive when faint or high Ga-67 uptake were observed. The correlation between the presence of CS positive pathology and each image examination was examined using Fisher's exact test. $P < 0.05$ was set as statistically significant. **Results:** Positive endomyocardial pathology rate was as low as 15% (6/39). In the 6 positive-biopsy patients, 83%(5/6) and 100%(6/6) patients were positive at Ga-67 SPECT and F-18 FDG PET, respectively. Meanwhile, in the 33 negative-biopsy patients, 91% (30/33) and 24% (8/33) patients were negative at Ga-67 SPECT and F-18 FDG PET, respectively. There was a significant association between the positive pathology and Ga-67 positive findings ($p < 0.05$). Meanwhile, no significant difference was observed between the positive pathology and FDG positive findings. **Conclusion:** Ga-67 SPECT has a clinical potential as gatekeeper prior to endomyocardial biopsy in patients suspected of CS, although further studies are needed. **References:** None.

EPS-168

Evaluation of F-18-Flutemetamol in hybrid PET-imaging of cardiac amyloidosis: A pilot study

L. Kessler[1], *M. Papathanasiou*[2], *A. Brainman*[1], *D. Kersting*[1], *P. Lüdike*[2], *M. Weber*[1], *A. Carpinteiro*[3], *T. Hagenacker*[4], *T. Rassaf*[2], *K. Herrmann*[1], *C. Rischpler*[1];
[1]*Department of Nuclear medicine, University-hospital Essen, Essen, GERMANY,* [2]*Department of Cardiology, University-hospital Essen, Essen, GERMANY,* [3]*Department of Hematology, University-hospital Essen, Essen, GERMANY,* [4]*Department of Neurology, University-hospital Essen, Essen, GERMANY.*

Aim/Introduction: Cardiac amyloidosis (CA) is a rising diagnosis in patients with severe heart failure. AL (light-chain) and ATTR (transthyretin) amyloidosis are mainly responsible for cardiac involvement of amyloidosis. However, diagnosing CA can be challenging and the gold standard still is endomyocardial biopsy (EMB). Amyloid specific PET-tracers may propose high potential for non-invasive diagnosis of CA and some tracers already showed promising results. Aim of this study was to evaluate F-18-Flutemetamol as PET-tracer for PET/MRI and PET/CT imaging of CA. **Materials and Methods:** Hybrid F-18-Flutemetamol-PET imaging was performed in 22 subjects with suspected cardiac amyloidosis (17 PET/MRI and 5 PET/CT). 13 of those 22 patients had a verified CA by EMB, imaging, or lab results. Mean injected activity was 183.7 ± 22.6 MBq and imaging was performed 68.7 ± 24.7 min p.i.. Myocardial SUVmean and SUVmax were measured and a background VOI was placed in the thoracic aorta for calculation of tracer-to-background ratios (TBRmean and TBRmax). Additionally, MR-based parameters such as late gadolinium enhancement (LGE), T1 mapping and extracellular volume (ECV) were evaluated. Results are reported as mean±SEM. **Results:** Mean patient age was 72.7±8.8 years. TBRmax and TBRmean were higher in patients with CA but did not reach statistical significance (TBRmax 1.3±0.2 vs. 0.95 ±0.03; TBRmean 1.3±0.2 vs. 1.0±0.07). On visual analysis, only 3 patients had positive PET scans with proven amyloidosis. There was no significant difference between TBRmax and TBRmean in patients with AL or ATTR subtypes. MR-based parameters showed a prolonged T1-time native in all patients (CA 1448±16ms vs. no CA 1364±30ms). Interestingly, the measured ECV showed significantly different results in CA and no CA patients CA 58.9±4.7 vs. no CA 35.1±2.5). **Conclusion:** Hybrid F-18 Flutemetamol PET/MRI is a novel tool for the assessment of cardiac amyloidosis. Our preliminary data shows a strong trend towards higher tracer-uptake in patients with cardiac amyloidosis. The combination with MR imaging beneficially adds morphological information and MR-based parameters, which can substantiate the diagnosis. Despite that only a small proportion of the verified patients had a visually enhanced tracer-uptake leading to the question if this tracer is feasible for the evaluation of CA. Further studies in a larger cohort of patients are warranted. **References:** None.

Scientific e-Posters

EP-01

Neuroimaging: Neurology

October 12 - 16, 2019 e-Poster Area

EP-0001

Disorders of Consciousness and visual fixation: a combined analysis with flash visual evoked potentials, MRI and PET/CT

G. Marotta[1], *D. Sattin*[2], *L. D'Incerti*[2], *D. Rossi Sebastiano*[2], *D. Guido*[2], *S. Tirelli*[2], *A. Bersano*[2], *D. Duran*[2], *S. Ferrraro*[2], *L. Minati*[2], *A. Nigri*[2], *C. Rosazza*[2], *M. Leonardi*[2], *R. Benti*[1];
[1]*Fondazione IRCCS Ca' Granda Ospedale Maggiore Policlinico, Milano, ITALY,* [2]*Fondazione IRCCS Istituto Neurologico Carlo Besta, Milano, ITALY.*

Aim/Introduction: Recent studies showed as visual responses to tailored stimuli seem to be one of the first evidence revealing that one patient is changing from Vegetative State (VS) to minimal consciousness (MCS). The aim of this cross-sectional study is to analyze the visual system in a selected group of patients in order to find useful markers for clinical classification of participants showing visual fixation ability. **Materials and Methods:** Flash visual evoked potentials (fVEPs), structural 3T magnetic resonance imaging (sMRI) and FDG-PET were analyzed in 58 inpatients. Forty-two (72%) patients out of 58 showed only visual blink reflex in the Coma Recovery Scale-Revised visual function subscale, twelve (21%) visual pursuit and four (7%) fixation scores. For FDG-PET, SUV maps were coregistered using SPM12 to individual volumetric T1 series, which were segmented to generate the normalization deformation field to be applied to the coregistered FDG-PET scan. The general linear model was used to perform a voxel-by- voxel univariate statistical test for groups comparison: a two-sample t-test was conducted between patients with the visual blink response only and patients with visual pursuit. The voxel-based statistical analysis was performed by applying a threshold of $p<0.001$ and considering clusters of at least 100 voxels. **Results:** A significant difference was also found between the two groups (voxel threshold= $p<0.001$ FDR-corrected) considering FDG-PET data. The cluster was composed of 389 voxels and it was localized in the right calcarine cortex (Broadmann area 17) and in the neighboring right lingual gyrus cortex (areas 18/19). The relationships between instrumental data (fVEPs, sMRI, PET) and sociodemographic variables and presence of visual blink to threat or visual pursuit responses were fitted in univariate and multivariable logistic regression models to predict visual pursuit behavior finding specific cut-off values. An AUC=0.902 was found using tailored cut-off values. Finally, a qualitative test of the best predictive model was made on four patients with visual fixation revealed in 3/4 patients a good probability to predict if fixation data could support/correlate to visual pursuit behavior or not, reducing diagnostic error using standard assessment scale only (25% in our small sample). **Conclusion:** The role of primary visual cortex area for the differentiation between blink and pursuit visual behavior seems to be important and our model could help clinicians to evaluate if visual fixation response supports or not the diagnosis of MCS. **References:** None.

EP-0002

Evaluation of reducing the [18F]FDG activity levels for clinical readings of PET/MRI scans of patients with non-lesional epilepsy

H. Kertesz[1], *T. Traub-Weidinger*[2], *J. Cal-Gonzalez*[1], *I. Rausch*[1], *O. Muzik*[3], *L. Shiyam Sundar*[1], *T. Beyer*[1];
[1]*QIMP Team, Center for Medical Physics and Biomedical Engineering, Vienna, AUSTRIA,* [2]*Division of Nuclear Medicine, Department of Biomedical Imaging and Image-guided Therapy, Medical University of Vienna, Vienna, AUSTRIA,* [3]*Department of Radiology, Wayne State University School of Medicine, The Detroit Medical Center, Children's Hospital of Michigan, Detroit, MI, UNITED STATES OF AMERICA.*

Aim/Introduction: To assess the combined effects of reducing injected [18F]FDG activity levels and applying novel image reconstruction techniques on clinical readings in patients with non-lesional epilepsy (NLE). **Materials and Methods:** Nine patients with NLE underwent a 60-minute dynamic [18F]FDG-PET/MRI examination on a fully-integrated Siemens Biograph mMR system. The mean injected activity was (305±95)MBq. Raw data was stored in list mode (LM) format and the last 10-minutes of the LM data was used for static image reconstructions. To evaluate the effect of decreased dose, four LM data sets were generated for each patient: LM data with 50%, 35%, 20% and 10% of the original counts by randomly removing counts from the original LM data. The data was reconstructed with two different image reconstruction techniques. First, the standard OSEM algorithm with resolution recovery (PSF) available from the vendor tools and, second with the Asymmetrical Bowsher (AsymBowsher) algorithm. The AsymBowsher algorithm takes advantage of the simultaneously acquired T1-MPRAGE MR information for the PET image reconstruction. Additionally, a 3mm FHWM Gaussian post-filter was applied to all reconstructions. The diagnostic quality of the PET images was evaluated visually by an experienced Nuclear Medicine specialist using a 5-point image quality scale: 5-(very good) to 1-(poor). The clinical readings were repeated after 4-months to assess the intra-reader agreement. Absolute differences between readings that did not exceed a score difference of ±1 were considered acceptable, higher deviations were reported. **Results:** For full count statistics, PSF image reconstruction was graded highest in both readings (mean value of 3.9 and 3.7 for the first reading and second reading respectively), while the filtered AsymBowsher received a score of (2.6 and 3.0). The results of the first reading were significantly lower than the second reading, especially at low count levels (35%-50%). The PSF reconstructions at 35% of the original counts received a mean grading of good (3). The intra-reader accuracy of the scores was 87% for PSF and 80% for AsymBowsher reconstructions. **Conclusion:** Our results indicate that [18F]FDG injected activity could be potentially reduced down to 35% of the original counts without loss of diagnostic value. Moreover, although PSF reconstructed images were initially preferred by the clinical reader, acceptance of images created using the AsymBowsher reconstruction increased after training. Thus, the full potential of AsymBowsher reconstruction might only be appreciated following extensive training with this type of images. The financial support of the Austrian FWF Project I3451-N32 is gratefully acknowledged. **References:** None.

EP-0003

Brain regions involved in cochlear implant user's speech comprehension: Insights from brain-perfusion-SPECT and EEG during a sentence discrimination task

M. L. Kessler[1,2], *I. Schierholz*[3,2], *M. Mamach*[4,2], *F. Wilke*[4], *A. Hahne*[5], *L. Geworski*[4], *F. M. Bengel*[1], *P. Sandmann*[6], *G. Berding*[1,2];
[1]*Department of Nuclear Medicine, Hannover Medical School, Hannover, GERMANY,* [2]*Cluster of Excellence Hearing4all, Hannover Medical School, Hannover, GERMANY,* [3]*Department of Otolaryngology, Hannover Medical School, Hannover,*

GERMANY, [4]Department of Medical Physics and Radiation Protection, Hannover Medical School, Hannover, GERMANY, [5]Saxon Cochlear Implant Center, University Hospital, Dresden, GERMANY, [6]Department of Otorhinolaryngology, University of Cologne, Cologne, GERMANY.

Aim/Introduction: The current study examines the underlying mechanisms of speech processing in CI patients using a multimodal approach. Data are collected by single photon emission tomography (SPECT) and electroencephalography (EEG). **Materials and Methods:** 21 post-lingually deafened CI patients (62±11y, 18 right-handed, 10 f) participated in the study with two sessions. One session includes a task in which sentences are classified as semantically correct or incorrect. During the task, a 96-channel EEG is being recorded. Two minutes after the start of the task, 740 MBq of 99mTc-HMPAO are injected intravenously. A SPECT scan 1.5 hours after injection shows the cortical activity during the task. A second session includes a SPECT scan after injection at rest. Image-based analysis was carried out with SPM8. **Results:** A larger N400 wave in the EEG was associated with enhanced activity in the middle temporal area revealed by the SPECT scan (task vs. rest). A higher working memory capacity was associated with increased activity in left-sided inferior, middle and superior temporal areas, as well as bilateral occipital and parietal areas. Contrasting CI users with higher and lower performance, using a median-split of scores in the Göttinger sentence test (speech reception threshold for 50% speech understanding in noise), a higher increase in perfusion in the bilateral high (pre)frontal lobe, Broca's area, as well as right-sided superior temporal, inferior temporal and temporopolar regions was observed in the group of lower CI performers considering difference images (stimulation-rest). The group of higher performers, in contrast, showed a higher increase in perfusion in occipital, left-sided middle and inferior temporal regions, as well as in the right-sided motor cortex. **Conclusion:** Combined SPECT/EEG measurements in the context of a speech processing task show the recruitment of a temporo-frontal network with differential activation patterns according to speech recognition abilities. The correct detection of semantic violations, as indicated by an enhanced N400 in the EEG, was related to higher perfusion in the middle temporal region, which is in line with findings in normal hearing subjects, providing further evidence that this region is the generator of the N400. **References:** None.

EP-0004

Extratemporal metabolic profile on FDG-PET in temporal lobe epilepsy as a predictor of surgical failure

***Y. Tang**, G. Liao, J. Li, T. Long, Y. Li, S. Hu;*
Department of PET Center, XiangYa Hospital Central South University, Changsha, CHINA.

Aim/Introduction: To evaluate whether the profile of extratemporal metabolic changes on FDG-PET could be used to predict seizure outcome in patients with drug-resistant temporal lobe epilepsy (TLE). **Materials and Methods:** We analyzed metabolic data with FDG-PET in 82 patients with unilateral intractable TLE (25.6 ± 10.6 years old at the time of surgery, 48 female participants, 37 left). Thirty age-matched controls were included. Patients were classified either as having seizure recurrence (Engel class II or greater, SZR) or becoming seizure-free (Engel class I, SZF) at least 1 year after temporal lobectomy. Pearson χ^2 tests were used to compare categorical variables including clinical, pathological, magnetic resonance imaging and FDG PET visual findings between two postoperative seizure outcomes. We compared regional abnormal glucose metabolism in inside and outside epileptogenic foci between each outcome group (SZR and SZF) and control group in each TLE side. Imaging processing was performed with statistical parametric mapping (SPM12). The volume, intensity and special brain areas of abnormal metabolism in temporal and extratemporal region visualized or quantified using xjView Matlab toolbox. **Results:** With a median follow-up 1.5 years (IQR 1.2-2.3), 60% of patients achieved SZF. Multivariate analyses demonstrated three predictors of seizure recurrence: left TLE (P =0.006), nonlesional pathology results (P=0.007) and extensive hypometabolism on FDG-PET (P = 0.03). All patients had hypometabolism in the temporal cortex ipsilateral to the epileptogenic region, but the surgical outcomes were not associated with the volume and intensity of ipsilateral temporal hypometabolism (P>0.05), whereas SZR correlated with extratemporal metabolic changes that differed according to the lateralization: In right TLE, compared with SZF patients, patients with SZR had larger volume of metabolic changes in extratemporal areas (P<0.05), the critical value of the volume of metabolic changes outside the right TLE foci calculated by ROC curve was 12580 mm^3, regional abnormal negative predictors were in the Cingulum_Ant_R/L, Frontal_Inf_Orb_R and Supp_Motor_Area_R(aal). In left TLE, SZR presented a volume of metabolic changes in extratemporal areas similar to right TLE, but the difference was not significant (P>0.05), whereas Cingulum_Ant_R, Precuneus_R and Frontal_Sup_Orb_L(aal) involvement metabolic changes correlated to a less favorable outcome. **Conclusion:** Extratemporal metabolic profile outside the seizure foci on FDG-PET may represent a prominent cause of temporal lobe surgery failure. Seizure control after epilepsy surgery might be improved by investigating areas of abnormal metabolism extratemporal as candidates for resection or neuromodulation. **References:** None.

EP-0005

FDG-PET in theevaluation of patients with drug-resistant focal epilepsy

***G. Capriotti**[1], P. Pizzichini[1], L. Carideo[1], G. Franchi[1], L. De Palma[2], D. Prosperi[1], A. Signore[1];*
[1]Sapienza University, Rome, ITALY, [2]Ospedale Pediatrico Bambino Gesù, Rome, ITALY.

Aim/Introduction: Interictal [18F]fluorodeoxyglucose-positron

emission tomography (FDG-PET) is useful in the presurgical evaluation of patients with drug-resistant focal epilepsy. Hypometabolism overlies the seizure-onset zone (SOZ) with a sensitivity of 86-90% in temporal lobe epilepsy (TLE) and of 45-60% in extra-TLE. We aimed at clarifying its relationship with ictal high-frequency oscillation (iHFOs), arterial spin labeling (ASL - an emerging non-invasive magnetic resonance imaging perfusion technique), and PET/CT. **Materials and Methods:** Twelve consecutive patients with cortical epilepsy for pre-surgical evaluation underwent a standardized assessment including video-electroencephalography (EEG) monitoring, structural MRI with ASL sequences and FDG-PET. We studied the correlation between epileptogenicity maps and FDG-PET and ASL. **Results:** we studied 12 patients [7 women and 5 man; mean age 23] for 12 total lesions. Of these 12 patients: 9 were affected by TLE and 3 by extra-TLE (2 patients with orbital epilepsy and 1 with cortical displasia). The frequency band of iHFOs was on average 81-139 Hz (lowest,30-60 Hz; highest, 160-210 Hz) and locolized the epilettogenic zone.PET scan identifies interictal hypometabolism in all patients with TLE and cortical displasia, whereas the scan were negative in the remains extra-TLE (orbital epilepsy). ASL-MRI identified abnormalities (hypoperfusion) were seen in 7 of 9 patients vith TLE and in 2 of 3 patients with extra-TLE. **Conclusion:** Conclusion: This finding suggests that interictal FDG-PET and ictal HFOs may share common underlying pathophysiologic mechanisms of ictogenesis in temporal lobe epilepsy.Interictal ASL is a non-invasive method that may help to localize the epileptogenic in extra-TLE zone showing hypo-perfusion in FCD. **References:** None.

EP-0006

Effects of different antihistamine drugs on energy consumption in the brain of healthy volunteers during cognitive study

M. Tashiro[1], *N. Suzuki*[1], *E. Chen*[1], *A. Kikuchi*[1], *A. Inami*[1], *A. Mohsen*[2,1], *S. Watanuki*[1], *M. Miyake*[1], *K. Takeda*[1], *K. Hiraoka*[1], *M. Maurer*[3], *K. Yanai*[4], *H. Watabe*[1];
[1]*Cyclotron and Radioisotope Center, Tohoku University, Sendai, JAPAN,* [2]*National Institutes of Biomedical Innovation, Health, and Nutrition, Osaka, JAPAN,* [3]*Department of Dermatology and Allergy, Charité—Universitätsmedizin Berlin, Berlin, GERMANY,* [4]*Department of Pharmacology, Tohoku University Graduate School of Medicine, Sendai, JAPAN.*

Aim/Introduction: Antihistamines often have sedating side effects on the brain of allergic patients. This side effect has been associated with certain accidents during car-driving or operating dangerous machinery. That is why this topic has been of social importance. In our previous study using positron emission tomography (PET) and [^{18}F]fluorodeoxyglucose, we observed that the brain energy consumption increased significantly after cognitive loads following antihistamine treatments in comparison to the results after the same cognitive studies following placebo treatment (1). But we could not separate the effect of antihismines to the baseline brain metabolism from that to the energy consumption to manage cognitive tasks. The aim of the present study, therefore, was to clarify the mechanism of this phenomenon. **Materials and Methods:** In this double-blind, placebo-controlled study-design, 18 healthy young Japanese men received single doses of non-sedative antihistamine (levocetirizine 5 mg) and sedative antihistamine (diphenhydramine 50 mg) at intervals of at least six days (Task group). Task performances and brain activity were evaluated during three cognitive tests (word fluency, two-back, and Stroop). Additional 6 healthy young Japanese men received the antihistamines and were tested in the same manner as Task group but without cognitive studies (Rest group). Regional cerebral glucose consumption changes were measured using positron emission tomography (PET) with [^{18}F]fluorodeoxyglucose, by scanning these subjects before and after antihistamine treatments. Then, brain energy consumption was examined in terms of standardized uptake value (SUV). **Results:** Energy consumption (SUV) in the prefrontal regions of Task group was significantly higher after antihistamines treatments (with levocetirizine and diphenhydramine) than that after placebo treatment. In Rest group, however, brain energy consumption in the prefrontal regions showed no-significant change before and after both antihistamines treatments and placebo treatment. As for the results of cognitive studyin Task group, Stroop test accuracy was significantly impaired by diphenhydramine although the performance after levocetirizine treatment was not impaired. **Conclusion:** These results suggested that the increased brain energy consumption observed in our previous study(1) was more associated with the increased energy demand to manage cognitive tasks during coginitive tests than with the increased energy consumption in the baseline state of the brain of subjects/patients. **References:**
1) Kikuchi A, et al. Effects of levocetirizine and diphenhydramine on regional glucose metabolic changes and hemodynamic responses in the human prefrontal cortex during cognitive tasks. Hum Psychopharmacol. 2018;33(2):e2655.

EP-0007

The Different Metabolic Patterns Of Brain 18f-FDG PET In Anti-nmda,anti-lgi1 And Anti-gabab Encephalitis

X. Zhao, *X. Li*, *Z. Qiao*, *K. Wang*, *Q. Chen*, *L. Ai*;
Beijing Tiantan hospital, Beijing, CHINA.

Aim/Introduction: Pathogenic auto-antibodies targeting the recently identified LGi-1, NMDA and GABAb induce autoimmune encephalitis. The comparison of brain metabolic patterns in ^{18}F-FDG PET of anti-NMDA,anti-LGi-1,and anti-GABAb encephalitis patients has not been performed yet in a larger sample and shall be helpful in differentiating these autoimmune encephalitis. **Materials and Methods:** The brain ^{18}F-FDG uptake of eleven anti-NMDA , twenty-eight anti-LGi-1 and seven anti-$GABA_b$ encephalitis patients admitted to Beijing Tiantan hospital between 2014 and 2018 was retrospectively analyzed. Group analysis by statistical parametrical mapping of ^{18}F-FDG shows significant ($p < 0.05$, two sample t-test uncorrected for

multiple comparisons and an extent threshold of 30 voxels) hypermetabolism and hypometabolism in different brain regions of these three types of encephalitis patients compared to forty-seven age and sex matched controls. **Results:** In general , the hypermetabolism brain regions of three types of encephalitis were observed in the cerebellum and basal ganglia. Group analysis of anti-NMDA encephalitis patients demonstrated regionally limited hypermetabolism in cerebellum contrasting hypometabolism in occipital and frontal lobes. The anti-LGi-1 was characterized by hypermetabolism in cerebellum and basal ganglia as well as an extensive frontal and parietal hypometabolism. The $GABA_b$ encephalitis patients showed hepermetabolism in medial temporal lobe and basal ganglia. **Conclusion:** This retrospective ^{18}F-FDG PET study provides novel evidence for distinct brain metabolic patterns in patients with anti-NMDA,anti-LGi-1 and anti- $GABA_b$ encephalitis. **References:** [1] Graus F, Titulaer M J, Balu R, et al. A clinical approach to diagnosis of autoimmune encephalitis.[J].The Lancet Neurology, 2016:S1474442215004019.[2] Solnes L B, Jones K M, Rowe S P, et al. Diagnostic Value of18 F-FDG PET/CT Versus MRI in the Setting of Antibody-Specific Autoimmune Encephalitis[J]. Journal of Nuclear Medicine,2017,58(8):1307-1313.[3] Baumgartner A, Rauer S, Mader I, et al. Cerebral FDG-PET and MRI findings in autoimmune limbic encephalitis: correlation with autoantibody types[J]. 2013,260(11):2744-2753.

EP-0008

Early diagnosis of Osmotic Demyelination syndrome with 18-FDG PET CT

N. K. Seniaray[1], *R. Verma*[1], *R. Ranjan*[2], *E. Belho*[1], *D. Malik*[1], *H. Mahajan*[1];
[1]*Mahajan Imaging Center, Sir Ganga Ram Hospital, New Delhi, INDIA,* [2]*Department of neurology, Sir Ganga Ram Hospital, New Delhi, INDIA.*

Aim/Introduction: Osmotic Demyelination Syndrome (ODS) which compasses both Central Pontine Myelinolysis (CPM) and Extrapontine Myelinolysis (EPM) is a rare neurological complication attributed to rapid correction of hyponatremia or rapid shifts of osmolality in certain metabolic and toxic states. It is characterized by destruction of the myelin sheath and oligodendrocytes in pons, cerebellum, hippocampus, basal ganglia, brain stem and thalamus without any inflammation and with relative preservation of the axons. Early diagnosis is imperative for adequate management of patients with Osmotic Demyelination Syndrome. MRI with its special sequences is the investigation of choice for the detection of the osmotic changes in the brain but sometimes is non contributory very early in the course of disease. 18-FDG PET shows areas of focal hypermetabolism in the pons, cerebellum, brain stem and bilateral medial temporal regions as early as within 24 hours of the disease and may be useful for establishing the diagnosis in clinically suspected ODS. **Materials and Methods:** 7 consecutive patients (3 males and 4 females) with suspected Osmotic Demyelination Syndrome, were evaluated with FDG PET/CT scan of the brain. The patterns of FDG uptake were recorded and comparison with normalized data was attempted. The areas of hypo/hypermetabolism that were two standard deviations from the mean were considered as abnormal. The patients were also analyzed based on the Z score surface maps of the 3D stereotactic surface projections (SSP) image and regional Z scores were evaluated. Post treatment follow-up scans, when available were compared with the pre-treatment scans. The FDG PET CT scans were compared with the diffusion weighted MRI scans and the areas of concordance recorded. **Results:** All patients had an abnormal pattern of FDG uptake, both on visual inspection and semiquantitative analysis. Variable degrees of focal hypermetabolism was noted in the pons, mid brain, thalami, basal ganglia, cerebellum, brain stem and bilateral medial temporal regions with or without associated cortical hypometabolism. Out of the 6 subjects, 3 patients had normal MRI at the time of clinical and scintigraphic diagnosis and 3 showed mildly restricted diffusion in the pons. All the subjects were positive for ODS on delayed MRI scans. On follow up, 2 out 6 showed improvement in the cerebral glucose metabolic pattern. **Conclusion:** FDG PET is a sensitive non invasive imaging modality which may contribute to the early diagnosis and management of patients with clinical suspicion of ODS, especially in the setting of non contributory/normal MRI. **References:** None.

EP-0009

FDG-PET assessment and metabolic patterns in Lafora disease: a multicenter retrospective study

A. Paccagnella[1], *A. Farolfi*[1], *F. Pondrelli*[2], *L. Muccioli*[2], *G. D'Orsi*[3], *R. Michelucci*[4], *E. Freri*[5], *L. Canafoglia*[6], *L. Licchetta*[2], *G. Marotta*[7], *F. Toni*[4], *T. Martino*[3], *P. Tinuper*[2], *F. Bisulli*[2], *C. Pettinato*[8], *S. Civollani*[8], *R. Bonfiglioli*[1], *V. Allegri*[1], *S. Fanti*[1];
[1]*S.Orsola Hospital, University of Bologna, Bologna, ITALY,* [2]*Department of Biomedical and Neuromotor Sciences, University of Bologna, Bologna, ITALY,* [3]*Epilepsy Centre, Clinic of Nervous System Diseases, University of Foggia, Ospedali Riuniti, Foggia, ITALY,* [4]*IRCCS Istituto delle Scienze Neurologiche di Bologna, Bologna, ITALY,* [5]*Pediatric Neurology, Fondazione IRCCS Istituto Neurologico Carlo Besta, Milano, ITALY,* [6]*Department of Neurophysiology and Diagnostic Epileptology, Fondazione IRCCS Istituto Neurologico Carlo Besta, Milano, ITALY,* [7]*IRCCS Ca' Granda Ospedale Maggiore Policlinico di Milano, Milano, ITALY,* [8]*Medical Physics Unit, Radiology Unit, S.Orsola Hospital, Bologna, ITALY.*

Aim/Introduction: Lafora disease (LD) is a rare, lethal, autosomal recessive progressive myoclonus epilepsy. ^{18}F-fluorodeoxyglucose positron emission tomography (FDG-PET) reports in LD patients are anecdotal, showing heterogeneous findings. Here we describe cerebral glucose metabolism pattern as assessed by FDG-PET in eight patients with LD. **Materials and Methods:** We included patients referred to three Italian epilepsy centers with genetically confirmed LD who underwent FDG-PET scan between April 2014 and January 2019. FDG-PET images were coregistered with MRI and evaluated by two independent

nuclear medicine physicians, with at least 3 years of experience in neuroimaging and unaware of clinical history. Furthermore, paired t-tests were performed for subgroups analysis on the basis of genetic (EPM2A vs. NHLRC1 mutations) and clinical features (presence of visual symptoms, stage of disease) employing SPM8 software. When possible, the examination was repeated during follow-up assessment. **Results:** Eight Italian patients (3M/5F) underwent FDG-PET examination after a mean of 6.6 years from disease onset (range: 1-9). Visually assessed FDG-PET was abnormal in 8/8 patients, with a substantial agreement (Cohen'κ 0.63) between two readers in the region-based visual analysis. Seven out of eight patients (88%) showed diffuse bilateral cerebral hypometabolism, more pronounced in advanced stages of disease. Most severely (moderate to severe) hypometabolic areas were parietal lobe (6/8 patients), temporal lobe (5/8), frontal lobe (5/8) and thalamus (4/8). Severe thalamic hypometabolism was a recurrent finding in our cohort. The SPM subgroup analysis found no significant differences between patients with EPM2A and NHLRC1 mutations, whereas a different pattern was found in patients with visual symptoms (bilateral hypometabolism in the parietal and temporal lobe) compared to those without. Moreover, higher stage of LD progression scale was positively associated with a more compromised and diffuse hypometabolism. In 3/8 patients (38%) the exam was repeated after a mean of 17 months (range: 8-36) showing a more pronounced hypometabolism compared to the baseline FDG-PET. **Conclusion:** FDG-PET seems highly sensitive to evaluate LD at any stage. Our findings may speculatively be related with LD pathogenesis (impairment of normal glycogen metabolism with consequent diffuse destruction of neurons and LBs accumulation). FDG-PET may also correlate with disease stage and be therefore useful to evaluate response to upcoming therapeutic strategies for LD. Further prospective studies would be useful to confirm the relation between FDG-PET findings and disease stage. **References:** None.

EP-0010

Brain Metabolism changes in patients with diffuse axonal injure after intrathecal cell therapy

J. Mucientes, J. Vaquero, M. Zurita, C. Fernandez, M. Mitjavila;
Hospital Universitario Puerta de Hierro, Majadahonda, Madrid, SPAIN.

Aim/Introduction: Neuroimaging in cell therapy in neurological disability is in its initial clinical stage. We describe our preliminary clinical experience with neurological FDG PET-CT before and after treatment in patients with defuse axonal injury (DAI) treated with cell therapy. **Materials and Methods:** Three patients with established neurological sequelae due to DAI received intrathecally autologous mesenchymal stromal cells MSCs. We performed a brain FDG PET before and a month after treatment. **Results:** All the three patients showed improvement after cell therapy, and subsequent studies with 18F-fluorodeoxyglucose (18F-FDG) positron emission tomography (PET) showed a diffuse and progressive increase in brain glucose metabolism **Conclusion:** Diffuse progressive increase in brain FDG activity may be related to the cell therapy and his clinical benefit. **References:** VaqueroJ,ZuritaM,RicoMA,BonillaC,AguayoC,Montilla J, et al. An approach to personalized cell therapy in chronic complete paraplegia: the Puerta de Hierro phase I/II clinical trial. Cytotherapy 2016;18:1024-35.Vaquero J, Zurita M. Functional recovery after severe central nervous system trauma: current perspectives for cell therapy with bone marrow stromal cells. Progr Neurobiol 2011;93: 341-9.

EP-0011

18F-FDG-PET in Focal, Drug-Resistent Epilepsy: An Important Tool for the Pre-Surgical Evaluation

F. Mattana[1]*, A. Farolfi*[1]*, A. Paccagnella*[1]*, G. M. Lima*[1]*, A. Lambertini*[1]*, V. Barone*[2]*, V. Allegri*[1]*, S. Fanti*[1]*;*
[1]*Metropolitan Nuclear Medicine, S. Orsola-Malpighi Hospital, University of Bologna, Bologna, ITALY,* [2]*IRCCS Bologna Institute of Neurological Sciences, University of Bologna, Bologna, ITALY.*

Aim/Introduction: Interictal [18F]fluorodeoxyglucose-positron emission tomography (FDG-PET) is used in the presurgical evaluation of patients with drug-resistant focal epilepsy. We aimed to understand the role of FDG-PET in individualizing the epileptogenic zone (EZ) and if it should be useful to guide the placement of electrodes in SEEG. **Materials and Methods:** We studied the correlation between FDG-PET and epileptogenicity maps in an unselected series of 25 consecutive patients. All patients underwent SEEG, as part of their pre-surgical evaluation. Period of reference was 2013-2015 with a minimum follow up of two years after surgery. **Results:** 16/25 (64%) had TLE: 9 with only temporal lobe involved, 6 with temporal and another extra temporal area involved, 9/25 (36%) patients had extra-TLE. The extra TLE was determined by a combined analysis of the ictal clinical semiology, EEG, MRI, SEEG, and FDG-PET. 13/25 (52%) patients were MRI positive and 12/25 (48%) patients were MRI negative for brain anomalies, while 23/25 (92%) were PET positive (defined from a presence of focal area of hypometabolism) and 2/25 (8%) where PET negative. Surgical resection was performed in all of these patients, and after a mean postoperative follow-up of 28 months (range 24-50 months), seizure outcome, according to Engel's classification, showed that 19 patients were in class I (76%), 3 in class II (12%), 1 in class III (4%), and 2 in class IV (8%). In 19 cases FDG-PET was concordant whit the SEEG (showing the presence of an hypometabolic area in the EZ was detected), whereas in 2 cases the hypo area was close to the EZ; in 2cases PET was negative in the EZ and in other 2 cases showed an hypo area without a corresponding EZ in SEEG. **Conclusion:** This study aimed to compare the localization of EZ on SEEG at seizure onset, with the interictal patterns of metabolism for each patient. We showed that hypometabolic regions correlate with the SEEG, not only in TLE as described in the previous literature, but also in the extra-TLE. This data could confirm the value of FDG-PET in the diagnostic process for focal, drug-resistent, complex cases of epilepsy. The power of these data is the very

good post-surgical outcame for most of enrolled patients, while the main limitations are the heterogeneity of the epileptogenic zone and the few number of the patients. **References:** None.

EP-0012

Multimodal imaging approach in epilepsy: PET-MRI software coregistration in the assessment of localization the potential epileptogenic focus

A. Mestre Fusco[1], *S. González-Ortiz*[2], *S. Medrano*[2], *M. Suárez-Piñera*[1], *M. Ley*[3], *A. Principe*[3], *J. Capellades*[2], *R. Rocamora*[3]; [1]*Nuclear Medicine, Hospital del Mar - Parc de Salut Mar, Barcelona, SPAIN,* [2]*Radiology, Hospital del Mar - Parc de Salut Mar, Barcelona, SPAIN,* [3]*Epilepsy Unit - Neurology, Hospital del Mar - Parc de Salut Mar, Barcelona, SPAIN.*

Aim/Introduction: Our aim is to evaluate the usefulness of the cerebral positron emission tomography (PET) and magnetic resonance imaging (MRI) images coregistration in order to identify the potential epileptogenic areas preoperatively in patients with drug-resistant epilepsy (DRE). **Materials and Methods:** We prospectively included 40 consecutive patients (January 2016-March 2018, mean 38 years-old, 19 male) with DRE both, PET and MRI, as part of the presurgical study. The 18F-FDG PET (Siemens Biograph 6 PET-CT) and MRI (Philips Achieva 3-Tesla), acquired separately, are coregistered with "integrated registration" application of the AW-server 2.0 software. FDG-PET and MRI are evaluated separately by a nuclear medicine and neuroradiologist and then the PET-MRI fusion is evaluated together in a second-look. We compare the localization of epileptogenic lesions by the three methods. The potential epileptogenic area determined by neuroimaging is compared with the electroclinical hypothesis and in some cases with the invasive EEG studies in patients who were implanted. **Results:** In 26 out of 40 patients (65%) the PET-MRI fusion second-look has changed the suspicious area either by a reduction in the spread of hypometabolism or by the detection of a new hypometabolic focus. Structural MRI showed no lesions in 16 patients. In these patients, PET-MRI fusion images showed a hypometabolic area in 13 (81%) patients that was concordant with clinical hypothesis or seizure onset zone on EEG. Localization of hypometabolism areas include temporal lobe (hippocampus, amydala or temporo-polar region), insula, frontal operculum, parietal lobe and parieto-occipital areas. Structural findings on MRI include focal cortical dysplasia, sclerosis, heterotopia and cortical asymmetries. **Conclusion:** The fusion of 18F-FDG PET-RMI is a useful method to detect or to delimit the potential epileptogenic zone and can be useful for planning invasive EEG studies or surgery. **References:** None.

EP-0013

Autoimmune encephalitis: utility of PET/CT with18F-FDG as the first diagnostic step

E. Fajardo Ordoñez[1], *R. Hernandez*[2], *J. Chavez Torres*[1], *D. Pachuca Gonzalez*[1]; [1]*Medica Sur, Ciudad de México, MEXICO,* [2]*Rodrigo Hernandez, Ciudad de México, MEXICO.*

Aim/Introduction: Assess the utility of PET/CT with ^{18}F-FDG, for the investigation of patients with suspected autoimmune encephalitis **Materials and Methods:** A retrospective study was conducted from June 2009 to February 2019. We reviewed ^{18}F-FDG PET/CT scans of patients with clinical diagnosis of acute encephalitis,18 cases were selected to be further reviewed for antibodies laboratory, historical information, diagnostic workup, medications administered, and neuroimaging findings **Results:** 18 patients (14 women, 4 men; mean age, 63 y) with clinical diagnosis of autoimmune encephalitis presented with acute altered mental status, with seizures, depression, visual hallucinations the most common neurological symptoms. All 18 patients had abnormal uptake with ^{18}F-FDG PET/CT showing hypermetabolism most commonly in the superior frontal, orbitofrontal, dorsolateral prefrontal, and parietal cortex, mesial temporal structures, cingulate, caudate and putamen. 6 patients had an abnormal radiopharmaceutical uptake as a suspicion of a primary tumor, which were subsequently confirmed as having malignancy. The rest of the patients were evaluated with EEG and CSF samples for the study of infections and paraneoplastic antibodies. CSF was positive in 1 patient for Borrelia burgdorferi infection. CSF was significant in 7 patients with elevation of white cell count in 5 patients and mild elevation of protein in 2 patients. 7 patients had paraneoplastic panel results available with 6 being negative for NMDA, anti-Hu, VGK antibodies, and 1 being positive for GAD65. All seven patients that had hypermetabolism with PET/CT were treated with immunoglobulin, which all improved clinically. MRI were available in 8 of the patients. 2 patients had hyperintensity on FLAIR weighted MRI, one located in bilateral internal frontal convolution cortex and the second at the bilateral mesial temporal lobe. The rest of MRIs were all unremarkable except development of isolated gliosis areas **Conclusion:** PET/CT is a useful tool in the diagnostic workup of patients with clinically suspected autoimmune encephalitis, to rule out neoplastic and infectious origin and to those who do not test positive for paraneoplastic antibodies. PET/CT should be performed in such patients, FDG-PET can be positive despite a normal brain MRI **References:** None.

EP-0014

18F-DOPA positron emission tomography features in brain tumefactive demyelinating lesions

S. Raffa[1], *M. Bauckneht*[2], *L. Roccatagliata*[1,3], *S. Capitanio*[2], *E. Sbragia*[4], *M. Pardini*[4,5], *C. Lapucci*[4], *M. I. Donegani*[1], *A. A. Miceli*[1], *A. Uccelli*[4,5], *M. Inglese*[4,5], *F. M. Nobili*[4,5], *G. Sambuceti*[1,2], *S. Morbelli*[1,2]; [1]*Department of health sciences (DISSAL), University of Genoa, Genoa, ITALY,* [2]*Nuclear Medicine Unit, IRCCS Policlinico San Martino, Largo R. Benzi 10, Genoa, ITALY,* [3]*Neuroradiology, IRCCS Ospedale Policlinico San Martino, Largo R. Benzi 10, Genoa, ITALY,* [4]*Clinical Neurology, Department of neuroscience (DINOGMI),*

University of Genoa, Genoa, ITALY, [5]Clinica neurologica, IRCCS Ospedale Policlinico San Martino, Largo R. Benzi 10, Genoa, ITALY.

Aim/Introduction: Tumefactive Demyelinating Lesions (TDLs), are defined as acute, large (>2 cm), tumor-like lesions in the central nervous system. These lesions are often associated with ring enhancement ad a T2 Hypointense rim, peripheral restriction on diffusion-weighted imaging ad venular enhancement, and presence of surrounding edema that causing mass effect. For these radiological characteristics, TDLs may mimic space-occupying lesions (SOLs). It has been suggested that positron emission tomography (PET), particularly with labelled amino acid tracers, could be useful in the differential diagnosis (d.d.) of TDLs, especially with primary brain tumors (PBTs), in particular with low-grade gliomas (LGGs) or primary brain lymphomas. Based on these considerations, we aimed to individuate specific 18F-DOPA-PET and MRIs features of TDLs in a retrospective case series including TDLs, LGGs and lymphomas. **Materials and Methods:** We retrospectively evaluated brain MRI and 18F-DOPA-PET performed between February 2018 and March 2019 in patients with SOLs whose d.d. included TDLs. MRIs were visually coregistered to 18-DOPA-PET images, and maximum standardized uptake (SUVmax) values within lesions and their mutual ratios with striatum were calculated. The final diagnosis was established based on histology or clinical/radiological follow-up at six months. **Results:** A total 8 patients were identified. In 3 patients the final diagnosis was TDLs. In the other 5 patients 4 were diagnose with LLGs (1 with gliomatosis cerebri pattern) and 1 primary brain B-cell Lymphoma (PBBCL). Mean SUVmax was 2,02 for TDLs (standard deviation s.d.- 0,48; range 1,31-2,42) and 4,48 (s.d. 0,86; range 3,19-5,53) for PBTs, with lowest value recorded in PBBCL (3,19). Mean ratios with striatum in TDLs were 0,7 (s.d. 0,17; range 0,6-0,9) and 1,5 (s.d. 0,44; range 0,9-2,1) for PBTs, with the lowest value recorded in PBBCL, overlapping with values of TDLs (0,9). **Conclusion:** The present case series support the potential usefulness of 18F-DOPA-PET in the differential diagnosis of TDL. For instance, there was no overlap in SUVratio in patients with TDLs with respect to LLGs. However, a gray-zone between TDLs and lymphomas was highlighted. Coregistration of PET and MRI data and more deep integration of 18F-DOPA-PET and MRI features might be of interest to better disclose the potential role of 18F-DOPA-PET in the differential diagnosis of TDLs. **References:** None.

EP-0015

Cerebral perfusion measured by ^{99m}Tc-HMPAO SPECT in a simulated microgravity model using a 5-day dry immersion

L. Guillon[1], *M. P. Bareille*[2], *E. Cassol*[1], *A. Beck*[2], *M. Beaurain*[1], *P. Peran*[3], *J. A. Lotterie*[1,3], *A. Pavy - Le Traon*[4,5], *P. Payoux*[1,3]; [1]*Nuclear Medicine Department of University Hospital of Toulouse, Toulouse, FRANCE,* [2]*MEDES, Toulouse, FRANCE,* [3]*TONIC, Toulouse NeuroImaging Center, University of Toulouse, Inserm, UPS, Toulouse, FRANCE,* [4]*Neurological Department of University Hospital of Toulouse, Toulouse, FRANCE,* [5]*I2MC - INSERM, Toulouse, FRANCE.*

Aim/Introduction: Regional cerebral perfusion (rCBF) may be modified during exposure to microgravity. Microgravity induces a rapid thoraco-cephalic fluid shift and generates a possible increase of intra-cranial pressure [1]. Dry immersion (DI) is a simulated microgravity model that reproduces the effects of microgravity on human fluids [2]. However, consequences on rCBF have never been directly assessed in real or simulated microgravity. **Materials and Methods:** Cerebral perfusion was measured 4 days before and at the end of a 5-day DI in 18 healthy male subjects (34.0 +/- 5.5 years old, 16 right dominant hand) using a single photon emission computed tomography (SPECT) with the radiopharmaceutical ^{99m}Tc-hexamethylpropylene amine oxime (HMPAO). SPECT-HMPAO were compared between the two groups using SPM 12, by paired t test statistical analysis with a threshold of $p < 0.005$. **Results:** DI induced a significant hypoperfusion in the cortex, mainly in the two temporal regions (right temporal peak level : $Z = 3,61$, $p_{uncorr} < 0,001$;left temporal peak level : $Z = 3,40$, $p_{uncorr} < 0,001$))and induced an increase in perfusion in subcortical regions (including left thalamus (peak level: $Z = 3,07$, $p_{uncorr} < 0,001$)). **Conclusion:** After 5 days of DI, subjects presented significant hypoperfusion mainly in the bilateral temporal regions and hyperperfusion in the left thalamus region, measured by SPECT-HMPAO. Hyperperfusion in the left thalamus may be related to a muscular biopsy in the right vastus lateralis performedthe day before the SPECT the end of DI. Hypoperfusion in the cortical regions might be due to the thoraco-cephalic fluid shift and/or to the unloading support induced by the DI model. To test these assumptions, we need to conduct analysis of other parameters such as indirect assessment of intracranial pressure and psychological tests. **References:** [1] Heer M, et al. Space motion sickness: incidence, etiology, and countermeasures. Auton Neurosci 2006; 129(1-2):77-9.[2] Navasiolava et al. 2011). Long-term dry immersion: review and prospects. Eur J Appl Physiol 2011;111(7):1235-60.

EP-0016

Brain perfusion SPECT imaging in comparison to brain MRI imaging and their correlation with clinical condition in patients with multiple sclerosis

M. Assadi[1], *H. Shooli*[1], *R. Nemati*[1], *N. Chabi*[1], *E. Jafari*[1], *H. Dadgar*[2]; [1]*Bushehr University of Medical Sciences (BUMS), Bushehr, IRAN, ISLAMIC REPUBLIC OF,* [2]*Imam Reza International University, Mashhad, IRAN, ISLAMIC REPUBLIC OF.*

Aim/Introduction: Multiple sclerosis (MS) is an inflammatory, disabling, and unpredictable disorder that involves the central nervous system (CNS) and results in the progressive neurological disturbance. The role of gray matter in Multiple sclerosis (MS) is increasingly evident. Both gray matter perfusion and volume reduction are correlated with cognition and ambulation impairment and other clinical disturbance. We aimed to compare quantitative brain perfusion SPECT with brain MRI imaging and their correlation with clinical tests. **Materials and Methods:** In this cross-sectional descriptive study, 19 patients with RRMS were recruited. They underwent brain perfusion SPECT imaging

and brain MRI imaging along with several clinical examinations including EDSS, MMSE, SPPB, rapid smell test, Wechsler memory test, word-color complex Stroop (software version). The intima layer thickness of the carotid artery measured by external ultrasound. The brain SPECT and brain MRI images quantitatively analyzed (grouped and individual) by SPM software employing VBM technique to identify abnormal areas in the brain. the location of areas with significantly reduced grey matter density or perfusion was detected by using AAL (Automated Anatomical Labeling) software. Data analysis was performed using SPSS version 22 software. **Results:** All of RRMS patients were cognitively unimpaired. Quantitative images analysis revealed SPECT imaging can detect broad abnormal areas on the brain better than MRI imaging except for areas deep in the brain (insula and basal ganglia) in which MRI imaging is better than SPECT imaging. Although both imaging modality correlated with clinical tests in cognitively unimpaired patients with RRMS, MRI imaging correlated with cognitive and ambulatory tests better than SPECT imaging but SPECT correlated with a more diverse spectrum of clinical tests. **Conclusion:** Quantitative brain perfusion SPECT imaging can be a complementary modality along with quantitative brain MRI imaging to either larger coverage of abnormality detection and early detection of cognition decline in cognitively unimpaired patients with RRMS before becoming clinically impaired. **References:** None.

EP-0017

Feasibility and Effectiveness of SISCOM With SPM To Locate Epileptogenic Focus in Clinical Practice

***C. Oliveira**, E. M. Souza, S. Brunetto, M. Alvim, F. Cendes, C. D. Ramos, B. J. Amorim, E. Etchebehere;*
Unicamp, Campinas, BRAZIL.

Aim/Introduction: Epilepsy is one of the most common neurological disorders and patients with drug-refractory seizures can be treated with surgical removal of the epileptogenic focus (EF). Visual comparison of ictal and interictal Single Photon Emission Computed Tomography (SPECT) images to locate EF can be difficult. To overcome the difficulties, softwares such as SISCOM that are capable of subtracting these ictal and interictal SPECT images and also combining the images to an MRI, can improve the localization of the EF. This study aim to demonstrate the feasibility of performing SISCOM using the free software Statistical Parametric Mapping (SPM), as an initial experience at an epilepsy reference center. **Materials and Methods:** Patients with refractory epilepsy were submitted to ictal and interictal SPECT images. All patients received 1110MBq of ^{99m}Tc-ECD prior to SPECT images. Images were acquired using the same acquisition parameters. Electroencephalogram (EEG) monitoring was performed during both ictal and interictal injections. Interictal injection was performed with the patient resting in a dark, quiet room. Ictal injection was undertaken at the beginning of a seizure while undergoing telemetry monitoring. SISCOM reconstruction was performed by a trained physician or physicist using the Statistical Parametric Mapping (SPM) software. The images were blindly analyzed both visually and with SISCOM by two experienced nuclear medicine physicians. The reference standard of EF location was defined by pathology and follow-up in operated patients. In non-operated patients the reference standard was determined by the set of patient's exams (seizure semiology, serial EEG, long-term-video-EEG, and MRI). Visual and SISCOM analyses were compared to reference standard and classified as concordant, discordant and partially concordant. **Results:** Ictal and interictal SPECT images were analyzed both visually and by SISCOM in twenty-four patients (13 women; 30.8 ± 13.3 years). In relation to the reference standard, SISCOM was concordant in 18 cases (75.0%), while visual analysis was concordant in 13 cases (54.2%). SISCOM increased by 20.8% the correct location of the EF. SISCOM was discordant in 5 (20,8%) and partially concordant in one patient. **Conclusion:** SISCOM with SPM is feasible in the clinical practice routine, and it can be a powerful tool in EF precise location, aiding in the surgical treatment of patients that are refractory to clinical treatment. **References:** 1.Chen T, Guo L. The role of SISCOM in preoperative evaluation for patients with epilepsy surgery: A meta-analysis. Seizure.2016;41:43-50. 2.Tamber MS, Mountz JM. Advances in the Diagnosis and Treatment of Epilepsy. Seminars in Nuclear Medicine.2012;42(6):371-86.

EP-0018

Syndrome of the Trephined: evaluating brain perfusion before and after cranioplasty using 99m-Tc HMPAO and SPECT-CT

***Á. Galiana**, S. Ruiz, I. Paredes, E. Gutiérrez, M. Tabuenca, M. Marín, E. Martínez, V. Godigna, D. Vega, J. Estenoz;*
Hospital Universitario 12 de Octubre, Madrid, SPAIN.

Aim/Introduction: The Syndrome of the Trephined (SoT) is a complication of craniectomy, responsible for multiple neurological symptoms in a period comprised between days and years after the surgery. The pathophysiology is still in discussion, although changes in brain perfusion are one of the principal hypothesis. Main symptoms include motor weakness (56,9%) as well as cognitive and language deficits (41,4% and 27,6%). Treatment of SoT is cranioplasty, which has demonstrated symptomatic improvement. This ongoing study aims to evaluate the changes in brain perfusion before and after cranioplasty using 99mTc-HMPAO and SPECT-CT imaging. **Materials and Methods:** The study involves 18 patients, aged 16 to 81, who had a craniectomy performed due to cranial traumas, and intracranial hemorrhages amongst other causes. The patients were diagnosed with SoT in our hospital, and were all eligible for cranioplasty. The cerebral perfusion of the patients was studied in three moments: before surgery, after one week and at least three months after the cranioplasty. Brain perfusion was evaluated both visually and quantitatively using QBrain© software, taking special attention to the non-surgically affected hemisphere, where automated analysis is less prone to errors caused by surgical alterations of brain parenchyma. Quantification was evaluated in 12 areas on each hemisphere.

Results were analyzed using multivariate analysis considering the changes in perfusion regarding the timeline of the study as well as the brain hemisphere (surgically affected hemisphere or not). The variables studied were the ratio comparing the region of interest with the pons (as the reference area) and Z-score (using QBrain© database of non-pathological brain as controls). **Results:** First results show a statistically significant increase in ratio of perfusion on both hemispheres (surgical and no-surgical) between the pre-surgical evaluation and the study obtained at least three months afterwards (ratios 1,11 and 1,14 respectively in non-surgical hemisphere). Same significance was obtained for Z-score (0,36 and 0,77 respectively in non-surgical hemisphere). Therefore, preliminary results show changes in 6 out of 12 areas, 2 of which were only significant in z-score values while the rest were significant in both z-score and ratio. **Conclusion:** According to our results, brain perfusion significantly changes in SoT patients before and after cranioplasty. This findings may be related to the pathophysiology of SoT. The increase in brain perfusion can also have implications in the clinical outcome of SoT after cranioplasty. The clinical relevancy of these findings needs to be furtherly evaluated in long term clinical studies. **References:** None.

EP-0019

FDG-PET/CT for Assessing The Cerebral Protective Effects of Hydrogen in Rabbits with Cardiac Arrest

Y. Tang[1], *G. Huang*[2], *J. Li*[1], *T. Long*[1], *Y. Li*[1], *S. Hu*[1];
[1]*Department of PET Center, XiangYa Hospital Central South University, Changsha, CHINA,* [2]*Department of Emergency, XiangYa Hospital Central South University, Changsha, CHINA.*

Aim/Introduction: To assess fluorodeoxyglucose (FDG)-positron emission tomography (PET) / computed tomography (CT) for evaluating the cerebral protective effects of hydrogen in rabbits with cardiac arrest. **Materials and Methods:** Male rabbits were divided into the hydrogen (n=6), control (n=6), and sham (n=3) groups. Cardiac arrest was induced by intravenous potassium chloride. During resuscitation, hydrogen/oxygen (1:24 v/v) and pure oxygen were inhaled by the hydrogen and control groups, respectively. Maximum standardized uptake values (SUVmax) measured by FDG-PET/CT at baseline and at 2 and 24h post-resuscitation. Blood samples were collected for UCH-L1 level measurements preoperatively, and at 24, 48, and 72h post-operation. After euthanasia (72h post-operation), brain tissues were extracted for Nissl's staining. **Results:** SUVmax values were first decreased before rising at 2 and 24h of resuscitation in hydrogen treated and control animals. SUVmax values in the frontal, occipital, and left temporal lobes as well as the whole brain were significantly different between the hydrogen and control groups, at 2 and 24h after resuscitation (P<0.05); NDS scores at 24 and 48h were lower in hydrogen treated animals (P<0.05). At 24h, serum UCH-L1 levels were increased in the hydrogen and control groups, but less pronounced in the hydrogen group (P<0.05). At 48 and 72h, UCH-L1 levels in the experimental and control groups were gradually decreased, with significantly lower values in experimental animals (P<0.05). Pathological data demonstrated reduced neuronal damage in the experimental group compared with controls at 72h. **Conclusion:** FDG-PET/CT could be used to monitor early cerebral damage and demonstrate the protective effects of hydrogen in brain after cardiac arrest. **References:** None.

EP-0020

Effects of bariatric surgery on brain glucose metabolism and cognitive function: insight from dynamic FDG PET/CT study

D. Volterrani*, G. Daniele, S. Mazzarri, F. Guidoccio, A. Dardano, L. Giusti, L. Fantechi, G. Manca, C. Morrone, S. Del Prato, G. Aghakhanyan;*
University of Pisa, Pisa, ITALY.

Aim/Introduction: We aimed to evaluate the impact of bariatric surgery (RYGB) on the brain glucose metabolism and the interplay between gut hormones/metabolomics, cerebral metabolic rate of glucose (CMRGlu) and cognitive function. **Materials and Methods:** Thirteen morbidly obese subjects with normal glucose tolerance (BMI 46±4.9 kg/m2; HbA1c 40.1±5.9 mmol/mol; age 42.4±9.8 years) planned for RYGB surgery were recruited. Theoral glucose tolerance test (OGTT) was performed, followed by 60 minutes FDG dynamic PET study.Continuous blood samples were drawn before and at 30, 60, 90, and 120 min for glucose, insulin, GLP, VIP, GIP and C-peptide measurements. The same venous blood samples were used for calculating radioactivity concentration in plasma. Fasting blood samples for metabolomics (leptin, brain derived neurotrophic factor, BDNF) were also collected and the homeostasis model assessment of insulin resistance (HOMA-IR) was calculated as an index of insulin resistance. The influx constant (Ki) and MRGlu were then quantified using the two tissue compartment Patlak approach with an imaged-derived input function (PMOD). Subsequently, the parametric CMRGlu images were created and spatially normalized in MNI space. The paired t-test and Spearman rank correlation were applied to assess changes and associations of voxel-wise CMRGlu and metabolomics. All patients underwent a battery of neuropsychiatric tests (MMSE, MoCA, Token test, TMT, etc) to assess cognitive function in several domains, before and 6 months after RYGB. **Results:** Six months after RYGB a significant BMI reduction (p<0.001) was achieved. Post-OGTT GLP1 was increased (p<0.01) as well as GIP (p<0.01). The HOMA-IR dropped significantly 6m after RYGB (p=0.02). Either whole brain and region-selective CMRGlu decreased 6m after surgery (15.9±4.6 to 10.5±5.1 µmol/min/100ml; p<0.01). Voxel-wise paired analysis displayed clusters of decreased CMRGlu 6m after RYGB in the widespread brain regions. In addition, we found a significant positive relationship between CMRGlu and HOMA-IR. All patients at baseline presented MMSE and MoCA scores in the normal range. However, 6 months after RYGB, the cognitive domains examined showed a trend of global improvement. MMSE score increased statistically significantly (p 0.002) as well as MoCA score (p <0.005). **Conclusion:** After bariatric surgery,

there are several modifications of multiple factors that play a role in the so-called "intestinal-brain cross-talk", in CMRGluand in cognitive function. CMRGluof morbidly obese subjects is abnormally enhanced in response to insulin. Bariatric surgery seems to reverse this insulin-mediated signal dysfunction and could produce significant CNS effects decreasing brain glucose over-consumption and promoting potential neuroprotective effects **References:** None.

EP-0021

Studying Rat Model of Herpes Simplex Virus type-1 Infection by [18F]FHBG in Accompanied by Neuroinflammation and Glucose Metabolism

N. Ghazanfari, E. E. F. J. de Vries, R. A. J. O. Dierckx, J. Doorduin; UMCG, Groningen, NETHERLANDS.

Aim/Introduction: Herpes simplex virus type 1 (HSV-1) is the most common cause of the Herpes simplex encephalitis (HSE) in humans. Animal studies have shown that HSV-1 enters the brain via the olfactory nerves, which are the only neurons with direct discloser to the environment. HSV-1 was found to affect the same brain regions as the ones affected in Alzheimer's and schizophrenia pathology. The aim of this study was to evaluate the feasibility of [18F]FHBG PET for studying HSV-1 infection of the brain and to monitor the accompanying inflammatory response and changes in glucose consumption with [11C]PK11195 and [18F]FDG PET. **Materials and Methods:** Male Wistar rats (n= 45) were inoculated with HSV-1 by the application of the virus on the nostrils, a similar approach with PBS was performed for controls (n=16). The onset of clinical symptoms of infection varied between animals. The presence and spread of active HSV-1 were analyzed by scanning animals (n=11) with [18F] FHBG at day 6 or 7. The occurrence of neuroinflammation due to infection was examined [11C]PK11195 PET (n=24) at day 5 or 7. [18F]FDG scans were performed longitudinally on infected animals (n=26) to evaluate glucose metabolism consumption on day 1, 3, 4, 5 and 6. 60-min dynamic PET acquisition was performed for all tracers. The statistical differences between control and HSV-infected groups for [18F]FHBG were analyzed using either the independent sample t-test (single measures) or the generalized linear model (repeated measures). The final values are considered to be significant at $P<0.05$ for all studies. **Results:** PET showed significant differences in [18F]FHBG uptake (SUV) in accumbens, cingulate cortex, prefrontal cortex, hippocampus, septum, striatum, thalamus, and midbrain. Differences in [11C]PK11195 uptake between day 5 and 7 were significant for all brain regions, except for cortical regions. [18F] FDG uptake on day 5 was significantly different from days 1, 3 and 4 in all the brain regions, while tracer uptake on day 4 was significantly different from days 1 and 3 only in the insula cortex. **Conclusion:** Scanning with [18F]FHBG showed mainly the virus path through the trigeminal nerve after inoculation via the nostrils. [11C]PK11195 and [18F]FDG showed the secondary effects accompanying an HSV-1 infection. **References:** None.

EP-0022

The Evaluation of Brain FDG PET Images in Temporal Lobe Epilepsy by Data Mining Methods in Terms of Lateralization of Epileptogenic Focus

Ü. Akdemir[1], I. Yildirim[2], U. Aydos[1], S. Gulbahar Ates[1], G. Kurt[3], L. Atay[1];
[1]Gazi University Medical Faculty Department of Nuclear Medicine, Ankara, TURKEY, [2]Gazi University Medical Faculty Department of Neurology, Ankara, TURKEY, [3]Gazi University Medical Faculty Department of Neurosurgery, Ankara, TURKEY.

Aim/Introduction: The aims of this study were to evaluate the relative metabolism values obtained from different brain regions by using data mining methods and to make a classification model for lateralization of epileptogenic focus in resistant temporal lobe epilepsy (TLE). **Materials and Methods:** Interictal brain FDG PET images of 53 patients with resistant TLE (mean age ± standard deviation = 27.1 ± 7.0) who had seizure control after surgical treatment at our hospital were evaluated retrospectively. The numerical analysis of PET images were done with SPM8 ("Wellcome Center for Human Neuroimaging") and WFU_PickAtlas ("ANSIR Laboratory, Wake Forest University School of Medicine") softwares. The AAL ("Automated Anatomical Labeling") atlas was used to obtain regional count values from spatially normalized PET images. The regional asymmetry indices [AI = (left hemisphere-right hemisphere) / (left hemisphere + right hemisphere) x 200] were calculated to eliminate the need for reference region and the need for count normalization of PET images. The patient group was randomized and divided into learning (n = 20) and test (n = 33) sets. A lateralization model was created with learning set in R software by using RWeka classification tool, definitive clinical lateralization information and asymmetry values of 13 different regions in which significant differences were observed in terms of lateralization. This model was then evaluated for the lateralization accuracy using the test data. The findings of this lateralization model was compared with the clinical outcome. **Results:** The clinical diagnoses (with regard to surgical procedures and clinical follow-up findings) were right TLE in 21 patients and left TLE in 32 patients. The asymmetry values of the 13 regions with significant asymmetry between regional metabolism values (mesial temporal lobe and functionally associated regions) were included in the classification analysis. When the classification model determined by RWeka (for Rolandic operculum, if AI> 2.06, right TLE; if AI ≤2.06, left TLE) was used on the test data for prediction, the results of the classification were found to be 90% consistent with definitive clinical lateralization (Cohen's kappa was 0.800; %95 CI 0.474 - 1.000; $p < 0.001$). **Conclusion:** In our patient group, the success rate of the metabolic asymmetry associated with rolandic operculum was found to be 90% in the lateralization of epileptogenic foci. The numerical analysis based on regional asymmetry of brain FDG PET findings in TLE can be used as an objective evaluation method with a very high diagnostic accuracy. **References:** None.

EP-0023

Target Volume Definition With ^{68}GA-DOTATOC-PET/CT And MRI For Patients With Meningiomas

M. Colandrea[1], *C. Garibaldi*[1], *M. E. Ferrari*[1], *A. Iannalfi*[2], *S. Pesente*[3], *S. L. Fracassi*[1], *L. Gilardi*[1], *A. P. Rocca*[1], *L. L. Travaini*[1], *D. Militano*[1], *S. Papi*[1], *A. S. Cascio*[1], *M. Cremonesi*[1], *C. M. Grana*[1];
[1]*Istituto Europeo di Oncologia, Milano, ITALY,* [2]*CNAO, Pavia, ITALY,* [3]*Tecnologie Avanzate, Udine, ITALY.*

Aim/Introduction: To investigate the potential impact of ^{68}Ga-DOTATOC PET/CT in addition to standard morphological imaging (MRI and CT) in gross tumour volume (GTV) delineation in patients affected by skull base meningiomas and treated with particle therapy. **Materials and Methods:** Sixteen patients (median age 51.4 y) with skull base meningiomas underwent ^{68}Ga-DOTATOC PET/CT for target tumor delineation followed by constract-enhanced (CE) MRI and CT for treatment planning with particle therapy. GTV for treatment was defined on the CE-MRI fused to the simulation CT (CTsim) integrating information from the PET/CT. Three methods to delineate the PET volume were evaluated: manual (PETman), semiautomatic (42% threshold of SUVmax, PETSUV42%) and an automatic adaptive thresholding method incorporating PET reconstruction parameters (PETauto) (iTA, TA, Udine). PETman volumes were delineated by the same nuclear medicine physician, while PETSUV42% and PETauto volumes were determined by medical physicists. The PET/CT, CE-RMI and CTsim were coregistered with a deformable image registration algorithm using the MIM Software (v. 6.1) and tumor volumes and positions were determined. The overlapping region of MRI and PETman resulted in GTVcommon. **Results:** The brain lesions had a median SUVmax of 12.1 ± 6.8 (range: 3.2-32.6). Overall, the GTV-MRI was larger than GTVPETman in 7 patients (43.8%), smaller in 6 (37.5%) and almost the same in 3 (18.8%). The median value of the different volumes were: GTV-MRI = 14.3 ± 37.2 cc, GTV-PETman = 14.4 ± 47.0 cc, GTVcommon = 12.2 ± 33.6 cc, GTV-PETSUV42% = 8.3 ± 18.3 cc, GTV-PETauto = 11.3 ± 26.2 cc. As expected, volumes determined by the fixed threshold technique were always smaller than GTV-PETman (Δ = - 51.0 ± 32.7%) and GTV-PETauto (Δ = - 21.5 ± 12.7%) since they do not take into account variations in tumor heterogeneity. The largest differences were observed for lesion showing a high SD of SUV. The median difference between GTV-PETman and GTV-PETauto was 39.6 ± 29.5 %. **Conclusion:** ^{68}Ga-DOTATOC-PET/CT seems to improve the target volume delineation in skull base meningiomas, often leading to a reduction of GTV compared with results from MRI. The automatic adaptive thresholding delineation method may provide robust and reliable tool to help physician in segmenting PET images, reducing inter- and intra-observer variability. **References:** None.

EP-02
Neuroimaging: Movement Disorders

October 12 - 16, 2019

e-Poster Area

EP-0024

Reliability of Dopamine Transporter PET Measurements with [^{18}F]FE-PE2I in Early Stage Parkinson´s Disease: A Preliminary Test-Retest Evaluation

V. Kerstens[1], *P. Fazio*[1], *M. Sundgren*[2,3], *G. J. Matheson*[1], *E. Franzén*[4,5], *C. Halldin*[1], *S. Cervenka*[1], *P. Svenningsson*[2], *A. Varrone*[1];
[1]*Department of Clinical Neuroscience, Centre for Psychiatry Research, Karolinska Institutet and Stockholm County Council, Stockholm, SWEDEN,* [2]*Department of Clinical Neuroscience, Neuro Section, Karolinska Institutet, Stockholm, SWEDEN,* [3]*Neuro Department, Karolinska University Hospital, Stockholm, SWEDEN,* [4]*Department of Neurobiology, Care Sciences and Society, Division of Physiotherapy, Karolinska Institutet, Stockholm, SWEDEN,* [5]*Function Area Occupational Therapy & Physiotherapy, Allied Health Professionals Function, Karolinska University Hospital, Stockholm, SWEDEN.*

Aim/Introduction: The reliable quantification of dopamine transporter (DAT) imaging in Parkinson's disease (PD) is important for diagnostic purposes as well as for potential evaluation of disease modifying treatment. [^{18}F]FE-PE2I is a suitable radioligand for imaging the nigrostriatal DAT in patients with PD (1). A test-retest study in young healthy subjects has shown that [^{18}F]FE-PE2I has a favourable low variability and good reliability of the measurements (2). However, the test-retest properties of [^{18}F]FE-PE2I in PD patients remains to be examined. Due to degeneration of dopaminergic neurons and thus loss of specific binding to DAT, higher measurement variability in PD might be expected. Therefore, the aim of this study was to examine the test-retest reliability of [^{18}F]FE-PE2I PET measurements in patients with early stage PD. **Materials and Methods:** Seven patients with early stage PD (5 men, 2 women; mean age 65.6±7.6 y; disease duration 8±3 y; Hoehn and Yahr 1-2; UPDRS 17.8±7.4) have so far been included. For each patient, two 93-minute PET-measurements with [^{18}F]FE-PE2I were performed within an interval between 7 and 28 days using a high resolution PET system (HRRT). On the day of PET, patients were examined in "off" with the MDS-UPDRS-III and for one week prior to each PET visit they wore a physical activity monitor (Actigraph GT3X+), to ascertain clinical stability within the study period. Parametric images of binding potential (BP_{ND}) were obtained with the wavelet-aided parametric imaging software using Logan graphical analysis and cerebellum as reference region (1). Regions of interest were caudate, putamen, ventral striatum, and substantia nigra. Test-retest reproducibility was determined with calculation of repeatability (absolute variability) and reliability (intraclass correlation coefficient, ICC). **Results:** The intrasubject variability was 6.1±4.4% for caudate, 8.6±9.8% for putamen, 8.1±6.6% for ventral striatum, and

10.7±14.7% for substantia nigra. The ICC for caudate, putamen, ventral striatum and substantia nigra were 0.97, 0.92, 0.87, and 0.79 respectively. **Conclusion:** These preliminary results show good reliability of DAT-PET measurements with [^{18}F]FE-PE2I in early stage PD patients. The results are in agreement with the results previously reported in younger, healthy subjects (2), indicating that [^{18}F]FE-PE2I-PET provides reliable estimates of DAT availability also in patients with PD. After completing the study, power-calculations can be made to estimate the sample size for future clinical trials using [^{18}F]FE-PE2I as DAT imaging marker. **References:** 1. Fazio et al. Mov Disord. 2018;33(4):592-599. 2. Suzuki et al. Nucl Med Commun.2014;35(3):231-7.

EP-0025

Dopaminergic and Metabolic Characteristics of Parkin Early Onset Parkinson's Disease: a Dual-tracer PET Study

J. Lu[1], *F. Liu*[2], *J. Ge*[1], *P. Wu*[1], *J. Wang*[2], *C. Zuo*[1];
[1]*PET Center, Huashan Hospital, Fudan University, Shanghai, CHINA,* [2]*Department of Neurology, Huashan Hospital, Fudan University, Shanghai, CHINA.*

Aim/Introduction: Mutation in Parkin is the most common cause of autosomal recessive Parkinson's disease(PD). Early onset PD (EOPD) is considered to have special disease progression. Dopaminergic and metabolic PET could provide nigrostriatal dopaminergic dysfunction and abnormal metabolic changes effectively. We aimed to investigate dopaminergic dysfunction and metabolic characteristics of Parkin EOPD and their associations with clinical ratings. **Materials and Methods:** We analyzed dopaminergic dysfunction ([^{11}C-CFT) and metabolism ([^{18}F-FDG) of 17 Parkin EOPD, 16 non-Parkin EOPD, 30 late onset PD (LOPD) patients and 18 normal controls at voxel, regional and network levels after age correction. Patient groups were matched for UPDRS motor ratings and H&Y scales. We analyzed relationships of dopaminergic, metabolic PET and clinical ratings in levels mentioned above. All analyzes were conducted in SPM 8 and ScanVP 7.1 implemented in Matlab8.4. **Results:** Three patient groups showed abnormal dopamine transporter (DAT) bindings and metabolic activities compared to normal controls. Parkin EOPD had lower DAT bindings than non-Parkin EOPD (P<0.05, post hoc: LSD) and similar DAT bindings with LOPD (P>0.05, post hoc: LSD) in striatum. Some of the abnormal metabolic regions were different among patient groups. Compared to non-Parkin EOPD group, Parkin EOPD group decreased glucose metabolism in superior and medial frontal gyrus, middle temporal gyrus, while increased in cerebellum, lingual gyrus and fusiform (P<0.01, uncorrected). However, three patient groups didn't show significant difference in network expressions (P=0.569, one-way ANOVA). It was noteworthy that Parkin EOPD had the lowest DAT binding and network expression among three patient groups which was in conflict with former impression of PD[1]. For correlations, DAT bindings had significant correlations with clinical ratings in whole PD, non-Parkin EOPD and LOPD groups (P<0.05), but none survived in Parkin EOPD group. Significant correlation between DAT bindings and PDRP expressions was only showed in LOPD group (P<0.05). **Conclusion:** In this dual-tracer PET study we demonstrated the unique dopaminergic dysfunction and cerebral glucose metabolic characteristics of Parkin EOPD patients at voxel, regional and network levels. This was the first FDG and CFT dual-tracer study in Parkin EOPD patients. Our findings might promote the understanding in further studies of pathophysiological and compensatory mechanisms in Parkin EOPD as well as non-Parkin EOPD, and demonstrated a brand-new idea for other kinds of studies in genetics of PD. **References:** [1] Liu FT, Ge JJ, Wu JJ, et al. Clinical, Dopaminergic, and Metabolic Correlations in Parkinson Disease: A Dual-Tracer PET Study. Clin Nucl Med. 2018;43(8):562-571.

EP-0026

Tc-99m TRODAT-1 SPECT Images in Diagnosis and Severity Evaluation of Parkinson's Disease using Deep Learning Model

P. Chuang[1], *C. Ko*[1], *C. Lin*[2], *R. Yen*[1];
[1]*Department of Nuclear Medicine, National Taiwan University Hospital, Taipei City, TAIWAN,* [2]*Department of Neurology, National Taiwan University Hospital, Taipei City, TAIWAN.*

Aim/Introduction: Dopaminergic transporter imaging using ^{99m}Tc-TRODAT-1 SPECT is known to reflect neurodegeneration in Parkinson's disease (PD) and served as clinical routine in differentiating PD from non-PD patients. Nevertheless, challenge is often encountered with inevitable interobserver variability. Semiquantitative analysis such as striatal-to-background uptake ratio and asymmetric index shows adequate performance however time and manpower consuming, especially in cases with variable anatomy or poor uptake activity. The aim of our study is to build suitable deep learning model aid in diagnosis and evaluate severity of PD. **Materials and Methods:** From January 2016 to December 2017, 313 consecutive patients diagnosed with idiopathic PD (iPD) or non-parkinsonism tremor referred for ^{99m}Tc-TRODAT-1 SPECT images were included retrospectively, all of which was closely followed at neurology department for at least 1 year to confirm diagnosis. Disease severity was categorized into early and late stage using Hoehn and Yahr scale with cutoff of 3. Every image was visual interpreted using 6-point score (with 0 stands for normal uptake and 5 for background activity) [1]. Patients were randomized into training (50%), validation (20%), and testing (30%) groups. The original SPECT were resampled into 128x128x64 matrix without any registration. We introduced random shift and rotation into training group to balance case number of each visual score. We built a convolutional neural network (CNN) with three convolution layers and two fully-connected layers to predict the score. Training was terminated when the validation group got the best performance. The comparisons were made on the testing group. **Results:** Characteristics including age, gender, diagnosis of iPD, disease severity, and visual score of training, validation, and testing groups were without significant difference using ANOVA. Using Kendall's tau correlation test,

the CNN-derived score showed fair correlation with visual score (r=0.6784, p<0.01). Diagnostic performance of CNN-derived score was non-inferior to visual score using receiver-operating-characteristic curve analysis by margin of 0.1, with area-under-curve 0.9163 and 0.9113 respectively (p=0.02), as well as indifferent correlation with clinical staging, r=0.6074 and r=0.5489 respectively (p=0.19). **Conclusion:** Our CNN model showed good diagnostic performance and fair clinical stage correlation which were comparable to routinely used visual interpretation of ^{99m}Tc-TRODAT-1 SPECT images. **References:** 1. Huang WS et al. Usefulness of brain ^{99m}Tc-TRODAT-1 SPECT for the evaluation of Parkinson's disease. Eur J Nucl Med Mol Imaging. (2004)31:155.

EP-0027

Comparison of ^{123}I-ioflupane SPECT imaging between the Veriton™ 360° CZT camera with striatum focusing and a conventional gamma-camera

M. B. Chawki, *M. Bordonné, T. Zaragori, G. Karcher, P. Marie, L. Imbert, A. Verger;*
CHRU de Nancy, Nuclear Medicine Department, Vandoeuvre-Lès-Nancy, FRANCE.

Aim/Introduction: The Veriton 360° CZT-camera (Spectrum Dynamics Medical) provides better performances in comparison to conventional gamma cameras owing to the properties of CZT detectors, and also to an original 360° geometry of detection allowing to focus the acquisition on striatum which could be particularly advantageous for ^{123}I-ioflupane SPECT imaging. This study aimed to compare the ^{123}I-ioflupane SPECT imaging with striatum focusing provided by the Veriton CZT-camera to imaging from a conventional gamma camera. **Materials and Methods:** ^{123}I-ioflupane SPECT acquisitions of 30 minutes, obtained with a conventional camera (Symbia T2, Siemens Healthineers) in clinical routine in 30 patients, were immediately followed by an additional 15 minutes acquisition focalized on striatum with the Veriton 360° CZT-camera. Tomographic count sensitivity was measured from projection images in counts/MBq/s after correction for the radioactive decay. SPECT images were reconstructed with previously optimized parameters and a comparison was planned between the 2 cameras for a visual classification as normal or pathological exam obtained by consensus of 3 experiences observers and for an automatic quantification of binding potentials of striatum structures on parametric images. **Results:** Tomographic count sensitivity from the Veriton camera was 50% higher than that of the conventional camera (397.3 ± 89.5 vs. 260.5 ± 54.1 counts/MBq/s, p<0.001). The visual classification as normal or abnormal was concordant between the 2 cameras in 87% of patients (26/30 patients, kappa coefficient of 0.73). Spearman correlation coefficients between the 2 cameras for the quantitative binding potentials of the right and left caudate and of the right and left putamen were respectively: 0.89, 0.84, 0.85 and 0.91 (p<0.001). **Conclusion:** ^{123}I-ioflupane SPECT images, obtained through a focused striatal recording of only 15 min with the Veriton 360° CZT-camera, provides a good diagnostic concordance with results from conventional gamma camera, both for visual and quantitative analyses. Furthermore, the high-count sensitivity of this camera gives the possibility of significantly reducing acquisition time and/or injected activity. **References:** None.

EP-0028

Corticobasal syndrome: is [^{18}F]FDG-PET a feasible tool to predict underlying Alzheimer's pathology?

A. M. N. Coutinho, *J. B. Parmera, M. R. Aranha, A. Studart Neto, C. R. Ono, E. R. Barbosa, R. Nitrini, C. A. Buchpiguel, S. M. D. Bucki;*
University of São Paulo, São Paulo, BRAZIL.

Aim/Introduction: Corticobasal Syndrome (CBS) is an atypical parkinsonian syndrome first considered a motor disorder but now also recognized as a cognitive disorder. The term CBS denotes the phenotype of multiple pathologies, including Alzheimer's disease (AD) and 4-repeat Tauopathies found on corticobasal degeneration (CBD). Accurate antemortem diagnosis is challenging, and diagnostic methods are being developed to predict the underlying pathology. Previous works with post-mortem analysis established [^{18}F]FDG-PET patterns closely related to AD underlying pathology and those commonly seen on CBD. The present study aimed to investigate the capacity of [^{18}F]FDG-PET to predict cortical amyloid deposition and cognitive features of AD in patients with CBS. **Materials and Methods:** Thirteen patients meeting criteria for probable CBS were prospectively evaluated and underwent both [^{18}F]FDG-PET and [^{11}C]PiB-PET scans to assess their brain amyloid status. According to their brain [^{18}F]FDG-PET metabolic patterns, patients were distributed in two groups: CBS likely related to AD (AD group) and CBS likely unrelated to AD (non-AD group). Participants were evaluated concerning their movement disorders and cognitive symptoms and underwent a complete neuropsychological evaluation. Clinical evaluation was performed blinded to the PET images. [^{18}F]FDG-PET and [^{11}C]PiB-PET scans were evaluated blindly to each other results and also to the clinical data. **Results:** Five patients with CBS had an AD pattern on [^{18}F]FDG-PET scans, and all of them (100%) tested positive for brain amyloid deposition. The remaining eight patients had a non-AD metabolic pattern, and 6 of them (75%) had negative [^{11}C]PiB-PET scans, all with typical features of CBD on [18F]FDG-PET. Two patients had non-AD brain metabolic patterns and positive [^{11}C]PiB-PET examinations. All cases of negative amyloid scans were blindly classified as having a non-AD-pattern. There were significant differences on the [^{18}F]FDG-PET AD and non AD subgroups on MMSE score, Clinical Dementia Rating (CDR), and Addenbrooke's Cognitive Examination-Revised (ACE-R) scales, with worst scores on the AD group (p<0.05). We also observed significant differences in MMSE and ACE-R according to the amyloid status (lower scores in individuals with positive [^{11}C]PiB-PET examinations). **Conclusion:** Patients with an AD pattern on [^{18}F]FDG-PET were predominantly positive on amyloid scans and had lower scores in cognitive scales despite age, gender, symptom duration, and

motor features, suggesting a higher functional decline related to AD pathology in CBS. Functional molecular imaging with [18F]FDG-PET might be a potential factor to predict CBS variants depicting their specific degeneration patterns. **References:** None.

EP-0029

Presurgical cognitive phenotype and its relation to brain metabolic pattern in the evaluation of the clinical outcome of Deep Brain Stimulation in Parkinson's Disease: an FDG-PET study

C. Polito, V. Berti, S. Ramat, F. Terenzi, G. Puccini, M. De Cristofaro, S. Sorbi, R. Sciagrà;
Università di Firenze, Firenze, ITALY.

Aim/Introduction: Deep Brain Stimulation (DBS) is not currently indicated for Parkinson's Disease (PD) patients with dementia. Several studies have addressed the cognitive and brain metabolic outcomes of DBS, but whether the presurgical cognitive phenotype and its relation to brain metabolism could affect the clinical outcome of DBS has been less explored. The aim of the present study is to identify the cognitive-metabolic profile of PD patients who could benefit the most from DBS. **Materials and Methods:** 36 consecutive PD patients (10F/26M mean age 59±7years), treated with DBS between 2008 and 2017 were selected. Clinical and neuropsychological profiles were collected before and one year after surgery. All patients underwent FDG-PET within a month before surgery. Patients were divided into three groups according to the cognitive phenotype: non-Mild Cognitive Impairment (non-MCI-PD, n=7, MMSE=29.29±0.9), MCI single non-amnestic domain (MCI-SD, n=12, MMSE=27.33±1.49), MCI multiple domain (MCI-MD, n=17, MMSE=26.76±2.30). Chi-Square and ANOVA were performed in order to explore presurgical clinical-demographic differences between groups, and paired t-test to assess DBS clinical outcome in each group. SPM12 ANOVA design was performed to investigate presurgical brain metabolic differences between groups, and multiple regression design to explore the relation between presurgical brain metabolism and the clinical variable showing the best response to DBS at follow-up in each group distinctively. **Results:** There were no differences between non-MCI, MCI-SD and MCI-MD in clinical and demographic variables. The motor part of the Unified Parkinson's Disease Rating Scale (UPDRSIII) and the Schwab And England Activities Of Daily Living Scale (SE-ADL) showed significant improvement after DBS in the Off-Therapy condition in MCI-SD and MCI-MD. At voxel-based analysis MCI-MD showed grater hypometabolism in bilateral Precuneus with respect to MCI-SD. UPDRSIII-Off-Therapy-post-DBS negatively correlated with presurgical brain metabolism in bilateral superior parietal gyrus in MCI-SD. The SE-ADL-Off-Therapy-post-DBS positively correlated with presurgical brain metabolism in bilateral parieto-occipital regions in MCI-SD. No significant correlation was found in MCI-MD neither for UPDRSIII nor for SE-ADL. **Conclusion:** In the present study MCI-SD PD patients showed presurgical preserved brain metabolism in bilateral precuneus, and after DBS preserved parieto-occipital brain metabolism seemed to predict better motor response and improvement in ADL. In MCI-SD PD preserved presurgical brain metabolism in bilateral precuneus and parieto-occipital regions could be useful to identify patients who could benefit most from DBS. **References:** None.

EP-0030

Utility of ^{18}FDG-brainPET for parkinsonisms diagnosis in daily clinical practice: our experience in a non-dedicated hospital

P. Santos-Holgueras, P. Garrastachu-Zumaran, C. Albornoz, X. Boulvard, L. Romero, A. Cabrera, F. Cañete, R. Delgado, R. Ramirez;
Nuclear Medicine and Molecular Imaging Division,
San Pedro Hospital-CIBIR, Logroño, SPAIN.

Aim/Introduction: Establishing the diagnosis in patients with parkinsonian syndromes is based on clinical diagnostic criteria, and many times is difficult at the early onset of the disease. To improve this, the use of different support biomarkers is proposed and beyond them appears ^{18}FDG-brainPET. This study aims to evaluate the validity of ^{18}FDG-brainPET in our daily clinical practice and its modulatory role in relation to the initial diagnostic suspicion. **Materials and Methods:** We selected patients with parkinsonian symptoms sent for ^{18}FDG-brainPET between 2012-2017. A visual analysis of ^{18}FDG-brainPET was performed by two independent observers, classifying images as atypical parkinsonism (AP), non-atypical parkinsonism (non-AP), and different atypical parkinsonisms subtypes, according to the accepted metabolic patterns. We analysed the validity of PET against clinical diagnosis in the follow-up, only in patients who had an established diagnosis by PET and by clinical assessment. Logistic regression models were used to estimate the probability of diagnosing parkinsonism according to the PET result adjusted for clinical suspicion of parkinsonism. A positive probability ratio was used to transform the previous probability of having parkinsonism only with clinical suspicion into the a posteriori probability once PET was done. **Results:** 68 patients (37 female, age 70, range 38-87) had undergone ^{18}FDG-brainPET. We finally analysed 54 patients with established diagnosis by PET and by clinical assessment. Validity of PET showed: sensitivity (S) 83,3%, specificity (E) 80%, positive predictive value 76,9%, negative predictive value 85,7% and accuracy 81,5%. Also high values were found when we analysed atypical parkinsonism subtypes: multiple system atrophy (S 85,7%, E 95,7%, accuracy 94,4%) and progressive supranuclear palsy (S 88,9%, E 97,8%, accuracy 96,3%). A logistic regression model showed that positive result in PET for AP is 2,7 times more likely to be an AP than PET with non-AP result, regardless of diagnostic suspicion. Probability of AP diagnosis with clinical suspicion was 60,7%, that rised to 86,6% if the PET is positive for AP, decreasing to 24,4% if the result was non-AP. **Conclusion:** Our results show that ^{18}FDG-brainPET accurately classifies patients with atypical parkinsonisms. This tool is useful in daily clinical practice, helping neurologists in clinical diagnosis. **References:** None.

EP-0031

Does aggregated tau moderate functional and structural connectivity profiles of the globus pallidus externus in progressive supranuclear palsy? Preliminary results of a [18F]PI-2620 PET/MRI study

G. Aghakhanyan[1,2], M. Rullmann[1], J. Rumpf[3], M. Schroeter[4], M. Patt[1], J. Classen[3], O. Sabri[1], H. Barthel[1];
[1]Department of Nuclear Medicine, University of Leipzig, Leipzig, GERMANY, [2]Regional Center of Nuclear Medicine, University Hospital of Pisa and Department of Translational Research on New Technologies in Medicine and Surgery, University of Pisa, Pisa, ITALY, [3]Department of Neurology, University of Leipzig, Leipzig, GERMANY, [4]Max Planck Institute for Human Cognitive and Brain Sciences, Leipzig, GERMANY.

Aim/Introduction: Progressive supranuclear palsy (PSP) is a primary 4R tauopathy predominantly affecting globus pallidus (GP), subthalamic nucleus and substantia nigra. The globus pallidus externus (GPe), the lateral component of the GP, is considered as a subcortical relay structure: Evidence suggests that GPe exhibits direct connections with associative, sensorimotor and limbic cortical areas (corticopallidal network). [18F]PI-2620 is a second-generation tau PET tracer with high binding affinity for aggregated tau in Alzheimer's disease (AD) and non-AD tauopathies. We aimed to assess the relationship between [18F]PI-2620 uptake and functional/structural connectivity (FC/SC) of the GPe. **Materials and Methods:** Six PSP patients with the predominant parkinsonian/cortico-basal phenotype (4 female, age 72±6 years) underwent 60 minutes dynamic PET imaging following 300 MBq bolus injection of [18F]PI-2620 with hybrid 3T PET/MRI. Ten age-matched controls were included for comparison of MRI data consisting of 3D T1, diffusion-tensor imaging (DTI) and resting-state fMRI. Regional [18F]PI-2620 standardized uptake value ratios (SUVr) were calculated using the cerebellum as a reference region by averaging 40 to 60 min p.i. dynamic frames. For FC analysis, the hypothesis-guided GPe-seed-based approach was applied. SC was estimated using probabilistic tractography calculating connection probability to frontal, temporal, parietal and occipital cortical targets for each GPe voxel. Hard segmentation of the GPe was performed by classifying seed voxels with the highest connectivity to each cortical target resulting in connectivity-defined regions (CDR). **Results:** PSP patients demonstrated focal [18F]PI-2620 uptake in the GPe (SUVr = 1.4±0.12). Compared to controls, the GPe displayed increased FC within the frontal network (right precentral/inferior frontal and left orbitofrontal cortices). The SC analysis depicted a trend towards decreased frontal and increased temporal CDR in the left GPe (p=0.08). Although frontal and temporal CDR in each hemisphere showed significant influence on the unilateral connectivity strength ($p < 0.05$), ANCOVA analysis did not reveal significant strength difference between groups. Interestingly, the SUVr in the GPe showed an inverse relationship with left frontal (r= - 0.83, p=0.05) and a direct relationship with temporal CDR (r=0.82, p=0.058). **Conclusion:** GPe-related [18F]PI-2620 uptake in PSP is associated with altered corticopallidal connectivity. We speculate that the decreased frontal CDR might be attributed to neurodegeneration, whereas increased FC and temporal SC might represent a potential adaptive mechanism. Conditional on replication in a larger PSP cohort, these hybrid tau PET/MRI results might lead to an improved understanding of tau-related connectivity dysfunction and adaptive mechanisms in PSP. **References:** None.

EP-0032

Preliminary Exploration of PET/MR Radiomics Features for Differential Diagnosis of Parkinson's Disease and Multiple System Atrophy

X. Hu[1,2], X. Sun[1,2], J. Guo[3], X. Lan[1,2], R. An[1,2];
[1]Department of Nuclear Medicine, Union Hospital, Tongji Medical College, Huazhong University of Science and Technology, Wuhan, CHINA, [2]Hubei Key Laboratory of Molecular Imaging, Wuhan, CHINA, [3]GE Healthcare (CHINA), Shanghai, CHINA.

Aim/Introduction: The study aims to preliminarily explore the value of ^{18}F-FDG and multi-MR sequence imaging from the integrated Time of Flight PET/MR system for differential diagnosis of Parkinson's disease (PD) and multiple system atrophy (MSA) by using radiomics analysis. **Materials and Methods:** 69 patients were included with 46 Parkinson's disease (PD) and 23 Multiple system atrophy (MSA). The final diagnosis was made according to the assessment of imaging findings, clinical symptoms, and follow-up with more than 1 year. Patients were performed ^{18}F-FDG PET/MR (GE SIGNA), and 3D-T1BRAVO, SWAN, T2FLAIR, T2PROPELLER were acquired at the same time. ^{18}F-FDG PET images were transformed to SUV images by normalized with dose/kg. Regions of interest (ROIs) of the bilateral putamen and caudate nucleus were drawn on each 3D-T1BRAVO image and mapped to other image sequences, which were then confirmed by experienced clinician. From 46 ROIs of PD patients' (first affected side) and 46 ROIs of MSA patients (bilateral sides), the radiomics features (396/side) were extracted with A.K. (Analysis-Kinetics, GE), and then feature selection was applied with spearman correlation and support vector machine-recursive feature elimination (SVM-RFE). Extremely randomized trees were applied to do modeling with each image and combinations of ^{18}F-FDG and MR images (train: test = 7:3, 5-fold cross-validation). The ability of PET/MR images to differentiate the diseases was evaluated with receiver operating characteristic curves, area under the curve (AUC), sensitivity, specificity and accuracy (ACC). **Results:** In the monomodal radiomics analysis, 36 features are selected for ^{18}F-FDG, which has the highest AUC (0.852) and ACC (0.75) as well as ideal sensitivity (0.714) and specificity (0.786). Besides, 3D-T1BRAVO and SWAN perform best sensitivity (0.857, AUC=0.827, ACC=0.75) and specificity (0.857, AUC=0.811, ACC=0.714), respectively. Combined ^{18}F-FDG with one of the MR sequences, the AUC, ACC, sensitivity and specificity are improved in different aspects, where ^{18}F-FDG combined 3D-T1BRAVO shows the higher sensitivity (0.857, AUC=0.847, ACC=0.786) and ^{18}F-FDG combined SWAN shows the better specificity (0.857, AUC=0.857, ACC=0.714). **Conclusion:** Radiomics

features of putamen and caudate nucleus from ^{18}F-FDG and MR 3D-T1BRAVO, SWAN, T2FLAIR and T2PROPELLER images could provide helpful information for differentiating PD and MSA. ^{18}F-FDG combined 3D-T1BRAVO showed better sensitivity, while ^{18}F-FDG combined SWAN demonstrated better specificity. More cases should be included for further identification.Funding: This study was supported by NSFC (81701759) and Key Project of Hubei Technological Innovation (2017ACA182). **References:** None.

EP-0033

Assessment of dopamine transporter imaging and olfactory testing in patients with Parkinson's disease: a semi-quantities analysis

M. Assadi, A. Moradi, E. Moradi, S. Farrokhi, H. Salimipour, N. Chabi, E. Jafari;
Bushehr University of Medical Sciences (BUMS), Bushehr, IRAN, ISLAMIC REPUBLIC OF.

Aim/Introduction: Parkinson's disease (PD) is a chronic progressive and degenerative disorder affecting about 1% of people over 65 years old. Olfactory disorder is one of the early non-motor symptoms in patients with Parkinson's disease. In this study, we investigate olfactory dysfunction in patients with Parkinson's disease with ^{99m}Tc-TRODAT, olfactory test and MRI. **Materials and Methods:** Patients with confirmed Parkinson's disease were enrolled in this study. Patients underwent the 40-item Smell Identification olfactory test and SPECT scans with ^{99m}Tc-TRODAT and MRI for measuring olfactory bulb. **Results:** 30 patients (19 (63%) males and 11 (37%) females) with Parkinson's disease were included in this study. ^{99m}Tc-TRODAT SPECT scan showed severe uptake reduction in 15 (78.9%) of males and 8 (72.7%) of females in left putamen and left caudate and 16 (84.2%) of males and 9 (81.8%) of females had a mild uptake reduction in right putamen and caudate. In the olfactory test of patients, 13 (68.4%) of males and 7 (63.7%) of females had severe hyposmia to anosmia. Comparison of olfactory bulb in patients with Parkinson's disease and healthy people didn't show any significant difference (P>0.05). There was significant relationship between 99mTc-TRODAT uptake reduction in right putamen and caudate with hyposmia (p<0.05). **Conclusion:** This study showed that a high percentage of patients with Parkinson's disease had olfactory dysfunction. And the uptake of ^{99m}Tc-TRODAT was decreased in these patients. Also, the olfactory test showed a decrease in odor identification in most people with Parkinson's disease. **References:** None.

EP-0034

Comparison of semiquantitative analysis of dopaminergic brain imaging

R. Durmo[1], B. Paghera[1], D. Albano[1], M. Bonacina[1], M. Gazzilli[1], E. Cerudelli[1], F. Dondi[1], A. Mazzoletti[1], F. Bertagna[2], R. Giubbini[2], P. Bellini[3];
[1]Nuclear Medicine, Spedali Civili Brescia, Brescia, ITALY, [2]Nuclear Medicine, University of Brescia and Spedali Civili Brescia, Brescia, ITALY, [3]University of Brescia, Brescia, ITALY.

Aim/Introduction: Brain SPECT is the most common used technique to differentiate degenerative parkinsonian syndromes from non-degenerative parkinsonism. The aim of our study was to directly compare, in the same population, the different performances of two methods of semiquantitative analysis data: one based on 2D ROI analysis (DaTSCAN 3-2 software; GE Xeleris workstation) and the other one based on 3D VOI method (the basal ganglia V2 software). **Materials and Methods:** 250 patients (146 male; 104 female) median age 65 who underwent a ^{123}I-Ioflupane SPECT in our Department for an as yet unclassified parkinsonian syndrome were retrospectively evaluated. At least after 2 year follow up a new clinical revaluation was made. SPECT were processed using two commercial programs to determine the relative uptake in the striatum. 1) DaTSCAN 3-2 software, an 2D operator depending software 2) the free software Basal-Ganglia Matching-Tool v.2 operator free 3D automatically software. A comparison of the results from the softwares was performed, together with a comparison with the visual assessment. **Results:** ^{123}I-Ioflupane striatal uptake was normal in 63/250 patients (25%) and abnormal in 187/250 patients (75%) with a mild, medium or severe unilateral or bilateral decreased uptake. In the cohort visual assessment showed a Sensitivity of 96.9%, Specificity of 100%, PPV of 98,5%, NPV of 89,4% for degenerative parkinsonism. The quantitative analysis was not obtained in 3 patients for the manual method and in 12 patient for the BasGan method. The mean caudate-occipital uptake ratio with 2D manual method was 3.21±0.65 for the right caudate and 3.22±0.64 for the left; with the BasGan respectively 3,18±0.97 for the right and 3.15±0.96 for the left. Putamen/occipital mean uptake ratio with the 2D manual ROI was 2.62±0.69 for the right and 2.6±0.72 for the left putamen; BasGan method was respectively 2.07±1.01 for the right and 2.09±1.00 for the left side. The ROC curve showed a sensitivity of 80,6% and specificity of 71.9 % with the Basal ganglia method and a sensitivity of 78,1% and specifity of 69.8% with the manual method. AUC for Basal Ganglia method was 0.827 for the caudate and 0.915 for the putamen. AUC for the manual method was 0.805 for caudate and 0.894 for putamen. No statistical difference between the two method was found (p=0.081 for the caudate and p=0.1 for the putamen). **Conclusion:** The two semiquantitative methods provide very robust results for routine evaluation of ^{123}I-Ioflupane scans and they are both remarkably accurate. **References:** None.

EP-0035

Characterization of the FDOPA Uptake of the Brainstem and Diencephalon in Parkinsonian Syndromes by PET / MRI

G. Demonceau[1,2], A. Tebbani[1], Q. Demonceau[1], V. Lebon[1,3];
[1]CEA-SHFJ Orsay, Paris, FRANCE, [2]Bois de l'Abbaye, Liège, BELGIUM, [3]University Paris Sud, Paris, FRANCE.

Aim/Introduction: FDOPA PET / CT is commonly used for the investigation of dopaminergic denervation, the diagnosis being based on striatal uptake. But other brain structures, including monoaminergic neurons of the brainstem and diencephalon, metabolize FDOPA and are likely to be affected. Using the values automatically generated by a homemade PET / MRI atlas, we looked for alterations in the FDOPA uptake in parkinsonian syndromes. We retrospectively selected 120 patients who underwent FDOPA PET / MRI examination, 49 with Parkinson's syndrome according to clinical and scintigraphic data, 71 others considered very unlikely to have this condition (the control group). **Materials and Methods:** the T1 images of each patient were registered on the T1 images of a model where 28 anatomical regions had been previously identified. The adjustment parameters were then applied to FDOPA images acquired 90 min after injection. In each region VOIs of different sizes were then generated: 1 voxel (1mm3), 27 voxels or a volume adapted to the size of the region to be studied. The mean SUV, alone or compared to that of the other regions, was used to distinguish the 2 groups, by the way of a Student's test. **Results:** the results were similar, using different sizes of VOIS. In the parkinsonian group, a significant reduction in SUV was observed in the substantia nigra ($p = 0.002$), amygdala ($p = 0.01$) and pulvinar ($p = 0.03$). We did not observe any significant difference in the A8 zone, the reticular or the raphe nuclei. In the supratentorial area, the occipital region was unaffected too, in contrast to the striatum. The best discriminations between parkinsonian and control groups, obtained by combining the activities of the whole regions, were provided by the difference between the SUV of, on the one hand, the putamen and, on the other hand, the A8 area, the hypothalamus, the pulvinar, the substantia nigra and the caudate nucleus, all with p less than 10^{-20}. **Conclusion:** for the first time in nuclear medicine, we think we have been able to automatically demonstrate the involvement of nuclei of the brainstem and diencephalon in Parkinson's syndrome. This opens perspectives in terms of early detection, staging and differential diagnosis of this disease. **References:** None.

EP-0036

Prognostic Role Of FDG PET Before Deep Brain Stimulation In PD Patients: A Voxel-Based Study

G. Puccini[1], *V. Berti*[1], *S. Ramat*[2], *F. Terenzi*[2], *C. Polito*[2], *M. De Cristofaro*[2], *S. Sorbi*[2], *R. Sciagrà*[1];
[1]*Nuclear Medicine Unit - University of Florence, Florence, ITALY,* [2]*Neurology Unit - University of Florence, Florence, ITALY.*

Aim/Introduction: Deep Brain Stimulation (DBS) is a neurosurgical procedure that could be a reliable tool for selected Parkinson's Disease (PD) advanced patients. Our aim is to identify the specific brain metabolic profile of PD patients who could benefit the most from this therapeutic option, in order to correctly select PD patients to treat with DBS. **Materials and Methods:** We selected a group of 35 consecutive PD patients (10F/25M mean age 59±7years) who were treated with DBS between 2008 and 2017. Clinical and neuropsychological profiles were collected before and after surgery. All patients had undergone FDG-PET within a month before surgery. We divided the patients into two groups depending on the Schwab And England Activities Of Daily Living Scale (SE-ADL) results during clinical follow-up of at least 1 year after surgery. The first group consist of 26 patients with a score of SE-ADL ≥ 90%, the second group include 9 patients with SE-ADL<90%. A SPM12 two-sample t-test (age and SE-ADL at baseline as nuisance variables) was performed comparing the two groups. **Results:** At voxel-based analysis subjects with SE-ADL <90% at follow-up showed significant hypometabolism in right occipital lobe (inferior and middle gyri) and left temporal lobe (middle gyrus), as compared to subjects with SE-ADL ≥ 90% at follow-up **Conclusion:** DBS has been an effective treatment for the majority of selected patients, but not for all. FGD-PET demonstrated a greater cortical hypometabolism in SE-ADL<90-group involving occipital and temporal lobe. This could suggest that an extensive impairment in these areas, assessed by pre-DBS FDG-PET, might be useful in identifying patients who could benefit less from the procedure. Instead patients with preserved metabolism in these areas seem to more likely benefit from surgery. Greater sample size is needed in order to confirm the pattern of the distribution of hypometabolism. **References:** - Walker Z et al. Clinical utility of FDG PET in Parkinson's disease and atypical parkinsonism associated with dementia. Eur J Nucl Med Mol Imaging. 2018; - Brajkovic L et al.The utility of FDG-PET in the differential diagnosis of Parkinsonism. Neurol Res. 2017;- Welter ML et al. Clinical predictive factors of subthalamic stimulation in Parkinson's disease. Brain 2002;- Rossi M et al. Challenges in PD Patient Management After DBS: A Pragmatic Review. Mov Disord Clin Pract. 2018.

EP-03

Neuroimaging: Psychiatry and Neurotransmission

October 12 - 16, 2019 e-Poster Area

EP-0037

Brain Dysfunction in Active and Abstinent Smoked Cocaine Addicts from Brazil and Uruguay

R. Ferrando[1], *C. Pascovich*[1], *S. Parra*[1], *M. Langhain*[1], *A. Silveira*[1], *P. Fielitz*[1], *A. Negrin*[1], *V. Esmoris*[2], *V. Martin*[1], *C. Rodríguez*[1], *F. Cadenas*[1], *E. Moreno*[3], *M. Bidegain*[3], *R. Ponde de León*[3], *L. Hopner*[4], *L. Mendes*[4], *F. Ornell*[4], *Y. Moreschi*[4], *N. Fares*[5], *M. Carballo*[3], *F. Kessler*[4];
[1]*Clinics Hospital, University of the Republic, Montevideo, URUGUAY,* [2]*Maciel Hospital, Montevideo, URUGUAY,* [3]*Catholic University, Montevideo, URUGUAY,* [4]*Clinics Hospital of Porto Alegre, Porto Alegre, BRAZIL,* [5]*University of Zurich, Zurich, SWITZERLAND.*

Aim/Introduction: Smoked cocaine (SC) has been linked to severe dependence, serious bio-psycho-social deterioration and criminal behavior, representing a big challenge for health,

education and public security. The drug is widely available in Latin America and impure forms are highly prevalent in the deprived population. The aim of the study was to evaluate brain dysfunction produced by chronic use of SC and its changes with abstinence in patients from two countries of our region. **Materials and Methods:** This prospective study recruited 166 subjects (127 from Uruguay and 39 from Brazil) divided in four groups: active SC users (G1, n=64), abstinent SC users (G2, n=34), active intranasal cocaine hydrochloride (CH) users (G3, n=33) and normal controls (NC) (G4, n=35). 91% of the users were male and ages ranged 17-37 years (27.0 ± 5.8, mean ± SD) without differences between groups or with NC. Mean dose of SC (3.1±3.3 g/day) did not differ from CH (2.2±1.7, p=0.11). Time of use was higher for CH (9.8±5.3 years) than SC (6.7±4.4, p=0.01). Mean time of abstinence in G2 was 4.5 months (range 1.0-22.3). Associated use of alcohol and cannabis without criteria for dependence was present in groups 1-3 in similar proportions. All subjects underwent resting 99mTc-ECD SPECT. Analysis was performed in SPM8. Country of origin was entered as a nuisance variable when necessary. Uncorrected voxel p-values lower than 0.001 and clusters > 100 voxels were reported. **Results:** G1 showed mesial frontal, anterior cingulate and ventromedial frontal hypoperfusion, and occipital and cerebellar hyperperfusion relative to NC. Hypoperfusion in G3 was more limited. G1 showed lower mesial prefrontal perfusion than G3. Brazilian SC users showed more prefrontal hypoperfusion than Uruguayan ones. The differences markedly reduced when controlling for time of substance use, which was longer in Brazilians. Mesial and dorsal prefrontal and posterior cingulate perfusion increased in G2 relative to G1, and occipital, cerebellar and anterior temporal perfusion decreased. **Conclusion:** SC abuse was characterized by greater dysfunction than CH in paralimbic prefrontal cortex comprising the reward system that play a major role in emotional control and adapted behaviour, providing a neural basis for the clinical profile described in addicts. Findings were similar in both countries despite possible regional differences in SC composition. Although some grade of brain dysfunction still persisted during abstinence, prefrontal activity increased, probably reflecting an improve in limbic balance, self-control and executive function, enhancing the probability of staying away from the drug. **References:** None.

EP-0038

Brain SPECT Perfusion Imaging With Brodmann Areas Mapping Of Psychotic Symptoms (Delusions And Hallucinations) In Patients With Alzheimer's Disease

V. Valotassiou[1], *N. Sifakis*[2], *C. Tzavara*[1], *E. Lykou*[3], *G. Angelidis*[1], *N. Tsinia*[4], *V. Kamtsadeli*[3], *I. Tsougos*[1], *D. Psimadas*[1], *S. Alexiou*[1], *S. Papageorgiou*[5], *P. Georgoulias*[1], *J. Papatriantafyllou*[3]; [1]*Dpt of Nuclear Medicine, University Hospital of Larissa, Larissa, GREECE,* [2]*Dpt of Nuclear Medicine, "Alexandra" University Hospital, Athens, GREECE,* [3]*IASIS Third Age Center, Athens, GREECE,* [4]*Aeginition Hosp., 1st University Psychiatric Clinic of Athens, Athens, GREECE,* [5]*2nd University Neurological Dpt., Attikon Hospital, Athens, GREECE.*

Aim/Introduction: Psychotic symptoms (delusions and hallucinations) are common and prominent features in Alzheimer's disease (AD) and their prevalence ranges from 30% to 50%. Delusions appear more frequently than hallucinations and the main forms are paranoid ideation and misidentification, while hallucinations are usually visual. Clinical evidence supports the hypothesis that degeneration of frontal cortex is responsible for the appearance of psychotic symptoms. The aim of this study was to evaluate perfusion in Brodmann areas (BAs) in AD patients with psychotic symptoms compared with healthy controls in order to detect areas implicated in the manifestation of these symptoms. **Materials and Methods:** We studied 65 consecutive patients (20 men, 45 women, age±SD 69.9±8.1 years, duration of disease±SD 3.4±2.4 years, education±SD 9.4±4.7 years) from an outpatient Memory Clinic. We used the established DSM-IV criteria for the diagnosis of dementia and the specific established criteria (NINCDS-ADRDA) for the diagnosis of AD. All the patients had a neuropsychological evaluation with a battery of tests including the mini-mental state examination (MMSE, mean 19.6±5.5) and the Neuropsychiatric Inventory (NPI). All the patients underwent a brain SPECT scan 20 min after the intravenous administration of 740MBq of ^{99m}Tc-HMPAO. We applied the NeuroGam™ software on the reconstructed data, for the comparison of brain perfusion in BAs in the right (R) and left (L) hemispheres with the software's normal data base consisted of healthy subjects of the same age. **Results:** Compared with normal subjects, psychotic symptoms in AD patients were correlated (p=0.05) with hypoperfusion in anterior and dorsolateral prefrontal cortices (BAs 8LR, 9LR, 10 LR, 46LR), left ventral and right dorsal posterior cingulate cortex (BA 23L, 31R), dorsal anterior cingulate cortex (BA 32LR), left anterior temporal gyrus (BA 22L), inferior frontal gyri, mainly on the left (BAs 44LR, 45L, 47LR), right supplementary somatosensory cortex (BAs 5R, 7R), left supramarginal gyrus (BA 40L) and right secondary visual cortex (BA 18R). **Conclusion:** Our findings support the hypothesis that impairment of frontal lobe is the underlying cause of psychotic symptoms in AD. Moreover, other connected regions in parietal, temporal and visual cortices, as well as cingulate cortex may be parts of a broader neural network underpinning the psychotic symptoms in AD. **References:** 1. Rosenberg PB, Nowrangi MA, Lyketsos CG. Neuropsychiatric symptoms in Alzheimer's disease: What might be associated brain circuits? Mol Aspects Med. 2015;43-44:25-37.2. Murray PS, Kumar S, Demichele-Sweet MA, Sweet RA. Psychosis in Alzheimer's disease. Biol Psychiatry. 2014 Apr 1;75(7):542-52.

EP-0039

Examinantion of brain perfusion and metabolism in metabolic diseases (focusing on diabetes and obesity)

K. Zita[1], *J. Varga*[2], *F. Nagy*[3], *M. Emri*[2], *M. Kaplar*[4], *C. Aranyi*[2], *I. Garai*[3]; [1]*University of Debrecen, Debrecen, HUNGARY,* [2]*Division of Nuclear Medicine and Translational Imaging, Medical Imaging Department, Faculty of Medicine, University of Debrecen, Debrecen, HUNGARY,* [3]*Scanomed Ltd., Debrecen, HUNGARY,* [4]*Department of Internal Medicine, Faculty of Medicine, University of Debrecen, Debrecen, HUNGARY.*

Aim/Introduction: Microcircular alterations that could already be observed in prediabetic state (obesity and insulin resistance) are supposed to have significant role in the developement of the consequences of diabetes mellitus. The main aim of our study was to compare the cerebrovascular microcirculation and metabolism of obese patients and patients suffering from type 2 diabetes mellitus. **Materials and Methods:** In our prospective study 57 patients with controlled type 2 diabetes mellitus (52±9,6 years) and 46 obese patients (50,6±7,9 years) were enrolled. BMI proved to be 34,06±5,94 in the diabetic group while it was 38,14±6,06 among the obese patients. Dynamic Tc99m-HMPAO study (AnyScanFlex, Mediso) was performed for evaluation of hemispheral perfusion using Patlak analysis. Then tomographic imaging was carried out at rest condition. Brain metabolism was estimated applying 18F-FDG PET/CT (AnyScan PC, Mediso). FDG and HMPAO scans were transformed to MNI152 brain map after T1 registration and used for SPM (Statistical Parametric Mapping) analysis. NeuroQ application (Syntermed) was used to evaluate regional differences. Statistical analysis (Shapiro-Wilk, Wilcoxon, Spearman correlation) was applied for assessment of group differences. **Results:** Hemispheral perfusion calculated with Patlak analysis showed positive correlation with BMI (rho=0.35, p=0.016). There were no significant differences in hemispheral and regional perfusion in T2DM and the obese group. However, we found hypometabolism in right and left cuneus (Br17) in T2DM with SPM analysis. NeuroQ analysis did not reveal significant regional perfusion or metabolic defects in either groups. **Conclusion:** Based on current literature hypometabolism in the region of the cuneus is a characteristic feature of neurodegenerative diseases. The reason why no significant perfusion defects were found could be explained by the fact that the enrolled diabetics were therapeutically well managed. Unexpected significant correlation with BMI is unclear, further investigation is required. **References:** None.

EP-0040

Scintigraphic low cerebral blood flow in first episode psychosis

C. Sioka, G. Georgiou, A. Karampas, P. Petrikis, A. Papadopoulos, S. Tsiouris, A. Fotopoulos;
University Hospital of Ioannina, Ioannina, GREECE.

Aim/Introduction: To evaluate brain perfusion abnormalities in antipsychotic-naive, first episode patients with psychosis. **Materials and Methods:** Cerebral blood flow (CBF) with ^{99m}Technetium-hexamethylpropyle (^{99m}Tc-HMPAO)-single photon emission computer tomography (SPECT) is an imaging method that may be useful to evaluate changes of regional cerebral perfusion (RCP). Fifteen patients (10 men, five women) were included in the study. They were experiencing their first psychotic episode, they were in the acute phase of the illness with prominent positive symptoms (delusions, hallucinations). All of them were antipsychotic naive, they received only benzodiazepines for less than a week. They were subjected to ^{99m}Tc-HMPAO-SPECT RCP. NeuroGam software was applied on SPECT studies. Abnormal areas were designated below 2 standard deviations of the normal mean uptake in area >50% pixels. Evaluation of the affected cerebral lobes was performed independently and according to the number of affected lobes. Thus, group 1 - G1 were patients with affected CBF in only one lobe, group 2 - G2 patients with low CBF in two lobes and group 3 - G3 patients with three or more affected lobes. **Results:** Reduced CBF was found in the limbic lobes in all patients. Participation of temporal, parietal and frontal lobes were noted in 8/15 (53%), 5/15 (33%) and 2/15 (13%) patients respectively. In G1 there were 7/15 (20%) patients with low CBF in limbic system. In G2 there was noted 3/15 (20%) patients with at least two hypoperfused CBF lobes and in G3 in 5/15 (33%) patients. **Conclusion:** Patients with first episode of psychosis, have low CBF, especially in the limbic system. This finding is of importance, since hypoperfusion may be a precursor of structural changes later in the course of the illness. The heterogeneity of the affected brain areas may be related to the duration of untreated psychosis (DUP or to other characteristics of the disease. The small study sample preclude us from drawing general conclusions. **References:** None.

EP-0041

From metabolic connectivity to molecular connectivity: application to dopaminergic pathways

A. Verger[1], T. Horowitz[2], M. Chawki[1], N. Girard[2], E. Guedj[2];
[1]CHRU Nancy, Nancy, FRANCE, [2]Timone, APHM, Marseille, FRANCE.

Aim/Introduction: This study aims to reveal the feasibility and potential of molecular connectivity based on neurotransmission in comparison to the metabolic reference with an application to dopaminergic pathways. For this purpose, we propose to compare the midbrain's connectivity and related dopaminergic pathways through a metabolic connectivity analysis using ^{18}F-FDG PET and neurotransmission connectivity analyses using ^{123}I-FP-CIT SPECT and ^{18}F-FDOPA PET. **Materials and Methods:** Images of 47 subjects for ^{18}F-FDG PET and ^{123}I-FP-CIT SPECT, and of 177 subjects for ^{18}F-FDopa PET, with absence of neurological or psychiatric disorder, were selected. Interregional correlation analysis was performed at the group-level to determine midbrain's connectivity with metabolic rate of glucose for ^{18}F-FDG PET imaging, and binding potential parametric images for ^{123}I-FP-CIT SPECT and ^{18}F-FDopa PET imaging. SPM-T maps of each radiotracer were generated, also with the use of masks to highlight the significant different findings obtained with each imaging modality and target. **Results:** ^{18}F-FDG PET, ^{123}I-FP-CIT SPECT and ^{18}F-FDopa PET imaging allowed revealing the nigro-striatal pathway (52.70, 14.36 and 55.16 cm^3, with respective T-voxel max of 14.96, 5.28 and 17.69), the meso-limbic pathway (8.36, 12.07, and 17.79 cm^3 with respective T-voxel max of 13.44, 5.12 and 16.41) and the meso-cortical pathway (3.59, 2.49 and 26.47 cm^3 with respective T-voxel max of 6.83, 2.49 and 7.05), at T-voxel threshold of 5.10, 2.80 and 5.10, respectively. Using a same T-voxel threshold of 5.10, SPM-T maps of ^{18}F-FDopa PET showed larger extended areas within the dopaminergic

pathways than ^{18}F-FDG PET and ^{123}I-FP-CIT SPECT (+38.25 and +99.42 cm^3 respectively), and less unspecific findings outside these pathways than ^{18}F-FDG PET (-46.85 cm^3). **Conclusion:** The present study illustrates the feasibility and interest to use molecular connectivity with ^{18}F-FDopa PET imaging for dopaminergic pathways. Such analysis can be applied to specific diseases involving the meso-telencephalic dopamine system, and potentially with other molecular SPECT/PET targets to other systems. **References:** None.

EP-0042

Factors influencing the cerebral 18F-DOPA uptake

A. Tebbani[1,2], *Q. Demonceau*[1], *V. Lebon*[1,2], *G. Demonceau*[1,3]; [1]*CEA-SHFJ, Orsay, FRANCE,* [2]*Université Paris Sud, Paris, FRANCE,* [3]*Bois de l'Abbaye, Seraing, BELGIUM.*

Aim/Introduction: besides the neurological diseases, others factors could influence the uptake of 18F-DOPA in the brain. Knowing their impact could ultimately lead to identify by quantitative measurements the neurological disorders. Therefore the impact of some of the most current physiological and pharmacological parameters has been evaluated in an almost normal population. **Materials and Methods:** 70 consecutive patients, referred for suspicion of Parkinson disease but by which the striatal F-DOPA uptake was normal on a PET/NMR examination, were included in the study. Age, gender, right- or left-handed, hypertension, diabetes and chronic intake of levodopa were retrospectively collected. For each patient, the SUV of 28 regions of interest of the trunk, the diencephalon and the cortex was measured from an automatic atlas based on the PET/NMR imaging. Briefly, the T1 images of each patient were registered on the T1 images of a reference model where several anatomical regions had been previously identified. The registration was carried out in a progressive way, in non-deformable and then deformable mode, after creation of a mask including the brainstem, the diencephalon and the striatum. The registration parameters were then applied to the 18F-DOPA images acquired 90 min after injection. The SUV of the 28 regions were finally related to the reticular SUV and the influence of the factors on them was statistically assessed by Student t-test. **Results:** influence of hypertension was the most prominent factor, increasing the ratio to reticular nuclei of the amygdala (+38%) and hypothalamus (+14%; p=0.009). The asymmetrical SUV of pulvinars decreased (-50%; p=0.004). Difference between SUV of substantia nigra and reticular nuclei increased (+36%; p= 0.002). The chronic intake of levodopa reduced the amygdala to reticular ratio (19%; $p=5.10^{-4}$). In male, the SUV ratio to reticular nuclei was higher in amygdala (+10%; p=0.01) and A8 region (+10%; p=0.005). Age, right-or left-handed and diabetes had no statistical influence in our population. **Conclusion:** Hypertension gender and the intake of levodopa are factors influencing the SUV to reticular ratio in different brain areas. These factors should be taken into consideration for quantitative discrimination between pathological and normal patients, chiefly for the analysis of the trunk, where the differences between pathology and normality are more subtle than in the striatum **References:** None.

EP-04

Neuroimaging: Dementia and Neurodegeneration

October 12 - 16, 2019 e-Poster Area

EP-0043

A Direct Comparison Between ^{18}F-FDG PET and Arterial Spin Labelling Perfusion MRI in Patients Referred for Differential Diagnosis of Dementia Using Simultaneous PET/MR

J. Ceccarini[1], *S. Bourgeois*[1], *K. Goffin*[1], *S. Sunaert*[2], *K. Van Laere*[1]; [1]*Department of Imaging and Pathology, KU Leuven; Nuclear Medicine and Molecular Imaging, University Hospitals Leuven, Leuven, BELGIUM,* [2]*Department of Radiology, University Hospitals Leuven, Leuven, BELGIUM.*

Aim/Introduction: [^{18}F]FDG-PET is an established tool to assist the clinical diagnosis and differentiation in the main forms of dementia syndromes, namely Alzheimer's disease (AD), frontotemporal dementia (FTD), Lewy body dementia (LBD), and vascular dementia. Arterial spin labelling (ASL) perfusion MRI has been proposed as a proxy marker for measuring neuronal dysfunction. The aim of the current study is to directly compare simultaneously acquired [^{18}F]FDG-PET with enhanced ASL (eASL)-MRI in the accuracy for differential diagnosis of dementia in a clinical prospective set of patients referred for differentiation of a dementing disorder. **Materials and Methods:** Twenty-seven patients with suspected neurodegenerative dementia disorder (age 64.3 ± 11.2 years, 14 M/13 F, MMSE 11-30) first underwent clinical routine 30-min brain [^{18}F]FDG-PET-CT scan (150.5 ± 11.5 MBq), and subsequently received a 20-min PET/MR scan, simultaneously acquired with an eASL-MRI acquisition on a 3T GE Signa PET-MR system. Thirty carefully screened age- and gender-matched healthy subjects served as controls (CON; age 63.9 ± 10.6 years; 14 M/16 F; MMSE 28-30; 40-60 min p.i static scan, 152.2 ± 11.1 MBq). [^{18}F]FDG-PET and eASL-MRI were compared by a standardized visual qualitative and semiquantitative regional analysis by two experienced nuclear medicine physicians, scoring activity/flow abnormalities using a 4-point scale. To determine group differences in glucose metabolism and blood flow, and to investigate the differences in statistical sensitivity and pattern deduction for both methodologies, voxel-based (t-test and 2nd level) analyses were performed in SPM12 (p_{FWE}<0.05 at cluster level). **Results:** The working diagnosis for the patient group consisted of 8 AD, 2 FTD, 1 LBD, 1 multiple system atrophy of the cerebellar type, 1 motor neuron disorder, 1 traumatic brain injury and 13 patients with no clear pre-PET

arguments for a neurodegenerative cause for the cognitive complaints. The visual analysis resulted in equal specificity (0.70) for differentiating normal and abnormal images between the two modalities, but in a higher sensitivity and confidence rating of the readers for FDG-PET (0.87) compared to ASL (0.60). Both VOI- and voxel-based analyses revealed reduced regional and quantitative hypometabolism and hypoperfusion between CON and AD, mainly in the mid-cingulate, posterior cingulate-precuneus cortices and parietotemporal areas as angular gyrus, although the pattern was more pronounced with FDG-PET and assessable on each individual patient. **Conclusion:** Overall, in a direct head-to-head comparison, FDG-PET has higher accuracy and confidence compared to eASL when differentiating patients referred for potential neurodegenerative causes, both visually as well as semiquantitatively (larger effect size). **References:** None.

EP-0044

SPM MRI-less 18F-Florbetaben PET for amyloid burden quantification and potential AD patients selection in clinical trials

P. Alongi[1,2], R. Laudicella[3,4], D. Sardina[5], S. Giliberto[2], G. Russo[5], A. Stefano[5], R. Coppola[6], M. Midiri[2], L. Grimaldi[6];
[1]Nuclear Medicine Unit, Fondazione Istituto G.Giglio, Cefalù PA, ITALY, [2]University of Palermo, Palermo, ITALY, [3]Department of Biomedical and Dental Sciences and of Morphofunctional Imaging, University of Messina, Messina, ITALY, [4]Nuclear Medicine Unit, Fondazione Istituto G.Giglio, Cefalù, ITALY, [5]Institute of Molecular Bioimaging and Physiology, National Research Council (IBFM-CNR), Cefalù PA, ITALY, [6]U.O.C. Neurologia, Fondazione Istituto G. Giglio, Cefalù PA, ITALY.

Aim/Introduction: To assess the impact of ^{18}F-Florbetaben (FBB)-PET/CT using a new processing-imaging-algorithm in correlation with clinical-data, neuropsychological-assessment and cerebrospinal-fluid (CSF) analysis to diagnose Alzheimer-disease (AD) in dementia's patients to be potentially included in clinical trials. **Materials and Methods:** Seventy-six patients with clinical evidence of dementia according to ENS-EFNS-criteria, underwent diagnostic FBB-PET/CT were retrospectively evaluated by a multidisciplinary-team (MDT). FBB-PET/CT results were correlated with clinical, cognitive-status, CSF-analysis and other imaging-technique. FBB-PET/CT images were processed with SPM-MRI-less and converted in standard-space (MNI-space) by normalizing them with tissue-probability-map as a template. Automated-anatomical-labeling atlas was used to mask each regional-VOI followed by extraction of SUVR, normalized on the cerebellar-grey-matter. The regional SUVR and scores from clinical and cognitive tests were used to create ROC-curves, obtaining the best thresholds for the clinical diagnosis. Leave-one-out cross-validation was carried out to validate the results. **Results:** At the qualitative-assessment, 48/76 patients (63%) showed an elevated amyloid burden at FBB-PET/CT scan,. In AD-detection and in comparison with conventional imaging (MR/CT), MDT evaluation and follow-up analysis, FBB-PET/CT resulted as true-positive in 40/76 (53%), true-negative in 23/76 (30%), false-positive in 3/76 (4%) and false-negative in 8/76 (11%). In terms of accuracy, FBB-PET/CT showed values of sensitivity, specificity, Negative predictive value, positive predictive value and global accuracy of 83%, 88%, 75%, 93% and 84%, respectively. At the semi-quantitative evaluation of FBB-PET/CT using our new processing imaging algorithm, a value of 1.006 in the inferior-frontal-cortex and of 1.03 in the precuneus-region, previously proposed in other study by our group (1), resulted the best cut-off SUVR-value, showing a good correlation with the diagnosis of AD. Based on FBB-PET/CT positivity (followed by other necessary features for inclusion criteria), 13/44 patients have been successfully enrolled in clinical trials using innovative monoclonal-antibodies therapy. **Conclusion:** SPM-normalized SUVR-analysis on FBB-PET/CT may allow better differential diagnosis of neurodegenerative disease in the clinical scenario. This new method could represent a valuable tool for the final diagnosis of AD and to correctly select patients into clinical trials using new target monoclonal-antibodies therapy. **References:** 1):Alongi P, Sardina DS, Coppola R, Scalisi S, Puglisi V, Arnone A, Raimondo GD, Munerati E, Alaimo V, Midiri F, Russo G, Stefano A, Giugno R, Piccoli T, Midiri M, Grimaldi LME. 18F-Florbetaben PET/CT to Assess Alzheimer's Disease: A new Analysis Method for Regional Amyloid Quantification. J Neuroimaging. 2019 Feb 3. doi: 10.1111/jon.12601.

EP-0045

Unveiling the Amyloid PET Patterns that Promote Cognitive Impairment among Amyloid-positive Subjects

A. Moscoso Rial[1], J. Silva-Rodríguez[2], J. Aldrey[3], J. Cortés[3], Á. Ruibal[3], P. Aguiar[1];
[1]University of Santiago de Compostela, Santiago de Compostela, SPAIN, [2]Fundacion Instituto de Investigación Sanitaria de Santiago (FIDIS), Santiago de Compostela, SPAIN, [3]University Hospital of Santiago de Compostela, Santiago de Compostela, SPAIN.

Aim/Introduction: Amyloid PET allows the detection of amyloid plaques in the neocortex, one of the defining neuropathological features of Alzheimer's Disease (AD). However, cortical plaques are also commonly found in cognitively normal elderly and therefore the clinical utility of amyloid PET is limited to exclude AD as the cause of cognitive impairment [1]. This study is aimed at (1) identifying the amyloid PET patterns that promote clinical symptoms among amyloid-positive (A+) subjects, and (2) implementing a new index from these patterns (Amy-Cog) to stratify A+ subjects into low/high cognitive impairment profiles. **Materials and Methods:** The Amy-Cog score was built using the amyloid PET uptake patterns that best discriminate between A+ cognitively normal (CN) subjects and A+ patients with mild AD. For this, we aggregated Florbetapir and PiB PET data from 3 observational studies (Alzheimer's Disease Neuroimaging Initiative, Australian Imaging Biomakers and Lifestyle Study of Ageing, and Open Access Series of Imaging Studies-3). Florbetapir scans from 131 A+ CN and 129 A+ mild AD subjects were used for optimal selection of uptake regions of interest (ROI) and model training. The model was then

evaluated in an independent sample of 235 A+ CN and 109 A+ mild AD individuals, and associations with the Amy-Cog status and longitudinal cognition were assessed in the A+ CN sample and in 322 A+ mild cognitive impairment (MCI) subjects. All the associations were adjusted by potential confounders, as well as by cortical amyloid burden and striatal uptake [2]. **Results:** The optimal set of amyloid PET uptake ROIs included allocortical, striatal, and white matter regions. Classification accuracy between A+ CN and A+ AD in the test set was high (AUC = 0.94), and superior to cortical amyloid burden and striatal uptake ($p < 0.001$). Among A+ CN subjects, the 14% Amy-Cog+ showed faster longitudinal cognitive decline (-0.36 MMSE points/year, $p < 0.001$) than Amy-Cog-. MCI Amy-Cog+ patients also showed faster cognitive decline and progression to AD dementia than Amy-Cog-. Both in A+ CN and MCI, longitudinal cognition was better predicted after including the Amy-Cog score in a model with cortical and striatal uptake alone ($p < 0.001$). **Conclusion:** The Amy-Cog score increases the value of a positive amyloid PET, providing a closer association between amyloidosis and clinical symptoms, and predicts cognitive decline in A+ CN and MCI subjects. **References:** [1] Johnson KA, et al. Alzheimers Dement. 2013 Jan; 9(1):e-1-16. [2] Hanseeuw BJ, et al. Alzheimers Dement. 2018 Oct;14(10):1281-1292.

EP-0046

^{123}I FP CIT Quantification in Older Subjects

A. Nicol;
Queen Elizabeth University Hospital, Glasgow, UNITED KINGDOM.

Aim/Introduction: ^{123}I FP-CIT imaging of striatal dopaminergic neuron terminals is used in the diagnostic pathway of Parkinson's Disease (PD) and Lewy Body dementia (DLB). Quantification is performed as an adjunct to visual assessment of images, using a normal database derived from healthy control subjects. Specific striatal binding is known to have a non-linear age dependency and corrections for age are applied. Databases are commonly produced using subjects up to age approx. 80 with interpolation for older subjects. This study aims to assess the accuracy of quantification for older subjects. **Materials and Methods:** Subjects referred for a ^{123}I FP-CIT scan which was subsequently reported as normal were collated. Fifteen consecutive subjects aged 80-90 (10F, 5M, mean age 85.0, SD 2.5) and fifteen subjects aged > 90 (11F, 4M, 92.5 (2.2)) were included. For reference, twenty subjects aged 60 - 80 were also assessed (14F, 6M, 67.4 (5.7)). Quantification was performed using age matched striatal Z scores from the European EARL database (Hermes BRASS). **Results:** The average striatal Z-scores for the groups of subjects aged 80-90 and > 90 were significantly different to zero ($p<0.05$, 80-90: mean 0.7, SD 1.4; >90: mean 0.7, SD 1.5). The average striatal Z-scores for the group aged 60-80 was not significantly different to zero (mean 0.1, SD 1.0). **Conclusion:** Quantification of ^{123}I FP-CIT scans may provide a useful adjunct to visual assessment. This uses databases which were developed with a focus on movement disorders and did not include many subjects older than age 80. The requirement for accurate reference data for these older subjects is highlighted. This may be of particular relevance in DLB referrals where a balanced loss of dopamine transporters is prevalent, and can be more challenging to detect visually. **References:** European multicentre Database of Healthy Controls for 123I FP-CIT SPECT (ENC-DAT): Age-related Effects, Gender Differences and Evaluation of Different Methods of Analysis. Varrone A et al. Eur J Nucl Med Mol Imaging (2013) 40: 213-227.

EP-0047

Individual brain metabolic connectome indictors predict the development of Alzheimer's dementia in mild cognitive impairment

I. L. Alberts[1], *M. Wang*[2], *J. Jiang*[3], *Z. Yan*[4], *J. Jiang*[4], *J. Ge*[5], *H. Zhang*[5], *C. Zuo*[5], *J. Yu*[6], *P. Cumming*[1], *A. Rominger*[1], *K. Shi*[1];
[1]*University clinic for Nuclear Medicine, Bern, SWITZERLAND,* [2]*Shanghai Institute for Advances Communication and Data Science, Shanghai University, CHINA,* [3]*Key laboratory of specialty fibre optics, Shanghai University, Shanghai, CHINA,* [4]*Shanghai University, Shanghai, CHINA,* [5]*Fudan University, Fudan, CHINA,* [6]*Huashan Hospital, Shanghai, CHINA.*

Aim/Introduction: The value of metabolic connectome approaches based on 18F-fluorodeoxyglucose (FDG) positron emission tomography (PET) has been demonstrated by numerous previous studies in neurodegenerative diseases. However, such metabolic networks are typically derived from groups of patients, with a resultant lack of individuality. We now present an individualised connectome approach to characterise brain-wide metabolic networks and explore the application in predicting the conversion of individuals with mild cognitive impairment (MCI) to Alzheimer's dementia (AD). **Materials and Methods:** We obtained FDG-PET data from the ADNI database consisting of 50 individuals without cognitive disturbance, 332 patients with stable MCI during 36 months' follow-up, 178 MCI patients who did develop AD within the follow-up interval, and 50 AD patients. The metabolic network for each individual was ascertained using connectome methodology based on Kullback-Leibler similarity. Furthermore, 457 network properties were derived from the individual metabolic network. We analyzed the metabolic network properties along with other clinical characteristics by the multivariate Cox proportional hazards technique. We also established four different Cox models, i.e. clinical characteristics, imaging pattern, imaging connectome and the combined model. Our proposed approach was compared with the spatial covariance mapping analysis. **Results:** The individual connectome analysis revealed brain metabolic network abnormalities, confirming a disruption of the network modular structure in the progression from MCI to AD. We found significant between-group differences in network properties across clinical groups in the precuneus, lingual, and temporoparietal cortices, precentral gyrus, and putamen. Metabolic connectome expression was a superior predictor of conversion than were other clinical or imaging pattern (HR, 3.80; 95% CI, 2.99-4.82; $P < 0.001$). The predictive performance

improved further when clinical and metabolic pattern variables were combined in the Cox model. The C-index scores in the test dataset were as follows: 0.728 (clinical), 0.749 (imaging pattern), 0.807 (connectome), and 0.827 (the combined model). **Conclusion:** Our individual brain connectome analysis identifies abnormal brain networks associated with conversion from MCI to AD, thus potentially constituting a clinically applicable imaging biomarker. **References:** None.

EP-0048

Task-specific regional cerebral metabolic pattern according to amyloid deposition in MCI patients: SPM analysis with paired FDG PET images

E. Lee[1], H. Youn[2], S. Lee[3], H. Jeong[2,4], J. Eo[1];
[1]Department of Nuclear Medicine, Korea University Guro Hospital, Korea University College of Medicine, Seoul, KOREA, REPUBLIC OF, [2]Department of Psychiatry, Korea University Guro Hospital, Korea University College of Medicine, Seoul, KOREA, REPUBLIC OF, [3]Department of Biomedical Sciences, Korea University Graduate School, Seoul, KOREA, REPUBLIC OF, [4]Korea University Research Institute of Mental Health, Seoul, KOREA, REPUBLIC OF.

Aim/Introduction: We investigated whether changes of the regional cerebral glucose metabolism (rCMglc) in resting and memory and attention task conditions are different according to amyloid deposition in MCI patients. **Materials and Methods:** Cognitively normal elderly peoples (NC) and MCI patients were prospectively enrolled and performed F-18 fluorodeoxyglucose (FDG) PET scanning in two different conditions, which were paired FDG PET image data. First basal FDG PET imaging was performed in the resting state with FDG injection in the lying position to minimize motor cortex activation. Second activation FDG PET imaging was performed after FDG injection during memory and attention tasks while lying on the PET bed. The tasks were continued until the end of the scanning to fully activate related cerebral regions during scanning. F-18 florbetaben (FBB) PET were also performed. MCI patients were classified into amyloid negative (MCIN) and amyloid positive (MCIP) groups based on FBB PET. FDG PET images were preprocessed using SPM12 with T1 MR images and estimated on a voxel-by-voxel basis. Basal and activation FDG PET images were compared within the subgroups and between subgroups (NC vs. MCIN, NC vs. MCIP and MCIN vs. MCIP) with statistical threshold of uncorrected P value <0.001 and extent threshold >100 continuous voxel size. **Results:** Ten normal control, 9 MCIN and 11 MCIP were recruited in this study. In activation PET compared with basal PET within the group, NC showed significantly increased rCMglc in the left precentral gyrus, right precentral gyrus, left lingual gyrus, left thalamus and left mid frontal gyrus, MCIN showed significantly increased rCMglc in the left mid temporal gyrus, right superior medial frontal gyrus, right superior temporal gyrus, right superior temporal pole, left precentral and right caudate, and MCIP showed significantly increased rCMglc in the right superior temporal gyrus and left superior frontal gyrus. In basal PET between NC and each MCI subgroup, only MCIP showed lower rCMglc in the right superior frontal gyrus. In activation PET between NC and each MCI groups, only MCIP showed lower rCMglc in the right mid frontal gyrus, right anterior cingulate gyrus, right inferior frontal gyrus, left inferior parietal gyrus and right superior parietal gyrus. **Conclusion:** During memory and attention tasks, cerebral metabolism changes compared with that in resting state. The patterns of this changes are different according to amyloid deposition in MCI patients. **References:** None.

EP-0049

Comparison of MR-based and PET-only quantification of tau load using [^{11}C]PBB3

E. Yousefzadeh-Nowshahr[1,2], G. Winter[2], P. Bohn[3], K. Kneer[2], C. von Arnim[4], M. Otto[4], C. Solbach[2], S. Anderl-Straub[4], D. Polivka[4], P. Fissler[4], V. Prasad[2], P. Kletting[1,2], M. W. Riepe[5], H. Braak[4], K. Del Tredici[4], M. Higuchi[6], A. Ludolph[4], A. J. Beer[2], G. Glatting[1,2];
[1]Medical Radiation Physics, Department of Nuclear Medicine, Ulm University, Ulm, GERMANY, [2]Department of Nuclear Medicine, Ulm University Hospital, Ulm, GERMANY, [3]Department of Nuclear Medicine, University Hospital Cologne, Köln, GERMANY, [4]Department of Neurology, Ulm University, Ulm, GERMANY, [5]Department of Psychiatry and Psychotherapy II, Ulm University, Ulm, GERMANY, [6]National Institute of Radiological Sciences, Chiba, JAPAN.

Aim/Introduction: [^{11}C]pyridinyl-butadienyl-benzothiazole3 ([^{11}C]PBB3) is a promising tracer developed for tau imaging in neurodegenerative diseases. Although MR-based quantification of tau load is commonly used as reference method, not all subjects necessarily have current MR images available in clinical routine. Here the ability of PET-only method for the quantification of [^{11}C]PBB3 tau tracer was evaluated and compared to the MR-based quantification. **Materials and Methods:** Eleven patients with suspected neurodegenerative disease were examined with [^{11}C]PBB3-PET and structural MRI. In the MR-based method, the MR images were normalized into the standard Montreal Neurological Institute (MNI) space using standard MRI templates. The estimated transformation matrix was then applied to the corresponding PET images. For the PET-only method, a [^{11}C]PBB3-PET template was created by averaging these PET images previously normalized to the MNI space. Then the PET images were registered into the [^{11}C]PBB3-PET template. The automated anatomical labelling (AAL) brain atlas was used to define masks for the frontal, temporal, parietal and occipital lobes in both methods. All regions of interest were masked for gray matter with a 30 % probability threshold. Standardized uptake value ratios (SUVRs) were calculated using the cerebellum as a reference region. Bland-Altman analysis was applied for comparison SUVRs from both methods. The correlations between SUVRs and mini-mental state examination (MMSE) were evaluated by Pearson's correlation analysis. A value of $p<0.05$ was assumed significant. **Results:** There was no significant difference between PET-only and MR-based quantification. In agreement with the MR-based method, the

[^{11}C]PBB3 uptakes obtained using the PET-only method were the highest in the temporal lobe and then followed by the occipital, parietal and frontal regions. For both methods, the significant correlations between SUVRs and mini-mental state examination (MMSE) were comparable in frontal (r_{MRI}=-0.81 vs. r_{PET}=-0.85); temporal (r_{MRI}=-0.76 vs. r_{PET}=-0.74); parietal (r_{MRI}=-0.84 vs. r_{PET}=-0.84); and occipital regions (r_{MRI}=-0.78 vs. r_{PET}=-0.85). Bland-Altman analysis showed lower and upper limits of agreement of -0.06 to +0.12 between global SUVRs of the MR-based versus the PET-only method. **Conclusion:** The PET-only approach provides accurate and precise [^{11}C]PBB3 load quantification without the need of MR images and it can be used for clinical diagnosis purposes, which might be of special relevance in a routine clinical setting. However, the MR-based method is more suitable for definition of the reference and gray matter regions. **References:** None.

EP-0050

A Brain PET staging system using Amyloid and Neurodegeneration Biomarkers for Individual Assessment in the Context of the 2018 NIA-AA Research Framework: an approach exploring clinical-biomarker mismatches and socio-demographic parameters

A. M. N. Coutinho, F. Porto, D. de Paula Faria, C. R. Ono, A. T. Garcez, P. Squarzoni, F. L. S. Duran, M. O. Oliveira, E. S. Tres, S. M. D. Bucki, O. V. Forlenza, R. Nitrini, G. Busatto Filho, C. A. Buchpiguel; University of São Paulo, São Paulo, BRAZIL.

Aim/Introduction: [18F]FDG-PET and [11C]PIB-PET are validated as neurodegeneration and amyloid biomarkers of Alzheimer´s disease (AD). We used a PET staging system based on the 2018 NIA-AA research framework to compare the proportion of amyloid positivity (A+) and hypometabolism (N+) in AD, amnestic mild cognitive impairment (aMCI) and healthy control groups in the specific context of a Latin-American Megacity. We also incorporated an additional classification of abnormal [18F]FDG-PET patterns and their co-occurrence with A+, exploring [18F]FDG-PET to generate hypotheses in cases presenting with clinical-biomarker "mismatches". **Materials and Methods:** Elderly individuals (N = 119) clinically classified as controls (N = 38), aMCI (N= 43) or early AD (N= 38) were included. We assessed their A(N) profiles and [18F]FDG-PET neurodegenerative patterns (classified as typical or atypical of AD), performing re-assessments of images whenever clinical classification was in disagreement with the staging (clinical-biomarker "mismatches"). We also investigated associations between "mismatches" and socio-demographic characteristics. **Results:** AD presented with higher rates of A+ and (N)+. aMCI and controls had similar "A" profiles, with a tendency of more individuals with neurodegeneration (N+) in aMCI. Amyloid positivity and typical (N)+ AD hypometabolic patterns were statistically associated. A non-AD pattern of hypometabolism was seen in all cases of neurodegeneration without amyloid (A-(N)+) in the clinically-defined AD group. All A-(N)- cases in the AD group had less than four years of formal education. **Conclusion:** The PET based A(N) staging system unveiled significant A(N) differences between AD and the other groups, whereas aMCI and controls had similar A profiles and minor differences in the (N) staging. [18F]FDG-PET could be used beyond simple (N) staging, since it provided alternative hypotheses to cases with clinical-biomarker "mismatches" and its AD hypometabolic pattern correlated with amyloid positivity. Low education was related to dementia in the absence of biomarker changes. **References:** None.

EP-0051

Agreement between amyloid-PET early phase images and FDG-PET: a single subject validation in amyloid positive and amyloid negative subjects

P. Santos-Holgueras[1,2], A. Dodich[3], P. Andryszak[4], B. Rakotomiaramanana[4], M. Scheffler[5], K. Lövblad[6], G. B. Frisoni[4], V. Garibotto[2,3];
[1]Nuclear Medicine and Molecular Imaging Division, San Pedro Hospital-CIBIR, Logroño, SPAIN, [2]Nuclear Medicine and Molecular Imaging Division, Diagnostic Department, Geneva University Hospitals, Geneva, SWITZERLAND, [3]NIMTlab, Neuroimaging and Innovative Molecular Tracers Laboratory, University of Geneva, Geneva, SWITZERLAND, [4]Memory Center and LANVIE - Laboratory of Neuroimaging of Aging, Department of Rehabilitation and Geriatrics, Geneva University Hospitals, Geneva, SWITZERLAND, [5]Radiology Division, Diagnostic Department, Geneva University Hospitals, Geneva, SWITZERLAND, [6]Neurodiagnostic and Neurointerventional Division, Diagnostic Department, Geneva University Hospitals, Geneva, SWITZERLAND.

Aim/Introduction: FDG-PET and amyloid-PET are validated biomarkers of neurodegeneration and of Alzheimer disease (AD) pathology. The acquisition of images immediately after injection for amyloid-PET (amy-PET_{ep}) offers the opportunity to measure cerebral blood flow, possibly representing an alternative to the evaluation of brain metabolism through FDG-PET. This study aims to evaluate the concordance of amy-PET_{ep} and FDG-PET in a large sample of amyloid positive and negative individuals using two different amyloid tracers. **Materials and Methods:** We selected 126 subjects (68 female, age: 71±7) from two ongoing studies at Geneva University Hospitals. All subjects performed both FDG-PET and amy-PET_{ep} (interval in months: 3±4.9; ^{18}F-florbetapir: 76, ^{18}Fflutemetamol: 50), spanning across the whole cognitive spectrum (6 unimpaired, 89 mild cognitive impairment, 31 dementia). 85 subjects were amyloid positive. All subjects had T1-weighted MRI images, used to normalize PET images. We computed standardize uptake value ratio (SUVR) images using cerebellum and pons/vermis as reference region for amyloid and FDG images, respectively. SUVR values were extracted from atlas-based regions of interests (ROIs) (bilateral frontal, temporal and parietal, anterior and posterior cingulate cortex). Correlation analyses between SUVR obtained from each region and from the mean SUVR across all regions between the early-phase ($SUVR_{epA}$) and FDG images ($SUVR_{FDG}$) through Pearson r index in the overall sample. Correlation

coefficients according to amyloid status and tracer were compared using the Fisher r-to-z transformation. FDG-PET and amy-PET_{ep} was evaluated visually as negative/non-AD/AD pattern by 2 independent readers, using statistical maps of single-subject comparison with a reference database of 30 FDG or 18 amy-PET_{ep} normal subjects, respectively. **Results:** We found significant correlations (p<0.005) in the overall group between $SUVR_{epA}$ and $SUVR_{FDG}$ in all the ROIs investigated, with r values ranging from 0.52 (left frontal) to 0.73 (right angular). The correlation was significant and did not differ between amyloid positive and negative subjects (r 0.68 and 0.52, respectively, p=0.2), nor between tracers (r 0.66 with florbetapir and 0.52 with flutemetamol, p=0.3). The agreement between raters in classifying patients according to the single-subject maps was good (Cohen's kappa: 0.69, SE: 0.056 CI95%: 0.58-0.80) **Conclusion:** Our results show that amy-PET_{ep} values are highly correlated with FDG-PET, in all ROIs analysed, for both tracers and also for both amyloid statuses. The good agreement observed in single subject analysis, comparable to the agreement reported for the interpretation of FDG-PET, supports the routine use of amy-PET_{ep} in clinical practice. **References:** None.

EP-0052

In vivo Amyloid Plaques quantification using F18-Flutemetamol PET/CT in 31 healthy controls and 130 MCI: SUVr methods's comparison and transposition in the centiloid scale

R. Lhommel[1], *B. Hanseeuw*[1], *V. Malotaux*[2], *L. Dricot*[2], *A. Ivanoiu*[1]; [1]*Cliniques Universitaires St-Luc, UCLouvain, Brussels, BELGIUM,* [2]*Institute of NeuroScience (IONS), UCLouvain, Brussels, BELGIUM.*

Aim/Introduction: F18-Flutemetamol PET is now a well validated surrogate biomarker to non invasively estimate the brain amyloid load of patient suspected of (pre-clinical) AD disease, either by visual or semi-quantitative SUVr analysis, approach less dependent of the operator's expertise and more appropriate to follow the amyloid variations under targeted investigational drugs. By proposing the centiloid scale approach in 2015, Klunk has pointed the importance to harmonize quantitative reports of Amyloid PET series. Therefore, we have planned to retreat our MCI patient's database to obtain individual centiloid SUVr and centiloid scale values (CSV) for each patient. The results of this centiloid analysis is reported here and compared to our previous SUVr computation methodology (still used for data consistency and comparison with our previous reports). **Materials and Methods:** Since 2011, 31 healthy controls (HC) and 130 MCI were imaged at baseline with Flutemetamol (target I.D 185 MBq; dyn 6X5min; 90min pi). Visual analysis (Sokoloff scale) and SUVr computation were performed using different evolution of the PNEURO workflows (PMOD, Zurich) from 3.2 to 3.9/4.0 version, natively implementing now the centiloid vois atlas. Historical $SUVr_{3.5}$ (=SUVneocortex/grey_cerebellum in PET space) were compared to $SUVr_{centiloid}$ values (= centiloid composite voi/GM+WM_cerebellum in MNI atlas space) and converted to CSV after PNEURO3.9 workflow validation (not detailed). Statistics were computed using PRISM8.0 and the Percentile 90 (PC90) of the control group defined as the cutoff reference for a «positive scan». **Results:** HC SUVr3.5 and $SUVr_{centiloid.}$ (mean±SD/median/PC90) were respectively 1.30±0.16/1.25/1.49 and 1.08±0.18/1.03/1.37 , both significantly different from the MCI group (1.55±0.34/1.45; p=0.0001***) and (1.34±0.37/1.30; p=0.008***). $SUVr_{centiloid.}$ were significatively lower than SUVr3.5 values (P<0.0001**** ; bias: -18.8%, SD of bias: 5.1). However, a good correlation was found between $SUV_{3.5}$ and $SUVr_{centiloid}$ (R^2:0.94 ; Y=1.0037*X-0.2665). A excellent correlation was found between SUVr 3.5 cutoff and the visual reading (only 4/161 visually borderline scans). The best fit of the Flut SUVr centiloid values in the centiloid scale was obtained using the equation (CSV= 116.0 x $SUVr_{centiloid}$ -113.9) derived from previous calibration steps (not detailed). The derived cutoff values (PC90 of the HC) were 1.374 for $SUVr_{centiloid}$ and 45.98 for the CSV. **Conclusion:** Despite lower values, Flutemetamol $SUVr_{centiloid}$ favorably compared with previous SUVr 3.5 but present the main advantage to be directly transposable in the centiloid scale for direct comparison with other study results. **References:** Klunk et al. Alzheimer Dement, 2015. http://www.gaain.org/centiloid-project

EP-0053

Multimodal Imaging of X-linked Adrenoleukodystrophies with [18F]Florbetaben PET/MRI

T. Gerhards, *M. Rullmann, H. Roicke, D. Lobsien, K. Hoffmann, J. Classen, M. Patt, O. Sabri, W. Koehler, H. Barthel; University Hospital Leipzig, Leipzig, GERMANY.*

Aim/Introduction: Leukodystrophies are a group of rare hereditary diseases characterized by impaired myelination or demyelination. In the case of X-linked adulthood cerebral adrenoleukodystrophy (X-ACALD), cerebral white matter (WM) changes are considered to be triggered by a gene defect that causes an insufficient degradation of very long chain fatty acids (VLVFA) with subsequent neurotoxic effects. Recently, we were able to show that the beta-amyloid PET Tracer ^{18}F Florbetaben which in addition to the actual target also binds to myelin has a great potential for improved imaging of WM diseases. The aim of this current pilot study was to evaluate for the first time the suitability of hybrid ^{18}F Florbetaben PET/MRI for imaging of X-ACALD. **Materials and Methods:** So far, we examined 4 patients with X-ACALD (mean age 43+/-7yrs, Loes score=9,8 ±2,6). 0-10min p.i. (perfusion equivalent) and 90-110min p.i. (myelin equivalent in WM) after application of about 300MBq ^{18}F Florbetaben, PET (SUVRs, global brain as reference), structural MR as well as DTI MR (FA values) images were simultaneously acquired on a 3T Siemens mMR hybrid PET/MR system. The WM signals were regionally analysed using the Johns Hopkins University WM tractography atlas (48 VOIs). Furthermore, we analysed a cross-sectional area of the outer lesion-rim and created profiles for the above imaging data. **Results:** Structural MRI revealed findings typical for X-ACALD with inflammatory demyelinating lesions in parieto-occipital, frontal or cerebellar

WM. In comparison with an age matched healthy control group, 28% of the DTI WM VOIs and 20% of the myelin PET WM VOIs showed pathologic values (more than 2STDEV). Regional myelin PET WM SUVRs were correlated with the regional WM FA values ($\bar{r}$ = 0.43). The cross-sectional profiles showed a clear increase of the FA levels in the transition zone from the lesion to the adjacent normal-appearing WM (NAWM). Here, perfusion PET showed a broader transition zone, while myelin PET revealed a steady increase from the centre of the lesion towards the adjacent NAWM. **Conclusion:** From these initial results it is concluded that multimodal ^{18}F Florbetaben WM PET/MRI could lead to a more specific characterization of the extent of the lesional burden and disease stage in X-ACALD as compared to MRI. This novel imaging approach would, thus, also be of great interest for monitoring re-myelination therapies. To confirm this assumption, however, larger case numbers and longitudinal imaging are required. **References:** None.

EP-0054

Radionuclide Cisternography revisited in the SPECT/CT era: applications in Normal Pressure Hydrocefalus and in the detection of Cerebrospinal Fistulas in comparison with Magnetic Resonance Imaging techniques

M. Waitman, A. M. N. Coutinho, R. F. Nunes, M. Trindade, E. C. Zaniboni, L. Bastos, M. Scaff, C. A. Buchpiguel;
Sírio Libanês Hospital, São Paulo, BRAZIL.

Aim/Introduction: Radionuclide cisternography continues being an important exam for the evaluation of both Normal Pressure Hydrocephalus (NPH) and cerebrospinal fluid (CSF) fistulas. NPH is characterized by the classic clinical triad of ataxia, urinary incontinence, and dementia, resulting from a change in the flow dynamics of CSF. The improvement of the symptoms tends to occur with a ventriculoperitoneal shunt (VPS). CSF fistulas result from multiple factors, including trauma, post-lumbar puncture or even spontaneously. However, most diagnostic techniques have limited sensitivity to investigate both conditions. The present study investigated the role of Radionuclide Cisternography with SPECT/CT (RC-SPECT/CT) in two scenarios: (1) prediction of VPS response in patients with suspected NPH; (2) in the detection of CSF fistulas. In both situations, we compared RC-SPECT/CT results with state-of-the-art MRI examinations. **Materials and Methods:** In scenario 1 we retrospectively included all patients with positive RC-SPECT/CT for NPH between the years 2006 and 2019 (N = 17). When at disposal, we also evaluated the MR results (callosal angle in 16 individuals and CSF dynamics in six). Patients had their charts reviewed to characterize the clinical response to VPS. In scenario (2), patients ate with a confirmed diagnosis and effective treatment of CSF fistulas (N = 10) had their results of RC-SPECT/CT and MRI retrospectively assessed to evaluate both the sensivity and the agreement between the methods. **Results:** In the NPH scenario, 88.2% of the patients with positive RC-SPECT/CT presented clinical improvement, and only two (11.8%) had no improvement in the symptoms after VPS placement. Sixteen patients had MRI evaluation. Among them, only 37.5% of the patients presented a narrowing of the callosal angle, and 60% showed alterations in CSF flow, findings associated with NPH. Regarding the confirmed CSF fistulas scenario, 70% of the patients had positive results on RC-SPECT/CT versus 50% on MRI. RC-SPECT/CT did not confirm only one CSF fistula detected by MRI. **Conclusion:** The present study suggests a high rate of prediction of response to VPS therapy by RC-SPECT/CT in NPH, apparently superior to the measurement of callosal angle and CSF dynamics by MRI, despite the low number of individuals with all the studies in the present sample. RC-SPECT/CT also identified a more significant percentage of patients with CSF fistula than MRI, in addition to more accurately detecting the level of extravasation of the CSF due to the use of SPECT-CT. **References:** None.

EP-0055

Clinical progression over one-year in mild cognitive impairment subjects with low ß-amyloid neocortical retention levels

E. Giovannini[1], G. Giovacchini[1], M. Riondato[1], S. Pastorino[1], O. Ferrando[1], V. Duce[1], M. De Biasi[2], C. Passera[2], E. Carabelli[1], A. Mannironi[1], L. Mansi[3], A. Tartaglione[2], A. Ciarmiello[1];
[1]Asl5, La Spezia, ITALY, [2]Memory Center, La Spezia, ITALY, [3]University, Napoli, ITALY.

Aim/Introduction: The rate of clinical progression of cognitive impairment in amyloid positive subjects with moderate retention levels is unknown. The primary aim of the study was to perform a 1-year follow-up on rate of cognitive decline in patients with mild cognitive impairment (aMCI) featuring moderate amyloid retention level with standardized uptake value ratio (SUVr) ranging from 1.3 to 1.5. The secondary objective was to compare the rate of cognitive decline in subjects with moderate amyloid positivity and negative ones. **Materials and Methods:** In this prospective phase III trial (EudraCT 2015-001184-39), 38 participants with aMCI underwent clinical, neuropsychological and PET amyloid imaging tests. Study participants were followed for 1 year to assess changes in global cognition and amyloid burden. PET images were scored as positive (Aß+) for amyloid retention using a standardized uptake value ratio ≥ 1.3, measured in grey matter, at baseline scan. The Mattis Dementia Rating Scale (MDRS) was used to assess clinical longitudinal changes of cognitive impairment. **Results:** Thirty-eight aMCI subjects completed the assessment according to study protocol. Amyloid positive subjects showed greater clinical worsening on MDRS score (p=0.006). Aß- showed no significant changes on MDRS scores over 1 year. We found significant MDRS score decrease in 37% of aMCI cohort (MDRS+), whereas in the remaining 63% MDRS were stable (MDRS-). Among subjects with cognitive deterioration 86% had positive amyloid scan and 14% were classified as amyloid negative while in MDRS- group 25% were Aß+ and 75% were Aß- (χ2=13; P=0.0003). Aß SUVr above 1.3 identified individuals with significant progression over one-year with a SS of 86% and a SP of 75%, as compared to

Aß- subjects. The PPV was 67% and NPV was 90%. **Conclusion:** This study demonstrates that, aMCI cognitive decline can be predicted at low retention amyloid level and above the threshold of SUVr=1.3 the rate of decline is increased. Detection of low amyloid deposition may help in selecting target population for preventive therapeutic interventions and to design treatment trial. **References:** None.

EP-0056

Evaluation of different methods for spatial normalization of PIB-PET brain images

F. Xie[1], *Q. Huang*[1], *D. Jiang*[1], *F. Hua*[1], *Y. Guan*[1], *Q. Guo*[2];
[1]*Huashan Hospital, Fudan university, Shanghai, CHINA,*
[2]*Department of gerontology, Shanghai Jiaotong university affiliated sixth people's hospital, Shanghai, CHINA.*

Aim/Introduction: PIB-PET can be used for detecting and quantitative measurement of the Aβ plaques. The precise of spatial normalization of PIB-PET images is important in quantitative measurements. So we evaluated the precise of spatial normalization methods regularly used PIB-PET images analysis, and try to recommend a more precise method for the quantitative measurements of PIB-PET. **Materials and Methods:** 21 AD patients ascertained by neurological physician were enrolled in this study. All subjects underwent FDG-PET, PIB-PET and MRI T1-weighted scanning. The PIB-PET images were normalized into MNI space by the following methods: (A) normalized to H_2O-PET template by SPM8; (B) FDG-based normalization by SPM8: co-registration of FDG-PET images of each subject to their corresponding PIB-PET images, then nonlinear normalization parameters were calculated between the co-registered FDG-PET images and the H_2O-PET template by SPM8 to transform the PIB-PET images to the MNI space; (C) MRI-based normalization by SPM8: co-registration of MRI to their corresponding PIB-PET images, then nonlinear normalization parameters were calculated between the co-registered MRI images and the MRI template by SPM8 to transform the PIB-PET images to the MNI space; (D) normalization to the dementia template[1]by SPM8; (E) FDG-based normalization to dementia template by SPM8; (F) normalization by SPM12; (G) FDG-based normalization by SPM12; (H) MRI-based normalization by SPM12. After normalization, the standard deviation (s.t.d) images were calculated, and the coefficient of variation (CV = s.t.d/mean) of the brain regions were calculated, including basal ganglia, frontal lobe, lateral parietal lobe, lateral temporal lobe, medial temporal lobe, occipital lobe, posterior cingulate gyrus and precuneus,. **Results:** The accuracy of normalization to H_2O and dementia template by SPM8 was 80.95% and 95.33%, no mismatches were found in other methods by visual inspection. Quantitative analysis showed the s.t.d and CV value of FDG-based normalization by SPM8 was minimum . **Conclusion:** FDG-based normalization of PIB-PET images by SPM8 was recommend for the measurements of PIB-PET image in AD studies. **References:** 1. Rosa, P.A.D., et al., A Standardized [18F]-FDG-PET Template for Spatial Normalization in Statistical Parametric Mapping of Dementia.Neuroinformatics, 2014. 12(4): p. 575-593.

EP-0057

Quantification of tau load using [^{11}C]PBB3: a voxel-wise statistical analysis

E. Yousefzadeh-Nowshahr[1,2], *G. Winter*[2], *P. Bohn*[3], *K. Kneer*[2], *C. von Arnim*[4], *M. Otto*[4], *C. Solbach*[2], *S. Anderl-Straub*[4], *D. Polivka*[4], *P. Fissler*[4], *P. Kletting*[1,2], *V. Prasad*[2], *M. W. Riepe*[5], *H. Braak*[4], *K. Del Tredici*[4], *M. Higuchi*[6], *A. Ludolph*[4], *A. J. Beer*[2], *G. Glatting*[1,2];
[1]*Medical Radiation Physics, Department of Nuclear Medicine, Ulm University, Ulm, GERMANY,* [2]*Department of Nuclear Medicine, Ulm University Hospital, Ulm, GERMANY,* [3]*Department of Nuclear Medicine, University Hospital Cologne, Köln, GERMANY,* [4]*Department of Neurology, Ulm University, Ulm, GERMANY,* [5]*Department of Psychiatry and Psychotherapy II, Ulm University, Ulm, GERMANY,* [6]*National Institute of Radiological Sciences, Chiba, JAPAN.*

Aim/Introduction: [^{11}C]pyridinyl-butadienyl-benzothiazole3 positron emission tomography ([^{11}C]PBB3-PET) has the potential to visualize and quantify accumulation and distribution of tau deposits in neurodegenerative diseases. Here we evaluated the ability of using [^{11}C]PBB3-PET in a routine clinical environment to detect and measure regional tau burden. **Materials and Methods:** 17 patients were examined with [^{11}C]PBB3-PET, 5 of them with advanced neurodegenerative diseases (ND) from the frontotemporal lobar degeneration (FTLD) or Alzheimers Disease (AD) spectrum (age: 64.0±8.1 y; mini-mental state examination (MMSE): 10-21) and 12 patients with mild cognitive impairment (MCI) (age: 63.8±7.1 y; MMSE: 23-30). The cerebrospinal fluid levels of tau (CSF_tau) and amyloid-β_{42} (CSF_Aβ) were assessed using a lumbar puncture. An automated PET-only method was developed to quantify tau pathology. To achieve this, all images were registered to a [^{11}C]PBB3-PET template, generated by averaging PET scans previously normalized to the standard Montreal Neurological Institute space. Statistical parametric mapping was used to perform a voxel-wise two-sample t-test analysis across groups. To compute target-to-cerebellum standardized uptake value ratios (SUVr) within 90 volume of interests (VOIs), the automated anatomical labelling brain atlas was used. All VOIs were masked for gray matter with a 30 % probability threshold. The correlation between SUVr values, MMSE, CSF_tau and CSF_Aβ were investigated by Pearson's correlation analysis. **Results:** Significantly higher [^{11}C]PBB3 binding was observed in patients with advanced ND compared to MCI patients in the inferior and middle temporal lobe (1.25±0.07 vs. 0.91±0.05, p = 0.02), and middle frontal lobe (1.23±0.07 vs. 0.88±0.05, p = 0.04). Although there was a substantial difference between groups in the left posterior cingulate (1.33±0.07 vs. 0.95±0.05), the results did not reach significance (p = 0.08). The regional analysis revealed that CSF_tau values were associated with occipital tau pathology (r = 0.64, p = 0.02), whereas CSF_Aβ values were related inversely to the increased tau burden in the parietal (r = -0.62, p = 0.03) and precuneus regions (r = -0.67, p = 0.02). MMSE showed significant inverse correlations in many regions with the strongest correlations in prefrontal, temporal, parietal, occipital and precuneus regions (r = -0.49 to -0.59, p < 0.05). **Conclusion:** Statistical voxel-wise analysis effectively

showed group differences in [11C]PBB3-PET tau signal. Both MMSE and CSF values had significant correlations with tau uptake in several brain regions, suggesting that [11C]PBB3-PET indeed is an effective surrogate parameter for tau load and disease severity. **References:** None.

EP-0058

Tremor and non-tremor Parkinson's disease show different patterns of 11C-CFT and 18F-FDG PET/CT imaging

M. Xin, C. Wang, J. Liu, G. Huang;
Renji Hospital, School of Medicine, Shanghai Jiao Tong University, Shanghai, CHINA.

Aim/Introduction: Parkinson's disease (PD) is a heterogeneous neurodegenerative disorder, including a tremor-dominant and a non-tremor (bradykinesia or rigid) subtypes. Tremor-dominant PD is generally prone to follow a benign disease course. To explore the relationship between the metabolic patterns and different PD clinical phenotypes, and whether the metabolic characteristics can reflect the PD disease progression, we investigated the dopamine transporter (DAT) and glucose metabolic PET imaging in patients with or without tremor. **Materials and Methods:** 11C-CFT together with 18F-FDG PET/CT scans of 33 consecutive patients with a clinical diagnosis of PD and abnormal DAT binding (24 with tremor, 9 without tremor) were analyzed both visually and semiquantitatively. **Results:** Caudate dopamine depletion in patients with tremor was milder than patients without tremor (P<0.05). Sorted by the modified Hoehn-Yahr (H-Y) stage, tremor-dominant PD patients with an early stage (H-Y: 1-2) showed less caudate dopamine depletion than non-tremor patients (P<0.05); while there were both severer dopamine depletions of anterior and posterior putamen in tremor-dominant PD patients with a late stage (H-Y: 2.5-5) than patients without tremor (P<0.01, respectively). In the 18F-FDG PET/CT imaging, the thalamus glucose uptake of patients with tremor showed more active than non-tremor PD patients (P<0.001). **Conclusion:** The dopamine and glucose metabolic phenotypes is associated with different clinical PD subtypes, as caudate dopamine function is less affected in the early stage of tremor-dominant patient. Multimode imaging may contribute to elucidate the mechanism of PD motor pattern and provide information of the disease prognosis. **References:**
1. Neudorfer C, Hinzke M, Hunsche S, El Majdoub F, Lozano A, Maarouf M. Combined Deep Brain Stimulation of Subthalamic Nucleus and Ventral Intermediate Thalamic Nucleus in Tremor-Dominant Parkinson's Disease Using a Parietal Approach. Neuromodulation. 2019. 2. Zeng Q, Guan X, Guo T, Law Yan Lun JCF, Zhou C, Luo X, et al. The Ventral Intermediate Nucleus Differently Modulates Subtype-Related Networks in Parkinson's Disease. Front Neurosci. 2019;13:202. 3. Akakin A, Yilmaz B, Kilic T, Rhoton AL, Jr. Anatomy of the subthalamic nucleus, with correlation of deep brain stimulation [RETRACTED]. J Neurosurg. 2015. 4. Eggers C, Kahraman D, Fink GR, Schmidt M, Timmermann L. Akinetic-rigid and tremor-dominant Parkinson's disease patients show different patterns of FP-CIT single photon emission computed tomography. Mov Disord. 2011;26:416-23. 5. Helmich RC, Hallett M, Deuschl G, Toni I, Bloem BR. Cerebral causes and consequences of parkinsonian resting tremor: a tale of two circuits? Brain. 2012;135:3206-26.

EP-0059

Imaging of tau deposition in neurodegenerative diseases of the FTLD/AD spectrum in a clinical setting using [11C] PBB3 PET/CT

G. Winter[1], P. Bohn[2], E. Yousefzadeh-Nowshahr[3], K. Kneer[1], C. A. F. von Arnim[4], M. Otto[4], C. Solbach[1], G. Glatting[3], S. Anderl-Straub[4], D. Polivka[4], P. Fissler[4], V. Prasad[1], M. W. Riepe[5], H. Braak[4], K. Del Tredici[4], M. Higuchi[6], A. Ludolph[4], A. J. Beer[1];
[1]Department of Nuclear Medicine, Ulm University, Ulm, GERMANY, [2]Department of Nuclear Medicine, University Hospital Cologne, Köln, GERMANY, [3]Medical Radiation Physics, Department of Nuclear Medicine, Ulm University, Ulm, GERMANY, [4]Department of Neurology, Ulm University, Ulm, GERMANY, [5]Department of Psychiatry and Psychotherapy II, Ulm University, Ulm, GERMANY, [6]National Institute of Radiological Sciences, Chiba, JAPAN.

Aim/Introduction: The accumulation of tau protein in the brain is a pathological hallmark of many neurodegenerative diseases. For positron emission tomography (PET) diagnostics, several tau-specific radiotracers have been developed in recent years, with [11C]PBB3 as one of the promising compounds. In this study, we retrospectively evaluated the first clinical experiences with PBB3 in a patient population with suspected neurodegenerative diseases, mostly from the AD and FTLD spectrum. **Materials and Methods:** The standardized uptake value ratio (SUVr) of [11C]PBB3 binding was determined for 27 patients based on a PET/CT examination in the region of individual lobes (frontal, temporal, parietal, occipital) and basal ganglia with cerebellar cortex as reference. Correlations between the SUVr and other clinical tests (mini-mental state examination - MMSE) and cerebrospinal fluid (CSF) parameters (CSF-Abeta; CSF-tau) were determined using the Pearson correlation. In addition, in 14 cases a [11C]PIB PET/CT and in 17 cases a [18F]FDG PET/CT were available for correlation analysis. The final diagnosis was based on the integration of all clinical and imaging data as well as the follow-up of the patients. **Results:** In 13 patients, no or only a weak accumulation of [11C]PBB3 was detected (PBB3-negative), while in 14 patients a moderate to pronounced uptake was found (PBB3-positive). Based on the visual assessment of tracer accumulation, the strongest PBB3 uptake occurred in the temporal lobe, followed by the occipital, frontal, and parietal lobes. In addition, basal ganglia uptake was observed in all patients. The determination of the Pearson correlation resulted in significant moderate correlations of SUVr for the respective lobes with MMSE (frontal: r = -0.54*; occipital r = -0.46*; parietal r = -0.57**) and CSF-tau (occipital r = 0.68*) (*p≤0.05; **p≤0.01). No correlation was found for basal ganglia. All PBB3-negative scans were also PIB-negative, while PBB3-positive scans were both PIB-positive and -negative. Most PBB3 scans were also FDG-positive. **Conclusion:** Uptake of [11C]PBB3 was most

pronounced in amyloidogenic neurodegenerative diseases, such as Alzheimer's disease, and correlated with CSF-tau. In these cases, typical uptake patterns were observed corresponding to the neurofibrillary tangle (NFT) stages III-VI. The uptake of [^{11}C] PBB3 correlated significantly with MMSE , suggesting that PBB3-PET might be a good parameter for disease severity. However, owing to the generally only moderate intensity of [^{11}C]PBB3 uptake, the clinical benefit at the individual patient level is still unclear and needs to be assessed in further prospective studies. **References:** None.

EP-0060

[18F] FBB Cortical Uptake Is Not Related To The Age Of Onset Of Alzheimer's Disease

A. Chiaravalloti[1], *A. E. Castellano*[2], *A. Martorana*[1], *M. Ricci*[3], *O. Schillaci*[1];
[1]*Department of biomedicine and prevention, University Tor Vergata, Rome, ITALY,* [2]*IRCCS Neuromed, Pozzilli, ITALY,* [3]*Department of Radiological, Oncological and Pathological Sciences, Sapienza University of Rome, Rome, ITALY.*

Aim/Introduction: To investigate the relationships between amyloid burden in brain and the age of onset of Alzheimer's disease (AD), exploring the differences between patients with early onset of Alzheimer's disease (EOAD, aged ≤ 65 years) and patients with late onset of Alzheimer's disease (LOAD, aged > 65 years). **Materials and Methods:** We examined 60 patients with clinical diagnosis of Alzheimer's disease according to NINCDS-ADRDA criteria. Of them 22 were EOAD, and 38 were LOAD. All of them underwent a brain Positron Emission Tomography (PET) scan 90 minutes after the injection of 4-[(E)-2-[4-[2[2-(2-fluoranylethoxy)ethoxy]ethoxy]phenyl]ethenyl]-N-methylaniline ([18F] FBB); 300 ± 10 MBq). Qualitative analysis of PET data was positive for increased amyloid burden in the brain in all the AD subjects. Relationships between amyloid burden in brain and age of onset of AD were assessed by means of Statistical Parametric Mapping (SPM) version 12, with the use of age as regression factor and sex, MiniMental State Examination (MMSE) as covariates in the regression analysis. Moreover, a two-sample t-test was used for comparison between EOAD and LOAD subjects. **Results:** There were no significant differences [18F] FBB uptake between EOAD and LOAD patients. Multiple regression analysis did not show any significant correlation between age of onset and brain amyloid deposition in AD subjects. **Conclusion:** In our study population, age of onset is not related to brain amyloid burden in AD patients. Other factors may be involved in explaining the clinical differences between EOAD and LOAD patients. **References:** None.

EP-0061

Impact of tracer retention level on visual classification of amyloid PET images

E. Giovannini, P. Lazzeri, E. Borsò, M. Riondato, A. Ciarmiello; Asl5, La Spezia, ITALY.

Aim/Introduction: Our aims were to test inter-rater agreement and concordance between visual and semiquantitative scoring at different amyloid retention levels in Mild Cognitive Impairment (MCI) patients. **Materials and Methods:** A sample of 71 amnestic MCI patients (AGE 73.96 ± 7.35 years, MMSE 24.23 ± 5.33, CDR-SOB 2.16 ± 2.14) underwent 18F-florbetaben PET/CT and clinical assessment. Amyloid positivity was assessed by semiquantitative approach by means of previously published threshold (SUV ≥ 1.3). Images were visually scored as positive or negative by three independent, certified readers blinded to neuropsychological result. Fleiss kappa coefficient was used to test inter-reader concordance on the whole population and on 3 subgroups with low (SUVr <1.1), medium (SUVr >1.1 <=1.5) and high (SUVr> 1.5) Aß burden. **Results:** Fleiss's kappa statistic was k=0.86,P <0.00001 on the whole sample. By evaluating the groups with different Aß burden separately, the inter-raters agreement changed according to tracer retention levels:k=0.85,P=0.0001; low Aß burden (SUVr <1.1)k=0.48,P=0.0001; medium Aß burden(1.1 <SUVr<=1.5) k=0.98,P=0.00001; high Aß burden (SUVr> 1.5) Moreover we found the lower reliability between visual and unsupervised evaluation of Aß positivity in the group with moderate retention levels ranging between SUVr =1.1 and 1.5. **Conclusion:** Inter-raters agreement of visual detection of amyloid positivity is high in low and high retention levels group but reduces in the range of 1.1<SUVr <=1.5, in these cases the support of semi-quantitative analysis would be necessary to reduce the risk of amyloid positivity misclassification. **References:** None.

EP-0062

Impact of MR-based head motion correction on amyloid PET diagnosis - A simultaneous PET/MRI study

M. Schürer[1], *T. Jochimsen*[1], *M. Rullmann*[1], *M. Patt*[1], *S. Tiepolt*[1], *M. Schroeter*[2], *C. Weise*[3], *D. Saur*[3], *K. Hoffmann*[4], *O. Sabri*[1], *H. Barthel*[1];
[1]*Department of Nuclear Medicine, University of Leipzig Medical Center, Leipzig, GERMANY,* [2]*Max Planck Institute for Human Cognitive and Brain Sciences Leipzig & Clinic for Cognitive Neurology, Leipzig, GERMANY,* [3]*Department of Neurology, University of Leipzig Medical Center, Leipzig, GERMANY,* [4]*Department of Neuroradiology, University of Leipzig Medical Center, Leipzig, GERMANY.*

Aim/Introduction: [18F]Florbetaben amyloid PET/MRI is a useful tool for early and differential dementia diagnosis. It is able to deliver, in a convenient way, dual amyloid pathology and neurodegeneration biomarker information [1]. One potential additional advantage of simultaneous PET/MR imaging is related to MR-based movement correction (MoCo) of the PET data [2]. As head movement can be a relevant problem in imaging cognitively impaired patients, we initiated the present study to evaluate the diagnostic relevance of MoCo in F18-florbetaben brain PET/MRI. **Materials and Methods:** We so far acquired simultaneous [18F]Florbetaben PET/MRI data (300MBq, 90-110min p.i., 3T Siemens mMR) of 13 cognitively impaired patients

(5 female, age=64±15yrs). In parallel to the PET acquisition, the vendor-provided BrainCompass MoCo (Biograph mMR E11P, Siemens Healthcare, Germany) was carried out. The MoCo PET vs. non-MoCo PET data were analyzed visually (standard BAPL scores for amyloid state and 5-point image quality scores) and semi-quantitatively (SUVRs, reference: cerebellar cortex, AAL template in SPM12). **Results:** 5/13 patients scored positive in the blinded read of the non-MoCo PET images. For the MoCo PET images, the BAPL scores were lower in our study population as compared to the non-MoCo PET images (1.62±0.96 vs. 1.77±1.01, p<0.001). In 1/13 patients, binary visual diagnosis changed from amyloid-positive to -negative via MoCo. MoCo led to an increase of image quality as compared to that of the non-MoCo data (4.38±0.51 vs. 4.00±0.82, p<0.05). The Cohen's d effect sizes for the regional SUVRs between the patients visually score amyloid-positive vs. -negative were higher for the MoCo images as compared to the non-MoCo images in 52/90 VOIs. Analyses of a potential association between the individual degree of head movement and the individual degree of PET signal/diagnosis change are ongoing. **Conclusion:** These preliminary results might point to a diagnostic benefit of MoCo in hybrid amyloid PET/MR imaging. This might be the case for both visual (special relevance for primary diagnosis) and semi-quantitative (special relevance for longitudinal assessments) [18F]Florbetaben PET data. Regardless, these early data encourage investigating more patients employing this technique. **References:** [1] Schütz, Lobsien, Fritzsch et al. Feasibility and acceptance of simultaneous amyloid PET/MRI. Eur J Nucl Med Mol Imaging 2016;43:2236-2243; [2] Catana, Benner, van der Kouwe et al. MRI-assisted PET motion correction for neurologic studies in an integrated MR-PET scanner. J Nucl Med 2011;52:154-161.

EP-0063

(99m)Tc-TRODAT-1 SPECT and (18)F-FDOPA PET in clinically suspected Parkinson's disease

***V. Baghel**, M. Tripathi, N. Damle, H. Goyal, P. Kumar, A. Sharma, C. Bal;*
All India Institute of Medical Sciences, New Delhi, INDIA.

Aim/Introduction: The current study aimed to assess the correlation between dopamine transporter imaging (DAT) using Tc-99m-TRODAT-1 SPECT/CT (TTDS) and FDOPA PET/CT in patients with clinically suspected Parkinson's disease (PD). The usual protocol followed in our department is to do TTDS to confirm presynaptic dopaminergic dysfunction (PSDD) in patients referred with parkinsonism. This is followed by FDOPA PET/CT in those cases where the reporting physician was not confident in reporting the TTDS and further correlation was felt useful. **Materials and Methods:** We undertook this retrospective review in 32 patients with clinical suspicion of PD who underwent both 99m Tc-TRODAT-1 SPECT/CT scan and (18)F-FDOPA PET/CT scan in our department between 2014-2018. SPECT images were acquired 4hrs after intravenous injection of 20-25 mCi of Tc-99m TRODAT, followed by CT acquisition on Symbia T6 dual head gamma camera (Siemens). Brain PET images, 3D emission scans of 15 minutes, were acquired 60 min after injection of 5 mCi of FDOPA intravenously on a Biograph mCT (Siemens) PET/CT scanner. Both scans were visually interpreted, SPECT scans before the PET scans and each independent of the other. Consensus was sought where interpretations differed. All the patients were telephonically interviewed to assess clinical outcome and treatment at a follow up that ranged from 6 months to four years. **Results:** A concordant result between TTDS and FDOPA PET/CT was obtained in 27/32 patients (84%). 24 of these patients (89%) with concordance on both modalities concurred with the clinical diagnosis and this included 17 patients with PD and 7 with non-neurodegenerative parkinsonism. In the remaining three patients (11%) the imaging diagnosis did not concur with the clinical follow-up. Discordant results were seen in 5/32 patients (16%). Of these in 2 cases (6.3%), the SPECT results concurred with the clinical follow-up while in the other 3 cases (9.3%), PET correlated better with the clinical follow up. **Conclusion:** Concordance of TTDS and FDOPA PET/CT with each other and the clinical diagnosis is good so TTDS as a single investigation is useful to evaluate PSDD that characterises PD. When the two modalities are discordant FDOPA PET correlates better with the clinical outcome. **References:** None.

EP-0064

Diagnostic and prognostic value of FDG-PET in AD patients with behavioural and psychological symptoms: is there a specific hypometabolic pattern?

***V. Berti**, C. Ferrari, P. Cappelletto, G. Puccini, C. Polito, G. Lombardi, G. Lucidi, M. De Cristofaro, A. Passeri, S. Sorbi, R. Sciagrà;*
University of Florence, Florence, ITALY.

Aim/Introduction: Behavioural and psychological symptoms in dementia (BPSD) represent a heterogeneous group of non-cognitive symptoms and behaviours that could occur in patients with Alzheimer's disease (AD), reducing the quality of life. This cross-sectional study investigated the relationships between BPSD in AD patients and cerebral metabolic activity as measured by FDG-PET. Our aim is to find a specific pattern of hypometabolism in AD patients with BPSD and in patients at risk of developing them, in order to use it as a prognostic factor. **Materials and Methods:** Sixty patients with AD diagnosis and brain FDG-PET were included in this study. Among them, 29 subjects were not affected by BPSD (AD-noBPSD), 17 presented BPSD (in the form of phsycosis, AD-BPSD) and 14 did not present BPSD but developed them (psychosis) after 1 year or more (AD-developer).FDG-PET scans of the 3 groups were compared with FDG-PET of 50 controls, and with each other using SPM software and multivariate ANOVA routine. Nuisance variables were age in the first analysis, and age and MMSE in the second analysis. **Results:** As compared to controls, all AD patients showed the typical AD pattern, with significant hypometabolism in bilateral posterior cingulate cortex (PCC) and precuneus, bilateral medial temporal and parieto-temporal cortices. The hypometabolic

pattern in AD-noBPSD involved mostly PCC and precuneus bilaterally, and left inferior parietal lobule and hippocampus. In AD-BPSD, the hypometabolic pattern involved also superior, middle and inferior temporal gyri bilaterally, in addition to bilateral PCC/precuneus. In AD-developer, the hypometabolic pattern involved PCC bilaterally, left parahippocampal gyrus and superior temporal gyrus bilaterally. AD-BPSD showed significant hypometabolism in right middle and superior temporal gyri as compared to AD-noBPSD, and only in middle temporal gyrus as compared to AD-developer. AD-developer showed significant hypometabolism in bilateral superior temporal gyrus as compared to AD-noBPSD. No other clusters of significant hypometabolism were found. **Conclusion:** Our results suggest a possible role of lateral temporal cortex, especially of the right hemisphere, in the development of BPSD in AD.The hypometabolic pattern specific of AD-BPSD patients is characterized by a widespread lateral temporal involvement. Besides, our results could suggest a possible role of superior temporal hypometabolism as a prognostic signature of future BPSD development, and an association of the progression of hypometabolism to more anterior temporal regions of the right hemisphere with the development of BPSD. **References:** None.

EP-0065

Relationships between neuropsychological assessment and cortical/subcortical [18F] FDG uptake in patients with Alzheimer's disease

***A. Chiaravalloti**, D. Di Biagio, A. Martorana, O. Schillaci;*
Department of Biomedicine and Prevention, University Tor Vergata, Rome, ITALY.

Aim/Introduction: The aim of the present study was to investigate the relationships between cortical and subcortical [18]F FDG uptake and neuropschological assessment in a cohort of subjects with Alzheimer's disease (AD). **Materials and Methods:** We evaluated 116 subjects with clinical diagnosis of AD (males=66;females=50) with a newly diagnosed with AD according to the NINCDS-ADRDA criteria. Mean age was 71,4±6 years old. All the subjects underwent a brain PET/CT scan using [18F]FDG, a complete neuropsychological assessment that included Mini Mental State Examination (MMSE); Rey Auditory Verbal Learning Test, immediate recall (RAVLT immediate); Rey Auditory Verbal Learning Test, delayed recall (RAVLT,delayed); Rey Complex Figure Test, copy (RCFT, copy); Rey Complex Figure Test, delayed recall (RCFT, delayed); Raven's Colored Progressive Matrices (RCPM); Phonological Word Fluency Test (PWF) and Stroop test. All the subjects were subjected to a cerebro spinal fluid (CSF) assay for amyloid, total tau and phopshorylated tau. The relationship between brain uptake of [18F] FDG and CSF biomarkers was analysed using statistical parametric mapping (SPM12; Wellcome Department of Cognitive Neurology, London, UK) implemented in Matlab R2018a using sex and age and CSF biomarkers as covariates. **Results:** The values of CSF amyloid, total tau and phosphorylated tau were respectively 363,6±162, 689±338,1 and 92,4±70,7. Neuropsychological assessment resulted in 22,6±8,6 for RAVLT, immediate; 71,4±5,9 for RAVLT, delayed;18,2±10,4 for RCFT, copy; 7,6±6 for RCFT, delayed; 18,8±9 (RCPM); 22,2±10,1 for PWF and 44,6±36,2 for Stroop test. We found a significant relationship between [18F]FDG uptake and performance in RAVLT immediate in a large portion of the left temporal lobe [positive correlation, Brodmann Area (BA)37 and BA22) and with RCFT, copy (positive correlation in left and right BA40 and left and right BA7). We did not find any significant relationships with other tests. **Conclusion:** The results of our study show that cortical and subcortical glucose consumption is moderately related to the neuropsychological assessment in patients with AD thus suggesting a limited impact on data analysis of brain metabolism in these subjects. **References:** None.

EP-0066

123I FP-CIT Image Characteristics in Parkinson's Disease and Lewy Body Dementia

***A. Nicol**[1], A. Spratt[2], R. Jampana[3], D. Grosset[3], E. Jackson[2], M. Sheridan[2];*
[1]Queen Elizabeth University Hospital, Glasgow, UNITED KINGDOM, [2]NHSGGC, Glasgow, UNITED KINGDOM, [3]INS, Queen Elizabeth University Hospital, Glasgow, UNITED KINGDOM.

Aim/Introduction: ^{123}I FP-CIT imaging of striatal dopaminergic neuron terminals is used in the diagnostic pathway of Parkinson's Disease (PD) and Lewy Body dementia (DLB). ^{123}I FP-CIT scans of a series of consecutive patients with PD or DLB who had ^{123}I FP-CIT imaging in their diagnostic phase were assessed. The frequency and characteristics of the patterns of ^{123}I FP-CIT uptake were determined. **Materials and Methods:** Patients were followed up clinically and PD or DLB subsequently confirmed. Clinical follow up was also performed on a group of subjects subsequently determined to have neither PD nor DLB. The ^{123}I FP-CIT scan appearances were assessed visually (normal, anterior-posterior gradient or balanced loss) and frequencies compared for the PD and DLB groups. Putamen-caudate ratios were calculated for the scans classified as normal, anterior-posterior gradient and balanced loss. **Results:** Subjects with PD (n=19, 14 M, 5 F, mean age 69 (SD 9.3)) had an anterior-posterior gradient pattern in 95% of cases, with the remaining scan a balanced loss. Subjects with DLB (n=13, 9 M, 4 F, mean age 77 (5.5)) had an anterior-posterior gradient in 46% of cases and a balanced loss in 54% of cases. The frequency of scan patterns was different for the PD and DLB groups (chi squared test of homogeneity, $p<0.01$). All the subjects subsequently determined to have neither PD nor DLB (n=22) had a normal ^{123}I FP-CIT scan. The putamen-caudate ratios of the striata in the normal (n=44, mean 0.94, SD 0.07), anterior-posterior gradient (n=48, mean 0.75, SD 0.10) and balanced loss (n=16, mean 0.87, SD 0.08) groups were significantly different (ANOVA, $p<0.01$). **Conclusion:** The frequency of ^{123}I FP-CIT scan patterns differs between PD and DLB. Knowledge of the prevalence of patterns of dopaminergic loss is critically important when clinically evaluating scans. **References:** None.

EP-0067

Usefulness Of Both 18F-FDG And Amyloid PET/CT In Patients With Cognitive Impairment: Is It Always Necessary To Perform Both Of Them?

M. Martínez de Bourio Allona[1], *L. Rodriguez-Bel*[1], *J. Mora-Salvadó*[1], *R. Reñé-Ramírez*[2], *J. Gascón-Bayarri*[2], *J. Campdelacreu-Fumado*[2], *J. Robles-Barba*[1], *L. Gràcia-Sánchez*[1], *C. Gámez-Cenzano*[1];

[1]*Department of Nuclear Medicine-PET (IDI). Hospital Universitari de Bellvitge-IDIBELL, L´Hospitalet de Llobregat (Barcelona), SPAIN,* [2]*Department of Neurology. Hospital Universitari de Bellvitge-IDIBELL, L´Hospitalet de Llobregat (Barcelona), SPAIN.*

Aim/Introduction: The aim of our study was to analyze the utility of performing both 18F-FDG and amyloid positron emission tomography (PET/CT) in patients with cognitive impairment in order to contribute to the final diagnosis. **Materials and Methods:** We performed a retrospective study of 43 patients with cognitive impairment (mean age: 70 years old; 21 men) who had undergone both 18F-FDG and amyloid PET/CT. 18F-FDG PET/CT was considered abnormal when pathological cortical and/or subcortical hypometabolism was seen supported by the semiquantitative analysis. The amyloid PET was considered positive or negative using the visual and quantitative analysis (Z-scores). **Results:** Out of the total patients studied, 70% (30/43) had an abnormal FDG-PET/CT. In 30% (9/30) of these, the FDG-PET/CT results were Alzheimer's disease (AD) versus Dementia with Lewy Bodies (DLB). Amyloid PET/CT was positive, with a diffuse pattern, in all of them, confirming AD in most of them. In 27% (8/30) of the cases, the FDG pattern was suggestive of frontotemporal dementia (FTD) versus atypical AD. Amyloid PET/CT was positive, confirming atypical AD, in 6 of them and negative in the remaining cases suggesting FTD and other causes (multifactorial, vascular…). In 7% (2/30) of the patients, the FDG-PET/CT differential diagnosis was corticobasal degeneration (CBD) versus AD: one had a positive amyloid PET/CT and was finally diagnosed of CBD related to AD. In the remaining 11 cases (36%) the FDG pattern was non-specific: one with findings suggestive of vascular disease supported by a negative amyloid study and the others (10/11) with low intensity FDG hipometabolism, 6 of them with a negative amyloid PET/CT and the others with a positive amyloid scan (diagnosed of early stage AD and mixed diseases). FDG-PET/CT was considered normal in 30% of the patients (13/43). Amyloid PET/CT was positive in 54% of these (7/13) and negative in the remaining cases, excluding AD. In the positive cases: 4 were finally diagnosed of early stage AD, 1 of mixed dementia and 2 had uncertain results. **Conclusion:** The use of amyloid PET/CT could be avoided if the symptoms, cognitive functioning examination and FDG-PET/CT are very suggestive of Alzheimer's disease. Nevertheless, in patients with similar or uncertain FDG pattern, it could be useful for making the differential diagnosis between AD and other diseases. In the negative FDG cases, more than 50% had a positive amyloid scan which means the importance of performing the amyloid study in these patients. **References:** None.

EP-0068

Regional brain metabolism assessed by ^{18}F-FDG PET/CT in patients with amnestic mild cognitive impairment: evolutive changes and comparison with ^{11}C-PIB PET/CT

J. F. Jimenez-Bonilla[1], *M. De Arcocha-Torres*[2], *R. Quirce*[2], *I. Martínez-Rodríguez*[2], *A. Pozueta*[3], *E. Rodríguez-Rodríguez*[3], *P. Sánchez-Juan*[3], *A. Sánchez-Salmón*[2], *F. Gómez-de la Fuente*[2], *I. Banzo*[2];

[1]*Nuclear Medicine Service, Marqués de Valdecilla Universitary Hospital, Molecular Imaging Group-IDIVAL, University of Cantabria, Santander, SPAIN,* [2]*Nuclear Medicine Service, Marqués de Valdecilla Universitary Hospital, Molecular Imaging Group-IDIVAL, University of Cantabria, Santander, SPAIN,* [3]*Neurology Service, Marqués de Valdecilla Universitary Hospital, Santander, SPAIN.*

Aim/Introduction: The purpose of this work was the evaluation of the regional brain metabolic pattern in patients with amnestic mild cognitive impairment (a-MCI) assessed by 18F-FDG PET/CT at initial diagnosis and at 5-year outcome, and its correlation with clinical evolution and 11C-PIB PET/CT scan. **Materials and Methods:** The study included 17 a-MCI patients (7 men; mean age: 67 years) who had ^{18}F-FDG and ^{11}C-PIB PET/CT scans at initial diagnosis and 5 years later. All patients were clinically re-evaluated at five years. A visual analysis of scans was performed by 2 experienced nuclear medicine specialists. The following cerebral areas were evaluated: cerebellum, temporo-parietal (TP), occipital, frontal, anterior and posterior cingulated, and basal ganglia. Brain ^{18}F-FDG PET/CT distribution was reported as normal or abnormal. Degrees of glucose hypometabolism were mild, moderate or severe. ^{11}C-PIB PET/CT cerebral retention was considered positive or negative. Sensitivity, specificity, positive predictive value (PPV) and negative predictive value (NPV) for Alzheimer's disease dementia (AD-D) were calculated considering TP hypometabolism as the key finding for ^{18}F-FDG PET/CT exam. **Results:** Thirteen out of 17 a-MCI patients evolved to AD-D and 4 out of 17 a-MCI patients did not. In the group of 13 patients who developed AD-D, visual analysis showed abnormal glucose distribution in 8 (unilateral TP hypometabolism in 6 and bilateral TP hypometabolism in 2). Two patients had also frontal hypometabolism. All 13 patients had positive ^{11}C-PIB PET/CT scans. In the group of 4 patients who did not evolved to AD-D, ^{18}F-FDG PET/CT was abnormal in 2 and normal in 2. In these 4 patients, PIB scan was positive in 1 and negative in 3. At 5-year, ^{18}F-FDG PET/CT showed more extensive glucose hypometabolism in all patients with initial abnormal scan. Moreover, ^{18}F-FDG PET/CT showed severe TP hypometabolism in 3 patients with initial normal scan. From these results, ^{18}F-FDG PET/CT has a sensitivity 66.6%, specificity 50%, PPV 90% and NPV 16.6% for diagnosing AD-D. On the other side, ^{11}C-PIB PET/CT had a sensitivity 100%, specificity 66%, PPV 92.8% and NPV 100%. **Conclusion:** ^{18}F-FDG PET/CT correctly predicted the type of dementia being TP hypometabolism the most frequent abnormality at initial diagnosis and linked to evolutive changes of the brain glucose metabolism pattern. The association of ^{18}F-FDG with amyloid ^{11}C-PIB PET/CT may improve the diagnostic yield for AD-D. **References:** None.

EP-0069

Imaging and CSF biomarkers for cognitive impairment

M. Agudelo, J. Bernal, B. Martinez-Sanchis, P. Sopena-Novales, A. Yepes-Agudelo, A. Utrera-Costero, P. Bello-Arques;
Hospital Universitario y Politecnico La Fe, Valencia, SPAIN.

Aim/Introduction: The diagnosis of Alzheimer's disease (AD) is based on postmortem anatomopathological findings. Currently a probable diagnosis of AD in vivo could be suggested based on biomarkers and clinical findings (IWG-2 criteria). Our aim is to assess the sensitivity and specificity of two biomarkers (Amyloid-PET and cerebrospinal fluid (CSF) biomarkers) for the detection of AD, taking as a gold standard the final clinical diagnosis in the follow-up by Neurology. Also to estimate the concordance and relationship between the findings on Amyloid-PET and CSF biomarkers **Materials and Methods:** A descriptive, retrospective study was carried out on patients with cognitive impairment referred to our center, who were evaluated with a brain amyloid-PET (18F-florbetapir, 18F-florbetaben or 18F-flutemetamol) and had a lumbar puncture for CSF biomarkers between 01/01/2016 and 03/31/2019. The results of the tests were compared with the final clinical diagnosis in the last available follow-up by Neurology (gold standard), standardized for our analysis as AD or not AD (NAD). We found 61 patients, who were evaluated with brain amyloid-PET. Only 34 patients had CSF analysis and clinical follow-up. The mean age was 68,26 years, 45% of the patients were women. In order to calculate the Kappa coefficient of concordance, sensitivity and specificity, the findings of amyloid-PET were classified as positive or negative for cortical amyloid deposit by visual assessment performed by a nuclear medicine specialist and the CSF markers were classified as positive if Aβ1-42 was decreased and at least one Tau marker was elevated according to reference values of our laboratory (otherwise negative). **Results:** The amyloid-PET showed a sensitivity of 100%, specificity of 83,3%, with 2 false positives. The CSF analysis had a sensitivity of 27,3% and specificity of 100%. The weighted Kappa coefficient between amyloid-PET and CSF biomarkers was 0.164 (95% CI). The level of concordance between amyloid-PET and CSF biomarkers was poor, indicating their complementary value in diagnosing AD. **Conclusion:** We found that amyloid-PET has high sensitivity. CSF biomarkers presented high specificity, but lower sensitivity. Low concordance between both biomarkers was found, supporting their combined use as mutually complementary tests in the in vivo diagnostic workup of AD to ensure a better sensitivity and specificity. **References:** None.

EP-0070

Perfusion Correlates Of Apathy In Patients With Alzheimer's Disease. A Brain SPECT Study With Brodmann Areas Mapping

V. Valotassiou[1], N. Sifakis[2], C. Tzavara[1], V. Kamtsadeli[3], G. Angelidis[1], E. Lykou[3], N. Tsinia[3], I. Tsougos[1], D. Psimadas[1], S. Papageorgiou[4], P. Georgoulias[1], J. Papatriantafyllou[3];
[1]Dpt of Nuclear Medicine, University Hospital of Larissa, Larissa, GREECE, [2]Dpt of Nuclear Medicine, "Alexandra" University Hospital, Athens, GREECE, [3]IASIS Third Age Center, Athens, GREECE, [4]2nd University Neurological Dpt., Attikon Hospital, Athens, GREECE.

Aim/Introduction: Apathy is one of the most common neuropsychiatric symptoms in patients with Alzheimer's disease (AD) affecting up to 80% of patients with moderate cognitive impairment. It is characterized by decreased motivation, initiative and interest, resulting in impaired functioning in daily living, early institutionalization and poor outcome of patients, as well as in great caregiver distress. Nevertheless, there is great controversy about its neural underpinnings in the literature and its neurobiological basis remains unclear. The aim of this study was to evaluate perfusion in Brodmann areas (BAs) in AD patients with apathy compared with healthy controls in order to reveal areas associated with this neuropsychiatric symptom. **Materials and Methods:** We studied 65 consecutive patients (20 men, 45 women, age±SD 69.9±8.1 years, duration of disease±SD 3.4±2.4 years, education±SD 9.4±4.7 years) from an outpatient Memory Clinic. We used the established DSM-IV criteria for the diagnosis of dementia and the specific established criteria (NINCDS-ADRDA) for the diagnosis of AD. All the patients had a neuropsychological evaluation with a battery of tests including the mini-mental state examination (MMSE, mean±SD 19.6±5.5) and the Neuropsychiatric Inventory (NPI, apathy mean±SD score 4±4.2). All the patients underwent a brain SPECT scan 20 min after the intravenous administration of 740MBq of ^{99m}Tc-HMPAO. We applied the NeuroGam™ software on the reconstructed data, for the comparison of brain perfusion in BAs in the right (R) and left (L) hemispheres with the software's normal data base consisted of healthy subjects of the same age. **Results:** Compared with normal subjects, apathy in AD patients was correlated (p=0.05) with hypoperfusion in right anterior prefrontal cortex (BA 10R), dorsolateral prefrontal cortices (BAs 8L, 9LR, 46R), ventral posterior cingulate cortices (BA 23LR), left dorsal anterior cingulate cortex (BA 32L), right entorhinal and perirhinal cortices (BAs 28R, 36R). **Conclusion:** Hypoperfusion of frontal and temporal cortices, as well as cingulated cortex may be the underlying neural correlates of apathy in AD patients. Functional nuclear imaging may contribute significantly to the understanding of the causative mechanisms and the improvement of patients' management. **References:** 1. Theleritis C, Politis A, Siarkos K, Lyketsos CG. A review of neuroimaging findings of apathy in Alzheimer's disease. Int Psychogeriatr. 2014;26(2):195-207 2. Rosenberg PB, Nowrangi MA, Lyketsos CG. Neuropsychiatric symptoms in Alzheimer's disease: What might be associated brain circuits? Mol Aspects Med. 2015;43-44:25-37.

EP-0071

Assessing the Effect of Noise on the Semi-Quantitative Analysis of Striatal Dopamine Transporter Imaging

E. Hesketh, P. Hillel, S. Redgate, J. Taylor;
Medical Imaging and Medical Physics, Sheffield, UNITED KINGDOM.

Aim/Introduction: There is conflicting guidance on the minimum required total counts for optimal SPECT imaging of ^{123}I-Ioflupane. The DaTSCAN (GE Healthcare) summary of product characteristics states 0.5million, SNM guidelines (SNM, 2012) recommend >1.5million, and EANM guidelines (EANM, 2009) state >3million. The local average is 1.7±0.54million. A combination of phantom and patient images were utilised to determine the required minimum total counts in order to avoid noise artefacts adversely affecting semi-quantitative results. **Materials and Methods:** A novel anthropomorphic 3D-printed phantom (J Taylor et al, 2018) was assembled with layers of radioactive ink patterns on paper, representing a realistic normal DaTSCAN.The phantom was scanned 8 times on a standard gamma camera (Discovery 670, GE Healthcare) using the clinical protocol but with 15seconds per projection. Images were summed together to simulate scans with 30, 45, 60, and 120seconds per projection. A normal patient scan with 3.4million counts was resampled using Poisson resampling software on an Xeleris workstation (GE Healthcare) to simulate images with 3, 2, 1.5, 1, and 0.5million total counts. Three resampled scans were produced with 3, 2, and 1.5million counts each. Ten resampled scans were produced with 1 and 0.5million counts. All scans were processed using in-house semi-quantitative software to calculate specific binding ratios, caudate-putamen ratios, and left/right symmetry parameters. Results were compared against locally-derived normal ranges. **Results:** Phantom Acquisitions: Total counts per scan for the 15 seconds per projection datasets were ~0.64 million counts per scan; 30 seconds- 1.27 million, 45 seconds- 1.9 million, 60 seconds- 2.56 million, and 120 seconds- 5.1 million. Of the eight 15seconds per projection scans, five (62.5%) had one or more quantitative parameters outside the normal range. Of the four 30seconds per projection scans, one (25%) had an abnormal semi-quantitative parameter. Patient scan: 60% of the 0.5million and 30% of the 1million counts scans had one or more abnormal semi-quantitative parameters, consistent with the rate of abnormality seen in the phantom acquisitions. For phantom scans reconstructed to ≥45seconds per projection (≥1.9million counts) and patient resampled scans with ≥1.5million counts, all results were within normal ranges. **Conclusion:** This study has demonstrated that there is the potential for misdiagnosis of ^{123}I-Ioflupane studies due to noise artefacts where the total counts acquired are below 1.5-2million. In order to achieve a consistent level of counts above this minimum, it may be advisable to implement patient-specific projection times based on the count-rate from a short pre-scan acquisition. **References:** None.

EP-0072

Semi-Quantitation in DaTSCAN SPECT: Preliminary Results of a Prospective Comparison of Cadmium Zinc Telluride (CZT) and Sodium Iodide (NaI) Detectors

F. Thiele[1], *J. M. Rogasch*[1], *C. Lange*[1], *W. Schäfer*[2], *J. Eßer*[2], *O. S. Großer*[3], *H. Amthauer*[1];
[1]*Charité – Universitätsmedizin Berlin, Klinik für Nuklearmedizin, Berlin, GERMANY,* [2]*Kliniken Maria Hilf Mönchengladbach, Klinik für Nuklearmedizin, Mönchengladbach, GERMANY,* [3]*Universitätsklinikum Magdeburg A.ö.R., Klinik für Radiologie und Nuklearmedizin, Magdeburg, GERMANY.*

Aim/Introduction: Cadmium zinc telluride (CZT) detectors offer improved sensitivity and noise characteristics over NaI detectors with a potential to reduce activity or acquisition time. This preliminary analysis of a prospective intraindividual comparison of CZT and NaI in dopamine transporter (DaT) SPECT with DaTSCAN™ focused on the potential for acquisition time reduction. **Materials and Methods:** Prospective analysis of 30 patients (20 males; age, 68 [range, 35-83] a) undergoing subsequent SPECT with a CZT and NaI system in a randomized order (GE Discovery NM/CT 670 CZT / Pro). SPECT was acquired for 30s per angular step (3°) after a median of 3.4 (2.6-4.5) h and 4.2 (3.6-4.9) h after injection of 180 (171-191) MBq DaTSCAN. CZT data were reconstructed (100% acquisition time, CZT100). CZT list mode data were used to simulate a shortened scan time (reduction of 25%, 50%, and 75%, CZT75, CZT50, CZT25). Signal-to-background ratios (SBR) and z-scores were automatically calculated for 4 regions (left/right caudate nucleus and putamen) using dedicated software (GE DaTQUANT), including a normal database from the Parkinson's Progression Markers Initiative. NaI represented standard of reference. **Results:** 11/30 patients had reduced putaminal DaT density (NaI z-score < -2). SBR and z-scores were each significantly lower with CZT100 than NaI in 4/4 regions (median SBR / z-score difference, -0.22 / -0.51), CZT75 vs. NaI in 2/4 regions (median, -0.23 / -0.53), CZT50 vs. NaI in 0/4 regions (median, -0.08 / -0.2), and CZT25 vs. NaI in 3/4 regions (median, +0.17 / +0.43; each $p<0.05$). The effect on clinical assessment was evaluated for each region defining a pathologic z-score < -2. Regardless of the CZT acquisition time, CZT and NaI results were discordant in ≥1/4 regions in up to 6 patients. CZT100 determined pathologic putaminal z-scores discordantly to CZT75 and CZT50 in 1/30 patients each. CZT100 and CZT25 were discordant in 3/30 patients. **Conclusion:** In this preliminary study of patients undergoing DaTSCAN SPECT, CZT resulted in systematically lower SBR than NaI which necessitates separate normal databases. Among different CZT acquisition times, high concordance in determination of pathologic putaminal activity may allow for acquisition time reduction of at least 25%. **References:** None.

EP-0073

Periodontal disease and PET amyloid imaging study

E. Triviño Ibáñez[1], *M. Gerez-Muñoz*[2], *M. Rashki*[1], *T. Rudolphi-Solero*[1], *A. González-Jiménez*[1], *J. Gil-Montoya*[2], *M. Gómez-Río*[1];
[1]*Department of Nuclear Medicine, University Hospital Virgen de las Nieves, Granada, SPAIN,* [2]*School of Dentistry, Granada Biohealth Research Institute, Granada, SPAIN.*

Aim/Introduction: Scientific evidence has shown an association between periodontal disease, a peripheral chronic infectious/inflammatory disease, and cognitive impairment, although a causative relationship between dementia and periodontitis has yet to be confirmed. The aim of this study is to determine whether clinical periodontitis is associated with the neuronal amyloid-β accumulation. **Materials and Methods:** We have designed a case-control study with cognitive impairment patients who meets appropriate use criteria (AUC) to perform PET-amyloid scan. Periodontitis disease it has been evaluated by measuring tooth loss, plaque and bleeding indexes, probing depths, and clinical attachment loss (CAL). **Results:** At this moment, the study includes 38 dentate adults (mean age: 62.95±7.2 years, 52.5% men). Amyloid-PET was positive in 22 patients (57.9%) and negative in 16 patients (42.1%). According with CAL, the 60.5% of patients had periodontitis. The percentage of patients with periodontitis who presented a positive result of amyloid PET was higher in comparison with the group of patients without periodontitis (72.7% vs 27.3% respectively), although there is not a significant association. **Conclusion:** Our preliminary results suggest that clinical periodontitis appears to be associated with positive result of amyloid PET, although results are not at the moment statistically significant. **References:** None.

EP-0074

Implementation of amyloid brain PET imaging biomarker in the diagnosis of Alzheimer's disease: our experience in a non-dedicated dementia clinic

P. Garrastachu Zumaran, P. Santos Holgueras, B. Matute Tobias, S. Lopez Álava, C. Albornoz Almada, X. Boulvard Chollet, L. Romero Robles, F. Cañete Sánchez, A. Cabrera Villegas, R. Delgado-Bolton, R. Ramirez Lasanta;
Fundacion Riojasalud. CIBIR, Logroño, Rioja, SPAIN.

Aim/Introduction: Amyloid PET imaging has been established as a biomarker for Alzheimer disease (AD). We analyse our first 22 months experience using amyloid brain PET imaging (AP) in our hospital in patients with mild cognitive impairment (MCI) **Materials and Methods:** We studied patients with MCI and suspicion of AD sent to our Department to undergone AP imaging. Patients underwent an extensive demographic, neurological, neuropsychological assessment (NPA) and brain MRI or CT scans. Some of them had also undergone FDG brain PET scan. AP was categorized as positive or negative by visual analysis using the rules proposed in each of the radiopharmaceutical leaflet.Besides, we analyze the concordance between the results obtained in AP and the FDG-PET scans positive or dubious for AD and the AP and the NPA with amnesic cognitive impairment with hippocampal pattern. **Results:** 92 amyloid PET imaging were performed (50 men, mean age 67(8sd). Of these, 75% had primary studies, 46% previous neurological or psyquiatric disordes, 64% cardiovascular risk factors, 30% family neurodegenerative background and 56% changes in RM/TAC . Amyloid PET imaging was positive in 60 patients (65,22%), confirming the suspected diagnosis of AD. Of these 60, 30 had also undergone FDG PET, and of those 30, 13(14%) had a metabolic pattern compatible with AD, 6 a dubious pattern, 2 a non-EA but neurodegenerative pattern and 3 had no significant hypometabolism. The kappa index between AP and the group of patients with definitive and dubious FDG-PET was 0,05 CI (-0,38- 0,5). The 92% of the patients with AP positive who were studied with NPA had a amnesic cognitive impairment with hippocampal pattern. Kappa index (0,14 ci -0.1-0.4).The 13% of the AP positive patients were included in pharmacological assays. PET amiloid imaging helped to decide to initiate pharmacological and cognitive stimulation in 52 and 43.7% respectively. Of the 32 AP negative patients, 17 had clinical and NPA suspition of AD. Follow up will confirm final diagnosis. **Conclusion:** PET amyloid was a useful biomarker to confirm the suspected diagnosis of AD in our daily clinical practice and allowed the prompt instauration of pharmacological treatment and cognitive stimulation. **References:** None.

EP-0075

A pilot study to assess the feasibility of utilising a dedicated cardiac gamma camera based on pin-hole collimated solid state detectors for Striatal Dopamine transporter imaging of the brain (DaTscan)

P. Hillel, S. Redgate, E. Lorenz, G. Armitage, J. Taylor, C. Romanowski, J. Himsworth, S. Wiles;
Sheffield Teaching Hospitals NHS Foundation Trust, Sheffield, UNITED KINGDOM.

Aim/Introduction: The GE Discovery NM 530c (D530c) is a dedicated cardiac camera utilising Cadmium-zinc-telluride (CZT) detectors to achieve high sensitivity, high spatial resolution SPECT images in a 19cm field of view. The study assesses its use for ^{123}I-Ioflupane imaging. **Materials and Methods:** Imaging of an anthropomorphic head phantom with fillable striatal inserts was employed to assess feasibility and determine the optimal head/scanner orientation and acquisition/reconstruction parameters. A pilot study was then performed on 20 patients being investigated for Parkinson's disease or Lewy Body Dementia (17 PD, 3 LBD; Age range 37 - 90y). Following administration of 185MBq ^{123}I-Ioflupane, patients were scanned on a standard dual-headed gamma camera directly before the D530c with acquisition times of 33min and 10min respectively. Patients completed a questionnaire to score for comfort/claustrophobia (1-5) following each scan and all images were blindly reported by four experienced reporters. **Results:** Optimal head orientation was found with the patient

positioned erect with the detector arc just above their head. This required the patients to be seated on a specially-designed chair with supporting headrest. The shorter acquisition time, lack of camera movement and unobstructed view meant patients generally preferred being scanned on the D530. Half scored this significantly better for comfort/claustrophobia than the standard camera whilst the other half found no significant difference (significance based on the score differing by 2 or more). The D530c generated mostly high quality scans. Blinded reporting revealed diagnostic agreement between scanners in 34/40 striata (85%). In 2/6 discordant cases the diagnosis changed from normal on the standard camera to abnormal on the D530c. In the other 4 cases, reports were equivocal from one of the scanners (the D530c in 3/4 of these cases). In 4/6 discordant cases, patients had a head tremor that resulted in greater head movement during the D530c scan where their head was less supported. **Conclusion:** Using a bespoke chair, patients could be scanned on the GE Discovery NM 530c cardiac camera to obtain high quality ^{123}I-Ioflupane brain scans. Overall, patients found this camera less claustrophobic compared with a traditional camera. Images showed good agreement with those obtained from the standard camera. Discordant cases are thought to be mainly due to greater head movement during the D530c scan as well as possible noise artefacts. Further investigation is warranted using a slightly longer imaging time and a re-designed imaging chair affording greater head stability. **References:** None.

EP-0076

Visual and semiquantitative analysis of regional brain metabolism in patients with amnestic mild cognitive impairment assessed by ^{18}F-FDG PET/CT: prognostic value after 5 years of evolution

J. F. Jimenez-Bonilla[1], *R. Quirce*[1], *M. De Arcocha-Torres*[1], *I. Martínez-Rodríguez*[1], *S. López-García*[2], *E. Rodríguez-Rodríguez*[2], *P. Sánchez-Juan*[2], *N. Martínez-Amador*[1], *A. Sánchez-Salmón*[1], *F. Gómez-de la Fuente*[1], *I. Banzo*[1];
[1]*Nuclear Medicine Service, Marqués de Valdecilla University Hospital, Molecular Imaging Group-IDIVAL, University of Cantabria, Santander, SPAIN,* [2]*Neurology Service, Marqués de Valdecilla University Hospital, Santander, SPAIN.*

Aim/Introduction: To evaluate the regional brain metabolic pattern in patients with amnestic mild cognitive impairment (a-MCI) assessed by 18F-FDG PET/CT and to correlate it with clinical evolution. **Materials and Methods:** Sixteen a-MCI patients (7 men; mean age: 67 years) and six healthy controls (3 men; mean age: 62 years) underwent 18F-FDG PET/CT after 30 minutes of i.v. injection of 185 MBq 18F-FDG and clinically re-evaluated five years later. Cerebellum, temporo-parietal, occipital, frontal, anterior and posterior cingulate areas and basal ganglia were visual and semi-quantitatively analyzed. Using the cerebellum as reference region, SUV ratios (SUVr) for each region were calculated in patients and controls. Mean of SUVr (mean SUVr) in regions was obtained in the control group. The normal range values of brain metabolism for each region was considered as the mean SUVr + 2 SD obtained in the control group. For semiquantitative analysis, the SUVr of each region in each a-MCI patient was compared to the normal range values previously established in the control group. Sensitivity, specificity and predictive positive value for Alzheimer's disease dementia (AD-D) were calculated considering temporo-parietal hypometabolism as key finding for visual and semiquantitative analysis and then, both were compared. **Results:** Thirteen a-MCI patients evolved to AD-D and 3 a-MCI patients did not (1 remained as A-MCI, 1 was diagnosed as normal pressure hydrocephallus and 1 as vascular a-MCI). All controls remained healthy after 5-year evolution. In the a-MCI who evolved to AD-D (n=13), visual analysis showed abnormalities in 8/13 (unilateral TP hypometabolism in 6 and bilateral TP hypometabolism in 2; moreover 2 patients associated a frontal hypometabolism). The semiquantitative analysis in those patients showed TP hypometabolism in 10/13 (unilateral TP hypometabolism in 5, bilateral TP hypometabolism in 5; moreover, frontal hypometabolism in 12/13; posterior cingulate hypometabolism in 4 and occipital hypometabolism in 5). In the a-MCI who did not evolved to AD-D (n=3), visual analysis did not show any abnormality and semiquantitative analysis showed unilateral TP hypometabolism in 1, and frontal hypometabolism in 2/3. Sensitivity, specificity and PPV of ^{18}F-FDG PET/CT to diagnose AD-D were 61.5%, 66% and 88% for visual analysis and 76.9%, 33.3% and 83% for semiquantitative analysis. **Conclusion:** ^{18}F-FDG PET/CT showed a limited prognostic value for AD-D in a-MCI patients. Visual and semiquantitative analysis provided similar PPV. The meaning of frontal, posterior cingulate and occipital abnormalities deserves deeper studies. A combination with amyloid PET/CT may be desirable for this purpose. **References:** None.

EP-0077

Changes of Cerebral Glucose Metabolism in Semantic Dementia: a ^{18}F-FDG PET Study

J. Lu[1], *K. Chen*[2], *J. Ge*[1], *Y. Zhu*[1], *J. Xiao*[1], *C. Zuo*[1], *Q. Guo*[3], *P. Wu*[1];
[1]*PET Center, Huashan Hospital, Fudan University, Shanghai, CHINA,* [2]*Department of Neurology, Huashan Hospital, Fudan University, Shanghai, CHINA,* [3]*Department of Geriatrics, Sixth People's Hospital, Shanghai Jiao Tong University, Shanghai, CHINA.*

Aim/Introduction: Semantic dementia (SD), characterized by progressive loss of semantic knowledge and relative preservation of grammatical aspects of language and episodic memory, is part of the disease spectrum of frontotemporal lobar degeneration (FTLD). MRI is the most widely used method to detect the characteristic anterior temporal lobe atrophy. Glucose metabolism of SD was seldom explored. This study aimed to investigate whether there were distinctive metabolic changes in SD patients using ^{18}F-FDG PET imaging. **Materials and Methods:** 15 SD (5 with predominance of right and 10 with predominance of left temporal atrophy) and 15 age-/gender-matched normal controls were enrolled. All subjects underwent

^{18}F-FDG PET and structural T1 MRI within 3 months in Huashan hospital, Shanghai, China. SPM 8 software implemented in Matlab8.4 was used for analysis. Scans with atrophy mainly located in the right hemisphere were flipped so that all patients had the left hemisphere of the brain as the major affected side. Each PET image was co-registered to individual structural T1 MRI and anatomically normalized into MNI152 standard space using DARTEL, and then smoothed. FDG Two-sample t test model was used to explore the regional metabolic differences between two groups. Voxel threshold was set at $P < 0.001$ (uncorrected). Clusters were also searched at FWE-corrected $P < 0.05$ level. A 4-mm radius spherical value of interest (VOI) was used to calculated the regional cerebral metabolic rate of glucose (rCMRglc) with ScanVP 7.1software. **Results:** Compared to normal controls, SD patients showed decreased glucose metabolism in left temporal lobe (BA 21) and bilateral parahippocampal gyrus while increased in bilateral frontal lobe (BA 4,6,9), bilateral parietal lobe (BA 3), bilateral occipital lobe (BA 18) and right cerebellum($P<0.001$, uncorrected). Left temporal lobe (BA 21), left parahippocampal gyrus, right frontal lobe (BA 6), right parietal lobe (BA 3), bilateral occipital lobe (BA18) and right cerebellum were survived at FWE $P<0.05$. As for rCMRglc, right parahippocampal gyrus and the regions survived at FEW $P<0.05$ except right occipital lobe (BA 18) showed significant differences ($P<0.05$, student t-test) between two groups, while differences in the rest regions were insignificant($P>0.05$, student t-test). **Conclusion:** Our study showed that SD patients had distinctive metabolic characteristics. ^{18}F-FDG PET might offer help in differential diagnosis of SD and other variants of FTLD, and even probable Alzheimer's disease. It may provide a new perspective for understanding brain regions involved in lexical and semantic processing. Future studies were needed to verify these observations. **References:** None.

EP-0078

Are there limitations in reporting brain PET for suspected neurodegenerative dementia in diabetic patients?

K. Mullin;
Belfast Health and Social Care Trust, Belfast, UNITED KINGDOM.

Aim/Introduction: Interpretation of 18F FDG PET CT brain in patients with suspected neurodegenerative dementia relies on the patterns of hypometabolism in the brain. In our institution we noted patterns of global hypometabolism, many of which appeared to be associated with diabetic patients, therefore we undertook a retrospective analysis to review these studies and identify any emerging trends. **Materials and Methods:** We conducted a review of all 18F FDG PET CT brain performed over a six month period. Diabetic patients and those patients reported with 'global hypometabolism' were evaluated further and information was obtained, including diabetic treatment, blood glucose level at the time of scanning and any further relevant clinical history. We compared findings from visual interpretation alongside computer assisted diagnostic software. **Results:** 152 PET brain scans were performed over a 6 month period. 16 Diabetic patients were identified. Of these 16, 6 had an abnormal study and 10 were considered negative for the presence of a neurodegenerative dementia. Of the 152 patients, global hypometabolism was reported in 7 patients, 5 of which were diabetic. **Conclusion:** There is an increased prevalence of global hypometabolism in diabetic patients, despite a normal blood glucose at the time of scanning. This can prove to be challenging and mask the characteristic patterns of hypometabolism that support the presence of an intrinsic neurodegenerative dementia. **References:** None.

EP-0079

Amyloid PET/CT for the diagnosis of Alzheimer's disease dementia and other dementias in patients with cognitive impairment and its relationship with cognitive functioning

L. Rodriguez-Bel[1,2]*, M. Martínez de Bourio-Allona*[1,3]*, J. Mora-Salvadó*[1,2]*, I. Rico-Pons*[4,2]*, R. Reñé-Ramírez*[5,2]*, J. Gascón-Bayarri*[5,2]*, E. Llinares-Tello*[1,2]*, I. Sánchez-Rodríguez*[1,2]*, J. Vercher-Conejero*[1,2]*, C. Gámez-Cenzano*[1,2]*;*
[1]*PET-Unit. Department of Nuclear Medicine, L'Hospitalet De Llobregat. Barcelona, SPAIN,* [2]*Hospital Universitari de Bellvitge-IDIBELL, Barcelona, SPAIN,* [3]*Hospital Univertario de Bellvitge-IDIBELL, Barcelona, SPAIN,* [4]*Department of Neurology, L'Hospitalet De Llobregat. Barcelona, SPAIN,* [5]*Department of Neurology, L'Hospitalet De Llobregat. Barcelona, SPAIN.*

Aim/Introduction: Diagnosis of Alzheimer's disease (AD) combines clinical criteria with biological markers. This study aimed to investigate the usefulness of amyloid positron emission tomography (PET) in the diagnosis of patients with cognitive impairment and its relationship with cognitive functioning. **Materials and Methods:** Eighty subjects were enrolled in the study (mean age: 69 years; range: 54-79y), including 58 Mild cognitive impairment (MCI), 11 dementia due to AD, 8 Atypical AD versus frontotemporal Dementia (FTD) and 3 possible non-AD dementia patients. They underwent ^{18}F-Flutemetamol PET/CT and an extensive cognitive functioning (MMSE and the Neuropsychological examination). The amyloid PET were dichotomized as positive or negative based on the visual PET reading and using a quantitative analysis (Z-scores). **Results:** Amyloid PET was positive in 50% of patients, mostly of them presenting a clinical MCI (amnestic subtype). The final clinical diagnosis according positive amyloid PETand additional clinical workup,was suggestive for dementia highly likely due to AD in 67,5 %, MCI due to AD with high likelihood in 30%, and Lewy Body Dementia in 2,5% of patients. In the dementia AD group, 63% of patients presented typical-AD, 22,2% atypical-AD and 14,8% mixed forms. Atypical variants of AD included: aphasic variants of AD , posterior cortical atrophy (PCA) and corticobasal syndrome underlying AD (CBS-AD). Positive amyloid PET studies showed a diffuse pattern and there were no differences in the distribution and intensity of amyloid deposition between different diagnostic groups. Mean MMSE was 21,8 (range 10-28) and the Neuropsychological examination showed a moderate or severe cognitive impairment in 67% of patients with a

Global Deficit Score (GDS: 4-5). In the negative amyloid group, the exclusion of AD diagnosis as a possible cause of cognitive impairment was made. Mean MMSE was 25,9 (range 14-30) and the neuropsychological examination showed a mild cognitive impairment in 66% of patients (GDS: 3). **Conclusion:** The use of amyloid PET was associated with improved diagnostic confidence, change in diagnosis and change in patient management in a majority of patients with MCI and patients with dementia. The most frequent change in clinical management involved the use of Alzheimer disease drugs. Amyloid PET was useful for discriminate AD dementia from non-AD dementia such as frontotemporal dementia. Nevertheless, the pattern of amyloid deposition was not useful for discriminate MCI due to AD from typical or atypical forms of AD. Neuropsychological examination was closed related to amyloid PET results and was helpful in the final diagnosis. **References:** None.

EP-0080

Brain ^{18}F-FDG PET qualitative and quantitative analyses in Atypical Parkinsonian Syndromes (APS) with Cognitive Clinical Symptoms (CCS)

S. F. Nuvoli[1], *M. R. Piras*[2], *G. Tanda*[1], *A. Lazzarato*[1], *A. Spanu*[1], *G. Madeddu*[1];
[1]*University of Sassari, Unit of Nuclear Medicine, Sassari, ITALY,*
[2]*University of Sassari, Unit of Neurology, Sassari, ITALY.*

Aim/Introduction: APS diagnosis is generally based on clinical criteria but often symptoms and signs may overlap in the different forms and particularly when cognitive disorders are present. Recent data suggest that brain ^{18}F-FDG PET could support clinical diagnosis since specific metabolic patterns are described.We further evaluated ^{18}F-FDG PET clinical usefulness in the diagnosis of CCS in APS patients. **Materials and Methods:** We investigated 18 consecutive patients with clinical symptoms attributable to APS already also ascertained with ^{123}I Ioflupane SPECT; moreover, each of these also referred slight to severe CCS. In particular, according to clinical and SPECT data, patients were classified in different groups:12/18 with evident signs of extrapyramidal disorders (Group 1), 2 with suspected corticobasal degeneration (CBD) Group 2), 2 with movement disorders and suspected behavior disorders (Group 3), and one of the remaining 2 cases had a suspect Lewy bodies dementia (LBD) with visual hallucinations and the other one a multisystem atrophy (MSA) with ideomotor slowdown (Group 4). All patients underwent brain ^{18}F-FDG PET/CT using GE Discovery tomograph. Images were evaluated both qualitatively and quantitatively with automated analysis program (Cortex Suite, GE Healthcare); brain metabolic map and normal age matched control group comparative analysis was produced. **Results:** ^{18}F-FDG PET showed different bilateral cortical hypometabolism patterns in the different groups. Group 1: 9/12 cases had reduced ^{18}FDG uptake in prefrontal and temporo-parietal areas attributable to Alzheimer Disease (AD), while the remaining 3/12 cases had normal metabolism despite CCS. Group 2: prefrontal and superior parietal hypometabolism in one case and temporo-mesial, temporo-lateral and cerebellum reduced uptake in the other, thus confirming CBD clinical suspect. Group 3: frontal and prefrontal hypometabolism in one case and temporo-parietal in the remaining one possibly attributable to AD in discordance with clinical symptoms (balance disturbance, ideomotor slowing with frontal aspects). Group 4: temporo-occipital hypometabolism in accordance with initially suspected LBD in one case and prefrontal reduced uptake compatible with CCS in the other case with suspected MSA. **Conclusion:** ^{18}F-FDG PET could be useful in correct CCS classification in APS patients since, in our casuistry although modest, the procedure confirmed the cognitive disorder clinical suspect in 77.7% of patients, while it excluded the presence or suggested an alternative diagnosis in respect of initial clinical classification in 22.3% of cases. According to these data an adequate cognitive disorder treatment has been started and the follow up with clinical and ^{18}F-FDG PET evaluations is currently in progress. **References:** None.

EP-0081

Assessing the Impact of Alternative ^{123}I Ioflupane Imaging Protocols on Image Interpretation for Complex Patients

E. Hesketh, J. Taylor;
Medical Imaging and Medical Physics, Sheffield, UNITED KINGDOM.

Aim/Introduction: The aim of this study was to identify alternative ^{123}I Ioflupane (DaTSCAN, GE Healthcare) scanning protocols that would be more tolerable for complex patients including those with excessive spine curvature (kyphosis), and claustrophobia. Phantom scans were performed to establish a suitable protocol that produces images of a similar diagnostic quality to those from the standard protocol. **Materials and Methods:** Five alternative scanning protocols were identified; 180° L-mode and 180° extended-detector H (EDH)-mode (A. Notghi et al, 2010), standard protocol with increased detector separation (kyphosis protocol), single-detector planar at vertex of skull, and a solid-state dedicated cardiac camera (CC) seated protocol (Hillel and Redgate, 2019). A novel 3D-printed anthropomorphic phantom (J Taylor et al, 2018) was constructed twice to represent a normal and a subtly abnormal pattern of tracer uptake. The phantom uses alternating attenuation slabs and paper built up into a head shape. The paper is printed with radioactive ink patterns that realistically represent striatal tracer uptake. Each phantom was scanned on a standard gamma camera (Discovery 670, GE Healthcare) using the standard 30-minute H-mode clinical protocol, alternative protocols, and on the cardiac camera. A group of 4 reporters scored the images on image quality, and diagnosis confidence where a score of 1 = "definitely abnormal", 3 = "equivocal", and 5 = "definitely normal". These were compared to scores for the standard protocol, and that which scored most closely was deemed the best alternative protocol. **Results:** Image quality was rated "good" for the standard and CC protocols, "poor - satisfactory" for EDH-mode, kyphosis, and L-mode protocols, and "unacceptable" for the vertex protocol. Diagnosis confidence scores for the normal

phantom were: standard protocol= 4.6±0.5, CC= 5±0, kyphosis= 3.4±0.9, EDH-mode= 3±1, L-mode= 2.8±1.3, vertex= 3±0. For the subtly abnormal phantom; standard protocol= 2.3±1.2, CC= 2±1.1, kyphosis= 1.8±0.7, EDH-mode= 1.6±0.9, L-mode= 3±1.1. EDH-mode protocol acquired 50% fewer counts than the standard protocol. **Conclusion:** The CC protocol rated most consistently with the standard protocol so is suggested as a suitable comfortable alternative for patients with claustrophobia and/or kyphosis. Both EDH-mode and L-mode protocols rated poorly therefore further work is required to determine a suitable alternative if no cardiac camera is available. **References:** A. Notghi et al, "Acquiring diagnostic DaTSCAN images in claustrophobic or difficult patients using a 180degree configuration," NMC, vol.31, no.3, pp.217-226, 2010.J.Taylor et al, "The subresolution DaTSCAN phantom: a cost-effective, flexible alternative to traditional phantom technology," NMC, vol39, pp268-275, 2018.

EP-0082

Contribution of the amyloid-PET to diagnosis Alzheimer disease

S. Perez Quiros, *B. Rodriguez Alfonso, S. Seijas Marcos, A. Sanfiel Delgado, M. Mitjavila Casanovas;*
Hospital Puerta de Hierro, Majadahonda, SPAIN.

Aim/Introduction: Alzheimer's disease has a high social impact for patients and their environment. Due to this is very important to have an early diagnosis in order to reduce its symptoms. The diagnosis is mainly made by clinical factors, although there are also available complementary imaging tests supporting the diagnosis for the neurology. The aim of our study is to analyze the contribution of the amyloid-PET to finding a final diagnosis in patients with possibility of having Alzheimer's disease. **Materials and Methods:** This observational retrospective study includes all amyloid studies which could be an Alzheimer's disease, having a previous complementary imaging brain test (18F-FDG-PET/TC or 99mTc-HMPAO-SPECT) from December/2014 until nowadays. Results from both diagnostic test was compared. A final diagnostic was established by the neurology, with a 18 months follow-up. We analyze if the diagnosis accuracy percentage was influenced by the amyloid data. **Results:** The inclusion criteria was in 46 studies. The average age of the patients was 60 years old. 82,6% of the patients had a SPECT-HMPAO previous and 76% of the patients had a FDG-PET with or without SPECT. The amyloid PET was positive in 28/46 of patients (61%). 18/28 of these patients had a previous complementary imaging test suggesting posterior neurological disease (64%). All these patients were finally confirmed with Alzheimer disease. The other 10 studies were not conclusive for posterior neurological disease (36%). 9/10 of patients were finally confirmed with Alzheimer disease, ando 1/10 of patients has "esclerosis mesial temporal". The amyloid PET was negative in 18/46 of patients (39%). 7/18 of these patients (39%) had a previous complementary imaging test suggesting posterior neurological disease, but confirming Alzheimer disease just in one. In the other 11/18 (61%) had a previous complementary imaging test not suggesting Alzheimer disease, and this one was ruled out in 10/11. Finally the amyloid PET was a helpful tool in 15/46 (32,6%) to have a more certain diagnosis of Alzheimer disease. **Conclusion:** PET/CT amyloid is a valuable tool for the diagnosis of Alzheimer's disease. It is capable of identifying a suspicious diagnosis in 32,6% of the patients, having a potential impact in therapeutic management. **References:** None.

EP-0083

Prognostic Value Of Brain Perfusion Spect In Patients With Atrial Fibrillation And Dementia

H. Hashimoto, *R. Nakanishi, S. Mizumura, Y. Hashimoto, Y. Okamura, K. Yamanaka, T. Ikeda;*
Toho University Faculty of Medicine, Tokyo, Japan, Oomori-nishi/Ootaku/Tokyo, JAPAN.

Aim/Introduction: Atrial fibrillation (AF) is the most common cardiac arrhythmia, and those afflicted have reduced quality of life, functional status, and cardiac performance. The patients with AF have a high risk of coronary heart disease and cardiovascular disease. Although the prevalence of AF is increasing, cognitive disorders are also on the rise in tandem with the aging of the population. The patients with dementia have also experienced lower the quality of life and have increased mortality. Technetium 99m ECD brain perfusion single photon emission computed tomography (99mTc-ECD brain perfusion SPECT) is a useful modality for diagnosing dementia and identifying high risk patients with mild cognitive impairment. However, there are few reports about the relationship between the value of Z score calculated by 99mTc-ECD brain perfusion SPECT and prognosis of patients with AF and dementia. The aim of this study was to evaluate the prognostic value of brain perfusion using 99mTc-ECD SPECT in patients with AF and dementia. **Materials and Methods:** Among 405 consecutive patients who were diagnosed as AF in cardiac outpatients and as dementia using Mini-Mental State Examination by neurologists or psychiatrists, we identified 170 patients (81±10 years) who underwent 99mTc-ECD brain perfusion SPECT. Of those, 73, 73, and 24 were diagnosed as Alzheimer's dementia (AD), vascular dementia (VD), and non-specified dementia respectively. Multivariate Cox model was used to assess if higher Z score by 99mTc-ECD brain perfusion SPECT and clinical parameters were associated with major adverse cardiovascular events (MACE) including cardiac death, myocardial infarction, hospitalization for heart failure, and stroke. Sub-analyses of multivariate Cox models by AD or VD were also assessed. **Results:** During a mean follow-up of 1258±1044 days, 62 MACE occurred. There was not significant difference of MACE between AD and VD (33%, vs. 44%, p=0.153). By multivariable Cox model, the higher Z score of temporal-occipital-pariental lobe was associated with increased MACE compared to the lower group (HR 2.521, 95% CI 1.465-4.337, p < 0.001). In a sub-analysis of patients with AD, Z score was the most significant prognostic factor for MACE (HR 3.969, 95% CI 1.374-11.468, p=0.011). The similar trend was observed in those

with VD (HR 2.247, 95% CI 1.028-4.913, p=0.043). **Conclusion:** This study demonstrated that the Z score of temporal-occipital-pariental lobe could be a potential prognostic value among patients with AF and dementia, regardless of type of dementia. **References:** None.

EP-0084

Application of the 2018 NIA-AA Research Framework to a large cohort of patients with cognitive impairment

G. Marotta, *T. Carandini, A. Arighi, G. G. Fumagalli, A. M. Pietroboni, L. Ghezzi, A. Colombi, M. Scarioni, C. Fenoglio, M. A. De Riz, E. Scarpini, D. Galimberti;*
Fondazione IRCCS Ca' Granda Ospedale Maggiore Policlinico, Milano, ITALY.

Aim/Introduction: The 2018 NIA-AA Research Framework use biological biomarkers to define Alzheimer's disease (AD) by its underlying pathologic process. Our aims were to assess the applicability of the 2018 NIA-AA Research Framework to a large cohort of patients with cognitive impairment (CI), and to evaluate correspondence between cerebrospinal fluid (CSF) and positron emission tomography (PET) biomarkers of Aβ deposition. **Materials and Methods:** We retrospectively analysed all patients who underwent CSF analysis from 2011 to 2017 in our Centre, receiving a diagnosis of CI, according to their clinical follow-up and neuroimaging. Patients were divided according to their CSF biomarkers, as defined by 2018-NIA-AA-RF. Prevalence of Normal, AD-continuum and Non-AD profiles in each clinical syndrome was calculated. When available, Aβ pathology was evaluated also with florbetapir-PET and correlation between PET and CSF data was performed. **Results:** CSF data were available from 628 patients. CSF analysis was available from 628 patients, of whom 49 underwent florbetapir-PET within 12 months. MRI/PET co-registration was obtained in 39 patients. Almost all patients with a positive florbetapir-PET 89% was classified as AD-continuum by their CSF data, 8% as non-AD, and 3% as Normal. Conversely, 43% and 28.5% of subjects with negative florbetapir-PET had Non-AD and Normal CSF profiles, respectively, but 28.5% was AD-continuum. Among patients diagnosed of AD, 87.3% were AD-continuum, whereas 11.3% were Non-AD. The AD-continuum profile was found also in 12% of frontotemporal dementia, 40% of Lewy bodies dementia, 16% of atypical parkinsonism, and 32% of vascular dementia. Amnesic MCI displayed a higher prevalence of AD-continuum compared to not amnesic (56.6% versus 36.4%). 50% of patients with negative FBP-PET were classified as AD-continuum according to CSF analysis, and no correlation between PET data and CSF Aβ levels was found. **Conclusion:** The AD continuum profile resulted a sensitive, but not specific, biomarker in detecting AD pathology. The incomplete agreement we found between CSF and PET Aβ biomarkers suggests that they are not perfectly interchangeable to quantify the Aβ burden, possibly because they assess different features of AD pathology. **References:** None.

EP-0085

A MRI-PET study between behavioral variant Frontotemporal Dementia and elderly Bipolar Disorder

G. Marotta, *G. Delvecchio, G. M. Mandolini, A. Arighi, C. Prunas, M. C. Mauri, A. M. Pietroboni, C. Cinnante, F. M. Triulzi, E. Scarpini, C. Altamura, P. Brambilla;*
Fondazione IRCCS Ca' Granda Ospedale Maggiore Policlinico, University of Milan, Milano, ITALY.

Aim/Introduction: Elderly Bipolar Disorder (BD) and Behavioral Variant of Frontotemporal Dementia (bvFTD) may exhibit similar symptoms and both disorders are characterized by selective abnormalities in cortical and subcortical regions that are associated with cognitive and emotional impairments.Aim of the study is to investigate common and distinct neural substrates of BD vs bvFTD by coupling, positron emission tomography (PET) and magnetic resonance imaging (MRI). **Materials and Methods:** FDG-PET and MRI scans were acquired for 23 bvFTD patients with mild cognitive impairments, 16 elderly BD patients and 68 healthy controls (48 for PET and 20 for MRI analyses). PET scans were obtained with a Biograph Truepoint 64 PET/CT scanner. MR images were acquired using a 3-Tesla Philips Achieva MRI scanner. For PET analyses, all FDG-PET images were subjected to affine and nonlinear spatial normalization into the MNI space with SPM12 using the dementia-optimized brain FDG-PET template and smoothed with an 8-mm Gaussian filter. For VBM analyses, all T1-weighted images were segmented and Dartel tools were then used to determine the nonlinear deformations for registering the GM and white matter images of all subjects, and the resulting images were spatially normalized into the MNI space and smoothed with an 6-mm Gaussian filter. Inference on the GM volumes and metabolic differences between groups was made using double-sided t-tests with a threshold of p<0.0 01. **Results:** bvFTD and BD patients exhibit different localization of gray matter (GM) reductions in the lateral prefrontal cortex (PFC), with the first group showing GM decrease in the ventrolateral PFC and the latter group showing GM reduction in the dorsolateral PFC and unique alterations within the orbitofrontal cortex. The bvFTD group also displayed unique volumetric shrinkage in regions within the temporo-parietal network together with greater metabolic impairments within the temporal cortex and more extensive volumetric and metabolic abnormalities within the limbic lobe. Finally, while the BD group showed greater GM volumes in caudate nucleus, bvFTD subjects displayed lower metabolism. **Conclusion:** The study explored structural and functional abnormalities in bvFTD and elderly BD patients, with the final aim of identifying the specific biological signature of these disorders, which might have important implications not only in prevention but also in differentiating diagnosis and treatment. **References:** None.

EP-0086

A Comparative PET Study for Assessing Abnormal Metabolic Brain Network Activity in Dementia with Lewy Bodies and Parkinson's Disease

P. Wu[1], *J. Ge*[1], *L. Li*[1], *Y. Zhu*[1], *J. Xiao*[1], *Q. Guo*[2], *C. Zuo*[1];
[1]*PET center, Huashan Hospital, Fudan University, Shanghai, CHINA,* [2]*Department of Geriatrics, Sixth People's Hospital, Shanghai Jiao Tong University, Shanghai, CHINA.*

Aim/Introduction: It has been debated for decades whether Dementia with Lewy bodies (DLB) and Parkinson's Disease (PD) are the same disorder. Previous studies with FDG PET have demonstrated PD is associated with a specific spatial covariance pattern (PDRP) and its individual expression could be used for differential diagnosis with atypical parkinsonism (multiple system atrophy and progressive supranuclear palsy) [1], In this study, we aimed to investigate whether an analogous pattern exists in DLB patients and how it characterizes the boundary issues between DLB and PD. **Materials and Methods:** We prospectively recruited 20 DLB patients and 20 age-/gender-matched healthy subjects to perform FDG PET imaging. 33 PD patients and 33 age-/gender-matched healthy subjects used to identify the PDRP [2] were also enrolled. DLB-related pattern (DLBRP) was identified by using SSM/PCA toolbox in the DLB patients and corresponding control subjects. The DLBRP was determined from a linear combination of select principal components (PCs) whose expression in individual scans gave the maximum separation between the patient and control groups. For each pattern (DLBRP&PDRP), the individual expression was computed and compared between groups. **Results:** For DLBRP identification, the first 3 PCs accounted for 57% of the subject × voxel variance. A logistic regression model including PC1 and PC3 yielded the lowest Akaike information criterion (AIC) value and their linear combination was disease-related, i.e., subject scores for this pattern best discriminated the two subject groups ($P<0.001$). DLBRP was characterized by metabolic increases in the bilateral putamen, premotor cortex and cerebellum accompanied by metabolic decreases in the bilateral caudate, thalamus, posterior cingulate and bilateral parietal-occipital regions. The topographic characteristics of DLBRP were similar to that of PDRP, but with an overall wider range. For each pattern (DLBRP/PDRP), subject scores measured in all subjects showed an effect of group (ANOVA; DLBRP: $F[3,102]=108.1$, $p<0.001$; PDRP: $F[3,102]=74.1$, $p<0.001$) with elevation in the DLB/PD patients ($p<0.001$, post-hoc tests) compared to the healthy controls. Moreover, network scores were similarly greater in the DLB patients than in the PD patients in both patterns ($p<0.001$). **Conclusion:** This is the first study to demonstrate the specific metabolic brain network corresponding to DLB using FDG PET imaging which presents a similar topography with PDRP but with wider range as well as higher quantitative expression. These results indicate that PD/DLB maybe under the spectrum of the same disease. **References:** [1] Tang et al. Lancet Neurol 2010 [2] Wu et al. Parkinsonism Relat Disord 2013.

EP-0087

Retinal and brain tau deposition evaluated by ^{18}F-Flortaucipir and its correlation with AD biomarkers in CSF

M. Meyer[1], *O. Rouaud*[1], *G. Allenbach*[1], *M. Nicod-Lalonde*[1], *V. Garibotto*[2], *A. Ampuero*[1], *G. Frisoni*[2], *N. Schaefer*[1], *J. Demonet*[1], *J. O. Prior*[1];
[1]*Lausanne University Hospital and University of Lausanne, Lausanne, SWITZERLAND,* [2]*University Hospitals of Geneva, Faculty of Medicine and University of Geneva, Geneva, SWITZERLAND.*

Aim/Introduction: The retina shares many common features with brain tissue, and changes in retinal neurons might mirror brain pathology. Previous studies have investigated the presence of pathological changes in human retinas in Alzheimer disease (AD). However, the detection of these changes was not consistent across studies. The aim of our study was to quantify ^{18}F-Flortaucipir in the retina and to investigate any correlation with brain tau deposition and AD biomarkers in Cerebro-Spinal Fluid (CSF). **Materials and Methods:** We prospectively analyzed ^{18}F-Flortaucipir PET/CT examinations from October 2018 to April 2019 (Siemens Biograph Vision 600). We measured retinal SUVmax, SUVmean and SUVratio (SUVR) using the cerebellar grey matter as a reference, on static images acquired 75 to 105 minutes after the injection of 180 MBq of ^{18}F-Flortaucipir. All brain regions of interest PET data were also converted to SUVRs using the cerebellar grey as a reference. A composite brain SUVR was calculated by averaging the SUVR of 6 cortical regions (frontal, occipital, parietal, lateral temporal and posterior and anterior cingulate cortex regions). AD biomarkers in CSF were collected for each patient (total-tau, phospho-tau and αβ-42). Correlation used the Spearman ρ. **Results:** 12 patients with cognitive impairment due to AD or suspected non-Alzheimers' pathology (SNAP) were included. 7 presented pathological brain tau deposition and 5 patients presented normal brain tau deposition, on the basis of visual inspection of PET images. Retinal SUVmax ranged from 1.41 to 4.99, retinal SUVmean from 0.79 to 2.58 and retinal SUVR from 1.21 to 3.97. There was no difference concerning retinal SUVmax, SUVmean and SUVR between patients with normal and pathological brain tau deposition ($p=0.88$, $p=0.64$ and $p=0.11$, respectively). Retinal SUVR presented negative correlation with occipital and lateral temporal SUVR ($\rho=-0.598$, $p=0.040$ and $\rho=-0.665$, $p=0.018$, respectively), but no significant correlation with composite brain SUVR ($\rho=-0.531$, $p=0.076$). Retinal SUVR presented negative correlation with total-tau in CSF ($\rho=-0.601$, $p=0.039$), but not with αβ-42 or phospho-tau. Composite brain SUVR presented negative correlation with αβ-42 in CSF ($\rho=-0.616$, $p=0.033$), but not with tau biomarkers. **Conclusion:** With this preliminary analysis, we have showed that ^{18}F-Flortaucipir deposition in the retina evolved a contrario to brain tau deposition, and to total-tau in CSF. Retinal signal with ^{18}F-Flortaucipir could represent an early non-invasive biomarker for AD. These results have to be confirmed with a larger population. **References:** None.

EP-0088

Metabolic Correlates of Dopaminergic Loss in Dementia with Lewy bodies

L. Beyer[1], *M. Huber*[1], *S. Morbelli*[2], *M. Unterrainer*[1], *A. Chincarini*[3], *R. Bruffaerts*[4], *M. Kramberger*[5], *M. Grmek*[5], *V. Garibotto*[6], *N. Nicastro*[6], *G. Frisoni*[7], *A. Pilotto*[8], *S. Garcia-Ptacek*[9], *I. Savitcheva*[9], *M. Pchoa-Figueroa*[10], *V. Camacho*[11], *D. Aarsland*[12], *P. Bartenstein*[1], *A. Rominger*[13], *M. Brendel*[1];
[1]*LMU, Munich, GERMANY,* [2]*University of Genoa, Genoa, ITALY,* [3]*National Institute of Nuclear Physics, Genoa, ITALY,* [4]*University of Leuven, Leuven, BELGIUM,* [5]*University of Ljubljana, Ljubljana, SLOVENIA,* [6]*University of Geneva, Geneva, SWITZERLAND,* [7]*LANVIE, Geneva, SWITZERLAND,* [8]*University of Brescia, Brescia, ITALY,* [9]*Karolinska Institutet, Stockholm, SWEDEN,* [10]*University of Linköping, Linköping, SWEDEN,* [11]*University of Barcelona, Barcelona, SPAIN,* [12]*University of Stavanger, Stavanger, NORWAY,* [13]*University of Bern, Bern, SWITZERLAND.*

Aim/Introduction: Striatal dopamine deficiency is a well-known phenomenon in Dementia with Lewy Bodies (DLB) and can be quantified in vivo by ^{123}I-FP-CIT single photon emission computed tomography (DaT-SPECT). DLB is further characterized by metabolic decline in distinct brain regions as accessible by ^{18}F-fluorodesoxyglucose positron emission tomography (FDG-PET). However, the linkage of dopamine deficiency to declining glucose metabolism and its role in the pathophysiological course of DLB are ill-understood. Hence, we made use of the hitherto largest dataset of combined DaT-SPECT and FDG-PET data in DLB to elucidate their associations during disease progression and to study metabolic connectivity as a function of degree of dopamine deficiency. **Materials and Methods:** We investigated 84 DLB patients of the European DLB consortium, all whom had undergone DaT-SPECT and FDG-PET investigations, along with molecular imaging data from historic healthy controls. After normalization of FDG-PET to the global mean uptake, we tested the correlation between striatal dopamine deficiency with relative glucose metabolism by region-based and voxel-based methods. Metabolic connectivity was analysed by inter-region coefficients at different stages of dopamine deficiency and compared to that in healthy controls. Data were controlled for center, age, gender, and educational level. **Results:** There was an inverse relationship between striatal dopamine innervation and relative glucose hypermetabolism in striatum. Regional and voxel-based methods revealed increasing relative glucose metabolism when dopaminergic function decreased in the basal ganglia and in limbic regions. With increasing dopamine deficiency, metabolic connectivity showed strong deteriorations in distinct brain regions implicated in DLB. However, the greatest disruptions of metabolic connectivity involved the basal ganglia and limbic system, spatially coincident with relative hypermetabolism. **Conclusion:** Combined analysis of dopamine-SPECT and FDG-PET in patients with DLB indicate pronounced associations of abnormality of the two biomarkers in the basal ganglia and limbic system. Greater dopamine deficiency correlated with increasing relative glucose metabolism, but decreasing metabolic connectivity of the afflicted regions. **References:** None.

EP-0089

PET/CT brain imaging using ^{18}F-FDG in patients with Creutzfeldt-Jakob disease

M. Grmek[1], *T. Rus*[2], *M. Popovič*[3], *M. Trošt*[2];
[1]*Department for Nuclear Medicine, University Medical Centre Ljubljana, Ljubljana, SLOVENIA,* [2]*Department of Neurology, University Medical Centre Ljubljana, Ljubljana, SLOVENIA,* [3]*Institute of Pathology, Medical Faculty, University of Ljubljana, Ljubljana, SLOVENIA.*

Aim/Introduction: Creutzfeldt-Jakob disease (CJD) is a fatal rapidly progressing neurodegenerative disorder presenting with cognitive decline and additional neurological signs caused by deposition of misfolded prion protein. Our aim was to identify and validate a specific multivariate metabolic brain pattern of CJD and to test its biological significance. **Materials and Methods:** 10 patients with rapidly progressing dementia and additional neurological signs (group CJD1; age 68.3 ± 12.4 years, survival from first symptoms 8.4 ± 10.6 months, Mini-Mental State Examination (MMSE) 19.9 ± 7.2) underwent diagnostic PET/CT brain imaging using 18F-FDG. All of them were diagnosed pathologically with CJD. 10 age-matched normal controls (NC) (group NC1; age 66.9 ± 5.4 years, MMSE 28.5 ± 1.2) were used as a control group. After spatial normalization into MNI space and smoothing performed in SPM5 (Wellcome Trust Centre for Neuroimaging), multivariate Scaled Subprofile Modeling/Principal Component Analysis (SSM/PCA) was performed using ScanVP software (http:// www.feinsteinneuroscience.org; Center for Neuroscience, Feinstein Institute for Medical Research, NY, USA) to identify a specific CJD related pattern (CJDRP). The stability of CJDRP was studied with bootstrapping algorithm. The pattern was validated on another cohort of 7 CJD patients (group CJD2; 6 patients with definite CJD, 1 with probable CJD, age 67.6 ±7.8 years, disease duration 4.8 ± 6.7 months, MMSE 10.4 ± 6.6) and 10 age-matched NC (group NC2). Expression of CJDRP was studied with TPR algorithm (ScanVP software) and was correlated with age, survival, disease duration, relative disease duration, cognitive (MMSE), clinical (CJD Neurological Status Scale), functional (MRC Prion Disease Rating Scale) scales and with cerebral-spinal fluid (CSF) tau, p-tau and amyloid beta concentrations in both the identification and validation groups. **Results:** The CJDRP was characterized by interconnected relative metabolic decreases in bilateral thalamus, caudate, cingulum, precuneus, frontal and parietal lobe. The CJDRP expression (z-scores) completely separated CJD patients in identification and validation cohorts from corresponding NC groups ($p<0.0001$). The pattern was stable on bootstrapping test (all but minimal areas of parietal lobe hypometabolism). Its expression correlated with relative disease duration, MMSE, clinical and functional scales but not with the CSF tau, p-tau nor amyloid beta. **Conclusion:** The CJDRP is a promising metabolic biomarker of CJD. It can help

clinician make a diagnosis in patients with suspected CJD. CJDRP expression correlates well with disease severity and progression and has therefore a potential to become a biomarker of CJD progression in the possible disease modifying clinical trials. **References:** None.

EP-05
Neuroimaging: Brain Malignant

October 12 - 16, 2019 e-Poster Area

EP-0090
Integration of dynamic parameters in the analysis of ^{18}F-FDopa PET imaging improves the prediction of molecular features of gliomas

T. Zaragori[1,2], *M. Ginet*[1], *P. Marie*[1,3], *V. Roch*[1], *G. Gauchotte*[4,5], *F. Rech*[6,7], *M. Blonski*[6,7], *Z. Lamiral*[3], *L. Taillandier*[7,8], *L. Imbert*[1,2], *A. Verger*[1,2];
[1]*Department of Nuclear Medicine & Nancyclotep Imaging plateform, CHRU Nancy, Lorraine University, Nancy, FRANCE,* [2]*IADI, INSERM U1254, Lorraine University, Nancy, FRANCE,* [3]*INSERM U1116, Lorraine University, Nancy, FRANCE,* [4]*Department of Pathology, CHRU-Nancy, Nancy, FRANCE,* [5]*INSERM U1256, Lorraine University, Nancy, FRANCE,* [6]*Department of Neurosurgery, CHRU-Nancy, Nancy, FRANCE,* [7]*Centre de Recherche en Automatique de Nancy CRAN, CNRS UMR 7039, Université de Lorraine, Nancy, FRANCE,* [8]*Department of Neuro-Oncology, CHRU-Nancy, Nancy, FRANCE.*

Aim/Introduction: ^{18}F-FDopa PET imaging of gliomas is routinely interpreted with standardized uptake value (SUV)-derived indices. This study aimed to determine the added value of dynamic ^{18}F-FDopa PET parameters for predicting the molecular features of newly-diagnosed gliomas. **Materials and Methods:** We retrospectively included 58 patients having undergone an ^{18}F-FDopa PET for establishing the initial diagnosis of gliomas, whose molecular features were additionally characterized according to the WHO 2016 classification. Dynamic parameters, involving time-to-peak (TTP) values and curve slopes, were tested for the prediction of glioma types in addition to current static parameters, i.e. tumor-to-normal brain or tumor-to-striatum SUV ratios and metabolic tumor volume (MTV). **Results:** There were 21 IDH-mutant gliomas, 16 IDH-mutant and 1p/19q co-deleted gliomas and 21 IDH-wildtype gliomas; dynamic parameters enabled differentiating the gliomas according to these molecular features, whereas static parameters did not. In particular, a longer TTP was the single best independent predictor for differentiating: 1) IDH-mutant gliomas from IDH-wildtype gliomas (area under the curve (AUC) of 0.789, global accuracy of 74% for the criterion of a TTP > 5.4min) and 2) IDH-mutant from 1p/19q co-deleted gliomas (AUC of 0.679, global accuracy of 69% for the criterion of a TTP > 6.9min). **Conclusion:** Prediction of the molecular features of newly-diagnosed gliomas with ^{18}F-FDopa PET, and especially of the presence or not of an IDH mutation, may be obtained with dynamic but not with current static uptake parameters. **References:** None.

EP-0091
The pentose phosphate pathway in glioma - a promising target for nuclear medicine?

E. Klebermass[1], *A. Woehrer*[2], *G. Ricken*[2], *S. Bucconi*[1], *A. Haschemi*[3], *T. Balber*[1], *M. Hacker*[1], *H. Viernstein*[4], *M. Mitterhauser*[1,5], *T. Traub-Weidinger*[1];
[1]*Department of Biomedical Imaging and Image-guided Therapy, Division of Nuclear Medicine, Medical University of Vienna, Vienna, AUSTRIA,* [2]*Institute of Neurology, Medical University of Vienna, Vienna, AUSTRIA,* [3]*Department of Laboratory Medicine, Medical University of Vienna, Vienna, AUSTRIA,* [4]*Department of Pharmaceutical Technology and Biopharmaceutics, University of Vienna, Vienna, AUSTRIA,* [5]*Ludwig Boltzmann Institute Applied Diagnostics, Vienna, AUSTRIA.*

Aim/Introduction: Gliomas account for 81% of malignant brain tumors, with glioblastomas being the most lethal and common ones (1). The pentose phosphate pathway (PPP) constitutes a major carbohydrate pathway in tumor metabolism that is exploited by tumor cells for nucleic acid synthesis and elimination of redox stress. Regarding glioma, most studies of the PPP have focused on the evaluation of glucose-6-phosphate dehydrogenase, the rate-limiting enzyme in its oxidative arm, and highlight a prognostic relevance (2). However, little is known about the impact of the non-oxidative arm, although its enzymes and the intermediate sedoheptulose-7-phosphate seem to play an important role in other malignancies (3, 4). We therefore aim to evaluate the role of sedoheptulose kinase (SHPK), a key regulator of carbon flux making sedoheptulose available for cells through phosphorylation. **Materials and Methods:** The anti-SHPK antibody (abcam, ab69920) was tested and validated on formalin-fixed paraffin-embedded healthy brain and glioma. Subsequently, immunohistochemical staining in a 1:500 dilution was performed on tumor biopsies of a heterogeneous cohort of 48 patients, having had [^{11}C] methionine and, in 21 cases, additional 2-[^{18}F]FDG PET scans. Hematoxylin was used as a counterstaining, colon and cervix FFPE tissues as positive- and negative controls, respectively. Expression was semi-quantitatively assessed using the following classification: positive cells 0-10%, 10-40%, and ≥ 50%. Staining intensity was rated from 1 to 4, 1 being the least intense. **Results:** 38/48 glioma biopsies showed expression in >10% of cells; 26 of them in ≥ 50% of cells. SHPK was detectable in tumor cells and microenvironmental cells such as microglia, macrophages and rare astrocytes. The majority of positive cells displayed a variable cytoplasmic staining (intensity 1-4), whereas tumor cells and macrophages occasionally exhibited a nuclear staining of higher intensity (3-4). Significant expression was present in 14/14 glioblastomas, and 11/18 low-grade gliomas (WHO grades I-II). Interestingly, 12/14 biopsies of completely

2-[18F]FDG PET-negative gliomas showed SHPK staining in >10% of cells. **Conclusion:** Evaluation of SHPK in glioma shows a significant expression in different tumor types across all grades of malignancy involving both tumor and microenvironmental cells. These encouraging results might open up new possibilities for metabolic imaging and/or treatment in these patients. **References:** (1) Ostrom QT., Bauchet L., Davis FG., et al. Neuro Oncol. 2014 Jul (2) Yang CA., Huang HY., Lin CL., et al. J Neurooncol 2018 (3) Ying H., Kimmelman AC., Lyssiotis CA., et al. Cell. 2012 Apr (4) Patra KC., Hay N. Trends Biochem Sci. 2014 Aug.

EP-0092

Volumetric assessment of gliomas: Comparison between 18F-FET and 68Ga-NODAGA-RGDyK

N. Testart[1], *F. Cicone*[1], *A. Hottinger*[2], *M. Nicod Lalonde*[1], *N. Schaefer*[1], *S. Gnesin*[3], *M. Meyer*[1], *P. Mitsakis*[1], *J. O. Prior*[1]; [1]*Nuclear Medicine and Molecular Imaging, Lausanne University Hospital and University of Lausanne, Lausanne, SWITZERLAND,* [2]*Neuro-Oncology, Lausanne University Hospital and University of Lausanne, Lausanne, SWITZERLAND,* [3]*Institute of Radiation Physics, Lausanne University Hospital and University of Lausanne, Lausanne, SWITZERLAND.*

Aim/Introduction: Amino acid PET with 18F-FET (FET) is becoming a standard functional imaging technique for the evaluation of glioma [1]. 68Ga-NODAGA-RGDyK (RGD) is a novel radiopharmaceutical targeting the integrin αvβ3 [2], which might provide additional information for stratifying patient prognosis and response to anti-angiogenic treatments. Our aim was to compare the tumour volumes identified by FET and RGD in a series of patients with glioma. **Materials and Methods:** Seven patients with newly diagnosed or recurrent glioma were referred for PET/CT examinations with both FET and RGD, less than one week apart. Images were registered with the software PMOD version 3.903 (PMOD Technologies, Zurich, Switzerland). After image registration, automatic tumour segmentation of both sets of images was performed using the average background signal in a large hemispheric VOI multiplied by 1.6 as a threshold for positivity. Tumour volumes identified by both modalities were compared and their spatial congruence calculated [3]. **Results:** The study population consisted of 7 patients (1F/6 M, mean age: 56y). According to the WHO 2016 classification of brain tumors, there were two glioblastomas (Grade IV, IDH wild-type), one ganglioglioma (Grade II IDH wild-type), two oligodendrogliomas (Grade II, IDH mutant, 1p19q co-deleted), one oligodendroglioma (Grade III, IDH mutant, 1p19q co-deleted) and one newly diagnosed non-enhancing, non-biopsied glioma. Magnetic resonance imaging showed presence of contrast enhancement in 3 out of 7 patients. On visual inspection, 100% (7/7) FET studies and 57% (4/7) RGD studies were positive. The tumour volume delineated using FET (FETvol 1.6) largely exceeded that of RGD (RGDvol 1.6). Median FETvol 1.6 and RGDvol 1.6 were 29.0mL (range, 10.8-207mL) and 2.95mL (range, 0-11.3mL), respectively (p=0.015). Overall, median overlapping volume was 2.95 ml (range 0-8.13mL), resulting in a median spatial congruence of 4.15% (range, 0-59.7%). RGD positivity was mostly located in tumour portions showing contrast enhancement at MRI. In two patients with high-grade tumours, there was RGD uptake extending to FET-negative tumour portions. One patient had a meningioma showing increased RGD uptake and negative FET. **Conclusion:** The information provided by FET and RGD PET are substantially different. FET PET identifies larger volumes than RGD. Some volumetric mismatch exists, whose significance should be further investigated in larger patient series with follow-up. **References:** 1) Albert NL, et al. Neuro Oncol. 2016;18:1199-208. 2) Gnesin S, et al. EJNMMI Res. 2017;7:43. 3) Cicone F, et al. Eur J Nucl Med Mol Imaging. 2015;42:905-15.

EP-0093

Correlation of [11C]Methionine PET Uptake With Ki-67 Immunohistochemistry In Patients With Untreated Gliomas

T. Skvortsova, D. Zakhs, Z. Savintseva, A. Gurchin, A. Kholyavin; N. P. Bechtereva Institute of the Human Brain of Russian Academy of Sciences, Saint-Petersburg, RUSSIAN FEDERATION.

Aim/Introduction: The aim of the study was to determine correlation between [11C]methionine uptake measured by positron emission tomography (PET) in newly diagnosed gliomas and tumor proliferative activity as measured by Ki-67 labeling index in tumor samples after surgery. Also analysis of matches between two biomarkers in each patient was performed. **Materials and Methods:** The glioma uptake of [11C] methionine (Met) was assessed using PET/CT (or PET) scanner in 214 patients between 18 and 75years of age (100 males, 114 females) with untreated gliomas. The final diagnosis was based on both histology and immunohistochemistry using Ki-67 antibodies. Tumor samples were classified as grade II gliomas (n=129; 97 astrocytomas, 32 oligodendrogliomas), grade III gliomas (n=66; 49 astrocytomas, 17 oligodendrogliomas) and glioblastomas (n=19). On PET-Met tumor-to normal brain uptake ratio (TBR) was calculated by dividing maximum Met uptake in the tumor (hot spot 10 mm in diameter) to activity concentration in the contralateral cortex. The Spearmen rank correlation test was used to analyze the relationships between TBR and Ki-67 labeling index (LI). **Results:** PET-Met analysis showed that TBR (mean±SD) of low-grade gliomas, anaplastic gliomas and glioblastomas were 1,67±0,64, 2,41±1,05, 3,45±1,03, respectively. The differences of TBR values between gliomas grade II vs III and grade III vs IV were significant (p<0,001). Among grades II-III gliomas Met uptake was higher in oligodendroglial tumors than in astrocytomas (p<0,01). The mean Ki-67 LI of low-grade and high-grade gliomas were 5%±4%, 14%±9%, respectively. Correlation analysis demonstrated weak correlation between Ki-67 LI and TBR values (r =0,50, p<0.05). With analyzing glioma subgroups TBR values correlated with Ki-67 LI in diffuse astrocytomas (r=0,52, p<0,05), oligodendrogliomas (r=0,34, p<0,05) and in high-grade gliomas (r=0,44, p<0,05) but not in low-grade gliomas. Higher Met

uptake in oligodendrogliomas compared with astrocytomas did not depend on Ki-67 LI. Comparison between TBR value and Ki-67 LI in each glioma showed a lack of coincidence in 24% of cases (high Met uptake but low Ki-67 LI and vice versa). The main reasons for such discrepancies were tumor molecular biology or incorrect biopsy target. **Conclusion:** The study showed that Met uptake in diffuse gliomas increases in parallel with the increase in their proliferative activity which justifies the use of PET-Met for glioma grading. In case of mismatch between two biomarkers one should rely on the indicator that implies a higher aggressiveness of the glioma. **References:** None.

EP-0094

^{18}F-DOPA uptake ratio correlates with Ki67 in gliomas at initial diagnosis, in a per-biopsy analysis

A. Girard[1], *X. Palard-Novello*[1], *P. J. Le Reste*[2], *A. Metais*[3], *F. Le Jeune*[1];
[1]*Centre Eugène Marquis, Rennes, FRANCE,* [2]*Neurosurgery - Universitary Hospital, Rennes, FRANCE,* [3]*Pathology - Universitary Hospital, Rennes, FRANCE.*

Aim/Introduction: Ki67 has been reported as a predicative factor for poor prognosis of glioma patients (1). At initial diagnosis, diffuse gliomas are highly infiltrative and heterogeneous tumors, and Ki67 expression varies spatially across each tumor. ^{18}F-DOPA PET might be a useful tool to target biopsies and guide tumor resection, but does not appear in this indication in the last EANM/EANO/RANO guidelines (2). We hypothesize that ^{18}F-DOPA uptake correlates with Ki67 expression, in a per-biopsy analysis. **Materials and Methods:** In these preliminary results of the GLIROPA study (NCT03525080) we prospectively included 8 patients with suspicion of diffuse glioma. ^{18}F-DOPA PET was performed before surgery in accordance with the last EANM/EANO/RANO guidelines (2). Based on ^{18}F-DOPA PET images, one to three 1mL volumes of interest (VOI) were defined for each patient, depending on the size and heterogeneity of the tumor. During surgery, biopsies were performed in these targets under neuronavigational control. The per-biopsy statistical analysis included bilateral Spearman's rank correlation coefficient between Ki67 and VOI-SUVmax (VOImax), VOI-SUVmean (VOImean) and VOI-SUVmax/Striatum-SUVmax ratio (VOI/Smax), respectively. **Results:** Six high grade gliomas (HGG) and two low-grades gliomas (LGG) were found at pathological analysis of tumors. There was ^{18}F-DOPA uptake in 7/7 HGG and 1/2 LGG. Sixteen biopsies were performed. In a per-biopsy analysis, Ki67 mean was 11% [range : 1% - 40%], VOImax 4.02 [range : 1.89 - 9.17], VOImean 2.51 [range : 1.26 - 4.79] , and VOI/Smax ratio 1.26 [range : 0.63 - 2.67]. Ki67 was significantly correlated with the VOI/Smax ratio (rho 0.52 ; p =0.037), but neither with VOImax (rho 0.48 ; p =0.058), nor with VOImean (rho 0.49 ; p =0.056). **Conclusion:** In a per-biopsy analysis, Ki67 was significantly correlated with the VOI/Smax ratio. These results strengthen the idea that ^{18}F-DOPA PET may be a useful tool to localize the most proliferative part of gliomas, and thus might help to target biopsies and guide tumor resection at initial diagnosis. **References:** 1) W.J. Chen , D.S. He , R.X. Tang, et al. Ki-67 is a valuable prognostic factor in gliomas: evidence from a systematic review and meta-analysis. Asian Pac J Cancer Prev. 2015;16(2):411-20. 2) I. Law, N.L. Albert, J. Arbizu, et al. EANM/EANO/RANO practice guidelines/SNMMI procedure standards for imaging of gliomas using PET with radiolabelled amino acids and [18F]FDG: version 1.0. Eur J Nucl Med Mol Imaging. 2019 Mar;46(3):540-557.

EP-0095

18F-FAZA PET and MRI for hypoxia, perfusion and diffusion assessment in high-grade glioma

P. Mapelli[1,2], *P. Scifo*[2], *G. Conte*[1,3], *F. Fallanca*[2], *A. Castellano*[1,3], *E. Incerti*[2], *V. Bettinardi*[2], *A. Coliva*[2], *V. Masiello*[2], *A. Compierchio*[2], *N. Anzalone*[1,3], *L. Gianolli*[2], *M. Picchio*[1,2];
[1]*Vita-Salute San Raffaele University, Milan, ITALY,* [2]*Nuclear Medicine Department, IRCCS San Raffaele Scientific Institute, Milan, ITALY,* [3]*Neuroradiology Unit and CERMAC, IRCCS San Raffaele Scientific Institute, Milan, ITALY.*

Aim/Introduction: 18F-FAZA PET/CT provides information on tumour hypoxic status, perfusion and diffusion weighted MRI (pw-MRI, dMRI) can further improve tumour characterization. The aim of the present study is to evaluate the complementary/additive role of 18F-FAZA PET and MRI, in assessing the functional status of high-grade glioma (HGG). **Materials and Methods:** Seventeen patients with brain MRI suggestive for HGG have been included. All patients underwent 18F-FAZA PET/CT, MRI (3D-T1w, T2w, FLAIR w pre- and post-contrast), diffusion (DTI) and perfusion (PWI) images; 11 pts have been considered for analysis in this preliminary work. PET-FAZA, pw-MRI and dMRI images were firstly co-registered to 3D-T1 MR. Ktrans, Vp and CBV maps were derived from PW images. Mean Diffusivity (MD) was obtained from DTI. 18F-FAZA SUV maps were calculated, divided by muscle value and a threshold of tumour-to-blood (T/B) >1.2 was used to define FAZA-based ROIs. Using these ROIs, Spearman correlations between FAZA SUV and PWI parameters were calculated. A second ROI was defined based on the Gd-enhanced regions on FLAIR images. Dice coefficient between the two ROIs was calculated to assess overlapping between them. Gd-based ROI was used to mask PWI and DTI maps, centers-of-mass (CoM) of ROIs in each single parametric map (Ktrans, Vp, CBV, MD, FAZA) were found and the relative distances were calculated. **Results:** No significant correlation between PET and PWI parameters (CBV, Ktrans and Vp) were obtained. The mean value of Dice coefficient among patients was 0.68±0.16. The CoMs of pw maps and MD in the ROIs defined by Gd-enhacement, were located slightly differently in the group of patients. The analysis of the relative 3D-distances between FAZA CoM and CoM in the 4 MRI maps in the 11 patients suggests that FAZA CoM is located in a position closer to the CoMs of DCE maps, but further away from CBV-CoM and MD-CoM. **Conclusion:** In the present cohort, 18F-FAZA PET/CT and MR parameters are not strongly related, suggesting the complementary role of these techniques in providing different information on tumour status. Among MR maps, CBV seems to provide the "most different" information compared to FAZA. The

limited number of patients might have hampered the statistical power of the analysis. Further analysis on larger cohorts are mandatory to deeply investigate these relevant aspects of HGG. **References:** None.

EP-0096

^{18}F-Fluorocholine PET/CT in the prediction of molecular subtypes and prognosis for gliomas

A. Garcia Vicente[1], *J. Perez-Beteta*[2], *M. Amo-Salas*[2], *G. A. Jimenez Londoño*[1], *F. J. Pena Pardo*[1], *M. Villena Martin*[1], *H. Sandoval Valencia*[3], *R. Barbella*[3], *J. M. Borras Moreno*[1], *E. Casillas Sagrado*[1], *V. Perez-Garcia*[2], *A. Soriano Castrejon*[1];
[1]*Hospital General Universitario de Ciudad Real, Ciudad Real, SPAIN,* [2]*Universidad de Castilla La Mancha, Ciudad Real, SPAIN,* [3]*Hospital General Universitario de Albacete, Albacete, SPAIN.*

Aim/Introduction: To study the association of metabolic features of ^{18}F-fluorocholine PET/CT in gliomas with histopathological and molecular parameters and prognosis. **Materials and Methods:** Prospective multicenter and non-randomized study (FuMeGA: Functional and Metabolic Glioma Analysis). Patients underwent a basal ^{18}F-fluorocholine PET/CT and were included after histological confirmation of glioma. Histological and molecular profile were assessed: grade, Ki-67, isocitrate dehydrogenase (IDH) status and 1p/19q codeletion. Patients underwent standard treatment after surgery/biopsy, depending on their clinical situation. Overall survival (OS) and progression free survival (PFS) were obtained.After tumor segmentation of PET images, maximum and mean standardized uptake value (SUV based variables), metabolic tumor volume and total lesion activity (volume-based variables), sphericity, surface, coefficient of variation and multilesionality were obtained. Relations of metabolic variables with histological and molecular profiles and prognosis were evaluated using Pearson's chi-square and t-student tests. Receiver operator caracteristic (ROC) curves were used to obtain the cut-off of PET variables and survival analysis was performed using Kaplan-Meier and Cox regression analysis. **Results:** 45 patients were assessed, 38 were diagnosed as having high-grade gliomas (HGG).Multilesionality was detected on PET in 11 cases (24.4%). Significant differences were found with respect to the IDH status and SUVmax and SUVmean, with higher values in IDH wild type as compared to IDH mutated tumors (SUVmax of 3.66±1.77; and 1.61±1.84, respectively; p=0.025 and SUVmean of 1.22±0.48 and 0.67±0.51, respectively; p=0.033). No significant relation was found with the other metabolic variables.The overall median PFS and OS were 5 and 14 months, respectively.Tumor grade, Ki-67, SUVmax and SUVmean were related to progression. SUVmax of 2.20 and 0.88 for SUVmean (AUC of 0.865, p=0.003 and AUC of 0.841, p=0.005, respectively) were the cut-off valid to predict progression.Kaplan-Meier analysis revealed significant association of SUVmax, SUVmean and multilesionaly with OS and PFS. SUVmean, sphericity and multilesionality were independent predictors of OS and PFS in Cox regression analysis.SUVmean (HR:4.61, p=0.002 for OS and HR: 3.64, p=0.001 for PFS), multilesionality (HR:3.58, p=0.009 for OS and HR: 2.67, p=0.012 for PFS) and sphericity (HR: 4.80, p=0.004 for OS). **Conclusion:** In patients with glioma, SUV-based variables, obtained from ^{18}F-fluorocholine PET/CT, showed association with histological and molecular characteristics of tumors.Some metabolic variables were stronger prognostic predictors than biological ones, as patients with tumors with higher SUVmean, lower sphericity and multiple foci on ^{18}F-fluorocholine PET/CT, had shorter PFS and OS. **References:** None.

EP-0097

MGMT methylation and IDH1 mutations do not affect [^{18}F] FDOPA uptake in primary brain tumors

A. Chiaravalloti[1], *A. Cimini*[1], *M. Zinzi*[2], *M. Salzillo*[2], *E. Di Giorgio*[2], *V. Villani*[3], *O. Schillaci*[1];
[1]*Department of biomedicine and prevention, University Tor Vergata, Rome, ITALY,* [2]*IRCCS Neuromed, Pozzilli, ITALY,* [3]*Neuroncology Unit, IRCCS Regina Elena National Cancer Institute, Rome, ITALY.*

Aim/Introduction: The aim of our study was to investigate the effects of methylation of the promoter of methyl guanine methyl transferase (MGMT) and isocitrate dehydrogenase (IDH1) mutations on amino acid metabolism evaluated with [^{18}F]-L-dihydroxyphenylalanine [^{18}F] FDOPA) Positron Emission Tomography/Computed Tomography (PET/CT uptake in primary brain tumors (PBT). **Materials and Methods:** 72 patients with PBT were enrolled in the study (33 women and 39 men; mean age 44±12 yo). All of them were subjected to PET/CT examination after surgical treatment. Of them, 29 (40,3%) were affected by grade II glioma and 43 (59,7%) by grade III. PET/CT was scored as positive or negative and standardized uptake value ratio (SUVr) was calculated as the ratio between SUV max of the lesion vs. that of the background. Statistical analysis was performed with the Mann Whitney U test. **Results:** Methylation of MGMT was detectable in 61 out of the 72 patients examined. Mean SUVr in patients without methylation of MGMT was 1.44±0.38 vs. 1.35±0.48 of patients with methylation (p=0.15). Data on IDH1 mutations were available for 43 subjects; of them, 31 had a deletion of IDH. Mean SUVr was 1.38±0.51 in patients with deletion and 1.46±0.56 in patients without deletion (p=0.79). **Conclusion:** MGMT methylation and IDH1 mutations do not affect [^{18}F] FDOPA uptake in primary brain tumors; thus representing a biomarker independent from the genetic patterns explored in our study. Analyses of quantitative uptake may not require adjustments for MGMT methylation and IDH1 mutations. **References:** None.

EP-0098

PET- and MRI-derived [^{18}F]FET PET parameters for the discrimination of low- and high-grade gliomas

S. Donche[1], *M. Henrotte*[1], *S. Bonte*[1,2], *J. Verhoeven*[3,1], *M. Acou*[4], *C. Van den Broecke*[5], *R. Van Holen*[6], *I. Goethals*[1];
[1]*Department of Nuclear Medicine, Ghent University Hospital,*

Ghent, BELGIUM, [2]Department of Electronics and Information Systems, Ghent, BELGIUM, [3]Department of Pharmaceutical Analysis, Ghent University, Ghent, BELGIUM, [4]Department of Radiology, Ghent University Hospital, Ghent, BELGIUM, [5]Department of Pathology, Ghent University Hospital, Ghent, BELGIUM, [6]Department of Electronics and Information Systems, Ghent University Hospital, Ghent, BELGIUM.

Aim/Introduction: Gliomas are the most frequent malignant primary brain tumours in adults and can be classified into either low-grade gliomas (LGG) or high-grade gliomas (HGG). There is an increasing interest in non-invasive diagnostic methods to support preoperative treatment planning, due to the risks associated with performing biopsies and resections. In this retrospective study, the role of different positron-emission tomography (PET)-based, and magnetic resonance imaging (MRI)-based O-(2-[18F]fluoroethyl)-L-tyrosine ([^{18}F]FET) PET-parameters in discriminating HGG from LGG was investigated. **Materials and Methods:** A pre-treatment [^{18}F]FET PET-scan and an anatomical MRI were performed in 30 patients (14 LGG and 16 HGG).Twenty-four PET-derived parameters were calculated using various SUV thresholds. Subsequently, an in-house developed segmentation algorithm [1] was used to label different tissue categories on both contrast-enhanced T_1-weighted and FLAIR MR images: necrosis (N), oedema (OE), non-enhancing tumour (NET) and contrast-enhancing tumour (CET). MR-derived tumour masks were applied to the PET-images to calculate 55 PET-parameters. PET- and MR-derived FET PET-parameters were compared between HGG and LGG. Significantly different parameters were analysed by ROC analysis. **Results:** Significant differences between HGG and LGG were found for 13 out of 24 and 17 out of 55 parameters for respectively the PET- and MR-derived PET-parameters. **Conclusion:** This study illustrates that various PET- and MRI tumour-derived [18F]FET PET-parameters are significantly different between HGG and LGG. Hence, these parameters may aid the pre-treatment diagnostic classification of gliomas. **References:** [1] Bonte, S., Goethals, I., & Van Holen, R. (2018). Machine learning based brain tumour segmentation on limited data using local texture and abnormality. Computers in biology and medicine, 98, 39-47.

EP-0099

Comparison of the diagnostic accuracy for intracranial germ cell tumours between ^{11}C-methionine and ^{18}F-fluorodeoxyglucose positron emission tomography/computed tomography

I. Kuji[1], *T. Suzuki*[2], *T. Yamane*[1], *A. Seto*[1], *E. Uchida*[2], *M. Shirahata*[2], *J. Adachi*[2], *K. Fukushima*[1], *K. Mishima*[2], *A. Sasaki*[3], *M. Yasuda*[4], *R. Nishikawa*[2];

[1]*Department of Nuclear Medicine, Saitama Medical University International Medical Center, Hidaka, Saitama, JAPAN,* [2]*Department of Neuro-Oncology/Neurosurgery, Saitama Medical University International Medical Center, Hidaka, Saitama, JAPAN,* [3]*Department of Pathology, Saitama Medical University, Moroyama, Saitama, JAPAN,* [4]*Department of Pathology, Saitama Medical University International Medical Center, Hidaka, Saitama, JAPAN.*

Aim/Introduction: Intracranial germ cell tumours (IGCT) are rare tumours occurring mostly in children and young adults. A few systematic reviews have reported the use of ^{11}C-methionine (^{11}C-MET) positron emission tomography/computed tomography (PET/CT) in the detection and follow-up of IGCT [1-2]. We compared the diagnostic accuracies of ^{11}C-MET and ^{18}F-fluorodeoxyglucose (FDG) PET/CT. **Materials and Methods:** The subjects were 36 patients (age: 5-59 years) with IGCT (25 with germinoma, 5 with mixed germ cell tumour, 3 with immature teratoma, and 3 with yolk sac tumour) who underwent ^{11}C-MET PET/CT before therapy and/or at serial follow-ups. There were 65 PET/CT scans showing 33 patients with tumours (TM+) and 32 without (TM-). A volume of interest analysis was performed on the tumours and on both intact contralateral brain and intact cerebellum. Indices of maximum standardised uptake value (SUV_{max}), tumour-to-normal-brain ratio (TNR), and tumour-to-cerebellar ratio (TCeR) were obtained from the measured values on ^{11}C-MET and ^{18}F-FDG PET/CT. The tumour size, human chorionic gonadotropin beta (hCGβ), alpha-fetoprotein (AFP), and tumour-free survival (TFS) were correlated with the PET indices. The PET indices in TM(+) and TM(-) were compared using receiver operating characteristic (ROC) curve analysis. **Results:** The areas under the ROC curve (AUCs) for SUV_{max}, TNR, and TCeR were 0.917 ($p<0.0001$), 0.925 ($p<0.0001$), and 0.936 ($p<0.0001$), respectively, on ^{11}C-MET PET/CT, while the AUCs were 0.732 ($p=0.003$), 0.684 ($p=0.017$), and 0.707 ($p=0,007$), respectively, on ^{18}F-FDG PET/CT. Moreover, the AUC for tumour size was 0.779 ($p<0.0001$) and for hCGβ was 0.599 ($p=0.197$). The AUC in both types of PET was higher for TNR than for TCeR. Among all the indices, the ^{11}C-MET-TCeR had the highest AUC. All AUCs on ^{11}C-MET PET/CT were higher than those on ^{18}F-FDG. The optimal threshold for the discrimination of TM(+) from TM(-) was 1.65 for SUV_{max}, 1.55 for TNR, and 1.05 for TCeR on ^{11}C-MET PET/CT. **Conclusion:** TCeRs on ^{11}C-MET PET/CT demonstrated the highest AUC (0.936) for the detection of intracranial germ cell tumours. The optimal threshold of TCeR was 1.05, with 77% sensitivity and 94% specificity on ^{11}C-MET PET/CT. **References:** [1]Fukuoka K, Yanagisawa T, Watanabe Y, Suzuki T, et al. Clinical interpretation of residual uptake in ^{11}C-methionine positron emission tomography after treatment of basal ganglia germ cell tumors: report of 3 cases. J Neurosurg Pediatr. 2015;16:367-71. [2]Okochi Y, Nihashi T, Fujii M, Kato K, et al. Clinical use of ^{11}C-methionine and ^{18}F-FDG-PET for germinoma in central nervous system. Ann of nucl med. 2014;28:94-102.

EP-0100

99mTc-DMSA (V) SPECT/CT scanning in patients with brain gliomas: diagnostic and prognostic utility

Y. G. Abdelhafez[1,2], *N. Ragab*[3], *W. Diab*[3], *W. Abd-El-Ghani*[3], *M. ElNaggar*[3], *M. Mekkawy*[3];

[1]*University of California Davis, Sacramento, CA, UNITED STATES OF*

AMERICA, [2]South Egypt cancer Institute, Assiut University, Assiut, EGYPT, [3]Faculty of Medicine, Assiut University, Assiut, EGYPT.

Aim/Introduction: Several PET and SPECT tracers are available for the differentiation between radiation necrosis and residual/recurrent glioma. PET with radio-labeled amino acids, has several advantages; however, it is expensive and not widely available, especially in developing world. SPECT has the advantages of being more widely-available and less expensive. Multiple SPECT tracers have been explored. The aim of this work was to evaluate the utility of post-therapy 99mTc-pentavalent dimercaptosuccinic acid (DMSA (V)) brain SPECT/CT in patients with glioma. **Materials and Methods:** Patients with pathologically or radiologically documented glioma were prospectively recruited for this study. 99mTc-DMSA (V) brain SPECT/CT scanning was acquired after a mean interval of 10 weeks from therapy, 2-3 h. after i.v. injection of 555-740 MBq of the tracer. Three nuclear medicine physicians (experience was 10, 22 and 15 years for readers 1, 2, and 3; respectively) independently and blindly interpreted the images visually as positive or negative for residual/recurrent disease. Agreement between two or more readers was considered a consensus. Reader 1 was asked to repeat the readings after 3 months interval to establish intra-reader agreement. All the readings were compared against the reference standard which was formulated based on subsequent clinical/neuroimaging follow up or pathology whenever performed. Overall survival was calculated from time of diagnosis till death or last follow-up. **Results:** Thirty-Four patients; (18 male,16 female; mean age 37.7±16, 82% of them with high grade glioma) were enrolled in this study. According to the reference standard, residual/recurrent disease was documented in 16 patients, while 18 patients were disease free. Consensus reading of 99mTc-DMSA (V) SPECT/CT successfully identified 13 true positive (sensitivity 81%, 95% confidence interval [CI]:54-96%) and 17 true negative cases (specificity 94%, 95% CI:73-100%). The overall accuracy was 88% (95% CI: 72-96%). Inter-observer kappa agreement between the three readers ranged from 0.71 to 0.82. Intra-observer agreement for Reader 1 was 0.76 (95%CI: 0.50-0.94). After 2-year of follow-up, 4/20 patients with negative DMSA (V) findings died compared to 7/14 with positive findings (overall survival was 65% compared to 0%, respectively, p=0.004). **Conclusion:** Post-therapy brain SPECT/CT with 99mTc- DMSA (V) is reliable and specific tool for assessment of patients with glioma after definitive therapy. Positive scans are linked to worse overall survival. **References:** None.

EP-0101

Comparison of diagnosis vaiue between PET/CT and PET/MR in brain tumors: a preliminary study

***Y. Xu**, J. Wang, S. Wang, C. Li;*
Hangzhou Universal Imaging Diagnostic Center, Hangzhou, CHINA.

Aim/Introduction: A retrospective study was done to explore the diagnosis value of PET/CT and integrated TOF PET/MR in brain tumors and the differences of two systems were compared. **Materials and Methods:** 32 patients with intracranial tumors done sequentially ^{18}F-FDG PET/CT imaging and PET/MR brain imaging on the same day were enrolled. Referring to the pathology and follow-up results, t test and χ2 test were used to compare the semi-quantitative value and the diagnostic performance between PET/CT and PET/MR. **Results:** A total of 78 lesions, including10 glioma, 11 lymphoma, 55 metastases, 1meningiomas, 1 pituitary. 31 additional lesions were found in PET/MR while not in PET/CT, and there was a statistically significant difference between the two (χ^2 =38.69, P<0.01). The SUVmax-MR and SUVmax-CT of 50 lesions whose 18F-FDG uptake were significantly higher than brain parenchyma were in good agreement (r=0.799). The T/B values of PET-MR were slightly higher but no statistically difference (t=1.297, p<0.05) with PET-CT. For other 28 lesions with comparable or lower uptake of brain parenchymal, PET/MR detected 17 more lesions than PET/CT, and the detection rates were statistically significant (χ^2 =28.76, P<0.01). There were 36 lesions with obvious edema found in both examinations, though 3 in PET/CT only found edema with no clear lesions. Among the 42 lesions with no edema, 28 more were found in PET/MR which is significant different with PET/CT (χ2=42.00, P<0.01). For 62 lesions with Dmax <3.0 cm, 31 more were found in PET/MR, demonstrating significant difference with PET/CT. **Conclusion:** Compared with PET/CT, better detection rate of intracranial lesions was obtained for lesions with mild uptake (comparative to brain parenchyma), with no obvious edema, and with Dmax <3.0 cm which benefit from the higher SNR of PET and excellent MR soft-tissue contrast in integrated PET/MR. **References:** None.

EP-0102

Value of quantitative Tc-99m Pentavalent (V) DMSA brain SPECT in predicting prognosis in patients with Glioblastoma Multiforme

***A. Kandeel**, A. Badawy, M. A. Abougabal, E. Abdelhady;*
Faculty of Medicine, Cairo University, Cairo, EGYPT.

Aim/Introduction: Introduction: Gliomas are the most common primary brain tumours, representing 40-50% of cases. GBM (WHO grade IV) is the most common type of primary gliomas; and also the most aggressive and resistant to treatment. The median survival time for malignant glioma grade IV by WHO is about 12 months. **Aim:** To evaluate the value of qualitative and quantitative 99m Tc (V)-DMSA uptake by the viable tumour tissue in patients with GBM before and after the end of therapy and correlating the SPECT results to the overall survival (OS) and progression-free survival (PFS). **Materials and Methods:** This prospective study included 40 patients (16 males and 14 females; mean age 47.8 ± 12.9 years) with pathologically proven Glioblastoma Multiform (GBM). Patients were clinically assessed for performance status to determine the treatment protocol. Brain SPECT studies were acquired early at 30 min

and late after 120 min after I.V injection of 15-20 mCi of ^{99m}Tc (V) DMSA at baseline as well as at least 4 weeks after the end of radiotherapy. SPECT images were interpreted qualitatively by visual assessment and semi-quantitatively by calculation of lesion/non-lesion (L/NL) ratio and retention index (RI). SPECT results in baseline and in follow up studies were correlated with the OS and PFS. The overall survival was calculated from the date of diagnosis (in the current study we considered it as the date of surgery) till the end of follow up period or death. The Progression-free survival was calculated from the date of diagnosis to the date of documented disease progression (clinical deterioration of the patients or radiological evidence of disease progression) or the date of death from any cause. **Results:** At baseline, enhanced ^{99m}Tc (V) DMSA uptake (either positive or negative) was significantly correlated with PFS at both early and late images (p 0.04 and 0.026, respectively) and with OS only at late images (p 0.036). Quantitatively, L/NL ratios at late images (mean 3.6±1.3) showed a statistically significant correlation with PFS and OS (p 0.021 and 0.025, respectively). RI had a significant positive correlation with only PFS (p 0.01). **Conclusion:** A a significant association between the degree of tumour uptake in ^{99m}Tc (V) DMSA brain SPECT and the overall & progression-free survival in patients with brain GBM. In addition ^{99m}Tc (V) DMSA brain SPECT may predict the prognosis of patients with brain GBM and can expect shorter progression-free survival in tumours with increased retention index. **References:** None.

EP-0103

Incremental values of FDG PET/CT by glucose loading for characterization and delineation of brain tumors

***D. Kim**, H. Ko, S. Lee, S. Kim, J. Chung, M. Yun;*
Yonsei University, Seoul, KOREA, REPUBLIC OF.

Aim/Introduction: F-18 fluorodeoxyglucose (FDG) PET/CT has been used successfully for diagnosis in patients with malignancy. However, FDG may not be the suitable tracer for detection of gliomas because of the high-rate of physiologic glucose metabolism in normal brain tissue. In this study, we aimed to enhance the value of FDG PET/CT for the detection and delineation of brain tumors by regulating blood glucose level. **Materials and Methods:** Nine patients with a suspicion of glioma underwent two FDG PET/CT scans; one with fasting and the other with glucose loading. For glucose loading, the patient was given intravenous infusion of 10% Dextrose water (DW) to obtain approximately 200mg/dL of blood glucose level. On each patient, standardized uptake value (SUV) and tumor-to-normal cortex (T/N) ratio on FDG PET/CT images were analyzed. In addition, FDG PET/CT of mouse glioblastoma (GBM) models were obtained on an animal PET and the correlation of T/N ratio with blood glucose level was assessed. Finally, FDG uptake of GBM cells (U87MG) and human neuron cells (HNC2) was compared under a different concentration of glucose in the media. **Results:** Based on the new 2016 World Health Organization (WHO) classification, there were 3 low grade gliomas and 7 high grade gliomas included. With glucose infusion, the tumor was delineated more clearly than the control in all high grade tumors. T/N ratio was 2.09 ± 0.55 under glucose loading and 1.70 ± 0.54 at fasting ($p < 0.05$) in high grade gliomas. In contrast, no remarkable FDG uptake was noted in low grade gliomas (T/N ratio with glucose loading vs fasting, 0.81 ± 0.03 vs 0.72 ± 0.07). Analysis of animal PET images also showed a significant positive correlation of T/N ratio over the blood glucose levels (R^2= 0.849). Similarly, at the cellular level, tumor to neuron ratio was 2.89 ± 0.49 in high glucose level and 1.74 ± 0.25 in low glucose levels ($P < 0.005$). **Conclusion:** In brain tumors, FDG PET/CT under glucose loading provided better tumor delineation compared with FDG PET/CT at fasting due to the lower background uptake in the normal cerebral cortex. FDG PET/CT methodology of regulating blood glucose can improve sensitivity for the characterization and volume delineation of brain tumor. **References:** None.

EP-0104

^{68}Ga-DOTANOC PET/CT in Meningioma

***S. Shamim**, G. Arora, J. Hussain, S. Somani, S. Datta Gupta, M. Tripathy, N. A. Damle, R. Kumar, C. Bal;*
All India Institute of Medical Sciences, Delhi, INDIA.

Aim/Introduction: Meningioma are the most common non-glial tumors and are mostly benign. Its incidence is higher in females and increases with age. The expression of somatostatin receptor in meningioma is well known that may be exploited for developing potent diagnostic and/or theranostic tool using ^{68}Ga-DOTANOC. Hence, we evaluated the diagnostic utility of ^{68}Ga-DOTANOC PET/CT in patients with meningioma. **Materials and Methods:** Fourteen patients (7 male, 7 female) of suspected or known meningioma, who underwent ^{68}Ga-DOTANOC PET/CT at our institute, were retrospectively evaluated. All patients were injected 3-5mCi of ^{68}Ga-DOTANOC intravenously. Whole body scan (vertex to mid-thigh) and an additional spot view of either brain or head and neckwas acquired for each patient on a dedicated PET/CT scanner (BiographmCT, Seimens, Germany or Discovery 710, GE, US) 60 minutes post-injection. PET/CT diagnosis was later corroborated with histopathology, clinical follow-up or conventional imaging suggestive of meningioma, assuming them as reference standard.Semi-quantitative analysis was done by estimating SUVmax of the lesion and the contralateral background. **Results:** Mean age of the patients was 41.8±15.7 years. Twelve out of fourteen patients (~86%) were positive for meningioma on PET/CT while two were negative. PET/CT findings were equivocal for glomus jugulare in one of the negative cases and for calcified granuloma in the other patient, with meningioma as the second differential in both the cases. The 12 PET/CT positive patients were also positive on the basis of reference standard. Amongst these 12 patients, 8 were biopsy proven while 4 others were confirmed by clinical data and conventional imaging. Therefore, it shows a strong correlation between PET/CT and other reference standard modalities in the detection of meningioma. Furthermore, the lesion to background ratio in these 12 patients was very high

with a median value of 17.85 indicating high SSTR expression in meningioma in contrast to normal brain parenchyma. **Conclusion:** ^{68}Ga-DOTANOC PET/CT can be an effective tool for the diagnosis of meningioma, owing to its high SSTR expression. Further evaluation with larger patient population, might be useful to study its theranostic application, especially in unresectable lesions. **References:** None.

EP-0105

Comparison between dynamic [18F]Fluoroethyltyrosine PET/CT and advanced MRI in cerebral high and low grade gliomas

L. Picori, U. Rozzanigo, D. Donner, M. Erini, P. Feraco, M. Recla, F. Chierichetti;
Santa Chiara Hospital, Trento, ITALY.

Aim/Introduction: To investigate if dynamic [18F]fluoroethyl-L-tyrosine [18F]FET PET/CT improves the diagnosis in patients with suspected new or recurrent cerebral gliomas, respect to advanced MRI techniques. **Materials and Methods:** We retrospectively evaluated 20 patients who performed [18F] FET by a PET/CT tomograph: 15 had an indeterminate brain lesion, 5 a suspect glioma recurrence. All patients underwent a 40 minutes dynamic [18F]FET PET/CT acquisition and two different sequences, between 5-15 minutes and 20-30 minutes. For dynamic studies time-activity and time to peak curves were extracted using different region-of-interest (ROIs) and volume of interest (VOIs) definitions. MRI was performed with a 1.5T scanner just before [18F]FET-PET/CT using perfusion (PWI) and diffusion (DWI) weighted imaging: afterwards rCBV and ADC values were calculated placing the VOIs on the solid components of the lesion. In case of doubt (13 cases) single-voxel MR spectroscopy was performed. Multimodality imaging by fusion of PET/CT and different MRI sequences was performed for a joint assessment (radiologist and nuclear physician). **Results:** Final diagnosis was based on histology in 8 patients who underwent neurosurgery (5 HGG, 3 LGG) and on follow-up imaging in 12 patients (8 tumor progression, 4 stable benign lesion). On the basis of [18F]FET-PET, 7 cases were classified as high uptake (2 glioma recurrence and 5 new diagnosis of HGG tumor), 8 as low uptake (4 glioma recurrence, 2 new diagnosis of LGG tumor, 1 tumor progression, 1 tumefactive demielinating lesion) and 5 as no uptake (1 new diagnosis of LGG tumor, 4 stable benign lesion). Sensibility for dynamic [18F]FET-PET was 93% and specificity was 80%. Multiparametric MRI was in agreement with [18F]FET-PET in all 7 cases of high uptake and in 5 cases of low uptake. [18F]FET-PET helped to classify 6 MRI indeterminate lesions (2 suspect radionecrosis with pathologic uptake, 4 benign lesions without uptake). In 2 cases there was a discrepancy between MRI and PET: 1 tumefactive demielinating lesion was classified by [18F] FET as low uptake lesion, 1 LGG confirmed at histology showed no uptake. **Conclusion:** In our experience, adding quantitative data, such as dynamic acquisition in PET/CT by aminoacid tracer like [18F]FET, to rCBV and ADC maps in advanced MRI is crucial for a better comprehension of tumor lesions and to assess grading. Dynamic [18F]FET-PET/CT and multiparametric MR imaging have a very high sensibility to detect new tumoral lesions or suspect glioma recurrence. Agreement between PET and MRI is essential to improve diagnostic specificity. **References:** None.

EP-0106

^{18}F-FET PET/CT In The Management Of Patients With Brain Tumor

M. Colandrea[1], *I. M. Milanesi*[2], *E. Lamperti*[2], *M. Schiariti*[2], *S. Alessi*[1], *M. E. Ferrari*[1], *S. L. Fracassi*[1], *L. L. Travaini*[1], *A. Silvani*[2], *L. Fariselli*[2], *P. Ferroli*[2], *A. S. Cascio*[1], *S. Papi*[1], *M. Fiorenza*[1], *C. M. Grana*[1];
[1]*Istituto Europeo di Oncologia, Milano, ITALY,*
[2]*Istituto Neurologico Besta, Milano, ITALY.*

Aim/Introduction: The aim is to present our experience with ^{18}F-FET PET as diagnostic tool in the initial staging of suspected glioma (for guiding biopsy or when biopsy is not feasible) or for differentiation of glioma recurrence from radionecrosis. **Materials and Methods:** We performed PET/CT with ^{18}F-FET in 30 patients with a doubtful MR imaging. Group A: 21/30 patients affected by brain tumors (1 GI, 7 GII, 8 GIII, 5 GIV according to WHO 2016) and already treated with surgery and radio-chemotherapy. These patients were evaluated by ^{18}F-FET PET in order to better define the nature of the lesions. Group B: 9/30 patients received ^{18}F-FET PET in the initial staging for guiding biopsy or when biopsy is not feasible. Manually drawn regions of interest over areas of maximal FET uptake were used to calculate tumor to background ratios (TBRmax). **Results:** 23 patients underwent 0-40 dynamic ^{18}F-FET PET scans and 7pts received a 20-40 min scan. TBRmax was assessed in the 20-40 min summation images in all patients, as well as in summation images from 5-20 min in 23 patients: no differences between early and late images in terms of TBRmax was found. Group A: 17/21 patients had positive PET consistent with recurrent disease (TBRmax > 1.6), 1 patient with suspected recurrence (TBR max >1.52) and 3 had negative PET consistent with radiation necrosis (no focal uptake). Moreover in 1 patient with two MRI lesions, PET discovered a third area of pathological uptake. 2/17 positive patients are still in good clinical conditions (false positive PET?), 3 in stable disease, 2 in progression disease, 4 died and 6 were lost at follow-up. The patient with doubdful PET is in stable disease. 2/3 PET negative patients are still in follow-up while 1 died after seven months (false negative PET?). Group B: 6/9 patients had positive PET suspicious for glioma. To date, 3 have died (1 GII, 1 GIV and 1 without histological data) and 3 are lost at follow-up (between them 1 GIII). 3/9 patients had negative PET, in 1 patient biopsy revealed gliosis and 2 were lost at follow-up. **Conclusion:** ^{18}F-FET PET/CT fused with functional and morphological images allows a better definition of areas of uptake. ^{18}F-FET PET/CT allows a conclusive recognition of recurrence or radiation necrosis and is a useful tool for guiding biopsy or helping in the diagnosis when biopsy isn't possible. **References:** None.

EP-0107

99mTc-MIBI SPECT/CT and multi-parametric MRI in patients with brain gliomas after therapy: initial results

Y. G. Abdelhafez[1,2], *E. Roshdy*[2], *H. Atta*[2], *M. ElNaggar*[3], *S. Gamal*[3], *A. Kandeel*[4], *Y. Mohamed*[4], *M. Abdel-Wanis*[2];
[1]*University of California Davis, Sacramento, CA, UNITED STATES OF AMERICA,* [2]*South Egypt cancer Institute, Assiut University, Assiut, EGYPT,* [3]*Faculty of Medicine, Assiut University, Assiut, EGYPT,* [4]*Faculty of Medicine, Cairo University, Cairo, EGYPT.*

Aim/Introduction: Several molecular imaging tracers and MRI techniques are investigated for differentiating radiation necrosis from residual/recurrent glioma. We aimed to explore the utility of post-therapy 99mTc-methoxy-isobutyl-isonitrile (MIBI) brain SPECT/CT and multiparametric MRI (mpMRI) in patients with glioma. **Materials and Methods:** Patients with pathologically or radiologically documented glioma were prospectively recruited for this study. 99mTc-MIBI brain SPECT/CT scanning was acquired 1 h. after i.v. injection of 666-925 MBq of the tracer. Lesion volume was quantified using isocontour threshold of 70% of the maximum pixel counts (volMIBI). mpMRI was performed on a 1.5 Tesla MRI machine within a median of two weeks from MIBI SPECT/CT study for a subset of patients. Techniques included perfusion, with calculation of relative mean transit time and relative cerebral blood volume (rCBV), spectroscopy, with calculation of choline/NAA ratio, and diffusion, with calculation of mean apparent diffusion coefficient (ADC). Qualitatively, the readings from both modalities were reported on a 5-point probability score as (1=definitely negative, 2=probably negative, 3=equivocal, 4=probably positive, and 5=definitely positive for residual/recurrent disease malignant). For the purpose of analysis, scores≥3 were considered positive. **Results:** Thirty-five non-consecutive patients; (25 male, 10 female; mean age 43.5±16.4 years, 86% of them with high-grade glioma) were enrolled in this study. 8/21 patients who were scored positive on MIBI SPECT/CT died by the time of analysis, compared to only 1/14 scored negative (p=0.056). volMIBI was significantly higher in high-grade compared to low-grade tumors (1.0±1.4 vs. 2.6±2.4;p=0.039), and in patients who died compared to those who were still alive (1.9±1.9 vs. 3.8±3.2;p=0.038). volMIBI was significantly predictive of mortality with AUC from ROC analysis of 0.76 (95%CI:0.56-0.97;p=0.02). 13/35 patients underwent mpMRI. volMIBI showed strong positive correlation with Choline/NAA ratio (r=0.872;p=0.054). Both MIBI SPECT/CT and mpMRI agreed on categorizing 4 benign and 7 malignant lesions. Two patients showed positive findings only on MIBI. Those two patients continued to demonstrate increasing uptake on subsequent follow-up MIBI SPECT/CT scanning. One of them progressed rapidly and died on disease. 19/35 patients had at least one additional follow-up MIBI SPECT/CT study. Among the 19, 3/8 patients with negative initial findings demonstrated positive uptake on subsequent scans while the remaining 11, who were originally scored positive, continued to show uptake impressive of residual/recurrent disease. **Conclusion:** In patients with glioma, post-therapy brain SPECT/CT with 99mTc-MIBI can provide useful diagnostic and prognostic information, that may complement the results obtained from mpMRI. **References:** None.

EP-0108

Comparison of diagnostic accuracy of aMRI, ^{201}Tl-SPECT and ^{18}F-fluorocholine PET/CT in the follow-up of low-grade gliomas

N. Testart, *E. Triviño Ibañez, M. Zurita Herrera, A. Jorques Infante, R. Luque Caro, A. Gonzalez-Jiménez, M. Rashki, A. Rodriguez-Fernandez, M. Gómez-Río;*
Hospital Universitario Virgen de las Nieves, Granada, SPAIN.

Aim/Introduction: The follow-up of treated low-grade glioma (LGG) requires the evaluation of subtle clinical changes and MRI results. When the result is inconclusive, additional procedures are required to assist decision-making, such as the use of advanced MRI (aMRI) sequences and nuclear medicine scans such as SPECT and PET. The aim of this study was to assess and compare the sensitivities and specificities of each imaging procedure and to determine whether incorporating ^{18}F-fluorocholine PET/CT in the follow-up protocol for treated LGG improves diagnostic accuracy and if it has a clinical impact. **Materials and Methods:** This was a retrospective analysis of a prospective cochort of consecutive patients with treated LGG during standard follow-up with indeterminate clinical and/or radiological findings of tumour activity. All patients underwent clinical evaluation, aMRI, ^{201}Tl-SPECT and ^{18}F-fluorocholine PET/CT. Images were interpreted by visual evaluation complemented with semiquantitative analysis. To determine its sensitivity and specificity, the imaging results were compared to a gold standard, either a surgical resection or a biopsy or a consensus based on a follow-up > 6 months. **Results:** Between January 2012 and December 2017, 34 patients (20 men and 14 women, mean ± SD age 41 ± 11.6 years (range 19 - 61 years) were included in this study. The final diagnosis was established by histology (eight surgical specimens, one biopsie) or by consensus of the Neuro-Oncology Group (25 patients) after a follow-up of >6 months (mean 16.7 ± 2.83 months). In our cohort, the sensitivity and specificity respectively for each test were: aMRI 95% and 66% ^{201}Tl-SPECT 62% and 80%; ^{18}F-fluorocholine PET/CT 89% and 86%. The global diagnostic accuracies were 91% for aMRI (36% inconclusive), 65% for ^{201}Tl-SPECT (28% inconclusive), and 88% for ^{18}F-fluorocholine PET/CT with no inconclusive studies. The performance of ^{18}F-fluorocholine PET/CT had a clinical impact with changes in the pre-test intended management in 64.7% of patients. Preliminary results from this cohort have previously been published in this journal [1]. **Conclusion:** Our results support the need to complement structural MRI with aMRI and nuclear medicine procedures in selected patients. ^{18}F-Fluorocholine PET/CT can be useful in the individualized management of patients with treated LGG with uncertain clinical and/or radiological evidence of tumour activity. **References:** [1] Gómez-Río et al. Eur J Nucl Med Mol Imaging. 2015 May;42(6):886-95.

EP-0109

Spatial relationship of 11C-Methionine PET and Gd-enhanced MRI in oncological brain lesions by using a fully hybrid PET/MRI system

P. Mapelli[1,2], *P. Scifo*[2], *F. Fallanca*[2], *V. Bettinardi*[2], *A. Castellano*[1,3], *M. Barbera*[1,3], *A. Falini*[1,3], *L. Gianolli*[2], *N. Anzalone*[1,3], *M. Picchio*[1,2];
[1]*Vita-Salute San Raffaele University, Milan, ITALY,* [2]*Nuclear Medicine Department, IRCCS San Raffaele Scientific Institute, Milan, ITALY,* [3]*Neuroradiology Unit and CERMAC, IRCCS San Raffaele Scientific Institute, Milan, ITALY.*

Aim/Introduction: 11C-Methionine (MET) PET and Gd-enhanced MRI regions are known to be both related with malignancy of brain neoplasms. In the present study their mutual relationship by using a fully hybrid PET/MRI system was explored in a group of patients with brain oncological lesions. **Materials and Methods:** Nine patients (13 lesions) with MRI suspicion for recurrent oncological disease underwent fully hybrid PET/MRI with MET. During the simultaneous acquisition of PET and MRI, the MRI protocol consisted of T2w, FLAIRw, 3D-T1w pre- and post-contrast, diffusion and Dynamic contrast enhanced (DCE) perfusion sequences. MET PET and MR perfusion were firstly co-registered to 3D-T1 MR. A volumetric region of interest (VOI) was used to measure standardized uptake value (SUV) max, metabolic tumour volume (MTV) and SUVmean for each lesion evident on MET images. A first analysis was performed by defining a second VOI based on the Gd-enhanced regions. Dice coefficient between the two VOIs was calculated to assess the overlapping between them. **Results:** Ten/13 lesions detected by MRI resulted positive (metabolically active) on MET PET images (mean SUVmax: 4,5; range: 2,5-10,8; mean SUVmean: 2,7; range: 1,5-6,5; MTV: 21,7, range: 0,5-94,6). The mean value of Dice coefficient among patients with both positive regions was 0.55±0.18. **Conclusion:** In patients affected by oncological brain lesions, MET PET is confirming its capability in differentiating between tumour active lesions and post therapeutic effects. From this preliminary spatial location analysis, it is evident that the areas defined by MET PET SUV and Gd MRI characterize different aspects of the tumour lesions (active lesions within non enhancing areas and viceversa) even if there is a quite good overlapping. Further analysis on the complete cohort of patients evaluating the quantitative perfusion and diffusion maps will be useful to deeply investigate these potentially relevant aspects of recurrent brain lesions. **References:** None.

EP-0110

Relationship Of Hearing Preservation Of Patients With Neurofibromatosis Type 2 With Tumor Maximum Standardized Uptake From The 11c-met Pet/ct Images

X. Zhao, *Z. Chen, S. Li, S. Zhang, C. Zhao, J. Zhang, X. Wang, F. Zhao, P. Liu, L. Ai;*
Beijing Tiantan hospital, Beijing, CHINA.

Aim/Introduction: Preoperative hearing test results was an important index for evaluating hearing functional preservation in Neurofibromatosis Type 2 (NF2) patients with bilateral vestibular schwannomas (VS) who underwent surgery resection. The aim of this study was to investigate the utility of SUVmax on ^{11}C-MET PET/CT in patients with NF2 to predict the change of hearing. **Materials and Methods:** Thirty young NF2 patients in a prospective natural history (17 men, 13 women; median age, 21.7 years) with 53 measurable hearing ears was minored by brain ^{11}C-MET PET/CT and MRI imaging from 2015 to 2018. The hearing function was classified by the American Academy of Otolaryngology-Head and Neck Surgery (AAO-HNS) criteria. Tumor maximum standardized uptake (SUVmax) was obtained from PET/CT images automatically . Cox regression were used to assess the association between PET/CT markers with hearing. **Results:** Eighteen ears maintained effective hearing (Class A and B) ears while 35 ears hearing significant loss (Class C and D) among 53 ears during follow-up. The SUVmax was correlated significantly with hearing grades (P=0.002, rs=0.324). In comparison with those patients with low metabolic activity in ^{11}C-MET PET/CT findings (SUVmax<2.75), a significant decrease of hearing was discovered in patients with high metabolic activity in ^{11}C-MET PET/CT findings (SUVmax>2.75) . The higher SUVmax was associated with hearing decrease on a univariate Cox model (hazard ratio = 0.433, P=0.002). **Conclusion:** The SUVmax was related to the patient's hearing in NF2, as an independent predictive factor of hearing loss in natural history. **References:** None.

EP-06

Translational and Molecular Imaging Therapy: Optimisation of Tracer Kinetics

October 12 - 16, 2019 e-Poster Area

EP-0111

First Reported SPECT/CT to Investigate Pharmacokinetics of Host Defence Peptides

K. Saatchi[1], *T. V. F. Esposito*[1], *D. Pletzer*[2], *C. Blackadar*[1], *C. Rodriguez-Rodriguez*[1], *R. E. W. Hancock*[2], *U. O. Häfeli*[1];
[1]*Faculty of Pharmaceutical Sciences, University of British Columbia, Vancouver, BC, CANADA,* [2]*Centre for Microbial Disease and Immunity Research, Department of Microbiology and Immunology, University of British Columbia, Vancouver, BC, CANADA.*

Aim/Introduction: Host defense peptides (HDPs) are short, cationic, amphipathic peptides with antimicrobial and immunomodulatory activity. HDPs present a promising alternative to existing antibiotics, which is of significance given the rise in antimicrobial resistance. Challenges, such as the aggregation of HDPs in biological media and lack of comprehensive pharmacokinetic assessments, have delayed

their translation into the clinic. This study presents the first detailed look at the biodistribution of lead HDPs and novel formulations using nuclear imaging techniques. **Materials and Methods:** HDPs (eg. IDR1002) and formulations thereof were radiolabeled with ^{67}Ga and characterized by standard techniques. The tracer was administered to healthy mice at different dose levels (2, 5 and 50 mg/kg) via subcutaneous, intravenous, intraperitoneal, and intratracheal delivery. Each mouse underwent serial SPECT/CT scans up to 48 hours to quantitatively track the distribution of the HDP. An ex vivo biodistribution was also conducted following the terminal scan. **Results:** ^{67}Ga- IDR1002 precipitated upon injection forming a local depot in the peritoneal cavity, subcutaneous fat, and lung parenchyma. The peptide was slowly absorbed systemically (i.e., subcutaneous absorption half-life was ~6h) and predominantly excreted renally. The peptide also precipitated into micron-size particles in the blood, which embolized in the lung capillaries and was lethal at higher doses. From the lung, the peptide cleared via the reticuloendothelial system and kidneys. **Conclusion:** This study is an important first step in examining the behaviour of HDPs in vivo. The tendency of IDR1002 for example to precipitate upon injection may be useful for some treatments, by forming a local depot of the drug and slowly releasing it thereafter. However, most indications and route of administration will require novel formulations of the peptide to overcome uncontrolled aggregations. **References:** None.

EP-0112

Comparison of the Physiological Uptake of ^{68}Ga-PSMA Between Early and 60-min Post-injection PET/CT Scans

T. Hekimsoy, S. Isgoren, G. Daglioz Gorur, H. Demir; Kocaeli University School of Medicine, Department of Nuclear Medicine, Kocaeli, TURKEY.

Aim/Introduction: The purpose in this study was to investigate the change in the physiological uptake of ^{68}Ga-PSMA between early (5-min and 15-min) and 60-min post-injection PET/CT scans. **Materials and Methods:** One hundred eighty male patients (mean age: 68.3±8.2) who underwent ^{68}Ga-PSMA PET/CT were analyzed. Patients were divided into two groups. PET/CT was performed at 5-min and 60-min in the first group (n=60) and at 15-min and 60-min in the second group (n=120) after administration of ^{68}Ga-PSMA. Physiological uptake was determined by calculating SUV_{max} for the lacrimal, parotid and submandibular glands, mediastinal blood pool, spleen, duodenum and SUV_{mean} for the liver and compared between early and 60-min images. Any 10% change in the SUV values was accepted as increase or decrease. The average SUV difference ($DIFF_{ave}$) between two datasets was calculated. The average percent differences ($\%DIFF_{ave}$) were calculated by dividing the SUV difference to the SUV value at 60-min post-injection. **Results:** In the first group (5-min); SUV_{max} of the lacrimal, parotid and submandibular glands was increased in 100% (n=60) of the patients and SUV_{max} of the duodenum was increased in 83.4% (n=50) of the patients in 60-min scans. Decrease of the uptake was observed in the spleen (55%, n=33), mediastinum (90%, n=54) and liver (100%, n=60). In the second group (15-min); SUV_{max} increased in the lacrimal glands (90.8%, n=109), parotid glands (100%, n=120), submandibular glands (85%, n=102) and duodenum (82.5%, n=99) in 60-min scans while decrease of the uptake was observed in the spleen (60.8%, n=73), mediastinal blood pool (75.8%, n=91) and liver (100%, n=120). $DIFF_{ave}$ of the lacrimal, parotid and submandibular glands, mediastinal blood pool, liver, spleen and duodenum were 3.8, 5.1, 4, 1.3, 1.7, 1,6 and 3.5 g/mL respectively for the first group and 3.5, 4.5, 3.9, 0.7, 1.3, 3.7, 3.6 g/mL respectively for the second group. $\%DIFF_{ave}$ of the lacrimal, parotid and submandibular glands, mediastinal blood pool, liver, spleen and duodenum were 36.2%, 29.6%, 22.4%, 48%, 43.2%, 21.9% and 28.9% respectively for the first group and 31.5%, 24.4%, 20.2%, 27.4%, 34%, 23.8%, 28.3% respectively for the second group. The correlation between early (5-min and 15-min) and 60-min post-injection scans was good ($P<0.01$) in all evaluated physiological uptake areas. **Conclusion:** It is observed that ^{68}Ga-PSMA uptake of lacrimal and salivary glands and gastrointestinal tract increases in time while uptake of liver, spleen and mediastinal blood pool tends to decrease. **References:** None.

EP-0113

Monitoring early vascular disrupting agent (VDAs) treatment response with 68Ga-DOTA-Heptap, an albumin binding tracer, in vivo PET/CT imaging

C. Huang[1], G. Chang[1], J. Lin[1], S. Hsu[1], W. Chang[1], F. Huang[2]; [1]Center for Advanced Molecular Imaging and Translation, Taoyuan, TAIWAN, [2]National Taiwan University, Taipei, TAIWAN.

Aim/Introduction: The dynamic tumor vasculature changes may be associated with tumor staging, treatment responds monitoring and prognostic evaluation. In this study, the feasibility of using novel blood pool tracer-68Ga-DOTA-Hepta as a surrogate biomarker for early detection of the functional status of tumor vasculature and whether such a biomarker can be used to monitor the treatment response after vascular disrupting agent treatment was evaluated in vivo. **Materials and Methods:** A subcutaneous tumor model was established by inoculation of 5×10^6 of U87MG tumor cells into the front flanks. The resultant tumors were allowed to grow for 3–5 weeks until they reached volumes of 200–500 mm^3. Tumor-bearing mice were treated with vascular disrupting agent CA4-P at a dose of 40mg/kg by intraperitoneal injection once a week for 2 weeks. As a control, saline (100uL) was injected into the control cohort of mice (n=5), repeating the same procedures. In addition to the PET/CT imaging assessment, the tumor growth was monitored every three days by caliper measurement of the perpendicular dimensions of each mass ($0.5\times$ length $\times$ width^2) during the experimental period. **Results:** Extremely high vessel density of glioblastoma U87MG tumor correlated with its high tumorigenic potential and blood pool volume justifies its role as a potential prognostic marker. The ^{68}Ga-DOTA-Heptap PET tracer longitudinally demonstrated prominent tumor uptake in

subcutaneous U87MG xenografts along with the steady growth of tumor size monitoring with the caliper. However, upon the administration of CA4-P, the immediate vessel collapse was observed with minimal tracer accumulation in PET imaging (2.74 ± 0.26 %ID/g) but rapidly restore and had even higher tracer uptake (6.75 ± 0.43 %ID/g) than the control group (5.1± 0.26 %ID/g) with the repeated PET imaging after 24 h post-treatment. These imaging analysis results correlated well with the subsequent tumor growth profile in which CA4-P treated group has an elevated tumor growth rate than the control group (2.5-fold), indicating that to compensate for the VDAs effects, tumor cells might recruit growth hormones or signals to revive the blood vessel growth and deteriorate the treatment prognosis. **Conclusion:** These results suggest that the proposed ^{68}Ga-DOTA-Heptap tracer is a promising surveillance biomarker for early malignant tumor detection as well as subsequent treatment effect monitoring. Thus, the non-invasive detection of tumor vascular leaking activity in vivo may permit a more precise definition of the roles of tumor vasculature status and yield insight regarding novel therapeutic strategies in the molecular level. **References:** None.

EP-0114

Influence of the degree of chelator conjugation on the physicochemical properties of Nanobody PET tracers

P. Debie[1], *H. Baudhuin*[1], *J. Puttemans*[1], *S. Hernot*[1], *C. Xavier*[1], *T. Lahoutte*[2];
[1]*Vrije Universiteit Brussel, Jette, BELGIUM,*
[2]*UZ Brussel, Jette, BELGIUM.*

Aim/Introduction: A first ^{68}Ga-labeled nanobody (Nb) for PET/CT imaging, targeting human epidermal growth factor receptor-2 (HER2), was translated to clinic, with other Nbs to follow. To date, these compounds are prepared by random conjugation with NOTA-chelator on the primary amines of their lysine residues, generating a heterogenous mixture with different chelator to Nb ratios (C/Nb). Different fractions may have differences in affinity and pharmacokinetics, which is relevant for their use in the clinic. We therefore evaluated different fractions of two clinically relevant Nbs, against HER2 and Macrophage Mannose Receptor (MMR), bearing 1, 2 or 3 chelators. Both binding capacity and in vivo biodistribution were investigated. **Materials and Methods:** Nbs were conjugated using standard procedures, at pH ~8.5 with 30* molar excess of NOTA. Conjugates were separated using anion-exchange chromatography, made possible due to the negative charge of the NOTA-chelator. Obtained fractions were assayed through, mass spectrometry and Surface Plasmon Resonance (SPR). Finally, the different fractions were radiolabelled with ^{68}Ga and injected in HER2+ tumor-bearing athymic, or MMR+ Macrophage-infiltrated tumor bearing C57Bl/6 mice. The anti-MMR nanobody is cross-reactive for murine and human MMR, whereas the anti-HER2 Nb has reactivity for the human homologue only. Ex vivo biodistributions (n=3/group) were determined 80 minutes post-injection. **Results:** Separation of different fractions was confirmed using mass spectrometry. SPR of HER2 specific Nbs showed a marginally decreasing (~5-9 nM) affinity with additional conjugated chelators, whereas SPR for MMR-specific Nbs is pending. In vivo biodistributions revealed typical biodistribution patterns, with minor differences between fractions. The MMR-specific fractions show similar tumor targeting (~2% IA/g) for increasing NOTA amounts, though decreased uptake can be seen in targeted organs such as spleen (4.9±0.8 to 1.7±0.01% IA/g), liver (6.2±1.9 to 3.6±1.5% IA/g) and bone (2.2±0.4 to 0.9±0.3% IA/g). Uptake in the kidneys appears to increase when going from 1 to 2 conjugated NOTA-chelators, though the difference is not significant. For the HER2-specific compounds, no off-target uptake is observed. There is, however, a significant difference in the uptake of the fractions in kidneys (40.2±5.4 to 24.0±1.7 % IA/g), with increasing C/Nb ratio corresponding to decreased uptake. Due to lacking growth of the HER2+ tumor model no statistical analysis was performed on tumor targeting. This experiment will therefore be repeated. **Conclusion:** Overall biodistribution of the different Nb-NOTA fractions matched the expected distribution for Nbs, with minor differences between fractions. Additional analyses will be performed for further evaluation. **References:** None.

EP-0115

Design and biodistribution of 64Cu_labelled liposomes bearing anti-CD44 aptamer in triple negative breast cancer murine model

F. Antoni[1], *H. Hillaireau*[2], *F. Hontonnou*[1], *B. Hosten*[1], *N. Vignal*[1], *L. Durand*[3], *S. Denis*[4], *V. Parietti*[5], *C. Chomienne*[6], *L. Sarda-Mantel*[1], *E. Fattal*[7];
[1]*Unité Claude Kellershohn Institut Universitaire d'Hématologie, Paris, FRANCE,* [2]*Institut Galien Paris-Sud, UMR CNRS 8612, Châtenay-Malabry, FRANCE,* [3]*UMR INSERM 1131 Institut Universitaire d'Hématologie, Paris, FRANCE,* [4]*Institut Galien Paris Sud, UMR 8612, Paris, FRANCE,* [5]*Département d'expérimentation animale, Institut Universitaire d'Hématologie, Paris, FRANCE,* [6]*UMR INSERM 1131, Institut Universitaire d'Hématologie, Paris, FRANCE,* [7]*Institut Galien Paris-Sud, UMR CNRS 8612, Paris, FRANCE.*

Aim/Introduction: Liposomes bearing anti-CD44 aptamers (anti-CD44 aptasomes) have recently demonstrated great potentialities for in vivo siRNA delivery to triple negative MDA-MB 231 breast cancer cells. This report attempts to evidence the whole biodistribution of such aptasomes by Positron Emission Tomography (PET) upon intravenous (IV) administration to mice xenografted with MDA-MB 231, in order to consider a companion imaging for further theranostic applications in patients. **Materials and Methods:** The strategy to obtain anti-CD44-NOTA-64Cu fluorescent aptasomes was first to develop a liposomal formulation containing both the metal chelator NOTA and fluorescein, then to post-insert a DSPE-PEG phospholipid coupled to an anti-CD44 aptamer (Apt1). Radiolabeling with Cu-64 was optimized. Fluorescent Cu-aptasomes were tested in-vitro for specific binding to CD44-expressing cells and cytotoxicity evaluation. Their in-vivo biodistribution was

quantified in comparison to that of NOTA-64Cu liposomes, using iterative microPET/CT imaging (from time of injection to 72h post-IV) in mice bearing MDA-MB 231 xenografts. Then tissular distribution of aptasomes and liposomes was studied ex-vivo by fluorescent microscopy. **Results:** NOTA was successfully attached to liposomes and demonstrated good chelatant properties without affecting aptamer attachment to CD44-expressing cells. Radiolabelling was achieved in 30 minutes without any purification step. Aptasomes' uptake in tumors was higher (2-fold) than that of non-targeted liposomes, and inhibited by the co-administration of CD44's natural ligand (hyaluronic acid). Histological studies evidenced the presence of liposomes and aptasomes inside tumor cells. **Conclusion:** Our anti-CD44 aptasomes showed higher tumor uptake than untargeted liposomes, related to specific interaction with CD44 in-vivo, so are good candidates for targeted anti-cancer therapy in patients with CD44-positive tumoral types. Also, antiCD44-Apt-Lip-NOTA-64Cu aptasomes can be used for companion PET imaging in this setting. **References:** Développement d›un agent théranostique liposomal anti-CD44 pour le traitement de cancer,Médecine Nucléaire, (2018) 42 (3) 154.

EP-0116

Optimizing affibody-mediated PET imaging of HER3 expression using long-lived radiocobalt for the next day PET image

S. Rinne[1], *C. Dahlsson Leitao*[2], *B. Mitran*[1], *V. Tolmachev*[1], *S. Ståhl*[2], *J. Löfblom*[2], *A. Orlova*[1];
[1]*Uppsala University, Uppsala, SWEDEN,* [2]*KTH - Royal Institute of Technology, Stockholm, SWEDEN.*

Aim/Introduction: Oncogenic signaling of human epidermal growth factor receptor type 3 (HER3) is a common cause of disease progression and therapy resistance in cancer. Imaging of HER3 expression could improve patient management. However, low target expression and endogenous expression, particularly in liver, limit the imaging contrast. We previously demonstrated feasibility of radiolabeled anti-HER3 affibody molecules for PET imaging in preclinical models. We observed that increased negative charge of the radiometal-chelator-complex reduces hepatic uptake and improves tumor-to-liver contrast. Aim of this study was to investigate the influence of charge of radiocobalt-chelator-complexes and compare the best radiocobalt-labeled variant of anti-HER3 affibody molecule $(HE)_3$-Z_{HER3} with the most favorable, recently optimized gallium-labeled variant. **Materials and Methods:** $(HE)_3$-Z_{HER3}-X (X=NOTA,NODAGA,DOTA,DOTAGA) was labeled with [^{57}Co]Co as a surrogate for ^{55}Co. Binding specificity and cellular processing were investigated in HER3-expressing cancer cell lines BxPC-3 and DU145. Binding affinity was measured on BxPC3 cells in real time. Biodistribution and targeting specificity of [^{57}Co]Co-$(HE)_3$-Z_{HER3}-X was studied 3h and 24h pi in Balb/c nu/nu mice with BxPC-3 xenografts and compared to [^{68}Ga]Ga-$(HE)_3$-Z_{HER3}-NODAGA. **Results:** $(HE)_3$-Z_{HER3}-X was stably labeled with radiocobalt and bound specifically to HER3 with subnanomolar affinity. Binding to cells was rapid, but internalized fraction was low for all conjugates and cell lines. Clearance of [^{57}Co]Co-$(HE)_3$-Z_{HER3}-X from blood was quick (<1%ID/g 3h pi). All conjugates specifically accumulated in the tumors and in organs with mErbB3 expression. The composition and charge of the Co-chelator-complex influenced the tumor and normal tissue uptake. Tumor uptake of NODAGA- and DOTA-conjugates with a single negative charge (-1) of the radiometal-chelator-complex was 2-3 fold higher than for Co-NOTA- (neutral charge) and Co-DOTAGA- (-2 charge) variants. [^{57}Co]Co-$(HE)_3$-Z_{HER3}-DOTA had the best tumor retention and significantly lower concentration in blood than the other conjugates at both time points, leading to superior tumor-to-blood (18 ± 5) and tumor-to-liver ratios (1.6 ± 0.3) at 24h pi. No significant differences between [^{68}Ga]Ga-NODAGA and[^{57}Co]Co-DOTA-labeled variants were observed 3h pi, but tumor-to-organ ratios improved with time for [^{57}Co]Co-$(HE)_3$-Z_{HER3}-DOTA suggesting [^{57}Co]Co-$(HE)_3$-Z_{HER3}-DOTA might be favorable for imaging of HER3 expression. **Conclusion:** [^{57}Co]Co-$(HE)_3$-Z_{HER3}-DOTA with a mononegative charge of the cobalt-chelator-complex was the most favorable cobalt-labeled variant. Further increase in negative charge had an adverse effect on biodistribution. The use of longer-lived PET nuclides, such as cobalt-55, might be a promising alternative to [^{68}Ga]Ga-labeled affibody molecules for imaging of HER3 expression with affibody molecules. **References:** None.

EP-0117

Pretargeted Radioimmunotherapy and SPECT Imaging of Peritoneal Carcinomatosis Using Bioorthogonal Click Chemistry: Probe Selection and First Proof-of-Concept

F. Degoul[1], *A. Rondon*[1], *S. Schmitt*[1], *A. Briat*[1], *N. Ty*[1], *M. Quintana*[1], *R. Membreno*[2], *B. Zeglis*[3,2], *I. Navarro-Teulon*[4], *J. Pouget*[4], *J. Chezal*[1], *E. Miot-Noirault*[1], *E. Moreau*[1];
[1]*UMR1240, Clermont-ferrand, FRANCE,* [2]*Department of Chemistry, Hunter College, City University of New York, New York, NY, UNITED STATES OF AMERICA,* [3]*Department of Radiology, Memorial Sloan Kettering Cancer Center, New York, NY, UNITED STATES OF AMERICA,* [4]*Institut de Recherche en Cancérologie (IRCM), U1194 – Université Montpellier – ICM, Radiobiology and Targeted Radiotherapy, Montpellier, FRANCE.*

Aim/Introduction: Pretargeted radioimmunotherapy (PRIT) based upon bioorthogonal click chemistry has been investigated for the first time in the context of peritoneal carcinomatosis using a 35A7 mAb bearing trans-cyclooctene (TCO) moieties and several ^{177}Lu-labeled tetrazine (Tz) radioligands. Starting from three Tz probes bearing PEG linkers of varying lengths between the DOTA and Tz groups (i.e. PEG_n = 4, 8, or 12, respectively, for Tz-1, Tz-2, and Tz-3), we selected [^{177}Lu]Lu-Tz-2 as the most appropriate for pretargeted SPECT imaging and demonstrated its efficacy in tumor growth control. **Materials and Methods:** An orthotopic model of PC was obtained following the intraperitoneal (i.p.) injection of A431-CEA-Luc cells in nude mice. Tumor growth was assessed using bioluminescence imaging. Anti-CEA 35A7 mAb was grafted

with 2-3 trans-cyclooctenes per molecule. Pretargeted SPECT imaging and biodistributions were performed to quantify the activity concentration of [^{177}Lu]Lu-Tz-1-3 in tumors and non-target organs to determine the best Tz probe for the PRIT of PC. **Results:** The pharmacokinetic profiles of radiolabeled [^{177}Lu]Lu-Tz-1-3 were determined using both SPECT imaging and biodistributions and demonstrated renal and hepatic clearances for [^{177}Lu]Lu-Tz-1, while [^{177}Lu]Lu-Tz-2 and [^{177}Lu]Lu-Tz-3 were mainly excreted renally. In addition, the longer the PEG, the more rapidly the Tz probe was cleared from the peritoneal cavity. In our PRIT study, we showed that 24 hours after the systemic injection of 35A7-TCO, the i.p. injection of 40 MBq of [^{177}Lu]Lu-Tz-2 significantly slowed tumor growth compared to control mice receiving only saline or 40 MBq of [^{177}Lu]Lu-Tz-2 alone. Ex vivo measurement of the peritoneal carcinomatosis index (PCI) confirmed that PRIT significantly reduced tumor growth (PCI = 15.5 ± 2.3 after PRIT vs 30.0 ± 2.3 and 30.8 ± 1.4 for the NaCl and [^{177}Lu]Lu-Tz-2 alone groups, respectively). **Conclusion:** Our results clearly demonstrate the impact the length of the PEG linker exerts upon the biodistribution of the ^{177}Lu-labeled Tz radioligands. Furthermore, we demonstrated for the first time the possibility of using bioorthogonal chemistry for both the pretargeted SPECT and PRIT of peritoneal carcinomatosis. **References:** None.

EP-0118

Structural Modification of Indolinone-Diene Analogues as Alpha-Synuclein Ligands and Its Structure-Activity Relationship Analysis

J. Lee, *J. Han, E. Nam, K. Chang, S. Lee;*
Neuroscience Research Institute, Gachon University, Incheon, KOREA, REPUBLIC OF.

Aim/Introduction: Development of novel radioligand for alpha-synuclein imaging is one of the most challenging topics in the diagnostic radiopharmaceutical research area. Although the early detection of neurodegenerative diseases is still not very practical, there are several promising agents for Alzheimer's disease (AD) targeting beta-amyloid, tau, and neuroinflammation, but none for Parkinson's disease (PD). Lewy body (LB) is a specific hallmark for PD, and to detect LB via a non-invasive method, a lot of research groups are striving to develop an effective small compound as an alpha-synuclein ligand. **Materials and Methods:** Indolinone-diene analogue[1] 1 was recently reported, showed not only a good binding affinity with synthetic alpha-synuclein fibrils but a high selectivity over beta-amyloid and tau fibrils (Ki= 2.1, 142, 80 nM, respectively, Thioflavin T assay result). Based on this structure, we designed several derivatives to increase binding affinity and selectivity but decrease lipophilicity to ensure better bioavailability. To keep the overall structural feature, we modified 1) indolinone core to other heterocyclic ring systems, 2) one double bond in diene to aromatic heterocyclic ring system and introduced 3) several indolinone N-substituents. Prepared compounds were tested its binding affinity using Thioflavin T as a competitive dye and structure-activity relationship analysis will be performed. **Results:** We could prepare total 13 compounds in reasonable yields and now we're working on the biological assay to confirm its binding affinity to alpha-synuclein fibrils. When we changed indolinone ring to thiazolidine-2,4-dione system, (E,E)-diene isomer, which is relevant to (Z,E)-diene of indolinone system, was exclusively formed and isolable. Since compound 1 is prone to Z/E isomerization in DMSO solution and (E,E) isomer is much less effective than (Z,E) isomer, we expect thiazolidine-2,4-dione system will show better activity and properties. **Conclusion:** Thioflavin T assay is now underway to confirm binding affinities of newly synthesized compounds and soon will be completed. Once we get the biological assay data, we'll analyze structure-activity relationship and propose possible binding mode via molecular docking study. **References:** 1. J. Med. Chem. 2015, 58, 6002–6017.

EP-0119

Identification of Peptide Ligands from Peptide Mixtures by Quantitative Analyses of Differential Cell Uptake Patterns

M. Parzinger, *H. Wester;*
Technical University of Munich, Garching bei München, GERMANY.

Aim/Introduction: The classical wet-chemical selection of a new peptidic lead structure for a given target is a time-consuming process that requires extensive synthetical and analytical efforts and subsequent in vitro assessment. To accelerate the classical selection process we investigated a screening method, based on the synthesis of a mixture of peptide ligands, followed by the differential analysis of the cellular uptake profile upon incubation of cells with the radiolabeled mixture of these peptide ligands. For proof-of-concept, CXCR4 was chosen as a model system in combination with a mixture of 25 peptides, including iodo-FC131 (IC_{50} = 2.07 ± 0.34 nM). **Materials and Methods:** A mixture of 25 cyclic pentapeptides with 5 variations at 2 positions was synthesized, isolated by preparative RP-HPLC and finally labeled with ^{125}I. Subsequently, CXCR4+ Jurkat cells were incubated at room temperature with the peptide mixture (1 nM plus 10 nM control). After removing the supernatant, the cells were washed with PBS and treated with a citrate buffer to isolate cell bound peptides. Supernatant and cell bound fractions were concentrated via StrataX SPE followed by RP-HPLC analysis. The peptide 'enrichment pattern' in the cell bound fraction was corrected for unspecific binding obtained in the control experiment. After comparison with the 'depletion pattern' in the supernatant fraction, the differential uptake of each peak in the original HPLC profile was determined and thus, after HPLC-MS, the peptides with the highest affinity towards CXCR4 were selected. **Results:** The selection process described above was validated by the successful 'selection' of iodo-FC131. In addition, the analytical data revealed a second peptide (peptide-B) with a twofold higher enrichment on the 1 nM test level. Analyses of the supernatants did not result in interpretable data since insufficient peak separation and thus complex peak integration did not allow for quantitative analysis. Affinity studies of the

two selected peptides resulted in IC_{50}'s of 79.3 ± 4.8 nM for the newly isolated peptide-B (cyclo(Gly-2-Nal-Dap-Arg-tyr)) and 2.07 ± 0.34 nM for the 'selected' iodo-FC131. **Conclusion:** The described cell-based screening method allowed to successfully isolate the well-known CXCR4 ligand iodo-FC131 and a newly described second peptide-B ligand from a mixture of 25 peptides. However, due to the limited sensitivity of the radiodetector, cross-evaluation of the supernatant and cell-bound fraction failed, making this method less valid and more complicated than initially expected. **References:** None.

EP-0120

^{99m}Tc Labeled Tetrazines for In Vivo Pretargeted Imaging

L. Bohrmann[1], *P. Biniecka*[1], *S. Karagiozov*[1], *C. Rodriguez-Rodriguez*[1], *M. M. Herth*[2], *K. Saatchi*[1], *U. O. Häfeli*[1];
[1]*University of British Columbia, Vancouver, BC, CANADA,*
[2]*University of Copenhagen, Copenhagen, DENMARK.*

Aim/Introduction: Targeted nuclear imaging using antibodies or nanoparticles often suffers from the drawback of requiring long-lived radionuclides owing to the slow pharmacokinetics of these targeting vectors. Using pretargeted imaging the biodistribution of the targeting vector and the radionuclide is separated in order to mitigate this shortcoming and to improve imaging contrast. In a first step, a tagged carrier is administered and allowed to accumulate at the target site. In a second step, a radiotracer is injected with the aim of specifically binding to the tagged carrier. Here we evaluate a panel of four ^{99m}Tc labeled tetrazines for use in pretargeted imaging with a trans-cyclooctene (TCO)-tagged bisphosphonate that accumulates at sites of active bone metabolism[1]. **Materials and Methods:** Two aromatic tetrazines linked to a novel chelator for labeling with ^{99m}Tc either directly or through an octaethyleneglycol-linker were synthesized using standard Pinner-like synthesis. Radiolabeling was performed using the commercially available IsoLink kit (Covidien, Petten, The Netherlands) to convert generator-eluted $^{99m}TcO_4^-$ into $[^{99m}Tc(CO)_3(H_2O)_3]^+$. Tetrazines were incubated with ^{99m}Tc tricarbonyl under mild conditions (70 °C, 30 min) to afford the labeled tracers in high radiochemical purity. For preclinical in vivo evaluation, healthy Balb/c mice were injected TCO-functionalized alendronate followed one hour later by the tetrazines. Mice were imaged 0, 2 and 6 h p.i.of the radiotracer and a full biodistribution study was performed after the last imaging time point. Control animals were injected saline prior to the tetrazines. **Results:** SUV analysis shows immediate accumulation of the tetrazines in knees and shoulders of mice that received TCO-tagged alendronate, which remains constant during the duration of the imaging study. These findings are confirmed by the biodistribution which shows up to 3.34 %ID/g of bone uptake, which is a factor of 27.8 higher than in control animals. Surprisingly, tetrazines containing an octaethyleneglycol performed worse than their counterparts without the hydrophilic linker. **Conclusion:** An established preclinical screening model for pretargeted imaging was used to identify a potential new ^{99m}Tc-labeled tetrazine. Due to the excellent nuclear properties with a half-life of 6 hours and a gamma energy of 140 keV this would be a valuable addition to the growing toolbox of pretargeted imaging applications and could help improve image contrast and reduce radiation burden to patients. **References:** 1. J. Med. Chem. 2016, 59, 20, 9381-9389.

EP-0121

Al^{18}F-NOTA-octreotide PET imaging of the somatostatin receptor: preliminary results of a human biodistribution, dosimetry and safety study

E. Pauwels[1], *F. Cleeren*[2], *T. Tshibangu*[2], *M. Koole*[1], *K. Serdons*[1], *K. Van Laere*[1], *G. Bormans*[2], *C. M. Deroose*[1];
[1]*Nuclear Medicine - UZ Leuven; Nuclear Medicine and Molecular Imaging - KU Leuven, Leuven, BELGIUM,*
[2]*Radiopharmaceutical Research - KU Leuven, Leuven, BELGIUM.*

Aim/Introduction: Implementation of ^{68}Ga-DOTA-peptide PET for somatostatin receptor (SSTR) imaging, the current gold standard, can be restricted due to the limited availability, high cost and relatively low throughput associated with ^{68}Ga-labeled PET tracers. Recent radiopharmaceutical developments have allowed to replace gallium-68 by fluorine-18 bound to aluminium (Al18F). Promising preclinical results with the Al18F-labelled somatostatin analogue NOTA-octreotide have been reported, with an affinity of 3.6 nM for the SSTR[1]. Our ongoing study aims to obtain preliminary human data supporting the feasibility of Al^{18}F-NOTA-octreotide PET in patients with neuroendocrine tumours (NETs). **Materials and Methods:** Three healthy volunteers were included so far (2M/1F; age 41-52 years). An IV bolus of 4 MBq/kg Al^{18}F-NOTA-octreotide was administered after a low dose CT. Tracer injection was followed by consecutive whole-body PET scans up to 90 minutes post-injection (PI), with additional scans at 150 and 300 minutes PI. Safety and tolerability were assessed through regular monitoring for adverse events, clinical evaluations and serial biochemical analysis. Images were analysed using MIM (MIM Software Inc, US). For dosimetry, all source organs with relevant activity were delineated on the PET images, with CT guidance. Time-activity curves were extracted and integrated to compute time-integrated activity. Individual absorbed organ doses and the effective dose were determined using OLINDA/EXM. **Results:** No adverse events were observed. Mean SUV_{max} at 60 minutes PI in the spleen, kidneys, liver, gall bladder, adrenal glands, pituitary gland, pancreas, bone marrow and muscle were 26.2±5.2, 29.9±10.8, 7.7±1.7, 7.7±1.5, 12.1±4.3, 8.6±1.5, 4.6±1.0, 1.2±0.4 and 0.8±0.4, respectively. Excretion was mainly renal. Overall, this biodistribution is similar to that of the ^{68}Ga-DOTA-peptides. The low bone uptake on the PET images indicates that free 18F-fluoride formation is not clinically relevant. In a first analysed subject, the highest dose was received by the spleen (0.184 mGy/MBq), followed by the urinary bladder wall (0.104 mGy/mBq) and the kidneys (0.046 mGy/MBq), with an effective dose of 0.021 mSv/MBq, which is comparable to ^{18}F-FDG. Biodistribution, dosimetry, safety in healthy volunteers

and initial findings in up to six patients with at least five SSTR positive lesions on routine ^{68}Ga-DOTA-peptide PET are planned. **Conclusion:** Administration of Al^{18}F-NOTA-octreotide was well tolerated and biodistribution and dosimetry are in line with the ^{68}Ga-DOTA-peptides. These preliminary results indicate that Al^{18}F-NOTA-octreotide shows promise for further human exploration in imaging SSTR. **References:** [1] Laverman J.Nucl. Med.2010;51(3).

EP-0122

Linker optimization to improve tumor uptake of PSMA binding radiopharmaceuticals

H. Kuo, Z. Zhang, H. Merkens, C. Zhang, N. Colpo, K. Lin, F. Bénard; Department of Molecular Oncology, BC Cancer, Vancouver, BC, CANADA.

Aim/Introduction: Various radiolabeled prostate-specific membrane antigen (PSMA)-targeting constructs have been designed and evaluated for endoradiotherapy of prostate cancer. ^{177}Lu-PSMA-617 is currently being studied in clinical trials for its therapeutic efficacy. To date, in current published series, the complete response rate was low. The goal of this study was to increase the tumor uptake to improve endoradiotherapeutic efficacy. Toward this goal, we investigated if substitution of the 2-naphthylalanine in PSMA-617 with other lipophilic amino acids could improve binding affinity and tumor uptake. **Materials and Methods:** Four new derivatives (HTK03026, HTK03027, HTK03029 and HTK03041) were synthesized on solid-phase. The 2-naphthylalanine in PSMA-617 was replaced with 2-aminooctanoic acid, 3-(2-anthryl)-L-alanine, 3-(1-pyrenyl)-L-alanine and 3-(9-anthryl)-L-alanine to generate HTK03026, HTK03027, HTK03029 and HTK03041, respectively. The binding affinity of non-radioactive standards to PSMA was determined by in vitro competition assays. ^{68}Ga labeling was performed in HEPES buffer (2 M, pH 5.0) with microwave heating (1 min). Imaging and biodistribution studies were performed in mice bearing LNCap prostate cancer xenografts. The best candidate was selected, radiolabeled with ^{177}Lu, and compared with ^{177}Lu-PSMA-617. **Results:** The binding affinities (K_i) of Ga-PSMA-617, Ga-HTK03026, Ga-HTK03027, Ga-HTK03029, Ga-HTK03041, Lu-PSMA-617 and Lu-HTK03041 to PSMA were 1.23, 12.5, 22.0, 16.6, 0.63, 0.24 and 1.88 nM, respectively. All ^{68}Ga-tracers enabled clear visualization of tumors in PET images. Tumor uptake values at 1h post-injection (p.i.) were 16.7±2.3, 12.9±2.9, 13.3±5.4 13.9±5.7 and 23.1±6.11 %ID/g for ^{68}Ga-PSMA-617, ^{68}Ga-HTK03026, ^{68}Ga-HTK03027, ^{68}Ga-HTK03029 and ^{68}Ga-HTK03041, respectively. At 3h p.i., uptake of ^{68}Ga-HTK03041 in tumor further increased to 28.2±9.2 %ID/g. SPECT imaging showed both ^{177}Lu-PSMA-617 and ^{177}Lu-HTK03041 had good tumor uptake and high target-to-background contrast, and were mainly excreted by the kidneys. Biodistribution results showed the tumor uptake of ^{177}Lu-PSMA-617 peaked at 1 h p.i. (15.1±5.6 %ID/g) and gradually reduced over time (7.9±2.8 %ID/g at 120h p.i.). Conversely, the tumor uptake of ^{177}Lu-HTK03041 at 4h p.i. was 18.7±3.0 %ID/g and remained stable over time (22.3±6.9 %ID/g at 120h p.i.). **Conclusion:** Replacing the 2-naphthylalanine in PSMA-617 had profound impact on PSMA binding affinity and tumor uptake. ^{68}Ga/^{177}Lu-HTK03041 showed higher tumor uptake than ^{68}Ga/^{177}Lu-PSMA-617, and the tumor accumulation remained stable over time. ^{177}Lu-HTK03041 warrants further investigation as an endoradiotherapeutic agent to treat metastatic prostate cancer. **References:** None.

EP-0123

^{68}Ga-labled N-Carboxymethyl-substituted PSMA ligands enhancing binding affinity

B. Lee[1], *S. Chu*[1], *W. Jung*[1], *H. Moon*[1], *H. Jeong*[1], *H. Kim*[1], *M. Kim*[1], *J. Kim*[1], *M. Kim*[1], *Y. Lee*[2], *K. Lee*[2], *S. Lim*[2], *D. Chi*[1,3], *K. Song*[2]; [1]*FutureChem, Seoul, KOREA, REPUBLIC OF,* [2]*Korea Instituted of Radiological & Medical Sciences, Seoul, KOREA, REPUBLIC OF,* [3]*Sogang University, Seoul, KOREA, REPUBLIC OF.*

Aim/Introduction: High uptake in tumor cells and low non-specific binding to normal organs are all important for the diagnostic and therapeutic efficacy of PSMA-targeted radioligand. However, it is not easy to find compounds that satisfy both of these factors at the same time. We made many efforts to solve this question and finally found that N-substituted methyl carboxylic acid of the lysine of Glu-urea-Lys enhances the binding affinity to PSMA protein. **Materials and Methods:** 22RV1 and PC3 PIP cell lines were used in vitro and in vivo experiments, respectively. Binding studies were performed by competition with ^{125}I-labeled MIP-1095. MicroPET images were acquired using an INVEON PET/CT scanner. **Results:** In order to confirm the effect of the carboxylic acid on the binding to PSMA, simple acetylated Glu-urea-Lys compounds were synthesized and tested in vitro. As a result, N-carboxymethyl substituted acetylated compound (Ki = 3.31±0.25 nM) was found to have 11.3-fold higher binding affinity than only acetylated compound (Ki = 37.3±2.31 nM). This is probably due to the salt bridge interaction with the arginine patch region in PSMA. DOTA chelator was then introduced in place of the acetyl group with a spacer of the appropriate length in between (FC694). A series of albumin binding moieties (phenyl, tolyl, and 4-iodophenyl butanoyl) groups were added to the FC694 compound using lysine to make FC701, FC703, and FC705, respectively. Binding affinities (Ki value) of these cold Ga-labeled DOTA-PSMA ligands were measured to be 12.9±0.49, 8.12±0.16, 5.82±0.11, and 3.00±0.11 nM for FC694, FC701, FC703, and FC705. ^{68}Ga-FC694 showed moderate uptake in tumor tissue of 4.05±0.64 %ID/g at 4.5 h, and rapid clearance from other organs including kidney (0.41±0.16 %ID/g at 4.5 h). On the other hand, ^{68}Ga-labeled FC701, FC703, FC705 showed tumor uptake of 7.20±3.39, 10.48±1.05, and 14.2±0.0 %ID/g at 4.5 h, respectively. The result was consistent with the relative albumin-binding ability of each compound. Although kidney retention seemed to gradually increase as albumin-binding ability increase, it is probably due to prolonged blood circulation. **Conclusion:** Carboxylic acid was found to increase the binding affinity of our new ligands to PSMA protein. It is probably due to the salt bridge interaction

with the arginine patch region. It also serves to reduce non-specific binding by maintaining the hydrophilicity of the compounds. MicroPET studies of ^{68}Ga-labeled PSMA ligands have shown that FC701 is suitable for PET imaging and FC705 is promising for therapeutic radioligand. **References:** None.

EP-0124

Application of ^{99m}Tc-3PRGD$_2$ imaging for early predicting pathological response to neoadjuvant chemotherapy in breast tumors and axillary lymph nodes

W. Miao, Z. Chen;
The First Affiliated Hospital of Fujian Medical University, Fuzhou, CHINA.

Aim/Introduction: The aim of this study was to investigate the value of ^{99m}Tc-3PRGD$_2$ imaging for predicting pathological response to neoadjuvant chemotherapy (NAC) in stage II-III breast cancer patients compared with ^{18}F-FDG imaging. **Materials and Methods:** Forty-one patients were underwent both ^{99m}Tc-3PRGD$_2$ imaging and ^{18}F-FDG imaging before NAC (baseline), after the first and fifth cycle of NAC. The tumor-to-background (T/B) ratios of ^{99m}Tc-3PRGD$_2$ imaging, standardized uptake values (SUV$_{max}$) of ^{18}F-FDG imaging in breast tumors and metastatic axillary lymph nodes (ALNs), and the relative changes of T/B (ΔT/B) and SUV$_{max}$ (ΔSUV$_{max}$) regarding to the baseline scans were calculated. A pCR (pathological complete response) was defined as the absence of residual invasive tumor cells in all breast and axillary node specimens. Statistical analysis was carried out by the univariate analyses, logistic regression, receiver operating characteristic (ROC) analysis and Z test. **Results:** A pCR was achieved in 13 of 41 patients after NAC in the prospective study. Logistic regression analysis indicated that tumor size and HER2 status were significantly associated with pCR (all $P < 0.05$). In ROC analysis for predicting pCR after first and fifth cycle, the area under curve (AUC) of ΔT/B in both tumors and ALN combined were 0.859 and 0.778, respectively (all $P < 0.01$). For ΔSUV$_{max}$, the ROC-AUC were 0.918 and 0.909, respectively (all $P < 0.01$). ROC-AUCs of ΔT/B in breast tumors for predicting the primary tumor pathological response were 0.827 ($P < 0.01$) and 0.687 ($P > 0.05$), and 0.859 ($P < 0.01$) and 0.713 ($P < 0.05$) for ΔSUV$_{max}$. The ROC-AUCs for predicting the ALN pathological response were 0.859 ($P < 0.01$) and 0.778 ($P < 0.05$) for ΔT/B, and 0.572 ($P > 0.05$) and 0.802 ($P < 0.01$) for ΔSUV$_{max}$. AUCs between ΔT/B and ΔSUV$_{max}$ after first cycle had no statistical difference for predicting breast tumors pathological response ($Z = 0.33$, $P = 0.74$). However, AUC of early ΔT/B was higher than ΔSUV$_{max}$ in ALN ($Z = 2.10$, $P = 0.035$). In HER2-positive patients, the early ΔT/B in responder group was higher than that of non-responder group. While early ΔSUV$_{max}$ in responder group showed higher than non-responder group in ER-positive patients. **Conclusion:** ^{99m}Tc-3PRGD$_2$ imaging and ^{18}F-FDG imaging showed a comparable prediction for pCR to NAC. ^{99m}Tc-3PRGD$_2$ imaging showed an earlier predictive value than ^{18}F-FDG imaging in ALNs pathological response. ^{99m}Tc-3PRGD$_2$ imaging may be earlier for predicting pathological response in HER2-positive patients. **References:** None.

EP-0125

Structure-activity-relationship investigation of an albumin-binding motif to improve tumor-to-kidney therapeutic index of PSMA-targeting agents

H. Kuo[1], *Z. Zhang*[1], *C. Uribe*[1], *H. Merkens*[1], *C. Zhang*[1], *F. Bénard*[1,2], *K. Lin*[1,2];
[1]*Department of Molecular Oncology, BC Cancer, Vancouver, BC, CANADA,* [2]*Department of Radiology, University of British Columbia, Vancouver, BC, CANADA.*

Aim/Introduction: Albumin-binder-conjugated prostate specific membrane antigen (PSMA)-targeting radiopharmaceuticals have been reported to improve tumor uptake and enhance treatment efficacy of prostate cancer. Recently we evaluated ^{177}Lu-HTK01169[1], a 4-(p-iodophenyl)butanoyl]-Glu-conjugated ^{177}Lu-PSMA-617 derivative, which delivered 8.3-fold higher absorbed dose to LNCaP tumor xenografts than ^{177}Lu-PSMA-617 and achieved single dose tumor eradication. However, ^{177}Lu-HTK01169 also resulted in higher absorbed dose to kidneys, leading to ~50% reduction in tumor-to-kidney therapeutic index compared to ^{177}Lu-PSMA-617. The aim of this study was to optimize the design of albumin binder to improve tumor-to-kidney therapeutic index while maintaining high absorbed dose delivered to tumors. **Materials and Methods:** 4-(p-R-substituted-phenyl)butanoyl]-Gly-conjugated (R=I, Br, Cl, F, CH_3, OCH_3, NO_2, NH_2, H) PSMA-617 derivatives were synthesized on solid phase. ^{68}Ga labeling was performed in HEPES buffer (2 M, pH 5.0). A biodistribution study was performed in LNCaP tumor-bearing mice. The best candidate was selected, radiolabeled with ^{177}Lu, and a dosimetry study was conducted in LNCaP tumor-bearing mice. Radiation dosimetry was calculated using the OLINDA v.1.2. **Results:** Blood retention (%ID/g at 1h and 3h pi) of ^{68}Ga-labeled albumin-binder-conjugated PSMA-targeting agents followed the lipophilicity order of the substituents: I(27.0±5.63, 23.9±1.03)≈Br(26.7±3.02, 21.2±2.21)>Cl(22.1±2.04, 17.4±1.15)>CH_3(16.8±2.14, 13.6±1.23)>OCH_3(12.1±0.60, 6.60±0.84)>NO_2(6.69±0.27, 2.52±0.69)≈F(5.73±0.93, 2.10±0.48)>H(4.68±1.09, 1.17±0.36)>NH_2 (1.74±0.11, 0.52±0.08). Conversely, the tumor uptake (%ID/g) at 1h pi was inversely correlated to the lipophilicity of the substituents: H(25.9±3.21)>NO_2(21.7±2.48)≈NH_2(20.7±3.79)>F(18.8±3.35)≈OCH_3(17.8±2. 89)≈Cl(17.2±1.67)>Br(11.2±3.33)>CH_3(8.54±0.74)>I(7.34±0.10). Tumor uptake was further increased from 1h to 3h pi for all compounds except the NH_2-substituted derivative. The Cl-substituted derivative (HTK03055) which showed relatively faster blood clearance, high tumor uptake (30.1±3.12 %ID/g at 3h pi) and lower kidney uptake (35.6±7.23 %ID/g at 3 h pi) was evaluated further with its ^{177}Lu derivative. Compared with ^{177}Lu-HTK01169, ^{177}Lu-HTK03055 had similar blood retention and peak tumor uptake (55.9±12.5 vs 53.4±1.53 %ID/g), but much lower kidney uptake (%ID/g) (1h (51.1±4.07 vs 31.7±5.13), 4h (85.7±7.11 vs 44.2±4.86), 24h (125±16.4 vs 26.2±4.69), 72h (37.8±18.7 vs 11.5±1.17), 120h (8.63±2.51 vs 2.86±1.08)). Dosimetry

calculations showed that compared to ^{177}Lu-PSMA-617, ^{177}Lu-HTK03055 delivered 8.9-fold higher absorbed dose to LNCaP tumor xenografts and an 1.85-fold improvement in tumor-to-kidney therapeutic index. **Conclusion:** We conducted structure-activity-relationship investigation on the 4-(p-R-substituted-phenyl)butanoyl]-Gly pharmacophore to optimize the selection of albumin-binding motif. We demonstrated that it was possible to maximize tumor uptake while improving the therapeutic ratio to normal organs with this strategy. This approach can lead to the development of therapeutic radiopharmaceuticals that require lower activities of expensive radioisotopes with potentially improved safety and efficacy profiles. **References:** Kuo H-T, et al. Molecular Pharmaceutics 2018;15:5183-5191.

EP-0126

Impact of global ultrasound-induced blood-brain barrier opening on the distribution of full monoclonal antibody cetuximab

C. Truillet[1], *V. Tran*[1], *A. Novell*[2], *M. Gerstenmayer*[1], *A. Bouleau*[1], *H. Nozach*[1], *B. Kuhnast*[1], *N. Tournier*[1], *B. Larrat*[1];
[1]*CEA, Orsay, FRANCE,* [2]*CNRS, Orsay, FRANCE.*

Aim/Introduction: Epidermal growth factor receptor (EGFR) involved in cell proliferation and migration, is overexpressed in 50% of glioblastomas. This suggests a relevance for molecularly-targeted therapy using anti-EGFR based strategies using monoclonal antibodies (mAb), such as cetuximab, for therapy. Clinical trials have shown the beneficial effects of cetuximab in various EGFR-expressing peripheral tumors, but failed in patients with recurrent glioblastoma.(1) One of the main issues is the poor penetration of mAb into the central nervous system (CNS) due to the presence of the blood-brain barrier (BBB). Recently, ultrasound (US) in combination with microbubbles has been used to transiently open the BBB and promote the delivery of therapeutic agent to CNS.(2) Non-invasive, dynamic and quantitative methods such as PET imaging using radiolabeled mAb may provide a translational imaging method to address the efficacy of US for the delivery of mAb into brain. **Materials and Methods:** Cetuximab was conjugated to DFO and labeled with ^{89}Zr at 0.5 MBq/µg. Affinity comparison between human and murine EGFR with cetuximab has been done. In vivo PET imaging and biodistribution were conducted in healthy nude male mice (no US vs US groups, n=8) in order to follow the kinetics of the ^{89}Zr-Cetuximab overtime. Brain uptake of ^{89}Zr-Cetuximab was initially monitored by dynamic PET, followed by static PET imaging at different time points post-injection. The time activity curves allowed the determination of the transfer rate constants between the blood and the brain. **Results:** Cetuximab exhibits an approximate 10-fold greater affinity with human EGFR compared to mouse counterpart. In control mice, the brain distribution of ^{89}Zr-Cetuximab was negligible (transfer rate = 0 ± 0.006 min^{-1}). The transfer rate increased up to 1.3 ± 0.23 min^{-1} when US were applied. The brain uptake without US remained constant at 0.7± 0.09 %ID/cc overtime whereas it reached 1.34± 0.15 %ID/cc at 1h and stay stable during 48 hours with US (1.36%± 0.16 %ID/cc). After 72h post-US, no significant difference between the US and the control cohorts was observed. Heterogeneity of the diffusion of 89Zr-Cetuximab within the brain was obvious and showed a maximum of accumulation under the area where US were applied. **Conclusion:** Here, PET was successfully combined with therapeutic US to demonstrate the efficiency of this strategy for mAb delivery into brain which raises potential application for tumor treatment. **References:** 1) Westphal, M., et al (2017), CNS Drugs; 31(9): 723-735. 2) Escoffre, J. M., et al. (2013), Mol Pharm 10(7): 2667-75.

EP-07

Oncology: PSMA Imaging and Therapy

October 12 - 16, 2019 e-Poster Area

EP-0127

Unexpected high incidence of positive 68Ga-PSMA-11 PET/CT performed during androgen deprivation therapy in biochemical recurrent patients, showing low PSA values (<0,5 ng/mL)

L. Muraglia[1,2], *F. Mattana*[1,2], *A. Farolfi*[1,2], *F. Ceci*[3], *P. Castellucci*[2,1], *L. Calderoni*[1], *V. Cervati*[1], *R. Mei*[1], *S. Fanti*[1,2];
[1]*Università di Bologna, Bologna, ITALY,* [2]*Metropolitan Nuclear Medicine, Policlinico Sant'Orsola-Malpighi, Bologna, ITALY,* [3]*Università degli studi di Torino, Torino, ITALY.*

Aim/Introduction: Primary aim of this retrospective single-centre analysis was to investigate the detection rate of 68Ga-PSMA-11 PET/CT in patients with prostate cancer (PCa) and PSA failure after radical prostatectomy (RP) and low but increasing PSA values (<0.5 ng/ml) during androgen deprivation therapy (ADT) at the time of PET/CT scan. **Materials and Methods:** 68Ga-PSMA-11 PET/CT is performed at our institution through a prospective, singlecenter, open label study (Eudract: 201500458927 OsSC). We retrospectively analysed consecutive PCa patients with biochemical recurrence whom referred to our institute for a PET/CT scan. Inclusion criteria were: PSA levels under 0.5 ng/ml at the time of the 68Ga-PSMA-11 PET/CT investigation, ongoing therapy with ADT and no prior ADT (abiraterone/docetaxel/enzalutamide or similar). 68Ga-PSMA-11 PET/CT performance was evaluated in terms of detection rate on a per-patient and a per-region basis (local vs distant lesions). **Results:** According with inclusion criteria, we enrolled 26 PCa patients (mean age 70 yo, range 53-83) with mean PSA level at the time of PET/CT of 0,28 ng/ml (median 0,29 ng/ml, range 0,10-0,50 ng/ml). T staging was ≥ pT3a in 23/26 cases (88%), N staging was pN1 in 14/27 cases (54%), Gleason Score was ≥8 in 17/26 cases (65%), mean time to relapse (TTR) was 17 months (range 1-70 months). PET/CT scan was positive in 17/26 patients (65%). PSMA pathologic uptake was observed only in the prostate bed or in pelvic nodes in 3/17 patients (18%), only in

extra-pelvic region in 12/17 patients (71%) and both in pelvic nodes and extra pelvic region in 2/17 patients (11%). Among positive patients, 15/17 (88%) were oligo-metastatic (≤ 3 lesions) and 2/17 (12%) multi-metastatic. PSMA positive findings were detected in the following subregions: 2 prostate bed, 4 pelvic nodes, 6 extrapelvic nodes, 19 bone. Mean SUVmax value of the lesions detected in our PET/CT scans was 18,2 (range 8-86). **Conclusion:** Our results showed that the detection rate of 68Ga-PSMA-11 PET/CT, in a population with low/moderate PSA values, is significantly higher than the one expected from literature in similar population showing low PSA values (< 0.5ng ml). This could be related to the influence of ADT on PSMA expression expecially in patients showing increasing PSA levels during ADT. Such elevated detection rate could influence greatly the therapeutic approach in such population allowing a prompt instauration of a personalized therapy. Main limitations of our study are the small number of patients enrolled and its retrospective design. **References:** None.

EP-0128

Location of biochemical recurrences after robot-assisted radical prostatectomy with sentinel node biopsy and lymph node dissection: analysis with PSMA-PET/CT and comparison with initial SPECT/CT

O. R. Brouwer[1], *E. Wit*[1], *P. J. van Leeuwen*[1], *F. W. B. van Leeuwen*[2], *H. G. van der Poel*[1];
[1]*The Netherlands Cancer Institute, Amsterdam, NETHERLANDS,* [2]*Leiden University Medical Center, Leiden, NETHERLANDS.*

Aim/Introduction: Robot-assisted radical prostatectomy (RARP) with extended pelvic lymph node dissection (ePLND) is generally applied as treatment for patients with intermediate and high risk prostate cancer (PCa). Sentinel node (SN) biopsy has the potential to increase the diagnostic accuracy of ePLND. Furthermore, it has been shown that incorporating SN biopsy in the procedure can lead to prolonged biochemical recurrence (BCR) free survival [1]. This study aimed to analyse the frequency and imaging results of patients with biochemical recurrence using PSMA-PET/CT. **Materials and Methods:** Follow-up data of patients who were included in a prospective randomized phase II study aiming to investigate the influence of the location of SN-tracer injection was analysed. Ethical Committee approval was obtained. All patients underwent RARP with SN biopsy followed by ePLND. The patients with a biochemical recurrence at follow-up were identified and evaluated. **Results:** Between 2013-2016, 113 patients were included. 37 patients had 1 or more tumorpositive lymph nodes at histopathology (33%). In 35 of these patients, the SN was als tumorpositive (95%, false negative rate 5%). Mean follow-up after surgery was 29,3 months (median 27,5). 29 patients developed BCR (26%). Additional imaging was performed in 25/29 patients (86%, PSMA-PET n=20, choline-PET n=4, nano-MRI n=1). Imaging revealed lymph node metastasis in 15/25 patients (60%). The recurrence was localised in a regional pelvic lymph node in the majority of patients (87%). 5/15 patients were stages pN0 at SN+ePLND (33%). Of these patients, 1 had non-visualisation of the SN on SPECT/CT, 1 also had distant metastases, and 3 had a recurrence on PSMA-PET/CT at the exact same location as the SN on SPECT/CT during primary treatment (SN not reached or excised). **Conclusion:** In 80% of pN0 patients who developed a BCR and showed a lymph node metastasis/recurrence on PSMA-PET/CT, this was due to a technically unsuccessful procedure or non-excised SN. This supports the accuracy of the SN procedure for lymph node staging in PCa patients and the potential importance of removing SNs outside the ePLND area. **References:** 1.Grivas N, Wit EMK, Kuusk T, KleinJan GH, Donswijk ML, van Leeuwen FWB, et al. The Impact of Adding Sentinel Node Biopsy to Extended Pelvic Lymph Node Dissection on Biochemical Recurrence in Prostate Cancer Patients Treated with Robot-Assisted Radical Prostatectomy. J Nucl Med. 2018 Feb;59(2):204-9.

EP-0129

Prospective evaluation of ^{68}Ga-PSMA-11 PET/CT sensitivity in patients with early biochemical relapse

O. Alonso Nunez[1,2], *G. dos Santos*[1,2], *M. Rodriguez Taroco*[1], *E. Silvera*[2];
[1]*Uruguayan Centre of Molecular Imaging (CUDIM), Montevideo, URUGUAY,* [2]*Clinical Hospital, University of Uruguay, Montevideo, URUGUAY.*

Aim/Introduction: We present our preliminary results as part of a prospective multicentre study sponsored by the IAEA (E13046) aiming to evaluate the diagnostic values of ^{68}Ga-PSMA-11 PET/CT in patients with prostate cancer and biochemical relapse after initial treatment. Our objective was to assess the sensitivity of this technique in patients with early biochemical relapse. **Materials and Methods:** We enrolled 86 patients between October 2017 and March 2019 with confirmed prostate cancer and biochemical relapse. From this sample, we analized 59 patients (median age: 66, range: 47-85 years) with PSA < 4.0 ng/mL (median: 0.61, range: 0.2-3.6 ng/mL) and with a follow-up of at least 3 months after PET/CT scanning (median: 11, range: 3-16 months). Images were acquired using a 16 or 64-slice PET/CT scanner with TOF correction and a dose of 2.0 MBq/kg ^{68}Ga-PSMA-11. Patients were initially treated with prostatectomy (n=50, 85%) or radiation therapy (n=9, 15%). PET results were validated by 3 blinded readers on a per patient basis and using a composite reference standard including histopathology (when available), conventional imaging or serum PSA behaviour after salvage therapy. The study was approved by our local review board and written informed consent was obtained from all patients. **Results:** ^{68}Ga-PSMA-11 PET/CT identified abnormal tracer foci in 30 patients (positivity rate: 51%) in the following sites: prostate gland (n=13), lymph nodes (n=36), bone (n=15) and lung (n=1). Forty-two patients were identified with prostate cancer relapse by means of the composite standard during follow up and PET correctly identified 28 patients (sensitivity was 0.67; 95% CI: 0.50-0.80). Sensitivity significantly increased with PSA: 0.48 for PSA ≤ 0.61 ng/mL to 0.86 for PSA > 0.61 ng/mL (P=0.020). **Conclusion:** Our single centre results suggest

that ^{68}Ga-PSMA-11 PET/CT has a clinically relevant sensitivity for the detection of prostate cancer lesions in the early biochemical recurrence setting with potential impact on prompt salvage therapy planning. **References:** None.

EP-0130

Retrospective Study Of Patterns Of Response To Androgen Deprivation Therapy On 68Ga-PSMA PET/CT In Prostatic Adenocarcinoma Patients

N. S. Mhatre, *V. Rangarajan, A. Agrawal, N. Purandare, S. Shah, A. Puranik;*
Tata Memorial Hospital, Mumbai, INDIA.

Aim/Introduction: With limited literature on the abilities of 68Ga PSMA PET/CT as a treatment response assessment tool in patients with prostatic adenocarcinoma, we explore the patterns of disease response on this modality with respect to biochemical response based on S.PSA, after medical or surgical androgen deprivation therapy. This may lead to further understanding of the in vivo effect on PSMA expression and disease volume, which may enhance its value in routine clinical practice. **Materials and Methods:** Whole Body PET/CT scans with 68Ga labelled PSMA-11 ligand, of 60 high risk prostatic adenocarcinoma patients who underwent a baseline scan for staging, followed by a follow up scan after androgen deprivation therapy (ADT) ,with mean interval of 5.7 months between 2 scans ,were included in this retrospective study. Treatment response on PSMA PET/CT based on quantitative volumetric PET parameter PSMA-Tumor Volume (PSMA-TV); in the lines of PERCIST criteria, was compared with biochemical response based on S.PSA levels ; by inter-rater agreement evaluation using Cohen's kappa coefficient. Lesion-wise response pattern was studied. **Results:** Overall PET based response with PSMA-TV showed no significant agreement with biochemical response measured with S.PSA (Cohen's kappa value (κ) being 0.07).Overall PET based response with PSMA-TV showed partial response in 64.2% and stable disease in 16.6 % of the patients with a complete biochemical response. Only 14.2% of patients who had complete biochemical response showed concordant results on PET/CT. 2 cases even showed progressive disease with complete biochemical response. Complete volumetric resolution of metastatic regional/distant lymph nodes in 50 % and skeletal lesions in 66% of the patients with the respective lesions. Primary site disease was the least responsive with 84% cases showing persistent or progressive disease. **Conclusion:** Discordance between the volumetric response on PET/CT (using PSMA-TV) and biochemical response endorses a possibility of the true objective representation of the post therapy disease burden by 68Ga PSMA PET/CT. Response to ADT differs lesion wise with primary disease showing persistence or progression in a strong majority of patients, whereas metastatic nodal and bony lesions show complete resolution in majority of the patients with the particular lesions respectively. Thus, post therapy PET/CT response may be used as a guide to plan local therapy with curative intent, following ADT. It is particularly useful in cases with low pre-therapy serum PSA levels. **References:** None.

EP-0131

Potential of molecular imaging with ^{99m}Tc-EDDA/HYNIC-iPSMA SPECT in brain tumors

P. Vallejo Armenta[1], *J. Soto Andonaegui*[1], *K. Contreras Contreras*[1], *G. Ferro Flores*[2];
[1]*Instituto Mexicano del Seguro Social, CDMX, MEXICO,* [2]*Instituto Nacional De Investigaciones Nucleares, Estado De México, MEXICO.*

Aim/Introduction: Brain tumors (BT) are highly treatment resistant and their marked angiogenesis attracts interest as a potential therapeutic target. Several researchers have proved that PSMA is expressed in the tumor-associated neovasculature of glioblastoma (GBM) and brain metastases (BM). Molecular imaging PET/CT is not as widely available; thus, a SPECT tracer is more cost-effective alternative.^{99m}Tc-EDDA/HYNIC-iPSMA radiopharmaceutical has been shown high radiopharmaceutical stability, specific receptor binding, high tumor uptake that due to the longer half-life (6.06 h) and increased lipophilicity[1,2]. The aim of the study was to assess the feasibility of using SPECT with 99mTc-EDDA/HYNIC-iPSMA for imaging BT. **Materials and Methods:** 21 patients with suspected BT underwent preoperative brain SPECT scan 3 hours after intravenous injection of 750 MBq 99mTc-EDDA/HYNIC-iPSMA: 13 with indeterminate brain tumor (IBT) and 8 with suspected glioma recurrence. Both visual and semiquantitative analyses were performed. Maximum target-to-background ratio(TBR_{max}) was calculated using contralateral tissue uptake as background. PSMA expression was assessed by immunohistochemistry (IHC) using PSMA monoclonal antibody. TBR_{max} was correlated with IHC findings and WHO grade tumor: low-grade glioma (LGG), high-grade gliomas (HGG). **Results:** 8 HGG (gliosarcoma, 2 anaplastic astrocytoma, 5 GBM); 2 LGG (oligodendroglioma, astrocytoma); 3 BM (breast cancer, poorly differentiated carcinoma); 6 recurrent gliomas and 2 reactive gliosis were found. Among the 13 cases with IBT, scan was positive in 8 patients with HGG (TBR_{max} 19±11.01) and 3 patients with BM (TBR_{max} 24.8±11.17), whereas 2 patients with LGG were negative. TBR_{max} was significantly correlated with glioma grading (Spearman r=0.92,p<0.001). Among the 8 cases with suspected recurrence, scan was positivein 6 patients with glioma recurrence (TBR_{max}7.1±3.78), whereas 2 patients with gliosis were negative. The optimal cut-off value of the TBR_{max} for the detection of malignant brain tumor (HGG, BM or recurrent glioma) was determined. By using 3.4 as the value for the threshold, the sensitivity and specificity were 89.5% and 100%, respectively. PSMA was highly expressed in the vascular endothelium of HGGand BM, while its expression in LGG was very low and completely absent in gliosis. **Conclusion:** 99mTc-EDDA/HYNIC-iPSMA brain SPECT is a feasible and potentially useful imaging tool for assessing of glioma grading (negative scan in LGG), to detect tumor recurrence (negative scan in treatment-related changes), planning treatment and biopsy guidance (the background uptake in normal brain parenchyma is absent, thus enhancing tumor detection). The PSMA binding

agents might be promising diagnostic and therapeutic option. **References:** 1. DOI: 10.1016/j.nucmedbio.2017.01.0122. DOI: 10.1016/j.nucmedbio.2017.05.005.

EP-0132

^{68}Ga-PSMA uptake variability: A test-retest study

J. olde Heuvel[1], *L. J. de Wit - van der Veen*[1], *M. L. Donswijk*[1], *C. H. Slump*[2], *M. P. M. Stokkel*[1]; [1]*Netherlands Cancer Institute Antoni van Leeuwenhoek, Amsterdam, NETHERLANDS,* [2]*Univ of Twente, Enschede, NETHERLANDS.*

Aim/Introduction: ^{68}Ga-PSMA-11 is an emerging imaging agent with unprecedented accuracy in prostate cancer (PCa) staging, yet repeatebility of uptake over time is unknown. The aim of this study was to assess the variability of ^{68}Ga-PSMA-11 uptake in primary prostate cancer (PCa) patients in a four-week interval. **Materials and Methods:** Inclusion criteria were age >18 years, histologically confirmed PCa and one of the following criteria to perform a ^{68}Ga-PSMA PET/CT scan: ≥cT3, Gleason score ≥7 or PSA ≥20 ng/mL. The first scan was performed on clinical indication, after which the second scan was scheduled approximately 4 weeks later. Patients were excluded if no substantial PSMA expression was visible in the prostate on the first scan or when treatment was started in between scans. Acquisitions were performed on a Vereos digital PET/CT system, 45 min after injection of 100 MBq ^{68}Ga-PSMA-11, from base of skull to mid-thigh. Acquisition time was 3 min per bed position for the pelvis and 2 min for the remainder of the scan range. Image reconstruction was performed using 3i15ss and 3mm Gaussian. Semi-quantitative measures (SUVmax, SUVmean) were determined in Osirix MD viewer using volumes-of-interest (>2cm diameter) in the prostate tumour, normal tissues, and blood pool. The difference between the scans was evaluated using Wilcoxon-signed-rank tests. **Results: Until April 2019,** 12 patients were included in this ongoing study. The median injected activity was not statistically different between the scans (99.4 MBq at scan 1 and 103.3 MBq at scan 2; p=0.08), as well as the time between injection and scan (45 and 47.5 min respectively; p=0.42). The median absolute difference in the prostate tumour uptake between both scans was 0.98 SUVmax (range 0.27-1.60) and 0.49 SUVmean (range 0.06-0.89). Median absolute differences in liver, parotid, and kidney uptake were 0.36, 1.23, 3.24 SUVmax, respectively and 0.35, 0.94, 1.95 SUVmean. Blood pool activity showed median absolute differences of 0.17 SUVmax and 0.11 SUVmean. Median variation of all measurements was below 11% for both SUVmax (range 5-31% tumour, 0-21% normal) and SUVmean (range 3-39% tumour and 0-46% normal) and none of the differences (tumour, normal tissues and blood pool) were statically significant. **Conclusion:** Preliminary results of test-retest 68Ga-PSMA-11 PET/CT scans in a four-week interval show that 68Ga-PSMA-11 uptake is comparable, with a clinical irrelevant variation in tumor and physiological distribution. Based on the presented repeatable uptake, 68Ga-PSMA PET/CT scans could potentially be used for surveillance and response monitoring. **References:** None.

EP-0133

Clinical Utility of ^{18}F-PSMA 1007 in Prostate Cancer

M. Joseph[1], *K. Vasan*[2]; [1]*Jeeyo PET-CT and Nuclear Imaging Centre, Mumbai, INDIA,* [2]*Jeeyo PET CT and Nuclear Imaging Centre, Mumbai, INDIA.*

Aim/Introduction: ^{68}Gallium (^{68}Ga) labelled prostate-specific membrane antigen (PSMA), a well-established tracer in the imaging of prostate cancer, has several shortcomings such as non-ideal energies, limited availability of the ^{68}Ga generator, requirement of high investment into synthesis modules and a high urinary excretion, which can obscure detection of the primary or residual disease. We present the clinical utility of ^{18}F-PSMA-1007 which has a longer half-life, high labeling yields, outstanding tumor uptake and fast, non-urinary background clearance. **Materials and Methods:** Total 68 patients were scanned with ^{18}F-PSMA-1007. Group A consisted of 50 patients that were suspected cases based on elevated PSA levels with high clinical suspicion. Histopathology was available in 40 patients, deemed as Group A1. Histopathology could not be traced of 10 patients, deemed as Group A2. Group B consisted of 18 patients who had proven disease, having received treatment, referred for disease status evaluation. **Results:** The sensitivity of ^{18}F-PSMA for detection of disease in group A1 was found to be 89.74%, PPV = 97.22%, accuracy = 87.50% based on pathological diagnosis. The SUVmax, SUVlbm and tumor background ratios, were found to have a small to medium correlation with pathological grade ($r < 0.3$) and cores involved ($0.3 < r < 0.5$). In Group A2, sensitivity, specificity, PPV and NPV based on PSA levels were found to be 100% with an accuracy of 100%. Loco-regionally advanced disease was found in 27 of both Group A1 and A2 (42% of 50) and metastases were found in 20 out of 50 (40%), resulting in upstaging in 94% of patients. In Group B patients, 15 out of 18 (83%) patients were found to have metastatic disease. There was no correlation between PSA values and the present or absence of a positive scan in this group ($r < 0.1$). ^{18}F-PSMA detected local recurrence in 3 out 4 (75%) patients who had undergone prostatectomy. Based on ROC analyses an SUVmax cutoff of > 4.1 was calculated to have the highest sensitivity, specificity (92.1%, 50% respectively) for detection of the primary disease in the prostate and SUVmax cutoff of > 3.5 was calculated for detection of nodal, lung and bone metastases (93.3% sensitivity, 100.00% specificity). **Conclusion:** ^{18}F-PSMA-1007 is a robust tracer, demonstrating good sensitivity for the detection of primary and metastatic disease, staging and re-staging in patients of prostate cancer. It overcomes practical limitations of ^{68}Ga-labelled PSMA targeted tracers. **References:** None.

EP-0134

Interobserver and Intraobserver Agreement for the Proposed miTNM Classification for the Interpretation of ^{68}GaPSMA-I&T PET/CT Imaging

A. Gültekin, *O. Yaylali, T. Şengöz, D. Yüksel, H. Şenol; Pamukkale University Medical Faculty, Denizli, TURKEY.*

Aim/Introduction: Prostate cancer(PCa) is the second most common cancer in men. Prostate spesific membrane anjigen(PSMA) is the most favorable tumor specific biomolecule found in molecular imaging studies. In recent years, ^{68}Ga-PSMA PET/CT has been used in diagnosis of PCa. This method is rapidly spreading due to the important clinical benefits. Before widespread clinical adoption of PSMA targeted PET imaging, its intraobserver and interobserver variability and agreement need to be established. There are very few studies on this subject. In this study, we aimed to determine the intra and inter observer agreement levels of ^{68}Ga-PSMA I&T PET/CT according to miTNM classification. **Materials and Methods:** Between March and June 2018, a total of 80 patients with ^{68}Ga-PSMA PET/CT with histologically proven PCa were evaluated twice, blindly by four nuclear medicine specialists at 4 weeks intervals. ^{68}Ga-PSMA synthesized in our department for PET/CT imaging was injected intravenously at a dose of 145-166mBq. After 60 minutes of injection, whole body scan images were created with the PET/CT device. PET/CT evaluations were performed according to miTNM classification over standard forms. We used Cohen's Kappa and Fleiss' Kappa analysis for to analyse agreement inter and intra observers. Statistical analysis was performed using R (version 3.4.3, Vienna, Austria) in RStudio (Version 1.1.463 - © 2009-2018 RStudio, Inc.). Package that we used for the analysis were "irr". **Results:** When ^{68}Ga-PSMA PET/CT findings are evaluated according to miTNM (tumor, lymph node, distant metastasis) classification, the obtained kappa values are as follows. Intraobserver Cohen's kappa coefficient was found to be 0.754±0.202 (substantial agreement), 0.907±0.007 (almost perfect agreement), 0.935±0.047 (almost perfect agreement) for miT, miN, miM, respectively. In interobserver assessment, interobserver adaptation for miT was good, agreement for miN, and agreement for miM was almost perfect. In the interobserver evaluation between four observers, the kappa coefficient was 0.502±0.295 for miT(moderate agreement), 0.722 ±0.149(substantial agreement) for miN, and 0.837± 0.062(almost perfect agreement) for miM. **Conclusion:** In the literature, there is no research on the intraobserver agreement study of ^{68}Ga-PSMA PET/CT. Our findings are the first results. The intraobserver agreement of PSMA PET/CT is almost perfect. PSMA PET/CT has moderate interobserver compliance in the evaluation of the primary tumor, but it has excellent interobserver agreement levels in local lymph node metastasis and distant metastasis evaluation. **References:** None.

EP-0135

Prospective comparison of hybrid ^{68}Ga-PSMA PET/CT and PET/MR in patients with biochemically recurrent prostate cancer

S. Jentjens[1], *C. Mai*[1], *L. De Coster*[2], *N. Ahmadi Bidakhvidi*[1], *N. Mertens*[1], *W. Everaerts*[1], *S. Joniau*[1], *R. Oyen*[1], *K. Van Laere*[1], *K. Goffin*[1];
[1]*University Hospitals Leuven, Leuven, BELGIUM,*
[2]*Europe Hospitals, Brussels, BELGIUM.*

Aim/Introduction: In patients with biochemically recurrent prostate cancer (PCa), highly sensitive localisation of recurrence is crucial, so patients may undergo salvage treatment as early as possible. ^{68}Ga-PSMA-PET/CT has become a routinely used technique in the evaluation of these patients. MRI is known to be superior to CT in soft tissue contrast and offers additional functional data through diffusion-weighted sequences, so the combination of PET with MRI might increase detection of recurrent disease. The aim of this prospective study was to investigate the incremental value of PET/MR versus PET/CT using ^{68}Ga-PSMA in patients with biochemically recurrent PCa. **Materials and Methods:** Patients were prospectively included and underwent routine ^{68}Ga-PSMA PET/CT (Siemens Biograph Truepoint 40; 69 min p.i., range 57-141min), followed by PET/MR (GE Signa 3T; 127 min p.i., range 80-167). All PET scans were evaluated by three nuclear medicine physicians for number of lesions, location and maximum and mean standardized uptake values (SUV). The CT and MR images were assessed by a uroradiologist. The findings were then combined in consensus to an overall PET/CT and PET/MR result. **Results:** A total of 34 patients were included with a mean age of 68 (± 7) years, mean PSA of 2.1 ng/mL and initial Gleason score between 6 and 9. 63 lesions were detected by PET_{CT}, 69 by PET_{MR}, 31 by CT only and 44 by MR only. All lesions detected by PET_{CT} were also detected by PET_{MR}, while 6 additional lesions were detected by PET_{MR} (69 vs 63, p = n.s.). No PET_{CT} detected lesions were missed by PET_{MR}. There was no significant difference in detection of local recurrence, bone or soft tissue lesions. Additional lesions to the PET_{MR} findings on MRI where two bone lesions. One patient showed multiple PSMA negative liver lesions on the MRI. An additional finding on CT was one PSMA negative lung lesion. Overall combined interpretation showed 72 lesions on PET/MR, PET/CT showed 66 lesions, but this difference was not significant. SUV_{mean} and SUV_{max} values were significantly higher on PET_{MR} than on PET_{CT} in lymph nodes (all $p < 0.01$), which may be related to the scan order (PET/CT first) and spatial resolution/contrast differences (time of flight on the PET/MR). **Conclusion:** In this prospective study, ^{68}Ga-PSMA PET/MR was able to detect localisation of biochemically recurrent PCa at least as accurate as PET/CT. **References:** None.

EP-0136

The Diagnostic Performance of ^{18}F-PSMA-1007 PET/CT In Prostate Cancer Patients With SuspectedRecurrence After Definitive Therapy

T. Lengana[1], *K. Kopka*[2], *I. Lawal*[1], *T. Boshomane*[1], *K. Mokoala*[1], *M. Vorster*[1], *F. Giesel*[3], *M. Sathekge*[1];
[1]*Department of Nuclear Medicine, Steve Biko Academic Hospital and University of Pretoria, Pretoria, SOUTH AFRICA,* [2]*Division of Radiopharmaceutical Chemistry, German Cancer Research Center, Heidelberg, GERMANY,* [3]*Department of Nuclear Medicine, Heidelberg University Hospital, Heidelberg, GERMANY.*

Aim/Introduction: The prostate bed is the commonest site of early recurrence of prostate gland. The currently used PSMA

ligands (^{68}Ga-PSMA and ^{99}mTc-PSMA) undergo early urinary clearance resulting in interfering physiological activity within and surrounding the prostate. This can result in sites of cancer recurrence being obscured.^{18}F-PSMA-1007 has an advantage of delayed urinary clearance thus the prostate region is reviewed without any interfering physiological activity.The aim of this study was to determine the diagnostic performance of ^{18}F-PSMA-1007 PET/CT in patients with biochemical recurrence after definitive therapy. **Materials and Methods:** Forty-six Prostate cancer patients (mean age 66.6±7.66, range 48-87 years) presenting with biochemical recurrence (mean PSA 2.37±2.81ng/ml, range 0.05 - 9.97) underwent non-contrast-enhanced ^{18}F-PSMA-1007 PET/CT. Areas of abnormal tracer uptake above background activity outside of organs with physiologic tracer biodistribution were considered as suggestive of prostate cancer recurrence. PET/CT findings were evaluated qualitatively and semiquantitatively (SUVmax) and compared to the results of histology, Gleason score, and conventional imaging. **Results:** Twenty-four of the 46 (52.17%) patients demonstrated a site of recurrence on ^{18}F-PSMA-1007 PET/CT. Oligometastatic disease was detected in 20 (43.5%) of these patients. Of these 9 (37.5%) demonstrated intra-prostatic recurrence, whilst lymph node only disease was noted in 8 (33.3%) whilst a single patient demonstrated isolated skeletal recurrence. The detection rates for PSA levels 0 - <0.5, 0.5-<1, 1-2, >2 were 31.3%, 25%, 55.6% and 76.5% respectively. 7 (29,2%) of the positive patients had been described as negative or equivocal on conventional imaging. Lowest detected PSA value was at 0.19ng/ml. **Conclusion:** ^{18}F-PSMA-1007 demonstrated good diagnostic performance detecting sites of recurrence at PSA values as low as 0.19ng/ml. Its superior ability to detect recurrence missed by conventional imaging will have a significant impact on patient management. **References:** None.

EP-0137

^{68}Ga-PSMA-11 PET surpasses clinical nomograms for prediction of lymph node metastasis in patients with intermediate to high-risk prostate cancer

D. A. Ferraro, U. J. Muehlematter, H. I. Garcia Schüler, N. J. Rupp, T. Hermanns, I. A. Burger;
University Hospital of Zurich, Zurich, SWITZERLAND.

Aim/Introduction: Radical prostatectomy with extended pelvic lymph node dissection (ePLND) is a curative treatment option for patients with clinically significant localized prostate cancer. The decision to perform an ePLND can be challenging because the overall incidence of lymph node metastasis is relatively low and ePLND is not free of complications. Using current prediction models to identify patients with nodal involvement, approximately 84-94% of ePLNDs performed are negative. The aim of this study was to compare the ability of ^{68}Ga-PSMA-11 PET with established nomograms to predict lymph node metastasis in men with prostate cancer. **Materials and Methods:** ^{68}Ga-PSMA-11 PET scans of 60 patients undergoing radical prostatectomy with ePLND were reviewed for qualitative (visual) assessment of suspicious nodes and assessment of quantitative parameters of the primary tumour in the prostate (SUV_{max}, total activity ($PSMA_{total}$) and PSMA positive volume ($PSMA_{vol}$)). Sensitivity and specificity of quantitative PET parameters to predict nodal metastasis were assessed with receiver operating characteristics (ROC) analysis. A multivariable logistic regression model combining visual nodal status on PET and primary tumour $PSMA_{total}$ was built. Net benefit at each risk threshold was compared with five nomograms: MSKCC nomogram, Yale formula, Roach formula, Winter nomogram and Partin tables (2016). **Results:** Overall, pathology of ePLND specimens revealed 31 pelvic metastatic lymph nodes in 12 patients. ^{68}Ga-PSMA-11 PET correctly detected suspicious nodes in 7 of them, yielding a sensitivity of 58% and a specificity of 98%. The area under the ROC curve for SUV_{max} was 0.70, for $PSMA_{total}$ 0.76 and for $PSMA_{vol}$ 0.75. The optimal cut-off for nodal involvement was $PSMA_{total} > 49.1$. The combination of a $PSMA_{total} > 49.1$ and visual positive nodes yielded a sensitivity of 100% and a specificity of 69% in our cohort. Furthermore, the PET model including those two PET parameters had a persistently higher net benefit compared to all clinical prediction models. **Conclusion:** Our model combining visual lymph node analysis on ^{68}Ga-PSMA-11 PET with $PSMA_{total}$ of the primary tumor performed better than currently used clinical prediction models to predict lymph node metastasis. Although this result has to be validated, ^{68}Ga-PSMA-11 PET showed the potential to improve patient selection for ePLND and reduce unnecessary surgical procedures. **References:** None.

EP-0138

Head To Head Comparison Of 18f-fch And 18f-psma-1007 Pet/ct In Biochemically Relapsed Prostate Cancer Patients - Preliminary Results

E. Witkowska-Patena[1,2], A. Giżewska[1,2], M. Dziuk[1,2], J. Miśko[2], A. Budzyńska[1,2], A. Walęcka-Mazur[3];
[1]*Military Institute of Medicine, Warsaw, POLAND,*
[2]*Affidea Mazovian PET/CT Medical Centre, Warsaw, POLAND,* [3]*Synektik Pharma, Kielce, POLAND.*

Aim/Introduction: The aim of the study was to prospectively compare diagnostic performance of 18F-FCH and 18F-PSMA-1007 PET/CT in patients with biochemical relapse (BCR) of prostate cancer and low prostate-specific antigen (PSA) levels. **Materials and Methods:** We prospectively enrolled 40 BCR patients after radical treatment of prostate cancer and PSA levels ≤2.0 ng/ml (median, 0.7 ng/ml, range, 0.01-2.00). 18F-FCH and 18F-PSMA-1007 PET/CT imaging was performed within a mean interval of 54±21 days. Skull to mid-thigh scans were done 87±10 min and 95±12 min after injecting 248±35 MBq and 295±14 MBq of 18F-FCH and 18F-PSMA-1007, respectively. Rate of negative, equivocal or highly suspicious of malignancy scan results was compared in per-patient analysis. Per-lesion, identified lesions were grouped as equivocal or highly suspicious for malignancy and then compared for their number, localisation (local relapse, lymph nodes, bones) and

SUVmax values. **Results:** 18F-FCH and 18F-PSMA-1007 PET/CT scans were positive (showed any lesions) in 17 (42.5%) and 35 patients (87.5%), respectively. Out of positive scans, 12% of 18F-FCH and 69% of 18F-PSMA-1007 PET/CT scans were highly suspicious of malignancy. The remaining 88% and 31%, respectively, were equivocal. Per-patient, 18F-FCH and 18F-PSMA-1007 PET/CT scan results were alike in 25% of cases. In 70% of scans, 18F-PSMA-1007 PET/CT upgraded 18F-FCH PET/CT results. 18F-PSMA-1007 scans also showed significantly more lesions (184 vs 63, p=0.0006). Local relapse, lymph node and bone lesions accounted respectively for 9%, 58% and 33% of 18F-PSMA-1007 and 5%, 89% and 6% 18F-FCH of PET/CT findings. Highly suspicious lesions accounted for 74% of 18F-PSMA-1007 and 11% of 18F-FCH PET/CT findings. In 18F-PSMA-1007 PET/CT, highly suspicious lesions accounted for 75%, 70% and 80% of local relapses, lymph node and bone findings, respectively. In 18F-FCH PET/CT all local relapses (n=3) and bone lesions (n=4) as well as 88% of lymph node findings were equivocal. SUVmax values of the assessed lesions are now undergoing statistical analysis. **Conclusion:** In early BCR patients 18F-PSMA-1007 showed higher detection rate than 18F-FCH PET/CT, especially of bone lesions. The former also showed more lesions in total, more highly suspicious lesions and less equivocal lesions. **References:** None.

EP-0139

Novel squaric acid coupled KuE-based PSMA inhibitors: Synthesis, radiolabeling with gallium68 and first in vitro and ex vivo evaluation

H. Lahnif[1], *L. Greifenstein*[1], *T. Grus*[1], *R. Bergmann*[2], *M. Schreckenberger*[3], *M. Miederer*[3], *S. Pektor*[3], *F. Roesch*[1];
[1]*Johannes Gutenberg University Mainz, Mainz, GERMANY,*
[2]*Helmholtz-Zentrum Dresden-Rossendorf, Dresden, GERMANY,*
[3]*University Medical Center Mainz, Mainz, GERMANY.*

Aim/Introduction: Introduction: Prostate cancer (PC) is one of the most common cancer types worldwide. Prostate-specific membrane antigen (PSMA) has been identified as an ideal target in diagnostic and therapy of PC since it is 1000-fold overexpressed in PC-cells. As target vectors for PSMA, urea-based-scaffolds have been established. KuE (L-lysine-urea-L-glutamate) moiety is the most used binding motif in PSMA inhibitors. **Aims:** In preliminary studies, we have identified the squaric acid (SA) as a promising linker moiety between the pharmacophore unit and radiolabeling unit. The application of SA as a coupling agent allows an easy synthesis, e.g. avoiding challenging protection group chemistry, and enables a fast and selective coupling. In this study, we investigate the impact of SA on the binding affinity and the pharmacokinetics of the potential PSMA ligands [^{68}Ga]Ga.AAZTA^5.SA.KuE, [^{68}Ga]Ga.DATA.SA.KuE and 4-[^{18}F]F Fluoroethoxybenzyl.SA.KuE. **Materials and Methods:** AAZTA^5.SA.KuE, DATA.SA.KuE, Ethylfluoride.SA.KuE and 4-Fluoroethoxybenzyl.SA.KuE were synthesized. Binding affinities of chelator.SA.KuE derivatives [^{nat}Ga]Ga.AAZTA^5.SA.KuE, AAZTA^5.SA.KuE, [^{nat}Ga]Ga.DATA.SA.KuE, DATA.SA.KuE and the fluoro-derivatives Ethylfluoride.SA.KuE and 4-Fluoroethoxybenzyl.SA.KuE were determined in a competitive cell assay using PSMA-expressing LNCaP-cells. LNCaP cells were incubated with 0.75 nM [^{68}Ga]Ga-PSMA-10 in the presence of different concentrations of the non-labeled PSMA-ligands. After incubation at RT and removal of free radioactivity, cell-bound activity was measured. PSMA-11 was used as reference. Data were analyzed in GraphPad Prism 5 using nonlinear regression. Male Balb/c nu/nu mice were subcutaneously inoculated with 5.10^6 LNCaP-cells. After i.v. administration of [^{68}Ga]Ga.DATA.SA.KuE (~10 MBq/nmol), the mice were sacrificed 1 h p.i. and the radioactivity of the organs was measured. % ID/g values were calculated. **Results:** Radiolabeling of AAZTA^5.SA.KuE and DATA.SA.KuE showed radiochemical yields of >95 % in 5 minutes for 10 nmol at RT. The IC_{50} values of AAZTA^5.SA.KuE and DATA.SA.KuE exhibit a nanomolar binding affinity (52.1 ± 4.0 nM and 51.1 ± 5.5 nM respectively). 4-Fluoroethoxybenzyl.SA.KuE shows a 7-fold higher binding affinity than Ethylfluoride.SA.KuE (40.8 ± 4.9 nM vs. 279.4 ± 3.7 nM). Tumor uptake of [^{68}Ga]Ga.DATA.SA.KuE was high (4.65 ± 0.58 %ID/g) and resulted in a high tumor-to-blood ratio of 9.3. Kidney uptake was remarkably low 12.82 ± 4.84 %ID/g. **Conclusion:** The results of the competitive binding assay on LNCaP cells showed a nanomolar binding affinity for the chelator.SA.KuE derivatives and 4-Fluoroethoxybenzyl.SA.KuE. Biodistribution data revealed the potential of SA in reducing kidney uptake. **References:** None.

EP-0140

Use of ^{68}Ga-PSMA-11 PET/CT in the detection of prostate cancer recurrence of non metastatic castrate-resistant patients: posivity rate and impact on patient management

M. Gauthé*, A. Fourquet, C. Aveline, F. Montravers, J. Talbot;*
Hôpital Tenon, Paris, FRANCE.

Aim/Introduction: We aimed to evaluate the detection rate and the impact on therapeutic management of PET/CT using prostate-specific membrane antigen ligand labeled with gallium-68 (PSMA-11) in non-metastatic prostate cancer (PCa) patients developing castration-resistance. **Materials and Methods:** Not metastatic PCa patients who were referred for PSMA-11 PET/CT because of a rise of prostate-specific antigen (PSA) serum level despite castrate serum testosterone inferior to 50 ng/dl between April 2016 and April 2018 were included. Abnormal foci detected on imaging were quoted in multiple anatomical areas (prostate/prostatic lodge, pelvic lymph nodes, paraaortic lymph nodes, supra-clavicular lymph nodes, bone and other locations) according to a 3-point scale (no suspicious uptake, equivocal uptake and pathologic uptake). Patients were categorized as metastatic if imaging detected at least a pathologic foci outside the prostate/prostatic lodge area, and oligometastatic if imaging detected at best 3 pathologic foci. The impact on therapeutic management was assessed by comparing changes decided during multidisciplinary meeting before and after PSMA-11 PET/CT. **Results:** Thirty-eight patients in total were included, among whom 25 (66%) had history of

prostatectomy. The mean age was 72 years-old and the median PSA serum level the day of the imaging was 3 ng/ml. The median follow-up time after imaging was of 12 months. PSMA-11 PET/CT was pathologic in 89%, equivocal in 3 % and negative in 8% of cases. At least one pathologic focus was found in 39% of cases in the prostate/prostatic lodge, 34% in pelvic lymph nodes, 32% in paraaortic lymph nodes, 8% in supra-clavicular lymph nodes, 26% in bone and 13% in other locations. Twenty-seven (71%) patients were categorized as metastatic and 14 (37%) as oligometastatic. PSMA-11 PET/CT results led to a change in management in 77% of cases (evaluated on 26 patients), statistically superior in oligometastatic patients by guiding stereotactic radiation therapy of metastasis. **Conclusion:** PSMA-11 PET/CT is useful in PCa patients developing a castration-resistance by identifying residual disease in 89% of cases. It also induces a change in therapeutic management of 3 patients out of 4, especially in oligomestatic patients. **References:** None.

EP-0141

Interobserver agreement in ^{68}Ga-PSMA PET/CT with structured PIP-RADS classification

L. van Kalmthout[1], *P. Kaldeway*[2], *A. Braat*[1], *M. Lam*[1], *H. van Melick*[2], *J. Lavalaye*[2];
[1]*Academic hospital, Utrecht, NETHERLANDS,* [2]*St. Antonius Ziekenhuis, Nieuwegein, NETHERLANDS.*

Aim/Introduction: Gallium-68 (^{68}Ga)-PSMA PET/CT has evolved as standard imaging procedure for prostate cancer (PCa) (re)staging due to its easy readability and presumed high interobserver agreement. To further optimize interpretation and subsequent clinical applicability of PSMA PET/CT, however, structured reporting methods are required. This study aims to determine interobserver agreement in PSMA PET/CT reporting, using the newly proposed PIP-RADS classification. **Materials and Methods:** From May 2015 up to June 2018, all consecutive ^{68}Ga-PSMA PET/CT scans for primary staging and restaging of PCa were retrospectively included in two institutions and evaluated by two blinded experienced nuclear medicine physicians. The prostate region, regional and distant lymph node sites, bone lesions and visceral lesions were scored on the PIP-RADS 5-point scale, with 1 being benign and 5 being highly suspicious of malignancy. Interobserver agreement was evaluated using Cohen's kappa, both on TNM-basis (prostate region (T-stage); regional lymph nodes (N-stage); distant lymph nodes (M1a-stage); bone lesions (M1b-stage) and visceral lesions (M1c-stage) and, more specific, on region-basis (including various anatomical lymph node sites). **Results:** A total number of 58 ^{68}Ga-PSMA PET/CT scans for primary staging and 60 for restaging of PCa were analyzed. Their clinical conclusions yielded a wide variety of terms. TNM-based evaluation of all patients according to the PIP-RADS classification showed substantial interobserver agreement for the prostate region (κ = 0.67); substantial agreement for regional lymph node sites (κ = 0.62); moderate agreement for distant lymph node sites (κ = 0.43). substantial interobserver agreement for bone lesions (κ = 0.62) and fair agreement for visceral lesions (κ = 0.22). Region-based analysis according to the PIP-RADS classification showed fair to substantial agreement for all tumor sites, except for visceral lesions (κ = 0.22). **Conclusion:** The structured PIP-RADS classification provides substantial interobserver agreement in localizing PCa tumor sites on ^{68}Ga-PSMA PET/CT and may be used to further optimize PET-interpretation in daily practice. **References:** None.

EP-0142

Can patient selection based on ^{68}Ga-PSMA-11 PET improve the outcome of radical prostatectomy in prostate cancer patients?

I. A. Burger, *D. A. Ferraro, U. J. Muehlematter, H. I. Garcia Schüler, D. Eberli, T. Hermanns;*
University Hospital Zurich, Zurich, SWITZERLAND.

Aim/Introduction: Accurate patient selection for invasive therapy is of major importance for patients with new diagnosed prostate cancer. Recently, the use of the new PET tracer targeting the prostate specific membrane antigen (PSMA) for staging was suggested for superior detection of metastatic disease. However, it is still unclear whether this superior sensitivity would translate into a significant impact on outcome. The aim of this study was to assess the biochemical recurrence (BCR) ratio in patients that underwent radical prostatectomy (RPE) after a ^{68}Ga-PSMA-11 PET for staging and compare it to recently published data reporting a BCR rate of 32% within 12 months after RPE[1]. **Materials and Methods:** In this retrospective analysis, approved by the local ethics committee, from 137 patients that underwent ^{68}Ga-PSMA-11 PET scans for staging intermediate or high-risk prostate cancer between April 2016 and May 2018, 116 patients gave written informed consent for retrospective analysis of their data. In 96 patients local therapy was considered an appropriate option after the PET scan and 58 of those patients underwent RPE with extended pelvic nodal dissection in our institution and were included in this analysis. PSA follow up was collected at 12 months after RPE, as well as information about the need of additional salvage radiotherapy due to PSA persistence or recurrence. A PSA level >0.2 ng/ml was considered BCR. **Results:** Twelve months after RPE additional salvage radiotherapy was necessary in 9 patients. 49 patients did not have any additional therapy after RPE. In 42 of them the PSA was undetectable after 12 months and 5 patients had a PSA below 0.2 ng/ml. Therefore, only 11 of 58 (19%) of patients selected for RPE based ^{68}Ga-PSMA-11 PET had biochemical recurrence after 12 months. Three patients with non-pathologically enlarged but ^{68}Ga-PSMA-11 PET positive common iliac lymph nodes were selected for RPE, all had an early BCR. If these three patients would not have been considered surgical candidates, only 8 of 55 (15%) would have had BCR after 12 months. **Conclusion:** With the current data we could show that there is some first evidence, that ^{68}Ga-PSMA-11 PET might reduce the rate of BCR in patients undergoing RPE from up to 30% to 15% after 12 months, despite the bias of a higher

risk patient population. **References:** Skove SL et al. Timing of Prostate-specific Antigen Nadir After Radical Prostatectomy and Risk of Biochemical Recurrence. Urology. 2017 Oct;108:129-134.

EP-0143

Advantages of ^{68}Ga-PSMA I&T PET/CT in primary staging of prostate cancer

W. Cytawa[1], *T. Bandurski*[1], *J. Tran-Gia*[2], *A. Schirbel*[2], *K. Fukushima*[2], *H. Wester*[3], *P. Lass*[1], *B. Brockhuis*[1], *W. Połom*[1], *A. K. Buck*[2], *C. Lapa*[2];
[1]*Medical University of Gdansk, Gdansk, POLAND,*
[2]*University Hospital Würzburg, Würzburg, GERMANY,*
[3]*Technische Universität München, Munich, GERMANY.*

Aim/Introduction: Prostate cancer (PCa) is the second most common malignancy in men worldwide. In spite of curatively intended treatment options in localized disease including radical prostatectomy (RP) or external beam radiation therapy (EBRT), up to 30% of patients will experience tumor recurrence. One of the key issues in clinical management of PCa patients is the accurate preoperative staging of the disease, in which conventional imaging yields unsatisfactory results.The aim of the study was to retrospectively assess the PSMA-avid distribution of PCa disease prior to planned definitive treatment in ^{68}Ga-PSMA I&T PET/CT. **Materials and Methods:** Eighty two patients with biopsy proven, treatment-naïve PCa were included in the study. All patients underwent ^{68}Ga-PSMA I&T PET/CT (PSMA I&T SCINTOMICS GmbH, Fürstenfeldbruck, Germany) for primary staging of the disease. Focal radiotracer accumulation within the prostate gland was considered as positive primary tumor uptake, whereas focally increased uptake within the lymphatic drainage areas was regarded as lymph node metastasis (LNMs). Bone metastasis (BMs) or other distant metastasis were also reported, according to PROMISE criteria. **Results:** Patients main characteristics: mean age 66.7 ± 7.3 years (range 53-83), median Gleason score (GSC) 7 (range 6 - 10), median PSA level 11.0 ng/ml (range 0.7-872.5). Low-risk disease was present in 11, intermediate-risk in 32, and high-risk in 39 patients (according to D'Amico classification). Sixty-six (80.5%) patients presented with positive primary tumor uptake. PSMA positive LNs were reported in 17 patients (20.7%). Distant metastases were found in 12 (14.6%) patients, predominantly in bones. Presence of N+ disease correlated considerably with GSC and PSA values, and hence with disease risk group: positive LNs were reported in 3/32 (9%) patients with intermediate-risk and 14/39 (36%) patients with high-risk disease. Similar to LNMs, incidence of distant lesions increased with disease risk group: 2/32 (6%) patients with intermediate-risk and 12/39 (31%) individuals with high-risk disease presented with retroperitoneal LNMs and/or BMs. No metastases were present in patients with low-risk PCa. We found a significant positive correlation (r=0.51, p<0.001) between the SUV_{max} of primary tumor uptake and PSA level, and between primary tumor SUV_{max} and GSC (r=0.38, p<0.001). Primary tumor uptake was also significantly higher in patients with LNMs (mean SUVmax 24.9±16.0) vs. patients without LNMs (mean SUVmax 14.1±12.6, p=0.039). **Conclusion:** ^{68}Ga-PSMA I&T PET/CT is a useful tool in primary staging of PCa with detection rates and PSMA expression of PCa lesions rising with GSC, PSA level and risk group of disease. **References:** None.

EP-0144

^{99m}Tc-PSMA-SPECT/CT in Patient With Prostate Cancer

I. Farkas, *Z. Besenyi, A. Maráz, Z. Bajory, A. Palkó, G. Sipka, S. Urbán, L. Pávics;*
University of Szeged, Szeged, HUNGARY.

Aim/Introduction: Several PSMA-specific ligands -mostly PET tracers - have been developed in the last few years. PSMA-PET/CT have higher detection rate than conventional imaging modalities to detect primary prostate cancer, tumor recurrences and metastases as well. We examined the clinical application of a ^{99m}technetium-labeled PSMA-radiopharmaceutical as part of the routine diagnostics of prostate cancer. **Materials and Methods:** We examined 61 male prostate adenocarcinoma (Gleason-score 8; 2-10), with suspicion of progression or recurrence of the disease (serum PSA level 3,05; 0,08 - 93,31). Whole-body PSMA-SPECT/CTs (Mediso AnyScan TRIO) and multiparametric MRIs (GE Healthcare Discovery MR750w 3.0 Tesla) of the prostate and the pelvic regions were performed within three weeks. We used 690 ± 97 MBq of ^{99m}Tc-mas3-y-nal-k(Sub-KuE) for the PSMA-SPECT scans. The images were evaluated visually and semi-quantitatively. **Results:** In case of 41 patients 77 PSMA-positive lesions were detected (10 primer prostate cancer; 11 local recurrence; 25 lymph node-, 28 bone- and 3 visceral metastases). 28 of them were localized outside, 49 were within the MRI's field of view. From these 49 lesions, 25 matched with the SPECT/CT. In case of ten lesions MRI raised suspicion of a metastasis but there was no associated pathological tracer uptake on the SPECT san. Six months follow up showed 4 of these were false positive findings. In 20 patients no PSMA abnormality was found. Despite the negative PSMA-SPECT/CT during the follow up period clinical data proved the presence of local recurrence in 12 cases. Tumor-to-normal activity concentration ratios were 30,32 ± 36,32 (3,34-193,77). The tracer uptake correlated with serum PSA level (Spearman's rank correlation; $P < 0.05$). No correlation was found between Gleason and tracer uptake. **Conclusion:** PSMA-SPECT/CT with 99mTc-mas3-y-nal-k(Sub-KuE) is a promising method in the evaluation of prostate cancer patients. It is capable of visualizing bone metastases, local recurrences and visceral metastases as well. Semiquantitative analysis revealed relationship between PSMA ligand uptake and disease activity. **References:** None.

EP-0146

Characterization And Targeting Of ^{177}Lu-PSMA617 Induced Prostate Cancer Cell Stress Response Signaling To Improve Therapeutic Efficacy

K. Lueckerath, A. D. Stuparu, S. Poddar, J. R. Capri, T. M. Le, K. Current, C. Cheng, C. G. Radu, J. Czernin; Univ. of California Los Angeles, Los Angeles, CA, UNITED STATES OF AMERICA.

Aim/Introduction: Only ~50% of patients with PSMA$^+$ tumors respond to PSMA directed radioligand therapy (RLT) and relapses occur uniformly in this group. We explored links between RLT-induced signaling alterations and actionable resistance mechanisms, and provide proof-of-principle for new, rationally designed RLT-based combination therapies using clinical stage inhibitors. **Materials and Methods:** ^{177}Lu-PSMA617 RLT-induced (phospho)proteomic alterations in the C4-2 PC mouse model were profiled using mass spectrometry. The relevance (i) of significantly altered pathways for mediating resistance to RLT, and (ii) of pharmacological targeting these pathways in combination with RLT was validated across a panel of PSMA$^+$ PC cells (immunoblot, flow cytometry, tumor cell growth inhibition), and in vivo using the C4-2 and 22Rv1 PC mouse models (treatment efficacy as determined by computer tomography). **Results:** Our (phospho)proteomic datasets revealed that activation of the DNA damage and replication stress response (DDR/RSR) and TP53-signaling can occur in response to RLT, and identified drugable key-effectors in these pathways such as ataxia telangiectasia and Rad3-related (ATR). In vitro, inhibition of ATR (ATRi) in combination with ionizing radiation (IR) sensitized PC cells to IR, by increasing DNA damage (pH2A.X) and cell death (Annexin V/PI), and impairing DNA damage signaling (pCHEK1/2) and colony forming capacity. In mice with C4-2 tumors, combining ^{177}Lu-PSMA617 RLT with ATRi resulted in synergistic tumor growth inhibition. However, tumors started to re-grow ~80 days post-RLT. Based on our phosphoproteomic dataset we hypothesized that adding inhibitors of ataxia-telangiectasia mutated (ATM) or poly ADP ribose polymerase (PARP) to the ATRi/RLT combination might improve therapeutic efficacy. In vitro, both triple combination regimens resulted in significantly enhanced DNA damage, cell death, and cell growth inhibition compared to ATRi/IR alone in all cell models tested. We are currently testing in two different PC mouse models (C4-2 [TP53$^{wt/wt}$, BRCA2$^{wt/wt}$], 22Rv1 [TP53$^{mut/wt}$, BRCA2$^{mut/mut}$] tumors) if concomitant administration of ATRi/ATMi and ATRi/PARPi, respectively, outperforms application of ATRi alone, and enhances the efficacy of RLT. **Conclusion:** Our study identified DDR/RSR signaling as liability of PC tumors that can be exploited to sensitize genetically divers PC models to RLT. We will expand our investigations to more stringent PC mouse models and analyses of biopsies from patients undergoing RLT. Our analytical approach may provide the rationale for future clinical trials of new RLT-based combination therapies. **References:** None.

EP-08
Inflammation & Infection: Molecular imaging in Infection and Inflammation

October 12 - 16, 2019

e-Poster Area

EP-0147

Clinical usefulness of 18F-FDG PET/CT in patient with cardiac implantable electronic device

C. Ferrari, A. Ungaro, A. R. Pisani, A. Gaudiano, V. Lavelli, C. Altini, A. G. Nappi, G. Rubini;
Nuclear Medicine Unit, Interdisciplinary Department of Medicine – University of Bari "Aldo Moro", Bari, ITALY.

Aim/Introduction: The use of cardiovascular implantable electronic device (CIED) has been increasing in the last decade. Long-term complications include device-related infections that may develop in the pocket, leads or cardiac valve. Currently, the diagnosis of CIED makes use of positive bacteriological samples associated with transthoracic echocardiography (TTE) and transoesophageal echocardiography (TEE) according to Duke's Criteria. 18F-FDG PET/CT is also performed for inflammatory processes in addition to oncologic purpose. The aim of this study was to evaluate the role of 18F-FDG PET/CT in patient with suspected infection of CIED. **Materials and Methods:** Fifteen patients who performed a 18F-FDG PET/CT from 2013 to 2019 for suspicion of CIED were retrospectively analyzed. The same number of patients (n=15), with implanted CIED, that underwent to PET/CT imaging for oncological reasons, which resulted negative and asymptomatic, was retrospectively evaluated as control group. Patients suspected of infection were previously evaluated according to Duke's criteria. 18F-FDG PET/CT studies were firstly visually analyzed on the basis of presence of hot spots around box or leads in the first group. Values of Sensitivity (Se) and Specificity (Sp) were estimated. A semiquantitative analysis was performed using the maximal standard uptake value (SUV_{max}) inside a region of interest (ROI) within the hotspots. Similar ROI were drowned in the control group on the boxes. The final diagnosis was obtained from the bacteriological data after device culture or during follow-up according to Duke's criteria, both considered as gold-standard. Concordance between gold-standard and 18F-FDG PET/CT was calculated with Fisher's Test. **Results:** All devices were implanted since at least 6 months. Cardiac device was harvested in 12/15 patients and confirmation of device culture was observed in 11/12 patients. The final diagnosis of the 3/15 patients left was based on negative follow-up according to Duke's Criteria. The agreement between 18F-FDG PET/CT and explantation or negative follow-up was statistically significant ($p< 0.05$). Se and Sp were respectively 91% and 75%. Semiquantitative analysis had shown in the control group a mild diffuse uptake around the box significantly higher than the opposite side: SUV_{max}: 1.97±0.5 vs 1.59±0.3; $p< 0.05$. Furthermore, patients with proven infection had higher uptake compared to control group SUV_{max}:

4.42±1.85 vs 1.5±0.34; p<0.01. A SUV value equal or > 2.47 discriminated all positive patients from controls. **Conclusion:** In agreement with literature, this study underlines the clinical usefulness of 18F-FDG PET/CT in patients with CIED infection due to its higher sensibility, repeatability and non-invasiveness. **References:** None.

EP-0148

^{99m}Tc-White Blood Cell Scintigraphy With SPECT/CT in the Diagnosis of Vascular Graft Infection

M. de la Rubia Marcos*, P. Garcia Alonso, C. Mena Melgar, B. Tagliatori Nogueira, A. Herrero Muñoz, C. Sandoval Moreno, C. Paniagua Correa, L. Castillejos Rodriguez, A. Ortega Valle, M. Balsa Breton;*
Hospital Universitario de Getafe, Getafe, SPAIN.

Aim/Introduction: Vascular graft infection is a rare complication that occurs in 1 to 6% of all prosthetic vascular procedures, with a high morbidity and mortality. It is associated with mortality rates of up to 75%, and 70% of peripheral prosthetic graft infection lead to limb amputation. Early diagnosis is essential to establish an adequate treatment. CT is generally considered the initial imaging modality of choice in these patients. However, ^{99m}Tc-HMPAO labeled white blood cell scintigraphy (^{99m}Tc-WBC) with SPECT/CT is showing promising results in improving imaging assessment of vascular graft infection. The aim of our study was to assess the accuracy of ^{99m}Tc-WBC scintigraphy with SPECT/CT in the diagnosis of vascular graft infection. **Materials and Methods:** We retrospectively analyzed thirty ^{99m}Tc-WBC scintigraphies with SPECT/CT performed in our center in thirty patients with suspicion of vascular prosthesis infection (3 women and 27 men, with an age range 33 - 87), between April 2014 to November 2018. Planar images were performed at 30 minutes, followed by delayed planar and SPECT/CT images at 2 hours. Studies were considered positive for graft infection if the intensity of activity involving the graft was the same as or greater than the liver or bone marrow activity (spine and pelvis). **Results:** Final diagnosis of infection was established in 10 patients, based on Fitzgerald criteria. Scintigraphy was positive in 11 patients, with only one false positive result. No false negatives were obtained. The values of sensitivity and specificity were 100% and 95% respectively, with a PPV of 91% and a NPV of 100%. 25 patients had a CT performed prior to scintigraphy, in 9 cases the result was positive and in the remaining 16 was negative. CT sensitivity and specificity obtained in our study were 62.5% and 76% respectively, with a PPV of 55.6% and a NPV of 81.3%. Diagnosis of infection led to prosthesis exeresis in 8 cases (all of them had a positive microbiological study of the extracted material), while the remaining 2 patients were treated with antibiotic therapy alone due to high surgical risk. **Conclusion:** Our results suggest a high accuracy for ^{99m}Tc-WBC scintigraphy with SPECT/CT in the assessment of clinically suspected arterial graft infection, even more than CT. **References:** None.

EP-0149

Role Of F-18 FDG PET-CT In The Evaluation Of Patients With Fever Of Unknown Origin

J. Mandarapu*;*
Continental Hospitals Limited, Hyderabad, Telangana, INDIA.

Aim/Introduction: Analysing whole body ^{18}F-FDG PET-CT in the evaluation of patients with FUO to Localise the source of FUO. Estimate the extent of involvement. Suggest the sites of biopsy, thereby usefulness in obtaining histopathological diagnosis. **Materials and Methods:** Study area : Department of Nuclear Medicine, Apollo Gleneagles PET/CT centre, Hyderabad. Study design : A prospective, observational study of 48 patients for a period of 24 months.Study population : 48 patients were included in the study among which 22 were male and 26 female. **Results:** Of the 48 patients male to female ratio is 0.8:1. PET-CT showed abnormalities (positive) in 36 patients and was normal (negative) in 12 patients. Among 36 PET-CT positive, 20(55.5%) patients were diagnosed as infective etiology. 15/20 (75%) were diagnosed as tuberculosis. Histopathology confirmed the diagnosis of tuberculosis in 7/15.In 8/15 patients where histopathology showed non diagnostic/in conclusive and in high clinical suspicious for tuberculosis, patient was started on ATT. In view of clinical response to ATT, the diagnosis of tuberculosis was confirmed. Imaging (CT/USG) guided drainage of abscess and pus culture and sensitivity confirmed the diagnosis of liver abscesses in 2/5(10%).PET/CT diagnosed as pneumonia in 1/5 patient (5%), cholecystitis in 1/5 patient (5%), bilateral polycystic kidney disease in1/5 (5%) patient and the diagnosis was confirmed with clinical improvement of the patients with higher antibiotics in all 3 patients. Neoplastic etiology was found in 5/36 (13.8%) patients. Histopathology confirmed the diagnosis of malignancy in all 5 patients.4/5 (80%) patients were diagnosed as Non Hodgkin`s lymphoma (NHL) and 1/5(20%) as gastro intestinal stromal tumour (GIST). Non infectious inflammatory diseases were found in 5/36 (13.8%) patients. Non specific false positive FDG uptake in small sub centimeter lymph nodes, spleen and bone marrow was seen in 5/36 (13.8%). Among 12 patients with PET-CT negative, 2(16.6%) patients were diagnosed to have infective etiology 1(8.3%) of the 12 patients had systemic lupus erythematous (SLE). In the rest 9/12 (75%) PET-CT negative patients, fever resolved and had uneventful course. **Conclusion:** Etiologies of FUO in the study were infection (45.83%), malignancy (10.41%), non infectious inflammatory diseases (12.50%), miscellaneous causes (2.08%) and undiagnosed fever (29.16%). Sensitivity, specificity, PPV and NPV of FDG PET/CT in FUO in the study were 91.1%, 64.2%, 86.1% and 75% respectively. PET/CT significantly contributed to the final definite diagnosis in 86.1% of the patients with FUO (P value = <0.05). **References:** None.

EP-0150

The role of "after washing imaging" in evaluation of tear drainage system by dacryoscintigraphy

R. Sadeghi*, T. Masoudi, H. Shayegani;*

Nuclear Medicine Research Center, Mashhad University of Medical Sciences, Mashhad, IRAN, ISLAMIC REPUBLIC OF.

Aim/Introduction: The aim of this study was to evaluate the efficacy of "after washing" imaging in interpretation of dacryoscintigraphy as a functional imaging technique used in evaluation of tearing problems. **Materials and Methods:** 300 nasolacrimal systems were studied. 100 µCi of technetium-99m sodium pertechnetate as drops of activity (10 µL) were placed into the inferior fornix of each eye. Dynamic images were obtained for 15 minutes in the sitting position. "After washing" phase was done by placing a drop (10 µL) of normal saline in each eye and external ocular massage for an additional 10 minutes. The imaging patterns for each eye in the first dynamic phase and after washing phase were recorded, separately. **Results:** First dynamic phase demonstrated a sensitivity of 97.4% and specificity of 22.6%. After washing phase showed a sensitivity of 91.2% and specificity 75.5%. After washing test, the obstruction pattern changed to "patent nasolacrimal duct" or "further progression" of the radiotracer to the nasolacrimal duct in the 25.1% and 24.4% of the nasolacrimal systems, respectively. **Conclusion:** After washing imaging is a useful method in dacryoscintigraphy which can improve the specificity of scan for diagnosis of lacrimal duct obstruction. It can also improve the localization of obstruction level in the lacrimal systems. **References:** None.

EP-0151

Progressive Accumulation of Radiolabeled White Cells in Scans Performed for Suspected Vascular Prosthetic Graft Infections

*J. Jooma, **A. G. G. Doruyter**, J. M. Warwick;*
Stellenbosch University, Cape Town, SOUTH AFRICA.

Aim/Introduction: Vascular prosthetic graft infection is a serious complication which can be diagnosed using radiolabeled white cell scintigraphy (WCS). Interpretation criteria proposed by a recent multicenter study, to diagnose or exclude soft tissue infection on WCS, have not been validated in suspected vascular prosthetic graft infections (SVPGI). No research has to date investigated whether assessment of progressive white cell accumulation improves the accuracy of WCS performed for SVPGI. **Materials and Methods:** A retrospective analysis was performed of all WCS scans performed for SVPGI between January 2004 and June 2018. Studies were only included if both 3-hr and 24-hr imaging were available. Initial 3-hr images were first classified as positive or negative on the basis of presence or absence of white cell activity at the site of the vascular graft. Next, by comparing 24-hr and 3-hr images, studies were scored as either positive or negative based on the presence or absence of progressive white cell accumulation: both visually, and by calculating an accumulation index using suitable regions of interest with count values corrected for decay. A composite reference standard according to which the final diagnosis was made was based on a combination of microbiological, clinical and imaging follow up. Accuracy of interpretation methods was compared using pairwise comparisons of receiver operating characteristic curves. **Results:** Twenty-three studies (n=23) of 24 SVGIs were included (21 patients, 8 female, mean age 62.3 years). Of all SVPGIs investigated, 18 were proven to be infected while in 6 infection was excluded. Visual interpretation of 3-hr images alone classified 23 cases correctly and resulted in 1 false positive. Visual interpretation of white cell accumulation over 24-hr classified 18 cases correctly and resulted in 1 false positive and 5 false negatives. Finally, interpretation based on an accumulation index alone correctly classified 12 cases but resulted in 3 false positives and 9 false negatives. Visual interpretation at 3-hr was statistically more accurate than visual assessment for accumulation over 24-hr ($p = 0.0265$). **Conclusion:** We found no evidence to suggest that assessment of progressive white cell accumulation improves diagnostic accuracy of WCS for SVPGI. To the contrary, early visual assessment at 3 hours appears to result in the highest accuracy in this context. **References:** None.

EP-0152

^{18}F-FDG PET/CT Assessment of Sarcoidosis Extension and Activity - A Single Center Experience

***M. Silvestre**, T. C. Ferreira, I. P. Carvalho, M. R. Carvalho, D. Ferraz, D. Fraga, F. N. Brandão, P. Ratão, R. Sousa, L. Salgado;*
Instituto Português de Oncologia de Lisboa, Lisbon, PORTUGAL.

Aim/Introduction: Sarcoidosis is a multisystemic disease of unknown cause, with formation of noncaseating granulomas during its course[1]. Our center is dedicated mainly to oncology, however ^{18}F-FDG PET/CT scans (PET) were performed for sarcoidosis evaluation during the past few years. The aim of this study is to retrospectively review our results assessing disease extension and activity using PET, in patients (pts) with sarcoidosis. **Materials and Methods:** From january-2014 until march-2019 we performed 64 PETs for sarcoidosis evaluation. We excluded re-evaluation scans or pts undergoing treatment (n=24) and pts with other possible diagnosis (n=1). Data from the remaining 39 PETs was collected regarding sites involved - intra-thoracic lymph nodes (LN), extra-thoracic LN, lungs, bone, muscle, spleen, skin, gastrointestinal tract, eyes, liver and pituitary - and respective standardized uptake values (SUVs). For cardiac sarcoidosis evaluation, we excluded PETs with unsatisfactory preparation (n=13). The remaining studies (n=26) were evaluated. **Results:** Our population had a mean age of 56 years (range 28-83) and 1:2 male to female ratio. Active disease was seen in 79% (n=31). From these, 55% had multisystemic disease (n=17). Sites most commonly affected were intra-thoracic LN (74%), extra-thoracic LN (42%) and lungs (39%). SUVs distribution for each site is on tables 1, 2, 3 and 4. Only 2 of the 26 pts had sarcoidotic cardiac disease, with SUVs 4,5 and 5,1. **Conclusion:** It is known that sarcoidosis affects primarily lungs and intra-thoracic LN[2]. However, our results show extensive involvement of extra-thoracic LN, being the second most affected site, with lungs on third place. Published

literature makes reference to a considerable amount of extra-pulmonary disease[3], although little is said regarding lymphatic system alone. The range of SUV values in sarcoidosis is not well established. High SUVs can be observed[3], and our results show that a wide range of uptake can be seen in all the sites, especially in lymphatic system. **References:** 1. Hunninghake GW, Costabel U, Ando M, et al. ATS/ERS/WASOG statement on sarcoidosis. American Thoracic Society/European Respiratory Society/ World Association of Sarcoidosis and other Granulomatous Disorders. Sarcoidosis Vasc Diffuse Lung Dis. 1999;16:149-173.2. Sobic-Saranovic D, Artiko V, Obradovic V. FDG PET Imaging in Sarcoidosis. Semin Nucl Med. 2013; 43:404-411.3. Soussan M, Augier A, Brillet P, et al. Functional Imaging in Extrapulmonary Sarcoidosis. Clin Nucl Med. 2014; 39:e146-e159.

EP-0153

Role of FDG PET/ CT in the Initial evaluation and Follow-up of Malignant Otitis externa

N. K. Seniaray, *R. Verma, E. Belho, D. Malik, H. Mahajan; Mahajan Imaging Center, Sir Ganga Ram Hospital, New Delhi, INDIA.*

Aim/Introduction: Malignant otitis externa is an aggressive infective disease with significant morbidity and disease specific mortality. The disease usually begins in the external ear and spreads to the adjacent bones resulting in associated temporal bone and skull base Osteomyelitis. Conventionally CT, MRI, gallium-67 and technetium-99m bone scan have been used for the pre-treatment evaluation, however each modality has its own limitations. 18F-FDG-PET/CT, which has been used primarily in oncology, is increasingly being used as a marker for localizing infective foci and can be used as an effective alternative to technetium-99m and gallium-67 scans for diagnosis, assessment of response and follow-up in patients with Malignant otitis externa. **Materials and Methods: :** A retrospective analysis of 22 patients clinically diagnosed with Malignant otitis externa was done. All the subjects underwent regional 18F-FDG-PET/CT scanning to evaluate the extent of involvement and localisation of infective foci. The disease was further evaluated based on the standardised uptake value (SUV Max) of FDG and extent of erosion and sclerosis within the involved skull bones on PET/CT. 4 patients underwent additional technetium-99m bone scan and the extent of skeletal lesions was compared with PET/CT. Follow up low dose regional 18F-FDG-PET/CT after antibiotic treatment was done in 6 patients. The data was analysed using appropriate statistical methods **Results:** FDG avid lesions were located in the external ear canal (n=18) with associated Osteomyelitis involving the petrous and mastoid temporal bones (n=21), sphenoid bone (n=7), temporo-mandibular joint (n=5) and nasopharyngeal regions (n=4). 6 patients underwent a second low dose regional PET/CT scan after active otitis resolved and after at least 6 weeks of antibiotic treatment. The scan demonstrated no or substantially reduced FDG uptake and treatment was stopped. One patient had significant uptake, and antibiotic treatment was continued until a third scan demonstrated no FDG uptake. **Conclusion:** 18F-FDG-PET/CT is a reliable imaging modality for the diagnosis, disease localization and extent, follow up, treatment response evaluation and in decision making regarding treatment cessation. 18F-FDG-PET/CT should be considered as the imaging modality of choice in the management of Malignant otitis externa. **References:** None.

EP-0154

Novel monitoring indices of osteomyelitis of the jaw using bone SPECT quantitative analysis: Preliminary study for patients with ARONJ

H. Hata[1], *T. Kitao*[2], *K. Imamachi*[1], *J. Sato*[3], *T. Asaka*[3], *N. Ohga*[3], *K. Hirata*[4], *T. Shiga*[5], *Y. Kitagawa*[3];
[1]*Dentistry and oral surgery, Hokkaido Cancer Center, National Hospital Organization, Sapporo, JAPAN,* [2]*Radiology Department, Hokkaido Cancer Center, National Hospital Organization, Sapporo, JAPAN,* [3]*Oral diagnosis and medicine, Graduate school of dental medicine, Hokkaido University, Sapporo, JAPAN,* [4]*Nuclear medicine, Graduate school of medicine, Hokkaido University, Sapporo, JAPAN,* [5]*Hokkaido Cancer Center, National Hospital Organization, Sapporo, JAPAN.*

Aim/Introduction: The number of patients with antiresorptive agent related osteonecrosis of the jaw (ARONJ) or osteomyelitis of the jaw (OMJ) is a growing social problem. However, the role of diagnostic imaging in the evaluation of ARONJ has not been adequately established without good index to assess the antiphlogistic effect in osteomyelitis. Development of quantitative analysis software has enabled several standardized uptake values (SUV) for analysis in SPECT bone scintigraphy. The present retrospective study was undertaken to evaluate the usefulness of SUV evaluations in SPECT to establish the curative effect of OMJ by comparing the states before and after the antiphlogistic therapy including hyperbolic oxygen therapy (HBO). **Materials and Methods:** Fifteen ARONJ patients participated in the study. The patients underwent SPECT prior to and after the pre-operative HBO. The baseline was assumed as that at the time of the SPECT imaging before the start of the preoperative HBO. We used the mean SUVmax of the bilateral cranial bones as the control [C] and attempted to adjust the SUVmax of the lesion [L] as expressed in the following equation: adjusted SUVmax (aSUVmax) = [L] - [C]. The optimum threshold to calculate the Metabolic bone volume (MBV) was determined to be [C] + 3. Retrospectively, we calculated the SUVmax and MBV of the SPECT using quantitative analysis software to evaluate the intensity and volume of inflammation in the OMJ. **Results:** The mean aSUVmax of all cases was significantly reduced from 11.53 to 9.16 after HBO ($p < .05$). Similarly, the mean MBV of all cases was significantly reduced, from 17.90cm^3 to 15.19cm^3, after HBO ($p < .05$). We compared the clinical course with the change in aSUVmax and MBV before and after the HBO for all patients. After the anti-inflammatory treatment including HBO, there were sharp decreases in values for 6 patients who had high aSUVmax (> 15) and/or had a large MBV (> 20cm^3) at the baseline. These cases were also subject

to clinically severe infections at the baseline. **Conclusion:** This is a first study applying SPECT quantitative analysis software to determine the curative effect of OMJ by comparing the states before and after antiphlogistic therapy including HBO. We propose two equations for the adjusted SUVmax and threshold SUV to enable data comparisons between cases. The overall aSUVmax and MBV were significantly reduced after HBO, and all of the SPECT quantification data reflected the specific clinical findings. **References:** None.

EP-0155

Polymyalgia Rheumatica as Paraneoplastic syndrome on ^{18}F-fluorodeoxyglucose Positron Emission Tomography/ Computed Tomography

G. Silov, *S. Karacavus, H. Gencer;*
Health Sciences University, Kayseri City Hospital, Department of Nuclear Medicine, Kayseri, TURKEY.

Aim/Introduction: Polymyalgia rheumatica (PMR) is characterized by inflammatory pain and stiffness of the shoulder and pelvic girdles, with biochemical evidence of inflammation. Polymyalgia rheumatica (PMR) is one of the inflammatory rheumatic diseases that can potentially be detected by positron emission tomography/CT. Several studies reported a PMR syndrome as a presenting manifestation of various malignant diseases. However, PMR patients have an increased risk of malignancies. In this study, we aimed to reveal relationship PMR and malign diaseases. **Materials and Methods:** We investigated 52 patients with any cancer history underwent 18-FDG PET/CT. FDG uptake in large joints, bursas and vertebral spinous processes was evaluated by calculating maximum standardised uptake values. **Results:** In cancer patients (16 lymphoma, 9 lung non small cell cancer, 8 breast cancer, 8 gynecological cancer, 7 GIS, 2 prostate adenocancer, 1 malignant melanoma, 1 lower lip SCC) were detected increased F-18 FDG uptake in ischial tuberosities (SUV max: 3.23 ± 1.43), greater trochanters (SUV max: 2.98 ± 0.73), and lumbar spinous processes (SUV max: 2.24 ± 1.04), shoulders (SUV max: 3.68 ± 1.62), sternoclavicular (SUV max: 2.14 ± 0.79). Positive results at two or more of these sites showed high sensitivity (86.5%) and specificity (89.2%) for the diagnosis of PMR. In this study remitting seronegative symmetrical synovitis with pitting edema (RS3PE) was seen in five patients including malignant melanoma, lower lip SCC, two non small cell lung cancer and prostat adenocancer. **Conclusion:** 18F-Fluorodeoxyglucose-PET/CT may be useful for the detection of unknown PMR lesions and RS3PE with cancer patients which are difficult to identify using other methods. Presence of RS3PE five cancer patients as a paraneoplastic syndrome, and thereafter concurrent with clinical presentation of PMR, suggests a common trigger factor for RS3PE from a these cancer and PMR. **References:** None.

EP-0156

Diagnostic Role Of Three-phase Bone Scintigraphy In The Differentiated Choosing Of The Component Of Endoprosthesis In Patients With Septic And Aseptic Osteoarthrosis Of The Hip Joint

P. Korol[1], *M. Tkachenko*[2];
[1]*Clinical City Hospital #12, Kiev, UKRAINE,* [2]*A.A. Bohomolets National Medical University, Kiev, UKRAINE.*

Aim/Introduction: To determine the diagnostic value of three-phase bone scintigraphy in the differentiated selection of endoprosthesis components ("friction units") in patients with septic and aseptic osteoarthrosis (OA) of the hip joints. **Materials and Methods:** 187 patients with septic and aseptic OA (109 women and 78 men) aged 34 to 75 years were imaged by bone scintigraphy: I stage - angiographic stage, II stage - early stage, 3 stage - delayed static phase. 3 hours after the intravenous administration of 740 MBq 99mTc MDP. **Results:** According to the results of microbiological analysis of diagnostic puncture of the hip joints, the patients were divided into two cohorts. The first cohort included 104 patients with aseptic OA of the hip joint, the second - 85 patients with septic OA (in 58 cases was detected S. aureus, in 27 cases - St. haemolyticus). A significant increase in arterial inflow ($t = 2.48$; $p < 0.05$) and integral perfusion ($t = 2.65$; $p < 0.05$) in the angiographic phase of patients with septic OA was determined due to intensification osteoblastic activity and angiogenesis, compared with patients with aseptic OA. In patients with septic OA, there was a significant predominance of retention ($t = 3.29$; $p < 0.05$) and specific accumulation of the radiopharmaceutical in the early ($t = 2.23$; $p < 0.05$) and delayed static phase of three-phase bone scintigraphy ($t = 2.36$; $p < 0.05$) as compared with indicators for aseptic OA. When endoprosthetics of patients with aseptic OA using the component of endoprosthesis - «ceramics-ceramics» in the postoperative period, no implant-associated complications were detected. In patients with septic OA, paraprosthetic complications were not recorded when using the «metal-ceramic» component. **Conclusion:** The parameters of the distribution kinetics of the radiopharmaceutical of three-phase bone scintigraphy have diagnostic value in patients with aseptic and septic OA of the hip joint when choosing the components of the endoprosthesis, especially when it is impossible to perform a diagnostic puncture of the hip joint. **References:** None.

EP-0157

FFDG PET/CT Identifies A Extra-Cardiac Target For Biopsy In Patients With Suspected Cardiac Sarcoidosis

D. Weinreb;
16 Birkdale Court, Slingerlands, NY, UNITED STATES OF AMERICA.

Aim/Introduction: The 2014 Heart Rhythm Society Guidelines allow for a diagnosis of cardiac sarcoidosis to be established in patients with a histologic diagnosis of systemic sarcoidosis

and for whom FDG PET demonstrates patchy, non-segmental hypermetabolism. These guidelines obviate the need for invasive endomyocardial biopsies. The objective of this study is to determine whether FDG PET may identify a relatively non-invasive target for biopsy to establish a histologic diagnosis of systemic sarcoidosis in patients presenting with non-ischemic cardiomyopathies. **Materials and Methods:** Eight cases of patients referred to FDG PET were retrospectively reviewed. None of these patients had an established histological or clinical diagnosis of systemic sarcoidosis. All presented with non-ischemic cardiomyopathies. FDG PET imaging was performed contemporaneously with stress-rest myocardial perfusion imaging. **Results:** In seven of the eight patients, the FDG PET study demonstrated both evidence of cardiac and extra-cardiac sarcoidosis. The classic pattern of patchy hypermetabolism in a non-segmental distribution was present in the cases. All seven cases also exhibited evidence for extra-cardiac sarcoidosis, including hypermetabolic supraclavicular, mediastinal and inguinal lymph nodes, as well as hepatic, splenic and intramuscular granulomas. One of the cases demonstrated intense FDG avidity involving the suprahepatic IVC as well as the femoral veins. Of note, the sites of supraclavicular and inguinal lymph nodes were not enlarged or intrinsically suspicious on CT and therefore would have not prospectively identified as targets for a biopsy in the absence of FDG PET imaging. The eighth patient exhibited no evidence of either cardiac or systemic sarcoidosis. **Conclusion:** These observations suggests that FDG PET is a valuable tool in establishing the diagnosis of sarcoidosis with cardiac involvement in a population of patients presenting with a non-ischemic cardiomyopathy. Specifically, FDG PET identifies sites amenable to relatively non-invasive biopsies to confirm the presence of non-caseating granulomas, while simultaneously demonstrating the classic pattern indicative of cardiac involvement. **References:** None.

EP-0158

Correlation between bone scan findings and echocardiography parameters in patients with cardiac amyloidosis

N. A. Martinez Amador[1], *O. Cuenca Vera*[1], *I. Martínez Rodriguez*[1], *M. De Arcocha Torres*[1], *R. Quirce*[1], *J. Jiménez Bonilla*[1], *A. Sánchez Salmon*[1], *M. Zarauza Navarro*[2], *G. Molina Mendoza*[1], *I. Banzo*[1];
[1]*Department of Nuclear Medicine. Marqués de Valdecilla University Hospital. Molecular Imaging Group (IDIVAL). University of Cantabria, Santander, SPAIN,* [2]*Department of Cardiology. Marqués de Valdecilla University Hospital. University of Cantabria, Santander, SPAIN.*

Aim/Introduction: To evaluate the correlation of the cardiac uptake in bone scan using 99mTc-DPD with the echocardiographic parameters of left ventricular ejection fraction (LVEF) and thickness of the interventricular septum (IVS) in patients with suspected cardiac amyloidosis. **Materials and Methods:** This retrospective study included 60 patients with suspected cardiac amyloidosis (48 men. mean age: 74.7±12.2 years) who underwent a whole body scan (WBS) in anterior and posterior projection after 3 hours of the i.v injection of 740 MBq 99mTc-DPD. A thoracic SPECT was also performed. Visual analysis of the cardiac uptake and the global distribution of the radiotracer following the Perugini scale were carried out by two nuclear medicine specialists. Visual scores 0-1 were considered negative for cardiac amyloidosis and scores 2-3 as positive. For semiquantitative analysis, ROI´s were drawn over the heart on the anterior projection of WBS. Number of counts in the heart was divided by the number of counts in WBS imaging, excluding the counts derived by bladder and kidneys, following the next index: Heart ROIc / WBS ROIc - (Bladder ROIc + Kidneys ROIc). The visual and semi-quantitative analysis of the cardiac deposit and the radiotracer distribution in WBS was correlated with the echocardiographic data of LVEF and thickness of IVS. **Results:** On visual analysis, 27 out of 60 patients (45%) had negative bone scan. On the other side, 33 out of 60 patients (55%) had positive bone scan .The semiquantitative analysis was only available in 57 patients. In the 27 patients who had negative bone scan the Heart/Whole body ratio (H/W) was 1.6±0.3. In the 33 patients who had positive bone scan the H/W mean value was 7.7±0.5 (p<0.0001). The LVEF did not show statistically differences between positive and negative patients (p=0.74). However statistically differences were observed between the thickness of IVS for positive and negative patients (19.17±2.94mm vs 14.85±5.01mm, p=0.005). **Conclusion:** Patients with cardiac uptake of 99mTc-DPD and high suspicion of transthyretin amyloidosis showed significantly greater IVS hypertrophy than whom were considered negative for cardiac uptake of radiotracer. A direct relationship was found between the uptake pattern in bone scintigraphy and the presence of myocardiopathy. No relationship was observed between LVEF and the cardiac uptake pattern on bone scan. **References:** None.

EP-0159

^{99m}-Technetium Diphosphonates in Transthyretin Cardiac Amyloidosis. Extracardiac Uptake Evaluation in Our Centre

A. Andres Gracia[1,2], *D. Nogueira Souto*[1], *L. Tardin Cardoso*[1], *M. Delgado Castro*[1], *P. Razola Alba*[1], *C. Lahuerta Pueyo*[3,2], *M. Aibar Arregui*[4,2], *E. Prats Rivera*[1], *D. Abos Olivares*[1];
[1]*Unidad Clínica Multihospitalaria de Medicina Nuclear de Aragon, Zaragoza, SPAIN,* [2]*IIS ARAGON, Zaragoza, SPAIN,* [3]*Servicio de Bioquímica Clínica. Hospital Universitario "Miguel Servet", Zaragoza, SPAIN,* [4]*Servicio de Medicina Interna-Hospital Clínico Universitario "Lozano Blesa", Zaragoza, SPAIN.*

Aim/Introduction: To evaluate the extracardiac deposit of ^{99m}Tc-labeled diphosphonates (DPD) in patients with suspected thransthyretin cardiac amyloidosis hereditary or wild-type. **Materials and Methods:** We performed 153 scans in 151 patients referred for clinical suspicion of cardiac amyloidosis (heart failure with preserved LVEF or with minimal repercussion 148 scans) or for being asymptomatic carriers of the disease (3 patients / 5 scans). Average age 74'72 (23-93 years), 66'7%

men and 33'3% women, from 11/21/2013 to 4/16/2019. All of them have been screened with ^{99m}Tc-DPD at 3 hours after its administration. For the evaluation of cardiac activity, Perugini's visual scale was used (0, 1, 2, 3), considering it positive in the cases of grade 2 and 3 uptake. Likewise, the locations of extracardiac radiotracer uptake have been evaluated (soft tissue, organs and osteoarticular) and a review of the clinical history and biopsy and analytical data was performed to check whether there was a histological evaluation of the affected organs. **Results:** In 153 exams, 72.5% corresponded to scans with score 0 (107) or 1 (4), while 27.5% corresponded to score 2 or 3 and therefore compatible with transtyrethin cardiac amyloidosis (aTTR) in the absence of free light chains. In 42 patients with positive scintigraphy, two patients had a positive genetic study (TTR gene (c.424G>A (p.Val122Ile) and c-220G>C(p.Glu74Gln)), in 18 patients the genetic study was negative (wild-type) and in 22 had not been determined. Most of the patients (82.3%) presented no pathological uptake or degenerative osteoarticular pathology. The remaining 27 patients (17.64%), 5 presented relevant bone pathology exclusively (2 cases of Paget's disease and 3 cases, metastatic bone disease), in 14 patients in soft tissues (gluteal region, pelvis, mediastinum, abdomen, pectoral muscles and left thigh), in 4 patients lung uptake, in 3 patients liver uptake and in 1 case thyroid uptake. In 22 patients with non-bone extracardiac uptake, a biopsy was performed in 6 patients. In the 3 cases in which the biopsy was performed on the site indicated by the scintigraphy, the result of the biopsy was positive for amyloidosis: one in abdominal fat, another in liver and another in mediastinal lymph nodes with a diagnosis of amyloid lymphadenopathy. As an interesting finding, all of the 4 patients with lung uptake had myocardial Perugini score 3 uptake. **Conclusion:** Non-bone extracardiac uptake of ^{99m}Tc-DPD- can guide the biopsy if histologic confirmation of amyloidosis is needed. **References:** None.

EP-0160

Contribution Of ^{18}F-FDG-PET/CT In Patients With Suspected Cardiac Implantable Device Related Infection

B. Rodriguez-Alfonso, A. Ramos-Martinez, V. Castro Urda, M. Cobo-Marcos, I. Sanchez-Romero, J. Toquero-Ramos, A. Restrepo-Cordoba, M. Mitjavila-Casanovas;
Hospital Universitario Puerta de Hierro, Majadahonda, SPAIN.

Aim/Introduction: Cardiac implantable devices (CID)-related infections are globally increasing. Echocardiography and modified-Duke criteria are the cornerstone in suspicion of CID-related infections, but their yield is suboptimal in this scenario, with a significant percentage of over or underdiagnoses. Because these processes constitute a life-threatening situation, a more prompt and accurate diagnosis is mandatory. The aim of this study was to evaluate the usefulness of ^{18}F-FDG-PET/CT in suspected CID-related infections in the clinical setting, analysing its performance and its influence over the final diagnosis. **Materials and Methods:** All ^{18}F-FDG-PET/CT studies carried out at our institution because of a suspected CID-related infection were included in this retrospective analysis. We calculated sensitivity (S), specificity (Sp) and positive and negative predictive values for the initial Duke classification, echocardiography, PET/CT and post-PET Duke classification. Post-PET Duke included ^{18}F-FDG uptake in leads, valves or endocardium as a major criterion. The gold standard was either the culture of explanted material or the final decision of the endocarditis team revised after 1-year follow-up. Net Reclassification Improvement (NRI) was used to assess the percentage of correct changes over the initial Duke classification based on PET/CT results. **Results:** Forty-five studies met inclusion criteria (mean age 66.9±13.9). The initial suspicion of CID-related infection was based on systemic (60%), local (35%) and mixed signs/symptom. Pacemaker was the most frequent CID (22 patients) and most had 2 or more leads. Prevalence of definite infective endocarditis (IE) was 56%. Infection limited to the pocket was established in 11% of patients and CID-related infection was ruled out in 33%. For the diagnosis of IE, post-PET Duke reached the highest S (0.92 (95%CI 0.82-1.0)) while PET/CT accounted for the highest Sp (0.94 (95%CI 0.84-1.0)). Echocardiography had the poorest S and Sp (0.42 and 0.67 respectively). S and Sp PET/CT for the detection of pocket infection were 0.84 and 0.92. According to NRI PET/CT improved the initial Duke classification in 52% of the cases. Also, PET/CT detected septic embolism in 31% of the cases, 3 unsuspected primary tumours and provided an alternative diagnosis in 4 out of 14 cases in which CID-related infection had been excluded. **Conclusion:** PET/CT constitutes an accurate diagnostic tool in suspicion of CID-related infections with good performance in the evaluation of IE as well as pocket infection. PET/CT results correctly re-classified more than a half of the initial diagnoses. PET/CT enables the detection of septic embolism, unsuspected primary tumour and alternative diagnosis **References:** None.

EP-0161

Contribution of ^{18}F-FDG-PET/CT in Treatment Decision Making in Patients with Suspected Cardiac Implantable Device Infection

B. Rodriguez-Alfonso, M. Mitjavila-Casanovas, L. Canales-Rodriguez, V. Castro Urda, M. Cobo-Marcos, A. Ramos-Martinez;
Hospital Universitario Puerta de Hierro, Majadahonda, SPAIN.

Aim/Introduction: Accurate diagnosis of the localization and extension of cardiac implantable device (CID) related infections enables the correct treatment decision. Definite infective endocarditis (IE) requires complete CID removal while in some cases of superficial infection or inflammation CID can be left in place. Patients who are at high risk for CID explant may be treated only antibiotics and, in these cases, it is also important to be aware of the infection severity to adjust duration. The aim of this study was to analyze the impact of PET/CT results on treatment choice and/or duration in patients with CID-related infection. **Materials and Methods:** We retrospectively analyzed the treatment choices in all the patients who underwent a PET/CT at our institution because of a suspected CID-related infection. We compared the initial attempt to treat with the final

treatment, after being aware of PET/CT results. Changes were registered as major changes when inter-modality (from explant to left in place or vice versa) and minor changes when intra-modality (adjustments in the duration of antibiotic therapy). **Results:** Forty-five patients met inclusion criteria. According to the initial suspicion, 15 patients were referred for superficial infection/inflammation or infection limited to the pocket, 13 for "possible EI-CID", 9 for "definite EI-CID" and 8 because unspecific systemic sings or symptoms. The first attempt to treat was complete removal of CID ± antibiotic therapy in 17 patients and antibiotic therapy or watchful waiting in 19. In 9 patients, although the most indicated treatment was removal of CID, it was not considered because of a high risk. After performing PET/CT studies, treatment strategies changed in 30 patients (66.7%). Inter-modality treatment changes happened in 11 patients, in 6 it changed from removal to antibiotic management and in 5 from antibiotic to removal. In 16 patients there were minor changes affecting the duration of antibiotics (it was shortened in 6 and increased in 10). In 3 patients the treatment focused on a different pathological entity not related to CID, which were considered as major changes. **Conclusion:** PET/CT is a very useful tool for the assessment of CID-related infections. Results of this imaging modality can lead to major changes in the therapeutic management in approximately 30% of patients. Minor changes occurred even more frequently, in approximately 35% of patients. **References:** None.

EP-0162

Musculoskeletical infections: contribution to definitive diagnosis of the semiquantitative analysis with 99mTc-besilesomab

P. Guardia Jimena, A. Castro López, M. Martínez del Valle Torres, R. Arenas Aguaza, M. Bermúdez Morales, E. Moratalla Aranda, R. Nieto Serrano, D. Becerra García;
San Cecilio University Clinical Hospital, Granada, SPAIN.

Aim/Introduction: Evaluate musculoskeletal infections through visual and semiquantitative analysis with 99mTc-Besilesomab. **Materials and Methods:** We included 56 patients with age ranges from 19 years to 84 years with suspicion of osteomyelitis due to the presence of articular prosthesis, osteosynthesis material or contagion via hematogenous route. Three phase bone scan (Tc-99m-oxidronate) was previously performed on all patients with positive result in all cases.The infection study was performed after injection of 555 MBq 99mTc-Besilesomab with static imaging 4 and 24 hours post injection, once the absence of human anti-murine antibodies (HAMA) was confirmed. The evaluation of the study was made visually and after semiquantitative analysis, making regions of interest (ROIs) on the suspicious areas of infection both in early and late images, with the same intensity scale in all images and considering the total counts of each ROI. The studies whose quantification was equal or superior in 24 hours images in comparison with 4 hours images were considered as positive, considering the decay of the radiopharmaceutical. The definitive diagnosis was made after the clinical monitoring of all patients either following the result of the microbiological culture or after response to the medical and/or surgical treatment. **Results:** 36 negative results (36 TN and 0 FN) and 20 positive results (17 TP y 3 PF) were obtained. According to these results, 100 % sensitivity, 92% specificity were obtained. A positive predictive value of 85 % and negative predictive value of 100 %. **Conclusion:** - The semiquantitative analysis of the studies with 99mTc-Besilesomab in the diagnosis of infectons of the musculoskeletal system supports the diagnostic decision after visual assessment and it contributes to the final decision in those cases in which the visual assessment is uncertain or not conclusive.- It is a reproducible procedure, not operator dependent which reduces intra-operator variability. **References:** None.

EP-0163

Odontogenic and non-odontogenic mandibular osteomyelitis: Differentiating findings on bone scintigraphy

K. Kawaji, M. Jinguji, M. Nakajo, A. Tani, T. Yoshiura;
Department of Radiology, Kagoshima University Graduate School of Medical and Dental Sciences, Kagoshima, JAPAN.

Aim/Introduction: Bone scintigraphy is often used to evaluate osteomyelitis of the mandible. The major causes of osteomyelitis in the mandible include dental infection (odontogenic) and adverse effects of external radiation therapy or bone resorption inhibitors (non-odontogenic). The purpose of this study was to investigate whether the pattern and degree of uptake in bone scintigraphy differ for the causes of mandibular osteomyelitis. **Materials and Methods:** This retrospective study included 20 consecutive patients with osteomyelitis of the mandible who underwent bone scintigraphy prior to treatment in our hospital from January 2013 to March 2019. Among these cases, 12 patients (8 males and 4 females; mean 57.0±4.5; range 41-73 years) were diagnosed as having odontogenic and remaining patients (6 males and 2 females; mean 70.1±11.4; range 63-78 years) were diagnosed as having non-odontogenic osteomyelitis. In all cases, bone scintigraphy was performed with 99mTc-HMDP. Regarding abnormal uptake in the mandible, the distribution was visually classified into three patterns (single nodular uptake, single long uptake, and multifocal uptake), and the degree of uptake was grade into 3 levels (grade 1: uptake equal to or less than surrounding bone; grade 2: uptake between grade 1 and 3; grade 3: uptake equal to or higher than the bladder). Furthermore, the lesion-to-orbit uptake ratio was calculated from the maximum counts within the region-of-interest. For the visual evaluation, the differences between odontogenic and non-odontogenic groups were evaluated using chi-square test. Lesion-to-orbit uptake ratio was compared between the two groups using Mann-Whitney U test. **Results:** The visual uptake pattern was significantly different between odontogenic (single-nodular: 66.7%, single-long: 33.3%, multifocal: 0%) and non-odontogenic (single-nodular: 12.5%, single-long: 12.5%, multifocal: 75.0%) groups

(P=0.001). As for the degree of visual uptake, there was no significant difference between odontogenic (grade 1: 0%, grade 2: 33.3%, grade 3: 66.7%) and non-odontogenic (grade 1: 0%, grade 2: 50.0%, grade 3: 50.0%) (P=0.648). However, the uptake ratio in odontogenic group (8.21±2.93) was significantly higher than that in non-odontogenic group (5.34±1.81) (P=0.016). **Conclusion:** In bone scintigraphy of mandibular osteomyelitis, odontogenic cases showed higher uptake ratio than non-odontogenic cases. In addition, non-odontogenic cases tended to present multifocal uptake pattern while odontogenic cases more often showed single uptake patterns. The pattern and degree of uptake in bone scintigraphy may provide clues about the causes of mandibular osteomyelitis. **References:** None.

EP-0164

^{18F}FDG-PET-CT in patients with spondylodiscitis: image, clinical and laboratory findings in 10 cases

J. Bernal, M. Agudelo-Cifuentes, B. Martinez-Sanchis, A. Yepes-Agudelo, A. Utrera-Costero, J. Fragio, P. Sopena-Novales, P. Bello-Arques;
Hospital La Fe, Valencia, SPAIN.

Aim/Introduction: Spondylodiscitis is the third cause of osteomyelitis in elderly patients. Although MRI is the gold standard imaging method at the diagnosis, ^{18F}FDG-PET-CT can be helpful when MRI is not clear or impossible to perform, providing unique metabolic parameters. Our aim is to describe ^{18F}FDG-PET-CT metabolic parameters along with clinical and laboratory findings in 10 patients with confirmed spondylodiscitis. **Materials and Methods:** Retrospective and descriptive study of patients with confirmed spondylodiscitis that had an ^{18F}FDG-PET-CT done in the work-up, between 2014 and 2019. We collected data from ^{18F}FDG-PET-CT image (number, localization of lesions, SUVmax, metabolic volume (MV), total lesion glycolysis (TLG), extraosseous foci), laboratory (CRP, pathogen), clinical history (duration of symptoms and antibiotic treatment before ^{18F}FDG-PET-CT, diabetes mellitus, infection foci) and MRI. **Results:** We had 10 patients and 13 lesions on ^{18F}FDG-PET-CT. The two diabetic patients presented with more than 1 lesion. Lesion localization was: 7 lumbar (54%), 4 thoracic (31%) and 2 cervical (15%), being L3-L4 space the most frequently affected (n=4). The main cause of spondylodiscitis was endocarditis (5 patients). The pathogen was detected in 9 patients: bacteria in 8 (E.Faecalis was the most frequent: 3 cases) and C.Albicans in 1. All ^{18F}FDG-PET-CT were positive, although most patients had antibiotic treatment (9/10). SUVmax and TLG were not lower in patients with long antibiotic treatment (>15 days before PET-CT). Mean SUVmax was 7,1 (4,6-12,7), mean MV was 41,4cm3 (15,2-122cm3), mean TLG was 166,1 (55-415,7). All patients that had ^{18F}FDG-PET-CT done early after the onset of symptoms (<2 weeks) had lesions with a higher SUVmax (above mean value). Most of lesions with high MV and TLG (above mean value) were found in patients with high levels of CRP (>75 mg/L). In 5 patients the ^{18F}FDG-PET-CT found extraosseous infective foci. All patients had MRI done in the diagnosis work-up. In 4 patients, the MRI was negative for spondylodiscitis, but became positive in an early control. **Conclusion:** In patients with spondylodiscitis, ^{18F}FDG-PET-CT can be more sensitive in detecting vertebral lesions and can show the origin and extension of the infection, even earlier than MRI. Our data suggest that antibiotic treatment may not affect ^{18F}FDG-PET-CT positivity and that the earlier the ^{18F}FDG-PET-CT is done after the onset of symptoms, the higher the SUVmax value in the lesion is. There may be a relationship between values of CPR and MV/TLG. We need more sample to confirm statistically the tendency of our data. **References:** None.

EP-0165

Bone extension of histiocytosis: Assessment with bone scan and FDG-PET/CT

A. Palomar Muñoz[1], M. Cortés-Romera[1], A. Sabaté-Llobera[1], L. Rubio-Álvarez[1], X. Solanich-Moreno[2], J. A. Narváez-García[3], J. J. Robles-Barba[1], J. Mestres-Martí[1], A. Rodríguez-Gasén[1], C. Gámez-Cenzano[1];
[1]Unit PET/CT (IDI)- Department of Nuclear Medicine. Hospital U. de Bellvitge-IDIBELL, L'hospitalet de Llobregat (Barcelona), SPAIN, [2]Department of Internal Medicine. Hospital U. de Bellvitge-IDIBELL., L'hospitalet de Llobregat (Barcelona), SPAIN, [3]Department of Radiology. Hospital U. de Bellvitge-IDIBELL., L'hospitalet de Llobregat (Barcelona), SPAIN.

Aim/Introduction: To determine the differences in the assessment of histiocytosis bone extension between bone scintigraphy (BS) and positron emission tomography/computed tomography with 18F-fluorodeoxyglucose (FDG-PET/CT). **Materials and Methods:** We retrospectively evaluated all the patients referred to our center with the diagnosis of histiocytosis, in which BS and FDG-PET/CT were available. The extension of the disease in skull, spine and limbs was assessed, as well as the number of areas with tracer uptake in both techniques. Radiotracer uptake was classified into three types of patterns: A) concordant (same locations and uptake areas), B) partially concordant (same locations but different uptake areas), and C) not concordant (different location). **Results:** Seven patients (2 women) were included in the study. Three of them had Erdheim-Chester disease, 3 Langerhans cell histiocytosis and 1 mixed histiocytosis. We observed 5 patterns A (71%), one B and one C. In the partially discordant pattern the FDG-PET/CT determined a greater number of uptake areas in the limbs but without additional locations. In the discordant patient, the BS showed uptake in a pelvic lesion and in the proximal tibia, both without clear evidence of FDG uptake (attributable to the disease and to post-surgical changes, respectively). In studies with concordant patterns, FDG-PET/CT additionally allowed assessing the soft tissue component associated with bone lesions in one of the patients, in addition to the assessment of extraosseous locations (4 patients, 57.1%). **Conclusion:** There were a 71% of concordant cases between both techniques. BS is very sensitive for the detection of bone disease in histiocytosis, but FDG-PET/CT was able to detect additionally soft tissue disease surrounding bone

lesions and demonstrates extraosseous locations (up to 57% of cases). **References:** None.

EP-0166

SPECT/CT imaging in dacryoscintigraphy for the anatomical localization of nasolacrimal duct obstruction

C. C. M. Fernandez[1], *K. Bayardo*[1,2], *E. Silvera*[1], *S. Rodriguez*[1], *A. Masso*[1,2], *R. Hitateguy*[2], *J. Vilar*[1,2], *R. Ferrando*[1,2];
[1]*Clinical Hospital, University of the Republic., Montevideo, URUGUAY,* [2]*Ferrari Ferrando Páez Nuclear Medicine Clinic, Montevideo, URUGUAY.*

Aim/Introduction: Nasolacrimal duct obstruction is more frequent in women over 40 years of age and may be due to infectious, inflammatory, congenital and/or traumatic causes. Dacryoscintigraphy is a dynamic method that allows non-invasive evaluation of lacrimal kinetics, contributing to the diagnosis and therapeutic management of the obstruction. Sometimes it can be difficult to determine the site of obstruction in planar images. The objective is to determine if SPECT/CT imaging adds information to define the location of nasolacrimal obstruction. **Materials and Methods:** Dacryoscintigraphy was performed by instilling 99mTc-pertechneciate in the lower fornix of both eyes, with dynamic images for 30 minutes, followed by a static image. SPECT/CT of the area of interest with low-dose CT was performed only if some grade of obstruction was identified in planar images. Finally, 22 patients (15 women, mean age 64 years, range 34-82) with diagnosis of epiphora (11 unilateral and 11 bilateral) were included. The studies were performed in two gamma cameras: Infinia Hawkeye 4 and Mediso AnyScan 16. **Results:** The topographic diagnosis of the lacrimal obstruction by planar images was concordant to that obtained by SPECT/CT in 15/22 patients. Planar images identified complete obstruction prior to the sac in 6 (5 right eyes [RE], 2 left eyes [LE]), partial obstruction prior to the sac in 3 (1 RE, 2 RE), complete obstruction in the sac in 3 (3 RE, 2 LE), partial obstruction in the sac in 8 (1 RE, 3 LE) and complete obstruction in the duct in 3 (1 RE, 3 LE). SPECT/CT detected partial obstruction prior to the sac in 1 patient (both eyes) with obstruction in the sac in the planar images, partial obstruction in the sac in 1 patient that had been identified prior to the sac, and passage to the nostril in 2 patients with partial obstruction in the sac and 3 cases with complete obstruction (1 prior to the sac, 1 in sac and 1 in duct) modifying the obstruction to partial. **Conclusion:** SPECT/CT can define the localization of the lacrimal obstruction more accurately than planar images. This information can help in the therapeutic decision selecting a non-invasive or surgical treatment depending on the site and magnitude of the obstruction. **References:** None.

EP-0167

^{18}F-FDGPET/CT with early and delayed imaging in infective endocarditis andimplantable cardiac electronic device infection

H. Navalon Martinez[1,2], *L. Vidal*[1,2], *S. Rubí*[1,2], *A. Morcuende*[1,2], *A. Repetto*[1,2], *N. Orta*[1,2], *B. Luna*[1,2], *M. Valiente*[1,2], *C. Medina*[1,2], *C. Peña*[1,2];
[1]*Hospital Universitario Son Esapases, Palma De Mallorca, SPAIN,* [2]*IdISBa, Palma de Mallorca, SPAIN.*

Aim/Introduction: Our aim was to evaluate the diagnostic accuracy of FDG-PET/CT in patients with suspected prosthetic valve(PV) infectious endocarditis(IE) and implantable-cardiac-electronic-device(ICED) infection, in whom modified Duke criteria were inconclusive; also assessing the added value of performing a delayed image acquisition. **Materials and Methods:** A retrospective study of 53 consecutive patients (total pool of 24PVs and 36ICEDs) where an FDG-PET/CT for suspected IE and ICED infection was performed between Jun-2015 and Jan-2019. Earlywhole-body (65min p.i.) and delayed thoracic (180min p.i.) FDG-PET/CT were acquired in all patients, following a myocardial uptake suppression with unfractionated heparin and diet. Considered positive if, at least, one of the early or late images demonstrates: intense-focal or markedly-heterogeneous uptake around the valvular plane (or around the subcutaneous generator on ICEDs), and negative if no-uptake or mild-moderate diffuse homogeneous uptake. Any focal or segmental uptake along the ICED wires was considered positive. The remaining was considered doubtful. Final IE or ICED infection diagnosis was established according to microbiologic analysis of explant samples when available, or clinical follow-up.Added value of delayed images was evaluated in terms of their capacity to change the final report of FDG-PET/CT, i.e. to provoke a switch from a negative or doubtful scan in the early imaging into a conclusive delayed positive or negative scan. SUV_{max} values when visually positive were also assessed. **Results:** From 60 studied devices, infection was confirmed in twenty-seven. Overall, FDG-PET/CT was positive in 17/60 devices and doubtful in 7/60, and showed a sensitivity, specificity, positive predictive value and negative predictive value of 63%, 97%, 94%, and 76%, respectively. In the ICED subgroup, FDG-PET/CT showed 8 positive studies, (7 generators and 1 proximal wire) where S, E, PPV and NPV were 67%, 100%, 100%, and 75%, respectively. In the PV subgroup FDG-PET/CT showed 9 positive studies, whit S, E, PPV and NPV were 60%, 95%, 100% and 77%, respectively. In 7 of 17 PET-positive studies (41%) there were morphological changes on late images, with 6 of 7 SUV_{max} augmentation. Overall, delayed images made possible a diagnostic change from doubtful to positive in 4 scans (finally confirmed as true-positives) and from doubtful to negative in 1 scan (finally deemed as a false-negative). **Conclusion:** FDG-PET/CT is a useful tool with a high specificity in the diagnosis of PV and ICED infections in patients with inconclusive previous Duke criteria,. The acquisition of a delayed image may improve the diagnostic certainty of infection. **References:** None.

EP-0168

The potential clinical role of ^{18}F-FDG PET-derived metabolic parameters in extrapulmonary tuberculosis among HIV-infected patients: An explorative prospective study

G. Boshomane, I. O. Lawal, T. Lengana, P. Rheeder, K. M. G. Mokoala, M. Vorster, M. M. Sathekge;
University of Pretoria, Pretoria, SOUTH AFRICA.

Aim/Introduction: 18F-FDG PET/CT is a useful imaging modality to quantify the extent of tuberculous in clinical practice. The baseline disease extent has been shown to be prognostic predicting response to standard regimen of anti-tuberculous treatment (ATT) as well as duration of treatment. HIV-infected individuals are susceptible to reactivation of old tuberculosis (TB) and the acquisition of new disease. We herein report our preliminary results on an-going study evaluating the role of ^{18}F-FDG in quantifying disease extent among HIV-infected and HIV-uninfected patients with extra-pulmonary TB. **Materials and Methods:** Thirty-three patients with extrapulmonary tuberculosis were prospectively recruited to undergo a ^{18}F-FDG PET/CT scan prior to the initiation of ATT. ^{18}F-FDG PET-derived metabolic parameters including SUVmax, SUVmean, MLV and TLG were computed for all tuberculous lesions in each patient. We compared these clinical characteristics and PET-derived metabolic parameters between HIV-positive and HIV-negative patients. **Results:** The mean age was 38.1 years. Twenty patients (60%) were female whilst thirteen (40%) were males. A total of 63.6% of the patients were HIV-positive. The HIV-infected patients were older compared with the HIV-uninfected patients (37.0 vs. 33.0). There was a preponderance of females among HIV-infected patients (66.7% of all HIV-infected patients) compared with HIV-uninfected patients (54.5% of all HIV-uninfected patients). Of the HIV-infected patients, only four patients were immunologically controlled with a CD 4 count >200 cells/uL. The median CD 4 count for the HIV-infected patients was 132 cells/uL (range: 32 - 1008). Subjects who were HIV-positive had a higher SUVmax (16.6 vs 9.8), SUVmean (4.4 vs 3.6), MLV (186.3 vs. 104.2) and TLG (757.5 vs. 369.9) when compared to HIV-negative patients suggesting higher disease burden in HIV-infected patients. **Conclusion:** Our preliminary data demonstrates the potential of ^{18}F-FDG PET-derived metabolic parameter in the assessment of disease extent in patients with extra-pulmonary TB. HIV-positive patients demonstrated higher disease burden compared with HIV-uninfected patients. This suggests that immunologically uncontrolled HIV-infected patients may respond less favourably to ATT and require longer treatment duration compared with HIV-uninfected patients. **References:** None.

EP-0169

MRI-based validation of 99mTc-HDP SPECT/CT in sacroiliitis - preliminary results

Z. Besenyi[1], *A. Bakos*[1], *G. Sipka*[1], *I. Farkas*[1], *S. Urbán*[1], *R. Hemelein*[2], *L. Kovács*[2], *L. Pávics*[1];
[1]*University of Szeged Department of Nuclear Medicine, Szeged, HUNGARY,* [2]*University of Szeged Department of Rheumatology, Szeged, HUNGARY.*

Aim/Introduction: Spondyloarthropathies (SpA) belong to the group of inflammatory arthritis which comprises the ankylosing spondylitis, reactive arthritis, psoriatic arthritis/spondylitis, and arthritis/spondylitis associated with inflammatory bowel diseases. Common finding between these different form of axial SpA is sacroiliac joint inflammation. The gold standard in diagnosis of sacroiliitis is magnetic resonance imaging (MRI). The aim of this study is to compare the efficacy of dual phase 99mTc-HDP-SPECT/CT and MR in diagnosis of sacroiliitis in axial- spondylarthritis (SpA) patients. **Materials and Methods:** Nineteen patients (8 females, 11 males, mean age: 36 years) were involved into the study. The patients were selected according to clinical features with inflammatory type low back pain raising the suspicion of axial SpA. All patients were therapeutic-naive for glucocorticosteroids, DMARDs or TNF-α inhibitors. First, sacroiliac MR examination was performed in the following sequences: T2- weighted STIR for the bone marrow edema (BME) and T1-weighted sequence for the fat metaplasia (FM). Within one-week 99mTc-HDP-SPECT/CT (Mediso, AnyScan Trio) were performed. SPECT/CT and MR images were evaluated visually by two independent observers. For quantitative evaluation MR slices were registered to CT (SPECT/CT). According to different structural lesions based on appropriate MR and CT slices VOI-s were determined manually. Bone marrow edema, which characteristic for active process, and chronical changes: fat metaplasia and sclerosis were contoured. As reference region an intact sacrum part was chosen. In each defined VOI average tracer uptake were calculated. **Results:** Six active sacroiliitis and 5 chronic sacroiliitis without active lesions were diagnosed according to the MR results. On the other 8 patients the sacroiliitis was excluded based on normal MR findings. By the 99mTc-HDP-SPECT/CT 6 active and 5 chronical sacroiliitis were found, in 8 patients there were no pathological changes characteristic for sacroiliitis. Intermodality analysis showed excellent agreement (Cohen-kappa, **ƙ**=0.84). In our patient group overall agreement was 89 %, in active sacroiliitis 89 %. On the bone SPECT tracer uptake was the highest in bone marrow edema, in sclerotic lesions was moderate and lowest in fat deposition. **Conclusion:** According to our initial results comparing MR and 99mTc-HDP SPECT/CT imaging in diagnosis of sacroiliitis we can state: 99mTc-HDP SPECT/CT is useful tool to detect active sacroiliitis in SpA patients. Furthermore, HDP-uptake can be helpful distinguish between early and chronic stages of sacroiliitis. Possible advantages of HDP-SPECT/CT compared to MR may include investigation of additional disease manifestation/joint involvement. Clinical relevance of this fact is under further study. **References:** None.

EP-0170

Diagnosis of infected hip and knee prostheses with Tc-99m Sulesomab: the utility of delayed (20-24hours) imaging

O. Mbakaza, O. A. Ayeni, K. Purbhoo, M. D. T. W. Vangu;
University of the Witwatersrand, Johannesburg, SOUTH AFRICA.

Aim/Introduction: To evaluate the clinical utility of a delayed (20-24hours) imaging in a dual-time acquisition with Tc-99m Sulesomab (LeukoScan) scintigraphy in the diagnosis of infection in painful hip and knee prostheses. **Materials and Methods:** Patients referred to the Nuclear Medicine Department of 2 tertiary hospitals affiliated with the University of the Witwatersrand, Johannesburg, South Africa with suspicion of infected hip and knee prostheses, who had dual-time acquisition protocol (4 hour and delayed 20-24 hour imaging) between January 2015 and November 2018 using Tc-99m Sulesomab scintigraphy were retrospectively enrolled in this study. All patients had clinical and/or biochemical suspicion of infection. The scintigraphic data was assessed visually by three nuclear medicine physicians blinded to laboratory and radiographic results. The images were independently reported as: positive, equivocal or negative for infection based on existing guidelines on data interpretation. The delayed images were compared to early images and visually graded as more intense, same intensity, less intense and no abnormal uptake. An increase in uptake intensity was considered consistent with infection, same intensity was considered equivocal, and less intense pattern was considered a negative result. In equivocal cases on delayed LeukoScan imaging, Tc-99m nanocolloid bone marrow scan was performed and the final result was determined thereafter. **Results:** There were 39 females and 22 males; mean age was 60.3 years. Sixty two percent (n=38) had hip prosthesis and 38 % (n=23) had knee prosthesis. Following visual analysis, early LeukoScan images were considered negative in 30% of studies. On delayed images, about half of the studies were negative, 15% positive, while a third were regarded as equivocal. There was non-conformity in the interpretation of images on direct comparison of early vs delayed images in more than half of the patients (55%). The difference in this early vs late comparison was significant ($p<0.001$). More than two thirds (69%) of the overall study had nanocolloid imaging as a final interpretative study. Both early and delayed images had a significant difference when compared to the final conclusion after nanocolloid imaging ($p=0.03$) and ($p=0.002$) respectively. **Conclusion:** Despite no concrete consensus on the use of delayed imaging with Tc-99m Sulesomab (LeukoScan) scintigraphy, our data suggest that the utility may be in reducing the number of false positive studies interpreted on early imaging. However, for cases considered positive on early images; delayed images may not be necessary if colloid imaging is readily available to improve specificity. **References:** None.

EP-09
Cardiovascular: Vascular Imaging

October 12 - 16, 2019

e-Poster Area

EP-0171

Medical mimics and incidental findings diagnosed on PET/CT for investigation of possible giant cell arteritis: a pictorial review

S. L. Ayesa, A. M. Sammel, R. Laurent, P. J. Roach, E. Hsiao, G. P. Schembri;
Royal North Shore Hospital, St Leonards, Sydney, AUSTRALIA.

Aim/Introduction: Giant cell arteritis (GCA) has a wide range of clinical manifestations including headache, scalp tenderness, jaw claudication, visual loss, aortic arch syndromes and stroke (1). With the increasing use of PET/CT for investigating GCA, medical mimics are often identified on imaging.We reviewed alternative diagnoses and significant incidental findings found on PET/CT during the prospective cross-sectional study of Giant Cell Arteritis and PET Scan (GAPS) (2). **Materials and Methods:** The prospective GAPS study imaged 64 new patients with suspected GCA with time-of-flight PET/CT from skull vertex to diaphragm, within 72 hours of commencing corticosteroids and prior to temporal artery biopsy. Images were read by PET experienced nuclear medicine physicians blinded to clinical history, biopsy and serology results. Incidental findings and/or alternative diagnoses were recorded, considered clinically significant if they lead to eventual diagnosis or treatment. **Results:** GCA was the clinical diagnosis in 21/64 patients, with biopsy proven GCA in 12/21. Incidental findings and/or alternative diagnoses were identified in 30/64 studies, the finding clinically significant in 13/30 patients. In 11/13, the alternative diagnoses contributed to patient presentation. 5 patients were diagnosed with malignancy - 4 with lung cancer (2 metastatic), and 1 with thyroid cancer. Lung malignancy was the final diagnosis in 3 patients, with 2 true incidental cancers detected (thyroid and lung). Typical polymyalgia rheumatica symptoms, of likely paraneoplastic cause, were recorded in 1 patient with a final diagnosis of lung cancer.7 diagnoses of infection included pneumonia (3), maxillary sinusitis (3) and cervical osteomyelitis (1). 2/3 patients with sinusitis were clinically diagnosed with biopsy negative GCA. 1 patient was diagnosed with clinically significant thyroiditis. The most common presenting symptoms in patients with a clinically significant alternative diagnosis was headache (12) and scalp tenderness (7). Jaw pain and scalp tenderness were present in all 3 patients with sinusitis. **Conclusion:** GCA is associated with a range of non-specific symptoms. The reporting physician should be alert to the range of possible alternative diagnoses for GCA and incidental findings, as many will be clinically relevant. **References:** 1. Salvarani C, Cantini F, Hunder G. Polymyalgia rheumatic and giant cell arteritis. Lancet. 2008;372:234-45.2. Sammel AM, Hsiao E, Schembri G, Nguyen K, Brewer J, et al. Diagnostic Accuracy of

PET/CT Scan of the Head, Neck and Chest for Giant Cell Arteritis: The Double-Blinded Giant Cell Arteritis and PET Scan (GAPS) Study. Arthritis Rheumatol. 2019 [ePub ahead of print, published online March 8 2010].

EP-0172

Relationships between the results of computed tomography coronary angiography and myocardial perfusion abnormalities on SPECT

K. Zavadovskiy, A. Maltseva, K. Kopeva, A. Mochula, E. Grakova; Cardiology Research Institute, Tomsk National Research Medical Centre, Russian Academy of Sciences, Tomsk, RUSSIAN FEDERATION.

Aim/Introduction: Currently myocardial perfusion imaging (MPI) is one of the most common methods to identify myocardial ischemia. Coronary computed tomography coronary angiography (CCTA) is well-established method of coronary atherosclerosis diagnosis, but it doesn't allow to identify myocardial ischemia. The purpose of this study was to assess the relationships between morphological CT-characteristics of coronary atherosclerosis and myocardial perfusion downstream in patients with intermediate pretest probability of stable coronary artery disease (SCAD). **Materials and Methods:** Materials and Methods: The study group comprised 68 patients (42 men, age 63 (56;68) years) who underwent coronary computed tomography angiography (CCTA) as well as stress-rest MPI (with CT attenuation correction) on the hybrid system GE Discovery NM/CT 570C equipped with with dedicated cardiac Cadmium-Zinc-Telluride gamma camera. The following CCTA features were assessed: Agatston calcium score, maximal stenosis degree, positive remodeling index, total atherosclerotic plaque length, the sum of stenoses, the presence of at least one stenosis >50%, plaque structure and geometry. The Segment Involvement Score, Segment Stenosis Score and CCTA based Syntax Score (CT_SS) were calculated as measures of global atherosclerosis burden. The patients were divided into two groups: 1) moderate and large stress perfusion defect extent (SSS≥9); 2. small perfusion defect extent (SSS<9). **Results:** The MPI parameters Summed Stress Score (SSS) and Summed Difference Score (SDS) had moderate correlation with CT-characteristics of coronary atherosclerosis: SSS with Segment Stenosis Score (ρ=0,25, p=0,0099), CT_SS (ρ=0,37, p=0,00003), the sum of stenoses (ρ=0,27, p=0,0033) and maximum stenosis (ρ=0,41, p=0,0002); SDS with CT_SS (ρ=0,31, p=0,00002) and maximum stenosis (ρ=0,34, p=0,0005). According to the univariate logistic regression, maximum stenosis (OR 1,04; CI 1,02-1,06; p=0,0001), the sum of stenoses (OR 1,01; CI 1,00-1,01; p=0,02), Segment Stenosis Score (OR 1,14; CI 1,04-1,25; p=0,04) and CT_SS (OR 1,32; CI 1,12-1,56; p=0,01), the presence of stenosis >50% (OR 5,4; CI 1,69-17,16; p=0,004), noncalcified (OR 1,79; CI 1,11-2,87; p=0,017) and circular features (OR 2,99; CI 1,48-6,04; p=0,002) of the atherosclerotic plaques were the independent determinants of moderate and large perfusion defect. By the results to multivariable logistic analysis the combination of several CT-characteristics of coronary atherosclerosis did not improve the prognostic model. **Conclusion:** Segment Stenosis Score, CT_SS as well as noncalcified structure and circular geometry of the atherosclerotic plaques are the most significant independent predictors of moderate and large stress perfusion defects. These CT morphological characteristics could be used for risk stratification in patients with intermediate pretest probability of SCAD. **References:** None.

EP-0173

Usefulness of 18-Fluordesoxiglucose PET/CT semi-quantification in the diagnosis of large vessel vasculitis: a retrospective study

D. Lisei Coscia, C. Vigil, O. Rodriguez, C. Salvat, A. Laverde, M. Domínguez, B. Fernandez, N. Martín, F. Gonzalez García; Hospital Universitario Central de Asturias, Oviedo, SPAIN.

Aim/Introduction: Large vessel vasculitis (LVV) is an arteries disease with two major variants, Takayasu arteritis and giant cell arteritis. Many arteries can be affected, mostly thoracic aorta and its main branches; with polymyalgia rheumatica (PMR) also belonging to this disease spectrum. The use of 18-Fluordesoxiglucose PET/CT (FDG-PET/CT) has been increasing in last years, although definitive diagnosis can be difficult due to the lack of accepted definitive criteria, which turns into a limitation of this technique. According to previous evidence using aorta to liver ratios, we decided to evaluate the use of FDG-PET/CT semi-quantification parameters in our series. **Materials and Methods:** We performed a retrospective analysis in a series of 33 patients with FDG-PET/CT. 22 of them have been previously diagnosed of LVV and 11 were considered as controls (most had symptoms of vasculitis or previous history of vasculitis/PMR, but without evidence of activity according to clinical, radiological, o laboratory parameters at the time of FDG PET/CT acquisition). Thoracic/main aorta branches SUVmax (SUVmax A) and right hepatic lobe SUVmax (SUVmax L) were obtained, plus erythrocyte sedimentation rate (ESR) and C-reactive protein (CRP) of all patients. Continuous variables were compared using T-Test, receiver operating characteristic (ROC) analysis was performed for SUVmax A absolute value and also for SUVmax A/SUVmax L ratio (A/L ratio). Pearson correlation was performed between CRP/ESR and SUVmax A. **Results:** No significant differences between case-control groups were found in demographic variables, ESR and CRP values. Aortic arch was the most frequently involved region visible in FDG-PET/CT. Significant differences were found between SUVmax A in LVV patients vs. controls: 3.86 (95%CI 4.12-3.59) vs. 3.12 (95%CI 3.47-2.77) (p<0.001) and between A/L ratio: 1.04 (95%CI 1.12-0.95) vs. 0.82 (95%CI 0.88-0.76) (p<0.001). In ROC analysis, the area under the curve (AUC) obtained for SUVmax A was 0.826 (p<0.003), enhaced when using A/L ratio: AUC= 0.872 (p<0.001). A mild positive correlation was found between SUVmax A and ESR r=0.538, p<0.01. **Conclusion:** The use of 18-Fluordesoxiglucose PET/CT allows an accurate diagnose in patients with suspected LVV with inflammatory activity. Among all parameters, the

semi-quantitative ratio using artery/liver uptake proved to be more precise than absolute SUVmax of the involved vessels. **References:** None.

EP-0174

Arterial inflammation detected with PET-TC ^{18}F-FDG at staging and end of treatment after ABVD for Hodgkin lymphoma

A. L. Gutiérrez Cardo[1], *B. Azzaoui Jiménez*[2], *A. J. Mesas Ruiz*[3], *M. Lillo García*[4], *M. A. Sánchez Chaparro*[2], *P. Valdivielso Felices*[2]; [1]*Hospital Regional Universitario de Málaga. Servicio Andaluz de Salud, Málaga, SPAIN,* [2]*Universidad de Málaga, Málaga, SPAIN,* [3]*Hospital Universitario Virgen de la Victoria. Servicio Andaluz de Salud, Málaga, SPAIN,* [4]*Fundación General de la Universidad de Málaga, Málaga, SPAIN.*

Aim/Introduction: Hodgkin lymphoma survivors are at increased cardiovascular risk. Positron emission tomography (PET) with ^{18}F-FDG is a potential predictor of long-term cardiovascular risk and at least two PET-CT scans are performed at staging and end-of-treatment. The purposes were to study the feasibility of performing vascular ^{18}F-FDG uptake in both scans and compare which study could show higher values: staging-PET affected by disease-induced inflammatory state or end-of-treatment PET after chemotherapy-induced endothelial damage. **Materials and Methods:** Scans from 23 patients with classic Hodgkin lymphoma, and complete remission after the last cycle of ABVD were included. Data recorded included sex, age, histological type, cardiovascular risk factors and time after last chemotherapy. Measurements of TBRmax and TBRmean were performed including thoracic aorta, common carotids and iliac arteries, SUV medium of VOIs traced in spleen and bone marrow (lumbar vertebrae) in initial and final PET. Data have been analysed with a Student's t-test for paired simples, Wilcoxon signed-rank test for non parametric data and Spearman's rank for time after chemotherapy and vascular uptake correlation. **Results:** Of the 23 studies carried out, 15 were men and 8 women, with an average age of 40 ± 18 years (14-82). Of these, 18 (78%) had no spleen involvement and 19 (82%) had no marrow involvement. In every patient vascular ROIs could be traced avoiding specific lymphomatous uptake. There was a significant increase in TBRmean in aorta and carotids in the second PET of 0.83 and a significant decrease in metabolic activity in spleen and bone marrow of 0.44 and 0.35 respectively, both including or excluding those with initial infiltration (5/23 22% spleen; 4/23 18% bone marrow). A weak negative correlation was found between time after chemotherapy acquisition and vascular uptake (-0,258 non significant). **Conclusion:** It is possible to measure vascular uptake for cardiovascular risk evaluation in Hodgkin lymphoma even in staging-PET.The increase of arterial inflammation after treatment, and the negative correlation between it and the time elapsed between the last cycle of ABVD and the PET performance could be due to the endothelial toxic effect of chemotherapy. **References:** None.

EP-0175

Molecular imaging of carotid artery atherosclerosis with pet: a systematic review

R. Piri, *O. Gerke, P. F. Høilund-Carlsen; Department of Nuclear Medicine, Odense University Hospital, Odense C, DENMARK.*

Aim/Introduction: Carotid artery atherosclerosis is the leading cause of cerebrovascular events. Therefore a decent opportunity is provided by investigating the carotid arteries before any adverse outcome. We conducted a systematic review of articles on PET imaging of carotid artery atherosclerosis with emphasis on clinical usefulness. **Materials and Methods:** Research articles in English reporting carotid artery PET imaging until November 2018 were systematically searched for in Medline/PubMed, Scopus, Embase, Google Scholar, and Cochrane Library. Duplicates, editorials, letters, case stories, conference abstracts, and patients with end-stage disease or receiving immunosuppressive medication were excluded. All eligible articles were reviewed by one observer (RP) to provide a PRISMA diagram. Included articles were grouped into the following categories: diagnostic performance, risk factors, laboratory findings, imaging modalities, or treatment, and the main information they provided was summarized. **Results:** Of 1718 primary hits, 57 studies were included. Being applied in 49 and 5 studies for imaging inflammation and microcalcification, respectively, 18F-fluorodeoxyglucose (FDG) and sodium fluoride (NaF) (5/57) were the most frequently used tracers. In summary, it has been shown that Normal carotid arteries have the lowest FDG uptake. Further that patients with symptomatic atherosclerosis have higher uptake than asymptomatic patients and that atherosclerotic carotid lesions ipsilateral to a cerebrovascular event had increased FDG uptake compared to the contralateral carotid artery, but that this difference tends to decrease with time, apparently due to reduced local inflammation in the ipsilateral carotid artery and increased inflammation in contralateral carotid artery. It was found that FDG uptake is significantly associated with increased age, male gender, body mass index (in healthy individuals), and with arterial hypertension, hypercholesterolemia, and diabetes mellitus. Histological assessment indicated a strong correlation between microcalcification and NaF uptake in symptomatic patients, but a negative correlation with FDG uptake. FDG uptake was associated with increased macrophage count and CD68 count, both accounting for increased local inflammatory response. FDG uptake was correlated with hypoechogenicity and microembolic signals on ultrasonography. FDG uptake was inversely correlated with CT-derived calcium score and directly with intima-media thickness on CT. In PET/MRI, FDG uptake correlated positively with necrotic lipid-rich core volume of plaques. **Conclusion:** While FDG-PET 'visualizes' the current status of carotid atherosclerosis inflammation and its possible clinical features enabling risk stratification of atherosclerotic plaques, NaF-PET appears to indicate long-term consequences of ongoing inflammation by 'visualizing' microcalcification enabling detection of atherosclerosis even in apparently normal carotid arteries. **References:** None.

EP-0176

Short-term discontinuation of vagal nerve stimulation alters ^{18}F-FDG blood pool activity in humans

E. Boswijk[1,2], *R. Franssen*[1], *G. H. E. J. Vijgen*[3], *R. Wierts*[1], *J. van der Pol*[1], *A. M. A. Mingels*[4], *E. M. J. Cornips*[5], *M. H. J. M. Majoie*[6,7,8], *W. D. van Marken Lichtenbelt*[9], *F. M. Mottaghy*[1,10], *J. E. Wildberger*[1,2], *J. Bucerius*[1,2,10];
[1]*Department of Radiology and Nuclear Medicine, Maastricht University Medical Center (MUMC+), Maastricht, NETHERLANDS,* [2]*Cardiovascular Research Institute Maastricht (CARIM), Maastricht University, Maastricht, NETHERLANDS,* [3]*Department of Surgery, Erasmus Medical Center, Rotterdam, NETHERLANDS,* [4]*Department of Clinical Chemistry, Maastricht University Medical Center (MUMC+), Maastricht, NETHERLANDS,* [5]*Department of Neurosurgery, Maastricht University Medical Center (MUMC+), Maastricht, NETHERLANDS,* [6]*Department of Neurology, Maastricht University Medical Center (MUMC+), Maastricht, NETHERLANDS,* [7]*Epilepsy Center Kempenhaege, Heeze, NETHERLANDS,* [8]*MHENS School of Mental Health & Neuroscience, Maastricht University, Maastricht, NETHERLANDS,* [9]*School of Nutrition and Translational Research in Metabolism (NUTRIM), Maastricht University, Maastricht, NETHERLANDS,* [10]*Department of Nuclear Medicine, University Hospital RWTH Aachen, Aachen, GERMANY.*

Aim/Introduction: Vagus nerve activation has a direct impact on inflammation. Therefore, we investigated whether vagal nerve stimulation (VNS) influences arterial wall inflammation as measured by ^{18}F-FDG uptake. **Materials and Methods:** Ten patients with left-sided VNS for refractory epilepsy were studied during stimulation (VNS-on) and in the hours after stimulation was switched off (VNS-off). In nine patients, ^{18}F-FDG uptake was measured in the right carotid, aorta, bone marrow, spleen and adipose tissue. Target-to-background ratios (TBRs) were calculated to normalize the respective standardized uptake values (SUVs) for venous blood pool activity. Median values are shown with their interquartile range and were compared using the Wilcoxon signed rank test. **Results:** Arterial SUVs were higher during VNS-off than VNS-on [SUV_{max} all vessels 1.8 (1.5-2.2) vs. 1.7 (1.2-2.0), p=0.051]. However, a larger difference was found for venous blood pool, reaching statistical significance in the superior cava vein [$_{mean}SUV_{mean}$ 1.3 (1.1-1.4) vs. 1.0 (0.8-1.1); p=0.011], resulting in non-significantly lower arterial TBRs during VNS-off than VNS-on [TBR_{max} all vessels 1.5 (1.4-1.6) vs. 1.7 (1.5-1.9), p=0.086]. Albeit in the same direction, differences in the remaining tissues were not significant. Insulin levels were increased after VNS was switched off (55.0 pmol/l (45.9-96.8) vs. 48.1 pmol/l (36.9-61.8); p=0.047]. However, the concurrent increase in glucose levels did not reach statistical significance [4.8 mmol/l (4.7-5.3) vs. 4.6 mmol/l (4.5-5.2); p=0.053]. **Conclusion:** Short-term discontinuation of VNS readily influenced arterial ^{18}F-FDG uptake. However, VNS significantly decreased the venous blood pool activity, possibly due to a systemic effect on glucose metabolism. The observed change in arterial ^{18}F-FDG uptake seems therefore less likely to be related to a direct effect on arterial inflammation. **References:** None.

EP-0177

Utility Of PET-CT With 18F-FDG In The Study Of Large Vasculitis

C. Mena Melgar, *C. Paniagua Correa, M. de la Rubia Marcos, B. Tagliatori Nogueira, A. Herrero Muñoz, C. Sandoval Moreno, P. Garcia Alonso, L. Castillejos Rodriguez, A. Ortega Valle, M. Balsa Breton;*
Hospital Universitario de Getafe, Getafe, SPAIN.

Aim/Introduction: To analyze the usefulness of PET-CT in the study of patients with suspicion or follow-up of the inflammatory process of the vascular system, focused on the involvement of large vessels. **Materials and Methods:** We retrospectively analyzed the PET-CT studies, performed during the last three years in our center, to 28 patients with suspicion or follow-up of vasculitis of large vessels (22 women and 6 men).A large number of requests (23) were made in the initial study of patients with suspected large vessel vasculitis, especially in cases with an atypical presentation and / or to assess the extent; while the rest of the included studies (5) were performed on patients with known pathology and suspected reactivation or response to treatment. All patients underwent PET-CT after the administration of 18F-FDG, with tomographic metabolic imaging at 45min post-injection and whole-body CT for attenuation correction and anatomical localization. For the analysis of the results, we compared the result of the PET-CT, using Meller's visual scale (which compares tissue uptake with respect to liver uptake, being an equal or superior uptake valid to evaluate the degree of inflammation and the activity of it); with the recognized gold-standard technique (arteriography for Takayasu arteritis and temporal artery biopsy in the case of giant cell arteritis) and / or with the clinical diagnosis made by the requesting physician. **Results:** Of the 28 patients, 18 had a negative PET-CT study, with 18 of them TN. Only 4 of them were considered as FN when the subsequent diagnosis was established by the clinician. Note that 3 of these 4 patients were in active treatment with corticosteroids at the time of PET-CT, which may be the cause of these FN.In the case of patients who were considered healthy at the end of the study, we found that all of them had a negative PET-CT study, showing a specificity of 100%.In turn, we observed that in all 6 patients with positive PET-CT study for vasculitis, all of them had this diagnosis confirmed by the gold-standard technique recognized, establishing a 100% PPV + in our study. **Conclusion:** PET-CT is very useful in the study of large vessel vasculitis, especially due to its high specificity and PPV +, identifying the patient with active pathology with sufficient certainty. **References:** None.

EP-0178

18F-FDG PET/CT and CT angiography in the evaluation of immunosuppressive therapy in large vessel vasculitis

M. M. S. Moragas[1], *M. Andreu*[2], *J. Martín*[1], *A. Caresia*[1], *M. Monteagudo*[3], *C. Diaz*[1], *A. Rodríguez*[1], *Z. Bravo*[1], *L. Bernà*[1];
[1]*Servei Medicina Nuclear. Parc Taulí Hospital Universitari, Sabadell (Barcelona), SPAIN,* [2]*Servei Radiologia. Parc Taulí Hospital Universitari, Sabadell (Barcelona), SPAIN,* [3]*Servei Medicina Interna. Parc Taulí Hospital Universitari, Sabadell (Barcelona), SPAIN.*

Aim/Introduction: 18F-FDG PET/CT (FDG-PET) and CT angiography (CTA) are useful in diagnosis of large vessel vasculitis (LVV), but more limited data are available on their contribution in treatment response assessment. The aim of the study was to compare FDG-PET and CTA in the evaluation of immunosuppressive therapy in LVV. **Materials and Methods:** 12 patients diagnosed of LVV have been studied twice with FDG-PET and CTA before (basal scan) and after treatment has been started or finished (monitoring scan). Patients were studied simultaneously in the same PET/TC device, with a mean follow up of 18 months. CTA diagnostic LVV criteria were circumferential aortic wall thickening >2 mm and >1 mm in aortic branches, and/or wall enhancement (> 40 UH), and/or irregular thickening extending to peri-vascular tissue, and/or structural vascular changes as complications. FDG-PET diagnostic LVV criteria were diffuse FDG uptake in aorta wall and/or its main branches using Meller visual scoring index, that compares vessel and liver uptake. Positive scan: score>2 for thoracic aorta and ≥ 2 for other vascular regions. Changes in basal and monitoring scans results were compared, and correlated with laboratory acute phase reactants (AFR). **Results:** Basal scan: All patients had a positive FDG-PET, 10 a CTA positive scan and 9 an AFR elevation. Monitoring scan: FDG-PET: 5 patients scan normalized in all vascular segments (complete response CR), 5 patients had reduction in number and/or metabolic activity of vascular segments (partial response PR), and 2 patients had increased in number and/or metabolic activity of vascular segments (progression P). Of 5 patients with FDG-PET CR, 2 had CTA CR (no inflammation nor structural changes), 1 had CTA PR (no inflammation or no estructural changes), 1 had no changes on CTA (no response NR) and 1 CTA was negative as basal scan. Of 5 patients with FDG-PET PR, 3 had a CTA PR, 1 NR, and 1 was negative as basal scan. Of 2 patients with FDG-PET R, CTA was also positive for R. There were not CTA CR with FDG-PET NR or PR. AFR only normalized in 3/9 patients, 1 RC, 1 PR and 1 P in FDG-PET. **Conclusion:** FDG-PET seems to be more sensitive than CTA and AFR in detecting CR in LVV. Both FDG-PET and CTA are sensitive in detecting progression. Value of FDG-PET PR has to be studied by following the patients, as it can be real response vs no response. **References:** None.

EP-0179

Measurement of epicardial adipose tissue with FDG-PET/CT in patients with type-2 diabetes mellitus

D. Dezso[1], *K. Zámbó*[1], *Z. Ritter*[1], *Z. Bán*[1], *Z. Szabó*[1], *B. Bódis*[2], *E. Várady*[3], *S. Szukits*[3], *A. Tóth*[3], *O. Nemes*[2], *K. Rucz*[2], *S. Szujó*[2], *E. Mezősi*[2], *L. Bajnok*[2], *E. Schmidt*[1];
[1]*University of Pécs Department of Nuclear Medicine, Pécs, HUNGARY,* [2]*University of Pécs 1st Department of Medicine, Pécs, HUNGARY,* [3]*University of Pécs Department of Radiology, Pécs, HUNGARY.*

Aim/Introduction: Type 2 diabetes (T2DM) is a leading risk factor of cardiovascular diseases. There is a strong correlation between coronary artery diseases and the volume of epicardial adipose tissue (EAT) deposits located between myocardium and visceral pericardium. This metabolically active ectopic adipose tissue is in strong relationship with visceral adipose tissue developmentally and correlates with its amount. EAT has been investigated intensively in the last few years, including its effect on cardiovascular risk. The aim of our work is to study the relationship between vascular calcification, subcutaneous adipose tissue and EAT in the diabetic population studied with FDG-PET/CT. **Materials and Methods:** Examinations of 18 T2DM patients' (8 men, 10 women, mean age 67±6.3) and 62 non-diabetic patients (35 men, 27 women, mean age 60±10.6) were investigated during our retrospective study. The volume of EAT was determined in 16 patients with coronary CT angiography (CTA) and FDG-PET/CT scans using Slicer 4.10.0 software (https://www.slicer.org, open source software package)[1]. In 64 cases only FDG-PET/CT data (Interview Fusion software, Mediso) were applied. SUVmax (Standardized Uptake Value), the volume of calcified arterial plaque (density above 130 Hounsfield Units) and EAT were measured and the results were evaluated using SPSS software. **Results:** Early results of our ongoing research showed no significant difference between BMI-corrected EAT volume ($p=0.465$) measured on CTA and FDG-PET/CT, however, the values were strongly correlated ($r=0.949$, $p<0.001$). Significant correlation was found between EAT volume and the calcification of the vascular system on the whole examined population ($r=0.266$, $p<0.05$). The amount of EAT ($p<0.001$), SUVmax ($p<0.05$) and the degree of vascular calcification ($p<0.05$) in patients with T2DM were significantly higher than in the control group. EAT SUVmax in both groups were significantly higher ($p<0.001$) than subcutaneous adipose tissue SUVmax, and the subcutaneous adipose tissue SUVmax was significantly higher ($p<0.05$) in T2DM patients compared to the control group. **Conclusion:** Based on our results, both CTA and FDG-PET/CT tests are suitable to quantify EAT. Patients with T2DM have significantly higher levels of EAT, higher FDG uptake, and vascular calcification. According to our results, the higher epicardial fat deposits may contribute to the higher cardiovascular risk in T2DM patients. **References:** [1] Fedorov A., Beichel R., Kalpathy-Cramer J., Finet J., Fillion-Robin J-C., Pujol S., Bauer C., Jennings D., Fennessy F., Sonka M., Buatti J., Aylward S.R., Miller J.V., Pieper S., Kikinis R. 3D Slicer as an Image Computing Platform for the Quantitative Imaging Network. Magnetic Resonance Imaging.2012 Nov;30(9):1323-41.PMID:22770690.

EP-10
Cardiovascular: Myocardical Perfusion Imaging

October 12 - 16, 2019

e-Poster Area

EP-0180
Myocardial ischemic patterns in patients with idiopathic pulmonary arterial hypertension

A. A. Ansheles[1], *I. G. Guryanov*[2], *T. V. Martynyuk*[1], *V. B. Sergienko*[1]; [1]*National Medical Research Center of Cardiology, Moscow, RUSSIAN FEDERATION,* [2]*National Economics Research Institute, Moscow, RUSSIAN FEDERATION.*

Aim/Introduction: According to Russian registry, 42% of idiopathic pulmonary arterial hypertension (IPAH) patients manifest with chest pain. The aim of current research was to assess myocardial perfusion in IPAH patients with ^{99m}Tc-MIBI SPECT, to justify LV/RV ischemia patterns as probable cardialgias substrate in this group. **Materials and Methods:** 74 patients with confirmed IPAH (70 women), mean age 38,2±9,4, formed group I (with cardialgia, n=36) and group II (without chest symptoms, n=38), all underwent myocardial perfusion CT-corrected ^{99m}Tc-MIBI SPECT at rest and after treadmill cardiopulmonary exercise test. LV perfusion abnormalities were evaluated using standard SSS/SDS parameters, RV was assessed visually, IVS/LW and RV/LV uptake ratios were calculated, in comparison with Holter and six-minute walking test (6MWT) results. **Results:** Group I demonstrated worse 6MWT results (439±107 vs 489±99m, p=0.04), higher rate of ischemic signs at Holter (22,2% vs 2,6%, p=0.03), shorter exercise duration (4,9±2,1 vs 5,9±2,4 min, p=0.06). Typical myocardial perfusion SPECT results, that did not differ in both groups, included visible, severely dilated RV (mean EDV=103±51 ml) with low EF (22±6%), diffusely inhomogeneous MIBI uptake. RV accumulation level was comparable to LV lateral wall (LW) (RV/LV ratio=0.60±0.09), that indicates RV hypertrophy. SSS/SDS values were somewhat higher in group I (8 [6-10] vs 6 [5-7], p=0.09, 3 [2-4] vs 2 [1-4], p=0.14, respectively). Stable perfusion defects were located in IVS in all cases, mean IVS/LW was lower in group I (0.56 ± 0.06 vs 0.60±0.07, p=0.01). Stable defects spread at stress images in 67% of patients in group I and in 32% of patients in group II. Moreover, 5 patients from group I (14%) demonstrated stress-induced apical and/or anteroseptal perfusion defects, that were suspicious for IHD, followed by coronary angiography, that showed intact coronary arteries in all cases. **Conclusion:** Myocardial perfusion impairments in IPAH include increased and inhomogeneous MIBI accumulation in dilated RV, impaired IVS perfusion presumably due to its compression by dilated RV, and perfusion defects spreading on stress images, in some cases involving not only IVS, but also adjacent LV segments. Those ischemic patterns are not due to direct damage of epicardial arteries, but due to combination of perfusion/demand disbalance in hypertrophied RV and microcirculatory impairments in compressed IVS, that get worse with myocardial pressure overload increase during physical exercise. After certain threshold those pathophysiological processes result in chest pain in IPAH patients, and assessment of those impairments as a pain substrate is useful with ^{99m}Tc-MIBI SPECT. **References:** None.

EP-0181
Visual identification of coronary calcifications on diagnostic chest CT improves diagnostic accuracy of Tl-201 CZT SPECT myocardial perfusion imaging

H. Chen, *Y. Chang*, *Y. Huang;* *Department of Nuclear Medicine, Kaohsiung Chang Gung Memorial Hospital, Kaohsiung, TAIWAN.*

Aim/Introduction: Single photon emission tomography (SPECT) myocardial perfusion imaging (MPI) can provide valuable diagnostic and prognostic information in patients with known or suspected coronary artery disease (CAD). Recently, the development of cadmium-zinc-telluride(CZT) SPECT MPI provided satisfactory sensitivity but suboptimal specificity for detecting CAD. Coronary artery calcification(CAC) is a useful CAD indicator when assessed by dedicated calcium scoring CT scan. Simultaneous CAC scoring with CZT SPECT MPI offered incremental diagnostic and prognostic information over CZT SPECT alone using Tc-99m sestamibi. The aim of this study is to assess diagnostic implications of CAC incorporated with Thallium (Tl)-201 CZT SPECT MPI. **Materials and Methods:** We retrospectively analyzed patients who underwent invasive coronary angiography (ICA) within 6 months of SPECT MPI. Patients who received diagnostic chest CT within 6 months prior to ICA were included (N=126). The MPI and CT images were interpreted by experienced nuclear medicine physicians and radiologists without knowledge of clinical history. For assessing the location and severity of perfusion defects, 17 segmentation scores and a 5-point scale were used. The global summed stress score (SSS) was calculated by adding all scores in 17 segments on stress images. MPI results were considered abnormal when SSS ≥4 . Identification of any calcified region (HU >130) within coronary artery territories on non-contrasted CT scan was defined as CAC positive. A coronary stenosis ≥50% on ICA was considered obstructive CAD. **Results:** The specificity of MPI plus CAC were higher than in MPI alone (86% vs 71%; p= 0.004). The sensitivity showed no significant difference between MPI plus CAC and MPI alone (75% vs 78%; p= 0.5). PPV of MPI plus CAC is 86% but only 76% in MPI alone (p<0.001). NPV showed no significant difference (75% vs 73%; p = 1.0). Both SSS and CAC were independent factors predicting obstructive CAD. **Conclusion:** CAC provides additional diagnostic values by improving the specificity of Tl-201 CZT SPECT MPI. **References:** **1.** Gimelli A, Liga R, Duce V, Kusch A, Clemente A, Marzullo P. Accuracy of myocardial perfusion imaging in detecting multivessel coronary artery disease: A cardiac CZT study. J Nucl Cardiol. 2017;24:687-695.2**.** Patchett ND, Pawar S, Miller EJ. Visual identification of coronary calcifications on attenuation correction CT improves diagnostic accuracy of SPECT/CT myocardial perfusion imaging. J Nucl Cardiol. 2017;24:711-

720.3**.** Mouden M, Ottervanger JP, Timmer JR, et al. The influence of coronary calcium score on the interpretation of myocardial perfusion imaging. J Nucl Cardiol. 2014;21:368-374.

EP-0182

Effect of Brown Adipose Tissue Activation on Myocardial [^{18}F]FDG Uptake

S. Alenezi[1], *S. Dannoon*[1], *N. Alnafisi*[1], *S. Asa'ad*[2], *M. Osman*[3], *A. Elgazzar*[1];
[1]*Kuwait University, Kuwait, KUWAIT,* [2]*Jaber Al-Ahmad Center for Nuclear Medicine and Molecular Imaging, Kuwait, KUWAIT,* [3]*St. Louis University, St. Louis, MO, UNITED STATES OF AMERICA.*

Aim/Introduction: The aim of this study is to investigate the relationship between brown adipose fat (BAT) activation and myocardial [^{18}F]FDG uptake in terms of intensity and patterns. **Materials and Methods:** The patients were divided into two groups; BAT and control group. The BAT group consists of 34 cases that showed BAT uptake. The control group, with no BAT uptake, included 68 patients that were matched for BMI, gender and season. The scans were retrospectively reviewed by two nuclear medicine physicians who visually evaluated the intensity of myocardial [^{18}F]FDG uptake. The myocardial [^{18}F]FDG uptake was visually classified into three patterns; diffuse, heterogeneous and focal. The regions of activated BAT distribution were noted. **Results:** The mean myocardial [^{18}F]FDG uptake was 2.50 ± 0.75 for the BAT group and 2.13 ± 0.88 for the control group with a statistically significant difference (P = 0.031). The myocardial [^{18}F]FDG uptake pattern was similar in the BAT and control groups with the diffuse pattern being the most common followed by the heterogeneous and less commonly focal. In the BAT group, the anatomical distribution of BAT was mainly in supraclavicular, paravertebral and axillary and to a lesser extent in cervical regions. **Conclusion:** BAT group had significantly higher intensity of [^{18}F]FDG myocardial uptake compared to control group. Presence of activated BAT did not affect the pattern of myocardial uptake. Knowledge of these findings may help in understanding the variability of myocardial [^{18}F]FDG uptake and consequently in avoiding misinterpretation of cardiac findings in PET/CT studies. **References:** None.

EP-0183

The evaluation of myocardial perfusion with CZT gamma camera in patients with intermediately stenosed left anterior descending coronary artery and estimated fractional flow reserve

S. Piszczek, *K. Tkaczewski, A. Mazurek, S. Osiecki, M. Dziuk;*
Military Institute of Medicine, Warsaw, POLAND.

Aim/Introduction: Fractional flow reserve (FFR) has become routinely performed in intermediate stenosis of coronary arteries to assess the hemodynamic significance. Left anterior descending artery (LAD) is one of the 3 main coronaries, LAD stenosis may be responsible for acute coronary syndromes. The aim of the study was to evaluate myocardial perfusion scintigraphy with cardiac dedicated CZT (cadmium-zinc-telluride) gamma camera in patients with intermediately stenosed LAD and estimated FFR. **Materials and Methods:** Twenty two patients (median age of 69 years) with intermediate (40-70%) stenosis in LAD on coronary angiography and normal left ventricular ejection fraction had estimated FFR under central vein adenosine infusion at 140µg/kg/min. Myocardial perfusion imaging (MPI) with cardiac dedicated CZT gamma camera was performed no later than 2 months post coronary angiography. Exercise treadmill stress test was performed in 15 out of 22 patients, the remaining 7 patients had pharmacological stress test with regadenoson injection. The rest MPI was performed when stress supine/prone images were classified as abnormal. The perfusion images were obtained approximately one hour post injection of 99mTc-sestamibi with activity of 296-592 MBq and were evaluated by two experienced nuclear medicine physicians. **Results:** In most of the stenosed LAD (16/22) FFR values were at or above 0.8 (normal). In remaining 6 patients FFR values ranged between 0.74 and 0.79 (range of 0.75-0.79 is considered as grey zone). MPI did not reveal significant perfusion abnormalities in the vast majority of patients (20/22). Only in two patients reversible perfusion abnormalities involved more than 10% of left ventricular myocardium (both had pharmacological stress test). In these two patients FFR values were at 0.75 and 0.8. One patient had subsequent percutaneous coronary intervention (PCI) with stent implementation into LAD stenosis and had no acute coronary syndrome or further PCI in course of 2-year follow-up observation. The second patient was excluded from further observation due to the lack of contact. **Conclusion:** The study showed good correlation between FFR and MPI results in the patients with intermediately stenosed LAD. Further studies with greater number of patients are necessary for appropriate statistical analysis to obtain reliable outcomes. **References:** None.

EP-0184

Evaluation of myocardial perfusion in patients with asymptomatic Beta-thalassemia major using myocardial perfusion SPECT and its possible association with severity of hematopoiesis

M. Assadi, *P. Rahimizadeh, A. Omrani, E. Jafari;*
Bushehr University of Medical Sciences (BUMS), Bushehr, IRAN, ISLAMIC REPUBLIC OF.

Aim/Introduction: Beta-thalassemia, a kind of hereditary blood disorders, is a chronic hemolytic anemia caused by impaired synthesis of the beta chain of hemoglobin. For survival, regular blood transfusion and chelation treatment are so important in these patients but these transfusions lead to siderosis in the myocardium which is the main cause morbidity and mortality in TM patients. Since heart failure can be detected with cardiac gated SPECT and also it can be used for evaluation of extent and intense of hematopoiesis in bone, we decided to evaluate

cardiac dysfunction in TM patients with ^{99m}TC-MIBI cardiac gated SPECT and hematopoiesis with whole body MIBI scan and compare cardiac gated SPECT with echocardiography and blood tests. **Materials and Methods:** Patients with TM who were referred for blood transfusion and checkup periodically, were included in this cross-sectional study. A questionnaire containing demographic data was provided from patients. then, myocardial perfusion scan, echocardiography and blood tests including LDL, HDL, Chol, Tg, ALT, AST, Hb, ferritin were performed for each patient. **Results:** 24 patients included 14 men (58.3%) and 10 women (41.7%) aged from 15-36 years and average of 24.3±6.5 years old were enrolled in this study. Myocardial perfusion scan (MPS) was normal in all patients. Mean of EF measured for patients was 58.88±13.45. Whole body MIBI was obtained mild for 19 patients (79.2%) and severe for 5 patients (20.8%). There was no significant relationship between scan EF with whole body mibi (p=0.825) and echocardiography EF (p=0.657). The results showed a significant relationship between the level of Hb with amount of blood transfusion (p=0.023) and the level of ferritin with amount of blood transfusion (p=0.002). **Conclusion:** Myocardial perfusion imaging was within normal limits in all asymptomatic patients but diastolic dysfunction was present in all cases. **References:** None.

EP-0185

Left ventricular mass index measured by myocardial perfusion scan: Correlation with echocardiography

M. Abdi[1], *Q. Naili*[1], *D. Djermane*[2], *M. Habbache*[1], *B. Said*[1]; [1]*Centre d'Imagerie Scintigraphique, Blida, ALGERIA,* [2]*CHU Mustapha Bacha, Algiers, ALGERIA.*

Aim/Introduction: Left ventricular mass index (LVMI) has a prognostic value of mortality and sudden death in patients with stable coronary heart disease, even when left ventricular ejection fraction (LVEF) is normal (1). The aim of this work is to evaluate the correlation between LVMI value calculated with a myocardial perfusion scan (MPS), and 2D echocardiography (Echo). **Materials and Methods:** Randomly selected, 50 patients that were oriented to our department for MPS, from July 2018 to January 2019, had an M-mode Echo the same week. There was 26 men and 24 women, with mean age of 63.96 ± 11.05 (±SD). MPS protocol was a stress-rest or stress only Sestamibi Gated SPECT. 32 patients had a normal scan, 8 myocardial infarction (MI), 5 ischemia, and 5 dilated cardiomyopathy (DCM). Left ventricular mass (LVM) was evaluated automatically, throw Corridor 4DM, on MPS. LVM was calculated in Echo according to Devereux's method, by an experienced cardiologist. Second lecture was done for all patients. LVMI was calculated by dividing LVM on body surface area, and expressed with g/m². **Results:** Mean value of LVMI calculated by MPS was lower than Echo (71.1 ± 15.94 and 78.88 ± 16.97, respectively). Same observation has been found on a previous study (2). MPS LVMI was plotted against Echo. Significant correlated has been found (y = 0.645x + 20.15, r = 0.68, p<00001). Correlation coefficient in our study was similar to an other study with 3D Echo (3). Increased LVMI has been found in 4 patients (1 normal, 1 ischemia, 1 DCM, and 1 MI) with MPS and 5 patients with Echo (superior to 88 in women and 111 in men). The patient with discordance between Echo and MPS had a concentric hypertrophy (normal MPS). **Conclusion:** LVMI calculated by MPS correlated significantly with Echo, but with smaller values. Similar results has been found in previous studies (2,3). This had not a significant impact in our group on the detection of increased LVMI. **References:** 1. Prognostic Significance of Increased Left Ventricular Mass Index to Mortality and Sudden Death in Patients with Stable Coronary Heart Disease (From the Heart & Soul Study) Mintu P. Turakhia, MD.2. Left ventricular mass index measured by quantitative gated myocardial SPECT with 99mTc-tetrofosmin: a comparison with echocardiography. Kaoru MARUYAM.3. Left ventricular mass measured by myocardial perfusion gated SPECT. Relation to three-dimensional echocardiography. Akinboboye O.

EP-0186

Lower Event Rate In Obese Patients With Transient Ischemic Dilatation Oof LV Cavity on Gmpi: Is Obesity Friend or Foe

N. Fatima[1], *M. u. Zaman*[1], *A. Zaman*[2], *U. Zaman*[2], *S. Zaman*[3]; [1]*Department of Radiology, Aga Khan University Hospital (AKUH), Karachi, PAKISTAN,* [2]*Civil Hospital, Karachi, PAKISTAN,* [3]*Dow Medical College, Dow University of Health Sciences (DUHS), Karachi, PAKISTAN.*

Aim/Introduction: Background: Obesity is considered as a major modifiable risk factor for coronary artery disease (CAD). But once CAD has been established, the correlation of obesity with all-cause mortality, cardiovascular mortality, infarction, and revascularization is unclear. Transient ischemic dilatation (TID) of left ventricular cavity (LV) in GMPI is a known predictor of severe CAD and worse prognosis. In this study we evaluated the impact of obesity (BMI ≥30) for fatal and non-fatal myocardial infarction (FMI and NFMI respectively) in patients with TID. **Materials and Methods:** Material and Methods: This is a continuation of a previously published study which revealed TID as a reliable predictor of multivessel CAD and NFMIs than FMIs. Patients with TID on GMPIs performed during 2008-2012 were categorized on the basis of BMI <30 (non-obese) and ≥ 30 (obese) and were followed till December 2017. During follow-up period data was collected about NFMIs, revascularization (PCI and CABG) and FMIs. Patients with significant change in BMI during follow up (from non-obese to obese and vice versa) were excluded from the cohort. **Results:** Results: During study period (2008-2017) 386 patients were found to have TID but 69 patients lost to follow-up. 36 patients who had significant change in BMI during study period were excluded. 281 patients constituted study cohort and 230 had BMI <30 (Non-obese; Mean BMI: 24.274 ± 2.982) while 51 had BMI ≥30 (Obese; Mean BMI: 37.433 ± 4.202). Mean age and male domination was not significant in two groups. Incidence of hypertension and dyslipidemia was significant higher in obese group. No significant difference was found for diabetes, family history and smoking in two groups.

GMPI was positive for perfusion abnormalities in 94% and 92% without significantly different fixed to reversible defect ratio between non-obese and obese groups. But obese group had higher mean left ventricular ejection fraction than non-obese group (%LVEF: 52 vs. 45%; significant p value). During follow-up period, NFMIs and FMIs were higher in non-obese with significant p-value for NFMIs only. **Conclusion:** Conclusion: Obesity (BMI ≥30) in patients with TID on GMPI is associated with lower FMI and NFMIs. Our findings will contribute to body of data favoring obesity paradox and reverse epidemiology in patients with CAD. In view of growing controversies about impact of obesity upon outcomes in patients with CAD, larger prospective trials are warranted. **References:** None.

EP-0187

Prognostic Value of Stress Gated MPI SPECT and Coronary Artery Calcium Score in Patients with Diabetes Mellitus

M. Havel[1], *M. Kaminek*[1,2], *P. Koranda*[1], *L. Quinn*[1], *I. Metelkova*[1], *M. Budikova*[1], *L. Henzlova*[1], *V. Kincl*[2];
[1]*Department of Nuclear Medicine, Faculty of Medicine and Dentistry, Palacky University Olomouc and University Hospital Olomouc, Olomouc, CZECH REPUBLIC,* [2]*International Clinical Research Center, Center of Molecular Imaging, Brno, CZECH REPUBLIC.*

Aim/Introduction: Patients with diabetes mellitus (DM) are in an increased risk of cardiovascular disease and cardiac death. Assessment of prognosis in such subjects could be essential for adequate therapy to minimise eventual unfavourable outcome. The aim of this study was to assess impact of Myocardial perfusion imaging (MPI) SPECT and its combination with coronary artery calcium score (CACS) for such purposes. **Materials and Methods:** We analysed retrospectively results of stress gated MPI SPECT and CACS evaluation in 334 patients with DM (average age 65 ± 10 years, 211 males). Adverse cardiac events as cardiac death, myocardial infarction (MI) or necessity of revascularization were recorded in this population and prognostic value of examination were statistically evaluated. **Results:** We recorded 77 CE during the median follow-up period of 17 months. CE were more often in patients with detected ischemia on gated SPECT MPI (75.3% vs. 15.2%, P < 0.0001), the CACS was significantly higher in such patient, too (median 225 vs. 977, P<0.0001). One-year CE rate was 42.2% for patients with ischemia vs. 3.3% without ischemia detected, 24.7% for patients with CACS >1000 vs 6.0% for CACS ≤ 1000. One-year CE rate in patients with negative MPI SPECT and CACS >1000 was 7.9% vs. 1.9% in those with CACS ≤1000. **Conclusion:** Gated MPI SPECT and CACS are both non-invasive methods suitable for CE predictions in population of patients with DM. What is more important, in patients with negative gated MPI SPECT, CACS score helped additionally to identify subjects with unfavourable outcome. **References:** None.

EP-0188

Interpretation of coronary collateral by myocardial perfusion gated spect

S. Ozdemir[1], *A. Barutcu*[2], *Y. Z. Tan*[1], *E. Aksit*[2], *A. Duygu*[2], *F. K. Ozturk*[1];
[1]*Onsekiz Mart Universty Faculty of Medicine Department of Nuclear Medicine, Canakkale, TURKEY,* [2]*Onsekiz Mart University Faculty of Medicine Department of Cardiology, Canakkale, TURKEY.*

Aim/Introduction: Coronary collateral circulation(CCC) is a natural anostomosis in response to ischemia caused by severe or total occlusion in coronary circulation. Well developed coronary collaterals are thought to reduce the severity of ischemia and infarct. Myocardial perfusion scintigraphy(MPS) is an accurate technique for the simultaneous evaluation of left ventricular wall perfusion, motion and thickening. For this reason the aim of this study was to retrospectively evaluate the effect of collaterals on myocardial perfusion, wall motion and thickening. **Materials and Methods:** Study patiens were retrospectively selected among patiens who underwent myocarial perfusion gated SPECT imaging and coronary angiography within 3 months, between 2015-2018. Only the patiens witj stenosis ≥80% in at least one of the major coronary arteries were included in this study. In total 96, patiens (69 men and 27 women, with a mean age of 63.12 ± 10.77 years) were included in the study. The patients were divided into two groups in accordance with coronary angiography results: Group1: who had not-well-developed collateral arteries (Rentrop grade 0-1) (n = 58). Group2: who had well-developed collateral arteries (Rentrop grade 2-3) (n = 38). **Results:** There were no statistically significant difference in summed stress score(p=0,531), summed difference score (p=0,634), wall motion score(p=0,957) and wall thickening score (p=0,717) parameters between the patients with and without CCC groups. **Conclusion:** Our study showed that CCC with different Rentrop grades, as shown by CAG, had no significant correlation with myocardial perfusion defined by MPS. **References:** None.

EP-0189

Interreader Reproducibility Between A Conventional And A CZT/SPECT Camera In The Myocardial Perfusion Scintigraphy (MPS): A Multicentric Study

N. Mansour[1], *E. Reyes*[2], *G. Angelidis*[3], *P. Georgoulias* [3], *C. Anagnostopoulos* [4], *P. Bravo*[5], *I. Bruno*[6], *A. Guarneri* [6], *A. Flotats* [7], *F. Fuentes-Ocampo*[7], *R. Di Dato*[8], *F. Keng*[9], *L. Kessler*[10], *M. Papathanasiou* [11], *R. Sciagrà* [8], *P. Soman* [12], *S. Nekolla*[1], *C. Rischpler*[10];
[1]*Nuklearmedizinische Klinik des Klinikums rechts der Isar, Munich, GERMANY,* [2]*Royal Brompton Hospital, London, UNITED KINGDOM,* [3]*Nuclear Medicine Department, University of Thessaly, Larissa, GREECE,* [4]*BRFAA - Biomedical Research Foundation Academy Of Athens, Athens, GREECE,* [5]*University of Pennsylvania, Philadelphia, PA, UNITED STATES OF AMERICA,* [6]*Fondazione Policlinico Universitario - IRCSS- "A. Gemelli", Rome, ITALY,* [7]*Hospital de la Santa Creu i Sant Pau, Barcelona, SPAIN,* [8]*Nuclear Medicine Unit, Department of Experimental and Clinical Biomedical Sciences "Mario Serio", Florence, ITALY,* [9]*National*

Heart Centre, Singapore, SINGAPORE, [10]University Hospital Essen, Department of Nuclear Medicine, Essen, GERMANY, [11]Department of Cardiology, West German Heart and Vascular Center, University Hospital, Essen, GERMANY, [12]University of Pittsburgh Medical Center, Pittsburgh, PA, UNITED STATES OF AMERICA.

Aim/Introduction: CZT camera systems are currently growing in popularity as a non-invasive cardiac imaging tool. They were reported to have higher sensitivity, neverthelessthere is still insufficient data to compare this technology with conventional SPECT cameras, especially in terms of interreader- and intrapatient- reproducibility. **Materials and Methods:** 83 patients with an indication for MPS, each of whom were examined using a CZT camera (D-SPECT, Spectrum Dynamics) as well as a conventional SPECT camera (Siemens E.CAM or Symbia T, Siemens Medical Solutions) were included in this study. The patients were recruited in the period between March and September 2013 during the clinical routine in the University Hospital Klinikum rechts der Isar in Munich. For 10 patients, results of a cardiac catheterization were also available. Anonymous standard stress/rest reports including static images and images of the short and horizontal/vertical long axes and polar maps were then distributed to 15 international readers varying in expertise: (Group A), Five readers with experience in both D-SPECT and conventional SPECT; (Group B), five readers with extensive experience in conventional SPECT ; and (Group C), five readers without extensive interpretation experience of MPS. The reports were then evaluated with respect to image quality, artefacts, diagnosis and diagnostic certainty. The readers had no access to patient's clinical data. **Results:** Both group A (p_s<0.05) and group C (p_s<0.05) reported the CZT systems to deliver a significantly better image quality than conventional SPECT. Consistent with these observations, conventional-SPECT images showed more attenuation artifacts (p_s<0.05). In Group A, the images from 33/83 patients were non-evaluable due to poor image quality. In contrast to CZT-SPECT with only 7/83 patient images were non-evaluable (p_s<0.05). Notably, no significant differences were evident between CZT-SPECT and conventional-SPECT in the remaining artefacts: signal-to-noise-ratio, liver- and bowel-activity, and low myocardial counts. As to the interreader variability, the diagnosis results of groups A and B (readers with experience) differed significantly from that of group C (inexperienced) (p_s<0.05).However, the diagnosis results within the expert groups showed no significant differences between CZT-SPECT and conventional-SPECT. **Conclusion:** Collectively, this study demonstrates that CZT camera systems show higher image quality with evidently less attenuation artifacts. The assessment and detection of ischemia and/or scar within the groups were not affected by the imaging systemruling out, thus, the necessity of a special training for the evaluation of images when introducing a CZT camera. **References:** None.

EP-0190

IInvestigation of clinical factors affecting the myocardial blood flow and flow reserve using Tl dynamic SPECT with a CZT gamma-camerain limited patients with normal summed stress score

***S. Shiraishi**, F. Sakamoto, N. Tsuda, K. Ogasawara, M. Nakagawa, Y. Yamashita, S. Tomiguchi;*
Kumamoto University, Kumamoto-city, JAPAN.

Aim/Introduction: Relative myocardial perfusion imaging can underestimate or misdiagnose "balanced" ischemia in patients with significant coronary artery disease (CAD) or microcirculatory disorders due to other clinical risk factors. Recently, some studies have demonstrated improved diagnostic accuracy for detecting CAD by using absolute quantification of the myocardial blood flow (MBF) or the myocardial perfusion reserve (MPR). In this study, we evaluated clinical factors affecting myocardial blood flow and flow reserve in specifically limited to patients with normal myocardial perfusion SPECT (summed stress score<3). **Materials and Methods:** We selected 125 consecutive patients that underwent coronary angiography (CAG) and both adenosine stress and rest with ^{201}Tl dynamic SPECT to calculate MBF using a CZT semiconductor gamma-camera. The MPR in the entire left ventricular myocardium was calculated by dividing stress-MBF by rest-MBF from the dynamic SPECT. We analyzed the correlation between various clinical risk factors including the number of CAD and quantitative values (rest-/stress- MBF and MPR). **Results:** In the multivariate regression analysis, the rest-MBF values showed statistically significant correlation with male gender (r=-0.341, p=0.01), estimated glomerular filtration rate (eGFR) (r=-0.268, p=0.001), and left ventricular ejection fraction (LVEF) (r=0.290, p=0.019), the stress-MBF values with HDL-cholesterol (r=0.326, p=0.001), LVEF (r=0.290, p=0.003), age (r=-0.191, p=0.002), male gender (r=-0.285, p=0.011), and the number of CAD (r=-0.279, p=0.034), and the MPR correlated with the number of CAD (r=-0.543, p=0.001), eGFR (r=0.279, p=0.002), and age (r=-0.347, p=0.004), respectively. **Conclusion:** This study suggests that microcirculatory disorders due to age, gender, HDL-CHO, GFR in addition to CAD are also important factors that affect the myocardial blood flow and flow reserve. **References:** None.

EP-0191

SPECT-CT 16 Slices Myocardial Perfusion Imaging vs Prone Acquisition In Minimizing Artifactual Defects Interpretation

***E. Papadaki**, N. Kapsoritakis, O. Bourogianni, M. Stathaki, A. Tsaroucha, M. Alefantinou, S. Koukouraki;*
Heraklion University Hospital, Iraklion - Crete, GREECE.

Aim/Introduction: Myocardial perfusion imaging (MPI) for coronary artery disease assessment often has false positive results due to attenuation correction mainly in the inferior and anterior myocardial wall. The aim of the study is to evaluate

myocardial perfusion attenuation defects using SPECT/CT 16 slices vs prone SPECT imaging for excluding false positive results in order to use it as a gate keeper for patients (pts) who will benefit from coronary angiography. **Materials and Methods:** From 12/2018-3/2019, 188 pts underwent a treadmill 99mTc-tetrofosmin MPI. 84/188 pts (group A) were subjected to scintigrams using a low-dose SPECT-CT γ-camera and 104 pts (group B) underwent SPECT in supine and prone position in order to clarify the inferior/anterior wall perfusion defects. The choice of each modality was random. The final diagnosis was based on coronary angiography. **Results:** Group A: In 68/84 pts (80.95%) SPECT/ CT managed to correct the perfusion defect qualitatively and quantitatively with an increase in Summed Stress Score (SSS:10-32). There was no need for an additional rest MPI study. 16/84 pts (19.04%) underwent a rest SPECT-CT. 4/16 had an unknown infarction of the inferior wall, 6/16 had ischemia of the inferior wall and 6/16 showed attenuation and scar. Group B: In 77/104 pts (73.1%) prone SPECT MPI managed to correct the perfusion defect (increase SSS 8-25). 27/104 pts (26.9%), underwent rest MPI study. 5/27 pts had an unknown infarction of the inferior wall, 8/27 pts had ischemia of the inferior wall and 7/27 pts showed attenuation and scar. In the remaining 7/27 pts prone interpretation was abnormal in spite of normal coronary angiography. **Conclusion:** The addition of SPECT/CT to stress MPI decreases false positive rates. Moreover it has a key benefit in reducing the number of rest studies and minimizing radiation exposure, investigation time, costs and unnecessary referrals to coronary angiograms. **References:** None.

EP-0192

Sensitivity of the treadmill stress test according to the risk stratification by clinical evaluation of the stable corany artery disease, confirmed whether by myocardial perfusion scan and coronary angiography

M. Habbeche[1], *Q. Naili*[1], *M. Abdi*[1], *B. Said*[1], *D. Djermane*[2];
[1]*Centre d'imagerie scintigraphique, Blida, ALGERIA,* [2]*Service de cardiologie CHU Mustapha Bacha, Alger, ALGERIA.*

Aim/Introduction: The treadmill stress test (TST) is know as one of the first line diagnostic test to detect the stable coronary artery disease (SCAD), due to its simplicity and lower cost.The aim of this study is to evaluate the sensitivity of this test related to the risk stratification by clinical evaluation of the SCAD, confirmed whether by myocardial perfusion scan (MPS) and coronary angiography (CA). **Materials and Methods:** From 2016 to 2018, 52 patients (41males and 11femele, sex ratio 3,7) has been enrolled for this study.The inclusion criteria were: Only the TST performed according the Bruce protocol has been validated . All the patients have a reversible ischemia more than 10% (2segments) detected on MPS. All the patients have a positive coronary angiography (stenosis ≥to 50%) performed less than 1month. Are excluded from the study patients with dilated cardiomyopathy. The patients were classified regarding the risk stratification by clinical evaluation (2013 ESC guidelines) on 3 groups :Pre test probablily (PTP) 16-65% , 66-85%, and >85% **Results:** Overall, the TST was positive on 38patients and negative on 14 (sensitivity= 73%). According to the PTP, the results were:Group PTP 15-65% :Over 14patients, 9 were positive TSTand 5 negative (Sensitivity =64%)Over the 5 negative TST, 4had single vessel disease involvement on CA, and 2 have a large reversible ischemia ≥ than 5 segments on MPS in LAD territory.Group PTP 66-85% : Among 28 patients , 21 were positive TST and 7negative (75% of sensitivity)On the negative TST group , all patients have multi-vessel involving (≥2) on CA and 2 have a large reversible ischemia (7/17 segments) on MPS in LAD territory.PTP >85% :Of the 10patients, 8 were positive TST and 2 négative TST (Sensitivity 80%)Among the patients with negative TST, all have ≥4 segments reversible ischemia on MPS and multi-vessels disease (≥2) involving in CA **Conclusion:** The overall sensitivity of the TST in patients with confirmed SCAD is 71% (67% in the literature (ACC/AHA Guidelines 2002)). This sensitivity increases with the initial clinical risk of coronary artery disease, it is therefore higher in case of high risk, or high intermediate. Some of the patients with negative TST , have a large extent of ischemia, with sometimes, a multi-vessel involving, especially in patients classified at high clinical risk of coronary disease. Therefore, a negative TST in high-risk patients does not rule out sometimes extensive or multi-vessel coronary disease **References:** None.

EP-0193

Could end-diastolic images in myocardial perfusion imaging performed on CZT camera determinate significant changes in ischemia assessment in Patients with diastolic dysfunction compared to Patients with normal diastolic function?

M. Bonacina[1], *D. Albano*[1], *M. Bertoli*[1], *F. Dondi*[1], *R. Durmo*[1], *A. Mazzoletti*[1], *E. Cerudelli*[1], *P. Bellini*[1], *M. Gazzilli*[1], *F. Bertagna*[2], *R. Giubbini*[2];
[1]*ASST Spedali Civili, Brescia, ITALY,* [2]*Università degli Studi di Brescia, Brescia, ITALY.*

Aim/Introduction: to evaluate in myocardial perfusion imaging (MPI) performed on a CZT camera if end-diastolic images can determinate significant changes in ischemia assessment in Patients with diastolic dysfunction compared to Patients with normal diastolic function. **Materials and Methods:** from October 2018 to March 2019 we included 34 patients without a previous diagnosis of CAD and without left bundle branch block, pacemaker or atrial fibrillation. Diastolic function was defined using echocardiogram as reference. Seventeen Patients (12 M, 5 F, mean age 68,5) had diastolic dysfunction (Group 1) and 17 (8 M, 7 F, mean age 75) had normal diastolic function. All images were acquired on a CZT camera, elaborated for both Groups with end-diastolic (Method 1) and routinely all-phases software (Method 2), and evaluated by 2 blind expert readers, who had to rate images with an ischemia scoring system (0 no ischemia, 1 mild, 2 moderate, 3 severe). For each reader, we registered if ischemia scoring increased, reduced or unchanged in both Groups with Method 1 compared to Method 2. A Yates test was

performed to compare the proportions of scoring changes in both Groups for both readers. **Results:** for reader 1 in Group 1, Method 1 increased ischemia score in 52,94% (9/17 Patients), was concordant in 29,41% (5/17 Patients) and reduced the ischemia in 17,65% (3/17); while in Group 2, Method 1 increased ischemia score in 41,18% (7/17 Patients), was irrelevant in 47,06% (8/17 Patients) and reduced ischemia in 11,76% (2/17). For reader 2 in Group 1, Method 1 increased ischemia score in 47,06% (8/17 Patients), was stable in 29,41% (5/17 Patients) and reduced ischemia in 23,53% (4/17); while in Group 2, Method 1 increased ischemia in 35,29% (6/17 Patients), was stable in 52,94% (9/17 Patients) and reduced ischemia in 11,76% (2/17). For both reader there was a significantly higher rate of ischemia score increasing in Group 1 compared to Group 2 with Method 1 (p 0,002 for reader 1 and p<0,001 for reader 2 respectively); there was no significant difference between the two readers scoring variation with Method 1 compared to Method 2 both in Group 1 (p 0,33) and in Group 2 (p 0,44). **Conclusion:** end-diastolic images caused major changes in ischemia assessment in myocardial perfusion imaging on CZT camera in Patients with diastolic dysfunction, further studies are needed to validate the clinical impact of these results**. References:** None.

EP-0194

Comparison of CZT-SPECT with A-SPECT and PETfor DiagnosingHemodynamically SignificantCoronaryArtery Disease: A Bivariate Meta-analysis

N. Dai, J. Ge;
Zhongshan Hospital of Fudan University, Shanghai, CHINA.

Aim/Introduction: This meta-analysis determined the diagnostic utility of single-photon emission computed tomography (SPECT) using cadmium-zinc-telluride (CZT) cameras (CZT-SPECT), positron emission tomography (PET) and conventional SPECT with Anger cameras (A-SPECT) versus FFR as a reference standard for detection of hemodynamically significant coronary artery disease (CAD) **Materials and Methods:** PubMed and EMBASE were searched for clinical studies comparing CZT-SPECT or A-SPECT or PET and FFR. Bayesian random effects analysis was used to compute pooled sensitivity, specificity, positive and negative likelihood ratios (LRs), and the summary receiver-operating characteristic curve of the index tests. The pre-test probability (PTP) ranges for each technique to rule-in or rule-out significant CAD were determined according to LRs. **Results:** On vessel-based analysis, CZT-SPECT had a similar sensitivity as PET (0.76 vs. 0.79, P=0.61) but higher sensitivity than A-SPECT (0.76 vs. 0.59, P=0.02); all CZT-SPECT, PET and A-SPECT demonstrated similar specificities (0.87 vs. 0.86 vs. 0.87, P>0.05), CZT-SPECT and PET showed trend of higher area under SROC (AUROC) than A-SPECT (0.86 and 0.89 vs. 0.83, P>0.05), but none of these achieved statistical significance. A-SPECT can rule-in and rule-out functionally significant CAD only when PTP is≥56% (48-63) and ≤ 27% (22-33), respectively. CZT-SPECT is able to rule-in functional CAD at a PTP ≥ 50% (40-60) and rule-out at a PTP ≤ 39% (32-44), indicating A-SPECT had relatively limited diagnostic power, especially in rule-out the functional CAD. The corresponding PTP values for PET were ≥ 51% (44-58) and ≤ 42% (32-54), respectively. **Conclusion:** CZT-SPECT demonstrated a similar sensitivity as PET but significantly higher sensitivity than A-SPECT in predicting FFR determined significant CAD; all CZT-SPECT, PET and A-SPECT had similar specificities on per-vessel analysis. Besides, they have different optimal performance ranges for ruling out and in functionally significant CAD. **References:** None.

EP-0195

Clinical impact of the use of ultralight exercise with adenosine stress myocardial perfusion imaging

***E. Tateishi**, K. Kiso, Y. Kawahara, S. Higuchi, T. Nishii, Y. Ota, A. Kono, T. Fukuda;*
National Cerebral and Cardiovasclar Center, Suita, Osaka, JAPAN.

Aim/Introduction: Adenosine is commonly used in pharmacological stress myocardial perfusion SPECT imaging (MPI); on the other hand, the side effects of adenosine occur with a high frequency. Recently, the combination of low-level exercise during adenosine infusion has been increasingly performed for the reduction of the adenosine-related side effects. However, the utility of very easy exercise with almost no intensity; ultralight exercise (UL-Ex), during adenosine infusion has not been well studied. We investigated the clinical impact of two types of UL-Ex in combination with adenosine stress MPI by evaluating the incidence of the side effects. **Materials and Methods:** Seven hundred and twenty-seven patients (68.7% male, mean age 76.3±9.0, range 27-96 years) underwent adenosine stress MPI with UL-Ex. Either supine leg ergometer with zero intensity (SE group, n=667) or handgrip exercise with 0.7kg strength (HG group, n=60) was performed during adenosine infusion. Adenosine was given as a continuous infusion of 120 micrograms/kg/min for 6 minutes. One hundred sixty patients undergoing adenosine stress MPI without any exercise were evaluated as controls. **Results:** Of the 727 patients who underwent adenosine stress testing with UL-Ex, 415 patients experienced the side effects of adenosine (57.1%), which was significantly lower than the incidence of the side effects in the control group (81.3%). The majority of the side effects were minor, such as chest discomfort (41.4%), flushing (30.9%), and headache (13.4%). Intermittent atrioventricular block was observed in 9 cases. The variability of systolic blood pressure was significantly smaller in patients with UL-Ex than in controls (-3.6±1.6 mmHg vs. -9.8±1.9 mmHg, p=0.014). No major side effects occurred requiring the interruption of adenosine infusion in either the SE or HG group. Comparing the SE and HG groups, there was no significant difference in the incidence of the side effects (57.6% vs. 51.7%, p=ns). **Conclusion:** Regardless of the type of exercise, the use of UL-Ex during adenosine stress testing is beneficial for the reduction of the adenosine-related side effects including drops in blood pressure. As a result, the addition of UL-Ex during pharmacological stress enables it to be performed more safely in patients with hypotension or

cerebrovascular diseases. Moreover, handgrip exercise is easy, and anyone can perform it in any position. It may be possible to apply UL-Ex in vasodilator stress myocardial perfusion imaging with not only SPECT but also other modalities. **References:** None.

EP-0196

Does prone myocardial perfusion imaging improve inferior and anterior perfusion defects?

Z. AL Bimani[1,2], *K. Whinfield*[1], *R. Klein*[1], *W. Zeng*[1];
[1]*University of Ottawa, Ottawa, ON, CANADA,* [2]*Oman Medical Speciality Board (OMSB), Muscat, Sultanate of Oman, OMAN.*

Aim/Introduction: Myocardial perfusion Imaging (MPI) traditionally images patients in supine position. The aim of this study was to assess the extent of perfusion defects improved by prone imaging and identify the subgroup of patients who might benefit the most from having prone images. **Materials and Methods:** Rest and stress supine and stress prone from 639 consecutive patients (age: 64.7±11.1, F:M=269:370) with suspected or known CAD were reviewed. Summed stress score (SSS) of the supine and prone and rest (SRS) of the inferior wall (3/17 segments) and the anterior wall (3/17 segments) was obtained on 4DM SPECT (INVIA, Ann Harbor, MI). The difference in SSS between the supine and prone images (DSSS) was evaluated for correlation with sex and BMI using Student's t test and Pearson's coefficient. **Results:** The mean summed score of the inferior wall was 1.72 ± 2.21, 1.64 ± 2.20 and 0.60 ± 1.59 for rest, stress supine and stress prone, respectively. The mean DSSS was 1.04 ± 1.67 ($p<0.001$), with a statistical difference between male and female (1.23 ± 1.76 vs. 0.78 ± 1.49, $p= 0.001$). There were similar findings in the infero-lateral wall. The mean summed score of the anterior wall was 0.50 ± 1.33, 0.42 ± 1.24 and 0.30 ± 1.09 for rest, stress supine and stress prone, respectively. The mean DSSS was 0.12 ± 0.86, with no statistical difference between sexes ($p= 0.61$). Of the 639 patients, 29 (5%) had larger, 317 had equal (50%), and 293 (45%) had smaller stress scores in the inferior wall on prone compared to supine. The median BMI was 27.1. The mean DSSS in the inferior wall was similar between BMI≥27.1 (0.94 ± 1.66) and BMI<27.1 (1.12 ± 1.65) with no statistical significance ($p=0.18$). There was negligible correlation between DSSS and BMI ($r=-0.01$, $p=0.015$). **Conclusion:** The addition of prone acquisition improves soft tissue attenuation artifact in the inferior wall region, as demonstrated by decreased perfusion defect score, in both male and female patients, but not in the anterior wall. BMI and sex do not predict changes in inferior wall defect scores by prone imaging. **References:** None.

EP-0197

Incidental Findings on Myocardial Perfusion SPECT/CT Images

I. El Bez, *R. Tulbah*, *I. Munir*, *F. Alghamlas*, *M. Alharbi*;
KFMC, nuclear medicine department, Riyadh, SAUDI ARABIA.

Aim/Introduction: Myocardial perfusion SPECT-CT plays a crucial role in the diagnosis of coronary artery disease, providing a noninvasive tool to monitor ischemia and infarction. The findings can have a profound impact on diagnosis and management in these patients. However, incidental noncardiac findings on low dose CT can also affect management. The intent of this study was to illustrate several subtle noncardiac abnormalities within nuclear cardiac imaging that can have an impact on patient management and follow-up. **Materials and Methods:** In this retrospective monocentric study, from December 2017 to April 2019, 200 patients referred for myocardial perfusion were reviewed. **Results:** Our analysis focused on 200 patients referred for myocardial perfusion. The overall prevalence of incidental extracardiac abnormalities was 47% (94 patients). Two patients (1%) have been identified with malignant lesions that have been taken care, one patient with lung cancer and one patient with breast cancer. For 20 patients (10%), extracardiac abnormalities explained the symptoms that motivated the realization of the myocardial TEMP. The most common abnormalities were micronodules and pulmonary nodules (70% of patients) who were most often classified as indeterminate and required follow-up, followed by hiatal hernia (20% of patients), thyroid nodules tracer avid (8% of patients), renal cycts (4% of patients), breast lesion (1% of patients), calcified axillary nodules (1% of patients), adrenal lesions (1% of patients), and liver lesions (1% of patients). **Conclusion:** The lack of interpretation of extracardiac structures, on the scanner performed for the attenuation correction, could cause delays diagnosis and management of malignant lesions. On the other hand, numerous abnormalities detected, which finally are benign, lead to the realization of additional investigations with dosimetric consequences and significant economic outcomes. **References:** None.

EP-11
Dosimetry: Dosimetry

October 12 - 16, 2019 e-Poster Area

EP-0198

Fast heterogeneous convolution algorithm used in absorbed dose calculation for beta emitters

A. Vergara Gil[1], *E. Mora Ramirez*[1,2], *J. Pouget*[3], *P. Kotzki*[3,4], *L. Santoro*[4], *E. Deshayes*[4,3], *M. Bardies*[1];
[1]*CRCT, UMR 1037, INSERM, Université Toulouse III, Paul Sabatier, Toulouse, FRANCE,* [2]*Universidad de Costa Rica, Escuela de Fisica, CICANUM, San Jose, COSTA RICA,* [3]*Institut de Recherche en Cancérologie de Montpellier, Montpellier, FRANCE,* [4]*Département de Médecine Nucléaire, Institut Régional du Cancer de Montpellier, Montpellier, FRANCE.*

Aim/Introduction: Absorbed dose calculations algorithms may be designed depending on the relationship between

activity spatial sampling and radiation range. The aim of this work is to propose a fast-heterogeneous convolution algorithm (FHCA) and compare dosimetric results with local energy deposition (LE), homogeneous convolution (FFT) and Monte Carlo (GATE) modelling, i.e. the 3 most frequently proposed approaches in a context of clinical dosimetry, for a medium range beta emitter such as ^{177}Lu. **Materials and Methods:** FHCA consists in a matrix convolution using an homogeneous absorbed dose kernel (HDK). The HDK was calculated using the dose point kernel approach[1] with GATE, up to 2cm from central voxel and activating the ion source implementation. This produced a 9x9x9 kernel matrix, small enough to be used in matrix convolution. While performing the first convolution, another kernel was considered to determine the influence of patient density (from the CT image) in the source-target path. The influence of the media for the HDK was removed by density multiplication. Absorbed dose rate results were compared in a context of clinical dosimetry of Lutathera[2] for the four mentioned algorithms, by considering only electronic emissions[3]. **Results:** For liver, spleen and L/R kidneys, relative differences to Gate in absorbed dose rate results varied from -6.6 to 3.1% for LE, -1.1 to 9.1% for FFT and -1.4 to 4.5% for FHCA, among all organs, for all time points. Calculation time for all time points were negligible for LE and FFT, lower than 10 minutes for FHCA but required more than 6 hours for Gate (on the same computer). **Conclusion:** Preliminary results in terms of accuracy vs. speed are encouraging. Further validation in more heterogeneous media (lungs, bones) is ongoing. **References:** 1Franquiz et al. Med Phys 30, 1030 2003; 2Mora-Ramirez et al. Eur J Nucl Med Mol Imaging 45(Suppl 1), S180 (2018); 3Eckerman and Endo. Radionuclide Data and Decay Schemes, SNM 2008.

EP-0199

Analysis of nuclide distributions of pre-therapeutic thyroid scintigraphies with I-131 and Tc-99m in comparison to intra-therapeutic I-131 scintigraphies in the context of radioiodine therapy in benign thyroid dysfunctions by means of parametric evaluation and 3D imaging

U. Lützen, S. Meyenburg, Y. Zhao, M. Marx, M. Jüptner, M. Zuhayra;
UKSH, Kiel, GERMANY.

Aim/Introduction: Prior to each radioiodine therapy (RIT), a thyroid scintigraphy with Tc-99m pertechnetate (Tc-99m) is made for the diagnosis of benign thyroid dysfunction. The radioiodine study with iodine-131 serves for the individual determination of the therapy activity. As is known, the two radiopharmaceuticals differ in their pharmacokinetics and dynamics. The aim of this work was to compare the differences in the intensity distribution of the tracers visually and by a new computer-aided quantification of the pre- and intratherapeutic scintigraphies by means of a subtraction analysis and a 3D representation. **Materials and Methods:** Pre- and intratherapeutic scintigraphies were performed with Tc-99m and iodine-131 in 48 patients (age: 42-94 years, median age: 74 years, 36 women and 12 men) suffering from Graves' disease (10), disseminated (5), unifocal (18) and multifocal autonomy (15). The image matrix and size of the scans were normalized and standardized. The intensity distribution of the tracers was calculated parametrically and displayed as 3D images. The processed scans were pairwise compared visually and computerized. **Results:** Pretherapeutic Tc-99m versus iodine-131 intratherapeutic scan: Visually, in two cases (4.2%) a comparable intensity distribution was shown, in 46 cases (95.8%) the intensity distribution was different. The computer analysis showed in 11 cases (22.9%) an equal intensity distribution, in 37 cases (77.1%), the intensity distribution was divergent. Pretherapeutic iodine-131 (radioiodine test scan) versus iodine-131 intratherapeutic scan: In seven cases (14.6%) a similar intensity distribution was visually evident; in 41 cases (85.4%) the intensity distribution was unequal. The calculation showed in 34 cases (70.8%) a consistent intensity distribution, in 14 cases (29.2%), the intensity distribution was different. **Conclusion:** The developed software allows an easy and reliable qualitative and quantitative comparison of the different scans. As it was to be expected our results reveal a good visual and especially a better computational comparability of the two I-131 scans in comparison to the pretherapeutic Tc-99m scan and I-131 scan performed intratherapeutically. Tc-99m scintigraphy provides a helpful guide to assess the function of the thyroid in order to make the preliminary diagnosis. We recommend the additional pretherapeutic I-131 scintigraphy in clinical routine that provides valuable additional information to verify and adjust the diagnosis by using the new program, and thus to optimize the determination of the individual therapeutic dose leading to a better outcome of the treatments of the patients. **References:** None.

EP-0200

Estimation Of The Absorbed Dose In Patients Treated With Ra223

M. Alonso Rodriguez, C. Andrés Rodríguez, J. Gómez Hidalgo, C. Gamazo Laherrán, B. Pérez López, V. De la Llana Granja, M. A. Ruíz Gómez, M. Agulla Otero, P. J. Turbay Eljach, N. Álvarez Mena, R. Torres Cabrera, R. Ruano Pérez;
Hospital Clínico Universitario de Valladolid, Valladolid, SPAIN.

Aim/Introduction: Preliminary experience acquired in estimating the absorbed dose in metastatic bone lesions of prostate cancer patients treated with Ra223 (Xofigo) in our center is shown. **Materials and Methods:** We studied a total of 50 lesions of 15 patients treated with Ra223 (Xofigo, Bayer Pharmaceuticals Inc., Germany). The usual treatment procedure is 6 intravenous administrations (with a separation between them of at least four weeks) of Ra223 for 55KBq/kg. In average, the activity injected was 4.0MBq. The images are acquired with an SPECT-CT system Siemens Symbia T2, which has been previously characterized in all its physical parameters. Prior to the first Ra223 administration, a bone scintigraphy and a SPECT-CT with Tc99m are adquired for the morphological characterization (size, density and depth) of the lesions. 48 and 168 hours after Ra223 administration, 20 minutes planar adquisitions are

taken (acquisition window of 82 keV ± 20%, Medium energy collimator). Through image analysis software, each lesion is localized in Ra223 images using the bone scintigraphy as a reference and the activity of Ra223 is quantified in each lesion. Subsequently, the absorbed dose and the effective half-life of the isotope are estimated following the MIRD methodology. Considering that a relative biological effectiveness (RBE) of 5 for alpha particles, the RBE-weighted absorbed dose (D_{RBE}) is also calculated. **Results:** The RBE-weighted absorbed dose in each lesion per Ra223 injection was, on average, 9.45±2.50 Gy, finding a big difference between lesions with a very low uptake (D_{RBE} below 1.25 Gy per injection) and other with a high absorbed dose (up to 27.5 Gy per injection). The resulting average D_{RBE} for the complete treatment was 56.7±15.0 Gy for each lesion. The half-life of the radionuclide in the lesion was 6.2±0.8 days. Due to the low activity injected, the number of Ra223 accounts detected in the lesion was sometimes below limit of detection with respect to the background, which made it difficult to accurately characterize the absorbed dose. On the other hand, intestinal uptake present in the 48h image can make it impossible to estimate the effective half-life in certain lesions. **Conclusion:** The procedure and preliminary results obtained in our center in the dosimetry of metastatic lesions treated with Ra223 are presented. The values obtained are similar to other preliminary studies about of dosimetry in this kind of treatments. **References:** None.

EP-0201

Partition method-based treatment planning in radioembolization with microspheres: software for tumor to normal tissue ratio calculation

F. Mañeru, D. Martínez, A. Fernández, L. Bragado, F. Caudepón, R. Estrada, N. Fuentemilla, M. Ribelles;
Complejo Hospitalario de Navarra, Pamplona, SPAIN.

Aim/Introduction: The Partition Method is a widely used option for dose estimations in liver radioembolization treatments with microspheres and its key parameter is the tumor to normal tissue uptake ratio (TN). The correct use of this method requires an accurate identification of the interface between health and tumor regions. This process has a high dependence on the chosen criteria to do so and even the user. The presented software offers a reproducible way to delimiting both regions and their uptake ratio. **Materials and Methods:** Tumor to normal tissue ratio is estimated from pre-treatment ^{99m}Tc macroaggregated albumin SPECT study (^{99m}Tc MAA SPECT). One of the bases of the partition method is that high, intermediate and low uptake regions match tumor, normal liver and non-irradiated areas respectively. From previously estimated liver and tumor volumes, the software obtains the thresholds count values corresponding to their boundaries. Then, total counts in each region are integrated and TN is derived as the quotient between uptake by volume in both regions. For all this process, software has been developed with Python code. The software is presented as an executable file and no previous installation is required. Program input data are the volumes of the healthy liver and the tumor and also the ^{99m}Tc MAA SPECT dicom file. All this information is processed and the obtained uptake threshold values are showed in order to make a visual validation of them in the SPECT-CT images if desired. Voxel size is also showed as additional information. The final output of the software is the tumor to normal tissue ratio. All the process can be delivered in a few seconds in a standard PC. **Results:** This tool allows a very reproducible estimation of tumor to normal tissue ratio and therefore of tumor and liver absorbed doses. Calculations are automatic and the only possible user dependence is derived from differences in previous volume measurements. For a safe use of the software, the threshold based segmentation validity is needed. This assumption may not be true in cases where SPECT is not an exact surrogate of the spheres distribution: widely spread metastases, presence of high necrosis areas or extrahepatic activity shunts. **Conclusion:** Simple and intuitive software is presented for the implementation of the Partition Method in hepatic radioembolization therapy. Standard calculation tools like this should help to reduce the derived from the user or institution dependence. **References:** None.

EP-0202

Different settings for the calculation of absorbed doses in therapy with radioactive somatostatin analogues

E. Grassi[1], E. Page[2,3], D. Finocchiaro[1,4], A. Versari[1], A. Filice[1], L. Braglia[1], M. Iori[1], J. Tipping[2], F. Fioroni[1];
[1]AUSL - IRCCS di Reggio Emilia, Reggio Emilia, ITALY,
[2]The Christie NHS Foundation, Manchester, UNITED KINGDOM, [3]University of Manchester, Manchester, UNITED KINGDOM, [4]Università di Bologna, Bologna, ITALY.

Aim/Introduction: the work was focussed on the comparison between the absorbed dose results obtained using different combinations of anthropomorphic phantoms (ORNL-type phantoms based on the Oak Ridge models, or NURBS-type phantoms based on the masses defined by ICRP89) and radionuclide decay dataset to produce the dose factors (legacy data versus decay series). These combinations are the same implemented in commercial software, such as OLINDA/EXM 2.0 and DOSEFX. **Materials and Methods:** a real dataset of 39 patients enrolled in a clinical trial for therapy with radioactive somatostatin analogues (labelled with ^{90}Y and ^{177}Lu) was considered. The absorbed dose calculation (for ^{90}Y and ^{177}Lu) was performed using the combinations: A) Legacy data and ICRP89 phantoms; B) Legacy data and ORNL phantoms; C) Decay series and ICRP 89. Input data for every combination were the same numbers of disintegrations for the time-activity-curves of liver, kidneys and spleen. The dataset was personalised for the real patient data (gender, weight of body and organs at risk) in all combinations for a more realistic approach. The statistical analysis was performed using R 3.3.3, studying also the Lin's agreement correlation coefficient for the comparisons: B versus A and C versus A for 90Y and 177Lu and for each organ. Confidence intervals (CI) were calculated considering a 0.95

confidence level. **Results:** Considering the Lin's coefficients for the various pairs of data, the concordance of the paired data is very high, also in relation to the respective CI, showing very similar results coming from different settings chosen for calculations. The coefficients lie in the range: for liver 0.82-0.99; for kidneys 0.97-0.99; 0.94-0.97. In all cases the values are included in the CI. **Conclusion:** the high agreement of the results obtained with different patterns of radionuclide decay data and phantoms show that the calculation of absorbed dose for the analysed organs (liver, spleen and kidneys) and for the two considered isotopes produce concordant values. **References:** [1] Josefsson A, Hobbs RF et al: Comparative Dosimetry for 68Ga-DOTATATE: Impact of Using Updated ICRP Phantoms, S Values, and Tissue-Weighting Factors; J Nucl Med 2018; 59:1281-1288 ; [2] - Cristy M, Eckerman KF. Specific Absorbed Fractions of Energy at Various Ages from Internal Photon Sources. III. Five-Year-Old. Oak Ridge, TN: Oak Ridge National Laboratory; 1987:1-42. ORNL/TM-8381/V3; [3] - Stabin M, Siegel JA RADAR Dose Estimate Report: A Compendium of Radiopharmaceutical Dose Estimates Based on OLINDA/EXM Version 2.0 J Nucl Med 2018; 59:154-160.

EP-0203

^{64}Cu/^{225}Ac-DOTA-rituximab internal dosimetry in mice using image-based Monte Carlo simulation

S. Woo[1,2], *W. Kim*[1], *C. Lee*[2], *I. Lim*[2], *K. Song*[3], *S. Lim*[2];
[1]*Division of applied RI, Korea Institute of Radiological and Medical Sciences, Seoul, KOREA, REPUBLIC OF,* [2]*Department of Nuclear Medicine, Korea Institute of Radiological and Medical Sciences, Seoul, KOREA, REPUBLIC OF,* [3]*Department of Urology, Korea Institute of Radiological and Medical Sciences, Seoul, KOREA, REPUBLIC OF.*

Aim/Introduction: Rituximab is used for non-Hodgkin's lymphoma, chronic lymphocytic leukemia and other autoimmune disease types of cancer. ^{64}Cu labeled DOTA-rituximab agent can be acquired PET image for non-Hodgkin's lymphoma (NHL) patients to monitor lymphoma therapy. The aim of this study was the evaluation of ^{64}Cu and ^{225}Ac labeled DOTA-rituximab internal dosimetry using Monte Carlo simulation. **Materials and Methods:** ^{64}Cu-DOTA-rituximab was administered intravenously (263 ± 32.0 μCi) in a mouse xenograft model (n=3). Small animal PET imaging was acquired on a dedicated small animal PET/CT system (Inveon™, Siemens Preclinical Solution, Knoxville, TN). PET data were acquired a 3-time points after the ^{64}Cu-DOTA-rituximab administration (2, 24, 48 hours). ^{64}Cu-DOTA-rituximab residence times were calculated via time-activity curves of the defined region of interest (ROI). Image-based internal dosimetry was calculated by residence time and Monte Carlo based S-value. S-value was calculated by Geant 4 Monte Carlo simulations. S-value was calculated self irradiation as well as cross irradiation with liver, kidney and tumor region. ^{225}Ac-DOTA-rituximab internal dosimetry was calculated by ^{64}Cu-DOTA-rituximab residence time and ^{225}Ac S-value which was include all decay chain (^{221}Fr, ^{217}At, ^{213}Bi, ^{213}Po, ^{209}Tl, and ^{209}Pb). The absorbed dose in all decay chain was summed up after applying weighting factors in the two possible pathways of the ^{225}Ac decay, 2 % for ^{209}Tl and 98 % for ^{213}Po. **Results:** ^{64}Cu-DOTA-rituximab self irradiation in live, kidney, and tumor were 2.12E-02, 6.77E-02, and 3.28E-01 mGy-g/MBq-hr, respectively. ^{225}Ac-DOTA-rituximab self irradiation in live, kidney, and tumor were 5.01E+00, 1.65E+01, and 2.75E+01 mGy-g/MBq-hr, respectively. The ^{64}Cu-DOTA-rituximab absorbed dose in liver, kidney, and tumor were 2.08E-02, 3.45E-02, and 1.05E-01 mGy-g/MBq, respectively. The ^{225}Ac-DOTA-rituximab absorbed dose in liver, kidney, and tumor were 2.08E-02, 3.45E-02, and 1.05E-01 mGy-g/MBq, respectively. Comparison of the tumor absorbed dose of ^{225}Ac labeled DOTA-rituximab has 58.7 fold change to ^{64}Cu-DOTA-rituximab tumor absorbed dose. **Conclusion:** In this study, evaluates the image-based ^{64}Cu and ^{225}Ac DOTA-rituximab internal dosimetry using self- and cross-irradiation of Monte Carlo simulation. This result of study applies to the monitor the NHL patient treatment as well as their targeted alpha therapy using ^{225}Ac-DOTA-rituximab. **References:** 1. Plosker, Greg L., and David P. Figgitt. "Rituximab." Drugs 63.8 (2003): 803-843.2. Forrer, Flavio, et al. "Radioimmunotherapy with 177Lu-DOTA-rituximab: final results of a phase I/II Study in 31 patients with relapsing follicular, mantle cell, and other indolent B-cell lymphomas." Journal of Nuclear Medicine 54.7 (2013): 1045-1052.

EP-0204

Accuracy of personalized kidney dosimetry in ^{177}Lu-DOTA-TATE based on a simplified single-time-acquisition with segmentation-free small-volume method

X. Hou[1], *W. Zhao*[2], *J. Beauregard*[3,4], *A. Celler*[1];
[1]*Radiology Department, University of British Columbia, Vancouver, BC, CANADA,* [2]*Department of Physics and Astronomy, University of British Columbia, Vancouver, BC, CANADA,* [3]*Department of Medical Imaging and Oncology Division of Research Center, CHU de Québec – Université Laval, Quebec, QC, CANADA,* [4]*Department of Radiology and Nuclear Medicine and Cancer Research Center, Université Laval, Quebec, QC, CANADA.*

Aim/Introduction: Peptide receptor radionuclide therapy (PRRT) with ^{177}Lu- radiolabeled-DOTA-TATE is an effective treatment option for inoperable neuroendocrine tumours (NETs). To ensure patient safety and improve treatment efficacy, a personalized kidney dosimetry has been suggested as a routine procedure in PRRT clinical studies. Dosimetry, however, requires complicated and time-consuming procedures, including multiple scans and challenging organ/tissue segmentations. Our study aims to propose a practical, yet accurate, dosimetry method to simplify segmentation procedures and minimize number of scans. **Materials and Methods:** Twenty-nine NETs patient data with forty-three ^{177}Lu-DOTA-TATE therapy cycles were analyzed. Three SPECT/CT scans, acquired at about 4h(D0), 23h(D1) and 70h(D3) after injection, were performed to measure the radiotracer biokinetics in kidneys. Segmentation-free small-volume (SV) kidney dosimetry was estimated based on our in-house-developed automatic, observer-independent method

for SV localization. The accuracy of SV doses, based on different location selections, was evaluated by comparing them with those from whole-kidney (WK) segmentation. Meanwhile, to simplify SPECT acquisition schedules, for each dataset, both WK and SV doses, based on a single-time-point (STP) method using a mono-exponential curve with the population mean effective half-life and normalized to kidney activities at D0 or D1 or D3 points, were calculated. The accuracy of WK+STP and SV+STP methods was evaluated by comparing the WK dosimetry with 3 time point acquisitions (WK+3TP). **Results:** The kidney effective half-lives obtained from SV+3TP agreed to within 10% with those obtained from the WK+3TP. The ratios of SV doses to WK doses were equal to 1.8±0.2. Comparing different methods of SV location selections, independently selecting SV in images from each of the three acquisitions has been proved to be the most accurate approach. For STP dosimetry, the errors of both WK and SV doses, normalized to the D3 scan, remained below 10% relative to those estimated using 3 time points. While, STP doses, normalized to D0 and D1 scans could be > 40%. The linear correlation coefficient between SV+STP dose (normalized to D3) and WK+3TP dose was about 0.9 ($p<0.001$). **Conclusion:** An automatic observer-independent SV location selecting method was developed and its good accuracy has been demonstrated by comparing it with the WK dosimetry. For STP dosimetry, mono-exponential curve, with the population-based mean effective half-life, normalized to the late data points (48-72h for kidneys) produced <10% errors. The clear linear relationship between SV+STP dose and WK+FT dose demonstrated its potential for use in clinical studies. **References:** None.

EP-0205

A Geant4-based Voxel S-value Generator For Radiopharmaceutical Therapy

B. Bednarz;
University of Wisconsin, Madison, WI, UNITED STATES OF AMERICA.

Aim/Introduction: Radiopharmaceutical therapy is experiencing tremendous growth due to the incorporation of novel radiopharmaceuticals into the armamentarium of oncologists. Accompanying this growth is a renewed interest in performing voxel-level dosimetry calculations in patients to help guide clinical decision making and optimize therapeutic efficacy. While voxel S-values (VSVs) provide an efficient way of performing voxel-level dosimetry, the availability of VSVs in the literature is sparse and limited to only a few isotopes. The purpose of this work was to develop a generalizable, multi-radionuclide VSV generator for clinical use. **Materials and Methods:** All S-values (Gy/MBq-s) were calculated using the Monte Carlo code Geant4.9.6. Radioactive decay was simulated by evoking the G4RadioactiveDecay class which models the decay of more than 2000 radioactive nuclei using the ENSDF database. Point-isotropic sources were defined at the center of a water phantom with a voxel size of 0.5 mm x 0.5 mm x 0.5 mm. Four different isotopes were considered ^{131}I, ^{177}Lu, ^{90}Y, and the decay chain of ^{212}Pb. The VsVs included both electron and photon contributions. A total of $3.2x10^8$ decays were sampled to achieve a statistical uncertainty of less than 5% in all voxels considered. In addition, the impact of decay position within the source voxel on VSVs was investigated by sampling the source uniformly within the source voxel. **Results:** All VSVs agreed well with values published in the literature for the same voxel resolution. The percent differences between the source VSVs calculated in this work and those used in the NukDose software(1) were 2.8%, 6.1% and 7.4% for ^{131}I, ^{177}Lu, and ^{90}Y, respectively. Assuming ^{212}Pb is in secular equilibrium with its daughter products, the VSVs for the source voxel of ^{212}Pb was two orders of magnitude higher than the other isotopes. The maximum percent differences between VSVs determined from sampling the source at the center of the source voxel versus uniformly within it was 52%, 54%, and 5.2% for ^{131}I, ^{177}Lu, and ^{90}Y, respectively. These discrepancies are dependent on the voxel resolution and the endpoint energies of the beta-particle emitted during decay. **Conclusion:** The tool presented in this work can generate VSVs for any radionuclide, at any voxel resolution, and using sampling distribution within the source voxel. The ultimate goal of this work is to make VSVs more readily available to the scientific community for clinical use. **References:** (1) Kletting P et al. Z Med Phys. 2015 Sep;25(3):264-74.

EP-0206

PRRT: standardized activity and dose quantification for dosimetry of NETs patients treated with ^{177}Lu

S. Di Biaso[1], E. Tonini[2], G. Di Domenico[1], A. Turra[2], L. Uccelli[3], A. Barboni[2], D. Farina[3], L. Lodi[3], E. Zappaterra[3], S. Zaccaria[3], S. Romani[3], E. Govoni[3], S. Bertelli[3], D. Bortolotti[3], A. Massimi[3], M. Bartolomei[3];
[1]Department of Physics and Earth Sciences, University of Ferrara, Ferrara, ITALY, [2]Medical Physics Unit, Sant'Anna University Hospital, Ferrara, ITALY, [3]Nuclear Medicine Unit, Sant'Anna University Hospital, Ferrara, ITALY.

Aim/Introduction: The Council Directive 2013/59/EURATOM fixes the necessity for a personalized dosimetry for patients treated with radionuclides. In order to fulfil the directive, an absolute quantification of the absorbed activity in organs of interests and in lesions becomes necessary: a correct activity estimation is, in fact, the base for a correct dose evaluation. Therefore, initially, counts need to be corrected for scatter, attenuation and CDR (Collimator to Detector Response); then, the Calibration Factor (CF) has to be evaluated for ^{177}Lu. Recovery Coefficients (RCs) need to be computed to correct for partial volume effect (PVE). Finally, the absorbed dose estimation through MIRD scheme has been evaluated. The aim of this study was to provide a complete and accurate procedure for absorbed dose estimation for the NETs patients treated in Sant'Anna University Hospital in Ferrara, enrolled under the FENET-2016 protocol (EudraCT:2016-005129-35). **Materials and Methods:** Attenuation, scatter and CDR was corrected by Symbia NET Workflow (Siemens' software to reconstruct and analyse SPECT/CT projection images). Moreover, CF computation can be done

using a uniform Jaszczak phantom. Then, RC evaluation study has been performed with a Nema image quality PET phantom with both hot spheres and filled pockets, in order to study volumes of clinical interest up to 1000 ml. In the last part of the work, the complete evaluation of the absorbed dose in kidneys and lesions has been computed, through the use of OLINDA 2.0 software. **Results:** The Calibration Factor for our SPECT/CT is equal to 17.2±0.8 cps/MBq. Moreover, a complete curve RCs vs Volume (ml) for Lutetium, with volumes up to 1000 ml, has been evaluated; its fit has been used to correct PVE for all volumes of clinical interest. The absorbed dose and its uncertainty have been evaluated for kidneys and lesions. **Conclusion:** Nowadays, a correct dose evaluation is important in order to quantitatively study the efficiency of the PRRT therapy on patient with NETs. Moreover, the precise knowledge of the absorbed dose and its uncertainty can help in making a decision over a possible re-treatment, verified that the total absorbed dose does not exceed critical values reported in literature. In this work, a reproducible and accurate procedure for a complete dose evaluation has been presented, in order to achieve the most personalized possible image-based dosimetry, given the boundaries of the MIRD scheme. **References:** None.

EP-0207

Thresholds in SPECT image for quantification in the planning of TheraSpheres™ Y90 treatments

M. Barquero Sanz, C. Andres, M. Martin Veganzones, R. Ruano, J. Velasco, C. Gamazo, A. Sainz, J. Gomez;
SACYL, Valladolid, SPAIN.

Aim/Introduction: In individualized dosimetry for SIRT with TheraSpheres™Y90 for hepatic tumor/MTX metastases it is necessary to determine the activity to be perfused A (GBq), the perfused and tumor volume V and the distribution of activity in each voxel within the tumor c. Planning consists in an arteriography study to determine the vascular pathway to access the tumor followed by the perfusion of 5-8 mCi ^{99m}Tc-MAA through this pathway to acquire an SPECT-CT study. The quantification of these SPECT images allows to determine regional or voxel-level activities to evaluate the absorbed doses in the later therapeutic perfusion of the 90Y u-spheres by the same vascular pathway. The optimal threshold that gives the best estimate of V is not necessarily the same as the threshold that gives the best estimate of A nor the best estimation of c. Then 3 thresholds are needed to estimate the corresponding recovery coefficients RC. As the volumes treated with TheraSpheres™Y90 (200-800 ml) are greater than those simulated with recent physical phantoms (0.5-200 ml), in this work we build a new phantom designed specifically for the correct determination of these thresholds. **Materials and Methods:** The phantom consists of 12 identical bottles of 30-40 ml each one united to simulate a heterogeneous tumor of ~450 ml and filled with an aqueous solution of 99MTc. The assembly is introduced into the IEC-Standard 61675-1 phantom filled with non-radioactive water. SPECT/CT image is acquired with a dual-head Siemens SYMBIA T-2 gamma camera, crystal thickness of 9.5 mm and LEHR collimators. SPECT is acquired with 32 frames, 30 s/frame, 128×128 matrix and 4.8 mm voxel. CT parameters are: 110 kVp, 63 mAs, 75 rpm. Reconstruction is done with Siemens Flash3D™, 8 iterations 4 subsets, CDR compensation, CT-derived Attenuation Correction and energy window-based Scatter Correction. Analysis of images were performed using IMAGEJ and Simplicity® **Results:** The best recovery coefficient for A, V and c are obtained with thresholds of 100%, 26% and 50%, respectively. We obtain reconstructions of high precision with total counts better than 90%. The distribution of activity at the voxel level is estimated well with the corresponding accounts with a 50% threshold. The percentage of true treated liver volume is estimated well with the voxels contained in the threshold image of 26%. **Conclusion:** The physical phantom developed can provide a good approach for the SPECT quantification to TheraSpheres™ Y90 dosimetry. **References:** None.

EP-0209

Torch: A Treatment Planning System for Personalized Radiopharmaceutical Therapy

***J. Grudzinski**, K. Sorensen, M. Gracz, B. Bednarz, P. Wickre;*
Voximetry, Middleton, WI, UNITED STATES OF AMERICA.

Aim/Introduction: Through many years of experience with external beam radiotherapy (XRT), it is well-known that patient-specific absorbed dose is an excellent predictor of treatment efficacy and toxicity. A similar approach of determining patient-specific absorbed doses to achieve clinical objective s for each patient can be used in radiopharmaceutical therapy (RPT). We have developed a proprietary treatment planning system, called Torch, for RPT that includes adaptation of single-photon emission computed tomography (SPECT) or positron emission tomography (PET) imaging to interface with computer hardware and specialty software algorithms. **Materials and Methods:** There are three main modules included in Torch: Torch-PK, Torch-MC, and Torch-Bio. Torch-PK uses nuclear medicine imaging data to model pharmacokinetic (PK) behavior of the radiopharmaceutical as a function of time to generate time activity curves (TACs) for each voxel within regions of interest (ROI). TAC's are then analytically integrated to determine the number of disintegrations that occur within each voxel. This data is then imported into Torch-MC where Monte Carlo radiation transport is performed to estimate the three-dimensional dose distribution in the patient. A simpler dose calculation method was also developed which uses dose-kernels (called Torch Lite). Torch-Bio uses the dose distribution generated from Torch-MC or Torch Lite to estimate biologically-equivalent dose metrics that are often used to characterize RPT. Torch will leverage the enormous computing power of graphics processing units (GPUs) to perform patient-specific dose calculations accurately and quickly for busy, resource-limited nuclear medicine and radiation oncology departments. **Results:** Torch-PK automatically fits the best PK model to each ROI. Torch

Lite computes voxel-based dosimetry in a matter of seconds by performing GPU-convolution of the cumulative activity map with MC generated dose-kernels e.g. ^{177}Lu, ^{131}I, ^{90}Y, ^{67}Cu, etc. Torch-MC performs MC radiation transport in a matter of minutes for beta, alpha, and Auger-electron emitting radionuclides. Dosimetry results are displayed as either cumulative or differential dose volume histograms. Voxel-based BED can also be exported to be combined with XRT dosimetry. Torch is radionuclide agnostic where dosimetry can be calculated for any radiopharmaceutical regardless of isotope, enabling greater flexibility/adaptability among treatment protocols. **Conclusion:** Torch will enable more precise and accurate treatment planning where optimal assessments can be completed in minutes, as opposed to tens of hours by leveraging the enormous computing power of GPUs coupled with MC simulation. For patients and clinicians, Torch enables a promise of personalized medicine yet to be realized in the field of nuclear medicine. **References:** None.

EP-0210

Idac-alpha - An Alpha Dosimetry Program For Healthy Tissue

M. Andersson;
Medical Radiation Physics, Malmö, SWEDEN.

Aim/Introduction: The aim of this project is to develop dosimetry for eight alpha emitting radiotherapeutics (Ac-225, At-211, Bi-212, Bi-213, Pb-212, Ra-223, Tb-149 and Th-227), including their progenies. Currently, it is usually assumed that the progenies decay in the same location as the parent nuclide. without further biokinetic transport. IDAC-Alpha is both a biokinetic and dosimetric software, which includes separate biokinetic transport models for all progenies. For progenies generated in the kidneys the software will include the retention from kidneys to the urinary content. **Materials and Methods:** IDAC-Alpha was applied on a compartmental model for Ra-223 dichloride in mCRPC patients (Taprogge J, et 2017). The software performs the absorbed dose calculations in two steps. First, a unique biokinetic model is created based on the input data of the biokinetic model of the parent. Secondly, the software modifies the data to create a full biokinetic model covering all decays which can therefore be solved numerically. Each nuclide and decay are tracked for each organ and absorbed doses are calculated. To keep the computational time below 1 second for both the dosimetric and biokinetic calculations the radionuclides are tracked for 1 year in the body, which is long enough to ensure that no significant activity is left in the body. Absorbed doses are calculated for the Ra-233 model for the mCRPC patients in two ways. A) all progenies decay at the same site as the Ra-233 and B) the progenies have separate biokinetic models. **Results:** The biggest differences in absorbed dose will be in the bone surface, the red marrow and the kidneys. This is due to the fact that the Ra-223 progenies have a lower bone uptake than their parent radionuclide. **Conclusion:** IDAC-Alpha is a biokinetic, user friendly software with a graphical interface, developed to perform more realistic alpha dosimetry calculations for healthy tissue. The software includes separate transfer of progenies and creates a unique biokinetic model based on the biokinetic parent data. Including the biokinetics of the progenies will often lead to a dose reduction as retention in the urine are included. **References:** Taprogge J, et al. Compartmental model for 223Ra-Dichloride in Patients with metastatic bone disease from castration-resistant prostate cancer.

EP-0211

Development and Verification of a Software Tool to Calculate Absorbed Doses at the Voxel Level in Molecular Radiotherapy Treatments

***T. Monserrat**, M. Peinado, N. Montenegro, D. Álvarez, J. Herrero, D. Bruzos;*
Hospital Universitario Central de Asturias, Oviedo, SPAIN.

Aim/Introduction: The treatment planning systems for molecular radiotherapy are a fundamental tool for the physicist responsible for dosimetry and they are in growing demand, especially after the publication of the 2013/59/EURATOM Directive. However, they require an economic investment and some of them are limited to a single radioisotope. Our objective was to develop a program to calculate doses at the voxel level directly on the clinical images of individual patients in molecular radiotherapy treatments with Lu-177, Y-90 and I-131. **Materials and Methods:** Software was developed in Python 2.7. It allows the user to load images from a hybrid SPECT/CT system, delineate the VOI (volumes of interest) and calculate the absorbed dose to each of them, following the MIRD methodology. As input data, the user must manually enter the isotope used (Lu-177, Y-90 or I-131), the calibration factor (MBq/count/s) and the residence time of each VOI. The partial volume effect correction factors can be incorporated in the quantification of activity in small VOI. The program loads the S-voxel factors corresponding to the voxel size of the SPECT images and the selected radioisotope. These S-voxel factors are taken from the database published in 2012 by Lanconelli et al. As a result, the program generates a dosimetric report with the average doses absorbed to all of the VOI and their corresponding dose-volume histograms. In order to test the accuracy of the calculated doses, different VOI were delineated on 12 phantom and 12 clinical images of Lu-177 with different activity concentrations. The dose calculated by the program was compared with the theoretical dose that would be received in each zone assuming self-absorption of the mean beta emission. **Results:** The doses estimated by the program are in good agreement with the theoretical ones, being on average (2.63 ± 0.69) % higher than those predicted by the theory. This overestimation is attributed to the fact that the theoretical doses have been calculated by making the assumption of beta emission only, while the program takes into account the whole spectrum of the isotope. **Conclusion:** The program presented calculates absorbed doses at the voxel level for different isotopes from SPECT / CT images of the patient, which allows us to perform individualized dosimetries and thus optimize treatments. **References:** None.

EP-0212

Iodine Internal Dosimetry using Anthropomorphic Voxelized Phantom in GATE

N. G. Cavedini, C. M. Dartora, A. M. Marques da Silva; PUCRS, Porto Alegre, BRAZIL.

Aim/Introduction: To investigate absorbed dose in organs at risk in iodine therapy using voxelized phantom. **Materials and Methods:** GSF Golem voxelized phantom (male, 38 years, 121 structures) was used in GATE Monte Carlo simulation application. β particles (89.3%, with 606 keV) and gamma photons (82.2% with 364 keV) from ^{131}I decay were simulated separated, to verify the contribution of each one in absorbed dose at risk organs. Thyroid gland was filled with homogeneous 0.1 MBq of ^{131}I. Risk organs studied were: thyroid gland (d=1.04 g/cm³), esophagus (d=1.05 g/cm³), trachea (d=1.03 g/cm³), spinal cord (d=1.03 g/cm³) and cervical vertebrae (d=1.92 g/cm³). **Results:** Thyroid absorbed dose per injected activity were 2.65 and 1.85 mGy/MBq for β- and gamma, respectively. This corresponds to a contribution of 58.91% of β- particle energy. Results for esophagus were $2.62.10^{-3}$ and $3.00.10^{-1}$ mGy/MBq for β- and gamma, respectively. Trachea absorbed doses were $3,02.10^{-3}$ for β- and $2,50.10^{-1}$ mGy/MBq for gamma. For spinal cord, the results showed absorbed doses of $1.16.10^{-3}$ mGy/MBq, for β-, and $2.14.10^{-1}$ mGy/MBq for gamma emissions. Results for cervical vertebrae were $1.96.10^{-2}$ and 1.50 mGy/MBq for β- and gamma, respectively. For adjacent organs of thyroid, contribution was mostly by gamma emission, representing 99.14%, 98.80%, 99.46%, 98.71% for esophagus, trachea, spinal cord and cervical vertebrae, respectively. Results are compared to Shahbazi-Gahrouei and Ayat (2015), with thermoluminescent dosimeters (TLD) in phantom neck above thyroid region and MCNP Monte Carlo simulation with mathematical phantom. Gamma absorbed dose measured with TLD ($8.53.10^{-1}$ mGy/MBq) in Shahbazi-Gahrouei and Ayat (2015) was 54% lower than that found in this work (1.85 mGy/MBq). MCNP simulation of thyroid absorbed dose (11.5 mGy/MBq) was 61% higher than than our work (4.50 mGy/MBq). The differences are due to the characteristics between mathematical and GSF voxelized phantom. **Conclusion:** Absorbed doses for thyroid gland, esophagus, trachea, spinal cord and cervical vertebrae were simulated with GATE Monte Carlo simulation. Thyroid gland gamma dose was comparable with previously published data, showing the appropriateness of GATE MC as an adequate tool for dose calculations, mainly with realistic voxelized phantoms. We did not find until now other papers showing the contribution of gamma and β-particle in iodine therapy at risk organs. **References:** Shahbazi-Gahrouei D, Ayat S. Determination of Organ Doses in Radioiodine Therapy using Monte Carlo Simulation. World J Nucl Med. 2015;14(1):16.

EP-0213

A Novel Patient-Based Dosimetric Approach for Y-90 Microsphere Treatment

F. Çakir[1], M. F. Bozkurt[2], A. K. Özden[2]; [1]Hacettepe University, Ankara, TURKEY, [2]Hacettepe University Faculty of Medicine, Ankara, TURKEY.

Aim/Introduction: Yttrium-90 (Y-90) microsphere treatment is an internal radiation treatment in which hepatic tumors are selectively targeted via arterial route owing to unique circulation pattern of the liver. One major questionable aspect of this treatment is the heterogeneity of intra-tumoral microcirculation and its effect on theraphy response as well as the amount of activity to provide maximum tumor dose along with minimum background dose. This study aims to give a vision to uncover these issues with use of a novel patient-based dosimetric approach. **Materials and Methods:** A total of 90 treatments which were performed with Y-90 glass microspheres in the same university hospital between the years 2012 and 2018 were re-planned retrospectively based on a novel personalised, patient-based dosimetric approach. During planning, a software that provides a voxel-based dosimetric approach through anatomical and functional sequence images of the patient was used. The retrospective dosimetric re-planning for each patient gave an evaluation in terms of targeted effective tumor dose and critical organ doses. The relation between Y-90 glass microsphere activities and perfused tissue volume, perfused tumor volume and absorbed doses was investigated. The planning steps of the software used in this study were reviewed in terms of parameters that would affect the dosimetric results, and a standard was specified for these parameters followed by comparison with those that were calculated pre-therapy with semi-dosimetric approach. **Results:** Novel patient-based retrospective plannings showed that the amount of Y-90 glass microsphere activity, which were used under current conditions and calculated taking a reference of absorbing a dose of 120 Gy of the lobar volume alone, were lower than the pre-calculated activity for 14 /90 (~%16) therapies and higher for 76 /90 (~%84) therapies when considering the critical organ tolerance doses. **Conclusion:** This study showed that the patient-based dosimetric approach, taking into account the anatomic variation of the relevant patient, different tumor size and its localization, is of vital importance with respect to provide maximum tumor dose along with minimum background dose in accordance with the logic of internal radiation treatment. The findings of this preliminary study will be expected to give rise to proceed with clinical studies in order to optimize treatment efficency. **References:** None.

EP-0214

Simple Bremsstrahlung SPECT Method for Whole-Liver Dosimetry in Treatments with ^{90}Y-Microspheres - Comparison with ^{90}Y PET

K. Knesaurek, S. Heiba, R. Pyzik, S. D. Pasik, L. Kostakoglu; Ichan School of Medicine at Mount Sinai, New York, NY, UNITED STATES OF AMERICA.

Aim/Introduction: Bremsstrahlung SPECT/CT (bSPECT/CT) is the most common method for post-therapy imaging in liver cancer treatment with ^{90}Y microspheres. However, quantitative bSPECT is very difficult due to scatter, septal penetration, the continuous nature of the bremsstrahlung energy spectrum,

and inefficient bremsstrahlung production. One way to address these limitations is to use Monte Carlo (MC)-based bSPECT reconstruction (ref. 1), which is not always practical. Here, we are proposing a simple approach for estimation of mean absorbed-dose to the liver using bSPECT/CT in patients undergoing treatment with ^{90}Y microspheres. **Materials and Methods: :** In our previous study comparing ^{90}Y dosimetry obtained using bSPECT/CT vs PET/CT, we found that there was a large difference between the mean doses to the liver. However, there was a high linear correlation between the doses, presenting an opportunity for quantitative assessment using bSPECT/CT ^{90}Y imaging, provided appropriate scaling and image enhancement. After treatment with ^{90}Y microspheres, 40 patients were immediately imaged on a dual-head Infinia SPECT/CT gamma camera and on a mCT PET/CT system . Local deposition method with known activity of ^{90}Y was used for dosimetry calculations utilizing MIM 6.8 software. Images from 25 of the patients, randomly selected, were used to calculate the correlation of mean liver doses obtained from bSPECT/CT vs. PET/CT. For the remaining 15 patients, the calculated correlation was used to estimate doses obtained from bSPECT/CT, which were then compared to the doses obtained from PET/CT, considered the gold standard for quantitative analysis. **Results:** From the 25 selected patients, the calculated linear correlation between bSPECT/CT and PET/CT ^{90}Y doses was high (r^2 =0.99), with a slope of 2.97 and an intercept of -3.43. This linear fit was used to calculate the bSPECT/CT doses for the remaining 15 patients. For these patients, the mean whole-liver dose obtained from bSPECT/CT fitted data vs that obtained from PET/CT were 47.3 Gy and 48.3 Gy, respectively. The average relative difference was 3.4 % (range -12.8 % to 13.0 %). **Conclusion:** Although quantitative bremsstrahlung imaging is difficult, as mentioned above, it is possible to calculate adequate estimates of whole-liver dosimetry from bSPECT/CT ^{90}Y imaging that is calibrated using its correlation with post-therapy PET/CT ^{90}Y images. **References:** Gustafsson J, Knešaurek K. Monte Carlo-Based Bremsstrahlung SPECT Reconstruction for Whole-Liver Dosimetry in Treatments with ^{90}Y-Microspheres - Comparison with ^{90}Y PET. EJNMMI 44, supp 2, S397, 2017.

EP-0215

Image-based 3D Dosimetry Techniques For Yttrium-90 SIRT Of HCC: Quantitative Comparison Of Tumor And Healthy Liver Absorbed Doses

J. Brosch, *A. Gosewisch, H. von Zimmermann, L. Kaiser, P. Bartenstein, H. Ilhan, A. Todica, G. Böning;*
Department of Nuclear Medicine, University Hospital, LMU Munich, Munich, GERMANY.

Aim/Introduction: Most of the dosimetric approaches for Yttrium-90-SIRT rely on 1D averaged tumor and healthy liver tissue doses, while 3D image-based dosimetry for treatment verification would be preferred. Depending on the institute, either ^{90}Y-bremsstrahlung-(BRS)-SPECT or ^{90}Y-PET is used for post-therapeutic imaging. Aim of this study was to investigate differences in absorbed dose values for ^{90}Y-PET and ^{90}Y-BRS-SPECT in comparison to a simplified Technetium-99m-MAA-SPECT based 3D dosimetry for institutions without access to ^{90}Y-PET Imaging. **Materials and Methods:** Seven patients (in total ten therapy cycles) suffering from unresectable hepatocellular carcinoma (HCC) received a ^{99m}Tc-MAA-SPECT/CT before ^{90}Y-SIRT and accordingly post-therapeutic ^{90}Y-BRS-SPECT/CT and ^{90}Y-PET/CT. The therapy volume was segmented from low resolution ^{90}Y-BRS-SPECT and the ^{99m}Tc-MAA-SPECT was scaled with the ^{90}Y therapy activity within this volume. This scaled ^{99m}Tc-MAA-SPECT based activity image as well as the ^{90}Y-BRS-SPECT and ^{90}Y-PET activity images were convolved with a pre-simulated ^{90}Y dose kernel for soft tissue to obtain 3D dose images. To compare tumor doses a spherical VOI (d=2cm) was drawn and placed in the tumor. Healthy liver doses were calculated for all patients showing activity uptake in healthy liver by averaging the doses of three spherical VOIs (d=2cm), which were placed in healthy liver tissue. **Results:** The mean tumor doses for all patients were found to be 133 (±34) Gy/GBq for the scaled ^{99m}Tc-MAA-SPECT dosimetric approach, 84 (±12) Gy/GBq for ^{90}Y-BRS-SPECT and 176 (±18) Gy/GBq for ^{90}Y-PET, respectively. The deviation of tumor doses in comparison to ^{90}Y-PET were 20% for scaled ^{99m}Tc-MAA-SPECT and 50% for ^{90}Y-BRS-SPECT. The mean healthy liver doses for all patients were found to be 19 (±8) Gy/GBq for the scaled ^{99m}Tc-MAA-SPECT dosimetric approach, 22 (±3) Gy/GBq for ^{90}Y-BRS-SPECT and 42 (±9) Gy/GBq for ^{90}Y-PET,respectively. The scaled ^{99m}Tc-MAA-SPECT values deviated 49% from ^{90}Y-PET while the ^{90}Y-BRS-SPECT based deviated 39%. **Conclusion:** With our study on seven HCC SIRT patients (10 therapy cycles), we observed a significant tumor dose underestimation for ^{90}Y-BRS-SPECT based 3D dosimetry. Dosimetry based on a scaled ^{99m}Tc-MAA-SPECT showed comparable tumor dose values within the given standard deviation. The deviation of scaled ^{99m}Tc-MAA-SPECT compared to ^{90}Y-PET tumor doses was overall smaller than those of ^{90}Y-BRS-SPECT based tumor doses. However, for healthy liver doses the scaled ^{99m}Tc-MAA-SPECT approach showed a larger deviation than the ^{90}Y-BRS-SPECT based values. We therefore conclude, that post-therapeutic 3D dosimetry based on scaled ^{99m}Tc-MAA-SPECT is feasible for tumor doses, while its application to healthy liver doses is limited. **References:** None.

EP-0216

The joint use of MAA SPECT/CT and CBCT enables better dosimetry planning for SIRT procedures

M. Rodríguez-Fraile, *M. Morales, A. Ezponda, M. Calvo, F. Grisanti, P. Berián, L. Sancho, A. Erhard, V. Morán, M. Iñarrairaegui, B. Sangro, J. Bilbao;*
Clínica Universidad de Navarra, Pamplona, SPAIN.

Aim/Introduction: To determine if MAA SPECT/TC and CBCT allow better dosimetry planning by means of a better definition of the target volume and the activity to be administered in each injection. **Materials and Methods:** 24 consecutive patients treated with SIRT using 90Y resin microspheres from 11/2018

to 03/2019 (20 hepatocellular carcinoma, 3 cholangiocarcinoma and 1 neuroendocrine tumor), were prospectively studied. Target volumes were obtained during SIRT planning from contrast-enhanced CT (CECT) in 23 patients, 99m-TC MAA SPECT/CT (MAA) in 24 and from cone-beam CT (CBCT) in 15, and were compared to the final target volume (FTV) obtained from 90Y-microspheres PET/CT (90YPET/CT) in all patients. For MAA and 90YPET/CT, target volumes were drawn using a VOI with isocontour (Syngo.via, Siemens). CBCT was also used to define the percentage of tumor volume perfused by each branch/artery. To assess agreement between studies, the Lin concordance coefficient correlation (CCC) was used and to define which study predicts better FTV, the determination coefficient (R^2) from the regression model. **Results:** In 75% of patients, SIRT was performed through segmental or tumor feeding arteries. Only in 4 patients (16%), MAA and SIRT administrations differed due to patient motion during SIRT (1), vasospasm (1) or minimal deliberate changes (2). Mean (SD) target volumes in ml were 749 (577) for CECT, 828 (521) for MAA, 806 (701) for CBCT and 1011 (562) for 90YPET/CT. Isocontour mode was 3% (range=1-9%) for MAA (67% patients) and 90YPET/CT (71%). In 25% of patients, CBCT defined percentage of tumor volume perfused by each artery (when >1 feeding artery) and consequently the percentage of activity to administer by each. The concordance with 90YPET/CT FTV was moderate for CBCT (CCC=0.6; IC=0.6-0.9) and substantial for CECT (CCC=0.7; IC=0.46-0.84). MAA reached maximal concordance (CCC =0.81; IC=0.64-0.91), being better when the 4 patients with changes in the administrations were excluded (CCC =0.85; (IC=0.68-0.93) Interestingly, MAA showed almost a perfect concordance with CECT in lobar or total administrations (CCC Lin=0.96; IC=0.8-0.99), in which anatomical volumes are accurately defined with CECT. The three studies predicted linearly the FTV with a weak R^2 for CBCT (R^2=0.5, p<0.05), moderate for CECT (R^2=0.65, p<0.01) and strong for MAA (R^2=0.8, p<0.01). **Conclusion:** MAA SPECT/CT predicts 90YPET/CT FTV better than CBCT or even than the conventional method (CECT). CBCT allows defining the activity to be administered through each artery. Therefore, the joint use of both techniques enables better dosimetry planning for SIRT procedures. **References:** None.

EP-0217

The 3D dosimetry-based treatment planning in clinical routine for SIRT: reality or illusion ?

J. Badel[1], *S. Parisse-Dimartino*[1], *F. Khayi*[1], *A. Martin*[1], *J. Labour*[1,2], *D. Sarrut*[1,2], *D. Kryza*[1], *C. Mastier*[1], *T. Mognetti*[1];
[1]*Centre Leon-Berard, Lyon, FRANCE,* [2]*CREATIS, Lyon, FRANCE.*

Aim/Introduction: The 3D dosimetry-based treatment planning in SIRT aims to optimize the tumor control by administering the highest possible activity in target volume while limiting complications irradiation to organs at risk. However, its clinical implementation is often perceived as complex and leads to its abandonment in favor of simplified dosimetric methods, so less optimized such as the BSA method for example [1]. Based on our clinical experience, we present the feasibility of a routine 3D-dosimetric planning for the management of SIRT patients. **Materials and Methods:** We have implemented a patient-specific dosimetry named yPOD (yttrium Personalized Optimized Dosimetry) for each patient in SIRT procedure. Our yPOD approach is a personalized voxel-based dosimetry using commercialized 3D dosimetry software. We defined a specific volume nomenclature to take into account all interest organs for the 3D dosimetry: Tumor(s) (T), Total Liver (TL), Lungs (L), Perfused Volume (PV=threshold segmentation set at 5% of the maximum count value), Healthy Perfused Liver (HPL=PV-T), Non-Perfused Liver (NPL=TL-PV). All these volumes are delineated on the pre-therapeutic 99mTc-macroaggregated-albumin SPECT/CT. The dose calculation is realized from voxel S-values dose kernel convolution algorithm. The density correction is applied even if hepatic heterogeneity has a low effect on the dose calculation. The mean absorbed dose is computed for each segmented volume and specific dosimetric criteria are further defined for the healthy perfused liver (HPL) and the tumor: the HPL volume to receive a dose of 70 Gy and the dose received by 95% of the tumor volume. The yPOD and the prescription of the administered activity to the patient are systematically validated by a medical-technical team composed of radiologist, nuclear medicine physician, radiopharmacist and medical physicist. **Results:** 15 patients have already benefited of an yPOD. Consequently, each of these patients has undergone a personalized and optimized SIRT by dosimetry-guided. The processing time for our 3D dosimetry method is on order of 1 hour including 15 minutes to prepare the dosimetric study, 40 minutes to delineate volumes and 5 minutes to obtain the dose-volume histogram. **Conclusion:** In the SIRT procedure, treatment planning based on 3D dosimetry in clinical routine is a reality, but it requires a significant resource, including a specific treatment planning system, a clinical dosimetry procedure and a dedicated time to medical-technical staff. **References:** [1] Stokke et al. "Dosimetry-based treatment planning for molecular radiotherapy: a summary of the 2017 report from the Internal Dosimetry task force" EJNMMI Physics 2017.

EP-0218

Normal organs and tumor absorbed doses of ^{188}Re-human serum albumin microsphere in GP7TB hepatoma model

L. Chen, W. Lee, C. Ho, Y. Chang, C. Chang;
Institute of Nuclear Energy Research, Taoyuan City, TAIWAN.

Aim/Introduction: The aim of this study was to investigate the dosimetry of ^{188}Re-human serum albumin microsphere (^{188}Re-HSAM) in GP7TB hepatoma model via intraarterial (i.a.) administration. **Materials and Methods:** Male F344 rats were intrahepatic inoculation with GP7TB 1 mm^3 cubes. At 26 days after tumor inoculation, dosimetry data was collected after injection of ^{188}Re-HSAM. Pharmacokinetic data of ^{188}Re-HSAM were obtained for estimation of absorbed doses in tumor and normal organs. Radiation dose estimates for normal tissues and tumor were calculated using the OLINDA/EXM program with

ICRP 30 GI Model and Voiding Bladder Model. **Results:** Based on excretion studies, urinary excretion was assumed to be 27% and intestinal excretion was assumed to be 16%. Higher absorbed doses in normal organs were observed in the liver (2.2 mSv/MBq), lower large intestine (1.8 mSv/MBq), upper large intestine (1.2 mSv/MBq) and kidneys (0.67 mSv/MBq). The red marrow absorbed dose was estimated to be 0.016 mSv/MBq. The effective dose was 0.36 mSv/MBq. The tumor radiation absorbed dose for the i.a. administration of ^{188}Re-HSAM was also calculated in this study. Tumor-absorbed doses for ^{188}Re-HSAM were 4.3 mGy/MBq at 1 g tumor sphere. The T-NT ratio was 1.9 in liver. **Conclusion:** The tumor-absorbed dose demonstrated obvious tumor localization and concentration of HSAM therapeutics loaded with ^{188}Re. Therefore, i.a. administration of ^{188}Re-HSAM could provide a benefit and it is a promising strategy for delivery of ^{188}Re-HSAM in oncology applications. **References:** None.

EP-0219

Quantification of ^{131}I activity in mouse kidneys using micro-SPECT and ex vivo gamma counting: experimental evaluation of uncertainties

C. Saldarriaga Vargas[1,2], *L. Struelens*[1], *M. D'Huyvetter*[2], *J. L. Eersels*[2], *V. Caveliers*[2], *P. Covens*[2];
[1]*Belgian Nuclear Research Centre (SCK-CEN), Mol, BELGIUM,* [2]*Vrije Universiteit Brussel, Jette, BELGIUM.*

Aim/Introduction: As opposed to conventional ex vivo gamma counting (GC) of dissected tissues, micro-SPECT offers the possibility to perform in vivo longitudinal studies on the same animal. In order to derive the pharmacokinetic parameters necessary for tissue dosimetry and the evaluation of the dose dependence of biological response, micro-SPECT must be quantitative and allow an accurate and reproducible assessment of the radiopharmaceutical activity in the relevant tissue. This study aims to evaluate the accuracy and reproducibility associated with the mouse pharmacokinetic assessment of ^{131}I-labeled single-domain antibody fragments (sdAb) using micro-SPECT, against GC ex vivo biodistribution studies. The focus is on the kidneys, where uptake of the ^{131}I-labeled sdAb is significant. **Materials and Methods:** Biodistribution studies were done on healthy C57BL/6 mice. The pharmacokinetic profile of ^{131}I-labeled sdAbs in the kidneys was determined from tissue activity measurements at different time points post injection, both with micro-SPECT and GC. SPECT/CT acquisitions were performed with a VECTor micro-SPECT/PET/CT (MILabs). Following the last SPECT acquisition, the activity of dissected tissues was assessed in a gamma counter (Cobra-II, Canberra-Packard). Several sources of uncertainties were evaluated experimentally for each technique. For SPECT: system performance in terms of activity recovery coefficients (phantom study) and measurement reproducibility, mouse inter-variability, and size of the image quantification ROI. For GC: device performance in terms of measurement reproducibility, cross-talk, sample volume effects and response linearity; as well as mouse inter-variability. Additionally, the accuracy and reproducibility of the activity calibration factors determined for each technique were evaluated. **Results:** For GC, the uncertainties due to device performance are mostly below 5% when using an appropriate measurement protocol. For SPECT, errors due to partial recovery of activity account for an underestimation of at least 20% of the kidney activity. Also the ROI size has a large impact on SPECT image quantification. SPECT measurements resulted in lower variability between time-specific kidney activities of different mice than GC, and resulted also in a lower variability in the estimated residence time (±10%, vs ±25% for GC). SPECT was also less prone to large (>15%) errors in the determination of the activity calibration factor. When using an appropriate SPECT ROI size, kidney activities from SPECT and GC agreed mostly within 20%. **Conclusion:** Micro-SPECT allows reproducible and reasonably accurate quantification of ^{131}I in murine kidneys. This opens the possibility to perform longitudinal biodistribution studies and kidney dosimetry for the same animals used for long-term toxicity studies. **References:** None.

EP-0220

Comparison of 6 MeV electrons scattering at the edges of metal and 3D-printed plastic collimators

S. Stuchebrov[1], *I. Miloichikova*[1,2], *Y. Cherepennikov*[1], *A. Krasnykh*[1], *B. Gavrikov*[3];
[1]*Tomsk polytechnic university, Tomsk, RUSSIAN FEDERATION,* [2]*Cancer research institute of Tomsk national research medical center of the Russian academy of sciences, radiotherapy department, Tomsk, RUSSIAN FEDERATION,* [3]*Moscow city oncology hospital №62, 1st Radiological department, Istra, RUSSIAN FEDERATION.*

Aim/Introduction: Electron external beam radiation therapy is a highly effective tool in cancer treatment. Currently, individual metallic collimators manufactured by cutting or melting are used to form complex electron fields. The authors propose an alternative approach to forming a transverse profile of the clinical electron beam fields by samples made of plastics using additive technologies. Plastic collimators are thicker than metal ones, so it is necessary to consider the effect of the edge scattering on the dose distribution. The purpose of this study is to compare the scattering effects for a 6 MeV electron beam at the edges of metal and plastic collimators. **Materials and Methods:** We experimentally obtain the dose field profiles for an ONCOR Impression Plus medical linear accelerator (the electron energy is 6 MeV) using GafChromic EBT3 dosimetry films. The metal collimator is melted in a special CIVCO furnace using an A-158 alloy consisting of bismuth (50%), lead (26.7%), tin (13.3%), and cadmium (10%), while the HIPS-plastic one is manufactured by rapid prototyping using Up!Plus2 printer. The thickness equals 15 mm for the metal sample and 40 mm for the plastic one. In the experiment, flat edged metal and plastic samples are placed in the path of the electron beam to block a part of the particle flux. A dosimetry film is placed at a 100 cm distance from the source. One part of the beam falls on the film

without an absorber, and the other part is completely absorbed in the material under study. This allows us to explore the blurred boundaries of these two areas for metal and plastic samples. **Results:** In accordance with the common approach, the beam penumbra (the distance between 80% and 20% isodoses) serves as a parameter to determine the electron boundary scattering. The penumbra of the beam formed by a plastic sample is on average 0.8 mm larger than that of the metal-formed one. The maximum difference does not exceed 1.0 mm. It is shown that the dose gradient does not differ for the region between 5% and 100% isodose. **Conclusion:** The comparison of the electron beam scattering at the edges of the metal and plastic collimators shows the applicability of plastic for the collimation of 6 MeV electron beams. The greater thickness of the plastic collimator has a negligible effect on the dose distribution. This work is supported by the Russian Science Foundation, project No. 18-79-10052. **References:** None.

EP-0221

Tumor Dosimetry And Radiobiological Study For High-Activity 131I-mIBG Therapy In The Management Of Refractory/Relapsed Neuroblastoma

C. Polito[1], *B. Cassano*[1], *E. Genovese*[1], *M. Longo*[2], *S. Donatiello*[1], *T. Insero*[1], *S. Valeri*[1], *M. F. Villani*[1], *A. Castellano*[1], *M. C. Garganese*[1], *V. Cannatà*[1];
[1]*IRCCS Bambino Gesù Children's Hospital, Rome, ITALY,*
[2]*Arcispedale Sant'Anna Hospital, Ferrara, ITALY.*

Aim/Introduction: Neuroblastoma is the most common paediatric neuroendocrine solid tumor. The tandem high activity therapy based on two administrations of 131I-meta-iodobenzylguanidine (131I-mIBG) is a modality of treatment now largely employed for patients having a wide range of tumor burdens and disease sites. The purpose of this study is to report dosimetric data on tumor absorbed doses in patients affected by neuroblastoma and to investigate on the biological effects associated to 131I-MIBG tandem therapy thorough biologically effective dose (BED) evaluation. **Materials and Methods:** This study included 28 131I-MIBG administrations given to 14 enrolled patients (with age varying from 4 to 20 years) treated for relapsed/refractory high risk neuroblastoma. All patients were treated twice (the mean interval between both administrations ranged from 15 to 21 days). The whole-body (WB) absorbed dose resulting from the first administration was used to determine the activity to inject during the second one in order to reach a total WB absorbed dose of 4 Gy. Absorbed dose to tumors having detectable 131I-MIBG uptake and measurable masses (evaluated through CT and MRI images) were calculated by conjugate-view planar imaging. In order to investigate the biological effects induced by high-activity 131I-MIBG therapies and to acquire suitable information for patient tailored therapy, a BED analysis was performed. The α/β radiobiological parameter value considered in this study was 13.08 Gy as found in literature for neuroblastoma, a kind of tumor having high cellular radiosensitivity. **Results:** The median value of injected activity per unit mass for the first administration was about 380 MBq/kg (ranging from 155 MBq/kg to 617 MBq/kg). Even if the injected activity per body mass for repeated treatments were roughly in the same order of magnitude, a high variability in tumor absorbed doses, ranging from 13 to 464 Gy (median: 255 Gy) was observed and the mean effective half-time was estimated as 39h in a range of 19h - 79h. Dosimetric data related to tumor absorbed doses were converted into BED values resulting in a mean value of 644 Gy. **Conclusion:** A personalized approach, combining patient-specific dosimetry, biological effects examination and clinical outcome, enables the delivery of as high as possible activities that can be tolerated by patients. For neuroblastoma treatments, WB and red-marrow absorbed doses could be individually prescribed, nevertheless, tumor absorbed dose values show high variability mostly depending on different 131I-MIBG uptakes and effective half-life in tumor lesions making difficult the outcome prediction. **References:** None.

EP-12

Clinical -> Diagnostic study -> Adult study -> Non-oncology study -> Endocrinology -> Endocrinology, benign

October 12 - 16, 2019 e-Poster Area

EP-0222

SPECT/CT with ^{99m}Tc-MIBI in Diagnosing Primary Hyperparathyroidism

P. O. Rumyantsev[1,2], *K. Slaschuck*[1], *M. Degtyarev*[1], *S. Serzhenko*[1], *A. Trukhin*[1], *Y. Sirota*[1], *P. Nikiforovich*[1], *M. Sheremeta*[1], *O. Baranova*[1];
[1]*Endocrinology Research Center, Moscow, RUSSIAN FEDERATION,*
[2]*Endocrinology Research Centre, Moscow, RUSSIAN FEDERATION.*

Aim/Introduction: Accurate anatomic localization of independent hyperfunctioning parathyroid glands allows performing radical surgery. SPECT/CTwith ^{99m}Tc-sestamibi (^{99m}Tc-MIBI) provides three-dimensional visualization of any hyperfunctioning gland(s) localized in the neck or mediastinum. In addition to surgical anatomy, the method allows evaluating the metabolic activity of hyperfunctioning parathyroid glands. **Materials and Methods:** Assessment of SPECT/CT diagnostic value in HTP visualization and improvement of management algorithms in patients with HTP. **Results:** Prospective study included 110 patients aged 21 - 80 years (mean age 57.1±2.7). Female to male ratio was 10:1. The follow-up period ranged from 3 to 24 months, the mean being 6 months. In all cases of biochemically confirmed HTP, the average preoperative levels were: Ca total - 2.85±0.05mmol/l; Ca ionized - 1.4±0.03mmol/l, PTH=196±52pg/ml; 25OH-VitD=23.3±4.7ng/ml. Scintigraphy was performed with SPECT/CT (GE model 670 NM/CT). Ultrasonography (US) was done with Voluson E8 (GE) by means of 10MHz linear probe. **Conclusion:** The exact localization

of hyperfunctioning parathyroid gland was identified in 102 (92.7%) out of 110 patients by means of SPECT/CT combined with neck US. All 102 patients had surgery, with the diagnosis being confirmed by histological examination: 90 adenomas (88%), four of which were multiple tumors from 2 to 4 parathyroid glands. 6 (6%) patients had hyperplasia; 4 (4%) patients had parathyroid carcinoma; 2 (2%) patients had atypical adenomas. HPT coexisted with papillary thyroid cancer, mostly microcarcinomas, in 6 patients. Ca and PTH levels normalized in all 102 (100%) operated patients; the other 8 patients are still under observation. The accuracy of neck US, planar SPECT and SPECT/CT methods in HPT visualization was 83.6%, 90.9, and 97.3%, respectively. Specificity of all methods was similar - 80%, while sensitivity was 84%, 92%, and 99%, correspondingly. PPV was comparable (97.7%, 97.9%, and 98%). However, NPV was 33.3%, 50%, and 88.9%, respectively. **References:** The study demonstrates that SPECT/CT is the most accurate method (97.3%) when combined with neck US. Modern intraoperative navigation techniques (gamma-probe and ICG-fluorescence) help to provide precise surgical removal of hyperfunctioning parathyroid gland(s). Further accumulation of clinical data and their advanced analysis are underway.

EP-0223

Digital PET/CT with 18F-Fluorocholine improves the detection of Occult Parathyroid Adenoma

D. A. Lopez Mora[1], *M. Sizova*[1], *A. Flotats*[1], *V. Camacho*[1], *A. Fernandez*[1], *F. Fuentes-Ocampo*[1], *J. Duch*[1], *A. Domenech*[1], *J. Perez*[2], *A. Moral*[2], *M. Estorch*[1], *I. Carrio*[1];
[1]*Nuclear Medicine Department. Hospital de la Santa Creu i Sant Pau, Autonomous University of Barcelona, Barcelona, SPAIN,* [2]*Department of Surgery. Hospital de la Santa Creu i Sant Pau, Autonomous University of Barcelona, Barcelona, SPAIN.*

Aim/Introduction: To compare the detectability of occult parathyroid adenomas (OPa) and image quality between digital and analog 18F-Fluorocholine PET/CT in patients with primary hyperparathyroidism (PHPT). **Materials and Methods:** Eleven patients (8 females; 63 ± 16 years) with PHPT (mean ± SD: parathyroid hormone 16.6pmol/L ± 11.4pmol/L; calcium 2.8pmol/L ± 0.1pmol/L) and negative (n=9) or inconclusive (n=2) 99mTc-MIBI scintigraphy and SPECT/CT were prospectively included from April to September 2018. All patients, who accepted to be scanned by the two systems, consecutively underwent a single day, dual imaging protocol (digital and analog PET/CT) after the intravenous injection of 18F-Fluorocholine. Three nuclear medicine physicians evaluated the lesion detectability identifying foci of radiotracer uptake suspected of OPa. Image quality was assessed using a 4-point scale (-1, poor; 0, fair; 1, good; 2, excellent). Differences were considered significant for a p value <0.05. **Results:** In 8 out of 11 patients, both systems detected OPa (PET+). The digital system was positive in 3 patients (27%) in whom the analog system did not detect OPa (PET-). There was no significant difference in the total number of OPa detected by the two systems (digital: 11 vs. analog: 8; p>0.05). Parathyroidectomy was performed in all patients, demonstrating solitary OPa in 82% of the patients. In the 3 patients with digital PET+ and analog PET-, all lesions were <10 mm. Moreover, in the patients with OPa confirmed by pathology the elevated baseline preoperative parathyroid hormone plasma levels decreased 10 minutes after the parathyroidectomy (16.6 pmol/L ± 11.4 pmol/L vs. 2.8 pmol/L ± 3.3 pmol/L). Improved imagen quality in the digital over the analog PET/CT was observed in 82% of the patients. The percentage of interrater concordance of detectability of OPa between both systems was 98%, with a high measure agreement between the observers (κ=0.9; p <0.0001). **Conclusion:** Digital PET/CT offers improved detectability and image quality in the assessment of occult parathyroid adenoma in patients with primary hyperparathyroidism. **References:** None.

EP-0224

An evaluation of a new TripleSPECT+ protocol for localisation of surgically proven parathyroid lesions, with assessment of both conventional and surface rendered image review

H. Ilyas[1], *H. Ahmad*[1], *S. Hafeez*[2], *J. Fowler*[1];
[1]*Guy's and St.Thomas' NHS Foundation Trust, London, UNITED KINGDOM,* [2]*Darent Valley Hospital, Dartford, UNITED KINGDOM.*

Aim/Introduction: To assess effectiveness of a TripleSPECT+ protocol in correctly localising parathyroid lesions compared to the original Planar+ protocol. **Materials and Methods:** Retrospective study with analysis of parathyroid scintigraphic scans in sequential patients with surgically proven parathyroid lesions. 30 patients scanned performed before and 30 after the introduction of the new TripleSPECT+ protocol were evaluated. The original Planar+ protocol: 400MBq intravenous 99mTc-MIBI with early and late planar images reviewed by the reporting physician who could request additional studies: SPECT, SPECT/CT and/or 80MBq pertechnetate thyroid planar scan. The new TripleSPECT+ protocol: 40 MBq pertechnetate thyroid SPECT study followed immediately with early MIBI SPECT after 900MBq 99m Tc-MIBI injection, with delayed MIBI SPECT-CT at 2 hours. TripleSPECT+ datasets could be viewed conventionally and also be used for advanced post processing including surface rendering according to the reporter's preference. Histopathology results were obtained from electronic patient records. Location of parathyroid lesions was compared with the scan report and the percentage of localised lesions in terms of right, left or ectopic was quantified as a percentage. For patients who were scanned according to the TripleSPECT+ protocol a comparison was made between those who had conventional image review and those which had also been surface rendered. **Results:** 30 patients were scanned using the Planar+ scan, with 53% of lesions being correctly localised (60% adenomas, 40% hyperplasia). 30 patients were scanned using the TripleSPECT+ scan, with 80% of lesions correctly localised (60% adenomas, 40% hyperplasia). Both protocols correctly localised adenomas in 78% of cases, however when conventional image review

was performed of TripleSPECT+ studies only 55 % of adenomas were correctly localised which increased to 100% when surface rendered were also considered.The correct side localisation of hyperplastic glands showed wide disparity between the protocols: 17% Planar+ compared to 83 % TripleSPECT+. Surface rendering did not show any advantage with both groups showing 83% positivity **Conclusion:** From this small pilot study, the new TripleSPECT+ protocol improved correct localisation of parathyroid lesions when compared to the Planar+ protocol from 53% to 80%. Inclusion of surface rendering resulted in further improvement in adenoma localisation with 100% correct localisation. We recommend a TripleSPECT+ protocol, with surface rendering being performed in cases where conventional review is unproductive. **References:** None.

EP-0225

Does the digital CZT detector improve the results of ^{99m}Tc-sestamibi/^{123}I subtraction SPECT/CT in parathyroid scintigraphy?

V. Tunninen[1], *M. Seppänen*[2], *T. Noponen*[3,4];
[1]*Department of Clinical Physiology and Nuclear Medicine, Satakunta Central Hospital, Pori, FINLAND,* [2]*Department of Clinical Physiology and Nuclear Medicine and PET centre, Turku University Hospital, Turku, FINLAND,* [3]*Department of Clinical Physiology and Nuclear Medicine, Turku University Hospital, Turku, FINLAND,* [4]*Department of Medical Physics, Turku University Hospital, Turku, FINLAND.*

Aim/Introduction: The major challenge in dual-isotope parathyroid SPECT/CT with ^{123}I and ^{99m}Tc-sestamibi is the close proximity of photon energies of these isotopes combined with the limited energy resolution of a traditional gamma camera. The aim of this preliminary phantom study was to evaluate whether the new digital CZT SPECT/CT camera with better energy resolution improves the outcome of ^{123}I/^{99m}Tc -sestamibi subtraction SPECT/CT in parathyroid scintigraphy when compared to a traditional gamma camera. **Materials and Methods:** For the purpose of this study, an antropomorphic phantom mimicking a parathyroid patient with two small adenomas (equivalent to 250mg and 130 mg adenomas in patient) was set up. The phantom was acquired using standard clinical protocols with Discovery NM/CT 670 CZT camera (GE Healthcare, Tirat Hacarmel, Israel) and with Symbia T6 SPECT/CT camera (Siemens Healthineers, Erlangen, Germany).Two subtraction SPECT/CT datasets were generated as in clinical practice (Hermes Medical Solutions, Stockholm, Sweden) and will be referred as traditional dataset and CZT dataset. Subtraction images were evaluated visually on the basis of adenoma appearance. For quantitative analysis, target-to-background -ratios were calculated for both adenomas with phantom background area as a background. The general appearance of subtraction artefacts was also evaluated. **Results:** Both adenomas were clearly visible in both datasets. The target-to-background -ratios of the 250 mg adenoma for the analog and the CZT camera were 8.0 and 11.0, respectively. The target-to-background -ratios of the 130 mg adenoma for the traditional and the CZT camera were 5.0 and 5.6, respectively. The edge artefact was faintly visible in both datasets with more emphasized appearance in the CZT dataset. **Conclusion:** The new digital CZT gamma camera appears to improve the target-to-background -ratio of the adenoma compared to a traditional gamma camera. However, this improvement did not have any clear effect on the visual appearance of these two targets representing small adenomas. Further studies are needed to find out if careful optimization of CZT camera acquisition parameters would further emphasize this difference and improve the visual appearance of an adenoma. **References:** None.

EP-0226

Self-comparison of ^{18}F-FDG PET/MRI and ^{18}F-FDG PET/CT in the Detection of Functional Pituitary Microadenoma with Inconclusive MRI Findings

H. Sui, *H. Wang, J. Zang, L. Lu, B. Hou, Q. Liu, Z. Zhu;*
Peking Union Medical College (PUMC) Hospital, Beijing, CHINA.

Aim/Introduction: To compare ^{18}F-fluorodeoxyglucose (^{18}F-FDG) positron emission tomography (PET)/magnetic resonance imaging (MRI) and ^{18}F-FDG PET/computed tomography (CT) in terms of image quality and lesion detection in patients with hormone-producing pituitary microadenoma. **Materials and Methods:** Twenty-nine patients with elevated pituitary hormone levels but inconclusive or negative MRI findings were recruited in this study. All patients underwent both brain PET/CT and PET/MRI scans after intravenous injection of ^{18}F-FDG (5.55 MBq/Kg body weight). Then, twenty-six patients accepted transsphenoidal adenomectomy within 2 weeks and pituitary microadenomas were confirmed in eighteen patients by surgical and pathologic findings, including 5 with primary pituitary microadenoma and 13 with recurrent pituitary microadenoma. Eight of the 26 patients were lack of confirmed pathologic findings in pituitary microadenoma. The remain three patients did not undergo surgeries. We detected the lesion by visual analysis and the maximum standardized uptake value (SUVmax) was measured. **Results:** For all these 18 patients pathologically diagnosed with pituitary microadenoma, PET/MRI provided definitive diagnosis in 18/18 (100.0%) patients, while PET/CT showed obvious lesions in 16/18 (88.9%) patients. The two patients with negative PET/CT findings were both recurrent. The SUV_{max} of ^{18}F-FDG PET/MRI was significantly correlated with that of PET/CT (P=0.000,r=0.893). The difference of SUVmax between the PET/MRI and PET/CT images was of no significance (5.4 ± 3.6 vs 4.6 ± 2.3, P=0.073). In comparison with PET/CT, PET/MRI performed superiorly in the image quality, and it showed more precise extent of tumor and provided greater detail in the evaluation of pituitary tumor. **Conclusion:** The use of PET/MRI is clinically feasible in pituitary microadenoma. Our study proved that compared with 18F-FDG PET/CT, ^{18}F-FDG PET/MRI displayed more accurate tumour location of functional pituitary microadenoma undetectable or inconclusive using contrast-enhanced MRI alone. **References:** None.

EP-0227

Preoperative accuracy in parathyroid adenoma localisation with contrast enhanced SPECT/CT

P. Sandqvist[1], *I. Nilsson*[1], *P. Grybäck*[1], *A. Sanchez-Crespo*[1], *A. Sundin*[2];
[1]*Karolinska University Hospital, Stockholm, SWEDEN,*
[2]*Uppsala University Hospital, Uppsala, SWEDEN.*

Aim/Introduction: Primary hyperparathyroidism is a common endocrine disease, mainly affecting elderly patients. The only known curative therapeutic approach is surgery. A good preoperative localisation is an important prerequisite for minimally invasive surgery. This in turn may decrease the risk for postoperative complications and need of inpatient care. The performance of multiphase contrast enhanced ^{99m}Tc-Sestamibi SPECT/CT for preoperative localisation of parathyroid adenoma remains to be determined. In this prospective study we aim to compare non-enhanced SPECT/CT with multiphase contrast enhanced SPECT/CT. **Materials and Methods:** 192 patients were eligible between May 2015 to May 2017. The patients underwent a one-stop shop preoperative examination with multiphase (native, arterial and venous phase) contrast enhanced ^{99m}Tc-Sestamibi SPECT/CT. The non-enhanced SPECT/CT image set was firstly reviewed, and findings recorded. Thereafter the same procedure was made using the complete examination image set. A clinical report was written as guidance for the surgeon. Surgical report, histopathological analysis of the surgical specimen and postoperative biochemical follow up, were used to confirm the initial parathyroid adenoma localisation. The likelihood for correct localisation was then investigated with regards to adenoma weight. **Results:** 149 patients with histopathological confirmation of at least one parathyroid adenoma and biochemical follow-up indicating cure, were finally included in the study. The median adenoma weight was 330 mg. The overall sensitivity and specificity for non-enhanced SPECT/CT were 81% and 96% respectively and for multiphase contrast enhanced SPECT/CT the corresponding results were 90% (p=0.003) and 98% (p=0.077). The gain in likelihood for correct detection using contrast enhancement compared to non-contrast enhanced SPECT/CT heavily increases with decreasing adenoma weight. Approximately above 500 mg, there is no differences in probability for correct adenoma localisation between non-enhanced and contrast enhanced SPECT/CT. **Conclusion:** Multiphase iodine contrast enhanced SPECT/CT outperforms non-enhanced SPECT/CT for preoperative localisation of small parathyroid adenomas. **References:** None.

EP-0228

Detectability Of 18F-Choline PET/MR In Primary Hyperparathyroidism With Negative Neck Ultrasound And Tc-99m MIBI Scintigraphy

M. Araz, *D. Nak, C. Soydal, E. Peker, I. Erden, S. Gullu, N. O. Kucuk;*
Ankara University, Ankara, TURKEY.

Aim/Introduction: i)To evaluate the power of 18F-FCH PET/MR in primary hyperparathyroidism ii)to compare with 18F-FCH PET/CT results, iii)to compare PET/MR and MR only results. **Materials and Methods:** Primary hyperparathyroidism patients with unlocalised disease who underwent 18F-FCH PET/MR were involved. Exclusion criteria were i)secondary or tertiary hyperparathyroidism ii)existence of chronic renal disease iii) evidence of any other malignancy including thyroid and parathyroid carcinoma. All PET/MR images were reevaluated by a nuclear medicine physician and all MR studies by a radiologist blinded to the PET data. Compatibility of the results of PET/MR and MR studies and comparative results of PET/MR and PET/CT in patients who also underwent PET/CT were investigated. **Results:** 34 patients (12M, 23F, mean age:49.5 ± 13.5 min:18 max:70) were enrolled. In 17/34 patients (50%) who had a negative 18F-FCH PET/CT study, PET/MR was performed. In 26/34 patients (76%), 18F-FCH PET/MR was reported as positive. In 18/26 patients (69%), confirmation was done histopathologically and in 2/26 patients (7%) by PTH washout. 6/26 patients (23%) were accepted as clinically true positive but surgery could not be performed and medical therapy was started. In 8/26 (30%) patients who had a negative PET/MR were clinically accepted as true negatives and taken under follow up. Explorative surgery was performed to none of them. In 23/34 patients (68%), 18F-FCH PET/MR and MR alone were concordant (K=0,31 p<0.05). In 11/34 patients (32%), 18F-FCH PET/MR and MR alone were discordant. In 7/11 discordant patients, MR findings were false positive, as confirmed by histology in 4/7 and clinically in 3/7 of them. In 4/11 patients, MR was false negative as the lesion which could not be specified as a parathyroid pathology with MR alone was 18F-FCH avid and surgical resection showed a parathyroid adenoma.Sensitivity, specificity, PPV, NPV and accuracy for MR alone evaluation and PET/MR were found as 80%, 50%, 70%, 64%,68% and 100%, 100%, 100%,100%,100% respectively. 17/34 patients underwent PET/MR following a negative PET/CT study. In 12/17 patients PET/MR was found positive. Confirmation was made by histopathology in 7/12, washout in 2/12 and clinically in 3/12 patients. In 5/12 patients, PET/MR was also negative. **Conclusion:** 18F-FCH PET/MR has an excellent performance for preoperative localisation of parathyroid adenomas and PET data has an important additive value over MR only imaging. 18F-FCH PET/MR may also considered as an effective tool in patients whom 18F-FCH PET/CT failed **References:** None.

EP-0229

Assessment of Intrahepatic Transplantation of Islet of Langerhans Grafts using Dynamic [^{68}Ga]Ga-NODAGA-exendin-4 PET Imaging

T. Jansen[1], *M. Buitinga*[1,2], *M. Boss*[1], *E. de Koning*[3], *M. Engelse*[3], *M. Nijhoff*[3], *O. Korsgren*[4], *O. Eriksson*[4], *M. Brom*[1], *M. Gotthardt*[1];
[1]*Radboud university medical center, Nijmegen, NETHERLANDS,*
[2]*KU Leuven, Leuven, BELGIUM,* [3]*Leiden University Medical Center, Leiden, NETHERLANDS,* [4]*Uppsala University, Uppsala, SWEDEN.*

Aim/Introduction: Patients with complicated type 1 diabetes (T1D) and unstable glycemic control can receive islet grafts via intrahepatic transplantation as treatment. This procedure results in an improved glycemic control and quality of life. Graft function will however deteriorate over time due to various factors. A tool to assess transplantation success and monitor islet survival and functionality would be of great clinical value. We applied dynamic PET imaging with the beta cell-specific tracer ^{68}Ga-labeled exendin-4 to study the presence of transplanted islets in T1D patients. **Materials and Methods:** Dynamic PET scans (60 min) were acquired after intravenous injection of [^{68}Ga]Ga-NODAGA-exendin-4 of 5 T1D patients who previously underwent intrahepatic islet transplantation (Tx-group: 2 men, 3 women). Graft function in these patients was biochemically proven prior to imaging with a mixed-meal tolerance test (MMTT). In addition, 3 control patients that awaited islet transplantation were imaged (2 men, 1 woman). Thresholding was applied to identify areas with high hepatic tracer uptake. Kinetic modeling was then used to measure the accumulation of the exendin-based tracer in these areas by determining the distribution volume. Islet function was expressed as the area under the curve of the measured c-peptide in the MMTT. Islet function was compared to the PET signal obtained from the analysis of the dynamic PET data. **Results:** The average transplanted islet equivalents (IEQ: measure for islet volume) in the Tx-group was $9.6*10^5 \pm 3.5*10^5$. The control and Tx-group did not differ in age (58.7±5.5 vs. 54±9.5 years, p=0.57), BMI (24.5±4.5 vs. 21.8±1.4 kg/m², p=0.57) and HbA1c (62.3±6.1 vs. 45.4±12.8 mmol/mol, p=0.14). Transplanted patients had a significantly higher c-peptide production during the MMTT (22.6 vs. 151.8 nmol.min/L, p<0.05). The distribution volume of the PET tracer obtained through kinetic modeling was significantly higher in the Tx-group (0.53±0.02 vs. 0.77±0.06, p=0.036), indicating an increased retention of the tracer in the liver i.e. the presence of intrahepatic islets. There was no significant correlation found in the Tx-group between Vt and IEQ, neither between Vt and c-peptide production. **Conclusion:** The data of this explorative study indicate that dynamic PET imaging using ^{68}Ga-labeled exendin-4 is a highly promising tool to assess intrahepatic transplantation of pancreatic islet grafts in T1D patients. This technique could offer the opportunity to further optimize islet transplantation protocols to improve islet survival. **References:** None.

EP-0230

Imaging of chemokine receptor type4 expression in primary aldosteronism using ^{68}Ga-pentixafor PET / CT

J. Ding[1], *L. Huo*[1], *Y. Luo*[1], *F. Li*[1], *H. Xing*[1], *A. Tong*[1], *J. Wen*[1], *Y. Zhang*[1], *X. Li*[2], *M. Hacker*[2];
[1]*Peking Union Medical College Hospital, Beijing, CHINA,*
[2]*Vienna General Hospital, Vienna, AUSTRIA.*

Aim/Introduction: Primary aldosteronism (PA) is the common surgically curable complication of hypertension which is challenging to accurately differentiate unilateral PA from bilateral PA as well as adrenocortical function by conventional CT imaging for therapeutic management. Chemokine receptor type4 expression elevated in aldosterone-producing tissue. We aimed to evaluate the diagnostic performance of ^{68}Ga-pentixafor PET/CT targeting CXCR4 in PA patients. **Materials and Methods:** We prospectively recruited twenty-five PA patients (10 males and 15 females, 46±10 years old) in our study. All patients initially underwent adrenal regional 68Ga-Pentixafor imaging prior to surgery (n=24) or adrenal venous sampling (AVS), (n=3) with follow-up time of 2-5 months. The SUV_{max} of lesions, lesion to liver ratio (LLR), and lesion to a contralateral ratio (LCR) were calculated and correlated with pathological and AVS results as wells as patients prognosis. Operating characteristic (ROC) analysis was performed to determine the threshold of SUV_{max} to differentiate aldosterone-producing adenomas (APA) from Non-APA. **Results:** Based on the visualization, 20(80%) patients were observed increased ^{68}Ga-Pentixafor focal uptakes. All patients were cured of hypertension post adrenalectomy of hot ^{68}Ga-Pentixafor lesions. 5(20%) patients present negative metabolic nodules, unilateral adrenal lesions were showed on CT in 4 patients and 1 were bilateral. 3 (75%) patients' symptoms didn't improved after surgery guided by CT. The analysis of these scans revealed an overall sensitivity of 95.2%, specificity of 100%, positive (100%) and negative predictive value (80%) for PA patients respectively. A total of 32 adrenal lesions in twenty-five patients were analyzed. The mean SUV_{max} =18.0±9.0 of APA was significantly elevated than unilateral or bilateral adrenal hyperplasia (3.3±1.1),(P<0.0001) and adrenal incidentaloma (4.4±1.1), (P=0.003). To differentiate APA from Non-APA, the threshold level of LLR ≥1.72 was associated with sensitivity (100%) and specificity (100%) and optimal cut-off of LCR ≥1.93 was associated with sensitivity (92.3%) and specificity (100%). **Conclusion:** ^{68}Ga-pentixafor PET/CT might be non-invasive approach to detect PA lesions, as well as could distinguish APA from Non-APA lesions, which representing a prognostic classification of PA patients. **References:** None.

EP-0231

Assisted visual reading using semi-quantitative analysis of pheochromocytoma and paraganglioma (PPGL) with 18F-FDOPA PET/CT

F. L. Grisanti, *M. I. Morales-Lozano, J. J. Rosales, E. Hernández-Acero, J. F. Bastidas, C. Perdomo, J. C. Galofré, C. Salvat, J. Arbizu;*
Clinica Universidad de Navarra, Pamplona, SPAIN.

Aim/Introduction: We aimed to define semi-quantitative parameters that could help visual reading of 18F-FDOPA PET/CT in the evaluation of patients with clinical, biochemical and/or conventional imaging characteristics suggestive of pheochromocytoma or paraganglioma (PPGL). **Materials and Methods:** Sixty patients (77% females, median age: 50 years [IQR 36.5-61]) with suspected PPGL and referred for a 18F-FDOPA PET/CT between 2011 and march 2019 were retrospectively evaluated. PET scans were analysed visually and semi-quantitatively by obtaining different parameters:

Tumor SUVmax, Tumor SUVmax/SUVmean liver (TLR), and Asymmetry Index (SUVmax pathologic adrenal gland/normal adrenal gland; AIndex). K-sample equality-of-medians test was performed to compare semi-quantitative values between PPGL and normal adrenal glands. Receiver operating characteristic curves were determined and areas under the curve were compared for different cutoffs of each parameter. The presence of a genetic predisposition was identified. Definitive diagnosis of paragangliomas and pheochromocytomas was achieved based upon biopsy or clinical follow-up. **Results:** Twenty-one out of 60 patients had a definitive diagnosis of PPGL (16 pathologically, and 5 through clinical follow-up): 26 lesions were paragangliomas and 9 lesions were pheochromocytomas. All of the PPGL identified pathologically were positive on 18F-FDOPA PET/CT scan by visual analysis (sensitivity=100%), and the specificity was 87,2% due to 6 false positives (n=1: adrenal hyperplasia, n=5 had subsequently normal biochemical tests). Median Tumor SUVmax and TLR for paragangliomas were 10.15 [IQR:6.09-17.3] and 5.81 [IQR 2.78 -8.93] respectively; whereas for pheochromocytomas they were 10.35 [IQR:8.63-19.4] and 5.64 [IQR: 4.85-9.89] respectively. These values were significantly higher than in normal adrenal glands (median SUVmax=1.79;[IQR 1.53-2.01]; median TLR=1,14; [IQR 0.96-1.33]; p<0.01). The median AIndex was significantly was higher in pheochromocytomas (2.61; [IQR 2.27-4.05]) than in normal adrenal glands (1.07 [IQR 1.02-1.14]; p<0.01). An AIndex > 1.57 had the highest diagnostic performance for pheochromocytomas (sensitivity, specificity and AUC=100%). For paragangliomas, TLR > 1.6 had a sensitivity of 100% and a specificity of 94.9% (AUC=0.99), while Tumor SUVmax > 2.94 had a sensitivity of 96.2% and a specificity of 94.9% (AUC=98%). Fourteen patients had positive genetic testing (67%): eleven patients (78%) had SDHD, two patients (14%) had NF-1, and one patient (7%) had RET mutation. **Conclusion:** Semi-quantitative analysis assists the visual reading of 18F-FDOPA PET/CT by increasing the diagnostic accuracy in the evaluation of PPGL. In spite of the limited sample size, the AIndex is a promising parameter for the evaluation of adrenal glands in pheochromocytomas, and TLR for paragangliomas. **References:** None.

EP-0232

Quantitative retrobulbar SPECT/CT measurement in Graves' ophtalmopathy

S. K. Barna[1], *I. Garai*[1], *L. Galuska*[2], *E. Nagy V.*[3], *J. Varga*[2]; [1]*Scanomed Ltd, Debrecen, HUNGARY,* [2]*Division of Nuclear Medicine and Translational Imaging, Department of Medical Imaging, Faculty of Medicine, University of Debrecen, Debrecen, HUNGARY,* [3]*Division of Endocrinology, Department of Medicine, Faculty of Medicine, University of Debrecen, Debrecen, HUNGARY.*

Aim/Introduction: Graves' ophtalmopathy (GO) in immunologically active or incative state requires different treatments. We have examined more than 1000 patients' retrobulbar uptake with [Tc-99m]DTPA in the last 15 years, evaluated by a custom software using manual ROIs on a standardized thick slice containing the retrobulbar space. The clinicians mainly used this method for differentiating active from non-active ophtalmopathy, with 10x10-6 ID/mL as threshold. We investigated the potential of quantitative SPECT/CT by more available software and more reproducible VOI positioning to simplify the method. **Materials and Methods:** SPECT projection images of twenty-six retrobulbar regions of 13 patients with suspected active GO were acquired 20 min after administering 400 MBq [Tc-99m]DTPA (128 projections x 30 sec, 128x128 matrix with ... mm pixel size); followed by a CT (120 kV, 40 mAs, 1.5 pitch, 90/min rotation with abdomen filter). OSEM iterative reconstruction included CT-based attenuation correction, Monte Carlo-based scatter correction, and resolution recovery. We drew three sets of VOIs, utilizing both SPECT and CT information. Method A: 2 cm diameter sphere to the retrobulbar area showing the highest uptake; method B: a cone covering the whole retrobulbar territory; and Method C: an 1 mL standard sphere to the highest activity in the retrobulbar area. The uptake was expressed as (a) activity concentration, (b) total VOI activity, or (c) maximal concentration; each normalized to the injected dose. The same parameters were tested when normalized to body weight as well. For each quantitative measure Pearson's r, and Kendall's tau-b correlation coefficients were calculated with the former method as reference. **Results:** Total and maximal VOI uptake values as well as measures corrected for body weight showed weaker correlation with the reference method than mean activity concentrations. We obtained better correlation with the larger sphere (2 cm vs. 1.2 cm diameter), and even slightly better with the conical VOI. **Conclusion:** We found that defining the retrobulbar area is much easier when utilizing the CT image as well. For the sake of simplicity and reproducibility, we select the sphere with 2 cm diameter as the VOI of choice, since drawing the conical region is more subjective. As the present analysis aimed at the best correlation with the reference method that did not take body size into account, we plan to consider activity concentration normalized to body weight as well during the forthcoming clinical evaluation based on a larger patient group. **References:** None.

EP-0233

Parathyroid Imaging With ^{18}F-fluorocholine PET/CT As A First Line Imaging Modality In Primary Hyperparathyroidism, A Retrospective Cohort Study

W. Broos, M. Wondergem, R. J. J. Knol, F. M. van der Zant; Northwest Clinics, Alkmaar, NETHERLANDS.

Aim/Introduction: ^{18}F-fluorocholine (FCH) PET/CT is a promising technique for visualizing hyperfunctioning parathyroid tissue in hyperparathyroidism. It is still under debate whether to use this technique as a first line imaging modality, or to use it when conventional techniques such as ^{99m}Tc-sestamibi scintigraphy or ultrasonography are inconclusive. This study evaluates FCH PET/CT as a first line modality. **Materials and Methods:** Patients with primary hyperparathyroidism, referred between June 2015 and December 2018 for FCH PET/CT as

first line imaging method, were included in this study. Baseline characteristics, clinical data, scan results and type of treatment were recorded. The detection rate was calculated on a per patient-based and a per lesion-based analysis. The reference standard comprised histopathological results, intraoperative response to parathyroidectomy and clinical follow-up. **Results:** Two hundred and seventy-two patients were included, of which 139 patients underwent parathyroidectomy, 47 were treated with calcimimetics and 86 patients received further follow-up without active treatment. For the surgical treatment group (77% women and 23% men, mean age 60 years, range 29-81), the detection rate was calculated. A single adenoma was detected in 127 scans, double adenoma in three scans, and in one scan three hyperfunctioning glands were detected. In eight scans, no lesions were visualized. A total of 154 parathyroid glands were surgically removed. Calculated patient-based detection rate was 95% and lesion-based detection rate was 90%. **Conclusion:** This retrospective cohort study shows high detection rates of FCH PET/CT in primary hyperparathyroidism, which is in accordance to literature. Use of FCH PET/CT as a first line imaging modality in preoperative planning of parathyroid surgery seems an appropriate choice. **References:** None.

EP-0234

^{18}F-Choline digital PET/CT Imaging for parathyroid adenoma detectability

C. Provost, R. Brahmi, C. Leite Nascimento, S. Hescot, L. Champion; Institut Curie, Saint Cloud, FRANCE.

Aim/Introduction: Primary hyperparathyroidism is a common endocrine disorder and about 85% is caused by a solitary adenoma of the parathyroid glands. In the 90s, PET modality was introduced to increase diagnostic performance for localization of parathyroid adenoma. Several PET tracers have been evaluated and one of them, choline-based PET tracer, a precursor for the biosynthesis of phospholipids, appears to be promising. In clinical practice, ^{18}F-choline PET/CT has acquired general acceptance to localize parathyroid adenoma but it remains unclear whether it could replace conventional scintigraphy with 99mTc-sestamibi SPECT/CT. In our preliminary study, ^{18}F-Choline is more efficient than conventional scintigraphy in parathyroid adenoma diagnostic, confirmed by pathology results. Moreover, digital PET/CT, equipped by new type of scintillation detector and digital photon counters increased the lesion detectability [1]. **Materials and Methods:** 7 patients, with a mean age of 73 years old [51-85], underwent ^{18}F-Choline PET/CT because of inconclusive diagnostic of suspicious parathyroid adenoma after normal 99mTc-sestamibi scintigraphy. For 5 patients, neck ultrasound was performed: 3 normal and 2 suspicious. PET images were performed in Vereos digital PET/CT (Philips) with 2.5 MBq/kg of 18F-Choline. Acquisition was centered on the cervicothoracic region (1 min/bed position), 20 minutes after tracer injection. Curative surgery was performed for 4 patients with pathology results, and planned for 3 patients. **Results:** PET/CT revealed 8 lesions in all 7 patients. Detected size lesions were between 2.5 x 5.5 mm and 7 x 11 mm. SUV max uptake values ranged from 3.4 to 12.9 with a mean of 6.7 and a median of 5.5. In our cohort, we detected at least one lesion in 7/7 patients (sensitivity of 100%). Pathology analysis confirmed the diagnosis for the 4 patients who underwent surgery. **Conclusion:** As already shown, ^{18}F-Choline PET/CT allows to detect hyperactivity of parathyroid glands before surgery. In the last 5 years, published studies generally described lesions above 5mm with scan duration between 2 to 10 min/bed position and dose between 1.5 to 3.5 MBq/kg. In our preliminary study, PET/CT was rapid and efficient, allowed to detect parathyroid adenomas of less than 3 mm with a dose of 1.5 MBq/kg and 1 min/bed position acquisitions. In addition, PET/CT was more sensitive than ultrasound imaging modality. **References:** [1] Degenhardt C, Rodrigues P, Trindade A, et al. Performance evaluation of a prototype positron emission tomography scanner using digital photon counters (DPC). IEEE Nucl Sci Symp Med Imaging Conf Rec. 2012:2820-2824.

EP-0235

Association Between ^{18}F-FDG PET/CT Findings and Bone Mineral Densitometry Results

A. Hassanzadeh-Rad, H. Amini, M. Eftekhari, B. Fallahi, A. Fard-Esfahani, A. Emami-Ardekani, D. Beiki;
Research Center for Nuclear Medicine, Shariati Hospital, Tehran University of Medical Sciences, Tehran, IRAN, ISLAMIC REPUBLIC OF.

Aim/Introduction: Osteoporosis is a major risk factor for skeletal fractures. Patients with malignancies are at risk for trabecular bone loss leading to osteopenia or osteoporosis. Hence, prompt diagnosis of osteopenia or osteoporosis has significant value to avoid fractures. Decreased bone marrow metabolism may be observed in subjects with decreased Bone Mineral Density (BMD), possibly in response to adipose tissue deposition in the bone marrow. We aim to correlate ^{18}F-FDG PET/CT findings with bone mineral densitometry results in order to suggest Dual-Energy X-ray Absorptiometry (DEXA) for some patients. **Materials and Methods:** After excluding patients with major confounding variables, 105 patients referred for ^{18}F-FDG PET/CT were included. Prior to FDG PET/CT study, bone mineral densitometry was performed by DEXA. Semi-quantitative and quantitative analyses were done on both DEXA and FDG PET/CT results. BMD, T-score, Z-score , Standardized Uptake values (SUVmax and SUVmean) and Hounsfield Units (HUmax and HUmean) were calculated for all three Regions Of Interest (ROIs) (trabecular bones of lumbar vertebrae and bilateral femoral necks). To find out correlation between these findings, statistical analysis was performed using SPSS version 22 (SPSS Inc, Chicago, IL). **Results:** Mean SUVmax,SUVmean,HUmax and HUmean were greatest in patients with normal BMD, followed by osteopenic and osteoporotic patients in all three ROIs (P-values < 0.0001) with significant positive Pearson's correlation between SUVs and T-scores. Using Receiver Operating Characteristic (ROC) curve analysis, trabecular lumbar vertebrae SUVmax could distinguish group of patients with diminished BMD from normal group with

L1-L4 SUVmax cut-off value=2.78 (sensitivity=78 %, specificity= 72 %, P-value < 0.0001). Considering left femoral neck SUVmax=1.59, ROC curve analysis was also able to distinguish two groups with normal and abnormal BMDs (sensitivity=80 %, specificity=82 %, P-value < 0.0001). More or less similar results were obtained with HUs and SUVs of all other corresponding ROIs. **Conclusion:** Findings of this study strongly suggest meaningful positive correlations between metabolic activities of trabecular bones in lumbar vertebrae and bilateral femoral necks and BMDs of these regions. By applying SUVmax cut-off values obtained in this study for all three corresponding ROIs, ^{18}F-FDG PET/CT may be used as a screening tool and in addition to main findings regarding metabolic activities of tumoral lesions, those patients with corresponding SUVmax below the cut-off values calculated in this study can be referred for DEXA, leading to prompt diagnosis of trabecular bone loss and may avoid osteoporotic fractures with earlier treatment. **References:** None.

EP-0236

Establishing F18- fluorocholine PET as a Second Line Imaging Technique in the Localization of Parathyroid Adenomas before Surgery in Patients with Primary Hyperparathyroidism and Negative or Inconclusive Neck Ultrasonography and Sestamibi Imaging

S. Röck[1], *C. Barkhausen*[2], *P. T. Meyer*[1], *C. Goetz*[1];
[1]*Department of Nuclear Medicine, Medical Center of the University of Freiburg, Faculty of Medicine, University of Freiburg, Freiburg, GERMANY,* [2]*EURO-PET GmbH, Medical Center of the University of Freiburg, University of Freiburg, Freiburg, GERMANY.*

Aim/Introduction: Localization of pathologic parathyroid glands in patients bearing primary hyperparathyroidism (PHPT) is recommended before carrying out targeted minimal invasive surgery in single parathyroid lesion thus potentially reducing the durations of surgery and the rate of complications. Preoperative localization may also prevent failures of surgical treatment related to multiglandular disease or ectopic parathyroid glands. Our aim was to investigate the accuracy of a choline-based tracer in localizing parathyroid adenoma (PTA) in case of negative or inconclusive ultrasound and scintigraphic results. **Materials and Methods:** A total of 37 patients (mean age 64 +/- 13 years, 70% female) biochemical diagnosed with PHPT and referred in our institution to localize PTA were retrospectively pooled. All included patients underwent neck ultrasonography and Tc99m-MIBI imaging prior to PET. Both methods failed to detect a PTA and an additional F18-fluorocholine PET with subsequent low-dose CT was performed before allowing a focused surgical approach. Mean Parathyroid hormone level were 134 pg/ml and Calcium 2.68 mmol/l. Early (15 minutes p.i.) and late (60 minutes p.i.) PET-images of the neck and upper mediastinum were acquired after injection of 165 +/- 26 MBq F18-fluorocholine (Vereos Digital PET/CT, Philips Medical Systems B.V., Eindhoven, The Netherlands) and iteratively reconstructed using PSF-modeling, scatter and attenuation corrections. Results were scored positive, inconclusive or negative after double blind reading and were compared to the surgical and pathological findings and the biochemical follow-up. **Results:** PTA could be clearly detected in 25 patients (68%) and all the location predicted by our hybrid PET/CT imaging matched surgical findings as well as follow-up. PET was rated as negative in 9 cases and 3 patients were rated as inconclusive or showed discordances between the two experienced readers. Only one of these negative patients was referred to neck dissection at the time of writing. Histological sections revealed lymph nodes in the retro-thyroid space, but no PTA. Late PET-imaging showed better diagnostic performance in detecting PTA (sensitivity, specificity, PPV and NPV were respectively 0.77, 1.00, 1.00 and 0.33 for early imaging and 0.88, 1.00, 1.00 and 0.50 for late imaging). No statistically significant difference was found between both readers. **Conclusion:** Our preliminary results demonstrate the high accuracy of F18-fluorocholine PET/CT to detect PTA in PHPT-patients with negative or inconclusive neck ultrasonography and sestamibi imaging. It may replace first line conventional imaging techniques in preoperative planning of parathyroid surgery. Larger, prospective studies are needed to confirm these findings. **References:** None.

EP-0237

Parathyroid imaging by ^{18}F-Fluorocholine PET/MR in patients with hyperparathyroidism

B. Emsen[1], *S. Mule*[1], *E. Evangelista*[1], *R. Braham*[2], *L. Baranes*[1], *J. Chalaye*[1], *L. Lerman*[1], *M. Abulizi*[1], *C. Dubouchet*[1], *O. De Barry*[1], *E. Calvo-Bota*[1], *S. Sahbai*[1], *J. Israel*[1], *A. Luciani*[1], *E. Itti*[1];
[1]*SyMPTOm PET/MRI platform, Henri Mondor Hospital, Créteil, FRANCE,* [2]*Department of Endocrinology, Henri Mondor Hospital, Créteil, FRANCE.*

Aim/Introduction: We sought to evaluate the diagnostic performance of ^{18}F-Fluorocholine (FCH) PET/MR imaging to identify parathyroid glands in patients with hyperparathyroidism (PHPT). **Materials and Methods:** 13 patients with PHPT were retrospectively included. PET/MR images were acquired on a Biograph mMR scanner (Siemens, Erlangen, Germany), 10 min after injection of 4.5 MBq/kg FCH, and consisted of 2 emission steps over the neck and chest for 15 min; simultaneously, MR imaging included T1 and T2 (STIR) weighted sequences, diffusion weighted sequences, and post-gadolinium T1 (VIBE) enhancement. Results were interpreted blindly by a radiologist and a nuclear medicine physician. Some patients already had a dual-isotope ^{123}I/^{99m}Tc-sestaMIBI parathyroid scintigraphy (n = 8) or/and neck ultrasonography (US) (n = 13). In some instances, FCH PET/MR was performed after inconclusive or discrepant results between these two modalities. **Results:** Average [extremes] patient age, calcium level and parathyroid hormone (PTH) level were 71 years [58-91], 2.82 mmol/L [2.53-3.45] and 118.89 ng/L [34-277], respectively. A positive PET (i.e. identification of abnormal FCH uptake) was found in 9 patients (69%), with an average SUVmax of 4.5 [2.6-9.1]. Only 4 patients underwent a parathyroidectomy, confirming the results of

PET. Higher parathyroid uptake was observed compared to physiological thyroid uptake (SUVmax = 2.96 [2.0-4.1], P = 0.01). Among the 9 positive PET, only 4 were positives on MR after blinded interpretation, but second unblinded interpretation (in view of the PET results) allowed the radiologist to identify the remaining 5 parathyroid glands. No case of positive MR but negative PET was observed. No case of ectopic mediastinal focus of uptake was observed. In only one patient, we founded 2 foci of abnormal uptake. PET was positive in 37.5% of patients with a negative sestaMIBI scintigraphy and in 66.7% of patients with negative US. Among the 3 patients with both negative sestaMIBI and US, PET was positive in 2 cases. A trend for higher PTH level was observed with positive PET (P = 0.05), whereas no significant difference was observed between calcium level and PET results (P = 0.40). No correlation was found between calcium or PTH levels and intensity of parathyroid uptake identified on PET. Intensity of physiological thyroid uptake did not depend on the delay between injection and beginning of PET acquisition (P = 0.68). **Conclusion:** FCH PET/MR appears to be a suitable imaging tool for the evaluation of PHPT, particularly in patients with a negative dual-isotope ^{123}I/^{99m}Tc-sestaMIBI scan. **References:** None.

EP-0238

Unsupervised Image Subtraction in Parathyroid Scintigraphy as a Prerequisite for Machine Learning

I. Marikova[1,2], *J. Trnka*[1,2], *D. Chroustova*[1,2], *D. Zogala*[1,2], *M. Samal*[1,2]; [1]*Charles University, 1st Faculty of Medicine, Prague, CZECH REPUBLIC,* [2]*General University Hospital, Prague, CZECH REPUBLIC.*

Aim/Introduction: Despite progress in imaging techniques and image processing, detection of parathyroid adenomas remains challenging. Therefore the examination is an obvious candidate for testing the machine learning approach using k-means clustering and classification methods. A prerequisite for machine learning is to select the features with good predictive power. The aim of our study was to test principal component analysis (PCA) of double-tracer parathyroid scintigraphy for automatic subtraction of 99mTc-pertechnetate from 99mTc-MIBI images. Our hypothesis was that PCA will emphasize differences between the two images regardless of their different scaling. **Materials and Methods:** In a pilot study, we have examined data of sequential double-tracer parathyroid SPECT in 15 consecutive patients selected from a database. Before principal component analysis, the data were registered in 3D using in-house written software. Principal component analysis was performed in Matlab (www.mathworks.com). With the two input images (99mTc-MIBI and 99mTc-pertechnetate), PCA results in two principal components (PC). In fact, it rotates original image coordinates (the axes of the graph with pixel values of the two images plotted against each other) in such a way that the first PC approximates the average image and the second PC the differences between the two original images. An advantage of PCA is that 'subtraction' does not need user interaction. PCA was applied to transversal, frontal and sagittal slices reconstructed from SPECT data and its results were visually compared with the results of routine interactive subtraction procedure. **Results:** In 15 patients, there was an agreement between visual assessment of PCA and standard difference images. Seven clearly positive findings were easily recognized with PCA, too. In 8 equivocal findings (low uptake, small lesions, tissue overlaps, residual misregistration artefacts) PCA did not help to resolve the problem producing equivocal results either. Visual assessment of interactively subtracted images seemed to be somewhat less sensitive to misregistration while PCA was much faster without any user interaction. **Conclusion:** In a pilot study, diagnostic information obtained from PCA was equivalent to that obtained by interactive subtraction procedure. Good performance of both methods requires perfect registration of input images. Image features extracted automatically by PCA are potentially useful in machine learning. Performance of machine learning procedures in double-tracer parathyroid scintigraphy will depend on their ability to differentiate residual misregistration artefacts from pathological uptake of the tracer in one of the two images. **References:** None.

EP-0239

Molecular Imaging to the surgeons rescue: 68Gallium-DOTA-exendin-4 PET/CT in pre operative localisation of Insulinomas

P. U N*, D. B Sen, D. Thakral;*
Fortis memorial research institute, Gurgaon, INDIA.

Aim/Introduction: Insulinoma is an islet-cell adenoma that secretes insulin. It is usually localized to the pancreas and is often the most common cause of endogenous hyperinsulinemic hypoglycaemia in non-diabetic adult patients. Surgical excision with a curative intent is the standard modality of treatment, and it requires precise localization of tumor tissue. 68Gallium-DOTA-exendin-4 PET/CT scan is a clinically reasonable and sensitive scan for the identification of insulinoma. The aim of this retrospective study was to determine the overall accuracy of 68Gallium-DOTA-exendin-4 PET/CT scan in the detection of insulinoma. **Materials and Methods:** Eight patients with fasting hyperinsulemic hypoglycaemia with neuroglycopenic symptoms were enrolled in this study. Whole body PET/CT scan was performed on a Philips time of flight PET/CT scanner, 60 minutes after injection of 68Gallium-DOTA-exendin-4. The imaging findings were compared to the histopathological diagnosis in six out of eight patients and to subsequent follow up in the remaining two patients who did not undergo surgery. **Results:** The sensitivity and specificity of 68Gallium-DOTA-Exendin-4 PET/CT scan in insulinoma detection was found to be 75% and 100% respectively. Overall accuracy was 87.5%. **Conclusion:** 68Gallium-DOTA-Exendin-4 PET/CT scan is highly sensitive for identification and exact localization of insulinoma which can guide better surgical exploration. However randomised controlled trials are needed to assess the accuracy of 68Gallium-DOTA-Exendin PET/CT scan in localization of insulinoma. **References:** None.

EP-0240

Optimizing ^{18}F-Fluorocholine PET/CT procedures in parathyroid imaging: a proposal

I. Bossert[1], *M. Hodolic*[2,3], *S. Chytiris*[4], *D. D'Ambrosio*[5], *A. Marchetto*[1], *C. Vellani*[1], *L. Croce*[4], *B. Rivolta*[6], *L. Chiovato*[4], *G. Trifirò*[1];
[1]*Nuclear Medicine Unit, Istituti Clinici Scientifici Maugeri Spa SB IRCCS, Pavia, ITALY,* [2]*Nuclear Medicine Research Department, Iason, Graz, AUSTRIA,* [3]*Nuclear Medicine Department, Faculty of Medicine and Dentistry, Palacký University, Olomouc, CZECH REPUBLIC,* [4]*Unit of Internal Medicine and Endocrinology, Istituti Clinici Scientifici Maugeri Spa SB IRCCS, Pavia, ITALY,* [5]*Medical Physics Unit, Istituti Clinici Scientifici Maugeri Spa SB IRCCS, Pavia, ITALY,* [6]*Endocrinology Unit, Istituto Clinico Città di Pavia, Pavia, ITALY.*

Aim/Introduction: Identification of pathological parathyroid glands in primary hyperparathyroidism, traditionally based on neck ultrasound (US) and/or ^{99m}Tc-SestaMIBI (MIBI) scintigraphy, is often challenging. PET/CT with ^{18}F-Fluorocholine (FCH) can improve detection of pathologic parathyroid glands, thanks to its better spatial resolution and lesion-to-noise ratio with respect compared to MIBI scan. Currently, Authors apply different protocols, with variations in administered activity, scanning time and bed time duration. The aim of our study was to propose a protocol for the FCH-PET/CT imaging which can optimize every variable preserving the good quality of the exam. **Materials and Methods:** We reviewed the literature of the past 4 years about FCH PET/CT in parathyroid imaging. On the basis of these results and of our PET/CT scanner (DIscovery 690 VCT, GE Healthcare) we decided to inject less than 2,5 MBq/kg of FCH, perform a dual-time point PET/CT acquisition at 15 and 60 minutes after the injection with a duration of 3 minutes per bed (neck and upper mediastinum), and to skip dynamic acquisition. To test our method we plan to enroll 50 patients with primary o tertiary hyperparathyroidism and negative or inconclusive conventional sestaMIBI scan. PET results will be confirmed with cito-hystological examination whenever possible. **Results:** We noticed a high eterogenity about injected activity, timing and protocol acquisition in literature. Until now, we prospectively enrolled 16 patients. We administered a median activity of FCH of 2,3 MBq/kg (range 2,1-2,46), for a median amount of activity of 173,6 MBq per patient (range 112,9-246,7). FCH-PET/CT was positive in 15 out of 16 patients. One patient had bilateral lesions (patient undergoing dialysis) and 1 patient had a focal FCH uptake in the supero-anterior mediastinum. So far only two patients had a cito-hystological confirmation of FCH PET result. **Conclusion:** Although we have a small number of patients, our method showed a good sensitivity allowing a reduction in patient's dose and exposure, bed time duration and avoiding dynamic acquisition, resulting in an easier patient's management. **References:** - J Endocrinol Invest. 2019 Apr;42(4):419-426. doi: 10.1007/s40618-018-0931-z. Epub 2018 Aug 9.PETC/CT with 18F-Choline localizes hyperfunctioning parathyroid adenomas equally well in normocalcemic hyperparathyroidism as in overt hyperparathyroidism.Bossert I, Chytiris S, Hodolic M, Croce L, Mansi L, Chiovato L, Mariani G, Trifirò G. - Nucl Med Commun. 2019 Feb;40(2):96-105. doi: 10.1097/MNM.0000000000000952. Choline PET/CT in parathyroid imaging: a systematic review. Broos WAM1, van der Zant FM, Knol RJJ, Wondergem M.

EP-13

Clinical -> Diagnostic study -> Adult study -> Non-oncology study -> Endocrinology -> Thyroid, benign

October 12 - 16, 2019 e-Poster Area

EP-0241

Patients with Hashimoto Nodular Goiter: Relation to Differentiated Thyroid Carcinoma and Outcome

J. Mihailovic, *J. Roganovic, V. Cimbaljevic, D. Stojanovic;*
Institute of Oncology, Sremska Kamenica, SERBIA.

Aim/Introduction: To analyze patients with Hashimoto nodular goiters, the relation between autoimmune disease and differentiated thyroid carcinoma (DTC) and outcome of DTC. **Materials and Methods:** This retrospective study included 4447 patients with thyroid nodules who were treated in a single institution between 2007 and 2018. Out of 4447 patients who underwent surgery, 700 were histologically confirmed as differentiated thyroid carcinoma (DTC), while 158/700 (22.6%) DTC patients had Hashimoto thyroiditis. Median patients' follow-up was 51.5 months (range, 2-134 months). A multivariate logistic regression analysis was used to analyze the Hashimoto thyroiditis as a predictive factor for thyroid malignancy. **Results:** Among 700 DTC patients, 158 (22.6%) patients had autoimmune disease [140 (88.6%) females and 18 (11.4%) males; <45 years= 33 (20.9%), ≥45 years=125 (79.1%) patients; mean age 57.8 years, (range, 22-88 years). All DTC patients underwent total thyroidectomy. Radioiodine therapy was applied in 45/158 (28.5%) patients, once or in several course if needed, according to the Tumor Board decision. Cumulative activity of I-131 ranged between 3.7-22.2GBq. The significant independent predictors of thyroid malignancy are: gender (p<0.001), age ≤45 years (p<0,001), and Hashimoto thyroiditis (p= 0.035). At the last follow up, all patients were alive. Complete remission was achieved in 111 (70.3%) patients, partial remission in 5 (3.2%) patients, stable disease in 3 (1.9%) patients, and proggressive disease in 39 (24.6%) patients. There were no disease-related deaths. **Conclusion:** Gender, age and Hashimoto thyroiditis are strong independent predictors for thyroid malignancy in patients with thyroid nodules. Adequate diagnostics is necessary in patients with thyroid nodules, in particular in males, elderly and Hashimoto thyroiditis. If treated properly, DTC patients related to Hashimoto nodular goiter have good prognosis, survival and outcome. **References:** 1. Jonklaas J, Sarlis NJ, Litofsky D, et al. Outcomes of patients with differentiated thyroid carcinoma following initial therapy. Thyroid 2006;16:1229-1242. 2. Haugen BR, Alexander EK, Bible KC, Doherty GM, Mandel SJ, et al. 2015 American Thyroid Association Management Guidelines

for Adult Patients with Thyroid Nodules and Differentiated Thyroid Cancer. The American Thyroid Association Guidelines Task Force on Thyroid Nodules and Differentiated Thyroid Cancer. Thyroid 2016;26:1-133. 3. Sawka AM, Brierley JD, Tsang RW, Thabane L, Rotstein L, Gafni A, Straus S, Goldstein DP. An updated systematic review and commentary examining the effectiveness of radioactive iodine remnant ablation in well-differentiated thyroid cancer. Endocrinol Metab Clin North Am 2008;37:457-480.

EP-0242

The Role Of Regulatory T Cells In Pregnant And Postpartum Women With Autoimmune Thyroid Disease

T. Bogovic Crncic[1], *S. Grbac Ivankovic*[1], *N. Girotto*[1], *I. Mrakovcic Sutic*[2];
[1]*Dept. of nuclear medicine, Clinical Hospital Centre, Rijeka; University of Rijeka, School of Medicine, Rijeka, CROATIA,* [2]*Dept. of physiology and immunology, University of Rijeka, School of Medicine, Rijeka, CROATIA.*

Aim/Introduction: Regulatory T cells (T regs) are a subtype of the adoptive immune cells that have unique immune modulating capabilities and play a central role in regulation of autoimmunity. These cells actively control, induce or suppress the function of other immune cells. The aim of our study was to investigate the changes of T regs in pregnant and postpartum women with autoimmune thyroid disease (AITD) and to compare the results to normal pregnancy and postpartum. **Materials and Methods:** The study included 185 pregnant women with no prior history of thyroid disease; 111 women in 1. half of pregnancy (6-20 weeks), 74 in 2. half of pregnancy (21-36 weeks) and 77 women in postpartum period (3 weeks-9 months after delivery). Peripheral blood and sera obtained from women were screened for thyrotropin, free thyroxine, free triiodothyronine values, titres of thyroid peroxidase and thyroglobulin autoantibodies as well as thyrotropin receptor stimulating antibodies. According to laboratory findings women were divided into 9 groups: normal pregnancy, normal postpartum women, euthyroid pregnant and postpartum women with AITD, pregnant women with autoimmune subclinical/clinical hypothyroidism and subclinical/clinical hyperthyroidism in pregnancy and postpartum and nonpregnant controls. Peripheral blood mononuclear cells were separated from blood samples by gradient centrifugation. Simultaneous staining of surface antigens on lymphocyte subpopulations was performed and analysed on fluorescence-activated cell sorter (FACS): CD4+CD25+FoxP3. **Results:** The percentage of T reg cells was significantly higher in normal pregnancy and in euthyroid pregnant women with AITD compared to nonpregnant women. Furthermore, the percentage of T regs was significantly higher in 1. and 2. half of pregnancy in women with autoimmune subclinical/clinical hypothyroidism and hyperthyroidism compared to normal pregnancy. The percentage of T regs was also significantly higher in euthyroid postpartum women with AITD and in postpartum women with autoimmune subclinical/clinical hypothyroidism and hyperthyroidism compared to control postpartum women. **Conclusion:** Significantly higher percentage of T regs in normal pregnancy indicates that these cells have a central role in regulating immune responses during pregnancy. Furthermore, our results suggest that T regs might be the key players in inducing the immune tolerance mechanisms in pregnant and postpartum women with AITD. **References:** None.

EP-0243

Diagnostic Algorithm for Assessment of Papillary Thyroid Carcinoma in Presence of Hashimoto Thyroiditis

V. Sukhov[1], *K. Zaplatnikov*[2];
[1]*NRCEM, St.Petersburg, RUSSIAN FEDERATION,* [2]*MAZ Nuclear Medicine Clinic, Nürnberg, GERMANY.*

Aim/Introduction: Papillary thyroid carcinoma (PTC) is not infrequently diagnosed yet not very aggressive form of thyroid cancers, especially in iodine-deficient areas. Hashimoto thyroiditis (HT) is a frequent autoimmune thyroid disease, known to be the most common cause of hypothyroidism in nonendemic goiter areas. Coexistence of these two diseases is possible but not often; although such cases are especially difficult for diagnostics in presence of so-called „gray zones": many hypoechogenic pseudonodules in HT, and poorly-differentiated PTC can show concurrent cancer types with foci of high grade changes (necrosis, focal loss of papillary-type nuclei, and foci with overall aberrant morphology). The fine needle aspiration is not possible for all patients, so we tried to establish algorithm for differential diagnosis. **Materials and Methods:** Patients with PTC/HT(+) (Gr.A, n=27) and PTC/HT(-) (Gr.B, n=32) were prospectively studied. We analysed age, sex, location, clinical data, tumor dimensions, angioinvasion, capsular infiltration, multifocality and lymphnode metastases, therapy history by means of consequentially performed clinical examination, thyroid hormone (fT4, fT3, TSH) and anti-TPO/anti-Tg antibodies levels assessment, thyroid sonography with Doppler DS, 99mTc-scitigraphy, MIBI-scitigraphy and FNAC. Every case of PTC was confirmed by patho-histological examination. **Results:** Statistically significant (P=0.001) difference in tumour size was found in two Groups: the average diameter was found to be 1.721+/-0.5812 and 1.145+/-0.871 cm in Gr.A and in Gr.B, respectively. Capsular infiltration was present only in Gr.A in 3 cases. The angioinvasion was found in 8 cases of Gr.A and 1 cases in Gr.B (P=0.310). Multifocality was found in 19 patients in Gr.A and in 2 in Gr.B (P=0.0009). There were no statistical differences in sex (P=0.423) and age (P=0.330). All pts in Gr.A expressed high levels of thyroid Abs. 51.5% Abs+ pts with US suspicious multifocal non-uniform thyroid goiter revealed scintigraphic cold lesion, in Gr.B 60% nodes were undetectable in scans. Informativity of 33% of Gr.A pts MIBI-scans was low for focal uptake by reason of high background in thyroid tissue and all pts of Gr.B had distinctive foci with retention at delayed images. More than 50% of Gr.A pts had nodules with histologicaly proven features of poorly-differentiated (solid variant) PTC. **Conclusion:**

We justified necessity of screening for PTC in population with concomitant HT, as potentially predisposable for malignization and assuming them to have more aggressive tumors. Combined data of clinical and laboratory examination, US with Doppler, 99mTc- and MIBI-thyroid scans, US guided FNAC (in some cases) will guarantee a precise diagnosis. **References:** None.

EP-0244

The Incidence of Thyroid Nodules Incresases with Age in Women of Reproductive Age

K. Zaletel[1], *E. Pirnat*[1], *T. Ušaj*[2], *K. Tuta*[2], *K. Bajuk Studen*[1], *N. Bedernjak Bajuk*[1], *M. Jesenko*[1], *N. Ostaševski Fernandez*[1], *S. Gaberšček*[3];
[1]*Department of Nuclear Medicine, University Medical Centre Ljubljana, Ljubljana, SLOVENIA,* [2]*Faculty of Medicine, University of Ljubljana, Ljubljana, SLOVENIA,* [3]*Department of Nuclear Medicine, University Medical Centre Ljubljana; Faculty of Medicine, University of Ljubljana, Ljubljana, SLOVENIA.*

Aim/Introduction: By ultrasound examination, thyroid nodules are found in 19 to 65% of unselected individuals. In the older age groups, the incidence of thyroid nodules increases with age. In the younger age groups as well as in pregnant women, data on the incidence of thyroid nodules is scarce. The aim of our study was to establish the incidence of thyroid nodules in pregnant and non-pregnant women of reproductive age. **Materials and Methods:** In this prospective clinical study we included 142 pregnant and 306 non-pregnant female volunteers of reproductive age. Women with the known thyroid disease were not included in the study. In every volunteer, thyroid ultrasound was performed using a 7.5-MHz linear transducer. The number of volunteers with thyroid nodules was detected. **Results:** Pregnant women were significantly older than non-pregnant women (32.9±5.1 and 29.8±7.1 years, respectively, $p<0.001$). Thyroid nodules were detected significantly more frequently in pregnant than in non-pregnant women (21.2% and 12.7%, respectively, $p=0.032$). Furthermore, in the larger group of non-pregnant women of reproductive age, the frequency of thyroid nodules significantly increased with age ($p<0.001$). In the age group up to 24 years, thyroid nodules were detected in 4.1% of women, in the age group 25-30 years, thyroid nodules were detected in 7.2%, in the age group 31-35 years, thyroid nodules were detected in 12.7%, and in the age group above 35 years, thyroid nodules were detected in 31.2% of women. **Conclusion:** Our results show that the incidence of thyroid nodules in women of reproductive age significantly increases with age. With the increasing age of pregnant women, beside Hashimoto's thyroiditis also thyroid nodules may represent a challenge in the screening strategy. **References:** None.

EP-0245

The Role of Pertechnetate Thyroid Scintigraphy in the Initial Workup of a Thyroid Diseases

T. Andjelkovic*, F. Velickovic, M. Rajic, M. Stevic, M. Vlajkovic;*
Center of Nuclear Medicine, Clinical center Nis, Nis, SERBIA.

Aim/Introduction: With the emergence of new echosography techniques accompanied by a thin needle biopsy, Tc-99m-perthnetate scintigraphy of the thyroid gland has lost its diagnostic primacy even though it is still almost routinely indicated in patients with thyroid gland diseases.The aim of this paper was to analyze the diagnostic contribution of the findings obtained by the Tc-99m-perthnetate scan in patients who are referred to thyroid gland scintigraphy during the initial workup. **Materials and Methods:** We retrospectively analyzed the findings of 350 subjects, 296 women and 54 men aged 56.4 ± 13.4 years in whom scintigraphy with Tc-99m-perthnetate was indicated for the first time due to suspected thyroid gland disease. Ultrasound examination of the thyroid gland was performed in all subjects, as well as some of the following laboratory analyses: thyrotrophic hormone, free thyroxin, thyroid-peroxidase and thyroglobulin antibody, thyroglobulin, calcitonin. **Results:** Multinodular goiter was the most commonly obtained scintigraphy finding on Tc-99m-pertechnetate scan, as it was diagnosed in 164 patients (46.9%), in 103 of whom the findings had additional diagnostic significance. In all 17 examinees (4.9%) with autonomous thyroid nodules findings and 26 (7.4%) with diffuse toxic goiter, the scintigraphic finding were useful for deciding on the further treatment either by radioiodine therapy or by surgery. Solitary cold nodules were detected in 87 subjects (24.9%), in 82 of whom scintigraphic findings had additional diagnostic significance for the evaluation of the nature of the nodules. Five subjects were diagnosed with smaller, insignificant nodules. An "empty" scintigram was detected in 10 subjects (2.9%) and all scintigraphy was of great significance for the confirmation of either subacute or amiodarone caused thyroiditis. Microscopic nodular goiter was detected in 46 subjects (13.1%) and the scan results showed additional diagnostic significance only in 18 patients. In the total of 256 subjects (73.1%) with thyroid gland diseases the Tc-99m-pertechnetate scan had additional diagnostic significance in the initial workup. **Conclusion:** The results of this study have shown that the scintigraphy Tc-99m-pertechnetate scintigraphy continues to be significant in the initial diagnostics of thyroid gland diseases. This simple procedure provides valuable information for reaching the final diagnosis as well as making the decision concerning additional testing or thyroid gland diseases treatment. **References:** None.

EP-0246

Ectopic Thyroid Glands - Presentation of Six Cases with Diagnostic and Therapeutic Approach

T. Jukic[1,2], *I. Mihaljević*[3], *I. Blažeković*[4], *M. Ivkić*[5], *M. Franceschi*[1,2];
[1]*University Department of Oncology and Nuclear Medicine, Sestre Milosrdnice University Hospital Centre, University of*

Zagreb, School of Medicine, Zagreb, CROATIA, [2]Faculty of Medicine Osijek, Josip Juraj Strossmayer University of Osijek, Osijek, CROATIA, [3]Clinical Institute of Nuclear Medicine and Radiation Protection, University Hospital Osijek , Faculty of Medicine Osijek, Josip Juraj Strossmayer University of Osijek, Osijek, CROATIA, [4]University Department of Oncology and Nuclear Medicine, Sestre Milosrdnice University Hospital Centre, Zagreb, CROATIA, [5]Unimedic Centre, Zagreb, CROATIA.

Aim/Introduction: Ectopic thyroid gland is a rare entity. It may be located anywhere from the base of the tongue to the mediastinum. Other locations are rare. Six patients (pts) with ectopic thyroid glands are presented: four with lingual and two with submandibular ectopic thyroid tissue. **Materials and Methods:** Median pts age at the time of presentation of lingual thyroid was 24 (15 - 36) years, while ectopic thyroid tissue in right submandibular region was recorded in 49-year old male and 57-year old female patient. Diagnostic approach included serum thyroid hormones and thyrotropin (TSH), thyroid scintigraphy with 99m-TcO4- or I-131 SPECT/CT, neck ultrasound (US), magnetic resonance imaging (MRI), fine needle aspiration biopsy (FNAB) and endoscopy. **Results:** Patients with lingual thyroid presented with swelling at the base of the tongue and dysphagia while pts with submandibular thyroid tissue presented with swelling in submandibular region. All pts with lingual thyroid and a male patient with submandibular thyroid had subclinical hypothyroidism at the time of diagnosis and L-thyroxine (L-T4) was introduced. A 25-year old female patient with large lingual thyroid and dysphagia was treated with laser surgery. A 28-year old female patient with lingual and pre-hyoid thyroid tissue and no symptoms is under follow up on L-T4 therapy during the last 5 years. Two male pts with lingual thyroid aged 15 and 36 years and dysphagia were referred to surgery. A 49-year old male patient with ectopic thyroid tissue in right submandibular region had previous diagnosis of congenital hypothyroidism. However, he stopped L-T4 before presentation. Ectopic thyroid was surgically removed and pathohistology revealed normal thyroid tissue. A 77-year old euthyroid female patient with ectopic thyroid tissue in right submandibular region has normally located right thyroid lobe while left lobe was surgically removed due to nodular goiter. Ectopic submandibular thyroid tissue was diagnosed 20 years ago and followed-up with US without progression in size. Thyroid scintigraphy with SPECT/CT diagnosed ectopic thyroid tissue in all pts. FNAB was performed in submandibular and pre-hyoid ectopic thyroid tissue locations. MRI was performed to reveal anatomic relations with other structures. Patients were followed-up with US and TSH. **Conclusion:** Subclinical hypothyroidism was common finding in pts with ectopic thyroid gland. Surgery is the preferred treatment of choice in pts with symptoms. However, pts without symptoms and signs of malignancy can be followed-up on L-T4 therapy. Ectopic thyroid tissue was diagnosed in adult age in almost all patients. **References:** None.

EP-0247

Scintigraphic findings in a patient with hyalinizing trabecular tumour of the thyroid

***J. Baumgarten**, C. Happel, K. Jung, D. Gröner, A. Sabet, F. Grünwald; University Hospital Frankfurt, Frankfurt, GERMANY.*

Aim/Introduction: Hyalinizing trabecular tumors (HTT) of the thyroid are relatively rare and mainly benign neoplasms.The lack of defined scintigraphic characteristics as well as the considerable resemblance to malignant entities in both ultrasound and cytological examination necessitates histopathological assessment. In this report we present scintigraphic findings in a patient with HTT. **Materials and Methods:** A 25-year-old female patient was referred with a recently diagnosed nodule in the right thyroid and pressure sensation. Ultrasound showed marked hypo-echogenicity, a regular margin demonstrating taller than wide shape with no microcalcifications (ATA 4) and considerable growth from 0.6 ml to 4.9 ml. $^{99m}TcO_4^-$ scintigraphy showed an increased uptake in the right lobe and a total uptake of 0.63 %. The TSH-level of 1.31 mU/l under goiter preventive medication with levothyroxine 75 µg/d and iodine 200 µg/d was not indicative of thyroid autonomy. ^{99m}Tc-MIBI scintigraphy demonstrated a markedly increased intra-nodular uptake after 10 min and a persisting retention after 60 min. Fine needle aspiration biopsy (FNAB) showed an oxyphilic transformation of a follicular neoplasm. **Results:** Given the presence of the cervical symptoms and for definite exclusion of malignancy, hemi-thyroidectomy was performed. Histopathological workup revealed a partly follicular, partly solid trabecular tumour with a prominent hyalinization. Immune histochemistry with Ki67 and TTF-1 positivity confirmed a HTT. **Conclusion:** This is the first description of scintigraphic features of a HTT. The presented case underlines the significance of $^{99m}TcO_4^-$ scintigraphy for the diagnostic workup of thyroid nodules, especially in patients with inconclusive FNAB. **References:** None.

EP-0248

Assessment of Somatostatin Receptor Expression in Thyroid Associated Orbitopathy with ^{68}Ga-DOTANOC PET/CT

***N. Damle**, M. Angamuthu, S. Arora, K. Lata, K. Shankar, R. Meel, S. Sharma, N. Tandon, C. Bal, M. Tripathi;*
All India Institute of Medical Sciences, New Delhi, INDIA.

Aim/Introduction: Somatostatin receptor expression is seen on lymphocytes and lymphocytic infiltration is known to play a role in Thyroid Associated Orbitopathy. To assess somatostatin receptor (SSTR) expression in thyroid associated orbitopathy using ^{68}Ga-DOTANOC PET/CT and correlate with clinical activity score. **Materials and Methods:** In this ethically approved prospective study, 8 patients underwent a Ga-68 DOTANOC PET/CT 45 minutes after intravenous administration of 3 mCi (111MBq) of tracer. Scans were obtained on a 64 slice PET/CT scanner with acquisition from vertex to manubrium. All patients

were also assessed for clinical activity score (CAS) The images were visually interpreted using the following criteria- • Thickening and radiotracer uptake in extraocular muscles (EOM) • Retro-orbital fat stranding and radiotracer uptake • Enlargement and radiotracer uptake in the lacrimal gland To quantify the uptake, a ratio of EOM/Fat/Lacrimal gland to pituitary and thyroid uptake was derived **Results:** The study group comprised of 4 male and 4 female patients. The median age was 35 years (16-65 years). Four patients had clinical activity score <4 and four had a clinical activity score ≥4. All the patients who had CAS more than 4 showed one or more extraocular muscle thickening, lacrimal gland enlargement with increased DOTANOC uptake and increased uptake ratios. Inspite of retroorbital fat stranding noted in all four patients, no significant DOTANOC uptake was seen. In patients with CAS less than four, no similar findings were noted except for one patient who had subtle extraocular muscle thickening, lacrimal gland enlargement, retroorbital fat stranding with no significant tracer uptake. Spearman correlation coefficient between CAS and SSTR expression was found to be 0.775, consistent with good correlation. **Conclusion:** SSTR expression, as assessed by ^{68}Ga-DOTANOC PET/CT in Thyroid Associated Orbitopathy has significant positive correlation with clinical activity score. It can therefore be used for the assessment of disease activity as well as response to treatment in an objective manner. This may also help in screening patients with steroid resistant ophthalmopathy who are likely to benefit from long acting octreotide as a therapeutic option. **References:** 1. Krassas GE. Octreoscan in Thyroid-Associated Ophthalmopathy. Thyroid. 2002 Mar;12(3):229-31. 2. Atkinson H, England JA, Rafferty A, Jesudason V, Bedford K, Karsai L, et al. Somatostatin receptor expression in thyroid disease. International Journal of Experimental Pathology. 2013 Jun;94(3):226-9.

EP-14

Clinical -> Diagnostic study -> Adult study -> Non-oncology study -> Other clinical studies -> Gastroenterology, benign

October 12 - 16, 2019 e-Poster Area

EP-0249

Improving Diagnostic Accuracy by Application of SPECT/CT on Hepatobiliary Scintigraphy: Pictorial Essay

J. Kim[1], *K. Yoo*[1], *S. Baek*[2], *S. Lee*[1], *Y. Choi*[1];
[1]*Hanyang University Medical Center, Seoul, KOREA, REPUBLIC OF,*
[2]*Kangdong Sacred Heart Hospital, Seoul, KOREA, REPUBLIC OF.*

Aim/Introduction: Hepatobiliary scintigraphy has been used to evaluate various GB disorder. However, sometimes it is difficult to diagnose by itself or leads to discordant result with the clinical findings. Recently, hybrid single photon emission computed tomography/computed tomography (SPECT/CT) is widely accepted modality providing both anatomical and functional information, and has been used in many nuclear medicine fields. Here, we would like to share some cases where we made accurate diagnosis by application of regional SPECT-CT on hepatobiliary scintigraphy. **Materials and Methods:** All patients underwent ^{99m}Tc-mebrofenin (185 MBq) hepatobiliary scintigraphy and successive regional SPECT/CT. The SPECT images before and after fatty meal administration over the liver area were acquired for 1 min followed by low-dose spiral CT images. **Results:** SPECT/CT increased the reliability in the diagnosis of typical acute cholecystitis and chronic cholecystitis. Moreover, SPECT/CT lead to more specific diagnoses from indeterminate or equivocal findings of planar hepatobiliary scintigraphy. It was possible to make the differential diagnosis for non-visualization of GB on hepatobiliary scintigraphy as follows: acute cholecystitis with cystic duct stone, GB collapse due to chronic cholecystitis, GB filling due to prolonged NPO state, and secondary edematous GB wall thickening from liver cirrhosis. It was also useful to detect chronic cholecystitis at distal part of bicameral GB, which was not possibly interpret on planar hepatobiliary scintigraphy. It was also helpful to detect and localize biliary leakage in postoperative patients. **Conclusion:** As illustrated here, the application of SPECT-CT on hepatobiliary scintigraphy could improve diagnostic accuracy in the evaluation of various GB disorders by exact localization of GB and by specifying the scintigraphy findings, which might also affect treatment and management of the patients. **References:** None.

EP-0250

Dynamic liver scintigraphy - quantitative tool in chronic liver disease?

D. Jocius[1], *D. Vajauskas*[2], *A. E. Tamosiunas*[1];
[1]*Vilnius University Hospital Santaros Klinikos, Vilnius, LITHUANIA,*
[2]*Lithuanian University of Health Sciences, Kaunas, LITHUANIA.*

Aim/Introduction: Chronic liver disease is multi-causal liver injury affecting significant amount of people in the world. Fibrosis (and cirrhosis) is a common pathway despite multiple different etiologic factors such as viral hepatitis B and C infection or chronic alcohol consumption. The diagnosis of chronic liver disease is made by laboratory tests, medical imaging and liver biopsy in selected cases. Transient elastography is the most widely used technique, with nowadays implemented new 2D shear-wave elastography and magnetic resonance elastography. Dynamic liver scintigraphy with 99mTc-mebrofenin (iminodiacetic acid derivate) has well established indications in liver imaging including functional assessment before liver surgery or acute cholecystitis and biliary atresia, but systemic use of 99mTc-mebrofenin in chronic liver imaging has never been used. The aim of this prospective study is to investigate the value of dynamic liver scintigraphy with 99mTc-mebrofenin in primary diagnosis of chronic liver disease and to compare it with both 2D-SWE and histologic examination of liver biopsy specimen. **Materials and Methods:**

We prospectively enrolled patients with primary diagnosis of chronic liver disease (viral hepatitis B and C) who were hospitalised for liver biopsy and who confirmed their agreement by signing informed consent. Liver dynamic scintigraphy was performed after injection of 99mTc-mebrofenin with planar static scintigraphy at 30 minutes. Several parameters including time to peak (TTP), time to half peak (1/2 TTP) and remaining liver uptake after 30 minutes were calculated. In addition liver 2D shear wave elastography measuring liver stiffness (in kPa) was performed to make head to head comparison between two imaging modalities. Live biopsy was performed shortly after both imaging tests. **Results:** Since now 32 patients with both HCV and HBV chronic infections were enrolled. In our preliminary results we found positive correlation between both scintigraphic parameters (TTP, remaining liver uptake at 30 min.) and 2D shear wave elastography. Also we found positive correlation between scintigraphic parameters and histological examination results. **Conclusion:** Recent quantitative radiologic methods (ultrasound and MR elastography) have little value evaluating liver parenchyma function. On the other hand liver scintigraphy with 99mTc-mebrofenin may show normally functioning liver cells trough receptor mediated uptake mechanism thus enabling to evaluate remaining liver function in chronic liver parenchymal disease. **References:** [1] Burden of liver disease in Europe: Epidemiology and analysis of risk factors to identify prevention policies. Journal of Hepatology. [2] SNM Practice Guideline for Hepatobiliary Scintigraphy 4.0" J. Nucl. Med. Technol.

EP-0251

Diagnosis of pleuroperitoneal communication as a complication of continuous ambulatory peritoneal dialysis by peritoneal scintigraphy - a case report

***A. N. B. Marques**, F. Abreu, C. Gaspar, S. Pintão;*
Hospital de Santa Cruz - Centro Hospital de Lisboa Ocidental, Carnaxide, PORTUGAL.

Aim/Introduction: Continuous Ambulatory Peritoneal Dialysis (CAPD) is an effective renal function replacement technique that can be complicated by the formation of hydrothorax, a potential life threatening complication.The main mechanisms of hydrothorax formation include mainly a primary diaphragmatic defect and anomalous lymphatic drainage motivated by increased intra-abdominal pressure.Peritoneal scintigraphy with technetium-99m macroaggregated human albumin (^{99m}Tc-MAA) helps to establish the diagnosis by evaluating possible dialysate leakage. **Materials and Methods:** Description of clinical case. **Results:** A 61-year old female patient undergoing CAPD treatment for three months, presented with dyspnea and right pleuritic chest pain accompanied by incomplete drainage of peritoneal dialysate, with a consequent increase in abdominal volume.Chest x-ray showed right pleural effusion. Peritoneal scintigraphy was performed. A dose of 185 MBq (5 mCi) of ^{99m}Tc-MAA was injected into a dialysate bag and instilled into the peritoneal cavity via the indwelling Tenckhoff catheter. Imaging was performed in a supine position using a gamma camera equipped with a high-resolution low energy collimator 4 hours after radiotracer administration. Scintigraphic imaging showed presence of tracer into the right hemithorax, confirming pleural peritoneal communication on the right side.Patient underwent surgical correction of the leakage. **Conclusion:** Peritoneal scintigraphy is a simple, safe and effective method for the identification of dialysate leakage in patients with CAPD. **References:** None.

EP-0252

SPECT/CT - solving the dilemma of hepatic hemangioma

***N. Manevska**, S. Stojanoski, T. Makazlieva, N. Bozinovska, D. Miladinova;*
Medical Faculty, Skopje, NORTH MACEDONIA.

Aim/Introduction: Hemangiomas, or hemangioma-like appearing lesions, are frequently detected in liver often as an incidental finding on computed tomography (CT) scans. Once detected, they can be a clinical dilemma as they need to be characterized. **Materials and Methods:** We retrospectively analyzed 108 patients, 62 females, (57.4%) and 45 males (41.67%), with mean age 50.05±11.92 years, sent to our Department for SPECT/CT of the liver to conclude or exclude the presence of hepatic hemangioma. Either ultrasound (US) or CT diagnostic scan, or both, were previously performed. SPECT/CT of the liver was performed with in vivo method, two hours after intravenously (i.v) administration of 550MBq 99mTcO4 labelled erythrocytes. **Results:** US was performed in 88 patients (81.48%), while CT in 74 patients (68.52%). Mostly the hemangiomas were localized in the right lobe. More than half of the patients (n=66, 61.11%) had one lesion only, while two or more lesions were seen on ultrasound or CT in (n=36, 33.33%). US demonstrated hyperechoic lesion, in some cases mixed echogenicity was seen, while CT scans described mostly hypodense liver lesions. The size of the lesion varied from to 6-140 mm (46.04 ± 27.1); 13 hemangiomas were giant. SPECT/CT confirmed hemangioma in 11 patients negative on US, and 4 patients negative on CT. In 40 patients hybrid imaging excluded the benign lesion of hemangioma. Most of the patients had benign diagnosis, while 12 had malignant diagnosis in whom in (n=7, 58.33%) metastasis was excluded and SPECT/CT detected hemangioma. Positive correlation between US and SPECT/CT, as well as between CT and SPECT/CT was detected in 43 patients (n=43, 39.81%) in both groups. CT together with US, had the highest sensitivity, accuracy and negative predictive value compared to SPECT/CT as refference, while CT alone and US alone had lower (94.4%, 72.6%, 71.2% vs, 91.5%, 68%, 66.7% vs, 79.6%, 64,4% and 54.2%, respectively). **Conclusion:** The hybrid imaging of SPECT/CT is a simple, efficient and useful method for detecting and localizing lesion of radioactivity concentration and solve the dilemma of differential diagnosis of hepatic hemangioma. **References:** None.

EP-0253

Gastrointestinal transit scintigraphy in patients with chronic constipation; an uncommon test. constipation; an uncommon test

M. Moreno-Caballero, J. Infante-de la Torre, A. Martínez-Esteve, J. Rayo-Madrid, P. Jiménez-Granero, A. Cobo-Rodríguez, J. Serrano-Vicente;
Hospital Universitario de Badajoz, Badajoz, SPAIN.

Aim/Introduction: Chronic constipation is a common pathology in children and adults. It is a serious condition that compromises quality of life, social functioning, and requires investigation including blood test, colonoscopy, radio-opaque marker study, and/or scintigraphy. The aim of this paper was to evaluate the usefulness of gastrointestinal transit scintigraphy in patients with chronic constipation. **Materials and Methods:** We evaluated 12 patients, 10 children (mean age 9, range 6-15) and 2 adults (49 and 58 year old), sent to our department with a diagnosis of chronic constipation refractory to treatment. All of them were subjected to clinical exam, biochemical determination, radiological imaging study and rectal biopsy. Clinical evolution time with constipation was at least 2 years. We performed a complete study protocol, including liquid gastric emptying scintigraphy and small and colonic transit times, following international guideline. Medications that affected gastrointestinal transit were withheld before and during the entire test. After oral administration of 37 MBq of 111In-DTPA in water accompanying with unlabeled standard solid meal, serial abdominal planar images were obtained for as long as 72 hours using a dual-head γ-camera. Regions of interest were defined in stomach, terminal ileum and in 6 regions of the large intestine together with determination of colon geometric center. **Results:** 11 patients showed altered scintigraphy study with a pattern of functional rectosigmoid obstruction in 5 of them, generalized slow colon transit pattern in 4, colonic inertia in 1 and slow gastric empty and slow small-bowel transit in 1. Normal radiological explorations were seen in 9 subjects. Radioisotopic study changed diagnosis in 8 patients and in other 3 patients contribute to clarify it, since discordance between normal radiological tests and/or abnormal rectal biopsy. One of the patients showed concordance between each imaging modality. The results of the test changed the therapeutic management in 8 cases. **Conclusion:** Gastrointestinal transit scintigraphy provided physiological, and useful information in the study of chronic constipation, been a reproducible and accurate method. This uncommon test determined both global and regional gastrointestinal transit time. The scintigraphy patterns are easily recognizable, can be evaluated quantitatively and help to determine appropriate therapeutic strategy in patients with constipation. **References:** None.

EP-0254

Clinical Utility Of Gallbladder Ejection Fraction: Is It Reliable By Itself?

J. Seo[1], J. Oh[2], H. Kim[1], J. Park[1];
[1]Fatima Hospital, Daegu, KOREA, REPUBLIC OF,
[2]Raphael Hospital, Daegu, KOREA, REPUBLIC OF.

Aim/Introduction: Hepatobiliary scintigraphy (HBS) with ^{99m}Tc-hepatoiminodiacetic acid (HIDA) has been a useful diagnostic imaging study for biliary pain and suspicious gallbladder (GB) abnormalities. Using cholecystokinin or a fatty meal, gallbladder ejection fraction (GBEF) can be easily calculated to assess GB contractility quantitatively. GBEF is commonly used as a biological parameter for selection of patients to undergo a cholecystectomy. So far, there are limited data about clinical impact of GBEF on patient management and follow-up. This study was to determine the usefulness of GBEF in the management of biliary pain or GB abnormalities. **Materials and Methods:** Among 225 patients who underwent HBS from January to June in 2016, 160 patients who had fatty meal HBS with GBEF calculation were enrolled. Subjects ingested 2 raw eggs (10 g fat) all at once. GBEF was calculated at 60 minutes after fatty meal intake. GBEF of ≥33% was used as the normal cutoff value according to previous reports. Patients had cholecystectomy or were treated medically. Patients were divided into groups on the basis of GBEF and management: EF_N-TX_C group with normal GBEF and cholecystectomy, EF_N-TX_M group with normal GBEF and medical treatment, EF_L- TX_C group with low GBEF and cholecystectomy, and EF_L- TX_M group with low GBEF and medical treatment. The follow-up period ranged 2-48 months. Blood samples were taken to analyze an association with GBEF and biochemical parameters. **Results:** Average GBEF was 67.20±31.04%. There was no significant difference in GBEF between men and women. In TX_C group, the histopathologic findings were not significantly different between EF_N and EF_L groups. In TX_M group, there was no significant difference in the follow-up of symptoms between EF_N and EF_L groups. However, serum total bilirubin, alanine aminotransferase (ALT), aspartate aminotransferase (AST), gamma-glutamyltransferase (γ-GTP) levels were significantly higher in EF_L group (p=0.0066, p=0.0039, p=0.0240, p=0.0303, respectively). Also, there was a negative correlation between serum total bilirubin, ALT, AST levels and GBEF (Pearson r=-0.1949, p=0.0135, Pearson r=-0.2013, p=0.0107, Pearson r=-0.1948, p=0.0136, respectively). **Conclusion:** The histopathologic findings of gallbladder and the symptoms after medical treatment were not different between patients with normal GBEF and low GBEF. GBEF levels were higher in patients with elevated liver enzymes or total bilirubin level. Also, there was a negative correlation between serum total bilirubin, ALT, AST levels and GBEF. Therefore, GBEF should be interpreted cautiously with hepatobiliary scan findings and other clinical features. **References:** None.

EP-0255

Utility of Bile Acid Malabsorption Test ^{75}SeHCAT in the Evaluation o Functional Chronic Diarrhea

V. Godigna Guilloteau, M. Marín Ferrer, E. Martínez Albero, A. Galiana Morón, D. Vega Pérez, A. Gardellini Guevara, S. Ruiz Solis, P.

Pilkington W, J. Esténoz Alfaro;
Hospital universitario 12 de Octubre, Madrid, SPAIN.

Aim/Introduction: To determine the impact of bile acid malabsorption test in the evaluation of funtional chronic diarrhea. **Materials and Methods:** We retrospectively analyzed data of 39 patients (p) with funtional chronic diarrhea (26 women and 13 men, average age 49.12 years (range 17-84 y) from January 2017 to April 2019, referred to the Nuclear Medicine department to rule out bile acid malabsorption (BAM). Past medical history: 3p atrophic gastritis, 2p Rheumatoid arthritis, 1p Lupus, 1p Myasthenia gravis, 1p Crohn's disease (CrD), 1p Multiple Sclerosis, 1p Ulcerative Colitis and 3p Hashimoto's disease. Past surgical history: 10 cholecystectomy, 3 ileal resection (1 CrD) and 2 right hemicolectomy with resection of ileum (<5cm). The following tests were performed: 39p colonoscopy, 33p lactose intolerance (LI) test, 19p bacterial overgrowth (BO) test, 32p celiac disease (CD) screening. Oral administration of 0.01mCi of 75-Selenium-homocholic acid taurine (75SeHCAT) was performed in all of them. We measured the abdominal retention of radiolabelled taurine-conjugated bile acid analogue after seven days (AR_7). AR_7 of <15% was considered positive for BAM: mild 10-15%, moderate <10-5% and severe <5%. Furthermore, BAM can be classified according to its etiology: ileal dysfunction (type I), idiopathic (type II) or associated with other gastrointestinal entities (type III). According to the final diagnosis, cholestyramine was administrated, analyzing its efficacy. The follow-up period ranged from 2 months to 2 years (average 8.2 months). **Results:** Positive BO test in 10/19p. Positive LI test in 11/33p. CDscreening positive in 1/32p. Colonoscopy: 11/39p with nonspecific changes, 8/39p diverticula-polyps and 1/39p collagenous colitis. ^{75}SeHCAT results were: Normal (16/39p): 5p LI (13.8%), 4p BO (11,3%), 1p collagenous colitis (2,7%), 3p Irritable Bowel Syndrome (8,4%) and 3p pending results. Positive (23/39p): 4p with mild AR_7, 8p with moderate and 11p with severe. 17p (47,2%) with only BAM, 6p (16,6%) with BAM associated with another pathology (4 LI, 1 autoimmune enteropathy and 1 multifactorial cause). These were classified as: Type: I (4p), II (10p) and III (9p). Twenty-two of 23p with positive ^{75}SeHCAT received cholestyramine, 16p improved symptoms, 1p with worse clinical symptoms and 5p pending clinical follow-up. **Conclusion:** SeHCAT is a usefull imaging test for the diagnosis of BAM and should be considered in all patients with functional chronic diarrea, specially when other tests are negative of inconclusive. **References:** None.

EP-0256

The Reliability of Manual Drawing for Salivary Gland Segmentation of Quantitative Tc-99m pertechnetate Salivary Gland SPECT/CT

W. Lee[1], *D. Oh*[2], *J. Kim*[2], *J. Han*[2], *J. Park*[3], *J. Lee*[3];
[1]*Seoul National University College of Medicine, Seong-Nam, KOREA, REPUBLIC OF,* [2]*Seoul National University College of Medicine, Seong-Nam, KOREA, REPUBLIC OF,* [3]*Seoul National University College of Medicine, Seoul, KOREA, REPUBLIC OF.*

Aim/Introduction: Salivary gland SPECT/CT (SG-SPECT/CT) is a promising nuclear medicine tool for functional evaluation of salvary glands. Quantitative approach for the SG-SPECT/CT would generate useful parameter of %injected dose (%ID). But manual drawing of individual salivary glands may elicit a problem of reproducibility because the glands are not well contrasted in SG-SPECT/CT without iodine-contrast. Here, we investigated the reproducibility of manual segmentation of salivary glands on the SG-SPECT/CT. In addition, we explored whether the early CT could be used for late SPECT %ID after mis-coregistration correction. **Materials and Methods:** Thirty patients (male:female=9:21, age=52.27±18.40y [mean±SD]) who underwent the SG-SPECT/CT (NMCT670, GE) from Aug 2017 to Sep 2018 were retrospectively enrolled. The SG-SPECT/CT protocol was Tc-99m pertechnetate (15mCi) injection, early SPECT/CT at 20min, sialogogue stimulation, and then late SPECT at 40min either with (n=19) or without CT (n=11). Quantitative SPECT approach was employed for the measurement of %ID using quantitative software (Q.Metrix, GE), which also provided the salivary volume data from corresponding CT. The reproducibilities of manual segmentation were assessed by intraclass correlation coefficient (ICC). Inter-operator and intra-operator ICCs were calculated using 30 patients (60 parotid and 56 submandibular glands) data of early SPECT/CT for %ID by SPECT and volume by CT. Additionally, in 19 patients with 38 parotid and 34 submandibular glands who had 40min CT available as a reference, 40min %IDs were calculated using 20min CT before and after correction for mis-coregistration, and the possibility for use of 20min CT for 40min %ID was examined. **Results:** Manual segmentation required multiple sessions of region-of-interest (ROI) drawings for parotid (~30 ROIs) and submandibular (~20 ROIs) glands on trans-axial CT images. The ICCs for intra- and inter-operator reproducibilities for %ID and volume were excellent. The ICCs for %IDs were greater than those for CT-derived volume, and the intra-operator ICCs were higher than inter-operator ICCs. The 40min SPECT %IDs derived from 40min CT as a reference were 0.087±0.041% for parotid and 0.071±0.038% for submandibular glands, while those from 20min CT before correction were 0.068±0.033% and 0.052±0.035%, and after correction 0.090±0.038% and 0.072±0.036%, for parotid and submandibular glands, respectively. Thus, bias±repeatability coefficients for %IDs before correction significantly improved after the correction. **Conclusion:** The reproducibility of salivary gland segmentation from manual drawing during the salivary gland SPECT/CT was excellent. Single CT scan may be sufficient enough to be applied to both pre- and post-stimulatory SPECTs, which may reduce radiation exposure to the patients. **References:** None.

EP-0257

Added value of SPECT/CT in localizing the correct site of gastrointestinal bleeding

F. Di Gregorio*, M. Rensi, D. Capobianco, M. Povolato, G. Ferretti, F. Giacomuzzi;*
Nuclear Medicine Unit - University-Hospital, Udine, ITALY.

Aim/Introduction: Blood loss from the gastrointestinal tract can be an acute and life-threatening event. In particular gastrointestinal bleeding can be occult with only positive fecal occult blood. For the treatment of gastrointestinal bleeding, it is important to accurately detect gastrointestinal bleeding and to localize the sites of bleeding. Bleeding scintigraphy is a useful imaging technique to detect gastrointestinal bleeding but planar imaging has a low accuracy in localizing the bleeding site. The aim of this study was to retrospectively assess the added value of SPECT/CT in the localize the correct site of gastrointestinal bleeding. **Materials and Methods:** A retrospective analysis in the past 5 years of 75 patients (44 males and 31 females; age range 48-90 years) with anemia and positive fecal occult blood was conducted. No evidence of gastrointestinal bleeding was identified by endoscopy during the clinical course. All patients underwent gastrointestinal bleeding scintigraphy with ^{99m}Tc-labelled red blood cells. Planar images of abdomen and pelvis were acquired initially with a blood perfusion phase dynamic imaging and after 60, 120, 240 and 360 minutes with static planar imaging. Abdominal SPECT/CT was performed after 24 hours or when an abnormal tracer uptake was evident at planar images. **Results:** Dynamic imaging was not able to identify bleeding site. Planar scintigraphy was positive in 64 patients and negative in 11 patients. In planar static imaging we found bleeding site on early images (< 120 minutes) in 16 out of 64 positive patients. SPECT/CT imaging was positive in 69 patients and negative in 6 patients. The source of bleeding was accurately diagnosed in 29 patients by the planar imaging and in 69 patients by the planar + SPECT/CT imaging.The diagnostic ability of planar and SPECT/CT imaging in detecting the site of bleeding was respectively 29% and 100%. **Conclusion:** Our data show that gastrointestinal bleeding scintigraphy in combination with SPECT/CT is a noninvasive and useful tool for the correct localization of gastrointestinal bleeding site. **References:** None.

EP-15

Clinical -> Diagnostic study -> Adult study -> Non-oncology study -> Other clinical studies -> Hematology, benign

October 12 - 16, 2019 e-Poster Area

EP-0258

^{18}FDG PET/CT in evaluation of patients with monoclonal gammopathy of undetermined significance (MGUS)

T. Rudolphi-Solero, R. Sánchez Sánchez, A. González Jiménez, M. Rashki, E. Triviño-Ibáñez, J. Llamas Elvira;
SAS, Granada, SPAIN.

Aim/Introduction: Monoclonal gammopathy of undetermined significance (MGUS) is an asymptomatic condition in which there is a presence of an abnormal M protein in the blood. It is important that these conditions be monitored, since increasing levels of this protein in addition to other tests may indicate a risk of progression to smoldering myeloma, myeloma, lymphoma, light-chain amyloidosis or Waldenstrom macroglobulinemia. The objective of this study is to evaluate the possible role of ^{18}F-FDG PET/CT in the correct classification and monitoring of these patients **Materials and Methods:** Retrospective analysis of patients who underwent ^{18}F-FDG PET/CT, after diagnosis of monoclonal gammopathy (2012/2016) classified in three subgroups according to the risk of progression to myeloma (low, intermediate, high). A positive PET/CT study for myeloma is considered if it presents areas of focal hypermetabolism outside of physiological distribution areas or diffuse increase in bone marrow of activity, superior to the background seen in patients without infiltration of the marrow. We have performed a statistical analysis describing the numerical variables as mean and standard deviation and the qualitative ones as frequencies. To compare the variables between the different groups, a bivariate analysis (Student's T-test and chi-square test) was performed, considering a p value <0,05 as significant. Analysis has been performed using the ROC curve in case of significance. SPSS 24. **Results:** A total of 156 patients with MGUS (81 men, 75 women) were included, mean age 68,8 years old. PET/CT was positive in 18, 9 in diagnosis and 9 in follow-up (average time to progression: 28 months). Significant differences were found, when comparing the groups with a positive and negative results in PET/TC, in the age (p=0,022) and the monoclonal component (0,015). There are no significant differences in sex, type of immunoglobulin, light chain ratio or risk classification. No relations were observed between the time to progression to myeloma and the qualitative variables. Using ROC analysis, the relation between the monoclonal component rate and the PET/CT result, with and area under the curve of 0,744, was studied. For cut-off point of 0,9 g/dL, figures of sensitivity of 77,8% and specificity of 59,2% were obtained. Additionally 22 incidentalomas were diagnosed, 7 of them confirmed by other diagnostic tests. **Conclusion:** The PET/CT study allows the correct classification of patients with MGUS. The age and the monoclonal component rate seem to be the variables most related to the probability of presenting a positive PET/CT for myeloma **References:** None.

EP-0259

Splenic volume assessment by heat denaturated red blood cells SPECT : validation against unenhanced low-dose SPECT/CT CT volumetry by OsiriX MD

G. Arsos[1], A. Siozopoylos[2], L. Kirkineska[1], S. Georga[1], A. Kalaitzogloy[1], K. Michailos[1], D. Katsampoukas[1], E. Moralidis[1], V. Perifanis[3], T. Vasiliadis[1];
[1]3rd Dept. of Nuclear Medicine, Aristotle University of Thessaloniki School of Medicine, Thessaloniki, GREECE, [2]Dept. of Anatomy, Democritus University of Thrace School of Medicine, Alexandroypolis, GREECE, [3]1st Propedeutic Dept. of Internal Medicine, Aristotle University of Thessaloniki School of Medicine, Thessaloniki, GREECE.

Aim/Introduction: Splenic volume (SV) is superior compared to the linear dimensions as a splenic size index. 99mTc-heat denaturated red blood cells (99mTc-hdRBC) is the ideal radiotracer for functional spleen imaging and Functional Splenic Volume (FSV) termed as the percentage of the injected activity of 99mTc-hdRBC per SV unit has been proposed for splenic function quantification. Thus, for FSV calculation, SV assessment is required. We aimed to compare a simple gamma-camera Nuclear Medicine segmentation tool applied on SPECT only data, against a validated, FDA approved, DICOM viewer software applied on CT data of 99mTc-hdRBC SPECT/CT scans, in SV assessment. **Materials and Methods:** Forty-two adult patients were enrolled, 37 with cirrhosis (Child-Pugh score 5-12, class A-C) for detection of functional hyposplenisn, 4 with normal liver function for definitive spleniculi characterization and 1 with ITP recurrence after splenectomy. All patients had 99mTc-hdRBC, low-dose, unenhanced SPECT/CT scans (64x64 matrix size, 60 steps, 15 sec/step, 120 kV, 30 mA) 2-3 hours post injection, with a dual-head GE NM/CT Optima 640 gamma-camera. SV were first assessed by applying the easy to use NM segmentation tool of the XELERIS (GE) work station to the SPECT data sets with a threshold value of 0.46 (SV-NM). Then, the DICOM CT data sets were transferred to a Mackintosh unit for segmentation and volumetric measurements using the OsiriX MD (v. 9.0) software. Due to low contrast between spleen and adjacent structures, manual segmentation was undertaken by tracing a ROI at the periphery of the spleen in every single slice in which it was visible and SV (SV-CT) was calculated by multiplying the sum of the areas outlined by slice thickness according to the Chavalieri's principle. Difference between SV-CT and SV-NM was assessed by Wilcoxon test, their relationship by linear regression analysis and their agreement by Bland-Altman analysis. **Results:** SV-CT ranged from 7 to 2.000 ml. SV-CT and SV-NM did not significantly differ (637±424 vs 634±418 ml, p=0.750) and closely correlated (SV-CT (ml) = 14,1 + 0.974 SV-NM, R=0.988, p<0.0001) and agreed each other (bias -3 ml, 95% CI -129 - 123 ml). **Conclusion:** Splenic volume assessment using SPECT data and inherent gamma-camera software only is as accurate and more convenient compared to a more sophisticated, validated CT volumetry software. Apart from spleen, the volume of other sharply delineated organs like the kidneys in 99mTc-DMSA scans could be potentially measured accurately with this simple method. **References:** None.

EP-0260

Comparison of blood volume calculation by radioisotopic dilution techniques with red lood cells abelled with Cr-51 and and Tc-99m administered simultaneously

A. Agudo Martinez, I. León-Asuero-Moreno, G. Sabatel-Hernández, M. Maniega-Pérez, P. de la Riva-Pérez, F. García-Gómez, I. Marín-Melero, C. Calvo-Morón;
Virgen Macarena University Hospital, Seville, SPAIN.

Aim/Introduction: The progressive extinction of the Cr-51makes imperative to adapt the blood volume calculation by isotopic dilution technique with red blood cells (RBC) labeled with Cr-51, considered gold standard, to Tc-99m technique. We assess its accuracy. **Materials and Methods:** Two blood samples (10ml) were obtained from healthy volunteer and were respectively labeled with 5,4MBq of 99mTcO4Na and 2,2MBq of 51CrO4Na. Both samples were centrifuged at 700g and washed with 40ml of physiological salt solution. A 1ml aliquot of each standard was taken and diluted in a 250ml flask, being the rest of the blood reinjected. 5ml of blood was extracted from the contralateral arm after 60 minutes. In order to obtain the final averaged values, activity (cpm) of 1ml of blood samples, 1ml of the diluted standard samples and background were measured in quadruplicate for each isotope the day of the test and two days later (Cr-51). Correct energy peak and window must be selected for both isotopes in the well counter for this purpose. The need to apply the Tc-99m decay correction during the counting was checked. The expression to obtain the total injected radioactivity (A) was: A=SRVs • S(cpm/ml): Radioactive concentration of diluted standard. • R: Weight(g) of labeled red cell suspension injected/Weight of labeled red cell suspension added to flask. • Vs: Dilution volume of standard. The expression for red cell volume (RCV) calculation was: RCV=AHv/B • Hv: Venous haematocrit. • B(cpm/ml): Radioactive concentration of blood sample. The expression PV=BV-RCV was applied for calculation of plasma volume (PV), where BV is blood volume calculated with BV=RCV/(f Hv). An average value of f=0,91 was considered. Results of RCV, PV and BV for each radioisotope were compared with predictions of normal blood volumes based on body surface area with formulas recommended by the Expert Panel on Radionuclides of the ICSH. **Results:** More than 10K counts were measured during the 5 minutes counting of the Tc-99m samples, being enough to get good statistical values. **Conclusion:** Measurement of the Tc-99m RCV after decay correction guarantees comparable results to the Cr-51 RCV. According to our results, the 1 minute counting would be enough being negligible the decay correction. **References:** 1. Gómez Perales JL. Blood volume analysis by radioisotopic dilution techniques: state of the art. Appl Radiat Isot. 2015; 96:71-82. 2. Perales JL. Mendoza AG. Development of a comprehensive software application for calculations in nuclear medicine and radiopharmacy. J Nucl Med Technol. 2010;38(3):153-62.

EP-0261

Comparison of two calculation methods for isotopic measurement of plasma volume

P. Orhon, M. Tempier, F. Cachin, S. Levesque;
Centre Jean Perrin, Clermont-Ferrand, FRANCE.

Aim/Introduction: Isotopic measurement of total blood volume is commonly used for diagnosis of polycythemia. In our clinical practice, red blood cell volume and plasma volume are determinate separately by isotope dilution methods to provide two independent measurements. Radioactive iodinated Serum Albumin is used for the Plasmatic Volume (PV) determination. ^{99m}Technetium-labelled red blood cells used to determine the

globular volume also allows, associated to the hematocrit, an indirect calculation of the PV. The present study was conducted to determine if these two methods for PV determination, on a statistically representative sample, provided similar results or not. **Materials and Methods:** From March 2017 to March 2019, data from 194 patients were retrospectively collected. For all of them, two independent isotopic measurements for red blood cell volume and PV were performed. For each patient, an Excel file was designed with the values of PV determined directly after injection of ^{125}I-serum albumin and those deduced by indirect calculation from the globular volume labelled with technetium-99m. These values were reported in a table for statistical Wilcoxon comparison test. **Results:** We collected 194 PV measurements using both ^{125}I-serum albumin and the indirect calculation method. The population studied consists of 163 men and 31 women with an average Body Mass Index (BMI) of 27.1 kg/m^2. An overall comparison of the PV values from these two measurements was performed with the Wilcoxon test (matched samples). The result of this statistical test reveals a significant difference between these two measurements ($p < 0.001$). As overweight and obesity can lead to changes in PV, we classify these patients into two sub-populations according to their BMI: 68 normo-weighted patients (BMI [18.5-24.9] kg/m^2) and 126 overweighted/obese (BMI >25 kg/m^2). This comparison with the sub classification depending on BMI highlights none statistical difference between PV measurements for the normo-weighted population whereas a statistical difference ($p < 0.001$) is observed in the overweighted/obese group. **Conclusion:** The independent measurement of PV by injection of ^{125}I-serum albumin could be considered as the reference method because it excludes the error on venous hematocrit. In clinical practice, this method may present inconvenience for the patient (repeated samplings of blood, radiation exposition and long liver period of iodine 125). Therefore, our results suggest that the indirect method may be sufficient for normo-weighted patients contrary to overweighted/obese patients. **References:** None.

EP-16

Clinical -> Diagnostic study -> Adult study -> Non-oncology study -> Other clinical studies -> Pulmonology, benign

October 12 - 16, 2019 e-Poster Area

EP-0262

The Mucous Plug Syndrome Mimicking A Unilateral Pulmonary Embolism Revealed By Lung SPECT CT: A Case Report

J. T. Zhang-Yin[1,2], *B. Durand*[2], *H. Lemasle*[2], *R. Ahond-Vionnet*[2];
[1]*Service de Médecine Nucléaire, Hôpital Tenon, Paris, FRANCE,* [2]*Service de Médecine Nucléaire, Hôpital Pierre Beregovoy, Nevers, FRANCE.*

Aim/Introduction: The mucous plug syndrome refers to an acute bronchial obstruction by mucous plugs. It could be manifested clinically by dyspnea, hypoxemia, and respiratory alkalosis mimicking pulmonary embolism. **Materials and Methods:** A 69 years old female patient was hospitalized for traumatic fall at home, she was diagnosed an amyotrophic lateral sclerosis one year before. Three days after hospitalization, she presented dyspnea, low oxygen saturation, tachycardia, hypoxemia, hypocapnia, and increased D-Dimer. In order to diagnose a pulmonary embolism, a single photon emission computed tomography ventilation/perfusion (SPECT/CT V/Q) was performed. It wasn't in favour of pulmonary embolism but showed a total abolished ventilation of the right lung. A bronchoscopy was performed and found a mucous plug (Fig 1) which was completely occluding the right main bronchus. The plug was removed by aspiration with Acetylcysteine. The symptoms disappeared and a control SPECT/CT V/Q was performed 2 days later, and showed a normalized ventilation and perfusion, in both lungs. **Results:** SPECT/CT perfusion (99m Tc-MAA) and ventilation (Technegas) images were acquired with a CZT dual head gamma camera (NM/CT 670 CZT, GE). A software of 3D lobar quantification (Q.Lung, GE) is used for calculating the distribution. The first SPECT/CT V/Q (Fig 2: upper line) shows a total abolished ventilation with relative conservation of perfusion of the right lung and without parenchymatous abnormality on the low-dose CT. The quantification (Fig 3) shows, for left vs right lung, a ventilation of 100% vs 0% and a perfusion of 74% vs 26%. This result highlights a total obstruction of the right bronchus, and a beginning decrease of the right lung perfusion. Two days after removing the mucous plug, the second SPECT/CT V/Q of control (Fig 2: lower line) shows a reestablished ventilation for the right lung, as the quantification illustrates (Fig 3): for left vs right lung, a ventilation of 46% vs 54% and a perfusion of 50% vs 50%. **Conclusion:** In patient with neuromuscular disease such as amyotrophic lateral sclerosis, bronchial mucous plugging is more common and represents the main precipitating factor of acute respiratory failure. As a differential diagnosis of pulmonary embolism, it is important to recognise it for not delaying its management. The lung SPECT/CT is a valuable tool in this situation, because the early accurate diagnosis prevents the complication such as lung collapse (1). **References:** 1. Nair, Pearson. Images in clinical medicine. Mucous plug in the bronchus causing lung collapse. NEJM 2002.

EP-0263

FDG PET/CT Findings in Cavitary Form of IgG4-Related Lung Disease

S. Kesim, *T. Öneş, S. Özgüven, K. Öksüzoğlu, S. İnanır, H. T. Turoğlu, T. Y. Erdil;*
Marmara University Istanbul Pendik Education And Research Hospital, Istanbul, TURKEY.

Aim/Introduction: Immunoglobulin G4 related disease (IgG4-RD) is a rare progressive fibroinflammatory disorder that recently defined in literature in which IgG4-positive plasma cells

and lymphocytes infiltrate single or multiple organs. Although various radiological findings of lung involvement has been reported in many IgG4-RD studies, the literature information is very limited for the type of cavitary form. Herein, we discuss FDG PET/CT findings of a case with cavitary form IgG4-related lung disease. **Materials and Methods:** A 50-year-old male patient was enrolled with cough, sputum and hemoptysis who did not response to the treatment of pneumonia. Biopsy was performed and the histopathological findings was consisted with IgG4-related lung disease. With this pathological diagnosis, the patient was referred to our department and FDG PET/CT was performed. **Results:** FDG PET/CT showed heterogeneous and intense FDG uptake (SUVmax = 8.2) in the areas of parenchymal consolidation and peribronchial ground glass opacities with occasional cavitary formation in the posterobasal segment of the left lower lobe. In addition, mild FDG uptake (SUVmax = 2.7) was observed in mediastinal lymph nodes of level 4L, 5 and 7 and the left hilar / peribronchial nodes, one inch in diameter. No other evidence of malignancy was noted elsewhere in the whole body images. With the pathology report, the findings were evaluated in favor of benign FDG uptake with chronic inflammatory response associated with IgG4. There was no evidence of systemic involvement in the rest of the body. **Conclusion:** IgG4-RD can mimic malignancy. In these cases, diagnosis is made by clinical evaluation, specific serum markers and finally histopathological validation. The gold standart treatment is steroids and immunosuppressive drugs. In the literature, it has been reported that FDG PET/CT is a useful diagnostic tool in the evaluation of the spread of the disease, in the detection of the lesion site for biopsy and in the follow-up of the treatment response. There are a few metabolic imaging studies evaluating lung findings for this disease. Our case was the first that discuss FDG PET/CT findings in cavitary form of IgG4 related lung disease. **References:** None.

EP-0264

Decrease in number of undetermined studies with ventilation/perfusion SPECT

J. Deportos, V. Vallejos, S. Lafuente, M. Solà, M. Salcedo, J. Riba, G. Moragas;
Hospital Universitari Germans Trias i Pujol, Badalona, SPAIN.

Aim/Introduction: to assess the number of undetermined studies with ventilation / perfusion SPECT in the suspicion of pulmonary thromboembolism. **Materials and Methods:** between March 9th and December 31st 2018 we retrospectively reviewed 559 patients (270 men, 289 women, 22 - 99 years) who underwent ventilation / perfusion SPECT to rule out pulmonary thromboembolism (PE). **Results:** 324 out of 559 patients were referred to rule out acute PE, 148 patients had a diagnosis of deep vein thrombosis (DVT), 58 patients had a diagnosis of pulmonary hypertension (PHT) and 29 of chronic PE. 21.1% out of 559 patients were positive for PE, 76% were negative and only 2.9% were undetermined. Out of 324 patients cited to rule out acute PE , 20.7% of them were positive, 75.9% were negative and 3.4% were undetermined. Patients with high D-dimer (more than 500 ng / mL) were positive in 22.4% cases, 75.3% were negative and 2,3% were undetermined. Patients with low D-dimer (less than 500 ng / mL) or without determination of D-dimer were positive in 18.7% cases , 76.6% were negative and 4.7% were undetermined. Out of 148 patients with DVT, 28.4% were positive, 69.6% were negative and 2% were undetermined. Out of 58 patients with PHT, 5.2% were positive, 91.4% were negative and 3.4% were undetermined. Out of 29 patients with chronic PE, 20.7% were positive and 79.3% were negative, without undetermined cases. **Conclusion:** with the experience in our center we can conclude that ventilation/perfusion SPECT obtains a percentage of positive studies comparable to the traditional planar study, while allowing a significant decrease in the number of undetermined results. **References:** None.

EP-0265

Evaluation of bronchopleural fistula with Technegas ventilation scintigraphy

Z. AL Bimani[1,2], S. Samaan[1], W. Zeng[1];
[1]University of Ottawa, Ottawa, ON, CANADA, [2]Oman Medical Speciality Board (OMSB), Muscat, OMAN.

Aim/Introduction: To Present a case of bronchopleural fistula diagnosed by the ventilation scan.To Review the presentation of bronchopleural fistula and associated radiological and nuclear medicine image findings. **Materials and Methods:** A bronchopleural fistula (BPF) is a direct connection between the bronchial tree and the pleural space, usually divided as central (involves the trachea or a lobar bronchus) and peripheral (involves a distal airway). The incidence of BPF ranges from 0.5% to 3.0% after lobectomy and from 2% to 20% after pneumonectomy. Although rare, a BPF is one of the most serious life-threatening complications of pulmonary resection. Therefore, prompt diagnosis and treatment are crucial. Nuclear medicine ventilation scan can accurately diagnose BPF by visualizing radiotracer at the pleural space, as described in the abstract. **Results:** A 72-year-old male presented with shallow breathing during sleep two weeks post right pneumonectomy for recurrent solitary fibrous tumor of the right pleura. His CXR showed increased lucency of the right hemithorax and CT chest showed large right pneumothorax associated with pleural effusion. Chest tube was inserted subsequently. The patient was suspected of having a BPF and a diagnostic ventilation scan was requested. The ventilation scan was performed following inhalation of approximately 37 MBq of Tc-99m Technegas. Both planar images and SPECT/CT of the chest were acquired. On the planar images, there was accumulation of Technegas at the right central airways with gradually increased uptake in the right plural space over time, confirmed by SPECT/CT, and indicative of a central BPF. The diagnosis of the BPF was subsequently confirmed by flexible bronchoscopy, which showed breakdown of the bronchial staple line in the lateral third of the right main bronchial stump at the site of the fistula. The patient was

managed by antibiotics and multiple exploratory thoracotomies for debridement, packing and Claggett window. The follow-up bronchoscopy demonstrated the healing of the right main bronchial stump. **Conclusion:** In this poster, the pathology and aetiology of the BPF will be discussed. The image findings from plain radiograph, CT and nuclear medicine ventilation scan will be discussed. **References:** None.

EP-0266

Spectrum of unilateral hypoperfusion or absent perfusion on pulmonary scintigraphy

N. Uyama[1], *H. Otsuka*[2], *Y. Otomi*[1], *M. Harada*[1];
[1]*Department of Radiology, Tokushima University Hospital, Tokushima, JAPAN,* [2]*Department of Medical Imaging/ Nuclear Medicine, Institute of Biomedical Sciences, Tokushima University Graduate School, Tokushima, JAPAN.*

Aim/Introduction: A finding of a globally diminished pulmonary artery blood flow to unilateral lung with or without an associated ventilatory abnormality is uncommon on lung perfusion scintigraphy (LPS). In the clinical setting, when these abnormalities are encountered, pulmonary embolism (PE) should be considered. However, PE is an infrequent cause, and any of a wide variety of diseases is the more likely culprit. In this exhibit, we consider the spectrum of unilateral lung hypoperfusion or the absence of perfusion altogether on LPS with combinations of additional imaging modalities, particularly contrast-enhanced computed tomography (CT). **Materials and Methods:** Between April 2010 and April 2019, we reviewed the scintigraphic and CT findings in the database and medical records of our institutes. A total of 634 lung scans were reviewed, and we identified 46 scans from 37 patients (men, 23; age, 42.2±31.3 years) with unilateral lung hypoperfusion or absent perfusion on LPS who had a clinical definitive diagnosis. **Results:** Of the 37 patients, 18 (men, 8; age, 13.1±16.6 years) were associated with congenital anomalies, such as a postoperative state of tetralogy of Fallot (TOF) or transposition of great arteries (TGA) or hypoplasia of the pulmonary artery or vein. Eleven patients (men, 10; age, 69.5±5.7 years) were associated with mediastinal and hilar masses, such as primary bronchogenic carcinoma, and metastatic tumors. Six patients (men, 5; age, 67.8±7.5 years) are associated with parenchymal lung disease, such as chronic obstructive pulmonary disease (COPD), idiopathic and secondary interstitial pneumonia, atelectasis from pleural effusion. Only 2 patients (both women; 74 and 81 years of age) with PE showed unilateral hypoperfusion or no perfusion, accounting for approximately 5% in our series. Large central emboli were able to be excluded, with alternative causes detected by contrast-enhanced CT. Unilateral lung hypoperfusion or absent perfusion is a more common finding in cyanotic congenital heart disease and mediastinal and hilar masses than in PE. **Conclusion:** A variety of diseases may present with unilateral lung hypoperfusion or absent perfusion on LPS; such findings are uncommon in cases of PE, and alternative causes should be considered in order to avoid a false-positive diagnosis. The correct diagnosis may be determined based on the correlation of lung ventilation scans, clinical history, and findings from additional imaging modalities, particularly contrast-enhanced CT. **References:** None.

EP-0267

Analyzing the influence of bronchodilators in ^{99m}Tc-MAA imaging

V. Mendi Barcina*, S. Rizkallal Monzon, B. Martinez De Miguel, E. Orihuela Pantoja, E. Dobra, H. Garcia Ruiz, E. Martinez Montalban; Hospital Universitario La Paz, Madrid, SPAIN.*

Aim/Introduction: Evaluate the clinical relevance of pharmacological interactions between different bronchodilators (glucocorticoids, anticholinergics, beta-2 adrenergic agonists) in pulmonary perfusion images with ^{99m}Tc-MAA. According to the specifications of the summary of product characteristics, bronchodilators can modify the biological distribution of ^{99m}Tc-MAA and thus alter the quality of the image and the diagnosis. Given the numerous patients with this treatment, we decided to assess the importance of this interaction and the possible modification of the treatment. **Materials and Methods:** Retrospective study of 50 patients underwent a pulmonary perfusion test with 185 MBq of ^{99m}Tc-MAA, between September 2018 and February 2019. The mean number of particles administered was 264.240,978 (±43.792,902). Bronchodilators were divided in 3 groups: 1=glucocorticoids, administered to 34% of patients (beclomethasone, fluticasone, budesonide), 2=anticholinergics to 36% (tiotropium, umeclidinium, ipratropium, glycopyrronium, aclidinium) and 3=Beta-2 adrenergic agonists to 42% (albuterol, terbutaline, salmeterol, formoterol, olodaterol, indacaterol, vilanterol). We evaluated the labeling activity with $^{99m}TcO_4^-$ of the different kits and the percentage of radiochemical purity (%RQP) by thin layer radiochromatography. % RQP must be ≥95%. Images acquisition was done with SPECT-CT (INFINIA HAWKEYE 4) and planar images using gammacamera (PHILPS BRIGTVIEW). The evaluation of the images quality was done by two independent nuclear physicians, classifying them in 3 groups: A=Good, B=Poor, C=Average. Statistical analisys was performed with SPSS program, using test of Chi-square with the exact test of Fisher. **Results:** The 3 groups of drugs present significant statistically association with the image quality: - (Group=0) Patients without bronchodilator treatment: 100% present group image (A). - (Group=1) Glucocorticoid vs. Image: p=0.047 64.7% presents group image (A) and 35.3% group image (C). - (Group=2) anticholinergics vs. Image: p=0.00 50% presents group image (A) and 50% group image (C). - (Group=3) beta-2 Agonists vs. Image: p=0.02 61.9% presents group image (A) and 38.1% group image (C).We didn't detect any differences between drugs in the same pharmacological group (i.e: albuterol vs. salmeterol). Labeling activity interval was 3.515-3.959 MBq, mean: 3.704,107 MBq. % RQP mean was 99.975% (±0.175). There was no statistical difference between the images obtained in each gammacameras (p>0.05). **Conclusion:** In the light of the evaluated cases, concomitant treatment of bronchodilator

drugs may interfere with the images quality obtained with ^{99m}Tc-MAA, so we should consider treatment suppression. It would be necessary to study how long we should suspend treatment before the study with ^{99m}Tc-MAA. On the other hand we didn't obtein any poor quality images(B). **References:** None.

EP-17

Clinical -> Diagnostic study -> Adult study -> Non-oncology study -> Other clinical studies -> Uro-nephrology, benign

October 12 - 16, 2019 e-Poster Area

EP-0268

PSMA PET imaging allows accurate determination of split renal function as compared with MAG-3 scintigraphy

M. Ries, P. Pauly, F. Rosar, F. Khreish, A. Schäfer, S. Ezziddin;
Universitätsklinikum des Saarlandes, Homburg, GERMANY.

Aim/Introduction: Split-renal function (SRF) determination, i.e. quantification of side-specific relative contribution of renal function, is valuable in various clinical settings including management of prostate cancer patients. Well-established methods are comprised of renal scintigraphy using ^{99m}Tc labelled MAG-3 and DMSA with dynamic and static imaging, respectively. Our aim was to evaluate the feasibility of SRF estimation by PSMA-PET/CT, as renal tubular PSMA expression seems to be an indicator of functioning parenchyma. **Materials and Methods:** PSMA-PET derived and MAG-3 scintigraphy based SRF were compared in n=98 patients with advanced prostate cancer who had PET/CT and renal scintigraphy in close temporal relationship (< 1 week apart). The PSMA PET derived split renal function (SRF_{PSMA}) was obtained from 68Ga-PSMA11 images acquired 60 min post-injection. The product of SUVmean and volume in a VOI with semi-automatical definition of 30% of SUVmax isocontour was calculated in both kidneys, resulting in relative proportions of each side. SRF_{MAG-3} was calculated with standard algorithms employing manual planar ROI selection and calculation of side-specific represention of the secretion phase of renogram. The values for the right kidney resulting from SRF_{PSMA} and SRF_{MAG-3} were compared and correlated. **Results:** Mean SRF of the right side was 50.5% (range: 11 - 96%) and 50.7% (range: 1.2 - 99.7%) using MAG-3 and PSMA PET, respectively. The correlation between both methods of SRF was good (r=0,89, p<0,001) and comparable to the correspondence of MAG-3 and DMSA scintigraphy. The correlation was good in both reduced as well as normal overall renal function. **Conclusion:** Renal tubular PSMA expression seems to be intra-individually proportional to renal function allowing to accurately assess split renal function by ^{68}Ga PSMA PET/CT imaging. Function loss of one kidney can be reliably indicated by PSMA PET and will be confirmed by functional renal imaging. **References:** None.

EP-0269

Comparison of Relative Renal Function with ^{99m}Tc-DMSA SPECT assessed by a CZT 360° VERITON and Anger cameras

C. Nganoa[1], A. Bouthiba[1,2], N. Roth[3], N. Aide[1,4], B. Enilorac[1], C. Lasnon[4], D. Agostini[1,2];
[1]Nuclear Medicine Department, University Hospital, Caen, FRANCE, [2]Normandy University, EA 4650, Caen, FRANCE, [3]Spectrum Dynamics Medical Ltd, Caesarea, ISRAEL, [4]INSERM 1199 ANTICIPE, Normandy University, Caen, FRANCE.

Aim/Introduction: ^{99m}Tc-Dimercaptosuccinic acid (DMSA) renal imaging is a useful and reliable mean for renal parenchyma analysis (urinary tract infection, unilateral or bilateral renal disease) and assessment of relative renal function. The aim of this study was to compare Relative Renal Function (RRF) with 99mTc DMSA SPECT between a conventional dual head ANGER camera (ECAM®, Siemens) and a CZT 360° VERITON camera. **Materials and Methods:** With the Ethical committee agreement, we evaluated patients who underwent routine static DMSA scan on a conventional dual head ANGER camera and agreed to perform 2 additional SPECT scans (Anger and CZT) the same day without CT or additional radiopharmaceutical injection. Anger and CZT SPECT data were respectively acquired for 10.7min and 11.73 ± 2.16min. Both studies were reconstructed using OSEM iterative algorithm (4iterations, 8subsets). Images were quantified automatically or semi-automatically using MIM software Renal SPECT workflow defining renal and cortical regions of interest for the left and right kidneys. A normal RRF is stated to be 45-55% for each kidney. We compared RRF values with Anger vs CZT using a semi-automatic and automatic workflow. RRF from planar clinical routine were compared to CZT SPECT **Results:** To date, DMSA renal SPECT imaging have been acquired in 7patients (age: 55±20 years, 5 females) injected with 108.5±8.0 MBq of ^{99m}Tc-DMSA. Mean RRF for left kidney on VERITON were 56.78%±25.48 for semi-automatic (observer1), 56.75%±25.12 for semi-automatic (observer2) and 57.96%± 24.74 for automatic. Friedman's test showed no significant difference between groups (p=0.867). Mean RRF for left kidney on ANGER were 57.13%±23.66 for semi-automatic (observer1), 57.08%±24.28 for semi-automatic (observer2), 58.26%± 24.50 for automatic and 59.61%±24.74 for planar images. On pairwise comparisons using Hollander & Wolfe's procedure, no significant difference was found. A statistical analysis combining both semi-automatic and automatic quantifications showed good correlation between VERITON SPECT and ANGER SPECT (R^2=0.9992). **Conclusion:** RRF assessed by CZT SPECT and ANGER SPECT show good correlation and Inter-user reproducibility. **References:** None.

EP-0270

DMSA scintigraphy in orthotopic kidneys: Do we really need to perform geometric mean assessment?

I. El Bez, R. Tulbah, I. Munir, F. Alghamlas, M. Alharbi;
KFMC, nuclear medicine department, Riyadh, SAUDI ARABIA.

Aim/Introduction: For assessment of split renal function of static renal scintigraphy with Tc-99m-dimercaptosuccinic acid (DMSA) the calculation of the geometric mean of counts from the anterior and posterior view is recommended. Aim of this retrospective study was to find out, if the anterior view is necessary to receive an accurate relative renal function (RRF) by calculating the geometric mean compared to calculating the split renal function using the counts of the posterior view only. Furthermore, we evaluated to what extent the patient's age influenced these differences. **Materials and Methods:** A total of 300 renal scintigraphies with 99mTc-DMSA performed at our Department in the last two years were studied. Only patients with orthotopic kidneys were included. The mean and standard deviation of the differences as well as the correlation coefficient between both methods were calculated. The scans were performed using a dual head gamma camera, low energy ultra high resolution collimator, matrix 256 x 256, 300 kcts/view. Background corrected values from both kidneys anterior and posterior were obtained. The difference between the right renal function in posterior view and the right renal function obtained using the geometric mean was calculated for all the patients. The Student's T test was applied to determine whether the differences between both methods were statistically different from zero. **Results:** The differential function of the right and the left kidney was no significantly changed when compared to the calculation of the geometric mean ($p<0.1$), for all age. **Conclusion:** The calculation of the RRF from the posterior view only was not statically different when compared to the calculation of the geometric mean in orthotopic kidneys, so that in these cases the anterior view is not necessary. **References:** None.

EP-0271

Effect of kidney depth correction in GFR measured by renal dynamic SPECT in patients with hydronephrosis

***Q. Zhao**, J. Cao, J. Tian, J. Luo;*
General Hospital of Ningxia Medical University, Yinchuan, CHINA.

Aim/Introduction: Kidney depth is one of the most important factors for the calculation of glomerular filtration rate (GFR) with ^{99m}Tc-DTPA dynamic SPECT imaging using Gates method, which defaults the Tonnesen formula to estimate the depth of the kidney. We compared the effect of kidney depth in GFR measured by renal dynamic SPECT imaging hydronephrosis patients . **Materials and Methods:** 64 patients (32 males, 32 females) with hydronephrosis who underwent renal dynamic SPECT imaging from January to December 2018 in General Hospital of Ningxia Medical University were retrospectively enrolled. The body mass index (BMI) and serum creatinine (Scr) level were recorded. The depth of kidney was calculated by Tonnesen formula (standard), Itoh formula (Itoh) and CT correction (CT) separately. Total and split renal GFRs were measured by renal dynamic SPECT imaging using Gates method using different kidney depths. The GFRs were compared and the correlations between GFRs and Scr level were analyzed. Kidney depth of underweight, normal, overweight and obesity groups according to the BMI range were compared. Intra class correlation coefficient (ICC) was employed to evaluate the relationship among kidney depths from standard, Itoh and CT correction. **Results:** The total GFR (mL/min) from standard (GFR_{std}), Itoh (GFR_{Itoh}) and CT (GFR_{CT}) correction were 75.53 ± 21.49, (89.38 ± 25.16 and 91.13 ± 27.32, respectively. Significant differences were found between GFR_{std} and GFR_{Itoh}, GFR_{std} and GFR_{CT} (all $p<0.001$). There was no significant difference between GFR_{Itoh} and GFR_{CT} ($p>0.05$). The same statistical results were found in the comparison of split GFR analyses. Comparison of GFRs, different kidney depths in hydronephrosis kidneys and non-hydronephrosis kidneys also showed no differences between Itoh and CT correction. The Scr level was not corelated with GFRs in hydronephrosis kidneys (all $p>0.05$). However, the correlation efficiency of Scr level and GFR_{std}, GFR_{Itoh} and GFR_{CT} in non-hydronephrosis kidneys was 0.45, 0.45 and 0.49, respectively (all $p<0.05$). There were no differences in kidney depths among different BMI groups (all $p>0.05$). ICC analysis showed correlation between GFR_{std} and GFR_{CT}, GFR_{Itoh} and GFR_{CT} ($r=0.91$, $r=0.91$, $p<0.05$) in non-hydronephrosis kidneys. **Conclusion:** GFR and kidney depth using Tonnesen formula were underestimated. Itoh formula had the similar estimation of kidney depth and GFR with CT correction, and could be used in hydronephrosis patients instead of CT correction. In hydronephrosis patients, Scr did not well corelate with GFR. No differences of kidney depth and GFR was found in hydronephrosis patients with or without normal BMI. **References:** None.

EP-0272

Is geometric mean calculation of renal split function applicable to patients with impaired renal function?

***O. K. I. Kotbi**[1,2], A. Albatly[1,3], B. Ziebarth[1], E. Leung[1], A. Rezk[1], R. Klein[1], R. Klein[1], W. Zeng[1];*
[1]The Ottawa hospital, Ottawa, ON, CANADA, [2]King Abdullah medical city in holy capital, Meccah, SAUDI ARABIA, [3]Prince Sultan Millitary Medical City, Riyadh, SAUDI ARABIA.

Aim/Introduction: The split renal function is routinely assessed by renal scan based on the posterior images. It is believed that geometric mean (GM) calculation could partially correct for soft tissue attenuation artifact due to the difference in kidney positioning. Dual-headed cameras have become routine equipment and enable GM calculation. In this study we assessed the split function by GM calculation in patients with normal and abnormal renal function, and compared the results from routine (posterior only) image measurements. **Materials and Methods:** We reviewed consecutive renal scans with ^{99m}Tc-MAG or ^{99m}Tc-DTPA from 103 patients who had both anterior and posterior images. For GM calculation, region of interest of each kidney and the background was drawn by 2 experienced operators blinded to clinical data on Hermes HybridViewer V2.6, in a similar manner as clinical routine. Serum creatinine closest to the renal scan date was obtained. 3 patients were excluded due to poor image quality and 12 cases with renal masses were

analyzed separately. Additional 10 patients were excluded due to the lack of recent creatinine (most with normal remote creatinine). The split function of the right kidney calculated from the posterior and GM were compared with student t-test. Continuous variables were presented as mean ± standard-deviation. **Results:** Of 78 patients with renal scans (age: 54.9 ± 14.8, F:M=39:39), 44 had normal creatinine (69.3±15.5, group 1) and 34 had abnormal creatinine (138.9±79.0, group 2), with the interval of 27.9±23.5 days. The mean split function of the right kidney was 51.6±12.1% from GM, compared to 51.0±12.5% from posterior for group 1, and 49.9±13.7% from GM, compared to 47.7±14.5% from posterior for group 2. The difference in right kidney split function between GM and posterior view was 2.26±1.77% for group 1 and 3.59±2.14% for group 2 (t-test, p=0.004). There was a moderate to strong correlation between kidney split produced by both operators (Pearson's correlation coefficient: 0.67). Of the 12 patients with renal masses, the difference between the GM and posterior view split function was 6.2±4.9%. **Conclusion:** The GM method is applicable to patients to patients with normal and abnormal renal function. The study demonstrated that GM calculation may be more clinically significant in patients with impaired than normal renal function (2.3% vs. 3.6% difference). Considering no additional radiation exposure or additional imaging time for the geometric method, it should be used in the routine assessment of renal split function. **References:** None.

EP-0273

DMSA scan versus MR imaging in pyelonephritis: A Meta-analysis

I. Sarikaya[1], *A. Sarikaya*[2], *A. Albatineh*[1];
[1]*Kuwait University Faculty of Medicine, Kuwait, KUWAIT,*
[2]*Trakya University Faculty of Medicine, Edirne, TURKEY.*

Aim/Introduction: The aim of this study was to compare the reported results of ^{99m}Tc-dimercaptosuccinic acid (DMSA) scan and magnetic resonance (MR) imaging in detecting renal parenchymal abnormalities in patients with pyelonephritis. **Materials and Methods:** Systematic searches of PUBMED and EMBASE databases were performed to extract studies performing both DMSA scan and MR imaging in patients with pyelonephritis. We used a search algorithm based on a combination of terms. Relevance of articles was assessed by two authors according to predefined in- and exclusion criteria. English-language publications were selected. Review articles, abstracts, case reports, editorials and studies in other diseases were excluded. Meta-analysis was performed in per-patient and per-kidney basis. **Results:** Seven (7) studies (164 patients) were analyzed. MR imaging was positive in 107 patients (65.2%) and DMSA scan was positive in 96 patients (58.5%). In acute pyelonephritis (95 patients), MR imaging was positive in 75 patients (78.9%) and DMSA scan was positive in 63 patients (66.3%). When assessing for scar (69 patients), MR imaging was positive in 32 patients (46.4%) and DMSA scan was positive in 33 patients (47.8). There were discordant results in 26 patients (MR positive/DMSA negative in 18 patients, and DMSA positive/MR negative in 8 patients). **Conclusion:** MR imaging is more sensitive than DMSA scan in detecting renal parenchymal abnormalities in acute pyelonephritis. In chronic pyelonephritis, MR imaging and DMSA scan has equal sensitivity in detecting scars. However, studies in larger number of patients with more established MR protocols can provide more accurate results on sensitivity of MR imaging and DMSA scan in detecting parenchymal abnormalities in pyelonephritis. **References:** None.

EP-0274

A comparison of the renographic results from living and cadaver donors in kidney transplantation

A. N. B. Marques, *F. Abreu, C. Gaspar, S. Pintão;*
Hospital de Santa Cruz - Centro Hospitalar Lisboa Ocidental, Carnaxide, PORTUGAL.

Aim/Introduction: The renographic evaluation of the renal graft in the immediate post-transplant period is a valuable method to provide graft information, such as the kidney transplant blood flow, function and possible complications, and can also be used as a baseline study for future comparative evaluations.We analyzed our hospital's renal transplant population and compared renographic evaluation results with donor status (living vs cadaver donor). **Materials and Methods:** We retrospectively analysed epidemiological data and up to 5 day post-transplant renal scan findings of all the patients submitted to renal transplantation since 2010 until now.Renographic images were acquired with ^{99m}Tc-MAG$_3$, according to the department protocol and a normal scan was considered one to be with preserved perfusion and time-activity curve. Epidemiological data were gathered from patient files.Statistical analyses were made using PAWS-23®. **Results:** 421 renal transplant recipients were studied, being 63.2% male, with a median age of 52 years old (16-68). The donors were 54% female, with a median age of 55 (4-77) and 79.1% of the renal grafts came from a cadaver donor.In renographic studies, 32.8 % of the transplant recipients had decreased perfusion and 59.7% showed signs of Acute Tubular Necrosis (ATN). Median Effective renal plasma flow (ERPF) was 177 (10-528). Median ERPF changed according to donor status [204 (living donor) vs 174 (cadaver donor), p=0.008]. The likelihood of having a normal renal scan did not changed according to donor status. **Conclusion:** The study concluded that the overall renal scan results of kidney transplants did not changed according to donor status. However, the graft function was better in the living donors than in the cadaver donors group. **References:** None.

EP-0275

Validation of the Glomerular Filtration Rate determination using Technetium-99m Diethylenetriaminepentaacetic acid instead of Chromium-51 Ethylenediaminetetraacetic acid

I. Romero, I. Gil-Viciano, L. Fernandez-Romero, P. Notta, L. Rubio-Alvárez, M. Ysamat-Marfà, C. Munuera-Sañudo, E. Pineda-Fernández, M. Bueno-Raspall, C. Gámez-Cenzano;
Nuclear Medicine-PET Unit, Hospital Universitari de Bellvitge, L'Hospitalet de Llobregat, SPAIN.

Aim/Introduction: In our department over 150 Glomerular Filtration Rate (GFR) determinations are performed yearly. The radiopharmaceutical that we used was chromium-51 ethylene diamine tetra-acetic acid (^{51}Cr-EDTA) is no longer available. There is a well-established alternative, the complex technetium-99m diethylene triamine penta-acetic acid (^{99m}Tc-DTPA). The aim of this study was to validate our procedure to determine GFR with ^{99m}Tc-DTPA by comparing the results obtained with both radiopharmaceuticals. **Materials and Methods:** Simultaneous measurements of the clearance rate of 3 MBq of ^{51}Cr-EDTA and 37 MBq of ^{99m}Tc-DTPA were performed in 27 patients. After the intravenous bolus administration of ^{51}Cr-EDTA followed by ^{99m}Tc-DTPA, blood samples were withdrawn from the contralateral arm at 2, 3 and 4 hours. After centrifuging, 1 ml of plasma samples in duplicate and standards in triplicate were counted in a gamma-counter Wizard 2 Perkin Elmer model, for each energy windows ^{99m}Tc and ^{51}Cr. For the ^{99m}Tc-DTPA, the dose measurements at dose calibrator and at well gamma-counter were decay corrected to time of administration.The GFR calculation was the slope-intercept method characterizing the late exponential and applying the Bröchner-Mortensen's correction for the missing fast exponential. The GFR was normalized to body surface area calculated by Dubois and Dubois formula. The calculated GFR (BSA corrected), using ^{99m}Tc-DTPA and ^{51}Cr-EDTA, was compared and the mean percentage of differences obtained. It was evaluated the correlation between the percentage of differences and the absolute value of GFR (BSA corrected). **Results:** The mean values of GFR were 84.9 (SD=19.7) ml/min/1.73m² for ^{51}Cr-EDTA and 87.6 (SD=21.1) ml/min/1.73m² for ^{99m}Tc-DTPA respectively. The linear regression showed a highly correlation (r=0,960) between the GFR values obtained with both radiopharmaceuticals. The mean percentage of paired differences was 3.2 % (SD= 5.9), systematically higher for ^{99m}Tc-DTPA. This result is consistent with published studies. No correlation was found between the percentage of difference and the GFR value. (r=0.023). **Conclusion:** The ^{99m}Tc-DTPA clearance is a validated alternative to the ^{51}Cr-EDTA in the assessment of GFR. The differences between the two radiopharmaceuticals are small enough to be clinical significance. **References:** None.

EP-0276

Does volume of distribution make a contribution to QC of GFR measurement?

J. M. Warwick, J. L. Holness;
Stellenbosch University, Cape Town, SOUTH AFRICA.

Aim/Introduction: Errors during GFR measurement fall into 3 categories: (type 1) failure of the single-compartment model; (type 2) whole curve measurement error; and (type 3) individual point measurement error [2]. Volume of distribution (v_{dist}) has traditionally been included as a quality control (QC) check for slope-intercept GFR (SI-GFR) measurements. However recent work has found v_{dist} to be both non-specific and insensitive for the detection of type 1 errors [1]. Type 2 and 3 errors are probably uncommon in research environments, but may be more frequent in clinical environments where GFR studies are performed by generically functioning technologists and/or trainees under supervision. The aim of this study was to evaluate v_{dist} for the detection of type 2 and type 3 errors. **Materials and Methods:** Using a dataset of 786 3-sample GFR measurements performed in patients with cancer, chronic kidney disease, and potential kidney donors, we introduced errors of varying size to (i) the standard counts (type 2) or (ii) one of the sample counts (type 3). Only "plausible" studies (GFR between 0 and 160 ml/min/1.73m2 and progressively decreasing sample counts) were included. GFR errors > 20% were considered significant. Cases in which v_{dist} in litres was beyond 8.19 times body surface area ±43% (2.5 SD) were considered to have failed QC [2]. **Results:** Despite using a donor-derived reference range for v_{dist} [2], it remained applicable in this pathologically mixed sample with 1.9% of unaltered studies being "falsely" positive. GFR changed significantly for type 2 errors >20%. For gross errors in the standard (< -50% or > 120%) v_{dist} had a sensitivity of > 80%. For significant type 3 errors, the correlation coefficient (r<0.985) was an excellent QC check, far more sensitive than v_{dist}. However for a 2-sample SI-GFR (where a correlation coefficient is unavailable), v_{dist} had a sensitivity of > 80% for large errors of the 2- or 3-hour samples (< -50% or > 40%). **Conclusion:** For SI-GFR measurements based on only 2 samples, or performed without injection site imaging, v_{dist} enables the detection of large type 2 and type 3 errors that may be otherwise undetectable. **References:** 1. McMeekin H, Wickham F, Barnfield M, Burniston M. Effectiveness of quality control methods for glomerular filtration rate calculation. Nucl Med Commun 2016; 37:756-766. 2. Holness JL, Fleming JS, Malaroda AL, Warwick JM. 99mTc-DTPA volume of distribution, half-life and glomerular filtration rate in normal adults. Nucl Med Commun 2013; 34:1005-1014.

EP-0277

SPECT/CT for detection of dialysate leakage in patients on continuous ambulatory peritoneal dialysis - a retrospective study

D. Chroustova[1], J. Trnka[1], M. Havrda[2];
[1]General University Hospital and 1st Faculty of Medicine, Charles University, Prague, CZECH REPUBLIC, [2]1st Department of Internal Medicine, Faculty Hospital Kralovske Vinohrady and Third Faculty of Medicine, Charles University, Prague, CZECH REPUBLIC.

Aim/Introduction: Continuous ambulatory peritoneal dialysis (CAPD) offers several advantages over hemodialysis, but some complications including dialysate leakage may occur. In this retrospective study we investigated the value of peritoneal scintigraphy using ^{99m}Tc-MAA SPECT/CT in evaluation of

dialysate leakage and its localization in patients undergoing CAPD. **Materials and Methods:** 23 patients (13 males 9 females, aged between 31 and 78 years with an average age of 54,7 years) underwent CAPD between 2010 to 2018, and those suspected to have dialysate leakage or dialysate retention in peritoneal cavity were enrolled into study. Peritoneal scintigraphy was performed after administration of 100 MBq ^{99m}Tc-MAA in dialysis solution into peritoneal cavity. Initial dynamic imaging and subsequent ANT/POST WB imaging and SPECT/ (low dose) CT examination using INFINIA Hawkeye gamma camera were performed. **Results:** Dialysate leakage was demonstrated by peritoneal scintigraphy in 10 patients. The pleuroperitoneal communication was detected in one woman, periumbilical leaks were found in three women, scrotal leakages in three men (one case on the right side and two cases on the left side), inguinal leaks in three men (two cases on right side and one case on the left side), vaginal leak was found in one woman. In five cases, a combination of abdominal wall defect with another leak type was found with advantage of hybrid CT image. The dialysate volume adjustment was performed in 12 non-leakage patients who had symptoms of the dialysate retention. They were investigated and followed for further mechanical complications: catheter obstruction or dislocation, or solution leakage around the catheter. **Conclusion:** Peritoneal scintigraphy is simple and effective method for detecting structural abnormalities and localizing the origin of leakage. According to our experience, SPECT/CT is very helpful for detection and more accurate localization of dialysate leakage, especially in cases of the leakage defects via abdominal wall, which are not always clearly visible on ANT/POST projections. **References:** None.

EP-0278

Practical attenuation correction in renal scintigraphy for precise split renal function measurements

R. Klein[1,2], *A. Rezk*[3], *O. Kotbi*[2], *A. Abdulrahman*[2], *E. Leung*[2], *B. Ziebarth*[1], *Z. Wanzhen*[2];
[1]*The Ottawa Hospital, Ottawa, ON, CANADA,*
[2]*University of Ottawa, Ottawa, ON, CANADA,*
[3]*Department of Physics, Ottawa, ON, CANADA.*

Aim/Introduction: Split renal function measurements using planar scintigraphy in living kidney donors and patients with suspected renal obstruction are vital metrics. They are typically performed using posterior imaging (PI) which assumes similar kidney tissue depths and hence similar photon attenuation. Attenuation corrections (AC), which may be especially important in abnormal kidney anatomies, have been previously proposed but their optimal clinical use is not conclusive. **Materials and Methods:** This retrospective study included patients which had undergone ^{99m}Tc-MAG3 or ^{99m}Tc-DTPA renal imaging on a dual-head gamma camera and had an abdominal region CT within 1 year. An experienced nuclear medicine physician classified each patient into normal or abnormal kidney anatomy groups by visual assessment. Right kidney differential function (RFK) was obtained from the area under the activity curve from 1-3 minutes post-injection using manually drawn regions-of-interest (ROIs) using the clinical renogram processing software (Hermes) both on posterior images (PI) and geometric-mean of anterior-posterior projections (GM). In addition, both PI and GM values were corrected for 140 keV photon attenuation using anterior and posterior soft-tissue depths of each kidney as measured on CT and assuming uniform linear attenuation of water (0.154 cm^{-1}) (ACPI and ACGM respectively). Balanced kidney function was assumed for 45%≤RFK≤55%. **Results:** Of the 80 patients included, 18 (23%) had abnormal kidney locations. GM estimated higher average RKF than PI (p=0.01) for both normal and abnormal groups (by 1.0% and 4.1% respectively). Similarly, ACPI had higher values by 0.9% and 4.5% (p<0.05 for both). GM and ACGM did not significantly differ (p>0.2) in either group, nor with ACGM and ACPI, indicating that GM sufficiently corrected for photon attenuation. Furthermore, smallest variability (standard-deviation) was achieved in GM-ACGM differences (2.2% and 3.7% for normal and abnormal groups) which used identical ROIs and AC influence was negligible. In comparison, variabilities of PI-GM were 2.8% and 5.8% and were even greater for ACPI-ACGM (3.9% and 8.6%) due to ROI variability and introduction of additional noise on depth measurements. Prevalence of balanced function increased from 57% with PI to 65% with GM in normal and from 33% to 50% in abnormal anatomies (p<0.01). **Conclusion:** Geometric-mean of anterior-posterior renal scintigraphy for split renal function measurements are more accurate than posterior imaging, and precision may be degraded by attenuation correction using CT-based depth measurements. Considering no additional radiation exposure or imaging time, geometric-mean should be used in routine assessment of split renal function. **References:** None.

EP-0279

Replacing 51Cr-EDTA with 99mTc-DTPA in GFR measurement : a prospective comparative study

G. Arsos[1], *E. Moralidis*[1], *A. Kalaitzogloy*[1], *D. Katsampoukas*[1], *C. Sachpekidis*[2];
[1]*3rd Dept. of Nuclear Medicine, Aristotle University of Thessaloniki School of Medicine, Papageorgiou Gen Hospital, Thessaloniki, GREECE,* [2]*Dept. Of Nuclear Medicine, Inselspital, Bern University Hospital, University Of Bern, Bern, SWITZERLAND.*

Aim/Introduction: 51Cr-EDTA is traditionally the main radiotracer for GFR measurement usually by the single injection-multiple sampling technique in Europe, while 99mTc-DTPA, alternatively proposed by the current guidelines, is less commonly used. Although similar, 99mTc-DTPA and 51Cr-EDTA may give significantly different GFR values, depending on DTPA exact formulation. Due to recent 51Cr-EDTA (GE) withdrawal**,** centers based upon this radiotracer and now shifted towards 99mTc-DTPA use, may experience problems of consistency in patients follow-up, GFR adjusted chemotherapy dosing and kidney transplant donation GFR cut-off values. The aim of our prospective study was to explore equivalence between one commercially available, widely used DTPA preparation

and 51Cr-EDTA (GE) in GFR measurement. **Materials and Methods:** Between 5/12/2018 and 22/2/2019, 42 consecutive patients aged 18-86 years, 15 F, referred for radionuclide GFR measurement had simultaneous GFR measurement with both $99mTcO_4^-$ labelled TechneScan DTPA (Mallinckrodt) and ready to use 51Cr-EDTA (GE) preparations. After simultaneous bolus i.v, administration of both radiotracers, 10 blood samples were obtained between 5 min to 4 hours post-injection and plasma 99mTc and 51Cr activities measured on the same and two days later respectively. For both radiotracers, GFR was calculated by : a) two-compartment bi-exponential kinetic analysis using 10 samples (GFR10, ml/min), allowing also for extracellular fluid volume (ECFV, l) assessment and b) by "slope-intercept", one-compartment mono-exponential analysis with 2 samples at 2 and και 4 hours post-injection and Brochner-Mortensen correction (GFR2, ml/min), according to British guidelines. GFR10, GFR2 and ECFV were scaled for body surface area (BSA) calculated according to Haycock formula (SGF10, SGFR2 both in ml/min/1.73 m² and SECFV in l/1.73 m² respectively). **Results:** 99mTc-DTPA and 51Cr-EDTA, values of GFR2 GFR10, ESV, SGFR2, SGFR10 and SESV were : 65.3±34.3 vs 64.6±34.0, p=0.047; 58.1±29.4 vs 57.5±29.2, ns; 72.6±35.9 vs 72.7±36.2, ns; 64.7±30.5 vs 64.6±30.5, ns; 14.9±3,2 vs 16.1±3.3, p less than 0.0001; 13.4±2.6 vs 14.4±2,7, p less than 0.0001, respectively. The corresponding 99mTc-DTPA-51Cr-EDTA correlations were strong with R² greater than 0.99 and p less than 0.0001 in all cases. 99mTc-DTPA GFR and ECFV values within the corresponding 51Cr-EDTA values ±10%, exceeded 95 and 83% respectively. **Conclusion:** GFR measurement with TechneScan DTPA (Mallinckrodt) shows values almost identical to those by 51Cr-EDTA (GE) in a wide range of renal function by both the "slope-intercept" technique and the 10 sample kinetic analysis. As expected by the slightly higher molecular weight of 99mTc-DTPA compared to 51Cr-EDTA, ECVF is slightly underestimated by appox. 1 l. **References:** None.

EP-0280

Simultaneous measurement of Glomerular Filtration Rate (GFR) with Tc-99m-labelled diaethylenetriaminepentaacetic acid (Tc-99m-DTPA) and Cr-51-labelled ethylenediaminetetraacetic acid (Cr-51-EDTA)

A. Agudo Martinez, A. Moreno-Ballesteros, F. García-Gómez, T. Cambil-Molina, R. Fernández-Sanz, C. Calvo-Morón;
Virgen Macarena Hospital, Seville, SPAIN.

Aim/Introduction: GFR can be measured through radionuclide-based techniques, being Cr-51-EDTA the gold-standard. The production of Cr-51 is decreasing, making imperative to adapt the Tc-99m technique. We compare GFR assessment through plasma clearance of Tc-99m-DTPA and Cr-51-EDTA following the same simple-injection technique, to assess its accuracy. **Materials and Methods:** Two healthy volunteers and one patient participated in this pilot study. Following hydration with 300ml water, 10MBq of Tc-99m-DTPA and 3MBq of Cr-51-EDTA were simultaneously injected. Standard doses of each radiotracer with half-dose were diluted in 1000ml of water. Patient and standard doses were measured by weighing of the syringes and the correction for residual dose by subtraction of empty from full syringe weights was done. Blood samples of 10ml were obtained from the contralateral arm at 120, 180 and 240min postinjection. Plasma samples were centrifuged at 1500g for 5min to isolate the plasma. Samples of 1ml of plasma, standard and water (background) activity (cpm), were counted per duplicated, in γ-counter the same day of study (Tc-99m-standard-samples) and two days later (Cr-51-standard-samples). Same set of plasma and background were used during the counting , after selection of correct energy peak. Decay correction was applied relative to time between counting of patient samples and standard samples. All samples were background-corrected. Plasma activity (P_t) disappearance reflects GFR and this one-compartimental model follows a single exponential: $P_t=P_0\ \exp(-Kt)$; P(t)=plasma concentration (cpm/ml) at t-time P_0=plasma concentration (cpm/ml) at injection-time K:constant of exponential clearance GFR=VdxK. V_d=volume of distribution.Slope-Intercetp Method by back extrapolation to zero-time was used to give the estimated activity per unit volume (P_o) in the volume of distribution, and $V_d=A/P_0$ where A=injected activity.To calculate A, the measurement of standard activity ($cpm/ml_{standard}$) and relation of patient ($W_{patient}$) and standard ($W_{standard}$) dose weights are used: $A=cpm/ml_{standard} x V_{standard} x (W_{patien}/W_{standard})$ The GFR was normalized by correction to surface area (BSA) of 1.73m2 and then the correction of Brochner-Mortensen (GFR_{corr}) was applied to allow the one-pool assumption. We also calculated half clearance as quality assurance check ($T_{1/2}(min)=Ln2/K(min^{-1})$). **Results:** Expected Vd in adult is 8 times the BSA (2-SD variation of +/-25%) and $T_{1/2}$ is between 100-120min. GFR measurement by both radiotracers were comparable. Vd and T1/2 values would improve by using Tc-99m according to expected if the first point was not taken into account. **Conclusion:** GFR measurement by Tc-99m-DTPA clearance is an accurate and feasible test using three-point monoexponential plasma method but we suggest starting plasma extraction after 120 minutes. **References:** None.

EP-0281

Renal Clearance Function Index - Preliminary Assessment of Clinical Usefulness of a New Dynamic Renal Scintigraphy Parameter

P. Cichocki[1], K. Filipczak[2], M. Surma[1], A. Płachcińska[2], J. Kuśmierek[1];
[1]Department of Nuclear Medicine, Medical University of Łódź, Łódź, POLAND, [2]Department of Quality Control and Radiological Protection, Medical University of Łódź, Łódź, POLAND.

Aim/Introduction: Split function of both kidneys (SF), one of the basic quantitative dynamic renal scintigraphy (DRS) parameters, has significant limitations. Its relative nature makes it unreliable for example in case of lack or a trace function of the other kidney, or bilateral renal disorders. This study aims to determine normative values of the original parameter reflecting renal

clearance in the absolute values - renal clearance function index (CFi), and preliminarily assesses its usefulness in selected clinical situations. **Materials and Methods:** Study included 2 groups: [1] - control - 20 healthy volunteers (40 kidneys); [2] - 41 patients with a single functioning kidney (with lack or trace function of the other kidney - SF <10%), and 15 patients (30 kidneys) with bilateral obstructive uro-/nephropathy - cumulative renographic curves with no or poor response to diuretic test, in total 56 patients (71 kidneys). DRS was performed according to a standard protocol - after intravenous administration of 111MBq ^{99m}Tc-EC, 120 sequential images were acquired (10s each). If necessary, study was extended by a diuretic test ("F+20" protocol). CFi was calculated for all kidneys using an in-house developed software. Its normative values were determined based on the control group (40 kidneys). In standard DRS evaluation, kidneys of patients from group 2 were classified as nephropathic if they met 2 out of 3 criteria: SF <45%, T_{MAX} >7min and/or peripheral cortical lesions in visual assessment. This routine diagnosis was compared with CFi results. **Results:** Mean CFi values in control group were 23,6 ± 4,4. CFi ≥15 (mean - 2SD) was determined as a normative limit. In group 2, 24/71 kidneys were classified as nephropathic according to classic criteria. Application of CFi changed the classification in 14/71 kidneys (20%) and affected 13 out of 56 patients (23%). This parameter was within normal range in 4/24 kidneys classified in conventional DRS as nephropathic and was below normal limit in 10/47 kidneys without features of nephropathy in conventional DRS. **Conclusion:** CFi, which reflects the clearance function of each kidney in absolute values, extends diagnostic capabilities of DRS. This parameter is particularly useful in situations when assessment of SF is unreliable. It was demonstrated that such situations may occur, among others, in patients with a single functioning kidney - to assess its actual performance, or with bilateral urinary tract obstruction - to differentiate between obstructive uropathy and nephropathy. **References:** None.

EP-0283

Can Glomerular Filtration Rate Estimation be Adapted for Local Oncology Patients?

J. L. Holness, H. M. Simonds, P. Barnardt, J. M. Warwick; Stellenbosch University, Cape Town, SOUTH AFRICA.

Aim/Introduction: Creatinine-based glomerular filtration rate (GFR) estimating equations tend to perform poorly in cancer patients. The Janowitz-Williams model is a new equation developed from a large Caucasian cancer population[1]. Our study evaluates the performance of this equation and three commonly used CKD equations in a genetically and socioeconomically diverse cancer population. It also evaluates the utility of a simple tool to improve GFR estimation by adapting the equations' parameters to better fit the data. **Materials and Methods:** GFR was measured from the plasma clearance of ^{99m}Tc-DTPA using the slope-intercept method. GFR was estimated (eGFR) from standardized serum creatinine levels using the original Cockcroft-Gault (CG), Modification of Diet in Renal Disease (MDRD), Chronic Kidney Disease Epidemiology Collaboration (CKD-EPI) and Janowitz-Williams (JW) equations. The population was then randomly and equally divided into development and validation sets. A Microsoft Excel add-in (Solver) was used to optimise the equations' parameters using the development set data. The bias, precision, accuracy and agreement of all original and adapted equations was determined using the validation set data. The impact that use of eGFR would have had on management decisions was also assessed. **Results:** Data of 435 patients were included. Of the original equations, the Janowitz-Williams was least biased and most precise. The original equations all overestimated GFR by 7.9 to 16.0 ml/min/1.73m². Bias of the adapted equations was significantly lower (-2.2 to 3.4 ml/min/1.73m², p<0.0001). The original equations had interquartile ranges (IQRs) of 21.8-30.4 ml/min/1.73m². Adapting the equations reduced the IQRs to 21.2-24.0 ml/min/1.73m². The accuracy, measured as P_{30} values, improved significantly from 57.1%-73.7% to 78.3%-82.9% after adapting the equations (p≤0.0001). The 95% confidence intervals (CI) were ± 42.3, 34.4, 32.9 and 33.3 ml/min/1.73m² for the adapted CG, MDRD, CKD-EPI and JW equations respectively. Using eGFR with a CI allows for reliable exclusion of patients with impaired renal function, however eGFR remains equivocal in a significant proportion of patients. **Conclusion:** The JW equation provides the most accurate unadapted estimate. Adapting the equations for a population of mixed ancestry improved their performance. While reliable to exclude low GFR when eGFR is normal to high, in the GFR range where most critical clinical decisions are made, the uncertainty of GFR estimates is large. In these cases there is no alternative to GFR measurement. **References:** 1. Janowitz T, Williams EH, Marshall A, et al. New model for estimating glomerular filtration rate in patients with cancer. J Clin Oncol. 2017;35(24):2798.

EP-0284

Is there a role for renal perfusion on the evaluation of urinary tract obstruction?

M. Monteiro[1], R. Silva[1,2], T. Saraiva[1], G. Costa[1,2], J. Pedroso de Lima[1,2,3];
[1]Centro Hospitalar e Universitário de Coimbra, Coimbra, PORTUGAL, [2]Faculdade de Medicina da Universidade de Coimbra, Coimbra, PORTUGAL, [3]Instituto de Ciências Nucleares Aplicadas à Saúde (ICNAS), Coimbra, PORTUGAL.

Aim/Introduction: Urinary tract obstruction (UTO) is a common clinical problem and a frequent cause of renal impairment. It is defined as a physical blockage to urine flow, which may result in hydronephrosis and ultimately renal parenchymal damage. Renal scintigraphy provides important functional data to assist in the diagnosis and management of patients with UTO, however renal perfusion has not been demonstrated to contribute to interpretation. With this retrospective work, we aim to assess the value of perfusion on diuretic renal scintigraphy in adults with suspected upper UTO (UUTO). **Materials and Methods:** One hundred and fifty diuretic renal scintigraphies with [^{99m}Tc]

Tc-MAG3, performed in adults between January and December 2018, were retrospectively reviewed. Patients with previous urologic surgeries or double J stent and with suspected lower UTO were excluded. Also, some scans were excluded due to technical errors (inconsistent time zero, patient motion and non-bolus injection). Drainage status, renal perfusion and function, both in absolute and differential terms, and all other relevant data, including demographic variables were recorded. A parenchyma to perfusion count ratio, corrected for background and time, was calculated. A ratio between parenchymal phase and vascular phase counts, adjusted for time and background, was calculated (F/P). Statistical analysis was performed using SPSS version 25.0. **Results:** 57 patients were selected (28 women, 29 men; age: 56.21±18.98, 19-95 years), with 114 kidneys, which were categorized as: group one - no suspected UUTO (31 right kidneys [RK], 26 left kidneys [LK]); group two - suspected UUTO without obstructive pattern (20 RK; 17 LK) and group three - suspected UUTO with obstructive pattern (6 RK; 14 LK). The median F/P was 3.63 (interquartile amplitude=1.65;1.14-10.84) for group one, 3.81 (interquartile amplitude=1.58;2.19-9.56) for group two and 2.23 (interquartile amplitude=1.72;0.95-5.77) for group three. Statistically significant differences for F/P were found between group three and the other two (Krustal-Wallis with Bonferroni correction, p<0.001 for both groups 3-1 and 3-2). No statistically significant difference was found between group one and two. **Conclusion:** Despite further larger and prospective studies are warranted, in our series, the F/P ratio seems to be statistically different between obstructed and non-obstructed kidneys. **References:** None.

EP-0285

Outcome of Kidney Function after Kidney Donation in Donors over 60 Years Old

M. A. E. Nicod Lalonde, J. Venetz, C. Geldhof, G. Allenbach, N. Schaefer, J. O. Prior, A. Boubaker;
University Hospital of Lausanne, Lausanne, SWITZERLAND.

Aim/Introduction: The aim of this study was to evaluate the outcome of kidney function following live kidney donation in donors aged over 60 years (>60y) compared to live donors under 60 years (<60y). **Materials and Methods:** We prospectively enrolled 27 living donors in the >60y group (15F/12M) with a mean age at kidney donation of 65±5y [range 60-78y] and 4 donors in the <60y group (4F) with a mean age of 44±5y [37-48y]. The enrollment of the <60y group was terminated early because of unavailability of Cr-51-EDTA. All but two donors had an estimation of renal function by I-123 hippuran renal scintigraphy (RS) prior to kidney donation. All but four donors had an estimation of glomerular filtration rate (GFR) by measuring plasma clearance of Cr-51-EDTA prior to kidney donation. A second assessment was made for all donors >6 months after kidney donation (mean 3.0±1.7y [0.6-5.7y] in the >60y group and mean 4.0±2.2y [2.4-7.2y] in the <60y group). The accumulation index (AI) acquired during RS (defined as the percentage of injected activity extracted by the kidney during 1 minute) was assessed. Data were processed using STATA. The two groups were compared using a Wilcoxon rank-sum (Mann-Whitney) test. **Results:** The mean GFR after donation was lower averaging 52±8.6ml/min/1.73m² in the >60y group vs. 69±9.6ml/min/1.73m² in the <60y group (p=0.01). The AI of the remnant kidney after kidney donation was 10.4±1.7% in the > 60y group vs. 12.5±0.8% in the <60y group (p=0.03). The increase of AI of the remaining kidney was lower in the >60y group (20±26% vs. 49±28% in the <60y group; p=0.04). The GFR decreased by 30±14% after donation in the >60y donors vs. 27±23% in the <60y (p=0.54). None of the patients in both groups had a GFR of less than 30ml/min/1.73m² after >6months after kidney donation. **Conclusion:** In our study, donors over 60y had a GFR decrease following kidney donation comparable to younger donors less than 60y. Thus, living kidney donation from older patients appears to be safe based on the pre-donation GFR and separate kidney function assessed by renography. The significance of the lower increase of AI of the remaining kidney in the >60y group remains to be further investigated. **References:** None.

EP-0286

Gravity-dependent Diuretic-renography: A Rational Approach For Functional Evaluation Of Urinary Diversion

G. Tartaglione[1], *N. Foschi*[2], *S. M. Recupero*[2], *M. Racioppi*[2,3], *R. Bientinesi*[2], *G. Palermo*[2], *M. Ragonese*[2], *L. Di Gianfrancesco*[2], *E. Sacco*[2], *F. P. Ieria*[1], *F. Pinto*[2], *P. F. Bassi*[2,3];
[1]*Nuclear Medicine, Cristo Re Hospital, Rome, ITALY,*
[2]*Department of Urology, Fondazione Policlinico Universitario "A. Gemelli" IRCCS, Rome, ITALY,* [3]*Urology, Università Cattolica del Sacro Cuore, Rome, ITALY.*

Aim/Introduction: Urinary diversion is anyone of several surgical procedures that divert the flow of urine to a replacement bladder (neobladder) or through an opening in the abdominal wall (stoma), connecting ureters with a tract of bowel. A stricture of the uretero-ileal anastomosis might appear in 1:5 of patients. The right identification of patients who would benefit from surgical treatment is a significant clinical challenge. We proposed Gravity-Dependent Diuretic-Renography (GDDR) with method F+10(sp) (Seated Position), in patients with urinary diversion and a suspected stenosis of the urinary tract. **Materials and Methods:** 39 patients with CT or ultrasound evidence of hydronephrosis in 44 Renal Units (RUs), and/or impairment of renal function parameters were enrolled. All subjects underwent GDDR with method F+10(sp) whereby the patient received IV a dose of MAG3-99mTc (150 Mbq, 0,3 mL) at time 0, drank 400 to 500 mL of water at the 5 minute, and received an IV injection of 20 mg of Furosemide as a bolus at the 10 minute after tracer injection [F+10 (sp)] during dynamic acquisition in seated position. Post-voiding static images at 20' and 60' were acquired. Test evaluation was based on Semi-quantitative parameters: Tmax (nv <7 min), Diuretic T1/2 (nv <8 min), Ratio 20min/peak (nv <0.25). The results were classified as: Dilation (Tmax >7 min, Ratio 20min/peak <0,25), Obstruction (Tmax >7

min, Ratio 20min/peak >0.25), or Equivocal. **Results:** F+10(sp) test showed: Dilation in 7/44 RUs (15.6%); Obstruction in 36/44 RUs (81.8%); Equivocal results in 1/44 RUs (2,3%). No side effects were reported. In 10 patients anastomosis stenosis caused RUs impairment and a nephroureterectomy was performed. In 7 out of 10 patients RUs failure occurred < 6 months after surgery. In selected patients, diagnostic work-up involved a retrograde cystography or a loop-graphy to confirm ileal-ureteral reflux. The equivocal result was related to an ileal-ureteral reflux. **Conclusion:** In urinary diversion the urine drainage is clearly dependent by patient position. The GDDR with method F+10sp exploiting gravity, better evaluates the gravity-dependent urine drainage, discriminating obstruction from simple urinary dilation. Thanks to a reduced dose of Furosemide (20 mg) and a better timing, the test avoids the side effects typical of other methods (bladder filling, disruption because voiding, and diuretic-related-hypotension) increasing accuracy. Considering the high rate of early stenosis (<6 months) of the uretero-ileal anastomosis, this diagnostic approach might be suggested during first months after surgery. **References:** 1) Taylor AT, et al Semin Nucl Med. 2018 Jul;48(4):377-3902.

EP-0287

Viability Of The Transplanted Renal Graft. Correlation Between Renal Biopsy And Isotopic Renogram 24h Post-Transplant

J. Gómez Hidalgo[1], *M. Ruiz Gómez*[1], *N. Álvarez Mena*[1], *P. Turbay Eljach*[1], *B. Pérez López*[1], *C. Gamazo Laherrán*[1], *M. Alonso Rodríguez*[1], *A. Sainz Esteban*[1], *M. Méndez Pascual*[2], *S. De Pablo Leonardo*[2], *M. González Soto*[1], *R. Ruano Pérez*[1];
[1]*Hospital Clínico Universitario de Valladolid. Medicina Nuclear, Valladolid, SPAIN,* [2]*Hospital Clínico Universitario de Valladolid. Unidad de trasplante renal, Valladolid, SPAIN.*

Aim/Introduction: to relate the histopathological assessment (SCORE) of the renal graft in patients transplanted with the isotopic renogram performed at 24 post-transplant. **Materials and Methods:** we studied 116 patients with cadaver kidney transplantation. The protocol of the histopathological assessment in the kidney transplant is by wedge biopsy; the processing of it is by freezing and is performed in those donors > 60 years old or between 40-60 years with hypertension and/or diabetes. The SCORE of the renal biopsy is obtained from the sum of 4 sections: percentages of glomerular sclerosis (0-3), intimal fibrous arterial hyperplasia (0-3), tubular atrophy (0-3) and interstitial fibrosis (0-3). Renal grafts with a total SCORE > 3 or one of the 4 sections with a score ≥ 2 are rejected. Twenty-four hours after transplantation we performed a 30 minutes renogram study focusing on the abdomen in anterior projection after the administration of 370 MBq of 99mTc-DTPA followed by planar images at 30 and 180 minutes. **Results:** we studied 116 patients (age: 61+/-12). In 39 transplanted grafts (33.62%) no biopsy was performed (not necessary). Of the rest of cases, only 1 presented a SCORE of 0 in the biopsy, 12 showed a SCORE of 1 (10.34%), 27 SCORE of 2 (23.27%) and 37 SCORE of 3 (31.89%). Of the 39 patients without biopsy, the renogram was normal in 14 patients (36%), 12 had discrete acute tubular necrosis (ATN) (30.77%), 11 moderate ATN (28.2%) and only 1 showed poor vascularization but it was secondary to intra-surgical hemorrhage. The only case with a SCORE 0 showed a normal renogram. Of the 12 patients with SCORE 1, 3 cases were normal (25%), 5 had discrete ATN (41.66%), 3 moderate ATN (25%) and 1 showed vascular thrombosis (8.33%). Of the 27 patients with SCORE 2, 5 cases were normal (18.5%), 12 discrete ATN (44.4%), 2 moderate ATN (7.4%), 7 severe ATN (26%) and 1 vascular thrombosis (3.7%). And of the 37 cases with SCORE 3, 9 patients presented a normal renogram (24.3%), 11 discrete ATN (29.72%), 9 moderate ATN (24.32%), 6 severe ATN (16.21%), 1 urine leak (2.7%) and 1 vascular thrombosis (2.7%). **Conclusion:** the renogram shows a good correlation with the SCORE obtained in the histopathology of the kidney graft biopsy. Higher SCOREs show more pathological scintigraphic findings (moderate-severe ATN and surgical complications): no biopsy (28.2%), SCORE 1 (33.3%), SCORE 2 (37.1%), SCORE 3 (45.93%). **References:** None.

EP-0288

Importance of 99mTc-DTPA renal scintigraphy in evaluating renal function in the pre-operative and post-operative elective F/BEVAR phases TAAAs

V. Frantellizzi[1], *L. Cosma*[1], *M. Ricci*[1], *M. Orrico*[2], *N. Mangialardi*[2], *M. Liberatore*[1];
[1]*Sapienza University of Rome, Rome, ITALY,* [2]*San Camillo Forlanini Hospital, Rome, ITALY.*

Aim/Introduction: The objective of this study is to evaluate any variation of renal function detected by dynamic renal scintigraphy with 99mTc-DTPA after elective fenestrated or branched endovascular aneurysm repair (F/BEVAR) for thoracoabdominal aortic aneurysms (TAAAs) and to assess whether branches and fenestrations have different early-term effects on renal function. **Materials and Methods:** Between January 2018 and March 2019, 26 patients (13 males, 13 females) underwent elective F/BEVAR for TAAAs. To assess renal function 99mTc-DTPA perfusion scintigraphy was performed two weeks pre-operatively and at 3 and 6 months post-operatively. Overall, 51 kidneys were analyzed: 19 in patients treated with branches and 32 with fenestrations. Primary end points were peri-procedural technical success, 30-days Medication administration errors (MAEs) and Glomerular Filtration Rate (GFR) variations between the pre-operative and the post-operative dynamic renal scintigraphy. Secondary end points were significant alterations of other parameters at the 99mTc-DTPA renal scintigraphy (time to peak, percentage of kidneys' perfusion and radioisotope uptake percentage). **Results:** The mean pre-operative global GFR was 53.2 ml/min (SD 20.2 range 18.02 - 95.5 ml/min). In 11 patients (4 treated with renal branches, 7 with renal fenestrations) the renal function was normal (pre-operative GFR > 60 ml/min); 11 patients (5 treated with branches, 6 with fenestrations) had mild to moderate chronic kidney disease (CKD) (pre-operative GFR

between 60 and 30 ml/min) and 4 patients (1 treated with renal branches, 3 treated with fenestrations) had severe CKD (pre-operative GFR < 30 ml/min). The GFR of the kidneys in which the renal arteries were managed by a side branch decreased significantly after 3 months (Z -2.03; p = 0.05) while no significant GFR's variations were noted after the treatment with fenestrations (Z -0.7; NS). The time to peak was also significantly reduced after the treatment with branches (Z -1.8; p = 0.05) but showed no significant modifications with fenestrations' (Z -1.5 ;NS). There were no further alterations regarding the remaining scintigraphic parameters. **Conclusion:** The use of branches for renal arteries is associated with a significant decrease of the GFR compared to the use of fenestrations and the alterations are evident at early stage. Longer follow-up on a larger population submitted to 99mTc-DTPA renal scintigraphy will be useful in evaluate separately renal function, clarifying the natural history of these alterations and their clinical implications. **References:** None.

EP-0289

^{51}Cr EDTA vs ^{99m}Tc DTPA vs inulin for GFR measurement: is there a systematic difference?

H. McMeekin[1], *F. Wickham*[2], *M. Barnfield*[3], *M. Burniston*[1];
[1]*Barts Health NHS Trust, London, UNITED KINGDOM,* [2]*Royal Free London NHS FT, London, UNITED KINGDOM,* [3]*Leeds Teaching Hospitals NHS Trust, London, UNITED KINGDOM.*

Aim/Introduction: The study aimed to investigate whether a systematic difference exists between ^{51}Cr EDTA and ^{99m}Tc DTPA for measurement of glomerular filtration rate (GFR), and to see how each tracer compares with modelled inulin clearance using the formula of Brochner-Mortensen and Rodbro.[1] **Materials and Methods:** GFR results from candidates attending the Royal Free Hospital nuclear medicine department for assessment of suitability for kidney donation during the period October 2008 to May 2015 were reviewed. The clinical protocol for GFR measurement had changed from using ^{51}Cr EDTA to ^{99m}Tc DTPA in October 2012, allowing the comparison of measured GFR distribution in the normal population before and after the change of radiopharmaceutical. A second cohort of oncology patients attending Leeds Teaching Hospitals NHS Trust underwent simultaneous GFR measurement with both tracers. **Results:** From the first cohort, 184 GFR studies performed with ^{51}Cr EDTA and 154 performed with ^{99m}Tc DTPA were included in the analysis. A systematic difference of 5.8% (95% confidence interval: 1.5% - 10.1%) was found in the normalised GFR, with ^{99m}Tc DTPA giving the higher result. This difference was found to be statistically significant, with a p-value of 0.008. From the second cohort, 50 patients underwent simultaneous GFR measurement with both tracers. A systematic difference of 2.9% (95% confidence interval: 1.8% -3.9%) was found in the normalised GFR, with ^{99m}Tc DTPA giving the higher result. This difference was found to be statistically significant, with a p-value of 0.00001. There was no statistically significant difference between the tracers when the GFR was calculated by full characterisation of the plasma clearance curve with 9-samples from 5 minutes to 8 hours post injection. For both cohorts, applying the formula derived by Brochner-Mortensen and Rodbro[1] to model inulin clearance to the ^{51}Cr EDTA measurements removed the difference with ^{99m}Tc DTPA. **Conclusion:** There is a small systematic difference between normalised GFR measured with ^{51}Cr EDTA and ^{99m}Tc DTPA, which is removed when GFR is calculated by full characterisation of the plasma clearance curve. However, this is not clinically significant in the context of intra-patient variability of GFR measurement, especially when GFR is measured without exercise restriction. ^{99m}Tc DTPA is more closely matched with inulin than ^{51}Cr EDTA. **References:** 1. Brochner-Mortensen, J. and P. Rodbro, Selection of routine method for determination of glomerular filtration rate in adult patients. Scandinavian Journal of Clinical & Laboratory Investigation., 1976. 36(1): p. 35-43.

EP-0290

Comparison Of Simultaneous Plasma Clearance Of ^{99m}Tc-DTPA And ^{51}Cr-EDTA - Can One Tracer Replace The Other?

L. Petersen*, T. Andersen, L. Jødal, N. Nielsen;*
Department of Nuclear Medicine, Aalborg, DENMARK.

Aim/Introduction: Aim: Both ^{99m}Tc-DTPA and ^{51}Cr-EDTA are widely used for determination of glomerular filtration rate (GFR), but direct comparative studies are few in numbers. Shortage of ^{51}Cr-EDTA makes a direct comparison highly relevant. The aim of the study was to investigate if there is any clinical relevant difference between plasma clearance of ^{99m}Tc-DTPA and ^{51}Cr-EDTA. **Materials and Methods: Materials and Methods:** Patients ≥ 18 years of age referred for routine GFR measurement by ^{51}Cr-EDTA were prospectively enrolled. The two tracers (10 MBq ^{99m}Tc-DTPA and 2.5 MBq ^{51}Cr-EDTA, both 0.5 mL) were intravenously injected at time zero. A standard 4-sample technique was applied with samples collected at 180, 200, 220, and 240 minutes if estimated GFR (eGFR) was ≥ 30 mL/min. Plasma clearance were calculated according to a one-pool model. **Results: Results:** Fifty-six patients (69% men) were enrolled into the study. All patients had an estimated GFR > 30 mL/min/ 1.73 m². No patients suffered from ascites or significant oedema. The mean ^{51}Cr-EDTA plasma clearance was 82 mL/min (range 16-226). Plasma clearances determined by the two methods were highly correlated (r=0.993). Plasma clearance of ^{51}Cr-EDTA was statistically lower when measured by ^{51}Cr-EDTA than ^{99m}Tc-DTPA (P=0.01), but the numerical difference was minimal (mean difference -1.4 mL/min; 95% limits of agreement (LOA) -6.6 to 9.4). The difference between the two methods was independent of the level of renal function. **Conclusion: Conclusions:** No clinically relevant difference was found between ^{99m}Tc-DTPA and ^{51}Cr-EDTA one-pool plasma clearance. Therefore, ^{99m}Tc-DTPA can replace ^{51}Cr-EDTA and vice versa when needed. **References:** None.

EP-0291

Accuracy of 24h Single Sample Measurement for Low GFR and Comparison with Same Day Slope-Intercept GFR

N. Sizer[1], *H. McMeekin*[1], *F. Wickham*[2], *B. Fongenie*[2], *M. Burniston*[1]; [1]*Barts Health NHS Trust, London, UNITED KINGDOM,* [2]*Royal Free London NHS Foundation Trust, London, UNITED KINGDOM.*

Aim/Introduction: The accuracy of a single sample GFR (SS-GFR) technique with a sample taken at 24 hours (24h) post-injection for patients with GFR lower than 30 ml/min/1.73m² was investigated. A comparison with the results from same day slope-intercept GFR (SI-GFR) was also performed. **Materials and Methods:** Data from patients referred for GFR assessment to inform the management of chronic kidney disease at the Royal Free Hospital were reviewed. 4-sample SI-GFR calculation with samples at 2h, 4h, 6h, and 24h post-injection was taken as the reference measurement to which the Gref and Karp SS-GFR (24h sample) [1] and same day SI-GFR (2h, 4h samples) were compared. In addition, 4-sample SI-GFR calculations with samples at 2h, 3h, 4h and 24h post-injection from patients with measured low eGFR at Barts Health NHS Trust will be reviewed for comparison with the Gref and Karp SS-GFR and same day SI-GFR. **Results:** 47 GFR examinations with reference GFR less than 30 ml/min/1.73m² were included in the analysis from the Royal Free Hospital. Bland-Altman analysis gave mean differences of 0.5 (95% confidence interval: -0.2 - 1.3) ml/min/1.73m² for SS-GFR (24h) and 2.4 (95% confidence interval: 1.3 - 3.6) ml/min/1.73m² for same day SI-GFR. 95% limits of agreement were -4.3 - 5.4 ml/min/1.73m² for SS-GFR (24h) and -8.1-12.9 ml/min/1.73m² for same day SI-GFR. Results from the Barts Health NHS Trust patient cohort will be presented at the conference. **Conclusion:** SS-GFR with a 24h sample is more accurate than same day SI-GFR in patients with GFR less than 30 ml/min/1.73m². Using SS-GFR with a 24h sample in routine clinical practice will result in clinically insignificant differences in GFR result compared with the reference technique, whereas a same day SI-GFR measurement could cause large inaccuracies. **References:** [1] Gref MC, Karp KH. Single-sample ^{99m}Tc-diethylenetriamine penta-acetate plasma clearance in advanced renal failure by the mean sojourn time approach. Nucl Med Commun 2009, 30:202-205.

EP-0292

Glomerular filtration rate can be estimated from the total bladder activity measured by quantitative ^{99m}Tc-DTPA SPECT-CT

C. Kim[1], *J. Cha*[1], *Y. Kang*[1], *D. Cha*[1], *K. Kang*[2]; [1]*Korea University Ansan Hospital, Ansan, KOREA, REPUBLIC OF,* [2]*Seoul National University College of Medicine, Seoul, KOREA, REPUBLIC OF.*

Aim/Introduction: A method using ^{51}Cr-EDTA is considered as a gold standard for measuring glomerular filtration rate (GFR). However, the availability of ^{51}Cr-EDTA is becoming more and more difficult in many countries, and another method using a 24-hour urine collection is sometimes inaccurate depending on the patient's cooperation. In this study, we showed the correlation between the GFR measured using ^{51}Cr-EDTA and the total bladder activity measured by quantitative ^{99m}Tc-DTPA SPECT-CT, and derived a formula estimating GFR. **Materials and Methods:** Among the patients who visited Korea University Ansan Hospital from November 2016 to April 2017 with decreased renal function, those who agreed were prospectively enrolled. There was no specific patient preparation except 500 ml of water was provided for good hydration. Quantitative SPECT images were acquired with Siemens Symbia Intevo SPECT-CT at 40 minutes after the intravenous administration of ^{99m}Tc-DTPA (290~444 MBq). The SPECT acquisition protocol was as follows: 30 views per each detector, 10 seconds per view, using a low-energy high resolution collimator in step-and-shoot mode over 360 degrees with circular orbit, and a 256*256 matrix. SPECT images were reconstructed using the xSPECT Quant method with 24 iterations, 2 subsets, and 10 mm Gaussian filter. Using MIM Maestro, the volume of interest (VOI) of bladder was drawn based on CT image, and a sphere with a diameter of 3 cm drawn in abdominal cavity was used to correct background activity. Mean percent of the injected dose per unit volume (%ID/ml) and the volume of each VOI were used for calculation. All the statistics were performed using GraphPad Prism, and Pearson correlation coefficients were obtained because all data sets were satisfactory with normality tests. **Results:** Among 22 enrolled patients, 2 patients had polycystic kidneys and 11 patients had previous kidney transplantation. The correlation coefficients for the groups of patients with transplanted kidney, without transplanted kidney, and all patients were 0.858, 0.892 and 0.877 respectively, showing good correlation and no significant difference between the groups. The following formula to estimate GFR from %ID of ^{99m}Tc-DTPA collected in bladder was obtained: GFR [ml/min] = 2.35* total bladder activity [%ID] +5.75. The Pearson correlation coefficient between the estimated GFR from this formula and the measured GFR using ^{51}Cr-EDTA was 0.877 (0.723~0.948; 95% C.I.). **Conclusion:** The total bladder activity measured by quantitative ^{99m}Tc-DTPA SPECT-CT shows good correlation with GFR measured using ^{51}Cr-EDTA, and can be a possible method to estimate GFR. **References:** None.

EP-18

Clinical -> Diagnostic study -> Adult study -> Oncology study -> General oncology -> Radioguided surgery

October 12 - 16, 2019 e-Poster Area

EP-0293

Sentinel lymph node biopsy in prostate cancer: a modified injection technique targeting the tumor index lesion

A. Mestre Fusco[1], *L. Fumadó*[2], *J. Abascal*[2], *L. Reixach*[3], *M. Suárez-Piñera*[1], *N. Juanpere*[4], *S. Vidal-Sicart*[1,5], *L. Cecchini*[2];

[1]*Nuclear Medicine, Hospital del Mar - Parc de Salut Mar, Barcelona, SPAIN,* [2]*Urology, Hospital del Mar - Parc de Salut Mar, Barcelona, SPAIN,* [3]*Universitat Autònoma de Barcelona, Barcelona, SPAIN,* [4]*Pathology, Hospital del Mar - Parc de Salut Mar, Barcelona, SPAIN,* [5]*Nuclear Medicine, Hospital Clínic, Barcelona, SPAIN.*

Aim/Introduction: The concept of sentinel lymph node biopsy (SLNB) in Prostate Cancer (PCa) was introduced in order to avoid the invasiveness of extended pelvic lymphadenectomy (ePLND). SLNB in PCa is still nowadays considered experimental. Our aim is to study a modified injection of 99m-Tc to the Index Lesion (IL) to perform sentinel node dissection in PCa. **Materials and Methods:** A prospective study performed between June 2016 and October 2018. The study involved a cohort of 41 patients diagnosed as intermediate to high-risk PCa. MRI was performed, with an IL and confirmed pathology. All patients underwent laparoscopic radical prostectomy (LP) with sentinel lymph node study (SLN) and ePLND. A preoperative lymphoscintigraphy with radiotracer 99mTc-colloid was performed (day before surgery, 240-300 MBq in 0.6 cc volume). Dose was injected to the IL and its peripheral area through cognitive fusion technique guided by transrectal ultrasound (TRUS). A lymphoscintigraphy was subsequently performed with planar images taken at 30 minutes and 3-4 hours post-injection. Radioactivity of SLN was intraoperatively measured by a gamma probe. Analysis included size and localization of the tumor, SLN drainage and histopathology findings. The outcome determined were sensitivity, specificity and PPV. **Results:** Lymphoscintigraphy demonstrated no uptake drainage in 2 patients. Sentinel nodes were positive in 10 patients (30.3%). No cases of negative sentinel nodes resulted in any pN1, this is a NPV of 100%. Sensibility, specificity and PPV were also 100%. A total of 524 lymph nodes were harvested, 108 (20.6%) sentinel nodes. In total, 24 were positive, 14 within the sentinel area. Mean surgical time for LP + SLNB + ePLND was 208 minutes (IQR 180-240). Although 13 patients suffered any type of intra or postoperative complication, only 2 cases are directly associates with SLNB procedure: first one a symptomatic UTI related to TRUS tracer injection and a second one, an ureteral injury that required surgical repair during the SLNB when a paraaortic SLN was being excised. **Conclusion:** Selective injection of radiotracer of 99mTc-nanocolloid to the prostate index lesion is a feasible and safe technique in prostate cancer, with excellent results in terms of patient staging. Negative SLNB is a predictor of negative ePLND. **References:** None.

EP-0294

Role Of Lymphoscintigraphy In The Assessment Of Lymphedema Of Extremities In Microsurgery Of Lymph Node Transfer

C. Sampol[1,2]*, O. Roca*[1,3]*, J. Estrada*[1,3]*, N. Orta*[1,2]*, A. Repetto*[1]*, M. Villar*[1]*, H. Navalon*[1]*, C. Peña*[1,2]*;*
[1]*Hospital Universitari Son Espases, Palma De Mallorca, SPAIN,* [2]*IdISBa, Palma de Mallorca, SPAIN,* [3]*Reconstructive And Plastic Surgery, Palma de Mallorca, SPAIN.*

Aim/Introduction: Secondary lymphedemas usually occur after lymphadenectomies and there is an increasing surgical possibilities in their treatment beyond microsurgery,as lymph node transfer,when conventional measures are inefficient. Our aim is to study the utility of lymphoscintigraphy in this context,evaluate patterns of lymphedema improvement after lymph node transfer and establish an intra-surgical role for lymphoscintigraphy. **Materials and Methods:** Reviewed 15p,14p lymphedema upper limb and 1p lower limb(grade II-III).Pilot protocol:lymphoscintigraphy pre-surgery,after interdigital injection of 4 mCi ^{99m}Tc-Nanocol in both extremities, followed by planar images after 15-30 min and 2 h(+SPECT-CT), and measurements(cms) of both limbs.Surgery day: 2mCi of ^{99m}Tc-Nanocol injected into donor lower limb("revers mapping").All donor areas were from inguinal lymph nodes. Intraoperative images of inguinal region are obtained by portable gamma camera(Sentinella) to mark the physiological drainage of the lower limb to design the flap,also confirmed with gamma probe. After cleaning fibrosis of the axillar receptor area, lymph node transfer was done.At 1-2y follow-up, measurements of upper limbs and lymphoscintigraphy underwent again.Pre and post-surgery drainage patterns are correlated with clinical and limb measurements. **Results:** 8/15p had presurgical lymphoscintigraphy:lymphatic drainage(4p), dermal backflow(6p), functioning lymph node levels II-III(3p) and supraclavicular activity(1p).5/8p underwent surgery,4 with revers mapping protocol.In 1p, an intra-surgical lymphoscintigraphy of the receptor axilla was also evaluated to safeguard funtioning lymph nodes.Counting radiation of the lymph node flap showed<10% of total activity of physiological lymph node drainage to be preserved.Postsurgical lymphoscintigraphy:drainage improvement in 2/5p(less dermal backflow, uptake in axillary lymph nodes level III not related to flap tissue), and correlating with clinical improvement in 3/5p, as well as reduction >1 cm in measurements on affected extremity. There is no case of iatrogenic lymphedema of the lower limb donor.7/15p had just postsurgical lymphoscintigraphies (2y follow-up):drainage improvement in all cases(uptake related to lymph node transfer tissue/surgical clips or in some dense tissue corresponding to lymphatics close to the flap or practical absence of dermal backflow).Clinical improvement was only seen in 5p but changes on measurements were not significant. **Conclusion:** Lymph node transfer procedure is useful in clinical improvement of chronic lymphedema.Lymphoscintigraphy seems to play a role in evaluating the viability of the lymph node flap based on changes in the lymphatic drainage, reduction of the dermal backflow or flap tissue uptake, and that correlates with clinical and morphological changes.Revers mapping protocol of the donor limb is essential to avoid iatrogenic.Also intraoperative lymphoscintigraphy of upper limb receptor axilla could be useful to preserve functional lymph nodes. **References:** None.

EP-0295

Feasibility Of The Radioguided Surgery During Transaxillary Endoscopic Parathyroidectomy

C. Sampol[1,2], *S. Pascual*[3], *J. Julian*[3], *J. Cifuentes*[3], *A. Repetto*[1], *N. Orta*[1,2], *B. Luna*[1], *M. Villar*[1], *C. Peña*[1,2];
[1]*Hospital Universitari Son Espases, Palma De Mallorca, SPAIN,* [2]*IdISBa, Palma de Mallorca, SPAIN,* [3]*Hospital Son Llatzer, Palma De Mallorca, SPAIN.*

Aim/Introduction: Radioguided surgery of the parathyroid glands using unilateral cervical exploration is widely established, replacing the bilateral cervical exploration. The technical improvement of gamma probes and the application of the sentinel node biopsy in laparoscopy would allow us to extrapolate that to endoscopic surgery of any pathology where a radioguided surgery has its application.The objective of our study is to assess the feasibility of parathyroid radioguided surgery using a minimally invasive surgical approach of the neck, which is the transaxillary endoscopic parathyroidectomy. **Materials and Methods:** Included 7p, 3M/5W, mean age 61yo,with a suspected diagnosis of primary hyperparathyroidism after an increase of PTHtest. All underwent cervical ultrasound/ scintigraphy 10min and 2h after injection of 20mCi ^{99m}Tc-MIBI, and early SPECT-CT. The surgery day we re-injected 10mCi of ^{99m}Tc-MIBI, and after transaxillary endoscopic approach of the neck, radioguided surgery of the adenoma was carried out using an endoscopic gamma probe. In 2 cases we used intravenous indocyanine green(ICG). Intraoperatively,at 5 and 10 min after removing the suspected gland,blood samples of PTHhormone level were obtained and finally the specimen was sent for anatomopathological confirmation. **Results:** All 7p had positive MIBI, predominantly left and inferior location. The ultrasound was clearly coincident in 2p, uncertain in 3p and negative in 2p. All adenomas in SPECT-CT were normotopic and directly related to the thyroid gland, excepting 1p which had an ectopic gland located in the thyro-thymic ligament. The mean basal PTH was 273.74pg/ml dropping to 25.4 pg/ml after removing the suspicious gland. Mean counts radiation of invivo adenoma (gammaprobe) were 1116.66cps and 446.66cps exvivo. Anatomopathological examination confirmed parathyroid tissue in all cases, with average weight of 0.71g(0.3-1.2) and average size 1.3cms. No remarkable complications during or immediately after surgery, including a patient with a pacemaker ipsilateral to the axillary approach. There were technical difficulties removing the ectopic gland due to the premediastinal location and the millimeter size, finally proceeding to unilateral anterior neck exploration. Both cases of using combination of radioactivity and ICG, the fluorescence clearly helped in the delimitation and removing adenomas. **Conclusion:** Transaxillary endoscopic radioguided surgery of parathyroid adenomas is feasible and safe method, similar to minimally invasive anterior cervical neck exploration, although it requires training, especially in ectopic location. The combined use of intravenous ICG helps and speeds up the process of identification and resection of the adenoma. The radioguided protocol for surgical intervention is the same, eliminating cervical scar. **References:** None.

EP-0296

Concordance Between Intracervical and Fundal Injections for Sentinel Node Mapping in Patients With Endometrial Cancer?: A Study Using Intracervical Radiotracer and Fundal Blue Dye Injections

R. Sadeghi[1], *M. Hassanzadeh Mofrad*[2], *M. Farazestanian*[2], *Z. Yousefi*[2], *S. Kadkhodayan*[2], *L. Zarifmahmoudi*[1];
[1]*Nuclear Medicine Research Center, Mashhad University of Medical Sciences, Mashhad, IRAN, ISLAMIC REPUBLIC OF,* [2]*Women's Health Research Center, Mashhad University of Medical Sciences, Mashhad, IRAN, ISLAMIC REPUBLIC OF.*

Aim/Introduction: Major controversy in sentinel node (SN) biopsy of endometrial cancer is the injection site of mapping material. We compared lymphatic drainage pathways of the uterine cervix and uterine body in the same patients by head-to-head comparison of intracervical radiotracer and fundal blue dye injections. **Materials and Methods:** All patients with pathologically proven endometrial cancer were included. Each patient received 2 intracervical injections of Tc-phytate. At the time of laparotomy, the uterus was exposed, and each patient was injected with 2 aliquots of patent blue V (2 mL each) in the subserosal fundal midline locations. The anatomical locations of all hot, blue, or hot/blue SNs were recorded. **Results:** Overall, 45 patients entered the study. At least 1 SN could be identified in 75 of 90 hemipelves (83.3% overall detection rate, 82.2% for radiotracer [intracervical] alone, and 81.1% for blue dye [fundal] alone). In 71 hemipelves, SNs were identified with both blue dye (fundal) and radiotracer (intracervical) injections. In 69 of these 71 hemipelves, at least 1 blue/hot SN could be identified (97.18% concordance rate). In 10 patients, para-aortic SNs were identified. All of these nodes were identified by fundal blue dye injection, and only 2 were hot. **Conclusion:** Our study shows that lymphatic drainage to the pelvic area from the uterine corpus matches the lymphatic pathways from the cervix, and both intracervical and fundal injections of SN mapping materials go to the same pelvic SNs **References:** None.

EP-0297

Findings in sentinel lymph node biopsy in 19 patients with ovarian cancer

A. Utrera*, M. Agudelo-Cifuentes, J. Bernal, P. Bello-Arques, L. Matute, V. Lago, A. Yepes-Agudelo, G. Figueroa, V. Vera;*
Hospital La Fe, Valencia, SPAIN.

Aim/Introduction: Our aim is to describe our experience with sentinel lymph node biopsy (SLNB) in ovarian cancer, between 2017 and 2019. **Materials and Methods:** We have carried out a study with 19 patients whose ages range from 26 to 74 years old (which average is 50 years old). The technique we used consisted in one injection of 1mCi of 99mTc-albumin nanocolloid in the ovarian ligaments or in the stump, during the surgery, followed by acquisition of static image with portable gamma camera to assess migration and further localization

of the sentinel nodes with gamma probe. In 53%, the surgical approach was laparoscopic. In all cases systematic aortic and pelvic lymphadenectomy (SAPL) was performed. **Results:** In 2 out of 19 patients, technical failures occurred regarding to the administration of radionucleid (extravasation and incomplete injection). The application of the tracer was performed in 63% of the cases in the stump and 37% were injected in the ovarian ligaments. We detected sentinel nodes in 88% of the patients, 57 % in abdominal lymphatic area and 43% in pelvic area. We removed a mean of 3 nodes (1-7). We classified the SLNB as: abdominal lymph nodes (paraortic, paracaval, interaortocaval) and pelvic lymph nodes (common iliac, external iliac, interiliac and obturator) In the anatomopathological study of the lesions, it could be verified that the majority of the tumour pieces corresponded to endometrial subtype with a frecuency of 35%, followed by 24% of clear cells, 18% serous, 6% mucinous, 12% borderline and others 6%. We had only one case of bilateral ovarian cancer; it was an atypical borderline tumor. From the sample studied, without taking into account two technical failures, the following results could be observed: In one case we didn't find any sentinel lymph node and the lymphadenectomy was negative for metastatic spread. One patient was positive for metastatic infiltration at lymphadenectomy despite negative sentinel node. Other case presented with a positive sentinel node, without invasion of the other nodes at lymphadenectomy, it was a borderline bilateral cancer **Conclusion:** In our experience the SLNB in ovarian cancer has shown promising results, with a high detection rate and specificity. It could lead to a future limitation of systematic lymphadenectomies in patients with ovarian cancer, avoiding its side effects. More sample and prospective studies are needed to collect stronger data. **References:** None.

EP-0298

Sentinel lymph node biopsy in patients with oral tongue cancer: prospective single center study

P. Krzhivitckii[1], *S. Novikov*[1], *S. Kanaev*[1], *Z. Radgabova*[1], *M. Kotov*[1], *O. Ponomareva*[1], *A. Artemyeva*[1], *M. Girshovitch*[1], *Y. Melnik*[1], *M. Bisyarin*[2];
[1]*N.N. Petrov National Medical Research Center of Oncology, St Petersburg, RUSSIAN FEDERATION,* [2]*N.N. Petrov Research Institute Oncology, St Petersburg, RUSSIAN FEDERATION.*

Aim/Introduction: The purpose of the study was to evaluate sensitivity and false negative rate of sentinel lymph node (SLN) biopsy compared to with the standard lymph nodes (LN) dissection in detecting metastatic disease. In addition, we tried determine optimal amount of LN sampling. **Materials and Methods:** All patients with T1-2N0 clinical stage of oral tongue cancer were eligible for inclusion in this prospective single center study. Lymph node mapping was obtained by injection of 99mTc-nannocolloids (100-150MBq in 0.3-0.4ml) in 4 points around the primary lesion. SPECT-CT visualization of sentinel lymph nodes started 60-120 min after injection. SLN biopsy started 8-12 hours after mapping and in all cases was followed by standard lymphodissection. Between 04.2015 and 12.2018, 37 patients were enrolled in the study **Results:** Sentinel lymph nodes were visualized in all but one patient. Bilateral lymph flow from the tongue cancer was detected in 17 (47%), monolateral - in another 19 (53%) patients. Among evaluated 36 patients, metastases in SLN were detected in 6 cases. Additional non-sentinel lymph nodes were involved in 5 of these 6 patients, in 4 cases metastases were detected distally from the level of involved SLN. In 4 patients with non involved SLN examination of LN removed by standard lymphatic dissection identified LN metastases. In all 4 cases these nodes were localized on the next level distally from the SLN basin. According to presented data sensitivity of SLN biopsy was 60%, false negative rate - 40%. If biopsy of SLN would be supported by dissection of SLN basins and one level distally than sensitivity of the procedure would reach 100% with false negative rate - 0%. **Conclusion:** In our patients with the oral tongue cancer (cT1-2N0M0) biopsy of SLN charachterised by low sensitivity (60%) and high false negative rate (40%) that can be explained by skip metastases one level distally. Combination of SLN biopsy with SLN basin dissection and dissection of LN one level distally can be promising tool for safety and not-traumatic treatment of these patients. **References:** None.

EP-0299

Sentinel node biopsy in breast ductal carcinoma in situ: our experience

P. Fernández-Rodriguez, Á. De Bonilla Damiá, R. Álvarez Pérez, R. Fernández López, D. Tamayo Carabaño, J. Jiménez-Hoyuela García;
Department of Nuclear Medicine. Universitary Hospital Virgen del Rocío, Sevilla, SPAIN.

Aim/Introduction: Ductal carcinoma in situ (DCIS) of the breast is a preinvasive neoplasm without periductal stromal invasion that represents about 20-25% of all breast malignancies. The incidence has experienced an important increase with the introduction of mammography screening. DCIS is a subtype of breast cancer theoretically unable to metastasize; therefore, sentinel lymph node biopsy (SLNB) procedure for DCIS is controversial and is not standard of care. However, nodal involvement for DCIS patients is reported. Aim of our study was to identify preoperative features predictive of nodal involvement in DCIS patients. **Materials and Methods:** We have retrospectively reviewed 78 patients with a median age of 55 years old [35-86] from January 2016 to December 2017 with a preoperative diagnosis of DCIS following a vacuum-assisted breast biopsy (VABB), and undergoing surgery with sentinel node biopsy. Only patients with a preoperative histopathology of pure DCIS without microinvasive disease and without ultrasound or MRI evidence of lymphadenopathy (pTis cN0) were included in the analysis. Variables distribution was compared between patients upstaged to invasive cancer at final pathology and patients with a confirmed DCIS, and between positive vs negative sentinel node patients. **Results:** Lymph node biopsy was positive in 15 (19.2%) patients, with 8 (53.3%)

macrometastases and 7 (46.6%) micrometastases. These patients presented several factors were predictive of nodal involvent like nuclear grade 2-3 (86,6%), Breast Imaging Reporting and Data System (BI-RADS) index >4 (93,3 %), lesion extension >20 mm (66.6%), cribiform and solid type (73,3%), and upstaging disease (66.6%), although upstaging could not be predicted preoperatively. Therefore, these factors should be considered for axillary evaluation. Axillary dissection was performed in 46,6% of these patients. **Conclusion:** The role of SLNB in DCIS patients is controversial, but routine abstention may increase the risk of understaging and subsequent undertreatment of some patients. The presence of macrometastatic axillary nodes in DCIS would change the subsequent adjuvant treatment, and even micrometastases could be suitable in order to plan a appropiate follow-up. A particular subgroup of DCIS with higher risk for positive SLNB could be identified, in which axillary evaluation would be required to define the most appropriate clinical management. **References:** None.

EP-0300

Radionuclide-guided sentinel lymph node mapping in urachal cancer

W. Cytawa, W. Połom, B. Brockhuis, P. Lass, M. Matuszewski;
Medical University of Gdansk, Gdansk, POLAND.

Aim/Introduction: Urachal cancer is a rare non-urothelial carcinoma with the incidence rate of 0.35 to 0.7 % of all bladder cancers and 22 to 35 % of adenocarcinomas of the bladder. It forms from the malignant transformation of enteric epithelium in the urachus (or its remnants) located between dome of the bladder and the umbilicus. The purpose of this study was to perform the radionuclide-guided mapping of lymphatic drainage with the use of preoperative lymphoscintigraphy and intraoperative gamma probe detection in patients with urachal cancer, and try to propose the lymphadenectomy template. **Materials and Methods:** A prospective study was conducted on 5 patients with urachal cancer. In each patient the region around the primary tumor was injected with ^{99m}Tc-nanocolloid during cystoscopy the day before surgery. SPECT/CT lymphoscintigraphy was performed using dual-head gamma camera short before surgery. The sites of focal tracer uptake were reported and verified intraoperatively using hand held gamma probe. All radioactive lymph nodes were considered sentinel lymph nodes (SLNs) and surgically removed during sentinel lymph node biopsy (SLNB) procedure. Lymphadenectomy of the remaining lymph nodes within a given lymphatic basin was additionally performed. **Results:** In all patients lymphatic outflow from the urachal tumor to the lymph nodes was present. Preoperative SPECT/CT revealed focal activity of radiotracer in the common iliac regions in all 5 patients, in 3 cases bilaterally, in the remaining 2 cases unilaterally. All preoperatively visualized lymph nodes were found with the use of gamma probe and excised during lymphadenectomy. None of the resected SLNs contained metastases. **Conclusion:** Radionuclide-guided mapping of the lymphatic drainage in urachal cancer is possible. Lymphatic outflow in urachal cancer can be bilateral or unilateral. Preoperative scintigraphic assessment of lymphatic drainage with hand held gamma probe verification of SLNs in urachal cancer allows minimally invasive, targeted lymphadenectomy. No recommendations about extension of lymphadenectomy were proposed. **References:** None.

EP-0301

Sentinel Lymph Node Detection in Patients with Melanoma on the Shoulder and Upper Trunk - a Guidance for Surgical Planning

M. Punda, I. Milas, J. Staničić, Z. Puljiz, M. Bosak-Butković, M. Šitum, M. Franceschi, T. Jukic;
UHC Sestre Milosrdnice, Zagreb, CROATIA.

Aim/Introduction: Cutaneous melanoma of the trunk shows potential to drain to multiple and uncommon lymphatic basins. The aim of the study was to determine the location of common and uncommon sentinel lymph nodes (SLNs) in patients with melanoma on the shoulder and upper trunk related to anatomic subareas of primary melanoma and its impact on surgical planning. **Materials and Methods:** The study included 172 patients (61.6% men, mean Breslow thickness 2.941±2.82 mm) who underwent SLN biopsy from January 2015 to January 2019. For the analysis, we defined six anterior and nine posterior anatomic sub-areas of the upper trunk and two of the shoulders. We considered all other locations outside of axilla as uncommon. After peritumoral injection of 99mTc-nanocolloid, dynamic and static planar imaging was performed. SPECT/CT was performed in 9.3% of patients. **Results:** Melanoma distribution was mainly in the upper sub-areas of the upper trunk: in 22/26 patients with anterior and among 104/121 patients with posterior location. Anterior melanomas showed axillary drainage in 24 (92.3%) of patients; 95.8% unilateral. Uncommon SLNs were detected in 5/26 patients: 3 supraclavicular, 1 infraclavicular and 1 subcutaneous SLN near the scar. Among patients with posterior melanoma, 93.4% had axillary drainage. Out of them, 43.4% had bilateral axillary drainage; 28.1% from medial trunk sub-areas. In 37/121 posterior melanomas we detected 47 uncommon SLNs: 22 supraclavicular, 12 inside the triangular intermuscular space, 8 nuchals and 5 in other locations. Melanoma on the shoulders (14 right, 11 left) in all but one patient drained to ipsilateral axilla, 4/25 patients had ipsilateral supraclavicular SLNs. In total, we identified 57 uncommon SLNs in 47 (27.3%) of patients, drained mostly (81% of SLNs) from the posterior upper trunk. Eleven (23.4%) of patients showed single uncommon SLNs, without axillary involvement. The neck region was a drainage basin for 42 uncommon SLNs among 31 patients. Out of 43 excised uncommon SLNs in 34 patients, 5 were tumor-positive. Fourteen uncommon SLNs in 13 patients were not removed by the surgeon as not identified; 4 patients out of them had tumor-positive axillary SLNs. **Conclusion:** Uncommon SLNs were detected in more than a quarter of our patients, mostly drained from the posterior upper trunk. The neck region was a drainage basin among two thirds of patients with uncommon

SLNs. We suggest that current multimodal approach in radio-guided surgery planning should be refined in order to achieve effective surgical treatment. **References:** None.

EP-0302

The comparative study of the validation for Tc-99m Tin-colloid and Tc-99m Phytate in sentinel node detection in breast cancer patients

J. Seok;
Chung-Ang University, Colleage of Medicine, Seoul, KOREA, REPUBLIC OF.

Aim/Introduction: Lymphoscintigraphy and sentinel node biopsy has become a standard method for detection of axillary lymph node metastasis in breast cancer patients, but the standard radiopharmaceutical was not prepared. About detection of axillary lymph node metastasis by lymphoscintigraphy and sentinel node biopsy in breast cancer patient, we compared the results of Tc-99m Tin-colloid and Tc-99m Phytate by subareolar injection. **Materials and Methods:** This study included 1,152 breast cancer patients who were performed operation during 2001-2019. Four hundred twelve patients were injected 0.8 ml of Tc-99m Tin-colloid (37-185 MBq) by subareolar injection. Seven hundred forty patients were injected 0.8 ml of Tc-99m Phytate (37-185 MBq). Lymphoscintigraphy was performed in supine position and sentinel node localization was performed by hand-held gamma probe in operation. **Results:** Among 412 patients by Tc-99m Tin-colloid, 374 cases (90.8%) were localized the sentinel node by lymphoscintigraphy and 367 cases (89.1%) were localized by gamma probe. Among 740 patients by Tc-99m Phytate, 723 cases (97.7%) were localized by lymphoscintigraphy and 725 cases (98.0%) were localized by gamma probe. The detection rate by lymphoscintigraphy and gamma probe was superior for Tc-99m Phytate compared to that for Tc-99m Tin-colloid, with a statistically significant difference. ($p<0.05$, $p<0.05$) **Conclusion:** Tc-99m Phytate is a better choice for localization of sentinel node than Tc-99m Tin-colloid in breast cancer patients. **References:** None.

EP-0303

Axillary Node Staging After Neoadjuvant Systemic Therapy Using Sentinel Node Biopsy and Radioiodine Seed Localization in Breast Cancer Patients. First Experiences in our Center

Á. Galiana*, M. Tabuenca, M. Marín, S. Aragón, E. Ciruelos, J. Torrens, S. Ruiz, E. Martínez, V. Godigna, D. Vega, J. Estenoz;*
Hospital Universitario 12 de Octubre, Madrid, SPAIN.

Aim/Introduction: Sentinel lymph node biopsy (SNLB) is a proven technique used for the axillary staging of breast cancer. With the surge of Neodajuvant Systemic Therapy (NST) axillary staging of these patients using only SNLB has demonstrated relatively high false negative results. Therefore other techniques have appeared such as Radioiodine Seed Localization (RSL), which uses 125-I titanium coated seeds introduced in pathological lymph nodes (clip-marked prior to NST) to help diminish false negative results compared with SNLB alone. These techniques are paving the way to the possible reduction of the number of axillary lymph node clearances (ALNC) needed. The aim of this study is to describe the first results obtained in our center using radioiodine seeds alone or in combination with SLNB to adequately perform the axillary staging in breast cancer patients after receiving NST. **Materials and Methods:** Eight breast cancer patients aged between 43 and 75 have been studied. Proven tumour positive axillary lymph nodes were localized using ultrasound and subsequently clip-marked. After the completition of NST and 24 hours before the surgery, a 125-I seed, was inserted using ultrasound in the clip-marked node. SNLB was performed using methylene blue, and 99m-Tc nanocolloids. In the operating room all the lymph nodes of interest were detected using a surgical gammaprobe and visual inspection for methylene blue colored nodes, and then examined by experienced pathologists. All patients had an ALNC. **Results:** 7 patients out of 8, had a radioiodine seed correctly placed in lymph nodes (2 patients had nodal conglomerates marked with one seed, 1 patient had 2 seeds placed). The remaining patient had an incorrectly inserted seed. Out of 7 patients with radiodine seeds adequately placed, only one patient had a false negative result in RSL localized node with one metastasis node found in its ALNC sample. The same patient was the only case of no migration with nanocolloids. No false negative case was found with SNLB techniques. Detection rate of axillary metastasis was 75% using RSL and 100% for SNLB, either alone or combined with RSL. Migration rate for nanocolloids was 87,5%. Coincidence rate of patients with nanocolloid positive nodes and radioiodine seeds was 71,43% (5/7). **Conclusion:** Preliminary results are promising, and show an adequate staging of axillary nodes, using both techniques. Further studies are being carried to establish more consistent conclusions. **References:** None.

EP-0304

Comparison of 1 day protocol and 2 day protocol of lymphoscintigraphy by subareolar injection in the detection of sentinel lymph nodes in breast cancer patients

J. Seok;
Chung-Ang University, Colleage of Medicine, Seoul, KOREA, REPUBLIC OF.

Aim/Introduction: Lymphoscintigraphy and sentinel node biopsy were used for the detection of axillary lymph node metastasis in breast cancer patients. We compared the results of subareolar injections on the day of surgery (1 day protocol) with injections the day before surgery (2 day protocol). **Materials and Methods:** This study included 1,152 breast cancer patients who underwent surgery between 2001 and 2019. For the 1 day protocol 0.8 ml of Tc-99m Tin-Colloid (37MBq) was injected in

789 patients in the subareolar region on the morning of the surgery. For the 2 day protocol 0.8 ml of Tc-99m Tin-Colloid (185MBq) was injected in 363 patients on the afternoon before surgery. Lymphoscintigraphy was performed in the supine position and sentinel node identification was performed by hand-held gamma probe during surgery. **Results:** Among 789 patients with the 1 day protocol, 757 cases (95.9%) were identified by sentinel node lymphoscintigraphy, and 762 cases (96.6%) were identified by gamma probe. Among the 363 patients, in the 2 day protocol, 340 cases (93.7%) had the sentinel node identified by lymphoscintigraphy, and 330 cases (90.9%) had the sentinel node identified by the gamma probe. There was no significant difference in the identification rate of the sentinel node between the 1 day and 2 day protocol by lymphoscintigraphy and the gamma probe. **Conclusion:** The results of the identification of the sentinel node according to 1 day or 2 day protocols showed no significant differences. Because the 2 day protocol allows for an adequate amount of time to perform the lymphoscintigraphy, it is a more useful protocol for the identification of sentinel nodes in patients with breast cancer. **References:** None.

EP-0305

Radioguided Occult Lesion Localization Plus Sentinel Node Biopsy After Neoadyuvant Chemotherapy In Breast Cancer

I. Cepedello Boiso, C. Ramirez Tortosa, J. Jimenez Anula, J. Ramirez Ferrol;
Complejo Hospitalario De Jaen, Jaén, SPAIN.

Aim/Introduction: The feasibility, accuracy and clinical significance of sentinel node and occult lesion localization (SNOLL) for patients with breast cancer after neoadyuvant chemotherapy has not yet determinate. The aim of this study was to investigate these questions. **Materials and Methods:** This is a prospective study performed from January 2009 to May 2019. Radioguided occult lesion localization plus sentinel node biopsy was performed after neoadyuvant chemotherapy in patients with breast cancer (tumor size > 3 cm or tumor size < 3 cm not suitable for breast-conserving surgery and axilary node negative). Axillary status was established by physical examination, ultrasound-guided core needle biopsy of any suspicious lymph node. SNOLL were carried out using standar 99mTc sulfur colloid (activity of 3 mCi and 0,2-0,5 ml volumen) injected directly into the lesion (guided by ultrasound or computer tomography) and in the cases of no lymphatic migration, realised subdermal injection. An intraoperative macroscopic examination of the specimen with margins evaluation was always performed. The Sentinel Lymp Node (SLN) were analysed by One-Step Nucleic Acid Amplification (OSNA). SLN was considered to be positive if macrometastases or micrometastases were found, and in such cases axillary dissection was consequently implemented. **Results:** A total number of 31 patients was recorded (all woman, 37-66 years old, mean age 49,32 years). SNOLL located all the occult breast lesions successfully. In 25 out of the 31 patients (80,6%), the breast specimen had clear and large margins. Despite intraoperative examination of the specimen, a total of 19, 4% (6 out of 25) patients required a second re-excision procedure for involved margin and in the all cases had finally clear margins. Lymphocistingraphy showed axillary drainage in every patients and 38 SLN samples (1,23 SLN/patient) were analyzed. Axillary lymph nodes were histologically negative in 25 patientes (80,6%) and positive in 6 patients (17,4%). Follow-up 10 years. Complete referal: 29 patients. Metastatic recurrence: 2 patients (one axillary recurrence, 31 month , treated with lymphadenectomy and other one pulmonary relapse, 24 month, treated with chemotherapy), both free of disease at the current time. **Conclusion:** Sentinel node and occult lesion localisation as a therapeutic option in breast cancer patients after neoadjuvant chemotherapy. **References:** None.

EP-0306

Study of Recurrence in Cervical Cancer after Selective Lymph Node Biopsy

M. Calderón Calvente, L. Nieto Morcillo, G. Guzmán Prudencio, M. Falgás Lacueva, P. Navarro Beltrán, L. De la Cueva Barrao, M. Sangrós Sahún, S. Álvarez Ruiz, D. Abós Olivares;
Hospital Universitario Miguel Servet, Zaragoza, SPAIN.

Aim/Introduction: In view of the recent evidence regarding survival and recurrence of patients treated with cervical cancer treated with a laparoscopic approach, our aim is to assess the effectiveness, relapse, and disease free survival (DFS) of patients who underwent laparoscopic surgery of cervical cancer with sentinel lymph node biopsy (SLNB). **Materials and Methods:** We retrospectively studied 25 consecutive patients, who had SLNB performed as part of the surgical treatment of cervical cancer from November 2013 to November 2018. The patients' relapse was studied until April 2019, with follow-up period ranging from 64 to 4 months. **Results:** 23 patients were included in our study. One patient underwent laparotomy and was therefore excluded. 24 of the 25 patients underwent a laparoscopic procedure, of those another patient was excluded from the study because he did not meet the ESMO guidelines recommendations for the performance of SLNB. We detected recurrence of the disease in 1/23 patients (8.3%). This patient had a negative result in SLNB and locally relapsed 22 months after surgery without signs of nodal invasion, showing no sign of disease at the time of revision. 2/23 (8.69%) of patients had a positive result in SLNB, and neither have shown signs of nodal or local disease in the follow up. Average DFS for patients treated with laparoscopy and SLNB was 60'76 months (IC95%:54.68-66.85). **Conclusion:** SLNB in the course of laparoscopic treatment of cervical cancer has proved to be a safe technique in our experience for nodal staging and a useful tool to make therapeutic decisions. **References:** None.

EP-0307

Tc-99m Phytate Lymphoscintigraphy In Breast Cancer: Comparison Of Different Injection Technique

B. Hung, P. Lee, Y. Huang;
Department of nuclear medicine, Koo Foundation Sun Yat-Sen Cancer Center, Taipei, TAIWAN.

Aim/Introduction: Breast cancer surgery has evolved towards minimizing morbidity and maximizing cure rates and sentinel lymph node (SLN) biopsy is becoming standard practice in most centers. However, there are still controversies about several aspects of lymphatic mapping for breast cancer, including injection site of radioisotope and the best agent to be used in this procedure. We aim to evaluate the efficacy of Tc-99m phytate lymphoscintigraphy in identifying SLN with subdermal and intradermal injection technique. **Materials and Methods:** A total of 1187 women with biopsy-proved breast cancer underwent Tc-99m phytate lymphoscintigraphy. The radioisotope (37-96 MBq in a volume of 0.2mL) was administered by subdermal injection over peri-tumoral and peri-areolar sites in 587 patients (group A) and intradermal injection over peri-tumoral and peri-areolar sites in 633 patients (group B). Five-minute static anterior-oblique images were obtained 0.5 to 6.5 hours after injection. Images were read independently and the SLN location was marked on the skin. A surgical handheld gamma probe was used to explore the SLNs in all patients. Surgical specimens were evaluated histopathologically. The SLN identification rate and comparison of groups were evaluated by chi-square test. A p-value of less than 0.05 was considered significant. **Results:** Among the 1187 patients (mean age 54.1 ± 10.6 years), ipsilateral axilla was the most common site of SLNs. Non-axillary drainage was uncommon and found only in 7(1%) patients in group A and 12(2%) patients in group B. The SLN identification rate by lymphoscintigraphy alone in group A and B were 72% and 93%, respectively. The SLN identification rate by lymphoscintigraphy combined with surgical gamma probe in group A and B were 94% and 99%, respectively. The SLN identification rate was superior with intradermal injection compared with subdermal injection to visualize the axillary SLNs ($p < 0.05$). The highest identification rate (99%) for the axillary drainage was obtained with combination of intradermal injection and surgical gamma probe. **Conclusion:** On the basis of this study, we conclude that intradermal injection of Tc-99m phytate combined with surgical gamma probe is an appropriate and useful method of identifying SLNs with very high successful rate. **References:** None.

EP-0308

Sentinel lymph node biopsy (SLNB) after neoadjuvant chemotherapy (A-NAC) in patients with locally advanced breast cancer (LABC). Preliminary results before validation of the technique

J. Espejo Niño, M. Nevares Herrero, R. Valverde Jorge, P. Cobos Baena, L. Andrés Álvarez, E. Rodeño Ortíz de Zarate;
Hospital Universitario Cruces, Barakaldo, SPAIN.

Aim/Introduction: SLNB is an important prognostic tool for nodal staging in patients with early breast cancer, although, in patients with LABC diagnosis treated with neoadjuvant chemotherapy, the technique continues in validation process because of the high false negative rates and the low detection rates.We evaluate in our center the successfully detection rate and the false negative rate(FNR) of SLNB performed after NAC in order to validate this valuable technique. **Materials and Methods:** Retrospective study (January/2012-April/2019). Inclusion criteria: consecutive patients, diagnosed with LABC (TNM-AJCC-7&8th-Edition); scheduled for neoadjuvant chemotherapy; with evaluation of the radiological response following RECIST 1.1 criteria; who underwent to mastectomy/lumpectomy, SLNB and axillary lymphadenectomy(LDN); with evaluation of the pathological response Miller&Payne criteria and Residual Cancer Burden calculation(RCB) and with a follow-up at least 6 months after chemotherapy. **Results:** 65 patients met the inclusion criteria, (average age: 50,3 years), 2 with bilateral involvement, in total 67 breasts. The initial T staging was: cT1: 11(16%); cT2: 37(55%); cT3: 14(21%); cT4: 6(9%); The initial N staging was: cN0: 26(39%) and cN(+): 41(61%). The cN(+) patients underwent to fine-needle aspiration biopsy(FNAB) and 35(85%) were FNAB(+) and 6(15%) FNAB(-). Histological subtypes included: infiltrating ductal carcinoma(IDC): 57(85%), infiltrating lobular carcinoma(ILC): 5(7%), IDC+Ductal Carcinoma in-situ(DCIS): 1(1,5%), HG-DCIS: 2(3%) and Medular Carcinoma: 1(1,5%). The prognostic biomarkers status were: Luminal A: 8(12%), luminal B: 16(24%), triple negative: 15(22%) and Her2: 28(42%). After chemotherapy the radiological responses by MRI were: 16(24%) complete responses(CR); 44(66%) partial responses(PR); 5(7%) stable diseases(SD); and 2(3%) progressions(PG). The pathological responses to NAC were: 20(30%) complete responses(G5-RCB-0) 4(6%); minimal residual disease(G2-RCB-I); 17(25%); moderate residual disease(G3,G4-RCB-II) and 25(37%) extensive residual disease(G1-RCB-III). 1 patient was non-valorable tumoral response for technical problems processing the T staging. 14(34%) de 41 cN+ presented nodal response to pN(0). The SLNB after chemotherapy results were: 26(39%) SLNB(+): 9 G3,G4-RCB-II and 17 G1-RCB-III. 34(51%) SLNB(-): 18 G5-RCB-0; 4 G2-RCB-I; 7 G3,G4-RCB-II and 4 G1-RCB-III. 7(10%) patients didn´t present tracer migration (NM): 2 G5-RCB-0; 1 G3,G4-RCB-II and 4 G1-RCB-III. The LDN results were: 20(31%) LDN(+): 12 SNLB(+); 4 SLNB(-) and 4 NM. 47(69%) LDN (-): 14 SLNB(+); 30 SLNB(-) and 3 NM. 1 SLNB(-) presented progression with bone and ovary metastasis. The 2 patients with radiological progression of the disease after chemotherapy were SLNB(+) and remain stable. **Conclusion:** In our center the SLNB detection rate was 89,5%. The FNR was 10%(7/67) according with previous studies. One of the SLNB (-) presented progression. **References:** None.

EP-19

Clinical -> Diagnostic study -> Adult study -> Oncology study -> General oncology -> Therapy response assessment

October 12 - 16, 2019 e-Poster Area

EP-0309

Metabolic parameters at baseline 18-F-FDG PET/CT and MYC expression for the assessment of clinical outcome and treatment response in diffuse large B-cell lymphoma

M. Cuzzocrea[1], *M. Spallino*[1], *E. De Ponti*[2], *I. Casaroli*[3], *S. Bolis*[3], *C. Landoni*[1], *L. Guerra*[1];
[1]*Nuclear Medicine Department, University Milan- Bicocca, Monza, ITALY,* [2]*Medical Physics Department, San Gerardo Hospital ASST Monza, Monza, ITALY,* [3]*Hematology Department, San Gerardo Hospital ASST Monza, Monza, ITALY.*

Aim/Introduction: The metabolic parameters assessed at baseline PET are promising prognostic tools in diffuse large B-cell lymphoma (DLBCL), as reported by recent papers. A growing interest is emerging about the biological characteristics of DLBCL, that are predictive biomarkers. We evaluate the prognostic value of metabolic parameters at baseline PET, also combining immunophenotypic evaluation of MYC, in DLBCL patients. **Materials and Methods:** We retrospectively evaluated 80 patients (48 men; mean age: 61 years, range 22-86) with newly diagnosed DLBCL, disease stage I-IV (8 stage I, 13 stage II, 19 stage III, 40 stage IV) referred to our Hospital between april 2011 and october 2017. The SUV derived parameters at baseline PET were calculated using a fixed threshold of 41% of the SUVmax. In a subgroup of 51 patients, we also evaluated phenotypic expression of MYC (14 pos, 37 neg) with immunohistochemistry. Sum rank test and receiver operating characteristics (ROC) curves were performed for statistical analysis. **Results:** The median of follow up was 25.5 months. In our series of 80 patients, 18 died and 19 relapsed. Among the semi-quantitative parameters, only tMTV was statistically significant. The mean ± SD, median, and range of tMTV in non relapsed vs relapsed patients were 314 ml ± 470, 107 ml (2-2067) vs 438 ± 435, 398 ml (22-1506) respectively (p value = 0.076). The mean ± SD, median and range of tMTV in alive vs dead patients were 335 ml ± 487, 115 ml (2-2067) vs 716 ± 1368, 203 ml (22-5501) respectively (p value = 0.065). A tMTV cut-off value of 400 ml showed a PPV and NPV of 33% and 88% for DFS and 30% and 84% for OS respectively. DFS was significantly different in patients with low vs high tMTV (p = 0.05). In the immunophenotypic sub-analysis, MYC negative patients with poor prognosis were associated to high tMTV both for DFS (p = 0.0019) and OS (p = 0.02). **Conclusion:** An optimal tMTV cut-off of 400 ml at baseline PET seems to be able to exclude disease recurrence or exitus with a good NPV (84% for OS and 88% for DFS) in DLBCL patients. High tMTV in MYC negative patients is associated with a worse prognosis. If these results will be validated in a larger population, tMTV and biological markers of DLBCL, can be used as benchmark to stratify patients for novel or risk-adapted therapies. **References:** None.

EP-0310

Role Of Pet-ct In The Evaluation Of The Effect Of Stereotactic Body Radiotherapy (sbrt) In Patients With Lung Metastases

I. Kostadinova[1], *G. Mateva*[1], *N. Nedev*[2], *M. Garcheva*[1], *A. Demirev*[1];
[1]*Clinic of nuclear medicine, Acibadem City Hospital-Oncology, Sofia, BULGARIA,* [2]*Clinic of Radiotherapy, Acibadem City Hospital-Oncology, Sofia, BULGARIA.*

Aim/Introduction: The purpose of this retrospective study is to assess the effect of SBRT in patients with oligometastatic disease of the lung, using PET -CT and CT and to compare the obtained information from the PET- and the CT part of the study. **Materials and Methods:** We retrospectively reviewed 20 patients with less than 3 lung metastases from different tumours treated with SBRT. The patient group included 7 patients with breast carcinoma, 6 with colorectal cancer, 4 with lung carcinoma, 2 with renal and 1 with gastric cancer. Prior to and after the radiotherapy (3-6 months after completion of treatment) the disease was evaluated with PET-CT. We have used PERCIST and RECIST criteria for evaluation of the results. The patients were treated on Varian TrueBeam STx™ linear accelerator, the respiratory motion was assessed with 4D-CT, The average BED 10 (biologically effective dose 10Gy) was 80.95Gy (range 59.5 - 198.72), delivered in 1 to 5 fractions. The effect of the treatment was evaluated with the change of SUVmax and the sizes of the lesions and the results were compared. **Results:** A local control, defined as lesions with complete response, partial response and stable disease, was achieved in 86%. The average SUVmax was 6.70 before treatment and dropped to 2.97 after the treatment. The decrease was statistically significant (p=0.03) with a strong correlation between the values prior to and after the SBRT (r=0.76). Using CT and RECIST criteria, there was the same ultimate therapeutic control - 86%, with a change of the average size of lesions - from 15.6 mm to 12.1mm, but the difference was not statistically significant comparing the pretreatment and post treatment sizes (p=0.39) with an average correlation (r=0.60). Therefore the changes in the PET part of the study, with SUVmax appear earlier and are more pronounced than morphological ones from CT-part. We did not find any correlation between the delivered dose (BED 10) and the change in SUVmax and between the BED 10 and the size of the lesions after the SBRT. **Conclusion:** SBRT is an effective treatment for patients with oligometastatic lung disease. PET is the more sensitive part of the hybrid study than CT for evaluation of treatment response. There is no correlation between the change of SUVmax and size of the lesion with the delivered dose. **References:** None.

EP-0311

Emphasizing role of post treatment surveillance PETCT scan for radically treated non metastatic squamous cell carcinoma of head and neck (SCHNC): Single Institution preliminary outcome.

*S. Gawde, **A. Kasat**, T. Basu, S. Parekh, A. Singhal;*
HCG Cancer Centre, Mumbai, INDIA.

Aim/Introduction: SCHNC is most common malignancy worldwide. For treatment response, accurate assessment is important since residual disease after radical chemoradiation (CRT) is present in 30±60% patients. Physical examination and conventional imaging alone is not sufficient. Aim is to evaluate diagnostic performance of PET/CT for detecting residual disease after radical CRT in patients with SCHNC. **Materials and Methods:** Single institutional retrospective analysis of predominantly locally advanced SCHNC treated with radical chemoradiation from October 2017 to December 2018 were evaluated, excluding metastatic and post operative cases at baseline. Patients had baseline radiological, physical, fiberoptic examinations and post-radical CRT PETCT imaging at 10-22 weeks of treatment completion. Two blinded nuclear medicine physician reviewed PETCT. Failures were categorized into local, nodal failure and distant metastases. PET scan results were compared with clinical, fiberoptic exams, EUA and pre-treatment PETCT scan. **Results:** 50 patients with median follow-up time of 7 months (range: 3-15 months) were analysed. Most were males (80.6%) with locally advanced (90.3%), Stage IVA-B 80.6%. HPV P16 available in 11 cases (only 4 HPV P16 +). T2, T3 and N2c (38.7%) were predominant T and N stage. 77.4% received concurrent chemotherapy and 22.6% had NACT. Majority (93.5%) received SIB-IMRT technique to dose of 66-70Gy. Baseline PETCT was available in 41.9% with SUV max ranging from 7.2 - 23.3. Post surveillance second PETCT was available only in 12.9%. At first follow up, complete response (CR) at primary site was seen in 77.4% on both fiberoptic laryngoscope (FOL) and PETCT. Residual local disease was seen in 22.6% on FOL and 38.7% (combined primary and nodal) on PETCT and distant metastasis was seen in 3 patients. There was significant concordance in assessing primary disease response between PET and FOL (88%), among that 71% cases showed CR on both PET and FOL. As per last follow up, 61.3% were locoregionally controlled and 38.7% had combined local and nodal residual disease on PET, out of which residual disease was biopsy proven in 32.3%. **Conclusion:** Surveillance PETCT shows high concordance with FOL for assessing primary disease and high sensitivity for detecting nodal disease. PETCT has potential to detect residual disease after radical CRT, with optimal time for scanning between 12-16 weeks after therapy followed by re-evaluation around 10±12 months later to detect late recurrences. Additionally, PETCT can guide decisions about neck dissection and identify patients with poor prognosis. **References:** None.

EP-0312

The role of 18F-FDG-PET/CT in the response evaluation of primary systemic therapy in breast cancer

J. Torok[1], S. Czibor[1], T. Tőkés[2], T. Gyorke[1];
[1]Semmelweis University, Nuclear Medicine Center, Budapest, HUNGARY, [2]Semmelweis University, Oncology Center, Budapest, HUNGARY.

Aim/Introduction: 18F-FDG-PET/CT have a crucial role in determining response to primary systemic therapy (PST) in breast cancer patients. The goal of our research is to compare the correlation between the visual and semiquantitative PET/CT response evaluation and the pathological remission detected after the PST. **Materials and Methods:** We performed 18F-FDG-PET/CT scans in 28 patients before and after PST, examining an overall number of 29 lesions (one patient had bilateral breast cancer). Core-biopsy was performed prior to treatment in every case, while PST was followed by surgery and histological examination to assess the response to therapy. We formed pathologic complete (pCR) and partial regression (pPR) subgroups based on the results of the latter. On PET/CT scans, FDG avidity of the primary tumor was evaluated using both visual assessment according to the Deauville-scale (DS) and semiquantatively (rPET, qPET, ΔSUVmax, ΔSUVpeak) based on standardized uptake values (SUV). These results were then compared to the postoperative histological findings. We calculated the areas under the receiver operating characteristic (ROC) curves (AUC) of the visual and semiquantitative methods thereafter determined optimal cut-off values. Specificity, sensitivity, positive (PPV) and negative predictive values (NPV) of each method were evaluated based on PET-response categories defined by these cut-offs. **Results:** The results of the ROC analysis were: AUC(DS)=0.76; AUC(rPET)=0.76; AUC(qPET)=0.78; AUC(ΔSUVmax)=0.85 and AUC(ΔSUVpeak)=0.85. The optimal cut-off values were 0.849 and 0.953 for rPET and qPET, and -82.7% and -80.7% for ΔSUVmax and ΔSUVpeak, respectively. Using chi² test, those patients who were deemed PET-positive or PET-negative using DS1-2 or any of the semiquantitative methods had a pCR or pPR result that significantly correlated with their PET-based category. Both ΔSUVmax and ΔSUVpeak methods had an 82.7% diagnostic accuracy, surpassing DS1-2(65%), rPET (65.5%) and qPET (68.9%) results. ΔSUVmax had the highest sensitivity (82.3%) and NPV (76.9%), while DS1-2, rPET and qPET had the highest specificity (100%) and PPV results (100%). DS1-2, rPET and qPET measurements had relatively high false negative results with an NPV below 60%. McNemar's test demonstrated that ΔSUVmax had significantly higher diagnostic accuracy than DS1-2, rPET and qPET. **Conclusion:** Response to therapy following PST can be evaluated with good accuracy by ΔSUV measurements between PET/CT examinations performed before and after PST. The evaluation of the post-PST PET/CTs in itself is less suitable to assess complete regression. **References:** None.

EP-0313

18F-FDG PET/CT Is Useful In The Evaluation Of Treatment Response With Tocilizumab In Patients With Large Vessel Vasculitis

E. Cerudelli[1], *G. Bosio*[2], *D. Albano*[2], *M. Gazzilli*[1], *M. Bonacina*[1], *R. Durmo*[1], *F. Dondi*[1], *A. Mazzoletti*[1], *P. Bellini*[1], *F. Bertagna*[1,2], *R. Giubbini*[1,2];
[1]*Università degli studi di Brescia, Brescia, ITALY,* [2]*Azienda Socio Sanitaria Territoriale degli Spedali Civili di Brescia, Brescia, ITALY.*

Aim/Introduction: 18F-fluorodeoxyglucose positron emission tomography (FDG-PET/CT) is useful in the detection of the arterial wall inflammation in patients affected by large-vessel vasculitis (LVV) as giant cell arteritis (GCA), Takayasu arteritis (TA) and aortitis. The aim of this study was to investigate the usefulness of FDG-PET/CT in the evaluation of therapy response with tocilizumab (TCZ), a humanized anti-interleukin-6 receptor antibody, in patients affected by LVV. **Materials and Methods:** We retrospectively evaluated 11 patients (7 female, 4 male; 56±19 years) with LVV treated with TCZ. FDG-PET/CT were performed at baseline and with an interval of 3-26 months (13,18±7,69) after the initiation of TCZ therapy. PET images were analysed visually and semi-quantitatively by measuring the maximum standardized uptake value (SUVmax) of the vascular wall of bilateral subclavian and common carotid arteries, ascending thoracic aorta, abdominal aorta and bilateral iliac arteries. Moreover, for each patient we selected the vessel with most increased uptake and we calculated the vessel-to-liver SUVmax ratio pre- and post-treatment. The ΔSUV ratio (pre-post treatment) was compared to changes of Erythrocyte Sedimentation Rate (ESR) and changes in glucocorticoid (GC) therapy, both considered as indices of disease activity. **Results:** Nine patients had a complete disease remission after TCZ, in two there was a reduction of vessels uptake. SUVmax ratio pre-treatment showed a strong correlation with blood levels of ESR (ρ 0,713; p 0,04). Vessel-to-liver SUVmax ratio was significantly decreased in post-treatment PET/CT (1,73±0,82 vs. 0,82±0,18; p=0,002). We observed a complete normalization of ESR in all cases after TCZ therapy. Mean GC dose was tapered from 28,86±15,06 mg/day to 7,09±4,66 mg/day (p<0,001). The ΔSUV ratio was significantly associated with reduction of GC therapy (p<0,001) and of ESR (p=0,007). **Conclusion:** Vessels FDG uptake decreased significantly after the initiation of TCZ therapy in LVV patients showing a good metabolic response. The reduction of FDG uptake is related to decrease of blood levels of ESR and of steroid therapy, confirming a reduction of disease activity. FDG-PET/CT could be used to evaluate treatment response in TCZ-treated patients. **References:** None.

EP-0314

"Overall PET Response" index based on ^{18}F-FCH PET/CT semiquantitative parameters: a useful method to evaluate 223Ra-dichloride therapy efficacy in mCRPC patients with bone metastases

C. Ferrari, *A. Niccoli Asabella, V. Lavelli, A. G. Nappi, S. Sisto, G. Sigrisi, M. Fanelli, G. Rubini;*
Nuclear Medicine Unit, Interdisciplinary Department of Medicine – University of Bari "Aldo Moro", Bari, ITALY.

Aim/Introduction: The endpoint of our study was to validate a reliable but simple method to evaluate 223Ra-dichloride (223Ra) therapy response in metastatic castration-resistant prostate cancer (mCRPC) patients with symptomatic bone metastases. We used ^{18}F-Fluorocholine (^{18}F-FCH) PET/CT semiquantitative analysis and compared PET parameters to bone scan (BS), conventionally considered as gold standard for 223Ra-therapy efficacy evaluation. **Materials and Methods:** 30 patients (mean age 75 years, range 57-89) with mCRPC underwent 223Ra-therapy at our Department, from February 2016 to September 2018. A retrospective analysis was performed, selecting 12/30 patients who completed the whole treatment (6 administrations, 55 kBq/kg each one) and performed both BS and ^{18}F-FCH-PET/CT at baseline and 2 months after therapy. We selected the 3 most metabolically active skeletal lesions (a total of 36) at baseline PET/CT and we monitored their post-treatment PET/CT changes, calculating 5 semiquantitative parameters (SUVmax, SUVmin, SUVav, MATV, TLA) and pre-/post-treatment Δvalue (ΔSUVmax, ΔSUVmin, ΔSUVav, ΔMATV, ΔTLA). We defined an Overall PET Response (OPR) for each of the 5 semiquantitative parameters, considering the trend of the 3 lesions Δvalues. Based on this index, we classified patients as PET responders (OPR-R) and PET non-responders (OPR-NR). Patients were considered responder for a specific parameter (OPR-$R_{\Delta SUVmax}$, OPR-$R_{\Delta SUVmin}$, OPR-$R_{\Delta SUVav}$, OPR-$R_{\Delta MATV}$, OPR-$R_{\Delta TLA}$) if at least 2 of the 3 lesions showed reduction or stability. The BS response to therapy was based on the difference between lesions' number in pre- and post-treatment examinations, dividing patients in BS responders (BS-R) and non-responders (BS-NR). The concordance between OPR and BS results was calculated by Cohen's K. P<0.05 was considered statistically significant. **Results:** According to BS, 4/12 patients were BS-R (33%) and 8/12 patients BS-NR (67%). Referring to OPR analysis, 7/12 patients (58%) were OPR-$R_{\Delta SUVmax}$, OPR-$R_{\Delta SUVmin}$, OPR-$R_{\Delta SUVav}$ and OPR-$R_{\Delta MATV}$; 8/12 patients (67%) were OPR-$R_{\Delta TLA}$. A statistically significant agreement between the two techniques was found for ΔSUVmax, ΔSUVmin and ΔSUVav (k=0.526; p=0.038). **Conclusion:** Our preliminary results suggest that ^{18}F-FCH-PET/CT evaluation by "Overall PET Response" index could be a summary but very useful method for 223Ra-therapy response assessment, with a special reference to ΔSUV parameters, which could represent a guide for a steady patient monitoring. **References:** None.

EP-0315

Intra Patient Sul Repeatability Of Background On ^{18}F-FDG PET/CT

R. Wang[1], *M. Su*[1], *J. H. Miller*[2];
[1]*West China hospital, Chengdu, CHINA,* [2]*Loma Linda University, School of Medicine, CA, CA, UNITED STATES OF AMERICA.*

Aim/Introduction: The background activity of normal soft tissues is often used as reference to assess tumor treatment response on ^{18}F-FDG PET/CT. Our objective was to find the preferred background through assessing the repeatability of different background activity, which was expressed by standardized uptake value normalized to lean body mass (SUL). **Materials and Methods:** Patients who have had two scans within several days were selected. Background SULs from aortic blood pool (ABP-SUL), liver (L-SUL) and muscle (M-SUL) were recorded. Intra-class correlation coefficients (ICCs) and Bland-Altman plots were used to evaluate the degree of repeatability between two scans. Then the intra-patient variation in SULs and factors which included blood glucose level (BGL), tracer uptake period and dose were calculated as relative changes between two scans. Finally, a linear regression model was used for analyzing all relative changes to identify which factor had correlation with SULs variability. **Results:** Seventeen patients were included. The SUL ICCs for ABP, liver and muscle were 0.66, 0.48 and 0.77 respectively. Similar results were obtained from Bland-Altman plots. According to liner regression analysis, there were positive correlations between variations of L-SUL and M-SUL and that of BGL (b=0.570and 0.492 respectively, p&lt0.05 altogether), and between variation of M-SUL and that of tracer uptake period (b=0.591, p=0.006). **Conclusion:** The SUL of liver is more sensitive to blood glucose level, therefore may not be suitable for the referential background. Activities within aortic blood pool and muscle are stable, and should be the preferred background for sequential patient evaluation. **References:** None.

EP-0316

Impact of PET Reconstruction Algorithms on Assessment and Quantification of FDG-PETCT Findings in Patients with Multiple Myeloma

S. Riaz, S. Arulogun, A. L. Smith, N. Rabin, S. Wan, J. Bomanji; NHS, London, UNITED KINGDOM.

Aim/Introduction: The purpose of this study is to assess how different PET image reconstructions may influence the clinical interpretation of FDG-PETCT studies, in patients with multiple myeloma. **Materials and Methods:** Standard of care FDG-PETCT scans performed for assessment in multiple myeloma patients were retrospectively reviewed. Scans were grouped under three broad indications: baseline assessment, response evaluation & suspected relapse. In each case, OSEM TOF and Bayesian penalized likelihood reconstruction algorithm (BPL) were available. A qualified nuclear medicine physician evaluated the following parameters on both sets of PET images: mediastinal and liver SUVmax, number of focal FDG avid lesions (skeletal and extramedullary) & SUVmax of up to 3 focal skeletal lesions per patient. SUVmax values were compared using paired t-tests. **Results:** In the period evaluated, 71 PET-CT scans were identified in 68 patients (average age: 64.3±10.3). Indications were: baseline assessment (n=17), treatment response evaluation (n= 27) and suspected relapse (n=27). In total, 112 skeletal lesions were identified.For mediastinal and liver measurements, in all three groups (baseline, response evaluation, suspected relapse), the SUVmax values are higher on OSEM TOF reconstruction - being 8.5%, 2.3% & 1.2% higher respectively in the mediastinum, and 10.2%, 7.5% & 8.9% higher respectively in the liver. For focal FDG avid skeletal lesions, average lesional SUVmax values are 1.9 ± 2.5, 2.1 ± 3.5, 2.0 ± 3.4 higher on the BPL reconstructions (24%, 12.8%, 27%, for baseline, response evaluation and suspected relapse groups respectively) (p<0.001 for all three groups). Additional focal avid skeletal sites are seen in 1 of the response evaluation and 5 of the suspected relapse cases on BPL reconstruction, not perceptible on routine TOF reconstructions. Adopting Deauville score as per IMPeTUs criteria[1], proposed for categorising treatment response, in the relevant group in our cohort would mean 8/27 (29.6%) of patients would be 'up-graded' if BPL reconstruction images were used for clinical assessment instead of routine OSEM TOF. **Conclusion:** A shift in PET reconstruction algorithm used in the FDG PETCT assessment of multiple myeloma patients would have a potentially significant impact in the clinical interpretation of the study findings. **References:** Nanni C, Zamagni E, Versari A, Chauvie S, Bianchi A, Rensi M, et al. Image interpretation criteria for FDG PET/CT in multiple myeloma: a new proposal from an Italian expert panel. IMPeTUs (Italian Myeloma criteria for PET USe). Eur J Nucl Med Mol Imaging. 2016 Mar;43(3):414-21.

EP-0317

Prognostic role of basal bone scintigraphy and ^{18}F-Fluorocholine PET/CT in patients with prostate cancer treated with ^{223}Ra

E. Casillas Sagrado[1], *A. M. García Vicente*[1], *N. Martínez Asensio*[2], *M. Amo-Salas*[2], *M. J. Tello Galán*[1], *I. García Carbonero*[3], *J. Cassinello Espinosa*[4], *R. Gómez Díaz*[1], *Á. M. Soriano Castrejón*[1]; [1]*Hospital General Universitario de Ciudad Real, Ciudad Real, SPAIN,* [2]*Castilla-La Mancha University, Ciudad Real, SPAIN,* [3]*Hospital Virgen de la Salud, Toledo, SPAIN,* [4]*Hospital Universitario de Guadalajara, Guadalajara, SPAIN.*

Aim/Introduction: To establish the prognostic value of bone scintigraphy (BS) and ^{18}F-Fluorocholine PET/CT (FCH-PET/CT) previous to ^{223}Ra (basal) and compare it to clinical variables, in patients with castration-resistant prostate cancer and bone metastases (CRPC-BM). **Materials and Methods:** Prospective and multicentre study started in 2015 (ChoPET-Rad). 63 patients with CRPC-BM were consecutively included. Clinical variables as Gleason score, basal PSA, LDH and AP, previous treatments and treatment failure were collected. Bone metastases characteristics as location (axial vs. axial plus extra-axial), number, blastic or not on CT, bone marrow involvement (super-scan pattern), tumor burden, FCH uptake above the hepatic pool, among others, were assessed. Patients underwent standardized follow-up and overall survival (OS) was obtained. The relation between imaging variables and OS was analyzed by Kaplan-Meier and Long Rank (Mantel-Cox) tests. Multivariate analysis was performed by Cox regression. **Results:** Median OS was 15 months. 39/63 patients

died during the follow-up.Treatment failure was observed in 55.6%. BS and FCH-PET/CT demonstrated axial plus extra-axial involvement in 61.9% and 56%, respectively. Polimetastatic disease was more prevalent in BS with respect to FCH-PET/CT (74.6 vs 64%, respectively). 34% of lesions had a non-blastic dominance on CT. Super-scan pattern was observed in 28% of BS and 24% of FCH-PET/CT. Multiple FCH-PET/CT variables were related to OS: axial plus extra-axial presence of metastases (HR=2.71;p=0.036), high tumor burden (HR=2.95;p=0.032), non-blastic dominance on CT (HR=3.26;p=0.030), super-scan pattern (HR=4.36;p=0.001), metastases with FCH uptake higher than liver (HR=3.90;p=0.004). In BS, only extent of disease and bone marrow involvement were associated to OS. On a multivariate analysis, only treatment failure (HR=6.06;p=0.003) and super-scan pattern on FCH-PET/CT (HR=4.57;p=0.004) were simultaneously predictors of OS. **Conclusion:** Basal ^{18}F-fluorocholine PET/CT offered additional information in the prediction of OS in patients with CRPC-BM treated with ^{223}Ra, being superior to BS and clinical variables. **References:** None.

EP-0318

Interim and end-of-treatment bone scintigraphy and ^{18}F-Flourocholine PET/CT in the prediction of response in patients with prostate cancer treated with ^{223}Ra

E. Casillas Sagrado[1], *A. M. García Vicente*[1], *N. Martínez Asensio*[2], *M. Amo-Salas*[2], *M. J. Tello Galán*[1], *I. García Carbonero*[3], *J. Cassinello Espinosa*[4], *R. Gómez Díaz*[1], *Á. M. Soriano Castrejón*[1];
[1]*Hospital General Universitario de Ciudad Real, Ciudad Real, SPAIN,* [2]*Castilla-La Mancha University, Ciudad Real, SPAIN,* [3]*Hospital Virgen de la Salud, Toledo, SPAIN,* [4]*Hospital Universitario de Guadalajara, Guadalajara, SPAIN.*

Aim/Introduction: To determine the aim of interim and end-of-treatment ^{99m}Tc-HDP bone scintigraphy (BS) and ^{18}F-Fluorocholine PET/CT (FCH-PET/CT) in the response evaluation of patients with castration-resistant prostate cancer and bone metastases (CRPC-BM) treated with ^{223}Ra. **Materials and Methods:** Prospective and multicentre ChoPET-Rad study. 63 patients with CRPC-BM were consecutively included. Basal, after 3 (interim) and 6 doses (final) BS and FCH-PET/CT were performed.Clinical variables [Gleason score, basal PSA, PA and LDH, previous treatments, treatment failure], and degree of response (progression or not) of bone metastases in both imaging techniques were assessed and their association with progression free survival (PFS), attending biochemical parameters, using Kaplan-Meier and Long Rank (Mantel-Cox) tests. **Results:** Of the patients included, 45% of them had Gleason score ≥ 8, 73% were in their third or consecutive line. Median of PFS was 3 months. 39/63 patients died during the follow-up.Neither clinical variables nor degree of response on BS were significant predictors of PFS. Interim and final degree of response assessed with FCH-PET/CT were related to PFS (Χ^2=6.01; p=0.014 and Χ^2=9.49; p=0.002, respectively).The patients identified as progression in final PET presented a risk of biochemical progression 4 times higher than the rest (p=0.012). Likewise, the patients categorized as progression in final BS had a death risk 5.2 times higher than the rest (p=0.004). **Conclusion:** Both interim and final ^{18}F-fluorocholine PET/CT were good predictors of the biochemical progression in patients treated with ^{223}Ra. Neither interim nor end-of-treatment bone scintigraphy were useful to predict biochemical response; nevertheless, progression in final bone scintigraphy was an adverse prognostic factor in terms of overall survival. **References:** None.

EP-0319

A Prospective Study In 613 Patients Seeking For Predictive Factors Of Physiological FDG Anal Uptake To Improve Post Chemo-radiotherapy PET Scans Interpretation In Anal Cancer

C. Lasnon[1,2], *N. Aide*[3,2,4], *C. Nganoa*[3], *B. Houdu*[3], *J. Kammerer*[1,4], *M. Galais*[1], *R. Ciapuccinni*[1], *L. Tainturier*[1,4];
[1]*Centre François Baclesse, Caen, FRANCE,* [2]*ANTICIPE, INSERM U1086, Caen, FRANCE,* [3]*Caen University Hospital, Caen, FRANCE,* [4]*Caen University, Caen, FRANCE.*

Aim/Introduction: Anal cancer is a relatively rare tumor whose incidence increases in developed countries. ^{18}F-FDG PET has been increasingly used for its post radio-chemotherapy evaluation. However, several authors reported the risk of local false-positive findings leading to low specificity and positive predictive values. These false positive results could result from post-radiotherapy inflammation or infection but certainly also from physiological anal canal uptake that is observed in a regular basis in clinical practice. The purpose of this prospective study (NCT03506529; HYPHYCA) was therefore to seek for predictive factors of physiological anal canal hypermetabolism in order to improve the specificity of post radio-chemotherapy PET evaluation. **Materials and Methods:** Over a two-month period, patients aged of 18 yo and more, referred for ^{18}F-FDG PET-CT at two EARL-accredited PET centres were included, after obtaining their informed and written consent. They were asked to fill in a questionnaire including seven closed questions about usual intestinal transit, ongoing medications relative to intestinal transit, history of digestive, anal and/or pelvic diseases. Age, gender, body mass index (BMI) were recorded.A single nuclear medicine physician visually and quantitatively analyzed anal canal uptake (SUV_{max_EARL}) and assessed visual rectal content (air, feces or both) and the largest rectal diameter (mm). **Results:** Six hundred and thirteen patients were included (sex ratio F/M=0.99) and 545 (89%) questionnaires were entirely fulfilled. Significantly more males presented with anal canal hypermetabolism (sex ratio (M/F) = 1.18 versus 0.85, p = 0.048). Moreover, patients with anal canal hypermetabolism had higher BMI (27.6 (5.7) kg/m^2 versus 23.9 (4.5) kg/m^2, p< 0.0001), higher rate of hemorrhoid history (43% versus 27%, p=0.016) and higher rate of rectum filled with only feces (21% versus 12%, p = 0.019) as compared to patients with no anal canal uptake. On logistic regression, all these variables were found to be independent predictors of the occurrence of an anal canal hypermetabolism. Odds ratio were 1.16 (1.12-1.20) per unit of BMI (kg/m^2) (p<0.0001), 1.48

(1.04-2.11) for males (p=0.029), 1.64 (1.10-2.45) for hemorrhoids history (p=0.015) and 1.94 (1.147-3.22) for the rectal filled with only feces (p=0.010). **Conclusion:** According to our study, the predictive factors of physiological anal canal hypermetabolism are high BMI, male gender, history of hemorrhoid and rectum filled with only feces. This paves the way to a more specific interpretation of post radio-chemotherapy PET evaluations of anal canal cancer and to the optimization of protocols by used of rectal enema. **References:** None.

EP-0320

18F-FDG-PET early response assessment of PD1-Immunotherapy in melanoma patients

D. Papamichail[1], *R. Hog*[1], *C. Sachpekidis*[1], *J. Hassel*[2], *A. Dimitrakopoulou-Strauss*[1];
[1]*Clinical Cooperation Unit Nuclear Medicine, German Cancer Research Center, Heidelberg, GERMANY,*
[2]*Universitätshautklinik, Heidelberg, GERMANY.*

Aim/Introduction: The aim of this ongoing study is to evaluate if 18F-FDG-PET has the potential to predict the response of patients with melanoma to PD1-therapy after two circles of therapy. **Materials and Methods:** From January 2015 to January 2019, 21 patients (13 females; average 56 y) with unresectable metastasized melanoma had a whole-body 18F-FDG-PET/CT examination at three time points: Before therapy start (t_1, base-line), after two circles of therapy (t_2, interim) and after completion of therapy (t_3, reference standard). Therapy response was assessed with European Organisation for Research and Treatment of Cancer (EORTC) criteria for PET/CT and PET Response Evaluation Criteria for Immunotherapy (PERCIMT) [1]. **Results:** According to EORTC criteria, of the 21 patients included in the study, 12 had disease progression (PMD) in PET at t_3. Ten of these patients (83.3%) had shown PMD in t_2, one patient had shown stable metabolic disease (SMD) and another patient partial metabolic response (PMR). Two patients who had complete metabolic response (CMR) in PET at t_3 had shown a complete response also at t_2. According to PERCIMT, 8 patients had PMD in PET at t_3. 5 of these patients (62,5%) had shown PMD in t_2, two patients had shown SMD and one patient had shown PMR. Again, two patients who had CMR in PET at t_3 had shown CMR also at t_2. Two-years follow-up of all patients remains for further evaluation. **Conclusion:** The preliminary results of our study indicate that 18F-FDG-PET after two circles of PD1-therapy can serve as a surrogate measure of therapeutic efficacy in stage IV melanoma patients. This might help to shorten therapy regimes or to consider earlier a different treatment strategy. The results will be validated based on long-term follow-up data. **References:** [1] Dimitrakopoulou-Strauss A. Monitoring of patients with metastatic melanoma treated with immune checkpoint inhibitors using PET-CT. Cancer Immunol Immunother. 2019 May;68(5):813-822.

EP-0321

One versus five lesions for response assessment by PERCIST in patients with lung cancer

S. Kwon, *J. O, I. Yoo, S. Kim;*
Seoul Saint Mary's Hospital, Seoul, KOREA, REPUBLIC OF.

Aim/Introduction: The number of lesions to evaluate when assessing treatment response is not validated for lung cancer. We compared one and five lesion measurements for response assessment by Positron Emission Tomography Response Criteria in Solid Tumors (PERCIST). **Materials and Methods:** Patients with lung cancer who had pre- and post-treatment FDG PET/CT from 2016 to 2017 were included and the standard uptake value corrected for lean body mass (SULpeak) of up to 5 hottest target lesions were measured. The percent change in the single hottest lesion (1-lesion-analysis), and percent change in the sum of up to 5 hottest lesions (5-lesion-analysis) were computed. Response category was designated: complete metabolic response (CMR) when no lesion with perceptible FDG uptake remained; partial metabolic response (PMR), stable metabolic disease (SMD), or progressive metabolic disease (PMD) determined using the PERCIST threshold of 30% and 0.8 unit change in SULpeak; unequivocal new lesion meant PMD. Regression analysis was used to investigate linearity between 1-lesion-analysis and 5-lesion-analysis, and the concordance for response categorization was assessed by kappa statistics. **Results:** Total 26 patients (13 non-small cell; 13 small cell) were included and all had FDG-avid lung cancer. The median interval between pre- and post-treatment PET/CT was 18.5 weeks (7.7 -37.4 weeks). Average of 3.4 target lesions were measured for 5-lesion-analysis at pre-treatment, and 3.6 at post-treatment. R^2 value was 0.48 ($p<0.001$) for all 26 patients, but increased to 0.92 ($p<0.001$) when one outlier categorized as PMD regardless of percent change due to new lesions was excluded. Response categorization with 1-lesion-analysis and 5-lesion-analysis was discordant in 1 patient (weighted kappa=0.94), who showed 30.4% decrease by 1-lesion-analysis and 28.6% decrease by 5-lesion-analysis. In 3 patients, the response was PMD despite less than 30% increase in SULpeak due to new lesions. Patients with CMR demonstrated SULpeak changes in range of -76.7% to -79.5% by 1-lesion-analysis and -74.3% to -80.8% for 5-lesion-analysis. **Conclusion:** Measuring single and up to five hottest lesions from FDG PET/CT for response assessment by PERCIST yielded high concordance rate in patients with lung cancer. **References:** None.

EP-20

Clinical -> Diagnostic study -> Adult study -> Oncology study -> Organ-based oncology -> Bone and soft tissues cancer primary and metastatic cancers

October 12 - 16, 2019 e-Poster Area

EP-0322

The Role Of ^{18}F-sodium Fluoride (Naf) PET/CT In The Evaluation Of Metastatic Bone Disease In Extremely Obese (super Obese) Patients

M. Usmani[1], *F. al Kandari*[1], *F. Marafi*[2], *G. Gnanasegaran*[3], *T. Van den Wyngaert*[4];
[1]*Kuwait Cancer Control Center, Kuwait, KUWAIT,* [2]*Jaber Al-Ahmad Molecular Imaging Center, Kuwait, KUWAIT,* [3]*Royal Free Hospital NHS Trust, London, UNITED KINGDOM,* [4]*Antwerp University Hospital Belgium, Antwerp, BELGIUM.*

Aim/Introduction: Obesity is an emerging public health crisis all around the world and presents with unique challenges for diagnostic imaging procedures, including the skeletal staging in cancer. The quality of conventional bone scintigraphy is generally poor in the obese patients. We have previously demonstrated that ^{18}F-NaF PET/CT has high diagnostic accuracy in morbidly obese patients (body mass index [BMI] >40kg/m^2) with cancer [1]. In the present work, we investigate whether these superior imaging characteristics are preserved in super-obese patients (BMI >50kg/m^2). **Materials and Methods:** Fifty-one extremely obese patients with BMI >50Kg/m^2 (mean weight 126.2±14.5 kg; BMI 54.57±4.8 kg/m^2; mean age 59.9 years [range 36 - 76]) and referred for ^{18}F-NaF PET/CT for the osseous staging of a newly diagnosed malignancy or suspected/proven recurrence were retrospectively analyzed. All patients underwent ^{18}F-NaF PET/CT scan after injection of 0.06 mCi/kg of ^{18}F-NaF according to EANM guidelines [2]. Images were interpreted using a 5-point scoring system as published previously [1]. Equivocal scores were classified as benign for the final analysis. The reference standard was based on the combination of confirmation of metastatic status by other imaging modalities or clinical follow-up. Diagnostic test characteristics were calculated using traditional methods. Means with standard deviations and proportions with 95% confidence intervals are reported. **Results:** The median duration of follow-up after imaging was 13 months (range 06-18). ^{18}F-NaF PET/CT was definitely benign in 25, possibly benign in 2, equivocal in 2, possibly malignant in 7 and definitely malignant in 15 patients. The overall prevalence of bone metastases according to the reference standard was 41.2% (95% CI 27.6-55.8%). The sensitivity, specificity, PPV, NPV and accuracy of ^{18}F-NaF PET-CT were 90.5% (95% CI 69.6-98.8%), 90% (95% CI 73.5-97.9%), 86.4% (95% CI 65.1-97.1%), 93.1% (95% CI 77.2-99.1%), and 90.2% (95% CI 78.6 - 96.7%), respectively. While few patients had BMI >60Kg/m^2 (n=6), similar results were seen in this subgroup. Osteoarthritic changes were commonly seen in super-obese patients mainly involving facet joints (76.5%), knees (74.5%), small joints of feet (47.1%), and ankle (21.6%). **Conclusion:** ^{18}F-NaF PET/CT retains its high diagnostic accuracy in super-obese patients (BMI >50Kg/m^2) resulting in a low number of equivocal findings and therefore offers high diagnostic confidence. It is less susceptible to artifacts induced by body habitus and may be the preferred functional imaging modality for this patient group. **References:** 1. Clin Nucl Med. 2017;42:829-836. 2. Eur J Nucl Med Mol Imaging. 2015;42:1767-1777.

EP-0323

Test-retest Reliability Of Quantitative Bone SPECT/CT Performed On Different Days

T. Yamane[1], *S. Shirotake*[2], *T. Okabe*[2], *K. Nishimoto*[2], *G. Kaneko*[2], *M. Oyama*[2], *A. Seto*[1], *K. Fukushima*[1], *I. Kuji*[1];
[1]*Department of Nuclear Medicine, Saitama Medical University International Medical Center, Hidaka, JAPAN,* [2]*Department of Uro-Oncology, Saitama Medical University International Medical Center, Hidaka, JAPAN.*

Aim/Introduction: While the advancement of SPECT/CT technology improved quantitative evaluation of the uptake, the reproducibility of the quantitative value has not yet been clarified. The aim of this study is to confirm the test-retest reliability of quantitative value calculated by a novel SPECT/CT of bone scans. **Materials and Methods:** This prospective study included eleven male patients with prostate cancer who performed SPECT/CT for the evaluation of bone metastasis. Written informed consents were acquired before enrollment in the study. Patients received a second bone scan (retest-scan) after 4-10 days of a first bone scan (test-scan). For the bone scans, images were acquired by a novel quantitative SPECT/CT scanner (Symbia Intevo, Siemens) after administration of [Tc-99m] methylene diphosphonate. SPECT/CT images from shoulder to pelvis were reconstructed by Ordered Subset Conjugate-Gradient Minimizer. We set regions of interests (ROIs) at visually increased uptake areas on metastasis and degeneration, as well as fundamental 12 normal areas. Uptakes of the ROIs were evaluated by standardized uptake value (SUV), and maximum SUV (SUVmax) and peak SUV (SUVpeak) were used. Intra-class correlation coefficient (ICC) was used to evaluate the difference of the 2 scans, and ICC of 0.8 or more was considered as almost perfect correlation. **Results:** We analyzed 212 ROIs including 163 normal, 25 degenerative, and 24 metastatic lesions. Percent differences (average ± standard deviation) for SUVmax were 11.7 ± 9.1% for normal, 18.0 ± 14.4% for degenerative, 10.4 ± 8.1% for metastatic, and 12.3 ± 9.9% for all lesions, respectively. Percent differences for SUVpeak were 11.0 ± 7.7% for normal, 16.0 ± 11.2% for degenerative, and 9.5 ± 8.0% for metastasis, and 11.4 ± 8.4% for all lesions, respectively. ICCs (and the 95% confidence interval in the parenthesis) of SUVmax were 0.91 (0.88—0.93) for normal, 0.92 (0.83—0.96) for degenerative, 0.80 (0.60—0.90) for metastatic, and 0.97 (0.96—0.98) for all lesions.

ICCs of SUVpeak were 0.94 (0.96—0.98) for normal, 0.94 (0.86—0.97) for degenerative, 0.86 (0.70—0.94) for metastatic, and 0.97 (0.96—0.98) for normal lesions, respectively. **Conclusion:** The novel quantitative SPECT/CT provides almost perfect test-retest reliability of SUVs among 2 bone SPECT/CT performed on different days. **References:** None.

EP-0324

Clinical Utility of hybrid versus planar images on bone scintigraphy for oncologic patients

I. El Bez, R. Tulbah, I. Munir, F. Alghamlas, M. Alharbi;
King fahd medical city, nuclear medicine department, Riaydh, SAUDI ARABIA.

Aim/Introduction: To evaluate retrospectively the additional diagnostic value of hybrid fused single photon emission computed tomographic with (SPECT-CT) images in assessing possible bone metastases. **Materials and Methods:** We identified 100 oncologic patients (75 female and 25 males). Bone scintigraphy including planar and SPECT-CT imaging were performed for all patients. First, we analyzed the planar images, then the fused images and focused on the additional value of fused images. Diagnostic confidence for each lesion was scored. On the planar images we classified as confident (malign, benign) or indeterminate **Results:** 100 oncological patients were included (75 women, 25 man; mean age, 52.4 years ± 10.7. The planar images demonstrate 245 foci: 211 were confidents (115 metastatic bone foci and 130 benign foci) and 34 were indeterminate. After review of fused images: for the confidents lesions: there were two benign lesions which became suspicious based on low dose CT. Almost all indeterminate became more confident in diagnosis with 25 benign lesions and 15 metastases. In addition, fused images demonstrated also 12 lesions non visualized on planar images. **Conclusion:** Results demonstrate the increased diagnostic confidence obtained with fused SPECT/CT images compared to planar images in differentiating malignant from benign bone lesions. **References:** None.

EP-0325

68Ga-PSMA-PET/CT vs Bone Scintigraphy in prostatic cancer; are we postponing the future?

S. Castro[1], G. Ferreira[1], L. Violante[1], L. Fonseca[2], I. Sampaio[1], C. Castro[1], H. Duarte[1];
[1]Instituto Português de Oncologia, Porto, PORTUGAL, [2]Centro Hospitalar Universitário do Porto, Porto, PORTUGAL.

Aim/Introduction: Prostate cancer is the second most common cancer in men and skeletal system is the most common site for distant metastasis. Therefore, it is very important in clinical practice to have sensitive imagiological methods that allow early detection of bone metastasis. The purpose of this study was to compare Gallium-68 prostate specific membrane antigen positron emission tomography/computed tomography (68Ga-PSMA-PET/CT) and Technetium-99m diphosphonate bone scintigraphy (BS) performance for bone metastases detection in prostate cancer patients. **Materials and Methods:** Retrospective study of 73 patients that underwent 68Ga-PSMA-PET/CT and BS between 01.01.2015 and 01.03.2019, with a maximum of 90 days between them and without any therapeutic change in that time period. The studies were classified as present, absent or suspected metastases. Global and per anatomic region analyses were performed. Cases suspicious of metastasis were redefined as positive and negative to allow for a scenario analysis. The best valuable comparator was defined based on follow up data, namely subsequent BS, 68Ga-PSMA-PET/CT, computerized tomography, magnetic resonance imaging, and histology when available. Specificity, sensitivity, positive predictive value, negative predictive value and accuracy were calculated using MedCalc software. Fisher test was used to assess the association between the accuracy of each exam and prostate specific antigen (PSA), alkaline phosphatase levels and clinical indication for performing the study (staging, biochemical recurrence and metastatic castration-resistant prostate cancer). **Results:** 68Ga-PSMA-PET/CT and BS were congruent in 58 (79.4%) patients, (40 negatives, 17 positives and 1 suspicious for metastasis) and differed in 15 (20.6%) patients. 68Ga-PSMA-PET/CT identified correctly seven (9.6%) patients with metastasis (BS negative) and BS identified correctly two (2.7%) patients with metastasis (68Ga-PSMA-PET/CT negative). Considering both scenarios, global specificity, sensitivity, positive predictive value, negative predictive value and accuracy varied between 97.7-100.0%, 89.5-93.1%, 96.4-100.0%, 93.6-95.6%, 96.0-96.0% for 68Ga-PSMA-PET/CT and 93.9-100.0%, 62.1-75.9%, 88.0-100.0%, 80.0-85.4%, 84.9-86.3% for BS, respectively. Comparing to BS, specificity, sensitivity, positive predictive value, negative predictive value and accuracy were higher in 68Ga-PSMA-PET/CT also per anatomic region analyzes. There was no correlation between diagnostic accuracy and clinical indication for performing the studies, PSA and alkaline phosphatase levels in both studies. **Conclusion:** In this review 68Ga-PSMA-PET/CT diagnostic performance for bone metastasis detection in prostate cancer was superior to BS. A larger sample and prospective randomized trials are needed in order to prove 68Ga-PSMA-PET/CT applicability in routine prostate cancer bone metastasis imaging. **References:** None.

EP-0326

Whole-body SPECT/CT: Could Replace Bone Scintigraphy in Cancer Patients?

F. Manchon Adsuar, R. Diaz Expósito, V. López Prior;
Fundación Instituto Valenciano de Oncologia, Valencia, SPAIN.

Aim/Introduction: SPECT-CT is commoly used after equivocal findings in the whole-body bone scan in the staging workup for cancer patients. Our objective was to investigate if whole-body SPECT-CT (3 FOV, field of view) could be applied and replace the planar bone scan in cancer patients, mostly prostate and breast cancer. Furthermore, our aim was to compare the sensitivity and specificity of both tests. **Materials and Methods:** In 29

patients (18 breast cancer, 10 prostate cancer, 1 rectum cancer), whole-body scan SPECT-CT and bone scan were prospectively performed for staging and re-staging. All data were acquired with 3 FOV SPECT-CT, Discovery NM/CT870 General Electric gamma camera. Subsequently, the follow-up was clinical and/or with other imaging modalities. **Results:** Based on planar image, 6 patients (20.69%) were positive for bone metastasis, and 23 (79.31%) were negative. The sensitivity and specificity was higher with whole-body SPECT-CT than with planar images to detect bone metastases (87.5% and 95.5% vs 77.7% and 95%). Whole-body SPECT-CT reclassified 3 negative bone scan patients into positives. The follow-up confirmed two of these patients. One positive patient by whole-body scan was downstaged by whole-body SPECT-CT to nonmetastatic disease. In all cases, whole-body SPECT-CT provided a better characterization of both benign and malignant lesions. **Conclusion:** Adding whole-body SPECT-CT images can result in a better patient management and a more precise identification of bone metastases. This technique could replace whole-body scan in the near future in selected cases. **References:** None.

EP-0327

Utility of SUV_{max}, SUV_{mean} AND SUV_{peak} values measured on baseline ^{18}F-FDG PET/CT to discriminate the high-grade from the low-grade soft tissue sarcomas

R. H. Reyes Marlés*, T. Moreno Monsalve, T. Rodríguez Locarno, J. Navarro Fernàndez, J. Puertas García-Sandoval, F. Santonja, L. Mohamed Salem, L. Frutos Esteban, J. Contreras Gutiérrez, G. Ruiz Merino, M. Claver Valderas;*
University Hospital Virgen de la Arrixaca, El Palmar, SPAIN.

Aim/Introduction: To analyze the utility of the SUV (SUV_{max}, SUV_{mean} and SUV_{peak}) values measured on a baseline ^{18}F-FDG PET/CT to discriminate between histological high-grade and low-grade soft tissue sarcomas (STS), according to the French Federation of Cancer Centers (Fédération Nationale des Centres de Lutte Contre Le Cancer, FNCLCC). **Materials and Methods:** A retrospective study was conducted in 83 patients with STS diagnosed between 2011-2018, having a baseline ^{18}F-FDG PET/CT, that employed the histological grade according to the French Federation of Cancer Centers (Fédération Nationale des Centres de Lutte Contre Le Cancer, FNCLCC). They were sorted out into two groups, high grade (grades 2 and 3) and low grade (grade 1). ROC curves were employed to evaluate the capacity of the baseline ^{18}F-FDG PET/CT SUV values to differentiate the high-grade from the low-grade lesions. **Results:** Statistical analysis using ROC curves found the following values as optimal cut-off points to discriminate high-grade from low-grade STS: -SUV_{max} 3.9 (AUC= 0.824; 95% CI = 0.717 - 0.931, sensitivity: 84%, specificity: 30%). -SUV_{mean} 2.5 (AUC= 0.798; 95% CI = 0.682 - 0.914, sensitivity: 81%, specificity: 30%). -SUV_{peak} 3.7 (AUC = 0.817; 95% CI = 0.708 - 0.926, sensitivity 81%, specificity: 30%). **Conclusion:** - The SUV_{max}, SUV_{mean}, and SUV_{peak} values measured on a baseline ^{18}F-FDG PET/CT allowed to differentiation between high-grade lesions from low-grade lesions in patients with STS. - ^{18}F-FDG PET/CT is a useful tool in the staging of patients with STS. **References:** Németh Z, Boér K, Borbély K. Advantages of (18) F FDG-PET/CT over Conventional Staging for Sarcoma Patients. Pathol Oncol Res. 2019 Jan;25(1):131-136. doi:10.1007/s12253-017-0325-0.

EP-0328

Role Of ^{18}F-FDG PET/CT In Management Of Malignant Peripheral Nerve Sheath Tumors (MPNST)

D. Yadav*, S. A. Shamim, S. Rastogi, C. Bal;*
All India Institute of Medical Sciences, New Delhi, INDIA.

Aim/Introduction: MPNST are malignant tumors arising from a peripheral nerve or in extraneural soft tissue and showing nerve sheath differentiation. They are rare and comprises about 5% of all soft tissue sarcomas. They are aggressive tumor associated with poor prognosis. 18FDG PET/CT has been used to differentiate between benign and malignant lesion in Neurofibromatosis (NF-1). The purpose of our study is to evaluate further role of 18FDG PET/CT in management of MPNST. **Materials and Methods:** We have performed a retrospective analysis to include 12 patients of MPNST who has undergone FDG PET/CT imaging for staging and restaging. Mean and maximum standardised uptake values (SUVmean, SUVmax) were measured for each primary/recurrent and metastatic lesion. For measuring the SUVmean of reference tissues, 1-cm diameter ROIs were placed on right liver lobe, aorta and left gluteal muscle, respectively. The SUVmax of PNSTs was normalised to mean liver uptake, yielding a (T/L) tumor-to-liver ratio (SUVmax Tumor/SUVmean liver). Univariate analysis was performed using the SPSS software package (version 23.0; IBM). **Results:** Twelve patients (9 males, 3 females) were enrolled in the study, out of which 3 patients (25%) of NF-1 underwent FDG PET/CT to differentiate between benign and malignant lesions. FDG PET/CT was done for staging in 5 patients, and it identified metastasis in 2 patients at baseline. Seven patients had recurrence post-surgical excision which was identified by FDG PET/CT imaging. In follow-up imaging done in 3 patients for response assessment, they had progressive disease which prompted treatment intensification. SUVmax of primary lesion showed correlation with histopathological grade (r=0.612, p=0.034). Metabolic Tumor Volume(MTV), Total lesion glycolysis (TLG) and SUVmax showed correlation with event free survival. **Conclusion:** In MPNST, FDG PET/CT can be used for staging, prognostication, restaging for recurrence and therapy response assessment, other than its already proven role in differentiating benign and malignant lesions in NF-1, predicting transformation of plexiform neurofibroma into MPNST in NF-1. **References:** 1. David Tovmassian, Muzib Abdul Razak, and Kevin London. The Role of [18F]FDG-PET/CT in Predicting Malignant Transformation of Plexiform Neurofibromas in Neurofibromatosis-1. Int J Surg Oncol. 2016; 2016: 6162182. 2. Salamon J1, Veldhoen S, Apostolova I, et al. 18F-FDG PET/CT for detection of malignant peripheral nerve sheath tumours in neurofibromatosis type 1: tumour-to-liver ratio is superior to an SUVmax cut-off. Eur Radiol. 2014 Feb;24(2):405-12.

EP-21

Clinical -> Diagnostic study -> Adult study -> Oncology study -> Organ-based oncology -> Breast, malignant

October 12 - 16, 2019 e-Poster Area

EP-0329

Prognostic Value Of F-18 FDG PET/CT In Invasive Ductal Carcinoma

S. Kang;
Catholic University of Daegu School of Medicine, Daegu, KOREA, REPUBLIC OF.

Aim/Introduction: To determine the prognostic implications of pretreatment F-18 FDG PET/CT (PET/CT) in patients with invasive ductal carcinoma (IDC), we evaluated the relationship between FDG uptake of the primary mass (pSUVmax) and known prognostic parameters of breast cancer. Prognostic significance of pSUVmax for the prediction of progression-free survival (PFS) was also assessed. **Materials and Methods:** Three-hundred eighty five female patients with IDC who underwent pretreatment PET/CT were enrolled from 2005 to 2016 year. The visual interpretation and pSUVmax of PET/CT was compared with clinicopathological parameters including ER, PR, HER2, axillary lymph node metastasis (LNM) and stage. The prognostic value of pSUVmax, for PFS was assessed using the Kaplan-Meier method. **Results:** Positive on tumor and axillary lymph node by visual interpretation of PET/CT can predict recurrence (P=0.0052, P<0.0001). pSUVmax was significantly higher in ERnegative tumors (P<0.0001), PR-negative tumors (P=0.0006), and positive LN metastasis (P=0.0001), but not different according to HER2 status. pSUVmax was significantly higher in patients with progression compared to patients who were disease-free (7.1±5.3 vs. 3.8±3.3, P<0.0001). A receiver-operating characteristic curve demonstrated a pSUVmax of 4.0 to be the optimal cutoff for predicting PFS (sensitivity; 69.4%, specificity; 66.8%). The patients with a high pSUVmax (more than 4.0) had significantly shorter PFS compared to patients with a low pSUVmax (P<0.0001). **Conclusion:** PET/ CT before treatment can be useful marker for the prediction of progression in patients with IDC. **References:** None.

EP-0330

FDG PET Findings In Invasive Ductal Carcinoma Of The Breast With And Without Coexisting DCIS

I. Sarikaya[1], *A. Sarikaya*[2], *A. Albatineh*[1], *E. Tastekin*[2], *Y. A. Sezer*[2];
[1]*Kuwait University Faculty of Medicine, Kuwait, KUWAIT,*
[2]*Trakya University Faculty of Medicine, Edirne, TURKEY.*

Aim/Introduction: Studies have reported that patients invasive ductal carcinoma (IDC) of the breast with coexisting ductal carcinoma in situ (DCIS) (IDC-DCIS) show lower metastatic potential and recurrence and better overall survival than the patients with pure IDC. In this study we further assessed F-18 fluorodeoxyglucose (FDG) positron emission tomography/computed tomography (PET/CT) images of patients with newly diagnosed IDC to determine if PET findings can predict the presence of DCIS and if there is any difference in PET findings in coexisting DCIS-positive and negative cases. **Materials and Methods:** FDG PET/CT images of patients with newly diagnosed IDC of the breast who subsequently underwent breast surgery and had histopathology result in our records were further evaluated. Tumor grade, pathological staging, presence of DCIS and its features were noted from the histopathology results. Maximum standardized uptake values (SUVmax) of the primary tumor, other hypermetabolic foci in the breast (multifocal uptake), and ipsilateral and contralateral normal appearing breast tissues were measured. Presence of axillary and distant metastases were noted. **Results:** Fifty seven (57) patients with IDC met the inclusion criteria. Histopathology showed the presence of coexisting DCIS in 44 patients (77.2 %). Coexisting DCIS was not present in 13 patients. Per histopathology, the primary tumor was unifocal in 33 DCIS-positive (75 %) and 12 DCIS-negative (92.3%) cases, and multifocal in 11 DCIS-positive cases (25 %), and 1 DCIS-negative case (7.7%). PET showed multifocal breast uptake in 20 of DCIS-positive cases (45.5 %) and 1 of DCIS-negative case (7.7%), and unifocal breast uptake (only in primary tumor) in 24 of DCIS-positive (55.5 %), and 12 of DCIS-negative (92.3%) cases. Axillary lymph node metastases were seen in all 13 DCIS-negative (100%), and 26 DCIS-positive (59%) cases. There was no significant difference in mean age, mean size of the tumor, mean SUVmax of the primary tumor, and mean SUVmax of normal breast in DCIS-positive and negative cases (p>0.05). **Conclusion:** Multifocal breast FDG uptake and multifocal tumor were more common in patients with IDC-DCIS than pure IDC. This preliminary finding may raise the question if there could be radiologically/pathologically undetected multifocal tumor in IDC-DCIS cases with unifocal tumor. **References:** None.

EP-0331

Impact of Patient Involvement on a Clinical Study: Experiences from a Study Analyzing FDG-PET/CT in Women with Advanced Breast Cancer

M. G. Hildebrandt[1,2], *M. Vogsen*[1,2], *S. Geneser*[1], *M. Rasmussen*[1], *M. Hoerder*[3], *PREMIO - Centre for Personalized Response Monitoring in Oncology;*
[1]*Odense University Hospital, Odense C, DENMARK,*
[2]*University of Southern Denmark, Odense, DENMARK,*
[3]*University of Southern Denmark, Odense C, DENMARK.*

Aim/Introduction: Patient involvement in health care research has become of increasing interest in recent years. Researchers, however, may be uncertain about the gain of involving patients in clinical studies. We aimed to evaluate the impact of patient

involvement on a clinical study of FDG-PET/CT in women with advanced breast cancer with regard to patient recruitment and change of attitude within our research team. **Materials and Methods:** Two patient representatives from the Danish Breast Cancer Organization were invited as partners of the research team. The patient partners were asked to contribute in particular to participator information as well as to evaluate ethical aspects in the study. The impact of patient involvement on patient recruitment was evaluated by comparing expected versus actual number of patients recruited, and by relating it to the patient recruitment from a previous study performed without patient involvement in a comparable patient population at the same institution from 2011-2014 (1). The expected patient recruitment in the current study has been registered at ClinicalTrials.gov (2). **Results:** The expected number of patients recruited was 135 patients per year (2). This number was based on patient recruitment in a previous study in which 33 patients were enrolled per year, only (1). Compared to this, 199 patients have been enrolled during the first year in the current study - i.e. 147 % of the expected number. Having patients as partners in the research team led to a major revision of the participator information material and the way ethical issues were addressed. An initial resistance within the research team was observed against inviting patients as partners of the team. The resistance resolved gradually during the process, and hence the most reluctant researchers from the beginning applauded the collaboration and the ideas generated by patient representatives in a later phase. **Conclusion:** Involving patients as partners in the research team resulted in major changes of the patient participator information material and had a significant, positive impact on patient recruitment for the study. Furthermore an improvement of ethical issues relevant for the patients was observed. Inviting and involving patients as partners of our research team changed the researchers' attitudes towards patient involvement in research in a positive direction. **References:** 1. Hildebrandt MG et al. [18F]Fluorodeoxyglucose (FDG)-Positron Emission Tomography (PET)/Computed Tomography (CT) in Suspected Recurrent Breast Cancer: A Prospective Comparative Study of Dual-Time-Point FDG-PET/CT, Contrast-Enhanced CT, and Bone Scintigraphy. Journal of clinical oncology. 2016;34(16):1889-97. 2. https://clinicaltrials.gov/ct2/show/NCT03358589?term=mestar&rank=1

EP-0332

Should prone ^{18}FDG- PET/CT be used to improve lymph node staging in breast cancer?

L. Sánchez Orduz[1], *M. Morales-Lozano*[2], *B. Aradas-Cabado*[3], *J. Rosales*[2], *J. Bastidas*[2], *F. Grisanti*[2], *M. Ochoa*[4], *M. Ribelles*[2], *M. Garcia-Velloso*[2], *M. Rodríguez-Fraile*[2];
[1]*SPECT medicina nuclear S.A.S, UNAB, Bucaramanga, COLOMBIA,* [2]*Department of Nuclear Medicine, Clínica Universidad de Navarra, Pamplona, SPAIN,* [3]*Department of Nuclear Medicine, Hospital Clínico Universitario de Santiago de Compostela, Santiago de Compostela, SPAIN,* [4]*Department of public health, Universidad Autónoma de Bucaramanga, Bucaramanga, COLOMBIA.*

Aim/Introduction: The aim was to compare the prone versus standard supine PET/CT acquisition for lymph node (LN) staging in patients with newly diagnosed breast cancer. **Materials and Methods:** This retrospective cohort study evaluated women with a recent diagnosis of breast cancer referred to our service for staging. All patients underwent dual time-point scans. The first acquisition was a supine whole-body scan from the head to the thighs performed 1 h after administration FDG (standard). The prone scan was perfomed with a mean delay of 25 minutes using the same breast MRI coil. The SUVmax, SUVmean, SUVmax ratio (SUVmax LN/SUVmax liver), SUVmean ratio (SUVmeanLN/SUVmean liver) at both time points in the lymph node and the retention index (prone SUVmax - standard SUVmax/standard SUVmax X100) were calculated. The final diagnosis was confirmed by pathology. **Results:** Seventy seven patients were finally included. The prevalence of confirmed lymph node involvement was 71,43%. Standard PET/CT SUVmax had excellent discriminatory power for lymph node metastasis (Sensitivity: 87,27% , Specificity: 95.45%, PPV: 98.00% NPV: 75,00%; correctly classified: 89,61% at 1,46, AUC ROC: 0,93) and also for prone PET/CT SUVmax (Sensitivity: 89,09% , Specificity: 86.36%, PPV: 94.22% NPV: 76,00%; Correctly classified: 88,31% at 1,32, AUC ROC: 0,92). Although prone PET/CT had a better sensitivity and higer SUVmax values than standard, there were not statistically significant differences in the predictive power of both standard and prone PET/CT (p=0,43). The criterion validity analysis of SUVmax ratio, SUVmean and SUVmean ratio values showed similar results and excellent discriminatory power for both standard and prone acquisitions. The absolute and percentage difference between prone and standard SUVmax, the SUVmean ratio values and the retention index showed statistically significant less discriminatory power than the standard PET/CT measurements. **Conclusion:** Although the prone PET/CT had a better sensitivity, both standard and prone PET/CT showed similar discriminatory power and criterion validity values for lymph node staging. The best diagnostic test for predicting lymph node involvement was the standard PET/CT SUVmax value, followed by prone PET/CT SUVmax value. **References:** None.

EP-0333

Should we insist on 18F-fluoride PET/CT for breast cancer patients? Review of experience and incidental findings

E. Mehdi[1], *F. Novruzov*[1], *J. Aliyev*[2], *L. Mehmetbeyli*[1], *S. Vatankha*[3];
[1]*Department of Nuclear Medicine, National Centre of Oncology, Baki, AZERBAIJAN,* [2]*Department of General Surgery, National Centre of Oncology, Baki, AZERBAIJAN,* [3]*Department of diagnostic radiology, National Centre of Oncology, Baki, AZERBAIJAN.*

Aim/Introduction: 18F sodium fluoride 18F-NaF PET/CT scan in patients with breast cancer is important in influencing clinical interpretation. Despite the numerous benefits of 18-F NaF PET/CT, it's being highly sensitive rather than specific and often cause challenges in clinical interpretation. Knowing the average uptake values for normal bone and frequency of benign skeletal

processes with influencing risk factors is important in diminishing the range of diagnostic false-positives. We provide valuable data of benign findings with 18F NaF PET/CT standardized uptake values (SUVs) seen in breast cancer patients. **Materials and Methods:** A retrospective analysis of 139 patient reports with the diagnosis of breast cancer who underwent 18F-NAF PET/CT at our EARL accredited institution between January 2019 and April 2019. All PET/CT scans were reviewed in consensus by two blinded nuclear medicine physicians. The findings were interpreted as benign if increased uptake correlated to endplates, within osteophytes and around the joints or radiological benign lesions seen on the morphologically oriented low dose CT images or follow-up magnetic resonance imaging. The maximum standardized uptake value (SUVmax) of region of interest and mean standardized uptake value (SUVmean) of bone marrows (sternum, lumbar vertebra and femur neck) were calculated per respective region. Statistical data analysis was made using SPSS Statistics and Modeler software. **Results:** The most common finding was osteophyte uptake seen in 47 patients (34%) with mean SUVmax=19.7 (SD=8.6). Facet joint uptake was in 34 patients (24%) with mean SUVmax=21.1 (SD=7.7). Endplate uptake was seen in 18 (13%) with mean SUVmax 19.2 (SD 5.5). The lowest coefficient of variation for bone marrow SUVmean was seen in lumbar vertebrae. There was negative correlation between SUVmean values of sternum and age. (r=-0.28, p=0.001). The weight was correlated significantly only with SUVmax values of knee joint uptake (r=-0.50, p=0.002) and presence of osteophyte uptake (p<0.05). **Conclusion:** Awareness of common benign findings knowledge in 18F-NAF PET/CT application is invaluable for correct diagnosis and achieves faster study interpretation time. **References:** None.

EP-0334

Comprehensive Analysis of Clinical Parameters used in Breast Cancer with F-18 FDG PET/CT Standardized Uptake Values

***E. Akgun**, O. O. Balkanay, H. B. Sayman;*
IUC Cerrahpasa Medical Faculty, Istanbul, TURKEY.

Aim/Introduction: Breast cancer (BC) is the first most common cancer in women after the skin cancer. The differentiation of molecular subtypes (MS) as well as histologic types of BC is important since they have different prognosis and response to therapy differently. In this study, we aimed to find out if there is a relationship between SUVs and moleculer subtypes of BC. **Materials and Methods:** In this retrospective study, we tried to find if SUVs obtained from 50 BC patients with different subgroups of molecular subtypes (Luminal A; Luminal B, HER2(-); Luminal B HER2(+); Triple negative/basal like) are with statistically significant difference or not. Moreover, we investigated the metabolic tumor volume (MTV) from the same PET data if it was also significantly different in between same groups. We also searched weather the maximum, mean or peak SUV differs between the histologic groups (HG) of BC such as ductal, lobular, mixed, papillary, mucinous, metaplastic, tubulary and anaplastic types or according to estrogen receptor (ER) or progesteron receptor (PR) positivity. Also the SUVs in a group of patients with lymph node metastasis (LNm) were investigated separately. The study patients divided into two groups according to Ki67 index by a subjective cutoff value of lower than 20 and equal or higher than 20 as well as according to the cerbB2 expression were also examined in terms of SUVs. Statistical analysis were made using ANOVA and students' t test by Microsoft SPSS v20.0 as appropriate. **Results:** 1. The maximum, mean and peak SUVs were found significantly different in MS (p=0.001). 2. There were no significant difference between MS in terms of MTV. (p=0.303) 3. SUVs were not found statistically significant fort he HG. 4. SUVs and MTV was not different in terms of ER or PR. 5. Maximum and peak SUVs were significantly different (p=0.004 and p=0.001 resp.), but not mean SUV (p=0.061) in patients with LNm. 6. Only maximum SUV was slightly different according to cerbB2 scores (p=0.034). 7. All SUVs were found significantly different in groups with Ki67 values lower or higher than 20, but not MTV. **Conclusion:** This extended analysis in a small number of patients with BC showed that SUVs are significantly different among MS but not in HG of BC. Additionally, there are differences of SUvs when other relevant clinical parameters of BC were individually considered. **References:** None.

EP-0335

Comparison of prone and supine 18F FDGPET parameters of locally advanced breast cancer

***E. Arslan**, T. Aksoy, T. F. Cermik;*
University Of Health And Science Istanbul Research and Training Hospital Clinic Of Nuclear Medicine, Istanbul, TURKEY.

Aim/Introduction: Prone position 18F fluorodeoxyglucose positron emission tomography/computed tomography (FDG-PET/CT) may improve the localization of the tumor, delineate the exact distance from areola which is utmost important for the surgical planning and separation of deep anatomic parts especially axillary lymph nodes. The aim of this study was to compare the PET CT metabolic and anatomic parameters by prone versus supine 18 FDG-PET in newly diagnosed breast cancer. **Materials and Methods:** Locally Institutional Review Board approved this prospective ongoing study. Total of 58 breast cancer patients whom newly diagnosed underwent both prone and supine FDG-PET/CT at the same scanning day. Two readers performed an independent review of all scans. Differences between the observers were resolved at a consensus reading session. Primary tumor SUVmax, SUV peak, SUVmean40%, MTV40%, TLG40, Thresh40, SUVmean70%, MTV70%, TLG70, and Thresh 70 values were calculated for both supine and prone positions. Also, differences between distance of primary tumor from the areola and pectoral muscle involvements and axillary lymph node status were evaluated by two interpreters. **Results:** Prone position mean primary tumor SUVmax was 11,34±6,79, supine position mean primary tumor SUVmax was 11,57±7,26. There was no significant difference

between prone to supine position primary tumor SUVmax (p: 0,549). Categorization of anatomic disease distribution has concordant between prone and supine scanning in 54 patients. Prone position; mean 40% MTV±STD:17,26±43,98 and mean 70%MTV±STD:2,04±2,83. Supine position mean40% MTV was 16,86±37,6 and mean70%MTV was 2,53±3,47. By far away prone position gives better anatomical location, exact distance from the areola and gives better visual assessment ability of pectoral muscle; as expected. In the 49 patients with breast and axillary disease, equal numbers of metastatic lymph nodes were identified on prone and supine scanning in 37 patients, whereas in the remaining 12 patients, prone scanning diagnosed in a higher number of visualized lymph nodes. **Conclusion:** Both prone and supine position FDG-PET/CT scanning gives identical information on locoregional disease distribution in Locally Advanced Breast Cancer. But prone position scanning may perform better than supine for assessing the number of metastatic lymph nodes, distance from the areola and delineation of pectoral muscle involvement. Prone position FDG-PET/CT may be useful for surgical planning in future clinical and research studies, including PET and magnetic resonance imaging (MRI) fusion applications. **References:** None.

EP-0336

Prevalence of focal incidental breast uptake on FDG-PET/CT and risk of malignancy: A Systematic Review and Meta-analysis

M. Naghavi-Behzad[1,2], *E. Aarstad*[1], *P. Nordhaug*[1], *L. Brønsro Larsen*[3], *M. Vogsen*[1,2,4], *O. Gerke*[2], *M. Grubbe Hildebrandt*[1,2];
[1]*Department of Clinical Research, University of Southern Denmark (SDU), Odense, DENMARK,* [2]*Department of Nuclear Medicine, Odense University Hospital, Odense, DENMARK,* [3]*Department of Radiology, Odense University Hospital, Odense, DENMARK,* [4]*Department of Oncology, Odense University Hospital, Odense, DENMARK.*

Aim/Introduction: FDG-PET/CT is increasingly used for oncologic and inflammatory diseases. Focal incidental FDG-uptake occurs rarely in breast tissue but has often significant consequences. This study aimed to systematically review literature regarding focal incidental breast uptake (FIBU) on FDG-PET/CT in order to yield an update on prevalence and risk of malignancy for FIBU. **Materials and Methods:** A systematic search for relevant articles published between 2012-2018 was performed through Medline, Embase, and Cochrane databases. Studies addressing detection of FIBU in patients without previous history of breast malignancy were included. The QUADAS-2 was used for quality assessment, and eligible data were pooled using a fixed-effects model. I^2 was calculated for the heterogeneity between studies. **Results:** Eight studies containing 180,002 scans were included in the systematic review. The median prevalence of FIBU for both genders was 0.52%(Range:0.18%-22.5%). Prevalence for women was mentioned separately in five studies and varied from 0.51%-23.5%. One study reporting a high prevalence was based on patients being staged for known malignancy, and the word "breast"was used in the search, which may have caused selection bias. Data from four studies (1-4) were eligible for meta-analysis; one of them was performed in a large screening population from Japan including 62,054 asymptomatic women. A high degree of heterogeneity was observed for prevalence data(I^2 of 97.5%), while moderate heterogeneity was observed for data on malignancy risk assessment(I^2 of 62.8%). The pooled prevalence of FIBU in women was 0.61%(Range:0.56-0.66%), and the pooled prevalence of malignancy of FIBUs was 38.7%(range:34.4-43.0%). The most commonly detected malignancy was invasive ductal carcinoma. **Conclusion:** FIBU occurs rarely on FDG-PET/CT although these results are dominated by a large study performed in a screening population. FIBU on FDG-PET/CT yields high risk of malignancy according to the results of published papers. Therefore, it should be considered relevant to further elucidate patients with incidentally detected FDG-uptake in breast in clinical practice. **References:** 1.Dunne,RM., et al., The role of the breast radiologist in evaluation of breast incidentalomas detected on 18-fludeoxyglucose positron emission tomography/CT.British Journal of Radiology.86(1026):20130034. 2.Lim,S., et al., Role of combined BI-RADS assessment using mammography and sonography for evaluation of incidental hypermetabolic lesions in the breast on 18F-FDG PET-CT.Acta Radiologica.54(10):1117-24. 3.Shin,KM., et al., Incidental breast lesions identified by 18F-FDG PET/CT: which clinical variables differentiate between benign and malignant breast lesions?Journal of breast cancer,2015.18(1):73-9. 4.Minamimoto,R., et al., Detection of breast cancer in an FDG-PET cancer screening program:results of a nationwide Japanese survey.Clinical breast cancer,2015.15(2):139-46.

EP-0337

Value Of Hybrid F-18 FDG PET/MRI In BIRADS 4 And 5 Breast Lesions: Preliminary Results Of An On-Going Study

L. L. Uslu[1], *R. Yılmaz*[2], *M. Velidedeoglu*[3], *O. E. Sahin*[1], *E. Akgün*[1], *S. Sager*[1], *H. B. Sayman*[1], *K. Sonmezoglu*[1];
[1]*Istanbul University-Cerrahpasa, Cerrahpasa Medical Faculty, Department of Nuclear Medicine, Istanbul, TURKEY,* [2]*Istanbul University, Istanbul Medical Faculty, Department of Radiology, Istanbul, TURKEY,* [3]*Istanbul University-Cerrahpasa, Cerrahpasa Medical Faculty, Department of General Surgery, Istanbul, TURKEY.*

Aim/Introduction: MRI is an efficient imaging modality for detection and characterization of primary breast lesions. Although it has high sensitivity in detection of malignant breast lesions it has limited specificity. Hybrid PET/MRI systems have the potential to further increase the diagnostic accuracy of MRI in primary breast lesions. The aim of our study is to compare the diagnostic value of hybrid FDG PET/MRI and MRI in patients with BIRADS 4 or 5 primary breast lesions. **Materials and Methods:** Twenty female patients with total 26 breast lesions, which were scored as BIRADS 4 or 5 using breast USG and mammography were prospectively enrolled in the study. All patients had whole-body hybrid TOF F-18 FDG PET/MRI in supine position

and additional breast PET/MRI using dedicated MRI sequences and DCE-MRI in prone position using a breast MRI-coil. Gold-standard was histopathology obtained after either tru-cut biopsy or breast surgery. Qualitative and quantitative analysis of PET data including SUVmax, SUVmean levels and BIRADS scores were recorded. Different cut-off levels for MRI were selected to calculate sensitivity and specificity of MRI: BIRADS-5 only, ≥ BIRADS-4C and ≥ BIRADS-4B. Combined PET/MRI data was evaluated according to the following criteria: All BIRADS-5 lesions and BIRADS-4 lesions with FDG uptake were scored as malignant. **Results:** Total 19 lesions were malignant and 7 lesions were benign. Mean SUVmax (8.36 versus 2.39) and SUVmean (5.12 versus 1.49) levels were significantly higher in malignant lesions compared to benign lesions (p=0.007 and p=0.008 respectively). Area under curve (AUC) for BIRADS-5, ≥ BIRADS-4C, ≥ BIRADS-4B, qualitative PET, SUVmax and SUVmean were 0.763, 0.876, 0.857, 0.759, 0.853 and 0.846 respectively. AUC for combined PET/MRI data was 0.759. Sensitivity and specificity of MRI BIRADS-5 only, ≥ BIRADS-4C and ≥ BIRADS-4B were 52.6%, 100%, 89.5%, 85.7%, 100% and 71.4%, respectively. Sensitivity and specificity of qualitative PET data and combined PET/MRI were 94.7%, 57.1%, 94.7% and 57.1%, respectively. SUVmax cut-off 2.62 has sensitivity and specificity of 84.2% and 85.7%, respectively for detection of malignant lesions. **Conclusion:** MRI is a sensitive and specific imaging modality for detection of malignant breast lesions with the highest AUC in our cohort. Combined PET/MRI for breast imaging may further increase the sensitivity of breast imaging. **References:** 1. Botsikas D et al. Eur Radiol. 2016;26:2297-307. 2. Jena A et al. Am J Roentgenol. 2017;209:662-70. 3. Pinker K et al. Clin Cancer Res. 2014;20:3540-9.

EP-0338

Added diagnostic value of FDG PET/CT in assessment of internal mammary nodal metastasis in breast cancer patients

E. El-kholy[1], *L. Khaled*[2];
[1]*Nuclear medicine unit, National cancer Institute (NCI) Cairo University, Egypt, Cairo, EGYPT,* [2]*Radiology department, Al-Azhar University, Egypt, Cairo, EGYPT.*

Aim/Introduction: to evaluate the role of FDG PET CT in detection of internal mammary nodal metastases in breast cancer patients and their prognostic value. **Materials and Methods:** Consecutive 110 female patients, mean age: 54.1±13 with pathologically proven breast cancer in whom initial (pre-operative) FDG PET/CT scan were retrospectively assessed. Internal mammary nodal lesions analysis were conducted in comparison to diagnostic CT. Pathological and clinical/radiological follow-up for 3-15 months duration served as standards of reference. **Results:** Internal mammary lymph node (LN) metastasis is reported in 10 patients (9%), their mean age was 53.6±13.8. Invasive duct carcinoma was the pathology in 9 among 10 patients. All 10 patients have epsilateral axillary nodal deposits, and 2 out of 10 have associated mediastinal nodal metastases. Only one of those patients shows distant bone metastases. The mean SUVmax value and size for evaluated internal mammary lymph nodes was 5.2 ± 2.27 and 1.3±0.17 cm (range,1-1.6 cm), respectively. The mean SUVmax of the associated primary breast tumor was 9.70 (SD, 4.4;range, 4.4-14.8). A total of 13 FDG avid internal mammary lymph nodes were detected. FDG PET CT had higher sensitivity, PPV and accuracy of 100%, 92.3%, and 38.5% versus 83.3% & 46.1%; for diagnostic CT; respectively. **Conclusion:** In an incidence of 9%, internal mammary lymph node metastasis in initial breast cancer staging is believed to be related to IDC pathology, presence of malignant axillary lymph nodes and high SUVmax of primary breast lesion. FDG PET CT seems to be superior to diagnostic CT in initial IM nodal detection with its subsequent alteration of therapy decisions and prognosis. **Key words**: FDG PET/CT, breast cancer, internal mammary, metastases. **References:** None.

EP-0339

Correlation Between Primary Breast Tumor Size And Prevalence Of Nodal And Distant Metastasis On FDG PET/CT at Initial Staging

N. Fatima[1], *M. u. Zaman*[1], *U. Zaman*[2], *A. Zaman*[2], *R. Tahseen*[3], *S. Zaman*[4];
[1]*Department of Radiology, Aga Khan University Hospital (AKUH), Karachi, PAKISTAN,* [2]*Department of Medicine, Dr Ruth Hospital,, Karachi, PAKISTAN,* [3]*Department of Radiation Oncology, Aga Khan University Hospital (AKUH), Karachi, PAKISTAN,* [4]*Dow Medical College, Dow University of Health Sciences (DUHS), Karachi, PAKISTAN.*

Aim/Introduction: patients with breast cancer, it is thought that the risk of developing metastases increases monotonically with tumor size, because the larger the cancer at diagnosis, the more cells are available to metastasize with increase disease specific mortality. Purpose of this study was to evaluate this linear relation between primary tumor size and metastases (nodal and non-nodal) using FDG PET/CT. **Materials and Methods:** We recruited 214 consecutive breast cancer patients who were referred for FDG PET/CT imaging for initial staging. Patients were categorized in to four groups based on primary tumor size (T1: ≤ 2 cm; T2: >2 cm and ≤ 5 cm; T3: > 5 cm; T4: any size involving chest wall or skin). For each group we determined ipsilateral axillary nodal, extra-axillary (including contralateral axillary) nodal, visceral and skeletal metastases seen on FDG PET/CT imaging. **Results:** 47/214 patients had T1 tumor and found to have 15% axillary, 47% extra-axillary, 68% visceral and 38% skeletal metastases. 104/214 patients had T2 tumor and found to have 21% axillary, 45% extra-axillary, 61% visceral and 37% skeletal metastases. 34/214 patients had T3 tumor and found to have 26% axillary, 47% extra-axillary, 76% visceral and 35% skeletal metastases. 29/214 patients had T4 tumor and found to have 45% axillary, 69% extra-axillary, 79% visceral and 41% skeletal metastases. On regression analysis, highest positive linear correlation was found for ipsilateral nodal metastasis (r =

0.945; significant p-value) followed by extra-axillary nodal (r = 0.772), visceral (r = 0.763) metastases. No significant correlation was found between primary tumor size and skeletal metastasis (r= 0.362). **Conclusion:** We found a linear correlation between primary tumor size and prevalence of metastases to nodes (highest for ipsilateral nodes) and viscera and favoring the conventional linear model. However, no linear correlation was found between prevalence of skeletal metastases and primary breast tumor size. **References:** None.

EP-0340

Dedicated breast PET and prone FDG PET-CT to characterise indeterminate breast lesions on MRI in patients with breast cancer

T. L. J. Wagner, C. Papagiorcopulo, D. Ghosh, C. Constantinou, C. Wickham, P. Tan, A. Malhotra;
Royal Free London NHS Trust, London, UNITED KINGDOM.

Aim/Introduction: Breast MRI in patients with breast cancer to assess extent of disease or multifocal disease can demonstrate indeterminate lesions requiring second-look ultrasound and ultrasound or MRI-guided biopsies. PET-Mammi is a hanging dedicated breast PET. Prone PET-CT is a dedicated acquisition performed with a breast-supporting device on a standard PET-CT scanner. We investigated if PET-Mammi and prone PET-CT were able to characterise these lesions further. **Materials and Methods:** Eleven patients with breast cancer and indeterminate lesions on breast MRI were included. Patients underwent prone PET-CT and PET-Mammi after injection of FDG subsequently on the same day. Patients then had second-look US, US- or MRI-guided biopsies and surgery. Imaging results were compared with biopsy and surgical pathology results. **Results:** PET-Mammi and prone PET-CT respectively identified 7/8 and 6/8 malignant index lesions that were present on MRI. Out of the 11 indeterminate lesions on breast MRI, 8 were malignant (3 x ductal carcinoma in situ, 2 x invasive ductal carcinoma (IDC), 3 x invasive lobular carcinoma (ILC)) and 3 were benign (3 fibroadenomas). PET-Mammi and prone PET-CT respectively identified 1/8 and 0/8 of the malignant lesions that were indeterminate on breast MRI. PET-Mammi and prone PET-CT identified 1/3 fibroadenomas that were indeterminate lesions on breast MRI. SUVmax was significantly inferior on prone PET-CT than on PET-Mammi, with a range of 20-58% of PET-Mammi SUVmax. One lesion that was close to the chest wall was identified on prone PET-CT but not on PET-Mammi. PET-Mammi identified two foci of malignancy that were not detected on prone PET-CT (18 mm IDC and 12 mm IDC). **Conclusion:** PET-Mammi and prone PET-CT were not able to characterise further indeterminate lesions on breast MRI. Most malignant lesions that presented as indeterminate lesions on breast MRI were not FDG-avid on PET-Mammi and PET-CT. 1/3 fibroadenoma that presented as indeterminate lesion on breast MRI was FDG-avid. **References:** None.

EP-22
Clinical -> Diagnostic study -> Adult study -> Oncology study -> Organ-based oncology -> Colorectal, malignant

October 12 - 16, 2019
e-Poster Area

EP-0341

Value of ^{18}F-FDG PET/CT metabolic parameters in patients with locally advanced rectal cancer

***L. García Zoghby**, M. Coronado Poggio, A. Obesso de Diego, A. Guzmán Cruz, D. Monachello Araujo, D. Travaglio Morales, S. Rizkallal Monzón, J. Cordero García, S. Rodado Marina, C. Lancha Hernández, C. Escabias del Pozo, C. Huerga Cabrerizo, L. Domínguez Gadea;*
Hospital Universitario La Paz, Madrid, SPAIN.

Aim/Introduction: The aim of this study was to assess the value of metabolic PET/CT parameters for predicting pathologic response in patients with locally advanced rectal cancer (LARC), undergoing neoadjuvant therapy. **Materials and Methods:** We retrospectively analyzed 29 patients (20 female, 9 male; mean age 67.6) with LARC, without metastatic disease. All patients were treated with neoadjuvant chemoradiotherapy followed by surgery, and were evaluated by ^{18}F-FDG PET/CT before neoadjuvant therapy, according to the standard protocol. Metabolic parameters such as metabolic tumor volume (MTV), total lesion glycolysis (TLG) and maximum standardized uptake value (SUVmax) were studied. Pathologic response to neoadjuvant therapy was assessed after surgery by tumor regression grade (TRG) classification by Dworak: 4 (no tumor cells), 3 (very few tumor cells), 2 (dominant fibrotic changes with few tumor cells), 1 (dominant tumor mass), 0 (no regression). We considered two different groups of patients depending on the pathologic response: "complete pathologic response" (TRG = 4) and "incomplete pathologic response" (TRG = 3 - 0). Correlation between basal PET/CT metabolic parameters and TRG was made using non-parametric tests (Kruskal-Wallis and Chi-squared test). Cut-off values of metabolic parameters were determined by receiver operating characteristic (ROC) curve analysis. Statistical significance was defined as $P < 0.05$. **Results:** We found "complete pathologic response" in 4 patients and "incomplete pathologic response" in 25 patients (TRG 3: 10 patients; TRG 2: 7 patients, TRG 1: 7 patients; TRG 0: 1 patient). Mean MTV was 12.19 cm³ (range, 3.83-26.13 cm³), mean TLG was 101 g/ml*cm³ (range, 40.54-249.96 g/ml*cm³) and mean SUVmax was 15.46 g/ml (range, 4.94-25.26 g/ml). Patients with "complete pathologic response" showed significantly lower MTV values than patients with "incomplete pathologic response" ($P = 0.023$). MTV cutoff value was 12.2 cm³ (AUC 86%). Patients with MTV < 12.2 cm³ showed better pathologic response to neoadjuvant therapy than patients with MTV > 12.2 cm³ ($P = 0.037$). We did not found significant correlation between TLG and SUVmax with TRG ($P > 0.05$). **Conclusion:** In patients with LARC, MTV in basal ^{18}F-FDG PET/CT is useful to predict pathologic response to neoadjuvant

therapy. **References:** Kim SJ, Chang S. Clin Nucl Med 2015; 40: 930-5.

EP-0342

Prognostic role of metabolic 18F-FDG PET/CT parameters and hematological prognostic indicators in patients with colorectal cancer

A. Cengiz[1], *Ö. Yersal*[2], *I. Kurt Ömürlü*[3], *Y. Yürekli*[1];
[1]*Adnan Menderes University, Faculty of Medicine, Department of Nuclear Medicine, Aydin, TURKEY,* [2]*Adnan Menderes University, Faculty of Medicine, Department of Medical Oncology, Aydin, TURKEY,* [3]*Adnan Menderes University, Faculty of Medicine, Department of Biostatistics, Aydin, TURKEY.*

Aim/Introduction: Inflammatory markers such as neutrophil to lymphocyte ratio (NLR) and platelet to lymphocyte ratio (PLR) may be prognostic biomarkers in solid tumors. Some tumor markers such as carcinoembryonic antigen (CEA), cancer antigen 19-9 (CA19-9), cancer antigen 125 (CA125) have also been used as the indicators for post-operative surveillance. The aim of this study is to evaluate the role of preoperative 18F-FDG PET/CT parameters including maximum standardized uptake value (SUVmax), metabolic tumor volume (MTV) and total lesion glycolysis (TLG) and hematologic prognostic indicators in patients with colorectal cancer (CRC) in terms of predicting prognosis. **Materials and Methods:** One hundred and one patients (35 F, 66 M) with newly diagnosed CRC and who had undergone 18F-FDG PET/CT for initial staging were evaluated retrospectively. SUVmax, SUVmean, MTV and TLG values were calculated for primary tumor. Patient data including pathologic stage at presentation, histology, tumor location (right/left colon), overall survival (OS) were analyzed. Complete hemogram analysis and serum CEA (ng/mL), CA-125 (U/mL) and CA19-9 (U/mL) levels obtained within two weeks of the PET/CT examination were used for hematological data. NLR and PLR were calculated in all patients. **Results:** 40 out of 101 patients died during the follow-up period. TNM stage, PET/CT parameters including SUVmax, MTV and TLG were found to be correlated with survival rate in univariate analysis ($p<0.05$). Although distant metastases were related with survival, LN metastases were not significantly correlated with survival time. Additionally, lesion location, histological type were not related with good prognosis. All hematological markers excluding PLR were also significantly associated with survival time. ROC analysis revealed that optimal SUVmax cutoff value for predicting survival time in patients with CRC was >17.9 (AUC=0.625; p=0.032). The calculated sensitivity and specificity values for this cutoff were 60% and 65.7%, respectively. To predict the survival time in these patients optimal MTV cutoff value was >34.29 (AUC=0.775; $p<0.001$), (sensitivity=85%, specificity=62.3%). The cutoff value for predicting survival time, optimal TLG value was >270.4 (AUC=0.790; $p<0.001$), (sensitivity=77.5%, specificity=68.9%). **Conclusion:** Preoperative 18F-FDG PET/CT metabolical parameters are useful to predict prognosis in patients with CRC. High preoperative NLR and high tumor markers were also shown to be negative independent prognostic factors in these patients. **References:** None.

EP-0343

^{18}F-FDG PET/CT And Tumor Markers In Reccurent Colorectal Cancer: Is There A Correlation?

F. Dondi[1], *D. Albano*[2], *D. Rexhep*[2], *M. Bonacina*[2], *A. Mazzoletti*[1], *E. Cerudelli*[2], *M. Gazzilli*[2], *P. Bellini*[1], *F. Bertagna*[1], *R. Giubbini*[1];
[1]*Università degli Studi di Brescia, Brescia, ITALY,*
[2]*Spedali Civili di Brescia, Brescia, ITALY.*

Aim/Introduction: Serum tumor markers (TM) are a widely accepted tool to monitor patients with previous diagnosis of colorectal cancer (CRC). ^{18}F-FDG PET/CT is increasing its utility in the evalutation of reccurent CRC. The aim of this study is to determine a possible correlation between tumor markers and semiquantitative PET/CT parameters in patients with CRC. **Materials and Methods:** We retrospectively included 72 patients (43 M, 29 F; mean age 65) who performed a total of 81 ^{18}F-FDG PET/CT scans in our department to evaluate possible reccurence of CRC after primary treatment. CEA and Ca 19.9 were collected within 3 months before or after PET/CT. PET images were evaluated visually and semiquantitatively collecting SUVmax, SUVmean, SUVbsa, SUL, MTV and TLG of the hypermetabolic lesions if present. A combination of clinical/imaging follow-up and/or histopathology was taken into account as reference standard. Chi-square test was used to correlate PET results and TM positivity or negativity. Kruskal-Wallis test was used to correlate PET results with TM values and TM positivity or negativity with semiquantitave PET parameters. ROC curve was applied to identify the best TM cutoff to determine recurrence of disease. Rank correlation was used to correlate semiquantitative PET parameters with quantitative TM values. **Results:** Among all PET/CT scans, 58 were positive (mean values: SUVmax 10,16, SUVmean 5,67, SUVbsa 2,57, SUL 7,50, MTV 32,4, TLG 312,93) and 29 were negative; after comparison with reference standard, 51 PET/TC were true positive, 20 true negative, 8 false positive and 2 false negative. Sensitivity was 96,23% (IC 87.02% to 99.54%), specificity 71,43% (51.33% to 86.78%). PPV 86,44% (77.98% to 91.99%), NPV 90,91% (71.57% to 97.54%) and accuracy 87,65% (78.47% to 93.92%). CEA values were available for 74 exams (mean values 20,84): in 52 patients were higher than normal cutoff and in 22 lower. CA19,9 values were available for 47 exams (mean values 455,9): in 21 was higher than normal cutoff while in 26 it was lower. We didn't found any correlation between all PET/CT parameters and tumor markers values or TM positivity/negativity. Applying the ROC curves analysis, we found a cutoff of 6,99 ng/mL for CEA (area under the curve 0,559) and a cutoff of 8 U/mL for Ca 19,9 (area under the curve 0,510). **Conclusion:** We demonstrated that ^{18}F-FDG PET/CT is a useful tool in the evaluation of recurrent CRC. We did not found any correlation between PET/CT parameters and tumor markers (CEA and CA19,9). **References:** None

EP-0344

Lesion size-SUVmax relationships in local recurrence and distant metastases of colorectal cancer

G. Arsos[1], *M. Lelegianni*[2], *E. Timotheadoy*[3], *E. Moralidis*[1], *V. Mpalaris*[1], *D. Katsampoukas*[1], *C. Papastergiou*[2]; [1]*3rd Dept. of Nuclear Medicine, Aristotle University of Thessaloniki School of Medicine, Papageorgiou Gen Hospital, Thessaloniki, GREECE,* [2]*Dept. of Radiology, Papageorgiou Gen Hospital, Thessaloniki, GREECE,* [3]*Dept. of Medical Oncology, Aristotle University of Thessaloniki School of Medicine, Papageorgiou Gen Hospital, Thessaloniki, GREECE.*

Aim/Introduction: 18F-FDG standardised uptake value (SUV) of the neoplastic lesions is the widely accepted measure of their glycolytic rate related (usually as SUVmax) to the malignant potential and aggressiveness of the neoplasms and its change may quantify early response to treatment. Apart from tumor type, histology and grade, known SUVmax determinants are body weight and composition and glucose blood levels, currently incorporated in modified SUV forms. Interestingly, lesion size seems to correlate with SUVmax value as has already been reported for non small cell lung cancer (NSCLC). This effect could potentially affect both malignancy SUVmax cut-off values as well as the accuracy of SUVmax changes for response to treatment assessment purposes. As evidence on this correlation in regard to local recurrence and distant metastases of colorectal cancer (CRC) is currently missing, the aim of the present study is to explore the relationship between 18F-FDG SUVmax and the size of local recurrence and distant secondary lesions in CRC patients. **Materials and Methods:** 18F-FDG-PET/CT scans of 138 adult patients with histologically proven CRC and evidence of hypermetabolic local recurrence and/or distant metastases were retrospectively analysed. Patients had been referred for 18F-FDG-PET/CT scan because of conventional imaging or biochemical suspicion of disease recurrence during the years 2016-2017. For each patient, local recurrence mass and/or the more hyperbolic (in case of multiplicity) pulmonary and/or liver lesion were analysed. For each examined lesion the SUVmax was calculated and its maximum diameter (Dmax) was measured on transverse CT slices. Correlation between Dmax and SUVmax was assessed by linear regression analysis. **Results:** Statistically significant positive linear correlation between Dmax and SUVmax was found in local recurrence mass (R^2=0.730, p less than 0.001), lung lesions (R^2=0.500, p less than 0.001).and liver lesions (R^2=0.283, p less than 0.001) **Conclusion:** Similarly to NSCLC, the size of the local recurrence mass and of the particular secondary CRC lesions, positively correlates to their SUVmax. This finding questions the accuracy of metabolic characterization of small lesions with low SUVmax in CRC and warrants further investigation. **References:** None.

Clinical -> Diagnostic study -> Adult study -> Oncology study -> Organ-based oncology -> Endocrine, malignant

October 12 - 16, 2019 e-Poster Area

EP-0345

Diagnostic Accuracy Of Somatostatin Receptor Scintigraphy In Patients With Suspected Tumor Recurrence By Increase In Chromogranin A

N. Alvarez Mena, B. Pérez López, J. Gómez Hidalgo, P. J. Turbay Eljach, C. Gamazo Laherrán, M. Alonso Rodríguez, M. A. Ruíz Gómez, M. J. González Soto, A. Sainz Esteban, R. Ruano Pérez; Hospital Clínico Universitario de Valladolid, Valladolid, SPAIN.

Aim/Introduction: To asses the diagnostic yield of Somatostatin Receptor Scintigraphy (SRS) to evaluate the possibility of recurrence of the primary neuroendocrine tumor after surgery and its relationship with levels of chromogranin A (CgA). **Materials and Methods:** Retrospective series of 51 monitored patients after neuroendocrine tumor surgery, from January 2017 to March 2019. They were classified into two groups: group A with suspicion of tumor recurrence due to increase in chromogranin A levels (36 patients) and group B with suspicion of relapse or for postoperative restaging without chromogranin A levels increased (15 patients). Variables such as age, gender, type of neuroendocrine tumor, levels of chromogranin A (CgA), scintigraphic result (SRS+/SRS-) and its concordance with CT and/or histology (H) were analyzed. **Results:** Average age 60 years (range 16-81 years); 57% women, 43% men. The primary tumors were 43 typical carcinoids, 7 atypical carcinoids, and 1 gastrinoma. **Group A** with suspicion of recurrence (CgA >100ng/ml): it was observed that in 16/36 patients (44.4%), the SRS was positive with histological confirmation (only 4 had CT before the SRS). In 19/36 patients (52.8%) the SRS was negative, of which 2 had a CT+ (small bowel carcinoid) or H+ (pulmonary carcinoid). **Group B** with suspicion of relapse or for postoperative restaging (CgA<100ng/ml): in 3/15 patients (20%) the SRS was positive (1 true positive concordant with CT+; 1 true positive not concordant with CT- but H+; and 1 false positive with CT- and H-). In 12/15 patients (80%) the SRS was negative. Only 1 of the 12 patients with SRS-, with inconclusive prior CT, had a non-concordant test with H+ (false negative). Comparing group A (CgA>100ng/ml) with group B (CgA <100ng/ml) the percentage of positivity of the SRS was 44.4% vs 20% (X^2, p <0.05). However, no differences were found in detection in patients with CgA> 500ng/ml vs CgA between 100-500ng/ml (38% vs 46%, p> 0.05). **Conclusion:** The SRS in patients with suspected tumor recurrence has a higher diagnostic yield with higher level of serum chromogranin A. In patients with CgA levels <100 ng/ml, a SRS should be avoided unless there is a morphological study that could increase the possibility of detecting the recurrence. **References:** None.

EP-0346

Comparison of ^{68}Ga DOTATOC PET/CT with morphological imaging in staging of neuroendocrine tumors

M. Finessi[1], *E. Pilati*[1], *R. Passera*[1], *V. Liberini*[1], *C. De Angelis*[2], *E. Arvat*[3], *N. Birocco*[4], *M. Brizzi*[5], *D. Campra*[6], *G. Giraudo*[6], *M. Bellò*[1], *G. Bisi*[1], *D. Deandreis*[1];
[1]*Nuclear Medicine Unit, Department of Medical Sciences, University of Turin, AOU Città della Salute e della Scienza di Torino, Turin, ITALY,* [2]*Gastroenterology Unit, Department of General and Specialist Medicine, AOU Città della Salute e della Scienza di Torino, Turin, ITALY,* [3]*Endocrine Oncology Unit, Department of Medical Sciences, University of Turin, AOU Città della Salute e della Scienza di Torino, Turin, ITALY,* [4]*Medical Oncology, Department of Medical Oncology, University of Turin, AOU Città della Salute e della Scienza di Torino, Turin, ITALY,* [5]*Medical Oncology, Department of Oncology, University of Turin, AOU San Luigi Gonzaga, Orbassano, Turin, ITALY,* [6]*Surgery Division, AOU Città della Salute e della Scienza di Torino, Turin, ITALY.*

Aim/Introduction: The aim of this study was to compare the performance of ^{68}Ga DOTATOC PET/CT in neuroendocrine tumor staging comparing to conventional imaging (CT or MRI). **Materials and Methods:** We retrospectively evaluated 35 consecutive patients that performed ^{68}Ga DOTATOC PET/CT scan from February 2017 to January 2019 for occult primary tumor detection of metastatic NET (28.6%, n=10) or for primary known tumor staging (71.4%, n=25); patient underwent CT (82.9%; n=29) and/or abdominal MRI (28.6%; n= 10). Concordance between ^{68}Ga DOTATOC PET/CT and conventional imaging (CI) was assessed and patients were divided in 3 groups both for CT and MRI: concordant PET+/CI+, discordant PET+/CI- and discordant PET-/CI+. **Results:** Among 35 patients, 40.0% presented with GEP-NET, 5.7% with lung, 28.6% with unknown site and 5.7% with other site (20.0% missing data); 40.0% had G1, 25.7% G2, and 5.7% G3 NET respectively. Of these patients 28.6% (n=10) presented with locally advanced, 31.4% (n=11) with metastatic disease (28.6% liver, 2.9% bone and 5.7% brain) at morphological imaging before PET evaluation. ^{68}Ga DOTATOC PET/CT scan was positive in 85.7% of cases (n=30/35), allowing the identification of primary lesion (T) in 71.4% of cases (n=25) including 7/10 cases of unknown primary site, lymph-nodal involvement (N) in 40.0% (n=14) and metastatic lesions (M) in 37.1% (n=13). A total of 29/35 patients underwent CT scan that was positive in 89.7% of cases allowing the identification of T in 72.4% of cases (n=21), N in 37.9% of patients (n=11) and M in 31% (n=9). MRI was positive in 10/10 patients, allowing the identification of primary lesion in 80.0% of cases (n=8), lymph-nodal and metastatic involvement in 70% of cases (n=7). Concordant findings PET+/CT+ were found in 17 patients (17 T, 5 N, 3 M); discordance PET+/CT- were found in 10 patients (4T, 2N, 5M); discordant findings PET-/CT+ were found in 4 patients (2T, 2N, 2M). Concordant findings PET+/MRI+ were found in 6 patients (6 T, 2 N, 2 M); discordant PET+/RM- in 3 patients (1T, 2N, 1M) and discordant PET-/RM+ in 2 patients (2M). **Conclusion:** Our data confirm the pivotal role of ^{68}Ga DOTATOC PET/CT in staging NETs, allowing the identification of occult primary site and unknown distant metastases. Despite CT is vastly available and MRI is preferred in case of liver metastases, ^{68}Ga DOTATOC PET should be always considered in NET patients staging. **References:** None.

EP-0347

Impact of Dual FDG and Ga68 DOTANOC PETCT on outcomes in patients with WHO Grade 2 GEP-NETs: Experience from Tertiary Care Cancer Center in India

A. Puranik*, V. Rangarajan, A. Agrawal, S. Shrikhande, V. Chaudhari, M. Bhandare, M. Bal, A. Ramaswamy, S. Shah, N. Purandare;*
Tata Memorial Centre, Mumbai, INDIA.

Aim/Introduction: WHO Grade 1 Gastro-enter-pancreatic Neuroendocrine Tumors (GEP-NETs) show high grade SSTR expression. FDG uptake is indicator of poor prognosis in tumors with Ki-67 greater than 20%. However, there is variable receptor expression seen in Grade 2 tumors which can impact management and outcome. We aimed at assessing outcome in patients with Grade 2 GEP-NETs who underwent dual imaging with FDG PET and Ga-68-DOTANOC PET/CT (DOTA PET/CT) **Materials and Methods:** Retrospective analysis of 170 patients (113 males, 57 females, age range - 47-74 years) with WHO Grade 2 (2010) GEP-NET who underwent whole body (base-skull to mid-thigh) FDG and DOTA PET/CT, between December 2014 and April 2016 was done. All 170 patients had Kennings score - 3/4 and were then referred for FDG PET. Scan positivity was based on visual score (uptake more than liver was positive scan). Patients received treatment according to decision of NET Joint-clinic as per established guidelines, and were followed up until death or till last out-patient visit upto August 2018. **Results:** Analysis was based on FDG uptake irrespective of Ki-67 values. 72/170 patients showed FDG positive scan while the rest showed negative study. Patients with FDG positive study showed poor outcome in the form of short overall survival (OS) of 8.6 months, whereas FDG negative cohort showed better outcomes, with OS not reached till the date of assessment. Other factors like age, size of primary, liver involvement were not considered. **Conclusion:** FDG PET should be performed in all Grade 2 GEP-NETs irrespective of Ki-67 values. FDG uptake, as described in the study becomes a significant determinant of prognosis and outcome in patients with somatostatin receptor-expressing WHO grade 2 GEP NET. **References:** Bucau M, Laurent-Bellue A, et al. Neuroendocrinology. 2018;106(3):274-282 18F-FDG Uptake in Well-Differentiated Neuroendocrine Tumors Correlates with Both Ki-67 and VHL Pathway Inactivation. Sampathirao N, Basu S. J Nucl Med Technol. 2017 Mar;45(1):34-41. MIB-1 Index-Stratified Assessment of Dual-Tracer PET/CT with 68Ga-DOTATATE and 18F-FDG and Multimodality Anatomic Imaging in Metastatic Neuroendocrine Tumors of Unknown Primary in a PRRT Workup Setting.

EP-0348

Pitfall upon ^{99m}Tc-EDDA/HYNIC-TOC interpretation: uterine leiomyomas

P. Valsamaki, G. Ntali, S. Michopoulos, V. Papantoniou; University General Hospital "Alexandra", Athens, GREECE.

Aim/Introduction: Somatostatin receptor (sstr) scintigraphy constitutes a sine qua non step with proven high sensitivity and specificity in the diagnostic armamentarium of neuroendocrine tumours (NET). The modality also indicates the option of targeted therapeutic "cold" or "hot" (radiolabelled) somatostatin analogue intervention. We herewith report cases of uterine leiomyoma(s) as a new pitfall upon sstr imaging interpretation. **Materials and Methods:** We present six cases of uterine leiomyomas incidentally discovered by ^{99m}Tc-EDDA/HYNIC-TOC (Tektrotyd) in women of different ages, referred due to suspected or biopsy-proven NET. Whole-body, static and tomographic imaging was conducted 75min up to 24h after injection of 740 MBq of the radiotracer. Sstr images with normal pelvic tracer distribution in women of corresponding age are presented as controls. **Results:** Regions of abnormally increased uptake in the pelvis were optically revealed by scintiscans with ^{99m}Tc-EDDA/HYNIC-TOC and semiquantitatively analyzed by using corresponding regions of interest (ROI) to estimate lesion-to-background (L/Bg) count ratio. Range of L/Bg was 1.5-2.5. Our results were co-evaluated with clinical, laboratory and other imaging findings, such as US, CT and/or MRI. Somatostatin receptors may be expressed in the uterus and in leiomyomas, irrespective of age. **Conclusion:** Our data underline the significance of this pitfall in the differential diagnosis of corresponding positive sstr scintigraphy and are compatible with limited existing literature reports. Moreover, the non-invasive identification of uterine leiomyoma(s) by sstr scintigaphy and the indicated threshold values, propounds the targeted application of somatostatin analogues in the non-invasive treatment algorithm of these benign, yet potentially irritating, disease entities. Further broader studies, both screening and follow-up, are warranted to define sstr scan sensitivity and specificity, as well as treatment effectiveness, ultimately avoiding surgical intervention. **References:** 1. Mena LM, Martin F, Jime'nez I, Ramos A. In-111 pentetreotide uptake in a uterine myoma. Clin Nucl Med. 2010;35:524-525.2. Zandieh S, Schu¨tz M, Bernt R, Zwerina J, Haller J. An incidentally found inflamed uterine myoma causing low abdominal pain, using Tc-99m-tektrotyd single photon emission computed tomography-CT hybrid imaging. Korean J Radiol. 2013;14:841-844. 3. De Leo V, La Marca A, Vegni V, Raggi CC, Maggi M, Petraglia F. Quantitative determination of sst2 and sst5 gene expression in uterine leiomyomata and the effect of treatment with somatostatin analogue. Fertil Steril. 2003;80:1058-1059. 4. Pirayesh E, Amoui M, Assadi M. ^{99m}Tc-Octreotide Uptake in the Uterus and a Subserosal Myoma Mimicking Tumoral Masses. J Nucl Med Technol 2014; 42: 77-78.

EP-0349

Relevance of different patterns of thyroid uptake of ^{18}F-fluorocholine in patients who undergo ^{18}F-fluorocholine PET/CT for detection of parathyroid disease

***E. Skorjanec Armic**, S. Rep, J. Jamsek, K. Zaletel, L. Lezaic; Department of Nuclear Medicine, University Medical Centre Ljubljana, Ljubljana, SLOVENIA.*

Aim/Introduction: Patients who undergo PET/CT with ^{18}F-fluorocholine (FCH) for detection of parathyroid disease demonstrate different patterns of thyroid uptake. The aim of the study was to determine the relevance of imaging findings and association with specific thyroid disease. **Materials and Methods:** We retrospectively analysed scans of 50 patients who underwent a dual-phase (5 min, 60 min p.i.) FCH PET/CT for detection of parathyroid disease and had a known or suspected thyroid disease (based on clinical examination, laboratory workup, ultrasound, pertechentate scintigraphy and fine needle aspiration cytology - FNAC). Patients were grouped according to thyroid pathology. The PET/CT images from the early scan were evaluated visually as well as semi-quantitatively (SUVmax) and then compared with thyroid findings. Results with $p < 0.05$ were considered statistically significant. **Results:** Euthyroid goiter: 14/28 patients had visible changes on PET (size > 2 × FWHM) with SUVmax 6.3 ± 1.8. Nine of these patients demonstrated focal uptake, while 5 had heterogeneous or homogenous uptake. Hashimoto thyroiditis: 11/13 patients showed homogenous uptake (SUVmax 7.7 ± 2.1). Graves' disease: one patient showed homogenous uptake (SUVmax 3.9). Intrinsic thyroid autonomy: out of 8 patients (2 with toxic multinodular goiter, 6 with single hyperfunctioning adenoma) 3 had diffuse and 5 had focal (2 increased and 3 decreased) patterns of uptake. Healthy euthyroid patients: 4 demonstrated homogenous uptake (average SUVmax 3.75) and 2 focal uptake (average SUVmax 6.1). Out of 14 patients with focal uptake 2 had toxic adenoma, 10 had visible nodules on imaging and 2 were healthy. Nine patients with focal uptake underwent FNAC: results showed benign lesions in 7 patients (SUVmax 4,9 - 7,3) and thyroid carcinoma in 2 patients (SUVmax 7,6 and 4,5). Specific thyroid pathologies had statistically significantly different patterns of FCH uptake (focal vs diffuse) on FCH PET/CT (chi-square $p = 0{,}000795$). Higher SUVs (One-Way ANOVA: $p = 0.006130$) were seen in patients with Hashimoto thyroiditis (homogeneous uptake) and visible nodules (focal uptake) compared to euthyroid patients. **Conclusion:** Our findings suggest that specific thyroid pathologies exhibit different patterns and intensities of FCH uptake, allowing for some inference on underlying etiology. Any focal changes or homogenous increase in uptake of FCH in the thyroid require referral to a thyroid specialist for clarification. **References:** None.

EP-0350

Spindle Cell Variant of Medullary Thyroid Cancer in Hashimoto's Thyroiditis

D. Šnajder[1], *V. Blažičević*[2];
[1]*Clinical Institute of Nuclear Medicine and Radiation Protection, Osijek, CROATIA,* [2]*Clinical Institute of Pathology and Forensic Medicine, Osijek, CROATIA.*

Aim/Introduction: Hashimoto's thyroiditis is a common autoimmune thyroid disease and often coexists with differentiated thyroid carcinomas, but the link between medullary thyroid carcinoma and Hashimoto's thyroiditis is not established, so the cases of these diseases occurring simultaneously are rare in the literature. Here we report a case of spindle cell variant of the medullary thyroid carcinoma in underlying Hashimoto's thyroiditis. **Materials and Methods:** A 65-year old female was followed up in our centre because of hypothyroidism due to thyroid autoimmune disease. On neck ultrasound after 18 years from initial diagnosis, an 11x7x9 mm hypoechoic nodule in the left thyroid lobe was found, and cytology was suggestive for spindle cell variant of medullary thyroid carcinoma. Calcitonin serum level was measured, and found elevated. **Results:** After total thyroidectomy, pathology was compatible with 10 mm spindle cell medullary thyroid carcinoma and Hashimoto's thyroiditis. Cancer cell were spindle-like formed with round to oval small nuclei with coarsely clumped chromatin. The pathological diagnosis of Hashimoto's thyroiditis was made based on islets of epithelial eosinophilic cells and extensive lymphocytic infilitrate with germinal centre formation around the tumour. **Conclusion:** Medullary thyroid carcinoma in Hashimoto's thyroiditis is rare, but must not be taken out of consideration when thinking about routine ultrasound check-ups in patients with non-nodular autoimmune thyroid disorder. **References:** None.

EP-0351

Secondary neoplastic involvement analysis in staging Neuroendocrine Tumors with PET/CT with ^{68}Ga-DOTATOC: Experience of 4 years

F. D. Kurkowski, L. M. P. Júnior, A. B. Sobrinho, R. R. Barra, G. A. Beckmann, M. M. Silva, A. S. F. Alves, A. M. Reis, B. C. Neves;
Imagens Médicas de Brasília, Brasília, BRAZIL.

Aim/Introduction: Neuroendocrine tumors (NET) are neoplasms considered rare and difficult of diagnose, which can produce symptoms that confuses with other diseases, are usually small (less than 1 centimeter) and don't have a defined risk group. They can present several organs as primary site, being the most common the gastrointestinal tract and lungs. The average time for the diagnosis is estimated between 5 to 7 years, which frequently results in the detection of associated metastasis, distant or locoregional. The purpose of this study consists in evaluating the secondary neoplastic involvement detected by the PET/CT with ^{68}Ga-DOTATOC, realized for primary staging, in a private clinic in the Federal Capital of Brazil, during a period of 4 years. **Materials and Methods:** Descriptive observational study of 499 PET/CT scans with ^{68}Ga-DOTATOC for the evaluation of NET were performed between 2015 and 2019. The exams were divided in 4 objectives: diagnosis, primary staging, follow-up and evaluation of therapeutic response. The focus of this study concerns in the evaluation of the exams requested for primary staging. **Results:** From the 499 scans, 132 (26,4%) were performed for primary staging of the disease after its histopathological diagnosis, via biopsy or surgical resection of the primary site (51%). The mean age of the patients was 54 years old (varying from 16 to 87 years) and 51% were female. The most common primary site was the rectum (26%), followed by small intestine and stomach (23% and 14%, respectively). From these patients, 25% already had findings suggestive of secondary involvement - locoregional or distant - with lymph node metastasis the most common site (present in 61% of the metastatic cases). **Conclusion:** In the early 2000s, the incidence of NET was estimated to be around 0,5% from all of the malignancies, however, nowadays, it is reported to correspond to about 2%. This rise is probably due to increase in knowledge about NETs and consequently to an earlier diagnosis. Our experience throughout these 4 years revealed metastatic involvement in 25% of the cases requested for primary staging. We can conclude the importance of early PET/CT scan with ^{68}Ga-DOTATOC to minimize the diagnosis in advanced stages of the disease. **References:** Oronsky B, PC Ma, Morgensztern D, Carter CA. Nothing But NET: A Review of Neuroendocrine Tumors and Carcinomas. Neoplasia. 2017;19(12):991-1002.

EP-0352

Do ^{68}Ga-DOTANOC PET/CT Have Incremental Value Over ^{131}I-mIBG Scintigrapy in the Management of Patients with Neuroendocrine Tumor?

J. Shukla, D. Singh, R. Walia, R. Vatsa, A. Chhabra, R. Kumar, B. R. Mittal;
Post Graduate Institute of Medical Education & Research, Chandigarh, INDIA.

Aim/Introduction: The primary aim of study was to compare diagnostic role of ^{131}I-MIBG and ^{68}Ga-DOTANOC PET/CT in NET patients. The secondary aims were to see the impact in management of patients, and association of gene mutation. **Materials and Methods:** ^{68}Ga-DOTANOC PET/CT and ^{131}I-MIBG whole body scans was performed in 106 patients (61 male, 45 female; mean age of 38.5 ± 16.2 years) of known or suspected NET. Following scans, 16 patients who were found positive for NET by histopathological examination were further evaluated for germline mutations. **Results:** ^{131}I-MIBG scans detected 41 lesions in 34 out of 106 patients with primary lesions in 29, regional lymph nodes in 2 and distant metastasis in 3 patients. However, ^{68}Ga-DOTANOC PET/CT scans detected 95 lesions in 55 patients and showed somatostatin receptor expressing lesions in 49 patients with mean SUVmax of 17.6 ± 26.5. It detected primary disease in 46, primary with regional lymph nodes in 1,

primary with distant metastasis in 3, regional lymph nodes in 1 and distant metastasis in 4 patients. The mean duration of follow up was 20.6 ± 16.5 months. Management following scans were: surgery in 35 patients, showed positive histopathology in 34 patients (^{131}I-MIBG positive in 24/34, ^{68}Ga-DOTANOC PET positive in 32/34, ^{68}Ga-DOTANOC PET/CT positive in all 34 patients) and negative histopathology in 1 patient; 177Lu-DOTATATE therapy in 2 patients and chemotherapy in 1 patient who showed metastatic disease; conservative therapy in 34 patients, no further therapy in 17 patients, 2 patients died following scans and 3 were lost to follow-up. Among 12 previously operated patients, 2 showed metastatic disease and 1 patient showed residual disease. ^{68}Ga-DOTANOC PET/CT demonstrated highest sensitivity and accuracy (Table) . The 15/16 patients underwent genotypic analysis underwent surgery; 8 patients were positive for germline mutations. Two gene mutations were detected in two patients. All these patients showed SSTR expressing lesions. Mutations in SDHB and MDH2 genes were most prevalent, followed by VHL, RET and SDHA. Deletion was observed in 1 patient in SDHB and substitution in all other mutations. Four novel mutations were observed in MDH2 (c.1005G>C, c.916G>A, c.580G>A) and SDHB (c.378_380delAAT). **Conclusion:** ^{68}Ga-DOTANOC PET/CT is better than ^{131}I-MIBG due to lower radiation exposure, decreased cost, better patient comfort, improved image quality, better diagnostic accuracy and therapy planning.^{68}Ga-DOTANOC PET/CT needs be considered as first line investigation for NET patients along with screening of germline mutations. **References:** None.

EP-0353

Impact of FDG PET/CT in directing management of well differentiated neuroendocrine tumours with Ki67 <5%

A. Agrawal, S. Choudhary, A. Puranik, V. Rangarajan, S. Shrikhande, M. Bal, V. Choudhary, M. Bhandare, A. Ramaswamy, N. Purandare, S. Shah;
Tata Memorial Hospital, Mumbai, INDIA.

Aim/Introduction: FDG PET/CT is traditionally used for staging poorly differentiated WHO grade III NET or to complement somatostatin receptor PET/CT in well differentiated NET with Ki67 ≥5%. Based on FDG positivity octreotide therapy or peptide receptor radionuclide therapy is complemented with chemotherapy in metastatic WD-NET. This study was undertaken to see the proportion of FDG PET/CT positivity in WD-NET with Ki67 ≤5% and whether it results in FDG directed management change. **Materials and Methods:** NET cases discussed in hospital multidisciplinary clinic from January 2018 to March 2019 were screened for this retrospective observational study. After going through the electronic medical records (EMR) of 207 patients, 56 patients were found to have Mib index of ≤5% and were included in the study. All these patients had dual imaging with 68Ga DOTANOC and FDG PET/CT at a fixed time point. Findings of each scan, reason for doing dual scan and whether there was a change in the management due to FDG PET/CT were noted from the EMR. **Results:** Out of 56 patients; 30 were grade I and 26 were grade 2 with Mib ≤5%. Median age was 52 years. All these were GEP NET cases. DOTANOC was positive in all patients. FDG was positive in 23 patients (41%). In rest of the 33 patients (59%) FDG was negative or weakly positive. FDG positivity changed management in only 6 patients (10.7%). In these patients, additional Capcetabine-Temozolamide chemotherapy was added. In only 10 patients (18%), there was a clear reason for doing dual scan. In 6 to decide on the need for additional chemotherapy along with PRRT and in 4 due to histological discrepancy in pathology report. In rest of the 46 patients (82%) there was no indication to do FDG PET/CT scan. **Conclusion:** Even though FDG positivity was seen in 41% of the cases, FDG directed management change was seen in relatively small number of patients. Moreover, there was no strong indication for doing dual scan in most cases. So, we recommend against routine FDG PET/CT for WD-NET with Ki67 ≤5%, and to reserve it for select few cases. **References:** None.

EP-0354

Three Cases Of Somatostatin Receptors Scintigraphy With 99mTc-Edda-Hynic-Toc Showing Exquisite Accuracy

D. De Palma, S. Casagrande, C. Gobbo, I. Schiorlin, S. Scotti;
Ospedale di Circolo, Varese, ITALY.

Aim/Introduction: Somatostatin receptor radiopharmaceuticals (SSR-RP) represent a well-established cornerstone of diagnostic evaluation of Neuroendocrine Tumors (NET). After about 30 years of 111-In labeled analogues monopoly, the radiopharmaceutical (RP) panel was enriched first with 68-Ga labeled PET RP (that need an "in house" production) and then with 99mTc- EDDA-Hynic-TOC (EHT). 68-Ga peptides availability improved with the registration of either generators and "cold" lyophilized kit, but the overall cost remains high for low-patients throughput departments. EHT is a definite step forward against Indium-labeled RP, offering better quality images with a 2/3rd lower radiation burden. Scanning 2 patients with a single kit reduces the cost, too. Its sensitivity is reported around 80-90%. Here we report 3 cases in which, in our opinion, EHT performed beyond expectations. **Materials and Methods:** We perform wholebody-addressed SPECT/CT of three patients with clinically suspect or histologically proven NET, using a Dual Head SPECT/CT equipped with a 2-slice CT (Symbia T2, Siemens), 4 hours after administration of 600 MBq of EHT. **Results:** The first was a 72-yo male with a MEN-1 syndrome, with a newly diagnosed malignant mass of the pancreatic tail and disease spread to abdominal lymphnodes and right adrenal. EHT scan showed an additional <10 mm liver lesion undetected by CT. The second was a 57-yo male with a recent removal of a malignant melanoma of the right arm and finding of two hepatic lesion and a mesenterial mass. FDG PET/CT showed uptake into liver nodules only. EHT was taken up by mesenterial and liver lesions and into an additional 11 mm-peritoneal node, not reported by CT. The third was a 66-yo male in which a NET focus was found after marsupialization of a liver cyst. The EHT scan correctly identified the primary neoplasm in the wall of the second portion

of the duodenum, together with a satellite lymphoadenopaty and a 9 mm lesion into the 6th liver segment. **Conclusion:** There are very few data in literature comparing accuracy of SPECT/CT and PET/CT SSR-RP scans against a true gold standard, and using both modalities at their best. In our cases EHT was able to pick up infracentimetric lesions also in anatomical positions in which movement artifacts or 2-slice CT reconstruction easily hampers visual analysis . EHT represents then a good option for overcoming a limited availability of 68-Ga labeled peptides. Its performance, more, is expected to improve with technologic refinement of SPECT/CT systems. **References:** None.

EP-0355

GEP neuroendocrine tumour staging: 68Ga-DOTANOC PET/CT versus conventional imaging

D. Calabro[1,2], *S. Telo*[1,2], *M. Guido*[2], *G. Argalia*[1,2], *E. Tabacchi*[1], *L. Zanoni*[1], *C. Mosconi*[3], *R. Casadei*[4], *C. Ricci*[4], *D. Campana*[4], *S. Fanti*[1,2], *V. Ambrosini*[1,2];
[1]*Nuclear Medicine, S. Orsola-Malpighi Hospital, Bologna, ITALY,* [2]*DIMES University of Bologna, Bologna, ITALY,*
[3]*Radiology, S. Orsola-Malpighi Hospital, Bologna, ITALY,*
[4]*DIMEC University of Bologna, Bologna, ITALY.*

Aim/Introduction: to assess conventional imaging (CI) and 68Ga-DOTANOC PET/CT concordance in the staging of gastroenteropancreatic (GEP) neuroendocrine neoplasm (NEN) patients(pts). **Materials and Methods:** Inclusion criteria were: i) pts' included in a CE-approved electronic archive; ii) either pathological confirmation or suspicion (on the basis of equivocal CI) of GEP-NEN; iii) CI (CT, MRI, CEUS) performed within three months of the PET/CT scan. PET/CT and CI concordance was evaluated for lesions sites and number. **Results:** Among 784 pts studied between September 2017 and March 2019, 104 performed 68Ga-DOTANOC PET/CT. Among 50 pts with confirmed GEP-NEN, in 32/50 (27 pancreas, 3 jejunum, 1 ileum, 1 stomach) CI data were available. Concordance was observed in 22/32 pts (69%): PET was positive in all but one pt (false negative for a millimetric pancreatic lesion). In the remaining 10/32 pts, PET/CT and CI were discordant. In 3/10 pts, PET/CT showed more lesions: multiple bone lesions in two pts, nodal metastasis in one pt (out of the EUS field of view). In 6/10 pts, CI showed more lesions (2/6 lymph-nodes, 2/6 pancreatic lesions (G2 and G3), 2/6 millimetric pancreatic lesions). In 1/10, PET/CT showed only one abdominal adenopathy, not reported in the CT which, on the contrary, showed multiple PET-negative splenic lesions. Of the 54 pts with suspected GEP-NEN, in 41/54 (10 ileum, 27 pancreas, 4 jejunum) CI data was available. In 23/41 pts (56%) PET/CT and CI were concordant: PET was positive in all cases and negative in one MRI-equivocal pt (pancreatic lesion, reported however more likely to be benign). In 18/41 pts (44%), PET/CT and CI were discordant. In two pts, PET/CT showed more lesions: bone lesions in one case and identified the ileal primary lesion in the other. In 16 pts, CI showed more lesions: two GIST and one pancreatic adenocarcinoma (3/16 truly negative PET/CT after histological confirmation), in 2/16 abdominal lymph-nodes, in 2/16 hepatic lesions, in 4/16 pancreatic lesions, in 2/16 ileal lesions and in 3/16 jejunum suspected lesions (however no histological confirmation was available for the latter three cases). **Conclusion:** Although recommended by current guidelines, 68Ga-DOTA PET/CT is not often performed for GEP-NEN staging. PET/CT and CI were discordant in approximately 40% of cases: PET/CT detected additional lesions mostly at bone level or outside CI field of view. Therefore, PET may provide useful information especially in pts with suspected widespread disease at first diagnosis. **References:** None.

EP-0356

18F-FDG and 68Ga-DOTANOC PET/CT imaging of lung NEN

S. Telo[1,2], *D. Calabrò*[1,2], *N. Daddi*[3], *M. Lugaresi*[3], *N. Bonazzi*[2], *G. Argalia*[1,2], *E. Tabacchi*[1], *L. Zanoni*[1], *D. Campana*[3], *S. Fanti*[1,2], *V. Ambrosini*[1,2];
[1]*Nuclear Medicine, S.Orsola Malpighi Hospital, Bologna, ITALY,* [2]*DIMES University of Bologna, Bologna, ITALY,*
[3]*DIMEC University of Bologna, Bologna, ITALY.*

Aim/Introduction: To evaluate double tracer PET/CT imaging (18F-FDG and 68Ga-DOTANOC) in pulmonary NEN patients (pts). **Materials and Methods:** Pts with confirmed pulmonary NEN who underwent 18F-FDG and 68Ga-DOTANOC PET/CT within 6 months and with clinical/imaging follow-up data were included in the study. Pts who underwent surgical or radio-chemo therapy with radical intent between the two examinations were excluded. Metabolic tumour volume (MTV) and receptor tumour volume (RTV) were evaluated with VCAR software (42% SUVmax threshold with manual adjustment when necessary) and the RTV/MTV ratio was calculated and correlated with pathology. **Results:** 26 pts were included: 16 typical carcinoids (TC), 8 atypical carcinoids (AC) and 2 large cells neuroendocrine carcinomas (LCNEC). Ki67% ranges were [1-3] for TC, [6-21] for AC and [30-60] for LCNEC. Most pts presented with local disease (18/26 pts with a single pulmonary lesion), 8/26 pts with metastatic disease (pulmonary, nodes, bone or liver). 68Ga-DOTANOC resulted true positive in 14/16 TC (SUVmax range: 2-80): 10/14 were also 18F-FDG positive (SUVmax range: 2,6-27,8). 18F-FDG and 68Ga-DOTANOC were concordant in 7/10 pts (lesions' number and site) while in 3/10 18F-FDG was falsely positive (inflammatory findings in 2 and non-NEN tumour in 1). 68Ga-DOTANOC was negative in 2/16 TC while 18F-FDG was faintly positive (uptake lower than the liver). In 5/8 AC 68Ga-DOTANOC was faintly positive: 18F-FDG showed more disease sites in 2 and the same lesions as 68Ga-DOTANOC in the remaining 3 (18F-FDG SUVmax range: 5,7-12,5). In 2/8 AC 68Ga-DOTANOC resulted positive (SUVmax: 6 and 18,3) and 18F-FDG negative. In 1/8 AC both tracers resulted positive for the same NEN lesions. Both radiopharmaceuticals were concordant and positive in the 2 LCNEC cases, although 18F-FDG uptake was higher. The RTV/MTV ratio was significantly different in TC and AC (p=0.004). The RTV/MTV ratio was>1 in 14/16 (87,5%) TC. The RTV/MTV ratio was <1 in 2/16 TC, in 8/8 AC and in 2/2 LCNECs. **Conclusion:** Despite all the limitations

of a small population, most pts presented uptake of both radiopharmaceuticals (although to a variable extent) and the RTV/MTV ratio significantly correlated with lung NEN pathology. **References:** None.

EP-0357

Added Value of ^{99m}Tc-Octreotide Scintigraphy and ^{18}F-FDG-PET/CT in Clinical Prognosis of Neuroendocrine Tumors (NET)

A. Cánoves-Llombart, I. Casáns-Tormo, H. Rodríguez-Parra, J. Sabater-Sancho, A. Amr-Rey, V. Carrero-Vásquez, M. Redal-Peña;
Nuclear Medicine, University Clinic Hospital, Valencia, SPAIN.

Aim/Introduction: In patients with NET we compare the detection of lesions with somatostatin receptors by ^{99m}Tc-octreotide planar and SPECT (with SPECT/CT fusion when possible), and metabolic activity by ^{18}F-FDG-PET/CT, and evaluate their relation with Ki-67 proliferation index, tumor differentiation, concordance and usefulness to assess disease progression. **Materials and Methods:** We retrospectively reviewed 25 patients with NET initial diagnosis, with both explorations in 75% of patients≤3months). They were excluded 10 patients by: chemotherapy between the two studies(2), no NET definitive diagnosis(3) and Ki-67 data not available(5). Finally, we analyzed 15 patients (42-75 y/o, 7 women), 10 lung NET and 5 gastroenteropancreatic. We consider well/poorly differentiated NET (based on NCCN 2017) and three groups according to Ki-67(<3%, 3-20%, >20%). Clinical follow-up after the last test: 9-35 months in 13/15 patients and <3 months in 2 patients (classified as non-evaluable (NE)). Non-progressive disease (NPD) if absence of new lesions by CT/MRI after 9 months. **Results:** 10/15 patients (66.6%) were positive with ^{99m}Tc-octreotide positive and 7/15 (46.6%) with ^{18}F-FDG, with general agreement between both tests in 12/15 patients (80%). Positive concordance (PC) in 7/15 (46.6 %), negative concordance (NC) in 5/15 (33.3%) and discordance(D) in 3/15, all of them with positive ^{99m}Tc-octreotide and negative ^{18}F-FDG. There were 5 patients with Ki-67<3%, 7 with 3-20% and 3 with >20%. In the group with Ki67<3%, 3 patients had NC (2NPD and 1NE), 1 PC(death by progression) and 1D with NPD. In the group with Ki-67 between 3-20%, 2NC with NPD, 3PC (3 progression-1 death) and 2D with NPD. Finally, in group with Ki-67>20%, 3PC: 1 progressed, 1 initial NPD but then deceased and 1 NE. Well differentiated NET(11)-poorly(4). Of the 11 well differentiated, 5NC(4 NPD and 1NE), 3PC (3 progression-2 death) and 3D(3 NPD). Of the 4 poorly differentiated, all of them where PC (2 progressed, 1 initial NPD, then deceased, and 1 NE). **Conclusion:** The general agreement between ^{99m}Tc-octreotide and ^{18}F-FDG was good. There were more NC in patients with lower Ki-67 proliferation index and with well tumoral differentiation, and more PC in patients with higher Ki-67 and poorly differentiation. However, combined assessment of both tests, especially in intermediate Ki-67 index, allows to improve the prognostic evaluation and individualizes the therapeutical decision making, although a larger number of patients must be evaluated. **References:** None.

EP-0358

The Use [18F]-DOPA-PET/CT in the Detection of Recurrence Localization in Patients with Biochemical Relapse of Medullary Thyroid Carcinoma

D. Ryzhkova;
National Almazov Medical Research Centre, St.Petersburg, RUSSIAN FEDERATION.

Aim/Introduction: The investigation of [18F]-DOPA-PET/CT diagnostic efficiency in the detection of localization of medullary thyroid carcinoma (MTC) recurrence in the patients with biochemical relapse. **Materials and Methods:** 19 patients (M:F 7:12; 43.5 years, range 30 - 71 years,) with increasing calcitonin level after total thyreoidectomy were included in the study. The median of calcitonin 2182.5 pmol/l (range: 191-18690 pmol/l) and the median of cancer embryonal antigen (CEA) 27 ng/ml (range: 5.8-164 ng/ml). All the patients underwent whole body PET/CT twice: 30 min and 60 min after administration of 300-350 MBq [18F]-DOPA. Additionally 5 patients with negative results of [18F]-DOPA PET/CT were referred to whole body [18F]-FDG PET/CT. **Results:** PET/CT with [18F]-DOPA was positive in 14 of the 19 patients. None had local recurrences of MTC. Neck and mediastinal lymph nodal involvement was observed in 9 patients. We found metastases in lung (2 patients), in liver (6 patients), and in bone (2 patients). We found the correlation between number of lesions and calcitonin (R Spearman = 0.65; p= 0.014) and CEA level (R Spearman = 0.79; p= 0.018). Moreover, we observed the relationship between SUV max and calcitonin level (R Spearman = 0.8; p= 0.005). Five patients with negative results of PET/CT with [18F]-DOPA and increasing calcitonin level [18F]-FDG PET/CT revealed metastases in lymph nodes (2 patient) and in liver (2 patient). PET/CT with [18F]-DOPA and [18F]-FDG both was negative in one patient. **Conclusion:** The results are demonstrated the usefulness of PET/CT with [18F]-DOPA in the detection of MTC recurrence in the patients with biochemical relapse. [18F]-FDG PET/CT provides with additional data in when tumor lost differentiation. **References:** None.

EP-0359

Value Of ^{99m}Tc-EDDA/HYNIC-TOC SPECT-CT Over Planar Scintigraphy In Gastroenteropancreatic Neuroendocrine Tumors

B. Luna[1], F. Cepa[1], C. Sampol[1,2], N. Orta[1,2], A. Repetto[1], M. Valiente[1], S. Rubí[1], J. Muncunill[1,2], C. Peña[1,2];
[1]Hospital Universitario Son Espases, Palma, SPAIN, [2]IdISBa, Palma, SPAIN.

Aim/Introduction: To analyze the value of SPECT-CT with ^{99m}Tc-EDDA/HYNIC-TOC vs planar scintigraphy in the initial staging and in the restaging by progression/recurrence of gastroenteropancreatic neuroendocrine tumors (GEP-NETs). **Materials and Methods:** A retrospective study of 26 patients (11women/15men; median age: 63.5 years) referred for ^{99m}Tc-EDDA/HYNIC-TOC scintigraphic evaluation in the initial staging,

and in the restaging by progression/recurrence, of GEP-NET from May 2015 to February 2019, was performed. Whole body planar scans (WBS) were acquired at 2 and 4 hours after intravenous administration of 666-740 MBq ^{99m}Tc-EDDA/HYNIC-TOC in all patients; a SPECT-CT of the abdominal region was completed after the planar study at 2 hours postinjection. The images were obtained using a double-head camera (NM/CT D670, GE). The total number of tracer deposits in the WBS and SPECT-CT was assessed. Any lesion with an uptake higher than hepatic activity was considered positive by visual analysis. The findings were correlated with the clinical, anatomopathological and/or radiological follow-up (mean: 13,38 months). **Results:** Primary NETs localization was pancreatic(13), gastric(7) and intestinal(6), 3 at small intestine and 3 at large intestine. All NETs had histological grade 1 (15) or 2 (11). Of the total number of patients, 11 were referred for initial staging and 15 patients for re-staging by progression/recurrence. Patient-based analysis showed: scintigraphy (S=69%, E=85%, PPV=82%, NPV=73% and accuracy=77%) and SPECT-CT (S=85%, E=100%, PPV=100%, NPV=87% and accuracy=92%). Lesion-based analysis showed that more lesions were detected with SPECT-CT (53) than with WBS (34). The statistical analysis showed: scintigraphy (S=92%, E=71%, PPV =82%, NPV =83% and accuracy=82%) and SPECT-CT (S=94%, E=100%, PPV =100%, NPV =91% and accuracy=96%). The group of patients referred for initial staging obtained: scintigraphy (S=67%, E=80 and accuracy =73%) and SPECT-CT (S=83%, E=100% and accuracy =91%). The group of patients referred for re-staging by progression/recurrence obtained: scintigraphy (S=71%, E=87% and accuracy =80%) and SPECT-CT (S=86%, E=100% and accuracy =93%). **Conclusion:** ^{99m}Tc-EDDA/HYNIC-TOC SPECT-CT is a reliable imaging method in the management of this type of tumors, with higher diagnostic accuracy and a higher lesion detection rate than planar imaging. In addition, it provides a better characterization and anatomical localization of lesions. **References:** None.

EP-0360

The impact of ^{99m}Tc-EDDA/HYNIC-TOC (Tektrotyd) SPECT/CT upon the clinical management of neuroendocrine tumors

G. Sipka, *Z. Besenyi, I. Farkas, A. Bakos, A. K. Augusztin, L. Pavics; University of Szeged, Department of Nuclear Medicine, Szeged, HUNGARY.*

Aim/Introduction: The somatostatin receptor (SSTR) scintigraphy is a valuable tool for neurendocrine cancers in staging and restaging. New therapeutic options become available after receptor positivity, which can serve as a curative solution. The purpose of our study was to compare the results of previous imaging studies with the Tektrotyd-SPECT/CT and establish how the obtained information influences the further treatment of patients. **Materials and Methods:** In our retrospective analysis, 51 histologically confirmed, various neuroendocrine cancer patients' (25 women, 26 male, mean age: 59 years) clinical data (CT, MRI, ultrasound, endoscopic images, histological findings, Ki-67 proliferation marker and serum chromogranin values) were compared with the Tektrotyd-SPECT/CT (Mediso AnyScan Trio) results. The average follow-up time was one and a half year (0,5-2,5 years) **Results:** The Tektrotyd-SPECT/CT was positive in 36/51 patients from a total of 257 identified tumour suspicious lesions. On the SPECT/CT 220 showed increased somatostatin receptor density. Only 197 pathological abnormalities were identified by the previous imaging studies. During the follow-up, we have seen a close correlation between the results of somatostatin receptor scintigraphy and the summarized results of subsequent studies used in the verification process (Chi-squared test, $p < 0.0001$). Most of the SSTR-positive lesions were found in the lymph nodes (70/220) and bones (76/220). The majority of SSTR-negative lesions were in the liver (19) and lung (14), while the majority of false positive cases were in the pancreas and small intestine. The Tektrotyd-SPECT/CT sensitivity was 88%, specificity was 78% and its accuracy was 84%. Based on the somatostatin receptor SPECT/CT the clinical treatment in 33 (65%) patients had changed, PRRT or other therapeutic interventions and drug modifications had been required. **Conclusion:** The Tektrotyd-SPECT/CT has high sensitivity and it makes it a suitable, easily accessible nuclear imaging method to detect neuroendocrine tumors. The treatment plan has modified in two thirds of the patients, which demonstrates the usefulness of this imaging modailty in patient care. However the relatively high number of false positive and negative lesions draw attention to the critical evaluation of Tektrotyd-SPECT/CT. **References:** None.

EP-0361

Impact of ^{68}Ga DOTATOC PET/CT in the Therapeutic Management of Neuroendocrine Tumors

E. Pilati[1], *M. Finessi*[1], *R. Passera*[1], *V. Liberini*[1], *C. G. De Angelis*[2], *E. Arvat*[3], *A. Piovesan*[3], *M. Gallo*[3], *L. Ciuffreda*[4], *N. Birocco*[4], *M. P. Brizzi*[5], *D. Campra*[6], *G. Giraudo*[7], *M. Bellò*[1], *G. Bisi*[1], *D. Deandreis*[1]; [1]*Nuclear Medicine Unit, Department of Medical Sciences, University of Turin, AOU Citta' della Salute e della Scienza di Torino, Turin, ITALY,* [2]*Gastroenterology Unit, Department of General and Specialist Medicine, University of Turin, AOU Città della Salute e della Scienza di Torino, Turin, ITALY,* [3]*Endocrine Oncology Unit, Department of Medical Sciences, University of Turin, AOU Città della Salute e della Scienza di Torino, Turin, ITALY,* [4]*Medical Oncology, Department of Medical Oncology, University of Turin, AOU Città della Salute e della Scienza di Torino, Turin, ITALY,* [5]*Medical Oncology, Department of Oncology, University of Turin, AOU San Luigi Gonzaga, Orbassano (Turin), ITALY,* [6]*4th General Surgery, Department of Surgical Sciences, University of Turin, AOU Città della Salute e della Scienza di Torino, Turin, ITALY,* [7]*1st General Surgery, Department of Surgical Sciences, University of Turin, AOU Città della Salute e della Scienza di Torino, Turin, ITALY.*

Aim/Introduction: The aim of this study was to assess the impact of ^{68}Ga DOTATOC PET/CT on therapeutic decision in patients with NETs in our multidisciplinary team. **Materials and Methods:** We retrospectively evaluated 160 consecutive

patients (91 men, 69 women) with NETs referred to our department from February 2017 to January 2019 to perform ^{68}Ga DOTATOC PET/CT scan for primary staging (n=57; 57.6%), including 10 patients for occult primary tumor evaluation, restaging (n=88; 55.0%) and follow up (n=15; 9.4%). 43/160 patients (26.9%) underwent also ^{18}F-FDG PET/CT to assess FDG avidity for high-grade NETs. The impact on therapeutic management was evaluated on the basis of multidisciplinary group PET guided decision: eligibility to locoregional therapies, indication for systemic therapies, Peptide receptor radionuclide therapy (PRRT) or association of locoregional plus systemic treatment. Median follow up after ^{68}Ga DOTATOC PET/CT was 12 months (range 1-23 months). **Results:** 53.8% of patients presented with GEP-NET, 13.1% with lung, 20.0% with other or unknown site respectively (13.1% missing data). 33.8% had G1, 34.4% G2 and 3.1% G3 NET respectively (28.8% missing data, including patients with suspected NET). 35.0% (n=56) presented with locally advanced NET and 21.9% (n=35) with metastatic disease; 55% of patients were treated with somatostatin analouges only and 16.3% received previously therapies such us chemotherapy, PRRT or interventional locoregional treatment. ^{68}Ga DOTATOC PET/CT was positive in 112/160 (70.0%) patients (38.8% primary lesion, 28.8% in lymph nodes, 36.9% in distant metastases). Among 48 patients negative to ^{68}Ga DOTATOC PET/CT scan, 5/48 were positive on ^{18}F-FDG PET/CT. ^{68}Ga DOTATOC PET/CT allowed the detection of occult primary lesion in 7/10 patients and an upstaging in 48/160 patients (30%). ^{68}Ga DOTATOC PET/CT affected the therapeutic management in 42.6% of patients (p<0.001): 30.8% were considered eligible for locoregional therapies, 44.2% sent to systemic therapies. 9.6% tp PRRT and 15.4% to locoregional plus systemic treatment. Of these 160 patients, 19 underwent to further ^{68}Ga DOTATOC PET/CT scan that was positive in 84.2% of these cohort of patients (n=16/19) and affected clinical decisions in 4 further patients. **Conclusion:** Our results from a monocentric large sample size, compared to available literature, confirm the pivotal role of ^{68}Ga DOTATOC PET/CT in the clinical management of NET patients and in the therapeutic decision of multidisciplinary team. **References:** None.

EP-0362

To assess the role of F-18 FDG PET-CT in management of adrenocortical carcinoma

N. Mohan, *S. Shamim, S. Arora, A. Passah, V. Baghel, R. Roma, S. Datta Gupta, S. Rastogi, C. S. Bal;*
All India Institute of Medical Sciences, New Delhi, INDIA.

Aim/Introduction: Adrenocortical carcinoma (ACC) is a rare endocrine neoplasm with an incidence of 1-2 per million population. Surgical resection is the mainstay of treatment, followed by adjuvant chemoradiotherapy. However, even with resection in non-metastatic patients, disease free 5-year survival is nearly 30%. Hence, post surgery restaging and surveillance is required for timely detection of residual, recurrent or metastatic disease. According to current NCCN guidelines FDG-PET/CT is not recommended for baseline evaluation or post therapy response assessment. Our objective was to evaluate the prospect of ^{18}F-FDG PET/CT in baseline staging and detection of residual and recurrent disease in ACC. **Materials and Methods:** Retrospective evaluation was done of consecutive ACC patients referred for FDG PET between Feb 2017 and April 2019. Patients were referred to our department for baseline evaluation, response to therapy or recurrent disease. Details from conventional imaging done were collected along with the reports of histopathology of biopsy or surgery specimens. PET/CT scans were visually assessed by two independent nuclear physicians. Ability of FDG-PET to detect primary, metastatic lesions and recurrence/residual disease was assessed. **Results:** In this study, data of 25 patients were analysed (8 females and 14 males) with median age of 39 years (range-2-57). All the patients were histopathologically proven cases of ACC and showed FDG positive lesions on PET-CT. Out of 25 patient, 12 patients were referred for staging and 13 for post therapy response assessment and restaging. Common sites of distant metastasis were lung, liver, abdominal wall and lymph nodes. PET/CT led to upstaging over conventional imaging in six patients, with detection of abdominal deposits and nodal metastases in three patients each. PET/CT revealed post-surgery residual disease in 4 out of 13 cases (31%) and new metastases in 7/13 (54%). Three patients with metastatic disease on chemotherapy are under follow-up with FDG PET/CT, of which one patient has shown partial response to therapy. **Conclusion:** FDG-PET/CT upstaged ACC at both baseline and post surgery in 24%, as well as detected residual disease in 31% of patients. PET was comparable to conventional imaging in detection of pulmonary and hepatic metastases and additionally detected missed abdominal wall deposits and nodes. Ability of FDG-PET in detecting new metabolically active lesions assists in restaging tumour and identifying residual disease, thereby optimizing management. **References:** Ardito A, Massaglia C, et al.18F-FDG PET/CT in the post-operative monitoring of patients with adrenocortical carcinoma. Eur J Endocrinol. 2015 Dec;173(6):749-56. doi: 10.1530/EJE-15-0707. Epub 2015 Sep 7.

EP-0363

68Ga-DOTA-exendin-4 PET/CT detects insulinomas in patients with endogenous hyperinsulinemic hypoglycemia in multiple endocrine neoplasia type 1 (MEN1)

K. Antwi[1], *G. Nicolas*[1], *M. Fani*[1], *F. Pattou*[2], *T. Heye*[1], *A. Grossman*[3], *P. Chanson*[4], *R. Jean Claude*[5], *P. Aurel*[5], *B. Gloor*[6], *D. Vogt*[1], *E. Christ*[1], *D. Wild*[1];
[1]*University Hospital Basel, Basel, SWITZERLAND,* [2]*Lille University, Lille, FRANCE,* [3]*University of Oxford, Oxford, UNITED KINGDOM,* [4]*Université Paris-Saclay, Paris, FRANCE,* [5]*University of Bern, Bern, SWITZERLAND,* [6]*University Hospital of Bern, Bern, SWITZERLAND.*

Aim/Introduction: Aim/Introduction: Surgical intervention is advised in patients with multiple endocrine neoplasia type-1 (MEN-1) with non-functioning pancreatic neuroendocrine

tumors (PanNET) and a size ≥20mm. Functioning PanNET such as patients with endogenous hyperinsulinemic hypoglycemia (EHH) due to (one or multiple) insulinomas should be treated surgically independent of size. Reliable preoperative localization of insulinomas is critical for surgical strategy. The aim is to evaluate feasibility and sensitivity of 68Ga-DOTA-exendin-4 PET/CT in the detection of relevant lesions in MEN-1 patients with EHH in comparison with magnet resonance imaging (MRI). **Materials and Methods:** Post-hoc subgroup-analysis of a larger prospective imaging study with 52 EHH patients.Six of 52 consecutive patients with EHH and genetically proven MEN-1 mutation were included. All patients received one 68Ga-DOTA-exendin-4 PET/CT and one MRI scan within 3-4 days. Thereafter, surgery was performed based on all imaging results. Lesion-based sensitivity of PET/CT and MRI were calculated. Readers were unaware of other results when reading the scans. Reference standard was surgery with histology and treatment outcome. True positive was defined as PanNET ≥20mm or insulinoma (=relevant lesions). **Results:** In six patients, 37 PanNET were confirmed by histopathology. Sensitivity (95% confidence interval) for combined PET/CT+MRI, MRI and PET/CT was 92.3% (64%-99.8%), 38.5% (13.9-68.4%) and 84.6% (54.6-98.1%), respectively (P-value=0.014 for the comparison of PET/CT+MRI versus MRI). After surgery, EHH resolved in all patients. **Conclusion:** ^{68}Ga-DOTA-exendin-4 PET/CT is feasible in MEN-1 patients with EHH. The combination with MRI is superior to MRI alone in the detection of insulinomas and may guide the surgical strategy. **References:** 1. Triponez F, Goudet P, Dosseh D, Cougard P, Bauters C, Murat A, Cadiot G, Niccoli-Sire P, Calender A, Proye CA, Group FETS. Is surgery beneficial for MEN1 patients with small (< or = 2 cm), nonfunctioning pancreaticoduodenal endocrine tumor? An analysis of 65 patients from the GTE. World J Surg. 2006;30(5):654-662; discussion 663-654. 2. Falconi M, Eriksson B, Kaltsas G, Bartsch DK, Capdevila J, Caplin M, Kos-Kudla B, Kwekkeboom D, Rindi G, Klöppel G, Reed N, Kianmanesh R, Jensen RT, participants VCC. ENETS Consensus Guidelines Update for the Management of Patients with Functional Pancreatic Neuroendocrine Tumors and Non-Functional Pancreatic Neuroendocrine Tumors. Neuroendocrinology. 2016;103(2):153-171 3. Vinik AI, Woltering EA, Warner RR, Caplin M, O'Dorisio TM, Wiseman GA, Coppola D, Go VL, (NANETS) NANTS. NANETS consensus guidelines for the diagnosis of neuroendocrine tumor. Pancreas. 2010;39(6):713-734.

EP-0364

Prognostic Validity of Dual Tracer PET/CT In The PRRT Enrollment of GEP-NET Patients

S. Pignata, *F. Minutoli, B. Catalfamo, H. Lanzafame, F. Panasiti, C. Mantarro, R. Filice, R. Laudicella, D. Cardile, S. Russo, M. Martino, S. Baldari;*
Nuclear Medicine Unit, Department of Biomedical and Dental Sciences and Morphofunctional Imaging, University of Messina, Messina, ITALY.

Aim/Introduction: To assess the ability of NET-PET-grade (1) in the prognostic stratification of gastro-entero-pancreatic-neuroendocrine-tumors (GEP-NETs) patients underwent peptide receptor radionuclide therapy (PRRT) with [^{177}Lu] DOTATOC. **Materials and Methods:** We retrospectively analyzed a series of 110 patients affected by advanced and progressive NETs who underwent PRRT at our department. Among them, 31 patients (M:F=18:13, median age 61 years, range 35-80) affected by advanced and progressive GEP-NETs underwent ^{18}F-FDG-PET/CT and ^{68}Ga-DOTATOC-PET/CT imaging within 31 days of each other. The patients have been divided into three groups, according to the WHO2010 classification: 1) G1 (proliferation index Ki67<3%): 16,1%, 2) G2 (Ki67 3-20%): 67,8%, 3) G3 (Ki67>20%) 16,1%. NET-PET-grade was applied to perform risk stratification for malignancies. **Results:** Taking as reference the NET-PET-grade stratification criteria, we classified patients in several prognostic groups, from P1 to P5, based on ^{68}Ga-DOTATOC and ^{18}F-FDG uptake. Among 31 patients, 12 had P1 grade (3/12 G1 e 9/12 G2), 5 had P2a grade (1/5 G1, 2/5 G2, 2/5 G3), 6 had P2b grade (1/6 G1, 3/6 G2, 2/6 G3), 4 had P3a grade (3/4 G2 e 1/4 G3), 2 had P3b grade (2 G2), 1 had P4a grade (1 G2), 0 had P4b grade and 1 had P5 grade (G2 with Ki67=12%). Within follow-up (median, 30 months; range 9 to 59), 5 G1 patients (P1-P2b) had Stable Disease (SD); while only one had a progression of the disease (PD) after 36 months. Among 21 G2 GEP-NETs patients, a heterogeneous response was registered. At a median observation time of 19 months (range 6-76), the best clinical responses were CR in 3 patients (14,2%), PR in 7 patients (33,3%), SD in 5 patients (24%) and PD in 6 patients (28,5%). The three patients with CR had NET-PET-grade p1 (Ki67=3%), p3a (Ki67=15%) and p3b (ki67=3%), while the only one patients p5 showed PD. In PD patients group, p1 patients had PFS ranging between 13-25 months, while the p3b patient had a shorter PFS. p1 patients with the best clinical response (CR+PR+SD) had a long follow-up (median, 27 months; range 12-76). All the G3 patients had a favorable NET-PET-grade-pattern (P2a-P3a). The clinical responses registered 1 CR, 3 SD, and 1 PD. **Conclusion:** Our preliminary results suggest that NET-PET-grade can be used for the prognostic stratification of GEP-NETs patients. **References:** 1) Chan DLH et al. Dual Somatostatin Receptor/FDG PET/CT Imaging in Metastatic Neuroendocrine Tumours: Proposal for a Novel Grading Scheme with Prognostic Significance. Theranostics.2017; 7(5):1149-1158.

EP-0365

68Ga-DOTANOC PET/CT: Qclear or not Qclear...that is the question..preliminary results in neuroendocrine patients

D. Calabro'[1,2], *S. Telo*[1,2], *S. Civollani*[3], *M. Lugaresi*[4], *E. Tabacchi*[1], *L. Zanoni*[1], *C. Pettinato*[3], *D. Campana*[4], *S. Fanti*[1,2], *V. Ambrosini*[1,2];
[1]*Nuclear Medicine, S. Orsola-Malpighi Hospital, Bologna, ITALY,* [2]*DIMES University of Bologna, Bologna, ITALY,* [3]*Medical Physics Unit, Radiology Unit, S.Orsola-Malpighi Hospital, Bologna, ITALY,* [4]*DIMEC University of Bologna, Bologna, ITALY.*

Aim/Introduction: to evaluate 68Ga-DOTANOC PET/TC with Qclear reconstruction compared to the standard reconstruction

(OSEM TOF+PSF) in neuroendocrine tumour patients. **Materials and Methods:** among the patients included in a CE-approved electronic archive, 68Ga-DOTANOC PET/CT scans acquired on DMI tomograph (GE Healthcare) between February and April 2019 were reconstructed with OSEM TOF+PSF (OSEM), Qclear with both beta800 and beta1000 values. Images were independently reviewed by five trained nuclear medicine physicians using Advantage Workstation (GE Healthcare). Images were assessed visually (lesions' number and image noise) and semiquantitevely, comparing mean and maximum OSEM SUV and Qclear SUV (QSUV) respectively for the liver background and the hottest lesion. **Results:** 24 68Ga-DOTANOC PET/TC scans of 24 pts were included. No statistical difference was found between healthy liver SUVmean and QSUVmean either with b800 and b1000 (p = 0.993). On a lesion number analysis, in 6/15 cases, PET/CT reconstructed with Qclear showed more positive areas than OSEM reconstruction (4/6 liver, 1/6 bone, 1/6 lymph nodes, 2/6 intestine). In 3/6, conventional imaging (ceCT), acquired within one month of the PET/CT scan, confirmed the presence of the supernumerary lesions (all millimetric in size). Based on visual analysis, all the nuclear medicine physicians agreed that Qclear b1000 reconstructed images were the easiest to read, showing less background noise. In 15/24 patients, PET/CT was positive. Although QSUV values of the hottest lesion showed a trend to increase compared to OSEM (delta OSEM vs 800Qclear: mean=17.6±17.1 [1.2 to 59.5%]; delta OSEM vs 1000Qclear: mean=11.3±14.4 [-4.2 to 42%]) no significant statistical differences were found between the hottest lesion SUVmax, QSUVmax b800 and QSUVmax b1000 and between QSUVmax b800 and b1000 (respectively p=0.702 and p=0.678). **Conclusion:** Although the analysis included a small sample, Qclear reconstructed images were the easiest to read, showing less background noise (especially the beta1000), resulting in the highest lesions detectability. Further studies are needed to assess the differences in SUV in CT-evident small lesions and to assess to what extent and clinical settings the higher lesions' number impacts the prognosis. **References:** None.

EP-23

Clinical -> Diagnostic study -> Adult study -> Oncology study -> Organ-based oncology -> Gynaecological, malignant

October 12 - 16, 2019 e-Poster Area

EP-0366

Prognostic role of early FDG-PET/CT in locally advanced cervical carcinoma patients (LACC): preliminary results

A. Di Paolo[1], *L. Carideo*[1], *A. Saccomanno*[1], *D. Anzellini*[2], *V. De Sanctis*[2], *P. Pizzichini*[1], *T. Lanzolla*[1], *G. Capriotti*[1], *A. Signore*[1], *D. Prosperi*[1];
[1]*Nuclear Medicine Department, Osp S. Andrea, Sapienza University, Rome, ITALY,* [2]*Radiotherapy Department, Osp S. Andrea, Sapienza University, Rome, ITALY.*

Aim/Introduction: To evaluate in patients with LACC the prognostic impact of FDG-PET/CT (early-PET) after exclusive chemoradiotherapy (CRT) and before intra-uterine brachitherapy. **Materials and Methods:** We included 24 pts with LACC (range 29-82 years) that referred to our institution between 2013 and 2019. Pts were treated with concomitant CRT and subsequent brachytherapy. FIGO STAGE: 1/24 was IB1, 3/24 were IIA, 14/24 IIB, 4/24 IIIB and 2/24 IVA. 10/24 pts had regional lymph node involvement and 1 pt had also positive lombo-aortic lymph nodes. 19/24 pts underwent radiotherapy and concomitant weekly chemotherapy with Cisplatin (40mg/mq2), 3 pts received also neoadjuvant chemotherapy and 2 patients only radiotherapy. 14/24 pts were treated with IMRT tecnique and 10 of them received IMRT-SIB (2.2 Gy x 28 fractions on GTV-cervix and GTV-LNs PET-positive, 1.8 Gy x 28 fraction on pelvis ± LN lombo-aortics). The total brachytherapy dose was 21 or 28 Gy in 3-4 fractions, 7 Gy per fraction, with the aim to obtain a total dose (EBRT plus BT) in the range of 85-90 Gy (6 pt 28 Gy, 2 pt 25 Gy, 16 pt 21 Gy). All pts performed FDG-PET/CT after CRT and before brachytherapy (early-PET). PET images were rated as positive when there was focal uptake with a SUV max >3. **Results:** At the end of CRT and before brachitherapy all pts performed early-PET: 18/24 were negative and 6/24 positive. 2/18 (11.1%) pts with negative early-PET showed a relapse: 1 pelvic nodal relapse after 15 months and 1 cervical, annexial and nodal relapse after 5 months from the end of brachytherapy. 3/6 pts (50%) with positive early PET-TC had progressive/relapse disease: 2 pts showed systemic (lung-heart) progressive disease after respectively 3-4 months and 1 pt showed nodal, cervical and bone relapse after 18 months from the end of brachytherapy. **Conclusion:** Our preliminary evaluation showed that early-PET before brachytherapy could have a predictive value in assessing the risk of recurrence/progression in LACC pts. Pts with positive early-PET at the end of CRT may benefit from adjuvant systemic treatment after brachytherapy. **References:** None.

EP-0367

Metabolic tumor parameters in F18- FDG PET/CT as a reliable predictor on overall survival in patients with cervical carcinoma

B. Pernthaler[1], *T. Nazerani Hooshmand*[1], *C. Gstettner*[1], *S. A. Herzog*[2], *R. M. Aigner*[1];
[1]*Medical University of Graz, Department of Radiology, Division of Nuclear Medicine, Graz, AUSTRIA,* [2]*Medical University of Graz, Department of Medical Informatics, Statistic and Documentation, Graz, AUSTRIA.*

Aim/Introduction: Determining the prognostic value of the metabolic tumor parameters, Metabolic Tumor Volume (MTV) and Total Lesion Glycolysis (TLG) in F18- FDG PET/CT in women with confirmed histopathological cervical carcinoma, as a predictor of treatment outcome and survival. **Materials and Methods:** In this retrospective study, January 2006 to July 2015, 69 women with cervical carcinoma were enrolled in our study. Age at the time of first manifestation, histopathology, SUV max

(Standardized Uptake Volume), SUV mean, MTV and TLG (SUV mean x MTV) were the parameters included to determine their impact on overall survival using Cox-Regression-Analysis. The extracted data of MTV and TLG were measured by receiver operating characteristic (ROC) curve. **Results:** Distant metastases were observed in 14 out of 69 patients (20,3%) with a mean age of 53,7 years old(SD ±16,4). The median follow up period was 1.5 years, in which 31,9% died due to the cancer. In the univariate Cox-Regression-Analysis show that age [> 60, HR 2.97; 95% CI 1.28 to 6.89; p = 0.011], MTV [HR 3.89; 95% CI 1.51 to 10.03; p = 0.005] and TLG [HR 3.25; 95% CI 1.35 to 7.81; p = 0.008] have an impact on overall survival of this series of patients , meanwhile no significant correlation between overall survival for metastasis, histology, SUV mean and SUV max was seen. **Conclusion:** Metabolic parameters MTV, TLG and age at the first manifestation of the disease correlated significantly with overall survival in women with cervical carcinoma underwent F18-FDG PET/CT. **References:** None.

EP-0368

^{18}F-FDG PET/CT in the assessment of suspected recurrence in ovarian cancer

P. García-Talavera San Miguel[1], *E. Alejo*[2], *S. Yañez*[3], *A. Verdú*[3], *P. Arias*[3], *A. C. Peñaherrera*[1], *J. C. Cañadas*[1], *M. E. Martín*[1], *P. Tamayo*[1]; [1]*Nuclear Medicine Department. Hospital Clinico Universitario de Salamanca, Salamanca, SPAIN,* [2]*Universidad de Salamanca, Salamanca, SPAIN,* [3]*Radiology Department. Hospital Clinico Universitario de Salamanca, Salamanca, SPAIN.*

Aim/Introduction: To evaluate the role of ^{18}F-FDG PET/CT in the re-staging of potentially resectable ovarian cancer recurrence, as well as in the clinically or biochemically suspected recurrence with negative or doubtful imaging techniques. **Materials and Methods:** Thirty patients were included; in 6 out of them, two PET/CT scans, at two different times, were acquired: 19 cases for re-staging and 17 for suspected recurrence. Histology: serous (27), endometrioid (2) and clear cells (1). Staging: I (5), II (2), III (17) and IV (6). Intravenous contrast CT (cCT) and PET/CT results were compared (maximum time interval between techniques: 1 month). Results were confirmed by means of radiological follow-up or histology. Spearman correlation was utilized to evaluate the association between size, number and uptake (SUVmax) of the lesions and tumor markers. ROC curve to calculate the optimal cut-off value of SUVmax for overall survival prediction was conducted. Survival analysis by means of Kaplan-Meier method was performed. **Results:** Twelve out of 36 PET/CT and cCT were concordant (33%): 11 positives (30 lesions). In one case both techniques were negative. In non concordant cases (24 cases; 67%) PET was positive in 19 and cCT in 21. In this group, PET detected 97 lesions and cCT 59. Out of them, 46 lesions were concordant (54.3%) and 64 non concordant (45.7%). In total, cCT detected 89 lesions and PET 127. Out of 89 lesions, 80 were confirmed (9 FP and 50 FN). Out of 127, all were confirmed (4 FN). Lesion detection rate was 96.9% for PET and 61% for cCT. There was no statistically significant correlation between tumor markers and number, size or SUVmax of the lesions. PET/CT modified the therapeutic management in 15 patients, with respect to cCT. In survival analysis, log-rank test shows statistically significant differences in patients with SUVmax > 11.8 (26.5 ± 4.6 months) and the group with SUVmax < 11.8 (36.2 ± 1.0 months). Incidental findings of PET-CT: invasive ductal carcinoma of the breast and intestinal diffuse large B cell lymphoma. **Conclusion:** ^{18}F-FDG PET/CT plays an important role in doubtful cases of suspected recurrence in ovarian cancer as well as in the re-staging of confirmed recurrence, with a detection rate for PET/CT of 96.9% vs 61% for cCT. PET/CT modified therapeutic management up to 41.7% of the cases and localized, furthermore, synchronic tumors in 6.7% of cases. Moreover, SUVmax could be a potential tool for prognosis prediction. **References:** None.

EP-0369

Dual Time FDG-PET versus Pelvic MRI in post-treatment evaluation of cervical cancer patients after chemoradiotherapy

A. Repetto, C. Sampol, N. Orta, H. Navalon, M. Valiente, S. Rubi, C. Peña;
Unversitary Hospital Son Espases - Nuclear Medicine Department, Palma de Mallorca, SPAIN.

Aim/Introduction: The aim of the study was to compare Dual Time FDG-PET and pelvic MRI findings in the evaluation of advanced cervical cancer. **Materials and Methods:** Prospective descriptive study from June 2017 to March 2019 of 18 women with locally advanced cervical cancer treated with radical chemoradiotherapy. Each patient had pelvic MRI and FDG-PET as imaging evaluation of post-treatment response realized at minimum 3 month after completed the treatment. We compared pelvic MRI with pelvic findings of FDG-PET and pelvic MRI with whole body findings of FDG-PET. We used SUV lean body mass as semicuantitative parameter. SUV of the lesions was calculated both in early (1 hour) and delayed scan (>2 hours) and a Retention Index % was obtained.The results of the images were classified in positive (partial response, progression, relapse) or negative (complete response, inflammatory changes).The final diagnosis was based on histopathology results (biopsy or cytology) and clinical data.The mean time of follow up pf patients was 11 months (4 - 21 months). **Results:** 18 women (mean age of 58 years old) with advanced cervical cancer were treated with radical chemoradiotherapy. At the diagnosis the most frequent histological subtype was squamous carcinoma (88%) and the FIGO stage varied from IB3 to IVA.Image studies were performed during an average of 3 months for both MRI and FDG-PET.On the base of final diagnosis, pelvic MRI had a Sensitivity of 67%, Specificity of 50%, VPP 22% and VPN of 87%. Pelvic Dual Time FDG-PET had Sensitivity of 33%, Specificity of 100%, VPP 100% and VPN of 88%. Whole body Dual Time FDG-PET had Sensitivity of 100%, Specificity of 93%, VPP 75% and VPN of 100%. The Retention Index values were divided into 3 categories of findings: negative if < -10%; indeterminate (from -10% to +10%);

positive > 10%, according to the interpretation of the FDG-PET. In the follow up of patients we observed a 30% of relapse in the negative group, 33% of relapse in the indeterminate one and 100% of death in the positive group. **Conclusion:** FDG-PET has higher Sensibility and Specificity than pelvic MRI.Retention Index in Dual Time FDG-PET could be a predictive factor of long term follow up response. Further investigations are needed to determine its role in clinical practice. **References:** None.

EP-24

Clinical -> Diagnostic study -> Adult study -> Oncology study -> Organ-based oncology -> Head and neck, malignant

October 12 - 16, 2019 e-Poster Area

EP-0370

18F-FDG PET/CT-based Nomogram for Predicting Individual Conditional Risk of 5-Year Recurrence before Initial Treatment of Nasopharyngeal Carcinoma

B. Gu[1,2,3], G. Ma[1,2,3], J. Zhang[1,2,3], Z. Yang[1,2,3], S. Song[1,2,3], Y. Zhang[1,2,3]; [1]Department of Nuclear Medicine, Fudan University Shanghai Cancer Center, Shanghai, CHINA, [2]Center for Biomedical Imaging, Fudan University, Shanghai, CHINA, [3]Shanghai Engineering Research Center of Molecular Imaging Probes, Shanghai, CHINA.

Aim/Introduction: To determine the value of intratumoral heterogeneity derived from ^{18}F-FDG PET/CT in long-term treatment outcome prediction in patients with primary nasopharyngeal carcinoma (NPC) and build a prognostic nomogram model for risk stratifications. **Materials and Methods:** A total of 171 primary NPC patients who underwent ^{18}F-FDG PET/CT before treatment were retrospectively enrolled. Data was randomly divided into training cohort (n=101) and validation cohort (n=70). The following PET parameters were analyzed: maximum and mean of standardized uptake value (SUVmax, SUVmean), metabolic tumor volume (MTV), total lesion glycolysis (TLG), and heterogeneity index (HI) for primary tumor and maximal neck lymph node using the absolute SUV threshold of 2.5 and relative SUVmax threshold of 70%. Cox analyses were performed on PFS in the training cohort (n=101). A prognostic nomogram based on this model was developed and validated. **Results:** The 5-year PFS rate for training and validation cohort were 79.21% and 68.57%, respectively. For the primary tumor, MTV and TLG with absolute SUV threshold of 2.5 and relative SUVmax threshold of 70% were significantly correlated with PFS. For the maximal neck lymph node, short diameter and HI were significantly correlated with PFS. Among the clinicopathologic parameters, M stage was significant prognostic factor for recurrence. In multivariate analysis, M stage (HR, 6.44; 95% CI, 1.72-24.08; P=0.006), TLG of the tumor with a relative threshold of 70% (HR, 1.02; 95% CI, 1.01-1.04; P=0.002), HI of the maximal neck lymph node (HR, 3.23; 95% CI, 1.22-8.54; P=0.018) were independent predictors. Based on this prognostic model (C-index, 0.74; 95% CI, 0.63-0.85), a nomogram was generated. For the cross validation, the C-index for this model was 0.73 (95% CI, 0.62-0.83) with the validation cohort. Three risk groups (high risk, intermediate risk, and low risk) were created based on this nomogram. Patients with a risk score of ≥111 had poorer survival outcomes than those with a risk score of 0-76 and 77-110. **Conclusion:** Intratumoral heterogeneity derived from ^{18}F-FDG PET/CT can predict long-term outcome in patients with primary NPC. A combination of PET parameters and the TNM stage enables better stratification of patients into subgroups with different PFS rates. **References:** None.

EP-0371

Clinical and prognostic value of staging ^{18}F-FDG PET/CT in laryngeal cancer

***D. Albano**, M. Bonacina, R. Durmo, E. Cerudelli, M. Gazzilli, F. Dondi, A. Mazzoletti, P. Bellini, F. Bertagna, R. Giubbini;*
Spedali Civili Brescia, Brescia, ITALY.

Aim/Introduction: Laryngeal carcinoma is one of the most common head and neck cancer with a high risk of relapse and death and seems to be crucial to stage accurately and assess prognostic features. The aim of this study was to investigate the diagnostic accuracy of 18F-FDG-PET/CT in laryngeal cancer and compared these results with conventional imaging (CI). The second point was to assess the value of preoperative 18F-FDG-PET/CT features to predict outcome survival. **Materials and Methods:** Fifty-four patients with histologically proven squamous cell laryngeal cancer were retrospectively enrolled; all patients underwent baseline 18F-FDG-PET/CT before any treatment. CI, as CT and MRI, was available for 49 patients. The PET images were analyzed visually and semi-quantitatively by measuring SUVbw, SUVlbm, SUVbsa, MTV and TLG of primary tumor (T) and total MTV (MTV total) and total TLG (TLG total). A combination of clinical follow-up/imaging follow-up and/or histopathology (when available) was taken as reference standard. PFS and OS were computed using Kaplan-Meier curves. **Results:** All primary tumours were clearly identified by CI, while 52 of 54 were recognized by 18F-FDG PET/CT with a sensitivity of 96.3%. Cervical nodal metastases were detected in 40/54 patients at 18F-FDG PET/CT and in 34/49 patients at CI. Sensitivity, specificity, positive predictive value, negative predictive value, and accuracy on a patient-based analysis for nodal disease were 100%, 86%, 95%, 100% and 96% at 18F-FDG-PET/CT, and 91%, 86%, 94%, 80%, 90% at CI with a better diagnostic performances of PET/CT. Instead diagnostic performances of PET/CT and CI were not significantly different on a side-by-side and level-by-level analysis. 18F-FDG-PET/CT recognized distant metastases in 7 patients allowing to upstage them. At a median follow-up of 27 months (range 4-75 months), relapse/progression of disease occurred in 31 patients with a mean time of 16.1 months and death occurred in 32 patients with a mean time of 38.25 months. The median PFS was 17.5 months and the median OS was 27 months. At

multivariate analysis, MTV T, MTV tot and TLG tot showed to be independent prognostic factors for PFS (p=0.002, p=0.001 and p=0.002). **Conclusion:** Both CI and PET/CT had good diagnostic performances for the staging of laryngeal cancer and baseline metabolic tumour features (MTV and TLG) showed an important prognostic value in assessing the rate of PFS. **References:** None.

EP-0372

[^{18}F]-Fluorodeoxyglucose PET/CT in predicting PD-L1 status in nasopharyngeal carcinoma

L. Zhao[1], *H. Chen*[1], *K. Fu*[1], *D. Fan*[2], *H. Wu*[1], *Y. Zhuang*[1], *Q. Lin*[3];
[1]*The First affiliated hospital of Xiamen University, Xiamen, CHINA,* [2]*Beijing Tiantan Hospital, Bejing, CHINA,* [3]*Xiamen Cancer hospital, The First affiliated hospital of Xiamen University, Teaching hospital of Fujian Medical University, Xiamen, CHINA.*

Aim/Introduction: Immunotherapy that blocks the PD-1/PD-L1 checkpoint pathway has shown promising antitumor activity in several phase I-II clinical trials of advanced nasopharyngeal carcinoma (NPC). Being the most wildly used molecular imaging in clinic, ^{18}F-FDG PET/CT provides multiple information of tumor biology. In this study, we aimed to investigate the association of PD-L1 expression with ^{18}F-FDG uptake and clinical features in patients with NPC. **Materials and Methods:** A total of 84 patients were initially histopathologically diagnosed with NPC between December 2016 and March 2019. All tissue specimens and PET/CT images were collected before any treatment. The PD-L1 antibody we used in this investigation was SP263 (Ventana, USA), which was the Blueprint PD-L1 IHC Assay Comparison Project recommended. High PD-L1 expression in tumor cells (TC) or tumor-infiltrating immune cells (TIIC) was defined as ≥50% of corresponding cells with membranous staining. **Results:** The values of tumor SUVmax and TLG in patients with positive TC PD-L1 expression were significantly higher than those of negative TC PD-L1 expression (SUVmax: 10.3±4.1 vs. 6.9±3.2; P < 0.001; TLG: 77.7±64.5 vs. 35.0±20.5; P < 0.001), whereas the SUVmax values and TLG in patients with positive TIIC PD-L1 expression is lower than those of negative TIIC PD-L1 expression (SUVmax: 7.0±3.4 vs. 9.7±4.1; P= 0.011; TLG: 29.1±14.4 vs. 71.3±61.2; P= 0.001). Univariate analysis showed that the expression of PD-L1 in TC was associated with tumor T stage (P= 0.044) but not with serum Epstein-Barr virus (EBV) load (P= 0.816). On the other hand, the expression of PD-L1 in TIIC was related to both T stage (P= 0.028) and serum EBV load (P= 0.003). In multivariate logistic regression analysis, PD-L1 expression in TC was positively associated with tumor SUVmax (P= 0.003) and TLG (P = 0.001), while PD-L1 expression in TIIC was negatively associated with SUVmax (P = 0.038) and serum EBV load (P=0.025). Through the ROC curve, the SUVmax cut-off value of 6.7 and the TLG cut-off value of 41.3 can be used to predict the PD-L1 status in TC with an accuracy of 78.6% and 71.4%, while the SUVmax cut-off value of 7.2 can be used to predict the PD-L1 status in TIIC with an accuracy of 72.6%. **Conclusion:** ^{18}F-FDG uptake within NPC lesions were positively correlated with PD-L1 expression in TC and negatively correlated with PD-L1 expression in TIIC. ^{18}F-FDG PET / CT imaging may be useful for predicting the PD-L1 status in patients with NPC. **References:** None.

EP-0373

FDG uptake in the mylohyoid muscle - a common misconception

D. Pizzuto[1], *P. Stolzmann*[1], *L. Husmann*[1], *E. Orita*[1], *C. Meerwein*[2], *G. K. von Schulthess*[1], *M. W. Huellner*[1];
[1]*Department of Nuclear Medicine, University Hospital Zurich, University of Zurich, Zurich, SWITZERLAND,* [2]*Department of Otorhinolaryngology, Head & Neck Surgery, University Hospital Zurich, University of Zurich, Zurich, SWITZERLAND.*

Aim/Introduction: The mylohyoid muscle is often believed to exhibit high physiologic FDG uptake [1,2]. The aim of this study was to use PET/MR for adequately assessing the normal FDG distribution in floor of mouth (FOM) muscles and neighboring major salivary glands (SG). **Materials and Methods:** Patients scanned with a simultaneous FDG PET/MRI system in our hospital for initial staging or follow-up of HN tumors were included. Patients with malignant lesions in SG or in FOM muscles were excluded. Volumes of interest (VOIs) were positioned separately for bilateral mylohyoid, digastric, genioglossus and geniohyoid muscles, based on T2-weighted and T1-weighted images, and fitted in all 3 planes. VOIs were placed separately for bilateral parotid, submandibular and sublingual glands in the same way. Absence of pathology in these regions was ensured by prior reviewing of PET/MR images and clinical patient data. Atrophic, fatty degenerated or previously resected glands were not considered for analysis. SUV_{max} was measured for each VOI. **Results:** Overall, 692 VOIs were positioned. FDG uptake in mylohyoid (SUV_{max}: 1.94 ± 0.37) and digastric muscles (SUV_{max}: 2.01 ± 0.37) were significantly higher compared to the geniohyoid (SUV_{max}: 1.67 ± 0.53) and genioglossus muscles (SUV_{max}: 1.75 ± 0.54) (Friedman Test; p<0.001). FDG uptake in the sublingual glands (SUV_{max}: 3.77 ± 1.63) was significantly higher compared to the parotid glands (SUV_{max}: 2.34 ± 0.60) and submandibular glands (SUV_{max}: 2.51 ± 0.59) (Wilcoxon signed-ranks test; p<0.001). Of all analyzed structures, the sublingual glands yielded the highest FDG uptake, which was also significantly higher than the FDG uptake in the mylohyoid muscles (p<0.001). FDG uptake in the parotid, submandibular and sublingual glands was inversely correlated to the age of subjects (Spearman' rho coefficient: -0.397 / p=0.004; -0.329 / p=0.021; -0.535 p<0.001; respectively), with higher uptake found in younger subjects. **Conclusion:** High FDG uptake in the mylohyoid muscle is a common misconception. The sublingual glands yield the highest physiologic FDG uptake in the floor of the mouth. A differentiation of these structures can easily be achieved using PET/MR. **References:** 1.Haerle SK, Hany TF, Ahmad N, et al. Physiologic [18F]fluorodeoxyglucose uptake of floor of mouth muscles in PET/CT imaging: a problem of body position during FDG uptake? Cancer imaging : the official publication of the International Cancer Imaging Society.

2013;13:1-7.2.Özülker T, Özülker F. Physiologic distribution of 18F-FDG. Atlas of PET-CT Imaging in Oncology: A Case-Based Guide to Image Interpretation. Heidelberg: Springer; 2015:3-19.

EP-0374

Evaluation of the use of fluorescent receptor-mediated tracers in specimens obtained from head & neck surgery

T. Buckle[1], *M. van Alphen*[2], *M. A. van Oosterom*[1], *D. M. van Willigen*[1], *M. van den Brekel*[2], *B. Karakullukcu*[2], *F. W. B. van Leeuwen*[1];
[1]*LUMC, Leiden, NETHERLANDS,* [2]*NKI-AvL, Amsterdam, NETHERLANDS.*

Aim/Introduction: Receptor targeted fluorescence-guided interventions are increasingly being applied in the surgical arena, with application in the head-and-neck (HN) area at the forefront of current innovations. Where the holy grail in image-guided surgery is direct identification of the primary tumor (margins) and/or metastases, fluorescence is currently most often used as a secondary means for identifying metastatic tumor spread, e.g. sentinel nodes. The few existing clinical proof-of-concept studies wherein receptor-mediated tracers were applied provide limited evidence for in vivo tracer performance and/or only provide evidence in a single indication. With the aim to limit the patient exposure to studies based on suboptimal image-guided surgery concepts, we explored the possibility of using ex vivo evaluation as intermediate step prior to initiation of clinical trials with new tracer candidates. **Materials and Methods:** Cy5 labeled tracers targeting Tyrosine-protein kinase Met (hepatocyte growth factor receptor; CMET; expression in 80% of HN tumors) or the epidermal growth factor receptor (EGFR; 66-84% expression) were evaluated in ten tissue samples obtained from five tongue tumor patients. Samples were incubated in tracer solution with increasing concentration (100-1000nmol; 5 minutes/concentration), washed for removal of unbound tracer, and imaged using a surgical grade Cy5 fluorescence camera equipped with custom image processing software. Tracers were evaluated for their ability to 1) enable fluorescence-based visualization of the tumor, 2) identify margins and 2) obtain a tumor-to-normal tissue-ratio of >2. Processed pathological specimens were evaluated using fluorescence imaging and related to H&E- and immunohistochemical staining. **Results:** Fluorescence imaging could be performed on all specimens, revealing differences in tracer uptake and fluorescence intensities between samples. While for the EGFR the tumor-to-normal-tissue ratio remained <2 at all tested concentrations, CMet-related tumor identification was successful in 5/5 samples and allowed assessment of the deeper margins of the tumor (250nmol). Next to aiding the selection of the best tracer candidates, the approach also helped to establish the most optimal conditions required for intraoperative imaging (e.g. minimal concentration required for detection). Fluorescence imaging of pathological samples allowed correlation between the stained tissue and receptor expression. **Conclusion:** The described ex vivo evaluation set up allowed study of tracer candidates for fluorescence-guided surgery without any risk to the patient. Clear difference between staining ability was seen between evaluated tracers, with CMet proving to be an interesting target for image-guided surgery applications in tongue tumor patients and thus, could potentially hold value for a clinical trial in oral cavity cancer. **References:** None.

EP-0375

Feasibility of Multiparametric Imaging with PET/MR in Nasopharyngeal Carcinoma: A Pilot Study

C. Cao[1], *Y. Xu*[2], *S. Wang*[2], *C. Li*[2];
[1]*Department of Radiation Oncology, Zhejiang Cancer Hospital, Hangzhou, CHINA,* [2]*Hangzhou Universal Imaging Diagnostic Center, Hangzhou, CHINA.*

Aim/Introduction: The aim of this pilot study was to explore the integrated Positron Emission Tomography and Magnetic Resonance imaging scanner (PET/MR) for biological characterization of nasopharyngeal carcinoma (NPC) and potential therapeutic applications of dose painting (DP). **Materials and Methods:** Twenty-one NPC patients with PET/MR were included in this study. Overlap of tumor volumes was analyzed on T2-weighted images (volume of interest, VOIT2), diffusion-weighted magnetic resonance imaging (VOIDWI) and 18F-fluorodeoxyglucose positron emission tomography (VOIPET). The overlap percentages of low-metabolic sub-region (cluster 1) and high-metabolic sub-region (cluster 2) in VOIPET and VOIDWI were analyzed by cluster analysis. **Results:** Both the VOIDWI and VOIPET were encompassed in the VOIT2, respectively 99.6% and 97.5%. The median tumor overlap was 94.4% (VOIDWI within VOIPET). The median overlap of cluster 2 in VOIPET and VOIDWI was 43.61%(27.67%-52.66%) and 21.86%(10.47%-40.89%), respectively. The median overlap of cluster 1 in VOIPET and VOIDWI was 48.03% (23.91%-63.15%) and 24.40 % (7.44%-51.44%), respectively. Separation between clusters appeared to be defined by a SUV value. **Conclusion:** For NPC, the VOIs of DWI and FDG PET were not overlapped completely and the volume defined by cluster-analysis might be meaningful for DP. **References:** None.

EP-0376

Impact of ^{18}F-FDG-PET/CT in the initial staging and changing the management intent in head and neck squamous cell carcinoma

A. Kandeel, *M. S. Mohamed*, *Y. A. Mohamed*, *M. A. Abougabal*, *H. Darwish*, *M. E. Aldaly*;
Faculty of Medicine, Cairo University, Cairo, EGYPT.

Aim/Introduction: To assess the role of ^{18}F-PET/CT in initial staging of head and neck squamous cell carcinoma and its role in changing the management compared to other conventional methods. **Materials and Methods:** A prospective study of 31 patients (21 male and 10 female), mean age 49.3 years

with histologically confirmed squamous cell carcinoma of the head and neck (nasopharynx was the commonest cancer in 15 patients (48.4%), poorly differentiated grade represented 64.5% of all tumors in 20 patients. Initial staging was achieved according to routine physical examination, endoscopy, CT, U/S, MRI, then ^{18}F-PET/CT was performed in a time interval less than 30 days. The findings of PET/CT were compared with those of the other conventional method. Correlation analysis between SUVmax of the primary tumor with tumor size, T staging and tumor grade was done as well as between SUVmax of the lymph node with lymph node size, N staging and tumor grade. **Results:** No significant difference between conventional methods and ^{18}F-PET/CT in both T and M staging (p=0.8 and 0.6, respectively). While N staging showed significant difference (p=0.034). The overall change in TNM staging by ^{18}F-PET/CT in relation to conventional methods was encountered in 15/31 patients (48.4%). ^{18}F-PET/CT changed; T staging in 3 patients, upstaging in 2 patients and downstaging in one patient. ^{18}F-PET/CT upstaged all 13/31 patients in N staging (41.9%). ^{18}F-PET/CT changed; M staging in 3/31 patients, upstaging in 2 and downstaging in one patient. PET/CT changed the intent of treatment from curative to palliative treatment in a 1 patient with nasopharyngeal carcinoma having multiple bone metastases. The results of ^{18}F-PET/CT modified radiotherapy in 21/31 patients (67.7%). ^{18}F-PET/CT detected intra-parotid nodule in 4 patients, one of them was detected by conventional CT so additional radiation was added. Retropharyngeal nodes were detected by ^{18}F-PET/CT in 3 patients that were missed by conventional imaging. ^{18}F-PET/CT detected two patients of thyroid papillary carcinoma and one case of sigmoid neoplasm confirmed by histopathology. A significant positive correlation was found between SUVmax of the primary lesion with the tumour size (r 0.395; p 0.03) and between SUVmax of the lymph nodes with lymph node size (r 0.794; p <0.001) and N staging (r 0.246; p <0.001). **Conclusion:** ^{18}F-FDG-PET/CT is considered a valuable imaging tool in head and neck squamous cell carcinoma in initial staging which change the staging and hence the radiotherapy planning and proper management. **References:** None.

EP-25

Clinical -> Diagnostic study -> Adult study -> Oncology study -> Organ-based oncology -> Hemato-oncology, malignant

October 12 - 16, 2019 e-Poster Area

EP-0377

The impact of PSF reconstruction algorithm on the early therapeutic response of lymphoma patients

B. Magyar, *E. Kristóf, S. Czibor, L. Jorgov, M. Barra, A. Fekésházy, Z. Varga, T. Györke;*
Semmelweis University, Nuclear Medicine Center, Budapest, HUNGARY.

Aim/Introduction: Interim 18F-FDG PET/CT is performed for monitoring the early therapeutic response of lymphoma patients treated with chemotherapy, and the PET images are visually evaluated by the Deauville criteria. Scores 1, 2 and 3 by the five-point Deauville criteria at interim PET/CT mean complete metabolic response (CMR), whilst scores 4 and 5 indicate partial/no metabolic response or progressive disease. Beside the conventional OSEM (Ordered Subsets Expectation Maximization), novel PSF (Point Spread Function) reconstruction using iterative Bayesian penalized-likelihood algorithms, like Q.Clear have recently been introduced to clinical practice. Q.Clear reconstruction method improves signal to background ratio with nearly the same signal to noise ratio and therefore can influence the visual assessment and so the Deauville scoring of smaller lesions, which might alter the evaluation of the early therapeutic response in lymphoma patients. **Materials and Methods:** During our study we evaluated 82 interim PET/CT examinations of lymphoma patients after 2-4 cyles of standard chemotherapy. The PET images were reconstructed both with OSEM (6 iterations, 6 subsets) and with Q.Clear (beta: 350) methods. After identifying the same target lesion on both reconstructed image sets we visually analysed them. Applying the five-point scale of Deauville criteria, we visually compared the FDG uptake of the target lesion to the tracer accumulation in the mediastinal blood pool and the liver. Finally we examined if the obtained scores differ by using OSEM or Q.Clear reconstruction algorithms. **Results:** Out of 82 examinations the two reconstruction algorithms resulted in different Deauville scores in 21 cases. In all the 21 cases Q.Clear reconstructed images presented higher scores. In 3 cases the score based on the visual evaluation increased from 1 to 2, in 10 cases from 2 to 3, in 6 cases from 3 to 4, and in 2 cases from 4 to 5. Consequently, in 6 cases using OSEM method resulted CMR, whilst applying Q.Clear reconstruction in these cases CMR was not achieved. **Conclusion:** In more than 25 % of the 82 interim PET/CT examinations evaulated, the OSEM and Q.Clear reconstructed images resulted different Deauville scores. In 6 cases applying Q.Clear instead of OSEM reconstruction, CMR could not have been declared. In conclusion, choosing the reconstruction algorithm could influence the interpretation of the early therapeutic response in 7 % of our cases. **References:** None.

EP-0378

Metabolic Tumor Volume Measurement In Early Hodgkin Lymphoma. Preliminary Results

M. Cortes Romera[1], *A. Palomar-Muñoz*[1], *E. Domingo-Domènech*[2], *G. Reynes-Llompart*[3], *J. Vercher-Conejero*[1], *P. Notta*[1], *A. Sureda-Balari*[2], *J. Mestres-Martí*[1], *C. Gámez-Cenzano*[1];
[1]*Unit PET/CT (IDI)- Department of Nuclear Medicine. Hospital U. de Bellvitge-IDIBELL, L'Hospitalet De Llobregat (Barcelona), SPAIN,* [2]*Department of Hematology. ICO. Hospital Duran i Reynals-IDIBELL., L'Hospitalet De Llobregat (Barcelona), SPAIN,* [3]*Department of Medical Physics .ICO. Hospital U. de Bellvitge-IDIBELL, L'Hospitalet De Llobregat (Barcelona), SPAIN.*

Aim/Introduction: The presence of bulky disease in Hodgkin lymphoma(HL), usually defined with one-dimensional measurement, can change patient´s risk grouping and thus the treatment approach. More recently, metabolic tumor volume(MTV) has also been identified as a promising baseline prognostic factor. Standardization of the methodology to evaluate MTV is crucial, and is needed to be available using commercial software and be robust and easy to use in daily practice. The aim of this study has been to assess, in patients with early stage HL, inter-observer variability in MTV measurement and to compare different methods of MTV measurement using FDG-PET/CT. **Materials and Methods:** Patients diagnosed with early stage HL were referred for FDG-PET/CT at initial staging/recurrence and at the end of treatment(EOT). Pretreatment MTV was measured, retrospectively, using different methods. We compared three methods(SUVmax>2.5 and SUVmax>41% per lesion, and SUVmax>41% per patient), using a PETVCAR software(General Electric). The relation between the presence of bulky mass(>=7cm) and MTV/TLG(Total Lesion Glycolysis) was assessed with Wilcoxon´s test. The intraclass correlation coefficient(ICC) and Bland-Altman Plot analysis(limits of agreement-LoA-) were used to measure the inter-observer correlation. It was evaluated the relation between MTV, SUVmax, SUVmean and SUVpeak in pretreatment-PET and the positivity observed in the EOT-PET defined by Deauville score(DS4-5) with lineal regression. **Results:** Twenty-eight patients with early stage HL(19 women; stage I in 5/ II in 23) were included. There were significant differences between MTV in patients with bulky versus no bulky disease($p<0.05$). As expected, patients with bulky disease presented with the highest MTV values. There was excellent concordance between the two observers when measuring the MTV by means of each one of the methods. ICCs were: 0.998 for SUVmax>41% per lesion, 0.996 for SUVmax>2.5 per lesion and 0.999 for SUVmax>41% per patient. Bland-Altman analysis showed higher differences between the two observers for SUVmax>41% per patient(LoA: -1.5+/-5.1) and SUVmax>2.5 per lesion(LoA:-6.2+/-21.8) than SUVmax>41% per lesion(LoA: 0+/-7.7), so this was the most reproducible method. Lineal regression showed a trend to a higher MTV for SUVmax>41% per lesion and per patient, which had more probability positive EOT-PET/CT. There was no correlation between SUVmax, SUVmean and SUVpeak and the positivity of EOT-PET/CT. **Conclusion:** There was excellent correlation between the two observers for measuring MTV with each of the methods. MTV-SUVmax>41% per lesion was the most reproducible method. Patients with higher MTV had a more positive EOT-PET/CT; however, more studies are needed in order to verify this point. **References:** None.

EP-0379

18F-FDG PET/CT in the evaluation of metabolic behaviour of solitary plasmacytoma and the progression to Multiple Myeloma

***M. Rashki**, R. Sánchez Sánchez, A. González Jiménez, T. Rudolphi Solero, E. Triviño Ibañez, J. Llamas Elvira;*
Hospital Virgen de las Nieves, Granada, SPAIN.

Aim/Introduction: Solitary plasmacytoma (SP) is an infrequent form of plasma cell dyscrasia that often evolves to multiple myeloma (MM), worsening the prognosis. Although, risk factors for progression to MM has not been clearly identified. Our aim was to evaluate the metabolic behavior of solitary plasmacytoma and the role of 18F-FDG PET/CT in predicting progression to myeloma. **Materials and Methods:** We retrospectively analyzed thirty patients affected by SP histological proven, who underwent 18-FDG PET/CT scan between 2009 and 2017. We divided them into staging group (pre-treatment) and follow-up group (post-treatment) and they were analyzed separately. The presence of multiple lytic lesions, a rate greater than 10% of plasma cells in bone marrow or the development of at least one CRAB symptoms (hypercalcemia, renal dysfunction, anemia) was considered progression to myeloma as established by the International Myeloma Working Group. The PET/CT images were analyzed visually and semi-quantitatively (maximum standardized uptake value body weight (SUVbw and SUV mean), body surface area (SUVbsa), metabolic tumor volume (MTV), total lesion glycolysis (TLG), tumor volume) and compared with age, sex, and site of the primary disease. We also registered the results from other image technics such as CT scan, MRI and bone scintigraphy. **Results:** Five patients were diagnosed with MM from the beginning and were discarded. Staging group (n = 11), the average age was 65 ±12 years, average SUV max 7,6 ± 4,4, MTV 44,3 ± 55,7 and TLG 88,6 ± 85,4. Two patients developed myeloma during follow-up (35 months) Follow-up group (n = 14), mean age 56,7 ± 7,6 years, mean SUVmax 6,9 ± 3,11 MTV 23,5± 21,6 and TLG 47,8 ± 40. Five of them evolved to MM. Comparing the patients who progressed to myeloma and the one who did not in terms of age, sex, the primary site of disease, semi-quantitative parameters (SUVmax, MTV and TLG) and tumor volume, there were no significant differences. Time to progression to MM was significantly shorter in patients with a higher value of SUVmax, MTV, TLG and tumor volume **Conclusion:** The PET/CT is a useful tool in the management of patients with solitary plasmacytoma, having a predictive role as the metabolic behavior of plasmacytoma seems to be related to a shorter progression time to myeloma. **References:** None.

EP-0380

Diagnostic Value Of Red Cell Mass Measurements And JAK2 V617F Mutation In Patients With Polycythemia Vera

***J. Stojanovic**, M. Todorović-Tirnanić;*
Center for Nuclear Medicine, Faculty of Medicine, University of Belgrade, Belgrade, SERBIA.

Aim/Introduction: Polycythemia vera (PV) is a myeloproliferative neoplasm characterized by absolute erythrocytosis with augmented total red cell mass (RCM) over 25% compared to its optimal value. Major criteria for diagnosis of PV (WHO 2016.) are: 1) increased RCM for more than 25 %, 2) present JAK2 V617F mutation. The aim of this study is comparing the results of JAK2 V617F mutation investigation and nuclear medicine method of RCM determination in patients with clinical diagnosis of

PV. **Materials and Methods:** Retrospective study including 111 patients with clinical suspicion of PV was performed. All 111 persons were tested for the presence of JAK2 V617F mutation, using a PCR-specific allele, and RCM was measured after autologous RBC labeling with chromom-51 in the form of sodium-chromate. **Results:** Based on RCM measurement results, the clinical diagnosis of PV was rejected in 43/111 (38.7 %) patients, and the group of 111 patients was devided into four subgroups: 1) confirmed diagnosis of PV: 68/111 patients (61.3 %). JAK2 V617F mutation was present in 49/68 patients (72.1 %); 2) apsolute erythrocytosis (RCM increased 11-25 % compared to optimal): 24/111 patients (21.6 %), JAK2 V617F mutation was present in 15/24 (62.5 %); 3) normal RCM: 16/111 patients (14.4 %), JAK2 V617F mutation was present in 7/16 (43.8 %); 4) anaemia (RCM lower than 10 % compared to optimal): 3/111 patients (2.7 %), JAK2 V617F mutation was present in 2/3 patients. The difference in the presence of JAK2 V617F mutation between patients with and without elevated RCM, as well as between the four subgroups of patients, was not statistically significant. **Conclusion:** Nuclear-medicine method of total red cell mass investigation is more precise and more specific than the presence of JAK2 V617F mutation, for PV diagnosis. **References:** None.

EP-0381

Prognostic value of baseline metabolic heterogeneity on ^{18}F-FDG PET/CT in primary mediastinal large B-cell lymphoma (PMBCL) treated with R-DAEPOCH chemotherapy

A. Alessi[1], *A. Guidetti*[2], *L. Devizzi*[2], *G. Argiroffi*[3], *A. Lorenzoni*[3], *G. Serafini*[3], *B. Padovano*[3], *A. Cicchetti*[4], *F. Scalorbi*[3], *V. Marasco*[2], *L. Farina*[2], *A. Dodero*[2], *P. Corradini*[2], *E. Seregni*[3];
[1]*Fondazione I.R.C.S.S. Istituto Nazionale Tumori, Milan, ITALY,* [2]*Department of Oncology and Hematology; Fondazione IRCCS Istituto Nazionale dei Tumori, Milan, ITALY,* [3]*Nuclear Medicine Unit; Fondazione IRCCS Istituto Nazionale dei Tumori, Milan, ITALY,* [4]*Fondazione IRCCS Istituto Nazionale dei Tumori, Milan, ITALY.*

Aim/Introduction: We investigated the prognostic value for predicting tumor response of baseline metabolic heterogeneity (MH) and of end of therapy (EOT) FDG PET/CT in a consecutive cohort of PMBCL pts treated with R-DAEPOCH. **Materials and Methods:** Forty-one PMBCL pts have been consecutively treated with 6 cycles of R-DAEPOCH. All pts underwent to PET/CT at baseline and at EOT. The disease was semi-automatically defined on PET images with a threshold of 25% of the SUVmax using a commercial software (PET VCAR, GE Healthcare). MH value was evaluated by estimating the coefficient of variation of the intratumoral FDG uptake. Cut-off of MH was established as the first quartile of the distribution in the study population. Patients were classified as responders and non-responders according to Deauville Score criteria (DS). **Results:** All but one patient received 6 cycles of chemotherapy, one pt only interrupted treatment for progressive disease (PD). Seven pts (17%) only received RT at EOT. With a median follow-up of 36 months (range, 5-112) the 3-years PFS and OS for all pts were 84% and 91%, respectively. Five pts (12%) presented relapse or PD at a median of 6 months (range, 4 - 9). EOT PET/CT was evaluable in 39 pts: 31 responders (DS 1-3) and 8 non responders (DS 4); in two patients the final reassessment is still ongoing. All but one relapsed or refractory patients presented DS4 at EOT. Twenty-seven pts were evaluable for MH. The cut-off discriminating high and low MH was 2.0 (median 2.12; range, 1.62 - 2.74). Seven pts presented a high MH whereas 20 pts a low MH. Three out of 7 pts with high MH relapsed or were refractory (43%) compared to only one refractory patient among low MH series (5%). The 3-years PFS was 95% for EOT PET negative pts and 96% for those with low MH. Due to the small number of pts with baseline high MH and DS4 PET at EOT the survival analysis in these subgroups is still inconclusive. **Conclusion:** PMBCL pts treated with R-DAEPOCH achieving a PET negativity and with a low MH at baseline have an excellent prognosis. Pts with baseline high MH and with DS4 EOT PET seem to be at high risk of progression, however an analysis on a larger cohort is needed in order to better define the prognostic role of both these parameters in order to plan a consolidation with RT. **References:** None.

EP-0382

Hepatosplenic T-cell lymphoma: clinical characteristics and imaging findings

F. Chao, X. Han;
The First Affiliated Hospital of Zhengzhou University, Zhengzhou, CHINA.

Aim/Introduction: Hepatosplenic T-cell lymphoma (HSTCL) is a rare, highly aggressive, rapidly lethal form of peripheral T-cell lymphoma. Patients present with extranodal disease involving the spleen, liver, bone marrow, and only rarely with lymphadenopathy. Because of the rarity of the disease, lacking specificity of clinical manifestations, laboratory examinations and imaging findings lack, it is easy to misdiagnose. **Materials and Methods:** 14 patients (9 females, 5 males; age range 10-71 years; median, 30.5 years) with hepatosplenic T-cell lymphoma pathologically confirmed were retrospectively analyzed. Clinical characteristics, imaging findings were reviewed. **Results:** One patients had a prior history of leucoderma for 23 years. Most of the patients presented with splenomegaly (100%), hepatomegaly (78%), pancytopenia (100%) and the B symptoms (93%) of lymphoma including weight loss, fevers, and night sweats. 6 patients were examined with ^{18}F-FDG PET/CT before chemotherapy. Among the 6 patients, 1 patient displayed hepatomegaly with diffuse increased FDG activity, while the other 5 patients is normal FDG activity. 3 patients displayed splenomegaly with high diffuse uptake of ^{18}F-FDG, while the other 3 patients undergone splenectomy before ^{18}F-FDG PET/CT imaging. 5 patients showed diffusely increased FDG activity in the bone marrow. Many enlarged lymph nodes and subcutaneous nodules were found in one patient who got 35 months CR after chemotherapy and autologous stem cell transplantation, which is a rare finding in HSTCL. Finally,

the disease progressed, and the patient died 56 months after diagnosis. While most patients died within two years (12/14). **Conclusion:** The clinical and imaging findings of hepatosplenic T-cell lymphoma in our study is similar to what was previously reported in the literature. Our cases show a variable pattern of FDG uptake at initial diagnosis. Therefore, the role of PET/CT in the diagnosis and follow-up of T cell lymphomas may need further study. **References:** None.

EP-0383

The Role Of PET/CT In Diagnosis And Follow Up Of Patients With Extranodal Localization Of Lymphoma

K. Mladenov[1,2], *V. Hadzhiyska*[2,2], *D. Vasileva*[3];
[1]*Clinic o nuclear medicine University Hospital Alexandrovska, Sofia, BULGARIA,* [2]*University Hospital Aleksandrovska, Sofia, BULGARIA,* [3]*National Specialized Hospital for Active Treatment of hematological diseases, Sofia, BULGARIA.*

Aim/Introduction: Accurate staging of Hodgkin's disease and non- Hodgkin's lymphoma is important for treatment management. The extranodal lesions is important parameter that affects the stage, prognosis and management of lymphoma patients. The aim of the study is to examine the accuracy of the PET/CT to determinate the extranodal additional involvement of tumour mass in newrly diagnognosed lymphoma and after therapy. **Materials and Methods:** A total patients aged 18 to 79 years. Were analyzed 92 With NHL and 92 with NHL. All patients were verified and staged by morphology and imaging methods. The patients were investigated by 18-F FDG PET/CT , according to the accepted protocol. **Results:** 32 patients (34,8%) with NHL were presented with extranodal primary lesions in stomach, nasopharynx and oropharynx, tonsils, testicles, lung and pleura, pancreas, brain, orbits, skin. In two patients with HL (2.6%) the tonsils were considered as an primary extranodal site. In 52 patients with NHL (56.5%) and 28 with HL(36.8%), nodal and extranodal lesions were found. The remaining patients with NHL and CL were with primary nodular disease localization. In all patients, polychichemotherapy was performed, consistent with the histological variant and the stages of the disease. Patients with HL, at 62 a complete response, in 8 - partial response, stable disease at 2 and at 4 with progression. After the therapy in patients with NHL, at 41 we achieved complete responses, at 24 - partial response, stable disease at 8 and progression at 19. In interim and next PET / CT during therapy with NHL patients we revealed new extranodal lesions in 11 patients. In case of partial response, high dose chemotherapy, radiotherapy and / or haematopoietic stem cell transplantation were performed. **Conclusion:** PET/CT is an accurate method for early detection of extranodal lymphoma involvement, which is important for treatment strategy. PET / CT along with histological verification is exclusively useful for differential diagnosis between non-lymphoproliferative malignant disease from limphoma. **References:** None.

EP-0384

Application value of ^{18}F-FDG PET/CT metabolic parameters in the prognostic prediction of Diffuse Large B-cell Lymphoma

J. Li, *X. Sun, Y. Li, J. Yang, Q. Zhao, P. Yang;*
General Hospital of Ningxia Medical University, Yinchuan, CHINA.

Aim/Introduction: To explore the predictive value and relationship with prognostic factors of baseline ^{18}F-FDG PET/CT imaging metabolic parameters SUVmax, MTV and TLG in patients with DLBCL. **Materials and Methods:** This study retrospectively analyzed 69 patients (32 males,37 females) with initially diagnosed DLBCL from January 2013 to September 2018. All patients were confirmed as DLBCL by pathology with complete clinical follow-up data (median follow-up time: 15.7 months), and all ^{18}F-FDG PET/CT scans were performed before chemotherapy. Using SUVmax=2.5 as the threshold, the value size of ^{18}F-FDG PET/CT imaging metabolic parameters SUVmax, MTV and TLG were obtained by using absolute threshold method. 69 patients with complete follow-up data were obtained, and the patient's age, gender, LDH level, IPI score, Ann Arbor staging, patient progression or recurrence time, and time of death were recorded . Through the above data, the patient's progression-free survival was collected. According to the follow-up results, the patients were divided into the progression/relapse group (20 cases) and the non-progression/ relapse group (49 cases). Statistical analysis was performed using SPSS22.0 software and t-test, ANOVA and ROC curve analysis were employed. The cutoff values of tumor recurrence/progression were predicted by SUVmax, MTV, TLG, respectively. Kaplan-Merier and Log-rank tests were used to analyze the prognostic value of prognostic factors. $P<0.05$ was considered statistically significant. **Results: 1.**There were significant differences in MTV and TLG between the LDH level normal group and the elevated group, the progression/relapse group and the non- progression/relapse group, and the Ann Arbor staging and IPI scores($P<0.05$),while there was no statistically significant difference in SUVmax values($P>0.05$). There were no significant differences in SUVmax, MTV and TLG between the two groups in terms of gender and age. **2.**The cutoff values of SUVmax, MTV, and TLG for predicting tumor progression/recurrence were 17.7, 330.6 cm^3, and 2553.2 g, respectively. There were significant differences in PFS of Ann Arbor stage, LDH level, MTV and TLG($P<0.05$). There was no statistically significant difference in PFS of gender, age, and SUVmax($P>0.05$). **Conclusion: 1.**The MTV and TLG values of DLBCL lesions were statistically significant between LDH level normal group and elevated group, progression/relapse group and non-progression/relapse group, Ann Arbor stage ,IPI score. **2.** ^{18}F-FDG PET/CT imaging metabolic parameters MTV and TLG were important prognostic factors of PFS in patients with DLBCL, while SUVmax predictive value was not significant. **References:** None.

EP-0385

Prognostic value of total metabolic tumor volume and total lesion glycolysis of baseline 18F-fluorodeoxyglucose positron emission tomography / computed tomography in Hodgkin lymphoma. Preliminary Results

C. A. Achury[1], *L. G. Diaz*[1,2], *C. Montes*[1,2], *R. Garcia*[1,2], *M. Peñarrubia*[3], *S. Fernandez*[4], *M. Vidal*[4], *J. Queizan*[5], *G. Hermida*[6], *D. Caballero*[1,2], *P. Tamayo*[1,2];
[1]*Hospital Universitario de Salamanca, Salamanca, SPAIN,* [2]*Biomedical Research Institute of Salamanca (Ibsal), Salamanca, SPAIN,* [3]*Hospital Universitario de Valladolid, Valladolid, SPAIN,* [4]*Complejo Asistencial Universitario de Leon, Leon, SPAIN,* [5]*Hospital de Segovia, Segovia, SPAIN,* [6]*Hospital Universitario de Burgos, Burgos, SPAIN.*

Aim/Introduction: To quantify total metabolic tumor volume (TMTV) and total lesion glycolysis (TLG) on pretreatment 18F-FDG PET/CT and analyze its prognostic value as predictors of response of treatment in patients diagnosed of Hodgkin lymphoma (HL). **Materials and Methods:** We here present 54 patients, of a prospective multicenter study carried out in newly diagnosed HL patients treated with 6 cycles of ABVD, who have completed the treatment and the response to the end of treatment has been evaluated. Median age of 59,3 years (range,14-81 years), with thirty-two men. All patients underwent at least two PET/CT studies with 18F-FDG, one at diagnosis (baseline) and the other at the end of treatment (EoT). TMTV and TLG parameters were quantified by three nuclear medicine physician blinded to a patient outcome on the semiautomatic free software "LIFEx" (http://www.lifexsoft.org) using an automatic segmentation of the lesions with a SUV > 3 with an adaptive threshold. To determine whether TMTV and TLG values predict the response to treatment univariate Cox regression analysis was performed. Statistical significance was considered at p<0,05. Data were analysed using SPSS software version 20. **Results:** Of the fifty-four patients, 41 patients (75,9 %) were in complete response at EoT with mean values of TMTV, TLG and SUVmax of 369,2 cm^3 (range 3-398), 2690,8 cm^3 (range, 5-2811) and 14,9 (range, 4-16), respectively. The mean values of TMTV, TLG and SUVmax in the 13 patients who did not reach complete response at the EoT were 437,1 cm^3 (range 3-1943), 4547,9 cm^3 (range, 5-25496) and 18,5 (range, 4-32), respectively. There were statistically significant differences between both group of patients with respect to TMTV (p<0.05) and TLG values (p<0.05), showing higher baseline TMTV and TLG values the patients that did not get complete response at the end of the treatment, but not with respect to SUVmax. **Conclusion:** Although our results are preliminary, they suggest that baseline TMTV and TLG values might predict the response of treatment in patients with HL. **References:** None.

EP-0386

Role of 18F-FDG PET/CT in the evaluation of bone marrow involvement in 3 different lymphomas subtypes: diffuse large B-cell, follicular and Hodking lymphoma

M. Suarez-Piñera[1], *E. Gimeno*[2], *I. Parraga*[2], *A. Mestre-Fusco*[3], *J. Ares*[4], *L. Colomo*[5], *B. Sanchez*[2], *A. Salar*[2];
[1]*Nuclear Medicine Department, Hospital del Mar, Parc de Salut Mar, Barcelona, SPAIN,* [2]*Hematology, Hospital del Mar, Parc de Salut Mar, Barcelona, SPAIN,* [3]*Nuclear Medicine Department, Hospital del Mar, Parc de Salut Mar, Barcelona, SPAIN,* [4]*Radiology, Hospital del Mar, Parc de Salut Mar, Barcelona, SPAIN,* [5]*Hematopathology, Hospital del Mar, Parc de Salut Mar, Barcelona, SPAIN.*

Aim/Introduction: Bone marrow involvement is an important parameter for staging and management of patients with lymphoproliferative disorders. During the last years bone marrow (BM) evaluation has changed since FDG-PET/CT has achieved and important role. However, this role might be different depending on the lymphoma subtype. The purpose of this study was to assess the ability of FDG-PET/CT to detect BM involvement in comparison with bone marrow biopsy (BMB) in 3 groups of patients with different lymphomas subtypes: Hodking lymphoma (HL), diffuse large B-cell lymphoma (DLBCL) and follicular lymphoma (FL). **Materials and Methods:** A retrospective study of 325 patients newly diagnosed of HL (n=102), DLBCL (n=160) and FL (n=63) was performed. Both a 18F-FDG PET/TC and an BMB was carry out in all of them. PET/CT was visually analysed and in some cases a semiquantitative (SUVmax) analysis was performed. FDG uptake in bone marrow was evaluated respect a reference region (other bones and/or liver). Distribution pattern was evaluated as well and classified as a diffuse, or patched (monofocal or multifocal). Visual analysis was always carried out by a nuclear medicine physician and occasionally by a radiologist. BMB was not guided and in most of the cases was carried out in the iliac crest. Sensitivity (S), Specificity (Sp), positive predictive value (PPV) and negative predictive value (NPV) were calculated. Change in the clinical management after PET/CT was collected as well. **Results:** Out of 325 patients, 70 (21%) patients had BM involvement by PET/CT criteria. BMB positive was found in 67 (20%). These results were not always concordant between both methods. S, Sp, PPV, NPV, of PET/CT in detecting BM involvement were: 75%, 89%, 37% and 97% in LH, 40%, 87%, 76% & 56% in FL and 67%, 86%, 53 % & 92% in DLBCL. In 14 patients clinical management was changed after PET results. **Conclusion:** The results of this study suggest that a negative ^{18}F-FDG PET/CT could predict absence of bone marrow infiltration in HL and DLBCL. In the rest of the situation the value of PET/CT is limited and BMB should be performed despite of the PET/CT results. PET/CT is a useful tool to guide the BMB procedure when it is needed, obtaining a higher profitability in BM evaluation. **References:** None.

EP-0387

Diagnostic Value of FDG PET/CT in Assessment of Bone Marrow Infiltration in DLBCL

A. Doma, B. Jezeršek Novaković, I. Žagar;
Institute of Oncology Ljubljana, Ljubljana, SLOVENIA.

Aim/Introduction: To determine the efficacy of FDG PET/CT in detecting bone marrow infiltration in diffuse large B-cell lymphoma (DLBCL) in comparison with bone marrow biopsy (BMB). **Materials and Methods:** 126 patients with histologically proven DLBCL who underwent pretreatment FDG PET/CT and BMB between December 2015 and January 2018 were retrospectively enrolled. PET images were visually analysed by an experienced nuclear medicine specialist, blind of BMB pathological results. Marrow involvement was classified as either diffuse, focal, or diffuse and focal. BM uptake on PET, exceeding the liver uptake, was deemed positive. BM uptake below the level of hepatic uptake was deemed negative. In all cases of positive PET and negative BMB, the posttreatment evaluation PET was reviewed to determine the presence of lymphoma deposits in BM on staging PET/CT. **Results:** 64 patients were male, 62 female, median age 63.5, age range 23 - 84 years. BM involvement was detected by PET/CT in 31 (25%) and by BMB in 18 (14%) cases. PET/CT and BMB were concordant in 105 (83%) cases, 16 with positive PET and BMB and 89 with negative PET and BMB. The sensitivity, specificity, positive and negative predictive value and accuracy of FDG PET/CT and BMB were 93.9%, 95.7%, 88.6%, 97.8%, 95.2% and 54.5%, 100%, 100%, 86.1% and 88.1%, respectively. The diffuse, focal and diffuse and focal increased pattern on PET was seen in 10, 23 and 2 patients and positive predictive value of PET was 60%, 100% and 100%, respectively. **Conclusion:** FDG PET/CT detects BM involvement in DLBCL in more patients than BMB. Sensitivity of BMB is low in the focal pattern of BM infiltration. Visualisation of focal BM involvement on PET/CT may avoid BMB. **References:** None.

EP-0388

The Role Of ^{18}F-FDG PET/CT In Detection Of Bone Marrow Involvement In Patients With Newly Diagnosed Non-Hodgkin's Lymphoma

C. Sandoval Moreno, P. García Alonso, M. de la Rubia Marcos, C. Mena Melgar, M. Tagliatori Nogueira, A. Herrero Muñoz, C. Paniagua Correa, L. Castillejos Rodriguez, A. Ortega Valle, M. Balsa Bretón;
Hospital Universitario de Getafe, Getafe, SPAIN.

Aim/Introduction: Nowadays ^{18}F-FDG PET/CT is being used for staging and follow up of lymphomas. We aimed to evaluate the efficacy of ^{18}F-FDG in detection of bone marrow involvement in Non-Hodgkin's Lymphoma (NHL). **Materials and Methods:** We reviewed records of all patients with newly diagnoses of NHL during 3 years. ^{18}F-FDG PET/CT and bone marrow biopsy (BMB) were performed simultaneously (time interval between both procedure less than 30 days) before treatment. We evaluated 59 patients (33 women and 26 male), the median age was 61.4 years (range 38 - 85 years) and 32.2% of them were histological classified as Follicular Lymphoma and 40.6% as Diffuse Larg B-Cell Lymphoma (DLBCL). ^{18}F-FDG PET/CT was performed using a standard protocol and BMB was doing in posterior left iliac crest. Visual evaluation was performed for ^{18}F-FDG PET/CT scan and we classified ^{18}F-FDG PET/CT results in negative (non bone uptake), positive (focal bone uptake) and diffuse positive (diffuse bone uptake). Finally, PET results were compared with histological data. **Results:** On the one hand, 34 of the 59 patients (57.6%) had a negative ^{18}F-FDG PET/CT study and negative BMB (true positive). On the other hand, 9 studies (15.2%) were false negative (non focal bone uptake and positive BMB), only one of them was DLBCL. These gave us a negative predictive value of 79%. Twelve patients (20.3%, 8/12 were DLBCL) had focal bone uptake: 5 of them had positive BMB (true positive) and 7 patients had negative BMB. In these 7 cases, ^{18}F-FDG PET/CT was negative in left iliac crest. One of them had positive FDG uptake and thoracic spine (T10) surgical biopsy was done with a result of bone marrow involvement. The other 6 patients had a negative ^{18}F-FDG PET/CT control after chemotherapy, so we considered them as a PET/CT true positive for bone marrow involvement. Finally, in our series, we classified 4 patients (6.8%) as a diffuse positive uptake. Two of them had a positive BMB. **Conclusion:** The role of ^{18}F-FDG PET/CT for bone assessment in the initial staging of NHL seems to be useful when focal positive bone uptake was observed. In these patients the visual assessment could have avoided BMB. In addition, PET/CT helps to locate lesions for biopsy. However, prospective and analytic studies are needed to prove this hypothesis, especially in negative cases in patients with DLBCL. **References:** None.

EP-0389

Comparison of Visual and Semiquantitative Methods in the Evaluation of Interim ^{18}F-FDG PET/CT Scans for the Assessment of Therapeutic Response in Diffuse Large B-cell Lymphoma Patients

S. Czibor[1], B. Bányai[2], L. Jorgov[1], Z. Varga[1], T. Györke[1];
[1]Semmelweis University, Nuclear Medicine Center, Budapest, HUNGARY, [2]Semmelweis University, Faculty of Medicine, Budapest, HUNGARY.

Aim/Introduction: Interim ^{18}F-FDG PET/CT scans are routinely performed for the evaluation of early therapeutic response in high-grade lymphoma patients. This assessment is most commonly based on the visual Deauville five-point scale (DS). However, recently, semi-quantitative methods, based on the standardized FDG-uptake value (SUV) have been introduced. Our aim was to compare the visual and semiquantitative assessment methods in interim PET/CT scans of diffuse large B-cell lymphoma (DLBCL) patients. **Materials and Methods:** Imaging and clinical data of 90 Chilean and Hungarian de novo DLBCL patients who participated in a clinical study organized by the International Atomic Energy Agency were retrospectively analysed. We measured SUV parameters in the most active residual lymphoma lesion and in an intrahepatic reference

volume of interest with a diamater of 3 cm. For semiquantitative evaluation, the modified qPET (m-qPET) was calculated as SUV_{peak}(lesion)/SUV_{mean}(reference), while the ratio-PET (rPET) was given as SUV_{max}(lesion)/SUV_{max}(reference). **Results:** Receiver Operating Characteristic (ROC)-analysis yielded a similar area under the curve (AUC) with each three methods (AUC DS: 0.7; AUC m-qPET: 0.73; AUC rPET: 0.72). Patients were divided into two groups according by each optimal cut-off value (m-qPET: 1.53; rPET: 1.54) obtained from the ROC-analysis (and by the conventionally used gouping og DS1-3 vs. DS4-5) and significantly different progression-free survival could be observed between each of the two groups (p<0,001). Positive predictive values were higher with both semiquantitative methods (m-qPET: 61% and rPET: 69% vs. DS: 52%), while negative predictive values remained similarly high with the visual and the semiquantitative approaches (m-qPET: 86%, rPET: 86% and DS: 88%). **Conclusion:** Semiquantitative evaluation of interim PET/CT scans has a better prognostic value than the visual score-based assessment. This - in conjunction with other biomarkers - could enable the early and precise identification of patients who need their treatment to be escalated or possibly de-escalated. **References:** Annunziata S, Cuccaro A, Calcagni ML, Hohaus S, Giordano A, Rufini V. Interim FDG-PET/CT in Hodgkin lymphoma: the prognostic role of the ratio between target lesion and liver SUVmax (rPET). Ann Nucl Med. 2016 Oct;30(8):588-92. Hasenclever D, Kurch L, Mauz-Körholz C et al. qPET - a quantitative extension of the Deauville scale to assess response in interim FDG-PET scans in lymphoma. Eur J Nucl Med Mol Imaging. 2014 Jul;41(7):1301-8.

EP-0390

Prognostic role of Interim PET in adult Hodgkin lymphoma

S. Pacella[1], *C. Landoni*[1], *C. Crivellaro*[1], *E. De Ponti*[2], *M. Arosio*[3], *F. Elisei*[3], *S. Bolis*[4], *L. Guerra*[3];
[1]*University of Milano Bicocca, Milano, ITALY,* [2]*Medical Physics Department, ASST Monza San Gerardo Hospital, Monza, ITALY,* [3]*Nuclear Medicine Department, ASST Monza San Gerardo Hospital, Monza, ITALY,* [4]*Haematology Department, ASST Monza San Gerardo Hospital, Monza, ITALY.*

Aim/Introduction: 18-Fluorodeoxyglucose (FDG) positron emission tomography/computed tomography (PET/CT) is an important tool for staging and for the response assessment in Hodgkin lymphoma (HL). It has been demonstrated that interim-PET (i-PET) has also a prognostic role and this study aimed to confirm this in patients with HL using the Deauville criteria; we also calculated the SUVmax and SUVpeak of the reference lesions. The results obtained with the two methods (semiquantitative and qualitative) were respectively correlated to disease free survival (DFS) and overall survival (OS). **Materials and Methods:** We retrospectively evaluated 83 patients (47 men, 36 women; mean age 40±14 years, range 20-73) with newly diagnosed HL, stage I-IV disease (27 stage I-IIA, 56 stage IIB-IVB). All patients underwent 18F-FDG PET/CT prior to treatment (baseline PET), after two cycles of chemotherapy (i-PET) and at the end of treatment. i-PET were qualitatively interpreted by two nuclear medicine physicians using the Deauville five-points scale with "the liver" as threshold: DS 1-3 classified i-PET as negative and DS 4-5 as positive. Lesions with the highest FDG uptake on i-PET were selected as "reference lesions" and SUVmax and SUVpeak of this were calculated. All datasets were correlated with DFS and OS. ROC curves were analyzed in order to find SUVmax and SUVpeak thresholds that better distinguish patients with good prognosis from the others. Kaplan-Meier method was used to evaluate DFS and OS. **Results:** The median follow-up was 36 months for DFS and 50 months for OS. i-PET scan resulted negative for 66 patients (79.5%) and positive for 17 (20.5%). The positive and negative predictive values of i-PET were 47,0% and 93,9%, respectively. The DFS and OS for positive i-PET and negative i-PET were 58.2% and 96.7% (p<0.0001), and 70.6% and 98.5% (p<0.0001) respectively. Cuts-off of 3.3 for SUVmax and of 3 for SUVpeak better distinguished good responders from the others and were also relevant for prognosis in terms of overall survival (OS) (p=0.014 and p=0.022, respectively). **Conclusion:** Interim PET/CT according to Deauville criteria with a threshold of 3 is a good predictor of outcome in patients with HL. Cuts-off of SUVmax < 3.3 and/or SUVpeak < 3 of the reference lesions are predictors of good prognosis in terms of overall survival (OS). **References:** Gallamini Andrea et al. "The predictive role of interim positron emission tomography for Hodgkin lymphoma treatment outcome is confirmed using the interpretation criteria of the Deauville five-point scale" Haematologica (2014).

EP-0391

Response Adapted Pet Ct Imaging In Hodgkin Lymphoma

K. Mladenov[1], *V. Hadzhiyska*[1], *D. Vasileva*[2];
[1]*University Hospital Aleksandrovska, Sofia, BULGARIA,* [2]*National Specialized Hospital for Active Treatment of hematological diseases, Sofia, BULGARIA.*

Aim/Introduction: With response-adapted therapy we measure the effect of treatment early in the course to distinguish the patients with treatment failure and modify the strategy. The aim of the study was to present our clinical experience to assess the role of interim PET/CT after chemotherapy for determination of the further management. **Materials and Methods:** Thirthy patients with HD were examined before and 20 days after 2/4 cycles of standard chemotherapy (ABVD or BEACOPP) by 18-F-FDG PET/CT. To assay the results we used 5-points Deauville scale and Lugano classification. **Results:** After 2/4 cycles of standard therapy, a negative interim PET results is obtained in 17 (58%) of the patients (score 1,2,3). These patients were in continuous complete remission. In the remaining 13 (42%) of the patients, interim PET varied from definitively positive to minimally positive (score 4, 5). By using the Deauville 5 point scale we found that the most frequently positive sites included the mediastinum, followed by superficial lymph nodes, abdominal nodes, lung nodes. All reported localizations of persistent residual uptake were at the original disease sites seen at baseline staging. In one patient was found a new site of

disease (score 5). In patients with HD there were two different treatment strategies, one starting with a less intensive regimen (ABVD) and another with a more efficacious regimen (BEACOPP), adopting opposite decisions by escalating or deescalating treatment based on interim PET results, while maintaining the original therapy for PET-negative and PET positive patients, respectively. **Conclusion:** 18-F-FDG PET is a well-established modality for interim assessment of tumor chemosensitivity early during therapy, rather than final therapy response at the time of evaluation, even proving to be a more accurate prognostic factor. PET-adapted strategy can modify management by individualizing therapy in the HD. Consequently, it is suggested that an adaptive therapy strategy based on interim PET results might distinguish high-risk patients who would benefit from escalated treatment regimens from low-risk patients whose treatment cycles could be abbreviated to minimize long-term adverse effects. **References:** None.

EP-0392

Efficacy of ^{18}F-FDG PET/CT in detection of bone marrow involvement in patients with newly diagnosed indolent Non-Hodgkin's Lymphoma

C. Sandoval Moreno, P. García Alonso, M. Tagliatori Nogueira, C. Mena Melgar, M. de la Rubia Marcos, A. Herrero Muñoz, C. Paniagua Correa, L. Castillejos Rodriguez, A. Ortega Valle, M. Balsa Bretón;
H. Universitario de Getafe, Getafe, SPAIN.

Aim/Introduction: In clinical practice, routine bone marrow biopsy (BMB) may no be necessary for all patients with Non-Hodgkin's Lymphoma (NHL). We aimed to evaluate the efficacy of ^{18}F-FDG in detection of bone marrow involvement in indolent Non-Hodgkin's Lymphoma. **Materials and Methods:** We reviewed records of all patients with newly diagnoses of indolent NHL (follicular lymphoma, marginal zone lymphoma and T cell lymphoma) during 3 years. ^{18}F-FDG PET/CT and bone marrow biopsy (BMB) were performed simultaneously (time interval between both procedure less than 30 days) before treatment. We evaluated 30 patients (18 women and 12 male), the median age was 62.3 years (range 38 - 82 years). ^{18}F-FDG PET/CT was performed using a standard protocol and BMB was doing in posterior left iliac crest. Visual evaluation was performed for ^{18}F-FDG PET/CT scan and we classified ^{18}F-FDG PET/CT results in negative (non bone uptake), positive (focal bone uptake) and diffuse positive (diffuse bone uptake). Finally, PET results were compared with histological data. **Results:** In our series, 21 patients (70%) had a negative ^{18}F-FDG PET/CT study: 15 of them had negative BMB (true negative). There were 6 false negative (positive BMB). These gave us a negative predictive value of 71%. We classified 5 patients as positive (focal bone uptake): 2 of them had a positive BMB (PET was positive in left iliac crest) and 3 of them had negative BMB. One case had a FDG guide surgical biopsy with a result of bone marrow involvement. All of them had a negative ^{18}F-FDG PET/CT control after treatment, so we considered them as a PET/CT true positive for bone marrow involvement. Finally, in our study, we classified 4 patients (13.3) as a diffuse positive uptake. Two of them had a positive BMB. **Conclusion:** The results of this study suggest that the ^{18}F-FDG PET/CT for bone assessment in the initial staging of indolent NHL seems to be useful when focal positive bone uptake was observed. In these patients, the visual assessment could have avoided BMB. In addition, PET/CT helps to locate lesions for biopsy. However, prospective and analytic studies are needed to prove this hypothesis, especially in negative and diffuse positive cases. **References:** None.

EP-0393

Opportunity Of ^{99m}Tc-1-thio-d-glucose SPECT Using In The Diagnosis And Staging Of Lymphomas

V. Chernov[1], *E. Dudnikova*[1], *R. Zelchan*[1], *V. Goldberg*[1], *T. Kravchuk*[1], *A. Danilova*[1], *A. Medvedeva*[1], *I. Sinilkin*[1], *O. Bragina*[1], *E. Stasyuk*[2], *V. Skuridin*[2];
[1]*Cancer Research Institute, Tomsk, RUSSIAN FEDERATION,*
[2]*Tomsk Polytechnic University, Tomsk, RUSSIAN FEDERATION.*

Aim/Introduction: To study possibility of ^{99m}Tc-1-thio-D-glucose (^{99m}Tc-TG) SPECT using for metabolic imaging and staging of malignant lymphomas. **Materials and Methods:** ^{99m}Tc-TG SPECT in 36 patients with newly diagnosed lymphomas were carried out. Sixteen patients had LH and twenty had aggressive forms of NHL: diffuse large B-cell lymphoma (15 cases), B-cell follicular lymphoma (2 cases), lymphoma from B cells in the marginal zone (1 case) and T-cell lymphoma (2 cases). In 3 patients IA stage was established, in 8 patients - IIA stage, in 4 patients - IIB stage, in 1 patient - IIE2 stage, in 4 patients - IIIA stage, in 2 patients - IIIB stage, in 6 patients - IVA stage and in 8 patients - IVB stage. **Results:** According to SPECT, pathological ^{99m}Tc-TG uptake in lymph nodes was observed in 31 (86%) of 36 patients. In 4 cases, the lymph nodes lesions also were not visualized by reference methods. In one patient enlarged submandibular lymph node (16 mm in size), determined by CT wasn't visualized by ^{99m}Tc-TG SPECT. Probably, this false-negative result is associated with the physiological enhancement of ^{99m}Tc-TG accumulation in the oropharyngeal region. Certain difficulties in the visualization of paratracheal, para-aortic and paracardial lymph nodes were noted. These difficulties were associated with a high background blood activity, which persisted even 4 hours after intravenous injection of ^{99m}Tc-TG. Software SPECT and CT fusion allowed visualizing nodal lesions of these localizations. In 5 cases, the lymph nodes lesions were visualized by ^{99m}Tc-TG SPECT, but were not detected by reference methods. According to the results of clinical and instrumental study, extranodal lesions were observed in 18 patients. Using ^{99m}Tc-TG SPECT extranodal hypermetabolic lesions were not detected in 4 (22%) of these patients: in the lung (1 case), in the liver (1 case) in the bone marrow (1 case) and in the stomach (1 case - ulcer less than 0.5 cm). In three patients, according to ^{99m}Tc-TG SPECT, a hypermetabolic lesions were visualized, which was not detected by CT results: in the lung (1 case), in the bone marrow (1 case) and in the soft tissue

(1 case). The ^{99m}Tc-TG SPECT using allowed changing the stage of disease (upstaging) in 4 (11%) patients. **Conclusion:** ^{99m}Tc-TG showed a high uptake in the nodal and extranodal lesions in malignant lymphomas patients. Therefore, we can consider ^{99m}Tc-TG SPECT as an additional diagnostic method for staging malignant lymphomas patients. **References:** None.

EP-0394

Prognostic Value of Total Metabolic Tumor Volume and Total Lesion Glycolysis of baseline 18F-Fluorodeoxyglucose Positron Emission Tomography/ Computed Tomography in Diffuse Large B-Cell Lymphoma

L. G. Diaz Gonzalez[1,2], *C. A. Achury*[1], *C. Montes*[1,2], *A. Martin*[1,2], *M. Peñarrubia*[3], *S. Fernandez*[4], *M. Vidal*[4], *J. Queizan*[5], *G. Hermida*[6], *D. Caballero*[1,2], *P. Tamayo*[1,2];
[1]*Hospital Clinico Universitario de Salamanca, Salamanca, SPAIN,* [2]*Biomedical Research Institute of Salamanca (Ibsal), Salamanca, SPAIN,* [3]*Hospital Clinico Universitario de Valladolid, Valladolid, SPAIN,* [4]*Complejo Asistencial Universitario de Leon, Leon, SPAIN,* [5]*Hospital de Segovia, Segovia, SPAIN,* [6]*Hospital Universitario de Burgos, Burgos, SPAIN.*

Aim/Introduction: To quantify total metabolic tumor volume (TMTV) and total lesion glycolysis (TLG) on pretreatment 18F-FDG PET/CT and analyze its prognostic value as predictors of response of treatment in patients diagnosed of diffuse large B-cell lymphoma (DLBCL). **Materials and Methods:** We here present 68 patients, of a multicenter prospective study carried out in newly diagnosed DLBCL patients treated with 6 cycles of R-CHOP, who have completed the treatment and the response to the end of treatment has been evaluated. Thirty-five men and thirty-three women with a median age of 60,2 years (range,24-82 years). All patients underwent at least two PET/CT studies with 18F-FDG, one at diagnosis (baseline) and the other at the end of treatment (EoT). TMTV and TLG parameters were quantified by three nuclear medicine physician blinded to a patient outcome on the semiautomatic free software "LIFEx" (http://www.lifexsoft.org) using an automatic segmentation of the lesions with a SUV > 3 with an adaptive threshold. To determine whether TMTV and TLG values predict the response to treatment univariate Cox regression analysis was performed. Statistical significance was considered at p<0,05. Data were analysed using SPSS software version 20. **Results:** Of the sixty-eight patients, 52 patients (76,5 %) were in complete response at EoT with mean values of TMTV, TLG and SUVmax of 554,2 cm³ (range 0,8-2340), 4689,2 cm³ (range, 2-11032) and 24,2 (range, 3-50), respectively. The mean values of TMTV, TLG and SUVmax in the sixteen patients who did not reach complete response at the EoT were 1468,25 cm³ (range 28-6626), 11026,2 cm³ (range, 229-31123) and 26,2 (range, 14-43), respectively. There were statistically significant differences between both group of patients with respect to TMTV (p<0.05) and TLG values (p<0.05), showing higher baseline TMTV and TLG values the patients that did not get complete response at the end of the treatment, but not with respect to SUVmax. **Conclusion:** Our results suggest that baseline TMTV and TLG values might predict the response of treatment in patients with DLBCL. **References:** None.

EP-0395

Prognostic role of baseline 18 F-FDG PET/CT parameters in MALT lymphoma: preliminary results

M. Rashki, *E. Triviño-Ibañez, J. López Ruiz, A. González Jiménez, T. Rudolphi Solero, J. LLamas-Elvira;*
Hospital Virgen de las Nieves, Granada, SPAIN.

Aim/Introduction: Mantle cell lymphoma (MCL) is a subtype of aggressive lymphoma with poor prognosis and high avidity of 18F-FDG in PET/CT (FDG-PET/CT), however, there are no validated criteria for FDG-PET/CT in the evaluation of treatment or the prediction of the tumor response. The aim of the study was to investigate whether the metabolic characteristics of FDG-PET/CT can predict the response to treatment and the prognosis in the MCL. **Materials and Methods:** We retrospectively enrolled 24 patients who underwent baseline FDG-PET/CT and 23 end of treatment FDG-PET/CT. The baseline PET images were analyzed visually and semi-quantitatively by measuring the maximum standardized uptake value body weight (SUVbw), metabolic tumor volume (MTV) and total lesion glycolysis (TLG). The end of treatment FDG-PET/CT was visually interpreted according to the criteria of the Deauville 5-point scale (DC). Survival curves were plotted according to the Kaplan-Meier method. **Results:** 24 patients (mean age: 67.1±9.8 years, 79.2% men, mean of follow-up: 35.4 months). Stage according to the Ann Arbor system: 5.3% stage II, 10.5% stage III and 84.2 % stage IV. B-symptoms were present in 18.2% of patients. International prognostic index (MIPI) score results demonstrated that 33.3% cases were in the low-risk group, 25% in the intermediate-risk group, and 41.7% in the high-risk group. Relapse/progression occurred in 33.3% of patients and death in 25%. Median OS and PFS were 25 months (IQR: 8.0-51.5 months) and 24.5 months (IQR: 8.0-49.8months) respectively. Baseline MTV and TLG were higher in patients with partial response compared to complete response group (124.3±427.0 vs 924.7±1297.3 and 734.0±2761.1 vs 3689.8±5195.0, respectively), although this differences did not reach statistical significance. In addition, patients with a high SUVmax had a worse outcome survival. Considering OS and PFS, the mean of survival was higher in patients with baseline SUVmax<5 compared with the group with baseline SUVmax≥5 (45.6±34.9 vs 30.3±39.6 months and 44.5±34.3 vs 24.2±20.8 months, respectively), although this differences did not reach statistical significance. **Conclusion:** Our preliminary results show that baseline FDG-PET/CT metabolic parameters were not significatly related to survival, although the patients with higher baseline SUVmax, MTV and TLG had worse outcome. **References:** None.

EP-0396

Response Assessment of Rosai-Dorfman Disease with ^{18}F FDG PET/CT

S. Shamim, *S. Datta Gupta, S. Tripathy, J. Hussain, G. Arora, C. Bal;*
All India Institute of Medical Sciences, Delhi, INDIA.

Aim/Introduction: Rosai-Dorfman disease (RDD) is a rare benign lympho-proliferative disorder of histiocytes, most often seen in lymph nodes. Approximately 25-43% of RDD present with extra-nodal manifestations, with skin being the commonest extra-nodal site. Usually a self-limiting inflammatory disorder, which remits with supportive care in the form of steroids or low dose thalidomide; rarely it may be aggressive in nature and not self-resolving, requiring chemotherapy. RDD lesions are known to be avid on ^{18}F-FDG PET. Use of PET/CT in evaluation of disease extent is well established; our aim was to assess the less explored possibility of use of^{18}F-FDG PET/CT in response assessment in RDD. **Materials and Methods:** Histopathologically proven cases of Rosai-Dorfman disease, referred by physician for ^{18}F-FDG PET/CT from June, 2014 to December, 2018 were retrospectively included in this study. Steroid was stopped for one week prior to scanning as per standard practice. Scan images were reported by two independent nuclear physicians and response was assessed as per PERCIST criteria. Patients were followed up clinically and management of patients was thereafter altered depending on scan findings. **Results:** Eleven patients with known RDD were included. Nine of the eleven included were male and two female, with mean age of 21 (±4.8) years. 10 out of 11 had extensive nodal disease at baseline and one had only cutaneous manifestations. The 10 patients with nodal involvement showed additional skeletal involvement in 2 cases, cutaneous manifestations in another 2 cases and pleural involvement in one. Three out of eleven had only post therapy ^{18}F-FDG PET/CT to look for residual metabolic disease. Remaining 8 patients had a median of three scans with a minimum of at least two (baseline and post therapy) scans. Treatment was discontinued in case of complete metabolic response (CMR), continued or altered in case of partial metabolic response or stable disease and altered in progressive disease as per the physicians' discretion. Patients with complete metabolic response at the end of treatment (3/11) were followed up with ^{18}F-FDG PET/CT surveillance. **Conclusion:** ^{18}F-FDG PET/CT appears to be a useful modality in guidance of patient management in Rosai-Dorfman disease and in assisting in screening for extra-nodal extension of disease. It allows timely cessation of treatment in the absence of metabolically active disease and change of treatment in non-responders. **References:** Warpe BM, More SV. Rosai-Dorfman disease: A rare clinico-pathological presentation. Australas Med J. 2014;7(2):68-72. Published 2014 Feb 28. doi:10.4066/AMJ.2014.1931.

EP-0397

^{18}F-FDG PET/CT imagingfeatures of renal lymphoma

Y. Yu, X. Han;
The First Affiliated Hospital of Zhengzhou University, Zhengzhou, CHINA.

Aim/Introduction: To investigate ^{18}F-FDG PET/CT imaging features and clinical manifestations of renal lymphoma. **Materials and Methods:** The clinical data and ^{18}F-FDG PET/CT imaging data of 99 patients with renal lymphoma (69 males and 30 females, aged 3-86 years) confirmed by pathology or multiple imaging were retrospectively analyzed. **Results:** All Ninety-nine cases of renal lymphoma were secondary, and ^{18}F-FDG PET/CT was positive. The diagnostic sensitivity was 100%(99/99). Among 99 cases of renal lymphoma, 97 cases were non-Hodgkin's lymphoma, 2 cases were Hodgkin's lymphoma, and 10 cases showed varying degrees of creatinine elevation.Renal lymphoma has a wide variety of manifestations, including multiple lesions, a solitary lesion,direct extension from retroperitoneal adenopathy,preferential involvement of the perinephric space,and diffuse infiltration of one or both kidneys , accounting for 35.4%, 22.2%, 12.1%, 5.1%, 3.0%, 17.2%, respectively. Mixed forms accounts for 5.1%. The SUV_{max} of the above types were 14.92 +8.69, 12.25 +5.78, 16.53 +8.01, 11.16 +3.54, 9.57 +4.45, 10.04 +5.44, and 14.32 +6.92 in the mixed presence. **Conclusion:** ^{18}F-FDG PET/CT imaging of renal lymphoma has high diagnostic sensitivity and plays an important role in the diagnosis, staging and evaluation of curative effect. **References:** None.

EP-0398

Validation of Multi-Foci Segmentation method for Measuring Metabolic Tumor Volume in Hodgkin's Lymphoma

M. R. F. Camacho[1], *E. Etchebehere*[1,2], *C. Ramos*[1,2,3], *A. Verçosa*[4], *N. Tardelli*[3], *M. Delamain*[5], *M. Takahashi*[6], *S. Brunetto*[7], *I. Metze*[5], *C. Souza*[5], *J. Cerci*[8];
[1]*MND Campinas, Campinas, BRAZIL,* [2]*Division of Nuclear Medicine, Department of Radiology, University of Campinas, Campinas, BRAZIL,* [3]*School of Medical Sciences, University of Campinas (UNICAMP), Campinas, BRAZIL,* [4]*UNICAMP, Campinas, BRAZIL,* [5]*Division of Hematology and Hemotherapy, Department of Internal Medicine, University of Campinas, Campinas, BRAZIL,* [6]*Institute of Physics, University of Campinas (UNICAMP), Campinas, BRAZIL,* [7]*Biomedical Engineering Center, University of Campinas (UNICAMP), Campinas, BRAZIL,* [8]*Quanta Diagnosis and Therapy Clinic, Curitiba, BRAZIL.*

Aim/Introduction: Calculation of metabolic tumor volume (MTV) and total lesion glycolysis (TLG) can be time-consuming.[1,2] The main objective of this study was to compare two methods of quantification: the multi-foci segmentation method (MFS), which is an automatic method, and the multiple VOI method (MV), which was used as reference standard. **Materials and Methods:** This was a prospective bicentric study in which 50 patients with Hodgkin's Lymphoma (HL) underwent staging 18F-FGD PET/CT. The exams were processed using the Syngovia VB20 software (Siemens Medical Solutions, Chicago, IL) in order to obtain MTV and TLG utilizing two fixed relative thresholds of 40% and 20% of the maximum standardized uptake value (SUV) of each lesion. All PET/CTs were processed using the MV and the MFS methods. Inter-class correlation coefficient and Bland & Altman plots were used for the statistical analysis. **Results:** The mean and the standard deviation values obtained for the MTV with MV and MFS were respectively 736 ± 856 mL and 660 ±

699 mL for the 20% threshold, and 313 ± 359 mL and 372 ± 434 mL for the 40% threshold. The time spent calculating the MTV was much lower with the MFS than with the MV (15 min. vs up to 4 hours, respectively) in patients with advanced disease. Time spent was similar in patients with localized disease. **Conclusion:** MTV and TLG calculations using MFS produce similar results to those obtained with MV and are much less timing consuming. Main differences between the two methods were related to difficulties in avoiding overlay of VOIs in the MV technique. MV and MFS perform equally well in lesions with very low uptake. **References:** 1. Im HJ, Bradshaw T, Solaiyappan M Cho SY Current Methods to Define Metabolic Tumor Volume in Positron Emission Tomography: Which One is Better? Nucl Med Mol Imaging. 2018 Feb;52(1):5-15.2.Song MK, Chung JS, Lee JJ, Jeong SY, Lee SM, Hong JS, Chong A, Moon JH, Kim JH, Lee SM, Kim SJ, Shin HJ. Metabolic tumor volume by positron emission tomography/computed tomography as a clinical parameter to determine therapeutic modality for early stage Hodgkin's lymphoma. Cancer Sci. 2013 Dec;104(12):1656-61.

EP-0399

Clinical and prognostic significance of FDG-PET derived biomarkers in high grade B cell lymphoma

Z. Ritter[1], *K. Zámbó*[1], *D. Dezső*[1], *Z. Szabó*[1], *Z. Bán*[1], *B. Kajtár*[2], *K. Farkas*[3], *Á. Szomor*[4], *A. Hussain*[4], *E. Schmidt*[1];
[1]*University of Pécs, Department of Nuclear Medicine, Pécs, HUNGARY,* [2]*University of Pécs, Department of Pathology, Pécs, HUNGARY,* [3]*University of Pécs Institute of Bioanalysis, Pécs, HUNGARY,* [4]*University of Pécs 1st Department of Internal Medicine, Pécs, HUNGARY.*

Aim/Introduction: Diffuse large B cell lymphoma (DLBCL) is the most common subtype of non-Hodgkin Malignant Lymphomas. There is a need to distinguish the high risk patients as early as possible for further intense therapy. For this purpose we aimed to evaluate the prognostic significance of biomarkers derived from baseline FDG-PET/CT and find their correlations with clinical and histological data. **Materials and Methods:** The baseline PET/CT of a total of 39 patients (25 women, 14 men) was performed between 2016-2018. The tumor volume was segmented by semi quantitative method using global threshold lesion detection software (Mediso). The detected biomarkers were: Standardized Uptake Value (SUVmax), Total Lesion Glycolysis (TLG), and Metabolic Tumor Volume (MTV). These data were correlated with the Revised International Prognostic Index (R-IPI), the Lactate Dehydrogenase (LDH) level and the Proliferation Index (MIB-1). All patients received standard R-CHOP treatment. During the treatment (3-4th cycle), and after the treatment was completed (6-8th cycles) PET/CT scan was repeated. The response to the therapy was evaluated by visual assessment, according to the Deauville 5 point scale criteria. Data were analyzed using the SPSS statistical software. **Results:** According to the interim PET/CT, 16 patients remained in Deauville 4 or 5 stages (group 1) and 23 patients (group 2) had complete metabolic remission (CMR). There was significant decrease in all three parameters (TLG: $p < 0.01$, MTV: $p < 0.01$ and SUVmax: $p = 0.05$) in patients with CMR. After completion of treatment further 9 patients from group 1 showed CMR, but in 7 patients stable disease was detected. In contrast, 3 patients from group 2 who were in CMR showed progression. Thus, at the end of the therapy, a total of 29 patients had CMR, 10 patients had detectable metabolically active tumor tissue. Based on these findings, we divided the patients into two new groups in which more significant difference in our biomarkers was found: TLG ($p < 0.001$), MTV ($p = 0.001$), SUVmax ($p < 0.05$). In addition, a significant positive correlation was found between MIB-1 and SUV max values ($p < 0.05$) and between TLG and LDH ($p < 0.001$) and MTV and LDH ($p < 0.001$) levels. **Conclusion:** Based on our results all three imaging parameters may be suitable for estimating response to standard therapy together with histological and laboratory data. We plan to expand our study with 80 patients to confirm our results. **References:** None.

EP-0400

Metabolic response of normal bone marrow in non-responders patients with Hodgkin Lymphoma: a FDG-PET/CT study

A. Borra[1], *R. Lai*[2], *M. Bauckneht*[1], *S. Capitanio*[1], *S. D. Morbelli*[1,3], *V. Ceriani*[1], *F. Fiz*[4], *S. Bruno*[5], *M. Piana*[6,2], *C. Cristina*[7], *D. Schenone*[6], *S. Maggio*[1], *F. Frassoni*[8], *C. Marini*[9,1], *G. Sambuceti*[1,3];
[1]*Nuclear Medicine Department, IRCCS Ospedale Policlinico San Martino, Genoa, ITALY,* [2]*SPIN Institute, CNR, Genoa, ITALY,* [3]*Department of Health Science, University of Genoa, Genoa, ITALY,* [4]*Nuclear Medicine Unit, Department of Radiology, University of Tuebingen, Tuebingen, GERMANY,* [5]*Department of Experimental Medicine, University of Genoa, Genoa, ITALY,* [6]*Department of Mathematics (DIMA), University of Genoa, Genoa, ITALY,* [7]*Department of Mathematics (DIMED), Padova University Hospital, Padua, ITALY,* [8]*Istituto Giannina Gaslini, Genoa, ITALY,* [9]*CNR Institute of Molecular Bioimaging and Physiology (IBFM), Milan, ITALY.*

Aim/Introduction: The present study aimed to verify whether metabolic response of active bone marrow (BM) to chemotherapy is correlated with treatment effect in patients with Hodgkin lymphoma. **Materials and Methods:** We studied 33 patients (10 female and 23 male, median age 42, range 19-78 years) with Hodgkin lymphoma. All patients underwent PET/CT imaging at baseline, after 2 cycles (interim) of ABVD (Adriamycin, Bleomycin, Vinblastine and Dacarbazine) and one month after treatment completion (EoT). Ten non-responders patients showed a positive interim scan (Deauville score ≥4) and were moved to BEACOPP scheme (Bleomycin, Etoposide, Adriamycin, Cyclophosphamide, Oncovin, Procarbazine and Prednisone). Patients with suspected BM involvement were excluded from the analysis. All PET/CT scans were analyzed to identify the intraosseous volume (IV) of all vertebral bodies at all time points. As previously described, an iterative optimization scheme was applied to each CT slice to identify the external bone border and thus to extract the IV and its metabolic activity from co-registered PET images. According to our previously

validated procedure, inactive BM was defined by IV voxels with a SUV <1.1, while voxels over this cutoff identified active BM. Volume of both BM components was estimated and expressed as % of total IV. **Results:** No differences in age, prevalence of male gender or disease extension were observed at baseline examination. Similarly, before treatment initiation, mean SUV of intraosseous voxels (1.83±0.34 vs 1.72±0.28, in responders and non-responders, respectively, p=ns) and extension of inactive BM (15±8% and 18±7%, respectively, p=ns) were not significantly different between the two groups. However, at the interim PET after the same two ABVD cycles, responders showed significantly lower extension of inactive BM with respect to non-responders (11±10% vs 26±15%, respectively, p<0.01). This difference even increased at EoT scan (18±10% vs 35±20%, respectively, p<0.01). By contrast, average SUV of either active and inactive BM did not show any significant difference at any study point between the two groups. **Conclusion:** ABVD failure is associated with a peculiar metabolic response by normal BM to chemotherapy characterized by a more evident loss of active BM in favor of its inactive counterpart. **References:** None.

EP-0401

Metabolic multiparametric analysis in PTLD baseline 18-FDG PET/TC: MTV, TLG, SUVmax, mean and peak can predict patient outcome after first line of treatment?

R. V. A. Vicinelli[1], *M. Spallino*[2], *C. Dolci*[2], *M. Nichelatti*[3], *A. F. Scarale*[2], *M. Bonacina*[1], *E. Preza*[1], *E. Gay*[2], *P. Minga*[4], *C. Rossetti*[2];
[1]*Nuclear Medicine Department, University Milano-Bicocca, Milan, ITALY,* [2]*Nuclear Medicine Unit, ASST Grande Ospedale Metropolitano Niguarda, Milan, ITALY,* [3]*Department of high formation, research and development, ASST Grande Ospedale Metropolitano Niguarda, Milan, ITALY,* [4]*Ematology Unit, ASST Grande Ospedale Metropolitano Niguarda, Milan, ITALY.*

Aim/Introduction: Post transplant lymphoproliferative disorders (PTLD) are a serious consequence of immunosuppression after solid organ transplantation. Aim of this study was to evaluate if some metabolic parameters extracted from baseline 18-FDG PET/CT such as maximum, mean peak, standard uptake values (SUVmax, SUVmean, SUVpeak), metabolic tumoral volume (MTV) and total lesion glycolysis (TLG) can predict response in PTLD after first line chemotherapy. **Materials and Methods:** 25 PTLD patients were retrospectively evaluated (19 males, mean age 45 years with range 22-84; with 75% of cases with B cell-lymphoma and 50% with EBV positivity). All patients underwent 18F-FDG PET/CT at baseline and after a first line of chemotherapy which was rituximab, cyclophosphamide, hydroxydaunorubicin, prednisone (R-CHOP) treatment for the majority of them as first choice. MTV, TLG, SUVmax, SUVmean, SUVpeak were calculated at baseline PET by using PET viewer add-on of Imaj2 FIJI software. Metabolic response was defined in post treatment scan as responder (CR, Deauville score 1-2) and non responder (NR, Deauville score 3-5) according to literature[1]. Classes of metabolic response were correlated to metabolic parameters at baseline by using Wald test. **Results:** Post treatment 18F-FDG PET/CT classified 16 CR, 9 NR. No significant differences between CR and NR in baseline 18F-FDG PET baseline were the found SUVmax (Median 24,6 ± 12,1 and 15,7 ± 16,77 respectively for CR vs NR, p 0.38), SUVmean (8,40± 5,65 and 5,35 ±6,77 respectively p 0,376) SUVpeak (21,77 ± 11,10 and 14,37 ± 14,19 respectively, p 0.83), MTV (210,3 ± 328,27 and 407,3 ± 312, p 0.41) and TLG (1790,69 ± 4227,75 and 3121,85 ± 2275,53 respectively, p 0.38). **Conclusion:** 18F-FDG PET metabolic parameters like MTV and TLG are nowadays widely studied as predictor of therapy response and prognosis in major type of lymphomas, e.g. B-cell type. In Our study there were no significant differences in multiparametric metabolic parameters extracted in baseline 18F-FDG PET/CT between CR and NR population affected by PTLD, suggesting they are not sufficient themselves to discriminate CR from NR. Further analysis with larger sample size with more biological and radiomics parameters could demonstrate the value of metabolic analysis in this kind of patients. **References:** 1 End-of-Treatment Positron Emission Tomography After Uniform First-Line Therapy of B-Cell Posttransplant Lymphoproliferative Disorder Identifies Patients at Low Risk of Relapse in the Prospective German PTLD Registry. Zimmermann H, Denecke T, Trappe RU.

EP-26

Clinical -> Diagnostic study -> Adult study -> Oncology study -> Organ-based oncology -> Liver, upper GI and pancreatic (non-endocrine), malignant

October 12 - 16, 2019 e-Poster Area

EP-0402

Digital PET/CT Improves the Detection of Liver Lesions in Cancer Patients

F. Fuentes-Ocampo[1], *D. López-Mora*[1], *A. Flotats*[1], *V. Camacho*[1], *L. Alarcón-Lagos*[2], *M. Sizova*[1], *A. Fernández*[1], *J. Duch*[1], *A. Domènech*[1], *M. Estorch*[1], *I. Carrió*[1];
[1]*Hospital de la Santa Creu i Sant Pau, Barcelona, SPAIN,*
[2]*Hospital Dr. Gustavo Fricke, Viña del Mar, CHILE.*

Aim/Introduction: The introduction of digital detectors in PET/CT may have a significant clinical impact with greater accuracy in the staging and follow-up of oncological diseases. Therefore, we sought to compare the detectability of liver lesions between a digital and an analog PET/CT in cancer patients. **Materials and Methods:** Twenty six oncological patients (14 women, 12 men; mean age of 69 ± 9 years; 10 lung cancer, 6 breast cancer, 5 colorectal cancer, 1 hepatocellular carcinoma, 1 melanoma, 1 prostate cancer, 1 urothelial cancer, 1 cancer of unknown primary origin) with liver lesions were prospectively included from February 2018 - March 2019. All patients, who accepted to be scanned twice, consecutively underwent a dual imaging protocol (digital and analog PET/

CT) in a single day. Three nuclear medicine physicians evaluated the detectability of liver lesions by counting the number of lesions with increased radiotracer uptake. Differences were considered significant for a p value <0.05. The STATA v15.1 was used for the statistical analysis. **Results:** There was a significant difference in the total number of liver lesions detected by the two systems (digital: 4.3 ± 5 vs. analog: 2.4 ± 3.4; p=0.024). In 17 out of 26 patients, both systems detected liver lesions (PET+). In 14 out of the 17 PET+ patients, the digital system detected more liver lesions than the analog system without reaching statistical significance (digital 6 ± 5.5 vs analog 3.7 ± 3.7; P>0.05). In the other three patients (of these 17 PET+) both systems detected the same number of liver lesions. Moreover, the digital system was positive in 7 patients (29%) in whom the analog system did not detect liver lesions (PET-). In these 7 patients, 80% of the lesions detected by the digital PET/CT (and not by the analog PET/CT) were <10mm (7.4±2.2 mm). Two patients were considered PET- by both systems. **Conclusion:** Digital PET/CT offers improved detectability of liver lesions in cancer patients over the analog PET/CT, even further for subcentimeter lesions. **References:** None.

EP-0403

Value of ^{18}F-FDG PET/CT in diagnosing pancreatic lesions:Comparison with CA19-9, enhanced CT and MR

S. Huang[1,2], *H. Chong*[2], *Y. Zhang*[2], *X. Lan*[2];
[1]*Cancer Hospital & Shenzhen Hospital, Chinese Academy of Medical Sciences and Peking Union Medical College, Shenzhen, CHINA,* [2]*Union Hospital, Tongji Medical College, Huazhong University of Science and Technology, Wuhan, CHINA.*

Aim/Introduction: To evaluate ^{18}F-FDG PET/CT in diagnosing pancreatic lesions, and compare it with CA19-9, contrast-enhanced CT (CECT) and contrast-enhanced MRI (CEMR). **Materials and Methods:** Cases of patients with suspected pancreatic lesions on ^{18}F-FDG PET/CT were retrospectively analyzed from Jan 2011 to June 2017. Inclusion criteria were as follows: (1) no pathological diagnosis, or any anticancer therapy including surgery, radiotherapy, or chemotherapy before any examination; (2) serum CA19-9, CECT or CEMR performed within 2 weeks of PET/CT if available; (3) complete medical history and follow-up data (> 6 months). Exclusion criteria were: (1) blood glucose >11 mmol/L before injection of 18F-FDG; (2) other malignant tumors in addition to the pancreatic lesions confirmed either before or after PET/CT scan; (3) pancreatic neuroendocrine tumors/cancers (NETs/NECs). Images were interpreted by at least two experienced nuclear medicines or radiologists. Visual analysis and semi-quantitative analysis (SUVmax) were utilized for PET/CT images. We compared the diagnostic efficacy of PET/CT with CA19-9, CECT and CEMR as well as combined tests. **Results:** A total of 467 cases were examined in this study, including 293 males and 174 females, with an average age of 57.79 ± 12.68 y (16-95 y). Cases in the malignant group (n=248) had significantly higher SUVmax (7.34±4.17 vs. 1.69±2.68, P <0.001) and CA19-9 (663.21±531.99 vs. 87.81±218.47, P <0.001) than those in the benign group (n=219). The sensitivity, specificity and accuracy of PET/CT were 91.9%, 96.3% and 94.0% respectively. Those for CECT were 83.6%, 77.8%, 81.2% respectively; and 91.2%, 75.0%, 81.7% were for CEMR. PET/CT corrected 14.7% (28/191) CECT and 11.9% (10/84) CEMR diagnoses. Diagnostic performances were not obviously improved when we combine CECT, CEMR or both with PET/CT. Although the diagnostic efficiency of CA19-9 was barely acceptable (80.0%, 69.0%, 74.9% respectively), the joint application of PET/CT and CA19-9 could significantly enhance the diagnostic efficiency compared with PET/CT alone (sen 97.4% vs. 91.9%, P = 0.026; spe 100.0% vs. 96.3%, P = 0.011). **Conclusion:** To our knowledge, this study reports the largest group of patients with suspected pancreatic lesions retrospectively evaluated by PET/CT, CA19-9, CECT and CEMR. Our results show that PET/CT has sensitivity similar to CEMR and significantly higher specificity and accuracy than CA19-9, CECT, and CEMR alone; and can help reduce false diagnoses of morphological images. Furthermore, combining PET/CT with CA19-9 could enhance diagnostic efficiency. **References:** None.

EP-0404

Utility of Metabolic Parameters on Baseline FDG PET/CT for Prognostication in patients with operable Esophageal Adenocarcinoma

R. Kakde, *N. Purandare, V. Rangarajan, A. Agrawal, S. Shah, A. Puranik;*
Tata Memorial Hospital & Research Center, Mumbai, INDIA.

Aim/Introduction: Metabolic parameters (SUV, MTV, and TLG) have been reported to be independent prognostic factors for survival in carcinoma of lung, ovary and head and neck cancers. Purpose of this study was to evaluate the utility of various metabolic parameters seen on FDG PET/CT in operable Esophageal Adenocarcinoma. **Materials and Methods:** Operated patients of esophageal adenocarcinoma who had undergone baseline staging with 18F-FDG PET/CT from 2005 to 2014 were included. Semi-quantitative parameters like SUV max, SUV mean, Total Lesion Glycolysis (TLG) and Metabolic Tumor Volume (MTV) of the primary site were correlated with overall survival (OS) and disease-free survival (DFS). Survival analysis was done considering the metabolic parameters using the Kaplan-Meier, ROC curve and the log rank test method. The cutoff point chosen based on ROC curve analysis was 16.2, 9.28, 17 and 157.10 for the SUVmax, SUVmean, MTV, and TLG respectively. **Results:** 104 operable Esophageal adenocarcinoma patients (M: F- 83: 21) were included in this retrospective study, age range: 22-82 years. Median follow up was - 40 months (range - 05-89 months) Mean follow up was - 42.19 months Median 5 year OS of the entire group was 44.3 % Median 5 year DFS of the entire group was 56 % There was a significant difference in OS in patients using TLG cutoff >157 (31% vs. 39.3%) (p=0.03). The difference in OS for SUVmax, SUVmean, MTV, and DFS for TLG values did not show a statistically significant correlation. **Conclusion:** Total Lesion Glycolysis (TLG) was significant predictor of overall survival in operated Esophageal Adenocarcinoma patients. Rest of the

metabolic parameters like MTV for OS and DFS and TLG for DFS showed a definite trend towards predicting clinical outcomes, though a statistical significance could not be demonstrated. **References:** None.

EP-0405

Fluorodeoxyglucose Positron Emission Tomography and computed tomography metabolic parameters in Oesophageal Carcinoma

K. G. M. Mokoala, *I. O. Lawal, T. M. G. Boshomane, T. Lengana, M. Voster, M. M. Sathekge;*
Steve Biko Academic Hospital / University of Pretoria, Pretoria, SOUTH AFRICA.

Aim/Introduction: Carcinoma of the oesophagus is a very ominous disease with an extremely poor prognosis with more than half of patients having unresectable disease at their first presentation. Nodal involvement is the poorest prognostic factor and survival rate drops dramatically with N2 or above disease. The aim of this study was to identify metastatic patterns of oesophageal carcinoma and to determine the abilities of FDG-PET/CT metabolic parameters in predicting the presence of distant metastasis and overall survival. **Materials and Methods:** Fourty-eight patients with histological diagnosis of oesophageal carcinoma underwent 18F-FDG PET/CT for staging. Maximum and mean standardized uptake values (SUVmax and SUVmean), metabolic tumor volume (MTV) and total lesion glycolysis (TLG) of the oesophageal cancer lesion were determined. We compared these parameters and determined their abilities to predict the presence of metastasis. **Results:** The mean age of the patients was 62 years ±13.94 with a 1:1 male to female ratio. The middle and distal thirds of the oesophagus were the most common sites of involvement, while only 20% of the tumours were in the proximal third of the oesophagus. The mediastinal lymph nodes were the most frequent (70%) site of nodal metastasis. There was no significant associations between MTV of the primary tumor and distant metastasis; however, TLG performed well in predicting the presence of distant metastasis. Both MTV and TLG were independent prognostic factors for overall survival. There was no correlation between SUVmax and SUVmean and metastasis. **Conclusion:** PET/CT metabolic parameters such as MTV and TLG can be predictors of overall survival in patients with oesophageal cancer, while TLG performed well in predicting the presence of distant metastases. **References:** None.

EP-0406

The Role Of 18F-FDG PET/CT For Evaluation Of The Efficiency Of Radiofrequency Ablation (RFA) Of Primary And Metastatic Tumors Of The Liver

G. H. Mateva, *I. Kostadinova, S. Handzhiev, A. Demirev, M. Garcheva - Tsacheva;*
Acibadem City Clinic Oncology Center, Sofia, BULGARIA.

Aim/Introduction: Radiofrequency ablation (RFA) of liver metastasis is non-invasive treatment option for patients with oligometastatic disease (up to 3 liver metastasis and no extrahepatic involvment). We aimed to share our preliminary data for the role of 18FDG PET/CT for treatment evaluation and early diagnosis of local relapse of liver metastasis after RFA procedure. **Materials and Methods:** We investigated 11 patients with total number of 20 liver metastasis.The primary tumors were as follows: 3 with colon cancer, 3 with pancteatic carcinoma, 2 with breast cancer, 2 with HCC and 1 with carcinoma of papila Vateri. The PET/CT studies were performed 2 months after the RFA, since the literature review showed it is the shortest interval of time that allows to assess the treatment effect with small chance of false positive lesions due to active post treatment necrotic and inflamatory changes. We have used mainly the change of SUVmax and the PERCIST criteria for interpretation of results. In all of the cases we performed contrast-enchanced ultrasound (CEUS) within 10 days after the PET/CT and compared it with the hybrid study. **Results:** In four patients (36%) we observed complete response, in one patient (9%) there was stable disease and in six of the patients (54%) - progressive disease (including 2 cases with extrahepatic involvement). When compared with CEUS we had disagreement in two cases, where PET/CT showed increased metabolic activity in lesions and progressive disease, while with CEUS the same lesions were evaluated as good therapeutic effect. As a result of the performed PET/CT study three of the patients underwent additional RFA for four lesions. **Conclusion:** In conclusion we suggest that PET/CT might be a valuable tool for early evaluation of efficiency of RFA of primary and metastatic lesions of the liver and planning of future treatment. However more investigations are needed for proving this consideration. **References:** None.

EP-0407

Does PET-CT scan play a role in the management of esophagus squamous cell carcinoma patient's? (about 41 cases)

O. Zakaria, *O. Amine, T. Sara, A. Hind, G. Amal;*
Nuclear medecine department, Ibn Rochd UH, Hassan II University, Casablana, MOROCCO.

Aim/Introduction: Esophageal cancer is a bad prognosis cancer. Its severity is related to its extension at the time of diagnosis. The total number of deaths in France estimated in 2010 was 3470. In the greater Casablanca region, esophageal cancer is estimated at 1.1% of all cancers in men. **Materials and Methods:** Retrospective study including cases of esophagus squamous cell carcinoma, explored by ^{18}FDG PET-CT from January 2011 to December 2017, in the nuclear medicine department of Ibn Rochd University Hospital in Casablanca, Morocco. **Results:** In total, forty-one patients were included . The average age was 42 years old. The exam was carried out as part of the extension assessment in 76% the cases, the postoperative evaluation report 2%, post-chemo-radiotherapy evaluation in 19%, recurrence suspicion 2%. ^{18}FDG PET-CT was

done according to eanm guidelines. The results of the ^{18}FDG PET-CT scan were, as part of the extension assessment, the disease was localized to the esophagus in 20%, local extension in 15%, lymph node extension in 45%, metastatic extension in 20%. As part of the treatment response assessment, after surgery: the response was partial in 100% of cases, post-chemo-radiotherapy: the response was partial in 50% of patients and progressive in the remaining 50%. In the context of suspected recurrence, PET was positive in all patients. In the four patients who has had two ^{18}FDG PET-CTs. The scan showed complete remission in one case, partial response in one case, and progressive disease in the remaining two patients. **Conclusion:** ^{18}FDG PET-CT scan is recommended in the initial extension assessment of esophageal cancers of non-metastatic forms after endoscopic ultrasound and CT scan; it allows evaluating the local, lymph nodes and metastatic extension. ^{18}FDG PET-CT scan also allows evaluation of the response to treatment, estimating the target volume for radiotherapy and confirming or reversing a tumor recurrence. **References:** None.

EP-0408

Detection Rate of Radiolabelled Choline PET or PET/CT in Hepatocellular Carcinoma: an Updated Meta-analysis

G. Treglia[1,2,3], *G. Signore*[4], *M. Nicod-Lalonde*[2], *J. O. Prior*[2], *B. Muoio*[5], *F. Bertagna*[6], *L. Giovanella*[1,7];
[1]*Clinic of Nuclear Medicine, Imaging Institute of Southern Switzerland, Ente Ospedaliero Cantonale, Bellinzona and Lugano, SWITZERLAND,* [2]*Department of Nuclear Medicine and Molecular Imaging, Lausanne University Hospital and University of Lausanne, Lausanne, SWITZERLAND,* [3]*Health Technology Assessment Unit, General Directorate, Ente Ospedaliero Cantonale, Bellinzona, SWITZERLAND,* [4]*School of Medicine, Sapienza University of Rome, Rome, ITALY,* [5]*Department of Internal Medicine, Ente Ospedaliero Cantonale, Bellinzona, SWITZERLAND,* [6]*Department of Nuclear Medicine, University of Brescia and Spedali Civili di Brescia, Brescia, ITALY,* [7]*Department of Nuclear Medicine, University Hospital Zürich and University of Zürich, Zürich, SWITZERLAND.*

Aim/Introduction: To date, different imaging methods have been used to detect hepatocellular carcinoma (HCC) and there are increasing literature data about the role of radiolabelled choline PET/CT in this setting. This method can detect HCC based on imaging the initial steps of phosphatidylcholine synthesis. We aimed to perform an updated meta-analysis about the detection rate (DR) of radiolabelled choline PET or PET/CT in HCC. **Materials and Methods:** A comprehensive computer literature search of studies published through December 2018 in PubMed and Cochrane library databases regarding the DR of radiolabelled choline PET or PET/CT in patients with HCC was carried out. The following search algorithm was used: A) "choline" OR "fluorocholine" OR "F-choline" OR "C-choline" OR "FCH" OR "CH" OR "FECH" OR "FMCH" AND B) "PET" OR "positron emission tomography" AND C) "HCC" OR "hepatocellular". Pooled DR of radiolabelled choline PET or PET/CT were calculated on a per patient- and on a per lesion-based analysis. Subgroup analyses taking into account the radiopharmaceutical used (^{18}F-choline versus ^{11}C-choline, and dual-tracer radiolabelled choline plus ^{18}F-FDG) were carried out. Statistical analyses were performed using StatsDirect software (Cambridge, UK). **Results:** Nine studies on the use of radiolabelled choline PET or PET/CT in 283 patients with HCC were included in the pooled analysis. The pooled DR of radiolabelled choline PET or PET/CT on a per patient- and on a per lesion-based analysis was 83% [95% confidence interval (95%CI): 75-89%] and 79% (95%CI: 72-86%), respectively. A significant heterogeneity among the selected studies was found on a per lesion-based analysis only. No significant publication bias was found. The subgroup analysis demonstrated a trend towards a higher DR when using ^{18}F-choline compared to ^{11}C-choline on a per patient- and on a per lesion-based analysis, without a statistical significant difference. Pooled DR of HCC by using dual tracer PET/CT (radiolabelled choline and ^{18}F-FDG) on a per patient- and a per lesion-based analysis was 91% (95%CI: 87-95%) and 89% (95%CI: 80-95%), respectively, without significant heterogeneity and publication bias. **Conclusion:** Radiolabelled choline PET/CT demonstrated a good ability in detecting HCC. The DR increases when dual tracer PET/CT is performed. Large multicenter studies and cost-effectiveness analyses are needed to strengthen the role of this imaging method in this setting. **References:** None.

EP-0409

Baseline metabolic parameters assessed with [18]FDG-PET/CT are predictive of early unresectable relapse after curative intended liver surgery of colorectal liver metastases

I. Duran Derijckere[1], *H. Levillain*[1], *A. Bohlok*[1], *C. Mathey*[2], *J. Nezri*[1], *R. Muteganya*[2], *N. Trotta*[2], *V. Lucidi*[2], *F. Bouazza*[1], *D. Germanova*[2], *G. Van Simaeys*[2], *S. Goldman*[2], *A. Hendlisz*[1], *P. Flamen*[1], *V. Donckier*[1];
[1]*Institut Jules Bordet, Brussels, BELGIUM,*
[2]*Hopital Erasme, Brussels, BELGIUM.*

Aim/Introduction: Accurate patient selection for curative intended surgery in with colorectal-liver-metastases (CRLM) remains challenging as predictive clinicopathologic factors and scores lack prognostic accuracy. Metabolic characteristics of CRLM, evaluated by 18FDG-PET/CT could contribute to better characterization of tumor biology and improve surgical selection. The aim of our study was to evaluate if metabolic baseline characteristics of CRLM assessed with ^{18}FDG-PET/CT at the time of diagnosis, before any preoperative treatment, could predict the benefit of surgery. **Materials and Methods:** In a series of 450 patients operated for CRLM, we retrospectively identified two groups 1) long-term survival group (LTS), as defined by a postoperative recurrence-free survival (RFS)≥5 years, i.e. the patients who benefited of surgery, and 2) early relapse group (ER), as defined by a RFS <1 year, i.e. the patients who did not benefit of surgery. ^{18}FDG-PET/CT was to be performed at the time of diagnosis of CRLM before any preoperative treatment. A total of 53 patients were analyzed, including 23 patients in the LTS group and 30 in the ER group. Clinicopathologic

characteristics, Clinical-Risk-Score (CRS) and baseline 18FDG-PET/CT metabolic parameters were analyzed. Low and high-risk CRS were defined by scores of ≤2 and ≥3, respectively. **Results:** No difference was observed between LTS (n=23) and ER (n=30) groups for clinicopathologic parameters, CRS and rates of low/high-risk CRS. However, all metabolic parameters, except for MTV, were significantly higher in ER patients, the ratio SUV_{max}/$SUV_{mean(liver)}$ was the most significantly different (median ER=4.21 vs LTS=2.82, p=0.008). The ROC curve analysis of SUV_{peak}/$SUV_{mean(liver)}$ ratios showed an area under the curve = 0.713 (95%CI 0.572-0.854). The definition of "positive test" was selected for predicting an early relapse. Evaluating the cut-off values of >4.0 and >6.5, we observed specificities of 73.9% and 95.7%, and sensitivities of 56.7% and 16.7%, respectively (PPV of 73.9% and 83.3%, respectively). Conversely, CRLM with no or low FDG uptake (ratio <1.43) were only seen in LTS patients (NPV=100%). **Conclusion:** In patients with CRLM, metabolic parameters assessed by ^{18}FDG-PET/CT may represent an early biomarker of intrinsic tumor biology, helping to predict the potential benefits of surgery. However, a single cut-off value may not take full advantage of the quantitative metabolic information provided by ^{18}FDG-PET/CT. **References:** None.

EP-0410

Prognostic Value Of Pretreatment Dual-time-point PET/CT Lean Body Mass-corrected Parameters In Patients With Hepatocellular Carcinoma

M. Sun[1,2,3], *G. Zhang*[3], *S. Hao*[3], *J. Guo*[3], *Z. Wang*[3], *G. Fan*[2];
[1]*Department of Nuclear Medicine, No. 4 Hospital of China Medical University, Shenyang, CHINA,* [2]*Department of Radiology, No. 1 Hospital of China Medical University, Shenyang, CHINA,* [3]*Department of Nuclear Medicine, General Hospital of Northern Theater Command, Shenyang, CHINA.*

Aim/Introduction: This study aimed to explore whether the pretreatment dual-time-point fluorine-18-fluorodeoxyglucose (^{18}F-FDG) PET/CT lean body mass (LBM)-corrected parameters could predict the overall survival (OS) in patients with hepatocellular carcinoma (HCC), and which imaging acquisition time point could provide more accurate predictive significance. **Materials and Methods:** We retrospectively investigated 46 HCC patients with pretreatment dual-time-point ^{18}F-FDG PET/CT. The patients' demographics, body index, clinical characteristics, and dual-time-point ^{18}F-FDG PET/CT LBM-corrected parameters (such as maximum standardized uptake value of the tumor, tumor-to-normal liver uptake ratio, metabolic tumor volume, total lesion glycolysis, etc.) were collected and included in the prognostic assessment for OS. The predictive significance of those indicators was analyzed by statistical software. **Results:** In the univariate analysis, aspartate transaminase (AST), Barcelona Clinic Liver Cancer (BCLC) staging, and dual-time-point ^{18}F-FDG PET/CT LBM-corrected parameters were significant predictors for OS. However, in multivariate and Kaplan-Meier analyses, only the LBM-corrected maximum standardized uptake value of the tumor obtained one hour after FDG injection ($lbmSUV_{max1h}$) higher than 3.65 g/ml, and AST greater than 46.19 U/l were significant independent predictors of poor OS. Additionally, in the comparison of dual-time-point PET/CT parameters using the BCLC staging system, the FDG uptake ratios of the tumor-to-normal liver increased significantly with time in both BCLC staging groups. **Conclusion:** Pretreatment dual-time-point ^{18}F-FDG PET/CT LBM-corrected parameters had significant prognostic value in patients with HCC. Furthermore, $lbmSUV_{max1h}$, as the independent prognostic factor for OS and the actual FDG uptake of the whole tumor, surpassed the prognostic worth of other LBM-corrected parameters obtained in the dual-time-point PET/CT imaging, although the delayed imaging could visualize the HCC lesion more effectively. **References:** None.

EP-0411

Diagnostic Performance Of Psma Pet For The Detection Of Hepatocellular Carcinoma

B. Noto[1], *A. Penning*[1], *S. Huss*[2], *A. Kanzog*[1], *M. Wildgruber*[3], *M. Schäfers*[1];
[1]*Clinic for Nuclear Medicine, Muenster, GERMANY,* [2]*Gerhard Domagk Institute for Pathology, Muenster, GERMANY,* [3]*Department of Clinical Radiology, Muenster, GERMANY.*

Aim/Introduction: To estimate the diagnostic accuracy of 68Ga-PSMA-11 PET for the detection hepatocellular carcinoma lesions using MRI as standard of reference. **Materials and Methods:** In this retrospective study 11 patients with hepatocellular carcinoma (HCC) which underwent ^{68}Ga-PSMA-PET/MRI from June 2018 to November 2019 prior to selective internal radiation therapy were enrolled. PET images were acquired over 40 minutes in one bed position of the upper abdomen beginning with injection of 2 MBq Ga-68-PSMA-11per kg body weight. MRI sequences were acquired concurrently including multiphase contrast enhanced MRI. All intraparenchymal liver lesions discernible on MRI were categorized according to LI-RADS criteria. Lesions with a LIRADS score ≥ 4 were rated as HCC, lesions with a score < 4 were rated as non-HCC. Tumor thrombus lesions in portal vein (LR-TIV) were excluded from analysis. Lesions were rated as positive on PSMA-PET if they visually showed a focal tracer uptake unequivocally above background or negative if uptake was on background level or less. **Results:** Including all Patients MRI showed 25 lesions ≥ LI-RADS 4 of which 19 showed increased tracer uptake and 12 lesions < LI-RADS 4 or LR-M of which 4 showed focal tracer uptake. Additionally, portal vein invasion was evident in 3 patients, showing intense tracer uptake in one. Sensitivity, specificity, positive likelihood ratio, negative likelihood ratio and respective 95 percent confidence intervals were calculated as 76.00% (54.87 - 90.64%); 66.67% (34.89 - 90.8%); 2.28 (0.99 - 5.23) and 0.36 (0.16 - 0.80). Kappa for agreement between MRI and PSMA-PET was 0.513 (p = 0.01). Increased uptake on PSMA-PET was strongly associated with arterial phase hyperenhancement on MRI (p = 0.01). The presence of PSMA uptake of lesions was also strongly associated with liver transplantation (p < 0.001). If patients with liver transplantation are excluded, sensitivity,

specificity, positive likelihood ratio and negative likelihood ratio for PSMA-PET are calculated as 95.00% (75.13 - 99.87%), 85.71% (42.13 - 99.64%), 6.65 (1.08 - 40.94) and 0.06 (0.01 - 0.40) respectively. **Conclusion:** ^{68}Ga-PSMA-11-PET shows good estimated sensitivity and specificity for HCC diagnostics and might therefore be a valuable tool in the diagnostics of focal liver lesions. However, ^{68}Ga-PSMA-11-PET might be of limited value in liver transplanted patients. **References:** None.

EP-27

Clinical -> Diagnostic study -> Adult study -> Oncology study -> Organ-based oncology -> Lung, malignant

October 12 - 16, 2019 e-Poster Area

EP-0412

Metabolic Active Tumour Volume Quantified on [^{18}F]FDG PET/CT Further Stratifies TNM Stage IV Non-Small Cell Lung Cancer Patients

H. C. Martins[1], *P. Lapa*[1,2], *B. Oliveiros*[3,4], *M. Silva*[1], *R. Silva*[1,5], *T. Saraiva*[1], *R. Ferreira*[1,5], *G. Costa*[1,2], *J. Pedroso de Lima*[1,2,5];
[1]*Centro Hospitalar e Universitário de Coimbra, Coimbra, PORTUGAL,* [2]*Faculty of Medicine, University of Coimbra, Coimbra, PORTUGAL,* [3]*Laboratory of Biostatistics and Medical Informatics, Faculty of Medicine, University of Coimbra, Coimbra, PORTUGAL,* [4]*Institute for Biomedical Imaging and Life Sciences, Faculty of Medicine, University of Coimbra, Coimbra, PORTUGAL,* [5]*Institute of Nuclear Sciences Applied to Health-ICNAS, University of Coimbra, Coimbra, PORTUGAL.*

Aim/Introduction: Lung cancer remains the leading cause of cancer mortality. The recently revised eighth edition of the TNM staging system defines new T and M descriptors and updates stage groupings, for non-small cell lung cancer (NSCLC), in the effort of improving prognostic accuracy. However, even with the new staging system, there are still substantial differences in the overall survival in patients in the same stage, with similar pathological and clinical characteristics. Stage IV consists of a very heterogeneous group of patients, with very different prognosis and an accurate estimate of the prognosis of patients with advanced NSCLC is essential before starting any palliative treatment strategy.The aim of this work was to investigate if the quantitative parameter whole body metabolic active tumour volume (MATV-WB) allows for improved stratification of TNM stage IV NSCLC patients. **Materials and Methods:** Initial staging [^{18}F]FDG PET/CT of 124 NSCLC TNM stage IV patients, performed between January 2010 and July 2018, 53 (42,7%) stage IVA and 71 (57,3%) stage IVB patients, 32 (25.8%) women, 92 (74.2%) men, aged 34-88 years (mean±SD: 66.1±10.6), were retrospectively evaluated, and MATV-WB was quantified. Each patient's follow-up time was recorded: 0.53-98.9 months (mean±SD: 17.0±16.8). An ideal MATV-WB cutoff was determined, and a binary variable was created: cutoff>MATV-WB≥cutoff. Subsequently, the MATV-WB, with the defined cutoff point, and TNM predictive capacity for overall survival (OS) time was evaluated and compared. The SPSS software (version 23; IBM Corp.) and R (R Foundation for Statistical Computing) software were used for the statistical analysis of the data. **Results:** MATV-WB was an independent and statistically significant predictor of OS (p<0.001). The OS predictive ability of MATV-WB was similar than TNM: MATV-WB C Index (95% CI)=0.653 (0,650-0.655); TNM stage C Index (95%CI)=0.562 (0.560-0.565); p (95%CI)=0.018 (0.015-0.021). The optimal cutoff point for MATV-WB was 114.5 (p<0.001). Estimated mean OS times of 29.5±4.0 (95%CI: 21.7-37.3) and 8.7±1.1 (95%CI: 7.5-11.8) (p<0.001), one-year survival rate (SR) (%) of 63.2±5.8 and of 35.7±6.4, and five-year SR (%) of 12.2±5.3 and no survivors, were determined, respectively, for patients with MATV-WB<114.5 and MATV-WB≥114.5. MATV-WB with the defined cutoff point seems to be a better predictor of the estimated mean OS time (MATV-WB: HR=2.541 (p<0.000); TNM: HR=1.476 (p<0.068). **Conclusion:** In NSCLC stage IV patients, MATV-WB, quantified on initial staging [^{18}F]FDG PET/CT, allows for improved stratification of these patients, which may contribute to the development of more personalized therapeutic strategies. **References:** None.

EP-0413

Joint compensation for motion and partial volume effects in PET/CT images of lung cancer patients: impact on quantification for different image reconstruction methods

S. Rezaei[1,2], *P. Ghafarian*[3,4], *A. Jha*[5,6], *A. Rahmim*[7,8], *S. Sarkar*[2], *M. Ay*[1,2];
[1]*Department of Medical Physics and Biomedical Engineering; Tehran University of Medical Sciences, Tehran, IRAN, ISLAMIC REPUBLIC OF,* [2]*Research Center for Molecular and Cellular Imaging, Tehran University of Medical Sciences, Tehran, IRAN, ISLAMIC REPUBLIC OF,* [3]*Chronic Respiratory Diseases Research Center, National Research Institute of Tuberculosis and Lung Diseases (NRITLD), Shahid Beheshti University of Medical Sciences, Tehran, IRAN, ISLAMIC REPUBLIC OF,* [4]*PET/CT and Cyclotron Center, Masih Daneshvari Hospital, Shahid Beheshti University of Medical Sciences, Tehran, IRAN, ISLAMIC REPUBLIC OF,* [5]*Department of Biomedical Engineering, Washington University in St. Louis, St. Louis, WA, UNITED STATES OF AMERICA,* [6]*Mallinckrodt Institute of Radiology, Washington University in St. Louis, St. Louis, WA, UNITED STATES OF AMERICA,* [7]*Departments of Radiology and Physics, University of British Columbia, Vancouver, BC, CANADA,* [8]*Department of Integrative Oncology, BC Cancer Research Centrer, Vancouver, BC, CANADA.*

Aim/Introduction: To develop and rigorously evaluate an image-based deconvolution technique for joint compensation of respiratory motion and partial volume effects (PVEs) for quantitative oncologic PET imaging, including studying the impact of different image reconstruction methods on quantification performance. **Materials and Methods:** An image-

based deconvolution technique was proposed, incorporating wavelet-based denoising within the Lucy-Richardson algorithm to jointly compensate for PVEs and respiratory motion. The method was evaluated using phantom studies with signal-to-background ratios (SBR) of 4 and 8, and using data from 10 patients with 62 lung lesions. In each study, PET images were reconstructed using four different methods: OSEM with time-of-flight (TOF) information, OSEM with point spread function modelling (PSF), OSEM with both TOF and PSF (TOFPSF), and OSEM without PSF or TOF (OSEM). Contrast to noise ratio (CNR), coefficient of variation (COV), and maximum standardized uptake values (SUV_{max}) were measured within the tumours, and compared to images that were not processed using the joint-compensation technique. Furthermore, variabilities arising due to the choice of the reconstruction methods were assessed. **Results:** In phantom images, for all reconstruction methods, CNR and SUV_{max} were higher in the images processed using the proposed compensation technique, particularly in small spheres. The mean CNR in all spheres was increased in our proposed method by 49.5%, 41.9 %, 44.9% and 38.9% for OSEM, PSF, TOF, and TOFPSF, respectively, in comparison with uncompensated images for 4:1 SBR, and by 30.6%, 27.4%, 38.0% and 33.6% for 8:1 SBR. Overall, incorporation of wavelet-based denoising within the Lucy Richardson algorithm improved CNR and COV in all cases. In patient data, the median values of the relative difference (%) of CNR for the compensated images in comparison to uncompensated images were 43.4%, 39.5%, 46.3% and 42.8% for OSEM-basic, PSF, TOF, and TOFPSF, respectively. Changes in motion amplitude, target size and SBRs in patient data resulted in significant inter-method differences in images reconstructed using different methods. Specifically, in small spheres, quantitative accuracy was highly dependent on the choice of the reconstruction method. **Conclusion:** Our results provide strong evidence that joint compensation, and in particular, incorporation of wavelet-based denoising, yielded improved quantification from PET images. The choice of the reconstruction method led to changes in quantitative accuracy, especially when the signal support is small. Overall, the reconstruction methods need to be carefully selected when applying compensation techniques. **References:** None.

EP-0414

SUV-derived Parameters Assessed on ^{18}F-FDG PET/CT and Serum Tumor Markers Predict EGFR Mutation: a Retrospective Study of 191 Patients with Lung Adenocarcinoma

R. Wang[1,2], *X. Liao*[1], *M. Liu*[1], *Y. Cui*[1], *X. Chen*[1], *J. Zhang*[1];
[1]*Peking University First Hospital, Beijing, CHINA,* [2]*Peking University International Hospital, Beijing, CHINA.*

Aim/Introduction: Epidermal growth factor receptor (EGFR) mutation in non-small cell lung cancer (NSCLC) shows a dramatic response to EGFR-tyrosine kinase inhibitors (EGFR-TKIs) therapy in the clinic. To explore a noninvasive method for evaluating EGFR mutation status in lung adenocarcinoma (ADC) patients, we analyzed the potential roles of standardized uptake value derived parameters from ^{18}F-FDG PET/CT combining with clinical characteristics. **Materials and Methods:** Data of 191 patients pre-treatment who underwent ^{18}F-FDG PET/CT and EGFR mutation test for diagnosed ADC were collected. Cutoff points for all measuring parameters were calculated using receiver operating characteristic (ROC) analysis. The relationship of EGFR mutant status with four parameters based on ^{18}F-FDG PET/CT [Maximum standardized uptake value (SUVmax), average of standardized uptake value (SUVmean), metabolic tumor volume (MTV), total lesion glycolysis (TLG)] and patients' clinical characteristics were evaluated respectively through univariate and multivariate Logistic regression. Predictive effectiveness of the model was obtained by using area under the curve (AUC) yielded by ROC analysis. **Results:** EGFR mutation-positive was showed in 33.0% of patients. EGFR mutation was found more frequently in patients with primary tumor of low SUVmean (< 5.29) (36.7% vs. 20.5%,), low MTV (< 8.13 cm³) (48.7% vs. 28.9%,), low TLG (< 256.37) (36.1% vs. 12.0%), and other clinical characteristics. In univariate Logistic regression analysis, SUVmean (< 5.29), MTV (< 8.13 cm³), and TLG (< 256.37) of the primary tumor were significantly relevant with EGFR mutation. Then the multivariate regression analysis with age adjustment revealed that women (OR = 2.106), low MTV (< 8.13 cm³: OR = 3.008), high CA19-9 (≥ 10.34 U/ml: OR = 2.066), and high proGRP (≥ 38.44 pg/ml: OR = 2.611), were independent significant predictor for EGFR mutation. The initial and adjusted AUC which was yielded by the ROC curve analysis for the predictive value of these factors were 0.721 and 0.723 respectively.The primary tumor size (p = 0.017) and MTV (p = 0.005) with in-frame deletion in exon 19were significantly higher than those with substitution mutation in exon 21. While there were no differences in the SUVmax, SUVmean and TLG between the different EGFR mutation types. **Conclusion:** Low SUV-derived parameters (SUVmean, MTV and TLG) might provide predictive value for EGFR mutation status to some extent. Especially, low MTV (<8.13cm³) was an independent predictor and could be integrated with other clinical factors (women, high CA19-9, and high proGRP) to enhance the discriminability on the EGFR mutation status in ADC patients. **References:** None.

EP-0415

^{18}F-FDG PET/CT In Pulmonary Sarcomatoid Carcinoma And Correlation With Clinicopathological And Genetic Results

L. Jiang;
Shanghai Pulmonary Hospital, Shanghai, CHINA.

Aim/Introduction: Pulmonary sarcomatoid carcinoma (PSC) is a rare subtype of non-small cell lung cancer with high aggression and poor prognosis. This study retrospectively investigated 2-deoxy-2-[18F]fluoro-D-glucose (^{18}F-FDG) positron emission tomography/computed tomography (PET/CT) imaging in PSC and correlation with clinicopathological and genetic findings. **Materials and Methods:** Pre-operative ^{18}F-FDG PET/CT findings were retrospectively analyzed in 24 patients with

PSC confirmed by post-operative pathology. The maximum standard uptake value (SUVmax), tumor location, size, TNM stage, serum tumor markers, pathology and genetic mutation were reviewed. **Results:** Total 24 lesions were detected in 24 patients (20 men; 4 women; average age: 62±9 years), without obviously abnormal serum tumor markers. Six patients had hilar PSC and 18 had peripheral (mean diameter: 47±14 mm). Eighteen lesions were in the upper lobes of bilateral lungs, and 22 exhibited necrosis. Five cases were TNM stage I, 12 stage II and 7 stage III. All 24 cases presented with intense ^{18}F-FDG uptake, and the mean SUVmax was 17.0±11.5 (range: 4.9-48.1). There was no correlation in SUVmax with serum tumor markers, location, size or TNM stage (P>0.05). Programmed cell death-ligand 1 (PD-L1) expression was detected in 21 cases and the positive rate was 87.5%. The SUVmax of lesions with PD-L1 ≥ 50% was obviously higher than those < 50% (21.2±10.1 vs 7.6±2.9, P<0.05). Six cases were detected with Kirsten rat sarcoma viral oncogene homolog gene (KRAS) mutation, and their SUVmax was significantly higher than those without mutation (27.3±13.2 vs 13.9±7.3, P<0.05). **Conclusion:** PSC tended to present with intense ^{18}F-FDG accumulation, which reflected high aggression and poor prognosis. The SUVmax of ^{18}F-FDG PET/CT could be useful for assessing PD-L1 expressive and KRAS mutative status of PSC. **References:** 1. Travis WD, Brambilla E, Nicholson AG, et al. (2015) The 2015 world health organization classification of lung tumors: impact of genetic, clinical and radiologic advances since the 2004 classification. J Thorac Oncol 10: 1243-1260.2.Takeuchi S, Khiewvan B, Fox P, et al. (2014) Impact of initial PET/CT staging in terms of clinical stage, management plan, and prognosis in 592 patients with non-small-cell lung cancer. Eur J Nucl Med Mol Imaging 41: 906-914.3. Mehrad M, Roy S, LaFramboise WA, et al. (2018) KRAS mutation is predictive of outcome in patients with pulmonary sarcomatoid carcinoma. Histopathology 73: 207-214.4. Lococo F, Torricelli F, Rossi G, et al. (2017) Inter-relationship between PD-L1 expression and clinic-pathological features and driver gene mutations in pulmonary sarcomatoid carcinomas. Lung Cancer 113: 93-101.

EP-0416

Molecular Imaging Of Pleomorphic Lung Carcinoma

L. Travaini, *M. Ferrari, M. Colandrea, G. Manfrinato, P. Maissoneuve, S. Papi, L. Spaggiari, G. Buonsanti, S. Fracassi, L. Gilardi, P. Rocca, S. Baio, C. Grana;*
IEO, Milano, ITALY.

Aim/Introduction: pleomorphic lung carcinoma is a rare form of lung cancer usually correlated with poor prognosis. Early recognition of patients could help the surgeon/oncologist to choose a more personalized treatment. The aim of this retrospective study was to assess the impact of metabolic features by fluorine-18 fluorodeoxyglucose PET/Computed Tomography ([18F]FDG-PET/CT) in the prediction of overall survival (OS) and disease free survival (DFS) in a series of patients with pleomorphic lung carcinoma submitted to radical surgery. **Materials and Methods:** we designed the analysis of consecutive patients referred to our hospital for staging of lung cancer. Inclusion criteria comprised age older than 18 years, diagnosis of pleomorphic lung carcinoma (WHO 2017) and staging by [18F]FDG-PET/CT performed less than 45 days from surgery. Metabolic parameters [maximum standardized uptake value (SUVmax), mean standardized uptake value (SUVmean), metabolic tumor volume (MTV), total lesion glycolysis and tumor/no tumor] were determined on [18F]FDG-PET/CT images. The SUV threshold for tumor segmentation was defined as the 41% of the SUVmax of the lesion. OS and DFS curves were plotted using the Kaplan Meier method and the log-rank test was used to assess differences in survival. Univariate and multivariable Cox proportional hazard regression adjusted for pathological stage (stage I, stage II, stages III-IV) was used to assess the association between PET parameters and survival. We performed receiver operating characteristic (ROC) curve analysis to illustrate the performance, measured with the area under the curve (AUC) of [18F]FDG-PET/CT parameters as predictors of mortality or tumor recurrence at 2 years. **Results:** the study included 49 patients equally distributed in stage I, II and III-IV with a mean aged=64.8±9.4 years. We found no significant differences between [18F]FDG-PET/CT parameters and tumor stage, indicating that cancers have highly intensive uptake also at initial stage. The two most important prognostic [18F]FDG-PET/CT parameters for OS at univariate and multivariable analysis were MTV (p=0.03) and the SUVmax (P=0.07). The ROC analysis of SUV-max and MTV for the prediction of 2-year mortality shows respective AUCs of 0.68 (95% CI 0.51-0.85) and 0.69 (0.53-0.84). **Conclusion:** MTV and SUVmax are the only two PET parameters which are prognostic for OS and DFS in patients with pleomorphic lung carcinoma, and that they have similar discriminatory ability. **References:** None.

EP-0417

Inter-observer agreement of the FDG PET CT visual Herder score for the assessment of solitary pulmonary nodules

K. Ordidge, *N. Gandy, M. Arshad, N. Soneji, K. Wallitt, S. Khan, T. Barwick;*
Charing Cross Hospital, London, UNITED KINGDOM.

Aim/Introduction: British Thoracic Society guidelines advise the use of a Herder visual score [1] for the assessment of SPN with FDG PET/CT [2]. There have been no studies to date looking at inter-observer agreement using the Herder scale. We investigated the inter-observer variability of its use in a single-centre retrospective study. **Materials and Methods:** The local PET/CT database was searched for 100 consecutive patients undergoing an FDG PET/CT for the evaluation of an SPN (inclusion criteria: SPN <8mm, blood glucose <11 mmol/L, exclusion criteria: documented malignancy in the past 5 years). All imaging was performed on a Siemens Biograph 64 PET/CT scanner with the same iterative reconstruction parameters. Anonymised images were reviewed independently by three consultant Nuclear Medicine Radiologists and the Herder score was documented, with a confidence score graded 1-3. Inter-

observer agreement was assessed using Interclass Correlation Coefficient modelling. **Results:** There was complete reviewer agreement in 81% cases, and interclass correlation with Cronbach's Alpha was excellent at 0.973 (95% CI, 0.962-0.981). The agreement between pairs of reviewers was good (Kappa scores for reviewer1v2= 0.764, 1v3= 0.874, 2v3 =0.748). There were 19 discrepant cases, of which in 8 patients the Herder risk calculations resulted in unchanged management plans. In the remaining 11 patients the changed risk calculations resulted in clinically significant different management plans, for example CT surveillance vs. consider image-guided biopsy. In these patients MDT discussions and records were followed up and in practice the clinical history or performance status guided patient management. Equivocal cases were most likely to be followed up with interval CT at 3 and 12 months. Confidence scores using the Herder scale were high, with reviewers giving a confidence score of 3 in an average of 78% of cases. **Conclusion:** Our study suggests excellent inter-observer agreement for use of the Herder scale in evaluating SPNs. Reviewer confidence scores were high reflecting high confidence in the use of the Herder scale for evaluating SPN. **References:** 1. Herder GJ, van Tinteren H, Golding RP, et al. Clinical prediction model to characterize pulmonary nodules: validation and added value of 18F-fluorodeoxyglucose positron emission tomography. Chest 2005;128:2490-62. Callister MEJ, Baldwin DR, Akram AR, et al. British Thoracic Society guidelines for the investigation and management of pulmonary nodules. Thorax 2015;70: ii1-ii54.

EP-0418

Diagnostic value of PET/CT in the determination of nodal status in patients with non small cell lung carcinoma

R. Czepczynski[1,2], *R. Giersz*[3], *M. Ruchała*[1];
[1]*Poznan University of Medical Sciences, Poznan, POLAND,* [2]*Dept. of Nuclear Medicine Affidea, Poznań, POLAND,* [3]*Greater Poland Centre of Pulmonology and Thoracic Surgery, Poznan, POLAND.*

Aim/Introduction: ^{18}F-FDG uptake as well as the enlargement of the mediastinal lymph nodes is not always caused by metastatic involvement. Moreover, even physiologically, size and ^{18}F-FDG activity vary among different anatomic groups of mediastinal lymph nodes. The aim of the study was to assess the diagnostic value of PET/CT in the determination of the nodal status with reference to its anatomic classification. **Materials and Methods:** 164 patients (102 men and 62 women) aged 44-85 yrs. (mean 63,5 yrs.) who had PET/CT for staging of NSCLC prior to surgery were included in the study. PET/CT was performed with Discovery ST scanner (GE Healthcare). The PET/CT images were retrospectively viewed and compared to the histopathological (HP) data of the nodes obtained by surgery (144 pts.), mediastinoscopy (33 pts.), and EBUS-guided biopsy (21 pts.). **Results:** Both, SUVmax measurement and HP verification was available for 419 lymph node groups in 164 pts. In 61 metastatic node groups (according to HP) the SUVmax was significantly higher (mean 3.3, median 2.2) than in the 358 negative node groups (mean 1.0, median 0.8); p=0.00001. The minimal number of false-negative and false-positive node groups (10.5%) was obtained with the cut-off value of SUVmax=1.7. With this cut-off sensitivity, specificity, PPV and NPV of PET/CT was 68.3%, 93.0%, 62.1%, 94.6%, respectively. The highest number of nodes evaluated with HP were available in anatomic groups: right paratracheal (4R; 92 pts.; 17 metastatic), subaortic (5; 54 pts.; 7 metastatic) and subcarinal (7; 132 pts.; 22 metastatic). Separate analysis of these node groups showed following SUVmax cut-off values: 1.7, 1.7 and 2.2, respectively. The metastatic lymph nodes measured at CT component of PET/CT had longer short axis (mean 12.9 mm; median 11 mm) than negative nodes (mean 7.9 mm; median 7 mm); p<0.00001. The short axis cut-off value of 17 mm presented with the lowest number of false interpretations. With this cut-off value sensitivity, specificity, PPV and NPV was 23.0%, 98.4%, 70.0%, 88.4%. Short axis cut-off value determined separately for 4R, 5 and 7 node groups was: 15 mm, 15 mm and 17 mm respectively. **Conclusion:** PET/CT more frequently overestimates than underestimates the nodal stage; therefore we postulate histopathological verification of all FDG-positive nodes. Morphological features of the nodes (short axis) should be taken into consideration as well. The obtained cut-off values may be helpful in more accurate interpretation of the nodal status. **References:** None.

EP-0419

Does positron emission tomography SUV_{max} reflects any predictive information in regard to the survival rate of advanced non-small cell lung cancer patients?

S. Lucic[1], *I. Djan*[1], *B. Zaric*[2], *A. Peter*[3], *D. Srbovan*[3], *M. A. Lucic*[1], *I. Novic*[4];
[1]*Medical Faculty, University of Novi Sad, Oncology Institute of Vojvodina, Sremska Kamenica, SERBIA,* [2]*Medical Faculty, University of Novi Sad, Institute for Pulmonary Diseases of Vojvodina, Sremska Kamenica, SERBIA,* [3]*Oncology Institute of Vojvodina, Sremska Kamenica, SERBIA,* [4]*Institute for Pulmonary Diseases of Vojvodina, Sremska Kamenica, SERBIA.*

Aim/Introduction: The aim of the study was to test the interconnection between maximum standardized uptake value (SUV_{max}) obtained by ^{18}F-FDG PET/CT and survival rate in the calculated non-small cell lung cancer (NSCLC) tumorous tissue volume. **Materials and Methods:** Fifty newly diagnosed patients (pts) (62.44±7.6 years (age range 42-80), 12 women (24%) and 38 men (76%)) with verified NSCLC in advanced stage (35 (70%) adenocarcinoma and 15 (30%) squamous cell carcinoma) underwent ^{18}F-FDG PET/CT examination. A region-of-interest (ROI), covering the tumour in each pts was determined and maximal standard uptake values (SUV_{max}) and tumour volumes were obtained. Depending on tumour volumes pts were grouped into group 1 (V_{max}<10cm^3; n=5), group 2 (10cm^3<V_{max}<20cm^3; n=9), and group 3 (V_{max}>20cm^3; n=36). Survival rate using death from any cause but mainly cancer was calculated with Kaplan-Meier method with a 95% confidence interval and log-rank test was used. Data sets were statistically analysed by Spearman's rank correlation coefficient

(ρ), with the level of confidence determined at p<0.05. **Results:** Survival curves were calculated by several factors, including age, sex, cancer type, SUV_{max}, and tumour volume. For age factor grouping, pts were divided as under or older than 70 years, and five-year survival rate of patients under and older than 70 years showed no statistical difference (p=0.35). Survival rates differences weren't found neither in different sex (p=0.764) and tumour volume (p=0.211) groups. For five year survival rate by tumour type no statistical significance was found (p=0.63), but for the strata label by tumour type, and calculated by volume groups, although not significant, log rank was p=0.142. Dependent on tumour type survival curves were calculated, and only by SUV_{max} factor showed borderline log-rank statistical significance of p=0.058. SUV_{max} value was divided into three groups (group 1: SUV_{max}<10; group 2: 10<SUV_{max}<20 and group 3: >20), and survival rate was calculated both for three and five-year survival with a significant log rank level of p=0.020 and 0.028, respectively. Survival curves for SUV max values with tumour type strata showed statistical significance (p=0.022). We found statistically significant correlation between SUV_{max} and tumour volume groups (ρ=0.377; p<0.05). **Conclusion:** Our results suggests that SUV_{max} in calculated cancer volume could be of significance in the assessment of prognosis and life expectance in advanced NSCL cancer patients, and may serve as a prognostic biomarker in the estimation of survival rate in NSCLC patients. **References:** None.

EP-0420

Utility of 18F-FDG PET/CT preceding CT-guided percutaneous biopsy for pulmonary lesions

H. Iwasa, Y. Murata, N. Hayashi, T. Yamagami;
Kochi Medical School Hospital, Nankoku, JAPAN.

Aim/Introduction: The use of 18F-FDG PET/CT (PET/CT) before CT-guided percutaneous biopsy provides both metabolic and anatomical positional information that assists with selecting the appropriate site for biopsy of a pulmonary lesion. The aim of this study was to evaluate the relationship between FDG uptake and the diagnostic success rate of CT-guided percutaneous biopsies of pulmonary lesions. **Materials and Methods:** Fifty-six consecutive patients with a localized pulmonary lesion who had undergone PET/CT before a CT-guided percutaneous biopsy at our hospital between November 2014 and February 2019 were evaluated retrospectively. The relationships between diagnostic success rate and lesion size and SUVmax on PET/CT were assessed. The patients were divided into three groups according to whether biopsy showed they had a malignant, benign, or inconclusive lesion. The final diagnosis was determined by either pathology of the excised lesion or 6-month clinical follow-up. **Results:** Of the 56 patients evaluated, biopsy showed 40 (71.4%) had a malignant lesion, 13 (23.2%) a benign lesion, and 3 (5.4%) an inconclusive lesion. All the 40 malignant lesions and 13 benign lesions biopsied showed accordance with the excision pathology or clinical course. Of the 3 inconclusive lesions resected, 2 were diagnosed as granulomatous lesions and 1 as an adenocarcinoma. Mean lesion size and SUVmax were 35.6 mm (range 8-98 mm) and 10.0 (range 1.5-32.7) for malignant lesions, 37.4 mm (range: 7-86 mm) and 4.7 (range 1.3-11.8) for benign lesions, and 18.7 mm (range 12-25 mm) and 1.9 (range 1.1-2.9) for inconclusive lesions, respectively. All FDG-avid lesions with a SUVmax >3.0 were diagnosed successfully, regardless of lesion size. However, all the biopsied inconclusive lesions were FDG-non-avid lesions. **Conclusion:** A diagnosis obtained by CT-guided percutaneous biopsy following PET/CT could be a diagnostic success, especially in cases of FDG-avid pulmonary lesions. **References:** None.

EP-0421

Delineating Metabolic Tumor Volume In NSCLC: Which Thresholding Method Should Be Used ?

H. N. M. Anwar[1], T. J. Vogl[2], M. A. Abougabal[1], F. Grünwald[2], P. Kleine[2], S. Elrefaie[1], N. A. Nour-Eldin[2];
[1]Cairo University, Cairo, EGYPT, [2]Frankfurt University, Frankfurt, GERMANY.

Aim/Introduction: The optimal method for delineation of the metabolic tumor volume (MTV) in lung cancer is still a matter of debate. The aim of the current study was to investigate the most accurate method for MTV measurement that can be used for the prediction of recurrence in early-stage NSCLC patients after curative surgical resection. **Materials and Methods:** We retrospectively reviewed 121 patients with pathologically documented stages I-IIIA NSCLC who had baseline ^{18}F-FDG PET/CT prior to receiving primary surgical treatment with a curative intent. MTV of the whole body tumor burden was obtained using the following thresholding methods: absolute 2.5 SUV ($MTV_{2.5}$), 50% of SUVmax ($MTV_{50\%}$) and liver SUVmean ($MTV_{liverSUVmean}$). Estimation of the cut-off value for MTV as a predictor of recurrence was determined using receiver operating characteristic (ROC) curve analysis and the Youden index. Patients were dichotomized above and below the calculated cut-offs, disease-free survival curves were generated for each group using the Kaplan-Meier method and the differences in survival between the subgroups were compared using the log-rank test. Sensitivity, specificity, positive predictive value, negative predictive value and overall accuracy of each thresholing method as regards prediction of recurrence were calculated. Comparison of accuracy was performed using Chi square test. p values less than 0.05 were considered statistically significant. **Results:** Median observation time of the patients after surgery was 24 months (range: 1- 74). The calculated cut-off using $MTV_{2.5}$ was 41.29 cm³, while that using $MTV_{50\%}$ was 9.75 cm³ and that using $MTV_{liver\ SUVmean}$ was 27.59 cm³. The difference in survival between patients above and below the calculated cut-off values was significant using all three thresholding methods. Overall, $MTV_{2.5}$ had the highest accuracy for the prediction of recurrence. Using this thresholding method, the sensitivity, specificity, positive predictive value, negative predictive value and overall accuracy were 65%, 75%, 57%, 81% and 72% respectively. Using $MTV_{50\%}$, the above mentioned

parameters were 68%, 62%, 46%, 80% and 64% respectively. Using $MTV_{liver\ SUVmean}$, the parameters were 68%, 69%, 53%, 80% and 69% respectively. However, none of the differences between the sensitivities, specificities and overall accuracies of the used thresholds was statistically significant. **Conclusion:** Among all the described thresholds for the measurement of MTV, the $MTV_{2.5}$ was most accurate in prediction of recurrence in early-stage NSCLC patients, followed by the $MTV_{liverSUVmean}$ and lastly the $MTV_{50\%}$ method.However, the difference in the accuracy between all the above mentioned methods was not statistically significant. **References:** None.

EP-0422

Correlation of Tumor Metabolism with Circulating and Tissue Levels of PD-L1 in Patients with NSCLC

E. Lopci, A. Castello, S. Rossi, E. Mazziotti, L. Toschi;
Humanitas Clinical and Research Hospital - IRCCS, Milano, ITALY.

Aim/Introduction: To evaluate the clinical and prognostic significance of circulating PD-L1 levels in patients with NSCLC. **Materials and Methods:** Overall, 40 patients with operated NSCLC (stage IA-IIIA) having a pre-surgical blood storage and undergoing staging FDG PET/CT were enrolled for the study. For the analysis, we determined plasma levels of PD-L1 (pg/ml), immune reactive areas (IRA%) covered by CD3, CD68, CD20, CD8, PD-1 and PD-L1 in tumor specimen, as well as metabolic parameters on FDG PET: i.e. SUVmax, SUVpeak, metabolic tumor volume (MTV) and total lesion glycolysis (TLG). All variables were statistically analyzed and associated to disease-free survival (DFS) for a median follow-up of 16.2 months. **Results:** The circulating levels of PD-L1 in the blood stream could be determined in 38/40 (95%) of the samples. The mean and median expression levels were 34.86 pg/ml and 24.83 pg/ml, respectively. No significant correlation could be determined between circulating PD-L1 and tissue expression of PD-L1/PD-1. A mild degree of positive correlation was observed for tissue PD-L1 and SUVmax (rho=0.390; p=0.0148). Hierarchical clustering combining circulating, tissue and metabolic parameters identified clusters of patients with high metabolic tumor burden or high expression of plasma PD-L1 levels (Z-score≥2) as having a poorer DFS (p= 0.033) compared to other clusters on log rank test. The multivariate analysis detected that stage and tumor metabolism (i.e. SUVmax and SUVpeak) resulted as independent prognostic factors to DFS. **Conclusion:** The plasma levels of PD-L1 result independent from the expression of PD-1/PD-L1 in NSCLC tumor tissue and, when combined with other clinic-pathological parameters, allow for the identification of clusters of patients with different outcome. Further prospective trials could determine a possible impact in NSCLC patients during the course of immunotherapy. **References:** Lopci E, et al. Eur J Nucl Med Mol Imaging. 2016 Oct;43(11):1954-61.

EP-0423

The relationship between PET parameters (SUVmax, SUVmean, MTV, TLG) and biomarkers which are effective in clinical applications (EGFR, ALK, MET, ROS-1, KRAS) in lung cancer patients

A. Arçay[1], A. Öner[2], H. Coşkun[3], E. Sürer Budak[4], M. Özcan[5], F. Aydın[1];
[1]Akdeniz University Nuclear Medicine Department, Antalya, TURKEY, [2]Afyon Kocatepe University Nuclear Medicine Department, Afyon, TURKEY, [3]Akdeniz University, Clinic of Medical Oncology, Antalya, TURKEY, [4]Antalya Training and Research Hospital, Clinic of Nuclear Medicine, Antalya, TURKEY, [5]Akdeniz University Pathology Department, Antalya, TURKEY.

Aim/Introduction: We aimed to determine the relationship between PET parameters (SUVmax, SUVmean, metabolic tumor volume and total lesion glycolysis) and the pathological gene mutations (EGFR, ALK, KRAS, ROS-1, BRAF) in lung cancer patients who had FDG PET/CT for staging. **Materials and Methods:** The total 488 patients who underwent mutation analysis (EGFR, ALK, KRAS, ROS-1, BRAF) in the pathology department of our university hospital between 2015 and 2018 were retrospectively reviewed. The mutation positive patients (33 patients) and all mutations negative patients (36 patients) who had FDG PET/CT at our department were included in the study. **Results:** The median age of 33 patients (19 male, 14 female) was 56 (38-86). The number of patients with positive EGFR, ALK, KRAS, ROS-1 and BRAF mutations were 21,5,5,1 and 1 respectively. The median values of SUVmax, SUVmean, MTV and TLG of EGFR positive patients were 13.44, 8.04, 6.47 and 67.33, respectively. The median values of SUVmax, SUVmean, MTV and TLG of ALK positive patients were determined as 10.86, 6.24, 8.19 and 41.22, respectively. The median values of SUVmax, SUVmean, MTV and TLG of KRAS positive patients were determined as 8.96, 5.51, 71.33, 311.71 respectively and there was no statistically significant difference between the PET parameters of these 3 groups (ANOVA, p> 0.05). However, in comparison of EGFR positive 21 patients with 36 patients who were not positive for any mutation, all PET parameters were higher in EGFR-positive patients (Mann Whitney, p = 0.011). No statistically significant difference was observed in other mutation groups. **Conclusion:** In our study, we found that SUVmax, SUVmean, MTV, TLG values obtained from PET examination for primary staging were not effective in showing biomarkers (EGFR, ALK, KRAS, ROS-1, BRAF) which are effective in treatment planning in lung cancer. However, we think that PET parameters may be helpful for patient selection because of the higher probability of EGFR mutation in patients with high metabolic activity. **References:** None.

EP-0424

Relation Between Metabolic Parameters In 18F-FDG PET/CT And Hematological Markers In Non-Small Cell Lung Cancer

S. Göksel[1], *A. Cengiz*[2], *H. Öztürk*[3], *Y. Yürekli*[2];
[1]*Recep Tayyip Erdoğan University Medical Faculty Education and Research Hospital, Department of Nuclear Medicine, Rize, TURKEY,* [2]*Adnan Menderes University Medical Faculty, Department of Nuclear Medicine, Aydin, TURKEY,* [3]*Adnan Menderes University Medical Faculty, Department of Biostatistics, Aydin, TURKEY.*

Aim/Introduction: Various inflammatory markers such as elevated neutrophil-to-lymphocyte ratio (NLR), platelet-to-lymphocyte ratio (PLR) and neutrophil count and low mean platelet volume (MPV) have been shown to be with poor prognosis in malignancies. Metabolic parameters in 18F-FDG PET/CT such as metabolic tumor volume (MTV) and total lesion glycolysis (TLG) have also been reported to be a prognostic marker in various cancers. The aim of this study is to evaluate the correlation between hematological markers and metabolic 18F-FDG PET/CT parameters in patients with non-small cell lung cancer (NSCLC). **Materials and Methods:** A total of 132 patients (122 male, 10 female) with NSCLC who underwent PET/CT for initial staging were evaluated retrospectively. Patients with hematological disease, infections, chemo/radiotheraphy or surgery history were excluded. Hematological parameters were measured within two weeks of the PET/CT imaging. Correlation between these parameters was evaluated with Spearman's correlation test. The prognostic significances of variables for overall survival (OS) were assessed by uni/multivariate analyses using Cox-regression model. $p<0.05$ was considered statistically significant. **Results:** There was statistically significant positive correlation between neutrophil (r:0.578, $p<0.001$), NLR (r 0.524, $p<0.001$), PLR (r:0.445, $p<0.001$) and MTV. While there was found positive correlation between neutrophil (r:0.593, $p<0.001$), NLR (r:0.540, $p<0.001$), PLR (r:0.460, $p<0.001$) and TLG, MPV was negatively correlated with TLG. SUVmax of primary tumor was not correlated with hematological parameters. While TLG, MTV, NLR and PLR were increased in advanced stages disease, MPV was decreased. Univariate Cox-regression analysis demonstrated that greater age ($p<0.05$), high neutrophil count ($p<0.001$), high NLR ($p<0.001$), high PLR ($p<0.001$), high MTV ($p<0.05$), high TLG ($p<0.05$), low MPV ($p<0.05$) values and advenced stage ($p<0.001$) were significant predictors of poor prognosis. Multivariate Cox-regression analysis revealed that NLR (HR:2.67; 95% CI, 1.74-4.08; $p<0.001$) and advanced stage disease (HR:7.77; 95% CI, 2.61-23.07; $p<0.001$) were significant independent predictors of poor prognosis. **Conclusion:** Prognostic hematological markers are significantly correlated with metabolic 18F-FDG PET/CT parameters in patients with NSCLC. These parameters can contribute to prognostic evaluation of patients with NSCLC in initial staging. **References:** None.

EP-0425

Study on SUV-derived parameters assessed on ^{18}F-FDG PET/CT for predicting EGFR mutation status and prognosis in Lung Adenocarcinoma

R. Wang[1,2], *X. Liao*[1], *M. Liu*[1], *X. Chen*[1], *L. Yin*[1], *B. Zhang*[1], *Y. Du*[1];
[1]*Peking University First Hospital, Beijing, CHINA,* [2]*Peking University International Hospital, Beijing, CHINA.*

Aim/Introduction: To explore valuable predictors for evaluating progression-free survival (PFS) in lung adenocarcinoma (ADC) patients, we analyzed the potential roles of standardized uptake value (SUV)-derived parameters from 18F-FDG PET/CT combining with epidermal growth factor receptor/anaplastic lymphoma kinase (EGFR/ALK) gene mutation state, and other clinical characteristics. **Materials and Methods:** Data of 84 ADC patients pre-treatment, who underwent ^{18}F-FDG PET/CT scans, EGFR gene mutations test, ALK rearrangement assay and other relative tests during the period of December 2011 to April 2016, were retrospectively collected. Then a series of clinical parameters including EGFR/ALK mutation status and SUV-derived features [maximum standardized uptake value(SUVmax), average of standardized uptake value (SUVmean), metabolic tumor volume(MTV), and total lesion glycolysis(TLG)]were evaluated. Best possible cutoff points for all parameters were calculated using receiver operating characteristic curve analysis. Survival analysis was performed using Cox proportional hazards model to determine the prognostic markers for PFS. Survival curves were obtained through Log-rank test and Kaplan-Meier curve. All data were analyzed with the SPSS software and p value less than 0.05 was considered as statistically significant. **Results:** The median follow-up period was 31months (24 to 58 months). It was found that SUVmax(≥ 3.01),SUVmean(≥ 2.25), MTV(≥ 25.41 cm^3), and TLG(≥ 55.02) of the primary tumorswere significant for PFS in univariate analysis. Then regardless of age, gender, co-morbidity, EGFR/ALK mutation status, and treatment program, TLG (≥ 55.02: HR = 4.965, 95%CI: 1.360-18.133), TNM stage (III/IV: HR = 7.811, 95%CI: 2.977-20.489), precursor of gastrin releasing peptide(proGRP) (≥ 45.65 pg/ml: HR = 4.070, 95%CI:1.442-11.487), tissue polypeptide antigen(TPA) (≥ 68.20 U/L: HR = 6.996, 95%CI:1.458-33.574), alkaline phosphatase (ALP) (≥ 82.50 IU/L: HR = 4.160, 95%CI: 1.416-12.219) and ratio of activated partial thromboplastin time (aPTTR) (≥ 1.16: HR = 4.58, 95%CI: 1.913-10.946) showed the independent prognostic factors through multivariate Cox proportional hazards analysis. The EGFR mutant ($p = 0.343$) and ALK rearrangement ($p = 0.608$) were insignificant either in survival analysis. **Conclusion:** High SUV-derived parameters (SUVmax, SUVmean, MTV and TLG) might provide prognostic value to some extent. Especially, high TLG (≥ 55.02) could be an independent prognostic factor and be integrated with other clinical features [TNM stage (III/IV), proGRP (≥ 45.65 pg/ml), TPA (≥ 68.20 U/L), ALP (≥ 82.50 IU/L), and aPTTR (≥ 1.155)] in predicting PFS of ADC patients. However, EGFR/ALK gene status could not be effective predictors for PFS in ADC patients. **References:** None.

EP-0426

FDG/PET SUVmax O F Percent Rate Of Subtype, size And Invasive Rate Of Pulmonary Adenocarcinoma

K. Hayasaka, T. Saitoh, H. Inoue, M. Fukasawa, M. Hiraga, Y. Shraishi, T. Tohgoh, M. Hiramatsu, K. Shimoda, K. Yoshimori, K. Ohta;
Fukujuji Hospital, Anti-tuberculosis Association, Tokyo, JAPAN.

Aim/Introduction: To determine the usefulness of SUVmax to determining the pathological rates of pulmonary adenocarcinoma subtypes, invasive size and rate. **Materials and Methods:** Between December 2015 and December 2018, this study enrolled 208 patients (233 sites) with a histological diagnosis of non-invasive and invasive adenocarcinoma exceptvariant. We calculated the pathological rates (%) of lepidic, acinar, papillary, solid and micropapillary components, as well as tumor invasion size (TIS) and rate (invasion size/tumor size) (TIR) invasive adenocarcinoma. All information was obtained from a retrospective review of medical records, PET findings and other sources, and statistically analyzed using SPSS version 11.0 software (SPSS Inc., Chicago, IL, USA). Statistical significance was set up $p < 0.05$. **Results:** The means (SD) of the tumor size (mm), TIS (mm), TIR and SUVmax of tumors were 24.7 (10.9), 14.2 (10.8), 0.548 (0.138) and 2.71 (2.60), respectively. Pearson correlation values were 0.269 ($p = 0.000$), 0.616 ($p= 0.000$) and 0.616 ($p= 0.000$) for SUVmax vs. tumor size, TIS and TIR, respectively. The pathological rates of lepidic, acinar papillary solid and micropapillary adenocarcinoma subtype were respectively, 46.8% (37.6%), 13.6% (18.5%), 30.9% (35.9%), 8.1% (23.6%) and 0.365% (1.08%). Pearson correlation values significantly differed at -0.587, 0.444 and 0.294 for SUVmax vs. rates of lepidic, papillary, solid ($p= 0.000$), and 0.214 micropapillary ($p=0.001$) component. Regression analysis significantly associated a decreased SUVmax with an increased rate (%) of the lepidic component. The SUVmax of the lepidic component was 3.98 (3.01) (< 50%; Lp < 50), 1.54 (0.514) (50% - 80%; Lp 50 - 80), 1.14 (0.554) (> 80% (Lp > 80), and the SUVmax of TIS was 0.867 (0.300) (0 mm; TIS 0), 0.936 (0.458) (0 - 5 mm; TIS 0 to < 5) and 3.18 (2.73) invasion size (> 5 mm; TIS > 5). Analysis of variance showed that differences were statistically significant for Lp < 50 vs. 50-80 and > 80 ($p = 0.000$), Lp 50 - 80 vs. > 80 ($p = 0.001$), TIS 0 vs. > 5 and 0 - 5 vs. > 5, ($p = 0.001$), but the difference was not statistically significant for TIS 0 vs. 0 - 5 ($p = 0.472$). **Conclusion:** The SUVmax of the rate (%) of the lepidic component and tumor invasion size could distinguish Lp < 50, from Lp 50 - 80 and > 80, and TIS 0 from 0 **References:** European Journal of Cardio-thoracic Surgery 2017; 51: 218.

EP-0427

Diagnostic Value of Total Lesion Glycolysis Evaluated by 18F-FDG PET/CT Added to SUVmax for Characterization of Solitary Pulmonary Nodule

S. Gungor, H. Keskin, H. I. Yakar, A. G. Akbiyik, I. N. Otken, H. Uslu;
Istanbul Medeniyet University School Of Medicine, Istanbul, TURKEY.

Aim/Introduction: Characterization of solitary pulmonary nodule (SPN) is necessary to choose an appropriate treatment approach on time. The aim of this study is to evaluate the diagnostic value of metabolic, volumetric, and metabolovolumetric parameters measured by 18F-fluorodeoxyglucose (18F-FDG) PET/computed tomography (CT) in differentiating malignant from benign SPNs. **Materials and Methods:** A retrospective review of 18F-FDG PET/CT scans from 80 patients with SPN confirmed by pathology or clinical follow-up were included. The diagnostic value of PET-CT metabolic, volumetric, and metabolovolumetric parameters to detect malignancy was calculated. In addition, maximum standard uptake value (SUVmax) and total lesion glycolysis (TLG) were combined and compared in terms of diagnostic accuracy. PET/CT parameters were assessed using the Mann-Whitney U-test, Independent Simple t Test, and Receiving Operating Characteristic analysis. **Results:** There were 38 benign and 42 malignant SPNs (median age:61±13 years, mean nodule diameter: 19.3 mm). The SUVmax, metabolic tumor volume (MTV), TLG, and CT volume showed significantly higher values in the malignant lesions compared with the benign lesions. Among the PET/CT parameters, the SUVmax and TLG had the highest area under the curve (AUC). The sensitivity, specificity, and accuracy of SUVmax, TLG, and SUVmax combined with TLG in the diagnosis of SPNs were 97.6%, 63.2%, 81.2%; 85.7%, 92.1%, 88.7%; and 85.7%, 94.7%, 90%, respectively. **Conclusion:** Traditional SUVmax method combined with the TLG can improve the diagnostic specificity and accuracy of SPNs particularly in infectious endemic regions. **References:** None.

EP-0428

Predictive value of PET-FDG derived lesion glycolisis values in Stage I non-small-cell lung cancer patients for selecting high risk patients

G. Santaguida[1,2], S. Pieropan[3,2], M. Cuzzocrea[1], E. Orunesu[1], L. Florimonte[1], D. Tosi[3], M. Castellani[1];
[1]Nuclear Medicine, Fondazione IRCCS Ca' Granda, Ospedale Maggiore Policlinico, Milano, ITALY, [2]Università degli Studi di Milano, Milano, ITALY, [3]Thoracic Surgery, Fondazione IRCCS Ca' Granda, Ospedale Maggiore Policlinico, Milano, ITALY.

Aim/Introduction: Aim of our study was to investigate the predictive value of F-18 fluorodeoxyglucose (FDG) PET/CT images in patients with stage I non small cell lung cancer regarding disease-free and overall survival, using different volume-based parameters of FDG uptake, independent of other histological features. **Materials and Methods:** We retrospectively evaluated 65 patients (34 males and 31 females; average age at PET/CT scan time of 68.2 years) with stage I lung cancer who underwent FDG PET/CT prior to surgery. All patients were treated surgically in our Institution between 2010 to 2017 and none of them had a previous adjuvant therapy. The median follow-up was 45 months from the surgery. Tumor maximum standardized uptake value (SUV max), metabolic tumor volume (MTV), total lesion glycolisis (TLG) were calculated along with

the performance of values, which were also normalized to average SUV of liver (SUVmaxLi; TLGLi) or controlateral lung (SUVmaxLu; TLGLu). TLG was calculated as MTV multiplied by the average SUV by using fixed threshold of 40% of the maximum intratumoral FDG activity. The prognostic importance of PET parameters, independent of other clinical or histologic features, was assessed by using Cox proportional hazard regression analysis of overall survival (OS) and disease free survival (DFS) for univariate analysis. **Results:** Overall survival (OS) and disease-free survival (DFS) were respectively 89.23% and 78.46%. Univariate analysis demonstrate that SUV max (p=0.03), MTV (p=0.002), TLG (p ≤ 0.001), SUVmaxLi (p=0.024), SUV maxLu (p=0.018), TLGLi (p ≤ 0.001), TLGLu (p ≤ 0.001), were all inversely correlated with disease free survival, independently of the age. We've found that overall survival was associated with TLG derived values only when normalized to healthy tissue. In particular among metabolic parameters only TLG normalized to average liver SUV was associated with unfavorable overall survival (p=0.024). **Conclusion:** All volume-based PET metrics all correlate with length of disease free survival. TLG normalized to average liver-uptake was the only parameter predictive of overall survival. We propose the use of these parameters for risk assessment in stage I-NSCLC. Patients with metabolically more active tumors and high level of total lesion glycolisis normalized to mean liver uptake, should be considered at higher risk for disease relapse and tumor related death and might be candidates for more aggressive treatment-schedules after surgery. **References:** None.

EP-0429

Prognostic value and patients'outcome evaluation using early FDG PET-CT in the assessment of Stereotactic Body Radiotherapy response in lung malignant lesions

L. Alarcon[1], *A. Fernández*[2], *N. Farré*[3], *D. López-Mora*[2], *J. Duch*[2], *A. Flotats*[2], *F. Fuentes*[2], *A. Soto*[3], *I. Carrió*[2], *V. Camacho*[2];
[1]*Nuclear Medicine department. Hospital Dr Gustavo Fricke, Viña del Mar, CHILE,* [2]*Nuclear Medicine Department. Hospital Sant Pau, Barcelona, SPAIN,* [3]*Radiotherapy department. Hospital Sant Pau, Barcelona, SPAIN.*

Aim/Introduction: Stereotactic body radiotherapy (SBRT) is a useful treatment in patients with non-surgical early lung cancer. The objective of our study was to determine the value of PET-TC in the assessment of pulmonary tumor one month after SBRT treatment in order to evaluate therapeutic response. **Materials and Methods:** This prospective study included 73 patients (65 men; mean aged 74, range, 45-93 years), with primary lung cancer (I and IIa stage) treated with SBRT (fractionated adapted dose 3/18 Gy 5/11 Gy or 8/7,5 Gy). All patients underwent two ^{18}F-FDG PET-CT scans (Phillips Gemini TF) before and after 1 month of SBRT. All PET-CT scans were reviewed and reported by consensus of 2 nuclear medicine physicians. SUVmax and size values were determined for each tumor. Overall (OS) and cause-specific (CSS) survival were evaluated with Kaplan-Meier curves after a mean follow up of 30 months (range 4 - 76 months). **Results:** At the early control, 26 (36%) patients presented complete response to SBRT (mean SUVmax from 7.5 to 1.3), 37 (50%) presented partial response (mean SUVmax from 9.6 to 4.4) and 10 (14%) showed stable disease (mean SUVmax from 4.5 to 4.4). None of the patients presented local progression after treatment. There were not statistically differences in OS and CSS between each group of patients. Nevertheless there was a statistically difference in OS (p<0.03) and CSS (p<0.01) in patients who presented <2.0 SUVmax value in control PET-CT. During follow up, 25 patients died (34%), 11 of them for specific causes related to lung cancer. **Conclusion:** Patients with complete normalization of FDG activity in early PET-CT evaluation have better overall and specific survival values after SBRT treatment of lung cancer. **References:** None.

EP-0430

Association between PD-L1 expression and histology with SUVmax on ^{18}FDG PET/CT in non small-cell lung cancer patients

E. Martínez Albero*, S. Ruiz Solís, L. Parrilla Rubio, V. M. Godigna Guilloteau, Á. Galiana Morón, D. Pérez Vega, J. Pilkington Woll, P. Sarandeses Fernandez, J. Estenoz Alfaro;*
Hospital Universitario 12 de octubre, Madrid, SPAIN.

Aim/Introduction: Programmed cell death-ligand 1 (PD-L1) is a protein expressed in many cancers, among them non small-cell lung cancer (NSCLC). The expression of PD-L1 protein in tumor cells could be a prognostic and predictive biomarker for response to antiPD-1/PD-L1 antibodies in lung cancer. Therefore we aim to study the association between the presence of PD-L1 expression and the maximum standardized uptake value (SUVmax) of ^{18}F-fluoro-2-deoxy-glucose (^{18}F-FDG) uptake in patients with NSCLC. **Materials and Methods:** We retrospectively analyzed 61 patients (p) with primary NSCLC who underwent ^{18}F-FDG PET/CT for initial diagnosis, from February 2013 to January 2018. Clinicopathological characteristics include gender, age, tobacco habit and tumor stage according to TNM 8thedition. PD-L1 protein expression was evaluated by immunohistochemistry. We studied the relationship between PD-L1 protein expression and histological subtypes using Fisher's exact test. Association between SUVmax and histological subtypes, PD-L1 expression and proportion of PD-L1 positive cells, was explained by linear regression model. We also analyzed if SUVmax could determine PD-L1 protein expression (ROC analyses) and its impact on 24 months survival. **Results:** The median age was 69.16 years (range: 38-83 years), 43 males (70.49%) and 51 smokers (86.44%). Adenocarcinoma was the most frequent histological subtype (72.13%), and nearly half (49.18%) were stage I in PET/CT. The mean value of SUVmax was 11,72 (range 0.89-43.99). Immunohistochemistry was performed in 57p. Nineteen had PD-L1 protein expression (33.33%). The percentage of tumors with positive PD-L1 protein expression was: 57.9% adenocarcinomas, 31.6% squamous cell cancer, 10.5% large cell carcinoma, but histological subtype could not be associated with PD-L1 (p= 0.0524). Our statistical analysis showed that SUVmax was significantly higher in patients

with PD-L1 expression (p=0.0125). In contrast, there was no correlation between SUVmax and histological subtypes and proportion of PD-L1 positive cells. A cutt-off value for SUVmax >11,03, was a predictor variable of PD-L1 expression with an area under the curve (AUC) 0,702 (Sensitivity 68% and Specificity 71%). No correlation was found between PD-L1 expression and advanced stages (p=0.21). We observed that patients with PD-L1 expression had less survival, but without statistical significance (Kapplan-Meier p=0.32). **Conclusion:** In NSCLC higher values of SUVmax were predictors of PD-L1 expression. SUVmax showed no correlation with histological subtypes or with the proportion of cells expressing PD-L1. Patients with PD-L1 expression tend to have less overall survival than patients without. **References:** None.

EP-0431

Diagnostic imaging of typical lung carcinoids: relationship between nuclear imaging and MDCT features and Ki-67 index

F. Linguanti[1], *V. Berti*[1], *E. Abenavoli*[1], *G. Danti*[2], *F. Mungai*[2], *V. Miele*[2], *V. Briganti*[1], *R. Sciagrà*[1];
[1]*Medicina Nucleare, Firenze, ITALY,* [2]*Radiology, Firenze, ITALY.*

Aim/Introduction: This study analyzes the capability of nuclear imaging (18F-FDG-PET/CT and somatostatin receptor scintigraphy/SPECT with 111In-pentetreotide) and contrast-enhanced multi-detector computed tomography (MDCT) to characterize typical carcinoids (TCs) of the lung, and the relationship of their findings with Ki-67 index. **Materials and Methods:** We analyzed 28 patients (17 males, 11 females, age range 43-86 years, mean age 67,2 years) with histological diagnosis of pulmonary TCs, who underwent both nuclear imaging (18F-FDG-PET/CT and somatostatin receptor scintigraphy/SPECT with 111In-pentetreotide) and MDCT at staging evaluation before surgery. FDG uptake was measured as the ratio between lesion SUVmax and liver SUVmean (SUVratio). In 111In-pentetreotide SPECT tumor/non-tumor ratio was measured at 4 and 24h post-injection and percent difference was calculated (T/NT%). The MDCT scan were reviewed for the following features: lesion location, size, margins, contrast enhancement, presence of calcifications, bronchial obstruction, lymph nodes and metastases. All imaging findings were correlated between them and with Ki-67 index. Nonparametric correlation analysis was performed using SPSS software. P<0.05 was considered significant. **Results:** Eighteen of the 28 lesions (64%) were in the right lung and mainly in the middle lobe. In MDCT scan lesions appeared as well-defined nodule in 21 patients (75%) and irregular mass in 7 patients (25%). Contrast enhancement was present in 11 patients (39%), calcifications in 7 patients (25%) and bronchial obstruction in 8 patients (28%). Lymph nodes and metastasis were present in 5 (17%) patients. Ki-67 index was negatively correlated with T/NT% (p<0.02) and positively with SUVratio (p<0.01); T/NT% and SUVratio were inversely correlated (p<0.05). The presence of lymph nodes and metastases was positively related to higher SUVratio (p<0.01). The presence of bronchial obstruction, lymph nodes and metastases was significantly correlated with higher grade of Ki-67 index (p<0.05). **Conclusion:** Nuclear imaging and MDCT are important to characterize lung TCs. We found a significant correlation between nuclear medicine features, some MDCT aspects and Ki-67 index. The association of nuclear medicine imaging and MDCT may be useful in predicting proliferative activity and prognosis of lung TCs. **References:** None.

EP-0432

Comparative analysis of lung perfusion scan with lung perfusion SPECT/CT for prediction of early postoperative lung function

H. Suh, S. Kim;
National Cancer Center, Goyang, KOREA, REPUBLIC OF.

Aim/Introduction: The aim of this study is to compare lung perfusion scan with single photon emission computed tomography/computed tomography (SPECT/CT) in the prediction of postoperative lung function and suggest appropriate preoperative modality for lung cancer patients. **Materials and Methods:** Forty two patients (male:female = 37:5, age = 68.7±8.9 years) with non-small cell lung cancer were recruited. Patients underwent technetium-99m macroaggregated albumin (Tc-99m-MAA) lung perfusion scan, SPECT/CT, and preoperative/postoperative pulmonary function tests within one month. Postoperative forced expiratory volume in the first second (postFEV_1) was predicted by remained lung after the operation, based on the radioactivity on lung perfusion scan and SPECT, and lung volume on CT. The % uptake of each lobe was derived from lung perfusion scan and SPECT. Correlation and paired comparison analysis were performed. **Results:** Actual postFEV_1 showed significant correlation with predicted postFEV_1 by lung perfusion scan (r=0.68, p<0.0001), SPECT (r=0.69, p<0.0001), and CT (r=0.74, p<0.0001). Predicted postFEV_1 by three methods showed no significant difference. The % uptake ratio of right to left lung between lung perfusion scan and SPECT were significantly correlated. Both lung perfusion scan and SPECT showed a strong correlation of each lobar distribution of % uptake, except for the right middle lobe (r=0.51, p<0.0001). **Conclusion:** Lung perfusion scan and SPECT/CT can predict early postoperative lung function, but SPECT/CT assess regional lung function more accurately than lung perfusion scan. We suggest SPECT/CT as a modality for prediction of postoperative lung function, where lung perfusion scan can substitute for SPECT/CT in patients planning pneumonectomy. **References:** None.

EP-0433

^{18}FDG-PET/CT in treatment monitoring and follow-up of lung tumors treated with stereotactic body radiotherapy

J. Vercher-Conejero[1], *P. Notta*[1], *A. Navarro-Martin*[2], *I. Sanchez-Rodriguez*[1], *E. Andia-Navarro*[1], *A. Palomar-Muñoz*[1], *L. Gracia-Sanchez*[1], *S. Padrones-Sanchez*[1], *C. Gamez-Cenzano*[1];
[1]*Hospital Universitari de Bellvitge-IDIBELL, L'Hospitalet de Llobregat (Barcelona), SPAIN,* [2]*Institut Català d'Oncologia, L'Hospitalet de Llobregat (Barcelona), SPAIN.*

Aim/Introduction: Stereotactic body radiation therapy (SBRT) is a relatively new treatment modality whose main indications are inoperable non-small-cell lung cancer and oligometastases to liver and lung. The aim of this study was to evaluate the usefulness of 18FDG-PET/CT in monitoring treatment response and in the follow-up of patients with pulmonary lesions treated with stereotactic body radiotherapy (SBRT). **Materials and Methods:** Ninety-one patients with lung lesions (stage I lung cancer or isolated pulmonary metastases from other tumors) were retrospectively studied with 18FDG-PET/CT before and after being treated with SBRT. The final analysis excluded 52 patients because an initial follow-up PET was not available or additional therapies were received. We finally included thirty-nine patients with pulmonary tumor lesions: 32/39 lung cancer and 7/39 colorectal metastases. PET/CT was performed <1 month prior SBRT, and after SBRT at 3 timepoints: <6, 6-18 and> 18 months. The clinical evaluation of the response was classified as stable disease (SD), including partial or complete metabolic response or progression (PD). **Results:** Primary lung tumors were adenocarcinomas (22) and squamous carcinoma (10), and adenocarcinomas (7) for colorectal cancer, presenting a baseline-SUVmax average of 6.9, 10.8 and 6.5 g/ml, respectively. SBRT dose ranged 34-60 Gy. SD was found in 76% although they showed a decrease in metabolic activity within the early evaluation without a significant reduction in size. Low diffuse metabolic uptake was observed in most patients due to inflammatory changes. 6 patients had PD by PET and CT, 3 in early evaluation, 2 in intermediate and 1 >18 months. **Conclusion:** Response evaluation with PET/CT seems to be more reliable than that observed only with CT in the follow-up of lung lesions treated with SBRT, probably because SBRT-induced CT changes may have a consolidation/mass-like appearance and therefore, differentiation from tumor recurrence can be challenging. However, it is important to keep in mind that diffuse hypermetabolism after SBRT may persist beyond 18 months after treatment without definitive evidence of recurrence. In our study, PET correlated with the clinical response and may be useful in predicting the response to SBRT and further research to determine optimal management is needed. **References:** None.

EP-0434

The value of semiquantitative FDG-PET parameters in the diagnosis of solitary pulmonary nodules with pre-test intermediate likelihood of malignancy: a single-centre study

A. Spanu, M. L. Stazza, S. Galassi, M. Rondini, P. Solinas, D. Sanna, F. Chessa, S. Nuvoli, G. Madeddu;
Unit of Nuclear Medicine, University of Sassari, Sassari, ITALY.

Aim/Introduction: Recent studies have demonstrated that the diagnostic accuracy of FDG-PET/CT in differentiating solitary pulmonary nodules (SPNs) is affected by the pre-test likelihood of malignancy of the nodule. The aim of the present single-centre study was to assess the value of some semiquantitative FDG-PET parameters in the diagnosis of SPNs with pre-test intermediate likelihood of malignancy. **Materials and Methods:** A consecutive series of 77 patients with SPNs with pre-test intermediate likelihood of malignancy, who underwent FDG-PET/CT examination, was retrospectively reviewed. PET images were acquired approximately 1 hour after the i.v. injection of 3.7 MBq/Kg of 18F-FDG using a hybrid PET/CT scanner (Discovery 710; GE Healthcare). SUVmax at 2.5 cut-off value was used to assess the accuracy of PET/CT in differentiating malignant from benign nodules. TLG and MTV parameters were also calculated and compared among the two groups of lesions and in the different histological types of malignant lesions using appropriate statistical methods. P value <0.05 was considered significant. All nodules were referred to definitive cytological/histopathological diagnosis after PET/CT. **Results:** Forty-six/77 nodules resulted malignant (primary lung carcinoma in all 46 cases), whereas 31/77 were benign. Using 2.5 as threshold SUVmax, FDG-PET/TC was true positive in 43/46 carcinomas (sensitivity: 94%), including seventeen ≤15 mm in size, and false negative in 3 (1 atypic carcinoid, 1 squamous cell carcinoma, 1 bronchoalveolar carcinoma; range size: 18-30 mm). The procedure was true negative in 23/31 benign lesions (specificity: 74%) and false positive in the remaining 8/31 lesions; among the latter, pneumoconiosis, fibrosis mixed with inflammation and mycosis were the commonest, with SUVmax ranging from 2.58 to 9.02. Overall accuracy, PPV and NPV of PET/CT were 86%, 84%, and 89%, respectively. SUVmax, TLG and MTV values were significantly higher (p<0.001) in malignant than in benign nodules. Moreover, SUVmax and TLG were higher in squamous cell carcinomas than in adenocarcinomas, whereas MTV was higher in the latter; however, differences were not statistically significant. **Conclusion:** In the present study carried out on a selected series of patients with SPNs with pre-test intermediate likelihood of malignancy, FDG-PET/CT proved a highly sensitive diagnostic method, even in the detection of small size carcinomas. With SUVmax <2.5, there is a 10% probability that a nodule is malignant. The addition of TLG and MTV might further help in differentiating malignant from benign nodules. However, semiquantitative parameters proved not useful in predicting the different histopathological types of primary lung carcinomas. **References:** None.

EP-0435

Prognostic value of ^{18}F-FDG PET/CT in patients with non small cell lung cancer treated with Stereotactic Body Radiation Therapy

P. García-Talavera San Miguel[1], E. González[2], C. Cigarral[2], F. Gómez-Caminero[1], J. G. Villanueva[1], C. Riola[1], L. G. Diaz[1], E. Martín[1], P. Tamayo[1];
[1]Nuclear Medicine Department. Hospital Clinico Universitario de Salamanca, Salamanca, SPAIN, [2]Radiotherapy Department. Hospital Clinico Universitario de Salamanca, Salamanca, SPAIN.

Aim/Introduction: To study the prognostic value of staging ^{18}F-FDG PET/CT (PET1) as well as ^{18}F-FDG PET/CT for response

assessment to the stereotactic body radiation therapy (SBRT) (PET2), in patients with non small cell lung cancer (NSCLC). **Materials and Methods:** Thirty two patients with NSCLC were included (Staging: 16 IA and 16 IB). They were diagnosed from May 2015 to April 2018 and treated with SBRT. Histology: squamous (17), adenocarcinoma (12), large cell carcinoma (1) and unclassified (2). The locations were: right upper lobe (12), middle lobe (3), right lower lobe (4), left upper lobe (6), lingula (1) and left lower lobe (6). In all of them, PET/CT for staging (PET1) and PET/CT at 4.2 ± 0.9 months of the end of the SBRT (PET2) were performed. The results of PET2 were correlated with radiological follow up (contrast CT), and 16 out of them with another PET/CT (PET3). SULpeak and TLG were calculated for all lung lesions in PET1 and PET2 (SULpeak1 and SULpeak2; TLG1 and TLG2). Progression free survival (PFS) curves were performed, by means of Kaplan Meir analysis and Log Rank test, after calculation of cut off values of the variables, based on ROC curves. **Results:** The following cut off values were selected as optimal: 6.9 for SULpeak1 (S=64.3%; Sp=78%), 41.5 for TLG1 (S=64.3%; Sp=78%), 2.7 for SULpeak2 (S=50%; Sp=72%) and 80.1 for TLG2 (S=54%; Sp=72%). In PFS curves, by means of Long Rank test, there were differences in mean PFS in all cases (TLG1: 13 ± 2.7 vs 23.2 ± 3.1 months; TLG 2: 15.5 ± 2.5 vs 23.9 ± 3.5 months; SULpeak2: 16.7 ± 3.7 vs 22.3 ± 3.1 months), but only significant differences were reached with SULpeak1 (p=0.05) (15 ± 3.2 vs 25.6 ± 3.3 months), maybe due to the small size of the sample. **Conclusion:** Calculated parameters (SULpeak and TLG) in staging ^{18}F-FDG PET-CT and ^{18}F-FDG PET-CT for response assessment are promising tools as prognostic predictors in patients with non small cell lung cancer stage I, treated by means of SBRT. **References:** None.

EP-0436

Prognostic Value Of Metabolic Parameters Of 18F-FDG PET/CT In Patients With Advanced (Non-Metastasic) Non-Small-Cell Lung Carcinoma

J. Villanueva, P. García-Talavera, A. Peñaherrera, J. Cañadas, C. Riola-Parada, F. Gómez-Caminero, J. González, J. Cascón, R. Cordovilla, P. Tamayo;
Hospital Clínico Universitario de Salamanca, Salamanca, SPAIN.

Aim/Introduction: To assess the utility of metabolic parameters of staging 18F-FDG PET/CT, total lesion glycolysis (TLG) and SUVmax, as prognostic factors of progression-free survival (PFS) and overall survival (OS) in patients with stage III non-small-cell lung carcinoma (NSCLC). **Materials and Methods:** 30 patients were included (23 men), mean age 67.6 ± 9.9 years, with stage III (56.7% IIIA, 40% IIIB, 3.3% IIIC) NSCLC (53% squamous, 47% adenocarcinoma) to whom a 18F-FDG PET/CT were performed between October 2014 and December 2017 for staging. Patients were treated with induction therapy followed by surgery or radiotherapy (16.7%) or concomitant chemotherapy/radiotherapy ± inmunotherapy treatment (83.3%). A clinical and radiological follow-up was done, collecting progression-free time from staging, and OS. Kaplan-Meier survival curves were created, according to SUVmax and TLG, calulating the optimal cutoff point by ROC curves. **Results:** 21 patients progressed during follow-up with a progression-free interval of 11.3 ± 9.8 months; 17 patients died, with a mean survival time of 18.9 ± 12.1 months; 9 patients remained disease-free with a median follow-up period of 29.8 ± 12.6 months. During the first year, global survival rate was 70% and progression-free rate was 53%. Progression sites were 52.9% locoregional and 47.1% distant metastasic disease (lung, adrenal, bone and liver). It was obtained significant differences (p=0.047) in mean time of PFS according to TLG, with a cutoff point of 265 (16.2 ± 3.2 months with TLG > 265 vs 31 ± 5.5 months with TLG < 265). On the contrary, it wasn´t obtained significant differences in OS according to TLG with the same cutoff point. In relation to SUVmax, with a cutoff point of 16.2, it was obtained differences in OS (26.5 ± 3.6 months with SUVmax > 16.2 vs 38.1 ± 5.2 months with SUVmax < 16.2) without reaching statistical significance. Neither was obtained statistical significance in PFS according to SUVmax, with a cutoff point of 14.6. **Conclusion:** The study confirms the utility of metabolic parameter TLG as a predictive factor in progression-free survival in patients with stage III non-small-cell lung carcinoma. **References:** None.

EP-0437

Improved detection of small pulmonary lesions using a digital PET/CT system compared with conventional analog PET/CT

A. Fernández León[1], A. Ruiz[2], V. Camacho[1], M. Estorch[1], A. Domenech[1], M. Sizova[1], I. J. Gich[3], I. Carrio[1];
[1]Nuclear Medicine Department. Hospital de la Santa Creu i Sant Pau, Barcelona, SPAIN, [2]Physics an Radioprotection Department. Hospital de la Santa Creu i Sant Pau, Barcelona, SPAIN, [3]Epidemiology Department. Hospital de la Santa Creu i Sant Pau, Barcelona, SPAIN.

Aim/Introduction: The aim of this study was to determine the impact of a new digital PET/CT (Vereos Phillips system) on the detectability of small lesions compared with analog PET/CT (Gemini Phillips system). **Materials and Methods:** We first performed a phantom study and subsequently a patient study. We analyzed 2 image-quality phantoms (Image Quality NEMA Phantom Set) in order to compare Recovery Coefficients (RC) in spheres with varying sizes using both digital and analog PETs. In the patient study 72 pulmonary nodules of less than 10 mm diameter were analyzed in 33 consecutive patients. Only lung lesions with positive FDG visual uptake on digital PET/CT were selected for comparison between digital and analog PET/CT. The order of study acquisitions was aleatory. For visual analysis, 2 experienced nuclear medicine physicians determined the PET positivity or negativity of nodules. For each lesion, we measured the mean and maximum standardized uptake values (SUVmean and SUVmax), based on the isocontour VOI at 40% of the maximum pixel value. We performed background measurements in the lung and in the liver, by drawing an spherical VOI of 30 mm. Quantitative values of each nodule were

corrected by hepatic activity, and contrast value was determined dividing SUVmax and SUVmean of nodules by lung activity. We used the Wilcoxon signed-rank test to compare visual detection and contrast values measurements in the nodules between two systems, and ROC curves to determine the minimum diameter of lesions we can detect in digital PET/CT but not in analog system. **Results:** Recovery coefficients in lesions less than 10 mm calculated in digital PET/CT were 58% versus 33% in analog PET/CT suggesting differences in detectability in the phantom study. In patients, digital PET was able to detect pulmonary lesions as positive (89,6%) in diameters between 3 and 4 mm compared with analog PET (AUC 0,866; p< 0.01). We observed statistically differences (p<0.01) in visual detection, global lesion contrast values (mean 1,35 in digital; mean 0.36 in analog) and in lesion contrast depending on its positivity in each system. **Conclusion:** Digital PET-CT resulted in higher detectability of small pulmonary nodules compared to analog PET/CT. **References:** None.

EP-0438

18F-FDG PET-CT quantitative parameters as prognostic factor in inoperable lung cancer

M. Moreno-Caballero, J. Cabrera-Rodríguez, J. Infante-de la Torre, J. Rayo-Madrid, C. Cruz, J. Serrano-Vicente, A. Martínez-Esteve, P. Jiménez-Granero, A. Cobo-Rodríguez;
Hospital Universitario de Badajoz, Badajoz, SPAIN.

Aim/Introduction: Standard management of lung cancer includes surgery and chemotherapy. However, stereotactic body radiotherapy (SBRT) is considered an appropriate treatment method in inoperable patients and early stage of the disease. The aim of the study was to evaluate the usefulness of FDG-PET-CT quantitative parameters as prognostic factors in inoperable lung cancer treated with SBRT. **Materials and Methods:** We retrospectively analyzed 55 patients (47 men, median age 75 years, range 56-99) diagnosed in the last 7 years with stage I primary lung cancer and treated only with SBRT (BED10 >110 Gy). After FDG-PET-CT scan, we determined the maximum standardized uptake value (SUVmax), metabolic tumor volume (MTV), and total lesion glycolysis (TLG) at different thresholds (SUVmáx 2, 2.5, 3, and 30%, 40% and 50% of SUVmax). The mean follow-up was 37 months. Prognostic factors for cancer-specific survival (CSS) and disease-free survival (DFS) were investigated by Cox regression model and survival curves using the Kaplan-Meier method. **Results:** Statistical analysis determined MTV2 (considering a threshold of SUVmax=2, p<0.02), TLG2 (threshold of SUVmax=2, p<0.02), and tumor size (p<0.001) as a significant predictive factors for both CSS and DFS. SUVmax, age and sex were not shown to be significant factors. ROC analysis estimated the appropriate cut-off value to these parameters (for CSS: MTV2=17.26, TLG2=51816, tumor size=29 mm; for DFS: MTV2=15.11, TLG2=51816, tumor size=22.5 mm). Kaplan-Meier survival analysis showed statistically significant differences in CSS and DFS between the groups of patients categorized by MTV2 and tumor size (p=0.001), and only in CSS between patient categorized by TLG2 (p=0.03). **Conclusion:** The pre-treatment quantitative assessment by FDG-PET-CT using metabolic parameters MTV2, TLG2 and tumor size proved to be prognostic factors for CSS and/or DFS in patients with inoperable primary lung cancer treated with SBRT. SUVmáx was not a significant predictor. The outcome of the study may help to personalize treatment administered to the patient. **References:** None.

EP-0439

Comparison of molecular oncological features and FDG uptake in lung cancer

F. Kiss[1], S. Czibor[1], C. Müller[2], É. Vaszilkó[1], Z. Varga[1], T. Györke[1];
[1]Semmelweis University, Nuclear Medicine Center, Budapest, HUNGARY, [2]Semmelweis University, Faculty of Medicine, Budapest, HUNGARY.

Aim/Introduction: Lung cancer is the most common malignant tumor in the world, and its prognosis and treatment depend significantly on the results of histological and molecular analysis. Taking samples is often difficult or unsuccessful (eg. due to extensive emphysema), in these cases imaging techniques can be helpful to create the final diagnosis. In our research, we examined whether there is a correlation between the molecular properties and the FDG uptake of the tumor. **Materials and Methods:** In our research, we analyzed the primary staging 18F-FDG-PET/CT scans made at our institute of 73 lung cancer patients (62 adenocarcinomas, 11 squamous cell carcinomas). We examined the presence or absence of K-Ras and PD-L1 mutations (53 K-Ras negative, 9 K-Ras mutants; 23 PD-L1 negative, 32 PD-L1 mutants), then we measured the maximum standardized uptake value (SUV_{max}) and the SUV peak (SUV_{peak}) in the tumors. We compared the results with a non-parametric statistical test (Mann-Whitney U test). We present the results as median ± interquartile range. **Results:** The FDG uptake of K-Ras and PD-L1 mutant tumors was significantly higher than non-mutant tumors (SUV_{max} for K-Ras: 21.4±9.7 vs. 13.6±6.3, SUV_{peak}: 18.4±7.8 vs. 10.6±5.5; SUV_{max} for PD-L1: 15.4±6.9 vs. 11.3±8.4, SUV_{peak}: 12.8±5 vs. 8.7±6.5). The FDG uptake of adenocarcinomas and squamous cell carcinomas did not differ significantly (SUV_{max}: 14.3±6.5 vs. 14.9±6.9; SUV_{peak}: 11.1±6.3 vs. 13.4±5.3). **Conclusion:** The semiquantitative evaluation of PET/CT scans can be helpful not only in conventional imaging diagnostics, but also in advanced molecular analysis. With the addition of other radiomic and molecular biomarkers, both SUV_{max} and SUV_{peak} may be appropriate parameters to facilitate more accurate histological stratification, and thus they also may help patients with proper diagnosis and consequently, adequate therapy. **References:** None.

EP-0440

The clinic study on the association between semiquantitative analysis for glucose metabolism imaging and proliferation-associated antigen Ki-67 in NSCLC

R. Wang[1,2], X. Liao[1], M. Liu[1], Y. Cui[1], Y. Fan[1], Z. Fu[1], J. Zhang[1], X.

Zhang[1], L. Di[1], X. Chen[1], Q. Jiang[1];
[1]Peking University First Hospital, Beijing, CHINA, [2]Peking University International Hospital, Beijing, CHINA.

Aim/Introduction: Although a large number of researches have reported the positive correlation between maximum standardized uptake value (SUVmax) and proliferation-associated antigen Ki-67, most of them only made a general analysis regardless of the diversity in pathological subtypes or TNM staging or both of them. The purpose of this study was to investigate the correlative association between the preoperative SUVmax of primary lesion measured on ^{18}F-FDG PET/CT and Ki-67 labeling index (Ki-67 LI) in non-small cell lung cancer (NSCLC) through a series of stratified analyses to relieve the influences from confounding. **Materials and Methods:** A hundred and eleven patients with histologically proven NSCLC by surgery and pre-operation ^{18}F-FDG performance were involved retrospectively in this research. For semi-quantitative analysis of ^{18}F-FDG PET/CT, SUVmax were estimated. The clinicopathologic parameters (gender, age, TNM stage, N stage, M stage, pathologic subtype, tumor size, Ki-67 LI of the primary tumor) were collected. Pathologic stage was assigned according to the seventh IASLC TNM staging system. The correlation between SUVmax and the clinicopathologic parameters was analyzed with multiple linear regression. Then the characters were categorized depending on clinicopathologic parameters respectively. The relevance between SUVmax and Ki-67 LI was studied by rank correlation analysis. All data were analyzed by the statistic software of SAS 9.2. P<0.05 was considered statistically significant. **Results:** 1. The SUVmax was related to the pathologic subtype, TNM stage, the size of tumor and Ki-67 LI significantly through the analysis of multiple linear regression. 2. Based on further correlation analysis with grouping, the significant relevance between SUVmax and Ki-67 LI was showed in the adenocarcinoma (r=0.42,P<0.001), the acinar predominant adenocarcinoma (r=0.48,P=0.009), the I stage (r=0.56,P<0.001), the N_0(r=0.65,P<0.001), the N_{1-3}(r=0.33,P=0.01), the M_0stage (r=0.49,P<0.001), the age ≤60 (r=0.46,P=0.001), and the age >60 years (r=0.42,P<0.001). The significant differences of SUVmax were displayed between the adenocarcinoma and squamous cell carcinoma in the same TNM stage, so were the difference of Ki-67 LI. **Conclusion:** The moderate relation exists between the value of semiquantitative analysis for glucose metabolism imaging and Ki-67 LI. Hence, primary prognoses on the proliferative features of tumor could be made according to the level of the glucose metabolism: the high level of SUVmax suggested the active tumor proliferation, and the poor prognosis could be made. **References:** None.

EP-0441

Role of texture parameters derived on ^{18}F-FDG PET/CT studies, in prediction of survival to therapy in lung carcinoma patients

***N. Rana**, B. R. Mittal, K. Agrawal, D. K. Dhawan;*
PGIMER, Chandigarh, INDIA.

Aim/Introduction: The advancements in medical imaging have led to development of tools for extracting information from images, that can be helpful in providing personalised patient care. Texture analysis is one such tool. Texture parameters on the basis of relation amongst image pixels can quantify various information regarding tumor heterogeneity. Clinical utility of these texture parameters require validation via multicenteric study. The aim of the present study was to see the role of texture parameters derived on ^{18}F-FDG PET/CT study in prediction of survival in lung carcinoma patients. **Materials and Methods:** A total of 30 patients (24 males, 6 females) with biopsy proven NSCLC, referred for ^{18}F-FDG PET/CT study for initial staging were included. Texture analysis was performed on PET/CT studies using a MATLAB based software package (CGITA-Chang-Gung Image Texture Analysis toolbox). A total of 59 texture parameters based on gray level co-occurrence matrix (GLCM) and normalised gray level co-occurrence matrix (NGLCM), neighbouring gray-tone difference matrix (NGTDM), gray level run length matrix (GLRLM), gray level size zone matrix (GLSZM), texture spectrum method (TS), texture feature coding method (TFCM), texture feature coding co-occurrence matrix (TFCCM) and neighbouring gray level dependence matrix (NGLDM) were calculated. Time for overall survival i.e. time between date of PET study and death of patient or time to last censoring from date of scan was noted. Kaplan Meir survival curve was used to find the median survival time. Ability of each texture parameter to predict survival time was evaluated using univariate and multivariate Cox regression models by studying the effect of texture parameters as covariates on Overall survival (OS). Differences in Kaplan-Meier survival curves were evaluated for parameters which had statistically significant association with survival using nonparametric log-rank test. **Results:** Median follow up time was 431.73 days (range, 28-1007 days) and median OS was 487 days (range, 28-640 days). Using univariate analysis, $Busyness_{NGTDM}$ and using multivariate Cox-regression analysis five texture parameters, $Run\ Percentage_{GLRLM}$, $Busyness_{NGTDM}$, $Complexity_{NGTDM}$, $Mean\ Convergence_{TFCM}$ and $Contrast_{TFCCM.}$ were found to be significantly associated with survival having p > 0.05. However, comparison using log rank for all the five texture parameters showed none of these had significant difference in association with survival in high and low value texture parameter group. **Conclusion:** Texture parameters in our study were not found to be able to predict survival in lung carcinoma patients. However, this needs further confirmation using larger number of patients. **References:** None.

EP-0442

N-staging in large cell neuroendocrine carcinoma of the lung: diagnostic value of ^{18}FDG PET/CT as compared to the histological gold standard

***H. Hautzel**[1], T. Plönes[2,3], Y. Alnajdawi[3], W. Fendler[1], C. Rischpler[1], L. Umutlu[4], K. Herrmann[1], C. Aigner[2,3];*
[1]University Hospital Essen, Dep. of Nuclear Medicine, Essen, GERMANY, [2]University Hospital Essen, Dep. of Thoracic Surgery, Essen, GERMANY, [3]Ruhrlandklinik Essen, Essen, GERMANY, [4]University Hospital Essen, Inst. of Radiology, Essen, GERMANY.

Aim/Introduction: The large cell neuroendocrine carcinoma of the lung (LCNEC) represents a rare entity occurring in less than 5% of all lung cancers. Due to its low differentiation (G3) it is FDG avid, thus PET/CT is suitable for staging of LCNEC. In early stages surgery with curative intent is the treatment of choice. Prerequisite for this is the correct lymphonodular staging. This study aimed at evaluating the diagnostic quality of FDG PET/CT against the histological gold standard gained by either surgical resection or mediastinoscopy. Additionally, our results were compared to literature-based findings in NSCLC with special respect to the N-staging. **Materials and Methods:** Between 03/13 and 02/19 31 patients with LCNEC were included. All underwent a FDG PET/CT for initial staging and subsequently either surgery (n=25) or mediastinoscopy (n=6). Per patient 15±8 lymph nodes were removed and histologically processed. Regarding the lymphonodular involvement, sensitivity, specificity, accuracy, positive predictive value (PPV) and negative predictive value (NPV) were calculated for the FDG PET/CT diagnostics using the final histo-anatomical N-staging (N0 to N3) as gold standard. **Results:** 24/31 patients had no LCNEC spread into the lymph nodes. 2/31 patients were finally staged N1. In 2/31 patients final outcome was N2 and in 3/31 patients N3. FDG PET/CT diagnosed a lymphonodular involvement of LCNEC with a sensitivity of 87.5%, a specificity of 87.0%, an accuracy of 87.1%, a PPV of 70.0% and a NPV of 95.2%. **Conclusion:** In LCNEC FDG PET/CT demonstrates both high sensitivity and specificity as well as a high NPV. However, PPV is slightly limited. The data shown here indicate that FDG PET/CT in LCNEC outperforms NSCLC FDG PET/CT diagnostics in terms of N-staging (NSCLC: sensitivity 62%; specificity 90%; PPV 63%; NPV 90%) (1). **References:** Silvestri, G.A., et al., Methods for staging non-small cell lung cancer: Diagnosis and management of lung cancer, 3rd ed: American College of Chest Physicians evidence-based clinical practice guidelines. Chest, 2013. 143(5 Suppl): p. e211S-50S.

EP-0443

Notch1-dependent targets in cancer stem cell resistance to EGFR inhibitors in oncogene-driven non-small cell lung cancer

F. Iommelli[1], *V. De Rosa*[1], *C. Terlizzi*[2], *C. A. Stewart*[3], *L. A. Byers*[3], *D. Piwnica-Worms*[4], *S. Del Vecchio*[2];
[1]*Institute of Biostructures and Bioimaging, National Research Council, Naples, ITALY,* [2]*Department of Advanced Biomedical Sciences, University "Federico II", Naples, ITALY,* [3]*Department of Thoracic/Head and Neck Medical Oncology, The University of Texas MD Anderson Cancer Center, Houston, TX, UNITED STATES OF AMERICA,* [4]*Department of Cancer Systems Imaging, The University of Texas MD Anderson Cancer Center, Houston, TX, UNITED STATES OF AMERICA.*

Aim/Introduction: Multiple molecular mechanisms may cause resistance of non-small cell lung cancer (NSCLC) to EGFR inhibitors including epithelial-mesenchymal transition (EMT) and presence of cancer stem cells (CSCs). Notch1 plays a key role in EMT and in the maintenance of CSCs. Upregulation and activation of Notch1 occurs in oncogene-driven NSCLC cells exposed to EGFR inhibitors. The aim of the present study was to test whether high levels of activated Notch1 can induce a reversible shift of oncogenic dependence from EGFR to Notch1 in NSCLC cells thus causing resistance to EGFR inhibitors. **Materials and Methods:** NSCLC H1975 cells bearing double mutant (L858R/T790M) EGFR were grown in adhesion (parental) and as tumor spheres to obtain an enriched cancer stem cell subpopulation. Parental cells and derived CSCs were then treated with erlotinib and WZ4002 to test cell viability and levels of EGFR signaling mediators. Markers of EMT and stemness included CD44, Notch1, Vimentin,E-cadherin and Oct3/4. The activation of Notch1 signaling and its cross-talk with EGFR was tested by binding assays with Notch1 agonist and western blotting. **Results:** Cell toxicity assays showed that tumor spheres were more resistant to treatment with erlotinib and WZ4002 as compared to parental cells. RT PCR array did not show any significant difference in the EGFR mutational status and copy number between parental cells and tumor spheres. A strong upregulation of Notch1, Notch1 intracellular domain (NICD), RBPSUH, c-Myc and Bcl-2 was found in tumor spheres and was associated with high levels of EMT and stemness markers. Furthermore a Notch-dependent increase of alpha5 beta1 integrin was found on the plasma membrane of CSCs. Analysis of EGFR pathways showed a strong downregulation of total EGFR in tumor spheres as compared to parental cells. When exposed to treatment with EGFR inhibitors, although a reduction of phospho-EGFR was observed in both cell populations, a less pronounced decrease of signaling mediators and cyclin D1 levels was found in tumor spheres as compared to parental cells. Binding assays of parental cells with increasing concentrations of DLL4 showed that EGFR downregulation simultaneously occurred with a dose-dependent increase of NCID, Hes1, Hey1, p53 and Sp1. **Conclusion:** Our findings indicate that high levels of activated Notch1 in CSCs subpopulation is associated with downregulation of EGFR and a higher resistance to EGFR inhibitors. Several potential targets were identified in Notch1 pathway that when simultaneously inhibited with EGFR may promote the escape of tumor cells from the staminal compartment. **References:** None.

EP-28

Clinical -> Diagnostic study -> Adult study -> Oncology study -> Organ-based oncology -> Melanoma, malignant

October 12 - 16, 2019 e-Poster Area

EP-0444

Whole-body 18F-FDG PET/CT in Uveal Melanoma Patients

D. M. Pursanova[1], *O. V. Mukhortova*[1], *I. P. Aslanidis*[1], *T. A. Katunina*[1],

S. V. Saakyan[2], K. V. Avakyan[2];
[1]A.N.Bakoulev National Medical Research Center of Cardiovascular Surgery of the Ministry of Health of Russian Federation, Moscow, RUSSIAN FEDERATION, [2]Helmholtz Moscow Research Institute of Eye Diseases of the Ministry of Health of the Russian Federation, Moscow, RUSSIAN FEDERATION.

Aim/Introduction: To investigate the usefulness of 18F-FDG PET/CT in uveal melanoma (UM) patients. **Materials and Methods:** This retrospective analysis included results of 18F-FDG PET/CT examinations performed in 72 UM patients: 28/72 patients examined before treatment for staging and 44/72 in 3-212 (mean 24,6±9) mo after radical therapy for detection of metastases. Examinations were done on PET/CT scanner (Biograph-64, Siemens) 90 min after 18F-FDG injection (180-200Mbq), in standard whole body mode including orbits. **Results:** The evaluation of local status in UM patients by PET/CT showed the high level of false-negative and equivocal results because of small tumor thickness, severe ocular muscles 18F-FDG uptake and motion artifacts. Overall, for detection of primary tumor PET/CT results were correct in 13/28 (46%) patients: in 0/4 with small, in 7/14 with medium and in 6/10 with large tumors according to COMS classification. The level of SUVmax in tumors was found from 1.6 to 4.3. There was no correlation of SUVmax with tumor size (p = 0.7). In the group of patients after radical treatment (n = 44) the local relapse was correctly diagnosed by PET/CT in 6/10 (60%) cases. The evaluation of distant areas identified 6/72 (8%) patients with other primary malignances (histologically confirmed): in 2/6 synchronous colon and breast tumors and in 4/6 metachronous tumors (lung, breast, thyroid, colon; in one patient - 3 other tumors). Distant metastases (in liver, bones, lungs, soft tissues, adrenal glands) were revealed in 11/72 (15%) patients: in 2/28 (7%) - examined for staging and in 9/44 (20%) in follow up group. Importantly, the oligometastatic distant lesions were detected in 3/11 patients and all of them had isolated hepatic involvement. False-negative PET results were received in 2/44 follow-up patients with small (up to 7 mm) hepatic metastases revealed by MRI. **Conclusion:** 18F-FDG PET/CT in UM patients is not useful for the assessment of status localis - primary tumors or local recurrences, but whole-body examination plays an important role in the personalized treatment approach. PET/CT results allow to identify patients for radical treatment, differentiate multiple and oligometastatic process, as well as detect second malignancies. **References:** None.

EP-0445

18 F-FDG PET/CT For Staging And Restaging Of Anorectal Melanoma

***A. N. Bakare**, A. Agrawal, S. Shah, N. Purandare, A. Puranik, V. Rangarajan;*
Tata Memorial Centre, Mumbai, INDIA.

Aim/Introduction: To evaluate diagnostic role of 18 F FDG PET/CT in initial staging and restaging of anorectal melanoma. **Materials and Methods:** This was a retrospective observational study, patients for initial staging and with clinical or radiological suspicion of disease recurrence referred for PET/CT from Jan-2006-Dec-2016, were included in the study. Diagnostic performance of PET/CT was evaluated for baseline staging and disease recurrence. Any area with intensity greater than background that could not be identified as physiological activity on PET images or which on CT correlation did not fit into benign (infective/inflammatory/degenerative) was considered to be suggestive of tumor on the PET study. PET/CT findings were correlated with histopathology results. When tissue diagnosis was not available, clinical or radiological follow-up was used as reference standard. **Results:** Total 61 patients who were referred for initial staging were included. PET/CT correctly detected primary lesion in 57 cases (93.44%), regional nodes in 46 cases (75.4%), non-regional nodes in 22 cases (36%) and distant metastases in 25 cases (41%). PET/CT was false negative in 2 cases which on surgical histopathological report revealed submucosal anorectal lesion. The sensitivity, specificity, positive predictive value, negative predictive value for primary lesion, regional nodes, non- regional nodes and distant metastases were 96.61%,100%,100%,50%; 97.87%,100%,100%, 93.33%; 100%,100%,100%,100% and 100%,100%,100%, 100% respectively. Total 24 patients were included for suspected recurrence/restaging. All the patients were treated previously by surgery, radiotherapy, or chemotherapy. PET/CT detected disease recurrence in 20 patients (83.3%).10 patients had recurrence at the primary site, 8 of whom also had distant metastases and 2 had only loco-regional metastatic nodes. In remaining 10 patients, there was no primary site recurrence, however, 2 patients had loco-regional nodal and distant metastases while 8 patients had only distant metastases. Histopathological confirmation was available in 6 patients whereas imaging and clinical follow-up confirmed recurrence in remaining patients. PET/CT was negative for recurrence in 3 patients. PET/CT was false negative in 1 patient which missed liver metastasis. Sensitivity, specificity, positive predictive value and negative predictive value of PET/CT was found to be 95%, 100%, 100%, 75% respectively with accuracy of 96%. **Conclusion:** 18 F FDG PET/CT demonstrates high diagnostic accuracy in the initial staging and detection of recurrent disease in cases of anorectal melanoma. **References:** None.

EP-0446

Metastatic melanoma response to combination therapy with BRAF and MEK inhibitors: a FDG PET/CT pilot study

***L. Burroni**, F. Fringuelli, G. Biscontini, A. Palucci;*
Nuclear Medicine, Ancona, ITALY.

Aim/Introduction: Melanoma is a highly metastatic neoplasm of the skin that has risen in incidence among white population over the past few decades. F^{18}-FDG PET/CT has become a cornerstone for staging disease, assessing therapy and determining prognosis in patients solid malignancies,

included advanced melanoma. Combination therapies for the treatment of metastatic melanoma are a matter of debate nowadays. We studied the early changes on F18-FDG PET/CT for patients with BRAF-mutant melanoma receiving BRAF and MEK inhibition therapy. **Materials and Methods:** 9 patients with advanced BRAF-mutant metastatic melanoma were included. All patients received combination BRAF and MEK inhibitors for the treatment of metastatic melanoma. In all patients F18-FDG PET/CT scans were performed at baseline and one month post treatment. All images were assessed visually to identify sites of increased uptake and SUVmax measures were calculated. HRCT was also performed in all patients. **Results:** The baseline PET/CT scan demonstrated multiple metastatic lesions in all patients. At follow-up 2 patients had a complete response, 3 had stable disease and 4 had progressive disease. In patients with progressive disease CT responses and clinical conditions have discouraged the execution of the follow-up PET/CT. **Conclusion:** Due to its ability in detecting metabolic changes before anatomic alterations take place, FDG PET/CT can be a powerful tool in personalized treatment management in advanced melanoma. In two cases with complete response, PET/CT played a significant role in patient monitoring and prediction of treatment response. In particular, change in SUV_{max} for the least responsive tumor and baseline performance may be useful prognostic indicators for progressive-free survival in patients with BRAF-mutant melanoma. **References:** None.

EP-29

Clinical -> Diagnostic study -> Adult study -> Oncology study -> Organ-based oncology -> Other malignant, including primary of unknown origin

October 12 - 16, 2019 e-Poster Area

EP-0447

Qualitative Assessment of Pericardial Metastasis in Oncologic F-18 FDG PET/CT

H. Lee, J. Kim;
Dongnam Institution of Radiological & Medical Sciences (DIRAMS), Busan, KOREA, REPUBLIC OF.

Aim/Introduction: Accurate diagnosis of the pericardial metastasis in F-18 FDG PET/CT is challenging especially in oncologic patients with multiple metastases. The aim of this study was to assess the qualitative analysis of pericardial metastasis in the F-18 FDG PET/CT in oncologic patients. **Materials and Methods:** Between Jan 2012 and Apr 2019, we reviewed 18,215 consecutive F-18 FDG PET/CT studies done for an oncologic indication (staging or follow-up) at our institution. 28 oncologic patients (range, 37-88 y; mean age, 63.2±12.9 y), who underwent F-18 FDG PET/CT for initial staging work-up or follow-up were enrolled in this study. F-18 FDG PET/CT images were reviewed by 2 experienced nuclear medicine physicians. A qualitative analysis was performed on the images. All pericardial metastases were scored for their extent and intensity using a 3-point scale (1 = low, 2 = moderate, 3 = high). Diffuse pericardial thickening with diffuse FDG uptake was considered as low-grade. Diffuse pericardial thickening with several hypermetabolic nodules was considered as moderate-grade. Intense hypermetabolic pericardial thickening was considered as high-grade. A final diagnosis of the pericardial metastasis was based on pericardial fluid cytology or clinical and imaging follow-up. **Results:** Among 28 oncologic patients with pericardial metastasis on F-18 FDG PET/CT, the most frequent primary tumor was lung cancer (12/28, 42.9%), followed by thymic carcinoma (3/28, 10.7%), breast cancer (3/28, 10.7%), gastric cancer (3/28, 10.7%), head and neck cancer (2/28, 7.1%), and five other malignancies (adenoid cystic carcinoma, pancreatic cancer, malignant B-cell lymphoma, malignant mesothelioma, and metastasis of unknown origin). Of 28 patients, the number of patients with pericardial metastasis which was diagnosed in initial staging work-up and follow-up (recurrence) was 11 and 17 patients, respectively. On qualitative analysis, the number of patients low-grade, moderate-grade and high-grade was 13 (46.4%), 8 (28.6%) and 7 (25.0%), respectively. In 7 patients with high-grade pericardial metastasis, the number of patients (5) who diagnosed in initial staging work-up was higher than that of patients (2) who in follow-up F-18 FDG PET/CT. However, in 13 patients with low-grade pericardial metastasis, the number of patients (8) who diagnosed in initial staging work-up was similar to that of patients (7) who in follow-up F-18 FDG PET/CT. **Conclusion:** In oncologic patients with F-18 FDG PET/CT, the most frequent primary tumor with pericardial metastasis was lung cancer. Patients with high-grade pericardial metastasis was initial staging work-up rather than follow-up on F-18 FDG PET/CT. **References:** None.

EP-0448

FDG-PET/CT is far superior to the Danish national standard of care diagnostic strategy in suspected occult cancer

R. Horvat, E. Døssing, S. Hess;
SVS Esbjerg, Esbjerg, DENMARK.

Aim/Introduction: Patients with non-specific symptoms and signs suggestive of occult cancer pose a clinical challenge; they are a heterogeneous population and the diagnostic strategy remains controversial. According to national guidelines in Denmark, the mainstay of the cancer fast-track program for these patients (referred to as suspected serious disease; SSD) is combined chest x-ray and abdominal ultrasound (CXR/US), whereas FDG-PET/CT may be added subsequently at the treating physicians' discretion. We have previously shown FDG-PET/CT to have high diagnostic yield in SSD when added to the diagnostic workup, but limited data compare CXR/US to FDG-PET/CT head-to-head. We retrospectively compared the relative diagnostic value of CXR/US and FDG-PET/CT in consecutive patients referred from family physicians to a dedicated SSD

outpatient clinic. **Materials and Methods:** All patients referred to the local SSD clinic during 2018 were included. Medical records were comprehensively reviewed for conclusions of CXR/US and FDG-PET/CT, histopathologic confirmation, and clinical conclusions. Scans were classified as true positive (TP; findings suggestive of malignancy or other severe systemic diseases confirmed by biopsy/clinical findings), false positive (FP; if subsequent investigations could not confirm such findings), true negative (TN; if findings were normal and the diagnostic process found no disease), or false negative (FN; if no abnormal findings were reported, but severe disease was subsequently diagnosed). **Results:** Ninety-five consecutive patients were included (43% males, mean age of 65 years (range 18-86)) and divided into three groups according to the diagnostic strategy at the SSD clinic; i.e. CXR/US only (n=31), FDG-PET/CT only (n=16), or CXR/US + FDG-PET/CT (n=48). In the latter group, eight patients were diagnosed with cancer (Breast (n=3), lung (n=2), prostate, head-neck, hematologic), and five with other severe systemic disease to explain their signs and symptoms (sarcoidosis (n=3) and large-vessel vasculitis (n=2)). All were correctly detected with FDG-PET/CT (13 TP, 8 FP, 27 TN, 0 FN). Thus, sensitivity, specificity, positive and negative predictive values, and accuracy was 100%, 77%, 62%, 100%, and 83%, respectively. In comparison, CXR/US only detected disease in one patient (malignant lymph nodes) yielding a sensitivity of only 8%. Similar sensitivities were found in the other two groups; i.e. 8% with CXR/US only, and 100% with FDG-PET/CT only. **Conclusion:** FDG-PET/CT is far superior to CXR/US in patients with clinically suspected occult cancer with sensitivity of 100% vs. 8%. If prospective data can substantiate these results, the national clinical guidelines should be revised and FDG-PET/CT should be the up-front first-line modality. **References:** None.

EP-0449

18F-FDG PET/CT In Peritoneal Carcinomatosis. Correlation With CT And Surgery In Evaluation Of Peritoneal Carcinomatosis Index (PCI)

A. Vallejo-Lesmes, *E. Rodriguez-Caceres, A. Santos -Bueno, J. Marquez-Fernandez, J. Prieto-Prieto, M. Guiote Moreno, J. Vallejo-Casas;*
Universitary Hospital Reina Sofia, IMIBIC, Cordoba University, Córdoba, SPAIN.

Aim/Introduction: Peritoneal carcinomatosis is the most common malignat process involving the peritoneum and results from metastatic dissemination into the peritoneal cavity, secondary to different tumors. Citoreductive surgery (CS) and hypermic intraperitoneal chemotherapy (HIPEC) has demostrated improve survival in this patient group. The success on this aproach relies primarily on the accurate selection of surgical candidates. This must be designed to exclude patients with extra-abdominal disease or abdominal disease not removable with surgery. AIM:To evaluate the clinical usefulness of the results obtained with the 18F-FDG PET/TC en the preoperative staging of patients with peritoneal carcinomatosis candidates for cytoreductive surgery (CS) and hyperthermic intraoperative intraperitoneal chemotherapy (HIPEC). **Materials and Methods:** A retrospective study comparing the values obtained with 18F-FDG PET/CT, CT and surgical evaluation (peritoneal carcinomatosis index or PCI, was considered as reference. Standard Uptake Value (SUV) maximun and peak, metabolic tumour volume (MTV) and total lesion glycolisis (TLG) were determined. Progression-free survival (PFS) and overall survival (OS) was assesed). Analysis using R software (V.3.5.1) was carried out to get the descriptive study and lineal regression to modeling the relationship between dependent variable (PCI) and PET/CT values. **Results:** We started the study with 80 patiens. 43 patients were excluded for extraabdominal disease, non surgical procedure or delay between PET/CT and surgery. We included 37 patients (7 men, 30 women). In 36/37 cases the PET/CT showed increase of metabolic tracer uptake. The mean PCI calculated in CT was 10,69 (SD 10,59), in PET/TC 11,57 (SD 11,13) and in surgical procedure 13,92 (SD 11,56). The mean MTV was 246,37 cm3 (SD 770,21) and TLG 348,26 (SD 623,43). The mean OS was 21 months and mean PFS was 12 months. 6 patients died at the end of study. Good correlation was found between surgical PCI and values obtained in CT (R2: 0,55; p<0,001, Pearson coefficient 0.74), and PCI calculted in PET/CT (R2:0,43; p<0.001, Pearson coefficient 0,66). The correlation for MTV and TLG was not stadistical signification. No correlation was obtained between OS and PFS with MTV and TLG. **Conclusion:** 18F-FDG PET/CT and CT showed good correlation with surgical PCI. We need more patients and more follow-up time to evaluated the real value of MTV and TLG in selection of patients with peritoneal carcinomatosis for CS and HIPEC **References:** None.

EP-0450

F-18 FDG-PET/CT in evaluating of the mediastinal tumours: The role of the metabolic and volumetric parameters

I. Ak Sivrikoz[1], *M. C. Sivrikoz*[2], *E. Durceylan*[2], *E. Gökçe*[2];
[1]*ESOGU School of Medicine Department of Nuclear Medicine, Eskişehir, TURKEY,* [2]*Eskıseşhır Osmangazi University School of Medicine Department of Thoracic Surgery, Eskişehir, TURKEY.*

Aim/Introduction: This study aimed to evaluate the role of pretreatment metabolic and volumetric F-18 FDG PET/CT parameters in the differentiation between benign and malignant mediastinal tumours. **Materials and Methods:** The 32 patients with mediastinal masses who underwent examination before operation were retrospectively reviewed (mean age 65 ±3,2 years, range 17-82 years). Histological examination indicated that 20 mediastinal tumours were benign, and 12 cases were malignant. To obtain quantitative PET parameters, we determined the maximum standardized uptake value (SUVmax), metabolic tumour volume (MTV), and total lesion glycolysis (TLG) for primary tumours. To define the contouring margins around the tumour, SUV cut-off value was considered at 2.5. If SUVmax of a tumour was equal to or less than the determined threshold,

MTV and TLG would be considered zero. The PET/CT patameters of benign and malignant tumours were compared using the Mann-Whitney U test. **Results:** The mean SUVmax, MTV and TLG of malignant mediastinal tumours were significantly higher compared to benign tumours (P<0.001). Mean SUVmax, MTV and TLG of benign mediastinal tumours were 2.4±1.2, 8.1±17.8 mL and 35.0±578.6 g, respectively. In malignant tumours, these values were determined at 8.2±3.4, 67.9±43.6 mL and 398.3±298.1 g, respectively). The mean SUVmax was significantly higher in invasive thymomas than those of non-invasive forms (P = 0.029). **Conclusion:** FDG PET/CT may be complementary for the evaluation of mediastinal masses. PET/CT may reduce unnecessary invasive investigations for diagnosis in patients with nonavid or low avid FDG lesions. However confirmatory tissue sampling is required to confirm PET positive findings for the definite diagnosis. **References:** None.

EP-0451

FDG PET with Low Dose CT versus Contrast Enhanced CT as Quantification Method to Assess the Extent of Peritoneal Carcinomatosis previous Cytoreductive Surgery-HIPEC: a Pilot Study

A. Repetto[1], *C. De Juan*[2], *M. Gimenez*[1], *J. Segura*[3], *R. Morales*[3], *M. Guillot*[4], *C. Peña*[1];
[1]*Universitary Hospital Son Espases - Department of Nuclear Medicine, Palma de Mallorca, SPAIN,* [2]*Universitary Hospital Son Espases - Department of Radiology, Palma de Mallorca, SPAIN,* [3]*Universitary Hospital Son Espases - Department of Digestive and General Surgery, Palma de Mallorca, SPAIN,* [4]*Universitary Hospital Son Espases - Department of Oncology, Palma de Mallorca, SPAIN.*

Aim/Introduction: The aim of the study was to compare FDG PET with Low Dose CT (FDG PET-CT) versus Contrast Enhanced CT (CE-CT) in pre-surgical quantification of peritoneal carcinomatosis using the Peritoneal Cancer Index (PCI) and to correlate both PCI values with surgical and histological (AP) findings. **Materials and Methods:** Retrospective study from 2014 to 2016 of 18 patients (11 women, 7 men; mean age 57 years old) with peritoneal carcinomatosis due to colon adenocarcinoma (8), ovarian serous carcinoma (9) and appendicular mucinous adenocarcinoma (1). All of them were candidate to cytoreductive surgery and HIPEC.The image studies were performed during the 3 months before the surgery. The extent of peritoneal carcinomatosis was quantified using PCI score (0-39) considering size and localization of the findings in 13 abdominal regions. PCI was calculated independently by a nuclear physician and by a radiologist in FDG PET-CT and in CE-CT respectively. A Pearson's correlation was calculated. **Results:** Median value of PCI was 6 [IQR 2-7] in FDG PET-CT, 3 [IQR 2-9] in CE-CT, 8 [IQR 4-12.7] in surgical PCI and 5.5 [IQR 2-12.7] in AP PCI.A positive correlation between PCI of FDG PET-CT and CE-CT was detected (r=0.63; p<0.01).Both FDG PET-CT and CE-CT PCI values resulted in a high positive correlation with surgical PCI (r=0.81 and r=0.83 respectively; p<0.01).Surgical PCI had a correlation with AP PCI (r=0.98; p<0.01). **Conclusion:** There is a good correlation between FDG PET-CT and CE-CT in pre-surgical evaluation of peritoneal carcinomatosis in patients candidate to cytoreductive surgery with HIPEC using PCI score. Surgical and histological findings have a good correlation with both imaging techniques with no differences.A combined FDG PET with Contrast Enhanced CT study could be the election technique in pre-surgical evaluation of patient with peritoneal carcinomatosis. **References:** None.

EP-0452

Positive Predictive Value of Suspected Primary Malignancy Localized on F-18 FDG PET-CT in Patients with Carcinoma of Unknown Primary (CUP)

B. Kumar*, H. Singh, R. Kumar, A. Bhattacharya, B. R. Mittal;*
Postgraduate Institute of Medical Education and Research (PGIMER), Chandigarh, INDIA.

Aim/Introduction: In cases of Carcinoma of Unknown Primary (CUP), F-18 FDG PET-CT is part of diagnostic workup for localizing the primary lesion when conventional imaging is negative. According to literature the primary detection rate of F-18 FDG PET ranges from 20-40% with higher sensitivity as compared to specificity. However, benign lesions may mimic primary lesions on F-18 FDG PET-CT. In the present study, our aim is to assess the positive predictive value of F-18 FDG PET-CT for PET positive lesions suspected to be primary in CUP. **Materials and Methods:** Patients who underwent F-18 FDG PET-CT for localization of primary site with histopathologically proven metastatic lesions and in whom primary site was suspected on basis of PET-CT were evaluated retrospectively. The results of F-18 FDG PET-CT were compared with the final histopathological findings as gold standard. The positive predictive value of F-18 FDG PET-CT was calculated. **Results:** A total number of 32 patients (mean age 53.9 + 14.14 SD, range 18 to 85; 21 males and 11 females) were evaluated for CUP by F-18 FDG PET-CT. Biopsy from the suspected site was done in all patients. Twenty two (66.7%) out of 33 patients were confirmed to have primary at a corresponding site suggested by F-18 FDG PET-CT. Primary lesions were confirmed in head and neck (n=4; 18.2%), bone marrow (myeloma, n=4; 18.1%), , lung (n=3; 13.6%), breast (n=2; 9.1%), lymphoma (n=2; 9.1%), esophagus (n=1; 4.5%), stomach (n=1; 4.5%), pancreas (n=1; 4.5%), prostate (n=1; 4.5%), adnexa (n=1; 4.5%), penis (n=1; 4.5%) and parotid (n=1; 4.5%) regions. Biopsy from rest of the 10 patients revealed no evidence of malignancy. Positive predictive value (PPV) of F-18 FDG PET-CT was 66.7%. **Conclusion:** F-18 FDG PET-CT has moderate positive predictive value for localization of primary site in patients with Carcinoma of unknown primary. **References:** 1. Kwee TC, Basu S, Cheng G, Alavi A. FDG PET/CT in carcinoma of unknown primary. Eur J Nucl Med Mol Imaging. 2009;37(3):635-644.2. Kwee TC, Kwee RM. Combined FDG-PET/CT for the detection of unknown primary tumors: systematic review and meta-analysis. Eur Radiol. 2008;19(3):731-744.

EP-30

Clinical -> Diagnostic study -> Adult study -> Oncology study -> Organ-based oncology -> Other urological, malignant

October 12 - 16, 2019 e-Poster Area

EP-0453

^{18}F-FDG PET/CT Value In The Detection Of Seminoma And Correlation To CT And Tumor Marker Levels - 8 Years Of Follow-up

J. Petrovic, *D. Sobic- Saranovic, N. Petrovic, S. Beatovic, S. Odalovic, I. Grozdic- Milojevic, M. Stojiljkovic, N. Rankovic, V. Artiko;*
Clinical Center of Serbia, Belgrade, SERBIA.

Aim/Introduction: Positron emission tomography/computed tomography using fluorine-18-fluoro- deoxyglucose (^{18}F-FDG PET/CT) is not used routinely in diagnostics of testicular carcinoma. Unlike CT that assess only anatomical structures and cannot confirm with certainty the nature of the lesions, especially in post-therapy setting, ^{18}F-FDG PET/CT evaluates active disease by detecting increased glucose metabolism within the lesions. Aim is to determine the role of ^{18}F-FDG PET/CT in detection of viable tumor tissue after orchiectomy, restaging after chemo/radiotherapy, as well as to determine diagnostic accuracy of this method as oppose to CT and tumor marker levels. **Materials and Methods:** Eighty-two men (age 39.80±10.14) after orchiectomy and histologically proven seminoma were referred to ^{18}F-FDG PET/CT. Indication were restaging after chemo/radiotherapy with positive/ uncertain CT, suspected recurrence based on CT or elevated serum tumor marker levels. All patients had tumor markers (LDH,AFP,β-HCG) and CT done prior to ^{18}F-FDG PET/CT, and clinical follow-up. Seventeen patients had a control ^{18}F-FDG PET/CT. The degree of metabolic activity was analyzed visually and semiquantitatively using SUVmax. **Results:** Out of 82 patients, 36 were considered true positive (43.9%), SUVmax 7.9+4.8. Recurrent disease was mostly found in retroperitoneal lymph nodes, distant metastases in lungs, bones, liver and 3 patients had local rest/recurrence. Six were false positive findings (posttherapy inflammation) and 3 false negative (lung micronodules, lymph nodes <1cm). All patients had clinical follow-up (up to 8 years) after the first PET/CT and 17 (20.7%) had a control scan. Sensitivity, specificity, accuracy of ^{18}F-FDG PET/CT were 92.3%, 86.04%, 89.02%, statistically higher than CT with sensitivity 60.3%, specificity 66.6%. Student t-test showed statistically significant correlation between levels of LDH and positive PET/CT findings (p=0.043). **Conclusion:** ^{18}F-FDG PET/CT is superior to CT in therapy response evaluation and detection of still active disease after therapy in normal size lymph nodes and residual tissue, due to its anatomical and functional assessment, as well as in cases when CT is negative and tumor markers are elevated. Elevated LDH is a useful indicator of relapse and it contributes to positive PET/CT findings. **References:** 1.Kassem T. Do we need 18F-FDG PET/CT scan in staging and management of testicular tumors? Egyptian J Radiology Nucl Med. 2016;47:445-452. 2.Cook G, Sohaib A, Huddart R, et al. The role of 18F-FDG PET/CT in the management of testicular cancers. Nucl Med Communication. 2015;36(7):702-708. 3.Fosså A, Fosså SD. Serum lactate dehydrogenase and human choriogonadotrophin in seminoma. Br J Urol. 1989;63:408-15.

EP-0454

Recurrent urinary bladder carcinoma- diagnostic and prognostic role of 18F FDG-PET/CT

S. Sakhale, *A. Agrawal, V. Rangarajan, S. Shah, N. Purandare, A. Puranik;*
Tata memorial hospital, Parel, Mumbai, INDIA.

Aim/Introduction: IRB approved retrospective study for the analysis of diagnostic and prognostic role of 18F FDG-PET/CT in urinary bladder carcinoma recurrence. **Materials and Methods:** 75 patients scanned between January 2013 and November 2015 were studied.Diagnostic accuracy was assessed compared to biopsy/cytology, and wherever these were unavailable, follow up imaging/clinical assessment were used. To eliminate bias due to urinary activity, delayed images (with/without Furosemide injection) were taken, wherever necessary.Median overall survival times were calculated using the Kaplan-Meier method. The differences in overall survival according to the PET(CT) result were analysed using the log-rank test. P values below 5% were considered significant. **Results:** Mean age of study population was 59 years +_ 10 years. 12 (16%) were females and 63 (84%) were males. Majority were high grade urothelial carcinomas 63/75 (84%) 41 patients had undergone cystectomy with/without chemo/radiotherapy. 27 had undergone TURBT with/without chemo/radiotherapy, while 7 had received chemo/radiotherapy without any surgical intervention. Recurrent bladder carcinoma was confirmed in 53/55 patients who were positive on FDG-PET/CT. In 18/20 patients with negative FDG-PET/CT scan, other imaging or follow-up clinical data confirmed absence of disease. For detection of recurrences, sensitivity and positive predictive value were found to be 96.36 % whereas specificity and negative predictive value were 90 %, with an accuracy of 94.67 %. Additional lesions were picked up in 16/75 (21%) patients. Treatment was modified in 9/75 (36%) patients. Median survival time was 38.7 months in patients with a negative FDG-PET/CT and 10.3 months in patients with a positive scan (p=0.001). 2-year overall survival was 83.3% for FDG-PET/CT negative and 47.5% for FDG-PET/CTpositive patients. **Conclusion:** 18F FDG-PET/CT shows a very good diagnostic performance in restaging patients of urinary bladder carcinoma with excellent sensitivity and accuracy. It shows excellent sensitivity in detecting occult nodal and distant metastasis. Additional lesions can also be picked up. Scan results also modify treatment strategy in considerable number of patients. Also it is a significant tool for predicting the overall survival. Our study also reveals that the problem of renal excretion of FDG can well be obviated by

delayed imaging with diuretic intervention. Thus, this should not be a hindrance in doing FDG-PET/CT studies for suspected bladder cancer recurrences. **References:** None.

EP-0455

The role of 18F-FDG PET/CT in the restaging of clear cell carcinoma patients after primary surgical treatment

M. Gazzilli[1], *R. Durmo*[1], *M. Bertoli*[1], *D. Albano*[1], *E. Cerudelli*[1], *M. Bonacina*[1], *F. Dondi*[1,2], *A. Mazzoletti*[1,2], *F. Bertagna*[1,2], *R. Giubbini*[1,2]; [1]*Azienda Socio Sanitaria Territoriale degli Spedali Civili di Brescia, Brescia, ITALY,* [2]*Università di Brescia, Brescia, ITALY.*

Aim/Introduction: In Europe, Renal Cell Carcinoma (RCC) represents 3% of all neoplasm. Prognosis in RCC depends on tumor extent, presence of metastasis, age and co-morbidities. 18Fluorine-Fluorodeoxyglucose Positron Emission Tomography/Computed Tomography (18F-FDG PET/CT) has suboptimal diagnostic performance in the initial staging of RCC due to physiological excretion of radiotracer in the kidney that can mask lesions uptake. More than 30% of the patients with a locally confined disease at diagnosis develop metastases after nephrectomy.The aim of our study is to establish the usefulness of 18F-FDG PET/CT in the restaging of clear cell renal (CCRC) carcinoma patients. **Materials and Methods:** From 2006 to 2019 we retrospectively analyzed 56 patients (Male:37, Female:19; median age: 64 years; range: 33-81 years) affected by CCRC who underwent radical or partial nephrectomy. (According to AJCC 8th edition at stage 19 patients were T1; 9 patients T2; 26 patients T3; 2 patients T4; according to Fuhrman grade: 1 patients was G1; 27 patients G2; 19 patients G3; 9 patients G4). All patients underwent 18F-FDG PET/CT for restaging purpose with the suspect of clinical or radiological relapse. Patients with positive 18F-FDG PET/CT results were considered as true-positives (TP) if further evaluations confirmed the malignant nature of lesions and false-positive (FP) if further evaluations showed no malignant lesions. Patients with negative 18F-FDG PET/CT results were considered as true negative (TN) if further evaluations confirmed no neoplastic lesions and false-negative (FN) if further evaluations showed malignant ones. **Results:** 18F-FDG PET/CT was positive in 34 patients (60.7%) and negative in 22 (39.2%). Sensitivity, specificity, positive predictive value (PPV), negative predictive value (NPV) and accuracy of F18-FDG PET/CT were 88.24, 85, 90.91, 80.95, 87.04 respectively. The most common site of lesions was mediastinal lymph nodes, lung, ipsilateral adrenal gland and bone. The lesion showed an intense 18F-FDG uptake with a value of SUV max and SUV mean between 2.6 and 16.1. **Conclusion:** Our preliminary study showed good sensitivity and specificity of 18F-FDG PET/CT for the restaging of patients with CCRC after primary surgical treatment, due to a high FDG uptake of the lesions. FDG PET/CT might replace conventional methods for restaging RCC because it is very accurate and examines all organ systems with high accuracy in one-stop-shop procedure detecting distant metastasis and in therapy monitoring. **References:** None.

EP-0457

Role Of Renoscintigraphy With ^{99m}Tc-DTPA In Determining Renal Function In Patients With Testicular Sertolioma After Cytostatic Therapy

P. Korol[1], *M. Tkachenko*[2];
[1]*Clinical City Hospital #12, Kiev, UKRAINE,* [2]*A.A. Bohomolets National Medical University, Kiev, UKRAINE.*

Aim/Introduction: The aim of the study to evaluate the diagnostic role of renoscintigraphy with 99mTc-DTPA parameters in assessing renal function of patients with non-herminogenic testicular tumors (testicular sertolioma) after cytostatic therapy. **Materials and Methods:** Renoscintigraphy with 99mTc-DTPA was used to study 64 male patients aged 8 to 51 year. All patients were divided into two cohorts. The first cohort included 41 patients with testicular sertolioma after cytostatic therapy (Cisplatin) at a rate of 20 mg/m2 body surface for 5 day, the second cohort included 23 patients who did not take this therapy. In all studied patients, the calculation of value of the glomerular renal filtration rate and effective renal plasma flow. The radionuclide parameters of the first cohort were compared with those of the second cohort. Renoscintigraphy was carried out in a dynamic mode (1 frame per minute) in 30 minutes, after intravenous injection of 99mTc-DTPA at the rate of 2 MBq/kg. **Results:** In patients of the first cohort mean value of the glomerular filtration rate of kidney was 107,2±0,14 ml/min., in patients of the second cohort the glomerular renal filtration rate was 61,2±0,18 ml/min. The mean parameters of effective renal plasma flow in patients of the first cohort were 568±0,27 ml/min, in patients of the second cohort were 417,0±0,24 ml/min. According to the results of statistical evaluation, the average parameters of the glomerular filtration rate, effective renal plasma flow in the first cohort of patients significantly increased relative to the calculated parameters of the second cohort of patients ($p < 0,05$). **Conclusion:** Renoscintigraphy with 99mTc-DTPA allows monitoring the changes in quantitative parameters of the functional activity of the kidneys and evaluating the effectiveness of cytostatic therapy in patients with testicular sertolioma and can be included in the protocol of diagnostic methods of studies. **References:** None.

EP-0458

F18 FDG PET CT in Restaging and Follow up of Seminomatus and Non Seminomatus Testicular Tumors

E. El-kholy, *O. Talaat;*
Nuclear medicine unit, National cancer Institute (NCI) Egypt, Cairo, EGYPT.

Aim/Introduction: to evaluate the role of FDG PET/CT in restaging and follow up of seminomatus and non seminomatus testicular tumors. **Materials and Methods:** 54 patients (mean age: 34.2 ±11.8) with pathologically proven testicular cancer in whom FDG PET/CT were retrospectively assessed. Total 89 PET/CT studies were conducted in comparison to diagnostic CT.

Pathological and clinical/radiological follow-up for 6-15 months duration served as standards of reference. **Results:** Seminomas type was more prevalent (64.8%). About 30% of patients did not developed metastases during their course of disease, while 38 patients, 31 (81.5%) had abdominal nodal deposits, 5 patients had distant sites and 2 patients presented by both. The lungs was the most common site for distant metastases. All 33 patient with seminomatous pathology had abdominal nodal deposits, while distant metastasis was confined to patients with Non Seminomatous pathology. FDG PET/CT had higher sensitivity, specificity, and accuracy of 94%, 86.5%, and 92.5% versus 76%, 85% 83%; for diagnostic CT in per patients analysis. A total of 90 lesions were reported, (62 nodal & 28 distant) metastatic lesions were analyzed. PET/CT showed good accuracy for the detection of residual/recurrent abdominal seminomatus lesions, with an overall sensitivity and specificity of 94.7 % and 93.3 %, respectively compared to 89.2% and 56.2% for diagnostic CT, their size mean+SD (3.9+-3.1) and SUVmax (7+-6.3). Non seminanomatus distant metastases showed comparable results for both PET/CT and diagnostic CT with dominant false negative small sized (mainly lung) lesions in PET/CT. 25 patient had single PET/CT, its results with diagnostic CT were comparable in 20 patients (84%), while 29 patients with repeated 64 PET/CT studies had comparable analysis to diagnostic CT in 22 patients (~76%). In the other 7 patients (~24%), a higher value of PET/CT in assessment of therapy response was noted. PET/CT shows CMR in 5 patients whom remain stationary in CT based on size difference analysis. **Conclusion:** The current study showed that 18FDG-PET/CT is useful in re-staging & assessment of response on testicular patients as compared to CT regarding seminomatus abdominal nodal lesions and non seminomatus distant disease. Key words: FDG PET/CT, testicular, restaging, therapy response, prognosis. **References:** None.

EP-31

Clinical -> Diagnostic study -> Adult study -> Oncology study -> Organ-based oncology -> Prostate, malignant

October 12 - 16, 2019 e-Poster Area

EP-0459

Impact of late PET/CT imaging with ^{68}Ga-RM2 in the characterization of prostate cancer

R. Schollhammer[1,2,3], *H. De Clermont Gallerande*[1], *G. Robert*[4], *M. Yacoub*[5], *F. Lamare*[1,2,3], *N. Balamoutoff*[1], *D. Vimont*[2,3], *E. Hindie*[1,2,3], *P. Fernandez*[1,2,3], *C. Morgat*[1,2,3];

[1]*Service de Médecine Nucléaire, CHU Bordeaux, Bordeaux, FRANCE,* [2]*Université de Bordeaux, INCIA, UMR 5287, Talence, FRANCE,* [3]*CNRS, INCIA, UMR 5287, Talence, FRANCE,* [4]*Service d'Urologie, CHU Bordeaux, Bordeaux, FRANCE,* [5]*Service d'Anatomopathologie, CHU Bordeaux, Bordeaux, FRANCE.*

Aim/Introduction: The GRP-R (Gastrin Releasing Peptide Receptor) is overexpressed on prostatic cancer cells and can be targeted with antagonist radiopharmaceuticals such as ^{68}Ga-RM2 (Touijer 2019). Its performances on PET/CT imaging of prostatic tumors have traditionally always been investigated 1 hour after injection. In this work we aimed to compare ^{68}Ga-RM2 PET/CT imaging at 1 hour and 2 hours in patients with prostate cancer at initial staging. **Materials and Methods:** We prospectively enrolled nine treatment-naïve patients with biopsy-confirmed prostate cancer (two Gleason score (GS) 6; three GS 7(3+4), one GS 7 (4+3) and three GS≥8). ^{68}Ga-RM2 PET/CT was performed before prostatectomy at 1 hour (RM2-1h) and 2 hours (RM2-2h) after injection of 2MBq/kg of ^{68}Ga-RM2. Each PET/CT was visually analyzed by two independent experimented nuclear physicians. Segmented PET images were then compared to histology (standard-of-truth). Prostatectomy samples were analyzed by an experimented pathologist who identified and staged each lesion according to GS. Each prostatectomy slice available was scanned for comparison between PET and histologic segmentation. Number of lesions detected and uptake intensity (SUV_{max} and Signal to Noise Ratio (SNR) relative to non-lesional prostate gland parenchyma) at each imaging time in each lesion were then analyzed. Lesions< 0.1cm³ were excluded. **Results:** On the 14 lesions confirmed by histology, both RM2-1h and RM2-2h detected 12 (85.7%) lesions. Fewer false-positive uptake on normal prostatic gland were seen with RM2-2h with a false positive rate of (1/9; 11.1%) compared with RM2-1h (2/9; 22.2%). Similar ^{68}Ga-RM2 uptake intensity was found at 1hour and 2hours: SUV_{max} = 6.2 ± 1.7 vs 6.3 ± 2.5 (p=0.66). However, a significant decrease of ^{68}Ga-RM2 was observed on normal prostatic gland: SUV_{max} = 2.8 ± 0.9 at 1 hour vs 1.8 ± 0.6 at 2 hours (p=0.01), conferring an increased SNR at 2 hours: 2.3 ± 0.9 vs 3.3 ± 1.1 (p=0.008). **Conclusion:** This small series is the first study comparing ^{68}Ga-RM2 PET/CT imaging at two different time points, 1 hour and 2 hours. Results showed greater signal-to-background of RM2 and fewer false-positive uptake at 2h than at 1h due to a faster wash-out from normal prostate gland. This finding is promising for a better characterization of prostate cancer lesions. **References:** Touijer KA, et al (2019). EurUrolOncol.

EP-0460

Novel F-18-siPSMA-14 shows favourable tracer kinetics for staging and restaging of prostate cancer patients

V. Prasad[1], *D. DiCarlo*[2], *J. Miksch*[1], *G. Fischer*[1], *F. Zengerling*[3], *C. Solbach*[1], *H. Wester*[2], *A. J. Beer*[1];

[1]*Department of Nuclear Medicine, University Hospital Ulm, Ulm, GERMANY,* [2]*Pharmaceutical Radiochemistry, Technical University Munich, Garching, GERMANY,* [3]*Department of Urology, University Hospital Ulm, Ulm, GERMANY.*

Aim/Introduction: To assess the biodistribution of F-18-siPSMA-14 in patients with histologically confirmed prostate cancer at different time points of imaging. **Materials and Methods:** Ten patients (71.1±8.1y; GS 6-9, mean PSA 73.4(0.18

- 667)ng/ml) referred for primary staging or restaging were examined with newly developed F-18-siPSMA-PET/CT (356±11 MBq, without furosemide). 7 patients were imaged at 60 (T1) and 120min (T3) p.i., 3 patients at 90min (T2), from head to mid-thigh (T1,T2) or from lower thorax to upper thigh (T3). SUVmax and SUVmean values were calculated for normal organs and normal prostate tissue, background (gluteus muscle and blood pool), and malignant lesions (intraprostatic tumor/residual tumor, bone, lymph and adrenal gland metastases). For determination of changes between early and late uptake only T1 and T3 were considered. Target/non target ratios were calculated by comparison of SUVmax and SUVmean with the blood pool activity. T test was performed to compare the difference in the mean of SUVmax and SUVmean in normal organs ($p<0.05$). **Results:** In all patients tumor lesions showed high F-18-siPSMA-14 uptake. The mean SUVmax(SUVmean) of prostatic lesions at T1/T3 were 14.2(6.0)/14.5(7.8); at T2 the mean SUVmax(SUVmean) of prostatic lesions were 43.3(24.6). The range of F-18-siPSMA SUVmax(SUVmean) in metastatic lesions at all time points was very high 11.1-42.6(6.9-24.3). In comparison to T1, metastatic lesions showed up to 20% increase in tracer uptake at T3. Other organs with physiologically high PSMA-expression (kidney cortex, duodenum) did not show any significant uptake difference at T1 and T3 [SUVmax(SUVmean) at T1/T3 = 35.3(18.0)/42.1(19.9) in kidney and 10.4(5.5)/12.2(6.0) in duodenum]. Strikingly, the liver and spleen SUVmax(SUVmean) ranging between 9.3-11.5 (6.8-8.2) remained stable/almost identical at all the three time points. Uptake in bone marrow at T1-T3 was variable but remained low (SUVmax<2) and almost unchanged. Only the low background activity (SUVmean gluteus muscle (<1) and blood (<2)) decreased significantly from T1-T3 ($p=0.000$) by up to 25%. Low, almost stable bladder uptake (SUVmax(SUVmean)=8.2-12.8 (6.6-9.2)) allowed excellent visualization of primary tumor or local residue. All (even <0.5cm) tumor lesions seen at T3 were also visible at T1. **Conclusion:** Biodistribution of F-18-siPSMA-14 is favorable, robust and allows depiction of very small metastases, clearly delineates the intraprostatic lesions and thus holds tremendous potential in staging and restaging of PC. Imaging at 90 min p.i. without furosemide injection is feasible. **References:** None.

EP-0461

Prospective evaluation of ^{18}F-DCFPyL in Patients with Biochemically Recurrent Prostate Cancer

A. Iagaru, H. Duan, H. Song, C. Harrison, K. Guja, B. Franc, F. Moradi, G. Davidzon;
Stanford University School of Medicine, Stanford, CA, UNITED STATES OF AMERICA.

Aim/Introduction: ^{18}F-DCFPyL is a promising PET radiopharmaceutical targeting expression of prostate specific membrane antigen (PSMA) in patients with biochemically recurrent (BCR) prostate cancer (PC). We present our experience in this single center prospective study evaluating the positivity rate of ^{18}F-DCFPyL PET/CT in BCR PC. **Materials and Methods:** We prospectively enrolled 55 men (52-91 year-old, mean±SD: 71.1 ± 7.2) with BCR PC after primary definitive treatment with prostatectomy (35 patients) or radiation therapy (20 patients). The presence of lesions compatible with PC was evaluated by two independent readers. Forty-six patients had concurrent scans with at least one other conventional imaging scan: CT (18 patients), MR (18 patients), bone scan (21 patients) or ^{18}F-NaF PET (12 patients), and ^{18}F-Fluciclovine PET/CT (11 patients). Findings from ^{18}F-DCFPyL PET/CT were compared with those from other modalities. Impact on management based on ^{18}F-DCFPyL PET/CT was recorded from chart review of clinical notes. **Results:** ^{18}F-DCFPyL PET/CT had an overall positivity rate of 84%, which increased with higher PSA levels (ng/mL): 33% (PSA < 0.5), 64% (0.5 ≤ PSA < 1), 100% (1 ≤ PSA < 2), 93% (2 ≤ PSA < 5) and 100% (PSA ≥ 5). ^{18}F-DCFPyL PET detected significantly more lesions than conventional imaging. For anatomic imaging, 18/36 (50%) of CT/MRI scans had congruent findings while ^{18}F-DCFPyL PET was positive in 16/36 (44%) of cases with negative CT/MRI. For bone imaging, 23/33 (70%) bone scan/^{18}F-NaF PET were congruent with ^{18}F-DCFPyL PET while ^{18}F-DCFPyL PET localized bone lesions in 7/33 (21%) patients with negative bone scan/^{18}F-NaF PET. In 5/11 (45%) ^{18}F-Fluciclovine PET had located the same lesions as the ^{18}F-DCFPyL PET. However, in 4/11 (45%) of patients with negative ^{18}F-Fluciclovine scan, ^{18}F-DCFPyL PET was positive, including two cases with uptake in single pelvic side wall lymph nodes and two cases with uptake in multiple sclerotic bone lesions. In the remaining 2/11 (18%) patients, ^{18}F-DCFPyL and ^{18}F-Fluciclovine scans had different findings. Lastly, 36 patients (65%) started new treatment after ^{18}F-DCFPyL PET and, most noticeably, 25% (14/55) of all BCR PC patients had lesion localization only on ^{18}F-DCFPyL PET, despite negative conventional imaging. **Conclusion:** ^{18}F-DCFPyL PET/CT is a promising diagnostic tool in the work-up of patients with BCR PC given the high detection rate as compared to currently available imaging modalities. Importantly, findings on ^{18}F-DCFPyL PET/CT imaging impacted actual clinical management in 65% of patients. **References:** None.

EP-0462

Diagnostic accuracy of 68Ga-PSMAHBED PET/CT and pelvic mp-3Tesla MRI in primary staging of patients with intermediate/high-risk prostate adenocarcinoma

M. Celli[1], F. Ferroni[1], R. Gunelli[2], M. Costantini[2], V. Di Iorio[1], D. Barone[1], P. Caroli[1], L. Fantini[1], A. Moretti[2], R. Galassi[2], M. Giganti[3], G. Paganelli[3], F. Matteucci[1];
[1]IRST, Meldola, ITALY, [2]Morgagni Pierantoni General Hospital, Forlì, ITALY, [3]Ferrara University, Ferrara, ITALY.

Aim/Introduction: to evaluate the diagnostic accuracy of whole-body 68Ga-PSMAHBED PET/CT (PSMA PET) and pelvic multi-parametric 3TeslaMRI (mpMRI) in primary staging of patients with intermediate/high-risk prostate adenocarcinoma (PCa). **Materials and Methods:** we prospectively enrolled 13 patients (age range: 49-72 years; median: 61 years) with biopsy-proven PCa (ISUP: 1 to 4; PSA range: 2.2-28.3ng/ml; biopsy T:

T2a-T2c) scheduled for radical prostatectomy. PSMA PET-CT and mpMRI were performed within six weeks prior to surgery and independently reported. Concordance between PSMA PET and mpMRI findings was assessed. A rigid co-registration of PSMA PET to T2-weighted MRI reporting all suspected PCa lesions onto the 12-segment prostate map was carried out. Post-prostatectomy pathology was the standard of truth for T and N staging; abdomen CT and bone scan for M staging. **Results:** pathologic prostate findings were documented in all 13 patients on mp-MRI and in 12 patients on PSMA PET. PCa tumour laterality (bilateral in 12 cases; monoloteral in 1 case) was correctly identified in nine patients by PSMA PET and in 10 patients by mpMRI. On a 12-prostate segment basis PSMA PET and mpMRI results were concordant in 115/156 segments (73.7%) being both positive for PCa in 30 segments and both negative for PCa in 85 segments. Concordant positive findings on PSMA PET and mpMRI resulted true positive (TP) on pathology in 80% (24/30 segments); concordant negative findings on both PSMA PET and mpMRI resulted true negative (TN) on pathology in 68% (58/85 segments).Discordant results were observed in 41 segments. Of these, 19 segments were positive on PSMA PET only (10 TP; 9 false positives); 22 segments were positive on mpMRI only (18 TP, 4 false positives). All patients resulted negative for nodal metastases on PSMA PET and mpMRI. Pelvic node dissection confirmed the N0 status. No distant metastases were demonstrated on PSMA PET and on pelvic mpMRI, nor suspicious lesions were documented on clinical bone scans and abdomen CTs. Tumours with ISUP 1, ISUP 2, ISUP 3 and ISUP 4 had a median SUVmax of 5.1, 10.3, 4.1 and 15.0, respectively. Median PCa SUVmax was 4.6 and 4.3 in patients with PSA starter < 10ng/ml and PSA starter > 10ng/ml, respectively. **Conclusion:** our preliminary results suggest that PSMA PET might have a role in PCA pre-operative staging. Obviously a larger number of patients is needed to understand the accuracy of PSMA PET compared to mpMRI. **References:** None.

EP-0463

Diagnostic performance of ^{68}Ga-HBED PSMA PET/CT in BCR prostate cancer: a single center study review

C. Reichel[1], *F. Lecouvet*[2], *B. Tombal*[3], *R. Lhommel*[1];
[1]*Nuclear medicine, Cliniques Universitaires Saint-Luc, UCL, Brussels, BELGIUM,* [2]*Medical imaging, Cliniques Universitaires Saint-Luc, UCL, Brussels, BELGIUM,* [3]*Urology Cliniques Universitaires Saint-Luc, UCL, Brussels, BELGIUM.*

Aim/Introduction: About 40% of all prostate cancer patients will have biochemical recurrence (BCR) in their lifetime. This BCR is defined as a rise of PSA > 0.2 ng/ml after radical prostatectomy. It is vital to identify these patients correctly as patient management will change accordingly. ^{68}Ga-HBED PSMA PET/CT has shown accurate identification of lesions in BCR settings, with up to 80% sensitivity and 100% specificity. The aim of this study was to review data of our center. **Materials and Methods:** 123 patients were retrospectively review and selected for inclusion. Patient PSA ranged from 0.2 to 400 ng/ml with a mean PSA of 14.5ng/ml. All patients were post radical prostatectomy or SRT radiotherapy and had received multiple lines of treatment. Images were acquired on a GEMINI TF PET-CT 64slices. All patients were reviewed by a nuclear physician in training and an expert reader in ^{68}Ga-HBED PSMA PET/CT. All positive lesions (prostate bed, lymph nodes, liver, lungs, bone) were reported. No a priori SUVmax cut-off was used for positivity (but SUVmax value at least > 2.0). **Results:** 27% of patients had positive lesions in the very-low PSA range (0.2-0.5ng/ml). Proportion raised when PSA raised respectively to 80% (0.5-1ng/ml) and 92% (>1ng/ml) in other ranges. In the very low PSA range, essentially lymph node lesions were identified. In the other categories, lymph nodes are still the most frequent lesions (up to 48%) but prostate bed and bone hot spots were reported for respectively 20% and 7% in the PSA range of 0.5-1ng/ml and respectively 38% and 17% in the PSA range >1ng/ml. As for size of lymph nodes, up to 70% of lesions were below classically described (DWI-)MRI-cut-off of 8mm. Lowest SUVmax was 2,9 and smallest positive lymph node was 1,7mm. If we pool patients, 83% had positive PET lesions : 24% only in lymph nodes, 21% only in prostate bed, 8% only in bone and-or lung. Other patients had multiple lesions. **Conclusion:** ^{68}Ga-PSMA PET/CT positivity degree raises with PSA levels. Limited degree of positivity was observed for low PSA (27% in PSA from 0.2 to 0.5ng/ml) but rapidly becomes relevant at higher PSA levels (80% for PSA 0..5-1ng/ml and 92% for PSA >1ng/ml). Up to 70% of lymph node lesions are below MRI-DWI size cut-off making it a vital imaging technique. **References:** None.

EP-0464

Role of [68Ga]-PSMA-11 PET/CT to target focal treatment in patients with biochemical relapse of prostate cancer

A. Skanjeti[1], *A. Dhomps*[2], *W. Sotlar*[2], *A. Ruffion*[3], *O. Chapet*[4], *J. Tordo*[2];
[1]*Nuclear Medicine, Hospices Civils de Lyon, Université Claude Bernard Lyon 1, Lyon, FRANCE,* [2]*Nuclear Medicine, Hospices Civils de Lyon, Lyon, FRANCE,* [3]*Urology, Hospices Civils de Lyon, Université Claude Bernard Lyon 1, Lyon, FRANCE,* [4]*Radiation Oncology, Hospices Civils de Lyon, Université Claude Bernard Lyon 1, Lyon, FRANCE.*

Aim/Introduction: Targeted therapy becomes more and more the treatment of choice in patients suffering from biochemical relapse of prostate cancer in order to postpone the start of systemic therapy and in particular hormonal treatment. Several studies have shown the higher sensitivity of [68Ga]-PSMA PET/CT over [18F]Fluorocholine PET/CT in prostate cancer, therefore, aim of this study was to evaluate the impact of [68Ga]-PSMA PET/CT in targeting focal treatment in case of biochemical relapse from prostate cancer and negative or inconclusive [18F]Fluorocholine PET/CT. **Materials and Methods:** Forty-two consecutive patients (age 71±6 years) in biochemical relapse of prostate cancer (mean PSA 8.9 ng/ml [0.21-58.49], mean PSA doubling time [dt] 8.7±7 months) were enrolled. All of them underwent a negative (31) or inconclusive (11) [18F]

Fluorocholine PET/CT three months or less before [68Ga]-PSMA PET/CT. The subsequent treatments were established preferentially in tumour boards. The efficacy of the targeted therapy was established by the oncologist based on follow-up longer than 3 months and two consecutive PSA analysis. **Results:** [68Ga]-PSMA PET/CT was positive in 37 patients (PSA 9.9 ng/ml, PSAdt 8.6months) and negative in 5 (PSA 1.2 ng/ml, PSAdt 10.1months, p=0.016 for PSA, ns for PSAdt). Eighteen patients underwent focal therapy based on [68Ga]-PSMA PET/CT (PSA: 2.3 ng/ml), in 22 a hormonal treatment was proposed (PSA: 13.8ng/ml, p=0.04), while in 2 patients was adopted a wait and see approach. Targeted therapy was radiation treatment for 13 patients and high intensity focused ultrasound in 6 (1 man underwent both treatments); it was successful in 16 men, (38% of the overall population). In 19 patients with PSA level≤2ng/ml [68Ga]-PSMA PET/CT successfully targeted focal therapy for 12 patients, while in 23 men with PSA>2 ng/ml [68Ga]-PSMA PET/CT successfully targeted focal therapy for only 4 men (p=0.0027). **Conclusion:** [68Ga]-PSMA PET/CT significantly impacted the management in about 2/5 of men with biochemical relapse of prostate cancer and negative or inconclusive [18F]Fluorocholine PET/CT. In fact, for patients with PSA level≤2ng/ml, [68Ga]-PSMA PET/CT was essential to propose a successful targeted treatment. Therefore, particularly for this cluster of patients with low PSA level, in which Choline PET/CT has shown a low detection rate, [68Ga]-PSMA PET/CT, if available, should replace Choline PET/CT. **References:** None.

EP-0465

Correlation among biochemical, biological characteristics and 18F-Choline PET/CT findings in a large cohort of 1225 prostate cancer patients

I. Ravelli[1,2], *L. Cuppari*[2], *P. Reccia*[2], *A. Cervino*[2], *M. Burei*[2], *M. Maruzzo*[3], *F. Zattoni*[4], *A. Guttilla*[5], *M. Gardi*[6], *L. Evangelista*[2];
[1]*Department of Nuclear Medicine, University of Padua, Padua, ITALY,* [2]*Nuclear Medicine Unit, Veneto Institute of Oncology IOV-IRCCS, Padua, ITALY,* [3]*Oncology 1 Unit, Veneto Institute of Oncology IOV-IRCCS, Padua, ITALY,* [4]*Department of Urology, Hospital of Udine, Udine, ITALY,* [5]*Department of Urology, Hospital of Camposampiero, Padua, ITALY,* [6]*Department of Urology, Hospital of Sant'Antonio, Padua, ITALY.*

Aim/Introduction: The aim of the present study was to assess the correlation among PSA, Gleason Score (GS) and 18F-Choline PET/CT results in a large cohort of patients with prostate cancer. **Materials and Methods:** Between October 2010 and March 2019, from a monocentric institutional database, we retrospectively recovered data for 1225 patients (age: 73±10 years) with prostate cancer who underwent 18F-Choline PET/CT. Data for GS and PSA level at PET time were collected. A patient-based and a site-based analysis for PET/CT findings were made. Chi-square test was used for the comparison between categorical variables. A p < 0.05 was considered statistically significant. **Results:** GS was lower than 6, equal to 7 and higher than 7 in 161 (13.1%), 340 (27.8%) and 563 (46%) patients respectively, while it was not available in 161 (13.1%). Median PSA level at PET time was 4.74 (IQR: 1.03-15.7) ng/mL. Two-hundred ten patients underwent PET/CT for the initial staging and 1015 (82.9%) for the biochemical recurrence of disease. The global detection rate for 18F-choline PET/CT was 76.6%, being equal to 71.7% for the restaging phase. In staging, 120 patients had a significant 18F-Choline PET/CT in the primary tumor, 72 (34.2%) in the lymph nodes and 47 (22.4%) in distant organs. The majority of patients with lymph node and distant metastases had a GS > 7 (48.5% and 29.7%, respectively; all p < 0.001), indepedently from the PSA levels. In recurrent setting, GS > 7 and PSA > 2 ng/mL was related to a detection rate of 78.6% and > 80%, respectively (all p < 0.001). Moreover, a PSA level > 5 ng/mL was associated with a positive 18F-Choline scan for distant metastasis in 62% of cases. **Conclusion:** GS is strongly correlated with 18F-Choline PET/CT findings both in staging and restaging. Conversely, PSA levels at PET/CT time play an important role for the selection of patients in the restaging phase. **References:** None.

EP-0466

Practical approach: description of three different patterns we found in 18 FCholine PET / CT in the diagnosis of bone metastasis for prostate carcinoma

M. Agolti, L. Solari, C. Aruga;
Centro Medicina Nuclear, Parana, ARGENTINA.

Aim/Introduction: To review the bibliography and our results in the value of 18 FCholine PET/CT in prostate cancer to diagnose bone metastasis. The 90% of patients with castration-resistant prostate cancer (CRPC) end up having bone metastases. 18 FCholine is a clearly better than bone scan in the diagnosis of bone metastasis. **Materials and Methods:** 18Fluorcholine (18FCH) PET/CT was performed in 30 patients with prostate cancer in our department, from January 31, 2017 to April 1, 2019; we included patients with biopsy proven prostate cancer with rise in PSA for restaging. **Results:** were correlated with clinical, biochemical and imaging follow up. We studied 30 patients. We found bone metastasis in 12 patients, 16 patients were high risk patients; considering high risk when PSA was 10 or more and Gleason was 7 or more. We saw 85 bone metastasis. In one pattern we found 57 hypermethabolic bone metastasis, with blastic or mixed CT images representing 67,05%. In the second pattern we found 12 blastic bone lesions in CT with normal 18 FCH uptake, representing 14,11% of the lesions , All these lesions were hyperdense on CT with a range of 500 to 845 HU . All these patients were under treatment with antiandrogenic therapy. The possible explanation for some experts is that these are really non-viable bone metastasis or other experts explain this situation as a low sensibility of the 18 Fluor Choline when detecting dense lesions due to diminished cancer cells or diminished perfusion, in these patients it would be useful to increase sensibility with Na fluoride PET/CT. In the third pattern we found 16 hypermethabolic lesions without changes in CT, accounting for 18,84 % of the lesions , regards this the explanation should be

that according to bibliography the image is done in early phases of sclerotic activity (microesclerosis), having no morphological changes. **Conclusion:** 18 FCH PET CT is a very useful method for diagnosing bone metastasis in Prostate Cancer biochemical recurrence. We can discribe Pattern one?: hypermethabolic and hyperdense/mixed bone metastasis in 67,05 % .Pattern two in 14.11 % was found when the lesions are very hyperdense in CT they may not uptake 18 FCH. The third pattern was found in 18.82% of the lesions where we found hypermethabolic lesions with normal CT. **References:** None.

EP-0467

68Ga-PSMA PET/CT in the evaluation of Prostate cancer patients with biochemical recurrence after radical therapy, a first multicentric study in Mexico

S. S. Medina[1,2], *O. Garcia*[1,3], *I. Soldevilla*[1,4], *U. Cancino*[1], *D. Cardosa*[1], *S. Lopez*[1], *A. Quintana*[1], *D. Hernandez*[1];
[1]*Instituto Nacional De Cancerologia, Mexico City, MEXICO,* [2]*Hospital Angeles Lindavista, Mexico City, MEXICO,* [3]*Hospital Médica Sur, Mexico City, MEXICO,* [4]*Centro Medico ABC, Mexico City, MEXICO.*

Aim/Introduction: The potential of 68Ga-PSMA PET/CT with high levels of serum prostatic specific antigen (PSA) is well known (> 10 ng/ml), for this reason, the of our prospective study is evaluate the diagnostic performance of 68Ga-PSMA PET/CT in restaging prostate cancer (PCa) patients with biochemical recurrence (BCR) following radical prostatectomy (RP) or radiotherapy (RT) **Materials and Methods:** Our prospective study starting from November 2017 to April 2019, we have enrolled 104 patients with BCR PCa. Our cohort included patients with PCa with initial Gleason Score (GS) ranging from 6 to 10, initially treated with either RP (48 patients), or RT (56 patients). All patients had a PSA values >0.2ng/ml (range 0.2 - 10 ng/ml) **Results:** 68Ga-PSMA PET/CT was positive in 83 patients (80%), equivocal in 6 patients (5%) and negative in 15 patients (15%). Particular findings were the following; local uptake (prostate bed or prostate gland) was observed in 67/104 patients (64%); 18 of these patients also showed nodal disease and 7 patients bone uptake co-existed. Nodal uptake was observed in regional sites in 20/104 patients (19%), and non-regional in 10/104 patients (9.6); and bone metastatic disease in 13/104 patients (12%). Only 16 patients (15%) showed recurrence outside the prostate bed or prostate gland, 12 exclusively nodal disease and 4 exclusively bone disease. A multivariate analysis showed that for PSA values 0.2 - 2 ng/ml 68Ga-PSMA PET/CT was positive in 69/83 patients (83%); a univariate analysis showed for 68Ga-PSMA PET/CT was positive for PSA values 0.2 - 1 ng/ml in 30/83 patients; 1.1 - 2 ng/ml in 39 patient; 2.1 - 4 ng/ml in 9 patients and 4.1 - 10 ng/ml in 16 patients. In addition we found a significant relationship between SUVmax values and GS, patients with GS 9 and 10 had higher SUVmax levels at recurrence sites (p = 0,005) **Conclusion:** We concluded that 68Ga-PSMA PET/CT as a highly sensitive and accurate tool in PCa patients with BCR even with low levels of PSA regardless of the initial radical treatment. With these findings we confirm the excellent potential of 68Ga-PSMA PET/CT granting earlier detection of BCR, improving patient care and better prognosis. **References:** 1.- Afshar-Oromieh A, Avtzi E, Giesel FL, Holland-Letz T, Linhart HG, Eder M, et al.The diagnostic value of PET/CT imaging with the (68)Ga-labelled PSMA ligandHBED-CC in the diagnosis of recurrent prostate cancer. Eur J Nucl Med Mollmaging. 2015;42:197-2092.

EP-0468

F-18-choline PET/CT in initial staging of prostate cancer patients

A. T. Golubic[1], *M. Gamulin*[2], *M. Solaric*[2], *T. Kulis*[3], *Z. Kastelan*[3,4], *D. Huic*[1,4];
[1]*Department of Nuclear Medicine and Radiation Protection, University Hospital Center Zagreb, Zagreb, CROATIA,* [2]*Department of Oncology, University Hospital Center Zagreb, Zagreb, CROATIA,* [3]*Department of Urology, University Hospital Center Zagreb, Zagreb, CROATIA,* [4]*University of Zagreb School of Medicine, Zagreb, CROATIA.*

Aim/Introduction: The aim of this study is to evaluate the role and value of F-18 choline PET/CT in initial staging and primary evaluation of prostate cancer extent. **Materials and Methods:** Hundred consecutive patients were scanned with F-18-choline PET/CT in from February 2012 to April 2018. Mean age of our patient population was 68 years (range 52 to 85 years). Mean PSA value at referral was 48,4 ng/ml (range 4,3 to 280,6 ng/ml). Patients had prostate biopsy performed prior to the scan, and were diagnosed with prostate adenocarcinoma, 41 in the high-risk group. Functional imaging was proposed after equivocal or negative conventional imaging findings (abdominal and pelvic MSCT), and equivocal findings of Tc-99m MDP bone scintigraphy. Results of Tc-99m MDP bone scintigraphy were available in 82 patients, most of them positive or equivocal for metastases, 89%. Mean administered activity was 209 MBq of F-18 choline (2-3 MBq/kg, IASOCholine, IASON GmBH). After the F-18 FCH scan patients had a minimum 6-month follow-up, ranging from 6 to 60 months. **Results:** Twenty four patients had localized prostate cancer with no positive metastases, while the majority of patients, 76%, had an F-18 FCH PET/CT scan positive for metastatic disease. Eight patients had a single positive pelvic lymph node, with a short axis diameter smaller than 1 cm. The other 68 patients had FCH positive metastatic disease, in seminal vesicles, lymph nodes and/or bone metastases. Fifty-six patients had lymph node metastases, with the mean SUVmax value was 6,4, ranging from 2 to 22. Twenty-five patients had bone metastases, with the mean value of SUVmax 10,7; ranging from 3,8 to 23,3. Sixteen patients had pathological uptake in the seminal vesicles. In the follow-up period change of management was observed in about two-thirds of patients, with a surgical approach chosen in ten patients with no FCH positive metastases. The majority of our patient population had a combination of radiotherapy and hormonal therapy, 60 %. Bilateral orchidectomy was performed in 12 patients, and 6 of them had an added docetaxel chemotherapy. Mean PSA levels

after six months of therapy and follow up was significantly lower than the baseline value, 2,1 ng/ml, ranging from undetectably low to the maximum value of 79 ng/ml. **Conclusion:** F-18-choline PET/CT provides clinicians with valuable information in the staging of prostate cancer. It has an important impact on therapeutic strategy, providing additional data necessary for the appropriate and individual patient management. **References:** None.

EP-0469

The added value of lumbopelvic SPECT/CT to negative planar 99mTC-Bone Scintigraphy in Prostate Cancer

M. Tagliatori Nogueira, P. García Alonso, M. De la Rubia Marcos, C. Mena Melgar, A. Herrero Muñoz, C. Sandoval Moreno, L. Castillejos Rodriguez, C. Paniagua Correa, A. Ortega Valle, M. Balsa Bretón; Hospital Universitario de Getafe, Madrid, SPAIN.

Aim/Introduction: Prostate cancer (PCa) is the second most commonly diagnosed cancer in men. The appropriate treatment planning requires accurate disease staging. In the last European Association of Urology guidelines (EAU-2018) is expressed that 99mTc-Bone scintigraphy has been the most widely used method for evaluating bone metastases of PCa. Nevertheless, the diagnostic yield is influenced by PSA level (2.3% with PSA<10 ng/mL, 5.3% with PSA 10.1-19.9 ng/mL and 16.2% with PSA 20.0-49.9 ng/mL), Tumoral Stage (6.4% organ-confined cancer and 49.5% locally advanced cancer), tumour Gleason (5.6% GS<7 and 29,9% GS≥8) and the presence of pain. A recent meta-analysis concluded that the SPECT has optimized the use of planar bone scintigraphy with sensitivity ranging from 87 to 92% and specificity of about 91% because of good morphological correlation. In the same year, The National Comprehensive Cancer Network (NCCN) coincided that 99mTc-Bone scintigraphy is a useful diagnostic tool in PCa when satisfying one of the following risk criteria for metastatic bone disease: Pain, PSA>20 ng/dl, T2 with PSA>10 ng/dl, GS≥8, T3-T4 or Biochemical progression with PSA>10 ng/dl.This study was conducted to assess the added value of lumbopelvic SPECT/CT to negative planar 99mTc-Bone Scintigraphy in PCa. **Materials and Methods:** After a negative planar 99mTc-Whole Body bone scintigraphy, a lumbopelvic SPECT/CT was acquired in 34 patients (between 66-89 years old) referred to Nuclear Medicine Department to rule out bone metastases. In addition, PSA level, Gleason and T-Stage was collected. **Results:** 27 of 34 patients were staging studies (79.4%), 6 were biochemical progression (17.6%) and 1 castration-resistant PCa (3%). We obtained 5 positive SPECT/CT for bone metastases and 29 negative studies. In view of these results, the therapeutic management changed in a 14.7% of the patients with negative planar scintigraphy. Analyzing the requests with the risk criteria for bone metastases (pain, PSA, T-stage, and tumour Gleason), we found that only 55,88% met risk criteria for rule out bone metastases and none of the ill-requested patients has yielded a pathological result. **Conclusion:** SPECT/CT increases the detectability of bone metastases and therefore the accuracy in the therapeutic management of patients with prostate cancer. Although it should be considered that the use of bone scintigraphy to rule out metastases is indicated only in highly selected patients. **References:** 1.National Comprehensive Cancer Network (NCCN). NCCN Clinical practice guidelines in oncology. https://www.nccn.org/professionals/physician_gls/pdf/aml.pdf.2.European Association of Urology (EAU). EAU-ESUR-ESTRO-SOIG Guidelines on Prostate Cancer V2, 2018. https://uroweb.org/guideline/prostate-cancer/

EP-0470

Difference in the spectrum of metastatic disease on 68Ga PSMA PET/CT after Radical Prostatectomy and after Radical Radiotherapy, in patients of Carcinoma Prostate with biochemical recurrence

N. K. Seniaray[1], *R. Verma*[1], *S. Khanna*[2], *E. Belho*[1], *D. Malik*[1], *H. Mahajan*[1];
[1]*Mahajan Imaging Center, Sir Ganga Ram Hospital, New Delhi, INDIA,* [2]*Department of Urology, Sir Ganga Ram Hospital, New Delhi, INDIA.*

Aim/Introduction: Radical prostatectomy (RP) and Radical radiotherapy (RT) are well established primary curative options for localized prostate cancer. Despite technical improvements, there is significant risk (15% to 40 % of all patients) of developing serum PSA-recurrence after radical prostatectomy and radiotherapy with differing disease patterns. Prostate-specific membrane antigen is increasingly being recognized as a novel target for the PET imaging of prostate cancer and 68Ga-PSMA has been suggested as a novel tracer for detection of prostate cancer relapse and metastases with high specificity and sensitivity. **Materials and Methods:** A retrospective analysis of subjects with carcinoma prostate, who had undergone definitive treatment (Radical prostatectomy or Radiotherapy) and presented with biochemical recurrence, was done by 68Ga PSMA PET/CT. The data collected was analysed to establish temporal occurrence and patterns of regional and distant metastatic disease in both the groups and correlated with serum PSA levels. **Results:** The study included 200 subjects with history of adenocarcinoma prostate. In the post radical prostatectomy group (n=144), median serum PSA was 1.8 ng/ml, the overall metastatic detection rate was 39.3% for PSA 0.2 to < 0.5 ng/ml, 47.3% for PSA 0.5 to < 1 ng/ml, 68.4% for PSA 1 to < 2 ng/ml and 93.1% for PSA ≥2 ng/ml. In this group local recurrence was identified in 28.73 % and lymph nodal metastases in 65.1%, with the pelvic lymph nodal metastases being the most common site of metastasis followed by bone metastases. The mean time for serum PSA recurrence in the radical prostatectomy group was 49.77±44.44 months (range 2-184 months). In the post radiotherapy group, median serum PSA was 5.2 ng/ml, the detection rate was 88.8 % for PSA 2 to < 4 ng/ml and 100 % for PSA ≥ 4 ng/ ml. Local recurrence after radiotherapy was present in 79.5 % of the group and 63.6 % had lymph nodal metastases. The mean time for serum PSA recurrence following radiotherapy was 49.15± 24.32 months, (range 12-111 months). **Conclusion:**

Radical prostatectomy and Radical radiotherapy are the two standard treatment options for localized carcinoma prostate. Although the extent and patterns of recurrence differed in the two groups, the temporal occurrence of metastatic disease remained comparable. **References:** None.

EP-0471

Diagnostic Efficacy of ^{18}F-PSMA-1007 in Staging of Prostate Cancer

K. Gourevich, A. Koskosi, Z. Keidar;
Rambam HealthCare Campus, Haifa, ISRAEL.

Aim/Introduction: Recent advances in imaging technologies such as using ligand targeting prostate-specific membrane antigen (PSMA) allow for better staging, restaging and treatment planning of patients with prostate cancer. Currently, ^{68}Ga-PSMA serves as the major PET tracer tool for the detection of prostate cancer. However, ^{68}Ga has several shortcomings as a radiolabel including short half-life and non-ideal energies. A novel promising ^{18}F-PSMA-1007 ligand may offer additional benefits, including availability, image resolution, and low urinal excretion of the ligand. This study aims to evaluate the diagnostic performance of ^{18}F-PSMA-1007 PET/CT in patients with newly diagnosed prostate cancer. **Materials and Methods:** Study population included 26 consecutive patients with biopsy proven prostate cancer that were referred for PSMA PET/CT staging study. All patients underwent whole-body (head to mid-thigh) PET/CT imaging at 60 minutes after injection ^{18}F-PSMA-1007 (average 333 MBq, range 284-418 MBq). ^{18}F-PSMA-1007 precursor, cassettes and reagents were obtained from ABX GmbH (Radeberg, Germany); the synthesis of the radiotracer was performed by Isotopia Molecular Imaging Ltd. (Petach Tikva, Israel) on a PET TRACE 16.4 Mev GE Cyclotron. The studies were review by Nuclear Medicine specialist for detection of prostate cancer sites. In addition, urinary uptake in the bladder was assessed and scored (0=no uptake, 1=mild uptake, 2=high urinary uptake). **Results:** From August 2018 to January 2019, 26 patients (age 56-81, Gleason Score 6-9, PSA 1.9-99.2) underwent ^{18}F-PSMA-1007 PET/CT. All patients showed at least one focus of pathological PSMA uptake in the prostate gland. 18/26 patients (69%) had localized disease in the prostate gland with no evidence of local or distant metastases. Four patients (15%) showed additional foci in the skeleton, one patient (4%) had a pathological uptake in a lymph node and 3 patients (12%) were found to have both bone and lymph nodes metastatic spread. Sixteen (62%) patients show no uptake in the urinary bladder (score 0), 7 (27%) patient was with slightly increased uptake (score 1), and only three (11%) patients show prominent uptake in the urine (score 2). **Conclusion:** ^{18}F-PSMA PET/CT had an excellent diagnostic performance with a detection rate of 100% in the prostate gland. The absence or minimal urinal excretion of the ligand in the majority of the patients (89%) can provide additional advantage for lower abdomen and pelvic imaging, especially in the prostate gland and the adjacent structures. **References:** None.

EP-0472

Assessment Of Bone Lesions With Ga^{68}PSMA Uptake Without Visible Bone Density Change On Corresponding CT

S. Tatlidil, F. Tamer, M. Gumus, Z. Ozcan;
Ege University, Izmir, TURKEY.

Aim/Introduction: In this study, morphological characteristics of bone lesions with increased Ga-68 PSMA affinity are reviewed in comparison with bone scintigraphy (WBS) and clinical follow-up findings in prostate carcinoma (PC) patients who underwent Ga-68 PSMA PET/CT for initial staging. **Materials and Methods:** The study group included patients in whom clinical records and other imaging methods were available for retrospective review. None of them had systemic therapy. The time interval between PET and WBS was < 4 months. PSMA avid bone lesions were divided into 3 groups according to the density pattern observed on CT as osteoblastic, osteolytic and lesions without visible density change. SUVmax and HUmax were measured over target lesion and in mirror symmetry considering cortex borders in order to get background values. Difference between target HUmax and background HUmax named as dHU as an indicator of degree of sclerosis. HU/SUV max values of lesions which were confirmed as metastasis by follow-up of imaging were analyzed statistically ($p<0,01$, t-test and $p<0.05$, Mann- Whitney U test). **Results:** There were 118 PSMA avid bone lesions in 42 patients. Typical osteoblastic pattern was observed in 55 lesions. There was no visible density change (NDC) in 52 lesions and 11 lesions were osteolytic. Patient based diagnostic references were clinical follow up, PSA, CT and WBS findings. All of NDC lesions showed sclerosis on follow-up CT. The mean SUV of PSMA positive lesions was 16.7 (3.2-59.0). There was no significant statistical difference between SUV max of the groups. There was no correlation between dHU and SUVmax values of osteoblastic lesions, whileas a moderate correlation was observed when all lesions included. Of the 70 lesions examined with both Ga-68 PSMA PET/CT and WBS, 49 lesions were (+) on both modalities. NDC lesions were divided into 2 groups as undetected (n = 10) and detected (n = 18) on WBS. The statistical analysis showed no significant dHU differences between two groups ($p>0.05$, Mann Whitney U test). Interestingly, HUmax values were higher >100 units than background in 75% of NDC lesions ($p<0.01$, t test). **Conclusion:** The study revealed that, bone metastases without typical osteoblastic pattern may be noted on Ga-68 PSMA PET/CT. It is assumed that these lesions may indicate early metastatic foci. Moreover the combined assessment of morphological and quantitative findings in addition to PSMA avidity may contribute to interpretation of bone lesions on Ga-68 PSMA PET/CT reporting. **References:** None.

EP-0473

Influence of urinary bladder activity on the detectability of local prostate cancer recurrence in ^{68}Ga-PSMA-PET/CT

I. L. Alberts[1], C. Sachpedikis[1], L. Dijkstra[1], E. Gourni[1], L. Meier[1], R. Cascato[1], S. Boxler[2], T. Gross[2], G. Thalmann[2], A. Rominger[1], A.

Afshar[1];
[1]*University clinic for Nuclear Medicine, Bern, SWITZERLAND,*
[2]*University clinic for Urology, Bern, SWITZERLAND.*

Aim/Introduction: Identifying prostate cancer (PC) lesions with ^{68}Ga-PSMA-11-PET/CT at early stages of recurrence is challenging. Increased bladder activity can obscure local relapse. While the addition of diuretics has been proposed to mitigate against this, there are no pre-existing studies examining the effect of bladder activity on detectability in local recurrence. **Materials and Methods:** 76 consecutive patients undergoing standard and additional late 68Ga-PMSA-11-PET/CT were retrospectively analysed. By institutional protocol, standard imaging was performed at 1.5h post injection (p.i.) of radiotracer, with 1L oral hydration with water beginning at 30min p.i. and 20mg of intravenous Furosemide at 1h p.i. Late imaging at 2.5h p.i. was not accompanied by additional Furosemide. First, a blinded consensus read of the two datasets was undertaken by two physicians. Then, an un-blinded read was performed, with measurement of standardised uptake values (SUV) in the bladder, in locally recurrent PC-lesions and in the background. **Results:** 40 locally recurrent PC lesions were identified in 46% (n=35) of patients, and at standard imaging in 49% (n=37) of patients. Increased PC lesion tracer uptake was observed at late imaging ($p<0.001$) and increased bladder activity ($p<0.001$). Such increased bladder activity obscured n=4 lesions. Analysis of SUV demonstrated that while the lesion activity is higher than bladder activity at standard imaging (immediately post diuresis), there is considerable overlap at late imaging, explaining the reduced detectability of lesions contiguous with the bladder. **Conclusion:** Furosemide in combination with hydration increases the detectability of locally recurrent PC in standard imaging. However, local tumour detectability decreases in additional late scans without re-administration of Furosemide and water. **References:** None.

EP-0474

Are PSA, Gleason score and tumor grade in prostate cancer associated with SUVmax values?

E. Karademirci*, G. Çapa Kaya, A. Aksu;*
Faculty of medicine, Izmir, TURKEY.

Aim/Introduction: The aim of the study was to investigate whether the relationship between SUVmax and PSA, tumor grade, Gleason Score that was obtained from Ga-68 PSMA PET/CT images taken with the purpose of staging in prostate cancer. **Materials and Methods:** Patients with Ga-68 PSMA PET/CT were retrospectively evaluated for staging in our center between February 2017 and October 2018.Patients with Gleason score (GS) and PSA values before treatment were included in the study. Patients were divided into risk groups according to GSS (GSR), grade (GSG), Ga-68 PSMA PET images according to their presence of metastases. The highest SUVmax of the prostate gland, lymph node and organ metastases were noted separately. Statistical analysis was performed using SPSS V22. **Results:** 93 patients with a mean age of 66 ±7 years were included in the study. 10 patients with GS 3+3 (10.8%) were classified as low-risk (GSDR). 83 patients with GS 3+4 and above (89.2%) were classified as high risk (GDP). According to GSG, 10 patients were divided into GSG1, 22 patients into GSG2, 15 patients into GSG3, 21 patients into GSG4 and 25 patients into GSG5. According to the results of the pet study, only 44 patients were followed up with PSMA involvement in the prostate , 18 patients were followed up with lymph node metastasis and 31 patients were followed up with distant metastasis. The mean prostate SUVs in GSDR were 5.2 ± 1.0 and 10.3 ± 1.0 in GSYR (p: 0.045). When patients with lymph node metastasis (18 patients) and only those with PSMA involvement in the prostate (44 patients) were compared, the prostate SUVmax values of the lymph node metastasis group were high ($p<0.001$), but there was no difference in PSA values.A statistically significant difference was observed between SUVmax and PSA values in patients with and without distant metastases(p: 0.003 ve 0.005, respectively). There was a weak correlation between GS and PSA values for all patients(p: 0.012, correlation coefficient: 0.26. There was a low correlation between GS and prostate SUVmax values($p<0.001$, correlation coefficient: 0.397). Low correlationwas found between prostate SUVmax values and PSA values($p<0.001$, correlation coefficient: 0.386). **Conclusion:** SUVmax values increase in high-risk patients and correlate with GS and PSA . Ga-68 PSMA PET imaging may be a more valuable parameter than PSA in detecting only the lymph node metastasis group **References:** None.

EP-0475

Primary staging of prostate cancer using ^{68}Ga-PSMA PET/CT

T. Graziani[1,2]*, M. Scarlattei*[1,2]*, G. Baldari*[1,2]*, S. Migliari*[1,2]*, A. Sammartano*[1,2]*, D. Gasparro*[3,2]*, U. Maestroni*[4,2]*, L. Ruffini*[1,2]*;*
[1]*Nuclear Medicine Division, University Hospital of Parma, Parma, ITALY,* [2]*Prostate Cancer Unit, University Hospital of Parma, Parma, ITALY,* [3]*Oncology Division, University Hospital of Parma, Parma, ITALY,* [4]*Urology Division, University Hospital of Parma, Parma, ITALY.*

Aim/Introduction: To assess the diagnostic value of [^{68}Ga]-PSMA PET-CT (PSMA-PET) in primary staging of patients with prostate cancer (PCa) and to assess PSMA-PET impact on patient management in the contex of a PCa Unit. **Materials and Methods:** We retrospectively analysed 170 PET/CT exams with 68Ga-PSMA performed in our istitution between April 2016 and March 2019, for staging biopsy-proven prostate adenocarcinoma. Results were available for 153 patients. Synthesis of [^{68}Ga]-PSMA-HBED-CC was performed using an automated module (Scintomics GRP®). ^{68}Ga was obtained from a IGG100 ^{68}Ge/^{68}Ga generator (Eckert & Ziegler). Mean yield of labelling was 65.53% and radiochemical purity 99.90% . Dynamic PET images of the pelvic region were acquired immediately after i.v. tracer injecton on a hybrid scanner Discovery IQ (GE Healthcare). Whole body PET/CT was acquired, from vertex to femur medium thigh, 60

min after tracer injection (150 Mbq). **Results:** At the moment of the PET scan mean PSA value was 13.82 ng/mL (range 1.4-124 ng/mL), Gleason Score (GS) was 7 in 71 pts and 8-10 in 52 pts. Moreover, PSMA PET was performed in 30 pts with GS 6 disease evaluated for active surveillance or wait&see. In 12/153 patients PET was performed during androgen deprivation therapy (ADT). PSMA-PET revealed at least one distant lesion (bone, lung or lymph node metastases) in 32/153 patients (20.9%) with PSA range 1.4-124 ng/ml, 3 of them with GS 6. In 125/153 patients PET showed PSMA uptake corresponding to the primary tumor. Oligometastatic disease (<3lesions) was assessed in 16/32 pts with distant lesions driving to localized treatment. In 6/12 patients during ADT PSMA-PET revealed distant metastases (bone, lung, abdominal and thoracic lymph nodes) and intraprostatic lesion in 9/12. PET scan was performed in 123 pts with intermediate/high-risk PCa with positive rate of 88.6% and distant lesion detection rate of 21.3% (26 pts). Number of distant lesions at PSMA-PET increased with Gleason Score and current ADT. **Conclusion:** In our cohort, 68Ga-PSMA PET/CT showed to identify patients with intermediate- to high-risk PCa and metastatic disease allowing lesion directed treatment in oligometastatic pts. Moreover, PSMA-PET allows to positively influence treatment management of pts candidate to active surveillance identifyng understimated metastatic lesions and eventually changing the planned treatment with more enlarged surgery. **References:** None.

EP-0476

Correlation of Ga68 PSMA PET/CT parameters, mpMRI parameters and histopathological grading in prostate cancer

A. Arçay[1], *F. Aydın*[1], *M. Aksu*[2], *A. Keven*[3], *E. Sürer Budak*[4], *C. Çevikol*[3], *A. Boz*[1];
[1]*Akdeniz University Faculty of Medicine, Nuclear Medicine Department, Antalya, TURKEY,* [2]*Akdeniz University Faculty of Medicine, Radiation Oncology Department, Antalya, TURKEY,* [3]*Akdeniz University Faculty of Medicine, Radiology Department, Antalya, TURKEY,* [4]*Antalya Training and Research Hospital, Clinic of Nuclear Medicine, Antalya, TURKEY.*

Aim/Introduction: Multiparametric (MP) MRI and biopsy are performed in the diagnosis of primary tumor in prostate cancer. However, in some cases, mpMRI may give false negative results, and biopsy is an invasive procedure. Ga-68 prostate-specific membrane antigen (PSMA) PET/CT has been performing for diagnosis of the recurrent disease and radionuclide therapy planning in recent years. In our study, we aimed to determine the relationship between Ga-68 PSMA PET / CT parameters (SUVmax, SUVmean, tumor volume: TV) and mpMRI parameters (ADC and PIRADS) in the detection of primary tumor in prostate cancer. **Materials and Methods:** Ga-68 PSMA PET/CT and mpMRI parameters of 31 patients with prostate cancer admitted to the radiation oncology department at our hospital were analyzed retrospectively. SUVmax, SUVmean, TV (cc) of the primary prostate tumor were calculated from PET/CT images. ADC values and PIRADS scoring were calculated from the MRI images which were performed within maximum period of 3 months with PET/CT. **Results:** Median PSA value of 31 patients were found to be 5 ng/ml (4-119). The number of patients with gleason scores 6,7,8,9 and 10 were 10,10,6,3 and 1 respectively. According to PIRADS scoring, 11 cases were classified as 5, 6 cases were 4, 4 cases was 3, 9 cases were 2 and 1 case was classified as 1. The median values for SUVmax, SUVmean, TV, ADC and PIRADS were 12.04, 6.14, 5.67, 640 and 5 respectively. There is positive correlation only between TV and PIRADS ($p \leq 0.05$, Spearman). There isn't any correlation between other PET/CT parameters and mpMRI parameters. There is also positive correlation between PSA levels and TV ($p \leq 0.05$, Spearman) **Conclusion:** According to our initial evaluation results, Ga-68 PSMA PET/CT imaging may be useful in the diagnosis of primary tumor in patients with prostate cancer, in which the mpMRI is negative and have high risk of malignancy and biopsy cannot be performed. **References:** None.

EP-0477

68Ga-PSMA-11 PET/CT in prostate cancer patients with biochemical persistence (BCP) after radical prostatectomy. Accuracy in localizing residual disease and impact on subsequent management

G. Polverari[1], *F. Ceci*[1,2], *M. Vada*[1], *P. Castellucci*[1], *A. Farolfi*[1], *L. Calderoni*[1], *F. Lodi*[1], *S. Fanti*[1];
[1]*Metropolitan Nuclear Medicine, S.Orsola-Malpighi Hospital, University of Bologna, Bologna, ITALY,* [2]*Nuclear Medicine, Department of Medical Sciences, University of Turin, Turin, ITALY.*

Aim/Introduction: The aim of the present study was to assess the accuracy of ^{68}Ga-PSMA-11-PET/CT to localize residual disease in prostate cancer (PCa) patients with persisting high PSA levels (BCP) after radical prostatectomy. Furthermore, we evaluated the impact of ^{68}Ga-PSMA-11-PET/CT on subsequent therapy management. **Materials and Methods:** ^{68}Ga-PSMA-11-PET/CT is performed at our institution through a prospective, single-center, open-label study (Eudract: 2015-004589-27 OsSC). We retrospectively evaluated clinical records of BCP patients (PSA nadir>0.1 ng/mL at 8 weeks after RP) who performed PET scan within 12 months from RP. Patients who already received salvage radiotherapy (SRT) were excluded by this analysis. Sixty-six (n=66) patients were analysed: median age=70 years-old (49-86); median initial-PSA=12 ng/mL (2.38-167.0); median PSA-nadir after RP=0.4 ng/mL (0.1-47); median PSA at PET scan=0.7 ng/mL (0.19-40.9); median PSAdt=3.2 months (-10.2 - 83.5). pT stage>=3a (n=42/66), <3a (n=24/66). Gleason-grade>=8 (n=40/66), <8 (n=26/66). 78.8% of patients performed lymph-node dissection together with RP and 15 resulted N1. Positive margins (R1) were present in 24/66 cases. Median time from RP to ^{68}Ga-PSMA-11-PET/CT was 168.5 days (51-349). 10/66 underwent concurrent hormonal-therapy (ADT) at time of imaging due to very high-risk disease. **Results:** ^{68}Ga-PSMA-11-PET/CT positivity rate was 59.1% (CI95% 46.3-70.8). Disease confined to pelvis only (prostate bed and/or pelvic lymph-

nodes) was detected in 22.7% of cases. The presence of at least one extra-pelvic lesion (extra-pelvic node and/or bone and/or visceral) was observed in 36.4%. PSMA positive findings were detected in the following sub-regions: 5 prostate bed, 23 pelvic nodes, 16 extra-pelvic nodes, 9 bone, 2 lung. Data regarding follow-up were available in 31/66 patients at this preliminary stage. Median follow-up was 15.5 months (4-36). 14/31 patients had negative ^{68}Ga-PSMA-11-PET/CT: 11 patients received SRT on prostate bed, 2 ADT, 1 active surveillance. 17/31 patients had positive ^{68}Ga-PSMA-11-PET/CT: 6 patients received pelvic SRT in an enlarged planned target volume (PTV) including PET positive nodes, 4 underwent stereotactic-body radiotherapy (SBRT) on PSMA positive lesions (3 nodes, 1 bone), 3 SBRT on PSMA positive nodes + ADT, 1 patient performed salvage lymph-node dissection, 3 underwent ADT. Compared to treatment planned prior to PET scan, overall changes in clinical management occurred in 58% of cases. **Conclusion:** This study confirmed the favourable efficacy of ^{68}Ga-PSMA-11-PET/CT to detect residual disease after RP in BCP patients, namely extra-pelvic disease not encompassed by primary therapy. In this specific clinical setting, ^{68}Ga-PSMA-11-PET/CT might influence the subsequent therapy management in the majority of patients. **References:** None.

EP-0478

Biochemical recurrence with low values of PSA in prostate carcinoma after radical therapy: sensibility of 68Ga-PSMA PET/CT

E. Fajardo Ordoñez, R. Hernandez, J. Chavez Torres, D. Pachuca Gonzalez;
Medica Sur, Ciudad de México, MEXICO.

Aim/Introduction: The purpose of this study was to study the sensibility of 68Ga-PSMA PET/CT in patients with prostate cancer with biochemical recurrence with low values of PSA after radical therapy **Materials and Methods:** A retrospective, cross-sectional and descriptive study was carried out with the aim of evaluate the sensibility of 68Ga-PSMA in patients with prostate cancer with biochemical recurrence following primary curative treatment. 53 patients with biochemical recurrence were scanned using 68Ga-PSMA during the period of October 2015 to February 2019. We selected 26 patients who had low values of PSA (&lt 2.5ng/ml). **Results:** The mean age of the study population was 66 years (range 49-85) with a mean prostate-specific antigen (PSA) level of 1.06 ng/ml (range 0.09-2.23). SUVmax mean found was 12.03 (range 1.9-100). 20 patients (76%) were treated with radical prostatectomy, and 6 (23%) with radiotherapy. 20 scans were positive, 6 were negative with 68Ga-PSMA PET/CT. The disease sites at the moment of the study was locoregional in 17(65%), and distant metastasis 9 (34%),13(50%) had abnormal uptake in prostatic bed. The Sensibility in group one:0.01-0.5 (71%), group two: 0.5-1 (80%), group three:1.01-1.5 (75%), group four: 1.6-2.5(83%). 68Ga-PSMA PET/CT has a high sensibility with levels of PSA as low as &lt 0.5ng/ml, and the sensibility increases with higher levels of PSA **Conclusion:** 68Ga-PSMA PET/CT have a high sensitivity in patients with biochemical recurrence with values of PSA as low as &lt 0.5ng/ml, to locate disease sites in prostate cancer. **References:** None.

EP-0479

^{18}F-Choline and ^{68}Ga-THP-PSMA Simultaneous PET/MRI for the Primary Staging of Prostate Cancer

M. Kulkarni[1], *A. Chandra*[2], *V. Glbson*[3], *J. Stirling*[4], *J. Joemon*[4], *S. Jeljeli*[4], *B. Challacombe*[5], *C. Brown*[5], *R. Popert*[5], *P. Dasgupta*[1], *P. Cathcart*[5], *V. S. Warbey*[3], *V. Goh*[4], *G. J. R. Cook*[4];
[1]*Department of Urology, Guy's and St Thomas' NHS Foundation Trust, and Dept of Cancer Imaging, King's College London, London, UNITED KINGDOM,* [2]*Department of Histopathology, Guy's and St Thomas' NHS Foundation Trust, London, UNITED KINGDOM,* [3]*Department of Nuclear Medicine, Guy's and St Thomas' NHS Foundation Trust, London, UNITED KINGDOM,* [4]*Department of Cancer Imaging, King's College London, London, UNITED KINGDOM,* [5]*Department of Urology, Guy's and St Thomas' NHS Foundation Trust, London, UNITED KINGDOM.*

Aim/Introduction: Preliminary results are presented from a single-centre prospective comparison of ^{18}F-choline and ^{68}Ga-THP-prostate specific membrane antigen (PSMA) PET/MRI to determine the accuracy of detection and characterisation of primary prostate cancer using histopathology as the reference. **Materials and Methods:** Thirteen men scheduled for radical prostatectomy underwent ^{68}Ga-THP-PSMA PET/MRI of the pelvis and 7 also had ^{18}F-choline PET/MRI scans. Imaging was performed 45-50 mins after injection of ^{68}Ga-THP-PSMA (mean163 MBq) or ^{18}F-choline (mean 319 MBq). T1, high-resolution T2 and diffusion-weighted (b 50, 800, 1500) 3T multiparametric MRI (mpMRI) scans were performed. Index lesions were located to a sextant and SUVmax and ADC values measured. These results were correlated with PSA, PSA density, 1.5T diagnostic mpMRI TNM stage, histopathological index site and highest Gleason score from prostatectomy specimens. **Results:** 13 patients (mean age 61 years, mean presenting PSA 9.41ug/L, mean PSA density 0.30ug/L/cm^3, Gleason score (GS) (range 3+3 to 4+4) have been recruited. All 7 ^{18}F-choline PET scans and 12/13 ^{68}Ga-THP PSMA PET studies demonstrated focal uptake within the prostate. There was a positive correlation between the location of the histologically-confirmed index tumour (demonstrated by the highest GS) and ^{68}Ga-THP-PSMA PET (as evaluated by SUVmax) in 8/13 scans (62%), for ^{18}F-choline PET in 5/7 scans (71%) and for 1.5T mpMRI in 8/13 scans (62%). For ^{68}Ga-THP-PSMA PET, the index lesion was concordant with the radiological TNM stage on mpMRI in 12/13 scans; 1 patient was upstaged. Greater ^{68}Ga-THP-PSMA PET SUVmax was associated with higher frequency of primary GS 4 (5 vs 2), higher PSA (11.8 vs 6.6 ug/L) and higher PSA density values (0.33 vs 0.25ug/L/cm^3). By comparison, the ^{18}F-choline PET SUVmax demonstrated concordance with radiological TNM stage on mpMRI in 6/7 scans (86%). Increased ^{18}F-choline PET SUVmax was associated with a higher frequency of GS 4 disease, higher PSA (18.3 vs 6.9 ug/L) and higher PSA density values (0.46 vs 0.22ug/L/cm^3). Lower ADC values were associated with higher

proportions of tumours of GS 4, higher PSA (13.5 vs 4.8ug/L and higher PSA density values (0.35 vs 0.18 ug/L/cm³). **Conclusion:** Hybrid PET/MRI with ^{68}Ga-THP-PSMA and ^{18}F-choline in the detection and location of primary prostate cancer index lesions appears promising but not perfect. In addition to showing a similar ability to detect index lesions to a 1.5T mpMRI, the molecular information that ^{68}Ga-THP-PSMA and ^{18}F-choline provide, correlates with disease-specific risk factors including PSA, PSA density and Gleason score. **References:** None.

EP-0480

Effect of androgen-deprivation therapy on the results of PET/CT with ^{18}F-fluciclovine in patients with biochemical recurrence of prostate cancer

T. Bach-Gansmo[1], *K. Korsan*[1], *T. V. Bogsrud*[2];
[1]*Oslo University Hospital, Oslo, NORWAY,* [2]*Tromsø University Hospital, Tromsø, NORWAY.*

Aim/Introduction: ^{18}F-Fluciclovine is an amino acid PET radiotracer approved in the US and in Europe for detection of recurrent prostate cancer. Androgen-deprivation therapy (ADT) is frequently used in the treatment of prostate cancer and is known to impact transporters involved in the uptake of radiotracers such as choline and ^{18}F-fluciclovine. As ADT is known to reduce the sensitivity of choline PET/CT, we examined the impact of ADT on the detection rate of ^{18}F-fluciclovine PET/CT in patients with recurrent prostate cancer. **Materials and Methods:** We conducted a retrospective review of data from patients who underwent ^{18}F-fluciclovine PET/CT for prostate cancer restaging at our institution and whose referral reported use of ADT for at least 3 months prior to imaging. All patients gave informed consent. **Results:** Of the 457 patients who underwent ^{18}F-fluciclovine PET/CT, 71 patients, contributing to a total of 73 scans, met the criteria for ADT use. Primary therapy for the 71 patients was radical prostatectomy (n=29), radiotherapy (n=30, 2 of whom had cryotherapy first), primary hormonal treatment (n=9), or unspecified (n=5). The median time to PET following surgery was 7 years and following radiotherapy was 6 years. Five scans (6.8%) were from patients with a baseline PSA < 0.5 ng/mL, while 17, 12, 15, and 19 were in the range 0.5-2, >2-6, >6-20, >20 ng/mL, respectively (missing data, n=5). Pre-scan Gleason scores were 5-6, 7, 8, 9 or 10 for 2, 26, 16, 19 and 2 scans, respectively (unknown=8). ADT prescriptions comprised Zoladex (n=18), Casodex (n=30), Zoladex plus Casodex (n=7), with Firmagon, Xtandi, Eligard, Procren and Zytiga (either alone, but more commonly in various combinations) being prescribed for the remaining patients. ^{18}F-Fluciclovine-avid lesions were found in 60/73 (82%) scans, with positivity in the prostate/bed in 33/73 (45%). Extraprostatic lesions were found in 46/73 (63%), including lesions in lymph nodes in 38/73 (52%) and in bone in 5/73 (6.8%). Two scans showed sclerotic non-avid lesions. The negative scans (n=13) included all 5 patients with PSA <0.5 ng/mL, 2 further patients with missing PSA data and 1 with evidence of sclerotic lesions. **Conclusion:** Rates of detection in these patients with recurrent prostate cancer who had been receiving ADT for at least three months were similar or higher than rates previously reported for ^{18}F-fluciclovine PET/CT. The data here suggest that it is not necessary to withdraw ADT from patients with prostate cancer before ^{18}F-fluciclovine PET/CT. **References:** None.

EP-0481

Comparison of PSMA-ligand PET/CT and multiparametric MRI for the detection of recurrent prostate cancer in the pelvis

A. Afshar-Oromieh[1], *B. Vollnberg*[1], *I. Alberts*[1], *A. Bähler*[1], *C. Sachpekidis*[1], *L. Dijkstra*[1], *F. Haupt*[1], *S. Boxler*[1], *T. Holland-Letz*[2], *T. Gross*[1], *G. Thalmann*[1], *J. Heverhagen*[1], *A. Rominger*[1], *K. Härmä*[1], *M. Maurer*[1];
[1]*University Hospital of Bern, Bern, SWITZERLAND,* [2]*German Cancer Research Center, Heidelberg, GERMANY.*

Aim/Introduction: Regarding the choice of MRI or PSMA-PET/CT for the detection of recurrent prostate cancer (rPC) still no clear recommendations exist in the guidelines. The aim of this evaluation was to compare PSMA-PET/CT and MRI for the detection of rPC in the pelvis. **Materials and Methods:** A retrospective analysis was performed for patients who were scanned at our institution with whole-body PSMA-PET/CT (tracer: 68Ga-PSMA-11) from 01/2017 until 09/2018 in order to detect rPC. Amongst them, 43 underwent an additional pelvic MRI within a time window of 2 months. Both modalities were compared as follows: a consensus read of the PET-data was performed by two nuclear physicians. All lesions were recorded with respect to their type and localization. The same was conducted by two radiologists for the pelvic MRI. Thereafter, both modalities were directly compared for every patient and lesion. **Results:** Overall, 30/43 (69.8%) patients presented with a pathologic MRI and 38/43 (88.4%) with a pathologic PSMA-PET/CT. MRI detected 53 rPC lesions (13 of them classified as "uncertain") and PSMA-PET/CT detected 75 pelvic lesions (3 classified as "uncertain"). The superiority of PSMA-PET/CT was statistically significant only if uncertain lesions were classified as "false-positive". **Conclusion:** PSMA-PET/CT demonstrated superiority over MRI for the detection of rPC in the pelvis. In order to detect rPC, a potential future scenario could be conducting first a PSMA-PET/CT. Combining the advantages of both modalities in hybrid PET/MRI scanners would be an ideal future scenario. **References:** None.

EP-0482

Extra skeletal incidental findings on CT part of NaF PET/CT in evaluation of prostate cancer

H. Nissen, *J. F. Lauridsen, P. Holdgaard, P. Dolliner, V. Ovchinnikova, K. M. Buch-Olsen, S. Tind, H. B. Jorgensen, J. B. Medhus;*
Department of Nuclear Medicine, Lillebaelt Hospital - University Hospital of Southern Denmark, Vejle, DENMARK.

Aim/Introduction: The advent of NaF PET/CT scans has led to various extra skeletal incidental CT findings (ESIFs) previously undiscovered by planar bone scans. These findings can be challenging with regards to further treatment and work-up. Literature disclosing findings for a North American population has been published [1] but similar literature is lacking for a Scandinavian demography. Our objective was to describe the prevalence of potentially clinically relevant ESIFs on whole-body low-dose non-contrast computed tomography (CT) as a part of NaF PET/CT, as well as detection rate of previously unknown malignancies. **Materials and Methods:** From start September 2018 until start December 2018 a total of 122 consecutive patients (men with a mean age of 73.8 years), all biopsy-proven prostate-cancer undergoing NaF PET/CT for osseous metastatic disease, were prospectively included in a database. The patients had no prior diagnostic imaging (CT, MR or PET/CT) done within the last three months and no scheduled diagnostic imaging in the near future . Examinations were independently reviewed and findings were subsequently categorized by clinical significance. Findings evaluated to have no clinical significance or no potential clinical significance was not registered. The CT was a low dose scan (120 kV; ref. mAs 20; iterative reconstructed) primarily intended for attenuation correction and localization. **Results:** A total of 43 ESIFs were detected on CT in 35 out of 122 patients (28.7%). 22 patients (18%) showed clinically significant findings that were previously unknown; Ten patients were found to have pelvic lymphadenopathy. One patient had multiple lung metastases. One patient had a fractured clavicula. One patient had an aneurismatic aorta. Other findings were mediastinal lymphadenopathy, lung nodules, hydronephrosis and hydroureter. Furthermore unknown primary malignancies were histologically proven in two patients (1.6%). **Conclusion:** Usage of low-dose non-contrast CT in NaF PET/CT performed for oncologic evaluation of prostate cancer may alter disease-staging and reveal clinically significant incidental findings requiring further evaluation and work-up. Our study showed clinically significant ESIFs in 18% of the population. Furthermore unknown primary malignancies were histologically proven in two patients (1.6%), of which one had no osseous metastatic disease from his prostate cancer. We conclude that ESIFs in this Scandinavian demography are significant and the CT part should be evaluated carefully even when used only for attenuation correction. **References:** [1] Guo HH[1], Moradi F, Iagaru A. Clinical significance of extraskeletal computed tomography findings on 18F-NaF PET/CT performed for osseous metastatic disease evaluation. Nucl Med Commun. 2016 Sep;37(9):975-82.

EP-0483

Incremental value of 68Ga PSMA PET/CT for preoperative risk stratification of Prostate Cancer

P. U N, *D. B Sen, D. Thakral, D. Pant;*
Fortis memorial research institute, Gurgaon, INDIA.

Aim/Introduction: Prostate cancer (PC) is the second most common cause of cancer. PC burden is growing worldwide and the most crucial part of patient management is precise local staging of disease. 68Ga PSMA PET/CT scan help in accurate staging of PC owing to its high PSMA avidity and specificity. The aim of this prospective observational study was to determine the accuracy of Gallium-68 Prostate-specific membrane antigen positron emission computed tomography (68Ga PSMA PET CT) in loco regional staging of intermediate and high risk prostate cancer using histopathology from radical prostatectomy specimens as a gold standard. **Materials and Methods:** 35 patients with biopsy proven prostate carcinoma were enrolled in this study. Whole body 68Ga-PSMA PET/CT scans were performed at baseline. The imaging findings were compared to the prostatectomy histopathology. These findings were also compared with multiparametric magnetic resonance imaging (mpMRI). **Results:** All 35 patients showed 68Ga-PSMA avid disease, of which 29 underwent radical prostatectomy, 1 underwent radiation therapy and 5 did not undergo surgery owing to metastases. Out of 29 patients, 13 had histologically prostate confined lesions where as 16 had extraprostatic lesions. 68Ga-PSMA PET/CT scan could detect prostate confined lesions in 12/13 and extra prostatic lesions in 11/16 patients. It could not detect extraprostatic lesions in 5/16 patients. We found concordance between 68Ga-PSMA PET/CT scan and histopathology in 22/29 and discordance in 6/29 patients. Overall sensitivity and specificity was 68.75% (38.46 % for mpMRI) and 92.3% (92.3% for mpMRI) respectively. **Conclusion:** 68Ga-PSMA PET/CT provided superior detection of locoregional preoperative staging of PC as compared to mpMRI in intermediate and high risk prostate cancer patients. **References:** Berger et al. 68Ga-PSMA PET/CT vs. mRI for locoregional prostate cancer staging: correlation with final histopathology. Prostate Cancer and Prostatic Diseases 2018;21: 204-211.

EP-0484

Paget disease as a potential pitfall in 68Ga-PSMA PET/CT imaging for prostate cancer: three case reports

S. Erhamamci[1], *N. Aslan*[2];
[1]*Baskent University Istanbul Health Practice and Research Center Hospital, Department of Nuclear Medicine, Istanbul, TURKEY,* [2]*Neolife Medical Center, Department of Nuclear Medicine, Istanbul, TURKEY.*

Aim/Introduction: 68Ga-PSMA imaging is a valuable tool in the workup of patients with prostate cancer presenting with the suspicion of metastatic disease. However, PSMA is expressed in nonprostatic tissues, as well as in other pathologic conditions. In this report, we describe the uptake of the PSMA in Paget's disease of bone, as a potential pitfall in 68Ga-PSMA-PET/CT in three cases with prostate cancer. **Materials and Methods:** All three patients had no history and complaint of bone disease. They underwent Tc99m-HDP bone scintigraphy and 68Ga-PSMA-PET/CT for primary staging. Case 1: A 63- year-old male presented with Gleason 3+4 prostate cancer. Bone scan demonstrated with increased tracer uptake in

the skull bone without any other abnormal tracer distribution on whole body. 68Ga-PSMA-PET/CT that showed heterogeneous PSMA uptake within the prostate gland that was consistent with prostate cancer, PSMA uptake in the left adrenal gland that was considered suspicious for metastasis, intense PSMA uptake in the skull bone. Case 2: A 59- year-old male presented with Gleason 4+3 prostate cancer. Bone scan showed diffusely increased osteoblastic activity in the right asetabulum, right inferior pubic ramus and right iliac bone. 68Ga-PSMA-PET/CT demonstrated PSMA uptake in the primary prostate lesion, as well as mild to moderate uptake was seen in the bone lesion similar to that seen in bone scintigraphy. Case 3: A 76-year-old male presented with Gleason 4+4 prostate cancer. Bone scintigraphy showed markedly increased tracer uptake in the right iliac bone, sacrum, L3 vertebra and the right proximal tibia. 68Ga-PSMA-PET/CT for initial staging demonstrated intense PSMA uptake in the primary site in the prostate, consistent with the known prostate cancer and PSMA uptake in the pelvic bones, mainly in the right hemipelvis, L1 to L3 vertebra, right proximal tibia and left scapula. **Results:** The diagnosis of Paget's disease was incidental, following both scintigraphic investigation performed for primary staging purposes. In all cases, radiotracer uptake was noted in the bones, corresponding to imaging findings on CT and bone scan consistent with Paget's disease of bone. **Conclusion:** In this report, we describe the uptake of the PSMA in Paget's disease of bone, a common condition in the same elderly male population that is at risk for prostate cancer. In light of the overlap in patients affected by prostate cancer and Paget's disease, it is important for nuclear medicine physicians to be aware of the potential for this diagnostic pitfall when interpreting PSMA-PET/CT scans. **References:** None.

EP-0485

Does ^{68}Ga-PSMA-11 PET/CT Detection Rate change during time? A single-center study

S. Telo[1,2], *S. Veneva*[3], *A. Farolfi*[1,2], *L. Calderoni*[1,2], *R. Mei*[1,2], *P. Castellucci*[1,2], *C. Fonti*[1,2], *F. Ceci*[4], *S. Fanti*[1,2];
[1]*Nuclear Medicine, S.Orsola Malpighi Hospital, Bologna, ITALY,* [2]*DIMES University of Bologna, Bologna, ITALY,* [3]*Nuclear Medicine, Alexandrovska Hospital, Sofia, BULGARIA,* [4]*Università degli studi di Torino, Torino, ITALY.*

Aim/Introduction: To evaluate if there is a detection rate (DR) trend of ^{68}Ga-PSMA-11 PET/CT in prostate cancer patients. **Materials and Methods:** We consecutively reviewed all ^{68}Ga-PSMA-11 PET/CT of patients who came to our center (S.Orsola Hospital, Bologna) for a 3 years period, from March 2016 to March 2019. ^{68}Ga-PSMA-11 PET/CT was carried out as part of clinical trials, and during this period, inclusion trial criteria were: 1) biochemical recurrence after radical therapy (radical prostatectomy or radical radiation therapy) with a PSA value ≥0.2 ng/mL or 2) castration-resistant prostate cancer patients with PSA progression. To evaluate a possible DR trend and to avoid the influence of monthly variations of the number of performed scans, patients were analyzed in groups of same numerosity (n=100) in chronological order. To study the DR, ^{68}Ga-PSMA-11 PET/CT findings were categorized in positive, negative and inconclusive/equivocal: this latter group was then re-evaluated by two expert nuclear medicine physicians in order to categorize them as positive or negative. **Results:** A total of 1600 ^{68}Ga-PSMA-11 PET/CT were included and divided in 16 consecutive groups. Mean and median DR were respectively 52 and 51 (range 41-64). Positive ^{68}Ga-PSMA-11 PET/CT were respectively 56, 48, 50, 52, 64, 52, 41, 49, 51, 44, 51, 59, 53, 53, 57, and 50/100 in the groups. **Conclusion:** We didn't find statistically significant variations in the detection rate during time of patients who underwent ^{68}Ga-PSMA-11 PET/CT for prostate cancer in our center. **References:** None.

EP-0486

The role of additional late PSMA-ligand PET/CT in the differentiation between lymph node metastases and ganglia

I. L. Alberts[1], *L. Dijkstra*[1], *G. Prenosil*[1], *E. Gourni*[1], *L. Meier*[1], *R. Cascato*[1], *S. Boxler*[2], *T. Gross*[2], *G. Thalmann*[2], *K. Rahbar*[3], *A. Rominger*[1], *A. Afshar*[1];
[1]*University clinic for Nuclear Medicine, Bern, SWITZERLAND,* [2]*University clinic for Urology, Bern, SWITZERLAND,* [3]*University clinic for Nuclear Medicine, Munster, GERMANY.*

Aim/Introduction: Differentiating between Prostate Cancer (PC) lesions and benign structures which exhibit radiotracer uptake in PSMA-ligand PET/CT can be challenging. Additional late imaging has been shown to be a powerful method for the discrimination between PC- and non-PC lesions, owing to the increasing tracer uptake of the former. Nevertheless, there are no pre-existing studies which describe the dynamic tracer uptake for ganglia, which this present study aims to address. **Materials and Methods:** 50 consecutive patients with PC who received standard and late 68Ga-PSMA-11-PET/CT (by local protocol at 1.5 and 2.5h p.i.) underwent retrospective evaluation. All lesions with a tracer uptake above local background indicative for ganglia as well as PC-lesions were analysed with regard to their maximum standardised uptake values (SUVmax) and localisation. **Results:** Overall, 82 PSMA-positive ganglia were identified at standard imaging (1.5h p.i.) in 70% of the patients with an additional four ganglia being revealed at late imaging only (total 86). 66 lesions suggestive for PC were detected in 44 patients (88%), of which 45% (n=30) were identified as lymph nodes. At late scanning, 73% of the LN exhibited an increase in SUVmax, whereas 65% of the ganglia exhibited a decreasing or stable SUVmax. **Conclusion:** Whereas the presence of increasing tracer uptake in potential PC lesions can provide additional data about the likelihood of malignancy, increasing SUVmax alone does not reliably differentiate between ganglia and PC lesions and is a potential diagnostic pitfall. We therefore recommend high resolution CT to enable morphological characterisation of ganglia. **References:** None.

EP-0487

Retrospective comparison of ^{68}Ga-PSMA-11 and ^{11}C-Choline performances in a cohort of selected prostate cancer patients after radical prostatectomy, presenting with low PSA levels and undergoing imaging with both modalities within 8 weeks

A. Farina[1], *I. De Nicola*[1], *A. Lambertini*[1], *F. Ceci*[2], *P. Castellucci*[1], *S. Fanti*[1];
[1]*Nuclear Medicine Department, Sant'Orsola-Malpighi Hospital, University of Bologna, Bologna, ITALY,* [2]*Nuclear Medicine, Department of Medical Sciences, University of Turin, Torino, ITALY.*

Aim/Introduction: The aim of this study was to assess the performance of ^{68}Ga-PSMA-11 (PSMA) and ^{11}C-Choline (Choline) PET/CT in a cohorts of selected prostate cancer (PCa) patients presenting with serum PSA levels (PSA) of 0.2 to 1.0 ng/mL after radical prostatectomy (RP). In order to minimise variability due to diverse clinical management, all patients underwent PET imaging with both radiotracers within 8 weeks of each other. **Materials and Methods:** All PCa patients referred to our center from February 2016 to February 2019 were retrospectively enrolled according to the following inclusion criteria: a) RP as primary therapy; b) Serum PSA levels between 0.2 and 1.0 ng/mL; c) PET imaging employing both PSMA and Choline, performed within 8 weeks of each other; d) Comprehensive clinical history and prior management data; e) Signed informed consent. Overall, 16 patients were enrolled in our study (mean PSA: 0.76 ng/mL, median PSA: 0,94 ng/mL; mean age: 71 years; median age: 71 years). All images were reviewed by at least two experienced nuclear medicine physicians and detection rate assessed for both tracers on a per-patient basis. **Results:** Choline imaging resulted positive in 4/16 (25%) and negative in 12/16 (75%) of cases. PSMA imaging was positive in 8/16 (50%) of cases and negative in 8/16 (50%) of cases. In 5/16 patients (31%) Choline detected no significant uptake, while PSMA imaging performed within 8 weeks identified at least one lesion, most commonly involving lymph nodes (50%), bone (37.5%) and the prostate fossa (12.5%). **Conclusion:** Our single-center, retrospective data shows consistency with the currently available literature, as we observed a higher detection rate of relapsing disease for ^{68}Ga-PSMA-11 PET/CT when compared to ^{11}C-Choline PET/CT, in a selected group of recurrent PCa patients with low PSA levels undergoing scanning with both modalities within a period of 8 weeks. **References:** (11)C-Choline PET/CT for restaging prostate cancer. Results from 4,426 scans in a single-centre patient series. $_{68}$Ga-PSMA-11 PET/CT in recurrent prostate cancer: efficacy in different clinical stages of PSA failure after radical therapy.

EP-0488

Performance of PSMA PET for Staging of Prostate Cancer

A. Guner[1], *K. Unal*[2], *H. Temiz*[2], *E. Kaya*[2], *E. Vardareli*[2], *M. Tuna*[3], *T. Doganca*[3];
[1]*Acibadem University, Istanbul, TURKEY,* [2]*Acibadem University Nuc Med Dept, Istanbul, TURKEY,* [3]*Acibadem University Urology Dept, Istanbul, TURKEY.*

Aim/Introduction: Ga68 PSMA PET is a promising modality to detect prostate cancer and its metastases. We aimed to evaluate its performance in preoperative staging by comparing with final pathologies after radical prostatectomy and pelvic nodal dissection. **Materials and Methods:** We retrospectively evaluated PSMA PET scans of 32 patients with radical prostatectomy and pelvic lymph node dissection. We compared final pathologies with PET images; uptake in prostate gland, Gleason scores and volumes, and size of nodal metastases. SUV's of PSMA uptake were additionally corrected for background normal prostate(SUV_bgcorr) and liver(SUV_lvcorr). **Results:** In 26/32(81%) of patients, PSMA correctly defined lesion with highest Gleason score. They were 3+4 in 13/26(50%), 4+3 in 9/26(35%), 4+4 1/26(4%) and 4+5 in 3/26(11%). Average SUV's of detected lesions were 15.4±13.1, SUV_bgcorr 4.1±3.9, and SUV_lvcorr 1.7±1.8. Average SUV's of detected lesions were for Gleason 3+4; 6.9±4.3; 2.5±1.2; 1±0.6, for 4+3; 21±17; 6.3±4.7; 2.6±2.2, and for 4+5; 22.5±32; 5.4±6.6; 2.6±3.3, SUVmax, SUV_bgcorr and SUV_lvcorr, respectively. Difference between SUV's (including both corrected SUV's) of 3+4 and 4+3, 3+4 and 4+5 were statistically significant, 4+3 and 4+5 lesions had higher SUV's than 3+4 lesions($p<0.001$). However, differences between SUV's of 4+3 and 4+5 lesions were not statistically significant. Average volume of lesions detected by PSMA were 3.8±4.8ml. Average volumes of missed lesions (6/32) were 2.9±1.5ml (Four had 3+4, rest 4+3 and 4+5). Volume difference was statistically not significant. For detected lesions volume correlation between PSMA and pathology was 0.337 ($p=0.09$). 8/32(25%) patients had lymph node metastases (average size 9.1±13mm's). PSMA PET detected at least one lymph node in 4/8(50%), average size was 16±16mm's. Of the four patients that lymph nodes not detected in PSMA, largest diameters were 4mm, 3mm, 1mm and 0.5mm (2.1±1.7). Difference in size between detected lymph nodes and missed lymph nodes was significant ($p=0.046$). **Conclusion:** PSMA PET correctly detected prostate lesions in majority of patients. Missed lesions had lower volumes, but difference was statistically not significant. In half of the patients with lymph node metastases, PSMA PET correctly detected at least one lymph node, achieving 50% sensitivity. Missed lymph nodes were statistically smaller in size, possibly reflecting PET scanner resolution limits. **References:** None.

EP-0489

Relationship Between PSA Levels and F-18 Sodium Fluoride Positron Emission Tomography Scan in Prostate Cancer Bone Metastasis

F. Abbaspour Raddakheli, *F. Kasraei, P. Maliha, N. Almanier, M. Leblanc, A. Alzahrani, V. Derbekyan, A. Ciarallo, R. Lisbona, J. Novales Dias, G. Abikhzar, M. Hickeson;*
McGill University, Montreal, QC, CANADA.

Aim/Introduction: F-18 Sodium fluoride PET (NaF) is increasingly used over Tc99m-MDP to assess bone pathology with more accuracy (1,2,3). In prostate cancer, rising PSA is often associated with bone metastasis, a poor prognosis factor. It is shown that PSA level more than 20 ng/ml is associated with a significant chance of bone metastasis detection in the Tc99m-MDP whole-body bone scan (4,5). Since there is no systematic review to correlate the result of NaF with PSA level, we reviewed NaF results of the last two years for prostate cancer and find out the relationship between PSA level and NaF results. **Materials and Methods:** A total of 237 NaF in 237 patients were retrospectively analyzed from May 2016 to December 2017. The population average age was 64 and the median PSA was 11.04 ng/ml. NaF results were categorized as a positive scan (presence of bone metastasis), negative scan (absence of bone metastasis) and suspicious (inconclusive for bone metastasis). ROC analysis was conducted. **Results:** There was a statistically significant correlation between NaF results and PSA values (P-value= 0.002). There is a significant difference between the PSA values in compared positive and negative NaF results (P-value= 0.003). There is a significant difference in PSA values between positive and suspicious NaF. (P-value = 0.023 respectively). The optimal cut-off value of PSA in a positive scan calculated at 14.14 ng/ml. (AUC= 0.592, P-value =0.025). **Conclusion:** With an appropriate understanding of the relationship between PSA and NaF PET results, we can further clarify the ideal time to investigate for bone metastasis. **References:** 1. Blau M et al. Fluorine-18: a new isotope for bone scanning. JNM. 1962;3:332-334 2. Ka Kit Wong et al. Dynamic Bone Imaging with 99mTc- Diphosphonates and NaF: Mechanisms and Applications JNM April 1, 2013 vol. 54 no. 4 590-599 3. Randi F Fonager et al. Diagnostic test accuracy study of NaF PET/CT, 99mTc diphosphonate SPECT/CT, and bone scintigraphy for bone metastases in newly diagnosed, high-risk prostate cancer. Am J Nucl Med Mol Imaging 2017;7(5):218-227. 4. Tanaka N, et al. Bone Scan Can Be Spared in Asymptomatic Prostate Cancer with PSA of ≤20 ng/ml and Gleason Score of ≤6 at the Initial Stage of Diagnosis. Japanese Journal of Clinical Oncology, Volume 41, Issue 10, 1 October 2011, Pages 1209-1213, 5. Kamaleshwaran K K, et al, Predictive value of PSA in detecting bone metastasis in prostate cancer using bone scintigraphy. Indian JNM 2012 Apr-Jun; 27(2): 81-84.

EP-0490

Detection Rate of ^{18}F-labeled PSMA PET/CT in Biochemical Recurrent Prostate Cancer: A Meta-analysis

G. Treglia[1,2,3], *S. Annunziata*[4], *D. A. Pizzuto*[5], *L. Ceriani*[1,5], *L. Giovanella*[1,5], *J. O. Prior*[2];
[1]*Clinic of Nuclear Medicine, Imaging Institute of Southern Switzerland, Ente Ospedaliero Cantonale, Bellinzona and Lugano, SWITZERLAND,* [2]*Department of Nuclear Medicine and Molecular Imaging, Lausanne University Hospital and University of Lausanne, Lausanne, SWITZERLAND,* [3]*Health Technology Assessment Unit, General Directorate, Ente Ospedaliero Cantonale, Bellinzona, SWITZERLAND,* [4]*Nuclear Medicine Unit, IFO Regina Elena National Cancer Institute, Rome, ITALY,* [5]*Department of Nuclear Medicine, University Hospital Zürich and University of Zürich, Zürich, SWITZERLAND.*

Aim/Introduction: The use of radiolabeled PSMA PET/CT for the evaluation of patients with biochemical recurrent prostate cancer (BRPCa) is increasing worldwide. Several articles and evidence-based data have been published about the role of ^{68}Ga-labelled PSMA PET/CT in this setting. Recently, ^{18}F-labeled PSMA agents have become available (^{18}F-PSMA-1007, ^{18}F-DCFPyL and ^{18}F-DCFBC). Labeling of PSMA agents with ^{18}F may offer numerous advantages, including longer half-life and improved image resolution. Furthermore, ^{18}F-labeled PSMA can be produced in larger amounts compared to ^{68}Ga-labelled PSMA increasing the availability and potentially reducing costs. We performed a systematic review and meta-analysis about the detection rate (DR) of ^{18}F-labeled PSMA PET/CT in BRPCa to provide evidence-based data in this setting. **Materials and Methods:** A comprehensive computer literature search of PubMed/MEDLINE, EMBASE and Cochrane Library databases for studies published through April 23, 2019 was performed using the following search algorithm: (A) "PSMA" AND (B) "DCFPyL" OR "DCFBC" OR "1007". Articles reporting information on the DR of ^{18}F-labeled PSMA PET/CT in BRPCa were included. Articles with possible patient data overlap were excluded. Pooled DR has been calculated on a per-patient basis, with pooled proportion and 95% confidence interval (95%CI) obtained using a random-effects model. Furthermore, DR of ^{18}F-PSMA PET/CT using different cut-off values of PSA has been calculated. **Results:** Six articles (645 patients) were selected and included in the meta-analysis. The pooled DR of ^{18}F-labeled PSMA PET/CT in BRPCa was 81% (95%CI: 71-88%). A statistically significant difference of DR was found using a PSA cut-off value of 0.5 ng/mL: the pooled DR was 86% for PSA ≥ 0.5 ng/mL (95%CI: 78-93%) and 49% for PSA < 0.5 ng/mL (95%CI: 23-74%). Statistical heterogeneity among the included studies was found, likely due to the different PSMA-agents used, with a trend towards a better DR by using ^{18}F-PSMA-1007 or ^{18}F-DCFPyL PET/CT as compared to ^{18}F-DCFBC PET/CT. **Conclusion:** ^{18}F-labeled PSMA PET/CT demonstrated a good DR in BRPCa, with similar results compared to those reported in the literature with ^{68}Ga-labeled PSMA PET/CT. The DR of ^{18}F-labeled PSMA PET/CT is related to PSA values with significant lower DR in patients with PSA < 0.5ng/mL. Prospective multicentric trials are needed to confirm these findings; nevertheless, ^{18}F-labeled PSMA PET/CT seems to be a promising cost-effective alternative to ^{68}Ga-labeled PSMA PET/CT in BRPCa. **References:** None.

EP-0491

Physiological ^{68}Ga-RM2 Uptake in Patients with Biochemically Recurrent Prostate Cancer: An Atlas of Semi-Quantitative Measurements

L. Baratto, *H. Duan, R. Laudicella, V. Ferri, A. Toriihara, N. Hatami, A. Iagaru;*
Stanford University, Palo Alto, CA, UNITED STATES OF AMERICA.

Aim/Introduction: ^{68}Ga-RM2 is a bombesin (BBN) analog that targets the gastrin releasing peptide receptors (GRPR) overexpressed in several cancer cells, including prostate cancer (PC). Here, we describe the distribution and range of physiological uptake of ^{68}Ga-RM2 in 85 patients with biochemically recurrent (BCR) PC. **Materials and Methods:** Eighty-five participants had simultaneous PET/MRI for BCR PC and were prospectively enrolled in this study. SUV_{max} and SUV_{mean} were measured in 24 normal anatomical structures for each participant. Three readers evaluated the images independently. Uptake in various normal tissues was classified into 4 different categories: no significant uptake if SUV_{mean} was less than SUV_{mean} of the Aortich Arch (AA); mild if SUV_{mean} was less or equal to 2.5, but higher than SUV_{mean} of the AA; moderate if SUV_{mean} was higher than 2.5, but less or equal to 5; intense if SUV_{mean} was higher than 5. **Results:** The highest activity was observed in the urinary bladder and renal collecting system, due to excretion of the radiotracer. No significant uptake was seen in the brain, salivary glands, lungs, myocardium, skeleton, muscles and fat. Liver, spleen and adrenal glands had mostly no significant uptake; the gastrointestinal tract had high physiological uptake, with pancreas being the organ with the highest SUV_{max} values (average SUV_{max} of 65.39). Moderate uptake was measured in the esophagus (average SUV_{max} of 3.98), while stomach, duodenum and rectum had mild uptake (average SUV_{max} of 2.54, 3.33 and 3.67, respectively). **Conclusion:** ^{68}Ga-RM2 is evaluated for PC detection. This atlas of normal biodistribution and SUV ranges in healthy tissues will help physicians distinguish between physiological vs pathological uptake, as well as plan future diagnostic and therapeutic studies using GRPR targeting radiopharmaceuticals. **References:** None.

EP-0492

68Ga-PSMA PET-CT: review of a population of prostate cancer patients at initial diagnosis

C. V. Pinto, C. Loewenthal, R. Vieira;
Hospital da Luz, Lisboa, PORTUGAL.

Aim/Introduction: To evaluate the impact of 68Ga-PSMA PET-CT results on the therapeutic management of patients at initial staging of prostate carcinoma. / Prostate carcinoma is the third most frequent neoplasm worldwide. At initial staging early detection and precise localization of cancer sites is determinant in therapy decision-making. Prostate-specific membrane antigen (PSMA) is a transmembrane protein expressed in prostatic tissues, including neoplastic tissue, with highest expression in undifferentiated, metastatic and hormone-resistant tumors. 68Ga-PSMA PET-CT detects lesions avid for PSMA and is currently one of the most sensitive and specific tests in disease detection, even at low PSA values. **Materials and Methods:** Retrospective evaluation of clinical electronic records of 102 patients (mean age 64.1 years, range 60-81) who underwent 68Ga-PSMA PET-CT for initial staging of prostate carcinoma between February 2017 and March 2019. Biochemical, clinical, imaging and pathological findings were reviewed. We compared results of prostate magnetic resonance imaging (pMRI) plus other imaging modalities combined, with PET-CT results, for staging prostate carcinoma, and evaluated clinical impact of PET-CT on treatment. **Results:** One hundred and two patients underwent 68Ga-PSMA PET-CT for initial staging of prostate carcinoma, approximately half of whom had pMRI (48 patients). The mean PSA initial value was 13.6 ng/ml (range 8.3-99). Gleason score was 6 in 1 patient, 7(3+4) in 8, 7(4+3) in 12, 8(4+4) in 17, 9-10 in 8 and in 2 wasn´t available. On PET-CT, 22 patients had disease confined to the prostate, 15 had locoregional disease (6 locally advanced and 9 regional lymph nodes), 10 had metastatic disease (2 distant lymph nodes, 7 bone metastases and 1 lung lesion) and 1 had no hypermetabolic lesions. PET-CT results didn´t change strategy in 32 patients (67%). In the remaining 16 patients, PET-CT changed TNM stage. In 5 patients, PET-CT resulted in down-staging, pathologically confirmed disease confined to the prostate without extraprostatic extension in 1, without regional lymph node extension in 2 and excluded bone metastases in 2. It resulted in up-staging 11 patients (detected lesions in regional lymph nodes in 3, non-regional lymph nodes in 2, bone metastases in 5 and lung nodules in 1). In 6/16 patients, PET-CT results were confirmed with pathological and other imaging findings. **Conclusion:** PET-CT with 68Ga-PSMA appears to bring added value at initial staging of patients with prostate cancer. A significant percentage of patients seems to benefit from the additional information provided, altering the therapeutic approach in one-third (33%) of patients. **References:** None.

EP-0493

The impact of 68Ga-PSMA PET/CT in prostate cancer patients with earlier biochemical recurrence

D. Has Simsek, Y. Sanli;
Istanbul University, Istanbul Faculty of Medicine, Istanbul, TURKEY.

Aim/Introduction: The goal of this study was to evaluate the diagnostic impact of 68Ga-PSMA PET/CT and its effect on therapy management of surgically treated prostate cancer (PC) patients with earlier biochemical recurrence (PSA ≤ 0.5 ng/ml). **Materials and Methods:** We analyzed 65 patients (median age:61 years, range: 45-89 years) who underwent 68Ga-PSMA PET/CT scans retrospectively with rising PSA values (range:0.03-0.5 ng/ml) after radical prostatectomy (RP). If the patients had received salvage radiotherapy (S-RT)/ stereotactic body radiotherapy (SBRT) and/or systemic therapy, they excluded the study. Images were analyzed by experienced nuclear medicine physicians and 68Ga-PSMA(+) suspicious areas were correlated by MRI, multiparametric MRI, histologic results or follow-up. The treatment strategy was evaluated according to 68Ga-PSMA PET/CT results based on NCCN guideline (2017) **Results:** At least one 68Ga-PSMA(+) tumoral lesion was detected in 26 of 65 (40%) 68Ga-PSMA PET/CT scans. 16 patients (24.6%) were oligometastatic, (n:8, pelvic , n:8 extrapelvic). 4 patients (6.1%) were multimetastatic (n:2, pelvic , n:2 extrapelvic). Metastatic lesions were detected in prostatic bed (n:7, 10.7%), pelvic lymph

nodes (n:14, 21.5%), abdominal lymph nodes (n:3, 4.6%), and bone (7/65 patients, 10.7%). Median PSA was 0.23 ng/ml and 0.244 ng/ml for 68Ga-PSMA negative and positive patients, respectively. According to 68Ga-PSMA PET/CT scan results, S-RT was planned to 45 patients (69.2%) and boost RT was added to 7 in these patients (10.7%). SBRT was planned to 8 patients (12.3%) for metastatic pelvic lymph nodes, SBRT + androjen deprivation theraphy (ADT) was planned to 10 patients (15.3) for extrapelvic oligometastatic disease and ADT was planned 2 patients (3%) for multimetastatic disease. Finally, the therapy management was changed in 27 of 65 (41.5%) patients. **Conclusion:** 68Ga-PSMA PET/CT could be useful, even in very low PSA levels, for detecting early recurrence and change the therapeutic approach. **References:** None.

EP-0494

Choline-PET Radiomic features to predict survival outcome in prostate cancer

P. Alongi[1,2], A. Stefano[3], P. Mapelli[4,5], R. Laudicella[6], R. Gentile[1], D. Sardina[7], G. Russo[8], S. Scalisi[1], G. Ganduscio[7], P. Toia[9,2], A. Vento[6], M. Picchio[4,5], S. Baldari[6], M. Midiri[10,2];
[1]Nuclear Medicine Unit, Fondazione Istituto Giglio, Cefalù, ITALY, [2]Department of Radiology, University of Palermo, Palermo, ITALY, [3]Institute of Molecular Bioimaging and Physiology, National Research Council (IBFM-CNR), Cefalu, ITALY, [4]Department of Nuclear Medicine, IRCCS San Raffaele Scientific Institute, Milan, ITALY, [5]Vita-Salute San Raffaele University, Milan, ITALY, [6]Department of Biomedical and Dental Sciences and of Morpho-functional Imaging, Nuclear Medicine Unit, University of Messina, Messina, ITALY, [7]Department of Surgical Oncological and Stomatological Sciences, University of Palermo, Palermo, ITALY, [8]Institute of Molecular Bioimaging and Physiology, National Research Council (IBFM-CNR), Cefalù, ITALY, [9]Dipartimento di Biopatologia e Biotecnologie Mediche, Policlinico "Paolo Giaccone", Palermo, Italy, Palermo, ITALY, [10]Dipartimento di Biopatologia e Biotecnologie Mediche, Policlinico "Paolo Giaccone", Palermo, ITALY.

Aim/Introduction: To investigate the potential application of texture analysis of restaging Choline-PET in prostate cancer (PC). To assess the predictive potential of quantitative imaging features on PC outcome **Materials and Methods:** 30 PC patients underwent 18F-Choline PET/CT for restaging purpose between 2014 and 2018 were evaluated. PET related structures containing volumetric segmentations (DICOM-RT) were imported in the open-source CGITA tool box implemented using MATLAB to extract imaging features from each lesion for T (primary or local relapse), N and M. ROC curves were generated to evaluate the discriminative ability of each parameter compared to FU status. OS and PFS were assessed through KM curves. **Results:** After a median FU period of 27 months (± 10.9), 24 (55%) patients had PD, and 19 (45%) showed SD. 105 features were extracted using CGITA tool box on PET images for each lesion selected for TNM status. ROC curves in prediction of outcome (PD vs SD) provide the best discriminative power for the parent matrix features as follow: T- SUV statistics Surface mean SUV 2 (AUC 0.91;Se 0.99; Sp 0.75), T - Voxel alignment Intensity variability and Run length variability (AUC 0.85;Se 0.83; Sp 0.87), N - SUV statistics Minimum SUV (AUC 0.77;Se 0.62; Sp 0.83); N - Normalized Cooccurance Entropy (AUC 0.67;Se 0.75; Sp 0.66), M - Normalized Cooccurance Entropy (AUC 0.77;Se 0.83; Sp 0.66), M - SUV statistics Surface SUV SD 3 (AUC 0.77;Se 0.66; Sp 0.83). KM curves on qualitative assessment of Choline PET showed a 3-yOS rate of 57% vs. 80% ($p < 0.05$) and 2y PFS rate of 36% vs. 80% ($p < 0.05$). KM Curve on best radiomics features showed worse cumulative survival rates in 3yOS and 2yPFS period as follow: T - Voxel alignment Intensity variability (3y-OS 20% vs. 80%; p=0.011; 2y-PFS 21% vs 83%); T- SUV statistics Surface mean SUV 2 (3y-OS 31% vs. 65%; p=0.28; 2y-PFS 32% vs 68%; p=0.28); N - SUV statistics Minimum SUV (3y-OS 40% vs. 72%; p=0.63; 2y-PFS 41% vs 67%; p=0.63); N - Normalized Cooccurance Entropy (3y-OS 39% vs. 73%; p=0.068; 2y-PFS 30% vs 77%; p=0.068); M - Normalized Cooccurance Entropy (3y-OS 49% vs. 67%; p=0.23; 2y-PFS 32% vs 68%; p=0.23). **Conclusion:** The goal of this work was to suggest the predictive potential of new Choline-PET quantitative imaging features on PC outcome. Several first order and second order features might be used for an accurate risk stratification in PC. **References:** None.

EP-0495

18F-Choline PET/CT in the Suspicion of Prostate Cancer Recurrence. Our Experience

C. Riola-Parada, P. García-Talavera, J. Villanueva, F. Gómez-Caminero, C. Achury, L. Díaz, J. Cañadas, A. Peñaherrera, P. Tamayo; Nuclear Medicine Department. Hospital Clínico Universitario de Salamanca, Salamanca, SPAIN.

Aim/Introduction: The aim of this study was to prove the usefulness of 18F-choline PET/CT in the suspicion of prostate cancer recurrence in our patients and to relate 18F-choline PET/CT detection rate with analytical and pathological variables. **Materials and Methods:** We prospectively analyzed 113 consecutive patients with prostate cancer (mean age 68 years, range 47-87 years) who received local therapy as primary treatment and who underwent 18F-choline PET/CT due to suspicion of recurrence (persistently rising serum PSA level). The patients were recruited from the Nuclear Medicine Department of Hospital Clínico Universitario de Salamanca, Spain, from November 2015 to February 2019. 18F-choline PET/CT findings were validated by anatomopathological analysis, other imaging tests or by biochemical response to oncological treatment. **Results:** 18F-choline PET/CT detected disease in 79 of 113 patients (detection rate 70 %). 19 patients (17%) presented exclusively local recurrence, 31 (27%) lymph node metastases, 28 (25%) bone metastases and 1 (0,01%) esplenic metastases. Mean PSA (PSAmed) at study time was 5.38 ng/mL (median 3.62, range 0.017-38 ng/mL). PSAmed in patients with positive PET/CT was 6.09 ng/mL (median 4.00, range 0.7-38 ng/mL), higher than in patients with negative PET/CT: PSAmed 3.71 ng/mL (median 2.89, range 0.017-15.90 ng/mL) ($p<0.05$). The percent of positive scans was 25% for PSA less than 1 ng/ml,

66,7% for PSA 1-1,9 ng/ml, 60% for PSA 2-2,9 ng/ml and 78% for PSA ≥3 ng/ml. PSA level could not differentiate between patients with local recurrence, lymph node metastases or bone disease. Mean total Gleason score at diagnosis was 6.89 (range 4-10). Mean total Gleason score in patients with a positive study was 7.04 (range 4-10) and in patients with a negative study was 6.57 (range 4-9), without statistically significant differences. **Conclusion:** 18F-choline PET/CT was able to detect disease in an important number of our patients (70%). PSA level could differentiate between positive and negative 18F-choline PET/CT. **References:** None.

EP-0496

Negative predictive value of the finding of non-metastatic disease with whole body 99m-Tc-HDP-SPECT-CT in prostate adenocarcinoma may be adequately high

E. E. Kauppila;
Seinäjoki Central Hospital, South-Ostrobotnian Health Care District, Seinäjoki, FINLAND.

Aim/Introduction: 18F-PSMA or 18F-fluorocholine PET are available for prostate cancer staging, but are expensive in comparison with whole body 99m-Tc-HDP-SPECT-CT, which may miss metastatic disease. Aim of this study is to evaluate the role of whole body bone SPECT-CT in staging of prostate adenocarcinoma. **Materials and Methods:** Clinical follow up of 202 patients with initial staging of N0M0 or N1M0 (n=11) disease with whole body bone SPECT-CT. **Results:** Imaging (for staging or re-staging) was performed for 202 patients (mean age 72.7 SD 8.4 years) with high risk prostate cancer or due to skeletal pain. Mean PSA was 15.3 (SD 17.3). For 8 patients follow up data were not available. After N0M0 or N1M0 staging with WB bone SPECT-CT PSA regression occured and remained low over one year in 157 (78.7 %) patients after the local treatment. PSA response less than 50 % was seen in 10 (5 %) and continuation of PSA progression in 25 (12.4 %) patients. In the latter two groups evidence of metastatic progression was found in 5 patients. There remaining 20 patients, whose PSA progression continued after the treatment with radical intention, may have local or metastatic progression of the disease. Thus, pessimistic NPV fell to 85 % and optimistic NPV to 97 %, respectively. **Conclusion:** Negative predictive value for metastatic progression of prostate adenocarcinoma using whole body bone SPECT-CT was high, 85-97 %, justifying its use for staging and re-staging of prostate adenocarcinoma in patients with high risk of metastatic disease. Complementary use of other imaging including PSMA and fluorocholine PET may be most useful in inadequte PSA-response, or progression, after treatment with radical intention. **References:** None.

EP-0497

^{18}F-Choline PET/MRI On The Therapeutic Approach For Prostate Cancer Patients Treated With Prostatectomy And Rising PSA Below 1 ng/ml

J. R. Garcia, A. Blanch;
CETIR, Viladomat (Barcelona), SPAIN.

Aim/Introduction: PET/CT with Choline analogues use remains controversial before small increases in prostate specific antigen (PSA) levels, due to its low detection rate in prostate cancer recurrence. Multiparametric MRI has shown higher detection rates for local recurrence. This study was aimed to evaluate changes in therapy approach for prostate cancer patients treated with prostatectomy who presented with rising PSA levels below 1 ng/ml, based upon the 18F-Choline PET/MRI findings. **Materials and Methods:** Our first 18 patients with prostate cancer treated with prostatectomy with rising PSA <1 ng/ml (range 0.2-0.9, mean 0.52), and who were referred for an 18F-Choline PET/MRI procedure were included in this study. A dual-phase study was acquired after intravenous administration of 185±10% MBq of 18F-Choline: 1) early imaging (immediately after tracer administration) of prostate area (emission PET/Multiparametric MRI). 2) whole-body imaging 1 h after tracer injection (emission PET/MRI: T1, T2, diffusion). Studies were read jointly by a Nuclear Medicine physician and a Radiologist, both with expertise in prostate pathology. The therapy approach was decided upon the Oncology Committee consensus: in those patients with oligometastatic disease, radiotherapy extent was based on tumor spread according to the PET/MRI findings, with a dose-escalation scheme. **Results:** Ten out of 18 patients (55.6%) were positive for the 18F-Choline PET/MRI study: 1) Recurrence was detected in 4 cases within the prostatectomy bed. 2) Recurrence was detected in 4 cases within infradiaphragmatic lymph-nodes (all of them with infracentimetric measurement). 3) A isolated bone metastatic lesion was detected in 2 cases. In 8 out of 18 patients (44.4%) 18F-Choline PET/MRI was negative and follow-up in active surveillance did not show evidence for recurrence (> 6 months). All those patients underwent radiotherapy on the prostate bed and on the Patient management based on the 18F-Choline PET/MRI findings has been: prostate radiotherapy in 22.2% of cases, extended radiotherapy with dose-escalation in 33.3%, active surveillance in 44.4%. **Conclusion:** In our series, hybrid 18F-Choline PET/MRI procedure showed a high detection rate for recurrence in prostate cancer patients treated with prostatectomy and rising PSA bellow 1 ng/ml, and 18F-Choline PET/MRI findings showed an impact on the therapeutic decision. **References:** None.

EP-0498

Diagnostic accuracy of 60min & 120min 18F-PSMA-1007 PET/CT in prostate cancer patients with biochemical recurrence. Initial results

E. Panagiotidis, *A. Paschali, P. Mitsakis, N. Papadopoulos, T. Kalathas, A. Pipintakou, V. Chatzipavlidou;*
PET/CT department, Theageneio Cancer Center, Thessaloniki, GREECE.

Aim/Introduction: The introduction of ligands targeting prostate-specific membrane antigen (PSMA), especially 68Ga-PSMA-11, revolutionized prostate cancer imaging, changing the management of patients with prostate cancer (PCa). 18F-labeled ligands can be produced in larger amounts and therefore can improve availability for a larger group of patients. 18F-PSMA-1007 was selected among several 18F-PSMA-ligand candidate compounds because it demonstrated high labeling yields, outstanding tumor uptake, and fast, non-urinary background clearance. The aim of our study was to evaluate the diagnostic performance of the recently introduced 18F-PSMA-1007 in PCa patients presented with biochemical recurrence. **Materials and Methods:** This is a retrospective analysis included 18 consecutive patients with biochemical relapse (mean age 65.7 ± 8.6 years) referred for PSMA PET/CT in our department. Whole-body PET/CT imaging was performed in all patients 60 & 120 min after injection of 328 ± 44 MBq 18F-PSMA-1007. Radical prostatectomy had been performed in 75%, Radiation Beam Therapy (RTH) of the prostate bed in 55% and androgen-deprivation therapy in 35% of the patients, respectively. The findings of the 18F-PSMA-1007 PET/CT scan were compared with the Gleason score (GS) and PSA level. **Results:** Sixteen out of 18 patients (88.8%) showed at least one pathological finding on 18F-PSMA-1007 PET/CT. The overall median PSA level was 1.63ng/ml (range 0,03-36.7 ng/ml). The tumor detection rate was positively correlated with PSA levels, resulting in detection rates of 75%, 80% and 100% among patients with PSA levels ≤1.0, 1.1-2.0 and > 2.0 ng/ml, respectively. The median GS was 8 (range 6-10). The rate of pathological scans in patients with GS>8 was 100%. Local recurrent cancer was present in 3 patients (18.75 %), lymph node metastases in 10 patients (62.5 %), and distant metastases in 6 patients (37.5 %). The median SUVmax value was 10.25 of the pathological findings. The median SUVmax increased from 10.25 to 13.2 between 60 and 120 min. However, all the pathological abnormalities depicted in both early (60min) and delayed (120min) acquisitions with no difference in detection rate. **Conclusion:** 18F-PSMA-1007 PET/CT is a powerful diagnostic tool that can detect recurrent PCa in patients with biochemical relapse, resulting in a significant impact on the management of this relevant group of patients. 18F-PSMA-1007 uptake of PCa lesions at 120 min compared to 60 min show an increase but with no clinical benefit, as no difference in detection rate demonstrated. **References:** None.

EP-32

Clinical -> Diagnostic study -> Adult study -> Oncology study -> Organ-based oncology -> Thyroid, malignant

October 12 - 16, 2019 e-Poster Area

EP-0499

Comparison between sonographic characteristics and cytopathologic findings of thyroid nodules detected incidentally at 18F-FDG PET/CT (18F-Fluorodeoxyglucose Positron Emission Tomography / Computed Tomography)

M. Waitman, *F. d. Barbosa, C. A. T. d. Mitteldorf, C. A. Buchpiguel, G. G. Cerri, C. d. Leite;*
Sírio Libanês Hospital, São Paulo, BRAZIL.

Aim/Introduction: 18F-FDG PET/CT has been increasingly used for staging/restaging neoplasms. Hence, incidentally thyroid nodules with radiotracer focal uptake, which were not the focus of the study, are commonly detected. Currently few data in the literature is available about how to manage these nodules. There is a consensus about the high probability of malignancy, so the Fine Needle Aspiration (FNA) assessment is strongly recommended. However, the sonographic characteristics of each nodule, based on standardized classifications such as Thyroid Imaging Reporting and Data System (TIRADS 2017), could select which nodule would need FNA, avoiding unnecessary procedures. There is also controversy about the value of PET Standardized Uptake Values (SUVs) and its correlation with malignancy. This study focused at sonographic characteristics of incidentally detected thyroid nodules with focal uptake at PET/CT and if TIRADS assessment could help to narrow the indications of FNA. We also analyzed the nodules SUV and its correlation with malignancy. **Materials and Methods:** We evaluated 28 patients submitted to oncologic PET/CT, which had incidentally radiotracer focal uptake in thyroid gland. 34 nodules were found with further ultrasound evaluation and biopsy with FNA was performed in all of them. Undetermined nodules classified on cytopathology were excluded from the analysis (10/34). For SUV correlation between malignant and benign nodules we applied T-student test with significance set at p<0,05. **Results:** We had 8 malignant (33,3%) and 16 benign (66,7%) nodules. For benign nodules, if previously applied TIRADS 2017 classification, five nodules would be submitted to FNA (68,8% reduction of FNA procedure). For malignant nodules, if previously applied TIRADS 2017 classification, four nodules would be submitted to FNA and another four nodules would not. However, three of the four nodules (75%) with no indication of FNA had just 0,8-1,0 cm in long axis, which according to current TIRADS, doesn't need to perform FNA, because they represent micropapillary carcinomas, a low grade malignancy that can be followed and treated when with larger sizes. There is no significant statistical difference (p=0,126) between malignant nodules SUVmax (mean:10,31 - range:3,7 - 27,6) and

benign nodules (mean:5,7 - range:2,6 - 16,7). **Conclusion:** The sonographic characteristics seems to have fundamental role in thyroid nodules FNA indication, even those with high focal uptake of FDG at PET/CT. The new classification of TIRADS 2017 presented good performance to avoid unnecessary FNA. SUV values did not demonstrate significant correlation with malignancy. **References:** None.

EP-0500

Correlation between Tg levels and 18 F-FDG PET/CT findings in follow up the group of radioiodine refractory disease DTC patients with negative PET/CT findings

D. J. Srbovan, S. Lucic, A. Peter;
Institute of oncology Vojvodina, Sremska Kamenica, SERBIA.

Aim/Introduction: To disclose place of negative 18F-FDG PET/CT findings in radioiodine refractory differentiated thyroid carcinoma patients (RRDTC) in the prediction the stable disease. We observe the group of RRDTC intermediate/high risk patients with high Tg levels in presence of high level of TSH (>25 microU/ml) and in absence of anti-Tg antibodies with negative PET/CT scan. **Materials and Methods:** 20 RRDTC intermediate/high risk patients with negative PET/CT scan were followed up for 12-60 month for the occurrence of recurrent disease or to confirm a stable disease. Tg were monitored every 6-12 months and control PET/CT was performed during follow up of the patient. The patients were under L-thyroxin therapy. We analyzed with Pearson, Kendalls and Spearmans bivariate correlation the significance of correlation between PET/CT findings,supressed Tg (Tg/LT4) and stimulated Tg levels (Tg/TSH). **Results:** 18 pts had papillary, 2 follicular (1 Hurthlle cell) thyroid cancer. Positive ^{18}F-FDG PET/CT scans was in 3(15%), negative^{18}F-FDG PET/CT scans in 17(85%).The location of pathological foci in positive ^{18}F-FDG PET/CT scans were retrotracheal, paratracheal and in lung. The range of serum Tg/LT4 was 0.4-67,9ng/mL in the negative PET/CT patients,7,5-24,8ng/mL in PET/CT positive group. The range of Tg/TSH in the negative PET/CT patients was 2,56-376ng/mL,31,3-932ng/mL in the PET/CT positive group. Pearsons bivariate correlation showed moderate significant positive correlation between Tg/TSH and PET/CT findings (r=0,509; p=0,022),Tg/LT4 and PET/CT findings (r=0,622;p=0,003).Spearmans correlation showed moderate significant positive correlation between Tg/TSH and PET/CT findings (r=0,449;p=0,047),Tg/LT4 and PET/CT findings (r=0,571;p=0,009). Kendall tau correlation showed also moderate significant positive correlation only between Tg/LT4 and PET/CT findings (r=0,479;τ=0,013). **Conclusion:** Bivariate correlation showed moderate significant positive correlation between Tg/TSH and PET/CT findings and Tg/LT4 and PET/CT findings wich suggests that PET/CT is a useful tool in the follow-up of this intermediate/high-risk RRDTC group of patients. **References:** None.

EP-0501

Contribution Of ^{131}I SPECT/CT To Planar Imaging In Post-Ablation Differentiated Thyroid Cancer

M. Quirce Pisano, J. Andres-Pacheco, J. Jiménez-Bonilla, I. Martínez-Rodríguez, N. Martínez-Amador, M. De Arcocha-Torres, A. Sanchez-Salmon, O. Cuenca-Vera, G. Molina-Mendoza, I. Banzo;
Department of Nuclear Medicine, Marques de Valdecilla University Hospital, Molecular Imaging Group (IDIVAL), University of Cantabria, Santander, SPAIN.

Aim/Introduction: The aim of this prospective study was to evaluate the value of 131I SPECT/CT in comparison to planar imaging in post-ablation setting of patients with differentiated thyroid cancer (DTC). **Materials and Methods:** The study included 33 patients (24 female, mean age 52 years) with DTC (29 papillary and 4 follicular) treated with total thyroidectomy. All patients received a dose of 1110 MBq 131I for ablation purpose in hypothyroidism status (endogenous TSH 77± 41 mUI/l). Serum levels of thyroglobulin (Tg) and antithyroglobulin antibody were also determinated. Whole body scan (WBS) and SPECT/CT scan were performed 5 days after the administration of 131I ablation. WBS included anterior and posterior projections from the head to feet. SPECT/CT of the region of interest was performed with a low-dose protocol (80 mAs, 130 KV, pitch 0.85, slice thickness 5 mm) acquiring 128 projections/20sec, matrix 128x128. The data were reconstructed using an iterative method (8 iterations, 4 subsets) using CT for attenuation correction. Images were interpreted by 2 experienced nuclear medicine specialists. The following anatomic regions were analysed: thyroid bed (TB), lateral of the neck and distant from the neck. Any increased 131I foci were considered abnormal both for WBS and SPECT/CT scans. **Results:** WBS showed 64 foci: 53 in TB, 10 in the laterocervical región and 1 in the thorax. SPECT/CT showed 72 foci: 56 in TB, 12 in the laterocervical region and 4 extracervical. Regarding the 53 foci in the TB detected by WBS, SPECT/CT identified 29 foci in TB, 22 foci in thyroglossal duct (TD) and 2 foci in cervical adenopathy. In addition, SPECT/CT detected 5 new foci in thyroglossal duct. Regarding the other locations, SPECT/CT identified 10 foci in lateral of the neck, 1 foci in mediastinum and 3 foci in lung. Overall serum Tg levels were 6.72 ± 9.77 ng/ml (ranging from <0.5 to 38), without positive titles of thyroglobulin-antibodies. Tg levels in the 5 patients with only uptake in TB were 10.58 ng/ml, being 2.05 ng/ml in the 4 patients with only uptake in TD. **Conclusion:** Compared to WBS, SPECT/CT provided valuable information for precise localization of 131I foci after ablation (mediastinum vs lung, thyroid remnant vs cervical adenopathy). Hybrid technique identified more number of foci than planar WBS. The more frequent location of thyroid remnants was in the TD (41.5% of foci). **References:** None.

EP-0502

Incremental value of cervico-thoracic SPECT/CT over planar imaging in postablation 131I scintigraphy for thyroid cancer

W. Amouri, E. Yakoub, S. Charfeddine, I. Jardak, B. Khrouf, M. Maaloul, F. Hamza, F. Kallel, K. Chtourou, F. Guermazi;
Nuclear medicine department, Habib Bourguiba Hospital, Sfax, TUNISIA.

Aim/Introduction: In patients with differentiated thyroid carcinoma, postablation 131I scintigraphy aims to detect residual disease. However, planar whole-body scan (WBS) has some limitations, such as low sensitivity and lack of anatomic landmarks. The aim of this prospective study was to evaluate the added value of cervico-thoracic SPECT/CT over WBS in postablation 131I scintigraphy. **Materials and Methods:** We prospectively reviewed planar 131I WBS and cervico-thoracic SPECT/CT imaging in 23 patients (20 women and 3 men, aged between 12 and 68 years) who underwent postablation scintigraphy five days after the administration of a therapeutic activity of 100 mCi 131I for differentiated thyroid carcinoma. WBS and SPECT-CT data were blindly reviewed and scored benign, positive, or indeterminate with respect of specific territories: thyroid bed, cervical lymph nodes and distant metastases. **Results:** Planar scintigraphy showed cervical uptake in 14 cases (61%); cervical and thoracic uptake in 9 patients (39%). The average number of foci per patient was 3 (1-7). The scan was classified indeterminate in 14 patients (61%) due to the presence of at least one equivocal uptake foci located outside the thyroid bed, benign in 5 patients (22%) showing thyroid bed uptake and positive in 4 patients (17%) with lateral cervical uptake and /or thoracic uptake suggesting metastatic disease. SPECT / CT images reduced the number of indeterminate lesions from 61% to 9% by allowing a better characterization of equivocal foci. Moreover, SPECT/CT confirmed metastatic disease in the 4 patients with a positive WBS and revealed a tumoral mass located to the thyroid bed in one patient with benign WBS. The final diagnosis was suggestive of metastatic disease in 13patients (56%). **Conclusion:** 131I SPECT/CT improved planar data interpretation by accurate anatomic localization and characterization of radioiodine uptake foci, and precise differentiation between tumor lesions and physiologic uptake. This hybrid imaging modality would have an impact on therapy decision-making and subsequent management of patients with differentiated thyroid carcinomas. **References:** None.

EP-0503

FDG-PET-positive incidental thyroid nodules - clinical implications and the role of thyroid scintigraphy

M. H. Reichkendler[1], K. Korsholm[1,2], L. Alslev[1], P. Oturai[1];
[1]Department of Clinical Physiology, Nuclearmedicine and PET, Rigshospitalet Copenhagen University Hospital, Copenhagen, DENMARK, [2]Department of Clinical Physiology and Nuclear Medicine, Bispebjerg and Frederiksberg Hospitals, Copenhagen, DENMARK.

Aim/Introduction: Incidental thyroid nodules (ITN) are defined as nodules detected on imaging studies performed in a patient with no thyroid-related clinical symptoms or suspicion of thyroid disease. Due to increased use of imaging, ITN are discovered more frequently, as thyroid nodules are common in the general Danish population. Focally increased metabolism - as visualized by FDG-PET - has been associated with thyroid cancer, however the reported prevalences of thyroid cancer in patients with FDG-positive ITN is highly varying (5-30%). **Materials and Methods:** The study is a retrospective analysis of patients who underwent a diagnostic FDG-PET/CT at department of Clinical Physiology, Nuclear Medicine & PET, Rigshospitalet, from 1st of January 2010 to 31st of December 2011. All FDG-PET reports were screened, and cases mentioning focal or diffuse high FDG-uptake in the thyroid were identified. Approximately 10,000 FDG-PET scans were performed in that period at our center. Results of further diagnostic investigations (thyroid scintigraphy, ultrasound, blood-analyses) were registered, in addition to any results of cytological and histological examinations of the thyroid. **Results:** 145 patients with incidental FDG-uptake in the thyroid were identified: 78 focal, 28 multifocal and 39 diffuse. In 59 cases (41%) a clinical follow-up of the ITN was performed. In 78 cases no clinical follow-up of the ITN was performed, and eight cases could not be identified. A thyroid scintigraphy was performed in 39 cases of which 14 showed a hypo-functioning nodule, either solitary (11) or dominating a multinodular goiter (three). The remaining were either normal or with no signs of potential malignancy. Biopsy was performed in 24 cases; in one case cytology was suspicious of malignancy; there were four cases of follicular neoplasia, 16 cases with no cells suspicious of malignancy, one case with atypical changes, and two cases where the biopsies failed. Excision of a thyroid lobe was performed in seven subjects. Histology showed three cases with nodular colloidal goiter, three cases with follicular adenomas and one case with inflammation of the thyroid. The case where biopsy showed cells suspicious of malignancy, the histological examination demonstrated follicular adenoma. **Conclusion:** In 145 patients with FDG-positive ITN we found no cases of thyroid cancer. This is, however, not in concordance with the literature where up to 30% malignancy is reported. Our findings might be due to the fact that a large number of patients (59%) did not undergo further investigations of the thyroid, or reflect different demographic conditions. **References:** None.

EP-0504

How accurate is serum thyroglobulin measurement in patients with differentiated thyroid cancer?

M. Tuncel, T. Telli, M. Çağlar Tuncalı;
Hacettepe University, Ankara, TURKEY.

Aim/Introduction: Serum thyroglobulin measurement is the method of choice in the follow-up of patients with differentiated thyroid cancer. However the need for TSH stimulation and optimal Tg level for determination of recurrent/persistent

disease has been the subject of debate. The aim of this study is to evaluate the accuracy of serum TG measurements as an indicator of tumor recurrence in patients with differentiated thyroid cancer (DTC) **Materials and Methods:** Seventy-seven metastatic patients treated with surgery for DTC were included in the study. (mean age:48, F/M:44/33 Papillary/Follicular/Poorly differentiated thyroid carcinoma: 65/7/5). Patients had stimulated and suppressed Tg within two months without any therapeutic intervention. Suppressed Tg>0,2 ng/ml or stimulated Tg>1 ng/ml was accepted as recurrent/persistent disease as suggested by the American Thyroid Association's excellent response criteria (1). The presence of local or metastatic disease was confirmed with biopsy or follow-up imaging **Results:** Forty-one and 36 patients have local and metastatic disease respectively. Median stimulated Tg and suppressed Tg was higher for distant metastases when compared to local disease (15 vs 153 ng/ml and 0,6 vs 38,7 (p<0,001). The detection rate of suppressed Tg for the presence of local disease was lower compared to distant metastases (63% vs. 97%). The detection rate of stimulated Tg was 83% for local disease and 97% for distant metastases. Local disease which was missed by suppressed was mostly due to small volume disease, lymph node metastases with a median number of 1 (1-9) and size of 9 mm (5-15). However all of these lesions were detected by ultrasonography. In one patient both thyroglobulin measurements were unable to detect the presence of bone metastases which had faint radioiodine uptake. **Conclusion:** Although serum Tg is a useful marker for the detection of DTC, its sensitivity of the test in small volume disease is limited especially when performed without TSH stimulation. Neck ultrasonography improves the diagnostic accuracy in those patients **References:** Haugen BR, Alexander EK, Bible KC, et al. American Thyroid Association Management Guidelines for Adult Patients with Thyroid Nodules and Differentiated Thyroid Cancer: The American Thyroid Association Guidelines Task Force on Thyroid Nodules and Differentiated Thyroid Cancer. Thyroid. 2016 Jan;26(1):1-133.

EP-0505

Comparison of Ga68 PSMA PET/CT and FDG PET/CT Findings In a Case with Follicular Thyroid Cancer

***C. O. Engur**, T. Öneş, S. Kesim, N. Filizoğlu, S. Özgüven, K. Öksüzoğlu, S. İnanır, T. Y. Erdil, H. T. Turoğlu;*
Marmara University Pendik Training and Research Hospital, Istanbul / Pendik, TURKEY.

Aim/Introduction: Prostate Specific Membrane Antigen (PSMA) is a type-2 membrane protein produced by the prostate epithelium and can also be expressed by nonprostatic tissues such as proximal renal tubules, salivary glands and colonic crypt neuroendocrine cells. PSMA PET / CT is a widely used imaging modality for the diagnosis, staging and re-staging of prostate cancer. Increased PSMA expression can be observed in some malignancies such as neuroendocrine tumors, renal cell carcinoma, breast cancer, colon cancer and primary differentiated thyroid cancers except prostate cancer. In the literature Follicular thyroid cancer has been reported to show PSMA expression. A case with same diagnosis with negative I-131 whole body scan with Ga-68 PSMA positive pulmonary and lymphatic metastatic lesions have been also reported. In this case report FDG PET/CT AND Ga-68 PSMA PET/CT imaging findings were discussed in a patient who was diagnosed as Follicular Thyroid Cancer. **Materials and Methods:** A patient who was diagnosed as Follicular Thyroid Cancer and operated several times for skeletal and brain metastases with negative I-131 whole body scan (with high thyroglobuline levels) has undergone PET/CT examinations in the same week both with FDG and Ga-68 PSMA. **Results:** The findings of the PET/CT examinations are shown in the table. **Conclusion:** FDG PET/CT imaging is a useful diagnostic tool for patients who was diagnosed as Follicular Thyroid Cancer with negative I-131 whole body scans. However, FDG is a nonspecific tracer and accumulates also in sites of infection and inflammation. At this stage, Ga-68 PSMA PET/CT may be useful for the assessment of clinically suspicious malignant lesions. Imaging with Ga-68 PSMA PET/CT may be useful in Follicular Thyroid Carcinoma patients who had negative I-131 total body scans and demonstrate high thyroglobuline levels. **References:** None.

EP-0506

Usefulness Of Post Treatment SPECT/CT In Whole Body Scan For The TNM Re-Staging In Patients With Well Differentiated Thyroid Cancer (WDTC)

***A. Yepes Agudelo**, S. Prado Wohlwend, R. Sanchez Vaño, M. Agudelo Cifuentes, J. Bernal Vergara, A. Utrera Costero, P. Olivan Sasot, P. Bello Arques, B. Martínez Sanchís;*
Hospital La Fe, Valencia, SPAIN.

Aim/Introduction: Evaluate the usefulness of the SPECT/CT in the whole body scan (WBS) after treatment with 131-I for the TNM re-staging in patients with well differentiated thyroid cancer (WDTC) **Materials and Methods:** We reviewed 176 patients (117 women) with WDTC treated in our center since 01/03/17 until 31/03/18. All of them with post treatment distribution WBS. Mean age was 52 years (10-82), the patients were referred from 13 hospitals, 152/176 where first treatments. SPECT/CT was performed in 61/176 patients, with inconclusive WBS or with focal uptake not suggestive of thyroid remnant. The post-surgical TMN was re-staged based in our image findings **Results:** In 9/61 patients the SPECT/CT showed not typical uptake of thyroid remnant. All of them were first treatments. 3/9 patients showed laterocervical involvement that wasn´t diagnosed previous to surgery . They didn't received cervical lymphatic emptying and were staged as T1b (two of them) and T2 in the TNM. In them the SPECT/CT modified their recurrence risk by the ATA2015 criteria (low to mid) conditioning the changes in the treatment and follow up. 2/9 patients showed laterocervical involvement, when only central ganglionar disease was previously known. 1/9 patient showed unknown bone metastatic compromise. 2/9 patients showed persistent disease at ganglionar levels previously removed. 1/9 patient showed an important thyroid

uptake related with incomplete surgery, despite surgical report of total thyroidectomy. Globally, in 6/9 patients the SPECT/CT modified the post surgical TNM stage, and in 3/9 modified the recurrence risk stage by the ATA2015 criteria. **Conclusion:** The SPECT/CT after non conclusive WBS, showed great usefulness in the TNM re-staging and in the review of recurrence risk levels among the ATA standards. The three patients changing the risk recurrence level, were all low risk cases. In that patients the lymph node involvement, in the absence of 131I therapy, would not have been detected. **References:** None.

EP-0507

Incidental Findings in the Thyroid Gland in PET-CT Studies with 18F-FDG

S. Garcia Martinez, A. Baena García, M. De Bonilla Candau, M. Cruz Montijano, J. Rodriguez-Rubio Corona, M. Pajares Vinardell; Puerta del Mar University Hospital, Cadiz, SPAIN.

Aim/Introduction: To analyze the thyroid alterations which have been visualized in the PET-CT studies with 18F-FDG, as well as the relationship with the patient's base pathology and their therapeutic management. **Materials and Methods:** Retrospective study from March 2016 to March 2018, including 114 explorations of 105 patients (67 women and 38 men) between 26-86 years old. A PET-CT study was performed based on different oncological pathologies (breast, lung , colon, thyroid ...). The analyzed variables were: oncological history, the focality or heterogeneity of the uptake, the laterality of the thyroid finding, SUVmax values, if the findings were already known, the performance of complementary tests after PET, the pathological anatomy of the finding and their therapeutic management. **Results:** Of the 105 patients, 14 had a history of thyroid cancer (15 studies) after PET acquisition and 91 patients had other types of non-thyroid cancers. Regarding the type of uptake, in 31/114 studies, diffuse uptake of FDG was visualized; only 17 explorations were evaluated: 16 by ultrasonography or CT diagnosed of MNB and 1 case was diagnosed of nodular hyperplasia due to FNAB. In 82/114 studies (73 patients), thyroid hypermetabolic foci were visualized: 32 studies in the left lobe, 27 in the right lobe, 3 in the isthmus, 7 studies with bilateral nodules and the rest (13 studies) were collections in the post-thiroidectomy: 7/13 due to locoregional adenopathies of which only 2 studies were confirmed as pathological; and 6/13 on suspicion of recurrence or progression, 4 of them were confirmed after that.Of these 82 studies, only 3 were diagnosed with thyroid cancer from a previously unknown hypermetabolic thyroid nodule: one with a history of melanoma (LTI), another with colon cancer (LTI) and another with leiomyosarcoma of the uterus (LTD). Regarding the uptake of FDG in PET, the lesion with greater glycidic activity (SUVmax 108g / mL) corresponded to thyroid infiltration by follicular lymphoma. The rest of the studies had values of SUVmax 2.4 - 7.9g / mL in cases of diffuse uptake and SUVmax 1.3 - 47.8g / mL in focal uptake. **Conclusion:** The most frequent thyroid finding in PET studies was hypermetabolic nodules. Only 3 of 114 studies (2.6%) were confirmed as incidental thyroid cancer, the rest of them were benign or not assessed findings, but without changes after 2 years. The highest FDG uptake corresponded to thyroid infiltration by follicular lymphoma. **References:** None.

EP-0508

18F-FDG PET-CT In Patients With Thyroid Cancer: Our Experience

A. Peñaherrera Cepeda[1], P. García-Talavera San Miguel[2], F. Gómez Caminero[2], C. Riola Parada[2], J. Villanueva Curto[2], E. Martín Gómez[2], J. Cañadas Salazar[2], C. Achury Murcia[2], P. Tamayo Alonso[2]; [1]Medicina nuclear, Complejo asistencial universitario de Salamanca, Salamanca, SPAIN, [2]Medicina nuclear, Complejo asistencial de Salamanca, Salamanca, SPAIN.

Aim/Introduction: To evaluate our preliminary results in several indications of 18F-FDG PET/CT in patients with thyroid cancer. Calculating if there are significant differences in the values of thyroglobuline in patients with suspected recurrence with positive and negative PET and the optimal cut-off value for the best accuracy of the technique. **Materials and Methods:** Sixty one patients with thyroid cancer (49 papillary, 6 medullary, and 6 others) were included (32 men; mean age: 56 ± 14 years old). 18F-FDG PET-CT was performed in all patients from January 2015 to February 2019 (87 studies). The indications were: staging (4), restaging (13), follow up (14), treatment response evaluation (11) and suspected recurrence (45). Mann-Whitney test and ROC curve were performed. **Results:** In all of the cases of staging, PET/CT was positive, contributing with useful information in ¾. In restaging group, in 9 cases PET detected more disease than other tecniques, and the findings of the ultrasonography and CT were confirmed in two cases; in addition, there was a false positive result and one doubtful case. In the follow up group, progression was detected in 8 cases and stability of the disease in 6. In the treatment response evaluation group, progression was detected in 5 cases, parcial response in 3, and stable disease in 2; one case was not fit to be evaluated. In the suspected recurrence group, 19 were PET positive (11 with histological confirmation), 15 negative, and 11 doubtful cases. Comparing the levels of thyroglobuline, significant differences were observed between positive and negative PET/CT groups ($U=65$; $p<0.032$). In the ROC curve analysis (AUC=0.727), considering a thyroglobuline cut-off of 10,4 ng/ml, sensitivity of 76.5% and specificity of 71.4% were obtained. **Conclusion:** In our study, the usefulness of 18F-FDG PET/CT in several indications was confirmed. Considering a thyroglobuline cut-off value of 10,4 ng/ml, we obtained sensitivity of 76.5% and specificity of 71.4%. **References:** None.

EP-0509

Papillary Carcinoma of Thyroid Associted with Thyrotoxicosis

K. Kota, N. Pandit;
JIPMER, Pondicherry, INDIA.

Aim/Introduction: Coexistence of thyrotoxicosis and thyroid cancer is rare. Hyperthyroidism may present as diffuse toxic goitre (DTG), toxic multinodular goitre or autonomously functioning thyroid nodule. In this study we report a series of cases having hyperthyroidism with coexisting papillary carcinoma of thyroid. **Materials and Methods:** In this study we observed 4 adult patients who presented with anterior neck swelling and thyrotoxic symptoms. Biochemically they were hyperthyroid and they underwent thyroid scan as a part of patient clinical work up. Thyroid scan was acquired after administration of 5 mCi of Tc-99m pertechnetate. Spot images of the neck and mediastinum in anterior and anterior oblique views were acquired after 20 minutes. Thyroid scan of 3 cases showed autonomously functioning thyroid nodule (AFTN) and they were planned for radio iodine ablation. Before giving therapy they underwent screening USG neck where suspicious hypo echoic nodules were found. FNAC from these nodules showed Bethesda category V and VI lesions. These three patients underwent total thyroidectomy along with central compartmental lymph nodal dissection. One patient biopsy is pending hence excluded from the study and in other two post-operative biopsy were reported as classical variant of papillary carcinoma of thyroid.Another patient's thyroid scan showed diffuse toxic goitre with no hypo-functioning areas. In view of gross thyroid swelling extending almost up to sternal notch, CT scan of neck was done, which showed tracheal compression. As tracheal compression was present, the patient underwent total thyroidectomy and post-operative biopsy came out as multifocal papillary carcinoma. **Results:** Out of 4 thyrotoxic cases reported, 3 had AFTN and 1 had DTG on thyoid scan. Histopathologically all these patients had papillary carcinoma of thyroid. According to the literature, carcinomas found in most of the AFTN's are either follicular carcinoma or follicular variant of papillary carcinoma. Here we have classical variant of papillary carcinoma along with AFTN which is a rare presentation. **Conclusion:** Thyroid carcinoma in thyrotoxicosis will alter the patient management hence careful clinical evaluation with ultrasound and FNAC may be necessary in selected cases. **References:** None.

EP-0510

Incidental discovery of thyroid cancer in scintigraphic studies of patients with hyperparathyroidism

V. Rodriguez Morales, B. Nuñez de De Oliveira, F. Loira Bamio, J. Muñoz, A. Renda, C. Martínez, D. Ruiz;
Hospital do Meixoeiro, Vigo, SPAIN.

Aim/Introduction: to assess the presence of thyroid cancer as an incidental discovery in patients with hyperparathyroidism that have discrepant MIBI/pertechnetate uptake in the scintigraphic study. **Materials and Methods:** a retrospective study was conducted using the medical histories and scintigraphic images of patients with hyperparathyroidism from January 2011 to January 2019. There were 47 cases selected that were studied with double-phase and double radiotracer parathyroid scintigraphy, with a dose of 740MBq of 99mTc MIBI and 185MBq of 99mTcO4, acquiring early images with MIBI (10 minutes) and late images (2 hours) with both radiotracers of the cervical region in anterior and anterior obliques projections with Pin-Hole collimator, which presented as a characteristic finding an area of hyper-uptake with MIBI and concordant hypocaptant image in the thyroid study; subsequently they underwent surgery (parathyroidectomy + total thyroidectomy / hemithyroidectomy) as definitive treatment. Patients who did not have post-surgical anatomopathological result were excluded. **Results:** once the exclusion criteria was applied to the 47 studies selected, the sample consisted of 33 patients, of whom 84.85% were women and 15.15% men, with an average age of 61 years (range from 38 to 87). The prevalence of multinodular goiter was observed in 96.97% of the cases studied. It was evidenced as a fortuitous discovery in the anatomopathological study of the surgical piece excised a papillary microcarcinoma in 9/33 patients (27.28%), of which 8 were women; coinciding the location of the tumor lesion with the same thyroid lobe in which the scintigraphic finding was observed in 5/9 patients (55.56%), while in the rest of the cases, the location of the lesion was contralateral. **Conclusion:** - Double-phase and double radiotracer parathyroid scintigraphy is a technique that allows the concomitant assessment of thyroid and parathyroid glands, without significant increase in exploration time and with low doses of radiation. - A scintigraphic pattern with MIBI /pertechnetate discrepant uptake in the presence of multinodular goiter could be considered an indirect data of underlying malignant thyroid pathology, highlighting the importance of expanding studies in these patients.- Due to the small size of the sample, it would be advisable to carry out new studies with a larger number of patients, in order to increase the evidence in favor of these findings. **References:** None.

EP-0511

Integrative Analysis Of Glucose Metabolism Signatures and Differentiation Of Thyroid Cancer: Diagnostic and Therapeutic Implications

H. Suh, H. Choi, J. Paeng, G. Cheon, J. Chung, K. Kang;
Seoul National University Hospital, Seoul, KOREA, REPUBLIC OF.

Aim/Introduction: F-18 fluorodeoxyglucose (FDG) PET and iodine scan of thyroid cancer have been clinically used based on the principle of loss of iodine uptake and increased glucose metabolism according to the dedifferentiation. However, understanding of their genomic background is lacking. We investigated the association between glucose metabolism and differentiation by using transcriptome data of advanced thyroid cancer as well as papillary thyroid cancer (PTC). **Materials and**

Methods: We used the RNA sequencing of PTC obtained from the Cancer Genome Archives and microarray data of poorly-differentiated and anaplastic thyroid cancer (PDTC/ATC). The signatures of GLUT and glycolysis were estimated to assess glucose metabolic profiles. The glucose metabolic profiles were associated with tumor differentiation score (TDS) and BRAFV600E mutation status. In addition, the survival analysis of glucose metabolic profiles was performed for predicting recurrence-free survival. **Results:** In PTC, the glycolysis signature was significantly correlated with TDS, while the GLUT signature was inversely correlated with TDS. The correlations were significantly stronger in BRAFV600E negative group than positive group. On the contrary, two glucose metabolism signatures were negatively correlated with TDS in PDTC/ATC. The high glycolysis signature was significantly associated with poor prognosis in PTC. The glycolysis signature was associated with recurrence-free survival independent of other clinicopathologic features. **Conclusion:** The glucose metabolic profiles are intricately associated with tumor differentiation in PTC and PDTC/ATC. In addition, as glycolysis was an independent prognostic marker, we suggest that the glucose metabolism features of thyroid cancer could be another progression marker different from differentiation and provide implications for risk stratification and therapeutic plan. **References:** None.

EP-0512

Correlation of mRNA-TSHR and mRNA-Tg with radioiodine whole body scan and ultrasound findings in thyroid carcinoma patients

T. Makazlieva[1], *O. Vaskova*[1], *T. Tripunoski*[1], *S. Stojanoski*[1], *N. Manevska*[1], *S. Risteski*[2], *H. Jovanovic*[2], *Z. Jakovski*[2], *A. Eftimov*[3];
[1]*Institut of pathophysiology and nuclear medicine, Skopje, NORTH MACEDONIA,* [2]*Institut for forensic medicine, criminology and medical deontology, Skopje, NORTH MACEDONIA,* [3]*Institut of pathology, laboratory of molecular pathology, Skopje, NORTH MACEDONIA.*

Aim/Introduction: Evolution of the differentiated thyroid carcinomas (DTC) is monitored mainly through evaluation of serum thyroglobulin (Tg), neck ultrasound (US) and whole body scan (WBS). Objective in our study was to evaluate the expression of TSHR-mRNA and Tg-mRNA in patients with DTC and to correlate the expression of the two transcripts with the findings from the WBS and neck US. **Materials and Methods:** Forty patients with DTC were included in the study. Neck US and WBS after radioiodine were performed and according detected progression or only remnant tissue presentation, findings were marked with gradual increase in the score. Total RNA was isolated from peripheral blood and used for two-step reverse transcriptase-polymerase chain reaction (rt PCR) with appropriate primers. Relative quantification using the ΔCt value, or difference between target gene and housekeeping gene was applied. Statistical analysis was performed with Spearman Rank Order Correlation. **Results:** We found significant negative correlation between ΔCt (Ct_{TSHR} - Ct_{GAPDH}) value and WBS/US findings (R= - 0,321; p<0,05) and also for ΔCt = (Ct_{Tg} - Ct_{GAPDH}) and WBS/US (R = -0,382, p<0,05), meaning that lower value of ΔCt for both genes, or higher expression of both transcripts, correlated with advanced disease findings either on US or WBS. **Conclusion:** Our data revealed moderate significant correlation between higher expression of TSHR-mRNA and Tg-mRNA with progression of the disease. Further studies with larger number of subjects are needed for understanding the real meaning of TSHR-mRNA and Tg-mRNA as biomarkers in DTC. **References:** None.

EP-0513

Treatment of Radio Iodine-Refractory well Differentiated Thyroid Carcinoma: Impact of PET-FDG on Decision Making

E. Lodi Rizzini[1], *E. Tabacchi*[1], *A. Farolfi*[1], *A. Morganti*[2], *F. Monari*[2], *S. Fanti*[1];
[1]*Nuclear Medicine Unit, S. Orsola-Malpighi University Hospital, Bologna, ITALY,* [2]*Radiation Oncology Center, S.Orsola-Malpighi Hospital, Bologna, ITALY.*

Aim/Introduction: the prognostic value of PET-FDG in non-avid-iodine well differentiated thyroid cancer(DTC) has been demostrated in literature with introduction of quantitative data such as SUVmax,SUVmean,metabolic tumor volume (MTV), total lesion glycolysis(TLG) which seem to correlate with progression-free-survival (PFS),overall survival (OS). PET-FDG can be a useful tool to avoid further toxic /ineffective radioiodine (RAI) courses and to select patients candidate to emerging systemic therapy such as TKI. **Materials and Methods:** we retrospectively evaluated 53 patients (pts) with well DTC treated with at least two RAI courses and that underwent PET-FDG-scan after a second RAI course (March 2012-May 2018)for suspect non-radioiodine-avid-lesion (negative/partial positive Rx-WBS-scan and high Thyroglobulin levels). We selected 19/53pts with positive PET-FDG scan after the second RAI course, with at least one hypermetabolic lesion. For each hypermetabolic lesion we calculated SUVmax, SUVmean, MTV,TLG. The follow-up of all pts(>=1year), clinical and laboratory data were collected . PFS was calculated. Students T-test was used to compare the means of the continuous variables calculated. **Results:** we included 19pts (mean age 56-years; 12F,7M). 62% of DTC were non aggressive histological types. 2/19pts were pT1, 1/19 was pT2, 11/19 were pT3,5/19 were pT4, 4/19 were pN0, 14/19 were pN1, 1/19 was pNx and 3/19 were M1. Rx-WBS after the second RAI course was negative in 8/19pts(42%). Positive PET-FDG uptake was observed in neck lymph nodes (53%), lung (26%) or in bone metastases (21%). 9/19 (47%) of the patients had a progression disease after the last therapeutic approach suggested by PET-FDG scan and 10/19 (53%) patients had a stable disease.Based on positive PET scan, therapeutic approaches were external-beam-radiation-therapy in 5/19pts (26%), surgery in 4/19(21%), observation in 9/19(48%), another RAI course in 1patient. Mean PFS of progression disease group and stable disease group were respectively 6 and 26.6 months. Mean TLG values were

significantly different between stable disease and progression disease group (p=0.045). No statistical significant differences between the other continuous variables(SUVmax, SUVmean, MTV)and PFS were found. **Conclusion:** PET-FDG guides us to decide the best therapeutic approach in pts with iodine-refractory disease, particularly in the case of high metabolic tumor burden disease, also to avoid further ineffective and toxic RAI courses. In our study more pts/follow-up are needed to find significant correlations between different metabolic parameters and PFS and to create prognostication-algorithms for pts with worse prognosis. **References:** Prognostic value of FDG-PET CT metabolic parameters in metastatic-radioiodine-refractory differentiated thyroid cancer. Manohar at al. ClinNuclMed2018; 43:641-647.

EP-0514

Is F-18 Fluorodeoxyglucose Positron Emission Tomography Useful In Thyroid Papillary Cancer With Positive Follow-up Radioiodine Scan And Elevated Serum Thyroglobulin Level?

J. Oh[1], *J. Seo*[2], *S. Bae*[1], *H. Kim*[1], *J. Bae*[1], *H. Jeong*[1], *W. Chang*[1], *H. Yoon*[1];
[1]*Raphael Hospital, Daegu, KOREA, REPUBLIC OF,* [2]*Daegu Fatima Hospital, Daegu, KOREA, REPUBLIC OF.*

Aim/Introduction: It has been well established that F-18 fluorodeoxyglucose PET/CT is useful for the detection of persistent or recurrent thyroid papillary cancer with negative follow-up radioiodine whole body scan (FUWBS) but increased serum thyroglobulin (Tg) level. We have investigated whether the PET/CT is also useful in thyroid papillary cancer with positive FUWBS finding and elevated serum Tg level. **Materials and Methods:** The patients who have undergone PET/CT due to elevated Tg level (> 2 ng/mL) at the time of FUWBS, were enrolled. All patients have been initially diagnosed with thyroid papillary cancer, and treated with total thyroidectomy and single radioiodine ablation therapy previously. A final diagnosis of persistent or recurrent disease has been confirmed with pathological evaluation or clinical and imaging follow-up. We compared the diagnostic performance of Tg and PET/CT in all patients. We have also compared the diagnostic performance of PET/CT in FUWBS-positive and FUWBS-negative groups. **Results:** The 41 eligible patients included 14 patients with positive FUWBS finding and 27 patients with negative FUWBS finding. A total of 14 out of 41 patients including five out of 14 FUWBS-positive and 9 out of 27 FUWBS-negative cases have been diagnosed with persistent or recurrent disease. The disease location involved thyroid bed in 1 patient, lateral neck in 10 patients, and lung in 3 patients. The sensitivity, specificity, positive predictive value (PPV), negative predictive value (NPV), and accuracy of PET/CT have been significantly higher compared with Tg (79, 85, 73, 88, and 83%, respectively, for PET/CT vs. 71, 52, 43, 78, and 59%, respectively, for Tg >7.11 ng/mL, P = 0.023). In subgroup analysis, the sensitivity, specificity, PPV, NPV, and accuracy of PET/CT in FUWBS-positive patients were comparable to those of FUWBS-negative patients (60, 89, 75, 80, and 79%, respectively, in FUWBS-positive vs. 89, 83, 73, 94, and 85%, respectively, in FUWBS-negative cases, P = 0.498). In the five FUWBS-positive cases with persistent or recurrent disease, all the radioiodine-positive lesions have been confined to the central neck, whereas malignant lesions have been located in the lateral neck or lung, which were not detected by FUWBS. **Conclusion:** PET/CT is useful for the detection of persistent or recurrent thyroid papillary cancer in patients with elevated serum Tg level regardless of FUWBS finding. **References:** None.

EP-0515

Utility of Radioactive Iodine ^{125} Seed as preoperative method for localization of cervical thyroid cancer recurrence

T. Cambil Molina, T. Martín Hernandez, C. Marín Velarde, J. Terron Leon, P. De la Riva Perez, J. Garcia Gomez, C. Calvo Morón;
Virgen Macarena University Hospital, Sevilla, SPAIN.

Aim/Introduction: The use of radioactive seeds (RSL)has recently been published for the localization of lesions in patients with recurrence or persistence of thyroid cancer.Our group wanted to evaluate its usefulness to improve the surgical result in patients re-operated of cervical metastasis of thyroid cancer. **Materials and Methods:** Six patients with papillary thyroid cancer (5/1 F/M) with a mean age of 54.5 years (43-68) with cervical lymphatic involvement due to recurrence/persistence evidenced by ultrasound and confirmed were studied, submitted to new surgical intervention with eradicating purpose. In the days prior to surgery an I-125 seed was placed, under aseptic conditions, in the target adenopathy using an 18G needle guided by ultrasound by an endocrinologist with experience in this disease Its correct position was verified by a radiation detector. In operating room, we used a gamma probe Navigator GPS) and a portable gamma camera (Oncovision Sentinella 102®) to detect the activity point in order to identify better approach for the suspicious lymph node. We locate this point within the surgical field, removing the target tissue and verifying that the seed was included in the excised tissue.An analysis of surgical procedure time, lesion localization as well as seed activity,radioactive exposure, advantages for the surgeon and degree of surgical resection were performed. **Results:** All the marked nodes were positive in histology. In 2 cases, it was necessary to perform flocculation of the adenopathy with physiological serum to isolate it from critical structures (carotid, recurrent nerve).The mean duration of the sonographic insertion procedure was 11±3,4 minutes.Time of placement prior to surgery was 4,3 days (3-7) and the average operating room time was 45(15-120) minutes. In our six patients we found 13 metastatic lymphadenopathies of 42 excised with an average nodal index of 0,69.The average maximum diameter of the histological specimen was 12,5±6.05 mm. The mean activity of the implanted seed was 65,53±21.1 (42,8-10) 5microCi.The level of Tg: 2,52±1,62 (0,2-3,98 ng/dl) significant decreased

after surgery a 0,15±0,13(0,04-0,36 ng/dl), p< 0.01 without positive antithyroglobulin antibodies.Tg stimulated in one case reached 4,3 ng/dl, and the other 5was <0,8 ng/dl.There were no complications or seed migration in any case. **Conclusion:** The initial experience of the introduction of the RSL in our unit has shown benefits for surgeons in the treatment the patients with repeated surgeries, it is been a safe and uncomplicated procedure, shortening the surgical time and improving the programming of the operating room activity. **References:** None.

EP-0516

Radioactive Iodine^{125} Seed as preoperative method for localization of cervical thyroid cancer lymphadenopathy. Preliminary results

T. Cambil Molina, *T. Martín Hernandez, J. Terrón León, C. Marín Velarde, P. De la Riva Perez, M. Molina Mora, I. León-Asuero Moreno, C. Calvo Morón;*
Virgen Macarena University Hospital, Sevilla, SPAIN.

Aim/Introduction: The use of radioactive seeds (RSL) has recently been published for the localization of lesions in patients with recurrence or persistence of thyroid cancer. Our group wanted to assess its performance in our hospital in order to improve surgical procedures on thyroid surgery. **Materials and Methods:** We studied four patients with differentiated thyroid cancer (3 papillary and 1 follicular carcinoma) with a mean age of 55 years (34-69) with only one clinical and ultrasound lateral cervical lymphatic involvement (diagnosed by cytology or Tg-FNAB) that had been programmed total thyroidectomy plus cervical lymphadenectomy. In the days prior to surgery, an I-125 seed was placed, under aseptic conditions and under local anesthesia, in the target adenopathy using an 18G needle guided by ultrasound by an endocrinologist with experience in the follow-up of thyroid cancer. Its correct position was later verified by a radiation detector. In operating room, we used a gamma probe (Navigator GPS®) and a portable gamma camera (Oncovision Sentinella 102®) to detect the activity point in order to identify the suspicious lymph node. We locate this point within the surgical field, removing the target tissue and verifying that the seed was included in the excised tissue. An analysis of surgical procedure time (complete lymphadenectomy), lesion localization as well as seed activity, radioactive exposure, advantages for the surgeon and degree of surgical resection were performed **Results:** All the marked nodes were positive in histology. Time of placement prior to surgery was 3.5 days (1-7) and the average operating room time was 44.25(32-65) minutes. In our four patients we found 8 metastatic lymphadenopathies of 54 excised with an average nodal index of 0,14±0,07. The maximum diameter of the histological specimen was 16±6.97 mm. The mean activity of the implanted seed was 73.2± 20.8 (43-89.9 microCi). In the implants performed, the average dose rate in contact and at a 1 meter from the patient, were 10.9 and 0.446 µSv/h, respectively (with a median of 7.2 and 0.4 µSv/h) In the three papillary carcinoma post surgery thyroglobulin levels were undetectable (< 0,11 ng/dl with negative antithyroglobulin antibodies). There were no complications or seed migration in any of the cases. **Conclusion:** The initial experience of the introduction of the RSL in our unit has shown benefits for the patients and surgeons and it is a safe and uncomplicated procedure, shortening the surgical time and improving the programming of the operating room activity. **References:** None.

EP-0517

Preliminary results of surveillance role of serum thyroglobulin without TSH-stimulation measured by an ultrasensitive kit : a prospective study

H. Kim[1], *S. Ha*[1], *Y. Park*[1], *J. Paeng*[1], *K. Kang*[1], *D. Lee*[1], *J. Chung*[2], *G. Cheon*[1];
[1]*Seoul National University Hospital, Seoul, KOREA, REPUBLIC OF,* [2]*National Cancer Center, Goyang, KOREA, REPUBLIC OF.*

Aim/Introduction: In papillary thyroid carcinoma (PTC), serum thyroglobulin (Tg) is routinely measured as a reliable tumor marker after surgery and ablation. Recently, second generation of immunoradiometric assay (IRMA) was developed to detect Tg with higher sensitivity of less than 0.1 ng/mL. The purpose of this study was to evaluate the possibility of basal ultrasensitive Tg (uTg) measured with new uTg IRMA to estimate clinically relevant thyroid-stimulating hormone (TSH)-stimulated Tg values and to validate adequate cut-off value of basal uTg for prediction of positive stimulated Tg levels. **Materials and Methods:** A total of 98 PTC patients were prospectively enrolled to measure paired sera of basal and TSH-stimulated Tg with two IRMA kits, RIAKEY Tg IRMA (Tg-RIAKEY) and Dynotest Tg-plus (Tg-plus). Reliability of the uTg kit, Tg-RIAKEY was evaluated in comparison with the conventional Tg (cTg) kit, Tg-plus. For the functional sensitivity of each kit, sensitivity, specificity, positive predictive value (PPV), and negative predictive value (NPV) were assessed in prediction of positive stimulated Tg. Optimal cut-off value of basal Tg was calculated from receiver-operating curve. **Results:** Tg-RIAKEY showed highly concordant results in comparison with Tg-plus (intraclass correlation coefficient, 0.931, P <0.001). The sensitivity, specificity, PPV, and NPV of Tg-RIAKEY with functional sensitivity cut-off value of 0.35ng/mL, were 73%, 77%, 52%, and 89% for positive stimulated Tg level over 1ng/mL. The optimal cut-off values for detecting positive stimulated Tg level of 1ng/mL were 0.35 ng/mL and 0.1 ng/mL for Tg-RIAKEY and Tg-plus, respectively. **Conclusion:** Basal uTg measured with the new IRMA kit may be used to predict positive levels of stimulated Tg during routine follow-up of PTC based on its high NPV, avoiding the inconvenience of TSH stimulation. **References:** None.

EP-0518

Evaluating Focal 18F-FDG Uptake In Thyroid Gland With Radiomics

A. Aksu, *N. P. Karahan Şen, G. Çapa Kaya;*
Dokuz Eylül Üniversitesi, Izmir, TURKEY.

Aim/Introduction: The aim of this study was to evaluate the ability of 18F-FDG PET/CT texture analysis to predict

the exact pathological outcome of thyroid incidentalomas. **Materials and Methods:** 18F-FDG PET/CT images between March 2010 and September 2018 were retrospectively reviewed in patients with focal 18F-FDG uptake in the thyroid gland and who underwent fine needle aspiration biopsy from this area. The focal uptake in the thyroid gland was manually drawn in 3D with 40% SUVmax threshold. Features were extracted from VOI using the LifeX package. Conventional, first and second order features were calculated from drawn ROI. The features obtained were compared in benign and malignant groups, statistically significant variables were evaluated by ROC analysis. The correlation between the variables with AUC value over 0.7 was examined; variables with correlation coefficient less than 0.7 were evaluated by logistic regression. **Results:** Forty-two patients (22 women) were included in the study. There was an average of 99.1 days between the PET/CT scan and the fine needle aspiration biopsy. Twenty of the patients (47.6%) had malignant pathology. The rates of malignancy were 65% and 31.8% in males and females, respectively; there was a statistically significant difference between males and females (p: 0.032). In univariate analysis, a statistically significant difference was observed in 6 conventional parameters, 5 first and 20 second order features between benign and malignant groups (p <0.05). The feature with the highest benign-malignant discriminating power was $GLRLM_{RLNU}$. When the cutoff was 68.6, the sensitivity , specificity , PPV , NPV and accuracy were 75%, 90.9%, 88.2%, 100% and 83.3%, respectively (AUC: 0.827, 0.693-0.962, 95% CI). A multivariate logistic regression analysis that included $GLRLM_{RLNU,}$ SUVmax and gender was performed to predict definitive pathology result (the stepwise regression method was used). Gender and $GLRLM_{RLNU}$ significantly contributed to the logistic model. Sensitivity, specificity, PPV, NPV and accuracy of the model in benign-malignant differentiation were calculated as 95%, 77.3%, 79.2%, 85% and 85.7%, respectively (AUC: 0.898, 95% CI 0.794-1.000). **Conclusion:** It is thought that, 18F-FDG PET/CT texture analysis may be useful in predicting the benign-malignant distinction of focal involvement in the thyroid gland and may prevent unnecessary biopsies in patients. Prospective studies with larger patient groups are needed. **References:** 1-Nioche C, Orlhac F, Soussan M, Boughdad S, Alberini J, Buvat I. A software for characterizing intra-tumor heterogeneity in multimodality imaging and establishing reference charts. Eur J Nucl Med Mol Imaging. 2016;43:S156-S157.

EP-33

Clinical -> Diagnostic study -> Paediatric study -> Benign (Diagnostic)

October 12 - 16, 2019 e-Poster Area

EP-0519

Benefits of hybrid CT-urography and dynamic nephroscintigraphy in children with obstructive uropathy

S. Kukushkina*, D. Fomin, A. Pavlov, O. Lugay, Y. Blanter;*

Federal State Budgetary Institution Russian Scientific Center of Roentgenoradiology, Moscow, RUSSIAN FEDERATION.

Aim/Introduction: Ultrasound and excretory urography can determinate obstructive uropathy reason less than in 50% cases. The CT-urography cannot be used routinely because of increased radiation dose. The hybrid CT-scintigraphy is based on the similarity of radiolabeled MAG3 and contrast agent kinetics. That allows continuous tracking of radioactive label via the urinary tract (UT) and when radiotracer appears in the zone of interest one (rarely two) directional CT-scans are performed. Therefore, one of CT-scintigraphy advantages is a radiation exposure declining several times. **Materials and Methods:** The study included 44 children, who underwent standard diagnostic protocol examinations: ultrasound examination of the kidneys, ureters and bladder, excretory urography and dynamic nephroscintigraphy, however the violation nature was undetermined. Patients were divided into two groups based on hybrid CT-scintigraphy data: 24 - hydronephrosis and 20 - ureterohydronephrosis. Administered activity of MAG3 was calculated according to the patience age (80-140 MBq), contrast volume —1,0-1,6 ml/kg. Both were administered simultaneously. The tracer transit was monitored continuously. In children with ureterohydronephrosis we used a single CT-scan, time-synchronized with tracer appearance in the ureterovesical anastomosis projection. The study was performed on the empty bladder. In patients with hydronephrosis, if renal calculi were suspected we performed a native CT-scan. If there were suspicion of a vascular anomaly according to ultrasonography the study was supplemented with the vascular phase. All investigation results were verified intraoperatively. **Results:** The hydronephrosis causes were ureteral-ureter segment stricture, calculus of ureteropelvic segment and renovascular conflict; ureterohydronephrosis - first two. Excretory urography had low informative visualization of renal calculi, ureteropelvic segment with contrast stasis or ureterovesical anastomosis when it shielded by contrast-filled bladder. Ultrasonography had low informative value determining stricture without ureter dilatation. Gas interposition in intestin and inability obtaining tight bladder filling blocked ureterovesical anastomosis visualization. CT-scintigraphy required one or two (bilateral defeat, obstruction severity) CTscans to established urodynamics violation causes. Average CT-scans number for all patients - 1.21. For differential diagnosis of obstruction nature the radiolabels transit through the UT was evaluated by a physiological evacuation test instead of delayed CT-scan. All obstructive causes, established by CT-scintigraphy, where confirmed intraoperatively. Average CT-scintigraphy effective dose over the entire examination period was 4,68±1.1 mSv what was less than in excretory urograpfy by 1,8±0,6 mSv, and in CT-urography by 4,8±1.1 mSv. **Conclusion:** Hybrid CT-scintigraphy can provide high quality of abnormal anatomical structure and functional state of urinary system visualization throughout all UT with reduced radiation dose. **References:** None.

EP-0520

Studying Fever of Unknown Origin in a 16-years old girl with 18-F FDG PET/CT

M. Gavra[1], *I. Sevaslidou*[2], *A. Malama*[1], *D. Verganelakis*[2], *G. Pitsoulakis*[1], *M. Chassiotou*[1];
[1]*Radiology, CT & MRI, Athens, GREECE,* [2]*Nuclear Medicine Department, Athens, GREECE.*

Aim/Introduction: Fever of unknown origin (FUO) along with unexplained sings of inflammation can be unresolved medical problems. FUO can be generated by either infection, or malignancies, or inflammatory diseases. This study demonstrates the usefulness of Fluorine-18fluoro-2-deoxy-d-glucose ([^{18}F] FDG)position emission tomography (PET/CT) towards diagnosis of FUO in a 16-years old girl. **Materials and Methods:** We report the case of a 16 year old girl presenting with high temperature (38,5ºC)of the last two months. No clear infection was neither diagnosed, nor peripheral lymphadenopathy, nor palpable hepatosplenomegalia. Laboratory tests revealed an increaseof inflammation markers ESR:85, LDH:274, CRP:15. Therefore, patient waschecked for: hepatitis, TOXO IgM/IgG, CMV IgM, EBV IgM, Wright, Mantoux, Ag Pl, laveran, immunoglobulins IgA/IgM/IgG. All indices were negative. Also, blood tests were normal, as well as tests for Listeria/Leismania were negative. Chest X-ray, CT-Thorax and US-heart provided no pathological findings. Abdomen CT and MRI showed splenomegalia and multiple lesions in the splenic parenchyma, in agreement with the abdominal US. Antibiotic therapy consisting of vancomycin and meropenem was prescribed, generating mildly decline of inflammation markers but no fever recession. Finally, a 18-F FDG PET/CT examination was performed as a last attempt to resolve the issue. The PET/CT demonstrated an increased uptake (SUVmax: 13,5) in the multiple focal lesions within the splenic parenchyma. A mild uptake (SUVmax:2,4) in small cervical, parasternal and inguinal lymph nodes was also noted. More important, multiple subcutaneous nodules at the lower extremities demonstrated hypermetabolic SUV values (SUVmax: 2,3).The above findings were attributed to inflammatory-granulomatous disease, with a minor probability of lymphoma. A spleen biopsy showed necrotizing granulomatous inflammation due to either mycobacterium of tuberculosis, or bartonellosis, or brucellosis and it excluded malignancy. Further tests, excluded tuberculosis and brucellosis. Finally, the Polymerase Chain Reaction (PCR) did not show bartonellosis, however immunoglobulin IgM was positive. **Results:** Considering the imaging findings by PET/CT & US and the laboratory results our patient was treated successfully for bartonellosis. **Conclusion:** The 18-F FDG PET/CT can be a valuable diagnostic non-invasive tool for the evaluation of fever of unknown origin in children. **References:** None.

EP-0521

Ectopic Thoracic Kidney

N. Filizoglu, *S. Özgüven, S. Kesim, C. Ö. Engür, K. Öksüzoğlu, T. Öneş, S. İnanır, H. T. Turoğlu, T. Y. Erdil;*
Marmara University Istanbul Pendik Education and Research Hospital, Istanbul, TURKEY.

Aim/Introduction: is a rare congenital anomaly and accounts for less than 5% of all renal ectopia. Intrathoracic kidneys are divided into four groups as intrathoracic renal ectopia with eventration of the diaphragm, closed diaphragm, diaphragmatic hernia and traumatic rupture of the diaphragm with renal ectopia. In this case report, a rare case of thoracic kidney with coexisting diaphragma eventration and herniation was presented. **Materials and Methods:** A 10-month-old girl patient whose left kidney was not seen in normal anatomic region on abdomen and pelvis ultrasonography was referred to Tc99m DMSA scintigraphy. **Results:** Tc-99m DMSA scintigraphy showed a normal localized right kidney with normal parenchymal function but no Tc99m DMSA uptake compatible with functional renal parenchyma was detected in the left renal region. Whereas left kidney with normal parenchymal function in the area compatible with the left hemithorax was noted in anterior posterior planar views of Tc99m DMSA scintigraphy. After static renal scan patient underwent thoracic CT and it revealed left hemidiaphragm eventration and thoracal herniation of the left kidney from the posterolateral defect (Bochdalek hernia). **Conclusion:** Thoracic renal ectopia is often asymptomatic and an incidentally recognized anomaly. It is suggested that delay in caudal migration of mesonephric tissue often leads to thoracic kidney. Thoracic ectopic kidneys usually have normal renal contours and collecting systems and Tc-99m DMSA scintigraphy enables the evaluation of the function of the incidentally detected thoracic ectopic kidney. In our case, the diagnosis of thoracic ectopic kidney which is a rare anomaly demonstrated by Tc-99m DMSA scintigraphy in a patient with unilateral renal agenesis reported in abdominopelvic USG. **References:** None.

EP-0522

Incremental value of intestinal transit scintigraphy in children with functional constipation

M. Pizzoferro[1], *R. Tambucci*[2], *M. F. Villani*[1], *T. Caldaro*[2], *P. De Angelis*[2], *F. Fusaro*[3], *M. C. Garganese*[1];
[1]*Nuclear Medicine Unit, Bambino Gesù Children's Hospital-IRCCS, Rome, ITALY,* [2]*Digestive Endoscopy and Surgery Unit, Bambino Gesù Children's Hospital-IRCCS, Rome, ITALY,* [3]*Department of Medical and Surgical Neonatology, Newborn Surgery Unit-IRCCS, Rome, ITALY.*

Aim/Introduction: Functional constipation (FC) is clinically diagnosed according to Rome IV criteria. However, in children experiencing symptoms despite conventional medical therapy, additional diagnostic tests should be considered to detect a possible underlying organic cause and tailor treatment. Colonic transit time (CTT) measurement can provide initial information to distinguish normal transit from rectosigmoid outlet obstruction (ROO) and slow-transit constipation

(STC). Despite colonic scintigraphy is considered as the most sensitive noninvasive method for the evaluation of colonic motility disorders its use in pediatric patients is far from routine and remains limited to few specialized centers. Aim of this retrospective study was to evaluate the clinical impact of colonic transit scintigraphic studies in children with FC. **Materials and Methods:** A retrospective chart review of children with FC, with or without soiling, unresponsive to standard medical treatment who underwent CTT with scintigraphy between 2016 and 2018 at Bambino Gesù Children's Hospital in Rome, Italy. ^{67}Ga citrate radiolabeled semiliquid meal was administrated. After a standard gastric emptying study, abdominal static images were acquired at 1-3-6-24-48-72 until 144 hours. Visual analysis and calculation of total transit time were performed. Classification was according to criteria based upon visual analysis: 1- NTT (normal transit time): nearly complete rectal emptying at 72 hours; 2- ROO: normal progression from right to left colon with radioisotope retention into the rectosigmoid colon at 72 hours; 3- STC: retention of radioisotope throughout the colon with failure of the activity to progress beyond the sigmoid colon at 72 hours. **Results:** Scintigraphy data were obtained from 45 constipated children (M/F, 23:22; median age 11.5 y [1-18 y]). Colonic scintigraphy showed NTT in 16 pts (36%), ROO in 10 pts (22%), and STC in 19 pts (42%). Among patients with NTT 12 children received anorectal manometry (ARM) showing normal anorectal dynamics. 7 patients (71%) with ROO underwent ARM, sphincter hypertonicity was observed in 4 (60%), the majority of them with a positive response after Botulinum Toxin (BT) injection. Among STC children further investigations were performed (ARM or colonic manometry) following by different therapeutic decisions (BT injection, surgery, osmotic/stimulant laxatives, transanal irrigations on-demand or continuously). **Conclusion:** Scintigraphic transit profiles may offer initial information on the pathophysiology of constipation, help in identify subgroups of children who deserve further investigation and finally may provide useful information for therapeutic decision-making. **References:** None.

EP-0523

Urea breath test in children

***I. El Bez**, R. Tulbah, I. Munir, F. Alghamlas, M. Alharbi;*
KFMC, nuclear medicine department, Riyadh, SAUDI ARABIA.

Aim/Introduction: The urea breath test (UBT) is generally considered the gold standard for the diagnosis of Helicobacter pylori infections in adults. The purpose of this retrospective study was to investigate the utility and accuracy of urea breath testing in children **Materials and Methods:** During a 7-year period, H pylori infection was investigated in 45 children admitted to our hospital. All patients had clinical gastritis manifestations as infant colics or recurrent abdominal pain for more than 3 months in whom, H pylori infection was suspected. A written parental consent was obtained for all children. **Results:** A total of 45 children were enrolled, mean age 11.3 years (aged 3 - 15years). The test was positive for 28 patients, indeterminate for 2 patients and negative for 15 patients. The 28 infected patients were treated and only 20 patients underwent follow up urea breath test, which was negative for all patients. **Conclusion:** Helicobacter pylori gastric infection in children is a public health problem. Classical diagnostic tools such as endoscopy are excessively invasive in the usual clinical context. Serology at this age has multiple drawbacks. The urea-13C breath test seems today the most appropriate alternative method and proved to be both simple and accurate for the diagnosis of H. pylori infections in children. The UHR method to calculate of (13) C-UBT result provided excellent results for children of all ages on both detection and follow-up of H pylori infection. **References:** None.

EP-0524

The applicability of the ICRP 128 kinetic model to pediatric patients at 3 hour time point post ^{99m}Tc-DMSA injection

***M. Pitkonen**, O. Sipilä, E. Hippeläinen;*
HUS Medical Imaging Center, Helsinki University Central Hospital, Helsinki, FINLAND.

Aim/Introduction: ^{99m}Tc-DMSA renal scintigraphy is one of the most common examinations applied to pediatric patients in our Nuclear Medicine department. According to the ICRP 128 biokinetic model of ^{99m}Tc-DMSA [1] radiopharmaceutical accumulates mostly into the kidneys and liver. Based on ICRP 128 kinetic model, the kidney to liver ratio is approximately 8.1 at 3 hours post injection. In our ongoing study, we compare ICRP 128 kinetic model to our pediatric patient population. We computed the kidney-to-liver ratio at one time point for both kidneys to compare how well the ICRP 128 kinetic model applies to our pediatric population. **Materials and Methods:** We analyzed retrospectively 46 pediatric patients that were chosen randomly. The patients ranged from 1 month old babies to 15 year olds who went through a ^{99m}Tc-DMSA scintigraphy. The ^{99m}Tc-DMSA activity dosage was based on the Dosage Card of the European Association of Nuclear Medicine [2], thus the effective dose is approximately the same for all body weights. Our scanning protocol consists of a 10 min dynamic gamma camera scan with both posterior and anterior views. The scan is started at 3 hours post injection. Motion correction was performed when necessary and ROI analysis was done on the summed image. The geometric mean was calculated from AP/PA images and the kidney-to-liver ratio was computed for both kidneys. The ratio was compared to ICRP 128 kinetic model's ratio. **Results:** The mean kidney-to-liver ratio of our patient data was 9,2 ± 4,4 and 7,7 ± 3,8 for right and left kidneys, respectively. The larger value of the right kidney is mostly due to the overlap of the right kidney and the liver. **Conclusion:** Our preliminary results of ^{99m}Tc-DMSA pediatric studies supports the ICRP 128 kinetic model. In the future we plan to conduct the same comparative analysis using a larger sample of pediatric patients. **References:** [1] ICRP, 2015. ICRP Publication 128. Ann. ICRP 44(2S) [2] Eur J Nucl Med Mol Imaging 2005 May; 32(5):581-8.

EP-34
Clinical -> Diagnostic study -> Paediatric study -> Oncology (Diagnostic)

October 12 - 16, 2019
e-Poster Area

EP-0525

A Diagnostic Use Of Post-therapy 131I-mibg Scintigraphy In Pediatric Patients With High-risk Neuroblastoma

H. Wakabayashi[1], *D. Kayano*[1], *A. Inaki*[1], *R. Araki*[1], *H. Maeba*[1], *R. Kuroda*[1], *N. Akatani*[1], *T. Yamase*[1], *S. Watanabe*[1], *T. Hiromasa*[1], *H. Mori*[1], *Y. Kunita*[1], *N. Nguyen*[1,2], *S. Kinuya*[1];
[1]*Kanazawa University Hospital, Kanazawa, JAPAN,* [2]*108 Hospital, Hanoi, VIET NAM.*

Aim/Introduction: ^{123}I-meta-iodo-benzyl-guanidine (^{123}I-MIBG) scintigraphy is useful to evaluate disease extent for children with neuroblastoma. ^{131}I-MIBGtherapy has been used for children with high-risk neuroblastoma, and post-therapy ^{131}I-MIBGscintigraphy may detect more lesions compared with diagnostic ^{123}I-MIBGscintigraphy. However, no study reveals a utility of post-therapy ^{131}I-MIBGscintigraphyfor high-risk neuroblastoma children with complete response to primary therapy as demonstrated by diagnostic ^{123}I-MIBG scintigraphy. We retrospectively examined a diagnostic utility of the post-therapy^{131}I-MIBG scintigraphy for patients who received ^{131}I-MIBGtherapy as consolidation therapy. **Materials and Methods:** Between June 2006 and March 2019, there were 19 high-risk neuroblastoma patients and 1 high-risk ganglioneuroblastoma patient with complete response to primary therapy as demonstrated by the diagnostic ^{123}I-MIBG scintigraphy. All patients received the ^{131}I-MIBG therapy without acute severe adverse effect [mean age: 7± 4 y.o., range 1-16 y.o., administration dose of ^{131}I-MIBG: high-dose (666MBq/kg, n=16), intermediate dose (444-555MBq/kg, n=2), and low-dose (< 444MBq/kg, n=2)]. The post-therapy^{131}I-MIBG scintigraphy was performed at 4 days after injection. Board certified physicians of nuclear medicine read the post-therapy^{131}I-MIBG whole-body images and single-photon emission tomography images for detecting residual diseases. We assessed the detection rate of a new lesion on the post-therapy^{131}I-MIBG scintigraphy. **Results:** On the post-therapy^{131}I-MIBG scintigraphy, the 6 (30%) of 20 children exhibited abnormal uptake. The site of abnormal accumulation was on the recurrence site in one case, operated sites in four cases, and bone metastasis in one case. **Conclusion:** The post-therapy^{131}I-MIBG scintigraphy could detect the residual disease that was not recognized by diagnostic ^{123}I-MIBG scintigraphy in 30% of pediatric patients with high-risk neuroblastoma and ganglioneuroblastoma. While the risks of radiation exposure must be considered, the diagnostic of post-therapy ^{131}I-MIBG scintigraphy can provide valuable information in planning treatment strategy. **References:** None.

EP-0526

Influencing factors of the first ^{131}I ablation therapy for children and adolescents differentiated thyroid cancer

L. Lina, *T. Tian, L. Bin;*
West China Hospital, Sichuan University, Chengdu, CHINA.

Aim/Introduction: To investigate predictors for successful ablation after first radioiodine therapy in children and adolescents with differentiated thyroid cancer. **Materials and Methods:** Patients aged ≤ 20 years were retrospectively analyzed. All patients underwent total or near total thyroidectomy with or without lymph node dissection. Response to treatment was evaluated 6 to 12 months after ^{131}I treatment. Successful ablation was defined as the absence of visible ^{131}I accumulation in the thyroid bed after whole-body scans, thyroglobulin levels <1 ng/ml in a TSH-stimulated state and normal results on neck ultrasonography, when performed. **Results:** 166 patients were studied: 138 (83.1%) girls, age 16.5±3.0 years, 163 (98.2%) papillary thyroid carcinomas. Tumor size was 3.0±1.6 cm. Successful ablation was achieved in only 61 patients (36.7%). Univariate analyses showed that age, LN metastasis ratio, ATA Risk, TNM, ^{131}I dose and ps-Tg were significantly associated with ablation failure ($P < 0.05$). Using logistic regression analysis, ps-Tg ($P < 0.05$) was the only significant factor in the prediction of ablation failure. The cutoff analysis of ps-Tg through ROC curve showed that the value of 16.1 ng/ml displayed 72.5% sensitivity and 98.6% specificity to predict ablation failure. **Conclusion:** The ps-Tg are significant predictors for the ablation failure and might be helpful on defining follow-up strategies in pediatric DTC. **References:** None.

EP-0527

PET/MR imaging of pediatric bone tumors: Case based review

K. Hawk, *C. R. N. Farrell, A. Pareek, A. Muehe, A. Pribnov, R. Steffner, R. Avedian, H. E. Daldrup-Link;*
Stanford University, Palo Alto, CA, UNITED STATES OF AMERICA.

Aim/Introduction: Imaging of pediatric bone tumors presents unique diagnostic challenges. 18F-FDG PET/MR has emerged as a valuable technique for initial assessment and management of these patients. Traditionally, plain radiography has been considered the first line imaging modality to assess presenting symptoms. Cross sectional imaging, most often MRI is then used for more detailed assessment, characterization and staging for oncologic management. 18F-FDG PET/MR not only provides excellent detailed anatomic assessment, but also provides an additional layer of information regarding the functional and metabolic biology of the neoplasm. This technique, therefore, provides detailed anatomic and functional imaging to assess staging and response to therapy. Particularly in the pediatric oncology population, this technique provides the added benefit of reduced radiation exposure when compared with 18F-FDG PET/CT techniques. Because this technology is relatively new, many practicing nuclear medicine physicians

may be unfamiliar with the nuances of the technique. This work provides an in-depth review of gold standards for 18F-FDG PET/MR imaging technique, reporting and classic imaging features of pediatric bone tumors. **Materials and Methods:** Following a comprehensive literature search on 18F-FDG PET/MR of pediatric bone tumors, we complied an extensive collection of most current evidence -based best practices in 18F-FDG PET/MR. This work presents our institutional approach over the past three years and experience with performing more than fifty 18F-FDG PET/MR scans of pediatric bone tumors, which will be demonstrated with a series of case examples. **Results:** The imaging protocol and reporting criteria for conducting 18F-FDG PET/MR imaging of pediatric and adolescent bone tumors will be detailed. Common osseous neoplasm with information on disease epidemiology, unique pathophysiology and classic 18F-FDG PET/MR imaging characteristics are provided. Neoplastic etiologies characterized include osteosarcoma, Ewing sarcoma, primary bone lymphoma, bone and bone marrow metastases, and Langerhans cell histiocytosis. Common imaging pitfalls including false positive results will also be demonstrated. Benefits and limitations of 18F-FDG PET/MR imaging when compared with 18F-FDG PET/CT will be detailed as we discuss research and clinical application directions of 18F-FDG PET/MR imaging. **Conclusion:** 18F-FDG PET/MR has emerged as a powerful tool in evaluation of pediatric bone tumors. This comprehensive case-based review details how 18F-FDG PET/MR can be used to evaluate the pediatric patient. Through explanation of 18F-FDG PET/MR imaging techniques, reporting mechanisms, disease pathophysiology, and classic imaging characteristics, this exhibit provides the learner with detailed understanding of applying 18F-FDG PET/MR to evaluate pediatric bone tumors. **References:** None.

EP-0528

MIBG Scintigraphy In Children With Neuroblastoma: Add Value Of Hybrid Images

***I. El Bez**, R. Tulbah, I. Munir, F. Alghamlas, M. Alharbi;*
King fahfd medical city, nuclear medicine department, Riyadh, SAUDI ARABIA.

Aim/Introduction: The purpose of our work is to illustrate the contribution of SPECT/CT in addition to the planar 123-I MIBG scintigraphy in the staging and the follow up of neuroblastoma in children. **Materials and Methods:** In this retrospective monocentric study, 44 children with neuroblastoma (aged 1 - 7 years) were studied to evaluate the accurate staging at the time of diagnosis or the follow up. All patients underwent whole body scintigraphy and hybrid SPECT/CT images of the involved sites, 24 h after intravenous 123-I MIBG injection. Patients were asked to discontinue any medication interfering with I-123 MIBG uptake before the study. **Results:** Planar MIBG images demonstrated primary tumors in 41/43 patients; Overall, SPECT/CT provided additional information in 30 of the 44 cases (68%): SPECT/CT images gave us most detailed information about the local tumor extent in all positive cases. Concerning metastatic lesions they showed many more foci, as to bone and bone marrow lesions in 14 cases and hepatic metastases in 2 cases. Finally, SPECT / CT allowed us to reclassify two patients, initially considered non-metastatic patients as liver metastasis. **Conclusion:** The MIBG scintigraphy is a simple, non invasive examination that has excellent sensitivity and specificity in detection, staging and follow up of neuroblastoma in childhood. The hybrid SPECT/CT imaging improves the performance of the planar scintigraphy as well in sensibility toward the deep and small lesions, and in specificity for foci poorly identified on planar imaging. **References:** None.

EP-0529

Differentiated Thyroid Carcinoma in Children and Teenagers

***I. El Bez**, R. Tulbah, I. Munir, F. Alghmlas, M. AlHarbi;*
King fahd medical city, nuclear medicine department, Riyadh, SAUDI ARABIA.

Aim/Introduction: Pediatric thyroid cancer is a rare disease with an excellent prognosis. The treatment consists on thyroidectomy and radioiodine ablation in the vast majority of patients, especially in patients with high risk of recurrence or death by thyroid cancer. Our objective was to evaluate presentation and long-term outcome in patients with pediatric differentiated Thyroid Carcinoma treated with radioiodine therapy in our institution. **Materials and Methods:** In this retrospective monocentric study, presentation, complications, and outcome of patients with pediatric differentiated Thyroid Carcinoma in Children and Teenagers DTC (age at diagnosis ≤19 y) treated in nuclear medicine department of king fahd medical hospital in Riyadh were assessed using medical records. No history of exposure to ionizingradiation or family history of CDT has been noted. **Results:** We identified 45 patients (35 females and 10 males). Extensive follow-up data were available for all patients. Median age at diagnosis was 12.2 years (range 7-19 y). At initial diagnosis, 15 the patients had cervical lymph node metastases; 4 patients had distant metastases. All patients underwent total thyroidectomy. Radioiodine was administered to 100%, with a median cumulative activity of 5.66 GBq (range 0.74-35.15 GBq). Overall, permanent surgical complications such as hypoparathyroidism were observed in 4 patients. There was no patient with damage to laryngeal nerves, neither recurrent laryngeal nerve nor superior laryngeal lesions. At last known follow-up, 19 patients had persistent disease and two experienced a recurrence. **Conclusion:** Survival of pediatric DTC is excellent. According to our results, we recommend radioactive iodine therapy for remnant ablation or residual disease for most children with DTC and a long-term follow-up because disease can recur decades after initial diagnosis and therapy **References:** None.

EP-0530

The Association Between Pathological Feautures and Resistant Disease In Paediatric Patients With Differentiated Thyroid Cancer

K. Kucuker, Z. Yapar, I. Guney, G. Buyukdereli;
Cukurova University, Adana, TURKEY.

Aim/Introduction: To reveal the associaton between post-operational pathological features and resistant disease in paediatric patients with differentiated thyroid cancer. **Materials and Methods:** Under 18 years old, 39 patients who had diagnosed as differentiated thyroid carcinoma and undergone one or more ^{131}I radioiodine thyroid ablation therapy between 2007-2018 at the Department of Nuclear Medicine, Cukurova University Balcali Hospital included in the study. After total thyroidectomy, ^{131}I radioiodine therapy was administered (1/3 of adult dose up to 5 years of age, 1/2 of adult dose up to 10 years of age, 5/6 of adult dose up to 15 years of age). Whole body radioiodine scan (WHRS) was performed with 1 milicurie (mCi) radioiodine at sixth month after therapy, serum thyroglobulin was also measured before and in third and sixth month after radioiodine therapy. The patients whose thyroglobulin value (according to our institution, <0.04 accepted negative) and WHRS were negative at the sixth month, evaluated as complete remission. Increasing of thyroglobulin level, positive WHRS and metastatic disease evaluated as resistant disease. The relationship between demographical and pathological features of patients and resistant disease was investigated. **Results:** Eight patients had resistant disease. All of the patients with resistant disease had papillary thyroid carcinoma. Four of them had classical variant, two of them had tall cel variant, one of them had oncosytic variant and one of them had follicular variant. In the time of diagnosis, all had lymphovascular invasion, seven of them had capsular invasion and metastatic lymph node. Of the eight patients, two had lung metastasis, two had residue tissue in servical region and four had serum thyroglobulin rise in the sixth month after therapy. There was no statistical correlation between resistant disease with gender (p value: 0,32), prepubertal and postpubertal age group (p value: 0,22), multicentricity of tumor (p value: 0,22), pathological type and subtype, capsular or lymphovascular invasion and metastatic lymph node existence. **Conclusion:** Despite encountering relatively rare, differentated thyroid carcinoma in paediatric population is critical issue due to its ability to emerge with distant metastasis, especially in lungs. It can also require multiple therapies due to resistant disease. Larger patient populations are needed to reach precise results about association between pathological characteristics and prognosis. **References:** None.

EP-0531

Response assessment in children with lymphoma underway checkpoint inhibitor therapy using 18 FDG-PET/CT

I. Vdovina, E. Kireeva, K. Chaurasiya, M. Chetchasova, L. Potapenko, N. Myakova, Y. Likar;
Dmitry Rogachev National Research Center of Pediatric Hematology, Oncology and Immunology, Moscow, RUSSIAN FEDERATION.

Aim/Introduction: Cancer immunotherapy with immune-checkpoint inhibitors is considered a promising strategy for cancer treatment. Checkpoint inhibitors, namely anti-PD1 antibodies, demonstrated efficacy across multiple types of cancer including relapsed or refractory lymphomas. Not surprisingly, flare reactions or delayed responses similar to those in patients with solid tumors have observed in patients with lymphoma. It is unclear how these reactions can be reliably identified and distinguished from the disease progression. Uniform response assessment criteria will help to make the right decision about response and it is critical for treating physicians to optimally use checkpoint inhibitor therapy in patients with lymphoma. ^{18}F-FDG PET/CT are widely used in early response evaluation conventional chemotherapy in patients with lymphoma and response assessment criteria are well established. While the response criteria applied ^{18}F-FDG PET/CT using checkpoint inhibitorscontinue to be studied.The aim of this study to determine time points of response assessment with ^{18}F-FDG PET/CT in children with lymphoma underway checkpoint inhibitor therapy. **Materials and Methods:** 10 patients with lymphoma received therapy anti-PD1 antibodies (Nivolumab). Nivolumab was administered at a dose 3 mg/kg every two weeks. 7/10 patients were with relapse of Hodgkin's lymphoma and 3/10 patients with relapse of diffuse B-cell large cell lymphoma. All patients underwent ^{18}F-FDG PET/CT before therapy with Nivolumab and for response assessment. The response was assessment in 2 patients after 3 injections, 7 patients after 4 injections and 1 patient after 5 injections of Nivolumab. The results of ^{18}F-FDG PET/CT were evaluated using LYRIC criteria. **Results:** CR was found in 2 patients after 4 injections; PR was found in 6 patients: 1 patient after 3 injections, 4 patients after 4 injections, 1 patient after 5 injections of anti-PD1; SD was found in 1 patient after 4 injections. Indeterminate response was found in 1 patient after 3 injections of Nivolumab which later was confirmed as a disease progression. **Conclusion:** Our preliminary results demonstrate the possibility to evaluate response in children with relapsed lymphoma who underway treatment with Nivolumab using ^{18}F-FDG PET/CT. However, the further studies need to be performed with more patient recruitment and analysis. **References:** None.

EP-0532

Prognostic value of 123I-MIBG scintigraphy in bone metastasic neuroblastoma

L. Nieto Morcillo, L. de la Cueva Barrao, M. Falgás Lacueva, M. Calderón Calvente, G. Guzmán Prudencio, S. Alvarez Ruiz, P. Navarro Beltrán, M. Sangrós Sahún, D. Abós Olivares;
Hospital Universitario Miguel Servet, Zaragoza, SPAIN.

Aim/Introduction: To analyse the prognostic value of 123I-MIBG

scintigraphy (MIBG) after induction chemotherapy in patients with bone metastasic neuroblastoma. **Materials and Methods:** We revised scintigraphies from patients with histopathological diagnosis of neuroblastoma from 2008 to the present, and established the existence of bone metastasis with MIBG uptake at the time of diagnosis as the criterion for inclusion. Skeletal SIOPEN score was calculated on 12 different bone regions, each scored 0-6 based upon disease extent, by 3 nuclear medicine physicians, clarifying differences by consensus and with the help of nuclear magnetic resonance. Each region was scored both at diagnosis and after induction chemotherapy, which was administered according to the SIOPEN/HR-NBL1 protocols. We registered the percentage change in SIOPEN bone score between scintigraphies taken at diagnosis and after induction in each patient, and stratified them based on score reduction &gt50% vs &it50%. We estimated OS and DFS in both groups. **Results:** 8/29 of the studied patients (28%) meet the criteria for inclusion, showing bone metastasis with MIBG uptake.In the 8 patients median OS was 49 months and median DFS was 26 months. In 6/8 patients (75%), Skeletal SIOPEN score decreased more than 50%, finding the average OS was 62 months and the average DSF was 61 months. In 2/8 patients (25%), Skeletal SIOPEN score wasn't reduced more than 50%, with an average OS of 36 months and an average DFS of 22 months. Both patients, finally died. There was no statistical significance difference between groups. **Conclusion:** In spite of the sample size, our results show that the lack of reduction of the metabolic activity after induction based on SIOPEN/HR-NBL1 protocol in stage IV patients with bone disease, appears to be related to worse prognosis for survival. **References:** None.

EP-0533

Spectrum of malignancies in patients with Neurofibromatosis (NF): role of FDG-PET/CT in detecting malignant transformation

M. Gavra[1], *K. Roka*[2], *I. Sevaslidou*[3], *D. Verganelakis*[3], *V. Lyra*[3], *M. Filippidou*[2], *A. Malama*[1], *A. Kattamis*[2];
[1]*Radiology, CT & MRI, Goudi, Athens, GREECE,* [2]*Oncology Department, NKUA, Goudi, Athens, GREECE,* [3]*Nuclear Medicine Department, Goudi, Athens, GREECE.*

Aim/Introduction: Neurofibromatosis type-1(NF1) and type-2(NF2) are distinct genetic-clinical-syndromes in which affected individuals develop both benign and malignant tumors that predominantly affect the nervous-system. Malignant peripheral sheath nerve tumours (MPSNT's) are uncommon, biologically aggressive soft tissue sarcomas of neural origin that pose tremendous challenges to diagnosis and effective therapy. In 50% of cases, they occur in the context of neurofibromatosis type I. In order to standardize and improve the clinical-care of patients with NF, the first Greek-national-center of reference was established in 1/1/2016. **Materials and Methods:** To describe the spectrum of malignancies, as well as implementation of PET-CT in diagnosing malignant transformation of plexiform neurofibromasin patients with NF examined from January 2016 until December 2018 in our NF-reference-center. Clinical diagnosis of NF1 was based to National-Institutes of Health diagnostic-criteria (NIH, 1988), while for NF2 to National-Neurofibromatoses-Foundation-Criteria (NNFF, 1997). Patients were evaluated from a multidisciplinary-team and underwent regular follow-up visits. **Results:** During the study period, 75 children (age 5-months - 17-years, 31 girls and 44 boys) were assessed, of whom 67 patients had NF1, 4 segmental NF1, 4 NF2. Molecular diagnosis was confirmed in 35 patients with NF1. The main clinical findings in patients with NF1 were: learning disabilities (83%); optic-pathway-gliomas (50%), pilocyticastrocytomas (3%); cutaneous neurofibromas (15%); plexiform neurofibromas (16%); scoliosis (26%); pseudoarthrosis (3%). Of notice 3 out of 12 patients with NF1 under regular follow up with known history of multiple plexifomneurofibromas underwent FDG PET-CT, due to progressive increase of size in certain lesions located in thoracic, abdominal and paraspinal lesions respectively. In all 3 patients with increased tracer uptake (SUV>6,6), pathology report after surgery confirmed the presence of MPSNT. Two of the patients remain in 1st remission 6 and 12 months after the end of chemotherapy respectively. In the 3rd patient with multiple plexiform neurofibromas after first line therapy for MPSNT, a 2nd MPSNT was suspected after PET-CT imaging and confirmed after surgery and pathology report. **Conclusion:** Patients with NF have a genetic predisposition to develop both benign and malignant neoplasms. Because of the disease burden, it is advisable not to perform biopsy in all plexiform neurofibromas, thus rational implementation of modern imaging techniques like PET-CT, could improve early selection of patients that need surgical excision and further treatment. **References:** None.

EP-0534

FDG PET/CT predictors of treatment response in patients with Osteosarcoma and Ewing's sarcoma

D. Volterrani, *G. Aghakhanyan, F. Guidoccio, L. Coccoli, T. Lupi, L. Caponi, S. Chiacchio, G. Casazza, A. Franchi, R. Capanna, I. Paglianiti;*
University of Pisa, Pisa, ITALY.

Aim/Introduction: To determine the relationship of serial [^{18}F] FDG uptake in the primary tumor with a histologic response and event-free survival in pediatric and young adult patients with osteosarcoma (OS) and Ewing's sarcoma (ES). **Materials and Methods:** Forty-one patients with OS and ES from a single institution (Pediatric Onco-Haematology Unit, University Hospital of Pisa), who underwent serial [^{18}F]FDG PET/CT imaging, including baseline (t0), after neoadjuvant (t1) and adjuvant chemotherapy (t2) were recruited. All patients were subdivided into 5 subgroups: localized ES, metastatic ES at the diagnosis, plurimetastatic ES at the diagnosis (Very High Risk Group), localized OS and metastatic OS. For all time-points, the serum lactate dehydrogenase and alkaline phosphatase activities, the PET-derived parameters, such as SUVmax, SUVmean, TLG and MTV for the principal lesion and the surrounding soft tissue

compartment and the postoperative histologic data, such as tumor grading and tumor response, were collected. Repeated measures ANOVA, linear regression and/or Pearson correlation analysis were applied between quantitative, ordinary and delta-encoded variables, as appropriate. Overall survival and event free survival were calculated using non parametric Kaplan-Meier test. Survival distributions were compared with logrank test. **Results:** Thirty-three out of the 41 patients underwent surgical treatment. According to histological response, all patients were categorized into responders (tumor necrosis > 90%, n. 15) and no-responders (tumor necrosis < 90%, n. 20). ANOVA showed mean affect across time with significant reduction of SUVmax at t1 ($p<0.0001$) and t2 ($p<0.01$). The degree of tumor necrosis hystopathologically assessed on the primary lesion showed a significant relationship with SUVmax and SUVmean at t1. Changes of SUVmax were also able to predict responders (tumor necrosis > 90%) with a sensitivity of 0.8 and a specificity of 0.78. Event-free survival was significantly worse in no-responders than in responders. A significant relationship was found between TLG and MTV values at the baseline (t0) PET/CT and the overall and the event-free survival. Moreover, a greater reduction of TLG and MTV values of the primary tumor after neoadjuvant chemotherapy was associated with a better prognosis. **Conclusion:** Metabolic changesof primary tumor after neoadjuvant chemotherapy assessed by [^{18}F]FDG PET/CT seem to act as predictors of histological response, stratifying, with good sensitivity and specificity, treatment responders from no-responders. Moreover, they seem to be also predictive of the overall and the event-free survival of patients with OS and ES. **References:** None.

EP-0535

Dosimetry in thyroid cancer paediatric patients

T. Kracmerova[1,2,3], *L. Mihaliova*[1], *V. Simonova*[1], *K. Taborska*[1];
[1]*University Hospital Motol, Prague, CZECH REPUBLIC,* [2]*Prague Medical Care Department, s.r.o., Prague, CZECH REPUBLIC,* [3]*Czech Technical University, FNSPE, Prague, CZECH REPUBLIC.*

Aim/Introduction: The Department of Nuclear Medicine and Endocrinology at Motol Univesity Hospital is the only facility in the Czech Republic dealing with the treatment of thyroid cancer in paediatric patients. From 2015 to April 2019, a total number of 29 newly admitted children under the age of 15 years was treated. We performed dosimetry on 24 of them. **Materials and Methods:** In total number of 24 patients with thyroid cancer (20 female, 4 male, 7-16 years of age, the average age of 12 years) who underwent theranostic application of ^{131}I-NaI, the dosimetry was performed. More than half of the patients were diagnosed with low-risk thyroid cancer (T1-T2 according to the 8th edition of TNM classification), 57% of the patients had no positive metastatic lymphatic nodes and only two patients were diagnosed with a lung metastatic process before hospitalization. TSH, TGL, and anti-TGL levels corresponded to the TNM classification. After the administration of diagnostic activity of 111 MBq, we performed organ dosimetry and whole-body dosimetry. Based on the dosimetric data, ultrasound findings and blood tests, the therapeutic dose was prescribed. Patients received therapeutic doses of 3.4 GBq - 5.7 GBq, with an average dose of 4.4 GBq. After the therapeutic administration, organ dosimetry was performed in selected group of patients with non-zero accumulation after diagnostic administration. **Results:** The whole-body dosimetry on paediatric patients was found not to be of significant relevance since the average dose for therapy was 0.08 Gy/GBq, which corresponds to an administred doses of 25 GBq at a whole-body dose of 2 Gy. Therefore, it is meaningful to perform whole-body dosimetry only on patients where bone-metastatic disease is suspected. Assuming that the dose was calculated correctly and that a sufficient therapeutic dose was applied (300 Gy to the thyroid remnants, 100 Gy to the nodes), it can be concluded that in 6 cases, the repeated therapeutic application was not predictable. As for these 6 cases, mostly aggressive forms of thyroid cancer were included. Totally 9 patients were repeatedly treated within 1 year. **Conclusion:** Organ dosimetry and its associated quantification of ^{131}I has many drawbacks - such as the effects of dead time, scattered photons, lesion volume determination and others. Considering these facts, we recommend performing organ dosimetry only in patients with metastatic lung disease. The first administered therapeutic dose should be maximised only on the basis of whole-body dosimetry while preserving the 2 Gy whole-body dose. **References:** None.

EP-35

Clinical -> Therapy study -> Adult study -> Other treatments -> Bone metastases, pain palliation

October 12 - 16, 2019 e-Poster Area

EP-0536

Usefulness of radium-223 in metastatic hormone-sensitive prostate cancer: a single centre experience

S. S. Medina[1,2], *O. Garcia*[1,3], *Z. Santana*[1], *N. Sobrevilla*[1];
[1]*Instituto Nacional De Cancerologia, Mexico City, MEXICO,* [2]*Hospital Angeles Lindavista, Mexico City, MEXICO,* [3]*Hospital Médica Sur, Mexico City, MEXICO.*

Aim/Introduction: Evaluate the feasibility of compassionate exemption Ra-223 treatment in metastatic hormone-sensitive high-grade prostate cancer (mHSHGPC) patients with concomitant androgen deprivation therapy (ADT). **Materials and Methods:** Seven patients with mHSHGPC, were treated with six cycles of Ra-223 plus ADT. All patients had undergone to 18F-NaF-PET/CT. A qualitative analyses of the 18F-NaF-PET/CT was performed in conjunction to the Alkaline Phosphatase (ALP), Lactate-dehydrogenase (LDH) and Prostatic-Specific Antigen (PSA) values. The mean of SUVmax values were used as a quantitative measure of tumoral burden. Changes in PSA,

ALP, LDH from baseline were evaluated, and were defined as an increase or a decrease of at least 30%. All patients received Ra-223 under the "compassionate use" clause of the Mexico. Written informed consent was obtained from each subject **Results:** Four patients showed a significant reduction in mean SUVmax after 3 cycles of Ra-223, and one after 6 cycles. Patients who showed reductions in mean SUVmax after Ra-223 also showed reductions in PSA, ALP and LDH. Four weeks after the last cycle of Ra-223 all patients had decreased total PSA, ALP and LDH values ≥30% also significant improvement on pain. Treatment-related adverse events were observed in two patients (patients with superscan); such as fatigue, diarrhea and nausea; meanwhile did not affect continuation of therapy. We found slight to moderate decreases in neutrophils and hemoglobin in two patients at the end of entire therapy. During treatment and at term, no patient required transfusion. One patient (with superscan) required prior to the last cycle administration of colony stimulating factor. None patient presented severe adverse event´s Grade III or IV according to Common Terminology Criteria for Adverse Events (CTCAE). No progress disease was documented after 14 ± 4 weeks. **Conclusion:** Ra-223 plus ADT can be safe and effectiveness in mHSHGPC; the semi-quantitative 18F-NaF-PET/CT as a method effective to monitor the treatment response in bone metastases. Due to concomitant administration of ADT, 18F-NaF-PET/CT cannot differentiate whether the findings were due to androgen blockade or the Ra-223; nevertheless, data supporting the efficacy of Ra-223 is the significant improvement on pain. **References:** Wenter V, Herlemann A, Fendler WP, Ilhan H, Tirichter N, Bartenstein P, Stief CG, la Fougère C, Albert NL, Rominger A, Gratzke C. Radium-223 for primary bone metastases in patients with hormone-sensitive prostate cancer after radical prostatectomy. Oncotarget 2017;8:44131-40.

EP-0537

Identifying Factors that Affect Patient Outcomes in Radium-223 Therapy: Retrospective Image Quantification of Bone Scans and Assessment of Blood Markers

J. Gray, *J. Scuffham, V. Prakash, R. Clauss, M. Shastry;*
Royal Surrey County Hospital NHS Foundation Trust, Guildford, UNITED KINGDOM.

Aim/Introduction: Radium-223 dichloride (Xofigo, Bayer) has been shown to reduce bone pain and increase overall survival (OS) in patients that present with metastatic castration-resistant prostate cancer (mCRPC) [1]. The aim of this study was to assess whether bone scan quantification and blood markers can be used to predict OS in these patients and how a patient responds to the therapy. **Materials and Methods:** 130 patients with mCRPC that were no longer on radium-223 therapy, either through completion of 6 cycles or through discontinuation, were retrospectively enrolled in this study. The metastatic involvement of the skeleton was quantified using the bone scan index (BSI), which was calculated using aBSI (EXINI Diagnostics AB). Kaplan-Meier analysis was performed to determine the prognostic power of the BSI at baseline (cycle 1), along with other clinical variables, including prostate-specific antigen (PSA) alkaline phosphatase (ALP) and haemoglobin (Hb). An experienced clinician classified a sub-sample of 41 patients with both pre- and post-therapy technetium-99m MDP bone scans into complete response, partial response, stable disease and progressive disease using modified Soloway criteria [2]. The relationship between the response classification and a) the change in BSI, PSA and ALP between baseline and cycle 6 and b) the values of BSI, PSA and ALP at baseline was investigated. **Results:** Median survival of the sample was 11.9 months. Increased OS post-therapy was found to be associated with BSI ≤ 3.0% (16.8 vs 8.8 months, $p = 0.016$), PSA ≤ 99 ng/ml (18.2 vs 9.2 months, $p = 0.003$), ALP ≤ 150 U/L (20.7 vs 9.0 months, $p < 0.001$), Hb > 110 g/L (18.2 vs 4.3 months, $p < 0.001$) at baseline. The change in BSI from baseline to follow-up was found to be significantly associated with the Soloway response classifications and was found to be superior to changes in PSA and ALP as a response marker. The BSI, ALP and PSA at baseline were found not to correlate with response classification. **Conclusion:** The BSI, PSA, ALP and Hb at baseline were found to be strong prognostic factors and the BSI emerged as the superior response marker. BSI is able to better reflect the heterogeneity of response than PSA and ALP, which only characterise the response on a global basis. The BSI, PSA and ALP at baseline were not indicative of response classification. **References:** [1] Sartor O. et al, Lancet Oncology 2014; 15:738-746 [2] Soloway M. et al, Cancer 1988; 61:196-202.

EP-0538

Role of FDG PET/CT in the prognostic stratification and response assessment of castration-resistant prostate cancer treated with radium-223 dichloride

M. Donegani[1], *S. Capitanio*[2], *M. Vitti*[1], *G. Fornarini*[2], *A. Miceli*[1], *E. Zanardi*[1], *M. Mencoboni*[3], *C. Marini*[2,4], *F. Boccardo*[1], *G. Sambuceti*[1,2], *S. Morbelli*[1,2], *M. Bauckneht*[2];
[1]*University of Genoa, Genova, ITALY,* [2]*IRCCS Policlinico San Martino, Genova, ITALY,* [3]*ASL3 Genovese, Genova, ITALY,* [4]*CNR Institute of Molecular Bioimaging and Physiology (IBFM), Milano, ITALY.*

Aim/Introduction: Radium-223 dichloride has emerged as the only bone-directed treatment option demonstrating an improvement in overall survival (OS) in metastatic castrate resistant prostate cancer (mCRPC). However, there is an urgent need for the identification of reliable molecular imaging biomarkers to non-invasively determine its efficacy (possibly improving patients' selection or identifying responders' after therapy completion). Generally, the FDG avidity is low in treatment naïve prostate cancer, increased in castration-resistant prostate cancer (mCRPC), and almost always present in chemotherapy-refractory mCRPC. Accordingly, FDG-PET/CT may represent an effective tool for measuring disease burden at baseline, performing prognostic stratification and assessing treatment response to radium-223 in mCRPC. **Materials and Methods:** All mCRPC patients underwent a baseline FDG-PET/CT for prognostic stratification before radium-223 treatment

initiation. Only patients with positive FDG-PET/CT at baseline were subsequently submitted to FDG-PET/CT after two months from radium-223 treatment completion. The following parameters were measured: SUVmax, SUVmean, metabolic tumor volume (MTV), total lesion glycolysis (TLG) per lesion and per patient bases. In patients who underwent post-therapy FDG-PET/CT, Deauville Score, PERCIST and EORTC criteria were applied to evaluate treatment response. Differences between LDH, ALP and PSA levels at the end of therapy with respect to baseline were also calculated (termed deltaLDH, deltaALP and deltaPSA). The correlation between PET- and biochemical-derived parameters with and OS were measured by Kaplan-Meier analyses. **Results:** 41 mCRPC patients who underwent both FDG-PET/CT scans were included in the final analysis (median interval between the two scans: 213 days). After a median follow-up of 12 months, 23/41 (56%) patients were still alive. At baseline, MTV and TLG significantly predicted long term OS independently from biochemical data. After therapy, deltaPSA, deltaLDH, PERCIST and EORTC scores were the most relevant predictors of OS. When combined, while PERCIST and EORTC classes were able to discriminate different OS in patients with deltaPSA and deltaLDH values within the first tertile including patients with reduction in PSA and LDH, their prognostic power disappeared in the two remaining tertiles in both groups, including patients showing biochemical progression during the course of treatment. **Conclusion:** FDG-PET/CT can represent a widely available method to directly measure active de-differentiated tumor burden in mCRPC patients' candidates to radium-223, providing prognostic information overpowering biochemical parameters. After treatment it can assess tumor load reduction particularly in patients included in the first tertile of deltaPSA and deltaLDH. **References:** None.

EP-0539

Three years' clinical practice of Radium-223 therapy in patients with symptomatic bone metastases from metastatic castrate-resistant prostate cancer: a single centre experience

M. Gazzilli[1], *R. Durmo*[1], *D. Albano*[1], *E. Cerudelli*[1], *M. Panarotto*[1], *E. Cossalter*[1], *F. Bertagna*[1,2], *R. Giubbini*[1,2];
[1]*Azienda Socio Sanitaria Territoriale degli Spedali Civili di Brescia, Brescia, ITALY,* [2]*Università di Brescia, Brescia, ITALY.*

Aim/Introduction: Bone is the most common site of distant metastasis in prostate cancer. Radium-223 was approved for the treatment of adult patients with castrate-resistant prostate cancer (mCRPC), symptomatic bone metastases and no known visceral metastases, in progression after at least two prior lines of systemic therapy for mCRPC, or ineligible for any available systemic mCRPC treatment. The aim of this study was to provide further characterization and sub-selection insights into the group of patients who would benefit most with treatment with Ra-223. **Materials and Methods:** We retrospectively analyzed a cohort of 38 patients treated with Radium-223 between July 2015 and December 2018. All patients underwent a baseline visit and a bone scintigraphy to prove the presence of bone metastases to assess the existence of AIFA requirements for treatment with Radium-223. Bone scan, ALP and PSA levels were repeated after third and after the end of alpha-emitter therapy. All patients were re-evaluated after two months from the end of therapy. Survival curves were plotted according to the Kaplan-Meier method and differences between groups were analyzed by using a two-tailed log rank test. **Results:** The response to the treatment in terms of pain reduction, according to NRS pain scale, was: pain reduction in sixteen patients; stable pain in fourteen patients and pain increased in eight patients. We arbitrarily established a cut off 10 bone lesions to evaluate the treatment response: patients with less than 10 bone metastasis had significant differences in PFS (p<0,001) compared to patients with more or equal to 10 metastases, no statistical significance was found considering the OS (p=0, 23) between the two groups. The same results was founded considering patients with baseline ALP<220 U/L, a cut off reported in literature showing a significant difference in PFS (p<0,001) and no statistical significance with OS (p=0,027). **Conclusion:** The results of our study showed that careful patient selection could play an important role in Radium-223 efficacy completing the whole treatment and obtaining the best response in term of symptom reduction with the fewer adverse effect. The most important founding of our study was the correlation between the number of bone metastasis and ALP with outcome. Patients with less than 10 bone metastasis and ALP<220 U/L at baseline had significant improvement in PFS (p<0,05). **References:** None.

EP-0540

Factors Contributing to Discontinuation of Radium-223 Dichloride Treatment in Patients with Castration Resistant Prostate Cancer (mCRPC) and Bone Metastasis. Single Center Experience

S. Kozak, O. Lang, R. Pichova, M. Mateju;
Nemocnice Kralovske Vinohrady, Klinika nuklearni mediciny, Prague, CZECH REPUBLIC.

Aim/Introduction: Radium-223 dichloride is a radionuclide used for treatment of men with castration-resistant prostate cancer with symptomatic bone lesions without visceral metastases. Patients receive the injection of Radium-223 dichloride 6 times in 4-week cycles with regular checkups in between (including blood count). In this study, clinical data and laboratory tests results of patient receiving Radium-223 were evaluated. Subsequently, the treatment success frequency was analysed to determine the factors contributing to treatment discontinuation. **Materials and Methods:** We retrospectively analyzed 17 men (mean age 69 years) treated with injections of Ra-223 dichloride at our department between June 2015 and February 2019. As a part of the analysis, the patients were divided into two groups: Group A, where 11 patients completed the treatment (they received all 6 injections), and Group B, where 6 patients did not complete the treatment (they received 1 to 5 injections). The data were analyzed for:

age, ECOG Performance Status (PS), reasons for discontinuation, Gleason score and results of laboratory tests - ALP, PSA, Albumin, Hemoglobin, Platelet count and Leukocyte count. Results from the two groups were compared using T-test. **Results:** Reasons for discontinuation in group B were: low hemoglobin and platelet count in 3 cases, death during the course of treatment in 2 cases and a new visceral liver metastasis in 1 case. There was no statistically significant difference between the groups in age, PS, Gleason score, values of ALP, albumin, leukocyte and platelets counts at the start of the treatment (p = 0,11 - 0,47). On the other hand, there was a statistically significant difference in PSA and hemoglobin. Group A had a lower PSA value (mean = 103 ng/ml, sd = 125) than Group B (mean = 503 ng/ml sd = 448) p = 0,04. The hemoglobin value in Group A was higher (mean =12,8 g/dl sd = 9) than in group B (mean = 11,3 g/dl sd = 18) p = 0,05. **Conclusion:** Overall 11 out of 17 patients (61 %) were able to complete the treatment. There were two factors contributing to discontinuation of treatment. Firstly, higher PSA values at the start of the treatment which could suggest more advanced disease. Secondly, lower hemoglobin values at the time of initial injection. These could further aggravate the Ra-223 dichloride negative effect on bone marrow, leading to low hemoglobin and platelets counts. **References:** None.

EP-0541

A Single Centre Experience with 223-Radium-Dichloride ($^{223}RaCl_2$) Therapy

R. Laudicella, F. Minutoli, A. D. Comis, A. Vento, H. Lanzafame, B. Catalfamo, F. Panasiti, C. Mantarro, S. A. Pignata, B. Pagano, S. Baldari;
Unit of Nuclear Medicine, Messina, ITALY.

Aim/Introduction: $^{223}RaCl_2$ is an alpha-emitter radiopharmaceutical approved for the treatment of patients affected by symptomatic bone metastases from castration-resistant prostate cancer (mCRPC), without any visceral metastases. In this study, we describe our experience evaluating the effectiveness, safety and haematological toxicity of $^{223}RaCl_2$ treatment. **Materials and Methods:** We retrospectively evaluated fifty-seven patients (mean age 73.03±7.38 years, range 57-89) with mCRPC, who received 55kBq/kg of $^{223}RaCl_2$, intravenously every 28 days for a maximum of 6 cycles (median 3.5, range 1-6). At enrolment, Gleason-Score was>6 in 67% and 40/57 patients (70%) had>10 bone lesions. 34/57 patients were previously treated with docetaxel. Computed-tomography (CT) and bone-scan were performed in all patients at enrolment and 3-months after the last administration. Complete blood counts, serum alkaline-phosphatase (ALP), prostatic-specific antigen (PSA), pain-score and painkiller drug-intake were evaluated at enrolment, before and after each $^{223}RaCl_2$ administration. **Results:** Overall, 237 administrations were performed in 57 patients; 35/57 patients received at least 4 administrations and 22/57 completed the 6 cycles of treatment. Mean PSA and ALP at enrolment were 429.64 ng/ml and 218.03 U/l, respectively. At baseline, mean values of pain-score, haemoglobin, white-blood cells and platelets-counts were 4.61±2.8, 12.37±0.92 g/dl, 3,966±485.19/mmc and 214,723±141.889/mmc, respectively. 34/57 (60%) patients experienced a condition of pain-relief/stabilization and reduced painkiller drug-intake, whereas 23/57 had mildly worsened the symptom. The percentage of patients showing a reduction in PSA values increased with the number of $^{223}RaCl_2$ administrations (R^2 =0.9975, P=0.0319). ALP values decrease was higher than PSA reduction, reaching a mean value of 79% after 4 administration (63% after 5 and 71% after 6 cycles). We registered only 1 skeletal-event (vertebral osteoporotic fracture). After last treatment, only one patient had severe anaemia (haemoglobin reduction between 6.5-7.9 g/dl); 11/15 patients with moderate-severe anaemia were previously treated with docetaxel (respectively, among them, mean haemoglobin levels at baseline and after last administration were 11.73±1.38 g/dl and 10.54±1.96 g/dl, P<0.001). Mild-moderate thrombocytopenia occurred in 9/57 patients (16%). At the imaging follow-up, we observed improvement/stabilization of bone lesions in 34/57 (59%) and a progression in 23/57 patients (41%). **Conclusion:** $^{223}RaCl_2$ can be safely used, with only a few cases of moderate/severe haematological toxicity (mainly in patients previously treated with docetaxel). This approach allowed to reach significant pain-relief with reduction of painkiller drug consumption, imaging response and biomarkers decrease in the majority of patients with a favourable hematologic toxicity profile; namely, in our experience, ALP% values declined earlier than PSA% values. **References:** None.

EP-0542

Value Of Dosimetry, Analytical Data And Imaging Tests In The Monitoring Of Bone Metastases Response Treated With ^{223}Radium (Xofigo) In Patients With Metastasic Castration-Resistant Prostate Cancer

M. Alonso Rodriguez, C. Andrés Rodríguez, B. Pérez López, C. Gamazo Laherrán, J. Gómez Hidalgo, M. A. Ruíz Gómez, V. De la Llana Granja, P. J. Turbay Eljach, N. Álvarez Mena, M. Agulla Otero, R. Torres Cabrera, R. Ruano Pérez;
Hospital Clínico Universitario de Valladolid, Valladolid, SPAIN.

Aim/Introduction: To assess the value of the absorbed dose of ^{223}Radium (Xofigo), analytical data and posttreatment imaging findings (bone scintigraphy and/or CT) in the evaluation of bone metastases response to treatment. **Materials and Methods:** We retrospectively reviewed 25 patients treated with ^{223}Ra from 2015 to 2019, of them 9 patients with completed full treatment (6 doses) were selected. Dosimetric calculation was done after each dose of ^{223}Ra . Total absorbed dose (Gy) of more intense uptake foci and total DRBE (relative biological effectiveness RBE-weighted absorbed dose) were calculated from whole body planar images and SPECT/CT performed 48h after the administration of ^{223}Ra and from images of relevant regions 168h after treatment. We collected analytical data (PSA and alkaline phosphatase), clinical data (improvement, stabilization, deterioration) and imaging findings in bone scintigraphy and/

or CT performed 2 months after treatment (partial response, stabilization or progression). **Results:** Of the 9 patients selected with dosimetric calculation after each dose of ^{223}Ra, one patient was not evaluated because of interposition of intense intestinal uptake. Average total absorbed dose (Gy) by lesion was 9.85 (range 1.7-28.6 Gy) and total DRBE (Gy) 49.25 (range 8.4-143.1Gy). Regarding PSA level, the 77.8% (7/9) of patients showed an increase (from 6 to 469 ng/ml posttreatment) and the 22.2% presented a decrease. All patients presented a significant decrease in alkaline phosphatase posttreatment levels (from 621 UI/L before treatment to 39 after treatment). Pain intensity collected from subjective data of patients and changes in their analgesic therapy showed improvement in 3 patients, stabilization in 5 and deterioration in 1. Regarding imaging evaluation 2 months after treatment, was performed with bone scintigraphy 7 and thoracic-abdominal-pelvic CT in 2. Imaging findings revealed partial response in 4 cases, stabilization in 1 and progression in 4. **Conclusion:** In the monitoring of bone metastases response to treatment, estimation of absorbed dose of ^{223}Ra along with clinical data of pain intensity shows an important value, because a higher DRBE is related with improvement or stabilization of pain, irrespective of PSA level and imaging findings after treatment. **References:** None.

EP-0543

Evaluation of the efficacy and safety of radio-223 dichloride in prostate Bone- metastatic Castration-resistant Prostate Cancer in our hospital

M. Asensio Ruiz[1], *Á. García Aliaga*[1], *A. Abella Tarazona*[1], *M. Soria Soto*[2], *M. Claver Valderas*[1], *M. Martínez Martínez*[1];
[1]*Hospital Clínico Universitario Virgen de la Arrixaca, Murcia, SPAIN,*
[2]*Hospital General Universitario Morales Meseguer, Murcia, SPAIN.*

Aim/Introduction: The indications in the product information of radio-223 dichloride were modified in June 2018, becoming third-line treatment in prostate Bone metastatic Castration-resistant Prostate Cancer (CRPC), as a result of these changes we have evaluated the efficacy and safety of this radiopharmaceutical in our hospital. **Materials and Methods:** Retrospective observacional study of all patients treated with radio-223 from December 2016 to April 2018 in our hospital. Demographic, diagnostic, therapeutic and clinical variables were collected. The response was assessed through the progression-free survival (PSF) and overal survival (OS). To asses the safety all treatment-related adverse events were recorded. **Results:** The studies were conducted on 36 men with CRPC treated with radio-223 dichloride with a mean age of 70.2 years (SD = 9.7), 42.4% ECOG 0-1, 36.4% ECOG 2-3. 5.6% received the treatment as first line, 61.1% as second line, 27.7% as third line and 5.6% as fourth line or higher. The mean dose that was administered was 4.6 MBq (SD = 0.7). 50% of patients did not complete the 6 cycles of radio-223 due to adverse reactions or worsening of the disease. 8.4% of patients reduced PSA by more than 40%. The mean of OS was 7.9 months (CI 6.3-9.5) and the PFS 4.1 months (IC 3.3-4.9). There is a significant correlation between the increase in OS and PFS with respect to the number of doses administered. The patients who received all the treatment (6 doses), had a higher OS compared to those who did not finish the treatment, 9.7 months versus 6.1 months respectively. 55.5% of the patients suffered thrombocytopenia, neutropenia and anemia grade 1-2, 8.3% thrombocytopenia and anemia in grade 3-4, 22.2% gastrointestinal effects such as nausea, vomiting and diarrhea and 11.1% noticed worsening in bone pain. **Conclusion:** PFS and OS observed in this study are lower than indicated in the clinical trials. This fact could be explained by a worse Performance Status and because approximately 40 % of patients were treated with radio-223 dichloride as third line or higher. Radio-223 was well tolerated, serious adverse hematological effects led to treatment interruption but the rest were clinically manageable. **References:** None.

EP-36

Clinical -> Therapy study -> Adult study -> Other treatments -> Local radionuclide treatments

October 12 - 16, 2019 e-Poster Area

EP-0544

Analysis of Prognostic Factors in Patients Who Received Transarterial Radioembolization for Unresectable Hepatocellular Carcinoma

C. Soydal, *D. Nak, M. Araz, P. Akkus, M. H. Baltacioglu, N. O. Kucuk;*
Ankara university medical faculty, Ankara, TURKEY.

Aim/Introduction: We aimed to analyze prognostic factors of patients who received transarterial radioembolization (TARE) for unresectable hepatocellular carcinoma (HCC). **Materials and Methods:** Eighty-six (73M, 13 F; mean age: 64.3±9.8) patients who received TARE for unresectable HCC were included to the analysis. Relationship between serum AFP and INR level, ALBI grade, NLR, presence of PVT, extrahepatic metastases, dimension of index lesion and overall survival was analyzed. **Results:** While 13 (15%) of patients had a history of liver surgery, 13 (15) and 12 (14%) had failure of previous radiofrequency ablation and TACE. Child-Pugh grade was calculated as A, B and C in 54 (67%), 24 (30%) and 3 (3%) of patients. Median serum AFP level was calculated as 24.4 (min-max: 1.4-49289). ALBI grade was 1 and 2 in 67 (78%) and 19 (22%) of patients. NLR was ≤5 in 76 (88%) and >5 in 10 (12%) of patients. PVT was detected in 30 (35%) patients. While 7 (8%) patients were in BCLC stage A group, 54 (63%) and 25 (29%) patients were in B and C groups, respectively. During pretreatment evaluation, extrahepatic metastases was detected in 20 (29%) patients. Resin and glass microspheres were used in 80 (93%) and 6 (7%) of patients. Sixty-two (72%) patients were died during mean 25.6±9.7 months follow-up period. Mean OS for all patients were calculated as 12.9±14.6 months. In univariate analysis,

ALBI grade (22.3±3.8 vs 11.6±4.2;p=0.03), NLR (21.8±3.6 vs 7.3±2.6;p=0.04), presence of extrahepatic metastases (30.1±5.4 vs 7.4±2.0;p=0.001) and PVT (26.5±4.8 vs 10.5±2.1;p=0.01). In multivariate analysis, serum INR level (p=0.005) and AFP level (p=0.004), ALBI grade (p=0.05), NLR (p=0.007), Child-Pugh score (0.006), presence of ascites (p=0.005) were significantly correlated with OS. **Conclusion:** Serum INR and AFP levels, ALBI grade, NLR, CP-score and presence of ascites seems to significant prognostic factors for patients who received TARE for unresectable HCC. **References:** 1. Rodolfo Sacco,Caterina Conte, Emanuele Tumino, Giuseppe Parisi, Sara Marceglia, Salvatore Metrangolo, Roberto Eggenhoffner, Giampaolo Bresci,Giuseppe Cabibbo, and Luca Giacomelli. Transarterial radioembolization for hepatocellular carcinoma: a reviewWorld J Gastroenterol. 2015 Jun 7; 21(21): 6518-6525. 2. Joseph Ralph Kallini, Ahmed Gabr, Riad Salem, and Robert J. Transarterial Radioembolization with Yttrium-90 for the Treatment of Hepatocellular Carcinoma Lewandowskicorresponding authorAdv Ther. 2016; 33: 699-714.

EP-0545

Beta-Emitting Lanthanoids (^{90}Y and ^{166}Ho) Labelled with Hydroxyapatite Particles: Formulation, Quality Control and Bio-evaluation for Radiosynovectomy

S. Batool[1,2], *M. Sohaib*[1], *S. Fatima*[2], *A. Ammar*[2], *K. Mir*[2], *M. Faheem*[2]; [1]*Pakistan Institute of Engineering and Applied Sciences (PIEAS), Islamabad, PAKISTAN,* [2]*Department of Nuclear Medicine, Nuclear Medicine, Oncology and Radiotherapy Institute (NORI), Islamabad, PAKISTAN.*

Aim/Introduction: The aim of this study was formulation and quality control of the lanthanoids (^{90}Y and ^{166}Ho) labelled with HA-particles along with their bio-evaluation in animal models for leakage out of joint space for possible use in the radiosynovectomy. **Materials and Methods:** These lanthanoids were prepared by (n, γ) reaction. Paper chromatography was used for radiochemical quality control of these lanthanoids. Hydroxyapatite particle size was determined with laser particle size analyzer. In-vivo bio-evaluation studies were performed in two rabbit models to assess leakages and biological half-lives. **Results:** Hydroxyapatite particles (95%) were in the range of 0.6µm-6.1µm. Adequate specific activities of these lanthanoids were produced by irradiating their natural targets. Radio-labeling efficiencies came out to be 99.5% for ^{90}Y-HA and 99.8% of ^{166}Ho-HA.They showed high stability at room temperature for 5 days. In vivo-bio-evaluation studies in rabbits showed no visual leakage of activity out of joint space after injecting the radiopharmaceutical. Average leakages measured indirectly from the residing time of the radiopharmaceuticals in the synovial cavity at third day post-injection were 11.5% & 3% for ^{90}Y-HA & ^{166}Ho-HA respectively. **Conclusion:** This study reveals HA particles labeled with the beta-emitting lanthanoids are suitable for use as therapeutic agents for radiosynovectomy for clinical management of synovitis. **References:** None.

EP-0546

Efficacy of radiosynoviorthesis after the surgery in pigmented villonodular synovitis of the knee

Z. Mangel[1], *G. Nagy*[1], *Z. Farbaky*[2], *M. Szentesi*[1]; [1]*Department of Rheumatology, Polyclinic of the Hospitaller Brothers of St. John of God, Budapest, HUNGARY,* [2]*Department of Radiology, Polyclinic of the Hospitaller Brothers of St. John of God, Budapest, HUNGARY.*

Aim/Introduction: Pigmented villonodular synovitis (PVNS) is a rare disorder with the benign tumoral proliferation of the synovium. The surgical treatment of PVNS alone in most cases is unsatisfactory, because if a few cells have not been removed, the disease will recur. Post-synovectomy adjuvant treatment with intra-articular injection of Yttrium-90 (^{90}Y) or Holmium-166 (^{166}Ho) yielded better results. The radiosynoviorthesis (RSO) is an effective way of treating the chronic synovitis, with this method we are eliminate the inflammation in 75 percent of the cases. **Materials and Methods:** Between May 1986 and August 2018, 17 patients (seven men and ten women aged 14-68 years) with diffuse PVNS were treated. All patients had monoarticular arthritis of the knee with histologically proved PVNS. The patients underwent 33 operations, two patients had four surgical procedures, one patient underwent three surgeries, eight patients had two surgeries and six patients had one surgical procedure. The radiosynoviorthesis was performed according to the method accepted in the national protocol.Yttrium-citrate injectable suspension marked by 185 MBq 90Y-citrate injectable suspension, and 40 mg of 1 ml triamcinolone acetonide and 1 ml of lidocaine 1%. Holmium-phytate injectable suspension marked by 600 MBq 166Ho-phytate injectable suspension, and 40 mg of 1 ml triamcinolone acetonide and 1 ml of lidocaine 1%.[1] Evaulation was based on the criteria as described by Müller, Rau and Schütte the score system was developed by the authors. The circumference of joint-swelling, the joint function, the measure of flexio-contracture, pain in state of rest and load on a pain analogue scale 1-10, joint warmth, walking capacity, the numbers of joint-punctions after the treatment, whether operation was necessary or not after the treatment were examined. **Results:** Mean follow-up time was 56 months (range from 4 to 144 months). All patients were followed up using clinical assesment. After the first injection excellent and good results were recorded in 41%. After the second radiosynoviorthesis thirteen patients (76%) showed excellent and good response. The mean functional evaluation score of 17 patients was 28 (range 16-34). Most of the ratings were excellent or good, in four cases moderate (24%). No complications were noticed after surgery or after the radiosynoviorthesis. **Conclusion:** A combination of debulking surgery with radiosynoviorthesis of Yttrium or Holmium for diffuse PVNS of the knee joint is a reliable treatment method, with good results. **References:** 1. EANM Procedure Guidelines for Radiosynovectomy, Eur J Nucl Med (2003) 30:BP12-BP16, Vol. 30, No.3, March 2003.

EP-0547

Therapeutic response of radiosynoviorthesis in knee haemarthrosis: a case series after total knee replacement

I. Iakovou, T. Kotrotsios, E. Giannoula, A. Kalaitzoglou, C. Sachpekidis, K. Michailo, G. Arsos;
Academic Dpt Of Nuclear Medicine, Papageorgiou Hsp, Thessaloniki, GREECE.

Aim/Introduction: Knee hemarthrosis is the result of injury, bleeding disorders, osteoarthritis, postoperative complications, neuropaticarthropathy, vascular disorders septic arthritis and tumors. Radiosynoviorthesis (RSV) is a technique of local and minimally invasive radiotherapy, being used for more than 60 years for the treatment of a range of refractory painful synovitis. Particularly in haemarthrosis, RSV has been proven safe and effective in the treatment of chronic, recurrent disease, mostly in the context of hemophilic arthropathy. **Aim:** Recurrent hemarthrosis after total knee replacement (TKA) is a rare but not uncommon complication.The aim of the current work is to present our experience of 12 cases of RSO in 9 patients after TKA complication as a safe and efficient alternative in the treatment of knee not haemophillic haemarthrosis. **Materials and Methods:** Nine patients with painful recurrent haemarthrosis after TKA underwent RSV with 90Y after failure of conservative and arthroscopic treatment. Three of them underwent 2 RSO procedures due to recurrent haemarthrosis. Pre treatment bone scintigraphy revealed hyperemic joints in 7 patients. Response to RSO was evaluated 1,3,6 months, with a maximum follow-up of 3 years by clinical examination to evaluate arhtralgia, range of motion and recurrent joint bleeding. **Results:** resposne to treatment and clinically pain relief was evident for 7 (77.8%) patients. Joint bleeding recurrence was reported in 3 (33.3%) cases and underwent a second RSV. Range of motion returned to normal for 7 (77.8%) patients. **Conclusion:** In cases of hemarthrosis after TKA, RSV should have place in the therapeutic armamentarium of the treating physician, as a minimally invasive, safe, and efficient therapeutic tool. **References:** J Arthroplasty. 2008 Sep;23(6):931-3. doi: 10.1016/j.arth.2007.07.012. Epub 2008 Mar 4.Recurrent spontaneous hemarthrosis after total knee arthroplasty successfully treated with synoviorthesis Kapetanos GA1, Papavasiliou KA, Makris V, Nikolaides AP, Kirkos JM, Symeonides PP.

EP-0548

Ecoguided Radiosynovectomy (RS). Therapeutic Effects

S. Menendez Sanchez, A. Garcia-Burillo, M. de Albert-de Delás, E. Carrillo-Villamizar, D. Villasboas-Rosciolesi, A. Cardozo-Saavedra, J. Castell-Conesa;
HUVH, Barcelona, SPAIN.

Aim/Introduction: Radiosynovectomy (RS) is an anti-inflammatory synovial treatment based on destruction of superficial synovial. Beta isotope emmisor is injected inside the joint without affecting bones, muscles or other structures. The aim of this study was to determinate the ecoguided RS in inflammatory joint pathologies after the failure of conventional treatments. The radionuclides used were 99mTc-90-Yttrium (90Y) , 99mTc-169-Erbium (169Er), 99mTc-186-Rhenium (186Re). **Materials and Methods:** 35 RS were evaluated between May 2016 and December 2018 that have taken place in 33 patients (24 women/9 men) affected by inflammatory joint pathology. We received 42 request but 7 were not recommended after ecography evaluation. The treatment used was 90Y in 22 knees pathology, 186Re in 9 medium size joints (5 elbows, 2 wrist, 2 ankles) and 169Er in 4 small size joints all of them metacarpophalangeals. The procedure of RS was always ecoguided and the properly radiopharmaceutical distribution was confirmed by scintigraphy images of the area. Patients had medical control with a nuclear doctor before and 2- 6 months after the precedure. They answered a subjective pain questionnaire using VAS scale. Pacients were classified in three groups according to their answers: VAS <4: Mild, VAS: 5-7: moderate and VAS >7: Severe. **Results:** Before treatment the patients were classified in two groups: 12/35 VAS moderate and 13/35 severe. Two months after the joint infiltration 22/35 VAS mild, 9/35 VAS moderate and 4/35 VAS severe. Six months after patients were classified as: 13/35 mild, 13/35 moderate and 9/35 severe. Three patients never changed their status from severe pain meanwhile 32 of them had a decrease pain, increase of movility and absence of swelling by the second month. 36.1% of the analized patients remained without symptoms by the sixth month. Immediate complications weren't detected for the 35 treatments. One patient registered a late complication as artrhitis of metacarpophalangeal even though once the infection episode was solved the patient reported clinal improvemt of the RS. **Conclusion:** Ecoguided RS is a safe procedure with a high therapeutic efficacy and low complications index. Effectiveness was shown in 91.6% of the cases by the second month. It represents a surgery and sclerosing treatments alternative although only 75% remain after 6 months. **References:** None.

EP-0549

Yttrium-90 Radioembolization for Unresectable/Recurrent Intrahepatic Cholangiocarcinoma

C. Pettinato[1], C. Mosconi[2], A. Cappelli[2], E. Tabacchi[3], E. Lodi Rizzini[4], F. Monari[4], S. Civollani[1], S. Fanti[3], L. Strigari[1];
[1]Medical Physics - AOU S. Orsola Malpighi - Bologna, Bologna, ITALY, [2]Radiology - AOU S. Orsola Malpighi - Bologna, Bologna, ITALY, [3]Nuclear Medicine - AOU S. Orsola Malpighi - Bologna, Bologna, ITALY, [4]Radiotherapy - AOU S. Orsola Malpighi - Bologna, Bologna, ITALY.

Aim/Introduction: Intrahepatic cholangiocarcinoma (ICC) is a rapidly progressing malignancy; only a minority of the tumors can be resected and the palliative regimens have shown limited success. The aim of this study was to assess overall survival, tumor response and the safety of radioembolization with yttrium-90 (^{90}Y-TARE) in patients with unresectable/recurrent ICC. **Materials and Methods:** Survival was calculated from the

date of the ^{90}Y-TARE procedure. Target and overall response were measured using EASL criteria. **Results:** Thirty five patients with unresectable ICC were treated with radioembolization using Y90 resin microspheres at a single institution from July 2010 to December 2018. Injected activity was calculated using MIRD model with three compartments, tumor, liver and lungs, based on pre-treatment 99mTc-MAA SPECT images.Mean injected activity, tumor dose, normal liver dose and survival were respectively 1.4 GBq (range: 0.6 - 2.4 GBq), 455.7 Gy (range: 72.3 - 1959.5 Gy), 13.9 Gy (range: 3.1 - 44.2) and 13.8 months (range: 1.9 - 34.7).In terms of overall survival 4/35 patients died within the firs three months: excluding these 4 patients from the analysis the mean survival was 15.3 months ranging from 4 up to 34.7 months. 7/35 patients showed a survival of less than 6 months, while 18/35 had a survival greater than 10 months. Treatment was well tolerated, and no mortality was reported within 30 days. **Conclusion:** In unresectable ICC, ^{90}Y-TARE is safe and offers a survival benefit and the majority of patients were good responders. **References:** None.

EP-0550

Current experience in our center with transarterial radioembolization (TARE) of inoperable liver lesions

M. Moreno-Caballero, A. Martínez-Esteve, P. Jiménez-Granero, A. Cobo-Rodríguez, J. Infante-de la Torre, J. Serrano-Vicente, J. Rayo-Madrid;
Departamento de Medicina Nuclear. Hospital Universitario de Badajoz, Badajoz, SPAIN.

Aim/Introduction: International guidelines recommend locoregional therapy, transarterial chemoembolization or systemic drugs as the first line of treatment in inoperable hepatic lesions. The use of Y-90 has become another well-accepted option, increasingly widespread in hospitals around the world. The aim of this work is to reflect the experience acquired in our center with the use of glass spheres of Y-90 (TheraSphere®). **Materials and Methods:** Descriptive study of case series, from April 2016 to May 2018. All patients included were decided in joint multidisciplinary committee. The existence of inoperable hepatic lesions (primary or metastatic) was considered for the treatment, when the other therapeutic alternatives presented limitations. In all cases, the liver constituted the organ with the greatest clinical impact. The planning studies were carried out with arteriography, scintigraphic planar images and SPECT/CT-MAA. Immediate control of the therapy was performed with abdominal PET/CT 24 hours after TARE, while the response evaluation was made with three-phase CT scan. **Results:** Ten patients, 6 men and 4 women were included, mean age 65 years [47-81]. Of them: 1 multiple metastases of colon adenocarcinoma (stage IVB), 1 multicentric cholangiocarcinoma (stage IVA) and 8 hepatocarcinomas, 2 of which had exclusive unilobar involvement and 6 were bilobar multicenter (intermediate and advanced stages of BCLC). Mean hepatopulmonary shunt of 4.9%; target volume average 1220 cc; activity average required in the administration of 1.8 GBq. In 1 patient, the cystic artery was embolized preventatively. Of the 8 patients in whom it was necessary to treat both lobes, 4 received sequential treatment in 2 times, with an interval of 30 days. In 1 of them there was neovascularization, with 80% non-correctable pulmonary shunt that made it impossible to complete the treatment. All patients treated presented concordance of SPECT/CT-MAA and post-therapy PET/CT images. Following response criteria in the first quarterly post-treatment control, 5 presented partial response (PR), 1 Stable Disease (SD) and 3 Progressive Disease (PD). There was only 1 mild complication due to cutaneous rash and post-radioembolization fever. The median survival was 9 months [2-18], being lower for the patient with multiple metastases of colon adenocarcinoma. **Conclusion:** In our experience, TARE showed good tolerance in all patients. The median survival was slightly lower than the data reflected in the literature; however we consider that the high global tumor burden conditioned our results. **References:** None.

EP-0551

Transarterial Radioembolization for the Treatment of Liver Metastases from Medullary Thyroid Cancer: Dose-Response Relationship and Estimate of the Radiobiological α Parameter

G. Boni, T. Depalo, I. Bargellini, L. Puleo, F. Bianchi, G. Lorenzoni, F. Guidoccio, A. Faranda, A. C. Traino, R. Cioni, R. Elisei, D. Volterrani;
University Hospital of Pisa, Pisa, ITALY.

Aim/Introduction: Liver metastases (LM) occur in 45% of patients with advanced medullary thyroid cancer (MTC). In some cases, LM cannot be treated with surgery or RFA/TACE, especially when a multifocal and a bilobar extension is present. Aim of this study is to investigate the efficacy of transarterial radioembolization (TARE) in patients with LM from MTC. **Materials and Methods:** Seven patients (6 M and 1 F; mean age 56±10 years) with predominant liver disease from MTC, previously selected by MRI or CT scans, underwent a pre-TARE planning angiography followed by a liver perfusion study with Tc99m-MAA SPECT/CT. TARE with Y90 resin microspheres was performed 7-14 days late and the administered activity was determined using the BSA method. Post-TARE Y90-PET/CT was performed within 24 hours. Post-treatment 3D dosimetry based on Y90-PET/CT allowed to calculate tumor average absorbed dose. Response to TARE was based on mRECIST criteria. Tumor volumes based on CT, serum calcitonin (Ct) and CEA levels were assessed before and after treatment. In selected cases, the radiobiological α parameter was calculated using a simplified linear quadratic model (LQM). **Results:** A total of 11 TARE procedures were performed (4 bilobar treatments and 3 unilobar treatments). The mean injected activity was 936±464 MBq. On CT at 4 months after treatment, we observed 2 CR (21.8%) and 5 PR (71.4%). A significant reduction of the treated tumor volume was also found (21.6±20.2 ml pre-TARE vs 2.1±1.8 ml post-TARE; $p = 0.002$). Serum Ct showed a significant reduction at one month after TARE (2982 vs 2657 ng/L; $p < 0.02$) and after 4 months of follow-up (2982 vs 2687 ng/L; $p < 0.04$).

In addition, mean CEA levels decreased at one month after TARE although not statistically significant (151 vs 111 µg/L; p = 0.08). The average absorbed dose to the tumor and to the healthy liver based on post-TARE 3D dosimetry resulted 239±173 Gy and 43±9 Gy, respectively. A significant direct relationship between the logarithm of tumor absorbed dose and its volumetric reduction was observed (r^2= 0.49; p < 0.03). The mean value of the estimated radiobiological α parameter was 0.013±0.007 Gy^{-1}. **Conclusion:** In our preliminary experience, TARE with Y90 microspheres seems to be an effective option for the treatment of LM in patients with advanced MTC. However, more data are needed to assess the long-term effects of TARE and the impact of this approach on the overall survival of these patients. **References:** None.

EP-0552

Knee Leackage Studies After Radiosinoviorthesis With Gamma Camera In Patients Treated With Chronic Synovitis

Z. Nagy[1], *E. Takács*[1], *Z. Mangel*[2], *P. Géher*[2], *M. Szentesi*[2];
[1]*Polyclinic of the Hospitaller Brothers of St. John in God Dept. of Nuclear Medicine, Budapest, HUNGARY,*
[2]*Polyclinic of the Hospitaller Brothers of St. John in God Dept. of Reumatlogy, Budapest, HUNGARY.*

Aim/Introduction: To analise the leackage percent of the injected radiopharmaceutical in the knee joint after 72 hours of radiosynoviorthesis with a planar gamma camera. **Materials and Methods:** 54 patient treated with Ho-166 labelled Phytate, 29 female and 25 male, mean age: 60±10.6 year. 81 patient treated with Y-90-citrate, 49 female and 32 male, mean age:58±13.5 year. In all of the 135 patients after 72 hours planar gamma camera images of the treated knee, the inguinal region and liver with the same parameters. Acquisition parameters for the Ho-166: 1 minute image with two peacks: 80keV and 110 keV, in a 128 matrix , for the Y-90: 5 min image at 80keV in a 128 matrix size. During the study we observed a large scale of different distribution of the injected isotopes in the knee joints so we added further scores: 1. the injected activity remained at the place of the injection, 2. the injected activity has been partially distributed in the knee and: 3. total distribution could be seen on the acquired images. **Results:** In all of the 135 patients a scatter from the knee region influenced the activity amount in the inguinal region however in some cases we could observed lymh nodules. The inguinal region activity in case of the Ho-166 isotope was: 11±4.3%, in case of the Y-90 isotope was: 15.8±14.8%. The liver activity was in case of Ho-166: 1,5±0.5%, in case of of Y-90: 4,11±1,5%. Overall the differnces between the two isotopes do not reflect the real leakage, becouse of the very different physical qualities. The most unexpected result of our study was the very different distribution of the injected isotope in the knee joint. The results regarding the point scores: in case of Ho-166: 2,6±0,6; in case of Y-90: 2,2±0,8. **Conclusion:** 1. in the analized 135 patients there is a no significant leakage using the isotopes availeble. 2. the analizis of the inguinal region can not be applied for routine leakage exam, but sometimes lymph nodes can be detected. 3. the imaging of the treated knee joint with RSO could show a very different distribution within the joint, therefore could have further clinical consecvencies. With other alternatives maybe that during the ultrasound exam the existing plicas within the knee joint could be a contraindication of RSO. This clinical study now is already runing in our Hospital. **References:** None.

EP-0553

Radioembolization of hepatic artery with 90 itrio cristal microspheres, for the treatment of patients with irresecable hepatic tumors

I. López Villar, *A. Martínez Lorca, P. Paredes Rodríguez, T. Navarro Martínez, P. Jane Soler, J. Bonilla Plaza, M. Orduña Díez;*
Ramón y Cajal University Hospital, Madrid, SPAIN.

Aim/Introduction: Unresectable liver tumors (primary or metastatic) obtain 80-100% of their blood supply from the arterial hepatic circulation, instead of the portal. Radioembolization RE with 90Y of the hepatic artery, is a therapeutic option for these tumors, as 2nd or more line in combination and / or alternative to biological agents. **Materials and Methods:** A retrospective study and follow-up of 47 RE, was carried out in Ramón y Cajal Universitary Hospital (November 2014- January 2019); We administered 47 RE in 36 patients (29 men- 7 women) with hepatocarcinoma primary 29 cases (1 single lesión 28 multicentric) and with metastatic (7 cases). Age (50-84 mean 61). Prior to therapy, the tumor irrigating vessels were mapped with 99m Tc-MAA 10-15 days before treatment. In the planning stage, the hepatic SPECT-CT study verified that the catheterized artery was the one that irrigated the tumor, in addition we estimated liver volume to be treated and evaluated the pulmonary shunt. Prophylactically selected artery was embolized to avoid extrahepatic deposition of microspheres. 90Y is a beta emitter with a half-life of 64.1 hours. After the treatment, the bremsstrahlung was explored to verify the distribution of the tracer administered. On 3 selected cases post 90Y SIRT (Selective Internal Radiation Therapy) imaging were scanned on PET/CT scanner. Line profiles through this sphere were taken on both the SPECT and PET images to compare how effectively each modality could recover the true activity distribution. Clinical and imaging follow up using MRI and/or CT. (3-12 moths in 36 cases) **Results:** In 30% patients (11/36) the treatment was rejected due to: shunt greater than allowed (10 p) and (1 p) patient died before SIRT. Eleven patients received 2 treatments in 2 years. The disease control rate was 72% (18/25 p) with: stable disease (12/25 p) and partial response (9/25 p). The disease progression rate was 28% (7/25 patients). Good initial tolerance except 6/25 cases (mild digestive symptomatology). There were no statistical difference between primary or metastatic lesions (50% vs 49%) with regards to progression disease p>0.05 not significant. **Conclusion:** 90Y crystal microspheres is a rescue therapy modality, efficient and safe, which lengthens the time to the progression of the disease. Research would be recommended in clinical situations in which the disease is

strictly limited to liver. Optimised PET/CT is a basis from wich to carry out individualised patient dosimetry in the present-future. Multidisciplinary collaboration is essential. **References:** None.

EP-0554

Radiosynovectomy in Refractory Synovitis - Initial Experience at Groote Schuur Hospital

S. More[1], *A. Cruickshank*[2], *B. Hodkinson*[3];
[1]*Division of Nuclear Medicine, Groote Schuur Hospital, Cape Town, SOUTH AFRICA,* [2]*Haemophilia Comprehensive Care Centre, Groote Schuur Hospital, Cape Town, SOUTH AFRICA,* [3]*Division of Rheumatology, Department of Internal Medicine, Groote Schuur Hospital, Cape Town, SOUTH AFRICA.*

Aim/Introduction: Radiosynovectomy (RSO) has been available for more than 50 years to alleviate the pain and swelling caused by chronic synovitis. We evaluated the efficacy of RSO performed at Groote Schuur Hospital in patients with haemophiliac arthropathy and other arthritides. **Materials and Methods:** Before RSO, all patients underwent joint sonography and bone scan to confirm active synovitis. A clinical exam, visual analogue scale (VAS) for pain and the HAQ-DI score were performed at baseline and 6 weeks post therapy. Adverse events and number of bleeds (in Haemophilia patients) were documented. **Results:** Since 2017, 13 patients have received RSO: Nine patients had severe Haemophilia A. In the remaining four patients, two had Rheumatoid Arthritis, one with an undifferentiated arthritis of the left knee confirmed on histology; one patient had a reactive arthritis of both knees - all these patients were refractory to their current therapies. Seven knees were treated with 185-222MBq of Yttrium90, two elbows and four ankles were treated with 74 - 111MBq of Rhenium 186 colloid.A significant reduction in pain VAS was seen in all the patients (Score 8(range 7-10) pre RSO to 1.0(range 1 -6) ($p<0.05$). In addition, a significant drop in the target joint bleeding was seen (6.6 bleeds per month to 0.7 bleeds per month)($p<0.05$) in the haemophilia patients. In all the patients who were not haemophiliac, there was an improvement in the HAQ scores (range 0.3 - 2.0) pre RSO to a (range 0.3 - 1.15) post RSO. No major adverse events were reported by any patient. **Conclusion:** In this small cohort, RSO was safe and effective in the short term. We plan to increase the cohort size and complete long term follow up **References:** None.

EP-0555

Determining factors of response to radioisotope synoviorthesis. Our experience over 10 years

E. Noriega, *W. R. Marínez Bravo, F. J. Pena Pardo, A. M. Gracía Vicente, G. Jiménez Londoño, M. E. Bellón Guardia, N. D. Disotuar Ruiz, E. Casillas Sagrado, A. M. Soriano Castrejón;*
University Hospital of Ciudad Real, Ciudad Real, SPAIN.

Aim/Introduction: University Hospital of Ciudad Real is the nuclear medicine referral hospital for radioisotopic synoviorthesis for all of Castilla-La Mancha. The objective of this study was to identify response factors to synoviorthesis in patients with refractory arthritis. **Materials and Methods:** Observational descriptive study of patients with refractory knee arthritis and indication of radioisotopic synoviorthesis performed between 2007 and 2017. Clinical data collected: age, gender, basic pathology (pigmented villonodular synovitis, rheumatoid arthritis, spondyloarthritis, osteoarthritis and nonspecific arthritis), previous treatments (analgesics, first line anti-inflammatory, second line corticosteroids and third line biologic treatment) and clinical follow-up of at least 6 months after the administration of radioisotope. Patients were considered in clinical remission, when they showed remission of the pain and normal clinical examination after the treatment. Frequencies were calculated for the categorical variables and their difference was measured by the Chi-square statistical test. Uni and multivariate analysis were performed to determine the factors associated with remission ($\alpha=0,05$ to be statistically significant). Descriptive analysis of the data was performed using the statistical program Stata 14.2. **Results:** Radiosynoviorthesis was performed in thirty patients (67.8% women, mean age of 46.9 and median of 49 years) referred by the Departments of Rheumatology and Traumatology with a scintigraphic confirmation for joint inflammatory process,. Two patients were excluded due to loss of follow-up. All patients were treated with Ytrium-90 (90Y) and none presented clinical complications after the procedure. The most frequent pathologies were: 42.9% pigmented villonodular synovitis, 25% rheumatoid arthritis, 14.3% spondyloarthritis, 11% osteoarthritis and 7.1% nonspecific arthritis. After 6 months, 60.7% of patients had clinical remission. In the univariate analysis, gender ($X^2=4.17$ $p=0.041$) and previous history of infiltration ($X^2=4.17$ $p=0.041$) were factors associated with remission (Table 1). In multivariate analysis, gender (OR: 0.12; 0.02-0.99, 95% CI) was the only independent factor associated with remission (Table 2). **Conclusion:** Radioisotopic synoviorthesis is a therapeutic strategy to be considered in patients with repetitive arthritis refractory to systemic treatment. Despite the small sample size, in our study, gender was the sole independent factor of remission. **References:** None.

EP-37

Clinical -> Therapy study -> Adult study -> Other treatments -> NET treatments, including mIBG and peptides therapy

October 12 - 16, 2019 e-Poster Area

EP-0556

Comparison of Best Therapy Response According to the Intraarterial Techniques performed in GEP NET Treated Patients in Relation to the Absorbed Dose, Ki-67 Index and Tumor Size Using n.c.a. Lu-177 Dotatate

G. Limouris[1], *M. Paphiti*[2], *R. McCready*[3];
[1]*Medical School, National and Kapodistrian University of Athens, Athens, GREECE,* [2]*National Health System, Athens, GREECE,* [3]*Cancer Research Institute, Sutton Surrey & Royal Sussex County Hospital, Brighton-Surrey, UNITED KINGDOM.*

Aim/Introduction: To compare best therapy response in GEP NET patients, treated with n.c.a. ^{177}Lu-DOTA-TATE in relation to the absorbed dose, Ki-67 index and tumor size, according to the different intra-arterial techniques performed (simple intra-arterial infusion or port-system temporal implantation). **Materials and Methods:** The study included 16 patients with non-functioning, unresectable liver-metastatic GEP-NETs, undergoing intra-arterial infusions with n.c.a. ^{177}Lu-DOTATATE (6 sessions with 7.2 GBq per cycle, at standard intervals of about 2 mo). Patients (9, originated from pancreas and 4, from lungs) were graded as (G1/G2) and (G3) and were under long-acting somatostatin analog treatment. The patients were classified in four groups according to their size, as follows: group A with tumor-size from 20 - 30 mm (main diameter), group B from 30 - 40 mm, group C from 40 - 50mm and group D from 50 up to 60mm. The infusion administration was performed intra-arterially either by direct simple infusion after catherization of the hepatic artery or by the temporal implementation of a port-system ending to the common hepatic artery. Response was evaluated according to RECIST criteria. Survival was analyzed based on Kaplan-Meier curve method. Cr-A was radio-immunologically measured and correlated with Ki-67 results. **Results:** The response rate of group A (6pts, mean tumor size 20-30mm, mean absorbed dose 450 Gy) was 50.0% as partial response (PR), of group B (3pts, mean tumor size 30-40mm, mean absorbed dose 150 Gy) was 70.0% as partial response (PR), of group C (4pts, mean tumor size 50-60mm, mean absorbed dose 450 Gy) was 20.0% as stable disease (SD) and group D (3pts, mean tumor size 6cm, mean absorbed dose 250 Gy) was 26.0% as stable disease (SD) . The median time of progression-free survival in group A was 53 mo, in group B, 58 mo, in group C 48 mo and 51 mo for group D. Cr-A values showed a parallel to Ki-67 values, level. **Conclusion:** The threshold absorbed dose is directly related to the tumor size and the Ki-67 index. The response of large tumors might be managed not only from a low Ki-67 index but additionally from the infusion technique, i.e., in favor to the implemented port since the radiopharmaceutical uptake is considerably elevated. **References:** None.

EP-0557

Long-Term Efficacy, Survival and Safety of Peptide Receptor Radionuclide Therapy (PRRT) in Metastatic Neuroendocrine Tumors of Unknown Primary (CUP-NETs)

J. Zhang[1], *W. Zhu*[2,1], *H. R. Kulkarni*[1], *A. Singh*[1], *C. Schuchardt*[1], *R. P. Baum*[1];
[1]*Theranostics Center for Molecular Radiotherapy & Precision Oncology, ENETS Center of Excellence, Zentralklinik Bad Berka, Bad Berka, GERMANY,* [2]*Department of Nuclear Medicine, Peking Union Medical College (PUMC) Hospital, Chinese Academy of Medical Science & PUMC, Beijing, CHINA.*

Aim/Introduction: The application of somatostatin receptor (SSTR)-PET provides a remarkable improvement in metastatic neuroendocrine tumors unknown primary (CUP) tumor detection, however, in a number of cases no primary tumor is found even with SSTR-PET and after prolonged follow-up. The purpose of this study was to analyze the long-term outcome, efficacy and safety of peptide receptor radionuclide therapy (PRRT) in patients with CUP-NETs after the introduction of SSTR-PET. **Materials and Methods:** A total of 144 eligible patients (F 75; age 28-85 y, mean age 60.0±12.0 y) with pathologically confirmed grade 1 (G1) or G2, progressive and metastatic CUP-NETs were enrolled. All subjects underwent ^{68}Ga-SSTR PET/CT and 105 patients underwent ^{18}F-FDG PET/CT. All patients received PRRT with lutetium-177 (^{177}Lu) and/or yttium-90 (^{90}Y) labeled somatostatin analogs (DOTATATE or DOTATOC). Among them, 108 patients (F 55; mean age 61.0±13.0 y) received more than 2 cycles of PRRT. Kaplan-Meier analysis was performed to calculate progression-free survival (PFS) and overall survival (OS), defined from start of PRRT. Treatment response, according to RECIST 1.1 (CT and/or MRI), and by molecular imaging criteria (EORTC). **Results:** 120 patients (83.3%) had liver metastases, whereas 85 (59.0%) with lymph node metastases, 13 (9.0%) lung, 56 (38.9%) bone, and 35 (24.3%) had metastasis of other organs. 31 (21.5%) had G 1 NETs, 72 (50.0%) had G2, and 41 (28.5%) were with unknown Ki-67 index. The median follow-up time was 92.8 months. The median PFS was 17.4 mo and median OS was 61.0 mo. For G1, G2, and unknown Ki-67 index CUP-NENs, the median PFS were 26.3 mo, 17.7 mo, 14.0 mo and median OS were 88.7mo, 71.6 mo, 54.6 mo, respectively. In the subgroup who received more than 2 cycles of PRRT, the median PFS was 22.6 mo and median OS was 72.3 mo. During the treatment and long-term follow up, grade 3 or 4 myelotoxicity (CTCAE), lymphopenia and thrombocytopenia occurred in three (2.1%) and one patients (0.7%). No grade 3 or 4 nephrotoxicity or any clinically significant decline in renal function after treatment was observed. There was no hepatic toxicity. **Conclusion:** PRRT is a favorable therapeutic option in patients with metastatic CUP-NETs that express somatostatin receptors, and tolerated well with few side-effects. PRRT has shown good response rates and results in encouraging long-term outcome in this large

cohort of patients with CUP-NETs with a follow up of up to 14 years after the commencement of both SSTR-PET and PRRT. **References:** None.

EP-0558

Somatostatin Receptor targeted radioligand therapy in head and neck paraganglioma

W. Roll[1], *M. Müther*[2], *B. Zinnhardt*[1], *L. Stegger*[1], *M. Weckesser*[1], *M. Schäfers*[1], *W. Stummer*[2], *K. Rahbar*[1];
[1]*Department of Nuclear Medicine, University Hospital Münster, Münster, GERMANY,* [2]*Department of Neurosurgery, University Hospital Münster, Münster, GERMANY.*

Aim/Introduction: Surgical resection is the therapy of choice in head and neck paraganglioma associated with significant morbidity depending on tumor size and localization. In case of progressive residual or recurrent disease, new and less aggressive therapeutic options are warranted. Somatostatin receptor (SSTR) targeted therapies pose a promising alternative, as SSTRs are upregulated in paragangliomas. However, only few studies provide evidence on efficacy of ^{177}Lu-DOTATATE therapy in these patients. The aim of this study was to evaluate the efficacy of peptide receptor radiotherapy (PPRT) with ^{177}Lu-DOTATATE for head and neck paragangliomas. **Materials and Methods:** A total of 7 consecutive patients (mean age: 60 years, range: 14-84) with progressive head and neck paragangliomas (3 carotid body tumors, 3 jugulotympanic paragangliomas, 1 both), treated with PRRT using ^{177}Lu-DOTATATE, were included in this retrospective analysis. Therapy response was assessed by interim and post-therapy ^{68}Ga-DOTATATE-PET-CT and, if available, MRI according to morphological (RECIST) and SSTR imaging parameters. Therapeutic uptake was classified on ^{177}Lu-DOTATATE scintigraphies 48h p.i. according to the Krenning scale. Additionally, longer-term clinical and imaging-based outcome was evaluated. **Results:** Patients received a median of 4 cycles (range: 3 to 5) of PRRT with ^{177}Lu-DOTATATE (mean injected dose 7.3 GBq). Interim and post-therapy staging showed at least stable disease in all patients. Tumor uptake in 48h p.i. ^{177}Lu-scintigraphies was moderate to high in all patients (Krenning scale; median: 3; range: 2-4). Furthermore, none of the patients showed progressive disease during the median follow-up time of 28 months (range: 6-37 months). **Conclusion:** SSTR targeted therapy using ^{177}Lu-DOTATATE shows promising efficacy and may lead to long lasting stable disease. **References:** None.

EP-0559

68Ga-DOTANOC uptake pattern as a prognostic factor in patients with non-functional well-differentiated G1/G2 pancreatic neuroendocrine tumours treated with 177Lu-DOTATATE

I. L. Sampaio[1], *G. Ferreira*[1], *L. Fonseca*[2], *J. Pedro*[3], *P. Gouveia*[4], *S. Castro*[1], *H. Duarte*[1];
[1]*Instituto Portugues de Oncologia do Porto, Porto, PORTUGAL,* [2]*Centro Hospitalar Universitário do Porto, Porto, PORTUGAL,* [3]*Centro Hospitalar São João, Porto, PORTUGAL,* [4]*Hospital Central do Funchal, Madeira, PORTUGAL.*

Aim/Introduction: Stage IV well-differentiated (WD) neuroendocrine tumours (NETs) of pancreatic origin can present a variable clinical behavior and, therefore, it's important to create predictive models of tumour aggressiveness. In this review we evaluated the pattern of somatostatin receptor expression in ^{68}Ga-DOTANOC PET/CT Maximum Intensity Projection (MIP) images and correlated it with patient outcome. The aim was to identify a model of somatostatin receptor expression pattern with prognostic value that could be easily used in clinical practice by both nuclear medicine and referring physicians. **Materials and Methods:** This review included 22 patients (12 men, 10 women, mean age 57y) with stage IV non-functional WD-NETs of the pancreas (5 G1, 15 G2, 1 unknown) treated with ^{177}Lu-DOTATATE (3 cycles, mean cumulative activity 19,03 GBq). Pre-treatment ^{68}Ga-DOTANOC PET/CT MIP images were reviewed by two nuclear medicine physicians and two endocrinologists. The majority of patients (21/22 cases) had more than 50% tumour burden with high ^{68}Ga-DOTANOC uptake (higher than liver and equal or superior to spleen/kidney uptake). MIP images were classified in two patterns: 1) homogeneous uptake- all lesions with high ^{68}Ga-DOTANOC uptake; 2) concomitant lesions with ^{68}Ga-DOTANOC uptake inferior to spleen/renal uptake. Inter-reader agreement was evaluated. Treatment outcome variables (time to progression-TTP and overall survival-OS) were evaluated and compared in both imaging patterns. Statistical evaluation was performed using SPSS version 24.0. Mann-Whitney test and Fisher´s exact test were applied. **Results:** Agreement in MIP imaging pattern classification was 100% between all four physicians. Fourteen patients (63.6%) had MIP images classified as heterogeneous uptake and 8 (36.4%) as homogenous uptake. Disease progression was registered in 37.5% (3/8) of patients with homogeneous uptake and in 85.7% (12/14) of patients with heterogeneous uptake (p= 0.052). Median time to progression was 25.0 (IQR 21.0-32.0) months in the homogenous group and 15.5 (IQR: 9.5-21.0) months in the heterogeneous group. Death events occurred in 12.5% (1/8) of cases in the homogeneous group and in 57.1% (8/14) of cases in the heterogeneous group (p=0.074). **Conclusion:** MIP imaging visual analysis can be a simple and reproducible method of evaluating tumour pattern uptake of somatostatin analogues (100% inter-observer agreement in our review). There was a tendency for longer time to progression and overall survival in patients with homogeneous uptake pattern in comparison with the heterogeneous group. A larger sample size is required to validate these results. **References:** None.

EP-0560

Long-term Outcomes After High-dose I-131 Mibg Therapy For High-risk Neuroblastoma: A Japanese Single-institution Experience

D. Kayano[1], *H. Wakabayashi*[1], *A. Inaki*[1], *A. Toratani*[1], *N. Akatani*[1], *T. Yamase*[1], *Y. Kunita*[1], *S. Watanabe*[1], *A. Takata*[1], *T. Hiromasa*[1], *H.*

Mori[1], S. Saito[1], N. T. Nguyen[1,2], S. Kinuya[1];
[1]Kanazawa University Hospital, Kanazawa, JAPAN, [2]108 Hospital, Hanoi, VIET NAM.

Aim/Introduction: High-dose iodine-131-labeled metaiodobenzylguanidine (I-131 MIBG) therapy for high-risk neuroblastoma has become common in recent years. Kanazawa University Hospital is the only institution which can perform the high-dose I-131 MIBG therapy for neuroblastoma in Japan. We investigated the long-term outcomes of high-dose I-131 MIBG therapy in patients with high-risk neuroblastoma. **Materials and Methods:** A total of 19 patients with high-risk neuroblastoma who underwent high-dose I-131 MIBG therapy at Kanazawa University Hospital between September 2008 and September 2013 were retrospectively analyzed. Eleven were males and 8 were females. The mean age at the I-131 MIBG therapy was 8.1 years old (range: 2-17 y. o.). All doses of I-131 MIBG were more than 444MBq / kg. The mean dose of I-131 MIBG was 587MBq / kg. We investigated the long-term outcomes and prognostic values of the high-dose MIBG therapy. This study was approved by the Institutional Review Board of Kanazawa University Hospital. **Results:** Following I-131 MIBG therapy, the 18 of 19 patients were performed chemotherapy and/or stem-cell transplantation. The initial response rate (complete response and partial response) was 37%. Event-free survival (EFS) rate at 1 and 3years after the I-131 MIBG therapy were 42% and 16%. Overall survival (OS) rate at 1 and 3 years were 58% and 42%. Estimated EFS rate and estimated OS rate at 5 years were 16% and 42%. The OS times were significantly longer for patients with less than 3 years for initial diagnosis to the MIBG therapy ($p < 0.05$) and for patients with complete response after I-131 MIBG therapy ($p < 0.05$). **Conclusion:** The high-dose I-131 MIBG therapy for high-risk neuroblastoma can provide favorable prognosis especially in patients with earlier I-131 MIBG therapy after initial diagnosis or with initial good response to I-131 MIBG therapy. **References:** None.

EP-0561

Manual labeling, Bio-distribution and Administration of ^{177}Lu-DOTATE: First Ever Trial from North Pakistan

***A. Ammar**, S. Fatima, Z. Khurshid, K. Bashir, S. Batool, N. Ahmed, M. Syed;*
Atomic Energy Cancer hospital, NORI AECH, Islamabad, PAKISTAN.

Aim/Introduction: Introduction: Peptide receptor radionuclide therapy (PRRT) using ^{177}Lu-DOTATATE for the treatment of gastroenteropancreatic tract (GEP) neuroendocrine tumors (NETs) is gaining worldwide momentum rapidly. It targets somatostatin receptors expressed on well-differentiated NETs. Analysis of clinical trials of PRRT shows its effectiveness in significantly decreasing the mortality and morbidity of patients. NET patient constitute 8% of our registered cancer patients every year. Owing to our limited budgeting and lack of highly sophisticated equipment, we performed manual labeling of ^{177}Lu-DOTATATE. **Aims and Objectives:** We performed the therapy as first ever clinical trial from Northern Pakistan region analyzing the manual labeling, bio-distribution, administration and clinical evaluation of ^{177}Lu-DOTATATE in GEP NET patients. **Materials and Methods: Materials and Methods:** ^{177}-Lu-DOTATATE was prepared manually according to the international guidelines. The study was designed under EANM protocols. Informed consent and ethical committee approval was obtained. Inclusion criteria comprised of patients having: Grade 1 well differentiated NET, Ki-67 index <20%, Karnofsky status 2 and a positive ^{99m}Tc-Octerotide or ^{68}Ga-DOTATATE scan. Fifteen patients were included in the preliminary study. Baseline work-up for every patient was completed. ^{177}Lu-DOTATATE therapy was preceded by amino-acids infusion. Whole body imaging with gamma camera, SPECT-CT and blood samples for marrow toxicity and electrolyte imbalance were performed at 4, 24 and 48 hours. Patients were discharged after 48 hours. **Results: Results:** ^{177}Lu-DOTATATE showed labeling efficiency of 99.2%. Normal physiological radio distribution was noted. Post-therapeutic scans showed higher tumor uptake, longer tumor residence time, and high tumor-to-kidney dose ratio. In metastatic GEP NETs the optimal target to non-target ratios ranged from 5.8% at 4 hours and exceeded to 12.7% at 24 hours. **Conclusion: Conclusions:** Our study showed effective labeling and bio-distribution of ^{177}Lu-DOTATATE. The manual labeling proved to be efficient, cost effective and feasible in our available resources. Tumor to non-tumor ratios showed very promising results. However, prospective studies are needed to analyze a large number of patients and thus establishing the clinical efficacy of therapy. Our on-going clinical trial will encompass response prediction and over-all survival analysis of patients. **References:** None.

EP-0562

PRRT Safety and Disease Control Persistence: the Feasibility of Retreatment

***M. Maccauro**, A. Capozza, G. Aliberti, J. Coppa, S. Pusceddu, F. Scalorbi, N. Prinzi, S. Bhoori, F. De Braud, V. Mazzaferro, E. Seregni;*
Foundation IRCCS Istituto Nazionale dei Tumori, Milan, ITALY.

Aim/Introduction: NETTER-1 trial definitely proved PRRT efficacy, with a total of 4 therapeutic administrations[1]. The possibility to continue PRRT after the 4th cycle should not be excluded a priori. In a population of patients (pts) with somatostatin receptors-expressing tumors, who previously underwent PRRT, we assessed the feasibility, the duration of disease control and the safety of PRRT re-challenge. **Materials and Methods:** We retrospectively analyzed a consecutive cohort of 22pts, previously treated with PRRT, who underwent and completed at least 1 additional PRRT cycle. First-line PRRT exploited tandem strategy (alternating 177Lu/90Y-DOTATOC), while re-challenge was performed with 177Lu-DOTATOC exclusively. Complete blood count and creatinine were monitored before, during and after PRRT until recovery. Hematological and renal adverse events were categorized

according to CTCAE 5.0. **Results:** Treated patients' mean age was 59 years. Eighteen presented gastroenteropancreatic (GEP)-NETs (55% ileal-NET, 45% pancreas-NET), of which 16pts had G1/2 NETs and 2pts G3. Among non-GEP NETs: 2 had bronchial-NET, 1 malignant pheochromocytoma and 1 thymoma. Mean number of PRRT administrations was 8 (range 6-12). The mean cumulative activity of Yttrium-90 was 8.15 GBq (range 2.59-15.88), with a mean number of 2 cycles/patient (range 1-6). Lutetium-177 mean cumulative activity was 33.23 GBq (range 11.01-61.54), with a mean number of 6 cycles/patient (range 2-11). Treatment was generally well-tolerated, no severe acute adverse events were observed. Hematological toxicity was transitory: anemia registered in 72% pts (G1 11/16, G2 5/16); thrombocytopenia in 4 (G1 3/4, G2 1/4); leucopenia in 50% (G1 in 9/11, G2 in 2/11); G1 neutropenia in 4pts. Increased creatinine values were documented in 82% pts (10/18 G1, 8/18 G2). Neither G3 nor G4 toxicity were experienced. Mean cumulative time to progression was 55 months (range 20-116). Selecting only the cohort of patients who didn't underwent different lines of treatment between PRRT challenge and re-challenge, the mean overall duration of disease control (between first-line PRRT and progression after PRRT-retreatment) was 67 months (range 24-119). **Conclusion:** PRRT retreatment appears to be a safe choice. In a cohort of patients with lack of alternative therapeutic options, it represents a potential treatment chance, with adequate response after initial cycles, showing relevant overall disease control duration. PRRT may represent a great advantage in terms of toxicity and reduction in health costs. Further advances towards this perspective should be embraced. **References:** Strosberg J, El-Haddad G, Wolin E, et al. Phase 3 Trial of 177Lu-Dotatate for Midgut Neuroendocrine Tumors. N Engl J Med 2017;376:125-135.

EP-0563

Does initial response to PRRT with ^{177}Lu-DOTA-TATE influence lesion progression? A lesion-based approach

L. Lemos[1], *R. Ferreira*[1,2], *A. Moreira*[1,2], *G. Costa*[1,3], *J. Pedroso de Lima*[1,2,3];
[1]*Nuclear Medicine Department, Centro Hospitalar e Universitário de Coimbra, Coimbra, PORTUGAL,* [2]*Instituto de Ciências Nucleares Aplicadas à Saúde (ICNAS), Faculdade de Medicina, Universidade de Coimbra, Coimbra, PORTUGAL,* [3]*Faculdade de Medicina, Universidade de Coimbra, Coimbra, PORTUGAL.*

Aim/Introduction: Peptide receptor radionuclide therapy (PRRT) has proven to be an effective, well-tolerated option in well-differentiated metastatic neuroendocrine tumors (mNETs), with substantial impact on progression-free survival. However, it is not clear how the responder lesions evolve when the disease progresses. The aim of this study was to evaluate, using a lesion-based approach, whether response to PRRT influences the future progression patterns. **Materials and Methods:** The clinical charts of patients with mNETs submitted to PRRT with ^{177}Lu-DOTATATE between July 2013 and March 2019 were reviewed. Treatment response was assessed on ^{68}Ga-DOTANOC-PET/CT. We only selected patients that, despite an initial response to PRRT, became progressive during the follow-up period. Therefore, each patient had, at least, three ^{68}Ga-DOTANOC PET/CT-scans: baseline (pre-PRRT-scan); post-therapy scan documenting complete or partial response (post-PRRTr-scan) and a third scan showing progression (post-PRRTp-scan). For each patient, lesions were counted and categorized according to their location on pre-PRRT-scan. Responding lesions were individually classified, by post-PRRTr-scan, as having had a complete (CR) or a partial response(PR). The post-PRRTp-scan were compared with the previous ones, and information regarding lesion progression status was recorded (number of new lesions, progression of previous stable lesions and progressing lesions which had responded to PRRT). Additional data such as age, gender, treatment cycles and administered activity was collected for each patient. Statistical analysis was conducted using SPSS Statistics 23. **Results:** Nine patients fulfilled inclusion criteria (7 male, 2 female, average age=68). Primary sites were lung(n=3), ileum(n=4) and pancreas(n=2). Each patient underwent 1-4 cycles of ^{177}Lu-DOTATATE, with an average cumulative activity of 585 mCi. Baseline scans showed 234 lesions: 13.7% lymph node(n=32); 0.4% lung(n=1); 50.9% liver(n=119); 3% pleural(n=7); 3% peritoneal(n=7) and 29.1% bone(n=68). On post-PRRTr-scan, 28.6% of the lesions (n=67) exhibited CR; whereas 40.6% (n=95) responded partially to the treatment. On the post-PRRTp-scan, 135 lesions fulfilled progression criteria, 2.2% of which were lymph node(n=3); 28.9% liver(n=39); 19.3% pleural(n=26) and 49.6% bone(n=67) metastasis. 61.5%(n=83) of progressing lesions were either new or did not initially respond to PRRT. 34.8% progressed after PR (n=47, 49.5% of initial PR), while 3.7% relapsed after early CR (n=5; 7.5% of initial CR). **Conclusion:** Despite the limitations of this study, our results suggest that, after a response to PRRT, either new lesions or lesions that had not shown an initial response to therapy are the main responsible for disease progression. Lesions that responded completely to the treatment showed low recurrence rate. **References:** None.

EP-0564

Efficacy and security of PRRT in neuroendocrine tumors: a single center experience in Mexico

S. S. Medina[1,2], *O. Garcia*[1], *J. Vargas*[1], *Q. Pitalua*[1];
[1]*Instituto Nacional De Cancerologia, Mexico City, MEXICO,* [2]*Hospital Angeles Lindavista, Mexico City, MEXICO.*

Aim/Introduction: Evaluate the efficacy and security of PRRT with [90Y-DOTA0,Tyr3]octreotide and [177Lu-DOTA0,Tyr3] octreotate, in patients after failure to first line treatment of NET´s. **Materials and Methods:** Seventy-four patients with progressive NET´s between December-2014 to December-2018 were analyzed; thirty-six patients had gastroenteropancreatic NET (48%), nineteen patients had bronchopulmonary NET´s (26%), and nineteen patients had other primary NET´s (26%). All patients were treated consecutively with 177Lu-DOTATOC and 90Y-DOTATOC mean activity 8.1 GBq (range

3.7 - 25.9). 274 treatments (247 with 177Lu-DOTATOC; and 27 with 90Y-DOTATOC) were administrated. Clinical responses were assessed 4-8 weeks after completing therapy and then after each of the 6-month intervals. The efficacy of PRRT was evaluated base on overall survival (OS) and progression-free survival (PFS) with Kaplan-Meier curves, radiological response was based on RECIST 1.1. Hormonal active tumors were evaluated with chromogranin-A serum (CgA); only gelofusine infusion over 4 hours was used for the kidney protection. **Results:** During a median follow up of 33 months (range 11-60 months) the observed PFS was 28 .6 months and OS was 33.6 months; 9 patients died (12%). The observed 5-years overall survival was 68%. Treatment response according to RECIST 1.1 criteria consisted of complete response in 2 patients (2%), partial response in 24 patients (33%), stable disease in 39 patients (53%) and progressive disease in 9 patients (12%). The disease control rate was 88%. Objective Response Rate (ORR), defined as proportion of patients achieving partial (PR) or complete response (CR), was 35%. Two patients (2%) revealed MDS five years, after receiving after total activity 25.9 GBq. No other hematological grade 3 and 4 was observed. Renal toxicity grade 3 was observed in four patients (5%), no grade 4 was observed. Univariate analysis showed that patients with highest average of SUVmax evaluate by 68Ga-DOTATOC-PET/CT (43.3% [IC 95%]) showed lower response rate compared with lowest average of SUVmax (56.7% [IC 95%]). Patients with less of 10 metastases showed better response (73.3% [IC 95%]) compared with patients with more than 10 metastases (26.7% [IC 95%). **Conclusion:** This study documents an important feature of the tumor response after treatment with 177Lu-DOTATOC and 90Y-DOTATOC is effective and safety treatment option for patients with disseminated or inoperable neuroendocrine tumors. Long term follow up revealed high disease control rate and long PFS with small number of side effects. **References:** None.

EP-0565

[^{68}Ga]-DOTATATE PET/CT parameters predict response to peptide receptor radionuclide therapy in neuroendocrine tumours

R. Sharma[1], *W. Wang*[1], *S. Yusuf*[2], *J. Evans*[1], *R. Ramaswami*[1], *F. Wernig*[1], *A. Frilling*[1], *F. Mauri*[1], *A. Al-Nahaas*[1], *E. O. Aboagye*[1], *T. D. Barwick*[1];
[1]*Imperial College, London, UNITED KINGDOM,* [2]*Imperial College NHS Healthcare Trust, London, UNITED KINGDOM.*

Aim/Introduction: [^{177}Lu]DOTATATE prolongs progression free survival (PFS) in metastatic neuroendocrine tumours (NETs). However, objective response rate is low. This, coupled with long duration of therapy and expense suggest need for better selection. We aim to assess whether baseline [^{68}Ga]DOTATATE-PET/CT parameters and RECIST 1.1 accurately predict clinical outcome to [^{177}Lu]DOTATATE. **Materials and Methods:** [^{68}Ga] DOTATATE-PET parameters (single lesion SUV_{max}, tumour to spleen and liver SUV ratios, and SUV_{max-av} using up to five target lesions in multiple organ sites) were determined at baseline and follow-up. Patients were followed 3-monthly until disease progression. Response was determined using RECIST 1.1. Baseline SSTR2 expression was assessed and compared with PET parameters. **Results:** In terms of treatment response to PRRT according to RECIST 1.1 28% of patients experienced a partial response (PR) 28%, stable disease (SD) was observed in 60% and progressive disease (PD) in 13%. RECIST 1.1 response was predictive of PFS such that patients having a PR had a PFS 2.5x that of SD, and almost 20x PD. Baseline, single lesion SUV_{max} predicted both response and PFS with SUV cut-off of 13.0 giving high sensitivity and specificity. No other PET parameter correlated with outcome. PET uptake correlated with tumoural SSTR2 expression. **Conclusion:** Response by RECIST 1.1 defines a subset of patients with markedly improved PFS. Baseline PET uptake predicts response to [^{177}Lu]DOTATATE such that a baseline SUV_{max} of 13.0 in the single most intense lesion defines a threshold below which patients have poor response to PRRT and worse PFS. This threshold should be taken forward into prospective studies. **References:** None.

EP-0566

An uncommon "pseudo-progression" pattern of morphological response, as early as after one cycle of PRRT, in siNET patients

I. Karfis, *G. Marin, P. Flamen;*
Jules Bordet Institute, Brussels, BELGIUM.

Aim/Introduction: Peptide Receptor Radionuclide Therapy (PRRT) is an effective, established therapeutic modality for patients with unresectable progressive Neuroendocrine Tumors (NETs), achieving disease control rates of more than 80-85%. 10-15% of treated patients fail to respond to PRRT. The aim of this communication is to report on a pattern of early morphological progression (documented on CT or MRI) after the first cycle of PRRT. **Materials and Methods:** We observe a morphological disease progression (volumetric lesion increase ± appearance of new lesions), as early as after the first PRRT cycle, in four of our treated patients. Three of them were included on LUMEN study (NCT01842165) and completed the planned four cycles of PRRT. The fourth patient is actually treated on a routine basis and he received already 2 cycles of PRRT. Two patients exhibit NET-related symptoms (flushing and watery diarrhea). All patients initiated PRRT due to progressive disease on a prevous CT or MRI. **Results:** All 4 patients had small intestinal NETs (3: ileum, 1: ileocaecal jonction) of low histological grade (3: Grade 1 and 1: Grade 2 with Ki-67: 5%, according to World Health Organization/ European Neuroendocrine Tumor Society criteria for small intestinal NETs). The range of disease progression prior to PRRT was 4-10 months. All patients had negative baseline FDG PET/CTs. The early morphological progression reported on the pre-cycle 2 assessment, was not confirmed on subsequent serial exams. None of the patients had worsened their Performance Status and the two symptomatic patients demonstrated improvement of their NET-related symptoms. Subsequent Ga-DOTATATE PET/

CTs were stable compared to baseline, except for the fourth patient who achieved partial response after 2 cycles of PRRT. Our main hypothesis is that this morphological progression reflects tumor dynamics, which was maintained at the early phase of the treatment, before PRRT begin to demonstrate his benefits. **Conclusion:** This uncommon "pseudo-progression" finding was not confirmed by subsequent morphological imaging, neither clinically, nor by subsequent Ga-DOTATATE PETs. Such patterns of morphological response in low grade siNET patients, should not lead to an early interruption of PRRT compromising his (rather medium to long-term) efficacy. **References:** None.

EP-0567

Targeted Molecular Therapy Using Radiolabelled Somatostatin Analogue (Dotatate): Initial Experience From A Tertiary Hospital In Singapore

***H. Huang**, W. Tham, D. W. M. Tai, D. C. E. Ng, S. X. X. Yan, K. Loke;*
Singapore General Hospital, Singapore, SINGAPORE.

Aim/Introduction: Lu-177 radiolabelled somatostatin analogues have been used for treatment of neuroendocrine tumors for more than a decade. We report our experience in our tertiary nuclear medicine referral centre. We aim to compare our results with previously published European and US data. **Materials and Methods:** Retrospective analysis of data from patients treated from January 2012 to October 2016 was performed. We recorded demographic information, type of tumour, and complications such as acute kidney injury, myelotoxicity, and hepatotoxicity. We also reviewed follow up Gallium-68 DOTATATE scans where available. **Results:** 66 patients were treated. 149 cycles of Lu-177 DOTATATE were administered in total. Doses ranged from 150 to 240 mCi. 17 patients had 2 cycles, 15 patients had 3 cycles, 9 had 4 cycles, 2 had 5 cycles and 1 had 6 cycles of therapy. 39 had follow up Gallium-68 DOTATATE scans. There was 1 complete response, 31 out of 39 (79%) patients showed stable or partial response whilst the rest showed progressive disease. We treated 29 male and 37 female patients. There were 50 patients with neuroendocrine tumours of various primary organs (commonest being the pancreas - 23 patients), 10 carcinoid tumours, 3 phaeochromocytomas and 3 paragangliomas. The longest duration of stable disease was 825 days. 9 patients out of 66 had acute kidney injury stage I or II. 7 had full recovery in 4 weeks. 12 out of 66 had minor myelotoxicity and 1 died due to myelotoxicity. 8 out of 66 had worsening liver enzymes. Most recovered to baseline over a mean of 2.5 months. 44 out of 66 (66%) patients had no recorded complications. There were 7 deaths due to disease progression. **Conclusion:** Lu-177 DOTATATE therapy is a safe and efficacious technique for treatment of somatostatin receptor positive tumours in Asian patients. **References:** Castaño JP, Sundin A, Maecke HR, et al. Gastrointestinal neuroendocrine tumors (NETs): new diagnostic and therapeutic challenges. Cancer Metastasis Rev. 2014;33(1):353-359. Kwekkeboom DJ, Krenning EP. Peptide receptor radionuclide therapy in the treatment of neuroendocrine tumors. Hematol Oncol Clin North Am. 2016;30(1):179-191. van der Zwan WA, Bodei L, Mueller-Brand J, de Herder WW, Kvols LK, Kwekkeboom DJ. GEPNETs update: radionuclide therapy in neuroendocrine tumors. Eur J Endocrinol. 2015;172(1):R1-8. Strosberg J, Wolin E, Chasen B et al. NETTER-1 Phase III in Patients with Midgut Neuroendocrine Tumors Treated with 177Lu-Dotatate: Efficacy and Safety Results. J Nuc Med. 2016; 57 (2): 629.

EP-0568

Efficacy of ^{177}Lu-DOTATATE Peptide Receptor Radionuclide Therapy in Patients with Inoperable/Metastatic, Progressing Neuroendocrine Tumors: Results of Our First Clinical Experience

***B. Gunalp**, A. Ucgun, U. Goker, S. Mahmudov, S. Ince, E. Alagoz;*
University of Health Sciences, Gulhane
Medical Faculty, Ankara, TURKEY.

Aim/Introduction: More than 50% of patients with Neuroendocrine Tumors (NETs) metastatic and inoperable at the time of diagnosis and progressive under conventional therapies with somatostatin analogs (SSA), everolimus, sunitinib, and chemotherapy. In these patients, Lu-177 DOTATATE Peptide Receptor Radionuclide Therapy (PRRT) can be a good treatment option. Our aim in this study is to investigate the efficacy of Lu-177 DOTATATE PRRT and factors affecting the outcome of these patients. **Materials and Methods:** Twenty-seven NETs patients (25 GEP-NETs & 2 bronchial NETs) with metastatic, inoperable disease, progressed on octreotide or lanreotide therapy and showing strong somatostatin receptor (SSTR) expression which determined by Ga-68 DOTATATE scan, included in this study. 5.5-7.4 GBq Lu-177 DOTATATE therapy was given every 8-12 weeks. Two to six cycles of treatment were applied**.** Cold octreotide was discontinued (long-acting 4 weeks, short-acting 24 hours) prior to the treatment. To prevent nephrotoxicity, a specific amino acid infusion is perfused 30-60 min before Lu-177 DOTATATE administration for at least 4 hours. In 5 patients somatostatin, LAR was continued between the therapy cycles. Patients were followed up for 30 months. **Results:** Objective response (partial remission and minor remission) was observed in 9 patients (33%) and stable disease in 12 patients (45%). No serious side effects (hematotoxicity, nephrotoxicity) were observed. Progression-free survival was determined median 31 months for GEP-NETs and 24 months for bronchial NETs. F-18 FDG PET/CT scan showed higher uptake than Ga-68 DOTATATE PET scan in tumor sites in patients with progression under treatment which represents dedifferentiation and poor prognosis for these patients. Conversely, a high SUV Max values at the tumor sites at the pre-treatment Ga-68 DOTATATE scan predicts good response to the Lu-177 DOTATATE therapy. **Conclusion:** It is concluded that Lu-177 DOTATATE therapy is effective as of 2nd and 3rd line therapy at this moment for metastatic, inoperable NET when conventional therapies are failed and could be more effective if therapy starts earlier stage of disease when a tumor has well-differentiated histology with higher SSTR expression. In progressive disease, additional cycles of Lu-177 DOTATATE

therapy can be given as a salvage therapy together with chemotherapeutic drugs as long as SSTR expression is shown by Ga-68 DOTATATE scan. **References:** 1. Kim S-J, et.al. The efficacy of Lu-177 DOTATATE RNT in patients with NETs: Eur J Nucl Med Mol Imaging (2015) 2.Brabander, et al. Peptide receptor RNT of NETs . J Best practice & research. Clinical endocrinology & metabolism 2016.

EP-0569

Cytoreductive Surgery And Lesion Excision As Treatment Of Choice In Intraperitoneal And Liver GEP NET Metastases Respectively, Followed By Radiopeptide Treatment

G. Limouris[1], *M. Paphiti*[2], *V. Krylov*[3], *M. Dolgushin*[4], *R. V. McCready*[5], *I. Kyriazanos*[6];
[1]*Medical School, National and Kapodistrian University of Athens, Athens, GREECE,* [2]*National Health System, Athens, GREECE,* [3]*Nuclear Medicine Department "A Tsyb" Medical Radiological Research Center, Obninsk, RUSSIAN FEDERATION,* [4]*"Blokhin's " Russian Oncological Research Center, Moscow, RUSSIAN FEDERATION,* [5]*Cancer Research Institute, Sutton Surrey & Royal Sussex County Hospital, Sutton-Surrey, UNITED KINGDOM,* [6]*I Surgery Dept, Army Naval Hospita, Athens, GREECE.*

Aim/Introduction: Introduction: We first report on adjuvant peptide receptor radionuclide therapy (PRRT) in 18 non-functioning pancreatic neuroendocrine tumours (NF-PNETs). Surgery preceded PRRT; (a) lesion excision was performed in liver metastases and (b) in rare cases where peritoneal secondaries were detected, peritonectomy, implemented as treatment of choice; both techniques adopted in our Institution, aiming to optimize PRRT for a longer-term survival. **Materials and Methods: Materials and Methods:** Eighteen NF-PNETs received adjuvant PRRT i.a., after transhepatic infusions; 6 of them received ^{111}In-Octreotide, in a dosage of 4.0 -7.0 GBq, (12 cycles with treatment intervals of 5-8 weeks) and 12 n.c.a.^{177}Lu-DOTATATE in a dosage of 7.4 GBq (6 cycles with treatment intervals also of 5-8 weeks), following their surgical excision as first-line treatment. Twelve patients underwent pancreato-duodenectomy and 6 distal pancreatectomy and splenectomy. Intraoperative liver ultrasonography was performed to enhance missed lesion detection. Peritoneal dissemination was detected in 2 and liver metastases [3 bilobar, 4 unilobar] presented in 7 patients. The former underwent cytoreduction maneuvers with complete removal of all macroscopic disease (CC-0). Following the principles of Cytoreductive Surgery, this was achieved with the use of standardized peritonectomy procedures and "en-bloc" resection of adjacent involved viscera whereas the latter underwent segmentectomy. Prophylactic cholecystectomy was planned to obviate adverse events due to the use of somatostatin analogues. Response assessment was classified according to RECIST criteria. Absorbed doses delivered to metastases, kidneys and red marrow were calculated according to OLINDA 1.0 program. CT/MRI were performed before and after the end of treatment and monthly US images for follow up. **Results: Results:** In all surgically treated cases immediately resulted in a significant down slowing of the tumor aggressiveness clinically and biochemically confirmed, accelerating the therapeutic efficacy, prolonging the survival rate assessed by Kaplan-Mayer curves (50,4 mo for surgically excised pts versus 33 mo in non-surgically treated pts). **Conclusion: Conclusion:** In pts with metastatic liver or peritoneal lesions, scheduled for surgical exeresis complementary, adjuvant radiopeptide therapy slows down the tumor aggressiveness, accelerates the therapeutic efficacy and improves the patients RECIST score assessment in favor to the partial remission scoring. The drawback of the concept is that regarding the peritonectomy and the surgical lesion liver debulking lurks the danger of tumor dissemination. The latter drives us to the skepsis that P R R T should precede the scheduled surgical excision by a therapeutic scheme of 2-3 cycles of n.c.a. ^{177} Lu-DOTATATE for tumor ablation. **References:** None.

EP-0570

Ki-67 expression index and early post-PRRT chromogranin A levels in NETs - Is there any correlation? Preliminary results

A. Mazurek[1,2], *M. Dziuk*[1], *S. Piszczek*[1,2], *M. Kolodziej*[2], *A. Gizewska*[1], *E. Witkowska-Patena*[1], *S. Osiecki*[1];
[1]*Military Institute of Medicine Department of Nuclear Medicine, Warsaw, POLAND,* [2]*Military Institute of Medicine Department of Endocrinology and Isotope Therapy, Warsaw, POLAND.*

Aim/Introduction: One of the treatment options for patients with neuroendocrine tumours (NETs) is peptide receptor radionuclide therapy (PRRT) with the use of yttrium/lutetium-labelled (90Y/177Lu) somatostatin analogues. Usually the patients with radiolabelled somatostatin-analogue avid NETs receive a four- cycles of PRRT. A few days after each PRRT course either increasing or decreasing CgA levels have been observed. Significance as well as factors determining early post-PRRT CgA levels dynamics remain unclear. The aim of the study was the estimation of potential correlation between Ki-67 expression indices and early CgA level dynamics after each cycle of PRRT in patients with NETs. **Materials and Methods:** A total number of 47 PRRT courses in 32 patients (24 females, mean age: 63 years) were assessed. The CgA levels were measured a one day prior to PRRT and two days after radionuclide administration. The patients received one (n=18), two (n=13) or three (n=1) PRRT cycles. Radionuclides administered were either 90Y (1.85 GBq) in combination with 177Lu (1.85 GBq) (34 courses) or 177Lu (7.4 GBq) alone (13 cycles). NETs originated from pancreas (9 patients), small intestine (6 patients), colon (6 patients) and lung (2 patients). In 9 patients the primary tumour site was unknown. Spearman's rho rank-order test was used to assess the correlation between Ki-67 expression and post-PRRT CgA kinetics. **Results:** The mean CgA level was 1309 ng/ml (range: 24.9-14335) at baseline and 1619 ng/ml (range: 28-14790) two days after PRRT cycle. Mean Ki-67 expression index was 5.4% (range: 1-20). CgA levels increased almost all except for 9 PRRT cycles. Spearman's rank coefficient for correlation between Ki-

67 expression indices and post-PRRT CgA kinetics values was 0.024957 (p=0.867751). **Conclusion:** We did not observe any statistically significant correlation between Ki-67 expression indices and early post-PRRT CgA level dynamics in patients with NETs. **References:** None.

EP-38

Clinical -> Therapy study -> Adult study -> Other treatments -> Other treatments

October 12 - 16, 2019 e-Poster Area

EP-0571

Peptide receptor radionuclide therapy for high-grade glioma brain tumors: Variable clinical response in a pilot study

M. Assadi[1], *R. Nemati*[1], *H. Shooli*[1], *M. Rekabpour*[1], *A. Amini*[1], *M. Ravanbod*[1], *H. Ahmadzadehfar*[2];
[1]*Bushehr University of Medical Sciences (BUMS), Bushehr, IRAN, ISLAMIC REPUBLIC OF,* [2]*University Hospital Bonn, Bonn, GERMANY.*

Aim/Introduction: This study aims to report our initial experience with an ongoing pilot study on the treatment of the brain tumors using intravenous administration of 177Lu-DOTATATE in 10 numbers of patients. **Materials and Methods:** In this prospective report, from 2017 to 2019, ten subjects suffering from high-grade glioma tumors were included to investigate the treatment efficacy with i.v. ^{177}-Lu-DOTATAE on high grade glioma tumors in these patients. Inclusion criteria are defined as radiological characteristics (on MRI) or histopathological confirmation of high-grade glioma tumors, Blood Brain Barrier (BBB) disruption as well as sufficient SSTRs expression on the surface of tumor cells. **Results:** A total of 10 subjects (6 male and 4 female) with a mean age of 58.8 years (±14.03) participated in this pilot study to assess the efficacy of the i.v. ^{177}Lu-DOTATATE in the treatment of high grade glioma tumors. Of those, 5 patients (50%) were newly diagnosed with high-grade glioma tumors and other 5 patients (50%) were affected with recurrent disease. The median KPS and ECOG performance status at entry was 48 and 2.8 ranging from 20 to 100 and 0 to 4, respectively. All patients have met the eligibility criteria and adequate laboratory test values. 7 patients (70%) showed large area of GAD-enhancement on MRI but 3 patients (30%) have small area with GAD-enhancement. Notably, the pattern of tracer uptake on PET or SPECT images was well corresponded to the areas with GAD-enhancement. The participants' response to the treatment were observed as 10% of complete remission (n=1), 30% of partial remission (n=3), 10% of stable disease (n=1), 40% of progressive disease (n=4), and 1 patient died of aspiration pneumonia before follow-up MR imaging **Conclusion:** The treatment was well tolerated and effective without no systemic toxicity although our participants were critically ill and disabled. Patients who had received radiotherapy shows less effective therapy which may be due to primary or acquired radioresistance. Regardless of the radiologic response in our patients improvement in quality of life were not significant since the long-standing mass effect have caused well-established ischemia to the critical structures in the their brain. Regarding our experience this treatment can be applied as pre-surgical therapeutic modality to shrink the tumor bulk which leads to feasible resection and may better outcomes. In total, i.v. ^{177}Lu-DOTATATE seems as a well-tolerated and attractive treatment in patients with high-grade glioma tumors that are eligible for further studies and clinical trials. **References:** None.

EP-0572

Quantitative kinetic analysis of Lu-177-DOTA-octreotate/octreotide treated patients with meningioma

L. Lehmonen[1,2], *E. Hippeläinen*[3], *V. Ahtiainen*[1], *L. Vaalavirta*[1], *V. Reijonen*[1];
[1]*Cancer Center, Helsinki University Hospital, Helsinki, FINLAND,* [2]*Department of Physics, University of Helsinki, Helsinki, FINLAND,* [3]*HUS Medical Imaging Center, University of Helsinki and Helsinki University Hospital, Helsinki, FINLAND.*

Aim/Introduction: Somatostatin-receptor (SSTR) targeted radionuclide therapy is a choice of treatment for patients with progressive, persistent meningioma and for multifocal disease. The treatment outcomes have varied, and a connection to the pre-therapeutic tumor uptake values in somatostatin PET-imaging has been observed [1,2]. In this work, we determine the tumor and kidney uptakes from post-therapeutic SPECT-CT images for patients with meningioma(s). **Materials and Methods:** We analyzed three patients treated with ^{177}Lu SSTR-targeted therapy at the Helsinki University Hospital. One patient (P1) with primarily grade 2 atypical recurrent meningioma with exceptionally high proliferation (MIB-1 30%) that later transformed to grade 3 malignant meningioma was treated with ^{177}Lu-DOTA-octreotate (cumulative activity A_{tot}=13.7 GBq in two cycles); one patient (P2) with fibrous grade 1 meningioma with coexisting grade 2 ileal metastatic neuroendocrine tumor (NET) was treated with ^{177}Lu-DOTA-octreotide (A_{tot}=28.5 GBq in four cycles); and one patient (P3) with multifocal, fibrous atypical grade 2 meningioma was treated with ^{177}Lu-DOTA-octreotide (A_{tot}=22.8 GBq in three cycles). The patients were imaged with Siemens Symbia Intevo T6 SPECT-CT at 24, 48, 72 and/or 168 hours after each treatment cycle. We measured the uptake in the tumor(s) and the kidneys at each time point, and subsequently calculated the effective half-lives t_{eff} and residence times t_{res} (tumor-to-kidney ratios). **Results:** The effective half-life of the tumor for the patient P1 was 58h, and for the kidneys 53h (cycle 2). The tumor-to-kidney residence time ratio was 0.5. For the patient P2, t_{eff} of the meningioma was 43h, t_{eff} of the largest NET tumor was 116h, and t_{eff} of the kidneys was 41h (cycle 1). The tumor-to-kidney t_{res} were 0.4 and 4.9, respectively. For the patient P3, t_{eff} of the largest meningioma focus was 55h and t_{eff} of the kidneys was 47h, and t_{res} was 0.2 (average of 3 cycles). The effective half-lives of the meningiomas appear shorter

compared to NETs, and the tumor-to-kidney uptake ratios seem considerably lower. The tumor residence time was approximately four times higher for P1 than for P2 and P3. This is due to the typically considerably higher affinity of ^{177}Lu-DOTA-octreotate compared to ^{177}Lu-DOTA-octreotide, which has been previously observed for NETs[3]. **Conclusion:** SSTR-targeted radionuclide therapy appears to be a well-tolerated treatment for progressive meningiomas. However, quantitative kinetic and subsequent dosimetric analysis is encouraged to further optimize and individualize the treatment. **References:** [1] Maricek et al. JNM 2015;55(2):171-176 [2] Kreissl et al. Radiat Oncol 2012;7:99-110 [3] Esser et al. EJNMMI 2006;33(11):1346-1351.

EP-0573

^{177}Lu-DOTATATE therapy in progressive meningioma

W. Roll[1], *M. Müther*[2], *B. Zinnhardt*[1], *L. Stegger*[1], *M. Schäfers*[1], *M. Weckesser*[1], *W. Stummer*[2], *K. Rahbar*[1];
[1]*Department of Nuclear Medicine, University Hospital Münster, Münster, GERMANY,* [2]*Department of Neurosurgery, University Hospital Münster, Münster, GERMANY.*

Aim/Introduction: Number of treatment options for meningioma decrease over time with disease progression. Neurovascular involvement and multifocal disease limit the success of surgical strategies. In addition, repeated radiation therapies are associated with increasing side effects. In progressive meningioma that overexpress somatostatin receptors (SSTR) peptide receptor radiotherapy (PPRT) with ^{177}Lu-DOTATATE is a promising alternative in heavily pretreated patients. The aim of the retrospective analysis was to evaluate the efficacy of^{177}Lu-DOTATATE PRRT in this patient cohort. **Materials and Methods:** Eight patients (median age 71 years; range: 56 - 77) with progressive meningioma (6 WHO I, 2 WHO II; 6 multifocal disease), all with prior repeated surgery and percutaneous radiotherapy, received ^{177}Lu-DOTATATE PRRT and were included in this retrospective analysis. Response to therapy was assessed by interim and post-therapy ^{68}Ga-DOTATATE-PET-CT and MRI according to morphological (RECIST) and SSTR imaging parameters. ^{177}Lu-DOTATATE scintigraphies 48h p.i. were evaluated according to Krenning scale. Additionally, clinical outcome and follow up imaging were analyzed for evaluation of time to progression. **Results:** Patients received a median of 3 cycles (range: 1 - 5) of PRRT with ^{177}Lu-DOTATATE (mean injected dose 7.1 GBq). Tumor uptake in 48h p.i. ^{177}Lu-Scintigraphies was heterogeneous (Krenning scale: median: 3, range: 1-4). Post-therapy staging scheduled 8-10 weeks after completion of therapy showed progressive disease in five patients; however, three patients had stable disease. The latter group's time of progression was 6, 10 and 25 months. **Conclusion:** In this cohort of eight progressive meningioma patients ^{177}Lu-DOTATATE therapy showed heterogeneous efficacy. **References:** None.

EP-39
Clinical -> Therapy study -> Adult study -> Other treatments -> Prostate cancer specific treatments

October 12 - 16, 2019
e-Poster Area

EP-0574

[^{177}Lu]-PSMA-617 in low-volume hormone sensitive metastatic prostate cancer: a prospective study

B. M. Prive[1], *S. Peters*[1], *C. H. J. Muselaers*[1], *P. Zamecnik*[1], *M. Janssen*[1], *T. W. J. Scheenen*[1], *M. W. Konijnenberg*[2], *J. F. Verzijlbergen*[1], *W. R. Gerritsen*[1], *N. Mehra*[1], *D. M. Somford*[3], *J. P. M. Sedelaar*[1], *I. M. van Oort*[1], *J. O. Barentsz*[1], *S. Heskamp*[1], *M. Gotthardt*[1], *J. A. Witjes*[1], *J. Nagarajah*[1];
[1]*Radboudumc, Nijmegen, NETHERLANDS,* [2]*ErasmusMC, Rotterdam, NETHERLANDS,* [3]*Canisius Wilhelmina Hospital, Nijmegen, NETHERLANDS.*

Aim/Introduction: 20-40% of localized hormone-sensitive prostate cancer (HS-PCa) patients present with disease recurrence after radical surgery or radiotherapy.[1] [^{177}Lu]-PSMA-radioligandtherapy (RLT) is a promising treatment for metastatic castration-resistant PCa. Based on the mode of action, patients in the HS-stage could potentially benefit too by postponing androgen deprivation therapy (ADT) or be a curative salvage option. We aimed to investigate the tolerability, dosimetry, and treatment response of [^{177}Lu]-PSMA-RLT in these early stage patients who presented with disease recurrence without conventional salvage options and had high expression on PSMA-PET/CT. **Materials and Methods:** In this ongoing prospective study (NCT03828838), 10 patients with HS, low-volume (<10 lesions) PCa and PSA doubling time <6 months will receive two cycles of [^{177}Lu]-PSMA-617 at an 8 (±1) week interval. All patients receive baseline ^{68}Ga-PSMA-PET/CT and MR-imaging. After the first cycle with 3GBq [^{177}Lu]-PSMA patients undergo intra-therapeutic dosimetry (whole-body and SPECT/CT 1, 24, 48, 72, and 144 hours p.i.) to perform dose calculations to the tumor and organs-at-risk. Based on these results the subsequent second [^{177}Lu]-PSMA injection will be adapted to 3-6GBq. Following both cycles, patients are monitored weekly for adverse events (AE; CTCAE 4.0) and blood analysis (hematology, chemistry and PSA). Baseline imaging is repeated at fixed timepoints (8, 20 and 32 weeks after cycle 1), as is the EORTC-QLQ-C30 questionnaire (monthly). **Results:** Currently, 4 patients have been included. All received prior salvage surgery/radiotherapy. Baseline metastases ranged from 1-10 and PSA levels were 0.43-20µg/l. All received 6GBq in the second cycle. After 3 months follow-up, none of 4 patients reported xerostomia or had significant changes on the EORTC-QLQ-C30 questionnaire. No high-grade (>2) AE were observed, however 3/4 patients reported temporarily G1-2 fatigue. Patient 1, 2, 3, and patient 4 had a PSA response from baseline of respectively -56%, +15%, -55% and +30% 12 weeks after cycle 2. Patient 1 had a complete response on both

PSMA-PET/CT and MRI 12 weeks after cycle 2. All organs-at-risk appeared to be within dose limitations during the primary analysis. At time of submission, the dosimetry is being finalized as are the 6 month post-treatment scans. **Conclusion:** [^{177}Lu]-PSMA-RLT appears to be safe in HS-PCa. All patients responded by at least temporarily stabilizing disease and postponing ADT. One patient showed complete radiological remission. RLT has the potential to become a new salvage option next to surgery or radiotherapy. **References:** Djavan B, et al. PSA progression following radical prostatectomy and radiation therapy. Eur Urol. 2003;43(1):12-27.

EP-0575

Combined PRLT using Ac-225 and Lu-177 labeled PSMA-617 (TANDEM-PRLT) in end-stage metastatic prostate cancer: a concept to reduce salivary gland toxicity?

T. Langbein[1,2], *H. R. Kulkarni*[2], *A. Singh*[2], *C. Schuchardt*[2], *J. Zhang*[2], *R. P. Baum*[2];
[1]*Technical University of Munich, School of Medicine, Department of Nuclear Medicine, Munich, GERMANY,* [2]*Zentralklinik Bad Berka, Theranostics Center of Molecular Radiotherapy and Molecular Imaging, Bad Berka, GERMANY.*

Aim/Introduction: First clinical data of Ac-225-labeled PSMA radioligand therapy in advanced metastatic prostate cancer (PC) demonstrated promising results (1). However, xerostomia became the dose-limiting toxicity. Recently, our group presented a protocol using lower administered activity of Ac-225-PSMA-617 applied with Lu-177-PSMA-617 to minimize adverse effects with potential synergistic efficacy (2). This study investigates salivary gland (SG) toxicity of this TANDEM-PRLT approach. **Materials and Methods:** 18 cases of end-stage PC patients selected for TANDEM-PRLT with available follow-up data at 2 months after treatment were investigated. Risk factors like previous taxane-based chemotherapy (7 of 18 pts), external radiotherapy to the head and neck region (2 of 18 pts) or Lu-177-PSMA (14 of 18 pts) were considered. 2.0 - 7.0 MBq of Ac-225 and 3.0- 7.2 GBq of Lu-177 were applied. Dryness of mouth was documented pre- and post-therapeutically according to CTCAE (v5.0) and the shorted xerostomia inventory (XI). A quantified salivary gland scintigraphy (SGS; maximum Uptake Umax; Ejection fraction EF) and SUVmax as well as the metabolic volume of the SG on the Ga-68-PSMA-11-PET/CT were compared. **Results:** Xerostomia increased significantly from grade 0 (max grade 1) to grade 1 (max grade 2; p= 0.001), the average XI rose from 10.73 (± 3.5) to 15.55 (± 4.18) (p= 0.003), however, no severe xerostomia was observed, no patient discontinued treatment. SGS revealed a significant decline of the EF in all SG (p< 0.001) while the Umax showed no significant changes. The Ga-68-PSMA uptake of all SG declined significantly (p< 0.05), while there were no strong significant changes of the metabolic volume detectable. Pretreatment with chemotherapy appeared to be a risk factor, although there was no significant correlation also with age. **Conclusion:** Despite limitations (number of patients, early follow-up setting) initial results propose a reduced SG toxicity of the TANDEM-protocol. Nevertheless, since findings confirmed a clear SG impairment when using Ac-225-PSMA, preventive strategies remain an urgent need, especially in subsequent alpha-PRLT cycles. **References:** [1] Kratochwil C, Bruchertseifer F, Rathke H et al. Targeted α-Therapy of Metastatic Castration-Resistant Prostate Cancer with (225)Ac-PSMA-617: Swimmer-Plot Analysis Suggests Efficacy Regarding Duration of Tumor Control. J Nucl Med. (2018) ;59(5):795-802 [2] Kulkarni HR, Schuchardt C, Langbein T et al. First Clinical and Dosimetry Results of Tandem Alpha-Beta PSMA Radioligand Therapy (TABPRLT) Using a Combination of Ac-225 and Lu-177 Labelled PSMA-617 for Progressive End-Stage Metastatic Prostate Cancer. Eur J Nucl Med Mol Imaging (2018) 45 (Suppl 1): S110.

EP-0576

Correlation between PSA response and response assessment with ^{68}Ga-PSMA-11 PET/CT-derived metabolic parameters in patients treated with ^{225}Ac-PSMA-617 for metastatic prostate carcinoma

I. O. Lawal[1], *A. Morgenstern*[2], *O. Knoesen*[3], *M. Vorster*[1], *G. O. Popoola*[4], *J. Mahapane*[1], *T. Lengana*[1], *T. M. G. Boshomane*[1], *K. M. G. Mokoala*[1], *F. Bruchertseifer*[2], *M. M. Sathekge*[1];
[1]*University of Pretoria, Pretoria, SOUTH AFRICA,* [2]*European Commission, Joint Research Centre, Karlsruhe, GERMANY,* [3]*Nuclear Technology Products (NTP), Pelindaba, SOUTH AFRICA,* [4]*University of Ilorin, Ilorin, NIGERIA.*

Aim/Introduction: PSA decline ≥50% is the validated criteria for assessing response to treatment in patients with prostate carcinoma. ^{68}Ga-PSMA-11 PET/CT-derived metabolic parameters such as SUVmax, SUVmean, whole-body tumor volume (PSMA-TV) and whole-body total lesion PSMA (TL-PSMA) are increasingly being reported as metrics for response assessment. We herein compare the response assessment using PSA decline versus ^{68}Ga-PSMA-11 PET/CT-derived metabolic parameters in patients treated with ^{225}Ac-PSMA-617 for metastatic castration-resistant prostate carcinoma (mCRPC). **Materials and Methods:** A total of 57 patients with mCRPC underwent ^{68}Ga-PSMA-11 PET/CT before and after completing treatment with ^{225}Ac-PSMA-617. SUVmax and SUVmean of lesions, as well as PSMA-TV and TL-PSMA of all malignant lesions, were determined. PET-derived parameters were tested for their correlation with baseline serum PSA and Gleason score. Metabolic response was defined for each PET metabolic parameter as a decline of ≥30% between baseline and post-treatment level. Serial PSA was done to monitor biochemical response. Biochemical response was defined as PSA decline ≥50% following treatment. Response assessment by PSA decline was compared with response assessment by PET-derived parameters. **Results:** Mean age of patients was 67.21 ± 8.96 years. There was a significant decline between baseline and post-treatment PSA (120.36 vs. 12.38), SUVmax (25.64 vs. 10.80), SUVmean (5.59 vs. 3.64), PSMA-TV (888.28 vs. 227.18) and TL-PSMA (4059.69 vs. 1109.93), all p<0.001. Baseline PSMA-TV and TL-PSMA showed significant correlation with PSA (p<0.001 in both cases) while SUVmax and SUVmean

did not (p>0.05). None of the PET-derived parameters showed a significant correlation with tumor Gleason score. Percentage of patients identified as responders by PSA=74, SUVmax=76, SUVmean=64, PSMA-TV=71, and TL-PSMA=75. Comparing response assessment by PSA versus PET-derived parameters, there was a significant level of agreement between PSA and PSMA-TV (K=0.40, p=0.002) as well as PSA and TL-PSMA (K=050, p<0.001). Response assessment by SUVmax and SUVmean did not show a significant level of agreement with PSA response assessment. **Conclusion:** Response assessment using ^{68}Ga-PSMA-11 PET/CT-derived PSMA-TV and TL-PSMA show good levels of agreement with biochemical response assessment by PSA decline of ≥50% in patients with mCRPC treated with ^{225}Ac-PSMA-617.PSMA-TV and TL-PSMA, therefore, have the potential to be used as imaging surrogate of response assessment in radioligand therapy of mCRPC. Our data suggest that the level of agreement between response assessment by SUVmax and SUVmean compared with PSA response assessment is not significant enough for these metrics to be used response assessment. **References:** None.

EP-0577

^{177}Lu-PSMA-617 Radioligand Therapy in Metastatic Castration Resistant Prostate Cancer: Safety, Efficacy and Quality of Life Assessment

M. P. Yadav, *C. Bal, S. Ballal, M. Tripathi, N. A. Damle;*
All India Institute of Medical Sciences, New Delhi, INDIA.

Aim/Introduction: The aim of this study was to evaluate the safety and efficacy of ^{177}Lu-PSMA-617 radioligand therapy (RLT) in metastatic castration resistant prostate cancer (mCRPC). **Materials and Methods:** In this prospective, single-arm, single-institutional study, 90 mCRPC patients with progressive disease on second-line hormonal therapy and/or docetaxel chemotherapy were recruited for the study. All patients underwent diagnostic ^{68}Ga-PSMA-HBED-CC PET/CT, prior to inclusion for therapy. Included patients underwent ^{177}Lu-PSMA-617 RLT at 8 -12 weekly intervals. Haematological, kidney function, liver function tests, and serum PSA levels were recorded before and after therapy at 2 weeks, 4 weeks and 3-month intervals. Biochemical response was assessed using trend in serum PSA levels. Radiographic and Molecular response were on diagnostic computed tomography (CT) and ^{68}Ga-PSMA PET/CT respectively. Clinical response was assessed by visual analogue score (VASmax), analgesic score (AS), Karnofsky performance status (KPS) and Toxicity and response criteria of the Eastern Cooperative Oncology Group (ECOG) criteria. Kaplan-Meier survival curves were used to derive, overall and progression-free survival. **Results:** The median age of patients was 66.5 years (range: 30-88 years). The median activity administered in the 90 patients was 111 ± 60.6 GBq ranging from 1-7 cycles and were followed-up over a median duration of 26 months. At 2-3 month interval after the first therapy and the end of assessment, >50% decline in PSA was observed in 32.2% and 45.5%, respectively. Univariate analysis did not reveal any patient parameters associated with PSA decline. Radiographic response by diagnostic CT revealed partial remission(PR) in 23% (16/69), stable disease (SD) in 54% (37/69), and progressive disease (PD) in 23% (16/69) of patients. Molecular tumor response by PERCIST 1 criteria revealed 19/69 (27.5%) patients with PR, 30/69 23% (43.5%) with SD, and 20/69 (29%) with PD. The disease control rate according to according to the radiographic and molecular response was 77% and 71% respectively. The median overall survival and median progression-free survivals were 14 and 11.8 months, respectively. The mean VASmax score decreased from 8 to 5. The mean analgesic score reduced from 3 to 2 after therapy. The mean KPS score improved from 60 to 70 after therapies. The mean ECOG performance status improved from 3 to 2 after therapy. Toxicities related to RLT were low and transient with no serious adverse effects. **Conclusion:** ^{177}Lu-PSMA-617 radionuclide therapy is a safe and effective approach to the treatment of mCRPC patients. **References:** None.

EP-0578

Safety and dosimetry of ^{177}Lu-PSMA radioligand therapy among patients with a single kidney as compared to patients with both kidneys with or without renal insufficiency before treatment

J. Zhang, *C. Schuchardt, H. R. Kulkarni, A. Singh, R. P. Baum;*
Theranostics Center for Molecular Radiotherapy & Precision Oncology, ENETS Center of Excellence, Zentralklinik Bad Berka, Bad Berka, GERMANY.

Aim/Introduction: The PSMA expression in the apical epithelium of the proximal tubules and high post-therapy uptake in kidneys after PSMA radioligand therapy (PRLT) raises concern about the tolerability and potential nephrotoxicity, especially in patients with already known renal insufficiency (RI). The aim of this study was to compare dosimetry and safety of ^{177}Lu-PRLT among prostate cancer patients with a single functioning kidney (sFK), patients with both kidneys (bFK) with or without baseline renal insufficiency. **Materials and Methods:** A total of 80 patients were included and retrospectively analyzed. All patients had PSMA-positive metastases confirmed on ^{68}Ga-PSMA PET/CT, had received at least 2 cycles of ^{177}Lu-PSMA-617 radioligand therapy. An established protocol practicable in our daily clinical routine was used for dosimetry calculation based on the MIRD-scheme. Mean absorbed doses was estimated using the software OLINDA 2.0. All parameters of renal and hematological toxicity profile were prospectively documented in a structured database and analyzed prior to each PRLT cycle and in follow-up. **Results:** In patients with sFK, the mean injected activity per cycle was 6.39 ± 1.05 GBq. Calculated radiation-absorbed doses of the kidney were 0.81 ± 0.32 Gy/GBq. The absolute doses to whole-body were 0.058 ± 0.027 Gy/GBq. In patients with bFK, the mean injected activity per cycle was 6.5±1.1 GBq. The dose estimations revealed a mean absorbed dose of 0.8 Gy/GBq for kidneys with effective half-life of 40 hours. The absolute doses to whole-body were 0.04 Gy/GBq with effective half-life of 42 hours. In patients with sFK, renal function (CTCAE G0:G1:G2)

were 50%:29%:21% before PRLT, 50%:43%:7% after the first cycle of PRLT, 50%:36%:14% after the second cycle of PRLT. In patients with bFK and normal baseline renal function, G0:G1:G2 were 100%:0%:0% before PRLT, 100%:0%:0% after the first cycle, and 98%:2%:0% after the second cycle of PRLT. No CTCAE-3 or 4 nephrotoxicity was observed. In patients with bFK, but already known RI before PRLT, hemoglobin grading (G0:G1:G2) were 23%: 69%:8% before PRLT, 23%:69%:8% after the first cycle, and 23%:62%:15% after the second cycle of PRLT. **Conclusion:** ^{177}Lu-PSMA-617 showed a comparable absorbed renal dose, and increased whole body dose in patients with a single kidney, as compared to patients with two kidneys. ^{177}Lu-PSMA-617 radioligand therapy is feasible and well tolerated without any signs of nephrotoxicity in patients with already known RI before PRLT including patients with a single kidney. No additional hematotoxicity was observed in this special patient group with baseline RI. Further long-term follow-up is warranted. **References:** None.

EP-0579

^{223}Ra-dichloride: Prognostic value of Baseline Quality of Life in mCRPC patients candidates to treatment

V. Frantellizzi, M. De Feo, C. De Angelis, G. De Vincentis; Sapienza University of Rome, Rome, ITALY.

Aim/Introduction: ^{223}Ra-dichloride(^{223}Ra) was approved for treatment of Castration Resistant Prostate Cancer patients with symptomatic bone metastases (mCRPC), owing to the palliative effect on bone pain and the significant improvement of overall survival (OS). The prognostic value of baseline data in predicting the survival prolonging effect of ^{223}Ra is still under investigation. The objective of this study was to investigate the impact of baseline quality of life (QoL) on OS in mCRPC patients treated with ^{223}Ra. The present study also evaluated the trend of patient-reported QoL during ^{223}Ra-treatment and post-therapy follow-up. **Materials and Methods:** 168 eligible mCRPC patients treated with ^{223}Ra (55 KBq/Kg 1q4wks for 6 cycles) were included in this non randomized study. Baseline QoL was assessed through the European Organization for Research and Treatment of Cancer Quality of Life Questionnaire C30 (EORTC QLQ-C30) and the Bone Metastasis Module (QLQ-BM22). Other baseline variables relevant to the OS analysis (age, height, weight, PLT,ECOG Performance Status,Hb, PSA, tALP), were taken into account. OS was established from the date of the first ^{223}Ra administration until the date of death. Data were retrospectively collected and summarized using descriptive statistics, univariate and multivariate analysis with Cox model, OS analysis stratified by score (ROC Curve) and Joint models. **Results:** Among 168 patients, 108 (64%) completed the scheduled administrations, 48 (29%) discontinued treatment because of progression disease or death, while 12 (7%) were still receiving ^{223}Ra at the time of the analysis. The mean follow-up time was 11±8 months. On univariate analysis, almost all items of both questionnaires were significantly correlated with OS, except for dyspnea, diarrhea and financial difficulties. In the multivariate analysis before PCA, baseline patients' Hb, tALP and two EORTC QLQ-C30 items were significantly associated with OS (physical functioning: HR=0.970, CI 0.960-0.980, p<0.001; dyspnea: HR=0.992, CI 0.986-0.999, p=0.023). In the resulting model of the multivariate analysis performed after PCA, baseline patients' Hb, tALP and global-QoL were independent significant predictors of OS (global-QoL: HR=0.995, CI 0.993-0.998, p=0.001). The OS analysis stratified by score of baseline QoL, showed a median OS of 5 and 12 months for scores respectively below and above the cut-off value (ROC Curve cut-off: -135.14) (log-rank test: p=0.01). The present analysis confirmed QoL deterioration over time, in accordance with previous studies. **Conclusion:** Baseline QoL is a significant predictor of OS, meaning that patients with better pretreatment QoL are more likely to obtain a marked survival prolonging effect from ^{223}Ra. **References:** DOI:10.1080/09553002.2019.1558301 DOI:10.1007/s12149-017-1228-6 DOI:10.3892/ol.2018.9785 doi:10.2217/fon-2018-0318.

EP-0580

High Activity ^{177}Lu-PSMA Therapy Of Metastatic Castration-resistant Prostate Cancer

C. Happel, W. T. Kranert, B. Bockisch, D. Gröner, K. H. Davis, J. Wichert, M. Stefanova, F. Grünwald, A. Sabet; University Medical Center Frankfurt / Department of Nuclear Medicine, Frankfurt, GERMANY.

Aim/Introduction: Recently ^{177}Lu labeled high-affinity prostate-specific membrane antigen (^{177}Lu-PSMA-617) has developed to a widely accepted and promising therapeutic option in patients suffering from metastatic castration-resistant prostate cancer (mCRPC). Current national and international guidelines recommend standard activities of 6GBq per cycles. In the German consensus protocol the cumulated maximum activity is specified to be18 GBq or in special cases 37GBq, limited by the kidney dose. **Materials and Methods:** Four patients with mCRPC were each treated with 10 cycles of ^{177}Lu-PSMA-617 to avoid tumor progression and disease specific complications. For dosimetry of the whole body and the kidneys as well as clinical monitoring of the course of therapy whole-body scintigraphy and SPECT were performed 24, 48 and 72h post intravenous administration of the radiopharmaceutical (scan speed: 12cm/min; matrix: 512x2048; 15s/step, 64steps). For further medical monitoring frequent PET/CT and functional scintigraphic imaging of the kidneys was performed. The corresponding remaining activity in the body was obtained from the geometric mean of measurements with an individually calibrated gamma probe twice a day. Kinetics was calculated by a least square fit using MS-Excel. It was used to calculate the mean whole body dose. Kidney mass was calculated out of CT Images. **Results:** Mean administered activity per cycle was 7.12GBq (Range 5.02-8.65GBq, according to tumor burden and kidney dose). Mean accumulated activity was 71.16GBq and ranged from 62.92GBq to 79.76GBq. Time between the first and the 10th administration ranged from 1.5 to 2.3 years. The mean whole body dose of the four patients was 243mGy per treatment (33mGy/GBq) and

2.4Gy (1.08Gy-3.86Gy) in total without any significant trend. The mean calculated kidney dose was 1.55Gy per treatment (0.22Gy/GBq) and 16Gy (13.5Gy-21.8Gy) in total, again without any significant trend. The cut off value for the kidneys of 23Gy was not exceeded. Blood parameters (haemoglobin, leucocytes and thrombocytes) as well as kidney function parameters (GFR, creatinine) did not change significantly over the whole period of treatment. **Conclusion:** Cumulated activities of nearly 80GBq within 1.5 to 2.3 years were well tolerated without any relevant complications. Therefore, dependent on kidney- and whole body dose, in consideration of the good therapeutic response and state of health an escalation of accumulated activity of up to 80GBq seems to be safe and effective. **References:** None.

EP-0581

Prognostic Value of Discordance Between ^{68}Ga-PSMA PET/CT and ^{99m}Tc-HDP SPECT/CT Bone Scintigraphy in Metastatic Prostate Cancer Patients Treated with ^{223}Ra-Dichloride

N. Plouznikoff[1,2], *C. Artigas*[1], *T. Gil*[3], *P. Flamen*[1];
[1]*Department of Nuclear Medicine, Institut Jules Bordet, Université Libre de Bruxelles (ULB), Brussels, BELGIUM,* [2]*Department of Nuclear Medicine, Centre Hospitalier de l'Université de Montréal (CHUM), Montreal, QC, CANADA,* [3]*Department of Oncology, Institut Jules Bordet, Université Libre de Bruxelles (ULB), Brussels, BELGIUM.*

Aim/Introduction: ^{223}Ra-dichloride is a calcium mimetic radiopharmaceutical targeting osteogenic cells currently indicated for metastatic castrate-resistant prostate cancer (mCRPC) patients with symptomatic bone metastases. A bone scintigraphy is usually performed prior to treatment to visualise targeted bone lesions. However, ^{68}Ga-labeled Prostate-Specific Membrane Antigen (PSMA) ligand PET/CT has shown better accuracy in detecting metastatic bone lesions, even before osteoblastic reaction. The purpose of this exploratory study was to investigate the prognostic value of a discordance between baseline ^{68}Ga-PSMA PET/CT and ^{99m}Tc-hydroxydiphosphonate (HDP) SPECT/CT bone scintigraphy on progression-free and overall survival (PFS/OS) in mCRPC patients treated with ^{223}Ra-dichloride. **Materials and Methods:** We retrospectively analysed 13 mCRPC patients treated with ^{223}Ra-dichloride (55 kBq/kg, up to 6 cycles every 4 weeks) at our institution who had a baseline ^{99m}Tc-HDP bone scintigraphy, as well as a baseline ^{68}Ga-PSMA-11 PET/CT to exclude extra-osseous disease. Bone scintigraphy included a SPECT/CT ranging from skull base to mid-thigh. Patients were classified as discordant if there was one or more bone lesion on PSMA-PET with no detectable corresponding uptake on ^{99m}Tc-HDP SPECT. Lesions <1cm³ on PET imaging (standard threshold of 42% of SUVmax used for volume determination) were excluded in order to account for the lower spatial resolution of SPECT. Clinical files were reviewed to obtain the date of disease progression (as recorded by tumor board) and eventual death. Survival was analysed using Kaplan-Meier curves, log-rank tests and the Cox proportional hazard model. **Results:** 4 patients were classified as discordant and 9 as concordant. All discordant patients at baseline stopped ^{223}Ra therapy after only 3 cycles due to clinical progression. Discordance was a univariate predictor of survival, with a shorter median survival for discordant vs concordant patients for both PFS (2.7 vs 5.7 months, 95%CI: 1.8-3.6 and 3.7-7.7 respectively, p<0.001) and OS (6.2 vs 13.0 months, 95%CI: 4.7-7.7 and 10.8-15.2 respectively, p=0.001). Discordance remained a predictor of OS in a multivariate analysis even after adjusting for the number of ^{223}Ra cycles received (p=0.038). **Conclusion:** Our study suggests that discordance between ^{68}Ga-PSMA PET/CT and SPECT/CT bone scintigraphy before ^{223}Ra-dichloride therapy could be a prognostic biomarker for PFS and OS. Patients with PSMA-positive but bone scintigraphy-negative bone metastases seem associated with a worse outcome, probably because those metastases are not effectively treated with ^{223}Ra. Prospective studies are required to investigate such discordances and determine if a baseline ^{68}Ga-PSMA PET/CT should routinely be performed for patients considered for Radium-223 radionuclide therapy. **References:** None.

EP-0582

Potential value of neuroendocrine differentiation serum biomarkers in prediction of response to radioligand therapy with Lu177 PSMA 617 for metastasized castrate resistant prostate cancer

V. Prasad[1], *M. Gruenert*[1], *F. Zengerling*[2], *J. Miksch*[1], *C. Bolenz*[2], *A. J. Beer*[1];
[1]*Department of Nuclear Medicine, University Hospital, Ulm, GERMANY,* [2]*Department of Urology, University Hospital, Ulm, GERMANY.*

Aim/Introduction: Radioligand therapy (RLT) with Lu-177 PSMA 617 of metastasized castrate resistant prostate cancer (mCRPC) patients can achieve good PSA response (>50% reduction in PSA value) in roughly 40-50% of patients. On the other hand about 30% of mCRPC can harbor neuroendocrine differentiation (NED) in metastases. Until now no literature exists on the value of Chromogranin A (CgA) and neuron specific enolase (NSE) in patients with mCRPC undergoing RLT. **Materials and Methods:** 13 consecutive mCRPC patients (68.9 y±6.2) undergoing RLT were followed up with PSA, CgA (upper normal limit UNL 102 ug/l) and NSE (UNL <17 ng/ml) prior to and at 6 weeks after RLT. Patients were treated with an average of 6 GBq every 6 weeks. Manny Whitney U test was performed to assess the hypothesis that both PSA responders and non-responders have same baseline CgA (CgAi), NSE (NSEi), ΔCgA, ΔNSE, ΔCgA/ΔNSE,% CgA above UNL, % NSE above UNL, and CgAi/NSEi. ROC analyses were performed to assess the best cut-off value for prediction of response RLT. **Results:** Mean±SD/median (range) baseline PSA was 758±1427 / 46.8 (0.50-5000). Baseline mean±SD / median (range) CgA and NSE values were 127.8±91.05 / 107 (36-357) and 16.5±4.4 / 17.5 (8.7-25.9). Baseline CgA values were elevated in 8/13 (61.5%) whereas NSE was elevated in 7/13 (53.8%) of patients. PSA based response evaluation could be performed in 11/13 patients; in remaining 2 patients the follow-up after 6

weeks is awaited. Seven out of 11 patients (63.4%) showed more than 50% reduction in PSA at 6 weeks. Only CgAi (p=0.012) ,% CgA above UNL (p=0.033) and CgAi/NSEi (p= 0.012) were found to be correlate significantly with PSA response. 100% of patients with elevated CgA achieved PSA reduction of more than 50% at 6 weeks interval but only 66.7% with elevated NSE. CgA of 101.5 or CgAi/NSEi ratio of 2.79 could predict PSA responders with sensitivity / specificity (%) of 86/100 and 100/100 respectively. Only 2 patients were on proton pump inhibitors; in both patients CgA was not elevated above UNL. **Conclusion:** In this explorative study in a limited number of patients elevated CgA as a marker for NED appears to be a good prognostic marker. In the next step, a multifactorial analysis in larger subgroup of patients will be performed to assess the added value of CgA over the known predictors of response to RLT. **References:** None.

EP-0583

The 68Ga / 177Lu-Theragnostic Concept in PSMA-Targeting of Metastatic Castration Resistant Prostate Cancer: Impact of Post-therapeutic Whole Body Scintigraphy in the Follow-Up

L. Scarpa[1], *J. Maffey-Steffan*[1], *A. Svirydenka*[1], *B. Nilica*[1], *S. Buxbaum*[1], *C. Mair*[1], *J. Bektic*[2], *E. von Guggenberg*[1], *C. Uprimny*[1], *W. Horninger*[2], *I. Virgolini*[1];
[1]*Medical University Innsbruck, Department of Nuclear Medicine, Innsbruck, AUSTRIA,* [2]*Medical University Innsbruck, Department of Urology, Innsbruck, AUSTRIA.*

Aim/Introduction: A targeted theragnostic approach based on increased expression of prostate-specific membrane antigen (PSMA) on prostate cancer (PC) cells is an attractive treatment option for patients with metastatic castration-resistant prostate cancer (mCRPC). **Materials and Methods:** Thirty-two consecutive mCRPC patients were selected for ^{177}Lu-PSMA617 therapy on the basis of PSMA-targeted ^{68}Ga-PSMA-HBED-CC PET/CT diagnosis showing extensive and progressive tumour load. Patients received 2 to 6 therapy cycles (each 6 GBq, 6 to 10 weeks apart) and were followed until death. PET/CT scans were compared to ^{177}Lu-PSMA617 24-hour whole-body scans and a detailed comparison of SUV_{max} values and absorbed tumour doses was performed. **Results:** ^{177}Lu-PSMA617 dosimetry indicated high tumour doses for skeletal (4.01±2.64 Gy/GBq; range 1.10-13.00 Gy/GBq), lymph node (3.12±2.07 Gy/GBq; range 0.70-8.70 Gy/GBq) as well as liver (2.97±1.38 Gy/GBq; range 0.76-5.00 Gy/GBq) metastases whereas the dose for tissues/organs was acceptable in all patients for an intention-to-treat activity of 24 GBq. Any PSA-decrease after the first therapy cycle was found in 24/32 patients (75%), after the second cycle in 22/32 patients (69%), after the third cycle in 16/29 patients (55%) and after the fourth cycle in 9/21 patients (43%). Post-therapy whole-body scintigraphy showed decreased tumor background ratios in 24/32 patients (75%) after the first therapy cycle, after the second cycle in 17/29 patients (59%) and after the third cycle in 12/20 patients (60%). The median progression free survival was 6 months and the median overall survival 12 months. Decreasing SUV_{max}-values were found for parotid (15.93± 6.23 before the treatment and after the treatment 12.33±4.07) and submandibular glands (17.65±7.34 before the treatment, 13.12±4.62 after the treatment) following each treatment, and transient xerostomia was found in 8/32 patients (25%). In 3/32 patients nephrotoxicity changed from Grade 2 to 3, whereas no Grade 4 nephrotoxicity or hematotoxicity was found. No significant correlation could be calculated for initial absorbed tumor doses and SUV_{max}-values of tumor lesions. However, in most patients visual whole-body scan and visual PET/CT scan interpretation exhibited a good correlation. Over the course of disease in 5/32 patients a mixed response pattern (i.e. disappearance of tumor lesions at one location and development of new lesions in a different location). **Conclusion:** Serial PSA measurements and post-therapy whole body scintigraphy are sufficiently accurate for the follow-up of ^{177}Lu-PSMA617-treated mCRPC-patients. **References:** None.

EP-0584

Radioligand Therapy with ^{177}Lu-PSMA in Metastatic Castration Resistant Prostate Cancer Patients: First case series in Iran

K. Aryana*, S. Zarehparvar Moghadam, G. A. Divband;*
Nuclear Medicine Research Center, Mashhad University of Medical Sciences, Mashhad, IRAN, ISLAMIC REPUBLIC OF.

Aim/Introduction: Prostate-specific membrane antigen (PSMA) is a promising theranostics for metastatic castration-resistant prostate cancer (mCRPC) patients. This study is designed to evaluate the effect of radioligand therapy with ^{177}Lu-PSMA in mCRPC patients **Materials and Methods:** 26 mCRPC patients, with an average age of 71.65 (±9.93) and a median Gleason score of 9, who had no other treatment options were selected for radioligand therapy with ^{177}Lu-PSMA between November 2016 and December 2018. 53% of the patients had an ECOG score of 2 to 4. **Results:** Twenty-six patients were treated with a total number of 57 cycles of ^{177}Lu-PSMA (total dose 341GBq, the median dose of 5.92 GBq). 19 patients (73%) showed some degree of PSA decline after the first cycle. 9 patients showed a PSA decline of ≥50% and 10 patients had a decline of <50%. Disease progression occurred in 7 patients. 13 patients underwent the second cycle of therapy out of whom PSA decline was observed in 8 patients (61.53%). 4 of them showed a decline of ≥50%. Five patients showed progression. Among the 7 patients who showed disease progression after the first cycle of therapy, 2 patients had progressive disease in the second cycle and one patient showed a PSA decline.15 patients had debilitating bone pain among whom 11 patients experienced reduced levels of pain between 10 to 14 days after the first cycle of treatment. No kidney and liver toxicity were noted. Two patients developed grade III anemia and two patients developed grade III thrombocytopenia. Three patients died in the follow up after the first cycle and 6 patients died during the follow-up period after the second cycle of therapy.

Conclusion: In our study, radioligand therapy with ^{177}Lu-PSMA in mCRPC cases showed to be an effective therapeutic option with minimal side effects which can result in a considerable decline in PSA values. Relatively high rates of mortality in our study could be due to advanced stages of disease in the referred patients. Side effects of previous treatments could have also contributed to the deterioration in patients' conditions before starting radioligand therapy. We conclude it is likely that Lu-PSMA could play an important role in prostate cancer management in earlier stages of the disease when a good bone marrow reserve is still preserved. However further studies must evaluate this theory **References:** None.

EP-0585

225Ac-PSMA-617 treatment and follow up in advanced stage metastatic castration resistant prostate cancer: First clinical experience from Azerbaijan

F. Novruzov[1], *J. Aliyev*[2], *F. Guliyev*[3], *B. Abbasov*[4], *L. Mehmetbeyli*[1], *E. Mehdi*[1];
[1]*Department of Nuclear Medicine, National Centre Of Oncology, Baku, AZERBAIJAN,* [2]*Department of General Surgery, National Centre Of Oncology, Baku, AZERBAIJAN,* [3]*Department of Urooncology, National Centre Of Oncology, Baku, AZERBAIJAN,* [4]*Department of Pathology, National Centre Of Oncology, Baku, AZERBAIJAN.*

Aim/Introduction: Prostate-specific membrane antigen is a unique target in metastatic castration resistant prostate carcinoma patients. PSMA is a good example of theranostic agent. A remarkable therapeutic efficacy has been demonstrated with 225Ac-prostate-specific membrane antigen (PSMA)-617 in heavily pre-treated metastatic castration-resistant prostate cancer patients. We report our clinical experience with 225Ac-PSMA-617 therapy in advanced stage metastatic prostate carcinoma. **Materials and Methods:** Nine patients with advanced castration resistant prostate cancer (Gleason score greater than 7) were selected for treatment using 225Ac-PSMA-617 at 2-month intervals, with initial activity of 6-8 MBq. 8 patients presented with both bone and lymph node metastases, while one patient had mucosal invasion of the bladder with severe hematuria and retroperitoneal conglomerate lymph node metastases. 5 patients had 2 treatment cycles administered. In one patient treatment was discontinued after one cycle due to good response. One patient with disseminated intense liver metastases received 8 MBq instead of 10 MBq for both cycles in order to evade possible liver insufficiency. PSA was measured every 2-4 weeks for PSA response assessment. 68Ga-PSMA-PET/CT was used for functional response assessment before each subsequent treatment cycle. Serial full blood count, renal function test, and liver function were obtained to determine treatment-related side effects. **Results:** Good antitumor activity assessed by serum PSA level and 68Ga-PSMA-PET/CT was seen in 8 of 9 patients. In 7/9 patients, PSA decline more than 4 times was seen after treatment. All patients had a more than 50% decline in the avidity of lesions for tracer on 68Ga-PSMA-PET/CT. One patient had complete resolution of all metastatic lesions (PSA nadir: 0.02 ng/mL), thus there was no need for treatment with an additional cycle. Grade 1-2 xerostomia were seen in 8 patients, and none was severe enough to lead to discontinuation of treatment. Bone pain relieved completely in 6 patients and 2 patients have declared significant fatigue following the first therapy course. **Conclusion:** Although, limited data are available on the clinical efficacy and side effects of 225Ac-PSMA targeted radionuclide treatment, it appears to provide hopeful and successful solutions for advanced prostate cancer. Further studies for informing clinical practice and clinical trial design are awaited. **References:** None.

EP-40

Clinical -> Therapy study -> Adult study -> Other treatments -> Radioimmunotherapy

October 12 - 16, 2019 e-Poster Area

EP-0586

Radioimmunotherapy with 90Y-ibritumomab. Twelve years experience

M. Lara Martinez*, F. Medina Romero, I. Cabrera Veloz, M. Canelas Subieta, S. Lakhwani Lakhwani, F. Fernandez Belmonte, M. Gonzalez Diaz, M. Gomez Rodriguez;*
Hospital Universitario de Canarias, Santa Cruz de Tenerife, SPAIN.

Aim/Introduction: Radioimmunotherapy in Non-Hodgkin Lymphoma is based on the use of conjugated monoclonal antibodies with a radioisotope in a radiotracer. This association produces a double effect on the lymphocytes expressing specific receptors by the combined effect of beta radiation and the antibody.The aim of this study is to evaluate our experience with treatments of 90Y-ibritumomab in Non-Hodgkin Lymphoma (NHL). **Materials and Methods:** Descriptive retrospective study of patients with NHL who were treated with Y90-ibritumomab from 2007 to 2019. In this period, 48 patients were selected, of whom 5 were excluded (follow-up time inferior to 3-4 months). In addition to demographic parameters, we analyzed treatment modality (refractory/relapse, consolidation, transplant conditioning), NHL type and stage and progression-free survival and overall survival. **Results:** We analyzed 43 patients treated with Y90-ibritumomab (34 men and 9 women), with a mean age of 60 years, with diagnoses of Mantle NHL (24 patients), Follicular NHL (16 patients) and Diffuse large B-cell NHL (3 patients), most of them in stage IV (38 patients), stages III (3 patients), II and I (1 patient of each). It was observed that the mean progression-free survival after treatment was 39 months and the mean overall survival was 52 months. We performed 4 patients with refractory NHL, 5 with indication of consolidation and 34 of transplant conditioning. **Conclusion:** Despite the heterogeneity of our sample, radioimmunotherapy with 90Y-ibritumomab is a feasible, effective and probably underused therapeutic

option. Its use in transplant conditioning is a promising field. **References:** None.

EP-41

Clinical -> Therapy study -> Adult study -> Thyroid treatment -> Thyroid treatments, benign

October 12 - 16, 2019 e-Poster Area

EP-0587

Correction Of Hyperfunctional Radiation Induced Stunning (CHRIS) In Pre-therapeutic Radioiodine-131 Uptake Test Of Patients Suffering From Multifocal Autonomous Thyroid Nodules

C. Happel[1], *I. Binse*[2], *B. Bockisch*[1], *A. Sabet*[1], *D. Gröner*[1], *W. T. Kranert*[1], *K. Herrmann*[2], *F. Grünwald*[1];
[1]*University Medical Center Frankfurt / Department of Nuclear Medicine, Frankfurt, GERMANY,* [2]*University Medical Center Essen / Department of Nuclear Medicine, Essen, GERMANY.*

Aim/Introduction: A reduced intrathyroidal uptake of radioiodine-131 after a previous diagnostic administration of radioiodine-131 is called thyroid stunning (TS). Possible explanations of this phenomenon are a dose dependant cellular inhibiting effect of the β^--radiation on the iodide transport mechanism as well as a release of thyroid hormones to the blood circulation due to radiation induced disposing of the thyroid follicles. Numerous studies describe TS in malignant thyroid diseases, but it is still controversial if the effect is also relevant in benign thyroid diseases. Therefore, the aim of this study was to evaluate TS caused by the radioiodine-131 uptake test (RIUT) in patients suffering from multifocal autonomous nodules (MAN) of the thyroid and correct this effect mathematically in order to improve accuracy of RIUT. **Materials and Methods:** 177 patients (median age 73 (34-92), 141 female) with MAN of the thyroid underwent RIT without thyreostatic medication. The variation of pre- to intra-therapeutic maximum radioiodine-131 uptake (MRU) dependent on pre-therapeutic radiation dose [Gy] was evaluated statistically and showed a reduced intra-therapeutic uptake of 8.2% per Gy administered dose in RIUT. Depending on the variation of pre- and intra-therapeutic MRU a correction of hyperfunctional radiation induced stunning (CHRIS) was conducted. The calculation of required radioiodine-131 activity to obtain a target dose of 150Gy was then re-evaluated in all 177 patients using CHRIS. **Results:** Median thyroid volume was 37ml (9-127ml) and median in RIUT-activity was 2.4MBq (range: 1.4-4.3MBq) resulting in a median dose of 0.54Gy (0.11-2.41 Gy). Median MRU in RIUT and in RIT was 36% (17-82 %) and 34% (17-69%) respectively. Therefore the mean ratio of RIT and RIUT MRU was 0.95 (0.63-1.59). A calculation using the pre-therapeutic calculated activity for a target dose of 150Gy, intratherapeutic EMU and effective halflife resulted in a mean target dose of 128Gy (56-258 Gy). A retrospective recalculation of the target dose using the CHRIS-modified activity revealed a significantly improved mean dose of 150Gy with a significantly smaller range of 98-239 Gy. The mean ratio of RIT and CHRIS-modified MRU was 1.00 (0.65-1.59). **Conclusion:** By the use of the CHRIS modification of the Marinelli equation intra-therapeutic intrathyroidal uptake can be predicted with significantly higher overall accuracy, leading to a better achievement of the planned dose in patients suffering from multifocal autonomous nodules of the thyroid. However, wether CHRIS is also leading to a higher success rate of RIT has to be evaluated in further studies. **References:** None.

EP-0588

Analysis of factors influencing the effective half-life of radioactive iodine in patients with hyperthyroidism by pretreatment with lithium carbonate

R. Wang, *B. Wu, Z. Yan, Y. Liu, X. Han, B. Liu;*
Nuclear Medicine Department, the First Affiliated Hospital of Zhengzhou University, Zhengzhou, CHINA.

Aim/Introduction: It was reported that lithium pretreatment combines with radioactive iodine treatment (RAI) might increase the cure rate and shorten the cure time for hyperthyroidism compared with RAI therapy alone. This might be explained by lithium decrease thyroid hormone synthesis or release and increase thyroidal uptake or retention of radioactive iodine (prolong the effective half-life, EHL). However, it has been found that lithium pretreatment does not retention radioactive iodine effective half-life in all patients with hyperthyroidism. In view of the narrow safe therapeutic window of treatment for lithium, it is very important to choose the right patients population before decide to lithium pretreat combined with RAI. This study is to investigate the influencing factors of the effective half-life of radioactive iodine before and after lithium carbonate pretreatment in hyperthyroidism. **Materials and Methods:** Qualified patients (EHL<5days, 4h /24h TRIU>85%) were recorded baseline characteristic as the possible influent infectors, such as gender, age, duration of diagnosed hyperthyroidism, radioactive iodine (RAI) treatment or anti-thyroid drug (ATD) treatment ever or not, serum thyroid hormones, serum thyroid antibodies, liver and kidney function, blood routine test, estimated thyroid volume, thyroid ^{131}I uptake value (TRIU). The patients were given 250miligram lithium orally, three times per day for seven days, and 2, 4, and 24h TRIU was measured before and after lithium treatment. Data were analyzed by t-test, χ^2-test, ANOVA, uni-variable linear regression, multi-variable linear regression using SPSS 21.0 statistical software (significance was defined as $P<0.05$). **Results:** Qualified patients were 225(72 males, 149 females). The effective half-life of radioactive iodine was prolonged (0.94±0.82)d in 147 patients (65.33%), while shortened (0.57±0.44)d in 78 patients (34.67%) after lithium carbonate treatment. Influential factors of ^{131}I effective half-life increase in thyroid with lithium treatment are age, FT3 level, TPO-Ab, 2h and 4h TRIU, EHL by uni-variable

linear regression analysis. By multivariable linear regression analysis, influential factors are age (X_1), FT3 (X_2), 2h TRIU (X_3), EHL (X_4), and the equation is $Y=4.465-0.069X_1-0.004X_3-0.277X_4$(in all patients), $Y=3.788-0.062X_1-0.135X_2-0.202X_3$(in male), $Y=4.386-0.006X_3-0.192X_4$(in female). **Conclusion:** Some factors can influent the change of EHL of radioactive iodine in thyroid after lithium treatment. Younger, lower 2h TRIU and shorter EHL are beneficial factors in all patients, while in male group, lower FT3 lever benefit to them additionally, EHL has no significant influence. **References:** None.

EP-0589

Personal Ablative Doses of Radioiodine in Young Patients with Grave`s Disease in Respect of Level of Anti-thyroid Antibodies

***M. Listewnik**, K. Jasiakiewicz, P. Gorczyca, H. Piwowarska-Bilska, B. Birkenfeld;*
Independent Public Clinical Hospital no 1, Szczecin, POLAND.

Aim/Introduction: The influence of radioiodine treatment (RIT) in ablative doses on thyroid volume and the level of anti-thyroid antibodies in patients up to 30 years old with Grave`s disease in 2012-2016 years. **Introduction:** In our Department of Nuclear Medicine records, the rate of patients up to 30 years old constituted 3% of the whole group subjected to RIT. Interestingly, increasing percentage of patients with elevated anti-thyroid antibodies is observed in developed countries. **Materials and Methods:** The group of 54 (40F and 14M) patients in average age 23.35±5.45 (range of 10-30; median 25) years, treated with the absorbed dose of 256 ±26.9 (range 200-350) Gy. Among them, 41(75.9%) patients were pretreated with antithyroid drugs in average period 25.9±26.8 months. The clinical, biochemical and dosimetry data and thyroid scintigraphy results were compared before and after RIT in the group under 18 (n=13; 24.1%)(U18) and over 18 (n=41; 75.9%)(O18) years of age. In 11 (20.4%) patients steroid protection was applied. Additionally, the group was divided backward according to a decline or an increase of thyroid receptors antibodies (TRAb) and anti-thyroid peroxidase antibodies (aTPO) concentration in reaction of RIT in one year follow -up. **Results:** Hyperthyroidism, normal function and hypothyroidism after RIT occurred in 10(18.5%), 6(11.1%) and 38(70.4%) patients, respectively. Absorbed dose and final results for U18 and O18 were similar (p=0.439, p=0.379, respectively). Steroid protection had no influence on final results. Baseline aTPO showed higher levels in serum concentration in U18 than O18 group (p value=0,040), but not for final aTPO. The final TRAb and baseline aTPO concentrations in backward analysis after RIT differs statistically (p=0.001, p=0.016, respectively). Before and after RIT, in O18 group, TRAb, thyroid volume reduction differs statistically for women (p=0.009, p=0.001, respectively), but in men only for aTPO (p=0.046). For OA group aTPO, TRAb, and thyroid volume before, and after RIT differs statistically (p=0.012, p=0.003, p=0.001, respectively). For the whole group, patients with backward TRAb decline no statistical difference was noted only for aTPO (p=0.878), and for those with backward a-TPO decline for TRAb (p=0.286). **Conclusion:** RIT in ablative doses is efficient for young patients. Young adults group and children group showed differences in anti-thyroid antibodies concentrations before and after RIT. The different kinetics TRAb as well as aTPO due to RIT requires more research. **References:** Lindgren O., Asp P., Sundloev A. The Effect of Radioiodine Treatment on TRAb, Anti-TPO, and Anti-TG in Graves' Disease. DOI: 10.1159/000495504.

EP-0590

An interim assessment of outcomes from long-term follow-up data of 12 years on radioiodine therapy in patients treated for Graves' disease

***G. Kumar**, A. Bhattacharya, B. Mittal;*
PGIMER, Chandigarh, INDIA.

Aim/Introduction: The study aims to evaluate outcomes in patients of Graves' disease treated with radioiodine. **Materials and Methods:** The ongoing retrospective study included 347 patients (254 females) after review of clinical records from 2001 to 2012. Patients underwent pertechnetate uptake scan and/or radioiodine uptake study before radioiodine therapy. Follow-up and outcomes were tabulated. Achievement of biochemical hypothyroidism or euthyroidism was considered as successful therapy. Continuous variables are presented as mean ± standard deviation (range). P value < 0.05 was considered statistically significant. **Results:** Mean age of the patients was 39.2 ± 11.7 (12 - 71) years. Symptom-onset duration was 4.7 ± 4.8 years (1 month - 25 years). Majority of patients (n=327; 94.8%) had history of antithyroid drugs (ATD) either continuously or intermittently since diagnosis. Biochemically, 271 patients (78.6%) were thyrotoxic at presentation; 66 and 8 patients were euthyroid and hypothyroid respectively. Pertechnetate scan was done in 323 patients, radioiodine uptake in 11 patients; eleven patients underwent both investigations. First dose of radioiodine administered (RAI-1) was 8.5 ± 8.3 (range 4.4 - 17) mCi. More than three quarters (n=273; 79.1%) were rendered hypo/euthyroid after first dose of radioiodine. Second and third doses of radioiodine were required in 63 (18.2%) and 9 (2.6%) patients respectively. Pertechnetate uptake was significantly higher (25.4 ± 13.7% vs 13 ± 9.9%, p<0.0005) in patients who needed ≥2 doses of radioiodine. No difference was noted in RAI-1 between these groups. Mean follow-up duration was 52.8 ± 37.5 (range 3 - 135) months. Radioiodine therapy was successful in 96.5%. Forty-two (12.1%) and 291 patients (84.3%) were rendered euthyroid and hypothyroid respectively. These outcomes were achieved in 12.7 ± 14 (1 - 90) months. Remaining 12 patients had refractory thyrotoxicosis. One-way ANOVA between outcome groups didn't reveal any significant differences in pertechnetate uptake, age, symptom-onset duration and RAI-1. However, in patients with hypo/euthyroidism at presentation (n=74; 21.4%), statistically significant (p=0.008) linear regression model was identified for duration to achieve hypo/euthyroidism following therapy; it was a function of age and ATD duration with a correlation of 36.5% between observed and predicted

outcomes. **Conclusion:** Radioiodine therapy has an excellent success rate with majority patients being rendered hypo/euthyroid after first dose. Pertechnetate uptake at presentation was significantly higher in patients requiring multiple doses of radioiodine. Duration to achieve hypo/euthyroidism after therapy was a linear function of age and ATD duration in patients who were hypo/euthyroid at presentation. **References:** None.

EP-0591

Radioiodine therapy and the induction of hyperthyroidism in patients with non-toxic goitre

***S. Abdelrazek**, P. Szumowski, J. Mysliwiec, M. Mojsak, M. Sankowski, N. Krolik;*
Department of Nuclear Medicine Medical
University of Bialystok, Bialystok, POLAND.

Aim/Introduction: Radioiodine therapy (RAIT) is non-invasive, safe and cost effective method of therapy for reduction of goitre. One of the early side effect is temporary hyperthyroidism, but some authors reported permanent hyperthyroidism after radioiodine therapy of non-toxic goitre, we also observed the induction of permanent hyperthyroidism in patients with non-toxic goitre. **Materials and Methods:** We treated 980 patients, aged 20-90 years; (76%) of them were female and (24%) male; the mean radioiodine uptake (RAIU) was 39% and thyroid volume ranged between 44-170 ml. Qualification of these patients were based on normal levels of serum fT3, fT4, TSH and characteristic appearance on thyroid scans and ultrasound. Malignant changes were excluded in all suspected nodules by fine needle aspiration biopsy. The activity dose was calculated by the use of Marinelli's formula and ranged between 200 -800 MBq. The mean absorbed dose was 199.4 ± 23.8 Gy. Thyroid ultrasonography, and thyroid scan with RAIU at 24hours was done before and after 12 months of RAIT. Follow up control for the evaluation of fT4, TSH was done every 6 weeks. **Results:** Permanent hyperthyroidism were induced in 12 patients (8 female and 4 male with a mean age 50 years) these patients had a mean thyroid volume of 58.3 ± 25.3 ml and a mean RAIU at 24hour of 48.2 ± 13.4% these patients received a mean radioiodine dose of 420 ± 147.2 MBq. Hyperthyroidism induced between four and six months after radioiodine therapy. TSH receptor antibodies were negative before RAIT, and were positive in all the patients after RAIT. RAIU at 24h increase in all the patients, and thyroid scintigraphy showed homogenous and diffuse uptake in both lobes with small reduction in the thyroid volume. All the patients received antithyroid drugs to control the hyperthyroidism, 4 patients were in euthyroid state and 8 patients received second dose of radioiodine, three patients achieve euthyroid state and five patients were in hypothyroidism. **Conclusion:** Radioiodine therapy is non-invasive, safe and cost effective method of therapy for reduction of goitre even in patient with low radioiodine uptake and should not be restricted to elderly, or to patients with high operative risk. In these cases radioiodine therapy induce hyperthyroidism, this may be due to the activation of silent Graves' disease in these patients. The induction of hyperthyroidism is a minor side effect and these can be treated easily with the second dose of radioiodine. **References:** None.

EP-0592

The efficacy of radioiodine therapy in patients with non-toxic nodular goitre with large cold nodule

***S. Abdelrazek**, P. Szumowski, J. Mysliwiec, M. Mojsak, L. Zukowski, P. Lisiewicz, M. Sankowski, N. Krolik;*
Department of Nuclear Medicine Medical
University of Bialystok, Bialystok, POLAND.

Aim/Introduction: Surgery is the first choice for the treatment of non-toxic goitre with large cold nodule. Most of the patients with the benign cold nodule refuse surgical operation. Radioiodine therapy (RAIT) is the choice for these patients. The aim of our study was to evaluate the efficacy of radioiodine therapy to reduce thyroid volume in patients with cold nodule, by the use of 2 doses of radioiodine therapy **Materials and Methods:** We treated 138 patients with non toxic nodular goitre with large cold nodule, aged 18-64 years; initial 24 h radioiodine uptake (RAIU) was ranged between 18-45%, and thyroid volume ranged between 48-120 ml. Qualification of these patients were based on normal levels of TSH and characteristic appearance on thyroid scans. Malignant changes were excluded in all prominent nodules by fine needle aspiration biopsy. The activity dose was calculated by the use of Marinelli's formula and ranged between 280-800 MBq. 80 patients received two doses of radioiodine and 58 patients received only one dose of RAIT. The absorbed dose ranged between 180 and 300 Gy. Thyroid ultrasonography, and thyroid scan with RAIU at 24 hrs was done before and after 6 and 12 months of RAIT. Follow up control was done every 6 weeks. **Results:** After 6 months RAIT in all the patients the large cold nodule changes to hot nodule. The size of whole gland decrease to 48%, in all the patients. In 58 patients the size of the thyroid gland decrease and no need to the second dose of radioiodine therapy. 80 patients received second dose of RAIT to decrease the nodule which was cold and turned to hot after the first dose. After 12 months of the second dose of radioiodine a mean thyroid volume reduction of 56% was achieved. After 12 months of RAIT euthyroidism persist in 58% of patients, and hypothyroidism develop in 42% of patients. All patients were highly satisfied; and the compressive symptoms relieved. **Conclusion:** Radioiodine is non-invasive, safe and cost effective method of therapy for goitre volume reduction in patients with cold nodule, and should be used in patients with benign nodule who refused surgical operation or patients with high surgical risk. The reduction of the cold nodule and the thyroid volume, were due to well accurate measurement of administered activity, relatively high effective half-life and well-organised follow up. **References:** None.

EP-0593

Quantitative assessment of hepatic uptake of I-131 during radioiodine therapy in patients with hyperthyroidism-related thyroid diseases

M. Jüptner, M. Marx, J. Ranjan, W. Schüler, M. Zuhayra, U. Lützen; University Hospital of Kiel, Kiel, GERMANY.

Aim/Introduction: Little is known about the pathophysiological mechanisms causing increased liver uptake of I-131 in patients receiving radioiodine therapy. To date, there is no known or proven correlation between increased liver uptake of I-131 and specific thyroid diseases. The aim of our study was to investigate a possible association between hepatic uptake of I-131 and hyperthyroidism-related thyroid diseases. **Materials and Methods:** 67 patients with Graves' disease and 37 patients with disseminated thyroid autonomy were studied during I-131 radioiodine therapy. In the posttherapeutic scintigraphic images, the counts in the liver were measured in ROI technique and compared to the counts measured in the whole body. Additionally, serological thyroid parameters and liver enzyme levels (TSH, T3, T4, TSH receptor antibodies, TPO antibodies, AST, ALT) were measured and compared to the individual liver uptake of I-131 by nonparametric correlation analysis. Moreover, the hepatic uptake of I-131 was compared between the patients receiving antithyroid drugs (Thiamazol, Carbimazol or Propythiouracil) and the patients without thyrostatic medication. **Results:** The liver uptake of I-131 was significantly increased in patients with Graves' disease compared to patients with disseminated thyroid autonomy (mean 2.33% vs. 0.81%; $p = 4.62 \times 10^{-11}$). In the patients with Graves' disease, a relevant positive correlation was observed between the hepatic uptake of I-131 and the level of thyrotropin receptor antibodies (Spearman's $r= 0.398$; $p= 8{,}4 \times 10^{-4}$). Furthermore, a significant negative correlation was found for the hepatic uptake of I-131 with TSH levels ($r= -0.258$; $p=0.035$) in patients with Graves' disease. Other serological parameters (T3, T4, TPO antibodies, AST, ALT) were not associated with the hepatic uptake of I-131. The intake of thyrostatic drugs had no significant impact on the hepatic uptake of I-131 (2.43% in the patients receiving antithyroid drugs vs. 2.18% in the patients without antithyroid medication; $p = 0.477$). **Conclusion:** Increased liver uptake of I-131 was associated with Graves' disease in our study and was not related to hyperthyroidism in general, suggesting that patients with Graves' disease are at increased risk for hepatic deposition of I-131 and potential subsequent radiogenic tissue damage. The specific thyrotropin receptor antibodies are supposed to play a crucial role in the pathogenesis of increased hepatic uptake of I-131 in patients with Graves' disease. **References:** None.

EP-0594

Assessment of the results of ^{131}I radioiodine therapy in patients with autonomously functioning thyroid nodules

Z. Adamczewski[1], J. Makarewicz[2], J. Kuśmierek[3], M. Adamczewska[1], P. Jarek[2];
[1]Department of Endocrinology and Metabolic Diseases, Medical University of Lodz, Lodz, POLAND, [2]Department of Nuclear Medicine and Oncological Endocrinology, Maria Sklodowska-Curie Memorial Hospital, Zgierz, POLAND, [3]Department of Nuclear Medicine, Medical University of Lodz, Lodz, POLAND.

Aim/Introduction: Most physicians consider ^{131}I as the first line treatment for toxic nodular goitre. Moreover, in patients with autonomously functioning thyroid nodules (AFTN) ("hot nodule") radioiodine treatment of hyperthyroidism is the method of choice. Aim: Assessment of the risk of hypothyroidism after radioiodine treatment in patients with AFTN, depending on the size of the nodule, the proportion of its volume to the volume of remaining thyroid gland, and administered activity of ^{131}I. **Materials and Methods:** Retrospective analysis was carried out in 202 patients (29-93 yo, average 66) diagnosed with „hot" nodule and treated with ^{131}I calculated dose dependent on size of the nodule and 24-h radioiodine uptake. Frequency of treatment success (defined as persistent euthyroidism), hyperthyroidism and hypothyroidism as assessed by serum TSH concentration, were analysed 6 - 12 months after ^{131}I therapy. **Results:** The volume of AFTN ranged between 1.1 and 105 cm³ (average 18.4 cm³), the volume of the thyroid gland was 7.5-221.1 cm³ (average 35.3 cm³), the proportion of AFTN to the thyroid volume was 0.04-0.98 (average 0.51). Therapeutic activities of 192-1554 MBq ^{131}I (average 694 MBq) were administered; what amounts to 8-611 MBq ^{131}I (average 70.7 MBq) per gram of AFTN weight. Hypothyroidism was diagnosed in 48 patients (23.8%). In hypothyroid patients the mean proportion of AFTN to thyroid volume was highest 0.61, SD 0.28 (vs euthyroid 0.46, SD 0.25, vs hyperthyroid 0.56, SD 0.28), p=0.005. Furthermore the risk of hypothyroidism is also increased in patients with smaller mean thyroid volume: hyperthyroid group 27.7 cm³, SD 17.7 vs euthyroid group 36.7 cm³, SD 25.6 vs hyperthyroid group 43.4 cm³, SD 24.2, p=0.025. No correlation was found between administered ^{131}I activity and the therapy outcome (p=0.65), also between AFTN volume and therapy outcome (p=0.09). **Conclusion:** Correlation, which was revealed between the therapy outcome and the proportion of the nodule to the thyroid volume, suggests the need to individualise activities of 131I used for therapy, or decide on other therapeutic procedure eg surgery, especially in patients with relatively large "hot" nodules and comparatively small thyroid volume. **References:** None.

EP-0595

I-131 therapy for Graves' disease with giant goiter

M. Jinguji, M. Nakajo, A. Tani, T. Yoshiura;
Department of Radiology, Kagoshima University Graduate School of Medical and Dental Sciences, Kagoshima, JAPAN.

Aim/Introduction: It has been reported that the treatment for Graves' disease with giant goiter is often difficult. The aim of this study is to summarize our experiences of . **Materials and Methods:** We reviewed 119 consecutive patients with Graves'

disease (101 females and 18 males, mean age 48.1 years, age range, 20-77 years) who underwent initial I-131 therapy in our hospital between September 2004 and March 2018 and were followed-up over 1 year. The I-131 dose was ≤ 518 MBq per treatment. Thyroid weight was estimated on CT. The patients were classified into either giant goiter (GG) group with thyroid weight ≥100g or non-giant goiter (NGG) group. Following factors were statistically compared between the two groups; interval between diagnosis of Graves' disease and initiation of I-131 therapy, age, sex, total I-131 dose, I-131 therapeutic effect after 1year, and number of I-131 therapies. For GG group, the states after two years were also examined. **Results:** Fifteen(12.6%) patients were classified into GG group (mean thyroid weight 179g, range 101-636g) and the remaining 104 were into NGG group (mean 39g, range 8-98 g) . Their age and sex were not significantly different. The interval between diagnosis and I-131 therapy was significantly longer in GG group (mean 13 years) than in NGG group (mean 4 years) (P<0.001). The number of I-131 therapies was significantly higher in GG group (mean twice; once 5, twice 7, three times 2, five times 1) than in NGG group (mean 1.1 times; once 86, twice 18) (P=0.002). The total I-131 dose in GG group (mean 896 MBq, range 475-2353 MBq) was significantly higher than that in NGG group (mean 235 MBq, range 48-666 MBq) (P<0.001). The thyroid weight reduction rate one year after I-131 therapy in GG group (mean 57.0%, range 55.8-96.8%) was significantly lower than that in NGG group (mean 69.4%, range 0-90.5%), (P=0.038). The fraction of patients in hyperthyroid states one year after I-131 therapy was significantly higher in GG group (57.1%) than that in NGG group (23.8%) (P=0.002). Two years after initial I-131 therapy, thyroid state was well controlled in 11 of 12 patients (91.7%) in GG group. **Conclusion:** The patients with Graves' disease who had giant goiter (weight ≥100g) often required multiple I-131 therapies with a dose of ≤ 518 MBq per treatment, but were generally well-controlled two years after initial treatment. **References:** None.

EP-0596

Outcome analysis after Radioactive Iodine-I131 Treatment in 424 patients with hyperthyroidism

M. Finessi[1], *A. Bisceglia*[2], *R. Passera*[1], *R. Rossetto Giaccherino*[2], *L. Pagano*[2], *G. Castellano*[1], *G. Bisi*[1], *D. Deandreis*[1];
[1]*Nuclear Medicine Unit, Department of Medical Sciences, University of Turin, AOU Città della Salute e della Scienza, Turin, ITALY,* [2]*Endocrinology, Diabetology and Metabolism Unit, Department of Medical Sciences, University of Turin, AOU Città della Salute e della Scienza, Turin, ITALY.*

Aim/Introduction: ^{131}I therapy (RAIT) represents a curative treatment for hyperthyroidism in toxic adenoma (TA), toxic multinodular goiter (TMG) and in Graves' disease (GD) in case of not controlled hyperthyroidism or disease recurrence after initial treatment with antithyroid drug (ATD) treatment. Aim of our study is to search for variables correlated with patient's outcome in a dosimetric based approach. **Materials and Methods:** We retrospectively analyzed 424 patients with hyperthyroidism referred to our department for RAIT between 2000 and 2018 (121 men and 303 women; TMG n=213, GD n=150, TA n=61). All patients underwent dosimetric approach by daily (6-24-48-72-96h) uptake measurement after administration of about 2 MBq of ^{131}I. Outcome was assessed at 6 and 12 months (m) and defined as response in case of euthyroidism and subclinical/overt hypothyroidism and no-response in case of persistent subclinical/overt hyperthyroidism. Association between outcome and baseline TSH values, ATD duration, posology and absorbed dose was evaluated by Mann-Whitney test. Risk factors for response vs no-response outcome were analyzed by binary logistic regression model. **Results:** At 6 and 12 months an overall cure rate of 78.7% and 83% was observed, respectively. TSH baseline values were higher in 6m and 12m response group compared to 6m and 12m no-response group (median 0.36 vs 0.08 mcUI/ml, p<0.001 and 0.34 vs 0.08 mcUI/ml, p<0.001 respectively). ATD duration and posology were lower in 6 and 12m response group compared to 6 and 12m no-response group (24 vs 36 months, p<0.004 and 5 vs 7.5 mg/die, p <0.014; 24 vs 32 months, p<0.043 and 5 vs 7.5 mg/die, p <0.005 respectively). Dose to target (D_T) was significantly lower in 6m responder compared to 6m no responder group (327 vs 373 Gy, p<0.003); conversely no statistical differences were found between D_T at 12m. Multivariate logistic models identify longer ATD duration and higher ATD posology as independent risk factors for no-response in GD group (ATD duration 6m-OR 1.01, p<0.04; 12m-OR 1.01, p<0.026 and posology 6m-OR 1.08, p<0.037; 12m-OR 1.09, p<0.059), in TMG group (ATD duration: 6m-OR 1.01, p<0.005; 12m-OR 1.01, p<0.012) and in TA group (ATD posology: 6m OR 1.28, p<0.06). **Conclusion:** Our data suggest that a more aggressive, older and uncontrolled disease revealed by longer duration and higher posology of ATD and low TSH levels is correlated to worse response. For these reasons RAIT therapy has to be considered earlier in patients management to allow better outcome and avoid ATD toxicity. **References:** None.

EP-0597

The effect of radioiodine therapy I-131 in patients with non-toxic nodular goitre

S. Abdelrazek, *P. Szumowski, J. Mysliwiec, M. Mojsak, L. Zukowski, M. Sankowski, N. Krolik;*
Department of Nuclear Medicine Medical University of Bialystok, Bialystok, POLAND.

Aim/Introduction: Simple goitre is defined as the enlargement of the thyroid gland, in the absence of autoimmune thyroid disease, malignancy, or inflammation, still constitutes a major diagnostic and therapeutic challenge. Radioiodine therapy (RAIT) is non-invasive, safe and cost effective method of therapy for goitre reduction. There is no consensus regarding the optimum treatment of benign non-toxic goitre. Randomised studies have shown that levothyroxine has poor evidence of efficacy and is inferior to radioiodine therapy regarding goitre

reduction. The aim of our study was to evaluate the short term efficacy of radioiodine therapy to reduce thyroid volume with minimal risk of hypothyroidism in patients with non-toxic nodular goitre. **Materials and Methods:** We treated 980 patients, aged 20-90 years; (76%) of the studied groups were female and (24%) male; the mean radioiodine uptake (RAIU) was 39% and thyroid volume ranged between 44-170ml. Qualification of these patients were based on normal levels of serum fT3, fT4, TSH and characteristic appearance on thyroid scans and ultrasound. Malignant changes were excluded in all suspected nodules by fine needle aspiration biopsy. The activity dose was calculated by the use of Marinelli's formula and ranged between 200 -800 MBq (459 ± 171 MBq). The mean absorbed dose was 199.4 ± 23.8 Gy, and was proportional to thyroid volume. Thyroid ultrasonography, and thyroid scan with RAIU at 24hours was done before and after 12 months of RAIT. Follow up control for the evaluation of fT4, TSH was done every 6 weeks. **Results:** After 12 months of radioiodine therapy a mean thyroid volume reduction of 48% was achieved. Approximately half of the effect is obtained within the first 3 months. Euthyroidism persist in 92% of patients, and hypothyroidism develop in 8% of patients. All patients were highly satisfied; with improvement in obstructive symptoms and exercise tolerance in the majority of patients. **Conclusion:** Radioiodine is non-invasive, safe and cost effective method of therapy for reduction of the goiter volume and should not be restricted to elderly patients, or to patients with high operative risk, but should be used as first choice in every patient with non toxic nodular goitre with thyroid volume > 40 ml especially in patients with special profession. Surgery should be reserved as first choice if malignancy is suspected. The reduction of thyroid volume with low percent of hypothyroidism, were due to well accurate measurement of administered activity, relatively high effective half-life and well-organised follow up. **References:** None.

EP-42

Clinical -> Therapy study -> Adult study -> Thyroid treatment -> Thyroid treatments, malignant

October 12 - 16, 2019 e-Poster Area

EP-0598

Survival pattern in differentiated thyroid cancer: A retrospective study from Sahloul University Hospital

H. Boudriga[1,2], *M. Ben Fredj*[1,2], *M. Ben Rejeb*[3], *A. Ezzine*[1], *K. Chatti*[2], *M. Guezguez*[1,2];
[1]*LR12ES02, University of Sousse, Medicine faculty of sousse, Sousse, TUNISIA,* [2]*Department of Nuclear Medicine, Sahloul University Hospital, Sousse, TUNISIA,* [3]*Department of Prevention and Care Safety, Sahloul University Hospital, Sousse, TUNISIA.*

Aim/Introduction: Survival rates for differentiated thyroid cancer (DTC) are excellent and reach up to 97% in 10 years. Despite appropriate treatment, some patients have a pejorative outcome and the management strategies of DTC remain controversial.The aim of this study was to analyse pathological findings, therapy, outcome and prognostic factors in patients with DTC. **Materials and Methods:** This is a retrospective survival analysis study carried out in a cohort of 312 patients.They were operated on and received radio-iodine (RAI) treatment. They were followed- up in the Nuclear Medicine department of Sahloul University hospital with a mean follow up period of 7.9 years. **Results:** Surgical treatment was total thyroidectomy for all of the patients. Lymph node dissection was performed in 83.3% of cases. All of them received RAI treatment after which they had measurement of serum thyroglobulin (Tg) levels and whole-body-RAI scan. At the time of diagnosis, 76.3% and 25.7% respectively belonged to I-II and III-IV disease stages according to the TNM/AJCC classification.According to ATA (American Thyroid Association) prognostic system, 41% of patients were low-risk patients, 41.3% were intermediate-risk patients and 17.6% were high-risk patients.At end of follow-up, the vast majority of the patients showed no evidence of disease (68.9%). Two of them (0.6%) died of cancer. The rest had disease persistence (27.9%) and recurrent disease (2.6%).The mean disease free-survival (DFS) was 12.27 years. The DFS rates at 5 and 10 years were respectively 89.2% and 71%.Independent prognostic factors for disease persistence/recurrence on multivariate analysis included: age >45 years, tumour size >4 cm, extra thyroidal extension, vascular invasion, and post-operative Tg level >7.75 ng/mL. **Conclusion:** A risk-categorisation approach should be used to guide the intensity of initial therapy and early follow-up recommendations (frequency of neck US, RAI WBS, cross sectional imaging and FDG PET scans). **References:** None.

EP-0599

The study of impact of iodine prohibition before radioiodine therapy on parathyroid hormone, vitamin D_3, electrolyte level of thyroidcarcinoma patients

Z. Gao, *J. Peng, Y. Zhang;*
Union Hospital,Tongji Medical College, Huazhong University of Science and Technology, Wuhan, CHINA.

Aim/Introduction: To observe and analyze the changes of serum PTH, vitamin D3 and electrolyte levels in patients with thyroid cancer which cured by total thyroidectomy before and after the iodine prohibition required by radioactive iodine therapy. **Materials and Methods:** A retrospective analysis was conducted on 566 cases (163 males, 403 females, with an average age of 40.00±11.43 yrs) of thyroid cancer patients receiving radioactive iodine therapy. The included patient data could be divided into three groups: (1) serum PTH value, total 25(OH)D value, serum Ca^{2+} value, serum P^{3+} value and serum Mg^{2+} value of the patients were measured (after iodine prohibition) before radioactive iodine therapy. (2)serum PTH value, total 25(OH)D value, serum Ca^{2+}, P^{3+} and Mg^{2+} of the patients with hyperparathyroidism were measured of whom

before radioactive iodine therapy (after iodine prohibition) as well as unaffected from iodine prohibition when the previous PTH value exceeded the normal upper limit. (3)PTH value and total 25(OH)D value, which were used as the baseline values for daily review of patients receiving radioactive iodine therapy, were compared with the corresponding values after iodine prohibition. The difference between PTH, total 25(OH)D and baseline values after iodine deprivation was recorded as "ΔPTH " and "Δtotal 25(OH)D" for correlation analysis. **Results:** 1. It was observed that PTH value was negatively correlated with total 25(OH)D value and serum P^{3+} value after radioactive iodine therapy with iodine prohibition. 2. Multiple linear regression was used to analyze the PTH value, total 25(OH)D value, serum Ca^{2+}, serum P^{3+} and serum Mg^{2+} value of patients after receiving iodine deprivation treatment. Take the PTH value as the dependent variable.3. There were significant differences in total 25(OH)D value and serum P^{3+} value of group of hyperparathyroidism after iodine prohibition and group of hyperparathyroidism which was not affected by iodine prohibition.4. The PTH and total 25(OH)D baseline values of patients were significantly different from those after iodine prohibition. 5. The negative correlation between ΔPTH value and Δtotal 25(OH)D value showed that the greater the decrease of Δtotal 25(OH)D value after iodine prohibition, the greater the increase of PTH value. **Conclusion:** The total value of 25(OH)D decreased after the patient received iodine prohibition before radioactive iodine therapy in hospital, which directly affected the level of PTH and indirectly affected the level of serum P^{3+}. **References:** None.

EP-0600

Differentiated Thyroid Cancer Ablation with fixed versus stage oriented dose. De-escalation strategy and follow up, since 1996 in 340 patients

S. Sophocleous;
Diagnostic center Agios Therissos, Strovolos, Nicosia, CYPRUS.

Aim/Introduction: Recent guidelines supported decreased doses of Radio Active Iodine (RAI) given for ablation for select populations with well-differentiated thyroid cancer (WTC). Starting work in Cyprus 1996, following at the time guidelines and knowledge, we treated thyroid cancer patients giving fixed dose von 100 mCi in nearly all patients. Starting 1998 we determined a low risk group (LRG) for tumor size <20 mm and an intermediate risk group (IRG) for tumor size <40 mm. **Materials and Methods:** The study was conducted on 340 patients who underwent ablative radioiodine therapy from August 1996 to August 2018. The LRG1 with TG level <2 ng/dl was treated with 30 mCi, the LRG2 with TG level >2 ng/dl was treated with 50 mCi. The IRG1 with Tg level <2 ng/dl was ablated with 60 mCi, the IRG2 with TG level> 2 ng/dl was ablated with 80 mCi After evaluation our results since 2007 we ablate the low risk patients with 60 mCi and the intermediate risk patients with 80 mCi. The success of ablation was determined six months after RAI therapy through thyroglobulin measurement and I-131 whole body (WB) scan. As success of ablation was evaluated at Tg<0.5 ng/dl stimulated and on WB scan no or hardly uptake on thyroid bed. **Results:** Between 1998 and 2006 On LRG1 ablation with 30 mci was not in all patients successful and a second dose was necessary. Ablation with 50 mCi in LRG2 was in nearly all patients successful. On IRG1 ablation with 60 mci was not in all patients successful and a second dose was necessary. Ablation with 80 mCi in IRG2 was successful in all patients. Between2007 and 2018 On LRG 60 mCi was in nearly all patients successful. On IRG 80 mCi was in all patients successful. **Conclusion:** ABLATION with stage oriented dose LRG 60 mCi and IRG 80 mCi is more than enough for successful ablation. Tg under stimulation and WB scan are indispensable for follow up. **References:** Cancer Archive.

EP-0601

SPECT-Ct Identifies Unsuspected Radio-iodine Refractory Disease in 4% Of Differentiated Thyroid Carcinoma Patients Presenting for Initial Remnant Ablation or Adjuvant I-131 Sodium Iodide Therapy

D. Weinreb;
16 Birkdale Court, Slingerlands, NY, UNITED STATES OF AMERICA.

Aim/Introduction: The addition of SPECT-CT to conventional planar imaging has been demonstrated to be consequential for I-131 NaI therapy planning and risk stratification. The goal of the present investigation was to determine whether SPECT-CT may routinely allow for the identification of unsuspected radio-iodine refractory disease not evident on either pre- or post-ablation planar imaging in patients with differentiated thyroid carcinoma. **Materials and Methods:** We retrospectively reviewed all radio-iodine therapies treated by the study investigator in the period between January 2017 and June 2018. A total of 95 therapies were performed. One patient with known osseous metastatic disease was excluded. None of the patients had been previously treated with radioiodine. The study population included all patients for whom the intent of the therapy was both remnant ablation and adjuvant therapy; inclusion of all such patients was necessary as the precise intent of the therapy could only be clarified after pre-ablation imaging was obtained. All patients were imaged with both planar and SPECT-CT imaging following the administration of either 4 mCi of I-123 NaI or 2 mCi of I-131 NaI. **Results:** Four cases of unsuspected radio-iodine refractory thyroid carcinoma were diagnosed based on the findings of SPECT-CT alone (4% of all patients), none of which demonstrated radio-iodine uptake outside of the thyroidectomy bed on planar imaging. These included two cases of non-RAI avid pulmonary nodules, one case of cervical lymphadenopathy and one case of mediastinal lymphadenopathy. None of the patients had prior imaging demonstrating the abnormalities evident on SPECT-CT. Only a single additional patient (1%) was diagnosed with unsuspected radio-iodine miliary pulmonary metastases, which were not apparent on an earlier diagnostic chest CT. Interestingly, an additional patient (1%) was incidentally diagnosed with a carcinoid tumor of the lung. **Conclusion:** Unsuspected radio-iodine refractory disease is routinely

encountered on the CT component of SPECT-CT images only. Although overall relatively uncommon, the frequency of radio-iodine refractory disease actually exceeded the frequency of radio-iodine avid disease in the study population. Patient management was significantly impacted as all of these patients underwent either external beam radiation or thoracic surgery within four months of diagnosis. The incidence of detection of radio-iodine refractory disease would have been significantly greater if patients undergoing remnant ablation only were excluded. **References:** None.

EP-0602

Prognostic factors and the health-related quality of life in patients with differentiated thyroid cancer

E. Olariu, M. Larg, K. Gabora, L. Hitu, E. Spinu, B. Gradinaru, G. Kermoison, G. Rusu, C. Pestean, D. Piciu;
The Oncology Institute "Prof. Dr. Ion Chiricuta", Cluj-Napoca, ROMANIA.

Aim/Introduction: Differentiated thyroid cancer in most cases has a favorable prognosis with a long-term survival rate. The multitude of prognosis factors that are presented to the patient as well as the communication of the risk group and the survival rate draws upon itself a certain physiological impact that can influence the quality of life. **Materials and Methods:** The first part of the study was a descriptive epidemiologic study type in which 5680 patients with thyroid neoplasia were analyzed from the data base of The Oncological Institute "Prof. Dr. Ion Chiricuta" Cluj-Napoca, Romania, new cases from the 2008-2017 period. The second part of this study was a cross-sectional study type, underwent by 66 patients with differentiated thyroid neoplasia, with ages between 20-80, with total thyroidectomy, new cases for their first appointment for ^{131}I therapy, with their TSH properly halted for their therapeutic break, in the September-December 2017 period. These patients were given the distress questionnaire found within the NCCN guide. The second part of the study benefited from a statistical analysis, both descriptive as well as a Pearson/Spearman correlation. **Results:** The first part of the study underlined a rise within the incidence of the thyroid cancer in the 2008-2017 period thus: in the year 2008=422 new cases up to the year 2017=731 new cases, with the predominance of differentiated thyroid cancers (5028/5680 new cases of thyroid cancer) and the feminine sex (4251 women with new cases of differentiated thyroid cancer/5028 patients with new cases of differentiated thyroid cancer). Distress was correlated with emotional problems (fear, sadness) r=0.376 with p<0.05. Distress was correlated with physical problems: fatigue (r=0.339, p=0.005) and appearance of prurience (r=0.253, p=0.04). Distress wasn't correlated with spiritual problems and most importantly there is no existing correlation between distress and the stages of the disease (r=-0.048, p=0.704). **Conclusion:** Distress is not influenced by the stage of the disease in which the patient is in, thus it isn't possible to draw conclusions related to the typology of a predisposed patient given his distress score who would require specific interventions. Patients with differentiated thyroid neoplasia at their first admission in the department of nuclear medicine tend to have a high distress score and implicitly a lower quality of life, the routine evaluation of patients related to the existence of problems tied to the thyroid neoplasia is obligatory. **References:** None.

EP-0603

Postoperativestimulated thyroglobulin level is a goodpredictor of the success ofthe first ^{131}I ablative therapyin patients with low risk differentiated thyroid cancer

M. Xiao Li, H. Xingmin, L. Baoping;
Department of Nuclear Medicine,The First Affiliated Hospital of Zhengzhou, Zhengzhou, CHINA.

Aim/Introduction: To determine the potential of postoperative-stimulated serum thyroglobulin levels (pre-Tg) immediately prior to initial I-131 ablative therapy (IAT) for predicting successful ablation in patients with low-risk differentiated thyroid carcinoma (DTC). **Materials and Methods:** Patients with DTC (n=662) treated with total or near-total thyroidectomy followed by immediate IAT were studied. Patients with positive anti-Tg autoantibodies, who did not meet the low-risk criteria, or with a recent history of iodine contamination were excluded. Patients were divided into three groups based: Pre-Tg levels ≤2 µg/liter, 2-10 µg/liter, and ≥10 µg/liter, using a threshold of 1 µg/liter for thyroglobulin levels at the time of the first D-WBS (Post-Tg). Diagnostic whole-body scans (D-WBS) and post-Tg levels were used to identify clinical outcomes (successful ablation, equivocal, or persistent disease). Various factors including age, sex, pre-Tg, and histopathology were analyzed to predict ablation success rates. **Results:** One hundred and fifty-eight patients fulfilled the inclusion criteria, with no drop-out, from December 2008 to April 2012. Successful ablation patients had significantly lower pre-Tg levels at the first IAT (P <0.001 vs. unsuccessful ablation). Pre-Tg was the only factor significantly related with ablation success rates. After the first D-WBS, of 32 patients with pre-Tg ≤2µg/liter, 28 (87.5%) showed successful ablation, one (3.1%) was regarded as "equivocal"; and three (9.4%) showed persistent disease. Of 126 patients with pre-Tg >2 µg /liter, successful ablation was observed in 59 cases (46.8%), 32 (25.4%) were regarded as "equivocal"; and persistent disease was observed in 35 (27.8%). Pre-Tg level were significantly correlated with the outcome of the initial IAT (three by three χ^2 test, χ^2=33, df=4, P <0.001). **Conclusion:** Pre-Tg ≤2 µg/liter is a promising factor predictive of successful ablation by the first IAT in patients with low-risk DTC. **References:** None.

EP-0604

A Single-centre Retrospective Review of Functional Metastases from Differentiated Thyroid Cancer

Y. Mathur, S. Singh, G. Kumar, A. Sood, A. Bhattacharya, B. Mittal;
PGIMER, Chandigarh, INDIA.

Aim/Introduction: Functional metastases from differentiated thyroid cancer (DTC) pose different diagnostic and therapeutic challenges. Extensive distant metastases are common findings in these patients and disease-specific mortality and long-term prognosis is still un-established due to limited literature which assesses behaviour of DTC with functional metastases. We aimed to retrospectively review data of patients presenting with suspicion of functional metastases from DTC in our institute in past 8 years to evaluate disease behaviour and response to radioactive-iodine therapy. **Materials and Methods:** We retrospectively reviewed data of patients with DTC who presented post total-thyroidectomy and had low TSH (<30mIU/L) levels (off thyroxine), grossly elevated serum Tg levels and minimal uptake in thyroid remnant on diagnostic I-131 whole-body scan (DxWBS). Demographic, clinical, biochemical, histopathological data, number and doses of I-131 therapies and subsequent follow-up data (with serum Tg, anti-Tg and DxWBS) of these patients was evaluated to study disease epidemiology, progression and response to I-131 therapy according to 2015 ATA Management Guidelines. **Results:** Twenty-nine patients (12 male) of age 50±14 years, satisfied the above-mentioned inclusion criteria, including 2 paediatric patients (age < 18 years). The initial TSH and thyroglobulin levels were 8.4±7.9 mIU/L and 3827±8520 ng/mL, respectively. The most common histopathologic subtype was follicular carcinoma thyroid (FCT) (62%, n=18), followed by papillary carcinoma thyroid (PCT) (38%, n=11). Subclinical hyperthyroidism (i.e. TSH<4mIU/L) was seen in 38% (n=11) patients; 73% (n=8) were of FCT subtype. Skeletal metastases were more prevalent in FCT compared to PCT (94% vs 67%). Metastases to uncommon sites like brain (10%, n=3), kidney (6.9%, n=2), liver, spleen and adrenal (6.9%) was also observed with FCT. A cumulative I-131 dose of 795 ± 356 mCi in 4.2± 1.8 cycles (range 1 - 7 cycles) was administered. Rank-Biserial correlation coefficients were extracted to evaluate correlation for histopathological subtypes (rho for PCT=0.19, FCT= -0.07) and age (rho=0.21) with therapy response at last follow-up and were not statistically significant (p>0.05). Survival rate of patients with functional metastases was 79% (n=23) at last follow-up. At last follow-up, 2 patients with PCT and 4 patients with FCT had died; there was no association between mortality and histopathologic subtypes (Fisher exact, p>0.05). **Conclusion:** FCT was not only the more commonly encountered histotype in patients with functional metastases, but also propensity towards advanced and atypical metastases. However there appears to be no difference in response to radio-iodine therapy or mortality between histopathologic subtypes and age of the presentation. **References:** None.

EP-0605

Therapeutic Response Prediction Using Iodine Scan-Corrected Serum Thyroglobulin in Patients with Differentiated Thyroid Carcinoma

S. Kwon[1], *M. Chowdhury*[1,2], *S. Jeon*[1], *A. Kim*[1], *J. Kim*[3], *H. Song*[3], *H. Bom*[1], *J. Min*[1];
[1]*Chonnam National University Hwasun Hospital, Hwasun-gun, KOREA, REPUBLIC OF,* [2]*Institute of Nuclear Medicine and Allied Sciences, Bangladesh Atomic Energy Commission, Bogra, BANGLADESH,* [3]*Chonnam National University Hospital, Gwangju, KOREA, REPUBLIC OF.*

Aim/Introduction: Pre-ablation serum thyroglobulin (Tg) has a limitation to reflect therapeutic effect of radioactive iodine (RAI) therapy in patients with differentiated thyroid carcinoma (DTC). We investigated whether the predictive performance of serum Tg for therapeutic response could be improved considering iodine uptake pattern in post-therapeutic scan and the thyroid tissue damage effect after RAI ablation therapy. **Materials and Methods:** A total of 319 DTC patients who underwent surgery and RAI ablation therapy with thyroid hormone withdrawal were included. Serum Tg level was measured just before RAI administration (D0Tg) and 7 days after RAI therapy (D7Tg). Ratio Tg (D7Tg/D0Tg) was used to reflect thyroid tissue damages, considering Tg after RAI therapy could be released from destroyed thyroid tissues. According to the presence of midline focal uptake above the thyroidectomy bed on iodine scan, the patients were classified into positive and negative uptake groups. Therapeutic responses were divided into excellent response (ER, negative imaging study and either suppressed Tg < 0.2 ng/ml or stimulated Tg <1 ng/ml) and non-excellent response. We sought to find the optimal combination of serum Tg by applying different cutoff values according to iodine uptake pattern followed by ratio Tg to improve the predictive performance for therapeutic response. **Results:** Among the 319 patients, 109 patients had midline focal uptake. Cutoff values of D0Tg for the prediction of ER were different according to iodine uptake pattern (negative group: 1.65 ng/ml, positive group: 3.30 ng/ml). Furthermore, the ratio Tg ≥ 9.0 ng/ml was also predictive to ER in the subgroup including patients with both positive midline uptake and D0Tg ≥ 3.30 ng/ml. Our combined approach using scan-corrected Tg showed better predictive performance for ER than D0Tg only (P < 0.001). **Conclusion:** Predictive performance of serum Tg for therapeutic response was significantly improved by applying different cutoff values according to iodine uptake pattern and the amount of released Tg after RAI ablation therapy. **References:** None.

EP-0606

Efficacy of Low and High dose Of Radioiodine For The Ablation Of Thyroid Remnant In Patients With Differentiated Thyroid Cancer Coexisting Chronic Lymphocytic Thyroiditis

M. Chao, *J. Xie, Z. Lv;*
Tenth People's Hospital of Tongji University, Shanghai, CHINA.

Aim/Introduction: Our prospective randomized trial found that **t**he low dose of 1850MBq radioiodine (RAI) is as effective as high dose of 3700 MBq for thyroid remnant ablation in patients with differentiated thyroid cancer (DTC). The aim is to further investigate the efficacy of low- and high-dose of RAI for thyroid remnant in patients with DTC coexisting chronic lymphocytic

thyroiditis (CLT). **Materials and Methods:** Inclusion criteria were an age of 16 years or older; total thyroidectomy or near total thyroidectomy; tumor-node-metastasis (TNM) stage of pT1-3 and any N stage, M0. All patients were randomly allocated to the high-dose group of 3700MBq and low-dose group of 1850MBq for RAI ablation therapy for DTC patients with and without CLT. Patients were prepared for ablation using thyroid hormone withdrawal. The thyroid remnant ablation outcome were evaluated according to ^{131}I diagnostic whole-body scan (DX-WBS), serum stimulated thyroglobulin (Tg-off), and thyroglobulin antibody (TgAb) level 6-9 months after ^{131}I ablation therapy. Ablation was considered to be successful if patients fulfilled the following criteria: no tracer uptake in the thyroid bed on DX-WBS and serum Tg-off <2ng/ml in patients with negative TgAb; no tracer uptake in the thyroid bed on DX-WBS, stable or decreasing TgAb in patients with positive TgAb. **Results:** A total of 336 DTC patients from January 2013 to October 2015 were included. 92 of 336 patients were concurrent with CLT while 224 patients had no CLT confirmed by pathology. Data could be analyzed for 83 cases, low-dose group, 40 patients, and high-dose group, 43 patients. There were no significant differences between the two groups in terms of baseline characteristics. The rate of initial successful ablation was 75.9 % in all patients, 70% and 81.4% in the low and high-dose group coexisting with CLT (p=0.225). 137 of 224 cases without CLT were treated with 1850MBq while 107 cases with 3700MBq. The low-dose patients without CLT(n=137) had a higher successful rate compared with those coexisting CLT, though no statistical significance(83.9% vs. 70%,P=0.05), and no difference was found in high-dose group between patients with and without CLT(n=107)(85.9% vs. 81.4%,P=0.48). **Conclusion:** In Chinese DTC patients coexisting with CLT, limited data suggested that the low dose of 1850 MBq RAI is as effective as high dose of 3700 MBq for thyroid remnant ablation. CLT is not a negative predictive factor for low-and high-dose initial successful ablation. **References:** None.

EP-0607

Is TSH suppression still necessary in intermediate- and high-risk papillary thyroid cancer patients with pre-ablation stimulated thyroglobulin <1 ng/mL before the first disease assessment?

T. Tian, R. Huang, B. Liu;
West China Hospital, Sichuan University, Chengdu, CHINA.

Aim/Introduction: Since papillary thyroid cancer (PTC) patients with pre-ablation stimulated thyroglobulin (s-Tg) < 1 ng/mL generally have a favorable prognosis, is TSH suppression still necessary in intermediate- and high-risk PTC patients with pre-ablation s-Tg < 1 ng/mL after initial therapy? The aim of this study was to assess the rate of disease recurrence in intermediate- and high-risk PTC patients with pre-ablation s-Tg < 1 ng/mL according to TSH levels measured 1 year after initial therapy. **Materials and Methods:** A retrospective series of intermediate- and high-risk PTC patients with pre-ablation s-Tg < 1 ng/mL was analyzed. Disease status was defined as the presence or absence of structural disease during late follow-up. Patients were grouped according to TSH level at 1 year: group 1, TSH < 0.1 mIU/L; group 2, TSH 0.1-0.5 mIU/L; group 3, 0.5-2 mIU/L; group 4, >2 mIU/L. **Results:** This study included 166 patients (78.3% females, median age 44 years) of whom the risk of recurrence was intermediate in 97 (58.4%) and high in 69 (41.6%). The response to initial therapy at 1 year was excellent in 163 patients (98.2%) and indeterminate in 3 (1.8%). Group 1 consisted of 63 patients (38%), group 2 of 47 (28%), group 3 of 28 (17%), and group 4 of 28 (17%). During a median follow-up duration of 5.8 years, disease recurrence was observed in only 4 patients (2.4%). The rate of disease recurrence was not significantly different between the TSH groups. **Conclusion:** TSH suppression before the first response to treatment assessment does not seem to influence the rate of disease recurrence after initial therapy in intermediate- and high-risk PTC patients with pre-ablation s-Tg < 1 ng/mL. **References:** None.

EP-0608

Intraoperative 123I-radionavigation as a method of objective control of the completeness of thyroidectomy and rational planning of subsequent adjuvant radioiodine ablation in patients with differentiated thyroid cancer

Y. Blanter, V. Solodkiy, D. Fomin, D. Galushko, O. Borisova, S. Kukushkina, O. Lyugay, A. Asmaryan, O. Avilov;
Federal State Budgetary Institution Russian Scientific Center of Roentgenoradiology (RSCRR) of the Ministry of Healthcare of the Russian Federation, Moscow, RUSSIAN FEDERATION.

Aim/Introduction: Contemporary clinical guidelines contain indications for adjuvant radioiodine therapy in patients with low and intermediate risks of recurrent/persistent differentiated thyroid cancer, allowing the use of the most sparing modes, but these are applicable only if the thyroid tissue is completely removed. The absence of a functionally significant thyroid remnant is determined by negative levels of thyroglobulin and anti-Tg antibodies. In this regard, the intraoperative detection of the thyroid residue is of a high interest. **Materials and Methods:** The study included adult 133 patients with thyroidectomy: the main group (n = 33 - using intraoperative gamma-detection), control group (n = 100 - with traditional visual control of the thyroid bed sanation). 123I-radionavigation techniques included the pre, intraoperative and postoperative stages; didn`t require special preparation of the patient and was based on the use of indicator activity 123I (0,5-1 mCi). The choice of 131I activity in the main and control groups was based on clinicopathological factors (tumor size, histology, lymphatic invasion, levels of postoperative unstimulated thyroglobulin) according to NCCN Guidelines Versions 1.2018. Patients of the main group were stratified by aggravating risk factors and received activity from 30 (no risk factors) to 50 mCi (identified risk factors). The activity in the control group was 50-100 mCi. **Results:** The absence of thyroid tissue on post-therapy scans after surgical treatment using 123-radionavigation was observed in 45.5%, and in 6% of observation when visual

control by thyroidectomy was used (p <0.0001); however, median uptake in main group 131I was 0.3% of the whole body, indicating a small thyroid remnant. In the control group, in 39% of patients, uptake in the thyroid bed was 10-22.6% of the whole body, which required a second course of radioiodine therapy. During the monitoring of patients after radioiodine therapy (> 1.5 years) and after performing of stimulation test 5% of patients had lymph node metastasis and 4% had an increase in thyroglobulin of more than 10 ng/ml, which required further treatment in the control group. There was no progression or recurrence of the disease in the radionavigation group. **Conclusion:** Using of 123I-radionavigation in thyroidectomy in the presence of complicating clinicopathological factors makes it possible to use careful treatment of radioiodine ablation and, in the absence of risk factors, refuse radioiodine ablation in favor of marker observation in patients with differentiated thyroid cancer. **References:** None.

EP-0609

The diagnostic value of serum TgAb value and its changes on the prognosis of DTC patients with positive TgAb

W. Hu, B. Liu;
The First Affiliated Hospital of Zhengzhou University, Zhengzhou, CHINA.

Aim/Introduction: To explore the influence of serum TgAb value and its changes rate(TgAb after thyroid surgery and ^{131}I treatment - TgAb before surgery)/TgAb before surgery ×100%) after thyroid surgery and ^{131}I treatment on the prognosis of DTC patients with preoperative positive TgAb, and determine its diagnostic cutoff value. **Materials and Methods:** A retrospective study was conducted on 478 DTC patients with preoperative TgAb positive (greater than the normal reference upper limit of 115IU/ml) from May 2013 to August 2018, including 63 males and 415 females aged 13 to 78(41. 0±12. 1) years. All patients underwent total or subtotal thyroidectomy and have complete clinical data. Serum Tg and TgAb under TSH stimulation(TSH>30IU/mL),together with cervical ultrasonography ,^{131}I-Dx-WBS were reviewed after 6 months of treatment. Median follow-up time was 24 months (range, 9-63 months). **Results:** 1.The cutoff value of TgAb for diagnosis of DTC persistence/recurrence was 295.2IU/ml, the sensitivity, specificity, positive predictive value, negative predictive value and accuracy were 79.1%, 70.6%, 30.5%, 95.4% and 71.8%, respectively. The cutoff value of TgAb change rate was -41.0%, the sensitivity, specificity, positive predictive value, negative predictive value and accuracy were 83.6%, 72.8%, 33.3%, 96.5% and 74.3%, respectively. The rate of DTC persistence/recurrence were 3.5% (11/310), 25.8% (25/97) and 43.7% (31/71), respectively in the decline rate of TgAb was more than 41.0%, less than 41.0% and TgAb increased (log-rank χ^2=99.056, P < 0.001). Pairwise comparison was statistically significant among the three groups (P < 0.017). 2.There was no significant difference in the diagnostic efficacy between the TgAb threshold and the TgAb rate of change threshold (both P > 0.05). The sensitivity, specificity, positive predictive value, negative predictive value and accuracy of coalition between two diagnostic methods can be improved to 92.5%, 84.7%, 49.6%, 98.6% and 85.8%. There was statistically significant difference compared with the cutoff value of TgAb alone (all P < 0.05). The specificity, positive predictive value and accuracy were statistically differenent compared with rate of change threshold alone(all P < 0.05). There was no statistically differenent in sensitivity and negative predictive value (all P > 0.05). **Conclusion:** 1. TgAb value and rate of change after thyroid surgery +^{131}I treatment can be used to monitor the persistence/recurrence of DTC. The diagnostic cutoff value was 295.2IU/mL, -41.0%, respectively. 2. The diagnostic efficacy of DTC persistence/recurrence between TgAb threshold and rate of change threshold are equivalent. The diagnostic accuracy can be improved when combined. **References:** None.

EP-0610

200mg vs 400mg daily dose of Sorafenib in radioiodine refractory differentiated thyroid cancer: A comparison of response and adverse effects

***A. Prashanth**, M. Angamuthu, M. Prabhu, K. Reddy, D. Chakraborty, S. Arora, C. Bal;*
All India Institute of medical sciences, New Delhi, INDIA.

Aim/Introduction: Sorafenib is a multi-kinase inhibitor approved for radio-refractory differentiated thyroid cancer. The recommended starting dose of sorafenib is 800mg per day. However due to multiple adverse effects many patients require dose reduction and interruptions. Starting with lower dose of sorafenib have been shown to have better compliance. The aim of the study was to compare the efficacy and adverse effects profile between 200mg and 400mg daily dose. **Materials and Methods:** In this retrospective study, 74 patients were included. 37 patients were prescribed 200mg once daily and 37 patients were prescribed 400mg daily dose. Patients were followed up at 6 weeks and thereafter every 3 months with complete blood counts, liver & renal function tests. Follow-up evaluations also included vitals, ECG and clinical examination to assess adverse effects. RECIST 1.1 was used to assess response on imaging. **Results:** There was no significant difference between the baseline characteristics (age, sex, Thyroglobulin levels, frequency and sites of metastasis) between the 200mg and 400mg groups. Median duration of follow-up was 17.5months (IQR: 10.8months). Radiological response was available in 49 patients (27 from 200mg group and 22 from 400mg group). Response in 200mg vs 400mg group revealed partial response (PR) in 18% vs 8%, stable disease (SD) in 10% vs 14% and progressive disease (PD) in 26% vs 22%. In 48 (64%) no change of dose was made throughout the study. A trial of dose escalation was made in 17 (22.6%) patients from 200mg to 400mg and 400mg to 800mg. Unable to tolerate higher dose, 8/17 patients were reverted back to their previous dose. Most common adverse effect noted was hand and foot skin reaction (HFSR), leading to dose reduction in 40% of patients on 400mg. No significant difference was seen between 200mg and 400mg groups in terms of adverse effects in

those continued on these dosages. **Conclusion:** Administration of 200mg daily dose of sorafenib has similar efficacy compared to 400mg, but with better tolerability. **References:** None.

EP-0611

Analysis of outcome of low risk differentiated thyroid carcinoma: a retrospective review and our experience of 6.5 years

H. Ahmed, M. Al Qahtani, H. Ilyas, F. Ul Hassan;
Guy's and St. Thomas' NHS Foundation, London, UNITED KINGDOM.

Aim/Introduction: To retrospectively analyse the clinical and biochemical outcome of the low risk differentiated thyroid carcinoma patients that were treated with total thyroidectomy and 1.1 GBq of radioactive iodine (RAI).. **Materials and Methods:** Computerised Radiology Information System (CRIS) was used to identify 68 patients that were treated with 1.1 GBq 131-I for differentiated thyroid carcinoma between September 2012 and December 2017. The patients' clinical history and blood tests were acquired from the Patient Electronic Record and clinic letters. Overall the patients were followed up between 1.25 - 6.5 years. **Results:** There were 52 females and 16 males. Median age for females was 48 years and 47 for males. Age range for females was 27-75 years and males 21-74 years. 21 patients underwent total or staged thyroidectomy without neck dissection and 45 patients had thyroidectomy with level VI neck dissection, 1 patient had bilateral neck dissection and 1 had level IV neck dissection. 66 patients were diagnosed as papillary thyroid carcinoma and 2 as follicular thyroid carcinoma. Patients with distant metastases (M1) and stage III and IV were excluded. T and N (tumour size and nodal spread) were: (as per TNM 7 classification), T1 (n=37), T2 (n=23) and T3 (n=8), N0 (n=41) and N1a (27). 8 patients were lost to follow up. Only 7% (n=5) of patients needed further treatment after initial surgery and RAI. Out of these 5 patients, one patient underwent further neck dissection for metastatic involvement of cervical lymph nodes and had only one additional RAI activity within a year of diagnosis.The rest of 4 patients had persistently raised stimulated thyroglobulin levels without any evidence of structural disease on dynamic risk stratification. One patient was treated with further radioiodine therapy and two patients were treated with two activities of radioiodine. One patient who was treated with further RAI was lost to followup. All 5 patients who needed further treatment were papillary carcinomas with TNM staging of T1 and two N1a and three N0. The rest of the 63 (93%) patients did not need any further treatment and remained in remission. **Conclusion:** Our study concludes that low activity 1,1 GBq 131 I is an effective treatment after surgery for low risk differentiated thyroid cancer. Only a small percentage of patients on follow up had recurrent disease needing surgery / further radioiodine treatments. **References:** None.

EP-0612

The Clinical Utility Of 18-f Fluro-Deoxy-Glucose Positron Emission Tomography Computed Tomography Concurrent With 131-I Therapy In Intermediate To High Risk Differentiated Thyroid Cancers

V. Malasani;
Fortis Memorial Research Institute, Gurgaon, INDIA.

Aim/Introduction: To determine incremental value of ^{18}F-FDG PET CT in post-operative risk stratification of patients with intermediate to high risk DTC over pathological staging and WBS and to determine whether the patients with FDG avid disease had a different clinical course compared to the others. **Materials and Methods:** 51 patients of DTC with post upfront thyroidectomy and patients who underwent secondary cytoreductive surgery for recurrent disease were included. All patients had serum TSH levels > 30 µIU/ml at the time of evaluation. Serum Tg, anti -Tg, 131-I WBS and^{18}F-FDG PET CT scan were performed. All these patients received RAI therapy and were followed up between 6- 12 months, with stimulated S. Tg , S.Anti Tg Ab , ^{131}I-WBS and ^{18}F-FDG PET CT scans. **Results:** Of the 51 patients, 36 had undergone primary thyroidectomy while 15 had undergone secondary cytoreductive surgery. PET CT scan done in the post primary surgical, pre -radioiodine therapy workup of patients enabled detection of additional positive findings in 5/36 patients and further changing their risk stratification. PET CT had additional benefit in detecting only 10/15 patients who had recurrence following RAI therapy. 24/51 had lymph nodal or metastatic disease at the base line. 4/24 underwent surgery and had no evidence of disease at follow up. 3/20 patients who had RAI neck nodes showed incomplete structural response, 1 patient who had iodine refractory disease showed progression, 1 patient who had additional iodine refractory cervical lymph nodes had persistent iodine refractory structural disease. Of the 15 patients who showed FDG and iodine avidity when followed up after radioiodine therapy, 6/15 stable disease, 4/15 partial response and 5/15 progressive disease on PET CT scan. There was an incremental value of PET CT scan over radioiodine scan in 11/15 patients, to detect the site of iodine refractory disease. **Conclusion:** Performing FDG PET CT scan as a routine in all intermediate and high-risk patients of DTC may help identify a more aggressive tumor biology earlier. FDG PET CT also has a significant incremental role over an I-131 whole body scan in detecting sites of structural disease, both during initial pre radioiodine therapy work up and especially in a recurrent setting. However whether this information can be translated into a change in management strategies leading to overall better outcomes, needs a larger study and longer follow up. **References:** None.

EP-0613

Does I-131 uptake in the subhyoid portion or lymph nodes affect the outcome of low-dose ablation therapy for patients with differentiated thyroid cancer?

S. Ito[1], S. Iwano[1], K. Kato[2], S. Naganawa[1];

[1]*Department of Radiology, Nagoya University Graduate School of Medicine, Nagoya, JAPAN,* [2]*Department of Radiological and Medical Laboratory Sciences, Nagoya University Graduate School of Medicine, Nagoya, JAPAN.*

Aim/Introduction: To evaluate the effect of I-131 uptake in the subhyoid portion or lymph nodes when performing low-dose ablation therapy for patients with differentiated thyroid cancer. **Materials and Methods:** This study included 196 post-operative patients (65 males, 131 women; age 53.6±14.1 y.o.) who underwent low-dose I-131 (1,110 MBq) ablation therapy. We conducted a retrospective review regarding cervical I-131 uptake sites, which were identified as the thyroid beds, subhyoid portion, or lymph nodes, using a post-therapeutic SPECT/CT. The response-evaluation scan was performed 6 - 8 months after I-131 ablation therapy, and the outcome of therapy was judged based on whether the I-131 uptake disappeared or not. Logistic regression analysis was performed to predict the outcome of I-131 ablation therapy on some risk factors. **Results:** Uptake only in the subhyoid portion was observed in 22 patients, while uptake only in the thyroid beds was observed in 87 patients. Forty-four patients had lymph nodes uptake. The success rate in the group that showed uptake only in the subhyoid portion was lower than that in the group that showed uptake only in the thyroid bed, but there was no significant difference between these two groups (64%, 82%, respectively; $p = 0.07$). In contrast, the success rate in patients with lymph nodes uptake was significantly lower than that in patients without lymph nodes uptake (43%, 70%, respectively; $p = 0.001$). Among the factors, such as ages, sex, utilization of recombinant human TSH, serum TSH-stimulated thyroglobulin level, uptake in the subhyoid portion, and uptake in lymph nodes; sex, uptake by the subhyoid portion, and uptake of lymph nodes were found to be significant predictors by univariate analyses. Multivariate analyses revealed that uptake in the subhyoid portion and lymph nodes were significant predictors. **Conclusion:** I-131 uptake in the subhyoid portion or lymph nodes can lower the success rate of low-dose ablation therapy for patients with differentiated thyroid cancer. **References:** None.

EP-0614

The role of metabolic-receptor imaging in selection of locally advanced dedifferentiated thyroid carcinoma patients for peptid-radioreceptor therapy

F. Velickovic[1], *T. Andjelkovic*[1], *M. Vidanovic*[1], *M. Stevic*[1], *M. Rajic*[1], *M. Vlajkovic*[1], *M. Matovic*[2];
[1]*University of Nis, Faculty of Medicine, Nis, SERBIA,* [2]*University of Kragujevac, Faculty of Medical Sciences, Kragujevac, SERBIA.*

Aim/Introduction: Loss of avidity for iodine, increased secretion of thyroglobulin, glucose metabolism disorder, and excessive expression of somatostatin receptors are the main features of the dedifferentiated thyroid carcinoma (DeDTC).The aim of this study was to assess the significance of somatostatin receptor scintigraphy (SRS) with Technetium-99m-HYNIC-[D-Phe1,Tyr3-Octreotide] (99mTc-Tektrotyd) and positron emission tomography with fluorine-18 fluor- deoxyglucose (18F-FDG-PET / CT) in the detection of recurrent disease and the selection of patients with DeDTC for peptide-radioreceptor therapy (PRRT). The secondary goal was the survival analysis after dedifferentiation in patients in whom the PRRT was applied. **Materials and Methods:** The study included 12 patients with DeDTC Patients were monitored 2-14 years (8.6 ± 3.7 years) following surgery and radioiodine ablation. The inclusion criteria for PRRT was the presence of focal accumulation on the SRS with 99mTc-Tektrotyde that was consistent with the finding of the 18F-FDG-PET / CT scan or if a greater number of pathological focuses were detected on the SRS compared to the 18F-FDG PET / CT scan in the same region. In 7 out of 12 subjects, 1-4 cycles of PRRT was applied. **Results:** One of 7 subjects treated with PRRT received a dose of 5.5GBq 90Y-DOTA0,Tyr3-octreotate (90Y-DOTATATE), while the other 6 were treated with tandem therapy using 2.75GBq 90Y-DOTATE and 2.75GBq 177Lu-DOTATATE. The RECIST response criteria showed a stabilization of the disease in 4, complete remission in one, and a progression of the disease in two, one of whom with fatal outcome. Out of 5 subjects who did not treated by PRRT, 2 had a stable disease while three died. Kaplan-Meier's analysis found that survival time in patients treated with peptide radioreceptor therapy was 102 ± 16 months after dedifferentiation, whereas in those who did not use this type of treatment, 38 ± 19 months. **Conclusion:** The results of our work have shown that the receptor-metabolic imaging using 99mTc-Tektrotyde and 18F-FDG PET / CT scans is extremely reliable for the selection of patients for PRRT. Also, the results have shown that PRRT is a promising therapeutic option for iodine negative thyroid carcinoma patients that can provide longer survival period after dedifferentiation. **References:** None.

EP-0615

"Unexpected uptakes" in post 131-I whole body scans in patients with differentiated thyroid cancer

D. Monachello Araujo, *S. Rodado Marina, A. Guzmán Cruz, L. García Zoghby, D. Travaglio Morales, M. Coronado Poggio, J. Cordero García, C. Escabias Del Pozo, C. Lancha Hernández, S. Rizkallal, L. Domínguez Gadea;*
Hospital Universitario La Paz, Madrid, SPAIN.

Aim/Introduction: To asses "unexpected uptakes" of 131-I in post-therapeutic whole body scans (WBS) of patients diagnosed with differentiated thyroid carcinoma (DTC). **Materials and Methods:** We retrospectively reviewed 535 patients diagnosed with DTC referred to our unit for treatment with 131-I between 2001-2010. We studied which of them had "unexpected uptakes" in the post-treatment WBS, excluding thyroid rests in the surgical site, and finally analyzing 111 patients with 125 "unexpected uptakes". In all of them concomitant SPECT-CT imaging was performed for better anatomic localization. We evaluated our findings with other imaging techniques results, serum tests, clinical evolution and, in some cases,

histological studies. Cases without a conclusive diagnosis were considered undetermined. **Results:** From the 111 analyzed patients with "unexpected uptakes" (20.7%) (23 males and 88 females; median age 48.9 years), 94 patients corresponded to papillary cancer, 11 to follicular cancer and 6 to Hürthle cancer. From the post-therapeutic 131-I WBS analyzed (111), 73 corresponded to first ablation treatment WBS and 38 to post-therapeutic WBS. We excluded, from the 125 "unexpected uptakes", physiologic processes (25) and contamination artifacts (13). Finally, we analyzed 87 "unexpected uptakes" outside the surgical site, classifying them in this way: other lesions/non-metastatic lesions: 20 (23%) (2 bone angiomas, 2 hepatic cysts, 1 neuroblastoma, 1 bone cyst, 6 dental processes, 5 bilateral nodular pulmonary diseases,1 bronchiectasis, 2 inflammatory lymphadenopathies); metastatic disease: 25 (29%) (pulmonary ± skeletal ± lymph nodes) and undetermined findings: 42 (48%), which were sorted by their localization (11 in the mediastinum, 20 in the neck/supraclavicular fossa, 3 in the thoracic outlet, 5 skeletal and 3 pulmonary). The thorax was the site with the majority of "unexpected uptakes" and undetermined diagnosis. **Conclusion:** There's a non-negligible percentage of patients with "unexpected uptakes" outside the thyroid surgical site in post 131-I WBS, the majority localized in the thorax.In about 50% of these patients we got to a final diagnosis, and in about 30% of these (metastatic disease) our test had a direct impact in their treatment and prognosis.The etiological knowledge of these uptakes is very useful in their correct interpretation, which will lead to a better treatment of these patients. **References:** None.

EP-0616

An Impact of Microscopic Positive Margin on Incomplete Response after I-131 Therapy in Differentiated Thyroid Cancer: A Retrospective Cohort Study

Y. Raruenrom, K. Sawangsri, C. Somboonporn, D. Theerakulpisut, N. Wongsurawat, T. Ratanaanekchai;
Khon Kaen University, Khon Kaen, THAILAND.

Aim/Introduction: Completeness of surgical resection is a determination of successful treatment in patients with differentiated thyroid cancer. Patients with grossly incomplete tumor resection are classified into high-risk of recurrence and had 56%-72% structural incomplete response after total thyroidectomy and I-131 therapy. However, an association between microscopic positive margin and incomplete response are still unclear. The recent standard guidelines did not mention about this issue. Thus, this research aimed to study an impact of microscopic positive margin on incomplete response after I-131 therapy in patients with differentiated thyroid cancer. **Materials and Methods:** This retrospective cohort study was conducted from January 2014 to February 2018 at Srinagarind Hospital, Khon Kaen University, Thailand. We included patients with differentiated thyroid cancer who underwent total thyroidectomy and received the first dose of I-131 therapy and excluded patients with gross residual tumor at the time of surgery or patients with distant metastasis. Thyroid specimens were re-evaluated by one pathologist who was blinded to clinical information to determine microscopic resection margin status. The positive microscopic resection margin was defined as the presence of tumor cells at the inked surgical margin. The treatment response was evaluated at 6-12 months after I-131 therapy and was classified according to the 2015 American Association Management Guidelines for Adults with Thyroid nodules and Differentiated Thyroid Cancer. Univariable and multivariable analyses were used to find an association between microscopic positive margin and incomplete response which included both structural incomplete response (SIR) and biochemical incomplete response (BIR). **Results:** One hundred patients (78 female; mean age 50.3 years) were included in the study. Ninety-three (93%) patients had papillary thyroid carcinoma. Microscopic positive margin was found in 27 (27%) patients. The mean I-131 dose was 4,743.4 MBq (128.2 mCi). After the median follow-up time of 10.3 months, 30 (30%) patients had incomplete response (20% SIR, 10% BIR). Univariable analysis showed a significant association between positive microscopic margin and incomplete response after I-131 therapy with odds ratio of 3.06 (95% CI: 1.21-7.75, p 0.018). After adjusted for important associated factors including tumor size, extrathyroidal extension, and cervical lymph node metastasis, microscopic positive margin still showed a significant association for incomplete response with adjusted odds ratio of 2.99 (95% CI: 1.04-8.63, p 0.042). **Conclusion:** Microscopic positive margin was found to be associated with incomplete response after I-131 therapy in patients with differentiated thyroid cancer. **References:** None.

EP-0617

Comparing High and Low dose I-131 Therapy in Intermediate and Low Risk Differentiated Thyroid Cancer Patients

T. Yasmin[1], *S. Adnan*[2], *M. N. Younis*[3], *A. Shahid*[3];
[1]*Institute of nucleay medicine and oncology lahore, Lahore, PAKISTAN,* [2]*Institute of nuclear medicine and oncology, Lahore, PAKISTAN,* [3]*Institute of Nuclear Medicine and Oncology Lahore, Lahore, PAKISTAN.*

Aim/Introduction: Although low dose I-131 has almost equal success rate as high dose in thyroid remnant ablation of low risk differentiated thyroid cancer (DTC) patients, an appropriate dose for the same is still a debate. We have conducted a prospective clinical research study to evaluate the role of low and high dose I-131 in intermediate and low risk DTC patients. To compare the effectiveness of low and high dose iodine -131 therapies in low and intermediate risk DTC patients. **Materials and Methods:** We studied effect of low and high dose I-131 DTC patients prospectively presented for thyroid remnant ablation. Group I (those who underwent high dose ablation (>100mCi)) and Group II (who were ablated with low dose iodine 131 (< 30mCi)). A definitive criteria of TG level < 2.0, USG of neck negative for residual thyroid tissue or suspicious regional lymph nodes and no I-131 avid lesion detected on

whole body scan was set to label patients as disease free at 6 months, 1 year and 2 years follow up. Data analyzed at SPSS 20, spearman correlation coefficient calculated between two groups. **Results:** Total 93 patients; Group I: Included 50 patients, 44 cases of papillary thyroid cancer (PTC) and 6 follicular thyroid cancer (FTC). 36 intermediate risk and 14 low risk patients were given high dose I-131 therapy. Six months follow-up revealed (30/50) 60 %, at end of one and two years (38/50) 76% disease free patients. Group II: Total 43 patients, 42 cases of PTC and 01 FTC. 22 intermediate and 21 high risk cases were ablated with low dose I-131 therapy. Six months follow-up revealed (29/43) 67% at end of one year (35/43) 81 % and end of two years (36/43) 84 % disease free patients. Statistically significant correlation was established among results of both the groups at different intervals. **Conclusion:** We conclude that high and low dose of radioactive Iodine-I-131 are almost equally effective therapeutic doses for ablation of differentiated thyroid cancer remnants in both intermediate and low risk patients. **References:** None.

EP-0618

A Follow Up Dose-rate Measurement Strategy for Patients Post ^{131}Iodine Ablation Therapy. Can We Improve the Post Treatment Restrictions Applied to the Patient on Discharge?

J. Weekes, M. Foley;
New Cross Hospital, Wolverhampton, UNITED KINGDOM.

Aim/Introduction: Patients on discharge post ^{131}Iodine Ablation Therapy are issued with radiation precautions (restrictions) depending on their remaining radiation dose-rate measured. These restrictions can have a huge influence on their family / work / life balance post discharge due to the need to:- The need to sleep separately from partner and children The need to keep a certain distance from family members and public. This can vary between 1-3 metres depending on the age of the childThe need to avoid close contact for any period of time (3 metres minimum distance) with pregnant femalesSuper hygiene methods in place to avoid spread or contamination of excreted ^{131}I The need to be signed off work The duration of restrictions put in place on discharge can span up to 27 days post discharge. As well as family life being affected, it can also have a considerable financial impact to the patient being unable to work during this period. **Materials and Methods:** A re-measurement service (15 minutes of staff time) was offered to 42 patients that received ^{131}I Ablation Therapy between 01/04/17 to 31/03/18 at The Royal Wolverhampton NHS Trust. 37 patients returned for their re-measurement on average 4 days post discharge. **Results:** 28 patients (76%) on day 4 post discharge had all their radiation restrictions lifted completely. 9 patients (24%) on day 4 post discharge had their restrictions reduced to a maximum of 4 further days thus dramatically reducing the original restrictions that were applied on discharge. **Conclusion:** From these results it can be shown that by offering a re-measurement service to patient's post ^{131}I Ablation Therapy we can show a significant benefit to the patient and their family thus improve the quality of the service **References:** Appendix 1 Restrictions for Patients Medical and Dental Guidance Notes, IPEM,P129.

EP-43

Preclinical and translational aspects, including radiopharmacy, radiochemistry and drug development -> Preclinical and translational aspects -> Preclinical aspects -> Animal models and in-vitro studies

October 12 - 16, 2019 e-Poster Area

EP-0619

A dual-labeled anti-FAP antibody for imaging and targeted photodynamic therapy of cancer associated fibroblasts in a pancreatic cancer mouse model

E. M. Smeets[1], *D. N. Dorst*[1], *S. A. M. Lith*[1], *A. Freimoser-Grundschober*[2], *C. Klein*[2], *M. Trajkovic-Arsic*[3], *M. Gotthardt*[1], *J. Siveke*[3], *E. H. J. H. Aarntzen*[1];
[1]*Radboudumc, Nijmegen, NETHERLANDS,* [2]*Roche Pharmaceutical Research and Early Development, Zurich, SWITZERLAND,* [3]*University Hospital Essen, Essen, GERMANY.*

Aim/Introduction: Pancreatic ductal adenocarcinoma (PDAC) is a prototype cancer dominated by an intense desmoplastic reaction, consisting of abundant extra-cellular matrix[1]. This impacts the metabolic and immune tumor microenvironment. Activated cancer associated fibroblasts (CAFs), expressing fibroblast activation protein (FAP), play a central role in this desmoplastic reaction[1]. Specific elimination of CAFs in PDAC potentially restores the aberrant tumor microenvironment, and therefore we developed a dual-labeled anti-FAP antibody for SPECT imaging and targeted photodynamic therapy (tPDT) of CAFs in PDAC. **Materials and Methods:** The anti-FAP monoclonal humanized IgG1 antibody 28H1 was conjugated with either DTPA only for imaging studies or with DTPA and the photosensitizer (PS) IRDye700DX for therapy studies. The irrelevant antibody DP47GS conjugated with DTPA and PS was used as a negative control. Ptf1awt/Cre;Kraswt/LSL-G12D;p53fl/fl (CKP) mice, developing spontaneous PDAC tumors, where injected with 10MBq [111In]-In-DTPA-28H1, dual-labeled [111In]-In-DTPA-28H1-IRDye700DX or [111In]-In-DTPA-DP47GS-IRDye700DX (50ug/mouse) and SPECT/CT imaging and biodistribution studies were performed 24h post injection. Five mice were subjected to tPDT by exposing the tumor to 50 J/cm2 690nm light at 24h post injection with 28H1 (n=3) or DP47GS (n=2). One hour after illumination, tumor tissue was collected and cell death was analyzed with immunohistochemistry. **Results:** Both [111In]-In-DTPA-28H1 (n=1) and dual-labeled [111In]-In-DTPA-28H1-IRDye700DX (n=4) are efficiently taken up by the tumor (24.32 %ID/g vs 13.12±3.55 %ID/g, respectively), and show low residual blood activity (12.09 %ID/g vs 8.22±4.17

%ID/g, respectively) after 24 hours. Conjugation of IRDye700DX to the antibody does cause increased accumulation in the liver (4.6 %ID/g vs 15.86±4.23 %ID/g, respectively), but this does not compromise tumor-targeting. Though there is some tumor uptake of [111In]-In-DTPA-DP47GS-IRDye700DX (11.37±4.38 %ID/g, n=3), tumor-to-blood ratio was significantly lower when compared to [111In]-In-DTPA-28H1-IRDye700DX, (1.76±0.3 vs 0.5±0.10, respectively (p=0.006)). Ex vivo fluorescence imaging showed that the IRDye700DX signal is only quenched in the part of the tumor that was exposed to light for both antibodies. However, only in the tumors treated with 28H1 tPDT specific cell death was observed in the tumor stroma, illustrated by increased expression of apoptosis marker cleaved caspase-3 and DNA double-strand break marker γH2AX, also in comparison to non-illuminated internal control tissue. **Conclusion:** The dual-labeled anti-FAP antibody targets PDAC tumors in mice with good signal-to-background ratios and favorable biodistribution. Furthermore, it efficiently induces cell death upon tPDT, indicating that FAP-tPDT is a feasible and promising approach to deplete CAFs in PDAC. **References:** Neesse, A., et al., Stromal biology and therapy in pancreatic cancer: a changing paradigm. (1468-3288 (Electronic)).

EP-0620

Impact of different tissues on Cerenkov luminescence imaging of positron emitters

E. Ciarrocchi[1,2], N. Belcari[1,2], S. Vitali[3], A. G. Cataldi[3], F. Bartoli[3], A. Marciano[3], A. Del Guerra[1,2], P. A. Erba[3,4];
[1]Department of Physics, University of Pisa, Pisa, ITALY, [2]Istituto Nazionale di Fisica Nucleare, Sezione di Pisa, Pisa, ITALY, [3]Department of Translational Research and of New Surgical and Medical Technologies, University of Pisa, Pisa, ITALY, [4]Azienda Ospedaliero-Universitaria Pisana, Pisa, ITALY.

Aim/Introduction: Cerenkov luminescence emitted by radionuclides in biological tissue depends on the energy spectrum of the beta particles and on the index of refraction and optical attenuation of the medium. The aim of this study is to perform ex-vivo Cerenkov luminescence imaging (CLI) of clinically relevant positron emitters in various tissues to determine the minimum detectable activity level as a function of the type of radioisotope and tissue. The final goal of our measurements is to define an optimal (organ- and radioisotope-specific) clinical protocol for intra-operative CLI of resected tumor specimens after whole-body PET/CT scanning, that includes the required injected activity and maximum allowed time delay for imaging. These results can be used also in other clinical imaging applications using Cerenkov radiation. **Materials and Methods:** Initial activities of 15 uCi of [^{18}F]FDG and 2 uCi of ^{68}Ga-citrate were diluted in 50 ul of water and placed inside clear plastic Eppendorfs. The empty portions of the Eppendorfs were covered with black tape to suppress the signal from this region. Slabs of various tissues (bovine lung and spleen, porcine heart and liver) of 2-3 mm thickness were placed around the Eppendorfs. The specimens were imaged for 1 minute inside a light-tight box with a cooled CCD camera and an f/0.95-25 mm lens. The minimum detectable activity level was determined as the value corresponding to SNR=2. **Results:** For ^{68}Ga-citrate, activity levels of 0.5 uCi or less were clearly detectable in all organs. For [^{18}F]FDG, ~10 uCi could be detected in lung and spleen, but not in liver and heart. Due to its higher positron endpoint energy, ^{68}Ga-citrate provided a SNR comparable to [^{18}F]FDG with roughly 13 times less activity. However, in clinical practice, this is partially compensated by [^{18}F]FDG longer half-life. If we consider a realistic time delay of 3 hours between radiotracer injection and patient imaging, ^{68}Ga-citrate activity will be 16% of the injected amount, whilst [^{18}F]FDG will be reduced to 32% of its original activity. **Conclusion:** These preliminary results suggest ^{68}Ga-citrate has the best performance in all tissues, including the effect of the time delay after injection. We will present the results of an extended systematic study to fully characterize the detection limits for both radioisotopes on a larger number of tissue specimens, investigating also the contribution of factors such as acquisition settings, and source depth and geometry. **References:** None.

EP-0621

Association between Brown Adipose Tissue Metabolism and Olfactory function in mice evaluated by ^{18}F-FDG micro-PET/CT imaging

Q. Lv[1,2], Y. Wei[1,2], X. Zhang[3], X. Li[4], T. Mou[3], Z. Zhu[3];
[1]Department of Otolaryngology, Beijing Anzhen Hospital, Capital Medical University, Beijing, CHINA, [2]Key Laboratory of Upper Airway Dysfunction-related Cardiovascular Diseases, Beijing Institute of Heart Lung and Blood Vessel Disease, Beijing, CHINA, [3]Department of nuclear medicine, Beijing Anzhen Hospital, Capital Medical University, Beijing, CHINA, [4]Department of Biomedical Imaging and Image-guided Therapy,Medical University of Vienna, Vienna, AUSTRIA.

Aim/Introduction: The systemic physiology effects of olfactory inputs still remain unclear. We aimed to assess the association between olfaction function and brown adipose tissue (BAT) metabolism by ^{18}F-FDG micro-PET/CT imaging in vivo. **Materials and Methods:** Animal models with allergic rhinitis and olfactory dysfunction (AROD group,n = 6) and toxic olfactory dysfunction (TOD group, n = 6) in adult BALB/c mice were established, respectively. After 12 weeks normal chow diet feeding, body weight, food intake, glucose level, triglyceride (TG) level, total cholesterol (TC) level and insulin resistance in blood were measured. Whole body imaging was acquired for 15 minutes at 50minutes post intravenous injection (37MBq/100g) by micro-PET/CT. Then, the maximum and mean standardized uptake values (SUV_{max} and SUV_{mean}) of BAT were measured. Standardized uptake value ratio (SUVR) values were corrected for background muscle activity. **Results:** Body weight was significantly reduced in mice with olfactory dysfunction. In comparison with the control group, body weight was significantly reduced in both AROD group (20%, $P < 0.001$) and TOD group (12%, $P = 0.019$), and food intake was reduced in both AROD and TOD groups

(AROD, 2.65 ± 0.64g; TOD, 2.55 ± 0.93g; Control, 4.93 ± 0.59g; P < 0.001) but without affecting the diurnal feeding pattern. The circulating TG level was decreased in both AROD and TOD groups (AROD, 43.49 ± 2.60 mg/dL; TOD, 41.41 ± 3.90 mg/dL; Control, 51.10 ± 4.53mg/dL; P < 0.001). The insulin resistance was improved in both AROD and TOD groups. SUV_{max} (AROD, 4.45 ±1.03; TOD, 3.83±1.82), SUV_{mean} (AROD, 1.71 ± 0.38; TOD; 1.37 ± 0.37)and SUVR (AROD, 6.11 ± 3.30; TOD, 10.00 ± 4.30) of the BAT was significantly increased in both AROD and TOD groups compared with control group(SUV_{max} 0.59 ± 0.39, SUV_{mean} 0.47 ± 0.30, SUVR 1.01 ± 0.70)(P < 0.001), indicating metabolism of the BAT in hyposmic mice was significantly increased. The Pearson's correlation showed that the level of TC and TG in all mice was significantly correlated with SUVmax (TC, r = -0.737, P = 0.001; TG, r = -0.501, P = 0.048) and SUVmean (TC, r = -0.713, P = 0.002; TG, r = -0.543, P = 0.030). **Conclusion:** Relatively short-term olfactory input may impact metabolic health by reduction of food intake, improvement of insulin sensitivity and energy expenditure of BAT activity which we detect via 18F-FDG micro-PET/CT in vivo. **References:** None.

EP-0622

^{18}F-FDG PET Imaging For Monitoring The Early Anti-tumor Effect Of Albendazole On Triple-negative Breast Cancer

H. Liu;
The First Affiliated Hospital of Soochow University, Suzhou, Jiangsu Province, CHINA.

Aim/Introduction: Breast cancer is the most common cancer in women worldwide. Triple-negative breast cancer (TNBC) accounts for 15-20% of all breast cancers, is valued due to its high malignancy, aggressiveness, high metastasis rate, high rate of recurrence, and poor prognosis. In addition to traditional chemotherapy, there is no clear standard treatment strategy for the treatment of TNBC, therefore, more effective treatment for TNBC is urgently needed. Albendazole (ABZ), an effective anthelmintic drug with low toxicity in human, can disrupt the microtubule in worms and exhibits anti-tumor potential in a variety of tumors. However, the therapeutic effect of ABZ on TNBC is unknown. In this study, we systematically investigated the inhibitory effect of ABZ on TNBC and monitored its early anti-tumor effect by ^{18}F-FDG PET. **Materials and Methods:** The effects of ABZ on TNBC cell lines were investigated in vitro using MTT, colony formation, wound-healing, transwell assays, western blotting, Cell cycle and apoptosis assay. In vivo treatment was conducted in a MDA-MB-231 tumor-bearing nude mice model. ABZ was administered through gastric perfusion. PET imaging was performed before and after 3 days of treatment. Tumor tissues were harvested for immunofluorescence analysis. Mouse body weight loss and survival rate were also evaluated. **Results:** ABZ treatment inhibited the proliferation and migration, while induced apoptosis and arrested cell cycle at the G2/M phase in MDA-MB-231 cells. Western blotting showed that ABZ induces autophagy and apoptosis in MDA-MB-231 cells via GLUT1/AMPK/P53 signaling pathway. In vivo ^{18}F-FDG PET imaging showed that 3-day ABZ treatment reduced SUVmax values in MDA-MB-231 xenografts compared to controls (SUV_{treat} = 7.60 ± 0.42, $SUV_{control}$ = 11.67 ± 1.80, P < 0.05), and immunofluorescence analysis showed lower TK1 expression, less GLUT1 membrane localization and more TUNEL-positive cells in the ABZ treated mice. Long-term treatment studies found that the tumor volume of the treatment group was smaller than that in the control group (V_{treat} = 632.03 ± 215.06,$V_{control}$ = 1142.16 ± 325.44,P < 0.01), and the survival time was prolonged. **Conclusion:** By inhibiting the GLUT1/AMPK/P53 signaling pathway, ABZ can induce autophagy and apoptosis, reduce glucose uptake, and ultimately inhibit TNBC. Our study suggests that ABZ can serve as a potential drug for TNBC treatment. **References:** None.

EP-0623

A Simple And Quantitative Method To Address The Synchronicity Between Uptake And Efflux Transporters In The Rat Liver Using ^{99m}Tc-mebrofenin Scintigraphy

S. Marie[1], *I. Hernández Lozano*[2], *L. Breuil*[1], *O. Langer*[2], *C. Truillet*[1], *N. Tournier*[1];
[1]*UMR 1023 IMIV, Service Hospitalier Frédéric Joliot, CEA, Inserm, CNRS, Université Paris Sud, Université Paris-Saclay, Orsay, FRANCE,* [2]*Department of Clinical Pharmacology, Medical University of Vienna, Vienna, AUSTRIA.*

Aim/Introduction: Imaging probes are needed to non-invasively and quantitatively assess the interplay between liver uptake and biliary secretion, which controls the clearance of many endogenous compounds and xenobiotics. ^{99m}Tc-mebrofenin is a readily available radiopharmaceutical for hepatobiliary scintigraphy. Previous studies performed in vitro and in transporter-deficient mice have shown that the hepatobiliary transport of ^{99m}Tc-mebrofenin involves organic anion-transporting polypeptide (OATP) transporters at the sinusoidal (blood-liver) interface, and the efflux transporter MRP2 at the canalicular (liver-bile) interface[1,2,3]. The aim of our study was to develop a simple quantification method to describe the activity of these transport systems in vivo. **Materials and Methods:** ^{99m}Tc-mebrofenin was injected into control rats (A_{inj}=42±6MBq; n=5) and immediately after a bolus of rifampicin (40mg/kg IV, A_{inj}=42±3MBq; n=5), a potent OATP/MRP2 inhibitor. Planar dynamic acquisitions were performed with a clinical Siemens Symbia gamma-camera during 40 minutes. Regions of interest were drawn over the heart (blood-pool), liver and intestine to obtain time-activity curves (TACs). Three quantification methods were tested: i)calculation of the transfer-rate constants between regions using integration plot analysis, ii)estimation of the area under the TAC ratio (AUCR) between regions and iii)compartmental modeling considering a mean volume for organs and a dual blood input function for the liver (hepatic artery and portal vein). Outcome parameters were compared using the Mann-Whitney test (p<0.05). **Results:** Rifampicin significantly decreased the blood-to-liver transfer-rate constant estimated with integration plot analysis from 0 to 2 minutes (linear part) (control=1.51±0.22min^{-1} vs

rifampicin=0.33±0.03min^{-1}). However, the liver-to-intestine transfer-rate constant could not be accurately determined with this method. $AUCR_{liver/blood}$ estimated from 0 to 2 minutes was significantly decreased by rifampicin (control=1.98±0.22 vs rifampicin=0.81±0.05). A significant decrease was also observed for $AUCR_{intestine/liver}$ estimated from 10 to 25 minutes (control=1.36±0.20 vs rifampicin=0.64±0.16). These results were confirmed by compartmental modeling, which identified a significant decrease for rifampicin-treated rats in k_1 (blood-to-hepatocyte exchange, control=7.37±1.62min^{-1} vs rifampicin=0.88±0.09min^{-1}), k_2 (hepatocyte-to-blood back-flux, control=0.15±0.08min^{-1} vs rifampicin=0.01±0.01min^{-1}) and k_3 (hepatocyte-to intrahepatic bile-duct exchange, control=0.15±0.08min^{-1} vs rifampicin=0.05±0.02min^{-1}) but not for k_4 (intrahepatic bile-duct to intestine, control=0.12±0.03min^{-1} vs rifampicin=0.64±0.88min^{-1}). **Conclusion:** ^{99m}Tc-mebrofenin planar scintigraphy offers a readily available method to study the interplay between sinusoidal and canalicular transporters in mediating hepato-biliary clearance in vivo. AUCR is a simple parameter to describe the respective activity of both transporter systems. Compartmental modeling enriched the interpretation of the data and revealed the importance of an additional transport system responsible for the back-flux of ^{99m}Tc-mebrofenin from liver to blood, most likely MRP3. **References:** None.

EP-0624

Eliminating Microglia in AD Mice Increases the Survival of Newborn Neurons in Dentate Gyrus and Enhances Pattern Separation

H. Yan[1], *W. Xiao*[1], *L. Wan*[2], *Q. Xie*[1];
[1]*Huazhong University of Science and Technology, Wuhan, CHINA,* [2]*Wuhan Raydata Technology Co., Ltd., Wuhan, CHINA.*

Aim/Introduction: Adult neurogenesis occurs in the subgranular zone (SGZ) of the dentate gyrus (DG) and takes part in the function of learning and memory. Only a minority of these newborn cells integrates into the network of hippocampus as functional mature neurons at last, while the majority of them suffer death because apoptosis or are engulfed directly by microglia, which implicates the possible pivotal role of microglia in the survival of neurogenesis in DG. **Materials and Methods:** Colony-stimulating factor 1 receptor (CSF1R) inhibitor. Triple transgenic mice. Immunochemistry. Positron emission tomography (PET). Water Morris. **Results:** Here, we showed that treatment with colony-stimulating factor 1 receptor (CSF1R) inhibitor, which results in quick removal of most microglia in the mouse brain, significantly increased the number of mature newborn neurons in aged C57BL/6 mice at the end of a 4 week period. Moreover, we uncovered that these mature newborn neurons owned more number of dendritic spines and the hippocampus tissue had higher glucose metabolism tested by PET in aged C57BL/6 mice after treatment by CSF1R inhibitor, and all the above phenomenon also recurred in the adult triple transgenic mouse model of Alzheimer's disease (3xTg-AD). Importantly, behavioural testing displayed that the treatment of CSF1F inhibitor improved the spatial pattern separation of aged C57BL/6 and adult 3xTg-AD mice. **Conclusion:** Collectively, these results demonstrate that eliminating microglia enhances the spatial pattern separation in adult AD mice by improving the potential of newborn neurons in DG. **References:** None.

EP-0625

An investigation for quantitative myocardial blood flow with Tc-99m MIBI by a graph plot analysis in rat with and without pharmacological stress agents

A. Okizaki*, M. Nakayama, K. Nomura, M. Ogata, Y. Nomura, M. Toda, A. Oya;*
Asahikawa Medical University, Asahikawa, JAPAN.

Aim/Introduction: We aimed to investigate the use of dynamic cardiac planar images to estimate myocardial blood flow (MBF) by a patlak plot analysis using time-to-peak (TP) map and compared it by the microsphere technique in rat. Positron emission tomography is considered the gold standard method, but is not available everywhere. By contrast, myocardial perfusion imaging (MPI) with single-photon tracers is more widely available. We reported that MBF estimation by a compartment model analysis using TP map could facilitate absolute MBF measurement in rats; however, a complicated mathematical calculation was necessary to perform the compartment model analysis. The TACs of input function and whole heart, both of them have a single peak in the first few phase of the acquisition. Where, the peak of whole heart may represent the activity from the left ventricle because the tracers may not be accumulated in the myocardium during the initial phases. We proposed using a patlak plot analysis for the time-activity curve (TAC) of myocardium, which obtained by a subtraction of left ventricle activity from whole heart activity, and hypothesized that this method could facilitate the measurement of absolute MBF by MPI in rat without the complicated mathematical calculation. **Materials and Methods:** Twenty-two normal rats were studied. Six rats were infused with a pharmacological stress agent (dobutamine in 3 rats, and propranorol in another 3 rats), and sixteen rats were infused with normal saline. Dynamic planar images with Tc-99m MIBI were obtained on a gamma imaging system for small animals (Inveon Multimodality System, Siemens, Germany), and input function and cardiac regions of interest were set using the TP map. The myocardial TAC was calculated with the following formula: myocardial activity = (whole heart activity) - (left ventricle activity). Moreover, left ventricle activity was obtained by curve fitting technique on the TAC of input function and whole heart in the first few phases. The MBF was estimated by a patlak plot analysis with the Renkin-Crone model and by the microsphere technique. **Results:** The MBFs with the patlak plot analysis and microsphere technique were significantly correlated. The peason's correlation coefficients was 0.73 ($p < 0.0001$). **Conclusion:** MBF estimation by a patlak plot analysis using TP map could facilitate absolute MBF measurement in rats with and without pharmacological stress agents. **References:** None.

EP-0626

Preclinical evaluation of apoptosis radiotracer [18]F-ML-10 in triple negative breast cancer

E. Jouberton[1,2,3], S. Schmitt[1], M. Roy[1], E. Chautard[1,2], N. Radosevic-Robin[1,2], A. Maisonial-Besset[1], J. Chezal[1], E. Miot-Noirault[1], Y. Bouvet[3], F. Cachin[1,2];
[1]Université Clermont Auvergne, INSERM, U1240 Imagerie Moléculaire et Stratégies Théranostiques, Clermont-Ferrand, FRANCE, [2]CLCC Centre Jean Perrin, Clermont-Ferrand, FRANCE, [3]Zionexa, Aubière, FRANCE.

Aim/Introduction: Standard treatment of early stage triple negative breast cancer (TNBC) is based on neoadjuvant therapy (NAT). A pathological complete response (pCR) associated to NAT is a predictive factor of patient survival. Methods for early evaluation of this response are needed, in order to readjust the therapeutic strategy in case of non-response. Apoptosis is a mechanism of cellular death induced by the NAT. Therefore, our team has evaluated in vitro and in vivo the capacity of an apoptosis radiotracer, the ^{18}F-ML-10 (2-(5-[^{18}F]fluoropentyl)-2-methylmalonic acid) to detect cell apoptosis in TNBC cells exposed to various cytotoxic agents. **Materials and Methods:** For in vitro studies, apoptosis was induced in two human TNBC cell lines (MDA-MB-468 and MDA-MB-231) by incubating cells with paclitaxel. Proportion of apoptotic cells were measured by flow cytometry (Annexin V / Propidium Iodide), western blotting (PARP activation) and TUNEL assay. ^{18}F-ML-10 cellular uptake was measured on the same cell lines, only treated with paclitaxel at different time. In vivo, TNBC xenograft or orthotopic mice models were randomized into three groups: respectively, with i.v. injections of one dose of paclitaxel (20 mg/kg, days 0), two doses of paclitaxel (20 mg/kg, days 0 and 3) and phosphate-buffered saline. PET imaging of apoptosis was performed before (day 0) and 72h after each treatment (days 3 and 6). ^{18}F-ML-10 uptake was quantified as change of tumor/muscle ratios (T/M) and %ID/g, and was compared with the amount of apoptotic cells determined by TUNEL immunohistochemistry assay and western blotting (cleaved PARP). **Results:** In vitro, treatment with paclitaxel induced a significant increase ($p<0.01$) of the apoptotic hallmarks of DNA fragmentation, membrane phospholipid scrambling and PARP activation in TNBC cells. ^{18}F-ML-10 uptakes were observed in these conditions compared to untreated cells for MDA-MB-468 (4.4) and MDA-MB-231 (2.1). For in vivo experiments, a higher accumulation of ^{18}F-ML-10 was observed, before treatment, in xenograft models ($T/M = 9.5 \pm 2.7$) compared to orthotopic tumors ($T/M = 2.0 \pm 0.4$). However, even if treated tumors exhibited significant apoptosis as evidenced by increased cleaved caspase-3 and apoptotic fraction, no significant increase in the ^{18}F-ML-10 tumor accumulation at days 3 and 6 post-treatment was observed. **Conclusion:** These first results highlighted that PET imaging using ^{18}F-ML-10 allows the visualization of apoptotic cells in TNBC models. However, it was not possible to detect an increased chemotherapy induced apoptotic response in our mice model. **References:** None.

EP-0627

Tailoring the sensitivity of PET tracers to detect P-glycoprotein-mediated drug-drug interactions at the blood-brain barrier: a comparative in vitro study

L. Breuil[1], S. Marie[1], M. Goislard[1], O. Langer[2], A. Del Vecchio[3], D. Audisio[4], F. Caille[1], N. Tournier[1];
[1]UMR 1023 IMIV, Service Hospitalier Frédéric Joliot, CEA, Inserm, CNRS, Université Paris Sud, Université Paris-Saclay, Orsay, FRANCE, [2]Department of Clinical Pharmacology, Medical University of Vienna, Vienna, AUSTRIA, [3]3 Service de Chimie Bio-organique et de Marquage, CEA-DRF-JOLIOT-SCBM, Université Paris-Saclay, Gif sur Yvette, FRANCE, [4]Service de Chimie Bio-organique et de Marquage, CEA-DRF-JOLIOT-SCBM, Université Paris-Saclay, Gif sur Yvette, FRANCE.

Aim/Introduction: PET imaging using radiolabeled substrates of P-glycoprotein (P-gp, ABCB1) have highlighted the importance of this efflux transporter in restricting the brain distribution of drugs across the human blood-brain barrier (BBB). So far, P-gp substrates with high transport capacity (avid substrates) have been employed to generate maximal contrast between baseline conditions and conditions with impaired P-gp function. However, the sensitivity of different radiolabeled P-gp substrates to detect small changes in P-gp function and/or predict the risk for inhibitor/substrate drug-drug interactions at the BBB remains to be compared. **Materials and Methods:** Standardized in vitro uptake assays were performed in MDCKII-MDR1 cells overexpressing human P-gp to compare the transport properties of the radiolabeled substrates ^{11}C-verapamil, ^{11}C-N-desmethyl-loperamide, ^{11}C-metoclopramide and the newly developed ^{11}C-domperidone. Cell-monolayers were incubated with buffer containing the tested compound (~1 MBq/mL) and the P-gp substrate calcein-AM (1 µM, fluorescent internal control for P-gp function). Six concentrations of the clinically validated inhibitors cyclosporine A (CsA, 0-25 µM) and tariquidar (TQD, 0-200 nM) were tested (n=4 per condition). After 30 min incubation, monolayers were washed and cell-lysate was counted for radioactivity and fluorescence. The transport ratio (TR) was estimated as the ratio of the maximal uptake (full inhibition) to the baseline uptake (no inhibition). Sensitivity to inhibition was described by the IC_{50} of CsA and TQD for each substrate, estimated from the sigmoidal Hill equation. Outcome values were divided by those of calcein-AM to provide relative (/R) values (IC_{50}/R and TR/R) in order to correct for inter-day variability and allow for comparison. **Results:** ^{11}C-metoclopramide (TR/R=0.22 and 0.23 for CsA and TQD, respectively) showed a lower transport capacity than ^{11}C-verapamil (TR/R=0.76 and 0.64), ^{11}C-N-desmethyl-loperamide (TR/R=0.54 and 0.39) and ^{11}C-domperidone (TR/R=1.22 and 0.86). Using CsA, the IC_{50} ranged from 2.4±0.5 µM (^{11}C-metoclopramide) to 6.4±0.6 µM (^{11}C-domperidone). IC_{50}/R was lower for ^{11}C-metoclopramide (IC_{50}/R=0.86)<^{11}C-N-desmethyl-loperamide (IC_{50}/R=0.96)<^{11}C-verapamil (IC_{50}/R=1.15)<^{11}C-domperidone (IC_{50}/R=1.89). Using TQD, IC_{50} ranged from 5.2±2.6 nM (^{11}C-metoclopramide) to 82±20 nM (^{11}C-domperidone). IC_{50}/R was lower for ^{11}C-metoclopramide (IC_{50}/R=0.23)<^{11}C-domperidone (IC_{50}/

R=0.82)<^{11}C-N-desmethyl-loperamide (IC_{50}/R=1.0)<^{11}C-verapamil (IC_{50}/R=1.15). **Conclusion:** Compared with the weak P-gp substrate ^{11}C-metoclopramide, avid P-gp substrates may lack sensitivity to detect small changes in P-gp function and fail to detect partial P-gp inhibition. Interestingly, the sensitivity to inhibition depends on the selected inhibitor. Standardized and normalized in vitro assays are therefore essential to select the radiolabeled substrate with the best ability to detect drug-drug interactions with P-gp inhibitors at the BBB in vivo. **References:** None.

EP-0628

[^{99m}Tc]Tc-HMPAO µSPECT/CT highlights cerebral blood flow enhancement and correlates with cognitive function improvements of chronic resveratrol exposure in aged rats

P. Garrigue[1], *A. Moyon*[1], *L. Balasse*[2], *Y. Mouhajir*[3], *J. Landrier*[3], *F. Dignat-George*[4], *M. Alessi*[4], *E. Seree*[3], *B. Guillet*[1];
[1]*C2VN INSERM1263 INRA1260 CERIMED Aix-Marseille Univ AP-HM, Marseille, FRANCE,* [2]*C2VN INSERM1263 INRA1260 CERIMED Aix-Marseille Univ, Marseille, FRANCE,* [3]*C2VN INSERM1263 INRA1260 Aix-Marseille Univ, Marseille, FRANCE,* [4]*C2VN INSERM1263 INRA1260 Aix-Marseille Univ AP-HM, Marseille, FRANCE.*

Aim/Introduction: Resveratrol is a natural stilbene found in grape skin and seeds, known for its antioxidant activity in the vascular and nervous systems. The present study investigated the influence of resveratrol on senescence in vivo, focusing on cerebral blood flow (CBF) µSPECT/CT imaging and cognitive function evolution. **Materials and Methods:** 3 months Sprague-Dawley rats (n=5 per condition) were fed with water supplemented with resveratrol 50 mg/L (Resv group) or with plain water (Control group), adlibitum for 5 months. At the age of 8 months, rats underwent a novel object recognition test (NOR) coupled with a [^{99m}Tc]Tc-HMPAO µSPECT/CT, respectively to evaluate the cognitive function itself, and to assess CBF during a cognitive stimulation. Right before the fourth NOR session, 20.9±2.8MBq of [^{99m}Tc]Tc-HMPAO were IV injected to the rat. Then the rat was returned to the arena and was allowed to explore both novel and familiar objects for 3min. 30min after [^{99m}Tc]Tc-HMPAO injection, the rat was anesthetized with 1.5% sevoflurane and a cerebral microSPECT/CT imaging was acquired for 20min on a calibrated NanoSPECT/CT+ camera (Mediso) to assess CBF. Image analysis was performed using InVivoScope® software (InviCRO). A volume of interest (VOI) was drawn over the whole brain for each animal, quantified and corrected by the tissue volume (MBq/µm3). All data were successfully tested for normality using a Shapiro-Wilk test and then analyzed with two-tailed, unpaired t-test. Experiments were performed according to an Ethics Committee agreement by trained and qualified operators. **Results:** Chronic resveratrol treated-group significantly increased the time spent on exploring the novel object compared to the control group (Resv: 89.8±12.2%; Control: 38.9±38.2%; *P=0.0416). The mean latency to first exploration of the novel object (LTF) was also significantly reduced in resveratrol-treated rats compared to the control group (Resv: 34.2±8.4s; Control: 93.8±29.1s; *P=0,0477), meanwhile no significant change was found on the usual object. A significantly higher cerebral [^{99m}Tc]Tc-HMPAO µSPECT signal was found in the resveratrol-treated rats (0.66±0.11%ID/µm3) compared to the control rats (0.36±0.09%ID/µm3, **P=0.0014). [^{99m}Tc]Tc-HMPAO µSPECT signal significantly correlated with the mean LTF (Pearson R^2=0.6547; **P=0.0046). **Conclusion:** Chronic exposure to resveratrol enhanced NOR performances of aged rats while enhancing their cerebral blood flow during NOR task. Micro-arrays performed on brain sections of the same animals showed a pronounced activation of anti-inflammatory and anti-oxydative genes in the resveratrol-treated group. [^{99m}Tc]Tc-HMPAO is a reliable and sensitive tool to assess the impact of drug candidates on the cerebral metabolism. **References:** None.

EP-0629

Biodistribution of PSMA-R2 in mice bearing prostate cancer

V. Muzio[1], *L. Ravasi*[1], *L. Sacchetti*[1], *L. Fugazza*[1], *S. Bacot*[2], *M. Debiossat*[2], *M. Ahmadi*[2], *C. Montemagno*[2], *C. Ghezzi*[2], *A. Broisat*[2];
[1]*Advanced Accelerator Applications, a Novartis company, Geneva, SWITZERLAND,* [2]*Univ. Grenoble Alpes, Inserm, CHU Grenoble Alpes, Grenoble, FRANCE.*

Aim/Introduction: Biodistribution assessment of Lutetium-177 PSMA-R2 in mice with prostate cancer grafts originating from tumor cells expressing or not the prostate specific membrane antigen (PSMA). **Materials and Methods:** PSMA positive-PC3-PIP tumor cells and PSMA negative-PC3-Flu tumor cells were respectively inoculated in right and left flank of five-week-old male athymic nude mice. Ex-vivo biodistribution consisted in assessing organ activity at 5, 15, 45min, 1, 4, 24, 48, 72h p.i. in the salivary glands, heart, lungs, spleen, stomach, small bowel, large bowel, liver, pancreas, adrenals, kidneys, bladder, urine, bone, skeletal muscle, thyroids, brain, PC3-PIP and PC3-Flu tumors. The corrected activity was expressed as a %ID/g or and as a %ID/organ (percentage of injected dose per gram of tissue or per organ). In-vivo biodistribution (%ID), was assessed on whole-body 30-min SPECT acquired at 15min p.i. after a 5-min CT. **Results:** The day of 177Lu- PSMA-R2 injection (7.2±0.2 MBq), PC3-Flu tumor mean volume was of 599±520 mm³, PC3-PIP was of 610±408 mm³ and mice weighted 26.7±2.6 g. At 5 min p.i., the activity was below 10% in all samples but kidneys (56.5±6.7), urine (90±18.9) and PC3-PIP tumors (10.4±3.3). At 1h, activity was 15.6±9.8 (kidneys), 485±218 (urine), 42.9±67.6 (bladder) and 27.6±12.3 (PC3-PIP). All other investigated organs were below 1%. At 4h, activity was 20.5±22.8 (urine) and 16.7±4.4 (PC3-PIP). At 24h, activity in PC3-PIP tumor was 13.7±4.4. At 48h and 72h p.i., activity was < 10% in all organs and< 1% in all organs except in the urine at 72h (1.06±0.8) and the PC3-PIP tumor with 8.2±3.3 at 24h and 5.9±1.4 at 72h. Thanks to this fast elimination through the kidneys, 177Lu-PSMA-R2 rapidly cleared from the blood. It was of 6.5±0.3%ID/g at 5 min, i.e. 11.1±0.9 %ID in total blood volume (TBV). At 4h, the blood activity (%ID/TBV) was

0.030±0.024 and 0.003 ± 0.001 %ID/TBV at 72h. Combination of fast clearance and high retention in PSMA-positive tissues yielded activity ratios of PC3-PIP to PC3-Flu, blood, liver or salivary gland > 1 at all time points. SPECT/CT quantification confirmed that 74.1±8.0 %ID was located in kidneys (9.6±5.4) or in urine (64.5±12.0). PC3-PIP tumor, SPECT quantifications (10.0%ID or 14.2%ID/g) accurately reflected that determined by gamma well counting at the same time point (10.0%ID or 12.4%ID/g). **Conclusion:** High uptake of 177Lu-PSMA-R2 was found in PC3-PIP in both in-vivo and ex-vivo studies, with a fast renal clearance and minimal uptake in the other investigated organs and fluids. **References:** None.

EP-0630

Optimization and comparison of cell labeling strategy with [^{89}Zr]Zr-complex for cell trafficking

M. Kim[1], *D. Kim*[1], *S. Lee*[1], *S. Kim*[2], *H. Soh*[2], *J. Ryu*[1], *S. Oh*[1];
[1]*Asan Medical Center, Seoul, KOREA, REPUBLIC OF,* [2]*Asan Institute for Life Sciences, Seoul, KOREA, REPUBLIC OF.*

Aim/Introduction: Assessment of cell behavior in vivo, such as distribution, retention to major organs, is important information for cell therapy. Radioisotope labeled cells and positron emission tomography (PET) are powerful tools to obtain quantitative information of cell trafficking. [^{89}Zr]Zr-DFO and [^{89}Zr]Zr-oxine are promising methods for cell labeling. We aim to optimize preparing condition of [^{89}Zr]Zr-complex and evaluate two labeling strategies with chimeric antigen receptor T (CAR-T) cell. **Materials and Methods:** [^{89}Zr]$ZrCl_4$ was prepared from [^{89}Zr]Zr-oxalate (Perkin Elmer) in the 1.0 M oxalic acid by trapping with QMA cartridge (Merck, Germany) and eluting with 1.0 N HCl. 0.7-7.0 nmol of DFO (DFO-Bz-NCS) and 0.02-2.0 μmol of oxine were used for preparation of [^{89}Zr]Zr-DFO and [^{89}Zr]Zr-oxine, respectively. CD19 CAR-Jurkat T cell was labeled with 0.08-0.24 kBq of each [^{89}Zr]Zr-complex. Labeling efficiency, cell viability, and production of cytokine IL-2 were assessed within 12 hr after cell labeling with [^{89}Zr]Zr-complex. Finally, we evaluated cell viability and cell proliferation rate of CAR-Jurkat T cell labeled with [^{89}Zr]Zr-DFO or [^{89}Zr]Zr-oxine up to 7 days. **Results:** Both 2.8 nmol of DFO and 2.0 μmol of oxine were shown 100% of chelation efficiency with 58.5±17.4 MBq of [^{89}Zr]$ZrCl_4$. CAR-Jurkat cell labeling efficiency with 0.08, 0.14, 0.19, 0.24 kBq of [^{89}Zr]Zr-DFO was 76.9±11.6%, 81.6±11.3%, 82.2±13.1% and 84.4±10.9%, respectively. And [^{89}Zr]Zr-Oxine showed labeling efficiency of 43.7±2.4%, 34.5±5.2%, 37.5±3.1% and 24.8±6.8% at the same dose points. Average cell viability after labeling with different dose of [^{89}Zr]Zr-DFO and [^{89}Zr]Zr-oxine was 93.5% and 91.6%, respectively. The [^{89}Zr]Zr-complex-labeled CAR-Jurkat cells similarly induced IL-2 release in positive target cell (Raji) at 70.7 ng/mL, compared to the unlabeled CAR-Jurkat cells (77.3 ng/mL). Up to day 7, the long term cell viability in the presence of 0.14 kBq [^{89}Zr]Zr-DFO and [^{89}Zr]Zr-oxine was around 88% and 20%, respectively. At the 0.08 kBq, the [^{89}Zr]Zr-DFO labeled cells were found to be more than 90% cell proliferative by day 3 and even more than 80% by day 7. [^{89}Zr]Zr-Oxine labeled cells showed only 56% capacity on day 1 and after day 3, the cell proliferation ability rapidly decreased in all doses. **Conclusion:** In this research, the preparation method of [^{89}Zr]Zr-DFO and [^{89}Zr]Zr-oxine with high chelation efficiency was optimized. Compared to CAR-Jurkat T cells labeled with [^{89}Zr]Zr-DFO and [^{89}Zr]Zr-oxine, [^{89}Zr]Zr-DFO labeled cells exhibited excellent cell viability and proliferation ability. **References:** None.

EP-0631

Feasibility of real-time in vivo ^{89}Zr-DFO-labeled CAR T-cell trafficking using PET imaging

S. Kim[1,2], *S. Lee*[1,3], *H. Soh*[1], *J. Chung*[1], *E. Cho*[1], *S. Lee*[1,2], *J. Ju*[4], *J. Shin*[4], *H. Kim*[1,2], *S. Oh*[1,2], *S. Lee*[4], *J. Chung*[5], *J. Ryu*[1,2];
[1]*Asan Medical Center, Seoul, KOREA, REPUBLIC OF,* [2]*University of Ulsan College of Medicine, Seoul, KOREA, REPUBLIC OF,* [3]*Hallym University Kangnam Sacred Heart Hospital, Seoul, KOREA, REPUBLIC OF,* [4]*National Cancer Center, Gyeonggi-do, KOREA, REPUBLIC OF,* [5]*Seoul National University, Seoul, KOREA, REPUBLIC OF.*

Aim/Introduction: Chimeric antigen receptor(CAR) T cell has been developed in recent years, producing impressive clinical reports in patients with hematologic malignancies. However, there is no standardized method available for cell trafficking and monitoring in vivo behavior of injected CAR T-cells. We assessed the feasibility of real-time in vivo ^{89}Zr-p-Isothiocyanatobenzyl-desferrioxamine B(Df-Bz-NCS, DFO) labeled CAR T-cell trafficking using PET. **Materials and Methods:** We constructed and produced CD19-targeting Jukat/CAR T-cells and T-cells obtained from human peripheral blood mononuclear cells(hPBMC). After synthesizing ^{89}Zr-DFO, cells were radiolabeled with 74~185 kBq in 5 × 10^6 cells/HBSS buffer at 37°C for 30 minutes. Then, we assessed the cell labeling efficiency, cell viability and function. For PET imaging of ^{89}Zr-DFO labeled CAR-T cells, we developed mouse xenograft models bearing both Raji(CD19 positive) and K562(CD19 negative) tumors in their bilateral franks. Serial images were acquired with PET/ magnetic resonance(MR) scanner from 1 hour to 7 days after injection of ^{89}Zr-DFO labeled cells. The biodistribution of CAR T-cells was also cross-confirmed by ex vivo tissue analysis with γ-counter, flow cytometry(FACS), Alu-PCR and immunohistochemistry(IHC), respectively. **Results:** The ^{89}Zr-DFO radiolabeling efficiency of Jurkat/CAR and hPBMC CAR T-cells was 70 ~ 79%, and radiolabeled activity was 98.1 ~ 103.6 kBq/10^6 cells. Cell viability after radiolabeling was > 95 %. There is no significant difference in function for IL-2 or IFN-γ secretion between unlabeled and labeled CAR T-cells. PET/MR images in xenograft models showed that most of the ^{89}Zr-labeled Jurkat/CAR T-cells were distributed in the lung(24.4 ± 3.4 %ID) and liver(22.9 ± 5.6 %ID) by 1 hour after injection. The cells gradually migrated to the spleen by day 1, where they remained stable until day 7(on day 7: lung 3.9 ± 0.3 %ID, liver 36.4 ± 2.7 %ID, spleen 1.4 ± 0.3 %ID). No significant accumulation of labeled cells was identified in tumors. A similar pattern was observed in ex vivo biodistributions on day 7(lung 3.0 ± 1.0%ID, liver 19.8 ± 2.2%ID, spleen 2.3 ± 1.7%ID). Similarly, the tracing of

^{89}Zr-labeled hPBMC CAR T-cells showed the same pattern. The distribution of CAR T-cells was also confirmed by FACS, Alu-PCR and IHC. **Conclusion:** We confirmed the feasibility of CAR T-cells trafficking in vivo using serial PET imaging after administration of ^{89}Zr-DFO labeling. Our results suggest that PET imaging of CAR T-cells, labeled with ^{89}Zr-DFO, can be used to investigate cellular kinetics, initial in vivo distribution, and safety profile of future CAR T-cell development. **References:** None.

EP-0632

In vivo Comparison Zr^{89} cell labelling techniques, internal Zr^{89}-Oxine labelling VS Zr^{89}-DFO-Bn-NCS cell surface labelling

S. J. Paisey, H. Almutairi, A. Dabkowski, C. Marshall, A. Ager; Cardiff University, Cardiff, UNITED KINGDOM.

Aim/Introduction: Two alternative strategies have been reported in the literature for the Zr^{89} labelling of cells. The most widely reported method involves the use of Zr^{89}-Oxine complexes to transport Zr^{89} across the cell membrane to internally label cells.[1] However, an alternative strategy has been published where a preformed Zr^{89}-Dfo-Bn-NCS complex is coupled to cell surface proteins.[2] Whilst both labelling methods have been used to good effect in specific cell types each method has the potential to adversely affect cells in different ways. Here we compare cell labelling and more importantly in vivo images of cells labelled via the 2 different methods in freshly extracted murine donor cells injected into wild type mice. **Materials and Methods:** Zr^{89} was produced and purified in house via adaptations of the methods of Walther et al[3],[4]. Murine cells extracted from the spleens of matched donor mice were split into 2 populations and simultaneously labelled with either Zr^{89}-Oxine via the methods of Ferris et. Al.[1] or Zr^{89}-Dfo-Bn-NCS via the methods of Bansal et. Al.[2]. Labelled the cells and immediately injected into wild type C57B/6 mice via tail vein (~5 x10^{6} cells, 0.8-2MBq). Mice were scanned for 1 hour under anaesthesia (isoflurane in O2, 1-2%) in a Mediso nanoscan PET/CT scanner up to 6 times post injection over a 15 day period. **Results:** Viable cell populations were obtained from both methods and showed similar biodistributions in vivo, however in our hands images of Zr^{89}-Dfo-Bn-NCS surface labelled cells contained anomalous concentrated hotspots of radioactive uptake randomly distributed throughout the body. **Conclusion:** More work is required to determine the exact cause of the anomalous hotspots of radioactivity derived from the Zr^{89}-Dfo-Bn-NCS surface labelled cells, however in the meantime caution should be exercised when imaging surface labelled cells particularly if the aim of the study is to show homing to metastases. **References:** 1) Ferris TJ, et al. Synthesis and characterisation of zirconium complexes for cell tracking with Zr-89 by positron emission tomography. Dalton Trans 2014;**43**:14851-7. doi:10.1039/C4DT01928H 2) Bansal A, et al. Novel 89Zr cell labeling approach for PET-based cell trafficking studies. EJNMMI Res 2015;**5**. doi:10.1186/s13550-015-0098-y 3) Walther M, et al. Implementation of 89Zr production and in vivo imaging of B-cells in mice with 89Zr-labeled anti-B-cell antibodies by small animal PET/CT. Appl Radiat Isot 2011;**69**:852-7. doi:10.1016/j.apradiso.2011.02.040 4) Dabkowski AM, et al. Optimization of Cyclotron Production for Radiometal of Zirconium 89. Acta Phys Pol A 2015;**127**:1479-82.

EP-0633

Cancer diagnostic imaging using the novel T cell that specifically attracted a cancer cell

Y. Nakagami[1], *D. Kano*[2], *S. Hosokawa*[3], *Y. Kaji*[1]; [1]*Dokkyo Medical University, Tochigi, JAPAN,* [2]*National Cancer Center Hospital East, Kashiwa, JAPAN,* [3]*Hirosaki University, Hirosaki, JAPAN.*

Aim/Introduction: Our collaborator previously established a novel cell line, termed HOZOT, derived from umbilical cord blood mononuclear cells. HOZOT cells actively penetrate into a variety of human cancer cell lines, but not into normal cell lines, and form apparent cell-in-cell structures. We established In-111-labeled and Tc-99m hexamethylpropylene amine oxime (HMPAO)-labeled HOZOT cells for the investigation of cancer. This study describes radiolabeling of HOZOT cells for the evaluation of cell trafficking in a model of human breast cancer in mice. **Materials and Methods:** Different labeling buffers and incubation times were evaluated to optimize In-111-oxine labeling conditions. Therefore, incubation with 0.011 MBq of In-111-oxine per million HOZOT cells in PBS (pH 7.4) for 20 min is the best condition that provides optimum labeling efficiency without affecting cell viability and functionality. On the other hand, The Tc-99m of 500MBq was added to 1 mg of HMPAO solution. The million HOZOT cells were incubated with 500 MBq of Tc-99m HMPAO at 37 degrees C for 5 minutes. The radiolabeled HOZOT cells were administered to mice with MDA-MB-468 human breast cancer cells from their tail veins, and the mice were sacrificed after 6 hours from the injection. The biodistribution of the radioactivity in each organ and cancer cells was counted. **Results:** The labeling efficiency of In-111-oxine labeled HOZOT cells was 99%. The labeling efficiency of Tc-99m-HMPAO labeled HOZOT cells was 60%. The biological activity of the In-111-oxine labeled HOZOT cells and Tc-99m-HMPAO labeled HOZOT cells was maintained because the radiolabeled HOZOT cells were not stained with trypan blue. The radioactivity according to each organ was high in order of kidneys, liver, spleen, gallbladder, lungs, and cancer cells. There was a little radioactivity of other organs. **Conclusion:** We developed the novel cell labeling method for HOZOT cells. The main discharge route of In-111 and Tc-99m from a body is guessed as kidney urinary tract system and biliary tract system. The radioactivity of the cancer cells was caught enough. If the radioactivity is suitable for imaging, this radiolabeling method will become a novel cancer imaging method. **References:** Takeuchi M, et al. Cell-in-cell Structures Formed between Human Cancer Cell Lines and the Cytotoxic Regulatory T-cell Line HOZOT. Journal of Molecular Cell Biology (2010), 2, 139-151.

EP-0634

Toxicity, efficacy and tumour imaging of ^{195m}Pt-cisplatin in mice

E. A. Aalbersberg[1], *L. de Wit - van der Veen*[1], *K. Codée – van der Schilden*[2], *O. Zwaagstra*[2], *E. Vegt*[1], *W. Vogel*[1];
[1]*Netherlands Cancer Institute, Amsterdam, NETHERLANDS,*
[2]*Nuclear Research and consultancy Group, Petten, NETHERLANDS.*

Aim/Introduction: Cisplatin is used in first-line treatment of many cancer types, but not all patients show response while toxicity can be severe. Radiolabeled cisplatin could theoretically enhance the therapeutic effect, or it could be imaged to aid treatment choices by selecting patients with adequate tumour uptake of cisplatin. The aim of this study was to determine the toxicity and efficacy of ^{195m}Pt-cisplatin compared to normal cisplatin, and to investigate ^{195m}Pt-cisplatin tumour imaging in mice. **Materials and Methods:** ^{195m}Pt-cisplatin (CISSPECT®) was obtained from NRG. Toxicity was evaluated in 69 mice, which received 6 mg/kg cisplatin containing 0%, 25%, 50%, or 100% (~10MBq) of ^{195}Pt-cisplatin. Toxicity was quantified by loss of body weight measured 2-3x/week, renal function measured with ^{99m}Tc-MAG3 after 1 day, 1 week and 1 month, and histopathology after 1 day, 1 week and 1 month. Treatment efficacy of ^{195m}Pt-cisplatin was compared to standard cisplatin in 20 mice with a mammary gland tumour, and was measured as PFS and OS. SPECT/CT imaging of ^{195m}Pt-cisplatin was performed in 5 mice with a mammary gland tumour at 1 and 24 hours post-injection of 5-12 MBq ^{195m}Pt-cisplatin. **Results:** Specific activity at the end of irradiation was 91 MBq/g Pt. Radionuclide purity of ^{195m}Pt-cisplatin was 96.1% at start of experiments; ^{197}Pt-cisplatin was the main impurity (3.9% of the total radioactivity). ^{195m}Pt-cisplatin did not lead to weight loss >10% for any of the applied doses. Some animals in every ^{195m}Pt-cisplatin dose group had a delayed excretion of ^{99m}Tc-MAG3 one month after administration. Histopathology of the kidneys demonstrated a small number of mild lesions after one month, but this was comparable to animals receiving normal cisplatin only. No differences in PFS and OS were found between mice receiving ^{195m}Pt-cisplatin or normal cisplatin. Tumour uptake on SPECT/CT was mild to moderate, with diffuse background uptake in normal tissues due to the binding of cisplatin to plasma proteins. **Conclusion:** In the applied mouse model, ^{195m}Pt-cisplatin did not prove more toxic or effective than normal cisplatin for the treatment of cancer. SPECT imaging of ^{195m}Pt-cisplatin uptake in tumour is feasible with adequate image quality in mice. **References:** None.

EP-0635

99m-Tc dimercaptosuccinic acid renal scintigraphy is correlated to fibrosis in a model of Chronic Kidney Disease in rats

M. Bobot[1], *G. Hache*[1], *S. Fernandez*[2], *L. Balasse*[2], *A. Moyon*[1], *P. Garrigue*[1], *S. Burtey*[1], *B. Guillet*[1];
[1]*Aix Marseille Université - CERIMED - Assistance Publique Hôpitaux de Marseille, Marseille, FRANCE,* [2]*CERIMED, Marseille, FRANCE.*

Aim/Introduction: Chronic kidney disease (CKD) increases cardiovascular events risk and mortality. Fibrosis is the hallmark of CKD and the severity of CKD usually correlates with the magnitude of kidney cortical fibrosis. Evaluation of interstitial fibrosis is crucial in preclinical research focusing on CKD, however post mortem histological staining is currently the gold standard for assessing fibrosis in rodents' kidneys. Therefore, approaches that allow longitudinal assessment of kidney structure are required to refine studies involving rodents. Thus, we investigated dedicated small-animal SPECT/CT renal imaging to monitor renal damage in vivoduring the induction a chronic kidney disease in rats. **Materials and Methods:** We induced CKD in Sprague-Dawley rats, by feeding them a diet containing 0.25% or 0.5% adenine (ARD) during 4 weeks. Kidney function was assessed by serum creatinine and urea. [^{99m}Tc]--dimercaptosuccinic acid ([^{99m}Tc]-DMSA) scintigraphy was performed once a week. At the end of the protocol (Day 35), histology was performed in kidneys with hematoxylin and eosine to establish a score of tubular lesions and Sirius red to quantify deposition of collagen 1 and 3. **Results:** Compared to control rats, we showed an increase in serum creatinine, serum urea from Day 14to Day 35 in 0.5% ARD rats but not with 0.25%ARD. ARD significantly decreased ([^{99m}Tc]-DMSA uptake in kidneys from Day 14to Day 35, in both 0.25% and 0.5% ARD rats ($p<0.01$ and $p<0.001$, respectively). Compared to control group,we showed an increase in the score of tubular lesions (ctrl: 0.5±0.4; 0.25%ARD: 1.9±0.4, $p<0.001$; 0.5%ARD: 2.9±0.4, $p<0.001$), and an increase in interstitial collagen I and III accumulation in renal cortex(ctrl: 1.8±0.8%; 0.25%ARD: 7.7±1.9%, $p<0.001$; 0.5%ARD: 29.5±4.3%, $p<0.001$). Interestingly, [^{99m}Tc]-DMSA uptake at Day 28 is negatively correlated to Sirius red stainingat Day 35 ($r=0,89$, $p<0,0001$, $R^2 = 0,67$) **Conclusion:** [^{99m}Tc]-DMSA scintigraphy was representative of cortical fibrosis in ARD rats. This imaging strategy enabled, beyond scare formation, longitudinal monitoring of kidney fibrosis and could be used as a non invasive prognosis outcome to estimate kidney fibrosis. **References:** None.

EP-0636

Towards Imaging Cisplatin Resistance with ^{64}Cu PET

F. Al-salemee, *J. Bartnicka, T. H. Witney, P. J. Blower;*
King's College London, London, UNITED KINGDOM.

Aim/Introduction: Cisplatin has been for decades the backbone of several chemotherapeutic regimens used in the treatment of various cancer types, including ovarian, testicular, lung and bladder cancer. However, the efficacy of this drug is often practically abolished by the development of resistance early in the course of chemotherapy, especially in ovarian cancer. Consequently, many patients receive several cycles of cisplatin, and suffer its debilitating side effects, in vain. A correlation between cellular accumulation of cisplatin and copper transporters (CTR1, ATP7A, ATP7B) has been reported in the literature on numerous occasions. In this work, we are investigating the possibility of utilising copper accumulation

in tumours, detected by positron emission tomography (PET) imaging with unchelated ^{64}Cu(II), as an indicator of cisplatin accumulation and hence sensitivity/resistance. **Materials and Methods:** Two variants of the human ovarian carcinoma cell line A2780, wild type (WT) and cisplatin-resistant (CisR), were incubated at 37°C with [^{64}Cu]$CuCl_2$ in 24-well plates (10KBq/well) for 10, 30, 60 and 120 minutes (accumulation); or 120 minutes followed by supernatant removal and replacement with fresh medium and re-incubation for 10, 30, 60 and 120 minutes (retention). The cells and the supernatants were then counted for radioactivity and the cell-associated fraction of radioactivity was calculated and, in case of accumulation, related to cell number. Cisplatin resistance was compared between the two cell lines using a Sulforhodamine B assay allowing the determination of the half-maximal inhibitory concentration (IC50). **Results:** The cell-associated radioactivity for WT cells was 0.54(±0.03), 1.2(±0.2), 3.7(±0.3) and 5.6(±0.4)Bq/10^{3}cell after 10, 30, 60 and 120 minutes, respectively; while it was 0.31(±0.05), 0.57(±0.05), 0.99(±0.03) and 1.24(±0.06) Bq/10^{3}cell for CisR cells (n=4). Retention values at 10, 30, 60 and 120 minutes were 58.6(±2.5), 53.3(±1), 39.7(±2.4) and 28(±1.5) % for WT cells, respectively; and 51.8(±2.4), 47.8(±0.6), 35.6(±1.9) and 21.3(±5.2) % for CisR cells (n=4). The IC50 for WT cells was 2.2(±0.55) µM, compared to 10.3(±1.44) µM for CisR cells (n=3). **Conclusion:** In this cell line there is a clear negative relationship between copper accumulation and acquired cisplatin resistance in vitro. The modest dissimilarity in copper retention between the two cell lines suggests that the difference in accumulation is mainly due to a difference in uptake rather than efflux. The results justify experiments to confirm this finding in vivo in mice bearing these cell lines with a view to assessing the prospects for clinical evaluation of this novel application of PET for imaging cisplatin drug resistance. **References:** None.

EP-0637

In vivo monitoring of human lymphoma using ^{64}Cu-DOTA-rituximab PET in mouse xenograft model for alpha-particle radioimmunotherapy

C. Lee, K. Kim, S. Woo, C. Kang, C. Kang, K. Lee, Y. Lee, K. Song, S. Lim, I. Lim;
KIRAMS, Seoul, KOREA, REPUBLIC OF.

Aim/Introduction: PET radiopharmaceuticals using rituximab are required because it can be used for selecting proper patients for rituximab treatment through imaging and for monitoring advanced radioimmunotherapy such as alpha particle. The aim of this study is to evaluate the targeted imaging of ^{64}Cu-DOTA-rituximab PET in human lymphoma model. **Materials and Methods:** CD20 expression was evaluated in lymphoma cell lines (Jurkat and Raji cells). DOTA-rituximab was conjugated in optimized conditions. ^{64}Cu was chelated to DOTA-rituximab. The number of chelators on rituximab conjugates was verified using MALDI-TOF MS for comparison of rituximab and DOTA-rituximab. Immunoreactivity was performed and analyzed using GraphPad Prism software. Tumor xenograft models were established in balb/c-nu mice using CD20 positive cells. Animal PET/CT imaging was obtained by INVEON scanner (Siemens) after tail vein injection with or without pre-dose received 2 mg cold rituximab. Specific binding of tumor was evaluated by organ biodistribution assay and autoradiography. CD20 expression in tumor tissue was evaluated by immunohistochemistry. **Results:** CD20 protein was highly expressed in Raji cells. Radiochemical purity of ^{64}Cu-DOTA-rituximab was more than 95%. Binding to Jurkat cells was not specific, whereas Raji cells was blocked with an excess of cold rituximab, which evaluating the specificity of binding. Immunoreactivity was more 75%. In PET/CT imaging, binding of ^{64}Cu-DOTA-rituximab was shown in tumors without pre-dose injection group. On the other hand, there was no signal in tumors with pre-dose injection group. Radioactivity of tumor was much higher than other organs. Tumor specific uptake of ^{64}Cu-DOTA-rituximab was related to CD20 expression. **Conclusion:** We demonstrated that human lymphoma was specifically visualized by ^{64}Cu-DOTA-rituximab PET in xenograft model. This suggest that alpha particle immunotherapy using ^{225}Ac-DOTA-rituximab is applicable to human lymphoma. **References:** None.

EP-0638

Early prognostic value of 99mTc-3PRGD2 scintimammography in acute Radiation-induced lung injury

L. Shi, Q. Bai, W. Zhang, M. Yuan, L. Wei;
Tangdu Hospital, Xi'an, CHINA.

Aim/Introduction: Acute radiation pneumonitis (RP) and radiation pulmonary fibrosis (RPF) are the most common treatment-related toxicities induced by thoracic radiation therapy (RT), but not all the patients with RP deteriorate into RPF without intervention treatment (such as glucocorticoids treatment, may cause a series of side-effects). Evidences showed acute radiation-induced lung injury (RILI) was accompanied by high expression of Integrin αvβ3. In this study, ^{99m}Tc-3(poly-(ethylene glycol), PEG)4-RGD2 (^{99m}Tc-3PRGD2) was used as a radiolabeling probe which could combine with the over expressed Integrin αvβ3 in RILI rats' modals. Histopathological examinations, immunohistochemistry examinations and image analysis were used to evaluate if the ^{99m}Tc-3PRGD2 scintimammography have the early potential prognostic value on acute RILI. **Materials and Methods:** The stability and radiochemical purity of ^{99m}Tc-3PRGD2 radiation molecular probe was verified by TLC and UPLC methods. A total of 50 female rats (8 weeks) were randomly divided into the normal control group (NC, n=10), 15Gy pulmonary radiation-induced injury group (15GyPI, irradiation dose=15Gy, n=40). Each rat had its own markers. All rats' exposure pulmonary field was assessed and marked by CT. Static and dynamic ^{99m}Tc-3PRGD2-SPECT data were collected every 5 days since RT assessed. 90th day post-irradiation, the lung samples were collected for Histopathological and immunohistochemistry examinations. **Results:** Pathological results verified that 3/39(8%) rats in the

group 15GyPI showed Grade 0 RPF, 5/39(13%) rats showed grade I RPF, 14/39(36%) rats showed Grade II RPF and 17/39(43%) rats showed grade III RPF. Combination of pathological and immunohistochemical results, more accumulation and faster metabolic rate of ^{99m}Tc-3PRGD2(after 5~30 days RT assessed) indicated worse prognosis. Especially Grade III RPF showed significant more accumulate and faster ^{99m}Tc-3PRGD2 metabolic rate than Grade II RPF (P<0.01). **Conclusion:** Compared to CT images or clinical symptoms, significant different were found in ^{99m}Tc-3PRGD2-SPECT data 4-10 weeks earlier. ^{99m}Tc-3PRGD2 scintimammography have the potential early prognostic value on acute RILI and this will be guiding our further therapy. **References:** 1.Wu, J.G., et al., Biometabolic Distribution of 99mTc-3PRGD2 and Its Potential Value in Monitoring Chemotherapeutic Effects. Molecular Imaging, 2015.14 (12): p. 11.2Ma, Q., et al., Differential diagnosis of solitary pulmonary nodules using 99m Tc-3P4-RGD2 scintigraphy. European Journal of Nuclear Medicine & Molecular Imaging, 2011.38 (12): p. 2145-2152 3.Yu, X., et al., Integrin alpha v beta 3-targeted small-animal SPECT/CT of the progression and recovery of liver fibrosis in a rat model. Journal of Nuclear Medicine, 2015.suppl 9(3).

EP-0639

Synthesis of ^{64}Cu-DOTA-T-DM1 and preliminary evaluation as a potential companion diagnostic agent for T-DM1

H. Kim, *I. Lee, E. Shin, E. Lee, R. Yoo, H. Chung, J. Shim;*
Korea Institute of Radiological & Medical Sciences, Seoul, KOREA, REPUBLIC OF.

Aim/Introduction: Trastuzumab-DM1 (T-DM1) is an ADC composed of the humanized HER2 antibody trastuzumab covalently linked to the cytotoxic agent emtansine (DM1), a potent treatment of HER2-positive metastatic breast cancer (mBC). Radiolabeling an ADC with copper-64(^{64}Cu), combined with positron emission tomography (PET) imaging enables non-invasive and tracking of ADC biodistribution. This approach can directly evaluate in both preclinical models and patients whether an ADC retains its mAb selective tumor targeting capability. Our objective was to develop ^{64}Cu-labeled-antibody drug conjugates (ADC) as immuno-PET-based companion diagnostic agents for that of ADC. **Materials and Methods:** T-DM1 was conjugated with DOTA or NOTA bifunctional chelator at 25ºC for 2 h. The DOTA-ADC and NOTA-ADC were purified with acetate radiolabeling buffer (pH 5.5) via size exclusion chromatography using PD-10 column. The ratio of chelator per ADC was confirmed by MALDI-TOF. The chelator conjugated ADCs were radiolabeled with $^{64}CuCl_2$ and formulated for intravenous administration. **Results:** The number of DOTA and NOTA conjugated on T-DM1 were 3.5 and 3.7, respectively. The labeling efficiencies were no less than 95%. Specific activities ranged from 3 to 20 mCi/mg. The ^{64}Cu-DOTA-T-DM1 and ^{64}Cu-NOTA-T-DM1 were more than 95% stable after 48 hours in human serum. The ^{64}Cu-labeled ADCs showed similar distribution when compared to their parental mAbs, and retained the same selective tumor accumulation as their mAbs. **Conclusion:** These radiolabeled ADCs were synthesized and examined as potential companion diagnostic agents. ^{64}Cu-DOTA-T-DM1 and ^{64}Cu-NOTA-T-DM1 are a stable and effective immuno-PET tracer for HER2 positive tumor imaging in vivo. **References:** None.

EP-0640

Decreased Striatal VMAT2 Binding in Type 2 Diabetes Rat by ^{18}F-FP-(+)-DTBZ PET-CT

F. Xie, *D. Jiang, Q. Huang, S. Ren, F. Hua, F. Hua, Y. Guan;*
Huashan Hospital, Fudan university, Shanghai, CHINA.

Aim/Introduction: Diabetes is a risk factor for Parkinson's disease, and they share similar pathogenic pathways in mitochondrial dysfunction, endoplasmic reticulum stress, inflammation, and alterations in metabolism. Vesicular Monoamine Transporter type 2 (VMAT2) has proven as a useful imaging marker for quantificationof dopaminergic integrity in Parkinson's disease, ^{18}F-FP-(+)-DTBZis a VMAT2 ligand which could apply to measure it. The aim of this study was to examine the expression of VMAT2 in the striatal of type 2 diabetic rat model. **Materials and Methods: Materials and Methods:** of age) and age-matched lean controls (n = 6, 8 wk of age) were randomly assigned to be fed with high-sugar and high-fat diets to raise the fasting blood glucose, and develop of type 2 diabetes. At 3, 6 and 12 months of age, PET/CT scans were performed at 60 min post intravenous injection of ^{18}F-FP-(+)-DTBZ. Imaging data were analyzed using PMOD 3.4 software. The striatal specific uptake ratio (SUr) was calculated as [(uptake in striatum - uptake in cerebellum) /uptake in cerebellum]. **Results:** The body weight of the two groups was statistically different at 6 months (454.33 ± 55.88, 380.17 ± 18.84) (P< 0.05), but there was no significant difference at 3 months (267.20 ± 9.42,202.00 ± 5.70) and 12 months (402.33 ± 19.45,442.67 ± 87.52) (P> 0.05). The fasting blood glucose of the T2DM group at 6 months and 12 months (10.58 ± 3.00 mmol/L, 15.63 ± 5.85 mmol/ L) was significantly higher than the control group (5.95 ± 0.75 mmol/L, 5.40 ± 0.49 mmol/L) (P<0.05, P<0.0001). In the T2DM group, ^{18}F-FP-(+)-DTBZ uptake in the striatum was significantly lower at 12 months (2.68 ± 0.24) than in the control group (3.46 ± 0.23) (P= 0.0002). There was a significant negative correlation between ^{18}F-FP-(+)-DTBZ uptake and fasting blood glucose in the striatum of the two groups at 12 months (r^2= 0.753,P= 0.001). **Conclusion:** The increase of blood glucose could decrease the expression of VMAT2 in the dopaminergic pathway in the brain. The expression of VMAT2 in the striatum of T2DM rats is also negatively correlated with fasting blood glucose. **References:** 1. Pagano G, Polychronis S, Wilson H, et al. Diabetes mellitus and Parkinson disease. Neurology. 2018;90(19):e1654-e1662.2. De Pablo-Fernandez E, Goldacre R, Pakpoor J, Noyce AJ, Warner TT. Association between diabetes and subsequent Parkinson disease. Neurology. 2018.

EP-0641

Synthesis And Pre-clinical Evaluation Of ^{124}Iodine-labeled Mucin1-folate Hybrid Peptide: Potential Theranostic Radiopharmaceuticals For Breast And Ovarian Cancers

I. Aljammaz, B. Alotaibi, F. AlRumayan, A. AlRabiah, S. Okarvi; King Faisal Spec. Hosp., Riyadh, SAUDI ARABIA.

Aim/Introduction: Epithelial mucin1 (MUC1) and folic acid (FA) are overexpressed by most epithelial cancers hence attracting increasing interest as potential targets for imaging and therapy. The high expression of MUC1 and FA on breast and ovarian cancers and low expression on normal tissues makes them potential targets for diagnosis and therapy of cancers. Different Ga-68 and F-18 labeled MUC1-FA-targeted PET tracers have been developed and demonstrated a high diagnostic efficacy. However, the short half-life of these radiotracers may limit distribution to distant imaging centers. Thus, as a part of our on-going research effort to develop theranostic radiopharmaceuticals, we here report the synthesis and preclinical evaluation of new $^{123/124/131}$I-MUC1-FA hybrid peptide conjugates. **Materials and Methods:** The synthetic approaches for the preparation of [$^{123/124/131}$I]-iodobenzene and pyridine MUC1-FA conjugates entailed sequence of reactions. The key precursors N-hydroxysuccinimide 3-tri-n-butylstannyl-benzoate and 3-tri-n-butylstannyl-pyridine carboxylate were radioiodinated using classical method involving 0.1% acetic acid/methanol, iodogen and NaI ($^{123/124/131}$I, 50 MBq) at room temperature. The N-succinimidyl-p-[I]-iodobenzoate ([$^{123/124/131}$I]-SIB) and N-succinimidyl-m-[I]-iodopyridine carboxylates ([$^{123/124/131}$I]-SIP) were purified using Sep-pak silica cartridge. MUC1-FA hybrid peptide was first reacted with [$^{123/124/131}$I]-SIB and [$^{123/124/131}$I]-SIP, followed by purification using C18 Sep-pak cartridge to furnish [$^{123/124/13}$I]-SIB- and [$^{123/124/131}$I]-SIP-MCU1-FA hybrid peptide conjugates. Radiochemical yields were >75% and synthesis times were ~45 min. **Results:** Radiochemical purity was always >98% without HPLC purification. The metabolic stability of [$^{123/124/131}$I]-SIB- and [$^{123/124/131}$I]-SIP-MUC1-FA peptide conjugates were determined in human plasma and revealed that these radioconjugates remained stable during incubation at 37ºC for at least 24 h. In vitro receptor binding tests on MCF7 as well as KB cell lines have shown that significant amount of the radioconjugates associated with cell fractions. In vivo characterization in normal mice revealed rapid blood clearance of these hybrid peptides with excretion by both urinary and hepatobiliary pathways. Initial in vivo biological characterizations in SCID and nude mice bearing MCF7 and KB cell line xenografts, respectively, demonstrated significant tumor uptake (>10%). The uptake in the tumors was blocked by excess injection of MUC1-FA hybrid peptide, suggesting a receptor-mediated process. **Conclusion:** These results demonstrate that these radioconjugates may be useful as precise theranostic radiopharmaceuticals for MUC1 and folate receptor-positive cancers and their metastasis. However, further evaluation is warranted. **References:** None.

EP-0642

In vivo longitudinal monitoring the permeability of the blood-spinal cord barrier in a dog hemisection spinal cord injury model using ^{13}N-NH_3 PET/CT

L. Zhang[1,2], Y. Jia[3], Y. Chen[1,2], X. Zhuang[3], H. Xia[1,2];
[1]Department of Neurosurgery, General Hospital of Ningxia Medical University, Yinchuan City, CHINA, [2]Ningxia Human Stem Cell Research Institute, General Hospital of Ningxia Medical University, Yinchuan City, CHINA, [3]Department of Nuclear Medicine, General Hospital of Ningxia Medical University, Yinchuan City, CHINA.

Aim/Introduction: Spinal cord injury is a devastating neurological disease that results in mechanical damage to the nervous and vascular structures, and thereafter the disruption of blood-spinal cord barrier (BSCB), which plays a protective and regulatory role for the spinal cord parenchymal [1]. And its disruption provides a unique opportunity for therapeutic intervention. A noninvasive and quantitative imaging method for evaluating the changes in BSCB permeability is crucial for the development of suitable therapeutic strategies for the treatment of SCI. **Materials and Methods:** Five male beagle dogs underwent a lateral hemisection on the tenth thoracic (T10) vertebra to build a hemisection SCI model. ^{13}N-NH_3 PET/CT was performed before SCI, and at 6 timepoints after SCI (1 day, 3 day, 7 day, 10 day, 14 day and 21 day). The uptake of ^{13}N-NH_3 in the spinal cord at T9-T10 was analyzed and quantitative assessed by maximum standardized uptake value (SUV_{max}) and mean standardized uptake value (SUV_{mean}). As an endogenous trigger of BSCB leakage[2], the expression level of monocyte chemoattractant protein-1 (MCP-1) in the serum at each timepoint was measured by canine cytokine antibody arrays. Correlation analysis was performed between the uptake of ^{13}N-NH_3 and MCP-1 levels. **Results:** Although BBB is permeable for ^{13}N-NH_3, ^{13}N-NH_3 could not across BSCB. Before SCI, the ^{13}N-NH_3 uptake in the spinal cord is at a very low level (SUV_{mean}=0.31 ± 0.18, SUV_{max}=0.36 ± 0.21). After SCI, the uptake gradually increased with time and peaked at 7 days (SUV_{mean}=0.97 ± 0.23, SUV_{max}=1.12 ± 0.28) after surgery, which showed the process of BSCB disruption. As the spinal cord self-healing, it showed a decrease in the uptake thereafter. But the uptake of ^{13}N-NH_3 in 21 days (SUV_{max}=0.67 ± 0.15, SUV_{mean}=0.79 ± 0.22) was still higher than the uptake before SCI ($P<0.05$). The SUV_{max} and SUV_{mean} value of ^{13}N-NH_3 were significantly correlated with MCP-1 (P=0.0073; P=0.0049). **Conclusion:** This study demonstrated that ^{13}N-NH_3 PET/CT is a feasible imaging method to assess the changes of BSCB permeability. Moreover, it possesses a wide prospect of clinical application for optimizing treatment protocols. **References:** 1. Bartanusz V, Jezova D, Alajajian B, Digicaylioglu M. The blood-spinal cord barrier: morphology and clinical implications. Ann Neurol 2011; 70:194-206. 2. Echeverry S, Shi XQ, Rivest S, Zhang J. Peripheral nerve injury alters blood-spinal cord barrier functional and molecular integrity through a selective inflammatory pathway. J Neurosci 2011;31:10819-10828.

EP-0643

Potentiality of ^{18}F-FDG easyPET-3D studies in mouse solid tumours

F. Ribeiro[1], *M. Lapo Pais*[2,3,4], *A. C. Santos*[3,5,4], *C. Ramos*[2], *A. Parma*[6], *A. L. M. Silva*[1,7], *I. F. Castro*[1,7], *P. M. M. Correia*[1,7], *P. M. C. C. Encarnação*[1], *N. C. Ferreira*[8], *D. A. Sá*[9], *I. Mohammadi*[1,10], *C. Nicolucci*[11], *D. Priolli*[11], *J. F. C. A. Veloso*[1,7];
[1]*University of Aveiro, Institute for Nanostructures, Nanomodelling and Nanofabrication (i3N) - Department of Physic, Aveiro, PORTUGAL,* [2]*Faculty of Sciences and Technology of University of Coimbra, Coimbra, PORTUGAL,* [3]*Institute of Biophysics of University of Coimbra, Coimbra, PORTUGAL,* [4]*Institute for Clinical and Biomedical Research (iCBR), Coimbra, PORTUGAL,* [5]*Faculty of Medicine, University of Coimbra, Coimbra, PORTUGAL,* [6]*Università degli Studi di Padova, Padova, ITALY,* [7]*RI-TE Radiation Imaging Technologies, Lda, Ílhavo, PORTUGAL,* [8]*Faculty of Medicine, Institute for Clinical and Biomedical Research (iCBR), Coimbra, PORTUGAL,* [9]*University of Coimbra, Institute of Nuclear Sciences Applied to Health (ICNAS), Coimbra, PORTUGAL,* [10]*Department of Basic Sciences, Faculty of Medicine, Sari Branch, Islamic Azad University, Sari, IRAN, ISLAMIC REPUBLIC OF,* [11]*Multidisciplinary Research Laboratory, São Francisco University, Bragança Paulista, BRAZIL.*

Aim/Introduction: The study of human diseases and the initial development of new drugs and therapeutics is often done using animal models. Preclinical PET scanners dedicated to small animal imaging allow evaluating the total period of radiopharmaceutical biodistribution. The same animal can be studied along time, representing its own control (inter-subject variability eliminated). In this context, the main application is oncology: to determine if the subject is a candidate for the study and to assess the response to therapy in tumoural models. Since glucose has a high uptake in certain organs and in tumours, ^{18}F-FDG has been one of the most used radiotracers for cancer imaging. However, the access to preclinical PET scanners is usually a problem for research centres mainly due to the high cost of the equipment and infrastructural requirements, associated to limited research budgets. EasyPET technology (a patented axial microPET system) represents a solution, since it allows a significant reduction in the number of components and thus in the final equipment cost, while achieving good sensitivity and state of the art spatial resolution in all the FOV. In addition, easyPET is highly portable and compact, requiring minimal lab space. The purpose of this study was to assess the potentiality of easyPET system to image mouse solid tumours with ^{18}F-FDG. **Materials and Methods:** In total, 35 BALB/c-nu/nu mice were used for scanning: 21 males were inoculated (subcutaneously) on the right flank with WiDr cells (human colon cancer, 2-3-wks. inoculation) and 14 females with MCF-7 cells (human breast cancer, 4-7-wks. inoculation). ^{18}F-FDG (8-26MBq/0.2-0.5mL) was intraperitoneally (i.p.) administered. 40 min latter, the animals were anaesthetized (i.p.) with a mixture of ketamine/largactil (3:1) diluted in saline. A scan with 10^6 counts was performed approximately 60 min after ^{18}F-FDG injection. PET images were reconstructed with the 3D MLEM-OSEM algorithm. **Results:** EasyPET was able of detect and characterize tumours in a very early stage (1-1.5mm), as well as to monitor their size through time, with its anatomopathology confirmed by histological studies. **Conclusion:** EasyPET technology was for the first time applied for in-vivo preclinical studies and showed great potential for applications in oncology. This study showed that easyPET scans provided an early diagnosis of tumours originated by human colon and breast cancer cells, all confirmed by histology. By detecting tumours before any external signs, easyPET allows an earlier treatment. Furthermore, easyPET allows a direct molecular assessment of treatment effects by follow-up imaging. **References:** None.

EP-0644

Radiofluorinated gases as regional ventilation markers: Application to a rat model of acute lung inflammation

J. Llop Roig, *V. Gómez-Vallejo, U. Cossío, A. Lekuona;*
CIC biomaGUNE, San Sebastian, SPAIN.

Aim/Introduction: Imaging methods visualizing local areas of impaired ventilation may become a powerful tool in the early/differential diagnose of lung diseases, as well as for the development of new therapeutic approaches. Currently, ventilation studies in the clinical arena are performed with single photon emission computerized tomography (SPECT) using radiolabelled aerosols [1]. However, these show central airway deposition and peripheral "hotspot" formation in patients with obstructive lung diseases. Moreover, SPECT has limitations in terms of sensitivity, spatial resolution and image quantitation. Recently, we have developed a fast an efficient method for the production of the radiofluorinated gases [^{18}F]SF_6 and [^{18}F]CF_4, which proved efficient in the visualisation of lung ventilation in healthy rodents using Positron Emission Tomography (PET) [2]. Here, we describe the investigation of [^{18}F]CF_4 as a ventilation marker in an animal model of impaired lung ventilation and correlate the results with [^{18}F]FDG-PET. **Materials and Methods:** [^{18}F]CF_4 was produced by a double irradiation process as recently reported [2]. Ventilation studies were carried out in a rat model of lung inflammation induced by intratracheal administration of lipopolysaccharide (LPS). Dynamic 10-min [^{18}F]CF_4-PET images were obtained in list mode at t=4 hours after administration of LPS, during inhaled administration of the radiofluorinated gas. [^{18}F]FDG-PET static images were also obtained for each animal 30 minutes after the finalisation of the first imaging study. Ventilation images were reconstructed by OSEM-3D iterative algorithm and voxel-by-voxel analysis was carried out to determine the coefficient of variation as a surrogate indicator of non-uniformity of gas distribution. [^{18}F]FDG-PET images were analysed to determine Standard Uptake Values in the lungs. **Results:** Ventilation studies in control groups showed uniform distribution of the radiofluorinated gas and fast elimination of the radioactivity after discontinuation of the administration. For LPS rats, the coefficient of variation was significantly higher than that obtained in the control group. Compared to controls, the mean [^{18}F]FDG uptake in the lungs of LPS rats was almost 2-fold greater at 4h. **Conclusion:** Our results suggest that [^{18}F]

CF_4 is an appropriate marker of regional lung ventilation and may find application in the early diagnose of acute lung disease. **References:** [1] Burch WM, Sullivan PJ, McLaren CJ. Nucl. Med. Commun. 1986, 7(12), 865. [2] Gómez-Vallejo V, Lekuona A, Baz Z, Szczupak B, Cossío U, Llop J. Chem Commun. 2016, 52(80), 11931.

EP-0645

A Computational Phantom of the Adult Labrador for Use in Preclinical Nuclear Medicine Dosimetry Studies

W. Bolch[1], *M. Sands*[1], *R. Milner*[1], *I. Dormehl*[2];
[1]*University of Florida, Gainesville, FL, UNITED STATES OF AMERICA,* [2]*University of Pretoria, Pretoria, SOUTH AFRICA.*

Aim/Introduction: With the completion of the canine genome project, dogs have been proven be an ideal species for pre-clinical investigations of both molecular imaging agents and therapy radiopharmaceuticals. There is thus an expressed need to establish computational anatomic models of dogs of different species to support the associated organ radiation dosimetry for these studies. In this work, we present a comprehensive hybrid computational anatomic and dosimetric model of the adult Labrador. This species is known to present with high incidence of osteosarcoma that is both genetically and phenotypically similar to human bone cancer. **Materials and Methods:** NURBS and polygon mesh models were constructed from high-resolution CT images of a 1.5-year Labrador imaged prior to euthanasia under an approved animal research protocol at the University of Florida. Bone samples from the skeleton were harvested and ex-vivo CT imaged at sub-millimeter resolution to obtain volume fractions of cortical bone, spongiosa, and medullary cavity space. Next, spongiosa bone cores were taken from 30 skeletal sites and subjected to microCT imaging at 30 micrometer resolution. The microCT images were segmented to assess volume fractions of trabecular bone and total marrow space of spongiosa. Voxel retagging procedures were applied to establish bone microstructures at varying marrow cellularities. Paired-image radiation transport was performed to assess values of monogenetic electron specific absorbed fractions across the canine skeletal sites. **Results:** A database of specific absorbed fractions (SAFs) has been assembled for both monoenergetic photons and electrons emitted within 32 different source tissues of the adult male Labrador phantom. Values of energy deposition to active marrow and skeletal endosteum were obtained via energy-dependent integration of the volumetric photon fluence in regions of trabecular spongiosa and newly developed canine-specific fluence-to-dose photon response functions. Canine-specific S values are presented for several key radionuclides used in diagnostic and therapeutic nuclear medicine. **Conclusion:** Dosimetric applications of the Labrador model are presented for model osteosarcoma tumors treated with ^{153}Sm-EDTMP or ^{153}Sm-PEI-MP. Based upon the ^{153}Sm S values established in this model, and a six-compartment biokinetic models of each agent (to include blood, urinary bladder content, kidneys, trabecular bone surfaces, cortical bone surfaces, and tumor), model tumor doses ranged from 16 to 50 Gy for ^{153}Sm-PEI-MP and from 8 to 25 Gy for ^{153}Sm-EDTMP. **References:** Biodistribution and pharmacokinetics of variously sized molecular radiolabelled polyethyleneiminomethyl phosphonic acid as a selective bone seeker for therapy in the normal primate model. Arzneimittelforschung 2001; 51, 258-263.

EP-0646

In vivo imaging of ^{68}Ga-labelled NOTA-EGFRvIII aptamer

J. Park, *Y. Cho, J. Chae, W. Kang;*
Yonsei University College of Medicine, Seoul, KOREA, REPUBLIC OF.

Aim/Introduction: Aptamers are synthetic single-stranded oligonucleotides that bind to a target molecule with high affinity and specificity. Glioblastoma is the most aggressive primary malignant brain tumors. Epidermal Growth Factor Receptor Variant III (EGFRvIII) is a most common extracellular EGFR mutation in glioblastoma. EGFRvIII has been considered as a promising target in cancer diagnosis and therapy because EGFRvIII is expressed only in tumor cells [1,2]. Herein, we investigate the biological characteristics of ^{68}Ga-NOTA- EGFRvIII aptamer as potential glioblastoma imaging agents. **Materials and Methods:** Ga-68 was concentrated using a NaCl-based ^{68}Ga eluate concentration method and labeled with NOTA conjugated EGFRvIII aptamers. Flow cytometry was performed on DKMG/EGFRvIII and U87-MG cell lines to confirm the expression of EGFRvIII. In vitro binding specificity of EGFRvIII aptamers was evaluated using confocal microscopy. In vivo PET/CT imaging of the ^{68}Ga-NOTA-EGFRvIII aptamer were determined in DKMG/EGFRvIII tumor-bearing nude mice. **Results:** ^{68}Ga- NOTA-EGFRvIII was prepared in 96-98% RCYs (decay-corrected, n = 10) with radiochemical purity above 98%. High levels of EGFRvIII expression was found in DKMG/EGFRvIII; however, EGFRvIII were not detectable in U87-MG cells. Confocal fluorescence microscopy images showed that Cy5-EGFRvIII aptamer bound specifically to EGFRvIII expressing DKMG/EGFRvIII cells, however, not bound to U87-MG cells. DKMG/EGFRvIII tumors were clearly visualized by microPET imaging in a tumor-bearing mouse at 60 after injection. **Conclusion:** NOTA EGFRvIII aptamer conjugate was successfully labeled with Ga-68. In vitro data showed that the EGFRvIII aptamer was selectively bound to target tumor cells. In addition, DKMG/EGFRvIII tumor xenografts in mice were clearly visualized on microPET imaging. Our study demonstrated that EGFRvIII may be a useful target molecule for the imaging of glioblastoma **References:** 1) Sampson JH, et al. Tumor-specific immunotherapy targeting the EGFRvIII mutation in patients with malignant glioma. Semin Immunol. 2008;20:267-275. 2) Bakas S, et al. In Vivo Detection of EGFRvIII in Glioblastoma via Perfusion Magnetic Resonance Imaging Signature Consistent with Deep Peritumoral Infiltration: The φ-Index. Clin Cancer Res. 2017;23:4724-4734.

EP-0647

Predictive and grading value of dynamic ^{99m}Tc-HYNIC-TPPTS-Tricine-3PRGD2 SPECT analysis on acute radiation-induced Pulmonary Fibrosis

L. Shi, Q. Bai, W. Zhang, M. Yuan, L. Wei;
Tangdu Hospital, Xi'an, CHINA.

Aim/Introduction: Acute radiation-induced pulmonary Fibrosis (RPF) is an important treatment-related toxicity after chest positioning radiotherapy. The evidence shows early stage RPF was accompanied by high expression of Integrin αvβ3. For these years, several researches set ^{99m}technetium-PEG4-E [PEG4-cyclo (arginine-glycine-aspartic acid)-D-phenylalanine-lysine)]$_2$ (^{99m}Tc-3PRGD$_2$) as a radiolabeling probe which could combine with the Integrin αvβ3. In this study, comprehensive analyses were used to evaluate if the ^{99m}Tc-3PRGD2 have the potential predictive and grading value on acute radiation-induced pulmonary Fibrosis. **Materials and Methods:** A total of 30 female rats (8 weeks) were randomly divided into the normal control group (NC, n=15) and the right lung radiation-induced injury group (RPI, irradiation dose=30Gy, n=15). HYNIC-TPPTS-Tricine-3PRGD$_2$ lyophilized kits were used for the preparation of ^{99m}Tc-HYNIC-3PRGD2 labeling. Immunohistochemistry methods were used to evaluate the expression of Integrin αvβ3. Histopathology examinations were performed after 60th days post radiation-treatment. computed tomography (CT) and Single photon emission computed tomography (SPECT) data were conducted post-radiation treatment. **Results:** The histopathology and immunohistochemistry results revealed that at the 60th day post-radiation treatment, the exposed right lung exhibited acute radiation-induced pulmonary fibrosis symptoms.Static whole-body SPECT scan showed significant differences in the ^{99m}Tc-HYNIC-3PRGD$_2$ accumulated between the exposed right lungs and normal left lungs 30min post-injection.In RPI, we also found that from the 9th day post-radiation treatment, the percentage clearance rate of ^{99m}Tc-HYNIC-3PRGD$_2$ in the right lung was significantly faster than that for the unexposed left lung. **Conclusion:** Overall, comparison of iconography (CT and SPECT) results, our data suggest that ^{99m}Tc-HYNIC-3PRGD$_2$ dynamic SPECT analysis have the potential predictive and grading value on acute radiation-induced pulmonary Fibrosis. **References:** 1.Trofimova, O.P., et al., [Radiation pneumonitis in the treatment of early-stage breast cancer]. Vopr Onkol, 2015.61 (1): p. 116-120. 2. N. Withofs , R.H. and R. Hustinx, Integrin avb3 and RGD-based radiopharmaceuticals. Retour Au Numéro, 2016. 3. Irina G. Luzina1, N.W.T., Natalia Nacu2, Virginia Lockatell2, Jung Choi2, Laura K. Hummers3 andSergei P. Atamas1,*, Regulation of pulmonary inflammation and fibrosis through expression of integrins αVβ3 and αVβ5 on pulmonary T lymphocytes. Arthritis & Rheumatism, 2009. 60(5): p. 10 4.Wu, J.G., et al., Biometabolic Distribution of 99mTc-3PRGD2 and Its Potential Value in Monitoring Chemotherapeutic Effects. Molecular Imaging, 2015. 14(12): p. 115.Yu, X., et al., Integrin alpha v beta 3-targeted small-animal SPECT/CT of the progression and recovery of liver fibrosis in a rat model. Journal of Nuclear Medicine, 2015. SUPPL.3(3)

EP-0648

easyPET-3D with ^{18}F-FDG: potentiality of quercetin in a cocaine exposure brain study in a mouse model

M. Pais[1,2,3], F. M. Ribeiro[4], C. Nicolucci[5], D. Priolli[5], C. Ramos[1], A. Parma[6], P. M. M. Correia[4], A. L. M. Silva[4], I. F. Castro[4], P. M. C. C. Encarnação[4], I. Mohammadi[4,7], J. F. C. A. Veloso[4], A. C. Santos[1,3,8];
[1]Institute for Clinical and Biomedical Research (iCBR), Coimbra, PORTUGAL, [2]Faculty of Sciences and Technology of University of Coimbra, Coimbra, PORTUGAL, [3]Institute of Biophysics of University of Coimbra, Coimbra, PORTUGAL, [4]University of Aveiro, Institute for Nanostructures, Nanomodelling and Nanofabrication (i3N) – Department of Physic, Aveiro, PORTUGAL, [5]Multidisciplinary Research Laboratory, São Francisco University, Bragança Paulista, BRAZIL, [6]Università degli Studi di Padova, Padova, ITALY, [7]Department of Basic Sciences, Faculty of Medicine, Sari Branch, Islamic Azad University, Sari, IRAN, ISLAMIC REPUBLIC OF, [8]Faculty of Medicine, University of Coimbra, Coimbra, PORTUGAL.

Aim/Introduction: Cocaine is one of the most commonly used drugs worldwide. In 2017, 3.5 million people in Europe, between the age of 15 and 64, used cocaine. Moreover, 17 million used cocaine at least once in their lifetime. During cocaine dependence, changes in brain's limbic system and in the central nervous system (CNS) occur, which may result in compulsive behaviour. The effects of this drug arise from the accumulation of dopamine in the synapses, resulting in euphoria that creates addiction. After opioids and cannabis, cocaine represents the most recurrent drug treatment. Flavonoids are a class of natural compounds with an increasing interest in the scientific and therapeutic fields. Quercetin is a flavonoid with a broad therapeutic action. The lack of specific treatment for chemical dependence brings up the need for alternatives to reduce cocaine addiction symptoms and quercetin can be the answer. Positron Emission Tomography (PET) images have a high sensitivity and can provide functional information at a molecular level. The acquisition of brain images using this technology and different radiopharmaceuticals, such as ^{18}F-fluorodesoxyglucose (^{18}F-FDG), allows the observation of brain regional changes. Animal models were proven to be an efficient way to predict drug addiction behaviour. Therefore, the present study intends to determine the influence of quercetin on cocaine exposure using a rodent's model. In this context, functional brain images using the easyPET system were acquired. **Materials and Methods:** 40 BALB/c mice were divided into 4 groups (control, cocaine, quercetin, cocaine+quercetin). ^{18}FDG (5.9-19.8 MBq in 0.2-0.5 mL) were intraperitoneally (i.p.) injected in the animals and 30 min after two stimuli (light and sound) were performed. 40 min after tracer administration, the animals were anesthetized (i.p.) with a mixture of ketamine/largactil (3:1) diluted in saline. Cocaine (0.5 mg/kg) and/or quercetin (50 mg/kg) were given also by i.p.. A scan with 10^6 counts was performed approximately 60 min after injection. **Results:** The analysis of cocaine exposure showed significant correspondence between the metabolically activated brain areas in mice and the ones mentioned for humans (striatum, thalamus, amygdala, brainstem and cerebellum). In mice it was also shown that quercetin triggered the same brain

areas. **Conclusion:** The easyPET system was able to identify the main brain areas in this animal model after cocaine exposure. In addition it was demonstrated that quercetin has potential to treat cocaine consumption. **References:** None.

EP-0649

99mTc-DTPA cerebral scintigraphy is associated with cognitive impairment in models of chronic kidney diseases in rats

L. Thomas[1], *M. Bobot*[2], *S. Fernandez*[3], *L. Balasse*[3], *A. Moyon*[2], *P. Garrigue*[2], *S. Burtey*[2], *G. Hache*[2], *B. Guillet*[2];
[1]*Aix Marseille Université - CERIMED, Marseille, FRANCE,* [2]*Aix Marseille Université - CERIMED - Assistance Publique Hôpitaux de Marseille, Marseille, FRANCE,* [3]*CERIMED, Marseille, FRANCE.*

Aim/Introduction: Recently, the importance of blood brain barrier (BBB) dysfunction has been highlighted as a key factor contributing to cognitive impairment in neurodegenerative disorders, and chronic kidney disease (CKD) patients have a higher risk of developing cognitive impairment. This risk is generally explained by the high prevalence of both symptomatic and subclinical ischemic cerebrovascular lesions. However, the influence of BBB dysfunction in this context has not been explorated so far. [99mTc]-diethylenetriaminepentaacetic acid ([99mTc]-DTPA) SPECT is a validated technique to assess BBB permeability. Thus, we conducted a preclinical study to determine whether quantitative evaluation of BBB permeability using the [99mTc]-DTPA SPECT can be associated with cognitive impairment. **Materials and Methods:** We induced CKD in male Sprague Dawley rats by Adenine rich diet (ARD) (0,5%) during 4 weeks or 5/6 nephrectomy, and evaluated BBB permeability by [99mTc]-DTPA SPECT/CT imaging during CKD and 2 months after cessation of ARD. CKD was assessed by biochemistry, indoxyl sulfate (IS) dosage in serum, and histology. We evaluated cognitive function by validated tests: working memory by the novel object recognition (NOR) test, spatial memory by the object location (OL) test, and social memory by the social interaction test (SI). **Results:** Compared to control, we described CKD in ARD rats throught i) an increase in creatininemia and urea in serum and an increased in fibrosis and tubuloinstestitial damage in kidneys. Interestingly, we demonstrated an increase in [99mTc]-DTPA uptake in brain (0.086±0.025%AI/g vs 0.003±0.010%AI/g; p<0.001; n=7), a decrease in the discrimination index in NOR (0.2±0.3 vs0.7±0.3; p<0.01; n=7), a decrease in the discrimination index in OL (0.02±0.09 vs0.39±0.07; p<0.01; n=11) and an increase in interaction time in SI (19.4±1.4s vs 7.6±1.6s, p<0.001, n= 12). [99mTc]-DTPA uptake in brain was correlated with and both the discrimination index in NOR (r=-0.86, p<0.01) and IS concentrations in serum (r=0.68, p<0.01). Similar results were observed in 5/6 nephrectomy rats (n=8). **Conclusion:** We report for the first time an increase in BBB permeability in two models of CKD in rats by [99mTc]-DTPA SPECT/CT imaging, which was correlated with cognitive impairment. This preliminary work highlights a potential involvement of CKD-induced BBB disruption in cognitive defect in CKD patients, as recently reported for chronic neurodegenerative diseases **References:** None.

EP-0650

MicroPET Imaging With [^{18}F]FP-(+)-DTBZ Reveals The Synergistic Neurotoxicity Of VMAT2 Inhibitor And MPTP To Dopaminergic Neurons

Y. Xu, *J. Tang*, *C. Liu*, *C. Zhao*, *H. Yu*, *Z. Chen*, *M. Xie*;
Jiangsu Institute of Nuclear Medicine, Wuxi, CHINA.

Aim/Introduction: Parkinson's disease is a common neurodegenerative disease characterized by progressive degeneration of dopaminergic pathways in nigrostriatal. Vesicular monoamine transporter 2 (VMAT2) is responsible for the storage and release of dopamine and alteration of its function is closely related to the viability of dopaminergic neurons and vulnerability to neurotoxins. In this study, using microPET imaging with 9-[^{18}F]fluoropropyl-(+)-dihydrotetrabenazine ([^{18}F]FP-(+)-DTBZ), the specific radioligand for VMAT2, we investigated the effects of inhibiting VMAT2 on 1-methyl-4-phenyl-1,2,3,6-tetrahydropyridine (MPTP)-induced death of dopaminergic neurons in mice. **Materials and Methods:** C57BL/6 mice were randomly divided into 5 groups: vehicle, dihydrotetrabenazine (DTBZ, a specific inhibitor of VMAT2, 5 mg/kg), low dose MPTP (10 mg/kg), DTBZ (5 mg/kg) & MPTP (10 mg/kg) and high dose MPTP (30 mg/kg) group. Drug delivery lasted for 10 days except that the high dose MPTP was administered from the sixth day. MicroPET imaging with [^{18}F]FP-(+)-DTBZ was performed 1 week before or after the drug delivery. Finally, tissues were dissected for analyzing the contents of dopamine (DA) and its metabolite, the expression levels of VMAT2 and tyrosine hydroxylase (TH), as well as the degeneration level of dopaminergic neurons using HPLC, western blotting and immunohistochemistry. **Results:** In contrast to the control, DTBZ and low dose MPTP treated mice, DTBZ&MPTP and high dose MPTP treated mice displayed substantially declined uptake of [^{18}F]FP-(+)-DTBZ in the striatum. Quantitative data indicated that compared with the control group (1.54±0.25), there is no significant difference in the striatal SUV of DTBZ (1.34±0.24, p=0.375) and low dose MPTP (1.22±0.09, p=0.143) alone treated mice, while the dramatic decrease was discovered in the DTBZ&MPTP treated mice (0.95±0.14, p=0.037). Correlation analysis indicated that SUVs are highly positive-correlated to the contents of DA and its metabolite 3,4-Dihydroxyphenylacetic acid (DOPAC) (r=0.8467 and 0.9003; p=0.0005 and p<0.0001, respectively), and also showed good correlation with the expression levels of VMAT2 and TH (r=0.7675 and 0.7714; p=0.0158 and 0.0149, respectively). Immunohistochemical results further demonstrated that after inhibiting the activity of VMAT2, the number of dopaminergic neurons was dreadfully decreased by low dose of MPTP (38.1±2.8% of the control values). **Conclusion:** MicroPET brain imaging with [^{18}F]FP-(+)-DTBZ in mice revealed that DTBZ co-administration significantly aggravates the neurotoxicity of MPTP to dopaminergic neurons. **References:** None.

EP-0651

^{18}F-FDG-PET/CT to monitor combination therapy with Xc- inhibitor sulfasalazine and Vitamin C in prostate cancer

Z. Li, Z. Zheng, G. Luo, X. Shi, Y. Long, W. Shen, X. Zhang;
The First Affiliated Hospital of Sun Yat-Sen University, Guangzhou, CHINA.

Aim/Introduction: The anticancer potential of pharmacologic ascorbic acid (AA) has been detected in over 50 cancer cell lines.Former studies has reported that the cancer cell selective cytotoxity of VC is induced from steady-state H_2O_2 level, produced from autoxidation. SAS can induce cytotoxic effect by suppressing the system Xc--cystine/glutamate antiporter (xCT) in cancer cells, also relates to glutathione (GSH) biosynthesis, which is critical during intracellular antioxidation. We hypothesized that targeting Xc^--transporter by SAS could improve anti-cancer activity of VC through intermission of GSH biosynthesis which results in accumulation of reactive oxygen species (ROS). And ^{18}F-FDG PET/CT could monitor the therapeutic response of the prostate cancer in vivo. **Materials and Methods:** We employed two Castration-resistant prostate cancer (CRPC), without PSA express, prostate cancer cell lines PC3 and DU145 to set up our study. Anti-proliferation effect of VC and/or SAS on prostatic cancer cells was detected using WST-8 assay and colony formation. We used Annexin V-FITC/PI FACS to monitor cell apoptosis induced by different treatment protocols. Then changes of cellular ROS and GSH were detected to prove our hypothesis. In vivo, BALB/c nude mice bearing prostate cancer xenograft were carried out to assess anti-cancer effect of single or combined therapy of VC and SAS. Small animal FDG PET/CT was performed before, one week after and two weeks after therapy administrations to monitor therapeutic response of tumors. We investigated the expression change of apoptotic related proteins, including cleaved-caspase-3, HMGB1 and the pro BAX, BCL-2 using immunohistochemistry in response to the single or the combined treatments. **Results:** Our study revealed that SAS could improve cytotoxicity of VC in prostate cancer cells. The synergistic effect of SAS and VC leads to significant depletion of cellular GSH, leading to an clear accumulation of ROS and this synergistic effect can be reversed by antioxidant N-Acetyl-L-cysteine (NAC). Moreover, the synergistic effect of SAS and VC was also found to block Xenograft tumor growth because of apoptotic and necrotic cell death, as determined by Immunohistochemistry. FDG-PET/CT also showed a clearly more reduced uptake in combination therapy group than single therapy groups with VC or SAS. **Conclusion:** Our results demonstrate that SAS, as a relatively non-toxic drug can target cystine transporter to improve therapeutic effect of VC and induce better therapy outcome contrasted to single treatment in prostate cancer. ^{18}F-FDG PET/CT is highly correlate with different therapeutic methods and could predict the different response of prostate cancer in vivo. **References:** None.

EP-0652

Radiolabeling, selection and evaluation of indium-111 labeled anti-mesothelins in human mesothelin-expressing xenografts

W. Hsu[1], K. Cheng[1], Y. Chang[1], C. Ho[1], C. Yu[2], S. Yang[2], H. Hsu[2], C. Yang[2], C. Chang[1];
[1]*Institute of Nuclear Energy Research, Taoyuan, TAIWAN,*
[2]*Development Center for Biotechnology, Taipei, TAIWAN.*

Aim/Introduction: Mesothelin (MSLN) is a 40 kDa cell-surface glycoprotein which is highly expressed in a variety of human cancers, and has great value as a target for antibody-based therapies. The aim of this study was to develop an indium-111 labeled anti-mesothelin as a novel companion diagnostic agent to detect MSLN-expressing tumors in vivo. **Materials and Methods:** Full-length and minibody of anti-MSLN antibodies obtained from Development Center for Biotechnology in Taiwan were conjugated with p-SCN-Bn-DTPA. The Drug to antibody ratio (DAR) was determined by matrix-assisted laser desorption/ionization time-of-flight mass spectroscopy. After radiolabeling with indium-111, the radiochemical purity, stability and immunoreactivity of ^{111}In-DTPA-anti-MSLNs were qualified before in vitro and in vivo studies. Cellular uptake and internalization studies of indium-111 labeled full-length of anti-MSLN antibodies were performed using KLM-1, OVCAR-3 and NCI-H226 cell lines. Two forms of ^{111}In-DTPA-anti-MSLNs were selected by nanoSPECT/CT molecular imaging in KLM-1, OVCAR-3 and NCI-H226 tumor bearing mice. The pharmacokinetics and in vivo tissue distribution of full-length of ^{111}In-DTPA-anti-MSLN were evaluated in normal and KLM-1 tumor-bearing mice, respectively. The dosimetry of ^{111}In-DTPA-anti-MSLN was evaluated by OLINDA software. **Results:** The DAR of DTPA-anti-MSLNs was range 1-4. The labeling efficiency and immunoreactivity of ^{111}In-DTPA-anti-MSLNs were >90% and >40%, respectively. The stability of ^{111}In-DTPA-anti-MSLNs was greater than 90% after 24 h at room temperature. Full-length antibody has longer circulation time than minibody. NCI-H226 cell show the higher cellular uptake of ^{111}In-DTPA-anti-MSLN than KLM-1 and OVCAR-3 cell lines in vitro. KLM-1 xenograft has a higher in vivo tumor uptake of ^{111}In-DTPA-anti-MSLN than NCI-H226 and OVCAR-3 xenografts. Tumor/muscle ratio of ^{111}In-DTPA-anti-MSLN was >10 performed by biodistribution studies during 24-96 h drug distribution in KLM-1 xenograft. The AUC of ^{111}In-DTPA-anti-MSLN was 7742 %ID/gh. Radiation absorbed dose study show the safety of 5 mCi ^{111}In-DTPA-anti-MSLN treated in human. **Conclusion:** We established in vitro and in vivo platforms to evaluate the novel indium-111 labeled anti-mesothelin antibodies successfully. The full-length of ^{111}In-DTPA-anti-MSLN showed high specific targeting and long term circulation in MSLN-expressing xenografts. The ^{111}In-DTPA-anti-MSLN may be a potential companion diagnostic agent for patient selection or monitoring of MSLN expression during therapy. **References:** None.

EP-0653

Optimisation of Conjugation for Radioimmunoconjugate Based Imaging of Intranuclear Eptiopes

M. Veal, *B. Cornelissen;*
University of Oxford, Oxford, UNITED KINGDOM.

Aim/Introduction: Antibody based radioimmunoconjugates (RICs) have great potential for a broad range of applications in medical imaging, offering unparalleled versatility, selectivity and specificity. Conjugation with cell penetrating peptides such as Tat (GRKKRRQRRRPPQGYG), and radionuclides allows imaging of a large array of intra-nuclear targets by PET or SPECT imaging[1]. Here, we developed a simplified and more efficient methodology for conjugating functional groups to antibodies through the use of SPAAC based click chemistry. **Materials and Methods:** Selected antibodies (anti-γH2AX, anti-GFP, anti-pATM, and a non-specific rabbit polyclonal IgG) were modified using the amine-reactive reagent DBCO-STP, introducing multiple azide-reactive DBCO groups. After removal of non-reacted starting product, the extent of DBCO labelling is determined by absorbance (309 nm). The antibody-DBCO conjugate is then reacted simultaneously with an azide modified chelating agent (N_3-Bn-DTPA), and cell penetrating peptide (N_3-Tat). The yield of the click reaction was determined by the relative reduction in absorbance (309 nm). After addition of $^{111}InCl_3$, radionuclide incorporation yield was determined by instant thin-layer chromatography (ITLC). A549 cells were exposed to ^{111}In-IgG-Tat or ^{111}In-IgG (without TAT) for 2 hours, and the uptake of 111In into cells was measured. Furthermore, flow cytometry will be used to compare the affinity of antibodies conjugated using the new conjugation process against previously used method and an unmodified antibody. **Results:** We successfully synthesised ^{111}In-labelled Tat-conjugated versions of several antibodies, including both polyclonal and monoclonal antibodies derived from both mouse and rabbit hosts. Internalisation assays with non-specific rabbit polyclonal antibodies have shown a >50 fold increase in cell associated radioactivity in comparison to a non-Tat modified control group, demonstrating the capacity for the RIC to penetrate the cell (4.634 ± 0.061 % vs. 0.075 ± 0.024 %, respectively; P = 0.003). Furthermore, this capacity for internalisation was considerably greater than results obtained using the previous conjugation technique (0.113 ± 0.011% vs. 0.028 ± 0.001 %; P < 0.001). **Conclusion:** We developed a simple and robust method for modifying antibodies for imaging nuclear epitopes, with reduced purification steps, reduced risk of antibody-antibody cross-linking and increased cell internalisation. **References:** 1. Knight, J.C., Koustoulidou, S. and Cornelissen, B., 2017. Imaging the DNA damage response with PET and SPECT. European journal of nuclear medicine and molecular imaging, 44(6), pp.1065-1078.

EP-0654

In vitro model system for biological quality control and functional research of radiopharmaceuticals used for Targeted Radionuclide Therapy

Z. Kalnina[1], *K. Shvirksts*[2,3], *E. M. Rubena*[4,1], *M. Grube*[2], *T. Kusins*[3,5], *R. Kovaldins*[6], *L. Mazkalnina*[3,4], *H. Rozensteins*[3,7], *A. Berzina*[5], *G. Kizane*[8], *A. Grinbergs*[3];
[1]*Latvian Biomedical Research and Study centre, Riga, LATVIA,* [2]*Institute of Microbiology and Biotechnology, University of Latvia, Riga, LATVIA,* [3]*Kodolmedicinas Klinika Ltd, Riga, LATVIA,* [4]*University of Latvia, Faculty of Biology, Riga, LATVIA,* [5]*Riga East University Hospital, Clinical Department of Nuclear Medicine, Riga, LATVIA,* [6]*University of Latvia, Faculty of Chemistry, Riga, LATVIA,* [7]*Institute of Biomedical Engineering and Nanomedicine, Riga Technical University, Riga, LATVIA,* [8]*Institute of Chemical Physics, University of Latvia, Riga, LATVIA.*

Aim/Introduction: In modern radio-oncology, proper diagnostics and control of metastatic prostate cancer (mPC) and neuroendocrine tumours (mNET) cannot be imagined without application of Ga^{68}-PSMA and Ga^{68}-DOTATATE radionuclide-guided PET/CT. In world's leading clinics, Lu^{177}-PSMA and Lu^{177}-DOTATATE - the theranostic counterparts of the above mentioned radiopharmaceuticals (RP) - are currently used for treating mPC and mNET when other therapeutic approaches fail. Such therapy is capable of substantially improving the patients' quality of life and overall lifespan. This theranostic approach represents a substantial step towards personalized targeted diagnostics and therapy. In this study, we aimed to develop a simple, sensitive and accurate in vitro test system based on cancer cell lines that could be used as fast internal biological quality control for the synthesized RP binding capacity and for the studying the above mentioned RP-induced physiological effects in cancer cells. **Materials and Methods:** Radiolabeling of Ga^{68} and Lu^{177} RPs (PSMA-I&T and HA-DOTATATE) was done in TEMA isolator using Scintomics GRP automatic synthesis module. The labeling efficiency and radiochemical purity were determined using radio thin-layer and high-performance liquid chromatography. Processes were done in accordance with "68-Ga-PSMA PET/CT: Joint EANM and SNMMI procedure guideline for prostate cancer imaging: version 1.0". The test system was based on stable cancer cell lines: PC3 ($PSMA^{+/-}$), LNCaP ($PSMA^{++}$), NCI-H69 ($SSTR2^{+}$), AR42J ($SSTR2^{++}$), CorL23 ($SSTR2^{-}$); human dermal fibroblast cell line Hs68 was used as a non-malignant control. The cell lines were validated for the target receptor PSMA and SSTR2 expression levels by immunocytochemistry and fluorescence microscopy and used for RP binding assays in following experiments. The RP treatment-induced biomolecular profile changes in the cell lines were evaluated by FTIR spectroscopy. **Results:** As a result, an in vitro test system suitable for express biological quality control of in-house synthesized RPs for their binding to PSMA and SSTR2 receptors was developed. The binding assay results were comparable with the receptor expression levels in the corresponding cell lines. Preliminary results indicated that the RP treatment of cancer cells positive for target receptor expression is linked with the increase of total carbohydrate content, not seen in receptor-negative cells. **Conclusion:** This study showed that by means of Ga^{68} and Lu^{177}-RPs, it is possible to assess the binding capacity to live cells both qualitatively

and quantitatively. Further elaboration of the developed in vitro test system and protocols is planned to enable the prediction of the RP binding efficacy in individual patient-derived biopsy material. **References:** None.

EP-0655

In vitro Evidence of Abnormal Glutamate to Glutamine Conversion in Astrocytes harvested from a Mouse Model of Amyotrophic Lateral Sclerosis: a potential Experimental Application of ^{13}N-ammonia

V. Cossu[1,2], *G. Sambuceti*[1,2], *T. Bonifacino*[3], *S. Bruno*[4], *S. Ravera*[4], *V. Ceriani*[2], *P. Piccioli*[5], *P. Castellani*[5], *M. Bauckneht*[1,2], *S. Capitanio*[1], *D. Gandolfo*[1], *S. Morbelli*[1], *M. Milanese*[3], *A. Democrito*[1], *C. Ghersi*[1], *G. Bonanno*[3,6], *C. Marini*[1,7];
[1]*Nuclear Medicine, IRCCS Ospedale Policlinico San Martino, Genoa, ITALY,* [2]*Department of Health Sciences, University of Genoa, Genoa, ITALY,* [3]*Department of Pharmacy, University of Genoa, Genoa, ITALY,* [4]*Department Experimental Medicine, University of Genoa, Genoa, ITALY,* [5]*Cell Biology Unit, IRCCS Ospedale Policlinico San Martino, Genoa, ITALY,* [6]*Pharmacology, IRCCS Ospedale Policlinico San Martino, Genoa, ITALY,* [7]*CNR Institute of Molecular Bioimaging and Physiology (IBFM), Milan, ITALY.*

Aim/Introduction: In the central nervous system, glutamate acts both as excitatory neurotransmitter and metabolic substrate channeled to the Krebs cycle after its conversion to alpha-ketoglutarate. Due to this double role, its extracellular concentration is tightly regulated. In particular, glutamate released by neurons in the synaptic cleft is removed by astrocytes and converted into glutamine to be transferred back to neurons for the conversion to glutamate configuring the so-called glutamate-glutamine cycle (GGC). Accordingly, the catalytic function of glutamine synthetase (GS) highly expressed in astrocytes plays a pivotal role in preventing glutamate toxicity. Although several studies reported an impaired GGC in amyotrophic lateral sclerosis (ALS), methods able to estimate glutamate processing rates by astrocytes are not available so far. Since the main fate of NH_3 taken up by cells is the production of glutamine by GS, we aimed to verify whether uptake kinetics of ^{13}N-NH_3 is altered in primary astrocytes harvested from SOD1^{G93A} mice as an experimental model of ALS. **Materials and Methods:** Astrocytes were isolated from brain harvested from neonatal (p2) wild-type (WT) and SOD1^{G93A} mice and cultured under standard conditions. Time-activity curves of cultured cells were defined using a dedicated instrument (LigandTracer, Ridgeview, SE) that consists of a beta-emission detector and a rotating platform harboring a Petri dish inclined at 30 degrees as to alternate cell position from nadir (for incubation) to zenith (for counting) every minute. For the experiments, astrocytes were incubated in saline enriched with 6 MBq/mL ^{13}N-NH_3 with or without glutamate 70 microM. Counting rate (counts per second, cps) of cultured cells was monitored for 30 minutes and normalized for both administered dose and cell number (C-Rate). **Results:** WT and SOD1^{G93A} astrocytes showed a similar ^{13}N-NH_3 uptake kinetics in the absence of glutamate and reached similar C-Rate values at 30 minutes (2.8±0.5 vs 2.9 ±0.6 cps, respectively, ns). By contrast, the presence of glutamate increased C-Rate to a greater degree in WT than in SOD1^{G93A} astrocytes (4.1±0.8 vs 2.7±0.8 cps, respectively, $p<0.01$). **Conclusion:** The present data suggest that monitoring NH_3 uptake might detect an abnormal GGC during the early disease stage of a mouse ALS model. This tool might complement the study of glutamate transporters and GS activity to clarify astrocyte role in ALS progression. **References:** None.

EP-0656

Biomarkers Exploration In a Small Animal Model of Cardiorenal Syndrome by 18FDG PET/MRI , Histology and Terahertz Imaging of the Kidney -Preliminary Results-

M. Furcea[1], *L. Agrigoroaie*[1], *C. Uritu*[2], *G. Stanciu*[2], *C. Mihai*[2], *I. Gardikiotis*[2], *R. Iliescu*[3], *C. Stefanescu*[3], *M. Gutu*[3];
[1]*University Hospital "Sf. Spiridon", Iasi, ROMANIA,* [2]*Advanced centre for research-development in experimental medicine - CEMEX, Iasi, ROMANIA,* [3]*University of Medicine and Pharmacy "Grigore T.Popa", Iasi, ROMANIA.*

Aim/Introduction: Cardiorenal syndrome is a clinical condition with a profound socio-economic burden, and elusive prognostic biomarkers. We present preliminary renal data of a rat model for the above pathology through multimodal imaging with 2-deoxy-2-[fluorine-18]fluoro-D-glucose (^{18}F-FDG) PET/MRI, histological analysis and terahertz (THz) spectrum reflectometry. **Materials and Methods:** We examined 24 male Wistar rats, divided into 3 lots: control (L1), heart failure (L2), cardiorenal group (L3). Heart failure was induced by intraperitoneal doxorubicin administration and renal failure by sub-total nephrectomy. ^{18}F-FDG PET/MRI scans were acquired at week 0 for L1, week 6 for L2 and week 18 for L3. Regions of interest were drawn on MRI images for kidneys and left ventricular cavity, which were used for volumetric assesment and VOI segmentation. PET derived GFR estimation was calculated based on the following formula: $GFR=Ki_{right}[min]*V_{right\ kidney}[ml]+Ki_{left}[min]*V_{left\ kidney}[ml]$. Ki is approximated as the slope of the linear regression of arterial tracer concentration by taking the renal activity as independent variable. A multi-flip spoiled GRE driven-equilibrium T1 relaxation time estimation sequence was employed for the study of ex vivo formalin-fixed rat kidneys. The histological assessment followed a standard hematoxilliyn-eozin protocol with 5 µm tissue slices, scoring the lesion progression on a visual scale from 0 to 4 (0-least affected, 4-severe disease). Paraffin-embedded renal tissue samples were further examined through THz pulsed-wave reflectometry, with resulting attenuation in the 0.2-3.3 THz range. **Results:** Through histological assessment, L1 was graded with a score of 0, L2 with a score of 1 (mild glomerular sclerosis, rare hyalinne cast-filled tubules, low inflammatory infiltration) and L3 with a score of 3 (moderate glomerular sclerosis, frequent hyalline casts, distorted tubular brush border and moderate inflammatory infiltration). The variation in arterial concentration explained by renal tracer dynamics for the 3 groups was $R^2_{L1}=0.97$, $R^2_{L2}=0.99$ and $R^2_{L3}=0.82$. Estimated GFR for

the L1, compared to literature (1.38 ± 0.1 ml/min), was within 1.26 ± 0.23 ml/min. L2 and L3 group deviated from L1 with values of 0.88 ± 0.14 ml/min, respectively of 0.52 ml/min. T1 renal parenchyma relaxation times were 403±42 ms for L1, 382±17 ms for L2 (suggested by increasead cellularity) and 301±22 ms for L3 group (expression of renal scarring) Study groups were differentiated by distinct patterns of the THz pulse attenuation. **Conclusion:** Our multimodal exploration of cardiorenal rat model was consistent in discriminating between study groups, hence confirming the hypothesis under study, with potential new non-invasive diagnostic avenues. **References:** None.

EP-0657

Radiobiological Evaluation of Copper-64 on Tumor Cells

D. Niculae, *R. Leonte, R. Serban, L. Chilug, D. Draganescu, M. Temelie, D. Savu;*
Horia Hulubei National Institute for Physics and Nuclear Engineering, Bucharest (Magurele), ROMANIA.

Aim/Introduction: Copper, as a natural bioelement in the human body, incorporated into a variety of proteins, is involved in key biological processes based on its redox properties. Its trafficking, accumulation and clearance are tightly controlled in normal health but often disturbed in disease states. These mechanisms can be exploited for both imaging and therapy, based on several radioisotopes of copper which are of certain medical interest. **Materials and Methods:** An automated process for the production and purification of copper radioisotopes produced by irradiating solid targets in a variable energy cyclotron has been developed, using an automated solid target system. To comparatively evaluate the biological effects we used a panel of tumor cell lines: U87MG (glioblastoma), AR2J (pancreatic cancer cells), HT29 (colon adenocarcinoma), A431 (epidermoid carcinoma) and DU-145 (prostate cancer cells) in comparison with non-tumoral, control cell lines (monocytes ATTC). We performed cytogenetic and radiocytotoxicity assays to evaluate the significant changes at cellular level induced by the exposure to 64CuCl2: cell viability by MTT/MTS, micronuclei testing genotoxicity and morphologic apoptosis and H2AX, when relevant. **Results:** A reliable process for production of ^{64}Cu by nuclear reaction ^{64}Ni(p,n), with low metallic impurities and of high specific activity, for biomedical application, is described. The process involves the plating of enriched ^{64}Ni (99.5%) on the target, pneumatic transfer to the irradiation station, mounted on a slope-down proton beam, irradiation at 14 MeV and uses automated module based on ion exchange chromatography to purify the resulted copper-64 chloride. Tumor cells were found to exhibit increased $^{64}CuCl_2$ comparing to normal cells; early DNA damage, higher cytotoxicity and genotoxicity were also observed in tumor cells, with different intensities for different cells tested. Double strain breakages were observed, which correlates with deficient DNA-damage repair capacity. The results contributes to elucidation of mechanisms involved, quantification of radiobiological effects and sustain the use of $^{64}CuCl_2$ for theranostic applications. **Conclusion:** The combination of positron, beta$^-$ and of high LET Auger electrons emissions imparts a high local radiation dose at the cellular level making it suitable for targeted radionuclide therapy, with high cytotoxic potency if the radionuclide is located within or close to cell nuclei. **References:** Qinghua Xie, Hua Zhu, Feng Wang, Establishing Reliable Cu-64 Production Process: From Target Plating to Molecular Specific Tumor Micro-PET Imaging, Molecules (2017); Avila-Rodriguez, M.A.; Nye, J.A. Simultaneous production of high specific activity 64Cu and 61Co with 11.4 MeV protons on enriched 64Ni nuclei. Appl. Radiat. Isot. (2007).

EP-0658

Radium-223 Inhibits Cancer Growth in Bone and Improves Survival in a Syngeneic Bladder Cancer Bone Metastasis Model

M. I. Suominen[1], *T. E. Kähkönen*[1], *J. H. E. Mäki-Jouppila*[1], *B. Sjöholm*[2], *I. Ahonen*[3], *D. Mumberg*[4], *K. Ziegelbauer*[4], *J. M. Halleen*[1], *S. Käkönen*[2], *A. Scholz*[4];
[1]*Pharmatest Services, Turku, FINLAND,* [2]*Aurexel Life Sciences Ltd., Askainen, FINLAND,* [3]*Vincit Oy, Turku, FINLAND,* [4]*Bayer AG, Berlin, GERMANY.*

Aim/Introduction: Radium-223 dichloride (Ra-223, Xofigo®) is a targeted alpha therapy which prolongs the survival of castration-resistant prostate cancer (CRPC) patients with symptomatic bone metastases. As a calcium-mimetic, Ra-223 selectively binds to hydroxyapatite and targets areas of high bone turnover such as bone metastases. The effects of Ra-223 on development and progression of osteolytic bone lesions and on survival in the syngeneic intratibial MBT-2 murine bladder cancer model in immunocompetent mice were investigated in this study. **Materials and Methods:** Female 5-7-week-old C3H/HeNHsd mice were inoculated intratibially with 5x10^5 MBT-2 cells on day 0. The mice were stratified based on body weight (n=40 per group) on day 5 and Ra-223 (300 kBq/kg, i.v.) or vehicle control was administered on days 5, 33, and 61. The tumor-induced osteolytic lesion area was imaged using radiography on days 10, 18, 25, 76, and at sacrifice. The mice were sacrificed when they met the predefined sacrifice criteria (> 20% body weight loss, palpable tumor outgrowth from the bone or general deterioration of health status). The study was terminated on day 158. **Results:** In this study, the first mice met the sacrifice criteria on study day 24 and the survival curves plateaued at 52% after 84 days in the control group and at 68% after 112 days in the Ra-223 treatment group. Survival on day 40 was significantly improved in the Ra223 treatment group compared to the vehicle control ($p< 0.001$), but the effect was not statistically significant at the end of the study. Based on X-ray imaging 25 days after cancer cell inoculation, Ra223 treatment also significantly decreased the bone lesion area compared to the vehicle treatment ($p=0.0041$). After initially sacrificing the mice with extensive bone lesions, tumor growth in bone was stabilized around day 25. The main reason for sacrifice at a later stage was breathing difficulties due to lung metastases, and in the Ra-223-treated mice only one mouse was sacrificed due to

bone metastases. Ra-223 treatment was well-tolerated; no body weight loss was observed. **Conclusion:** In summary, radium-223 dichloride (Xofigo®) demonstrates moderate single agent in vivo efficacy in the intratibial MBT-2 murine bladder cancer model of osteolytic bone metastasis. Retaining a functional immune system in syngeneic mouse models is particularly relevant for the characterization of potential immune-stimulatory effects of Ra-223. The promising results obtained in this model warrant further investigation of Ra223 in combination with immuno-oncological treatments like checkpoint inhibitors. **References:** None.

EP-0659

Imaging [^{18}F]olaparib in malignant glioma models

S. L. Hopkins, M. Mosley, P. Isenegger, J. Baguña Torres, F. Guibbal, A. Pacelli, R. Hueting, V. Gouverneur, B. Cornelissen;
University of Oxford, Oxford, UNITED KINGDOM.

Aim/Introduction: Imaging of the DNA damage repair enzymes, poly(ADP-ribose) polymerases (PARP), using a radiolabeled PARP inhibitor has been proposed for cancer patient selection, outcome prediction, dose optimisation, genotoxic therapy evaluation, and target engagement validation. We previously reported the synthesis of a radiolabelled structural equivalent of the FDA-approved PARP inhibitor, olaparib, to allow PET imaging in preclinical pancreatic tumour models.[1] Here, we have investigated the effect of administered dose on tumour uptake and target engagement of [^{18}F]olaparib in U87MG and U251MG malignant glioma models. **Materials and Methods:** The U87MG and U251MG cells and tumours were characterised for PARP1, PARP2, and PARP3 expression using Western blot and/or immunofluorescence. In vitro, specificity of [^{18}F]olaparib cell uptake was determined using an excess of unlabelled olaparib. In vivo, PET/CT images were acquired, 1 h after an intravenous bolus injection of 0.5, 1.0, 4.0, or 8.0 µg [^{18}F] olaparib and ex vivo biodistribution studies were subsequently performed. Separately, specificity of tumour uptake was evaluated by blocking of [^{18}F]olaparib using an excess of cold olaparib. **Results:** In vitro, [^{18}F]olaparib showed similar uptake across U87MG and U251MG cell lines. Cell uptake of 1 µM [^{18}F] olaparib could be blocked by more than 70% by addition of an excess of cold olaparib. In vivo, tumour uptake of [^{18}F]olaparib in both U87MG and U251MG mouse xenografts was higher for lower doses (0.5 and 1.0 µg) compared to higher doses (4.0 and 8.0 µg). Ex vivo biodistribution analysis showed U251MG and U87MG tumour uptake of 7.1 ± 1.5 and 6.5 ± 0.9 %ID/g, respectively for 1.0 µg dose vs. 3.3 ± 0.4 and 1.7 ± 0.2 %ID/g for 8 µg ($P < 0.001$). In a separate study, blocking decreased U251MG and U87MG tumour uptake from 6.1 ± 0.6 and 7.4 ± 0.9 %ID/g, respectively for 1.0 µg [^{18}F]olaparib to 1.2 ± 0.3 and 1.2 ± 0.2 %ID/g, respectively for 20 µg olaparib + 1 µg [^{18}F]olaparib ($P < 0.0001$). **Conclusion:** Taken together, we have demonstrated that [^{18}F]olaparib tumour uptake is dependent on administered dose, can measure PARP levels in glioma models, and is specific in vitro and in vivo. **References:** 1. Wilson, T. C. et al. PET imaging of PARP expression using [^{18}F]olaparib. J. Nucl. Med. **60,** 504-510 (2019).

EP-0660

Radiosynoviorthesis Using Sn-117m Colloid to Treat Canine Elbow Osteoarthritis Demonstrates Efficacy and Safety

C. A. Doerr[1], J. M. Donecker[1], N. R. Stevenson[1], G. R. Gonzales[1], J. C. Lattimer[2];
[1]*Serene, LLC, The Woodlands, TX, UNITED STATES OF AMERICA,*
[2]*University of Missouri, Columbia, MO, UNITED STATES OF AMERICA.*

Aim/Introduction: Homogeneous Sn-117m colloid (HTC) was studied in order to determine the safety and efficacy of radiosynoviorthesis (RSO) injections for the treatment of mild to moderate, and moderately severe canine osteoarthritis (OA). As a result of these trials, HTC is being commercialized in the US as a treatment for OA in dogs, and clinical trials in human arthritis using ascorbic homogeneous Sn-117m colloid (AHTC) will commence in Canada in 2019. **Materials and Methods:** Study 1 prospectively enrolled 44 dogs (45 elbows) with mild-moderate elbow OA into three randomized dosing arms, and Study 2 prospectively enrolled 15 dogs (27 elbows) with moderately severe elbow OA treated by a single dose. All dogs were followed up to 12 months. Therapeutic success by canine brief pain inventory (cBPI) was defined as either (1) improvement of >1 for pain severity score (PSS) AND >2 for pain interference score (PIS), or (2) improvement of >1 for PSS OR >2 for PIS. Therapeutic success by clinician's lameness examination (CLE) was defined as significantly improved p values between the two assessment time points. In Study 1 a force plate analysis was also evaluated with therapeutic success defined as improvement of >5% at any time point in the peak vertical force (PF) or the mean vertical impulse (IMP). Safety was assessed by analysis of CBC and blood chemistry, joint fluid, UA, and by owner and clinician assessment. **Results:** Study 1 (per protocol 34 elbows) demonstrated success in cBPI, CLE and force plate in the medium dose group which was selected as the only dose used for Study 2. Study 2 (per protocol 25 elbows) showed therapeutic improvement in cBPI and CLE. cBPI success using PSS AND PIS demonstrated improvement over baseline of up to 70.0%, over 12 months. cBPI success using PSS OR PIS demonstrated improvement over baseline of up to 81.8% over 12 months. CLE showed statistical improvement compared to baseline at day 90. Force plate evaluation demonstrated improvement in PF or IMP of up to 66.7% in either elbow over 180 days. No safety issues were noted. **Conclusion:** The therapeutic success and safety of HTC for OA in dogs supports the use of AHTC in upcoming human trials. **References:** None.

EP-0661

Validation of á2ä1 as cancer stem cell marker for molecular imaging using 1B50-1 mAb probes : A preliminary study on Hepatocellular Carcinoma

X. Guo, G. An, W. Zhao, Z. Zhang, H. Zhu, Z. Yang;
Peking University Cancer Hospital & Institute, Beijing, CHINA.

Aim/Introduction: In previous research, we identified a new antibody named 1B50-1 targeting α2δ1 which specifically expressed in cancer stem cells (CSCs). These α2δ1+ tumor-initiating cells (TICs) with stem cell-like properties, might be the cell of origin for HCC recurrence. Herein, we investigated whether near-infrared fluorescence (NIR) imaging Cy5.5-1B50-1 and positron emission tomography (PET) radiotracer ^{64}Cu-NOTA-1B50-1 were sensitive approaches for non-invasively detecting and quantitating of CSCs on hepatocellular carcinoma. **Materials and Methods:** 1B50-1 antibody was labeled with either an Cy5.5 or ^{64}Cu (using NOTA-NCS as bi-functional chelator).1B50-1+ Hep-12 cell lines and Huh7 cell lines culture and/or xenografted on NOD-SCID mice for ^{64}Cu-NOTA-1B50-1 evaluation. Binding affinity and binding specificity of ^{64}Cu-NOTA-1B50-1 were evaluated by various cellular researches. NIR imaging of Cy5.5-1B50-1 was performed in Hep-12 models at 4, 24, 48, 72 and 96 h post-injection. Micro-PET imaging of ^{64}Cu-NOTA-1B50-1 was performed in Hep-12 models or Huh7 models at 2h, 12h and 36h post-injection. Immunofluorescence (IF), immunohistochemistry (IHC) and autoradiography of tumor and main organ were carried out to confirm the expression of α2δ1. **Results:** The radiolabeling yield for 64Cu-NOTA-1B50-1 was 85±0.5 % (n = 5). The average specific activity was 8.2 GBq/μmol (n = 5). The mean radiochemical purity was 98.6 ± 0.6% (n = 5). In Hep-12 cellular uptakes studies, uptake of ^{64}Cu-NOTA-1B50-1 was significantly higher than that of Hep-11 ($P < 0.0001$); higher than the uptake of ^{64}Cu-NOTA-mIgG3 ($p < 0.0001$). The Bmax and Kd values of ^{64}Cu-NOTA-1B50-1 in Hep-12 cells were determined to be 0.9312 nM and 2.7 nM, respectively, showing high binding constant of the radiotracer in the cell line. In NIR images, higher tumor uptake of Cy5.5-1B50-1 could be visualized at all-time points measured (4-96 h) than that of Cy5.5-mIgG3. Furthermore, in micro-PET imaging studies, 64Cu-NOTA-1B50-1 showed a significant higher tumor uptake compared with 64Cu-NOTA-mIgG3 ($p<0.0001$, n=5),and the tumor uptake of ^{64}Cu-NOTA-1B50-1 decreased significantly with 0.5 mg cold 1B50-1 ($p < 0.0001$) further confirmed the specificity. The small lesions (0.3-0.4 cm) were successfully detected by ^{64}Cu-NOTA-1B50-1 PET imaging, and the tumor uptake of α2δ1+ low expression Huh7 models showed 9.90 ± 0.21ID%/g at 36 h. **Conclusion:** We successfully synthesized and evaluated ^{64}Cu-NOTA-1B50-1/Cy5.5-1B50-1 in α2δ1+ Hep12 models. And ^{64}Cu-NOTA-1B50-1/Cy5.5-1B50-1 had a great potential for non-invasive, real-time detection, staging, and follow-up supervision of the dynamic changes of α2δ1+ cells in vivo. It may be possible to early warning of recurrence of HCC at cellular level. **References:** None.

EP-0662

Using Radiolabelled APOMAB® For Non-Invasive ImmunoPET Imaging of Tumour Cell Death Following Chemotherapy

V. Liapis[1], W. Tieu[2], P. Takhar[2], A. Evdokiou[3], M. P. Brown[4], A. H. Staudacher[4];
[1]University of South Australia, Adelaide, AUSTRALIA, [2]Molecular Imaging and Therapy Research Unit, South Australian Health and Medical Research Institute, Adelaide, AUSTRALIA, [3]Discipline of Surgery, Breast Cancer Research Unit, Basil Hetzel Institute and Centre for Personalised Cancer Medicine, University of Adelaide, Adelaide, AUSTRALIA, [4]Translational Oncology Laboratory, Centre for Cancer Biology, SA Pathology and University of South Australia, Adelaide, AUSTRALIA.

Aim/Introduction: Early detection of tumour treatment responses represents an unmet clinical need with no approved non-invasive methods. APOMAB® is an antibody targeting Lupus associated antigen (La/SSB). La is over-expressed in malignancy and selectively targeted by APOMAB in cancer cells dying from DNA-damaging anti-cancer treatment. Therefore, APOMAB is a unique diagnostic tool that detects dead cancer cells in this clinical setting and thus could distinguish between treatment responsive and non-responsive patients.The aim of this study is To evaluate tumour and normal tissue uptake of Zirconium-89-labelled APOMAB in untreated and chemotherapy-treated tumour-bearing mice by whole body positron-emission tomography (PET) imaging. **Materials and Methods:** Mice bearing subcutaneous syngraft or human xenograft tumours were untreated or given cisplatin chemotherapy followed 24h later by intravenous injection of Zr89-APOMAB. Tumour treatment response was monitored using bioluminescence imaging and Zr89-APOMAB uptake was measured using an Albira SI PET imager. **Results:** Although tumour uptake of APOMAB was detected in untreated mice, uptake significantly increased in both syngeneic and human tumours of lung and ovarian cancers after chemotherapy but not in normal tissues. **Conclusion:** APOMAB® is a selective in vivo marker of chemotherapy-induced tumour cell death in both syngeneic and xenograft tumours. Given that tumour tissue, rather than normal tissues, was targeted after chemotherapy, these results support the clinical development potential of APOMAB® as both a predictive marker of treatment response and a theranostic imaging agent, which might guide delivery of APOMAB®-directed antibody radio or drug conjugate therapies. **References:** None.

EP-0663

"Theranostics" - Radioimmunodetection and Radioimmunotherapy for Metastatic Colorectal Cancer in Preclinical Cancer Models

T. Cuda[1], P. Thomas[2], S. Rose[3], S. Puttick[3], J. Hooper[1], Cancer Cell Biology Team, Mater Research Institute- The University of Queensland;
[1]The University of Queensland - Mater Research Institute, Brisbane, AUSTRALIA, [2]Royal Brisbane and Women's Hospital, Brisbane, AUSTRALIA, [3]CSIRO, Brisbane, AUSTRALIA.

Aim/Introduction: Worldwide, colorectal cancer is the third most common malignancy and forth leading cause of cancer-related death. The five-year survival for localised disease is 90%, but this plummets to 10% for metastatic disease[1]. The non-specific nature of current chemotherapeutic regimes results in varying degrees of systemic toxicity and myelosuppression, limiting disease control and survival[2]. Our laboratory has employed a monoclonal antibody (mAb) to a transmembrane glycoprotein, known to be overexpressed on the surface of colorectal cancer cells with minimal expression in normal tissue, in a theranostic approach for colorectal cancer. This project assessed the novel radiolabelled mAb as a cancer-specific PET imaging radioligand and a therapeutic radioligand for colorectal cancer in preclinical cancer models. **Materials and Methods:** As a diagnostic radioligand, we assessed the avidity during PET imaging of our Zirconium-89 (^{89}Zr)-mAb in detecting colorectal cancer in a range of mouse models. In a therapeutic phase, we performed tumour burden and survival experiments on mice carrying patient-derived colorectal cancers randomised into the following groups: 1) no treatment; 2) 5-fluorouracil (5FU) - a chemotherapy used as current standard of care; 3) a single dose of the therapeutic radioligand Lutetium-177 (^{177}Lu)-mAb; or 4) combination therapy of 5FU and a single dose of ^{177}Lu-mAb. **Results:** During the diagnostic PET imaging phase, we found that ^{89}Zr-mAb demonstrated significantly higher avidity than control radioligands for colorectal cancer. In the therapeutic phase of the study, a single dose of ^{177}Lu-mAb was significantly more effective than three doses of the chemotherapy regime 5FU at slowing tumour growth. ^{177}Lu-mAb improved the efficacy of chemotherapy thus opening the possibility of using the radioligand as a single agent or concurrently with chemotherapy. **Conclusion:** The current overall survival of patients with metastatic colorectal cancer is dismal. The emerging field of theranostics may offer a new therapy for patients with metastatic colorectal cancer. This study demonstrates proof of concept of a radiolabelled mAb specific to a transmembrane glycoprotein as both a radioimmunodetection and radioimmunotherapy agent for the prognostication and treatment of colorectal cancer in preclinical mouse models. Our future prospects will work towards eventual clinical trial. **References:** 1. Belov L, Zhou J, Christopherson RI. Cell surface markers in colorectal cancer prognosis. International journal of molecular sciences 2010; 12(1): 78-113.2. Master AM, Sen Gupta A. EGF receptor-targeted nanocarriers for enhanced cancer treatment. Nanomedicine (London, England) 2012; 7(12): 1895-906.

EP-0664

^{68}Ga labeling, quality Control and preliminary Biological Evaluation of tumor PDL1 targeting Molecular NOTA-WL12

J. Jiang, *Z. Hua, Y. Zhi;*
Peking University, Beijing, CHINA.

Aim/Introduction: tumor immunotherapy is a new method of tumor treatment after surgery, radiotherapy and chemotherapy, but only some solid tumor patients can benefit from it. It is of great significance to screen the positive patients who have curative effect response to tumor immunotherapy. In this paper, a new polypeptide NOTA- WL12, with PD-L1 targeting was designed and synthesized, and the radioactivity labeling, quality control and preliminary biological evaluation of ^{68}Ga were carried out. It is expected that ^{68}Ga-NOTA- WL12 can be used to screen patients with tumor clinical immunotherapy as soon as possible **Materials and Methods:** in this project, 14 amino acid cyclic sequences WL12, were synthesized and obtained by peptide automatic synthesizer, and the target molecular probes which could be used for radiation labeling were obtained by means of amino coupling bifunctional chelating agent NOTA. NOTA-WL12, the peptide was confirmed by HPLC and MS. Then, the radionuclide ^{68}Ga was labeled and the ^{68}Ga -NOTA-WL12 PET molecular probe was obtained. The labeling efficiency was determined by Radio- HPL/TLC and the stability in vitro and in vivo was studied. The metabolism of HT29 and MDA-MB- 231mice in vivo was observed by Micro-PET equipment. **Results:** the NOTA-WL12 HPLC retention time 9.26 Min of 10mg grade, which can be used for radiochemical labeling, was synthesized in this project. Radio-HPLC analysis showed that the labeling rate was more than 95% and the radiochemical purity was more than 99%. The ^{68}Ga-NOTA-WL12 probe showed good radiochemical properties with a specific activity of 27.8-111.2 GBq/umol. In vitro stability studies showed that it remained 90% stable in 5% calf serum buffer for 4 h. Micro-PET imaging was performed at 1.0h after intravenous injection of 5.5 MBq . In the tumor lesions of mice with high expression of PD-L1, the radioactivity uptake was significantly increased, but no obvious radiation community was found in the tumor lesions of the negative control group. **Conclusion:** NOTA-WL12 peptide was designed and synthesized in this study. the PDL1 targeted NOTA-WL12 was radiolabeled by ^{68}Ga, and the ^{68}Ga-NOTA-WL12 molecular probe was obtained. The probe has good radiochemical properties, in vitro stability and good metabolic properties. The synthesis and preliminary biological evaluation of ^{68}Ga-NOTA- WL12 probe show that it is expected to be used in the screening of patients with tumor clinical immunotherapy. **References:** None.

EP-0665

Combined PET and MR imaging of HET-CAM xenografts for evaluation of targetspecific binding of radioligands

G. Winter[1], *A. B. F. Koch*[1], *J. Löffler*[1,2], *C. Solbach*[1], *G. Glatting*[3], *V. Rasche*[2], *A. J. Beer*[1];
[1]*Department of Nuclear Medicine, Ulm University, Ulm, GERMANY,* [2]*Center for Translational Imaging, Internal Medicine II, Ulm University, Ulm, GERMANY,* [3]*Medical Radiation Physics, Department of Nuclear Medicine, Ulm University, Ulm, GERMANY.*

Aim/Introduction: Specificity to the target structure is one of the main selection criteria in the development of new specific agents for oncological diagnosis and therapy. These data are obtained from tests in mice and an appropriate animal

experiment permit is required. The Hens egg test-chorioallantoic membrane (HET-CAM) model offers an excellent alternative in terms of animal welfare according to the 3R principles (Replacement, Reduction, Refinement) and does not require an animal experiment permit. An undeveloped immune response system allows the growth of vascularized tumor xenografts on the membrane surface and a determination of the target-specific accumulation of the drug of interest. [^{68}Ga]PSMA-11 was used to demonstrate the principle of the HET-CAM model for assessing specific radiotracer accumulation. **Materials and Methods:** Tumor xenografts were established by application of PSMA-positive cell line LNCaP C4-2 (1x10^6 cells) and the PSMA-negative control PC-3 (7.5x10^5 cells) in combination with matrix (40%, v/v) in silicon rings on the CAM on embryo development day (EDD)7. Between EDD12 to 14 MR and PET imaging was performed. Anatomical information was obtained by high-resolution imaging using a small animal MR (BioSpin 117/16, Bruker) [1]. For PET imaging 150µl [^{68}Ga]PSMA-11 solution was prepared and injected into a CAM vessel, followed by a dynamic 60-minute PET scan (Focus 120, Concorde Microsystems Inc.). Quantitative evaluation of tumor accumulation was achieved by gamma counter measurements (COBRA II, Perkin Elmer). Using reference point registration in 3D slicer software [2] MRI and PET data were superimposed. **Results:** Tumor growth could be successfully visualized by MRI. In PET, accumulation of [^{68}Ga]PSMA-11 was observed in the PSMA-positive tumor and in the chick embryo. According to the gamma counter measurements there was a significantly higher accumulation of [^{68}Ga]-PSMA-11 observed in LNCaP C4-2 tumors in comparison to PC-3: (0.26±0.71) %ID (LNCaP C4-2); (0.07±0.05) %ID (PC-3); (n=20). A ratio of (4.2±4.0) (PSMA-specific/non-specific) was calculated. Time-activity curves demonstrated an increasing tracer accumulation over time of (8.5±2.6) % in LNCaP C4-2. **Conclusion:** Quantitative evaluation of the specificity of radiotracer accumulation by PET using the HET-CAM model with xenografts was successfully demonstrated. Fusion of PET and MR images allowed for combined analysis of molecular PET data and high-resolution anatomical information. According to the 3R principle, the HET-CAM model could be used for the evaluation of new radiopharmaceuticals as an alternative for mouse experiments. **References:** [1] Zuo, Z. et al. 2017 and 2015. [2] Fedorov, A. et al. 2012.

EP-0666

Radiobiological effect of in vitro ^{99m}Technetium labelling of red blood cells. Study with micronucleus assay in human peripheral blood lymphocytes

A. Abella Tarazona[1], *M. Asensio Ruiz*[1], *Á. García Aliaga*[1], *T. Chivato Martín-Falquina*[2], *M. Martínez Martínez*[1];
[1]*Hospital Clínico Universitario Virgen de la Arrixaca, Murcia, SPAIN,* [2]*Hospital General Universitario Santa Lucía, Cartagena, SPAIN.*

Aim/Introduction: The purpose of this study is to evaluate by the cytokinesis-blocked micronucleus assay the degree of cytological radiation damage to lymphocytes occurring after in vitro Tc-99m labelling of red blood cells. **Materials and Methods:** The blood obtained from healthy voluntary donors (n=4) was processed and radiolabelled with different activities (3.7, 37, 185, 370 MBq and 740MBq) following the Procedure Guideline from the Royal Spanish Pharmacopea. After radiolabelling, 1ml of each sample, together with 1 ml of control sample and 1 ml of stannous control, were added respectively to 7 ml lymphocyte-selective medium and cultured at 37ºC for 72h. Cytochalasin B at a final concentration of 6 µg/ml was added 44h after the beginning of the culture to block cytokinesis. At the end of the incubation the cells were harvested, treated with a hypotonic solution containing 0.075 M KCl and fixed with a mixture of methanol:glacial acetic acid (3:1). Slides were stained with Giemsa at 5% and micronuclei were scored in 1000 binucleated cytokinesis-blocked cells. **Results:** Labelling efficiency was 92.7 ±2.6 (n= 20) The number of micronucleus scored in 1000 binucleated cells was 7±4 for control and 10±6 for stannous control. After incubation of isolated lymphocytes with 3.7, 37, 185 and 370 MBq, micronucleus scored in 1000 binucleated cells were 8±7, 19±4, 45±19, 102±25. Scoring of micronucleus was not posible in the labelling experiments with 740 MBq due to an almost complete impairment of the proliferation capacity of lymphocytes. **Conclusion:** The damage produced during the labelling of red blood cells with Tc-99m was slightly higher compared to the control and stannous control and it was proportional to radiolabelling activity.Compared with leukocyte labelling, the damage obtained in our results were much lower and agrees with the results of other authors in the evaluation of external leukocyte irradiation. It is an aspect to take into account in case of pediatric patients, with whom smaller activities are used and there is the possibility of injecting aberrant lymphocytes. **References:** Radiopharmaceutical Procedure Guideline Number 6. Royal Spanich Pharmacopea Available at: https://www.aemps.gob.es/medicamentosUsoHumano/farmacopea/informacionRFE/guia6.htm [Accessed 24 April 2019] Thierens HM, Vral AM, Van Haelst JP, Van de Wiele C, Schelstraete KH, de Ridder LI. Lymphocyte labeling with Technetium-99m-HMPAO: A radiotoxicity study using the micronucleus assay. J Nucl Med 1992;33(6):1167-74. Miñana E, Roldan M, Chivato T, Martínez T, Fuente T. Quantification of the chromosomal radiation damage induced by labelling of leucocytes with [18F]FDG. Nucl Med Biol 2015;42:720-723.

EP-0667

Preclinical evaluation of ^{68}Ga-DOTA-NT-20.3: A promising PET imaging probe to discriminate human pancreatic ductal adenocarcinoma from pancreatitis

A. Prignon;
Sorbonne Universite, Paris, FRANCE.

Aim/Introduction: Neurotensin receptor 1 (NTSR1) is overexpressed in human pancreatic ductal adenocarcinoma (PDAC). Specific non-invasive PET imaging probes may improve diagnostic accuracy and the monitoring of therapy for patients with PDAC. Here, we report the use of the ^{68}Ga-

labeled neurotensin (NTS) analogue DOTA-NT-20.3 to image human PDAC in animal models and to discriminate tumors from pancreatitis. **Materials and Methods:** PET imaging, biodistribution, blocking and histology studies were performed in subcutaneous AsPC-1 pancreatic tumor-bearing mice. In addition to the preclinical study, two tissue microarrays slides, constructed by small core biopsies (2 to 5) from standard paraffin-embedded tumor tissues were used to confirm the high (78%) positivity rate of NTSR1 expression in human PDAC. **Results:** ^{68}Ga-DOTA-NT-20.3 PET images showed rapid tumor uptake and high contrast between tumor and background with a fast blood clearance and a moderate accumulation in the kidneys. Ex vivo biodistribution showed low uptake in normal pancreas (0.22 %IA/g) and in remaining organs at 1 h post-injection, kidney retention (5.38 ± 0.54 %IA/g), fast clearance from blood and confirmed high uptake in tumors (5.28 ± 0.93 %IA/g) leading to a tumor-to-blood ratios values of 6 at 1 h post-injection. The significant decrease of tumor uptake in a blocking study demonstrated the specificity of ^{68}Ga-DOTA-NT20.3 to target NTSR1 in vivo.PET imaging was also conducted in an orthotopic xenograft model that allows tumors to grow in their native microenvironment and in an experimental pancreatitis model generated by caerulein injections. As opposed to ^{18}F-FDG, ^{68}Ga-DOTA-NT-20.3 distinguishes PDAC from pancreatitis. **Conclusion:** Thus, ^{68}Ga-DOTA-NT-20.3 is a promising PET imaging probe for imaging PDAC in humans. **References:** None.

EP-0668

Role of Syndecan Gene in the Pathogenesis of Liver Damage in Radioactive Iodine-131 Therapy

N. Yumusak[1], *A. Yigin*[2], *H. Atilgan*[3], *A. Kalayci Yigin*[4], *G. Koca*[5], *R. Yilmaz*[1], *M. Korkmaz*[5];
[1]*Department of Pathology, Harran University Faculty of Veterinary Medicine, Sanliurfa, TURKEY,* [2]*Department of Genetic, Harran University Faculty of Veterinary Medicine, Sanliurfa, TURKEY,* [3]*Department of Nuclear Medicine, Mustafa Kemal University, Hatay, TURKEY,* [4]*Cerrahpasa Medical Faculty, Istanbul University, Istanbul, TURKEY,* [5]*Department of Nuclear Medicine, Ankara Training and Research Hospital, Ankara, TURKEY.*

Aim/Introduction: The aim of this study was to investigate the presence of Syndecan gene in iodine-131(^{131}I) induced liver damage of rats after high-dose treatment. **Materials and Methods:** Fifty Wistar Albino rats were divided into five, as ten rats in each group. 111 Mbq/kg ^{131}I was administered to each rat in all experimental groups except the control. The control group consisted of rats with no intervention. 6th h, 24th h, 7th day and 30th days on the study the animals were sacrificed, and the evaluation of biodistribution and histopathological studies were performed on the livers removed. Western-blot, Real-time PCR and immunohistochemistry were carried out for Syndecan gene expression, and the differences between the groups were statistically evaluated. **Results:** Syndecan gene expression was observed to increase in the all ^{131}I-administered (6th h, 24th h, 7th day and 30th days) groups (P<0.01), whereas there was no expression in the control group. Immunohistochemical staining pattern in the extracellular source was observed in the overexpressed Syndecan groups (P<0.01). Histopathologically, there was difference for hyperemia, double nucleus, perivascular fibrosis, inflammatory cells and capsule thickening parameters in terms of incidence between the control and ^{131}I groups that shows the harmful effect of ^{131}I (P<0.01). **Conclusion:** The expression level of Syndecan gene was significantly upregulated in the ^{131}I administered groups. These results suggested that Syndecan genes might play a role in ^{131}I induced liver damage. **References:** None.

EP-0669

In-vivo ^{18}F-fluoro-thymidine Positron Emission Imaging For Disease Monitoring In A Mouse Model Of High-risk Myelodysplastic Syndrome

L. Sarda-Mantel[1], *F. Hontonnou*[2], *B. Hosten*[1], *N. Vignal*[1], *C. San*[1], *M. Pla*[3], *P. Fenaux*[4], *P. Kriet*[3], *C. Chomienne*[4], *R. Padua*[3];
[1]*Unité Claude Kellershohn, IRSL, Université Paris Diderot, APHP Lariboisière Saint-Louis, Paris, FRANCE,* [2]*Unité Claude Kellershohn, IRSL, Université Paris Diderot, Paris, FRANCE,* [3]*Inserm U1131, IRSL, Université Paris Diderot, Hôpital Saint-Louis, Paris, FRANCE,* [4]*Inserm U1131, IRSL, Université Paris Diderot, APHP Hôpital Saint-Louis, Paris, FRANCE.*

Aim/Introduction: High-risk myelodyspastic syndrome (HR-MDS) is characterized by decreased apoptosis of bone marrow precursors which correlates with expression of BCL-2 protein , and is at risk of evolving to acute myeloid leukemia with increased bone marrow blasts. This disease occurs in elderly patients and has a poor prognosis in the absence of efficient treatment. The evaluation of new therapeutic agents in animal models of the disease is hampered by the absence of accurate in vivo biomarkers to follow the effect of the treatments, because bone marrow biopsy is not easy in mice. ^{18}F-fluoro-thymidine Positron Emission Tomography (FLT-PET) allows in vivo quantification of cell proliferation and has been suggested for the diagnosis and follow-up of myelodysplastic disorders in patients. Our aim was to evaluate the ability of FLT-PET to monitor bone marrow involvement in our triple transgenic MMTVtTA/TetoBCL-2/MRP8NRASD12 mouse model of HR-MDS. **Materials and Methods:** We investigated 3 groups of mice (FVB/N strain): normal controls (G1, n=7), 2-months old HR-MDS mice (G2, n=8), and 3 months-old HR-MDS mice (G3, n=8). All mice underwent FLT-PET/CT imaging (Inveon microPET/CT, Siemens), after intravenous injection of 7-10 Mbq of [^{18}F]FLT. Static acquisitions were acquired 1h15 after radiotracer injection. [^{18}F]FLT uptake in femoral bone marrow was quantified and normalized by the background blood pool activity, by using volumes of interest drawn on the femurs and the heart. Just before PET/CT, peripheral blood samples were taken for blood counts, and for BCL-2 and Mac-1hi/Gr1lo (blast cells) expression measurements. **Results:** Peripheral blood platelet counts were 1055±221, 895±118 and 823±181 x10^3/mm^3 in G1, G2 and G3

respectively (NS). BCL-2 expression was 1.2±1.1% in G1, 18±4% in G2 (vs G1: p<0.001) and 33±13% in G3 (vs G1: p<0.02, vs G2: p<0.05). Mac-1hi/Gr1lo expression was 1.3±1.8% in G1, 15±10% in G2 (vs G1: NS) and 24±2% in G3 (vs G1: p<0.002; vs G2: NS). [^{18}F]FLT-PET images of HR-MDS mice showed asymetric hot spots in femoral diaphyses, and sometimes in humerus. PET contrast in femoral bone marrow was 1.07±0.21 in G1, 1.62±0.67 in G2 (vs G1: p<0.03) and 2.07±1.08 in G3 (vs G1:p<0.02; vs G2:NS). **Conclusion:** [^{18}F]FLT-PET imaging shows femoral bone marrow abnormalities in HR-MDS mice, with intensity increasing with age, BCL-2 and Mac-1hi/Gr1lo blood expressions whereas platelets counts inversely decrease. These results suggest that [^{18}F]FLT-PET imaging is a surrogate non-invasive quantitative marker of HR-MDS bone marrow involvement and may be used for therapy monitoring in our mouse model. **References:** None.

EP-0670

Developing Peptide based Nanoconstructs as Potential Theranostic Agents

I. U. Khan[1], *E. Achilli*[2], *R. Zahoor*[1], *A. Fatima*[1], *M. Sohaib*[1], *A. Shahid*[1], *C. Flores*[2], *M. Grasselli*[2], *A. R. Jalilian*[3];
[1]*Institute of Nuclear Medicine and Oncology (INMOL), New Campus Road, Lahore, PAKISTAN,* [2]*Laboratorio de Materiales Biotecnológicos, Universidad Nacional de Quilmes-IMBICE (CONICET), Bernal, ARGENTINA,* [3]*Department of Nuclear Science and Applications, International Atomic Energy Agency (IAEA), Vienna, AUSTRIA.*

Aim/Introduction: The acronym THERANOSTICS epitomizes the inseparability of diagnosis and therapy, the pillars of medicine and takes into account personalized management of disease (usually based on nanomedicine) for a specific patient. Nanomedicines, especially in round shape particles or nanoparticles (NPs), are studied for application in the field of diagnosis and treatment of cancer. In this research work, we report on developing novel hybrid NPs (HNPs) prepared with a gold core and a multilayer coating of albumin (Alb) stabilised by a novel radiation-induced crosslinking method. The resultant bioconjugate thus possesses characteristics that make it highly biocompatible and a multifunctional platform for covalent immobilization of peptides. **Materials and Methods:** HNPs were decorated with a DOTA-Bombesin synthetic peptide in order to address cancer cells which overexpress GRP receptors. For fluorescence detection experiments, NPs were labeled with NHS ester BODIPY 630/650. Confocal microscope pictures were captured with Olympus FV300/BX61 microscope. Flow Cytometry analyses were performed with a BD FACSCalibur® cytometer. Briefly, cells were incubated for 1, 2 or 4 h with NPs diluted in the complete medium. Data acquisition and analyses were performed using the BD CellQuest Pro software package, recording 20,000 events. Radiolabeling was done with ^{177}Lu/^{68}Ga and tested the biological compatibility of novel radio-bioconjugate in rabbit animal models. **Results:** The conjugation of novel albumin-gold NPs with DOTA-BBN was characterized by the plamon peak and absorbance at 280 nm. The increment of absorbance at 280 nm shows the conjugation of peptide with albumin-gold nanoparticles. Flow cytometry analysis and confocal microscopy were applied to study the in-vitro specific interaction of these nanoconstructs to PC-3 and NCI-H460 cell lines. Furthermore, we tested the cytotoxicity of novel nano constructs by using 3T3 and Hela cells. The binding affinity of the decorated HNPs to gastrin-releasing peptide (GRP) receptor was tested by using PC-3; which was found in nanomolar range. The radiolabeling yield in most cases was >90%. The clinical potential of these radiolabeled nano bioconstructs was ultimately evaluated in tumor-bearing mice that showed siginificant uptake in tumor xenografts. **Conclusion:** Novel radiolabeled nanoconstructs based on gold NPs stabilized with many Alb layers may have great potential to be further evaluated as feasible tumor-seeking agents. This approach might be further extended to a tumor-specific targeting by using various neuropeptide derivatives as carrier of chemotherapeutic agents and should be tested in various malignancies beyond prostate cancer, thus ultimately, used as a future tool for Peptide Receptor Radionuclide Therapy. **References:** None.

EP-0671

Preclinical translational bridge studies supporting advancement of ^{111}In-Bn-DTPA-NLS-trastuzumab to Phase I clinical trial in patients with HER2-positive breast cancer

C. Chan[1], *Z. Cai*[1], *S. Done*[2,3], *R. Reilly*[1,4];
[1]*Departments of Pharmaceutical Sciences and Medical Imaging, University of Toronto, Toronto, ON, CANADA,* [2]*Laboratory Medicine and Pathobiology, University of Toronto, Toronto, ON, CANADA,* [3]*Laboratory Medicine Program, University Health Network, Toronto, ON, CANADA,* [4]*Toronto General Research Institute, University Health Network, Toronto, ON, CANADA.*

Aim/Introduction: ^{111}In-Bn-DTPA-NLS-trastuzumab is a novel Auger electron-emitting RIT agent for HER2-positive breast cancer (BC). Our aim was to conduct preclinical translational bridge studies (pharmacokinetics (PK), radiation dosimetry, biodistribution and acute toxicity) to support the advancement of ^{111}In-Bn-DTPA-NLS-trastuzumab to Phase I clinical trial in patients with HER2-positive BC that will evaluate tumour and normal tissue uptake and dosimetry by SPECT imaging. **Materials and Methods:** Biodistribution studies were performed up to 144h p.i. in Balb/c mice injected i.v. with ^{111}In-Bn-DTPA-NLS-trastuzumab (60 µg; 6.1 MBq). Tissue uptake was expressed as %ID/g and converted to %ID/organ using organ weights. Cumulative radioactivity ($\tilde{A}_s$) in each source organ up to 144h p.i. was calculated by integrating the radioactivity vs. time curves. $\tilde{A}_s$ values were used to project radiation doses to target organs in humans using OLINDA/EXM. PK studies were performed after i.v. injection of ^{111}In-Bn-DTPA-NLS-trastuzumab (60 µg; 5.8 MBq). Blood samples were obtained up to 144h p.i. and ^{111}In concentration vs. time plotted and fitted to a 2-compartment PK model. Standard PK parameters were estimated. Acute toxicity studies were performed in Balb/c

mice injected i.v. with ^{111}In-Bn-DTPA-NLS-trastuzumab (60 μg; 0.9 MBq) which corresponded to 21-times and 30-times the planned radioactivity and mass doses, respectively for the Phase 1 trial on a MBq/kg and mg/kg basis. Toxicity was assessed by body weight, serum alanine aminotransferase (ALT) and creatinine (SCr), complete blood counts (CBC), hemoglobin (Hb), hematocrit (Hct) and histopathological examination of tissues at 14 days. **Results:** Organs with the highest uptake were blood, muscle and bone (21.1±2.1, 3.4±0.6 and 2.5±0.4 %ID/organ, respectively at 144h p.i.) The projected whole body dose to humans for ^{111}In-Bn-DTPA-NLS-trastuzumab was 0.052 mSv/MBq corresponding to 5.8 mSv for the Phase I dose (111 MBq; 5 mg). The highest normal organ doses were received by the bone, kidneys and liver (0.205, 0.08 and 0.07 mSv/Bq, respectively). ^{111}In-Bn-DTPA-NLS-trastuzumab exhibited biexponential elimination from blood with an α-phase half-life of 2.2h and β-phase half-life of 50.3h. There was no significant difference in body weight of mice receiving ^{111}In-Bn-DTPA-NLS-trastuzumab compared to mice treated with unlabeled Bn-DTPA-NLS-trastuzumab or normal saline. Similarly, there were no significant differences in CBC, Hb, Hct or serum ALT or SCr in mice treated with ^{111}In-Bn-DTPA-NLS-trastuzumab compared to control groups. No morphological changes in tissues were observed. **Conclusion:** Preclinical translational bridge studies indicate that ^{111}In-Bn-DTPA-NLS-trastuzumab will be safe to administer to patients with HER2-positive BC at an amount of 111 MBq (5 mg). **References:** None.

EP-0672

Evaluation specific infection in severe acute pancreatitiswith a novel probe ^{18}F-FDS

Z. Zhu[1,2], *Q. Peng*[3], *J. Li*[4], *Q. Wang*[5], *X. Zhang*[4], *X. Su*[5], *S. Hu*[1,2];
[1]*Department of PET Center, Xiangya Hospital, Central South University, Changsha, CHINA,* [2]*National Clinical Research Center for Geriatric Disorders (XIANGYA),* *Xiangya Hospital, Central South University, Changsha, CHINA,* [3]*Department of Pharmacy, Xiangya Hospital, Central South University, Changsha, CHINA,* [4]*School of Public Health, Xiamen University, Xiamen, CHINA,* [5]*Department of Nuclear Medicine,Zhongshan Hospital ,Xiamen University, Xiamen, CHINA.*

Aim/Introduction: Severe acute pancreatitis (SAP) is the most serious type of acute pancreatitis associated with high morbidity and mortality.Even more,when there is a secondary infection,it will be more dangerous.So it is very important to diagnose whether SAP is associated with secondary infection or not at an early stage. But so far there is no ideal method for initial clinical diagnosis.In this study, we utilize 2-^{18}F-fluorodeoxysorbitol (^{18}F-FDS) as a PET/CT tracer and try to identify SAP with kinds of infections on PET imaging at early stage. **Materials and Methods:** 36 male Sprague-Dawley rats were randomly divided into 3 groups and were injected with sodium tauronate firstly and then followed by 3 kinds of bacterias (Escherichia coli, Staphylococcus aureus and Inactivated Escherichia coli) respectively to induce SAP model with infections. Blood samples were collected at 3 time points for 0h,1h,3h after modeling to detect serum amylase and do blood routine analysis.Then the rats were performed with the PET/CT scan with ^{18}F-FDS and ^{18}F-FDG respectively at 3h and 6h(3 rats for ^{18}F-FDG or ^{18}F-FDS PET imaging each time point).After that,the animal welfare was executed, and the autoradiography, biodistribution were analyzed.HE staining and Graman staining were performed as well. **Results:** In the early 3h of PET/CT imaging after modeling, ^{18}F-FDS was observed to accumulate in the pancreatic site of E. coli-infected SAP model rats, and it was more evident at 6 h after modeling, and the diffusion range was greater.No significant was seen in the others. PET SUV values of ^{18}F-FDS in Escherichia coli, Staphylococcus aureus and inactivated Escherichia coli were 2.7±0.06, 1.03±0.19 and 0.67±0.18, respectively. There is a significant difference between the values of the E. coli group and the others (E.coli vs S.aureus, q=8.96, p<0.01; E.coli vs inactivated E.coli q=9.35, p<0.01). ^{18}F-FDG showed significant aggregation in each group (2.07±0.21 in the E.coli group, 2.30±0.53 in the S.aureus group, and 1.80±0.11 in the inactivated E.coli group).No significant differences were noted (F=1.69, p=0.26). Biodistribution results also showed that the ^{18}F-FDS of E. coli group had a pancreatic tissue distribution value of 1.25±0.17% ID/g;which is higher than the others(0.50±0.16% ID/g and 0.47±0.09%ID/g,F=28, P=0.0009).While the ^{18}F-FDG Biodistribution results showed no significant difference among these groups (1.34±0.11%ID/g,1.39±0.12%ID/g,1.21±0.12%ID/g;F=1.923, P=0.2263). **Conclusion:** ^{18}F-FDS PET imaging maybe is a promising method for evaluating of specific secondary infection in severe acute pancreatitis at an early stage.The imaging characteristics can be recognized as early as 3h after SAP onset. **References:** None.

EP-0673

RGDyc Peptide-modified Pamam Dendrimer Conjugates Labeled With Radionuclide ^{131}I For SPECT Imaging And Radiotherapy Of Lung Carcinoma

Z. Jinhe;
General Hospital of Southern Theater Command, PLA, Guangzhou, CHINA.

Aim/Introduction: Arginine-glycine-aspartic acid-tyrosine-cysteine (RGDyC)-modified PAMAM dendrimer labeled with radionuclide iodine-131 (^{131}I) was synthesized and utilized for targeted single photon emission computed tomography (SPECT) imaging and radiotherapy of cancer. **Materials and Methods:** In this study, amine-terminated poly(amidoamine) (PAMAM) dendrimer of fifth generation (G5) was used as a platform to conjugate with PEGylated arginine-glycine-aspartic acid-tyrosine-cysteine(RGDyC) peptide, followed by acetylation of the remaining terminal amines. Then the dendrimer was labeled with radioactive ^{131}I to form the targeted nanoplatform ^{131}I-RGDyC-PEG-PAMAM. The targeting and therapeutic effects were subsequently evaluated in vitro and in vivo. **Results:** We show that the PAMAM platform possesses approximately 33 PEG and 5.7 RGDyC moieties on each PAMAM. The dendrimer

platform can target human lung carcinoma A549 cells over expressing αvβ3 integrin due to the attached RGD. With the attached tyrosine moiety having the phenol group, the dendrimer platform can be effectively labeled with ^{131}I with high radiochemical purity and good stability. Importantly, the ^{131}I labeling renders the dendrimer platform with an ability to be used for targeted SPECT imaging and radiotherapy of an αvβ3 integrin-overexpressing lung carcinoma model in vivo. **Conclusion:** The developed targeted theranostic dendrimeric nanoplatform ^{131}I-RGDyC-PEG-PAMAM may hold promise to be used for targeted theranostics of human carcinoma. **References:** Shih YW, Chien ST, Chen PS, et al. α-Mangostin Suppresses Phorbol 12-myristate 13-acetate-Induced MMP-2/MMP-9 Expressions via αvβ3 Integrin/FAK/ERK and NF-κB Signaling Pathway in Human Lung Adenocarcinoma A549 Cells. Cell Biochemistry & Biophysics. 2010;58(1):31-44.Ding GB, Wang Y, Guo Y, et al. Integrin α(V)β(3)-targeted magnetic nanohybrids with enhanced antitumor efficacy, cell cycle arrest ability, and encouraging anti-cell-migration activity. ACS applied materials & interfaces. 2014;6(19):16643.

EP-44

Preclinical and translational aspects, including radiopharmacy, radiochemistry and drug development -> Preclinical and translational aspects -> Preclinical aspects -> Biology, benign disease

October 12 - 16, 2019 e-Poster Area

EP-0674

On the reduction of uptake of radiolabeled DARPins in kidneys

A. Vorobyeva[1], *M. Altai*[1], *J. Garousi*[1], *S. S. Rinne*[1], *A. Schulga*[2], *S. Deyev*[2,3];
[1]*Uppsala University, Uppsala, SWEDEN,* [2]*Shemyakin & Ovchinnikov Institute of Bioorganic Chemistry, Moscow, RUSSIAN FEDERATION,* [3]*National Research Nuclear University "MEPhI", Moscow, RUSSIAN FEDERATION.*

Aim/Introduction: Designed ankyrin repeat proteins (DARPins) are small engineered scaffold proteins with molecular weight of 14-18 kDa. Radiolabeled DARPins 9_29 and G3 demonstrated high-contrast imaging of HER2 at the day of injection in preclinical studies. Their small size provides fast extravasation into tumors and efficient renal excretion enables rapid achievement of high tumor-to-organ ratios. However, high renal accumulation of activity for DARPins labeled with residualizing labels is a limitation for targeted radionuclide therapy. Better understanding of the mechanisms behind kidney uptake of DARPins could aid in the development of strategies to reduce it. In this study we have investigated whether the renal uptake of [^{99m}Tc]Tc(CO)$_3$-G3 could be reduced by administration of compounds that act on various parts of the reabsorption system in kidney. **Materials and Methods:** Biodistribution and renal uptake of [^{99m}Tc]Tc(CO)$_3$-G3 was measured ex vivo in healthy female NMRI mice 4 h after injection of the tracer. The effect of lysine and gelofusine (megalin ligands), colchicine (microtubule inhibitor), probenecid (organic anion transport inhibitor), mannitol (osmotic diuretic), furosemide (loop diuretic) as well as sodium maleate and fructose (decrease intracellular ATP) on renal uptake of [^{99m}Tc]Tc(CO)$_3$-G3 was investigated. The effect of maleate was additionally studied for another DARPin variant, [^{99m}Tc]Tc(CO)$_3$-9_29. Autoradiography of kidney sections was used to study the localization of activity in kidneys. **Results:** Co-injection of lysine or gelofusine was not effective for reduction of kidney uptake of [^{99m}Tc]Tc(CO)$_3$-G3. Administration of sodium maleate before the injection of [^{99m}Tc]Tc(CO)$_3$-G3 reduced its kidney-associated activity by 60.4 ± 10.3%, while administration of fructose reduced it by 46.9 ± 7.6% compared to the control. The decrease in kidney uptake provided by sodium maleate was also observed for [^{99m}Tc]Tc(CO)$_3$-9_29. Pre-injection of colchicine, probenecid, mannitol or furosemide had no effect on kidney uptake of [^{99m}Tc]Tc(CO)$_3$-G3. Kidney autoradiography showed mainly cortical accumulation of activity for all studied groups. **Conclusion:** The ineffectiveness of lysine to lower the kidney uptake of [^{99m}Tc]Tc(CO)$_3$-G3 suggests that its re-uptake is not driven by megalin receptor system. Both fructose and maleate lower the cellular ATP level in proximal tubule cells and their reduction of kidney re-uptake indicates the involvement of an ATP-driven mechanism of uptake. The decrease provided by maleate for both DARPins, G3 and 9_29, indicates that their uptake proceeds through a mechanism independently of DARPin scaffold composition. **References:** None

EP-45

Preclinical and translational aspects, including radiopharmacy, radiochemistry and drug development -> Preclinical and translational aspects -> Preclinical aspects -> Tumor biology

October 12 - 16, 2019 e-Poster Area

EP-0675

Application of ^{18}F-FMISO in Determination of Hypoxia Level in Murine CT26 Tumors During Various Stages of Development

L. Kiraga[1], *L. Cheda*[2], *B. Taciak*[1], *K. Różańska*[1], *K. Tonecka*[3], *A. Szulc*[3], *K. Kilian*[2], *E. Górka*[1], *Z. Rogulski*[2], *T. P. Rygiel*[3], *M. Król*[1];
[1]*Warsaw University of Life Sciences, Warsaw, POLAND,* [2]*University of Warsaw, Warsaw, POLAND,* [3]*Medical University of Warsaw, Warsaw, POLAND.*

Aim/Introduction: The aim of this research was to determine levels of hypoxia at various stages of tumor development using positron emission tomography (PET) and to compare

different methods of hypoxia evaluation in pre-clinical CT26 tumor model. **Materials and Methods:** For the experiments, BALB/c mice (females, 8-12 weeks old) were used. Each mouse was inoculated intramuscularly with CT26 cells (murine colonorectum carcinoma) in the right lower leg. Evaluation of hypoxia level was performed by intravenous administration of [^{18}F]fluoromisonidazole ([^{18}F]FMISO) followed by PET-CT imaging at the day 5, 7, 9, 12, 14, 16, and 18 after cancer cells transplantation. Tumor shapes on fused PET-CT images were contoured on each slide consisting part of tumor. Obtained VOI (volume of interest) was quantitatively analyzed using PBAS module of PMOD software. In each time-point images of 6-9 mice were analyzed. Intensity of hypoxia in tumor tissue was evaluated by counting SUV (standardized uptake value), and %ID/ml (per cent of injected dose per ml of VOI). The results were compared with two other methods of hypoxia determination: the molecular method based on the qPCR analysis of selected genes expression related to hypoxia and a fluorescence microscope imaging of pimonidazole (PIMO)-positive tumor areas. **Results:** Both PET and fluorescence microscopy methods showed that hypoxia increased till day 14 of tumor growth, whereas qPCR results showed that tumor hypoxia at molecular level was relatively high at early stage of tumor development. Additionally, necrotic regions dominated the tumor tissue at later stages of development, decreasing the number of hypoxic areas and completely eliminating normoxic regions (observed by PET). Comparing our results with available studies concerning tumor hypoxia we may conclude, that during tumor development the level of hypoxia fluctuates and two peaks of hypoxia occur. The first one is observed at the initial stage of tumor growth and the second one - in terminal stage, when chronically ischemic, hypoxic tissue starts to transform into necrosis. **Conclusion:** These results showed that molecular, gene expression-related methods of hypoxia determination are more accurate to prove changes undergoing at cellular level, however in order to visualize and count volumes of hypoxic regions in the investigated area, especially at further stages of tumor development, PET is the recommended tool. Furthermore, we noted interesting principle - during development of tumor, two peaks of hypoxia occur. **References:** None.

EP-0676

In vivo investigation of APN/CD13 inhibitors in tumor bearing animal models using 68Ga-NODAGA-cNGR radiotracer

A. Kis[1], *J. P. Szabó*[1], *T. Nagy*[1], *N. Dénes*[1], *I. Kertész*[1], *S. Lakatos*[2], *K. Halmi*[1], *E. Berényi*[1], *G. Trencsényi*[1];
[1]*Division of Nuclear Medicine and Translational Imaging, Department of Medical Imaging, Faculty of Medicine, University of Debrecen, Debrecen, HUNGARY,* [2]*Division of Radiology and Imaging Science, Department of Medical Imaging, Faculty of Medicine, University of Debrecen, Debrecen, HUNGARY.*

Aim/Introduction: Several malignant tumors, such as prostate, ovarium, pancreas carcinomas, melanomas and fibrosarcomas are positive for Aminopeptidase N (APN/CD13) receptor, which play an important role in neo-angiogenic process and metastatic tumor cell invasion. Our previous studies have already shown that ^{68}Ga-labeled NGR peptides bind specifically to APN/CD13 expressing tumor cells. ^{68}Ga labeled NGR peptides enable the investigation of the neo-angiogenic process with Positron Emission Tomography (PET). APN/CD13 inhibitors are potential chemotherapeutic agents in APN/CD13 positive tumors. The aim of this study was to investigate the effect of APN/CD13 inhibitors in subcutan and orthotopic HT1080 tumor bearing animal models using ^{68}Ga-NODAGA-cNGR. **Materials and Methods:** On day 0. CB17 SCID mice (n=30) were inoculated subcutan (n=15) with 1,5x10^6/animal/150 µl and orthotopically (n=15) with 1x10^6/animal/10 µl HT1080 (human fibrosarcoma) cells. Three days after inoculation the animals were randomly distributed into three groups (control, Bestatin [15 mg/kg] treated, Actinonin [5 mg/kg] treated). The daily intraperitoneal Actinonin or Bestatin treatments were administered for 7 days.^{18}FDG or ^{68}Ga-NODAGA-cNGR PET scans were taken on the 5th, 6th and 10th day to monitor tumor growth. On the 10th day 90 min after intravenous injection of 10±0,3 MBq ^{68}Ga-NODAGA-cNGR PET or PET/MRI scans and ex vivo biodistribution studies were made. Data were statistically analysed using unpaired Student's test. **Results:** On the 10th day PET scans were taken using ^{68}Ga-NODAGA-cNGR. In the case of subcutan HT1080 tumor bearing animals significant (p≤0,05) differences were observed in SUVmean values between Bestatin treated (SUVmean= 0,01±0,009) and control (SUVmean= 0,114±0,045) groups. Also singnificant (p≤0,05) heterogeneities were noticed among SUVmean values in orthotopically transplanted HT1080 tumor bearing animals, where SUVmean values were 0,009±0,006 in Actinonin treated groups and 0,026±0,013 in control groups. In subcutan tumors tumor/muscle (T/M) ratios - which were received from ex vivo biodistribution studies - are well correlated with in vivo T/M SUVmean ratios. However this kind of correlation was not observed during the investigation of orthotopically inoculated tumors. **Conclusion:** In the case of subcutan HT1080 tumor bearing animals' Bestatin treatment, while orthotopically inoculated HT1080 tumor bearing animals' Actinonin treatment reduced the ^{68}Ga-NODAGA-cNGR uptake in tumor in proportion to control group. This project was supported by the ÚNKP- 18-3-I-DE-32 new national excellence program of the ministry of human capacities. **References:** None.

EP-0677

Epigenetic Treatment with Histone Deacetylase Inhibitor Increases Uptake of [^{111}In]In-DOTA-TATE by Neuroendocrine Tumor Cells

I. Klomp*, S. U. Dalm, P. M. van Koetsveld, F. Dogan-Oruç, M. de Jong, L. J. Hofland;*
Erasmus MC, Rotterdam, NETHERLANDS.

Aim/Introduction: The somatostatin-2 receptor (SST2) is highly expressed on neuroendocrine tumor (NET) cells making it a suitable target for peptide receptor radionuclide therapy (PRRT)

using radiolabeled somatostatin analogues. Although PRRT has proven its value for treatment of NETs, treatment efficacy can be further improved by upregulating SST2. Epigenetic processes, such as histone acetylation, are highly involved in regulating gene transcription. Since histone acetylation is linked to transcriptional activation, histone deacetylase inhibitors (HDACis) may increase SST2 expression, and thus the efficacy of PRRT. We aimed to study the effect of the HDACi valproic acid (VPA) on SST2 expression and uptake of radiolabeled somatostatin analogues. **Materials and Methods:** Studies were performed in the human pancreatic NET cell line BON-1. Cell growth assays were performed to determine the EC_{50} of VPA after 7 day treatment. Subsequently, cells were treated for 7 days with the EC_{50} of VPA to study the effect on SST2 mRNA expression and uptake of [^{111}In]In-DOTA-TATE. Cells were trypsinized and cultured in 12-well plates on day 5. On day 7, different assays were performed: (1) RT-qPCR to determine the amount of SST2 mRNA expression and (2) uptake and internalization studies by incubating cells for 4h at 37ºC with 1nM [^{111}In]In-DOTA-TATE, +/- 1µM octreotide. The measured radioactivity was expressed as percentage added dose (%AD)/mg DNA. Additionally, reversibility of VPA treatment was determined. Cells were treated for 7 days with VPA, after which VPA-supplemented medium was replaced by medium without VPA to day 10. Samples for RT-qPCR were collected directly after treatment on day 7 (control + VPA-treated cells) and day 10 (only VPA-treated cells). **Results:** We found an EC_{50} value for VPA of 1mM. Seven day treatment with 1mM VPA resulted in both significant increased uptake and internalization of [^{111}In]In-DOTA-TATE compared to untreated BON-1 cells ($p<0.01$). In line with this, mRNA expression levels of VPA-treated cells were significantly upregulated after treatment ($p<0.05$). Moreover, reversibility of HDACi treatment was demonstrated by two-fold decreased SST2 mRNA expression levels 3 days after discontinuation of VPA when compared to SST expression directly after treatment ($p<0.05$). **Conclusion:** Results show that VPA is capable of inducing a reversible upregulation of SST2 expression and to enhance uptake of [^{111}In]In-DOTA-TATE. Therefore, the combination of VPA and PRRT potentially improves treatment efficacy. This combinational treatment will be evaluated further. **References:** None.

EP-0678

Radiogenomics in Ewing Sarcoma: Integration of Functional Imaging and Transcriptomics Characterizes Tumor Glucose Uptake

C. Prexler[1], *M. S. Kesper*[1], *M. Mustafa*[2], *W. Seemann*[2], *O. Schmidt*[1], *K. Gall*[1], *K. Specht*[3,4], *H. Rechl*[5], *C. Knebel*[5], *K. Woertler*[6], *W. Weichert*[3,4,7], *G. H. S. Richter*[1,4,7], *M. Schwaiger*[2,4,7], *I. von Luettichau*[1,4], *W. Weber*[2,4,7], *S. Burdach*[1,4,7];

[1]*Department of Pediatrics and Children's Cancer Research Center, Kinderklinik München Schwabing, Klinikum rechts der Isar, Fakultät für Medizin, Technische Universität München, Munich, GERMANY,* [2]*Department of Nuclear Medicine, Klinikum rechts der Isar, Technische Universität München, Munich, GERMANY,* [3]*Institute of Pathology, Klinikum rechts der Isar, Fakultät für Medizin, Technische Universität München, Munich, GERMANY,* [4]*CCC München - Comprehensive Cancer Center, Munich, GERMANY,* [5]*Department of Orthopedic Surgery, Klinikum rechts der Isar, Fakultät für Medizin, Technische Universität München, Munich, GERMANY,* [6]*Department of Diagnostic and Interventional Radiology, Klinikum rechts der Isar, Fakultät für Medizin,Technische Universität München, Munich, GERMANY,* [7]*DKTK German Cancer Consortium Munich, Munich, GERMANY.*

Aim/Introduction: The radiogenomics methodology, which combines imaging data with omics data like transciptomics, was already applied to diverse adult cancer types, revealing correlations of molecular characteristics of the tumors based on features extracted from images. To the best of our knowledge pediatric cancer has not been assessed by functional radiogenomics so far, although the prognostic value of glucose uptake in PET in sarcoma has already been proven[1]. **Materials and Methods:** In our project we conduct a large-scale analysis of gene expression in Ewing sarcoma tumor tissue with respect to image features from 18F-FDG PET-CT or PET-MRI. We compare tumors with low glucose uptake (low SUVmax) to tumors with high glucose uptake (high SUVmax) in 11 Ewing sarcoma patients using differential expression analysis and machine learning. **Results:** Eight genes were significantly upregulated in tumors with low SUV compared to tumors with high SUV in Ewing sarcoma: ABCA5, ARHGAP18, GSTM3, KL, NAF1, NPY5R, PLSCR4 and SFMBT1. Some of these are already known predictive markers for survival in other cancer types, but not in Ewing sarcoma so far. Noteworthy, NPY and its receptors NPY1R and NPY5R are known targets of the fusion transcript EWS-FLI1 that is characteristic of Ewing sarcoma. It was shown before that NPY signaling via receptors 1/5 promotes cell death, whereas under hypoxic conditions signaling switches from 1/5 to 2/5, which rather promotes malignancy[2]. In our 11 patients NPY, NPY1R and NPY5R are all upregulated in tumors with low glucose uptake. Therefore, the mechanism of NPY signaling promoting cell death seems to be more active in tumors with low glucose uptake. **Conclusion:** We characterize Ewing tumors with respect to their glucose uptake on gene expression level, thereby contributing to a better understanding of tumor biology with regard to differentiation, inflammation and metabolism. As several studies state an association between lower SUVs and improved survival, the eight genes found to be differentially expressed may be predictive for outcome in Ewing sarcoma and provide potential targets for treatment, especially in tumors with high SUV having poor prognosis. By additional integration of more image features from first and second order in the future we aim to examine in more detail which molecular characteristics of Ewing tumors can be inferred from the imaging data. Furthermore, we want to improve prediction of outcome by combination of expression data and imaging data using machine learning methods like random forest. **References:** [1] Raciborska, ClinTranslOncol, 2016. [2]Tilan, Oncotarget, 2013.

EP-0679

GRPR mRNA Expression Levels to Select Patients Suited for GRPR-mediated Radionuclide Imaging and/or Therapy

S. Dalm, K. Ruigrok-Ritstier, C. M. Beaufort, J. W. M. Martens, C. H. M. van Deurzen, M. de Jong, A. M. Sieuwerts;
Erasmus MC, Rotterdam, NETHERLANDS.

Aim/Introduction: The gastrin releasing peptide receptor (GRPR) is overexpressed on estrogen receptor positive (ER+) breast cancers (BCs), making it a biomarker predictive for peptide receptor radionuclide imaging and therapy using GRPR radioligands. BCs can be diagnosed and characterized (e.g. hormone receptor expression) using histopathology and immunochemistry, respectively, on excised tumor material. Ideally this tumor material can also be used to characterize GRPR-expression on the cancer cells, and thus determine whether patients are suited for GRPR-directed interventions. However, a number of previous studies by ourselves and others using GRPR antibodies failed to correctly determine GRPR-expression, and standard immunohistochemistry staining protocols in our hospital using different GRPR antibodies produced debatable results. Therefore the aim of this study was to determine whether we can use GRPR mRNA expression to identify BCs suitable for GRPR-mediated interventions. Since the GRPR is also expressed on healthy breast tissue we aimed to determine a cut-off value for GRPR positivity. **Materials and Methods:** Tumor material and corresponding healthy tissue of 13 ER+ BCs were analyzed for GRPR-expression by RT-qPCR and in vitro autoradiography. For RT-qPCR, RNA was isolated and GRPR mRNA expression was evaluated and quantified relative to the average expression of 3 reference genes using the deltaCq method. For comparison in vitro autoradiography was performed. Tissue slices were incubated with 10^{-9}M of the GRPR radioligand ^{111}In-JMV4168, after which the percentage added dose (%AD) of the radioactivity bound to the tissue was quantified.Hematoxylin and eosin staining was performed to localize tumor cells and to determine the percentage of tumor cells present. **Results:** Both analyses were successfully performed in 11/13 cases. The %AD was significantly correlated with GRPR mRNA expression (Spearman's R=0.57, p=0.018). A cut-off was determined at 0.1 for relative GRPR mRNA expression (sensitivity:75%, specificity:82%) to detect GRPR transcripts selectively in tumor tissue. Eight cases had low (<0.1) expression in healthy tissue and high (≥0.1) expression in corresponding cancer lesions, however in 2/8 differences were small. In 1 case we found an inverse result and in 2 cases both tumor and normal were below cut-off. GRPR positive samples determined by RT-qPCR had a significantly higher %AD (p=0.005) and a higher percentage of tumor cells (p=0.02). **Conclusion:** With the help of the cut-off value determined in our study GRPR mRNA expression can potentially be used to screen ER+ BCs for GRPR-mediated nuclear imaging and/or therapy. More studies will be performed now to further validate these findings. **References:** None.

EP-0680

Loss of PSMA during neuroendocrine differentiation of prostate cancer is associated with elevation of metabotropic glutamate receptors as an alternative diagnostic target

M. K. Bakht[1,2,3], *K. F. Stringer*[4,1], *J. M. Lovnicki*[5], *A. Pillon*[1], *F. Shahbazi-Raz*[6], *J. J. Hayward*[6], *S. Oh*[2,3], *J. F. Trant*[6], *G. Cheon*[2,3], *C. Kwak*[7], *C. Jeong*[7], *K. Kang*[2,3], *Y. Wang*[5], *X. Dong*[5], *L. A. Porter*[1];
[1]*Department of Biological Sciences, University of Windsor, Windsor, ON, CANADA,* [2]*Department of Nuclear Medicine, Seoul National University College of Medicine, Seoul, KOREA, REPUBLIC OF,* [3]*Laboratory of Molecular Imaging and Therapy, Cancer Research Institute, Seoul National University College of Medicine, Seoul, KOREA, REPUBLIC OF,* [4]*Department of Pathology, Cincinnati Children's Hospital Medical Center, Cincinnati, OH, UNITED STATES OF AMERICA,* [5]*Vancouver Prostate Centre, University of British Columbia, Vancouver, BC, CANADA,* [6]*Department of Chemistry and Biochemistry, University of Windsor, Windsor, ON, CANADA,* [7]*Department of Urology, Seoul National University College of Medicine, Seoul, KOREA, REPUBLIC OF.*

Aim/Introduction: Prostate-specific membrane antigen (PSMA) protein is encoded by the FOLH1 gene and is highly expressed in most of the prostate adenocarcinomas (AdPC). PSMA cleaves vitamin B9 to stimulate PI3K-Akt signaling through metabotropic glutamate receptors (mGluR) [1]. Its expression mostly correlates inversely with survival. However, the poor prognostic neuroendocrine (NE) prostate cancer (NEPC) lesions have suppression of the PSMA gene [2]. Treatment-induced NEPC (t-NEPC) is an emerging drug-resistant phenotype, and its visualization is a high priority. The possible alternative imaging options for NEPC has not been fully explored. In this work, we demonstrate that in PSMA-suppressed NEPC have elevated levels of most of mGLuR genes family members. **Materials and Methods:** We evaluated the transcript abundance for PSMA and mGluR family members including GRM1to 8 genes as well as SRRM4 (t-NEPC marker) across 909 tumors. We employed patient-derived xenograft (PDX) models to study the alterations of GRM1-8 in during NE-transdifferentiation of PSMA-positive AdPC. We also investigated changes of GRM genes in well-established prostate cancer cell lines including NCI-H660 as an NEPC model and LNCaP, DU145 and PC3 as AdPC models. **Results:** A significant elevation of GRM genes in NEPC patient samples and AdPC samples with high expression of NE marker genes was observed. There is a significant direct correlation between GRM1-6 and SRRM4 gene expression. Kaplan-Meier survival analysis of GRM genes showed high expressions of GRM1,3-4,5, and 8 genes are associated with poor outcome (log-rank p<0.05). PSMA-negative NCI-H600 as a model of NEPC has significantly higher levels of GRM1-4, 7, and 8 while NE-negative cell lines showed minimal expression of GRM genes. The PDX model of NE-transdifferentiation demonstrated a significant gradual elevation of GRM2-4 and 6 during the suppression of the PSMA gene. **Conclusion:** This work represents the loss of PSMA as an imaging target in NEPC is associated with an elevation in the expression of mGLuR genes family members.

The observed elevation of mGluR gene expression in NEPC demonstrates the possible ability of mGluR targeted imaging for follow-up imaging of low-PSMA patients and monitoring for NEPC development. **References:** [1] Kaittanis, Charalambos, et al. "Prostate-specific membrane antigen cleavage of vitamin B9 stimulates oncogenic signaling through metabotropic glutamate receptors." Journal of Experimental Medicine 215.1 (2018): 159-175. [2] Bakht, Martin K., et al. "Neuroendocrine differentiation of prostate cancer leads to PSMA suppression." Endocrine-Related Cancer 26 (2019): 131-146.

EP-0681

Metabolic changes of melanoma assessed by [^{18}F]FDG and [^{18}F]FLT PET during immune checkpoint inhibitor treatment: potential role as a predictive imaging biomarker

S. Oh, H. Youn, J. Paeng, Y. Kim, K. Kang, G. Cheon, J. Chung; Seoul National University, Seoul, KOREA, REPUBLIC OF.

Aim/Introduction: Immune checkpoint inhibitors (ICI) are immunotherapy agents that induce active inflammation against cancer cells, with target proteins like programmed cell death ligand-1 (PD-L1). While [^{18}F]FDG is widely used for cancer imaging by visualizing glucose metabolism, [^{18}F]FDG uptake of tumor may be variable in ICI treatment because both tumor and immune cells affect [^{18}F]FDG uptake. The aim of this study was to assess change of tumor glucose and nucleic acid metabolism using [^{18}F]FDG and [^{18}F]FLT PET during ICI treatment, to develop a potential imaging biomarker for monitoring and predicting response of tumor to ICI therapy. **Materials and Methods:** B16F10 murine melanoma cells (1×10^6) were inoculated to C57BL/6 mice and anti-PD-L1 antibody (10 mg/kg) was daily injected i.p. starting from day 5 after inoculation when tumor diameter was 2-3 mm. [^{18}F]FDG and [^{18}F]FLT PET scans were performed at day 6 and 7 (early phase), and also at day 13 and 14 (late phase). Tumor uptake of [^{18}F]FDG and [^{18}F]FLT was measured as target-to-background ratio on each images and compared between treated tumors (n = 26) and control tumors (n = 20). Tumor size was followed up and tissue was obtained at day 14. **Results:** Tumor growth was suppressed in the treatment group and tumor size was significantly different between the two groups on day 14 (463.77 ± 300 vs 181.52 ± 128.05 mm^3, p = 0.0049). At early phase, [^{18}F]FDG uptake of the treatment group was higher than that of control group (p = 0.0089), whereas [^{18}F]FLT showed insignificant difference between the two groups. However, at late phase, [^{18}F]FDG uptake presented similar uptake in both groups, whereas [^{18}F]FLT uptake of control group was markedly increased to a higher level than that of treatment group (p < 0.0001). When FDG-FLT uptake ratio was calculated, it was higher in treatment group than control group at early phase (p = 0.0035) as well as late phase (p < 0.0001). **Conclusion:** In ICI-treated group, [^{18}F]FDG and [^{18}F]FLT uptakes are varied at different phases. However, the FDG-FLT ratio (glucose metabolism-to-tumor proliferation ratio) is constantly higher in ICI-treated group, probably due to active inflammation. The results suggest that combination of [^{18}F]FDG and [^{18}F]FLT PET images can be a more effective imaging biomarker than [^{18}F]FDG and [^{18}F]FLT PET alone, in predicting and monitoring response to ICI. **References:** None.

EP-0682

SPECT Imaging of Endogenous Tumor Hypoxia Marker Carbonic Anhydrase IX with^{111}In-labeled VHH B9

S. A. M. van Lith[1], F. J. Huizing[1], B. A. W. Hoeben[1], S. Doulkeridou[2], M. Gotthardt[1], P. M. P. van Bergen en Henegouwen[2], J. Bussink[1], S. Heskamp[1];
[1]Radboudumc, Nijmegen, NETHERLANDS, [2]Utrecht University, Utrecht, NETHERLANDS.

Aim/Introduction: Hypoxia is present in the majority of solid tumors and is associated with poor outcome and radioresistance. Carbonic anhydrase IX (CAIX) is a transmembrane enzyme that is upregulated by cells under hypoxic conditions. Therefore, non-invasive imaging of CAIX could be of prognostic value and it may allow radiotherapy planning and treatment effect monitoring. The aim of this study was to validate and optimize SPECT imaging of CAIX expression in a head-and-neck squamous cell carcinoma model using an anti-CAIX variable domain of heavy chain antibody (VHH). **Materials and Methods:** VHH B9 was conjugated site-specifically with maleimide-DTPA and labeled with ^{111}In. The binding affinity and internalization of [^{111}In]In-DTPA-B9 was analyzed using SKRC-52 cells, which ubiquitously express CAIX. Subsequently, a dose-escalation study was performed in athymic nude mice with subcutaneous SCCNij153 head-and-neck cancer xenografts. Targeting specificity was determined by blocking specific uptake with unlabeled VHH B9, and by analyzing tumor uptake of an ^{111}In-labeled irrelevant VHH R2. A subgroup of mice was co-injected with plasma expander gelofusin, to reduce renal retention of [^{111}In]In-DTPA-B9. Tracer uptake at 4 hours after injection was determined by ex vivo radioactivity counting and SPECT/CT scans. Furthermore, spatial correlation between tracer uptake on autoradiography images and immunohistochemical staining of CAIX expression was analyzed. **Results:** DTPA-B9 was radiolabeled with ^{111}In at a specific activity of 4 MBq/µg. [^{111}In]In-DTPA-B9 bound to SKRC-52 cells with high affinity (IC_{50} = 11.3 nm, K_D = 27.2 nM) and the internalization rate of the tracer was relatively low (K_e = 0.01). A protein dose of 5 µg resulted in the highest uptake in SCCNij153 tumors in vivo (1.05±0.14%ID/g), with tumor-to-blood and tumor-to-muscle ratios of 11.5 and 24.7, respectively. Unlabeled B9 reduced tumor uptake to 0.30±0.03%ID/g and irrelevant [^{111}In]In-DTPA-R2 showed tumor uptake of 0.20±0.14%ID/g. Gelofusin did not significantly alter kidney uptake of [^{111}In]In-DTPA-B9. Immunohistochemistry and autoradiography images showed co-localization of [^{111}In]In-DTPA-B9 and expression of CAIX. **Conclusion:** [^{111}In]In-DTPA-B9 VHH shows specific targeting of CAIX expression in head-and-neck cancer xenografts. In ongoing studies we will determine if a fusion protein of B9 with an albumin binding domain shows improved tumor uptake compared to B9 alone. Furthermore

we will compare B9 to other CAIX imaging tracers and we will determine its potential for treatment selection and monitoring of hypoxia responses to therapy. **References:** None.

EP-0683

The Elusive Link between ^{18}FDG uptake and Glycolytic Flux explains the Preserved Diagnostic Accuracy of PET-CT in Diabetic Cancer Patients

V. Cossu[1,2], *M. Bauckneht*[1,2], *S. Bruno*[3], *A. Orengo*[1], *L. Emionite*[4], *F. Di Giulio*[1], *S. Capitanio*[1], *E. Balza*[5], *P. Castellani*[5], *P. Piccioli*[5], *A. Miceli*[2], *S. Raffa*[2], *A. Borra*[2], *M. Donegani*[2], *S. Morbelli*[1], *S. Ravera*[3], *G. Sambuceti*[1,2], *C. Marini*[1,6];
[1]*Nuclear Medicine, IRCCS Ospedale Policlinico San Martino, Genoa, ITALY,* [2]*Department of Health Sciences, University of Genoa, Genoa, ITALY,* [3]*Department Experimental Medicine, University of Genoa, Genoa, ITALY,* [4]*Animal Facility, IRCCS Ospedale Policlinico San Martino, Genoa, ITALY,* [5]*Cell Biology Unit, IRCCS Ospedale Policlinico San Martino, Genoa, ITALY,* [6]*CNR Institute of Molecular Bioimaging and Physiology (IBFM), Milan, ITALY.*

Aim/Introduction: The present study aims to verify whether the link between [^{18}F]-2-deoxy-glucose (FDG) uptake and activity of the reticular enzyme hexose-6P-dehydrogenase (H6PD) contributes to preserve PET/CT diagnostic power in experimental models of streptozotocin-induced diabetes mellitus (STZ-DM). **Materials and Methods:** The study included 72 Balb/c mice subcutaneously implanted with colon (CT26, n=36) or breast (4T1, n=36) cancer cells. Each cohort was subdivided into two clusters ("control" and "STZ-DM") that were further subdivided into three groups treated with saline or metformin (MTF) at low or high doses (10 or 750 mg/Kg daily, respectively). Two weeks after cancer cells inoculation, all mice were submitted to micro-PET imaging. After sacrifice, enzymatic pathways and response to oxidative stress were evaluated in harvested tumors. Finally, competition by 2-deoxy-glucose (2DG) on cell uptake of FDG and the fluorescent analogue 2-[N-(7-nitrobenz-2-oxa-1,3-diazol-4-yl)amino]-2-deoxyglucose (2NBDG) was studied in cultured cells. **Results:** At microPET imaging, 4T1 and CT26 cancer volumes and average metabolic rate of glucose (MRGlu) were superimposable in "control" mice and showed a similar reduction under MTF treatments. In STZ-DM group, both cancer volumes and MRGlu were slightly, yet significantly, lower than control ones, while MTF capability to decelerate lesion growth and MRGlu was virtually abolished. This metabolic reprogramming was not explained by any change in expression or activity of hexokinases, phosphofructokinase or glucose-6-phosphate-dehydrogenase while it closely agreed with the response of H6PD catalytic function. Differently from glucose, coincubation with 2DG virtually abolished FDG uptake in cultured cells and their capability to concentrate 2NBDG within the endoplasmic reticulum. **Conclusion:** These data challenge the current dogma linking 2DG/FDG uptake to the glycolytic rate and introduce a new model to explain the relation between glucose analogues uptake and hexoses reticular metabolism. This selective fate of FDG contributes to the high sensitivity of PET imaging despite moderate hyperglycemia. **References:** None.

EP-46

Preclinical and translational aspects, including radiopharmacy, radiochemistry and drug development -> Preclinical and translational aspects -> Translational aspects -> Cardiology

October 12 - 16, 2019 e-Poster Area

EP-0684

^{18}FDG-PET, MRI Relaxometry And Terahertz Reflectometry in a Multimodal Imaging Heart Study of a Cardiorenal Syndrome Small Animal Model

L. Agrigoroaie[1], *D. Furcea*[1], *C. Uritu*[2], *G. Stanciu*[2], *C. Mihai*[2], *I. Gardikiotis*[2], *R. Iliescu*[1], *C. Stefanescu*[1], *M. Gutu*[1];
[1]*University of Medicine and Pharmacy "Gr. T. Popa", Iasi, ROMANIA,* [2]*Advanced Center for Research and Development in Experimental Medicine CEMEX, Iasi, ROMANIA.*

Aim/Introduction: Cardiorenal syndrome is a intricate clinical condition, with reliable prognostic biomarkers still lacking. We present preliminary cardiac data of a cardiorenal syndrome rat model through 2-deoxy-2-[fluorine-18]fluoro-D-glucose (^{18}F-FDG) PET/MRI multimodal imaging, MRI relaxometry and terahertz (THz) spectrum reflectometry. **Materials and Methods:** We examined 24 male Wistar rats, partitioned into 3 lots: control (L1), heart failure (L2), cardiorenal group (L3). Heart failure was induced by intraperitoneal doxorubicin administration and renal failure by sub-total nephrectomy. ^{18}F-FDG PET/MRI scans were acquired at week 0 for L1, at week 6 for L2 and at week 18 for L3. Tracer kinetics were analysed by calculating standardized uptake values (SUV) and washout times at 50% (T50) and at 75% (T75) of peak SUV.The ex vivo formalin-fixed rat hearts were studied under a multi-flip spoiled GRE driven-equilibrium single pulse observation of T1 relaxation MRI sequence. For histological assessment, standard hematoxilyn-eosin staining of 5 µm tissue slices was used, scoring the progression of pathognomonic signs on a visual scale from 0 to 4 (0-no abnormality, 4-severe disease). Paraffin-embedded heart tissue samples were further examined through THz pulsed-wave reflectometry, with resulting attenuation in the 0.2-3.3 THz range. **Results:** Qualitative histological evaluation observed progression of heart disease from a score of 0 for L1 to a score of 2 for L2 (sparse areas of myocardial fibrosis, atherosclerosis, intracellular doxorubicin-induced vacuolisations) to a score of 4 in L3 group (extensive myocardial fibrosis, atherosclerosis, intra- and intercellular vacuolisations).In ^{18}F-FDG PET data, L1 and L2 displayed a statistically significant difference only in myocardial T75 (mean $T75_{L1}$=1.1 vs. $T75_{L2}$=1.9 min, $p<0.05$). In contrast, subjects from L3 vs. L1 exhibited prolonged myocardial washout times at T75 and at T50 (mean $T75_{L1}$=1.1 vs. $T75_{L3}$=40

min, p<0.001; mean $T50_{L1}$=3.5 vs. $T50_{L3}$=40 min, p<0.001); moreover, comparing L3 vs. L2 still yielded a significantly distinct temporal dynamics (mean $T75_{L2}$= 1.9 vs. $T75_{L3}$= 40 min, p<0.001; mean $T50_{L2}$=5.9 vs. $T50_{L3}$=40 min, p<0.05).T1 left ventricular muscle relaxation times were 374±23 ms for L1, 439±9 ms for L2 and 262±11 ms for L3 group, suggesting hypertrophic cardiomyopathy for L2 and dilatative cardiomyopathy for L3. Distinct patterns of the THz pulse attenuation were observed, differentiating the groups within the studied THz range. **Conclusion:** Our multimodal imaging investigations of a cardiorenal rat model were consistent in discriminating between study groups, confirming the hypothesis under study, and also suggests a potential for new diagnostic tools worth exploring. **References:** None.

EP-47

Preclinical and translational aspects, including radiopharmacy, radiochemistry and drug development -> Preclinical and translational aspects -> Translational aspects -> Neurology

October 12 - 16, 2019 e-Poster Area

EP-0685

[^{18}F]GE180-µPET Depicts Drug-induced Changes of Glial Activation by the TSPO-Agonist Etifoxine during Vestibular Compensation in the Rat

A. Krämer[1,2], *C. Branner*[1,2], *M. Lindner*[1,2], *M. Grosch*[1], *A. Gosewisch*[1,2], *R. Oos*[2], *P. Bartenstein*[2], *S. Ziegler*[2], *A. Zwergal*[1,3]; [1]*German Center for Vertigo and Balance disorders, DSGZ, University Hospital, LMU Munich, Munich, GERMANY,* [2]*Department of Nuclear Medicine, University Hospital, LMU Munich, Munich, GERMANY,* [3]*Department of Neurology, University Hospital, LMU Munich, Munich, GERMANY.*

Aim/Introduction: Initial symptoms after acute unilateral vestibular loss ameliorate over days to weeks due to central vestibular compensation (VC). Glial activation in the ipsilesional vestibular nerve and nucleus has been reported during VC, but its functional role for recovery remains unclear. The aim of the current study was to investigate, whether modulation of glial activation by the TSPO-agonist etifoxine (ETX) changes the course of behavioral recovery during VC in the rat model of unilateral labyrinthectomy (UL) and can be visualized by serial [^{18}F]GE180-µPET. **Materials and Methods:** 21 male SD rats underwent an irreversible chemical UL by transtympanic instillation of bupivacaine and p-arsanilic acid. 11 animals were treated with ETX (25 mg/kg body weight i.p. per day) for 7 days after UL, a control group (n=10) with saline injections. Behavioral symptoms of vestibular asymmetry were scored clinically (nystagmus, postural asymmetry) and by apparative testing in an open field (gait instability) on days 1,2,3,8,15,22,29 post UL. [^{18}F]GE180-µPET was recorded one week before and 1,8,15,22,29 days after surgery. The PET scans started 45 min after i.v. injection of 50 MBq [^{18}F]GE180 with a 15 min transmission, followed by a 30 min emission. Images were compared in a voxel-wise manner between time points and conditions using SPM8. **Results:** Nystagmus peaked on day 1 and ceased until day 8 post UL with no differences between groups. Postural asymmetry significantly ameliorated between days 5 and 15 in the ETX-group (p=0.008) and days 5 and 22 in the control group (p<0.001). Comparison of postural asymmetry scores between groups showed relatively lower values in the ETX-group on days 15 (p=0.032), 22 (p=0.002) and 29 (p=0.021). The ETX-treated group moved relatively more along the borders of the open field from day 8. In both groups, [^{18}F]GE180 uptake was increased from day 1 to 29 in the ipsilesional vestibular nucleus and bilateral hippocampus compared to baseline. ETX-treated rats showed a lower [^{18}F]GE180 uptake in the ipsilesional vestibular nucleus on days 8,15,22,29 and in the hippocampus after day 15 post UL compared to controls (p<0.005). **Conclusion:** Improvement of postural asymmetry by the TSPO agonist ETX is accompanied by a decreased glial activation in central vestibular networks during intermediate VC. This data suggest that the course of glial activation follows the recovery of vestibular function. [^{18}F]GE180-µPET is a feasible and sensitive method to depict and monitor drug-induced changes of glial reactions over time in vivo. **References:** None.

EP-0686

Cerebral Glucose Metabolism Differs According To Future Weight Change

K. Pak[1], *S. Kim*[2]; [1]*Pusan National University Hospital, Busan, KOREA, REPUBLIC OF,* [2]*Pusan National University Yangsan Hospital, Yangsan, KOREA, REPUBLIC OF.*

Aim/Introduction: The brain is known to play a central role in controlling the desire to eat. We aimed to evaluate the brain regions that might have a long-term effect on eating behavior and weight changes. Therefore, we utilized the data of cognitively normal subjects who are examined by several neurologic tests, and followed-up for 36 months from Alzheimer's Disease Neuroimaging Initiative (ADNI) database, and investigated to search the brain regions that are associated with future weight change. **Materials and Methods:** The weight of each subject was measured on each visit at baseline (W0), 36 (W36) months after brain ^{18}F-Fluorodeoxyglucose (FDG) positron emission tomography (PET). Percentage (%) change of weight was calculated as follows: [(W36-W0)/W0]*100. We classified each subject's change into one of three categories: weight loss, stable, and weight gain. Dynamic 3-dimensional scans of six 5-min frames were acquired 30 mins after injection of 185 MBq of FDG. Image analysis was done using Statistical Parametric Mapping 12 **Results:** Ninety-six subjects were included in this study (male 54, female 42). Subjects with future weight gain showed hypometabolism in left cerebellum compared with

those with future weight loss & stable. Percentage change of weight was positively associated with brain metabolism in right insula, and right caudate nucleus **Conclusion:** Subjects with future weight gain showed hypometabolism in left cerebellum, and the more cerebral Glucose Metabolism of right insula and right caudate nucleus the subjects have, the more weight will be gained in the future. This study raises the possibility that the brain glucose metabolism precedes the future weight change **References:** None.

EP-0687

A simultaneous FDG-PET/fMRI does not reveal neural plasticity following a working memory training

I. Ripp[1], *M. Emch*[2], *Q. Wu*[3], *J. Cabello*[1], *K. Koch*[2], *I. Yakushev*[1];
[1]*Department of Nuclear Medicine, Klinikum Rechts der Isar, Technical University Munich, Munich, GERMANY,* [2]*Department of Neuroradiology, Klinikum rechts der Isar, Technical University Munich, Munich, GERMANY,* [3]*Department of Neuroradiology, Klinikum rechts der Isar, Technical University Munich, Munich, Munich, GERMANY.*

Aim/Introduction: The concept of working memory (WM) training yielding improvements in even untrained cognitive domains is widely debated in the literature. These training effects have been ascribed a potential role delaying age- and disease-related cognitive decline. The relationship between these so called transfer effects and changes on the network level remain unclear. We studied the effects of an extensive 8 weeks long online supervised visual and verbal n-back WM training at the behavioral and neuroimaging level in 61 middle-aged healthy participants. **Materials and Methods:** To understand potential training induced neural plasticity, we acquired simultaneous 18F-fluorodeoxyglucose (FDG) PET and MRI data studying potential changes in metabolic and functional characteristics at a network and a single voxel level. Using a purely data driven approach, an independent component analysis (ICA), we extracted a number of neurocognitive networks (NCNs), as well as sensory networks as reference. Altered connectivity of NCN such as the default mode network (DMN) and central executive network (CEN), was hypothesized. Network integrity measurements were compared for each network of interest between pre- and post-training. At a single voxel level FDG-uptake was compared between pre- and post-training. **Results:** Based on both fMRI and FDG-PET imaging modality the anterior and posterior DMN, CEN and salience network were extracted. No difference in network integrity measures was found. Mass univariate analysis at the voxel level did not reveal significant training induced changes in FDG uptake. The evaluation of nine different neurospychological tests aqcuired before and after the training period revealed a significant practice effect, but no transfer effects, i.e. an improvement in tasks other than the trained tasks. **Conclusion:** In summary, our multimodal neuroimaging approach did not reveal WM induced changes. In accordance, our behavioural results reveal no transfer effects following a training suggesting to revise the concept of WM training. **References:** None.

EP-0688

The amount of HF-rTMS sessions modifies the SERT availability and determines an increase or decrease in central homovanillic acid and 3,4-dihydroxyphenylacetic acid

R. Dockx[1,2], *K. Peremans*[1], *D. De Bundel*[3], *A. Van Eeckhaut*[3], *L. Vlerick*[4], *I. Polis*[4], *N. Van Laeken*[5], *G. Pauwelyn*[5], *I. Goethals*[6], *F. De Vos*[5], *A. Dobbeleire*[1], *J. H. Saunders*[1], *C. Baeken*[2];
[1]*Department of Veterinary medical imaging and small animal orthopaedics, Faculty of Veterinary Medicine, Ghent University, Merelbeke, BELGIUM,* [2]*Department of Psychiatry and Medical Psychology, Ghent Experimental Psychiatry (GHEP) lab, Ghent University, Ghent, BELGIUM,* [3]*Department of Pharmaceutical Chemistry, Drug Analysis and Drug Information (FASC), Research group Experimental Pharmacology, Center for Neurosciences (C4N), Vrije Universiteit Brussel, Brussels, BELGIUM,* [4]*Small Animal Department, Faculty of Veterinary Medicine, Ghent University, Merelbeke, BELGIUM,* [5]*Laboratory of Radiopharmacy, Faculty of Pharmaceutical Sciences, Ghent University, Ghent, BELGIUM,* [6]*Department of Radiology and Nuclear Medicine, Ghent University Hospital, Ghent, BELGIUM.*

Aim/Introduction: Repetitive transcranial magnetic stimulation (rTMS) is thought to exert its anti-depressant action through the serotonergic and dopaminergic system. Nonetheless, only the immediate effects on these systems have been thoroughly studied. Therefore, this study aimed to evaluate the effects - immediate and long-lasting - of an acute and chronic accelerated high frequency repetitive rTMS (aHF-rTMS) on serotonin transporter (SERT), dopamine and its metabolites in the cerebrospinal fluid (CSF) and serum of healthy beagle dogs. **Materials and Methods:** 22 dogs were randomly divided into 3 unequal groups: 5 active sessions (n=10), 20 active sessions (n=8), and 20 sham sessions (n=4). Each dog received an anatomical MRI, neuronavigation and a baseline [^{11}C]DASB PET scan, followed by an aHF-rTMS treatment over the left frontal cortex. 24 hours, 1 month and 3 months after the last stimulation session [^{11}C]DASB PET scans were acquired. After each scan, a CSF and serum tap was performed. The SERT binding index (BI) of 23 brain regions was calculated. The concentrations of dopamine (DA), homovanillic acid (HVA), 3,4-dihydroxyphenylacetic acid (DOPAC) in the CSF and serum were analysed on a reversed phase liquid chromatography system with electrochemical detection. Linear mixed models were used to analyse the data. **Results:** An acute (24 hours post) increase in SERT BI in the region containing the raphe nuclei (P-value = 0.04) was seen within the 20 active sessions group. In addition, the BI decreased in the subgenual cortex (P-value = 0.002), pre-subgenual cortex (P-value = 0.02) and left thalamic area (P-value = 0.04) one month after stimulation. Immediate (24 hours post) differences in SERT BI, were noticed between both active protocols in the left thalamic area (P-value = 0.04) and the pre-subgenual cortex (P-value = 0.01). Within the 5 active sessions group HVA was increased 24 hours (P-value = 0.02), 1 month (P-value = 0.04) and 3 months (P-value < 0.001) after the stimulation. A decrease in HVA was seen for the 20

sessions active group 1 month (P-value = 0.01) and 3 months (P-value = 0.04) after the stimulation. **Conclusion:** Both active protocols were able to modify the SERT BI, central DOPAC and HVA concentrations. Administering more sessions of an aHF-rTMS protocol induces changes in SERT BI in different brain regions other than when applying fewer sessions. The results imply that a single and four-day active HF-rTMS over the left frontal cortex provoke contrasting effects on the dopaminergic system. **References:** None.

EP-0689

Effects of Chronic Alcohol Self-Administration on Striatal Phosphodiesterase 10A Availability Are Associated with Poor Decision-Making

J. Ceccarini[1], *Y. E. Klingl*[2], *B. de Laat*[1], *G. Schroyen*[3], *M. Ooms*[4], *G. Bormans*[4], *K. Van Laere*[1];
[1]*Nuclear Medicine and Molecular Imaging, University Hospitals Leuven; Department of Imaging and Pathology, KU Leuven, Leuven, BELGIUM,* [2]*Department of Neurosciences, KU Leuven, Experimental Neurology and Leuven Brain Institute (LBI); Center for Brain & Disease Research, Laboratory of Neurobiology, VIB-KU Leuven, Leuven, BELGIUM,* [3]*Department of Imaging and Pathology, KU Leuven, Belgium, Leuven, BELGIUM,* [4]*Radiopharmaceutical Research Laboratory, KU Leuven, Leuven, BELGIUM.*

Aim/Introduction: Phosphodiesterase 10A (PDE10A) is a dual substrate enzyme highly enriched in dopaminoreceptive striatal medium spiny neurons, which are involved in psychiatric disorders such as addiction. Preclinical studies suggest a correlation of PDE10A in neuronal and behavioral responses to alcohol intake and preference[1,2]. However, little is known about the effects of alcohol exposure on PDE10A activity. We performed a longitudinal microPET [^{18}F]JNJ42259152 study to evaluate changes on PDE10A availability in rats subjected to different stages of alcoholization, in combination with behavioural assessments. **Materials and Methods:** Nine adult Wistar rats were monitored over a 10-week alcohol abuse reinstatement model[3], including 6 weeks of alcohol exposure, 2 weeks of withdrawal, followed by 1 week of relapse. Animals who reported an alcohol preference ≥30% during the first exposure phase were defined as alcohol-preferring rats. Decision-making and anxious behaviour were assessed with the rat Iowa Gambling Task and open field test over the 10-weeks´ time. Dynamic 60-min PDE10A [^{18}F]JNJ42259152 microPET scans were performed at alcohol exposure week 2, 4 and after relapse. In order to evaluate the effects of 6 weeks of alcohol exposure, a sham control group of 9 rats was added to the experiment. Parametric PDE10A BP_{ND} images were generated using a Logan reference tissue model with cerebellum as reference region[4], and were analyzed using VOI- and voxel-based approach. **Results:** Alcohol preference increased over time especially during week 3 and 6 of alcohol exposure, and during relapse (32±14%, 22±7%, 33±19%). Animals that showed poor decision making and higher anxiety levels displayed a greater alcohol preference. The first weeks of alcohol exposure resulted in an increased striatal PDE10A binding (12±16%), compared to controls. Comparing PDE10A BP_{ND} after 4- versus 2-weeks of exposure, showed a decreased PDE10A in the caudate-putamen and NuAc ($P_{FWE\text{-}corrected}$:0.02-0.003). This striatal PDE10A decrease was mostly present in alcohol-preferring rats (alcohol preference:30-70%), and was associated with impaired decision-making over the last exposure phase and abstinence (r_s>0.7). A similar regional decrease in PDE10A availability towards normalization was observed after one week of relapse ($P_{FWE\text{-}corrected}$:0.002-0.008). **Conclusion:** Chronic alcohol self-administration induces a reversible increased PDE10A enzymatic availability in the striatum that is related to higher alcohol preference and poor decision-making. These data implicate that PDE10A mediated signaling plays an important role in modulating the reinforcing effects of alcohol, suggesting that PDE10A inhibition may have beneficial behavioural effects on alcohol intake. **References:** 1.Logrip ML,Alcohol.2015;49:795-802. 2.Logrip ML.Front Integr Neurosci.2014;8:8-30. 3.Simms JA.Alcohol Clin Exp Res.2008;32:1816-1823. 4.Celen S.Neuroimage.2013;82:13-22.

EP-48

Preclinical and translational aspects, including radiopharmacy, radiochemistry and drug development -> Preclinical and translational aspects -> Translational aspects -> Oncology (Translational)

October 12 - 16, 2019 e-Poster Area

EP-0690

F-18 labeled FAPI-74 in patients with lung cancer: biodistribution at 3 imaging time points

F. L. Giesel[1], *T. Lindner*[1], *S. Adeberg*[2], *F. Staudinger*[1], *P. Flechsig*[1], *H. Rathke*[1], *M. Röhrich*[1], *J. Debus*[2], *U. Haberkorn*[1], *C. Kratochwil*[1];
[1]*Department of Nuclear Medicine, University Hospital Heidelberg, Heidelberg, GERMANY,* [2]*RadioOncology, University Hospital Heidelberg, Heidelberg, GERMANY.*

Aim/Introduction: Recently, ^{68}Ga-labeled FAPI-04 was reported a promising tracer for imaging several tumor-entities (Ref-1). To overcome supply limitations of short-half-life (1h) generator nuclide ^{68}Ga with longer half-life (2h) cyclotron produced ^{18}F, the preclinically favorable ligand FAPI-74 was utilized as [^{18}F]AlF (Aluminium-Fluorid) complex. This retrospective analysis investigates the biodistribution and tumor-uptake of patients examined with clinical indication at different imaging time-points. **Materials and Methods:** FAPI-74 was successfully used for imaging of 5 patients (median age 52) with lung cancer undergoing to delineate target volume for planned external-beam radiotherapy. For all patients emission scans at 10 min, 1h and 3h after injection of mean 220 MBq ^{18}F-FAPI-74 were acquired. Normal organ distribution and tumor uptake (primary tumor, LN and distance Metastases, respectively) were evaluated

per SUV at each time-point. **Results:** In primary cancer average SUVmax was 12.5 at 10 min; 13.5 at 1h and 11.4 at 3h; in lymph node metastases it was 9.8, 12.1, and 11.4; in distant metastases 10.3, 10.9 and 11.8. So, for most lesions the uptake peaked later than 10 min. p.i. but there was already some wash-out between 1h and 3h p.i.. Biodistribution, pharmacokinetics and tumor-to-background ratios are comparable to the previous ^{68}Ga-labeled compound. **Conclusion:** The [^{18}F]AlF-labeled ligand FAPI-74 presented comparable tracer-characteristics to the recent published ^{68}Ga-FAPI-04. **References:** Giesel FL, Kratochwil C, Lindner T, Marschalek MM, Loktev A, Lehnert W, Debus J, Jäger D, Flechsig P, Altmann A, Mier W, Haberkorn U. ^{68}Ga-FAPI PET/CT: Biodistribution and Preliminary Dosimetry Estimate of 2 DOTA-Containing FAP-Targeting Agents in Patients with Various Cancers.J Nucl Med. 2019 Mar;60(3):386-392. doi: 10.2967/jnumed.118.215913. Epub 2018 Aug 2.

EP-0691

In-111 Labeled Cd166-targeted Peptide For Detecting Colorectal Cancer Stem-like Tumor In Vivo

S. Guan, T. Luo, C. Peng, T. Liao;
Institute of Nuclear Energy Research, Longtan District, Taoyuan, TAIWAN.

Aim/Introduction: Cancer stem cells (CSCs) involved in drug resistance, metastasis and relapse of cancers, which can significantly affect tumor therapy. Therefore, it is important to develop specific therapies targeted probe at CSCs for improvement of survival and quality of life of cancer patients. Studies have indicated that the CD166 protein has been considered as a specific marker for colorectal CSCs (CCSCs) detection. In this study, we attend to use polyethylene glycol (PEG) linked CD166-targeted peptides (CD166P-PEG) as a nuclear imaging agent probe for CD166 detection in CCSC xenograft animal model. **Materials and Methods:** The CD166+ HCT15 cells were obtained by Magnetic-activated cell sorting. The CD166 and stem cell markers expression were detected by using western blot. Tumor sphere assay was performed for stem cell characteristics assay. The CD166 anti-peptide (CD166ap) was discovered by using Phage display peptide library kit, Ph.D.™-12. The CD166ap was conjugated with PEG and DTPA (DTPA-PEG-CD166ap) for detecting the cell binding ability. The DTPA-PEG-CD166 and DTPA-PEG were labeled with In-111 (^{111}In-DTPA-PEG-CD166, ^{111}In-DTPA-PEG) for tumor detection in animal model. **Results:** In this study, CD166+ cells were successfully isolated from the HCT-15 CRC cell line using magnetic activated cell sorting (MACS) and presented CSC characteristics. Subsequently, we designed the CD166P-PEG which was comparable to CD166 antibody as a CCSC probe during cell binding assay and confirmed the CD166+ targeting ability. Finally, we further observed that the DTPA conjugated CD166P-PEG with indium-111 labeling (^{111}In-DTPA-PEG-CD166P) was significantly enhanced in tumors tissue site of CD166+ HCT-15 xenograft mice as compared with non-CD166P-PEG control. **Conclusion:** The radioisotope-labeled CD166-PEG may be useful to apply in CRC patients for CD166 nuclear medicine imaging. **References:** None.

EP-0692

Clinical translation of the PepProtect concept: Improved detection of cancer and metastases, applied in medullary thyroid cancer patients with [^{111}In]In-MG11 scanning during neprilysin inhibition

R. Valkema[1], *A. C. Froberg*[1], *T. Maina*[2], *B. A. Nock*[2], *E. de Blois*[1], *M. Melis*[1], *M. W. Konijnenberg*[1], *S. L. W. Koolen*[1], *R. P. Peeters*[1], *W. W. de Herder*[1], *M. de Jong*[1];
[1]*Erasmus Medical Center, Rotterdam, NETHERLANDS,* [2]*Molecular Radiopharmacy, INTRASTES, NCSR "Demokritos", Athens, GREECE.*

Aim/Introduction: Many tumour-targeted radioabelled peptides are (partially) instable in vivo, due to enzymatic degradation. It is known from preclinical studies that neprilysin (neutral endopeptidase, NEP) is a key enzyme in this process. In situ NEP inhibition by administration of a suitable inhibitor can stabilize circulating biodegradable radiopeptides, resulting in clearly enhanced tumour targeting [1]. The present ongoing first-in-human study investigates the effects of the oral NEP-inhibitor racecadotril (RAC) on the in-vivo stability of the CCK_2-receptor (CCK_2R) specific radiopeptide (([^{111}In]In-DOTA)D-Glu^{10})-gastrin(10-17), or [^{111}In]InMG11, and on the tumour uptake in patients with medullary thyroid carcinoma (MTC). [^{111}In]InMG11 has high affinity for CCK_2R-positive tumours, but it is instable in-vivo. RAC is a commercially available and safe NEP-inhibitor, registered as an anti-diarrhoea drug for adults and children. **Materials and Methods:** Until now, first 2 out of 12 planned MTC patients completed all 3 assessments: Base-1: RAC (only toxicity); Base-2: InMG11 scintigraphy and quantitative SPECT-CT (toxicity, [^{111}In]InMG11 stability, tumour uptake); Combination: RAC + [^{111}In]InMG11 scintigraphy and quantitative SPECT-CT (toxicity, stability, tumour uptake). A single dose of 400mg RAC was given orally 90 min before i.v. injection of [^{111}In]InMG11 (185 MBq/10 nmol peptide). **Results:** Patient 1 (female, 57y), 15 yr after neck surgery, serum calcitonin (Ct) 300 ng/L without known lesions: at Base-2, intact serum [^{111}In]InMG11 was 6% at 10 min after i.v. infusion, 1 neck lymph node (LN) was faintly visible on the planar 24h scan, with SUVmax 0.13 on quantitative SPECT-CT. Given in Combination, with RAC, intact serum [^{111}In]InMG11 impressively increased to 54% and the LN was clearly visible (SUVmax 0.40). Additional suspicious lesions were noted. Patient 2 (male, 48y), after recent irradical surgery for T4aN1bMx MTC, serum Ct 1188 ng/L: at Base-2, intact [^{111}In]InMG11 was 8%, with visible (index) tumour remnant (SUVmax 0.28); additional LNs and suspicious metastases were faintly seen. At Combination, intact [^{111}In]InMG11 was 73%, with much better visible tumour (SUVmax 1.29) and clearly visible LNs and metastases . Both patients had no grade-2/3/4 toxicity during the studies. **Conclusion:** We present first clinical proof of concept of the PepProtect concept in MTC patients in this preliminary study. Oral RAC effectively protected [^{111}In]InMG11 against enzymatic degradation, resulting in an impressive 3-4x

higher uptake in human MTC lesions. **References:** [1] J Nucl Med;55:121-7;2014.

EP-0693

[^{68}Ga]Ga-NODAGA-Il2 for imaging activated T-cells

I. Antunes[1], *E. L. van der Veen*[2], *F. V. Suurs*[2], *R. A. J. O. Dierckx*[1], *M. N. Lub-de Hooge*[3], *E. G. E. de Vries*[2], *E. F. J. de Vries*[1];
[1]*University of Groningen, University of Medical Center of Groningen, Dept. of Nuclear Medicine and Molecular Imaging, Groningen, NETHERLANDS,* [2]*University of Groningen, University of Medical Center of Groningen, Dept. of Medical Oncology, Groningen, NETHERLANDS,* [3]*University of Groningen, University of Medical Center of Groningen, Dept. of Hospital and Clinical Pharmacy, Groningen, NETHERLANDS.*

Aim/Introduction: Interleukin-2 (IL2) is a 15.5 kDa glycoprotein that binds with high affinity to IL2 receptors (IL2R) that are overexpressed on activated T-cells, which can play a major role in the tumor immune response. We have developed N-(4-[^{18}F]fluorobenzoyl)interlekin-2 ([^{18}F]FB-IL2) which has been successfully used for detecting activated T-cells in rodents[1] and currently in human studies. We now developed a simplified method to label IL2 with ^{68}Ga to allow usage in centers lacking a cyclotron. Here we present the synthesis of [^{68}Ga]Ga-NODAGA-IL2 and its in vitro and in vivo evaluation. **Materials and Methods:** NODAGA-NHS was conjugated with IL2 at pH 8.5 for 2 h at room temperature. The conjugate was purified and kept at -80^{0}C until the radiolabelling day. For the radiolabelling method, different parameters were tested in order to get the optimal synthesis method. The stability was tested (TCA precipitation) in human plasma. To evaluate the in vivo properties of the new PET tracer, an ex-vivo biodistribution of [^{68}Ga]Ga-NODAGA-IL2 (0.55±0.13 MBq) was performed in immunocompetent BALB/c mice (n=6). In addition, to evaluate its selectivity towards activated T-cells, a 60 min dynamic PET scan of [^{68}Ga]Ga-NODAGA-IL2 (0.44±0.18) followed by ex-vivo biodistribution was performed in severe combined immunodeficiency (SCID) mice inoculated with activated peripheral blood mononuclear cells (PBMCs). **Results:** When using small volumes of ^{68}Ga (20-50MBq-100 uL) in the presence of NaOAc (pH4.5) or HEPES (pH4.5), the [^{68}Ga]Ga-NODAGA-IL2 was obtained with 90% yield and radiochemical purity (>95%) within 30 min. However, with larger volumes of ^{68}Ga (600-300 MBq-1 mL) the yield of [^{68}Ga]Ga-NODAGA-IL2 was ≤ 10%. Nevertheless [^{68}Ga]Ga-NODAGA-IL2 could be obtained with high radiochemical purity (>95%) within 60 min. [^{68}Ga]Ga-NODAGA-IL2 showed high stability in human plasma with >90% of the tracer remaining intact after 60 min. Biodistribution of [^{68}Ga]Ga-NODAGA-IL2 in BALB/c mice showed high uptake in kidneys (162.8±18.9 %ID/g-60 min), spleen (19.8±3.5 %ID/g-60 min), liver (22.9±4.3%ID/g-60 min) and bone marrow (9.3±2.7 %ID/g-60 min). As for the PET study in SCID mice inoculated with activated PBMCs, the images clearly showed binding of the tracer to activated PBMCs. The [^{68}Ga]Ga-NODAGA-IL2 uptake was found to be higher in activated PBMCs (1.1±0.5 %ID/g) when compared with the uptake in the Matrigel itself (0.5±0.2 %ID/g). **Conclusion:** The new [^{68}Ga]Ga-NODAGA-IL2 showed increased binding towards activated T-cells, indicating that this tracer might be used to image activated T-cells in centres lacking a cyclotron. **References:** [1] Di Gialleonardo et al., J Nucl Med, **2012**, 53:679-86.

EP-0694

Imaging benign and malignant intracranial tumors with ^{18}F-fluoroglutamine PET

X. Xu[1], *H. Zhu*[1], *L. Zhu*[2], *H. Kung*[3], *Z. Yang*[1];
[1]*Beijing Cancer Hospital, Beijing, CHINA,* [2]*Beijing Normal University, Beijing, CHINA,* [3]*University of Pennsylvania, Philadelphia, PA, UNITED STATES OF AMERICA.*

Aim/Introduction: To prospectively determine whether differences between benign and malignant intracranial tumors can be depicted with ^{18}F-(2S,4R) 4-fluoroglutamine (^{18}F-FGln) PET and compared with enhanced MRI. **Materials and Methods:** 33 patients (16 women, 17 men; age range, 26-79 years) with solitary intracranial tumors underwent dynamic or static whole-brain ^{18}F-FGln PET/CT after giving informed consent in this institutional review board-approved. Histopathologic diagnoses were made in all cases (15 high-grade gliomas, 9 metastases to the brain, 3 primary brain lymphoma and 6 benign lesions). In 6 benign lesions, 1 was cerebral infarction, 2 was chromophobe cell pituitary adenomas and last 3 were meningiomas. The maximum standardized uptake value (SUVmax) for lesion and peritumoral regions was measured on PET images was calculated. Differences were assessed with one-way analysis of variance, Fisher exact, and Student t tests. **Results:** Differences in SUVmax between high-grade gliomas (5.18±1.14), metastases (3.11±1.68), and primary brain lymphomas (7.01±1.39) were significant ($P < 0.05$). These differences were also significant at pairwise analysis. The time activity curve (TAC) of dynamic ^{18}F-FGln PET/CT in the three groups of malignant tumors show that lymphomas with a rapid increase in the early phase (0~5min. pi), and a consistent in the middle (5~15min.pi) and late phase (15~30min.pi); the high-grade gliomas with a low level in the initial phase, a slow increase in the middle and late phase; the metastases with a slow increase in the first and middle phase, and a consistent in late phase. In six benign lesions, there was high radioactive uptake in 3 meningiomas (SUVmax=5.32±1.34), moderate uptake in 2 pituitary adenoma (the SUVmax were 3.68±1.20) and mild radioactive uptake in the lesion edge of cerebral infarction (SUVmax=2.17). **Conclusion:** High-grade gliomas, metastases, and lymphomas may be distinguished on the basis of measured ^{18}F-FGln uptake and TAC. Higher uptake of ^{18}F-FGln is a significant feature of primary brain lymphomas. The uptake of ^{18}F-FGln in some benign tumors, such as the pituitary adenoma, and meningiomas requires special attention and further study. **References:** None.

EP-0695

Radiolabeling and biodistribution in the tumor xenograft

of ^{211}At-labeled anti-CXCR4 antibody for cancer stem cell targeted alpha-particle therapy

N. Oriuchi[1,2], S. Zhao[1], M. Aoki[1], C. Tan[1], S. Sugawara[1], K. Nishijima[1], S. Shimoyama[1], K. Washiyama[1], K. Takahashi[1], T. Ikezoe[3], H. Ito[1,4]; [1]Advanced Clinical Research Center, Fukushima Medical University, Fukushima, JAPAN, [2]Department of Nuclear Medicine, Fukushima Medical University, Fukushima, JAPAN, [3]Department of Hematology, Fukushima Medical University, Fukushima, JAPAN, [4]Department of Radiology, Fukushima Medical University, Fukushima, JAPAN.

Aim/Introduction: C-X-C chemokine receptor type 4 (CXCR4) is known to express in the various cancer stem cells. Aim of the study was to test the biokinetics of ^{211}At-labeled anti-CXCR4 antibody (^{211}At-CXCR4) in the tumor xenograft to see the possibility of cancer stem cell targeted radioimmunotherapy. **Materials and Methods:** Human acute leukemia cell line (U937) was maintained for in vivo examination. ^{211}At was produced via ^{209}Bi(α, 2n)^{211}At nuclear reaction using cyclotron MP-30 in our facility. Anti-CXCR4 monoclinal antibody was labeled with ^{125}I and ^{211}At. Radiochemical yield was evaluated by SE-HPLC and then purified with PD-10 column to secure radiochemical purity.Suspension of 1 x 10^7 cells in 100 µL PBS (-) were injected subcutaneously in the dorsal flank of the athymic Balb/c nude mice to prepare for in vivo biodistribution study. The animal studies were approved by the Local Animal Care Committee and were performed in accordance with our institutional guidelines. When the tumors were ~8-15 mm in diameter, ^{125}I, or ^{211}At-CXCR4 were injected intravenously into the animals. At 1 min, 1 hr, 6 hr, 24 hr, and 48 hr after injection, mice were euthanatized, and aliquots of blood were collected. Organs of interest were excised and weighed, and the radioactivity counts was measured to expressed as % injected dose/gram (%ID/g). **Results:** Blood clearance of ^{211}At-CXCR4 was slow; 66.9%ID/g at 1 min, 38.3%ID/g at 6 hr, and 20.4%ID/g at 24 hr in the serum, Biodistribution of ^{211}At-CXCR4 as well as tumor uptake was similar to that of ^{125}I-CXCR4. Radioactivity in the thyroid gland was slightly increased up to 24 hr. **Conclusion:** Although blood clearance of ^{211}At-CXCR4 was slow due to IgG nature compared with the physical half-life of ^{211}At, and the affinity of the antibody to tumors used in the present study was low, ^{211}At-labeled anti-CXCR4 antibody was stably radiolabeled and biodistribution including tumor uptake was similar to ^{125}I-labeled antibody, suggesting possibility of radioimmunotherapy targeting cancer stem cells. **References:** None.

EP-0696

Translational proof-of-concept with 68Ga-NeoBOMB1 in the Management of Gastrointestinal Stromal Tumor Liver Metastasis Treated with Interventional Radiology Methods

R. De Juan Rubio[1], M. Pretze[2], L. Reffert[2], F. Orlandi[3], J. Schmaljohann[1], S. Diehl[2], K. Büsing[2], N. Rathmann[2], S. Schönberg[2], C. Decristoforo[4], P. Hohenberger[2], B. Wängler[2]; [1]Universitätsklinikum, Mannheim, GERMANY, [2]Medical Faculty Mannheim, Heidelberg University, Mannheim, GERMANY, [3]Advanced Accelerator Applications, Colleretto Giacosa, ITALY, [4]Medical University, Innsbruck, AUSTRIA.

Aim/Introduction: Ga^{68}-NeoBOMB1 is a novel DOTA-coupled gastrin-releasing peptide receptor (GRPR) high affinity antagonist with excellent in vivo stability. Our study aim was the translation of preclinical results and experience with the preparation of Ga68-NeoBOMB1 using a GMP kit approach and a licensed 68Ge / 68 Ga generator. Furthermore, we explored the application of ^{68}Ga-NeoBOMB1 in patients with gastrointestinal stromal tumors (GIST) before and/or after interventional treatment methods (selective internal radiotherapy (SIRT), electroporation, microwave) of liver metastases. **Materials and Methods:** Contrast-enhanced PET/CT studies were performed on a 40-slice PET/CT scanner with 80 ml arterial i.v. contrast. Images were obtained 45 minutes (early) and 120 minutes (delayed) following a ^{68}Ga-NeoBOMB1 injection of 1,5-2 MBq/kg (135-229 MBq) into the antecubital vein. We examined three patients (2f, 1 m; 51-77) with liver metastases prior to SIRT therapy. Image acquisition, attenuation correction, fusion, reconstruction and post-processing were performed on a dedicated workstation. SUVmax was determined both on the early and delayed imaging. Patients were followed clinically and with MR quarterly. **Results:** A validation of the production (radiosynthesis) and quality control were performed before starting the GMP production of ^{68}Ga-NeoBOMB1 for patient use. Six independent batches of ^{68}Ga-NeoBOMB1 were produced, all held the quality criteria with a radiochemical yield of >95% and radiochemical purity >95%. Patient one (f,77) (liver, peritoneum) had an isolated lesion in S8 (SUVmax early 11,2 delayed 16,6) and underwent electroporation with confirmed complete response after 11 month follow-up. Patient two (m, 57) (multiple liver) had a PET/CT before and after SIRT therapy , which showed response in S8 lesion (SUVmax 1,4 late 3,3) and persistence in S 2/3 (SUVmax 6,3 late 16,1). The patient underwent electroporation on the left lobe, and developed progressive disease at 3-month follow-up. Thus, PET-CT distinguished recurrence from response. Patient three (f, 51) (multiple liver) had SIRT and microwave therapy was followed by PET/CT 3 months with no residual uptake, however progressive disease was demonstrated at 3 months MR follow-up. **Conclusion:** We successfully introduced ^{68}Ga-NeoBOMB1 in our clinical environment and are now capable of routine production under GMP conditions for routine patient care of patients with GIST metastatic liver disease. The lesion-to-background contrast allowed staging and restaging of metastatic liver disease. PET/CT with ^{68}Ga-NeoBOMB1 seems to be useful in pre- and post-therapy assessment in GIST liver metastases which were treated by interventional treatment methods. **References:** None.

EP-0697

Comparison of ^{18}F-(2S, 4R) 4-fluoroglutamine imaging between healthy and tumor subjects

X. Xu[1], H. Zhu[1], L. Zhu[2], N. Li[1], H. Kung[3], Z. Yang[1]; [1]Beijing Cancer Hospital, Beijing, CHINA, [2]Beijing Normal

University, Beijing, CHINA, [3]University of Pennsylvania, Philadelphia, PA, UNITED STATES OF AMERICA.

Aim/Introduction: The purpose of this study was to compare dynamic PET/CT imaging of ^{18}F-FGln between healthy and oncological subjects and explore the optimal imaging time in different cancer types. **Materials and Methods:** 13 healthy volunteers and 27 oncological patients underwent ^{18}F-FGln and ^{18}F-FDG PET/CT scans separately within one week. Distribution of ^{18}F-FGln in major organs of healthy and oncological subjects were analyzed and compared with those of ^{18}F-FDG. In addition, tumor ^{18}F-FGln avidity versus ^{18}F-FDG avidity in patients with paired PET scans (n=27) was evaluated. The SUVmax and SUR of tumors with ^{18}F-FGln were compared between two scan phases (early(10min), late(60min)) **Results:** ^{18}F-FGln activity (SUVmean) of most normal organs in cancer patients were lower than that of healthy subjects, especially in lung, muscle, spleen and heart ($p<0.05$). Additionally, FGln-avid tumors weren't uniformly with FDG-avid and vice versa. Overall, 24 of 27 pathological primary lesions suggestive of malignancy on both (early and late) ^{18}F-FGln PET/CT images, however, there was a significant decrease in SUVmax on late images in most cancer ($p=0.005$) while the SUR of lung cancers ($p=0.021$) and thyroid cancers ($p=0.386$) showed increase from the early to the late acquisition, but decrease was seen in breast lesions ($p=0.022$). **Conclusion:** Images provided by ^{18}F-FGln may further supplement the diagnosis of ^{18}F-FDG in cancer patients and detect the metabolic changes in different tumors. Furthermore, imaging time for ^{18}F-FGln PET/CT in different cancer types may need to be optimized to improve contrast resolution for visualization and quantification of tumors. **References:** Dunphy MPS, Harding JJ, Venneti S, Zhang H, Burnazi EM, Bromberg J, et al. In Vivo PET Assay of Tumor Glutamine Flux and Metabolism: In-Human Trial of (18)F-(2S,4R)-4-Fluoroglutamine. Radiology. 2018;287:667-75.

EP-0698

PSMA expression a promising biomarker to predictdifferentiated thyroid cancer aggressiveness and outcome

M. Sollini[1], *L. Di Tommaso*[1], *M. Kirienko*[1], *C. Piombo*[2], *M. Erreni*[2], *A. G. Lania*[1], *L. Antunovic*[2], *A. Chiti*[1];
[1]*Humanitas University, Pieve Emanuele, ITALY,* [2]*Humanitas Clinical and Research Center, Rozzano, ITALY.*

Aim/Introduction: Prostate specific membrane antigen (PSMA), a type II integral membrane protein, is overexpressed in prostate cancer and on the endothelial cells of tumor neovessels of several solid malignancies, including differentiated thyroid cancer (DTC)[1].We aimed to test the potential role of PSMA as biomarker for DTC aggressiveness and outcome prediction, in terms of earlier recurrence/progression, iodine refractoriness, and presence of disease at last follow-up. **Materials and Methods:** We retrospectively screened all patients who underwent thyroidectomy between 01/01/2010 and 31/12/2017 in our institution. Applying the inclusion (a-histologically proved thyroid cancer, b- tissue availability) and exclusion criteria (a- no clinical or follow-up data, b- medullary thyroid cancer) a cohort of 59 patients (mean age 53.12±16.76 years) was selected. The monoclonal mouse anti-human PSMA antibody, that binds an epitope present on the extracellular portion of PSMA, was used to stain the tissue sections. The 3-points scale [2] was used to score PSMA positivity: 0-5% expression was considered as negative (score 0), 5-50% as moderately positive (score 1) and 50-100% as highly positive (score 2). A cumulative score (0-10%, 11-79% and 80-100%) was also explored. Univariate and multivariate logistic regression were performed to predict the presence of distant metastases, chosen as endpoint of aggressiveness. The area under the curve (AUC) was calculated. Cox models were built to predict patient outcome in terms of recurrence, iodine refractoriness, and status at last follow-up, calculated using the Kaplan-Meier failure function. **Results:** At immunostaining 12/59, 25/59 and 22/59 of patients had score 0, score 1 and score 2, respectively. According the cumulative score, PSMA expression was ≤10% in 17/59 cases, 11-79% in 31/59 cases and ≥80% in 11/59 cases. At multivariate analysis age, sex, histotype, vascular invasion, T and N parameters and PSMA positivity resulted significant predictors of distant metastases (AUC=0.92). Recurrence or progression occurred in 14/59 and 5/59 patients, respectively; median DFS was 23 months (range 3-82); 12 patients developed RAI refractoriness with a median time of 19.5 months (range 2-32); one patient died of DTC; 46 among the 58 patients alive at last follow-up were disease-free. The final multivariate model to predict RAI refractoriness included as covariates stage, high PSMA expression (≥80%), and the interaction between moderate PSMA expression (11%-79%) and stage. **Conclusion:** PSMA, a marker of neovasculature formation, expressed by DTC resulted to contribute to predict tumor aggressiveness and to be promising in outcome prediction. **References:** 1. Br J Pharmacol. 2016;3041-79.2. Sci Rep. 2017;7:5202.

EP-0699

Entresto®-treated mice show superior targeting of PC-3 xenografts vs. controls after injection of the SPECT tracer [^{99m}Tc]DB4

P. Kanellopoulos[1,2], *A. Kaloudi*[1], *M. de Jong*[3], *E. P. Krenning*[4], *T. Maina*[1], *B. A. Nock*[1];
[1]*Molecular Radiopharmacy, INRASTES, NCSR "Demokritos", Athens, GREECE,* [2]*Molecular Pharmacology, School of Medicine, University of Crete, Heraklion, GREECE,* [3]*Department of Radiology & Nuclear Medicine, Erasmus MC, Rotterdam, NETHERLANDS,* [4]*Cyclotron Rotterdam BV, Erasmus MC, Rotterdam, NETHERLANDS.*

Aim/Introduction: The gastrin-releasing peptide receptor (GRPR)-directed radiotracer [^{99m}Tc]DB4 (^{99m}Tc-[N_4^0,Pro[1],Tyr[4],Nle[14]] BBN, BBN: bombesin) has shown specific uptake in prostate cancer lesions in mice and in man. It is assumed that the tumor values achieved thus far may further improve by enhancing the metabolic stability of [^{99m}Tc]DB4. In situ metabolic stabilization

of [^{99m}Tc]DB4 may be achieved by co-injection of a suitable neprilysin (NEP) inhibitor, as previously shown for a series of BBN-like theranostic radioligands. In the present study, we compared the biological profile of [^{99m}Tc]DB4 in mice bearing PC-3 xenografts, treated or not with the FDA approved drug Entresto®, aiming to clinical translation of the NEP-inhibition concept. **Materials and Methods:** [^{99m}Tc]DB4 was injected in healthy Swiss albino mice without or with co-injection of the NEP-inhibitor sacubitrilat (0.3 mg sacubitrilat/kg body weight); a third mice group received a slurry of the FDA-approved drug Entresto® (containing 50 mg of the sacubitrilat-prodrug sacubitril/kg body weight) by oral gavage 30 min in advance. Blood samples collected 5 min postinjection (pi) were analyzed by RP-HPLC. Biodistribution was conducted in SCID mice bearing PC-3 xenografts in their flanks. [^{99m}Tc]DB4 was injected alone in mice 30 min after orally receiving Entresto®, or in untreated mice, or together with sacubitrilat; animals were sacrificed at 4 h pi and biodistribution was conducted. **Results:** While 26.3±2.9% (n=5) of [^{99m}Tc]DB4 were detected intact in peripheral mouse blood at 5 min pi, by Entresto® or sacubitrilat-treatment the percentage of intact radiotracer reached 71.5±1.8% (n=4) and 74.3±7.1% (n=4), respectively. A likewise impact of orally administered Entresto® or iv-injected sacubitrilat was observed on the uptake of [^{99m}Tc]DB4 in the PC-3 xenografts, which notably increased at 4 h pi from 6.5±1.2%ID/g (n=4) to 16.4±4.3%ID/g (n=3) and 16.2±0.7%ID/g (n=3), respectively. Uptake doubled in the GRPR-rich mouse pancreas, but intestinal and renal values were little affected by such treatment. **Conclusion:** This study has shown that oral administration of the FDA-approved drug Entresto® or iv-coinjection of the respective NEP-inhibitor sacubitrilat in mice substantially improved the stability of [^{99m}Tc]DB4 in peripheral mice blood. As a result, the uptake of [^{99m}Tc]DB4 in the implanted PC-3 tumors was favourably enhanced as well. The in-situ NEP-inhibition concept warrants translation in the clinic and is currently pursued. **References:** None.

EP-49

Preclinical and translational aspects, including radiopharmacy, radiochemistry and drug development -> Preclinical and translational aspects -> Translational aspects -> Therapy

October 12 - 16, 2019 e-Poster Area

EP-0700

Theranostic $^{64/67}$Cu SARTATE Clinical Trial - Imaging and PRRT of Patients with Meningioma:Preliminary safety data

G. P. Schembri, S. Dave, D. Chan, E. Hsiao;
Royal North Shore Hospital, St Leonards, AUSTRALIA.

Aim/Introduction: ^{67}Copper sartate is a novel agent with therapeutic applications across a number of somatostatin expressing tumours. We report preliminary safety findings in a first in human trial utilising 67Cu-Sartate. **Materials and Methods:** ^{67}Cu-SARTATE is being evaluated in a Phase I-IIa multidose trial with recurrent or progressive grade I-III meningioma (ACTRN12618000309280). Participants receive up to 4 therapy cycles (6-12 weeks apart) of approximately 5GBq of 67Cu-SARTATE, given concurrently with renoprotective amino acids. Safety visits occur between each cycle at fortnightly intervals. The last follow-up visit is planned for 12 weeks after administration of the last cycle. Adverse events were graded using CTCAE v4.03 criteria. **Results:** 11 cycles of therapy in 3 patients (4,4 and 3 cycles) have been completed at this time. All ^{67}Cu Sartate infusions were completed without incident. There were no reported clinical events related to blood pressure, heart rate, temperature or oxygen saturation. One patient developed sinus tachycardia attributed to thyroxine overdosage.There were no changes in renal function with stable creatinine and eGFR. Baseline eGFR 91 , post treatment 91. Total WCC were stable however reductions in lymphocytes counts were evident in all three patients though not with every cycle. PRRT has been noted to suppress B lymphocyte counts, though usually with ^{90}Yttrium. This typically resolves within 90 days. Dexamethasone (given as premedication) may be a contributing factor. The lowest value recorded was 0.4 X 10^9/L (grade 3 toxicity). This patient had a prexisting low platelet count suggesting underlying bone marrow dysfunction. The other two patients had grade 2 toxicity. No change in other FBC indices were evident. INR remained stable and urinalysis was unremarkable. Physical examination remained stable.Adverse effects (AE) were reported by all three patients. All the reported AEs were grade 1. Examples include minor rash and non trial related drug effects.Those potentially associated with therapy were metallic taste post treatment and transient blurred vison after 1 cycle. **Conclusion:** In this small phase 1 trial, initial results suggest therapy with ^{67}Cu Sartate is well tolerated with no directly related side effects requiring treatment. Minor grade 1 AE's, most not considered directly due to therapy. Grade 2/3 reduction in lymphocytes noted. Ongoing follow-up to trial endpoint required to confirm significance and resolution of this finding. **References:** 1. Sierra ML et al: Lymphocytic toxicity in patients after peptide-receptor radionuclide therapy (PRRT) with 177Lu-DOTATATE and 90Y-DOTATOC. Cancer Biother Radiopharm. 2009 Dec;24(6):659-65. doi: 10.1089/cbr.2009.0641.

EP-0701

Evaluation of Non-Small Cell Lung Cancer by PET/CT with $^{64}CuCl_2$: initial experience in humans

S. S. Medina[1,2], O. Garcia[1,3], S. Lopez[1];
[1]Instituto Nacional De Cancerologia, Mexico City, MEXICO, [2]Hospital Angeles Lindavista, Mexico City, MEXICO, [3]Hospital Médica Sur, Mexico City, MEXICO.

Aim/Introduction: Evaluate the diagnostic potential of the use of the PET/CT with $^{64}CuCl_2$ in patients with non-small cell lung cancer without mutations before to initiate therapy. **Materials and Methods:** Eleven patients with NSCLC without gene

mutations was included, baseline 18F-FDG-PET/CT and 64CuCl2 PET/CT imaging was performed. We calculate and compare the DRs of the $^{64}CuCl_2$ PET/CT with the standard imaging ^{18}F-FDG PET/CT. DRs were calculated as the ratio between the number of positive lesions visualized by $^{64}CuCl_2$ PET/CT and the total number of lesions visualized by ^{18}F-FDG PET/CT. **Results:** Overall, 8 out of 11 patients (73%) demonstrated high focal uptake of 64CuCl2 on PET/CT images. 36% patients showed higher uptake in the primary tumor. 27% patients showed tracer uptake in lymph nodes metastases, of which 18% patients do not demonstrated metastatic sites a when compared with previous 18F-FDG PET/CT. In 2 patients (18%) very low uptake was observed in the primary tumor in lung; and 3 patients (27%) very faint focal uptake was noted in previous non-pathologic bone fractures which was considered to be a nonspecific inflammatory process. To determine the DR of two radiotracers in detecting lesions, we performed a lesion-based analysis. A total 68 lesions were detected by 18F-FDG PET/CT, 24 of which were in the lung, 30 regional lymph-node metastases, 17 distant non-bone metastases (including non-regional lymph-node metastases) and 14 bone metastases. 64CuCl2 PET/CT showed significantly lower DRs than did18F-FDG PET/CT. A complete match was found with a previous 18F-FDG PET/CT study in 2 patients. No difference in bone metastases DR was observed between 18F-FDG PET/CT and 64CuCl2 PET/CT. The difference between the DR of 64CuCl2 PET/CT and that of 18F-FDG PET/CT was not statistically significant (P = 0.108). All patients was initially treated with therapy based in platinum agents, the four patients who showed the highest uptake in the primary tumor with 64CuCl2 PET/CT, presented partial metabolic response in the response evaluation (3-4 cycles, mean 3 cycles), and only one of them showed partial response by RECIST and PERCIST criteria visualized with 18F-FDG PET/CT. **Conclusion:** This study reports the first in-human application of a $^{64}CuCl_2$ PET/CT, in the primary staging of patient's with NSCLC chemo-naïve; these results may represent that $^{64}CuCl_2$ PET/CT uptake is based on the expression of CTR1 transporters seeking to differentiate between those patients who may benefit from platinum-based therapy. More studies are necessary for confirm these findings. **References:** None.

EP-0702

Metabolic Alternation in Liver Tumor and Parenchyma with ^{18}F-FDG PET and NMR Metabolomics in A Mouse Model

Y. S. Chung, G. Lin, T. Yen;
Chang Gung Memorial Hospital, Tao-Yuan, TAIWAN.

Aim/Introduction: Radiation induced liver disease (RILD) is thought as a limitation of radiation treating liver cancer. The mechanisms underlying the radiation response to the liver parenchyma and hepatocellular carcinoma (HCC) still remain the prosperous research subjects. The purpose of this study was to investigate the metabolites alternations of the liver parenchyma and tumor in a mouse model after receiving irradiation. **Materials and Methods:** The mice were implanted BNL liver tumor xenografted in right liver lobe, underwent 15 Gy irradiation. The ^{18}F-FDG PET images of liver parenchyma and tumor lesion were retrospectively evaluated in irradiated mice (RT, n=7) and non-irradiated mice (non-RT, n=6) served as a control at day 1 and day 3 after radiation. The independent metabolic study was carried out the tissues removing of the right liver parenchyma, left liver parenchyma and tumor after the mice with or without irradiation in 1 day (n=6, RT v.s.non-RT) and 3 days (n=6, RT v.s.non-RT). The metabolites of tissues and tumors were analyzed with nuclear magnetic resonance (NMR) techniques. **Results:** The SUVmax FDG uptake of the right liver parenchyma, left liver parenchyma and tumor regions were increased at day 1 and/or day 3 after receiving radiation. But, there is no statistical significant difference between RT and non-RT groups. The score plots from PCA metabolites analysis of right and left liver parenchyma and tumors revealed separate clusters of the RT and non-RT mice, indicating the differences on metabolites composition. In sophisticated metabolites analysis results, the glucose and acetate were significant elevated 12.3 ($p<0.001$) and 2.5 ($p<0.01$) folds of the right liver parenchyma in RT mice, respectively at day 1 after irradiation. The associated pathways induced by irradiation in right liver parenchyma were starch and sucrose metabolism ($p<0.027$), galactose metabolism ($p<0.036$), pyruvate metabolism ($p<0.032$) and glycolysis and gluconeogenesis ($p<0.036$) found significantly activated after irradiation in 1 day. **Conclusion:** The metabolites alternations of the liver parenchyma and tumor in a mouse model are found on as early as one day after receiving irradiation. The elevated glucose metabolism in liver parenchyma and tumor region after irradiation demonstrated with concurrently ^{18}F-FDG PET and metabolite analysis NMR techniques. **References:** None.

EP-0703

Use Of Whole Body SPECT/CT To Study Biodistribution Of [^{67}Cu]SARTATE In Subjects With Meningioma - Preliminary Results

D. L. Bailey[1], *K. P. Willowson*[1], *G. P. Schembri*[1], *A. Hedt*[2];
[1]*Royal North Shore Hospital, Sydney, AUSTRALIA,*
[2]*Clarity Pharmaceuticals, Sydney, AUSTRALIA.*

Aim/Introduction: Copper-67 SARTATE ([^{67}Cu]MeCOSAR-Tyr3-Octreotate, Clarity Pharmaceuticals, Sydney, Australia) is currently being trialled for treatment of somatostatin-expressing tumours. We have undertaken a first-in-human non-randomised, open label clinical trial in subjects with unresectable meningioma to study the biodistribution of the radiopharmaceutical in organs apart from brain, where there is no disease. **Materials and Methods:** To date, three subjects have had 11 cycles each of 5 GBq [^{67}Cu]SARTATE administered with simultaneous amino acid infusion. Imaging is performed using whole body SPECT/CT at time points 1, 4, 24 and 96 hrs after administration. All scans are performed on a dual-head gamma camera (Siemens Intevo.6) using an energy window on the 185 keV gamma photon of ^{67}Cu (Branching Ratio = 0.49). Organs of

interest were defined on the CT scan and from these the decay corrected percentage injected dose (%ID) in the target organs was measured at each time point. The remaining percentage in the rest of the body was also determined. The biological half-life ($t_{½(b)}$) of the radiopharmaceutical was determined by fitting exponential functions to the retention data. **Results:** Averaged over all cycles in the three subjects the peak %ID in the organs of interest, ranked in decreasing order, were: muscle - 13.3%, liver - 9.4%, kidneys - 4.1%, spleen - 3.4% and bone marrow - 1.6%. The effective half-lives measured were: blood pool - 22.5 hrs, muscle 22.6 hrs, bone marrow - 40.9 hrs, liver - 41.6 hrs, spleen - 43.1 hrs, kidneys - 48.5 hrs with the remainder clearing with a $t_{½(b)}$ = 47.1 hrs. **Conclusion:** Whole body SPECT/CT at multiple time points has allowed precise organ definition for evaluating biodistribution in multiple organs. These data will be used to assess whole body and organ dosimetry and can further be used to personalise the prospective individual dose of therapeutic radiopharmaceutical for the subject. **References:** None.

EP-0704

Feasibility and initial safety of $^{86/90}$Y-NM600 theranostics in a canine patient with metastatic osteosarcoma

R. Hernandez, I. Marsh, J. Grudzinski, E. Aluicio-Sarduy, M. Turek, J. Engle, Z. Morris, B. Bednarz, D. Vail, J. Weichert;
University of Wisconsin, Madison, WI, UNITED STATES OF AMERICA.

Aim/Introduction: Over the last three decades, survival for metastatic osteosarcoma (mOSA) patients has not improved substantially, thus novel combination therapies to treat mOSA are direly needed. Our study investigated the feasibility and toxicity profile of [^{90}Y]Y-NM600 for the treatment of mOSA in a translationally relevant companion canine model of mOSA. **Materials and Methods:** A 45 kg mastiff companion dog presented with wide-spread metastatic osteosarcoma (mOSA) was recruited through the UW-Madison veterinary clinic. Clinical examination, complete blood count (CBC), urinalysis, and comprehensive metabolic panel (CMP) were performed at entry. A [^{86}Y]Y-NM600 185 MBq (5 mCi) intravenous bolus was administered to the patient followed by the acquisition of serial PET/CT scans in a clinical PET/CT scanner at 2, 24, and 48h post-injection. Blood samples were collected prior each imaging timepoint to assess [^{86}Y]Y-NM600 blood clearance. Region-of interest analysis of the PET images was performed to determine [^{86}Y]Y-NM600 uptake -presented as standardized uptake value (SUV)- and clearance in the tumor and normal organs, and to estimate the dosimetry of therapeutic [^{90}Y]Y-NM600. A conservative 592 MBq (16 mCi) [^{90}Y]Y-NM600 activity was administered to investigate initial safety. Clinical examination, CBC, urinalysis, and CMP were performed regularly after the administration of both the imaging and TRT agents. **Results:** Selective uptake and prolonged retention of [^{86}Y]Y-NM600 in the primary and metastatic lesions was observed by PET/CT. Mean and maximum SUV in the tumor peaked at 4.6 and 7.6, respectively, at the 48 h post-injection timepoint. Blood circulation ($t_{1/2}$ = 9.3 hours) and hepatobiliary excretion of the radiotracer was evidenced by the initially elevated blood radioactivity and gradual distribution to the gallbladder and feces. Patient-specific dosimetry using a voxel-based dose calculation platform determined a tumor to bone marrow dose ratio greater than 2, for both the primary and the lung metastatic lesions. Administration of a [^{90}Y]Y-NM600 activity, delivering <1 Gy to the bone marrow, did not cause any acute and sub-acute adverse events (AEs). Serial CBC, CMP, urinalysis, and client-documented quality of life questionnaires documented no significant clinical or clinicopathologic AEs after [^{90}Y]Y-NM600 treatment. No clinically significant changes in serum biochemistry profile were noted and all hematologic cell lines remained constant or higher than baseline. **Conclusion:** Our data demonstrates the feasibility and safety of $^{86/90}$Y-NM600 theranostic approach in canines and provides guidance for further dose escalation studies in dogs and future Phase-1 human clinical trials. **References:** None.

EP-50

Preclinical and translational aspects, including radiopharmacy, radiochemistry and drug development -> Radiopharmacy, radiochemistry, drug development -> Drug development -> New biological targets and ligands

October 12 - 16, 2019 e-Poster Area

EP-0705

Assessment of In Vivo Glucagon Receptor Engagement in Rat Liver

I. Laitinen[1], *S. Jones*[1], *V. Derdau*[1], *O. Eriksson*[2], *T. Haack*[1], *L. Johansson*[2], *P. Larsen*[3], *C. Loewe*[1], *S. Pierrou*[2], *O. Plettenburg*[4], *M. Schudok*[1], *I. Velikyan*[5], *M. Wagner*[1];
[1]*Sanofi-Aventis Deutschland GmbH, Frankfurt am Main, GERMANY,* [2]*Antaros Medical AB, Uppsala, SWEDEN,* [3]*Grünenthal GmbH, Aachen, GERMANY,* [4]*Helmholtz Zentrum München, Neuherberg, GERMANY,* [5]*Department of Medicinal Chemistry, Uppsala University, Uppsala, SWEDEN.*

Aim/Introduction: The glucagon receptor (GCGR) is a G protein-coupled receptor that is expressed primarily in the liver, where it plays a vital role in regulating glucose production and in maintaining glucose homeostasis. It has emerged as an interesting target in the development of pharmacological weight-loss therapies in recent years, particularly as part of poly-agonists that combine the benefits of GCGR agonism with agonism at the glucagon-like peptide-1 receptor. Determining in vivo target engagement of these dual-agonists has been a challenge. Here we describe the use of a novel GCGR targeting radiotracer [1] to visualise the interaction of glucagon receptor-targeting molecules with the glucagon receptor in a rodent

model. **Materials and Methods:** Healthy SD female rats were administered single i.v. bolus of [^{68}Ga]Ga-DO3A-S01-GCG over a range of different doses (n=39), with or without a prior s.c. or i.v. injected glucagon receptor binding compounds. Sixty minute dynamic PET scans were performed with a Siemens INVEON small animal PET/CT scanner. Uptake in tissues was calculated, and the volume of distribution (V_T) were estimated from a Logan plot using image-derived blood input function. **Results:** High specific accumulation was observed in the liver (1.49±0.17 %ID/g, < 0.25 µg/kg) compared to blood (0.19±0.04 %ID/g) at 60min after tracer injection. Liver uptake was shown to be dose dependent, with an in vivo K_d of 0.7 µg/kg and a mass effect of 0.15 µg/kg. The volume of distribution was significantly lower in rats dosed (s.c. 45min prior to tracer injection) with 0.75 mg/kg of a long-lasting glucagon-receptor agonist (2.75±1.47) compared to animals administered with tracer alone (7.25±2.49) (p=0.0488). Rats dosed (i.v. 15min prior) with 28 µg/kg of a murine acting dual-agonist showed significantly reduced V_T in the liver (2.66±0.24, p=0.0161). **Conclusion:** We show, for the first time, the ability to observe GCGR engagement of a GCGR agonist or dual GLP-1R/GCGR agonist in rodent liver in vivo. **References:** 1) Velikyan I, et al. First-in-class Positron Emission Tomography tracer for the Glucagon receptor. EJNMMI Res (2019) 9(1):17.

EP-0706

Preparation of I-125 labeled TAT peptide using stable iodination linker for White Blood Cell radiolabelling

T. Choi, B. Kim;
KIRAMS, Seoul, KOREA, REPUBLIC OF.

Aim/Introduction: HIV TAT-derived peptides as cell penetrating peptides(CPP) are promising tools for transducing therapeutic molecules which possess low membrane permeability. Radioiodine is commonly employed to prepare radiolabeled peptides. A major shortcoming of radioiodinated peptides prepared by direct labeling methods is their deiodination in vivo. For the preparation of more stable radioiodinated peptides, we introduced a new linker (3-ADIBO-3-oxopropyl-3'-[tributylstannyl]benzamide) to azido-TAT peptide. **Materials and Methods:** Bu_3Sn-TAT was synthesized with ADIBO-azide click chemistry in 50% acetonitrile and purified by prep-HPLC. I-125 was added to Bu_3Sn-TAT and followed by adding 10 µg of chloramine T. I-125 labeled TAT was purified by HPLC. Stability of reconstituted I-125 labeled TAT after nitrogen purged drying was evaluated in DMSO. THP-1, a monocytic leukemia cell line, was used to evaluate cell radiolabelling ability of I-125 labeled TAT peptide. **Results:** The radiolabelling yield was 93% at the maximum. I-125 labeled TAT was more stable at 4 ℃ than 40 ℃. For 14 days, approximately, 4% and 11% of I-125 labeled TAT was degraded at 4C and 40C, respectively. Cellular uptake was measured with carrier-free I-125 labeled TAT of carrier-added I-125 labeled TAT. Cellular uptake ratio of carrier-free I-125 labeled TAT was 1.4%.Cellular uptake ratios of carrier-added were 4.5%, 10.6%, 19.6%, 23.8%, and 19.8% at cold I-TAT 2.5, 5, 10, 25 and 50 µM concentrations, respectively. **Conclusion:** TAT peptides were successfully radioiodinated and penetrated into the cell. Intracellular uptake of HIV-derived TAT was thought to be influenced by cold I-TAT concentration to stimulate cell membrane endocytosis in order to intracellular intake via energy-dependent endocytosis. **References:** Enhanced tumor retention of radioiodinated anti-epidermal growth factor receptor antibody using novel bifunctional iodination linker for radioimmunotherapy, 2016. Oncology Reports 35: 2159-3168.

EP-0707

LDLR targeting for radiotheranostic drugs in glioblastoma

C. Malicet[1], *I. Tworowska*[2], *J. Nowak*[1], *P. Lécorché*[1], *L. G. Flores II*[2], *R. Zielinski*[3], *M. Khrestchatisky*[4], *J. Temsamani*[1], *E. Delpassand*[2];
[1]*Vect-Horus, Marseille, FRANCE,* [2]*RadioMedix Inc., Houston, TX, UNITED STATES OF AMERICA,* [3]*MD Anderson Cancer Center, Houston, TX, UNITED STATES OF AMERICA,* [4]*Aix-Marseille Université, Centre National de la Recherche (CNRS), Institute of Neurophysiopathology (INP), Marseille, FRANCE.*

Aim/Introduction: The prognosis of patients with glioblastoma is poor with an average life expectancy of 12-15 months from diagnosis. Permeability of the blood-brain barrier (BBB) is one of the factors that limit efficacy of the drugs. The low-density lipoprotein receptor (LDLR) expressed at the BBB mediates the transport of endogenous ligands through the BBB. VECT-HORUS has identified and chemically optimized a family of peptide-vectors targeting the LDLR and able i) to cross the BBB and ii) to target tumors such as U87MG glioblastoma that express high levels of the human LDLR. The objective of this study was to determine the LDLR targeting properties of ^{68}Ga/^{177}Lu-radiolabeled peptide vectors using the U87MG glioblastoma model. **Materials and Methods:** The LDLR targeted DOTA-conjugates (VH-DO31, VH-DO33) and NODAGA conjugate (VH-NO31), (10-30ug, Vect-Horus, France) were labeled with 68Ga (1.5mCi) eluted from 68Ge/68Ga generator (ITG GmBH, Germany) or with 177Lu n.c.a (1mCi, ITG GmBH, Germany). The LDLR targeting properties of these conjugates were thus determined in vitro in U87MG cellular uptake studies, as well as in vivo in U87MG xenografted mice. The PET/CT images of U87MG xenografts generated in athymic nude mice (10 weeks, n=3) were acquired using G4 PET/Xray camera (Sofie Biosciences; 10min/scan) at 1h, 2h, 3h, and 4h post-injection. **Results:** All 68Ga/177Lu-labeled conjugates were synthesized with radiochemical purity higher than 91 % (radio-HPLC). Radiolytic stability was increased using C18 ethanol purification of the final products. 177Lu-VH-DO33 showed the highest retention of the agent in U87MG cell line at 1h (13.88± 1.6 %ID/mg) and 21h incubation time (8.7± 4 %ID/mg) compared to 177Lu-VH-DO31 (8.28 ±6.2 %ID/mg). The microPET imaging studies showed rapid accumulation and retention of all VH derivatives in the tumor as monitored up to 4h post-injection. All agents were eliminated through bladder and kidneys. There was no accumulation of agents in the bone marrow. The image-based biodistribution studies of 68Ga-VH-DO31, 68Ga-VH-DO33

and 68Ga-VH-NO31 showed that the tumor to muscle ratios (SUV ratio) after 30 min post-injection were 4.12, 5.07 and 3.88, respectively and remained at the same levels up to 3h post-injection. The SUV ratios of tumor to kidneys were as follows: 68Ga-VH-DO31 (0.46), 68Ga-VH-DO33 (0.84) and 68Ga-VH-NO31 (0.46) confirming renal elimination of the agents. **Conclusion:** VH derivatives showed favorable hLDLR targeting properties in vitro and in vivo in U87MG models. These preliminary results suggest that hLDLR may serve as a target for the development of radiotheranostic drugs for glioblastoma. **References:** None.

EP-0708

^{99m}Tc-labeled hydroxyapatite nanoparticles as potential tracers for solid tumors

Z. Novy[1], *V. Lobaz*[2], *M. Vlk*[3], *J. Kozempel*[3], *M. Hruby*[2], *M. Hajduch*[1], *J. Drymlova*[4], *R. Navratil*[4], *M. Petrik*[1];
[1]*Palacky University in Olomouc, Olomouc, CZECH REPUBLIC,* [2]*Institute of macromolecular chemistry, CAS, Prague, CZECH REPUBLIC,* [3]*Czech Technical University, Prague, CZECH REPUBLIC,* [4]*University Hospital Olomouc, Olomouc, CZECH REPUBLIC.*

Aim/Introduction: The aim of this work was to label newly prepared hydroxyapatite nanoparticles (HAP-NP) with 99mTc using clinically established radiotracer 99mTc-HDP, further verification of radiochemical stability of such labelled nanoparticles in vitro and mainly to describe their biodistribution in healthy and in tumor mice employing SPECT/CT as well as gold standard ex vivo biodistribution approach. Five different variants of nanoparticles were tested with specific biopolymer coating on the surface. **Materials and Methods:** Radiolabeling of nanoparticles was done under mild conditions, i.e. room temperature and pH 7.4, followed by quality control step represented by radiochemical purity check by iTLC in order to reveal labeling efficiency and in vitro stability of the tracer. Ex vivo studies were performed on healthy and tumor mice (1h, 6h, 24h p.i.). The biodistribution of labeled nanoparticles was also monitored by μSPECT/CT system 1h, 3h, 6h a 24h post injection for two different application approaches. First, in vitro prelabeled nanoparticles and second, 99mTc-HDP applied with various time intervals after unlabeled nanoparticles. We have studied influence of antiangiogenic therapy with bevacizumab to HAP-NP biodistribution in tumor-bearing mice too. **Results:** The HAP-NPs were labeled with high radiochemical purity and sufficient stability for their in vivo applications. Ex vivo biodistribution studies revealed dominant accumulation in the liver and spleen. The favorable tumor/blood ratio was determinated from tumor mouse study. In vivo imaging showed mainly the same organs as ex vivo study, i.e. liver and spleen. Ex vivo data from bevacizumab-treated tumor animals reported significant differences in HAP-NP accumulation in kidneys and heart, but not in the tumor. **Conclusion:** Tested HAP-NPs could be relatively easily labeled with 99mTc-HDP. Their in vitro stability is on satisfactory level. Biodistribution studies revealed high accumulation of NPs in liver and spleen. These findings were confirmed by SPECT/CT imaging in healthy and in tumor mice. In case of two-phase application approach, there were positive results for time intervals from three to six hours between injection of HAP-NP and 99mTc-HDP. But tumors were not visualized in SPECT scans. This project was supported by the Ministry of Health of the Czech Republic (grant No. 16-30544A). **References:** None.

EP-0709

In Vitro Evaluation of [^{18}F]FPA as a Fatty Acid Synthase-targeting Imaging Agent for Breast Cancer and its In Vivo Whole-Body Biodistribution in Normal Mice

Y. Huang[1], *C. Tsai*[1], *B. Ho*[2], *H. Ho*[2], *Y. Chang*[1], *C. Wu*[3], *R. Yen*[1,3], *C. Shiue*[1,3];
[1]*PET Center, Department of Nuclear Medicine, National Taiwan University Hospital, Taipei, TAIWAN,* [2]*Department of Anesthesiology, Wan Fang Hospital, Taipei Medical University, Taipei, TAIWAN,* [3]*Molecular Imaging Center, National Taiwan University, Taipei, TAIWAN.*

Aim/Introduction: Fatty acid synthase (FASN) is a key enzyme in fatty acid synthesis pathways and its expression has been known to be an indicator of poor prognosis in breast cancer (BC). Recently, a hypothetical model for FASN-regulated estrogen receptor(ER)-signaling in BC cells has been suggested. As one of the short fatty acids, [^{18}F]2-fluoropropionic acid ([^{18}F]FPA) has been proved as a promising oncological imaging agent. In order to clarify FASN-targeting uptake mechanism of [^{18}F]FPA in BC, we have studied its in vitro binding with ER$^+$ and ER$^-$ BC cells along with its whole-body biodistribution in normal mice using microPET imaging. **Materials and Methods:** [^{18}F]FPA was automatically synthesized based on reported methods with FLEXLAB module(iPhase). Briefly, fluorination of methyl 2-bromopropionatewith K[^{18}F]/$K_{2.2.2}$ in anhydrous MeCN at 110 ^{0}C for 10 min gave the radiofluorinated intermediate. After NaOH hydrolysis and H_2O dilution, the crude product was purified with a semi-preparative HPLC and the isolated [^{18}F]FPA solution was formulated and passed through a 0.22 μm sterile filter to give [^{18}F]FPA for QC, in vitro binding assay with ER$^+$ and ER$^-$ BC cells and in vivo uptake in normal mice. In vitro binding assays of [^{18}F]FPA with ER$^+$ and ER$^-$ BC cells were performed. MicroPET imaging were performed with normal ICR mice (20-30 g, n=3) using small-animal Argus PET/CT scanner. **Results:** The RCY of [^{18}F]FPA was 39.1±12.6 % (n=6, EOB after HPLC isolation) and the synthesis time without formulation was about 85 min at end of synthesis. The radiochemical purity was > 90 % as determined by analytical HPLC and TLC methods. Compare to previous results of FASN-targeting [^{11}C]Acetate, our results indicated that [^{18}F]FPA had significant uptake in both ER$^+$ and ER$^-$ BC cells at 15, 30 and 60 min. In addition, microPET images in normal mice showed that [^{18}F]FPA had significantly accumulation in bladder. **Conclusion:** [^{18}F]FPA has been automatically synthesized with Flexlab module. In vitro binding assay showed that [^{18}F]FPA had significant uptake in both ER$^+$ and ER$^-$ BC cells and its FASN-blocking studies are ongoing. MicroPET images in normal mice showed that [^{18}F]FPA had significantly accumulation in bladder

and its radiation dosimetry will be evaluated for incoming human studies. The evaluations of [^{18}F]FPA as potential imaging agent for BC and other diseases continue. **References:** None.

EP-0710

Structural Optimization of the Arecaidine Diphenylmethyl Ester Scaffold for Muscarinic Acetylcholine Receptor PET Tracer Development

M. Ozenil[1], *K. Pacher*[1], *C. Vraka*[1], *H. Spreitzer*[2], *M. Hacker*[1], *M. Mitterhauser*[1,3], *W. Wadsak*[1,4], *V. Pichler*[1];
[1]*Department of Biomedical Imaging and Image-guided Therapy, Division of Nuclear Medicine, Medical University of Vienna, Vienna, AUSTRIA,* [2]*Department of Pharmaceutical Chemistry, University of Vienna, Vienna, AUSTRIA,* [3]*Ludwig Boltzmann Institute Applied Diagnostics, Vienna, AUSTRIA,* [4]*CBmed GmbH - Center for Biomarker Research in Medicine, Graz, AUSTRIA.*

Aim/Introduction: Several neurodegenerative diseases are associated with altered functions of muscarinic acetylcholine receptors (mAChRs), which makes them an interesting target for neuroimaging. At EANM 2018, we reported on the tremendous gain in mAChR affinity of DPMARE (arecaidine diphenylmethyl ester) and FDPMARE (arecaidine bis(fluorphenyl)methyl ester) compared to arecoline itself. Regarding the affinity and subtype selectivity, these compounds feature promising characteristics for mAChR PET tracer development. Nevertheless, limited stability against human liver microsomes and pronounced nonspecific binding of [^{11}C]DPMARE and [^{11}C]FDPMARE observed in binding studies on living cells motivate us to further improve pharmacokinetic and accordingly physico-chemical properties prior to in vivo studies. **Materials and Methods:** Several new tracer candidates and their corresponding precursors based on the structure of DPMARE and FDPMARE were synthesized. Conjugates of arecaidine with the M1-prefering drug pirenzepine were prepared by nucleophilic substitution with a β-chloro amide (**1**, **2**). Compounds featuring different, generally more polar aryl substituents were synthesized by esterification of arecaidine with benzoin (**3**), (4-bromophenyl)(4-fluorophenyl) methanol (**4**), bis(6-fluoropyridin-3-yl)methanol (**5**), furan-2-yl(phenyl)methanol (**6**) and bis(4-methoxyphenyl)methanol (**7**). These novel potential mAChR ligands were characterized by 2D-NMR, ESI-MS, UV-HPLC and by X-ray crystallography if applicable. A competitive radioligand binding assay using [methyl-^{3}H]-N-methylscopolamine was performed to assess the in vitro binding affinity of the compounds. The most promising compounds were labelled with carbon-11 and were tested for their human liver microsome metabolism and plasma protein binding. **Results:** The K_i values of the newly synthesized compounds were in the order **1**, **2**, **7** > **3**, **6**, **5** > **4**, with the last compound offering a promising affinity in the low nanomolar range. The affinity was in close relation to the lipophilicity. LogP values were in the range of 0.57 up to 4.12 with the following trend: **1**, **2** < **5** < **3** < **7** < **6** < **4**. N-methylation of respective precursor molecules with [^{11}C]CH_3I as radiosynthon facilitated carbon-11 labelling in excellent yields. **Conclusion:** The major limitation of previously synthesized compounds was the high unspecific binding. For this set of compounds, we significantly reduced the lipophilicity. The most promising candidate for PET tracer development offers affinity in the low nanomolar range for M1 and M3-M5, with a 40-fold subtype selectivity of M1 over M2. The next step is to substitute arecaidine with 4-methylmorpholine-2-carboxylic acid, which allows to reduce lipophilicity on another part of the molecule and potentially reach further subtype selectivity. **References:** None.

EP-0711

Development of radiofluorinated CYP11B2-Inhibitors for the differential diagnosis of primary aldosteronism

A. Schirbel[1], *B. Heinze*[2], *P. Maier*[1], *M. Schneider*[1], *S. Samnick*[1], *A. K. Buck*[1], *B. Streile*[1], *K. Marienfeld*[2], *S. Hahner*[2];
[1]*University Hospital Würzburg, Department of Nuclear Medicine, Würzburg, GERMANY,* [2]*University Hospital Würzburg, Department of Endocrinology, Würzburg, GERMANY.*

Aim/Introduction: Primary aldosteronism is a frequent cause of secondary hypertension. It is associated with increased morbidity and mortality compared to hypertensive controls. The central diagnostic problem is the differentiation between bilateral and unilateral disease. This classification is crucial for further treatment as unilateral disease may be cured by surgery while patients with bilateral hyperaldosteronism receive lifelong medical treatment. The enzyme aldosterone-synthase (CYP11B2) is expressed exclusively in the adrenal cortex and is overexpressed in aldosterone producing adenomas. This enzyme should represent a highly suitable target for specific molecular imaging. A problem is the high expression of 11ß-hydroxylase (CYP11B1), which shows high homology to CYP11B2. Our aim was therefore to develop radiofluorinated inhibitors of CYP11B2 with high affinity and selectivity. **Materials and Methods:** Based on 3,5-disubstituted pyridines as known inhibitors we synthesized more than 100 compounds. In vitro analysis of the inhibitors was performed in the human adrenocortical carcinoma cell line NCI-H295 and in murine adrenocortical Y1 cells that were stably transfected with the respective human CYP11B enzymes. Suitable tracers were labelled with F-18 and evaluated in cell uptake experiments and frozen tissue imaging using slices of different human adrenal tumors. **Results:** 19 fluorinated inhibitors showed IC_{50}-values in the low nanomolar range for inhibition of CYP11B2 and selectivity factors up to 100. The corresponding radiofluorinated tracers were synthesized with high RCY and showed a variable cell uptake up to 30% in NCI-h295-cells. Frozen tissue imaging revealed a very high and selective uptake of six tracers in slices of aldosterone producing adenomas. **Conclusion:** For the differential diagnosis of primary aldosteronism we developed six suitable radiofluorinated tracers with high affinity and selectivity which will be evaluated in PET-studies using humanized mice. **References:** None.

EP-0712

1,5-Disubstituted 1,2,3-Triazole-based peptidomimetics: Synthesis and Application to Minigastrin

I. Valverde[1], *N. M. Grob*[2], *M. Béhé*[3], *T. L. Mindt*[4,5]; [1]*Institut de Chimie Moléculaire de l'Université de Bourgogne, Dijon, FRANCE,* [2]*Center for Radiopharmaceutical Sciences ETH-PSI-USZ, Institute of Pharmaceutical Sciences ETH, Zürich, SWITZERLAND,* [3]*Center for Radiopharmaceutical Sciences ETH-PSI-USZ, Paul Scherrer Institute, Villigen, SWITZERLAND,* [4]*Ludwig Boltzmann Institute of Applied Diagnostics, Vienna, AUSTRIA,* [5]*Medical University of Vienna, Department of Biomedical Imaging and Image Guided Therapy, Vienna, AUSTRIA.*

Aim/Introduction: Regulatory peptides have been shown to be suitable vectors for the specific delivery of radioactivity to tumors and metastasis for diagnostic and therapeutic applications in nuclear oncology. A potential drawback of such vectors is represented by their instability in vivo as the result of rapid degradation by intra- and extracellular peptidases. In the past, we have shown that the use of 1,4-disubstituted 1,2,3-triazoles as protease resistant trans-amide bond surrogates leads to an enhanced stability in radiolabeled bombesin and neurotensin derivatives and to an improved tumor uptake in vivo.[1] 1,5-disubstituted 1,2,3-triazoles have been considered as cis-amide bond and turn mimics. Moreover, structural studies support the evidence that some GPCR receptors prefer turn conformations in peptide/protein ligands.[2] One of these receptors is the CCK2 receptor (CCK2R), which is overexpressed in medullary thyroid carcinoma or small cell lung cancer. We herein wish to report the synthesis of analogs of a CCK2 receptor binding conjugate, [Nle[15]]MG11, containing a 1,5-disubstituted 1,2,3 triazole moiety in different backbone positions. **Materials and Methods:** Unlike previously described,[1a] the 1,5 disubstituted 1,2,3-triazole scaffold was introduced in the peptide sequence as a dipeptide mimic building block. This particular protease resistant moiety was synthesized by ruthenium-catalyzed azide-alkyne cycloaddition (click chemistry).[3] Triazole-substituted peptide conjugates were synthesized by classical solid phase synthesis methods. The optimization of the cycloaddition conditions and the synthesis of the building blocks used in the elaboration of the peptidomimetics will be discussed. **Results:** We have synthesized "clickable" azido acids and amino alkynes by straightforward procedures from commercial amino acids. These building blocks were successfully used for the synthesis of a series of analogs of the CCK2R-targeting [Nle[15]] MG11 conjugate. In vitro and in vivo studies to establish if the conjugates have retained biological activity are currently ongoing. **Conclusion:** Combination of solution and solid phase synthesis led to the synthesis of novel 1,5-disubstituted 1,2,3-triazoles-substituted MG11 analogs. To the best of our knowledge, this is the first report of the replacement of amide bonds with 1,5-disubstituted triazoles in a peptide-based conjugate for its use in radiopharmacy. **References:** 1) a) Valverde, I. E.; et al. Angew. Chem. Int. Ed. 2013, 52, 8957; b) Mascarin, A.; et al. Bioconjug. Chem. 2015, 26 (10), 2143-2152. 2) Ruiz-Gómez, G.; et al. Chem. Rev. 2010, 110 (4), PR1-PR41. 3) Boren, B. C.; et al. J. Am. Chem. Soc. 2008, 130, 8923.

EP-0713

Biological evaluation of radiolabelled peptides for oestrogen positive tumour theranostics

M. Gano, *F. Vultos, C. Fernandes, F. Silva, F. Mendes, J. D. G. Correia; Centro de Ciências e Tecnologias Nucleares, Instituto Superior Técnico, Universidade de Lisboa, Bobadela, PORTUGAL.*

Aim/Introduction: The oestrogen receptor (ER) is an important biomarker for prognosis and guiding treatment of breast cancers (BC). It has also been used as target for molecular imaging and therapeutics. Despite the enhancement in the BC survival rate due to new clinical strategies, there is still a need for more effective and personalized treatments. Theranostics is particularly suitable for that purpose. Radiolabelled peptides containing the LXXLL sequence have demonstrated high ER affinity and favourable behaviour in cellular and animal models. Thus, our aim was to compare the biological performance of two ^{111}In-LXXLL-peptide derivatives (single peptide and peptide coupled to an antitumoral agent, ER3AO) to assess their theranostic value in ER positive tumours. **Materials and Methods:** LXXLL-peptide derivatives were synthesized and conjugated to the bifunctional chelators by microwave-assisted solid phase synthesis. ^{111}In-complexes were obtained by reaction with $^{111}InCl_3$. Radiochemical purity and in vitro stability of ^{111}In-peptides were evaluated by HPLC. ER binding affinities were evaluated by a fluorescent polarization assay with the corresponding inactive In(III) complex peptide. Cellular uptake was assessed in MCF-7 (ER+) and MDA-MB-231 (ER-) human BC cells. The internalization rate of the ^{111}In-peptides into the cell nucleus was also evaluated. The ability to induce DNA damage in vitro was tested by incubation with double-stranded plasmid DNA for 140 hours. Biodistribution and in vivo stability was assessed in Balb/c mice with MCF-7 xenografts. **Results:** ^{111}In-peptides were obtained with high radiochemical yield and purity at high specific affinity. The ^{111}In-peptides demonstrated high in vitro stability. Both radiolabelled peptides have showed rapid and high uptake in MCF-7 cells (ER+). The ^{111}In-ER3AO, has had high nuclear internalization (higher than 50%) in MCF-7 cells and demonstrated ability to cause direct damage in DNA. Biodistribution studies of both ^{111}In-peptides in tumour-bearing mice indicated rapid clearance from blood and main organs, high kidney uptake and specific uptake in the ER-rich organs and tumours. Favourable target / non-target tissues radioactivity ratios were found. Differences in the biodistribution profiles of each ^{111}In-peptide derivative were mainly assigned with the involvement of each excretory pathway. High in vivo stability of the complexes was confirmed by HPLC analysis of urine and blood samples. **Conclusion:** Biological evaluation of both ^{111}In-peptide derivatives in cancer cells and tumour-bearing mice indicate promising features suggesting that is worthwhile to modify the peptidic derivative to improve the biodistribution/excretion profiles and further explore the potential for theranostic applications. **References:** None.

EP-0714

Development of O-[^{11}C]Methyl Ester Derivative of Sacubitril for PET Imaging of Neprilysin

V. Teyssier[1,2], *J. Simard*[2], *D. Petrenyov*[2], *F. Tournoux*[1,2], *J. N. DaSilva*[1,2];
[1]*Université de Montréal, Montréal, QC, CANADA,* [2]*Centre de recherche du centre hospitalier de l'Université de Montréal, Montréal, QC, CANADA.*

Aim/Introduction: Neprilysin (NEP), also known as CD10, is a cell surface membrane peptidase overexpressed in heart failure (HF) and in numerous malignant tumors. It is thus a target of choice for PET imaging. We have recently reported the radiosynthesis of the novel 11C-methylated derivative of LBQ657 (active metabolite of the antihypertensive drug sacubitril, an NEP inhibitor (NEPi) FDA approved in combinaison with valsartan to reduce the risk of cardiovascular death and hospitalization for HF in patients with chronic HF (NYHA Class II-IV) and reduced ejection fraction). Here, we present the development and initial autoradiographic evaluation of the novel [^{11}C]methylated derivative of Sacubitril, [^{11}C]SacOMe, for PET imaging of NEP. **Materials and Methods:** The O-[^{11}C]methyl ester analog was produced by O-[^{11}C]methylation of Sacubitril with [^{11}C]methyl triflate in the presence of K_{222} and potassium carbonate for 3 min at 50 °C using a Synthra® MeIplus Research platform. The reaction was then quenched and purified by semi-prep HPLC. [^{11}C]SacOMe was collected into MQ water, transferred through a light C18 Sep-pak, reformulated in<10 % EtOH/Saline and filtered. The identity of [^{11}C]SacOMe was confirmed by co-elution on analytical HPLC with unlabeled fully characterized standard SacOMe. In vitro autoradiography was performed on 20 µm-thick slices of rat kidney incubating [^{11}C]SacOMe (5nM) with or without NEPi (10 µM of thiorphan or Sacubitril) in a HEPES-buffered saline with BSA pH 7.4 for 20 min at 37 °C to discriminate total and non-specific binding, respectively. **Results:** [^{11}C]SacOMe was produced in 12±2 % radiochemical yield (32±3 % decay-corrected from [^{11}C]CO_2, n= 5) within 30 minutes. The radiochemical purity was >99% and molar activity was high at 407±92 GBq/µmol. The high signal observed in the renal NEP-rich outer medulla was completely blocked (>99.9%) in the presence of NEPi, demonstrating specific binding of [^{11}C]SacOMe to NEP. **Conclusion:** The one-step synthetic and purification automated process was optimized to produce the [^{11}C]SacOMe in high yields, purity and molar activity. High uptake and specific binding to NEP-rich areas of kidney slices suggest potential for PET imaging. Micro-PET, metabolism and selectivity binding studies are currently in progress. This innovative research is translatable to humans. **References:** None.

EP-0715

Design and validation of a 68Ga-radiolabelled PET imaging agent for in vivo evaluation of APJ expression

B. Louis[1], *A. Moyon*[2], *A. Bouhlel*[1], *L. Balasse*[1], *S. Fernandez*[3], *S. Simoncini*[4], *P. Brige*[5], *C. Souihi*[6], *G. Hache*[2], *F. Dignat-George*[7], *P. Garrigue*[2], *B. Guillet*[2];
[1]*C2VN INSERM 1263 INRA 1260 CERIMED Aix-Marseille Université, Marseille, FRANCE,* [2]*C2VN INSERM 1263 INRA 1260 CERIMED Aix-Marseille Université APHM, Marseille, FRANCE,* [3]*CERIMED Aix-Marseille Université, Marseille, FRANCE,* [4]*C2VN INSERM 1263 INRA 1260 Aix-Marseille Université, Marseille, FRANCE,* [5]*LIIE, CERIMED, Aix-Marseille Université, Marseille, FRANCE,* [6]*APHM, Marseille, FRANCE,* [7]*C2VN INSERM 1263 INRA 1260 Aix-Marseille Université APHM, Marseille, FRANCE.*

Aim/Introduction: This study aimed at developing a ^{68}Ga-radiolabelled PET imaging agent for assessing tissular APJ receptor expression. APJ has recently been reported to be overexpressed in various cancer types and especially during angiogenesis induction. To date, several APJ-targeted therapeutic strategies are explored. In this work, we designed AP747 as a potent specific ligand of APJ for PET/CT imaging of its expression in oncological applications. **Materials and Methods:** [^{68}Ga]gallium chloride solution was obtained from fractionated elutions of a Galliapharm generator (Eckert&Ziegler). AP747 was designed, produced, and radiolabelling was set up (pH5, 5min at room temperature). Radiochemical stability in NaCl0.9% and human serum was validated up to 2h after synthesis by radiochromatography on iTLC-SG and sodium citrate 0.1M pH5 (n=3). In vitro characterization of [^{68}Ga]Ga-AP747 specificity towards APJ was performed on APJ-overexpressing human colon carcinoma T84 cells, as verified by western-blot. Blocking was performed using a 50-fold excess of APJ ligand. Quantification of radioactivity was realized on background-corrected autoradiographs (n=3, Cyclone Perkin-Elmer). 4-month-old Swiss-nude mice were subcutaneously xenografted with 10^6 T84 cells (n=6) and rested for 4 weeks. 5.1±1.1MBq/50µL of [^{68}Ga]Ga-AP747 were IV injected (n=6), µPET/CT acquisitions performed 1h after radiotracer injection on a NanoScan PET/CT (Mediso). 24h later, in vivo blocking was realized by injecting 50µg of non-radioactive APJ ligand 30min before injecting [^{68}Ga]Ga-AP747 (n=6). Image analysis was performed using VivoQuant® software (InviCRO). Regions of interest were drawn over tumor and muscle for each animal quantified and corrected by the tissue volume (Mbq/mm3). Experiments were performed according to an Ethics Committee agreement by trained and qualified operators. **Results:** [^{68}Ga]Ga-AP747 was produced with a radiochemical purity of 96.7%±2.0 and stability in serum evaluated at 2h (95.0±1.5%). Autoradiographs showed APJ selective biding of [^{68}Ga]Ga-AP747 on T84 cells (16.64±10.98%) reversed by blocking (4,09±7.35%, *P=0.0183). Dynamic PET imaging showed favorable pharmacokinetic profiles with fast renal clearance and low background in liver, lungs, and digestive system. µPET/CT imaging of mice ectopic colon adenocarcinoma xenografts showed a high [^{68}Ga] Ga-AP747 tumor-to-muscle ratio (7.93±2.17) reversed after blocking in the same animals (1.03±0.31, *P=0.0235, n=6). Immunohistochemistry confirmed APJ expression in explanted tumor tissues. **Conclusion:** This proof of concept shows [^{68}Ga]Ga-AP747 might be a useful candidate for imaging APJ expression in tumors. [^{68}Ga]Ga-AP747 showed a specific and

strong uptake in colon adenocarcinoma tumor model in vitro and in vivo, and a low background in healthy organs. Upcoming studies will focus on the interest of this tracer for theranostic purposes. **References:** None.

EP-0716

Gallium-68 Labelled Radiotracer Based On Dota-curcumin For Imaging Of Colon-rectal Carcinoma

M. Asti[1], *G. Orteca*[2], *F. Pisaneschi*[3], *S. Rubagotti*[1], *T. W. Liu*[3], *G. Biagiotti*[4], *D. Piwnica-Worms*[3], *M. Iori*[1], *P. C. Capponi*[1], *E. Ferrari*[2];
[1]*AUSL-IRCCS Reggio Emilia, Reggio Emilia, ITALY,* [2]*University of Modena, Modena, ITALY,* [3]*MD Anderson Cancer Center, Houston, TX, UNITED STATES OF AMERICA,* [4]*University of Firenze, Firenze, ITALY.*

Aim/Introduction: Colorectal cancer is the third most commonly occurring cancer in men and the second most commonly occurring cancer in women worldwide. In the present study, we report a new gallium-68 labelled curcumin derivative (namely ^{68}Ga-DOTA-C21) and its initial validation as marker for early detection of colorectal cancer. **Materials and Methods:** The precursor and non-radioactive complexes were synthesized and deeply characterized by analytical methods then the curcuminoid was radiolabelled with gallium-68. The in vitro stability, cell uptake, internalization and efflux properties of the probe were studied in HT29 cells, and the in vivo targeting ability and biodistribution were investigated in mice bearing HT29 subcutaneous tumour model. **Results:** DOTA-C21 was synthesized with a 38% yield through a tree steps reaction and characterized by ESI-LC/MS and ^{1}H/^{13}C NMR spectroscopy. Post-processing of the generator elution was performed by cation exchange purification and $^{68}Ga^{3+}$ was incubated with 10 nmol of precursor in ammonium acetate buffer (pH 4). Kinetics were fast and the incorporation yield was 97±2 % after 5 min at 95 °C (n = 3). ^{68}Ga-DOTA-C21 exhibits decent stability (57±3 % after 120 min of incubation) in physiological media and a curcumin-mediated cellular accumulation in colorectal cancer cell line (121±4 KBq/mg of protein within 60 min). In HT29 tumour-bearing mice, the tumour uptake of ^{68}Ga-DOTA-C21 is 3.57±0.3 % of the injected dose per gram of tissue after 90 min post injection with a tumour to muscle ratio of 2.2±0.2. High amount of activity (12.73±1.9 % ID/g) is recorded in blood and significant uptake of the radiotracer also occurs in the intestine (13.56±3.3 % ID/g), lungs (8.42±0.8 % ID/g), liver (5.81±0.5 % ID/g) and heart (4.70±0.4 % ID/g). **Conclusion:** Further studies are needed to understand the mechanism of accumulation and clearance; however, ^{68}Ga-DOTA-C21 provides a productive base-structure to develop further radiotracers for imaging of colorectal cancer. **References:** None.

EP-0717

Development of a novel high affinity ^{89}Zr-Anticalin radiotracer directed against human CD98hc for diagnostic PET tumor imaging

V. Morath[1,2], *F. Deuschle*[1,3], *A. Schiefner*[1,3], *M. Heider*[1,4], *S. Ballke*[1,5], *C. Brandt*[1,3], *S. Reder*[1,2], *K. Steiger*[1,5], *F. Bassermann*[1,4], *M. Schwaiger*[1,2], *W. Weber*[1,2], *A. Skerra*[1,3];
[1]*Technische Universität München, München, GERMANY,* [2]*Department of Nuclear Medicine, München, GERMANY,* [3]*Lehrstuhl für Biologische Chemie, Weihenstephan, GERMANY,* [4]*Department of Medicine III, München, GERMANY,* [5]*Institute of Pathology, München, GERMANY.*

Aim/Introduction: Increased amino acid supply and dysregulated integrin signaling constitute two hallmarks of tumor biology and are pivotal for metastatic transformation of cells. In line with its involvement in both pathophysiological processes, overexpression of the cluster of differentiation 98 heavy chain (CD98hc) is clinically observed in various cancers, rendering it a promising tumor target. Hence, development of a ^{89}Zr-ImmunoPET radiotracer that targets corresponding heterodimeric amino acid transporters holds promise for deeper insight into tumor physiology and as a potential tool for in vivo diagnostics. **Materials and Methods:** An Anticalin (~20 kDa) with picomalor affinity (K_D = 50 pM) towards the human CD98hc ectodomain (hCD98hcED) and optimized plasma half-life using PASylation technology was labeled with $^{89}Zr^{IV}$ and subsequently used for preclinical PET imaging of xenograft tumor-bearing mice. **Results:** Our in vitro studies demonstrate specific binding of the radiolabeled Anticalin to several CD98hc-expressing human cancer cell lines, suggesting broader applicability in cancer research. Positron emission tomography (PET) imaging of mice bearing human prostate carcinoma, multiple myeloma or B-cell lymphoma using the ^{89}Zr-Anticalin radiotracer revealed strong and specific tracer accumulation in the xenograft tumors. For example, a biodistribution study with PC3 prostate carcinoma at t=24 h post injectionem revealed high accumulation of the radiotracer (8.6±1.1% ID/g) in the tumor, versus 5.4±1.1% ID/g in the cohort blocked with an excess of unlabeled Anticalin (p=0.0032), and a favorable tumor-to-muscle ratio of 11.8. **Conclusion:** So far, molecular imaging of amino acid transporter activity with ^{18}F-labeled amino acid mimetics such as FET or ACBC is an established diagnostic approach in clinical practice. The present study constitutes a first attempt to specifically target CD98hc for in vivo imaging in a preclinical setting. Our findings provide a proof of concept for the non-invasive diagnostic CD98hc-imaging. Consequently, the anti-CD98hc Anticalin radiotracer opens interesting biomedical applications in the area of cancer theranostics. **References:** None.

EP-0718

Development of a multivalent NPY analogue for selective nuclear delivery of terbium-161

A. Chastel[1,2,3], *D. J. Worm*[4], *I. D. Alves*[5], *D. Vimont*[2,3], *M. Petrel*[6], *P. Fernandez*[1,2,3], *E. Hindié*[1,2,3], *A. Beck-Sickinger*[4], *C. Morgat*[1,2,3];
[1]*Nuclear Medecine Department, University Hospital of Bordeaux, Bordeaux, FRANCE,* [2]*University of Bordeaux, INCIA, UMR5287, Bordeaux, FRANCE,* [3]*CNRS, INCIA, UMR5287,*

Bordeaux, FRANCE, [4]Institut für Biochemie, Universität Leipzig, Leipzig, GERMANY, [5]Institute of Chemistry & Biology of Membranes & Nanoobjects (UMR5248 CBMN) CNRS - Universite Bordeaux - Institut Polytechnique Bordeaux, Bordeaux, FRANCE, [6]Pôle d'Imagerie Electronique - Bordeaux Imaging Center UMS 3420 CNRS US4 INSERM, Bordeaux, FRANCE.

Aim/Introduction: Neuropeptide Y (NPY) receptor subtype-1 (Y_1) is known to be overexpressed in numerous tumors making radiolabelled NPY-analogues of interest for imaging and therapy [1].^{161}Tb is an interesting alternative to ^{177}Lu to deliver radiations, due to its emission spectrum rich in Auger electrons [2]. Here, we describe the combination of a receptor-targeting peptide with a releasable NLS-DOTA unit for the development of a subcellular active radiopharmaceutical. **Materials and Methods:** By solid phase peptide synthesis, the Y_1-preferring [F^7,P^{34}]-NPY was modified at Lys^4 with a fatty acid for stabilization, as well as a sequence consisting of an intracellularly cathepsin B-cleavable linker, a NLS and a DOTA chelator (pb12). The non-receptor binding control conjugate (pb13) was also synthetized. Following labelling with native terbium-159 (^{nat}Tb), plasmon waveguide resonance (PWR) was performed on MCF-7 cells. Receptor activation (IP_3 accumulation) and internalization were performed on COS7 cells stably co-expressing the Y_1 or Y_2 and the chimeric G-protein $G\alpha_{\Delta 6qi4myr}$ for pb12, pb13, ^{nat}Tb-pb12, and ^{nat}Tb-pb13 peptides. Furthermore, radiolabelling of the peptides with ^{111}In as surrogate for ^{161}Tb was conducted. Specific internalization and nuclear uptake of ^{111}In-pb12 into MCF-7 cells were determined. Finally, the ability of ^{nat}Tb-pb12 to convey terbium into MCF-7 cells was quantified using Particle-Induced X-rays Emission (PIXE). **Results:** pb12 and ^{nat}Tb-pb12 are full agonists at the Y_1 with an EC_{50} of 1.6 nM and 1.2 nM respectively while there were only able to activate the Y_2 at high concentration (10 µM). ^{nat}Tb-pb12 was able to stimulate internalization of the Y_1 whereas no internalization of the Y_2 was observed. Using PWR, binding affinities of pb12 and ^{nat}Tb-pb12 were 3.1±0.8 nM and 30.3±3.7nM respectively but pb13 and ^{nat}Tb-pb13 have no affinity regarding Y_1. On binding assays, affinities of ^{111}In-pb12 and ^{111}In-pb13 were 5.06 ± 3.52 nM and >1000 nM, respectively. Y_1-mediated internalization was 24.05 ± 8.15 % for ^{111}In-pb12 at 2h ($p = 0.006$). ^{111}In-nuclear fraction from ^{111}In-pb12 was 7.75 ± 2.44% and 4.60 ± 1.35 % of total binding at 2h without/with the cathepsin-B inhibitor CA-074Me ($p = 0.004$). Finally, PIXE experiments demonstrated the ability of ^{nat}Tb-pb12 to convey 2.27 fold more terbium into Y_1-expressing MCF-7 cells than non-exposed cells ($p = 0.041$). **Conclusion:** Our results demonstrate that the multivalent pb12 compound is a promising construct to deliver terbium in Y_1-expressing tumor cells. **References:** 1. Körner M, Reubi JC. Peptides. 2007;28:419-25 2. Hindié E, Zanotti-Fregonara P, Quinto MA, Morgat C, Champion C. J Nucl Med. 2016;57:759-64.

EP-51
Preclinical and translational aspects, including radiopharmacy, radiochemistry and drug development -> Radiopharmacy, radiochemistry, drug development -> Drug development -> Radiopharmacokinetics and drug development

October 12 - 16, 2019

e-Poster Area

EP-0719
Whole-body dynamic PET-MR imaging unveils the biodistribution and tissue kinetics of ^{11}C-buprenorphine in humans

A. Pinon[1], *C. Leroy*[1], *F. Caillé*[1], *P. Gervais*[1], *S. Jan*[1], *C. Comtat*[1], *Z. Chalampalakis*[1], *B. Fernandez*[2], *M. Bottlaender*[1], *N. Tournier*[1]; [1]*UMR 1023 IMIV, Service Hospitalier Frédéric Joliot, CEA, Inserm, CNRS, Université Paris Sud, Université Paris-Saclay, Orsay, FRANCE,* [2]*GE Healthcare, Applications & Workflow, Orsay, FRANCE.*

Aim/Introduction: Buprenorphine is a partial agonist of the µ-opioid receptors used for the management of severe pain or opioid-addiction maintenance therapy. PET imaging using radiolabeled buprenorphine offers a unique tool to non-invasively study the brain and tissue distribution in vivo and provide information regarding the clinical pharmacokinetics (PK) of this compound. We here report the first-in-human use of ^{11}C-buprenorphine obtained from a preliminary study in healthy subjects (EudraCT n°2017-001897-41). **Materials and Methods:** Buprenorphine was radiolabeled with carbon-11 at its O-methyl position to provide pharmaceutical grade ^{11}C-buprenorphine (9.7 GBq/µmol). Three healthy male volunteers (mean age 27 years) received an i.v. bolus of ^{11}C-buprenorphine (208.3±72.4MBq). Injection was immediately followed by repeated whole-body PET-MR scans acquired on a GE Signa PET-MR system during 90 min. PET images were reconstructed in order to provide whole-body dynamic PET images (with frames ranging from 2 to 16 min) automatically co-registered to MRI. Volumes of interests were drawn using Pmod software to yield decay-corrected time-activity curves in selected organs. Maximal uptake of the radioactivity in organs is expressed as the percentage of injected dose per volume (%ID.cm^{-3}±standard deviation). **Results:** In early and intermediate frames, prominent distribution sites were the liver (0.0108±0.0040%ID.cm^{-3}) and the gallbladder and bile ducts (0.1652±0.1873%ID.cm^{-3}), consistent with the known hepato-biliary clearance of buprenorphine. ^{11}C-buprenorphine was then secreted in the duodenum and progressively moved to the jejunum (0.0185±0.0162%ID.cm^{-3}) at the final frames. Accumulation of the radioactivity in the urinary bladder was relatively low (0.0353±0.0184%ID.cm^{-3} at final frame) suggesting a modest urinary excretion. The distribution of ^{11}C-buprenorphine to the brain cortex was obvious (0.0028±0.0002%ID.cm^{-3}) and consistent with the distribution of µ-opioid-receptors. A so far unreported uptake of ^{11}C-buprenorphine was observed in the myocardium

(0.0021±0.0002%ID.cm^{-3}). None of the 3 subjects experienced any adverse effects. **Conclusion:** This pilot clinical PET-MR study revealed the tissue kinetics ^{11}C-buprenorphine for the first time in humans. Imaging data are consistent with the known PK features of buprenorphine. This study confirmed the favorable safety profile of the procedure and the adequate brain uptake for opioid receptors imaging. The binding of ^{11}C-buprenorphine in the myocardium is consistent with the local expression of opioid receptors and the opioidergic regulation of cardiovascular function and myocardial stress resistance [1]. This may pave the way for the study of opioid-receptor systems in organs other than the central nervous system. **References:** [1] Headrick, J.P., See Hoe, L. E., Du Toit, E.F. and Peart,J.N. (2015), Opioidergic cardioprotection. Br J Pharmacol,172:2026-2050.

EP-0720

Preparation and Initial Evaluation of ^{18}F-labeled PSMA for Prostate Specific Membrane Antigen (PSMA) targeted PET imaging of Prostate Cancer

S. Okarvi, I. AlJammaz;
King Faisal Specilist Hospital and Research Centre, Riyadh, SAUDI ARABIA.

Aim/Introduction: Prostate specific membrane antigen (PSMA) expressed by most of the prostate cancers is a promising molecular target for prostate cancer diagnostic imaging and targeted radionuclide therapy. Although ^{68}Ga-PSMA-11 has been shown great potential for efficient targeting of prostate cancer in clinical settings. However, ^{68}Ga-PSMA-11 has some constraint due to its renal elimination, as radiotracer accumulation in the urinary tract may reduce the diagnostic confidence in the area of the ureter and effect the detection of local recurrence after radical prostatectomy. Additionally**,** half-life of ^{68}Ga (68 min) and limited amount of ^{68}Ga elution from the generator somewhat limited the doses for a larger group of patients. The purpose of this study was to develop a new generation PSMA ligand radiolabel with most clinically relevant and relatively longer half-life (110 min) PET radioisotope^{18}F. **Materials and Methods:** PSMA ligand, Glu-NH-CO-NH-Lys-pharmacophore was prepared by standard solid-phase peptide synthesis and linked to Ahx residue as spacer group. We have used 4-[^{18}F]fluorobenzaldehyde ([^{18}F]FB-CHO) as a synthon to prepare ^{18}F-PSMA. Aminooxy-functionalized PSMA was incubated with ([^{18}F]FB-CHO) in NH_4OAc buffer at pH 4 in the presence of MeOH at 90°C for 15 min. The resulting ^{18}F-labeled PSMA ligand was evaluated for its potential as a PET imaging probe in xenograft models expressing PSMA. Also, in vitro cell-binding was conducted on PSMA expressing LNCaP prostate cancer cell line. **Results:** The Aminooxy-functionalized PSMA was radiolabeled efficiently with ^{18}F in two-step and a high yield synthesis method to generate ^{18}F-labeled PSMA, which showed high metabolic stability in human plasma. Tumor cell binding indicated the high affinity and specificity of ^{18}F-PSMA towards PSMA-positive LNCaP prostate cancer cell line, with the binding affinity of 3.79±1.03 nM. In nude mice with LNCaP xenografts, ^{18}F-PSMA displayed efficient clearance from the blood and uptake and retention in all the major organs (excluding kidney) was found to be low to moderate (below 5%ID/g). The tumor uptake was 2.93% ID/g at 1 h p.i., with good tumor to blood and muscle ratios. **Conclusion:** Site-specific ^{18}F-labeled PSMA ligand against PSMA expression has been synthesized via chemoselective oxime formation between an aminooxy-functionalized PSMA and ^{18}F-FB-CHO moiety. Initial favorable in vitro and in vivo properties justify further preclinical studies of this PET radiotracer. **References:** None.

EP-0721

Evaluation Of Several Newly Designed Affibody-based Drug Conjugates Using Radionuclide-based Techniques: A Powerful Tool For Drug Development

M. Altai[1], *H. Ding*[2], *S. Rinne*[3], *A. Vorobyeva*[1], *T. Gräslund*[4], *V. Tolmachev*[1], *A. Orlova*[3];
[1]*Immunology, Genetics and Pathology, Uppsala, SWEDEN,* [2]*Department of Protein Science, KTH Royal Institute of Technology, SWEDEN,* [3]*Department of Medicinal Chemistry, Uppsala, SWEDEN,* [4]*Department of Protein Science, Stockholm, SWEDEN.*

Aim/Introduction: Targeted delivery of cytotoxic small drug molecules using antibody-drug conjugates is a promising strategy for treatment of disseminated cancer. However, the large size of antibodies results in poor tumour penetration of the constructs. We have recently constructed a novel drug conjugate based on engineered scaffold-protein HER2-binding affibody molecule (7 kDa) fused with an albumin binding domain ABD_{035} for half-life extension. The construct was site-specifically coupled to the small drug molecule DM1. The affibody-drug conjugate (AffiDC) was designated as ($Z_{HER2:2891}$)-ABD-MC-DM1. Using radionuclide-based techniques it was possible to gather information about binding specificity, processing, in vivo kinetics and tumour targeting properties of our AffiDC. Treatment with the novel AffiDC was well tolerated and resulted in twice longer survival compared to control groups. Biodistribution studies revealed that AffiDC had high hepatic uptake. Hepatic toxicity is one of the major complications observed for many drug candidates in the clinic. We have therefore designed hydrophilized variants of our previously investigated AffiDC, containing polyglutamate spacers. The use of hydrophilic spacer for reduction of hepatic uptake was evaluated using radionuclide-based techniques. **Materials and Methods:** The three HER2-binding AffiDCs ($Z_{HER2:2891}$)-ABD-MC-DM1, ($Z_{HER2:2891}$)-ABD-E_3-MC-DM1 and ($Z_{HER2:2891}$)-ABD-E_6-MC-DM1 were site-specifically labelled with ^{99m}Tc using tricarbonyl chemistry. The binding specificity to and cellular processing by HER2-expressing cells was studied using SKOV-3 cell line. The influence of the presence or absence of glutamate spacer on the hepatic uptake was evaluated. In vivo tumour targeting properties was compared in mice bearing SKOV-3 xenografts injected with the respective radiolabelled AffiDCs and sacrificed at 4, 24 and 46 p.i. An additional group of mice bearing RAMOS xenografts (HER2-negative) was injected with the radiolabelled-AffiDCs

to confirm HER2 mediated uptake. **Results:** All three AffiDCs were efficiently labelled with ^{99m}Tc with preserved specificity of binding to HER2-expressing cells. The incorporation of the hydrophilic glutamate spacer reduced the liver uptake by 36% for both ($Z_{HER2:2891}$)-ABD-E_3-MC-DM1 and ($Z_{HER2:2891}$)-ABD-E_6-MC-DM1 compared to the parental ($Z_{HER2:2891}$)-ABD-MC-DM1 (8.7±0.2 and 8.6±0.9 vs. 13.4±0.8 %ID/g, 4 h p.i.). The newly designed hydrophilized AffiDCs targeted HER2-expressing xenografts in mice specifically. The tumour uptake was comparable to that of the parental AffiDC, ($Z_{HER2:2891}$)-ABD-MC-DM1, at all studied time points. **Conclusion:** The newly designed hydrophilized AffiDCs demonstrated reduced hepatic uptake, long residence in circulation and specific targeting of HER2-expressing xenografts. A particular advantage of radionuclide-based-techniques is that it enabled to compare the properties of several drug candidates in a quantitative manner. Thus, it represents a powerful tool for drug development. **References:** None.

EP-0722

HMGB1 expression in leukocytes as a marker of cellular stress induced by 99mTc-HMPAO-labelling procedure: a pilot study

G. A. Follacchio[1,2], *V. Manganelli*[3], *A. Pala*[1], *F. Monteleone*[1], *T. Garofalo*[3], *M. Liberatore*[1];
[1]*Sapienza University of Rome, AOU Policlinico Umberto I, Nuclear Medicine Unit, Rome, ITALY,* [2]*Department of Molecular Medicine, Sapienza University, Rome, ITALY,* [3]*Sapienza University of Rome, Department of Experimental Medicine, Rome, ITALY.*

Aim/Introduction: Autologous White Blood Cells (WBC) scintigraphy, the gold standard imaging procedure for diagnosis of infection, is characterized by an elaborate sequence of cell separation and radiolabelling. Besides in vivo imaging quality control, no molecular tool is available to evaluate WBC damage secondary to cell manipulation. High Mobility Group Box 1 (HMGB1) is a 30KDa protein of the alarmins family [1]. HMGB1 is secreted by activated monocytes and passively released from the nucleus of damaged cells following different types of injury [2, 3]. Aim of this study was to evaluate HMGB1 levels in plasma from patients with suspect of prosthetic joint infection (PJI), and in WBC cytosolic extracts (CE) before and after 99mTc-HMPAO labelling procedure, as a marker of induced WBC damage. **Materials and Methods:** Patients with suspect of PJI referred for WBC scintigraphy were prospectively enrolled. HMGB1 levels were evaluated in plasma at baseline (t_0), and in CE obtained from patients' leukocyte concentrate before (t_1) and after 99mTc-HMPAO labelling (t_2) by Immunoblotting analysis. In addition, blood samples from healthy donors without history or signs of acute/chronic illness were included as controls and evaluated under the same procedure. **Results:** Four patients and three healthy subjects were enrolled. Immunoblotting revealed that HMGB1 levels were significantly increased in plasma (t_0) from patients compared to healthy donors, due to the underlying disease (p=0.0028). Similar results were obtained in WBC-CE from patients (t_1) compared to healthy donors (p=0.0107). Moreover, HMGB1 levels in WBC-CE from 99mTc-HMPAO-labelled leukocyte concentrate (t_2) did not show significant changes compared to the cold cellular sample (t_1) (p=0.3369). **Conclusion:** These preliminary findings showed increased HMGB1 levels in plasma from patients with suspect of PJI. Furthermore, for each subject, HMGB1 levels evaluated in WBC-CE after radiolabelling with 99mTc-HMPAO did not show significant changes compared to those before 99mTc-HMPAO treatment. Prospective evaluation of a larger cohort of patients and controls is currently ongoing to test the results of this pilot study. **References:** 1. Goodwin GH, Sanders C, Johns EW. A new group of chromatin-associated proteins with a high content of acidic and basic amino-acids. Eur J Biochem 1973;38:14-9 2. 2. Manganelli V, Signore M, Pacini I, et al. Increased HMGB1 expression and release by mononuclear cells following surgical/anaesthesia trauma. Critical Care 2010;14:R197 3. Manganelli V, Truglia S, Capozzi A, et al. Alarmin HMGB1 and Soluble RAGE as New Tools to Evaluate the Risk Stratification in Patients With the Antiphospholipid Syndrome. Front Immunol 2019;10:460.

EP-0723

Molecular Mechanisms of Radium-223 Uptake in the Gastrointestinal Tract and Pharmacological Modulators to Improve Therapeutic Outcome

D. Abou[1], *N. Benabdallah*[1], *A. L. Villmer*[1], *M. Doucet*[2], *D. Chesner*[3], *N. C. Zachos*[2], *R. C. Riddle*[2], *D. L. J. Thorek*[1];
[1]*Washington University School of Medicine, Saint Louis, MO, UNITED STATES OF AMERICA,* [2]*Johns Hopkins University School of Medicine, Baltimore, MD, UNITED STATES OF AMERICA,* [3]*Johns Hopkins School of Medicine, Baltimore, MD, UNITED STATES OF AMERICA.*

Aim/Introduction: Radium-223 dichloride is a first in class alpha particle emitting radionuclide formulation that targets sites of bone remodeling at bone metastases. It is approved for castrate resistant metastatic prostate cancer (mCRPC). An alkali earth metal series under Calcium, Radium-223 homes to the bone; however clinical experience has shown significant and rapid sequestration in the gut. Approximately 50% of the administered activity is concentrated in the duodenum several minutes after infusion. This leads to cases of gastrointestinal (GI) distress, drug cessation, and a reduction of the absorbed dose at sites of disease. We have investigated the distribution of Radium-223 in advanced small animal models of disease. Our work has shown that these model organisms recapitulate the clinical distribution of the radionuclide; and was used to elucidate mechanisms involved in uptake and transport of Radium-223. **Materials and Methods:** Radium-223 was produced using an in house microgenerator from radiochromatographic purification from source Actinium-227/Thorium-227. Naïve, male, skeletally mature, C57Bl/6 mice were administered 3.7kBq of Radium-223 dichloride in 30mM citrate for biodistribution at appropriate times after injection; excised organs were counted for activity; for autoradiographic localization in tissues; histological evaluation of radiotoxicity

in the GI was performed with immunofluorescence (IF) of TUNEL and gH2AX. Functional human gut epithelial organoids were used in a transwell assay of Radium-223 transport to evaluate a 75 compound library of ion channel modulators. Lead compounds that increased (positive control) or blocked Radium-223 transport were selected for in vivo testing of effect on distribution. **Results:** As with men, a significant proportion of administered Radium-223 was found in the intestinal tract of mice within 15min and excreted by 24h. DNA damage and cellular apoptotic cascades were observed in the duodenum and cecum at 24h in animals that had been exposed to the radionuclide therapy. Ex vivo testing of Radium-223 transport revealed an active process of transepithelial transport that could be inhibited with select pharmacophores. Lead ion-channel inhibitors were tested in vivo with coadministration of Radium-223. Biodistribution data demonstrated a decrease in early gut accumulation, renal excretion and a commensurate doubling of Radium-223 fixation in the bone. **Conclusion:** This work has detailed cellular transport processes in the intestinal epithelium that contributed to Radium-223 sequestration in this soft-tissue compartment. Pharmacological modulators from an in vitro organoid screen have in vivo efficacy. Several of these compounds are clinically approved and may contribute to improved patient management for mCRPC patients on Radium-223 dichloride. **References:** None.

EP-0724

QSAR Studies in the Identification of Chemical Compounds with Affinity for Dopamine Transporter: a Possible Method of Selection of New Radiotracers in the Parkinson's Disease Diagnosis

M. Soria Merino[1], *J. Castillo Garit*[2], *M. Romero Otero*[1], *F. Pérez Giménez*[3], *R. Maestre Cutillas*[1], *P. Ponce Ortega*[4], *A. Amr Rey*[5], *J. Sabater Sancho*[5], *A. Cánoves Llombart*[5], *V. Carrero Vasquez*[5], *I. Casáns Tormo*[5], *H. Rodríguez Parra*[5], *M. Redal Peña*[5], *J. Padilla Sánchez*[5], *V. Pérez Doñate*[6];
[1]*Radiopharmacy Unit, Hospital Clínico Universitario de Valencia, Valencia, SPAIN,* [2]*Experimental Toxicology Unit, Universidad de Ciencias Médicas de Villa Clara, Santa Clara, CUBA,* [3]*Research Unit of Radiopharmacy and Stability Drugs, Universidad de Valencia, Valencia, SPAIN,* [4]*Hospital Pharmacy Service, Hospital Clínico Universitario de Valencia, Valencia, SPAIN,* [5]*Nuclear Medicine Service, Hospital Clínico Universitario de Valencia, Valencia, SPAIN,* [6]*Microbiology Service, Hospital Universitario de la Ribera, Valencia, SPAIN.*

Aim/Introduction: Parkinson's disease (PD) is a neuro-degenerative disorder characterized by the degeneration of dopaminergic nigrostriatal connections. The dopamine transporter (DAT) serves as a selective marker of dopamine terminal innervations in the striatum. DAT has been extensively studied through in vivo imaging by Single-Photon Emission Computed Tomography (SPECT) and Positron Emission Tomography (PET). Quantitative Structure-Activity Relationship (QSAR) analysis constitute a method for molecular design and screening of new chemical structures that has been shown to be highly effective in the prediction of physicochemical and/or pharmacological properties. In our case, we use the affinity constant to DAT binding as discriminant property. **Materials and Methods:** We have performed a QSAR analysis using a series of 65 drugs with different pharmacological properties, from which we have obtained the value of the affinity constant for DAT binding, from bibliographic reports. This property is an important requirement for the PET and SPECT radiotracers that are used to map DAT in the neuroimaging of PD. We have calculated a large number of molecular descriptors of these compounds using the DRAGON software and we have used the QSARINS software and genetic algorithm techniques to obtain the multiple linear regression (MLR) models. **Results:** The best results were obtained for the MLR model with four variables, among which are molecular descriptors related to the capacity of formation of hydrogen bonds and the lipophilic character. The values of R^2 (0.7554), Q^2 leave-one-out (0.6800) and external R^2 (0.7090) of the model, confirm its stability and robustness in predicting the value of the affinity constant DAT binding. **Conclusion:** The research for new compounds with the desired physicochemical properties requires enormous human resources and high economic cost. The proposed theoretical model can be a useful tool in predicting the binding affinity to DAT and therefore in the search for new PET and SPECT radiotracers used in the neuroimaging of PD. **References:** Brooks DJ, Pavese N. Imaging biomarkers in Parkinson's disease. Progress in neurobiology. 2011;95(4):614-28. Gini G. QSAR: What Else? Computational Toxicology: Springer; 2018. p. 79-105. Tatsumi M, Groshan K, Blakely RD, Richelson E. Pharmacological profile of antidepressants and related compounds at human monoamine transporters. European journal of pharmacology. 1997;340(2-3):249-58. Carlier PR, Lo MM, Lo PC, Richelson E, Tatsumi M, Reynolds IJ, et al. Synthesis of a potent wide-spectrum serotonin-, norepinephrine-, dopamine-reuptake inhibitor (SNDRI) and a species-selective dopamine-reuptake inhibitor based on the gamma-amino alcohol functional group. Bioorganic & medicinal chemistry letters. 1998;8(5):487-92.

EP-0725

Theranostic Nanomedicine for Imaging and Treatment of Multiple Joints in Rheumatoid Arthritis

Z. Nosrati, *T. V. Esposito, M. Bergamo, C. Rodriguez-Rodriguez, K. Saatchi, U. O. Häfeli;*
Faculty of Pharmaceutical Sciences, University of British Columbia, Vancouver, BC, CANADA.

Aim/Introduction: Rheumatoid arthritis (RA) patients are frequently given anti-arthritic drugs including nonsteroidal anti-inflammatory drugs, glucocorticoids, disease-modifying anti-rheumatic drugs and biologics, or combinations thereof. Many patients fail to respond satisfactorily to these treatments or experience side effects. The main reason for non-ideal treatment is that insufficient drug doses reach the joints, therefore higher and more frequent doses needed.

To improve the drug pharmacological profile and direct the anti-inflammatory activity to the site of disease, i.e., the inflamed joints, we synthesized a pro-drug that increased circulation time resulting in sustained release when it reaches the microenvironment -of the inflamed joints. **Materials and Methods:** Our methods encompass the chemical syntheses of the polymeric prodrugs and the investigation of their stability and release kinetics. The pharmacokinetics of the prodrug was established after radiolabeling with In-111, and preclinical SPECT/CT imaging in an RA mouse model. The efficacy of the prodrugs is also established in the same RA model and compared to the free drug given in the same form/ timing as it is currently administered to patients. In vitro stability measurements of the prodrugs in human synovial fluid from rheumatoid arthritis patients is ongoing to better understand the impact of the local environment of an inflamed joint and how that influences drug release. **Results:** Results show that delivering methotrexate (MTX) bound to a carrier polymer produces a significant increase in drug uptake in the inflamed joints. When MTX was delivered as a prodrug, a 4x lower dose given every two weeks was just as effective as two standard dosages per week of free MTX. In addition, attaching folic acid (a targeting ligand that selectively binds to folate receptors) to the polymeric carrier helped to keep the active drug longer in the targeted lesion. **Conclusion:** In this study, using SPECT/CT we show our prodrug approach delivers higher concentrations of anti-arthritic drugs to inflamed joints than has previously been possible, despite lower and less frequent drug doses. Current studies include to utilize and test our novel pro-drug delivery system with other effective RA drugs to further improve their pharmacological profile in patients with RA. **References:** None.

EP-0726

Improvement and Comparison of Immobilized Artificial Membrane Chromatography (IAM) in Brain PET-Tracer Development: A Potential High Throughput Method to Predict Blood Brain Barrier Penetration?

C. Vraka[1], *S. Gloimueller*[1], *S. Mijailovic*[2], *L. Nics*[1], *M. Hacker*[1], *M. Mitterhauser*[2], *W. Wadsak*[1,3];
[1]*Radiology and Nuclear Medicine, Vienna, AUSTRIA,* [2]*Ludwig Boltzmann Institute Applied Diagnostics, Vienna, AUSTRIA,* [3]*CBmed, Graz, AUSTRIA.*

Aim/Introduction: In 2006 it was shown by Tavares et al. that permeability (Pm) measurements using immobilized artificial membrane chromatography (IAM) show a better correlation to the percent injected dose in brain than other in vitro parameters, e.g. logP [1]. Therefore, it was concluded that IAM measurements have a predictive value on blood brain barrier (BBB) penetration. In contrast, our group couldn't demonstrate any differences in Pm values between BBB penetrating and non-penetrating compounds using an extended dataset. Moreover, we found relatively high standard deviations (SD) of the Pm values caused by column batch differences and the calculation using an extrapolation to 100% aqueous phase [2]. Hence, the aim of this study is to evaluate the gradient IAM HPLC method described by Valko et al. [3] and the comparison with the described isocratic method [1,2] with regard to prediction of BBB penetration. **Materials and Methods:** For all measurements, an Agilent HPLC system (Series 1100/1200) was used. Injection volume was 5 µL of a 0.5 mg/mL reference standard solution, flow-rate was 1.0 mL/min and the linear gradient started from 0% acetonitrile (AcN) and 100% 50 mM ammonium acetate buffer (pH 7.4) to 100% AcN in 10.5 min, then keeping 100% AcN for 1 min and back to initial conditions within 0.5 min with an equilibration time of 5 min. The column (IAM P.C. DD2, 150x4.6mm) was calibrated with 8 reference compounds. Almost 100 compounds, categorized in BBB penetrating and non-penetrating drugs, will be tested. **Results:** So far, SD of the retention times are in the same range for all groups. The run time was reduced dramatically (one 15 min run in contrast to 4 different runs). However, K_{IAM} of the Tavares method show higher SD values for each compound caused by the extrapolation calculation. Additionally, no significant differences were found between the drug groups using the isocratic method. Preliminary data indicate also no significant differences between the drug groups using the gradient method. **Conclusion:** Preliminary data show a higher accuracy of the gradient method in comparison to the isocratic method. However, the results regarding the different drug groups should be compared and prediction of BBB penetration based on in-vitro IAM data has yet to be clarified. **References:** [1] Tavares AAS et al. Nucl Med Biol 2012;39:127-35. [2] Vraka C et al. Expanding LogP: Present possibilities. Nucl Med Biol 2017;58:20-32. [3] Valko K et al. J Pharm Sci 2000;89:1085-96.

EP-0727

Development of a potential theranostic candidate for PET imaging and Boron Neutron Capture Therapy

E. Jestin[1], *S. Bénard*[1], *V. Meneyrol*[1], *I. Ait-Arsa*[1], *J. Andries*[1], *F. Gimié*[1], *N. Goonoo*[2], *A. Bhaw-Luximon*[2];
[1]*GIP CYROI, Sainte Clotilde, FRANCE,* [2]*Biomaterials, Drug Delivery and Nanotechnology Unit, Center for Biomedical and Biomaterials Research (CBBR), University of Mauritius, Réduit, MAURITIUS.*

Aim/Introduction: Boron Neutron Capture Therapy (BNCT) is a promising radiotherapy for cancer treatment whose specificity is to deliver a precise and high dose of radiation while preserving the surrounding healthy tissue. We report here a boron containing tool that was also radiolabeled for PET imaging. **Materials and Methods:** Curcumin-BF_2 (CUR-BF_2) was synthetized. A new formulation process with copolymer PEG-b-PCL containing 1.1mg/ml of CUR-BF_2 was set up using an ethanolic formulation. No dialysis was needed to remove any organic solvent. The self-assembled polymeric micellar solution was then filtered at 0,22µm. Nanovectors size were determined with dynamic light scattering (DLS). Several in vitro IC_{50} were tested using MTT assay on MIA PACA tumor cells lines. CUR-BF2 was radiolabeled with a $^{18}F/^{19}F$ isotopic exchange method in a Tracerlab FX-FN module. The radioactive fluoride was eluted

from QMA cartridge with tetrabutylammonium bromide and dried by azeotropic distillation with acetonitrile to provide [^{18}F] TBAF. CUR-BF_2, triflic anhydride and tert-Butanol were added to the reaction vessel in acetonitrile and heated at 50°C for 15 min. The mixture was evaporated to dryness and dissolved in ethanol. Analytical HPLC measurements were performed to control the radiochemical purity, the specific activity and stabilities of the radiotracer. [^{18}F]CUR-BF_2 was formulated with copolymer PEG-b-PCL. Preliminary PET imaging studies were performed with control mice to visualize the biodistribution in organs. 7±5 MBq were injected intravenously. PET imaging acquisitions were performed during 60 min after injection. **Results:** Starting with 60GBq, [^{18}F]-CUR-BF_2 was obtained with an automation system with 97±0.5% radiochemical purities and up to 53 GBq/mg. Stabilities have shown no degradation, confirming their use for mice injection. The copolymer PEG-b-PCL allows the dissolution of up to 1.1 mg/ml of non-radioactive hydrophobic product for intravenous injection. Curcumin-loaded polymeric nanomicelles have a size distribution of 130±10 nm. PET imaging have shown accumulation in gallbladder, intestines, bladder and knee joint. **Conclusion:** A Boron-containing precursor was quantitatively radiolabeled on automated module through a ^{18}F/^{19}F isotopic exchange method with excellent RCP and SA. PET imaging are ongoing with several tumor models. **References:** None.

EP-0728

Compatibility of HYNIC-chelator with ^{99m}Tc-based Somatostatin Receptor Antagonists

R. H. Gaonkar[1], *F. Wiesmann*[1], *G. P. Nicolas*[2], *L. Del Pozzo*[1], *R. Mansi*[1], *M. Fani*[1];
[1]*Division of Radiopharmaceutical Chemistry, University Hospital Basel, Basel, SWITZERLAND,* [2]*Division of Nuclear Medicine, University Hospital Basel, Basel, SWITZERLAND.*

Aim/Introduction: PET imaging of somatostatin receptor (sstr)-expressing neuroendocrine tumors with ^{68}Ga-labeled sstr-antagonists showed improved sensitivity compared with^{68}Ga-labeled sstr-agonists[1]. Nevertheless, ^{99m}Tc remains the workhorse of diagnostic nuclear medicine. Therefore, the development of ^{99m}Tc-based sstr-antagonists is attractive and clinically relevant. Hydrazinonicotinamide (HYNIC) is a well-established chelator for ^{99m}Tc-labeling, performing excellently in combination with the sstr-agonist Tyr^3-octreotide (^{99m}Tc-HYNIC-TOC). Unexpectedly, when combined with the sstr2-antagonist SS01,^{99m}Tc-HYNIC-SS01 showed no uptake in sstr2-expressing cells[2], indicating loss of receptor recognition. The aim of this work was to determine whether HYNIC is a suitable chelator for the development of ^{99m}Tc-based sstr-antagonists. Herein we report the compatibility of HYNIC when employing spacers of different length. **Materials and Methods:** We coupled the peptide SS01, 4-Cl-Phe-cyclo(D-Cys-Tyr-D-Trp-Lys-Thr-Cys)D-Tyr-NH2,with the spacers β-Ala, Ahx (aminohexanoic), Aun (aminoundecanoic acid) or PEG4 and conjugated it with HYNIC at the N-terminus. We labeled all conjugates with 99mTc, using edda as co-ligand. We determined their hydrophilicity by partition coefficient experiments and checked their stability up to 4h on RP-HPLC. We determined in vitro cellular uptake, internalization and fate of the sstr2-surface bound radiopeptidefractionof each radio-conjugate using HEK-hsstr2cells. SPECT/CT imaging studies in HEK-hsstr2 bearing mice are in progress and will be reported. **Results:** The ^{99m}Tc-labeled conjugates formed single radioactive components with high radiochemical purity (~ 95%), which remained stable for at least 4h. The introduction of β-Ala, Ahx or PEG_4 did not significantly affect the hydrophilicity but resulted in a substantial improvement in receptor recognition, compared with^{99m}Tc-HYNIC-SS01. ^{99m}Tc-HYNIC-PEG_4-SS01 showed the highest hydrophilicity compared to ^{99m}Tc-HYNIC-Ahx-SS01 and ^{99m}Tc-HYNIC-β-Ala-SS01 (LogD= -2.03±0.13 versus -1.96±0.06 and -1.91±0.19, respectively). The introduction of Aun resulted in a very lipophilic conjugate, which was therefore excluded from further evaluation. The Ahx conjugate showed the highest uptake, with more than twice (36.60±0.19%) than that of β-Ala-(14.42±0.02%) and PEG_4- conjugates (14.77±1.93%) at 4h. Internalization rate was <14% for all conjugates, indicative of their antagonistic properties. Head-to-head SPECT/CT images of the β-Ala, Ahx and PEG_4 ^{99m}Tc-labeled conjugates will be presented. **Conclusion:** The chelator HYNIC can be considered for the development of ^{99m}Tc-based sstr2 antagonists when combined with appropriate spacers. Among the tested spacers, Ahx showed the best in vitro performance. Confirmatory studies with other analogs are on-going. **References:** 1. Nicolas G et al., J Nucl Med 2018;59:915 2. Abiraj K et al., EJNMMI Research 2018;8:75.

EP-0729

Differential ex vivo uptake analysis: an efficient method for tracer selection

M. Konrad, *M. Parzinger, A. Wurzer, R. Beck, H. Wester;*
Technical University of Munich, Garching, GERMANY.

Aim/Introduction: Typically the selection of promising candidates from a series of potential radiopharmaceuticals relies on the determination and comparative assessment of various parameters determined by in vitro and in vivo studies. A final decision is especially difficult if the candidates hardly or only marginally differ from each other, e.g. in the case of a series of peptide or peptidic diastereomers. Based on our experience that biodistribution studies even on large cohorts of animals often do not allow to accurately quantify small differences in the in vivo behavior of such compounds, we investigated whether the differential ex vivo radio-HPLC analysis of relevant tissue samples after coinjection of 4 diastereomeric ^{18}F-labeled PSMA tracers in a small cohort of mice could overcome this limitation. **Materials and Methods:** The 4 ^{18}F-PSMA inhibitors to be assessed were labeled as mixture, formulated and injected into LNCaP tumor bearing CB17-SCID mice (n=4). The relevant organs were dissected 0.5 h p.i. and homogenated using buffer with competitor (20 µM PMPA) and cell lysing components (HEPES, 1 M/NaCl, 1 M; 17:2) by means of a Potter-Elvehjem tissue grinder or a ball mill. The resulting extraction efficiencies were

calculated after centrifugation at 17,000 g and concentration of the supernatant over a StrataX SPE cartridge. The extracted solutions, containing the 4 diastereomers, were analyzed and relative percentage of each diastereomer quantified by radio-HPLC. Thereafter, the differential uptake of each diastereomer was calculated by comparison with the relative percentage of the diastereomers in the initially injected solution. **Results:** Deviating extraction efficiencies were observed for the relevant tissues and body fluids resulting in efficiencies of 90.5 ± 4.5% for blood, 48.0 ± 12.0% for kidney, and 44.0 ± 13.0% for tumor (all n=4). Quantification of radio-HPLC analyses revealed significantly different and reproducible uptake patterns for the 4 diastereomers and thus allowed for the selection of the candidate with the best tumor and lowest blood, and kidney uptake. **Conclusion:** A straight forward method was developed to identify a single peptide tracer in a mixture of 4 diastereomers as the one with the most favorable biodistribution by means of the analysis of their differential uptake patterns. This method not only delivers more accurate selection criteria of tracers with very similar in vivo behavior, but also helps to diminish the number of mice needed in preclinical evaluation. **References:** None.

EP-0731

Development of Dual sstr2- and sstr5-specific Radiolabelled Somatostatin Analogues

R. Mansi[1], *G. Nicolas*[2], *K. Abid*[3], *E. Grouzmann*[3], *A. Harris*[4], *M. Fani*[1]; [1]*Division of Radiopharmaceutical Chemistry, University Hospital Basel, Basel, SWITZERLAND,* [2]*Division of Nuclear Medicine, University Hospital Basel, Basel, SWITZERLAND,* [3]*Catecholamine and Peptides Laboratory, University Hospital of Lausanne, Lausanne, SWITZERLAND,* [4]*Somtheranostics SARL, Chemin du Midi 6, CH-1053 Cugy, SWITZERLAND.*

Aim/Introduction: Clinically approved radiolabelled somatostatin analogues show high affinity for the somatostatin receptor (sstr) subtype 2 (sstr2). Neuroendocrine tumours (NETs) mainly overexpress sstr2, however, co-expression of the subtype 5 (sstr5) has been reported in 20-50% of intestinal or bronchial NETs[1]. Therefore, dual sstr2- and sstr5-targeting has the potential of enhancing the radiotracer uptake on NET cells, the image contrast and the tumour absorbed dose. In this study, we report on the development of a new somatostatin analogue as a radio-theranostic agent for dual sstr2- and sstr5-targeting. **Materials and Methods:** We selected the 2-iodo-aminoacid analogue G02113 ((4-amino-3-iodo)-D-Phe-c[Cys-(3-iodo)-Tyr-D-Trp-Lys-Val-Cys]-Thr-NH_2)[2] with high sstr2 and 5 affinity, conjugated it with the chelator DOTA and labelled it with ^{68}Ga and ^{177}Lu. We characterized both radiotracers in vitro and in vivo using HEK cells with stably transfected human sstr2 (HEK-hsstr2) and sstr5 (HEK-hsstr5). We determined the affinity of ^{68}Ga-/^{177}Lu-DOTA-G02113 to each receptor subtype and studied their biodistribution, pharmacokinetics and imaging with dedicated micro PET/CT and SPECT/CT scanners. In our study, we used ^{68}Ga-/^{177}Lu-DOTA-NOC as reference. **Results:** ^{nat}Ga- and ^{nat}Lu-DOTA-G02113 have a similarly high affinity for sstr2 (IC_{50} = 0.32 and 0.35 nM, respectively), while the one for sstr5 is higher for ^{nat}Ga-DOTA-G02113 than for its ^{nat}Lu-counterpart (IC_{50}= 1.86 and 3.5 nM, respectively). Compared to ^{nat}Lu-DOTA-NOC, ^{nat}Lu-DOTA-G02113 has slightly better affinities for both receptor subtypes, however lower internalization rate (26.8±1.5% vs 18.1±0.7%, at 4h in HEK-hsstr2) with comparable externalization rate (40-50% within 4h). ^{68}Ga-DOTA-G02113 showed a high uptake in sstr2- and sstr5-expressing tumours (26.3±8.2 and 14.9±5.9 %IA/g, 1h p.i., respectively), similarly to ^{68}Ga-DOTA-NOC (30.1±8.2 and 11.6±5.0 %IA/g, respectively). There was a substantial kidney uptake (14.1±3.7 %IA/g at 1h p.i.), indicating renal excretion, and a noticeable liver uptake (6.4±1.9 %IA/g), possibly due to the lipophilicity of the radiotracer (log D = -0.95±0.1). ^{177}Lu-DOTA-G02113 reached its maximal uptake at 1h p.i. on sstr2- and sstr5-tumour (14.2±1.8 and 1.8±0.3 %IA/g, respectively), while about 60% remained in both tumours at 24h p.i. The mean time-integrated activity coefficient of ^{177}Lu-DOTA-G02113 was 8.6 h and 0.8 h in sstr2- and sstr5-expressing tumours, respectively. **Conclusion:** ^{68}Ga-DOTA-G02113 reveals its ability to target both receptor subtype sstr2 and sstr5 with high affinity, while in vivo results suggest suboptimal pharmacokinetic properties of ^{177}Lu-DOTA-G02113 for targeting sstr5. **References:** 1. Reubi JC et al. Eur J Nucl Med Mol Imaging, 2003;30:781-93. 2. Moor SB et al. J Med Chem, 2005;48:6643-52
.

EP-52

Preclinical and translational aspects, including radiopharmacy, radiochemistry and drug development -> Radiopharmacy, radiochemistry, drug development -> Radiochemistry -> Radionuclide production

October 12 - 16, 2019 e-Poster Area

EP-0732

Comparison of two potential ^{47}Ca/^{47}Sc radionuclide generator systems

D. Pawlak, W. Wojdowska, M. Żółtowska, I. Cieszykowska, J. L. Parus, P. Garnuszek, R. Mikołajczak;
Radioisotope Centre POLATOM, National Institute for Nuclear Research, Otwock, POLAND.

Aim/Introduction: Scandium-47 ($T_{1/2}$ = 3.35d, $E_{\beta max}$ = 600 keV), beta emitter with energy higher than that of ^{177}Lu ($T_{1/2}$ = 6.73d, $E_{\beta max}$ = 498 keV), is an attractive therapeutic radionuclide. It can be produced by irradiation of ^{46}Ca with thermal neutrons in ^{46}Ca(n,γ)^{47}Ca→^{47}Sc nuclear reaction or in cyclotrons via ^{48}Ca(p,2n)^{47}Sc channel. Due to the longer half-life of ^{47}Ca ($T_{1/2}$ = 4.54d) the ^{47}Ca/^{47}Sc system can serve as radionuclide generator. The aim of this work was to compare two methods of ^{47}Sc separation from ^{47}Ca allowing multiple separation of ^{47}Sc solution of high radionuclidic and chemical purity suitable for radiolabeling of DOTA-peptides. **Materials and Methods:**

$CaCO_3$ targets (40 mg, 5.0% enrichment in ^{46}Ca) were irradiated for 150 h in thermal neutron flux of 1.2 10^{14} $cm^{-2}s^{-1}$ in Maria reactor. Targets dissolved in HCl were loaded either on the extraction chromatography column with TBP (tributylphosphate) resin or the DGA (N,N,N′,N′-tetra-n-octyldiglycolamide) resin (Triskem Int). ^{47}Sc was eluted from DGA with 0.05 M HCl, and was used as such for radiolabelling of DOTATATE while ^{47}Sc was eluted from TBP with water and passed through the cation exchange column (AG50W-X8) to decrease its acidity. Subsequent separations of ^{47}Sc were carried out after about 4 days needed for ingrowth of ^{47}Sc. Target material was recovered via precipitation of calcium carbonate for repeated irradiation. **Results:** Irradiation of ^{46}Ca enriched targets resulted in radioactivity up to 400 and 300 MBq at EOB for ^{47}Ca and ^{47}Sc, respectively. Separation yields of ^{47}Sc in 4 consecutive separations were: about 80% for the TBP and about 90% for the DGA. The only measured radionuclidic impurity was ^{47}Ca with the concentration below 0.1% for both methods. DOTATATE labeling yields were above 90% and were comparable for both methods. **Conclusion:** Both tested extraction chromatography resins, DGA and TBP, allow to obtain ^{47}Sc with high yield and purity suitable for preparing radiopharmaceuticals. In addition, we demonstrated that ^{47}Sc can be effectively separated from ^{47}Ca up to 15 days after EOB. Acknowledgements: This project was supported with the funds awarded by the Ministry of Science and Higher Education in Poland within the agreement No. 3639/FAO/IAEA/16/2017/0, IAEA Research Contract No. 20496 and CERAD project, financed under Smart Growth Operational Programme 2014-2020, Priority IV, Measure 4.2. **References:** None.

EP-0733

SPE on tributyl phosphate resin as an alternative method of ^{47}Sc separation from ^{47}Ca

M. Zóltowska, D. Pawlak, W. Wojdowska, I. Cieszykowska, J. L. Parus, R. Mikołajczak;
Radioisotope Centre POLATOM, National Centre for Nuclear Research, Otwock, POLAND.

Aim/Introduction: ^{47}Sc ($T_{1/2}$ = 3.35d) is an attractive theranostic radionuclide due to its twin radionuclides emitting positrons ^{43}Sc and ^{44}Sc. It can be produced in $^{46}Ca(n,\gamma)^{47}Ca \rightarrow ^{47}Sc$ nuclear reaction with thermal neutrons. However, separation of ^{47}Sc from excess of Ca is a challenge, since the mass ratio of ^{47}Sc to Ca in the irradiated target ranges 1 to 10^6 - 10^8. In our experience, out of several methods investigated for separation of Sc from Ca, the extraction chromatography on tributyl phosphate (TBP) resin was found to be promising. Herein, in order to facilitate the separation process, we determined the separation coefficients (ion distribution between the resin and the solution in equilibrium, D_w) for Sc on TBP resin and HCl at various concentrations. **Materials and Methods:** Natural $CaCO_3$ (Sigma Aldrich), TBP resin (tributyl phosphate, TrisKem), 36% HCl, Fluka and ^{46}Sc ($T_{1/2}$ = 83.8 d) as a tracer were used. TBP distribution coefficients D_w were determined as described by Horwitz et al. [1]. In brief, three reference solutions of ^{46}Sc were prepared, against which the sorption efficiency of ^{46}Sc on TBP was investigated. Eppendorf vials with 50 mg TBP resin were weighed and 1 mL HCl of appropriate concentration was added. After soaking the resin, 40 µL (5ng) of ^{46}Sc solution was added, vials were shaken for 1 h and left for 10 minutes to stabilize the phases. Supernatant was separated by centrifugation and radioactivity of 100 µl aliquots was measured. **Results:** The calculated D_w values indicated that ^{47}Sc separation from Ca is most efficient in the HCl concentration range from 7.5 to 10 M. These findings were confirmed by separation of nuclear reactor produced ^{47}Sc on TBP resin from 9 M HCl solution with the 82% yield. The obtained ^{47}Sc was used to radiolabel DOTATATE with 95% radiochemical purity and specific activity 5.8 MBq/nmol. The influence of calcium excess on D_w values was also examined. **Conclusion:** Separation of Sc in HCl is most effective on TBP resin when using HCl in the concentration range 7.5-10 M. This was confirmed by ^{47}Sc separation with the yield higher than 80% when using 9 M HCl. Acknowledgements: This project was supported with the funds awarded by the Ministry of Science and Higher Education in Poland within the agreement Nr 3639/FAO/IAEA/16/2017/0 and CERAD project, financed under Smart Growth Operational Programme 2014-2020, Priority IV, Measure 4.2. **References:** [1] E.P. Horwitz et al. Appl Radiat Isot. 2005;63:23-26.

EP-0734

Development of a solid target system

D. Szikra[1], V. Forgács[1], G. Nagy[2], A. Vágner[2], A. Fekete[1], G. Trencsényi[1];
[1]University of Debrecen, Faculty of Medicine, Medical Imaging Department, Division of Nuclear Medicine, Debrecen, HUNGARY, [2]Scanomed Ltd., Debrecen, HUNGARY.

Aim/Introduction: Automatized production of radiometals for PET imaging is becoming more important, as the theragnostic concept gains broader application in the treatment of oncological patients. Working with cyclotron produced isotopes on a daily basis always calls for automatization of every possible process in order to decease personnel dose. Handling of the irradiated targets is causing the highest doses from the irradiated material and from the high backdround of the cyclotron bunker. Our aim was the development of a simple pneumatically actuated shuttle type solid target handling system for the production of 44Sc, 68Ga, 52Mn and other isotopes. **Materials and Methods:** A GE PETtrace 800 Cyclotron is used for daily production of 18F and 11C in our institute. The solid target system was designed not to disturb the routine isotope production The target system was constructed by using the beam entrance and foil holder parts of an old GE water target. Onto these parts a pneumatically actuated aluminum block was attached, that accepts the shuttle with the target material. When the shuttle is slided to the beam line by the metal block, it cooled from the back with a water cooling chamber. **Results:** Solid calcium pellet was pressed into the 8mm diameter cavity of the target shuttle and irradiated with beam currents up to 40 uA for 60-120 minutes without

any noticeable overheating or degradation. Irradiated calcium could be readily dissolved from the aluminum (AlMgSi1) shuttle with 4ml 3M HCl. Solid chromium, zinc powder or lead foil were also successfully applied for the production of ^{52}Mn, ^{68}Ga and $^{205/206}$Bi, respectively. **Conclusion:** The prepared target shuttles can be inserted into a shuttle port outside the cyclotron bunker, and transported through flexible tubing into the irradiation port. Irradiated shuttles can be transported back and dropped directly into a lead pot after irradiation, minimizing personnel dose. **References:** None.

EP-0735

[^{89}Zr]ZrOx/Cl preparation on commercial cassette base synthesis module

E. Cazzola[1], *J. Amico*[1], *A. Kotliarenko*[2], *D. Peruzzi*[1], *O. Azzolini*[2], *A. D'Angelo*[1], *M. Malachini*[1], *G. Keppel*[2], *G. Gorgoni*[1];
[1]*Ospedale Sacro Cuore, Negrar, ITALY,* [2]*National Institute of Nuclear Physics -INFN LNL, Legnaro, ITALY.*

Aim/Introduction: [^{89}Zr]Zirconium is one of the emergent isotope due to the favorable PET imaging characteristics (β+max 0.395 MeV; 22.7%) and halflife (T½78.4h) ideal to labeling Antibodies. Monoclonal antibodies (MAbs) are the most approved biopharmaceutical in the word with a multiple and selective targets.The immunoPET can facilitate the approval for new MAbs and can help on patient selection. Due of this needs a robust production, purification and labelling procedure should be optimized on automatic modules in order to minimize the operator dosimetry and increase the reproducibility.Aim of this work is based on easy modification of automatic, cassette base, commercial module in order to dissolve and purify the [89Zr]Zirconium in both formulation currently used from sputtered target. The single use cassette reducing the possibility to accumulate metal impurities in the purification step due to missing cleaning step mandatory on synthesis modules based on fixed tubes technology. **Materials and Methods:** A Eckert&Ziegler cassette base module were used to set up an automatic dissolution and purification procedure. The Sputtered [89Y]Yttrium targets were bombarded on TR-19 cyclotron at 12.5 MeV without degrader at different current 20-60 μA for a variable time 30-240 minutes. The coins were transferred on dedicated coated hotcell and finally insert on a EZAG module in order to dissolve and purify the [89Zr]/[89Y] material in a single use cassette. A 2 N HCl solution was used to dissolve the target material, the solution was transfer to ZR resin (Triskem) and recovered on vial in oxalate or chloride forms. **Results:** Ten sputtered target were processed after bombardment and final impurities profile were evaluated by γ-spettrometry and by ICP-MS. Molar Activity were calculated by tritation with DFO for booth chemical forms. **Conclusion:** What we described on this work is one of the possible way to optimize the [89Zr]Zirconium production starting from [89Y]Yttrium sputtered target, with a simple and single use cassette recovery process based on EZAG module to minimize the impurities. **References:** None.

EP-0736

US DOE Tri-Lab Research and Production Effort to Provide Accelerator-Produced ^{225}Ac for Radiotherapy: 2019 Update

K. John;
Los Alamos National Laboratory, Los Alamos, NM, UNITED STATES OF AMERICA.

Aim/Introduction: The current availability of accelerator produced ^{225}Ac from the US Department of Energy Isotope Program's Tri-Lab (ORNL, BNL, LANL) Research and Production Effort to Provide Accelerator-Produced ^{225}Ac for Radiotherapy will be presented. **Materials and Methods:** The Tri-Lab effort produces ^{225}Ac via the ^{232}Th(p,x)^{225}Ac nuclear reaction leveraging the US DOE high-energy accelerator facilities at Brookhaven National Laboratory (200 MeV at 165 μA) and Los Alamos National Laboratory (100 MeV at 275 μA). Targets are processed and final product is distributed from Oak Ridge National Laboratory. **Results:** To date, the Tri-Lab effort has produced and distributed over 250 mCi of accelerator-produced ^{225}Ac to end users for overall product evaluation including a variety of dosimetry, toxicity and biodistribution studies. Results of these studies suggest that the impact of the ^{227}Ac co-product on patient dosimetry will be minimal. Challenges remain with respect to the logistical considerations associated with the ^{227}Ac co-product including facility licensing and disposition of patient waste. **Conclusion:** The US DOE Tri-Lab effort is routinely distributing accelerator-produced ^{225}Ac for pre-clinical R&D with the aim of supporting clinical studies. Short term effort is focused on development of a Drug Master File with long term effort focused on development of processing capabilities aimed at supporting Ci-scale batches. **References:** (1) J.W. Weidner et al., Appl. Radiat. Isot. 70 (2012) 2602 (2) J.W. Engle et. al., Phys. Rev. C. 88 (2013) 014604 (3) J.W. Engle et. al., Radiochim. Acta 102 (2014) 569 (4) V. Radchenko et. al., Journal of Chromatography A 1380 (2015) 55 (5) J.R. Griswold et. al., Appl. Radiat. Isot. 118 (2016) 366 (6) V. Radchenko et. al., Talanta 175 (2017) 318.

EP-53

Preclinical and translational aspects, including radiopharmacy, radiochemistry and drug development -> Radiopharmacy, radiochemistry, drug development -> Radiochemistry -> Radiopharmaceutical preparation

October 12 - 16, 2019 e-Poster Area

EP-0737

^{68}Ga-Labeling of PSMA-11: Which Technique is the Best?

S. Pfaff[1,2], *V. Pichler*[1], *E. Schaier*[1,2], *F. Girschele*[1], *C. Philippe*[1], *M. Hacker*[1], *M. Mitterhauser*[1,3], *W. Wadsak*[1,4];
[1]*Medical University of Vienna, Vienna, AUSTRIA,* [2]*University of Vienna, Vienna, AUSTRIA,* [3]*Ludwig-Boltzmann-Institute*

Applied Diagnostics, Vienna, AUSTRIA, [4]CBmed GmbH - Center for Biomarker Research in Medicine, Graz, AUSTRIA.

Aim/Introduction: ^{68}Ga-radiolabeling is probably one of the most interesting applications for radiopharmacy facilities, since this nuclide is easily available through ^{68}Ge/^{68}Ga-generators and the popularity of [^{68}Ga]Ga-PSMA-11 is flourishing. Besides conventional ^{68}Ga-complexations via synthesizing modules that are usually cassette-based or fixed-tubing-based, exotic techniques like microwave assisted- or microfluidic synthesis are available for radiolabeling. Recently, a KIT for ^{68}Ga-labeling of PSMA-11 was developed that does not need any synthesizers or energy supply. However, choosing the best approach among these possibilities is demanding and needs conscientious research. Consequently, this study aimed to compare a microfluidic-, microwave assisted-, KIT-, cassette-and fixed-tubing-based ^{68}Ga-labeling regarding their applicability and efficiency. **Materials and Methods:** PSMA-11 was purchased from ABX (Radeberg, Germany) and the KIT was provided by ANMI (Liege, Belgium). Gallium-68 was obtained from a ^{68}Ge/^{68}Ga-generator (GalliaPharm® from EZAG, Berlin, Germany or Galli Eo™/Ad from IRE Elit, Fleurus, Belgium). The applied synthesizers were SynChrom R&D (Elysia-raytest, Straubenhardt, Germany), GRP+ (Scintomics, Fürstenfeldbruck, Germany), PET-wave (CEM, Kamp-Lintfort, Germany) and NanoTek (Advion, Ithaca, USA) and the applied precursor concentrations were 2.5, 1.4, 0.42 and 0.5 µg/mL, respectively. The radiochemical conversion rate (RCR, determined by TLC and HPLC), radiochemical yield (RCY, content of product related to the starting activity, corrected for decay) or/and RCY not corrected for decay (RCY ncd) were determined. **Results:** ^{68}Ga-complexations of PSMA-11 using a microfluidic device resulted in a RCR of 93.3±7.5%. A RCR of 91.0±2.1% was achieved via microwave assisted synthesis in less than 1 min. The cassette-based-system resulted in a RCY ncd of 45.3±2.3% and shows overall synthesis time of more than 30 min. The fixed-tubing-based synthesizer achieved a RCY ncd of 73.7±6.2. KIT-based labeling gave a quantitative RCY ncd ≥ 90.3±2.6% within 5 min with minimal handling requirements. **Conclusion:** Microfluidic synthesis of [^{68}Ga]Ga-PSMA-11 was performed using low precursor amounts. Due to the ability of performing numerous syntheses consecutively, this approach could be feasible for a dose-on-demand approach using higher activities of cyclotron produced gallium-68. Microwave assisted synthesis achieved quantitative RCRs within <1 min using a remarkable low precursor amount. Hence, this approach is worth pursuing for clinical routine productions. The cassette-based-system achieved a good RCY, but the synthesis duration of >30 min reduces the activity yield. In contrast, the fixed-tubing-based system enabled high RCY in <20 min. The KIT needs a higher precursor amount, but enables a broad implementation of [^{68}Ga]Ga-PSMA-11 in radiopharmacy facilities due to its convenient applicability and low technical effort. **References:** None.

EP-0738

[^{18}F]FET production with a modified gallium-68 automated synthesizer in a Radiopharmacy without cyclotron facility

M. Riondato, *S. Pastorino, E. Giovannini, O. Ferrando, P. Lazzeri, V. Duce, A. Ciarmiello;*
Nuclear Medicine Department, La Spezia, ITALY.

Aim/Introduction: Among PET imaging applications, O-(2-[18F]fluoroethyl)-L-tyrosine ([^{18}F]FET) is gaining attention for the assessing brain tumors. [^{18}F]FET is an established radiopharmaceutical not commonly available in Italy, used by few hospital radiopharmacies with a cyclotron facility or purchased by other countries. The aim of this study is to demonstrate that a radiopharmacy without a cyclotron facility, but implemented with an automated synthesizer typically dedicated for 68Ga chemistry and a fully equipped Quality Controls (QCs) laboratory, can prepare [^{18}F]FET according to the European Pharmacopoeia(PhE) monograph starting from an external supply of [^{18}F]fluoride for radiolabeling. **Materials and Methods:** [^{18}F]FET radiosynthesis was carried out using a standard Modular-Lab PharmTracer (Eckert & Ziegler, EZ) in the typical setting for the production of gallium-68 peptides, implemented with a commercially available chemical vacuum pump (Laboport) and an external additional 3-way valve (Burkert). EZ disposable cassettes for 68Ga-peptide synthesis are reassembled and the reactor replaced with a glass MX-Tracerlab (GE). All reagents were purchased by ABX. All purifications were performed with on-line cartridges (QMA-Light, C18-Plus Long and Alumina N cartridges, Waters). [^{18}F]fluorine for radiolabeling (PhE grade), initially used to assess critical steps of radiosynthesis was 7.5-12 GBq. **Results:** [^{18}F]fluoride was automatically transferred (pneumatic system) from the shipped vial to an anionic exchange cartridge. After elution and azeotropic distillation, TET precursor (10 mg in 3.5 ml ACN) was added to the activated [18F]fluoride and the mixture heated at 100°C for 500 sec. Best hydrolysis condition was found in 1N HCl (3.5 ml) at 100°C for 15 min. Diluted and cooled reaction mixture was transferred on a C18-Plus Long cartridge and washed with water. Cartridge containing [^{18}F]FET was then eluted with 9 ml of ethanol/water (5:95 v/v). First 2 ml were discarted, while the rest collected after purification on Alumina N cartridge. The product was reformulated with saline to the standard final batch volume of 20 ml, and sterilized and collected. [^{18}F]FET was obtained during validation syntheses in a non-decay corrected yield of 24.1%±3.1% (n=8). After QCs all batches of [^{18}F]FET respected the monograph specifications. For the evaluation of enantiomeric purity, an easy, cheap and fast thin layer chromatography (TLC) method was proposed and successfully carried out. **Conclusion:** This work presents an initial experience of [^{18}F]FET production using an automated synthesis module, commonly applied for 68Ga-tracers. Synthetic strategy details and final purification without a HPLC are presented. **References:** None.

EP-0739

[^{131}I]ICF01012 automated radiosynthesis for first human targeted radiotherapy of metastatic melanoma

M. Cosson[1], *S. Levesque*[1], *M. Tempier*[1], *S. Tarrit*[2], *M. Galmier*[2], *J. Chezal*[2], *E. Miot-Noirault*[2], *F. Cachin*[1], *P. Auzeloux*[2];
[1]*Centre Jean Perrin - Service médecine nucléaire, Clermont Ferrand, FRANCE,* [2]*INSERM UMR1240 – Imagerie moléculaire et stratégies théranostiques (IMoST) – Université Clermont Auvergne (UCA), Clermont Ferrand, FRANCE.*

Aim/Introduction: [^{131}I]ICF01012 is a candidate for targeted radiotherapy of metastatic melanoma.[1-4] To complies with the current Good Radiopharmacy Practice, as well as for radiation protection, we developed a fully automated radiosynthesis on AllinOne tracer synthesizer (Trasis). We present here the main chemical and pharmaceutical data necessary for achieving the Investigational Medicinal Product Dossier (IMPD). **Materials and Methods:** Both radioactive precursor (Na^{131}I solution, Izotop) and chemical stannyl precursor (ERAS Labo) are GMP grade. The radiolabelling step is a nucleophilic substitution in acidic (HCl) conditions in presence of hydrogen peroxyde as oxydazer. Purification is achieved on a C18 cartridge. Finally, the product is eluted with an ethanol/water solution (15:85, v/v). Final sterilisation is conducted by filtration (0.22 µm filter). The synthesis module is located in a shielded hot cell that ensure a grade B environment in a grade C laboratory. The disposable cassette and program lines were specifically designed for this production. Eleven tests were checked on the final product: appearance, pH (paper), identification and radionucleidic purity (gamma spectrometer, Ortec), filter integrity (AiO, Trasis), endotoxin (Endosafe-PTS, Charles River). We use radio-HPLC (Shimadzu, Kinetex C18 column, Phenomenex) for identification, radiochemical and chemical purity of [^{131}I]ICF01012 solution. The only externalise tests are the determination of residual solvents and the sterility test. **Results:** Three consecutives synthesis of [^{131}I]ICF01012 were carried out for IMPD. The total radiosynthesis procedure time is less than 30 minutes. The mean radiochemical yield is 70% (64-76%). The HPLC method (12 min) is validated and allows to obtain identification of [^{131}I]ICF01012, chemical and radiochemical purity, and specific activity. The radiochemical purity is 97.7±0.5%, with an average specific activity of 31 GBq.µmol^{-1}. The chemical purity measurement showed that the residual amount of stannane chemical precursor is below the limit of quantification (50 ng.mL^{-1}). All intern release tests are carried out in less than 30 minutes after the end of production. Radiochemical stability was evaluated during the first 4 hours, without any de-iodation observed. **Conclusion:** Process validation was successfully performed by preparing and controlling three consecutive batches of [^{131}I] ICF01012. Our IMPD was validated in 2018 by the national French authority (ANSM). The clinical trial is active since January 2019. **References:** 1-Chezal JM et al., brevet PCT WO2008012782, 2008. 2-Chezal JM et al., J. Med. Chem., 2008, 51, 3133-3144. 3-Degoul F et al., Int. J. Cancer 2013, 133, 1042-1054. 4-Cachin F et al., Medecine Nucleaire 2015, 39(5), 458-464.

EP-0740

Radiolabeling of an anti-CD66 antibody with diagnostic and therapeutic radionuclides and biological evaluation

G. Fischer, *C. Hamp, J. Wenz, G. Winter, G. Glatting, A. J. Beer, C. Solbach;*
University Hospital, Ulm, GERMANY.

Aim/Introduction: Electron emitter-labeled anti-CD66 antibodies can be used for radioimmunotherapy within the concept of myeloablation prior to stem cell transplantation, with the aim of reducing side effects compared to conventional strategies. In addition to radiotherapy, radiolabeling with In-111 or Ga-68 enables diagnostic SPECT- or PET-imaging i.a. for dosimetry. Due to manufacturer-related antibody-modifications, the chelator conjugation procedure and the radiolabeling procedure needed to be re-established with respect to the radiometals Ga-68, In-111 and Y-90. Moreover, the biological evaluation of the antibody quality was extensively adapted. **Materials and Methods:** The conjugation chemistry of the antibody and the chelator DTPA (via p-SCN-Bn-CHX-A″-DTPA) was performed in 0.05 M HEPES buffer at pH 8.5 for 2 h at ambient temperature and was subsequently stored for 15 h at 4-8°C. SEC-LC followed by ultrafiltration was performed for antibody purification. An aliquot of the radionuclide (up to 788 MBq for Y-90 and up to 52 MBq for In-111 or Ga-68) in hydrochloric acid was adjusted with sodium-, ammonium-acetate or HEPES-buffer to a pH of 5 to 6, followed by the addition of 50-200 µg antibody in 15-214 µl of 0.9% NaCl-solution. Radiolabeling succeeded within a reaction time of 10 min at ambient temperature (Ga-68 and Y-90) or 1 h at 37°C (In-111). The chelator-to-antibody ratio (antibody/Arsenazo III competition test) and the antibody concentration were determined by spectrophotometric evaluation. The immunoreactivity of the antibody was determined by cell binding assay (granulocytes). Serum stability tests were performed by adding an aliquot of antibody to human serum at 37°C with subsequent analysis by radio-HPLC. **Results:** Chemical purities of the antibody conjugated with DTPA after purification were >95%. Radiolabeling yields were up to 96% for Y-90, 80% for Ga-68 and 74% in case of In-111. Ultrafiltration increased the radiochemical purities of In-111 and Y-90 labeled antibodies to >95%. The determined antibody-chelator-ratios were in the range of 4-6. Final antibody concentrations of 1-4 mg/ml were obtained by the purification procedure. Immunoreactivity tests showed that up to 90% of the Y-90 and 70% of In-111 labeled antibodies still bind to CD66 surface-proteins of granulocytes. In-111 labeled antibodies showed a high biological stability in human serum (88% intact after 24 h). **Conclusion:** The antibody-conjugation, the radiolabeling procedure and the biological tests were successfully re-established and transferred into a protocol-based, validated and GMP-compatible procedure. **References:** None.

EP-0741

High yield synthesis of [^{11}C]Methionine via [^{11}C] Methyltriflate by use of the Loop Method

C. Solbach, F. Arndt, R. Gratzl, A. J. Beer, G. Fischer, J. Wenz;
Clinic for Nuclear Medicine, University of Ulm, Ulm, GERMANY.

Aim/Introduction: [^{11}C]Methionine ([^{11}C]MET) is one of the most applied PET-radiopharmaceuticals. It is successfully used for the evaluation of brain tumors by PET. The corresponding radiosyntheses for the production of [^{11}C]MET use L-homocysteinethiolactone (HCTL) or L-homocysteine (HC) as precursors and [^{11}C]methyliodide ([^{11}C]MeI) as labelling precursor. Although these well-established production methods content a final chromatographic method as solid phase extraction or radio-HPLC for the separation of the product [^{11}C]MET from the reaction mixture, a clear contamination of the final radiopharmaceutical product solution with „cold" chemical impurities (e.g. HC, HCTL) may still occur. The application of the "loop-method" by use of the highly reactive C-11 labelling precursor [^{11}C]methyltrifluoromethylsulfonate ([^{11}C]MeOTf) for the production of [^{11}C]MET may reduce the content of cold impurities significantly due to a clearly reduced precursor amount. Moreover, the use of [^{11}C]MeOTf should lead to high radiochemical yields of [^{11}C]MET in a clearly shortened process time. **Materials and Methods:** $^{11}CO_2$ is produced by use of the ^{14}N(p,α)^{11}C-nuclear reaction (PETtrace 800 cyclotron, GE) followed by automated transformation into [^{11}C]MeI (MeI microlab, GE) and on-line conversion into [^{11}C]MeOTf by use of silvertriflate (on Graphpac GC) at 200 ° C. By passing the gaseous and highly reactive [^{11}C]MeOTf in a moderate inert gas flow (He 6.0, 50 ml/min) through the reaction loop (l: 700 mm, i.d.: 1mm, polyethylene; containing a solution of 375 µg (2.45 µmol) of L-HCTL and 1.8 mg (45 µmol) NaOH in 100 µl EtOH/H_2O 70/30 v/v) of a TRASIS All in one cassette module the desired product [^{11}C]MET is build. The labelling step is then followed by rinsing the reaction loop with 15 ml of PBS via 2 conditioned C-18 Sep Pak Plus SPE cartridges (Waters) and subsequently sterile filtration through a 0.22 µm sterile filter into a sterile septum sealed product container. **Results:** The loop method succeeds within 18 min after EOB (end of bombardment) and in excellent radiochemical yields of 37-50 % with respect to $^{11}CO_2$ allowing absolute yields of up to 35 GBq of [^{11}C]MET. The radiochemical purity of the final radiopharmaceutical solution was always >99%. The content of HCTL was always below the detection limit whereas the content of HC was always <22 µg/ml (<330 µg/batch). **Conclusion:** An effective and rapid method for the production of highly pure [^{11}C]MET allowing multi-patient application has been developed. Additionally, the reaction is characterized by the use of disposable products, whereby the reaction can be performed GMP compliant. **References:** None.

EP-0742

Investigation of automated radiofluorination methods for oxidatively sensitive aryl systems

A. McDonald[1,2,3], Y. W. Goh[1,2], J. M. White[3], A. Scott[1,2,4], U. Ackermann[1,2,4];
[1]Olivia Newton John Cancer Research Institute and La Trobe University, Heidelberg, AUSTRALIA, [2]Department of Molecular Imaging and Therapy, Austin Health, Heidelberg, AUSTRALIA, [3]School of Chemistry and Bio21 Institute, The University of Melbourne, Parkville, AUSTRALIA, [4]Department of Medicine, The University of Melbourne, Parkville, AUSTRALIA.

Aim/Introduction: Radio fluorination of aryl systems has been a significant challenge in the area of radiochemistry for some time. As more methods are developed, it is important to select the appropriate system for the target molecule at hand. A molecule of interest to our research group was the N-(4-chlorobenzyl)- indole-3-carbaldehyde, denoted Oncrasin-1, due to its potential as a radiotracer for oncology. Fluorination of this system was investigated, with radio fluorination of the benzyl ring at 3 different positions being to determine the optimal lead compound. This work investigates two precursor classes for radiolabelling; iodonium salts have been popular, with a variety of methods for forming them, compared with relatively new in boronic acid/ester precursor radiofluorination. **Materials and Methods:** Precursor synthesis was envisioned through coupling between an appropriate iodobenzyl halide and the indole-3-carbaldehyde, followed by oxidation to the iodonium salt. Successful synthesis of the iodobenzyl intermediate was followed by attempts to form a precursor utilizing multistep and one pot procedures were unsuccessful. Boronic acid pinacol ester precursors were synthesized through both a miyaura borylation with the iodine precursor previously synthesized as well as a sodium hydride coupling of the indole-3-carbaldehyde and the appropriate boronic ester benzyl bromide. Radiolabelling of this system was undertaken in an automated Flexlab module and utilized a custom potassium triflate eluent in combination with a copper triflate catalyst and pyridine co-solvent to produce radiofluorinated products. **Results:** Iodonium salt forming reactions were investigated using a benzyl iodide precursor. These reactions were unsuccessful however a multistep synthesis utilizing a diacetoxy-iodo intermediate produced a ring opened structure indicating that these conditions were preferentially oxidizing the indole structure over the desired benzyl iodide. Methods utilizing boronic acid pinacol ester precursors in combination with a copper triflate catalyst system initially produced no labelled products prior to fluoride elution optimization; standard bicarbonate and carbonate eluent systems result in alternative reactions. A potassium triflate eluent system was developed with a preconditioned carbonate QMA. Further optimization of the system was undertaken, with a preformed copper catalyst being less effective than the catalyst system formed in situ. Yields of 10-18% were obtained for the three precursors. **Conclusion:** Radiolabelling of aryl systems containing electron rich indole scaffolds should consider avoiding traditional iodonium salt forming reactions as oxidative

side reactions appear to be favoured over the iodonium salt forming reaction. Instead, boronic acid ester precursors offer an attractive alternative route for radiofluorination of these systems. **References:** None.

EP-0743

Synthesis and Complex Chemistry of the Bifunctional HBED-NN Chelator

A. Makarem, K. Klika, G. Litau, Y. Remde, K. Kopka;
German Cancer Research Center, Heidelberg, GERMANY.

Aim/Introduction: Radiometal-based radiopharmaceuticals bearing bifunctional HBED chelators are powerful tools for cancer diagnosis and therapy.[1] Bifunctional HBED chelators make strong complexes with trivalent gallium, and additionally, can be conjugated to bioactive molecules.[2] In this context, the copper(I)-catalyzed azide-alkyne cycloaddition (CuAAC) reaction is one of the popular conjugation methods for linking complexing agents to bioactive molecules.[3] We hereby introduce di-tert-butyl 2,2'-(ethane-1,2-diylbis{[5-(2-azidoethyl)-2-hydroxybenzyl]azanediyl})diacetate (in short: HBED-NN) as the first bifunctional HBED chelator with two terminal azide groups for direct "click" conjugation. We also studied this chelator for its potential use in gallium-based radiopharmaceuticals. Although the pharmaceutical profile of the hexadentate [Ga(HBED)] framework has been studied multiple times in other researches,[4] the exact structure of this complex has not been confirmed yet. For this reason, we investigated the complex chemistry of the [Ga(HBED)] coordination sphere and determined its structure geometry. **Materials and Methods:** The HBED-NN chelator entered into defined CuAAC reactions as well as complexation reactions under various conditions. In this context, we simulated the general synthetic route of HBED-based radiopharmaceuticals[5] for the preparation of the hexadentate [^{nat}Ga(HBED-NN)] complex. The structural features of this complex was studied by NMR techniques (1D, 2D, variable temperature). **Results:** The synthesis of HBED-NN (ester-protected) was accomplished in 5 steps. We next studied the click chemistry of this chelator using small terminal alkynes. For investigating the complex chemistry, we employed a representative vector model with an uncomplicated spectral pattern in the ^{1}H NMR spectrum especially in the upfield region where protons of the chelate cage appear. Phenyl acetylene met these requirements and therefore its "click" product was used as the overall complexing agent. Complete NMR characterization of [Ga(HBED-NN)] confirmed an octahedral structure with the carboxylate oxygens trans to each other and the phenolic oxygens cis to each other for this complex. **Conclusion:** We have introduced HBED-NN as a diazide variant of the bifunctional HBED chelator which enables "click" coupling without using linkers. Also, we determined the geometry of the [Ga(HBED)] chelate cage. This study shows that the HBED-NN chelator-type is potentially an excellent candidate for the development of new radiopharmaceuticals. **References:** (1) Afshar-Oromieh, A. et al. Eur. J. Nucl. Med. Mol. Imaging 2014, 41, 11-20. (2) Schuhmacher, J. et al. Nucl. Med. Biol. 1992, 19, 809. (3) Makarem, A. Synlett 2018, 29, 1239. (4) Eder, M. et al. Pharmaceuticals 2014, 7, 779. (5) Zha, Z. Bioconjug. Chem. 2016, 27, 1314.

EP-0744

Robust cobalt cage assemblies as anionic radioisotope chelating agents: Efficient radiolabelling using the [^{99m}Tc]TcO_4^- anion and beyond

B. Burke[1], W. Grantham[2], V. Nail[1], I. Renard[1], D. Roberts[1], P. J. Lusby[2], S. J. Archibald[1];
[1]University of Hull, Hull, UNITED KINGDOM, [2]University of Edinburgh, Edinburgh, UNITED KINGDOM.

Aim/Introduction: Synthesis of ^{99m}Tc agents for SPECT imaging involves the chemical reduction of the [^{99m}Tc]TcO_4^- anion using methods which are often incompatible with chelator-biomolecule conjugates, limiting the potential applications. This reliance on redox reactions is a consequence of the assumption that the chemical reactivity of the pertechnetate anion is negligible; it does not bind to any ligand.[1] Here, we present the use of a robust self-assembled supramolecular cage structures for reduction-free encapsulation of [^{99m}Tc]TcO_4^-. Other anions also being assessed include [^{18}F]SO_3F^-, [^{18}F]BF_4^-, [^{123}I]I^-, [^{131}I]I^- and [^{188}Re]ReO_4^- for both nuclear imaging and radioisotope therapy applications. **Materials and Methods:** A supramolecular cage assembly terminating in amine groups was synthesised using a "assembly-followed-by-fixing" method which involves post-assembly oxidation of dynamic Co^{II} species to give a non-equilibrium Co^{III} analogue.[2] Radiolabelling was carried out using [^{99m}Tc]TcO_4^- directly from a ^{99}Mo/^{99m}Tc generator (Curium, UK) for 5 minutes at room temperature - extending the time does not improve radiochemical yield. Radiochemical stability measurements were carried out by adding individual competing anions, or serum, to pre-labelled cage for various times. SPECT imaging of the radiolabelled cage assembly was carried out in naïve mice and biodistribution compared to free [^{99m}Tc]TcO_4^-. **Results:** Radiolabelling with [^{99m}Tc]TcO_4^- was carried out to determine a radiolabelling EC_{95} value of 1.9 µM. Stability measurements demonstrated consistent equilibrium based anion competition and serum stability. When [^{99m}Tc]TcO_4^- labelled cage was imaged using SPECT in comparison with free [^{99m}Tc]TcO_4^-, a difference in biodistribution was observed, with significant uptake noted in the liver. These imaging results are consistent with the radiochemical stability data, in which the cage is reaching equilibrium with blood-based anions, releasing a small amount of free pertechnetate, causing some NIS mediated thyroid and stomach uptake. **Conclusion:** While the use of self-assembled carrier systems in nuclear medicine is still in its infancy, we have demonstrated a clear step forward, showing both the robustness of an amino terminating $Co^{III}_4L_6$ cage in vivo and that binding the [^{99m}Tc]TcO_4^- anion significantly affects its biodistribution.[3] This is the first step towards the development of reductant-free kit bioconjugates for targeted SPECT imaging. The approach is currently being translated to other anions for both PET imaging and radioisotope

therapy applications. **References:** [1] I Zolle. Technetium-99m Pharmaceuticals: Preparation and Quality Control in Nuclear Medicine; Springer: Berlin, Heidelberg, New York, 2007. [2] M.J. Burke et al., J. Am. Chem. Soc. 2016, 138, 9308. [3] B.P. Burke et al., J. Am. Chem. Soc., 2018, 140, 16877.

EP-0745

Critical impact of the conjugation strategy on the stability of ^{89}Zr-labeled immunoconjugates towards radiolysis

P. Adumeau, M. Moreau, L. Da Costa, C. Bernhard, A. Dubois, V. Goncalves, F. Denat;
Universite de Bourgogne, Dijon, FRANCE.

Aim/Introduction: For immunoPET imaging, zirconium-89 is very enticing for the radiolabeling of antibodies due to its radioactive half-life (3.3 days) matching the biological half-life of the protein. The radiolabeling of biomolecules with ^{89}Zr first implies the modification of the biomolecules to introduce a chelating agent, like desferrioxamine - DFO, the gold standard for ^{89}Zr radiolabeling.[1] Among the numerous bioconjugation strategies available, the most widely used is undoubtedly the random conjugation of lysine residues with isothiocyanate moieties, leading to the formation of a thiourea linker. The ionizing radiation generated by the radioelement can however degrade this linker, leading to its rupture and the release of the chelator/radiometal complex, and the thiourea linker has proven particularly sensitive to this phenomenon in the past.[2,3] Rudd et al. have proposed to use squaramate as an alternative to isothiocyanate, as it offers many advantages over the latter.[4] However, the behavior of the squaramide linker toward radiolysis has never been thoroughly investigated. **Materials and Methods:** In order to investigate the putative improved behaviour of the squaramide linker toward radiolysis, we have synthesized several trastuzumab-based conjugates bearing DFO derivatives via either a thiourea or a squaramide linker. These conjugates were then radiolabeled with ^{89}Zr using standard radiolabeling procedures, and the stability of the radioconjugates was investigated over the course of 7 days using size-exclusion chromatography. **Results:** The radiolabeling of the different conjugates yielded the radioconjugates with comparable yield (>95 %), radiochemical purity (>99 %) and specific activity (50 GBq/g). However, squaramide- and thiourea-based radioconjugates clearly showed different behaviours upon incubation at 37°C for 7 days, with the thiourea conjugates dropping to up to 60 % of integrity while the squaramide-based conjugates remained above 95 % of integrity. **Conclusion:** These preliminary results demonstrate that the squaramide linker is indeed more stable than the thiourea, and therefore the squaramate should replace advantageously the isothiocyanate moiety for the conjugation to lysine residues in the radiochemistry field. We are currently in the process of synthesizing more conjugates to confirm these results and extend these findings beyond trastuzumab-based conjugates. **References:** 1. Heskamp, S. et al. Bioconjug. Chem. 28, 2211-2223 (2017).2. Liu, C. et al. Nucl. Med. Biol. 30, 207-214 (2003).3. Vosjan, M. J. W. D. et al. Nat. Protoc. 5, 739-743 (2010).4. Rudd, S. E. et al. Chem. Commun. 52, 11889-11892 (2016).

EP-0746

A Simple Azeotropic Drying Free Synthesis of [18F] FET Via Fluorination of Chiral NiII Complex Precursor In Conjunction With Tetrabutylammonium Tosylate

T. Skvortsova, O. Fedorova, R. Krasikova, V. Orlovskaya;
N. P. Bechtereva Institute of the Human Brain of Russian Academy of Sciences, Saint-Petersburg, RUSSIAN FEDERATION.

Aim/Introduction: [^{18}F]FET is an important and specific tracer for PET diagnostics of cerebral tumors. The number of [^{18}F]FET PET examinations is expected to increase in the next few years due to its logistical advantages over L-[^{11}C-methyl]methionine. We earlier developed a convenient synthesis of [^{18}F]FET via kryptofix mediated raduifluorination of a chiral Ni^{II} complex of an alkylated (S)-tyrosine Schiff base, Ni-(S)-BPB-(S)-Tyr-OCH_2-CH_2OTs (**I**). Radiochemical yield (RCY) of [^{18}F]FET was 26% (EOS) within 45 min synthesis time, using Scintomics Hotbox^{one} automated module. Here we optimize the ^{18}F-fluorination process via substituting kryptofix/carbonate with an inert phase transfer catalyst (PTC), tetrabutylammonium tosylate (TBAOTs). The novel protocol was adapted to GE TRACERlab FX N Pro, a commonly used ^{18}F-radiolabeling platform. **Materials and Methods:** [^{18}F]fluoride was eluted from QMA carb. cartridge with solution of 5 mg TBAOTs in 2 mL of ethanol. The solvent was evaporated; 2 mg of (**I**) in 0.9 mL of acetonitrile was added. Fluorination was performed at 100ºC for 5 min following removal of reaction solvent to dryness. After acidic hydrolysis (0.5M HCl/EtOH, 125ºC, 5 min) the pH of reaction mixture was adjusted to 9.0. Resulting turbid solution was passed through filtration column and three tC18 Light cartridges connected sequentially. [^{18}F]FET was eluted with 10 mL of sodium acetate (5 mM, pH 4) containing 3% of EtOH and further purified by passing through CM Plus cartridge to remove any residual nickel. **Results:** By using the chemically inert TBAOTs for radiofluorination of **I** a better RCY (40.6±3.4%, n=5, EOS) was achieved applying only 2 mg of precursor. [^{18}F]FET was obtained with radiochemical purity >99% and enantiomeric purity 95-96%. All results of the quality control were within the limits established by the European Pharmacopoeia. **Conclusion:** A simple, fast and azeotropic drying free automated synthesis procedure for [^{18}F] FET using **I** as a labeling precursor, was developed. The use of TBAOTs for elution of [^{18}F]fluoride and following fluorination resulted in over 40% practical yield of [^{18}F]FET within 35 min synthesis time. We believe that the benefits of this chemically inert PTC are worth evaluating in the preparation of other useful fluorine-18 labelled radiotracers. We acknowledge Russian Foundation of Basic Researches (RFBR, project N 18-29-01015) for financial support. **References:** None.

EP-0747

A Modified Procedure For The Synthesis Of A Potential Tau Imaging Agent [F18]-THK5351 Employing A Sumitomo Semi-automatic Chemical Synthesizer F121R

J. M. Cheung, *N. Ng, K. Liu, C. Ho;*
Hong Kong Sanatorium & Hospital, Hong Kong, HONG KONG.

Aim/Introduction: [^{18}F]-THK5351 is a promising tau tracer of arylquinoline derivative for PET imaging of neurofibrillary pathology in Alzheimer's disease (AD). It demonstrates high binding affinity for hippocampal homogenates of AD brains and less non-specific retention in white matter. However, repeated attempts to synthesize [^{18}F]-THK5351 following the literature procedure resulted in two inseparable products in HPLC purification with low yield. We, therefore, proposed a modified procedure that is more effective in the synthesis of this compound. **Materials and Methods:** With the Sumitomo F121R synthesizer, the protected precursor, (2S)-3-((2-(6-(methylamino) pyridin-3-yl)quinolin-6-yl)oxy)-2-((tetrahydro-2H-pyran-2-yl)oxy) propyl-4-methylbenzenesulfonate was fluorinated at various temperature settings (110-125ºC) to compare the product yields. The amount of precursor compound was systematically reduced to compare the yields under the same reaction conditions. To avoid forming two compounds and to keep the solvent homogeneity, a larger volume of potassium acetate with a higher concentration was used to neutralize the reaction mixture after acid hydrolysis, and the solid phase extraction solvent aqueous ethanol was diluted with HPLC mobile phase before proceeding to HPLC purification. **Results:** We were able to reduce the precursor compound proposed in the literature reference from 3 mg to 1 mg. The optimal temperature for the fluorination reaction was found to be 125ºC. After acid hydrolysis, the crude product mixture was neutralized with potassium acetate of a higher concentration (1.6M) in a larger volume (1.5 mL). Upon dilution of the aqueous ethanol eluent from the purification Sep-Pak light Oasis HLB with 0.6 mL HPLC mobile phase, the HPLC purified product [^{18}F]-THK5351 was eluted at 9 minutes as a single sharp peak. The radiochemical identity of the product was verified by spiked standard analysis, and the radiochemical purity was >99% by analytical HPLC with a reaction yield of 32.8±11.6%. The HPLC purified fraction was formulated into an injectable solution, which passed all quality control requirements, thus suitable for patient administration. **Conclusion:** The tau imaging agent [^{18}F]-THK5351 was successfully synthesized using a Sumitomo F121R synthesizer in our radiopharmacy laboratory at a yield of 32.8±11.6% (n=3) and >99% radiochemical purity though with less precursor (1 mg). These could be achieved by making modifications in the reaction temperature, adjustment on the pH of the crude reaction mixture followed by dilution with HPLC mobile phase before HPLC purification. **References:** None.

EP-0748

Study on Chelator-Free Zr-89 Labeling of PAMAM Dendrimers

G. Kim[1], *J. Lee*[1], *K. Yu*[2], *S. Kim*[1];
[1]*Dongguk Univ., Gyeongju, KOREA, REPUBLIC OF,*
[2]*Dongguk Univ., Seoul, KOREA, REPUBLIC OF.*

Aim/Introduction: The aim of the present study is to bind Zr-89 to oxygen sites of dendrimers without using a chelator in order to easily and stably coordinate Zr-89 to polyamidoamine (PAMAM) dendrimers 5G, which is widely studied as a drug delivery system. PAMAM dendrimers are promising nanomaterials because they are biocompatible and can carry drugs stably at the terminal amine sites. Zr-89 is a radioisotope that can be used as a diagnostic radionuclide using PET since it emits positron and has a relatively long half-life and is suitable for long-term study of drug delivery system. **Materials and Methods:** Polyamidoamine (PAMAM) dendrimers 5G and $ZrCl_4$ were purchased from Sigma-Aldrich and Zr-89 was supplied by Korea atomic energy research institute. A simple method is as follows: 1) Zirconium is introduced at room temperature using a chelator at the terminal amine sites of the dendrimer, and 2) zirconium is introduced into the dendrimer at room temperature without chelating, and confirming the yield and proceeding with biological evaluation. **Results:** The zirconium-bound dendrimers without chelator showed higher yields and showed a high label stability of ≥98% after the introduction of Zr-89. Cellular uptake of MDA-MB-231 cells was up to 40% ID. **Conclusion:** In conclusion, it has been confirmed that direct coordination of Zr-89 with dendrimer branches is effective in the study of diagnostic drug delivery using dendrimer, and thus it is possible to utilize more amine groups at the terminal of dendrimer when carrying the drug. **References:** Eszter Boros et al., Chelate-free radiolabeling of metal ion binding and heat-induced iron oxide nanoparticles, Chem. Sci., 2015, 6, 225.

EP-0749

Development of novel ^{68}Ga chelators for PET imaging

D. Sneddon[1], *W. T. Stuber*[2], *S. Faulkner*[2], *B. Cornelissen*[1];
[1]*Radiobiology Research Institute, University of Oxford, Oxford, UNITED KINGDOM,* [2]*Department of Chemistry, University of Oxford, Oxford, UNITED KINGDOM.*

Aim/Introduction: Gallium-68 (^{68}Ga, $t_{½}$ = 68 min) is a positron emitting radioisotope used clinically for positron emission tomography (PET) imaging. Typically, coordination of ^{68}Ga requires high temperatures and rigorous pH control, limiting its application, making it unsuitable for sensitive peptides and small molecules. Therefore, we have designed a series of novel macrocyclic and acyclic chelators and have investigated their coordination of ^{68}Ga. A panel of novel NOTA-based chelators, appended with mixed picolyl, nitrobenzene or longer chain carboxylic acid pendant arms were evaluated. **Materials and Methods:** Gallium-68 (220 MBq, 5.5 mL, 0.1 M HCl) was

eluted from an E&Z ^{68}Ge/^{68}Ga generator and the volume was reduced via a DGA resin. ^{68}Ga was eluted in H_2O (500 µL) and the pH adjusted to pH 4.5-5 using ammonium formate buffer (~100 µL, 5 M, pH 4.5-5). The chelator of interest (1 µmole) in H_2O or DMSO was added and the reaction mixture heated to 95°C for 10 min. Radiolabelling efficiency was measured by radio-iTLC and HPLC. After radiolabelling had been confirmed, the reaction conditions, including buffer, pH, temperature and time, were optimised. Competition studies were undertaken to assess relative complexation efficiencies of each chelator and compared to standard ^{68}Ga chelators, 1,4,7-triazacyclononane-1,4,7-triacetic acid (NOTA) and 1,4,7,10-tetraazacyclododecane-1,4,7,10-tetraacetic acid (DOTA). **Results:** Under standard labelling conditions (pH 4.5-5, 95°C), macrocyclic compounds were successfully radiolabelled, as determined by radio-iTLC and HPLC. Non-optimised yields varied but reached >80% for some compounds. Optimal radiolabelling conditions are being investigated to improve these yields. Stability assessments are currently underway. **Conclusion:** A series of novel chelators were successfully radiolabelled with ^{68}Ga. These results have allowed us to pinpoint necessary structural features for ^{68}Ga coordination, resulting in the design of a second generation of chelators for ^{68}Ga. **References:** None.

EP-0750

A simplified method for the radio-synthesis of [^{18}F]-flumazenil

P. Kumar, R. Joshi, N. Rao;
National Institute of Mental health and Neurosciences, Bengaluru, INDIA.

Aim/Introduction: [^{18}F]-flumazenil (FMZ) has been synthesized by various strategies involving complex purification by on-line high-performance liquid chromatography (HPLC) and also by solid phase cartridges. [^{18}F]-FMZ has been used for the assessment of the gamma amino butyric acid (GABA) receptors by positron emission tomography (PET). We have tried various solid phase extraction (SPE) cartridges combinations and calculated yields. Objective: To standardize and synthesize [^{18}F]-flumazenil using various combinations of the solid phase cartridges in order to minimize the loss of radiochemical yield during purification. **Materials and Methods:** [^{18}F] was produced by standard nuclear reaction using [H_2O^{18}] as a target material. The precursor nitormazenil was procured from ABX, Germany. The radio-fluorination was standardized for various parameters like temperature (130-160°C), precursor concentration (3-5 mg), various combination of SPE cartridges (HLB, tC18, C18 and alumina). the crude mixture was diluted with acidic water and passed through various combinations of the SPE cartridges (HLB + tC18, HLB + C18, C18 + Alumina) and final product eluted by using 2.0 mL of 20% ethanol/ phosphate buffer (pH-4.0). The mechanism of labeling is nucleophilic substitution and carried out in FX2N Tracerlab module. The combination of various cartridges and labeling parameters are established outside the module and then an automated protocol has been designed in FX2N module for clinical use. **Results:** The labeling was found to be maximum by using K^{18}F/kryptofix complex in the DMF at 160°C for 30 min. An equimolar concentration of [K/K2.2.2]$^+$18F$^-$/precursor was used and the incorporation of 18F in the flumazenil was found to be 19 ± 3%. The combination of C18 and alumina cartridges gave a better yield (5 ± 2 %) as compared to 1-2% by the other two combinations. The radiochemical purity was 95 ± 3 % as evaluated by Radio-HPLC with retention time at 15.4 ± 0.3 min (n = 10). This method was adopted for automation and a sequence (for FX2N) was created by us to run the protocol for clinical production of the [^{18}F]-flumazenil. **Conclusion:** [18F]-flumazenil was synthesized with higher radiochemical purity and a simple automated method has been developed for the clinical use. **References:** Vaulina D, Nasirzadeh M, Gomzina N. Automated radiosynthesis and purification of [^{18}F]flumazenil with solid phase extraction. Appl Radiat Isot. 2018 May;135:110-114. Ryzhikov NN, Seneca N, Krasikova RN, et al. Preparation of highly specific radioactivity [18F]flumazenil and its evaluation in cynomolgus monkey by positron emission tomography. Nucl Med Biol. 2005 Feb;32(2):109-16.

EP-0751

Upgrading a basic dose calibrator: development of an automatic decay-calculator

T. Chivato Martín-Falquina[1], *E. Miñana Olmo*[2], *M. Martínez Ramírez*[2];
[1]*Hospital General Universitario Santa Lucía, Cartagena, SPAIN,*
[2]*Hospital Universitario San Juan De Alicante, San Juan, SPAIN.*

Aim/Introduction: Dose calibrators are essential instruments in radiopharmaceutical practice. They allow for the accurate measurement of radioactivity required for radiopharmaceutical preparation and dispensing. Most modern devices include a decay function so the technician can easily prepare doses in advance. However, simpler or older dose calibrators may lack this feature, making the use of formulas or decay tables necessary in order to manually calculate the decay. We present a simple and affordable solution for those devices that feature a serial communication port, such as VDC-404 and VDC-603 (Veenstra Instruments, Netherlands), Atomlab 400 (Biodex Medical Systems, USA) or Curiementor 3 (PTW, Germany). **Materials and Methods:** Decay calculation was done with a Raspberry pi zero WH, a credit card size single board computer running Raspbian 9, connected to the dose calibrator (VDC-404, Veenstra Instruments, Netherlands) by a RS-232 DB9 to TTL adapter. We used a numeric keypad and a 16x2 I2C LCD display for input and output respectively. Software consists of a Python 3 script with the decay constants for ^{99m}Tc, ^{123}I, ^{131}I, ^{67}Ga, ^{90}Y, ^{51}Cr, ^{111}In and ^{18}F. To validate the device we prepared 30 doses set to different times and compared the decayed activity obtained via manual and automatic calculation. **Results:** The Raspberry receives the data about isotope, activity and measurement unit from the dose calibrator in real time, displaying it on the LCD. The operator can change the desired "use time" and the Raspberry will act as a decay calculator, showing in the display the resulting activity at

the new reference time. No difference was found in the decayed activity values regardless of the calculation method: manual or automatic. **Conclusion:** We have developed a modified dose calibrator that provides the operator with an instant and accurate value of the decayed activity, simplifying the task and reducing the risk of miscalculation that arises using calculators and decay tables. The device has minimal footprint, requires an investment of less than 40€ and compatibility with other dose calibrators models is possible with just slight changes to the script. All these characteristics make this device an interesting solution for Radiopharmacies still relying on manual decay calculations. **References:** Schematics, manual and code are available at https://github.com/tchivato/Decay_calculator

EP-0752

An Efficient Automated Radiosynthesis And Bioactivity Confirmation Of [^{18}F]FP-(+)-DTBZ As A VMAT2 Tracer

Z. Chen, *C. Zhao, C. Liu, J. Tang, Y. Xu, M. Xie;*
Key Laboratory of Nuclear Medicine, Ministry of Health, Jiangsu Key Laboratory of Molecular Nuclear Medicine, Jiangsu Institute of Nuclear Medicine, Wuxi, CHINA.

Aim/Introduction: PET imaging with [^{18}F]fluoropropyl-(+)-dihydrotetrabenazine ([^{18}F]FP-(+)-DTBZ) has shown its potential for tracing vesicular monoamine transporter type 2 (VMAT2) for related disorders such as Parkinson's disease. This study focused on the optimization of the radiolabeling method of [^{18}F]FP-(+)-DTBZ to fulfill the demands of pre-clinical and clinical application. **Materials and Methods:** Optimized labeling conditions were carried out through manual radiosynthesis of [^{18}F]FP-(+)-DTBZ by altering the molar ratio of the precursor to base (P/B), base species, solvents, reaction temperature, reaction time and precursor concentration. The method with highest radiochemical yield (RCY) were applied to automated radiosynthesis. Purification of the crude product was conducted with a Sep-Pak Plus C18 cartridge. Quality control and stability of [^{18}F]FP-(+)-DTBZ were carried out by HPLC. In vitro cellular uptake and blocking assays were performed in human neuroblastoma cell line SH-SY5Y. In vivo imaging with small animal positron emission tomography (microPET) was performed with normal Sprague-Dawley rats along with VMAT2 blocking test. **Results:** An RCY (as determined with HPLC) of 88.7 % was obtained with 1.0 mg precursor under the optimized condition (P/K_2CO_3 =1:8, heating at 120 °C for 3 min in dimethyl sulfoxide). This ^{18}F-labelling condition were successfully applied to an commercially available automated module and gave a high activity yield (AY) of 30-55 % (non-decay corrected) in ~40 min with a >99.0 % radiochemical purity (RCP) and a > 44.4 GBq/μmol molar activity (A_m). Stability test displayed that the RCP retained >98.0 % in 8 h both in saline and in phosphate buffer saline (PBS; pH 7.4). In vitro cellular uptake assay showed accumulation of [^{18}F]FP-(+)-DTBZ in SH-SY5Y cells, which could be significantly inhibited by VMAT2 inhibitor DTBZ. Rat brain microPET imaging displayed that the striatum has the highest uptake in brain with a standardized uptake value (SUV) of 2.74 ± 0.21 at ~70 min. Furthermore, the striatum SUV deceased 73% when [^{18}F]FP-(+)-DTBZ was co-injected with DTBZ (1.0 mg/kg), confirming the specificity of [^{18}F]FP-(+)-DTBZ to VMAT2. **Conclusion:** We optimized the radiolabeling method of [^{18}F]FP-(+)-DTBZ and successfully applied it to a commercial available module. The automated synthesis gave a high AY and high RCP of [^{18}F]FP-(+)-DTBZ. In vitro SH-SY5Y cell assay and in vivo rat microPET imaging confirmed its specific binding to VMAT2. Our optimized radiosynthesis of [^{18}F]FP-(+)-DTBZ facilitated its preclinical and clinical routine application for VMAT2 imaging. **References:** None.

EP-0753

AAZTA^5-squaramide ester: a promising tool for ^{177}Lu-labeling of monoclonal antibodies under mild conditions concerning immuno-based endoradiotherapeutic applications

B. Klasen, *E. Moon, F. Roesch;*
Institute of Nuclear Chemistry, Mainz, GERMANY.

Aim/Introduction: Combining the advantages of both cyclic and acyclic chelator systems, AAZTA is well suited for complexation of various diagnostic and therapeutic radiometals such as gallium-68, scandium-44 and lutetium-177 under mild conditions. Due to its specificity for primary amines and pH dependent binding properties, the squaric acid (SA) moiety represents an excellent tool for selective coupling of the appropriate chelator to different target vectors[1]. Therefore, the aim of this study was to evaluate radiolabeling properties of the novel bifunctional AAZTA^5-en-SA being coupled to a model antibody (bevacizumab) in comparison to DOTA-en-SA using the therapeutic nuclide lutetium-177. **Materials and Methods:** As proof-of-concept, bevacizumab was functionalized with a tenfold molar excess of either AAZTA^5-en-SA or DOTA-en-SA resulting in a ratio of 0.2-0.7 bound chelator moieties per protein. The corresponding immunoconjugates AAZTA^5-en-SA-mAb and DOTA-en-SA-mAb were purified twice via fractionated size exclusion chromatography (SEC) and subsequently radiolabeled with lutetium-177 at pH 7 and ambient temperature as well as 37° C. In vitro complex stability of [^{177}Lu]Lu-AAZTA^5-en-SA-mAb was investigated in human serum and PBS at 37 °C over a period of 15 days. **Results:** After 90 min, ^{177}Lu-labeling of AAZTA^5-en-SA-mAb resulted in almost quantitative radiochemical yields of > 98 % at ambient temperature and > 99 % at 37 °C, respectively. After purification via SEC, the radioconjugate [^{177}Lu]Lu-AAZTA^5-en-SA-mAb could be obtained with a purity of > 99 % and an apparent specific activity of 4.1 GBq/μmol. In contrast, ^{177}Lu-labeling of DOTA-en-SA-mAb showed negligible low radiochemical yields of < 2 % both at ambient temperature and 37 °C. Complex stability measurements of [^{177}Lu]Lu-AAZTA^5-en-SA-mAb in human serum indicated > 99 % protein bound activity within 15 days. In PBS, formation of a by-product led to slightly decreased stability of > 93 % intact conjugate over the same period. **Conclusion:** Coupling of AAZTA^5-en-SA to the monoclonal antibody bevacizumab could be confirmed via

successful ^{177}Lu-labeling with almost quantitative radiochemical yields both at ambient temperature and 37 °C. Within 15 days, the resulting radioconjugate indicated high in vitro stability of > 99 % in human serum and > 93 % in PBS, respectively. In contrast, no significant complexation of lutetium-177 via the DOTA functionalized analogue could be observed under identical conditions. Therefore, AAZTA^5-en-SA is a promising tool for ^{177}Lu-labeling of sensitive biomolecules such as antibodies for theranostic applications. **References:** [1] K.-H. Glüsenkamp, W. Drosdziok, G. Eberle, E. Jähde, M. F. Rajewsky, Zeitschrift für Naturforsch. C 1991, 46, 498-501.

EP-0754

Radiolabelled multifunctional hybrid magnetic nanoparticle probe for dual-modality (SPECT and MRI) medical in vivo imaging

G. Dodi[1], *C. M. Uritu*[1], *I. Gardikiotis*[1], *C. T. Mihai*[1], *L. Agrigoroaie*[2], *M. Furcea*[2], *B. I. Tamba*[1], *C. Stefanescu*[3];
[1]*Advanced Research and Development Center for Experimental Medicine, Grigore T. Popa University of Medicine and Pharmacy, Iasi, ROMANIA,* [2]*Department of Nuclear Medicine, University Emergency Hospital "Sf. Spiridon" Iasi, Iasi, ROMANIA,* [3]*Department of Biophysics and Medical Physics, Nuclear medicine, Faculty of Medicine, Grigore T. Popa University of Medicine and Pharmacy, Iasi, ROMANIA.*

Aim/Introduction: The development of non-invasive, high sensitive, high-resolution, and quantitative all-in-one multifunctional candidates that can be detected by multimodal techniques, namely single-photon emission computed tomography and magnetic resonance imaging (SPECT and MRI) represents a challenge in nanomedicine imaging. The main objective of this paper is to develop multifunctional hybrid magnetic- based nuclear imaging probes for evaluating their behaviour in biological systems in vitro and in vivo. **Materials and Methods:** An innovative strategy divided in several steps, was employed for achieving dual-modality candidate:- first, hybrid magnetic nanoparticles were synthesised using iron oxide core obtained by partial oxidation method and multifunctional silica shell chains; - then, cytotoxicity of the multifunctional hybrid magnetic tracer was investigated on normal V79 cell line; -further, the amine groups on the hybrid magnetic nanoparticles surface were radiolabelled with ^{99m}Tc, eluted from a ^{99}Mo/^{99m}Tc Drytec Generator system as $Na^{+99m}TcO_4^-$;- in vivo biodistribution of the obtained radiolabelled multifunctional hybrid magnetic nanoparticle probe was determined after intravenous administration on healthy experimental animals by in vivo SPECT imaging and ex vivo gamma counting of the excised tissues; - dual-modality imaging evaluation of the synthesised nanotracer was obtained by SPECT and MRI comparison studies. **Results:** The structure, external morphology, size distribution, colloidal and magnetic properties were characterised by FT-IR, TEM, XRD, DLS and VSM analyses. The characterization results confirmed the formation of well-defined crystalline magnetite conjugates with broad distribution, relatively high saturation magnetization and irregular smooth surface. In vitro cell viability assay displayed good biocompatibility of the conjugates with the percent of viable cells exceeding 80% after 48 h incubation for normal cell line. The magnetic amine functionalized Fe_3O_4 nanoparticles were successfully labeled with ^{99m}Tc using standard radiolabeling methods as reveled by the radiolabeling yield (≈ 90%) assessed using instant thin layer chromatography. Both the ex vivo biodistribution and in vivo SPECT imaging on healthy animals showed a similar pharmacokinetic biodistribution profile for ^{99m}Tc- amine Fe_3O_4 nanoparticles. **Conclusion:** In summary, we have developed new molecular imaging probes based on hybrid magnetic nanoparticles radiolabeled with the diagnostic radionuclide ^{99m}Tc for SPECT imaging and evaluated their biodistribution profiles in healthy animals.The obtained results opened opportunities to extend this new nanotracer for therapeutic use due to its versatile functions to link different molecules to the same core. **References:** Acknowledgement: This work was supported by a grant of Ministry of Research and Innovation, CNCS - UEFISCDI, project number PN-III-P1-1.1-PD-2016-1642, within PNCDI III.

EP-0755

Automated synthesis of [^{11}C]SC560 with Synthra® synthesis module

C. Kwizera, *I. F. Antunes, R. Zijlma, E. de Vries;*
Umcg, Groningen, NETHERLANDS.

Aim/Introduction: ^{11}C labeled 5-(4-chlorophenyl)-1-(4-methoxyphenyl)-3-(trifluoromethyl)-1H-pyrazole ([^{11}C]SC560) is a PET tracer that selectively binds to COX-1that is overexpressed in inflammatory conditions[1]. In order to potentially use this tracer in a clinical settings we developed an automated syntheses of the tracer. Therefore, this study aimed to describe the automated [^{11}C]SC560 production in a Synthra synthesis module and the evaluation of [^{11}C]SC560 selectivity towards a COX-1 expressing ovarian cancer cell line (OVCAR3)[2]. **Materials and Methods:** [^{11}C]SC560 was prepared by O-[^{11}C]methylation of the phenolic precursor with [^{11}C] methyl triflate in 0.25 ml dry acetone containing 5 µL of NaOH (1M). The reaction was performed in a Synthra synthesis module at room temperature for 3 min. Subsequently , the mixture was diluted with 1.3 ml of a solution containing HCL0.1M/ACN/WFI (9:1:1) and purified by High-performance-liquid-chromatography (HPLC, µBoundapak C18(5µm, 8x 300 mm)-mobile phase acetonitrile/ water (70:30 v/v), at flow rate of 3 ml/min). The radioactive product with a retention time of 14 min was collected and formulated in ethanol/WFI (containing 6µL of Tween20). The formulated tracer was submitted to quality control. For the in vitro studies, 0.1×10^6 OVCAR3 cells were plated in a 12 well plate 24 h before the experiment. SC560 (COX-1), Indomethacin (COX-1 and COX-2) and Celecoxib (COX-2) were added in triplicate to the cells. 30 min after the incubation with the inhibitors, [^{11}C]SC560 was added (<1MBq) and left to incubate at 37°C and 5% CO_2 for 30 min. Afterwards the cells were washed with cold PBS, trypsinazed, resuspended and transferred to tubes for the measurement of

radioactivity by gamma counter and cells counted by the trypan blue method. **Results:** The total automated synthesis time of [^{11}C] SC560 was 50 min with a radiochemical yield of 25%, a molar activity of ± 50000 GBq/µmol (n =3) and radiochemical purity was greater than 95%. The uptake of [^{11}C]SC560(6.15±0.69 %uptake/million cells) in OVCAR3 cells was significantly reduces in the presence of cold SC560 (4.47±0.22 %uptake/million cells, p=0.02) or Indomethacin (3.13±0.33 %uptake/million cells, p=0.015) but not with Celecoxib (5.31±0.88 %uptake/million cells, p=0.26). **Conclusion:** [^{11}C]SC560 can be produced reproducibly in an automated Synthra synthesis module. As a proof-of-principle we were able to demonstrate selectivity of of [^{11}C]SC560 in OVCAR3 cells. Further studies are ongoing to have a better understanding of this PET tracer for COX-1 expression. **References:** [1] Fujisaki et al., Ann. Nucl Med, 2005, 19:617-625. [2] Gupta et al., Cancer Res, 2003,63:906-911

EP-54

Preclinical and translational aspects, including radiopharmacy, radiochemistry and drug development -> Radiopharmacy, radiochemistry, drug development -> Radiopharmacy -> Quality control & quality assurance

October 12 - 16, 2019 e-Poster Area

EP-0756

Initiation Of A Prospective Clinical Multicentre Trial With Local Production Of A Short-Lived PSMA-PET-Radiopharmaceutical In The D-A-CH-Region: Chances And Experiences

O. Neels[1,2], *C. Zippel*[1,2], *F. L. Giesel*[3,2,1], *K. Kopka*[1,2];
[1]*German Cancer Research Center, Heidelberg, GERMANY,*
[2]*German Cancer Consortium (DKTK), Heidelberg, GERMANY,*
[3]*University Hospital Heidelberg, Heidelberg, GERMANY.*

Aim/Introduction: The development of innovative radiotracers targeting PSMA for non-invasive imaging of prostate cancer and successive treatment results in an increasing number of multicentre clinical trials using the most promising PSMA ligand candidates. For prospective studies with short-lived radiopharmaceuticals like [^{68}Ga]Ga-PSMA-11, a regulatory and country-specific structure has to be established before recruitment of patients is possible. This structure allows the decentralized manufacturing of the investigational medicinal product (IMP) according to Good Manufacturing (GMP) and subsequent implementation of the respective tracer compliant with Good Clinical Practice (GCP). **Materials and Methods:** For the multicenter clinical trial (phases-I/-II) „Ga-68-PSMA-11 in high-risk prostate cancer" (NCT03362359) within DKTK a harmonized decentralized radiotracer production in multiple radiopharmacies has been set up for the very first time in the German speaking Radiopharmacy/Nuclear Medicine Community. In this prospective clinical study Nuclear Medicine physicians, radiopharmacists, urologists, pathologists and study related experts like lawyers and study nurses out of eleven study sites within the so-called D-A-CH region (Germany-Austria-Switzerland) have been involved. The basis for the accurately specified radioactive IMP manufacturing procedure was defined by EU-GMP requirements plus national standards (e.g. Medicinal Products Act and Radiation Protection Law). **Results:** For the recruiting study sites the required allowances, e.g. manufacturing authorization from local authorities as well as approval from ethics committees and national regulatory bodies such as BfS and BfArM in Germany, BASG in Austria as well as BAG and Swissmedic in Switzerland, have been obtained. The challenge of manufacturing a short-lived radiopharmaceutical at each of the participating geographically different sites with identical specification by adaption of production and quality control processes and parameters according to the IMP dossier (IMPD) during the starting phase of the clinical trial under a centralized quality assurance management has been achieved. **Conclusion:** The initiation and establishment of a multicentre clinical trial including the manufacturing of a short-lived radiopharmaceutical IMP across local study sites is very complex, but manageable. In view of the high European and national regulatory and legal burdens and the number of involved partners it is feasible in a defined time frame. Based on the achieved structures, the decentralized manufacture of novel short-lived radiopharmaceuticals can be established in the D-A-CH region and even on a European level for further investigator initiated multicentre clinical trials. We estimate our experiences important for the development of the field Nuclear Medicine at the national and international level taking into account the new EU regulation No 536/2014. **References:** None.

EP-0757

3D printing of SPECT phantoms using resin monomers radiolabeled in a one-pot process

L. Meier, *T. Läppchen, M. Fürstner, G. Prenosil, T. Krause, A. Rominger, B. Klaeser, M. Hentschel;*
Clinic of Nuclear Medicine, Inselspital, Bern University Hospital, University of Bern, Bern, SWITZERLAND.

Aim/Introduction: We aimed to develop a simple approach to 3D print radiolabeled phantoms. The clinical routine of PET and SPECT/CT is becoming increasingly important due to the possibility of determining tracer concentrations quantitatively. For multicenter clinical studies, scanners must be tested to allow comparability between diverse scanner types, or brands. Different phantom types are in use (Nema-, Jaszczak-, Derenzo-phantoms), requiring radioactive liquids filled into hollow phantoms. Recently, 3D printing technology has been introduced to print such phantom. An approach to use radiolabeled starting materials for 3D printers does not exist, yet [1]. Two general concepts of radiolabeling are applied to radiolabel molecules

either by covalently binding radioisotopes or using a chelator group to bind multivalent radioactive cations. Here, we followed a new one-pot approach of radiolabeling resin monomers in a phase transfer process: an aqueous solution of γ-emitter technecium-99m was mixed with hydrophobic 3D printer resin monomers, hydrophobic ligand additives were added and the water was chemically removed. Then, the phantom was printed with a standard SLA 3D printer. **Materials and Methods:** The following procedure was implemented: Pertechnetate solution was directly added to the resin monomer resulting a two-phase mixture. (A) A reducing agent also serving as a ligand was added to induce a phase transfer of the radiocation into the hydrophobic phase, (B) an anionic monomer amplified the phase transfer and (C) a chemical drying agent removed the residual aqueous phase. This radiolabeled starting material was directly used to print a radiolabeled phantom on a Projet1200 3D SLA printer. **Results:** A one-pot phase transfer procedure has been developed to radiolabel resin monomers by technecium-99m. A hydrophobic-hydrophilic balance of >100:1 was achieved as determined by a gamma counter (Wizard 2470). Radiolabeled 3D phantoms of different shapes (spheres, cylinders etc.) were printed. Homogenous distribution of the radioisotope in the polymer was confirmed by autoradiography and SPECT/CT of slices of a printed cylinder. Stable binding in the matrix was tested by washout cycles in ethanol at 50°C and in 0.1mol/l HCl overnight. No significant amount of radioactivity was washed out. **Conclusion:** 3D-printing of phantoms incorporating the radioisotope Tc-99m is feasible. When adapting the process to radiolabel longer living radioisotopes, the approach will enable reproducible quality control. **References:** [1] Filippou V. Med Phys 45, e740-760(2018).

EP-0758

Challenging The Validity Of Retrospective Sterility Testing

I. Koslowsky[1], *E. Schirrmacher*[2], *K. Logan Smith*[1];
[1]*Alberta Health Services, Calgary, AB, CANADA,*
[2]*University of Alberta, Edmonton, AB, CANADA.*

Aim/Introduction: Retrospective sterility testing has been part of the quality assurance program for radiopharmaceuticals for many years. The current approach is to let radiopharmaceuticals decay before sterility testing. Depending on the decay characteristics of the isotope, the sample may need to be retained for several months before it can be sent for testing: the applicability of the sterility test becomes questionable. The aim of this study was to determine whether microorganisms can sustain viability over time. **Materials and Methods:** The tests for sterility were performed using the &lt71&gt Sterility Tests methodology in the United States Pharmacopoeia. Growth promotion and method suitability studies were performed to confirm compatibility between the media, microbes, and products. Viability studies were performed using the following products: Tc99m-Medronate (MDP), FDG, and 10% Ethanol. Ethanol was selected, as it is a commonly used diluent in PET production; FDG and MDP are common imaging agents. Products were 'contaminated' with 30 or 90 cfus of 6 strains of organisms (3 aerobes, 1 anaerobe, 2 fungi). Aliquots were withdrawn at 30 hours, 4 days or 10 days for FDG and ethanol; and 4 days, 10 days, and 30 days for MDP. Fluid thioglycollate and tryptic soy broth media were inoculated, in triplicate, with the contaminated aliquots and incubated for 14 days at 30°C or at room temperature (20 to 25°C). Media were observed for growth at 5 days and 14 days. **Results:** Microorganisms were inconsistent in viability between products and time periods. Therefore microbes and replicates were pooled for each product (18 samples per time period per product). With FDG, 5 of 18 replicates exhibited growth at 30 hours with 3 of 18 replicates demonstrating growth at 10 days. Ethanol initially showed better sustainability (11 of 18 viable) at 30 hours; however only 1 replicate demonstrated growth at 4 days. MDP was more consistent in the type of microbes sustained and the length of time with 9 replicates growing at 4 days and 8 replicates sustained at 30 days. **Conclusion:** The current required method for testing sterility of radiopharmaceuticals is not sufficiently robust: there is reasonable risk in generating a false negative result. The number of false negative results in this study challenges the value retrospective sterility testing offers in a quality assurance program. Other techniques that establish and validate a sterile environment during production may bring more meaning to a quality assurance program. **References:** &lt71&gt Sterility Tests, USP41-NF36, 2018.

EP-0759

Time-lapse And Long-term Stability Of " RGD "lyophilized Kit

S. Lee, *S. Lo, S. Wang, S. Lo, S. Chen, M. Li;*
Institute of Nuclear Energy Research Atomic Energy Council, Taoyuan, TAIWAN.

Aim/Introduction: Integrin $\alpha_v\beta_3$ has been listed as an excellent candidate for cancer therapy, because of participate in tumor angiogenesis, and regulate the course and metastasis of cancer. Tripeptide RGD (Arg-Gly-Asp) is well known that can specific bind to integrin $\alpha_v\beta_3$, so many scientists have developed a cyclic pentapeptide (cRGDfK) for cancer drugs research. Previous study, we used this structure and combination with EB to develop a new tracer ^{111}In-DOTA-EB-cRGDfK with high affinity of albumin and $\alpha_v\beta_3$. NanoSPECT/CT image also confirmed that ^{111}In-DOTA-EB-cRGDfK had high accumulation amount at tumor site in MDA-MB-231 and 4T1 breast cancer animal model. Therefore, we development a DOTA-EB-cRGDfK lyophilized kit for ^{111}In labeled purpose. The aim of this study was to evaluate the time-lapse and long-term stability of lyophilized kit. **Materials and Methods:** The DOTA-EB-cRGDfK kit contents of the vial were lyophlized and sealed under nitrogen. This product is stored in the refrigerator at -20°C.Three batches of DOTA-EB-cRGDfK kit were inject 1~2mL of In-111 solution in 0.1N HCl (with 6~9 mCi). Shake vigorously, let the contents in the vial will be completely dissolved. Then, place the vial into a dry-heater for 15 minutes at 95°C.Let the vial stand for approximately 10

minutes, so it reaches room temperature. After preparation, the pH of the final products (^{111}In-DOTA-EB-cRGDfK injection) is 6~7. Final products are stand at room temperature for 0, 1, 2, 3, 4, 8, and 24 hours, the radiochemical purity of each time are analyzed by radio-high performance liquid chromatography. Three batches of DOTA-EB-cRGDfK lyophilized kit were taken out after 0, 1, 2, 3, 4, and 5 months after storage at -20°C. Then follow described above preparation methods to analyze the final products at that month. **Results:** The radiochemical purity of three batches of ^{111}In-DOTA-EB-cRGDfK radioactive products at the 0th, 1, 2, 3, 4, 8 and 24 hour was 97.9%±0.4, 98.0%±0.6, 98.0%±0.5, 97.8%±0.5, 97.7%±0.5, 97.6%±0.4 and 97.5%±0.5. The time-lapse stability results show that the ^{111}In-DOTA-EB-cRGDfK radioactive products had considerable stability within 24 hours. The radiochemical purity of ^{111}In-DOTA-EB-cRGDfK radioactive products that prepared from DOTA-EB-cRGDfK lyophilized kit can still >90% after 5 months. **Conclusion:** We demonstrated that the DOTA-EB-cRGDfK lyophilized kit have high degree of product stability, both in term of time-lapse and long-term analysis. The DOTA-EB-cRGDfK lyophilized kit can be more valuable in the marketing of breast cancer diagnostic drugs in the future. **References:** None.

EP-0760

Various Detection Techniques for ^{225}Ac

E. Arponen, T. Oikari, V. Haaslahti;
Hidex OY, Turku, FINLAND.

Aim/Introduction: Targeted alpha therapy (TAT) is a promising approach for treatment of cancer. The demand for suitable radioisotopes is strong. ^{225}Ac is an alpha particle emitting radionuclide with a 10 d half-life. ^{225}Ac yields several daughter radionuclides in its decay scheme and a net of four alpha particle emissions. The parent and the daughters are each individually lethal to cells. Recent studies of ^{225}Ac-PSMA617 for the therapy of metastatic castration-resistant prostate cancer have shown the clinical potential of targeted alpha therapy (1). The aim of this work is to study various detection techniques for quality control and radiation safety purposes of ^{225}Ac and its daughters. **Materials and Methods:** ^{225}Ac samples were measured with Hidex Triathler. Three different detection modes were applied in this study: liquid scintillation counting using alpha/beta separation electronics, high energy beta detection by solid plastic scintillator adapter and gamma detection by a well type NaI(Tl) crystal detector. In liquid scintillation counting, samples were mixed with AquaLight AB scintillation cocktail which provides optimal pulse length difference for separation of alpha emitters from beta emitters. With the plastic scintillator adapter and gamma detector samples were unharmed. **Results:** Triathler is a portable single-sample counter, which has a multichannel analyzer (MCA) and optional alpha/beta separation. The alpha decays can be clearly separated from the betas and yield a very low background as no natural alphas are present. Plastic scintillator adapter is sensitive to beta radiation and is only little affected by gamma background. The samples can be measured non-destructively in microtubes. The advantage of NaI(Tl) detector is that gamma spectrum shows also different gamma emitters. **Conclusion:** Triathler with alpha/beta separation and the plastic scintillator adapter is suitable for measuring ^{225}Ac and its daughters. Alpha/beta separation is however best suited to studying individual alpha and beta isotopes. The advantage of plastic scintillation adapter and gamma detector is that both liquid and solid samples such as TLC strips can be measured without the need for sample preparation. Further studies are planned for the development of detection methods for quality control purposes. Triathler can also be used as a wipe test counter to measure for possible radioactive contamination in laboratory areas. **References:** 1. Kratochwil C, Bruchertseifer F, Giesel F.L. et al. J Nucl Med 2016; 57:1941-1944.

EP-0761

Evaluation of ^{99m}Tc-tilmanocept retention in different syringes at different times

C. Franco Monterroso[1], B. Santos Montero[2], M. Hernández Fructuoso[2], E. Romero Herrera[1], S. Ruiz Llama[1], J. Castell Conesa[1];
[1]*University Hospital Vall d'Hebron, Barcelona, SPAIN,*
[2]*University Hospital Vall d'Hebron - IDI, Barcelona, SPAIN.*

Aim/Introduction: ^{99m}Tc-tilmanocept is a new radiopharmaceutical for imaging and intraoperative detection of sentinel lymph nodes. It has been widely reported that several radiopharmaceuticals are retained or adsorbed by plastic syringes to different extents. A high retention suggests a subsequent inadequate dosing (a lower administered dose) and can cause image quality problems (false negative) and even increase the cost. The aim of this study was to determine the ^{99m}Tc-tilmanocept retention percentage in the preparation vial after reconstitution and in different types of plastic syringes at different times. **Materials and Methods:** Six tilmanocept lyophilized vials (Lymphoseek®) were reconstituted with 222MBq of freshly eluted sodium pertechnetate in 0,7 ml sodium chloride 0,9%. 24 doses of 37MBq were dispensed: 12 doses in 1 ml Luer-Lock Chirana syringes (type A), and 12 in 1ml BD Plastipak™ syringe (type B). All dispensed doses were stored at room temperature (approximately 20-22 ºC).The activity in the syringes was measured immediately before and after simulated injections. The residual activity percentage in each syringe ((residual activity/initial activity) x100) was determined at t=0h, t=1h, t=2h and t=6h. The percentage of residual activity in labelled vials after dispensation was also evaluated ((residual activity/labelled activity) x100). A Capintec CRC-55tR dose calibrator was used to measure initial and residual activity. Results are reported as mean±SD for all samples. The level of significance was set at $P<0.05$ (Student's t-test). **Results:** The labelling efficiency of all vials used during this study were more than 98%.The percentage of residual activity in vials after doses dispensation was 8.40%± 2.56. The percentage of residual activity in type A syringes at t=0h, t=1h, t=2h and t=6h were 18.01% ±7.20, 19.71%±8.07, 22.32±4.08% and 39.95%±17.84 respectively.The percentage of residual activity in type B syringes

at t=0h, t=1h, t=2h and t=6h were 15.42%±8.59, 19.15%±9.64, 23.06%±10.65 and 31.91% ±12.25 respectively. There were not statistically significant differences between both types of syringes at all times: t=0h p=0.139, t=1h p=0.300, t=2h p=0.445, t=6h p=0.181. **Conclusion:** Both types of syringes show a high retention percentage, potentially causing underdosing and poor image quality. This retention is probably due to a mechanism of adsorption. We recommend the dispensation of 15-18% extra activity in every dose to compensate the retention and dispense doses immediately before injecting.The results show that measurement of retention in syringes should be regarded as an essential aspect of quality to assure the administered dose and avoid image quality problems. **References:** None.

EP-0762

Pharmacovigilance and Nuclear Medicine : French adverse event reports related to Radiopharmaceuticals

S. Langlet[1], *D. Pascal-Ortiz*[1], *D. Hillaire-Buys*[2], *I. Couret*[3]; [1]*Médecine nucléaire, Centre hospitalier, Perpignan, FRANCE,* [2]*Centre régional de pharmacovigilance, CHU Lapeyronie, Montpellier, FRANCE,* [3]*Médecine nucléaire, CHU Lapeyronie, Montpellier, FRANCE.*

Aim/Introduction: In nuclear medicine, the number of examinations is increasing (1.5 million in 2017 in France) and new radiopharmaceuticals (RP) become available. However, pharmacovigilance data remain scarce. The objective was to study RP-related adverse events (AE) reported in the French pharmacovigilance database since 1989. **Materials and Methods:** French pharmacovigilance reports involving the Anatomical Therapeutic Chemical classes V09 "Diagnostic RP" (DRP) and V10 "Therapeutic RP" (TRP) were screened from June 1989 to April 2018. 434 cases in which an RP was rated as unique "suspect" or "interaction" were identified and analysed. **Results:** Among the 434 cases, 150 (34%) were severe, including 13 deaths. DPRs were involved in 323 cases (74%), including (i) 264 cases (82%) of clinical and/or biological manifestations (CBM) among which 68 (25%) serious AE and 2 deaths, (ii) 43 cases (13%) of image alteration (IA), and (iii) 16 cases (5%) of medication errors (ME). Dermatologic (190, 41%) and general or injection-related (60, 13%) reactions were the most frequently reported CBM using DRPs, mainly ^{99m}Tc-HDP and ^{18}F-FDG. IA led to uninterpretable data in 34 cases (80%), mainly using ^{99m}Tc-DMSA, ^{18}F-FDG, and ^{99m}Tc-HDP. Several factors altering DRP biodistribution and responsible for IA were identified: (i) preparation (18/43, 42%), (ii) manufacture (7/43, 16%), (iii) injection (2/43, 5%), (iv) physiopathological factors (1/43, 2%), (v) prior treatment (1/43, 2%), and (vi) drug interactions (3/43, 7%). Concerning ME, a reversal of the DRP was identified in more than half of the cases. TRP were involved in 111 cases (26%) and concerned exclusively CBM, among which 68 (61%) serious AE and 10 deaths. ^{177}Lu-dotatate and ^{131}I-sodium iodide were the most frequently reported. CBM were mainly hematologic (64, 28%) (related to ^{177}Lu-dotatate), respiratory (40, 17%), and gastrointestinal (29, 13%). **Conclusion:** There is likely an important underreporting of RP-related AE given the low number of reports and the increasing number of examinations. CBM are less frequent but more serious in therapy than in functional imaging. Since preparation issues may impact RP biodistribution, pre-administration quality control should be performed as much as possible. Nuclear medicine teams need to be sensitized to RP-related AE notification, including IA and ME. **References:** None.

EP-0763

Patient-reported adverse events of diagnostic radiopharmaceuticals

N. Schreuder[1,2], *P. L. Jager*[3], *J. G. W. Kosterink*[1,4], *E. P. van Puijenbroek*[1,5]; [1]*University of Groningen, Groningen, NETHERLANDS,* [2]*GE Healthcare Radiopharmacy Zwolle, Zwolle, NETHERLANDS,* [3]*Isala Hospital, Zwolle, NETHERLANDS,* [4]*University Medical Center Groningen, Groningen, NETHERLANDS,* [5]*Netherlands Pharmacovigilance Centre Lareb, 's-Hertogenbosch, NETHERLANDS.*

Aim/Introduction: Adverse events (AEs) of radiopharmaceuticals can occur, but the reported frequency of 0.0023 - 0.011% is low [1,2]. However, this information originates from voluntary identification and reporting, which may decrease the rate. In addition, as there is usually no follow-up contact between the patient and the nuclear department, post-test adverse events may remain undetected. This study aims to investigate the type and frequency of adverse events of diagnostic radiopharmaceuticals as reported by patients within one week after administration. **Materials and Methods:** A validated questionnaire was used to collect data from patients undergoing a nuclear medicine procedure. We collected demographic data and analysed AEs occurring immediately after administration as well as those occurring later. Adverse events were analysed, coded and assessed for causality by two independent researchers. For the causality assessment, we used the Silberstein algorithm [2] that is specifically designed for AEs of radiopharmaceuticals. **Results:** In total, 1002 patients completed the questionnaire. A total of 186 patients (18.6%) reported a total of 379 AEs. Most reported AEs were general disorders, administration site conditions (42%), nervous system disorders (17%) and gastrointestinal disorders (9%). Most adverse events (80%) occurred shortly after administration of the radiopharmaceutical and 90% of those resolved without any sequelae within a median time of 15 minutes (IQR 2 - 120 min). However, 20% occurred later after the patient had left the nuclear medicine department. Of the reported AEs, 168 (99 patients) were determined to be possibly or probably related to the radiopharmaceutical. In the latter group, 113 AEs (68 patients) could probably also be attributed to the stress agent that is used with myocardial perfusion scans and were thus excluded from further calculations. AEs were mainly reported for most-used radiopharmaceuticals: Tc-99m oxidronic acid, F-18 fludeoxyglucose, and Tc-99m tetrofosmin. The overall frequency of patients experiencing adverse events

possibly or probably related to diagnostic radiopharmaceuticals was determined to be 2.72% (31/1002). **Conclusion:** Adverse reactions with diagnostic radiopharmaceuticals can occur, and the frequency as reported by patients was found to be 2.7% and higher than reported in the existing literature. **References:** (1) Hesslewood SR, Keeling DH. Frequency of adverse reactions to radiopharmaceuticals in Europe. Eur J Nucl Med 1997; 24:1179-1182. (2)Silberstein EB, Ryan J: Prevalence of adverse reactions in nuclear medicine: Pharmacopeia Committee of the Society of Nuclear Medicine. J Nucl Med 1996; 37:185-192.

EP-0764

In vitro analysis of ^{99m}Tc-EDDA/HYNIC-TOC bonding to blood clots and comparison with other radiopharmaceuticals

***M. Valiente**, M. Villar, F. Cepa, S. Rubi, B. Luna, H. Navalon, C. Medina, F. Vega;*
Hospital Universitario Son Espases, Palma, SPAIN.

Aim/Introduction: Unexpected small hot spots were found in scintigraphic planar lung images with 99mTc-EDDA/HYNIC-TOC performed in our department in 9 neuroendocrine tumor studies, which could lead to diagnostic errors. Quality controls for testing radiochemical purity resulted normal, and a problem with injection technique was thus suspected. Several previous publications refer to formation of small thrombi that would embolize pulmonary arterioles when blood is aspired into the syringe during venous puncture. In order to determine if blood clot bonding exists, we have tested ^{99m}Tc-EDDA/HYNIC-TOC in coagulated and anticoagulated blood samples and also other radiopharmaceuticals under identical conditions as control experiments to support our in-vitro analysis. **Materials and Methods:** Tested radiopharmaceuticals were ^{99m}Tc-EDDA/HYNIC-TOC, ^{99m}Tc-MIBI and sodium pertechnetate (^{99m}TcO4$^-$) eluted from a ^{99}Mo/^{99m}Tc generator. All radiopharmaceuticals labelling and quality controls were developed according to summary of product characteristics. Whole blood samples were extracted from healthy adults. An heparinized tube was used as anticoagulant for half of the extracted blood and 1ml samples of both anticoagulated and non-anticoagulated blood were collected and incubated at room temperature with 200µl of radiopharmaceutical with an activity of 3'7-24MBq during 30min. Total activity was measured and non-bound activity was washed twice with 3ml of saline by removing supernatant after centrifugation at 1000g during 10min. Finally, bound activity was measured in sediment of both clotted samples and blood cells (mainly RBCs) of anticoagulated samples. Activity measurements, corrected by background and radioactivity decay were determined using a dose calibrator. **Results:** Results showed low activity fraction of ^{99m}Tc-EDDA/HYNIC-TOC bound to blood clots (9'4±2'6%; n=22) with no statistical significance in relation to activity retained in anticoagulated samples (p>0.05). MIBI (29'3±6'9%;n=15) and TcO4$^-$ (31'5±12'3%;n=8) showed higher fraction of activity bound to blood clots evidencing also a significant increase over fraction bound to RBCs in anticoagulated samples (12'4±2%,n=16, for MIBI and 10'6±2'5%,n=8, for TcO4$^-$). **Conclusion:** We found no evidence of ^{99m}Tc-EDDA/HYNIC-TOC bond to clots in our in-vitro experiment. Other radiopharmaceuticals as ^{99m}Tc-MIBI and TcO4$^-$ revealed increase of retention in contact with clots possibly explained by non-specific trapping and also, in case of ^{99m}Tc-MIBI, by interaction with hydrophobic fibrin involved in coagulation process. Our results are consistent with the fact that ^{99m}Tc-EDDA/HYNIC-TOC is a peptide which does not diffuse through cell membrane nor does it have a specific transporter. Further evaluation with larger sample size and considering other factors could be developed to characterize those increased uptake foci on scintigraphic images. **References:** None.

EP-0765

Development and validation of a HPLC method to determine chemical purity and radiochemical purity of [^{68}Ga]-DOTA-Pentixafor (PET) tracer

***S. Migliari**, A. Sammartano, M. Scarlattei, G. Baldari, G. Serreli, C. Ghetti, L. Ruffini;*
AZ. OSP. Universitaria Di Parma, Parma, ITALY.

Aim/Introduction: Due to its overexpression in a variety of tumor types, the chemokine receptor 4 (CXCR4) represents a highly relevant diagnostic and therapeutic target in nuclear oncology. Recently, [68Ga]-DOTA-Pentixafor has emerged as an excellent imaging agent for positron emission tomography (PET) of CXCR4 expression in vivo. Preparation conditions may influence the quality and in vivo behaviour of this tracer and no standard procedure for the quality controls (QCs) is available. Aim of this study was to develop a new rapid and simple HPLC method of analysis for the routine QCs of [68Ga]-DOTA-Pentixafor to guarantee the high quality of the finished product before release. **Materials and Methods:** A stepwise approach was used, based on the quality by design (QbD) concept of the ICH Q2 (R1) and Q8 (Pharmaceutical Development) guidelines in accordance with the regulations and requirements of EANM, SNM, IAEA and WHO. The developed analytical test method was validated because a specific monograph in the Pharmacopoeia is not available for [68Ga]-DOTA-Pentixafor. **Results:** The purity and quality of the radiopharmaceutical obtained according to the proposed method resulted high enough to safely administrate it to patients. Excellent linearity was found between 0.5 and 4 µg/ml, with a correlation coefficient (R2) for calibration curves equal to 0.9995, the average coefficient of variation (CV%) resulted <2% (0.14%) and the average bias% value was 100.21%. **Conclusion:** The developed method to assess the radiochemical and chemical purity of [68Ga]-DOTA-Pentixafor is rapid, accurate and reproducible allowing routinely use of this PET tracer as diagnostic tool for imaging CXCR4 expression in vivo, also assuring patient safety. **References:** Migliari S, Sammartano A, Scarlattei M, Serreli G, Ghetti C, Cidda C, Baldari G, Ortenzia O, Ruffini L. Development and Validation of a High-Pressure Liquid Chromatography Method for the Determination of Chemical Purity and Radiochemical Purity of a [(68)Ga]-Labeled Glu-Urea-Lys(Ahx)-HBED-CC (Positron Emission Tomography) Tracer. ACS Omega. 2017.

EP-0766

Risk management in a radiopharmacy: implementation of a microbiological contamination program based on a risk-assessment

M. Riondato, S. Pastorino, G. Giovacchini, E. Borsò, A. Ciarmiello; Nuclear Medicine Department, La Spezia, ITALY.

Aim/Introduction: One of the main risk in a radiopharmacy is the loss or reduction of sterility assurance and the subsequent microbiological contamination of injectable preparations. Clean-room and hot-cell environments must be periodically monitored and European Pharmacopoeia and Eu-GMP, which are the main guidelines in this context, have been recently implemented towards the determination of the acceptable levels of risk to ensure an appropriate radiopharmaceutical (RPh) quality. A Quality System driven by risks represents a crucial advance in legislation, now placing its emphasis on prevention of incidents rather than cure.The aim of the study is to develop an appropriated sampling layout for our radiopharmacy using risk analysis and experimental approaches. Results will be evaluated in order to implement the routinely inspections, to justify the microbiological monitoring frequencies and to propose risk-reducing measures. **Materials and Methods:** The number of monitoring points for a pharma-grade area depends on the size of each isolated environment (UNI EN ISO 14644-1), while their locations are driven by the risk level of contamination for the product quality. Sampling point risk levels were assessed using the failure mode and effect analysis (FMEA) approach. Room surfaces and gloved fingertip and workbench sampling were monthly monitored with TSA Petri dishes, two times per day (begin and the end as the worst case). After sampling dishes were incubated at 25°C/35°C and the number of colony forming units (cfu) counted. Criteria for evaluation of the results was based on current legislation. **Results:** A selection of representative points was identified for each environment. Kind of manipulation, infrastructure aspects, routinely practice and adequacy of cleaning specified in our procedures were considered in the assessment, as well as 4 years of historical data. Low, Mid and High risk level of contamination were addressed for 46 potential sampling points. 19 spots with significant severity were identified and the microbiological contamination tested at rest and in operation, both for bacteria and fungi growth. Clean-rooms respected the environmental requirements. Results for hot-cells were satisfactory, however 2 of the 5 isolators showed a slight deviation (gloved fingerprints at the end of the day) from the imposed criteria, probably due to the high frequency of entrance of disposable materials. **Conclusion:** The radiopharmacy has achieved compliance to guidelines implementing the microbiological contamination control program using a risk-assessment approach, confirming the 6 months monitoring frequency. Due to experimental evidence, the cleaning and disinfecting procedures applied to isolators have been implemented. **References:** None.

EP-55
Preclinical and translational aspects, including radiopharmacy, radiochemistry and drug development -> Radiopharmacy, radiochemistry, drug development -> Radiopharmacy -> Radiopharmaceuticals - PET

October 12 - 16, 2019

e-Poster Area

EP-0767

Application of production and quality control procedures of 18F-PSMA-1007: dominant in diagnosis of prostate cancer, through Synthera V2

***R. Shukurov**, M. Balashov, Z. Dadashov, M. Valiyev, E. Mehdi, F. Novruzov;*
Department of Nuclear Medicine, National Centre of Oncology, Baku, AZERBAIJAN.

Aim/Introduction: 68Ga-PSMA-11 is one of the tracer that successfully used in diagnosis of prostate cancer. However the limitation such as short half-life and radioactivity amount of 68Ga, getting from Ge-68\Ga-68 generators motivate scientist to develop new radiotracers for diagnosis of prostate cancer. 18F-PSMA-1007 is an attractive alternative to 68Ga-PSMA-11 and 18F-DCFPyL. Here in we presented synthesis of 18F-PSMA-1007 and quality control of this final product in vast quantities per batch, 18F-PSMA minimizes the need for daily multiple tracer syntheses and allows transfer to satellite centers. **Materials and Methods:** Fluorine produced in cyclotron was trapped in QMA cartridge (Synthera V2 module, IBA). Consequently, trapped 18F is eluted using TBA-HCO3. Drying was accomplished by azeotropic distillation using acetonitrile. After drying processes were over, labelling took place by adding precursor to the reaction vial. Solution were purified from chemical and radiochemical impurities by running through on C18 cartridge several times. The product was subsequently eluted with 30% EtOH, then passed through SCX cartridge. The main activity transferred to final product vial which obtained the phosphate buffered solution. 18F-PSMA radiochemical purity analyses are determined by HPLC and TLC methods. 18F-PSMA-1007 reference standard (ABX, Germany) was solved with 1ml ultra-pure water. The HPLC analyses were performed on C18 (4.6x250mm) column. The HPLC mobile phase was a mixture of acetonitrile/water/0.1% trifluoroacetic acid (TFA) (30:70:0.1) (Rf-7.5-8.0). Mobile phase for TLC analysis was acetonitrile/ water (60:40) mixture. **Results:** Yield of 18F-PSMA-1007 was 40%. Unlike HPLC analysis obtained by gradients for 18F-PSMA, in this HPLC analysis method suitable result was obtained by using isocratic solution. **Conclusion:** The radiochemical purity analysis with HPLC method has been improved and it makes possibility doing analysis without gradient pump. The chromatographic results which obtained from the standard and final product using isocratic buffer solution confirm reliability of this method. **References:** 1. Cardinale J1, Martin R2, Remde Y3, Schäfer M4,

Hienzsch A5, Hübner S6, Zerges AM7, Marx H8, Hesse R9, Weber K10, Smits R11, Hoepping A12, Müller M13, Neels OC14,15, Kopka K16,17. Procedures for the GMP-Compliant Production and Quality Control of [18F]PSMA-1007: A Next Generation Radiofluorinated Tracer for the Detection of Prostate Cancer. Pharmaceuticals (Basel). 2017 Sep 27;10(4)2. Kambiz Rahbar,1 Ali Afshar-Oromieh,2,3 Robert Seifert,1 Stefan Wagner,1 Michael Schäfers,1 Martin Bögemann,4and Matthias Weckesser1 / Diagnostic performance of 18F-PSMA-1007 PET/CT in patients with biochemical recurrent prostate cancer / Eur J Nucl Med Mol Imaging. 2018; 45(12): 2055-2061.

EP-0768

Simultaneous production 18F-FDG and other 18F based (18F-NaF, 18F-FES, 18F-PSMA 1007, 18F-FET) radiopharmaceutical drug by a single run of medical cyclotron

Z. Dadashov, M. Valiyev, R. Shukurov, M. Balashov, F. Novruzov; Department of Nuclear Medicine, National Centre of Oncology, Baku, AZERBAIJAN.

Aim/Introduction: 18F-FDG is currently the most common used PET radiopharmaceutical in clinical oncology. Another Fluorine-18 based radiopharmaceuticals (NaF, FES, 18F-FET and F-PSMA) were popular for diagnostic methods using PET/CT in last few years. The objective of this study was to establish an easy, convenient and simultaneous production method for 18 Fluoride based molecules during routine synthesis of 18F-FDG production by using single run of cyclotron. **Materials and Methods:** The main core of this method to arrange level of F-18 input line into the V-vial. It can be clearly seen that, the amount of F-18 into V-vial. In general, 2.2 ml of transferred activity of radioactive fluorine from cyclotron collected inside V-vial.The first stage of production: 1.5 ml F-18 activity will be directly extract from the V-vial by the first synthesis module (SYNTHERA-A, IBA) for FDG synthesis; the second stage of production: 0.7 ml F-18 activity will be extract by second synthesis module (SYNTHERA-B, IBA) for NaF, FES or F-PSMA production. If there are several available synthesis modules in facility it should be possible to get several 18F-Fluorine based radiopharmaceuticals drug by single irradiation of enriched water by the cyclotron. The input line can be moved to any position in V-vial based on the required activity. The very important point of this procedure are to adjust the estimated bulk and properly arrange the F-18 input lines going to the different synthesis modules. **Results:** With this method, both synthesis processes can be performed simultaneously without any radiation exposure and it is possible to send the both product safely to the dispensing system. The process ends without any loss of activity. **Conclusion:** This is very appropriate and financially efficient method. To avoid cross contamination it should be better to make a separate dispensing system. In this method without using extra enriched water to get two radiopharmaceutical drugs and also saving production time. **References:** None.

EP-0769

^{89}Zr labelled nanoparticle coating with biotin inserted cell membrane as a biomaterial for enhancing long-term circulation and tumor targeting

***J. Lee**, P. Choi, M. Hur, S. Yang, Y. Kong, E. Lee, H. Song, J. Park; Korea Atomic Energy Research Institute, Jeollabuk-do Jeongeup-si, KOREA, REPUBLIC OF.*

Aim/Introduction: The final goal of nanomedicine is blood long-term circulation and effective drug delivery for diagnosis and treatment of various diseases. However, phagocytosis by macrophages is a critical issue indeed for delivering the drug to the target site. In order to solve this problem, camouflaged nanoparticles used with the natural erythrocyte membrane (Em). These cell membrane can overcome the immune barriers because CD47 proteins on Em are recognized by SIRP-alpha receptor of macrophage as a"Don't eat me" signal. In addition, biotin receptor s are overexpressed in many cancer cells, leukemia, ovarian, colon, mastocytoma, lung, renal and breast cancer cell lins[1]. Accordingly, we inserted biotin as the tumor active targeting ligands on Em surface. Their synergistic strategy is to enable long-term circulation and tumor targeting. **Materials and Methods:** Synthesized hollow mesoporous silica nanosphere (HMSN) was dispersed in a HEPES buffer (pH 7.5) at various concentrations. Zirconium-89 (^{89}Zr) has been incorporated with an advantageous half-life ($t_{1/2}$: 3.3 days) for long-term tracking of nanoparticles. The pH of ^{89}Zr-oxalate or chloride (~20 MBq) was adjusted to pH 7.5–8. After stirring with HMSN and ^{89}Zr at room-temperature for 24 hours, labeling efficiency was confirmed by radio-iTLC using 50 mM DTPA as the mobile phase. Em of the mice was isolated by a modified cell membrane extrusion method[2]. Biotin-DSPE-PEG was inserted on Em surface for tumor active targeting. Finally, Biotin-Em (BE) and ^{89}Zr labelled HMSN were co-extruded using mini-extruder. **Results:** BE camouflaged HMSN was successfully synthesized and characterized for in vivo long-term behavior and tumor active targeting. ^{89}Zr was incorporated under the mild condition with labeling efficiency of >96% on the silanol group of HMSNs by chelator free method[3]. After BE coating, the release of ^{89}Zr was decreased for long-term tracking. That means BE-^{89}Zr-HMSN can be used for the candidate of long-term tracking. Compared to the 89Zr-HMSN and Em-^{89}Zr-HMSN, BE-^{89}Zr-HMSN was accumulated effectively and rapidly in the tumor site. **Conclusion:** Having distinguished potentials viz. non-release of ^{89}Zr, long-term circulation and effective tumor targeting ability in biological systems this strategy can be applied extensively to identify the long-term in vivo behavior and tumor targeting of nanomedicine while enhancing their biocompatibility. **References:** [1] Russell-Jones G et al., Australia: Access Pharmaceuticals Australia Pty. Ltd; 2004. PCT WO2004/045647. [2] Xiaoqing R et al., Biomaterials; 2016, 92, 13-24. [3] Shreya G et al., Advanced science; 2016, 3, 1600122.

EP-0770

Fully Automated Radio Synthesis Of [18F]MK-6240 For Clinical Use

J. Toyohara[1], *T. Tago*[1], *K. Nishino*[1,2], *M. Sakai*[1,2], *K. Ishii*[1];
[1]*Tokyo Metropolitan Institute of Gerontology, Itabashi-ku, Tokyo, JAPAN,* [2]*SHI Accelerator Service, Shinagawa-ku, Tokyo, JAPAN.*

Aim/Introduction: Fluorine-18 labeled 6-(fluoro)-3-(1H-pyrrolo[2,3-c]pyridine-1-yl)isoquinolin-5-amine ([18F]MK-6240) is a second generation selective PET radiopharmaceuticals for detecting human neurofibrillary tangles, which are made up of aggregated tau protein. Herein, we report the fully automated two-step, one-pot radiosynthesis of [18F]MK-6240 using a commercially available radiosynthesis module, SHI CFN-MPS200 and its validation for clinical use. **Materials and Methods:** The cassette for [18F]MK-6240 synthesis was designed with compact and efficient routing, and the programs were developed to control the synthesis. Nucleophilic fluorination of the 5-di-Boc-6-Nitro precursor NGMA-239 with [18F]KF/K.222 complex was carried out using a stepped gradient temperature protocol [1], followed by acid deprotection, neutralization, SPE pre-purification [2] and semi-preparative HPLC (eluent: 425/20/500 ethanol/0.5M sodium phosphate corrective injection/water for injection). The radioactive fraction was collected, diluted with sterile saline and sterile filtered into a pyrogen-free collection vial as an ethanol containing saline solution. Three consecutive batches of [18F]MK-6240 were produced and all quality control tests were performed on the final product: appearance, radionuclide identity, radiochemical purity, chemical purity, molar activity, pH, shelf-life for 8 hours, residual solvents, filter integrity, sterility and bacterial endotoxins were analyzed. **Results:** The total synthesis time was within 90 min form the end of bombardment. Decay-corrected radiochemical yields were 7.5-14.1% based on formulated product (1750-3810 MBq). The radiochemical purity was ≥98% at end of synthesis and the product could be stored for 8 hours without too much radiolysis (radiochemical purity remained >97%). The use of SPE pre-purification and the preparative HPLC purification resulted in pure, sterile product with barely detectable levels of residual solvents, and extremely low levels of total chemical impurities (<0.3 µg/mL) and bacterial endotoxins (<0.1 EU/mL). Using the fluoride-free materials composed cassette such as silicon tube and polypropylene connectors, resulted in high molar activity (943-1541 GBq/µmol at the end of synthesis) of the product. Three consecutive productions of [18F]MK-6240 complied with the product specifications and process was confirmed to be appropriate for the production of [18F]MK-6240. Formulated [18F]MK-6240 maintained radiochemical purity, chemical purity, molar activity (≥37 GBq/µmol), as well as clarity and a pH over a period of 8 hours. **Conclusion:** [18F]MK-6240 was validated for clinical use with a SHI CFN-MPS200 radiosynthesis module. The methodology described herein can facilitate multi-center trials and widespread use of this radiopharmaceutical for imaging tau protein in vivo. **References:** [1] Collier TL, et al, J Label Compd Radiopharm 2017; 60:263-269. [2] Mulligam RS, et al, WFNMB2018 abstract, 20-24 April 2018, Melbourne.

EP-0771

[18F]FPEB is a substrate for Pgp and Bcrp in the rodent brain

J. Choi, *K. Jung, S. Oh, K. Kang, S. Han, K. Nam, K. Lee, Y. Lee;*
Korea Institute of Radiological and Medical Sciences, Seoul, KOREA, REPUBLIC OF.

Aim/Introduction: [18F]-3-fluoro-5-[(pyridin-3-yl)ethynyl] benzonitrile ([18F]FPEB) is a specific PET radiotracer for the metabotropic glutamate receptor 5 (mGluR5). Although its biological effectiveness were validated in the preclinical and clinical trials, the effect of efflux transporters on the brain uptakes of [18F]FPEB has not been reported. Therefore, the purpose of the present study is to determine whether the brain uptakes of [18F]FPEB is influenced by efflux transporters (i.e. P-gp and/or Bcrp) in the rodent **Materials and Methods:** Male Sprague-Dawley (260-300 g, n=5 for each group) rats were used. Male FVB (wild-type), Mdr1a/b$^{(-/-)}$, Bcrp1$^{(-/-)}$ and Mdr1a/b$^{(-/-)}$Bcrp1$^{(-/-)}$ genetic background were used (n=4 for each group). After animals were anesthetized, catheters were inserted into the tail veins. For mice, [18F]FPEB (7.4- 9.2 MBq) was injected to the tail vein. For rats, tariquidar (6 mg/kg) was bolusly injected to inhibit P-gp activity, followed by administration of [18F]FPEB (14.8-16.6 MBq). For attenuation correction, micro-CT imaging was conducted. Cortex, hippocampus, striatum and cerebellum were defined as volumes of interests. The obtained uptake value was represented as the standardized uptake value (SUV). **Results:** In the pharmacological inhibition model, P-gp blocked group with tariquidar showed 8 to 12% increase in the brain uptake compared with the control group. In the genetic ablation models, P-gp knockout mice such as Mdr1a/b(–/–) and Mdr1a/b(–/–)Bcrp1(–/–) there was a 8 ~ 53% increase in [18F]FPEB uptake compared with that in the wild-type mice. In contrast Bcrp knockout mice showed a decrement of 5 ~ 12% uptake and P-gp/Bcrp knockout group displayed an increment of 5 ~ 17% compared with wild-type. **Conclusion:** [18F]FPEB is a substrate of P-gp and Bcrp, where it is more affected by P-gp. **References:** 1. Hamill, T. G., Krause, S., Ryan, C., Bonnefous, C., Govek, S., Seiders, T. J. O. N., ... Burns, H. D. Synthesis , Characterization , and First Successful Monkey Imaging Studies of Metabotropic Glutamate Receptor Subtype 5 (mGluR5) PET Radiotracers. Synapse 2005;216; 205-216.2. Wang, J.; Tueckmantel, W.; Zhu, A.; Pellegrino, D.; Brownell, A. Synthesis and Preliminary Biological Evaluation of 3- [18F] Fluoro-5-(2-Pyridinylethynyl) Benzonitrile as a PET Radiotracer for Imaging Metabotropic Glutamate Receptor Subtype 5. Synapse 2005, 961, 951-961.

EP-0772

Non-invasive whole-body imaging of immune checkpoints using PET-labeled small molecules as predictive biomarker for response to therapy

M. Wazynska[1], *R. Butera*[2], *M. de Bruyn*[1], *A. S. S. Domling*[2], *P. H. Elsinga*[1], *H. W. Nijman*[1];
[1]*University of Groningen, University Medical Center Groningen,*

Groningen, NETHERLANDS, [2]University of Groningen, Faculty of Science and Engineering, Groningen, NETHERLANDS.

Aim/Introduction: PD1/PD-L1 blockade have transformed the landscape of oncology with unprecedented long term disease remission, and even cure in hard-to-treat cancers. Nevertheless, PD1/PD-L1 inhibitors are only effective in a subset of patients and predictive biomarkers for treatment efficacy are urgently needed. Positron-emission tomography (PET) is exquisitely suited as a biomarker as it offers an excellent sensitivity, high spatial resolution and can overcome the obstacles such as tumor heterogeneity, sampling errors and dynamic changes in checkpoint expression. Moreover, development of small molecule PD1/PD-L1 PET tracers would be highly beneficial, since available PD1/PD-L1 antibody based PET tracers are characterized by long biodistribution time, higher radioactivity burden, lower permeability and high production cost. **Materials and Methods:** We developed a potent class of small molecule PD-L1 antagonists based on PD1/PD-L1 blockade disruption bioassay, as well as NMR-based fragment screening approach to achieve high affinity, selectivity for PDL1, good stability and solubility. The lead compound was further modified to allow radiolabeling. Modifications included methylation and aromatic fluorine substitution. Synthesis of cold reference compounds and their precursors, PET-labelling, HPLC purification and formulation allowed to test selected tracer ([^{11}C]RB66, [^{18}F]RB67) in biological system. For binding experiments CHO.PD-L1, CHO.PD1, H292 and H358 cell lines were chosen. CHO cell lines were transfected with PD-L1 protein and PD1 (negative control). H292 and H358 were cancer cell lines with endogenous expression of PD-L1 (low and intermediate expression of PD-L1 respectively). H358 cell line was engineered into PD-L1 knock out using CRISPR/Cas9 technique. **Results:** Successfully synthesized PET-tracers did not exhibit significant binding towards CHO.PD1 and CHO.PD-L1. Testing [^{18}F]RB67 with H292 and H358 has shown no binding to negative control (H292) and a significant uptake in PD-L1 expressing cell line (H358). To further investigate the nature of this binding, [^{18}F]RB67 was tested on H358 PD-L1 knock out cell line and H358 PDL1 wild type cell line in condition allowing internalization (37 °C incubation) and other preventing it (4°C). Experiments has shown significant cell uptake at 37 °C, no binding to knock out cell line and cell line at 4°C. **Conclusion:** Results suggest that there is high binding of [^{18}F]RB67 to H358 PD-L1 expressing cells, no significant off-target binding and internalization is the main way for tracer uptake, however further investigation to fully confirm stated hypothesis is needed to be able to proceed with in vivo model. **References:** None.

EP-0773

Effective Surface Modification of the Zr-89 labeled Iron Oxide Nanocluster and tracking Biological Behavior for Tumor Xenograft Mouse Model

***P. Choi**, J. Lee, Y. Gong, E. Lee, S. Yang, H. Song, M. Hur, J. Park;*
Korea Atomic Energy Research Institute, Jeongeup, KOREA, REPUBLIC OF.

Aim/Introduction: Nanoparticles having the properties to target cancer cells by Enhanced Permeability and Retention (EPR) effect are used to study in vivo behavior and track their pharmacokinetics by zirconium-89 due to relatively long half-life. It is important to understand or to examine how surface properties of the nanoparticles affect the in vivo behavior. In this study, we select three of biocompatible coating materials which are easily coated on iron oxide nanoparticles and clearly unknown for its in vivo behavior such as polyethyleneimine (PEI), polyvinylpyrrolidone (PVP) and bovine serum albumin (BSA). After the surface modification, we could confirm what the coating materials are expected to help tumor target through measuring PET. **Materials and Methods:** Firstly, we synthesized the ^{89}Zr labelled iron oxide nanocluster (^{89}Zr-IONCs) by hydrothermal direct-labeling synthetic method. In order to change the surface properties of ^{89}Zr-IONCs for improvement of colloidal stability in biological environments and effective tumor target, the surface of ^{89}Zr-IONCs was coated by PEI, PVP and BSA through electrostatic interaction and hydrogen-bonding, respectably. Characterization for the surface coating was confirmed by DLS/Zeta-potential equipment. To examine biological behavior of each surface coated ^{89}Zr-IONCs, we performed colloidal stability experiment, cellular uptake and measurements of PET images for CT-26 tumor xenograft mouse. **Results:** The colloidal stability in biological medium such as PBS (pH 7.4), DMEM and serum was significantly high for 24 h after completion of all surface modification while non-coated ^{89}Zr-IONCs was shown to tend to aggregate in the solution (>600 nm). The surface charge of ^{89}Zr-IONCs was changed depend on the coating materials (^{89}Zr-IONCs@PEI : +18 mV, ^{89}Zr-IONCs@PVP : +0.12 mV, ^{89}Zr-IONCs@BSA : -32 mV) which affect for in vivo behavior after intravenous injection. Utilizing measurements of PET images, PVP and BSA coated ^{89}Zr-IONCs was rapidly reached in tumor site and continuously increased until 24 h. In contrast, no tumor uptake was shown for PEI coated ^{89}Zr-IONCs and bared ^{89}Zr-IONCs. Another one important thing is that liver uptake of ^{89}Zr-IONCs@PVP drastically decreased after 2 h of i.v. injection. **Conclusion:** Neutral or negative surface charge and higher colloidal stability of the nanoparticles was effective for tumor uptake rather than the other. Especially, PVP coating is expected to target cancer cells in the field of nanomedicine that was confirmed by PET images using Zr-89. **References:** None.

EP-0774

Development of novel ^{68}Ga-Labeledlong noncoding RNA MALAT1 probes for in vivo tumour imaging

***M. Dong**[1], Z. Liu[1], M. Yang[2], Y. Xu[2], D. Pan[2], G. Wang[1], T. Hu[1];*
[1]The First Affiliated Hospital, College of Medicine, Zhejiang University, Hangzhou, CHINA, [2]Jiangsu Institute of Nuclear Medicine, Wuxi, CHINA.

Aim/Introduction: With the advent of next-generation sequencing technology, there is rapidly increasing interest in long noncoding RNAs (lncRNAs). The objectives of this study were to develop a novel ^{68}Ga-Labeled long noncoding RNA

MALAT1 probes to evaluate the characteristics of the imaging probe in vitro and to determine whether it can be used for imaging MALAT1 expression in malignant tumours. **Materials and Methods:** ^{68}Ga- MALAT1 ASO positron molecular probes were prepared in a one-step protocol starting from the precursor (NOTA-chelated oligonucleotides).The new ^{68}Ga- MALAT1 ASO binding to PBS solution and to human plasma proteins was examined by means of ultrafiltration. The biodistribution and biokinetics were evaluated in vivo in normal rats and athymic rat bearing HCC-LM3 tumor. Dynamic micro-PET imaging lasting up to 480min was performed immediately after intravenous injection of ^{68}Ga- MALAT1 ASO positron molecular probes. Blank studies were performed using ^{68}Ga-DOTA alone without oligonucleotide. The ^{68}Ga-antisense oligonucleotide uptake in tumors was also compared with ^{68}Ga-sense oligonucleotide uptakes. **Materials and Methods:** ^{68}Ga- MALAT1 ASO positron molecular probes were prepared in a one-step protocol starting from the precursor (NOTA-chelated oligonucleotides).The new ^{68}Ga- MALAT1 ASO binding to PBS solution and to human plasma proteins was examined by means of ultrafiltration. The biodistribution and biokinetics were evaluated in vivo in normal rats and athymic rat bearing HCC-LM3 tumor. Dynamic micro-PET imaging lasting up to 480min was performed immediately after intravenous injection of ^{68}Ga-MALAT1 ASO positron molecular probes. Blank studies were performed using ^{68}Ga-DOTA alone without oligonucleotide. The ^{68}Ga-antisense oligonucleotide uptake in tumors was also compared with ^{68}Ga-sense oligonucleotide uptakes. **Results:** The average radiochemical yields of ^{68}Ga- MALAT1 ASO was 50% (not corrected for radioactive decay) ranging 15 to 20min, and radiochemical purity was large than 98%. Intravenously injected ^{68}Ga- MALAT1 ASO positron molecular probes revealed high-quality PET images, allowing quantification of the biokinetics in major organs and in tumors. The biodistribution and biokinetics of intravenously administered ^{68}Ga- MALAT1 ASO positron molecular probes showed high uptake in the tumor tissues (3.04±0.11%ID/g, 2.04±0.04%ID/g at 30min, 60min respectively). Tumor/blood and tumor/muscle odds were 8.47±0.02, 8.1725±0.12 respectively at 60min after intravenously injected 100 uCi ^{68}Ga-MALAT1 ASO positron molecular probes. **Conclusion:** Our results provide evidence that ^{68}Ga-MALAT1 ASO is a convenient approach, and these novel probes can serve as novel specific molecular probes for in vivo imaging of tumour expressing MALAT1. **References:** None.

EP-0775

Development of novel [^{18}F]thiosemicarbazone metal fluoride complexes as potential neuroimaging agents

D. Stimson[1], *T. K. Venkatachalam*[1], *G. K. Pierens*[1], *P. V. Bernhardt*[2], *K. Mardon*[3], *D. C. Reutens*[1], *R. Bhalla*[1];
[1]*Centre for Advanced Imaging, University of Queensland, Brisbane, AUSTRALIA,* [2]*School of Chemistry and Molecular Biosciences, University of Queensland, Brisbane, AUSTRALIA,* [3]*National Imaging Facility, University of Queensland, Brisbane, AUSTRALIA.*

Aim/Introduction: The SPECT imaging agent [^{99m}Tc]HMPAO (Ceretec) is both neutral and lipophilic[1] (logP of 1.9) enabling blood brain barrier (BBB) permeability. Labelling strategies utilising stable metal-^{18}F bonds have been reported,[2,3] however these metal-^{18}F complexes are hydrophilic and will unlikely cross the BBB. Our interest is to develop ^{18}F-labelled agents with comparable properties to Ceretec as potential neuroimaging agents for PET. **Materials and Methods:** A series of structurally related indium chlorido complexes of bis-thiosemicarbazones were prepared, starting from the appropriately substituted bis-thiosemicarbazones[4]. Aliphatic groups were introduced into the structure to reduce the liphophilicity of the molecule. Fluoride was introduced into the coordination sphere using a halogen exchange strategy by replacement of chloride with nitrate (using $AgNO_3$) then treating the nitrato complex with potassium fluoride. Radiolabelling with fluorine-18 was achieved using a similar approach. Similarly, gallium chlorido complexes of bis-thiosemicarbazones were prepared and converted to their corresponding nitrate complexes before radiolabelling with fluorine-18. Complexes of both the indium and gallium compounds were characterised with NMR and X-ray crystallography[5,6]. Lipophilicity of gallium-fluoride complexes was assessed by measuring the octanol/water partition coefficient. Imaging studies of [^{18}F]diphenylthiosemicarbazone gallium fluoride in mice were performed using preclinical PET/CT. **Results:** The measured logP of [^{19}F]diphenylthiosemicarbazone gallium fluoride is 1. Imaging studies in mice with PET indicate that the [^{18}F]diphenylthiosemicarbazone gallium fluoride is stable in vivo and showed rapid uptake of the complex in the brain. **Conclusion:** To our knowledge, we have synthesised the first indium-^{18}F complex and report the first Ga-^{18}F complex studied in vivo. Our work highlights the potential of using ^{18}F-labelled indium and gallium fluoride compounds for neuroimaging with PET. **References:** 1. Moretti J, Caglar M, Weinmann P, J Nucl Med, 1995; 36:359-363. 2. McBride W, Sharkey R, Goldenberg D, EJNMMI Research 2013; 3:36. 3. Bhalla R, Darby C, Levason W, Luthra S, McRobbie G, Reid G, Sanderson G, Zhang W, Chem Sci, 2014; 5:381. 4. Venkatachalam T, Bernhardt P, Pierens G, Stimson D, Bhalla R, Reutens D, Aust J Chem. 2019 (online early). 5. Venkatachalam T, Pierens G, Bernhardt P, Stimson D, Bhalla R, Lambert L, Reutens D, Aust J Chem. 2016; 69 (9). 6. Venkatachalam T, Bernhardt P, Stimson D, Pierens G, Bhalla R, Reutens D, Aust J Chem. 2017; 71 (3).

EP-0776

Establishing a GMP-compliant 89-Zirconium radiopharmaceutical production capability at the Royal Marsden Hospital Foundation Trust, UK

J. Tan[1], *C. Da Pieve*[2], *G. Smith*[2], *D. Turton*[2], *W. J. G. Oyen*[2];
[1]*Royal Marsden Hospital Foundation Trust (RMH), Sutton, UNITED KINGDOM,* [2]*Institute of Cancer Research (ICR), London, UNITED KINGDOM.*

Aim/Introduction: Owing to their high target affinity and specificity, radiolabelled antibodies have been extensively

investigated for the imaging of receptor expression in tumours. The long-lived positron emitter zirconium-89 has a half-life ($t_{1/2}$ = 78.4 hrs) compatible with the biological half-life of antibodies (mAbs). Positron Emission Tomography (PET) with zirconium-89-mAbs showed great potential to provide information about tumour targeting/target expression, and is a promising tool for personalized medicine and for accelerating/improving drug development. Although zirconium-89-mAbs have been prepared and clinically used for more than a decade in countries such as The Netherlands and USA, the stringent regulatory environment in the UK has delayed the GMP-compliant production of such radioimmunoconjugates. Herein we summarise the implementation of the general process described by Vosjan et al.[1] for the GMP-compliant preparation of mAb conjugates and their radiolabelling at the Royal Marsden Hospital (RMH) NHS Foundation Trust, UK. **Materials and Methods:** The production of a zirconium-89-mAb consists of two main phases: the preparation of the DFO-mAb conjugate and subsequent radiolabelling. Each phase, requiring extensive manual manipulations, was developed using the available infrastructure and services at RMH and the ICR, UK. Both processes were entirely carried out in a Grade A environment using commercially available mAbs. Risk assessments were produced when ready-to-use reagent or buffers were not available. Quality control, characterisation and quantification of the products were performed either at RMH Radiopharmacy and ICR expert laboratories, or external specialists. Zirconium-89 was purchased from BV Cyclotron VU, NL. **Results:** Although most of the processes followed standard radiopharmaceutical preparation techniques, some non-standard procedures required particular attention: PD10 desalting columns were tested to determine the removal of the storage germicide, and the content of oxalate/HEPES in the final product. UV-Vis measurements demonstrated germicidal removal according to manufacturer-suggested protocol. Ion-exchange HPLC was a reliable technique for the quantification of oxalate and HEPES levels. Facilities at the ICR were suitable for DFO-to-mAb ratio determination by ESI-MS, mAb quantification by UV, and Lindmo assay. RMH facilities were used for sterility and endotoxin determination, filter-integrity testing, and QC analysis by ITLC and SEC-HPLC. **Conclusion:** Our goal is to establish the RMH and ICR as a UK centre of excellence for the development and production of GMP-compliant zirconium-89-mAbs. The RMH-ICR team has already investigated the applicability of crucial steps with the objective of positive engagement with local regulators in the near future. **References:** 1. Vosjan MJWD et al. Nat. Protoc. 2010, 5, 739 ADDIN EN.REFLIST.

EP-0777

^{18}F-Labeled PET Tracers Derived from Angiotensin II type 1 Receptor Antagonists

X. Chen[1], *M. Hoffmann*[2], *R. A. Werner*[1], *K. Arimitsu*[3], *H. Kimura*[3], *M. Decker*[2], *T. Higuchi*[1];
[1]*University Hospital of Würzburg, Würzburg, GERMANY,*
[2]*Julius Maximilian University Würzburg, Würzburg, GERMANY,*
[3]*Kyoto Pharmaceutical University, Kyoto, JAPAN.*

Aim/Introduction: Angiotensin II type 1 receptors (AT_1R) are involved in various diseases progress as well as the therapeutic applications, such as hypertension, heart failure, nephropathy and inflammation. ^{18}F&#8211labelled radiotracers derived from clinically used AT_1R antagonists using positron emission tomography (PET) technology can reflect the functionality of the renin&#8211angiotensin system by monitoring the pathophysiological distribution and alteration of AT_1R. **Materials and Methods:** By studying the structure&#8211activity relationship, fluorine was introduced to different positions of the aliphatic side chain of valsartan and irbesartan. Precursors and the corresponding cold references have been synthesized and evaluated in CHO&#8211K1 cell lines expressing human AT_1R. After successful radiolabeling, biodistribution and blocking studies were performed in rats and pigs. **Results:** The fluorine derivatives of valsartan and irbesartan showed almost identical IC_{50} values at AT_1R, 14.6 and 6.6 nM, respectively, as compared to their leads, 11.8 and 1.6 nM, respectively, as well as Angiotensin II 2.0 nM. Successful radiolabeling of both radiotracers in a one&#8211pot two steps procedure enabled in vivo PET imaging. Distinct kidney uptake could be observed using both radiotracers with specificity proved by blocking studies using either valsartan or irbesartan. **Conclusion:** The results demonstrated the strategy of deriving novel AT_1R PET tracers from clinically used AT_1R antagonists with the least structural modification. Both ^{18}F&#8211valsartan and ^{18}F&#8211irbesartan may serve as tracers for renal imaging, inflammatory assessment and cancer diagnosis by providing information regarding the distribution and alteration of AT_1R under pathophysiological conditions. **References:** 1. Hoffmann M, Chen X, Hirano M, Arimitsu K, Kimura H, Higuchi T, Decker M. ^{18}F&#8211Labeled Derivatives of Irbesartan for Angiotensin II Receptor PET Imaging. ChemMedChem 2018, 13, 2546-2557.2. Chen X, Hirano M, Werner RA, Decker M, Higuchi T. Novel ^{18}F&#8211Labeled PET Imaging Agent FV45 Targeting the Renin-Angiotensin System. ACS Omega 2018, 3, 10460-10470.3. Chen X, Higuchi T, Decker M, Hoffmann M. Sartan Analogue, Patent PCT/EP2018/077897, 12.10.2018.

EP-0778

First Phantom-based Quantitative Assessment of Scandium-44 in a Commercial PET Device

T. Lima[1,2], *S. Gnesin*[2], *E. Nitzsche*[3], *C. Müller*[4], *N. van der Meulen*[5,4];
[1]*Radiation Protection Group, Aarau Cantonal Hospital, Aarau, SWITZERLAND,* [2]*Institute of Radiation Physics, Lausanne University Hospital, Lausanne, SWITZERLAND,* [3]*Institute of Nuclear Medicine and PET, Aarau Cantonal Hospital, Aarau, SWITZERLAND,* [4]*Center for Radiopharmaceutical Sciences ETH-PSI-USZ, Paul Scherrer Institute, Villigen-PSI, SWITZERLAND,* [5]*Laboratory of Radiochemistry, Paul Scherrer Institute, Villigen-PSI, SWITZERLAND.*

Aim/Introduction: Scandium (Sc) is a good candidate for theranostic applications, suitable for both imaging (Sc-43 and Sc-44) and therapy (Sc-47) [1]. A "proof-of-concept" study regarding first-in-human use of Sc-44 for imaging metastatic

neuroendocrine tumours was reported recently [2]. To date, quantitative Sc-44 PET imaging was not evaluated, however. The aim of this study was, therefore, to evaluate quantitative capabilities of Sc-44 PET in a commercial device. **Materials and Methods:** The NEMA/IEC body phantom was scanned using a Siemens mCT Biograph PET-CT. Sc-44 was produced at PSI's research cyclotron [2]. A single-bed list-mode (LM) acquisition (150s scan duration) was performed using the vendor-based Sc-44 setup and reconstructed according to the local clinical protocol used for whole-body oncologic [^{18}F]FDG PET examinations. In addition, we characterised the signal recovery according to the number of iterative updates (iterations from 1 to 10). For all reconstructions, pertinent image corrections (normalization, dead time, activity decay, random coincidence and attenuation) were applied. Presently, Sc-44 prompt-gamma and scatter corrections were not optimized and would potentially result in quantitative bias. To investigate this point, we reconstructed the acquired data with different scatter corrections available (no correction, relative correction and absolute corrections) [3].System cross-calibration with the local dose calibrator (BGcal) and image noise, expressed by the coefficient of variation (COV) were evaluated on the homogeneous background region (5kBq/mL) of the NEMA/IEC phantom. Maximum (RCmax) and 50% threshold corrected for background (RCA50) recovery coefficients were measured for all spherical inserts (25kBq/mL) present in the phantom. **Results:** Acceptable image noise (COV<15%) was achievable with low iteration numbers (it<3). System-to-dose calibrator differences were large, BGcal ranged from 66.3 to 68.1 % of the expected value, regardless of the scatter correction method applied. Despite the effect of over correction due to the applied scatter corrections, RC values measured in lesions exceeded the RC range recommended by the EARL/EANM for [^{18}F]FDG procedures [4]. For the tested range of iterations, RCA50 ranged from 29.9% to 59.9% for the smallest lesion (10 mm diameter), [45.5%:80.3%], [66.4%:75.6%], [71.7%:75.7%], [75.1%:78,6%] and [76.7%:80.9%], respectively, for the 13, 17, 22, 28 and 37 mm spherical inserts in the NEMA/IEC phantom. **Conclusion:** The results of this study show that clinical Sc-44 PET imaging has the potential to provide signal recovery in lesions of different sizes comparable with present F-18 PET standards. Nevertheless, the quantitative accuracy of Sc-44 PET still requires optimized scatter and prompt-gamma corrections. **References:** (Picture with references deleted)

EP-0779

New approach to production and quality control of 16α-[18F] fluoroestradiol ([18F] FES: The effective functional molecular imaging probe for positive estrogen receptors breast cancer

Z. Dadashov, *R. Shukurov, M. Valiyev, K. Eryilmaz, M. Balashov, F. Novruzov;*
Department of Nuclear Medicine, National Centre of Oncology, Baku, AZERBAIJAN.

Aim/Introduction: Hormonal therapy is one of the crucial methods in treatment of breast cancer with positive estrogen receptors. FES is an estrogen analogue and it is a radiopharmaceutical that enables detecting of estrogen receptor expression, also predicts response to hormonal therapy and manages to identify positive estrogen receptors with PET/CT imaging. Our aim was to develop a reliable, easy-to-use, remotely controlled synthesis for non-carrier added 16α -[18F]FES by nucleophilic substitution using a disposable FDG cassette for "Synthera V2". **Materials and Methods:** Production and purification processes executed using two FDG cassettes by changing their design and commands in sequences sections. FES reagent kit for "GE TRACERlab MX" (ABX®) was used during synthesis process. For purification process of final product usually HPLC system is required. Because not all production facilities are equipped with HPLC purification system we have solved this issue without HPLC using second synthera module. The purification process successfully executed by adjusting FDG cassettes' design and sequence commands in "Synthera V2" (IBA) synthesizer. Purification of the crude product accomplished using solid phase extraction cartridges (WAX, HLB Plus, Sep-Pak C18 and Light Alumina N). Formulation of the final product is implemented in the automatic synthesis. **Results:** TLC and HPLC were used to identify radiochemical purity of 18F-FES. Radiochemical and chemical purities were determined using the following HPLC conditions: Agilent 1200 HPLC, Kromasil 100-5- C18 column (4,6x250mm) eluted with 1 mL/min acetonitrile (50%) in water (50%) (Wavelength 254 nm, injection volume 20 mL). Reference standard (FES) has a Rf value of 7.58 and the Rf value of 18F-FES is 7.65 (Figure 1).Radio TLC was performed on F254 glass-backed silica plates (Merck), (eluent acetonitrile/H2O=95/5) and radioactivity was detected with a miniGita from Raytest. Rf value of 18[F] (0-0.1) and the Rf value of product is (0.7-0.8) (Figure 2). **Conclusion:** The purification of FES synthesis process is possible with 2 combined "Synthera V2" devices without HPLC. Production process took 60 minutes with 25% yield. Radiochemical purity of final product was 98% for both HPLC and TLC methods. **References:** 1.J Pharm Pharm Sci. 2007;10(2):256s-265s. Clinical production, stability studies and PET imaging with 16-alpha-[18F]fluoroestradiol ([18F]FES) in ER positive breast cancer patients. Kumar P(1), Mercer J, Doerkson C, Tonkin K, McEwan AJ. 2.European Pharmacopoeia, 7th edition, 2011. 3.K. E. Knott; D. Grätz; S. Hübner; S. Jüttler; C. Zankl; M. Müller. Simplified and automatic one-pot synthesis of 16α[^{18}F] fluoroestradiol without HPLC purification. Journal of Labelled Compounds and Radiopharmaceuticals, v.54,pp.749-753(2011).

EP-0780

In vivo visualisation of GLP-1 receptor expression with PET/CT in patients with morbid obesity undergoing bariatric surgery

L. Deden[1], *M. Boss*[2], *F. Berends*[3], *M. Brom*[2], *E. Hazebroek*[1], *M. Gotthardt*[2];
[1]*Rijnstate, Vitalys, Arnhem, NETHERLANDS,* [2]*RadboudUMC, Nijmegen, NETHERLANDS,* [3]*Rijnstate, Arnhem, NETHERLANDS.*

Aim/Introduction: An approach for in vivo beta cell imaging is targeting the glucagon-like peptide-1 receptor (GLP-1R) by radiolabeled exendin-4, a glucagon-like peptide-1 (GLP-1) analogue. However, the role of GLP-1 is wider than stimulating insulin secretion from the beta cells. For example: GLP-1 induces satiety and many effects of gastric bypass surgery are related to an increase in GLP-1 levels. Signaling mechanisms of GLP-1 in these effects are not completely understood yet, but involvement of GLP-1R is expected. Therefore, the aim of the study is to determine in vivo GLP-1R expression by assessing the distribution of ^{68}Ga-exendin-4 in human. **Materials and Methods:** Distribution of ^{68}Ga-exendin-4 uptake on PET/CT was analyzed in bariatric patients who underwent GLP-1R imaging between September 2015 and January 2019. PET/CT was performed one hour after injection of ^{68}Ga-exendin-4 (100±5 MBq). **Results:** In total 24 patients were included in this analysis, 10 patients prior to and 14 patients at least one year after Roux-en-Y gastric bypass surgery. Clear tracer uptake was observed in pancreas and duodenum in all patients. Most patients showed uptake in the salivary glands and pituitary (70-90%). In a part of the patients, tracer uptake was observed in breast tissue, small intestine, uterus and ovary and cardiac tissue (8-40%). **Conclusion:** GLP-1R expression was observed in several tissues in the human body in vivo. This biodistribution was not described before in human. GLP-1 is hypothesized to have an important role in many metabolic functions, however the exact mechanism of GLP-1R signalling is unknown. For example, GLP-1 may have an effect on hypothalamus-pituitary-adrenal axis via pituitary GLP-1 receptors. Effects of GLP-1 on cardiac function and blood pressure may be facilitated by GLP-1 receptors in cardiac tissue. Further research is needed to understand the role of GLP-1 and GLP-1R in these tissues and for this GLP-1R imaging may be a valuable tool. **References:** None.

EP-0781

Quantitative Clinical Imaging of ^{89}Zr: Developing the Patient Pathway

A. Fenwick[1,2], *L. Bartley*[2], *D. Deidda*[1], *W. Evans*[2], *K. M. Ferreira*[1], *S. Paisey*[2], *A. P. Robinson*[1], *C. Marshall*[2];
[1]*National Physical Laboratory, Teddington, UNITED KINGDOM,* [2]*Wales Research & Diagnostic Positron Emission Tomography (PET) Imaging Centre, School of Medicine, Cardiff University, Cardiff, UNITED KINGDOM.*

Aim/Introduction: The popularity of ^{89}Zr has increased in recent years, partly due to applications in the diagnosis and treatment of non-Hodgkin's lymphoma[1] and other immuno-PET studies[2]. This is of particular interest in patient treatment planning, where ^{89}Zr-labelled antibodies may be used as a dosimetry planning vector for ^{90}Y antibody therapies. Additionally, due to its relatively long half-life (78.42h), the tracking of tumour response to antibody therapy over several days is possible and shows future potential for this radionuclide. The successful implementation of these applications rely on the accuracy of the activity distribution determined using PET. This study investigated the quantitative accuracy of clinical PET systems for ^{89}Zr imaging. **Materials and Methods:** A 6L cylindrical phantom and a standard NEMA-IEC-PET body phantom were filled with solutions of ^{89}Zr with activities varying between 50 and 100MBq that were standardised by the National Physical Laboratory to determine the activity concentration. The phantoms were measured on a GE-690-PET/CT and a Mediso-Anyscan-Trio-PET/CT. Repeat measurements over 4 weeks were performed to confirm device stability. Different volumes of interest were manually drawn to assess partial volume effect and quantification accuracy. **Results:** Both systems demonstrated an ability to determine the activity within the selected regions to within 10% for large volumes, increasing to 20% for volumes down to 1mL when using an independent OSEM-based reconstruction method[3]. Manufacturer supplied software showed deviations of up to 20% on large volumes and up to 40% for volumes down to 1mL however these differences were dependent on the reconstruction. A major source of error was found to be the use of incorrect nuclear data within the manufacturer supplied software and therefore a simple post-processing correction method was developed. Standard uncertainties on the activity determination of 5-10% for the spheres in the NEMA phantom were calculated. **Conclusion:** The first traceable measurements of ^{89}Zr were performed on clinical PET/CT systems. Methods for calculating and propagating uncertainties are presented alongside protocols for creating suitable test phantoms in a traceable manner. The accuracy of two clinical imaging systems in the determination of activity uptake was assessed, and recommendations made for the verification of activity uptakes in different clinically relevant geometries aiding the use of this radionuclide in the clinical arena. **References:** [1] DOI:10.1007/s00259-006-0160-0. [2] DOI:10.1155/2014/203601 [3] DOI:10.1088/0031-9155/57/4/867.

EP-0782

Instrumentation and Infrastructure for Setting up Advanced PET/CT Services beyond F18-FDG in a Developing Country

A. Fatima*, A. Parveen, I. Khan, A. Shahid;*
INMOL Cancer Hospital, Lahore, PAKISTAN.

Aim/Introduction: Our aim in this study is to share our experience in setting up advanced PET CT services beyond ^{18}FDG, including instrumentation and infrastructure. Our primary focus is to provide a cyclotron-independent solution, primarily ^{68}Ge/^{68}Ge generator as a one-stop shop comprehensive tool in an emerging economy. Due to resemblance of co-ordination chemistry of ^{68}Ga, ^{177}Lu and ^{90}Y, it is possible to use the same vector molecule for subsequent radionuclide therapy. **Materials and Methods:** ^{68}Ga is an easily-available generator-derived diagnostic trivalent radio metal with convenient labeling characteristics. Our center has launched a GMP compliant, fully automated click and start cassette-based synthesis system with easy handling (ITG, Germany) for the daily routine production of ^{68}Ga labeled radiopharmaceuticals. Since it was a new set-

up so all regulatory parameters, e.g., license commitments (including generator set-up, elution, drug preparation, ^{68}Ge breakthrough testing, final disposition), radiation protection program including development and implementation of written emergency procedures for leaking or damaged generators, have been well validated, documented and fully implemented. We have established the clinical practice by using DOTA-NOC for imaging of NETs and Prostate-Specific Membrane Antigen (PSMA) for imaging of prostate cancer, followed by treatment with ^{177}Lu-DOTATATE and ^{177}Lu-PSMA. Quality control parameters of ^{68}Ga/^{177}Lu-biomolecules were assured according to European pharmacopoeia. **Results:** We are able to establish a reliable, highly-efficient and medically approved high quality ^{68}Ge/^{68}Ge generator system with a shelf-life of at least 1 year, low ^{68}Ge breakthrough (not more than 0.005%), narrow elution profile and low metal-ion contamination. The elution efficacy of our ^{68}Ga/^{68}Ge generator is approximately 97±2.2%, while labeling efficacy of ^{177}Lu-biomolecules is 98±1.2%. One elution was able to provide doses for 3 to 4 patients. Unfortunately, the short half-life of ^{68}Ga limits the consumption duration. However, this drawback was compensated by the fact that the injected dose can be as low as 100 to 150 MBq still resulting in high quality images and the generator can be eluted repeatedly within 1-2 hour interval. **Conclusion:** ^{68}Ga appears to be a PET analogue of ^{99m}Tc with added value of better sensitivity, resolution, quantitation and personalized medicine. It is a cost-effective complement to cyclotron-based tracers. It can enable PET CT studies in remote hospitals without access to accelerators thereby promoting PET technique for earlier and better diagnostics. We have successfully validated and implemented a programme of advanced diagnostics and therapeutics using ^{68}Ga and ^{177}Lu ligands. This approach can be used in other developing countries." **References:** None. none

EP-0783

2-[^{18}F]FDG: The working horse trapped in the cell's metabolic network

E. Klebermass[1], *M. Mahmudi*[1], *V. Pichler*[1], *A. Miller*[2], *C. Vraka*[1], *T. Balber*[1], *A. Haschemi*[2], *W. Wadsak*[1,3], *M. Hacker*[1], *H. Viernstein*[4], *M. Mitterhauser*[1,5];

[1]*Department of Biomedical Imaging and Image-guided Therapy, Division of Nuclear Medicine, Medical University of Vienna, Vienna, AUSTRIA,* [2]*Department of Laboratory Medicine, Medical University of Vienna, Vienna, AUSTRIA,* [3]*CBmed GmbH - Center for Biomarker Research in Medicine, Graz, AUSTRIA,* [4]*Department of Pharmaceutical Technology and Biopharmaceutics, University of Vienna, Vienna, AUSTRIA,* [5]*Ludwig Boltzmann Institute Applied Diagnostics, Vienna, AUSTRIA.*

Aim/Introduction: It is current knowledge that 2-[^{18}F]FDG is trapped in cells as 2-[^{18}F]FDG-6-phosphate. However, there is growing evidence that its accumulation in cells is not only a function of glucose transporter abundance and hexokinase activity, but the result of more complex cellular processes. Studies showed that metabolism of 2-[^{18}F]FDG can go way beyond the formation of its 6-phosphate derivative, suggesting glycogen metabolism and pentose phosphate pathway (PPP) to be involved (1). Additionally, Marini et al have proposed 2-[^{18}F]FDG accumulation to be strongly dependent on the endoplasmic PPP enzyme hexose-6-phosphate dehydrogenase (H6PD) (2). Therefore, this study aims at further elucidating the metabolic mechanisms and pathways involved to create a basis for a better understanding of 2-[^{18}F]FDG accumulation kinetics, 2-[^{18}F]FDG-negative tumours and efflux phenomena. **Materials and Methods:** The HPLC method by Rokka et al was modified, comprising all known and potential metabolites of 2-[^{18}F]FDG (3). Metabolism studies of 2-[^{18}F]FDG were performed with three different human cancer cell lines HT1080, Huh7 and HT29, using the PPP enzyme inhibitors dehydroepiandrosterone and carbenoxolone (CBX), or different starving times and cell culture media to influence metabolism. For each setting, 2 MBq/mL 2-[^{18}F]FDG were applied to the respective cells, which were then incubated for 1 h, lysed and analysed with radio-HPLC. Accumulation experiments were performed with similar conditions, where the overall retention of 2-[^{18}F]FDG in cells was determined. **Results:** 11 intracellular metabolites different from 2-[^{18}F]FDG-6-phosphate reached up to 95%, depending on the experimental setting. A shift in metabolism was particularly prominent under glucose withdrawal and pre-treatment with PPP inhibitors. In contrast to previous findings (2), the H6PD inhibitor CBX only significantly reduced 2-[^{18}F]FDG accumulation in Huh7 cells under starving conditions (-15 ± 2% compared to vehicle control, $p < 0.05$). Moreover, this was the only case where CBX pre-treatment lead to both a reduction of the H6PD metabolite 2-[^{18}F]FD-phosphogluconate and a lower intracellular 2-[^{18}F]FDG accumulation. **Conclusion:** 2-[^{18}F]FDG metabolism is extremely variant and strongly depends on internal and external influences. The interplay between 2-[^{18}F]FDG metabolism and PPP, as well as the potential impact of its metabolism need to be thoroughly investigated to get the whole picture of 2-[^{18}F]FDG retention. **References:** (1) Southworth R., Parry CR., Parkes HG., et al. NMR Biomed. 2003 Dec (2) Marini C., Ravera S., Buschiazzo A., et al. Sci Rep. 2016 Apr (3) Rokka J., Grönroos TJ., Viljanen T., et al. J Chromatogr B Analyt Technol Biomed Life Sci. 2017 Mar.

EP-0784

Preparation and biological assessment of ^{64}Cu-NOTA-anti EGFR as a Radioimmunoconjugate for Diagnosis of EGFR^{+} ESCC by PET

B. Alirezapour, h. Yousefnia, A. Bahrami Samani;
Nuclear Science and Technology Research Institute, Tehran, IRAN, ISLAMIC REPUBLIC OF.

Aim/Introduction: Immuno-PET provides valuable information about tumor location, phenotype, susceptibility to therapy, and treatment response, especially to targeted radioimmunotherapy. In this study, we prepared anti Epidermal Growth Factor Receptor (EGFR) antibody via identical chelator, NOTA (p-SCN-Bn-NOTA)

labeled with ^{64}Cu and performed preliminary biodistribution studies in mouse bearing ESCC to evaluate the EGFR expression levels using immuno-PET in an Esophageal Squamous Cell Carcinoma (ESCC) model. **Materials and Methods:** Cetuximab was conjugated with NOTA (Macrocyclics B-605), the average number of the chelator conjugated per mAb was calculated and total concentration was determined by spectrophotometrically. NOTA-Cetuximab was labeled with ^{64}Cu then Radiochemical purity and immunoreactivity by TE-8 cell line and serum stability of ^{64}Cu-NOTA- anti-EGFR were determined. The biodistribution studies and radioimmunoscintigraphy were performed in female BALB/c mouse bearing ESCC (^{64}Cu-NOTA- Anti-EGFR i.v., 100 µl, 20±5 µg mAb , 6, 12, 24 and 48 h). **Results:** ^{64}Cu-NOTA-anti-EGFR was prepared (RCP >98% ± 0.7, Specific activity 4.8 ± 0.7 µCi/µg). Conjugation reaction of chelator (50 molar excess ratio) to antibody resulted in a product with the average number of chelators attached to a mAb (c/a) of 3.4 ± 0.3. Labeling yield with ^{64}Cu in 400µg concentration of bioconjugate was 93.8% ± 1.1. Immunoreaction of ^{64}Cu-NOTA-anti-EGFR complex towards EGFR antigen was determined by RIA and the complex showed high immunoreactivity towards EGFR. In vitro and in vivo stability of radioimmunoconjugate was investigated respectively in PBS and blood serum by RTLC method. In vitro stability showed more than 91% ± 2.2 in the PBS and 79% ± 1.7 in the serum over 24 h. The Immunoreactivity of the radiolabeled anti-EGFR towards TE-8 cell line was done by using Lindmo assay protocol. Under these conditions, the immunoreactivity of the radioimmunoconjugate was found to be 0.78. The biodistribution of ^{64}Cu-NOTA- anti-EGFR complex in the mice with normal and ESCC at 6, 12, 24 and 48 h after intravenous administration, expressed as percentage of injected dose per gram of tissue (%ID/g). Biodistribution and imaging studies at 24 and 48 h post-injection revealed the specific localization of complex at the site of tumors. **Conclusion:** ^{64}Cu-NOTA- anti-EGFR is a potential compound for molecular imaging of PET for diagnosis and follow up of EGFR expression in oncology.Keywords— Anti- EGFR, Copper-64, Monoclonal Antibody, ESCC. **References:** None.

EP-0785

Radioimmunoimaging of EGFR with pretargeting Cetuximab in triple negative breast cancer

X. Lan, *L. Yuan, Y. Gai, R. An, Y. Zhang;*
Union Hospital, Tongji Medical College, Huazhong University of Science and Technology, Wuhan, CHINA.

Aim/Introduction: Breast cancer is the second leading cause of morbidity and mortality in women. Triple negative breast cancer (TNBC) has special biological behavior and poor prognosis, and high expression of epidermal growth factor receptor (EGFR) plays an important role. Radioimmunoimaging (RII) is an important technique for tumor imaging. However, because of large molecular weight and long circulation time, monoclonal antibody (mAb) is not suitable for short half-life radionuclides. Pretargeting technique is a method of labeling mAb in vivo, which could increase the tumor/background ratio and make it possible for short half-life radionuclide. The objective was to explore the feasibility of ^{68}Ga PET imaging of EGFR with pretargeting Cetuximab in TNBC. **Materials and Methods:** Strained transcyclooctene (TCO) and electrond eficient tetrazine (Tz) have inverse electron-demand Diels-Alder reaction. Cetuximab-TCO was obtained by modifying Cetuximab with TCO-NHS. The radioligand ^{68}Ga-L-NETA-Tz was prepared by using L-NETA as a chelating agent. Human basal breast cancer cells MDA-MB-468 and MDA-MB-231 were cultured, and EGFR expression of the two cell lines were identified. Nude mice bearing xenografts of the two cell lines was established. 50 µg of Cetuximab-TCO was injected into the tumor-bearing mice in advance, and after different time (12, 24, 36 and 48 h), 150 µCi ^{68}Ga-L-NETA-Tz was injected. The "click chemistry" of TCO and Tz was realized in vivo. Small-animal PET imaging and biodistribution were performed to evaluate pharmacokinetic properties. Two control groups, MDA-MB-468 mice without injection of Cetuximab-TCO (C1) and MDA-MB-231 mice with negative expression of EGFR (C2), and one blocking group (MDA-MB-468 mice pretreated with 100 folds of excess Cetuximab) were also performed animal PET imaging for specificity study. **Results:** ^{68}Ga-L-NETA-Tz molecular probe was successfully prepared with high labeling yield of >95%. The expression of EGFR in MDA-MB-468 was much higher than that in MDA-MB-231. PET imaging and biodistribution results showed that the best imaging results were obtained at 36 h pre-injection of Cetuximab, in which the highest tumor uptake was achieved after 1 h injection of ^{68}Ga-L-NETA-Tz with optimal tumor/muscle ratio 4.67±0.46. However, there was no significant tumor uptake in the blocking group and two control groups. **Conclusion:** We successfully explored RII of monoclonal antibody with short half-life radionuclide. Pretargeting with Cetuximab-TCO for 36 h, ^{68}Ga-L-NETA-Tz could detect the high expression of EGFR in vivo, which provided a novel method for PET imaging of TNBC. Funding: This study was supported by NSFC 81630049. **References:** None.

EP-56

Preclinical and translational aspects, including radiopharmacy, radiochemistry and drug development -> Radiopharmacy, radiochemistry, drug development -> Radiopharmacy -> Radiopharmaceuticals - SPECT

October 12 - 16, 2019 e-Poster Area

EP-0786

Comparison of two HAES sedimantation agents for leukocyte separation in radiolabeling procedure

A. Socan, *T. Debelak, M. Kroselj, P. Kolenc Peitl;*
University Medical Centre Ljubljana, Ljubljana, SLOVENIA.

Aim/Introduction: HAES (2-hydroxyethyl starch), a plasma expander, in molecular weight 200/0.5 (mean molecular weight of 200kDa), has long been a sedimentation agent of choice for leukocyte radiolabeling in routine clinical practice. Due to serious side effects connected with HAES as plasma expander, today only HAES with lower molecular weight 130/0.4 (mean molecular weight of 130kDa) is available on the market and potential usage for radiolabeling of leukocytes. Our aim was to compare effectiveness in obtaining leukocytes for radiolabeling from blood using both types of HAES. **Materials and Methods:** 30 mL of venous blood from 18 individuals was withdrawn into 50 mL syringes containing 13 mL of sedimentation agent and 10 mL of anticoagulant (ACD-A) and allowed to sediment in the syringe for 60 min in accordance with EANM guidelines for leukocyte radiolabeling with ^{99m}Tc-HMPAO. 3 mL of venous blood was withdrawn into the vacutube with EDTA to gain erythrocyte, leukocyte and platelet numbers. After sedimentation LRP (leukocyte rich plasma) volume was assessed. During radiolabeling, samples (0.5 mL) of LRP and LPP (leukocyte poor plasma), after 10 min centrifugation of LRP at 150G, were collected. Number of different cell types present in each of the samples were measured by automatic haematology analyzer (Advia 120, Siemens), and leukocyte numbers available for radiolabeling and other cell types in cell sample were determined. **Results:** With usage of HAES 200/0.5 as sedimentation agent average volume of LRP for radiolabeling was 32.3±3 mL. Average number of leukocytes in cell sample available for radiolabeling was 4.2×10^9/L (54.8% of the average number of leukocytes in the whole blood - AWBL). The average number of erythrocytes in the sample used for radiolabelling was 2×10^{10}/L (0.5% of average erythrocyte number in the whole blood - AWBE), while average number of the platelets was 9×10^9/L (4% of average platelet number in the whole blood - AWBP) respectively. With HAES 130/0.4, the average volume of LRP was 20.2±6.1 mL, average number of leukocytes for radiolabeling was 4.8×10^9/L (66.5% AWBL), number of erytrocytes was 2×10^{10}/L (0.6% AWBE) and number of platelets was 5.5×10^{10}/L (24.8% AWBP). **Conclusion:** We can conclude that HAES 130/0.4 can be used as sedimentation agent for leukocyte radiolabeling instead of discontinued HAES 200/0.5. Sedimentation time of 60 min enables collection of leukocytes in numbers suitable for radiolabeling with erythrocytes and platelets numbers sufficiently low for good images to be acquired. **References:** None.

EP-0787

Contribution of 131-I NP-59 Planar and SPECT/CT Imaging in Patients with Hypersecretory Adrenal Syndromes and Incidentally Discovered Adrenal Masses

A. Sainz Esteban*, M. Ruiz Gómez, C. Gamazo Laherrán, J. Gómez Hidalgo, P. Turbay Eljach, N. Álvarez Mena, M. González Soto, B. Pérez López, M. Alonso Rodríguez, R. Ruano Pérez;*
Hospital Clinico Universitario, Valladolid, SPAIN.

Aim/Introduction: To assess the contribution of radioiodinated I-6-ßiodomethyl-19-norcholesterol (NP-59) imaging in hypersecretory adrenal syndromes and characterization of incidentally discovered adrenal masses in terms of diagnostic accuracy and anatomic localization. **Materials and Methods:** We include 37 patients (20 men, age: 60±11) investigated for adrenal hypersecretory syndromes, with or without adrenal nodules, (15 patients with ACTH-independent Cushing's disease, two hyperandrogenism and 18 hyperaldosteronism) and for characterization of incidentally discovered adrenal masses (two patients) using NP-59 scintigraphy with SPECT/CT imaging. Sequential anterior and posterior images of the upper abdomen were acquired between 2 and 7 days following intravenous injection of 37 MBq I-131 NP-59. Saturated solution of potassium iodide was given to block free radioiodine thyroid uptake. Twenty three patients with suspected hyperaldosteronism or ACTH-independent Cushing's disease received pharmacological adrenosuppressive preparation with dexamethasone. SPECT/CT imaging was performed on day 5 postinjection. Clinical and imaging data were reviewed to evaluate whether additional information derived from near-simultaneous anatomic localization aids study interpretation. The final diagnosis was obtained with clinical follow-up, other imaging tests and/or pathological studies when available. **Results:** Taking the final diagnosis as a final result, the NP-59 imaging produced 31 true-positives, one false-positive, three true-negatives, and two false-negatives (adenoma and bilateral adrenal hiperplasia). Sensitivity, specificity, positive predictive value, negative predictive value, and accuracy were 93.9, 75.0, 96.8, 60.0, and 91.9%, respectively. Of the 15 patients with suspected Cushing's disease, eight showed in the NP-59 scintigraphy hyperfunctional adrenal nodules, one nonfunctioning adrenal nodule, six bilateral adrenal hyperplasia and one normal scan. Of the two patients with suspected hyperandrogenism, one presented with a carcinoma and one with a hyperfunctional adrenal nodule. Of the 18 patients with suspected hyperaldosteronism four presented with hyperfunctional adrenal nodule, 10 with bilateral adrenal hyperplasia and four patients were normal. Of the two patients with incidentally discovered adrenal masses, one presented a bilateral adrenal hyperplasia and one with a hyperfunctional adrenal nodule. SPECT/CT assisted study interpretation by localizing focal uptake in small adrenal adenomas in two patients, by localizing focal uptake small bowel and gall bladder and distinguishing malignant radiological pattern on the CT in one patient. In the rest of the patients SPECT/CT confirmed adrenal origin of activity increasing reader confidence but did not change the planar interpretation of the study. **Conclusion:** NP-59 scintigraphy provides useful information on the functional status of hypersecretory adrenal syndromes. Besides, SPECT/CT imaging allows precise localization of the functional activity improving diagnostic interpretation. **References:** None.

EP-0788

The Possibility of ^{99m}Tc-1-thio-d-glucose Spect Using For Detection of Residual Tumor Tissue After Non-radical Surgical Treatment and Visualization Of Recurrence in Patients With a Brain Tumor

R. Zelchan[1], *A. Medvedeva*[1], *I. Sinilkin*[1], *O. Bragina*[1], *A. Ryabova*[1], *E. Stasyuk*[2], *A. Rogov*[2], *V. Skuridin*[2], *V. Chernov*[1], *E. Choynzonov*[1], *E. Mishina*[3];
[1]*Tomsk National Research Medical Center of the Russian Academy of Sciences includes the following Research Medical Institutes: Cancer Research Institute, Tomsk, RUSSIAN FEDERATION,* [2]*National Research Tomsk Polytechnic University, Tomsk, RUSSIAN FEDERATION,* [3]*Siberian State Medical University, Tomsk, RUSSIAN FEDERATION.*

Aim/Introduction: to study the possibility of ^{99m}Tc-1-thio-D-glucose (^{99m}Tc-TG) SPECT using for metabolic imaging of a residual tumor after non-radical surgical treatment and detection of recurrence in patients with a brain tumor. **Materials and Methods:** the study included 10 patients after non-radical surgery for a brain tumor and 9 people with a brain tumor recurrence. All patients underwent ^{99m}Tc-TG SPECT 2 hours after intravenous administration of the radiopharmaceutical at a dose of 500 MBq. The study was performed according to standard protocols; 32 projections were recorded in a matrix of 256x256 pixels without hardware magnification. During processing, the tumor/background index was calculated as the ratio of the intensity of radiopharmaceutical accumulation in the area of interest and the symmetric zone of the intact brain tissue. MRI with contrast and PET / CT were used as reference methods. **Results:** It was possible to visualize residual tumor tissue 14 days after surgery using ^{99m}Tc-TG SPECT in all 10 patients. The sensitivity of ^{99m}Tc-TG SPECT was 100%. The mean values of the tumor/background index were 1.55±0.27. Brain tumor recurrence was also detected in all patients (n = 9). In the group of patients with recurrent tumors, the values of the tumor/background index were 3.50 ± 0.43. The presence of residual tumor tissue after non-radical surgery, as well as the presence of recurrent brain tumor was confirmed by MRI and PET/CT data with ^{11}C-methionine. It should be noted, that in the study ^{99m}Tc-TG uptake only in tumor tissue were found. Also a physiological accumulation of the radiopharmaceutical in the projection of the soft tissues of the aponeurotic helmet, choroid, mucous membranes of the nasal and oral cavities was visualized. **Conclusion:** This study demonstrated that the ^{99m}Tc-TG selectively accumulates in a brain tumor. High values of the tumor/background index allow obtaining contrast images of the tumor tissue, which simplifies the diagnostic process. ^{99m}Tc-TG SPECT can be considered as a promising method of metabolic imaging of malignant brain tumors and their recurrences. It should be noted that with similar parameters of diagnostic efficacy with PET/CT, ^{99m}Tc-TG SPECT is advantageously characterized by simplicity of execution and low cost of the procedure itself. **References:** None.

EP-0789

^{99m}Tc-labelled ketal based nucleolipid nano assembly as SPECT-trackable Drug delivery system for CNS

S. Chaturvedi[1], *S. Swastika*[1,2], *A. Kaul*[1], *P. Panwar Hazari*[1], *S. Pal*[1], *B. Singh*[2], *P. Barthélémy*[3], *A. K Mishra*[1];
[1]*Institute of Nuclear Medicine and Allied Sciences (INMAS), Delhi, INDIA,* [2]*Department of Chemistry, Banaras Hindu University, Varanasi, INDIA,* [3]*ARNA laboratory, Univ. Bordeaux, INSERM U-1212, UMR CNRS 5320, F-33000, Bordeaux, FRANCE.*

Aim/Introduction: Nucleolipids are bioinspired hybrid molecules wherein nucleosides are modified using long lipidic chains. The result is an ampiphilic molecule bearing polar and non-polar heads capable of supramolecular association. The structural similarity of nucleolipids with cellular membranes, allow the nucleolipids to diffuse through the cells leading to enhanced cellular internalization. Extending the concept, we hypothesize that nucleolipid can be exploited as drug delivery systems for central nervous system (CNS). Design of drug delivery systems which can effectively cross the blood brain barrier for effective delivery of drugs remains a challenge. We aimed to explore the potential of nucleolipid nano-assemblies as a blood brain barrier permeable vehicle for the delivery of hydrophilic drugs and reactivators along with SPECT based tracking of the assemblies. **Materials and Methods:** The uridine based nucleolipid appended with two C_{15} lipid chains and bearing pH labile ketal linkage was synthesised using multi-step synthesis. Synthesis involved activation of 2′, 3′ hydroxyl followed by addition of palmitone. The 5′ position was tosylated and converted to amine for subsequent bioconjugation with chelator (diethylenetriaminepentacetic acid) for ^{99m}Technetium (^{99m}Tc) labelling. The compounds and intermediates were characterised using spectroscopic techniques. Nano-assemblies were formed through routine procedure and characterized for size along with physicochemical assessment through quenching and potentiometric studies. Various encapsulation parameters were evaluated. The nano-assemblies were ^{99m}Tc-radiolabelled. **Results:** After having encouraging results from our earlier work with standalone nucleolipids (brain uptake = 0.2 %ID/g, excellent radiolabelling, good biocompatibility), we have developed nucleolipid nano-assemblies with mean particle size distribution of 100-200 nm. Physicochemical characterization showed low non-specific protein binding and optimum stability. The encapsulation efficiency of hydrophilic drug, methotrexate, in nucleolipid nano-assemblies was found to be approximately 72%. Drug release kinetics was also assessed for a period of 24 h. Radiolabelling of nucleolipid nano-assemblies has been carried using ^{99m}Tc with more than 97 % specific activity. Animal biodistribution studies indicate stable formulation with predominantly hepatobiliary route of excretion. Encapsulation of hydrophilic reactivators oxime and release kinetics as function of time and pH is in process. Future studies will concentrate on real time tracking using SPECT imaging of drug loaded nucleolipids in mice models and subsequent assessment of brain uptake. **Conclusion:** If successful the nucleolipid nano-assemblies can be a novel drug delivery approach for delivery of drugs and reactivators in brain. **References:** None.

EP-0790

N-terminal position of histidine-glutamate-containing tag improves biodistribution of [^{99m}Tc]Tc-labeled DARPin G3

A. Vorobyeva[1], *A. Schulga*[2], *E. Konovalova*[2], *R. Güler*[3], *J. Löfblom*[3], *M. Sandström*[1], *J. Garousi*[1], *V. Chernov*[4], *O. Bragina*[4], *A. Orlova*[1], *V. Tolmachev*[1], *S. M. Deyev*[2,5];
[1]*Uppsala University, Uppsala, SWEDEN,* [2]*Shemyakin & Ovchinnikov Institute of Bioorganic Chemistry, Moscow, RUSSIAN FEDERATION,* [3]*KTH Royal Institute of Technology, Stockholm, SWEDEN,* [4]*Cancer Research Institute, Tomsk National Research Medical Center Russian Academy of Sciences, Tomsk, RUSSIAN FEDERATION,* [5]*National Research Nuclear University "MEPhI", Moscow, RUSSIAN FEDERATION.*

Aim/Introduction: Radionuclide molecular imaging of human epidermal growth factor receptor 2 (HER2) expression in disseminated cancer enables stratification of patients for HER2-targeted therapies. A small engineered scaffold protein DARPin G3 (molecular weight 14 kDa) is a possible agent for imaging of HER2. Based on experience with other scaffold protein, affibody molecules, we hypothesized that composition (hexahistidine H_6 or histidine-glutamate $(HE)_3$) and position (C- or N-terminus) of histidine-containing tags could influence the biodistribution of [^{99m}Tc]Tc$(CO)_3$-labeled DARPin G3 and might be used for optimization of its imaging properties. **Materials and Methods:** Four G3 variants containing a tag either at N-terminus (H_6-G3, $(HE)_3$-G3) or at C-terminus (G3-H_6, G3-$(HE)_3$) were recombinantly produced and labelled with [^{99m}Tc]Tc$(CO)_3$. Labelling yield, label stability, specificity and affinity of the binding to HER2-expressing cell lines, biodistribution and tumour targeting properties of these variants were compared. In vivo targeting was compared in BALB/C nu/nu mice bearing HER2-positive SKOV-3 xenografts at 4 and 24 h after injection. HER2-negative Ramos xenografts were used for specificity control. **Results:** All four G3 variants were labelled with an isolated yield of 50-70% and had radiochemical purity higher than 97%. All labels were stable under histidine challenge. Binding of all labelled variants to HER2-expressing cells in vitro was specific and dissociation equilibrium constants were similar, approximately 90 pM. The uptake in SKOV-3 xenografts was similar (7- 9 %ID/g at 4 h and 5-8 %ID/g at 24 h after injection) for all variants. The uptake in HER2-negative Ramos xenografts was significantly ($p<0.05$) lower than in SKOV-3 xenografts. Position and composition of histidine-containing tags had a strong influence on uptake in normal tissues. The tumour-to-liver ratio for [^{99m}Tc]Tc$(CO)_3$-$(HE)_3$-G3 (4.9 ± 0.3 at 4 after injection) was significantly ($p<0.05$) higher than tumour-to-liver ratios for [^{99m}Tc]Tc$(CO)_3$-H_6-G3, [^{99m}Tc]Tc$(CO)_3$-G3-H_6 and [^{99m}Tc]Tc$(CO)_3$-G3-$(HE)_3$ (1.6 ± 0.7, 1.8 ± 0.3, and 2.2 ± 0.3, respectively). [^{99m}Tc]Tc$(CO)_3$-$(HE)_3$-G3 provided also significantly higher tumour-to-lung, tumour-to-bone and tumour-to-muscle ratios. Better contrast of HER2 visualization using [^{99m}Tc]Tc$(CO)_3$-$(HE)_3$-G3 was confirmed by gamma-camera imaging. **Conclusion:** Position and composition of histidine-containing tags have a strong influence on biodistribution of [^{99m}Tc]Tc$(CO)_3$-labelled DARPins and can be used for optimization of their targeting properties. [^{99m}Tc]Tc$(CO)_3$-$(HE)_3$-G3 variant provided the highest tumour-to-tissue ratios, which should improve sensitivity of HER2 imaging in common metastatic sites. **References:** None.

EP-0791

Imaging of EpCAM expression in pancreatic cancer using radiolabelled DARPin Ec1

A. Vorobyeva[1], *A. Schulga*[2], *A. Abouzayed*[1], *E. Konovalova*[1], *T. Gunther*[1], *H. Ding*[3], *T. Graslund*[3], *A. Orlova*[1], *S. M. Deyev*[2,4], *V. Tolmachev*[1];
[1]*Uppsala University, Uppsala, SWEDEN,* [2]*Shemyakin & Ovchinnikov Institute of Bioorganic Chemistry, Moscow, RUSSIAN FEDERATION,* [3]*KTH, Stockholm, SWEDEN,* [4]*National Research Nuclear University "MEPhI", Moscow, RUSSIAN FEDERATION.*

Aim/Introduction: Efficient treatment of disseminated pancreatic cancer remains an unmet clinical need. One possible target for treatment is epithelial cell adhesion molecule (EpCAM). Intense EpCAM overexpression was found in 23-37% of pancreatic cancers. Several EpCAM-targeting therapeutics are currently in clinical trials. A precondition for their successful application is identification of patients having tumours with high EpCAM expression. Radionuclide molecular imaging offers a non-invasive approach for stratification of patients for EpCAM-targeting therapies. Designed ankyrin repeat proteins (DARPins) are promising candidates for targeting vectors for radionuclide imaging. Their small size (molecular weight of 14-18 kDa) creates potential for a high-contrast imaging at the day of injection. Particularly of interest is DARPin Ec1, which binds to EpCAM with affinity of 68 pM. The aim of the study was to evaluate the feasibility of imaging of EpCAM-expressing pancreatic cancer xenografts using radiolabelled Ec1. **Materials and Methods:** Ec1 was indirectly radioiodinated using N-succinimidyl-3-methylstannyl-benzoate to ensure rapid excretion of radiometabolites. EpCAM-expressing BxPC3 pancreatic cancer cell line was used for characterisation of [^{125}I]I-PIB-Ec1 in vitro and in vivo. Biodistribution of [125I]I-PIB-Ec1 was measured in BALB/C nu/nu mice bearing BxPC3 xenografts at 3 and 6 h after injection. EpCAM-negative Ramos xenografts were used as a negative control. MicroSPECT/CT imaging was used to confirm the biodistribution data. **Results:** EpCAM Ec1 was labelled with a radiochemical yield of 22±4%. The radiochemical purity was 99±0%. [^{125}I]I-PIB-Ec1 retained high specificity and picomolar affinity of binding to EpCAM expressing cells in vitro. The uptake of [^{125}I]I-PIB-Ec1 in BxPC3 xenografts was 66-fold higher ($p<0.0005$) than in EpCAM-negative Ramos xenografts, which demonstrated specificity of targeting. The [^{125}I]I-PIB-Ec1 cleared rapidly from blood and non-specific compartments. Already at 3 h p.i., the tumour uptake (3.8±0.9% ID/g) exceed by far the uptake in normal tissues (except kidneys), resulting in e.g. tumour to-blood ratio of 18±4 and tumour-to-pancreas ratio of 32±11. The tumour uptake did not decrease by 6 h, while there was an additional decrease of uptake in normal tissues. This resulted in a further increase of tumour-to-organ ratios. For example, the tumour-to-blood ratio increased to 43±12 and the tumor-to-pancreas ratio increased to 99±40. MicroSPECT/

CT imaging confirmed high-contrast visualization of BxPC3 xenografts. **Conclusion:** Indirectly radioiodinated DARPin Ec1 provided high-contrast imaging of EpCAM a few hours after injection. This can be utilized for imaging of EpCAM expression using SPECT (using iodine-123) and PET (using iodine-124). **References:** None.

EP-0792

Comparative Evaluation Of Tumour-targeting Properties Of An Antagonistic Bombesin Analogue Labelled With Residualizing (^{111}In-DOTA) And Non-residualizing (^{125}I-Tyr) Labels

M. Oroujeni, *A. Abouzayed, B. Mitran, V. Tolmachev, A. Orlova, U. Rosenström;*
Uppsala University, Uppsala, SWEDEN.

Aim/Introduction: Gastrin releasing peptide receptor (GRPR) is overexpressed in many cancers such as prostate, breast, pancreatic and lung. Bombesin analogues are short peptides with a high affinity to GRPR. Radiometal-labelled antagonistic bombesin analogues demonstrated good targeting of GRPR-expressing tumours. Internalization of bombesin antagonists by cancer cells was slow. We hypothesized that the residualizing properties of the label are not critical for a good tumour retention but a non-residualizing label would provide quicker clearance of activity from normal tissues. The aim of this study was to evaluate targeting properties of ^{125}I-Tyr-PEG2-RM26 and compare it directly with the properties of ^{111}In-DOTA-PEG2-RM26. **Materials and Methods:** The bombesin analogue Tyr-PEG2 [D-Phe^{6}, Sta^{13}, Leu^{14}] Bombesin[6-14] (denoted as Tyr-PEG2-RM26) was synthesized by standard manual solid-phase peptide synthesis. Tyr-PEG2-RM26 was labelled with ^{125}I using Iodogen at room temperature. In vitro stability of ^{125}I-Tyr-PEG2-RM26 in 1mM of NaI and half-maximal inhibitory concentration (IC50) were evaluated. In vitro binding specificity of ^{125}I-Tyr-PEG2-RM26 bound to two GRPR-expressing cell lines with a different level of expression, PC3 and DU-145 was tested by a saturation assay. The cellular processing of the labelled conjugate bound PC3 cell line was evaluated using an acid wash method. The biodistribution of ^{125}I-Tyr-PEG2-RM26 and ^{111}In-DOTA-PEG2-RM26) in Balb/c nu/nu mice bearing PC3 tumours was measured at three time points (0.5, 3 and 24 h). In vivo specificity of both radioconjugates was confirmed by saturation of GRP receptors with PEG4-RM26 as a blocking agent. **Results:** The labelling of Tyr-PEG2-RM26 with ^{125}I resulted in 75% radiochemical yield and 95% purity. ^{125}I-Tyr-PEG2-RM26 was stable in PBS and NaI. ^{125}I-Tyr-PEG2-RM26 retained binding specificity to GRPR expressing cell lines. The IC50 values of Tyr-PEG2-RM26 and DOTA-PEG2-RM26 were determined to be 1.5±0.6 nM and 3.1±1.1 nM, respectively. The cellular processing of ^{125}I-Tyr-PEG2-RM26 by PC3 cell line was characterized by fast internalization during the first hour of incubation followed by rapid leakage of radioactivity from cells. Biodistribution showed that the uptake in the pancreas and tumour was GRPR-specific for both radioconjugates. The blood clearance of ^{125}I-Tyr-PEG2-RM26 was appreciably slower and the activity accumulation in all organs was significantly higher than of ^{111}In-DOTA-PEG2-RM26. Tumour uptake of ^{111}In-DOTA-PEG2-RM26 was significantly higher than ^{125}I-Tyr-PEG2-RM26, resulting in significantly higher tumour-to-organ ratios at all studied time points. **Conclusion:** An introduction of a hydrophobic tyrosine moiety at N-terminus of RM26 could change cellular processing and biodistribution of antagonistic bombesin analogue in an unfavourable way. **References:** None.

EP-57

Preclinical and translational aspects, including radiopharmacy, radiochemistry and drug development -> Radiopharmacy, radiochemistry, drug development -> Radiopharmacy -> Radiopharmaceuticals - Therapy

October 12 - 16, 2019 e-Poster Area

EP-0793

Kit Based Re-188 Microspheres for Selective Intra-Arterial Radionuclide Therapy (SIRT) of Unresectable Liver Cancer

J. Shukla, *N. Kalra, A. Duseja, A. Chhabra, Y. Rathod, M. Parmar, R. Kumar, H. Singh, B. R. Mittal;*
Post Graduate Institute of Medical Education & Research, Chandigarh, INDIA.

Aim/Introduction: Unresectable primary and metastatic liver cancer have limited options for the treatment. Selective Intra-Arterial Radionuclide Therapy (SIRT) has been proved as a valuable option when the tumor is large, multinodular, portal vein is thrombosed, etc. SIRT may offer reduced toxicity profile, highly effective tumor responses, prolong survival and improved quality of life. **Materials and Methods:** Microsphere kit was developed and Re-188 microspheres have been prepared and underwent quality control procedures to qualify for human use. Clearance from Institutional ethics committee was obtained, and the patients (n=20) were assessed by hepatologist, interventional radiologist and nuclear medicine physician prior to the procedure. Pre-therapy assessment included clinical history, complete blood counts, LFT, serology for hepatitis B or C infection and triple phase CT/MRI/PET-CT for treatment planning. Child's score, alpha feto protein and portal vein status were documented. After informed written consent, a catheter was placed and a scout dose of 3-5 mCi Tc-99m / Re-188 microspheres was delivered. Whole body image was acquired under gamma camera. The ROI counts on anterior, posterior images were noted to calculate lung shunt fraction and tumour to normal liver ratio (TNR). The therapy dose (mCi) was calculated so that the maximum absorbed dose to lung, normal liver and bone marrow should not exceed 12 Gy, 30 Gy and 1.2 Gy respectively. For personalized dosimetry, whole body and SPECT/CT images were acquired

at 24 and/or 48 hours post therapy and the radiation absorb dose (Gy) to various organs was calculated by MIRD method. The response to SIRT was assessed on TPCT/PET-TPCT after 8-12 weeks post therapy by mRECIST. **Results:** Re-188 microspheres were easily administered; no gastroduodenal reflux and no procedure related complications/adverse events were noted. The localization of Re-188 microspheres in lesion was more than 75% of the administered dose. Out of 20 pts, 5 patients are surviving. Complete response was achieved in three patients, one patient underwent transplant surgery and doing well. The max survival was 30 months. 2 patients died before follow-up. The clinical condition of patients was improved on follow up.. **Conclusion:** Kit based Re-188 microspheres are cost-effective and convenient option for SIRT. **References:** 1. Shukla J et al. Two cases of Rhenium-188 microspheres for inoperable hepatocellular carcinoma. Clin Nucl Med. 2019;44: e93-e95. 2. Vadi SK,...Shukla J et al. Demonstration of treatment response to trans-arterial radio-embolization (TARE) on 68Ga-DOTANOC PET/CT in a patient with metastatic neuroendocrine tumor. Clin Nucl Med. 43 (9), e312-13.

EP-0794

Preparation and evaluation of biodegradable polymer micelle for brachytherapy

A. Makino, T. Mori, H. Okazawa, Y. Kiyono;
University of Fukui, Eiheiji-cho, Yoshida-gun, Fukui, JAPAN.

Aim/Introduction: Recently, injectable thermo-sensitive hydrogels have attracted increasing attention as carriers for tumor therapies (brachytherapy) since they are possible to retain therapeutic radionuclides at the injected site over a long period. In this study, a thermo-sensitive polymer micelle was newly designed as a carrier for brachytherapy. **Materials and Methods:** The thermo-sensitive micelle was prepared from the newly synthesized amphiphilic block polymer (PNnPG-b-PLLA), whose hydrophilic (thermosensitive) and hydrophobic units are consisted from poly(N-n-propyl glycine) and poly(L-lactic acid), respectively. PNnPG-b-PLLA was synthesized via N-carboxy anhydride (NCA) polymerization using PLLA as a macroinitiator and polymer length on hydrophilic and hydrophobic chains was determined by NMR. Micelle was prepared by injecting the polymer solution dissolved in acetone to the ice-cooled aqueous solution. Diameter of the micelle was determined by dynamic light scattering (DLS) method. The thermosensitive micelle encapsulating ^{64}Cu was co-incubated with LNCaP human prostate adenocarcinoma cell line, in vitro anti-tumor activity of the micelle was evaluated. **Results:** PNnPG and PLLA polymer unit lengths of the synthesized amphiphilic polymer (PNnPG-b-PLLA) were 70 mer and 30 mer, respectively. The micelle diameter at 15 degrees Celsius was 50-60 nm. The micelle showed thermosensitive behavior around 20-25 degrees Celsius, and character of the PNnPG unit was changed from hydrophilic to hydrophobic. Caused by the micelle surface hydrophobization, the micelles were quickly gathered by intermiceller hydrophobic interaction and formed submicron size aggregation. Importantly, the micelle directly injected to the transplanted tumor region of the model mouse showed effective retention behavior as expected, which was caused by the aggregation. To the hydrophobic core region of the micelle, beta-ray emitting ^{64}Cu could be encapsulated in high yield (>95%), and ^{64}Cu could be stably encapsulated into the micelle up to 96 h. In vitro study, cytotoxicity was observed depending on the dose of ^{64}Cu activity administrated. **Conclusion:** The newly prepared thermo-sensitive polymer micelle has basic characters as a carrier for brachytherapy. We are currently undergoing in vivo evaluation using tumor- bearing mice. **References:** None.

EP-0795

Magnetic properties of 2,3-dicarboxypropane-1,1-diphosphonic acid coated magnetite nanoparticles and radiolabeling with ^{99m}Tc and ^{90}Y for possible theranostic application

***A. A. Vukadinovic**, M. Peric, M. Radovic, M. Mirkovic, D. Jankovic, D. Petrovic, Z. Milanovic, S. Vranjes-Djuric;*
University of Belgrade, Vinca Institute of Nuclear Sciences, Belgrade, SERBIA.

Aim/Introduction: Combining the effects of hyperthermia and radiation therapy represents a new approach for possible application in cancer treatment. In this study, the heating efficiency of 2,3-dicarboxypropane-1,1-diphosphonic acid (DPD) coated magnetite nanoparticles in the presence of various ionic strengths has been explored. This allowed more profound understanding of magnetic behavior of Fe_3O_4-DPD MNPs. Radiolabelling method with γ emitter ^{99m}Tc and β emitter ^{90}Y was used as a reliable and powerful tool for determination of in vivo behavior. **Materials and Methods:** Fe_3O_4 MNPs were prepared by coprecipitation method, DPD water solution was added and the coating reaction was carried out overnight at room temperature. Radiolabeling of Fe_3O_4-DPD MNPs was performed with ^{99m}Tc using $SnCl_2$ as a reducing agent. ^{90}Y labeling of Fe_3O_4-DPD MNPs was performed using $^{90}YCl_3$ solution. The magnetic hyperthermia efficiency of Fe_3O_4-DPD MNPs was tested under alternating magnetic field (30 mT) and the resonant frequencies between 252-577 kHz. The in vitro stability of radiolabeled MNPs was tested in different solutions: saline (0.9 % NaCl), human serum and 0.01 mol/dm3 DTPA. Biodistribution studies were carried out in healthy male 4-week old Wistar rats. **Results:** In the magnetic hyperthermia studies, the temperature increase of Fe_3O_4-DPD MNPs (2 mg/ml) as a function of time was evaluated under different frequencies 252-577 kHz and magnetic field strength of 30mT. From the temperature curve it was observed that Fe_3O_4-DPD MNPs reach hyperthermia temperature even at lower frequencies. During in vitro stability studies, the radiochemical purity of ^{99m}Tc-Fe_3O_4-DPD MNPs determined after 24 h incubation in saline, human serum and DTPA was 92.9%, 84.2% and 91.5%, respectively, showing that ^{99m}Tc-Fe_3O_4-DPD MNPs exhibits excellent in vitro stability, regardless the incubation conditions. After 72h of incubation

in all tested media ^{90}Y-Fe_3O_4-DPD MNPs showed radiochemical purity of 87.6%, 79.4% and 91.3% for saline, human serum and DTPA, respectively. Biodistribution after i.v. injection showed a high accumulation of MNPs in the liver 1h after administration (16.03% ID/g for ^{99m}Tc-Fe_3O_4-DPD and 11.28% ID/g for ^{90}Y-Fe_3O_4-DPD MNPs) as well as the long-term retention in the same organ. Low accumulation of both radiolabeled nanoprobes in lungs was observed. **Conclusion:** Radiolabeling of Fe_3O_4-DPD MNPs with gamma emitter ^{99m}Tc, and beta emitter ^{90}Y, seems to hold great potential for future applications in different imaging techniques and radionuclide/hyperthermia therapy. Furthermore sufficiently high hyperthermia temperature even at lower frequencies, pave the way towards the possible theranostic application of Fe_3O_4-DPD MNPs. **References:** None.

EP-0796

Development of new radopharmaceutical based on ^{177}Lu-labeled HEDP, DPD and IDP for the potential palliative treatment of painful bone metastases

Z. Milanovic, *M. Radović, M. Mirković, D. Stanković, D. Janković, M. Perić, A. Vukadinović, D. Petrović, S. Vranješ Đurić;*
Vinca Institute of Nuclear Sciences, Belgrade, SERBIA.

Aim/Introduction: Aim/Introduction: Bone seeking radiopharmaceuticals are important option in the management of metastatic bone pain. Due to some negative characteristics of routinely applied therapeutic radiopharmaceuticals, there is still much potential for the improvement. The aim of the present study was to investigate ^{177}Lu-labeled ligands: 1-hydroxyethane 1,1-diphosphonic acid (HEDP), 2,3-dicarboxypropane-1,1-diphosphonic acid (DPD), and imidodiphospha tetetrasodium salt (IDP), as potential bone pain palliation agents. **Materials and Methods: Materials and Methods:** Complex formation between non-radioactive lutetium ($LuCl_3$) and tested ligands was examined, using conductance and cyclic voltammetry measurements. Labeling of ligands with ^{177}Lu was confirmed by three different methods ITLC, HPLC, and electrophoresis. Biodistribution and bone accumulation was determined by ex vivo measurement of radioactivity in organs followed by in vivo imaging studies in healthy Wistar rats. Radioactivity in organs was measured in a well counter and obtained results are expressed as a percentage of injected dose per gram (%ID/g). **Results: Results:** Results revealed that all three examined ligands are capable to form stable complexes with ^{177}Lu in high radiolabeling yield (> 90%) forming in vitro stable complexes. The most critical parameters, with highest influence on the radiolabeling were concentration of ligands and pH. Determined by electrophoresis, radiolabeled complexes were electronegative molecules. Bone accumulation and retention after 0.5, 2, 96, and 168 h for the ^{177}Lu-HEDP, ^{177}Lu-DPD, ^{177}Lu-IDP were: 1.13±0.22%, 2.18±0.23%, 3.62±0.55% and 6.3±0.01%, respectively. The highest selective bone accumulation with relatively low uptake in soft tissue (less than 1% at all 4-time points), was observed only for ^{177}Lu-HEDP. Unlike ^{177}Lu-HEDP, other two ^{177}Lu-labeled ligands showed insignificant bone (<1%) and high liver (>1.5%) and spleen (>2%) uptake. **Conclusion: Conclusion:** Obtained results suggest that different functional groups beside phosphonate/phosphate groups present in the HEDP, DPD and IDP significantly affect the bone accumulation of ^{177}Lu-labeled complexes. This implicates that among examined complexes, only^{177}Lu-HEDP is suitable for further preclinical investigations. **References:** None.

EP-0797

Radiolabeling of Gold Nanoparticles With Lu-177 as a Platform for Cancer Theranostics

N. Daems[1], *M. Ooms*[2], *T. Cardinaels*[2], *S. Baatout*[3], *C. Michiels*[4], *S. Lucas*[5], *V. Karen*[2], *A. Aerts*[3];
[1]*SCK-CEN/UNamur, Mol, BELGIUM,* [2]*Radiochemistry expert group, Nuclear Materials Science, SCK-CEN, Mol, BELGIUM,* [3]*Radiobiology Unit, Biosciences, Environment, Health and Safety, SCK-CEN, Mol, BELGIUM,* [4]*Unité de Recherche en Biologie Cellulaire-NARILIS, UNamur, Namur, BELGIUM,* [5]*Research Center for the Physics of Matter and Radiation-NARILIS, UNamur, Namur, BELGIUM.*

Aim/Introduction: In cancer radiotherapy, gold nanoparticles (AuNPs) have emerged as promising radiosensitizers, which accumulate in the tumor and increase the effectiveness of external beam radiotherapy by local production of reactive oxygen species (ROS) and secondary electrons upon irradiation. Five nm gold nanoparticles surrounded by an organic shell of polyallylamine (PAA) are produced by plasma vapor deposition and are conjugated to anti-EGFR-antibodies (Cetuximab-Ctxb) for active tumor targeting (AuNPs-PAA-Ctxb). In order to increase the therapeutic effect of the AuNPs-PAA-Ctxb, we aim to radiolabel the nanoparticles with ^{177}Lu. **Materials and Methods:** The labeling approach would be to first link Ctxb with bifunctional chelators (BFCs), DOTA or DTPA, followed by conjugation of Ctxb-BFC to AuNPs-PAA. The final step comprises the radiolabeling of the AuNPs-PAA-Ctxb-BFC complex with ^{177}Lu. **Results:** MALDI-ToF MS analysis indicated that a 20, 40 and 80 molar excess addition of BFCs to the labeling reaction, leads to an increasing BFC:antibody ratio of 2, 3 and 5, respectively. However, a 40 and 80 molar BFC excess profoundly reduced the binding capacity of Ctxb to EGFR-overexpressing A431 cells. A radiochemical purity of > 95% was achieved after 3h at 50°C for Ctxb-DOTA-^{177}Lu or instantly at room temperature for Ctxb-DTPA-^{177}Lu. Moreover, both radiolabeled immuno-complexes were stable for at least 3 days in serum at 37°C. In addition, we showed that Ctxb-BFCs retain their target binding capacity when conjugated to AuNPs-PAA. **Conclusion:** When successful radiolabeling of AuNPs-PAA-Ctxb with ^{177}Lu is achieved and the target binding capacity of the nanoconjugates is preserved, further experiments can be conducted to investigate the specificity of the enhanced cancer cell killing effect on EGFR-overexpressing A431 cells. Furthermore, the biodistribution and the therapeutic effect of the radiolabeled AuNPs-PAA-Ctxb-^{177}Lu could be assessed after injection in tumor-bearing mice. **References:** None.

EP-58
Preclinical and translational aspects, including radiopharmacy, radiochemistry and drug development -> Radiopharmacy, radiochemistry, drug development -> Radiopharmacy -> Radiopharmaceuticals ? Multimodal / optical probes

October 12 - 16, 2019
e-Poster Area

EP-0798
Development of a bimodal (PET/NIR) tumor tracer for non-invasive staging and fluorescence guided surgery of prostate cancer

C. S. Kramer, T. Kanagasundaram, K. Kopka;
German Cancer Research Center (dkfz), Heidelberg, GERMANY.

Aim/Introduction: Prostate cancer is the second most common cancer type in men, thus modern treatment and diagnostic methods are needed especially for progressed stages. The detection of distant metastases and local lymph node metastases is not only important for oncological staging and therapeutic decision making, but also for oncological surgery. To provide a tracer that can be used for oncological staging in PET and for fluorescent light-guided surgery, we developed a PSMA-specific HBED-dye conjugate (1). To reduce the overall molecular weight we want to develop the next generation PSMA-specific tracer with a newly designed PET-activatable near-infrared (NIR) dye. While the PET-activated „hot" tracer enables oncological staging and preoperative planning, the NIR modality of the „cold" tracer can be used during surgery to detect more precisely lymph node metastases and enabling R0 resection while protecting healthy structures. **Materials and Methods:** Two different dye families (silicon rhodamines and silicon pyronines) were de-novo synthesized in high overall yields. Both classes of dyes are small molecules unifying the dye property and the radiolabel at an average MW of 500 g/mol. The silicon atom is not only crucial for the dye properties but fluorine can covalently bind to it, thus PET activation can proceed via a fluorine isotopic exchange. Therefore the silicon atoms needed to be decorated with a fluorinatable leaving group and a tert-butyl group that hampers hydrolysis. **Results:** The silicon pyronines possesses fluorescence properties in visible light with a high stokes shift from over 200 nm and can easily be radiolabeled via fluorine isotope exchange with up to 75% conversion. Initial stability experiments show water stability for at least 3.5 h. It is known that pyronines can be converted into NIR dyes in one step; experiments for this transformation are ongoing. The silicon rhodamines exhibit NIR properties (λ $_{abs}$ = 659 nm, λ $_{em}$ = 685 nm) with quantum yields up to 0.50 and initial experiments showed that PET nuclide labeling of this dye is possible. Furthermore, this dye class was also successfully coupled to a PSMA binding motif to enable first biochemical binding experiments. **Conclusion:** We could successfully synthesize de-novo two families of fluorescent dyes that can be "activated" for PET-imaging in an one step reaction whereby one dye class possesses NIR properties. The dye property and the radiolabel could so be reduced to an average molecular weight of 500 g/mol. **References:** (1) Kopka et al., J. Nucl. Med. 2018, 59, 639-645.

EP-0799
11ß-Ethylestradiol-PEG-DOTA: A novel highly affine estrogen a receptor ligand for radio-metalation

F. Braun[1], *S. Muñoz*[1], *V. Marmann*[1], *T. Fischer*[1], *H. Endepols*[1], *M. Pietsch*[2], *M. von Brandenstein*[3], *A. Drzezga*[1], *K. Schomäcker*[1];
[1]*University of Cologne, Clinic of Nuclear Medicine, Cologne, GERMANY,* [2]*University of Cologne, Institute of Pharmacology, Cologne, GERMANY,* [3]*University of Cologne, Clinic of Urology, Cologne, GERMANY.*

Aim/Introduction: Estrogen Alpha Receptors (ERα) are promising targets for radioactive estrogen-based vectors. After receptor binding, the radioactive estrogen is internalized and localized in the proximity of the DNA. This makes ERα an attractive target for use in the targeted radionuclide treatment. Up to this point, estrogens have mostly been labeled with radioactive halogens such as isotopes of iodine and fluorine. To overcome the obstacles of in vivo dehalogenation, 11ß-ethylestradiol (Ees), a much more affine ligand [1] than native Estradiol (Es), is labeled with radioactive metal ions such as ^{68}Ga and ^{177}Lu. **Materials and Methods:** Ees and Es were coupled to DOTA using a polyethylene glycol (PEG) linker and radiolabeled with ^{68}Ga and ^{177}Lu. The PEG-DOTA modified estrogens (EesPD and EsPD) were tested by a commercially available fluorescence polarization ligand binding assay in order to compare the affinity of the new compounds. The K_d-values of the corresponding radiolabeled compounds were determined by a newly developed binding assay basing on an ERα immobilisation on a high-adsorption plastic matrix (Brand). **Results:** The labeling of EsPD and EesPD yielded a radiochemical purity of >98% for ^{177}Lu and >96% for ^{68}Ga with a specific activity of 40 MBq/nmol. After 48h, stability of >89% in human serum was found in the case of [^{177}Lu] EsPD and -EesPD. The affinity experiments of non-radioactive precursor EsPD and EesPD revealed K_d-values of 70nM and 24nM. The binding assay with the corresponding radioactive estrogens labeled with ^{177}Lu resulted in K_d values of 610nM and 29nM. **Conclusion:** The modification with PEG-DOTA showed an obvious decrease in the receptor-affinity for both Ees and Es. However, EesPD also revealed that the presence of the ethyl group in the 11ß position of the steroid led to a higher affinity (factor 3). Labeling with radioactive lutetium resulted in a significant loss of affinity for EsPD (without ethyl group). In EesPD, this effect was not observed. The new compound EesPD appears to be an interesting precursor for use in targeting of BC with ERα overexpression. It shows potential for use in diagnosis as [^{68}Ga]EesPD as well as in therapy as [^{177}Lu]EesPD. **References:** Anstead GM, Carlson KE, Katzenellenbogen JA. The estradiol pharmacophore: ligand structure-estrogen receptor binding affinity relationships and a model for the receptor binding site. Steroids. 1997 Mar;62(3):268-303. Review.

EP-0800

Multimodal nanoparticles for integrated PET/MR imaging and therapeutic purposes

A. Deshotel[1,2], F. Bouraleh Hoch[1], V. Thakare[2], G. Laurent[1], C. Bernhard[2], A. Dubois[2], M. Moreau[2], A. Oudot[3], F. Brunotte[3], R. Bazzi[1], F. Denat[2], S. Roux[1];
[1]UTINAM, UMR 6213, CNRS, Université de Bourgogne Franche-Comté, 16 Route de Gray, 25030, Besançon, FRANCE, [2]Institut de Chimie Moléculaire de l'Université de Bourgogne, UMR 6302, CNRS, Université de Bourgogne Franche-Comté, 9 Avenue Alain Savary, 21000, Dijon, FRANCE, [3]Georges-François LECLERC Cancer Center - UNICANCER, 1 Rue Pr Marion, 21079, Dijon, FRANCE.

Aim/Introduction: In molecular imaging, overcoming limitations of some techniques by associating them with complementary advantages of others seems to be a promising strategy. Among the diverse options, allying the exceptional sensitivity of Positron Emitting Tomography (PET) with the high resolution of an anatomical modality like Magnetic Resonance Imaging (MRI) was the strategy chosen in this work. The development of imaging devices integrating those two modalities is in itself a major challenge as is the design and synthesis of multimodal probes. **Materials and Methods:** The synthesis of different theranostic nanoprobes for PET/MR imaging has been developed considering that the nanoparticles were to accumulate in unhealthy organs through EPR effect and to be eliminated by renal clearance. To get multimodal objects capable of immobilising different metal ions used in imaging (Gd^{3+} or ^{68}Ga) ultra-small gold nanoparticles were coated with different types of organic molecules. Macrocyclic chelators were coupled with a dithiolated anchoring part to get simple bifunctional ligands used to get a mixed layer on the surface of the nanoparticles. To overcome the complicated characterisation of these nanoparticles, three-way orthogonal platforms functionalised by two macrocyclic ligands and by a dithiolated grafting site were developed. To lessen the fast renal clearance of these objects, gold nanoparticles were grafted on biodegradable maghemite nanoflowers (negative contrast for MRI). The biodistribution of these nano-objects was studied in mice after radiolabelling using a preclinical PET/MR scanner. **Results:** The reduction of a gold salt in the presence of different dithiolated chelators provides ultra-small gold nanoparticles (core size: 2-3 nm, hydrodynamic diameter: 6-8 nm). After complexation of gadolinium, the nanoparticles were radiolabelled with ^{68}Ga. With a single intravenous injection, the biodistribution of these nanoparticles was followed simultaneously by T_1-weighted MRI (Gd^{3+}) and by PET (^{68}Ga) in mice with a PET/MR preclinical imaging device. Golden nanoflowers obtained by grafting gold nanoparticles on superparamagnetic iron oxide nanoflowers were followed in mice by T_2-weighted MRI (iron oxide) and PET (β^+ emitters) using the same imager as before. **Conclusion:** The different nanoprobes successfully behaved as imaging agents for integrated PET/MR imaging and were removed from the body through renal clearance in most cases. Owing to the therapeutic properties of the nanoparticles: radiosensitisation for the gold ones and magnetic hyperthermia for the iron oxide; the study of their biodistribution is a key step for their use as theranostics. **References:** Laurent et al. Nanoscale 2016, 8, 12054. Lartigue et al. ACS Nano 2012, 6, 10935.

EP-0801

^{99m}Tc-^{68}Ga-ICG MAA and Nano Colloid of human serum albumin: a tri-modal imaging agent

M. Marenco[1], M. G. Persico[1,2], G. Ferrarazzo[1], G. Cavenaghi[1], C. Aprile[3], L. Lodola[1];
[1]Fondazione IRCCS Policlinico San Matteo, Pavia, ITALY, [2]University School for Advanced Studies IUSS, Pavia, ITALY, [3]National Center for Oncological Hadrontherapy CNAO), Pavia, ITALY.

Aim/Introduction: Recent developments in sentinel lymph node (SLN) and in radio occult lesion localization (ROLL) suggest the need for a multi-modal contrast agent providing a better pre-surgical imaging via PET and an intra-operative mapping via fluorescence detection. For that reason, we have characterized a tri-modal SLN/ROLL targeting agent ^{99m}Tc-^{68}Ga-Indocyanine Green (ICG) with macroaggregated or nanocolloidal human albumin (^{68}Ga-^{99m}Tc-ICG-MAA/NC-HSA), based on SPET, PET and fluorescence imaging. **Materials and Methods:** Radiolabelling. Commercially available kits of MAA and NC-HSA particles are used for radiolabelling with ^{68}Ga and ^{99m}Tc. A buffered solution of ^{68}Ga-chloride is added to the MAA/NC kit previously dissolved in 2 mL saline. The ^{68}Ga-MAA/NC suspension is incubated in a heat block at 75 °C for 30 min. Then ^{99m}Tc Pertechnetate in saline is added to the labelling vial, incubated at room temperature for 20 min. Fluorescent tagging. A vial of ICG Pulsion® (25 mg) is dissolved in 5 mL water. 100 µL of this ICG solution is added to the ^{68}Ga-^{99m}Tc-ICG-MAA/NC-HSA vial (incubation at room temperature for 5 min). Quality control. The radiochemical purity (RP) after radiolabelling was assessed with ITLC, mobile phases MetOH:H_2O 85:15 and tribasic-citrate solution 0.1 M, pH 6 for ^{99m}Tc and ^{68}Ga respectively. Fluorescent purity was measured by the same iTLC method (MetOH:H_2O 85:15) scanned with a PDE (PhotoDynamicEye) probe. **Results:** The RP for the ^{68}Ga and ^{99m}Tc labelled MAA and NC was ≥ 97 %. without significant radioactivity at the solvent front (^{99m}Tc pertechnetate and free or hydroxylated ^{68}Ga) with the respective mobile phases. Fluorescent purity was affected by a variable amount (5-20%) of unbound dye. Additional in vitro stability tests of the hybrid imaging agent assessed with DTPA challenge, dilution test and incubation in human plasma confirmed the compound stability. Polycarbonate membrane (50-30 nm pore size, Nuclepore) filtration confirmed the absence of agglutination of NC after labelling procedure. **Conclusion:** This first attempt shows the possibility to obtain a SPET/PET/fluorescence imaging agent starting from commercially available kit, with a simple procedure and no additional pre- or post- purification steps. PET imaging with ^{68}Ga could provide a quantitative pre-operative map for surgical planning with a better spatial resolution and the possibility to predict signal intensity during surgery. The presence of Tc-99m could be useful to assess the validity of the

model proposed, in vitro at first and then in clinical practice. **References:** None.

EP-0802

^{68}Ga-DTPA-FITC-Silk Fibroin Nanoparticles, a Promising Agent for Positron Emission Tomography and Fluorescence Dual Modal Imaging

M. Asensio Ruiz[1], *A. Garcia Aliaga*[1], *A. Abella Tarazona*[1], *A. Lozano Pérez*[2], *J. Cenis*[2], *T. Martinez Martinez*[1];
[1]*Unidad de Radiofarmacia, Hospital Clínico Universitario Virgen de la Arrixaca, Murcia, SPAIN,* [2]*Departamento de Biotecnología, Instituto Murciano de Investigación y Desarrollo Agrario y Alimentario (IMIDA), Murcia, SPAIN.*

Aim/Introduction: In the last decades the Silk Fibroin Nanoparticles (SFNs) have received considerable attention not only for their ability to act as active vehicle for low bioavailability drugs and/or biomolecules, but also for their highly biocompatible and non-antigenic nature. On the other hand, ^{68}Ga has also attracted the attention though the increasing development of generator-based ^{68}Ga targeting vectors and their wide applications for diagnosis and treatment, especially, theragnosis. The purpose of this work is the dual labeling of SFN with fluorescein (FITC) and ^{68}Ga diethylene pentaacetic acid (DTPA), as a diagnostic agent with improved sensitivity and accuracy, and a new platform for future theragnostic applications. **Materials and Methods:** SFNs were prepared by nanoprecipitation in MeOH. The DTPA-functionalized silk fibroin nanoparticles (DTPA-SFNs) were prepared by amide coupling reaction using the EDC/NHS activating system. DTPA-FITC-SFNs were prepared by adding FITC in DMSO to DTPA-SFN in carbonate buffer. After the washing steps, DTPA-FITC-SFNs were dispersed in ultrapure water, autoclaved (121 ºC 30 min) and kept refrigerated and protected from light until use. For the optimization of radioisotope loading, aqueous suspensions of DTPA-FITC-SFNs from 1 to 10 mg/ml were incubated with up to 74 MBq of $^{68}GaCl_3$ in 0.1 M HCl from a ^{68}Ge/^{68}Ga generator. In order to improve the radiolabeling yield, different loading conditions (buffered aqueous loading media, incubation time and effect of temperature) were tested. Labeling yield was calculated as radioactivity in SFNs divided by total radioactivity. Stability of the labeling was tested by incubation in saline under stirring, at room temperature for 1 hour. The hydrodynamic characterization of the nanoparticles was performed by DLS technique and Zaverage (d.nm), PdI and Zpotential (ζ, mV) were determined before and after radiolabeling. **Results:** Radiolabeling yield was SFN concentration dependent, ranging from 16.31 ±1.38 % (n=6) to 58.00±2.63% (n=8), with a residual activity in supernatants after incubation from 2% to 12% (n=16). The radioactivity loading content varied from 11 MBq/mg SFNs to 4 MBq/mg SFNs (n=24). The size of the loaded nanoparticles slightly decreased after radiolabeling and the Z potential shifted to less negative values due the effect of positive charges contributed by the ^{68}Ga ions bounded to the DTPA in the nanoparticles. **Conclusion:** ^{68}Ga-DTPA-FITC-SFNs are a promising dual modal imaging agent. Further studies, including stability tests, cytotoxicity in cell cultures and in vivo distribution are needed in order to determine the actual performance and their effectiveness in nanomedicine. **References:** None.

EP-0803

Folate Receptor Targeted Dual-modality Imaging Agent For Molecular Imaging And Fluorescence-guided Surgery

D. Kim, M. Kim, S. Kim;
Wonkwang University School Of Medicine, Iksan, Jeollabuk-do, KOREA, REPUBLIC OF.

Aim/Introduction: Folate receptor (FR) is an ideal target for cancer imaging because it is frequently overexpressed in major types of human tumor, whereas its expression in normal organs is highly limited. Combining nuclear and fluorescence imaging techniques provides a novel approach for cancer imaging and monitoring surgery. In the present study, we developed Tc-99m Folate-Gly-His-Glu-Gly-Glu-Cys-Gly-Lys(-5-Carboxy-X-rhodamine)-NH_2 (Folate-ECG-ROX) as a dual modality imaging agent to target FR-positive tumor cells. Simultaneous labeling with Tc-99m and ROX could provide both nuclear and fluorescent imaging. The diagnostic performance and surgical usage of Tc-99m Folate-ECG-ROX as a dual-modality imaging agent for tumor was also evaluated in a murine model. **Materials and Methods:** Folate-ECG-ROX was synthesized using Fmoc solid-phase peptide synthesis. Radiolabeling of Folate-ECG-ROX with Tc-99m was done using ligand exchange via tartrate. Binding affinity and in vitro cellular uptake studies were performed. Gamma camera imaging, biodistribution and ex vivo imaging studies were performed using KB and HT-1080 tumor-bearing murine models. Tumor tissue slides were prepared and analyzed with immunohistochemistry staining and confocal microscopy. Surgical removal of tumor nodules in murine models with peritoneal carcinomatosis was performed under the fluorescence imaging system. **Results:** After radiolabeling procedures with Tc-99m, Tc-99m Folate-ECG-ROX complexes were prepared in high yield (> 97%). The K_d of Tc-99m Folate-ECG-ROX for KB cells was estimated to be 6.9 ± 0.9 nM. Gamma camera imaging revealed substantial uptake of Tc-99m Folate-ECG-ROX in KB tumors. Specific uptake of Tc-99m Folate-ECG-ROX was assessed by biodistribution, ex vivo imaging and immunohistochemistry staining studies. Under real-time optical imaging, the removal of visible nodules was successfully performed. **Conclusion:** We developed Tc-99m Folate-ECG-ROX as a dual modality imaging agent targeting FR of tumor. In vivo and in vitro studies demonstrated substantial and specific affinity of Tc-99m Folate-ECG-ROX for FR. Nuclear imaging using Tc-99m could allow quantitative assessment of organ distribution and tumor accumulation while fluorescent imaging using ROX could provide microscopic, ex vivo, and in vivo fluorescent imaging. Thus, Tc-99m Folate-ECG-ROX could provide both pre-operative molecular imaging and intra-operative guidance. Its feasibility was simulated in murine models. Taken together, results of the present study suggest that

Tc-99m Folate-ECG-ROX is a potential dual-modality imaging agent for diagnosis and surgical guidance of FR-positive tumor. **References:** None.

EP-59

Technical aspects -> Instrumentation and data analysis -> Data analysis -> Artificial intelligence and Radiomics

October 12 - 16, 2019 e-Poster Area

EP-0804

Prospective evaluation of a Novel Deep Learning Algorithm (PSMA-AI) in the assessment of 99mTc-MIP-1404 SPECT/CT in patients with low or intermediate risk prostate cancer

F. Pouliot[1], K. Sjöstrand[2], N. Stambler[3], J. Richter[2], K. Gjertsson[2], K. Johnsson[2], V. Wong[3], J. Jensen[3], L. Edenbrandt[2,4], A. Anand[2,5]; [1]Université Laval, Quebec City, QC, CANADA, [2]EXINI Diagnostics, Lund, SWEDEN, [3]Progenics Pharmaceuticals Inc, New York, NY, UNITED STATES OF AMERICA, [4]Gothenburg University, Gothenburg, SWEDEN, [5]Skane University Hospital, Lund, SWEDEN.

Aim/Introduction: ^{99m}Tc MIP-1404 (1404) is a PSMA targeted imaging agent for the detection and staging of clinically significant prostate cancer. Manual assessment of tracer uptake in SPECT/CT images introduces inherent limitations in inter- and intra-reader standardization. The study objective was to evaluate the performance of PSMA-AI assisted reads over manual assessment and known clinical predictors. **Materials and Methods:** The study analyzed 464 evaluable patients with very low-, low-, or intermediate- risk prostate cancer, whose diagnostic biopsy indicated a Gleason grade of ≤ 3+4 and/or who were candidates for active surveillance (1404-3301). All subjects received an IV injection of 1404 and SPECT/CT imaging was performed 3-6 hours post-dose. Three independent readers evaluated the images. All subjects underwent either voluntary RP (low- and intermediate-risk) or prostate biopsy (very low-risk) post dosing. Clinically significant disease was declared in subjects with Gleason grade 7 or higher. The PSMA-AI was developed and locked prior to the analysis. Three different independent readers used PSMA-AI to obtain quantitative expression of 1404 in the prostate against the background (PSMA-Index). PSMA-Index for all readers and subjects were compared to the histopathological reference, yielding 6 receiver operating characteristic (ROC) curves (3 manual reads + 3 PSMA-AI assisted reads). The clinical performance of the 1404 PSMA-AI assisted read was also evaluated by comparing the Area Under the ROC Curve (AUC), of a multivariate model (PSA, clinical staging and diagnostic Gleason score) with and without PSMA-Index. **Results:** The manual reads demonstrated AUCs of 0.62, 0.62 and 0.63. The reads with PSMA-AI demonstrated AUCs of 0.65, 0.66 and 0.66. The PSMA-AI performance in terms of AUC was higher than manual in all 3*3=9 pairwise comparisons between the two reader groups, with statistically significant improvement observed in five cases (nominal p<0.05), not accounting for multiple comparisons. The predictive ability of the baseline multivariate model, without PSMA-Index, was at AUC 0.74. Upon adding of PSMA-Index, the model predictive ability increased to AUC 0.77. The logistic regression model indicated that PSMA-Index (p=0.004), pre-surgery PSA (0.018) and % positive cores (p=<0.001) were significantly associated with clinically significant disease. When measuring reproducibility, log (PSMA-Index) correlation coefficients for pairs of PSMA-AI readers were 0.94, 0.97 and 0.98. **Conclusion:** The study demonstrated that PSMA-AI provides a standardized platform to generate reproducible quantitative assessment of 1404. The PSMA-AI assisted read demonstrated an additive improvement over manual assessment and other known predictors for identifying men with clinically significant disease. **References:** None.

EP-0805

18F-FDG PET/CT radiomic features for the prediction of clinical outcomes in locally advanced breast cancer (LABC)

A. Bettinelli[1], L. Evangelista[2], A. Zorz[1], L. Cuppari[2], M. Paiusco[1]; [1]Medical Physics Department, Veneto Institute of Oncology IOV - IRCCS, Padua, ITALY, [2]Nuclear Medicine Unit, Veneto Institute of Oncology IOV - IRCCS, Padua, ITALY.

Aim/Introduction: Current metabolic information, alongside immunohistochemical parameters, cannot accurately predict the clinical outcomes in LABC. Radiomic metabolic features extracted from 18F-FDG PET/CT may prove to be stronger predictive factors for determining neoadjuvant chemotherapy (NAC) outcomes, capturing the intratumoral heterogeneity which is considered to be strongly associated to treatment response. As a preliminary step, the relationship between tumor clusters, as defined by radiomic metabolic features, and histopathologic characteristics, tumor response to NAC, disease free survival (DFS) as well as overall survival (OS) in LABC patients has been investigated. Furthermore, we sought to identify an image-derived signature that can stratify patients into low/high survival groups. **Materials and Methods:** 18F-FDG PET/CT images of 72 LABC patients were retrospectively analyzed for metabolic radiomics. Immunohistochemical parameters included Ki67, ER, PR, and HER2. Primary tumors were delineated by a semi-automatic tool and checked by two expert nuclear medicine physicians. From PET images 168 features has been extracted in a 3D approach; IBEX software was employed for the task. Consensus clustering was used to group tumors that exhibit similar radiomic metabolic patterns. Chi-square test was applied in comparing the proportion of ER-positive (>10%), PR-positive (>10%), HER2-positive (+++), high Ki67 expression (>20%) and pathologic complete response (pCR) among clusters. Wilcoxon based, Fisher Score and Minimum-redundancy-maximum-relevance (mRMR) filter type methods were employed for feature selection. Four features were selected, for each method, as covariates for the COX proportional hazard

ratio model. Survival curves were obtained by Kaplan-Meier method. Patients were followed for at least 5 years. Analysis was performed by using Matlab and R-software. **Results:** Out of 72 patients, 40(55%) had a ER-positive LABC, 54(74%) showed a tumor proliferation index (Ki67)>20%, 19 (26%) were responders to NAC, 24 (33%) had a recurrence of disease and 18 (25%) died. A significant difference emerged for Ki67 expression among clusters, while any difference was found for other clinical data. The median value of each signature was able to stratify patient survival; in particular, according to the Fisher Score, patients with a value lower than the signature median threshold showed a better OS than the counterpart (p-value = 0.015). The stratification achieved with the identified signature outperform the one obtained with PR-positive status (p-value = 0.077), the most predictive immunohistochemical parameter. **Conclusion:** Radiomic features defining the signature, which capture metabolic phenotype, add valuable information for both LABC stratification and outcome prediction. Validation of the results is ongoing on a different sample. **References:** None.

EP-0806

Comparison of machine learning methods for automated [^{18}F]-FDG PET based hydrocephalus classification

M. Grosch[1], *L. Kaiser*[2], *S. A. Ahmadi*[1], *P. Bartenstein*[2], *A. Zwergal*[1,3], *S. Ziegler*[2];
[1]*German Center for Vertigo and Balance Disorders, University Hospital, LMU Munich, Munich, GERMANY,* [2]*Department of Nuclear Medicine, University Hospital, LMU Munich, Munich, GERMANY,* [3]*Department of Neurology, University Hospital, LMU Munich, Munich, GERMANY.*

Aim/Introduction: Machine learning methods aiming at enhanced medical image analysis are subject to ongoing research. In this study, [^{18}F]-FDG PET data from patients with normal pressure hydrocephalus (NPH) and healthy controls were processed to test the capability and accuracy of automated hydrocephalus classification. **Materials and Methods:** A total of 49 [^{18}F]-FDG PET datasets were included in the study, consisting of a study group with 25 NPH patients and a control group with 24 healthy subjects. Image data were normalized to percent injected dose per ml (%ID/ml) and average values in 83 brain regions were determined based on the Hammersmith atlas (n30r83; implemented in PMOD image analysis software). These were taken as input parameters for subsequent analysis. Univariate statistical analysis was performed using SPSS and multivariate analysis using scikit-learn software implemented in Python. Three different classification models (random forest (rf), logistic regression (lr), support vector machine (svm)) were implemented with 5-fold nested-cross-validation (nCV), feature reduction (FR) and principle components analysis (PCA) aiming to identify hydrocephalus patients. **Results:** Univariate SPSS analysis of input features in corresponding brain regions between groups yielded significant differences for 13 brain regions, which were exclusively located in the periventricular zones (e.g. caudate nucleus, thalamus, cingulate gyrus) ($p < 0.005$; Mann-Whitney-U-test). The classification accuracy averaged over 5 nCV folds was 0.87 (rf), 0.97 (lr), 0.95 (svm) without performing FR/PCA. FR to 10 features, based on an ANOVA calculation, without subsequent PCA resulted in an accuracy of 0.89 (rf), 0.83 (lr), 0.85 (svm) and with additional PCA to 5 components in an accuracy of 0.85 (rf), 0.91 (lr), 0.91 (svm). Extracting 5 components by applying PCA to all 83 features without FR provided a classification accuracy of 0.91 (rf), 0.93 (lr), 0.93 (svm). **Conclusion:** This pilot study indicates that advanced machine learning methods based on [^{18}F]-FDG PET features allow to classify NPH against healthy controls with high accuracy. Similar performance across applied classification models was found. Larger patient cohorts are needed to account for overfitting in training procedures. In addition, classification algorithms will be applied to patient groups with different cerebral pathologies in order to investigate them in clinically relevant questions. **References:** None.

EP-0807

A questionnaire-assist deep learning method to classify dementia diseases by using Tc-99m ECD SPECT image

F. Tseng[1], *Z. Lin*[1], *P. Chiu*[2], *G. Hung*[3], *Y. Ni*[1];
[1]*Institute of Nuclear Energy Research, Taoyuan City, TAIWAN,* [2]*Department of Neurology, Show Chwan Memorial Hospital, Changhua City, TAIWAN,* [3]*Chang Bing Show Chwan Memorial Hospital, Changhua City, TAIWAN.*

Aim/Introduction: Recently deep learning is a powerful tool in image classification. Tc-99m ECD single photon emission tomography (SPECT) images with a convolutional neural network can be applied to the classification of dementia diseases. However, it is not easy to acquire a large number of nuclear medicine images for training. In this study, we analyze the feature importance of dementia questionnaires with a deep neural network (DNN) and try to use the information to improve the convolutional neural network (CNN). **Materials and Methods:** For preparing materials of training data, data aggregation and data cleaning will be applied on seventy Tc-99m ECD SPECT images and five thousand questionnaires data from different sets of patients. After data pre-processing, we have trained five thousand questionnaires with DNN and seventy SPECT images with CNN. In the training process, transfer learning method was used in the CNN model such as ResNet50. Finally, we will concatenate feature vectors of DNN model into the flatten layer of CNN. **Results:** In the dementia questionnaires, the diseases divided into four cases: Alzheimer Disease (AD), Parkinson Disease (PD), Normal control (NC) and others. The preliminary predicted results of DNN model shown that the accuracy of AD, PD, and NC were 84%, 79% and 73% on the validation set of questionnaire. Since the number of Tc-99m ECD SPECT images was insufficient, we froze the weights of the CNN model for first several layers and fine-tune the neural network. We will adjust the parameters of the neural network and use cross-validation to obtain better predictive performance. **Conclusion:** Deep learning is a data-driven technology that

performs better as the number of training data increased. But medical nuclear images are expensive and difficult to obtain, especially in the normal database. The dementia questionnaires were expected to provide additional information to improve the training process. We believe that the method could increase the predictive performance of nuclear medicine images classification in the small-scale datasets. **References:** Yiming Ding, Jae Ho Sohn and Michael G. Kawczynski and et al., "A Deep Learning Model to Predict a Diagnosis of Alzheimer Disease by Using 18F-FDG PET of the Brain", Radiological, 2018. Andre Esteva, Alexandre Robicquent, Bharath Ramsundar and et al., "A guide to deep learning in healthcare", nature medicine, 2019.

EP-0808

Reinforcement Learning for Automated PET Image Segmentation

R. L. Smith, *L. Bartley, S. Paisey, C. Marshall;*
Cardiff University, Cardiff, UNITED KINGDOM.

Aim/Introduction: To utilize quantitative information provided by PET it is necessary to differentiate abnormal tissue from surrounding areas; accurate image segmentation is therefore paramount. A popular image segmentation technique is thresholding which relies on the intensity of images and is suitable in PET due to the low resolution and high contrast. Large variability in intensities of pathologies and noise make defining a consensus on the optimal thresholding level difficult. To address these problems, we for the first time set PET image thresholding in a Reinforcement Learning (RL) paradigm. RL is inspired by behavioral psychology where an artificial agent makes actions (A_t) in an environment (E) described by its current state (S_t) seeking to maximize a reward (R) to perform a desired task. This sequential decision making is formulated as a Markov Decision Process (MDP). Q learning used in this work is a form of model free RL where the agent may select the best action based on values learned in a Q table during exploitation, or to explore the environment by taking random actions. With successive iterations the Q table is updated using the Bellman equation until optimal Q values and hence action selection policies are learned in the Markovian domain. **Materials and Methods:** RL for PET image segmentation of five spheres from the NEMA Image quality phantom was performed. 20MBq of Fluorine-18 was inserted into the background. Five spheres with varying inner diameter [37mm, 28mm, 22mm, 17mm, 13mm] were filled with 5MBq/ml of 18F. Image thresholding of PET images was framed as an MDP; S_t was defined as the thresholding value; A_t as increasing or decreasing the threshold value; R as the negative absolute difference between the ground truth volume and the segmented volume. Q learning was performed until the terminal state was reached. **Results:** The percentage difference between the ground truth volume and that calculated from the segmentation allows a measure of accuracy to be determined. This error value for the five spheres in descending volume was 1.3%, 0.8%, 0.01%, 1.6% and 2.0% respectively; exceeding performance of previous reported thresholding segmentation in the literature. **Conclusion:** The final paper will perform analysis of the method in-vivo using 18F studies where the ground truth will be obtained from organ dissection of the preclinical model. RL for PET thresholding provides an attractive option for image segmentation. **References:** None.

EP-0809

Low Dose CT to Assess Performance of Deep Learning Pre-Clinical Medical Image Segmentation for Automated Organ-wise Delineation of PET

R. L. Smith[1], *N. Evans*[1], *V. Florence*[2], *S. Paisey*[1], *E. Fittock*[1], *F. Siebzehnrubl*[1], *C. Marshall*[1];
[1]*Cardiff University, Cardiff, UNITED KINGDOM,*
[2]*Polytech Marseille, Marseille, FRANCE.*

Aim/Introduction: Micro-PET-CT allows non-invasive monitoring of biological processes, disease progression and therapy response. Morphological information provided by CT allows organ / tissue delineation for subsequent quantification of physiological information depicted by PET. Deep learning with convolutional neural networks (CNNs) has achieved state-of-the-art performance for automated medical image segmentation and utilized successfully by our group in Micro-PET-CT. The robustness of such approaches in the presence of noise addition / dose reduction of the CT data has not been explored. We thus simulate dose reduction of pre-clinical CT images using a Poisson noise model and evaluate the effect of segmentation performance with increasingly lower dose for 6 regions (skeleton, kidney, bladder, brain, lung, muscle and fat). **Materials and Methods:** Negating electronic noise and subject anatomy, variance in x-ray images may be asserted to quantum noise allowing a model for simulated image noise versus dose (mA) to be constructed. With a mono-energetic x-ray source the mean number of photons (N) incident on the detector is $N=N_o\exp^{(-projections)}$; N_o represents x-ray intensities. N is modelled as a Poisson process ($\lambda=N$) a term for the projection noise is thus $\log(N/N_o)$. Modulating N_o serves as a variable to control noise levels ($\sim 1/N_o$) in projections. A linear relationship between image variance in a central region of an example image and $1/N_o$ was found. As image variance ~ 1/mA, systematically reducing N_o has the effect of simulating a percentage dose reduction in mA. Simulated dose reduction of 5 test cases (50kVp, 300mA, 0.25x0.25x0.25mm) was performed in the sinogram domain allowing reconstruction of noisy simulated CT images. Dose reduction was performed from 10% - 100% in increments of 10%. Test images were segmented using our previously trained model for whole body pre-clinical image segmentation. The Dice coefficient of the six segmented regions for each test case and each dose reduction was assessed. **Results:** The percentage reduction in DICE from the ground truth serves as a measure of the reduction in performance of the segmentation with increasing noise. A 50% dose reduction was for all 5 test subjects resulted in a mean (across all 6 organs) percentage reduction in DICE <25%. **Conclusion:** The pattern in reduction in performance of segmentation as dose was reduced was

similar for each tissue. This may have implications for utilizing reduced dose CT coupled with a deep CNN for segmentation if the CT component is used to anatomically locate physiology on PET data. **References:** None.

EP-0810

Determining the influence of patient's positioning in prone/supine breast PET/CT examination on the selection of the contouring algorithm using radiomics features

D. Borys[1], *I. Gorczewska*[1], *K. Matusik*[2], *M. Jarzab*[3], *A. d'Amico*[1]; [1]*Department of PET Diagnostics, Maria Sklodowska-Curie Memorial Cancer Center and Institute of Oncology, Gliwice Branch, Gliwice, POLAND,* [2]*Silesian University of Technology, Gliwice, POLAND,* [3]*III Department of Radiotherapy and Chemotherapy, Maria Sklodowska-Curie Memorial Cancer Center and Institute of Oncology, Gliwice Branch, Gliwice, POLAND.*

Aim/Introduction: Any PET/CT study in standard clinical routine is performed in a supine position. Breast examination in MRI scan is executed in a prone position with a breast coil to improve the signal to noise ratio. This difference in patient position results in large deformation of the region of interest and impedes comparison of PET/CT study with MRI. We have compared the outcome of PET/CT scan in a supine and prone position. For both positions, a radiomic features of the lesion were determined using three contouring algorithms. Our question was how the selection of the algorithm influences the radiomic features and how the situation changes in both positions. **Materials and Methods:** 225 patients with lesions in breast were selected and double PET/CT series were performed in both positions: supine and additional prone. Mean age of patients was 46.2 years +/- 11 (range 21 to 72). Prone position was achieved using a homemade pad, with the shape of breast coil in MRI. Regions of interest including lesions were contoured using three segmentation methods: adaptive contouring, 41% maximum and 2.5 SUV implemented in Philips IntelliSpace station. Using pyRadiomics (v2.1.0), for the original image, 100 features were computed in groups: shape, first order and texture based (GLCM, GLRLM, GLSZM, GLDM). Data analysis was performed using python to compare above-mentioned parameters if they differ significantly regarding the algorithm used. Tests were performed for each position separately. Statistical significance was determined using Friedman's non-parametric test with p-value less than 0.05 considered as significant. **Results:** For both positions, we have observed significant differences for selected contouring algorithms in a various number of radiomic features. For supine, there were 63 parameters statistically different while in prone 64. 58 parameters were tatistically different in both positions, 32 had p-value above 0.05 meaning that there were no differences. In 10 parameters position of the patient during the study was crucial, because the statistical concluding was different - we have observed the change in p-value regarding the supine/prone position (varying from below to above-established level of statistical significance). **Conclusion:** Statistical significant differences were observed in more than half of analyzed radiomic features independently of the patient position. Based on the results we can conclude that the position of the patient during the PET/CT study in breast cancer imaging and the selection of the contouring algorithm may affect the variability of the determined radiomic features. **References:** Acknowledgment: Grant No. STRATEGMED2/267398/4/NCBR/2015.

EP-0811

Stability of PET Radiomic Features: A Preclinical Study

E. Alsyed[1], *R. Smith*[2], *C. Marshall*[2], *S. Paisey*[2], *E. Spezi*[1,3]; [1]*School of Engineering, Cardiff University, Cardiff, UNITED KINGDOM,* [2]*Wales Research & Diagnostic PET Imaging Centre, Cardiff, UNITED KINGDOM,* [3]*Velindre Cancer Centre, Cardiff, UNITED KINGDOM.*

Aim/Introduction: Extracting quantitative features from medical images is known as radiomics. Several studies support the claim of using radiomic features as biomarkers in cancer treatments. Defining the volume of tumour or region of interest (ROI) is one of the most critical steps in the radiomic process. Radiomic output may vary with different delineation size. The objective of this study is to evaluate the stability of PET image radiomic features with different tumour delineation volumes. **Materials and Methods:** Eight mice with 4T1 tumours injected with 10.0 ± 2.0 MBq of 18F-FDG, 50 minutes post injection they were imaged (by Mediso Nanoscan PET/CT) for 20 minutes. Four regions of interests (ROIs) were defined by four different systematic 3D-Contour sizes (4, 4.5, 5, 5.5 mm). Seventy-eight 3D-radiomic features were extracted using SPAARC (Spaarc Pipeline for Automated Analysis and Radiomic Computing an in-house developed tool built on Matlab) for each volume. The intra-class correlation coefficient (ICC) was calculated for each feature [2]. **Results:** Forty-two (54%) features show ICC ≤ 0.50. Only one feature (infoCorrelation1) of GLCM3D shows ICC ≥ 0.80. Thirty-five (45%) features exhibited 0.80 > ICC ≥ 0.50. **Conclusion:** Robustness and stability of PET image radiomics in tumour volume is feature-dependent. Different volumes of tumours affect the radiomic output. Further studies are needed to evaluate the influence of the partial volume effect on PET/CT image radiomic features. Radiomic features with high ICC can be safely used while features with low or medium ICC should be used with caution especially during patient management. **References:** 1. Cook, G. J. R., Siddique, M., Taylor, B. P., Yip, C., Chicklore, S., & Goh, V. (2014). Radiomics in PET : principles and applications, 269-276. https://doi.org/10.1007/s40336-014-0064-0 2. Parmar C, Rios VE, Leijenaar R, Jermoumi M, Carvalho S, Mak RH, Mitra S, Shankar BU, Kikinis R, Haibe-Kains B, Lambin P, Aerts HJ. Robust Radiomics feature quantification using semiautomatic volumetric segmentation. Plos One 2014;9:e102107 3. Tong, S., Alessio, A. M., & Paul E Kinahan. (2010). Image reconstruction for PET/CT scanners: past achievements and future challenges. Imaging in Medicine, 2(5), 529-545. https://doi.org/10.2217/iim.10.49.Image 4. Zwanenburg, A. et al, 2019, The image biomarker standardisation initiative, <https://arxiv.org/abs/1612.07003>.

EP-0812

Precision and Accuracy of Radiomics Analysis at Poor Noise Conditions: a Phantom Study Using 3D Printed 'Tumor' Inserts

A. Somasundaram[1], *E. Pfaehler*[1], *J. van Sluis*[1], *D. Vállez García*[1], *E. G. E. de Vries*[1], *R. A. J. O. Dierckx*[1], *R. Boellaard*[1,2];
[1]*University Medical Center Groningen, Groningen, NETHERLANDS,* [2]*Amsterdam University Medical Centers, Amsterdam, NETHERLANDS.*

Aim/Introduction: ^{89}Zr-MAb PET, used in oncological studies to predict targeting of MAbs, suffers from poor signal-to-noise ratio, which affects quantitative radiomic metrics. In order to obtain an optimal ^{89}Zr PET radiomics analysis, it is important to identify those features least sensitive to noise. High versus low noise phantom studies were performed using 3D printed phantom inserts reflecting realistic tumor shapes and tracer uptake, to study radiomic feature accuracy and precision. **Materials and Methods:** A NEMA image quality phantom containing ^{18}F-FDG filled inserts was scanned for 30 minutes. From the list-mode scan, ten frames each for 5s and 120s frame durations were reconstructed. The noise conditions in 5s scan are comparable to those typically seen in ^{89}Zr PET. All images were reconstructed using three different reconstruction protocols with varying degrees (full width at half maximum in mm) of Gaussian smoothing: EARL1 (6.5 mm), EARL2 (5.0 mm), and clinical (2.0 mm). Volumes of interest (VOI) were manually defined on the low dose CT images. VOI perturbations of one voxel, including erosion, dilation, and translation, were applied to simulate segmentation errors. Intraclass correlation coefficients (ICC) were calculated between the ten frames for each frame duration. A similarity distance metric (SDM) measuring within-subject similarity was used to calculate the difference of the short frame duration feature as well as of the perturbed VOI feature from the original 30 minute scan feature. ICC and SDM above 0.75 were regarded as high. **Results:** For the different reconstructions, a high ICC was observed in 95-99% of features for the 120s frames, and in 84-90% of features for the 5s frames. In the 120s scan, 43%, 76%, and 86% of features yielded a high SDM for clinical, EARL2, and EARL1 reconstructions respectively. The percentages for the 5s scan dropped to 12%, 16%, and 21%, correspondingly. VOI translation yielded a high SDM for 87-99% of features for all reconstructions. VOI dilation or erosion by one voxel resulted in a high SDM for only 59-78% of features for EARL and 75-81% for clinical reconstructions. **Conclusion:** Although a majority of features from ^{89}Zr PET-like noisy images are similar between them, these features show a large bias compared with those from optimal noise conditions. VOI dilation and erosion have a larger impact on radiomic feature performance than VOI translation. Because increased smoothing results in lower noise, EARL reconstruction seems to result in a more favorable radiomic feature performance. **References:** None.

EP-0813

Image-based biomarkers for resectable NSCLC using F-18-FDG-PET/CT: evaluation of a novel Matlab based algorithm for better characterisation of radiomics features

K. Kneer[1], *J. Steinacker*[2], *N. Eberhardt*[1], *E. Yousefzadeh-Nowshahr*[1], *J. Raacke*[1], *S. Rüdiger*[3], *C. Kropf-Sanchen*[3], *M. Beer*[2], *V. Prasad*[1], *G. Glatting*[1], *A. Beer*[1];
[1]*University Hospital, Department of Nuclear Medicine, Ulm, GERMANY,* [2]*University Hospital, Department of Diagnostic and Interventional Radiology, Ulm, GERMANY,* [3]*University Hospital, Department of Internal Medicine II, Ulm, GERMANY.*

Aim/Introduction: Predictive and prognostic parameters from texture analyses (TA) of F-18-FDG-PET/CT in NSCLC are often calculated based on Cox proportional hazard method (CoxM). However, the value of some of the parameters in case of non proportional hazards can be challenging. In this work we evaluated a new Matlab based algorithm to determine the optimal prognostic threshold of these parameters. **Materials and Methods:** Pre-therapy PET/CT data of 81 patients (66a, f21, m60) with histologically confirmed NSCLC with a median follow-up of 4.6a were retrospectively analysed. A volume of interest defined for the primary tumor was analysed for PET and CT using MIPAV. We focused on the following imaging parameters: CT-volume and solidity, circularity, kurtosis, excentricity, SUVmax for PET. CoxM and our novel Matlab based methods were used to determine the prognostic values of aforementioned parameters. On Matlab, the optimal thresholds were determined as follows: 1.patient data were sorted in ascending order of the investigated parameter. Then different thresholds were defined using Matlab. Both groups as divided by the threshold were tested for significance (log-rank-test, $p<0.05$). 2.Best threshold was defined as the one with the lowest p-value. 3.We compared four groups by combining two parameters, e.g. SUVmax and CT-volume. P-value was calculated with the log-rank test. **Results:** None of the analysed image based parameters showed proportional hazard on CoxM. Poor negative prognostic value was observed for CT-volume >1434 mm³ (p=0.018). PET-parameters showed significant negative prognostic value for SUVmax >12.2 (p=0.003), solidity >0.9810 (p=0.004) or circularity >0.1966 (p=0.009). For small CT-volumes, prognosis was excellent independent of other PET/TA parameters. In larger tumors different subgroups could be defined by combining CT-volume and SUVmax/TA-parameters of PET. Tumors with larger volume and higher SUVmax showed significantly worse prognosis compared to tumors with smaller volume and lower SUVmax. Similar, tumors with larger CT-volume and higher PET-Solidity showed worse prognosis than those with higher volume and lower PET-Solidity (p=0.014). Poor prognosis was seen in patients with higher SUVmax and higher PET-Solidity compared to lower SUVmax and lower PET-Solidity (p=0.016). **Conclusion:** We successfully applied a novel algorithm for determination of optimal parameters and their prognostic threshold for TA data not showing proportional hazard as assumed in the Cox proportional hazard model. Powerful prognostic parameters could be defined for CT and

PET using TA of FDG PET/CT even for this homogenous low-risk NSCLC population. SUVmax, PET-solidity and CT tumor volume were found to be the best predictive factors. **References:** None.

EP-0814

The comparison of radiomics features on FDG PET/CT acquisition between supine and prone position

I. Gorczewska[1], *D. Borys*[2], *M. Jarzab*[3], *A. d'Amico*[1];
[1]*Department of PET Diagnostics, Maria Sklodowska-Curie Memorial Cancer Center and Institute of Oncology, Gliwice, POLAND,* [2]*Institute of Automatic Control, Silesian University of Technology, Gliwice, POLAND,* [3]*III Department of Radiotherapy and Chemotherapy, Maria Sklodowska-Curie Memorial Cancer Center and Institute of Oncology, Gliwice Branch, Gliwice, POLAND.*

Aim/Introduction: Combination of PET and CT allows the functional PET and anatomical CT images to be acquired under identical conditions. The standard study is performed in supine position. The major roles for PET/CT in breast cancer are detecting, localizing metastasis, monitoring the response to treatment and early detection of recurrence. Patient with breast cancer undergo the MRI study in a prone position. In this study we have compared 18F-FDG PET/CT scans performed in supine and additional prone position to verify if the radiomic features of lesion change significantly regarding to position of the patient. **Materials and Methods:** 225 patients with lesions in breasts were selected and two PET/CT series were performed in following positions: standard supine and additional prone. Mean age of analysed women was 46.2 years +/- 11 (range: 21 to 72 years). Prone position was achieved using a self-made pad, replicating the shape of breast coil in MRI. Regions of interest including lesions were contoured using three segmentation methods: adaptive contouring, 41% maximum value and 2.5 SUV implemented in Philips IntelliSpace station. Using pyRadiomics (v2.1.0), for the original image, 100 radiomic features were computed in groups: shape, first order and texture based (GLCM, GLRLM, GLSZM, GLDM). Data analysis was performed using python numpy, scipy and pandas modules to compare parameters if they differ significantly in both positions. Statistical significance was determined using Wilcoxon matched-pairs signed rank test. A p-value less than 0.05 was considered significant. **Results:** Each tested contouring method present significant differences in both positions (prone vs supine). For adaptive contouring there were 46 parameters statistically different. In the other 54 considered features the p-value was equal or greater than the assumed level of statistical significance. The method'41% of maximum level'had the following proportion of results with and without differences: 47 to 53 parameters. Evaluated proportion of results for 2.5 SUV method was 54 significant and 46 non-significant. From among 100 examined radiomic features, there were 25 with statistical differences with position as a differentiating variable in all algorithms at the same time. The common part in the insignificant parameters for all considered contouring methods were 20 parameters. **Conclusion:** Statistical significant differences were observed in almost half of analyzed radiomic features independently of the contouring method. Based on the results it is appropriate to conclude that the position of the patient during the PET/CT study in breast cancer imaging is very important. **References:** Acknowledgment: STRATEGMED2/267398/4/NCBR/2015.

EP-0815

Validation of an open source Natural Language Processing (NLP) and an in-house developed python script for named entity recognition from radiology reports of lung carcinoma cases

S. Mithun[1], *A. K. Jha*[1], *U. B. Sherkhane*[1], *V. Jaiswar*[1], *R. V. Prasad*[2], *C. M. Ortiz*[3], *S. Puts*[4], *V. Rangarajan*[1], *A. Dekker*[5], *L. Wee*[5];
[1]*Tata Memorial Hospital, Mumbai, INDIA,* [2]*Philips innovation campus, Philips India, Bangalore, INDIA,* [3]*Netherlands eScience Center, Amsterdam, NETHERLANDS,* [4]*MAASTRO Clinic, Maastricht, NETHERLANDS,* [5]*Department of Radiation Oncology, MAASTRO Clinic, Maastricht, NETHERLANDS.*

Aim/Introduction: With increasing cancer incidences and treatment direction going towards personalised medicine, increasing research in the field, it is becoming increasingly important to capture maximum information related to disease processes, treatments, outcomes etc. All imaging reports are documented as free text discourse. Extraction of relevant information from free text biomedical reports is very cumbersome. Several open source NLP systems are available which make it less time consuming to extract information from radiology reports. In this study, we have validated a python script created in house for named entity recognition (NER) for specific disease identification phrases related to lung cancer diagnosis in a corpus of free text radiology reportsand compared it with an open source NLP system, cTAKES. **Materials and Methods:** This study has been approved by our institutional ethics committee. 100 expert-generated free text PET/CT and 100 CT scan reports from Tata Memorial Hospital performed on lung carcinoma patients were anonymized and cleaned to extract only the findings and impression using Python. Initially, we used cTAKES analysis engine AggregatePlainTextFastUMLS to extract around 12 disease identification phrases from the reports.An in house developed python script was simultaneously used for the same. We validated the output from both softwares against a gold standard of manual identification by a human reader. We specifically looked at recall (Sensitivity), specificity and accuracy of detecting reportsfor both the python script as well as cTAKES. **Results:** The overall recall, specificity and accuracy for NER by cTAKES for PET/CT reports were 0, 1 and 0.507 respectively and for CT scan reports was 0.069, 1 and 0.611. However, the same for our python script was 0.99, 0.99 and 0.99 respectively for PET/CT reports and 0.928, 1 and 0.970 respectively for CT scan reports. **Conclusion:** cTAKES recall and accuracy for NER for disease identification phrases lung cancer from PET/CT& CT scan reports is very poor due to the use of abbreviations and colloquial terminologies which are not mapped in dictionaries.

However the python script was more customized and hence worked very well for extracting these terms. These results may be used for modifying cTAKES script to ensure better performance. **References:** None.

EP-0816

Is there any correlation between the radiomic features extracted from CT and PET Images

A. K. Jha[1,2], *S. Mithun*[1,2], *U. B. Sherkhane*[1], *V. Jaiswar*[1], *N. C. Purandare*[1], *V. Rangarajan*[1], *A. Dekker*[2,3], *L. Wee*[2,3];
[1]*Tata Memorial Hospital, Mumbai, INDIA,* [2]*GROW-School for Oncology and Developmental Biology, Maastricht University Medical Center, Maastricht, NETHERLANDS,* [3]*Department of Radiation Oncology (MAASTRO Clinic), Maastricht, NETHERLANDS.*

Aim/Introduction: Use of visual interpretation of CT image and semi-quantitative parameters of PET image has been established in planning, interim evaluation and follow-up of patient in oncology. Although semi-quantitative parameters like SUVmax, TLG and MTV are used to prognosticate the disease as well as early treatment response.Radiomics analysis of PET and CT images suggest potentially informative features, which may be used for personalized treatment selection in oncology. The influence of CT image acquisition and reconstruction on radiomic features extraction requires investigation. The aim of this study was the correlation between radiomic features extracted from CT and PET images. **Materials and Methods:** 104 NSCLC patients with pre-treatment PET/CT scans were included in this study. The lung tumor in PET was delineated by SUV threshold (42%) and the same contour were copied to co-registered CT images. Subsequently, 1093 radiomic features were extracted from each tumor segment and for each image modality. The bin width for CT and PET radiomic analysis were 25 and 0.5 respectively. Correlation between the radiomic features extracted from CT and PET images was assessed by calculating the concordance correlation coefficient (CCC) between the two imaging modalities. **Results:** 54% of PET and CT radiomic features have mutually positive correlation and 46% have negative mutual correlation. 91(8.33%), 69(6.3%) and 51(4.67%) features, respectively, have CCC greater than 0.5, 0.7 and 0.9. only 32 (2.93) radiomic features had CCC equals to or more than 0.98. In top twenty features ten features are shape based features. Table one shows top ten radiomic features excluding shape based features with CCC values.Table 1: Top tan features having best correlation excluding shape based features **Conclusion:** Our study suggests that majority of PET and CT radiomic features are not correlated to each other. And majority of highly correlated features are shape based features. **References:** None.

EP-0817

Methionine PET Imaging For Differentiation Between Recurrent Brain Tumor And Radiation Necrosis: Radiomics Approach With Random Forest Classifier

M. Hotta[1], *R. Minamimoto*[1], *K. Miwa*[2];
[1]*National Center for Global Health and Medicine, Tokyo, JAPAN,* [2]*International University of Health and Welfare, Tochigi, JAPAN.*

Aim/Introduction: Distinguishing radiation necrosis from recurrent brain tumor is important for selecting an appropriate treatment strategy. However, an accurate diagnosis often remains challenging in conventional imaging. Although the lesion-to-background ratio (L/B ratio) using 11C-methionine (MET) PET provides good diagnostic performance in the diagnosis of recurrent brain tumor from radiation necrosis, this methodology still yields false-positive or -negative cases. The purpose of this study was to investigate the efficacy of MET PET using a radiomics approach with a random forest classifier for differential diagnosis between recurrent tumor and radiation necrosis. **Materials and Methods:** We enrolled 42 patients (age: 55.8±13.2 years) with glioma (n=21) and brain metastasis (n=21) who underwent MET PET between October 2014 and June 2016 due to suspected recurrence on MRI after radiation therapy. A total of 44 lesions showing abnormal MET uptake were used for analyses. Surgical histopathological analysis or more than 6 months of follow-up with MRI was the reference standard. For calculating the L/B ratio, the maximum standardized uptake value (SUV) of the lesion and the mean SUV of the normal brain cortex using 1.0 cm^3 sphere were measured. For radiomics analysis, the three-dimensional volume of interest was set to encompass the lesion, and the area with a SUV of more than 1.3 times of the normal brain cortex was automatically contoured; 42 textual features were extracted and used for machine learning. A random forest classifier was applied to separate the radiation necrosis from recurrent tumor after balancing the number of lesions in both radiation necrosis and recurrent tumor using the synthetic minority oversampling technique. Gini importance was used to identify relevant textual features for classification. **Results:** Thirty-three and 11 lesions were confirmed as recurrent tumor and radiation necrosis, respectively. For the differentiation between tumor recurrence and radiation necrosis, the L/B ratio evaluation and radiomic classifier demonstrated an area under the curve of 0.72 and 0.98, sensitivity of 66.7% and 90.1%, specificity of 63.6% and 93.9%, accuracy of 79.5% and 92.2%, positive predictive value of 84.6% and 95.2%, and negative predictive value of 38.9% and 88.6%, respectively. Gray level co-occurrence matrix (GLCM) dissimilarity was the most relevant textual feature for the diagnosis. **Conclusion:** A radiomics approach using MET PET yielded excellent results for differentiating radiation necrosis from recurrent tumor, which was superior to the L/B ratio evaluation. These findings should be validated on a larger scale using independent data for future clinical translation. **References:** None.

EP-0818

AI-based Tools for Automated Quantification of PET/CT Studies

L. Edenbrandt[1], *J. Ulen*[2], *O. Enqvist*[2,3], *E. Trägårdh*[4];
[1]*Sahlgrenska University Hospital, Gothenburg, SWEDEN,* [2]*Eigenvision, Malmö, SWEDEN,* [3]*Department of Electrical Engineering, Chalmers University of Technology, Gothenburg, SWEDEN,* [4]*Skane University Hospital, Malmö, SWEDEN.*

Aim/Introduction: Deep learning, a subfield of artificial intelligence, has become the method of choice for image analysis applications and therefore gained increased usage also in medical imaging. Automated deep learning-based quantification of PET/CT studies has the potential to improve or substitute current methods of assessing extent and activity of cancer in the human body. RECOMIA is a nonprofit organization with the objective of promoting research in this field by providing academic researchers with . **Materials and Methods:** The first step in automated quantification of PET/CT studies is usually to segment the organs of interest in CT. In this work two convolutional neural networks (CNN) were trained to segment 75 different organs. The networks were designed to handle the fact that the number of vertebrae and ribs can vary between different subjects.The organs included: 56 bones (skull, mandible, humeri, femuri, cervical vertebrae, thoracic vertebrae, lumbar vertebrae, sacrum, hip bones, ribs, scapulae, clavicles and the sternum) and 19 soft tissue organs (brain, lungs, heart, aorta, liver, gallbladder, ventricle, spleen, pancreas, adrenal glands, kidneys, urinary bladder, prostate, rectum and gluteus maximus muscles).A dataset of approximately 10,000 manual organ segmentations in 231 images were used to train the CNNs. Not all organs were annotated in all images, which had to be handled in the training process. The CT scans were split into training (80%) and validation (20%) groups. **Results:** The CNN-based segmentations were compared to the manual segmentations on the validation group. The overall recall was 93.4%, that is, there was agreement on 93.4% of the voxels that were manually labelled. Similarly, the overall precision was 95.3%. Another way to measure accuracy is by the per-organ Dice index. The average Dice index over the 75 organs was 0.91, (0.85 for the soft tissue organs and 0.93 for the bones).The run time of the CNNs was about 2 minutes on a desktop computer. **Conclusion:** AI-based tools can provide highly accurate and reproducible organ segmentations, similar to those obtained manually by radiologists, but much faster. We continue to train new CNNs to continuously improve performance. The tools developed in this project are available on request at www.recomia.org for research purposes. **References:** None.

EP-0819

Preliminary Results of Whole Liver Segmentation with Deep Learning for SIRT

X. Tang[1], *E. Jafargholi Rangraz*[1], *W. Coudyzer*[2], *J. Bertels*[1], *D. Robben*[1], *G. Schramm*[1], *W. Deckers*[2], *C. M. Deroose*[1,2], *K. Baete*[1,2], *M. J. Gooding*[3], *J. Nuyts*[1];
[1]*KU Leuven, Leuven, BELGIUM,* [2]*University Hospitals Leuven, Leuven, BELGIUM,* [3]*Mirada Medical Ltd, Oxford, UNITED KINGDOM.*

Aim/Introduction: For radiation dose calculation in selective internal radiation therapy (SIRT), an accurate liver segmentation is required. Our aim was to investigate the feasibility of using a convolutional neural network (CNN) for liver segmentation for SIRT patients. **Materials and Methods:** A multi-scale CNN [1] was modified for liver segmentation for SIRT patients. The CNN was trained on 230 datasets from three liver segmentation challenges, including Medical Segmentation Decathlon (MSD), LiTS17, and SLIVER07, and 12 SIRT patient datasets from UZ Leuven. Validation was performed on 12 datasets from LiTS17 and SLIVER07 challenges, and 13 SIRT patient datasets. The model was tested on 20 datasets from the MSD challenge and 32 datasets from 30 SIRT patients, which were not used in training and validation. The CTs from the three challenges are contrast-enhanced (CE) and some CTs from the SIRT patients are non-CE. The results are evaluated through the dice score (DSC) and the volume ratio (RV) of the CNN segmentation to manual delineation. **Results:** The trained model achieved a median DSC and RV of 0.97 and 0.99 on the challenge data for testing. This result was comparable to the highest DSC of 0.95 reported for the MSD challenge. A median DSC and RV of 0.94 and 0.93 were achieved on the 32 SIRT test datasets. CNN had poor performance for two SIRT test datasets, with DSC of 0.84 and 0.62. **Conclusion:** The CNN model trained on general data of liver cancer achieved good results on the SIRT data with relatively normal liver shapes and low disease burden, only slight adjustment may be needed for clinical use. However, the trained model failed on SIRT data with high tumor burden, diffuse tumor involvement, and low-dose CT, since these cases are not adequately represented in the training data. The lower performance on SIRT patients may result from a difference in manual delineation strategy between the clinical SIRT data and the challenge data. The experiments could also indicate some diversity between the SIRT data and the challenge data, resulting in worse segmentation of SIRT data using the model mainly trained on the challenge data. To solve the latter, collection of a larger (multi-institutional) datasets of representative SIRT work-up cases may be required. A more detailed analysis of the observed performance difference is ongoing. (This projected is funded by H2020-ITN project HYBRID.) **References:** [1] Kamnitsas et al., Medical Image Analysis 2017.

EP-0820

A Machine Learning Segmentation Approach For The Extraction Of Radiomic Features In PET Studies

P. Alongi[1,2], *A. Stefano*[3], *A. Comelli*[4], *S. Bignardi*[5], *M. Sabini*[6], *A. Yezzi*[7], *M. Ippolito*[8], *G. Russo*[3];
[1]*Fondazione Istituto Giglio, Cefalù, ITALY,* [2]*Univ. of Palermo, Palermo, ITALY,* [3]*Inst. of Molecular Bioimaging and Physiology, National Research Council (IBFM-CNR), Cefalù, ITALY,* [4]*Department of Industrial and Digital Innovation, Univ. of Palermo AND Fondazione Ri.MED, Palermo, ITALY,* [5]*Department of Electrical and Computer Engineering, Georgia Institute of Technology, Atlanta, GA, UNITED STATES OF AMERICA,* [6]*Medical Physics Unit, Cannizzaro Hospital, Catania, ITALY,* [7]*1Department of Electrical and Computer Engineering, Georgia Institute of Tech., Atlanta, GA, UNITED STATES OF AMERICA,* [8]*Nuc. Med. Department, Cannizzaro Hospital, Catania, ITALY.*

Aim/Introduction: Radiomics on PET, including semiquantitative, first-order intensity, shape and textural features extracted from the tumors, provides information about tumor biology and behavior to get a better prognosis, and treatment response prediction in oncological patients. In this context, we present an innovative machine learning approach which purpose is to tackle the real-time, 3D tumor segmentation task in a nearly full automatized way. **Materials and Methods:** The proposed algorithm identifies a user-independent ROI around the tumor in the PET slice containing the SUVmax. The volume is then reconstructed using a slice-by-slice marching approach until a suitable automatic stop condition is met. The segmentation is performed using an enhanced local active contour based on the minimization of a novel energy functional which integrates the information provided by a machine learning component based on k-nearest neighbor classification method. As a result, the whole algorithm is automatic and the output segmentation is user independent. Five phantom experiments for a total of 30 radioactive spheres, and 41 clinical cases comprising 12 lung, and 29 head & neck cancers were used in our study. To train and validate the machine learning component, fixed ROIs were placed by three expert physicians in a subset of 3 phantom spheres and 6 patient lesions from the initial PET dataset with the purpose of identifying 3 different areas: tumor, background and border-line regions. The remaining data were used to assess the performances of the segmentation algorithm. The physicians performed manual segmentations around each lesion, and a ground truth estimation tool was employed to define a consolidated reference starting from different manual delineations. **Results:** Phantom performance results were divided considering small spheres with diameters < 22 mm and large spheres with diameter > 17 mm. In the smaller spheres, the mean dice similarity coefficient (DSC) was 78,84±6,18%. In the larger spheres, mean DSC increased to 90,36±2,75%. Clinical cases showed high agreement with the gold standard (R2 = 0.98). The mean DSC was 87,14±3,31% and 87,88±3,89%, in head & neck and in lung cancers. In order to confirm that the method was operator-independent, a sub-dataset of 5 head & neck, and 5 lung cancers was segmented by the three physicians. The result consisted of identical volumes. **Conclusion:** the proposed method can be efficiently applied in the clinical routine for tumor segmentation, and to extract radiomic features with potential benefit to improve tumor phenotyping, prognosis, and treatment response prediction, noninvasively. **References:** None.

EP-0821

AI-Based PET-to-PET Alignment Enabling Individual Tumour Tracking and Multi-Tracer Analysis

E. Tragardh[1], *J. Ulén*[2], *O. Enqvist*[2], *L. Edenbrandt*[3];
[1]*Skåne University Hospital, Malmo, SWEDEN,* [2]*Eigenvision, Malmo, SWEDEN,* [3]*Sahlgrenska University Hospital, Göteborg, SWEDEN.*

Aim/Introduction: In the clinic, multiple PET-CT scans from the same patient are often acquired and the value of these types of analyses has been illustrated in recent studies (1-2). However, tools for automatic analysis of dual PET/CT studies are lacking. For instance, tracking individual metastases in consecutive PET/CT studies is very time-consuming, making the evaluation of treatment response expensive. The aim of this study was to develop a method for automated comparison of PET tracer uptake in dual PET/CT studies. **Materials and Methods:** The CNN-based bone segmentation in (3) can be used to segment 56 individual bones from CT images. Given two PET/CT studies of the same patient, this method was applied to each CT image. Next, for each bone, a standard alignment software (Elastix) was used to estimate the (rigid) motion of that bone between the two studies. Using each motion on the corresponding voxels, allows us to align one PET image to the other with voxel precision. Using a fixed metastasis criterion, this allows tracking individual metastases between two different scans, speeding up the evaluation process. **Results:** We analyzed two cases to highlight the possibilities of the new technique. Patient A with prostate cancer and bone metastases underwent both an 18F-sodium fluoride (FLUR) and an 18F-fluorocholine (CHOL) PET/CT. The automated method detected 20 hotspots in the skeleton. Hotspots likely to represent metastases by visual analysis had SUVmax FLU/CHOL ratios less than 7 whereas most of those representing degenerative disease had higher ratios. Patient B with lymphoma underwent two 18F-FDG-PET/CT studies with 2 months interval. The automated method detected 19 hotspots in the skeleton. Four hotspots showed a decrease and 10 an increase of SUVmax of more than 10%. In five of the hotspots SUVmax differed less than 10% between the studies. **Conclusion:** We present a deep learning-based approach to segment the same object in two images and estimate a transformation between them. The method could be a tool to evaluate treatment response or for assessment of disease heterogeneity. The automated AI tool is available on request for research purposes at www.recomia.org. **References:** 1 Davis JC, et al. 18F-FDG Uptake During Early Adjuvant ... J Nucl Med. 2018;59:25-30. 2 Fox JJ, et al. Positron Emission Tomography/Computed Tomography-Based Assessments ... JAMA Oncol. 2018;4:217-224. 3 Lindgren Belal S, et al. Deep learning for segmentation of 49 selected bones ... Eur J Radiol. 2019 Apr;113:89-95.

EP-0822

Evaluation of radiomics quantification using a multi-compartment multimodality imaging phantom

K. M. Meijer[1], *I. Hernández-Girón*[1], *W. M. Brink*[1], *A. Webb*[1], *C. H. Slump*[2], *L. F. de Geus-Oei*[1,2], *D. V. Kuznetsov*[3], *D. R. Schaart*[4,5], *F. H. P. van Velden*[1], *W. Grootjans*[1];
[1]*Leiden University Medical Center, Leiden, NETHERLANDS,* [2]*MIRA Institute for Biomedical Technology and Technical Medicine, University of Twente, Enschede, NETHERLANDS,* [3]*Electronic and mechanical support division, Delft University of Technology, Delft, NETHERLANDS,* [4]*Radiation Science and Technology, Delft University of Technology, Delft, NETHERLANDS,* [5]*Holland Proton Therapy Centre (HollandPTC), Delft, NETHERLANDS.*

Aim/Introduction: Accurate quantification of intratumor heterogeneity using radiomics features is becoming increasingly important for precise characterization of cancer lesions. In this study, the performance of PET, CT and MR imaging for depicting heterogeneous uptake and enhancement patterns was investigated. **Materials and Methods:** Multi-compartment 3D printed imaging phantoms, that can be inserted in the casing of the NEMA-NU2 PET image quality phantom, were used to simulate heterogeneous uptake and enhancement patterns in PET (Vereos digital PET scanner (Philips, Medical Systems)), CT (Aquilion One (Canon Medical Systems)), and MR (Philips Ingenia 1.5T (Philips Medical Systems)) imaging. Three different phantom inserts, consisting of cylindrical volumes containing different rectangular compartments (L-shape, stair-shape, and U-shape), were filled with different concentrations (ratios of 2:4:8:16 with respect to the background) of ^{18}F-fluorodeoxyglucose (FDG), iodinated contrast, and gadolinium contrast. The rectangular shapes were created at different scales, consisting of cubes with dimensions of 10×10×10 mm, 7.5×7.5×7.5 mm and 5×5×5 mm, respectively. Image acquisition was repeated 5 times (standard abdominal imaging protocols). Furthermore, high resolution CT imaging was performed for generating a ground-truth reference in order to determine the accuracy of radiomics quantification. A total of 54 radiomic features were extracted using PyRadiomics. **Results:** Regarding the test-retest analysis, features extracted from MR had the highest reproducibility (only 1 feature had more than 20% variation), followed by CT (17 features >20%) and PET (28 features >20%). The First-Order (FO), Gray Level Co-occurrence Matrix (GLCM), Gray Level Run Length Matrix (GLRLM), Neighboring Gray Tone Difference Matrix (NGTDM) features were reproducible on all imaging modalities, with variations below 20%. Furthermore, analysis showed that the scale of the heterogeneous structure significantly affected the absolute value of almost all radiomics features. PET was affected to a lesser extent by heterogeneity scale than CT and MR, with the GLCM feature group least affected. Finally, the absolute value of most FO, and GLCM features showed less than 20% deviation from the high-resolution ground-truth, whereas the GLRLM, Grey Level Size Zone Matrix (GLSZM) and NGTDM features showed significant deviations. **Conclusion:** This study showed that heterogeneous uptake and enhancement patterns can be simulated on PET, CT and MR imaging using a multi-compartment imaging phantom. The three imaging modalities showed different performances regarding test-retest reproducibility and accuracy of radiomic quantification. **References:** None.

EP-0823

A Novel Automated Deep Learning Algorithm for Segmentation of the Skeleton in Low-Dose CT for [(18)F] DCFPyL PET/CT Hybrid Imaging in Patients with Metastatic Prostate Cancer

K. Gjertsson, *K. Johnsson, J. Richter, K. Sjöstrand, L. Edenbrandt, A. Anand;*
EXINI Diagnostics AB, Lund, SWEDEN.

Aim/Introduction: [(18)F]DCFPyL (PyL-PSMA) PET/CT hybrid imaging is one of the most promising diagnostic assessments for prostate cancer patients. For accurate diagnosis and treatment planning the manual delineation of organs in three-dimensional hybrid imaging is essential but it is also a highly labor-intensive process. Our objective was to automate the process of accurate bone segmentation in whole body low-dose CT of PyL-PSMA PET/CT scans for subsequent automated detection of lesions in bone. **Materials and Methods:** We developed a deep learning algorithm based on cascaded deep convolutional neural networks for semantic segmentation of the 49 bones in 12 skeletal regions (thoracic- and lumbar vertebrae, sinister/dexter ribs, sternum, sinister/dexter clavicle, sinister/dexter scapula, sinister/dexter ilium, and sacrum). A training set (N=90) and validation set (N=22) of pairs of low-dose CT images and manually crafted segmentation maps were used to develop the deep learning algorithm. The algorithm's performance was further assessed on a test set (N=10) of low-dose CT drawn from a PyL-PSMA study with corresponding manual segmentations of five representatively chosen body parts (sinister ilium, lumbar vertebrae, sinister ribs, dexter scapula, and sternum) used as ground truth. The Sørensen-Dice score was used to evaluate the performance of the segmentation in PyL-PSMA PET/CT. **Results:** The segmentation algorithm required less than 120 seconds to generate a complete segmentation of a whole body low-dose CT of PyL-PSMA PET/CT scan and achieved a Sørensen-Dice score mean and standard deviation of 0.95 and 0.024 on the training set and 0.93 and 0.036 on the validation set. On the test set the algorithm achieved mean (and standard deviation) of 0.94 (0.016) for dexter clavicle, 0.91 (0.013) for sinister ribs, 0.92 (0.019) for sternum, 0.94 (0.033) for lumbar vertebrae and finally 0.97 (0.0033) for sinister ilium. Performance overall skeletal regions in the test set was 0.94 (0.027). **Conclusion:** The study has demonstrated the efficiency and effectiveness of our fully automated segmentation algorithm of the 49 bone in the 12 skeleton regions of whole body low-dose CT in PyL-PSMA PET/CT images. Future work includes automated lesion detection and categorization in PyL-PSMA/CT as well as further evaluation of the clinical utility. **References:** None.

EP-60
Technical aspects -> Instrumentation and data analysis -> Data analysis -> Cardiology: data analysis and imaging systems

October 12 - 16, 2019
e-Poster Area

EP-0824
Favorable Image Reconstruction for Adequate Myocardial Perfusion Imaging Using Rubidium-82 on a Digital PET System

S. S. Koenders[1,2], *J. D. van Dijk*[1], *P. L. Jager*[1], *H. Arkies*[1], *J. R. Timmer*[3], *M. Mouden*[3], *C. H. Slump*[2], *J. A. van Dalen*[4];
[1]*Isala hospital, Department of Nuclear Medicine, Zwolle, NETHERLANDS,* [2]*Technical Medicine Centre, University of Twente, Enschede, NETHERLANDS,* [3]*Isala hospital, Department of Cardiology, Zwolle, NETHERLANDS,* [4]*Isala hospital, Department of Medical Physics, Zwolle, NETHERLANDS.*

Aim/Introduction: The use of myocardial perfusion imaging (MPI) with Rubidium-82 (Rb-82) PET for the detection of coronary artery disease is increasing rapidly. Recently, PET systems with digital photon counting technology have become available. As these systems have an increased temporal and spatial resolution it is unknown which reconstruction settings are best to use for MPI assessment. Our aim was to determine an image reconstruction that provides sufficient defect visibility in MPI using a digital PET system. **Materials and Methods:** We retrospectively included 30 consecutive patients who underwent rest and regadenoson-induced stress Rb-82 PET/CT (Vereos, Philips Healthcare). PET data were reconstructed with a 3D ordered subset expectation maximization (OSEM) algorithm, using 4 combinations of iterations, subsets and Gaussian post-smoothing filters: 2 iterations, 15 subsets and filtering of 4 mm (2i15s4mm), 2i15s6mm, 3i15s8mm and 3i15s12mm. These settings were selected out of 15 settings that comprised a range of scan quality from excessively smooth to excessively noisy, where the extreme ones were rejected. For each patient, the four reconstructions were shown randomly and side-by-side to two expert teams consisting of a nuclear medicine physician and cardiologist. The readers ranked scan quality from best (score 1) to worst (score 4) and as adequate or inadequate. **Results:** The scan quality of the 2i15s6mm reconstruction was better than that of the reconstructions using 2i15s4mm or 3i15s12mm ($p \leq 0.001$). The mean scan quality was 2.4 ± 0.8, 1.7 ± 0.4, 2.1 ± 0.8 and 3.8 ± 0.4 for the reconstructions using 2i15s4mm, 2i15s6mm, 3i15s8mm and 3i15s12mm, respectively. All scans reconstructed with 2i15s6mm were scored as adequate. For the scans reconstructed with 2i15s4mm, 3i15s8mm and 3i15s12mm, 3% of the scans were scored as inadequate. **Conclusion:** Adequate scan quality can be obtained using the OSEM reconstruction algorithm in PET MPI using Rb-82 on a digital system. The combination of 2 iterations, 15 subsets and a Gaussian post-smoothing filter of 6 mm was preferred for defect visibility. **References:** None.

EP-0825
The Influence of Attenuation Artefacts Caused by Metallic Injection Ports in Breast Tissue Expanders on the Calculation of LVEF in MUGA Studies

A. Hughes;
Christie Medical Physics & Engineering, Royal Preston Hospital, Preston, UNITED KINGDOM.

Aim/Introduction: Breast cancer patients who have undergone mastectomy as part of their treatment are frequently fitted with tissue expanding implants to aid breast reconstruction. These devices have metallic injection ports which can cause attenuation artefacts in radiological images. Such patients may subsequently receive chemotherapy and undergo serial MUGA studies to detect changes in cardiac performance. The aim of this study was to investigate the impact of artefacts caused by breast tissue expanders on the calculation of left ventricular ejection fraction (LVEF). **Materials and Methods:** Through retrospective analysis of MUGA studies on patients fitted with tissue expanders a computer programme was written which could simulate the size and intensity of the observed attenuation artefacts and could be added to any location within an image. 20 MUGA studies of female patients without breast tissue expanders were then selected and the computer simulated artefact was added to one of five locations over the left ventricle: at the centre of the chamber and at the borders of the septal wall, lateral wall, valve plane and apex. For each patient, the original study and the five additional studies containing an artefact were processed using the EF Analysis software on a Xeleris 4.0 computer (GE Medical Systems), using automatic and manual edge detection methods. **Results:** The computed LVEF of the 20 patients in the original studies ranged from 44 to 75% (mean=59.5%). For those studies processed using automatic edge detection there was a general increase in calculated LVEF when the artefact was positioned over the centre of the chamber (mean=68.2%, range 37-79%). With the artefact over the boundary of the left ventricle the change in LVEF was much lower at all locations. With automatic processing the ventricular borders and identification of the end systolic frames were largely incorrect. In some patients the addition of the artefact caused the calculated LVEF to change by as much as ±25%. With manual edge detection the impact of artefacts located over the centre of the left ventricle were greatly reduced (mean LVEF=60.2%, range 46-75%). Furthermore, end systolic frames were correctly identified and the artefact caused individual discrepancies in LVEF of ±5%. **Conclusion:** Artefacts associated with breast tissue expanders can interfere with automatic edge detection routines leading to erroneous calculation of LVEF. However, with careful manual definition of the ventricular borders these errors can be avoided and reliable estimates of LVEF obtained, even in the presence of these artefacts. **References:** None.

EP-0826

Prevalence, Characteristic And Pronostic Value Of Extra-cardiac Uptake Of 99mtc-hydroxythylene Diphosphonate In Cardiac Amyloidosis

M. Abulizi[1], *N. Malka*[1], *M. Kharoubi*[2], *T. Damy*[3], *E. Itti*[1];
[1]*Hospital henri-mondor, medecine nuclear departement, Créteil, FRANCE,* [2]*Hospital henri-mondor, cardiologie departement, Créteil, FRANCE,* [3]*Hospital henri-mondor, cardiologie departement, Créteil, FRANCE.*

Aim/Introduction: Systemic amyloidosis is a serious disease resulting from extracellular deposition of amyloid fibrils within organs. The two main forms of cardiac amyloidosis (CA) are AL amyloidosis due to light chains, and transthyretin amyloidosis (TTR). Diphosphonate scintigraphy has demonstrated performance in assessing myocardial involvement in amyloidosis, particularly in TTR patients, with a worse prognostic in its presence. The prevalence, characteristics and prognostic value of extracardiac diphosphonate uptake have been poorly described. **Materials and Methods:** This retrospective study included all consecutive patients referred to the Amylose Mondor French reference center for suspicion of cardiac amyloidosis (CA) who underwent ^{99m}Tc-HMDP scintigraphy between October 2012 and December 2016. Whole-body images acquired at early phase (10 min post-injection) were analyzed for the presence of cardiac or extracardiac uptake and the patients were classified according to a new classification "MADI" (Methodological Amyloidosis Diagnosis Index), defined as follows: no uptake (MADI 0), exclusive extracardiac uptake (MADI 1), exclusive cardiac uptake (MADI 2) or both (MADI 3). Patient characteristics as well as their prognosis were compared according to their MADI classes. **Results:** 308 patients including 247 with CA, among whom 75 hTTR,107 wtTTR and 65 AL. 61 patients han no CA formes a control group. 187 patients (75.7%) with CA demonstrated significant myocardial uptake, including 182 TTR (100%) and 5 AL (7.7%). 72 patients (38.5%) with CA also demonstrated extracardiac uptake. The most common site of involvement was the pleuropulmonary field. Uptake in the digestive tract, kidneys, muscles and thyroid was described whereas spleen, liver and lymph nodes uptake was only observed in the AL group. 2 controls had pulmonary uptake. No TTR patients were found in the MADI 0 and MADI 1 classes. The MADI 1 class led to the conclusion of an AL form and the scintigraphic involvement (MADI 1 to 3) had a pejorative prognosis value ($p = 0.02$). In the TTRs, particularly the wtTTRs, the MADI 3 class had a pejorative prognosis value ($p < 0.0001$). **Conclusion:** Extracardiac uptake of^{99m}Tc-HMDP is quite common and seen in almost 30% of patients with CA. The MADI classification is likely to guide the clinician regarding the diagnosis, to guide the carrying out of complementary examinations and to stratify the prognosis according to the typing of amyloidosis. **References:** None.

EP-0827

Evaluation of washout rate with crosstalk correction between ^{123}I-BMIPP and ^{201}TlCl for triglyceride deposit cardiomyovasculopathy (TGCV)

T. Kamiya[1], *T. Watabe*[2], *K. Fujino*[1], *M. Chimura*[2], *K. Hirano*[2], *Y. Sakata*[2], *J. Hatazawa*[3];
[1]*Osaka University Hospital, Suita, JAPAN,* [2]*Osaka University Graduate School of Medicine, Suita, JAPAN,* [3]*Osaka University, Suita, JAPAN.*

Aim/Introduction: Triglyceride deposit cardiovasculomyopathy (TGCV) is aberrant TG accumulation in both coronary arteries and myocardium. In the diagnosis guide of TGCV, its criteria of washout rate (WOR) is less than 10% in ^{123}I-BMIPP scintigraphy. Because there is an interference between 159 keV gamma-lay emitted from ^{123}I and 167 keV gamma-lay emitted from ^{201}Tl in dual-isotope study with scintillation camera, WOR of ^{123}I-BMIPP includes error for their quantification. We evaluated the effect of crosstalk correction (CTC) between ^{123}I and ^{201}Tl in calculating WOR of ^{123}I-BMIPP for the diagnosis of TGCV. **Materials and Methods:** The cardio-hepatic phantom (Kyoto Kagaku Co.) was filled with ^{123}I and ^{201}Tl solution. For obtaining of CTC coefficient, which was defined the accurate or crosstalk detectability proposed by previous report[1), 2)], each single-isotope phantom study (^{123}I or ^{201}Tl) was acquired with dual energy window. After the calculation of the CTC coefficient, simultaneous dual-isotope phantom was scanned at early and delayed phase (20 hours). Radioactivity of ^{123}I and ^{201}Tl at early phase was each 100 kBq/mL and was left until delayed phase. The time-dependent count change with decay correction was defined in WOR. **Results:** CTC[^{123}I-^{123}I], CTC[^{123}I-^{201}Tl], CTC[^{201}Tl-^{123}I] and CTC[^{201}Tl-^{201}Tl] coefficients were 56.5, 22.3, 8.7 and 32.2 counts/MBq/sec, respectively. Compared to theoretical value (0.0%), the WOR without CTC was -21.0 ± 4.1%. On the other hands, the WOR corrected by CTC was 3.0 ± 0.6%. **Conclusion:** By applying CTC, WOR can be calculated more precisely in dual-isotope scintigraphy. **References:** 1) Jpn J Nucl Med Tech, 12. 8-14 (1992) 2) Radioisotopes, 43. 520-530 (1994).

EP-0828

Improved accuracy in diagnosing cardiac amyloidosis through increased myocardial 99mTc-DPD uptake associated with increased LV mass

L. Monaco[1], *A. Scarale*[2], *R. Sara*[2], *C. Popescu*[2], *M. Spallino*[2], *C. Dolci*[2], *M. Cuzzocrea*[1], *G. Cabrini*[2], *E. Gay*[2], *M. Milella*[2], *F. Musca*[2], *F. Caobelli*[3], *C. Rossetti*[2];
[1]*Università degli studi di Milano Bicocca, Milano, ITALY,* [2]*ASST Grande Ospedale Metropolitano Niguarda, Milano, ITALY,* [3]*Universitatsspital Basel, Basel, SWITZERLAND.*

Aim/Introduction: Cardiac involvement in systemic amyloidosis leads to progressive cardiomyopathy, therefore new therapeutic strategies are now available. ^{99m}Tc-DPD scintigraphy, based on Perugini qualitative-score, allows to identify

cardiac amyloidosis (CA) through a non-invasive procedure. However, a quantitative approach is desirable. Our purpose was to identify a semiquantitative parameter to improve the diagnostic accuracy in patients with suspected CA. **Materials and Methods:** We retrospectively evaluated 29 patients with suspected CA since January 2017 to September 2018. Each patient underwent comprehensive clinical evaluation, transthoracic echocardiography (TTE) and whole-body ^{99m}Tc-DPD scintigraphy. TTE estimated LV volumes, function and ventricular mass. In addition to Perugini' score visual interpretation, each scan was also semiquantitatively evaluated through cardiac uptake normalized to background activity (nCU), defined as [total counts (myocardial ROI) / total counts (right hemithorax background ROI)]. ROIs dimensions were identical in the same patient. Biopsy (7/29) or clinical follow-up determined CA final diagnosis. **Results:** A significant correlation between Perugini' score and nCU (r=0.89, p<0.001) was detected. nCU was unrelated to BMI (p=0.56). CA was confirmed histologically in 7/29 patients. A good diagnostic performance of nCU (AUC=0.675) was demonstrated by ROC curves, optimal threshold was 1.38 (sensitivity 85.7%, specificity 54.5%). An optimal threshold of 317.5 g/m2 was shown for LV mass (sensitivity 50.0%, specificity 78.6%). The simultaneous presence of nCU and LV mass above limits led to improve accuracy (global chi-square 15.75, p=0.03). **Conclusion:** In this small cohort semiquantitative nCU resulted at least non-inferior than the widely accepted Perugini visual score. Myocardial ^{99m}Tc-DPD uptake combined with LV mass improved diagnostic accuracy. **References:** None.

EP-0829

Assessment of three software packages in the estimation of left ventricular volumes and ejection fraction with resolution recovery algorithm in gated myocardial perfusion SPECT vs cMRI: preliminary results of a single centre

E. Calandri[1], *F. Guana*[2], *L. Conversano*[1], *S. Gallina*[1], *S. Leuzzi*[3], *E. Soligo*[4], *S. Debernardi*[4], *M. Liberatore*[5], *G. Chiorino*[2], *M. Pultrone*[1]; [1]*Department of Medicine and Urgency, Nuclear Medicine Unit, Ospedale degli Infermi, Ponderano, ITALY,* [2]*Laboratory of Cancer Genomics, Fondazione Edo ed Elvo Tempia, Biella, ITALY,* [3]*Department of Medicine and Urgency, Unit of Cardiology, Ospedale degli Infermi, Ponderano, ITALY,* [4]*Department of Medicine and Urgency, Radiology Unit, Ospedale degli Infermi, Ponderano, ITALY,* [5]*Department of Radiology, Oncology and Human Pathology, Nuclear Medicine Unit, "Sapienza" University, Rome, ITALY.*

Aim/Introduction: To evaluate the performance of three software in the quantification of left ventricular end-diastolic (EDV), end-systolic volume (ESV) and ejection fraction (LVEF) from ECG-gated perfusion SPECT applying a resolution recovery (RR) algorithm (GE Myovation Evolution), respect to cardiac MRI (cMRI) gold standard. **Materials and Methods:** We retrospectively analyzed 18 patients (13 men, 5 women; age range: 42-81), with suspected (12) or known (6) coronary artery disease. All patients underwent a dual-day gated-SPECT (8 gates/cardiac cycle) and cMRI (30 gates/cardiac cycle), with a mean interval of 10,5 months ± 8,4, without any health change or revascularization procedure between the two procedures, no arrhythmias or artifacts. Gated-SPECT was performed on a conventional γ-camera 60' after 99mTc-MIBI or 99mTc-tetrofosmin injection at rest (652 Mbq ± 81). Images were reconstructed by FBP and by RR protocol (OSEM, 12 iterations, 10 subsets, RR). EDV, ESV and LVEF were calculated employing Quantitative gated SPECT (QGS), Myometrix (MX) and Corridor 4DM (4DM). Statistical analysis was performed using R version 3.5.3. Mean values of EDV, ESV and LVEF were tested for significance using Wilcoxon or paired t-test (assumption of normality assessed using Shapiro-Wilk test). Agreement between imaging reconstruction algorithms and between gated-SPECT software packages and cMRI was studied with Pearson's (r) or Spearman's (R) correlation coefficients and Lin's concordance correlation coefficient (LCC). **Results:** Concerning EDV and ESV, a significant difference was noticed between imaging reconstruction algorithms for all parameters and between each software and cMRI (p<0,05), except for 4DM-FBP vs 4DM-RR(ESV) (p=0,074). Concerning LVEF, no significant difference was observed in QGS-FBP vs QGS-RR (p=0,086), 4DM-FBP vs 4DM-RR (p=0,269), MX-FBP vs cMRI (p=0,383). Concordance and correlation between imaging reconstruction algorithms were always >0,9; respect to cMRI, the concordance was always lower using RR compared to FBP. **Conclusion:** Despite of some limitations, such as the low number of patients and the retrospective approach, that do not allow to draw definite conclusions, our study suggests that 4DM-FBP vs 4DM-RR shows the best concordance for EDV and ESV, and QGS-FBP vs QGS-RR shows the best concordance for LVEF. Respect to cMRI, RR algorithm is always associated with a lower concordance if compared to FBP reconstruction. Significance tests suggest that no significant differences between imaging reconstruction algorithms for 4DM-FBP vs 4DM-RR in ESV evaluation, for QGS-FBP vs QGS-RR and for 4DM-FBP vs 4DM-RR in LVEF evaluation, occur. EF from MX-FBP is the only parameter that doesn't significantly differ from cMRI. **References:** None.

EP-61

Technical aspects -> Instrumentation and data analysis -> Data analysis -> Data analysis and management

October 12 - 16, 2019 e-Poster Area

EP-0830

Noninvasive Tracer Kinetic Analysis of Brain ^{18}F-Florbetaben PET: a Comparison of Kinetic Models

S. Ferreira[1,2,3], *F. P. M. Oliveira*[1], *M. Silva*[1], *Â. Silva*[1], *C. Oliveira*[1], *J. C. Castanheira*[1], *S. C. Vaz*[1], *N. Matela*[3], *J. Sanchez-Gonzalez*[2], *D. C. Costa*[1]; [1]*Champalimaud Centre for the Unknown, Champalimaud Foundation, Lisboa, PORTUGAL,* [2]*Philips Healthcare Iberia, Madrid, SPAIN,* [3]*Institute of Biophysics and Biomedical Engineering, Faculty of Sciences of the University of Lisbon, Lisboa, PORTUGAL.*

Aim/Introduction: Currently, most of the brain ^{18}F-Florbetaben PET studies are only analyzed visually and/or using standardized uptake value ratios on late (90 minute post-injection) acquisitions. Although adequate for clinical practice, accurate amyloid PET burden cannot be quantified this way. Our aim was to compare four of the most popular reference region based kinetic methods on dynamic acquisitions. **Materials and Methods:** Twelve consecutive brain dynamic ^{18}F-Florbetaben PET studies acquired in the Philips Vereos Digital PET/CT were selected. Five had 60 minutes and seven 45 minutes duration starting immediately post-injection. Four patients had a clinical amyloid positive scan, while the remainders had a negative scan. Four kinetic methods were compared: simplified reference tissue method (SRTM2), modified reference tissue method (MRTM2), Logan plot and Patlak plot. Cerebellar grey matter was always the reference region. Comparison criteria were: (a) mean normalized residuals of the time activity curves fitting in 10 brain regions of interest (ROI) -mesial temporal cortex, prefrontal cortex, anterior cingulate, posterior cingulate, putamen, precuneus, caudate, occipital cortex, parietal superior cortex, parietal inferior cortex- (b) visual classification of the amyloid burden based on the parametric images generated by the methods and (c) visual evaluation of the parametric images noise level. **Results:** Very good fitting was achieved in all ROIs. Normalized mean residuals were approximately 2% for all methods, without statistical significance among them (Friedman ANOVA, $p = 0.212$). Visual evaluation of the amyloid burden based on the parametric images was concordant and identical to the clinical evaluation. Visually, the K parametric images from Patlak method displayed less noise compared to the distribution volume ratio (DVR) from Logan method, binding potential from MRTM2 (BP-MRTM2) and binding potential from SRTM2 (BP-SRTM2). In the 10 ROI considered, there were high to very high correlations among the DVR, BP-MRTM2 and BP-SRTM2 ($0.778 \leq r \leq 0.998$). The correlation between the K and the DVR, BP-MRTM2 and BP-SRTM2 varied between low and very high ($0.445 \leq r \leq 0.950$). The perfusion like parametric images V_0 (Patlak) and R_1 (MRTM2 and SRTM2) were of very good quality; with no visual differences among them. Very high correlation ($r>0.9$) was obtained in all 10 ROI considered. **Conclusion:** All four kinetic methods originated very good fitting and similar visual amyloid burden classification. Patlak K parametric images presented differences when compared to the DVR and BP images. Further studies are encouraged to tease out potential physiological or methodological reasons to explain these differences. **References:** None.

EP-0831

Standardization of PET MBF Quantification through Development of a One-for-all Software Tool

S. Nesterov[1,2], *R. Buechel*[3], *J. Dickson*[4], *V. Dilsizian*[5], *H. Gewirtz*[6], *A. Manrique*[7], *J. O. Prior*[8], *R. Sciagrà*[9], *M. Smith*[5], *A. Thomassen*[10], *J. Knuuti*[1];
[1]*Turku PET Centre, Turku, FINLAND,* [2]*IEPhB RAS, St.Petersburg, RUSSIAN FEDERATION,* [3]*Univ. of Zurich, UZH, Zurich, SWITZERLAND,* [4]*Univ. College London, Institute of Nuclear Medicine, London, UNITED KINGDOM,* [5]*Univ. of Maryland School of Medicine, Baltimore, MD, UNITED STATES OF AMERICA,* [6]*Harvard Medical School, Boston, MA, UNITED STATES OF AMERICA,* [7]*Univ. Caen Normandie, CHU de Caen, GIP Cyceron, Caen, FRANCE,* [8]*Centre Hospitalier Univ. Vaudois, Lausanne, SWITZERLAND,* [9]*Careggi Univ. Hospital, Florence, ITALY,* [10]*Odense Univ. Hospital, Odense, DENMARK.*

Aim/Introduction: Reported stress MBF values for the healthy volunteers can be 1.50±0.74 mL/min/g (1) while patients with CAD can have 3.18±0.85 mL/min/g (2), the range of CFR normal cutoffs is from 1.44 (3) to 2.74 (4). The quantitative PET MBF analysis field is fragmented; the results cannot be safely pooled, and diagnostic cutoffs remain relatively institution-specific. One main reason of this variability—and the one we can affect—is that PET quantification is done with different software tools. We aim at building a free, open-source quantitative PET MBF image analysis software that can become a global standard. **Materials and Methods:** Experts from 11 centers worldwide were involved in the designing such a software. During the first iteration, they de novo generated product requirements and defined the currently problematic areas in MBF quantification. These items were compiled and fed back to the centers during the second iteration — to estimate the importance of each item—academic and practical—as well as evaluating the implementation priority of the features. A rating scale was used where 2 stood for extreme importance, 1 stood for moderate importance, and zero for no importance at all. **Results:** A list of 202 items in 19 categories was generated. Apart from certain obvious requirements, such as utilizing 17-segment LV polar plot, Q/R from PACS, DICOM read and write, etc., the majority of items had a greater variance in their ratings. For example, in tissue segmentation, the automatic one with manual adjustment scored 3.4 times higher the second most popular option of fully automatic segmentation. A human operator was preferred to start the segmentation process with manual definition of LV axes and the ability to correct and adjust contours for every single frame of the dynamic acquisition was required as well. The LV base was considered the best place for the blood pool ROI definition, followed by the left atrium and then the LV cavity. In the tool´s validation, the most important factors were evaluating operator and test-retest variability and standardization of acquisition and analysis protocols for tracers in current clinical use, followed by evaluating the tool´s prognostic value. **Conclusion:** The collective minds of experts in the field of quantitative PET MBF analysis are designing a software tool that can significantly advance knowledge in the field by becoming a global standard. **References:** (1) Krivokapich et al., 1989; (2) Zervos et al., 1999; (3) Morton et al., 2012; (4) Muzik et al., 1998.

EP-0832

Dependence of dead-time correction factors on attenuating conditions in the object

W. Zhao[1,2], *C. Caldwell*[3], *A. Celler*[2];
[1]*Department of Physics and Astronomy, University of British Columbia, Vancouver, BC, CANADA,* [2]*Medical Imaging Research Group, Department of Radiology, University of British Columbia, Vancouver, BC, CANADA,* [3]*Department of Medical Imaging, University of Saskatchewan, Saskatoon, SK, CANADA.*

Aim/Introduction: For post-injection SPECT scans of patients undergoing ^{177}Lu DOTATATE therapy, the high flux of photons may result in camera dead-time. In order to perform personalized dosimetry, quantitative measurement of activities in patients must be performed. Since images are reconstructed from primary photons (corrected for attenuation and scatter), dead-time correction must account for primary photon losses. However, for the same injected activity, these dead-time losses will be different for patients of different size, thus exhibiting different amounts of attenuation. The dead-time correction factor is usually determined using phantom experiments, where the photon attenuating conditions are obviously different from those in patients. Consequently, the correction factors obtained from these experiments may not accurately recover the dead-time count losses occurring in patient studies. Our aim was to propose a dead-time correction method that is less dependent on the photon attenuating conditions. **Materials and Methods:** Twelve planar scans (Siemens Symbia Intevo) were performed, using vials with ^{177}Lu activity and four different thicknesses of photon attenuating medium (0 to 20 cm thickness of solid water). The activities of sources ranged from 11 to 10585 MBq. Data were acquired into six energy windows: one photopeak, two scatter windows and additional three windows to cover the entire spectrum. The triple-energy-window method was used to remove scatter from and calculate the observed primary counts in the photopeak. The true primary counts for the scans with high activity were determined from the primary counts observed in scans with low activity (<1042 MBq), using linear extrapolation. For each attenuating condition, the primary photon count loss due to the dead-time, (defined as the percentage of true primary counts), was analyzed as functions of photon count-rates in A: the photopeak, B: the sum of the photopeak and scatter windows and C: the entire spectrum, as these three count-rates are easily obtained during patient scanning. **Results:** For the maximum investigated activity (~10.6 GBq), the difference between the primary photon dead-time count losses determined using the four photon attenuating slabs was the smallest when count-rates in the entire spectrum were considered. The values of these differences amounted to 9.4% for case A, 7.6% for case B and only 3.5% for case C. **Conclusion:** The dead-time correction factor for primary photons should be analyzed as a function of observed photon count-rate in the entire spectrum, as in this case its value is less dependent on the photon attenuating conditions in the object/patient. **References:** None.

EP-0833

Using phase space for SPECT Monte-Carlo simulation

D. Sarrut[1,2], *T. Baudier*[1], *J. Labour*[1,2], *J. Badel*[2];
[1]*CREATIS, Lyon, FRANCE,* [2]*Centre Léon Bérard, Lyon, FRANCE.*

Aim/Introduction: Detailed Monte-Carlo (MC) simulation of tomographic SPECT image acquisition remains a long process, in particular due to the very low sensitivity: only one gamma detected for about 1e5 emitted. Several Variance Reduction Techniques or fast GPU-based algorithms have been proposed [1-5]. However, the process still remains complex for large source activity distribution. Moreover, two specific issues remain. First, the tracking of the gammas inside the CT is performed for all acquisition angles. Secondly, the patient to detector distance is narrowed for each gantry angle and, during simulation, geometrical overlaps may arise between detector and CT volumes. **Materials and Methods:** Inspired from the Linac phase-space (PHSP) method and assuming that constant activity for all projection angles, we propose to perform the tracking of the gamma in the CT only once and to store the particles emerging the patient in a PHSP, avoiding to redo the tracking for all angles. With realistic activity, the PHSP size would be very large, around 100GB for 5e9 emitted gamma (about 150 MBq of In111). Instead, we proposed to exploit the ARF-nn method[2] to obtain similar image characteristic with about 10 times less particles. Moreover, a new tool that allows to store the gamma in PHSP when they just emerge from the patient skin, via a mask, was developed. From this PHSP, it is now possible to perform tomographic simulation varying the spect head distance without volume collision. **Results:** A complete detailed tomographic SPECT MC simulation have been performed using the two steps method described above. It allows to store a PHSP of 8 GB, from which all 30 angles projections can be simulated, avoiding to redo gamma patient tracking and allowing varying skin-to-detector distance without volume collision. All methods were implemented in GATE[5] and will be available to the community in the next version. **Conclusion:** We propose a two steps methods for detailed SPECT MC simulation based on adapted phase space and ARF-nn. **References:** [1] Ljungberg. "A Monte Carlo program for the simulation of scintillation camera characteristics." CMPB, 29:257-272-1989[2] Sarrut. "Learning SPECT detector angular response function with neural network for accelerating Monte-Carlo simulations." PhysMedBiol. 17;63(20):205013-2018[3] Rydéen. "Fast GPU-based Monte Carlo code for SPECT/CT reconstructions generates improved 177Lu images". EJNMMI, 5(1)-2018.[4] Cajgfinger. "Fixed-Forced-Detection for fast SPECT Monte-Carlo simulation". PhysMedBiol, 63(5)-2018.[5] Sarrut. "A review of the use and potential of the GATE Monte Carlo simulation code for radiation therapy and dosimetry applications." MedPhys, 41(6):064301-2014.

EP-0834

Can SPECT Resolution Be Considered Invariant in Partial Volume Correction?

R. Gillen[1,2], *A. M. Denis-Bacelar*[2], *S. J. McQuaid*[1], *K. Erlandsson*[1], *K. Thielemans*[1], *B. F. Hutton*[1];
[1]*Institute of Nuclear Medicine, University College London, London, UNITED KINGDOM,* [2]*National Physical Laboratory, Teddington, UNITED KINGDOM.*

Aim/Introduction: Most partial volume correction (PVC) methods assume spatially invariant resolution. In SPECT imaging, however, the resolution may change under different imaging conditions: position in the field of view, acquisition and reconstruction parameters (application of resolution modelling (RM) and number of iterations), activity distribution and attenuation. This work aimed to investigate the bias introduced by PVC when assuming spatially invariant resolution. **Materials and Methods:** STIR [1] was used to generate digital phantoms, of varying complexity, with 'point sources' at four positions. STIR was then used to forward project (Technetium-99m SPECT with LEHR collimators) and reconstruct these data (using OSEM). 2D Gaussians were fitted to the Point Spread Function (PSF) of each reconstructed point source, giving Full Width at Half Maximum (FWHM) values in radial and tangential directions for different phantoms and conditions. A second set of phantoms, of the same shape and attenuation as above, were also generated with hot regions representing tumours of different sizes. These were convolved with two different kernels; one representing an appropriate PSF for the specific imaging conditions, and one representing a 'standard' PSF measured at the centre of a uniform cylinder. The bias introduced by applying PVC with an inappropriate PSF was estimated by comparing the Recovery Coefficients calculated from convolving the phantom with the standard kernel versus convolution with the specific kernel. **Results:** Resolution varied significantly depending on position within an object. For example, tangential resolution measured in an elliptical object was 13.4mm at the centre, and 7.7mm at a position 12cm from the centre. There were differences of up to 36% between radial and tangential resolution, depending on the shape and attenuation of the object, and position within the object. Resolution was also affected by the distribution of activity. Applying RM improved the resolution in most cases but introduced ringing artefacts and took longer to converge. Using a standard PSF for PVC introduced a bias which depended on lesion diameter and tumour to background ratio (TBR). For a TBR of 11, a bias of under 6% was measured for tumour diameters of 4cm or larger, but biases of 8-33% were demonstrated for smaller lesions (diameters between 3cm and 0.9cm). **Conclusion:** The common assumption of spatial invariance is inappropriate for PVC of SPECT imaging and may lead to inaccurate quantification. Measurement of the PSF, specific to patient and position, is required for accurate PVC. **References:** 1.Fuster et al 2013, https://doi.org/10.1118/1.4816676

EP-0835

Reproducibility Study of Lesion Features Extracted from ^{18}F-FDG PET Images of the Same Patients Acquired on Two Philips PET/CT Scanners: Digital VEREOS versus GEMINI TF

C. S. Constantino[1,2], *F. P. M. Oliveira*[1], *M. Silva*[1], *C. Oliveira*[1], *J. C. Castanheira*[1], *Â. Silva*[1], *S. C. Vaz*[1], *P. Vieira*[2], *D. C. Costa*[1];
[1]*Champalimaud Centre for the Unknown, Champalimaud Foundation, Lisbon, PORTUGAL,* [2]*Faculdade de Ciências e Tecnologia, Universidade Nova de Lisboa, Lisbon, PORTUGAL.*

Aim/Introduction: The recent addition of digital equipment to the clinical armamentarium of PET/CT leads to some concerns regarding inter-device data variability. Our aim was to compare the performance of two PET/CT devices (Philips Digital Vereos -VEREOS- and GEMINI TF -GEMINI-) on consecutive imaging data from the same subjects after a single administration of FDG. **Materials and Methods:** ^{18}F-fluorodeoxyglucose (FDG) PET images from 41 oncological patients (studied twice) were included (23 Females and 18 Males, with 65 ± 9 years old). Image acquisition was obtained with VEREOS and GEMINI scanners after a single radiotracer injection (246 ± 60 MBq). 22 subjects were examined first on the VEREOS, and 19 on the GEMINI. Immediately after the first examination, followed the second acquisition in the other scanner. Image reconstruction was applied with default clinical parameters (VEREOS: 4x4x4 mm³, OSEM 3 iterations and 15 subsets, relax factor 1.0; GEMINI: 4x4x4 mm³, OSEM 3 iterations and 33 subsets, relax factor 0.7). FDG avid lesions were identified by an experienced nuclear medicine physician first on the VEREOS data, unaware of the image source. Afterwards, all annotations were transposed to GEMINI data. An automatic segmentation algorithm, based on Bayesian classifier, was applied to all images. From the segmented lesions, first order statistics and geometric features were extracted [1]. The intraclass correlation coefficient (ICC) for absolute agreement between the correspondent features was assessed using IBM SPSS 20. **Results:** 164 FDG avid lesions were identified on VEREOS images. Of those, 161 lesions were confirmed and delineated on GEMINI images. The main anatomical localizations of the lesions included breast, liver, and lungs. A high agreement (ICC > 0.7) was demonstrated for most of the features, both in the first order statistics and those related to geometry. Energy, metabolic tumor volume, tumor lesion glycolysis, surface area, and SUVpeak revealed an excellent agreement (ICC > 0.9). SUVmax, a frequently used feature in the clinics, showed high agreement (ICC = 0.89). On average, this feature was statistically higher in VEREOS than in the GEMINI (95% confidence interval: 0.20-0.67). **Conclusion:** There is high agreement between most of the first order and geometric features extracted from both devices imaging data. Under controlled acquisition and reconstruction parameters, these features can be used in multi-scanner studies (including longitudinal patient evaluation), using VEREOS and GEMINI PET/CT devices. **References:** [1] H. Aerts et al., "Decoding tumour phenotype by noninvasive imaging using a quantitative radiomics approach," Nat. Commun., 5:4006, 2014.

EP-0836

Is it valid to simulate a decrease in the administered activity by a reduction in the acquisition time of a PET scan?

J. M. Martí-Climent[1], *E. Prieto*[1], *P. Aguilar*[1], *A. García*[1], *V. Morán*[2];
[1]*Clínica Universidad de Navarra, Pamplona, SPAIN,*
[2]*Clínica Universidad de Navarra, Madrid, SPAIN.*

Aim/Introduction: Short acquisition scan times are frequently used as a surrogate for the evaluation of low activity protocols in PET studies. The aim of this study was to evaluate the validity of this assumption. **Materials and Methods:** NEMA anthropomorphic image quality phantom with hot spheres (10, 13, 17, 22, 28, 37 mm) was scanned (192 s acquisition time) with a Biograph mCT TrueV PET/CT system with 3 sphere contrasts (8:1; 4:1 and 2:1) and decreasing background concentrations (Cn = 5.3/2^n kBq/mL, n: 0 to 6). The first acquisition (C0) was resampled to simulate acquisition times down to 3 s (Tn = 192/2^n s, n: 0 to 6). For each contrast and concentration-time combination, 3 consecutive scans were acquired. PET images were reconstructed with OSEM+TOF+PSF (3 iterations, 21 subsets, 2 mm Gaussian filter) and with a reconstruction fulfilling EARL criteria (OSEM+TOF with 3 iterations, 21 subsets, 5 mm Gaussian filter). A spherical volume of interest (VOI) with a diameter equal to the internal diameter of each sphere and centered on it was drawn on each sphere. For background, 9 circular regions of interest (ROI, 37 mm diameter) were drawn in the central plane of the spheres and in ± 2 and + 4 planes beyond. Images were analysed by means of background variability, and signal to noise ratio (SNR) and contrast recovery (CR) for each sphere. Person's correlation and Lin's concordance correlation coefficient (rho) were evaluated between pairs of acquisitions with equal concentration*time product (C0T1-C1T0, **…**, C0T6-C6T0). **Results:** CR values increased as the size of the spheres increased. SNR values increased when the size of the spheres increased, decreased when the contrast decreased and decreased when the acquisition time decreased. Analysis of the visible spheres showed rho values higher than 0.953 (CR) and 0.993 (SNR) for the 6 pairs of EARL reconstructions, and higher than 0.911 (CR) and 0.993 (SNR) for 5 pairs of OSEM+TOF+PSF reconstructions. **Conclusion:** Simulation of PET tracer activity reduction is possible with short acquisition protocols. The phantom study has shown the interchangeability of the images in terms of signal to noise ratio and contrast recovery, especially for the reconstruction meeting the EARL criteria. **References:** None.

EP-0837

Impact of the Bayesian Penalized Likelihood (BPL) algorithm on hypoxia PET/CT in patients with lung neoplasia

S. Hapdey[1], *E. Texte*[2], *P. Gouel*[2], *B. Barres*[3], *P. Bohn*[1], *S. Thureau*[4], *P. Vera*[1];
[1]*Nuclear Medicine dept, Centre Becquerel & QuantIF-LITIS EA 4108, Rouen Medical University, Rouen, FRANCE,*
[2]*Nuclear Medicine dept, Centre Becquerel, Rouen, FRANCE,*
[3]*Nuclear Medicine dept, Centre J. Perrin, Clermont-Ferrand, FRANCE,* [4]*Radiotherapy dept, Centre Becquerel & QuantIF-LITIS EA 4108, University of Rouen, Rouen, FRANCE.*

Aim/Introduction: To determine the impact of the Bayesian Penalized Likelihood (BPL) reconstruction algorithm in comparison to OSEM on hypoxia PET/CT images using ^{18}F-MIZO and ^{18}F-FAZA radiopharmaceuticals. **Materials and Methods:** First, a Jaszczak phantom with 6 fillable spheres (35-1000µL) with a low sphere-to-background radio (SBR=3) was scanned on a GE710 PET/CT and reconstructed with OSEM and BPL to determine the best BPL β parameter among 300, 350, 400, 500 and 600. Twenty patients with lung neoplasia suspicion were included. Each patient benefitted from ^{18}F-MISO and/or ^{18}F-FAZA PET/CT exams (i.e 38 lesions), reconstructed with OSEM and BPL (with β=300, 350 and 400). Lesion was considered as hypoxic if the lesion SUVmax ≥ 1.4. A blind evaluation of lesion detectability and image quality was performed on a set of 78 randomized BPL and OSEM images by 10 nuclear physicians. SUVmax, SUVmean and hypoxic tumor volumes (using three different segmentation methods: i/ fixed SUV≥1.4 thresholding (HTV1.4); 60% thresholding of SUVmax (HTV60%); 1.5*Mediastinum SUVmax thresholding (HTV1.5med)) were measured and compared for each reconstruction. **Results:** The phantom analysis showed a significant increase of quantitative parameters using BPL compared to OSEM (+37%, +28% and +22% with β=300, 350 and 400 resp.) but had no impact on sphere detectability. The optimal β determined by the phantom analysis was β350. Regarding patient data, as for phantom analysis, all quantitative parameters showed a significant increase with BPL compared to OSEM (+15% in SUVmax with β=350). However, BPL had no significant impact on lesion detectability (mean detectability score for the 10 observers of 32.9/38 and 32.2/38 for OSEM and BPL resp.) and the image quality analysis did not show a clear trend in favour of BPL or OSEM. There was no correlation between SUVmax increase with BPL and either SUV or hypoxic volume from the initial OSEM reconstruction. Only one lesion was additionally considered as hypoxic with BPL. HTV1.4 was not impacted by BPL reconstruction (whatever the beta parameter), while HTV60% and HTV1.5med were both smaller than the hypoxic volume measured with OSEM reconstruction. **Conclusion:** BPL allows a significant increase in quantitative parameters and contrast without significantly improving the lesion detectability or image quality. The variation in hypoxic volume by BPL depends on the method used but SUV≥1.4 thresholding seems to be the more robust method, not impacted by the reconstruction method (BPL or OSEM). This segmentation method must be preferred if hypoxia PET-guided radiotherapy boost are envisaged. **References:** None.

EP-0838

Constructing Bland-Altman plots in small to moderate sample sizes: use rather a factor between 2 and 2.4 than 1.96

O. Gerke, *Odense Agreement Working Group;*
Odense University Hospital, Odense C, DENMARK.

Aim/Introduction: Bland-Altman Limits of Agreement (BA LoA) are well known and widely applied in methods comparison and in observer variation studies on quantitative outcomes. Assuming normally distributed differences, usually the 97.5 percentile of the Standard Normal distribution (i.e. 1.96) is employed in their construction. Alternatively, the factor 2 was proposed earlier as appropriate approximation in practical applications, whereas the factor $t_{0.975,n-1}\sqrt{((n+1)/n)}$ was indicated to secure the property of BA LoA to represent a prediction interval with 95% coverage. The aim was to contrast the factors 1.96, 2, the respective t-quantile $t_{0.975,n-1}$, and the exact factor $t_{0.975,n-1}\sqrt{((n+1)/n)}$ in the construction of BA LoA with respect to their actual coverage probability in small to moderate sample sizes. **Materials and Methods:** In a simulation study, we investigated the probability of BA LoA constructed with abovementioned factors to cover the next observation when sampling from the Standard Normal distribution. Sample sizes were varied from n=10 to n=700, and we generated (n+1) observations from the Standard Normal distribution 10,000 times for each sample size. The first n observations of each fictive trial were used to derive BA LoA to which the last observation was compared to. The coverage probability was then the number of cases out of 10,000 fictive trials where the LoA comprised the last observation. **Results:** For the classical factor of 1.96, coverage probabilities circulated closely around the nominal level of 0.95 from n=400 onwards, whereas this was the case from n=70 on for both the approximate factor of 2 and the respective t-quantile $t_{0.975,n-1}$. The application of the approximate factor 2 kept, though, more conservatively the nominal coverage level than the respective t-quantile $t_{0.975,n-1}$ did as the empirical coverage exceeded the nominal level of 0.95 for all sample sizes n≥70 apart from n=160 for factor 2. Applying the exact factor of $t_{0.975,n-1}\sqrt{((n+1)/n)}$, the coverage probability varied only slightly around 0.95 for all sample sizes investigated. As $\sqrt{((n+1)/n)}$ converges to 1 with increasing sample size, $t_{0.975,n-1}$ and $t_{0.975,n-1}\sqrt{((n+1)/n)}$ implicated close to identical coverage probabilities for sample sizes of at least n=180. **Conclusion:** In order to retain prediction intervals with a coverage probability of at least 0.95, BA LoA should be constructed using rather $t_{0.975,n-1}\sqrt{((n+1)/n)}$ for n≤70 and 2 for n>70 than 1.96. Only if the sample size exceeds n=400 will the coverage probability of BA LoA employing the factor 1.96 be close to the nominal level of 0.95. **References:** None.

EP-0839

Nonparametric alternatives to Bland-Altman Limits of Agreement in case of non-normally distributed data

O. Gerke[1], *M. E. Frey*[2], *H. C. Petersen*[2], *Odense Agreement Working Group;*
[1]*Odense University Hospital, Odense C, DENMARK,*
[2]*University of Southern Denmark, Odense M, DENMARK.*

Aim/Introduction: The assessment of agreement in method comparison and observer variability analysis on quantitative measurements is usually done by means of Bland-Altman Limits of Agreement (LoA) for which the paired differences are implicitly assumed to follow a Normal distribution. Whenever this assumption does not hold, the respective 2.5% and 97.5% percentiles of the distribution of paired differences must be assessed by quantile estimation. In the literature, simple empirical quantiles have been used before. The aim of this project was to (a) compare 14 different quantile estimators as to which extent these successfully serve as prediction intervals for the next observation and (b) propose robust alternative quantile estimators to Bland-Altman LoA when the assumption of Normality does not hold. **Materials and Methods:** In a simulation study with 2,000 fictive trials per sample size and distributional assumption, both sample quantile estimators, subsampling quantile estimators, Kernel quantile estimators, and other methods for quantile estimation were applied. Sample sizes were n=30, 50, 80, 100, and 150, and six different distributions were used for the paired differences: Normal; Normal with 1%, 2%, and 5% outliers; Exponential; and Lognormal. The performance of the 14 estimators in generating prediction intervals was measured by their respective coverage probability for one newly generated observation. **Results:** For n=30, a sample quantile estimator based on one order statistics (namely using the smallest and largest observed difference as estimates for the 2.5% and 97.5% percentiles, respectively) outperformed all other estimators. Another sample quantile estimator that employed a weighted average of two order statistics around the respective target percentiles of 2.5% and 97.5% was the only estimator to achieve a coverage probability of at least 95% in all distributional scenarios for the remaining sample sizes. The Harrell-Davis subsampling estimator and estimators of Sfakianakis-Verginis type achieved the nominal level of at least 95% coverage for all investigated distributions for sample sizes of at least N=80, except for the Exponential distribution where the coverage probability was 94% instead. **Conclusion:** Simple sample quantile estimators based on one and two order statistics can be used when deriving nonparametric LoA for sample sizes of up to 50 and at least 50 observations, respectively. For sample sizes exceeding 80 observations, more advanced quantile estimators that make use of all observed differences are equally applicable, but may be considered intuitively more appealing than simple sample quantile estimators that are based on only a few observations from the sample. **References:** None.

EP-0840

What are the effects of respiratory gating method on measurement accuracy of SUVmax with respect to lesion size? An anthropomorphic phantom study

B. Serrano[1], *M. Salva*[1], *Y. Ben Ahmed*[1], *N. Garnier*[1], *R. Amblard*[1], *B. Paulmier*[2], *R. Villeneuve*[1], *F. Hugonnet*[2], *V. Nataf*[2], *M. Faraggi*[2];
[1]*Princess Grace Hospital Center, Medical Physics Department, Monaco, MONACO,* [2]*Princess Grace Hospital Center, Nuclear Medicine Department, Monaco, MONACO.*

Aim/Introduction: Standardized Uptake Value (SUV) measurement of lung lesions is impaired by both partial volume effect (PVE) and respiratory motion that induce lesion blurring. Those additional effects affect more the smallest lesions. We aimed to compare two methods of gating, an automatic amplitude-based gating (AABG) and a conventional 4 phase-based respiratory gating (PBRG), on SUVmax measurement on different sizes of lesions using an anthropomorphic phantom simulating breathing. **Materials and Methods:** This study was performed on a PET/CT (Siemens mCT), fitted with four rings and time of flight (TOF). We used an anthropomorphic TORSO phantom representing a patient. Ten spheres of various inner diameters (6 to 33mm) were introduced into the lungs (air density) with the possibility of adding an axial mechanical device simulating breathing movement with a frequency of 15 cycles/min. Concentration in the spheres was the same for all diameters. We varied the concentration between 5 to 100 kBq/ml. The background and liver activities were respectively (39±2) and (14±1) MBq. We studied 4 different PET acquisitions: a standard 2.5min acquisition without movement (SA) as our reference of "true SUVmax", a 2.5min acquisition with simulated breathing movement (BMSA) without any gating and a 10min BMSA with respectively PBRG and AABG correction. Gated acquisitions were monitored with a pressure sensor system (Anzai Medical Corporation). Parameters reconstructions were: 2 iterations, 21 subsets, gaussian filter (FWHM=2mm), matrix size 200x200 pixels, TrueX algorithm (OSEM+PSF) and TOF. The largest sphere (diameter 33mm) was considered as the reference for results normalization. **Results:** The reproducibility for each acquisition of SUVmax was high (r=0.96, p=0.0003). For all the acquisitions and all the tracer concentrations within the spheres, the smallest detectable sphere's diameter was 12mm indicating the effect of PVE. Compared to the reference SUVmax values obtained with SA, SUVmax decreased significantly in all spheres below 27mm diameter with non-gated BMSA acquisitions (Δ=-34±11%, $p<10^{-4}$), in all spheres below 18mm diameter with PBRG acquisitions (Δ=-13±7%, $p<10^{-3}$) while average loss on SUVmax was moderate with AABG in all spheres below 12mm (Δ=3±4%, $p<10^{-3}$). **Conclusion:** PVE mostly impaired detectability of spheres diameters below 12mm corresponding to 3 times the spatial resolution of our camera. SUVmax measurement accuracy was impaired for spheres below 18mm with PBRG and 12mm with AABG. Furthermore, this impairment was at least four times less marked with AABG compared to PBRG. **References:** None.

EP-0841

Software development and validation for Salivary Gland Scintigraphy using Gamma Camera

A. K. Jha, *S. Mithun, A. D. Puranik, S. Shah, A. Agrawal, N. C. Purandare, V. Rangarajan;*
Tata Memorial Hospital, Mumbai, INDIA.

Aim/Introduction: Radiation induced damage of salivary gland parenchyma leading to impairment of salivary function is known for years. Iodine-131 radionuclide therapy as well as external beam radio therapy (EBRT) leading to impairment of salivary functions and xerostomia has been reported in literature. Modalities such as CT, MRI and sonography provide morphological information, where as sialography and scintigraphy provide functional information of salivary glands. Since, radiation induces functional damage of salivary gland, hence functional assessment by sialography or scintigraphy becomes imperative to perform in this scenario. Salivary scintigraphy being a relatively non-invasive procedure is preferred widely. However, unavailability of standardized software makes salivary scintigraphy a cumbersome process. Aim of our study was to develop and validate software for salivary scintigraphy processing. **Materials and Methods:** Software was developed in Alladin Editor available on Xeleris 4.1 workstation, GE medical system. An anterior dynamic imaging was performed for 30 min (15 sec/frame; matrix: 128X128; zoom:2) after injection of 7 to 10 mCi of $^{99m}TcO_4^-$ intravenously. Sialagogue was administered orally 14 min after injection.Upon loading dynamic image in the software a composite image from 10 to 13 min displayed in view port. Software prompts to draw ROI over parotid and submandibular salivary gland as well as background on brain on composite image. Time activity curves are generated for all the salivary gland from the contour. Point of sialagogue administration and nadir is localised on the graph by the two localizers. Uptake as well as ejection fraction of salivary glands are calculated automatically by using standard formula. Software was validated on 30 patients' data by comparing uptake and ejection fraction calculated by salivary software with manual method on 30 patients. **Results:** Average uptake value for two parotid and two sub-mandibular glands were 0.41, 0.38, 0.28, 0.26 by software and 0.44, 0.36, 0.31, 0.29 were that of manual method. Likewise, average excretion fraction for two parotid and two sub-mandibular glands were 52%, 49%, 37%, 39% by software and 50%, 46%, 35%, 36% by manual method respectively. The overall percentage difference in estimation of salivary uptake and excretion fraction by two methods were 5% and 5.6% respectively. **Conclusion:** This software simplifies the salivary function estimation by scintigraphy method. This software also performs well on all the parameters and accurately calculates salivary uptake as well as salivary excretion function. **References:** None.

EP-0842

Evaluation of Atlas Based Attenuation Correction in Bone Scintigraphy

F. P. Oliveira[1], *Â. Silva*[1], *J. C. Castanheira*[1], *A. Canudo*[1], *S. Mairos*[1], *M. Silva*[1], *J. Cruz*[1], *A. Domingues*[2], *D. Veiga*[2], *M. Ferreira*[2], *D. C. Costa*[1];
[1]*Champalimaud Centre for the Unknown, Champalimaud Foundation, Lisboa, PORTUGAL,* [2]*Neadvance - Machine Vision, S.A, Braga, PORTUGAL.*

Aim/Introduction: Bone scintigraphy is widely used to map bone metabolism, in particular searching for osteoblastic bone lesions. In clinical practice, this is currently done qualitatively based

on visual inspection. Geometric mean of anterior and posterior projections is frequently computed for quantification purposes. However, this quantification method does not take into account real photon attenuation and sensitivity of gamma cameras. In this work, we propose an atlas based attenuation correction method to quantify radiopharmaceutical distribution. **Materials and Methods:** Whole-body CT acquisitions from 18 females referred for clinical reasons were used to build an attenuation atlas dataset. Another dataset was built with 10 minutes post-injection (610±56 MBq of ^{99m}Tc-Oxidronate) bone scintigraphy from 35 females. This dataset was used for validation. To create the attenuation atlas, the attenuation map on anterior-posterior direction was created from each whole-body CT, considering the photon energy of the ^{99m}Tc. Each 2D attenuation map was then geometrically aligned with a female bone scintigraphy atlas previously built. Then the attenuation atlas was obtained by averaging all 2D attenuation maps. The second step was the implementation of the attenuation correction and validation. The bone scintigraphy atlas was aligned with each patient's bone scintigraphy and then the geometric transformations found were applied to the attenuation atlas built. Since the attenuation profile of each patient depends on the anterior-posterior body thickness, before applying the attenuation map to the geometric mean of the anterior and posterior projections, a patient specific correction was performed. This was based on a linear regression model taking into account the patients' height and weight. Finally, the correction for the gamma camera sensitivity was applied. Validation was done by comparing the theoretical whole-body activity (injected activity corrected for the decay) with the estimated whole-body activity using the proposed methodology. **Results:** High agreement between the theoretical and estimated activities was achieved (intraclass correlation coefficient of 0.856, $p < 0.001$). Mean and median absolute deviations were 3.9% and 2.7%, respectively. There were four cases with a deviation equal or superior to 10%. **Conclusion:** The herein proposed methodology proved to have potential to be used in the estimation of the radiopharmaceutical body distribution. Further studies are imperative using late (more than 2 hours post-injection) acquisitions. Potential sources of error also need to be thoroughly investigated. **Financial support:** Project LISBOA/NORTE-01-0247-FEDER-017685 - BTSCAD (Bone Tumor Scan - CAD) under the PORTUGAL 2020 Partnership Agreement, through the European Regional Development Fund. **References:** None.

EP-0843

Outsourced Teleradiology in the swiss medical system: a financial analysis for a promising concept

F. Caobelli[1], *N. Schöni*[2];
[1]*Universitätsspital Basel, Basel, SWITZERLAND,*
[2]*University of Zürich, Zürich, SWITZERLAND.*

Aim/Introduction: Teleradiology is feasible and yields similar quality of traditional reporting. Only a few papers have investigated the financial impact of teleradiology, and only considering in-house systems for remote reporting, thus reporting high costs and limited impact on personal management. Conversely, an outsourced management of teleradiology is expected to provide major advantages in terms of organization of department workload, personnel management and cost optimization. We here report a financial analysis based on an innovative teleradiology model, wherein the reporting is outsourced to an external society. **Materials and Methods:** Costs were quantified using insurance reimbursements of swiss medical system as reference. A cost-minimization analysis was conducted considering a representative Institution performing among other investigations 50 FDG-PET/CT, 150 Thorax-Abdomen CT und 40 Thorax-Abdomen MR each week, employing 10 nuclear medicine physicians (2 engaged in PET) and 20 radiologists (2 engaged in CT, 2 in MR). The following aspects were considered: 1) the need of reassigning MD to different diagnostics in case of personnel shortage (PS) 2) the maximum number of scans that a MD can report in one day without loss of quality, with consequent need for reducing department's workflow 3) insurance reimbursement 4) the costs of outsourced teleradiology. Three scenarios of MD-PS (illness, congresses, vacations) were considered: 1=10%; 2=20% and 3=30%, **Results:** Total revenue per week in the representative Institution is 80,000 CHF for PET/CT, 72,990 CHF for CT and 43,830 CHF (=196,820 CHF/week). In Scenario 1, overall loss was 22,115 CHF/week. In Scenario 2, the loss increased to 39,364 CHF/week. Finally, in Scenario 3 the total loss reached 93,532/week. Assigning the canceled investigation to outsourced teleradiology allowed to limit money loss to 4,955 CHF in scenario 1 (-77%), 8,828 CHF in scenario 2 (-78%) und 21,022 CHF in scenario 3 (-79%). **Conclusion:** A flexible system for teleradiology accounting for fluctuating PS allowed to reduce the potential loss due to canceled scans. This is expected to financially impact even more those Institutions with less employees. It may be foreseen that a comparable increase in revenue can be obtained by optimizing the scanners utilized capacity without the need of increasing fix costs. **References:** None.

EP-0844

Study of different quantitative uptake metrics in F18-FDG PET/CT imaging in breast cancer: impact of workstation and segmentation method

M. Ibañez, *J. Navarro Fernández, L. Frutos Esteban, J. Contreras Gutiérrez, L. Mohamed Salem, F. Hernández Almagro, J. Villa Sánchez, I. Sime Loayza, M. Tomás Redondo, T. Rodríguez Locarno, T. Moreno Monsalve, R. Reyes Marlés, M. Castellón Sánchez, F. Nicolás Ruiz, E. Para Vergara, R. Mears Baño, M. Claver Valderas;*
Clinic Universitary Hospital Virgen de la Arrixaca, El Palmar, Murcia, SPAIN.

Aim/Introduction: There is increased interest in various new quantitative uptake metrics beyond standardized uptake value (SUV) in oncology PET/CT studies. The purpose of this study is to investigate the variability of several quantitative metrics

in breast cancer using F18-FDG PET/CT different workstation and segmentation methods focused on the breast lesion. **Materials and Methods:** Twenty patients with early to locally advanced breast cancer were studied. F18-FDG PET/CT were performed using a Philips Ingenuity TF64 (Cleveland, OH, USA). Two minutes/bed position and list-mode time of flight (TOF) adquisition were used. Image reconstruction was performed using 3 iterations and 33 subsets, 3D ordered subset expectation maximization (BLOB-OS-TF) being reconstructed in two types of matrices: 144x144 matrices with voxel size 4x4x4mm (standard voxels) and 288x288 matrices with voxel size 2x2x2mm (Small voxels) without PSF resolution recovery.The imagen analysis was reviewed using two worksations: IntelliSpace Portal 7.0 and Syngo.Via VB20A. Three automated segmentation methods were applied: adaptive thersholding method for IntelliSpace Portal 7.0 and 40% threshold of SUVmáx form IntelliSpace Portal and Syngo.Via.The quantitative metrics evaluated were SUVmax, SUVmean, SUVpeak, MTV and TLG by drawing region of interest (VOI) on the breast lesion. **Results:** For uptake metrics SUVmax, SUVmean, SUV peak, similar values for workstation as well as for 4mm and 2mm voxel size segmentation methods were obtained. SUVmax values were identical in all methods. While the MTV 4mm showed the greatest variability, MTV measured al 40% in IntelliSpace was 3-fold higher (15.2 CI95%:4.0-26.4) than in Syngo (5.8 CI95%: 4.4-7.2). A similar situation was observed for TLG 4mm data, since the IntelliSpace showed a 2-fold value than Syngo platform, although there were no statistically significant differences (p=0.126 for MTV and p=322 for TLG). SUVpeak was calculated only in 8 patients at 2mm by adaptive threshold and at 9 by threshold 40% used IntelliSpace Portal being limitation of this software. **Conclusion:** Although both workstation and segmentation methods render similar data for all variables, significant differences were obtained regarding MTV and TLG data. Therefore, in those studies in which these parameters are of interest, the software used must be taken into account since there is a possibility of unrealiability. **References:** None.

EP-0845

Comparison of different quantitative uptake metrics in ^{18}F-FDG PET/CT in breast cancer according to voxel size using different workstation and segmentation method

M. Ibañez, *J. Navarro Fernández, L. Frutos Esteban, J. Contreras Gutiérrez, L. Mohamed Salem, F. Hernández Almagro, J. Villa Sánchez, I. Sime Loayza, M. Tomás Redondo, T. Rodríguez Locarno, T. Moreno Monsalve, R. Reyes Marlés, M. Castellón Sánchez, F. Nicolás Ruiz, E. Para Vergara, R. Mears Baño, M. Claver Valderas; Clinic Universitary Hospital Virgen de la Arrixaca, El Palmar, Murcia, SPAIN.*

Aim/Introduction: There are several methods to quantify different uptake metrics to diagnose the tumor lesion severity. These values can be slightly modified attending to the segmentation methods, workstation employed, but specially to the voxel size. Therefore, the objective of the present study was to compare the similarity degree among the different uptake metrics according to the voxel size. **Materials and Methods:** Twenty patients with early to locally advanced breast cancer were studied. ^{18}F-FDG PET/CT were performed using a Philips Ingenuity TF 64 (Cleveland, OH, USA). Two minutes/bed position and list-mode time of flight (TOF) adquisition were used. Image reconstruction was performed using 3 iterations and 33 subsets, 3D ordered subset expectation maximization (BLOB-OS-TF) being reconstructed in two types of matrices: 144x144 matrices with voxel size 4x4x4mm (standard voxels) and 288x288 matrices with voxel size 2x2x2mm (small voxels) with out PSF resolution recovery. Two Workstation were used: IntelliSpace Portal 7.0 and Syngo.Via VB20A. Three automated segmentation methods were applied: adaptive thresholding method for IntelliSpace Portal 7.0 and 40% threshold of SUVmax for IntelliSpace Portal and Syngo via. Uptake metrics determined were SUVmax, SUVmean, SUVpeak, MTV and TLG for 4mm and 2mm voxel size. **Results:** Considering all methods as a whole, our data showed statistically significant differences for all parameters studied ($p<0.001$) excepting MTV and TLG. Specifically, the data obtain using 2mm voxel size were higher than 4mm voxel size for SUVmax, SUVmean, SUVpeak. Moreover, attending to the specific segmentation method, further differences were revealed. For instance, in the adaptive threshold method, MTV and TLG data were also significantly different depending on the voxel size. In addition, there were also statistically significant differences depending on the workstation used to determine the tumor lesion. In this regard, the IntelliSpace Portal 7.0 using 40% threshold of SUVmax showed no differences regarding MTV and TLG parameters and voxel size; however, the MTV data in the Syngo.Via was significantly higher at 4mm than 2mm ($p<0.001$). **Conclusion:** The voxel size modifies the quantitative uptake metrics in most parameters employed for tumor diagnosis. Therefore, data obtained by one or the other voxel size are not fully comparable. **References:** None.

EP-0846

Partial Volume Correction for Lymph Nodes in 18F-PSMA PET Images

J. Schaefferkoetter, *C. Ortega, P. Veit-Haibach, U. Metser; University Health Network, Toronto, ON, CANADA.*

Aim/Introduction: Partial volume effects in medical imaging result from limited scanner resolution and heterogenous tissue types within voxels. These effects degrade resolution and quantitative accuracy and are especially problematic for PET imaging. This is an important consideration for PSMA-PET as lymph node (LN) SUV measurements can be a key indicator for grading prostate disease. The work here investigates partial volume correction (PVC) for LNs in PET images. **Materials and Methods:** LN regions of interest (ROIs) were contoured on both CT and on PET volumes by a radiologist - these were used to generate mask volumes. The CT mask was the basis for the PVC and was transformed to the PET space by interpolation onto its corresponding voxel coordinate grid, accounting for any possible translational misregistration. Once transformed into

the PET space, each ROI in the mask was scaled to reflect its actual contrast, since this determines the local spill-over effect. Each contrast was found empirically, searching over a large range for the correct value. The ROI-scaled anatomical mask was then smoothed with a 3D kernel approximating the scanner response function - dividing the original anatomical volume by the smoothed data then yielded a map of PVC factors, which was applied directly to the PET volume. **Results:** The effects of the PVC were evaluated in a population of 74 patients and 241 LNs for both unsmoothed and 5mm Gaussian post-smoothed images. The PVC significantly affected region mean and max SUV measurements in the unsmoothed images. The trend showed good correlation between SUV increase and volume, generally following an exponential curve, with regions of 0.01 cm3 volume realizing an max SUV increase over 150% and those with 1 cm3 volume showing an increase around only 5%. The changes in corrected SUVs measured in the smoothed images were less pronounced. In fact, region mean was notably unchanged by the PVC for all LNs in the post-smoothed images. **Conclusion:** This work evaluated an approach to obtain partial volume effect-corrected SUVs for LNs, based on the volumes measured in their high resolution, anatomical images. However as expected, this work showed that any PVC for these small structures is less effective when when using image post-smoothing, which is often the case in clinical PET. As clinical guidelines focus on reference measurements for disease staging and grading, higher degrees of accuracy in image quantification may help to standardize patient management. **References:** Erlandsson, et al. 2012.

EP-0847

New Nuclear Functional Imaging Data in NET$_s$Theragnostic Approach

C. R. Stolniceanu[1], *C. Ungureanu*[1], *C. Preda*[1], *C. Volovat*[1], *S. Volovat*[1], *T. Ionescu*[2], *E. Chifor*[2], *A. Statescu*[2], *M. Gutu*[1], *M. Matovic*[3], *C. Stefanescu*[1];
[1]*University of Medicine and Pharmacy U.M.F „Grigore T. Popa", Iasi, ROMANIA,* [2]*University Emergency Hospital "Sf. Spiridon", Iasi, ROMANIA,* [3]*Center of Nuclear Medicine, Kragujevac, SERBIA.*

Aim/Introduction: Tektrotyde somatostatin receptor imaging is an essential step in neuroendocrine tumors (NETs) theragnostics, tailoring the eligibility for Peptide Receptor Radionuclide Therapy. This prospective PhD step NETs study aims to evaluate and compare the statistical differences of the pathological quantitative uptake radiolabeled somatostatin analogues (RSA) patterns between gastro-intestinal (GI-NETs) and pancreatic NETs (P-NETs). **Materials and Methods:** We studied, over a 12-month period, 53 patients, with a female/male ratio of 0.39:1, mean (±standard deviation (SD)) age 53.9-year-old (±10.3), histologically proven GI- and P-NETs, from 2 nuclear medicine centers. Study design: (gamma camera Siemens e cam Dual Head, LEAP collimator, appropriate software): dynamic scintigraphy (60 images, 1 image/second, 128x128 matrix), spot scintigraphy (10 minutes/image, 256x256 matrix), whole body scintigraphy (matrix 256x1024, 6cm/min bed movement) and SPECT (128x128 matrix, 132 images). Images were acquired at 10 minutes, 2-4 and 24 hours after i.v. administration of 10.57 MBq/kg bw ^{99m}Tc-Tektrotyd. Regions of interest (ROI$_s$) for each hot pathological area were defined. The uptake was quantified (counts/pixel) and the following indices were calculated: I_1=tumor/liver, I_2=tumor/spleen, I_3=tumor/lung, I_4=tumor/right thigh. Uptake kinetics graphs for all indices and the tumor heterogeneity graphs were compared. Statistical correlations were calculated to evaluate the pathological quantitative uptake indices differences between GI- and P-NETs. **Results:** Our data demonstrated the statistical correlations regarding the pathological quantitative uptake RSA patterns, with the next values: statistically significant negative correlation for I_4 (p=0.05, Pearson coefficient R -0.5, coefficient of determination R_2 0.24 and Spearman's coefficient R_s -0.47), with the mean I_4 GI-NETs 5.09, (2.88-8.80), variance (V) 3.25, SD 1.8, standard error of the mean SEM 0.31, respectively the mean I_4 P-NETs 4.6 (3.22 -5.94), V 0.94, SD 0.97, SEM 0.21. V 0.94, SD 0.97, SEM 0.21. For I_3 indice, was found a statistical positive correlation (R 0.32, R_2 0.104, Rs 0.25), with a mean I_3 GI-NETs 3.38, (1.12-5.73), V 1.60, SD 1.26, SEM 0.22, respectively a mean I3 P-NETs 2.15, (0.34-3.92), V 1.09, SD 1.04, SEM 0.23. For I_1 and I_2, the values were not statistically significant correlated (R 0.37, R_2 0.14, Rs 0.1053 for I_1, respectively R -0.02, R_2 0.15 and Rs 0.2). **Conclusion:** From our study, best indices to be calculated would be I_3 and I_4. Although, were not statistically significant correlations for all four indices the uptake kinetics analysis next to the tumor heterogeneity graphs represent important nuclear functional imaging features in NETs theragnostic approach. **References:** None.

EP-0848

Study of different quantitative uptake metrics in ^{18}F-FDG PET/CT imaging from malignant lymph node in breast cancer: impact of workstation and segmentation method

M. Ibañez*, J. Navarro Fernández, L. Frutos Esteban, J. Contreras Gutiérrez, L. Mohamed Salem, F. Hernández Almagro, J. Villa Sánchez, I. Sime Loayza, M. Tomás Redondo, T. Rodríguez Locarno, T. Moreno Monsalve, R. Reyes Marlés, M. Castellón Sánchez, F. Nicolás Ruiz, E. Para Vergara, R. Mears Baño, M. Claver Valderas; Clinic Universitary Hospital Virgen de la Arrixaca, El Palmar, Murcia, SPAIN.*

Aim/Introduction: The purpose of this study is to investigate the variability of several quantitative metrics in malignant lymph node breast cancer using ^{18}F-FDG PET/CT with different workstation and segmentation methods focused on the lymph nodes. **Materials and Methods:** Seventeen patients with locally advanced breast cancer (N1-N3) were studied. ^{18}F-FDG PET CT were performed using a Philips Ingenuity TF 64 (Cleveland, OH, USA). Two minutes/bed position and list-mode time of flight (TOF) adquisition were used. Image reconstruction was performed using 3 iterations and 33 subsets, 3D ordered subset expectation maximization (BLOB-OS-TF) being reconstructed in two types of matrices: 144x144 matrices with voxel size

4x4x4mm (standard voxels) and 288x288 matrices with voxel size 2x2x2mm (small voxels) without PSF resolution recovery. The image analysis was reviewed using two Workstation: IntelliSpace Portal 7.0 and Syngo.Via VB20A. Three automated segmentation methods were applied: umbral adaptative and 40% of the maximun tumor value as a thresthold with IntelliSpace Portal and segmentation 40% of the maximun tumor value by Syngo via. The quantitative uptake metrics evaluated were SUVmax, SUVmean, SUVpeak, MTV and TLG by drawing region of interest (VOI) on the breast lesion. **Results:** For uptake metrics SUVmax, SUVmean and SUVpeak, similar values for work stations as well as segmentation methods for both 4mm and 2mm voxel size were obtained. While the MTV 4mm showed the greatest variability, MTV measured at 40% in IntelliSpace was 4-fold higher (11.7 CI95%:1.7-21.7) than in Syngo (2.9 CI95%: 1.8-4). A similar situation was observed for TLG 4mm data since the IntelliSpace showed a 2-fold value than Syngo platform, although there were no statistically significant differences (p=0.05 for MTV and p=0.165 for TLG). SUV peak was calculated only in 4 patients at 2mm by adaptive threshold and at 3 by threshold 40% used intelliSpace Portal being limitation of this software. **Conclusion:** Although both workstation and segmentation methods render similar data for all variables, significant differences were obtained regarding MTV and TLG data. Therefore, in those studies in which these parameters are of interest, the software used must be taken into account, since there is a possibility of unreliability. **References:** None.

EP-0849

Quantitative assessment of joints affected by rheumatoid arthritis using [^{11}C]DPA713 PET

M. Yaqub[1], *N. Verweij*[2], *S. Pieplenbosch*[1], *R. Boellaard*[1], *C. van der Laken*[2], *A. A Lammertsma*[1];
[1]*Amsterdam UMC, Vrije Universiteit Amsterdam, department of radiology and nuclear medicine, Amsterdam, NETHERLANDS,* [2]*Amsterdam UMC, Vrije Universiteit Amsterdam, department of reumatology, Amsterdam, NETHERLANDS.*

Aim/Introduction: Rheumatoid arthritis (RA) is a systemic connective tissue disease that affects up to 2-4% of adults in developed countries. An accurate tool for both early diagnosis and monitoring of treatment could contribute to early instalment of effective therapy and reduction of permanent physical damage. The macrophage is an excellent imaging target for RA, because of its early infiltration in the synovium of RA patients and reflection of disease activity throughout the course of the disease. [^{11}C]DPA713 is a promising macrophage tracer for RA[1]. The aim of the present study was to develop an accurate plasma input kinetic model for quantification of [11C] DPA713 PET studies of arthritic joints in RA patients. A second aim was to use this model to assess the performance of various simplified quantitative approaches. **Materials and Methods:** Dynamic [^{11}C]DPA713 PET scans (60 min) were performed in 5 RA patients, including arterial and venous sampling. Using CT images, volumes of interest (VOIs) were drawn manually within the boundaries of RA active joints, healthy joints, and bone marrow regions. [^{11}C]DPA713 data were analysed using various plasma input models, i.e. single tissue (1T2k), and reversible (2T4k) and irreversible two tissue compartment models (2T3k), all including an additional fit parameter for blood volume. In addition, linearized/simplified methods were evaluated, i.e. Logan, Patlak, standardized uptake values (SUV) and target to blood ratios (TBR) averaged over various intervals, by comparing results with those of the optimal plasma input model. **Results:** Whole blood activity and plasma to whole blood activity ratios showed good agreement among patients and between arterial and venous samples. Visual assessment showed acceptable fits for all models in all segmented regions, except for the 1T2k model that didn't fit well in the bone marrow time activity curves. The Akaike goodness of fit criterion preferred the 2T3k model for all regions. Patlak K_i provided good agreement (R^2 = 0.83) with this non-linear 2T3k approach. SUV correlated highly with K_i (R^2=0.82) and showed a significant difference in uptake between unaffected vs affected RA regions (p=0.018). **Conclusion:** The optimal quantitative model for assessment of [^{11}C]DPA713 uptake in RA joints is 2T3k. K_i based on this 2T3k analysis showed good correlation with clinical levels of RA. Furthermore, SUV (at 30-60 min pi) is the preferred simplified quantitative method showing similar performance in identifying affected versus non-affected RA regions as K_i. **References:** [1] Gent Y et al, Arthritis Res Ther 2014 16:R70.

EP-0850

Development of PET in Europe

A. N. Stevens;
Medical Options, London, UNITED KINGDOM.

Aim/Introduction: To track the development and use of PET in Europe. The provision and level of scanning of PET (PET, PET/CT and PET/MR) in Europe varies widely both between and within countries where workload volume differs between providers. The large differences between facilities in terms of scan volumes and the range of tracers in use precluded a simple sampling approach and required identification of all European PET providers. **Materials and Methods:** Facilities with PET and or cyclotron(s) were identified from a number of sources primarily equipment manufacturers and sites providing PET. Sites were invited to describe their operation including their equipment profile, the number and types of patient studies performed and their use of radiotracers. We were able to identify over 95% of the PET cameras and cyclotrons operating in Europe. Over 50% of these sites provided workload numbers for 2018. To project total workload we employed a segmentation scheme for each country or region which identified ten types of facility allowing us to estimate more accurately patient numbers at sites who did not contribute workload data. **Results:** In 2018 there were 799 providers of PET and/or CT or MR in Europe of which 18 were mobile. PET/CT accounted for over 90% of the installed systems. PET cameras which comprised 2.2% of the total and PET/MR 5.3% were almost entirely operating in research

settings. FDG studies accounted for 88% of the total patient workload with oncology examinations accounting for 89% of FDG scans. Tracers other than FDG accounted for 12% of studies and of these Fluorine 58%, Gallium 27%, and Rubidium 9% were the significant nuclei in use. Characterising prostate disease accounted for 53% of the studies with F-Choline, 18F and 68Ga PSMA accounting for 96% of these investigations. Scan numbers rose by 9.0% from the 1.73m scans estimated for 2016 versus 7.8% between 2014 and 2016. There are wide variations across Europe both in terms of scans performed and patient throughput. In some cases this is due to reimbursement and in others working practices and patient catchment. **Conclusion:** Across Europe the number of FDG studies continues to grow as the proportion of patients in countries with low adoption levels chases that of the high adopters. In these countries oncology examinations are levelling off. Compounds other than FDG offer the major opportunity to expand the use of a PET. **References:** We thank the sites contributing to this study.

EP-0851

Multicenter study of rapid bone-SPECT/CT image acquisition

K. Miwa[1], *T. Murata*[2], *N. Miyaji*[3], *T. Kamiya*[4], *Y. Owaki*[5], *T. Okamoto*[6], *R. Emura*[7], *M. Takahashi*[8], *R. Kobayashi*[1], *T. Iimori*[2];
[1]*Department of Radiological Sciences, International University of Health and Welfare, Tochigi, JAPAN,* [2]*Department of Radiology, Chiba University Hospital, Chiba, JAPAN,* [3]*Department of Nuclear Medicine, Cancer Institute Hospital of Japanese Foundation for Cancer Research, Tokyo, JAPAN,* [4]*Department of Medical Technology, Osaka University Hospital, Osaka, JAPAN,* [5]*Office of Radiation Technology, Keio University Hospital, Tokyo, JAPAN,* [6]*Department of Radiology, Tsugaru General Hospital, Aomori, JAPAN,* [7]*Department of Radiology, Kimitsu Central Hospital, Chiba, JAPAN,* [8]*Department of Central Radiological Technology, Saitama Medical University Hospital, Saitama, JAPAN.*

Aim/Introduction: The addition of SPECT/CT to whole-body bone scintigraphy is time-consuming and can prolong the procedure by approximately 15 min per bed position. The duration of acquisition needs to be reduced without decreasing image quality and negatively affecting diagnostic confidence. This multicenter study aimed to determine the feasibility of rapid bone-SPECT/CT imaging for detecting bone metastases. **Materials and Methods:** We scanned NEMA body phantoms comprising six spheres (diameter: 10, 13, 17, 22, 28 and 37 mm) containing ^{99m}Tc solutions with a sphere-to-background ratio of 6 at seven institutions. We investigated image quality and the quantitative accuracy of GE Infinia Hawkeye4, GE Optima NM/CT640, GE Discovery NM/CT670, NM/CT670 CZT, Siemens Symbia T6, Intevo16 and Philips BrightViewX with XCT SPECT/CT systems. The duration of image acquisition varied from 1 to 30 (1, 2, 3, 4, 5, 10 and 30) minutes. Data were reconstructed using GE Evolution for bone, Siemens Flash 3D or xSPECT Quant and Philips Astonish, ten subsets, and a varying number of iterations. The smallest visually detectable sphere in reconstructed images acquired over different durations was identified. We then measured the %contrast and background variability of 17-mm spheres recommended by the Japanese Society of Nuclear Medicine Technology (JSNMT) bone-SPECT guidelines and standardized uptake values (SUV). **Results:** The 17-mm hot spheres were obvious on SPECT images acquired overa period of 3 min using all scanners. The %contrast increased with the number of iterations but became almost saturated starting from five iterations. The balance between %contrast and background variability differed among scanners. Three- and four-min SPECT image acquisitions were needed to optimize the number of iterations required to meet the JSNMT criteria. Smaller lesions were detected more effectively over longer acquisitions using the Discovery NM/CT670 CZT and Symbia Intevo16, although background noise was significantly higher than that of other scanners when acquisitions were ≤ 4 min. The SUV were relatively stable during 4-min acquisitions. **Conclusion:** Rapid bone SPECT/CT is technically feasible without loss of image quality and quantitative ability to detect potential bone metastases. **References:** None.

EP-62

Technical aspects -> Instrumentation and data analysis -> Data analysis -> Image reconstruction

October 12 - 16, 2019 e-Poster Area

EP-0852

Added Value of Siemens xSPECT Bone Algorithm in Reading Musculoskeletal SPECT/CT

N. Gandy, *J. Phillips, K. Wallitt, Z. Win, M. Arshad, K. Ordidge, A. Gomes Moura, L. M. Perry, N. Soneji;
Imperial College Healthcare NHS Trust, London, UNITED KINGDOM.*

Aim/Introduction: To determine whether use of the CT as frame-of-reference for image reconstruction (xSPECT bone) improves diagnostic confidence and detection of bone metastases or pain generators compared with iterative reconstruction with resolution recovery (Flash 3D) SPECT reconstruction when evaluating musculoskeletal SPECT/CT. **Materials and Methods:** 20 patients (30 more patients to be evaluated) referred for bone scans with musculoskeletal pain suspected to have bone metastases and/or degenerative pain generators were identified. Bone SPECT/CT scans were acquired using a Siemens Intevo Bold gamma camera at our centre. Data was reconstructed with both xSPECT (xSPECT/CT) and Flash 3D (F3D SPECT/CT) algorithms. Two consultant radionuclide radiologists performed a retrospective review of the reconstructions. The reviewers were blinded to the clinical indication and independently reviewed anonymised F3D SPECT/CT followed by xSPECT/CT datasets. Each case was given

a diagnostic confidence (1 to 3, low to high) and image quality (1 to 5, low to high) score. **Results:** The initial 20 cases included 8 cases for metastatic bone disease in known malignancy and 12 cases for pain generators. Inter-observer agreement for presence or absence of metastases and pain generators was 90% and 85% respectively. Average image quality score by both readers increased from 3.0 for F3D SPECT/CT to 4.7 for xSPECT/CT ($p<0.0001$). Diagnostic confidence for Reader 1 changed from 2.95 with F3D SPECT/CT to 2.98 with xSPECT/CT ($p=0.6663$), and from 2.77 to 2.95 for Reader 2 ($p = 0.0165$). Reader 2 identified an average of 2.3 more lesions on xSPECT/CT vs F3D SPECT/CT compared to Reader 1 with an average of 0.05 more lesions. xSPECT/CT helped identify low grade uptake within smaller joints compared to F3D SPECT/CT, although overall diagnosis was unchanged for the majority of cases. Only one discrepant metastasis case was identified demonstrating mottling of marrow uptake on xSPECT/CT due to tiny sclerotic metastases otherwise only visible on the CT component and not identifiable on F3D SPECT/CT images. **Conclusion:** The xSPECT/CT reconstruction provides potential scope to identify more subtle areas of radiopharmaceutical uptake with better anatomical localisation given the improved image quality. However, our findings demonstrate variable improvement of diagnostic confidence between readers and limited change in overall diagnosis. Further studies are needed to assess the improved clinical efficiency of xSPECT/CT reconstructions. **References:** None.

EP-0853

Optimized PET reconstructions: Can they be harmonized as well?

H. Vosoughi[1,2], *P. Geramifar*[3], *A. Rahmim*[4], *F. Emami*[2], *M. Hajizade*[1], *M. Momennezhad*[1];
[1]*Department of Medical Physics, Mashhad University of Medical Science, Mashhad, IRAN, ISLAMIC REPUBLIC OF,* [2]*Nuclear Medicine Department, Razavi Hospital, Imam Reza International University, Mashhad, IRAN, ISLAMIC REPUBLIC OF,* [3]*Research Center for Nuclear Medicine, Shariati Hospital, Tehran University of Medical Science, Tehran, IRAN, ISLAMIC REPUBLIC OF,* [4]*Departments of Radiology and Physics, University of British Columbia, Vancouver, BC, CANADA.*

Aim/Introduction: PET/CT images are extensively utilized for diagnosis, (re)staging and monitoring treatment response. Preferred protocols should have optimal image quality and detectability with accurate quantification, and as such reconstruction protocols should be optimized. There are significant variations in PET quantification due to differences in scanner hardware and reconstruction algorithms. To tackle the challenge of variability in quantitative values between PET images obtained using different scanners, determination of harmonized reconstruction is very important. **Materials and Methods:** Data acquisition of IQ-NEMA phantom with SBR 4:1, 6:1, 8:1 and 10:1 was performed on a SIEMENS Biograph6 TrueV PET/CT scanner. Raw PET data were reconstructed using 6 different iterations (x subsets) and Gaussian post-smoothing filters with FWHM 2, 4, 6, 8 and 10 mm. In addition, image reconstruction was performed with/without PSF modeling (HD and 3D mode). CNR, COV, percentage difference of CNR, RC_{max}, $RC_{A50\%}$ and RC_{peak} were evaluated for standardization, and were compared with EARL specification reference values. **Results:** CNR and COV improved using smoother filters and fewer iterations. COV was less than cutoff (15%) for all reconstructions of frames >3min. Percentage difference of CNR between FWHM 4 and 6mm for all reconstructions was more than other sequential filter pairs. Though in SBR4:1, the maximum value of CNR of the smallest sphere was 8, it was barely visible, but in SBR6:1, CNR increased to 15. Iterations 30-60 with suitable post-smoothing Gaussian filters harmonized quantitative PET data. There were no difference in RC curves between 3D and HD mode in SBR 4:1. In HD mode, RC_{max} and $RC_{A50\%}$ were overestimated in higher SBRs and higher iterations. Positive bias in RC_{max} and $RC_{A50\%}$ was observed for 13, 17, 22mm spheres caused by PSF-modeled reconstruction, creating edge artifact. However, applying 6mm Gaussian filter and/or using RC_{peak} reduced this bias. Furthermore using CNR as a surrogate for image quality demonstrated that 6 mm Gaussian filter can be appropriate towards optimized as well as harmonized imaging. **Conclusion:** Image quality and detectability in PET images strongly depends on activity to background ratios, reconstruction parameters and post-smoothing filter. The optimized post-reconstruction filter was found to minimize variations of RC in comparison to EARL references. In addition, accurate quantification is feasible utilizing PSF modeling when utilizing appropriate filters. **References:** None.

EP-0854

Regularized Reconstruction Improves Signal-to-noise and Quantification for ^{18}F- PSMA PET/CT Imaging

C. F. Uribe[1], *N. Colpo*[1], *E. Rousseau*[2], *F. Lacroix-Poisson*[2], *D. Wilson*[1], *A. Rahmim*[1,3], *F. Bénard*[1,3];
[1]*BC Cancer, Vancouver, BC, CANADA,* [2]*Universite de Sherbrooke, Sherbrooke, QC, CANADA,* [3]*University of British Columbia, Vancouver, BC, CANADA.*

Aim/Introduction: The popular ^{18}F-labeled PSMA-targeting PET tracer, ^{18}F-DCFPyL, has shown to be significantly superior in detecting metastatic prostate cancer than ^{18}F-FDG. Accurate quantification of ^{18}F-DCFPyL images can enable evaluation of therapeutic efficacy, comparison between centres, and the potential to build outcome predictive models. Ordered subsets expectation maximization (OSEM) is commonly used to generate PET images, but noise is amplified at high number of iterations. As such, limited iterations are used in practice to maintain adequate image quality; however, this may not be sufficient to achieve convergence and leads to lower standardized uptake values (SUV). The block sequential regularized expectation maximization (BSREM) algorithm, also called Q.Clear (GE Healthcare), allows convergence while avoiding noise amplification at higher number of iterations. In

this study, we perform quantitative comparison of OSEM and BSREM-based ^{18}F-DCPFyL images on a cohort of prostate cancer patients. **Materials and Methods:** Whole-body ^{18}F-DCFPyL PET/CT imaging was performed on 30 patients with biochemical recurrence following curative-intent therapy for prostate cancer. Images were reconstructed using OSEM (32 subsets, 2 iterations) and BSREM (32 subsets, 25 iterations, gamma=2, beta=400) including attenuation and scatter correction. Images were interpreted by experienced nuclear medicine physicians. Regions of interest (ROIs) for the 3 most active lesions were drawn using MIM (MIM Software) and fixed 40% threshold. Each ROI was cloned and shifted to a region in the vicinity of the lesion to determine the maximum, mean, and standard deviation (s.d.) of the background (bg) activity. SUVmax, SUVmean, signal-to-noise ratio (SNR, calculated as lesion_SUVmean/bg_s.d.), and contrast (calculated for both SUVmax and SUVmean w.r.t. bg_SUVmean) were compared between the two algorithms. As distributions were skewed, a $\log_{10}$ transformation was applied and the Shapiro-Wilk normality test suggested that the transformed data was normally distributed. A paired t-test was used to determine statistically significant differences. Values are reported as (mean, [95% confidence interval]). **Results:** Mean BSREM SUVmax=(17.4, [13.0-23.2]), SUVmean=(9.6, [7.5-12.2]), SNR=(53.7, [41.0-70.3]), contrast_max=(19.5,[13.2-28.7]), and contrast_mean=(10.0,[7.0-14.4]) were 28.9%, 15.7%, 34.9%, 17.5%, and 2.0% higher, respectively, than OSEM SUVmax=(13.5, [10.5-17.3]), SUVmean=(8.3, [6.6,10.4]), SNR=(39.8,[31.8-49.9]), contrast_max=(16.6,[11.9-23.1]), and contrast_mean=(9.8,[7.1-13.5]). Statistically significant differences between algorithms were observed for SUVmax ($p=8.0\times10^{-8}$), SUVmean ($p=7.8\times10^{-8}$), SNR ($p=3.9\times10^{-7}$), and contrast_max ($p=1.8\times10^{-2}$), but not for contrast_mean (p=0.7). **Conclusion:** Use of regularized reconstruction can achieve significantly higher lesion SUVmax, SUVmean, SNR, and contrast_max for prostate cancer imaging using an ^{18}F-labeled PSMA PET radiotracer. This may lead to improved image quantification and clinical task performance in prostate cancer patients imaged with ^{18}F-DCFPyL. **References:** None.

EP-0855

Does Bayesian penalized likelihood reconstruction (Q.Clear) for FDG-PET always outperform image quality of OSEM-based reconstruction?

J. M. M. Rogasch[1], *F. Hofheinz*[2], *S. Suleiman*[1], *M. Lukas*[1], *H. Amthauer*[1], *C. Furth*[1];
[1]*Charité-Universitätsmedizin Berlin, corporate member of Freie Universität Berlin, Humboldt-Universität zu Berlin, and Berlin Institute of Health, Department of Nuclear Medicine, Berlin, GERMANY,* [2]*Helmholtz-Zentrum Dresden-Rossendorf, Institute for Radiopharmaceutical Cancer Research, Dresden, GERMANY.*

Aim/Introduction: Bayesian penalized likelihood reconstruction for PET (e.g. GE Q.Clear) aims at improving convergence of lesion activity while ensuring sufficient signal-to-noise ratio (SNR). This study evaluated reconstructed spatial resolution, peak recovery (RCpeak) and SNR of Q.Clear compared to OSEM with time-of-flight (TOF) with and without point spread function (PSF). **Materials and Methods:** The NEMA IEC Body phantom was scanned for 3 min each (GE Discovery MI) for five times every 30 min (3.1, 2.6, 2.1, 1.8, and 1.5 kBq/ml F18) with spheres filled with 4- or 8-fold the background activity concentration (SBR 4:1, 8:1). Reconstruction with Q.Clear (beta, 150/300/450), "PSF+TOF 2.0" (in-plane filter, 2.0 mm; iterations, 2; subsets, 17), "OSEM+TOF 2.0" (identical), "PSF+TOF 6.4" (in-plane, 6.4 mm; 4/8) and "OSEM+TOF 6.4" (6.4 mm; 2/8) was performed. Spatial resolution was derived from 3D sphere activity profiles. RCpeak as ((sphere SUVpeak/background SUVmean) / true SBR). SNR as (background SUVmean/background SUVstddev). **Results:** Spatial resolution of Q.Clear 150/300/450 was each significantly higher than for all conventional algorithms (Wilcoxon, each $p<0.05$; except for Q.Clear 450 vs. OSEM+TOF 2.0 at SBR 4:1). Median spatial resolution at SBR 8:1 for Q.Clear 150, Q.Clear 300, PSF+TOF 2.0 and OSEM+TOF 2.0 was 3.6, 4.2, 5.0 and 5.1 mm compared to SBR 4:1 with 4.4, 4.9, 5.7 and 5.6 mm. SNR for Q.Clear 150 and OSEM+TOF 2.0 were similar at both SBR ($p>0.05$) but Q.Clear 150 showed higher RCpeak for the small spheres by +6.3 to 10.8% (diameter, 10 to 17 mm). SNR of Q.Clear 300 and PSF+TOF 2.0 were similar as were RCpeak (difference, +0.3 to 4.1%). Compared to PSF+TOF/OSEM+TOF 6.4, Q.Clear 150/300/450 each showed lower SNR (-79.7 to -35.9%) but higher RCpeak (+4.6 to 27.8%) at both SBR. **Conclusion:** Q.Clear improves reconstructed spatial resolution at high and low SBR compared to PSF+TOF and OSEM+TOF with both investigated iteration and filter settings. For specific conditions this resulted in higher RCpeak for small spheres at comparable SNR (Q.Clear 150 vs. OSEM+TOF 2.0). Highest RCpeak were achieved with PSF+TOF 2.0 and Q.Clear 150, but at the cost of lowest SNR. **References:** None.

EP-0856

Impact of Radiation Dose Reduction of CT component in Whole-Body PET/CT Protocols on CT Image quality

I. Ali[1], *Y. Mohamed*[2], *I. Naser*[1], *M. I. Amin*[1], *H. Abdel Gawad*[3], *M. Hamdy*[4];
[1]*Zagazeg university faculty of medicine, Zagazeg, EGYPT,* [2]*Cairo university faculty of medicine, Cairo, EGYPT,* [3]*Cairo university hospitals, Cairo, EGYPT,* [4]*Cairo university Hospitals, Cairo, EGYPT.*

Aim/Introduction: We aim to reduce radiation dose of CT component in the whole-body PET/CT protocols, without compromising the image quality, aided by advanced iterative reconstruction technique.Regarding the issue of radiation dose, it is worth noting the recent progress and further advancements that can reduce the dose to the patient from CT exams. Important dose reductions have already been obtained through the development of optimized imaging protocols, smarter and more efficient x-ray beam collimation, advanced reconstruction algorithms, and by control of the x-ray flux illuminating the object. **Materials and Methods:** Forty eight patients underwent CT imaging with two different doses

during Whole-body PET/CT exams. All patients were scanned using a similar technique except for the changes done for CT dose optimization. Effective dose (ED) from the CT component of the examination was estimated using dose-length product (DLP) values from reports generated by the scanner and the anatomy-specific conversion factor for the whole body (the K factor). Image processing of the low CT dose images was also done with advanced iterative reconstruction technique. The studies were randomized and blinded for experienced two CT readers who graded the imaging quality of anatomic structures. **Results:** CT protocol optimization resulted in reduction of the mean DLP, CTDI and ED from 1296.8±291.9, 13.6±2.6 and 19.45 to 796.5±165.3, 8.2±1.7 and 11.96 with 38.6% reduction of the mean CT radiation dose. The blinded analysis of image quality showed no clinically significant degradation of the lower-dose study that showed comparable means of image noise, contrast, edge detection and overall quality with the high dose study (3.0±0.42, 2.9±0.44, 2.96±0.31 and 2.98 ±0.5 versus 2.87±0.45, 2.83±0.35, 2.84±0.5 and 2.86±0.45 respectively). The lung parenchyma was better visualized on the higher-dose CT scans. **Conclusion:** We can significantly reduce the CT radiation dose in whole-body PET/CT protocols with maintenance of the image quality by using the advanced iterative reconstruction technique. **References:** None.

EP-0857

Dual Asymmetric Detection Heads Of A Novel Compact Molecular Breast Imaging System For Early Breast Cancer Diagnosis

G. Poma[1,2], *E. Cisbani*[3], *F. Garibaldi*[3], *F. Giuliani*[3], *T. Insero*[4], *M. Lucentini*[3], *A. Marcucci*[5], *P. Musico*[6], *J. Nuyts*[7], *F. Santavenere*[3], *C. Sutera*[1];
[1]*Istituto Nazionale di Fisica Nucleare, Catania, ITALY,* [2]*Dipartimento di Fisica ed Astronomia, Università degli Studi di Catania, Catania, ITALY,* [3]*Istituto Superiore di Sanità, Roma, ITALY,* [4]*Ospedale pediatrico "Bambin Gesù", Roma, ITALY,* [5]*Aernoautica Militare Italiana, Roma, ITALY,* [6]*Istituto Nazionale di Fisica Nucleare, Genova, ITALY,* [7]*KU Leuven, Leuven, BELGIUM.*

Aim/Introduction: Breast cancer is the most common cancer in women, and its early detection is a crucial aspect for an effective therapy. Mammography (MMG) is the most used technique for screening, able to identify small-size tumours; nevertheless MMG showed reduced performance in case of dense breast. MRI, US and Molecular Breast Imaging (MBI) techniques have been proposed as complementary to MMG. MBI, based on the use of radionuclides and gamma camera, provides functional, sensible and specific informations, appropriate to dense breast. It may represent a promising support to mammographic screening. **Materials and Methods:** In order to maximize the Signal-to-Noise Ratio (SNR) and spatial resolution in a MBI image, a new compact system, consisting of a two asymmetric (different geometries and collimations) detectors, has been developed. The two detector heads face each other in anti-parallel viewing direction, either mildly compressing the breast and allowing: spot-compression: a PMMA breast-phantom (with four spherical tumoral lesions inside, different sizes) is resting on the big detector (LH) and the small one points the lesion moving on the phantom; Limited-Angle Tomography (LAT): the LH and phantom are fixed and the SH rotates over an arc. A full scale prototype based on matrices of Position Sensitive PhotoMultiplier Tube (PS-PMT), coupled to segmented NaI(Tl) scintillators with parallel and pin holes optics has been constructed to evaluate the expected performances. Monte Carlo (MC) simulations using the GATE framework have been performed to evaluate the best detector configuration, in terms of sensitivity and spatial resolution, and data and image processing solutions; the detectors provide complementary planar images that shall be properly combined to get enhanced, diagnostic information with high specificity and sensitivity. **Results:** Preliminary lesion detectability outcomes show approximative 5 mm diameter as lower limit, confirmed by MC. Good correspondence of reconstructed and real tumor depth was found in LAT modality: trade-off between larger span and number of view, clinical session time and complexity need to be evaluated. The analysis of simulated and real data is ongoing to optimally exploit the MBI images in the different procedures and combine them to the mammographic/tomographic outcomes. **Conclusion:** After a description of the system, we will present the results of the performed measurements, in different modalities, including comparison with MC simulations and the LAT, at different lesions positions and with a diagnostic range of uptakes. Status of the analysis of the optimal MBI and mammographic image fusion will be also reported. **References:** None.

EP-0858

A preliminary assessment of metallic artefact reduction strategies for quantifying FDG activity around cardiac implantable electronic devices

M. Memmott[1], *I. S. Armstrong*[1], *J. Jones*[2], *V. J. Panin*[2];
[1]*Manchester University Hospitals NHS Foundation Trust, Manchester, UNITED KINGDOM,* [2]*Siemens Medical Solutions USA, Inc. Medical Imaging, Knoxville, TN, UNITED STATES OF AMERICA.*

Aim/Introduction: CT artefacts caused by high density objects in the field of view propagate through to attenuation-corrected PET reconstruction, causing significant positive and negative bias around the object, potentially leading to false positive or negative results. Two options for metallic artefact reduction (MAR) are available for the Siemens Biograph Vision; Cardiac MAR (CMAR) and iMAR. The former is a global attenuation correction (AC) map based algorithm derived to account for high-frequency metallic lead motion. The latter is a parameter-dependent iterative CT-sinogram based method. The iMAR algorithm has a preset available for cardiac implantable electronic devices (CIEDs) to improve CT quality but the impact of the algorithm on the accuracy of PET data around metallic devices has not been studied. This preliminary phantom work aimed to evaluate the accuracy of PET quantification around

CIEDs. **Materials and Methods:** A CIED was suspended in a water filled phantom containing ^{18}FDG and PET-CT data acquired using a standard clinical protocol. CT data were reconstructed with standard and iMAR algorithms, using all available presets. PET AC was performed using CMAR algorithm (standard CT) and iMAR CT. In addition, a method developed to better match AC and PET, based on time-of-flight consistency conditions, the maximum likelihood attenuation correction factor (TOF-MLACF) [1], was also investigated. The excellent time-of-flight performance of this system makes TOF-MLACF an interesting option to explore in this context. For each dataset, uniform PET slices were used to generate a statistical distribution of expected voxel values. The percentage of voxels outside the 95% confidence intervals of this distribution was calculated as a measure of artefact reduction. The first 10 focal hot-spots were also automatically identified using the maximal average of a 7-voxel regional cluster. **Results:** All reconstructions with the exception of $iMAR_{dental}$, TOF-MLACF and CMAR demonstrated one or more focal hot-spots adjacent to the device. The CMAR algorithm produced a global reduction in uptake in the presence of the device, with the greatest percentage of voxels (6.9%) outside the uniform distribution. The $iMAR_{dental}$ and TOF-MLACF reconstructions gave the lowest percentage of voxels outside the uniform distribution (6.2 % and 4.4%). **Conclusion:** This phantom study demonstrates that effective MAR in PET data could be achieved in the clinical setting using the $iMAR_{dental}$ preset, allowing interpretation of attenuation-corrected PET data. Results from the current TOF-MLACF prototype show promise, warranting further investigation. **References:** [1] Bal H et al. Phys Med Biol 2017; 62:2542-2558.

EP-0859

The Effect of Different Time Per Bed Position on Image Quality and Semi-Quantitative Measurements in ^{68}Ga-RM2 and ^{68}Ga-PSMA11 PET/MR Images

L. Baratto, H. Duan, H. Gandhi, M. Khalighi, A. Iagaru;
Stanford University, Palo Alto, CA, UNITED STATES OF AMERICA.

Aim/Introduction: PET/MR is used for assessment of prostate cancer because of its high soft tissue contrast recovery and high-quality PET images. Here, we evaluated the impact of different PET acquisition times (time per bed) on image quality, lesion detectability and quantification in a cohort of prostate cancer patients. **Materials and Methods:** We retrospectively analyzed data from 90 prostate cancer patients who underwent either ^{68}Ga-RM2 (n=45) or ^{68}Ga-PSMA-11 (n=45) PET/MR. The raw PET data were retrospectively reconstructed using different time per bed position (TpB): 30 seconds (s), 1minute (m), 2m, 3m and 4m. Each reconstruction was reviewed and qualitatively scored using a Likert scale (1 - poor, 5 - excellent quality). SUV_{max} values were measured from ^{68}Ga-RM2/PSMA PET/MR for up to 6 lesions compatible with prostate cancer. Uptake in gluteal muscles was also collected in all patients as a measure of image noise. **Results:** The mean±SD injected dose was 3.82±0.15 and 4.39±0.79 mCi for ^{68}Ga-RM2 and ^{68}Ga-PSMA11, respectively. The mean BMI was 26.49 and 27.71 for patients who underwent ^{68}Ga-RM2 and ^{68}Ga-PSMA11, respectively. The mean±SD scores for ^{68}Ga-RM2 PET images were 1.04±0.21 for TpB=30s reconstructions, 2±0.3 for TpB=1m, 3.07±0.45 for TpB=2m, 4.64±0.53 for TpB=3m and 4.78±0.42 for TpB=4m. The mean±SD scores for ^{68}Ga-PSMA11 PET images were 1.18±0.39 for TpB=30s reconstructions, 2.22±0.42 for TpB=1m, 3.40±0.58 for TpB=2m, 4.87±0.40 for TpB=3m and 4.91±0.36 for TpB=4m. A total of 129 lesions (66 on ^{68}Ga-RM2 and 63 on ^{68}Ga-PSMA11) were detected and the mean SUV_{max} measurements were: 11.07, 10.19, 9.57, 9.43 and 9.42 for the ^{68}Ga-RM2 TpB of 30s, 1m, 2m, 3m and 4m, respectively; 14.69, 12.82, 12.11, 11.72 and 11.52 for the ^{68}Ga-PSMA-11 TpB of 30s, 1m, 2m, 3m and 4m, respectively. The mean SUV measurements in gluteal muscles were: 0.32, 0.22, 0.19, 0.17 and 0.15 for the ^{68}Ga-RM2 TpB of 30s, 1m, 2m, 3m and 4m, respectively; 0.35, 0.27, 0.23,0.20 and 0.18 for the ^{68}Ga-PSMA-11 TpB of 30s, 1m, 2m, 3m and 4m, respectively. **Conclusion:** Here we shown that 3 or 4 minutes per bed position for both radiopharmaceuticals result in excellent image quality. Even data acquired at 2 minutes per bed resulted in diagnostic images (average score >3). **References:** None.

EP-0860

Optimisation of TOF and PSF PET Reconstruction for the Detection and Quantification of Metastatic Tumour Lesions in the Liver

Y. Bouchareb[1], N. Tag[2], H. Sulaiman[1], M. El-zain[1], A. Al-Jabri[2], Z. Jawa[2], H. Al-Dhuhli[2];
[1]Sultan Qaboos University, Muscat, OMAN, [2]Sultan Qaboos University Hospital, Muscat, OMAN.

Aim/Introduction: To optimise TOF and PSF-based PET reconstruction for an accurate estimation of F-18 FDG uptake within metastatic tumour lesions in the liver. **Materials and Methods:** Phantom PET/CT scans were performed on the mCT 128 slices Siemens scanner. The detection and quantification of metastatic tumour lesions in the liver requires the use of optimal number of iterations, number of subsets, filter size and matrix size in the iterative image reconstruction process. The NEMA image quality phantom was used; spheres 10, 13, 17, 22, 28 and 37 mm diameters and the background compartment were filed with F-18 activity. Spheres-to-background (2.1 kBq/mL) ratio was 4:1 (total activity was 29.8 MBq). Three types of reconstructions: OSEM-TOF-PSF (routine reconstruction), OSEM-PSF and OSEM-TOF were optimised by means of varying number of iterations (1 to 5 iterations), number of subsets (8 to 24 subsets), filter size (2 to 7mm) and matrix size (128x128 to 400x400 pixels). For each reconstruction, contrast recovery coefficients (CRC) were calculated for all spheres and compared to the expected EANM/EARL CRC values using the mean percentage difference (MPD) for all spheres. The resulting optimal reconstruction and the routine reconstruction (OSEM-TOF-PSF using 2 iterations, 21 subsets, 3mm filter size and 400x400 pixels) were also applied to 15 FDG PET/CT scans. SUVmax, SUVpeak and MTV (Metabolic Tumour Volume) were calculated for both reconstructions.

Results: From the CRC analysis, OSEM-TOF-PSF (2 iterations, 21 subsets, 3mm filter and 400x400 pixels), OSEM-PSF (2 iterations, 24 subsets, 3mm filter and 400x400 pixels) and OSEM-TOF (2 iterations, 12 subsets, 3mm filter and 256x256 pixels), found to be optimal in each type of reconstruction, provided an MPD of 13%, 7% and 4%, respectively. The latter was considered to be the optimal reconstruction. On patient data, the mean percentage differences, calculated within 24 lesions (15 patients), in SUVmax, SUVpeak and MTV between the routine reconstruction and OSEM-TOF (2 iterations, 12 subsets, 3mm filter and 256x256 pixels) were 8%, 7%, 30%, respectively. The visual assessment of reconstructed images by two NM physicians was in favour of OSEM-TOF-PSF (2 iterations, 21 subsets, 3mm filter and 400x400 pixels) in 80% of the lesions. **Conclusion:** The OSEM-TOF (2 iterations, 12 subsets, 3mm filter and 256x256 pixels) provides a better quantitative accuracy compared to routine reconstruction. However, for image quality purposes the OSEM-TOF-PSF (2 iterations, 21 subsets, 3mm filter and 400x400 pixels) offers better appearance of metastatic tumour lesions in the liver. **References:** None.

EP-0861

Comparison of two strategies for mitigation of gross misregistration of CT and PET in PET/CT imaging

T. Pan, B. Simon, R. Millican;
The University of Texas, Houston, TX, UNITED STATES OF AMERICA.

Aim/Introduction: Respiration induced gross misregistration between CT and PET can compromise the quality of PET/CT imaging. A solution to mitigate the issue is to perform repeat limited field-of-view PET/CT scan, which prolongs the scan time and incurs additional CT radiation exposure to the patient. The purpose of the study is to evaluate if average CT can achieve registration with the PET data, can avoid the repeat scan time, and can reduce CT radiation exposure to the patient. **Materials and Methods:** We reviewed 5 PET/CT studies with a repeat PET/CT scan due to gross misregistration between CT and PET at or near the diaphragm on a GE PET/CT scanner. Maximum misregistration was 4.75 cm. Both scan time and CT dosimetry of the PET/CT and repeat PET/CT were recorded. Extents of misregistration in the original and repeat PET/CT images were measured. Instead of repeat scan, we used an average CT scan of 5 sec to combat gross misregistration of CT and PET, and acquired 20 patient scans with the average CT. Comparison of average CT and repeat PET/CT on scan time, CT radiation dose, misregistration and impact to workflow was made. **Results:** For the 5 patients with a repeat PET/CT scan of 3 to 4 beds over the abdominal area, scan time was increased by 9 to 12 mins from PET, CT dose was increased by 3.4±1.7 mSv, and misregistration of 1.3 cm remained in 1 patient study, suggesting that it may not be reliable to remove misregistration with repeat scan. For the 20 patients with an average CT scan instead of repeat PET/CT, CT dose was increased by 2.1±1.5 mSv. Misregistration measured at the diaphragm was corrected on all 20 patients without additional PET data acquisition. The processing time of average CT was less than 2 min. **Conclusion:** Using average CT to combat misregistration between CT and PET of PET/CT imaging can save scan time by 9 to 12 mins, can reduce radiation exposure to the patient from 3.4±1.7 mSv of repeat CT to 2.1±1.5 mSv of average CT, and can be realized without any impact to patient throughput. Average CT was also more reliable than repeat CT to mitigate the gross misregistration problem between CT and PET. **References:** Pan et al, Attenuation correction of PET cardiac data with low-dose average CT, Medical Physics, 2006.

EP-0862

Taking Advantage of STIR Open Source Software in clinical PET Image Reconstruction Using the raw data obtained from a Commercial PET/CT Scanner

H. Jozi[1], P. Geramifar[2];
[1]Science and Research Branch, Islamic Azad University, Tehran, IRAN, ISLAMIC REPUBLIC OF, [2]Research Center for Nuclear Medicine, Shariati Hospital, Tehran University of Medical Science, Tehran, IRAN, ISLAMIC REPUBLIC OF.

Aim/Introduction: One of the most important components in Positron Emission Tomography (PET) imaging, is image reconstruction. At this point all raw data are converted into images that represent activity distribution in body using different iterative or analytical reconstruction methods. Modern imaging systems with their own commercial softwares and reconstruction algorithms, are alike a black box, which give no access to their users in modifying the parameters in reconstruction or correction algorithms. On the other hand, STIR[1] is an open source software that has never been used instead of commercial software in clinical routine. The aim of this study is to reconstruct PET raw data obtained from a Commercial PET/CT scanner using STIR. **Materials and Methods:** In this study, the header of PET scanner in the Siemens Biograph6 PET/CT imaging system was defined in accordance with existing parameters. In this modeling, parameters such as the number of segments, axial compression and maximum and minimum ring difference per segment ... were adjusted according to the michelogram of an actual scanner. Thereafter, the raw data of a patient's whole-body PET scan in the sinogram mode was extracted and reconstructed using STIR. The images were then compared with the ones reconstructed using commercial software of SIEMENS scanner (Syngo) as the gold standard. The algorithms used in image reconstruction were (1) FBP, (2) OSEM iterative algorithm with 2 iterations and 21 subsets and (3) iterative algorithm with 8 iterations and 21 subsets. The uptake difference was measured in various ROIs in normal tissues including the liver, lungs, heart as well as in pulmonary tumors. **Results:** The activity concentration obtained from the STIR reconstructed images in normal tissues of liver, lungs, heart and pulmonary tumors (after applying normalization), has a good conformity with those measured in clinical images reconstructed by the Syngo commercial software. **Conclusion:** The results shows the potential of using STIR open source software in the reconstruction of three-dimensional PET raw

data obtained from a commercial PET/CT system. Thus, STIR provides the possibility of improving different algorithms such as scatter correction, resolution recovery or motion correction in the commercial scanners. **References:** [1] Thielemans, Kris, et al. "STIR: software for tomographic image reconstruction release 2." Physics in Medicine & Biology 57.4 (2012): 867.

EP-0863

Quantitative Evaluation of TOF Benefits on the Simulated PET/CT Images Using Mont Carlo Study

H. Jozi[1], *P. Geramifar*[2];
[1]*Science and Research Branch, Islamic Azad University, Tehran, IRAN, ISLAMIC REPUBLIC OF,* [2]*Research Center for Nuclear Medicine, Shariati Hospital, Tehran University of Medical Science, Tehran, IRAN, ISLAMIC REPUBLIC OF.*

Aim/Introduction: Time-of-flight (TOF) capability would improve the signal-to-noise ratio (SNR) and Noise Equivalent Counting Rate (NECR) of PET scanners. This improvement is mainly depend on the scintillator decay time, time response of coincidence circuits and front-end electronics. In this regard, we simulated a non-TOF clinical PET/CT scanner capable of TOF using GATE Monte Carlo simulation to quantitatively assess the possible advantageous of TOF in image SNR and improvement in counting performance of PET scanner. **Materials and Methods:** In this study, we simulated the Siemens Biograph6 true points PET/CT scanner (SIEMENS, Erlangen, Germany), using GATE Monte Carlo package with 500 ps timing resolution and 4.5 ns coincidence window. Simulated data were reconstructed in STIR, using both filtered back projection (FBP) and Iterative reconstruction (OSEM) methods. Attenuation correction was applied in both models (TOF and non-TOF) in the digital XCAT anthropomorphic phantom. Moreover, hyper-metabolic lesions were simulated. The images were compared in terms of contrast improvement (CNR), SNR, noise and coefficient of variations (CV) for TOF evaluation purpose. **Results:** It was shown that TOF information improves the image quality in terms of SNR and CNR, and it can significantly improve the fast convergence of the OSEM algorithms. Moreover, improved SNR in TOF reconstructed images demonstrate the benefit of TOF in high random fraction coincidences. Our simulated SNR_{gain} followed a recent model developed by Erikson, with a proportionality constant measured to be α^2=0.6. **Conclusion:** The results confirmed the advantages of TOF information in image reconstruction including better identification of image details, better contrast, and image noise reduction in terms of CV. Thus, the SNR_gain can be predicted for Iterative reconstruction methods, by means of a reliable Monte Carlo simulator. **References:** None.

EP-0864

Scan time optimisation of PET/CT examinations in case of patients in pain

A. Zagorska, *V. Kouykin*, *A. Tsonevska*;
Acibadem City Clinic Cancer Center, Sofia, BULGARIA.

Aim/Introduction: Cancer patients are staged or followed-up by PET/CT examinations. It is not uncommon to examine patients with pain that makes difficult the proper conduction of the study. The aim of this study is to investigate whether a reduced in comparison to the typically applied scanning time in a standard PET/CT protocol can be used in case of patients with difficulties to stay immobile during the examination. **Materials and Methods:** Two groups of 10 patients each referred for F-18 FDG scans on a Discovery™ IQ (GE Healthcare) PET/CT system were included in this study. The administered activity was 3 MBq kg-1. Patients were scanned in list mode at 2 minutes per bed position. Data were rebinned to simulate 1.75 min (retro reconstruction A), 1.5 min (retro reconstruction B) and 1 min (retro reconstruction C) per bed position acquisitions, without changing the other parameters. VPHD (iterative reconstruction algorithm) and Q.Clear (Bayesian penalized likelihood reconstruction algorithm) were applied. Subjective assessment of image quality for both groups was made by two experienced physicians using a three-point scale in the first stage of the study. In the second stage measurements of SUVmax in the liver, mediastinum, lung and a patient lesion were carried out. The differences between measured data for the primary examination and the retro reconstructions A and B were calculated. **Results:** Results from the first stage of the study showed that retro reconstructions A and B were with similar quality as the primary examination. The retro reconstruction C was not acceptable. Results presented as median, minimum and maximum in parenthesis and average of the differences for retro reconstruction A were as follows: SUV_{max}(mediastinum) 1% (-2%, 7%), 2%; SUV_{max}(liver) 1% (-2%, 7%), 2%; SUV_{max}(Lung) 2% (-2%, 6%), 2%. Results for retro reconstruction B were: SUV_{max}(mediastinum) 4% (0%, 12%), 5%; SUV_{max}(liver) 5% (-3%, 14%), 5%; SUV_{max}(Lung) 6% (-4%, 8%), 4%. Results for selected lesion were: VPHD, retro reconstruction A: SUV_{max} 0% (-3%, 3%), 0%; retro reconstruction B: SUV_{max} 2% (-2%, 4%), 2%. For Q.Clear, retro reconstruction A: SUV_{max} 1% (-3%, 5%), 1%; retro reconstruction B: SUV_{max} 0% (-3%, 8%), 2%. **Conclusion:** According to the present study, the time for patient examination can be reduced in case of severe disease to minimize the patient movement during the examination and/or interruption of the studies due to patients in pain. **References:** None.

EP-63
Technical aspects -> Instrumentation and data analysis -> Data analysis -> Neurology: data analysis and quantification

October 12 - 16, 2019
e-Poster Area

EP-0865

Partial volume corrected image derived input functions for kinetic modelling of FDG PET brain studies

H. Keijzers, S. S. V. Golla, M. Yaqub, N. Scheltens, P. Scheltens, M. Hofman, R. Boellaard;
Amsterdam UMC, Amsterdam, NETHERLANDS.

Aim/Introduction: Cerebral metabolic rate of glucose (CMRglc) is an important biomarker in studies of Alzheimer's disease and can be obtained with FDG PET. By kinetic modelling the influx rate constant (Ki) of FDG can be determined, which is proportional to CMRglc. Kinetic modelling requires an arterial input function (AIF), normally derived by arterial blood sampling. Efforts have been made to omit arterial sampling by determining the input function directly from cerebral vasculature visible in PET images. However, partial volume effects caused by limited spatial resolution results in inaccurate image derived input functions (IDIFs). Partial volume correction (PVC) can improve the accuracy. This study assesses the accuracy of Ki determination with PVC IDIFs, by calculation of correlation and agreement between Ki derived using PVC IDIFs and Ki derived using AIFs. **Materials and Methods:** Forty-eight dynamic 18F-FDG PET scans with minimal patient motion, arterial blood sampling data and arterial manual samples, were selected from a group of 92 scans acquired in 46 patients in the NL-ENIGMA study (1). PVC was applied to the original PET images using Van Cittert iterative deconvolution combined with a highly constrained back-projection (HYPR) denoising method (2). Cerebral vasculature was segmented by threshold-based volume of interest (VOI). Using this VOI, IDIFs were extracted from the original PET images and the PVC PET images. All IDIFs were calibrated to the manual blood samples. Patlak analysis was performed to obtain Ki using AIFs and IDIFs. Correlation was assessed using linear regression, agreement was assessed with Bland-Altman plots. **Results:** Linear regression analysis shows very strong correlation between Ki derived using PVC IDIFs and AIFs ($r = 0.88$), and strong correlation when non-PVC IDIFs are used ($r = 0.63$). Bland-Altman analysis shows significant ($p<0.01$) bias in both cases (PVC; Ki mean difference = -0.0019 min^{-1}, non-PVC; Ki mean difference = -0.0043 min^{-1}), and limits of agreement (LOA) are smaller when PVC IDIFs are used (PVC; LOA = 0.0041 min^{-1}, and non-PVC, LOA = 0.0079 min^{-1}). **Conclusion:** Partial volume correction and calibration improves correlation and agreement between Ki derived using IDIFs and Ki derived using AIFs. It also reduces the bias, which remains significantly different from zero. The origin of the bias of Ki values by PVC IDIF is subject of further investigation. Other future directions include calibration of PVC IDIFs to venous manual samples.

References: (1). Scheltens et al. Alzheimer's Dement (N Y). 2016; 2:223-40(2). Golla et al. EJNMMI Research (2017) 7:36.

EP-0866

Validation of reference regions for [^{18}F]Flortaucipir and [^{18}F]Florbetapir brain PET studies using non-invasive simplified metrics

S. S. V. Golla[1], B. M. de Vries[1], T. Timmers[1,2], E. E. Wolters[1,2], R. Ossenkoppele[1,2], S. Verfaillie[2], R. C. Schuit[1], P. Scheltens[2], W. M. van der Flier[2,3], A. D. Windhorst[1], B. N. van Berckel[1,2], R. Boellaard[1];
[1]Department of Radiology & Nuclear Medicine, Amsterdam UMC, Amsterdam, NETHERLANDS, [2]Alzheimer Center & Department of Neurology, Amsterdam UMC, Amsterdam, NETHERLANDS, [3]Department of Epidemiology & Biostatistics, Amsterdam UMC, Amsterdam, NETHERLANDS.

Aim/Introduction: Simplified reference tissue methods (SRTM) are applied for quantification of brain PET studies, particularly because they eliminate the need to perform arterial cannulation. SRTM requires a validated reference region. Ideally, a proper validation of a reference region would be to perform blocking or displacement studies along with histopathological assessments on post-mortem tissue samples usually resulting in complex study designs and cumbersome procedures. An alternative is to compare the distribution volume (V_T) of the reference region between patients and controls and/or before and after intervention/displacement. However, performing dynamic scans and arterial sampling is not always possible, specifically in elderly subjects and advanced disease stages. The aim of this study was therefore to determine if simplified non-invasive approaches could be used to verify if a previously validated reference region for [^{18}F]Flortaucipir and [^{18}F]Florbetapir PET imaging is still valid in subjects groups under conditions where verification using plasma input is not feasible. **Materials and Methods:** Dynamic 130 minutes [^{18}F]Flortaucipir PET scans, obtained from nineteen subjects (10 Alzheimer's disease(AD) patients and 9 controls(C)) and 90 minutes [^{18}F]Florbetapir dynamic scans obtained from fourteen subjects (8 AD patients and 6 C) were included in this study. Regional V_T's estimated from a reversible two tissue compartmental model (with V_B) for both tracers was considered as a standard for validating an optimal reference region. Semi-quantitative measures (standardised uptake value corrected for body weight(SUV_{BW}), lean body mass(SUL) and body surface area(SUV_{BSA})) were obtained by using part (early, middle, or late) of the dynamic scans. Simulations were also performed to evaluate the effect of flow and specific binding (BP_{ND}) on the semi-quantitative metrics. **Results:** Late uptake SUV_{BW}, SUL and SUV_{BSA} correlated well with V_T for [^{18}F]Flortaucipir and [^{18}F]Florbetapir. $SUL_{(80\text{-}100\ min)}$ (AD: r^2= 0.97; C: r^2=0.95) and $SUV_{BSA\ (50\text{-}70\ min)}$ (AD: r^2= 0.96; C: r^2=0.77) correlated best with V_T for [^{18}F]Flortaucipir and [^{18}F] Florbetapir respectively. A $SUL_{(80\text{-}100\ min)}$ less than 1 for [^{18}F] Flortaucipir and $SUV_{BSA(50\text{-}70\ min)}$ less than 0.03 for [^{18}F]Florbetapir suggests absence of specific binding. Simulations confirmed that SUL and SUV_{BSA} were only slightly (<5%) affected by 25%

changes in flow. Changes in SUL and SUV_{BSA} are predominantly related to the presence of specific binding. **Conclusion:** In situations where dynamic scanning and arterial sampling is not feasible $SUL_{(80\text{-}100\ min)}$ for [18F]Flortaucipir and $SUV_{BSA\ (50\text{-}70\ min)}$ for [18F]Florbetapir can be used to evaluate the use of a previously validated reference region. **References:** None.

EP-0867

A quantitative approach for the diagnosis of nonconvulsive status epilepticus from brain perfusion SPECT images

G. Reynés-Llompart[1,2], S. Jaraba Armas[3,4], J. Mora[2], J. Sala-Padró[3], L. Rodriguez-Bel[2], M. Veciana[5], J. Suils Ramón[2], M. Falip Centelles[3], C. Gámez-Cenzano[2];
[1]Medical Physics Department. Institut Català d'Oncologia, L'Hospitalet de Llobregat, SPAIN, [2]Nuclear Medicine-PET Department. Hospital Universitari de Bellvitge-IDIBELL., L'Hospitalet de Llobregat, SPAIN, [3]Neurology department, Epilepsy unit, Hospital Universitari de Bellvitge-IDIBELL. Universitat de Barcelona, L'Hospitalet de Llobregat, SPAIN, [4]Neurology department, Hospital de Viladecans, Viladecans, SPAIN, [5]Neurophysiology department, Hospital Universitari de Bellvitge-IDIBELL. Universitat de Barcelona, L'Hospitalet de Llobregat, SPAIN.

Aim/Introduction: Diagnosing status epilepticus (SE) is a challenging task, as EEG patterns can be difficult to interpret, and the absence of an EEG correlate does not rule out the definitive diagnosis. In this setting, the value of neuroimaging tools is crucial. The present work aims to develop a quantitative approach using 99mTc-HMPAO-SPECT in patients with clinical suspicion of SE. **Materials and Methods:** A total of 54 patients with clinical suspicion of SE were retrospectively included (39% women, median age 64.5 years). All of them underwent a perfusion HMPAO-SPECT. The final diagnosis of SE or no-SE (35 vs 19 patients), was based on clinical, therapeutical image and EEG results. Two experienced neurologists reviewed all the data. The radiopharmaceutical was administered during the clinical episode suspected to be a SE. SPECTs were acquired in a Philips Skylight and reconstructed in a dedicated station. Each reconstruction was normalized to the SPM SPECT template. We used in-house software to obtain a Z-score map comparing each individual SPECT to an external healthy normal database. Only the voxels inside a brain mask (excluding the sublobar area) were considered; all clusters of less than 100 pixels were also excluded. From the resulting map the maximum value (Z_{max}), the number of significant voxels with Z-score>2.5 (N), and the anatomical region with the maximum value were recorded. The latter was obtained using the AAL human brain atlas. The dataset was randomly split in a train (n=30) and test group (n=24). A univariate analysis of the train data was performed to find the relevant variables related to the final diagnosis of SE. Then, a logistic regression was fitted to predict SE. The model was validated using the training dataset by means of the receiver-operator characteristic curve (ROC) and its area under the curve (AUC). **Results:** The number of significant voxels N and the Z_{max} were highly correlated (r=0.89), thus only the latter was included in the logistic model as it was the one with the lower p-value (p=0.08, using a t-test). The anatomical region was statistically significant (p=0.01, using a Fisher exact test) as well as the patient age (p=0.01, using a t-test). For the logistic regression, the AUC for the train data was 0.88 and for the test data was 0.80, showing a good fit with the observed results. **Conclusion:** The proposed quantitative approach to diagnose SE using 99mTc-HMPAO-SPECT, shows a good correlation with the final diagnosis. **References:** None.

EP-0868

The Impact Of Reference Region Choice On The Apparent Ordering Of Amyloid Deposition

F. Heeman[1], M. Yaqub[1], L. Collij[1], S. Ingala[1], G. Salvadó[2], A. Wink[1], P. Visser[1], B. N. M. van Berckel[1], J. D. Gispert López[2], F. Barkhof[1,3], A. A. Lammertsma[1], I. Lopes Alves[1], o. the AMYPAD consortium.[1];
[1]Amsterdam UMC, Vrije Universiteit Amsterdam, Radiology and Nuclear Medicine, Amsterdam Neuroscience, Amsterdam, NETHERLANDS, [2]BarcelonaBeta Brain Research Center, Barcelona, SPAIN, [3]Institute of Neurology and Healthcare Engineering, University College London, London, UNITED KINGDOM.

Aim/Introduction: Capturing the initial stages of amyloid-beta accumulation is essential both for improving diagnosis of early Alzheimer's disease and selecting individuals for secondary prevention trials. To this end, several studies have attempted to identify the first regions that show amyloid pathology. Some of these developed staging frameworks, showing a temporal ordering of regions becoming amyloid positive[1]. Major differences in methodology between these studies exist, especially with respect to the reference region used for normalization. Therefore, the aim of this study was to assess the impact of different reference regions on the apparent ordering of regional amyloid pathology. Furthermore, since the standardized uptake value ratio (SUVr) may be biased by confounders, corresponding models were developed for the non-displaceable binding potential (BP_{ND}). **Materials and Methods:** Dual-time-window [18F]flutemetamol-PET scans and T1-weighted MR images (N=189, Table1) were included and preprocessed as described previously[2]. SUVr (90-110 minutes post injection) and parametric BP_{ND} images (obtained using receptor parametric mapping (RPM)[3]) were generated based on three reference regions ((RR), cerebellar grey matter (CBGM), whole cerebellum (WCB) and cerebral white matter (CRWM)). To this end, RPM's basis function (BF) settings were optimized, by correlating BP_{ND} obtained for all sets of BF settings, per RR, with regional BP_{ND} obtained using the simplified reference tissue model (SRTM) with CBGM as RR. Resulting images were warped into MNI space and global and regional values were extracted. For each set of global BP_{ND}+1 and SUVr values, Gaussian Mixture Modeling was used to define positivity cut-offs as the mean +2SD of the left (low amyloid) distribution. Next, these cut-offs were applied to all regions and those were ordered according to the frequency of positivity across the cohort. Finally, the

resulting ordering was compared between reference regions and metrics (SUVr vs BP_{ND}) using Spearman's rank correlation. **Results:** Orderings derived from BP_{ND} and SUVr images, using CBGM as RR, showed high correlation (ρ=0.93). Furthermore, this BP_{ND} derived ordering showed a high correlation with BP_{ND} derived orderings using WCB and CRWM as RR (ρ=0.97), the same was true for the SUVr derived ordering (CBGM) compared to SUVr derived orderings using WCB and CRWM as RR (range of ρ=0.98 and 0.99). **Conclusion:** The ordering of regional amyloid positivity appears to be robust against the choice of reference region. **References:** 1.Grothe et al.(2017)Neurology 89(20),2031-2038 2.Konijnenberg et al.(2018)Alzheimer's research therapy 10(1),75. 3.Gunn et al.(1997)Neuroimage 6(4),279-287.This work has received support from the EU-EFPIA Innovative Medicines Initiatives 2Joint Undertaking (grant No115952).

EP-0869

MR-guided partial volume correction of 3D PET images using a split Bregman optimized parallel level set framework

Y. Zhu[1,2], *A. Rahmim*[2,1];
[1]*Johns Hopkins University, Baltimore, MD, UNITED STATES OF AMERICA,* [2]*University of British Columbia, Vancouver, BC, CANADA.*

Aim/Introduction: Quantitative accuracy of PET images is influenced by the partial volume effect. In this work, we propose and evaluate a post-reconstruction partial volume correction (PVC) method with subtle MR-based guidance through parallel level set (PLS) regularization. The objective function is minimized with a non-smooth optimization technique, which avoids blurring of recovered images compared to smooth optimization. We compare performance against PLS solved with conventional smooth optimization and region-based voxel-wise (RBV) PVC. **Materials and Methods:** We utilized least-squares fidelity term (having knowledge of the blurring point spread function (PSF) kernel) along with MR-guided PLS regularization to formulate post-reconstruction PVC of PET images. To solve the minimization problem, we developed a non-smooth optimization technique based on the split Bregman method. An auxiliary variable was introduced to decouple the non-smooth part from the original problem. The non-smooth subproblem could then be efficiently solved with soft-thresholding. For the rest of the problem, we reached the approximate solution with a one-step steepest descent method to enable efficient 3D implementation. The proposed method was then assessed using the BrainWeb phantom and realistic PET simulations (n=20 noise realizations), followed by OSEM reconstruction (10 subsets, 24 iterations). Different PVC algorithms were assessed. Since RBV requires segmentation of MR images, we investigated both perfect segmentation and realistic segmentation obtained by segmenting BrainWeb MR images using SPM12. Mean percentage bias and coefficient of variability (COV) were computed. For comparison, regularization parameters in PLS methods were tuned to generate matched COV relative to RBV method. **Results:** For matched COV values (~18% for gray matter (GM) and ~42% for white matter (WM)), both RBV and PLS provided reduced bias compared to results obtained directly from pure OSEM reconstruction (27.5% for GM and 48.8% for WM). Among these methods, RBV with exact segmentation generated lowest bias (6.0% for GM and 7.4% for WM). The quantitative accuracy of non-smooth optimized PLS (bias: 11.9% for GM and 21.7% for WM) was significantly ($p<0.01$; paired t test) better relative to RBV with SPM12 segmented MR (13.8% for GM and 23.6% for WM) as well as smooth optimized PLS (18.0% for GM and 31.9% for WM). **Conclusion:** We propose a non-smooth optimized PLS method for post-reconstruction PVC of PET with subtle MR-guidance. The method shows better performance relative to smooth optimized PLS and RBV for realistic segmentations. **References:** None.

EP-0870

[18F]FDG PET/MR brain studies: Dependency of image-derived input function on the defined volume-of-interest and its radiotracer environment

L. Shiyam Sundar[1], *O. Muzik*[2], *L. Rischka*[1], *A. Hahn*[1], *R. Lanzenberger*[1], *M. Hienert*[1], *E. Klebermass*[1], *M. Bauer*[1], *I. Rausch*[1], *E. Pataraia*[1], *T. Traub-Weidinger*[1], *T. Beyer*[1];
[1]*Medical University of Vienna, Vienna, AUSTRIA,*
[2]*Wayne State University School of Medicinme, Detroit, MI, UNITED STATES OF AMERICA.*

Aim/Introduction: To show that accurate modelling of the tracer distribution in the volume-of-interest (VOI) and its corresponding background is necessary to perform an effective partial volume correction (PVC), for the purpose of calculating an accurate Image-derived input function (IDIF). **Materials and Methods:** Ten healthy controls underwent test-retest [18F] FDG brain PET/MRI examinations in a fully-integrated PET/MR (Siemens Biograph mMR). The imaging protocol consisted of a 60-min PET list-mode acquisition along with parallel MR acquisitions comprising of a 3D time-of-flight MR angiography (MRA), T1-MR and high-speed MR navigators for monitoring subject motion. Arterial blood samples (AIF) were collected as reference standard. A low-dose CT scan was performed for the purpose of attenuation correction. An automatic segmentation algorithm was used to segment three different regions (petrous, superior cervical and inferior cervical) of the internal carotid arteries from the MRA images. A brain mask was calculated from T1-w MR using SPM 12. This was done to correct for the spill-out from the brain to the artery. Motion vectors from MR navigators were used for motion correction. To recover the apparent tracer activity in the carotids, an iterative Mueller-Gartner PVC algorithm, which is aware of the spatial and temporal variability of the petrous background region was used. This bias was specifically introduced to identify the dependency of VOI and its radiotracer background on the calculated IDIF. Absolute percentage differences of the area-under-the-curve (AUC) between the IDIFs obtained from the different VOIs and AIF were calculated and reported. **Results:** Assessment of the percentage difference between AUC of IDIFs and AIF was

(1.5 ±1.0) % for petrous, (10 ±10) % for superior portion of the cervical and (30 ±20) % for the inferior portion of the cervical. **Conclusion:** The implemented PVC performed the best for petrous, with the IDIF deviating from AIF by less than 3%. Since the PVC was implemented only with the accurate modelling of the petrous region's tracer environment, the PVC performed better in the petrous region, in comparison to superior or inferior cervical. Based on our results, we have identified that, to obtain an accurate IDIF, a PVC with an accurate modelling of the VOI and its radiotracer environment is necessary. **References:** None.

EP-0871

MRI-guided Voxel-based Automatic Semi-quantification of Dopamine Transporter Imaging

J. Trnka, P. Dusek, D. Zogala, V. Ptacnik;
General University Hospital and Charles University, Prague, CZECH REPUBLIC.

Aim/Introduction: Functional imaging with ^{123}I-FP-CIT SPECT (DaTScan™) suffers from poor spatial resolution resulting in partial-volume effect in the striatal regions, which affects the subsequent semi-quantification. Definition of regions of interest for semi-quantification is further subject to user's experience and inter-observer variability. The aim of this work has been to develop an automatic method for definition of volumes of interest and partial-volume correction using patient-specific MRI and providing complete contrast recovery. **Materials and Methods:** The procedure consists of spatial pre-processing (MRI and SPECT/CT image registration and segmentation), partial-volume correction in SPECT images, and calculation of uptake indices in striatal regions. Spatial preprocessing was implemented in FMRIB software library. Partial-volume correction was performed by region-based voxel-wise (RBV) technique provided by PETPVC tool. Expected spatial resolution required by RBV method was estimated using anthropomorphic striatal phantom. Uptake indices were calculated for the whole striata, caudate nuclei, and putamina. Linearity and reproducibility were assessed. **Results:** It was possible to find a value of expected spatial resolution which provided complete contrast recovery in striatal phantom measurements for given acquisition and reconstruction conditions. Deviation of uptake indices from expected linear behavior was less than 0.15 in terms of RMSE. The reproducibility between repeated measurements was 3-7% depending on the simulated uptake ratio. Due to its nature, the method did not exhibit any inter/intra-observer variability. **Conclusion:** The proposed method provides complete recovery of striatal uptake. It can reduce inter/intra-observer variability, accurately define and localize volumes of interest, and effectively suppress partial-volume effect. Its results can be used for research purposes. The method can be reproduced using publicly available software. **References:** None.

EP-0872

Estimation of the spatial resolution of [^{18}F]-FDG brain PET(MR) scans using phantom measurements and human scan data

A. Marques da Silva[1], *G. Schramm*[2], *J. van Aalst*[2], *N. Mertens*[2], *K. Van Laere*[2], *M. Koole*[2];
[1]*PUCRS, Porto Alegre, BRAZIL,* [2]*KU Leuven, Leuven, BELGIUM.*

Aim/Introduction: Three practical approaches were compared to directly measure the spatial resolution of [^{18}F]-FDG brain PET(MR) using either the NEMA image quality (IQ) phantom, the Hoffman brain (HB) phantom or human PET/MR datasets. **Materials and Methods:** All scans were performed on a GE Signa PET/MR. IQ phantom data were obtained as part of NEMA acceptance procedures (10min acquisition, with 8:1 sphere to background ratio). HB phantom data were acquired using a 20min PET-only protocol. Five [^{18}F]-FDG human brain PET/MR datasets were obtained by the simultaneous acquisition of a 20min PET and anatomical MRI. For IQ and HB phantoms, attenuation correction (AC) was performed using a built-in template and a CT-based attenuation map, respectively. For human PET/MR data, a template-based MR-AC map was used. PET reconstructions were based on TOF information and OSEM (192x192x89 matrix, 1.6x1.6x2.8mm voxelsize), with 4 iterations, 28 subsets, and resolution modeling. An isotropic Gaussian postfilter with varying Full Width at Half Maximum (range: 3-8mm FWHM) was used to generate PET data with different spatial resolution. For IQ phantom, the reconstructed PET resolution was determined as the optimal Gaussian filter to match the measured radial profile through the different spheres, with the underlying theoretical profile modeling the sphere size, cold sphere edge and 8:1 sphere to background ratio. For the HB phantom, the compartments mimicking gray matter (GM), white matter (WM) and cerebrospinal fluid (CSF) were segmented using a CT scan and the PET resolution was determined as the optimal Gaussian filter for a partial volume correction using GM, WM and CSF maps to reconstruct the GM activity concentration [1]. For the human PET/MR data, an SPM12-based segmentation of the anatomical MR was performed, and the PET resolution was estimated as the optimal Gaussian filter for the segmented GM and WM tissue maps to reconstruct the PET data while assuming constant GM and WM activity concentrations. **Results:** For a clinically relevant Gaussian postfilter of 5mm FWHM, the estimated PET resolution was 5.7, 5.6 and 5.6 mm FWHM for the IQ phantom, HB phantom, and human PET/MR data, respectively. Additional values in the table included. **Conclusion:** Since all approaches provided very similar spatial resolution estimates, human PET/MR datasets can be considered to evaluate or monitor the spatial resolution of reconstructed [^{18}F]-FDG brain PET (MR) datasets and to align [^{18}F]-FDG brain PET(MR) imaging protocols in terms of resolution across centers and PET(MR) systems. **References:** [1] Muller-Gartner et al. JCBFM 1992.

EP-0873

Pharmacokinetic analysis of dynamic [18F]3-Fluoro-5-[(pyridin-3-yl)ethynyl] Benzonitrile[18F]FPEB PET In Asian Population

W. X. Xie[1], *S. Yu*[2], *C. T. Yang*[1], *S. B. Tai*[3], *K. Riffel*[4], *W. Li*[4], *C. L. Chin*[5], *A. B. M. A. Asad*[6], *K. S. H. Loke*[1], *W. W. C. Lam*[1], *D. C. E. Ng*[1];
[1]*Singapore General Hospital, Dept of Nuclear Medicine and Molecular Imaging, Singapore, SINGAPORE,* [2]*Proton Therapy Pte Ltd, Singapore, SINGAPORE,* [3]*Ministry of Health, Singapore, SINGAPORE,* [4]*Translational Biomarkers, Merck & Co., Inc., West Point, PA, UNITED STATES OF AMERICA,* [5]*Translational Biomarkers, Merck LLC, South San Francisco, CA, UNITED STATES OF AMERICA,* [6]*Translational Biomarkers, MSD, Singapore, SINGAPORE.*

Aim/Introduction: [18F]FPEB is a radioligand that affords high specific binding to metabotropic glutamate V receptors (mGluR5) in early clinical trials (1). We aim to evaluate the pharmacokinetics of [18F]FPEB and quantify regional brain distribution of mGluR5 in healthy Asian individuals. **Materials and Methods:** Five healthy volunteers (HVs) completed one or two [18F]FPEB dynamic 90 min PET scans. Arterial blood samples were collected for arterial input function and metabolite correction. Twelve cerebral region of interests (ROIs) were defined using magnetic resonance imaging (MRI) brain atlases and individual anatomical images, which included the neocortex (frontal, temporal, parietal and occipital cortices), subcortical regions (putamen, caudate) and limbic regions (amygdala, hippocampus, thalamus and the cingulate gyrus), the pons and cerebellum. One- and two-tissue compartment models (1TC, 2TC) and the Logan plot were applied to the regional time activity curves (TACs) to calculate regional distribution volumes (V_T) and binding potential (BP_{ND}). The simplified reference tissue model (SRTM2) was also used to estimate BP_{ND}. The pons was used as a reference region, as it showed low receptor expression. **Results:** The tissue TACs peaked within 5 minutes of tracer injection, with varying degrees of retention across regions. The highest uptake was seen in the putamen and insula, and lowest uptake in the pons. The 2TC and the reference tissue models showed a good fit to the data, but poor fitting was observed with the 1TC model. Good correlation between the V_T estimated by 2TC and the plasma reference graphical analysis (PRGA) was found. The PRGA showed the best fit for V_T across all regions, with standard errors <10% in > 75% of fits. The reference tissue models showed consistent estimates of $BP_{ND,}$ The BP_{ND} (SRTM2) of the basal ganglia, in the regions of the caudate nucleus and thalamus are 1.38 ±0.54 and 0.88±0.17 respectively, while the BP_{ND} of the insula and cortices, in the frontal, parietal and temporal lobes are 1.85±0.37, 1.55±0.32, 1.48±0.32, 1.54±0.31 respectively (2). **Conclusion:** We observed consistent values of V_T and BP_{ND} using PRGA and SRTM2 methods; these are appropriate models for analysing quantitative [18F]FPEB dynamic PET imaging of mGluR5 in the Asian population. **References:** 1. de Laat B, et al Preclinical Evaluation and Quantification of 18F-FPEB as a Radioligand for PET Imaging of the Metabotropic Glutamate Receptor 5. 2. Wong DF, et al. 18F-FPEB, a PET radiopharmaceutical for quantifying metabotropic glutamate 5 receptors: a first-in-human study of radiochemical safety, biokinetics, and radiation dosimetry.

EP-0874

Assessment of Brain Regional Hypometabolism in Metastatic Breast Cancer Patients with ^{18}F-fluorodeoxiglucose: Influence of the Reference Region

S. D. Almeida[1,2], *F. P. M. Oliveira*[2], *D. C. Costa*[2], *J. C. Castanheira*[2], *M. Silva*[2], *J. C. Reis*[1], *P. Almeida*[1], *L. Travado*[2];
[1]*Instituto de Biofísica e Engenharia Biomédica, Faculdade de Ciências, Universidade de Lisboa, Lisbon, PORTUGAL,* [2]*Champalimaud Centre for the Unknown, Champalimaud Foundation, Lisbon, PORTUGAL.*

Aim/Introduction: Quantitative assessment of the central nervous system metabolism with FDG-PET is usually calculated via standardized uptake values (SUV), and/or SUV ratios (SUVr). The choice of the denominator reference region influences data reliability within and between patients. As part of a larger project DistressBrain to examine associations between negative affect and brain regional metabolism in metastatic breast cancer (mBCa) patients, we investigated the optimal SUVr reference region in these patients. **Materials and Methods:** Forty-four female mBCa patients (60±11 y.o.) without brain metastases underwent two brain FDG-PET exams on the same day, 30-45 minutes and 3 hours post-injection (p.i.). A dataset of FDG-PET images acquired 30-60 minutes p.i. from a healthy group of twenty-eight female (76±5 y.o.) from the Alzheimer's Disease Neuroimaging Initiative was used as control group. All images were spatially registered to the Montreal Neurological Institute space. Voxel-wise statistical analysis was performed using the statistical parametric mapping (SPM12) toolbox. A paired t-test was used to search for SUV differences between 30-45 minutes and 3 hours p.i. Then, several reference regions were tested for intensity normalization: whole-brain, thalamus, striatum, pons and cerebellum. A two-sample t-test, with correction for age, was used to compare metabolic uptake patterns between the mBCa 30-45 min p.i. versus controls, per each reference region. A voxel-wise p-value of 0.05 with family-wise error correction for multiple comparisons was applied. **Results:** Overall brain SUVs were higher at 3 hours than 30-45 minutes p.i. with statistically significant differences only in the occipital cortex. Pons and cerebellum normalization originated significant higher SUVr values at 3 hours in all cortical and subcortical regions. mBCa patients showed insular, striatal and inferior frontal gyrus (BA 44, 45) hypometabolism compared to controls using the pons as reference region. Whole-brain and cerebellum normalization only depicted a small hypometabolic region in the insula. Normalization to the thalamus or striatum originated no significant differences between patients and controls. There was no area of significantly higher SUVr in the mBCa group in comparison with the controls whatever reference region used. **Conclusion:** mBCa patients showed higher occipital FDG uptake at 3 hours than 30-45 minutes p.i. Therefore, this brain region is not adequate for denominator reference to calculate SUVr.

Normalization by the pons appears more sensitive to distinguish brain metabolic pattern differences between mBCa and controls than other reference regions tested. This suggests no significant influence of mBCa patients' treatments in pons uptake. Financial support: FCT; PTDC/MHC-PSC/3897/2014. **References:** None.

EP-0875

Impact and correction of white matter spill-in counts on amyloid PET quantification

J. Silva-Rodríguez[1], *F. J. López-González*[2], *A. Moscoso*[1], *N. Efthimiou*[3], *P. Aguiar*[2];
[1]*Health Research Institute of Santiago de Compostela, Santiago de Compostela, SPAIN,* [2]*Universidade de Santiago de Compostela, Santiago de Compostela, SPAIN,* [3]*University of Hull, Hull, UNITED KINGDOM.*

Aim/Introduction: The partial volume effect (PVE) is one of the most prominent issues of amyloid(Aβ) PET quantification. PVE produces the spill-in of white matter (WM) counts into the gray matter (GM). This effect will be especially relevant in amyloid-negative images (low GM counts), such as those used for the estimation of SUVR thresholds, and highly dependent on WM uptake. In this work, we are aimed at providing a systematic study of the impact of WM spill-in counts on these cases and to evaluate the performance of different PVE correction methods. **Materials and Methods:** We examined 122 AV-45 PET images from cognitively normal patients recruited for ADNI2. Resolution standardization was carried out by smoothing to a resolution of 8-mm (ADNI) and by applying two PVE corrections: iterative Yang (iY) and regional voxel-based (RBV). SUVR values were normalized by using the cerebellum GM ($SUVR_{CGM}$) and the whole cerebellum ($SUVR_{WC}$) as reference regions. Amyloid-positive patients according to ADNI's $SUVR_{WC}$=1.11 were excluded. WM SUVR values were obtained for both the segmented and eroded WM ($SUVR_{WM}$ and $SUVR_{EWM}$). The variability of $SUVR_{WM}$ across the sample was studied. The correlations between SUVR and WM uptake were studied for all cases. We also tested a simple analytical correction based on the linear fitting of a subset of the data. **Results:** $SUVR_{WM}$ followed a Gaussian distribution with an average of 1.79 and a standard deviation of 0.24. Linear correlations were observed between $SUVR_{WM}$ and $SUVR_{CGM}$ (slope=0.28, Pearson's r=0.82) and $SUVR_{WC}$ (slope=0.13, r=0.64) for the smoothed data. These correlations were independent of using the whole WM or the eroded WM. When applying PVC, we observed a reduction on this effect (r=0.24 for iY, r=0.31 for RVB, both for $SUVR_{CGM}$). As a counterpart, PVC significantly biased SUVRs, which would invalidate the usage of SUVR thresholds calculated without PVC. The proposed analytical correction decreased the dependence of $SUVR_{CGM}$ (r=0.29) and $SUVR_{WC}$ (r=0.22) with $SUVR_{WM}$, while maintaining similar SUVR values, which makes it interesting to correct previously preprocessed data. **Conclusion:** We observed a significant variability of SUVR associated with the variations on WM uptake across patient samples and harmonization approaches. Resolution harmonization by image smoothing increased the effect significantly. These results can be helpful when designing new harmonization strategies, and might also explain some recent results showing that reference regions including WM (as in $SUVR_{WC}$) provide better quantification results, as the inclusion of WM will partially compensate the spill-in counts. **References:** None.

EP-0876

Feasibility of a Brainstem and Diencephalon Atlas in FDOPA PET / MRI Imaging

G. Demonceau[1,2], *Q. Demonceau*[1], *V. Lebon*[1,3];
[1]*CEA-SHFJ Orsay, Paris, FRANCE,* [2]*Bois de l'Abbaye, Liège, BELGIUM,* [3]*University Paris Sud, Paris, FRANCE.*

Aim/Introduction: to constitute an atlas of FDOPA uptake in the brainstem and diencephalon from images acquired in PET / MRI: the registration of the images on a reference model was carried out in MRI and then applied to PET images, the validation of the results taking place mainly in PET. **Materials and Methods:** we retrospectively selected 35 patients who underwent FDOPA PET / MRI: 15 considered as positive for dopaminergic denervation (visually decreased putaminal activity), 20 considered as normal (the control group). After reconstruction of the tomographic sections, the T1 images of each patient were registered on the T1 images of a reference model where several anatomical regions had been previously identified. The registration was carried out in a progressive way, in non-deformable and then deformable mode, after creation of a mask including the brainstem, the diencephalon and the striatum. The registration parameters were then applied to the FDOPA images acquired 90 min after injection. The choice of the optimal method of registration was based on the analysis of the dispersion of the activity in the summed image of the control group. A score was created, multiplying each SUV of each voxel of a predefined area by the spatially corresponding SUV in the model. Eight areas of the brainstem were used to create the final score. We finally investigated the correlation between the scores of 70 deformable registrations and the ability of specific brain regions to discriminate, using those registrations, the parkinsonian from the normal patients. **Results:** visually the images of the brainstem, diencephalon and striatum are correctly replaced after registration in all patients, without deformation. No manual correction was needed. A significant inverse correlation (Pearson's coefficient; p-values less than 0,0001) was found between the 70 scores and the corresponding p-values of a Student t-test comparing the control and patient groups in 5 non-striatal regions: the epiphysis, the hypothalamus, the pulvinar, the raphe nuclei and the substantia nigra. Furthermore, using the registration method with the highest score, two of those regions (the substantia nigra and the hypothalamus) exceeded the level of signification. Those statistical characters were also observed in well validated regions in Parkinson's disease, the caudate and the putamen. **Conclusion:** using the hybrid PET / MRI technique, it

is possible to reliably achieve an automatic analysis of FDOPA uptake in brainstem and diencephalon nuclei. The method is independent of the injected tracer, which broadens its scope. **References:** None.

EP-0877

Is I-123-MIBG cardiac SPECT-CT with attenuation and scatter correction a useful tool for the diagnosis of prodromal Lewy body disease compared to planar scintigraphy?

G. Roberts[1], *J. Lloyd*[2], *G. Petrides*[2], *K. Howe*[2], *T. Ali*[2], *R. Durcan*[1], *S. Lawley*[1], *H. Kain*[1], *P. Donaghy*[1], *J. O'Brien*[3], *A. Thomas*[1];
[1]*Newcastle University, Newcastle upon Tyne, UNITED KINGDOM,* [2]*Newcastle upon Tyne Hospitals, Newcastle upon Tyne, UNITED KINGDOM,* [3]*University of Cambridge, Cambridge, UNITED KINGDOM.*

Aim/Introduction: 123-I MIBG (meta-iodobenzylguanidine) cardiac imaging for sympathetic denervation is a validated diagnostic biomarker for dementia with Lewy bodies (DLB) and is listed as an indicative biomarker in the 2017 international consensus criteria for DLB diagnosis. There has been very little research in the diagnostic accuracy of cardiac MIBG in the prodromal stages of DLB or in the advantage of attenuation and scatter corrected SPECT-CT compared to planar imaging. We aimed to evaluate this in subjects with either MCI due to Lewy body disease (MCI-LB) or due to Alzheimer's disease (MCI-AD). **Materials and Methods:** An anthropomorphic chest phantom was filled with I-123 solution using activities typical of healthy subjects. The phantom was scanned on a Siemens Intevo with MELP collimators using both planar and SPECT-CT techniques. Further scans were acquired with a PMMA chest plate added, then breasts. The SPECT-CT images were reconstructed using OSEM with resolution recovery, attenuation and scatter correction (ACSC) applied.Twenty-nine healthy controls, 24 MCI-AD and 32 MCI-DLB subjects aged over 60 years were recruited and assessed clinically as part of a research study. Their diagnoses were confirmed by a panel of three expert old age psychiatrists. All were administered 111±10% MBq I-123-MIBG and imaged at 4 hours ±30 minutes using standard planar imaging, followed by SPECT-CT. SPECT images were reconstructed as above. The heart-to-mediastinum ratios on planar images (HMR_planar) were calculated using a circular cardiac region and rectangular mediastinum region, with corresponding spherical and cuboid regions for HMR_SPECT. **Results:** Phantom HMR_planar decreased by 20% with the PMMA plate added; 39% with plate and breasts. Cardiac counts with ACSC SPECT showed less dependence on phantom size than SPECT without ACSC (5% vs 33%). There was a significant linear relationship between HMR_planar and BMI ($p<0.01$, $R^2=0.44$) in healthy controls, but no significant relationship for HMR_SPECT ($p>0.1$, $R^2=0.03$). Healthy controls were used to provide reference ranges for HMR_planar and HMR_SPECT (mean±2SD). 20/24 MCI-AD cases had normal scans with planar and 21/24 with SPECT-CT. 17/32 MCI-LB cases were abnormal on both planar and SPECT-CT. The difference between mean HMR for normal and abnormal scans was much greater for SPECT-CT than planar. **Conclusion:** By reducing variation due to patient size, SPECT-CT improves separation between normal and abnormal cardiac MIBG scans, with a small improvement in MCI diagnostic accuracy. In clinical practice, SPECT-CT may be useful in borderline cases where the planar image result is unclear. **References:** None.

EP-0878

Comparison of Cortical Parcellation Based Asymmetry Index Calculation Methods in PET/MRI Epilepsy Diagnostic

D. Fajtai[1], *Z. Tóth*[1], *A. Fekésházy*[1], *Á. Csóka*[1,2], *A. Takács*[1], *Z. Vajda*[2], *I. Repa*[2], *PET/MR Epilepsy diagnostic multidisciplinary research team, M. Emri*[3];
[1]*Somogy County Moritz Kaposi Teaching Hospital, Medicopus Nonprofit Ltd., Kaposvár, HUNGARY,* [2]*Somogy County Moritz Kaposi Teaching Hospital, Dr. József Baka Diagnostic, Radiation Oncology, Research and Teaching Center, Kaposvár, HUNGARY,* [3]*University of Debrecen, Faculty of Medicine, Department of Medical Imaging, Division of Nuclear Medicine and Translational Imaging, Debrecen, HUNGARY.*

Aim/Introduction: Interictal ^{18}F-FDG PET has currently acknowledged the primary imaging modality for the presurgical metabolic assessment for focal epilepsy. Because of the localisation of the epileptic focus needs to be assessed at the individual patient level the Statistical Parametric Mapping (SPM) may be the best method for semi-quantitatively comparing a patient to a healthy database. Unfortunately, large datasets from healthy subjects are not yet available for ^{18}F-FDG PET/MRI, limiting the possibility of providing an accurate statistical evaluation of individual patient data. As an alternative, for quantifying the differences between hemispheres, the proposed application is the Asymmetry Index (AI) based seizure-zone localisation. The simultaneously measured functional and anatomical PET/MRI images and the availability of most advanced neuroimaging software allows the automatic evaluation of regional AI data in native space and MNI152 atlas space, as well. We aimed to compare the sensitivity of the native- and atlas space-based regional AI (rAI) calculation techniques with the SPM results in a selected temporal lobe epileptic patient's group. **Materials and Methods:** From our lab's FDG-PET/MRI Epilepsy Database we selected 36 patients (age ranges between 15 and 57, mean = 29.7 ± 10.1) whose large (> 3 cm^3) lateralised hypometabolic area was identified in the temporal lobe by SPM after the comparison with the control population of 19 subjects. In parallel with the SPM analysis, we generated Harvard-Oxford cortical atlas-based rAI data in MNI152 space (HO-rAI), and FreeSurefer segmentation (based on Desikan-Killiany Atlas) induced rAI in native-space (FS-rAI). We characterised the sensitivity of a rAI calculation methods by the maximal absolute value of rAI data measured in the temporal lobe regions. Because of the non-normality of data, we applied the paired Wilcoxon test to compare the rAI values, and Spearman's rank correlation coefficient to assesses the relationship between rAI and SPM's

t-max value. **Results:** We found that the rAI calculation in atlas space resulted in significantly (p = 0.0006) higher rAI values than the native-space parcellation technique. We also found a strong correlation between t-max and HO-rAI (rho= 0.547, p< 0.0001) and FS-rAI (rho= 0.603, p< 0.0001). **Conclusion:** Although we consider the cortical parcellation in native space as a subject-specific region delineation method, the usage of these regions for detecting asymmetry in FDG-PET images is not so sensitive than the rAI calculation in MNI152 space. (Acknowledgement: This research was granted by the EFOP-3.6.2-16-2017-00008 project.) **References:** None.

EP-0879

Correction of head motion and attenuation map realignment in PET/MR studies: comparison between PET-image based and EPI-image based methods

C. R. Brambilla[1,2,3], O. Zeusseu[1,4], J. Scheins[1], E. R. Kops[1], L. Tellmann[1], N. J. Shah[1,5,6], I. Neuner[1,7,6], C. Lerche[1];
[1]Institute of Neuroscience and Medicine 4, INM-4, Forschungszentrum, Jülich, GERMANY, [2]Department of Psychiatry, Psychotherapy and Psychosomatics, RWTH University, Aachen, GERMANY, [3]Faculty of Medicine – Faculty 10, RWTH University, Aachen, GERMANY, [4]Department of Medical Physics, HTW des Saarlandes, Saarbrücken, GERMANY, [5]Institute of Neuroscience and Medicine 11, INM-11, JARA, Forschungszentrum Jülich, Jülich, GERMANY, [6]JARA - BRAIN - Translational Medicine, Aachen, GERMANY, [7]Department of Psychiatry, Psychotherapy and Psychosomatics, RWTH Aachen University, Aachen, GERMANY.

Aim/Introduction: Dynamic PET is a method to analyze metabolic aspects of the brain using the time course of the activity distribution for deriving quantification parameters. In these studies, as data acquisition frequently lasts more than 1.0 h, head motion can degrade accuracy of the time activity curves (TACs), leading to erroneous quantification results. In addition, it also can lead to mismatches between the attenuation map and the subsequent PET frames affecting the final quantification. The aim of this work was to evaluate two head motion correction (MC) methods in a PET/MR study with [^{11}C]ABP688 bolus-infusion protocol. **Materials and Methods:** PET-image based method (M1): PET images were reconstructed according to a predefined framing scheme without attenuation and scatter corrections. For these dynamic images (non-MC), co-registration with respect to a reference image was done with PMOD [1] and the inverse rigid movement parameters were extracted and applied to each of the single attenuation maps. Subsequently, the Multiple Acquisition Frame (MAF) method [2] was used for image reconstruction using the matched attenuation maps. In a last step, the rigid transformation was applied to the attenuation corrected PET images generating the MC images. EPI-image based method (M2): EPI images (3 volumes) were repeatedly acquired during the dynamic PET study. They were acquired before and after the T1 anatomical acquisition (AC reference) at several timepoints before and after further MR sequences as part of an fMRI study during the last 30 minutes of the PET acquisition. For all EPI images, a realignment with respect to the very first EPI image was done with SPM12 [3] and inverse rigid movement parameters were extracted and applied to the static attenuation map. Subsequently, MAF was used for image reconstruction using the newly created dynamic and matched attenuation maps. Finally, rigid transformation was applied to the AC PET image frames of the entire dynamic acquisition. **Results:** We have evaluated the M1 method for a measurement using [^{11}C]ABP688 with 2.5 minutes frames during 65 minutes of PET acquisition [4]. After applying M1, visible misalignment between images disappeared and "jumps" in TACs were reduced. The M2 method is currently being analyzed. **Conclusion:** Both methods allows semi-automatic detection and compensation of inter-frame motion without additional tracking hardware. Both methods are expected to improve the accuracy of TACs in case of subject's motion in dynamic PET studies. **References:** [1] www.pmod.com/web/ [2] IEEE TMI, 16, 1997, 137-144. [3] ww.fil.ion.ucl.ac.uk/spm/software/spm12/ [4] DGN 2019, abstract P107.

EP-0880

Acquisition period of amyloid PET imaging using [^{18}F]Florbetapir can be compressed without alteringstandardized uptake value ratios

K. Wgatsuma[1], M. Sakata[1], K. Ishibashi[1], K. Miwa[2], N. Kojima[1], Y. Osuka[1], H. Kim[1], K. Ishii[1];
[1]Tokyo Metropolitan Institute of Gerontology, Tokyo, JAPAN, [2]International University of Health and Welfare, Otawara, JAPAN.

Aim/Introduction: The durations of uptake and acquisition time for the positron emission tomography (PET) image using [^{18}F]Florbetapir differ according to the purpose. The recommended uptake time ranges from 30 to 50 min post-injection, then image acquisition takes 10 - 20 min thereafter. Therefore, the duration of the entire procedure can range from 40 to 70 min. The present study aimed to evaluate the accuracy of quantitative PET measures acquired over a shorter scanning using [^{18}F]Florbetapir. **Materials and Methods:** Images were acquired from nine individuals (mean age, 84.4 y) using a Discovery MI PET/CT system (GE Healthcare). The mean injected dose of [^{18}F]Florbetapir was 352.1 MBq and two 20-min scans were performed starting at 30 and 50 min post-injection. The datasets were reprocessed to produce the following sets of sinograms: 30 - 35, 30 - 40 and 30 - 50 min and 50 - 55, 50 - 60, and 50 - 70 min after radiopharmaceutical administration, then the images were reconstructed under clinical conditions. All [^{18}F]Florbetapir images were separately normalized to a standard [^{18}F]Florbetapir template using Amygo neuro software (FUJIFILM Toyama Chemical Co. Ltd.). Anatomical volumes of interest (VOI) were automatically placed on seven regions. Mean cortical (cSUVR) and regional (rSUVR) SUVR were calculated with the cerebellar value as the reference. A cSUVR of > 1.10 was defined as amyloid positive. Significant differences among cSUVR and rSUVR were determined using repeated measures one-way analysis of variance and Friedman tests. Values with

P< 0.05 were considered significant. **Results:** The mean (± SD) cSUVR in nine individuals for 30 - 35, 30 - 40, 30 - 50, 50 - 55, 50 - 60, and 50 - 70 min procedural durations were 1.00 ± 0.11, 1.00 ± 0.11, 1.01 ± 0.12, 1.03 ± 0.13, 1.03 ± 0.13, and 1.03 ± 0.13. The SUVR in amyloid-positive patients increased slightly over time even after 30 min post-injection. The amyloid positivity of two individuals was inconsistent by uptake duration. The mean cSUVR and rSUVR did not significantly differ according to multiple comparisons except for those of the medial frontal regions. **Conclusion:** [^{18}F]Florbetapir imaging offers stable quantitative values even over durations as short as 5 min because the standard [^{18}F]Florbetapir protocol includes a larger dose and shorter uptake duration than PET imaging with other approved [^{18}F] labeled amyloid tracers. However, differences in uptake duration might affect the diagnostic outcomes of amyloid PET. **References:** Tiepolt S, et al. EJNMMI.2013;40:238-44.

EP-0881

Test-retest reliability of adenosine A_{2A} binding in the human brain with ^{11}C-preladenant-PET

M. Sakata[1], *K. Wagatsuma*[1], *T. Tago*[1], *K. Ishibashi*[1], *K. Ishii*[1], *K. Ishiwata*[1,2,3], *J. Toyohara*[1];
[1]*Tokyo Metropolitan Institute of Gerontology, Tokyo, JAPAN,* [2]*Southern Tohoku Research Institute for Neuroscience, Koriyama, JAPAN,* [3]*Fukushima Medical University, Fukushima, JAPAN.*

Aim/Introduction: The aim of the present study was to evaluate the reproducibility of cerebral adenosine A_{2A} receptor (A2AR) quantification using ^{11}C-preladenant and PET in a test-retest study. **Materials and Methods:** Dynamic ^{11}C-preladenant PET scans (90-min) were performed twice for each subject in eight healthy male volunteers (26 ± 10 y.o.) using D710 PET/CT scanner (GE Healthcare). The subjects were asked to refrain from caffeine over half-day, and the time of the scans were roughly matched in each subject to avoid the effect of diurnal variation. The injected dose was 705 ± 46 MBq and the specific activity was 65 ± 19 MBq/nmol. During the scan, arterial blood was sampled at various time intervals, and the fraction of the parent compound in plasma was determined by HPLC analysis. ROIs were placed on the cerebellar cortices (as the reference region), putamen, and head of the caudate nucleus (as the target regions). According to the previous work[1], total distribution volume ratio (DVR) was estimated by Logan reference tissue method. Absolute test-retest variability (aTRV), and intra-class correlation coefficient (ICC)[2] were calculated as the index of repeatability. **Results:** The DVRs (mean ± SD (min - max), n = 8) were 5.6 ± 1.6 (2.4 - 6.9) at test scan and 5.3 ± 1.7 (1.8 - 6.9) at retest scan in putamen, and 4.4 ± 1.4 (1.8 - 6.2) at test scan and 4.1 ± 1.4 (1.4 - 5.3) at retest scan in caudate. The aTRVs of putamen and caudate were 18 ± 8 % and 18 ±9 %, respectively. The ICCs of putamen and caudate were 0.77 and 0.77, respectively. The smallest outlier of DVR was the result of the oldest (51 y.o.) subject. **Conclusion:** In this study, "moderate" test-retest reproducibility, and large inter-subject differences of ^{11}C-preladenant-PET were observed. These variances might be attributable to competition by endogenous A2AR binding ligands. The analysis of plasma caffeine concentration would be included in further studies. **References:** [1] Sakata, M, et al., JNM, 58:9, 2017. [2] Shoukri, MM, et al., BMC Med Res Methodol, 6:24, 2006.

EP-0882

Assessing regional FDG uptake in the brain in normal, low and high blood glucose levels

I. Sarikaya[1], *A. Albatineh*[1], *A. Sarikaya*[2];
[1]*Kuwait University Faculty of Medicine, Kuwait, KUWAIT,*
[2]*Trakya University Faculty of Medicine, Edirne, TURKEY.*

Aim/Introduction: Various studies have been performed to assess global or regional F-18 fluorodeoxyglucose (FDG) uptake in the brain, mainly in normo and hyperglycemia. In this study, using whole body F-18 FDG positron emission tomography/computed tomography (PET/CT) images, we assessed regional FDG uptake in multiple regions of the brain in normal, low and high blood glucose levels to understand if there are regional differences. **Materials and Methods:** In this retrospective study, whole body F-18 FDG PET/CT images were used to analyse the brain. Inclusion criteria included adult patients (age range 18-65 year-old) with no history of diseases or symptoms affecting the brain, no abnormal findings in the brain on both PET and low dose CT images, no image artefacts and no other factors affecting FDG uptake in the brain. Maximum standardized uptake values (SUVmax) were measured in lateral and medial frontal, temporal, parietal, and occipital cortices, lateral cerebellar cortex, posterior cingulate cortex, caudate nucleus, putamen, thalamus, brain stem, and scalp in patients with normal blood glucose (91-100 mg/dl), low blood glucose (61-70 mg/dl), and high blood glucose (171-200 mg/dl) levels. In each blood glucose range, fifteen (15) F-18 FDG PET images were analyzed (total 45 images). Mean ± SD of SUVmax of the brain regions for each blood glucose range was calculated and statistical analysis of the values were performed. **Results:** Mean **S**UVmax in all the assessed brain regions was significantly lower in hyperglycemia ($p<0.001$), and not different in hypoglycemia ($p> 0.05$) as compared to normoglycemia. In all blood glucose levels, FDG uptake is highest in lateral frontal cortex and lowest in medial temporal cortex and brain stem as compared to other regions of the brain. At blood glucose range of 171-200 mg/dl, hyperglycemia induced reduction in regional FDG uptake/SUVmax ranged from 55.9 % to 63.7 % (mean 60 ± 2.4) which was below 60% in medial temporal cortex, cerebellum and brain stem and above 60% in other brain regions. Mean scalp activity was lower in hyperglycemia ($p<0.001$), and not different in hypoglycemia ($p> 0.05$) as compared to normoglycemia. **Conclusion:** Gross assessment of regional glucose metabolism in the brain shows that hyperglycemia induced reduction of FDG uptake is approximately same in various regions of the brain which could be slightly less in medial temporal cortex, cerebellum and brain stem than other regions. Hypoglycemia does not seem a significant effect on regional or global FDG uptake in the brain. **References:** None.

EP-0883

Comparing Automated Regional Analysis Techniques of Neurologic ^{18}F-Fluoro-L-DOPA Images

D. Fajtai[1], *Z. Tóth*[1], *A. Fekésházy*[1], *Á. Csóka*[1,2], *A. Takács*[1], *I. Repa*[2], *M. Emri*[3];
[1]*Somogy County Moritz Kaposi Teaching Hospital, Medicopus Nonprofit Ltd., Kaposvár, HUNGARY,* [2]*Somogy County Moritz Kaposi Teaching Hospital, Dr. József Baka Diagnostic, Radiation Oncology, Research and Teaching Center, Kaposvár, HUNGARY,* [3]*University of Debrecen, Faculty of Medicine, Department of Medical Imaging, Division of Nuclear Medicine and Translational Imaging, Debrecen, HUNGARY.*

Aim/Introduction: PET imaging with ^{18}F-Fluoro-L-DOPA (F-DOPA) tracer provides a promising approach for examining various brain diseases, like Parkinson's disease (PD) which is a neurodegenerative disorder resulted as a progressive loss of dopaminergic neurons in the basal ganglia. In the case of PD, the neurons in the putamen were the most impaired compared to other segments of basal nuclei, and this can help to distinguish PD from other movement disorders. The decreased tracer intake in the putamen can be detected with proper segmentation and intensity normalisation, while the hemispherical differences can tell more about the severity of the PD. With the simultaneously acquired functional and anatomical PET/MRI images the problem of spatial registration of the MRI and PET images is theoretically solved, which simplifies the segmentation of basal ganglia, and so provides the automatization of the atlas-based regional analysis (AROI). For AROI calculation we implemented two techniques: a fast, less-accurate segmentation algorithm (F-AROI) and a slow, anatomically accurate method (S-AROI). We aimed to examine how the usage of the F-AROI and the S-AROI technique influence the calculated regional values. **Materials and Methods:** We used nine patient's T1 MR and F-DOPA PET image, examined with PET/MR in our facility. In both methods after the T1-based segmentation, we calculated the normalised ROI values using the mean F-DOPA uptake of the occipital fusiform gyrus as a normalisation factor. In the segmentation part of F-AROI we used the components of the FSL package, while in the S-AROI we applied the "recon-all" pipeline of FreeSurfer. Using these methods we evaluated the normalised ROI value of the dorsal and ventral putamen, caudate nucleus (CN), nucleus accumbens (NACC) and the CN+NACC region, in both hemispheres of all subjects. Because of the non-normality of data, we applied the paired Wilcoxon test with FDR correction to compare the normalised ROI values. **Results:** The statistical tests resulted that the choice of the algorithm has no significant effect ($p > 0.91$ in all cases) on the measured regional averages. **Conclusion:** The faster FSL based algorithm can reproduce the results of the FreeSurfer based slower method. On the other hand, we have found that the FreeSurfer segmentation process may tend to fail because of high volume structural abnormalities inside the brain, while the FSL based algorithm can serve useful results if the basal ganglia is not affected by the anomaly. (Acknowledgement: This research was granted by the EFOP-3.6.2-16-2017-00008 project.) **References:** None.

EP-0884

Optimization of time acquisition of dopaminergic scan on a 360° CZT camera

P. Payoux[1], *E. Cassol*[1], *P. Blanc*[2], *N. Roth*[3], *A. Hitzel*[1], *P. Gantet*[1];
[1]*CHU Purpan, Toulouse, FRANCE,* [2]*CHG Albi, Albi, FRANCE,* [3]*Spectrum Dynamics Medical Ltd., Caesarea, ISRAEL.*

Aim/Introduction: The innovative 360-degree CZT detectors system (VERITON, Spectrum Dynamics system) proposes a higher photon sensitivity, allowing for decreased scan times and/or reduced doses. In dopaminergic assessment the minimal counts admitted for QC is up to 1.5 million. In this work, we have determined the mean time necessary to obtain this threshold. **Materials and Methods:** During March 2019, 68 subjects (38 males, 30 females) were addressed to our nuclear medicine department for dopaminergic scintigraphy. All underwent a DaTSCAN SPECT (185 MBq +/- 10%) on a Veriton system with a time acquision of 20 minutes (ref) in brain focus mode. Reconstruction parameters were following: OSEM3D 6 iterations 8 subsets; pre-iteration filter: convolution smoothing frequency 2, smoothing factor 0.125; post-filter: median filter, support 3. No correction of scatter and no correction of attenuation was applied. For each subject, an image corresponding to 1.5 million counts was extracted from the list-mode acquisition data and the time to obtain this image was calculated. Pre-time 20 minutes images and pre-counts 1.5 million counts images were analysed by 3 observers and binding potential (BP) was calculated by the DaTsoft3D quantification software. For all images, observers determine the final diagnosis, image quality and confidence. **Results:** Mean of total counts for 20 minutes acquisition was 2.4 M (>1.5 Mcounts). Pre-counts 1.5 M counts duration was 13.3 minutes on average (+33% time gain). Image analysis was similar for the original and the 1.5 Mcounts images and there was an excellent correlation of BP for the two sets of Data (0.970 for caudate nucleus, 0.988 for putamens). A small difference of the mean of binding potentials was observed: 0.12 ($p<0.0001$) for caudate nucleus and 0.06 ($p=0.0019$) for putamens. These differences are very small (in relative value 3% for caudate nucleus and 2% for putamens) and have no incidence on analysis. **Conclusion:** Based on brain focus, pre-counts 360° CZT acquisition should reduce the acquisition time of dopaminergic scan to 13.3 minutes on average with enough counts. With this acquisition mode, no modifications of diagnosis was observed compared to 20 minutes pre-time acquisitions. **References:** Assesment of a CZT camera (360°) 12 detectors for dopaminergic neurotransmission assesment. Payoux et al. Abstract in Médecine Nucléaire, 43, Issue 2, March-April 2019.

EP-0885

The Utility Of Technetium-99m ECD Brain Spect Using NeuroGam Software In Children With Autism Spectrum Disorder

P. Mohan[1], *G. Shroff*[2], *V. Mahajan*[3], *H. Mahajan*[3];
[1]*Mahajan Imaging Centre, New Delhi, INDIA,* [2]*NuTech Mediworld, New Delhi, INDIA,* [3]*CARING, Mahajan Imaging, New Delhi, INDIA.*

Aim/Introduction: Autism Spectrum Disorder (ASD) is one of the most prevalent disorders in child and adolescent psychiatry. The purpose of the study was to investigate perfusion patterns in children with ASD. In order to avoid missing brain lesions, we applied brain processing software NeuroGam with SPECT to evaluate and analyze the brain cerebral cortical blood flow. **Materials and Methods:** Forty children (36 boys, 4 girl; mean age: 6.9+/-1.7 years) with ASD disorder defined by DSM-III-R criteria were included in the study. Age- and sex-matched control group was also included in the study. Before arrival, patients were instructed to avoid caffeine, tea, or other drugs known to affect cerebral blood flow (CBF). To avoid head movement during scanning (20-30 min), the patient were made comfortable and relaxed. The uncooperative patients needed sedation. Tracer injection preceded sedation to avoid sedation-induced blood flow changes. Brain perfusion images were obtained 45 minutes after the intravenous injection of an adjusted dose of Tc-99m ECD to children. Visual and semiquantitative evaluations using NeuroGam software were performed. **Results:** NeuroGam software offers each corresponding region of interest expressed as a percentage of the mean pixel value in the entire volume, including the anterior cerebral, middle cerebral, and vertebral terrain. Significantly lower cortical activity was noted in the ASD group, particularly in the prefrontal regions, temporal and parietal lobes. **Conclusion:** NeuroGam software can help identify areas of cerebral cortex having significant hypoperfusion indicating decreased neuronal activity in children with ASD. Brain SPECT scan is simple, noninvasive, involves minimal radiation, and may serve as a cost-effective tool to identify children with ASD. **References:** None.

EP-64

Technical aspects -> Instrumentation and data analysis -> Data analysis -> Quality control, performance and standardization

October 12 - 16, 2019 e-Poster Area

EP-0886

Determination of the activity of 99mTc-HMDP to be injected in adults to optimize the quality of the image

E. A. L. Bathily[1], *C. Meyer*[2], *O. Diop*[1], *F. Besson*[2], *B. Ndong*[1], *M. S. Djigo*[1], *A. Forbes*[2], *G. Grimon*[2], *K. Guèye*[1], *G. Thiaw*[1], *C. V. De Labriolle*[3], *M. Mbodj*[1], *E. Durand*[2];
[1]*Université Cheikh Anta Diop, Dakar, SENEGAL,* [2]*Biophysics and Nuclear Medicine Department, Kremlin Bicetre Hospital, Paris, FRANCE,* [3]*Nuclear Medicine Department, Armand Trousseau Hospital, Paris, FRANCE.*

Aim/Introduction: Our study is to review the habit that most often occurs to adapt the injected activity only to the patient "weight" (MBq/kg in adults), in an approach that aims to obtain a same image quality in all patients. Indeed, a large patient has a larger volume of distribution and a greater attenuation thickness; to detect the same flow of photons, it is necessary to inject more. General objective: propose an optimization of activity to be injected, by appreciation of the distribution volumes and attenuation thicknesses (AT). Specifically: - propose alternative formulas according weight, height and gender, allowing to homogenize the outgoing photon flux - compare these models to the recommendations and look at their dosimetric impact. **Materials and Methods:** The following data were recorded for130 patients who have done a 99mTc-HMDP scintigraphy at the Bicêtre hospital nuclear medicine department: gender, age, weight, height, injected activity, delay between injection and acquisition and image quality. We measured activities detected in counts/cm² at lumbar vertebra L3. Thanks to the CT, AT with regard to L3 were measured. Using linear regression analysis with R studio software, we were able to estimate the AT from the measured values. Extracellular volume (ECV) was calculated using the Christensen and Groth's formula:ECV=8117 ml / m2 x 0.00718 x (Weight) $^{0.425}$ x (Height) $^{0.725}$ - 28 ml **Results:** The measured activity in L3 was 806± 450 counts/cm². The Signal (counts / (min.cm)= surface concentration(counts/cm²) * scanning speed (cm / min). To have good image, the target signal (average) was 13140 and the target Theoretical Plasma Concentration (TCP) was 12.3 KBq / mL. The estimated AT was= 11,76905 + 0,079454* Weight - 5,133455* Height. The activity who must be injected to detect the same photon flux (Q_{target}) is thus calculated by the relation: $Q_{target} = 12.3* ECV *2^{3/6} *e^{(0,11 *AT estimated).}$ $Q_{target}= 12.3 * 8117* (0,00718 * (Weight)^{0,425} * (Height)^{0,725}) - 28 * 1,41 * e^{(0,11 * 11.76905 + 0.079454 * Weight - 5.133455 * Height).}$ Q_{target} ranged from 403 to 1400 MBq (40 to 140 kg) and between 9.2 to 11.2 MBq / kg for the weight Q_{target}. **Conclusion:** Our formulas are good alternatives in determining the activity who must be injected to minimize irradiation while optimizing image quality. Values are consistent with recommendations and diagnostic reference levels. **References:** None.

EP-0887

Comparison the ^{18}F-FDG regional size dependent PET segmentation method for texture analysis

S. Woo[1], *M. Cho*[1], *W. Kim*[1], *H. Sheen*[1], *K. Song*[2], *I. Lim*[1];
[1]*Division of applied RI, Korea Institute of Radiological and Medical Sciences, Seoul, KOREA, REPUBLIC OF,* [2]*Department of Urology, Korea Institute of Radiological and Medical Sciences, Seoul, KOREA, REPUBLIC OF.*

Aim/Introduction: Texture features are quantitative image

heterogeneity using ROI analysis. The regional segmentation method for ROI definition can affect the texture features. The aim of this study was to compare the PET image texture features depending on segmentation methods. **Materials and Methods:** NEMA IEC body phantom was used for PET image. ^{18}F-FDG were injected into the spheres with diameter of 22, 17, 13 and 10 mm. The ^{18}F-FDG PET image regional segment methods were used SUV 1.5, 2.0, 2.5 region growing, and edge detection. To optimize the reconstruction parameters were applied the 16, 21 subsets and TrueX with 2 iteration. Compare the calculated volume in each segment method with size of phantoms spheres. Texture features such as energy, kurtosis, and entropy were calculated using LIFEx software. To evaluate the difference of texture feature according to the segmentation method, reference segmentation method and relative change amount were calculated. **Results:** SUV 2.0 with 16 subsets and 2 iteration was no significantly difference between the actual size of phantom's spheres exclude 10 mm diameter sphere. Entropy PET images of SUV 2.0 segment methods with diameter of 22, 17 and 13 mm calculated as 0.96, 0.94 and 0.78 respectively. Energy of SUV 2.0 were calculated as 0.11, 0.12 and 0.18 respectively. Kurtosis of SUV 2.0 were obtained as 1.73, 1.89, 2.41 respectively. Entropy, energy, and kurtosis relative change with SUV 2.0 and edge detection was 0.53%, 0.85% and 2.97% change in 13 mm sphere of phantom. **Conclusion:** The result of this study was shown that optimized spheres segmentation method is SUV 2.0 in IEC phantom PET image with 16 subset and 2 iteration. The segmentation method should be considered for texture features analyzing. **References:** 1. Orlhac, Fanny, et al. "Tumor texture analysis in 18F-FDG PET: relationships between texture parameters, histogram indices, standardized uptake values, metabolic volumes, and total lesion glycolysis." Journal of Nuclear Medicine 55.3 (2014): 414-422.

EP-0888

The Prevelence of Severely Altered FDG Biodistribution - Addressing the Issue of Potentially Nondiagnostic FDG-PET/CT Scans

M. Weiler-Sagie[1], *S. Halperin*[2], *Z. Keidar*[1,2];
[1]*Rambam Health Care Campus, Haifa, ISRAEL,* [2]*Technion, Haifa, ISRAEL.*

Aim/Introduction: Changes in FDG biodistribution can reduce lesion detectability in FDG-PET/CT imaging. The prevelance of FDG PET/CT scans with severely altered biodistribution (SABD) is unclear. Insulin is known to alter FDG biodistribution and patients are therefore instructed to fast 4-6 hours prior to the scan. Hyperglycemia is known to alter FDG biodistribution and therefore SNMMI and EJNMMI guidelines recommend measurement of blood glucose level (BGL) before FDG injection and advise re-scheduling in patients with BGL > 200 gr/dL. The aim of the study was to assess the prevalence of scans with severely altered FDG biodistribution and test for correlation with BGL and other patient related and imaging related parameters. **Materials and Methods:** Two-hundred fifty-five consecutive skull-base to mid-thigh FDG-PET/CT scans from a single center were retrospectively re-reviewed. All patients are routinely instructed to fast 4-6 hours before the scan and the fasting status is re-confirmed before FDG injection. Scans were assessed by visual qualitative inspection of PET axial, coronal, sagital and MIP images for SABD. Severly altered biodistribution was defined as markedly increased diffuse muscular uptake that raises the reviewing physicians concern for a potentially non-diagnostic PET portion of the scan due to reduced lesion detectability and/or unreliable lesion standard uptake values (SUVs). Liver uptake was measured as SUVmean and SUVmax in a fixed volume of interest in the right lobe. Patients parameters including BGL measured immediately before FDG injection, age, gender, height, weight, and referral indication, were recorded. Correlation of SABD with BGL, body mass index (BMI) and liver SUVs was calculated. **Results:** Severly altered FDG biodistribution was present in 3% of scans (8 of 255). Referal indication was oncologic in 98% of the scans. The population consisted of patients 5-95 years of age. The male to female ratio was 1:1. BGL range was 68-290 mg/dL, with 151 patients (59%) with BGL >100 mg/dL, of them 8 (3%) with BGL >200 mg/dL. There was no correlation between SABD and BGL levels;(r=0.153), fasting hyperglicemia of BGL > 100 mg/dL (r=0.104), BGL > 200;(r=0.097), BMI (r=0.206), liver SUVmean (r=-0.040) or liver SUVmax (r=-0.011). **Conclusion:** The prevelance of severly altered FDG biodistribution was 3%. No correlation was found between SABD and BGL, BMI or liver SUV. Blood glucose level of > 200 gr/dL could not predict these potentially non-diagnostic scans, questioning the need for BGL measurement before FDG PET/CT scans in routine clinical practice. **References:** None.

EP-0889

Evaluation of SPECT Systems Performance using Carlson Phantom

R. Y. Aimazrou[1], *T. O. Aimutairi*[2], *A. K. Alosaimi*[3], *S. F. Aianazi*[4];
[1]*King Faisal Specialist Hospital and Research center, Riyadh, SAUDI ARABIA,* [2]*King Abdullah Hospital, Bisha, Bisha, SAUDI ARABIA,* [3]*King Faisal Medical city for Southern Region, Abha, SAUDI ARABIA,* [4]*Prince Mohammad Bin Abdulaziz Hospital, Riyadh, SAUDI ARABIA.*

Aim/Introduction: Evaluation of tomographic systems is essential procedure to obtain a reliable system with high-quality single photon emission computed tomography (SPECT) images. AAPM report numbers 52 recommend using Jaszczak phantom to evaluate the SPECT total performance. Whereas, many countries are using a Carlson phantom to evaluate their SPECT systems. This study is establishing reference values for the Integral uniformity (IU), root-mean-square noise (rms) and contrast measurement using a Carlson phantom as well as the number of resolved objects. **Materials and Methods:** In this study, measurement of the IU and rms of the uniform area and the contrast of the largest three spheres following the procedure described in AAPM report No.52. These measurements applied on twenty SPECT studies with and without using Chang and CT attenuation corrections. The phantom was injected with about

15-20mCi of Tc-99m activity. The phantom centered on the imaging bed. The LEHR collimators mounted on the camera. The acquisition parameters are; 140KeV peak, 20% energy window, 128x128 matrix, step and shoot mode, 128 views, 360º orbit, 400 K Counts/view, with non-circular orbit. Uniformity correction was applied to all the studies. Images were reconstructed by FBP algorithm with Butterworth filter, 0.5 cutoff frequency and order of 5. For each study, reconstructed images were evaluated visually looking for any distortion or ring artifact in the uniform area. The resolved spheres, cold and hot rods were counted, the straightness of the lines in the Mesh area were assessed. Three transverse slices were summed in the uniform region, and a 21X21 ROI pixel area used to calculate the IU and rms noise. The best slice of the spheres selected for the calculation of contrast. **Results:** Most of the studies in the uniform area showed uniform slices clear from any artifacts. The number of objects was increased when the attenuation correction was applied. Mesh squares showed straight lines in all the studies. IU and rms noise values showed a wide variation. Contrast decreased with decreasing sphere diameter. Contrast for the largest sphere was decreased when Chang AC applied while it was increased for the CT AC studies. For the smaller spheres, all the AC studies showed increased values. **Conclusion:** In this study, reference values for the evaluation of the SPECT systems were produced using Carlson phantom. This phantom has represented significant results to evaluate the performance of SPECT and SPECT/CT systems. **References:** AAPM report no. 52.

EP-0890

Thrombosis as incidental finding in ^{18}F-FDG PET/CT scan performed in oncologic patients: usefulness of intravenous contrast-enhanced CT

L. Garcia, C. G. Wakfie Corieh, E. Rodriguez Gallo, L. Landaeta Kancev, A. Blanes, R. Valhondo Rama, M. Garcia Garcia-Esquinas, M. J. Pérez Castejón, J. L. Carreras Delgado;
San Carlos Clinical Hospital, Madrid, SPAIN.

Aim/Introduction: The main indication for ^{18}F-FDG PET (Positron Emission Tomography) is the evaluation of cancer. Scientific evidence shows that oncologic patients have a hypercoagulable state due to malignant cells producing factors with procoagulant activity. Since at our institution we generally perform ^{18}F-FDG PET with intravenous (IV) contrast-enhanced computed tomography (CT), we aimed at evaluating the value of this combined technique in the detection of unknown thrombotic process. **Materials and Methods:** A retrospective study was carried out reviewing the medical records of patients who had undergone an IV contrast-enhanced ^{18}-FDG PET/CT scan from November 2014 to December 2017. A total of 120 patients diagnosed with thrombosis were included, what entailed an average of 4 patients/month with unknown thrombotic disease at the moment of undergoing the scan. Images were interpreted independently by two specialists with wide experience, a nuclear physician and a radiologist. **Results:** From the whole of patients, 57.5% were women and the average age was 59 years. The most frequent type of cancer was the colorectal one (23.3%), followed by lung and breast tumors, head and neck cancer and lymphoma. The 46.7% presented distant metastasis at the time of exploration, while the 13.3% had just regional lymph nodes involved. Out of the 120 patients, 71 (59.2%) presented pulmonary embolism (segmental pulmonary arteries were the most common location) and the remaining 49 (40.8%) were diagnosed from thrombotic disease in another location (jugular, cava or portal vein thrombosis were the most frequent findings). **Conclusion:** It is proved that oncologic patients have an increased risk of thrombosis and that treatment is different in cancer and non-cancer patients; therefore performing the ^{18}F-FDG PET/CT scan using IV enhanced-contrast could provide additional value for a correct diagnosis, ensuring that the optimal treatment is offered having a direct impact in the survival rate. However, further randomized controlled trials are required before firm conclusions can be made. **References:** None.

EP-0891

Imaging Protocol Optimisation for ^{223}Ra on Conventional Clinical Devices

T. Lima[1], R. F. P. Simões[2], L. Vasconcellos de Sá[3], B. Trimpin[1], E. Nitzsche[1];
[1]Aarau Cantonal Hospital, Aarau, SWITZERLAND, [2]National Cancer Institute - INCa, Rio de Janeiro, BRAZIL, [3]Institute of Radiation Protection and Dosimetry - IRD, Rio de Janeiro, BRAZIL.

Aim/Introduction: ^{223}Ra is used in the treatments of bone metastases (BM) from castration-resistant prostate cancer (CRPC). Attempts on extending the clinical indication have been proposed and evaluated, for example, in breast cancer patients presenting with metastatic bone lesions [1,2]. For CRPC, prescription and dosimetry are based on patient's weight [3], and research of the administration of a higher activity per weight has shown poor results [4]. The availability of imaging protocols would enable the evaluation of different treatment strategies in BM benefiting from individualised dosimetry. Different imaging protocols have been published [5,6,7,8] but the common energy window (EW) recommended includes a low EW which comprises of the emission from the ^{223}Ra and the lead characteristic X-Rays originated (RXC) from collimator. The aim of this work was to evaluate an optimized EW, to exclude contributions from RXC [9], in a conventional clinical device. **Materials and Methods:** For this work, a Siemens Symbia Gamma Camera was used. We evaluated the 4 proposed energy windows in 3 different planar acquisitions set-ups. First acquisition set-up consisted of three capillary tubes of 1 mm diameter and one with 6 mm diameter positioned directly in the patient bed. Subsequently set-ups consisted of two of the 1mm tubes and the 6 mm tube being placed in the PTW Head phantom with holders for capillary with an empty phantom and with water (mimicking scatter), respectively for the second and third set-up. For all acquisition the low energy all-purpose collimator was used and time was used as stopping condition. Profiles and signal to noise ratio

(SNR) were analysed for all evaluated energy windows. **Results:** The main difference between the energy windows evaluated was the energy peak used for the lower window either including or not including the RXC. For all set-ups noise was slightly lower at the proposed window (reduction of 12.5%, 12.3% and 14.9% for set-up one, two and three, respectively). The proposed energy window with 89keV also showed improvements in terms of SNR with gains ranging from 2 to 16% in the first set-up, 4 to 8% in the second and 5 to 30% in the third set-up. The lower the gains were found at more scatter conditions. **Conclusion:** The proposed energy window taking into account contributions from the lead collimator characteristic X-Rays has shown a potential to improve image quality in Ra-223 patient. Reduced improvements have been found on conditions with higher contributions from scatter. **References:** (Picture with references deleted)

EP-0892

Intercomparison of radionuclide calibrators used in the main Lithuanian hospitals with the secondary standard ionization chamber

K. Skovorodko[1], *A. Gudelis*[2];
[1]*Vilnius University Hospital Santaros Klinikos, Vilnius, LITHUANIA,* [2]*State research institute the Center for Physical Sciences and Technology (FTMC), Vilnius, LITHUANIA.*

Aim/Introduction: The accuracy of measuring radiopharmaceutical activity must comply with international standards and guidelines. The aim of this study was to assess the uncertainty of measured activities by radionuclide dose calibrators, which are used in Lithuanian hospitals for prescribed radiopharmaceutical dosage administration of commonly applied radionuclides for diagnostic and therapy procedures, with the help of the secondary standard radionuclide calibrator. **Materials and Methods:** Responses of twelve radionuclide calibrators that are used in three main hospitals' daily practice were compared with the readings of the secondary standard radionuclide calibrator Capintec CRC-15R (4π γ ionization chamber) brought to hospitals by the Ionizing Radiation Metrology Laboratory of the Center for Physical Sciences and Technology (FTMC) that is the National Metrology Institute (NMI) in Lithuania. Radionuclides ^{18}F, ^{99m}Tc, ^{131}I, ^{137}Cs, ^{57}Co and ^{223}Ra were selectively measured in two standard geometries: in 3 ml syringes and P6 vials. Ten readings of experimental values were taken with each instrument, corrections for the decay and for the background were applied. Then differences between experimental mean values and reference values were determined, the uncertainties were calculated. **Results:** The results of the intercomparison showed that the uncertainty for check sources was up to 8 % for ^{137}Cs and 2 % for ^{57}Co, uncertainties for diagnostic radionuclides ^{99m}Tc and ^{18}F in P6 vial geometry were found up to 13 % and 5 %, respectively; the uncertainty was within 15 % for ^{99m}Tc and 4 % for ^{18}F in syringe geometry, while uncertainties for therapy radionuclides ^{131}I and ^{223}Ra in P6 vial geometry were within 4 %, and within the tolerance of 5 % of the reference value in syringe geometry. **Conclusion:** The intercomparison measurements with secondary standard reference chamber and traceable radioactive sources could identify problems in accuracy of measurements done by radionuclide calibrators in hospitals, especially for different source geometry effects, at low energy or for lower activities. Hospital results revealed that regular check of radionuclide calibrators is necessary in order to meet the recommendations to be within 5 % (at k = 2 level) with the reference values for therapy radionuclides and within 10 % of the prescribed dosage for diagnostic procedures. **References:** None.

EP-0893

Acceptance and Quality Tests in Thyroid Uptake Systems

D. Verganelakis[1], *T. Makri*[1], *I. Sevaslidou*[1], *V. Lyra*[1], *M. Gavra*[2], *M. Chassiotou*[2];
[1]*Nuclear Medicine Department, Oncology Clinic 'Elpida', Children's Hospital "Aghia Sofia", Athens, GREECE,* [2]*CT & MRI Department, Children's Hospital "Aghia Sofia", Athens, GREECE.*

Aim/Introduction: The aim of this work is to suggest a protocol regarding acceptance and quality tests for all available types of thyroid uptake systems. Currently, there numerous types of thyroid uptake systems available in nuclear medicine departments worldwide dating back to 1980's until today's most recent models. Quality control (QC) tests vary amongst models with older systems to require more user involvement and time consuming processes. In recent uptake systems there are software embedded QCs that cover certain types of tests with variable ranges of errors, with minimum user involvement and minimum requirement of time. In order to achieve comparable results amongst different nuclear medicine facilities, further standardisation of QC tests is required. **Materials and Methods:** Three different types of thyroid uptake systems were used along with a set of test rods of Cs137 & Eu152. The uptake systems had different: i) number of channels, ii) software and algorithms, iii) maximum count rates, iv) differential and integral linearities, v) other hardware and physical characteristics. For all of them, Background, Contamination, Autocalibrate, System, Resolution, Constancy, Minimum Detectable Activity and Chi-Square tests were performed. **Results:** Each thyroid uptake system produced the same Background and Contamination result, but slightly different results in the Autocalibrate, System, Resolution, Constancy, Minimum Detectable Activity and Chi-Square test. The range of variation amongst results was between 0.5% to 6%. Varying certain parameters for each test, such as Counting time, Number of Repetitions, Duration of measurements, Precision factor, Correction factor, etc. produced statistically more convergent results amongst the various types of systems. **Conclusion:** There is a need for further standardisation and harmonisation of the Quality Acceptance and Control tests of the various thyroid uptake systems that are today available in order to reach comparable results of high accuracy and reliability amongst different nuclear medicine departments. **References:** None.

EP-0894

Development of Simulation Environment for bone SPECT imaging using SIMIND

H. Daisaki[1], *M. Shimizu*[2], *T. Iizuka*[2], *H. Shimada*[3], *T. Ino*[4], *T. Saito*[1], *I. Kuromori*[1], *H. Masuko*[1], *S. Fukai*[1,5], *K. Shimizu*[1], *T. Nakahara*[6], *K. Kashikura*[1];
[1]*Gunma Prefectural College of Health Sciences, Gunma, JAPAN,* [2]*Fujioka General Hospital, Gunma, JAPAN,* [3]*Gunma University Hospital, Gunma, JAPAN,* [4]*Gunma Cardiovascular Center, Gunma, JAPAN,* [5]*The Cancer Institute Hospital Of JFCR, Tokyo, JAPAN,* [6]*Keio University Hospital, Tokyo, JAPAN.*

Aim/Introduction: In Japan, the SPECT imaging guideline for bone scintigraphy was published in 2018, and the clinical use and image quality standardization of the SPECT imaging for bone scintigraphy are now spreading. Also, in recent years, quantitative evaluation using, for example, SUV using SPECT/CT camera has been used clinically. It may be useful to use simulation for standardization of image quality and evaluation of quantitative accuracy of the SPECT imaging. **Materials and Methods:** A digital phantom with Hot/BG ratio=6 was created by modifying QIBA-DRO (Washington University). And, a Monte Carlo simulation environment that simulates bone SPECT imaging was constructed using SIMIND[1)] (Ver 6.1.2) and the digital phantom. The simulation accuracy was verified in comparison with bone SPECT images acquired using NEMA body phantom filled with ^{99m}Tc solutions of BG=10.8kBq/ml and E-CAM (Siemens Healthcare) SPECT camera. The verification was physically performed using 17mm Hot sphere contrast ($Q_{H,17mm}$), background variability using 17mm ROI ($N_{B,17mm}$), and contrast noise ratio (QNR). **Results:** The bone SPECT image obtained by our constructed simulation had a difference of -1.9% at $N_{B,17mm}$, 5.2% at $Q_{H,17mm}$, and 7.6% at QNR, compared to the measured SPECT image. It was a relatively good agreement under conditions with sufficient statistics. However, in the conditions of acquisition duration with 10min/bed (20sec/step, 30 step) corresponding to a clinical situation, the image quality shows large variations among multiple simulations of 12.6% at $Q_{H,17\ mm}$, 12.7% at $N_{B,17mm}$, and 14.3% at QNR. **Conclusion:** The construction of a simulation environment simulating bone SPECT imaging was possible with relatively good accuracy. In the future, it may be applied to the evaluation of quantitative variability and the optimization of image quality. However, because physical indicators of image quality show variation depending on count statistics, it is necessary to pay attention to the variation in the case of imaging optimization. **References:**
1) https://www.msf.lu.se/research/the-simind-monte-carlo-program

EP-0895

Improving the Assessment of Dose Calibrator Linearity for the Clinical Activity Range

D. O'Keeffe;
Medical Physics and Bioengineering, Christchurch Hospital, Christchurch, NEW ZEALAND.

Aim/Introduction: Demonstration of the linearity of a radionuclide dose calibrator gives confidence that the accuracy of activity measurements can be maintained across the clinical range of activities typically used for imaging when only low or high activity calibration standards are available. Absolute activity accuracy is important for the control of patient dose, but the linearity is also important when performing relative measurements such as standardised uptake values (SUV) in PET and more recently in nuclear medicine imaging. Linearity as a performance measurement is well-known, but how to analyse the data when measuring it remains inconsistent across publications for the decaying source method, even in recent standards [1]. The aim of this investigation was to see if the decaying source method of linearity assessment could be improved for measurements in the clinical range of activities. This range was chosen because within this range the dose calibrator electrometer performance is more important than linearity changes due to saturation effects that are typically only observed when measuring high activities. **Materials and Methods:** Automated activity measurements were taken every 10 seconds for an 11 GBq Technetium-99m source decaying to 1 MBq in two models of dose calibrator that employed a microprocessor controlled multi-range electrometer. The activity variance versus mean activity was measured using a sliding analysis window of 10 readings (100 seconds). The linearity was measured using a linear fit to the logarithm of the activity readings versus time, and two models of decay were forced by performing the same fit for the decay fraction and by using the average decay corrected readings. **Results:** The variance measurements showed the range changes of the multi-range electrometers employed in the dose calibrators. These changes were subtle for high activities, but much clearer for low activity measurements. The fitting of the linearity measurement data varied depending on the degree of dose calibrator non-linearity, but the forced fit, using the decay fraction or decay corrected readings, gave consistent results. **Conclusion:** Multiple measurements of activity over the clinical range can provide useful information on the range changing of the dose calibrator electrometer. This can help with planning activity measurement points in other linearity assessment methods such as by dilution or attenuation sleeves. Combined with using fitting of activity data to the decay fraction or decay correction, the decaying source linearity assessment can be improved. **References:**
[1] IEC TR61948-4(2019) "Nuclear Medicine Instrumentation - Routine Tests - Part 4: Radionuclide Calibrators.

EP-0896

Proposal for National Quarterly Quality Control Tests for the SPECT/CT Systems

R. Y. Aimazrou[1], *S. F. Alanazi*[2], *T. O. Almutairi*[3], *A. K. Alosaimi*[4];
[1]*King Faisal Specialist Hospital and Research center, Riyadh, SAUDI ARABIA,* [2]*Prince Mohammad Bin Abdulaziz Hospital, Riyadh, SAUDI ARABIA,* [3]*King Abdullah Hospital, Bisha, SAUDI ARABIA,* [4]*King Faisal Medical city for Southern Region, Abha, SAUDI ARABIA.*

Aim/Introduction: Several international agencies have published numerous guidelines for QC tests for the SPECT and SPECT/CT systems. Most of third world countries lack any recommendations for routine testing of these systems. This study aims to propose a national quarterly QC (QQC) tests for the SPECT and SPECT/CT systems that guarantee the system reliability and optimized performance. **Materials and Methods:** Eight QQC tests were performed by a qualified medical physicist immediately after the PPM. The COR and intrinsic uniformity calibrations were acquired before conducting these tests. Up-to-date, more than 25 QQC tests have been conducted on five systems at King Faisal Specialist Hospital and Research Center. They include; intrinsic and extrinsic flood field uniformity, system spatial resolution and linearity, whole body system spatial resolution without scatter, total tomographic performance and SPECT/CT spatial registration tests. They are practical and consume about 3 hours. The required radionuclides and phantoms such as Carlson and two sizes quadrant bar phantoms were used. All these tests were evaluated visually and using the vendor software for the uniformity tests and COR calibrations. **Results:** These tests evaluate the performance of the system quantitatively and qualitatively using several performance indicators which demonstrates its suitability for clinical use. Several times it was found that the photopeaks needed to be adjusted. Uniformity tests showed consistent behavior of the systems with some abnormalities in some occasions. These were resolved by either acquire the uniformity calibration tables or retune the system. Consistently, 3-and-5 millimeters bars were determined for the system and whole-body spatial resolution tests, respectively and always the resolved bars were look linear. Most of the tests showed consistent behavior in resolving different objects of Carlson phantom. Three spheres, seven rods and four pairs of hot lesions inserts were usually resolved. Often, the uniform area looks uniform but with the occasional appearance of ring artifacts. Moreover, the linearity part shows straight lines in both directions. For SPECT/CT systems, the accuracy of image registration was evaluated visually by displaying the fused slices of SPECT and CT images of Carlson phantom. **Conclusion:** The proposed national QQC tests are suggested to be performed for the SPECT and SPECT/CT systems in order to offer a set of tests that have been constantly examined and could guarantee the system reliability. Tests results occasionally showed deficiencies in image quality or SPECT performance. Most of the issues were solved and modified by the user and/or service personnel. **References:** None.

EP-0897

Is there any ^{18}F-FDG PET/CT BAT pattern in oncological patients?

W. Jalloul[1], *E. Chifor*[1], *A. Tarca*[1], *M. Gutu*[1], *D. Chetan*[2], *C. Ștefănescu*[1], *A. Naum*[2];
[1]*Nuclear Medicine Laboratory, County Emergency Hospital „Sf. Spiridon", Iasi, ROMANIA,* [2]*Nuclear Medicine Laboratory, Regional Institute of Oncology, Iasi, ROMANIA.*

Aim/Introduction: Brown Adipose Tissue (BAT) represents an endocrine metabolic active tissue with complex pathological implications, demonstrating high uptake of ^{18}F-FDG. Consequently, ^{18}F-FDG PET/CT, highly used in cancer evolution assessment, proved to be an essential tool for its detection and quantification. The purpose of this study is to evaluate BAT ^{18}F-FDG PET/CT possible pattern characteristics in oncological patients as well as possible factors which can influence BAT activation. **Materials and Methods:** The BAT imaging pattern, with qualitative and quantitative statistical analysis, was realized in 48 ^{18}F-FDG PET/CT scans performed for 41 patients who were referred to our Nuclear Medicine Laboratory between July 2017 and April 2019, for different oncological diagnosis. **Results:** The median value (m_v) of patients age with ^{18}F-FDG BAT positive scans was 33.7 years. This tissue was active more often in female patients (58.5%), the m_v Body Mass Index (BMI) was 24.39, and the Blood Glucose (BG) level was normal (m_v = 90 mg/dl). In 58% of cases the initial diagnosis was Hodgkin's lymphoma and 51.2% of patients have received surgical treatment and chemotherapy. We noticed that 65.9% of cases were reported in cold seasons (autumn and winter), even if the scan room temperature was always the same. BAT was unilateral in 2.4% of cases, the rest being bilateral, with symmetric distribution in 68.3%, homogeneous in 43.9%. In 12.19% of cases the localization was unique, all the rest being multiple. We mention that the maximum value of SUV_{max} was calculated in paravertebral localization but supraclavicular SUV_{max} had the best Pearson correlation (ρ) with thoracic aorta SUV_{max} (used like reference). A statistical significant ρ (direct and low intensity, Sig<0.05) was found between BMI and BG level, and between latero-cervical SUV_{max} and SUV_{max} latero-thoracic. **Conclusion:** Complex BAT data can result from the ^{18}F-FDG PET/CT scans analysis, making evidence of multiple factors which could contribute to BAT activation. These data could be useful both for a correct image interpretation and for making new treatment strategies based on this type of tissue. **References:** None.

EP-65

Technical aspects -> Instrumentation and data analysis -> Instrumentation -> General aspects

October 12 - 16, 2019 e-Poster Area

EP-0898

Variable Density 3D-grids for Non-uniform Activity Distributions in PET and SPECT Phantoms: a Proof of Concept

C. F. Uribe*, R. Ataya, R. Coope, A. Rahmim, F. Bénard;*
BC Cancer, Vancouver, BC, CANADA.

Aim/Introduction: Radiomics, extraction of extensive

quantitative features from radiological images, has generated recent interest promising improved assessment of disease and prediction of outcome. A challenge is that many radiomic features cannot be properly correlated to existing PET and SPECT phantoms which use compartments filled with uniform distributions of activity. This study presents a method to generate 3D-printed meshes of variable density, that, when immersed in a uniform tracer concentration, create predefined non-uniform activity distributions. The problem is to maximize the dynamic range between high and low activity concentrations, within the limitations of 3D-printing technology and system spatial resolution so gradients appear smooth. **Materials and Methods:** We developed MATLAB scripts that create 3D-meshes with two components: a 3D-grid of thin bars, and cubes centred at each node of the grid. The bars hold the cubes in position. Activity concentration (AC) is varied by cube size, specified by values in a three dimensional matrix with the elements representing concentration at each node. The symmetry of this geometry is exploited to minimize the number of stereolithography triangles and therefore its file size. Linear-gradients with grid spacing of 3, 4, 5, and 6mm were printed by Shapeways (Eindhoven Netherlands) using selective laser sintering (SLS). These phantoms were immersed in a solution with ^{18}F-FDG and scanned using a GE D690 PET scanner (GE Healthcare, USA). Imaging revealed a limit of ~.75mm between cube faces beyond which printer support material could not be removed. At 5mm grid spacing, the dynamic range varied from 1/2 to 1/8 of maximum activity. Spherical linear-gradients and uniform spheres were printed using 5 and 6mm grid spacings. **Results:** The optimal grid spacing was found to be 5mm, balancing image smoothing with the ability to create printable geometry. Initial measurements using a maximal AC of 125 kBq/mL on a linear-gradient phantom witha 5mm grid-spacing, showed decrease concentration of 1.1%/mm vs. a predicted 1%/mm. Gradient and uniform spheres ranging, for example, from 100% AC (at the centre) to 40% AC (periphery) likewise performed as expected. In this particular example, 44% AC was observed in the periphery relative to the maximum AC in the hot sphere. **Conclusion:** We have demonstrated a method for developing non-uniform distributions of activity with the potential to more realistically represent non-uniform features observed in patient images and for use towards radiomic feature applications. This approach can be used to create complex geometries with variable activity concentrations. **References:** PMID 28766726.

EP-0899

A web-based platform for collecting, researching and presenting molecular hybrid imaging artefacts

O. Roesner, M. Rullmann, B. Sattler, O. Sabri;
University Hospital Leipzig, Department for Nuclear Medicine, Leipzig, GERMANY.

Aim/Introduction: Imaging artefacts affect image quality and quantifiability and, thereby, may hamper the diagnostic interpretation. The possible reasons for and solutions to particular hybrid imaging artefacts should be made available to the users in the form of a representative collection of cases. Currently, this mainly exist as print media, coming with high logistic and temporal efforts in collecting and preparing, processing and provision of artefact cases. The instructive presentation of the cases is limited by inflexibility and impracticability due to the static nature of such media. These observations render the identification of a reason or adaptation of a solution strategy for an artefact based on print media almost impossible. **Materials and Methods:** A web-based platform was developed (http://www.ipet-science.de/artifacts/). An upload-mask has been implemented that captures artefact cases with all case-related data and images. Submitted cases will then be moderated by experts and scientifically processed. For cases with unknown reasons or solutions, a comment section where these aspects can be processed or discussed with other users is included. The user can search an increasing number of cases and adapt solution approaches for his own problem. A pilot-phase was performed. Invited users uploaded cases from the literature or their own clinical routine. Feedback was recorded in the form of an integrated questionnaire. **Results:** Over two months a total of 25 artefact cases were uploaded. The average time to upload was 13 min. The upload-mask reduces time needed to collect data and enables a sustainable and complete data collection. The database enables the structured collection of larger amount of data. The database and search-mask allow for a specific and faster research. 15 questionnaires could be evaluated. 80% rated the operability being very instructive, 75% the performance very practical and 85% the overall performance and necessity very interesting. **Conclusion:** The platform and the underlying software are stable. In terms of effort, completeness and sustainability, it shows clear advantages over the presentation in the form of print media. It will be a very useful toll in clinical practice to assist with artefacts in hybrid molecular imaging. The next steps include the ability to upload DICOM data. As the number of uploaded cases increases, an AI-based evaluation of the database is sought and then should assist the user in finding most reliable solution strategies for their own case very quickly. As legal data security issues are solved, the platform will enter wider test period. **References:** None.

EP-0900

[^{11}C]PBR28 and [^{11}C]UCB-J Blood Metabolite Analysis by Solid Phase Extraction

M. Huiban, S. Moz, M. A. Ali, G. Searle, R. Gunn, E. A. Rabiner, J. Passchier;
Invicro, A Konica Minolta Company, London, UNITED KINGDOM.

Aim/Introduction: Quantitative analysis of PET scans often requires the measurement of radioligand concentration in plasma over time. Chromatographic methods have been mainly used for this purpose in the past, in which blood samples may require pre-treatment or the use of online trapping column with column-switching HPLC methods to overcome plasma protein binding [1]. More recently, Solid Phase Extraction (SPE)

methods have been reported as an alternative [2], [3]. With these methods, typically plasma samples do not need to be pre-treated, as plasma proteins can be washed off the SPE cartridge using micellar solvents. Here we report our comparison of such SPE methods, using an automated sample processing system, against the gold standard HPLC methodology, for the analysis of [^{11}C]PBR28 and [^{11}C]UCB-J human plasma metabolites. **Materials and Methods:** Sample analysis was performed using the Biotage® Pressure+ 48 manifold system and Oasis® HLB 3cc 60mg flangeless cartridges. Plasma samples were diluted with micellar eluent consisting of a solution of 40mM SDS at pH 7.0 containing 5% of 1-BuOH. After loading of the samples, cartridges were rinsed with either water, or mixtures of water and methanol to wash away residual proteins and any polar radio-metabolites. Parent fraction of the radiotracer was left on the cartridges. Washed fractions and cartridges were measured for radioactivity content in well-counters, and parent fractions estimated as the ratio of these counts. Methods (e.g. volumes and composition of the rinsing solutions) were optimised for each tracer, comparing results with the parent fraction as determined by HPLC analysis (column switching method). **Results:** Average differences between HPLC and SPE for the parent fractions of [^{11}C]PBR28 and [^{11}C]UCB-J were 2.2% (n=5) and 1.9% (n=6) respectively. Highly reproducible results were obtained at each time-points, providing overall good agreement between radioligand parent curves. **Conclusion:** Excellent correlation was obtained for these two tracers between the HPLC and SPE methods. This methodology is currently being extended to [^{18}F] BCPP. The simplicity of these methods is very attractive, avoiding the need for complicated and expensive infrastructure, and opens up the use of these research tracers to a wider range of imaging facilities. **References:** [1] Hilton et al., Nucl. Med. Biol., 2000, 27, 627.[2] Katsifis et al., Nucl. Med. Biol., 2011, 38, 137.[3] Nakao et al., Nucl. Med. Biol., 2013, 40, 658.

EP-0901

Assessment of image quality comparing 2 acquisitions speeds in whole body bone scan with new generation of collimators and processing software

C. Garcia[1], *N. Gohimont*[2], *H. Sanon*[3], *R. Muteganya*[4], *M. Tondeur*[5]; [1]*CWaPi, Tournai, BELGIUM,* [2]*CHUB Hopital Erasme. Université Libre de Bruxelles, Bruxelles, BELGIUM,* [3]*Centre Hospitalier Universitaire Yalgado Ouédraogo, Ouagadougou, BURKINA FASO,* [4]*Clinique de l'Europe, Bruxelles, BELGIUM,* [5]*CHU Saint Pierre. Université Libre de Bruxelles, Bruxelles, BELGIUM.*

Aim/Introduction: Introduction: New generation of Cameras using LEHRS collimators and new processing image software C2D are reputed to enable decreasing scan times and/or administered activity without compromising image quality. C2D processing is applied to planar images with purpose to diminish statistical noise without degradation of image resolution and contrast. It combines a linear non-anisotropic edge preserving iterative filter with contrast enhancement procedure. The filtering procedure iteratively updates each pixel using signal strength and local variation in the pixel neighboring area. The contrast enhancement is done by deconvolution with empirical point spread function. At the last stage -the processed image is linearly blended with original image to preserve noise texture. **Materials and Methods:** Four nuclear medicine specialists independently and blinded concerning the acquisition characteristics, compared quality images of 38 patients using 2 speed acquisitions 15cm/min and 20cm/min. All examinations were scored with a 5 levels scale (1: poor/not clinically acceptable - 5: excellent quality). After this first analysis, the quality of the same WBS acquisitions were compared using 5 levels of C2D (no Clarity®, 20, 40, 60, 80 and 100% blending). All WBS were scored with the same scale and finally, a "best choice" concerning quality was made by each observer. **Results:** User preference between WBS at 15cm/min vs 20cm/min without any other intervention was 117 for slower speed and 44 for the quicker speed. The rate is 117/161 in favor of the slower one, (95% confidence interval: 65%-79%). Quality: only 30 examinations were scored non-diagnostic (poor quality). For the speed: no detectable difference was found (p=0.79), for both speeds the median C2D level preferred blending is 60%. Concerning the observer; we found statistically significant differences (p<0.0001). If we split the population following BMI: normal <=25 vs. overweighted > 25 patients, there is no detectable difference, (p=0.26). Multivariate analysis: The observer is the only factor impacting significantly on the choice of the blending parameter (p<0.0001). **Conclusion:** In our study, WBS at slower speed was preferred. There is a strong impact of the observer on the preferred blending value for choosing a parameter for the Clarity software. No obvious preferences for the level of blending of C2D were found, with a median "best choice" at 60% at both speeds. **References:** None.

EP-0902

Modern and Efficient Management in the Nuclear Medicine Departments: the Lean Approach

L. Metello[1], *P. Ratao*[2], *A. Roda*[3], *M. Capoulas*[4], *J. Nery*[5], *M. Nunes*[6], *A. S. Moreira*[7], *L. Cunha*[7]; [1]*ESS-IPP & IsoPor-Azores, Lda, Angra do Heroismo - Azores, PORTUGAL,* [2]*NM Dept, IPOFG-Lisboa & IsoPor-Azores, Lda, Angra do Heroismo - Azores, PORTUGAL,* [3]*Med Physics Dept, IPOFG-Coimbra & IsoPor-Azores, Lda, Angra do Heroismo - Azores, PORTUGAL,* [4]*Pharmacy Dept, HBA - Loures & IsoPor-Azores, Lda, Angra do Heroismo - Azores, PORTUGAL,* [5]*NM Dept, HGSA-Porto & IsoPor-Azores, Lda, Angra do Heroismo - Azores, PORTUGAL,* [6]*NM Dept, Unilabs-Porto & IsoPor-Azores, Lda, Angra do Heroismo - Azores, PORTUGAL,* [7]*IsoPor-Azores, Lda, Angra do Heroismo - Azores, PORTUGAL.*

Aim/Introduction: Healthcare Management is a highly challenging task, full of dilemmas regarding prioritization of investment and cost containment while always keeping the maximum quality of care. Therefore, tools are required to help managers to deal with such dynamic and complex challenges. "Lean Management" is one of them, proving its place by adding

value into a variety of industries over the last decades. In our specific case, starting a new NM Department was considered as the perfect opportunity to introduce Lean methods and technics and embedding them in our Quality Management System was considered a natural "step further", defining the Lean approach as a "quality improvement method that focuses on maximizing activities that are valued by the costumer and eliminating waste that hinders efficiency in the workplace". **Materials and Methods:** The first step was providing staff an overview about Lean methods and philosophy. Then, we went through the eight classical steps process for Lean implementation: 1) All staff levels were adequately involved; 2) Careful observation of the "gemba", with analysis of processes where they occur; 3) Efforts for elimination of all forms of waste (defined as "steps that do not add value in a process"); 4) Standardization of Practices: Standard Operating Procedures (SOPs) were adopted for every procedure (from patient reception to clinical reports release); 5) Flow improvement of all processes; 6) Use of visual cues for communication; 7) Add value to the customer; 8) Application of Lean tools for data collection and analysis, improving processes and sustaining change. Detailed practical specific examples of all and each of these steps will be given. **Results:** The seven categories of waste were analyzed and actions to minimize them were implemented, p.e.: optimizing the agenda (careful booking, patient instruction and follow-up about previous preparation for scans), close stock control, avoiding expired drugs and supplies, placing required supplies in each room at the right time and amount. Moreover, via adoption of the "5S Tool", we ended up by having a better organized and cleaner workplace, with "a place for everything, everything in its place". **Conclusion:** The implementation of Lean Management in Nuclear Medicine Departments shouldn´t be an end by itself: it is a continuous improvement process that seeks continuous attention, distinguishing Lean Management from conventional management systems by the involvement of every single collaborator, who is empowered to identify problems, propose and implement solutions, creating an overall culture for change (the kaizen principle). **References:** None.

EP-0903

Atomlab 100plus dose calibrator adjustment by 177Lu calibrated source in a phase I/II study for treatment of NH lymphoma with 177Lu-DOTA-HH1

P. Saletti[1], *S. Cardo*[2], *S. Raspanti*[2], *G. Belli*[1];
[1]*AOU Careggi, Florence, ITALY,* [2]*University of Florence, Florence, ITALY.*

Aim/Introduction: A radiopharmaceutical that will be soon used at Careggi University Hospital in a phase I/II study for NH lymphoma treatment is 177Lu-DOTA-HH1, even though 177Lu is not inserted in control unit of dose calibrators currently used at our Nuclear Medicine department in order to measure activity to be administered. The aim of present work is the determination of the specific calibration factor of 177Lu for an accurate activity measurement of radiopharmaceutical to be administered in current study. **Materials and Methods:** Biodex Atomlab 100plus is the dose calibrator involved in the present study together with a calibrated 177Lu source, a 20ml vial containing a 177Lu solution at 0.04M, that was sent to our department with a calibration certificate of National Physical Laboratory (Middlesex, UK). The activity was 214.3MBq (1% expanded uncertainty) at 12:00 of 31 july 2018 UTC. Measurements were performed in vial and calibration factor was adjusted until a difference of less than 2% was achieved. Later, 8 ml of solution were moved in a 10ml syringe and a similar procedure was repeated with the same requirement, i.e. a deviation of less 2%. **Results:** A deal setting value of 118 for the vial and of 116 for the syringe were found at the end of the whole procedure, both leading to a difference of less than 1% from activity expected values. Moreover, such values differ less than 1% from 117, the setting value suggested in operator manual of dose calibrator according to specific firmware in use. **Conclusion:** A simple procedure was actuated in order to adjust the calibration factor of Biodex Atomlab 100plus dose calibrator to be used in a phase I/II study for NH Lymphoma treatment. Obtained results are within 1% of expected activity values according to protocol procedure. This also confirm the worth of the dose calibrator in use because a deviation of less than 1% was highlighted with different investigated geomteries, 20ml vial and 10ml syringe and both in good agreement deal setting value in operator manual. **References:** Biodex - Atomlab 100 plus Operator Manual.

EP-66

Technical aspects -> Instrumentation and data analysis -> Instrumentation -> Imaging guided surgery

October 12 - 16, 2019 e-Poster Area

EP-0904

Freehand fluorescence tomography - Extending the hybrid image-guided surgery concept

M. N. van Oosterom[1,2], *P. Meershoek*[1,3], *M. M. Welling*[1], *F. Pinto*[4], *P. Matthies*[4], *H. Simon*[5], *T. Wendler*[6], *N. Navab*[7], *C. J. H. van de Velde*[2], *H. G. van der Poel*[3], *F. W. B. van Leeuwen*[1,3,8];
[1]*Interventional Molecular Imaging Laboratory, Department of Radiology, Leiden University Medical Center, Leiden, NETHERLANDS,* [2]*Department of Surgery, Leiden University Medical Center, Leiden, NETHERLANDS,* [3]*Department of Urology, Netherlands Cancer Institute-Antoni van Leeuwenhoek Hospital, Amsterdam, NETHERLANDS,* [4]*SurgicEye, Munich, GERMANY,* [5]*Eurorad, Eckbolsheim, FRANCE,* [6]*Computer Aided Medical Procedures, Technical University Munich, Munich, GERMANY,* [7]*Computer Aided Medical Procedures, Johns Hopkins University, Baltimore, MD, UNITED STATES OF AMERICA,* [8]*ORSI Academy, Melle, BELGIUM.*

Aim/Introduction: Within the field of image-guided surgery,

hybrid- or dual-modality-based guidance technologies have been successfully applied to integrate the complementary qualities of radioactive guidance (i.e. in-depth localization) and fluorescence guidance (i.e. superficial and high-resolution localization). In this study, we investigate how the generation of a novel freehand fluorescence (fhFluo) imaging method can complement freehand SPECT (fhSPECT) in a hybrid setup, providing intraoperative augmented reality displays of the tracer distribution and virtual reality surgical navigation towards features defined in these images. **Materials and Methods:** An opto-nuclear detection probe (capable of gamma and fluorescence tracing) was integrated with a declipseSPECT surgical navigation platform. In this setup, near-infrared optical tracking was used to determine the position and orientation of the hybrid opto-nuclear probe, while recording its measurements at every location. Dedicated look-up table models were generated and used to reconstruct this information towards 3D fhSPECT and fhFluo reconstructions. Image resolution of both freehand imaging modalities was compared in a phantom setting, while in-tissue signal penetration was evaluated in flat-surfaced human skin explants. Finally, the combined potential of the fhSPECT and fhFluo technologies was evaluated in prostate and lymph node specimens obtained from five prostate cancer patients directly after sentinel lymph node dissection and prostatectomy. These patients received either separate injections of indocyanine green (ICG) and ^{99m}Tc-nanocolloid, or the hybrid tracer ICG-^{99m}Tc-nanocolloid. As reference, all conditions were also imaged with a handheld gamma camera and surgical fluorescence camera. **Results:** After hard- and software integration, the devised hybrid imaging and navigation setup was capable of creating 3D nuclear and fluorescence tomography scans. With a 1 mm imaging resolution, fhFluo was superior to fhSPECT (6 mm). However, the fluorescence modalities were restricted to a maximum tissue-depth of 0.5 cm, while the nuclear modalities were applicable at all evaluated depths (i.e. depths <2 cm). Both fhSPECT and fhFluo modalities enabled augmented- and virtual-reality navigation towards tracer hotspots. This also included relative hotspot quantification with an accuracy of 3.9% (fhSPECT) and 4.1% (fhFluo). Evaluation of prostate cancer specimens confirmed that fhSPECT provided in-depth detectability at low resolution, while fhFluo provided a superior resolution while being restricted to superficial detection. **Conclusion:** This study showed that when radioactive and fluorescent tracer features are combined, fhFluo provides complementary value to fhSPECT. By applying freehand technologies, a unique hybrid modality is created that supports intraoperative 3D imaging, augmented reality display and surgical navigation. **References:** None.

EP-0905

Simultaneous ^{125}I-seed and ^{99m}Tc guided breast cancer surgery : from probes characterization to clinical trial

C. Hoog, P. Koulibaly, J. Gal, T. Desdoits, C. Dejean, C. Chapellier, J. Haudebourg, J. Darcourt, E. Barranger;
Antoine Lacassagne Center, Nice, FRANCE.

Aim/Introduction: ^{125}I-seeds can be used as landmarks to localize non-palpable breast lesions instead of implanting metal wires (harpoons). This new technique is known to be more efficient and more comfortable for the patient, but requires a nuclear probe usually employed for ^{99m}Tc sentinel node detection. This study aimed to compare the performances of different probes to valid the feasibility of simultaneous ^{125}I and ^{99m}Tc detection and to present the preliminary results of the clinical trial "IODINE BREAST" comparing ^{125}I-seed and harpoon techniques. **Materials and Methods:** 3 probes were characterized according to the NEMA NU3-2004 standard (linearity, sensitivity, spatial resolution tests) for both ^{99m}Tc punctual sources and Ø 0.8 mm × 4.5 mm ^{125}I-seed (IsoSeed® - Eckert & Ziegler) emitting gamma emission of 140 and 27 keV respectively. Impact of ^{99m}Tc scatter (from injection point and sentinel node) on ^{125}I-seed detection was also assessed while performing in vitro simulations of clinical cases.The clinical trial comparing harpoon and ^{125}I-seed techniques is a prospective single-center, non-inferiority and randomized study with stratification according to histological status. The intermediary analyze concerned the first 116 patients. 60 harpoons and 56 ^{125}I-seeds (from 5 to 10 MBq) were implanted under imaging control (ultrasound or stereotactic mammography) within 24 hours (harpoon) or 10 days (seed) before surgery. ^{99m}Tc colloid areola injections for the sentinel node detection were scheduled the same day or the day before surgery. **Results:** The three probes presented heterogeneous performances but were all suitable for simultaneous ^{99m}Tc sentinel node and ^{125}I-seed detection. A ^{125}I-seed implanted just below an ^{99m}Tc injection point is the only case in wich ^{99m}Tc scatter may impact the seed localization.Intermediary results of the clinical trial confirmed the non-inferiority of the ^{125}I-seed technique compared to the gold standard harpoon technique and a gain of comfort (based on VAS scale) for the patient 3 to 24 hours after surgery ($p<0.003$) as well as a shortening of radiological and surgical durations ($p<0.03$). **Conclusion:** The non-significative impact of ^{99m}Tc scatter on ^{125}I-seed detection makes this relevant guided breast surgery possible with a single one nuclear probe. **References:** None.

EP-0906

Feasibility of PSMA-mediated fluorescence imaging at tracer dose

D. van Willigen[1], *A. W. Hensbergen*[1], *M. N. van Oosterom*[1], *F. A. van der Wijk*[1], *K. Bauwens*[2], *H. G. van der Poel*[3], *F. W. B. van Leeuwen*[1,2,3], *T. Buckle*[1,3];
[1]*LUMC, Leiden, NETHERLANDS,* [2]*ORSI Academy, Melle, BELGIUM,* [3]*NKI-AvL, Amsterdam, NETHERLANDS.*

Aim/Introduction: Fluorescence-guidance is an upcoming methodology to improve surgical accuracy. However, the ability to provide intraoperative fluorescence-guidance is 1) dependent on the amount/concentration of the fluorescent dye accumulated in the lesion(s) of interest and 2) hampered by tissue-dependent signal attenuation. This generally results

in application of relatively high doses, which can have negative impact on toxicity and costs. While tracer dose application (100 ug) is the mainstay in nuclear medicine, to date there is still controversy about the feasibility of receptor-mediated fluorescence imaging in vivo at tracer dose levels. Following validation of the performance of new bimodal tracer designs for PSMA in mouse tumor models we have set-out to validate the performance of fluorescence-guidance in a large animal (pig) model with increased translational character. Reasoning that basal PSMA levels in the prostate should already allow evaluation of the feasibility of PSMA-mediated fluorescence imaging in vivo, we evaluated the ability to identify the prostate in vivo after administration of a tracer dose PSMA-targeted tracer. **Materials and Methods:** A high affinity (19.2 ± 5.8 nM) Cy5-functionalized PSMA targeting tracer (EuK-(SO_3)Cy5-MAS_3; 100 ug) was administrated intravenously in five male and three female pigs (35-40kg). Blood and urine samples were obtained during 240 minutes. In vivo imaging and robot assisted prostatectomy were performed at four hours post injection in combination with Cy5 imaging using a clinical Cy5-modified laparoscopic system. Following in vivo imaging, tracer uptake in excised tissues (prostate, kidney, ureter, liver, abdominal fat, muscle, splenic tissue and salivary gland) was evaluated ex vivo using fluorescence confocal microscopy. **Results:** Presence of fluorescence in the blood was detected at early time points after tracer administration (t=5 - 20 minutes) with decreasing intensity over time. Urinary clearance was observed, with fluorescence still present in the urine at the time of imaging and subsequent prostatectomy (120 min). Robot-assisted prostatectomy could be aided by fluorescence imaging based on tracer uptake in the prostate. Confocal microscopy of excised tissues confirmed tracer uptake in the kidney and prostate and revealed a faint tracer-related fluorescence signal in the ureter. No fluorescence was detected in the liver, abdominal fat, muscle, splenic tissue or the salivary gland. **Conclusion:** Our findings indicate that intraoperative PSMA-mediated fluorescence imaging using a tracer dose regime is feasible. The applied approach in (non-tumor bearing) pigs widens translation opportunities from molecule to man and decreases the chance of applying non-successful image-guidance approaches in patients. **References:** None.

EP-67

Technical aspects -> Instrumentation and data analysis -> Instrumentation -> Metric and intervention

October 12 - 16, 2019 e-Poster Area

EP-0907

Validation of NaI detector for whole body counting of thorium-227 / radium-223

I. Murray[1], *B. Rojas*[1], *R. Callister*[1], *A. Cleton*[2], *G. Flux*[1];

[1]*Royal Marsden NHSFT, Sutton, UNITED KINGDOM,*
[2]*Bayer AG, Clincial Pharmacology, Berlin, GERMANY.*

Aim/Introduction: Thorium-227 is an alpha emitting radioisotope with potential therapeutic applications in molecular radiotherapy. Thorium-227 decays to radium-223, which may have an independent biodistribution to that of the parent thorium-227 radiopharmaceutical. Pharmacokinetic measurements made with sodium iodide (NaI) detectors could introduce the potential for cross-talk between neighbouring gamma photopeaks as well as from scattered gamma photons due to their limited energy resolution. The aim of this work was to validate the use of a spectral analysis technique to distinguish the relative contribution of each isotope to a measured photon spectrum. **Materials and Methods:** A NaI detector was connected to a pulse height analyser positioned ~2 m above a phantom containing a mixture of thorium-227 and radium-223. Multiple energy spectra measurements were made over 14 days. Energy spectra per unit activity arising from unscattered thorium-227 photons and Ra-223 photons as well as from scattered photons were modelled. These spectra were scaled until the combination of these component spectra resulted in the closest match to the measured data. The scaling factors were assumed to be estimates of the activity in the phantom. **Results:** Measured estimates of activity followed the expected decay curves. The mean errors in estimating thorium-227 and radium-223 were -2.8% ± 6.6% and 2.5% ± 10.1% respectively. The differences between the integrals of the theoretical and estimated time activity curve were -2.3% and 1.6% for thorium-227 and radium-223 respectively. **Conclusion:** Whole body counting of thorium-227 / radium-223 can be achieved using a conventional sodium iodide detector. **References:** None.

EP-0908

Use of The Silicon Photomultiplier (SiPM)-based PET/CT Results in lower FDG Uptake in Mediastinal Blood Pool Compared to The Conventional PET/CT

Y. Toyama;
Tohoku university, Sendai city, JAPAN.

Aim/Introduction: The purpose of this study was to investigate whether FDG uptake of the liver and the mediastinal blood pool changes depending on the type of PET/CT. **Materials and Methods:** 177 patients, who underwent both conventional (no Time-of-Flight) and SiPM-based FDG-PET/CT (on another day) at our institution for the follow up after acute treatment were investigated. We excluded the cases with differences in patient's conditions between two scans. In SiPM-PET, respiratory gating was used around the diaphragm. We set VOIs (30mm in diameter) and measured the SUVmax / mean in the right hepatic lobe, further we set VOIs (10mm) and measured the SUVmax / mean in the blood pool of ascending aorta (at the height of sternum angle). Also, as a control, we set VOIs (10mm) and measured

the SUVmax in the aortic wall at the same level of blood pools. Furthermore, the contrast ratio (SUVmax in aortic wall/ SUVmean in blood pool) was measured to investigate the difference in contrast between aortic wall and blood pool. **Results:** Finally, 142 patients were investigated (72males. mean age at the time of SiPM-PET: 63.9 ± 13.6). There were no significant differences in the body mass index or blood glucose between two PET scans. The SUVmean (2.45 ± 0.34 vs 2.48 ± 0.40) and SUVmax (3.08 ± 0.44 vs 3.06 ± 0.49) of liver and the SUVmax of the ascending aortic wall (2.27 ± 0.29 vs 2.29 ± 0.34) were no significant difference between SiPM-PET/CT and conventional-PET/CT. However, in the blood pool of ascending aorta, SUVmean (1.60 ± 0.24 vs 1.76 ± 0.30, p<0.0001) and SUVmax (1.80 ± 0.27 vs 1.94 ± 0.32, p=0.0003) of SiPM-PET/CT were significantly lower than conventional. Therefore, the contrast ratio of SiPM-PET/CT was singnificantly higher than that of conventional (1.44 ± 0.23 vs 1.31 ± 0.15, p<0.0001). **Conclusion:** It is assumed that FDG accumulation of the ascending aorta became possible to separate into the wall and the true blood pool because of the improved resolution of the SiPM-PET camera, furthermore, the SiPM-PET/CT provided high contrast for aortic wall compared to the conventional PET/CT. However, there was no difference in liver accumulation between different resolutions. In conclusion, the present study has demonstrated that it is necessary to be careful to use blood pool as references for therapeutic response assessment or comparison of lesion between different PET/CTs. **References:** None.

EP-68

Technical aspects -> Instrumentation and data analysis -> Instrumentation -> Optical imaging

October 12 - 16, 2019 e-Poster Area

EP-0909

Intraoperative real-time visualization of nerves using a novel nerve-specific tracer

T. Buckle[1], *A. W. Hensbergen*[1], *D. M. van Willigen*[1], *K. Bauwens*[2], *H. G. van der Poel*[3], *F. W. B. van Leeuwen*[1];
[1]*LUMC, Leiden, NETHERLANDS,* [2]*ORSI Academy, Melle, BELGIUM,* [3]*NKI-AvL, Amsterdam, NETHERLANDS.*

Aim/Introduction: Surgically induced nerve damage is common in oncological surgery, but can result in debilitating side-effects. Unfortunately, intraoperative nerve delineating techniques that provide real-time guidance are still unavailable. The anatomical variation between individual patients and what is presented in common anatomical atlases strengthens the demand for approaches that enable intraoperative nerve imaging. In an attempt to address this unmet clinical need, fluorescent tracers that specifically target myelin in the peripheral nervous system were developed, and their targeting- and nerve visualization ability was evaluated. **Materials and Methods:** Based on its (photo)physical- and targeting properties, the lead peptide sequence OP10' was selected from a matrix of different targeting peptides. OP10'was C-terminally functionalized using the visible dye Fluorescein or the far-red Cy5 dye, yielding OP10'-FITC and OP10'-Cy5. Myelin-related affinity was evaluated in vitro using myelinating Schwannoma cells (flow cytometry and confocal imaging). Specificity was confirmed through co-staining with a myelin-specific antibody. Binding was further evaluated in dorsal root ganglia (DRG) derived from THY-1 YFP mouse embryos. Microscopic and macroscopic nerve imaging was performed in THY-1 YFP mice following a local tracer administration. The intrinsic YFP signal expressed in axons of these mice was used as a control. The in vivo biodistribution of OP10' was evaluated after intravenous administration of a ^{111}In-radiolabeled version of the peptide (^{111}In-DTPA-OP10'). The ability of OP10'-FITC to visualize nerves in the hypogastric plexus surrounding the prostate was further evaluated in vivo in male pigs and ex vivo in human prostate tissue obtained after prostatectomy using a clinical imaging set-up. **Results:** OP10'-Cy5 displayed a nanomolar affinity for myelin (97±20 nM) and confocal microscopy indicated co-localization of peptide staining with myelin presence on the cell surface of myelinating Schwann cells. Binding to could further be confirmed on DRG's and ex vivo nerve tissue. Following local administration OP10'-Cy5 allowed for fluorescence imaging of the sciatic nerve in vivo (Figure 1), enabling clear discrimination from the background tissue. Biodistribution data revealed that OP10' does not enter the central nervous system (CNS) and as such has a minimal toxicity threat. Both in pigs and ex vivo human prostate tissue OP10'-FITC allowed of detection of the hypogastic plexus. **Conclusion:** OP10' has proven to be a potent nerve-specific tracer that is able to target myelin both under in vitro, ex vivo, and in vivo conditions. Biodistribution data further underlines that this particular nerve tracer does not pose a threat for the CNS. **References:** None.

EP-69

Technical aspects -> Instrumentation and data analysis -> Instrumentation -> PET and PET/CT

October 12 - 16, 2019 e-Poster Area

EP-0910

Phantom-based image quality assessment of clinical ^{18}F-FDG protocols in digital PET/CT and comparison with conventional PMT-based PET/CT devices

S. Gnesin[1], *C. Kieffer*[1], *K. Zeimpekis*[2], *J. Papazyan*[3], *R. Guignard*[4], *J. O. Prior*[5], *F. R. Verdun*[1], *T. V. M. Lima*[6];
[1]*Institute of Radiation Physics, Lausanne University Hospital, Lausanne, SWITZERLAND,* [2]*Department of nuclear medicine, Zürich Universitätsspital, Zurich, SWITZERLAND,* [3]*Radiology and medicine nuclear department, Genolier Clinique, Genolier, SWITZERLAND,* [4]*Department of Nuclear medicine, La Tour Medical Group, Meyrin, SWITZERLAND,* [5]*Department of*

nuclear medicine and molecular imaging, Lausanne University Hospital, Lausanne, SWITZERLAND, [6]Department of nuclear medicine, Aarau Kantonsspital, Aarau, SWITZERLAND.

Aim/Introduction: We assessed and compared image quality obtained with clinical ^{18}F-FDG whole-body oncologic PET protocols used in three different, state-of-the-art digital PET/CT and two conventional PMT-based PET/CT devices. The goal was to evaluate improved trade-off between administered activity (patient dose exposure/signal-to-noise ratio) and acquisition time (patient comfort) while preserving diagnostic information achievable with the recently introduced digital compared to the previous analogue PET technology. **Materials and Methods:** We performed 300s list-mode (LM) PET acquisitions of a NEMA/IEC NU2 phantom, with activity concentrations of 5kBq/mL and 25kBq/mL for the background (9.5L) and sphere inserts respectively. Adopting the local clinical protocol setup, in each device, reconstructions were obtained varying the image statistics (10, 30, 60, 90, 120 and 180 s from LM data) and the number of iterations (range: 1 to 10). Quantitative cross-calibration, image noise on the uniform background assessed by the coefficient of variation (COV), recovery coefficients (RCs) evaluated in hot spheres and a cold contrast (in a lung insert) were measured per each reconstructed dataset. The characteristic time-activity-product (TAP), that is the scan time per bed position × mass-activity administered (in min.MBq/kg) was compared across datasets. **Results:** Good system cross-calibration was obtained for all tested datasets, <6% deviation from the expected value was observed. For all clinical protocol setups, image noise was compatible with clinical interpretation (COV<15%). Digital PET showed improved signal-to-noise compared to conventional PMT-based PET. RCs were comparable between digital and PMT-based PET datasets. Compared to PMT-based PET, digital systems provided comparable image quality with lower TAP (average ~40%, up to 70% less). **Conclusion:** This study compared the achievable clinical image quality in three state-of-the-art digital PET/CT devices (from all possible vendors [N=3]) as well as image quality obtained in two conventional PMT-based PET. Reported results show that a comparable image quality is achievable with a TAP reduction of ~40% in digital PET. This could lead to a significant reduction of the mass-activity administered and/or scan time with direct benefits in terms of dose exposure, image quality and patient comfort. **References:** None.

EP-0911

Monolithic PET detectors with sub-mm transverse and 6 layer DOI identification for next generation high resolution clinical PET scanners

***M. Stockhoff**, R. Van Holen, S. Vandenberghe;*
Ghent University, Gent, BELGIUM.

Aim/Introduction: Future high resolution PET systems are likely to depart from the pixelated detector design and move to monolithic scintillation crystals. This design allows high resolution 3D event positioning while maintaining high sensitivity, energy and timing resolution [1]. In a small market study, we found that the monolithic crystal is also more economical when compared to a pixelated detector design with < 2 mm pixel sizes (e.g. 0.5mm pixels > 3-4 times more expensive). Previously we demonstrated the 2D spatial resolution and the effect of sensor array related parameters [2]. The aim of this work is to use optical simulations to determine the depth resolution of a monolithic detector and explain the depth dependent resolution degradation. Furthermore, we demonstrate the uniformity over the whole detector and the spatial resolution when simulating a Derenzo-like collimator. **Materials and Methods:** In simulations, a 50x50x16mm^3 lutetium-yttrium oxyorthosilicate (LYSO) crystal is coupled to an SiPM array and calibrated in 1mm steps with a perfect 511keV pencil beam source. Per position the calibration data is organized in six depth-layers. Events are then positioned with a nearest neighbor algorithm. The ground truth DOI is extracted from the simulation data and compared to the determined depth layer. The hypothesis for depth dependent resolution degradation is varying amounts of statistical noise on the SiPM pixels. This is tested by simulating different scintillator light yields. The uniformity is evaluated with a flood source. The Derenzo-like phantom is simulated as pencil beams of 0.45-1.8mm diameter. **Results:** The layer classification accuracy is 72%. The mean depth positioning error is 1.6mm. The effect of depth-dependent resolution degradation clearly diminishes with increasing number of photons. Spatial resolution is generally improving with more light photons per scintillation event. In the Derenzo setup sources up to 0.6mm can be distinguished from one another. The flood source histogram shows artifacts in the form of hot spots and edge non-uniformities. **Conclusion:** This study demonstrates the 3D resolution that can be obtained with this detector without being constrained by practical limitations of experimental setups. In the future, these optical simulations may be used as a more precise (e.g. perfect calibration source) and fast method to obtain calibration data for real monolithic detectors. **References:** [1] Berg E et al. 2018 Semin. Nucl. Med. 48 311-31[2] Stockhoff M et al. submitted 03/2019 to PMB-108741 Advanced optical simulation study on the spatial resolution of a thick monolithic PET detector.

EP-0912

PET2020: Combination of clinical routine PET and molecular research in one compact and cost-efficient high resolution long axial FOV PET scanner

***S. Vandenberghe**[1], M. Stockhoff[1], C. Thyssen[1], N. Efthimiou[2], M. Akl[1], Y. D'Asseler[1], E. Achten[1], C. Vanhove[1], K. Muylle[3], E. Vansteenkiste[1], V. Keereman[1], J. Karp[4], R. Van Holen[1];*
[1]Universiteit Gent, Ghent, BELGIUM, [2]University of Hull, Hull, UNITED KINGDOM, [3]Vrije Universiteit Brussel, Brussel, BELGIUM, [4]University of Pennsylvania, Philadelphia, PA, UNITED STATES OF AMERICA.

Aim/Introduction: We describe a European long axial FOV

whole body PET imager using high-resolution, depth-encoding monolithic detectors. These detectors outperform current pixelated PET detector technology in clinical and Total Body PET. This detector technology has been used extensively in commercially available preclinical imaging systems. The combination of advanced positioning algorithms and fine SiPM sampling leads to high intrinsic spatial resolution (< 0.8 mm) and excellent DOI (6 layers). This was shown in the thin (8 mm) preclinical detectors and now translated into thicker (16 mm thick) clinical detectors with minimal degradation (still sub mm resolution and 6 DOI layers). Pixelated systems for clinical systems have in best case 2.8 mm x 2.8 mm pixels with no DOI information. **Materials and Methods:** For clinical routine FDG imaging, throughput and an acceptable system cost is important and therefore we present a simple compact and cost-efficient base system design of 70 cm bore (based on current clinical routine) and 70 cm axial length. The system consists of 14 rings with each ring composed of 40 blocks of 50x50x16 mm monolithic LYSO blocks coupled to analog SiPM. **Results:** By using an axial length of 70 cm the sensitivity increase (about a factor of 3) for single organ imaging is close to its maximum. This system will have a PET component cost that is 'only' a factor 2-2.5x higher than a current high-end state of the art clinical PET-CT (20 cm axial FOV) but will be 8 x more sensitive for clinical routine FDG body imaging. An isotropic spatial resolution of 2-2.5 mm is expected over the complete field-of-view based on the excellent spatial resolution of the detectors in combination with positron physics (mostly acolinearity). **Conclusion:** As the total component cost remains limited, the final price of this system will be comparable to that of current PET-MR systems. The first version of this system is funded by FWO Flanders and will be installed and used in a multidisciplinary environment (large and medium animals, human volunteers and plants). This combination of acceptable cost and superior performance can bridge the gap between clinical system and Full Total body PET systems. It can serve not only as a high-end imaging system for research but also as a general high throughput clinical imaging system, potentially gradually replacing current short axial FOV PET-CT, as it will be a more cost-efficient system over its full lifetime. **References:** None.

EP-0913

Physical Performance of a PET Scanner Prototype with Extended Axial Field of View using Sparse Detector Module Rings Configuration: A Monte Carlo simulation study

S. Zein, *N. A. Karakatsanis, A. Gupta, J. R. Osborne, S. A. Nehmeh;*
Weill Cornell Medical College, New York, NY, UNITED STATES OF AMERICA.

Aim/Introduction: To assess the physical performance of an extended axial field of view (AFOV) PET scanner prototype with sparse detector module rings configuration. **Materials and Methods:** The Siemens Biograph Vision (Bio-Vis) PET/CT scanner encompasses 8 rings of 38 LSO detector modules. Each module comprises 2 (axial) x 4 (transaxial) blocks. Each block includes 5x5 LSO crystals (3.2x3.2x20 mm^3) optically coupled to an array of 2x4 SiPMs. The axial length of each detector module ring is 32 mm, thus yielding a total AFOV of 256 mm. The Bio-Vis AFOV was extended to 480mm (Ex-PET) by interleaving the detector modules with 32mm physical gaps corresponding to the axial dimension of the Bio-Vis detector module. Lead shields of 3mm axial and 20mm radial dimensions were inserted in the gaps in between the detector module rings to reduce inter-crystal scattering. Monte Carlo models of the Bio-Vis (gold standard) and Ex-PET were developed using the Geant4 Application for Tomography Emission (GATE). Performance measurements of the two PET configurations were performed using GATE simulations and following the NEMA NU 2-2012 standards. The NEMA Image Quality (IQ) phantom was simulated using a target-to-background ratio of 4:1, and the corresponding images were reconstructed with a 3D-OSEM algorithm (3 iterations, 19 subsets, 431x431 matrix, and 1.6 mm slice thickness). For Ex-PET, a table flow motion approach, as per Bio-Vis option, was adopted to compensate for the count loss due to the gaps. **Results:** Reduction of less than 5% in the axial and transverse spatial resolutions were observed between Ex-PET and Bio-Vis. The Ex-PET model showed a system sensitivity of 19.37 cps/kBq, compared to 19.58 cps/kBq for Bio-Vis. No image artifacts were observed in the IQ phantom, and all spheres were detected. The contrast recovery of Ex-PET deviated by less than 4% from that of Bio-Vis for all spheres. The Ex-PET background variability was higher by ~30% for the 10mm sphere with the difference reduced to ~12% for the 22mm sphere. **Conclusion:** The proposed Ex-PET sparse module rings configuration allowed extending the PET AFOV from 256mm to 480mm without increasing the number of detector modules, while maintaining comparable contrast recovery and image quality to those of Bio-Vis. An increased, yet more uniform, background variability was observed with Ex-PET across the AFOV. **References:** None .

EP-0914

Assessment of the Prompt Gamma Coincidence Correction Approach Using Iodine-124: a Comprehensive Phantom Study

W. Jentzen[1], *H. Bal*[2], *R. Hofferber*[1], *P. Costa*[1], *R. Wierts*[3], *I. Rausch*[4], *A. Berger*[4], *T. Beyer*[4], *M. Conti*[2], *K. Herrmann*[1];
[1]*Clinic of Nuclear Medicine, University of Duisburg-Essen, Essen, GERMANY,* [2]*Siemens Medical Solutions USA, Inc., Knoxville, TN, UNITED STATES OF AMERICA,* [3]*Maastricht University Medical Centre, Department of Radiology and Nuclear Medicine, Maastricht, NETHERLANDS,* [4]*QIMP Team, Center for Medical Physics and Biomedical Engineering, Medical University of Vienna, Vienna, AUSTRIA.*

Aim/Introduction: ^{124}I is an increasingly used radionuclide in positron emission tomography (PET) imaging. The PET data are used, e.g., in pretherapy dosimetry, requiring (absolute) image quantification. However, ^{124}I PET quantification is impaired by the presence of prompt gamma coincidences. The objective

of this study was to assess the value of the prompt gamma correction (PGC) approach using phantom setups mimicking challenging conditions similar to what clinically observed in antibody and somatostatin receptor imaging. **Materials and Methods:** All measurements were performed on a Siemens Biograph mCT PET/CT system with ^{124}I (and ^{18}F for reference purposes). Three types of phantoms were used: (a) a soft-tissue tumor phantom (consisting of spheres of varying sizes mounted in an abdominal phantom) that mimics tumors embedded in a warm background, (b) a bone-lung tumor phantom that simulates tumors in cold lung and cortical bone tissues, where the activity was filled only in spheres and in the abdominal cavity, but not in the lung and cortical bone compartments, and (c) an organ phantom that simulates organs in a warm background with activity filled in spine, kidney and liver inserts as well as the abdominal cavity. A standard clinical acquisition protocol (low counting statistics) and a reference acquisition protocol (high counting statistics) were performed using an emission time of 240 s and 1 h, respectively. All ^{124}I data were reconstructed with (PGC_{on}) and without prompt gamma correction (PGC_{off}). The percentage differences between imaged and activity meter-based activity concentrations (ACs) were determined for PGC_{off} and PGC_{on} (and ^{18}F) images. **Results:** For all phantom setups, ^{124}I image quantification with PGC_{on} was close to the expected value (≤10%) and was comparable to that of ^{18}F images . AC deviations between PGC_{off} and PGC_{on} (ΔPGC) images were similar for both acquisition protocols. For phantom (a), the sphere (background) ΔPGC was, on average, -14% (-30%). For phantom (b), sphere in cortical bone inserts (lung insert) ΔPGC ranged from -90% to -60% (-1% to -4%). For phantom (c), ΔPGC for the spine, kidney, liver inserts were about -15%, -10%, -25%, respectively. The underestimation of the ACs in PGC_{off} images was a consequence of the scatter overcorrection when the prompt gammas are not modeled. **Conclusion:** PGC is effective and mandatory for reconstructing ^{124}I images to obtain higher quantitative accuracy, in particular for background, bone lesions and extended organs. The ACs (and thus the absorbed doses) are underestimated without applying a PGC. **References:** None.

EP-0915

Recovery of Missing Data in Partial Geometry Dedicated Breast PET Scanner Using Compressive Sensing

A. Emami[1,2,3], *P. Ghafarian*[4,5], *H. Ghadiri*[1,2], *P. Geramifar*[6], *M. Ay*[1,2];
[1]*Research Center for Molecular and Cellular Imaging, Tehran University of Medical Sciences, Tehran, IRAN, ISLAMIC REPUBLIC OF,* [2]*Department of Medical Physics and Biomedical Engineering, Tehran University of Medical Sciences, Tehran, IRAN, ISLAMIC REPUBLIC OF,* [3]*International Campus, Tehran University of Medical Sciences, Tehran, IRAN, ISLAMIC REPUBLIC OF,* [4]*Chronic Respiratory Diseases Research Center, National Research Institute of Tuberculosis and Lung Diseases (NRITLD), Shahid Beheshti University of Medical Sciences, Tehran, IRAN, ISLAMIC REPUBLIC OF,* [5]*PET/CT and Cyclotron Center, Masih Daneshvari Hospital, Shahid Beheshti University of Medical Sciences, Tehran, IRAN, ISLAMIC REPUBLIC OF,* [6]*Research Center for Nuclear Medicine, Shariati Hospital, Tehran University of Medical Sciences, Tehran, IRAN, ISLAMIC REPUBLIC OF.*

Aim/Introduction: Most breast positron emission tomography (bPET) scanners consist of tightly packed discrete detector rings to improve scanner efficiency. In this study, we aimed to use new compressive sensing (CS) techniques and image inpainting in breast PET imaging to investigate the feasibility of decreasing the number of detectors while maintaining image quality. Conventional reconstruction methods generate severe artifacts in the reconstructed images. **Materials and Methods:** A dedicated breast PET scanner is based on LYSO crystals coupled with SiPM, and it consists of 14 compact modules with a transaxial field of view (FOV) of 180 mm in diameter and 50 mm axial FOV. Different methods for data recovery were investigated using simulated data in breast PET scanners with partial geometry (introducing gaps). A new CS technique was developed to recover missing observations in breast PET data acquisition. The methods used for filling the crack structure in sinogram PET data include partial differential equation based methods (PDE). A simulation experiment was performed to evaluate the proposed CS recovery algorithm. The simulation dataset consists of six disks of various sizes in a uniform background with an activity concentration of 5:1. Seven detector blocks (50%) turned off, and then the proposed CS algorithm was applied to recover the missing PET data. Also, different levels of noise were simulated to assess the performance of the proposed algorithm. The partially acquired sinograms were then retrieved using the proposed algorithm. For large gap structure, new CS produces better results. Comparisons were made by calculating the spatial resolution and contrast. **Results:** Both CS and image inpainting are skillful of recovering PET images with good quantitative accuracy from partially sampled data. So, an approach can be used to potentially reduce the cost of dedicated breast PET scanners while sustaining excellent image quality. The results of the Contrast Recovery (CR) for the recovered images was improved by more than 22%. The simulation results showed that the new CS algorithm could control gap artifacts, as well as Poisson random noise, and recovered spatial resolution. **Conclusion:** Our results showed that whether a large part of a whole of data is unknown, new CS techniques adjoined with the reconstruction in image space were the best strategy. Estimation of missing data in the inpainting method can improve the quality of recovered images, especially for small gap structures. **References:** None.

EP-0916

Quantitative gated PET and CT imaging of mice and rats using a fully integrated animal monitoring system

P. Mollet, *S. Neyt*, *B. Vandeghinste*;
Molecubes NV, Gent, BELGIUM.

Aim/Introduction: In cardiac research, non-invasive measurement of left ventricular end-systolic (ESV), end-diastolic volume (EDV) and left ventricular ejection fraction (LVEF) is a useful tool to evaluate and monitor cardiac function in health and disease. Respiratory gating techniques are useful to exclude

breathing artefacts which is beneficial for lung research. We evaluated the feasibility of cardiac, respiratory and dual gated PET and CT for mice and rats on the Molecubes B-CUBE PET and X-CUBE CT systems. **Materials and Methods:** In order to obtain physiological signals, Molecubes developed dedicated animal beds for mice and rats with fully integrated cardiac, respiratory and temperature monitoring capabilities. The electronics are equipped with a high precision clock to allow synchronisation of the monitoring signals with the PET and CT systems. For cardiac gated PET, a rat was injected with 14 MBq of 18F-FDG 60 min prior to scanning. A PET acquisition of 45 minutes was done. 3 ECG-leads connected to the rat front legs and left hind leg were used to obtain the cardiac signal. Additional the integrated pressure pad and carbon heat pad in the animal bed were used to capture the respiratory signal and maintain body temperature. A peak detection algorithm was implemented to identify the peak locations of the cardiac signal. For each cardiac cycle, 8 gates were defined and for each gate a PET image was reconstructed using the OSEM algorithm with default settings as provided by the Molecubes software. ESV, EDV and LVEF were calculated using PMOD PCARD v4.0. For respiratory gated CT imaging, the default respiratory gated CT protocol was used. The data was reconstructed using ISRA algorithm and a voxel size of 100 µm. End-inspiration and end-expiration aerated lung volumes were calculated with HU based segmentation with Horos. **Results:** For cardiac gated PET, a left ventricular ejection fraction of 58% was calculated based on EDV and ESV in a healthy rat. Respiratory gated CT imaging in mice showed that there was a 34% difference in aerated lung volume between end-expiration and end-inspiration phase of the respiratory cycle. **Conclusion:** Our results demonstrate the possibility of using the integrated monitoring system for both gated PET and CT imaging. Thanks to the high spatial resolution of the PET system, cardiac function can be visualised and quantified. µCT imaging has proven to be useful in determining the difference in aerated lung volume between end-expiration and end-inspiration phase of the respiratory cycle. **References:** None.

EP-0917

Metabolic Response Assessment Following Stereotactic Ablative Radiotherapy (SABR) in oligo lung metastases - How early we get to see!

A. Kasat, *S. Gawde, S. Parekh, A. Singal, S. Vangipuram; HCG Cancer Centre, Mumbai, INDIA.*

Aim/Introduction: FDG PET-CT is a well established cancer imaging tool for diagnosis, staging and response assessment. It is also well known that, post chemotherapy or radiotherapy, metabolic response precedes morphologic response which is based on size criteria. However, earliest time needed for the maximum metabolic response post radiosurgery has never been assessed. Present study evaluates the trend in metabolic regression post SABR with serial FDG PET-CT scans in patients with oligo lung or mediastinal metastases. **Materials and Methods:** 5 patients with oligometastatic lung tumors (Primaries: Colorectal cancer - 2, Breast - 2 and Head and neck cancer- 1) were planned for SABR by Deep inspiratory breath hold technique using Active breath controller & risk fractionated protocol. Doses delivered were in the range of 110-116gy biologic equivalent dose (BED). All patients underwent diagnostic pre- and post-treatment PET-CT scans. Post SABR PET-CT scans were timed serially at 48hrs, 7, 30, 60 and 90 days post treatment. PET-CT scans were reviewed in order to determine the pre- and post- treatment maximum standardized uptake value (max SUV) of the lesion, including "complete resolution" of FDG-avidity. Corresponding morphologic variations of the target lesions were studied on the corresponding CT images. **Results:** All the 5 patients showed serial regression in metabolic activity, with maximum regression in metabolic activity occurring at 1week post SABR. The observed metabolic regression was between 40-54% (median - 50%) at 48 hours and 67-82% (median 80%) at 1week post SABR. During the evaluation period, there was no significant change in size of the lesion. After 1 week of SABR, there was no further decrease in metabolic activity, most probably due to initiation of inflammation. **Conclusion:** In cases of recurrent solitary lung or mediastinal metastases, the metabolic response precedes morphologic response, with maximum response seen at 1 week post SABR. This is the first study reported in literature which looked into the trend of metabolic regression following SABR. **References:** None.

EP-0918

Systematic Error On The Displayed Delivered Activity Of The Medrad® Intego Pet Infusion System

A. Wenger, *C. Weyermann, M. Hofbauer, M. Christen, K. Zeimpekis; Universitätsspital Zürich, Zürich, SWITZERLAND.*

Aim/Introduction: The MEDRAD® INTEGO PET Infusion System is used worldwide in order to minimize the occupational dose of PET technologists. As of 2017, more than 400 units have been installed worldwide. This device prepares a ^{18}F-FDG solution and injects it to the patient, allowing the technologists to remain at distance during the injection, hence decreasing their occupational dose. The prescribed activity is based on a standardized protocol per kilogram of body weight. It is derived from an agreement between the PET/CT vendor and the local medical team, taking into consideration the sensitivity of the scanner, the minimum desired image quality and the desired acquisition time. Too low activity would result in noisy images and too high activity would result in unnecessary dose to the patient: a trade-off between both resulted in the aforementioned protocol. The accuracy of the activity preparation is therefore of high importance: a too low activity could result in a misdiagnosis due to a too low SNR. The aim of this work is to test the vendor's claim which guarantees a delivered activity within 10% error margin. **Materials and Methods:** We simulated patient injections of ^{18}F-FDG with three independent MEDRAD® INTEGO PET Infusion Systems, each of them used in our clinical routine. A wide range of activities

were ordered, from 100MBq to 300MBq, reflecting our clinical practices. The injected activities were collected in large vials. We withdrew samples from the vials and measured their activity in the activimeter of our local hotlabs. Several samples of different volumes and dilutions were prepared in order to exclude any volume effect or random errors from the activimeter measurements. After the initial study, we repeated a simpler version of the measurements for six months with a time interval of approximately 30 days. **Results:** We have found a systematic overestimation of the delivered activity displayed on the Intego system compared to the activity measured with our activimeters. This systematic deviation remains within the 10% margin and is linearly correlated with the prescribed activity. Hence, we could extract a correction factor, currently used in our clinical practice to correct for the device's activity overestimation. We have found that the correction factor is device dependent. **Conclusion:** We recommend every center currently using the MEDRAD® INTEGO PET Infusion System to introduce an analogous step in their QA protocol in order to correct for the device's systematic overestimation of the injected activity. **References:** None.

EP-0919

Phase Ia intra-individual comparison study of osteoblastic metastases using rapid high definition whole-body Na^{18}F digital photon counting PET/CT

C. L. Wright, K. Binzel, J. Zhang, E. Folefac, D. A. Diaz Pardo, D. G. Stover, J. P. Monk III, M. V. Knopp;
The Ohio State University, Columbus, OH, UNITED STATES OF AMERICA.

Aim/Introduction: Oncologic and non-oncologic bone imaging with sodium fluoride (Na^{18}F) PET/CT is used clinically for the detection and characterization of osteoblastic lesions. For those patients with symptomatic bony disease, standard Na^{18}F PET image acquisition times (60 - 120 s/bed) for whole-body assessment are longer than desired and new approaches to substantially reduce whole-body PET image acquisition time are needed. The recent introduction of clinical PET/CT systems equipped with digital photon counting PET (dPET) detectors enable new PET imaging approaches for reduced PET image acquisition times, PET imaging with reduced radiotracer doses and higher definition PET image reconstruction. The aim is to assess a substantially faster, whole-body, high-definition Na^{18}F PET imaging approach for the detection and characterization of osteoblastic lesions using dPET/CT technology. **Materials and Methods:** A Phase Ia intra-individual comparison of whole-body Na^{18}F dPET/CT imaging (Vereos, Philips) was performed using a target Na^{18}F dose of 185 MBq in 22 male oncologic patients. We performed investigational dPET acquisitions at a substantially faster 30 s/bed (at ~70 min post injection) and at the standard 90 s/bed (at ~85 min post injection). All image data sets were reconstruction using high-definition (voxel volume = 2x2x2 mm^3) and Time-of-Flight. All individual and matched data sets were reviewed using an Intellispace Portal workstation by a blinded reader panel to evaluate lesion detectability, overall image quality and background quality. **Results:** All patients had evaluable dPET images (n = 44) for qualitative assessment of ^{18}F biodistribution and osteoblastic lesions. ^{18}F-avidity within normal bone and osteoblastic lesions was visually comparable with faster 30 s/bed acquisitions to the standard 90 s/bed acquisitions. No discordant ^{18}F-avid osteoblastic lesions were identified between the 30 s/bed and 90 s/bed acquisitions. Quantitatively, the average SUVmean values were comparable for 30 s/bed and 90 s/bed acquisitions in terms of background skeletal muscle and normal vertebral bone. The average SUVmax of 39 osteoblastic lesions were also comparable for 30 s/bed and 90 s/bed acquisitions (30 ± 26 and 33 ± 28, respectively). **Conclusion:** Digital photon counting PET technology allow for 3x faster whole-body high-definition Na^{18}F PET imaging without loss of overall image quality, lesion conspicuity or quantitative accuracy. Faster PET image acquisition for patients with symptomatic bony disease remains an unmet clinical need and this Phase Ia study demonstrates rapid whole-body high-definition Na^{18}F PET imaging is readily achievable with dPET/CT technology. **References:** None.

EP-0920

Variability in NEMA NU 2-2012 Sensitivity Measurements of GE Discovery MI Digital Time-of-flight PET-CT Systems

A. Moreno, E. Ilan, M. Lubberink;
Uppsala University Hospital, Uppsala, SWEDEN.

Aim/Introduction: There is considerable variability in NEMA NU 2-2012 sensitivity values for identical scanners, which makes meaningful comparison difficult. For four identical Discovery MI PET-CT scanners recently installed at Uppsala University Hospital, variations in sensitivity during acceptance testing between scanners were > 10%. The aim of this work is to evaluate and compare the sensitivity according to the NEMA protocol in order to assess whether the variability in the results is due to experimental aspects or to actual differences in scanner performance. **Materials and Methods:** In order to isolate the source of variability, combinations of the NEMA sensitivity test were performed. Sensitivity was measured for all four scanners using a single phantom filling. The test was repeated in one of the scanners using a single filling while the phantom set-up was mounted and un-mounted completely in every measurement in order to assess the uncertainties introduced from it. Finally, sensitivity was measured repeatedly in a single scanner, with a single filling and a single set-up so random error could be evaluated. All tests were performed by the same medical physicist and the results were compared to those from the acceptance tests performed by the manufacturer´s specialist. **Results:** The mean sensitivity of the four scanners based on a single phantom preparation was 13.61 ± 0.14 cps/kBq, as compared to the 13.9 ± 0.71 cps/kBq in the acceptance tests. The sensitivity in one scanner using a single filling and introducing a set-up variation was 14.04 ± 0.15 cps/kBq. The sensitivity in that same scanner with a single set-up and a single filling was 13.58 ± 0.01 cps/kBq. **Conclusion:** Differences

in the NEMA sensitivity measurements between scanners was lower in our measurements using a single phantom filling as compared to the acceptance tests (coefficient of variation 1.0% versus 5.1%). According to the other tests, random errors between measurements are negligible (0.02%) while the set-up manipulation introduces an uncertainty (0.85%) which is comparable to the variability we measured between scanners. Differences in the acceptance tests arise therefore mainly from experimental errors and lack of reproducibility of setting up the experiment, and not from difference in actual scanner performance. **References:** None.

EP-0921

Accuracy of the Siemens Biograph Vision 600 for Radiotherapy planning; technical aspects and extra acceptance testing

E. Raaijmakers, S. Schip, van Het, E. Gerrits; Institute Verbeeten, Tilburg, NETHERLANDS.

Aim/Introduction: In 2018 Institute Verbeeten installed a new PET-CT scanner, the Biography Vision 600, for both Nuclear Medicine and Radiotherapy use. The RT scans are used for contouring and planning. It is therefore essential that volumes can be accurately outlined and can be translated to linac coordinates. During the acceptance testing we have paid special attention to the RT requirements. The aim of this study is to report on specific issues for this new scanner in relation to the Radiotherapy planning. **Materials and Methods:** Acceptance testing was done according to AAPM TG66. Table sag was measured with kettle belts placed on specific points on the RT bed. Sag was measured at different points on the table and compared to the zero position as well as the position in unloaded condition. This was done for weights up to 120 kg. Contouring accuracy was measured with the NEMA image quality phantom. The phantom was filled with different concentrations for the background. The known volumes of the bowls was compared to the different volumes acquired with the planning system Eclipse (Varian). Contouring was done on a percentage of SUV max. Also 4D CT and PET was tested using the Cirs thorax phantom with Na-22 sources as moving objects. **Results:** All table measurement were well within the AAPM standards. Table Sag, even with 130 kg, sag was less than 2 mm. For contouring the best value representing the volume was 30 % of SUV max. (older scanners typically use 42 %) 4D gating protocols were made clinically available. For that purpose timing between PET and CT was optimized. **Conclusion:** The scanner is well suited for RT applications. However, due to better resolution , contouring parameters of old- analogue- scanners cannot be used for the new scanners. Volumes will be underestimated if done so. **References:** Quality assurance for computed-tomography simulators and the computed tomography- simulation process: Report of the AAPM Radiation Therapy Committee Task Group No. 66. Mutic et al. Med Phys 2003;30:2762-2792.

EP-0922

Performance Evaluation of a Newly Designed SiPM-based Preclinical Scanner Based on NEMA-NU4 2008

M. Amirrashedi[1,2], S. Sarkar[1,2], P. Ghafarian[3,4], R. Hashemi Shahraki[1,2], P. Geramifar[5], H. Zaidi[6,7,8], M. Ay[1,2];
[1]Tehran University of Medical Sciences, Tehran, IRAN, ISLAMIC REPUBLIC OF, [2]Research Center for Molecular and Cellular Imaging, Tehran University of Medical Sciences, Tehran, IRAN, ISLAMIC REPUBLIC OF, [3]PET/CT and Cyclotron Center, Masih Daneshvari Hospital, Shahid Beheshti University of Medical Sciences, Tehran, IRAN, ISLAMIC REPUBLIC OF, [4]Chronic Respiratory Disease Research Center, NRITLD, Masih Daneshvari Hospital, Shahid Beheshti University of Medical Sciences, Tehran, IRAN, ISLAMIC REPUBLIC OF, [5]Research Center for Nuclear Medicine, Shariati Hospital, Tehran University of Medical Sciences, Tehran, IRAN, ISLAMIC REPUBLIC OF, [6]Division of Nuclear Medicine and Molecular Imaging, Geneva University Hospital, Geneva, SWITZERLAND, [7]Geneva University Neurocenter, Geneva University, Geneva, SWITZERLAND, [8]Department of Nuclear Medicine and Molecular Imaging, University of Groningen, University Medical Center Groningen, Groningen, NETHERLANDS.

Aim/Introduction: Recent years have witnessed widespread interest and increased popularity in translational molecular imaging-based biomedical research stimulated largely by the availability of dedicated small-animal scanners. Among the promising animal imaging modalities, Positron Emission Tomography (PET), as a highly versatile research tool, has further enabled the quantitative assessment of disease progression and metabolic evaluation of cellular biology. Xtrim-PET is a newly designed Silicon Photomultipliers (SiPMs)-based prototype PET scanner dedicated for small laboratory animal imaging. Optimizing scanning protocols can be achieved through reliable system performance characterization and tuning. In this work, we present the performance evaluation of the Xtrim-PET according to the National Electrical Manufacturers Association (NEMA) NU-4 2008 standard. **Materials and Methods:** NEMA standard was used for measurement of spatial resolution, sensitivity, counting rate performance, scatter fraction and image quality. The in vivo imaging capability of the scanner is also showcased through scanning a normal mouse injected with ^{18}F-FDG. Furthermore, the performance characteristics of the developed scanner are compared with commercially available systems and current prototypes. **Results:** The volumetric spatial resolution at 5 mm radial offset from the central axis of the scanner is 6.81 µl whereas a peak absolute sensitivity of 2.99% was achieved using a 250-650 keV energy window and a 10 ns timing window. The peak noise-equivalent count rate (NECR) using a mouse-like phantom is 113.18 kcps at 0.34 KBq/cc with 12.5% scatter fraction, whereas the NECR peaked at 82.76 kcps for an activity concentration level of 0.048 KBq with a scatter fraction of 25.8% for the rat-like phantom. An excellent uniformity (3.8%) was obtained using NEMA image quality phantom. Recovery coefficients of 90%, 86%, 68%, 40% and 12% were calculated for rod diameters of 5, 4, 3, 2 and 1 mm, respectively. Spill-over ratios for air-filled and water-filled

chambers were 35% and 25% without applying any correction for attenuation and Compton scattering effects. **Conclusion:** The results demonstrated that the system has good spatial resolution and sensitivity, which makes it suitable for small animal studies. The quantitative capability of the system is being improved through the implementation of dedicated data correction techniques, including attenuation and scattering as well as statistical image reconstruction with accurate system modeling to further enhance overall image quality. Overall, our assessment proves practical and technical suitability of the Xtrim-PET for use in the preclinical imaging domain using molecular imaging probes. **References:** 1. National Electrical Manufacturers Association 2008 NEMA Standards Publication NU 4 - 2008.

EP-0923

Use of insulin to avoid false-negative for FDG-PET Imaging in cancer patients with high blood glucose level: a prospective cross-over study

H. Gauthier, E. Gobaert, N. Penel;
Centre Oscar Lambret, Lille Cedex, FRANCE.

Aim/Introduction: To determine whether insulin can improve the image quality and tumour uptake of 18-fluorodeoxyglucose (FDG) in patients with concurrent uncontrolled diabetes mellitus and cancer, and avoid false-negative results. **Materials and Methods:** Twenty-two patients with various malignancies (13 colon cancer patients, 7 lung cancer patients, 1 lung sarcoma patient, 1 unknown primary tumor patient) and high blood glucose level at the time of imaging (mean 14 +/- 3 mmol/L; mean glycosylated hemoglobin: 9,6%) were included. All patients underwent two PET studies (mean delay 12 ± 6 d). The first PET study was performed under fasting conditions for patients without known diabetes (n=3). Patients with known diabetes mellitus (n=19) continued to eat their standard meals and take their oral medication. The second PET study was performed under fasting conditions without diabetic medication for all patients. Patients received a sub-cutaneous insulin injection prior to the PET scan, and patient blood glucose levels were monitored until the levels were below 8.8 mmol/L. A visual assessment of the image quality of each PET scan (defined by the signal-to-background ratio) was performed by two independent observers who were blinded to the exam conditions. The mean peak of the standard uptake value (SUV) was measured at the tumor sites. **Results:** Blood glucose levels at the time of PET 2 after insulin therapy (mean: 7.2 mmol/L) were significantly lower ($p<10^{-4}$) than the blood glucose levels at either PET 1 (mean: 14 mmol/L) or PET 2 before insulin injection (mean: 12.7 mmol/L). The image quality of PET 2 scans was better than PET 1 scans in 14 cases, unchanged in 6 cases and worse in 2 cases. Patient tumors were visualized in 14 out of 21 patients. For these patients, the SUV of the tumor was significantly higher on PET 2 than on PET 1 ($p = 0.0001$). Only one false-negative result was observed (minimum follow-up of 6 months). For three patients, metastases that were not visualized on PET 1 appeared on PET 2. Improvement of the image quality was not influenced by body mass index, a decrease in the blood glucose level or the rate of glycosylated hemoglobin. **Conclusion:** This study confirmed that liver metastasis could be missed even if primary tumor or others metastatic sites are observed. Diabetic patients with hyperglycemia (≥ 160 mg/L) at the time of PET examination must beneficed of an insulin protocol. **References:** None.

EP-0924

Assessment of a Monte Carlo simulation of PET recordings from the fullly-digital Vereos camera

J. Salvadori[1], P. Marie[2,3], G. Karcher[3], L. Imbert[1,3];
[1]IADI UMR-1154, Nancy, FRANCE, [2]INSERM UMR-1116 DCAC, Nancy, FRANCE, [3]CHRU-Nancy, Nuclear Medicine, Nancy, FRANCE.

Aim/Introduction: Digital PET systems, involving solid-state silicon photomultipliers instead of conventional photomultipliers, allows improving time-of-flight capability and shortening dead time and piles-up effect. Furthermore, they were recently shown to enhance contrast-to-noise-ratio, lesion detectability and ultimately diagnostic confidence over a wide range of activity concentration. However, acquisition and reconstruction parameters need to be further optimized to fully benefit from this technology leap and Monte-Carlo simulations may constitute a useful tool for this purpose. The objectives of this study was to elaborate a Monte-Carlo modeling of the Vereos digital PET with the GATE platform and to assess this simulation by direct comparison between simulated and actual recorded data from the NEMA NU-2 2018 protocol. **Materials and Methods:** The Vereos system geometry was modeled together with its signal processing chain, according to the manufacturer's specifications and while taking into account background noise, energy blurring, temporal resolution, dead time and coincidence processing. The GATE simulation results were compared to actual recorded data obtained based on the NEMA NU-2 2018 protocol, with post-processing being provided by a homemade software. Simulated and actual data were both reconstructed with the open-source tomographic reconstruction software CASToR and identical parameters. **Results:** The simulated count-rate curves were fitted in order to match the actual ones using the dead-times and piles-up effects as adjustment parameters**.** Up to an activity concentration of 60 MBq/ml, a higher than 99 % agreement was obtained for single event rates, with maximal differences of 4 %, 6%, and 3 % for respectively total, random and true coincidence count-rates. This resulted in a lower than 10 % difference between the noise equivalent count rate (NECR) obtained from simulated (172 kcps at 49.7 MBq/ml) and actual (161 kcps at 55 MBq/ml) recordings. Lower than 5% differences were documented between simulated and actual recordings for axial sensitivity profile, as well as for timing and energy resolution over a wide range of activity concentration. The background relative noise and contrast recovery coefficients obtained from the spheres of an IEC phantom, were very close between simulated and actual

recordings, with maximum relative differences of 5% and 6%, respectively. **Conclusion:** PET recordings from the fully-digital Vereos camera can be simulated with the GATE software with high concordance relative to the actual physical properties of this camera. **References:** None.

EP-0925

Qualitative and Quantitative Assessment of Reducing the Scan Time for ^{18}F-flurodeoxyglucose (^{18}F-FDG) Wholebody PET/CT to 2 min/bed

A. McCann, D. Maguire, A. Dowling, L. Harris, R. P. Killeen, J. Lucey; UCD-SVUH PET CT Research Centre, St Vincent's University Hospital, Dublin, IRELAND.

Aim/Introduction: A pilot study of 20 ^{18}F-flurodeoxyglucose(^{18}F-FDG) patients was performed to investigate if quantitative PET/CT values in clinical images can be maintained with a reduced acquisition time (scan time reduced from 3min/bed to 2min/bed). The results of the pilot study confirmed that there was good correlation between the quantitative metrics associated with the mediastinal blood pool, cerebellum, bladder and metabolically active tumours for both scan times. However, a statistically significant difference was found in the quantitative metrics of the liver. This study expands the pilot study to a larger cohort of patients to investigate if the results found in the pilot study are representative of that of a larger population and determine if the reduced scan time is feasible without impacting quantitative metrics. **Materials and Methods:** Patients were administered 3 MBq/kg ^{18}F-FDG up to a maximum of 300MBq. Following a one hour uptake period, wholebody images were acquired on a Siemens Horizon PET/CT scanner. Listmode acquisition facilitated the reconstruction of 3min/bed and 2min/bed images. All images were iteratively reconstructed with time of flight. Images were analysed with Siemens Syngo. Via image software. Using well-defined regions of interests for both data sets, the SUVmax, SUVmean and metabolic volume of the primary tumour and the bladder were assessed. The liver signal-to-noise ratio (SNR) was calculated and the uptake in the cerebellum and mediastinal bloodpool compared. The clinical image quality was visually assessed by a board certified Nuclear Medicine Physician/Radiologist and rated using the Likert scale, with the observer blinded to the acquisition type. **Results:** A comparison of the quantitative metrics of both scan times in the pilot study found that the percentage difference in the SUVmax of the mediastinal blood pool, cerebellum and bladder were not statistically different with p-values > 0.05 (95% CI). However, the SNR of the liver and the liver SUVmax were found to be statistically different with p-value <0.05 (95%CI). The absolute value of the liver SNR for both scan times compare very well to those published in literature, which indicates that even with a reduced acquisition time the PET/CT is achieving acceptable image quality. Further results of the larger patient cohort will be presented and their clinical significance discussed. **Conclusion:** This study will determine, based on the results of the larger cohort of patients, whether a 33% reduction in scan time for ^{18}F-FDG whole body scans is feasible, without significantly impacting image quality. **References:** None.

EP-0926

In vitro detection limit of ^{89}Zr-labelled cells using a human PET system

L. Lechermann[1]*, R. Manavaki*[1]*, T. D. Fryer*[2]*, B. Attili*[1]*, D. Lau*[1]*, L. B. Jarvis*[3]*, L. Aloj*[1]*, B. Basu*[4]*, N. Patel*[5]*, M. Cleveland*[5]*, J. L. Jones*[3]*, F. I. Aigbirhio*[2]*, F. A. Gallagher*[1]*;*
[1]*Department of Radiology, University of Cambridge, Cambridge, UNITED KINGDOM,* [2]*Wolfson Brain Imaging Centre, University of Cambridge, Cambridge, UNITED KINGDOM,* [3]*Department of Clinical Neurosciences, University of Cambridge, Cambridge, UNITED KINGDOM,* [4]*Department of Oncology, University of Cambridge, Cambridge, UNITED KINGDOM,* [5]*GSK Medicines Research Centre, Stevenage, Hertfordshire, UNITED KINGDOM.*

Aim/Introduction: Imaging and in vivo tracking of cells can provide much needed information and help non-invasively to improve the accuracy, efficacy and safety of cell- and novel immune modulator therapies. Zirconium-89 ($t_{1/2}$=78.4 h) has been used recently to synthesize [^{89}Zr]Zr(oxinate)$_4$[1], a suitable radiotracer for cellular tracking and imaging using Positron Emission Tomography (PET)[2-4].This work presents an in vitro approach to quantify and determine the detection limit of T cells labelled with [^{89}Zr]Zr(oxinate)$_4$ utilizing a human PET system. **Materials and Methods:** [^{89}Zr]Zr(oxinate)$_4$ was synthesized according to published methods[4]. Jurkat cells were labelled with different amounts of [^{89}Zr]Zr(oxinate)$_4$ by a 30 min incubation in both PBS and complete RPMI 1640 medium at room temperature to generate different specific activities (SA) on cells (kBq/10^6). Labelled cell suspensions of 10^4, 10^5, 10^6 cells per well were seeded on 6-well plates. Plates were imaged on a GE Signa PET/MR and GE D690 PET/CT scanner for 30 min and reconstructed using parameters from a standard clinical protocol. The total activity in each well (n=34, 7 independent experiments) was determined by drawing regions of interests over each well on coronal images. Cell suspensions were transferred into 1.5 mL Eppendorf tubes after the scan, measured in a Triathler Gamma Counter (Hidex) and correlated with imaging data. In addition, cells were counted on a hemocytometer and checked for viability by trypan blue exclusion after each scan. **Results:** [^{89}Zr]Zr(oxinate)$_4$ was synthesized at a yield of >95% in an aqueous solution. The specific activity (SA) of labelled cells ranged from 0.4 kBq/10^6 cells to 41.2 kBq/10^6 cells. Cells could be visualized and quantified on PET images above a signal to background ratio of 20. Using this in vitro model, 5.20x10^5 cells with a SA of 2.18/10^6 cells could be visualized; in contrast, the lowest cell number that could be detected was 6.75x10^4 when the specific activity was 27.8 kBq/10^6 cells. **Conclusion:** The results show the feasibility of quantifying and detecting Jurkat T-cells labelled with [^{89}Zr]Zr(oxinate)$_4$. Cell detection using PET/CT or PET/MR depends on at least 3 factors: signal to background, cell number and specific activity per cell. This work has important

implications for human cell labelling procedures, particularly when using radiosensitive cells such as T-cells which require detection of low cell numbers while minimizing dose per cell. **References:** [1] Dalton Trans. 2014; 43(39): 14851-14857 [2] Clin Cancer Res. 2017; 23(11): 2759-2768 [3] Mol. Ther. 2018; doi:https://doi.org/10.1016/j.ymthe.2018.10.006 [4] J Nucl Med. 2018; 59(10): 1531-1537.

EP-0927

Optimization of CT acquisition protocol in brain 18F-FDG PET/CT

A. Loi[1,2], S. Zucca[3], P. Guglielmo[4], M. Bassu[2], M. Carta[2], N. Pisu[4], S. Sanna[4], S. Loi[3], F. Portesani[2], S. Aste[2], D. De Vittor[2], M. Boero[4];
[1]Centro PET, Cagliari, ITALY, [2]Alliance Medical, Cagliari, ITALY, [3]S.C. Fisica Sanitaria AOB, Cagliari, ITALY, [4]S.C. Medicina Nucleare AOB, Cagliari, ITALY.

Aim/Introduction: Optimize the CT acquisition parameters for brain PET/CT examination tailoring to to the specific diagnostic task: a low dose CT scan used for attenuation correction and anatomical alignment only and a medium dose CT scan with superior diagnostic imaging quality. **Materials and Methods:** Morphological imaging can provide guidance in the evaluation of the functional information related to the 18F-FDG uptake of the brain. A phantom study was carried on with a CATPHAN600 CT phan (CP). HU mean value and standard deviation, SNR and CNR were evaluated on the images of the uniform and low contrast test object were acquired with different $CTDI_{vol}$(1.1 mGy, 1.6 mGy, 3.3 mGy, 6.6 mGy, 13.1 mGy, 24 mGy, Body 32 cm phantom). In order to test the attenuation correction, PET/CT acquisition of a NEMA PET phantom (NU-94) was performed. The phantom was filled with a background solution with 8 kbq/ml18F-FDG while the two internal cylinders were filled with4 kbq/ml (Les1) and 16 kbq/ml (Les2). NU-94 acquisitions were performed varying $CTDI_{vol}$and using a list-mode PET acquisition time.The mean value and the standard deviation of the concentration were evaluated in the background region (ROI_b), and in the two cylinders ($ROI_1$and ROI_2). **Results:** As expected, the CT noise evaluated in the uniform section of CP decreased when $CTDI_{vol}$increased (std=24 HU @ 1.1 mGy and std=5.75 HU @ 24 mGy), leading to an increase of the SNR (from 0.5 to 2). CNR improved with the increase of CT dose. The modulation of CT tube current had no effect on the PET images of the NU-94 phantom. Concentration mean values were also not affected by the CT dose levels, giving similar image quality. Two CT acquisition protocols were defined. A CT acquisition with low dose level ($CTDI_{vol}$1.6 mGy) is performed for attenuation correction purpose only. The medium dose level CT protocol ($CTDI_{vol}$13.1 mGy) can be performed for better image quality. **Conclusion:** Two different CT acquisition protocols were defined for brain PET/CT. The CT low dose level protocol is judged adequate for attenuation correction purpose when a recent diagnostic or MR study is available and can be registered with the PET dataset supporting morphological evaluation. A medium dose level CT protocol is preferred when no complementary imaging is available as the improve image quality justifies the increase in patient dose. **References:** None.

EP-0928

Low Dose 68 Ga DOTA Zoledronate Bone PET/CT Scan on a High Definition Digital PET Scanner-First Technical Feasibility Study Done in Kuwait

B. M. Alenezi;
Jaber Alahmed For Molecular Imaging Center, Kuwait, KUWAIT.

Aim/Introduction: Gallium-68 zoledronate [^{68}Ga] Ga-DOTA^{ZOL} is a potent bisphosphonate PET tracer for evaluation of metastatic bone disease. We aim to assess the technical feasibility of doing a low dose 68Ga DOTA zoledronate bone PET/CT in a high definition digital PET/CT scanner and assess the image quality of the various image reconstructions parameters. **Materials and Methods:** Three patients who were referred for PET bone scan as a part of evaluation for metastatic bone disease were included in the study. All 3 patients were injected with 0.06mCi per kg of 68Ga zoledronate. The whole-body blood pool and delayed skeletal phase whole-body images were acquired using the advanced digital PET/CT system (GE Discovery MI). The acquisition time was 0.5 min/bed for whole body blood pool images and 3 min/bed for delayed whole-body images. Delayed whole body images were reconstructed at different time points (0.5 min/bed, 1 min/bed , 2min/bed and 3min/bed) and each data set was reconstructed with six different beta (β) values (150, 300, 450, 600, 800 and 1000) by using Bayesian penalized likelihood reconstruction (Q.Clear). The images were assessed by two different senior nuclear medicine physicians for the best image quality for the different reconstructions. **Results:** Whole body blood pool images showed high uptake in kidneys and urinary bladder as organs of excretion and faint uptake in heart blood pool and the vascular blood pool. The nuclear medicine physicians felt that the blood pool images are of high quality comparable to whole body blood pool of 99mTc MDP. After comparing all the reconstructed data sets using various bed positions and beta values the nuclear medicine physicians had a consensus opinion that one min per bed acquisition is as good as three minute per bed acquisition with respect to image quality for clinical reporting. Comparison of Beta values with Q.Clear revealed that 450 and less of beta values made the images noisy and more than 800 made it over smoothened. Hence a beta value of 600 to 800 gave the best images. **Conclusion:** Use of low dose of [^{68}Ga] Ga-DOTA^{ZOL} based bisphosphonates for metastatic bone scan imaging appears technically feasible. One min per bed position gave good quality images comparable to three min per bed on the high definition digital PET scanner. Best beta values for Q.Clear reconstruction appears to be between 600-800. **References:** None.

EP-0929

EasyPET-3D, a super high spatial resolution and cost-effective PET scanner for training and preclinical applications

F. Castro[1,2], *P. M. C. Correia*[1,2], *P. M. C. C. Encarnação*[1], *A. L. M. Silva*[1,2], *F. M. Ribeiro*[1], *I. Mohammad*[1], *A. I. Veloso*[3], *A. C. Santos*[4], *J. F. C. A. Veloso*[1,2];
[1]*Departamento de Fisica da Universidade de Aveiro & i3N, Aveiro, PORTUGAL,* [2]*RI-TE Radiation Imaging Technologies, Lda, Ílhavo, PORTUGAL,* [3]*DigiMedia, Universidade de Aveiro, Aveiro, PORTUGAL,* [4]*iCBR Coimbra Institute for Clinical and Biomedical Research, Coimbra, PORTUGAL.*

Aim/Introduction: EasyPET technology is an original concept for high-resolution 3D PET imaging that uses 2 opposite detector arrays rotating synchronously with 2 degrees of freedom and very high granularity, being capable to scan millions of lines of response (LORs) in minutes and perform full body mouse axial imaging with only a small number of detector cells. EasyPET achieves a great level of detail and spatial resolution that is very uniform in all the field of view (FoV) due to the intrinsic capacity to mitigate parallax errors, since its detector arrays are always collinear, unlike ring-based PET scanners. EasyPET-3D detector arrays can have different geometries and each scan can be performed with different parameters in order to achieve different sensitivity, level of desired detail/speed and image specific regions within the FoV, which is also a unique ability of this scanner when compared with existing systems. This study aims to characterize the performance of EasyPET-3D following NEMA NU 4-2008 standards. **Materials and Methods:** The tested EasyPET-3D system uses 2 arrays of 16x2 LYSO crystals of 2x2x30 mm^3 pixel size coupled to corresponding arrays of silicon photomultipliers with 1.3 mm^2 active area, covering an axial FoV of 35 mm length and maximum radial FoV of 50 mm diameter. A dedicated 3D reconstruction method was developed based in OSEM and MLEM algorithms, taking into account the original geometry of the scanner and the high number of possible LORs. **Results:** Based on NEMA standardized methods for performance evaluation of preclinical PET scanners, NEMA IQ and NEC phantoms filled with 18F-FDG and a point-like 22-Na source were imaged, in order to determine spatial resolution, sensitivity, uniformity and other NEMA parameters achieved by EasyPET-3D. Results and images will be presented. **Conclusion:** EasyPET-3D system results are very promising showing the high potential of this system for training and preclinical imaging research applications. EasyPET technology has the best cost/performance ever achieved in the history of PET imaging and thus systems based in this technology, such as the EasyPET-3D, have the potential to become the most affordable high-quality PET scanners in their class, which is not only limited to training and preclinical imaging applications but can also be upgraded to organ-specific clinical imaging such as positron emission mammography. Furthermore, EasyPET technology can be seamlessly integrated with CT or optical imaging to build hybrid scanners. **References:** Patent WO/2016/147130.

EP-70
Technical aspects -> Instrumentation and data analysis -> Instrumentation -> PET/MR

October 12 - 16, 2019
e-Poster Area

EP-0930

PET/MR, the optimal imaging tool for quantitative biodistribution studies in nanoparticle research

A. Courteau[1], *M. Moreau*[2], *P. M. Walker*[3,1], *M. Guillemin*[4], *C. Drouet*[4], *A. Oudot*[4], *L. Carchon*[5], *S. Roux*[6], *J. McGrath*[7], *R. Garipov*[7], *A. Cochet*[1,4,3], *F. Brunotte*[1,4,3], *J. M. Vrigneaud*[1,4];
[1]*ImViA laboratory, EA 7535, University of Burgundy, Dijon, FRANCE,* [2]*Institut de Chimie Moléculaire de l'Université de Bourgogne, UMR CNRS 6302, Dijon, FRANCE,* [3]*CHU François Mitterrand, Dijon, FRANCE,* [4]*Georges-François Leclerc Cancer Centre, Unicancer, Dijon, FRANCE,* [5]*Georges-François Leclerc Cancer Center, UNICANCER, Dijon, FRANCE,* [6]*Institut UTINAM, UMR CNRS 6213, University of Franche-Comté, Besançon, FRANCE,* [7]*MR-Solutions Ltd, Guildford, UNITED KINGDOM.*

Aim/Introduction: Due to their size, nanoparticles can be easily labeled with several atoms bearing optical, radioactive and magnetic properties. MRI is sensitive to variations in T1 and T2* induced by nanoparticles and PET allows a highly sensitive and linear response to nanoparticles concentration. Therefore, PET/MRI is a technique of choice for the purposes of imaging and quantitating. This study aims at validating microPET/MR imaging both with phantoms and small animals for the study of nanoparticles. **Materials and Methods:** 7 mice were installed on a heated bed with respiratory gating before an intravenous injection of 5.2 ± 0.8 MBq of nanoparticules labelled by ^{68}Ga and gadolinium. Imaging was performed 15 min post-injection on a 7 T fully integrated PET/MR system with a helium-free magnet and SiPM-based PET insert. Fast spin echo images were acquired with TR of 1000 ms, TE of 11 ms, 4 averages, matrix of 256^2, and a field of view of 40 × 40 mm^2. List-mode PET data were acquired simultaneously during 30 min and then reconstructed using 3D-OSEM algorithm with the following corrections: random, scatter, dead time, normalization, and radioactive decay. Phantoms acquisitions were performed with ^{68}Ga. A homogeneous mouse-like cylinder was used to assess both signal to noise ratio (SNR) in MR imaging and PET count rate linearity. Image quality metrics were acquired with the NEMA-IQ phantom and spatial resolution was assessed using an ultra micro hot spot phantom. Just after imaging, the animals were sacrificed and ex vivo counting was then compared to in vivo PET quantification in four organs for each animal. **Results:** Phantom data showed that the count rate versus radioactive concentration relationship was linear up to 50 MBq. Qualitatively, a signal enhancement was visible on the liver and kidneys of mice. No significant differences were found between in vivo and ex vivo counting data. At high activities, the acquisition of PET data caused a detectable increase of the noise in simultaneously acquired spin echo images but did not affect the overall quality

of MR images. **Conclusion:** Using proper calibrations, PET/MR imaging of nanoparticles labelled with ^{68}Ga and gadolinium was performed easily with excellent spatial resolution and quantitative accuracy. **References:** None.

EP-0931

The effects of ^{18}F-FDG dose reductions on quantification and diagnosis in whole body PET/MRI

Y. Xu[1], *J. Guo*[2], *F. Li*[1], *C. Li*[1];
[1]*Hangzhou Universal Imaging Diagnostic Center, Hangzhou, CHINA,* [2]*GE Healthcare(CHINA), Shanghai, CHINA.*

Aim/Introduction: The study aims to investigate the effects of reduced tracer dose on the semi-quantification and clinical diagnosis in ^{18}F-FDG wholebody integrated PET/MR imaging. **Materials and Methods:** 20 patients (38.5±22y; BMI 20.13±3.84)with malignant tumors were performed 6min/bed whole body PET/MR(GE SIGNA)imagingwith respiratory gating at 45.29±9.22minafter injected standard dose (3.7MBq/kg). The imagingofreduced doses wassimulated byTOF and non TOF reconstruction with100%, 75%, 50% and 25% of the original data.The signal-to-noise ratio (SNR), SUVmax and SUVmean of liver background in each simulated dose were analyzed by paired t test while theSUVmax, SUVmean, metabolic tumor volume(MTV) and total lesion glycolysis(TLG) of the lesions by Wilcoxon test. Reconstructed images wererandomly assigned to four observation groups, with three observers in each group. χ^2 testwas used to do the statistical analysis forthediagnosis. **Results:** The image SNR decreases significantly ($P < 0.01$) with reduced dose. No significant difference was found both in SUVmeanof liverand 56 lesions(2-3 lesions/patient;D 22.88±15.09mm)at each dose,as well as in liver SUVmaxand lesions' SUVmax, MTV, TLG at 100%, 75%, and 50% simulated dose ($P > 0.05$). Yet SUVmax at 25% simulated dose was significantlyhigher than that of 100% ($P < 0.01$)..while MTV and TLG of lesions were lower ($P < 0.05$). Except 25% dose, the lesion detection rate from other doses and all the observers are consistent ($P > 0.05$).However, higher false positive rate of small lesions caused by increased noise at 25% doseresults in reading divergence among observers ($P < 0.05$, in comparison with 100% dose).In addition, the lesion detection rates of TOF images are higher than that of non-TOF images in each simulated dose($P < 0.05$). **Conclusion:** A 50% of standard dose can be feasible in ^{18}F-FDG PET/MR 6min/bed whole body examination. The lesion detection rate and the semi-quantitative are relativelyconsistentwith decreased SNR except at 25% dose. It's suggested to prolonge scan time when dose less than 50% in case of potential deviated SUVmax, MTV and TLG,degraded images quality and misdiagnosis of small lesions.Compared with non-TOFimages, TOFimages own improvedlesion detection rate,andgood consistency under various simulated doses. **References:** 1.Sah B R , Ghafoor S , Burger I A , et al. Feasibility of18F-FDG dose reductions in breast cancer PET/MRI[J]. Journal of Nuclear Medicine, 2018, 59(12):jnumed.118.209007.2.Sekine T , Delso G , Zeimpekis K G , et al. Reduction of\r, 18\r, F-FDG Dose in Clinical PET/MR Imaging by Using Silicon Photomultiplier Detectors[J]. Radiology, 2017:162305.

EP-0932

Feasibility of Ultra-Low Dose Ultra-High Definition PET/MR for Assessment of ACL Graft Healing

K. Binzel*, C. Kaeding, R. Magnussen, D. C. Flanigan, B. Sanders, M. V. Knopp;*
The Ohio State University Wexner Medical Center, Columbus, OH, UNITED STATES OF AMERICA.

Aim/Introduction: PET/MR for the assessment of ACL graft healing post-reconstruction surgery has been proven feasible. We have previously shown the ability to perform ultra-high definition (UHD) 1 mm isotropic voxel PET image reconstruction based upon the sensitivity and time of flight performance of next-generation digital photon counting systems. Here we aimed to simulate and test the feasibility of performing ultra-low dose imaging while maintaining the image quality and quantitative robustness previously experienced. **Materials and Methods:** 12 patients post-surgical ACL graft reconstruction had an MRI on a 3T Ingenia CX using the dedicated 16 channel knee coil, with both knees imaged sequentially. Dynamic PET/CT imaging was performed on a digital photon counting system (Philips Vereos) continuously for 75 minutes post-injection of 111 MBq ^{18}F-FDG. Listmode data were reconstructed using the 576x576 matrix 1mm^3 voxel volume protocol, with both PSF and Gaussian filter enabled. Default dynamic frame times of 5 minutes per frame were used, as well as 2.5 min/frame secondary reconstructions, simulating a 50% dose reduction by reducing the count data by the same fraction. Regions of interest were placed over the graft, bone tunnels, quadriceps muscle and PCL, as well as in the contralateral healthy knee, also imaged. **Results:** Excellent image quality and robust quantification resulted from the 2.5 min/frame, 50% dose reduction simulation reconstructions. SUVs measured on the low dose images were not significantly different ($p>0.25$) from full dose, 5 min/frame data in all regions except the muscle, where activity concentrations are extremely low and varied among patients. Since this evaluation, an additional 10 patients have now been imaged using an average dose of 48 MBq. Initial assessment shows that equivalent image quality can be produced, while still using the UHD reconstruction protocol. Quantification also appears robust and dynamic uptake curves from the graft signal appear similar to those seen in matched patients from the higher dose group. **Conclusion:** Next-generation digital PET/CT systems will allow for significant reductions in image acquisition time as well as injected radiotracer dose. Our already low-dose knee imaging has been further optimized to utilize an FDG injection below 50 MBq while maintaining visual and quantitative precision. The preserved ability to apply an ultra-high definition reconstruction protocol provides exceptionally detailed insight into the graft healing process post-reconstructive surgery, offering a non-invasive imaging methodology for sports medicine and other non-oncologic applications limited by concerns over patient

radiation exposure. **References:** None.

EP-0933

EPI distorsion correction for Lung PET-MRI oncology

F. L. Besson[1,2], B. Fernandez[3], S. Faure[4], A. Seferian[5], O. Mercier[6], X. Mignard[5], F. Parent[5], S. Bulifon[5], D. Montani[5], S. Mussot[6], E. Fadel[6], D. Mitilian[6], E. Blanchet[7], A. Chetouani[7], F. Bouderraoui[7], H. Cherkaoui[8], D. Planchard[9], C. Naltet[9], C. Le Pechoux[9], C. Caramella[9], B. Besse[9], C. Comtat[10], P. Gervais[7], V. Lebon[7], E. Durand[1,2];
[1]*Department of Nuclear Medicine Hopitaux Universitaires Paris Sud, APHP, Le Kremlin-Bicêtre, FRANCE,* [2]*IR4M unit UMR8081 Paris Sud-CNRS, Orsay, FRANCE,* [3]*GE Healthcare, Orsay, FRANCE,* [4]*CNRS UMR 8628, Université Paris Sud Institut de Mathématique d'Orsay, Orsay, FRANCE,* [5]*Department of respiratory medicine, Hopitaux Universitaires Paris Sud, APHP, Le Kremlin-Bicêtre, FRANCE,* [6]*Thoracic Oncology Institute, Université Paris-Sud, Hopital Marie Lannelongue, Le Plessis-Robinson, FRANCE,* [7]*Department of Nuclear Medicine, Service Hospitalier Frederic Joliot, Université Paris Sud, CEA, Orsay, FRANCE,* [8]*Neurospin, CEA, Orsay, FRANCE,* [9]*Thoracic Oncology Institute, Université Paris-Sud, Gustave Roussy, Villejuif, FRANCE,* [10]*IMIV, CEA, Orsay, FRANCE.*

Aim/Introduction: To evaluate the impact of geometric distortions inherent to diffusion weighted imaging (DWI) in the field of PET-MRI lung oncology. **Materials and Methods:** 10 patients were prospectively recruited and underwent an 18F-FDG PET-MRI for lung oncology purpose. For all patients, the imaging protocol included several thoracic PET-MRI acquisitions: a PET acquisition performed one hour after the intra veinous injection of 18F-FDG; a set of DWI acquisitions with anterior-posterior phase encoding (b values of 0,500, 800 s/mm²) and reverse-phase encoding polarity (b value = 0 s/mm²); a high resolution post contrast-enhanced 3DT1-weighted FSPGR sequence. DWI data were corrected for geometric distortions using the reverse phase encoding method. All the DWI data (non corrected and corrected from the distortion) were warped to the same T1 weighted PET-MRI isotropic reference space before analyses. Quality of the co-registrations to the reference T1 PET-MRI was quantitatively assessed using mutual information metric. The percentage gain compared to non-warped DWI data was also computed. ADC feature maps of each lung lesion were computed from the DWI data non-corrected and corrected from the distortion, and voxel-wise percent differences together with paired t-test were computed. Finally, regional ADC-SUV monotonic correlations were explored from optimal realigned DWI-PET data. **Results:** Quality of the co-registration between DWI and T1 PET-MRI data was significantly improved by the reverse phase encoding method (relative gain on mutual information compared to non-warped DWI data : 4-46%, vs 0.4-27% for warped data without distortion correction, p inferior to 0.05). The between-ADC feature maps regional differences ranged from -100% to more than +150%. Regional correlations between ADC and SUV computed from optimal realigned DWI-PET data revealed only weak monotonic relationships between the two features at the voxel level (spearman coefficients inferior to 0.5 in all the cases). **Conclusion:** DWI-related distortions are significant in thoracic PET-MRI, and should be corrected for accurate DWI-PET multimodal analyses. ADC and SUV showed weak monotonic relationship at the voxel level, emphasizing their complementarity. **References:** Chang H, Fitzpatrick JM. A technique for accurate magnetic resonance imaging in the presence of field inhomogeneities. IEEE Trans Med Imaging 1992;11(3):319-29. Turner R, Le Bihan D et al. Echo-planar imaging of intravoxel incoherent motion. Radiology 1990;177:407-14. White NS, McDonald C et al. Diffusion-weighted imaging in cancer: physical foundations and applications of restriction spectrum imaging. Cancer Res 2014;74(17):4638-52.

EP-0934

Quantitative T1 and T2 mapping for multimodal PET-MRI lung oncology purpose

F. L. Besson[1,2], B. Fernandez[3], S. Faure[4], G. Guillot[2], A. Vignaud[5], O. Mercier[6], A. Seferian[7], S. Mussot[6], E. Blanchet[8], D. Mitilian[6], A. Chetouani[8], S. Bulifon[7], F. Bouderraoui[8], X. Mignard[7], C. Le Pechoux[9], D. Montani[7], V. de Montpreville[6], A. Levy[9], E. Fadel[6], D. Planchard[9], B. Besse[9], P. Gervais[8], C. Comtat[8], V. Lebon[8], E. Durand[1,2];
[1]*Department of Nuclear Medicine Hopitaux Universitaires Paris Sud, APHP, Le Kremlin-Bicêtre, FRANCE,* [2]*IR4M unit UMR8081 Paris Sud-CNRS, Orsay, FRANCE,* [3]*GE Healthcare, Orsay, FRANCE,* [4]*Laboratoire de mathématiques Université Paris Sud-CNRS, Orsay, FRANCE,* [5]*CEA-Neurospin, Saclay, FRANCE,* [6]*Thoracic Oncology Institute, Université Paris-Sud, Hopital Marie Lannelongue, Le Plessis-Robinson, FRANCE,* [7]*Department of respiratory medicine, Hopitaux Universitaires Paris Sud, APHP, Le Kremlin-Bicêtre, FRANCE,* [8]*Service Hospitalier Frederic Joliot, Université Paris Sud, CEA, Orsay, FRANCE,* [9]*Thoracic Oncology Institute, Université Paris-Sud, Gustave Roussy, Villejuif, FRANCE.*

Aim/Introduction: To assess the T1/T2-mapping approach for PET-MRI multimodal tissular characterization in the field of lung oncology. **Materials and Methods:** Two phantom session including T1/T2-mapping methods (IR,VFA,SMART1 / MEFSE) were performed on the same PET-MRI. Accuracies of T1/T2 mapping methods were assessed by the error measures against the phantom ground truths. Reliabilities were assessed by computing the intraclass correlation coefficients estimates of the phantom measures (ICC, mixed effect model, absolute agreement). For clinical validation, 8 patients underwent a PET-MRI for suspected lung cancer, including PET, DWI and T1/T2-mapping acquisitions. For all lesions, images were warped into the same isotropic reference space before features maps computation. Voxel-wise spearman correlations were performed to explore monotonic relationships between T1, T2, ADC and SUV features. Considering the 4 features, the lesions were partitioned using an unsupervised gaussian mixture approach. Finally, features profiles were explored at the cluster level. **Results:** Based on phantom analyses, SMART1 was the most accurate T1-mapping method for T1 relaxation times above 500ms ($SMART1_{error}$ less than 10% for the two sessions, ranging from 11 to 103% for the others methods). IR

and SMART1 were the most reliable (ICC = 0.999;$_{95}$CI = 0.99-1 for both). MEFSE was highly accurate for T2 relaxation times ranging from 23 to 278ms, with high reliability (ICC = 0.986, 95CI = 0.86-1). The 8 clinical lung lesions all showed T1 and T2 relaxation times in the ranges 1090-2209.5ms and 57.1-99.8ms respectively. For all the lesions except 2, absolute r values were inferior to 0.5 for all the features pairs. Unsupervised clustering provided 2 components for 6 lesions, and 1 component for two highly homogeneous lesions. At the regional level, features profiles were significantly different, as well as their monotonic relationships. **Conclusion:** T1/T2-mapping is feasible for PET-MRI lung oncology purpose. The multimodal profiles of T1, T2, ADC and SUV features emphasized their potential respective contribution for the lesion characterization at the regional level. **References:** Damadian R. Tumor detection by nuclear magnetic resonance. Science 1971. 171 (3976): 1151-3 Damadian R, Zaner K, Hor D, DiMaio T. Human tumors detected by nuclear magnetic resonance. Proc Natl Acad Sci USA 1974;71(4):1471-3. Yarnykh VL. Actual flip angle imaging in the pulse steady state : a method for rapid three-dimensional Mapping of the Transmitted Radiofrequency field. Magn Res Med 2007; 57:192-200 Nikola Stikov, Mathieu Boudreau et al. On the accuracy of T1 mapping: Searching for common ground. Magn Reson Med 2015; 73(2):514-22.

EP-0935

Cardiac Misalignment In PET/MR Attenuation Correction - A Frequent Artifact In Myocardial Perfusion Imaging, Which Is Enhanced By Adenosine-Stress

E. von Felten, G. Benetos, D. Patriki, D. Benz, A. Giannopoulos, G. P. Rampidis, A. Pazhenkottil, C. Gräni, T. Fuchs, P. Kaufmann, R. Buechel;
Department of Nuclear Medicine, Zürich, SWITZERLAND.

Aim/Introduction: Misalignment of positron emission tomography (PET) datasets and maps for attenuation correction (AC) is a well-known potential source of artifacts in myocardial perfusion imaging (MPI). A hybrid PET/MR scanner offers inherent spatial co-registration of the PET dataset an AC-maps from MRI (MRAC). Therefore, occurrence of misalignment may seem unlikely. We aimed to evaluate the prevalence and the impact of MRAC-misalignment during MPI with PET/MR using adenosine-stress. **Materials and Methods:** Twenty-eight patients underwent 13N-ammonia PET MPI during adenosine-stress and at rest. We acquired Dixon MR sequences for creation of MRAC-maps immediately prior to the stress and rest dynamic PET acquisition, respectively. Of note, the stress MRAC-map was therefore acquired during fully effective adenosine-stress. For both, stress and rest, we performed a 7-minute dynamic, followed by a 10-minute static PET acquisition. After reconstruction of PET data based on the original co-registration (non-shifted images), we examined cardiac contours from the summed static PET dataset and the MRAC-map for spatial misalignment. If necessary, we performed manual adjustment to assure optimal cardiac co-registration (shifted images). We calculated a shift-vector indicating the summed shift distance of PET against MRAC in x-, y- and z-axis. We assessed summed stress, rest and difference scores (SSS, SRS, SDS) in non-shifted and shifted datasets. Additionally, we assessed the difference in z-axis of the diaphragm's location between rest and stress MRAC-maps. **Results:** Manual correction of co-registration was necessary in 25 (89.3%) stress and in 12 (42.9%) rest PET datasets. Median shift-vector was significantly higher in stress than in rest datasets (14mm [IQR 11-19] vs. 0mm [IQR 0-8]). Median SSS, SRS and SDS were significantly higher in non-shifted than in shifted images (SSS: 12 [IQR 8-13] vs. 7 [IQR 5-9]; SRS: 7 [IQR 4-9] vs. 5 [IQR 4-6]; SDS: 5 [IQR 4-8] vs. 3 [IQR 1-5]; all p<0,01). The difference of the diaphragmatic position in the MRAC-map between rest and stress, indicating different breathing-levels during and after adenosine-stress, correlated with the difference of SSS between shifted and non-shifted images (r=0.405, p=0.012). **Conclusion:** Spatial misalignment between PET and MRAC datasets occurs frequently during MPI, even if performed on a hybrid PET/MR scanner. Our findings indicate that breathing levels differ depending on the presence or absence of adenosine-stress lead to MRAC-misalignment particularly due to the "upward creep" phenomenon. Systematic review for cardiac misalignment and its eventual correction by execution of a manual MRAC-shift should be implemented in every cardiac PET/MR protocol. **References:** None.

EP-0936

Ultra-fast Dynamic Perfusion ^{18}F-NaF PET in Prostate Cancer as Enabled by Digital Photon Counting PET/CT - A Feasibility Demonstration

K. Binzel, T. Porter, C. L. Wright, E. Folefac, J. P. Monk III, D. Diaz Pardo, D. G. Stover, I. Hsieh, J. Zhang, M. V. Knopp;
The Ohio State University Wexner Medical Center, Columbus, OH, UNITED STATES OF AMERICA.

Aim/Introduction: To assess the feasibility of ultra-fast frame rate dynamic perfusion of Na-^{18}F PET/CT for patients with advanced prostate cancer. **Materials and Methods:** Ten patients with suspicion of recurrent prostate cancer were imaged as part of this initial feasibility and methodology development study. Patients were imaged over one bed position at the site of suspected tumor for 15 minutes immediately following injection of 185 MBq Na-^{18}F. Imaging was performed on a digital photon counting system (Vereos Philips, dPET) with continuous listmode acquisition. The patients spent the remaining uptake period in the injection suite followed by whole body imaging at 75 minutes post-injection as per standard of care. Listmode data from the dynamic acquisition was clipped and reconstructed with various time frames from 1 second per dynamic frame to 15 seconds per frame. Regions of interest were placed over any present bone tumor as well as degenerative regions and a region of healthy bone within the dynamic field of view. **Results:** The ultra-short dynamic reconstructions produced evaluable data sets for all acquisitions. Using the longer acquisitions for reference, regions of interest were placed in a reliable manner.

Physiologic motion could readily be corrected for, however very little motion was observed. An adaptive reconstruction approach was utilized to minimize image noise which otherwise would have led to degradation of image quality due to the considerable reductions in count density. All this was accomplished while preserving quantitative accuracy due to the performance characteristics of the digital photon counting system, as validated by listmode data clipping simulations. The ultra-short 1 and 9 sec/frame dynamic curves gave exceptionally detailed views of the perfusion in both bone lesions and areas of degenerative changes. **Conclusion:** In this feasibility demonstration, we have demonstrated that one second per frame image reconstruction of dynamic perfusion Na-^{18}F PET/CT data is robustly achievable. By anatomic correlation to the CT, quantification of tumor features such as vascularity and perfusion appear to be robustly and accurately assessed. This methodology may be applied to assess perfusion characteristics of bone tumors where the PET based measurement of tumor microcirculation may help guide therapy planning. Additionally, response to therapy may potentially be assessed via follow up measurement of changes in rates of bone lesion perfusion. **References:** None.

EP-0937

Metal artifact reduction in ^{68}Ga-PSMA-11PET/MRI for prostate cancer patients with hip joint replacement using multiacquisition variable-resonance image combination

K. Kudura;
Nuclear Medicine Department, Zürich, SWITZERLAND.

Aim/Introduction: PET/MRI has a high potential in oncology imaging, especially for tumor indications where high soft tissue contrast is crucial such as genitourinary tumors. One of the challenges for PET/MRI acquisition is handling of metal artifacts. In addition to conventional methods more innovative techniques have been developed to reduce those artifacts such as the selective multi-acquisition variable-image combination (MAVRIC SL). The aim of this study is a quantitative and qualitative assessment of metal artifact reduction in ^{68}Ga-PSMA-11 PET/MRI for prostate cancer patients with hip joint replacement using a selective MAVRIC SL sequence for the whole pelvis. **Materials and Methods:** Retrospectively analyzed were data of 20 men with 37 metal hip implants diagnosed with PCA, staged or restaged by ^{68}Ga-PSMA-11 PET/MR from June 2016 to December 2017. Each signal cancellation per side or metal implant was analyzed in the LAVA-FLEX sequence, considered as the reference sequence, as well as T1-weighted FSE and MAVRIC-SL. Two reviewers reported independently on a four-point scale (0= not assessable, 1= only partially visible, 2= visible with substantial blurring, 3= good depiction of anatomical structures) whether abnormal pelvic ^{68}Ga-PSMA-11 uptake could be assigned to an anatomical structure in the tested sequences. **Results:** The smallest averaged signal void was observed on MAVRIC SL sequences with a mean artifact size of 26.17 cm2 (range 12.63 to 42.93 cm2, $p < 0.001$). The best image quality referring to anatomical assignment of pathological PSMA uptakes in the pelvis reported on a four-point scale by two independent readers was noted on MAVRIC SL sequences compared to T1-weighted FSE and LAVA-FLEX sequences with excellent interreader agreement. **Conclusion:** MAVRIC SL sequence allows better image quality in the surrounding of hip implants by reducing signal voids and increasing so the accuracy of anatomical assignment of pathological ^{68}Ga-PSMA-11 uptakes in prostate, pelvic lymph nodes and bones over LAVA-FLEX and T1-weighted FSE sequences. **References:** None.

EP-0938

Technical limitations of 18F-FDG PET/MR in pediatric oncology: Case-based review of false positive findings

K. Hawk, A. Muehe, F. Siedek, A. J. Theruvath, H. E. Daldrup-Link;
Stanford University, Palo Alto, CA, UNITED STATES OF AMERICA.

Aim/Introduction: 18F-FDG PET/MR has quickly become a powerful tool for staging, follow up and surveillance of pediatric cancer patients. The significantly reduced radiation exposure compared to 18F-FDG PET/CT and superior anatomic detail of the nervous system and soft tissues are among the many benefits of 18F-FDG PET/MR imaging in pediatric care. Nonetheless, 18F-FDG PET/CT has technical limitations. The nuclear medicine physician must have an intrinsic understanding of these limitations and be able to understand and recognize possible false positive findings. Inadvertent misclassification of normal or benign PET-avid findings as malignancy can have a great impact on further treatment and prognosis. This case-based work is designed to educate nuclear medicine physicians about the technical limitations of 18F-FDG PET/MR and potential false positive findings in pediatric cancer patients. **Materials and Methods:** Following a comprehensive literature search on current techniques in 18F-FDG PET/MR in pediatric oncology, we complied an extensive collection of most current evidence -based best practices in 18F-FDG PET/MR. This work presents our institutional approach and experience with performing more than 150 18F-FDG PET/MR scans of pediatric patients with a series of case examples detailing technical limitations and false positive findings. **Results:** The imaging protocol and reporting criteria for conducting 18F-FDG PET/MR imaging of pediatric oncology patients will be detailed. Classical technical limitations of the 18F-FDG PET/MR imaging technique are provided. Non-neoplastic etiologies including infection, inflammation, physiologic hypermetabolism and iatrogenic causes are detailed as potential false positive findings. Benefits and limitations of 18F-FDG PET/MR imaging when compared with 18F-FDG PET/CT will be detailed as we discuss research and clinical application directions of 18F-FDG PET/MR imaging. **Conclusion:** 18F-FDG PET/MR has emerged as a powerful tool in evaluation of pediatric oncology patients. This comprehensive case-based review details how 18F-FDG PET/MR can be used to evaluate the pediatric oncology patient. Through explanation of 18F-FDG PET/MR imaging techniques, reporting mechanisms,

technical limitations, and classic false positive findings, this exhibit provides the learner with detailed understanding of applying 18F-FDG PET/MR to evaluate pediatric tumors and how to accurately identify false positive findings in order to provide excellent patient care. **References:** None.

EP-0939

Validation Of Aseptic Filling Process Of A New Automated Dispenser, Karl 100

S. Emery, C. Rémy, M. Razzouk-Cadet, C. Grangeon-Chapon; CHUN, Nice, FRANCE.

Aim/Introduction: Positron-emission is a nuclear medicine functional imaging that needs sterile radiopharmaceutic injections. For radioprotection purposes, dose preparations are often performed by dispensing machines whose operation must ensure sterility of dispensed doses. The aim of this study was to test the aseptic filling process of a new automated dispenser used to prepare fluorinated tracers doses, Karl100. **Materials and Methods:** In order to validate Karl100 aseptic process, 12 media fill tests were performed replacing both radiopharmaceutical vials and sodium chloride 0.9% infusion bags by suitable TSB (Tryptic Soy Broth) packaging. All fluid handling operations were done by the automated dispenser in accordance with its usual operating procedure. 12 Rad-Inject syringes filled with TSB were obtained and were finally transferred in sterile vials as follow: -9 samples of 6 mL using only a needle for the transfer, -3 samples of 6 mL using the specific infusion set of the Rad-Inject which includes a 0.22 µm filter. Aninfusion bag of TSB was used for the 3 tests using an infusion set for transfer. In order to increase media fill tests sensitivity, the final samples were then filtered (0.45 µm) throught Steritest EZ system (Merck Millipore; Molsheim, France) and cultured for fourteen days in two different growth media, one for aerobic and fungal microorganisms (Bact/Alert SA 259789; Biomérieux, Craponne, France)at room temperatureand the other for anaerobic microorganisms (Bact/Alert SA 259790; Biomérieux, Craponne, France) at 35°C. **Results:** At the end of 14 days of incubation, all samples remained sterile without microbial growth: media fill tests were successful. **Conclusion:** Although preparation of the Rad-Inject syringe requires disassembly of the plunger under non-sterile conditions, thesesimulation tests validated the aseptic filing process of Karl100. The 0.22 µm filter on infusion set provides an additional protection against microbial contaminations even if radiopharmaceutical is already sterile in Rad-inject syringe. Futhermore this filter includes a mandatory bubble trap to remove the air of the Rad-Inject tubing. In conclusion, Karl100 and its disposable devices can be used safely for radiopharmaceuticals dispensing in nuclear medicine departments. **References:** None.

EP-71

Technical aspects -> Instrumentation and data analysis -> Instrumentation -> SPECT and SPECT/CT

October 12 - 16, 2019

e-Poster Area

EP-0940

Simultaneous Ventilation/Perfusion SPECT Acquisition: Diagnostic Accuracy

N. Gandy, N. Soneji, J. Phillips, L. M. Perry, M. Woodward, K. Wallitt, H. Tam, D. Gopalan;
Imperial College Healthcare NHS Trust, London, UNITED KINGDOM.

Aim/Introduction: To determine whether simultaneous acquisition of perfusion and ventilation components of VQ SPECT utilising Tc99m-MAA and Kr-81m-gas has equivalent image quality and diagnostic accuracy as sequentially acquired perfusion and ventilation studies. **Materials and Methods:** VQ SPECT studies were acquired on a Siemens Symbia T16 gamma camera. The original report was based on a sequential perfusion (10sec/view) followed by ventilation SPECT (20sec/view) (SVQ). A Tc99m window with lower and upper scatter was included during ventilation SPECT acquisition to acquire simultaneous perfusion data. The simultaneous perfusion SPECT was reconstructed with dual-energy (DEW) and triple-energy window (TEW) scatter correction. 10 anonymised studies (5 positive and 5 negative for pulmonary embolus (PE)) were retrospectively reviewed by three consultant radionuclide radiologists independently (40 more cases pending). The reviewers were blinded to acquisition and reconstruction methods for the perfusion study. Studies were scored for image quality (1-4) and perfusion defects were documented as matched, mismatched or reverse mismatched. Overall diagnosis was documented as positive for PE if at least one mismatched defect was identified. The original report for the SVQ acquisition of each study was taken as the gold standard. **Results:** A total of 90 reads were completed by the three reviewers. Average image quality score of perfusion images was 2.8 (SVQ), 2.9 (DEW) and 3.0 (TEW). Overall inter-observer agreement for presence of PE was 93.3% with two discordant readings for one case. This case was reviewed by a consultant cardiothoracic radiologist and diagnosed as positive on all three acquisitions. Intra-observer agreement for presence of PE between the three different acquisitions was 90% for Readers 1 and 2 and 100% for Reader 3 - total of 1 discordant reading by SVQ and 2 by TEW. The average sensitivity for positive PE diagnosis across all three readers was 86.7% for SVQ acquisition, 93.3% for DEW and 73.3% for TEW. Specificity for PE diagnosis was 100% for all three reconstructions. Accuracy for each type of reconstruction, SVQ, DEW and TEW was 93.3%, 96.7% and 86.7% respectively. There is no significant difference in sensitivity or accuracy between the different reconstructions. **Conclusion:** This study demonstrates equivalent diagnostic accuracy of simultaneous perfusion and

ventilation acquisitions in comparison to sequential acquisitions with preserved specificity and no significant change in image quality or sensitivity when scatter correction is applied. Implementation of simultaneous acquisition in daily practice will decrease acquisition time for VQ SPECT and improve departmental efficiency and patient comfort. **References:** None.

EP-0941

Phantom study for activity quantification of ^{177}Lu SPECT/CT imaging

O. Ferrando[1], *A. Chimenz*[1], *M. Riondato*[2], *G. Rambaldi*[1], *F. Foppiano*[1], *A. Ciarmiello*[2];
[1]*Department of Medical Physics - ASL5 Spezzino, La Spezia, ITALY,* [2]*Department of Nuclear Medicine - ASL5 Spezzino, La Spezia, ITALY.*

Aim/Introduction: To assess the of activity quantification with ^{177}Lu phantom studies on our SPECT/CT scanner (SYMBIA T2 - Siemens Healthcare). SPECT-based activity quantification is necessary for personalized image-based dosimetry in target radionuclide therapy as recommended by the EURATOM 2013/59 directive. **Materials and Methods:** Quantitative SPECT/CT studies with ^{177}Lu was performed using the methodology proposed in [1]. The scanner calibration factor and the recovery coefficients for different spherical objects in different radioactive backgrounds were evaluated. The used instrumentation consists of an uniform cylindrical phantom (5860 mL) and an IEC NEMA torso-phantom containing hot sphere inserts with volumes in the range (0.5 - 25) mL. The spheres were filled with a solution of ^{177}Lu with an activity concentration of 2.9 MBq/mL. Background activity concentrations were in the range (0.04 - 0.18) MBq/mL with the following sphere to background ratio: 67.1:1, 32.6:1, 19.4:1, 12.8:1. Images were reconstructed using the proprietary OSEM 3D algorithm (FLASH 3D, Siemens Healthcare), CT-based attenuation correction, energy window-based scatter correction and resolution recovery. **Results:** The scanner calibration factor was 5.1 cps/MBq. Mean recovery coefficients vary from 73% (for volumes of 25 mL) to 12% (for volumes of 0.5 mL) with variations in the range of 1% - 5%. The number of subsets and iterations and filtering applied to image reconstruction were chosen based on a previous study [2] and were set to 8iterations/8subset/no image filtering since these parameters seem to improve activity recovery and limiting the background variability. Background activity concentratrions were determined with errors between -3.5% and 4.2%. **Conclusion:** Following the indications of the EURATOM 2013/59 directive, concerning activity quantification for personalized dosimetry in radionuclide therapy, a scanner calibration factor and the activity recovery coefficients were found for ^{177}Lu applications. Our results show that activity in phantom can be determined with a difference less than 5% respect to the true activity. These results have to be validated in further studies with different object sizes and shapes and also with patient scans. **References:** [1] J. Zeintl et all. "Quantitative accuracy of clinical 99mTc SPECT/CT using ordered-subset expectation maximization with 3-dimensional resolution recovery, attenuation and scatter correction". Journal of Nuclear Medicine, Vol.51, no. 6m pp. 921-928, 2010. [2] O.Ferrando et all. SPECT-CT activity quantification in 99mTc-MAA acquisitions. Journal of Diagnostic Imaging in Therapy. 2018; 5(1):32-36. http://dx.doi.org/10.17229/jdit.2018-0624-034.

EP-0942

Sensitivity comparison between normal, fast and super-fast Low Dose SPECT/CT in order to localize and discriminate the nature of doubtful findings to complete whole-body bone scintigraphy in cancer patients

A. Farina[1], *R. Bonfiglioli*[1], *M. Maccagnani*[1], *S. Zoboli*[2], *S. Fanti*[1];
[1]*Nuclear Medicine Department, Sant'Orsola-Malpighi Hospital, University of Bologna, Bologna, ITALY,* [2]*Nuclear Medicine Department, Maggiore Hospital, Bologna, ITALY.*

Aim/Introduction: The aim of this retrospective study was to assess the performance (sensibility) between different Low Dose SPECT/CT in a cohort of oncological patient who undergone to whole body bone scintigraphy in order to clarify doubtful findings. **Materials and Methods:** This is a single centre retrospective review on patients selected between subjects sent to our operating unit to be undergone to bone scintigraphy from September 2016 to March 2019 according to the following inclusion criteria: a) comprehensive clinical history and prior management data; b) observe of doubtful findings by nature or location during whole body bone scintigraphy; c) execution of segmental LD-SPECT/CT to complete the study; d) acquisition data of LD-SPECT/CT (normal: 3º every 15'; fast: 6º every 15'; super-fast: 9º every 5'); e) obtaining informed consent. All images were reviewed by two experienced nuclear medicine physicians. Technical data of LD-SPECT/CT acquisition were reviewed by one senior radiologic technologist. Overall, 169 patients were enrolled in our study (92 female, 77 male): 110 undergone to normal LD-SPECT/CT (Group A); 34 undergone to fast LD-SPECT/CT (Group B); 25 undergone to super-fast LD-SPECT/CT (Group C). The districts examined through LD-SPECT/CT were head and neck (16/169), chest (44/169), lumbar spine (36/169), pelvis (62/169) and legs (11/169). **Results:** In Group A we found 37 new findings of whom 22 confirmed by subsequent radiological investigations (59%). In Group B we found 12 new findings of whom 5 confirmed by subsequent radiological investigations (42%). In Group C we found 9 new findings of whom 7 confirmed by subsequent radiological investigations (78%). In every groups we were able to clarify the anatomic location of the doubtful finding and to provide bone structural information independently by subsequent radiological investigations. **Conclusion:** Fast and super-fast LD-SPECT/CT had a sensibility comparable to normal LD-SPECT/CT, but it permits to obtain the diagnostic information in shorter time (5-10 minutes vs 20 minutes). The mainly advantage is for frail patients who experience reduced discomfort due to a complex diagnostic investigation. **References:** None.

EP-0943

Comparative study of IQ-SPECT and conventional SPECTGated Myocardial Perfusion Imaging

D. Biao;
The Frist Affiliated Hospital of ZhengZhou University, Zhengzhou, CHINA.

Aim/Introduction: To compare the left ventricular semi-quantitative perfusion results and cardiac function parameters of IQ-SPECT equipped with SMARTZOOM collimator and conventional SPECT system equipped with low energy high resolution collimator (LEHR), and to explore the difference between the results of the two imaging methods. **Materials and Methods:** A total of 35 subjects with severe arrhythmia were excluded from November 2016 to April 2017. The resting-gated myocardial perfusion imaging (G-MPI) was performed by IQ-SPECT and conventional SPECT acquisition methods, respectively. A low dose CT scan was performed after the last acquisition for attenuation correction. Five-stage semi-quantitative visual analysis of images was performed by two senior nuclear medicine physicians using a double-blind method. Cardiac function parameters were obtained by the Cedars QGS software automated analysis software. Finally, the resting perfusion total score (SRS), ejection fraction (EF), end-diastolic volume (EDV), end-systolic volume (ESV), peak ejection rate (PER), and peak-time filling were obtained by the two acquisition methods. Rate (PFR). Analysis was performed using SPSS 22.0 software using paired sample t-test or paired sample rank sum test (Wilcoxon test). **Results:** The resting perfusion score of the IQ-SPECT system was higher than the conventional score [SRS: 4(6) and 3(6)]. The EF calculated by IQ-SPECT was reduced [EF: (58.14 ± 17.10)% and (62.66 ± 21.13)%]. IQ-SPECT calculated lower EDV [EDV: 73 (57) ml and 85 (46) ml]. The PER calculated by IQ-SPECT is low [(2.34±0.92) EDV/s and (3.15±1.15) EDV/s]. The PFR calculated by IQ-SPECT is low [(2.35±0.93) EDV/s and (2.58±1.15) EDV/s]. The difference in ESV between the two was not statistically significant [ESV: 30 (30) ml and 27 (41) ml]. **Conclusion:** Conclusion The new IQ-SPECT system can shorten the acquisition time and / or reduce the dose of radiopharmaceuticals injected into patients. When comparing the semi-quantitative perfusion results and functional parameters of the left ventricle obtained by IQ-SPECT with the conventional SPECT system, we found that Significantly, the SRS describing the myocardial perfusion index was higher in IQ-SPECT with lower EF values, EDV, PER, and PFR. **References:** None.

EP-0944

Performance characteristics of ^{225}Ac produced gamma and X-rays SPECT imaging with medium-energy collimator

S. Woo[1,2], *W. Kim*[1], *H. Sheen*[1], *C. Lee*[2], *K. Song*[3], *S. Lim*[2], *I. Lim*[2];
[1]*Division of applied RI, Korea Institute of Radiological and Medical Sciences, Seoul, KOREA, REPUBLIC OF,* [2]*Department of Nuclear Medicine, Korea Institute of Radiological and Medical Sciences, Seoul, KOREA, REPUBLIC OF,* [3]*Department of Urology, Korea Institute of Radiological and Medical Sciences, Seoul, KOREA, REPUBLIC OF.*

Aim/Introduction: Alpha emitted radioisotopes have a high radiation weighting factor. For this reason, the acquisition of acceptable quality of the alpha emitted radioisotope image has highly challenging. The aim of this study was the acquisition of ^{225}Ac produced gammas and X-rays for SPECT image with a medium-energy collimator. **Materials and Methods:** The National Electrical Manufacturers Association (NEMA) standard NU 4-2008 phantom filled with 115.7 μCi of a ^{225}Ac was scanned by Inveon multimodality scanner (Siemens Preclinical Solution, Knoxville, TN). The NEMA NU 4-2008 phantoms is a 50-mm-long, 30-mm-diameter cylinder and consist of different regions to analyze 3 distinct aspects of image quality. The first 20 mm of the phantom body are solid, with 5 fillable rods with diameters of 1, 2, 3, 4, and 5 mm. SPECT data acquired using 3 mm medium energy pinhole collimator. Two photopeak energy window setting was acquired as 86 (± 20% from ^{225}Ac, ^{213}Bi), 218 (± 20% from ^{221}Fr, ^{213}Bi), 440 (5% ^{213}Bi) keV. To correct the scatter and background, performed the triple-energy-window method. The acquired data were reconstructed by maximum a posteriori (MAP) 3D reconstruction (iteration 16 and subset 6) with point spread function (PSF) mode. The evaluation of images quality was performed by uniformity and full width half maximum (FWHM). In addition, we acquired ^{225}Ac SPECT mice image. **Results:** We are able to visualize the 2, 3, 4, and 5 mm diameter rods in the 86 keV X-ray image whereas 1, 2, 3, 4, and 5 mm diameter rods are visualized in gamma-ray image. The uniformity of 86, 218, and 440 keV with PSF were 0.50, 0.84, and 0.54, respectively. The FWHM of 86, 218, and 440 keV were 1.78 ± 0.12, 1.89 ± 0.07, and 1.50 ± 0.05 mm, respectively. The relative change of 86 keV compare to 440 keV uniformity and FWHM were 7.5 % increase and a 15 % decrease. According to the acquired ^{225}Ac SPECT of mice image, the radioisotope was highly uptake in liver area. **Conclusion:** X-ray image produced ^{225}Ac decay chain was similar uniformity as well as FWHM of its gamma-ray. The result of this study presented the importance of X-ray production of ^{225}Ac decay chain to improve the SPECT image quality with a medium-energy collimator. **References:** Robertson, A. K. H., et al. "Multi-isotope SPECT imaging of the 225Ac decay chain: feasibility studies." Physics in Medicine & Biology 62.11 (2017): 4406.

EP-0945

Beyond Nema For Modern Spect Cameras

A. Alosaimi[1,2], *S. Patford*[3], *J. Smith*[3];
[1]*King Fasial Medical City for Southern Region, Riyadh, SAUDI ARABIA,* [2]*Queensland University of Technology, Brisbane, AUSTRALIA,* [3]*Royal Brisbane and Women's Hospital, Brisbane, AUSTRALIA.*

Aim/Introduction: National Electrical Manufacturer Association (NEMA) published several standards to provide uniform

quality control (QC) tests for scintillation camera performance. Unfortunately, these guidelines do not include tests for the SPECT/CT systems, particularly the involvement of CT in the SPECT images. Therefore, this study aims to develop an extension to NEMA NU 1 standard to include additional QC specification. These are: (1) SPECT/CT Spatial registration, (2) CT attenuation correction accuracy and (3) whole-body SPECT/CT scan uniformity. **Materials and Methods:** Test (1) was performed by using either plastic IV tube filled with oral CT contrast solution mixed with ^{99m}Tc or 1 mm diameter metallic line sources filled with only ^{99m}Tc. The fusion registration misalignments were quantified with the scanner software in 6 degrees of freedom. Test (2) was accomplished by using a 20 cm diameter cylindrical phantom, which was filled with approximately 200 MBq of ^{99m}Tc. ROI of areas ranging from 0.7 cm^{2}to 13 cm^{2}centred on the trans-axial slices were used. Test (3) was performed by acquiring a SPECT of a line source over two contiguous bed positions. The uniformity line profile was obtained by taking the sum of the counts in each SPECT slice as a function of slice location. **Results:** It was found that the software needed adequate contrast for both SPECT and CT images to accurately detect the two line sources for fusion. The counts in a ROI on the non-CT attenuation corrected SPECT image was compared to the same ROI on the CT attenuation corrected SPECT image. The maximum deviation from the average counts and its slice location were reported as percentage non-uniformity. **Conclusion:** In order to achieve accurate registration result, the metallic line source phantom is recommended. The accuracy of attenuation coefficient for water applied can be imperially determined. The maximum non-uniformity artefact result was satisfied. **References:** 1.Chakraborty, D., Bhattacharya, A., Gupta, A. K., Panda, N. K., Das, A., & Mittal, B. R. (2013). Skull base osteomyelitis in otitis externa: The utility of triphasic and single photon emission computed tomography/computed tomography bone scintigraphy. Indian journal of nuclear medicine: IJNM: the official journal of the Society of Nuclear Medicine, India, 28(2), 65. 2.NEMA (2013) NEMA Standards Publication NU 1-2012. Performance Measurements of Gamma Cameras. National Electrical Manufacturers Association Virginia 3.Bailey D, Humm J (2014) Nuclear Medicine Physics: A Handbook for Teachers and Students. IAEA4.Cherry SR, Sorenson JA, Phelps ME (2012) Physics in nuclear medicine, vol4th;4;. vol Book, Whole. Elsevier/Saunders, Philadelphia

EP-0946

Dual-Isotope Peptide Receptor Radionuclide Therapies with ^{177}Lu and ^{90}Y: Is Quantitative Imaging Possible?

C. Miller[1], *A. Rahmim*[1,2,3], *A. Celler*[2];
[1]*Department of Physics, University of British Columbia, Vancouver, BC, CANADA,* [2]*Department of Radiology, University of British Columbia, Vancouver, BC, CANADA,* [3]*Department of Integrative Oncology, BC Cancer Research Centre, Vancouver, BC, CANADA.*

Aim/Introduction: Peptide receptor radionuclide therapy using DOTATATE labeled with ^{177}Lu or ^{90}Y is a promising treatment for neuroendocrine tumours. However, Kunikowska et al. (2011) has shown that using these two isotopes simultaneously results in better patient outcomes. As ^{90}Y emits higher energy β- particles than ^{177}Lu, personalized dosimetry should be performed to not exceed dose limits to critical organs while optimizing tumour control. Kidneys are the critical organs in this therapy, and large variations in their doses have been observed. Assuming identical biodistributions of ^{177}Lu- and ^{90}Y-DOTATATE, dosimetry can be performed using ^{177}Lu SPECT imaging. Only ^{177}Lu emits suitable photons for imaging, while ^{90}Y is a pure β- emitter and cannot easily be imaged. Moreover, Bremsstrahlung photons created by ^{90}Y can cloud the ^{177}Lu spectrum, making activity quantification inaccurate. This work aims to determine if dosimetry based on quantitative imaging of ^{177}Lu in the presence of ^{90}Y is possible. **Materials and Methods:** Monte Carlo GATE simulations were performed of spheres containing ^{177}Lu, ^{90}Y, or both placed in a phantom filled with cold water, water with ^{90}Y, or water with ^{90}Y+^{177}Lu. Eighteen different concentrations of ^{177}Lu and/or ^{90}Y in the spheres and seven different background configurations were imaged with a simulated Siemens Symbia camera. Concentrations of each isotope were chosen based on injected activities which would not exceed dose limits to critical organs. The quantification accuracy and noise distribution were determined for every configuration. **Results:** With no background in the phantom, quantification error of ^{177}Lu remained below 12% for low concentrations of ^{177}Lu (0.3 MBq/ml) and 3% for high concentrations (2 MBq/ml) for all ^{177}Lu to ^{90}Y sphere ratios. With ^{90}Y+^{177}Lu background, the error ranged from 6% for low background ratios (1:10 background to ^{177}Lu-source) to 24% for high ratios (1:3 background to ^{177}Lu-source). The noise levels ranged from 20% for low concentrations of ^{177}Lu in the sphere to below 5% for high concentrations. **Conclusion:** Activity quantification of ^{177}Lu in the presence of ^{90}Y is achievable with an acceptable margin of error (< 15%) at low and high ratios of ^{177}Lu to ^{90}Y-sphere activity (maximum ratio 1:6) and moderate ratios of background to ^{177}Lu-source activity (maximum ratio 1:5). Errors are high (> 20%) with high background ratios (1:3) but this is rarely seen in patients. This suggests that quantitative dosimetry in dual isotope PRRT is possible. **References:** Kunikowska et al., Eur J Nucl Med Mol Imaging, 2011. 38(10):1788-97.

EP-0947

Shorter Dynamic Planar Scintigraphy to Estimate Myocardial [^{123}I]-MIBG Washout Rates

Y. Kumakura, Y. Shimizu, K. Ichikawa, N. Yoshida, K. Nomura; Saitama Medical Center, Saitama Medical University, Kawagoe, JAPAN.

Aim/Introduction: The heart-to-mediastinum ratio (HMR) and washout rate (WR) have served as simple semi-quantitative indices of myocardial [^{123}I]-MIBG scintigraphy for more than two decades. However, it is burdensome and inconvenient for patients with Parkinsonian symptoms to undergo the conventional scanning protocol, which demands two scans

approximately three hours apart. We introduced a short (30 min) dynamic planar imaging procedure, and have just completed scanning of approx. 240 patients suspected of Lewy body diseases. A pharmacokinetic model similar to a [^{18}F]-FDOPA inlet-and-outlet model (Kumakura et al., 2007) was applied to the TACs after correction for plasma and myocardium-specific counts. Then, we investigated the relationship between the semi-quantitative indices and the new kinetic indices indicative of [^{123}I]-MIBG loss from myocardium as well as unidirectional uptake to catecholamine storage vesicles. **Materials and Methods:** For now, a total of consecutive 130 patients suspected of LBDs were analyzed and reported here. We used a conventional two-detector SPECT camera (GE Discovery NM 630) equipped with ELEGP collimators. The dynamic imaging was started immediately after a bolus injection of 111 MBq of [^{123}I]-MIBG. To obtain TAC-based "input functions", we used mediastinum TACs after smoothing with a three-phase exponential decay function, a population-based blood-to-plasma ratio (BPR) curve, and a population-based metabolite correction (PBMC) curve. The two correction curves were published by another group. (Wu et al., 2016). We subtracted the smoothed mTACs from the hTACs to isolate myocardium-specific TACs. Then, we calculated magnitudes of three new indices representing unidirectional uptake (iUp), loss rate (iLoss), and non-specific distribution to myocardial interstitial space (iNs) for comparison with those of HMR and WR. **Results:** No patient failed. Linear regression analysis revealed that iUp/iLoss (an index of vesicular storage) was a significant predictor of delayed HMR (slope: 0.375, P< 0.0001, R2: 0.97) as well as early HMR (slope: 0.264, P< 0.0001, R2: 0.97). We found that 0.693/iLoss (min: pharmacological half life of [^{123}I]-MIBG trapped in myocardium) was a significant predictor of WR (slope: -0.0545, P< 0.0001, R2: 0.71). The mean of 0.693/iLoss was 15 min. **Conclusion:** In view of replacing the conventional 3h protocol, we confirmed that the HMRs and WR can be predicted from the new indices obtained from the 30 min planar dynamic procedure. It proved to be clinically feasible and well suited to quantitation of [^{123}I]-MIBG turnover and storage capacity in the sympathetic myocardial nerve terminals. **References:** Kumakura et al., PMID: 17652599; Wu et al., PMID:27081169.

EP-0948

"Fast" SPECT/CT, a new possibility for the assessment of bone metastasis as add-on to planar bone scintigraphy. Preliminary study in 31 patients

A. Baena[1], *M. Cruz-Montijano*[2], *S. García-Martínez*[2], *M. Pajares-Vinardell*[2], *J. Freire-Macias*[2], *M. De Bonilla*[2], *F. Partida-Palma*[2], *T. Gutierrez-Amares*[2];
[1]*Hospital Universitario Puerta del Mar, Cadiz, SPAIN,*
[2]*Hospital Universitario Puerta del Mar, Cádiz, SPAIN.*

Aim/Introduction: The aim of this study is to assess whether a "fast" acquisition SPECT/CT (SPECT-CT-F) can replace the standard SPECT/CT (SPECT/CT-S) study for the investigation of suspicious bone metastases after a whole-body bone scan (WB-BS). **Materials and Methods:** A total of 31 patients with a history of oncological disease and metastasis suspicion in a WB-BS that needed a SPECT/CT-standard and also underwent a SPECT-fast were included. Of the total number of patients, 60% were women. 38% had breast cancer, 29% prostate cancer, 16% other cancers and 16% suspected oncology. All studies were performed using a single low-dose CT scan, which was used for both rapid and standard SPECT. SPECT parameters were the following: a) SPECT-standard: 128x128 matrix, zoom factor 1, 20 s/view, 60 views; b) SPECT-fast: 128x128 matrix, zoom factor 1, 10s/view, 30 views. Obtaining total acquisition times of 14 min and 7s for the SPECT-standard and 3 min and 50 s for the SPECT-fast. The studies were independently evaluated by 3 nuclear medicine doctors with more than 20 years of experience, who independently judged each study (standard and fast SPECT). Findings were classified as metastatic, equivocal, benign or normal (negative for metastasis). The agreement between observers and intra-observer concordance between SPECT-standard and SPECT-fast was calculated. Statistical analysis of the results was performed using Cohen's Kappa. **Results:** Using SPECT/CT-S, 22 patients (71%) were classified as benign findings, 7 patients (22.6%) were classified as malignant findings and 2 patients were classified as equivocal findings (6.4%). There was a 80% (25/31) of agreement between the three evaluators (same diagnosis) in WB-BS and SPECT-standard. Of these 25 studies, 84% were benign findings and 16% were classified as malignant. A 100% of agreement was found between standard and fast SPECT for the same evaluator. **Conclusion:** This preliminary study can conclude that SPECT-fast may be useful in bone scintigraphy studies for discrimination between a benign and malignant finding in the context of oncological patients with suspicion of a single bone metastasis, making it possible notably reduce the SPECT acquisition time without compromise diagnostic value. **References:** Palmedo H, Marx C, Ebert A, Kreft B, Ko Y, Turler A, et al. Whole-body SPECT/CT for bone scintigraphy: diagnostic value and effect on patient management in oncological patients. Eur J Nucl Med Mol Imaging. 2014;41:59-67.

EP-0949

A rapid protocol to evaluate myocardial flow reserve with myocardial scintigraphy using CZT camera and Regadenoson

J. Pinaquy, *Q. Ceyrat*, *T. Couffinhal*, *H. Douard*, *F. Debordeaux*, *L. Bordenave*;
CHU, Bordeaux, FRANCE.

Aim/Introduction: Cardiac positron emission tomography (PET) is superior to single-photon emission computed tomography(SPECT) thanks to its quantitative analysis capabilities, especially for measuring myocardial blood flow (MBF) and myocardial flow reserve (MFR). The recent development of new cadmium zinc telluride (CZT) gamma cameras has enabled dynamic acquisition, allowing measurement of MBF and MFR.This prospective study

aimed to validate a rapid protocol, using Regadenoson, and to analyse the standard images from myocardial perfusion imaging (MPI) without any loss of information. **Materials and Methods:** From February to June 2018, 10 patients were prospectively enrolled in our study to evaluate the MBF and MFR. Patients were imaged using a solid-state dedicated cardiac camera (Discovery NM530c). All patients underwent a 1-day gated rest-stress protocol. Concomitant with the intravenous bolus administration of the resting ^{99m}Tc-tetrofosmin dose of 2.5 MBq/kg, a list-mode acquisition was started for 6 min immediately prior to the standard 10 min acquisition. On completion of the resting state images, pharmacological stress was induced using regadenoson. At the vasodilation peak , the second dose of ^{99m}Tc-tetrofosmin of 8 MBq/kg was injected, and 6 min of list-mode data was collected at the time of the injection, after which the standard acquisition of stress MPI over 5 min was realized. List-mode dynamic data were reformatted and reconstructed using Corridor4DM software(INVIA) into five different reconstruction models: three of 6 min (test 1: 21×3s, 1×9s, 1×15s, 1×21s, 1×27s, and 7×30s [32 frames]; test 2: 30×3s and 18×15s [48 frames]; and test 3: 60x 3s and 6x30s [66 frames]); and two of 4 and 3 min (20x3s and 6x30s [26 frames]; and 20x3s and 4x30s [24 frames], respectively). The primary endpoint was the difference between the five models, the secondary endpoint the image quality of the MPI. **Results:** The average age of the patients was 68.5 years and 40% were female. The study population had an average body mass index (BMI) of 28.4 kg/m²and all of the patients had at least one cardiovascular risk factor.The 6-min tests highlighted no significant difference in the flow measurement and MFR (p=0,15), and appears by decreasing acquisition time (<4 min). The image quality did not differ significantly (p=0.6) between dynamic acquisition and standard acquisition. **Conclusion:** We determined a fast (12 min), reliable and reproducible protocol with minimal mobilization of the patient, to flow measurements. This will enable reliable analysis MFR while maintaining both qualitative visual and functional data. **References:** None.

EP-0950

Evaluation of Veriton™ 360° CZT-camera performances for quantitative Dopamine Transporter (DaT) Imaging: a SPECT study based on quality and anthropomorphic phantoms

E. Cassol[1,1], *P. Gantet*[1], *P. Payoux*[1,2];
[1]*Department of Nuclear Medicine, University Hospital of Toulouse Purpan, Toulouse, FRANCE,* [2]*ToNIC Toulouse Neuroimaging Center, Toulouse University, Inserm, Toulouse, FRANCE.*

Aim/Introduction: Dopamine Transporter (DaT) imaging can be performed in SPECT on Anger-cameras either equipped with parallel (LEHR) or convergent collimators (Fan-Beam). Last year, a 3D Cadmium-Zinc-Telluride (CZT)-camera became commercially available. The VERITON™ system (Spectrum Dynamics Medical), uses 12 independent detector arms to provide 360° coverage. Our aim is to evaluate the performances of Veriton on Jaszczak phantom and to test acquisition modes and reconstruction parameters impact for binding potentials (BP) quantification in a striatal phantom. **Materials and Methods:** The Jaszczak Phantom™ containing the cold rods insert and 6 cold-spheres was filled with 267MBq of Iodine (^{123}I). Acquisitions were successively performed on Veriton and on DiscoveryNM/CT670 (General Electric Healthcare) with LEHR and Fan-Beam collimators. The striatal anthropomorphic phantom (Radiology Support Device, RSD) was filled with 28MBq of ^{123}I to achieve the following BP: 6.0 for right and left caudate nuclei, 6.0 for the right putamen and 2.4 for the left-one. On Veriton, acquisitions were performed in "non- brain- and striatum-focus modes" on Discovery670, with LEHR and Fan-Beam in 4 and 8 minutes. Iterative reconstructions were performed with different number of iterations. For each configuration, the number of counts was recorded. Image quantification was done with DaTsoft3D (Imsoft, Toulouse) to determine integral-non-uniformity percent, Contrast-to-Noise ratio (CNR) and BP. CNR variation was studied with sphere-diameter and number of iterations. The mean absolute error (MAE) was calculated between expected and measured BP values. **Results:** Image quality is improved with Veriton except for the spatial resolution observed to be more accurate on Fan-Beam images. The integral non-uniformity is lower and the volumetric sensitivity is 6.99×10^{6}cps/(MBq.ml^{-1}) versus 3.17×10^{6}cps/(MBq.ml^{-1}) for LEHR-Discovery. For all spheres, the CNR-value increases with the number of iterations (up to the 20th). Veriton-CNR is higher, from 1.5 to 2 times for spheres between 12 and 25mm diameter even though the small sphere remains difficult to detect due to its low CNR-value. In RSD, the relative pixel count-rate is 2.54; 1.93; 1.44; 1.71 for respectively striatum, brain, non "focus modes" and FB (1 is for LEHR). With "low" counts level, the MAE increases over 6 iterations but MAE is minimized with the "Brain-Focus" acquisition mode (under 0.2). **Conclusion:** For same acquisition-time, thanks to the focus mode, pixel-count is strongly increased when compared to LEHR-Discovery. ^{123}I-DaTscan image quality is not improved with Veriton when compared to Fan-Beam-Discovery. Binding potentials in brain compartments can be quantified with good accuracy if image-statistics are over 1.5Mcts. **References:** None.

EP-0951

Impact of acquisition and reconstruction parameters on cardiac perfusion imaging using the new 360° CZT VERITON camera

A. Manrique[1,2], *A. Bouthiba*[1], *B. Enilorac*[2], *P. Tager*[2], *C. N'Ganoa*[2], *N. Roth*[3], *D. Agostini*[1,2];
[1]*Normandie Université - EA 4650, Caen, FRANCE,* [2]*CHU de Caen, Caen, FRANCE,* [3]*Spectrum Dynamics, Caesarea, ISRAEL.*

Aim/Introduction: The Veriton camera (Spectrum Dynamics, Caesarea, Israel) is a multi-purpose SPECT scanner that uses 12 independent CZT detector arms to provide 360-degree coverage with minimal photon loss. The aim of this study was to assess the impact of a focus mode that allows a cardiocentric acquisition to increase sensitivity and resolution compared

to conventional circular orbit. **Materials and Methods:** We used the anthropomorphic torso phantom (Data Spectrum, Hillsborough, NC) with the cardiac insert filled with a solution of 99mTc (myocardium: 22 kBq/ml, liver: 35 kBq/ml, mediastinum: 1.2 kBq/ml). A defect (5,4 ml) filled with cold water was placed successively in inferolateral and anteroseptal positions. A series of 10 min list mode acquisitions was performed using successively automatic or manual body contour, with both circular orbit and cardiac focus. Acquisitions were reframed to 4 different acquisition durations (2.5, 5, 7.5 and 10 minutes) and processed using OSEM alone (40 iterations) or after applying a proprietary (Spectrum Dynamics) cardiac model (SD). Defect size and cardiac volume were measured using QPS and QGS. Resolution, assessed as the FWHM of the defect-free wall, and contrast-to-noise ratio (CNR) were calculated using ImageJ. Statistical analysis was performed using linear model (body contour, cardiac focus and acquisition duration were forced in the model). **Results:** Count statistics were increased by cardiac focus ($p<0.0001$), automated body contouring ($p<0.0001$) and acquisition duration ($p<0.0001$). FWHM was independently improved by using automated body contouring ($p<0.0001$) and SD reconstruction ($p<0.0001$). CNR was only increased by using SD reconstruction. The measurement of defect size was improved by cardiac focus ($p<0.001$), automated body contouring ($p<0.0001$) and increased acquisition duration ($p<0.05$). Finally, ventricular volume was overestimated by SD vs. OSEM (74±5.3 ml vs. 63±4.8 ml, $p<0.0001$) and to a lesser extent by automated vs. manual body contouring (70±7ml vs. 67±7 ml, $p<0.01$). **Conclusion:** When using the new 360° CZT Veriton camera, cardiac focus and automated body contouring improved both count statistics and resolution and resulted in an improved assessment of perfusion defects. Using a cardiac model in the reconstruction process improved contrast-to-noise ratio and resulted in an increased ventricular volume. **References:** None.

EP-0952

GATE-based simulations of the performance of the Symbia Intevo SPECT/CT system for evaluating novel image reconstruction algorithms

H. Kertesz[1], *N. Denisova*[2], *M. Ondar*[2,3], *J. Cal-Gonzalez*[1], *I. Rausch*[1], *P. Schaffarich*[1], *T. Beyer*[1];
[1]*QIMP Team, Center for Medical Physics and Biomedical Engineering, Vienna, AUSTRIA,* [2]*Khristianovich Institute of Theoretical and Applied Mechanics, Siberian Branch of Russian Academy of Sciences, Novosibirsk, RUSSIAN FEDERATION,* [3]*Novosibirsk State Technical University, Novosibirsk, RUSSIAN FEDERATION.*

Aim/Introduction: To model and evaluate the performance of a state-of-the-art SPECT/CT system (Siemens Symbia Intevo) using GATE simulations as part of an ongoing project for the validation of a novel image reconstruction algorithm using local regularization (MAP-L). **Materials and Methods:** The SPECT system is made of two NaI-based detector heads (59.1x44.5x0.95cm³). The useful field-of-view (UFOV) is 53.3x38.7cm.Low-energy high-resolution (LEHR) collimator was modelled, which is made of lead with hexagonal holes (diameter of 1.11mm, height 24.05mm, septal thickness 0.16mm).The SPECT model was evaluated following the NEMA NU1-2007 protocol for system planar sensitivity (SPS) and intrinsic spatial resolution (ISR). For the evaluation of the SPS a Petri dish (diameter 150mm, height 15mm) filled with 125MBq ^{99m}Tc was used. The evaluation of the ISR was done with the NEMA X-Y phantom made of a 3mm thick lead plate with 1mm slits positioned at a distance of 30mm. A point source (1GBq activity ^{99m}Tc) was placed in a lead shielded holder at a distance of 270 cm from the detector. The full-with half-maximum (FWHM) and full-width tenth-maximum (FWTM) were calculated for the UFOV and the central field-of-view (CFOV) corresponding to 75% of the UFOV. The simulated values were compared to the measured reference values that were obtained previously during the acceptance test of the system. The ISR in Y direction was not available in the acceptance test. **Results:** The simulated SPS with the LEHR collimator at 10cm distance was 92.8 (measured 88.7) cps/MBq and 93.8 (89.0) cps/MBq for detector 1 and 2, respectively. The ISR in X direction was 3.3mm (3.5mm) FWHM for both UFOV and CFOV, 6.3 (6.8mm) FWTM for UFOV and 6.4 (6.8mm) FWTM for CFOV. In Y direction the simulated ISR was 3.1mm FWHM and 6.1mm FWTM for both UFOV and CFOV. **Conclusion:** The proposed SPECT model showed good accuracy with less than 6% discrepancies in comparison to the measured reference values. The application of the model for the evaluation of novel image reconstruction algorithms in simulated numerical phantoms is work in progress. The model will be extended and validated with the high-energy collimator for ^{131}I simulations and will be available online. The financial support of the Austrian FWF Project I3451-N32 is gratefully acknowledged. **References:** None.

EP-0953

Head to head comparison of General Electric Swiftscan solution versus Siemens Symbia in bone scintigraphy on NaI-camera

M. Bailly, *F. Thibault*, *G. Le Rouzic*, *G. Metrard*;
CHR Orléans, Orleans, FRANCE.

Aim/Introduction: General Electric (GE) Swiftscan solution combines a new Low Energy High Resolution and Sensitivity collimator (LEHRS) with image processing (Clarity 2D) and tomographic step and shoot continuous mode. The aim of this study was to compare clinical and physical performances of this new technology in bone scintigraphy with Siemens Symbia. **Materials and Methods:** Physical phantom measurements were performed using GE pre-production LEHRS, GE Low Energy High Resolution (LEHR) and Siemens LEHR collimators, followed by a prospective clinical study approved by an ethic committee. 67 patients referred for bone scintigraphy were enrolled from February to July 2018. Whole-body, static acquisitions, and when needed SPECT were performed 2 hours after injection of 9.25

MBq/kg Tc-99m-methylene-diphosphonate (MDP). Each patient underwent two acquisitions consecutively on GE and Siemens gamma-camera, using respectively pre-production Swiftscan and LEHR collimator (order of passage was randomized). All the images were anonymized and blind-analyzed by 2 board certified nuclear medicine physicians. Image quality was visually scored and contrast over nose ratio was measured on whole-body scans. **Results:** Maximum sensitivity was 100 cts/MBq for Siemens LEHR on planar acquisitions. GE SwiftScan LEHRS and GE LEHR maximum sensitivity were respectively 9% and 22% lower. Using Clarity 2D, GE Swiftscan LEHRS spatial resolution was the best with 9.2 mm versus 10.1 mm and 10.6 mm for GE LEHR and Siemens LEHR collimators. In tomographic mode, the sensitivity of GE Swiftscan solution was superior to both LEHR systems (16% and 25% respectively for Siemens and GE). There was no significant difference in spatial resolution. In clinical use, signal was higher on Siemens system and noise was lower on GE Swiftscan solution. Contrast-to-noise ratios were not significantly different between the two systems. There was a significant image quality improvement with GE SwiftScan in planar images ($p<0.001$ for both observers) and in whole body scan ($p<0.05$ for one of the observers). No significant difference in image quality was observed on SPECT images. **Conclusion:** GE SwiftScan collimator design improved sensitivity compared to "classical" GE LEHR collimator without compromising resolution. Adding Clarity 2D, SwiftScan solution strongly enhances whole-body and planar image quality. In SPECT mode, it improves volumetric sensitivity without impacting image quality and can lead to time or dose reduction. **References:** None.

EP-0954

Effects of acquisition time, energy window width and matrix size on image quality in bone SPECT acquired using a general-purpose CZT gamma camera

S. Arvola[1], *M. Seppänen*[1,2], *T. Noponen*[1,3];
[1]*Department of Clinical Physiology and Nuclear Medicine, Turku University Hospital, Turku, FINLAND,* [2]*Turku PET Centre, Turku, FINLAND,* [3]*Department of Medical Physics, Turku University Hospital, Turku, FINLAND.*

Aim/Introduction: Cadmium zinc telluride (CZT) gamma camera has superior spatial resolution, energy resolution and sensitivity compared to conventional NaI(Tl) scintillator camera. The purpose of this study was to evaluate the effects of shorter acquisition time, narrower energy window and larger image matrix on the image quality of bone SPECT acquired using a CZT gamma camera. **Materials and Methods:** Ten prostate cancer patients at high risk of bone metastases underwent ^{99m}Tc-HMDP SPECT/CT examinations using Discovery NM/CT 670 CZT camera (GE Healthcare, Tirat Carmel, Israel). The data were acquired in list mode with three bed positions, 13 s/projection (about 48 min total acquisition time), ±7.5% energy window centered at 140 keV, and a 128 x 128 matrix. The SPECT data were reframed using Lister program of Xeleris 4.0 server (GE Healthcare, Tirat Carmel, Israel) to produce data sets with the total acquisition times of about 40, 30, 25, and 20 min, with the energy window widths of ±5, ±4, ±3, and ±2%, and with a 256 x 256 matrix size. From the reconstructed images, skeletal lesions were segmented using an SUV threshold which varied between different lesions but was constant for the same lesion in different images. Areas of normal appearing bone adjacent to the lesions were segmented to evaluate lesion contrast and background noise. Volumes and mean, peak and maximum SUVs of the lesions were also measured. **Results:** A total of 50 lesions were analyzed. Shorter acquisition time did not significantly affect lesion contrast. Narrower energy windows of ±5, ±4, ±3, and ±2% increased lesion contrast on average by 3, 7, 6, and 11%, respectively. Matrix size did not significantly affect lesion contrast. Noise was significantly higher in all reframed images. The mean SUVs, peak SUVs, and lesion volumes were significantly different only between the original images and the images corresponding to 256 x 256 matrix. Maximum SUVs were not significantly different between the original and any of the reframed images. **Conclusion:** Based on this study, shorter acquisition time and larger image matrix do not significantly affect lesion contrast, while narrower energy window slightly increases lesion contrast in bone SPECT acquired using a CZT camera. Lesion volumes and SUVs are only affected by larger image matrix. A more thorough analysis based on visual evaluation by experienced nuclear medicine physicians will reveal the optimal acquisition parameters, which provide images with sufficient contrast-to-noise ratio. **References:** None.

EP-0955

Monte Carlo simulations of pre-clinical SPECT systems with ^{99m}Tc and ^{188}Re sources

M. Beliš[1,2], *K. Van Hecke*[1], *T. Cardinaels*[1,3], *S. Vandenberghe*[2];
[1]*SCK•CEN, Mol, BELGIUM,* [2]*Ghent University, Ghent, BELGIUM,* [3]*KU Leuven, Leuven, BELGIUM.*

Aim/Introduction: Rhenium-188 (^{188}Re) is a β^-emitting radionuclide ($t_{1/2}$ = 17.0 h, E_{max} = 2.1 MeV), suitable for radiotherapeutic applications. In addition, it emits a 155 keV γray (15 %), which can be used for imaging with current SPECT (single-photon emission computed tomography) systems. However, several high-energy γrays in emission spectrum of ^{188}Re, together with radiation produced by β^-particles (Bremsstrahlung), may complicate quantitative imaging. The aim of our research is to simulate the spectra of detected events with ^{188}Re sources and compare with the SPECT gold standard, technetium-99m (^{99m}Tc). These simulations provide useful information about the amount of contamination, their origin, the scatter fraction and the detection efficiency with various parameters of a collimator. **Materials and Methods:** GATE software (Geant4 Application for Tomographic Emission) was used to execute Monte Carlo simulations. Point and volume sources of ^{99m}Tc and ^{188}Re were used in the simulations, either directly or wrapped in water-filled phantoms. Single-crystal NaI detectors (50×50×4 mm) were positioned at several distances from the center of the system. Various setups were simulated,

with no collimator present in the system, or using simplified tungsten collimator plates. The low-energy collimator plates had 1 or 20 lofthole openings (a gradual change from a circular aperture to a rectangular end). Novel high-energy collimator with loftholes was used for comparison as well. **Results:** Current results show an acceptable effect of the high-energy γ-rays from the ^{188}Re emission spectrum in the optimal energy window around 155 keV. However, a decrease of the spatial resolution in these small systems may be caused by penetration of high-energy photons or by the primary β$^-$particles reaching the detector. More than 60 % of the detected events in the energy window 155 ± 15 keV are primary events. On the other hand, scattering in the collimator is significantly low (4 % of the events). Most of the scattered photons are coming from the scattering in the phantom and the detector itself (crystal and backscatter from the electronics). These results will be confirmed by phantom studies with ^{188}Re and compared to experiments with ^{99m}Tc. **Conclusion:** Obtained results are promising for usage of ^{188}Re as a theranostic agent - both for the therapy and imaging - without the necessity of administration radiopharmaceuticals with pure diagnostic radionuclides. **References:** None.

EP-0956

Image quality and SUV accuracy evaluation of bone SPECT-CT images using new available techniques: xSPECT Bone® and xSPECT Quant®

V. Moran[1], *P. Aguilar*[2], *E. Prieto*[2], *E. Guillén*[1], *L. Sancho*[1], *J. Richter*[2], *J. Martí-Climent*[2];
[1]*Clinica Universidad De Navarra, Madrid, SPAIN,* [2]*Clinica Universidad De Navarra, Pamplona, SPAIN.*

Aim/Introduction: xSPECT-Bone® (xB) and xSPECT-Quant® (xQ) are new reconstructions that produce quantitative ^{99m}Tc-HDP-SPECT images. The aims of this study were to assess xB and xQ image quality in comparison to Flash-3D (F3D), and to compare SUV accuracy of SPECT images for both xB and xQ. **Materials and Methods:** A NEMA image quality phantom was scanned using a Symbia-Intevo SPECT-CT (Siemens). The phantom was filled with ^{99m}Tc, resulting in a sphere-to-background ratio of 5.3:1 and the spheres were also loaded with CT contrast to achieve around 350 HU in the CT image. SPECT-CT images were acquired with 1.5 and 4.5 million total counts for both 128 and 256 matrix size. Images were reconstructed with xB, xQ and F3D at 12, 24, 48 and 96 updates, 10mm postsmoothing, with attenuation and window based scatter corrections. A qualitative evaluation of image quality was performed with fixed reconstruction settings (48i, 1s, FWHM=10mm). Background variability (BV), hot-sphere-contrast (Q_H) and mean signal-to-noise ratio (SNR_{mean}) for each sphere, reconstruction and acquisition were measured. Mean recovery coefficient (RC_{mean}) was also measured for different diameters using xB and xQ. **Results:** xB reported better spatial resolution than xQ and F3D. Spheres with ø ≥ 22, 28 and 37 mm were detected in xQ, F3D and xB images (4.5-Mcounts). Spheres with ø≥28 mm were perceptible for both xQ and F3D and with ø≥37 mm for xB (1.5-Mcounts). BV was similar for xQ and xB, and higher than for F3D. For all spheres and updates, BV was within the range [6.4%-25.3%], [6.0%-26.6%] and [2.9%-10.2%] with xQ, xB and F3D (4.5-Mcounts); and [3.1%-37.6], [2.9%-39.4%] and [5.2%-20.9%] in 1.5-Mcounts images. Q_H was only above 70% for spheres with ø≥17 mm (xB) and ø≥37 mm (xQ). Q_H with F3D was below 70% regardless the updates for all spheres. SNR_{mean} was lower for xQ than for xB and F3D, regardless total counts. There was no substantial difference between SNR_{mean} for F3D and xB. SUV accuracy (RC_{mean}) was better for xB than for xQ. xB offered much higher recovery for the largest sphere (>85% for 1.5-Mcounts, >90% for 4.5-Mcounts) than xQ (>75% for both acquisitions). **Conclusion:** xB performance was better than xQ and F3D. Image quality did not differ significantly between xQ and F3D. SUV accuracy of bone SPECT images using xB is better than using xQ. Overall, xB did not only produces considerably better image quality, but also yield more accurate SUV value. **References:** None.

EP-0957

Synthetic planar bone scans reprojected from SPECT/CT data have better image quality than original planar bone scans

S. Arvola[1], *A. Sohlberg*[2], *M. Seppänen*[1,3], *T. Noponen*[1,4];
[1]*Department of Clinical Physiology and Nuclear Medicine, Turku University Hospital, Turku, FINLAND,* [2]*Laboratory of Clinical Physiology and Nuclear Medicine, Joint Authority for Päijät-Häme Social and Health Care, Lahti, FINLAND,* [3]*Turku PET Centre, Turku, FINLAND,* [4]*Department of Medical Physics, Turku University Hospital, Turku, FINLAND.*

Aim/Introduction: The purpose of this study was to evaluate the image quality of synthetic planar bone scans reprojected from SPECT/CT data. **Materials and Methods:** Fifteen prostate cancer patients at high risk of bone metastases underwent ^{99m}Tc-HMDP planar bone scintigraphy and SPECT/CT examinations using Discovery NM/CT 670 CZT camera (GE Healthcare, Tirat Carmel, Israel). SPECT/CT was performed immediately after bone scintigraphy. The SPECT data were acquired in list mode with three bed-positions, 120 projections, 13 s/projection, ±7.5% energy window centered at 140 keV, and a 128 x 128 matrix. The SPECT data were reframed using Lister program of Xeleris 4.0 server (GE Healthcare, Tirat Carmel, Israel) to reduce the time per projection into 5 s, which corresponds to a total acquisition time of about 25 min. The total acquisition time for planar bone scintigraphy was about 20 min. The SPECT data were reconstructed and reprojected into synthetic anterior and posterior planar images using HybridRecon-Oncology 3.0 software (HERMES Medical Solutions AB, Stockholm, Sweden). Benign and malignant skeletal lesions visible in both original and synthetic planar images were segmented using equally sized circular regions of interest (ROIs). Normal bone adjacent to lesion was sampled to calculate lesion to normal bone contrast-to-noise ratio (CNR). Circular ROIs were also placed on a normal rib and adjacent lung tissue to evaluate rib to lung CNR. **Results:** A total of 50 lesions and 15 normal ribs were analyzed.

The synthetic planar bone scans had significantly higher ($p < 0.001$) lesion to normal bone and rib to lung CNRs compared to the original planar bone scans. The median difference between synthetic and original planar bone scans was 205% for lesion to normal bone CNR and 244% for rib to lung CNR. **Conclusion:** Synthetic planar bone scans have better image quality than original bone scans. Therefore, it is possible to synthesize high-quality planar bone scans when only SPECT/CT is acquired decreasing the total acquisition time. Synthetic planar bone scans may also speed up the reading of whole-body SPECT/CT images significantly. **References:** None.

EP-0958

Effect of reconstruction iterations on the SUVs of ^{99m}Tc-HDP SPECT/CT

S. Arvola[1], *I. Jambor*[2], *M. Seppänen*[1,3], *T. Noponen*[1,4];
[1]*Department of Clinical Physiology and Nuclear Medicine, Turku University Hospital, Turku, FINLAND,* [2]*Department of Diagnostic Radiology, University of Turku, Turku, FINLAND,* [3]*Turku PET Centre, Turku, FINLAND,* [4]*Department of Medical Physics, Turku University Hospital, Turku, FINLAND.*

Aim/Introduction: The purpose of this study was to evaluate the effect of changing the number of iterations in ordered subsets expectation maximization (OSEM) reconstruction on the standardized uptake values (SUVs) of ^{99m}Tc-HDP SPECT/CT. **Materials and Methods:** SPECT data from three-bed ^{99m}Tc-HDP SPECT/CT examinations of nine patients acquired on Symbia T6, True Point SPECT/CT scanner (Siemens Healthineers, Erlangen, Germany) were reconstructed using HybridRecon-Oncology (version 2.1, Hermes Medical Solutions, Stockholm, Sweden) OSEM algorithm with 15 subsets and 1, 2, 3, 4, 5, 10 and 20 iterations. The reconstructions included corrections for photon attenuation, scatter and collimator detector response. Counts were converted into SUVs using the SUV SPECT package (Hermes Medical Solutions, Stockholm, Sweden). From the reconstructed images, a total of 52 skeletal lesions, including bone metastases and benign findings, were analyzed. A lesion was first segmented from the reconstructed image (iterations = 1) using a visually appropriate SUV threshold ranging from 5 to 12. Next, the resulting volume of interest (VOI) was copied into other differently reconstructed images of the same patient. Maximum, peak and mean SUVs (SUV_{max}, SUV_{peak} and SUV_{mean}) of the lesions were measured from the VOIs and compared between images reconstructed using different numbers of iterations. The patients also underwent ^{18}F-NaF PET/CT scans within two weeks of ^{99m}Tc-HDP SPECT/CT scans. The SUVs of same lesions were measured from the PET images and used as reference values. **Results:** The median $SUVs_{max}$ were 22.0, 26.6, 29.6, 29.9, 31.2, 34.5 and 36.5, the median $SUVs_{peak}$ were 18.7, 21.9, 23.4, 23.9, 24.4, 26.1 and 27.1, and the median $SUVs_{mean}$ were 14.5, 16.6, 17.3, 17.5, 17.7, 18.3 and 18.5 for SPECT with 1, 2, 3, 4, 5, 10 and 20 iterations and 39.0 ($SUVs_{max}$), 28.5 ($SUVs_{peak}$) and 23.1 ($SUVs_{mean}$) for PET, respectively. All three SUV measures were statistically different between differently reconstructed SPECT images and between SPECT and PET according to Wilcoxon matched-pairs signed rank test ($p < 0.001$). **Conclusion:** The SUVs of ^{99m}Tc-HDP SPECT/CT increase with the number of reconstruction iterations, and a very high number of effective iterations (subsets x iterations) is required to calculate SUVs that are completely converged and close to the corresponding SUVs of ^{18}F-NaF PET/CT. Increasing the number of iterations from 10 to 20 increased the SUVs of ^{99m}Tc-HDP SPECT/CT by less than 6%, suggesting that the SUVs are almost converged by 10 iterations and 15 subsets, with still clinically acceptable processing time of five minutes. **References:** None.

EP-0959

Feasibility and time reduction of I-123 MIBG planar imaging using a CZT-based whole-body camera: phantom study, and clinical study for patients with suspected or known Lewy body diseases

N. Okano[1], *I. Osawa*[1], *S. Tsuchihashi*[1], *K. Fukushima*[2], *I. Kuji*[2], *I. Matsunari*[3];
[1]*Department of Radiology, Saitama Medical University Hospital, Saitama, JAPAN,* [2]*Department of Nuclear Medicine, International Medical Center, Saitama Medical University, Saitama, JAPAN,* [3]*Division of Nuclear Medicine, Department of Radiology, Saitama Medical University Hospital, Saitama, JAPAN.*

Aim/Introduction: Myocardial sympathetic innervation imaging using 123I-metaiodobenzylguanidine (MIBG) has recently been used to diagnose Lewy body diseases (LBD). Using novel "whole-body" cadmium-zinc-telluride (CZT) camera (Discovery NM/CT 670 CZT), the heart-to-mediastinum uptake ratio (HMR) can be directly measured from planar imaging. However, evidence for the feasibility of high-speed cardiac SPECT imaging using CZT-based SPECT systems has been mostly limited to "cardiac-dedicated" CZT-cameras, such as D-SPECT and Discovery 530C. We aim to disclose properties of the novel whole-body CZT scanner in phantom study, and subsequently, explore feasibility and potential time reduction in clinical study. **Materials and Methods:** In phantom study, difference of HMRs according to types of scanners/collimators was evaluated. Images were acquired with referenced collection time/window width, and later, reframed to produce images with different collection times/window widths using Lister-tool to compare their HMRs.In clinical study, MIBG planar imaging was performed in 36 patients with suspected or known LBD. Images with a collection time of 300 seconds were obtained, followed by reframing to produce images with shortened collection times, and HMRs were compared to evaluate collection time-dependent difference. **Results:** In phantom study, the HMRs obtained from the CZT-based camera were lower than those obtained from the Anger camera with medium-energy general-all-purpose collimators, but were comparable to those obtained from the Anger camera with low-energy ultra-high-resolution collimators. The difference in HMRs between the normal and disease models were reduced as the window widths increased. The HMRs almost unchanged when the collection time was >

50 seconds. The HMRs for patients with clinically diagnosed LBD were significantly lower than those without (1.63 ± 0.08 versus 2.21 ± 0.08 at early phase ($p < 0.001$), and 1.54 ± 0.09 versus 2.08 ± 0.09 at delayed phase ($p < 0.001$)). There was good consistency in HMRs between the 300- second images (reference) and the 200-second (intra-class correlation (ICC) coefficients > 0.99), 100-second (ICC coefficients > 0.97) and 50-second (ICC coefficients > 0.89) images. **Conclusion:** In planar images with a whole-body CZT-based scanner, the HMRs of patients with LBD were significantly lower than those without. HMRs with the collection time > 50 seconds showed good consistency with those of 300 seconds (which was consistent with phantom study). Although, standardisation of the HMRs measured by whole-body CZT-based detectors may be required, these findings indicate a clinical utility and potential time reduction of this novel scanner for HMR measurements. **References:** None.

EP-0960

Comparison Of The Quality Of Brain Images Obtained With ^{99m}Tc-HMPAO Aquired Using Either The Veriton 360° CZT Camera Or A Conventional Anger Camera, And With An ^{18}F-FDG Analog PET System

M. Bordonne, *M. Chawki, T. Zaragori, V. Roch, R. Grignon, G. Karcher, P. Marie, L. Imbert, A. Verger;*
CHRU Nancy, Nuclear Medicine Department, Vandoeuvre les Nancy, FRANCE.

Aim/Introduction: The Veriton 360° CZT-camera (Spectrum Dynamics Medical) provides better performances in comparison to conventional gamma-cameras owing to CZT detectors features and also to an original 360° geometry of detection that allows acquisitions focused on the brain, which is particularly advantageous for brain SPECT imaging. This study aimed to assess the quality of the perfusion brain images provided by the 360° CZT-SPECT system, as compared with those provided by conventional Anger-SPECT and additionally, compared to analog PET recording of ^{18}F-FDG brain images. **Materials and Methods:** We retrospectively selected 3 groups of 21 patients matched for sex, age (±10 years) and who had undergone a brain ^{99m}Tc-HMPAO SPECT acquisition with either the 360° CZT-SPECT camera (Group 1) or a conventional Anger-SPECT system (Symbia T2, Siemens Healthineers, Group 2) or a brain ^{18}F-FDG recording with an analog PET camera (Biograph 6, Siemens Healthineers**,** Group 3). Images from each system were reconstructed with a similar level of convergence of the iterative reconstruction process, with corrections for attenuation and diffusion and with the recommended voxel sizes. Tomographic count sensitivity was measured from the projection SPECT images with the total recording counts corrected for the decay for each camera. Spatial resolution, assessed with a sharpness index in the frontal cortex; and grey (occipital)/white (semi-oval center)-matter contrast were obtained with an automatic algorithm. **Results:** Tomographic count sensitivity was 114% higher with 360° CZT acquisitions compared to those obtained with conventional SPECT camera (304±61 vs. 142±20 counts/MBq/s, $p<10^{-11}$). Image quality from the CZT-camera was: 1) much higher than that from conventional gamma-camera with, on average, a 30% higher sharpness index (10.5±2.4mm vs. 8.1±1.1mm, p=0.006) and a 40% higher contrast (1.23±0.47 vs. 0.88±0.36, p=0.005) and 2) close to that of FDG PET for which sharpness index was only 23% higher on average (13.0±2.7mm, p=0.01) and contrast was similar (1.03±0.27, p=NS). **Conclusion:** Image quality of perfusion brain SPECT images is markedly higher with the Veriton 360° CZT-camera, in comparison with that provided by Anger-SPECT camera, and it is even close to that observed for ^{18}F-FDG brain images from an analog PET camera. In addition, the high-count sensitivity of the 360° CZT-camera gives the possibility of significantly reducing acquisition time and / or injected activity. **References:** None.

EP-0961

Evaluation Of Early Vs. Standard Delayed Imaging Protocol In ^{99m}Tc- Sestamibimyocardial Perfusion Scintigraphy Using A Czt Based Gamma Camera

H. Sachani;
Narayana Hrudayalaya, Bangalore, INDIA.

Aim/Introduction: Myocardial perfusion scintigraphy has pivotal role in assessment of ischaemic state of the heart. It's an accurate, non-invasive imaging modality for assessment of significance of coronary artery stenosis and provides diagnostic & prognostic information in patients with suspected/ diagnosed coronary artery disease. Scans acquired on traditional dual detector have lengthy acquisition times (~15 minutes); ASNC imaging protocol prescribes minimum wait of 30 minutes between the exercise stress and stress imaging and 60 minutes between the rest injection and rest imaging reducing patient compliance because of lengthy acquisition time & long duration of entire examination (~4-5 hours). Early imaging could result in shorter waiting times for patients and be important in clinical situations like suspected ACS, where time is critical for therapeutic interventions. Aim of this study was to compare quality of early time point acquired ^{99m}Tc-Sestamibi MPI images with standard delayed acquisition protocol and to assess diagnostic performance on the basis of perfusion defects and quantitative parameters between two sets of images. **Materials and Methods:** 126 patients referred for clinically indicated myocardial perfusion imaging (MPI) study were enrolled. MPI was performed on CZT camera according to early imaging protocol (within 15 minutes of tracer injection) and repeat images were taken at 60 minutes post tracer injection. Image processing and reconstruction was done and quality was visually analysed by experienced NM physician. Summed stress score, summed rest score & summed difference score and quantitative MPI parameters like LVEF, ESV & EDV were compared between the two sets of images. Perfusion defects were assessed and compared between two sets of images taking coronary angiography findings as gold standard. **Results:** Early and delayed image sets compared for image quality showed moderate to substantial agreement. The

SSS, SDS, SRS and quantitative parameters had no statistical difference between two sets of images. Territory wise diagnostic accuracy of perfusion defects in two sets of images showed almost perfect agreement. **Conclusion:** Study concluded that images acquired at early time-point (under15 minutes post injection) are similar in terms of quality, quantitative data and territory wise diagnostic accuracy for detection of perfusion defects to images acquired at standard delayed time-point (~60 minutes post injection). Clinical information provided by early image is equivalent to that provided by standard delayed scan. Hence, adopting an early protocol can enhance patient compliance by reducing waiting time for imaging, overall length of examination and augment logistics of nuclear cardiology laboratories. **References:** None.

EP-0962

Comparing the use of IQ-SPECT versus LEHR-SPECT on the influence of abdominal radiotracer uptake in myocardial perfusion SPECT-CT

***A. de Vries**, J. van Rijs, J. E. Huijbregts;*
Gelre Hospitals, Apeldoorn, NETHERLANDS.

Aim/Introduction: IQ-SPECT (Siemens Medical Solutions) is a technology that allows short-time acquisition imaging of the heart by using a multi-focal collimator, a cardiocentric orbit, and advanced iterative reconstruction. The zoom effect of the so called SmartZoom collimators of IQ-SPECT may however also zoom in on unintended activity near the heart, e.g. radiotracer uptake in the gastric wall or biliary system[1], leading to an unreliable diagnostic value. The aim of this study is to investigate the use of IQ-SPECT versus LEHR-SPECT on the influence of abdominal radiotracer uptake in myocardial perfusion SPECT-CT. **Materials and Methods:** Unpaired data of 2 groups of patients (n=50 each) were compared in a retrospective study. The first group was scanned using conventional LEHR collimators on a Infinia Hawkeye SPECT-CT system (GE Healthcare) and reconstructed with filtered back projection. The second group was scanned with IQ-SPECT collimators on a Symbia Intevo 6+ and iteratively reconstructed. Only rest scans were compared, as those are more likely to be effected by nearby activity. Scans were scored by 2 observers on a 3-point Likert scale, 1) Good; 2) Average but reliable; 3) Unreliable. Statistical analyses was performed using the Mann-Whitney U-test for the non-attenuation-corrected (NAC) as well as the attenuation-corrected (AC) images. In addition to comparing patient data, a phantom study was designed. The Amsterdam gated (AGATE) dynamic cardiac phantom (Vanderwilt Techniques) was supplemented with a chamber representing the fundus of the stomach. ^{99m}Tc concentrations were 150 kBq/ml for the myocard compartment as well as the gastric wall compartment and 4.5 kBq/ml for the bloodpool. Scans were performed using IQ-SPECT (Symbia Intevo) and subsequently using LEHR-SPECT on the Infinia Hawkeye. Scans were scored on a 3-point Likert scale by 2 observers. **Results:** Mann-Whitney U-test resulted in no significant difference between IQ-SPECT and LEHR-SPECT with p-values of 0.055 for the NAC images and 0.716 for the AC images. No significant difference was observed (NAC p=0.402, AC p=0.656) when looking at the reliable scans (group 1 and 2) and unreliable scans (group 3). The phantom study confirmed the results of the patient study. **Conclusion:** No significant difference was observed between the assessability of the myocardial perfusion scans using IQ-SPECT or LEHR-SPECT. **References:** [1] Van Dongen A.J., Van Rijk P.P., J Nucl Med 2000; 41(8); 1315-7.

EP-0963

A whole-body bone SPECT of a high quality may be recorded in less than 20 minutes with the Veriton 360° CZT-camera

***L. Imbert**[1], M. Chawki[1], A. Bahloul[1], S. Melki[1], G. Karcher[1], A. Verger[1], F. Paycha[2], P. Marie[1];*
[1]CHU Nancy Hopital Brabois Adultes, Vandoeuvre les Nancy, FRANCE, [2]APHP, Hôpital Lariboisière, Paris, FRANCE.

Aim/Introduction: The Veriton™ 360° CZT-camera (Spectrum Dynamics Medical) is equipped with 12 swivelling high-resolution detectors covering an axial field-of view of 32 cm and assembled with a helicoidal CT in a hybrid system. The detectors may be positioned close to any part of the body and the overall detection system provides a much higher count sensitivity than current Anger-SPECT cameras. This study aimed to determine whether whole-body bone SPECT/CT acquisitions could be recorded using the Veriton camera: 1) with a comparable total recording-time to that of current whole-body bone planar scintigraphy (15 to 20 min) and 2) with a high enough image quality as compared with the bone SPECT currently obtained with 3.7 fold longer recording times on Anger cameras (10 vs. 3 min per bed position). **Materials and Methods:** Additional Veriton SPECT recordings of only 3-min per bed position were scheduled in 9 patients, who were initially referred to a conventional whole-body planar scintigraphy on an Anger camera equipped with parallel-hole collimators (Symbia, Siemens Medical Healthineers) and among whom, 6 had additionally undergone an 10-min Anger-SPECT recording centered on the pelvis. SPECT images were reconstructed for both cameras with dedicated iterative algorithms, corrections for diffusion and for attenuation with the CT map and additionally for the Veriton, with an original algorithm for partial volume correction (PVC). **Results:** Image quality, provided by the 3-min CZT-SPECT recordings centered on the pelvis, was comparable to that provided by the 10-min Anger-SPECT recordings with especially, equivalent image contrast (for lumbar vertebrae: 1.79±0.12 vs. 1.80±0.07, and for iliac crests: 1.83±0.20 vs. 1.76±0.11), and with equivalent spatial resolution assessed through a sharpness index (for lumbar vertebrae: 6.1±0.6% vs. 6.0±1.5% and for iliac crests: 9.9±2.3% vs. 9.1±1.0%). When reconstructed with the PVC algorithm, the sharpness index of the Veriton SPECT images was significantly enhanced (lumbar vertebrae: 8.5±0.7% and iliac crests: 11.4±2.0%; p = 0.001 and p = 0.002 for the comparisons vs. conventional SPECT

and vs. Veriton SPECT without PVC, respectively), whereas image contrast was not enhanced (for lumbar vertebrae: 1.75±0.13 and for iliac crests: 1.80±0.25). **Conclusion:** A whole-body bone SPECT recording, achieved with the Veriton 360° CZT-camera in no more than 20 min, could advantageously replace current bone scanning protocols associating planar whole-body and SPECT acquisition workflows. **References:** None.

EP-0964

Diagnostic performance of 360° CZT SPECT compared to a conventional camera in lung perfusion scintigraphy

K. Anindita[1,2], K. Delaunay[3,4], B. Mahida[4], K. Doyeux[4], F. Rouzet[4,3,1];
[1]Inserm 1148, Paris Diderot University, Paris, FRANCE, [2]ENSAM Paris Tech, Paris, FRANCE, [3]Paris Diderot University, Paris, FRANCE, [4]Department of Nuclear Medicine, Bichat Claude Bernard University Hospital, APHP, Paris, FRANCE.

Aim/Introduction: Lung perfusion scintigraphy is widely used in the diagnosis of pulmonary embolism (PE) and quantification of perfusion prior to lung surgery (Surg). Tomographic acquisitions have proved superior to planar ones but are time consuming. Cameras with CZT detectors constitute a technological leap forwards for SPECT imaging with greater sensitivity compared to conventional NaI cameras. The aim of this study was to assess whether the new generation Veriton CZT-camera (Spectrum Dynamics Medical) equipped with 12 detectors around 360° would allow acquisition time reduction without impairment of diagnostic and quantitative performances. **Materials and Methods:** 14 consecutive patients (age: 68 ± 15 years, males: 6, informed consent obtained) referred to our centre for lung scintigraphy were enrolled. After injection of 185 ± 19 MBq 99mTc-labelled macroaggregated human albumin, 10min SPECT (60 steps/detector, 10 sec/step) was acquired on a conventional camera Discovery NM/CT 670 (General Electric Healthcare). Immediately after completion of conventional imaging, patients were asked to move to Veriton for a 10min acquisition (list mode). Optimized clinical iterative reconstruction was performed with both systems and an additional reconstruction with acquisition duration reduced to 5 and 2.5 min on Veriton. The following parameters were recorded: 1/ Number of segmental perfusion defects (18 segments, PE group); 2/ Relative uptake quantification in each pulmonary lobe (5 lobes, Surg group) using the same CT-based segmentation. The outcome criteria were: 1/the reproducibility of the number of segmental perfusion defects (PE group, blinded readers, Intraclass Correlation Coefficient-ICC) and 2/the difference of relative quantification (Surg group, Bland-Altman plot). **Results:** In the PE group, the absolute agreement between conventional camera (CC) and Veriton CZT camera was excellent with ICC [95% CI] = 0.986 [0.746 - 0.999] for 10min acquisition duration on conventional camera and 2.5 min acquisition on Veriton (other results available in Table). In Surg group, the comparison lobe by lobe of relative perfusion showed no difference between acquisitions, with a mean difference [95% CI limits of agreement]: 0% [-3.8 ; +3.8] for 10min acquisition duration on CC and 2.5min on Veriton. **Conclusion:** Greater sensitivity of the Veriton compared to conventional camera offers the opportunity to decrease acquisition duration up to 75% without loss in diagnostic (PE) and quantitative (Surg) performances. **References:** None.

EP-72

Technical aspects -> Radiation protection and dosimetry -> Dosimetry and radiobiology -> Clinical studies -> Clinical dosimetry

October 12 - 16, 2019 e-Poster Area

EP-0965

Dosimetric aspects with TL dosimetry in 99mTc-nanocoll lymphoscintigrafy in pregnant women

P. Saletti[1], M. Fedi[1], L. Ballati[2], A. Falivene[1], L. Vaggelli[1], G. Belli[1];
[1]AOU Careggi, Florence, ITALY, [2]University of Florence, Florence, ITALY.

Aim/Introduction: Lymphoscintigraphy in pregnant women requires a specific approach due to radioprotection constraints for the foetus. The aim of present work is to investigate if a reduced amount of radiopharmceutical could lead a good diagnostic result and verify, by TLD dosimetry, radioprotection compliance. **Materials and Methods:** A set of 6 pregnant women participated the study in the period 2015-2019 and a mean activity of 12MBq was administered (ranging from 6 to 20MBq) according to AIMN Guidelines. Before 99mTc-nanocoll injection, 3 stripes of 4 TLD each (12 in total) were placed in correspondance with womb; their removal was carried out before surgery. Lymphoscintigraphies were performed at Siemens e.cam gammacamera with LE-HR collimators and 15% energy window in orthogonal and oblique projection. TLD LiF100 were then read at Harshaw 6600 system and measured glow curves were lastly compared with 10 background TLD. **Results:** All obtained images were completely satisfactory from diagnostic point of view and an accurate indication of the sentinel lymphnode was always given for surgery. Mean TLD background resulted in 1.7nC (ranging from 0.7 to 3.0nC) while a mean of 1.6nC (ranging from 0.7 to 3.3nC) was measured in TLD placed on women. Taking into account related background of each TLD set, none among all TLD measured a real dose (i.e. no difference from background) proving that no radiological impact is connected with such modified approach to lymphoscintigraphy. **Conclusion:** The results pointed out with the present work have two main implications. First of all, absorbed dose by the foetus was completely irrelevant, as expected, due to reduced 99mTc-nanocoll administered activity even though scintigraphic images were absolutely adequate. Secondly, these evidences could be the starting point for a radioprotection programme involving all lymphoscintigraphic examination, even in non pregnant patients, if logistics such as scheduling time and hospital organisation could make it

possible. **References:** AIMN guidelines for Lymphoscintigraphy in Melanoma and Breast cancer.

EP-0966

Development of I-131 Radionuclide Therapy Patient Monitor with Predictive Exposure Rate Capability

C. Munoz-Ferrada;
Gammasonics, Lane Cove, AUSTRALIA.

Aim/Introduction: Patients receiving large doses of radionuclides for therapy often require admission to a specialized ward of the hospital where they can be isolated from staff and the public until their external radiation exposure rates have decreased to acceptable levels. The development of a ceiling-mounted radiation monitors which connects to the hospital IT network and allows, the exposure rates to be monitored from any PC that can access the detector, either internally or externally. **Materials and Methods:** A radiation detector has been developed which is housing in a small case, it is activated by Power Over Ethernet (POE) and has an Ethernet network interface to connect to the hospital LAN. The software has been developed to address the output of the device on a COM channel of a PC. The system is located and calibrated at a given distance above the patient bed, but the detector adjusts at the "exposure rate of 1 m" and is calibrated independently. Multiple detectors in different rooms can be supported on one PC. The software performs real-time curve fitting (assumed monoexponentially) and extrapolation to estimate when the radiation exposure from the patient will be lower than the local regulatory limit. **Results:** In considering a typical patient trace over approx. 36 hours (not shown), abrupt drops in exposure rate are observed with voiding with a final drop to zero when the patient was discharged from the room. Extrapolation from the high initial levels of the decreasing exposure rate allows estimation of the earliest possible time for discharge, thus improving efficiency of room use and patient satisfaction whilst providing colour-coded feedback to local staff (nurses etc) about current exposure rates. **Conclusion:** This cost-effective device helps to optimally manage patients admitted after radionuclide therapy. It can be used for any radionuclide that emits photons where minimising exposure of the public must be ensured. **References:** None.

EP-0967

Uncertainty in Reference Phantom-Based Dosimetry Calculations: Impact of Number of Source Organs

A. Josefsson[1], *J. J. Siritantikorn*[1], *M. Tatit Sapienza*[2], *W. E. Bolch*[3], *G. Sgouros*[1];
[1]*Johns Hopkins University School of Medicine, Baltimore, MD, UNITED STATES OF AMERICA,* [2]*São Paulo University, São Paulo, BRAZIL,* [3]*University of Florida, Gainesville, FL, UNITED STATES OF AMERICA.*

Aim/Introduction: Dosimetry for diagnostic agents is typically performed using the MIRD Committee, S-value method with a particular anatomical reference geometry. S-value based dosimetry methods provide the mean absorbed to a reference target geometry from a collection of source organs. The number of source organs considered, and their nature impacts the estimated effective dose value. In this work, we investigate how the number of source organs used impacts the effective dose for two different reference phantom geometries. **Materials and Methods:** Previously collected patient imaging data were used in the investigation. Two to four whole-body diagnostic PET/CT-images was acquired for 16 patients (5 male and 11 female) after administration of ^{68}Ga-DOTATATE. Volumes of interest (VOIs) were drawn for normal tissues on the PET/CT-images for the spleen, liver, kidneys, adrenal glands, brain, heart, lungs, thyroid gland, pituitary gland, salivary glands, testes, red marrow (L1-L5), muscle (right thigh) and whole-body. Dosimetric calculations were performed using the ICRP 110 voxelized phantoms, ICRP 133 specific absorbed fractions and ICRP 103 tissue weighting factors. Representing the Cristy-Eckerman (CE) stylized phantoms OLINDA/EXM version 1 using ICRP 60 tissue weighting factors was used. Three different approaches were used to evaluate the effect of what normal tissues where included in the dosimetric calculations: Based on 1) the organ weight (decreasing: muscle, liver etc.), 2) the tissue weighting factor (decreasing: lungs, red marrow etc.) and 3) the highest increase or impact on the effective dose coefficient. The whole-body activity was subtracted with the activity of the respective organs included and was used as the remainder-of-body activity in all calculations. **Results:** As the number of source organs included in the calculation was increased from 1 to 13, the effective dose coefficient, e, increased from 0.017 to 0.023 mSv/MBq for the ICRP phantom and the corresponding range for the CE phantom calculation increased from 0.012 to 0.027 mSv/MBq. The number of source organs required for e to converge to its final value was similar; 6 and 5 for ICRP and CE phantoms, respectively. **Conclusion:** Depending upon the reference phantom chosen and the number of source organs in included, effective dose estimates can vary by more than a factor of 2. Results obtained will also depend on the normal organ distribution of the imaging agent. **References:** None.

EP-0968

Establishment of National DRL for CT in Hybrid Imaging Studies "The First National NM CT (PET) Dose Audit for KW population"

M. Masoomi[1], *I. Al-Shammeri*[1], *J. Al-Shammeri*[2], *H. Elrahman*[1], *3 Farwaniya Hospital - Kuwait, 3 Mubarrak Al Kabeer Hospital -Kuwait, 3 Al-Jahra Hospital - Kuwait, 3 Chest Diseases Hospital - Kuwait, 3 Kuwait Cancer Control Center Hospital - Kuwait, 3 Jaber Al Ahmed MI - Kuwait;*
[1]*Nuclear Medicine Department, ADAN Hospital, Kuwait City, KUWAIT,* [2]*Nuclear Medicine Department, Faculty of Medicine, Kuwait University, Kuwait City, KUWAIT.*

Aim/Introduction: Diagnostic reference levels (DRLs), for CT part used in PET examinations are limited. Published DRLs from other countries may not be directly relevant to the state of Kuwait (KW). The aim was to propose a national DRL for CT part of PET imaging operating in KW, in support of optimization and dose reduction. **Materials and Methods:** The research was a multicentre collaborative study with participation of 7 PET-CT centres in KW. The data collection was restricted to adult oncology patients due to a limited number of the other studies. The study was based on the UK - IPEM methodology and the upper limit of entries for each centre was set to 30 with a total of 195 patients. The CTDIvol, DLP and scan length (SL) were recorded and Mean, Median, Standard Deviation, Minimum and Maximum values, 75th percentile as well as WB effective dose (ED) were calculated. All centres except one (Philips) accommodated GE PET/CT scanners with an integrated 64 slices CT, and applied AEC. **Results:** Dose and scan length statistics for the half body (HB) accounted for 51.5% of the total (195) and combined (WB +HB) examinations presented together with the Proposed local DRLs and Achievable doses. The CT data were used for AC and localization. Patient dose varied considerably, with a maximum of twofold variation in DLP. The ratio of maximum to minimum mean doses between different centers for HB and (WB+HB) for the same clinical studies varied between 1.1 - 3.7 for HB and 2.3 -6.2 for (WB+HB). There were variations of proposed and achievable local DRL in practice between 7 centers highlighting the need for national DRL. Third quartile DLP (mGy. cm) and CTDIvol (mGy) values (set for NDRL) for the HB PET/CT was (570, 5.2) which was higher than the current UK NDRL (400, 4.3) but lower than the Swiss National NDRL (620, 6). Comparatively, the Proposed NDRLs for (WB+HB) was (643, 4.6) which was lower than Swiss National Data (720, 5.0). The results were in reasonable agreement with the both centers, though, SWISS had entries of 5000 (HB), 706 (WB) and the UK had 370 (HB). Calculated ED varied from 5.4 to 13.4 mSv, with a mean value equal to 8.4 mSv. **Conclusion:** The study demonstrated the need for national CT DRLs for PET/CT and it has been proposed in KW for oncology examinations based on data collected from 7 centers. **References:** None.

EP-0969

Assessment the activity incorporated by the patient's caregivers after Iodine-131 thyroid therapy

M. J. Carapinha[1,2,3], *M. Reis*[4], *L. Silva*[4], *M. Santos*[4], *G. Costa*[5], *M. Silva*[5], *J. Isidoro*[5], *C. Nunes*[2,6], *A. Tavares*[2], *P. Teles*[4];
[1]*Escola Superior de Tecnologia da Saúde de Lisboa, Lisboa, PORTUGAL,* [2]*Escola Nacional de Saúde Publica, Universidade Nova de Lisboa, Lisboa, PORTUGAL,* [3]*H&TRC - Health & Technology Research Center, ESTeSL - Escola Superior de Tecnologia da Saúde, Instituto Politécnico de Lisboa, Lisboa, PORTUGAL,* [4]*Centro de Ciências e Tecnologias Nucleares, Instituto Superior Técnico Universidade de Lisboa, Lisboa, PORTUGAL,* [5]*Serviço de Medicina Nuclear, Centro Hospitalar e Universitário de Coimbra, EPE, Coimbra, PORTUGAL,* [6]*Centro de Investigação em Saúde Pública, Av. Padre Cruz, 1649-016, Lisboa, Lisboa, PORTUGAL.*

Aim/Introduction: Evaluate the activity incorporated by the caregivers of the patients undergoing thyroid cancer (TC) therapy with iodine-131 (131I), based on the amount of 131I excreted in the urine. **Materials and Methods:** An observational study was performed using a sampling of 22 patients and 34 caregivers. The patients, submitted to 131I treatments for TC, were discharged from hospital 48h after therapy. All caregivers received instructions on radiation protection, based on Euratom recommendations. A urine sample was collected from every caregiver, about 70h after dischargement of the patients. The samples of urine were analyzed by gamma spectrometry. A biokinetic model was used for the 131I according to the ICRP Publication 78 to quantify the activity incorporated by the caregivers, based on the concentrations of 131I present in the urine. All ethical principles of the investigation were respected. **Results:** The average activity of 131I given to the patients was 3207.3±1184.8 MBq. When the patients were discharged, the average effective dose rate measured at 1 meter distance was 8.2±6.1 μSv.hr-1 (1-25 μSv.hr-1). In the 34 caregivers with average of 48.1±18.6 years only in 3 caregivers wasn't detected 131I in the urine. The mean activity concentration of 131I founded in the urine samples has 97.4 Bq.L-1(range: 0.0-1146 Bq.L-1) and the mean H_T(thyroid) was 0.81±2.38 mSv, with a median of 0.03 mSv, a minimum of 0 mSv and a maximum of 9.46 mSv. The specific activity of 131I in urine: it is not the same among on the classes of the administered activity (p=0.019); it is not the same on the different classes of caregivers ages (p=0.470); it is not the same on the different degree of relationship (p=0.744). We observed a moderate correlation between the specific activity of 131I in the urine and the activity administered to the patients (ρ_{sp}=0.540; p=0.001); and a high correlation between the specific activity of 131I in the urine and the effective dose rate in the patients (ρ_{sp}=0.730; p<0.001). CI of 95%. **Conclusion:** The patients are a radioactive source that can increase the exposure of the caregivers to ionizing radiation. The specific activity of 131I in the urines of the caregivers is related to the activity administered to the patients. It is clear that caregivers of patients submitted to radioiodine therapy can be subject to internal contamination. The 131I concentration in the urine due to internal contamination do not represent a radiological hazard for the exposed individuals. **References:** None.

EP-73

Technical aspects -> Radiation protection and dosimetry -> Dosimetry and radiobiology -> Clinical studies -> Clinical radiobiology

October 12 - 16, 2019 e-Poster Area

EP-0970

The Protective Effect of Vitamin D Against Radioiodine (RAI) Therapy Damage to Male Fertility

C. Cebi Sen[1], *A. Akbulut*[2], *G. Koca*[2], *A. Kirmit*[1], *H. Atilgan*[3], *B. Nacir*[2], *N. Yumusak*[1], *M. Korkmaz*[2];
[1]*Harran University, Sanliurfa, TURKEY,* [2]*Ankara Training*

and Research Hospital, Ankara, TURKEY, [3]Kahramanmaras Necip Fazil City Hospital, Kahramanmaraş, TURKEY.

Aim/Introduction: We evaluated evaluate antioxidant effects of active vitamin D (calcitriol) against high-dose radioiodine (RAI) therapy-associated damage of male fertility. **Materials and Methods:** Wistar albino rats were used and randomly into three groups (n=12). The first group was appointed as the negative control group and received no RAI or medication. The second group (RAI group) was administered only received 3 mCi/kg (111 MBq/kg) RAI by gastric gavage as the positive control group and the last group (RAI+calcitriol) was the treatment group that received 3 mCi/kg RAI by same method and calcitriol (200 ng/kg/day) by intraperitoneal route. Seven days after, intracardiac blood samples were taken for hormone analysis and testis samples were removed for the evaluations of histopathologic, total oxidant status (TOS), total antioxidant status (TAS), spermatological parameters. Caspase-8, and caspase-9 were used to show increased apoptosis resulting from testis damage and the terminal deoxynucleotidyl transferase mediated deoxyuridine triphosphate nick end labeling (TUNEL) assay was used to determine the frequency of possible DNA breaks because of treatment. **Results:** RAI led to significant increase in tissue TOS levels and significant decrease TAS levels ($p<0.05$ for each). It was demonstrated a significant decrease in epididymal spermatozoa viability and motility in all of the treatment groups, in comparison with the control group ($p <$ 001). A significant decrease was also detected in sperm DNA fragmentation, follicle-stimulating hormone (FSH) level in the RAI+calcitriol group when compared to the radioiodine group. The staining intensity of caspase-8,and caspase-9 antibodies was found to be statistically more significant in the RAI+calcitriol group than in the RAI group ($P <0.05$). The nuclear highlighting shown by the TUNEL was more increased in the RAI group than in the RAI+calcitriol group ($p <0.05$). **Conclusion:** Vitamin D demonstrated potent antioxidant and radioprotective effects on testis against RAI-induced oxidative damage. **References:** None.

EP-0971

The Evaluation of Bone Marrow Suppression and Secondary Malignancy Risk after Radioiodine Treatment in Patients with Thyroid Cancer after 10 Years Follow Up

***K. Toplutas**, S. Sager, R. Uslu Besli, S. Asa, S. Khosroshahi, H. Sayman, I. Uslu, K. Sonmezoglu;*
Istanbul University-Cerrahpasa,Cerrahpasa Medical Faculty Department of Nuclear Medicine, Istanbul, TURKEY.

Aim/Introduction: Radioiodine(I-131) treatment may have some adverse effects to non-thyroid tissue due to its energy and cumulative effect. Studies have shown a significant increase in the development of leukemia and salivary gland cancer after radioiodine treatment. The aim of our study was to examine the frequency of bone marrow suppression and secondary tumor growth in patients received high-dose radioiodine in our clinic before 2010 due to thyroid cancer. **Materials and Methods:** A total of 3000 patients with thyroid cancer were retrospectively reviewed. Patients were followed up for an average of ten years period in our department. The study included 74 patients(F=51,M=23) who received radioiodine ≥600 mCi. Patients were divided into two groups 600 mCi - 1000mCi(n=50), and ≥1000mCi(n=24). 71,6% of the patients were papillary thyroid carcinoma, 16.2% with follicular thyroid carcinoma, 5.4% had poorly differentiated thyroid carcinoma, 4% no detailed data was found on the pathology. **Results:** The mean age of the patients was 48.7 years. According to the first pathology reports, 10.8% (n = 8) of the patients had pT1, 8.2% (n = 6) pT2, and the remaining group of patients had pT3 and pT4 tumors.There were 44 patients with lymph node metastasis, 24 patients with lung metastasis and 14 patients with bone metastasis during diagnosis and treatment. Also brain metastasis was detected in 2 patients and liver metastasis in 2 patients. Among the group receiving 1000mCi or more(max 1700mci), 6 patients died and 8 patients were alive. For the group receiving 600-1000mCi, 8 of them died, 33 of them were alive. Only 3 out of our patients(700,750,1350mCi) developed bone marrow suppression. One patient had leukopenia. One patient had pancytopenia and another patient had bicytopenia. The patient with bistopenia had dysplastic changes in the peripheral smear. Treatment of 2 patients with bone marrow suppression was stopped accordingly. Four patients from all patients were recently diagnosed with a second primary malignancy including one patient with prostate cancer(1300mCi), one with larynx cancer(600mCi), one with lung cancer(1600 mCi), and the other patient received rectum cancer(850mCi) diagnoses. **Conclusion:** Although bone marrow suppression was seen in 6.1%(n=3) of the patients, secondary leukemia and treatment-related solid tumor development was not detected. The number of patients with solid tumors were not significantly different from the normal population. Complete blood count follow-up still useful test to prevent possible complications and side effects in patients receiving high iodine doses. **References:** None.

EP-74

Technical aspects -> Radiation protection and dosimetry -> Dosimetry and radiobiology -> Preclinical studies -> Preclinical dosimetry

October 12 - 16, 2019 e-Poster Area

EP-0972

Evolution and evaluation of effective dose in the context of diagnostic nuclear medicine

***J. C. Ocampo Ramos**[1], E. Mora-Ramirez[2], M. Bardiès[1];*
[1]CRCT, UMR 1037, INSERM, Université Toulouse III Paul Sabatier, Toulouse, FRANCE, [2]Universidad de Costa Rica, Escuela de Fisica, CICANUM, San Jose, COSTA RICA.

Aim/Introduction: Small or medium differences are noted when the effective dose (ED) is calculated using different available software, tools, and methodologies. The calculation of the effective dose could be a little be tricky considering the different approaches, approximations and information available. A guideline about how to put a new diagnostic radiopharmaceutical into the market is missing, especially if it is a gender-specific drug. **Materials and Methods:** We used different inputs, available commercial, academic and in-house developed tools to test and evaluate the effective dose in an accurate way and being ICRP compliance. Biokinetics of several radiopharmaceutical were used and sex-specific inputs were considered when they were available. **Results:** The inappropriate input, use of software and the misinterpretation of the effective dose could yield to errors up to 10% in the ED assessment. The results in this work could be useful as a guideline of how to compute the effective dose properly in the context of diagnostic nuclear medicine for clinical and preclinical studies. **Conclusion:** Despite significant numeric differences in the organ absorbed dose, the effective dose is a robust quantity. Direct and wrong use of tools without the proper understanding and the definition of the ED is a major source of miscalculation. Care must be taken to ensure that the quantity calculated is clearly reproducible and in line with the ICRP recommendation. **References:** ICRP, 1991. 1990 Recommendations of the International Commission on Radiological Protection. ICRP Publication 60. Ann. ICRP 21 (1-3). ICRP, 2007. The 2007 Recommendations of the International Commission on Radiological Protection. ICRP Publication 103. Ann. ICRP 37 (2-4). ICRP, 2015. Radiation Dose to Patients from Radiopharmaceuticals: A Compendium of Current Information Related to Frequently Used Substances. ICRP Publication 128. Ann. ICRP 44(2S).

EP-75

Technical aspects -> Radiation protection and dosimetry -> Radiation protection -> Radiation exposure & protection

October 12 - 16, 2019 e-Poster Area

EP-0973

Ultra-low Dose CT for PET Attenuation Correction

E. Prieto[1], *B. Aguilar*[1], *V. Morán*[1], *M. Pérez-Macho*[2], *C. Castellet-García*[3], *J. M. Martí-Climent*[1];
[1]*Clínica Universidad de Navarra, Pamplona, SPAIN,* [2]*Hospital Universitario Marqués de Valdecilla, Santander, SPAIN,* [3]*Consorcio Hospitalario Provincial de Castellón, Castellón, SPAIN.*

Aim/Introduction: Some clinical scenarios require several PET/CT studies in a short time interval (follow up, clinical trials, multi-tracer studies...). If CT image is redundant for localization/diagnosis, CT patient dose could be reduced substantially. The aim of this study is to explore the CT protocol for minimum patient dose without compromising accurate attenuation correction and PET image quality. **Materials and Methods:** Scans were acquired in Biograph mCT TrueV PET/CT and reconstructed with EARL parameters. A cylindrical uniform phantom (diameter 20 cm) was filled with 164 MBq of FDG and placed within a parallelepiped container (section 17x34 cm) filled with non-radioactive water. Twenty-one CT images were acquired (Tube potential: 80, 100, 120 kV; current-time product: 10, 20, 40, 60, 80, 100, 120 mAs, without AEC). A 300s PET image was reconstructed using each of the 21 mu-maps. CTs, mu-maps and PET images were visually inspected to identify and quantify potential artifacts. Additionally, a NEMA anthropomorphic phantom with 43 MBq in the background compartment containing two non-radioactive spheres and 4 hot spheres (contrast 8:1) was scanned with the clinical protocol for oncology (120s). PET images were corrected for attenuation using the clinical CT (120kV-80mAs-AEC) and the lowest achievable dose CT (according to the previous experiment). PET image quality was evaluated according to the NEMA NU-2 standard. **Results:** Cylindrical uniform phantom: CTDI ranged from 0.2 to 8.7 mGy. Only the two lowest CTDI conditions (80kV-20mAs and 80kV-10mAs) produced artifacts in CT images and mu-maps that caused a non-uniformity artifact in the PET Images. For all the rest PET images (CTDI ≥ 0.43 mGy), the mean uptake value in the most affected area varied less than 2% respect to the reference value. Noise level of CT images and mu-map was clearly dependent on CTDI, but noise in PET image did not vary significantly. NEMA anthropomorphic phantom: CTDI values were 5.57 mGy for the clinical CT (120kV-80mAs-AEC) and 0.82 mGy for the low dose CT (80kV-40mAs-noAEC). Contrast recovery coefficients for cold and hot spheres varied less than ±0.5%. The average lung residual varied from 9.98 % to 9.09% (increase of 1.2%). Background variability varied less than 2%. **Conclusion:** It has been demonstrated, with a wide phantom, that CTDI can be reduced to 0.43 mGy without any perceptible qualitative or quantitative degradation in corrected PET image. Using the NEMA phantom, a CTDI reduction of 85% did not degraded PET image quality. **References:** None.

EP-0974

Personal dose equivalent $H_p(10)$ in patient's family members after ^{131}I therapy in thyroid cancer and benign thyroid diseases

M. J. Carapinha[1,2,3], *T. C. Ferreira*[4], *M. T. Rézio*[4], *L. Salgado*[4], *S. Vaz*[4], *G. Costa*[5], *R. Ferreira*[5], *J. Isidoro*[5], *C. Nunes*[2,6], *A. Tavares*[2];
[1]*Escola Superior de Tecnologia da Saúde de Lisboa, Lisboa, PORTUGAL,* [2]*Escola Nacional de Saúde Publica, Universidade Nova de Lisboa, Lisboa, PORTUGAL,* [3]*H&TRC - Health & Technology Research Center, ESTeSL - Escola Superior de Tecnologia da Saúde, Instituto Politécnico de Lisboa, Lisboa, PORTUGAL,* [4]*Instituto Português de Oncologia de Lisboa, Francisco Gentil, EPE, Lisboa, PORTUGAL,* [5]*Centro Hospitalar e Universitário de Coimbra, EPE, Coimbra, PORTUGAL,* [6]*Centro de Investigação em Saúde Pública, Av. Padre Cruz 1649-016, Lisboa, PORTUGAL.*

Aim/Introduction: The aim is to quantify the personal equivalent dose $H_p(10)$ of the family members (FMs) of patients submitted to iodine-131 therapy (RAIT): thyroid cancer (TC) or benign thyroid diseases (BTD) and compare $H_p(10)$ values of children and adults. **Materials and Methods:** An observational study was performed in FMs of patients treated in two hospitals (83 FMs of 48 patients). After receiving instructions on radiation protection, based on Euratom recommendations, all FMs used a whole body thermoluminescent dosimeter (TLD) during 21 days. The FMs were divided in two groups: TC-Group, 65 FMs (5 children <10 y) of 37 patients treated for TC (average activity = 3369.6 MBq; range 1110-5920 MBq); BTD-Group, 18 adults FMs of 11 patients treated for BTD (average activity = 365.4 MBq; range 185-555 MBq). The TC patients were discharged 48h after therapy and BTD patients were treated as ambulatory patients. All ethical principles of the investigation were respected. **Results:** In the TC-Group, FMs had an Body Mass Index (BMI) of 26.1 ± 5.5 $Kg.m^{-2}$ and the mean of $H_p(10)$ was 0.14 mSv (range 0.00-3.37 mSv). At discharge, patients in this group had a mean effective dose rate measured at 1 meter distance of 10.4 $\mu Sv.h^{-1}$ (range 2-28 $\mu Sv.h^{-1}$). In the BTD-Group, FMs had a BMI of 26.8 ± 3.7 $Kg.m^{-2}$ and the mean of $H_p(10)$ was 0.37 mSv (range 0.01-2.40 mSv). The $H_p(10)$ value correlated with the degree of relationship and the age of the FMs. In both groups, the $H_p(10)$ of the FMs showed a moderate correlation to the RAIT activity (ρ_{sp}=-0.450; p=0.010) and no correlation with patients effective dose rate (ρ_{sp}=0.171; p=0.173) or BMI of FMs (ρ_{sp}=-0.074; p=0.585). In the TC-Group a moderate correlation was found between the effective dose rate and the RAIT activity administered (ρ_{sp}=0.342; p=0.009) and a non-statistically significant correlation between the effective dose rate and the BMI (ρ_{sp}=0.237; p=0.088). CI 95%. **Conclusion:** The FMs of the patients submitted to RAIT for BTD received higher doses when compared to FMs of TC patients. The $H_p(10)$ of the FMs was correlated to the degree of relationship and the age of the FMs. In the patients submitted to ^{131}I therapy for TC or BTD, the $H_p(10)$ of the FMs is associated to the ^{131}I administered activity. It is important to underline that the personal dose equivalent in these FMs does not reach the limits recommended by ICRP 97 and ICRP 94. **References:** None.

EP-0975

Radiation Exposure to Carers and Comforters from patients undergoing ^{18}F-FDG-PET/CT

E. Kalogianni, D. Levart, N. Heraghty, S. Soares, A. Cheetham, B. Corcoran, N. Mulholland, M. Vadrucci, G. Vivian;
King's College Hospital, London, UNITED KINGDOM.

Aim/Introduction: The UK legislative implementation of the new European Commission Basic Safety Standards (BSS) (Ionising Radiation (Medical Exposure) Regulations {IR(ME)R} 2017) were introduced to protect patients against the hazards associated with the use of ionising radiation in medical settings. The exposure of carers and comforters is now considered a medical exposure, falling within the scope of IRMER17. Under the regulation the employer is responsible to establish dose constraints with regard to the protection of carers and comforters and all exposures should be justified. The aim of this study was to estimate the in-hospital radiation exposure of carers and comforters accompanying patients undergoing PET-CT examinations and to establish guidance for radiation safety. **Materials and Methods:** 23 patients (13 females, median age was 62 years (30 - 93), median weight: 76 kg (48 - 130)) undergoing a FDG-PET/CT scan during a period of 4 weeks were randomly selected. Patients were injected with 4.5 MBq/kg of ^{18}F-FDG to a maximum of 400 MBq and rested in a quiet environment until scanning. All patients had equivalent dose rate measurements recorded at 1 m and 10 patients had additional equivalent dose rate measurements recorded at 0.5 m and 0.1 m from the mid abdomen.Measurements were performed using a Tracerco PED+ Personal Electronic Dosimeter, which records equivalent dose rate and cumulative dose, during the patients resting period and a series 900 Mini-Instruments survey meter. All measurements were corrected for background, measured in the same room without the patient. **Results:** The median injected activity was 342 MBq (224 - 425). The median resting period was 51 min (43 - 61). The median dose rates per unit of injected activity measured at 1m, 0.5 m and 0.1 m were 0.07 µSv/h/MBq (0.04 - 0.09), 0.20 µSv/h/MBq (0.11 - 0.50) and 0.75 µSv/h/MBq (0.40 - 0.89) respectively. The median cumulative dose received during resting period measured at 1m, 0.5 m and 0.1 m was 20 µSv (12-39), 76 µSv (34 - 201) and 234 µSv (167 - 301) respectively. The 95th percentile for these measurements were 33 µSv, 152 µSv and 286 µSv. **Conclusion:** Doses to comforters and carers were within the dose constraint recommended by the International Commission on Radiological Protection (Publication 103) of 5mSv per occurrence. This study confirms that comforter and carer radiation exposure levels from FDG PET-CT examinations practice are acceptably low. **References:** None.

EP-0976

Life quality improvement in Pediatric Patients submitted to Radioiodine Therapy for a return to daily life As Fast As Reasonably Achievable

M. Pizzoferro[1], *C. Polito*[2], *B. Cassano*[2], *M. F. Villani*[1], *M. Longo*[2], *E. Genovese*[2], *A. Castellano*[3], *A. Grossi*[4], *M. C. Garganese*[1];
[1]*Nuclear Medicine Unit, Bambino Gesù Children's Hospital-IRCCS, Rome, ITALY,* [2]*Medical Physics Unit, Bambino Gesù Children's Hospital-IRCCS, Rome, ITALY,* [3]*Oncology Unit, Bambino Gesù Children's Hospital -IRCCS, Rome, ITALY,* [4]*Endocrine Unit, Bambino Gesù Children's Hospital -IRCCS, Rome, ITALY.*

Aim/Introduction: Radioiodine (^{131}I) therapies on children with differentiated thyroid cancer and neuroblastoma can be a discouraging experience requiring an isolation period due to radiation safety concerns. Post-therapy radiation isolation depends on the value of dose-rate on the day of discharge (estabilished by Radiation protection97 and Italian regulation). Pediatric patients usually have dose-rate values on discharge involving a month of school absence and no contacts with other peers in order to avoid unduly irradiation. However, each patient

has an individual kinetic of radioactivity excretion depending on extension and uptake of disease, renal function and other individual parameters. The aim of our study is to improve patient quality of life reducing as much as possible the radiation isolation period after discharge by implementation of a specific patient radiometric protocol. **Materials and Methods:** Children affected by thyroid cancer or neuroblastoma are treated in our Istitution in a child-friendly therapy room, accompanied by their parents, for 3-4days. A well established dosimetric protocol is routinely applied including measurement of patient dose-rate at a distance of 1 meter by radiation detector up to 7days after radioiodine administration. All radiometric data are collected and analyzed to assess individual radiotracer excretion/retention time. For each patient radiation isolation period is calculated according to Italian regulation considering the dose rate on discharge. An update on 7thday after therapy administration (when ^{131}I-Whole Body Scan is scheduled) is also performed on the basis of relative emission rate value. **Results:** 69treatments were performed in our Istitution (2016-2018): 35 with high-administered activity of ^{131}I-MIBG and 34 ^{131}I-NaI administrations (13 thyroid remnant ablations, 21 metastatic treatments). Median age was 13years (range 3-20yrs); median weight was 47kg (range 12-123kg). Median administered activities were: 11GBq for ^{131}I-MIBG (range 3.1-18 GBq), 2GBq (range 1.11-2GBq) of ^{131}I-NaI for thyroid remnant ablation, 5.5GBq (range 2.2-10.8 GBq) of ^{131}I-NaI for metastatic treatments. Relative difference between dose rate measured on discharge vs updated value on 7thday led to a reduction of isolation period of: 24(range 6-34) days for ^{131}I-MIBG treatments, 10(range 0-26) days for thyroid remnant ablations; 18(range 2-32) days for metastatic thyroid treatments. **Conclusion:** Our protocol, routinely applied in clinical practice, makes the experience of the isolation period easier and positive for both patients and parents, from hospitalization in therapy room to a faster return to daily life. Radiometric data updated on 7th day safely allow reducing radiation isolation period, improving life quality in children submitted to radioiodine therapy. **References:** None.

EP-0977

Optimal shielding specification for ^{68}Gallium - validation by Monte Carlo Simulations and Empirical Measurements

A. McCann[1,2], *S. Cournane*[1], *A. Dowling*[1], *D. Maguire*[1], *R. P. Killeen*[1], *J. Lucey*[1], *L. L. Vintro*[2];
[1]*UCD-SVUH PET CT Research Centre, St Vincent's University Hospital, Dublin, IRELAND,* [2]*School of Physics, University College Dublin, Dublin, IRELAND.*

Aim/Introduction: Significant improvements in the design and availability of Gallium (^{68}Ge/^{68}Ga) generators has resulted in their increased presence in PET/CT facilities. Vial and syringe shields originally designed for ^{18}F are now routinely used with ^{68}Ga; however, ^{68}Ga has a more complex decay scheme than the pure positron(β+) emitter ^{18}F. Positrons from ^{68}Ga possess an energy (1899keV, 96.7%) significantly higher than those of ^{18}F (633keV, 96.8%). The ^{68}Ga positrons have a longer path length and result in more intense Bremsstrahlung radiation. In addition to the 511keV annihilation photons, ^{68}Ga also decays with gamma emissions of 1077keV(3.2%) and 1883keV(0.14%) which can further complicate the shielding requirements. The potential skin dose due to contact with an unshielded syringe has been reported to be approximately 11 times higher for ^{68}Ga than ^{18}F attributable to higher energy positrons[1]. Optimal shielding for ^{68}Ga should stop the positron emissions and significantly attenuate the gamma and Bremsstrahlung emissions. This study will compare simulated and measured transmission data for ^{18}F and ^{68}Ga and determine optimal shielding requirements for ^{68}Ga. **Materials and Methods:** Monte Carlo simulation (EGSnrc, Canada) and Radiological Toolbox V3.0(NRC, USA) will be used to generate radiation transmission data and model beta particle effective path length data for ^{68}Ga and ^{18}F through tungsten, lead, perspex and various combinations of these materials. Modelling will be complimented by empirical dose rate measurements performed with a variety of commercially available gamma and beta detectors, while energy spectra will be examined using the Ortec Digidart-LF portable MCA detector. **Results:** Commercially available PET syringe shields typically have a wall thickness of 7.5-9mm. PET Syringe shields are typically specified in terms of ^{18}F attenuation, with no specification given for ^{68}Ga. However, ^{68}Ga positrons are modelled to have a much longer effective path length in both tungsten and lead, compared to ^{18}F. Simulated results will characterize the gamma radiation of ^{68}Ga as it traverses through these materials, the interactions of its high energy positrons and their resulting bremsstrahlung radiation. Further theoretical and measured results will be presented in detail. **Conclusion:** This study compares simulated and measured transmission data for ^{18}F and ^{68}Ga for a range of commonly used vial and syringe shields towards presenting the optimum shielding requirements for ^{68}Ga. The accuracy of a range of commercially available dose rate meters for use with ^{68}Ga is also assessed. **References:** 1 Kemerink et al. Extremity doses of nuclear medicine personnel: a concern. EJNMedMol Imaging. 2011;39(3):529-32.

EP-0978

External radiation exposure to the patient's environment after treatment with Cu-67 SARTATE

J. Preston[1], *E. Lengyelova*[1], *C. Biggin*[1], *M. Parker*[1], *M. Harris*[1], *E. van Dam*[1], *E. Bailey*[2], *D. Bailey*[2], *G. Schembri*[2];
[1]*Clarity Pharmaceuticals, Eveleigh, AUSTRALIA,* [2]*Royal North Shore Hospital, St Leonards, AUSTRALIA.*

Aim/Introduction: Cu-67 SARTATE, a beta and gamma-emitting therapeutic radiopharmaceutical is in clinical development as a potential treatment for a range of different SSTR-2 expressing cancers including meningioma, neuroblastoma and neuroendocrine tumours. Other Cu-67 based radiopharmaceuticals are also in development using different targeting moieties including GRPr (Bombesin) and PSMA analogues. An important component of radiopharmaceutical development is the assessment of radiation safety risks to the

patient's environment, including risk to the family, caregivers and the general public. This assessment also involves development of suitable radiation safety instructions, that balance the requirement of minimising radiation exposure to the family and carers without impacting on patient care and wellbeing; whilst also maintaining adherence and compliance to US radiation safety guidelines. **Materials and Methods:** Estimates of external radiation exposure from patients were obtained from predictive modelling using published dose coefficients for Cu-67 and preclinical estimates of effective half-life of Cu-67 SARTATE in the patient. According to these estimates, a series of radiation safety instructions were developed to ensure the radiation exposure to the patient's environment remains below acceptable radiation safety limits. The modelled estimates were subsequently compared to actual data utilising dose rate measurements acquired from the first-in-human clinical trial of Cu-67 SARTATE. **Results:** The radiation safety instructions developed applying the modelled estimates were shown to offer sufficient protection to the patient's family, caregivers and general public. The observed preliminary external dose rate measurements from an ongoing clinical trial with Cu-67 SARTATE verified that adherence to the radiation safety instructions ensure that radiation exposure to others remains below the acceptable limits. **Conclusion:** The radiation safety instructions following treatment with Cu-67 SARTATE in patients with meningioma have been shown to be sufficient, the external radiation exposure to family, caregivers and general public were below the generally accepted levels of 1mSv to children and pregnant/nursing mothers and the general public; and 5mSv for primary caregivers. Additionally, the preliminary dose exposure rates indicate that Cu-67 SARTATE can be given as an outpatient treatment, which is in line with NUREG 1556, Vol 9, Rev 2 (Table U.1). **References:** None.

EP-0979

Development of a quantitative annual risk assessment model for Nuclear Medicine: simulating radiation doses to hospital staff cohorts and members of the public

S. Cournane*, N. McArdle, J. McCavana;*
St Vincent's University Hospital, Dublin 4, IRELAND.

Aim/Introduction: Annual radiation risk assessments are performed to assess radiation doses that hospital staff, patients and members of the public are liable to receive. When radiation doses in excess of a 0.3mSv dose constraint from a single source are identified, practices are reviewed with the aim of reducing exposure and/or introducing additional dose monitoring where required. Nuclear medicine patients can be a source radiation exposure for their family, staff and members of the public within and outside of the hospital environment. Previous studies have calculated doses to different cohorts from patients based on proximity models and interaction patterns combined with dose rates and biokinetic models for single interactions; however, there is very little data or methodology available towards performing annual quantitative risk assessments. Accordingly, this study estimates, for a university teaching hospital and tertiary referral centre for breast and liver disease, the annual doses to the various staff groups and members of the public by examining the referral source frequency and pathways of patients attending for scans. **Materials and Methods:** Throughput, patient scanning frequency, injected activities, patient biokinetics, excreted activities, occupancy patterns, patient interaction patterns for various staff and patient cohorts, staff work rostering, workflow patterns and ward/clinical area design were examined to inform on parameter inputs to the quantitative risk assessment model. Information gained was through radiological information system, survey and interview techniques. **Results:** Modelled doses received and proximity models of staff from nuclear medicine patients will be compared to those presented in the literature, while estimated doses to family members will also be presented. Examples of annual modelled doses, per staff member, include those for ICU nurses (<15μSv), cancer day ward nurses, (<60μSv) and porters (<65μSv). In addition, theoretical scenarios simulated to examine the radiation exposures received from those staff members involved in, for example, pathological sampling from surgery (Sentinel node; <25μSv), nuclear medicine waste pipe leaking/bursting (<90μSv), and blood-sampling in phlebotomy (<10 μSv), will be presented, **Conclusion:** A risk assessment template quantifying risks as mentioned above has been developed, appropriate for current work practices. Annually, it can be populated with the breakdown of annual workload including referral sources to identify any groups at risk or workflows that require review. This tool has proved invaluable when educating staff cohorts throughout the hospital about the estimated typical doses that they receive in an environment, where sometimes the perceived risks are not commensurate with the real risks. **References:** None.

EP-0980

Comparison of correction factors for assessment of skin exposure of workers' hands in specific operations with selected radiopharmaceuticals

J. Hudzietzova[1]*, M. Fulop*[2]*, J. Sabol*[3]*, J. Doležal*[4]*, J. Kubinyi*[5]*, O. Kraft*[6]*, P. Povinec*[7]*, A. Vondrák*[8]*, L. Foltinová*[9]*;*
[1]*Czech Technical University in Prague, Kladno, CZECH REPUBLIC,* [2]*Slovak Medial University, Bratislava, SLOVAKIA,* [3]*Faculty of Security Management PACR, Prague, CZECH REPUBLIC,* [4]*Department of Nuclear Medicine, University Hospital Hradec Králové, Hradec Králové, CZECH REPUBLIC,* [5]*IZOTOPCENTRUM, s.r.o, Nitra, SLOVAKIA,* [6]*Department of Nuclear Medicine, University Hospital Ostrava, Ostrava, CZECH REPUBLIC,* [7]*PET centre BIONT, a.s., Bratislava, SLOVAKIA,* [8]*IZOTOPCENTRUM, s.r.o, Bratislava, SLOVAKIA,* [9]*UEBA, University of Economics in Bratislava, Bratislava, SLOVAKIA.*

Aim/Introduction: The correction factor, corresponding to the ratio of the skin exposure at the most exposed location and the exposure measured at the position of the finger dosimeter, may differ depending on working situations and conditions. The aim of the paper is to highlight possible differences in the

size of this factor during relevant specific procedures involving use of various radiopharmaceuticals and also to refer to the possible difference in its values in case of insufficient syringe shielding. **Materials and Methods:** The study included workers from selected nuclear medicine department engaged in using radiopharmaceuticals labelled with ^{18}F and ^{131}I (a total of 111 measurements). A similar pilot investigation was also carried out with ^{11}C and ^{68}Ga. Based on the monitoring using 12 TLDs fixed on workers' hands, the correction factor was calculated for workers handling the same radiopharmaceuticals. Its values referred to the position on the second index finger. In the case of ^{18}F measurements the effect of insufficient shielding was observed. **Results:** Following our present results, the correction factor referring to the index finger root was found to be significantly different for individual radionuclides. Based on our assessment, the correction factor involving ^{18}F and ^{131}I amounted to 3.5 and 1.9, respectively. From the pilot measurements involving ^{68}Ga, the correction factor was found to be 6.2 while in the case of ^{11}C its value was 2.8. In the specific case, when during the ^{18}F applications the insufficient shielding was used, the correction factor was up to three times higher than that under normal standard conditions. **Conclusion:** Preliminary results indicate that for different radiopharmaceuticals the correction factors may differ significantly. For this reason, it would be appropriate to verify the correction factors for each radiopharmaceutical and group of workers using the same radiopharmaceuticals. The correction factor assessed for standard situations should not be used in cases where the workers repeatedly use insufficient shielding. In such cases it is recommended to examine the values of the correction factors taking into account the influence of the insufficient shielding. Acknowledgments: The study has been partially supported by the project SGS18/100/OHK4/ IT/17 project. **References:** None.

EP-0981

Comparison of eye lens and hand skin exposures during handling ^{18}F, ^{11}C and ^{68}Ga radiopharmaceuticals

M. Fulop[1], *J. Hudzietzová*[2], *J. Sabol*[3], *P. Ragan*[1], *A. Vondrák*[4], *L. Foltínová*[5];
[1]*Slovak Medical University, Bratislava, SLOVAKIA,* [2]*Czech Technical University in Prague, Kladno, CZECH REPUBLIC,* [3]*Faculty of Security Management PACR, Prague, CZECH REPUBLIC,* [4]*IZOTOPCENTRUM, s.r.o, Nitra, SLOVAKIA,* [5]*UEBA, University of Economics in Bratislava, Bratislava, SLOVAKIA.*

Aim/Introduction: At present, in addition to ^{18}F-FDG radiopharmaceuticals, new PET radiopharmaceuticals labelled with ^{11}C and ^{68}Ga radionuclides are introduced in nuclear medicine. These radiopharmaceuticals emit the same penetrating gamma photons of 511 keV. Therefore, the optimized radiation protection for working with the ^{18}F labelled radiopharmaceutical is usually considered as sufficient approach also for these new radiopharmaceuticals. However, the ^{11}C and ^{68}Ga radionuclides emit positrons of higher energy than ^{18}F and the range in biological tissue of these positrons by several mm longer. The aim of the paper is to point out the importance of controlling the compliance with radiation protection requirements in PET workplaces for newly introduced positron radiopharmaceuticals where routine procedure applicable to handling of ^{18}F, ^{11}C and ^{68}Ga may result in higher skin and/or eye lens exposure. **Materials and Methods:** In nuclear medicine, a radiopharmaceutical is routinely administered to a patient via a cannula. The comparison of the exposure due to gamma photons and positrons of hand holding the infusion tube leading into the cannula with radiopharmaceutical solutions ^{18}F, ^{11}C and ^{68}Ga is simulated by the Monte Carlo code MCNP6 using a hand voxel phantom. In the same administration of the radiopharmaceutical, the administering person is inclined above the injection site and observes the infusion tube filling with the radiopharmaceutical while exposing the eyes to the gamma radiation and the positrons penetrating the infusion tube. The equivalent dose of the eye lens in the head voxel phantom is compared to the $H_p(3)$ calculations of the personal TLD dosimeter placed on the chest of the MIRD chest phantom for the same irradiation geometry. **Results:** Monte Carlo simulations with the phantom of the hand holding the infusion tube showed that when replacing the ^{18}F radiopharmaceutical with ^{11}C, the skin irradiation on the hands is increased by a factor of 2. The confusion of the ^{18}F radiopharmaceutical ^{68}Ga is more prominent, with a 4-fold increase in skin irradiation at the same actions hands. In the case of irradiation of the eye lens with an unshielded ^{68}Ga radiopharmaceutical at a distance of 50 cm, Monte Carlo simulations showed that the equivalent dose is a factor of 2 higher than the $H_p(3)$ value obtained by a personal chest dosimeter. **Conclusion:** The efficiency of radiation protection measures introduced when handling the ^{18}F radiopharmaceuticals should be carefully checked when introducing ^{11}C and ^{68}Ga labelled radiopharmaceuticals. Acknowledgements: Study has been supported - SGS18/100/OHK4/1T/17 project. **References:** None.

EP-0982

Incorporation Of ^{177}Lu During Care Of ^{177}Lu-PSMA And ^{177}Lu-DOTATATE Therapy Patients

C. Happel[1], *W. T. Kranert*[1], *B. Bockisch*[1], *U. Kratzel*[2], *J. Baumgarten*[1], *C. Nguyen Ngoc*[1], *E. Garayev*[1], *F. Grünwald*[1], *A. Sabet*[1];
[1]*University Medical Center Frankfurt / Department of Nuclear Medicine, Frankfurt, GERMANY,* [2]*Bavarian Environment Agency, Office Kulmbach, Kulmbach, GERMANY.*

Aim/Introduction: The determination of the annual effective ^{131}I dose of the nursing staff caused by incorporation on a nuclear medicine therapy ward is required in Germany. Since the establishment of ^{177}Lu-PSMA-617 for treatment of metastatic castration-resistant prostate cancer and ^{177}Lu-DOTATATE for neuroendocrine tumors the patient spectrum on nuclear medicine wards has changed, but currently routinely performed incorporation monitoring of ^{177}Lu is not prescribed. The reason is the absence of volatility of ^{177}Lu compared to ^{131}I. In a routinely performed incorporation analysis the 208keV

gamma-peak of ^{177}Lu was unexpectedly detected and a closer analysis was performed to estimate the effective dose for the employee concerned. Aim of this study is to present these data and to discuss the possibility of ^{177}Lu incorporation and potential reasons. **Materials and Methods:** Activity concentration in urine samples (collection for 24h) of the nursing staff of a nuclear medicine therapy ward was routinely examined fortnightly. During a week with two ^{177}Lu-PSMA patients (accumulated activity: 16.9GBq) and two ^{177}Lu-DOTATATE patients (accumulated activity: 10.9GBq) the 208keV gamma-peak of ^{177}Lu was detected in two 24h urine samples (0.88l and 3.5l respectively). ^{177}Lu is known to be not volatile, therefore the exact reason of the incorporation and the incorporation pathway remains unknown. Preparation was done in a flue and the direct contact of the nurses to the patients was restricted to a necessary Minimum. **Results:** For calculation of the dose a single ingestion with total resorption in the gastrointestinal tract and the biochemical behavior of ^{177}Lu-DOTATATE (which is previously described in several studies) was assumed. The calculated supply of activity using these presumptions corresponds to a proportion of 10^{6} of the administered activity. The detected ^{177}Lu activity in the urine samples was 70.9 and 14.4Bq leading to a concentration of 80.6 and 4.11Bq/l. The dose coefficient of ^{177}Lu-DOTATATE for the effective dose is $5.2*10^{-11}$Sv/Bq. The dosimetric evaluation of the measured values led to effective doses of $2.56*10^{-3}$mSv and $2.64*10^{-4}$mSv respectively. **Conclusion:** Due to biochemical behavior of ^{177}Lu and preparation in a flue, inhalation of the radiopharmaceutical is implausible. Incorporation by penetration due to unnoticed skin contamination is implausible as well because frequent contamination measurements were performed. In the follow-up samples of the employees concerned no ^{177}Lu was detected confirming the hypothesis of a unique incorporation by unnoticed ingestion. A systematic incorporation by inhalation can therefore be excluded. However, routine analysis of ^{177}Lu in incorporation monitoring might be reasonable. **References:** None.

EP-0983

Iodine 131 Excretion In Saliva And Bronchial Secretion In Differentiated Thyroid Carcinoma

B. Bockisch[1], *B. Sauter*[2], *M. Etzel*[3], *W. T. Kranert*[1], *S. Wagner*[1], *A. Sabet*[1], *F. Grünwald*[1], *C. Happel*[1];
[1]*University Hospital Frankfurt, Department of Nuclear Medicine, Frankfurt, GERMANY,* [2]*Kreiskliniken Darmstadt-Dieburg, Darmstadt, GERMANY,* [3]*Radiologie Darmstadt, Darmstadt, GERMANY.*

Aim/Introduction: Knowledge of radioiodine pharmacokinetics in ablative radioiodine-131 therapy of differentiated thyroid carcinoma (DTC) and its excretion is particularly important for the evaluation of potential contaminations and dosimetry. I-131 excretion of the salivary glands during radioiodine therapy of DTC is currently not adequately examined. Therefore, the aim of this study was a quantitative determination of this issue. **Materials and Methods:** A 68 year-old patient with DTC and tracheostoma was treated in our department with 3.45 GBq I-131 (i.v. administration). Suctioning of the bronchial secretion was necessary due to the tracheostoma. Bronchial secretion was highly contaminated with saliva because of esophagus obstruction with a esophago-bronchial fistula. Measurement of the remaining whole body I-131 activity was performed using a gamma probe calibrated for I-131. The complete saliva contaminated bronchial secretion was collected over 4 days, each suctioning separately, and measured in aliquots of 1 ml in a well counter (1,659 - 2,399 ml/fraction; saliva-contaminated bronchial secretion and lavage liquids). The resulting activity kinetics in saliva-contaminated bronchial secretion was compared to the I-131 whole body activity. **Results:** Measurements of the saliva-contaminated bronchial secretion showed a biexponential progression with effective half-life of 0.2 d (fast phase) and 1.16 d (slow phase). In parallel the activity kinetic of the whole body showed a biexponential progression as well with effective half-life of 0.28 d (fast phase) and 0.98 d (slow phase). ICRP calculated whole body dose amounted to 250 mSv. Assuming a continuous saliva excretion of 1.5 l/d, the activity concentration in saliva-contaminated bronchial secretion decreased from 2 MBq/ml on the first day to 30 kBq/ml on the fourth day after administration. The overall excreted I-131 activity in the cumulative saliva contaminated bronchial secretion was 2.1 GBq (60% of the administered activity). **Conclusion:** I-131 excretion in saliva contaminated bronchial secretion corresponds with whole body activity. I-131 activity excreted with the saliva is high due to almost absent remaining thyroid tissue (DTC: excretion 60%, uptake thyroid bed: ~1%). Especially during the first 24h after administration special radiation protection precautions are required in handling saliva, the resulting sewage water and waste as well. Saliva contaminated bronchial secretion leads to an increased radiation exposition of the respiratory tract. **References:** None.

EP-0984

CT optimisation and LDRLs for SPECT/CT in a Paediatric Hospital

E. Morris[1,2], *A. Rose*[1,2], *M. Easty*[2], *L. Biassoni*[2];
[1]*Barts Health NHS Trust, London, UNITED KINGDOM,* [2]*Great Ormond Street Hospital for Children NHS Foundation Trust, London, UNITED KINGDOM.*

Aim/Introduction: Diagnostic Reference Levels (DRLs) are required by European Council Directive 2013/59/EURATOM (1), to provide a benchmark for the radiation dose expected for typical examinations in typical patients. If a comparison of local patient's radiation doses to the DRLs shows the DRL to be consistently exceeded, an investigation and optimisation of the examination or corrective action to improve clinical practice can be implemented. Paediatric patients are especially sensitive to ionising radiations. In the last 15 years the radiology community have been trying hard to perform imaging tests of diagnostic quality with the minimum radiation exposure to the patient. After the installation of a new 16 slice SPECT/CT in our specialised

paediatric hospital, a project was initiated to optimise the CT protocols, both for attenuation correction and localisation of SPECT studies and use as a standalone CT scanner. The aim was to compare radiation dose and image quality with the standalone CT scanner in the hospital and national or international diagnostic reference levels, where available. **Materials and Methods:** The SPECT/CT scanner was initially set up using historical protocols. Image quality measurements were performed using a CATPHAN 500 and ATOM® Dosimetry Verification Phantoms in different paediatric sizes. Image noise measurements and contrast to noise ratios were compared against various scan parameters to identify the minimum required image quality at the lowest possible radiation dose. Radimetrics™ Radiation Dose Management software was used to record patient study parameters for setting LDRLs. Weight groups were used for all body examinations LDRLs, and age groups for head exam LDRLs. **Results:** Patient exposure parameters were gradually adjusted and image quality assessed by a Nuclear Medicine Physician and a Consultant Radiologist in an iterative process. The image quality and radiation dose received by the patients was comparable between the SPECT/CT and the standalone CT scanner. LDRLs have been set for selected examinations for some weight and age groups of patients. However, some weight and age categories are less well represented in the referred paediatric patient population and the threshold for sufficient patient numbers to set an LDRL in these categories has not yet been reached. **Conclusion:** LDRLs have been set for the most commonly used SPECT/CT examinations in the department with satisfactory image quality and low radiation exposure. **References:** European Commission. Council Directive 2013/59/EURATOM [internet]. [cited 18th April 2019] Available from https://eur-lex.europa.eu/legal-content/EN/TXT/?uri=CELEX%3A32013L0059#ntr4-L_2014013EN.01000101-E0004

EP-0985

Challenging Radioiodine Therapies: The art of not tripping over your feet whilst looking up at the stars

***R. Fernandez**, A. Nunes, F. Hassan, V. Lewington, S. J. Allen;*
Guy's & St Thomas' Hospital, London, UNITED KINGDOM.

Aim/Introduction: Radioactive iodine (^{131}I) has been used to treat benign and malignant thyroid conditions for over sixty years. With advances in medicine, an increasing number of patients with complex co-morbidities are being referred for ^{131}I treatment. Treating this patient cohort brings challenges around minimisation of radiation dose to at-risk groups and management of radioactive waste generated during/after treatment. Patients in four different challenging situations were successfully treated after careful planning by multi-disciplinary teams experienced in delivery of radioiodine. **Materials and Methods:** Three patients with end-stage renal disease on dialysis were referred for radioiodine treatment (one patient treated with 3.7GBq following total thyroidectomy, two patients treated with 800MBq for benign thyroid disease). Of the latter group, one patient had significant mobility issues requiring assistance from a carer upon hospital discharge, whilst another was registered blind and dependant on her partner for home care. Another patient treated with ^{131}I for thyroid cancer developed chest pain shortly after hospital discharge and required care in the Emergency Department. A teenage patient with thyroid cancer who had swallowing difficulties and gastric motility complications required IV radioiodine administration and assistance from a carer during her inpatient stay. Another young patient with Graves' disease was referred for radioiodine treatment whilst an inpatient in a secure mental health unit (MHU). **Results:** Following each dialysis (with 2 day interval between dialysis sessions), decrease in residual ^{131}I activity varied between the malignant/benign patient groups [Range: 19-53%]. Instantaneous dose-rate, measured in rooms adjacent to treated patients was highest for the dialysis patient treated with 3.7GBq and was 11microSv/hour. Maximum occupational whole-body (WB) dose was 66microSv, recorded by a renal nurse attending to the patient during a 4 hour dialysis session. In the MHU an Occupational therapist received 42microSv WB dose during a group therapy session. Carers & Comforters wearing WB dosimeters for the contact period duration recorded minimal radiation dose [Maximum received was 1.8mSv by the blind patient's carer]. Maximum ^{131}I activity in generated solid radioactive waste (e.g. dialysis tubing) was 1MBq. This residual waste activity decreased by 50-60% with each subsequent dialysis. Solid radioactive waste retained from the MHU contained 0.2MBq ^{131}I. **Conclusion:** This study presents a number of very different, complex clinical scenarios, each involving patients requiring ^{131}I administration who presented with challenging comorbidities/complications. Careful planning of treatments by teams experienced in the delivery of radioiodine ensures that patients in these groups have equitable access to treatment. **References:** None.

EP-0986

Management Of Extravasation Of Lutetium 177 Dotatoc

***A. C. Bekker**, P. F. Staanum, H. Bluhme, A. K. Arveschoug;*
Department of Nuclear Medicine and PET, Aarhus University Hospital, Aarhus, DENMARK.

Aim/Introduction: In June 2018, a 68-year old woman with metastatic neuroendocrine tumor received the first out of four treatments with 7,5 GBq Lutetium-177-Dotatoc. The radioactive pharmaceutical was injected via intravenous catheter in cubital fossa in the left arm. Treatment was performed in a shielded room at The Department of Oncology, Aarhus University Hospital. Immediately after end of infusion, the nurse noticed a swelling in the upper left arm, proximal to the injection site. The patient confirmed having felt a slight discomfort during infusion. Action was now taken as to confirm an extravasal injection. **Materials and Methods:** A Rados RDS-120 surveymeter was used to measure radiation dose rate close to the injection site. A few minutes after end of injection, the dose rate was approximately 5000 microSv/hour. The patient was immediately transferred to

The Department of Nuclear Medicine and PET Centre in order to perform a wholebody-scan and a Spect-CT, including the upper left arm, using a Siemens Symbia T16 Spect-CT. The patient was transferred back to The Department of Oncology, a compression bandage was applied combined with bags with heated gel in order to stimulate the lymphatic drainage. Furthermore, the patient was instructed in elevating the arm while activating the venous pump by flexing and stretching the elbow, using an elastic cotton string tied to something stable. During the day the compression bandage was re-applied, as the swelling decreased. The patient continued exercising the left arm. **Results:** The post injection scans confirmed that the entire treatment dose was located in the patients upper left arm. Approximately 6 hours post injection, measurement of the radiation dose rate close to the injection site now showed a 5-fold decrease to 910 microSv/hour. 24 hours post injection the dose rate had decreased further to 104 microSv/hour, at day 4 to 49 microSv/hour and finally at day 7 to 29 microSv/hour. Wholebody and Spect-CT confirmed the decrease of activity in the arm and was now showing high uptake in the neuoendocrine tumour cells and uptake in the kidneys. **Conclusion:** With an immediate recognition and appropriate management it is possible to reverse an extravasal injection of Lu-177-Dotatoc by elevation, compression, heat and venous pump exercises. Thereby, it was possible to avoid any further discomfort to the patient including additional treatments. **References:** None.

EP-0987

I-RISK: A Mobile Application for Patient-Specific Instruction and Effective Dose Estimation for Family Members and Member of thePublic for Patients Receiving Iodine-131 Therapy

***K. Chuamsaamarkkee**, P. Charoenphun, M. Panawech, K. Thongklam, S. Vittayachokkitikhun, W. Chamroonrat;*
Division of Nuclear Medicine, Department of Diagnostic and Therapeutic Radiology, Faculty of Medicine Ramathibodi Hospital, Mahidol University, Bangkok, THAILAND.

Aim/Introduction: Radioiodine (^{131}I) therapy has been used for thyroid diseases for many decades and it is the most common therapeutic radioisotope. Following radioiodine therapy, several concerns regarding to radiation safety are rising, for instance; post-discharge patient instructions and the effective dose to family members and member of the public. Unfortunately, several concerns are not well managed due to lack of standard regulatory guidance. Therefore, I-Risk mobile application aims to provide the patient-specific instructions based on the ATA (American Thyroid Association) and IAEA (International Atomic Energy Agency) guidelines. I-Risk also provides the effective dose estimation for family members and public with user-defined scenario for duration and distance of ^{131}I treated patient contact. **Materials and Methods:** I-Risk classifies the users into two groups (a) the ^{131}I treated patients or their family members and (b) the healthcare practitioners. The ^{131}I treated patients or their family members are required to fill in the following parameters; type of disease (hyperthyroid or thyroid cancer), activity and date of treatment. For the healthcare practitioners, the radiation exposure of ^{131}I treated patient measuring by a survey meter is used as a primary input. The occupational factor and distance are also the crucial factors to estimate the effective dose. The thyroidal and extrathyroidal uptake fraction values are derived from the US NRC (United States Nuclear Regulatory Commission) recommendation. The effective half-life which depend on administration activity and time-point of measurement is taken from the published literatures based on Asian population data. **Results:** Patient-specific instruction based on the type of disease, administered activity and treatment date could be generated from I-Risk displaying in user-friendly interface. In addition, the total effective dose equivalent (TEDE) could be calculated using a dose rate data from survey meter fitted on the Asian population data. **Conclusion:** In conclusion, I-Risk can provide the individual specific instruction for ^{131}I treated patients. The healthcare practitioners can use I-Risk as a guidance to manage the radiation safety concerns. Subsequently, family members and public will get less unnecessary radiation exposure from the patients who received ^{131}I therapy. Additionally, I-Risk also provides the Q&A (question and answer) section which the users can directly enquire their questions to the experienced medical physicist. **References:** None.

EP-0988

Pattern Of Myocardial ^{18}F-FDG Uptake Related To Radiation Dose Before And After Radiotherapy In Patients With Esophageal Cancer

***X. Sha**[1], C. Han[2], G. Gong[1], Y. Yin[1];*
[1]Department of Radiation Oncology, Shandong Cancer Hospital Affiliated with Shandong University, Jinan, CHINA,
[2]Turku PET Centre, Turku University Hospital, Turku, FINLAND.

Aim/Introduction: With increased long-term survival in esophageal cancer patients with radiotherapy, radiation-induced cardiac toxicity happens more frequently. The purpose of this study was aiming to investigate change of myocardial [18F]FDG uptake before and after radiotherapy, and relationship between this change and radiation dose on myocardium during therapy. **Materials and Methods:** Ten patients with thoracic esophageal cancer with radiotherapy were enrolled in Shangdong Tumor Hospital, Jinan, China during 2016-2018. [18F]FDG PET imaging was performed 1-2 week before radiotherapy and 2-3 months after radiotherapy. Prior to PET imaging, patients were fasted over 12 hours.PET imaging data were analyzed using Carimas (developed in Turku PET Centre, Turku, Finland). Radiation dose data were outputted as Dicom image data format (each pixel represents radiation dose). Then it was fused with FDG PET imaging. Left ventricular myocardium (LV-VOI) was segmented based on FDG PET images. Using same LV-VOI, corresponding radiation dose was extracted from radiation dose image. Finally, the relationship between change of FDG PET uptake and radiation dose for left ventricular myocardium was calculated. **Results:** Three myocardial

accumulation patterns of FDG PET uptake related to radiation dose were categorized. Uptake of FDG was increased in high radiation dose in four patients, meanwhile, uptake of FDG was decreased in high radiation dose in another four patients. In last two patients, uptake of FDG was not significantly changed with radiation dose. Since without clinical data, it is not possible to correlate the FDG PET uptake pattern with cardiac toxicity in current study. **Conclusion:** In patients with esophageal cancer with radiotherapy, accumulation of FDG is complicated with increased, decreased or no-change modes related to radiation dose. **References:** [1] Evans J D, Gomez D R, Chang J Y, et al. Cardiac 18F-fluorodeoxyglucose uptake on positron emission tomography after thoracic stereotactic body radiation therapy[J]. Radiotherapy and Oncology, 2013, 109(1):82-88. [2] Fang W, Zhao L, Xiong C, et al. Comparison of 18F-FDG uptake by right ventricular myocardium in idiopathic pulmonary arterial hypertension and pulmonary arterial hypertension associated with congenital heart disease[J]. Pulmonary Circulation, 2012, 2(3):365-372. [3] Taylor C, McGale P, Brønnum D, Correa C, Cutter D, Duane FK, et al. Cardiac structure injury after radiotherapy for breast cancer: cross-sectional study with individual patient data. J Clin Oncol 2018;36:2288-96.

EP-0989

A Significant Reduction Of The Radiation Exposure Of Medical Personnel In The Context Of Radioiodine Therapy By An Alternative Effective, Reliable And Accurate Method For Measuring The Pre-therapeutic Activity Of The [^{131}I]-iodine Capsule

***J. Ranjan**, U. Lützen, Y. Zhao, M. Jüptner, M. Marx, M. Zuhayra;*
Nuclear Medicine, UKSH, Kiel, GERMANY.

Aim/Introduction: The handling of the iodine-131 (I-131)-capsules in the context of the Radioiodine Therapy (RIT) leads to a significant radiation exposure of the medical personnel, especially their hands during the obligatory pre-therapeutic measurements. This study proves a significant reduction in the radiation exposure of medical personnel by determining the radioactivity of the I-131-capsules in an alternative measurement, which keeps the I-131-capsule itself in the shielded lead container during measurement. **Materials and Methods:** I-131-capsules are delivered in closed shielded lead containers. Hp(10) dose rates were measured on the surface of the lead container using a commercially available dose rate meter (Bertold Umo LB 123) and 4 mm steel fixation devices to ensure exact and reproducible measurement geometry on the surface of the lead container in two positions, the top and the side. The exact activity of the I-131-capsule was subsequently measured conventionally using a dose calibrator. Calibrating curves were created by linear correlation between the results obtained in [MBq vs. µSv/h]. The Hand Hp(0.07) and whole body doses were determined with thermo luminescent ring dose meters (TLD) and Optically stimulated luminescence dose meters (OLS) during measuring the activity of 115 I-131-capsules (cumulative activity 197 GBq) by using the two measurement methods within a period of 6 months. **Results:** The linear calibration curves show determination coefficients of R^2 0.999. The total relative measurement uncertainty of the method is ±6.1% and lies below the threshold limit for the maximum allowed uncertainty of ±10% for measuring radioactivity in radioactive drugs according to the European pharmaceutical regulations. The hand dose during the measuring period of 6 month was for the conventional measuring of the I-131-capsule in the dose calibrator 9.570 mSv (0.0486 mSv/GBq). Our new method for measuring the I-131-capsule using the fixing device and Bertold Umo LB 123 led only to 0.279 mSv (0.0014 mSv/GBq). This means a reduction of the hand dose by nearly 35 fold. The effective dose (whole body) for both measuring methods was under the detection limit of the dose meter. **Conclusion:** During the clinical routine the introduction of our new measuring method leads to a distinct reduction of the radiation exposure of the hands of the medical staff and allows an accurate determination of the activity of the [131I]-capsules prior to application. **References:** None.

EP-0990

Common Errors and Misconceptions in Radiation Protection

J. Cortese;
British Columbia Institute of Technology, Burnaby, BC, CANADA.

Aim/Introduction: There are many common misconceptions in the application of radiation safety principles and practices in Nuclear Medicine. Through a 20-year career in radiation safety training, auditing, inspecting and investigating, common errors have been observed in Nuclear Medicine departments across Canada. Discussing some of these errors and misunderstandings can be useful to promote best practice in Radiation Safety. **Materials and Methods:** Years of observations, inspections, investigations, interviews and audits have revealed common misconceptions among Nuclear Medicine practitioners. Through anecdotal evidence, explanation of the physical properties of radiation, physical measurements around radioactive sources, dose estimations and shielding calculations it can be demonstrated that some common practices in Nuclear Medicine are ineffective and some commonly neglected safety equipment can be very useful in the clinical setting. **Results:** Technologist explanations of dose and risk to patients are often incorrect. Lead aprons are often used when ineffective, and often the wrong type of lead aprons are purchased. Syringe shield use is often dismissed because of incorrect assumptions. Contamination monitoring programs are often set up improperly. **Conclusion:** Sharing expertise, physical measurements, scientific data and years of experience can prevent many common misconceptions in the application of radiation safety in Nuclear Medicine and promote best practice. Discussing the pros and cons of safety equipment and practice is an effective way to enhance the safety culture within the Nuclear Medicine community. **References:** None.

EP-0991

Absorbed Dose Estimation To Co-Habitants And Co-Travellers Of Patients Treated With Radioiodine For Differentiated Thyroid Carcinoma

I. Iakovou[1], *K. Hatziioannou*[2], *K. Badiavas*[2], *E. Papanastasiou*[3], *A. Zapros*[3], *G. Arsos*[1];
[1]*3rd Nuclear Medicine Laboratory, Aristotle University of Thessaloniki, Papageorgiou General Hospital, Thessaloniki, GREECE,* [2]*Medical Physics Department, Papageorgiou General Hospital, Thessaloniki, GREECE,* [3]*Medical Physics Laboratory, Aristotle University of Thessaloniki, AHEPA University Hospital, Thessaloniki, GREECE.*

Aim/Introduction: Thyroid remnant ablation with radioiodine is a well-established treatment for patients with Differentiated Thyroid Carcinoma (DTC) after thyroidectomy. After hospitalization of approximately 3-4 days these patients return to their homes presenting a possible radiation hazard to the people around them, such as co-travellers and co-habitants. This work aims to estimate the possible radiation burden to the people, both co-travellers and co-habitants, which came in contact with the patients after their release from the hospital, analyzing data obtained during their hospitalization. **Materials and Methods:** Over a period of 8.5 years data from 1066 patients were used to estimate the possible radiation burden to family members and people that came in contact with the patients, grouping them according to their age, type of contact with the patient (co-traveller, co-habitant) and patient family status, assuming different exposure scenarios for each group and based on the written precautions given to all patients before discharge. Possible correlations between the iodine effective half-life (Teff), estimated from patient dose rate measurements during hospitalization, patient age and the method used for thyroid preparation for ablation (Thyroid Hormone Withdrawal-THW or administration of recombinant human thyroid stimulating hormone-rhTSH) were also investigated. **Results:** Mean absorbed dose to adult cohabitants was estimated to be 15 μSv (range 0.1-117 μSv), to babies (0-5yr) and small children (5-10yr) 20 μSv (range 0.8-196 μSv), to children (10-18 yr) 15 μSv (range 0.5-117 μSv) and to co-travellers 9 μSv (range 0.2-115 μSv). The highest doses to co-habitants were estimated in the few cases where the patient was a single parent of one or more children (mean children dose 64 μSv, range 11-279 μSv). No statistically significant difference in Teff between THW (mean Teff: 16.0 hrs) and rhTSH (mean Teff: 15.5 hrs) groups was observed. **Conclusion:** Provided necessary precautions are followed, radiation burden to the family members and co-travellers of DTC patients treated with radioiodine following thyroidectomy can be kept well below the corresponding dose limits and constraints. **References:** None.

EP-0992

Radiation Exposure of Nurses Including Eye Lens in PET Facility in Association with Performance Status of Patients

M. Hosono, *N. Takahara*, *Y. Yakushiji*, *K. Sakaguchi*, *Y. Yamada*, *H. Kaida*, *K. Ishii*, *Y. Nishimura*;
Kinki University Faculty of Medicine, Osaka-Sayama, JAPAN.

Aim/Introduction: Radiation protection is an important issue for nurses who take care of patients in PET facilities, and equivalent dose to the lens of the eye should be assessed as well as effective dose. Radiation exposure of nurses may be increased when patients have problems in activities of daily living (ADL) and need intensive nursing care. We measured individual dose of nurses in consideration of performance status of patients. **Materials and Methods:** Individual dose of nurses was measured during PET practices through injection of FDG, nursing care, to patients' discharge from the facility. Each nurse wore 2 individual dosimeters (MYDOSE PDM-111, Hitachi Aloka Medical) on the chest and abdomen. Performance status of patients was recorded using Katz index of independence in ADL, which is a standard method to assess ADL by categorizing into 7 grades from Index 6 (good) to Index 0 (poor). Radiation doses and contact time were recorded and analyzed. Equivalent dose to the lens of the eye was measured using thermoluminescent dosimeter at the bilateral angles of the eye as Hp(3) for 5 nurses who cared totally 167 patients. **Results:** Nurses cared overall 902 consecutive patients, who were grouped into Index 6 of 825 patients (91.5%), Index 5 of 41 (4.5%), Index 4 of 13 (1.4%), Index 3 of 7 (0.8%), Index 2 of 6 (0.7%), Index 1 of 3 (0.3%), and Index 0 of 7 (0.8%). Mean contact time of nurses to patients was 1 min to 10 min for Indices 6 to 0. Radiation doses of nurses were correlated with ADL of patients. On the basis of these results, the weighted average of exposure of a nurse was 0.25 μSv/patient. The mean equivalent dose of the lens of the eye of the nurses was 1.7 and 2.2 μSv/patient on the right and left, respectively. **Conclusion:** This approach of considering ADL of patients for dose evaluation of nurses was useful to optimize radiation protection. In our facility, patients with poor ADL account for a small fraction of patients, then, how to reduce radiation exposure from good ADL patients is important for reducing overall radiation exposure. Equivalent dose of the lens of eye would be under the dose limit (20mSv/y) even if a nurse would care 5,000 patients/year. **References:** Katz S et al. N Engl J Med 1983;309:1218.Perez ME et al. Optimization of radiation doses received by personnel in PET uptake rooms. Health Phys 2014;107(5 Suppl 3):S198-201.

EP-0993

Radiation safety instructions given to all household contacts significantly reduce radiation exposure from illiterate patients treated with low dose radioactive iodine (I -131)

K. Salman[1], *S. Wagieh*[2], *A. Bakhsh*[1], *M. Al-Ezzi*[2], *T. Munshy*[1];
[1]*King Abdullah Medical City-Makkah, Makkah,*

SAUDI ARABIA, [2]King Abdullah Medical City-Makkah (Oncology Center), Jeddah, SAUDI ARABIA.

Aim/Introduction: Radiation safety instructions (RSI) represent a cornerstone in I-131 therapy. Illiteracy may be an obstacle in proper understanding of these instructions and may decrease ability of conveying these instructions accurately to family members and household contacts. **Aim**: To evaluate the significance of giving RSI to all household contacts of illiterate patients treated with low dose I-131 therapy **Materials and Methods:** 23 illiterate patients with thyroid cancer presented for post- operative ablation with 30 mCi (1110 MBq) I-131 were included. 11 patients received direct RSI from radiation safety officer (RSO) to convey them to their 51 household contacts .On the other hand, for the 54 household contacts of the remaining 12 patients an arrangement was done to meet all contacts by the RSO to give RSI directly. Thermoluminescent dosimeters (TLD's) were dispensed to all household contacts to measure radiation exposure. TLD's were collected on the fifth day and radiation exposure figures to household contacts were measured. **Results:** Radiation exposure figures to all household contacts were below 1 mSv, ranging from 143uSv to 535uSv. The first group of contacts had a mean exposure of 373± 139 (range: 218 to 535 uSv) .These figures for the second group of contacts , who received direct RSI from RSO were 193 uSv ± 91 (range :143-291 uSv) respectively, with a statistically significant difference between both figures (P<0.05) **Conclusion:** Radiation exposure to all contacts was below the radiation exposure constraint of 1mSv. Yet, radiation exposure figures were significantly less for household contacts who received direct RSI from RSO compared to those who received these instructions from the patient .Our results emphasize the value of giving direct radiation safety instructions to all household contacts of illiterate patients treated with I-131 to reduce radiation exposure figures and to achieve the ALARA principle. **References:** -Martin R., Silva F., Colon MA., Roman D., Gonzalez TB: Evaluation of Household Radiation Exposure and Safety after Ambulatory Radioiodine Ablation therapy. Journal of thyroid cancer .2016,1(1): 35-41. - Kuo S., Ho T., Liou M. , Lin K. , Cheng R., Chan S. , Huang B., Ng S., Liu F. , Chang H.,Hsieh S., Chiang K. , Chen H. , Lo T., Lin C. , Lin J. Higher body weight and distant metastasis are associated with higher radiation exposure to the household environment from patients with thyroid cancer after radioactive iodine therapy. Medicine, September 2017;96(35) pe7942.

EP-0994

Iodine 131 In Ascites After Radioiodine Therapy (RIT)

B. Bockisch[1], *M. Etzel*[2], *B. Sauter*[3], *C. Happel*[1], *W. T. Kranert*[1], *N. Mader*[1], *A. Sabet*[1], *F. Grünwald*[1];
[1]*University Hospital Frankfurt, Department of Nuclear Medicine, Frankfurt, GERMANY,* [2]*Radiologie Darmstadt, Darmstadt, GERMANY,* [3]*Kreiskliniken Darmstadt-Dieburg, Darmstadt, GERMANY.*

Aim/Introduction: Pharmacokinetics of Iodine-131 and its excretion are important for dosimetry and to control possible contamination pathways. Biodistribution of Iodine-131 in patients with ascites has not been examined to date. Ascites occurs by pass over of fluids from blood vessels to the abdominal cavity and may therefore be contaminated with I-131. Concentration of I-131 in ascites was measured. **Materials and Methods:** A 57-years-old male patient with ascites suffering from Graves' disease received oral RIT (510 MBq, intratherapeutic thyroid uptake 83 %). Four days after administration scintigraphic imaging of the abdomen followed by a puncture of the ascites was done. 8 litre ascites of an estimated total volume of 20 l were removed and a sample of 1 ml analysed in a calibrated well counter. 15 days after administration, the puncture was repeated (8 l removed, estimated total volume of 14 l). **Results:** Activity concentration in punctured ascites 4 d and 15 d after administration was 0.165 kBq/ml (total of 1.32 MBq) and 0.35 kBq/ml (total of 2.8 MBq), respectively - corresponding to 1.5 % and 3.2 % of total extrathyroideal activity as measured by whole body and partial body (thyroid) activity with a calibrated gamma probe. An increased activity in ascites was not detectable in scintigraphic imaging compared to the surrounding tissue. **Conclusion:** Ascites is contaminated with I-131 in patients treated with RIT and may exceed the local contamination limits. Because most of the ascites of the first puncture was generated prior to radioiodine-131 administration, increased activity in the second puncture was detected. Activity concentration in ascites will depend on administered dose as well as individual bio-kinetics. Therefore, a puncture of ascites should be performed prior to RIT. If this is not possible it should be performed during inpatient treatment, as ascites has to be handled and disposed according to local radiation protection regulations. **References:** None.

EP-0995

Effective finger dose for the staff performing in house production of ^{68}Ga-PSMA and ^{68}Ga-DOTATOC

K. Dalianis[1], *K. Gogos*[1], *G. Kollias*[1], *E. Oikonomou*[2], *R. Efhtimiadou*[2], *V. Prasopoulos*[2];
[1]*Medical Physics Department, Hygeia SA, Athens, Marousi, GREECE,* [2]*PET/CT Department, Hygeia SA, Athens, Marousi, GREECE.*

Aim/Introduction: The PET/CT applications have been continuously increasing. Development and availability of radiopharmaceuticals is a key driving force of nuclear medicine establishment and expansion. New radiopharmaceuticals specific for particular diseases is one of the driving forces of the expansion of clinical PET. Although such an increase is a positive trend for the benefit of patients, the associated risk of radiation exposure of staff needs to be properly evaluated. The aims of this study were to estimate the effective finger dose for the staff involved in in house production of ^{68}Ga-PSMA and ^{68}Ga-DOTATOC. **Materials and Methods:** To estimate the effective dose from external exposure, all 5 members of the staff (2 nurses, 2 medical physicists, 1 radio pharmacist) worn ring thermoluminescence

dosimeters (TLDs). We use 1850 MBq Ge68/Ga68 generator which is eluted daily by the medical physicist. The synthesis is performed by the radio pharmacist. The doses were derived by the medical physicists. The injected activity per patient is 185-200 MBq . **Results:** A total of 22 examinations were performed . The collective finger doses received by all 5 members of the PET/CT staff were the following: Nurse 1 received 1.56 mSv as a finger dose and Nurse 2 received 2.25 mSv finger dose respectively. Medical Physicist 1 received 2.96 mSv finger dose and Medical Physicist received 2 3.12 mSv respectively. Radio pharmacist received 3.98 mSv finger doses. **Conclusion:** The personnel dose results are significantly lower than the recommended annual dose by International Commission for Radiological Protection. Ring dosimeters must be worn for the safety of the nuclear medicine personnel involved in synthesis and injection of Ga-68 peptides. **References:** [1] Dalianis K, Malamitsi J, Gogou L, Pagou M, Efthimiadou R, Andreou J, Louizï A, Georgiou E Dosimetric evaluation of the staff working in a PET/CT department, Nuclear Instruments and Methods in Physics Research A 569, 548 - 550. [2] Biran T, Weininger J, Malchi S, Marciano R, Chisin R. Measurements of occupational exposure for technologist performing 18F FDG PET scans. Health Phys 2004; 87:539-44 [3] Amaral A, Itie C, Bok B, Dose Absorbed by Technicians in Positron Emission Tomography Procedures with FDG, Brazilian Archives of Biology and Technology 50: pp.129-134, Semptember 2007.

EP-0996

Dosimetric evaluation to medical workers operating in a PET/CT department after the use of in house production of Ga-68 peptides

K. Dalianis[1], *K. Gogos*[1], *E. Oikonomou*[2], *G. Kollias*[1], *R. Efhtimiadou*[2], *V. Prasopoulos*[2];
[1]*Medical Physics Department, Hygeia SA, Athens, Marousi, GREECE,* [2]*PET/CT Department, Hygeia SA, Athens, Marousi, GREECE.*

Aim/Introduction: Positron Emission Tomography is considered one of the most relevant diagnostic imaging techniques that provides both functional and morphological information for the patient. Due to the high-energy tracers emitting 511 KeV used in PET/CT departments and considering the risks associated to ionizing radiation that have been derived from previous studies, special attention is needed when dealing with radiation protection aspects in a PET/CT modality . Since the new era of in house production with synthesis modules new radiopharmaceuticals such us [68Ga]-PSMA and [68Ga]-DOTATOC new measurements concerning the doses to medical staff are needed. The aim of this study was to measure the effective wholebody dose of the personnel. **Materials and Methods:** The estimation of equivalent dose from external dosimetry for all three members of the staff was monitored with the use of TLDs badges and electronic dosimeters worn at the upper pocket of their overall (two medical physicists and one radiopharmacist). The average workload of the department is 3 patients per week. 19 patients were examined. Data were collected day-to-day concerning the interaction of the staff during synthesis procedures. **Results:** The elution of Ga-68 generator is done on daily bases by medical physicist and synthesis is performed by the radiopharmacist. The collective effective doses received by all 3 members of the staff were the following: Medical Physicist1 received 0.15 mSv whole body dose per month, Medical Physicist2 received 0.12 respectively. Radiopharmacist received 0.18 mSv whole body dose per month. **Conclusion:** Regulations exist to ensure safety of the medical workers according to ALARA principles. From our results we can observe that although there is an increase of the doses for technologists and nurses the numbers are significantly lower than the recommended annual dose limit. **References:** [1] D. Keskintepe AYO: A Study on Personnel Dosimeters.Fabad J Pharm Sci. (2004); 29:77-80.[2] Rollo.F.D. Nuclear medicine physics, instrumentation,and agents first edition . (1977).[3] Council Directive 96/29/EURATOM of laying downBasic Safety Standards for the Protection of the Healthof Workers and the General Public against the Dangersarising from Ionizing Radiation. Official Journal of theEuropean Communities. (1996); 39:1-114.[4] WILLIAMS ED, LAIRD EE, FORSTER E. Monitoringradiation dose to the hands in nuclear medicine: locationof dosemeters. Nuclear Medicine Communications. (1987); 8:499-503.[5] MACKENZIE A. Reduction of extremity dose in theradiopharmacy. Nuclear Medicine Communications(1997), 18:578-581.[6] Pant GS, Sharma SK, Bal CS, Kumar R, Rath GK:Radiation dose to family members of hyperthyroidismand thyroid cancer patients treated with 131I. RadiationProtection Dosimetry. (2006); 118:22-27.

EP-0997

Rotating duties among nurses to reduce occupational radiation exposure during PET/CT procedures

Y. Nishii, Y. Murata, N. Hayashi, N. Akagi, H. Iwasa, C. Komatsu, M. Hamada, T. Yamagami;
Kochi Medical School Hospital, Kochi, JAPAN.

Aim/Introduction: Reduction of radiation exposure and maintaining patient safety are important issues for nursing staff carrying out PET/CT examinations. The objective of this retrospective study was to evaluate the effect of nurses rotating their duties on exposure to occupational radiation during PET/CT procedures. **Materials and Methods:** Three nurses performing PET/CT procedures in our institution from January 2016 to December 2017 were included in this retrospective study. A total of 3,907 continuous PET/CT examinations were performed by the conventional duty method in 2016, while 3,598 examinations were performed using an improved duty method in 2017. The improved duties for PET/CT were divided into the following three roles of the examination procedure: A) precautions related to the examination and guidelines of the facilities; B) securing the route of the blood vessel; and C) measurement of blood sugar level, operation of the automated injector, and escort of the patient to the waiting room. The 3 nurses rotated each role one after another in succession,

resulting in each nurse carrying out all 3 roles, 4-6 times every day. The dose of radiation exposure of each nurse was measured every day using a pocket dosimeter. **Results:** There was a small difference in examination numbers in the years before and after the improvement in duties. However, the dose of radiation exposure of each nurse was reduced significantly following the improvement in duties (mean 3.19±0.56 μSv/day in 2016 vs. 2.21±0.33μSv/day in 2017, p<0.001). **Conclusion:** Rotating duties by sequential role sharing in nurses results in a reduction in occupational radiation exposure during PET/CT procedures. **References:** None.

EP-0998

Radiation exposure of staff from PET/CT performed with ^{18}F-FDG

M. Zdraveska Kochovska, S. Nikolovski, Z. Filipovski;
JZU UI PET, Skopje, NORTH MACEDONIA.

Aim/Introduction: The PET CT facility and cyclotron unit was established in Skopje at the end of 2016. The institution has own production unit with cyclotron manufactured by General Electric Medical Systems and three fully equipped radio pharmacy laboratories. The aim of this study is to present radiation doses to whole body and extremities received by technologists, physicists and radio pharmacists working in production unit during ^{18}F-FDG preparing and dispensing and also technologists working in diagnostic part during administration of the doses and positioning the patients for PET/CT scan. **Materials and Methods:** During this period about 1800 patients has been performed for PET/CT scan and number is increasing every year. TLD model Panasonic UD-802AS was used to measure Hp (10) the whole-body radiation doses and UD-807 calibrated to measure the personal dose equivalent Hp (0,07) for extremities. TLD reader is Panasonic UD-705, calibrated with source Cs-137 has gamma energy range of 33 keV to 1,3 MeV and dose display range from 85 μSv to 200 mSv. **Results:** The results show that all involved staff received about (1,98±0,05) mSv for whole body dose. For the extremity dose the difference was found between radio pharmacists working in QC laboratory and other staff. Maximum registered value of effective dose for one year was registered to one of the technologist working in a QC lab and it was 14,39 mSv. The results were compared with dose limits proposed by International Commission on Radiation Protection (ICRP, 2007) for whole body 20 mSv and maximum skin dose limit for extremities 500 mSv. **Conclusion: :** Following the basic rules of radiation protection and having on mind the inverse-square law with increasing the distance between radiation source and personnel and reducing the time of activity, absorbed dose decreases substantially. The results show that the staff is working in safety environment and follow the rules about radiation protection. **References:** 1. International Commission on Radiological Protection. The 2007 Recommendations of the International Commission on radiological Protection. ICRP Publication 103, Ann.ICRP 37 (2-4) (2007). 2. International Commission on Radiological Protection. Radiation dose to patients from radiopharmaceuticals- Addendum 3 to ICRP publication 53. ICRP Publication 106. Ann. ICRP 38 (1-2). Annex E (2008) 3. Covens,P., Berus, D., Buls, N., et al. Personal dose monitoring in hospitals: global assessment, critical applications and future needs. Radiat. Prot. Dosim. 124 (3) 250-259 (2007).

EP-0999

Uptake of I-131 to the thyroid of infant mice administered to mothers and substances affecting the uptake

T. Hongyo, Y. Sawai, Y. Ueda;
Osaka Univercity, Suita, JAPAN.

Aim/Introduction: Large doses of radioactive iodine in the nuclear accident etc. may cause thyroid dysfunction and thyroid cancer in children due to internal exposure. This is because radioactive iodine is specifically incorporated into the thyroid and the younger the age, the more sensitive it is. Since infants absorb nutrients only through mother's milk, it is important to examine the degree of uptake of radioactive iodine taken into the infant thyroid and the substances that affect its uptake. **Materials and Methods:** Besides stable iodine tablet (potassium-iodide, 2μg/g BW), we used two different types of iodine inclusion to examine their suppression effect of the I-131 uptake: dried seaweed (50μg/g BW) and diluted iodine gargle (30 times diluted (3.3%); The iodine content was 2.33μg/g BW). Each iodine inclusion was given to the ICR mothers of the newborn baby mice, through a feeding tube, and I-131 (74kBq/mouse) was given 6 hours after the iodine inclusions, and the thyroid uptake suppression-effect of I-131 through breast milk was examined. The 0, 1, 3, 5, 7, and 10-day-old infants were euthanized 24 hours later, and the suppression effect of the I-131 uptake by iodine inclusions were examined with use of gamma scintillation-counter. The percentage of I-131 taken into the thyroid per body weight was evaluated. Moreover, we searched for materials without iodine which can possibly be a substitute for stable iodine tablet when iodine inclusions cannot be used. **Results:** The thyroid uptake rate per weight of I-131 was the highest at 0 day of age. When the mother was given the iodine inclusions, thyroid uptake of I-131 of the baby was significantly suppressed. However, the younger the baby was, the weaker the degree of suppression was. In 0-day-old infants, dried seaweed was more effective than potassium-iodide in suppressing thyroid uptake. As a substance that does not contain iodine, potassium perchlorate (22.3μg/g BW) was shown to suppress the uptake of I-131, and administration of cow milk to the mother significantly increased thyroid uptake rate per weight of I-131 in the infants. **Conclusion:** In the case of 0-day-old infants, the thyroid uptake rate per body weight of I-131 is the highest, so it is considered that it is necessary to pay attention to the protection of radioactive iodine internal exposure particularly immediately after delivery and under such circumstances, it is better to ingest dried seaweed rather than potassium-iodide and mothers should refrain from cow milk intake. **References:** None.

EP-1000

A Useful Pump To Inject Lutathera®

C. Rouet, M. Chassel, C. Blambert, R. Gaston, M. Coutier, A. François Joubert;
Centre Hospitalier Métropole Savoie, Chambery, FRANCE.

Aim/Introduction: Lutathera® (Lutetium [^{177}Lu]-oxodotreotide) must be administered by slow intravenous infusion over 30 minutes. The recommended administration method is the gravity method [1], which is not very intuitive and requires the staff to stay near the patient during the procedure in order to monitor the flow of Lutathera®. We provide a new method of administration by using the Plum 360™ (ICU Medical) [2], an active pump, able to infuse drugs from a glass vial kept straight. **Materials and Methods:** The pump, provided with two infusion lines, was first connected to 500 mL saline in bag. This tube connected the IV bag to the pump and the pump to an empty IV bag (to simulate the patient). The second line was connected from the pump to a glass vial (used to simulate Lutathera®). This vial was kept upright, in a shielded vial. Some medical devices were tested to provide the best infusion conditions. The system was approved by simulation of ^{99m}Tc (6 vials : 200-400 MBq / 22 mL in each, before assays) and ^{177}Lu (1 vial : 3000 MBq / 22 mL) infusion in the empty IV bag. Activities of the vials were measured before and after assay, with and without flushing the vials with saline. A study of costs was also carried out. **Results:** The pump was connected to the vial by adding a male-male connector with at its end, a long needle inserted into the vial cap. The vial had to be kept at an angle in order to keep the needle in the bottom of the vial. An air intake in the vial was required to replace the vacuum created (needle with a 0,22 µm filter). No radioactive leaks and contaminations were noticed. Without flushing the vial, the amount of residual activity was on average 2.8 % (+/- 0.7 %, n=3) with ^{99m}Tc and 2.6 % with ^{177}Lu (n=1). By flushing the vial, the residual activity was brought down to 0.6 % (+/- 0.5 %, n=3). The pump is also equipped with alarms in case of occlusion or presence of air in the system. The pump costs less than 1400 € and disposable materials are around 5 € per patient. **Conclusion:** The Plum 360™ is a useful and cost-effective pump to infuse radiopharmaceutical in vials, especially Lutathera®. **References:** 1. Lutathera® Summary of product characteristics. 2018 2. Plum 360™. ICU Medical. 2017.

EP-1001

Assessment of Occupational Radiation Doses in Different Diagnostic and Interventional Radiology and Molecular Imaging Services

Y. Bouchareb[1], I. Al-Maskery[1], H. Al-Zeheimi[1], A. Al-Rasbi[1], N. Al-Makhmari[2], A. Al-Haji[2], H. Al-Dhuhli[2];
[1]Sultan Qaboos University, Muscat, OMAN, [2]Sultan Qaboos University Hospital, Muscat, OMAN.

Aim/Introduction: Personal radiation dose monitoring, assessment and records keeping is a legal requirement in ionising radiation regulations for radiation workers in the different diagnostic imaging and therapeutic occupational groups. The purpose of this study was to assess occupational radiation doses in different diagnostic, interventional and therapeutic radiology and molecular imaging services, aiming to reduce personnel radiation doses further. **Materials and Methods:** Personal radiation doses recorded over the last three years were collected (n=104) from our TLD dosimetry service. Personal radiation doses were monitored on a monthly basis. Five different occupational groups were considered: diagnostic radiology (conventional x-rays and computed tomography), interventional radiology, nuclear medicine technologists and radiographers, medical physicists and nurses. For the sake of an objective assessment, only effective whole body doses measured using TLDs during the full 36 months in each speciality, were included in this study. Average mean doses, maximum and cumulative doses per year in each occupational group were estimated and compared against maximum permissible doses and the local dose investigation levels, which consists of 6 mSv per year for each occupational group. **Results:** Personal radiation analysis performed for the five occupational groups over three years resulted in an average personnel radiation doses of 1.23 mSv for nuclear medicine, 0.6 mSv for both diagnostic and interventional radiology, 0.45 mSv for medical physicists, 0.5 mSv for nurses. Over the three years, maximum whole body doses received by the nuclear medicine, diagnostic radiology, interventional radiology, medical physicists and nurses personnel were 7.4 mSv, 0.9 mSv, 0.5 mSv, 1.4 mSV and 2.1 mSv, respectively. Similar trends of average and maximum whole body doses were observed on a year-to-year basis. The higher maximum whole body dose in the nuclear medicine occupational group is believed to be due to the significant increase of the number radionuclide therapy sessions in the last two years (30% increase in number of patients). **Conclusion:** Personnel radiation doses for all occupational groups are well below maximum permissible doses setup in the ICRP and IAEA safety standards and the dose investigation levels currently applicable for radiation workers at our institution. These findings suggest, at the exception of nuclear medicine staff for whom the dose investigation level should be adjusted, lower dose investigation level for all other occupation groups without compromising the quality of service offered to patients. **References:** None.

EP-1002

The Quantitative Analysis of Uranium Isotopes in the Urine of an Ammunition Clean-up Worker deployed on Dutch North Sea Islands

F. Klimaschewski;
Uranium Medical Research Institute, London, UK, UNITED KINGDOM.

Aim/Introduction: Military target practice training sites on the Dutch Islands Vlieland and Terschelling in the North Sea include the use of uranium weapons. Civilians are employed

on those islands to collect projectiles, debris and remove tank wrecks. **Materials and Methods:** One subject involved in the clean-up reported severe multiple health problems (i.e. general weakness, problems with lung function and blood cells/leukemia) as a consequence of only two weeks of work on the testing sites. 24-hour urine analysis with ICP-MS was performed by Jülich laboratory four years after exposure to determine the concentration and precise isotopic composition of three uranium isotopes (^{234}U, ^{235}U, ^{238}U) in the urine specimen. **Results:** The analysis measured a ^{234}U concentration of 5.6E-04 ng/l (1.3E-4 Bq/l) and a ^{238}U concentration of 1.13E+01 ng/l (1.4E-4 Bq/l).) The ^{238}U/^{234}U ratio was 17 417, normally indicative of natural uranium. ^{235}U reported as non-detectable indicates a rather unusual result inconsistent with other population studies. **Conclusion:** The total uranium concentration measured in the urine of the subject years after exposure is below the mean concentration of uranium urine excretion in Germany (approx. 21.5 ng/d). However, this does not rule out the possibility of initial contamination of the lung with uranium from weapon systems at time zero that exceed permitted levels since uranium might have been metabolized several years after inhalation. Further research, especially into the environmental contamination, is warranted. **References:** None.

Technologists e-Poster Presentation Sessions

804-1

Technologists: Technologist e-Poster Presentation Session 1

Monday, October 14, 2019, 11:30 - 13:00 Room 133/134

TEPS-01

Development of a M4 PAM PET radioligand - [^{11}C]PF-06885190 - for a study in nonhuman primates

S. Nag[1], *R. Arakawa*[1], *K. Maresca*[2], *C. Butler*[2], *L. Chen*[2], *Z. Jia*[1], *E. Lachapelle*[2], *M. Jahan*[1], *T. McCarthy*[2], *L. Zhang*[2], *C. Halldin*[1]; [1]*Karolinska Institutet, Stockholm, SWEDEN,* [2]*Pfizer Inc, Cambridge, MA, UNITED STATES OF AMERICA.*

Aim/Introduction: Muscarinic acetylcholine M4 receptor functions as inhibitory auto-receptors for acetylcholine, and its activation inhibits acetylcholine release in the striatum. It is reported that within the striatum M4 receptor activation acts antagonistically with dopamine D_1-like receptors and indicate that M_4 receptors may be a potential target for the treatment of Parkinson's disease and other relevant central nervous system disorders. PF-06885190 has been identified and evaluated by Pfizer as a novel M4-selective PET ligand candidate with high affinity (human binding Ki = 0.16 nM, rat binding Ki = 7.15 nM) and selectivity. In this study, our aims were a) to radio-label PF06885190 with C-11 b) to evaluate the brain distribution of [^{11}C] PF06885190 as a PET radioligand for M4 in nonhuman primate (NHP) and assess whether the brain uptake of [^{11}C]PF06885190 can be blocked by a selective M4 PAM compound PF06852231 and c) to analyze radiometabolites in blood plasma of NHP. **Materials and Methods:** Precursor PF06898527 and reference standard PF-06885190, were synthesized in multi-step syntheses. Radiolabeling of [^{11}C]PF06885190 was performed in two steps via N-methylation of the precursor, PF06898527, followed by deprotection using HCl (0.5 N, 200 µL). Two PET measurements were performed using a male cynomolgus monkey, one at baseline and another after pretreatment with a selective M4 PAM compound PF06852231. The V_T of [^{11}C]PF06885190 was examined using Logan graphical analysis with arterial input function. Radiometabolites were analyzed in monkey blood plasma using gradient HPLC system. **Results:** Radiolabeling of [^{11}C]PF06885190 was accomplished successfully with moderate radiochemical yield and high radiochemical purity which was above 99%. Molar activity was 312 ± 128 GBq/µmol at the time of administration. The radioligand were found to be stable in the formulation with radiochemical purity exceeding 99% after 1h of end of the synthesis. In vivo, the whole brain uptake of [^{11}C] PF06885190 in NHPs was 4.1 SUV at the peak of the baseline condition. However, it showed fast wash-out as it dropped to half of the peak at around 10 minutes. The percent change of V_T from baseline was approximately -10% after pretreatment of a M4 PAM, PF06852231. Radiometabolite studies showed relatively fast metabolism, but still demonstrated that 17-20% of [^{11}C]PF06885190 remain unchanged in blood plasma at 90 min post-injection. **Conclusion:** Radiolabeling of [^{11}C]PF06885190 was performed successfully. Although sufficient brain uptake of [^{11}C]PF06885190 was observed, these data suggest that [^{11}C] PF06885190 might have low specific binding in the NHP brain. **References:** None.

TEPS-02

An efficient method for the labeling procedure of ^{68}Ga-PSMA and ^{68}Ga-DOTA-TATE

E. Poel, M. F. Lam, Y. Chahid;
Amsterdam UMC, location AMC, Amsterdam, NETHERLANDS.

Aim/Introduction: The increase in clinical use of ^{68}Ga-PSMA PET-CT and ^{68}Ga-DOTA-TATE PET-CT results in more commercially available labeling procedures of those peptides. The aim of this study was to obtain an easy method for ^{68}Ga-PSMA and ^{68}Ga-DOTA-TATE productions. Without the use of a labeling module and when commercial kits are not available. **Materials and Methods:** 1.1 ml ^{68}Ga solution in 0.1 M HCl was generated using a $Ti0_2$ based ^{68}Ge /^{68}Ga generator (Galli Eo, IRE ELit, Belgium). The sodium acetate buffer was made from European Pharmacopoeia (Ph. Eur.) sodium acetate buffer solution (Fischer Chemical, United Kingdom) and NaCl 0.9%. In case of ^{68}Ga-PSMA: 30 µg PSMA-11 (ABX, Germany) was solved in different buffer solutions, added to the 1.1 ml ^{68}Ga-solution and reacted for 5 minutes at room temperature. In case of ^{68}Ga- DOTA-TATE: 50 µg DOTA-TATE(ABX, Germany) was solved in different buffer solutions, added to the 1.1ml

^{68}Ga-solution and heated at 95°C for 7 minutes. Radiolabeling efficiency was obtained using a radio high-performance liquid chromatography (radio-HPLC) and thin-layer chromatography (TLC). **Results:** A radiolabeling efficiency >99% was obtained for both peptides using different dilutions of the Ph. Eur. buffer. In case of ^{68}Ga-DOTA-TATE the optimal buffer was obtained by diluting 5.0 ml of Ph. Eur. buffer with 95 ml NaCl 0.9%. The use of 3.0 ml of this buffer solution in the labeling procedure of ^{68}Ga-DOTA-TATE resulted in the highest radiolabeling efficiency (>99%). In case of ^{68}Ga-PSMA the optimal buffer was obtained by diluting 25 ml of Ph. Eur. buffer with 75 ml NaCl 0.9%. The use of 2.0 ml of this buffer in the labeling procedure of ^{68}Ga-PSMA resulted in the highest radiolabeling efficiency (>99%). **Conclusion:** An efficient method, without the use of a labeling module, for the labeling of ^{68}Ga-PSMA and ^{68}Ga-DOTA-TATE was obtained from the peptides and an easy made buffer solution. **References:** None.

TEPS-03

Quality assurance audit of in-house prepared 68Ga labelled radiopharmaceuticals: 5 years of institutional experience

***B. S. Shetye**, P. Monteiro, M. Pathan, S. Mithun, A. Jha, V. Rangarajan;*
Tata Memorial Hospital, Mumbai, INDIA.

Aim/Introduction: The progressive development of 68Ge/68Ga generator system, compatible gallium radiochemistry, ease of synthesis methods emerged with a new era of in-house labeled PET radiopharmaceuticals. The automated synthesis method is error free but expensive. Proper implementation of necessary measures before and during the procedure turns manual synthesis into reliable and cost-effective option. Hence, we assessed the performance of 68Ge/68Ga generators (n=9), labeling efficiency, quality control parameters of 68Ga-DOTANOC and 68Ga-PSMA prepared by manual synthesis. **Materials and Methods:** Total 1230 (DOTANOC n = 415, PSMA n= 815) synthesis were performed using nine ITG 68Ge/68Ga generators (30 mCi n= 7, 50 mCi n= 2). Rinsing was done using 5 ml of 0.05N HCl (n=100) 25µg of DOTANOC and 5µg of HBED-CC-PSMA in 0.025M sodium acetate buffer was used for labelling. It was done manually using IQs 68Ga fluidic module following standard procedure using 0.05N HCl as eluant. PSMA synthesis was done using GMP certified PSMA labelling kit. All reagents were prepared using Millipore water. Contamination of the stock solution was prevented by discarding leftover solutions. Cartridge and Millipore filter were conditioned just before the beginning of synthesis. The proper temperature was maintained throughout the synthesis. Delivery of 68Ga in a reaction vessel and loading of product over the cartridge were ensured by measuring the surface dose rate over a reactor and cartridge. RCP was measured by ITLC method using 0.1M sodium citrate. Labelling efficiency and stability of the product, radionuclidic purity were assessed. **Results:** Elution yield was 70 to 75%. Low yield between 25 to 56 % was reported for DOTANOC (n=75) and PSMA (n= 29). It got corrected by preparing reagents after every 15 days. Labelling efficiency for DOTANOC was 80 % (n= 350, STDEV = 0.004, pH= 5.5) and PSMA 84 % (n=786, STDEV=0.003, pH= 5.5). RCP of DOTANOC was > 97% and PSMA was > 99%. Radiochemical stability of product was studied up to 4 hrs. It was >94%. Product was measured after 36 hrs to rule out 68Ge breakthrough. No activity was observed in it. **Conclusion:** Our data showed reliable RCP results and consistent labeling efficiency by following proper measures as indicated above. Manual synthesis permits the use of a generator more cost-effectively and as per our own requirement. **References:** None.

TEPS-04

A High Yield Automated Synthesis Of ^{18}F-FLT On PET-MF-2V-IT-I Module With SPE Purification

***W. Hongyong**, P. Zou, M. Xie, Y. Liu, J. Wu, H. Wu;*
Jiangsu Institute of Nuclear Medicine, Wuxi, Jiangsu, CHINA.

Aim/Introduction: 3'-deoxy-3'-18F-fluorothymidine (^{18}F-FLT) is a thymine analog that is currently recognized as the best indicator of growth in assessing the proliferation of tumors and normal tissues. In one of these applications, this utility has been demonstrated in a variety of tumor models, such as lung cancer, colorectal cancer, and lymphoma. The synthesis of ^{18}F-FLT was automatically optimized by a solid phase extraction column (SPE) purification using a PET-MF-2V-IT-I synthesizer (PET-MODULE Technology Co., Ltd, Beijing). **Materials and Methods:** ^{18}F ion (352MBq) was adsorbed to the QMA column, and the K2.2.2/K_2CO_3 solution was rinsed. Under the nitrogen condition, the eluent was heated under acetonitrile at 120 ° C for 5 minutes, dried, and then 3-N-Boc-5'-O-dimethoxytrityl-3'-O-nosyl-thymidine(N-BOC-FLT) was dissolved. Acetonitrile was added to the reaction mixture, and heated at 100 ° C for 10 min; then hydrochloric acid (1 M) was added, and hydrolysis was carried out at 105 ° C for 5 minutes, the solution was neutralized with sodium hydroxide (1 M). Then, the resulting mixture removes excess fluoride ions through the aluminum column. The reaction mixture was washed with 20 ml of water and purified by C18 column, solid phase silica gel column, CM solid phase column or PS-2 solid phase column through ethanol. Finally, after aseptic filtration, ^{18}F-FLT was obtained. **Results:** The synthesized ^{18}F-FLT was purified by SPE using a domestic PET-MF-2V-IT-I synthera synthesizer. The precursor N-BOC-FLT requires 10 mg compared to other literature reports. In this reaction, although the precursor N-BOC-FLT used only 5 mg, ^{18}F-FLT was synthesized in a high yield, and the by-products were few. The synthesis method tested four SPE columns (C18, CM, Silica, PS-2) to purify ^{18}F-FLT. The yields of the automatically synthesized ^{18}F-FLT were 21%, 36%, 13% and 16% (EOS), respectively. Radiochemical purity ≥ 98%. The total reaction time using the SPE column is about 25 minutes and does not require HPLC for purification. From the results, the purification method using CM solid phase column is the most effective. **Conclusion:** We have developed a high-volume method for automated synthesis of ^{18}F-FLT. ^{18}F-FLT was synthesized automatically by means of a domestic PET-MF-

2V-IT-I module, a small number of precursors and SPE column purification method. **References:** None.

TEPS-05

Outstanding cleaning method for the reliability of the automated synthesis module with non-cassette type

H. Park, J. Kim, H. An, H. Lee, G. Lee, B. Lee, W. Lee, S. Kim;
Seoul National University Bundang hospital, Seongnam-si, Gyeonggi-do, KOREA, REPUBLIC OF.

Aim/Introduction: A commercialized available automated module (e.g., TracerLab FX_{FN} made by GE Healthcare) is used for easy and efficient production of ^{18}F-labeled radiopharmaceuticals. In case of non-cassette type module, the cleaning step is vitally required for maintaining yields of radiotracer after completing radiolabeling including acid or base treatment. Herein we present an efficient cleaning know-how acceptable in the TracerLab FX_{FN} platform to avoid unexpected production failures. **Materials and Methods:** After [^{18}F]FET production, the used 2N HCl and sodium acetate buffer in the deprotection occurred the serious contamination of parts in the module and then caused the decreasing the yield or generated the failure in the next production. The optimized cleaning procedure is performed as follows: i) All used reagent vials (No. 1-6) and reactor are rinsed by 2 mL distilled water (DW); ii) The reactor and O-ring are disassembled from the module, followed by sonication in acetone for 20 min; iii) After equipping to the module, the reactor except O-ring added 10 mL acetonitrile (ACN) and heated at 100 ºC for 5 min; iv) After cooling, the reactor including O-ring is heated at 100 ºC for 5 min again in the condition of lowered the reactor needle and opened two-way valve and reagent vials. At this time the distilled ACN efficiently cleanses all tubings as well as valves connected on the reactor; v) Finally, the reactor and reagent vials are rinsed with 2 mL ACN and 2 mL DW, respectively, followed by drying with the help of acetone and N_2 gas. Other formulation parts cleansed through the recommended method in the manual. **Results:** While the previous radiochemical yield (RCY) of [^{18}F] FET recorded in 20 ± 15% with a failure rate of 10% (n = 20), new cleaning method enhanced significantly RCY of [^{18}F]FET (35 ± 5%) with no production failure (n = 50). The prepared [^{18}F] FET satisfied all quality control test standards for clinical uses. **Conclusion:** The automated radiosynthesis equipped with new cleaning method provides high and reproducible yields of [^{18}F] FET suitable for routine clinical use. **References:** None.

TEPS-06

Determination of Aluminum in Pertechnetate and Perrhenate Solution in eluate of ^{99}Mo / ^{99m}Tc and ^{188}W/^{188}Re Generator

M. Karamivand[1], *F. Farajbakhshmamaghani*[2], *M. Davarpanah*[2];
[1]*Pars Isotope Co, Tehran, IRAN, ISLAMIC REPUBLIC OF,*
[2]*Pars Isotope, Tehran, IRAN, ISLAMIC REPUBLIC OF.*

Aim/Introduction: The ALUM-PARS kit provides a rapid, easy and inexpensive way to test aqueous solutions, particularly pertechnetate generator eluate, for trace quantities of aluminum. The United States Pharmacopeia 38-NF33 allows a concentration of aluminum ion in an injection ≤ 10 micrograms per milliliter (10 µg/ml) in technetium 99m eluate. **Materials and Methods:** This kit content chromazurol S, citric acid-sodium citrate buffer and saline 0.9% and was optimization parameters by spectrophotometry method. Freeze-dried ALUM-PARS kit by removing the water from the material and sealing it in a vial, the material can be easily stored, shipped, and later reconstituted to its original form for injection. Added 1 mL of pertechnetate eluate of ^{99}Mo / ^{99m}Tc or ^{188}W/^{188}Re generator to lyophilized ALUM-PARS kit and compared the intensity reference color. Also results of the analysis aluminum ion solution in eluate of ^{99}Mo / ^{99m}Tc and ^{188}W/^{188}Re generator by proposed procedure were found to be in excellent agreement with those obtained by atomic absorption spectrophotometric method. **Results:** Amount aluminum in pertechnetate solution eluate of ^{99}Mo / ^{99m}Tc and ^{188}W/^{188}Re generator determinate, hence was color change ALUM-PARS kit from yellow to violet (0 µg/ml to 40 µg/ml aluminum). **Conclusion:** Aluminum complex formation with ALUM-PARS kit, the intensity of the color is directly proportional to the amount of aluminum in the solution and this method is quick and easy application for Semi-quantitative determination of aluminum in Pertechnetate and Perrhenate Solution eluate of ^{99}Mo / ^{99m}Tc and ^{188}W/^{188}Re Generator. **References:** None.

TEPS-07

The "Radiopharmacy of errors": a serious game to strenghten quality

T. Martin, C. Maurel, N. Sapin, I. Benard-Thiery;
Radiopharmacy department, Centre Antoine Lacassagne, Nice, FRANCE.

Aim/Introduction: Manufacturing of radiopharmaceuticals must comply with certain quality standards and strict rules of radiation protection. Deviations from good practices and procedures are sometimes observed in current radiopharmacy practice. Therefore operator training has to be developed. Simulation is a source of innovative pedagogical developments in health care. The use of a "room of errors" constitutes a useful learning tool to reinforce the radiopharmacy technician skills and knowledge. **Materials and Methods:** Four radiopharmacy technicians took part in real-life situations characterized by a defined number of errors. Those were set up according to the internal procedures and the risk mapping of the radiopharmacy department. Two still scenes representing the daily work in a PET-lab and a SPECT-lab were created. In each scene, several mistakes could be found concerning hygiene, preparation and dispensation of the radiopharmaceuticals, quality control of the preparations, radiation protection, and transport of radioactive packages. In addition, a moving scene was played out, consisting in the preparation of a radiopharmaceutical in the SPECT-lab. In this scene, technicians had to find manipulation

errors. The radiopharmacy technicians had to report every error they could find. A debriefing was carried out to discuss and explain each situation afterwards. **Results:** In the PET-lab the radiopharmacy technicians found 58% (mean=7.5/13) of the errors. None of them detected the prescription error or knew the rules to indicate a radioactive contamination on the floor. 73% (mean=11/15) of the errors were discovered in the SPECT-lab. For example, technicians did not notice the low pressure of the shielded enclosure or the wrong batch number of an Iodine-131 capsule. During the moving scene 67% (mean=8.5/12) of the manipulation errors were detected. **Conclusion:** This work evaluated the potential benefits of creating a "room of errors" in a high risk process such as the radiopharmacy practice. This process represented an effective way to provide an update concerning good practices and a reminder concerning critical endpoints. The impact over the long term has yet to be evaluated. Nevertheless, direct purposeful experiences close to reality are the best way to learn and retain. The development of the "Radiopharmacy of errors" in other departments could be introduced to train technicians and evaluate practices. **References:** None.

TEPS-08

Quality Improvement of Patient Safety and Images through Analysis and Compliance with Standard Operating Procedures in ^{18}F-FDG PET/CT scan

S. Yoon, J. Ryu;
Asan Medical Center, Seoul, KOREA, REPUBLIC OF.

Aim/Introduction: This study aimed to improve patient safety culture and image quality through improvement activities such as analysis and compliance with standard operating procedures (SOPs). Asan Medical Center implemented standards of the international guidelines by establishing SOPs to ensure the accuracy and reliability of ^{18}F-FDG PET/CT scans. **Materials and Methods:** Patients who received ^{18}F-FDG PET/CT scan at Asan Medical Center from January 2014 to October 2015 before and after improvement activities were compared with respect to dose and uptake time of ^{18}F-FDG. Several causal factors, such as technologists, time zones, PET/CT equipment, and patient age and height were analyzed to find decisive fundamental factors to solve problems. Dose compliance rate and uptake time were measured. **Results:** Compliance rate for dose was 97.48%, an improvement of 7.31% compared to that before improvement activity. Deviation between actual and reference dose was 4.18%, 1.08% less than that before improvement activity. Over-dosing was 0.47%, 3.39% less than that before improvement activity. Average uptake time was 60 ± 2.10 min, 3.22 min less than that before improvement activity. **Conclusion:** The role and responsibility of the radiological technologist is to examine the proper dose and precise uptake time of ^{18}F-FDG in compliance with SOPs within the acceptable range and to constantly analyze performance to reduce deviations. This should be applied to quality management of the entire nuclear medicine examination and the PET/CT scan, and a series of efforts like this could eventually improve the patient safety culture and quality of examination. **References:** None.

TEPS-09

Appreciation of patients' feeling about the environment of a new digital PET-CT room

M. Pappon, P. Genoud, M. Meyer, J. Prior;
CHUV, Lausanne, SWITZERLAND.

Aim/Introduction: Since 20 years, advances in PET technology have been significant, with important benefits for the patients in term of diagnosis performances, but also patients' comfort. Many factors have been identified as affecting patients' experience of PET/CT: scan time, environmental temperature, discomfort in the waiting area, interactions with staff, pain and discomfort during the scan, symptoms of claustrophobia or duration of waiting time.The aim of our study was to compare patients' experience of PET/CT with our 2 PET/CT devices: a conventional PET/CT (GE Discovery 690, installed 2011), and a latest-generation digital PET/CT (Siemens Vision 600, installed 2018). **Materials and Methods:** Data were collected during 1 week in 51 consecutive patients for each PET/CT room. The patients filled one self-report questionnaire directly after the PET/CT imaging. The questionnaire comprised questions related to 5 different parts: room, table comfort, examination time, scanner and NM technologist help with 2-5 questions for each part. A four-point Likert scale was used for the response. **Results:** Concerning the PET/CT room, less patients were cold (score 1 or 2) with the water-cooled digital PET/CT as compared to conventional air-cooled PET/CT (19.6% vs 64.7%, p<0.001). Concerning the PET/CT comfort, more patients found the table comfortable (score 4) in digital PET/CT as compared conventional PET/CT (65% vs 43%, p=0.050). Moreover, contention material seemed better adapted (score 4) in digital PET/CT as compared conventional PET/CT (77% vs 61%, p=0.088).Concerning scanner duration time, there was no difference among group; however, more patients found that they did wait only shortly after the PET/CT acquisition (score 3 or 4) in the digital PET/CT as compared to conventional PET/CT, due to quicker image reconstruction time (86% vs 69%, p=0.034).Concerning the PET/CT camera, less patients found that ring diameter was too small (score 1) and so very stressful in the digital PET/CT as compared to conventional PET/CT (0% vs 10%, p=0.042).Concerning the technologists' help, there was no differences between scanners. **Conclusion:** Our study highlights that patient experience of PET/CT is heterogeneous, but in most cases, patients are satisfied or very satisfied. We found that room conditions, materials and organization of the examination of our latest-generation digital PET/CT are better adapted to optimize patient's comfort and reduce the examination stress. **References:** None.

TEPS-10

One instruction for all-managing pediatric protocols across departments

H. Søgaard, R. N. H. B. Christensen;
Aarhus University Hospital, Aarhus N, DENMARK.

Aim/Introduction: Children diagnosed with cancer are treated with chemotherapy. Due to the kidney toxicity of these drugs, they are examined with a GFR (glomerular filtration rate) test, as a part of their treatment protocol. The examination takes part at the Department of Pediatrics and Adolescent Medicine, and is performed as a collaboration between a nurse and a technologist from the Department of Nuclear Medicine. When attending these examinations, we observed that the procedure was different due to the individual nurse. The aim of this work is to provide the nurses with a valid protocol that is easily accessible and in detail describes how to perform the GFR test correctly. In addition, the protocol describes the procedures performed by the technologists. **Materials and Methods:** In 2018, 56 cancer diagnosed children were examined with a GFR test. A tracer of 20 MBq Tc99m-DTPA or 2 MBq Cr51-EDTA were injected and 5 blood samples were drawn at set times, within 2 hours from the injection. The children all had a central venous catheter (CVC), a central line catheter (PICC-line) or implantable port for tracer injection and blood sample drawing. The nurse handled the CVC. Tracer injection was always supervised by the technologist. The protocol was prepared in cooperation with a nurse specialist, and safe handling of the CVC, dead space and level of information, were all taken into consideration to obtain the right protocol beneficial for both the nurses and technologists. **Results:** Having one joint protocol we have observed that all the examinations are performed in a uniform way, regardless of which nurse is drawing the blood samples. The frequency of corrective actions and the risk of unsuccessful examinations are reduced. Due to the protocol there is no longer frustration or uncertainty in the team of nurses on how to perform the examination. Nor for the technologists, as the full procedure now is described in an approved document. **Conclusion:** It is now possible for nurses and technologists easily to find the applicable protocol in the hospital documentation files. Following this protocol, the examination is performed in a uniform way regardless of which nurse is performing the test. In the Department of Nuclear Medicine, we know with much more certainty that the blood samples received meets the requirements of the examination. **References:** None.

TEPS-11

Cost Saving of PET/CT and Contrast Enhanced CT in Lymphoma Patients

C. Vazzana, R. Sanco, M. Trevisan, F. Lincetto, A. Biscotto, L. Evangelista;
Istituto Oncologico Veneto IRCCS, Padova, ITALY.

Aim/Introduction: In modern oncology, combined imaging based on PET/CT plays a central role in the diagnosis, staging and post-treatment follow-up of patients with neoplastic disease. The possibility of performing TNM staging with a single examination PET/CT and contrast enhanced (ce)CT, provides a full diagnosis immediately and reduces the time required for the patient to undergo separate diagnostic examinations. The aim of our study was to analyse the impact of medical and nonmedical costs of PET/CT with simultaneous ceCT, in a cohort of patients with lymphoma. **Materials and Methods:** From October to November 2018, a total of 32 patients with Hodgkin and non-Hodgkin lymphoma referred to our institute was administered a questionnaire to evaluate the nonmedical costs of fluorodeoxyglucose (FDG) PET/CT. The questions elicited current working status at the time of the questionnaire, the type of work done, the distance from home to the institute, and the means of transport used. In the case of private transport, they were asked to provide the type of vehicle. Moreover, to evaluate the costs of informal care, they were asked to indicate whether someone accompanied them to the institute and the type of work done by the person. In addition, the medical costs related to PET/CT performed with ceCT, PET/CT with low-dose nonenhanced CT and separate ceCT were also recovered. The analysis of costs for PET/CT, and ceCT separately, and the hypothetical PET/ceCT costs were estimated. **Results:** The costs for ceCT, PET/CT, PET/ceCT in all patients, were 7767,68 euro, 21982,08 euro and 26177,92 euro, respectively. The expense for all 32 patients was 2387,62 comprising the working day, transport, and caregiver. The medical costs were 929,68 euro for PET/CT with separate ceCT, and 816,06 euro for PET/ceCT in a single session. Therefore, the economic recovery for each patient was equal to 12% . However, in our study population, the cost saving was equal to 17% , because the reduction of the number of hospital visits required by patients undergoing diagnostic imaging can improve the global costs. **Conclusion:** Our results show that FDG PET/CT performed with standard dose ceCT in a single session, in patients with lymphoma, provides benefits in terms of both medical and nonmedical costs **References:** Role and Cost Effectiveness of PET/CT in Management of Patients with Cancer Muhammad Wasif Saif,a,* Ifigenia Tzannou, Nektaria Makrilia, and Kostas Syrigosa.

TEPS-12

Managing patients and working spaces during facilities upgrade: a single-center experience

M. Maccagnani[1], D. Pedrini[2], A. Farina[1], A. Lambertini[1], S. Fanti[1], S. Barbieri[3];
[1]Nuclear Medicine Department, Sant'Orsola-Malpighi Hospital, University of Bologna, Bologna, ITALY, [2]Tecnical Department, Sant'Orsola-Malpighi Hospital, University of Bologna, Bologna, ITALY, [3]Department anesthesia Intensive Care, University of Padova, Padova, ITALY.

Aim/Introduction: Due to a recent structural upgrade to the working spaces of our PET-Centre within the department of Nuclear Medicine (Sant'Orsola-Malpighi-University-Hospital,

Bologna, Italy), we investigated potentially beneficial changes to patient management, clinical flow and radiotracer delivery, taking place in parallel with active renovation works. We aimed at drafting a set of guidelines to help managing future scenarios involving periodically occurring renovations in a setting of continued clinical activities. **Materials and Methods:** A preliminary inspection of the planned working sites within the ward was performed by the technologist team, in order to establish clear boundaries and border areas of the active renovation sites. The size of the patient population needing access to the ward (as well as that of the active medical and tech staff) within the planned time-frame of activities was estimated. All procedural alterations were discussed in a series of meeting with all the involved members of the medical management, medical physics and tech teams. Buffer and dedicated treatment zones were planned to guarantee proper care to patients with special needs, while capacity and location of public spaces were planned in accordance to current legislation (0.4pts/mt² within 40 meters of viable emergency exits). In addition, we also considered radiation exposure due to sharing waiting spaces with our conventional nuclear medicine ward (mixing of patients injected with different radionuclides). Temporary re-location of patients from the immediate vicinity of the active sites to our conventional nuclear medicine ward was initiated, without significantly modifying the timing of tracer delivery and image acquisition. The least flow-disruptive options were selected after a final consultation. Modifications to current hospital guidelines were drafted accordingly into a special directive. **Results:** Structural renovations within our PET-Centre took place between July 30th 2018 and progressed for the next 7 weeks. All changes to the usual clinical activities were implemented in accordance with the newly developed guidelines. No unexpected disruptions to the clinical flow occurred and no complaints were reported by either patients or health professionals up to the end of renovation works. **Conclusion:** Our single-centre study resulted in the drafting of a set of guidelines which allowed for a successful continuation of all clinical activities within our nuclear medicine department in parallel with major building renovations and tech upgrades. Those healthcare institutions facing periodical renovations, and especially high-volume imaging centers may also consider its adoption to minimize down-time and thus guaranteeing acceptable waiting times for patients. **References:** None.

TEPS-13

Discovery, A New Zealand Nuclear Medicine Department voyage that has made a real difference

P. E. Lamerton;
Hawkes Bay District Health Board, Hastings, NEW ZEALAND.

Aim/Introduction: This presentation will cover the change in work processes and management for staff and patients following the installation of the GE Discovery 650 NM/CT highlighting the benefits for a regional hospital. **Materials and Methods:** Hawkes Bay Memorial Fallen Soldiers Hospital is the only public hospital in Hawkes Bay region of New Zealand. Located on the east coast of the North Island it has a current population of 166,000. The radiology department has a main CT as well as the NM/CT providing a SPECT/CT service to this area with no PET/CT. The Nuclear Medicine department offers a wide range of scans maintaining considerable growth in numbers and variety of scans over the past 10 years. The business case for installation of the Discovery 650 NM/CT in late 2013 focused on having the CT as a backup CT scanner. It soon became apparent that this was only one of the many benefits following its installation such as helping the hospital to keep within the government fast track cancer targets. **Results:** Key changes were implemented which included NM technologists undertaking diagnostic CT training to extend their scope of practice, allocation of a dedicated CT session weekly, allocation of a CT member to work on the hybrid CT, modifying booking templates and creating an adaptive NM and CT team. **Conclusion:** In conclusion the results have been very positive for the management of the radiology department as a whole including NM and CT staff interaction and most beneficial for the patients as we now have one visit for the Nuclear Medicine scan and staging CT. For the patient this means one IV line for the visit and one point of contact which is less demanding and eases their journey through Nuclear Medicine. We have adapted our Nuclear Medicine service to meet growing demands in both modalities under severe economic restraints that control our NZ Public Health Hospitals. **References:** None.

TEPS-14

Tracer extravasation in PET/CT: could we predict it?

M. Trevisan*, A. Biscotto, F. Lincetto, M. De Rossi, F. Ruffo, P. Reccia, A. Cervino, M. Burei, L. Cuppari, A. Carraro, L. Evangelista;*
Nuclear Medicine Unit, Veneto Institute of Oncology IOV - IRCCS, Padua, ITALY.

Aim/Introduction: Primary end-point of the present study was to evaluate the incidence of tracer extravasation in a large cohort of patients undergoing PET/CT or PET/contrast enhanced (ce) CT examinations for oncological requests. Secondary end-point was to assess if the correction of the routine procedures can reduce the tracer extravasation rate. **Materials and Methods:** Data from 1100 patients undergoing PET/CT exams were prospectivelycollected. Patients were affected by oncological disease (i.e. lymphoma in 19.3%, breast cancer in 15.5%, colon-rectal cancer in 5.3%, lung cancer in 14%, prostate cancer in 11.5% and other in 34.5% of cases).The majority of patients underwent 18F-FDG PET/CT or PET/ceCT (n=995; 86.8%). The following iinformation were recovered: age of patients, size of cannula (in gauge), injection site, the intensity of extravasation (low, moderate and severe), prediction of extravasation before PET/CT acquisition andeffects of extravasation on the semiquantitative evaluation in terms of standardized uptake value (SUV). **Results:** Median age was 67 years (range: 12-93 years). PET/CT was performed in 1075 patients (98%),while PET/ceCT in only 25 cases. The tracer extravasation was reported in

63 (5.7%) patients. It was defined as low in 25, moderate in 21 and intense in 17 subjects (39.7%, 33.3% and 30%, respectively). The presence of a tracer extravasation was predicted in 44.4% of cases; therefore 61% of patients performed a PET/CT examination with their arms raised above the head. SUV was considered as measurable in 64% of cases.Furthermore, a 25/27 gauge cannula and the antecubital venous access were correlated with tracer extravasation in 40% and 63% of patients, respectively. **Conclusion:** The rate of extravasation is low in a large cohort of patients, being inferior to 6%. However it can be further reduced by including specific procedures, in example the choice of cannula size and the injection site. **References:** None.

TEPS-15

Lutetium (177Lu) Oxodotreotide Therapy - Increasing Capacity and Demand

E. Seal;
University Hospital Birmingham, Birmingham, UNITED KINGDOM.

Aim/Introduction: On 29th August 2018 the National Institute for Health and Care Excellence (NICE) published guidance stating that Lutetium (177Lu) oxodotreotide (Lutathera) was now a recommended treatment option for neuroendocrine tumours. This meant that funding was now available to certain NHS patients which fitted the specific criteria set out in the NICE Guidelines. A departmental review of capacity and demand was carried out to determine the maximum number of patients that could be treated every year and what resources would be required to achieve maximum capacity. **Materials and Methods:** In previous years funding was limited to mainly private patients and patients taking part in clinical trials so the highest number of Lutathera treatments performed in one year was 37. Once the guidance from NICE had been issued and funding approved the Neuroendocrine Tumour team estimated there would be roughly 25 patients eligible every year for treatment, this would equate to 100 Lutathera treatments each year. With this being almost 3 times more Lutathera treatments than before several factors were taken into consideration to decide when the department would be able to manage with the demand: 1) There would be increased pressure on the gamma cameras due to more imaging slots being needed to image the patients after their treatment 2) Extra staff would need to be employed in order to run the service smoothly and efficiently 3) Staff doses have to be estimated to ensure suitable radiation protection could be provided and utilized 4) The rooms used for in-patient treatment are only free at certain times so calculations to work out how many nights are free a week would be done 5) Could Lutathera be administered as an out-patient, how would this work and what set-up costs would there be? 6) A national tariff had been applied to the procedure, was the funding enough to be able to supply the service to a standard the department were happy with? **Results:** All of these issues were discussed a plan was put into place. There were new staff hired, new protocols written and schedules created to allow for the 100 Lutathera treatments a year. **Conclusion:** This study aims to show how the service was changed in order to facilitate such an increase in demand for Lutathera treatment and what provisions were made to support the service. **References:** None.

TEPS-16

Estimate of thyroid volume aimed at radiometabolic treatment of hyperthyroidism

R. Russo, *L. Tommasi, E. Pomposelli, H. Rouhanifar, R. Piva, O. Gandini, M. Muratori, D. Maranzana, H. Belloni, G. Cuccu, D. Valentini, A. Muni;*
SS.Antonio Biagio e Cesare Arrigo hospital, Alessandria, ITALY.

Aim/Introduction: In the calculation of tailored dose for radiometabolic treatment of hyperthyroidism, an essential parameter is the estimate of the total thyroid volume or of the hyper-functioning nodule volume. In the daily routine the ultrasound (US) is the golden standard in the calculation of this crucial parameter. However evidences from the literature show that nuclear medicine techniques such as NaI-131 and ^{99m}Tc scintigraphy have the advantage of directly estimate the hyper-functioning glandular volume. Thus the aim of our study is to compare US, NaI-131 and ^{99m}Tc scintigraphy in the calculation of thyroid volume. **Materials and Methods:** We enrolled 10 patients with hyperthyroidism (8 patients with Basedow disease and 2 patients with Plummer disease) candidate to undergo radiometabolic treatment. For the analysis of scintigraphic data we used Siemens software "Esoft Thyroid Upatke Processing" that allows to estimate the percentage of thyroid tracer uptake, area, volume and weight of the gland. This software was previously set by performing measurements of images acquired on an antropomorphic thyroid-shape phantom containing ^{99m}Tc. From these measurements we found out 40% as the desaturation threshold that best reflects the real dimensions of the gland. Thus, after the application of this cutoff value on patients' scintigraphic images, we drawn minor and major axis on the corresponding isocontour. These values were imputed in the dedicated software in order to obtain the size of each lobe. **Results:** The thyroid volumetry data obtained with the different calculation methods underwent to statistical analysis by Excel and for each distribution the arithmetic average, median and standard deviation values were calculated. The inferential statistical analysis was then completed by obtaining the graphs of the distributions with the relative coefficients of determination R^2 and of correlation R. In particular the graphs were obtained by comparing the volume data between ultrasound and planar scintigraphy with ^{99m}Tc, planar scintigraphy with ^{99m}Tc and scintigraphy with NaI-131 and ultrasound with planar scintigraphy with NaI-131. The results show a strong correlation between the volume data of the three methods, as shown by the value of R which was always elevated and above 0,9. **Conclusion:** US, NaI-131 and ^{99m}Tc-scintigraphy can be used indifferently in the calculation of personalized radioiodine dose to be administered in hyperthyroidism treatment. However, in this scenario, ^{99m}Tc-scintigraphy demonstrated a higher

accuracy in the evaluation of thyroid volume respect to NaI-131 scintigraphy. ^{99m}Tc scintigraphy glandular volume showed a strong correlation with the values found with US. **References:** None.

TEPS-17

Biodistribution Mapping of ^{223}Radium Dichloride during the course of Treatments 2 to 6. A Patient Case Study

***J. Weekes**, I. Sayers, M. Foley;*
New Cross Hospital, Wolverhampton, UNITED KINGDOM.

Aim/Introduction: To evaluate the biodistrution of ^{223}Radium Dichloride (Xofigo) at 36 set anatomical sites (anterior and posterior) in Patient X over a period of at least 22 days post administration. This was performed for treatments 2 - 6 of Patient X's ^{223}Radium Dichloride therapy. The aim of this unique study was to look at the Effective and Biological half -life of ^{223}Radium Dichloride during the individual treatments and evaluate any changes in the half-life's that occur over the course of Patient DN's therapy. **Materials and Methods:** By using a scintillation counter, readings were acquired over set anatomical sites (anterior and posterior) for treatments 2-6. The readings were taken at the skin surface and the mean counts per second during a 20 second observation period were recorded for all sites. Background readings were also acquired and recorded. The data was recorded into identifiable Excel files eg.,treatment number etc., The whole analysis was done with R, a statistical programming language. Activity / time curves were plotted for each anatomical measurement site. **Results:** A Biphasic decay curve was observed in 98 % of sites on a $\log_{10}$ scale. Using all the data points over the treatments, it shows that the estimated gradients or effective half-life's increase with the number of treatments. **Conclusion:** Why would there appear to be a longer biological uptake of ^{223}Radium Dichloride at sites of disease as a result of increase treatments which naturally increases the effective half -life of ^{223}Radium Dichloride therapy. **References:** 1.CRUK website. Accessed 09/03/2019 2.Tannock I, et al. N Engl J Med. 2004;351:1502-1512 3. Goh P, et al. Curr Oncol. 2007;14:9-12 4. Parker C, et al. N Engl J Med. 2013;369(3):213-23 5.Henriksen G Cancer Res. 2002 Jun 1;62(11):3120-5 6. Yoshida K Ann Nucl Med 2016; 30: 453-460.

TEPS-18

Referral Rates and Overall Survival of Patients Receiving Ra223 Therapy for mCRCP at the Beatson West of Scotland Cancer Centre

***I. Kerr**, C. Brown, C. Findlay, G. Buchanan;*
Beatson West of Scotland Cancer Centre, Glasgow, UNITED KINGDOM.

Aim/Introduction: In May 2016, the Beatson Oncology Centre (BOC) opened a Ra223 therapy service treating mCRPC patients in the West of Scotland. This catchment area includes referrals from six Health boards, and a population of 2.8M. The aim of this work was to review the referral patterns and the outcome of patients in the three years since the service was established. **Materials and Methods:** The date of patient referrals to the service were audited to establish any trends in patient throughput. The Overall Survival (OS) of patients that completed all six cycles of Ra223 were compared with published data from the Alsympca trial. **Results:** A total of 178 patients were referred between May 2016 and April 2019. The audit of patient treatments revealed an initial referral rate in the first six months (8.4+/-6.2 per month) which was higher compared to the overall mean of the data (4.9+/-6.2 per month). This higher rate corresponds to a backlog of patients waiting for the service to open. As these patients were more likely to have progressed while waiting for treatment, they were more symptomatic and, therefore, less patients completed all six fractions (40% compared to 52%). Of note, following the Pharmacovigilance Risk Assessment Committee (PRAC) guidance which relegated Ra223 to third line treatment in July 2018, from September 2018 onwards, referrals have approximately halved. Of those patients completing all six fractions 51 out of 87 patients are now deceased, their OS was 9.7 months. This is not comparable with Alsmypca, which reported 14.9 months. This difference may be due to less stringent clinical criteria for treatment, a smaller sample size, and a proportion of patients treated with six fractions that are still alive. **Conclusion:** Deceased patients that completed all six cycles of treatment showed a lower OS than that found in the Alsympca trial. Additionally, the number of patients being referred to the service has been significantly impacted by the new PRAC guidance. The overall survival of this new cohort of patients has not yet been evaluated. **References:** None.

TEPS-19

Impact of TOF(Time of Flight) reconstructions on SUVmax(Standard uptake value) in AD(Alzheimer Disease)/PD(Parkinsonism Disease) patients:Using of ^{18}F-FDG,^{11}C-CFT and ^{11}C-PIB

***D. Wimalarathne**[1,2], X. Lan[1], Y. Zhang[1], W. Ruan[1], R. An[1], X. Sun[1], F. Hu[1];*
[1]Department of Nuclear Medicine,Union Hospital,Tongji Medical College,Huazhong University of Science and Technology, Wuhan, CHINA, [2]Department of Radiography and Radiotherapy,Faculty of Allied Health Sciences, General Sir John Kotelawala Defence University, SRI LANKA.

Aim/Introduction: This study evaluated the impact of TOF reconstruction on SUVmax among ^{18}F-FDG, ^{11}C-CFT and ^{11}-C-PIB suspected Alzheimer's patients. The use of SUVmax value plays an important role in neuro positron emission tomography magnetic resonance imaging (PET/MRI).TOF reconstructions have a significant impact on SUVmax, presenting a challenge for centres with well-defined protocols for diagnosis of Alzheimer's classifications based on SUVmax. This has led to the slow adoption of TOF reconstructions. **Materials and Methods:** Total

71 patients, the median age of 63±8.7 years old and median BMI (Body mass index) 23.91±3.34 (Kg/m2)) with suspected Alzheimer's disease underwent simultaneous PET/MR (SIGNA, GE Healthcare, USA) after injection of ^{18}F-FDG (2-deoxy-2-(^{18}F)fluoro-D-glucose), ^{11}C-CFT(Dopamine transporter/DAT) and ^{11}C-PIB(Pittsburgh compound). 22 ^{18}F-FDG, 24 ^{11}C-CFT and 25 ^{11}C-PIB patients' brain were scanned 15-20 min with arms down supine position. Each PET LIST mode data was reconstructed with and without TOF respectively using the system default three dimensional ordered subset expectation maximization iterative reconstruction algorithm (3D-OSEM). SUVmax of selected brain volume of interest (VOI) were measured using the PMOD 3.906 PNEURO module in both TOF and non-TOF images. T1 weighted MRI was employed for segmentation and brain was segmented to Frontal Lobe(FL), Temporal Lobe(TL), Parietal Lobe(PL), Occipital Lobe(OL), Caudate Nuclei(CN), Nucleus Accumbens(NA), Putamen(PU), Thalamus(Th), Pallidum(PA), Corpus Callosum(COC), Substantia Nigra(SN), Insula(IN), Anterior Cingulate Cortex(ACC), Posterior Cingulate Cortex(PCC), Cerebellum Cortex(CC), Cerebellum Medulla(CM), Brain Stem(BS) and White Matter(WM). TOF and non-TOF SUVmax values were assessed by paired t-test in SPSS 23.0. **Results:** SUVmax of each ^{18}F-FDG ^{11}C-CFT and ^{11}C-PIBs' selected brain volume in TOF images showed higher than those in non-TOF images. For all brain regions, the average SUVmax in ^{18}F-FDG ^{11}C-CFT and ^{11}C-PIB increased by 6.09%, 7.47% and 5.54% respectively in TOF reconstructions. The average SUVmax in ^{18}F-FDG TOF was significantly higher than in non-TOF images in all brain segments (i.e. $p<.05$). In ^{11}C-CFT, FL,TL,PL,OL,CN,NA,Th,PA,SN, ACC, PCC, CC, BS and WM showed significantly higher average SUVmax in TOF than in non-TOF (i.e. $p<.05$). The average SUVmax in ^{11}C-PIB TOF was significantly higher than in non-TOF in FL, TL, PL, OL, CN, NA, Th, IN, ACC, PCC and BS (i.e. $p<.05$). **Conclusion:** The quantitative differences of segmented brain volumes are apparent in TOF and non-TOF PET/MRI images. Depending on a greater quantitative effect from TOF reconstruction, simultaneously PET/MRI will positively impact the proper diagnosis of Alzheimer's disease. This study was supported by the Key Project of Hubei Province Technical Innovation (2017ACA182) **References:** None.

TEPS-20

Validation of Standardized Uptake Value about Hardware Components in Integrated PET/MRI

B. Kim[1], *M. Kim*[2], *I. Moon*[1], *H. Lee*[1], *G. Noh*[1];
[1]*Department of Nuclear Medicine, Seoul National University Hospital, Seoul, KOREA, REPUBLIC OF,* [2]*Department of Radiology, Seoul National University Hospital, Seoul, KOREA, REPUBLIC OF.*

Aim/Introduction: A cross calibration of PET is to identify discrepancies between PET scanner and dose calibrator to ensure the standardized uptake value (SUV). An MR based attenuation correction (MRAC) of PET/MRI needs to be considered in human body as well as in hardware components for MR imaging. However, the cross calibration of the integrated PET/MR has been only performed regardless of hardware components. The purpose of this study was to evaluate the SUV on the impact of hardware components in integrated PET/MRI. **Materials and Methods:** For performing the cross calibration between PET/MRI scanner and dose calibrator, we used a cylindrical water phantom, a Ge-68 cylindrical phantom, and a 3.0T integrated PET/MRI (Biograph mMR, Siemens, Germany). A cylindrical phantom of 9.52 L was filled with demineralised water, 59.2 MBq fluoride-18 solution, 0.2 mM Gadolinium-DTPA as a T1 relaxation modifier, and 150 mM NaCl as a conductivity to avoid artifacts from MR imaging. The cross calibration correction factor (CCCF) was produced by scanning the prepared phantoms regardless of the hardware components such as a patient table and RF body surface coils. After applying the CCCF, we obtained PET/MR images for the water phantom to check the accuracy of attenuation correction according to presence of the hardware components (hwc, non-hwc). DIXON sequences for MRAC were acquired simultaneously with PET. All PET images were reconstructed using 3D OSEM. A total of 103 regions of interest were drawn to measure mean SUVs (SUV_{hwc}, $SUV_{non\text{-}hwc}$) for the water phantom on each image. Statistical analyses were performed to compare SUV measurements on both images. **Results:** The CCCF obtained by the cross calibration using the water phantom and the Ge-68 phantom was 0.96. The SUV_{hwc} and $SUV_{non\text{-}hwc}$ which reflected the CCCF were measured as 0.922±0.016, and 0.998±0.010, respectively. SUV_{hwc} was identified as significantly smaller than $SUV_{non\text{-}hwc}$ ($P< 0.05$). The Difference between $SUV_{non\text{-}hwc}$ and SUV_{hwc} showed 0.076±0.018. **Conclusion:** The hardware components such as s patient table and RF body surface coils may have a considerable impact related to the underestimation of the SUV in integrated PET/MR imaging. The SUV validation which included the hardware components is able to ensure the accuracy of quantitative analysis. So, we suggest including hardware components when performing the cross calibration between PET/MRI scanner and dose calibrator. **References:** KELLER, Sune H., et al. Cross-calibration of the Siemens mMR: easily acquired accurate PET phantom measurements, long-term stability and reproducibility. EJNMMI physics, 2016, 3.1: 11.

TEPS-21

Optimization of Bayesian penalized likelihood reconstruction parameters for quantitative brain Positron Emission Tomography (PET) imaging

D. Ribeiro[1], *W. Hallett*[1], *O. Howes*[2,3,4], *R. McCutcheon*[2,3,4], *M. Nour*[2,3,4], *A. A. S. Tavares*[5];
[1]*Invicro, London, UNITED KINGDOM,* [2]*Institute of Psychiatry, Psychology & Neuroscience, London, UNITED KINGDOM,* [3]*Medical Research Council London, Institute of Medical Sciences, London, UNITED KINGDOM,* [4]*Institute of Clinical Sciences, Faculty of Medicine, Imperial College London, London, UNITED KINGDOM,* [5]*Edinburgh Imaging, The University of Edinburgh, Edinburgh, UNITED KINGDOM.*

Aim/Introduction: Nuclear medicine technologies have

recently seen advances in scanner hardware and reconstruction algorithms. Q.Clear is a Bayesian penalized likelihood reconstruction algorithm that presents improvements in the Positron Emission Tomography (PET) image signal-to-noise ratio (SNR)[1]. This study aims to evaluate the performance of Q.Clear against the ordered subset expectation maximization (OSEM) and filtered back-projection (FBP) algorithms, in dynamic brain PET images. **Materials and Methods:** Contrast recovery (CR) and background variability (BV) were investigated with the National Electrical Manufacturers Association (NEMA) Image Quality (IQ) phantom and resolution, axial uniformity and SNR were investigated with the Hoffman phantom, both filled with ^{11}C- or ^{18}F-labelled solutions. Data collection and reconstruction was performed using a Siemens Biograph 6 TruePoint PET-Computed Tomography (CT) and General Electric SIGNA PET-Magnetic Resonance (MR). The non-displaceable binding potentials (BP_{ND}) for the Substantia Nigra (SN), Striatum (St), Globus Pallidus (GP), Thalamus (Th), Caudate (Cd) and Putamen (Pt) from seven [^{11}C]PHNO PET-MR datasets were investigated. Intraclass correlation coefficients, repeatability coefficients (RC), coefficients of variation and bias from Bland-Altman plots were reported. Statistical analysis was conducted using a 2-way ANOVA model with correction for multiple comparisons. **Results:** For the Q.Clear reconstructions, as the β parameter increases, CR and BV decrease in the NEMA IQ phantom. The CR results are lower for FBP and OSEM versus Q.Clear. The BV results are higher for Q.Clear versus OSEM. For the Hoffman phantom, low β levels provide the best resolution and high β levels provide the best uniformity and SNR. When comparing a standard OSEM reconstruction of 6 iterations/16 subsets and 5mm filter with Q.Clear with different β values, the quantitative bias and RC were lower for Q.Clear with β=100 for the SN, Th and GP and with β=200 for the St, Cd and Pt. The Q.Clear with β=100, 200 and 400 are the only reconstructions across all structures that don't present statistically significant differences ($p<0.001$) when compared to the standard OSEM reconstruction. **Conclusion:** Q.Clear improves CR and provides better in plane, axial resolution and SNR in the PET-MR, in comparison to OSEM, and FBP in the PET-CT. Quantitative brain PET studies using [^{11}C]PHNO are more accurate when using Q.Clear with β<400 which is the value used for clinical ^{18}F-FDG whole-body studies. **References:** [1] Teoh EJ, McGowan DR, Macpherson RE, Bradley KM, Gleeson FV. Phantom and clinical evaluation of the Bayesian penalized likelihood reconstruction algorithm Q.Clear on an LYSO PET/CT system. J Nucl Med. 2015 Sep;56(9):1447-52.

TEPS-22

Correlation of the Standardized Uptake Value(SUV) and the Apparent Diffusion Coefficient(ADC) Value in Breast Carcinoma with Simultaneous [18F]-FDG PET/MRI

M. Kim[1], *B. Kim*[2], *H. Jung*[1], *Y. Bang*[1];
[1]*Department of Radiology, Seoul National University Hospital, Seoul, KOREA, REPUBLIC OF,* [2]*Department of Nuclear Medicine, Seoul National University Hospital, Seoul, KOREA, REPUBLIC OF.*

Aim/Introduction: Both the apparent diffusion coefficient (ADC) value and standardized uptake value (SUV) indirectly represent the biological characteristics of cancer. Our study attempt to evaluate the mutual association by comparing SUVs and mean and minimal ADC values at the same region in breast carcinoma. **Materials and Methods:** 40 patients (mean age: 41.64±7.95 years, range: 32-62 years) with breast cancers underwent F-18 FDG PET/MRI (Biograph mMR, Siemens, germany) examinations at our institute during a period from July in 2018 to March in 2019 were enrolled in this study. PET images were acquired 60 min after administration of F-18 FDG (5.18MBq/kg of body weight). We evaluated whether there was a correlation among the SUVs, ADC(b values; 0 and 1000 seconds/mm2)mean, and ADCmin values in the same region as maxSUV, peakSUV, and meanSUV. Pearson correlations were calculated to investigate the association between SUVs and mean and minimal ADC values. **Results:** 40 lesions were detected. The mean SUVmax, ADCmean and ADCmin were 8.53 ± 5.46 (range, 1.01-26.85), 956.20 ± 234.40 × 10−6 mm2/s (range, 425.70-1278.00 × 10−6), and 851.96 ± 222.32 × 10−6 mm2/s (range, 373.00-1211.00 × 10−6), respectively. We found a weak positive correlation between maxSUV and mean and minimal ADC values(correlation coefficient r=0.232, p=0.150 and r=0.302, p=0.059, respectively). **Conclusion:** Our study demonstrates a weak positive correlation between SUVs and mean and minimal ADC values at the same region of max, peak, and meanSUV in patients with breast cancer. we found that correlations could play an important role in assessing the tumor condition in a specific region of interest. **References:** Kitajima K, Yamano T, Fukushima K, Miyoshi Y, Hirota S, Kawanaka Y, Miya M, Doi H, Yamakado K, Hirota S. Correlation of the SUVmax of FDG-PET and ADC values of diffusion-weighted MR imaging with pathologic prognostic factors in breast carcinoma. European journal of radiology. 2016 May 1;85(5):943-9.Wetter A, Lipponer C, Nensa F, Heusch P, Rübben H, Schlosser TW, Pöppel TD, Lauenstein TC, Nagarajah J. Quantitative evaluation of bone metastases from prostate cancer with simultaneous [18 F] choline PET/MRI: combined SUV and ADC analysis. Annals of nuclear medicine. 2014 Jun 1;28(5):405-10.

804-2

Technologists: Technologist e-Poster Presentation Session 2

Monday, October 14, 2019, 11:30 - 13:00 Meeting Room 120/121

TEPS-23

Case-by-case Evaluation of Clearance of Waste contaminated with Residues of the Radiopharmaceutical Xofigo

O. Nitzsche[1], *S. Thierfeldt*[1], *R. Kunz*[1], *K. Wittke*[2];
[1]*Brenk Systemplanung GmbH, Aachen, GERMANY,*
[2]*Bayer AG, Wuppertal, GERMANY.*

Aim/Introduction: Depending on the residual activity and the time it will take for decay of this activity below clearance levels, waste contaminated with radiopharmaceuticals can either be treated as radioactive waste or can be cleared and then disposed of as conventional waste (usually by incineration). Some radiopharmaceuticals contain radionuclides with half-lives that will not allow decay to activities below unconditional clearance levels within reasonable time. The radiopharmaceutical preparation Xofigo® with the active ingredient $^{223}RaCl_2$ is manufactured and marketed by Bayer AG (Bayer). The active ingredient of the preparation is Ra-223 with a half-life of 11.4 d. Xofigo® also contains Ac-227 with half-live of 21.8 a and its daughter nuclide with half-live of Th-227 18.7 d respectively, due to the manufacturing process. **Materials and Methods:** In this paper, a case-by-case analysis in accordance with German regulations is reported for waste contaminated with residues of Xofigo® with the aim of enabling the release of the waste without further restrictions. It is taken into account that the resulting waste have to be collected in a closed container and incinerated in waste incineration plants. The case-by-case assessment demonstrates that the potential exposure of persons of the general public will not exceed 10 µSv per calendar year. Especially for employees of waste incineration plants, it is further proven that the exposure to be expected for these persons is significantly below 1 µSv per calendar year. This ensures that no dose of more than 10 µSv/a can be obtained even in the case of superimpositions with exposures from releases for disposal from other sources. Exposure calculations were performed on the basis of the generic radiological model prepared for the deriving clearance levels for disposal of cleared wastes on landfill disposal sites or in incineration plants with appropriate adjustments to the model to account for the significantly lower quantities of Xofigo® waste and the special features of Rn-219 (daughter nuclide of Ra-223). The calculation is based conservatively on a substantial increase of the current annual applications in Germany. **Results:** The calculations of the potential exposure indicate that a decay time of 150 days should be observed. Also for the activity concentration of the long living mother nuclide Ac-227, the pharmaceutical release specification is used as a very conservative upper limit. **Conclusion:** Release of Xofigo® residues after decay of the short living nuclides Th-227 and Ra-223 towards the equilibrium with Ac-227 is possible without further requirements. **References:** None.

TEPS-24

A sensitive analytical method for the determination of the long-lived impurity ^{227}Ac in production batches of Xofigo® has been developed in order to allow for unconditional release of clinical waste after decay-in-storage

J. Gay[1], *I. Hunnes*[2], *A. K. Pearce*[3], *P. Ivanov*[3], *K. Wittke*[4];
[1]*Bayer AG, Berlin, GERMANY,* [2]*Bayer AS, Oslo, NORWAY,* [3]*National Physical Laboratory, Teddington, UNITED KINGDOM,* [4]*Bayer AG, Wuppertal, GERMANY.*

Aim/Introduction: Radiopharmaceuticals are produced according to high quality standards, however, the medical isotopes used, e.g. ^{68}Ga, ^{90}Y, ^{99m}Tc, ^{111}In, ^{123}I, ^{153}Sm, ^{177}Lu, ^{223}Ra or ^{225}Ac may be contaminated with long lived radionuclidic impurities. Although these contaminants typically account for less than 0.01% of the total radioactivity, they need to be considered for waste disposal and in many cases require setting up costly and tedious disposal concepts. In principle, the short half-lives of ^{223}Ra (11.4 days) and its daughter nuclides allow for decay-in-storage of Xofigo® related waste. However, traces of the long-lived mother nuclide ^{227}Ac of ^{223}Ra production potentially present in Xofigo® drug solution might require setting up a specific waste management pursuant to local regulations on waste disposal. Being able to determine ^{227}Ac as a weak ß-emitter next to a high excess of ^{223}Ra and its progeny (predominantly emitting α, but also β and γ) is analytically challenging. According to the current specification for drug release, the maximum content of ^{227}Ac is ≤0.004% relative to ^{223}Ra. A level that guarantees patient's safety related to exposure from ^{227}Ac being present only in traces, if at all. On the other hand it doesn't meet the requirements for unconditional release of Xofigo® related waste in some European countries due to very strict ^{227}Ac limits for waste disposal. Therefore, Bayer has developed a sensitive analytical method dedicated to waste management. **Materials and Methods:** The method consists of a radiochemical separation of potential traces of ^{227}Ac from ^{223}Ra with use of extraction columns following detection with liquid scintillation counting (LSC). **Results:** This method allows proof of ^{227}Ac levels below 0.000001% relative to ^{223}Ra, and thus unconditional release of Xofigo® related clinical waste. Results of ^{227}Ac measurements on Xofigo® production batches are provided to Xofigo® users on request. **Conclusion:** In summary, development of a sensitive analytical method to determine ^{227}Ac traces in Xofigo® production batches resulted in ecologically and economically improved waste management. **References:** None.

TEPS-25

Differentiated thyroid cancer patiens treated with radioiodine-therapy and individualized recommendation of radioprotection

C. Moisescu-Goia, *A. Sabo, C. Pestean, I. Cecan, M. Crisan, E. Olariu, D. Piciu;*
Oncological Institute of Cluj-Napoca, Cluj-Napoca, ROMANIA.

Aim/Introduction: Patients with differentiated thyroid cancer who receive necessitate hospitalization. Radiological safety standards for nuclear medicine practice issued by CNCAN require that patients receive recommendations on radiation protection measures that have to be meet immediately after discharge. The purpose of the study is to highlight the importance of the individual recommendations that patients receive at discharge depending on the measured flow. **Materials and Methods:** The study was conducted on a sample of 11 patients with differentiated thyroid cancer admitted to the

Nuclear Medicine Laboratory of the Oncology Institute "Prof. Dr. Ion Chiricuta"Cluj-Napoca within one months. The subjects (two men and nine women) had T1b to T4c stage lymph node and lung metastases, aged between 23-80 years. I-131 activity was between 1.1GBq administrated and 3.7 GBq, with a mean of +/- SD +/- 2.78 GBq 0.96GBq. Measurements were performed on consecutive days (for 2 or 3 days) of patient flow, and on the day of discharge even the flow of personal lingerie used by patients during hospitalization was measured. **Results:** The 11 patients hospitalized were measured repeatedly, and the recorded flow at 1m distance was between 77.4 to 17 µSv/h on the first day post I-131administration therapy; to reach values between 10.4 and 1.8 µSv/h after 3 or 4 days of hospitalization. On discharge day of each patient the personal ligerie used during hospitalization was mesured. The recorded values were between 2.34 to 41.7 µSv/h, with a weight of 54.5% below 10 µSv/h. The results of the measurements revealed the lack of statistically significant correlations with the activity of I-131 administered, p = 0.736. **Conclusion:** The study highlighted the importance of the individualized recommendations on radiation protection based on measured flow values for discharged patients not the administered activity of I-131. **References:** None.

TEPS-26

A Phantom Study on Radiotracer Dose Reduction in Integrated PET/MR System

J. Zhuang, M. Bai;
Xuanwu Hospital, Capital Medical University, Beijing, CHINA.

Aim/Introduction: The purpose of the current study was to explore the feasibility of radiotracer dose reduction in the integrated PET/MR system achieved by the application of time-of-flight (TOF) method with phantom, while the image quality (IQ) was not inferior to its original level. **Materials and Methods:** Measurements were performed on GE SIGNA PET/MR following National Electrical Manufacturers Association (NEMA) NU 2-2007 protocol using IQ phantom. The hot-sphere-to-background activity concentration ratio was 4:1. All data were periodically acquired in list-mode format with an acquisition time of 11 minutes. The scans successively started at 0, 1/2, 1, 3/2, 2 half-lives of ^{18}F-FDG. The activity concentration of the hot spheres was 2.12×10^4 Bq/ml at the beginning of the scan. A CT-based attenuation map was used to carry out the attenuation correction. PET images were reconstructed using both TOF method and point spread function (PSF) correction, TOF method only, PSF correction only, neither TOF method nor PSF correction. The obtained PET images were quantitatively evaluated by contrast recovery, background variability, and signal-to-noise ratio (SNR) of hot spheres. A paired t-test was performed to assess the difference between the images acquired at lower radiotracer activity reconstructed with TOF method and those acquired at higher radiotracer activity reconstructed without TOF method. **Results:** The contrast recovery remained almost constant over the 2 half-life periods of ^{18}F-FDG, meanwhile the background variability displayed a rising tendency, and the SNR dropped as the radiotracer activity decreased. Using TOF to reconstruct could improve the contrast recovery ($p<0.05$) and SNR ($p<0.05$) significantly, and reduce the background variability ($p<0.05$). When the radiotracer activity decreased to 50%, background variability ($p>0.05$) and SNR ($p>0.05$) of the PET images reconstructed with TOF had no significant difference with the corresponding PET images acquired at 100% radiotracer activity reconstructed without TOF, while the PET images acquired at 50% radiotracer activity reconstructed with TOF had superior contrast recoveries to those acquired at 100% radiotracer activity reconstructed without TOF ($p>0.05$). **Conclusion:** The image quality of the PET images deteriorates with the radiotracer activity decaying. While the radiotracer activity decreasing to 50%, the decline of image quality can be compensated by using TOF method. Therefore, the application of TOF method can reduce at least half of the dose to patients from PET/MR examinations. **References:** 1. National Electrical Manufactures Association (NEMA). Standards Publication NU 2-2007. Performance Measurements of Positron Emission Tomographs. Rosslyn, VA: NEMA; 2007.

TEPS-27

Examination of the Correlation between patient-dependent parameters and radiation dose rates measured around patients undergoing PET/CT imaging using 18F-FDG

S. Alqahtani[1], *K. Soliman*[2], *A. Alenezi*[3];
[1]*PSMMC, Riyadh, SAUDI ARABIA,* [2]*Medical Physics Department, PSMMC, Riyadh, SAUDI ARABIA,* [3]*Faculty of Applied Medical Sciences, KSU, Riyadh, SAUDI ARABIA.*

Aim/Introduction: Patients undergoing 18F-FDG PETICT imaging are considered as external sources of radiation. Accurate dose rate estimation is important for conducting realistic risk assessments and performing dose reconstruction in cases of accidental exposures. The patient radiation self-attenuation factor is assumed to be a function of the patient's body size metrics; but can we use these metrics to predict the dose rate around the patients with accuracy in situation where direct dose rate measurements are not possible?. The objectives of this work were to measure the patient attenuation factor by performing direct dose rate measurements from patients, to study the possible correlation between the measured dose rate constant from the patients and their body size metrics and to measure the patients' voiding factor. Five different body size metrics were tested for correlation in this study **Materials and Methods:** We have measured the dose rate at one meter anterior to the patient body surface from 57 patients just before voiding and also immediately after voiding using a calibrated ionization chamber; the injected activity measured with a properly calibrated clinical dose calibrator used in the nuclear medicine department was corrected for decay and used to calculate the dose rate per unit activity **Results:** The measured average dose rate per unit activity was 92.2 14 $\mu Sv.hr^{-1}.GBq^{-1}$. This result is with close agreement with the value recommended by AAPM TG-

108. There was no statistically significant correlation between the dose rate constant per unit activity and the 5 patient body size metrics tested in the table below. The measured patient voiding factor was found to be equal to 0.89+0.06. **Conclusion:** Patient bladder voiding before scanning reduced the measured dose rate at one meter from the patient by about 11%. Patient body size metrics cannot be used solely to predict the dose rate levels expected from individual patient. The activity normalized dose rate constant of 92 (uSv/h/GBq) measured at one meter anterior to the patient can be used with confidence to estimate dose rates from patients undergoing PET/CT imaging using FDG because it includes patient body attenuation and scatter factor. The presented data can be used by medical physicist working in nuclear medicine for optimization of protection and justification of locally applied radiation safety measures. **References:** Madsen, M.T., Anderson, J.A., Halama, J.R., Kleck, J., Simpkin, D.J., Votaw, J.R., Wendt III, R.E., Williams, L.E. and Yester, M.V. (2006) AAPM Task Group 108: PET and PET/CT Shielding Requirements. Medical Physics, 33, 4-15., https://doi.org/10.1118/1.2135911.

TEPS-28

Typical patient doses from CT part of PET/CT examinations in Slovenia and comparison with other countries

J. Peric[1,2], *I. Zagar*[1], *D. Zontar*[3];
[1]*Institute of Oncology, Ljubljana, SLOVENIA,* [2]*Faculty of Health Sciences, University Ljubljana, Ljubljana, SLOVENIA,* [3]*Slovenian Radiation Protection Administration, Ljubljana, SLOVENIA.*

Aim/Introduction: In hybrid PET/CT imaging, the CT part (due to attenuation correction) allows for more precise determination of the activity in the selected volume and greater accuracy and reliability in lesion localization. Despite several important benefits, it should be noted that the addition of CT to the PET system increases radiation load in PET/CT imaging. Many previous studies emphasized a great need to optimize radiation exposure and radiation protection. However, the diagnostic reference level (DRL) for CT in hybrid systems in Slovenia has not yet been determined. **Materials and Methods:** The study involved 540 patients who had a PET/CT examination. We selected 180 patients per each nuclear unit in Slovenia. The first 60 patients had PET/CT from the top of the head to the middle of the thigh, the other 60 patients had a PET/CT from the base of the skull to the middle of the thigh and the last 60 patients had PET/CT of the entire body. The selected patient population had body weight 70 to 90 kg and average BMI 27.05 ± 2.8. The average value of Dose Length Product (DLP) was calculated for each individual protocol and compared between NM units in Slovenia and with already published diagnostic reference levels. **Results:** We found a statistically significant difference in the DLP between protocols carried out by different NM in Slovenia, taking into account the error possibility of 5%. The average DLP in the University Clinical Center Ljubljana was 20% lower than DLP at the Institute of Oncology Ljubljana and 40% lower at the University Clinical Center Maribor. On average NM units in Slovenia have lower (> 22%) DLP compared with DRL in Australia for all three protocols. The research also showed that height and gender had a statistically significant impact on the patient's dose. **Conclusion:** The results of the research will be a good basis for proposing the predicted diagnostic reference dose levels for hybrid PET/CT imaging in Slovenia, in order to optimize and improve work practice. **References:** None.

TEPS-29

CT Dose Optimization

B. Gillman;
British Columbia Institute of Technology, Vancouver, BC, CANADA.

Aim/Introduction: Computed tomography (CT) is not only ubiquitous in modern clinical environments but also a vital tool in obtaining diagnostic information. But rising concerns of CT radiation exposure have prompted many dose optimization and reduction strategies to be developed. Technologists should be aware of the techniques and technologies available to them to help reduce CT dose to patients. **Materials and Methods:** When investigating dose optimization, there are a number of essential aspects to consider. First, it is important to be familiar with how CT dose is measured and know the limitations involved these dose metric estimates. Second, learn what dose reduction strategies are available to you. These are a combination of actions the technologists can do (such as modifications of scanning parameters based on individual patient considerations), as well as built in features of the scanner itself (such as recent technological innovations such as Specific Organ Dose Adaption and Reduction protocol - SODAR) that can be taken advantage of. With these strategies in mind, the technologist can help optimize CT dose during three key phases of the scan: before, during, and after. During each of these phases, some of the most significant dose reduction techniques will be highlighted. Finally, it is equally important to look at methods for evaluating your departments current radiation usage and able to track changes (and hopefully improvements) over time. **Results:** Radiation dose metrics such as Dose-Length Product (DLP) should be monitored in clinical practice using Diagnostic Reference Levels (DRLs). DRLs are an established, effective technique to not only track changes, but also set guidelines for imaging radiation dose. **Conclusion:** It is important to know your scanner and understand the dose reduction technologies available to you as a technologist. Utilizing these strategies as they become standard of practice will reduce CT radiation exposure to your patients. **References:** None.

TEPS-30

Evaluation in animal imaging of the new generation of pre-clinical all-digital PET/CT

W. Xiao[1], *H. Yan*[1], *L. Wan*[2], *Q. Xie*[1];
[1]*Huazhong University of Science & Technology, Wuhan, CHINA,* [2]*Wuhan Raydata Technology Co., Ltd., Wuhan, CHINA.*

Aim/Introduction: It's well known that positron emission tomography(PET) has wildly extended its application area and proved more importance in both clinical diagnose and pre-clinical research. Here, in order to assess application of the new generation of all-digital animal PET/CT system - Trans-PET Discoverist 180, we performed a series of experiments to evaluate animal imaging performances. **Materials and Methods:** Materials: male wild type C57BL/6J mice, male myocardial infarction(MI) mice, male rats, rabbit 2-Deoxy-2-(^{18}F)fluoro-D-glucose (^{18}F-FDG) Trans-PET Discoverist 180 (Raycan Technology Co., Ltd, Suzhou, China) Methods: First, we performed scans for single wild type mouse and rat. Before experiment, animals were fasten overnight. For mice experiment, 200μCi of ^{18}F-FDG or ^{18}F-NaF was injected via tail vein. 60 minutes(min)(for FDG) or 120min(for NaF) after injection, the mice were placed on scan bed for 10min's PET static scan(10min/bed,inhaled anesthesia with 2~3% isoflurane) followed by normal mode CT scan. Rats experiments had the same protocol except the injected dose was 500μCi and the PET mode was set in whole body for 20min (10min/bed, 2 beds). We also performed scans for 4 mice or 2 rats in one scan. Next, MI mice without fasting were scanned and compared the data with wild type mice. We also performed dynamic scans for mouse and rat using ^{13}N-Ammonia to observe the blood flow in heart and brain. Last, we performed large animal scans on rabbits. 1mCi/kg ^{18}F-FDG was injected via ear vein. Rabbits were scanned 120min after ^{18}F-FDG injection for 20min in whole body mode(5min/bed, 4 beds). Data analysis: After PET scanning and image reconstruction, dicom data was processed with software Carimas(Turku PET center, Turku, Finland). **Results:** Trans-PET Discoverist 180 is a useful tool in pre-clinical research. PET image of single mouse is of high quality. The axial length of FOV is 10cm and enough for scanning of one whole mouse body. The large radial FOV enables 4 mice or 2 rats in one scan, that can be very helpful in short half-life radiotracer imaging. Mice heart imaging is clear and data can easily be processed and recognized by other software, such as Carimas. Dynamic scanning enables realtime and dynamic monitoring of pharmacokinetics in whole mice body or majority rat body. **Conclusion:** The large FOV of Trans-PET Discoverist 180 makes it a unique animal PET scanner for large animal, that has wildly extended its application area. And it's also able to do PET scan for monkey brain. **References:** None.

TEPS-31

Conventional vs. digital Philips PET/CT: evaluation of phantom data

A. Ebbens, T. Kuijer, E. Martens, B. J. de Wit-van der Veen; Netherlands Cancer Institute, Amsterdam, NETHERLANDS.

Aim/Introduction: A new digital PET/CT scanner was recently introduced at our department, enabling more detailed imaging and either dosage or acquisition time reduction. In a clinical setting, however, it is important that the quantitative performance of both our digital and conventional PET/CT scanners is comparable. Therefore, the aim of this study is 1. to compare reconstructions on both conventional and digital PET/CT and 2. to find optimal quantitative reconstruction parameters for the digital 2mm PET/CT. **Materials and Methods:** The NEMA NU2-2007 Image Quality phantom was filled with 3.9 Bq/mL ^{18}Fluorine (^{18}F)-FDG in the background and 18.1 Bq/mL ^{18}F-FDG in the six spheres (inner diameters between 10 to 37mm), to result in a 4.7:1 sphere-to-background ratio. A two bedposition (bp) scan of two and ten minutes per bed were performed on both conventional (Philips Gemini) and digital (Philips Vereos) PET/CT. Conventional scans were reconstructed according to standard 4mm-EARL (3 iterations (i) and 33 subsets (s)). Digital PET/CT reconstructions were the following: 4mm-EARL (3i15s and 3.0mm Gaussian), 2mm-3i7s, 2mm-3i11s and 2mm-3i17s, all without Gaussian or PSF. Recovery coefficients of the maximum voxel value (RC_{max}) were determined for each sphere using the EARL software tool. Accordingly, the RC_{max} was normalised to the largest sphere for all reconstructions. RC's were compared to the EARL-specifications. **Results:** The absolute RC_{max}-values of the EARL reconstructions at 10 minutes per bp of the conventional and digital PET/CT were within EARL-specifications, whereas all 10 minute 2mm recons were positioned above the maximal RC_{max}, especially for the two smallest spheres (10 and 13mm). The shape of the normalised curves for all reconstructions for the digital PET/CT were similar; the curve of the conventional scanner was generally lower for the two smallest spheres (10 and 13mm), and slightly higher for the 17mm sphere. **Conclusion:** In general, the digital PET/CT shows better recovery of the smallest spheres (<17mm), and remains within EARL specifications with the 4mm-EARL-recon. Quantification using the 2mm 3i7s reconstruction maintains a good recovery for small spheres, and corresponds best to conventional 4mm-EARL-PET/CT. Accordingly, quantitative comparison with the conventional PET is possible, however further optimization of the digital PET/CT protocols could be achieved using point spread function reconstruction and Gaussian filters. **References:** None.

TEPS-32

PET-CT acquisition protocol optimization with a new digital PET-CT

S. Cola[1], F. Fioroni[2], A. Palmieri[1]; [1]Nuclear Medicine S. Maria Nuova Hospital, Reggio Emilia, ITALY, [2]Physical Department S. Maria Nuova Hospital, Reggio Emilia, ITALY.

Aim/Introduction: In june 2018 a new G.E. Discovery MI has been installed in our departement.The aim of this study is to optimize the ratio between time acquisition and injected dose in relation with patient BMI index. **Materials and Methods:** In our institution the baseline protocol, for oncological PET-CT examination, consisted of the administration of 3.7 MBq/kg of FDG and an acquisition of 3.5 min/bed. In the new proposal WB FDG scan the activity was reduced to 3.0 MBq/kg and the acquisition time varies from 2 to 3 minutes depending on patient BMI index.The baseline perfusional brain protocol consisted of the administration of 2.8 MBq/kg FDG and 20

minutes acquisition. In the new proposal brain scan the activity was reduced to 2.5 MBq/kg and 15 minutes acquisition time in list mode method. We are going to reduce to 10 minutes the time of acquisition.The overall image quality was subjectively rating by the referring physician. **Results:** The examination were analized. In most cases the first data show that the examination quality was find good and has been scored as interpretable . We are going to analize all the data thorough way. **Conclusion:** The PET-CT high sensitivity allow to reduce PET doses and acquisition time without modify the image quality. It is important to pay attention to the BMI index of the patient **References:** None.

TEPS-33

Quantitative harmonization of Biograph mCT systems using post-reconstruction filter (EQ. Filter) and its validation in clinical studies for whole body ^{18}F-FDG

A. Hurtado de Mendoza, C. Soza, J. Flores, S. Lopez, J. Spuler, H. Amaral;
Center for Nuclear Medicine & PET/CT Positromed, Santiago, CHILE.

Aim/Introduction: To harmonize SUV metrics in different mCT systems including Time-of-Flight (TOF) and Point Spread-Function (PSF) technologies through the implementation of an EQ-filter tool to decrease intervariability across clinical protocols. **Materials and Methods:** To obtain a corrected ECF a uniformity phantom was used to cross calibrated two PET/CT Siemens systems: mCT FLOW (mCT1) and Biograph mCT 20 (mCT2). An image quality test with standard NEMA IQ phantom NU2-2007 according to EARL specifications was performed. An isocontour-VOI (41% and 50%, respectively) with unfiltered ultraHD (PSF + TOF) 2 iterations, 21 subsets, pixel size 4.07 mm² for mCT1 and unfiltered iterative + TOF 2 iterations, 21 subsets, pixel size 4.07 mm², for mCT2 was used to find the RCs for SUVs max and mean. To adjust RC curves an EQ-filter algorithm was applied smoothing the reconstructed images. Then a shorter scan was performed to find the minimal scan-time acquisition ensuring COV values (1) under 15% in the background of phantom. To correlate our results with the standard clinical whole-body 18F-FDG protocol for SUV max and peak in each scanner, we analyzed 10 lung and mediastinum lesions (< 3 cm of diameter) in four patients and tested using the Spearman´s rank test. **Results:** The harmonized parameters for mCT1 was ultraHD 2 iterations, 21 subsets, EQ.filter 7.6 mm, with an absolute error of 3.5% for RCs max and 1.4% for RC mean; for mCT2 was iterative + TOF 2 iterations, 21 subsets, EQ filter 5.6 mm, with an absolute error of 1.8% and 4.6% respectively. In both systems the absolute error for RCs max and mean for 17, 13 and 10 mm spheres was close to 2.4%. However, in the case of the RCs mean in mCT1, we obtained 0% of the of absolute error. The minimum time for mCT2 was 2 min for bed-acquisition providing 10% COV in the uniform background compartment and 0.7 mm/seg bed-velocity and 11.6% COV for mCT1. After harmonization we observed a consistent reduction in the values measured for SUV max and peak in comparison to the clinical protocol for each system, with a high correlation between them. **Conclusion:** EQ-filter harmonize the reconstructed parameters regardless the use of PSF and TOF capabilities decreasing the discrepancy and variability between SUV max, mean and peak quantifications in our intra-center context. **References:** 1. Koopman et al. EJNMMI Physics (2016) 3:22.

TEPS-34

Image quality of 18F-FDG for patients with a high body mass index examined on Si-photomultiplier based PET

B. Olsson[1], J. König[2], E. Trägårdh[1], J. Oddstig[3];
[1]Clinical Physiology and Nuclear Medicine, Skåne University Hospital and Lund University, Malmö-Lund, SWEDEN,
[2]Department of Radiology, Central Hospital, Kristianstad, SWEDEN, [3]3Radiation Physics, Skåne University Hospital and Lund University, Malmö-Lund, SWEDEN.

Aim/Introduction: Due to photon absorption and scatter the image quality for high body weight patients that undergoes ^{18}F-FDG PET examinations may be lower compared with normal-weight patients. In our clinical protocol, patients are administered an activity of 4 MBq/kg body weight, maximum 500 MBq, and for patients < 100 kg images are acquired for 1.5 min/bed position. To compensate for attenuation factors the acquisition time is prolonged for the overweight patients. The aim was to investigate if there is any difference in image quality for patients with a BMI above respectively below 30 kg/m² and if prolonging the acquisition time for patients with BMI ≥30 kg/m² would equalise the image quality for the high BMI patients. **Materials and Methods:** The study included 32 patients with a BMI ≥ 30 kg/m² and from a previous study we extracted 21 patients, referred to as the control group, who had a BMI < 30 kg/m² and a weight < 100 kg. The patients were injected with 4 MBq/kg, maximum 500 MBq, and imaged after 60 minutes on a Discovery MI (GE Healthcare, Milwaukee, WI, USA) PET-CT using a block-sequential regularization expectation maximization reconstruction algorithm (Q.Clear, GE Healthcare) with a beta-value of 550. The acquisition time for patients in the control group was 1.5 min/bed position. For patients with high BMI the acquisition time was 4 min/bed position, acquired in listmode, which allowed the studies to be truncated to six different acquisition times of 1.5 - 4 min/bed position with 30 sec intervals. Three regions-of-interest (ROIs) in the liver were drawn in each patient. Using the ROIs in the liver, the average signal-to-noise ratio (SNR) was calculated for each patient. **Results:** Patients with BMI ≥ 30 kg/m² had a mean BMI of 34.3 (30-49) kg/m² and for patients with BMI < 30 kg/m² was the mean BMI 23.6 (16-29) kg/m². For patients with a BMI ≥ 30 kg/m² SNR increased with increasing acquisition time, ranging from 10.4 to 16.8. An acquisition time of 1.5 min/bed position yielded a mean SNR of 10.3 for patients with BMI < 30 kg/m² and 10.4 for patients with BMI ≥ 30 kg/m². **Conclusion:** The quantitative analysis showed no significant difference in SNR between patients with BMI > 30 kg/m² and the control group for acquisition times of 1.5 min/bed position. The image quality should be confirmed by qualitative analysis of experienced nuclear medicine physicians. **References:** None.

TEPS-35

Studies On Decision Of The Cut-off Standardized Uptake Values For Normal Bones In ^{18}F-fluoride Pet/ct And ^{18}F-fdg Pet/ct

R. Ono[1], *N. Fujita*[1,2], *C. Hasegawa*[1], *Y. Ito*[1], *T. Tada*[1], *R. Murayama*[1], *Y. Tsutsumi*[1,2], *T. Odagawa*[1], *M. Tamura*[1], *S. Abe*[2], *K. Kato*[1]; [1]*Departmemt of Radiological and Medical Laboratory Sciences, Nagoya University Graduate School of Medicine, Nagoya, JAPAN,* [2]*Department of Radiological Technology, Nagoya University Hospital, Nagoya, JAPAN.*

Aim/Introduction: For the detection of bone metastases, ^{18}F-fluoride (NaF) PET/CT and ^{18}F-FDG PET/CT are used as imaging modalities. If the standardized uptake values (SUVs) of normal bone are known, they can be used in differentiation of normal bones and bone metastases and have the potential to evaluate treatment response. To our knowledge, however, no reports have been published on the cut-off SUV to label a finding either normal or metastatic in ^{18}F-NaF PET/CT and ^{18}F-FDG PET/CT. The aim of this study is to determine SUVs from normal bones in ^{18}F-NaF PET/CT and ^{18}F-FDG PET/CT. **Materials and Methods:** Our study subjects were 7 patients who underwent ^{18}F-NaF PET/CT and ^{18}F-FDG PET/CT between April 2008 and July 2018 at our Hospital. In this study, normal bones were defined as those from which bone lesions such as cancer, fracture and metabolic bone diseases were excluded. We measured SUVmax and SUVpeak from the normal vertebral bodies of the cervical, thoracic, and lumbar vertebrae in 7 patients, and calculated mean SUVmax and SUVpeak, and coefficient of variation of each vertebral body. **Results:** The mean SUVmax and SUVpeak in ^{18}F-NaF PET/CT were 8.7 and 7.3 in the cervical vertebrae, 9.8 and 7.7 in the thoracic vertebrae, and 11.0 and 8.2 in the lumbar vertebrae, respectively. Those in ^{18}F-FDG PET/CT were 2.3 and 1.9 in the cervical vertebrae, 3.1 and 2.4 in the thoracic vertebrae, and 3.8 and 2.8 in the lumbar vertebrae, respectively. The coefficients of variation of SUVmax and SUVpeak in ^{18}F-NaF PET/CT were 0.27 and 0.24. Those in ^{18}F-FDG PET/CT were 0.28 and 0.27, respectively. **Conclusion:** Different normal vertebrae had different SUVs in ^{18}F-NaF PET/CT and ^{18}F-FDG PET/CT. The highest SUV was found in the lumbar vertebrae, followed in order by the thoracic and cervical vertebrae. It would be better to decide the cut-off values for each vertebral region. In order to decide the cut-off values to label a finding either normal or metastatic, both SUVmax and SUVpeak can be used. **References:** None.

TEPS-36

Verification of acquisition condition in dynamic imaging using continuous bed motion PET/CT

T. Umezawa, *T. Iimori, T. Murata, K. Sawada, Y. Masuda, T. Uno; Chiba University Hospital, Chiba, JAPAN.*

Aim/Introduction: PET/CT, which is capable of continuous bed motion (CBM) acquisition, can perform a wide range of dynamic acquisition, including Step & Shoot (SS). This method can be used with motion artifact of a patient or if the scan was aborted. If the scan suddenly stops, image noise increases due to the decrease in acquisition count. Thus, the use of normal reconstitution conditions could affect quantitative accuracy. In this study, we verified the optimal acquisition conditions in a dynamic collection using CBM. **Materials and Methods:** In this study, the PET/CT system used was the Biograph mCT Flow 20 R-4, manufactured by Siemens Healthineers (Erlangen, Germany). Physical evaluation of the dynamic acquisition was performed using the NEMA body phantom and image analysis software with the PET quality control tool, which was PET quact (Nihon Medi-Physics, Tokyo Japan). By reading several articles about dynamic acquisition methods, we determined that the dynamic acquisition pass number was seven. We calculated the contrast ratio (QNR_{10mm}) of the 10-mm hot sphere for the evaluation of both the Gaussian filter size and iteration and the subset number. Additionally, contrast ($Q_{H,10mm}$), background variability (N_{10mm}), contrast ratio (QNR_{10mm}), and Recovery Coefficient (RC) were calculated with and without image reconstruction at the time of flight and the point spread function. **Results:** Regardless of the Gaussian filter value, the noise tended to decrease gradually when greater than four sums, and the QNR_{10mm} exceeded the standard value when greater than four sums (the standard value of the Gaussian filter is less than 9 mm). In the evaluation of the recovery rate, four sums or greater showed a smaller value than did the standard. In the case of three sums or less, the 10-mm hot sphere could be identified by increasing the Gaussian filter value. However the 10-mm hot sphere could not be recognized at the Gaussian filter value of over 9 mm. **Conclusion:** By using the optimal acquisition conditions for each iteration number, we found that image quality that meets the criteria of image analysis values could be obtained even with passes of 4 sums or less. **References:** Yamamoto H, Takemoto S, Maebatake A, et al. Verification of image quality and quantification in whole-body positron emission tomography with continuous bed motion. Ann Nucl Med. 2019;33:288-294.

TEPS-37

Evaluation of Respiratory Motion Correction on Liver Kinetic Analysis for Dynamic PET Imaging

Y. Shao[1], *J. Wang*[2], *X. Wang*[2], *J. Cui*[3], *N. Li*[3], *L. Huo*[2], *H. Zhang*[1]; [1]*Department of Biomedical Engineering, Tsinghua University, Beijing, CHINA,* [2]*Department of Nuclear Medicine, Peking Union Medical College (PUMC) Hospital, Chinese Academy of Medical Science and PUMC, Beijing, CHINA,* [3]*SinoUnion (Beijing) Healthcare Technologies Co., Ltd, Beijing, CHINA.*

Aim/Introduction: In PET imaging, respiratory motion is known to cause reduced accuracy in the localization as well as the quantitation of PET abnormalities. However, its impact on dynamic PET imaging has not been adequately investigated. This study aims to evaluate the effects of respiratory motion correction on the liver kinetic analysis. **Materials and Methods:** Two patients with hepatic cancer, and two patients

with cholangiocarcinoma (one with liver metastases) after interventional therapy underwent 60-minute dynamic ^{18}F-FDG PET imaging after low-dose CT scan. All the patients' respiratory motion was recorded simultaneously using the Anzai respiration gating system. For each PET scan, 23 frames (10×60s, 5×120s, and 8×300s) were reconstructed using time-of-flight (TOF) ordered subsets expectation maximization algorithm (OSEM) without motion correction (NMC). To correct for respiratory motion (MC), list-mode PET data were sorted into 6 respiratory phases, and for each phase, 23 frames were reconstructed in the same way as described above. Two spherical regions of interest (ROIs), with 20mm diameter each, were placed manually in the normal tissue at the apex of liver (UpNor) and in the middle of liver (MidNor). Time activity curves (TACs) of the maximum standardized uptake value (SUV_{max}) were extracted. TACs of the 6 gated phases were averaged to obtain a MC TAC. Kinetic analysis was performed with a 2-tissue-compartment model using PMOD (PMOD Technologies Ltd, Zürich, Switzerland) to obtain K_1, k_2, k_3, and K_i for the NMC and MC cases respectively. **Results:** Obvious liver motion could be observed for all the patients in the gated dynamic PET images. For the UpNor and MidNor ROI, comparing the MC case to the NMC case, K_1 increased by 20.95%±34.24% and 12.88%±35.27% respectively; and k_3 decreased by 39.47%±16.08% and 13.80%±6.43% respectively; and K_i, equaling $k_1 \times k_3/(k_2+k_3)$, decreased by 34.67%±13.91% and 17.34%±6.40% respectively. **Conclusion:** Respiratory motion can be clearly observed in dynamic PET imaging. With MC, the obtained kinetic parameters changed substantially compared with the NMC cases. Continued studies will be carried out in the future to include more clinical data. **References:** Choi Y, Hawkins R A, Huang S C, et al. Evaluation of the effect of glucose ingestion and kinetic model configurations of FDG in the normal liver. J Nucl Med. 1994;35:818-823. Yu Y, Chan C, Ma T, et al. Event-by-event continuous respiratory motion correction for dynamic PET imaging. J Nucl Med. 2016;57:1084-1090.

TEPS-38

Bayesian penalized-likelihood reconstruction algorithm in the advanced digital PET/CT system for 18F-NaF PET/CT in morbidly obese patients

M. Al-Daas[1], *L. Ali*[2], *A. Sasikumar*[3], *A. Esmail*[3], *F. Marafi*[3];
[1]*Jaber Al-Ahmad Center for Molecular Imaging, Shuwaikh, KUWAIT,* [2]*Kuwait universty, Jabriya, KUWAIT,* [3]*Jaber Al-Ahmad center for molecular imaging, Shuwaikh, KUWAIT.*

Aim/Introduction: Q.Clear, a Bayesian penalized-likelihood reconstruction algorithm for PET, was recently introduced by GE Healthcare on their PET scanners to improve clinical image quality and quantification. Our aim in this work is to determine the optimum penalization factor (beta) for clinical use of Q.Clear using advanced PET/CT system and compared it with the standard PET reconstructions. **Materials and Methods:** Ten morbidly obese patients (body mass index, 45.28 ± 4.45 kg/m2) referred for NaF PET-CT for evaluation of bone metastases were retrospectively analyzed. All the patients underwent a whole body 18F-NaF PET/CT scan using an advanced digital PET/CT system (GE Discovery MI) in JACMMI. All the patients were injected with 0.06 mCi/kg of 18F-NaF using a digital injector and imaged at 60 minutes post injection. Images were acquired for 2 minutes per bed and then reconstructed using Bayesian penalized likelihood reconstruction (Q.Clear) with different beta (β) value of 200, 400, 600, 800 and 1000. Signal-to-noise-ratio were measured in the third lumbar vertebra and in a representative lesion and were reviewed along with the visual quality of the images. The images were assessed by two different senior nuclear medicine physicians for the image quality for the different reconstructions. **Results:** All ten patients had interpretable 18F-NaF studies using conventional reconstruction. Both the nuclear medicine physicians had consensus opinion on the quality of the images obtained with the different beta values of reconstruction using Q.Clear reconstruction. All the Q.Clear reconstructions with various beta values had image quality comparable with conventional reconstructions. Reconstructions with beta values of 200, 400 and 600 gave noisier images. Images reconstructed with beta values of 1000 had excessively smooth images which the nuclear medicine physicians felt could affect the interpretability when compared with the conventional reconstruction. The SNR values progressively increased with increase in beta value. Q.Clear reconstructions with beta value of 800 gave the best image quality. **Conclusion:** Q.Clear reconstructions with beta value of 800 gives the best image quality while imaging morbidly obese patients using 18F-NaF. **References:** 1. Teoh EJ, McGowan DR, Macpherson RE, Bradley KM, Gleeson FV. Phantom and Clinical Evaluation of the Bayesian Penalized Likelihood Reconstruction Algorithm Q.Clear on an LYSO PET/CT System. 2. Usmani S, Marafi F, Ahmed N, Esmail A, Al Kandari F, Van den Wyngaert T. Diagnostic Challenge of Staging Metastatic Bone Disease in the Morbidly Obese Patients: A Primary Study Evaluating the Usefulness of 18F-Sodium Fluoride (NaF) PET-CT.

TEPS-39

Influence of statistical fluctuation on the accuracy and stability of SUV and TBR - A phantom study

X. Xie*, M. Yun, H. Mi, X. Zhang;*
Department of Nuclear Medicine, Beijing Anzhen Hospital, Beijing, CHINA.

Aim/Introduction: The aim of this study was to evaluate the impact of statistical fluctuation on the accuracy and stability of SUV and TBR using phantom data. **Materials and Methods:** The image quality phantom with 4 hot spheres and 2 cold spheres in warm background was scanned. The activity ratio of the hot spheres to the background was 4:1. The PET data were acquired in list mode for 1800s, from which data were extracted to generate 10 images with different pixel sizes for each of the 60_s, 90_s, 120_s, 150_s, 180_s scanning times. Different scanning times correspond to different statistical fluctuation. SUVs (SUVmax and SUVpeak) and TBRs (TBRmax-max, TBRmax-avg, TBRpeak-peak and TBRmax-peak) of the three hot spheres

(diameter of 22 mm, 17 mm, 13 mm) were calculated. The relative differences (RD) between these quantitative values and their references were also calculated to evaluate the accuracy and reliability of these metrics under different noise levels. **Results:** The SUVs of the background were overestimated as the scan duration was shortened, especially for images with small pixel size. The RD of SUVmax with the pixel size of 2mm×2mm had the range of 87%-186% (corresponding scan duration of 180_s and 60_s). The SUVpeak was more stable than SUVmax, with the RD range of 30%-50%. For hot spheres, the SUVmax had similar but weaker trend as that of the background. The SUVmax of hot spheres had the RD range of 44-69%, 34-46% and 36-46% respectively. The SUVpeak of hot spheres had the RD range of 12-15%, -1-1% and -14--13%. As the TBRs, TBRmax-peak was the most accurate value under different statistic noise. The TBRmax-peak of 13-mm-diameter sphere which represents small lesions had the RD range of -2%-6%. TBRmax-max was generally underestimated and increased as the scan time and pixel size increased. TBRmax-max of 13-mm-diameter sphere had the RD ranged from -47% to -27%. TBRmax-avg was overestimated as the scan duration was shortened, which had the same tendency as the SUVmax. **Conclusion:** The SUVmax was overestimated as the scan time and pixel size decreased which gave rise to image noise. SUVpeak was less sensitive to image noise and had higher reproducibility and reliability under different statistical fluctuation. The TBRmax-peak is the most accurate and stable metric among a wide variety of TBR. **References:** None.

TEPS-40

Optimization of image reconstruction for rapid image acquisition by ^{18}F-NaF bone PET: Comparison of OSEM and Bayesian penalized likelihood algorithms

T. Yoshii[1], *K. Miwa*[1], *K. Wagatsuma*[2], *M. Yamaguchi*[1], *M. Suga*[1], *Y. Kamitaka*[1], *T. Yamao*[1], *S. Hiratsuka*[1];
[1]*International University of Health and Welfare, Tochigi, JAPAN,* [2]*Tokyo Metropolitan Institute of Gerontology, Tokyo, JAPAN.*

Aim/Introduction: The Bayesian penalized likelihood reconstruction algorithm (BPL), commercially marketed as Q.Clear (GE Healthcare), is a reconstruction algorithm that allows for a full convergent iterative reconstruction leading to better image quality and quantitative accuracy while limiting noise. The BPL has been optimized as a reconstruction parameter for PET images with various tracers, but ^{18}F-NaF bone PET has not yet been evaluated. The present study aimed to determine the optimal image reconstruction of OSEM and BPL for rapid ^{18}F-NaF PET image acquisition. **Materials and Methods:** A custom-designed body phantom consisting of lung, soft tissue, normal spine, and a model metastatic bone tumor was scanned using a Discovery MI (GE Healthcare). The phantom allows optional adjustment of the activity distribution, tumor size and line attenuation coefficient. Bone PET images were reconstructed using OSEM + PSF + TOF (1 to 16 iterations, 17 subsets and a 4-mm Gaussian filter), BPL + TOF (β = 200 - 700) and scan durations of 30 to 120 (30, 45, 60, 90 and 120) seconds. We calculated signal to noise ratios (SNR) and contrast as indicators of image quality, recovery coefficients (RC) and count rate characteristics as indicators of quantitative accuracy. **Results:** At a scan duration of 120 sec, the optimal reconstruction parameters of OSEM + PSF + TOF and BPL+TOF were two iterations and β = 400, respectively. At 90 sec, SNR and contrast reconstructed using BPL + TOF increased by 24% and 18%, respectively, at the same noise level of OSEM + PSF + TOF applied to the optimal reconstruction. The BPL + TOF was superior to OSEM + PSF +TOF in terms of RC and count rate characteristics regardless of ^{18}F-NaF PET scan duration. The quantitative performance of BPL + TOF was better than OSEM + PSF + TOF because measured values of BPL + TOF were close to true values in terms of count rate characteristics. **Conclusion:** The present study determined the optimal reconstruction parameters for ^{18}F-NaF Bone PET at various acquisition durations. Our results suggested that BPL + TOF (β = 400) can maintain excellent image quality and quantitative accuracy over a shorter duration of acquisition. **References:** None.

TEPS-41

Development of a fully automatic analytical program for the ^{123}I- MIBG myocardial uptake measurement method

R. Sako[1], *Y. Uchiyama*[2], *Y. Kamiya*[3,1], *S. Ito*[2];
[1]*Graduate school of health sciences, Kumamoto University, Kumamoto, JAPAN,* [2]*Faculty of Life Sciences, Kumamoto University, Kumamoto, JAPAN,* [3]*Chibana Clinic, Okinawa, JAPAN.*

Aim/Introduction: Iodine-123 metaiodobenzylguanidine (^{123}I-MIBG) has been used to evaluate the cardiac sympathetic nerve in Lewy body diseases (LBDs) including Parkinson's and dementia with Lewy bodies. We recently developed a new method for ^{123}I-MIBG myocardial uptake measurements. However, this method is time-consuming because it uses several nuclear medical image analytical programs and requires manual operations. Therefore, a fully automatic analytical program is required to improve reproducibility, shorten operation time, and simplify analytical operations. The purpose of this study is to develop a fully automatic program for the ^{123}I- MIBG myocardial uptake measurement method. **Materials and Methods:** The ^{123}I-MIBG uptake index was calculated by dividing the output function by the input function. The input function was determined using the administered dose obtained by analyzing the count-time activity curve (TAC) of the pulmonary artery (PA) on dynamic chest images. The automatic region of interest (ROI) setting program for the PA was developed based on an image phase analysis of dynamic chest images. The integrated counts were obtained from the area under the curve (AUC) of the TAC on the PA-ROI, which was fitted using the gamma function. The gamma function fitting program based on mixed gamma distributions was developed using an expectation-maximization algorithm that analyzed the time activity curve of dynamic chest images. The output function was determined by the ^{123}I-MIBG single-photon computed-tomography counts on the polar map created by an automatic program that employs

circumferential analysis of short-axis images. To confirm the clinical usefulness of this program, 77 patients were examined using the automatic method and the results were compared with those obtained through the manual method. **Results:** The coincidence ratio between the location of the PA-ROI by the automatic program and that by manual methods was 90.4%. A good correlation was observed between the ^{123}I-MIBG myocardial uptake values obtained by the automatic and manual setting methods. The repeatability and reproducibility of the input function determination operations dramatically improved when using the automatic program. The time required for fitting analysis using the automatic method was 2-3 s as compared to 10 min for the current analytical method. **Conclusion:** We developed a fully automatic myocardial uptake quantification analytical program for the ^{123}I-MIBG myocardial uptake quantification method. This program contributes to improving reproducibility and reducing the time of analysis of the method. **References:** None.

TEPS-42

Accuracy of Planar Scan based and SPECT/CT based Quantification Methods in Bone Scintigraphy

D. Sercic[1,2], *A. Doma*[1], *I. Zagar*[1], *D. Skrk*[3];
[1]*Institute of Oncology Ljubljana, Ljubljana, SLOVENIA,* [2]*Faculty of Health Sciences, University of Ljubljana, Ljubljana, SLOVENIA,* [3]*Slovenian Radiation Protection Administration, Ljubljana, SLOVENIA.*

Aim/Introduction: Main purpose was to compare the results of the planar scan based and SPECT/CT based technique of activity quantifications and to determine the existence of possible correlations. In addition, to determine the potential impact of different patient based or acquisition dependent variables. **Materials and Methods:** The retrospective study included 90 osteoblastic skeletal lesions in 66 patients (30 males, 36 females) who had planar whole body bone scintigraphy and regional SPECT/CT performed at our institution between November 2017 and December 2018. Mean age of patients was 63 (17 - 89) years. Mean BMI was 28.7 (20.1 - 36.9) kg/m². The mean time between planar scan and SPECT/CT was 52 (22 - 166) min. The activity in lesions on planar images was calculated from measured activity in two opposite 2D projections against a known activity (standard source): $[ACTIVITY_{lesion}/((COUNTS_{lesionAP}-COUNTS_{bgdAP})+(COUNTS_{lesionPA}-COUNTS_{bgdPA}))/2=ACTIVITY_{std}/((COUNTS_{stdAP}-COUNTS_{bgdAP})+(COUNTS_{stdPA}-COUNTS_{bgdPA}))/2]$. Data was corrected for radioactive decay, absorbed and scattered counts accordingly. The commercially available SPECT/CT Q.Metrix quantification software (GE Healthcare inc.) was used to calculate quantification in SPECT/CT (3D) data. Several variables were analyzed: patient's gender, age, body mass index (BMI), measured activity in lesion (% of injected activity), time between application of radiopharmaceutical and the beginning of data acquisition, time between planar and SPECT data acquisition. Wilcoxon test of 2 samples was used for comparison of two methods of quantification. Depending on the data normality, independent samples T - test and Mann-Whitney U test were used to determine potential impact of different variables. **Results:** The difference between two quantification methods was statistically significant ($p \leq 0.001$). Difference in quantification between two methods (Mean ± STD) was 16.9% ± 28.2 (absolute difference 27.8 ± 17.3). There was a strong linear correlation between both quantification methods (the Pearson correlation value = 0,952). Based on linear regression analysis, the model was defined ($Q_{SPECT}=-0.032+1.536\times Q_{Planar}$; $R^2=0.91$) to predict the result of one method of quantification using the result of the second method. The level of measured activity in skeletal lesion affected the difference in results between both quantification methods ($p=0.008$). Other tested variables were not statistically significant. **Conclusion:** The difference between two methods of activity quantification was statistically significant. Quantifications based on planar scans and SPECT acquisition were in strong linear correlation. Quantification results are however unreliable in lesions with high osteoblastic activity on bone scans. Quantification of activity in skeletal osteoblastic lesions is independent of other tested variables. **References:** None.

TEPS-43

Evaluation of cingulate island sign ratios for the differentiation of dementia with Lewy bodies versus Alzheimer's disease using ^{123}I-IMP SPECT

N. Hayashi, *Y. Murata, A. Hirota, N. Akagi, H. Iwasa, K. Ito, H. Kazui, T. Yamagami;*
Kochi Medical School Hospital, Nankoku, JAPAN.

Aim/Introduction: Preserved activity in the posterior cingulate gyrus relative to the precuneus is called the cingulate island sign (CIS), which has been reported as a characteristic finding in dementia with Lewy bodies (DLB). Recently, the CIS ratio has been suggested to differentiate DLB from Alzheimer's disease (AD). The CIS ratio using ^{18}F-FDG PET or ^{99m}Tc-ECD SPECT, could be useful; however, that by ^{123}I-IMP SPECT has not been established. Therefore, the goals of this study were as follows: 1) to optimize image reconstruction and volume of interest (VOI) placement for calculating the CIS ratio, and 2) to determine the accuracy and cut-off value for ^{123}I-IMP SPECT. **Materials and Methods:** Seven patients with DLB and 17 patients with AD (including probable) underwent ^{123}I-IMP SPECT in this retrospective study. SPECT imaging was performed for 28 minutes after ^{123}I-IMP administration. Five images were generated using different image reconstruction methods (Flash 3D™ and FBP) and different correction methods (attenuation and scatter). Each image was evaluated by 3 VOIs. The CIS ratios were calculated as a ratio of posterior cingulate to occipital activity. The CIS ratio to distinguish DLB from AD was evaluated using the area under the curve (AUC) of the receiver operating characteristic (ROC). **Results:** The largest values for the AUC and accuracy were obtained from Flash 3D (CTAC+, SC+) and FBP (Chang+, SC+). The cut-off value, AUC, and accuracy were 0.901, 0.765, 83.3% and 0.936, 0.790, 79.2%, respectively. **Conclusion:**

Our results would provide a foundation for use of the CIS ratio on ^{123}I-IMP SPECT. The CIS ratio on ^{123}I-IMP SPECT could be useful with a cut-off value of 0.901 using Flash3D (CTAC+, SC+) in our institution. **References:** None.

TEPS-44

Introduction of a New 3D Analysis for the DATscan and the Realisation of a larger and more up to date Reference Set

A. Gelderblom[1], *P. Brinks*[2], *J. Habraken*[1], *J. Lavalaye*[1], *J. Salcedo*[1], *M. Vredenduin*[1];
[1]*St Antonius Hospital, Nieuwegein, NETHERLANDS,*
[2]*Diakonessenhuis, Utrecht, NETHERLANDS.*

Aim/Introduction: Dopamine transporter (DAT) scan analysis is now performed using a 2D software package with regions of interest in caudate nucleus and putamen. This requires several manual acts and is laborious and time-consuming. Manual processing may also cause differences in outcome due to inter-observer variance. A new software package - the BRASS analysis - can execute a fully automated 3D analysis. This project was set up to implement this new analysis. **Materials and Methods:** We selected a consecutive series of 149 patients with DAT scans between 2014 and 2016, allowing for at least two years of follow-up. The final diagnosis of the neurologist was used as a gold standard. 59 patients were clinically diagnosed with Parkinson's disease (PD), 65 were labelled normal. We excluded 25 patients, mostly because of a different diagnosis. The 124 patients were analysed with the BRASS programme. We related the resulting uptake values of the normal scans to the patient's age. With these results, we created four trend lines with a confidence interval of 2 SD. We then plotted the PD scans against these trend lines to assess how many would fall within the confidence interval. **Results: Conclusion:** The new BRASS method provides a semi-quantitative analyses that gives results matching clinical outcome but without the manual manipulations. This diminishes inter-observer variance and will therefore improve outcome reliability. **References:** None.

804-3

Technologists: Technologist e-Poster Presentation Session 3

Monday, October 14, 2019, 11:30 -13:00 Meeting Room 130

TEPS-45

Cut-Off Frequency Optimization on Hot Bone Spine Lesions in 99mTc-HDP SPECT-CT

C. Ferreira, *C. Low*, *N. Rao*, *J. Cullis*;
University Hospital of Coventry and Warwickshire, Coventry, UNITED KINGDOM.

Aim/Introduction: Bone scans are the most commonly used imaging protocol in nuclear medicine. SPECT-CT is used to provide anatomic localisation of the detected lesions and has higher sensitivity than planar imaging alone. It also has a lower cost than PET-CT. When optimising SPECT-CT it is important to consider the reconstruction process because of the degrading imaging effects, like attenuation, scatter and depth-dependent resolution. The aim is to investigate the effects of varying cut-off frequencies on the contrast, signal-to-noise ratio and visual analysis whilst maintaining the order of the Butterworth filter constant. **Materials and Methods:** SPECT-CT bone scans are locally acquired on a GE Discovery 670 using a 20% energy window centred at 140 keV, LEHR collimators, 120 projections and 25 seconds per projection. These images are reconstructed using an iterative algorithm (2 iterations and 10 subsets) and filtered using a Butterworth filter (cut-off and order of 0.48 cycles.cm^{-1} and 10 respectively). The SPECT-CT images from 25 patients (12 males, 13 females, average age of 61.5±13.9 years) with spine lesions were reconstructed with different Butterworth frequency cut-offs (0.38, 0.48 and 0.68 cycles.cm^{-1}) and compared. Images were compared both subjectively by three consultants and quantitatively using contrast and signal-to-noise ratio. **Results:** The contrast increased significantly ($p<0.005$), but the signal-to-noise ratio decreased significantly ($p<0.005$) when the cut-off frequency was increased. Subjective assessment by three consultants inferred that the cut-off frequency of 0.68 cycles.cm^{-1} was considering optimal as this cut-off allowed for the detection of more lesions. The size of the lesions was also taken into consideration. Lesions with a larger size had increased contrast and a decreased signal-to-noise ratio, with the opposite being verified for small lesions. **Conclusion:** Before selecting the cut-off frequency it is important to take into account the size, intensity and localisation of the lesion. Image quality and clinical analysis of the images were found to be improved with a cut-off of 0.68 cycles.cm^{-1} in patients with spine lesions as it increased the number of detected lesions and the contrast of the images. **References:** Sayed, Inayatullah Shah & Syahirah Mohamed Nasrudin, Nor. (2016). Effect of Cut-Off Frequency of Butterworth Filter on Detectability and Contrast of Hot and Cold Regions in Tc-99m SPECT. International Journal of Medical Physics, Clinical Engineering and Radiation Oncology. 5. 100 -109. 10.4236/ijmpcero.2016.51011.

TEPS-46

The Influence Of Attenution Correction On The Image Quality In Single Photon Emission Computed Tomography

S. Rep[1], *N. Frelih*[1], *L. Lezaic*[1], *J. Zibert*[2];
[1]*University Medical Centre Ljubljana, Ljubljana, SLOVENIA,* [2]*Faculty of Health Sciences, University of Ljubljana, Ljubljana, SLOVENIA.*

Aim/Introduction: Attenuation has a strong influence on the data and consequently on the quality of the image. Attenuation correction corrects the weakening of the rays in various depths. The non-diagnostic, low-dosage CT is usually used for the attenuation correction when the images are taken with the

SPECT/CT. The aim of this master's thesis is to find out how the attenuation correction in the case of the SPECT/CT influences the quality of the image. **Materials and Methods:** The Phantom NEMA IEC BodyPhantom was filled with the isotope technetium-99m. Eight images were captured, each with a different ratio of the specific activity between the phantom background and the spheres. The images were reconstructed in the program called Oasis by three different reconstructions: the filtered back projection, the non-corrected iterative reconstruction, and with the attenuation correction using the CT. The number of counts in the background and in all six spheres was measured. This was followed by the comparison of the contrast in images that were reconstructed using different methods. According to evaluated data, appropriate statistical analyses were performed: descriptive statistic, repeated measures ANOVA and Wilcoxon signed-rank test were conducted in Matlab. **Results:** On the images that were processed by the filtered back projection or the iterative reconstruction, the background is not homogeneous. On the images that were corrected using the CT, the number of counts is evenly spread across the entire background of the phantom, thus making the background homogeneous. The statistical analysis showed that contrast is typically significantly divergent among the different methods of reconstruction ($p < 0.005$). **Conclusion:** It was discovered that the increase in the number of counts, and consequently the image contrast, is proportional to the size of the sphere, and to the increased ratio of activity between the background and the sphere with all three types of reconstruction. The CT-AC images have the best contrast; images with iterative reconstruction are second best; images processed by the filtered back projection are third. Because the CT-AC images are of better quality than the non-corrected images, it is recommended that the CT-AC be used for all tests; however, due to the removal of artefacts caused by attenuation correction, it is also important to examine the non-corrected images every time. **References:** Grosser O S, Kupitz D, Ruf J et al. (2015). Optimization of SPECT-CT Hybrid Imaging Using Iterative Image Reconstruction for Low-Dose CT: A Phantom Study.

TEPS-47

Usefulness of partial volume effect correction in ^{201}Tl/^{123}I dual-isotope myocardial SPECT on CZT-SPECT camera

D. Ichioka[1], *S. Shiraishi*[2], *S. Tomiguchi*[3];
[1]*Graduate School of Health Science, Kumamoto, JAPAN,*
[2]*Kumamoto University Hospital, Kumamoto, JAPAN,*
[3]*Faculty of Life Sciences, Kumamoto, JAPAN.*

Aim/Introduction: A cadmium zinc telluride (CZT) detector single photon emission computed tomography (SPECT) device (CZT camera) has better energy resolution than a conventional NaI detector SPECT device, so it is reported its usefulness on dual-radionuclide imaging. However, affect of partial volume effect (PVE) to quantitative assessment of the myocardial radioactivity has not been evaluated enough. The aim of this study was to evaluate the usefulness of PVE correction for the estimation of ^{201}Tl and ^{123}I myocardial radioactivity in ^{201}Tl/^{123}I dual-isotope myocardial SPECT using CZT-SPECT camera by phantom study. **Materials and Methods:** ^{201}Tl, ^{123}I and ^{201}Tl+^{123}I water solutions were injected into the various sizes of rods in rod phantom and myocardial part of a chest myocardial phantom, respectively. SPECT data were acquired with list mode using a CZT-SPECT camera (Discovery NM 530c, GE). Each SPECT image was reconstructed with CT attenuation correction and scatter correction using triple energy window (TEW) method. Recovery coefficient (RC) curve for full width at half maximum (FWHM) was obtained from rod phantom images, and PVE correction was performed using RC corresponding to FWHM of the myocardial wall thickness using myocardial part in the chest phantom. The relative error was calculated by using the estimated value of myocardial radioactivity concentration and the measured true value. **Results:** Underestimation of myocardial radioactivity concentration was observed in under 20mm diameter of ^{201}Tl and ^{123}I rods. Relative error after PVE was within 10% between the estimated and true value of each rod size. **Conclusion:** PVE correction using RC in addition to attenuation and scatter correction was suggested to be useful for quantitative estimation of myocardial radioactivity in ^{201}Tl/^{123}I dual-isotope myocardial SPECT. **References:** None.

TEPS-48

The Evaluation of the impact of ^{99m}Tc gamma rays on x-ray detectors during a CT low dose acquisition

A. Resende Geao, *A. Santos;*
Hospital CUF Descobertas, Lisboa, PORTUGAL.

Aim/Introduction: The objective of this study was to study the potential impact of gamma photons with energy of 140Kev from ^{99m}Tc decay in ^{99}Tc, in CT for anatomical reference or for attenuation correction, considered low dose CT. Both x-ray and gamma ray are electromagnetic radiation and both have similar chemical and physical characteristics. With the newest SPECT/CT equipment installed on our Nuclear Medicine department we wanted to evaluate the impact of gamma rays on x-ray detectors during SPECT/CT and the possibility of gamma-generated noise on CT images. **Materials and Methods:** To evaluate the contribution of photons from technetium, gamma photons with an energy of 140 kV, in low dose CT, when a SPECT / CT is performed. Acquisitions were made in every combinations possible of mA and kV for the new GE 850. First with the phantom filled with water and then 740MBq (20mCi) of ^{99m}Tc were added and the same acquisitions were performed. The study was performed on our Gamma Camera (SPECT/CT) with the Jaszczak Phantom. **Results:** After reviewing the images for each acquisition parameter of low dose CT, with and without ^{99m}Tc activity, no significant different values were found in any of these images. These results suggest that any scattered radiation emitted from the phantom was eliminated and excluded by CT detectors. **Conclusion:** Although theoretically unlikely for gamma rays to affect CT acquisition, this study was performed to test the possibility that gamma rays can cause increased noise on CT images. After reviewing the images and comparing

hounsfield units and the standard deviation of the ROI values, no obvious noise was found. The number of x-ray photons is very high compared with gamma photons even for the low dose CT aqqisition and a high ^{99m}Tc activity. **References:** None.

TEPS-49

The effect of metal artifact reduction on quantitative SPECT/CT imaging

T. Konishi[1], *T. Shibutani*[2], *K. Okuda*[3], *H. Yoneyama*[1], *R. Moribe*[1], *M. Onoguchi*[2], *K. Nakajima*[4], *S. Kinuya*[5];
[1]*Department of Radiological Technology, Kanazawa University Hospital, Kanazawa City, JAPAN,* [2]*Department of Quantum Medical Technology, Institute of Medical, Pharmaceutical and Health Sciences, Kanazawa University, Kanazawa City, JAPAN,* [3]*Department of Physics, Kanazawa Medical University, Kahoku-gun, JAPAN,* [4]*Department of Functional Imaging and Artificial Intelligence, Kanazawa University, Kanazawa City, JAPAN,* [5]*Department of Nuclear Medicine, Kanazawa University Hospital, Kanazawa City, JAPAN.*

Aim/Introduction: Metal implants have been proven to cause severe artifacts on computed tomography (CT) images, which can affect CT attenuation correction (CTAC) for quantitative single-photon emission computed tomography (SPECT)/CT. Several studies have reported that metal artifact reduction (MAR) technology has improved image quality of CT and the quantitative accuracy of the standardized uptake values (SUVs) of positron emission tomography /CT. Recently, MAR technology has been introduced for SPECT/CT and may prove to be useful. This study aimed to evaluate the effect of MAR on quantitative SPECT/CT. **Materials and Methods:** We used an elliptic cylinder phantom filled with Tc-99m uniform solutions in which two artificial hip prostheses were set to acquire SPECT/CT images. Radiotracer concentration was 64.7 kBq/ml. The artificial joints comprised femoral stem, femoral head, and acetabular components, which were made of metal alloy. SPECT/CT images were reconstructed using CT data processed with and without MAR for CTAC. Quantitative SPECT/CT images with and without MAR were created and compared. Total 44 circular regions of interest (ROIs) were set on the CT and SPECT/CT images with a diameter of 13.5 mm (5.0 pixels). Fourteen ROIs were placed in the dark streak areas in which Hounsfield units (HUs) could be underestimated, 19 in the white streak areas in which HUs could be overestimated, and 11 in the non-artifact areas. We compared mean SUVs (SUV_{means}) obtained from quantitative SPECT/CT images with and without MAR to evaluate the effect of MAR on quantitative SPECT/CT. **Results:** There was a remarkable reduction in metal artifacts on CT images processed with MAR. For ROIs in the dark streak areas, the use of MAR increased SUV_{mean} from 0.91 ± 0.15 to 1.03 ± 0.06 ($P < 0.001$), whereas for ROIs in the white streak areas, the use of MAR decreased SUV_{mean} from 1.07 ± 0.05 to 1.04 ± 0.05 ($P < 0.001$). There was no significant difference in SUV_{mean} with and without MAR in the non-artifact areas. We observed errors in SPECT/CT quantification from −29.1% to +16.7% without MAR, depending on the ROI localization. When MAR was used, these errors were reduced to a range between −7.45% and +13.1%. **Conclusion:** Results of this study indicated that MAR could improve the quantitative accuracy of SPECT/CT. MAR can serve as a practicable technique for quantitative SPECT/CT in patients with metal implants. **References:** None.

TEPS-50

Performance Evaluation of a New Collimator Optimized for ^{177}Lu Preclinical SPECT Imaging

N. Colpo[1], *C. Uribe*[1], *J. Rousseau*[1], *C. Kamphuis*[2], *F. Beekman*[2,3], *F. Bénard*[1,4];
[1]*BC Cancer, Vancouver, BC, CANADA,* [2]*MILabs B.V., Utrecht, NETHERLANDS,* [3]*Delft University of Technology, Delft, NETHERLANDS,* [4]*University of British Columbia, Vancouver, BC, CANADA.*

Aim/Introduction: There is growing interest in radiopharmaceutical development for radioligand therapy; ^{177}Lu is a popular radioisotope for this purpose. This study aims to design and evaluate a new collimator optimized for ^{177}Lu imaging. Performance was also evaluated for other isotopes. **Materials and Methods:** We designed a collimator (XUHS-BM) for the MILabs U-SPECT^{+}/CT with a larger bore to accommodate bigger/mature mice with subcutaneous xenografts. An increased bore thickness was used to reduce penetration from higher energy gammas. Qualitative Jaszczak hot rod phantom and quantitative line sources (0.38mm diameter) with ^{99m}Tc, ^{177}Lu, ^{111}In and ^{67}Ga were scanned for 1h using a rat/mouse collimator (UHR-RM, previously used to image larger mice) and the new XUHS-BM. Images were reconstructed (20% wide photopeak windows: ^{99m}Tc (140kev), ^{177}Lu (208keV), ^{111}In (173 and 247keV), ^{67}Ga (93, 184 and 300keV) using the similarity regulated ordered subset expectation maximization algorithm (64 subsets, 3 iterations) with scatter correction and 0.4mm voxel size. Spatial resolution was determined by visually inspecting the rods in the Jaszczak image (0.85, 0.95, 1.1, 1.3, 1.5, 1.7mm) and by calculating the full width half maximum (FWHM) of the line sources. The energy spectra of different bed positions from uniform cylinder scans were added to determine the total detected events for each photopeak. The total events, measured activity, and scan time provided the sensitivity in cps/MBq. The system energy resolution of each photopeak in the energy spectrum was determined by calculating the FWHM. **Results:** The spatial resolutions of XUHS-BM were 0.7mm (^{99m}Tc), 0.8mm (^{67}Ga) and 0.9mm (^{177}Lu, ^{111}In). Rods in the Jaszczak were better visualized with XUHS-BM than UHR-RM images, due to improved count statistics. The sensitivity of XUHS-BM was 3.6 times greater for ^{99m}Tc, ^{111}In and ^{177}Lu and 2.1 times greater for ^{67}Ga compared with UHR-RM. System energy resolutions for each photopeak/isotope slightly improved with the XUHS-BM compared to the UHR-RM (from 10.3% to 9.8% for ^{177}Lu, 208keV). Significant improvements in image quality were seen including ^{177}Lu at low activity levels. **Conclusion:** A custom-designed collimator showed higher sensitivity and excellent qualitative

spatial resolution compared to a rat/mouse collimator, resulting in superior image quality for a variety of radiopharmaceuticals. Improved system energy resolution could be due to lower septal penetration. Our results suggest that the new XUHS-BM collimator is an interesting alternative to image larger mice with SPECT radioisotopes using low levels of injected activity. **References:** None.

TEPS-51

Repeatability and stability evaluation of ^{177}Lutetium quantification

***M. C. Dekker**, D. M. V. Huizing, B. J. de Wit - van der Veen;*
Antoni van Leeuwenhoek, Amsterdam, NETHERLANDS.

Aim/Introduction: The aim of this study is to evaluate the repeatability and stability of ^{177}Lutetium (^{177}Lu) quantification on our Siemens Symbia TruePoint SPECT-CT. **Materials and Methods:** A vial (~20 ml) with a known amount of ^{177}Lu was positioned next to the patient during post-therapy planar gamma and SPECT-CT acquisitions, after intravenous injection of 7400 MBq ^{177}Lu-DOTATATE. Planar gamma images acquired 0.5, 4, 24 and 72 hours post-injection were used for repeatability evaluation. A ROI with a diameter of 5 cm was drawn in the middle of the vial on both posterior and anterior view to determine the sum of the counts. Accordingly, the geometric mean was calculated to correct for different detector distances. The geometric mean was correlated to the activity in the vial at the time of the acquisition. SPECT-CT scans performed 24 hours after injection were used to evaluate quantification stability over time. A cylindrical VOI with a diameter of 4cm radius was drawn around the vial and the sum of counts in the VOI was compared with the activity in the vial at the time of acquisition. All analysis was performed using PLANET Onco (DOSIsoft, Cachan, France). **Results:** Planar imaging series of 9 patients were used to assess quantification repeatability, with a mean activity of 94.1 MBq (range 39.4-141.6) in the vials. The first scan at 0.5h post-injection was used as the reference time point. A mean difference of 13.7% between the first and all other scans was observed, with differences ranging from 0.4% to 51.4%. A total number of 36 SPECT-CT scans (of which 24 were usable) performed between March 2016 and January 2019, were used to evaluate quantification stability. The mean activity in the vials was 72.4 MBq (range 30.0-122.0). The quantification stability assessment shows a steady line between the know amount of radioactivity and measured sum of counts over time, with a coefficient of variation of 6.8%. Two vials with high amounts of radioactivity (122.0 and 104.4 MBq) both underestimated the mean ratio between count and activity in de vial. **Conclusion:** Vial measurements on planar and SPECT-CT imaging showed repeatable and stable quantification for ^{177}Lu during three years. These results indicate that quantification with our Siemens Symbia TruePoint SPECT-CT is suitable for potential dosimetric analysis. This method is a reliable way to determine the stability of the camera. **References:** None.

TEPS-52

Agreement between functional parameters of myocardial perfusion assessed with gated IQ-SPECT and conventional SPECT/CT

***W. Martínez**, V. Poblete García, E. Noriega Álvarez, E. Casillas Sagrado, A. García Vicente, Á. Soriano;*
Servicio de Medicina Nuclear. Hospital General Universitario de Ciudad Real, Ciudad Real, SPAIN.

Aim/Introduction: Aim: to compare values obtained with gated IQ-SPECT system with those obtained with a conventional device with low-energy high-resolution (LEHR) collimators. **Materials and Methods:** Methods: we prospectively evaluated 28 patients [mean age= 52.8-year-old (18-80), 27 men], with suspected coronary artery disease. All patients underwent a myocardial perfusion study (only stress for 24 patients and stress+rest for 4 patients) using both gamma-cameras consecutively. Each patient underwent a single injection of 20mCi of ^{99m}Tc-tetrofosmin. IQ-SPECT was equipped with Smartzoom collimators and images were acquired over 208º cardio-centric orbit with 17 views per detector and 9 seconds/view, zoom of 1, matrix of 128x128 and tolerance window of 40%.The conventional gamma-camera equipped with LEHR collimators was considered as the reference method. Gated-SPECT images were acquired over 180º thoraco-centric orbit, with 60 views of 35 seconds, matrix of 64x64, zoom of 1.3 and tolerance window of 40%. Uncorrected images and corrected (by CT) images were obtained.Mean and SD values of left ventricular ejection fraction (LVEF), end-systolic (ESV) and end-diastolic volumes (EDV) and SDs were calculated for each method. Mann-Whitney was performed to compare the values obtained with both techniques. p-values <0.05 were considered statistically significant. **Results:** Results: the total acquisition time was around 5 minutes using the IQ-SPECT, being shorter than 20 minutes used with conventional technique. The perfusion images were normal in all patients and they were similar with both techniques.The mean of LVEF, ESV and EDV obtained with conventional technique and IQ-SPECT were respectively: LVEF = 52.9% (49.2-56.6) and 48.1% (43.8-52.4); EDV = 114.8ml (100.9-128.7) and 108.4ml (94.6-122.2); and ESV = 56.8 ml (45.8-67.8) and 58.6ml (47.9-69.2). Not significant differences were found between these values (LVEF p = 0.08, EDV p = 0.50, ESV p = 0.81). Agreement degree on the functional parameters between both systems was 0.648 for the LVEF, 0.873 for the ESV and 0.934 for the EDV. **Conclusion:** Conclusions: our findings suggest a tendency of IQ-SPECT to produce smaller LVEF than conventional LEHR myocardial perfusion imaging. These findings are consistent with previous studies. **References:** None.

TEPS-53

Development of cardiac phantom for evaluation of fusion image of Myocardial perfusion imaging and CT-A

***A. Kikuchi**[1], Y. Honma[1], H. Honma[2], A. Andou[2], M. Kitama[1], G. Okuyama[1];*
[1]Department of Radiological Technology Faculty

of Health Sciences, Sapporo, JAPAN, [2]Ono Memorial Hospital, Sapporo, JAPAN.

Aim/Introduction: The usefulness of fusion images of CT angiography (CT-A) and Myocardial perfusion imaging (MPI) has been reported. However, MPI and CT-A fusion image accuracy has not yet been reported when creating fused images. That is because there was no phantom for CT-A, MPI image evaluation corresponding to both devices. Therefore, we developed a CT and MPI compatible hybrid phantom. **Materials and Methods:** The heart and trunk created a phantom using acrylic considering radiation absorption.In the lung part, a phenol resin was used in consideration of absorption.For the blood vessel model of the heart, the material of EPDM in consideration of the CT value at the time of imaging was used.Three 10 mm diameter acrylic markers are placed in the myocardium to verify the alignment accuracy of MPI and CT-A.We have verified marker detectability due to differences in imaging conditions such as pixel size, CT-A detectability has due to differences in CT imaging conditions, and verification of fusion image accuracy using images.As for the difference in detectability, MPI performed visual evaluation for circumferential-curve by axial image and verification of fusion image accuracy of processor.. **Results:** In the case of the pixel size of 3 mm, MPI was able to draw all the markers when the pixel size was 3 mm, but partially not able to be drawn when the pixel size was 6 mm. The CT-A model was able to be drawn regardless of the difference in imaging conditions. Fusion image accuracy was performed on CT-A and MPI, which differ in image conditions, but there was no discrepancy between CT-A and MPI in visual evaluation. From this, we were able to verify the Fusion image accuracy of the processor used this time. **Conclusion:** It has been confirmed that the CT-MPI hybrid phantom we developed are phantoms that did not use contrast agents and that could be used to verify the accuracy of fusion images. This said that to be because the installation position and size of the myocardial marker were appropriate in consideration of the resolution of the myocardial image. In the future, I would like to proceed with verification under more imaging conditions. **References:** Piccinelli M, Santana C, Sirineni GKR, et al. Diagnostic performance of the quantification of myocardium at risk from MPI SPECT/CTA 2G fusion for detecting obstructive coronary disease: A multicenter trial. J Nucl Cardiol. 2018 Aug;25(4):1376-1386.

TEPS-54

Examination of myocardial extraction using Semantic Segmentation by Deep learning

K. Okada[1], *A. Kikuchi*[1], *T. Kawakami*[1], *Y. Honma*[1], *K. Nakajima*[2], *H. Yoneyama*[3];
[1]*Hokkaido University of Science, Sapporo, JAPAN,* [2]*Kanazawa University, Kanazawa, JAPAN,* [3]*Kanazawa University Hospital, Kanazawa, JAPAN.*

Aim/Introduction: In the examination using 99mTc preparation in cardiac nuclear medicine, extra-cardiac activity often affects myocardial image, and various measures have been reported. We apply the image processing technology using artificial intelligence, and report as we developed a method to extract only the myocardial region necessary for diagnosis at the image level. **Materials and Methods:** As myocardial extraction program, Semantic Segmentation 1) by Deep Learning model U-Net 2) was used. The data we used was an axial image, and pixels in images were manually labeled the myocardium, liver, small intestine, and BG. Accuracy and loss were examined using 1920 images as training data and 480 images as test data and 360 images as data for verification. Furthermore, since the pixels in images of BG was very large among the data as the number of training data, compared Dice coefficients with and without Class Weight. **Results:** In the result of the learning model which does not consider the difference in the number of learning, accuracy was close to 1 at around 100 epoch, but validation accuracy converged at around 0.9 Although loss decreased to near 0, validation loss increased and finally divergence at around 1.5. The same tendency was confirmed in any learning model. On the other hand, in the examination of the presence or absence of Class Weight which consider the difference in the number of learning, It was shown that there was almost no difference in Dice coefficients and it was found that it was not necessary to consider Class Weight. **Conclusion:** In this result, all learning models used this time, the accuracy and loss both show the same tendency, and it was found that which largely depends on the data used this time. In the future, it will be necessary to create a learning model using multicenter clinical data. **References:** [1] Jonathan Long, Evan Shelhamer, Trevor Darrell, "Fully Convolutional Networks for Semantic Segmentation", 2014.[2] Olaf Ronneberger, Philipp Fischer, Thomas Brox, "U-Net: Convolutional Networks for Biomedical Image Segmentation", 2015.

TEPS-55

mcARM An Automated Motion Correction Algorithm For MPI Spect

A. Szucs[1,2], *Z. Fegyvári*[2], *B. Kári*[3,4,2], *O. Pártos*[4];
[1]*Eotvos Lorand University, Budapest, HUNGARY,* [2]*Mediso Medical Imaging Systems, Budapest, HUNGARY,* [3]*Semmelweis University, Department of Radiology, Budapest, HUNGARY,* [4]*Semmelweis University, Nuclear Medical Center, Budapest, HUNGARY.*

Aim/Introduction: In myocardial perfusion imaging patient motion can introduce hazardous effects in the reconstructed image volumes. The change in reconstructed left ventricle (LV) values can alleviate or increase total perfusion deficit (TPD) scores in patients, leading to repeated acquisition or misdiagnosis of patient data. A fully automatic image space method working in complete field-of-view (FOV) is created applying image analysis on the projection frames and the reconstructed volume as well. The combined techniques (image space and reconstructed volume space) are designed to increase accuracy of the detected motion vectors. **Materials and Methods:** We

propose an image based automatic method that estimates motion vectors based on a multi-stage pipeline. As a first step, a sub-pixel accurate registration method is applied in an inter frame manner to detect larger (>= 2 pixels) movements on complete FOV projection images. In the second step, the motion corrected frames are reconstructed and we apply an automatic LV segmentation algorithm (ARM) on the reconstructed volume. The segmented LV mask is reprojected on each frame. As the third step, we run local Lucas-Kanade Optical Flow in a small neighborhood of the reprojected LV mask to capture smaller (<2 pixels) movements in the projection images. To handle sub-pixel accuracy motion correction, bilinear interpolation scheme is applied on the projection frames. The mcARM method was validated using physical phantom and patient studies as well using 99mTc MIBI, 99mTc Tetrofosmin radiotracers. Thirty-seven patients were evaluated following tracer injection on Mediso AnyScan systems. The performance of mcARM was compared against Cedars-Sinai MoCo method using OSEM reconstruction method. The detectability of perfusion defects caused by motion artifacts were evaluated quantitatively calculating the TPD scores, aided by visual interpretation of the sinogram and linogram of the corrected studies. **Results:** The proposed method (mcARM) showed significant improvement over MoCo based on our findings on both phantom and patient studies calculating the TPD scores and by visual interpretation. With a median age of 53.95 years and body weight of 81 kgs, the method was evaluated on 37 patients, 17 male and 20 female. The algorithm showed an improvement of 20% in the calculated TPD scores compared to MoCo and relative error of 10% compared to manually corrected images. **Conclusion:** A fully automatic complete FOV motion correction algorithm is introduced, with fast running times (2-4 seconds). Evaluation on patient and phantom studies showed promising results for future developments in automatic SPECT motion correction. **References:** None.

TEPS-56

The use of effervescent granules in myocardial perfusion imaging; the full secret to a man's heart

J. Goh[1], *M. Ng*[1], *M. Chang*[1], *K. Tan*[1], *Y. Wong*[1], *Z. Huang*[2], *J. Tan*[2], *K. Tong*[3];
[1]*Sengkang General Hospital, Singapore, SINGAPORE,*
[2]*National Heart Centre, Singapore, SINGAPORE,*
[3]*Singapore General Hospital, Singapore, SINGAPORE.*

Aim/Introduction: Myocardial perfusion imaging (MPI) plays an integral role in diagnosing, managing and long-term follow up of patients with coronary artery disease (CAD). Radiopharmeceutical ^{99m}Technetium-sestamibi, is administered intravenously to depict the distribution of blood in the myocardium in MPI studies. Increased activity in subdiaphragmatic organs adjacent to the heart, especially bowel uptake, often interferes with the evaluation of the inferior myocardial wall. It results in either an underestimation or overestimation of the uptake in the inferior myocardial wall. Hence, a revised MPI technique with introduction of a sufficient quantity of not highly attenuating gas (4g EZ-GAS granules) into the stomach of patients to distend the stomach and consequently displace the organs adjacent to the heart was investigated. The aim of this study is to investigate if a distended stomach will aid in removing the gastrointestinal (GI) attenuation artefact and consequently, eliminate the false positive inferior wall defect seen in MPI. **Materials and Methods:** A prospective study of 120 patients undergoing either dipyridamole myocardial perfusion or RAMP exercise protocol or myocardial perfusion rest was conducted. Patients were allowed 100ml of water and 100ml of choice beverage with creamer prior to the SPECT scan. They were scanned at 30 - 60 minutes post ^{99m}Technetium-sestamibi injection. 4g of sodium bicarbonate-citric acid-simethicone effervescent granules (EZ-GAS) with 30ml of water was given to each patient after the first scan and a repeat scan was performed immediately. The presence of activity in the liver, bowel and stomach were determined visually on reconstructed images. A reduction by 3 or more reconstructed image slices with visible GI activity between the initial and repeated scan was assumed as bowel displacement by distension of stomach. Image interpretation was conducted by 2 independent nuclear physicians. **Results:** 25 of the patients (approximately 20%) showed negligible to no change in the GI activity seen on the initial and repeated scan images. 58 patients (approx. 50%) demonstrated slight to moderate changes in the GI activity seen between the initial and repeated scan images. The remaining 37 patients (approx. 30%) were reported with noticeable changes in the GI activity between the initial and repeated scan images. **Conclusion:** A distended stomach does reduce the frequency of "hot" GI activity seen on the reconstructed images slices, thereby improving the activity counts of the inferior myocardial wall. **References:** Van Dongen, A. J., & Van Rijk, P. P. (2000). Minimizing liver, bowel, and gastric activity in myocardial perfusion SPECT.

TEPS-57

Diagnostic utility of 99mTc-DPD scintigraphy in patients with suspected cardiac amyloidosis

E. N. Andersen[1], *A. Hodt*[1], *E. Gude*[2], *T. Bach-Gansmo*[1];
[1]*Oslo University Hospital Ullevål, Departement of Radiology and Nuclear Medicine, Oslo, NORWAY,* [2]*Oslo University Hospital Rikshospitalet, Departement of Cardiology, Oslo, NORWAY.*

Aim/Introduction: The aim of this prospective investigation was to determine the diagnostic utility of ^{99}mTc-3,3-diphosphono-1,2-propanodicarboxylic- acid (DPD) scintigraphy in patients referred with echocardiographic signs of myocardial hypertrophy potentially related to amyloidosis. **Materials and Methods:** The study was performed at Oslo University Hospital and was performed on all patients who underwent evaluation for suspected cardiac amyloidosis in the period of November 2018 and April 2019. Of approximately 50 planned patients, 11 patients (8 males, and 3 females, median age 71) have so far been included with written consent. At the time of writing

cardiac biopsy has been performed in 6 patients. Patients were scanned using one Siemens hybrid SPECT/CT (Symbia Intevo Bold) with a low-energy high-resolution (LEHR) collimator after intravenous injection of 700 MBq of 99mTc-DPD. Whole body (WB) scintigraphy was performed approximately 3 hours post-injection. SPECT/CT was performed in patients with visually detectable uptake in the myocardium. The whole body scans was visually scored with the grading devised by Perugini et al.[1] **Results:** Of the 11 99mTc-DPD patients, the WB were clearly negative in 8 patients, slightly positive in 1 patient (Perugini grade 1), positive in 1 (Perugini grade 2), and strongly positive in 1 patient (Perugini grade 3). Cardiac biopsy was positive for transthyretrin (TTR) in the Perugini grade 3 case, and Perugini Grade 1 patient had light chain (AL) amyloid deposits. For the patients with negative DPD scintigraphy, 1 was positive for light chain amyloidosis, and 3 patients had negative biopsies with regards to amyloidosis. **Conclusion:** The incidence of TTR is low in our population of patients with hypertrophic cardiomyopathy, and some uptake of DPD can be visualized in patients with light chain amyloidosis. **References:** Perugini, E., Guidalotti, P. L., Salvi, F., Cooke, R. M., Pettinato, C., Riva, L., ... & Fallani, F. (2005). Noninvasive etiologic diagnosis of cardiac amyloidosis using 99mTc-3, 3-diphosphono-1, 2-propanodicarboxylic acid scintigraphy. Journal of the American College of Cardiology, 46(6), 1076-1084.

TEPS-58

Analysis Of Influence Factors And Correlation For Quality Of Wholebody Bone Scan Imaging

T. Lu, G. Yang;
Shandong Cancer Hospital affiliated to Shandong University, JInan In ShanDong province, CHINA.

Aim/Introduction: Whole-body bone is the most common examination in nuclear medicine. It can clearly show the bone morphology and reflect bone metabolism; good image quality is critical to clinical diagnosis. This paper aims to analyze the influencing factors and correlation of the quality of whole-body bone imaging, and propose improvement measures to improve image quality. **Materials and Methods:** A retrospective study was selected on 1524 patients who received whole-body bone scan in nuclear medicine department from Apr 1 2018 to Aug 30 2018 in Shan Dong Tumor Hospital; The image quality was classified into A(good quality), B(normal quality) and C(poor quality) according to the clinical evaluation index of SPECT/CT instrument; Summarizing gender, age, blood calcium, urea nitrogen, creatinine, body mass index (BMI), injection to imaging interval, nuclide abnormal concentration at the injection site, treatment measures, bladder filling status, soft tissue intake, foreign bodies and nuclide contamination, etc; measurement data who have influence on image quality are further grouped and compared between groups; using variance analysis and graded logistic regression analysis to analyze influencing factors and correlation for quality of whole-body bone scan imaging, and proposing improvement methods. **Results:** In this study, 40% patients had good imaging quality, 50.3% patients with general imaging quality and 9.7% patients with poor imaging quality. The quality of the whole-body bone scan was correlated with gender(X^2=65.642,p=0.010), age (X^2=9.227,p=0.002), blood calcium(X^2=4.615,p=0.032), BMI(X^2=8.975, p=0.003), injection to imaging interval(X^2=20.890, p=0.001), nuclide abnormal concentration at the injection site(X^2=9.227. p=0.002), radiotherapy(X^2=3.115, p=0.003), bladder filling state(X^2=15.644, p=0.001) and soft tissue uptake(X^2=35.642, p=0.001); urea nitrogen, creatinine, foreign body and nuclide contamination were not statistical correlation with image quality. The first influencing factor was injection technique, accounting for 10.8%, followed by high soft tissue intake and bladder filling, accounting for 7.4% and 6.6%, respectively. Comparison between BMI and serum calcium showed that patients with ages less than 45 years and BMI less than 23.9 had better imaging quality, and there was no statistical difference between blood calcium groups. **Conclusion:** There are many factors affecting the quality of whole-body bone scan images in clinical work; the main factors are injection site and technique, soft tissue intake, bladder filling state, injection to imaging interval; followed by gender, age, BMI and blood calcium. Improving injection techniques, reducing soft tissue intake and emptying the bladder before examination can significantly improve the quality of imaging. **References:** None.

TEPS-59

Performance And Analysis Of Vertebral $^{99}Tc^{M}$-mdp Uptake After Chest Tumor Radiotherapy

T. Lu, G. Yang;
Shandong Cancer Hospital affiliated to Shandong University, JInan In ShanDong province, CHINA.

Aim/Introduction: To analyze the changes in vertebral 99Tcm-MDP uptake and the correlation with clinical radiotherapy parameters in chest tumor patients. **Materials and Methods:** A retrospective study was conducted in 110 patients who underwent chest tumor radiotherapy in our hospital from April 20, 2014 to October 31, 2018; and performed whole-body bone scan before and after radiotherapy. The clinical information, tumor factors and radiotherapy plan were analyzed by semi-quantitative analysis. We divided the results of bone scan into normal vertebral uptake group and abnormal vertebral uptake group, meanwhile analyzed the change in vertebral body 99Tcm-MDP uptake and the correlation with clinical radiotherapy parameters. Calculated (T/N前) - (T/N后)/(T/N前), draw ROC curve, and found the best diagnosis threshold of vertebral 99Tcm-MDP uptake abnormality. **Results:** In 110 patients, 48(43.6%) patients had local poor vertebral radioactivity uptake, with minimum vertebral exposure dose 1039.5cGy, maximum dose 4480cGy, and average dose 2139.5cGy; the shortest imaging interval was 61 days; and the remaining 62(56.4%) patients had no obvious abnormal radioactive uptake. The degree of vertebral body uptake was correlated with radiotherapy dose(X2=4.401,p=0.036),

radiotherapy frequency(X2=2.241,p=0.027), vertebral body irradiation dose(X2=5.913,p=0.015) and the imaging interval before and after radiotherapy(X2=12.542,p=0.013); and was no statistical correlation with age, gender, BMI, single radiotherapy dose, PTV, PTV dose, vertebral irradiation volume and the distance from radiotherapy target center to vertebral center. Grouped imaging intervals and compared between groups, we found that there was a difference between 3-6 months and 7-12 months in vertebral body uptake, abnormal vertebral 99Tcm-MDP uptake at intervals less than 6 months accounted for 2/3. The sensitivity and specificity of evaluating the 99Tcm-MDP uptake abnormality were 74.6% and 82.9% respectively. The area under the curve was 0.934 by ROC curve, indicating that (T/N前) - (T/N后)/(T/N前) was better for evaluating change rate of 99Tcm-MDP uptake in vertebral body, and the optimal diagnostic threshold for 99Tcm-MDP uptake abnormality in vertebral body was 0.161. **Conclusion:** 99Tcm-MDP uptake in vertebral after radiotherapy with chest tumor is closely related to radiotherapy dose, radiotherapy frequency, vertebral irradiation dose and imaging interval. With radiotherapy dose, radiotherapy frequency and vertebral body irradiation dose increased, the probability of abnormality of 99Tcm-MDP uptake is greater; and the earlier imaging time after radiotherapy, the higher detection rate of vertebral injury. The change of vertebral body 99Tcm-MDP uptake can reflect the degree of radioactive vertebarl damage to some extent. **References:** None.

TEPS-60

Quantitative accuracy of standardized uptake value (SUV) for xSPECT Bone technology using new supine phantom

T. Shibutani[1], *M. Onoguchi*[1], *T. Konishi*[2], *H. Yoneyama*[2], *H. Ichikawa*[3], *K. Okuda*[4], *K. Nakajima*[5];
[1]*Department of Quantum Medical Technology, Institute of Medical, Pharmaceutical and Health Sciences, Kanazawa University, Kanazawa city, JAPAN,* [2]*Department of Radiological Technology, Kanazawa University Hospital, Kanazawa city, JAPAN,* [3]*Department of Radiological Technology, Toyohashi Municipal Hospital, Toyohashi city, JAPAN,* [4]*Department of Physics, Kanazawa Medical University, Kanazawa city, JAPAN,* [5]*Department of Functional Imaging and Artificial Intelligence, Kanazawa University, Kanazawa city, JAPAN.*

Aim/Introduction: Standardized uptake value (SUV) of bone SPECT using xSPECT Bone technology has clinically been used as a quantitative index. Although some fundamental research of xSPECT Bone technology has been reported, the phantom study simulated human body has not been performed. We demonstrated the quantitative accuracy of SUV for xSPECT Bone algorithm using the phantom simulated human body. **Materials and Methods:** Phantom was used as a Sim² bone phantom (Kyoto Kagaku, Co., Ltd., Japan), which simulated the thorax portion including spine and lung. The supine is composed different 5 tumor regions (the diameter of the sphere: 13, 17, 22 and 28mm, and whole vertebral body: diameter of 36mm and length of 35mm) in the vertebral body. We prepared K_2HPO_4 solution of cortical and soft bone regions (CT value: 1000 and 300 HU) for the phantom. Tumor and normal bone parts were filled with a mixed solution of ^{99m}Tc and K_2HPO_4 of 300 and 50 kBq/mL, respectively. The body part was also filled with a ^{99m}Tc solution of 8 kBq/mL as background (BG). Radioactive concentration ratio of tumor, normal and B.G were 6:1:0.16. SPECT/CT scanner used a dual-head Symbia Intevo BOLD (Siemens, Erlangen, Germany) equipped with a low-energy high resolution (LEHR) collimator. SPECT data were acquired with 256×256 matrices, 2.4 mm of pixel size, the circular orbit of 360° in 3° increments. SPECT images were reconstructed using ordered subset conjugate gradient minimization method incorporating xSPECT Bone algorithm. The volume of interests(VOI) were drawn on tumor parts and normal bone using GI-Bone software, and mean SUV was calculated. We calculated the recovery coefficient (RC) of other tumor region as a reference of the tumor region of the whole vertebral body. Mean SUV ratio (SUVR) of the tumor and normal bone parts was used to evaluate the contrast. **Results:** The SUV_{mean} for tumor region of the whole vertebral body and normal bone were 5.78 and 1.03 for soft bone, and 5.77 and 1.08 for cortical bone, respectively, and relative error was within 3-8%. The RCs of 13, 17, 22 and 28mm tumor regions were 33.7, 44.5, 58.9 and 77.2 for soft bone, and 32.9, 47.7, 62.3 and 82.8 for cortical bone, respectively. The SUVR of each tumor region was 1.9-5.6 for soft bone and 1.8-5.4 for cortical bone. **Conclusion:** The SUV calculated by xSPECT Bone algorithm showed high quantitative accuracy and could be a good basis for further clinical application. **References:** None.

TEPS-61

Creation Of A Labeled Technetium-99m Colloid Drug For The Detection Of Guarding Lymph Nodes

A. Rogov, *E. Stasyuk, E. Nesterov, V. Sadkin, E. Shelikhova;*
National Research Tomsk Polytechnic University, Tomsk, RUSSIAN FEDERATION.

Aim/Introduction: Lately the interest to use of radioactive colloidal nanomaterials in medicine has been grown. They found their application for labeling autoleucocytes, to carry out lymphoscintigraphy and to identify "sentinel" lymph nodes. The most suitable radionuclide for labeling nanoparticles is short-lived technetium-99m, which is today used for diagnosis in almost all areas of medicine. Preliminary studies have shown that stable colloidal compounds can be obtained by a simple way by means of adsorption of reduced technetium-99m on gamma-aluminum oxide. Selection for the use of aluminum oxide as a carrier of technetium-99m is its low toxicity and good adsorptive properties, availability, and low cost. At the same time, a crucial factor for success is not their chemical composition, but the size of nanoparticles.Aim:Obtaining suitable for tagging with technetium-99m aluminum nanopowder with particle size in the range of 50-100 nm. **Materials and Methods:** As the object of study the was used nanopowder gamma-oxide Al_2O_3. It prepared from nanopowder of aluminum hydroxide by its was gradually heating to 400°C for 2 hours. The particle

size was determined using electron microscope Philips SEM515. The average particle size is in the range of 100-200nm. Before the adsorption technetium-99m on oxide Al_2O_3 it was carried out acidizing. In this regard, were found the optimal conditions of oxides acidizing which maximum adsorption of ^{99m}Tc. The maximum of radionuclide adsorption is observed on oxide treated with HCl in an amount of $2 \cdot 10^{-4}$ mol/g. Technetium-99m presenting in the original eluate in the highest degree of oxidation (+7) and does not have a sorption capacity. **Results:** Therefore, research was made to of reduced technetium-99m in lower degrees of oxidation (+5) and it is more chemically active. To of reduced technetium-99m we used Tin(II) chloride dihydrate ($SnCl_2 \cdot 2H_2O$). When carrying out the synthesis of the drug used ultrasonic and vial with preparation was heated in a water bath (70-80°C) for 30min. In a finished pharmaceutical the particle size was determined by photons cross-correlation spectroscopy using analyzer of particle size Nanophox produced by company «Sympatec GmbH» **Conclusion:** The measurement showed that 85% of the particles are in the range of 95-150nm. These figures confirm suitability of the drug and the feasibility of conducting trials of the drug on laboratory animals in accordance with the European Convention for the Protection of Vertebrate Animals used for Experimental and other Scientific Purposes (Strasbourg, 1986). **References:** None.

TEPS-62

Lymphoscintigraphy and sentinel node localization in gynaecological cancers into practice: a UK single-centre protocol

L. Pereira, K. Brooks, T. Barnden, O. Devaja, A. Corrigan;
Maidstone and Tunbridge Wells NHS Trust, Maidstone, UNITED KINGDOM.

Aim/Introduction: In the ESMO 2017 guideline on cervical cancer, the sentinel node (SLN) dissection is pointed as standard in the treatment of vulvar cancer. It also mentions that there is increasing evidence suggesting an important role in cervical cancer. Finally, it emphasises that the nuclear procedure for the detection of SLN (in addition to the blue dye) should only be done in centres with enough expertise and training. Despite this relevant reference, gynaecological SLN is not performed routinely in most European centres. Aim: To share this centre's experience in setting up and performing lymphoscintigraphy and sentinel node location in gynaecological cancer patients. **Materials and Methods:** A total of 381 female patients have undergone one of the procedures (vulvar or cervical SLN scintigraphies) between January 2011 and April 2019. While the protocol has been updated in line with the 2014 EANM guideline, the department developed it in a way that would meet the service needs and reflect a personalised approach. **Results:** This presentation will entail two parts: a brief clinical overview, which will include common indications and examples of imaging results; and a technical description and explanation of the protocol, which will comprise: delivery of a patient-centred service through liaison with oncology specialist nurses, surgeon and the patient and its relatives; the detailed preparation of the facilities, exemplified and illustrated with pictures; radiopharmaceutical proprieties, biodistribution and handling; dose preparation and types of administration; hybrid imaging acquisition parameters and radiation protection considerations. **Conclusion:** This work presents our current gynaecological protocol, which has been adapted over the years in in view of the department's experience and the guidance and literature available on this matter. Furthermore, it clarifies the technologist's role in this process and highlights the importance of a multidisciplinary team effort when dealing with this particularly sensitive pathology. **References:** Marth, C. Landoni, F. Colombo, N. Mahner, S. McCormack, M. Gonzalez-Martin, A. 2017. "Cervical Cancer: ESMO Clinical Practice Guidelines for Diagnosis, Treatment and Follow-Up." Annals of Oncology, ESMO Guidelines Committee 28: iv72-iv83.

TEPS-63

Net Administered Activity As A Surrogate Quality Control Indicator For Non-Imaging Breast SLNB Procedures

L. Wason, A. Nicol, J. Dennis, C. Flynn;
NHS Greater Glasgow And Clyde, Glasgow, UNITED KINGDOM.

Aim/Introduction: Many centres perform non-imaging sentinel lymph node biopsy (SLNB) to accurately stage axillary lymph node involvement in breast cancer. The aim is to administer adequate activity of radiopharmaceutical to ensure the sentinel nodes can be detected in theatre using a gamma probe. These intradermal administrations can be challenging - small volume, high concentration radiopharmaceutical, dead space in syringe, high pressure and respiratory movement could all be significant factors in determining if the target net activity is administered. As imaging is not used to confirm tracking of the radioisotope from the injection site to the axilla, an alternative method of confirming administration of the appropriate activity to each patient is sought. Anecdotal communication from theatre indicates it is possible to have a situation of no radiopharmaceutical detected in the axillary nodes. In the absence of imaging to directly check radiopharmaceutical tracking to the lymphatic system we propose the net administered activity as an alternative quality control indicator of satisfactory radiopharmaceutical administration. **Materials and Methods:** Consecutive patients undergoing breast SLNB over a period of seven months were reviewed. The dispensed and residual activity was collected for 58 patients and the net activity administered calculated. The administered activities and percentage residuals were compared to the DRL for both same day (20MBq) and next day (40MBq) procedures. The maximum and minimum values for each were also obtained. The residual was converted into a percentage of the net administered activity. Mean, median and standard deviations were obtained for the percentage residuals for all administrations. **Results:** The mean±stdev administered activity for same day and next day procedures was 20.8MBq ± 2.0 and 38.7MBq ± 3.3 respectively. The results show that 69% of administrations were within 10% and 95% within 20% of the

DRL. All administrations were within 25% of the DRL. The mean residual activity as a percentage of administered activity was 12.5±9.0%, with a maximum of 48.5% and a minimum of 2.8%. **Conclusion:** This investigation demonstrates that there are technical challenges associated with breast SLNB intradermal injections and there may be a role for a check on administered activity by measuring residuals. This must be balanced against the potential safety risk associated with measuring residual activities. Further work will include inter-operator assessment and raising operator awareness. **References:** None.

TEPS-64

Clinical Effectiveness Of Sentinel Node Biopsy In Early Oral Cavity Carcinoma

Y. Herrera-Martinez, Á. Bonilla De Damiá, V. Pachón Garrudo, D. Tamayo Carabaño, R. Álvarez Pérez, J. Jiménez-Hoyuela García; Hospital Universitario Virgen del Rocío, Seville, SPAIN.

Aim/Introduction: This study investigates the effectiveness of sentinel lymph node biopsy (SNLB) in patients with oral carcinoma without clinically and radiographically cervical lymph nodes involvement. **Materials and Methods:** Prospective study in 34 patients with T1-T2N0M0 squamous cell carcinoma of the oral cavity. Lymphoscintigraphy was performed after the administration of four peritumoral injections of 3 mCi of ^{99m}Tc-nanocolloid. The sentinel lymph node (SNB) was detected by the acquisition of dynamic, early, delayed, SPECT/CT images. The day after the SLN detection, its intra-operative recognition was carried out using a Navigator GPS® scintigraphic probe. The first sentinel node was excised, and subsequently elective deferred lymphadenectomy was performed if tumor infiltration of the SNB was observed. Follow-up was performed on average 9 months (range 2-21 months). **Results:** Thirty-four patients (16 men and 18 women) were included in the study with an average age of 59,2 years. Lesions were localized in the tongue in 22 cases (64,7%), 10 (29%) in the floor of the mouth and 2 (5%) in the gum. A mean of 2,29 SLN was excised per patient. The bilateral drainage of the radiotracer was observed in 7 patients (20,5%). The SLN was localized in all patients (100%). Metastases were found in 9 of the 34 patients (26%); in those patients with initial negative SLN, recurrence was observed in only one case during the follow-up. Cervical lymphadenectomy was avoided in 74% of the patients. **Conclusion:** SLNB allows a correct cervical staging of oral cavity carcinomas, avoiding unnecessary cervical lymphadenectomy. **References:** None.

TEPS-65

Quantitative estimation of the renal tubular function with ^{99m}Tc- MAG3: comparative software approach using two methods in a pediatric population

M. J. Carapinha[1,2,3], R. Silva[1], F. Silva[1], S. Figueiredo[1,3], L. Vieira[1,3]; [1]Escola Superior de Tecnologia da Saúde de Lisboa, Lisboa, PORTUGAL, [2]Escola Nacional de Saúde Publica, Universidade Nova de Lisboa, Lisboa, PORTUGAL, [3]H&TRC - Health & Technology Research Center, ESTeSL - Escola Superior de Tecnologia da Saúde, Instituto Politécnico de Lisboa, Lisboa, PORTUGAL.

Aim/Introduction: The ability to quantify function by Effective Renal Plasma Flow (ERPF) using camera based Technetium-99m mercaptoacetyltriglycine (^{99m}Tc-MAG3) clearance methods is an accurate and time-saving technique as compared with the standard laboratory tests. Often providing information not possible with the conventional radiological modalities, this quantitative assessment can be determined by a linear formula - Modified Gates Method (MGat) - or a quadratic approach - Modified Schlegel Method (MSch). The aim of this work was to evaluate the effect of the MGat and MSch methods on the absolute value of ERPF in ^{99m}Tc-MAG3 dynamic renography. **Materials and Methods:** A retrospective study with a non-probabilistic sample of twenty one children (9.5 ±3.1 years; 32.1±10.7 kg) referred for diuretic (12.8 ± 4.8 mg of furosemide) ^{99m}Tc-MAG3 (120.0 ± 27.5 MBq) renogram was used. Data were available in Xeleris GE™ workstation database at Lisbon School of Health Technology (ESTeSL) and were processed using Renal Analysis application. To obtain the ERPF (mL/min) parameter by the MSch and MGat methods, all the studies were manually processed by the same operator considering the following regions of interest (ROI): left kidney (LK), right kidney (RK), peri-renal background (BKG), aorta artery (AA) and injection site (IS). Additionally, right and left kidney Area (A), uptake (Up) and $T_{1/2}$ quantitative parameters were assessed for each method. To evaluate the significance and association between the variables, the Shapiro-Wilk, Wilcoxon and Spearman correlation tests were used, considering α=0.05. **Results:** Paired samples Wilcoxon test found significant differences in ERPF MGat and MSch ($p<0.01$); RKA MGat and MSch ($p<0.05$); LKA MGat and MSch ($p<0.05$). Contrarily, there were not significant differences for Uptake ($p>0.05$) and for $T_{1/2}$ parameter ($p>0.05$), considering L and R kidneys, when MGat and MSch methods were applied, though higher significance values were found in Up parameter. **Conclusion:** Results suggest that the applied method may possibly influence the obtained ERPF absolute value. MGat and MSch methods originate different ERPF and A values, despite similar metrics for the Up and $T_{1/2}$ parameters. The effect of location of the kidneys (L-R) seems to slightly affect method association criteria for all the parameters with more impact in the LK values. **References:** None.

TEPS-66

Comparison of Single and Dual Isotope Imaging for 3D Lung Lobar Quantification with SPECT-CT

T. Sousa, S. Gregg, K. Wechalekar; Royal Brompton and Harefield Foundation Trust Hospital, London, UNITED KINGDOM.

Aim/Introduction: Chronic obstructive pulmonary disease affects 400 million individuals worldwide and is predicted to be the third leading cause of death by 2020. Lung volume reduction

surgery (LVRS) is an established means of targeting hyperinflation in patients with severe emphysema. Preoperative evaluation of regional lung function is essential to planning and predicting the outcomes of surgery. Our previous work [1] established the ability to perform 3D lung lobar quantification (3DLLQ) using hybrid CT + sequential lung perfusion and ventilation (VQ) SPECT offering accurate quantitation at lobar level. The purpose of this study is to compare 3DLLQ analysis between sequential and simultaneous dual isotope VQ SPECT-CT. **Materials and Methods:** 20 patients (14 Male, 6 Female, mean age 65, range: 39-79 years) referred for lung lobar quantification were included. Initially, perfusion (^{99m}Tc) and Ventilation (^{81m}Kr) SPECT-CT scans were acquired sequentially followed by simultaneous dual isotope VQ SPECT-CT acquisition. Scans were performed using a general purpose dual head gamma camera (GE Infinia Hawkeye). Hybrid Recon for Lung and 3DLLQ applications (Hermes Medical Solutions) were used to reconstruct the attenuation-corrected SPECT images and to calculate the percentage contribution of each lobe to total lung function for each technique as demonstrated previously [1]. **Results:** Bland-Altman plots for the assessment of right and left lung function demonstrate excellent agreement between single isotope and dual isotope imaging techniques (+3.1 and -3.2 for Q and +3.9 and -3.9 for V) In lobes, the limits of agreement were very good for both Q and V quantification (+4.4 and -4.7 for Q and +3.4 and -3.5 for V). There was an excellent correlation between the two imaging techniques for the assessment of differential lung function ($r>0.98$, $P<0.001$ for both V and Q) with a mean ±SD difference of 0.05±1.6 for Q and 0.0±2.0 for V. Also, correlation between the techniques for lobar contribution was very good ($r > 0.97$, $P< 0.001$ for both V and Q). The mean ±SD difference between techniques for all the lobes was 0.14±2.3 (Q) and 0.02±1.8 (V). **Conclusion:** Our investigation demonstrates that simultaneous dual isotope VQ SPECT-CT acquisition is feasible in 3DLLQ. This reduces the acquisition time considerably, resulting in increased patient comfort. In addition, image quality is improved due to reduction in motion artefacts and mis-registration between perfusion, ventilation and CT. **References:** [1] Thillainathan AV,2013, EANM, SPRINGER, Pages: S292-S293, ISSN:1619-707.

804-4

Technologists: Technologist e-Poster Presentation Session 4

Monday, October 14, 2019, 11:30 - 13:00 Meeting Room 118/119

TEPS-67

Assessment of 2-hour Images for ^{99m}Tc-HYNIC-TOC Studies Using Image Interpretation and Image Analysis

S. Tavares[1], *M. Jessop*[1], *D. Pencharz*[1], *E. Manca*[1], *N. Singh*[1], *S. Figueiredo*[2];
[1]*Royal Sussex County Hospital, Brighton, UNITED KINGDOM,*
[2]*Lisbon School of Health Technology, Lisbon, PORTUGAL.*

Aim/Introduction: Scintigraphy with ^{99m}Tc-HYNIC-TOC (Tektrotyd®) is valuable for the diagnosis of neuroendocrine tumours (NETs), particularly those expressing a high density of somatostatin receptors. The aim of this retrospective study was to examine our current local Tektrotyd® imaging protocol, assessing the usefulness of 2-hour whole body imaging. **Materials and Methods:** Whole body scintigraphy was performed in seventeen patients at 2 and 4 hours after intravenous administration of 740MBq ^{99m}Tc-Tektrotyd®. SPECT-CT was performed in all cases at 4 hours. 10/17 patients had positive findings. The whole-body images were independently assessed by two experienced Nuclear Medicine Physicians and judgement was made in each case on whether the 2-hour imaging was felt necessary for accurate diagnostic interpretation. In addition, Image Quality Metrics (IQM) were used to evaluate target-to-background-ratio (TBR) (right dome of liver/ right calf) on the Xeleris™ v.3.0 workstation, and image texture analysis i.e. contrast, energy (uniformity), correlation, entropy and homogeneity, was performed using LIFEx software with a region of interest (ROI) over the right dome of liver. **Results:** To standardize image comparison, the liver was chosen as the image feature for analysis. Image texture analysis showed very little difference between the 2 and 4-hour images for homogeneity (average of 2%), uniformity (average of 1%) and correlation (average of 2%). Entropy decreased (average of 23%) by the 4-hour image as biodistribution stabilized, and contrast was far more variable depending on the individual patient. TBR increased from 2 to 4-hour by an average of 19%. Both Nuclear Medicine Physicians agreed that for 16/17 patients the 2-hour image was not necessary for accurate diagnostic interpretation. **Conclusion:** Following assessment of the usefulness of 2-hour images in ^{99m}Tc-Tektrotyd® studies, as part of the imaging protocol for diagnosis and staging of patients with NETs, it can be concluded that the 2-hour imaging adds little additional diagnostic information, and is less useful than 4-hour imaging where pathological areas become more prominent. In addition, if SPECT-CT is available for further clarification of lesions, the 2-hour images could safely be omitted, resulting in more streamlined imaging, reducing patient inconvenience and improving scanner and staff efficiency. **References:** 1. Al-Chalabi H, et al. Feasibility of a streamlined imaging protocol in technetium^{99m}-Tektrotyd somatostatin receptor SPECT/CT. Clin Radiol [Internet]. 2018 Jun. Available from: https://linkinghub.elsevier.com/retrieve/pii/S0009926018300084. 2. Nioche C, et al. LIFEx: A Freeware for Radiomic Feature Calculation in Multimodality Imaging to Accelerate Advances in Characterization of Tumor Heterogeneity. Cancer Res [Internet]. 2018 Jun. Available from: http://cancerres.aacrjournals.org/lookup/doi/10.1158/0008-5472.CAN-18-0125.

TEPS-68

Quantification Of Technetium-99m Sestamibi Thyroid Scintigraphy In Ait Type I And Ii

E. Kranenborg, *M. v Rutte, J. Lavalaye, J. Habraken;*
St. Antonius Hospital, Nieuwegein, NETHERLANDS.

Aim/Introduction: Amiodarone induced thyrotoxicosis

(AIT) is a thyroid disease, caused by the use of amiodarone. Amiodarone is medication against cardiac arrhythmias. AIT can be divided into 3 types. Type I is an excessive production of the thyroid hormone. Type II is a destructive thyroiditis. Type III is a combination of type I and II. The treatment of AIT is difficult and not always successful. Distinguishing between type I and II is important to optimize the treatment. Currently there is no gold standard to diagnose AIT. Technetium-99m sestamibi thyroid scintigraphy (^{99m}Tc-STS) is regularly applied to differentiate between the different types of AIT. However, these images are only assessed visually. It may be of added value to quantify these images, to give more specific determination between type I en II. **Materials and Methods:** ^{99m}Tc-STS was performed with 185 MBq sestamibi and acquisition of static images 2, 10, 15 and 60 min after injection. 18 AIT patients who underwent ^{99m}Tc-STS, were retrospectively assessed. For every patient a fixed ROI was placed in the middle of one thyroid lobe. For every single patient the same ROI location was used on all planar images. A background ROI was drawn to correct for background radiation. The average number of counts in every image was plotted in a graph. **Results:** 14 Patients were diagnosed as type II and 2 patients as type I. 2 patients were visually indistinguishable (type III). All type I en II patients corresponded with the follow up diagnosis. The type III patients were after follow up diagnosed as type I (1 patient) and type II (1 patient). The quantification results were plotted against the diagnosed type of AIT. The graphs show a clear difference between type I and II, especially at 15 min. The results at 15 min images are between 0.91 - 2.3 cts/pixel (type I) and 0.24 - 0.62 cts/pixel (type II). The results of type III who turned out to be type II was 0.57 and type I was 0.94. The results at 15 min are always above 0,8 cts/pixel for type I and always below 0,8 cts/pixel for type II. **Conclusion:** This study has shown that ^{99m}Tc-MIBI quantification is a reliable and easy method for diagnosis and classification of AIT. It is possible to define a clear cut-off between type I and II. The quantification method for these patients is in full correspondence with the clinical follow-up. **References:** None.

TEPS-69

Serum creatinine measurement as a predictor for single sample GFR using 99mTc-DTPA

***G. Hilland**, A. Matos, C. Findlay;*
NHS Greater Glasgow and Clyde, Glasgow, UNITED KINGDOM.

Aim/Introduction: Radionuclide measured Glomerular Filtration Rate (mGFR) assessment using 99mTc-DTPA (Diethylenetriamine Pentaacetic Acid) is widely used in Nuclear Medicine for patients pre-nephrotoxic chemotherapy or assessment of potential live kidney donors (PLKD). British Nuclear Medicine Society (BNMS) guidelines published in 2004 recommended using a 4-sample slope intercept GFR protocol (SI-GFR). However updated BNMS guidelines published in 2018 recommend a single sample GFR measurement (SS-GFR) for patients without ascites, oedema or other expanded body space. The recommended single sample time should be based on the best available estimate of body surface area normalised GFR. One such measurement is the estimated GFR (eGFR) based on serum creatinine concentration. The purpose of this audit was to compare SI-GFR and the SS-GFR measurements to aid confidence in transitioning to a SS-GFR method. We also wished to look at the validity of using eGFR as a single sample time predictor. **Materials and Methods:** Using 4-sample SI-GFR measurements, the equivalent SS-GFR was calculated using the single sample time point identified in the guidelines. The patient's most recent eGFR measurement was used to identify which of the 4 blood samples would be the SS equivalent. **Results:** Thirty 99mTc-DTPA SI-GFR patients were retrospectively reviewed. The thirty patients comprised 21 pre-chemotherapy assessment and 9 PLKD patients with an average eGFRs of 84.9 ± 61.8 mL/min/1.73m². The average SI-GFR and SS-GFRs were 84.2 ± 50.4 and 83.9 ± 53.5 mL/min/1.73m² respectively. Time between eGFR and mGFR was 23 ± 83 days. Comparison of eGFR measurements with SI-GFR and SS-GFR were statistically different. Recommended single sample times for eGFRs > 50 mL/min/1.73m2 demonstrated no clinical significance between SI-GFR and SS-GFR (p>0.05) however SS-GFRs for patients with eGFRs of 25-50 mL/min/1.73m2 were consistently higher than SI-GFRs. Average time between eGFR and mGFR for all patients was 11.7 ± 4.4 days. **Conclusion:** Preliminary findings using eGFR to determine single sample times for 99mTc-DTPA mGFRs gave mixed results. As anticipated eGFR is not a good predictor of SS-GFR or SI-GFR measurements. With regard to mGFR methods, SS-GFRs at 2, 3 and 4 hours do correlate with SI-GFRs. However low GFRs estimated at 25-50 mL/min/1.73m2 (6 hour SS-GFR) give significantly different results from SI-GFRs. It may be that using the 6 hour single sample improves accuracy for lower GFRs. **References:** None.

TEPS-70

End of Chromium-51 availability: Setting-up of a new protocol, validation and impact analysis

***S. A. Figueiredo**, G. Allenbach, J. O. Prior, J. Delage, J. Costes;*
CHUV, Lausanne, SWITZERLAND.

Aim/Introduction: Chromium-51 (^{51}Cr) was used for red blood cells (RBC) volume determination until December 2018, when its production stopped. Re-infusion of RBC labeled in vitro with technetium-99m (^{99m}Tc) followed by dilution measurement is also a documented alternative method. The aim of this work is to compare these two techniques in terms of labelling efficiency, accuracy and impact in our daily practice. **Materials and Methods:** Simulation tests were performed to validate the alternative calculation method. Blood samples were collected from healthy volunteers and RBC labeled with ^{99m}Tc reduced by PYP. Then, labeled cells were injected in a two-liter flask of water. Flask samples were withdrawn at three time points (20, 30 and 40 minutes) and measured by gamma counter to calculate the flask volume. Results were compared with the theoretical two-liter flask volume. ^{99m}Tc method was compared to ^{51}Cr method regarding to: labelling efficiency, processing time, supplies costs

(PYP kits vs. ^{51}Cr) and wastes management. **Results:** After two washing steps, the labelling efficiency of RBC with ^{99m}Tc (n=4) was significantly superior than the labelling with ^{51}Cr (98.9 ± 0.47%, vs 87.5 ± 2.5[1], p>0.0005). Flask volume estimation with ^{99m}Tc labelled RBC (n=3) was 2,112 ± 15 mL for a theoretical volume of 2000 mL (+5.6%). ^{99m}Tc leakage from cells was not measured during this study, but will be measured in the first patient for improving calculation accuracy. ^{99m}Tc procedure for RBC volume calculation is longer than ^{51}Cr procedure (3.5 hours vs 2.5 hours) due to the ^{99m}Tc PYP reduction step and the multiple washing steps to remove extracellular PYP. ^{99m}Tc procedure is more economical compared to ^{51}Cr, even if processing time is longer. Moreover, ^{99m}Tc generator allows a much easier ^{99m}Tc supply than ^{51}Cr. Finally, the ^{99m}Tc half-life (6.02h) makes the wastes management much easier in comparison to ^{51}Cr (27.8d). **Conclusion:** This study validates ^{99m}Tc RBC labeling in vitro as an alternative method to ^{51}Cr for RBC volume determination with high reproducibility. Volume measurement accuracy will be further improved by correcting for the bias introduced by ^{99m}Tc RBC leakage. **References:** 1: Richard J. Kowalsky, Steven W. Falen; Radiopharmaceuticals in Nuclear Pharmacy an Nuclear Medicine; Second Edition; p.753-756.

TEPS-72

Glomerular filtration rate: Comparison of two tracers

L. Janus, T. Andersen, K. Thilsing-Hansen, D. Roholdt, C. Led, P. Andersen, H. Thomsen, O. Gerke, P. Høilund-Carlsen, J. Simonsen; Odense University Hospital, Odense C, DENMARK.

Aim/Introduction: At our department, we used to measure glomerular filtration rate, GFR, with Cr-51-labelled ethylenediaminetetraacetate (Cr-51-EDTA). Since the supplier at short notice closed down the production of this tracer, we were forced to replace it. The choice fell on Tc-99m-labelled diethylenetriaminepentaacetate (Tc-99m-DTPA) which is also a well-established GFR tracer. However, no direct comparison between the two seemed to exist. We therefore made a head-to-head comparison in patients referred to us for a medical indication. **Materials and Methods:** During the last four weeks with Cr-51-EDTA available we administered both Cr-51-EDTA (GE Healthcare) and Tc-99m-DTPA (Mallinckrodt Pharmaceuticals) to most of our patients. Injections were consecutive (3.7 MBq of Cr-51-EDTA, 8 MBq of Tc-99m-DTPA) and the standard number of blood samples were drawn. A well counter (2470 Wallac Wizard 2™, Perkin Elmer) registered energy peaks for both Cr-51 and Tc-99m, and the two were counted simultaneously. **Results:** A total of 54 patients were examined with this dual-isotope method; 51 of them with single-sample GFR measurement (blood samples 3 h p.i.) and three of them with the multiple-sample method (blood samples 3h, 4h, and 5h p.i.). Results for the 51 single-sample measurements are presented. Mean GFR measured with DTPA (GFR_{DTPA}) did not differ from that determined with EDTA (GFR_{EDTA}); the mean [95% CI] difference was 0.40 [-0.40;1.19] mL/min. The difference ranged from -7.30 to 7.31 mL/min; 95% Limits of Agreement according to Bland & Altman were [-5.12;5.92]. However, a regression line revealed that GFR_{DTPA} exceeded GFR_{EDTA} at high GFR values (difference<0 at GFR_{EDTA}>80 mL/min) and vice versa (difference>0 at GFR_{EDTA}<80 mL/min). **Conclusion:** GFR_{DTPA} can replace GFR_{EDTA} since the difference between the two lies within few GFR units that most often will have no clinical consequence. However, data indicated that the two tracers are not handled completely similarly in the body and that differences become more marked at the extremities of the GFR spectrum. Hence, a more detailed comparison between the two tracers, especially at poorer renal function, is warranted. **References:** None.

TEPS-73

Association between TNM staging and primary tumor parameters assessed in ^{18}F-FDG-PET/CT study in NSCLC patients

K. Pietrasz[1], P. Cegla[1], K. Witkowska[2], R. Czepczynski[3], M. Bryl[4], W. Cholewinski[5,1];
[1]Nuclear Medicine Department, Greater Poland Cancer Centre, Poznan, POLAND, [2]Affidea Medical Center, Poznan, POLAND, [3]Department of Endocrinology, Metabolism and Internal Medicine, Poznan University of Medical Science, Poznan, POLAND, [4]Oncology Department at Regional Centre of Lung Diseases in Poznan and Department of Thoracic Surgery, Poznan University of Medical Sciences, Poznan, POLAND, [5]Chair and Department of Electroradiology, Poznan University of Medical Science, Poznan, POLAND.

Aim/Introduction: Lung cancer is the leading cause of death in Poland and worldwide in both sexes and around three million new cases are diagnosed worldwide. The aim of the study was to compare the TNM stage of the cancer with biological parameters of primary tumor as SUV_{max}, MTV and TLG in patients with NSCLC. **Materials and Methods:** Retrospective analysis was performed on a group of 79 newly diagnosed lung cancer patients. PET scans were acquired on Gemini TF PET/CT scanner between 60-90min after injection of ^{18}F-FDG with the mean activity of 364±75 MBq, with the area being examined from calvaria to half way down the thigh. The reconstructed PET images were evaluated using MIM 6 Software for SUV_{max}, MTV and TLG values. For MTV calculation a 3D lung phantom study was performed for simulation of the variety of activity and volume. **Results:** In the whole analyzed group, 31 patients were women, while 48 patients were men. In 38 patients NSCLC were diagnosed in the left lung, while in 41 patients in right lung. The analysis of the cancer stage showed stage IA2 in 8 patients, stage IA3-6 pts, stage IB-4pts, IIA-3 pts, 15 patients with stage IIB, stage IIIA-17 pts, IIIB-5, IIIC-5, IVA in 7 patients and stage IVB in 9 patients. The lowest TLG values were observed in stage IA2 (11.31±15.27) and the highest in stage IIIC (1003.20±953,59). The lowest value of SUV_{max} and MTV were found in stage IA2 (6.8±3.8 and 1.37±0.42 respectively). The highest value of SUV_{max} was found in stage IIA (13.4±11.4) and MTV in stage IIIC (108.15±127.24). **Conclusion:** Metabolic parameters of the tumor and proliferative process expressed with MTV and TLG represent different from TNM

staging system biological description of lung cancer, which may be important for the treatment and prognosis. **References:** None.

TEPS-74

Assessment of ^{18}F-FDG PET/CT texture analysis to discriminate NSCLC from radiation pneumonitis after CIRT

M. Suga[1,2], *R. Nishii*[3], *K. Yamazaki*[3], *Y. Kamitaka*[1,2], *K. Miwa*[2], *R. Kohno*[4], *K. Tanimoto*[1], *T. Higashi*[3], *H. Tsuji*[1];
[1]*QST hospital, National Institute of Quantum and Radiological Science and Technology, Chiba, JAPAN,* [2]*Department of Radiological Sciences, International University of Health and Welfare, Tochigi, JAPAN,* [3]*Department of Molecular Imaging and Theranostics, National Institute of Radiological Sciences, QST, Chiba, JAPAN,* [4]*Department of Accelerator and Medical Physics Therapy Systems Section, National Institute of Radiological Sciences, QST, Chiba, JAPAN.*

Aim/Introduction: The differentiation of local recurrence from a primary tumor and radiation pneumonitis (RP) is critically important for selecting optimal clinical therapeutic strategies to manage post carbon-ion radiotherapy (CIRT) in patients with non-small cell lung cancer (NSCLC). Although 18F-FDG PET/CT (FDG-PET/CT) plays a key role in the metabolic imaging of patients with NSCLC who require CIRT management, PET/CT diagnosis based on SUVmax cannot always distinguish between NSCLC and RP. The present study aimed to determine whether FDG-PET/CT texture parameters can differentiate NSCLC from RP after CIRT. **Materials and Methods:** We retrospectively analyzed FDG-PET/CT image data from 32 patients with histopathologically proven NSCLC who were scheduled to undergo CIRT, and 31 patients who were diagnosed with RP after CIRT (50.0 Gy (RBE) in single fraction). Radiation pneumonitis was diagnosed by biopsy or at clinical follow-up > 1 year after CIRT. Volumes of interest (VOI) on tumors were delineated using a threshold of 40% of the maximum standard uptake value (SUVmax) in each lesion. The SUV parameters of SUVmax, SUVpeak, SUVmean, metabolic tumor volume (MTV), total lesion glycolysis (TLG) and seven typical texture parameters of FDG-PET/CT were determined using PETSTAT image-analysis software. Data were statistically compared between NSCLC and RP using nonparametric Wilcoxon rank sum tests. Diagnostic accuracy was assessed using ROC curves. **Results:** Among SUV parameters, MTV ($p < 0.0001$) and TLG ($p = 0.001$) significantly differed between NSCLC and RP. The feature quantities of texture parameters, namely, GLRLM, GLSZM, NGLCM3D, NGLCM and NGTDM significantly differed between NSCLC and RP. The areas under the receiver operating characteristics (ROC) curves (AUC) were as follows: SUVmax 0.64, MTV 0.86, TLG 0.75, GLRLM 0.83, GLSZM 0.76, NGLCM3D 0.71, NGLCM 0.72 and NGTDM 0.82. Diagnostic accuracy was better using GLRLRM or NGTDM than SUVmax ($p < 0.01$). **Conclusion:** The texture parameters of FDG-PET/CT were useful to differentiate NSCLC from radiation pneumonitis after CIRT, and GLRLM and NGTDM in particular would be promising parameters with excellent diagnostic accuracy. **References:** None.

TEPS-75

Impact of respiratory and ECG gated ^{18}F-FDG PET/CT for cardiac sarcoidosis

K. Hanaoka, *S. Watanabe*, *Y. Shibata*, *H. Kaida*, *K. Ishii*;
Institute of Advanced Clinical Medicine, KINDAI University, Osaka-sayama, JAPAN.

Aim/Introduction: Myocardial accumulation of ^{18}F-FDG is affected by respiratory and cardiac motion. The aim of this study was to estimate the impact of respiratory and ECG gated ^{18}F-FDG PET/CT on the diagnosis of cardiac sarcoidosis. **Materials and Methods:** Eighteen patients were acquired on a GE Discovery 710 PET/CT equipped with a Varian RPM respiratory gating system and ECG system. Non-gated PET images and two kinds of gated PET/CT images, Respiratory-gated PET (PET events during inhalation were reduced and reconstructed with conventional helical CT) and ECG-gated PET (16 bin ECG gated PET reconstructed with conventional helical CT) were created from list-mode clinical 18F-FDG PET/CT data. These data were analyzed using a polar map divided according to the 17-segment model of the American Heart Association. The SUVmax of cardiac volume data, accumulation pattern on polar map, and wall motion on ECG-gated PET were measured and compared. **Results:** The average rate of SUVmax improvement from nongated PET on respiratory-gated PET and ECG-gated PET at ES and ED showed 4.0, 28.7 and 3.8%, respectively. Compared with non-gated PET, accumulation in respiratory-gated PET was more localized and shifted to the center of the polar map. Three patients with the high accumulation showed regional wall motion abnormalities in same segment. **Conclusion:** For a ^{18}F-FDG PET/CT scan for cardiac sarcoidosis, both respiratory-gated and ECG-gated PET/CT scans are recommend to localize regions of accumulation in the polar map and to detect the myocardial wall motion abnormalities. **References:** 1) Advanced imaging of cardiac sarcoidosis. Schatka I, Bengel FM. J Nucl Med. 2014 Jan;55(1):99-1062) Usefulness of respiratory-gated 18F-FDG PET/CT scan protocol in patients having positive myocardial 18F-FDG uptake. Watanabe S, Hanaoka K, et.al., Nucl Med Commun. 2019 Mar;40(3):235-241.

TEPS-76

Correlation of HPV status and biological parameters assessed in ^{18}F-FDG-PET/CT study in head and neck cancer patients

P. Cegla[1], *E. Majchrzak*[2], *R. Czepczynski*[3], *K. Pietrasz*[1], *A. Kaczmarek*[1], *W. Golusinski*[2];
[1]*Nuclear Medicine Department, Greater Poland Cancer Centre, Poznan, POLAND,* [2]*Department of Otolaryngology, Head and Neck Surgery and Oncology,Greater Poland Cancer Centre, Poznan, POLAND,* [3]*Department of Endocrinology, Metabolism and internal Medicine, Poznan University of Medical Science, Poznan, POLAND.*

Aim/Introduction: Head and neck cancer still remain a significant public health problem taking sixth place in the frequency of morbidity and mortality and they are a serious diagnostic problem both in Poland and worldwide. Despite

the newer treating methods many patients die because of the primary tumor resistance to treatment. PET/CT is a modern method of functional imaging, which enables the assessment of a variety of biological processes. HPV positive cancer are epidemiologically distinct from HPV negative. The aim of the study was to assess the influence of HPV infection on biological parameters obtained in ^{18}F-FDG-PET/CT study in patients with head and neck cancer. **Materials and Methods:** Retrospective analysis was performed on a group of 55 patients with newly diagnosed head and neck cancer. PET scans were acquired on Gemini TF PET/CT scanner 60min after IV injection of ^{18}F-FDG with the mean activity of 364±75 MBq, with the area being examined from calvaria to half way down the thigh. Several PET biological parameters in primary tumor include SUV_{max}, SUV_{mean}, TotalSUV, TLG and MTV were assessed and the correlation between HPV$^+$ and HPV$^-$ patients was checked. For statistical analysis T-test and Mann-Whitney test were used and the materiality level $p<0.05$ were considered significant. ROC curves were used to obtain best cut-off point between HVP$^+$ and HPV$^-$ patients in all assessed parameters. **Results:** HPV$^-$ patients showed higher values for all assessed parameters compared to HPV$^+$ group but without any statistically significant differences: for SUV_{max} 9.3±3.7 vs 8.5±3.3 (p=0.52), for SUV_{mean} 5.2±2.0 vs 4.8 vs 2.2 (p=0.47); for TotalSUV 1694.0±1948.7 vs 1141.5±1251.7 (p=0.36); for TLG 108.34±124.69 vs 73.06±80.11 (p=0.36); for MTV 20.30±25.86 vs 14.04±12.62 (p=0.42). The best cut-off value determining HPV$^+$ and HPV$^-$ patients for SUV_{max} was 9.7, for SUV_{mean} 4.4, for TotalSUV 3921.9, for TLG 251.00 and for MTV was 34.52. **Conclusion:** In this limited study we did not observe any statistically significant differences between HPV$^+$ and HPV$^-$ patients, however HPV$^-$ patients tend to show higher values for all assessed parameters which may be helpful in differentiation and diagnosis of patients with head and neck cancer. The best cut-off level was found and might be helpful to differentiate the high-risk HPV negativity subtypes from positivity. **References:** None.

TEPS-77

Parametric Whole Body FDG PET Scan: Just Do It!

H. Danielsen, *M. F. Pedersen, L. C. Gormsen, O. L. Munk;*
Aarhus University Hospital, Aarhus, DENMARK.

Aim/Introduction: Whole-body ^{18}FDG PET imaging (WB-PET) is routinely used for the assessment of malignant diseases based on standard uptake values (SUV) and requires that the patient lies still for 10-15 minutes. FlowMotion Multiparametric PET is a new dynamic WB-PET (DWB-PET) protocol introduced by Siemens that allows imaging of the rate of tracer uptake and apparent distribution volume, which are more quantitative measures than SUV. However, DWB-PET requires that the patient is injected in the scanner and remains still up to 70 minutes. This is a review of our experiences and recommendations for patient handling during DWB-PET. **Materials and Methods:** 35 patients were scanned in the Siemens Vision 600 PET/CT scanner. Patients with clear signs of tremors, pains, claustrophobia or nervous bladder were excluded. On arrival, we informed the patient about the entire procedure and stressed the importance of lying still during the extended scan. Patients were placed head first supine with arms along the body, a peripheral venous catheter (PVC) was placed and blood-glucose was measured. Positioning aids were carefully placed to make patients feel comfortable. The patient line (PAS) from the automated FDG-injector was coupled with the PVC. The examination involved a topogram, AC-CT, 6-minutes scan of the chest region started at tracer injection, and a series (9-12) WB-PET where the last WB-PET scan correspond to clinical routine WB-PET at 60 min p.i. **Results:** We found that image artifact could be reduced by optimizing the patient handling: 1) Hand movements led to pelvis artifacts, which could be minimized by instructing the patient to hold two small wedges; 2) Head movements were reduced with a special head-holder, a pillow and wedges on the side; 3) Effect of residual FDG in PAS was avoided by moving the PVC from the antecubital fossa to the dorsal side of the hand and by removing the PAS right after injection. For all scans, the AC-CT and DWB-PET were visually inspected for movement, and divided into two groups; Acceptable movement and non-acceptable movement for both head and hand. When comparing groups of patients with antecubital PVCs (N=17) with hand PVCs (N=18), we found a reduction in hand-movements from 29.4% to 17.6% resulting in less image artifacts. **Conclusion:** For extended-acquisition DWB-PET examinations, it is essential to allocate time to inform and position the patient and to use positioning aids to reduce movements and thus artifacts in the parametric image. **References:** None.

TEPS-78

18F-FDG PET/CT prone vs. supine

D. Boon, *C. de Haan;*
Dijklander ziekenhuis, Hoorn, NETHERLANDS.

Aim/Introduction: The aim of this study is to compare prone (hanging breasts) and supine acquired 18F-FDG PET/CT for visualisation of primary tumours and regional lymph nodes in breast cancer patients. The patients did not have prior surgery or any other treatment. **Materials and Methods:** Twenty-six patients were included from September 2018 to April 2019. All patiënts signed an informed consent form. One hour after injection of 150-250 MBq (depending on the bodyweight) 18F-FDG PET/CT was performed, primarily PET/CT images from orbitae to sinus pleurae were acquired in prone position, with the help of a breast-support board. Subsequently, a standard PET/CT in supine position from skull to knees was acquired. The scan time per bed position was three and a half minutes for both procedures. A nuclear medicine physician compared both scans to assess diagnostic differences. **Results:** Generally there is no difference in diagnosis between prone and supine, however some cases in prone position shows a better lesion detection because there is less compression of breast tissue. In 46,2% (n = 12) there is no difference between prone and supine. In 23% (n = 6) there is a improved view of the primary tumour, 15,4%

(n = 4) shows a better view of the lymph nodes and 7,7% (n = 2) a better view of the primary tumour and the lymph nodes. However, in 7,7% (n = 2) the nuclear medicine physician assesses the supine position as superior in lesion detection. **Conclusion:** Prone position PET/CT improves the visualization of the primary tumour and the number of detected axillary lymph nodes. Therefore, it is a valuable addition to standard supine PET/CT for locoregional assessment of breast cancer patients. **References:** S.C. Teixeira et all, Additional prone 18f-fdg pet/ct acquisition to improve the visualization of the primary tumour and regional lymph node metastases in stage ii /iii breast cancer. In: S.C. Teixeira; Breast cancer tailored staging using molecular imaging. University of Amsterdam; 2016: p. 43-59.

TEPS-79

The effect of image based motion correction on the HRRT scanner

R. B. Bertelsen, M. L. F. Schwartz;
Nuclear Medicine and PET, Skejby, DENMARK.

Aim/Introduction: The aim of this study is to uncover for how many patients it is necessary to use HRRT_users_software_1.2 for image based motion correction on the HRRT. The scanner has a high resolubility of 2.5 mm which can cause the smallest movement to affect the image quality. Most of the patients scanned on the HRRT are diagnosed with either Parkinson's disease (PD) or Alzheimer's disease (AD). Because of the side effects from those diseases it is difficult for the patients to lie completely still during the scan. **Materials and Methods:** To narrow down the data we have chosen to focus on patients from three different projects: Project1 involving PD patients and healthy individuals all experiencing REMsleep behavior disorder (RBD). The patients where scanned with ^{18}F-Dopafor 20 minutes. Project2 involving PD patients with or without RBD scanned for 90 minutesusing ^{11}C-Mener. Project3 wanted to exam the effect of ketones in the brain. The patientswhere scanned for 120 minutes using ^{18}F-FDGfor the last 60 minutes. The data was collected during the period May 2014 to March 2019. To map the movement of the patients we analyze the data with a Motion QC program, which is a part of HRRT_users_software_1.2. To determine if the images should be motion corrected we calculate the RMS displacement and maximum displacement. If the results exceed the determined references, we will make an image based motion correction using the Motion Correct program from the HRRT_users_software_1.2. **Results:** Project 1 showed that none of the patients had moved so much that an image based motion correction was necessary. Project 2 showed the need for motion correction in close to 18 % of the scanned patients. In project 3 we saw an even higher range of movement during the scans. It showed that 41 % of the scans needed to be motion corrected. **Conclusion:** The longer the patients has to lie in the scanner the harder it gets to stay completely still. Therefore the use of image based motion correction is justified for the long scans. Because the image based motion correction is a further image processing and it puts the results further from the original raw data, we recommend making the scans as short as possible. **References:** None.

TEPS-80

^{18}F-FDG PET/MR multiparametric measurement of head and neck cancer patients underwent modern 3D based radiotherapy - preliminary results

A. Kedves[1,2,3], Z. Tóth[4,5], T. Pintér[2], B. Sánta[1], Z. Cselik[6], V. Koczka[7], D. Sipos[1,5,2], F. Omar[5], G. Bajzik[2], J. Hadijev[2], I. Repa[2], M. Moizs[8], Á. Kovács[1,5];
[1]Department of Medical Imaging, Faculty of Health Sciences, University of Pécs, Kaposvár, HUNGARY, [2]Dr. József Baka Diagnostic, Radiation Oncology, Research and Teaching Center, "Moritz Kaposi" Teaching Hospital, Kaposvár, HUNGARY, [3]Department of Health Economics and Health Care Management, University of Pécs,, Pécs, HUNGARY, [4]PET Medicopus Nonprofit Ltd. "Moritz Kaposi" Teaching Hospital, Kaposvár, HUNGARY, [5]Doctoral School of Health Sciences, University of Pécs, Pécs, HUNGARY, [6]Oncoradiology, Csolnoky Ferenc County Hospital, Veszprém, HUNGARY, [7]Department of Health Promotion and Public Health, University of Pécs, Kaposvár, HUNGARY, [8]"Moritz Kaposi" Teaching Hospital, Kaposvár, HUNGARY.

Aim/Introduction: PET/MR imaging provides a unique opportunity to acquire structural, metabolic and functional data simultaneously. The purpose of this study was to assess the predictive value of multiparametric PET/MR imaging data in head and neck cancer patients treated with radiotherapy. **Materials and Methods:** Twenty patients with histopathologically proven head and neck squamous cell carcinoma (HNSCC) treated with modern 3D based radiotherapy in our institutions were enrolled in this retrospective survey. FDG PET/MR imaging was performed before and after the therapy for all the subjects. Pretreatment tumor SUVmax, SUL_{peak}, total lesion glycolysis (TLG), and metabolic tumor volume (MTV) PET parameters and diffusion-weighted MR based ADC_{mean} parameters were measured. According to the result of post-therapy imaging 2 patient subgroups were created: 1.: patients achieving complete response (CR) and 2: subjects with post-treatment viable tumor tissue (Non-CR). Pretreatment imaging parameters were correlated with therapy response. Statistics included Spearman's correlation and Mann-Whitney U test using SPSS 25 software. **Results:** After completion of radiotherapy, imaging showed complete response for 8 patients while metabolically active tumor tissue was observed in 12 cases. We were unable to find statistically significant difference between the pretreatment SUV_{max} (p=0,135), SUL_{peak} (p=0,343), TLG (p=0,135) and ADC_{mean} (p=0,734) values of CR and Non-CR patient groups, although pre-therapy MTV parameter proved to be significantly higher in Non-CR group (p=0,007). Between the evaluated pretreatment PET and MR parameters, a weak correlation was only observed for PET SUVmax and MR ADC_{mean} values (r= -0,346 p= 0,135). **Conclusion:** According to our preliminary results pretreatment PET SUV_{max}, SUL_{peak}, TLG and MR ADC_{mean} parameters were unable to predict therapeutic response, while MTV seems to be more

accurate for this purpose. Further examination with involving more patients to the study could be essential to validate these preliminary results. **References:** Wang, K., Mullins, B. T., Falchook, A. D., Lian, J., & He, K. (2017). Evaluation of PET/MRI for Tumor Volume Delineation for Head and Neck Cancer, Front. Oncol. 7 (January), 1-8. https://doi.org/10.3389/fonc.2017.00008Min M., Lee MT., Lin P., Holloway L., Wijesekera D., Gooneratne D. (2016), et al. Assessment of serial multi-parametric functional MRI (diffusion-weighted imaging and R2*) with 18F-FDG-PET in patients with head and neck cancer treated with radiation therapy. Br J Radiol 2016; 89: 20150530. https://doi.org/10.1259/bjr.20150530

TEPS-81

Comparison And Evaluation Of The Effectiveness Between Respiratory Gating Method Applying The Flow Mode And Additional Gated Method In PET/CT Scanning

D. Jang, *Y. Park, G. Lee, H. Cho;*
Seoul national university bundang hospital, Bundang-Gu, Seongnam-Si, Gyeonggi-Do, KOREA, REPUBLIC OF.

Aim/Introduction: The present study aimed at assessing the effectiveness of the respiratory gating method used in the flow mode and additional localized respiratory-gated imaging, which differ from the step and go method. **Materials and Methods:** Respiratory gated-imaging was performed in the flow mode for twenty patients with lung cancer (10 patients with stable signals and 10 patients with unstable signals), who underwent PET/CT scanning of the torso using Biograph mCT Flow PET/CT (Siemens, Germany) at Bundang Seoul University Hospital between June 2018 and September 2018. Additional images of the lungs were obtained by using the respiratory gating method. SUVmax, SUVmean, and Tumor Volume (cm^3) of non-gating images, gating images, and additional lung gating images were found with Syngo,bia (Siemens, Germany). A paired t-test was performed with GraphPad Prism6, and changes in the width of the amplitude range were compared between the two types of gating images. **Results:** The following results were obtained for all patients when the respiratory gating method was applied: $SUV_{max} = 9.43 \pm 3.93$, $SUV_{mean} = 1.77 \pm 0.89$, and Tumor Volume $= 4.17 \pm 2.41$ for the non-gating images, $SUV_{max} = 10.08 \pm 4.07$, $SUV_{mean} = 1.75 \pm 0.81$, and Tumor Volume $= 3.56 \pm 2.11$ for the gating images, and $SUV_{max} = 10.86 \pm 4.36$, $SUV_{mean} = 1.77 \pm 0.85$, Tumor Volume $= 3.36 \pm 1.98$ for the additional lung gating images. No statistically significant difference in the values of SUV_{mean} was found between the non-gating and gating images, and between the gating and lung gating images ($P>0.05$). A significant difference in the values of SUV_{max} and Tumor Volume were found between the aforementioned groups ($P<0.05$). The width of the amplitude range was smaller for lung gating images than gating images for 12 out of 20 patients (3 patients with stable signals, 9 patients with unstable signals). **Conclusion:** In PET/CT scanning using the respiratory gating method in the flow mode, any lesion movements caused by respiration are adjusted. In addition, the width of the amplitude range decreased according to the stability of respiration to a more significant degree in the additional lung gating images than the gating images. We found that gating images provide information that is more useful for diagnosis than the one provided by non-gating images. For patients with irregular signals, it may be helpful to perform localized scanning additionally if time allows. **References:** None.

TEPS-82

Technical acquisition modality of cerebral PET/CT images in patients with memory disorders

L. Pavanello, *F. Sciume, M. Cucca, D. Grigolato, M. Zuffante, E. Biggi, M. Ferdeghini;*
Azienda Ospedaliera Universitaria Integrata di Verona, Verona, ITALY.

Aim/Introduction: This study wants to evaluate the importance of acquisition modality images in patients with memory disorders using a method with dynamic frames imaging. **Materials and Methods:** 26 adults patients (14 men, 12 women, range: 55-72 years) were studied between February 2018 to March 2019. All the patients were administered with the same 18F-amyloid tracer and PET/CT Philips Gemini TF Big Bore was used for acquisition images. Head scan was performed at 90 minutes post-injection of 300 MBq 18F-amyloid tracer. Patients have been positioned supine with the head and neck relaxed in the special support, the scanner laser aligneed to the orbital-meatal and median sagittal planes, arms along the body and support under the knees to maintain greater stability and comfort. Brainstem and cerebellum must be understood in the fiel of view. The CT parameters were: 120 KV, 70 mAs pitch 0.813, 16x1.5mm collimation, thickness 5, FOV 600, the acquisition field from vertex to the base of the skull, rotation time 0.5 sec. PET images were acquired with 4 dynamic bed position, each acquisition was of 5 min/bed, start delay from bed of 5 sec, FOV 256 mm. **Results:** 3/26 patients were necessary to interrupt the examination due to patients limited collaboration. 1/3 patients repeat all the images scan because he moves during the first frame and 2/3 patients were possible elaborate images by removing final frames in which the patients had moved. In all other cases it was possible to merge the 4 frames and obtain a single 20 minute image. **Conclusion:** Dynamic acquisition technique with 4 frames makes it possible to reduce repeating the exam because images elaboration allows to exclude the final frames in cases patient may have moved the head. **References:** None.

TEPS-83

Caloric Restriction improves Established Proteinuria in Adriamycin-Induced Nephropathy:A N^{13}-ammonia PET study

J. W. A. Sijbesma[1], *A. van Waarde*[1], *A. Klooster*[2], *R. H. J. A. Slart*[1], *H. H. Boersma*[1], *R. A. J. O. Dierckx*[1], *H. van Goor*[3], *S. J. L. Bakker*[4];
[1]*NMMI, Groningen, NETHERLANDS,* [2]*Dept. of Pathology, Pathologie Friesland, Leeuwarden, NETHERLANDS,*
[3]*Pathology and Medical Biology, Groningen, NETHERLANDS,*
[4]*Nephrology, Groningen, NETHERLANDS.*

Aim/Introduction: Reduction of proteinuria is an important strategy to prevent loss of kidney function. Preclinical studies suggest that caloric restriction (CR), induced at a young age, protects against age-related proteinuria. We hypothesized that CR in established proteinuria reduces urinary protein excretion (UPE). The current study investigated the effect of CR in established renal disease using N^{13}-ammonia PET for kidney perfusion assessment. **Materials and Methods:** Male Wistar rats (n= 56; age 12± 2 week) were intravenously injected with 2.1mg/kg Adriamycin (doxorubicin) as a model with induced renal dysfunction. At 6 weeks after injection, baseline UPE was measured. Mean arterial blood pressure was determined followed by a 10 minute positron emission tomography (PET) scan with N^{13}-ammonia (45.3± 5.6MBq). At 7 weeks after Adriamycin injection rats were randomly assigned to 4 groups: An ad libitum (AL) and a CR group (60% of ad libitum food intake) fed with a 12% protein diet (12%AL, 12%CR) and an ad libitum and a CR group fed with a 20% protein diet (20%AL, 20%CR). All groups were treated for 12 weeks. UPE was measured at week 9 and 12. The blood pressure measurement and PET scan were repeated at the end of the study. PET scan was used to determine the mean standard uptake value (SUVmean) of N^{13}-ammonia in the cortical and medullar region. **Results:** At baseline UPE was similar in all groups ($p>0.20$) with a median value of 495 and an interquartile range of 127mg/24h. After 12 weeks of diet, all animals exposed to CR had a 20.3% lower UPE ($p=0.003$) compared to ad libitum fed animals. At week 9 this effect was only seen in the 12%CR group. SUVmean was significantly higher in the 12%CR group compared to the 12%AL group for the cortical ($p<0.001$) and medullar region ($p<0.05$) at the end of the study. Compared to baseline SUVmean was significantly increased in the 12%CR group in both regions ($p=0.001$). The opposite effect was seen in the 12%AL group where SUVmean was decreased. ($p<0.05$). Blood pressure in animals exposed to caloric restriction was 21.2% lower ($p<0.0001$) compared to AL fed animals. **Conclusion:** CR lowers UPE and blood pressure in rats with established proteinuria. Increasing SUV in the 12%CR group indicates improved kidney function on PET imaging. CR was most effective if applied in combination with protein restriction. These results may guide future intervention studies in patients with proteinuric and obesity-related nephropathy. **References:** None.

TEPS-84

Influence of intravenous diuretics on the detectability of local prostate cancer recurrence in ^{68}Ga-PSMA-11 PET/CT

L. Dijkstra, *I. Alberts, G. Prenosil, A. Rominger, A. Afshar-Oromieh;*
Nuclear Medicine Inselspital, Bern, SWITZERLAND.

Aim/Introduction: Generally, 68Ga-PSMA-PET/CT is performed at 1h post injection of radiotracer (p.i.). While numerous studies show that delayed imaging increases tumour detectability, increased bladder activity can make the detection of locally recurrent lesions more difficult. In this study, we investigate the effect of an examination protocol including oral hydration and diuretics, and determine the effect on tumour detection. **Materials and Methods:** This retrospective study evaluated 76 patients referred to our centre for 68Ga-PSMA-11 PET/CT. Our protocol was as follows: 30 min p.i. patients were given oral hydration with 1L of water, and at 1h p.i. 20mg of Furosemide was administered intravenously. Additional late imaging without further hydration or diuresis was performed at 2.5h p.i. Two physicians read the standard and late datasets in a blinded and un-blinded read to determine the detectability of locally recurrent lesions. **Results:** At standard imaging 40 lesions of locally recurrent PC were identified in 35 patients. At late imaging, 44 lesions were identified in 37 patients. In later imaging, the bladder activity (standardised uptake value) SUV was observed to increase. In four cases, the activity in the bladder at later imaging was seen to mask the PC lesions. Although these lesions also showed higher SUV at late imaging, the increase was seen to overlap with the bladder, explaining the reduced detectability. **Conclusion:** The addition of oral hydration and furosemide to our examination protocol resulted in increased detectability of PC lesions at standard imaging. In the late imaging, however the detectability decreases when no second injection of furosemide and water is given. Further studies are required to optimise the examination protocol of such patients. **References:** None.

TEPS-85

Tracer Uptake Of Hepatocellular Carcinoma In Psma Pet Is Associated With Arterial Phase Hyperenhancement In Mri

A. Kanzog, *L. Stegger, M. Schaefers, B. Noto;*
Department of Nuclear Medicine, Münster, GERMANY.

Aim/Introduction: To investigate if tracer uptake of hepatocellular carincoma lesions in PSMA-PET is associated with arterial phase hyperenhancement in MRI. **Materials and Methods:** 11 patients with proven hepatocellular carcinoma which underwent 68Ga-PSMA-PET/MRI from 06/2018 to 11/2019 in preparation for selective internal radiation therapy were enrolled. 2 MBq Ga-68-PSMA-11per kg body weight were injected. PET images were acquired over 40 minutes in one bed position of the upper abdomen beginning with injection. MRI sequences were acquired concurrently including multiphase contrast enhanced MRI. All liver lesions discernible on MRI with a

LI-RADS score ≥ 4 were considered HCC lesions and noted. HCC lesions were categorized as showing tracer uptake in PSMA-PET if they visually showed a focal tracer uptake unequivocally above background. HCC lesions were categorized as showing arterial phase hyperenhancement in MRI if they showed increased intensitiy in arterial phase images compared to native images and were unequivocally more intense than surrounding liver parenchyma in arterial phase images. Statistical analyses were performed using IBM® SPSS®, Version 24. Fisher's exact test was used to assess association of tracer uptake of lesions in PET and arterial phase hyperenhancement in MRI. **Results:** 25 lesions with a LI-RADS score ≥ 4 were detected and considered to represent HCC lesions. Of those 19 showed tracer uptake in PSMA-PET of which all also presented with arterial phase hyperenhancement in MRI. 6 lesions showed no tracer uptake in PSMA-PET of which only one presented with arterial phase hyperenhancement in MRI. Fisher's exact test showed a strong association of tracer uptake in PSMA-PET and arterial phase hyperenhancement in MRI ($p < 0.001$). **Conclusion:** Tracer uptake of hepatocellular carincoma lesions in PSMA-PET is strongly associated with arterial phase hyperenhancement in MRI. **References:** None.

TEPS-86

SUVmax in Organ Confined Prostate Cancer and Its Correlation with PSA level and Gleason Score. A Single Center Study

M. Khaskhali;
Sindh Institute of Urology and Transplantation, Karachi, PAKISTAN.

Aim/Introduction: The early management of Prostate Cancer is a challenging issue, for the appropriate tumor staging in newly diagnosed Prostate Cancer (PC). Prostate Specific Antigen and Gleason Score are considered to be major parameters for treatment planning. The novel radio tracer Ga-68 Prostate Specific Membrane Antigen (PSMA)-11 PET-CT shows increased metabolic activity in PC and provides reliable information about tumor grading. The increased metabolic activity of Ga-68 PSMA-11 is defined as Standardized Uptake Value (SUV)max. **Materials and Methods:** The retrospective analysis of 77 patients who were referred to department of Nuclear Medicine and Molecular Imaging for Ga-68 PSMA-11 PET-CT from September 2017 to February 2019. All of them had biopsy proven organ confined adenocarcinoma and their PSA level were obtained 4-5 weeks prior to Ga-68 PSMA PET-CT scan. **Results:** There were total 77 patients included in our study with mean age of 66.33 years having histologically proven Prostate cancer. The GS of all patients ranges from 6 to 10. The mean PSA for all patients was 37.24 ng/ml ranging from 1.2 to 239 ng/ml with a median value of 22 ng/ml. Mean SUVmax of all patients was 17.33±14.59 with a median of 14.03 ranging from 2.03 to 81.35. SUVmax in PC was higher in patients having PSA level more than 10 than those whose PSA level is <10. Correlation of SUVmax with PSA and GS showed significant correlation (rSpearman 0.306 & 0.367) having p-value 0.01. **Conclusion:** The SUVmax of organ confined tumor correlates well with PSA level and Gleason Score. The intensity of focal radiotracer activity clearly differentiates disease site from healthy part of organ and can be a reliable guide for needle biopsy. We also found that median SUVmax and median PSA values increase with increasing GS. So we recommend that PSMA PET-CT can be performed in cases of organ confined tumors with GS of 6 and PSA level of <10 also as they show significant radiotracer uptake in tumor. **References:** None.

TEPS-87

The addition of late PSMA-ligand PET/CT imaging for the differentiation between benign and malignant PSMA uptake

L. Dijkstra*, I. Alberts, G. Prenosil, A. Rominger, A. Afshar-Oromieh;*
Nuclear Medicine Inselspital, Bern, SWITZERLAND.

Aim/Introduction: PSMA ligand PET/CT has commonly been performed at 1h post injection of radiotracer. However, additional late imaging has been shown to be a powerful method for the discrimination between lesions of prostate cancer (PC) and non-PC lesions, such as nerve ganglia. Nevertheless, there are no pre-existing studies which show the pattern of tracer uptake at late imaging, which this present study aims to address. **Materials and Methods:** 50 patients were retrospectively analysed who underwent standard (1.5h) and late (2.5h p.i.) ^{68}Ga-PSMA-11-PET/CT. Lesions with tracer uptake greater than background as well as PC-lesions were identified by two physicians in an unblinded consensus read of both sets of imaging. The localisation and standardised uptake values (SUV) for the lesions was noted. A thin-slice CT enabled the morphological characterisation of the lesions as ganglia, bone metastases, locally recurrent PC lesions or lymph node metastases. **Results:** We identified 82 PSMA-positive ganglia at standard imaging (1.5h p.i.) in 70% of our patients with an additional four ganglia being revealed at late imaging only (total 86). We identified 66 PC lesions in 44 patients (88%). Of these, we identified 45% (n=30) as lymph nodes. At late scanning, 73% of the LN exhibited an increase in SUVmax, whereas only 65% of the ganglia exhibited a decreasing or stable SUVmax. **Conclusion:** We noted that at late imaging, increasing tracer uptake provides additional diagnostic information aboutn the likelihood of malignancy. However, increasing SUVmax alone cannot reliably differentiate between LN and ganglia, since 35% of ganglia also exhibited increasing SUVmax. Reliance on these values alone therefore is a potential diagnostic pitfall, and we draw attention to our thin slice CT protocol which allowed for better morphological characterisation of ganglia. **References:** None.

TEPS-88

Correlative assessment of lumbar intervertebral disc degeneration in alkaptonuria patients using quantitative analysis in 18F-NaF PET/CT and MRI grading systems

E. H. Alawadhi[1]*, A. Mistry*[2]*, S. Vinjamuri*[3]*, J. Gallagher*[1]*, R.*

Lakshminarayan[4], *J. Dillon*[1];
[1]*Institute of Ageing & Chronic Disease, University of Liverpool, Liverpool, UNITED KINGDOM,* [2]*Department of Radiology, Royal Liverpool and Broadgreen University Hospitals, Liverpool, UNITED KINGDOM,* [3]*Department of Nuclear Medicine Royal Liverpool University Hospital, Liverpool, UNITED KINGDOM,* [4]*Liverpool Clinical Laboratories, Royal Liverpool & Broadgreen University Hospitals Trust, Liverpool, UNITED KINGDOM.*

Aim/Introduction: Alkaptonuria (AKU) is a metabolic bone disease characterised by elevated homogentisic acid (HGA). Over time HGA deposits in connective tissue forming cartilage pigmentation leading to advanced premature arthritis. Quantitative and qualitative assessment from 18F-NaF-PET/CT and MRI can be used to evaluate lumbar intervertebral disc degeneration in AKU patients. The aim of this study was to evaluate the relationships between the 18F-fluoride uptake from PET/CT and morphological MRI data by measuring maximum standardised uptake value (SUV_{max}) and Pfirrmann grading systems at lumbar intervertebral discs and assess the effect of gender and age on these values. **Materials and Methods:** A total of 203 lumbar discovertebral units (DVUs) from 34 AKU patients (19 men,15 female) who underwent whole body 18F-NaF PET/CT and MRI were analysed. Mean age of subjects was 48.38 ± 10.04 years, with no age difference between genders. Subjects were separated into four groups stratified by decade of life. Image viewing and analysis software HOROS was used. The ROI were drawn over the lumbar DVUs on three sagittal CT slices covering the disc plus endplate of the two adjacent vertebrae, from segment T12/L1 to segment L5/S1, then correlated to PET images in order to measure the SUV_{max}. Lumbar disc degeneration was assessed from MRI using 8 level validated modified Pfirrmann grading system. The measured values were compared with each other. The effect of gender and age for SUV_{max} and Pfirrmann score was tested. **Results:** Lumbar disc spaces were more likely to be degenerative when SUVmax and Pfirrmann score for DVU were higher. There was a correlation between SUVmax and Pfirrmann scores at all lumbar DVU levels ($p < 0.05$) except at L2/L3. However several cases showed that despite an advanced grade 8 Pfirrman score there was decreased 18F-NaF uptake. Female subjects had lower SUV_{max} values and Pfirrmann scores than male subjects. Although SUV_{max} for all DVU showed no correlation with age ($p > 0.1$), there were significant correlations between Pfirrmann score and age ($p < 0.0001$). **Conclusion:** Lumbar intervertebral disc degeneration of patients with ochronotic arthropathy was associated with increased 18F-fluoride uptake on PET and high Pfirrmann score on MRI. Several advanced grade 8 Pfirrman score discs showed little corresponding SUV_{max} on PET/CT. These cases were more likely to have fusion at the interbody level with inactive calcification. This study demonstrates the correlation between functional PET and anatomical MRI findings until intervertebral disc fusion occurs in ochronotic patients. **References:** None.

TEPS-89

Relationship between standardised uptake values, Hounsfield Units and bone density value of vertebral body in the lumbar spine: a study in alkaptonuria subjects using 18 F-NaF PET/CT and DEXA scan

E. H. Alawadhi[1], *S. Vinjamuri*[2], *J. Gallagher*[1], *R. Lakshminarayan*[3], *J. Dillon*[1];
[1]*Institute of Ageing & Chronic Disease, University of Liverpool, Liverpool, UNITED KINGDOM,* [2]*Department of Nuclear Medicine Royal Liverpool University Hospital, Liverpool, UNITED KINGDOM,* [3]*Liverpool Clinical Laboratories, Royal Liverpool & Broadgreen University Hospitals Trust, Liverpool, UNITED KINGDOM.*

Aim/Introduction: Alkaptonuria (AKU) or black bone disease is a metabolic bone disease characterised by elevated homogentisic acid (HGA), which causes severe osteoarthropathy. An abnormal active bone lesion in the spine can be evaluated by 18F-NaF PET/CT. This study aimed to clarify the differences in 18F-NaF uptake and bone attenuation coefficients according to the bone densitometry reports at the lumbar spine levels (L1-L4) using semi-quantitative maximum standardised uptake values (SUVmax) and Hounsfield Units (HU) from PET/CT images. **Materials and Methods:** We analysed the data of 38 patients with alkaptonuria (mean age ± SD, 50.3 ± 10.9) who underwent 18FNaF PET/CT and DEXA scans. To evaluate the relationship between the distribution of sodium fluoride (18F-NaF) uptake and bone density values, SUVmax from PET, mean HU from CT and T-score from DEXA of lumbar vertebrae body were compared. In order to determine HU for each lumbar vertebra body (L1-L4), ROI was drawn covering the trabecular bone region in the sagittal slice section at three different anatomical locations. The exact ROI was copied to PET images to measure the SUVmax. The average HU and SUVmax for each lumbar level were generated. **Results:** According to the DEXA report, thirty-one patients (75.6%) of the 38 AKU patients had a normal bone mineral density at the average lumbar vertebral body (L1-L4), noting that mean SUVmax value measured from PET was 12.22 ± 38.9 and mean HU measured from CT was 159.1 ± 82.7. Five patients (12.2%) had osteopenia, with measured SUVmax of 11.54 ± 3.9 and mean HU of 99.6 ± 38.9. Only one patient (2.4%) had osteoporosis at lumbar spine with SUVmax 9.99 and mean HU 18.2. There was a moderate correlation between SUVmax and T-score at upper lumbar vertebral bodies (L1 and L2) $p < 0.05$, and no clear correlation at L3 and L4 ($p = 0.67$ and 0.63). A strong relationship was noted between HU and T-score at all lumbar vertebral bodies ($p < 0.001$). SUVmax at lumbar vertebral bodies proportionally increases at the higher values of vertebral HU. These observations were more significant in L1 and L2 and less so at L3 and L4. **Conclusion:** Lower bone mineral density at the lumbar spine was associated with decreased 18F-NaF uptake in PET imags and less bone attenuation coefficients in CT images. Radiographic quantitative methods from 18F-NaF PET/CT can highlight areas of higher bone metabolism and give structural information in AKU patients. **References:** None

AUTHORS INDEX

EUROPEAN ASSOCIATION OF NUCLEAR MEDICINE

20

FOCUSMEETING.EANM.ORG

EANM FOCUS 3

MOLECULAR IMAGING AND THERANOSTICS IN NEUROENDOCRINE TUMOURS

ATHENS, GREECE

JAN 30 - FEB 01, 2020

EANM® European Association of Nuclear Medicine

BIOMEDICAL IMAGING AND THERAPY FOR PERSONALIZED HEALTHCARE

ESMIT

European School of Multimodality Imaging and Therapy

Level 1

Educate yourself online!

No Limits, Full Education

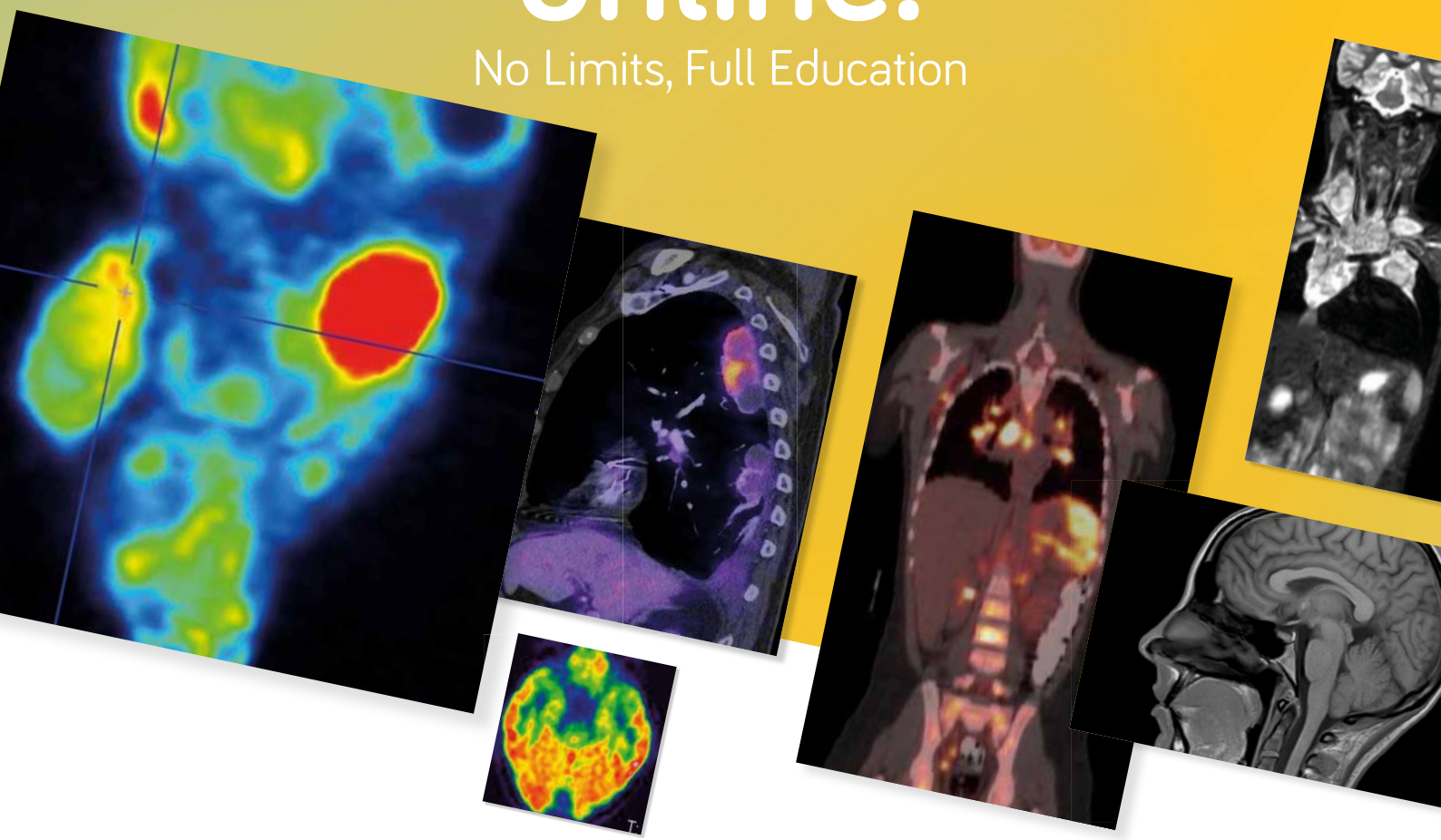

Recorded Sessions

Webinars

Preparatory eTeachings

e-Poster Area

Corporate Educational Platform

elearning.eanm.org